DFI-EFFC

GEOTECHNICS REIMAGINED

International Conference on Deep Foundations and Ground Improvement

The Bruges Meeting & Convention Centre

Proceedings



MAY 21-23

2025

BRUGES, BELGIUM

dfi-events.org/dfi-effc25

DOI: 10.37308/DFIEFFC.2025

Invited Lectures

Response of Pile Groups to Applied Load And General Subsistence Per the Unified Method and US Vs. EU Codes
Bengt H. Fellenius 1

Revolutionizing Foundations: Advances In Thermo Active Piling Engineering
Lyesse Laloui, Lausanne, Elena Ravera, Alessandro F. Rotta Loria 19

The Second Generation of Eurocode 7 – A Modern Basis For The Design of Piled Foundations and Ground Improvement
Christian Moormann, University of Stuttgart 1076

Digitisation, Monitoring and Data Analysis

Low-Strain Impact Testing of Piles – AI Analysis
Joram.M. Amir, Erez .l. Amir, Gil Amihai 29

The Embodied Carbon of Continuous Flight Auger, Auger Displacement (CHD) And Precast Driven Displacement Piles in Cohesive Ground
Jon Ball, Faye Dandy, James Cowburn 37

Novel Analytical Methods for Predicting the Response of Bored Piles in Sand
Raffaele Cesaro, Raffaele Di Laora, Alessandro Mandolini 44

Deep Learning Algorithms for The Monitoring and Control of Drilling and Grouting Works
Andrea Danzi, Giuseppe Di-Salvo, Alberto Flor, Raffaella Granata 54

A Semi-Analytical Model for Elastic Settlements of End-Bearing Piles in Inhomogeneous Soils
Armando Della Corte, Aggelos Tsikas, Stijn François, George Anoyatis 66

Thermal Integrity Testing; New Scenarios and Methods
Anthony Fisher, Qianchen Sun, Chris Barker 74

Comparing Thermal Integrity Test Data With as -Built Conditions
Fiona E. Hughes, Robert Jackson, Peter Ingram 84

Towards Axial Capacity Predictions Through MWD Data: What Can We Learn From Installation Efforts of Drilled Displacement Piles
Anne Lemnitzer, Genesis Figueroa, Morgan NeSmith 94

The Practical Challenges of Processing Measuring-While-Drilling (MWD) Data and Correlation Study With Grouting Data
Mehdi Mahmoudysepehr, Sandro Gomes, Sandra Coelho 104

Thermal Integrity Profiling of Deep Foundations
Nasser Massoudi 111

Investigating The Unseen Flow of Concrete in Deep Foundation Construction
Thomas Mitchell, Chris Barker, Christopher Wilkes, Chenfeng Li 123

Qualified Pile Load Testing Campaigns as a Key Aspect for the Sustainable Design of Piled Foundations For Infrastructure Projects
Christian Moormann, Axel Ruiken, Olaf Stahlhut 134

The Impact of Long Opening Times on Shaft Friction in Cohesive Soil
Duncan Nicholson, João Ferreira, Anton Pillai, Xiangbo Qiu 147

Incorporating Distributed Fibre Optic Sensing and Machine Learning into Dry Deep Mixing
Stefan Ritter, Sølve Hov, Priscilla Paniagua 163

Evaluation of Vibration Measurement in Jet Grouted Elements
Nikolaus Schneider, Elisa Kant 173

A Case Study of Utilising Digitalisation Techniques to Achieve Efficiency and Carbon Benefits During Piling Projects
Ian Chong, Michael Trubshaw, Kalisha Sejpar, Sofia Michelaki 183

3D Ground Model Neder-Betuwe Levee Reinforcement Project in the Netherlands
N.S. Walrave, M. Hop, J. van der Kop, K.M. Hermann, A. Haile, E. Ünal, J.W.T.A. Schuringa 192

Digital Measurement Technology In Foundation Works / In-Process Monitoring to Ensure Quality
Patrik Wenzl 202

Embracing Sustainability Through Materials And Equipment

Undertaking A Life Cycle Assessment to Calculate the Environmental Footprint of Repurposed Secondary Market Steel Tubulars for Foundations
Bill Baillie, Robert W. J. Holdway, Mark P. Dowling 209

Doubling Sustainability of Concrete Foundation Piles Through Enlarged Bases and Screw-In Displacement Methods
Przemyslaw A. Zakrzewski, Stephen Buttling 219

The Tremie Guide – About Concrete Performance and Sustainability
Rabea Barhum, Karsten Beckhaus, Chris Harnan 228

Investigation, Trial and Use of Cem Vi (C Vi) Concrete for A Sustainable Deep Foundation Future
Chris Barker, Fragkoulis Kanavaris, Titusz Tomor, Jonathan Ly 238

Evaluating Environmental Impacts of Deep Foundations: A Life Cycle Approach for Sustainability
André V. A. Borgatto, Guilherme A. F. Silva, Belmira Neto, Castorina S. Vieira 250

Comparative Analysis of Carbon Footprint Between Pile Foundation Type: A Perspective on the Construction Procedure
Ricardo B. Born, Luis F. P. Sales, Renan E. Cordeiro, Marcus V. A. Belloli, Gabriel M. Corrêa 260

Limestone Filler Implementation in Geotechnical Concrete Mixes
Hugo Chapin, Christophe Justino, Sivilay Sayavong 270

Comparison of Propagation Efficiency Between Tube-A-Manachette and Multi-Strainer Chemical Grouting Methods In Granular Soils
S.-H. Cheng, Ricky K.-N. Wong, Isaac T.-Y. Wong, H.-W. Cheng, K. Imakura, H.-M Huang 279

Simplified Circularity Assessment Model for Soil Mixing Applications
Brian J Freilich, Kimberly K Martin 287

Pile Group Settlement Analysis for Weak Rock Foundation Sockets Designed Using a Modified Correlation Factor
Sujatha Manoj, Harry G Poulos 298

The Application of CO_2-Fixed Recycled Fine Aggregate as Filler of Sand Compaction Piles
Sho Nishiie, Takao Kono, Ryohei Ishikura, Adel Alowaisy 308

Influence of Anchoring Systems and Their Manufacturing Processes and High-Strength Steels On CO_2 Reduction
Andreas Schiller 314

A Look into the Future of Self-Hardening Slurries in A De-Carbonizing World
Gilbert R. Tallard, Gregory E. Thomas 325

The Innovation of a New Pile System to Reduce Environmental Impacts: The Prefabricated Concrete Screw Pile
Peter Wardinghus, Paul M. Wiltcher, Jakob T. Udengaard, Søren D. Otte 333

Towards Sustainable Ground Improvement: A Life Cycle Assessment of Stone Columns and Dry Soil Mixing In Norwegian Clays
Nejla Y.H., Simon O., Robert T., Vincent W. 344

Impact of Deep Foundation Works on Urban or Natural Environments

Coordination of Complex Geotechnical Works at A Tideway Site in Central London
Sophie Vicard, Sivilay Sayavong, Adrian Bugea, Vasileios Papastathis, David Kwong 354

Analysis of the Lateral Pressure of Wet Concrete on Neighboring Foundations
Amira Chouikh, Stéphane Guérineau, Cristophe Justino, Maxime Fonty 364

Dewatering With Artificial Recharge for the Construction of A Multifunctional Complex
Nicolas Denies, Griet Goossens, Bert Creve, Eric Leemans 376

Serviceability Limit State Design: Base Response of Screw Injection Piles
Kevin J. Duffy, Ken G. Gavin 386

The Role of Mechanized Shaft Sinking with VSM In Inner-City Applications
Stefan Frey, Julian Binder 394

First Experiences of a New Generation of Trench Cutter – Contributing to Reducing Carbon Emissions
Franz-Werner Gerressen, Alexander Blatt, Joao Nunes 403

Remedial Works to Arrest the Differential Settlement of Foundations of Sabic Building
Haytham T. S. Hamdan 411

Removeable Ground Anchors Using Pyrotechnics – Innovative, Sustainable and Safe
Florian Hude 421

Field Measurement of Airborne Noise Emission During Impact Piledriving on Land and The Effect of Reduced Stiffness at The Impact Interface
Maarten in ‘t Veld, Jort van Wijk 432

Support Fluids for Piling in Urban Areas: Preparation, Operation and Specification
Stephan A. Jefferis, Chris Barker, Daniel P. McNamara, Brian B. Sheil 442

Reimagining Foundation Design in The Electric Power Transmission Industry
Peter Kandaris, Prasad Yenumula 456

Design Oosterweel Link with Preservation of a Historically Protected Building Samga Silo A
Bart Rombauts, Ramses Verachtert 468

Elephant And Castle Town Centre Development - Engineering Within the Harwich Formation In Close Proximity to Tunnels
Tony P. Suckling, Sajjad R. Peima 478
Innovative Applications of Shoring Techniques for Deep Excavation in Downtown San Francisco
Sam Yao, M. Ali Naeem 488

New Developments in Deep Foundations and Special Applications

Comparing Theoretical Predictions and Guidelines Against Pile Test Data for CFA Piles in Glauconitic Sands in Belgium
Grégoire, Olgu Orakci, Hannes Claes, Hanne Vanhaekendover, George Anoyatis 498

Re-Evaluation of The Design During Construction with Monitoring Data and Utilization of The Observational Method in Shoring Works
Cihat A, Önder A. Nuray İ. Ç. Canberk A Numan V. 509

Bored Piles in Rock: Recent Design Lessons Learned
Paul Axtell 518

Pile Load Testing and Data Collection Advances in The Last Ten Years and The Case for Design Optimisation
Zoe Baldwin, Anthony Fisher 528

Execution of Bored Piles Under Polymer Fluid Support – Sustainable and Flexible Concept for A Mega Project
Rabea Barhum, Rowena Verst, Karsten Beckhaus 538

Acceptance Criteria to Optimize the Foundation Design and Installation
Marcel W. Bielefeld , Eelco van der Sloot, Rob F. van Dorp 547

Optimizing Foundations Based on CSM Panels Using Rapid Load
Marcel W. Bielefeld, Rob F. van Dorp, Jurgen Houben, Oskar H.J. de Kok, Frits Huijbrechts 560

Assessment And Mitigation of Crosshole Sonic Logging Anomalies In Large Diameter Bored Piles
Patrick Casey, Chris Barker 569

Piling For Solar Farms
John R. Davie, José L.M. Clemente 580

Deep Foundations Difficulties Solved by Customized Grouting
Russell J. Denny, David Martel 590

Barrette Bi-Directional Preliminary Load Test Up To 148750 KN
Federico Fanti, Claudio as ioli Davide Benvenuto 600

Foundation Architecture: A New Approach for Realizing Infrastructure from The Ground Up
Boyoung Yoon, Morgan NeSmith, Anna C. Frost, J. David Frost 608

Deep Mixing Method for Stabilization of Coal Combustion Residual Material
Raffaella Granata Lorenzo Faedi Mohamed Elgouhary 617

Threaded Displacement Piles – A Comparison with Continuous Flight Auger Piles in Cork, Ireland
David Hard Kevin McDonnell 628

Bearing Capacity of Pile Groups Under Generalized Loading Condition
Raffaele Di Laora Raffaele Cesaro, Chiara Iodice, Maria Iovino, Luca de Sanctis, Alessandro Mandolini 636

The EFFC/DFI Support Fluid Task Group Field Research Study
Christophe Justino Chris Harnan 645

Evaluation of Slump Flow and Slump Flow Velocity Test Method for Deep Foundation Concrete
Christophe Justino 654

High Modulus Walls in Updated En 12063
Antti J. Perala 664

PIV Analysis of The Ground Behavior at Pile Tip by Vertical Load Test of Model Piles with And Without Expanded Bottom as A Variable
Kazuto K. Author Shuichi S., Yasuhiro G., Toshiaki A., Kenta K. 674

Investigation of Soil Reaction Curves Extracted from 3D FE Models.
A. Kheffache, B. Stuyts 686

Lessons Learnt from Back-Analysis of Offshore Monopile Lateral Response
Bruno Stuyts, Wout Weijtjens, Christof Devriendt, Carlos Sastre Jurado 695

Field Investigation on The Characteristics of Clayey Soil Close to Diaphragm Walls
Diethard König Duncan Nicholson, Rowena Verst, Chris Harnan 704

Systematic Laboratory and Field Investigations on the Soil-Concrete Interface of Diaphragm Walls and Bored Piles with Focus on The Influence of Wall Roughness
Rowena Verst, Diethard König, Jiarui Du, Achim von Blumenthal, Matthias Pulsfort, Torsten Wichtmann 715

Performance And Load Distribution in Stabilized Soil as Support for An Excavation in Marine Clay
Marit S. Løyland, Egil J. Monsås, Anders G. Nore, Ana P. Paniagua 727

Cpt Based Design Method for Horizontal Capacity of Piles Installed by The Rotary Cutting Press-In Method
S.M.K. Pasha, Y. Ishihara, M. Eguchi, Y. Toda 736

New Concepts for Sustainable Application of Deep Vibratory Compaction
K. Rainer Massarsch 747

Enhancements to the Coupled Hydro-Mechanical Hypoplastic Model for Unsaturated Soils
Shanujah Mathuranayagam, William Fuentes, Samanthika Liyanapathirana 765

Base Capacity Design for Piles in Extremely Weak to Very Weak Mercia Mudstone
Hiram M. Goncalves, Michael Vance, Sarah Pye, Imran Farooq 774

Displacement Pile Group Efficiency Assessment for a Technically and Economically Sustainable Design of Pile Groups in Non-Cohesive Soil
Felix Mitlmeier, Christian Moormann 784

Micropiled Precast Foundation Design for Transmission Line Projects in Australia
Bora Okumusoglu**,** Joaquin Sanchez, Robin Zeybek, Dr Matthew Sentry, Carel Nagel, Pablo Alvarez 794

Review of CPT Direct Design Methods for Driven Cast-In-Situ Pile Capacity Using Instrumented Pile Load Tests to Failure
Megan Packer 809

State of Practice for Quality Control in Drilled Foundations
George Piscsalko, Dr.-Ing, Jon Sinnreich 821
Incorporating Cyclic Degradation into Pile Design for the Gull Wing Bridge, Lowestoft
Scott A Reid, Paul J R Morrison, Cameron J Hughes 837

How Embracing Engineering Challenges Unlocked the Reduction in Embedded Carbon at The Sstc3 Soil Nailing Project
Ash Rogers, Cerys Orriss 847

The Second Edition of the EFFC/DFI Guide to Working Platforms – Design Aspects
Moritz Schleeh, Christian Moormann, Christian Moormann, James De Waele 857

Measurement of Pile Set and Impact Velocity for Driven Pile Acceptance
Julian P. Seidel, Hossein A. Ahmadi 868

Design Optimization with Bi-Directional Push-Out Load Tests of Bored Piles in Angola
Alberto Silva, Porto, Dr. Melvin England, Fugro, Wallingford, Maarten Profittlich, Fugro, Leidschendam 877

Numerical Simulation of Ground Improvement using Stone Column in Silts
Shivangi Singh, Ashwathy MS 887

Installation of Precast Reinforced Concrete Piles as Part of The Expansion of Existing Industrial Buildings and Technical Infrastructure
Filip Sokołowski 897

Comparison Analysis of Pile-Supported Lumped Mass and Actual Buildings Under Dynamic Loadings
Sangseom Jeong, Sumin Song 909

Modeling of vibrations induced by Mecca-Medinah high-speed train and earthquake mitigation analysis
Ahmed M. Taha, Ikrema A. Hassan, Farid Rehimi, Abdulrahman Yussef, Talal Merghelani, Hany El Naggar 917

Method For Evaluating the In-Plane Shear Strength of Wall-Type Ground Improvement With H-Steel Installation
Takao Kono, Yuki Kageyama, Jun Hamada 927

Self-Hardening Slurry Filtration Test and The End of The Api Test Dead End
Gilbert R. Gregory E 937

CPT-based Analysis on Vertical and Lateral Capacity of Steel Sheet Piles Installed by the Press-in with Auger
Tamboura H.H., Ishihara Y., Eguchi M., Mori, A. 947

Reducing The Carbon Footprint of Pile Construction: The Impact of Innovative Technologies
Mario A. Terceros H., Mario Terceros Arce; Walter Paniagua Paniagua, Antonio Marinucci 957

Context And Challenges of Deep Foundations in Urban Environments: A Case Study
Adrien Dumont, Grégory Laurent, Thomas Wulleman 967

Reinventing our Business and Contractual Environment

Development And Implementation of An Ai-Backed Human Detection Safety System for Piling Rigs and Cranes
Andrew Bell, David Fowle, Jason Dobson 976

The Use of The Enviro-Wall-Mat Combination in Soft Soil Conditions for Marshalling Areas, Crane Hard Stands and Lay Down Areas
J.W.R. Brouwer, H.W.H. Engelen 986

Bridging Physical and Digital Realms: The Role of Digital Twins in Geotechnical Engineering
Dr. Ehsan Moradabadi 993

How Geotechnics Can Speed Up Decarbonisation with The Help of Clients
Paul Vidil, Soletanche Bachy, Rueil-Malmaison 1013

Engineering People Centric Sustainability
S Briggs-North, Head of Human Resource 1020

Re-Using & Strengthening Existing Foundations

Pile Capacity Testing for Reusing the Existing Foundation
Marcel W. Bielefeld 1026

The Reuse Potential and Sustainability of Locally Reclaimed Sand in Levees
K.M. Hermann, Fugro 1036

Risk Sharing

Design Versus Load Testing: A Case Study On 127 Load Tests
Henri de Chaunac, Fondytest, Brussels, Joachim Clabau, Thomas Wulleman 1044

Modelling The Impacts of Climate Change on Geotechnical Companies
Luke R, Alexander Bridge, Isis Bliah, Sillion 1056

The Mayor and the Geotechnical Engineer – Challenges Obtaining Approval For Use of Alternative Fill Materials to Accommodate Sea Level Rise in the City of San Francisco
Lori A., Scott A. Walker, PE, GE 1066

RESPONSE OF PILE GROUPS TO APPLIED LOAD AND GENERAL SUBSISTENCE PER THE UNIFIED METHOD AND US vs. EU CODES

Bengt H. Fellenius, Dr. Tech., Sidney, BC, Canada

ABSTRACT

The forthcoming update of the US AASHTO Specs will agree with the Canadian building code and the US Corps of Engineers code in regard to the analysis and design of piled foundations. Case histories on observations on full-scale piled rafts are reviewed and show that the response of interior and perimeter piles differ. Single piles and perimeter piles engage the soil from the ground downward. In contrast, interior piles engage the soil from the pile toe level upward. Interior piles and soil have strain compatibility, which determines the distribution of load between the piles, the raft contact stress, and the load-transfer movement. Particularly so in subsiding environment, because perimeter piles are subjected to downdrag and drag forces, while neither downdrag nor drag force will affect the interior piles to any appreciable degree. The difference will affect the load distribution and bending moment response across the raft, which is also governed by the degree of rigidity of the raft and by the difference in dishing at the pile toe level and in the dishing of the actual raft. Contact stress under the raft, be it large or small, is incidental to the response of a piled foundation and cannot be considered to reduce the effect of the load applied to the foundation.

Keywords: piles, settlement downdrag drag force, codes

INTRODUCTION

For the last several decades, the North American codes addressing pile foundations have shown a bewildering variety. Some are stuck to the old system of determining an "allowable load" from dividing the pile "capacity"—determined by a test or calculation—by a factor of safety, in effect, declaring that "if the capacity is good enough, then, the settlement is good, too". That some codes incorporate load-and-resistance-factor-design and, as a few do, add some serviceability factors, changes nothing. Plainly, a design aiming for a satisfactory ratio (factor of safety or resistance factor) between the sustained load and a perceived "capacity" does not necessarily establish a safe condition. The "capacity"-plus-factor approach is particularly inadequate where settlement additional to that from the supported structure is caused, for example, by fills, excavations, site subsidence etc.

Through the years, the perceived adverse effect of soil settling in relation to the piles accumulating to drag force was simply addressed by adding the drag force to the load from the supported structure, subtracting it from the "capacity", and requiring that the reduced "capacity" pile be "safely" larger in order for it to accept this load. This is the approach taken by the Eurocode, which still adds drag force to the load from the structure. However, starting in the 1960s, numerous full-scale studies of the phenomenon of negative skin friction developing drag force have been conducted showing that the mentioned approach to incorporating drag force (and downdrag) is invalid, indeed, very costly, and yet not always resulting in a safe foundation. This was recognized in the Ontario Highway Bridge Design Code 1992 (which in 2002 developed into Canadian Highway Bridge Design Code for Foundation, CSA-S6-06). The 1992 Ontario code recognized drag force as an environmental force only of importance for the pile axial strength and inconsequential for the geotechnical response of a pile. In 2012, the US Army Corp of Engineers, Design Guidelines stated that the drag force "*does not decrease the bearing capacity (geotechnical capacity) of the pile*". In contrast, the AASHTO Specs continued to add the drag force to the sustained load included the statement (terms adjusted): "*pile resistance available to support structure loads plus drag force shall be estimated by considering only the positive side and toe resistance below the lowest layer contributing to downdrag*". This unfortunate clause is applied in the US not just to the design of foundations for highway structures, but also to foundations for buildings and other structures. Regrettably, it is frequently applied also in Canada and Mexico.

 © DFI International Bruges 2025

The North-American situation has not been favorable to economical and safe piled foundation. To resolve the issues, the US Federal Highway Association, FHWA, established a committee to review the current design of a piled foundation in settling ground and propose a more rational approach. In 2024, the committee delivered an NCHRP report (Coffman et al. 2024), which, by the end of 2025, will be officially incorporated in the next edition of the AASHTO Specs. The main thrust of the NCHRP Report was to approach the long-term response of a pile to load and general subsidence and bring it closer to the codes of Canada and the US Corps of Engineers.

The NCHRP Report offers two methods, called Method 1 and Method 2 for the analysis of single piles. Both apply the unified method for pile analysis and design (Fellenius 1984; 1988, 2004). Method 1 accepts a simplified plastic ("ultimate") soil response for the pile shaft and pile toe resistances. Method 2 incorporates the shear-movement response of the pile shaft and pile toe resistances, so-called t-z and q-z functions. The following introduces the unified method as applied to single piles and to piled foundations comprising pile groups.

SINGLE PILES
t-z/q-z functions

The precursor to a settlement analysis of a pile is determining the movement of the pile due to an applied load and the associated distribution of axial force in the pile, making use of the available information on the pile, the soil, and, as is often needed, the results of an instrumented static loading test. A pile responds to applied load by moving a small distance, which generates shaft resistance and, when the applied load is sufficiently large, also toe resistance. Figure 1 shows six typical functions, describing the shaft and toe resistances vs. movement, called t-z and q-z functions, respectively. The functions can display quite an array of force-movements, depending on soil type and soil response. In the figure, all curves have been normalized to show both movement and force to go through an arbitrarily assigned common point, "**Target Point**". A single function coefficient applicable to each type of function alternative determines the shape of the selected function before and after the Target Point. The mathematics of the functions are presented in my Red Book (Fellenius 2025).

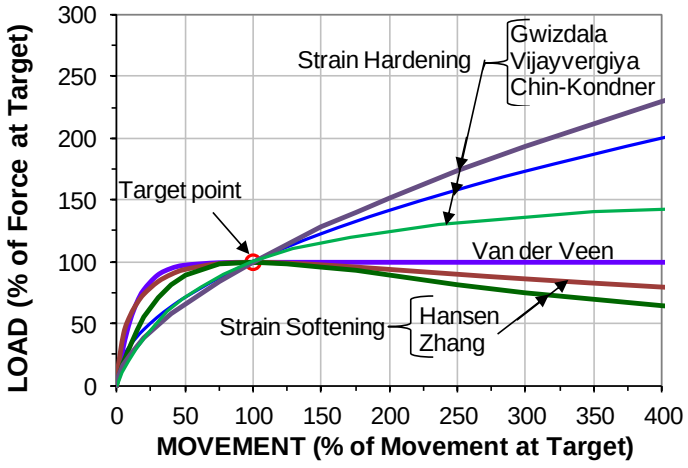


Fig. 1. Typical t-z and -z function curves

The t-z functions can range from strain-softening to strain-hardening. The simplest analysis is with the shaft resistance response assumed to be elastic- plastic similar to the vander Veen function. However, most often the actual response is hyperbolic (Chin-Kondner; Vijayvergiya) or parabolic (Gwizdala), i.e., initially steep and then gently increasing. Sometimes, the shaft resistance reduces (softens) with increasing movement (Hansen; Zhang). Sometimes, but far from always, a distinct change of slope, or curvature, appears at a force-movement, here termed "Target Point", but often not and the movement of the Target Point can be small or large. The t-z function depends on the soil type, soil densities, soil geologic origin (i.e., how created or formed), and mineralogy. Therefore, it is difficult, when faced with a design or analysis case, to choose a representative

 © DFI International Bruges 2025

function type and coefficient, and target movement without well-founded experience, including back-analyses of pile tested under similar conditions in the particular geology.

Piles are made up of a series of pile-elements and the t-z/q-z curves represent the force-movement response of an element to an applied force. Where the response can be represented by the vander Veen, Hansen, or Zhang functions, an ultimate resistance, a logical "capacity" value, can be assumed represented by the indicated peak resistance, here the Target point. Others would be decided by some arbitrary definition.

"Capacity" assessed from the Gwizdala, Vijayvergiya, and Chin-Kondner functions have no visual relation to the shape of the force-movement curve and require a specific definition to identify an ultimate value. There are many such definitions around and most are rather randomly chosen; the profession has neither an agreed-on definition to apply, be it a specific force-movement t-z curve for a pile element or a pile-head load-movement. Note, also, that the accumulated sum of the "capacities" of the individual pile elements is not the "capacity" of the pile other than in the rare event that all pile elements have plastic resistance (vander Veen function).

The toe function (q-z) is always strain-hardening and usually best simulated as a Gwizdala function, showing ever increasing resistance with increasing pile-toe movement. The pile toe is not fully engaged until all pile elements have mobilized significant shaft resistance. Once the shaft resistance of the pile element encompassing the pile toe is mobilized, most of the additionally applied load is normally pile-toe resistance. The response of the pile-toe element is obviously very important.

The Unified Method for Single Piles

The principles of the Unified Method (Fellenius 1984; 1988; 2004; 2025) are very basic. Figure 2A shows distributions of axial force, N.B. unfactored, for a series of applied loads to 30 m long pile installed in a two-layer soil deposit. (The curves should be thought of as originating from the pile toe). The portion of the applied load reaching the pile toe, i.e., the toe resistance (R_t), is indicated at the pile toe. The dotted force curve starting from an assumed sustained load, Q_d, indicates axial force that increases with depth due to accumulated negative skin friction. Each intersection of the latter curve with a force distribution curve is a potential "force equilibrium"—a "neutral plane" (first reported observed in full-scale tests by Johannessen and Bjerrum 1965 and Endo et al. 1969). A horizontal line is drawn from each such intersection. The curves of the example trend to be parallel, indicating that the soil response is plastic once the pile toe is engaged.

Figure 2B shows the horizontal lines from the potential force equilibriums intersecting with the expected long-term settlement distribution ("soil subsidence") curve. Each such intersection indicates a potential settlement equilibrium, i.e., depth where the settlement of the pile is equal to the settlement of the soil, with the sloping straight line representing the pile compression and its value at the pile toe level and at the pile head level indicating the pile toe movement (δ_t) and corresponding pile head settlement, respectively.

A true force equilibrium can only occur at a depth where there is no movement between the pile and the soil, i.e., the settlement of the pile is equal to the settlement of the soil, the intersections of pile-force line and subsidence curve, the "settlement equilibrium". The figure shows an infinite number of force and settlement equilibriums. Only one of these equilibriums is true, which is when the toe force in Figure 2A is the toe force that results in a pile-toe movement for one of the "settlement equilibrium" intersections shown in Figure 2B is at the same depth as the force equilibrium, when the particular q-z relation of toe force and toe movement is satisfied. The depth for which this condition is satisfied is the depth of the "Equilibrium Plane" ("neutral plane").

 © DFI International Bruges 2025

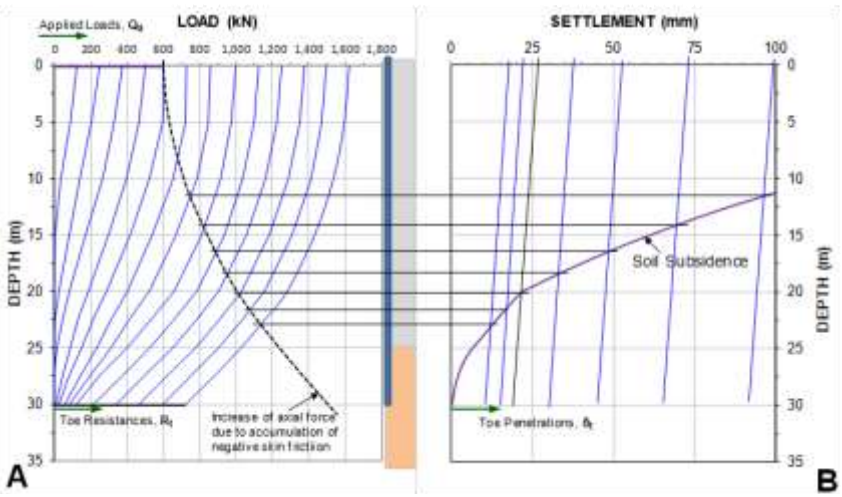


Fig. 2. Distributions of pile-force, pile-settlement, and soil subsidence

Figure 3 uses a graphical procedure to illustrate the principles of the Unified Method and how to determine the depth to the Equilibrium Plane and the long-tem pile settlement—the objective of the analysis. For conditions of plastic soil response, the force distributions curves are essentially parallel, equal, but for the fact that they rise from increasing values of toe resistance. Therefore, the analysis can be carried out using a simple spread sheet, a somewhat time-consuming effort, however.

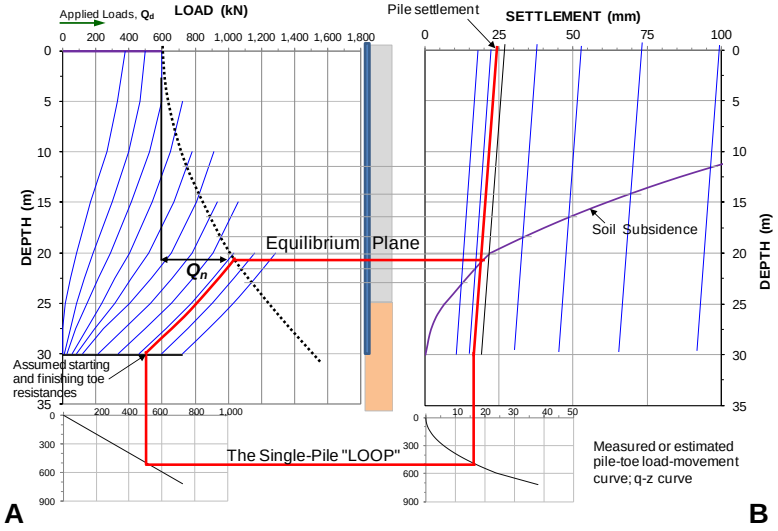


Fig. 3. Loop" determining the Equilibrium depth and the pile settlement

For any toe resistance value, the force equilibrium depth is relatively simple to determine as it is not that dependent on the t-z function. However, unless the soil response is plastic, it will be difficult to get the maximum force right, but that matters less (the maximum force establishes the drag force, but that is a factor for assessment in regard to structural strength and of no concern for the geotechnical analysis). The pile settlement, a more or less straight vertical line, is therefore easy to determine. Its intersection with the soil settlement line determines the settlement equilibrium. The key action is a trial-and-error procedure applying different toe forces and toe movements per the q-z relation to establish where the force and settlement equilibriums appear at the same depth, constituting the Equilibrium Plane. Method 1 applies plastic shaft resistance and Method 2 considers that shaft resistance follows a t-z relation, usually a hyperbolic strain-hardening function (c.f. Figure 1).

 © DFI International Bruges 2025

The graphical process is to, first, draw a force distribution curve downward from the pile head, i.e., a diagram of force versus depth (Figure 3A). The curve starts with the applied sustained load and increases with the load due to negative skin friction accumulated along the entire length of the pile—the dotted curve. Second, a series of force distribution curves are drawn upward from a couple of potential pile toe forces, showing the axial force increasing with accumulated positive shaft resistance. Each intersection of the downward increasing force distribution curve and an upward increasing curve is a force equilibrium and a potential Equilibrium depth. The analysis is best performed using effective stress. Stress-independent analysis (i.e., fixed shaft shear; undrained shear strength values) can give very misleading results.

Third, the soil subsidence is plotted in a diagram of settlement versus depth (Figure 3B). The soil settlement curve can be established from calculations in the same spread sheet or obtained separately from other source. (The important matter is that the settlement is calculated for the actual pile location as the soil is affected by the various fills, loads, and excavations determined by, say, Boussinesq distribution).

The Settlement Equilibrium depth is where the pile settlement line (i.e., toe movement plus compression, and it is only approximately straight) intersects with the soil settlement curve. (The pile settlement line is determined from the pile compression calculated from the axial force distribution and rising from a toe movement correlated to the pile toe force). That is, the Equilibrium depth is where the "Loop" (red lines shown in the figure), satisfies the force and movement relations for the pile, primarily, the q-z function. The 'satisfying' "Loop" starts at a pile toe force, rises to intersect with the downward force distribution, proceeds horizontally to intersect with the subsidence curve, goes downward to the pile toe, indicating a pile toe penetration that matches the force per the q-z relation. The settlement indicated at the pile head is the downdrag for the pile under the loading conditions and the double-arrow indicates the associated drag force, Q_n.

The drag force is of no concern for the response of the piled foundation; only of concern in regard to the structural strength of the pile. The transfer from negative skin friction to positive shaft resistance occurs gradually in a transition zone that reduces the magnitude of the drag force so no "kink" appears in the force curve. However, this is not shown in the figure.

N.B., even when the t-z response is plastic, the manually produced spread-sheet assisted solution will likely require investing several hours of work. Manual spread-sheet calculation for non plastic t-z relations, the more common condition, is still possible, but would need investing considerable time.

The unified method applies equally well to analysis of piled foundations where the long-term settlement is minimal, essentially comprising small secondary compression or "creep" settlement. Those cases will show small shaft resistance, in either negative or positive direction, along an upper length of the pile and some shedding of force along the lower length due to shaft resistance and, then, the balance, the toe resistance. The pile long-term settlement will be the pile-toe movement plus the pile compression.

PILE GROUPS, WIDE AND NARROW

It was once common to design pile groups by assuming the capacity of the group to be equal to the capacity of same number of single piles reduced by an "efficiency coefficient", defined as the ratio of the group-capacity to the sum of the individual piles. This approach originated in the fact that a group of piles will sometimes induce appreciable settlement in the soil below the pile toe level while well spread-out single piles do not. Thus, at equal load per pile, the group will settle more than the single pile. The "group efficiency" approach, e.g., Converse-Labarre equation (Bolin 1941) and others, attempt to adjust to this fact by an oblivious transfer from difference in settlement to a presumed difference in "capacity". Yet, the response of a single pile tested within a group is about the same as that of a single pile tested outside the group. Design by applying a

 © DFI International Bruges 2025

group bearing efficiency factor is not realistic. For example, Terzaghi and Peck (1948) stated: *Attempts to evaluate group action by efficiency equations are likely to be misleading. ... therefore, efficiency equation should not be used.* On the same subject, in the third edition (1996) they added: *It is preferable to evaluate the settlement of a proposed pile foundation on the basis of physical properties of the soil into which the load is transmitted by the piles*. Regrettably, the neat mathematics of the efficiency approach still appeals to many, it seems, because efficiency equations still pop up in actual designs. However, the response of a pile group to an applied load, be the group small or large, narrow or wide, has to be analyzed in terms of settlement, which involves the distribution of forces between the interior and perimeter piles in the group, the shaft rigidity, the raft stress, the settlement below the pile-toe level, the interaction between pile-toe and pile-shaft, and the outside features, such as fills, excavations, site subsidence, etc. There are not many full-scale observations on piled raft settlement, but the few available do illustrate the response of pile groups to load.

Contact Stress and Strain Compatibility

That the contact stress below a piled raft cast on the ground in-between the interior piles would contribute to the bearing of the raft is a widespread fallacy. However, just like the stress distribution between rebars and the concrete in a reinforced concrete column, the distribution of the raft load to the piles ("rebars") and to soil ("concrete"), respectively, follows the principle of strain compatibility per the respective areas and E moduli of the materials. That is, the force in the piles and in the soil will be according to each total area and E modulus, the strain, ϵ, being equal for the soil and pile. The total contact load for a pile group comprising closely spaced piles will be smaller than for groups with widely spaced piles. This is, of course, because the free soil area, A_{soil}, is smaller where piles are closely spaced and larger where the piles are widely spaced, determining the ratio between the load portion on the soil and that on the piles, $E_{soil}\ A_{soil}\ \epsilon$ and $E_{pile}\ A_{pile}\ \epsilon$, respectively. For case records showing this, see Auxilia (2009) and Yamashita (2011; 2012; 2013) and Fellenius et al.(2019).

Moreover, while the E-modulus of the pile does not change with depth, the E-modulus of the soil will likely differ between the various soil layers. Therefore, the contact stress (by definition immediately under the raft) is usually large, because, there the soil is usually engineered backfill with an E-modulus much larger than that of the natural soil. Further down in the natural soil, the E_{soil} is small, therefore, the force in the soil will be smaller and the axial force in the piles will be correspondingly larger than just below the pile head. This is independent of whether the total area of the piled foundation and the total area of the piles, the Footprint Ratio, is small or large. Fellenius et al. (2019) reported a full-scale static loading test on a pile group comprising thirteen 300 mm diameter, 9.5 m long pressure-grouted bored piles installed in silty sand and connected to a rigid pile raft. Figure 4A shows a diagram of the average load-movement of the pile group and of perimeter and interior piles measured in the test and Figure 4B shows a schematic distribution of axial force from the pile head down to the pile toe for an interior pile. Note that the E-modulus in the natural soil being smaller than that of the engineered backfill, resulted in a reduction of the soil force and an increase of the strain represented by increase of axial force—i.e., a transfer of force to the piles—establishing a new strain equilibrium for the unchanged total force, pile and soil.

Distribution of Load between Interior and Perimeter Piles

Figure 4B also shows that pile shaft was engaged from the pile toe upward and that no shaft resistance developed along the upper length of the pile. Indeed, as first stated by Franke (1991), when load is applied to a group of piles, the shaft resistance on interior piles is not mobilized from the head downward, the way it is in a single pile, but from the toe to upward. This means that for an interior pile, in contrast to that for a perimeter pile, shaft resistance does not develop along the upper length of the pile. For a flexible raft and uniformly distributed load, therefore, both the compression and pile toe penetration will be larger for an interior pile than for a perimeter pile. However, because perimeter piles are affected by shaft resistance starting at the ground surface, their response is stiffer than that of the interior piles. Therefore; in case of a rigid raft, the perimeter piles will receive a larger sustained load as opposed to the interior piles. In case of

 © DFI International Bruges 2025

ongoing subsidence of the area around the pile group with a rigid raft, the reverse will occur: the perimeter piles will move (compress) more, due to downdrag, and the interior piles will receive the portion unloaded from the perimeter piles.

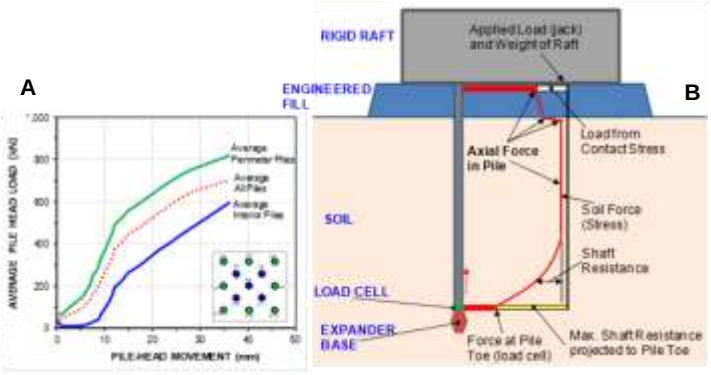


Fig. 4 Pile-head load-movement curves and interior pile distribution of axial force

The Franke principle is illustrated in the following hypothetical example comprising a wide piled-raft foundation supported on 355 mm diameter, round concrete piles at a three-diameter spacing in a square grid and constructed to 22 m depth in a soft soil transitioning to a dense sand at 20 m depth. The applied unfactored sustained load is 800 kN/pile. The live load is 200 kN/pile. A small fill placed across the area outside the foundation footprint will result in long-term subsidence at the site amounting to about 25 mm. Figure 5A illustrates the analysis procedure for where the toe force is equal to the upward movement (compression) of the soil in-between the piles. According to the Franke principle, the shaft resistance is then equal to the balance between the toe force and the applied load. The blue curve shows the pile toe resistance versus toe movement, the q-z curve, as determined in a test or by 'informed' analysis. The burgundy curve shows the applied load subtracted by the shaft resistance engaged upward from the pile toe plotted against the pile toe movement—this curve can be obtained in a bidirectional static loading test, real or simulated, as shown in Figure 5B, for the bidirectional cell placed right at the pile toe (had the test been real, the downward curve would have to be extrapolated beyond about 500 kN).

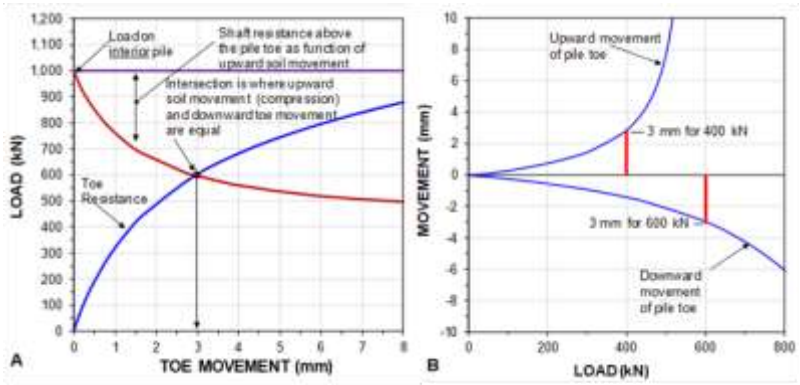


Fig. 5. The Fellenius-Franke method for determining the load-transfer toe-movement and toe-force for interior piles

The strain compatibility principle, i.e., that the strain is the same in the interior pile and the soil, means that the applied load causes no relative movement between the pile surface and the soil in the interior of a pile group. Thus, there is no shaft resistance along the interior piles and the latter piles will transfer their full share of the load to the pile toe. This is similar to absence of shear force between rebars and concrete due to the applied load in the reinforced concrete column. (The toe response is addressed below). In contrast to the interior piles, the perimeter piles will shed load due to shaft resistance.

 © DFI International Bruges 2025

As the load reaches the pile toe level, the pile toe moves down, which is the same mechanism as when pushing the soil upward starting at the pile toe level. The pile toe response depends on the pile toe soil stiffness (force-penetration relation, i.e., the particular q-z function). The distance the pile toe moves into the soil (the pile toe penetration) is equal to the soil's upward movement along the pile. The process generates shaft resistance in the zone immediately above the pile toe, which reduces the force reaching the pile toe.

Obviously, the response of interior versus perimeter piles will be insignificant in a 3 by 3 group of piles: 8 perimeter piles versus 1 interior pile. Similarly, a 4 by 4 group will have 12 versus 4 piles and a 5 by 5 group will have 14 versus 9 piles. A design of a pile group, must therefore differ between narrow group (groups with four or fewer rows of piles) and wide groups (groups of five or more rows).

The response of an interior pile in a wide piled foundation differs from that of the piles in a narrow piled foundation. The response of a perimeter pile, i.e., the outermost row—sometimes, also the next row in—is similar to that of a single pile.

The mentioned difference was first observed by Okabe (1977) when measuring axial force distribution in interior and perimeter piles driven through compressible clay to bearing in dense sand. Figure 6 presents the records in four instrumented piles in the group and a single pile nearby after 4.5 years. The site was subjected to general subsidence due to water mining that developed general subsidence and significant drag force in the single pile. Measurements of axial force in the perimeter pile showed it to have a drag force about equal to that for the single pile. However, the interior piles were neither affected by negative skin friction nor by positive shaft resistance. Note that the perimeter pile did not support the raft, but instead showed a pull force at the foundation raft level. Also that my moving the perimeter-pile force-distribution curve to start from zero pile-head load in the figure (dashed curve less the circled point), shows that its response was practically the same as that of the single test pile.

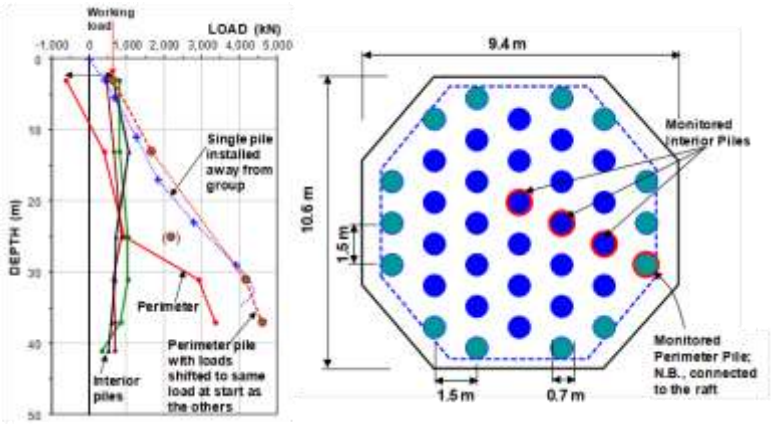


Fig. 6. Axial pile loads measured 4.5 years after construction (Okabe 1977)

A raft can be either rigid or flexible (and anything in between). Figure 7 shows typical (qualitative) load-movement response for a perimeter pile and an interior pile. For a certain total pile load applied to the raft, if the raft is rigid, the pile head movements are equal for all piles. Then, because the shaft resistance for a perimeter pile develops from the raft level (or ground surface), the response of the perimeter pile is stiffer than that of the interior piles and, therefore, the load at the head of the perimeter pile will be larger than that of the interior pile. If the raft is flexible, the loads will be equal, and, because of the response of the perimeter pile is stiffer, its movement will be smaller than that of the interior pile. (The plotted movements do not include the effect of the settlement below the pile toe level). As a raft is never totally rigid or totally flexible, the actual load of any case will be somewhere in-between the extremes, as the red circles indicate in the figure.

 © DFI International Bruges 2025

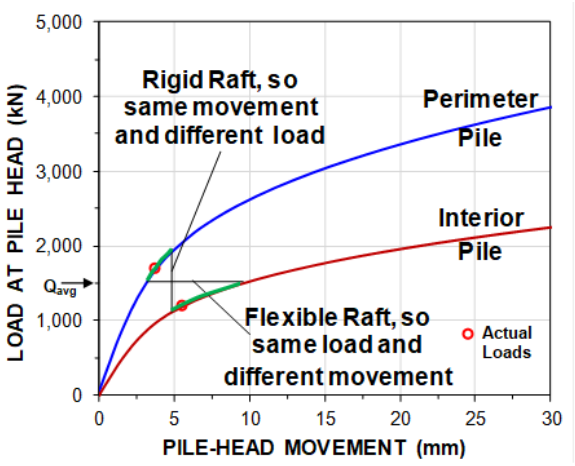


Fig. 7 Comparison of loaded distribution for a perimeter pile and an interior pile in a wide pile group

Fellenius (2019) reported a numerical analysis of load and settlement for an 8.4-m diameter, rigid piled raft supported on a wide group of 49 piles in a 50 m thick deposit of silty sand with a 40-MPa soil E-modulus and a ß-coefficient of 0.56 (from an assumed 35-degree internal friction angle and an earth stress coefficient, K_0= 0.8). Linear soil response was assumed with plastic shear after 5 mm movement. The numerical analysis (Plaxis) imposed a series of 10-mm raft movements to a 40 mm maximum raft settlement. The raft was cast on the ground surface.

Figure 8A shows the calculated soil settlement distributions and the calculated pile movement. The 40-mm pile-head movement (raft settlement) was the same across the raft (it being rigid). i.e., same for all piles. Because of the relatively small pile compression, all pile toe movements were just about slightly less than the 40 mm imposed for the pile head. For the interior piles, there was minimal movement between the pile and the soil, but for a length along the lowest part (up from the pile-toe level). In contrast, the perimeter piles moved more than the soil, thus, engaging shaft resistance and this stiffer response caused them to receive a larger portion of the sustained load and a larger pile compression

Zhang et al. (2025) did a similar numerical analysis of a large pile group, 1,600 21 m long piles, supporting an 80 m wide LNG tank (flexible raft above ground). Similarly to the foregoing analysis, the results showed that the perimeter piles engaged the soil from the pile-head downward, while the interior piles engaged the soil from the pile-toe upward. That is, both numerical analyses agreed with the presented principles of response of wide pile groups to applied load.

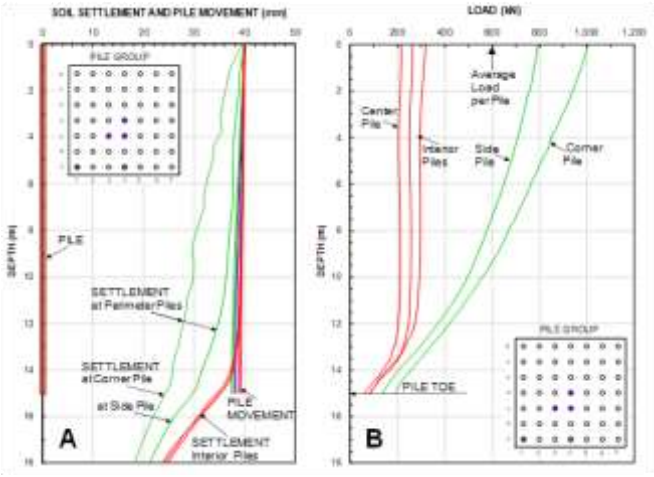


Fig. 8 Results of numerical analysis.
A. Soil settlement and pile movement. B. Axial pile loads

 © DFI International Bruges 2025

Settlement below the pile toe level

Be the spacing or the contact stress large or small, the response of the piled raft, of any rigidity, is compression of the equivalent pier system (piles and soil) plus settlement of the soil below the pile toe level. The compression of the pier system is determined by E_{pier}, the combined E-moduli (E_{pile} and E_{soil}) in relation to the respective areas of piles and soil (Fellenius 2016; 2025). The settlement of the soil below the pile toe level can be calculated as that of a flexible equivalent raft at the pile toe level loaded by the same stress as applied to the foundation raft, as shown in Figure 9. Note, the analysis must include the influence of stress changes due to adjacent other foundations, fills, excavations, and changes of groundwater table.

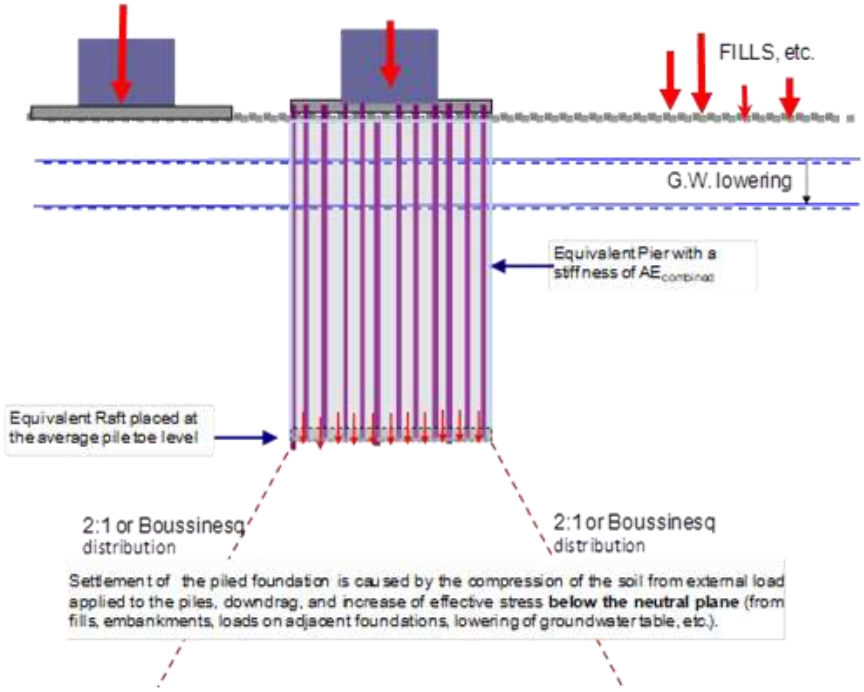


Fig. 9. The equivalent raft for calculation of settlement below the pile toe level

"Floating piles", i.e., shaft-bearing piles in soft compressible soil, can drastically reduce total and differential settlement of a raft or embankment placed on the piles. Broms (1976) reported settlement measured for two rectangular embankments on a 15 m thick deposit of compressible soft clay. One of the two embankments was supported on a grid of 500-mm diameter, 6 m deep lime-columns ("soft piles") placed at a center-to-center spacing of 1.4 m (2.8×column-diameter). The Footprint Ratio, i.e., ratio between total column ("pile") area and total footprint area, was about 10 %, an important parameter, because the E-modulus of the equivalent pier is about equal to the pile E-modulus times the Footprint Ratio (Fellenius 2019; 2025).

Figure 10 combines the measurements from the two embankments taken at 16, 65, 351, and 541 days, respectively, after constructing the embankment. "Column Area" shows records under the embankment supported on 6 m long lime-columns and "Reference Area" shows records from an adjacent embankment with no columns. The measurements established that the settlement for the column-supported embankment was not only smaller, but also more uniform than under the no column reference area. The settlement records of both embankments can be fitted in a back-calculation, using the same set of soil parameters for both and applying the equivalent raft concept.

 © DFI International Bruges 2025

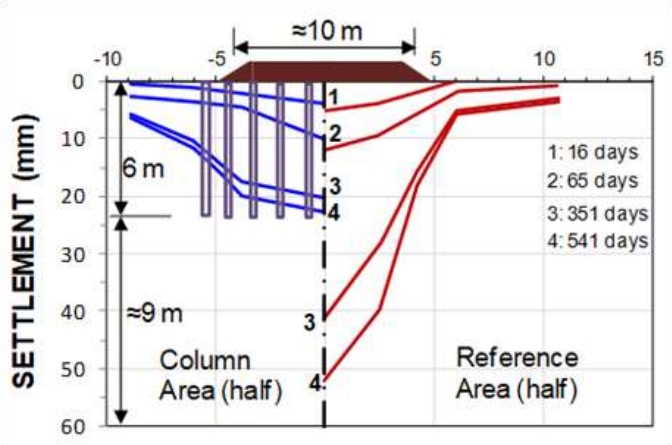


Fig. 10. Settlement of lime-column supported and unsupported embankments on soft compressible clay (data from Broms 1976)

However, Figure 11 compiles a case records presented by Badellas et al. (1988) of a flexible silo raft in Thessaloniki founded on piles, again confirming the equivalent raft approach (also addressed by Georgiadis et al. 1989 and Savvaidis 2003).

Gwizdala and Kesik (215) reported observations on the Gdansk Millennium Bridge. The main bridge component is a single tower, a 100-m tall reinforced concrete pylon, consisting of a 52.4 x 22.4 m concrete slab supported on 50 bored piles of 1,800 mm diameter and 30 m embedment. The total unfactored load was 480 MN and the unfactored working load per pile was 9,600 kN. The soil profile consisted of 25 m of interbedded clay and sand deposited on sand. The foundation lies close to and parallel to the river, which meant that the effective stresses on the river side are smaller than on the opposing side (Figure 12). Starting after the casting of the slab, the pylon settlement was monitored over time. Settlement analysis considering the non-equal distribution of the initial effective overburden stress agreed well with the observed differential settlement shown in Figure 13 between the wider side and the land side, demonstrating the importance of the analysis to take into account any difference in effective stress distribution below the raft area.

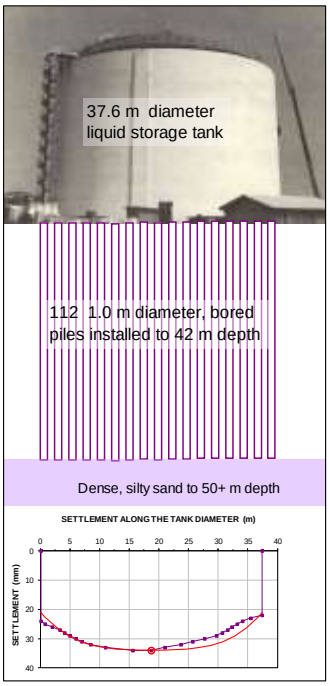


Fig. 11 Layout of the piles and measured and calculated settlements for the Thessaloniki tank along the tank diameter. (Data from Badellas et al. 1988)

 © DFI International Bruges 2025

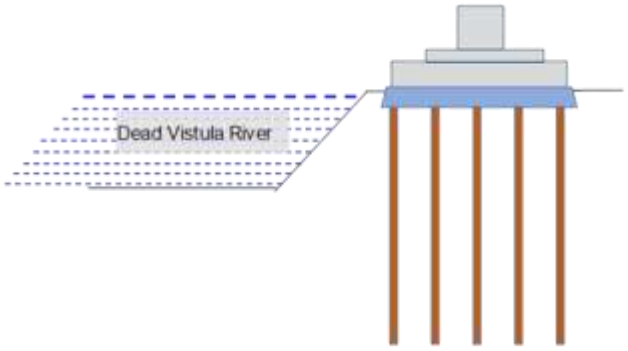


Fig. 12. Vertical section and geometry of the pier.

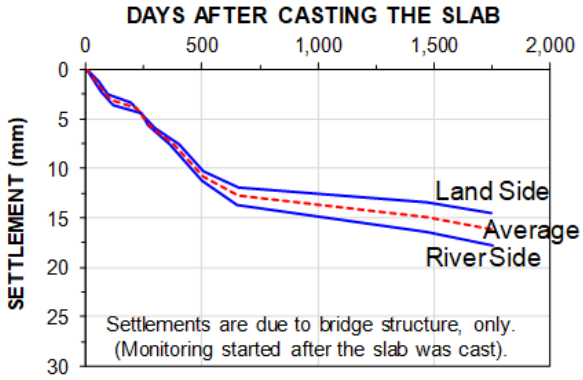


Fig. 13. Measured settlements (data from Gwizdala and Kesik 2015).

A pile group comprises perimeter piles and interior piles. Most piled foundations have more perimeter piles than interior piles. For example, to include an equal number of perimeter and interior piles, a rectangular pile group has to have 48 piles; 6 rows and 8 columns. Of the perimeter piles, the corner pile has the maximum exposure to the shaft resistance development. Therefore, it can be expected that the corner pile will, at first, take on larger load from the superstructure. Then, in the long-term, as the surrounding soil consolidates and settles, negative skin friction will reduce the shaft resistance and make the perimeter piles appear to become softer, thus, some of the load will be transferred to the interior piles.

Mandolini et al. (2005) and Russo and Viggiani (1995) reported measurements of the response of a wide pile group comprising 144 driven 406 mm diameter pipe piles supporting a bridge abutment. The pile axial load applied to 35 piles was monitored as the bridge was constructed and over about 10 months afterward. Figure 14 shows that interior piles under the raft carried 60% of the load carried by perimeter piles after the construction of the bridge had been completed. Then, because the perimeter piles were affected by general subsidence, adding drag force, pile compression increased. The rigid bridge cap ensured that some on the load on the perimeter piles, notably the corner pile, was transferred to the interior piles.

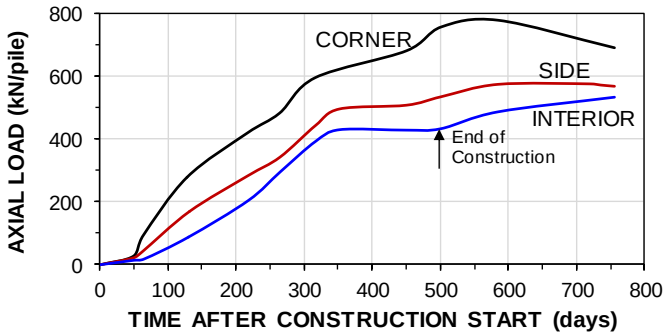


Fig. 14. Measured axial load during and after construction (from Russo and Viggiani 1995)

 © DFI International Bruges 2025

Cooke et al. (1981) reported similar results from monitoring a 43 m long, 20 m wide piled foundation comprising 450-mm bored piles constructed at 1.6 m c/c. The building was designed with perimeter and interior walls as bearing walls. Figure 15 shows the average pile-head loads monitored during and after the construction for eight instrumented piles: perimeter piles at corner and side piles, and interior piles. The load at both the head and toe was measured with a 360 mm wide, 100 mm thick cell cast in the pile that measured force using eight cylinders between two steel plates with vibrating-wire gages for determining imposed strain that was calibrated to force. The difference to the 400 kN/pile monitored total average load implied a total contact load of 14 MN, correlating to 16 kPa contact stress. Assuming a pile E-modulus of 30-MPa, the $E_{pile}A_{pile}$ parameter becomes 5 GN correlating the stress to 80-με axial pile strain. The soil underneath the raft, engineered fill or natural London clay, likely experienced the same 80-με strain and the 16 kPa stress correlates to E_{soil} = 250 MPa, which is a realistic value both for an engineered fill and the overconsolidated London clay. In contrast to the case of Okabe (1977), no general subsidence affected the piles.

Hansbo (1984; 1993) and Hansbo and Jendeby (1998) reported a remarkable case history of long-term response of two four-storey buildings in Göteborg, Sweden, supported on 300 mm diameter piles, driven to 28 m depth in a thick deposit of soft clay. One building was constructed on a grillage of beams (contact area was not reported) and the other on a raft. The buildings were on opposite sides of a street. The nominal total average load over each building footprint corresponded to 66 kPa and 60 kPa, respectively—very similar values. The as-designed average axial working loads were 220 kN and 520 kN/pile, respectively—quite different values. The conservatively estimated pile "capacity is stated to have been 330 kN, smaller than the sustained load per pile supported by Building 2. At the end of construction, measured pile loads were about 150 and 300 kN/pile, respectively, again, values quite different from each other. As shown in Figure 16, the measurements over a 13 year period showed that the buildings settled on average a very similar amount, about 40 mm,. The equivalent-pier shortening was smaller for Building 1, reflecting its smaller average pile load (and larger pier EA-parameter), but, because of the average stress across the footprint being larger, this difference was compensated by the larger footprint stress resulting in larger settlement below the pile toe level.

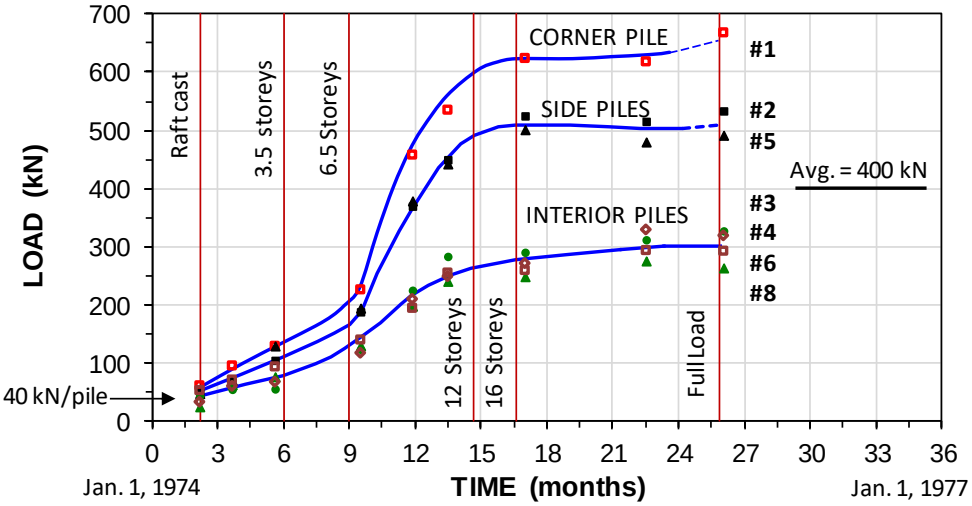


Fig. 15 Load at head of monitored piles over two years

 © DFI International Bruges 2025

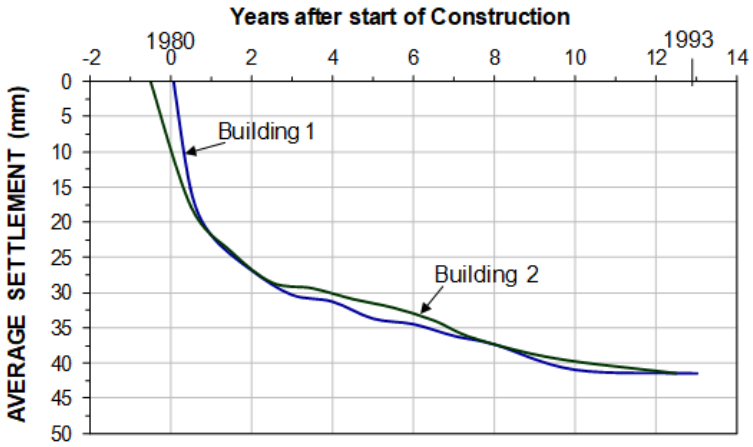


Fig. 16. Settlement measured for the two buildings over 13 years

Fellenius (2019) compiled settlement for storage tanks records of hydro testing of oil tanks 33,000 m^3 in volume, 19 m tall oil tanks, each place on a piled raft supported on 422 piles (case history by van Impe et al. 2018). The piles were 460-mm diameter, 21.6 m long screw piles (Omega piles). The average pile load was estimated to 780 kN (about 200 kPa average across the tank) and a static loading test to 3,500 kN maximum load showed no sign of failure. Tank 1 was tested first to measured 180 kPa, which caused a 20 mm, quite uniform, settlement along the tank perimeter as indicated in Figure 17. The water was then pumped over to Tank 2 resulting in measured 184 kPa stress. The settlement ranged from 15 through 20 mm with the smallest value along the side nearest Tank 1 (at Gages #10 to #11) and the largest diametrically opposite. It is obvious that the load on Tank 1 preloaded the soil under Tank 2 and caused some initial settlement, which, unfortunately, was not measured (the purpose of the tests was to the check the tanks, not to monitor settlement). Analysis of the measured settlements of the two tanks applying an equivalent raft at the pile toe depth and using the same parameter input for both analyses fitted both settlement records.

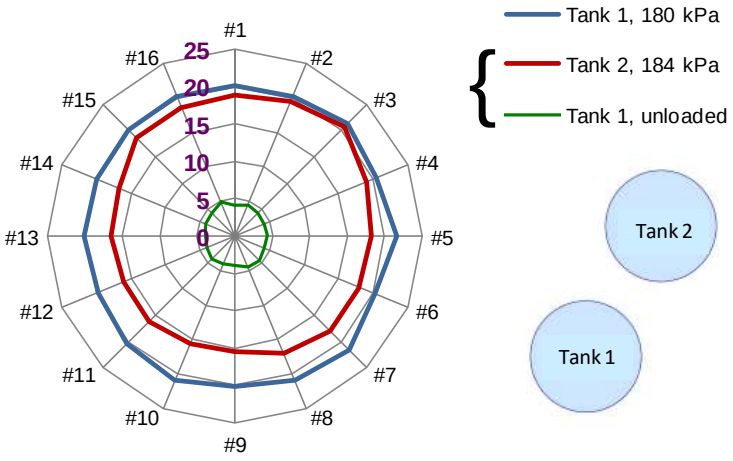


Fig. 17. Measured perimeter settlements for Tanks 1 and 2 and remaining settlement of Tank 1 after unloading. (Data from van Impe et al. 2018).

Buttling et al. (2024) reported result of nine years of monitoring a 3.0 to 3.5 m thick pile raft foundation for pile loads and settlement supporting a 200 m tall tower in Bangkok. The piles were 1,000 mm diameter, 4.5 m long bored piles. After end of construction, the load on the perimeter piles was larger loads than on the interior piles. Figure 18 shows the measured settlement across the 36 m wide raft. The load-movement during the construction was about 100 mm and, due to the general subsidence at depths below the pile-toe level, the post-construction settlement over the nine years of monitoring amounted to about 40 mm. The differential settlement across the raft half-width at the end of construction was 15 mm. Because of ongoing general subsidence, the perimeter

 © DFI International Bruges 2025

piles were affected by downdrag and, therefore, some of the loads on these piles was transferred to the interior piles, thus, as shown in the figure, not only reducing the differential settlement, but reversing the raft from showing a sagged shape (bowl) at end of construction to become hogging some six years later.

The technical literature includes very few full-scale case histories on pile group response, but the foregoing survey is not exhaustive. For example, Inoue et al. (1977) presented an additional and equally educational case history of settlement due to downdrag. Kakurai et al. (1987) reported measured long-term distributions of axial force.

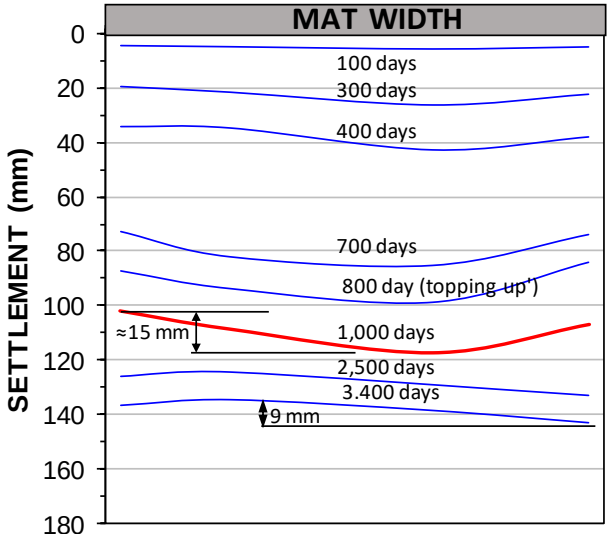


Fig. 18. Settlement measured for the tower raft over 3,400 days—9 years

CLOSURE

Designing a piled foundation based on the concept of "capacity" is fraught with much uncertainty. A more reliable design approach is to instead emphasize settlement and apply the Unified Method (Fellenius, 1984, 1988, 2025), which recognizes the particulars of single piles and of interior and perimeter piles in pile groups, and whether the groups are narrow or wide. The settlement analysis is particularly important for piles at sites experiencing subsiding soil.

Before engaging in analysis, compile all soil information (geology and mineralogy, densities, layering compressibility, GW and pore pressure distribution (also well below the expected pile toe level), and pile data. Information on past and planned excavations, fills and loads is vital.

The design will start with back-calculating the response of a pile subjected to a static loading test: the t-z/q-z functions and force distribution. Then, it involves determining the response of a single foundation-pile subjected to initial loading, long-term loading, general subsidence, etc. For a pile group, also the distribution of applied load across the raft and between piles, and the pile group settlement, total and differential must be assessed.

If a change in the distribution of effective stress around foundation piles is expected to occur during the life of a structure supported on a pile foundation, e.g., basement excavation and/or fills, this must be included in the analysis. Therefore, analysis using stress-independent shear parameters (i.e., "alpha-method"; total stress analysis; undrained shear strength; "ultimate shaft resistance") have limited use and the analysis is best performed with effective stress parameters. For example, the results of a back-analysis of a static loading test executed from the ground surface with the shaft isolated from the soil within a future excavation depth for basements will considerably overestimate the long-term conditions for the piled foundation, if the analysis is made with stress-independent parameters.

 © DFI International Bruges 2025

The Unified Method analysis can be carried out manually. However, for other than a very simple case, it would, even when aided by a spread sheet, involve much time and require unrepresentative short-cuts and simplifications. Software exists that will save time and allow for input of all case data, e.g., soil parameters, t-z/q-z functions, pore pressure distribution, geometry, pile type (size, length, loads, properties), area loads, fills, excavations, etc.. The output needed for design assessment comprises distributions of effective and total stress, distributions of axial force and settlement due to sustained loads and general subsidence, simulation of a static loading test, etc. The software must enable quick calculation of effect of changes in soil layering, type of pile, loading, etc. Personally, I use the software pair UniSettle and UniPile by www.unisoftGS.com. All case analyses presented in this paper have been produced with this software pair.

The one thing that a structure cares about is that the settlement not be larger than it can accept. To assure this, a design needs to be based on estimated settlement of the piled foundation related to the settlement that would bring about distress. First, such approach requires collaboration between the structural and the geotechnical engineers, Second, the geotechnical engineer should correlate forces and movement (t-z/q-z relations) and pile compression with settlement of the soils due not just an applied load but also due to other factors, such as fills, load units, excavation, groundwater lowering, etc.

Currently, the EuroCode's approach differs from the North-American approach. I strongly believe it would be advantageous for the Users of the EuroCode, if the code would be edited to address design of piled foundations in a manner closer to the unified method.

References

Auxilia, G.B., Burke, P., Duranda, M., Ulini, F., Buffa, L. Terrioti, C., Dominijanni, A., and Manassero, M., 2009. Large storage capacity cement silos and clinker deposit on a near-shore sandy fill using piles for soil improvement and settlement reduction. 17th ICSMGE, Alexandria, October 5-9, 2009, Vol. 3, pp. 1181-1184.

Badellas, A., Savvaidis, P. and Tsotsos, S., 1988. Settlement measurement of a liquid storage tank founded on 112 long bored piles. Second International Conference on Field Measurements in Geomechanics, Kobe, Japan, Balkema Rotterdam, pp. 435-442.

Bolin, H.W., 1941. The pile efficiency formula of the uniform building code. Building Standards Monthly, 10(1) 4-5.

Broms, B.B., 1976. Pile foundations—pile groups. Report on Session III to the 6th ECSMFE, Vienna, Vol. 2.1 pp. 103-132.

Buttling, S., Fellenius, B.H., and Pinijpol, N. 2024. A case history of nine years of monitoring a wide pile group. Institution of Civil Engineers, ICE–Geotechnical Engineering, 177(2) 13 p.

Coffman, R.A., Blanchard, J.D., Stuedlein, A.W., Jana, A., and Budge, A.S., 2024. Design of piles for downdrag. NCHRP 1112, The Unified Method, TRB, Wa, 353 p.

Cooke, R.W., Bryden-Smith, D.W., Gooch, M.N., and Sillett, D.F. 1981. Some observations of the foundation loading and settlement of a multi-storey building on a piled raft foundation in London Clay. Proc. Inst. Civ. Engrs, Part I-70, pp. 433-460.

Endo M., Minou, A., Kawasaki T, and Shibata, T, 1969. Negative skin friction acting on steel piles in clay. Proc. 7th ICSMFE, Mexico City, August 25 29, Vol. 2, pp. 85-92.

Fellenius, B.H., 1984. Negative skin friction and settlement of piles. Proceedings of the Second International Seminar on Pile Foundations, Nanyang Technological Institute, Singapore, 18 p.

Fellenius, B.H., 1988. Unified design of piles and pile groups. Transportation Research Board, Washington, TRB Record 1169, pp. 75-82.

 © DFI International Bruges 2025

Fellenius, B.H., 2004. Unified design of piled foundations with emphasis on settlement analysis. Honoring George G. Goble—Current Practice and Future Trends in Deep Foundations. Geo-Institute Geo-TRANS Conference, Los Angeles, July 27-30, 2004, Edited by J.A. DiMaggio and M.H. Hussein. ASCE Geotechnical Special Publication, GSP125, pp. 253-275.

Fellenius, B.H., 2006. Results from long-term measurement in piles of drag load and downdrag. Canadian Geotechnical Journal 43(4) 409-430.

Fellenius, B.H., 2015. The response of a "plug" in an open-toe pipe pile. Geotechnical Engineering Journal of the SEAGS & AGSSEA 46(2) 82-86.

Fellenius, B.H., 2016. The unified design of piled foundations. The Sven Hansbo Lecture. Geotechnics for Sustainable Infrastructure Development – Geotec Hanoi 2016, edited by Phung Duc Long, Hanoi, November 23-25, pp. 3-28.

Fellenius, B.H., 2019. Observations and analysis of wide piled foundations. Canadian Geotechnical Journal, 56(3), 378-397. doi.org/10.1139/cgj-2018-0031.

Fellenius, B.H., 2021. Long-term response of piled foundations to sustained load. Independent Project Analysis, IPA, Invited Special Contribution, 6(2), p. 4-12.

Fellenius, B.H., 2025. Basics of foundation design—a textbook. Electronic Edition, www.Fellenius.net, 572 p.

Fellenius, B.H., Terceros, H.M., Terceros, A.M., Massarsch, K.R, and Mandolini, A., 2019. Static response of a group of 13 piles tested simultaneously. 4th Bolivian International Conference on Deep Foundations, Santa Cruz de la Sierra, Bolivia, May 23-24, 13 p.

Franke E., 1991. Measurements beneath piled rafts. International Conference on Deep Foundations, Ecole National des Ponts et Chaussees, Paris, March 19-21, pp. 599-626.

Georgiadis, M., Pitilakis, K., Tsotsos, S., and Valalas, D. 1989. Settlement of a liquid storage tank founded on piles. Proceedings of the 12th International Conference on Soil Mechanics and Foundation Engineering, Rio de Janeiro, August 13-18, Vol. 2, pp. 1057–1060.

Gwizdala, K. and Kesik, P., 2015. Pile group settlement, methods, examples of calculations referred to measurement results carried out in field tests. 16th ICSMGE, Edinburgh, September 13-17, pp. 1091-1096.

Hansbo, S. 1984. Foundations on creep piles in soft clays. First International Conference on Case Histories in Geotechnical Engineering, St. Louis, May 6-11, 1984, pp. 259-264.

Hansbo, S., 1993. Interaction problems related to the installation of pile groups. Proceedings of the 2nd International Geotechnical Seminar on Deep Foundations on Bored and Auger Piles, Ghent, 1–4 June, 1993, pp. 119–130.

Hansbo, S. and Jendeby, L., 1998. A follow-up of two different foundation principles. Foundations on friction creep piles in soft clays. International Conference on Case Histories in Geotechnical Engineering. St. Louis, March 9-12, 259 264.

van Impe, W.F., van Impe, P.O., and Manzotti, A., 2018. Pile design and group behaviour—a case study of large tank foundations in soft soil conditions. Geotechnical Engineering Journal of the SEAG & AGSSEA, 49(1) 15-29.

Inoue, Y., Tamaoki, K., Ogai, T., 1977. Settlement of building due to pile downdrag. Proc. 9th ICSMFE, Tokyo, Vol. 1, pp. 561–564.

Kakurai, M., Yamashita, K., and Tomono, M., 1987. Settlement behavior of piled raft foundations on soft ground. Proceedings of the 8th Asian Regional Conf. on SMFE ARCSMFE, Kyoto, 20 -24 July 1987, Vol. 1. pp. 373 -376.

Mandolini, A., Russo, G. and Viggiani, C. (2005). Pile foundations: experimental investigations, analysis, and design. Proc. 16th ICSMGE, September 12 -16, Osaka, Japan, pp. 177-213.

 © DFI International Bruges 2025

Okabe, T., 1977. Large negative friction and friction-free piles methods. 9th ICSMFE, Tokyo, July 11-15, Vol. 1, pp. 679 682.

Russo, G. and Viggiani C. (1995). Long-term monitoring of a piled foundation. Fourth Int. Symposium on Field Measurements in Geomechanics, Bergamo, pp. 283–290.

Savvaidis, P., 2003. Long-term geodetic monitoring of the deformation of a liquid storage tank founded on piles. Proc. 11th FIG Symposium on deformation measurements, Santorini, Greece, May 25-28, 2003, 8p.

Terzaghi, K. and Peck, R.B. (1948). Soil Mechanics in Engineering Practice. 1st Edition, John Wiley & Sons, New York, 566 p.

Yamashita, K. Hamada, J., Takeshi, Y., 2011. Field measurements on piled rafts with grid-form deep mixing walls on soft ground. Geotechnical Engineering Journal of the SEAG & AGSSEA, 42(2) 110.

Yamashita, K. Hamada, J., Onimaru, S., Higashino, M., 2012. Seismic behavior of a piled raft with ground improvement supporting a base-isolated building on soft ground in Tokyo. Soil and Foundations 52(5) 1000-1015.

Yamashita, K., Wakai, S., and Hamada, J. 2013. Large-scale piled raft with grid form deep mixing walls on soft ground. Proc. 18th ICSMGE, September 2 6, Paris, France, Vol. 3, pp. 2637-2640.

Zhang, W., Shi, J., Lin, G., and Lin, C., 2025. Settlement analysis of a large pile group supporting an LNG storage tank.

 © DFI International Bruges 2025

REVOLUTIONIZING FOUNDATIONS: ADVANCES IN THERMO ACTIVE PILING ENGINEERING

Lyesse Laloui, Swiss Federal Institute of Technology in Lausanne, EPFL, Laboratory of Soil Mechanics, Lausanne, Switzerland, lyesse.laloui@epfl.ch
Elena Ravera, GEOEG consulting, Lausanne, Switzerland, elena.ravera@geoeg.net
Alessandro F. Rotta Loria, Northwestern University, Department of Civil and Environmental Engineering, Subsurface Opportunities and Innovations Laboratory, Evanston, USA, af-rottaloria@northwestern.edu

ABSTRACT

The urban subsurface is an increasingly critical resource for addressing the growing demands of modern societies, particularly in the realms of energy and infrastructure development. This paper focuses on energy geostructures—innovative foundations that leverage underground renewable energy in a cost-effective and efficient manner. These systems integrate geotechnical engineering principles with energy functionality, providing dual benefits: structural stability and heating/cooling capabilities for buildings and infrastructure. Their performance is governed by interactions between thermal and mechanical loads, which pose challenges to address their analysis and design. Over the past 30 years, substantial research has advanced the understanding of energy piles, barrettes, walls and slabs, resulting in practical tools for their engineering applications. This study synthesizes these advancements and bridges the gap between theoretical research and real-world implementation. It presents core theoretical frameworks for evaluating energy foundations and examines a case study of a real-world installation, offering critical in-sights into their operational performance.

Keywords: energy geostructures; real-world installation; geothermal energy; thermo-active foundation

INTRODUCTION

Energy geostructure technology

The pressing challenges of climate change, driven by greenhouse gas emissions and resource depletion, highlight the critical need for a transition to a sustainable, low-carbon economy. In 2022, almost half of the energy demand in buildings was used for space and water heating, resulting in approximately 2,400 Mt of direct CO_2 emissions and 1,700 Mt of indirect CO_2 emissions, maintaining similar levels to the previous year. Despite the growing role of efficient and low-carbon heating technologies, over 60% of heating energy demand is still met by fossil fuels. Furthermore, energy consumption for cooling has more than tripled since 1990, contributing to increased electricity grid stress, higher greenhouse gas emissions, and the exacerbation of urban heat islands (International Energy Agency, 2023).

A promising opportunity to address these challenges lies in utilizing the untapped energy potential of the subsurface. Over the past three decades, energy geostructures have emerged as an innovative technology within shallow geothermal systems (Laloui and Rotta Loria, 2019). These technologies integrate geothermal heat exchangers into earth-contact structures. Starting with pile foundations, the technology has now expanded to different types of earth-contact structures, such as walls, slabs, and barrettes. By leveraging the stable, low-enthalpy thermal energy of the shallow subsurface, energy geostructures can provide renewable heating and cooling for buildings, domestic hot water production, and seasonal thermal storage. They can also prevent ice formation on pavements and slabs for roads, bridges, and runways or reduce ventilation needs in underground infrastructures. Energy geostructures are currently deployed in geothermal heat pump systems, but the rise of fifth-generation district heating and cooling networks offers a pathway to scale their use. These networks, which connect multiple energy users, allow energy geostructures to function as low-temperature, ground-coupled energy sources and storage systems, improving network sustainability, flexibility, and resilience (Meibodi and Loveridge, 2022).

 © DFI International Bruges 2025

Constructed primarily from reinforced concrete, energy geostructures incorporate heat exchanger tubes—typically made of high-density polyethylene—that are attached to the reinforcement cage or integrated into drainage paths during construction (Fig. 1). These tubes, with diameters of 10 to 40 mm, circulate a thermal transfer fluid, usually water with antifreeze or a salt solution, to exchange heat with the surrounding ground. Proper thermal insulation is often applied to the initial pipe sections to minimize climatic influences and enhance efficiency. Pipe configurations in energy geostructures vary depending on the system design, affecting installation, operation, and maintenance costs. For instance, energy walls, and slabs exchange heat with both the ground and air, and their efficiency depends on the strategic placement and insulation of the pipes. With careful design and integration, energy geostructures offer a cost-effective, sustainable solution to decarbonizing the built environment, addressing both structural and energy needs in a single system (Laloui and Rotta Loria, 2019).



Fig. 1. Installation of heat exchanger tubes on reinforcement cages of foundation structures before pouring concrete or integrated into drainage paths (image source: GEOEG (www.geoeg.net)).

Environmental, social, and economic aspects of energy geostructures

The use of energy geostructures for thermal energy needs in buildings and infrastructure has proven to be environmentally sustainable, socially beneficial, and economically viable. These systems are considered low-carbon technologies that contribute to decarbonization by significantly reducing CO_2 emissions. Energy geostructures align with international policies, regulations, and agreements promoting sustainability and can complement other renewable energy technologies to create highly efficient and flexible systems. Traditional heating systems powered by gas or electricity emit approximately 200 gCO_2eq/kWh. In contrast, renewable systems offer a lower environmental impact, with life-cycle emissions ranging from 4 to 46 gCO_2eq/kWh (Edenhofer et al., 2011). Recent advancements in renewable technologies have further improved these figures: poly-Si photovoltaic panels emit 12–20 gCO_2eq/kWh (Louwen et al., 2016), low-temperature solar thermal panels emit 5.8 gCO_2eq/kWh (Pfadt-Trilling et al., 2023), and energy geostructures emit approximately 15 gCO_2eq/kWh. From an environmental perspective energy geostructures require no additional soil

 © DFI International Bruges 2025

excavation; furthermore, embedding heat exchanger circuits in the concrete reduces the risk of pipe damage or groundwater pollution. Concerns about subsurface temperature variations are mitigated as temperature disturbances from energy geostructures are typically limited to a distance of 5–10 m. These systems also enable the recovery of otherwise wasted heat, creating highly efficient energy storage solutions (Laloui and Rotta Loria, 2019). In urban areas undergoing the effects of subsurface heat islands, shallow geothermal systems have also been shown to achieve higher heating efficiency due to excess subsurface heat from human activity (Zhu et al., 2010; Bayer et al., 2019; Benz et al., 2022; Rotta Loria, 2023).

From a social perspective, energy geostructures offer numerous benefits, including quieter and more hygienic cooling systems compared to conventional air conditioning, improved hygrothermal performance for sensitive environments like museums, and enhanced personal comfort through radiant heating of walls and floors (Brandl, 2016).

Economically, energy geostructures provide reliable returns on investment, typically within 2–10 years, with stable costs unaffected by volatile energy markets (Brandl, 2016; Singh et al., 2019). Their low maintenance requirements further shorten payback periods (Brandl, 2016; Sani et al., 2019). Compared to other geothermal systems, they are more cost-effective since heat exchangers are integrated into structural elements already needed for construction, reducing excavation costs and administrative burdens. Studies have shown that operational costs for buildings over 50 years often exceed initial construction costs, highlighting the importance of energy-efficient concepts for long-term economic and environmental benefits (Brandl, 2016). On a national scale, energy geostructures reduce energy imports, decreasing dependence on external economic or political factors.

Synopsis

Over the past decades, scientific research has laid the groundwork for understanding and designing energy geostructures, resulting in a range of tools from simplified calculations to sophisticated computational models. A landmark contribution to this field, presented by Laloui and Rotta Loria (2019), consolidates the theoretical and practical knowledge required to design and implement these systems effectively. This article builds on these foundations, bridging the gap between academic advancements and practical applications. It first explores key design methodologies, offering insights into sound scientific analysis and design approaches. Subsequently, it presents a real-world case study that demonstrate the practical implementation of energy geostructures and their role in advancing building and urban energy management.

DESIGN OF ENERGY GESOTRUCTURES

The design of energy geostructures requires a comprehensive understanding of the thermo-hydro-mechanical interactions that govern their geothermal and structural functions. These systems involve complex phenomena where heat transfer induces mass transfer and deformation. To accurately model these behaviors, it is necessary to solve the relevant balance and constitutive equations, which allow the calculation of temperature distributions, flow fields, displacement fields, and stress fields. The continuity and momentum equations are, respectively.

$$\rho_f \nabla \cdot \boldsymbol{v_f} = 0 \quad [1]$$

$$\rho_f \left(\boldsymbol{v_f} \cdot \nabla\right) \boldsymbol{v_f} = \nabla \cdot [-p\mathbf{I} + \boldsymbol{K}] + \boldsymbol{F} \quad [2]$$

Where ρ_f is the fluid density, $\boldsymbol{v_f}$ is the velocity vector, p is the pressure, $\boldsymbol{K}$ is the viscous stress tensor, and $\boldsymbol{F}$ is the volume force vector. The energy conservation equation when convection and conduction characterize the heat transfer reads:

$$\rho_f c_{p,f} \boldsymbol{v_f} \cdot \nabla T - \nabla \cdot (\lambda \nabla T) = Q \quad [3]$$

 © DFI International Bruges 2025

where $c_{p,f}$ is the heat capacity at constant pressure, λ is the thermal conductivity, T is the temperature, and Q is the heat source. Solving Eq. 3 alongside the mass conservation equation allows to address conduction-convection heat transfer problems and highlights the thermo-hydraulic coupling between heat and mass transfer. The momentum conservation equation, when simplified by neglecting the influence of body forces, becomes:

$$\nabla \cdot \boldsymbol{\sigma} = \mathbf{0} \quad [4]$$

where $\nabla \cdot$ is the divergence operator and $\boldsymbol{\sigma}$ is the total stress tensor. The stress tensor can be expressed as

$$\boldsymbol{\sigma} = \boldsymbol{D} : [\boldsymbol{\varepsilon} + \boldsymbol{\beta}(T - T_0)] \quad [5]$$

where $\boldsymbol{D}$ is the elastic stiffness tensor, which contains the material parameters (i.e., Young's modulus, E, and Poisson's ratio, ν), $\boldsymbol{\varepsilon}$ is the total strain tensor, $\boldsymbol{\beta}$ is a vector that comprises the linear thermal expansion coefficient of the material, α, and $T - T_0 = \Delta T$ is the applied temperature variation.

Energy piles and energy barrettes, typically surrounded by soil or rock, primarily engage in heat transfer through conduction. Convection with the surrounding ground will occur in presence of significant groundwater flow. The mechanical behavior of energy piles is characterized by axial forces due to the vertical loads and thermal expansion. The schematic in Fig. 2a illustrates the heat transfer modes in energy piles, emphasizing the axial mechanical response and the interaction between the pile and the ground. For energy walls and slabs, the thermal and mechanical behaviors are more complex due to their interaction with both the ground and the air. These structures not only exchange heat with the surrounding soil, but also with the air, allowing for the collection of both geothermal and aerothermal energy. The heat transfer in these elements involves a combination of conduction through the ground and convection with the air, and the mechanical behavior is dominated by bending rather than axial forces. This bending response is a result of thermal expansion combined with external mechanical loads. The schematic in Fig. 2b shows the deformation of energy walls and slabs under combined thermal and mechanical loading, highlighting the predominant bending deformation.

The analysis and design of energy geostructures can be categorized based on the theoretical approaches employed. Critical aspects of their thermo-hydro-mechanical behavior can be effectively addressed through analytical and semi-analytical modeling methods. However, as the design or analysis progresses, numerical modeling approaches become indispensable for obtaining a comprehensive understanding of the heat transfer, mass transfer, and deformation phenomena that define the behavior of energy geostructures (Rotta Loria, 2020). The following is a summary of theory that can serve the understanding of the behavior and performance of energy geostructures, providing an overview of the expertise available on energy geostructures.

 © DFI International Bruges 2025

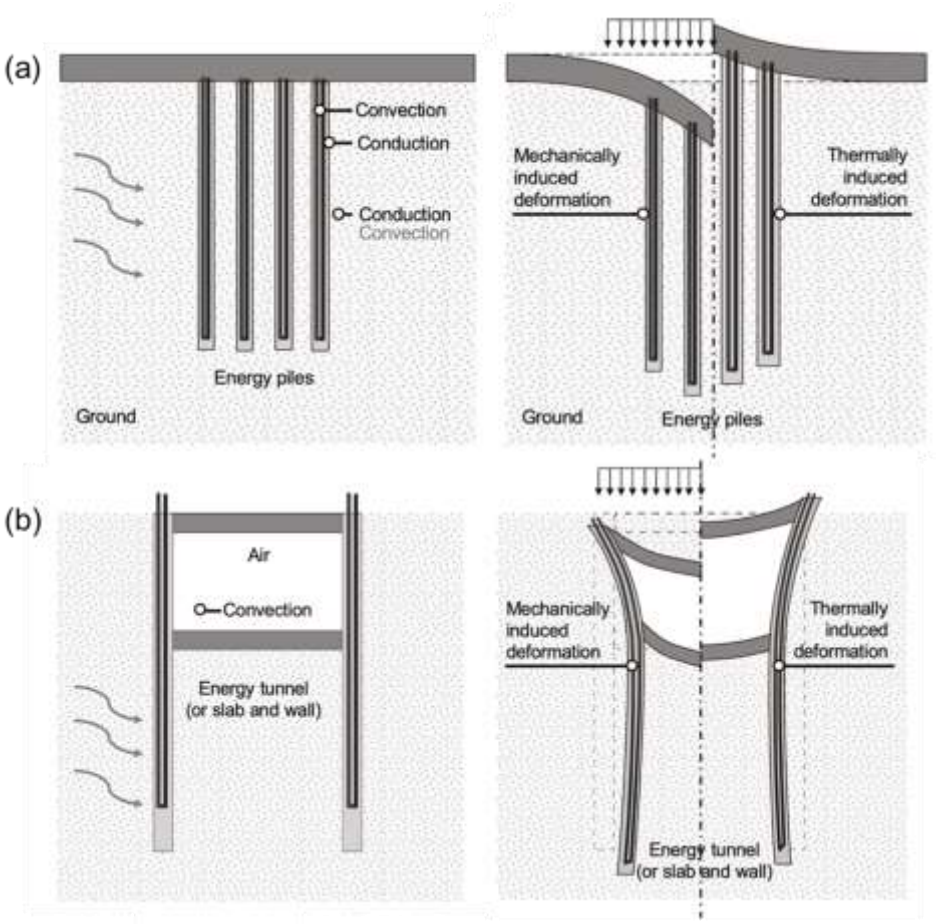


Fig. 2. Heat transfer modes and schematic of deformations (for positive temperature variations) characterizing (a) energy piles and barrettes and (b) walls and slab (modified from Rotta Loria, 2020).

Analyti

Analytical methods provide practical tools to address various aspects of energy geostructure behavior. These approaches are particularly valuable for initial assessments and conceptual design due to their efficiency and relative simplicity. In the following, methods are presented that consider the three interconnected aspects of the behavior of energy geostructures, i.e., energy, structural and geotechnical aspects.

From an energy perspective, thermal performance can be assessed using thermal power charts and thermal resistance models.

Thermal power charts for estimating the thermal power that can be extracted or injected from energy geostructures are available for energy piles, barrettes and walls (Rotta Loria, 2020). These charts consider the characteristics of the site, the configuration of the pipes, the effective thermal conductivity of the soil, the presence, extent and direction of groundwater flow, and the presence and extent of air flow in underground built environments. An example of a thermal power chart proposed by Zannin et al. (2022) for energy wall characterised by different groundwater flow conditions is shown in Fig.3a. These charts can be useful for gathering preliminary information on the energy potential of some energy geostructure installations (e.g., SIA D0190, 2005; Batini et al., 2015; Zannin et al., 2022; Rotta Loria et al., 2023). They give conservative estimates of thermal power because they refer to steady-flux energy operations (i.e., associated with lower bounds on the actual values of thermal power that can be exploited).

 © DFI International Bruges 2025

Thermal resistance models are a more advanced analytical approach to evaluating the energy performance of energy geostructures and involve utilizing the concept of thermal resistance. This includes both time-dependent and time-independent thermal resistance formulations. To address the limitations of traditional solutions designed for heat exchangers in vertical boreholes, specific thermal resistance models have been proposed for energy piles (e.g., Li et al., 2012; Loveridge et al., 2014). Additionally, complementary analytical solutions have been developed for other geostructures such as energy walls (e.g., Kurten et al., 2015).

Analytical models addressing structural behavior include stress charts, continuum analysis models, and load-transfer models:

Stress charts initially developed for conventional piles subjected only to mechanical loads have been adapted for energy piles and barrettes subjected to thermal loads (e.g., Garbellini and Laloui, 2019; Laloui and Rotta Loria, 2019; Rotta Loria et al., 2023). These charts provide estimates of vertical stresses for variables that include different soil and geostructure properties as well as structural constraints. The importance of estimating vertical stress, which characterizes energy geostructures such as energy piles, barrettes, walls, and slabs, lies in the need to control this variable to ensure the required structural performance.

Continuum analysis models are more advanced methods for analyzing geostructures based on simplifications of the continuum thermo-elastic theory (e.g., Laloui et al., 2003; Zannin et al., 2020). Thermal loads arise from temperature variations occurring within and around energy geostructures during their geothermal operations. These variations are typically non-uniform and can be idealized as consisting of two components: a uniform temperature variation that induces axial deformation and a linear temperature variation that causes bending. Uniform temperature variations are considered independently in the analytical modeling of cylindrical energy geostructures, such as piles. In contrast, both uniform and linear temperature variations are considered together in the analytical modeling of planar geostructures, such as walls. Preventing these temperature-induced effects results in axial loads and bending moments, respectively.

In load-transfer models any modeled geostructure is discretized into several elements. These elements interact with the soil via springs that follow a given constitutive law (e.g., determined theoretically or experimentally). Load transfer models can thus better account for the influence of mechanical and thermal loads compared to charts-based approaches. These models are available to describe the behavior of isolated energy piles, groups of energy piles, as well as energy walls and slabs subjected to mechanical and thermal loads (e.g., Knellwolf et al., 2011; Ravera et al., 2020a; Zannin et al., 2020).

The geotechnical behavior of energy geostructures is analyzed using displacement charts, interaction factors charts, and continuum-based methods:

Displacement charts, similar to stress charts, provide estimates of vertical displacements (e.g., Rotta Loria et al., 2016; Rotta Loria et al., 2017a; Rotta Loria et al., 2023). Fig. 3b shows an example of a chart indicating the vertical displacement of the head of a single cylindrical energy pile subjected to a thermal load in an elastic soil mass. The displacement values provided are expressed per unit of applied thermal load. The thermally induced displacement is reported in absolute value to be representative of the heating and cooling thermal loads, which involve reversible conditions for the soil.

Interaction factors charts are available to account for interactions occurring when piles are grouped and quantify the degree of mechanical interaction between energy piles located sufficiently close to one another and subjected to mechanical and thermal loads. These charts are applicable to scenarios both without a slab at the head of the piles and with a slab connecting the piles (e.g., Rotta Loria et al., 2016; Rotta Loria et al., 2017a; Ravera et al., 2020b). The degree of interaction is quantified through a displacement interaction factor, which measures the effects caused by the loading of a source pile on a receiver pile. Displacement interaction factors are provided in tables for uniform soils as well as for

 © DFI International Bruges 2025

scenarios involving the presence of a finitely or infinitely rigid bearing layer. An example of a chart presenting interaction factors for energy piles subjected to a thermal load is shown in Fig. 3c.

Continuum analysis models that incorporate the geotechnical aspects have been developed for groups of energy piles, utilizing Mindlin's equations (e.g., Rotta et al., 2017b). A key advantage of this approach over chart-based methods is its ability to define interaction factors as a function of depth rather than being limited to the pile head.

The load-transfer method described in the section on structural aspects for defining stresses also addresses geotechnical aspects by providing information on displacements and soil-structure interface resistance.

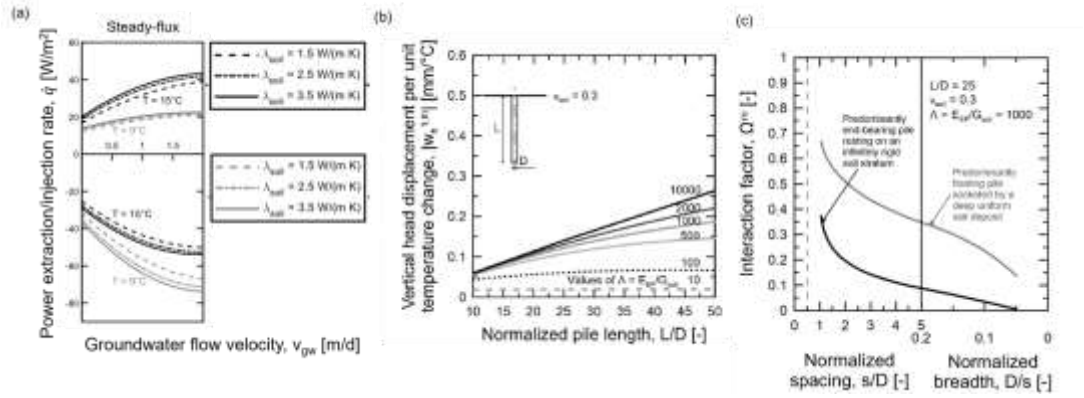


Fig. 3. Examples of (a) power charts (modified from Zannin et al., 2022), (b) displacement charts, and (c) interaction factor charts (modified from Rotta Loria, 2020).

Numerical methods

Numerical analysis is the most advanced approach for analyzing and designing energy geostructures, encompassing energy, structural, and geotechnical aspects. For energy performance, simulations model heat and mass transfer characteristics, often using temperature or thermal power variations applied to the geostructures. Advanced software facilitates modeling of embedded tubes and heat transfer interactions with the built environment. Time-dependent simulations are essential, as thermal loads in energy systems vary over time. Structural aspects are simulated by applying forces or displacements, with structural elements or simplified stiffness quantifications. Concrete behavior is typically modeled as linear thermoelastic, but advanced analyses may include thermal creep and tensile resistance. Geotechnical simulations incorporate soil properties to realistically represent heat transfer, mass transfer, and deformation phenomena, with a focus on thermal expansion coefficients to estimate thermally induced deformations and stresses.

APPLICATION AND DEVELOPMENT OF ENERGY GEOSTRUCTURES

This section expands on a case study involving the development and application of some of the previously discussed methods related to a real project case. An experimental and computational study about the performance of a real-world installation of a complex energy geostructure foundation is summarized here concerning Testimonio II building located in the Principality of Monaco (Rotta Loria et al., 2023).

The Testimonio II real estate complex is located in the Principality of Monaco. Testimonio II includes 348 housing units in two residential towers, a 50-place nursery, and a new site for the International School of Monaco, which accommodates 700 students. The building also features several levels of underground parking, constructed on complex foundations with different base levels depending on the location on the site. The foundation of Testimonio II includes barrettes, piles, diaphragm walls, and slabs. Some of these foundation elements have been thermally activated to harness geothermal energy from the ground and supply the building in combination with a vertical geothermal borehole field

 © DFI International Bruges 2025

drilled beneath the structure. The geostructure system consisting of 165 energy piles and approximately 9,500 m² of energy barrettes was analyzed, designed, and tested to meet the building's energy needs.

During the design phase, field experiments and three-dimensional time-dependent thermo-hydro-mechanical analyses of energy barrettes were conducted. The field experiments included thermal performance tests, in which thermal loads were applied to geothermal heat exchangers to observe their behavior under varying geometric, site, and operational conditions. These tests were conducted to investigate the thermal behavior of energy barrettes based on pipe configurations and the location of the heat exchangers on the site. The results validated the models used during the design phase (Fig. 4).

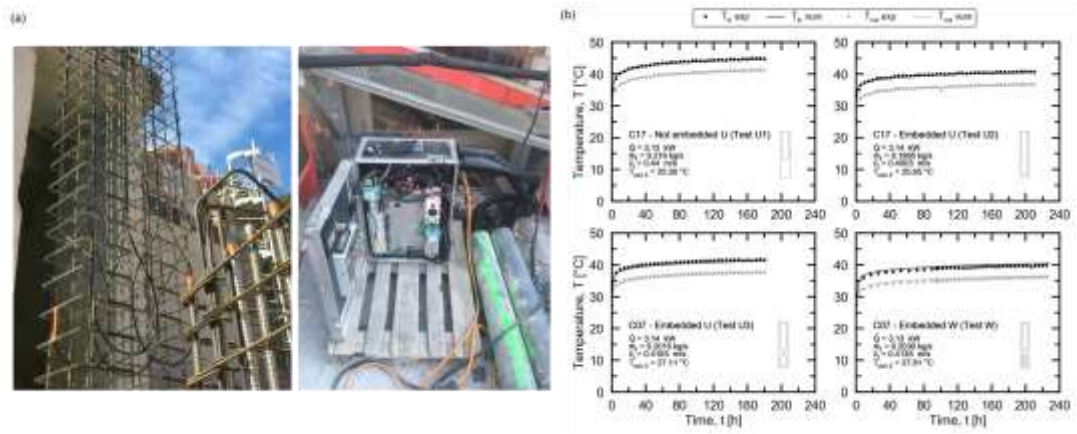


Fig. 4. (a) photograph of one of the energy barrettes supporting the considered building ensemble and testing equipment; (b) comparison between the experimental and simulation results (modified from Rotta Loria et al.. 2023).

The numerical analyses modeled the energy geostructures, the soil, and the integrated pipes, enabling a deeper understanding of thermal interactions and their effects on the overall system performance (Fig. 5). The results provided new insights into the behavior of energy barrettes under a variety of practical conditions, highlighting significantly non-uniform temperature fields within and around the foundations. This analysis led to the development of the first design charts for this type of energy geostructure (Rotta Loria et al., 2023). However, as noted earlier, while these charts are useful tools for an initial energy assessment, numerical analyses remain essential. Fig.5 shows that in cases involving complex foundation geometries, thermal and mechanical interactions can only be accurately analyzed through time-dependent three-dimensional thermo-hydro-mechanical modeling. Neglecting these interactions may result in diametrically opposed performance outcomes for energy geostructures, leading to marked traps, particularly when dealing with the performance of complex energy geostructures (Ravera et al., 2024).

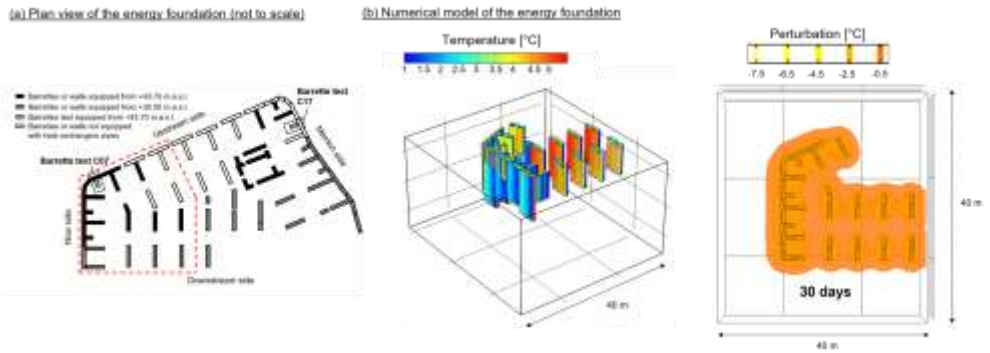


Fig. 5. (a) plan view of the energy foundation supporting the ‘‘Centrale’’ portion of the ensemble; (b) numerical model used to predict the behavior of selected energy barrettes — temperature profiles in the exchanger tubes and temperature perturbation in the surrounding soil (image source: GEOEG (www.geoeg.net)).

 © DFI International Bruges 2025

CLOSURE

Over the past thirty years, research initially focused on understanding the behavior and performance of energy piles has gradually expanded to include other types of foundations, such as barrettes, walls, and slabs. This progression marks the field's evolution from its early focus on specific elements to a comprehensive maturity encompassing all foundation types. Building on this extensive body of knowledge, the present work offers experimental and computational study that shed light on the real-world performance of energy geostructures systems. The findings of this study underline the practicality and efficiency of energy geostructures in all their forms, demonstrating their capacity to deliver sustainable and effective energy solutions across a variety of urban applications. This highlights their role as a fully viable and mature pathway toward more sustainable cities and infrastructures.

REFERENCE

Bayer, P., Attard, G., Blum, P., and Menberg, K. 2019. The geothermal potential of cities. Renewable and Sustainable Energy Reviews, 106, 17–30.

Batini, N., Rotta Loria, A.F., Conti, P., Testi, D., Grassi, W., and Laloui, L. 2015. Energy and geotechnical behaviour of energy piles for different design solutions. Applied Thermal Engineering, 86, 199-213.

Benz, S.A., Menberg, K., Bayer, P., and Kurylyk, B.L. 2022. Shallow subsurface heat recycling is a sustainable global space heating alternative. Nature Communications, 13(1).

Brandl, H., 2016. Geothermal geotechnics for urban undergrounds. Procedia engineering, 165, pp.747-764.

I.E.A. International Energy Agency 2023. Tracking Clean Energy Progress (TCEP).

Edenhofer, O., Pichs-Madruga, R., Sokona, Y., … Zwickel, T. 2011. Renewable Energy Sources and Climate Change Mitigation, Summary for Policy Makers. 1075.

Garbellini, C. and Laloui, L., 2019. Three-dimensional finite element analysis of piled rafts with energy piles. Computers and Geotechnics, 114, p.103115.

Knellwolf, C., Peron, H. and Laloui, L. 2011. Geotechnical analysis of heat exchanger piles. Journal of Geotechnical and Geoenvironmental Engineering, 137(10), pp.890-902.

Kürten, S., Mottaghy, D. and Ziegler, M. 2015. A new model for the description of the heat transfer for plane thermo-active geotechnical systems based on thermal resistances. Acta Geotechnica, 10, pp.219-229.

Meibodi, S.S. and Loveridge, F. 2022. The future role of energy geostructures in fifth generation district heating and cooling networks. Energy, 240, 122481.

Laloui L, Moreni M, and Vulliet L. 2003. Comportement d'un pieu bi-fonction, fondation et échangeur de chaleur. Canadian Geotechnical Journal. 40(2): 388-402.

Laloui, L. and Rotta Loria, A.F. 2019. Analysis and Design of Energy Geostructures.

Li, M. and Lai, A.C. 2012. New temperature response functions (G functions) for pile and borehole ground heat exchangers based on composite-medium line-source theory. Energy, 38(1), pp.255-263.

Louwen, A., van Sark, W.G J.H.M., Faaij, A.P.C., and Schropp, R.E.I. 2016. Reassessment of net energy production and greenhouse gas emissions avoidance after 40 years of photovoltaics development. Nature Communications, 7(1), Article 1.

 © DFI International Bruges 2025

Loveridge, F. and Powrie, W. 2014. 2D thermal resistance of pile heat exchangers. Geothermics, 50, pp.122-135.

Pfadt-Trilling, A.R., Widyolar, B.K., Jiang, L., Brinkley, J., Bhusal, Y., Winston, R., and Fortier, M.O.P. 2023. Life cycle greenhouse gas emissions of low-temperature process heat generation by external compound parabolic concentrator (XCPC) solar thermal array. Renewable Energy, 205, 992–998.

Ravera, E., Sutman, M. and Laloui, L. 2020a. Load transfer method for energy piles in a group with pile–soil–slab–pile interaction. Journal of Geotechnical and Geoenvironmental Engineering, 146(6), p.04020042.

Ravera, E., Sutman, M. and Laloui, L. 2020b. Analysis of the interaction factor method for energy pile groups with slab. Computers and Geotechnics, 119, p.103294.

Ravera, E., Rotta Loria, A.F. and Laloui, L. 2024. Performance of complex energy geostructures. Geomechanics for Energy and the Environment, 38, p.100536.

Rotta Loria, A.F. and Laloui, L. 2016. The interaction factor method for energy pile groups. Computers and Geotechnics, 80, pp.121-137.

Rotta Loria, A.F. and Laloui, L. 2017a. Displacement interaction among energy piles bearing on stiff soil strata. Computers and Geotechnics, 90, pp.144-154.

Rotta Loria, A.F., Vadrot, A. and Laloui, L. 2017b. Effect of non-linear soil deformation on the interaction among energy piles. Computers and Geotechnics, 86, pp.9-20.

Rotta Loria, A. F. 2020. Energy geostructures: theory and application. In E3S web of conferences (Vol. 205, p. 01004). EDP Sciences.

Rotta Loria, A. F. 2023. The silent impact of underground climate change on civil infrastructure. Communications Engineering, 2(44).

Rotta Loria, A.F., Ravera, E. and Laloui, L. 2023. Thermo-hydro-mechanical behavior of energy barrettes: field experiments and numerical simulations. Geomechanics for Energy and the Environment, 34, p.100451.

Sani, A.K., Singh, R.M., Amis, T. and Cavarretta, I. 2019. A review on the performance of geothermal energy pile foundation, its design process and applications. Renewable and Sustainable Energy Reviews106,54–78

SIA-D0190. 2005. Utilisation de la chaleur du sol par des ouvrages de fondation et de soutènement en béton. Guide pour la conception, la réalisation et la maintenance. Zurich, Switzerland

Singh, R.M., Sani, A.K. and Amis, T. 2019 An overview of ground-source heat pump technology. Managing Global Warming,455–485.

Zannin, J., Ferrari, A., Larrey-Lassalle, P. and Laloui, L. 2022. Early-stage thermal performance design of thermo-active walls implemented in underground infrastructures. Geomechanics for Energy and the Environment, 30, p.100218.

Zannin, J., Loria, A.F.R., Llabjani, Q. and Laloui, L., 2020. Extension of Winkler's solution to non-isothermal conditions for capturing the behaviour of plane geostructures subjected to thermal and mechanical actions. Computers and Geotechnics, 128, p.103618.

Zhu, K., Blum, P., Ferguson, G., Balke, K.-D., and Bayer, P. 2010. The geothermal potential of urban heat islands. Environmental Research Letters, 5(4), Article 044002.

 © DFI International Bruges 2025

LOW-STRAIN IMPACT TESTING OF PILES - AI ANALYSIS

Joram.M. Amir, Piletest.com Ltd., Netanya, Israel, (+972)9891 1899, jmamir@piletest.com
Erez .l. Amir, Piletest.com Ltd., Netanya, Israel, (+972)9891 1899, erezam@piletest.com
Gil Amihai, Data Scientist, Kadimah-Tzoran, Israel, (+972)523331300, gil.amihai@gmail.com

ABSTRACT

Low-strain integrity testing of foundation piles is a widespread method for the integrity testing of deep foundations. The equipment used is relatively low-cost, the pile head requires little preparation, and the net testing time is short. Due to these properties, the method is especially suited to 100% testing of piling sites. The method is standardized (ASTM 2016), that defines "integrity" as *"The qualitative evaluation of the physical dimensions, continuity of a pile, and consistency of the pile material"*.
The Artificial Intelligence (AI) model presented in this paper was trained to assess the pile lengths on a database of real test results, individually analyzed by an experienced engineer. The resulting model was then validated using test results obtained from several independent testing laboratories. In the first stage, the pile length was the only physical dimension parameter that we investigated. So far, the results are encouraging and justify further development.

KEYWORDS: Pile, Integrity, Analysis, Artificial Intelligence, AI, Machine Learning, ML

INRODUCTION

Developed by Beylich (1963), the low-strain impact testing method involves tapping the pile head with a hand-held hammer while an accelerometer is pressed against the head. Each hammer impact creates a one-dimensional acoustic wave that travels downwards and is then reflected upwards from the pile toe. During this process, the resulting pile head displacements are monitored by an accelerometer, connected to a portable computer that stores and analyzes the time-history of pile head velocities. Inspecting this time-history can indicate the pile integrity, namely the pile length and any variation from its cross section.

While field testing is relatively simple, interpreting the method's test results is not always straightforward and should be performed by suitably experienced geotechnical engineers. The method proposed in this paper lowers the need for such experienced engineer by automating the analysis.

RESEARCH GOAL

The research goal was to build an AI model that can analyze the test results as well as a human expert. Ideally, the model should be able to:

- Predict the pile length (by placing the length marker at the correct toe reflection)
- Assess the pile's integrity
- Set up display parameters such as amplification, filter, etc.
- Categorize the pile into one of the following categories: good/questionable/problematic/inconclusive
- Provide textual analysis

PILE LENGTH

Establishing the actual pile length is of utmost importance to confirm that the pile has sufficiently penetrated the planned bearing layer and will develop the required geotechnical capacity. In most cases, the length also serves as the basis for payment to the piling contractor. Nevertheless, for bored and cast in-situ piles, the actual length is usually unknown. The four available values are as follows:

 © DFI International Bruges 2025

1 $L_{planned}$ - the planned length, i.e., the length shown in the contract drawings

2 L_{asmade} - the as-made length measured in situ and reported by the site supervisor

3 L_{expert} - the length obtained by the low-strain impact test and reported by a qualified testing engineer

4 L_{model} - the length predicted by the proposed AI model

The last two items are a direct function of the wave speed assumed by the tester. For a given site, the wave speed is also unknown. Therefore, testers may be guided by the following methods:

1. Published correlations, based on the concrete compressive strength and age (Amir 1988).
2. If available, an average representative number of as-made lengths on the specific site.

Statistical analysis (Amir and Amir 2008) has shown that the wave speed assumed by most testers is 4,000 m/s, plus or minus 10 percent.

METHODOLOGY

Machine Learning Methods

Machine Learning (ML) model training is an iterative process in which the model goes over the input data, and "learns" the patterns by minimizing the "loss" (or error) between its predictions (output) and the real target (input). The training (Fig. 1) is stopped when the error reaches the minimum, but overfitting (learning specific instead of general patterns) should also be controlled.

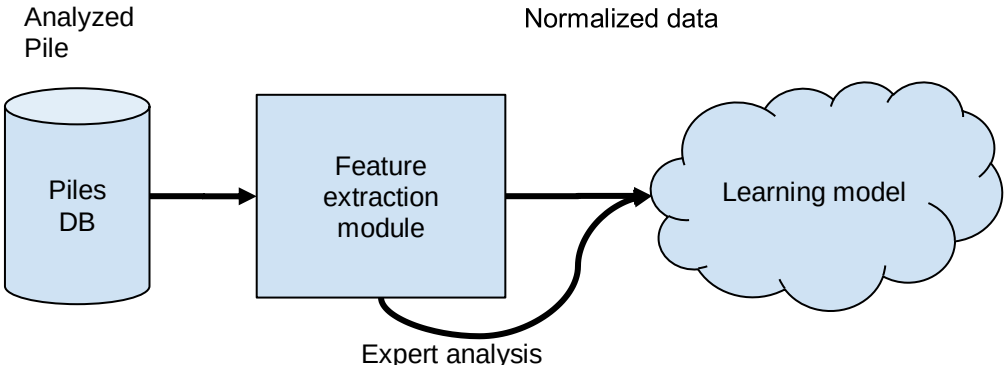


Fig 1: Training phase

At the end of the training phase, the model weights are saved, so the trained model can be used for inference-making predictions on new data (Fig.2).

We tried two types of ML models: decision-tree-based (e.g., XGBoost [5]) and Deep Learning [6]). As expected, the performance of all models improved as the amount of data increased. The deep learning model performed better, so we chose it for final training and validation.

The data

A testing agency gave us access to its test results database (590,000 test results), reflecting the products of six teams over twenty years. Eighty percent of those were randomly picked for the training stage of the ML model, using several machine learning (ML) approaches. The remaining twenty percent were saved for model inference validation.

 © DFI International Bruges 2025

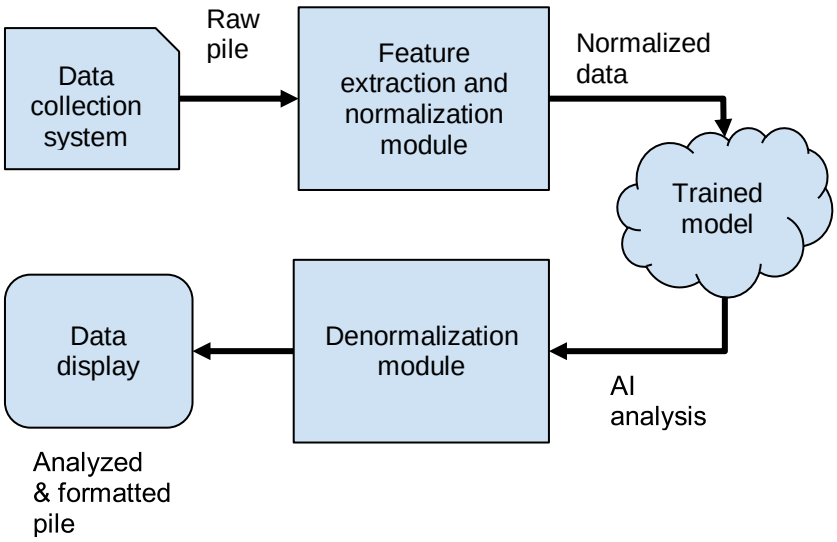


Fig. 2: Inference phase

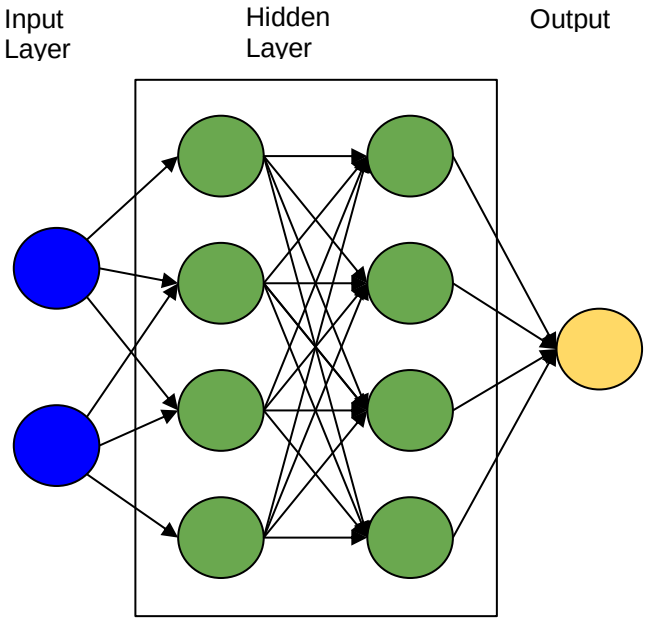


Fig. 3. Schematic deep learning network structure

The inputs of the *trained* model for each tested pile were as follows:

- Accelerometer time series vector - data at fixed time intervals according to the sample rate $_{planned}$ [m]
- The wave speed c [m/s]. This is a major unknown and in order to remove the complexities involved from the model, we have switched to a time-only model and converted $L_{planned}$ to $T_{planned}$ (time), according to Equation 1.
- $L_{planned}$ (m).

$$T_{planned} = 2 \cdot \frac{L_{planned}}{c} \quad [1]$$

 © DFI International Bruges 2025

Preprocessing

After a few failed attempts, we realized that the data needed to be pre-processed using default parameters and passed on to the model in the same form as it appeared to an expert when analyzing it.
A quick-reject script scanned all input data for user entry errors. The script also rejected extreme cases such as very short or very long piles, piles with very high amplification, or piles where the user collected an abnormally high number of impacts (indicating this is an exceptionally hard-to-test case). In total, 81k test results, or 14% of the raw data, were rejected.

Amplification

A typical amplification factor for a 30m long pile is 100-200. Without proper amplification, the time series appears "flat" without apparent features.
Based on Amir & Amir (2008), who studied the relationship between planned length and amplification, we have set the amplification for all piles to 10 + $L_{planned}$ * 3 (for example, 70 for a 20m pile)

Data duration

The system acquires the data for a much longer time than later displayed. This is done for cases in which the user does not know the planned length or wants to examine second reflections. Presenting the whole time- series to the model resulted in poor results (since most of the trace beyond the toe reflection contains little information and adds noise to the system).
Based on the dataset analysis, we clipped the time series to 1 millisecond beyond the planned length. At a typical wave speed of 4000m/s, this is equivalent to 2m of data.
Next, we diluted the time series to 100 points - a good compromise between size and resolution.

Other parameters

All display parameters, such as low-pass filtering, sharpening, etc., were set to zero. Next, we normalized the clipped and amplified time series to the range of 0…1 (where 0.0 is the time of the hammer impact and 1.0 is $T_{planned}$ + 1 millisecond). $T_{planned}$ was also normalized to the same range.

Evaluation Criterion

We used the mean absolute percentage error (MAPE) as the success criterion. MAPE (Eq. 2) indicates the absolute distance from the expert's prediction in percentage of the AI model prediction. For example, if the expert reached a figure of 10m and the AI model predicted 10.5m (or 9.5m), the MAPE is 5%.

$$MAPE = \frac{100}{n} \cdot \sum_{i=1}^{n} \frac{L_{model} - L_{expert}}{L_{expert}} \quad [2]$$

RESULTS

The model was tested on the remaining ~20% (110,000) and the results (Fig. 4) show a correlation (R^2) of 0.9757 between L_{model} and L_{expert} analysis, with a MAPE of 1.6% relative to the human experts' analysis L_{expert}. In other terms, 90% of the AI models' predictions were not more than 2% shorter or longer in relation to the human expert's analysis.

 © DFI International Bruges 2025

Note that the abnormal data points cannot be classified as “outliers” as it is impossible to tell if the error is due to the expert, the model (or both) without re-evaluating each of the 110,000 data points. The main value of (Fig. 4) is demonstrating the correlation. At this testing phase, model errors can only be quantified, but the reasons for the error cannot be obtained.

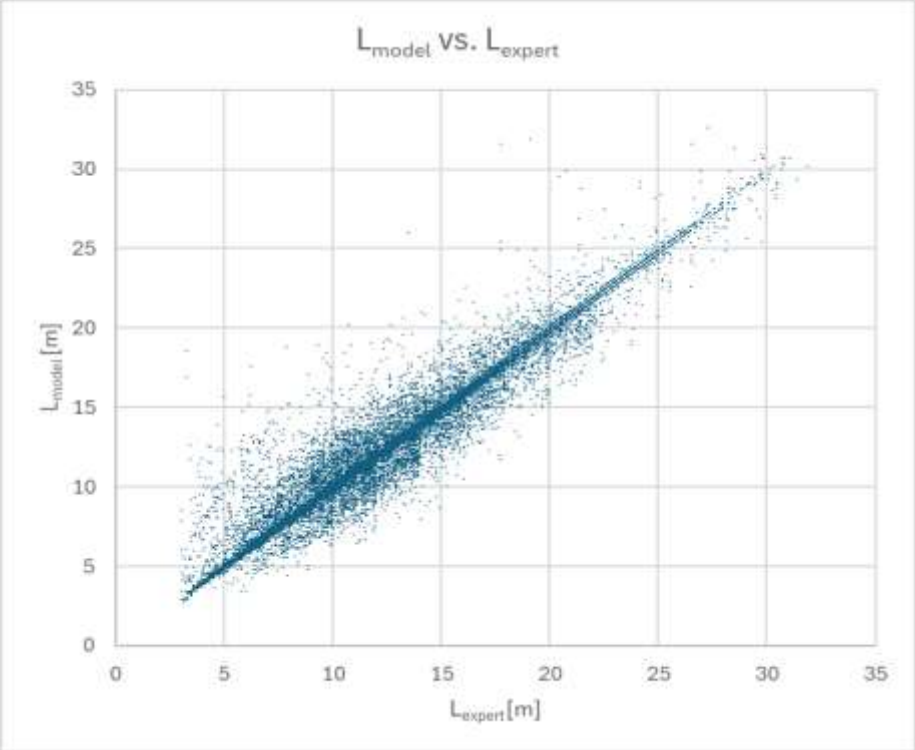


Fig. 4: ML prediction compared to experts’ analysis

The model-predicted length mark L_{model} was compared to two "naive" predictions:

- The planned length $L_{planned}$. Although an input to the system, this value can also be used as a naive predictor.
- The deepest trough (toe reflection) in the signal after the initial hammer impact - $L_{minimum}$. Under ideal conditions, the deepest trough is defined as the toe reflection, so this naive predictor works well in most piles (in this research, about 85% of the piles).

To study the scatter in more detail, we plotted the accumulated percentage of the predictions (L_{Model}, $L_{planned}$, and $L_{minimum}$), against L_{expert}.
The prediction distribution (Fig. 5) shows that the AI model performs better than the two other naive predictors. To clarify that, we have highlighted a few points on the graph with a large red dot.

90, 94, and 96 percent of the model’s predictions L_{model} are accurate to within 2, 5, and 10 percent (respectively) of the expert-predicted length L_{expert} (or better).
The ML prediction accuracy is better than the values considered acceptable by the industry (Amir and Amir 2008).

CLASSIFICATION OF THE RESULTS

For simplicity, the AI results may be classified as:

1) "Good" predictions - within 5% of L_{expert} (About 94% of the results) (Fig. 6)

 © DFI International Bruges 2025

2) "Better" results, where the model result was clearly better than the expert's (Fig. 7)
3) "Wrong" results (Fig. 8)
4) "Inconclusive" prediction - Different from L_{expert} by more than 5% but could have been picked up by another expert (Fig. 9). In Figures. 6-9, the upwards-pointing green triangle is L_{model} and the vertical red line is L_{expert}.

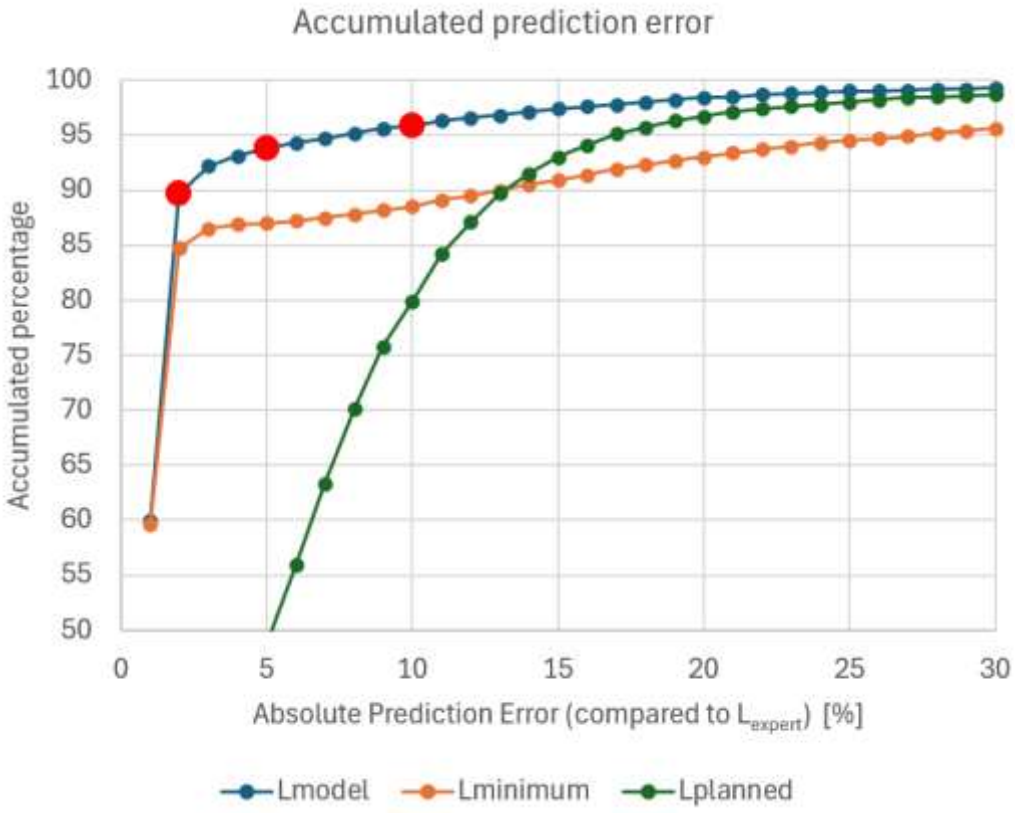


Fig. 5 - Prediction error [%] of AI model L_{model}, planned length $L_{planned}$ and the deepest trough $L_{minimum}$ - compared to the expert's analysis L_{expert}



Fig. 6 - "Good" example: $L_{expert} \cong L_{model}$

 © DFI International Bruges 2025

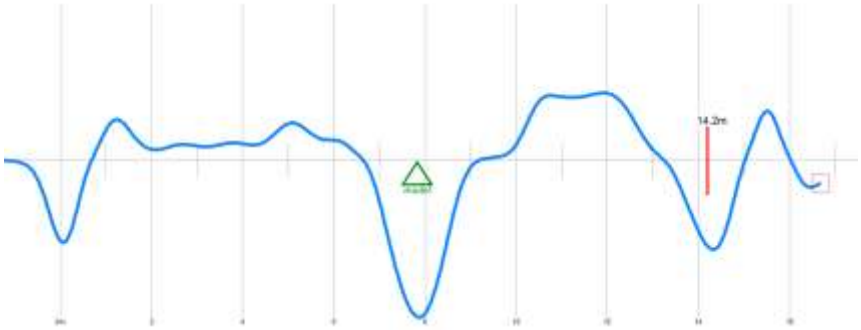


Fig 7. "Better" example: L_{model} is a better choice than L_{expert}

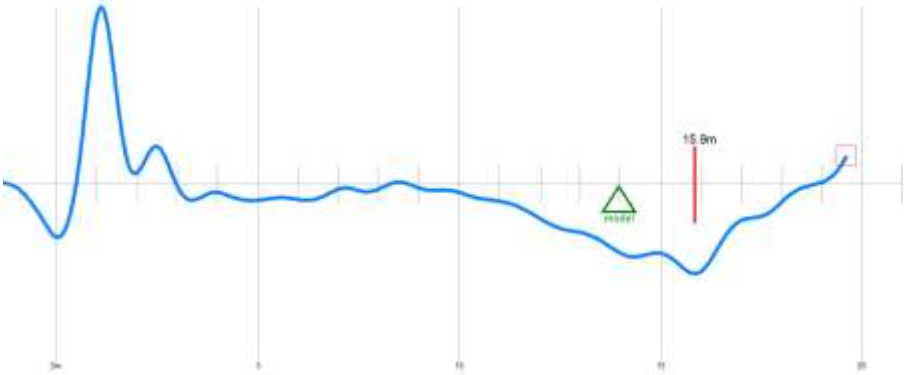


Fig 8: "Wrong": L_{model} does not select the right location

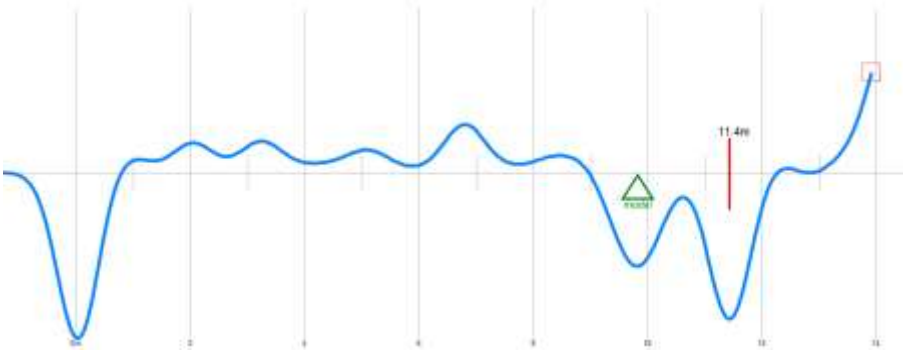


Fig. 9: "Inconclusive" example: on another day or another expert could have agreed with L_{model}

SUMMARY AND CONCLUSIONS

- The AI model predicted the lengths of 90% of all test results with an accuracy of 2% or better - compared to L_{expert} (human expert's analysis). This is better than that considered acceptable by the industry.
- It is likely that by improving the AI models' architecture and training, and by gathering more data, the prediction quality would improve.

 © DFI International Bruges 2025

- A well-performing AI model could point to erroneous human analyses or be used for training novice analysts.
- The potential of using AI to replace human analysis is promising. However, as mistakes are inherent in any AI inference, AI cannot replace solid engineering judgment.
- Further development is required to achieve more of the research goals:
    - Identify anomalies as related to changes in the pile impedance and provide textual analysis.
    - Categorize the pile test results into one of the following categories: good/questionable/problematic/inconclusive
- The AI model should be expanded using test results from a variety of test agencies and experts.

ACKNOWLEDGMENTS

The authors are indebted to Dr. L. Sharshevski and Y. Neeman (Isotop Ltd.), who provided valuable access to their vast databases.

REFERENCES

1. Amir, J.M (1988): Wave velocity in young concrete, Proc 3rd Intl Conf on Application of stress-wave theory to piles, Ottawa, pp. 911-912.

2. Amir, E.I & Amir, J.M (2008): Statistical Analysis of a Large Number of PEM Tests on Piles, Proc. 8th Intl. Conf on Application of Stress Wave Theory to Piling, Lisbon, pp. 671-675.

3. ASTM (2016) : D5882 Standard Test Method for Integrity Testing of Deep Foundations by Low Strain Impact, ASTM, W. Conshohocken, PA.

4. Beylich, M. (1963): Types de Fondation Classiques – Controle des Pieux, LCPC

5. Introduction to boosting trees: https://xgboost.readthedocs.io/en/stable/tutorials/model.html.

6. What is deep learning: https://aws.amazon.com/what-is/deep-learning/

 © DFI International Bruges 2025

THE EMBODIED CARBON OF CONTINUOUS FLIGHT AUGER, AUGER DISPLACEMENT (CHD) AND PRECAST DRIVEN DISPLACEMENT PILES IN COHESIVE GROUND.

Prof Jon Ball, Roger Bullivant Piling, Swadlincote, Derbyshire, UK. 07966394391, jon.ball@roger-bullivant.co.uk

Faye Dandy, Roger Bullivant Piling, Swadlincote, Derbyshire, UK. 07977058059, faye.dandy@roger-bullivant.co.uk

James Cowburn, Roger Bullivant Piling, Swadlincote, Derbyshire, UK. 07971131664, james.cowburn@roger-bullivant.co.uk

ABSTRACT

Historically, design of foundations has rarely considered the carbon consumption associated with construction. However, with the advent of the European Federation of Foundation Contractors' (EFFC) Carbon calculator, championed by the Federation of Piling Specialists in the UK, there is now a reliable benchmarking technique available to compare and understand this aspect of the process better. This paper will present a comparison of three pile drilling construction methods in the same cohesive ground conditions in relation to their relative carbon consumption. A comparison of Continuous flight auger (CFA), Displacement auger (CHD) and Driven precast displacement (PCC) will be used to illustrate the relative carbon consumption of each drilling method. To assist with the comparison, two efficiency techniques will be used to assist with the discussion. First, the drilling methods will be normalised in relation to load and then they will be normalised against cost to society. The implications of these two efficiency techniques; carbon/load and carbon/cost will be discussed. It will be concluded that displacement auger (CHD) is the most efficient piling method, in regard to carbon efficiency.

INTRODUCTION

It is becoming increasingly common in the UK that funders are placing greater emphasis in the tender process on the magnitude of carbon consumption which takes place to complete the project. Cost and carbon consumption are increasingly given equal weight when considering the successful selection of subcontractor in the award process.

It has become necessary for funders, clients and subcontractors to consider not only the most efficient foundation solution from a cost perspective, but also from a carbon consumption perspective too. Therefore, it is exceedingly useful to understand the most efficient foundation system from a carbon perspective at an early stage in the process.

The purpose of this paper is to bring together a comparison of various types of piles installed on sites in the UK, in similar ground conditions, to understand the relative sustainability benefits of each foundation type. This exercise has been facilitated using the EFFC carbon calculator version 5.0 (https://www.effc.org/content/uploads/2025/03/EFFC-DFI-CC_v5-7.xlsm), which has rapidly become the UK piling standard tool for this type of investigation.

Three different pile types will be reviewed, Continual Fight Auger (CFA), Driven Precast (PCC) and Auger Displacement Piles (CHD), all commonly installed in the UK. In Table 1 and 2 below are the variable input parameters used in the EFFC carbon calculation sheet for the two different sites one in central Scotland, the Second in the South of England. Comparisons will be made between the carbon consumption for each method, normalised against geology, load bearing and the impact of the process as a cost to society.

 © DFI International Bruges 2025

Table 1. Variable input parameters for site A

	PCC	CFA	CHD
Concrete volume (m^3)	1.35	2.39	2.08
Cement UK designation	CEM III/A	CEM III/B	CEM III/B
Total cementitious content (kg/m^3)	193	143	143
GGBS (%)	50	73	73
Aggregate	1195	812	812
Sand	615	823	823
Water	124	200	200
Waste (t)	N/A	3	0.25

Table 2. Variable input parameters for site B

	PCC	CFA	CHD
Concrete volume (m^3)	0.72	2.26	1.9
Cement UK designation	CEM III/A	CEM III/B	CEM III/B
Total cementitious content (kg/m^3)	193	150	150
GGBS (%)	50	73	73
Aggregate (kg/m^3)	1195	785	785
Sand (kg/m^3)	615	782	782
Water (kg/m^3)	124	224	224
Waste (t)	N/A	2.83	0.25

The values contained within tables 1 and 2 are derived from insitu volume measurement and concrete mix designs provided by the concrete supplier for each of the projects under review.

GEOLOGY

Both sites are dominated by cohesive material throughout and briefly summarised in Table 3 below.

Table 3. Geotechnical summary

Site reference	Shear Strength (kPa)	Bulk Unit Weight (kN/m^3)	Description	Age
Southern UK (Site A)	80-220	19	Fissured, over-consolidated CLAY	Cretaceous
Central Scotland (Site B)	45-150	21	normally consolidated (Glaciolacustrine) CLAY	Pleistocene

EMBODIED CARBON

Both Driven Precast piles (PCC) and continual flight auger (CFA) piles have been available in the UK for many years and are common throughout the industry. Less common is the Auger Displacement (CHD) pile, successfully developed in the late 1990's in the UK market.

Like CFA, Auger Displacement piles are cast insitu, but without the associated surface arisings generated by CFA piles. The soil displaces around the CHD tool resulting in improved pile performance due to the non-uniform cross section along the pile length. The specialised drill tool

 © DFI International Bruges 2025

pushes the soil outwards, enhancing the efficiency of the pile to carry load and significantly removing the production of surface spoil. The method is noted to be most suited for use in congested urban environments (van Impe, 2004) as well as suitable where there is contaminated ground (Wade et al., 2012)



Figure 1. Auger Displacement (CHD) pile

Geotechnical pile designs have been produced for each site to quantify the required length of each pile type for a single serviceability state. BSEN 1997-1 (2004+A1:2013) and UK National Annex has been followed for the purposes of design on both occasions. Comparisons have been made between piles of a specific length to determine the embodied carbon for each. This information is contained in Table 4 with Figure 2 showing this information is graphical format. The embodied carbon analysis has been assessed using the EFFC carbon calculator (EFFC V5, 2024).

Material Based Emissions

Table 4. Comparative carbon consumption normalised to pile length.

Pile Type	Site	Pile Length (m)	Embodied Carbon per Pile (Kg)
CFA	A	15	0.286
CHD	A	15	0.208
PCC	A	15	0.095
CFA	B	8	0.271
CHD	B	8	0.19
PCC	B	8	0.05

 © DFI International Bruges 2025

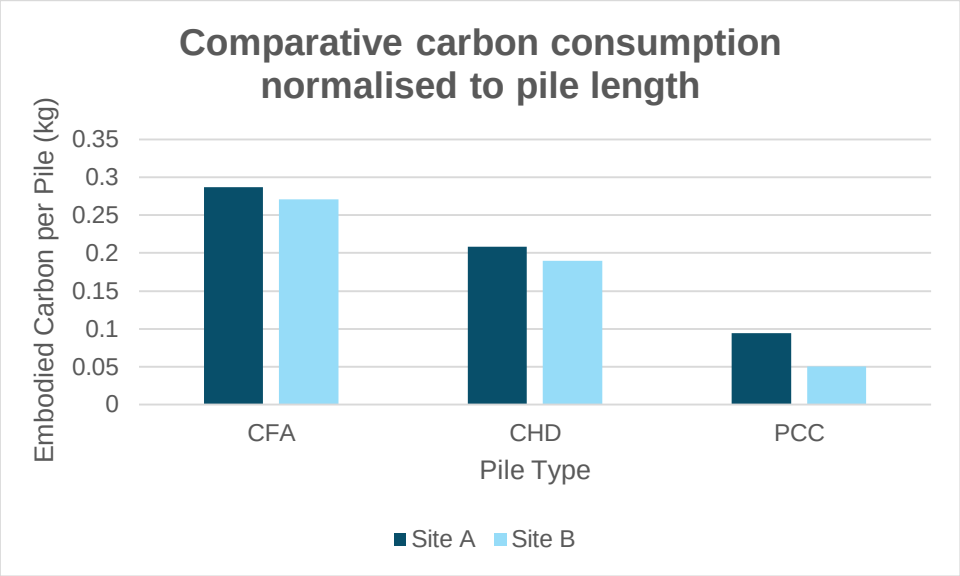


Figure 2. ***A bar graph showing comparative carbon consumption normalised to pile length.***

It can be seen from Table 4 and Figure 2 that the lowest emissions for a fixed pile length are those from a driven Precast pile (PCC). However, whilst a direct comparison of each pile can be made from the information contained in Table 4 above, this information is highly influenced by the concrete mix used; carbon efficient mixes will return lower values of consumption for the same pile length compared with those mixes that are less efficient. This is therefore a straightforward and useful tool to design and refine the carbon emissions of the materials used in producing similar dimensioned piles across numerous sites.

Load Based Emissions

The writers assert that the assessment of material-based emissions is not sufficiently detailed to fully consider the comparative emissions of different piling methods as the relative geotechnical benefits of each installation process are not considered in a material only assessment, which could lead the funder's engineer to select an inefficient piling method.

The information contained in Table 4 does not consider the geotechnical design length required to support a specific serviceability limit state (SLS) otherwise known as the geotechnical efficiency. The values of embodied carbon normalised against load is contained in Table 5 for each pile type is intended to highlight the impact of this parameter. In this analysis, the benefits of individual bearing capacity efficiencies are included together with material-based emissions.

Table 5. Carbon emissions normalised to load.

Pile Type	Site	Pile Length (m)	Embodied Carbon per kN (Kg/kN)
CFA	A	15	0.18
CHD	A	15	0.07
PCC	A	15	0.16
CFA	B	8	0.20
CHD	B	8	0.09
PCC	B	8	0.16

It can be seen from the information contained in Table 5 that the most efficient piling method from the perspective of load capacity combined with carbon emissions is that of the CHD pile.

 © DFI International Bruges 2025

As can be perceived from Figure 3 below, a normalised load assessment is a significantly more powerful approach and considers that for the same load, the appropriate design of CFA piles is longer than driven precast, which in turn is longer than CHD which returns the shortest length for the notional SLS in the same ground conditions.

Many instances where ultimate load capacity of the CHD pile has significantly exceeded current design predictions (Jeffrey et al., 2010) which has its origins in CFA pile design which is shown to be conservative (Gavin et al., 2009) therefore it stands to reason that along with other similar types of displacement piles that have been found to perform well in terms of load settlement behaviour (Bell, 2010) the CHD pile is the most efficient out of the 3 pile types.

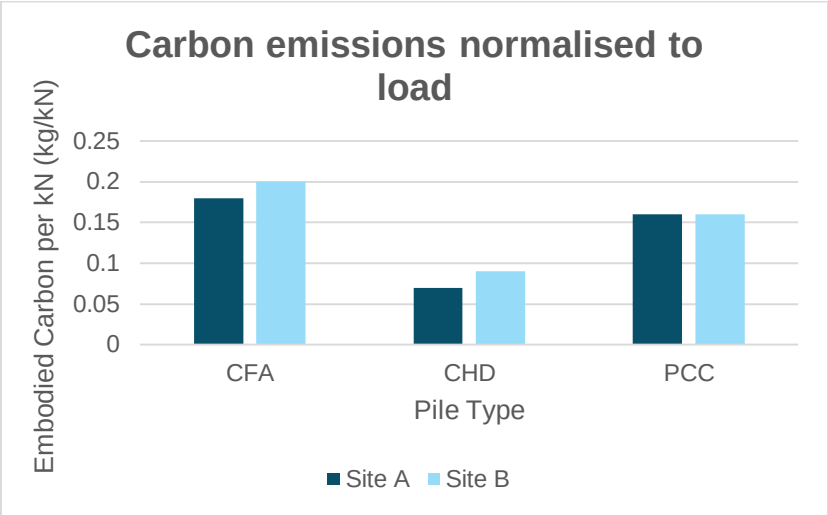


Figure 3. A bar graph showing carbon emissions normalised to load for CFA, PCC and CHD piles.

Using the same data, slightly different results are highlighted which indicate that the most efficient pile is in fact CHD. CHD is consistently lower in regards embodied carbon according to the EFFC assessment method. The low value reflects the significantly higher bearing capacity efficiency offered by CHD when compared with the other installation methods listed reflecting the efficiency in both load bearing, associated reduced length and resulting carbon emissions.

SOCIETAL IMPACT

The writers have noted that in discussions with some clients, comprehension of magnitudes of emissions are sometimes difficult to grasp in a commercial environment. A recent study by Rennert (2022) gives insight as to the costs incurred by society to repair the damage done by carbon emissions. Including these costs in the normalised load assessment allows a degree of financial comparison of installation methods, pile efficiencies and overall volumes. The results of this review for a typical 100 pile project designed for an Ultimate limit state of 1500kN are contained in Table 6.

Table 6. Societal impact

Pile Type	Site	Embodied carbon per kN (Kg/kN)	Impact ($/T/kN)
CFA	A	0.18	5049.91
CHD	A	0.07	2028.83
PCC	A	0.16	4494.48
CFA	B	0.20	5540.45
CHD	B	0.09	2506.45
PCC	B	0.16	4363.63

 © DFI International Bruges 2025

It can be seen in Figure 4 that the most expensive method used is that of CFA piling, followed by Driven Precast. The least expensive approach is that of CHD.

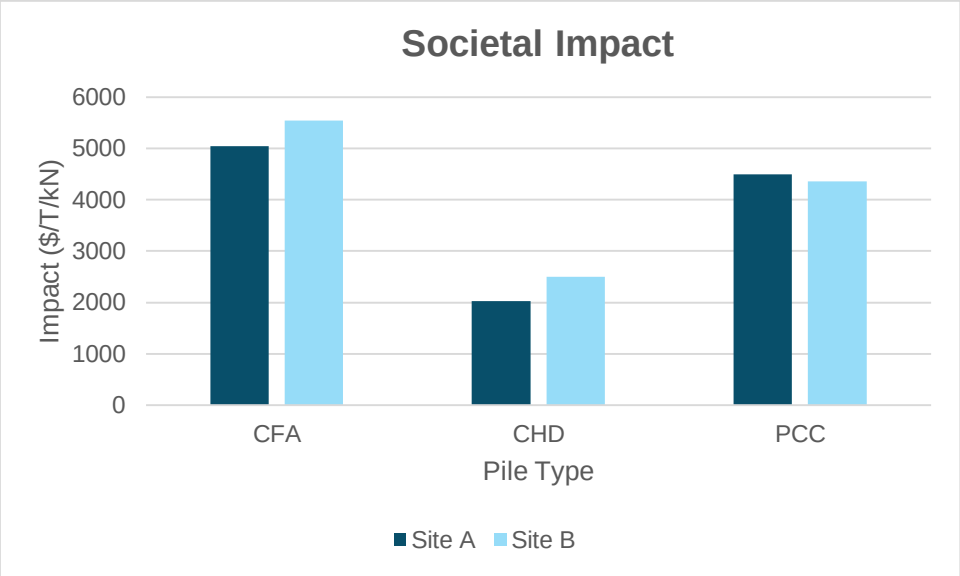


Figure 4. A bar graph showing societal impact of the carbon emissions produced by the installation of CFA, PCC and CHD pile types.

CONCLUSIONS

As the inclusion of embodied carbon is becoming increasingly equally weighted to overall costs it is essential for both funders and specifying engineers to have a clear path to understand not only the material-based emissions, but also include the efficiency of the installation method regarding load bearing too. And whilst it is well understood that not all piling methods are applicable for all loads in all geotechnical environments, where there is overlap, the approach detailed above is promoted as a clearer method to achieve that clarity of understanding. Using these approaches, for this study CHD appears to be the most efficient approach.

The introduction of financial societal costs facilitates further understanding and comparison, allowing the less involved to understand the repercussions of their choices in terms that are easy to understand.

ACKNOWLEDGEMENTS

The authors would like to thank their colleagues, staff and site teams at Roger Bullivant Piling, the University of Dundee and finally, our families for the support and expertise given in assisting the writing of this paper.

REFERENCES

Bell A (2010) Foundation solutions for the urban regeneration of Glasgow city centre. In Proceedings of the DFI and EFFC 11th International Conference: Geotechnical Challenges in Urban Regeneration, London, UK. EMAP Networks, Peterborough, UK, pp. 120–129.

British Standards Institution, BS EN1997-1:2004+A1 :2013 Eurocode 7: Geotechnical design – Part 1 general rules.

 © DFI International Bruges 2025

British Standards Institution, BS EN1997-1:2004+A1 NA :2014 National Annex to Eurocode 7: Geotechnical design – Part 1 general rules.

EFFC/DFI Carbon calculator V5 (2024), (https://www.effc.org/content/uploads/2025/03/EFFC-DFI-methodological-and-user-guide-v2.2.pdf).

Gavin KG, Cadogan D and Casey P (2009) Shaft capacity of continuous flight auger piles in sand. ASCE Journal of Geotechnical and Geoenvironmental Engineering 135(6): 790–798.

Jeffrey J.R., Brown M.J., Adam J., et al., 2016 CHD pile performance part I- physical modelling. Proceedings of the institute of Civil Engineers: Geotechnical Engineering, Vol 169, Issue 5, pp421-435, (https://doi.org/10.1680/jgeen.15.00131).

Jeffrey JR, Schwamb T, Brown MJ and Ball J (2010) Understanding CHD pile performance in granular soils. In Proceedings of the DFI and EFFC 11th International Conference: Geotechnical Challenges in Urban Regeneration, London, UK. EMAP Networks, Peterborough, UK, pp. 130–138.

Knappett J.A., Caucis K., Brown M.J et al, 2016 CHD pile performance part II- numerical modelling. Proceedings of the institute of Civil Engineers: Geotechnical Engineering, Vol 169, Issue 5, pp436-454, (https://doi.org/10.1680/jgeen.15.00132).

Rennert, K., Errickson, F., Prest, B.C. *et al.* Comprehensive evidence implies a higher social cost of CO_2. *Nature* **610**, 687–692 (2022). https://doi.org/10.1038/s41586-022-05224-9Sharif, Y. U., Brown, M. J., Ciantia, M. O., Cerfontaine, B.,Davidson, C., Knappett, J., Meijer, G. J. & Ball, J. (2021b).Using DEM to create a CPT based method to estimate the installation requirements of rotary installed piles in sand. Can. Geotech. J. 58, No. 7, 919–935, (https://doi.org/10.1139/cgj-2020-0017).

van Impe WF (2004) The Overview of Almost Two Decades of Full Scale Research on Screw Piles. Laboratory of Soil Mechanics, Ghent University, Ghent, Belgium.

Wade S, Handley B and Martin J (2012) Types of bearing piles. In ICE Manual of Geotechnical Engineering, Volume II: Geotechnical Design, Construction and Verification (Burland J, Chapman T, Skinner H and Brown M (eds)), 1st edn. ICE Publishing, London, UK, pp. 1191–1223.

 © DFI International Bruges 2025

NOVEL ANALYTICAL METHODS FOR PREDICTING THE RESPONSE OF BORED PILES IN SAND

Raffaele Cesaro, University of Campania "Luigi Vanvitelli", Italy, raffaele.cesaro@unicampania.it
Raffaele Di Laora, University of Campania "Luigi Vanvitelli", Italy, raffaele.dilaora@unicampania.it
Alessandro Mandolini, University of Campania "Luigi Vanvitelli", Italy, alessandro.mandolini@unicampania.it

ABSTRACT

In this work simple methods are proposed for the prediction of the load-settlement response of the bored piles in sandy soils. First, an analytical solution, based on the well-known similarities between the pile tip behaviour and that of an expanding spherical cavity in an elasto-plastic medium, is proposed. Second, the paper describes an effective framework for the evaluation of the shaft load-settlement response accounting for the horizontal stress increase during the loading process produced by the dilatancy occurring in the shear band. The proposed methods require standard input parameters, available from ordinary in situ and laboratory tests performed in current practice.

Keywords: Bored piles, Base resistance, Shaft friction, Settlement, Axial load, Sand

INTRODUCTION

In the last decades great research efforts have been made to develop and improve design tools for pile groups and piled rafts (Randolph, 2003). However, arguably any prediction about the pile group behaviour is function of the analysis of the single pile response under axial load, that represents the first step of any pile-foundation design process. Nevertheless, they all use as the key ingredient the response of the single pile, which has received much less attention in the last years, despite the current state of practice is far from being considered reliable and accurate. As a matter of fact, designers rely upon outdated solutions and empirical correlations and/or rules with limited insight on the underlying physical mechanisms, which results in great uncertainties (Fellenius, 2017).

With the aim of providing physically-based models to be directly applied in practice, this work presents analytical solutions for the prediction of the load-settlement response of the pile base and the pile shaft, under axial load, limited to bored piles in sandy soils. Each solution requires standard input parameters, given the ordinary in situ and laboratory tests employed in the current practice.

The base resistance of piles in sand is generally assessed by theoretical approaches based on the limit equilibrium method. Several expressions for the well-known bearing capacity factors are available from literature; among these, the ones proposed by Berezantzev et al. (1961) are perhaps the most employed in current practice. However, contrary to the assumption made by such methods, experimental evidence shows that distinct failure surfaces are not observed beneath piles in sand (Vesic, 1977). As a consequence, as stated by Vesic (1977), "*the ultimate load is rarely well defined, in many cases there is no visible collapse of the foundation and no clearly defined peak load*". Centrifuge load tests, which allow testing to very large settlements, clearly show that even for base settlements exceeding 100% of the pile diameter a limit resistance cannot be clearly identified, especially for bored piles. In reality, the base resistance mobilization of bored piles in sandy soils is strongly affected by the soil stiffness. In this regard, the first contribution worth of note is the solution proposed by Vesic (1977) based on the well-known similarities between the punching mechanism at the pile tip and the expansion of a spherical cavity in an elasto-plastic medium. To use the cavity expansion theory to predict the pile base load-settlement behaviour, (a) analytical solutions to compute the pressure-expansion behaviour of the cavity are needed and (b) semi-analytical correlations are required to relate

 © DFI International Bruges 2025

the end bearing resistance to the cavity pressure and the pile base settlement to the cavity expansion. For the step (a) in this work the solution proposed by Yu & Houlsby (1991) is employed.

On the other hand, open issues still remain about the prediction of shaft friction at failure. Therefore, a physically based analytical model is presented for the evaluation of the shaft friction, based on that suggested by Mascarucci et al. (2016), accounting for the horizontal stress increase during the loading process produced by the dilatancy occurring in the shear band.

Thus, adopting both proposed solutions, it is possible to build up a complete framework for the evaluation of the single pile load-settlement response exploiting the suggestions by Fleming (1992).

PILE BASE RESPONSE

From observations made in deep punching of metals, several authors concluded that the pressure required to produce a deep hole in an elastic-plastic medium is proportional to that necessary to expand a cavity of the same volume and under the same conditions. Moreover, Yasufuku & Hyde (1995) argue that many authors have observed that the deformation bulb beneath a loaded pile tip strongly resembles a spherical cavity expanded in an infinite medium. The computation of the pressure-expansion behaviour of cavity may be performed through different solutions available in literature. This work adopts the solution by Yu and Houlsby (1991), based on the hypothesis of elastic-plastic soil with Mohr-Coulomb yield criterion with a non-associated flow rule; moreover, no restrictions are imposed on the magnitude of the deformations. Thus, the properties of the soil are defined by the Young's modulus E, Poisson's ratio ν, cohesion c, angle of friction φ and angle of dilation ψ. Since the response prediction of cast-in-situ piles in sandy soils is the focus of this work, the cohesion is always assumed as equal to zero. Due to space limitations, the mathematical formulation of the above solution is not shown herein.

Note that in Yu & Houlsby (1991) solution the friction and dilation angles are assumed to be constant. Although this is a simplified approximation, since both angles depend on the stress history, Collins et al. (1992) have shown that adopting average values between the initial state ($\varphi = \varphi_{max}$, $\psi = \psi_{max}$) and ultimate state ($\varphi = \varphi_{cv}$, $\psi = 0$) leads to realistic results. Following this suggestion and the work of Bolton (1986) on the dilatant behaviour of sands, Randolph et al. (1994) proposed to estimate the friction and dilatant angles directly from the relative density D_R and the mean effective stress p_0'.

The correspondence between the pile base resistance and the cavity pressure is obtained assuming, as proposed by Vesic (1977) that during the penetration of the pile a rigid cone of soil is formed at the pile base, the vertical section of the cone is a triangle with a base angle α equal to $45°+\varphi/2$, and that the normal pressure acting on the lateral surface of the cone is equal to the cavity expansion pressure (Fig. 1).

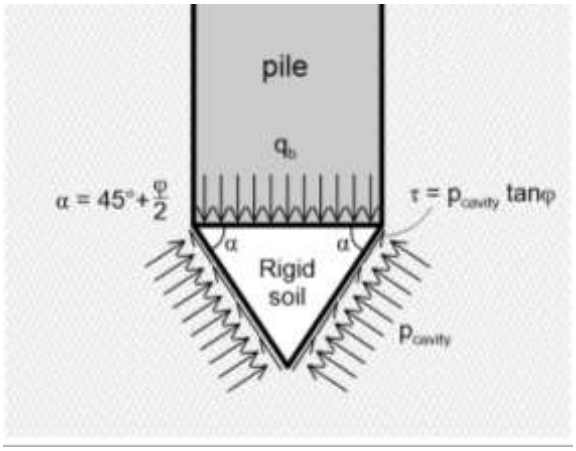


Fig. 1. Correlation between cavity expansion pressure and pile base normal stress.

 © DFI International Bruges 2025

It follows that the relationship between the pile base normal stress and the cavity pressure is given by (Randolph et al., 1994; Yasufuku & Hide, 1995):

$$q_b = p_{cavity} \frac{1}{1 - sin\varphi} \quad [1]$$

It should be pointed out that the adoption of equation 1 for the prediction of the load-settlement curve implies implicitly full shear strength mobilization over the conical surface from the early stages of the process.

Furthermore, some simplified hypotheses are adopted in this work:
(a) the initial radius of the cavity is equal to that of the pile
(b) the pile tip settlement is equal to the increase in the cavity radius
(c) the elastic stiffness of the pile base k_b is equal to that of a rigid disk on an elastic half space:

$$k_b = \frac{2dG_0}{1-\nu} \quad [2]$$

where G_0 is the shear modulus of the soil at low strains, d is the pile diameter and ν is the Poisson's ratio.

Given the hypotheses (a) and (b), the condition (c) is implemented by simply modifying the shear modulus, to get an equivalent G_{cavity} satisfying the equation:

$$\frac{G_{cavity}}{G_0} = \frac{(1 - sin\varphi)}{\pi(1-\nu)} \quad [3]$$

It can be observed that, given the ordinary values of the friction angle and the Poisson's ratio, the above stiffness is typically equal to 0.14÷0.225 G_0.

The reliability of this method was checked by Cesaro et al. (2023) and Cesaro (2024) against 50 well-documented in-situ pile load tests performed worldwide, cast in situ (bored, Continuous Flight Auger-ing and Full Displacement Pile) in sandy soils. For each load test the load-settlement curve at pile base is available and the subsoil condition are well known. The pile load test database involves several piles geometries (diameters from 0.4 m to 2 m and lengths from 6 m to 91 m). Cesaro et al. (2023) reported for each case history the reference, pile type, pile geometry and soil.

In Figure 2 the good performance of the proposed method is shown for 4 case histories involving very different pile geometries and different installation technologies.

 © DFI International Bruges 2025

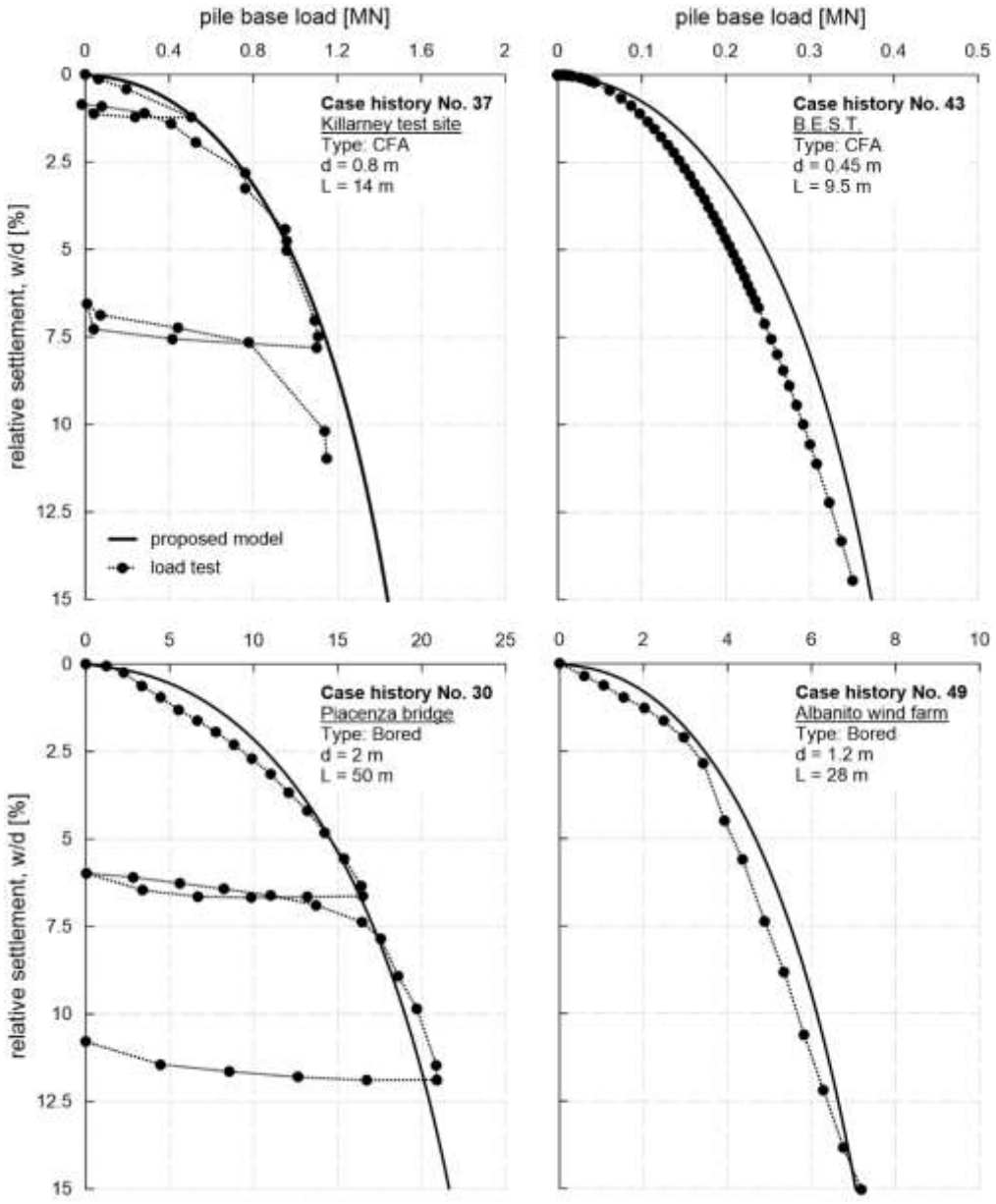


Fig. 2. Load test results against load-settlement curve predicted by the proposed cavity expansion-based model, employing Yu & Houlsby (1991) solution for 4 case histories from Cesaro et al. (2023).

PILE SHAFT RESPONSE

It has been observed that, knowing the initial shaft stiffness k_s and the ultimate resistance Q_s, the shaft load-settlement response can be easily mathematically described through a hyperbolic equation (Fleming, 1992):

$$Q = \frac{w}{\frac{1}{k_s} + \frac{w}{Q_s}} \quad [4]$$

Alternatively, several laws for the description of the shaft load-settlement response can be employed (Bateman et al., 2022). For instance, it is possible to adopt a linear-power law with a gap, since it is more flexible compared to the hyperbolic law given the presence of 2 fitting parameters, b and w_{50}:

 © DFI International Bruges 2025

$$\begin{cases} Q = wk_s & w \le \dfrac{Q_i}{k_s} \\ Q = \dfrac{Q_s}{2}\left(\dfrac{w}{w_{50}}\right)^b & w > \dfrac{Q_i}{k_s} \end{cases} \quad [5]$$

where,

$$Q_i = \left(\frac{Q_s}{2}\right)\left(\frac{2k_s w_{50}}{Q_s}\right)^{\frac{b}{b-1}} \quad [6]$$

Note that w_{50} is the settlement related to 50% of the shaft resistance, as shown in Figure 3, whereas b affects the rate of stiffness degradation, in particular, the higher the b value, the stiffer the load-settlement response.

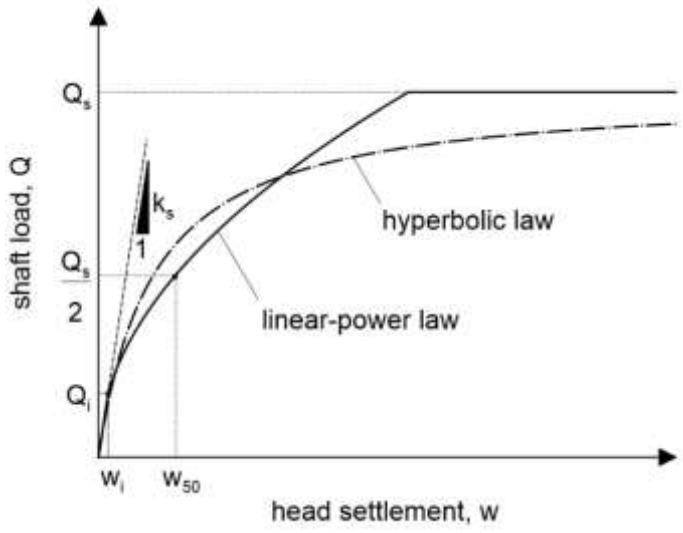


Fig. 3. Load-settlement laws adopted to describe the pile shaft response.

To evaluate the elastic shaft stiffness k_s different approaches can be adopted. In general terms the available methods can be classified in two categories: continuum models and independent springs models. The springs-based approach has the advantages that although requires smaller computational effort than rigorous continuum-based formulations, yields predictions that are in satisfactory agreement with more complex solutions. The original solution proposed by Randolph & Wroth (1978) is perhaps the most widespread (Fleming et al., 2008) given its effectiveness despite the simple mathematical formulation. According to the authors, the initial shaft stiffness k_s can be estimated trough the following expression:

$$k_s = \frac{2\pi L G_{L/2}}{\zeta} = \frac{2\pi L G_{L/2}}{\ln\left\{\left[0.25 + \left(2.5\frac{G_{L/2}}{G_L}(1-\nu) - 0.25\right)\frac{G_L}{Gb}\right]\frac{2L}{d}\right\}} \quad [7]$$

where, G_L and G_b are the soil shear moduli (at low strains) at the depth L and underneath pile base, respectively, whereas $G_{L/2}$ is the soil shear modulus (at low strains) at the depth $L/2$.

 © DFI International Bruges 2025

As regards the ultimate resistance Q_s, for bored piles embedded in cohesionless soils, under the hypothesis of negligible influence of the installation process and of the Poisson's effect, the ultimate shaft friction can be computed as:

$$q_s = (\sigma'_{h0} + \Delta\sigma'_h)\tan\varphi_{cv} \quad [8]$$

During the loading process, the soil shearing localizes in a thin shear band close to the pile, where the shear deformations imply volumetric strains depending on the soil dilation potential. The horizontal stress increment $\Delta\sigma_h'$ is due to the confinement exerted by the soil surrounding the shear band. Modeling the shear band as an expansive cylindrical cavity the surrounding soil can be represented as a linear spring with a stiffness $k = 4G/(d + 2t_s)$, where t_s is the shear band thickness. It follows that the horizontal stress increment is proportional to the stiffness of the "equivalent spring" and to the radial displacement u of the shear band, function of the angle of dilation ψ. For the sake of simplicity, Mascarucci et al. (2014, 2016) proposed to adopt a linear reduction for ψ with γ (from peak, where $\psi = \psi_p$, to critical state conditions, where $\psi = 0$) since experimental results show a regular reduction of soil dilatancy during shearing, and although the linearity between tan ψ-γ can be considered a simplification, more complex functions would increase the number of parameters without significantly altering the results. In light of the above the total radial displacement of the shear band can be estimated as:

$$u = \int_0^{\gamma_{cv}} \tan\psi\, t_s\, d\gamma = t_s \tan\psi_p \frac{\gamma_{cv}}{2} \quad [9]$$

where γ_{cv} is the shear strain at critical state. Thus, the ultimate shaft friction is equal to:

$$q_s = \left[\sigma'_{h0} + t_s \tan\psi_p \frac{\gamma_{cv}}{2} \frac{4G}{(d + 2t_s)} \right] \tan\varphi_{cv} \quad [10]$$

The angle of dilation at peak ψ_p is computed through the equation proposed by Bolton (1986).
Three ingredients need therefore calibration, namely t_s, γ_{cv} and G.

Given the high relative roughness of bored piles, the shear band is completely developed in the soil, as consequence its thickness t_s is not affected by the pile surface characteristics but only by the soil properties. It is well known that t_s primarily depends on soil particle size, typically ranging between 5 and 25 times the mean particle grain size, D_{50}. However, Cesaro (2024) collected several laboratory tests on different sands from the specialized literature, where the shear band thickness was measured, while the grain size distribution and the critical state friction angle were known for each tested material. From the results of these tests, the normalized shear band thickness can be estimated through the following expression:

$$\frac{t_s}{D_{50}} = 9.75 \left[\left(\frac{D_{50}}{1mm} \right)^{0.9} \left(\tan\varphi_{cv} \right)^{-1.5} C_u^{\,0.25} \right]^{-0.55} \quad [11]$$

where C_u is the coefficient of uniformity.

As regards the shear strain at critical state, Okuyama et al. (2003) carried out several plane strain compression tests (PS) on 9 different sands and analyzed the results together with that provided by Yoshida & Tatsuoka (1997) and concluded that the displacement required to achieve critical state conditions, w_{cv} (= γ_{cv} t_s), mainly depends on the mean particle size. In light of this, they show that

 © DFI International Bruges 2025

considering the average value of w_{cv} for each sand it is possible to detect a clear trend of variation as function of D_{50}. Following the hint of Okuyama et al. (2003) and considering the direct shear tests results collected by Mascarucci et al. (2016), it can be observed that the critical state shear displacement can be estimated through the following expression:

$$w_{cv} = 4.215 D_{50} + 1.85 \quad [12]$$

with w_{cv} and D_{50} in mm. It is worth of note that since in the test results provided by Yoshida & Tatsuoka (1997) and Okuyama et al. (2003) the shear band thickness is known, the shear strain at critical state γ_{cv} can be directly computed without further assumptions. A range of $\gamma_{cv} \simeq 40\% \div 180\%$ with an average value about equal to 100% is obtained. As a side comment, Mascarucci et al. (2016) suggested to adopt a conservative value equal to 60%.

In order to take into account the non-linear behaviour of the soil, in eq. 10 a secant stiffness should be adopted. Cesaro (2024) carried out a wide parametric study employing the Yu & Houlsby (1991) solution, for each theoretical case the secant stiffness was computed against the cavity expansion normalized with the yielding cavity expansion u_y and proposed the following regression law:

$$\begin{cases} \dfrac{G}{G_0} = 1 & if \quad u \le u_y \\ \dfrac{G}{G_0} = \left(\dfrac{u}{u_y} \right)^{-0.425} & if \quad u > u_y \end{cases} \quad [13]$$

where for cohesionless soil,

$$\frac{u_y}{D} = \frac{p_0' \sin\varphi}{4 G_0} \quad [14]$$

The effectiveness of the presented analytical framework was checked by Cesaro (2024) against the results from 5 full scale load-tests. In Figure 4 the comparison is shown between the predicted load settlement curves with the measured ones from the load test results provided by Viggiani & Vinale (1983).

The authors reported pile load tests results performed for the design of the foundation of the Naples Law Courts' Building. The foundation consists of a reinforced concrete slab resting on 241 bored piles with a length of 42 m and diameters ranging between 1.5 and 2.2 m. The two piles analyzed in this work have respectively d = 1.5 m (pile A) and d = 2 m (pile B). The fundamental properties of the soil are reported in Viggiani & Vinale (1983).

TOTAL LOAD-SETTLEMENT RESPONSE

Employing the solutions presented in this work, the simplest way to obtain the total-load settlement curve of the single pile under axial load, is to adopt the hypothesis of rigid pile. Thus, it is possible at first to estimate the load settlement curve at pile base. Note that the proposed method for the evaluation of the pile base response is load-driven. Then, since the rigid pile hypothesis implies that the settlement at pile base w_b is equal to the settlement at the pile head w_h, it is possible to compute the load at the pile shaft for each settlement level trough eq. 4 or 5. The total load Q is equal to the sum of the pile tip load Q_b and the shaft load Q_s. It follows that the elastic pile stiffness is the sum of the pile base elastic stiffness from eq. 2 and of the pile shaft elastic stiffness from eq. 7 and is thereby overestimated, since the pile shortening is neglected.

 © DFI International Bruges 2025

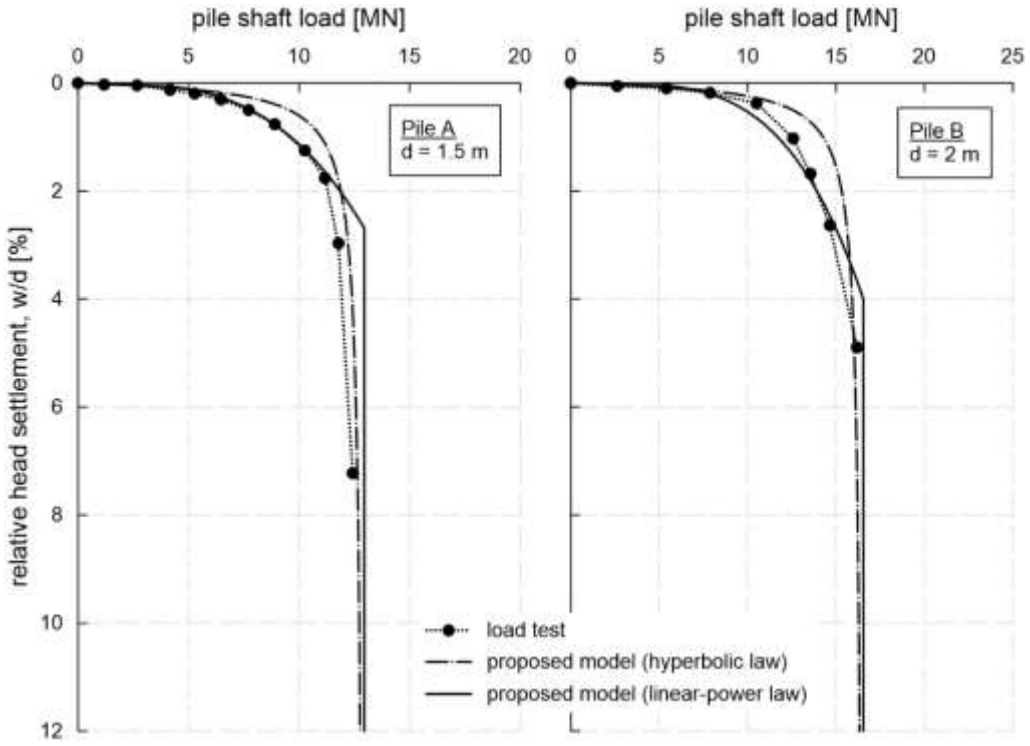


Fig. 4. Comparison between measured and predicted shaft load-head settlement curves.

In order to take into account the pile compressibility employing the proposed solutions, it is possible to adopt the simplified method proposed by Fleming (1992). The author states that the elastic shortening of the pile under axial load is an additional settlement to that calculated with the rigid pile hypothesis and must depend on the relative development of load transfer between the pile and soil along its length, as well as on the load being transferred at the pile base. It can be assumed that the shortening occurs in two different stages:

(a) the first stage represents the elastic shortening which takes place during the load increase up to the complete mobilization of shaft friction and can be computed as the shortening of the concrete column having length equal to the distance from the pile head of the centroid of the friction load transfer diagram $K_E L$ (Fig. 5). For instance, for uniform friction the elastic shortening will be at most equal to that of a column of length $0.5L$. However, since friction takes place more rapidly at the upper part of the pile than at its base, the author suggests to adopt an effective column length slightly lower than $K_E L$. It follows that:

$$\Delta w_s = \frac{4\alpha_L K_E L Q}{\pi d^2 E_c} \qquad if \quad Q < Q_s \qquad [15]$$

where, α_L is the effective length reduction factor and E_c is the concrete Young's modulus. The author suggests to adopt αL = 70%-80%.

(b) the second stage represents the elastic shortening that occurs when the applied load exceeds the ultimate shaft load:

$$\Delta w_s = \frac{4L}{\pi d^2 E_c}\left[\alpha_L K_E Q_s + (Q - Q_s)\right] \qquad if \quad Q \geq Q_s \qquad [16]$$

Dividing the soil medium into n layers, each of them corresponding to a depth z_i and a shaft friction q_i, given a generic friction load transfer diagram, the centroid depth is equal to:

 © DFI International Bruges 2025

$$K_E = \frac{\sum_{i=1}^{n} \frac{\left(q_{s,i} + q_{s,i-1}\right)\left(z_{s,i}^2 - z_{s,i-1}^2\right)}{4}}{\sum_{i=1}^{n} \frac{\left(q_{s,i} + q_{s,i-1}\right)\left(z_{s,i} - z_{s,i-1}\right)}{2}} \quad [17]$$

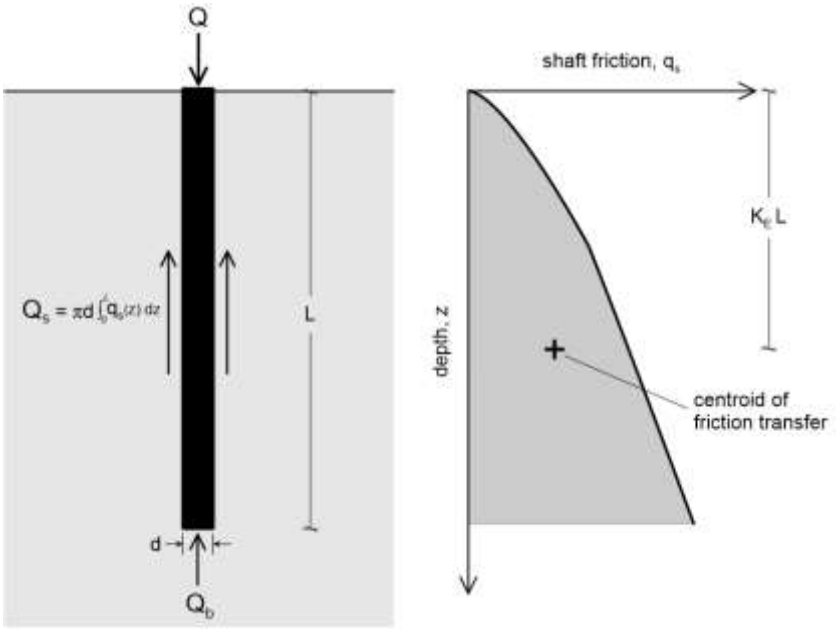


Fig. 5. Simplified method of calculating elastic shortening.

CONCLUSIONS

In this paper analytical solutions are provided to predict the load-settlement response of the bored piles in sandy soils under axial load. As regards the pile base response, exploiting the similarities between the pile tip punching behaviour and that of an expanding spherical cavity in an elasto-plastic medium, an analytical solution is proposed, for the prediction of the entire load-settlement curve at pile tip. Furthermore, a physically based framework for the evaluation of the shaft load-settlement response for bored piles embedded in sandy soils is presented, accounting for the horizontal stress increase during the loading process produced by the dilatancy occurring in the shear band. The proposed methods require standard input parameters, given the ordinary in situ and laboratory tests employed in the current practice. Since the two contributions are computed separately, a "combination criterion" is required to obtain the total settlement response. For this aim, the simplified method proposed by Fleming (1992) can be adopted. It is worth highlighting that the prediction of load-settlement response of the single pile, besides serviceability checks, may be needed also for the definition of the capacity, given that this is often referred to a certain settlement level.

REFERENCES

Bateman, A. H., Crispin, J. J., Vardanega, P. J., Mylonakis, G., 2022. Theoretical t-z curves for axially loaded piles. Journal of Geotechnical and Geoenvironmental Engineering, ASCE, 148(7), 04022052.

Berezantzev, V. G., Kristoforov, V., Golubkov, V., 1961. Load bearing capacity and deformation of pile foundations. Proceedings of the Fifth International Conference of Soil Mechanics and Foundation Engineering, Vol. 2, Paris, pp. 11–15.

Bolton, M. D., 1986. The strength and dilatancy of sands. Géotechnique, 36(1): 65–78.

 © DFI International Bruges 2025

Cesaro, R., Di Laora, R., Mandolini, A., 2023. A novel method for assessing pile base resistance in sand. In: Ferrari, A., Rosone, M., Ziccarelli, M., Gottardi, G. (eds) Geotechnical Engineering in the Digital and Technological Innovation Era. CNRIG 2023. Springer Series in Geomechanics and Geoengineering. Springer, Cham.

Cesaro, R., 2024. Innovative design methods for piles and pile groups. PhD thesis, University of Campania “Luigi Vanvitelli”, Italy.

Collins, F., Pender, M. J., Yang, W., 1992. Cavity expansion in sands under drained loading conditions. Int. J. Numer. Anal. Methods Geomech. 16, 3-23 (1992).

Fellenius, B. H., 2017. Report on the B.E.S.T. prediction survey of the 3rd CBFP event. Proceedings of the 3rd Bolivian International Conference on Deep Foundations, April 27-29, Vol. 3, 7-25, Santa Cruz de la Sierra, Bolivia.

Fleming, W. G. K., 1992. A new method for single pile settlement prediction and analysis. Géotechnique 42, No. 3, 411–425.

Fleming, W. G. K., Weltman, A. J., Randolph, M. F., Elson, W. K., 2008. Piling engineering. CRC Press.

Mascarucci, Y., Miliziano, S., Mandolini, A., 2014. A numerical approach to estimate shaft friction of bored piles in sands. ACTA Geotech., 9(3), 547–560.

Mascarucci, Y., Miliziano, S., Mandolini, A., 2016. 3M analytical method: evaluation of shaft friction of bored piles in sands. J. Geotech. Geoenviron. Eng., ASCE.

Okuyama, Y., Yoshida, Tetuya, Tatsuoka, F., Koseki, J., Uchimura, T., Sato, N. and Oie, M., 2003. Shear banding characteristics of granular materials and particle size effects on the seismic stability of earth structures. Proc. 3rd Int. Symp. on Deformation Characteristics of Geomaterials, IS Lyon 03 (Di Benedetto et al. eds.), Balkema, September, 2003.

Randolph, M. F., Wroth C. P., 1978. Analysis of deformations of vertically loaded piles. J. Geotech. Engng Div., ASCE 104, No. GT12, 1465-1488.

Randolph, M., Dolwin, J., Beck, R., 1994. Design of driven piles in sand. Geotechnique 44 (3), 427–448.

Randolph, M., 2003. Science and empiricism in pile foundation design. Géotechnique, 53:10, 847-875.

Vesic, A.S., 1977. Design of Pile Foundations. Highway Practice No 42, TRB NRC, Washington D.C.

Viggiani, C. and Vinale, F., 1983. Comportamento di pali trivellati di grande diametro in terreni piroclastici. Rivista Italiana di Geotecnica. 17 (2), 59-84.

Yasufuku, N., Hyde, A.F.L., 1995. Pile end-bearing capacity in crushable sands. Geotechnique 45 (4), 663–676.

Yoshida, T. and Tatsuoka, F., 1997. Deformation property of shear band in sand subjected to plane strain compression and its relation to particle characteristics. Proc. 14th ICSMFE, Hamburg, 1, 237–240.

Yu, H. S. and Houlsby, G. T., 1991. Finite cavity expansion in dilatant soils: Loading analysis. Géotechnique 41(2), 173–183.

 © DFI International Bruges 2025

Deep Learning Algorithms for the Monitoring and Control of Drilling and Grouting Works

Andrea Danzi, Systra S.p.A., Trento, Italy, adanzi@systra.com
Giuseppe Di-Salvo, Trevi S.p.A., Cesena, Italy, gdisalvo@trevispa.com
Alberto Flor, Systra S.p.A., Trento, Italy, aflor@systra.com
Raffaella Granata, Trevi S.p.A., Cesena, Italy, rgranata@trevispa.com

ABSTRACT

Efficient logging and precise control of drilling and grouting operations are essential in construction of tunnels, dams, levees, and confinement of polluted areas. With the growing demands of digital solutions supporting the construction process, the integration of advanced logging and automated control systems of grouting parameters emerges as an innovative strategy to enhance quality and productivity in project execution. This study delves into the potential of employing machine learning models to accurately predict and regulate the pressure and flow rate within a grouting system. We introduce an innovative data logging system capable of producing extensive datasets on grouting parameters suitable for Deep Learning algorithms. Leveraging two distinct datasets gathered at the Mosul Dam (Iraq) and Rogun Dam (Tajikistan) Projects, we implemented a recurrent Artificial Neural Network architecture using long short-term memory (LSTM) cells. To the best of our knowledge, these datasets are larger than any other state-of-the-art (over 55,000,000 data points from approx. 7000 grout holes for Mosul Dam and 8,500,000 data points from approx. 6000 grout holes for Rogun Dam). Having such large datasets allowed us to obtain a realistic estimation of the model performance, without potential bias due to missing ground features.

Keywords: Dam Safety, Grouting, Artificial Neural Networks, LSTM

INTRODUCTION

The paper's main contributions include:

- Developing one of the largest datasets for grouting operations (63 million data points) to train machine learning models.
- Applying Long Short-Term Memory (LSTM) models to predict and regulate key grouting parameters, such as pressure and flow rates.
- Improving grouting process efficiency and safety by automating pressure and flow rate regulation based on real-time data.
- Adapting AI-driven predictive models for complex environments, including the Mosul and Rogun Dam projects with varying geological conditions.
- Integrating AI with automated control systems like "T-Grout" to manage grouting operations remotely.

These contributions advance the use of AI in civil engineering, particularly in automating and optimizing critical processes in dam construction and repair.

BACKGROUND

Mosul Dam, Iraq

Mean Features of the Project

Mosul Dam is located on the Tigris River about 60 km north-west from the city of Mosul (Iraq). The Dam was built in the first half of the 1980s as a multipurpose project conceived for irrigation, flood control, water supply and hydropower generation. It is a zoned embankment dam (Fig. 1), which includes a 5-gate service spillway, a hydropower facility rated to 750 MW and features a bottom outlet structure with two gates and an emergency spillway. The Dam is 3500 m long and up to 113 m high, with the crest at El.+343 m above sea level. The designed maximum water level in the reservoir is at El.+335 m, the minimum operating level is at El.+300 m. The storage capacity of the reservoir is about 11.1 billion cubic meters.

 © DFI International Bruges 2025

The foundation rock comprises gypsum, anhydrite, marl, dolomite, and limestone strata. Over the years, the structural integrity of the dam and its operational capacity gave cause for severe concerns, principally because of phenomena of dissolution in water of gypsum and anhydrite layers occurred in the bedrock foundation. In consideration of the critical situation characterizing the dam, in 2015 the Iraqi Government issued an international invitation to tender with an emergency procedure for the maintenance and safety of the dam. Trevi S.p.A. was awarded the tender: the contract included works for the repair of manufactured structures in correspondence of the bottom outlet and grout injections aimed at repairing the grout curtain. Concurrently, the design and the supervision of the works were entrusted to the USACE, acting as Engineer for the project (Granata and Bateman, 2022).

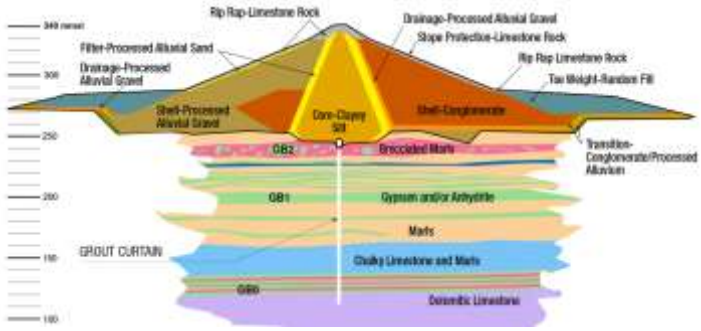


Fig. 1. Mosul Dam - Typical Cross Section

The drilling and grouting works had to be carried out both from the dam crest and from the grouting gallery, with the goal of injecting mixes able to intercept and plug the fissures and voids, mainly derived from dissolution and karst phenomena. The end purpose of the emergency grouting program was to install a grout curtain along the full length of the grouting gallery (2200 m), connected to curtains to be installed from the crest of the Dam, east of the spillway and on west abutment (490 and 220 m). A further piece of curtain was installed from the crest of the Main Dam in the 280 m immediately right of the spillway, to grout the rock between the base of the embankment and the top of the grouting tunnel extrados (where the grouting gallery enters the foundation rock). Because of the stratigraphy and design considerations, it was necessary to drill and inject holes to a depth of 150 m and over. Due to the water level in the reservoir, the gallery activities were further complicated by the need to operate in the presence of a significant waterhead (up to 100 m).

Drilling and grouting works were performed 24 hours per day six days per week. The drilling and grouting program, from November 2016 through July 2019, included a total 667,800 m of rotary drilling/redrilling, 85,000 m of coring, 35,450 m predrilling in the embankment. A total of 5390 boreholes were injected with 40,800 m3 of grout, corresponding to 27,000 t of cement (Fig.2). The grouting involved 404,000 m of hole length, with an average grout take of 102 l/m (Granata et Al., 2022).

Drilling and Grouting Method

According to the analysis, studies and outcomes of the Risk Assessment Findings (USACE, 2016), the Dam's foundation was divided into "Critical Areas", which defined the grouting priorities. The drilling and grouting methods were based on a "flexible approach", since the rock conditions vary significantly within very short distances and depths. These variable conditions include solution features of different sizes and orientations, joints and widened joints, irregular slopping, rock fissures, irregular top of rock, and varying combinations of these structures. The presence of flowing water under artesian pressures was typically encountered when drilling and grouting from the gallery.

At Mosul Dam, the grout curtain included three alignments: Downstream, Midstream and Upstream, 0.6 m spaced. Locally in the gallery, the grout curtain was integrated with an additional row of boreholes downstream inclined. Sometimes, new boreholes were instructed (in position, and depth), based on the grouting results, in accordance with the observational method. Each line included

 © DFI International Bruges 2025

Primary to Quaternary holes, split spaced from 12 m to 1.5 m. Some Quinary holes were drilled in between, mainly for coring and verification purposes.

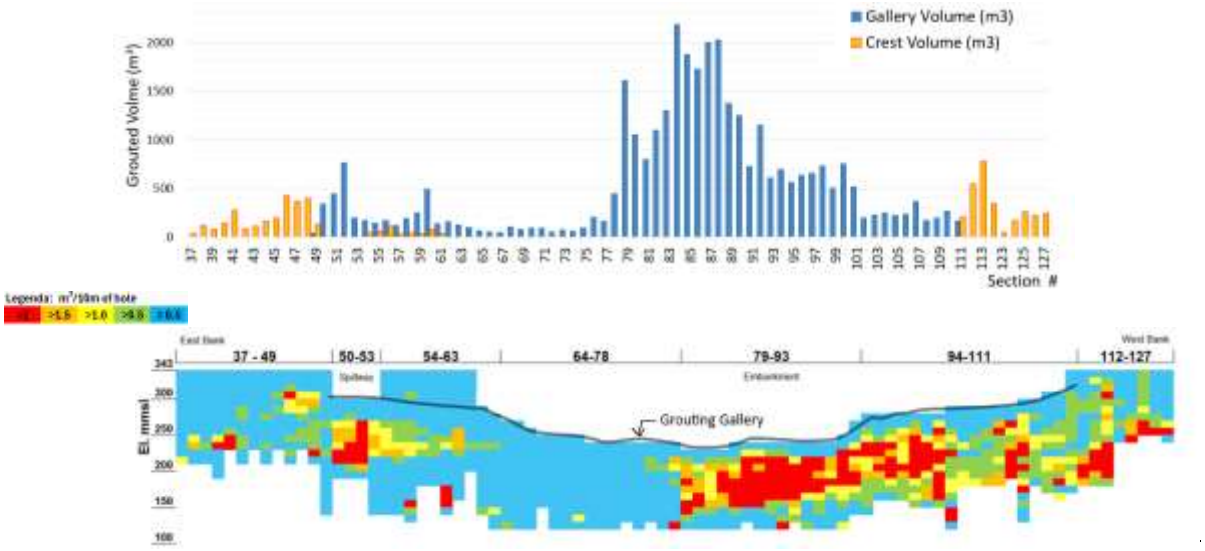


Fig. 2. Grout takes along the Grout Curtain; each Section includes all holes along 36 m of Curtain. Above: Grout takes in each Section. Below: Average grout take in each hole (Granata et Al., 2022).

Almost all the boreholes were grouted to a depth ranging between 100 and 150 m depth. The upstage method (≤ 5 m long stages), was the most applied grouting method. The downstage and downstage-zone methods were also used based on field observations and geology. For all cases, each borehole was pressure grouted using a single packer, lowered in the hole at top of the stage to be grouted (Granata et Al., 2022).

The grouting of each stage started with a thin grout (both in density and viscosity), and continued with thicker grouts, with increasing cement content and setting fastener. The grouting volume for each type of mix was directed by a flowchart defining the relationship between the effective pressure recorded during grouting and the volume of mix being injected. The grouting pressure and methodology varied along the dam, based on encountered geology and observed issues while drilling. Depending on the stage depth and borehole location, the final neat pressure to reach ranged between 4 and 40 bar. The closure criteria for each stage were based on the designed refusal pressure and flowrate, which had to be reached and maintained constant for a prefixed time. Once the closure condition was reached, further waiting time was spent to allow the complete dissipation of the final backpressure.

All the grouting operations were controlled, monitored and managed by "T-Grout", a Trevi proprietary Automated Control System of the Grouting Process (Fig. 3 left) developed with the fundamental IT support of SWS (now Systra S.p.A.). The grouting software directly governs the whole grouting process and triggers mix changes based on pre-set criteria for pressures or volumes within the bounds of the refusal criteria. With the help of the T-Grout system, which is a computer-automated web application (allowing the remote management of grouting activities) more than 150,000,000 data samples were recorded and stored. This huge amount of data made possible deep analyses of the grouting behavior and foundation rock responses. The data were also input in the USACE Information Systems for Construction Monitoring and Risk Assessments (Bateman et Al., 2018).

Electronic data acquisition devices were set up for each injection hole, both at the grout pump and at the grout header (flowmeter and pressure gauge), to gather pressure and flow data. All the collected data were transmitted to the grouting software, which in turn regulated the pump pressure and flowrate to maintain their values within the required limits. The software automatically computed the effective pressure, correcting the "raw value" measured at the borehole collar, taking into consideration all the dynamic and static head losses/gains. A centralized control room was setup to manage and monitor the grouting operations across the dam from a single location. At the grouting place, technical operators

 © DFI International Bruges 2025

were allowed to check all the parameters and the grouting behavior through tablets, directly connected to the “grout header” and the “control room”. Wireless hotspots with internet connection were set up across the entire dam to enable communication among teams working simultaneously throughout the dam and the offices. To this aim, the entire gallery and crest were equipped with a Local Area Network (LAN) using 3000 m of newly installed fiber-optic cable. The system structure is shown in (Fig. 3).



Fig. 3. Structure of the System Computerized Control System of Grouting and the Control Room

Rogun Dam, Tajikistan
Mean Features of the Project

The Rogun Dam Project in central Tajikistan involves the construction of a rock-fill dam along the Vakhsh River near the city of Rogun (about 100 km east of Dushanbe). The 3600 MW Rogun HPP is a world record project that includes the construction of the highest embankment dam in the World (335 m high). A general section at the Main Dam axis is sketched in Fig. 4, which shows the geological setting: over the entire dam footprint, the two main geological units are the Sandstone and the Siltstone / Argillite, in alternating strata and steeply inclined bedding. The rock permeability can be due to the joints and to other rock mass defects interpreted as result of internal tectonic movement.

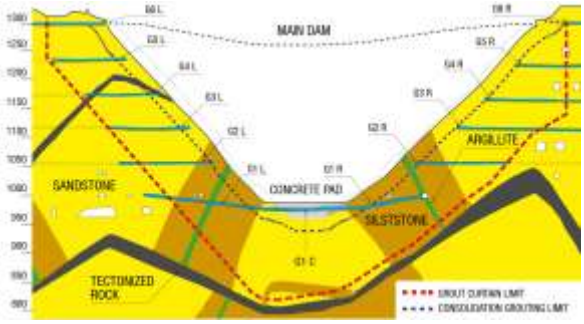


Fig. 4 Section at the Main Dam Axis

The construction of the Main Dam and relevant works are part of Contract Lot 2, awarded to Webuild S.p.A. (WB). As part of the Main Dam construction, drilling and grouting works are required for the consolidation and waterproofing of the dam foundation rock. The drilling and grouting works for the consolidation grouting of the RCC Pad and around the galleries, and for the installation of the grout curtain in the grouting galleries were awarded to Trevi S.p.A.. The grouting activities started in July 2022. At the time of writing this paper, the grouting activities are still in progress.

 © DFI International Bruges 2025

The grout curtain shall reduce and control the seepage through the dam foundation. The consolidation grouting below the concrete pad is conceived to reduce the hydraulic gradient in the slightly distressed shallow foundation area. The grout curtain for the Main Dam is installed mainly from the grouting galleries, excavated on 6 levels in both left and right banks and in the precast concrete at the riverbed. The curtain is drilled towards upstream, perpendicular to the grouting galleries, to intersect those discontinuities that may allow water leakage after the impounding. The grout curtain in the grouting galleries requires boreholes drilled with different inclinations, to grant its continuity (see Fig. 5). The near-surface rock mass of the distressed shallow foundation at the two banks will be treated by dedicated holes drilled from the surface.

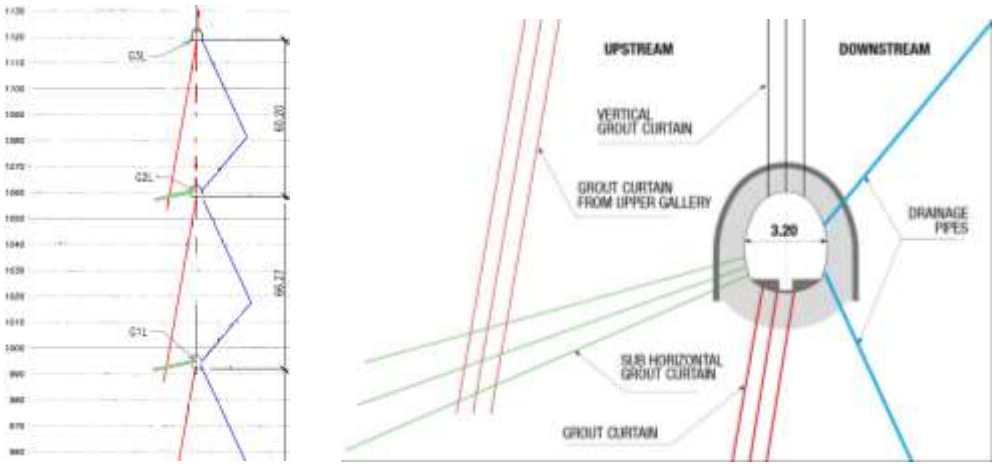


Fig. 5 Borehole setting for the Grout and Drainage Curtains

Drilling and Grouting Method

The grout curtain includes 3-lines of boreholes (max length 200 m); final spacing on each line is 2.0-2.5 m (depending on lithology). Below elevation 1120 mmsl the design foresees the use of the GIN method, with GIN 2500 and Pmax 40 bar, except the uppermost stage with Pmax 20 bar. The method to apply above elevation 1120 will be defined in the next future. The consolidation of the rock behind the galleries lining is performed using the Pmax criterion (5-10 bar) through dedicated boreholes 10 m long. At the time of drafting this paper (September 2024), Trevi grouted a total of over 6000 boreholes, over a total length exceeding 137,000 m.

Since the T-Grout was successfully used at Mosul Dam, Trevi decided to use this system at Rogun Dam as well. For the same reason, it was decided to involve Systra S.p.A. for support in the T-Grout adaptation and IT management. Unfortunately, at Rogun Dam Project it was impossible to install a Local Area Network (LAN) in the grouting galleries. Therefore, the system had to be modified to Stand Alone setting. The operators upload (via USB) the grouting instructions and parameters in the T-Grout at the grouting plants, where they can monitor the grouting behavior. Once per day, the recorded data is downloaded and transferred to the master computer, to update the data-manager, edit the daily report, print the report and diagram for each grouted stage, update the drawings.

DATA COLLECTION

For our study, we consider data coming from the two projects described in the previous section. The data collected from the two projects are stored in a NoSQL database with the same structure providing the data storage of a Software Architecture designed for supporting the collection of a huge amount of data. The T-Grout Automated Control System has been designed to collect data in real-time and store it in an enterprise level database. The architecture follows an extended model-view-controller (MVC) pattern described in the diagram below (Fig. 6):

 © DFI International Bruges 2025

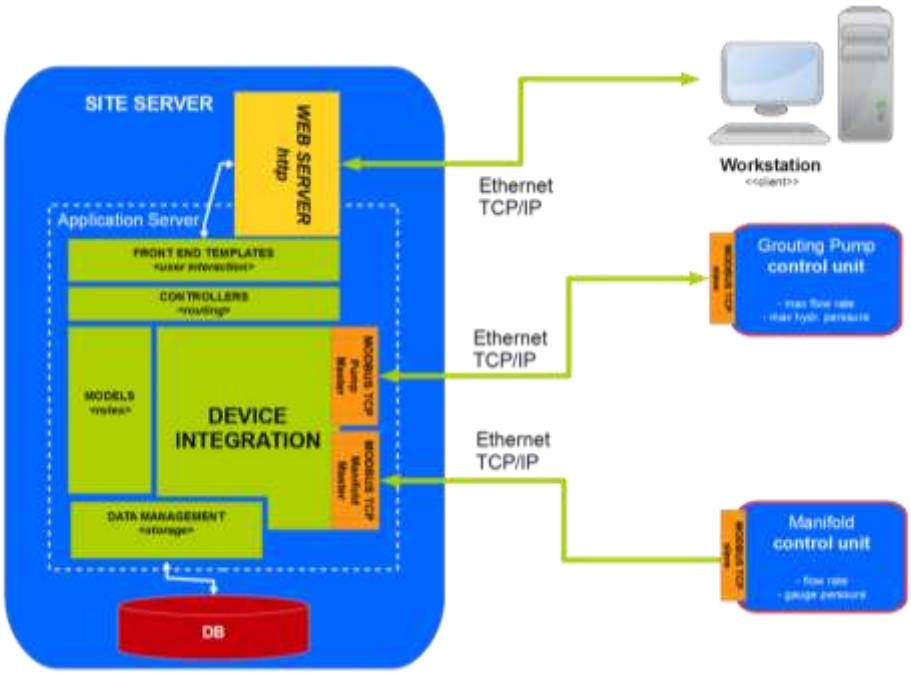


Fig. 6 Architecture following an extended model-view-controller (MVC)

The T-Grout follows a modular, event-driven, component-based architecture. It uses regions, composite views, controllers, and application objects to manage complexities in real-time data collection. NoSQL database stores data in a flexible, document-oriented format. This allows for dynamic and scalable data management, unlike traditional relational databases (RDBMS). The database is schema-less, meaning each document can have a different structure. The T-Grout has been designed with the following models:

- Boreholes: 3D geometry of grouting activity.
- Stages: grouting design parameters.
- Timeseries: real-time data from grouting equipment.

Models handle data synchronization with a REST API, managing attributes and emitting events when data changes. Data flows to the backend using an Object Data Modeling (ODM) component for the specific DB. The architecture includes:

- Controller objects separating route definitions from route-handling logic.
- Views responsible for rendering templates and filling them with data from models.
- Models representing individual data entities, handling data synchronization.

The NoSQL database's flexible structure allows for easy adaptation to changing data structures. As the amount of data grows, architecture can scale out by adding more machines to handle the load. In some implementations (e.g., Mosul and Rogun), additional features such as LAN connectivity or rugged laptops acting as Site Servers are used to enhance data collection and management.

ARTIFICIAL INTELLIGENCE METHODOLOGY APPLIED TO GROUTING DATA

Designing AI algorithms for making predictions on data stored in a NoSQL, database involves several key steps (Fig. 7):

1. Data Extraction: Extracting relevant data from a NoSQL database using PyMongo and structuring it into a suitable format for machine learning (e.g., Pandas DataFrame).

2. Data Preprocessing: Cleaning, normalizing, and transforming the raw data into numerical formats to ensure it is ready for input into the neural network.
3. Neural Network Architecture: Designing a neural network architecture tailored to the type of prediction task (e.g., regression or classification) using a feedforward neural network or specialized architectures like RNNs or CNNs.
4. Model Training: Training the preprocessed data using suitable loss functions and optimizers, such as Adam or SGD, with libraries like TensorFlow or PyTorch.
5. Prediction: Using the trained model to make predictions on new data, potentially integrating it with the NoSQL database for real-time or batch predictions.

In this section, we describe in detail the artificial intelligence methodology we use for predicting and driving the grouting parameters as managed by the T-Grout Automated Control System.

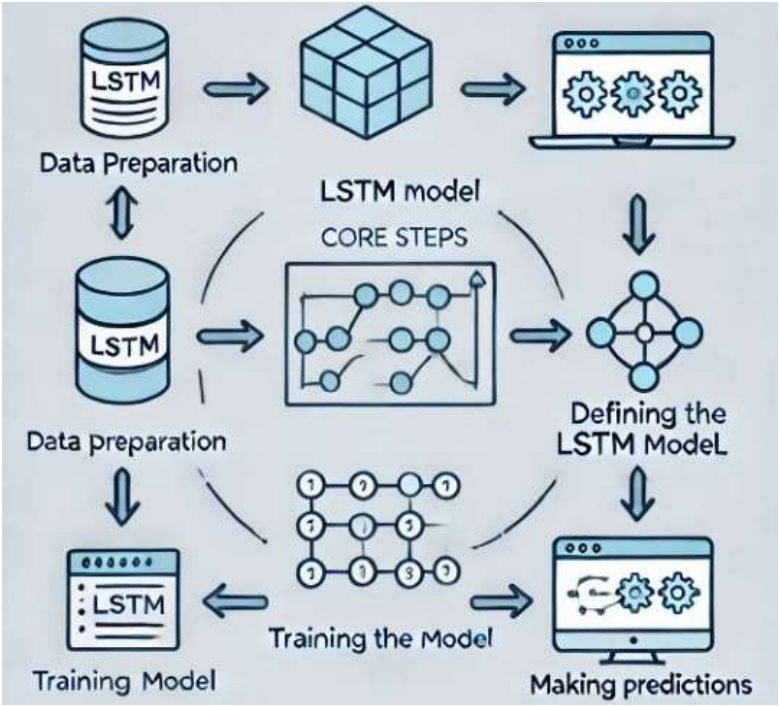


Fig. 7 – Designing AI algorithms for making predictions on data stored in a NoSQL

Data extraction

Data extraction and Data preprocessing are all performed with the Python programming language, using packages for reading data from NoSQL databases (e.g. PyMongo) and managing them as dataframes (e.g. Pandas) to give the data the right shape for machine learning algorithms.

Data Preprocessing

Before feeding our data to the LSTM, the dataset undergoes several transformations to prepare it for modelling. The first step is to identify the relevant features that will be used in the model. In this case, we have four independent variables: "Input pressure (bar)", "Input flow rate (s/min)", "Flow rate (l/min/m)", and "Effective pressure (bar)". We also have one target variable, which is "Effective pressure (bar)". The correlation matrix (Fig. 8) was used to select features from the grouting parameters. In the Matrix, the correlation coefficients between variables, range from -1 (perfect negative correlation) to 1 (perfect positive correlation); the diagonal elements are always 1, as each variable is perfectly correlated with itself; the matrix is also symmetrical since correlation between quantity A and B is a symmetric

 © DFI International Bruges 2025

property. The reason for selecting these variables is that they all contribute to understanding the behavior of the system we are trying to model and have high correlation with the target variable.

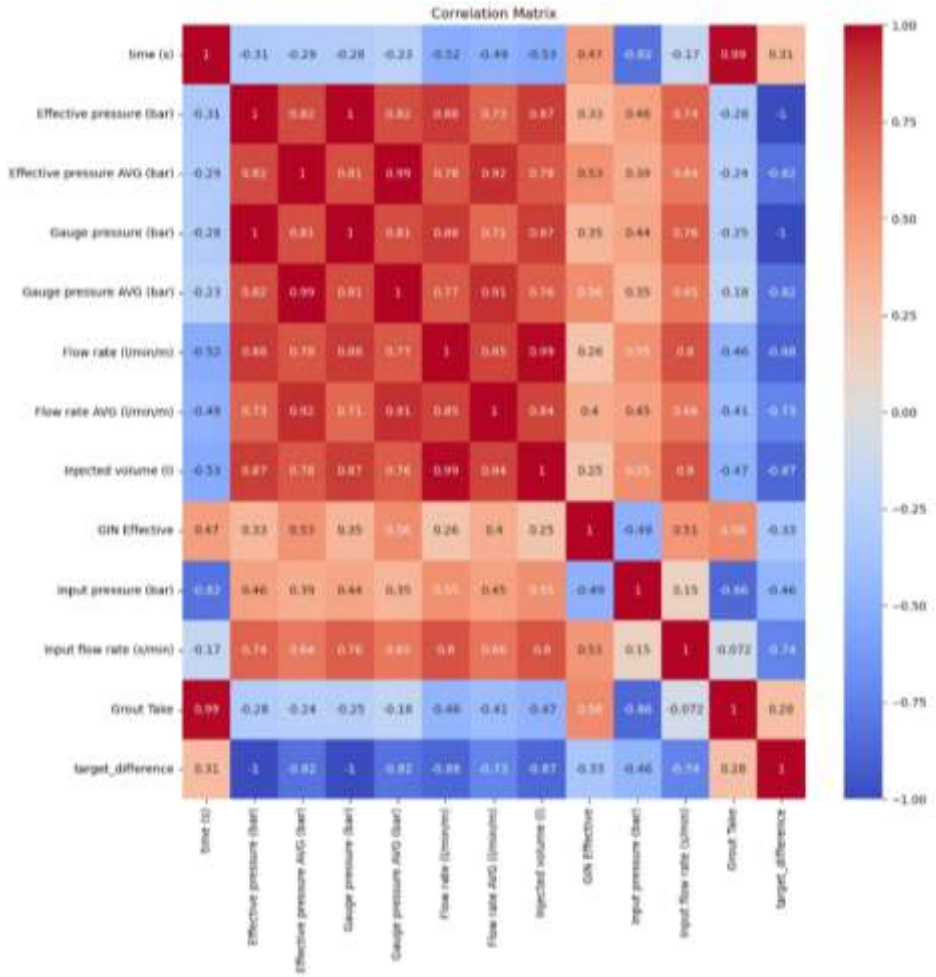


Fig. 8. Correlation Matrix

Next, we deal with any missing values from the dataset. If the missing values are few in between long series of data, we are just linear interpolate the missing points. If the missing values represent a long interval of time, then we split the dataset into two new datasets, before and after the missing points, so that we do not mix data too far apart temporarily. This processed data will be used as input for our machine learning model.

The dataset also undergoes scaling using a MinMaxScaler. This step is necessary because many machine learning algorithms are sensitive to the scale of their input data. Scaling ensures that all features have similar magnitudes, which can improve the stability and performance of the model.

The lookback variable is also defined: it determines how many past time steps we consider when making predictions. In this case, it is set to 10, meaning our model will only use the last 10 timesteps to make a prediction for the target at the successive step. The training and testing datasets are paired into sequential pairs, where each pair consists of four feature vectors with 10 timesteps each, followed by a single target value representing the expected outcome at the subsequent time step.

Finally, the dataset is split into training and testing sets. This is crucial because it allows us to evaluate the performance of our model on unseen data. The ratio of training to testing data can be adjusted depending on the specific needs of the problem at hand. In this case, we have set aside 20% of the data for testing.

 © DFI International Bruges 2025

Neural Network Architecture

In this work we use a type of Recurrent Neural Network (RNN) called Long Short-Term Memory (LSTM). Unlike traditional Artificial Neural Networks (ANNs), LSTMs can process sequential data by maintaining a hidden state that preserves information about past elements. LSTMs have feedback connections and gates, including input, output, and forget gates, which help the model retain long-term dependencies and learn complex patterns in sequences of data. The LSTM architecture has already been successfully implemented in engineering contexts (Flor et Al. 2023).

The architecture consists of three layers: an input layer, two LSTM layers, and a dense output layer. The first LSTM layer has 50 units and uses the ReLU activation function. This means that it will learn a representation of the input data that captures its most notable features. The second LSTM layer also has 50 units but uses the tanh activation function. This allows the model to learn more nuanced relationships between inputs and outputs. Finally, the output layer is a single unit with a linear activation function, which produces an output that can be interpreted as a value (Fig. 9).

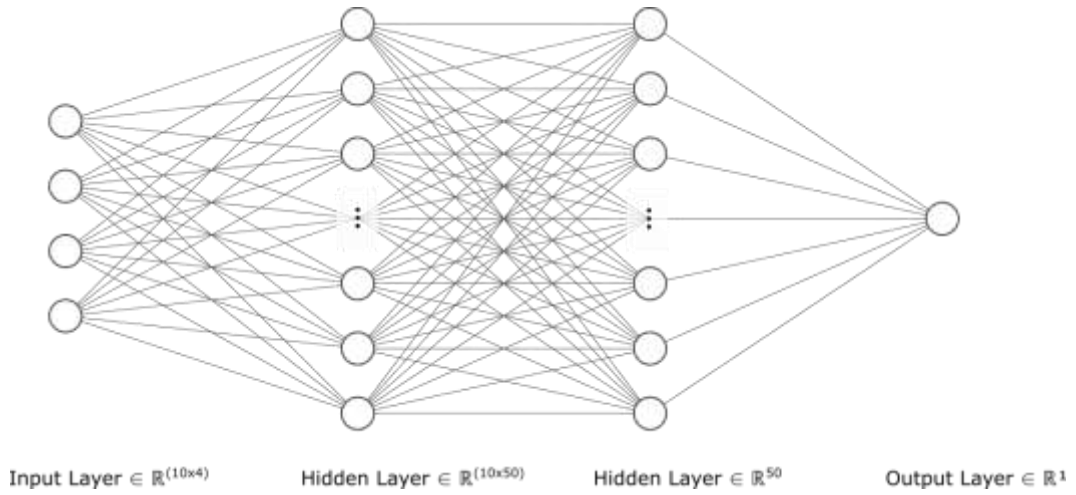


Fig. 9. Schematic representation of the LSTM neural network employed

One of the key features of this architecture is the use of dropout regularization during training. Dropout helps prevent overfitting by randomly dropping out units during training, which forces the model to learn more robust representations of the data. The Adam optimizer is also used, which is a popular choice for RNNs because it adapts the learning rate to the individual unit's needs.

Another important aspect of this architecture is the look-back parameter, which determines how many past time steps we consider when making predictions. In this case, the lookback is set to 10, meaning our model will only use the last 10 timesteps to make a prediction. This allows us to capture some of the dynamics in the data without relying on historical trends. We used Keras with Jax backend to construct the architecture and model the data.

Model Training

After defining the neural network architecture, training is initiated using the Adam optimizer (initial learning rate 0.001 and batch size 32) for 20 epochs. This allows the model to refine its understanding of patterns in the data without overfitting. The Mean Squared Error (MSE) regression loss function provides feedback on how well the model's predictions match actual target values, enabling it to adjust its internal parameters through backpropagation and optimization.

After generating predictions, the MSE loss function is applied to compare predicted outputs with actual values. It calculates the average of squared differences between predicted and actual values,

 © DFI International Bruges 2025

penalizing larger errors more heavily due to squaring. Finally, the trained model makes predictions on the testing data.

Grouting Prediction: Performance and Evaluation

The LSTM model demonstrated excellent performance in predicting the effective pressure, achieving a low MSE of 0.00183. This indicates that the model's predictions closely align with the actual values in the test data. The ability of the LSTM to learn the intricate relationships between past and present values in the time series contributed to its superior performance compared to the simpler linear regression and ARIMA models.

In conclusion, the LSTM neural network proved to be a valuable tool for predicting the effective pressure in our grouting system. Its capacity to learn long-term dependencies and complex patterns in time-series data makes it a promising approach for tackling similar prediction tasks in various domains.

In Fig. 10, Fig. 11, Fig. 12 (next page) are some examples of how well the proposed architecture fits the prediction on the Effective Pressure. Charts are paired two by two; the first chart displays in blue the data used for training the neural network and from a certain point onwards shows in orange the actual value vs the predicted value in green. The second chart is a zoom into the slice of data where the actual value (blue) is compared with the predicted value (orange). Notice the difference between the training part (leftmost part of the data) and the test part (rightmost). This is a clear indication of the precision of the algorithm to understand the relationship between features and target. This is an expected, but important, consequence of the non-deterministic nature of machine learning techniques.

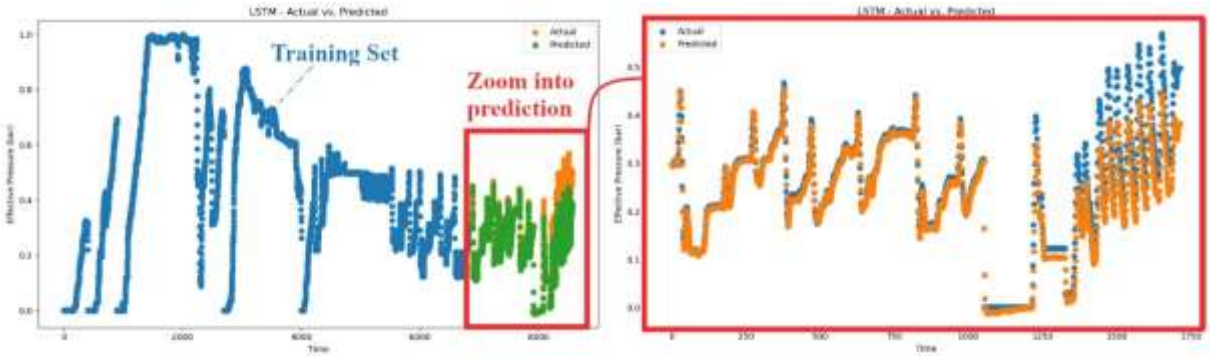


Fig. 10. Dataset A.1: (Left) Training data in blue, Actual in orange, Predicted in green. (Right) Zoom into A.1: actual in blue and predicted in orange with a MSE of 0.00183

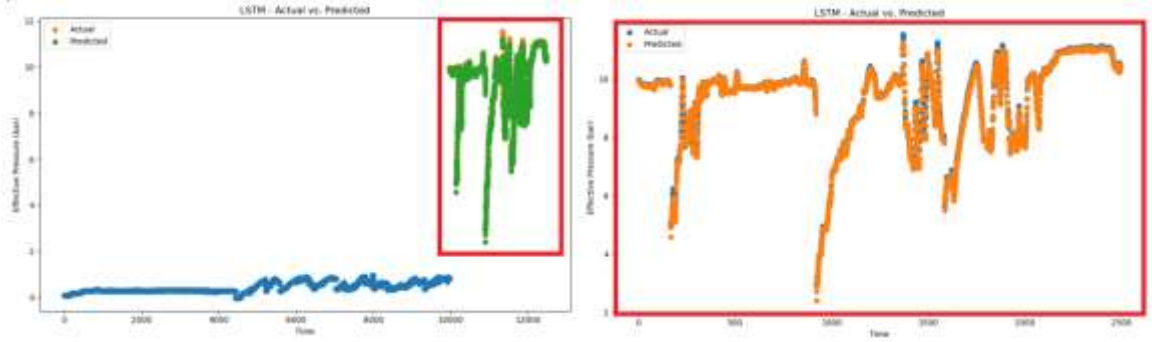


Fig. 11. (Left) Dataset B.2: Training data in blue, actual data in orange, predicted data in green. (Right) Zoom into B.2: actual data in blue and predicted data in orange, with a MSE of 0.0324

 © DFI International Bruges 2025

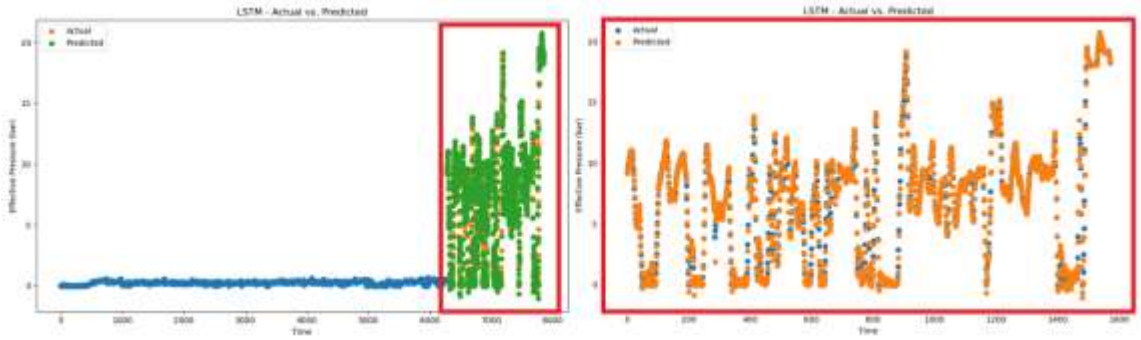


Fig. 12. (Left) Dataset C.4: Training data in blue, actual data in orange, predicted data in green. (Right) Zoom into C.4: actual data in blue and predicted data in orange, with a MSE of 0.0526

CONCLUSIONS

Our research leverages extensive datasets from the Mosul Dam and Rogun Dam projects to demonstrate the benefits of employing Long Short-Term Memory (LSTM) models in optimizing grouting processes.
What we developed is a model that can predict critical parameters such as pressure and flow rate. The machine learning model enables more precise control, reducing errors and ensuring enhanced safety during critical infrastructure operations.

The exceptional performance of LSTM models in capturing sequential dependencies makes them well-suited for time-series data like that generated by grouting systems. The integration of these AI models into the "T-Grout" system represents a significant milestone in the automation of construction technologies, offering improved project execution and quality management.
While our preliminary results are encouraging, there is still room for further development and exploration:

- Generalizability across various engineering fields: We propose applying our deep learning models to foundation work or compensation grouting projects to determine their applicability across different disciplines.

- Enhanced model accuracy through additional variables: Incorporating drilling data from before the grouting phase into the model could improve prediction accuracy and robustness.

- Real-time integration with geotechnical instrumentation: Seamlessly integrating our AI models with real-time data from ground settlements monitoring systems and other geotechnical instrumentation will enable dynamic predictions and adjustments during grouting operations, ultimately enhancing on-the-fly decision-making."

REFERENCES

Amemiya, T., Powell, J.L. (1981). A comparison of the box-cox maximum likelihood estimator and the non-linear two-stage least squares estimator. Journal of Econometrics 17, 351–381.

Bateman, V.C., Worsham, B.M., Blackman, L.E., Williams, N.D., Sells, B.S. (2018), “Mosul Dam – Building 2D & 3D Project Information Systems for Construction Monitoring and Risk Assessments”, DFI & EFFC Proceedings, International Conference on Deep Foundations and Ground Improvement, Rome, Italy, June 6-8, 2018.

 © DFI International Bruges 2025

Flor A., Sassi F., La Morgia M., Cernera F., Amadini F., Mei A., Danzi A. (2023). Artificial intelligence for tunnel boring machine penetration rate prediction. Tunnelling and Underground Space Technology, Volume 140, 105249.

Granata R., Bateman V. (2022). “2022 OPA Winner: Mosul Dam Rehabilitation Project”, DFI 47th Annual Conference on Deep Foundations, 4-7 October 2022, National Harbor, Maryland, USA. Published on Deep Foundation Magazine, Sept/Oct 2022, pp.16-21

Granata R., Crippa C., Di Salvo G. (2022). Remedial Grouting at Mosul Dam, Iraq “. 6th International Conference on Grouting and Deep Mixing”, New Orleans, LA., postponed 15-18 January 2023.

USACE (2016). Potential Failure Modes Analysis and Semi-Quantitative Risk Assessment, Mosul dam, October 2016.

Uzair, M., Jamil, N. (2020). Effects of hidden layers on the efficiency of neural networks, 2020 IEEE 23rd international multitopic conference (INMIC), IEEE. pp. 1–6.

 © DFI International Bruges 2025

A SEMI-ANALYTICAL MODEL FOR ELASTIC SETTLEMENTS OF END-BEARING PILES IN INHOMOGENEOUS SOILS

Armando Della Corte, KU Leuven, Bruges, Belgium. armando.dellacorte@kuleuven.be
Aggelos Tsikas, Quantum Neural Technologies QNT, Athens, Greece. ait@monogramgroup.eu
Stijn François, KU Leuven, Leuven, Belgium. stijn.francois@kuleuven.be
George Anoyatis, KU Leuven, Bruges, Belgium. george.anoyatis@kuleuven.be

ABSTRACT

In this study, a novel approximate static solution is derived for the elastic settlements of end-bearing piles in vertically inhomogeneous soils. Following the seminal work of Nogami and Novak (1976) and previous work by some of the authors, the pile is modelled as a rod, and the soil as an approximate continuum of the Tajimi type. Soil inhomogeneity is introduced via a generalized power law variation of the soil shear modulus with depth. The eigenvalues and the associated soil modes are now obtained by solving a generalized eigenvalue problem that emerges from the use of appropriate shape functions in the solution, which satisfy the boundary conditions of the pile-soil system. Unlike existing models for homogeneous soil, the associated Fourier coefficients are now coupled and obtained as solutions to a set of simultaneous algebraic equations of equal rank to the number of modes considered. The solution is expressed in terms of generalized Fourier series and includes: (1) displacements and stress fields within the soil and along the pile-soil interface; (2) displacements and normal stresses along the pile length, and (3) static pile head stiffness. The results obtained from the proposed solution compare well against results from available methods in the literature.

Keywords: Static pile stiffness; semi-analytical model; soil inhomogeneity; soil-pile interaction, end-bearing piles

INTRODUCTION

In piling engineering design, the analysis of pile settlement is a classical problem that has long been a subject of extensive research. Over the years various methods, such as boundary element solutions (Davis and Poulos (1968); Banerjee and Davies (1978)), finite elements (Ottaviani (1975); Syngros (2004)), simplified t-z models (Kraft et al. (1981)), several hybrid formulations (Chin and Poulos (1991); Mandolini and Viggiani (1997)), and semi-analytical models (Mylonakis (2001); Anoyatis and Mylonakis (2012); Anoyatis et al. (2019); Anoyatis et al. (2023); H. Liu and H. Liu (2024); Della Corte et al. (2024a); Della Corte et al. (2024b)) have been proposed to address the problem. Despite the significant advancements made, key aspects of the problem such as the influence of pile-soil stiffness contrast, pile slenderness, the response of end-bearing versus floating piles and soil inhomogeneity remain poorly understood, mainly because of the lack of pertinent analytical tools.

On one hand, powerful finite element commercial software can handle a variety of complex soil–pile configurations; however, such tools can be computationally expensive. On the other hand, analytical models provide a cost-effective alternative solution for soil–pile interaction analysis, offering valuable insight into the physics of pile-soil interaction and serving as a benchmark solution to verify more complex finite element models (FE). Winkler and plane strain models fail to capture key aspects of the problem, such as the continuity of the medium and the attenuation of soil displacements and stresses with radial distance from the pile. Moreover, the fundamental problem in the implementation of Winkler models lies in the assessment of the Winkler springs (Anoyatis et al. (2013)). In contrast, three-dimensional analytical models can provide more realistic predictions compared to Winkler and plane strain models.

The solution proposed in this work considers the three-dimensional nature of the problem by modelling the soil as an approximate continuum of the ‘Tajimi type’, following the seminal work of Nogami and Novak (1976) and previous work by some of the authors. Such model reduces the number of dependent variables by eliminating certain stresses and displacements in the governing elastodynamic equations. Key to the Tajimi approach in axial mode is the physically motivated

 © DFI International Bruges 2025

assumption that the vertical normal, σ_z, and vertical shear stresses, τ_{rz}, in the soil, are controlled solely by the vertical soil displacement u_z. The equilibrium in the radial direction is not satisfied with this approach. This reduces the two equations of classical axisymmetric elasticity to one, which satisfies the equilibrium only in the vertical direction.

The approximate static solution derived in this paper extends the pioneering solution of Nogami and Novak (1976) and represents an alternative solution to the one derived by Anoyatis et al. (2019) for the analysis of static axially loaded end-bearing piles. Unlike the closed-form solution of Anoyatis et al. (2019), the proposed model captures the soil modes (eigenfunctions) of the problem along the vertical coordinate by using simpler cosine functions compared to the more complicated modified Bessel functions used in Anoyatis et al. (2019), reducing significantly the computational complexity. The soil-pile system response is expressed in terms of a generalized Fourier series. Apart from its intrinsic theoretical interest, the proposed model has distinct advantages over available two-dimensional models accounting for soil inhomogeneity as it accounts for the continuity of the medium, accounts for soil inhomogeneity in the vertical direction, accounts for compressibility of the soil material and is free of empirical constants. The accuracy of the proposed static model is verified through comparisons with available models in the literature.

MODEL DEVELOPMENT

The problem considered in this study is shown in Fig. 1, it consists of a single solid vertical pile of length L and circular cross section of diameter d that is embedded in an inhomogeneous soil deposit. The pile is modelled as a rod, following the classical strength-of-materials solution, rests on a bedrock and is subjected to an axial static force F. The pile is modelled as an elastic rod of Young's Modulus E_p and mass density ρ_p. The soil is modelled as Tajimi type continuum and is characterised by its soil mass density ρ_s, Poisson's ratio ν_s. Soil inhomogeneity is introduced through the following depth-dependent shear modulus function

$$G_s(z) = G_{sH}\left[b + (1-b)\left(\frac{z}{H}\right)\right]^n \quad [1]$$

where z is the vertical coordinate, n and b are dimensionless inhomogeneity parameters that control the shape of the stiffness distribution. b links the stiffness at the surface of the layer G_{s0} to the stiffness at its bottom G_{sH}, that is, $b = (G_{s0}/G_{sH})^{1/n}$.

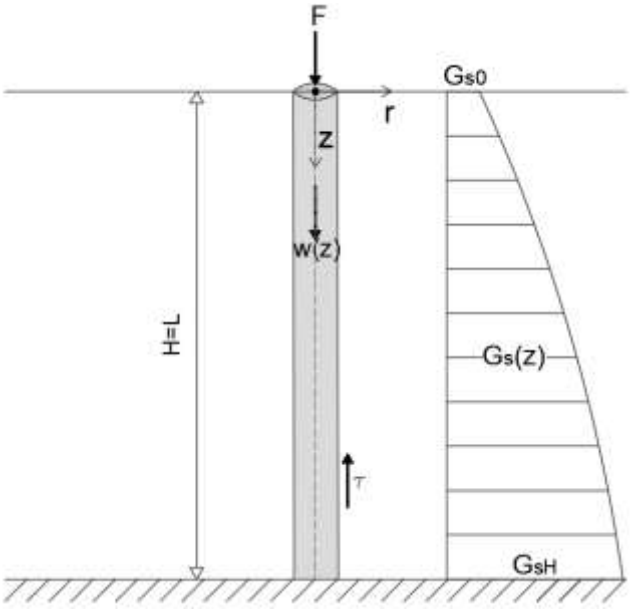


Fig. 1 Problem considered.

 © DFI International Bruges 2025

Soil analysis

The equilibrium of vertical forces acting on a soil element in axisymmetric conditions in cylindrical coordinates yields the governing differential equation:

$$\frac{\partial(\tau\, r)}{\partial r} + r\,\frac{\partial \sigma}{\partial z} = 0 \qquad [2]$$

where $\tau = \tau_{rz}(r,z)$ and $\sigma = \sigma_z(r,z)$ are the vertical soil shear and normal stresses. The stress-displacement relations for axisymmetric deformations in a Tajimi-type continuum are (Nogami and Novak (1976); Mylonakis (2001); Anoyatis et al. (2019)):

$$\sigma \approx -\eta_s^2\, G_s \frac{\partial u}{\partial z} \qquad [3]$$

$$\tau \approx -G_s \frac{\partial u}{\partial r} \qquad [4]$$

where $\eta_s^2 = 2(1-\nu_s)/(1-2\nu_s)$ is a compressibility parameter related to the Tajimi approximation, and relative discussion is provided in the earlier works of Mylonakis (2001) and Anoyatis et al. (2019).

Substituting Equations [3] and [4] into Equation [2] the equilibrium of vertical forces acting on a soil element can be expressed in terms of soil displacement (Anoyatis et al. (2019)):

$$\frac{1}{r}\frac{\partial}{\partial r}\left(r\frac{\partial u}{\partial r}\right) + \eta_s^2 \frac{\partial^2 u}{\partial z^2} + \eta_s^2 \left[\frac{1}{G_s}\frac{\partial G_s}{\partial z}\right]\frac{\partial u}{\partial z} = 0 \qquad [5]$$

where $u = u_z(r,z)$ is the vertical soil displacement. The solution to Equation [5] can be expressed as the product of the solutions of the two ordinary differential equations that arise from the application of the classical method of separation of variables:

$$R'' + \frac{1}{r}R' - q^2 R = 0 \qquad [6]$$

$$(\bar{G}_s \Phi')' + \lambda \bar{G}_s \Phi = 0 \qquad [7]$$

where $\bar{G}_s = G_s/G_{sH}$ expresses in a dimensionless form the profile of soil stiffness. q and λ are variables that emerge from the application of the method of separation of variables, and they are linked through the compressibility coefficient as $q = \eta_s\sqrt{\lambda}$. The solution to Equation [6] has been given in the work of Mylonakis (2001). Equation [7] is a Sturm-Liouville equation and its solution has been obtained in the work of Anoyatis et al. (2019) by using modified Bessel functions of the first and second kind. The solution proposed in this study captures the soil modes $\Phi = \Phi(z)$ by employing simpler trigonometric functions that allow the proposed model to be computationally less expensive than the one proposed by Anoyatis et al. (2019). In this regard, the soil modes are expressed in terms of Fourier series:

$$\Phi_m = \sum_{k=1}^{\infty} S_k^m\, \Psi_k \qquad [8]$$

where S_k are the Fourier coefficients, and $\Psi_k = cos(\alpha_k z)$ is a cosine function. $\alpha_k = (\pi/2H)(2k-1)$ is derived from the boundary condition of zero displacement at the pile tip. Substituting Equation [8] into Equation [7], making use of the orthogonality identity of the cosine functions and the weak formulation concept, yields the following eigenvalue problem:

 © DFI International Bruges 2025

$$\sum_{k=1}^{\infty} S_k^m \int_0^H \bar{G}_s \, \Psi_k' \, \Psi_n' \, dz \; - \sum_{k=1}^{\infty} S_k^m \, \lambda_m \int_0^H \bar{G}_s \, \Psi_k \, \Psi_n \, dz = 0 \qquad [9]$$

The solution of which gives the eigenvalues λ_m of the problem and the desired S_k^m Fourier coefficients. The corresponding soil modes $\Phi_m(z)$ can now be computed using Equation [8]. Displacements and shear stresses in the soil can be expressed in terms of Fourier series as:

$$u = \sum_{m=1}^{\infty} B_m \, K_0(q_m r) \, \Phi_m \qquad [10]$$

$$\tau = \sum_{m=1}^{\infty} G_s \, B_m \, q_m \, K_1(q_m r) \, \Phi_m \qquad [11]$$

where B_m are Fourier coefficients, and K_0 and K_1 are the modified Bessel functions of the second kind, zero and first order, respectively.

Soil-pile interaction analysis

The equilibrium of vertical forces acting on a pile segment yields the equation of the pile motion:

$$-E_p A_p \frac{\partial^2 w}{\partial z^2} + \pi d \tau_0 = F \qquad [12]$$

where A_p is the pile cross sectional area and $\tau_0 = \tau(r = d/2, z)$ is the vertical soil shear stress at the soil-pile interface. $F = F(z)$ can be expanded in Fourier series as:

$$F = \sum_{m=1}^{\infty} f_m \, G_s \, \Phi_m \qquad [13]$$

where the coefficients f_m are obtained by applying the orthogonality of the soil modes:

$$f_m = \int_0^H F \, \Phi_m \, dz \, / \int_0^H G_s \Phi_m^2 \, dz \qquad [14]$$

Substituting Equations [10], [11] and [13] into Equation [12], considering perfect bonding at the soil-pile interface and utilising the weak form concept, yields the following system of $m \times k$ of equations that can be expressed in a more compact form as:

$$E_p A_p \sum_{m=1}^{\infty} B_m \, K_0(s_m) \int_0^H \Phi_m' \Phi_k' \, dz \; + 2\pi \, s_k \, B_k \, K_1(s_k) \int_0^H G_s \Phi_k^2 \, dz = F \Phi_k(0) \qquad [15]$$

where $m = 1,2,3 \ldots N$ and $k = 1,2,3 \ldots N$, in which N is the number of modes considered in the analysis, and $s_m = q_m d/2$ is a dimensionless parameter. Unlike the solution for homogeneous soils, in the proposed model the Fourier coefficients B_m are coupled and are obtained by solving [15]. The pile displacement can now be obtained from Equation [10] by setting $r = d/2$:

 © DFI International Bruges 2025

$$w(z) = \sum_{m=1}^{\infty} B_m \, K_0(s_m) \, \Phi_m \qquad [16]$$

With the pile displacement obtained, the evaluation of the static pile head is straightforward and is given by:

$$K_{head} = F \Big/ \sum_{m=1}^{N} B_m \, K_o(s_m) \, \Phi_m(0) \qquad [17]$$

NUMERICAL RESULTS AND MODEL VERIFICATION

Figure 2 shows the variation of the first three static soil modes with the depth. Each mode is normalised to be unitary at the surface, $z = 0$. The results refer to a soil deposit with a linear variation of the stiffness with depth. The ratio between the stiffness at the surface and the stiffness at the bottom of the soil layer is $G_s/G_{sH} = 0.25$. The results obtained from the proposed solution are compared with the results obtained from the more rigorous solution of Anoyatis et al. (2019) and show excellent agreement, demonstrating the predictivity power of the proposed model.

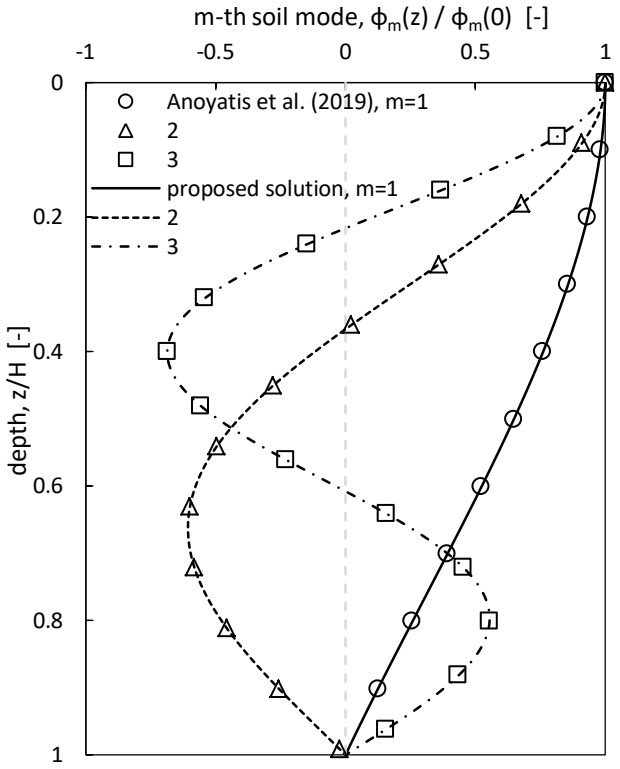


Fig. 2 First three static soil modes. Comparison of the proposed solution against the more rigorous solution of Anoyatis et al. (2019). $\boldsymbol{n = 1,\ b = 0.25, \nu_s = 0.4}$.

Figure 3 plots the variation of the normalised pile head stiffness with normalised pile slenderness for stiff E_p/E_{sH} =100 and E_p/E_{sH} =1000 soft soil deposits. The results pertain to a soil deposit with zero stiffness at the surface and linear variation of shear modulus with depth. The results from the proposed solution are compared against the results from Anoyatis et al. (2019) and show very good agreement.

As expected, the pile head stiffness drops with increasing pile slenderness L/d and it is higher for stiff soils E_p/E_{sH} =100.

 © DFI International Bruges 2025

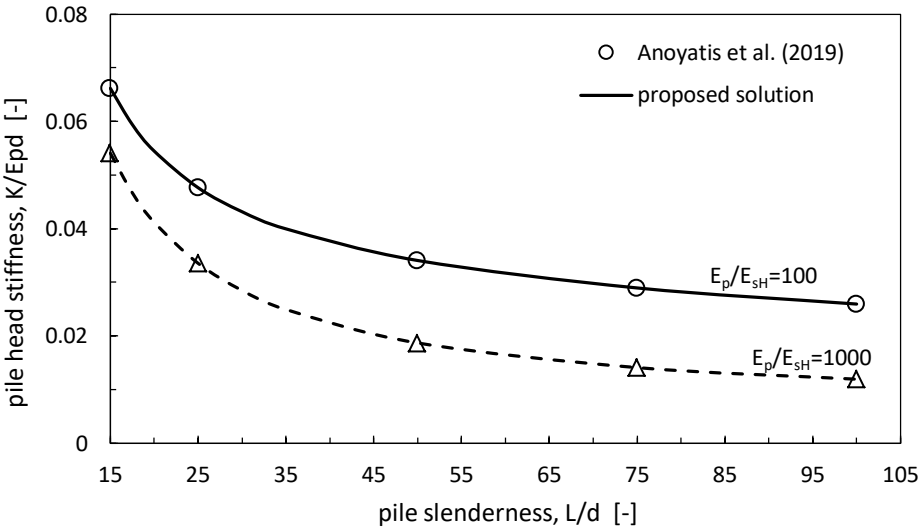


Fig. 3 Variation of normalised pile head stiffness. Comparison of the proposed solution against the solution of Anoyatis et al. (2019). $n = 1,\ b = 0, \nu_s = 0.4$.

Figure 4 shows normalised soil displacement (a) and normalised shear stress (b) contour plots in the $r - z$ plane for a Gibson soil ($n = 1,\ b = 0$). As expected, both soil displacement and shear stress attenuate with increasing radial distance from the pile. Vertically, soil displacement decreases and becomes zero at the bottom of the layer, due to the presence of the bedrock. In general, the shear stress remains finite at the soil surface due to the approximate nature of the model. However, in the case of a soil deposit with zero stiffness at the surface, the shear stress would also be zero according to the proposed approximate model (Equation [11]), as observed in Fig. 4(b).

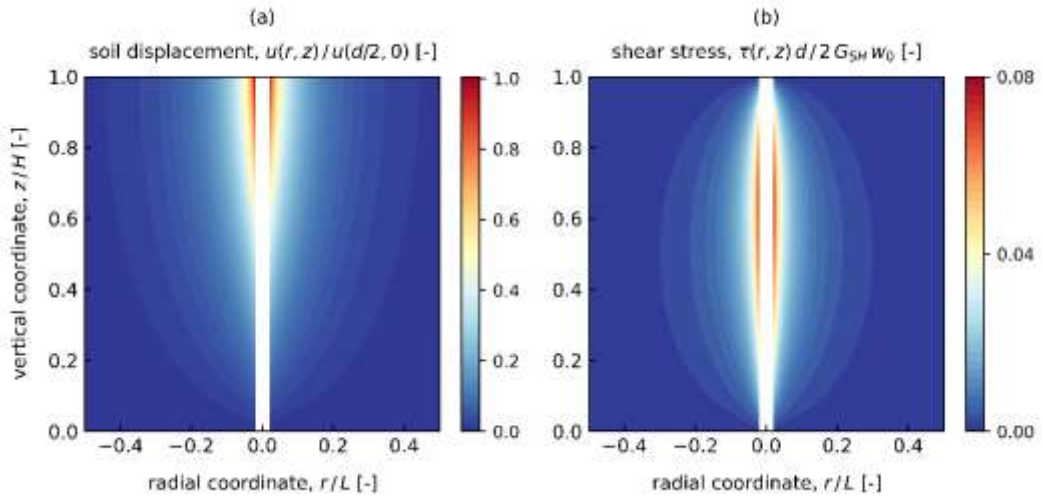


Fig. 4 Variation of normalised soil displacement (a) and normalised shear stress (b) along both r and z coordinates. $n = 1,\ b = 0, \nu_s = 0.4, E_p/E_{sH} = 100, L/d = 25$.

CONCLUSIONS

In this work, a semi-analytical solution for elastic settlements of end-bearing piles in inhomogeneous soils under static vertical load is derived. The equilibrium of forces in the horizontal direction is not satisfied in this approach, nor is the boundary condition of zero shear stresses at the soil surface; however, these approximations have a minor influence on the solution. In the proposed approximate-continuum solution simple cosine functions are used to accurately capture the soil modes. This technique generates results that are in perfect agreement with the more rigorous model of Anoyatis et al. (2019) and significantly reduces the computational complexity compared to the modified Bessel

 © DFI International Bruges 2025

functions of the first and second kinds employed in the solution of Anoyatis et al. (2019). Furthermore, the proposed approximate model with pertinent modifications could be employed to address other problems such as piles subjected to kinematic load and dynamic pressures of retaining walls with generalized soil inhomogeneity.

The Python scripts and data of this study will be made openly available on the KU Leuven webpage titled 'Soil–Structure Interaction Toolkit', at the URL: https://bwk.kuleuven.be/projects/SSItk/, which aims to host scripts and data for a wide range of commonly met soil-pile interaction problems.

ACKNOWLEDGMENTS

The research proposed in this paper was supported by KU Leuven through the project "ATHENA Analytical & programming efficiency in geoTecHnical ENgineering Applications" (C24E/22/009), KU Leuven Internal Funds. The authors are grateful for this support.

REFERENCES

Anoyatis, G., and Mylonakis, G., 2012. Dynamic Winkler modulus for axially loaded piles. Géotechnique, 62(6) 521-536. doi.org/10.1680/geot.11.P.052.

Anoyatis, G., Di Laora, R., Mylonakis, G., 2013. Axial kinematic response of end-bearing piles to P waves. Int J Numer Anal Methods Geomech, 37(17) 2877-2896. doi.org/10.1002/nag.2166.

Anoyatis, G., 2013 Contribution to kinematic and inertial analysis of piles by analytical and experimental methods. PhD Thesis. GR: University of Patras.

Anoyatis, G., Mylonakis, G., and Tsikas, A., 2019. An analytical continuum model for axially loaded end-bearing piles in inhomogeneous soil. Int J Numer Anal Methods Geomech, 43(6) 1162-1183. doi.org/10.1002/nag.2886.

Anoyatis, G., François, S., Orakci, O., and Tsikas, A., 2023. Soil-pile interaction in vertical vibration in inhomogeneous soils. Earthquake Engng Struct Dyn, 1-20. doi.org/10.1002/eqe.3968.

Anoyatis, G., Della Corte, A., Orakci, O., Di Laora, R., Tsikas, A., and François, S., 2024. Kinematic response of end-bearing piles in inhomogeneous soils under P-wave excitation. 8th International Conference on Earthquake Geotechnical Engineering (8ICEGE), Osaka, Japan, May 7-10, 2024, Japanese Geotechnical Society Special Publication, 10 (55) 2078-2083. doi.org/10.3208/jgssp.v10.OS-44-05.

Anoyatis, G., François, S., Letizia, N., Della Corte, A., Orakci, O., and Tsikas, A., 2024. Seismic soil pressures on rigid walls retaining inhomogeneous backfills. Proceedings of the 18th World Conference on Earthquake Engineering (WCEE2024). Technical Session: GEO - geotechnical earthquake engineering and site response. Milan, Italy, June 30 to 5th July 2024.

Banerjee, P.K., and Davies T.G., 1978 The behaviour of axially and laterally loaded single piles embedded in nonhomogeneous soils. Géotechnique. 28(3) 309-326.

Chin J.T., and Poulos H.G., 1991. Axially loaded vertical piles and pile groups in layered soil. Int J Numer Anal Methods Geomech, 15(7) 497-511.

Davis, E.H., and Poulos, H.G., 1968. The use of elastic theory for settlement prediction under three-dimensional conditions. Géotechniqu,18(1) 67-91.

 © DFI International Bruges 2025

Della Corte, A., Orakci, O., Tsikas, A., François, S., and Anoyatis, G., 2024a. A semi-analytical model for axial soil-pile interaction in generalized inhomogeneous soils. Proceedings of the XVIII European Conference on Soil Mechanics and Geotechnical Engineering (ECSMGE24), Lisbon, Portugal, August 26-30, 2024, 438-443.

Della Corte, A., Orakci, O., Letizia, N., Tsikas, A., François, S., and Anoyatis, G., 2024b. An overview of semi-analytical models for soil-structure interaction: model development and toolkit. Proceedings of the 17th PAN-AMERICAN CONFERENCE ON SOIL MECHANICS AND GEOTECHNICAL ENGINEERING. 2nd LATIN-AMERICAN REGIONAL CONFERENCE OF IAEG, La Serna, Chile, November 12-16, 2024.

Gazetas, G., 1984. Seismic response of end-bearing single piles. Int J Soil Dynam Earthq Eng,3(No. 2) 82-93.

Gibson, R.E., 1967. Some results concerning displacements and stresses in a non-homogeneous elastic half-space. Géotechnique, 17(1) 58-67.

Kraft Jr L.M., Ray R.P., and Kagawa T., 1981. Theoretical tz curves. Journal of Geotechnical and Geoenvironmental Engineering, 107(ASCE 16653):GT11.

Mandolini A., and Viggiani C., 1997. Settlement of piled foundations. Géotechnique, 47(4) 791-816.

Mylonakis G., 2001. Winkler modulus for axially loaded piles. Géotechnique.51(5):455-462.

Nogami, T., and Novak, M., 1976. Soil-pile interaction in vertical vibration, Earthquake Engineering & Structural Dynamics, 4(3) 277-293. doi.org/10.1002/eqe.4290040308.

Ottaviani, M., 1975. Three-dimensional finite element analysis of vertically loaded pile groups. Géotechnique, 25(2) 159-174.

Poulos, H. G., and Davis, E.H., 1980. Pile foundation analysis and design, Wiley.

Randolph, M.F., and Wroth, C.P., 1978. Analysis of deformation of vertically loaded piles. J Geotech Eng, 104(12) 1465-1488.

Syngros K., 2004. Seismic response of piles and pile-supported bridge piers evaluated through case histories. PhD Thesis: City University of New York.

 © DFI International Bruges 2025

THERMAL INTEGRITY TESTING; NEW SCENARIOS AND METHODS

Anthony Fisher, Cementation Skanska Ltd, Doncaster, UK, anthony.fisher@skanska.co.uk.
Qianchen Sun, ARUP, London, UK, jason.sun@arup.com.
Chris Barker, ARUP, London, UK, chris.barker@arup.com

ABSTRACT

Thermal integrity testing has become one of the standard non-destructive tests used on deep foundations with guidance documents and model specifications widely available. It's detailed investigation of the foundation's perimeter can provided new insights into the as-built pile and the ground in which it is formed. As the adoption of this test has increased, so has the range of situations in which it has been employed. These now include thermal testing of deep CFA piles, testing of piles which use low cement concrete mixes and testing of piles installed in marine environments. The method of carrying out thermal integrity testing has also varied and now includes distributed fibre optic sensing alongside the more established use of digital temperature sensors.

For these new situations and techniques, establishing a theoretical and practical framework for the use of thermal integrity testing is an essential precursor for its success. This paper presents recent case histories and data, highlighting how the technique can be successfully deployed in the situations highlighted. Comparison of measured data with numerical simulation is used to create a sound framework for both the implementation of the test and interpretation of the collected data

Keywords: Thermal Integrity Testing, Distributed Fibre Optic Sensing

INTRODUCTION

The purpose of integrity testing, is to independently verify the quality and structural soundness of deep foundation elements, by utilising non-destructive testing methods to identify any potential flaws, defects, or deterioration that could affect their load-bearing capacity, thereby ensuring the safety of the structure built on top of them; essentially acting as a quality check without causing damage to the foundation element itself.

Like all risk mitigation measures, the integrity testing selected for a particular project needs to appropriate to both the likelihood and severity of the risk, a judgement which can only be made if the ability of the test to identify those features or flaws which could be a defect is understood. Any factors which can reduce or increase the sensitivity of the test method also needs to be considered. The evaluation of new techniques and re-evaluation of existing ones is, therefore, an important and continuous process to ensure that understanding grows in step with development in testing technology and industry practice.

The most recent of integrity testing techniques to be used for this purpose is thermal integrity testing. This test takes advantage of the exothermic chemical reactions in the hydration of cement. By measuring the temperature of concrete during its initial curing the presence of such reactions can be confirmed and anomalous areas, where such reactions are noticeably different, identified. Early publications of this technique such as Mullins and Winters (2011), deployed this test on rotary bored piles using an infrared sensor lowered into a reservation tube within a pile.

More recently, an alternative method, the use of thermal wire, manufactured by PDI, has become more widespread due to the advantages it offers, as described in Boeckmann et al. (2022). Case studies of its use are presented in publications such as Mullins and Piscsalko (2012) and Coleman and Belardo (2017), which cover a variety of piling situations and diameters. Additionally, a further method of carrying out the technique using distributed fibre optic sensing (DFOS) has been developed and is described by Fisher and Bell (2017).

In response to this continued evolution, this paper addresses three new scenarios in which thermal integrity testing has been deployed, the use of low carbon cement, deep Continuous Flight Auger (CFA) piles and marine piles. This paper also considers the technique of using distributed fibre optic sensing (DFOS) to carry out the test. This will allow clients and specifiers to select appropriate mitigation measures for the risks associated with foundation integrity.

 © DFI International Bruges 2025

LOW CARBON CEMENT

With the linkage between global warming and carbon dioxide emissions firmly established at an international and political level, the proportion of emissions attributable to construction is under increasing scrutiny. Amongst these emissions, the production of concrete, particularly the manufacture of Portland cement clinker is a significant contributor. In the UK, the Department for Business, Energy & Industrial Strategy (2022) report that 1.5% of the UKs emissions arise from the manufacture of cement, however, globally, estimates by Lehane and Felix (2018) put that contribution at as much as 8%. Reducing these emissions is, therefore, a significant priority for the foundations industry. In the UK one way of achieving this has been to replace a proportion of the cement used in foundations with supplementary cementitious materials (SCMs).

Ground Granulated Blast furnace Slag (GGBS) is a by-product of the steel industry and is often viewed as a sustainable SCM. Alongside the technical and economic reasons for its inclusion, it is increasingly being used in low carbon concretes. BS EN 197 – 1(2019) defines a CEM IIIA cement which can include between 36 to 65% replacement and CEM IIIB cement which can include between 66 to 80% replacement of clinker with GGBS and this is now regularly used in foundation mixes. Other alternative mixes using alkaline activated cementitious material and geopolymer technologies also rely on high proportions of GGBS, according to Arnold et al. (2023). Even though the long-term use of GGBS may decrease as alternative methods of steel production are introduced, in the medium term, the use of GGBS replacement is likely to continue. This is significant for thermal integrity testing because of the way in which GGBS affects concrete heat generation.

Compared with Portland cement or indeed other SCMs such as Pulverized Fuel Ash (PFA), GGBBs mixes, as described by De Shutter and Taerwe (1995), produce heat more slowly and so both the peak temperature and the rate of temperature change in a deep foundation can be significantly reduced. This will make defects harder to detect. To investigate this issue, Figure 1 presents measured changes in temperature from piles of different diameters and using different concrete mixes, including CEM IIIB. These results have been selected from pile installed in similar ground conditions and the measurements include both thermal wire and fibre optic cables.

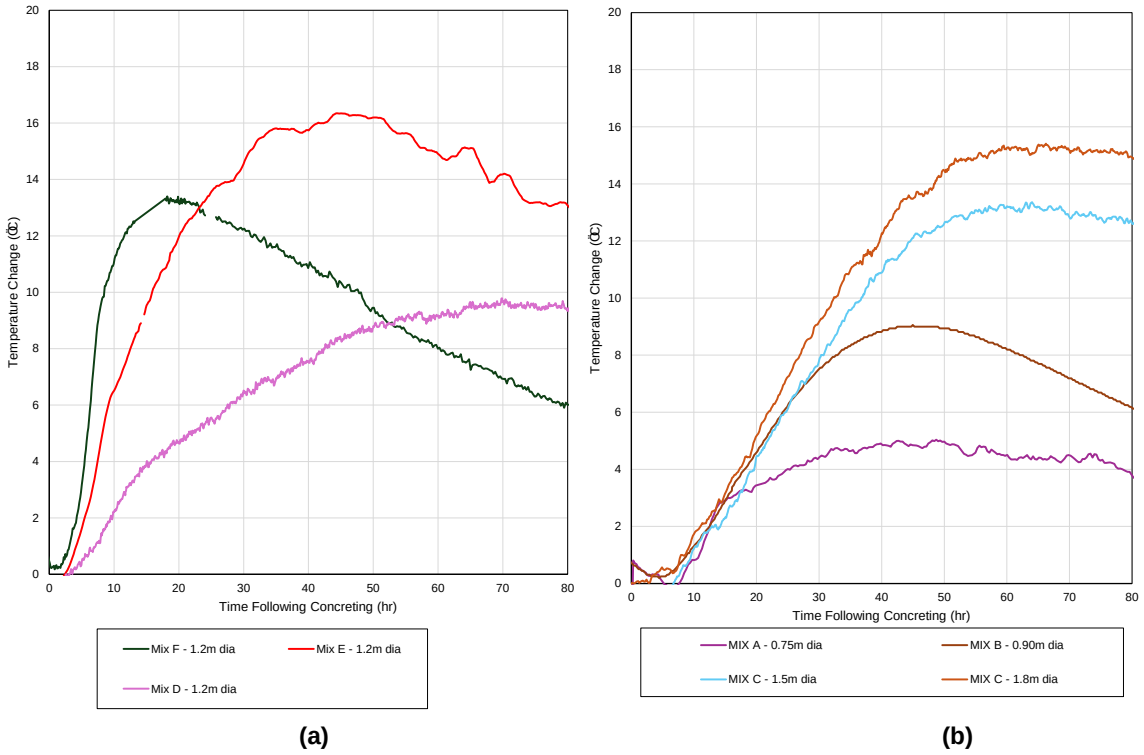


FIG. 1 (a) Temperature change vs time for 1.2m diameter piles with different cement types. (b) Temperature change vs time measured in different sized piles using CEM IIIB Cement.

The first important observations from this data is that the presence of high proportions of GGBS increase the time required for concrete to reach its peak temperature. For the 1.2m diameter piles presented, the time to peak temperature increases from 20 hours for a CEM IIIB mix in which PFA is used as a SCM to 70 hours for a CEM IIIB mix. It is important, therefore, that the data capture time is increased for these

 © DFI International Bruges 2025

high replacement mixes. This is discussed by Mullins et al. (2021) who presents a formula for calculating the appropriate time range for thermal integrity testing measurements based on pile diameter and GGBS content. Whilst appropriate for the larger diameter piles, for CEM IIIB mixes, the data presented would suggest that the calculated window should be increased for small diameter piles. The mixes presented do not include retarding admixtures and it is important to note that these can significantly increase the time to peak temperature.

The second observation is that the both the peak temperature change and the time to reach the peak temperature decrease for smaller diameter piles. From the data in figure 1, it can be seen that a reduction in diameter from 1.8m to 0.75m has resulted in a significant decrease in temperature change. It is also evident that that the relationship between diameter and peak temperature change is not linear, with more significant reductions in peak temperature change with progressive reductions in diameter. This is apparent in the theoretical data presented by Sun et al. (2022) and reproduced in figure 3, which calculates that peak temperature measurements from thermal integrity testing will reduce from a constant value for diameters above 1.2m to increasingly lower values at smaller diameters.

Whilst applicable for all concrete mixes, this effect is of particular importance where high levels of cement replacement have been employed. Given that the effectiveness of a thermal integrity test relies upon the difference in temperature between a flaw and sound concrete, if the heat produced by the concrete reduces, the visibility of a flaw is similarly reduced. In the case of CEM IIIB mixes, it is this authors experience that sufficient heat is still produced in piles above 0.9m in diameter but that tests carried out on smaller diameters will be less sensitive.

Table 1. Concrete mix designs referred to in this paper.

Mix Name	Cement Type	Cement Content (kg/m^3)	GGBS Content (% of total Cementitious material)
Mix A	CEM IIIB	420	67%
Mix B	CEM IIIB	420	70%
Mix C	CEM IIIA	400	75%
Mix D	CEM IIIB	450	70%
Mix E	CEM IIA	460	50%
Mix F	CEM IIB	320	0%
Mix G	CEM IIIA	427	40%

DEEP CFA PILES

Since the development of modern hydraulic piling rigs, the ability to install deep and large foundations has rarely been limited by equipment alone. Instead, it is additional drivers such as the congestion of brownfield urban sites and increasing land values that have made their use more common. CFA piles have long presented practitioners with the need for an appropriate integrity testing method due to the risk of errors in the concreting process, during which the auger is withdrawn at an appropriate rate with respect to the volume of concrete or grout being pumped into it. An undersupply of concrete will result is a pile with a smaller cross-sectional area than intended whereas an oversupply may, in soft ground, cause excessive overbreak or collapse.

Conventionally formed in diameters of up to 1.2m, these piles have often been tested using a low strain methods such as pulse echo (time domain) or transient dynamic response (frequency domain). Whilst these tests are well suited to CFA piles and able to detect significant necking and cracks with relative ease, their ability to test deep piles is limited due to attenuation of the signal as it passes down the pile. Practically the penetration is limited to a maximum depth over diameter ratio of 30 as described by White et al. (2008) although this requires optimum conditions and preparation to achieve. With CFA piles now being regularly installed in excess of 25m, a new approach to testing is required.

The CFA installation process dictates that any reinforcement is plunged into the pile after the augers are withdrawn. This places limits on the length and density of reinforcement which can be installed and often prohibits the inclusion of the ducts which would be needed to allow cross hole sonic to take place. In UK practice, reinforcement of these piles is seldom full length with short cages plunged into the concrete after the augers are withdrawn. In these situations, thermal integrity testing sensors, installed on a central bar

 © DFI International Bruges 2025

which is plunged into the fresh concrete offers a practical solution. It achieves a full length test whilst maintaining constructability of the pile. This method has been used widely and is reported in Becker et al. (2015), up to 22.3m and in Rui et al. (2021) up to 25m.

As part of the foundations for an energy from waste facility in Scotland, 29m CFA piles were installed at a diameter of 600mm. The project also included a preliminary test pile which was loaded to four times its working load. Given the risk of a structural failure at these loads, a thermal integrity testing was carried out on this pile using DFOS. To successfully plunge the fibre optic instrumentation to depth, a 63.5mm GEWI bar was used with the sensing cables tied to it. The diameter of the bar was chosen to ensure that there was sufficient weight to aid penetration through the concrete and sufficient rigidity to prevent the bar from buckling and snagging on the sides of the pile. However, this bar was also chosen due to a surplus being available on the construction site and, subject to the consideration of rigidity and penetration, there would be no requirement for such a high grade of steel or diameter of bar to be used on other projects.

Figure 2 presents the results of the thermal integrity testing on central bars in 600mm diameter CFA piles. The pile was concreted with a CEM IIIA mix (Mix G in Table 1) and so, despite its relatively small diameter, meaningful thermal data could still be collected from the central portion of the pile. Peak temperatures were reached within 18 hours.

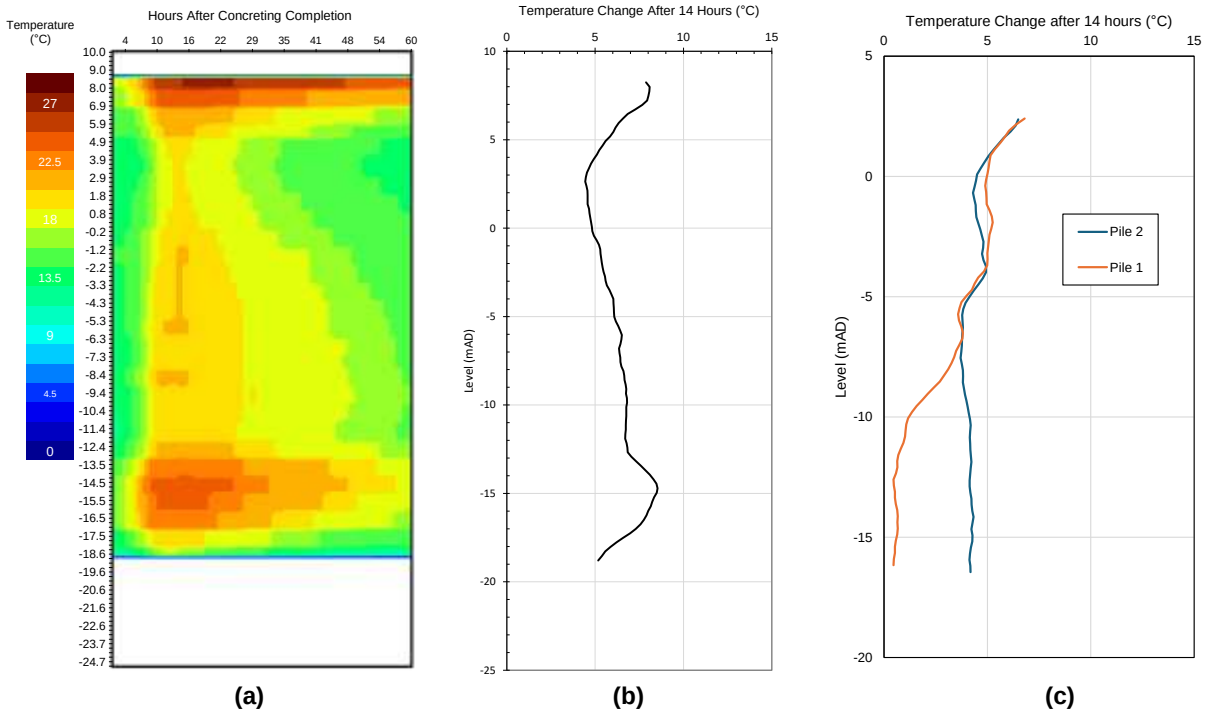


FIG. 2 (a) Measured temperature in a CFA pile with time and level. (b) Temperature change in a CFA pile at peak temperature. (c) Comparison between temperature changes measured in a normal (Pile 1) and defective (Pile 2) CFA pile.

Whilst the use of a central bar presents practical and economic advantages, it is important to consider the impact this may have on the results and how they will differ from those collected from sensors attached to the reinforcement cage of a pile. This can be understood by considering the distribution of temperature across a piles section. Peak temperatures are experienced in the centre of a pile and, in large diameter piles, across a central region. There is then a rapid reduction in temperature through the cover zone of a pile. This distribution has been verified both experimentally and theoretically by Sun et al. (2022) and is presented in Figure 3.

 © DFI International Bruges 2025

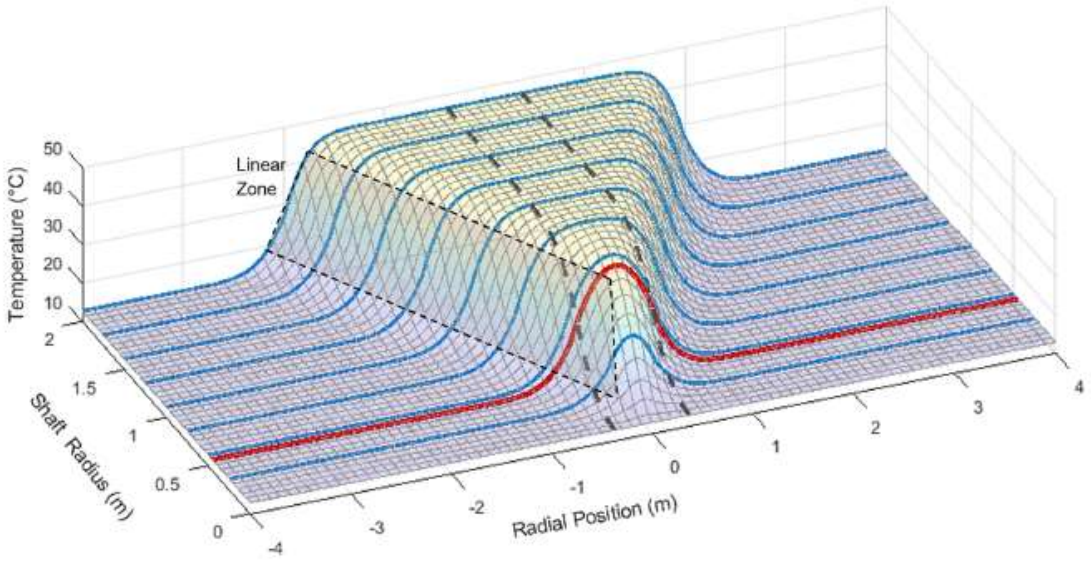


FIG. 3 Numerical model of peak temperature measured in a pile as a function of shaft radius and sensor position. (Sun et al., 2022)

One advantage of measurements made on a conventional reinforcement cage in which sensors are placed at opposite sides is that eccentricity of this cage will be readily detectable. A reinforcement cage moved to one side of a pile will experience a decrease in temperature on the side moved towards the edge of the pile and an increase on the side which moves towards the centre. Examples of this are presented in Piscsalko and Ellis (2022). With a central string of sensors, eccentricity may appear as gradual reductions in temperature that is indistinguishable from a defect.

To illustrate this problem, Figure 2 (c) presents a defect in a 600mm diameter CFA pile which was caused by an undersupply of concrete in the lower half. The thermal integrity test results from this pile are presented alongside those of an adjacent pile which was installed successfully. Whilst this was not measured using a central bar, it illustrates the temperature signature of such a defect and demonstrates that it is one which would be difficult to distinguish for bar eccentricity. It is essential, therefore, to ensure that the bar is centralised within the pile and is not going to buckle. This is a more significant consideration for smaller diameter piles due to the smaller central region of consistent temperature.

A second consideration is that changes in pile radius will be less apparent with thermal measurements in the centre of a pile than they would be if measured at the extremities. Conversely to the issue of eccentricity, this issue is more pronounced for larger diameter piles where central temperatures plateau and are less affected by changes in the cover zone. In scenarios where a central bar is used alongside a short, top reinforcement cage, it is often beneficial to instrument both separately in order to avoid an offset shift in the position of the thermal wire in the pile to more simply assess the pile integrity. In these cases, it is important to be aware of the different types of measurement and their sensitivity to different variations in the pile.

MARINE PILES AND GROUND WATER

Deep foundations are often installed in ground which includes water bearing strata. In the UK, in central London, alluvial gravel deposits typically overlay the dominant London clay formation. These deposits can rapidly become saturated following periods of rainfall and this has a significant effect of the thermal conductivity of the strata, reducing the measured concrete temperatures within them. In these cases, affected areas may be flagged as anomalies, however, an engineering consideration of the ground conditions will be required to reach a satisfactory explanation.

In more extreme examples, foundations are installed in rivers or even the sea, where the cased top section of the pile is exposed to water, which can sometimes be flowing. Typically, these piles are constructed through a permanent section of casing, allowing the pile shaft to be formed, reinforcement installed and then concrete placed. In the UK this has been the case in reclaimed dockland environments such as Canary Wharf as well as for the creation of new port structures. In order to interpret the results of thermal integrity testing of these foundations, the effect of these features needs to be considered.

 © DFI International Bruges 2025

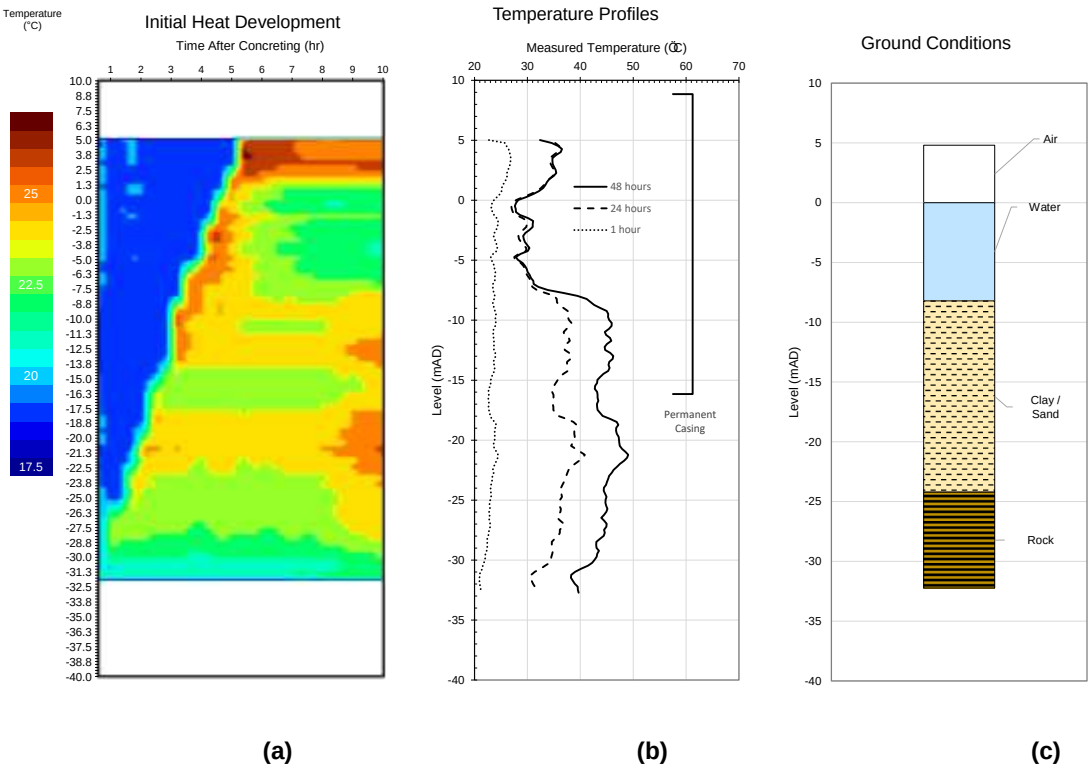


FIG. 4 (a) Measured temperature during concreting and initial curing of a marine pile with level and time. (b) Measured temperature vs level (c) Ground conditions.

The pile presented in Figure 4. was constructed in a tidal dock through a permanent casing with a 5m up stand above water level. It was installed through approximately 9m of water down to the level of the dock bed. Thermal integrity testing was carried out using DFOS. Conventional analysis of thermal integrity testing identified significantly reduced temperature in the sections of the pile within the water, with those sections measuring virtually no temperature change. This result was not unexpected and has been reported on other similar projects such as the Portal North Bridge in New Jersey (Muchard et al., 2024). As previously stated, with a reduction in temperature change, the sensitivity of a thermal integrity test can be significantly reduced.

Given the challenges mentioned and following a number of marine piling projects in the UK, a new method of investigating the integrity of foundations has been developed. This method is applicable to foundations constructed using support fluids. Support fluid within the bore will typically reach a temperature which approaches that of the surrounding ground. This will often be several degrees cooler than the fresh concrete. Temperature measurements made during concreting can readily identify the rise of the concrete within the bore. Any inclusions or mixing with the support fluid will show up as cooler locations, even prior any heat generation happening within the concrete. In the example presented in Figure 4, it can be seen that the concrete poured within the permanent casing is initially hotter than the concrete below bed level. It can also be seen how the concrete exposed to the water cools more rapidly than the concrete exposed to the air. Combining this information with concreting records and drilling observations greatly increase the amount of information which can be obtained from the pile for assessment of integrity.

DISTRIBUTED TEMPERATURE SENSING

The earliest examples of thermal integrity testing were reported by Mullins and Winters (2015) and these made use of a temperature probe, lowered into a foundation through a reservation tube, cast in with the reinforcement. This method, whilst convenient when reservation tubes are present has now been superseded by the use of thermal wire which, amongst other advantages, permits continuous remote measurements of concrete temperature. Whilst both of these methods are covered in ASTM D7949, ASTM International (2016), thermal wire has been broadly recognized as a superior method in publications such as Boeckmann (2022). Like many NDT methods, however, the practice of thermal integrity testing has continued to evolve with the development of new technology. This has recently included the use of Distributed Temperature Sensing (DTS), a subset of DFOS, as described by Fisher and Bell (2017).

 © DFI International Bruges 2025

It would be misleading to describe DTS as a new method, it is simply a different method of collecting temperature data. DTS in of itself is not new and has been used in many fields since the 1980s as described by Ukil et al. (2012). There is, therefore, already a body of work dedicated to the difference between collecting temperature using point sensors and collecting data using a DTS.

The principal difference with DTS data is that each measurement is not a point measurement, rather, it is an average temperature measured across a length of fibre optic cable, for example 0.5m, 1.0m or 1.5m. This length is commonly referred to as the spatial resolution of the measurement. According to Selker et al. (2013), this average is not a simple linear one but is closer to a Gaussian distribution. As a result, a distributed measurement can be considered as a centre weighted average over the spatial resolution. Selker et al. (2013) report that the real world performance of most DTS systems is considerably better than the simple gaussian assumption. Where DTS is to be used as a method of thermal integrity testing it is important to consider the impact of the measurement characteristics on the results of the test. This impact can be assessed both theoretically and practically.

For applications where temperature vary significantly over short distances (with respect to the spatial resolution) the impacts of using DTS may be considerable, however, for the purposes of thermal integrity testing, it is widely reported that the variations in temperature are not instantaneous but gradual, and increasingly so as time elapses and as the effects of heat transfer within the materials occur.

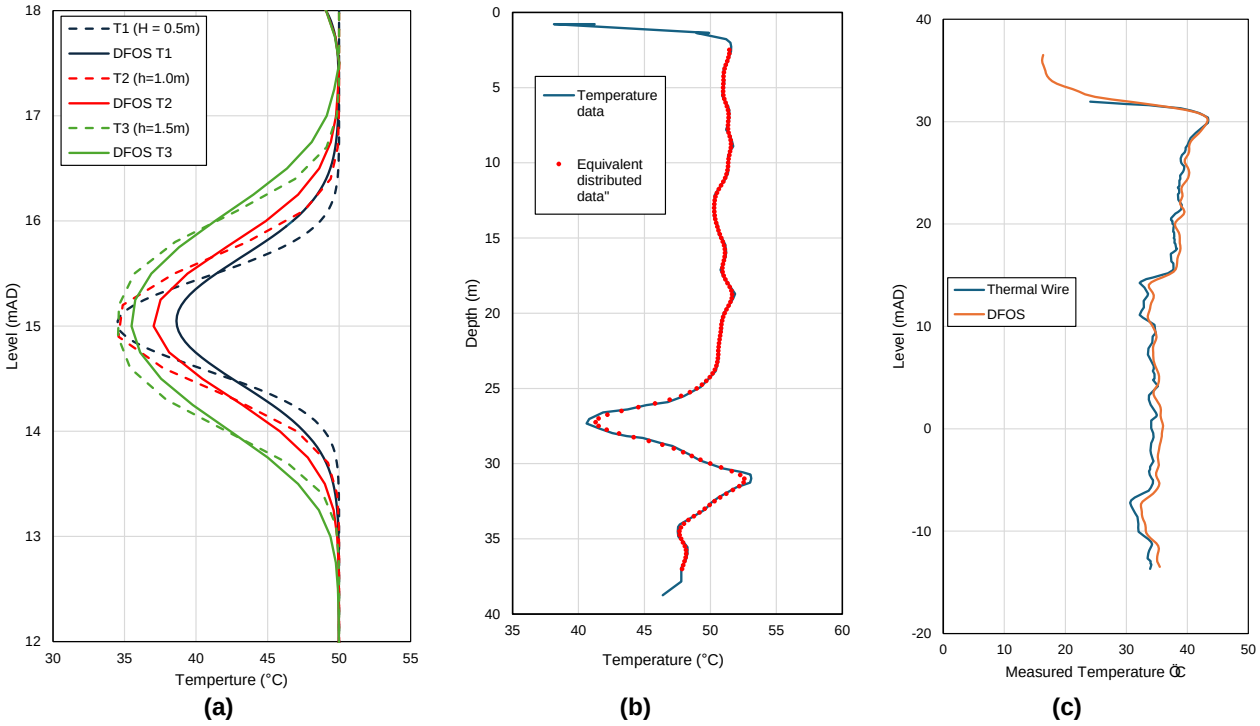


FIG. 5. (a) Theoretical comparisons between values of simulated temperature and equivalend distributed temperature measurements for flaws of different heights. (b) Real temperature data of a flaw, reproduced from Piscsalko et al (2016) compared to equivalent distributed data. (c) Measured data from TIP wire and DFOS for a rotary bored pile..

Figure 5 (a) firstly presents a comparison between the simulated temperatures surrounding a theoretical flaw (dashed lines) with the equivalent distributed measurements. The simulated temperatures have been calculated by assuming a flawed zone within a pile having a fixed temperature, with surrounding concrete have having a distinct, higher temperature. To model the effect of heat transfer from adjacent zones, a spatial average of temperature has been calculated at each location with the weightings of adjacent temperatures corresponding to a normal distribution. Whilst this is not based on actual numerical modeling of the problem, it is sufficient to investigate and illustrate the effect of distributed measurements. Finally, the equivalent distributed measurements have been calculated, using a spatial resolution of 1m and presented alongside the simulated temperature values.

The cases presented in Figure 5. illustrate the effect of spatial resolution and highlight that the difference between the simulated measurements and the equivalent DTS measurements is dependent on the vertical extent of temperature variation caused by the flaw. Where this is less than the spatial resolution, the impact is most noticeable.

 © DFI International Bruges 2025

These calculations illustrate the measurement differences to be expected from temperature variations with a very small extent. It is important to note that the majority of real flaws reported in piles cause temperature variations over a much greater extent. Figure 5. also presents data from a real flaw identified between 25 and 35m by Piscsalko et al. (2016). This has been overlain with the calculated, equivalent distributed data from which it can be seen that, whilst present, the differences are small.

Finally Figure 5 (c), also presents data from a UK project where measurements were made using both DTS and thermal wire. As can be seen, the two sets of measurements are in good agreement. A similar result was noted by Boekman et al. (2022) and this served to strengthen the conclusion that for the purposes of thermal integrity testing, the effect of DTS measurements, whilst important to consider, are not significant.

As previously noted, the nature of the spatial resolution is an important parameter in assessing the effect of using DTS data. When quoting the spatial resolution of a measurement system, it is common to refer to the distance between measurements in which 80% of an instantaneous temperature rise is captured. This method is further explained in IEC 61757-1-2023. Most commercially available DTS systems used for thermal integrity testing are able to measure with a spatial resolution of 1.0m, however, it is important that manufactures are able to define how this has been calculated for their instrument. With an increasing number of instrument manufactures developing DTS systems, it is likely that the availability of instruments with smaller spatial resolutions will increase and the cost of such instruments will continue to fall.

The adoption of a consistent definition for spatial resolution is important, not only to ensure that the quality of the measurements made are sufficient for use in thermal testing, but also because, once understood, they allow the conventional formula developed to correct for the roll of in temperature at the top and bottom of a pile presented in Mullins et al. (2020) to be reformulated to account for distributed data. In the examples presented in Figure 5 (b) and (c), a 1m spatial resolution has been used, based on the IEC definition and adopting a gaussian distribution of data.

DISCUSSION

Having considered four different ways in which the practice of thermal integrity testing is being adapted and evolved, it is appropriate to discuss the impact these changes have on the sensitivity of the test. This information will allow an informed, project specific decision to be made on whether the test method is appropriate for the risk.

Two scenarios have been presented in which the amount of heat produced by a pile is significantly reduced, through the use of concrete mixes and in the exposed sections of a marine pile. In the case of CEM IIIB mixes, piles above 0.9m in diameter are relatively unaffected and can be effectively tested by simply extending the measurement period. However, for smaller diameter piles the impacts are more significant and, in these cases, the sensitivity of the test will be significantly reduced. For marine piles of all diameters and concrete mixes, the amount of heat loss in the exposed sections of the pile will be significant and will, in most cases, reduce the sensitivity of the test in these regions. It is important to note that the sections of a pile which are within the ground below water level are typically unaffected.

For CEMIII/B mixes, an alternative testing strategy may be required for smaller diameter piles because the reduced temperatures will not yield sufficient information to readily detect those flaws which could result in a defect. Whilst the loss of sensitivity of the test in the exposed section of a marine pile is no less severe, it should also be considered that the concrete within the permanent casing of such a pile is less vulnerable to flaws arising from the ground conditions and so the reduced sensitivity of the test in these regions may be of no consequence. In some circumstances, additional information can be obtained from tests in low temperature situations through commencing monitoring of temperature prior to pile concreting or through testing the central section of the pile.

For deep CFA piles, a thermal integrity test carried out using a central bar will be less sensitive than testing carried out on a reinforcement cage. However, if adequately centralized and if consideration is given to the expected distribution of temperatures across the piles section, the test can still allow evaluation of large defects from of the lower part of the pile which would otherwise go untested. The central bar thermal test is currently the best option for a deep CFA pile for which a full-length test is a requirement.

The use of DFOS for thermal integrity testing is a valuable extension to the discipline. Provided that the spatial resolution of the instrument is appropriately specified, DTS measurements are more than sufficient for thermal integrity testing purposes and are sensitive enough for the tests carried out to be effective.

 © DFI International Bruges 2025

CONCLUSION

The adoption and adaption and thermal integrity testing has continued to extend industry capability to verify the integrity of deep foundations. However, as has been shown, there are multiple factors which influence the sensitivity of a thermal integrity test and these need to be properly considered in both the selection of appropriate testing and interpretation of the results. Whilst some limits to the effectiveness of thermal integrity testing have been established, alternative ways to both deploy the sensors and interpret the data can be used to increase the available information from testing in these situations.

With these limitations understood, thermal integrity testing can continue to be used as an effective test method for a wide range of deep foundations.

REFERENCES

Arnold, W., Astle, P. Drewniok, M., Forman, T., Gibb, I., Kanavaris, F., Khosravi, N., Martin, B., Mulholland, A., Munro, I., Scrivener, K., de Silva, M. and Wake, G. 2023. The efficient use of GGBS in reducing global emissions.

ASTM, 2016. Standard Test Methods for Thermmal INtegrity Profiling of Concrete Deep Foundations, Online: ASTM International.

Becker, M. L., Coleman, T. L. and Belardo, D.S. 2015. Thermal Integriy Profiling of ACIP Piles. Proceedings of The International Foundations Congress and Equipment Expo, San Antonio, TX.

Boeckmann, A., Yeskoo, A. R. and Axtell, P. 2022. Use of Thermal Integrity Profiling (TIP) in Drilled Shaft Evaluation. Misouri Department of Transportation, Research Report number cmr 22-002.

British Standards Institution. 2019. Cement. Part 1: Composition, specifications and conformity criteria for common cements. BSI, London.

Coleman, T., and Belardo, D. 2017. Thermal Integrity Profiling accelerates construction of railroad projects. AREMA

De Schutter, G. and Tawrew, L. 1995. General hydration model for portland cement and blast furnace slag cement. Cement and Concrete Research, Vol 25, No3, pp. 593 – 604.

Department for Business, Energy & Industrial Stategy. (2022). UK greenhouse gas emissions by Standard Industrial Classification (SIC) 1990-2022.

Fisher, A. 2022. Developments in Thermal Integrity Testing Practice and Interpretation. Washington DC, Deep Foundations Institute.

Fisher, A. and Bell, A., 2017. The Application of Fibre Optic Sensor Technology in the Integrity Testing of Deep Foundations. Rome, Deep Foundations Institute.

IEC. 2023. International Standard, Fibre optic sensors- Part 1-2: Strain measurement – Distributed sensing based on Brillouin scattering. Switzerland.

Institution of Civil Engineers, 2017. ICE Specification for Piling and Embedded Retaining Walls. 3rd Edition ed. London: ICE Publishing.

Lehane, J. and Felix, Preston. 2018. Making Concrete Change. Innovation in Low-carbon Cement and Concrete. The Royal Institute of International Affairs, Chatham House Report.

Muchard, M., Glider, J., Faust, P. 2024. Drilled shaft construction and some NDT surprises at the portal north bridge. Deep Foundations. Colorado, Deep Foundations Institute.

Mullins, G., Winters, D. 2011. Infrared Thermal Integrity Testing Quality Assurance Test Method to Detect Drilled Shaft Defects. Washington State Department of Transportation, Research Report WA-RD 770.1.

Mullins, G. and Piscsalko, P. E. 2012, Thermal Integrity Profiling: An innovative Technique for Drilled Shafts. Deep Foundations Magazine, DFI.

 © DFI International Bruges 2025

Mullins, G., Johnson, K, R., Winters, D., Hilferding, H. and Kupselaitis, K. 2021. Selection of thermal integrity data regression parameters. Geotechnical Testin Journal, Vol. 44, No. 3, pp741-755.

Piscsalko, P. E., Ellis, M. 2022. Advantages in using Thermal Integrity Profiling. Proceedings of the 11th International Stress Wave Conference, Rotterdam.

Rui, Y., de Battista, N., Kechavarzi, C., XU, X. and Yin, M. 2021. Distributed fibre optic monitoring of a CFA pile with a central reinforcement bar bundle. Frontiers of Structural and Civil Engineering.

Selker, J. S., Tyler, S. and van de Giesen, N. 2013. Comment on "Capabilities and limitations of tracing spatial temperature patterns by fibre-optic distributed temperature sensing" by Liliana Rose et al. Water Resources Research.

Sun, Q., Elshafie, Z. E. B., Barker, C., Fisher, A., Schooling, J. and Rui, Yi. 2022. Integrity monitoring of cast in-situ piles using thermal approach: A Field case study. Engineering Structures 272 114586.

Ukil, A., Braendle, H. and Krippner, P. 2012. Distributed Temperature Sensing: Review of Technology and Applications. IEE Sensors Journal, Vol. 12, No. 5, pp 885 – 892.

White, B., Nagy, M. and Allen, R. (2008). Comparing cross-hole sonic logging and low-strain integrity testing results. Proceedings of the 8th International conference on the applications of stress wave theory to piles, Lisbon.

 © DFI International Bruges 2025

COMPARING THERMAL INTEGRITY TEST DATA WITH AS-BUILT CONDITIONS

Fiona E. Hughes, Arup, Birmingham, United Kingdom, +447929672037, fiona.hughes@arup.com
Robert Jackson, Strabag, London, United Kingdom, robert.jackson@strabag.com
Peter Ingram, Arup, London, United Kingdom, peter.ingram@arup.com

ABSTRACT

The use of thermistor-based methods to assess the integrity of deep foundations is increasing across the industry. There are many benefits of thermistor-based testing, which include the test results being available whilst construction works are ongoing, enabling the project team to react to any anomalies whilst the foundation contractor is still mobilised, and health and safety benefits compared to alternative methods that require instrumentation within the reinforcement cage. However, there are few references which compare the thermal test data to the as-built conditions of deep foundations, which leads to the potential for misinterpretation of test results. In this paper, the thermal integrity test data from diaphragm wall panels constructed to form two deep shafts in London are presented and compared to the conditions encountered during excavation of the shafts. It is widely understood that lower temperatures during curing can indicate reductions in the concrete section, however this review of as constructed diaphragm wall panels identified that the construction process and detailing of the structural elements can also affect the temperature generated during curing of the diaphragm wall panels. This paper highlights that it is essential to review not only the thermal test outputs, but also the corresponding design and construction information. Recommendations are given as to the essential outputs required in the test report to enable this comprehensive review.

Key words: thermal integrity, diaphragm wall panels

INTRODUCTION

Integrity testing is routinely undertaken to assess the quality of cast-in-situ foundations, such as piles and diaphragm wall panels, and identify significant anomalies that could have a structural significance with regard to performance and durability. The traditional method employed in diaphragm wall panels and piles has been the use of cross-hole sonic logging, however the use of thermal -based methods to assess the integrity of deep foundations is increasing across the industry (EFFC/DFI 2018).

This paper describes real life examples of thermal integrity profiling in diaphragm walls and highlights how the temperature profile is to be interpreted. This interpretation is then compared to construction information. The majority of the discussion in this paper is as equally applicable to bored piles as it is to diaphragm walls.

It is important to remember that at the time of assessing the thermal data the excavated face of the diaphragm wall is usually not visible, and other available information should be used in tandem to conduct the assessment including, but not limited to, concreting records detailing tremie pipe embedment and level of concrete surface.

WHAT AFFECTS THE TEMPERATURE PROFILE?

The premise of thermal integrity testing is that by considering the change to temperature measurement of the concrete within the diaphragm wall panel (or pile) one can determine the location of potential anomalies. The temperature recorded is a result of the heat of hydration of the concrete. In simple terms, any areas where higher temperatures are recorded compared to the average temperature line indicate greater heat and likely increased concrete cover, the reverse can be said for lower temperature than the average can indicate reductions in the concrete cover.

This review of as constructed diaphragm wall panels identified that the construction process and detailing of the structural elements can also influence the results. This paper highlights that it is essential to review not only the thermal test outputs, but also the corresponding design and construction information to enable a comprehensive review.

 © DFI International Bruges 2025

The key benefits of thermal integrity testing are realised when the results are available as early into the construction cycle as possible, whilst construction works are ongoing, as this enables the project team to react to any anomalies whilst the foundation contractor is still mobilised. This allows improvements to be made to construction methodologies for future works should an issue be identified in constructed elements and facilitates timely repairs to any defects.

PROJECT DETAILS

In this paper, data from the design and construction of two deep shafts in London are presented. The stratigraphy at the site comprises: a superficial layer of Made Ground which overlies; London Clay; Harwich Formation; Lambeth Group; and Chalk.

The shafts are formed of 46m deep, single bite, overlapping diaphragm wall panels as the primary earth retaining structure in a circular shape (Fig**.** 1). A total of 48no. panels, with plan dimensions of 1.0m by 2.8m were constructed. The diaphragm wall panels were excavated using a combination of rope grab and cutter. Bentonite slurry was used to support excavation of the diaphragm wall panels.

The reinforcement cages were prefabricated off site with the Thermal Integrity Profile (TIP) wires attached on site. The reinforcement cages in secondary panels were rectangular in plan, whilst in primary panels they were trapezoidal in shape (as shown in Fig**.** 2 and Fig. 3) to avoid steel extending into sections subsequently broken back during formation of the secondary panels. Skid spacers were attached to the reinforcement cages to provide 75mm cover. Couplers were installed at the base slab level of the shaft but without a box-out due to concerns this may inhibit concrete flow around the couplers and cause an imperfection.

Design specification requirements.

The ICE Specification for Piling and Embedded Retaining Walls, Third edition (Institution of Civil Engineers, 2016) was used as the basis for the asset specific specification. The specification permitted either cross-hole sonic logging testing or thermal integrity testing as the method for assessing the integrity of the diaphragm wall panels. The Contractor selected thermal integrity testing due to the test results being available whilst construction works were ongoing (enabling the project team to react to any anomalies whilst the foundation contractor was still mobilised), and health and safety benefits compared to alternative methods that require instrumentation within the reinforcement cage (Federation of Piling Specialists 2023).

The asset-specific specification required that initially all the diaphragm wall panels were to be integrity tested. Subject to the review of early findings and results of the first 10no. diaphragm wall panels, the specification permitted the frequency of testing to be reduced to at least 10% of the remaining panels. For the shafts discussed in this paper, the satisfactory results of the first 10no. diaphragm wall panels enabled the frequency of testing to be reduced. The Contractor identified the remaining panels to be tested so that they were evenly distributed through the remainder of the construction programme and included both primary and secondary panels.



Fig. 1 Photo at base of shaft showing good alignment of couplers.

 © DFI International Bruges 2025

Installation of thermal sensor cables

Every diaphragm wall panel tested was instrumented with 6no. thermal sensor cables with thermistors at 300mm to 400mm centres for the full length of the reinforcement cage. The cables were split into sections equal to the length of the 4no. reinforcement cages and were spliced at each connection. The location of the thermal sensor cables is shown in Fig. 2.

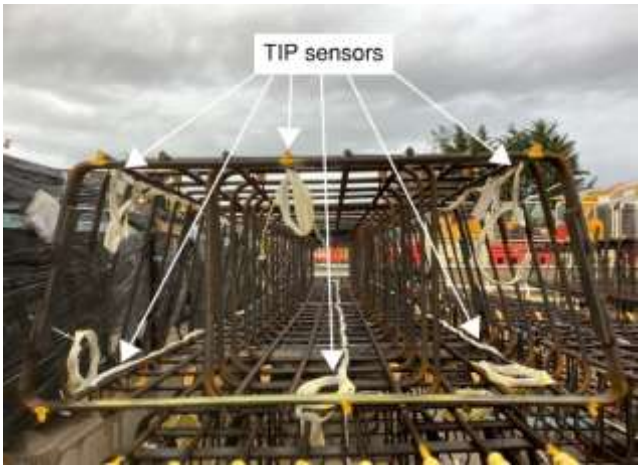


Fig. 2 Thermal sensor cables installed on a primary diaphragm wall panel reinforcement cage.

A total of 23no. diaphragm wall panels were instrumented, each with 6no. thermal sensor cables. Of these, 18no. panels had at least 4no. sensors working throughout the construction process, with 3no. panels having no working sensors. In total, 70% of the installed cables survived the construction process. It was found that cables attached to the reinforcement cages with tie-wire guns had a greater frequency of failure than cables attached using zip wires. Fibre optic cables have been found to be more reliable in this regard.

REVIEW OF THERMAL INTEGRITY TEST DATA

In the following section, the thermal test data are compared to the as-built conditions to identify aspects of the construction process and detailing of the structural elements that affect the temperature generated during curing of the diaphragm wall panels. The thermal cable numbering shown in Fig. 3 will be used.

Comparison between primary and secondary panels.

Before assessing the panels, it is imperative that one understands the geometry of the reinforcement cage within the concreted panel and the predicted impact of the temperatures seen at each location.

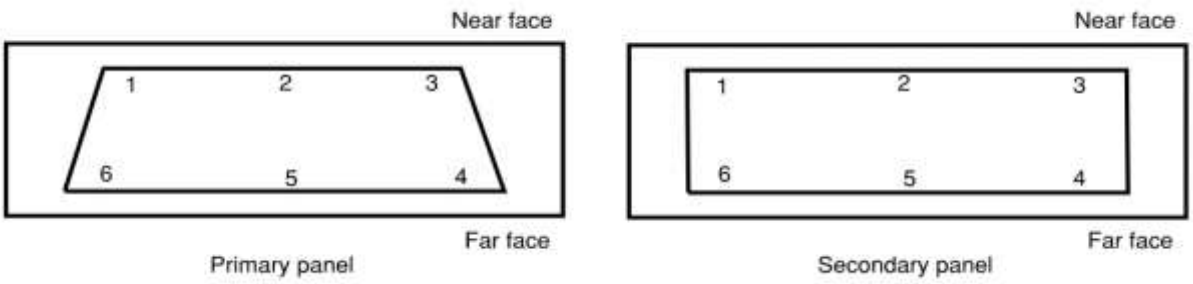


Fig. 3 Schematic of thermal sensor cable locations and numbering.

 © DFI International Bruges 2025

The design location of the cages is the centre of the corresponding panels. For secondary panels, cables 1, 3, 4, and 6 should have similar temperatures recorded. Cables 2 and 5 should have similar temperatures but are likely to be lower than 1, 3, 4, and 6 by virtue of less concrete surrounding the wires. Should the cage move within the panel the concrete cover experienced by individual cables changes and temperature will change, either higher where there is more cover or lower where there is less cover. Primary panels are similar to secondary panels, however cables 1 and 3 are expected to have higher temperature due to the presence of larger concrete cover.

Influence of end condition of panels

The mean peak temperature of the 12no. primary panels tested was 45.1°C, compared to 49.9°C for the secondary panels. This difference can be explained by the difference in the thermal properties of the materials surrounding the panels, through which heat is dissipated. All four sides of a primary panel are surrounded by in situ ground. In contrast, only two sides of secondary panels are in contact with in situ ground, with the other two in contact with constructed primary panels, which themselves will still be dissipating heat.

A good general check is to measure the overall temperature recorded for each panel type to ensure reasonable consistency of temperatures and clarify the right concrete mix is installed in each panel type.

Influence of temporary formwork

In shafts constructed without stop-ends the cutter is used to cut into the adjacent concrete panels to provide the watertight joint. However, for the cutter pumps to work correctly the cutter must be immersed into the bentonite prior to operation. To facilitate this, a temporary stop-end/formwork, 4-6m deep, was installed into the top of either side of the primary panels so that the initial 4-6m of the adjacent secondary panels can be excavated with the grab (refer to Fig. 4 and Fig. 5). Once installed, the top of the temporary steel formwork sat approximately 300mm above the top of the guide wall.

In this instance the top 6m of the thermal cables 1, 3, 4, and 6 on primary panels recorded peak temperatures of 30°C compared to approximately 40-45°C recorded on cables 2 and 5. Inspection of the quality of concrete was undertaken on site, and it was observed that there was sound concrete at the location of recorded lower temperatures.

Review of the construction methodology identified that the lower recorded temperatures were at the locations of temporary steel formwork. The thermal conductivity of steel is an order of magnitude greater than that of London Clay, which is approximately 1.2 W/m°C (Midttømme et al. 1998), therefore heat generated during hydration of the concrete was dissipated more quickly through the steel than through the adjacent ground, resulting in lower temperatures on thermal wires 1, 3, 4, and 6.

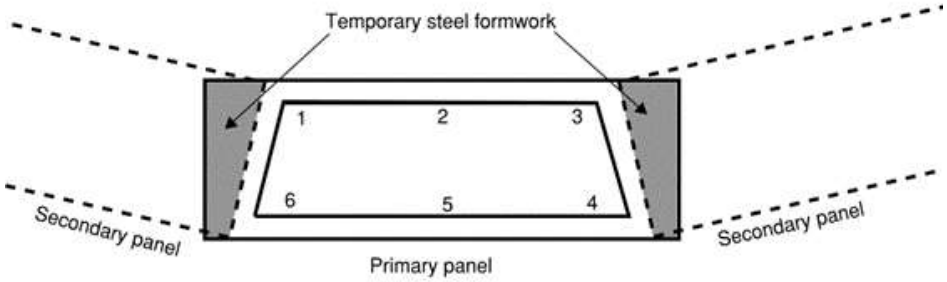


Fig. 4 Plan layout indicating location of formwork /stop-end.

 © DFI International Bruges 2025

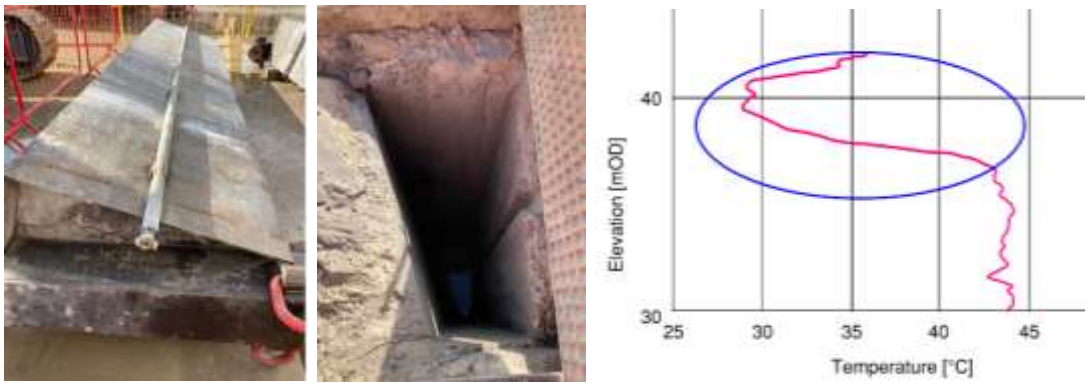


Fig. 5 Left - Photographs of formwork/stop-end and void formed in primary panel. Right – lower peak temperature in cable 4 at the top of the panel.

Influence of couplers

Couplers were installed in the all the diaphragm wall panels of the larger shaft at 15m above the toe of the panels to form a structural connection to the base slab. A void former was attached to the end of each coupler to prevent concrete blocking the thread and to enable the couplers to be located during subsequent stages of construction, as shown in Fig. 6.

A temperature reduction of 2-3°C was recorded on the thermal cables located on the Near Face (NF) (cables 1, 2, and 3), see Fig. 6. Inspection of the panel during excavation identified that this reduction in temperature was not due to an inclusion of debris stuck in or above the couplers. It is therefore logical to conclude that the reduction in temperature was due to a higher density of steel at this location, and therefore a lower volume of concrete.

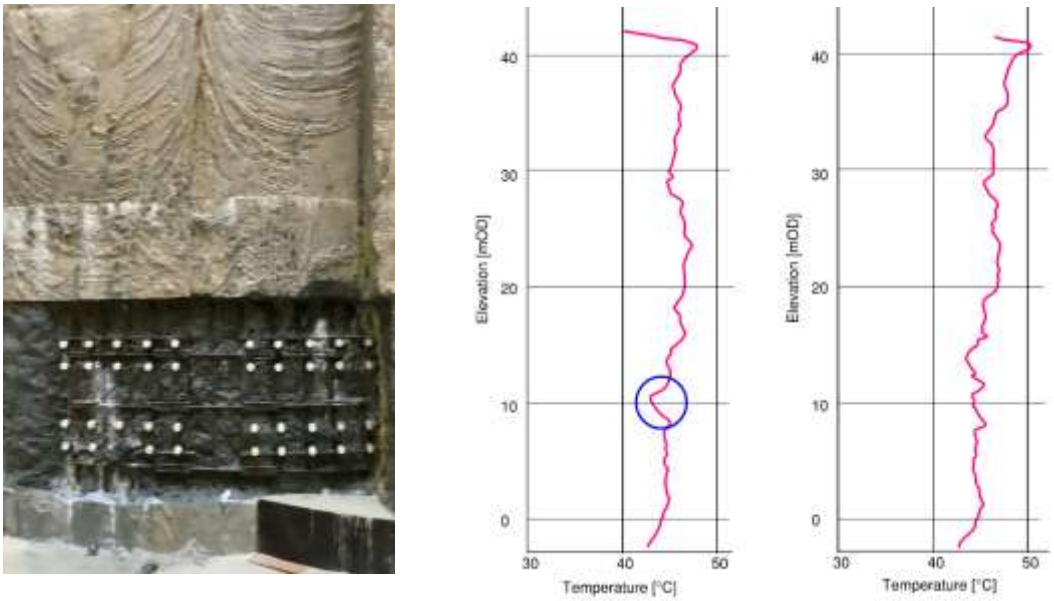


Fig. 6 Left – Photograph of couples in secondary panel. Centre - Near Face peak temperature profile highlighting a slightly lower temperature at the coupler location but – right – Far Face showing no lowering of temperature.

 © DFI International Bruges 2025

Absence of aggregate.

A localised section with an absence of aggregate was identified at the top of 1no. diaphragm wall panel when breaking back the panel to cut off level (

Fig. 7). The cause of the absence of aggregate has not been confirmed, but is likely due to surging of the tremie pipe when it was removed from the top of the panel, causing the concrete to segregate. On review of the TIP test data, it was shown that the TIP cable located closest to this (cable 2) showed a peak temperature of 49°, 4-5° degrees higher than the rest of the length of the thermal cable, and cables in the equivalent position in other panels. The increased percentage of cement due to the absence of aggregate is likely to have resulted in a higher heat of hydration compared areas of well mixed concrete.

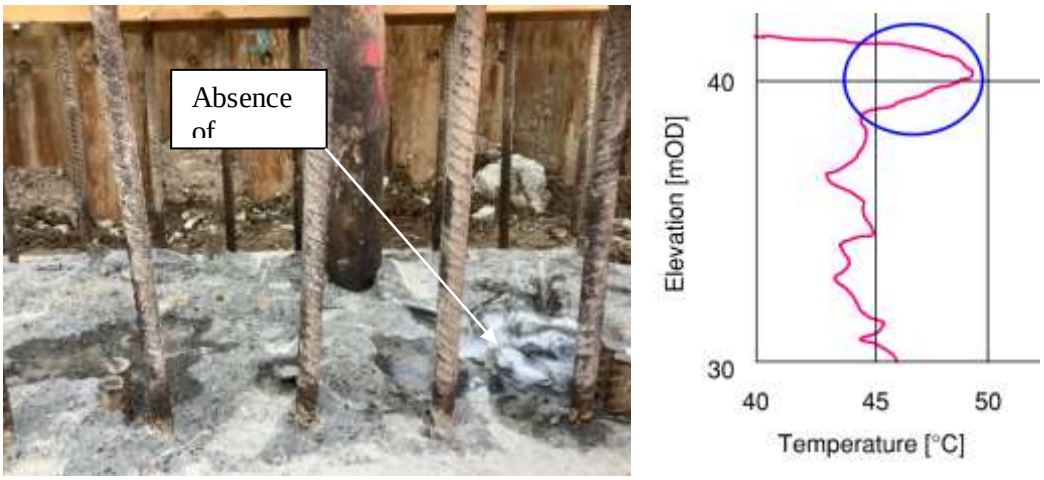


Fig. 7 Absence of aggregate at cut off level highlighted by thermal profile.

Cage translation.

On 1no. secondary panel, thermal cables on the near face (cables 1, 2, and 3) recorded peak temperatures consistently ~5°C lower than cables 4, 5, and 6 (

Fig. 8). During excavation of the shaft, it was found that skid spacers were visible through the near face of the concrete on this panel. The reduction in temperature recorded by the thermal cables on the near face is therefore considered to be due to a reduced cover on the near face.

In this instance, reduced cover on the Near Face was not an issue for durability as a secondary lining was to be cast against the Near Face of the diaphragm wall panels above the base slab level. It is worthwhile noting that a reduction in cover may impede concrete flow and increase the likelihood of inclusions in the cover zone, so should therefore be avoided.

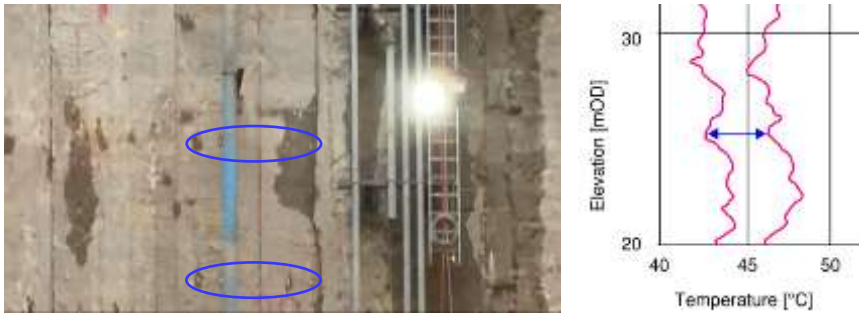


Fig. 8. Temperature difference between Near Face (NF) and Far Face (FF) cables due to loss of cover on NF.

 © DFI International Bruges 2025

Base conditions

Fig 9 indicates a reduction in temperature at the base of the panel. Temperature reduction at the toe of a panel is common due to an increase in panel surface area in contact with the ground. A reduction in temperature at the toe of a panel can also be caused by debris on the base of a panel due to ineffective base cleaning, or mixing of the support fluid and concrete (often caused by not keeping the two separate with a plug of material when starting concreting). Careful review of the thermal data from all tested panels should be undertaken to establish the thermal "signature" for the site conditions and panel geometry and used to identify anomalies. Whether the diaphragm wall is load bearing or not will determine the extent of further assessment if an anomaly is identified. A review of the tremie techniques and base cleaning would be appropriate to attempt to eliminate this feature in subsequent panels. Determining the extent of over dig will also inform the assessment of this feature.

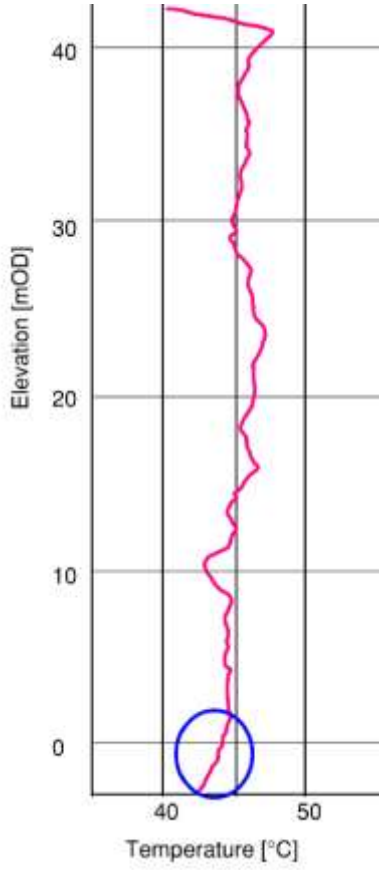


Fig 9. Reduction in temperature at the base.

Concrete rise during construction

Should an anomaly be detected it is possible to review the development of the concrete pour with time and see the height of the concrete at particular times. An example is shown in Fig**.** 10 where the step change in temperature from 15°C (which equates to the temperature of bentonite support fluid in a diaphragm wall panel) to 19°C shows the elevation of the concrete throughout the casting of the diaphragm wall panels. The temperature of the concrete is low as it has yet to start the heat of hydration process which is delayed further in high percentage cement replacement (e.g. replacement with Ground Granulated Blast-furnace Slag, GGBS) mixes. This temperature data can be used in conjunction with the concreting records to look at probable causes of anomalies, for example the entrapment of debris due to uneven concrete level rise across the panel. For this review to be feasible,

 © DFI International Bruges 2025

accurate construction records are required with times for concrete volume installed, the measuring dips to concrete surface, and lengths of tremie pipe being removed. The level of the concrete surface should be measured and recorded at multiple spacings across the panel – it is recommended that at a minimum this should be either side of each tremie pipe, equating to a total of n+1 locations (where n is the number of tremies being used for concreting the panel). Consistent accuracy may be obtained by using the same equipment - commonly a weighted tape - and a single operator.

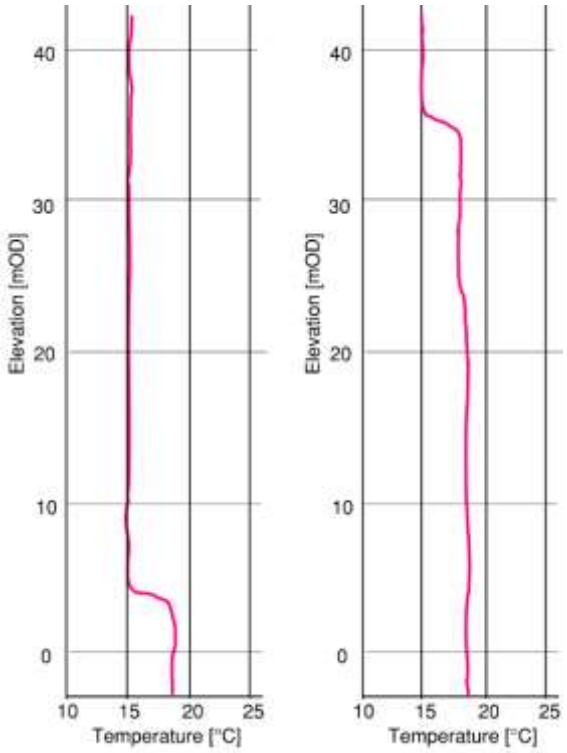


Fig. 10 Concrete pour levels during construction.

SUMMARY AND RECOMMEDATIONS

The review presented in this paper has shown that the construction process and detailing of the structural elements can affect the temperature generated during curing of the diaphragm wall panels. Discussions between the Designer and Contractor during the review of thermal based testing has identified several recommendations to enable a comprehensive review of the thermal data, which are detailed below. It is recommended that the thermal test outputs are reviewed against the design and construction details presented below to enable a thorough review of the thermal data.

Report production and presentation.

The authors believe there are two aspects to the reporting.

1. The data presentation, and
2. The assessment of the data in regard to the actual construction techniques.

Generally, the data presentation report is conducted by an independent testing house or third-party who most likely does not get provided with the full construction details to be able to assess the profile adequately.

A standardised reporting methodology across the industry would help reduce defects (or improve the detection of misidentified defects) and increase the likelihood of assured quality records being accepted by the project teams.

 © DFI International Bruges 2025

Recommendations

The following is recommended:

- Provide the "initial" temperature readouts in good time to influence the ongoing construction of panels/piles. It is recommended that this data is provided within 24 hours of reaching peak temperature.
- Highlight obvious anomalies due to change of temperature of more than 5°C.
- Provide a report of temperature versus depth in graphical form (temperature on x-axis, depth on y-axis).
- Provide full report within 7 days of completion of construction of the foundation element.
- The following should be made available as required:
    - Time-lapse temperature profile to aid further investigation of any anomalies.
    - Temperature against depth data in excel format to allow the contractor to produce own graphs for detailed presentation if required.

The Specialist contractor shall, in conjunction with the construction records, review the initial report immediately upon receipt to look for evidence of anomalies and undertake a review of the construction techniques employed to eliminate potential anomalies. This will hopefully avoid similar anomalies in subsequent panels. These changes to technique shall be recorded clearly and shared with the Client for future records in case a dispute arises as to the causes of the anomalies.

The specialist contractor should then produce a full integrity/quality record that assesses the panels that have been thermally evaluated against those that have not been tested, based on highlighting any outliers within the construction records similar to those that have been found on the tested panels that have shown anomalies. In this way the specialist contractor can assess whether similar anomalies may be present in the untested panels.

It is recommended that the following parameters are considered:

- Overall element dimensions.
- Open life of panels.
- Bentonite fluid properties:
    - Fluid sampling of top middle and bottom of panel after completion of digging.
    - Bentonite properties just before concrete at base of panel through the tremie pipe.
- Time to de-sand each panel.
- Time between completion of excavation to first concrete placement.
- Concreting records.
- Overbreak.
- Ground conditions.

 © DFI International Bruges 2025

REFERENCES

EFFC/DFI, 2018. Guide to Tremie Concrete for Deep Foundations 2nd Edition. https://www.effc.org/media_corner/effc-dfi-guide-to-tremie-concrete-for-deep-foundations-2nd-edition/. Accessed 09-24-24.

Federation of Piling Specialists, 2023. Guidance Note – Considerations For Specifying Crosshole Sonic Logging Tests forumcourt.sharepoint.com/FPS RZ/Forms/AllItems.aspx?id=%2FFPS RZ%2FWebsite%2FSafety Guidance %28Members%29%2FFPS - Guidance Note Considerations For Specifying Crosshole Sonic Logging Tests - R1 - for TC comment %28002%29%2Epdf&parent=%2FFPS RZ%2FWebsite%2FSafety Guidance %28Members%29&p=true&ga=1 Accessed 09-23-24.

Institution of Civil Engineers, 2016. ICE specification for piling and embedded retaining walls. ICE Publishing.

Midttømme, K., Roaldset, E. and Aagaard, P., 1998. Thermal conductivity of selected claystones and mudstones from England. *Clay Minerals*, *33*(1), pp.131-145.

 © DFI International Bruges 2025

TOWARDS AXIAL CAPACITY PREDICTIONS THROUGH MWD DATA: WHAT CAN WE LEARN FROM INSTALLATION EFFORTS OF DRILLED DISPLACEMENT PILES

Genesis Figueroa. Graduate Student Researcher, Univ. of California Irvine, Irvine, CA, USA
Kevin Duffy. Post-doctoral Researcher, Delft University of Technology, South Holland, The Netherlands
Morgan NeSmith. Director of Engineering, Berkel & Company Contractors, Inc., Atlanta, GA, USA
Anne Lemnitzer. Associate Professor, Univ. of California Irvine, Irvine, CA, USA, Corresponding author: alemnitz@uci.edu

ABSTRACT

The future of performance-based foundation design involves integrating Measurement-while-Drilling (MWD) data to enhance the resilience and construction efficiency of pile foundations. During the installation of Drilled Displacement Piles (DDPs), measurements include penetration speed (v_z), rotational speed (v_r), downward thrust, torque (T) or hydraulic pressure (P_{drill}). With these measurements in mind, data from 32 DDPs across 10 project sites in the US and Europe were collected and analyzed. A generalized formulation for installation effort was developed to compare existing pile databases with the data gathered by the authors. The proposed method uses a decomposed installation effort model that separately accounts for the shaft and toe portions of the pile. A regression analysis of the dataset shows the potential of using installation effort to predict pile capacity and provides fundamental knowledge towards establishing a basic framework for estimating pile load capacities during DDP installation. This application highlights the value of real-time monitoring data in performance-based foundation design.

Keywords: drilled displacement piles, measurement while drilling, axial capacity, screw displacement piles.

INTRODUCTION

During pile installation, data acquisition systems provide a significant amount of real-time information, commonly known as measurement-while-drilling (MWD) data. Building on the capability of this data is a rapidly growing research area in the industry (NeSmith and NeSmith, 2008). For drilled displacement piles (DDPs, also known as screw displacement piles in Europe), MWD data can be leveraged to (i) assess soil variability at the site (ii) quantify soil improvement, (iii) develop axial capacity predictions and (iv) optimize pile construction by balancing installation efficiency with satisfactory operational performance.

The drilling tool of a DDP consists of several auger flights near the tip, followed by an enlarged displacement body further along the pile length. Several different DDP designs and installation procedures are available in the industry, however, regardless of the type of drilling tool, each design aims for a combination of soil removal around the pile tip and soil displacement around the enlarged body, maximizing both installation efficiency and the pile's ultimate capacity. Key measurements during this process include penetration speed, rotational speed, crowd force on the pile head, and torque. Upon tool extraction, concrete volume and grout pressure are recorded, if applicable.

Installation procedures can have a significant effect on the pile capacity, as shown in both drilled displacement piles (van Impe, 2001; Siegel et al., 2007; Hird and Guymer, 2011; Pucker and Grabe, 2012) and in screw anchors and auger piles (Brown, 2005; Cerfontaine, 2023). For instance, the theoretical framework and model tests by Slatter (2000) show how the radial stresses acting on a DDP depend on the combined process of soil transport, soil displacement, and the installation torque during pile installation. However, no industry-wide consensus has been established on how DDP installation

 © DFI International Bruges 2025

and tool geometry impact the pile's ultimate capacity, largely due to the lack of publicly available, full-scale, pile load tests where the pile base and shaft resistances have been directly measured.

Towards the goal of exploring the effect of drilling parameters on the capacity of full-scale DDP piles, this paper presents the first step of the authors' research by revisiting and building upon existing correlations between the installation effort and pile capacity, showing how MWD data could be used to quantify installation efforts with more certainty and how to make them a useful tool to aid in the design of drilled displacement piles in the future.

DDP DATABASE AND ANALYSIS

Data analyzed in this paper was generously provided by members of the Deep Foundation Institute's ACIP and DD technical committee and the archives of TU Delft in the Netherlands. In these projects De Waal, Auger Pressure Grouted Displacement (APGD), and Omega piles were constructed, and drilling data was recorded. Static axial load tests following the American (ASTM D1143) and Dutch (NPR 7201) codes were performed to determine the axial capacity of the DDPs. The authors reviewed all project data to ensure uniform site information and consistent data quality across all projects, including: the type of displacement tool, in-situ soil testing, the availability of groundwater table locations, and the availability of key MWD data such as the penetration speed (v_z) and the hydraulic pressure (P_{drill}). When pile load testing on the site exhibited a clear, in-situ, plunging behavior, the ultimate bearing capacity of the piles (Q_u) was calculated using the Modified Davisson Offset Limit method adjusted for other pile types following Perlow's (2020) recommendations. Van der Veen's (1953) method was applied to extrapolate test data when no failure was observed experimentally. The axial load at a pile head settlement equal to 10%D ($Q_{10\%D}$) was also recorded when available (Table 1). DDPs in the database were installed in different soil profiles such as homogeneous cohesionless soils, homogeneous cohesive soils, and stratified soil profiles. Therefore, both, friction piles as well as end-bearing piles, were represented.

Data analysis

NeSmith and NeSmith (2008) introduced an "Installation Effort" (Eq. 1) and compared it to the pile's total capacity (Q_u) observed in the field. This database was entirely developed for Berkel's APGD piles. The authors considered two key drilling parameters: the Torque Index (*TI*) calculated from the hydraulic drilling pressure, and the Penetration Rate Index (*PRI*) calculated from the penetration speed (v_z) of the drilling tool. The coefficients in Eq. 1 were defined based on the company-specific drill rig. The base penetration rate (PR_{base}) is the rate at which the gearbox moves vertically with no resistance and was defined as 0.1 m/s (20 ft/min). The base torque (T_{base}) is the required torque to turn the gearbox with no soil resistance at maximum rotation rate. This parameter was defined as 10 MPa (100 bars). The cumulative installation effort (IE_{cum} - Eq. 2) was calculated by summing the IE for every 30 cm (1 ft) along the pile.

To compare the new database collected by the authors to the original NeSmith & NeSmith (2008) database, the installation effort proposed by NeSmith & NeSmith (2008) was modified to remove the rig-specific fitting coefficients PR_{base}, and T_{base}. A new Cumulative Installation Effort was defined as IE_{2cum}. Eqs. 3-5 explain the derivation of this modified installation effort, where *PR* (or v_z) and T (or P_{drill}) are in ft/min and bar, respectively. In Eq. 3 the terms PR_{base} and T_{base} were removed from the summation as they are common factors at each depth. By solving for PR_{base}, and T_{base} equal to 0.1 m/s (20 ft/min) and 10MPa (100bars), respectively, Eq. 4 is obtained. Eq. 5 shows the new IE_{2cum} and its relationship with NeSmith and NeSmith (2008) IE.

 © DFI International Bruges 2025

Table 1. Overall information of each project site and tested piles

Project Site	Pile	GWT Depth [m]	Tool	D [cm]	L [m]	Grout Factor	Average vz [m/s]	Average Pdrill [MPa]	Qu [kN]		$Qu_{10\%D}$ [kN]
PS1	P1	1.2	Omega	40.6	20.3	1.2	0.06	16.9	2139	*	-
	P2	**1.2**	**Omega**	**40.6**	**19.8**	**1.2**	**0.07**	**17.6**	**1601**	*	-
	P3	**1.2**	**Omega**	**40.6**	**19.6**	**1.1**	**0.13**	**15.8**	**1334**	*	**1334**
	P4	1.2	Omega	40.6	19.6	1.1	0.08	17.0	1512	*	-
PS2	P5	5.2	APGD	40.6	22.9	1.3	0.03	21.5	5649		-
	P6	5.2	APGD	40.6	21.3	1.3	0.04	18.3	5084		-
	P7	5.2	APGD	40.6	19.8	1.3	0.03	15.8	5178		-
PS3	**P8**	**3.0**	**DeWaal**	**35.6**	**16.5**	**1.2**	**0.04**	**12.7**	**2945**		**1196**
	P9	3.0	DeWaal	35.6	15.2	1.2	0.04	12.8	3114		1744
	P10	3.0	DeWaal	35.6	14.9	1.2	0.05	11.9	2242	*	-
	P11	3.0	DeWaal	35.6	13.1	1.2	0.05	11.2	1794	*	2242
	P12	3.0	DeWaal	35.6	11.6	1.2	0.05	10.5	1146	*	-
PS4	P13	1.2	DeWaal	45.7	9.1	1.2	0.05	16.4	1001	*	1036
	P14	1.2	DeWaal	45.7	16.8	1.2	0.04	17.2	1753	*	1893
	P15	1.2	DeWaal	61.0	9.1	1.2	0.05	18.6	1570	*	1475
PS5	P16	2.4	DeWaal	40.6	8.5	1.2	0.04	21.0	1794	*	1789
	P17	2.4	DeWaal	40.6	10.1	1.3	0.06	20.7	1873	*	1875
PS6	P18	3.7	DeWaal	45.7	15.2	1.3	0.10	14.4	1654	*	1794
	P19	3.7	DeWaal	45.7	15.2	1.3	0.08	13.8	1694	*	1702
PS7	P20	6.1	DeWaal	35.6	9.1	1.2	0.04	6.4	3089	*	2740
	P21	6.1	DeWaal	35.6	7.9	1.2	0.05	3.3	2431	*	2204
PS8	P22	0.5	DeWaal	40.6	23.8	1.2	0.06	16.6	2765		-
	P23	0.5	DeWaal	40.6	21.6	1.2	0.06	16.5	2541	*	2508
	P24	0.5	DeWaal	35.6	24.4	1.3	0.06	17.5	3090		-
	P25	0.5	DeWaal	35.6	22.3	1.3	0.05	17.3	2989		-
PS9	P26	1.5	DeWaal	40.6	17.4	-	0.13	13.6	2402	*	2370
	P27	1.5	DeWaal	40.6	17.9	-	0.13	14.1	2406	*	-
	P28	1.5	DeWaal	40.6	17.4	-	0.12	13.8	2306	*	2306
	P29	1.5	DeWaal	40.6	17.9	-	0.11	14.8	2157	*	2158
PS10	P30	1.5	DeWaal	35.6	16.0	-	0.09	13.8	1487	*	1485
	P31	1.5	DeWaal	35.6	16.5	-	0.11	13.2	1157	*	1092
	P32	1.5	DeWaal	35.6	16.5	-	0.10	13.9	996	*	945

*: Pile reached an in-situ axial load failure

$$IE = PR_{index} * T_{index} = \left[\frac{1}{\sqrt{PR/PR_{base}}}\right] * \left[2.7815 * \left(\frac{T}{T_{base}}\right)^{1.3629}\right] \quad [1]$$

$$IE_{cum} = 2.7815 * \sum \frac{1}{\sqrt{PR/PR_{\text{base}}}} * \left(\frac{T}{T_{\text{base}}}\right)^{1.3629} \quad [2]$$

$$IE_{\text{cum}} = 2.7815 * \frac{\sqrt{PR_{\text{base}}}}{T_{\text{base}}{}^{1.3629}} * \sum_{z=0}^{z=L} \frac{T_z{}^{1.3629}}{\sqrt{PR_z}} \quad [3]$$

$$IE_{\text{cum}} = 0.00234 * \sum_{z=0}^{z=L} \frac{T_z{}^{1.3629}}{\sqrt{PR_z}} \quad [4]$$

$$\frac{IE_{\text{cum}}}{0.00234} = \sum_{z=0}^{z=L} \frac{T_z{}^{1.3629}}{\sqrt{PR_z}} = IE_{2.\text{cum}} \quad [5]$$

 © DFI International Bruges 2025

Figure 1 presents the results of the IE_{2cum} calculations. Fig. 1(a) plots the cumulative IE_{2cum} vs. the piles' ultimate capacity Q_u, and Fig. 1(b) presented the cumulative IE_{2cum} vs. the pile capacity at a displacement corresponding to 10% of the pile diameter ($Q_{10\%D}$). Both graphs suggest that high variability exists for a given installation effort. For example, as shown in Fig. 1a, an $IE_{2,cum}$ of 30,000 corresponds to a pile capacity ranging from 1500 to 4000 kN. The high variability in measured pile capacity may suggest that local geology or minerology, pile tip resistance, ground water conditions and tool geometry can have an influence on the installation-capacity correlation (NeSmith and NeSmith, 2008). It also cautions a general application of a method that simply sums MWD data without the consideration of local geology.

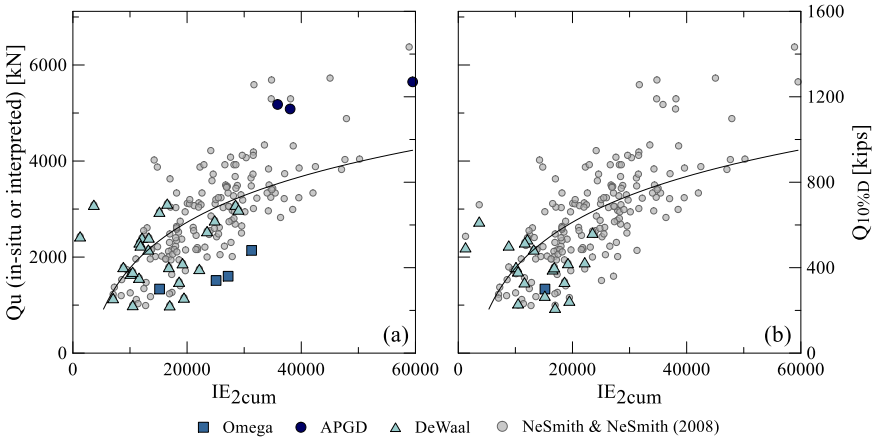


Fig. 1. IE_{2cum} vs. (a) Ultimate axial load (Qu), (b) at a settlement equal to 10%D ($Q_{10\%D}$).

Analysis of three pile installations

To illustrate the impact of site-specific factors on the installation effort, three representative sites were selected from the database, as shown in Fig. 2-4. These sites were chosen to assess piles with different IE_{2cum} reaching a similar axial failure load (P2 and P3), and piles with a similar IE_{2cum} but different axial load behavior (P3 and P8). Cone penetration tip resistance (q_t in Fig. 2-4) suggests that all piles (P2, P3 and P8) are installed in similar, primarily clayey soils sites. The soil behavior type index I_c (Robertson 2014) ranges between 2.5-3.5.

Piles P2 and P3 have nearly identical pile geometries (D, L) and were installed at the same project site using the same displacement tool. Pile P2 was installed with a consistent downward speed v_z of 10 cm/sec until a stronger layer was encountered (~10 m depth). Consequently, the installation speed decreased, and the drilling pressure increased. Thereafter, the drilling tool continued with the same initial linear downward trend observed in the upper layer (Fig. 2c).

Pile P3 was advanced at a much faster rate, reaching a penetration speed 1.5 times higher than pile P2 (Fig. 3d). The same installation trends can be observed as P3 enters the strong layer at 10m depth, however slightly less drilling pressure was applied due to the initially higher downward speed. (i.e., faster advancement through the stronger layer). P3 therefore has a lower IE_{2cum} due to the inverse relationship of v_z in the IE_{2cum} equation.

Pile P8 was installed with a much slower downward advancement of only 5cm/sec (or less) and tipped in a stronger bearing layer starting around 12m of depth. A reduction in penetration speed (v_z) and increase in drilling pressure (P_{drill}), is evident when entering the strong bottom layer of site P8 (see Fig. 4(a) and (c)).

Figure 5a-c shows the individual IE_2 with depth during the installation of P2, P3, and P8. The individual IE is the installation effort required to penetrate one foot of soil, and is represented by one data point every foot. Figure 5d shows the cumulative (total) Installation Effort2 (IE_{2cum}-Fig. 5d) of all three piles. This value represents the sum of the installation effort up to the respective pile length/depth. Hence, the last data point represents the effort to install the entire pile length. Fig. 5 also shows the soil behavior type defined based on the I_c (Robertson 2014).

 © DFI International Bruges 2025

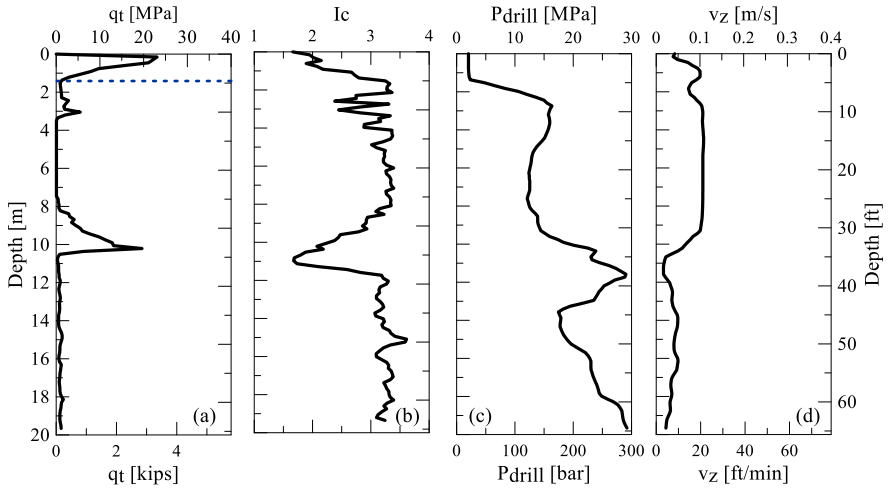


Fig. 2. P2 data: (a) q_t, (b) I_c, (c) P_{drill}, (d) v_z.

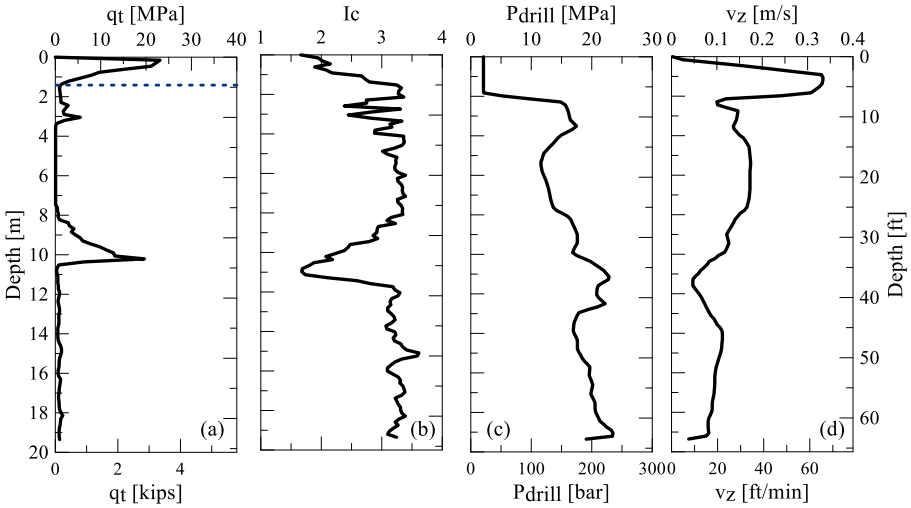


Fig. 3. P3 data: (a) q_t, (b) I_c, (c) P_{drill}, (d) v_z.

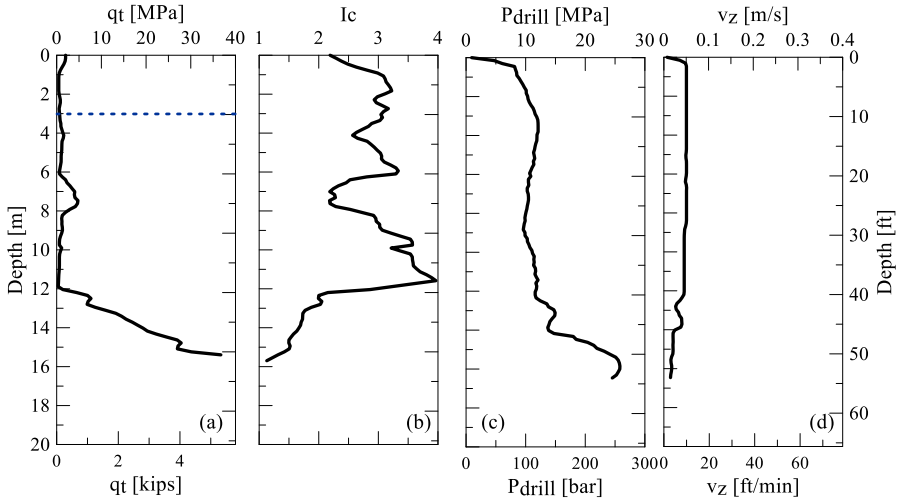


Fig. 4. P8 data: (a) q_t, (b) I_c, (c) P_{drill}, (d) v_z.

 © DFI International Bruges 2025

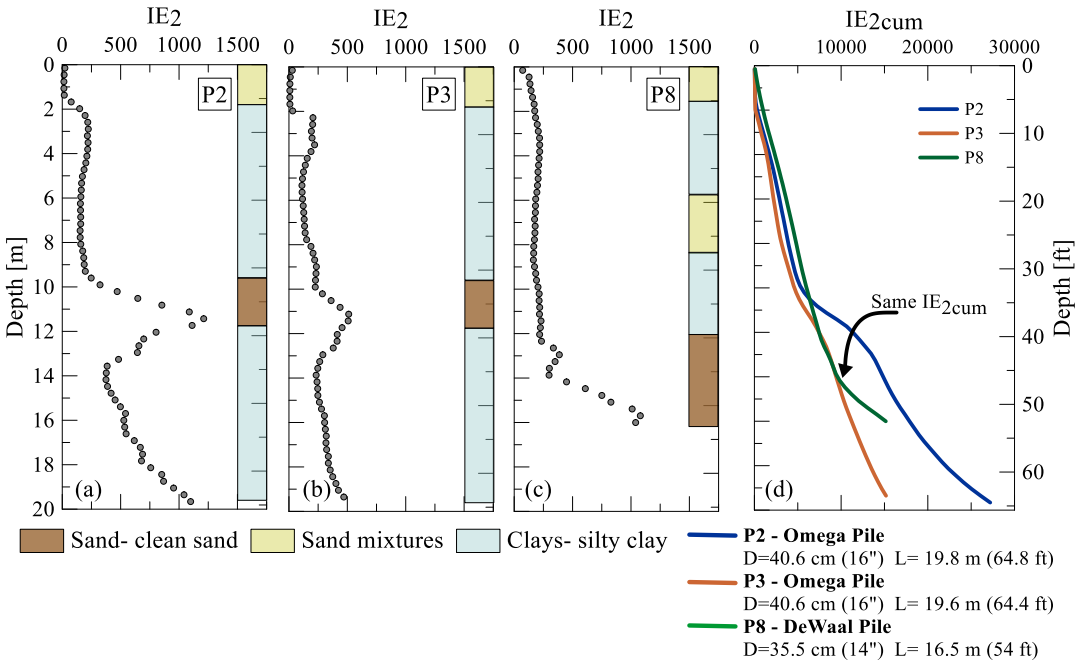


Fig. 5. IE_2 at all depths for (a) P2, (b) P3, and (c) P8. IE_{2cum} for all three piles.

Piles P2 and P3 have an intermediate clean sand layer from 9.5 to ~11.5m with a q_t ranging from 5 to 20 MPa; a significant increase in the IE_2 can be observed at this depth for both piles as the tool pushes through the stronger layer (Fig. 5). Pile P8 also has a sandy layer from 6 to 8 m, however this layer has an average q_t of less than 5MPa, and consequently, not much variation of the IE_2 is observed at this depth. A significant increase of the IE_2 can be observed when P8 reached the clean sand layer at 12m (target bottom layer for pile tip).

Figure 5d shows that piles P2 and P3 follow a very similar cumulative installation effort IE_2. For instance, at a depth of 14m the cumulative IE_2 is the same for P3 and P8 regardless of which layers are along the pile shaft; i.e., the cumulative installation effort does not recognize whether the pile passes through an intermediate (strong) bearing layer or whether this layer is reached at the end (e.g. for Pile 8). Pile P8 only begins to show a significant increase in installation effort after reaching the bottom clay layer.

In contrast, when comparing P2 and P8 (Fig. 5d), both piles show a similar installation effort until about 10m of depth, followed by a divergence of IE due to the speed and pressure applied to P2 while passing the stronger sand layer. At about >16m depth, both piles approach similar installation efforts.

These discrepancies can lead to a wrong interpretation of the axial load capacity for both P3 and P8 (Fig. 6).

Although IE_{2cum} for P2 (~28000) is almost twice the IE_{2cum} for P3 (~15000), the axial load tests on both piles show similar capacities. On the other hand, when comparing P3 and P8, both piles were installed at different sites under different installation conditions and geometries. Both piles have similar IE_{2cum} but significantly different failure capacities. P8 has more than twice the capacity of P3. Given the soil conditions at both sites, it's likely that both piles mobilized their base and shaft capacities very differently—with P3 predominantly a shaft-bearing pile and P8 predominantly an end-bearing pile. Hence it is important to understand the mechanisms which contribute to developing the total axial pile capacity (friction or end-bearing). When the cumulative installation effort is calculated, the location of a strong layer does not play a significant role since all the effort is lumped into a single value (IE_{2cum}).

 © DFI International Bruges 2025

Decomposition of installation effort

While the concept of cumulative installation efforts captures the overall pile installation effort, recognizing individual contributors, such as end-bearing, shaft friction, or overburden stresses is critical. Separation of parameters is also important for developing future correlations between the IE and axial design capacities; especially since most design approaches rely on increased resistance with increasing depths. To demonstrate this further, the installation effort was decomposed into friction and end-bearing components.

To reiterate, the piles' individuals IE_2s were calculated at foot-long increments (Fig. 5a-c – Eq. 5) and the cumulative value (IE_{2cum}) was calculated by summing the IE_2 along the pile depth until the desired pile embedment is reached (Fig. 5d). The cumulative effort IE_{2cum} was divided into pile shaft and pile toe . The effort attributed to the pile toe was taken as the sum of IE_2 in a zone 4D above the pile toe.

Figure 7 shows the $IE_{2.shaft.cum}$, $IE_{2.toe.cum}$, and the IE_{2cum} for piles P2, P3, and P8. It is evident that piles P2 and P8 require a substantial installation effort in the region of the pile toe, which agrees with the individual installation effort variation shown in Fig. 5. This observation is likely associated with the effects of overburden pressure and soil densification at lower depths and does not necessarily imply that the pile is an end-bearing pile (see example of P2). Figure 7 shows the percentage contribution of the $IE_{2.shaft.cum}$, $IE_{2.toe.cum}$ in the total cumulative IE_{2cum}. It can be observed that for P8 (end-bearing pile) the cumulative installation effort in the toe area represents a quarter of the total effort when constructing the pile.

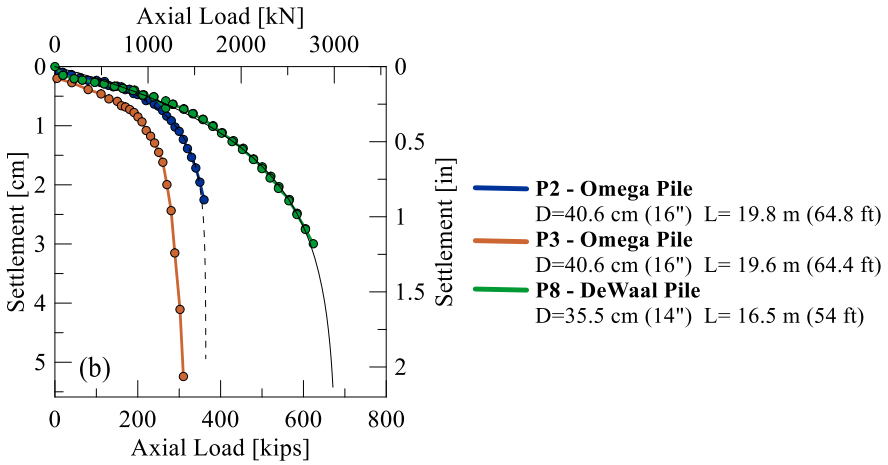


Fig. 6. Comparison between P1, P3, and P12 (a) IE_{2cum}, and (b) axial load test results.

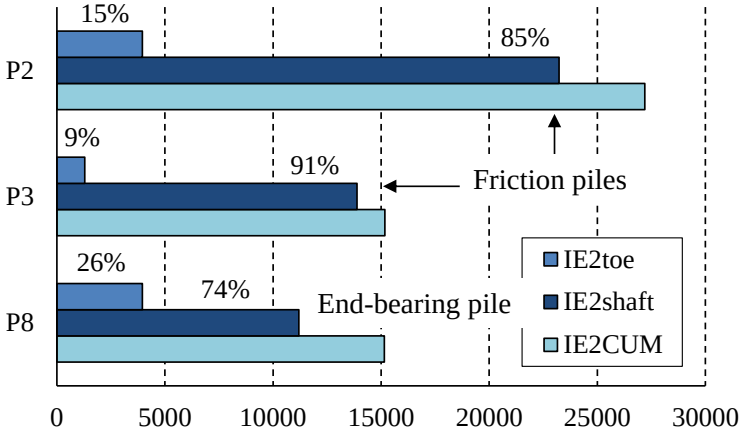


Fig. 7. $IE_{2.shaft}$, $IE_{2.toe}$, and IE_{2cum} for piles P2, P3, and P8.

 © DFI International Bruges 2025

The average IE_2 in the shaft ($IE_{2.shaft.ave}$) and toe area (4D above pile toe - $IE_{2.toe.ave}$) was obtained to compare the overall effort in both zones. A simple linear regression analysis of $IE_{2.shaft.ave}$, $IE_{2.toe.ave}$, and IE_{2cum} was carried out to understand the importance of each IE_2 component when predicting the axial load capacity of the piles. This purely mathematical analysis led to the derivation of Equation 6. Equation 6 presents a prediction of ultimate pile capacity and the components of the installation effort in terms of shaft friction and toe resistance. This equation was only derived for P2, P3, and P8, and is intended to emphasize the importance of the distinction between the shaft and toe IE_2. The weighted factors preceding each component shown in Eq. 6 demonstrate the significance of the installation effort while drilling in the toe area, ≈4 times the IE_2 at the pile's shaft. To reiterate this does not mean that the pile is necessarily an end-bearing pile, the weighted factor simply accounts for the stronger (and likely more compressed) soil layers at greater depths. It indirectly accounts for the effects of overburden pressure on the soil-pile resistance and follows the same linear trend as shown by the general increase of drilling pressure (P_{drill}) with depth (Figs 2-4). Table 2 compares the predicted capacity ($Q_{u.MWD}$) calculated with Eq.6 with the measured capacities in the field. Pile capacities calculated from the installation efforts yielded predictions within 5% accuracy of the measured failure load on site.

$$Q_{u.MWD}[kN] = \frac{10000*(4.46IE_{2.\text{toe.ave}}+1.13IE_{2.\text{shaft.ave}})}{IE_{2.\text{cum}}} \quad [6]$$

Table 2. Predicted ultimate load ($Q_{u.MWD}$) with $IE_{2.shaft}$, $IE_{2.toe}$, and the $IE_{2cum.}$

Pile	$Q_{u.test}$ [kN]	$IE_{2shaft.ave}$	$IE_{2toe.ave}$	IE_{2cum}	$Q_{u.MWD}$ [kN]
P2	1627	370	931	27194	1682
P3	1356	222	392	15178	1320
P8	2992	221	955	15156	2977

The close agreement between predictions and in-situ measurements is expected, given the limited number of case histories in the regression model, but it highlights the potential of this analytical approach. It also demonstrates the use of decomposed installation efforts to predict the axial load capacity of drilled displacement piles.

SUMMARY AND CONCLUSION

The future of performance-based foundation design integrates MWD data to improve pile foundation resilience and efficiency. During Drilled Displacement Pile (DDP) installation, key parameters such as penetration speed, rotational speed, thrust, torque, and hydraulic pressure are measured. Data from 32 DDPs across 10 sites in the US and Europe were analyzed. The analysis of a cumulative installation effort revealed that in order to establish a reliable method for using installation effort as correlation between axial pile capacity and MWD parameters, a simplified 2D analysis (IE_{2cum} vs. axial capacity) is insufficient. While the cumulative installation effort effectively represents the total energy exerted during pile installation by summing parameters up to a given depth, it is essential to consider its individual contributions.

A regression analysis performed on the three case histories presented in this paper demonstrates how the separation of installation effort in shaft and toe installation efforts changes the predictive accuracy. A prototype equation to estimate axial pile capacities, currently only applicable to the small dataset presented herein, demonstrates the potential of more accurately estimating the axial pile capacity compared to previously developed correlations. Using the equation proposed herein, a predicted pile capacity within 5% of the measured capacity in the field was obtained.

The authors aim to refine and expand this model by incorporating key geotechnical parameters (e.g., σ_z, or GWT) and additional soil characterization indices. Geological variability, soil angularity, and site-specific factors also affect the improvement achieved by the displacement tool, influencing axial load and settlement performance. Operator skill and rig-specific features further contribute to variability, particularly in drilling pressure and tool geometry. As such, the authors are actively expanding their pile database and refining this framework to develop a predictive design model, capable of integrating high-quality site data and MWD records for diverse soil conditions and DDP

 © DFI International Bruges 2025

tools. Ongoing work includes data collection and analysis, as a larger database will help refine the general functional relationships between the DDP tool, geometry, MWD data, and pile behavior.

ACKNOWLEDGEMENTS

This research was primarily supported by the DFI Technical Committee fund. Partial support was also obtained from grant CMMI 1752303 sponsored by the National Science Foundation of the United States. We gratefully acknowledge the following professionals and companies for their support of this project and their willingness to share data generously: Sam Warren (Farrell Design-Build, Inc.), Piyush Sharma and Danny Cohen (formerly @ Morris-Shea Bridge Co., Inc.), Tim Siegel (Dan Brown & Associates), and Berkel & Company Contractors, Inc.

REFERENCES

ASTM (American Society for Testing and Materials) (2020). *Standard Test Methods for Deep Foundation Elements* Under *Static Axial Compressive Load*. ASTM International, Standard D1143M. West Conshohocken, PA. doi: 10.1520/D1143_D1143M-20.

Basu, P., Prezzi, M., Basu, D. (2010). Drilled displacement piles: Current practice and design. DFI Journal - *The Journal of the Deep Foundations Institute* 4(1):3–20. https://doi.org/10.1179/dfi.2010.001

Brown, D. A. (2004). Practical considerations in the selection and use of continuous flight auger and drilled displacement piles. *Advances in Designing and Testing Deep Foundations*, 251-261. https://doi.org/10.1061/40772(170)4

Cerfontaine et al. (2023). Control of screw pile installation to optimize performance for offshore energy applications. Géotechnique, 73(3), 234-249. https://doi.org/10.1680/jgeot.21.00118

Figueroa, G., Vrugt, J., Lemnitzer, A. (2024). Evaluation of soil improvement surrounding drilled displacement piles through pre- and post-installation CPT data. *Manuscript in review, Acta Geotechnica*

Hird, C.C., Ni, Q., Guymer, I.: Physical modeling of deformations around piling augers in clay. *Geotechnique* 61(11), 993–999 (2011)

NEN (Dutch Standardisation Insitutue) 2020. Geotechniek-Bepaling van het axiaal draagvermogen van funderingspalen door middel van proefbelastingen [Geotechnics–Determination of the axial capacity of foundations pile through load tests]. [In Dutch.] NPR 7201:2017 +A1. Delft, Netherlands: NEN.

NeSmith, W. M., & NeSmith, W. M. (2006). *Anatomy of a data acquisition system for drilled displacement piles*. GeoCongress 2006, 1-6. https://doi.org/10.1061/40803(187)67

NeSmith, W. M., & NeSmith, W. M. (2008). I*nstallation Effort: Current Calculation Methods and Uses in Design and Construction in the U.S*. 5th International Geotechnical Seminar on Deep Foundations on Bored and Augered Piles. Ghent, Belgium.

Perlow M. (2020). *A soil quake Davisson Offset Method for Drilled Foundations*. Deep Foundation Institute 45th Annual Conference, USA, Red Hook, NY, 183

Pucker, T., Grabe, J.: Numerical simulation of the installation process of full displacement piles. *Comput. Geotech*. 45, 93–106 (2012)

Robertson, P. K., Cabal K. L. (2014). Guide to Cone Penetration Testing for Geotechnical Engineering. Gregg Drilling & Testing, Inc., p 108-116.

Siegel, T. C., NeSmith W. M., NeSmith W. M., Cargill, P. E. (2007). *Ground Improvement resulting from Installation of Drilled Displacement Piles*. Proceedings, DFI's 32nd Annual Conference on Deep Foundations, Colorado Springs, CO, October 11-13, 2007.

Slatter, J. W. (2000). The fundamental behaviour of displacement screw piling augers. PhD Thesis, Monash University. pp 193.

Van der Veen, C. (1953). *The bearing capacity of a pile*. Proceedings of the 3rd International Conference on Soil Mechanics and Foundation Engineering, 2, 84-90.

Van Impe, W.F. (2001). Considerations on the influence of screw pile installation parameters on the overall pile behaviour. Proceedings of the Symposium on Screw Piles. Brussels, Belgium, 127-149.

 © DFI International Bruges 2025

THE PRACTICAL CHALLENGES OF PROCESSING MEASURING-WHILE-DRILLING (MWD) DATA AND CORRELATION STYUDY WITH GROUTING DATA

Mehdi Mahmoudysepehr, VSL system UK, London, UK, phone +447385466736, mehdi.mahmoudysepehr@vsl.com
Sandro Gomes, VSL system UK, London, UK, sandro.gomes@vsl.com
Sandra Coelho, Independent consultant, London, UK, smscoelho@gmail.com

ABSTRACT

This article deals with processing of drilling parameters obtained during the execution of fissure grouting works for the construction of cross-passages in a tunnel project in the United Kingdom. The intent of this research was to use Measuring-While-Drilling (MWD) data as a work planning tool by providing insight to the ground conditions, optimizing drilling inputs and investigating how that allows to forecast the grouting stage. MWD whilst not a new technique, can currently benefit from the potential of data-driven methods and software that can support faster analysis of the MWD data, but challenges remain in:

- defining the rules for the initial cleaning of data (to remove non-relevant data points caused by the drilling process) as there are no clearly defined rules for this operation,
- the initial exploratory analysis of the data to choose the most relevant characteristics or parameters for that specific ground.

There is ample bibliography regarding techniques to explore MWD data (e.g establishing correlations with ground characteristics or grouting) but background work to use these techniques can be daunting and scare users away from exploring MWD on a construction site. This paper presents an example of the basic work that needs to be done, which is not often reported or mentioned in passing in technical documents, and how relevant information can be initially obtained using simple tools (Python data analytics libraries and spreadsheets). It further discusses the next steps in the ongoing investigation.

KEYWORDS: Measuring-while-drilling, drilling, grouting, data-processing, exploratory analysis, visualisations.

INTRODUCTION

The information used in this study comes from drilling and grouting data for fissure grouting in cross passages built for a tunnel in the United Kingdom; the tunnel goes through mostly, various chalk formations. The aim was to seek a methodology that could, in a short time:

- allow for the forecast of grout quantities to be injected into the ground based on the drilling data, and
- establish if drilling data in secondary and tertiary holes could evidence the improvement of the formation characteristics after grouting of the primary boreholes.

MWD involves the continuous recording of parameters such as depth, time, penetration rate, torque, rotation speed and pressure, which can be analyzed to infer subsurface conditions and optimize ground improvement operations.

Despite its advantages (demonstrated in the studies presented below), implementing MWD in real-life scenarios presents several practical challenges:

- ensuring dimensional consistency (data pre-processing),
- initial cleaning to remove irrelevant points caused by the drilling process (the absence of standardized international guidelines complicates the establishment of consistent data cleaning and normalization protocols),

 © DFI International Bruges 2025

- understanding what drilling or compound parameters are the most useful for that particular ground and the investigation goals.

With the present big data platforms and technologies, one could be tempted to rush using those techniques. But they are still difficult to implement, time and resource consuming. Simpler tools such as Python data analytics libraries and spreadsheets can prove useful at an initial stage and provide insights and leads to future work.

BACKGROUND LITERATURE

Schunnesson (1998) investigated why percussive drill monitoring was not used for rock characterisation in the underground industry despite its reliable hardware and low operational costs. Modern drill rigs' operator adjustments and automated control systems make it difficult to extract accurate geological information from raw drilling data. Schunnesson suggested step-wise normalisation to isolate rock-dependent variations from external factors. Normalisation eliminated hole length-dependent variations, thrust-dependent variations, and penetration rate's effect on torque pressure. Normalised data improved rock property predictions like ore boundaries and fracturing at three Swedish crystalline rock sites.

Van Eldert et al. (2020) discussed tunnel excavation MWD data complexity and the need for efficient normalisation and filtration for accurate rock mass characterisation. Existing methods ignored collaring and extension rod coupling. The paper introduced a stepwise algorithm that filters operational parameters and normalises data using production factors and rock drill settings, yielding reliable results across drilling conditions. Van Eldert et al. (2020) used the MWD Fracturing Index to characterise rock mass conditions for grouting in a 1.9 km Stockholm bypass tunnel. Grouting reduces tunnel water ingress and depends on fracture apertures and frequency. The study divided rock mass into six quality, apparent fracturing, and grout consumption groups. These categories were compared to the penetration rate and rotation pressure-derived mean fracturing index. The fracturing index predicted grout consumption 85% of the time and diagnosed rock conditions 93% of the time. A conceptual method using the MWD fracturing index and water loss tests optimised grouting, potentially reducing grouting by 59% in the case study.

Overall, the literature emphasizes the importance of data cleaning, normalization, and the integration of data-driven techniques to enhance the reliability and usefulness of MWD data.

DATA PRE-PROCESSING AND TRANSFORMATION FOR DRILLING OPERATION ANALYSIS

Whilst the works mentioned above present techniques and approaches to evaluate and use MWD data in a systematic way, they can also become daunting in that they require a great deal of time and investigation to understand the techniques behind them. Also, reference to “removal of outliners” is frequent but for those dealing with MWD for the first time, what this means might not be clear at first.

The authors consider that the first important step is understanding where the sensors are installed in the drilling rig and the units in which they are measured. A standard set of data would include time (h: min: s), depth (m), moving speed (m/h), injection pressure (bar) (this being the pressure of the drilling fluid measured inside the hole), tool or thrust pressure (bar) (measured in the hydraulic system), rotation torque (bar) (measured in the hydraulic system) and rotation speed (rpm). Other systems using different units can exist and understanding the exact characteristics of the data set needs to be the first step.

The preprocessing commenced by standardizing units across the dataset. "Moving speed" was converted from meters per hour to meters per minute to ensure temporal consistency. The equations to convert the thrust and torque pressures are provided by the manufacturers of the equipment (Fig. 1). It must be noted that, for the torque, the relationship is dependent on the gear used during drilling;

 © DFI International Bruges 2025

although sensors are already available to record the gear, when these are not installed an accurate conversion (or an educated guess) relies on information provided by the drillers.

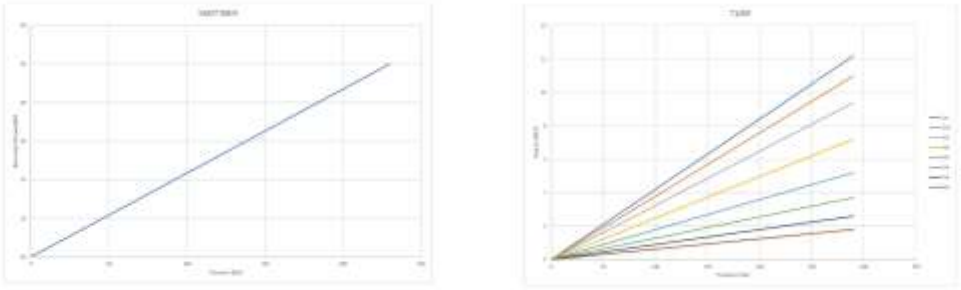
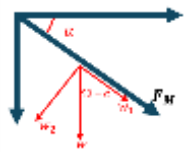


Figure 1 Conversion graphs for the force (left) & torque (right)

The effective thrust applied to the ground also depends on the weight of the drill bit and the total weight of the rods at any given stage; furthermore, for upward holes, the weight of the rods reduces the force, for downward holes, it increases it. This requires the decomposition of the vertical weight of the rods into vectors so that the correspondent force aligned with the rods is added (downward holes) or subtracted (upward holes) to the thrust force (Fig. 2).



$$w_1 = w \times Cos\,(90 - \alpha)$$

$$F_{net} = F_M \pm w_1$$

Figure 2 An example of vectorial decomposition of the weight of the rods

Depth categorization was achieved by segmenting the drilling depth into intervals of 0.75 meters (the length of the rods in this specific case) up to a maximum depth, facilitating targeted analysis at specific depth ranges. The total weight of the drill rods was calculated based on the number of rods in use, and their vertical projection was determined using the borehole's inclination angle, sourced from a predefined dictionary.

The "penetration per revolution" (PPR) was computed by dividing the adjusted "moving speed" by the "rotation speed," providing insights into drilling efficiency per drill bit rotation.

Compound parameters were calculated to be evaluated in correlation with raw parameters. In this case, the drilling energy proposed by Teale (1964) and the Somerton Index as defined by Somerton (1959) were used.

METHODOLOGY FOR REMOVAL OF DATA ASSOCIATED ONLY WITH THE DRILLING PROCESS

Ideally, the sensors gather data throughout the entire drilling process, capturing information on manoeuvres for adding or extracting rods, flushing, and redrilling. These data points should be excluded as they do not pertain to the ground's actual response to the data. The raw data was processed utilising Python data analytics libraries. The Python script utilised for data cleaning applied filters to eliminate records with "moving speed" less than or equal to zero and "rotation speed" less than or equal to one, as these likely indicate non-operational intervals or inaccurate sensor data.

An algorithm was developed to classify drilling operation data into four distinct phases: "Drilling," "Flushing," "Redrilling," and "Rods extraction." It systematically analyses each data point,

 © DFI International Bruges 2025

concentrating on variations in depth as well as speed to precisely determine the phase of operation. The algorithm initially tracks the maximum depth attained during drilling and assesses whether the drilling phase has ended according to a specified depth threshold. During active drilling, the maximum depth is updated whenever a new, deeper measurement is obtained. For each data point, the algorithm computes the variation in depth from the preceding entry. If the depth increases and the speed exceeds a minimum threshold, the operation is classified as "Drilling," signifying active penetration into new material. If the depth is increasing while the current depth is below the previously recorded maximum (indicating re-entry into an already drilled section), and the moving speed is adequate, the operation is classified as "Redrilling." A reduction in depth indicates "Flushing," which denotes the temporary retraction of the drill bit for the purpose of debris removal or adjustments. Upon surpassing the established depth threshold, indicating the conclusion of the drilling phase, the algorithm modifies its classification parameters. Positive depth alterations are categorised as "Drilling" or "Redrilling" depending on whether the present depth exceeds the maximum depth documented. Negative depth changes are now classified as "Rods extraction," signifying the removal of drill rods upon the conclusion of drilling.

Through the systematic application of these rules, the algorithm efficiently eliminates non-drilling activities, isolating data relevant to the actual drilling process. This improves the precision and dependability of later evaluations of drilling performance and subsurface conditions, without addressing specific variables or technical particulars. The dataset was refined by isolating data points categorised as "Drilling," thereby including only information pertinent to the actual drilling process. This preprocessing step is essential to guarantee that subsequent analyses and interpretations are founded on precise and significant data, accurately representing the ground's response to the drilling operations. The cleaned and updated dataset (Fig. 3) now offers a more dependable basis for subsequent analysis.

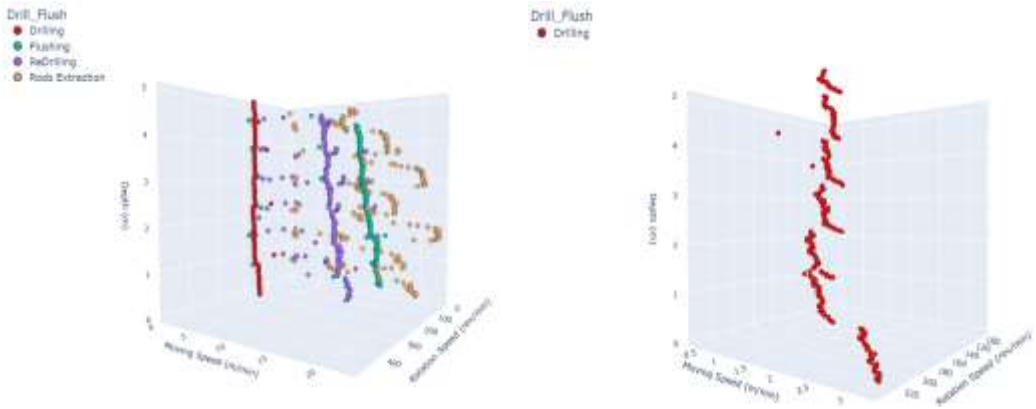


Figure3 3D visualization of raw, transformed data (left) and only drilling phase (right)

INITIAL EXPLORATORY ANALYSIS

The preparation of robust databases and analysis methodologies and algorithms is not an easy or quick task, but more simplified analysis can be performed to get an insight at the drilling process and whether that can affect the data being collected. In this case, the data from each borehole was cleaned using Phyton and then transported to spreadsheets to allow the creation of multiple graphs using average data from different stages and phases of drilling.

One of the parameters that drillers often change while drilling to optimize the process is the rotation speed. The data from cross-passages (CP) 12 and 21 are plotted in Fig. 4: CP12 was drilled without any particular requirements being given to the drillers who were free to choose whatever rotation speed was suitable, which led to a wide range of rotations. When they were asked to drill for CP21, ideally, in the range of 200 to 250 RPM, the correlation between the average drilling speed and the

 © DFI International Bruges 2025

average Somerton Index (Somerton, 1959) improved. One of the variables had been almost removed from the analysis of the rock mass response to drilling.

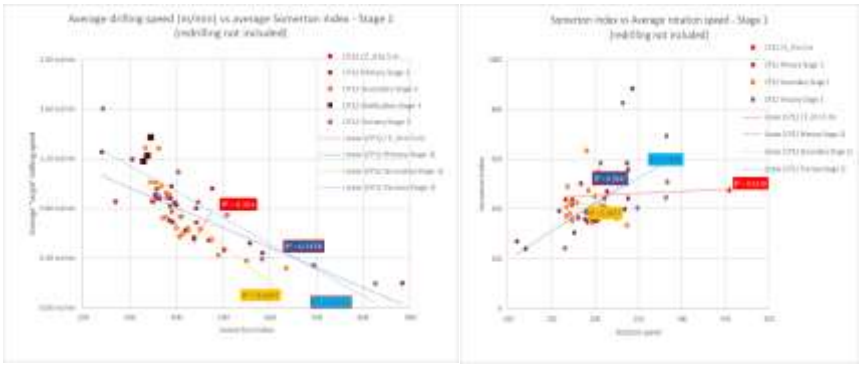


Figure 4A: Visualization of the relationships between the Somerton Index and the drilling speed and rotation speed for CP12

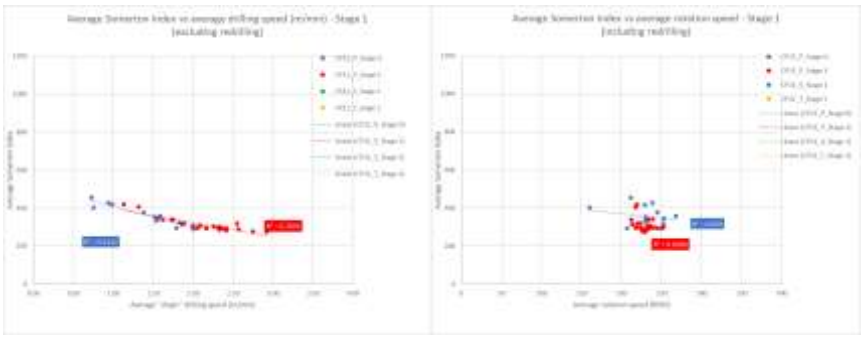


Figure 4B: Visualization of the relationships between the Somerton Index and the drilling speed and rotation speed for CP21

Following the simplified analysis above, correlation matrixes have been constructed for various CPs (CP12, CP20, CP21, and CP22) using Phyton. For CP12 and CP20, there was no steering guidance for the drill rig operators; however, for CP21 and CP22, the operator was requested to maintain a constant rotation speed (as far as possible) during operation. To create the correlation matrixes, the cleaned data is examined individually, and a consolidated dataset is compiled for all boreholes of each CP. Fig. 5 shows that maintaining a constant rotation speed enhanced some of the correlations, particularly between rotation speed and advance speed, net force and drilling energy.



Figure 5A CP12 and CP20 Correlation Matrix

 © DFI International Bruges 2025

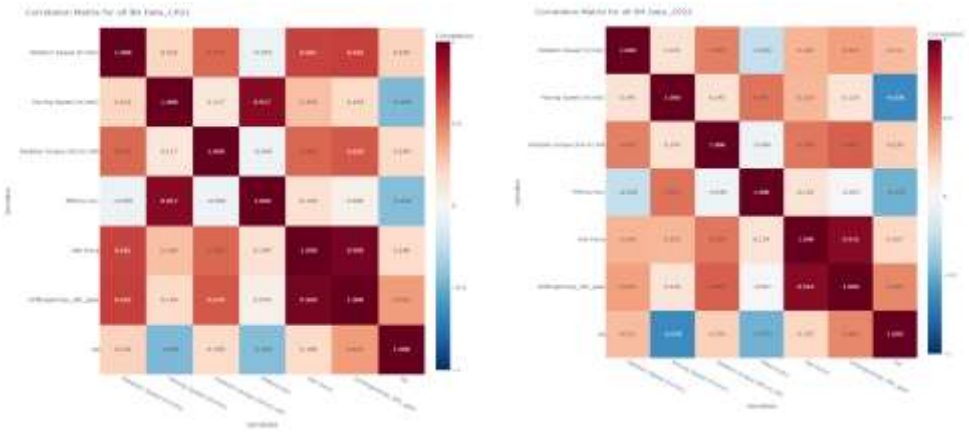


Figure 4B CP21 and CP22 Correlation Matrix

One the main aims of this study was to correlate drilling and grouting data. Several correlations were attempted without much success. An example of said attempts is presented in Fig. 6 where the coefficient Volume x pressure in the last 30 s of grouting was plotted against the average Somerton Index for the respective drilling Stage.

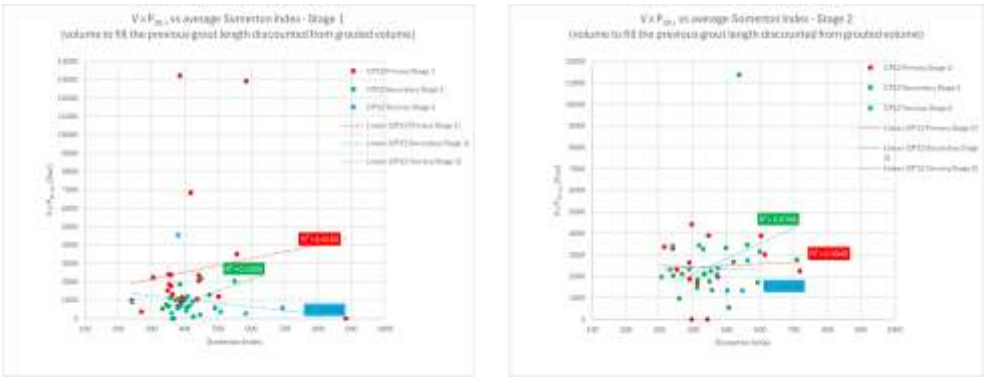


Figure *6 Correlation between Vx $P_{30\ s}$ vs average Somerton Index*

The graphs show very weak correlations. However these are one to one correlations and, considering that drilling is a complicated process with multiple actions occurring simultaneously, there is a possibility that correlations exist for between the ground and grouting when more drilling parameters are considered simultaneously.

In order to explore grouting / drilling relations, the next step is to explore potential correlations using the method proposed by Sapronova and Marcher (2023) where a correlation analysis of compositional data was followed by unsupervised clustering to detect outliers and reduce data volume and dimensionality.

RESULTS & DISCUSSIONS

This paper presents a review of previous publications that show the potential in the use of MWD in geotechnical engineering, despite its implementation requiring time and investigation to understand the techniques behind them. It also discusses in detail the rules applied in the preprocessing and cleaning of MWD data in order to extract the information relevant to posterior analysis. The use of algorithms can be implemented in tools that are now commonly available, such as Phyton data analytics libraries, to perform data cleaning. Additionally, it shows that sophisticated correlation analysis across multiple parameters confirms more simplified one-to-one analysis done using simple

 © DFI International Bruges 2025

spreadsheets and, most importantly, confirm the simple assumption that reducing the number of variables during drilling enhances the relevant data for posterior use.

Combining drilling and grouting presents its own challenges and several iterations of correlations and methods need to be undertaken to understand which one, for this particular case, provides insights between drilling and the following grouting volumes and pressure. This research work is still ongoing, the next step involves preparing and transforming the total volume of data on a big data platform. Subsequently, machine learning algorithms must be evaluated to attain the primary objective of forecasting grouting data and enhancing the overall efficiency of ground improvement operations.

REFERENCES

- Somerton, W.H. (1959) 'A laboratory study of rock breakage by rotary drilling', Journal of Petroleum Technology Vol. 216, pp 92-97
- Teale, R (1964) 'The concept of specific energy in rock drilling', Journal of Rock Mechanics and Mining Science, Vol 2, pp 57-73
- SCHUNNESSON, H. (1998) Rock characterisation using percussive drilling, Int. J. Rock Mech. Min. Sci. Elsevier Science Ltd., pp. 711–725. https://doi.org/10.1016/S0148-9062(97)00332-X.
- Van Eldert, J., Schunnesson, H., et al. (2020) 'Improved filtering and normalizing of Measurement-While-Drilling (MWD) data in tunnel excavation,' Tunnelling and Underground Space Technology, 103, p. 103467. https://doi.org/10.1016/j.tust.2020.103467.
- Van Eldert, J., Funehag, J., et al. (2020) 'Drill Monitoring for Rock Mass Grouting: Case Study at the Stockholm Bypass,' Rock Mechanics and Rock Engineering, 54(2), pp. 501–511. https://doi.org/10.1007/s00603-020-02279-w.
- Sapronova, A. and Marcher, T. (2023) 'Correlational Analysis for Extracting Patterns in Geotechnical Data'https://www.issmge.org/events/ismlg

 © DFI International Bruges 2025

Thermal Integrity Profiling of Deep Foundations

Nasser Massoudi, Ph.D., P.E. 1
[1] Bechtel Corp., 12011 Sunset Hills Drive, Reston, VA 20190; e-mail: nmassoud@bechtel.com

ABSTRACT

Thermal integrity profiling (TIP) methodology is reviewed and case histories for cast-in-place concrete foundations are presented. Results from several TIP tests are compared with pile integrity testing (PIT) results. The applications include 1.5m (5ft) diameter and approximately 10m (33ft) long caissons, 36cm (14in.) diameter and approximately 25m (80ft) long augered cast-in-place (ACIP) piles, and 0.9m (3ft) diameter and 12m (40ft) long caissons. Detailed information is presented on the foundations, test set up, and test outcome. Results show both variations and similarities in findings from the two test methods. It is concluded that TIP is superior to PIT for the assessment of foundation integrity, particularly for long ACIP piles; for TIP is not limited by the piling length to diameter condition, and it can offer additional useful quality information.

Keywords: ACIP, Augercast, Caisson, Foundation, Integrity, Pile, PIT, Shaft, Thermal, TIP

INTRODUCTION

Quality assessment of cast-in-place concrete foundations requires validation of their integrity, which includes verification of diameter, length, shape, reinforcement, and concrete quality. These features control the foundation performance in many ways, including load distribution. Yet, the actual pile condition is typically hidden below ground as deep foundations are mostly constructed in a manner that does not allow direct inspection of their features. In past decades, crosshole sonic logging (CSL) and PIT, among other methods, have been used for obtaining the necessary validation. The CSL method is intrusive, relatively costly, and takes 4-7 days to process the final results; therefore, it enjoys limited use. PIT is fast and inexpensive; however, it has limitations, particularly for longer and slender foundations. TIP is becoming more commonplace; for it offers many of the advantages of the CSL, without the higher cost, delayed results, and installation issues associated with CSL, and is also devoid of PIT limitations. Hyatt et al. (2019) summarized a comparison of CSL and TIP testing for several caissons, including cost and schedule, showing advantages of TIP.

In this paper, a brief description of the TIP and PIT methodology is given, followed by review of example applications. The acronym "TIP" is intentionally underlined in this paper for the reader's ready visual distinction from the acronym "PIT."

REVIEW OF TIP AND PIT METHODS

TIP Method. TIP is a non-destructive testing method that relies on temperature development from the cement heat of hydration in the concrete or the grout. TIP has no pile length limitation. It evaluates the entire cross-section of the pile, does not have a length to diameter (L/D) limitation (can be used for any length pile with proper wire length), can provide input on reinforcing cage alignment, and can provide input on the adequacy of concrete/grout cover over the reinforcing cage.

 © DFI International Bruges 2025

An overview of the TIP methodology, development, test procedure, and analysis are provided in Mullins (2010). The TIP technology was developed by the University of South Florida. The technology was licensed to Foundation & Geotechnical Engineering, LLC that teamed with Pile Dynamics, Inc. which manufactures and distributes the equipment. TIP uses thermal probes (TP) or thermal wires (TW) for temperature measurement. TP is used inside a steel or PVC casing; the data is recorded at specified intervals. TW is attached to the pile reinforcement (rebars) and temperature is typically recorded at intervals of 15 minutes. Thermal measurements are typically made at intervals of 0.3m (1ft) along the pile. Temperature variations of ±4 deg. F. should be expected due to variations in TW locations and shifting of reinforcement in the pile. Both TP and TW provide temperature information which is correlated to areas of rapid or slow heat loss in the pile, indicative of pile shape, integrity, and location of the reinforcement cage. Pile condition assessment can be made typically about 24-48 hours after concrete/grout placement in the pile, although this time can vary based on pile diameter and other factors. Piscsalko et al. (2016) provide a case history where TIP readings continued for 120 hours. Piscsalko (2014) and Bixler et al. (2016) describe TIP in detail and provide examples of applications for caissons and ACIP piles. Becker et al. (2015) describe a case history of TIP application for ACIP piles. Piscsalko et al. (2016) propose guidelines as acceptance criteria for caissons tested using TIP. A Satisfactory (S) condition is assigned when the pile shows 0-6% reduction in effective radius and the concrete cover criteria is met. A Probable Defect (PD) condition is assigned when the effective radius is reduced by more than 6% or the concrete cover criteria is not met. Even when a pile is classified as PD, a structural evaluation of the pile is recommended to assist with establishing the extent of condition and any corrective measures sought.

Mullins and Johnson (2016 and 2017) describe the results of a test program for augercast piles. Among others, they conclude that (1) the shape of augercast piles can be estimated relatively accurately by making thermal measurements from the center bar; however, the predication is highly dependent on grout volume used in data reduction, (2) measurements may not detect deviations in alignment of the center bar, (3) pile shape and alignment can be detected as long as four thermal sensors (TP or TW) are used, and (4) a minimum of four thermal sensors should be used on the rebar cage for piles greater than 61cm (2ft) in diameter. In addition, good agreements between actual (exhumed) and predicted pile radius from thermal measurements were obtained only when the actual pile volume from exhumed piles was used (Mullins and Johnson, 2017). In other words, the volume of reported grout (or concrete) greatly affects pile size prediction and should be corrected to exclude the initial pumped volume and that portion of the grout (or concrete) which is wasted on the ground surface upon auger extraction.

In general, shortage of competent concrete/grout (necking or inclusion) is registered in TIP results as regions of cooler temperature whereas extra concrete (bulging) is registered as warmer temperature. Temperature values are readily affected by cage eccentricity as well as surrounding cover. A cage closer to one side of the excavation exhibits cooler temperature than the average temperature of all sensors since the cage is closer to the soil. When the cage is closer to the pile center, temperatures are warmer. Since pile diameter and temperature relationship is strongly linear in the cage region, a plot of average temperature mimics the actual shape of the pile. The average temperature can be correlated with volume of concrete/grout installed in a pile. It is expected that the temperature profile vs. depth will be uniform for a uniform pile with no defects and with a centered rebar cage (a perfect pile). Presence of defects in the pile or eccentricity of the cage will disrupt the uniformity of temperatures. Presence of soil inclusions or necking in the pile results in a sudden drop in temperature at the depth of occurrence. Examples of expected temperature signatures are provided by Sellountou et al. (2013). The pile is considered uniform in shape and quality if

the average temperature vs. depth is consistent. Bulges in piles manifest as localized increases in average temperature. Reduction in pile section, necking, or inadequate concrete quality manifests as a localized decrease in average temperature. In general, anomalies are indicated by abrupt changes in temperature profile. However, anomalies can be discerned when they generally exceed more than 10% of the cross-sectional area of the pile. Rebar cage verticality can be assessed by comparing an individual temperature profile from a particular TW string vs. the average profile; higher individual temperature indicates the cage is closer to the center of the pile, and conversely, lower individual temperature indicates the cage is closer to the pile face. Given enough thermal measurements, a 3D profile of the pile can be produced, showing variation along the pile. Modelling of temperature measurements includes making corrections for thermal roll-off at the top and bottom of the pile, due to concrete-air and concrete-soil interface, respectively. The correction (usually within one pile diameter) is necessary as temperatures in these regions of the pile are non-linear. Calibrations have been made by exhuming a 46cm (18in.) diameter, 20m (65ft) long ACIP pile and comparing the actual geometry of the pile with information obtained from TW installed in the pile (GRL, 2018); results showed that overall, the effective pile diameter from TIP results varied by about 2% from actual measurements.

PIT Method. PIT is a non-destructive testing method that relies on the concept of wave propagation. It is also referred to as the low strain method, in comparison to the dynamic testing of piles, for PIT involves impacting the pile head using only a small hand-held hammer. When the pile top is struck, waves propagating down the pile are reflected back to the top when an impedance change is encountered, such as from the pile toe. In such cases, pile integrity is verified, i.e., stresses travel through a known pile length to the pile toe of known concrete quality with only minor variations in recorded amplitude between impact and toe reflection. In general, sharply defined velocity reflections are attributed to clear impedance changes; and slowly changing reflections are caused by gradual changes in impedance; however, they can also be caused by soil strength variations. In PIT testing, a clear pile toe reflection is generally taken as an indication of acceptable pile integrity. When toe reflection is not observed, it is not possible to draw clear conclusions on pile integrity.

Details on the development of PIT are described in various sources (Rausche and Goble, 1979; Reiding et al., 1984; and Rausche et al., 1992). Massoudi and Teferra (2004) provide case histories of piles tested using PIT, including testing of unknown piles for determining pile length. Webster et al. (2011) provide recommended guidelines for classification of concrete piles from PIT records. Bungenstab and Beim (2015) provide an overview of PIT testing and background theory for augercast piles.

Advantages of PIT are that it is a very quick test, very economical, many tests can be done by one person in one day, and preliminary results can be viewed almost in real time. Limitations of PIT are that it is generally not applicable to piles with L/D ratios exceeding about 30 (for diminishing propagation of the input wave from interface friction along the pile), any pile exceeding 50m (160ft) in length, timber piles exceeding 15m (50ft) in length, piles embedded in existing structures, steel piles (due generally to typically high L/D and high surface area to pile volume that causes the input waves to be quickly dampened by surrounding soils), and open-ended pipe piles (although concrete-filled steel piles can be tested). PIT is also very much subject to the experience and judgement of the person performing the test and analysis of the data. Vaidya and Likins (2014) show possible abuses of PIT and how defective piles can be shown as acceptable. Additionally, PIT application is least desired as the only means for assessing integrity of ACIP piles due their generally large L/D ratio. Webster et al. (2011) reference a German study on integrity testing of in-situ concrete piles where 18% of about 3,700 piles showed “considerable quality deficiencies.”

 © DFI International Bruges 2025

Many factors can influence the interpretation of PIT records, leading to incorrect assessments, e.g., bulges in the pile (negative velocity reflections), high soil resistance (strong soils) along the pile shaft, pile length relative to its diameter, numerous cross-sectional changes, etc. A defect is generally indicated by a large positive velocity reflection before the toe. A positive velocity could also indicate a reduction in elastic modulus of the pile. Also, PIT is typically limited to identification of major pile defects or concrete/grout quality changes such as major cracks, necking, soil inclusions, or voids in the pile. These PIT limitations can be overcome by use of TIP for the assessment of foundation integrity.

CASE HISTORIES

Findings from several PIT and TIP tests on caissons and ACIP piles are presented below.

Case History No. 1: Caisson with Misaligned Cage

Foundation. A 1.5m (5ft) diameter, 9.7m (32ft) long caisson, plus 1.5m (5ft) of stickup. The caisson L/D is about 8. The subsurface conditions and the caisson are shown in Figure 1.

Caisson Installation. The caisson was installed using a 1.5m (5ft) diameter, full length steel casing. The steel casing was temporary with the goal of preventing hole collapse until concrete placement was completed. The design compressive strength of the concrete was 31MPa (4,500psi). In addition to the reinforcement cage, the finished caisson included a 2.5m (8ft) long permanent steel casing extending 1.5m (5ft) above the ground surface.

Installation of the reinforcing cage in the caisson did not go as planned. When the temporary casing was pulled out, the cage settled about 1.1m (4ft) deeper than planned and shifted in location. These introduced changes in the caisson that were not intended.

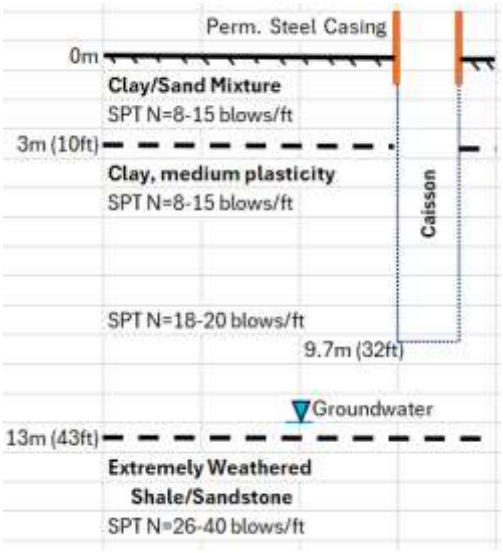


Figure 1. Subsurface Conditions and Caisson No. 1.

PIT. PIT tests were not performed.

TIP. Tests were performed following ASTM WK34326, i.e., a "working – WK" document. Currently, the reference ASTM standard for TIP testing is ASTM D7949. Five (5) strings of TW were installed on the reinforcement cage, each extending to the bottom of the caisson. The TW consisted of temperature sensors, spaced at 30cm (1ft) intervals. TIP data from each TW string was collected via a Thermal Acquisition Port (TAP). Automatic data acquisition started once concrete was poured. The reported volume of concrete below the ground surface was used for data interpretation. The TIP results are shown in Figure 2.

 © DFI International Bruges 2025

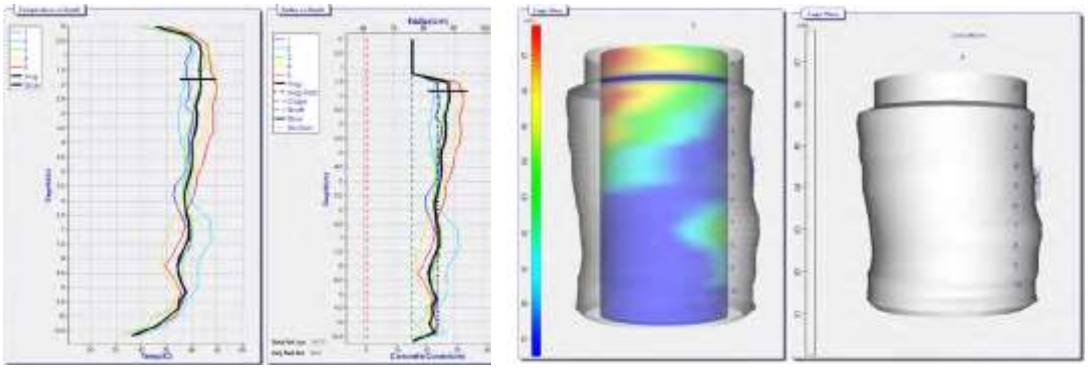


Figure 2. TIP Results for Caisson No. 1: (a). Temperature vs. Depth, (b). Estimated Radius vs. Depth, (c). 3D Image with Rebar Cage in Color, (d). 3D Caisson Image without Cage.

Figure 2(a) shows the measured temperature from each TW vs. depth (lines numbered 1 through 5), including an average value based on all TWs (thick black line marked as "Avg"). The average temperature line appears reasonably uniform along the caisson length, with minor reduction with depth increase, and with no apparent sudden changes. Figure 2(b) shows the estimated radius of the caisson vs. depth based on each TW reading and also an average radius line from all TWs (shown in thick black line), as well as a reference line for position of the cage (shown as the dotted red line) and the design shaft diameter (shown as the dotted green line). The average radius line appears fairly uniform along the length of the caisson, with only minor variations, changing from about 88cm (35in.) at the top of the caisson to about 83cm (33in.) at bottom of the caisson, or a difference of about 5cm (2in.). Additionally, the average radius line indicates that the caisson is larger than the design value of 75cm (30in.), or about 13cm (5in.) and 8cm (3in.) larger at the top and at the bottom, respectively. Also, the results show no noticeable reduction in the caisson diameter in comparison with the design. Figure 2(c) shows a 3D interpretation of the caisson with the rebar cage design position superimposed in color, and a visual illustration of estimated cage position and concrete cover over the reinforcing cage along the caisson length.

As noted previously, the rebar cage shifted during removal of the temporary casing. Results in Figure 1(a) show a small misalignment (shifting) in the rebar cage, manifesting in cooler temperatures in the upper half and warmer temperatures in lower half of TW#2, while TW#4 and TW#5 show the opposite. Despite the cage misalignment, TIP results show that the estimated concrete cover for the cage exceeds 15cm (6in.), satisfying the design requirement of a minimum of 7.5cm (3in.).

Case History No. 2: Caisson with Correct Cage Alignment

Foundation. Following the unexpected cage shift in Caisson No. 1, a second caisson (Caisson No. 2) was installed for verification of adequate construction methodology. Caisson No. 2 was 1.5m (5ft) in diameter, 10.4m (34ft) long, plus a 1.5m (5ft) stickup. The caisson L/D was about 8. The subsurface conditions at Caisson No. 2 are similar to Caisson No. 1.

Caisson Installation. Installation of Caisson No. 2 was similar to Caisson No. 1, however, without the rebar cage mishap. The upper 3m (10ft) of the caisson were permanently cased with about 1m (3.3ft) of the steel casing as stickup.

 © DFI International Bruges 2025

PIT. Tests on Caisson No. 2 were performed following ASTM D5882 seven days after foundation installation. The concrete had achieved a compressive strength of about 40MPa (5,800psi) on the day of testing, based on laboratory compressive strength tests. The top of the caisson was prepared, and 5 different locations were tested. An example PIT record is shown in Figure 3, suggesting strong toe reflection and no significant impedance decrease over the caisson length, indicative of Sound Shaft Integrity. A slight over-sizing of the caisson may be indicated by the negative velocity signature (increasing impedance) from about 9m (30ft) extending to the foundation bottom which is corroborated by the TIP results in Figure 4(b).

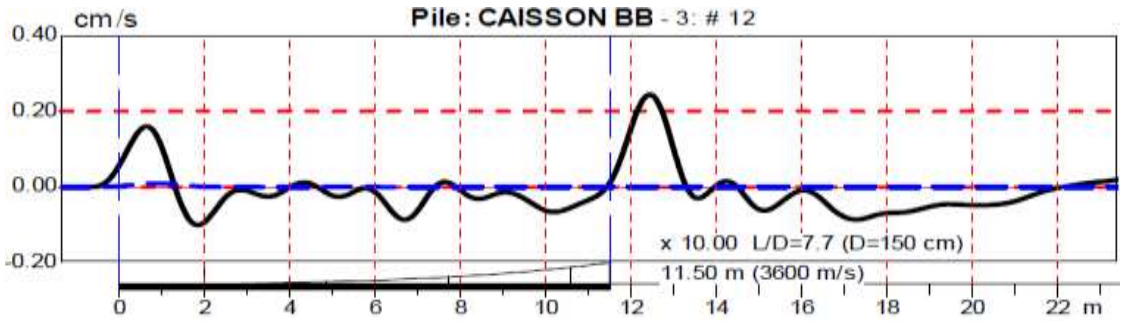


Figure 3. PIT Results on Caisson No. 2.

TIP. Tests on Caisson No. 2 were performed using 5 TW and TAP configurations similar to Caisson No. 1. The TIP results are shown in Figure 4. Figure 4(a) shows the measured temperature from each TW vs. depth (lines numbered 1 through 5), including an average value based on all TWs. The average temperature line appears very uniform along the caisson length, with no apparent sudden change. Figure 4(b) shows the estimated radius of the caisson vs. depth, the average line, as well as reference lines for the position of the cage and design diameter. The average radius line appears reasonably uniform along the length of the caisson, with only minor variations, changing from about 88cm (35in.) at top of the caisson to about 81cm (32in.) at bottom of the caisson, or a difference of about 7cm (3in.). Additionally, the average radius line indicates that the caisson is larger than the design value of 75cm (30in.), or about 13cm (5in.) and 6cm (2in.) larger at the top and at the bottom, respectively. Also, results show no noticeable reduction in the caisson diameter in comparison with the design. Figure 4(c) shows a 3D interpretation of the caisson with the cage design position superimposed in color, and a visual illustration of actual cage position and the concrete cover over the reinforcing cage along the caisson length. As indicated in Figure 4(a), minor temperature differences among TWs indicate a generally concentric rebar cage relative to the caisson diameter.

Overall, TIP results suggest a relatively consistent caisson cross-section and concentric rebar cage. Also, the estimated concrete cover meets or exceeds the design requirement of a minimum of 7.5cm (3in.).

 © DFI International Bruges 2025

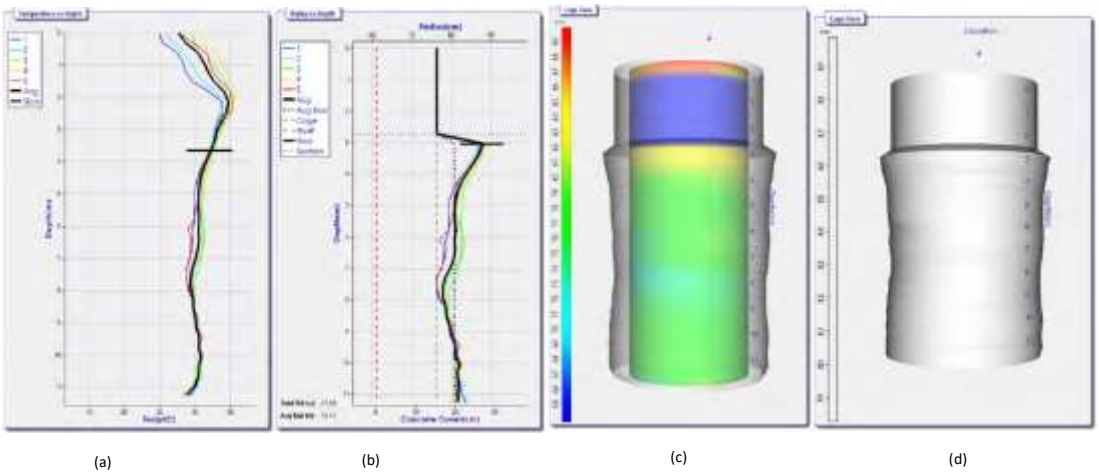


Figure 4. TIP Results on Caisson No. 2: (a). Temperature vs. Depth, (b). Estimated Radius vs. Depth, (c). 3D Image with Rebar Cage in Color, (d). 3D Caisson Image without Cage.

Case History No. 3: ACIP Pile Foundations

Foundation. Four 36cm (14in.) diameter ACIP piles were installed to depths ranging from about 23-26m (75-85ft) in length. Both PIT and TIP tests were performed on all 4 piles. All piles were constructed using grout with design compressive strength of 28MPa (4,000psi). Each pile included a reinforcement cage, as well as a center bar on which a full-length TW string was attached. The piles L/D ranged from 64 to 73. The upper 0.6m (2ft) of piles were cased with a thin-wall metal casing. The subsurface conditions and the ACIP pile are shown in Figure 5.

PIT. Tests were performed following ASTM D5882. The 7-day compressive strength of the grout was 31MPa (4,500psi). A wave speed of 3,800m/sec (12,500ft/sec) was assumed for reducing the velocity records. PIT data were collected from several hammer blows to the pile tops. An immediate assessment of pile quality was made in the field upon data collection. More refined analysis of the velocity data was performed later, adjusting for amplification and filtering, as needed. Representative PIT results are shown in Figure 6(d). Understandably, they show no clear pile toe reflection due to the very large L/D ratios in the 60-70 range.

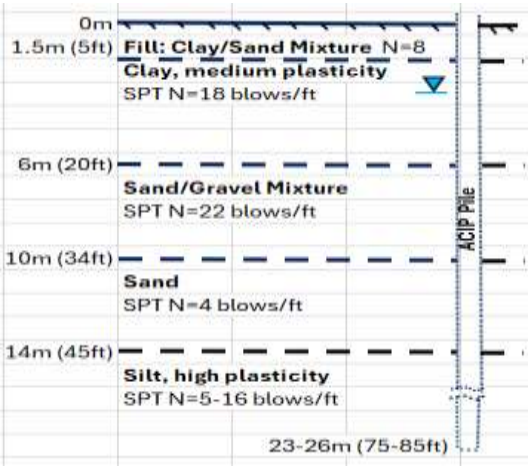


Figure 5. Subsurface Conditions and the ACIP Pile.

 © DFI International Bruges 2025

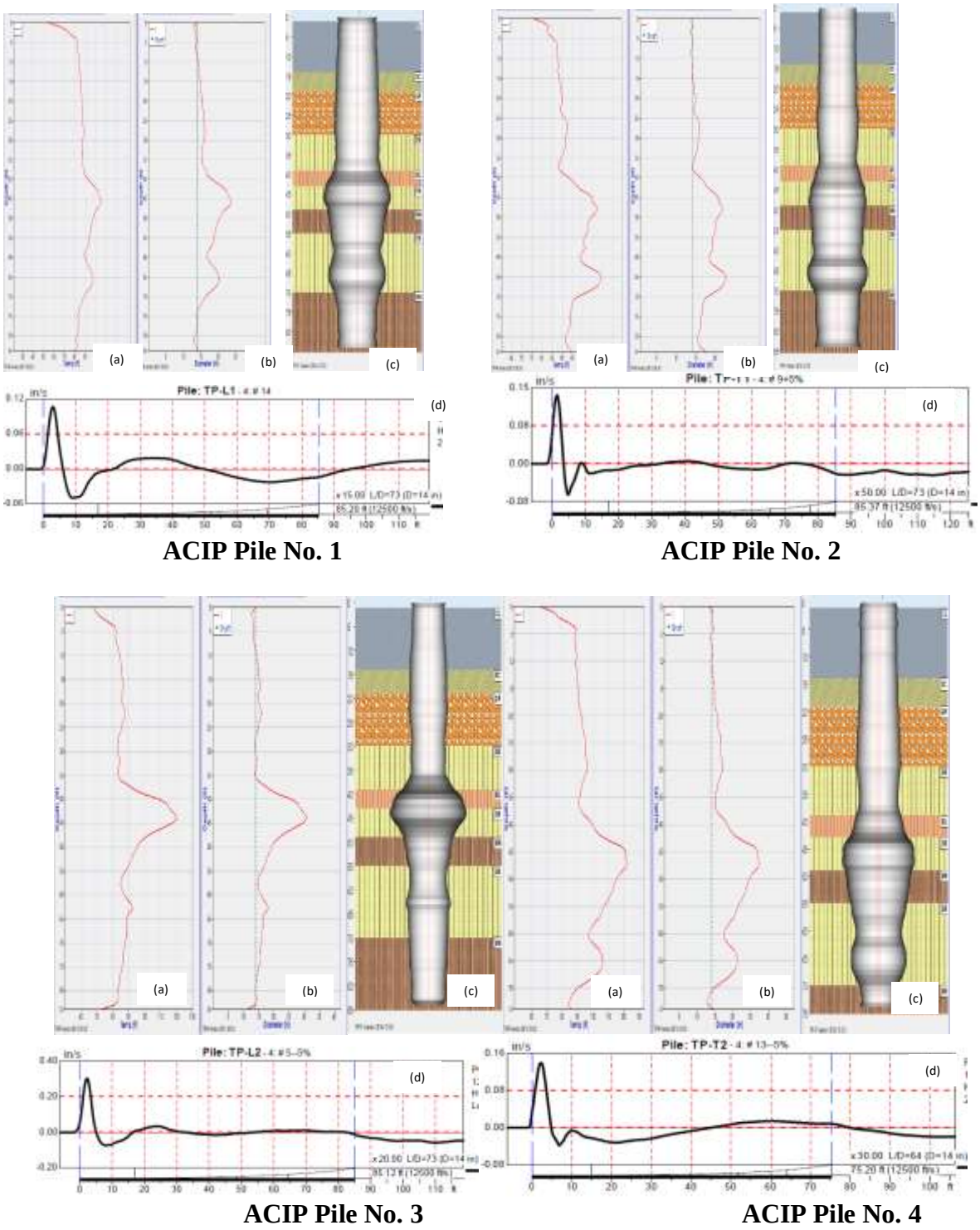


Figure 6. TIP and PIT Results on ACIP Piles No. 1 Through No. 4: (a). TIP Temperature vs. Depth, (b). TIP Estimated Diameter vs. Depth, (c). TIP 3D Image, (d). PIT Results.

Notwithstanding the absence of a clear pile toe reflection, the PIT results do not indicate a major impedance reduction. Therefore, all piles fall into the category AB40, meaning that the piles have acceptable shaft integrity (i.e., no major defects) to a depth of approximately 12m (40ft). Interpretation of the records beyond the 12m (40ft) length is not possible due to absence of toe reflection.

 © DFI International Bruges 2025

TIP. Tests were performed following ASTM D7949. A single string of TW was attached to the center rebar in each pile, extending from top to bottom of the pile. The TW consisted of temperature sensors, spaced at 30cm (1ft) intervals. TAP boxes started data acquisition once the pile was installed. Peak grout temperature was reached in about 8-11 hours after grout placement. The temperature data was downloaded from the TAP boxes and used in conjunction with the reported volume of grout for interpretation. TIP results are shown in Figure 6.

All thermal profiles in Figure 6 show measurements and interpreted pile diameters that are indicative of continuous piles larger than the design diameter (design diameter is shown as the green dotted line in Figure 6(b)). Also, no abrupt reduction in temperature is shown which would be indicative of a major reduction in pile diameter. In fact, the opposite is indicated in depth ranges of about 12-21m (40-70ft), i.e., higher temperatures manifest within these depths, indicative of larger pile diameter (bulge). Based on reported grout volumes, pile diameters at isolated depths are estimated to approach 58-66cm (23-26in.), as shown in Figure 6(c). Pile No. 3, which shows bulges in the 11-20m (35-65ft) depth range, shows an estimated diameter that approaches approximately 79cm (31in.). It should be noted that the dramatic appearance of bulges in Figure 6(c) is the result of roughly 10-fold exaggerated graphical scale.

Case History No. 4: Caisson Foundations in Variable/Strong Ground

Foundation. Two clusters of 24 caissons were installed, each caisson 0.9m (3ft) in diameter, 12m (40ft) long. The caisson L/D is about 13. The subsurface conditions and the caissons are shown in Figure 7.

Caisson Installation. The caissons were installed using full length temporary steel casing with the goal of preventing hole collapse. The concrete design compressive strength was 41MPa (6,000psi). The caisson locations had already been partially excavated for other purposes. Prior to caisson installation, the area was backfilled with cemented-treated fill (CTF), for a maximum depth of about 9m (30ft). The CTF was placed in lifts and compacted, achieving an average moist density of about 21kN/m^3 (134pcf) at 13% moisture. Laboratory testing of CTF material indicated an average unconfined compressive strength of about 0.83MPa (275psi) at 28 days. Caisson installation proceeded as planned, with each caisson penetrating both the CTF and the native soils, albeit by various amounts, as shown in Figure 7.

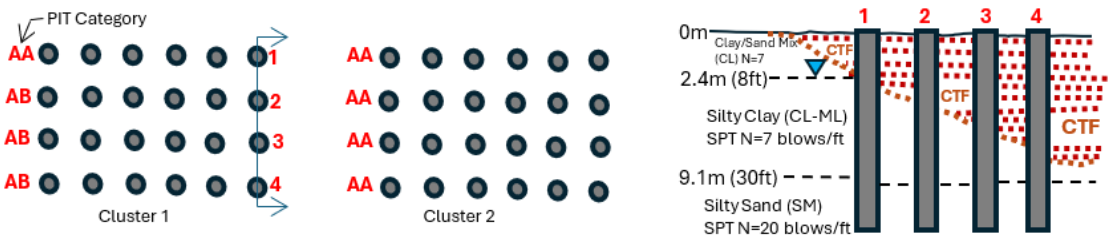


Figure 7. Caisson Foundations and Subsurface Conditions in Variable/Strong Ground.

PIT. Each cluster of caissons included 15 PIT tests, performed following ASTM D5882 about 10-15 days after caisson installation. In Cluster 1, all tested caissons with the shortest length in the CTF (about 2.7m (9ft), or 23% of its length) resulted in the AA Category (i.e., acceptable toe reflection, sound integrity); however, PIT tests on all other caissons resulted in the AB Category (i.e., toe reflection not seen, integrity inconclusive - when toe reflection is not observed, it is not possible to draw clear conclusions on pile integrity). The Category AB caissons had 38% to 64% of their lengths within the CTF. In Cluster 2, all 15 tested caissons resulted in the AA Category,

 © DFI International Bruges 2025

regardless of location or length in the CTF, suggesting strong toe reflection and indicative of sound integrity. This was despite similar ground conditions, caisson geometry, and installation method in both clusters. The discrepancy in PIT results between the two clusters could not be readily explained. It is known that strong materials, such as the CTF, can interfere with PIT signals reaching the foundation toe and render the results "inconclusive," however, similar ground conditions also existed at Cluster 2, yet they did not produce "inconclusive" results. Examples of Category AB records from PIT tests in Cluster 1 caissons are shown in Figure 8.

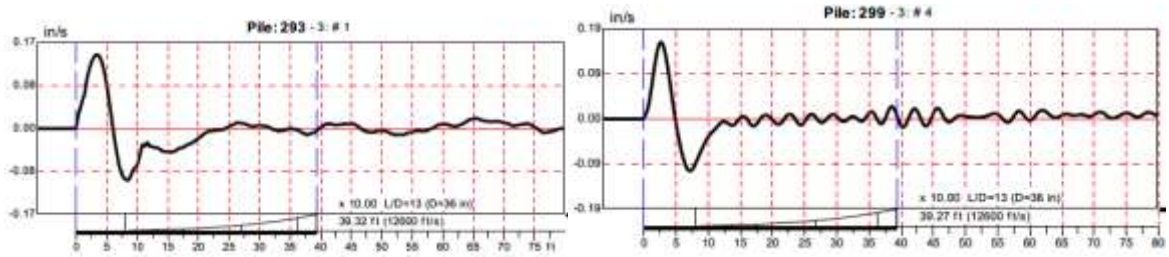


Figure 8. Example 'PIT Category AB' Records from Cluster 1 Caissons.

TIP. Tests on Cluster 1 and 2 caissons were performed using a 4 TW and TAP configuration. One caisson in Cluster 1 and 3 caissons in Cluster 2 were tested. Peak temperatures were reached in about 18 to 30 hours after concrete placement. The TIP results for one of the caissons in Cluster 1 (that indicated Category AB from PIT testing, i.e., integrity inconclusive) is shown in Figure 9.

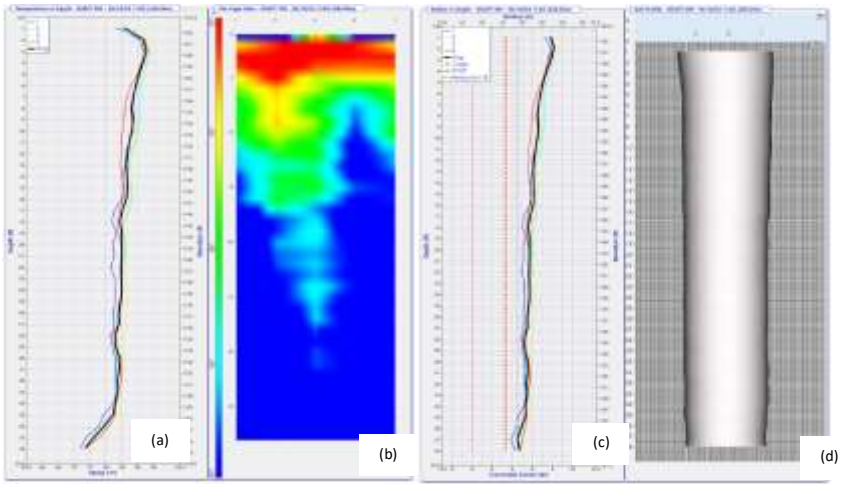


Figure 9. TIP Record of 'PIT Category AB' Caisson: (a). Temperature vs. Depth, (b). Flat Cage View vs. Depth, (c). Estimated Radius vs. Depth, (d). 3D Caisson Rendition.

Figure 9(a) shows the measured temperature from each of the 4 TWs vs. depth, including an average value based on all TWs. The average temperature (black) line appears very uniform along the caisson length, with no apparent sudden changes. Figure 9(b) shows the flat cage view of temperature vs. depth. Figure 9(c) shows the estimated radius of the caisson vs. depth, the average line, as well as reference lines for position of the cage and design diameter. The average radius line appears reasonably uniform along the length of the caisson, except in the upper approximately 3.3m (10ft) suggesting a larger diameter caisson. Figure 9(D) shows a 3D interpretation of the caisson. Overall, TIP results suggested relatively consistent caisson cross-section, concentric rebar cage, and concrete cover exceeding the design requirement of a minimum of 7.5cm (3in.), with no abnormality in measured temperatures, indicative of caissons

 © DFI International Bruges 2025

with sound integrity. Without such TIP results, the "inconclusive" PIT results on the same caissons would have necessitated additional unnecessary investigations to confirm integrity or remedial measures for many caissons.

CONCLUSIONS

Both PIT and TIP are non-destructive tests for assessing the integrity of pile foundations. For typical piles, TIP can generally be completed within 12-48 hours after pile installation. This is a major advantage in accelerating quality verification of foundations. TIP provides information on additional foundation features that PIT cannot, e.g., information on concrete/grout cover condition and rebar cage alignment. Further, TIP does not have the L/D limitations that PIT has.

Despite advantages over PIT, there are uncertainties in TIP data reduction that can lead to errors, as such reductions rely on other input than just concrete/grout temperature. Example input that could exacerbate errors include overlooking correction of reported concrete/grout volume, center bar not initially positioned near the center of the pile, or roll-off corrections for pile top and bottom shape due to air and annual average soil temperatures. These affect TIP data interpretation and influence estimating pile diameter, verticality, and reinforcement cover. Fortunately, their contribution can be minimized with proper control.

For ACIP piles, grout/concrete volume input greatly affects interpretation of TIP results. The volume of reported grout should be corrected prior to use, excluding from the reported total the initial pumped volume (used to fill the lines and build pressure in the system) and the grout that is wasted on the surface upon auger removal. Accounting for grout that represents the auger volume, at time of grout return, is reasonable and should be considered. For caissons, excluding from the reported volume the volume to fill the tremie pipes and any waste is reasonable.

PIT is a quick and relatively inexpensive test to perform. Preliminary results can become available in the field almost immediately. PIT works well for piles with limited L/D (typically below 30), and uniform grounds. High resistance soils further limit the L/D to lower than 30 and the depth to which a pile can be assessed. Also, PIT results are only as accurate as the presumed pile material wave speed which can be affected by variations or defects in pile material. Additionally, PIT cannot detect misalignments in pile reinforcement or model reinforcement cover. Further, piles that produce complex PIT signatures, e.g., those with multiple or highly variable impedance (cross-section), are difficult or impossible to analyze.

Few ACIP piles have relatively low L/D ratio, making PIT testing success questionable, except under certain conditions such as short and "fat" piles and/or combined with soft soil conditions. Therefore, TIP testing should be the leading method of choice for integrity testing of typical ACIP piles. Particularly, TIP provides additional information on pile integrity (cage alignment and concrete cover) that PIT is unable to provide.

Testing limitations should be considered before selecting the method of integrity testing. Interpretation of testing records require thorough familiarity with the test method. Good understanding of wave propagation concept is important for evaluation of PIT records. Good judgement by qualified professionals is key for reasonable interpretations. It is not ideal to assign such testing scope to the foundation contractor; however, should any portion of PIT or TIP data collection be delegated to them for logistical reasons, their expertise must be vetted first.

Neither TIP nor PIT is intended, or should be used, in lieu of load testing for assessing the load carrying capability of piles. Neither TIP nor PIT results should be the only data used for qualifying, accepting, or rejecting foundations. Such decisions should also rely on other

 © DFI International Bruges 2025

foundation installation information, including inspection, concrete/grout quality and quantity, pile production records particularly the volume of concrete/grout vs. depth, and soil boring logs.

REFERENCES

ASTM D5882. Standard Test Method for Low Strain Impact Integrity Testing of Deep Foundations. ASTM International, West Conshohocken, PA.

ASTM D7949. Standard Test Method for Thermal Integrity Profiling of Deep Foundations. ASTM International, West Conshohocken, PA.

ASTM WK34326. Proposed Standard. Test Method for Integrity Testing of Concrete Deep Foundations by Thermal Profiling. ASTM International, West Conshohocken, PA.

Becker, M., Coleman, T., and Belardo, D. (2015). Thermal Integrity Profiling of ACIP Piles. Proceedings of The International Foundations Congress and Equipment Expo 2015.

Bixler, M., Belardo, D., and Piscsalko, G. (2016). Case Histories Using TIP for Foundation Quality Assurance. Proceedings, GeoVancouver 2016, Vancouver, B.C.

Bungenstab, F.C.I., Beim, J.W. (2015). Continuous Flight Auger (CFA) Piles–A Review of the Execution Process and Integrity Evaluation by Low Strain Test. Proceedings, 15th Pan-American Conference on Soil Mechanics and Geotechnical Engineering: Buenos Aires.

GRL (2018). Pile Diameter Modelled Using Thermal Integrity Profiling with Extracted Pile Measurements. GRL Engineers, Inc. and Pile Dynamics. Newsletter 87, March 2018.

Hyatt, T., Belardo, D., Melker, R., Webster, J. (2019). Cost and Technical Comparison on Non-Destructive Test Methods for Drilled Shafts. DFI Annual Conference, October 2019.

Mullins, G. and Johnson, K. (2016). Optimizing the Use of the Thermal Integrity System for Evaluating Augercast Piles. Report No. BDV25-977-09 to FLDOT. July 2016.

Mullins, G. and Johnson, K. (2017). Thermal Integrity System for Augered Cast-In-Place Piles, Part II, Implementation Plan. Report No. BDV25-977-34 to FLDOT. August 2017.

Piscsalko, G., Likins, L., Mullins, G. (2016). Drilled Shaft Acceptance Criteria Based upon Thermal Integrity Profiling. Proceedings, 41st Annual International Conference on Deep Foundations, Seepage Control and Remediation, October 2016, New York, NY.

Piscsalko, G. (2014). Non-Destructive Testing of Drilled Shafts and CFA Piles-Current Practice and New Method. Proceedings, DFI/EFFC 11th International Conference on Piling and Deep Foundations, 2014, Stockholm, Sweden.

Sellountou, E.A., Alvarez, C., Rausche, F. (2013). Thermal Integrity Profiling: A Recent Technological Advancement in Integrity Evaluation of Concrete Piles. Proceedings, First International Conference, Seminar on Deep Foundations: Santa Cruz, Bolivia, 2013.

Vaidya, R., Likins, G.E. (2014). Guidelines for Successful High Strain Dynamic Load Tests & Low Strain Integrity Tests for Bored Piles. Proceedings, Indian Geotechnical Conference: Kakinada, India, December 2014.

Webster, K., Rausche, F., Webster, S. (2011). Pile and Shaft Integrity Test Results, Classification, Acceptance and/or Rejection. Compendium of Papers of the 90th Annual Meeting of the Transportation Research Board, 2011.

 © DFI International Bruges 2025

INVESTIGATING THE UNSEEN FLOW OF CONCRETE IN DEEP FOUNDATION CONSTRUCTION

Thomas Mitchell, Swansea University, Swansea, United Kingdom
Chris Barker, Ove Arup and Partners Ltd, London, United Kingdom
Christopher Wilkes, Ove Arup and Partners Ltd, London, United Kingdom
Chenfeng Li, Swansea University, Swansea, United Kingdom

ABSTRACT

Computation Fluid Dynamics (CFD) based numerical modelling has proven to be a powerful tool for simulating the unseen flow of tremie concrete in deep foundation construction. This paper reports a parametric study of the relationship between concrete consistence and cover zone depth, revealing how they affect concrete flow mechanisms within bored piles. Flow features observed from the numerical simulations are linked to the likelihood of physical defect generation. The open-source CFD software OpenFOAM is used to model the tremie concrete as a non-Newtonian Bingham fluid. A gravity-driven approach is implemented with a high-fidelity, 3D geometry to capture both the gravity-pour process of the tremie method and detailed flow around the reinforcement and cover zone. Reducing the cover zone size and using lower consistence concrete contribute to an increase in the severity of negative flow features – meaning an increase in the likelihood of generating defects such as mattressing, voids and inclusions.

Keywords: tremie concrete, computational fluid dynamics, defects, bored piles, cover zone

INTRODUCTION

The flow mechanisms of concrete from the base of a tremie pipe and subsequent filling of the pile bore have not been well understood until recently. This is primarily due to this process occurring unseen tens of metres below ground surface. Historically, understanding of such mechanisms was inferred indirectly and occasionally from construction observations made when difficulties arose. Over past decades, there has been much conjecture over what happens at the base of a tremie pipe, but there has been little clear evidence to substantiate theories. Only relatively recently has our understanding of the key fresh tremie concrete properties of yield stress and viscosity been effectively correlated with slump-flow and slump-flow velocity (EFFC/DFI, 2024), allowing the avoidance of undesirable fresh concrete mixes that have a higher propensity to lead to defects by pre-construction and production concrete testing.

Due to the scale of foundation elements, full-size experimental investigations of the tremie process to investigate what conditions lead to the generation of defects are prohibitively costly. However, numerical modelling can now be utilised as a cost-effective alternative, which is becoming a growing area of research in the literature. Additionally, details are available from numerical models that are not readily attainable from physical experiments – information such as velocity vectors, stress, and strain values throughout the simulation domain. These models also enable various parametric comparisons to be conducted. Such capabilities can offer a greater insight into the root cause of flow mechanisms and their links to the creation of defects.

Some small-scale numerical studies have been conducted regarding concrete flow in bored piles, but the parameters investigated lack grounding in industry specifications and the flow mechanisms observed are not linked to defect generation. The study presented here utilises Computational Fluid Dynamics (CFD) based numerical modelling to better understand the concrete flow mechanisms that lead to defects in bored piles, addressing this gap in the literature. A parametric study examines the influence of concrete consistency and cover zone size on concrete flow within bored piles. These flow mechanisms are then connected to the probability of defect generation, and the numerical results are compared to observed flow phenomena observed in constructed foundations.

 © DFI International Bruges 2025

BACKGROUND

Upon exposure of deep foundation structures, defects and imperfections, including mattressing, bleed channels, voids, inclusions, insufficient cover, necking and bulging, are occasionally revealed as discussed by Beckhaus et al. (2011) and Flemming et al. (2009). An imperfection that adversely affects the foundation's performance and thus requires repair before incorporation into the permanent works is considered a defect. The existence of a defect within a deep foundation can lead to the reduction of the structure's performance, reliability and lifespan, as investigated by Yao et al. (2024). The process of remedying such defects is costly and time-consuming.

The tremie method is a common but challenging construction technique for placing concrete in submerged conditions, where sidewall stability of the pile bore is necessary to prevent ground collapse. Support fluids, typically mineral or polymer-based, are used to achieve this by filling the excavations of deep foundations during digging. As shown in Figure 1, the concrete is placed by gravity feed using a hopper and vertical tremie pipe to fill the excavation bottom-up. The key feature of this method is that the tremie pipe is constantly submerged in fresh concrete to reduce the direct contact between the concrete and support fluid. Increased direct contact leads to more mixing of the concrete and support fluids, reducing the concrete quality (EFFC/DFI, 2024).

The type of concrete used in this process is referred to as ‘tremie concrete’. It is a specific concrete type with particular fresh properties, widely used to construct deep foundation elements such as bored piles and diaphragm wall panels due to its superior post-hydration compressive strength and high level of workability, as reported by Wilkes et al. (2023). The term ‘workability’ has been replaced by the word ‘consistence’ in European standards, but not in the United States. Both words are often used interchangeably and refer to fresh concrete’s ability to flow and the ease with which it can be mixed and poured (EFFC/DFI 2024). For clarity, the term consistence will be used throughout this paper.

When the pile design, fresh concrete properties, and construction methodology are incompatible, a departure from desired concrete flow mechanisms occurs, leading to imperfections and possible defects. The mechanisms generating such defects within these structures have previously not been fully understood, but they were believed to be caused by concrete's inability to flow easily into the cover zone (EFFC/DFI 2024; Brown et al. 2007; Beckhaus et al. 2011). These mechanisms have now been investigated using numerical methods and are discussed below.

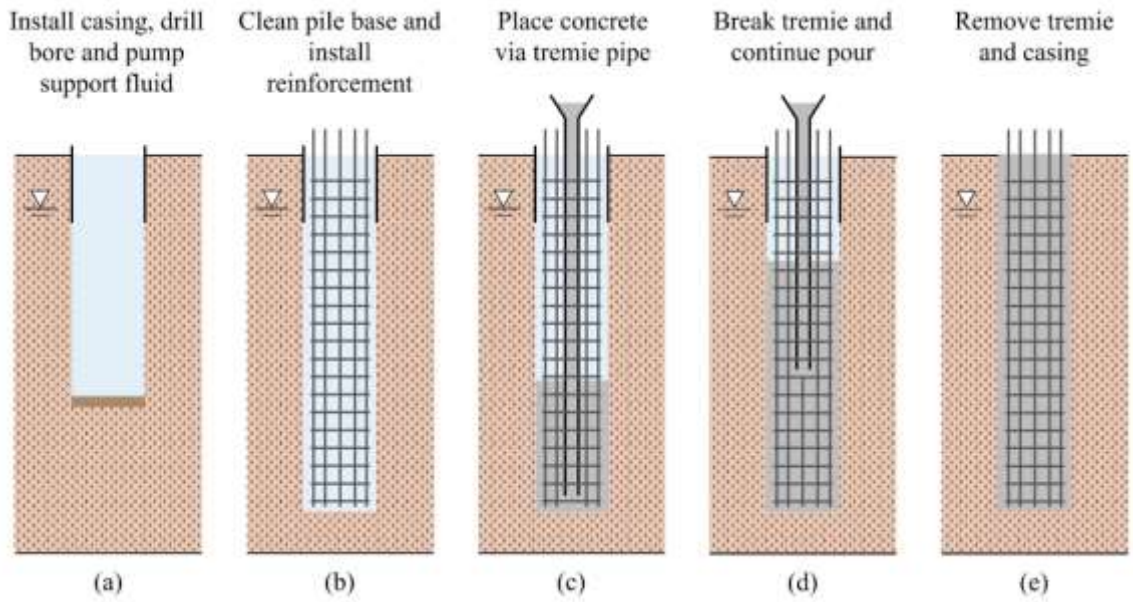


Figure 1. Schematic diagram of the cast-in-place bored pile construction process using the tremie method.

 © DFI International Bruges 2025

Tremie concrete consistence is critical in the construction of deep foundations, as the concrete is required to flow easily down the tremie pipe under its own weight and then up and around clustered reinforcement without the use of vibration. Research by Kränkel and Gehlen (2018) has demonstrated a correlation between slump-flow tests and the dynamic yield stress of tremie concrete and is, therefore, the preferred consistence test to be performed on-site to ensure adequate consistence of the concrete mix prior to pouring. The test involves a standard slump cone placed on a base plate and filled with fresh concrete. The cone is lifted smoothly over 1-3s, the concrete spreads, and its final rest diameter is measured – this value is referred to as the slump-flow. BS-EN-12350 (2019) describes the details of the test procedure.

MODELLING METHODOLOGY

The parametric study of the relationship between concrete consistence and cover zone depth was undertaken to reveal how these parameters affect tremie concrete flow mechanisms during the concreting of bored piles. Understanding flow features observed from the numerical simulations would better inform the likelihood of physical defect generation. Modelling methodology and assumptions are discussed below.

Numerical Model

The numerical modelling conducted in this paper uses the open-source CFD software OpenFOAM, specifically, the multiphaseInterFoam solver. This solver is capable of modelling n-phase incompressible, immiscible, and isothermal flow problems and has been validated for simulating fresh concrete flow with laboratory testing by Wilkes (2021) and Fierenkothen et al. (2016, 2019b). Three fluid phases are required in the model to capture air, support fluid and concrete. The volume of fluid (VOF) method captures the interface regions between these fluids. The fresh concrete is modelled as a homogeneous Bingham fluid, so aggregate-dependent flow features such as segregation and blockage are not captured. This assumption is valid in the context of this study, as the bulk flow behaviour is likely a dominating factor regarding defect generation (EFFC/DFI 2024).

Model Geometry

The simulated pile has a depth of 8.2 m and a diameter of 1.5 m. The reinforcement is constructed with 40 mm diameter vertical bars with 100 mm clear spacing and 16 mm diameter horizontal bars with 200 mm clear spacing. The cover zone size is variable, with a lower limit of 25 mm and an upper limit of 250 mm. The tremie exit is 200 mm from the base of the pile and has a diameter of 250 mm. Such values are typical pile parameters defined in SPERWall (ICE 2016).

To maintain a computationally feasible model while capturing the flow features of interest, the focus of concrete flow within the pile is limited to the base 1 m. As shown in Figure 3 (a), the base 1 m contains the reinforcement cage and has a full diameter of 1.5 m. Above this region, the pile diameter decreases, and reinforcement is no longer modelled to reduce the total number of elements. The simulation concludes once the concrete level inside the pile reaches 0.95 m so that the change in geometry does not influence the flow. The total depth of the pile is considered in the model so that the boundary conditions capture the pressure differential caused by the difference in concrete level inside the tremie pipe and pile, which is the driving force for concrete flow in the tremie method. To further reduce the computation cost, a 60° wedge is modelled, and rotational symmetry is assumed – this approach is typical when modelling such systems (Fierenkothen et al. 2016; Jeyaraj et al. 2023).

Boundary Conditions

Figure 3 (b) shows the boundary conditions applied to the model. A shortened pile is visualised in the figure for clarity in the labelling. The hopper region comprises four main components: the concrete inlet, concrete overflow, atmosphere and hopper walls. Concrete fills the hopper at a fixed rate via the concrete inlet, representing the pumps that transfer concrete between the transit mixer and pile. A flow

 © DFI International Bruges 2025

rate is chosen to ensure the hopper is filled with concrete throughout the duration of the simulation – any additional concrete leaves the system via the concrete overflow, maintaining a constant fluid head of concrete. The atmospheric boundary conditions at the pile opening allow the support fluid to leave the system as it is displaced by concrete. All walls are prescribed no-slip boundary conditions. This boundary condition setup leads to the pressure differential driving concrete flow. The domain is initialised with support fluid in the pile, concrete filling the tremie and hopper, and air in the region above the hopper.

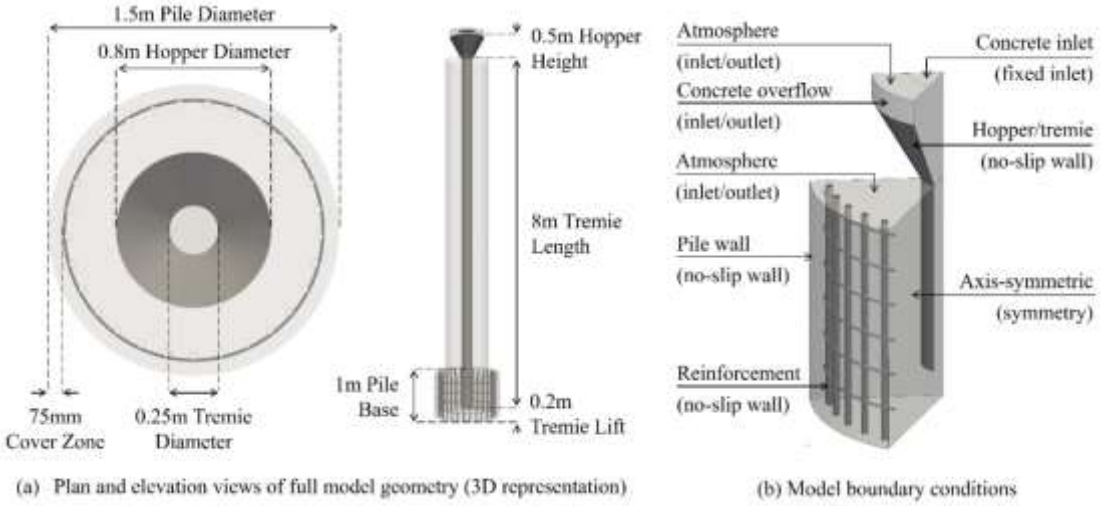


Figure 2. Model geometry and boundary conditions.

Modelling Concrete Rheology

The constitutive Bingham model has been shown throughout the literature to capture fresh concrete's bulk flow behaviour (Fierenkothen et al. 2019b; Wilkes 2021). Two key parameters govern the fluid's behaviour: yield stress, which represents the stress required to initiate flow, and plastic viscosity, a measure of the fluid's resistance to flow. The equation below describes the relationship between stress and strain as defined by the Bingham model.

$$\tau = \tau_0 + \mu\dot{\gamma} \quad [1]$$

Where τ is the shear stress, τ_0 is the yield stress, μ is the viscosity, and $\dot{\gamma}$ is the strain rate. If the fresh concrete undergoes shear stress below its yield stress, it acts as a rigid body. Applied stresses larger than the yield stress cause the fluid to behave as a viscous fluid with constant viscosity.

The yield stress and viscosity values of tremie concrete must be balanced to provide adequate performance in deep foundation construction. Yield stress must be suitably low to provide sufficient form-filling but high enough to displace the support fluid above within the pile and resist the shearing forces that lead to segregation (EFFC/DFI 2024). Similarly, the viscosity must be low enough to ensure acceptable flow rates for a timely construction process but not so low as to introduce stability issues. An unstable mix leads to the inability to maintain water within the concrete matrix under the significant hydrostatic pressures observed in deep foundations (Larisch 2019).

Parametric Study Parameters

The EFFC/DFI (2024) recommend a target slump-flow range of 400 to 550mm for tremie concrete. As such, the concrete parameters in this study have been selected to cover a range beyond this, from 350 mm to 590 mm - equivalent to a range of consistency classes from F2 to SF1 as specified in BS 8500-1 (British Standards Institution 2023). A suitably wide range of concrete consistencies allows general trends to be observed based on these parameters. The Bingham properties (viscosity and yield

 © DFI International Bruges 2025

stress) for these concrete mixes have been obtained from Wilkes (2021) and Fierenkothen (2019a), as shown in Table 1. These studies conducted laboratory slump flow tests with various concrete mix designs, followed by equivalent numerical simulations in OpenFOAM to validate the Bingham parameters of these mixes. The support fluid Bingham properties used throughout this study are τ_0 = 7 Pa, and μ = 0.03 Pa.s and density of ρ = 1075 kg/m3, correlating to a clean bentonite slurry (Wilkes 2021).

Table 1. Concrete Bingham properties, equivalent slump-flow values and references.

Slump Flow (mm)	Viscosity, μ (Pa.s)	Yield Stress, τ_0 (Pa)	Author
590	35.8	54	C. Wilkes (2021)
500	30.2	130	C. Wilkes (2021)
430	25	170	C. Fierenkothen (2019a)
385	30	295	C. Fierenkothen (2019a)
350	50	390	C. Fierenkothen (2019a)

The term cover zone refers to the region between reinforcement and the pile surface - its primary function is to provide a layer of protection for the reinforcement against external elements. There are two factors to be considered during the design phase of the cover zone: the need for a particular concrete cover during the structure's service life and the need for a minimum concrete cover during construction to allow for adequate concrete flow and the removal of any temporary casing.

For the execution of deep foundations using concrete poured by the tremie method, execution standards covered in BS EN 1536 (British Standards Institution 2010a), BS EN 1538 (British Standards Institution 2010b), and ACI 301 (American Concrete Institute 2016) require a suitable amount of cover to allow for concrete flow around reinforcement, leading to complete embedment of the steel. The nominal cover is defined in Equation 2.

$$c_{nom} = c_{min} + \Delta c_{dev}, \quad where\ c_{min} \geq max \begin{vmatrix} c_{min,structural} \\ c_{min,execution} \end{vmatrix} \qquad [2]$$

Where c_{nom} is the nominal cover, Δc_{dev} is the allowance for construction tolerance and c_{min} is the greater of the minimum required cover for durability, bond and execution. A nominal concrete cover of at least 75mm is recommended by the EFFC/DFI (2024) (e.g. a minimum cover over 50mm plus a tolerance of 25mm). A report by Brown et al. (2018) on behalf of the U.S Federal Highway Administration suggests cover zone values dependent on pile diameter: 75mm cover for piles with a diameter less than or equal to 1m, 100m cover for diameters between 1m and 1.5m, and 150mm cover for diameters above 1.5m.

Based on these industry specifications, cover zone sizes of 25mm, 75mm, 150mm and 250mm were selected to be investigated within this parametric study to go beyond the recommended specification ranges. The geometries of these cover zone values are visualised in Figure 3 – the transparent grey shows the pile domain, and the dark grey represents the reinforcement cage and tremie pipe. Combined with the five variables for concrete consistence, this yields a total of 20 simulation configurations.

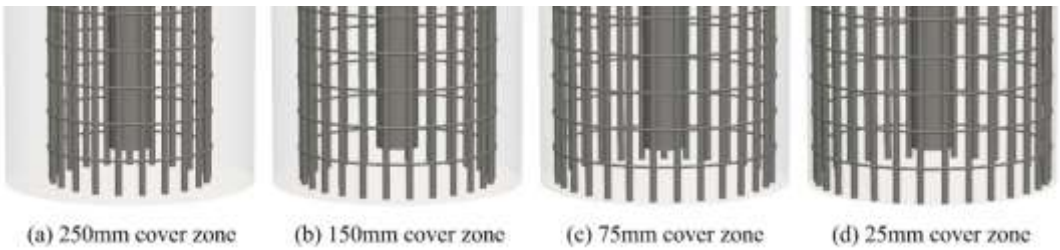


Figure 3. Visualisation of various concrete cover zone sizes.

 © DFI International Bruges 2025

RESULTS AND DISCUSSION

General Flow Mechanisms

Figure 4 shows a cross-section through the centre of the pile, focusing on the bottom one metre of the element. The case shown has a 75 mm cover zone, and the concrete has rheological properties equivalent to a slump-flow of 590 mm. The left side of each sub-image is a slice between two vertical reinforcements, and the right side is a slice directly through the vertical reinforcement. The dark grey represents the reinforcement and tremie pipe, the transparent grey represents the pile domain, and the coloured regions are the concrete phase. The concrete colouring denotes its velocity magnitude, where dark red is relatively fast flowing, and dark blue is stationary. The black arrows show the velocity vectors throughout the fluid. Whilst the pile also contains support fluid, for clarity, only the concrete phase is visualised in this figure.

Figure 4 (a) shows the concrete state shortly after flow initiation. At this point, horizontal flow dominates as the concrete spreads radially to fill the cover zone. Upon entering the cover zone, flow rapidly slows and becomes stationary, as shown by the dark blue regions in Figure 4 (b) and (c). Once stationary within the cover zone, the concrete effectively becomes locked in place and is not disturbed by the fresh concrete entering the pile.

Figure 4 (d) shows the fully developed, general flow mechanism observed within reinforced bored piles. Concrete enters the pile via the tremie, is redirected 180°, and exhibits vertical flow confined within the reinforcement cage. This continues until the concrete reaches the flow front, which refers to the concrete region at the concrete-support fluid interface. At the flow front, the horizontal flow component grows, leading lateral flow through the reinforcement cage and filling of the cover zone. Concrete at the flow front is continuously consumed into the cover zone, exposing fresh concrete to the support fluid. This flow mechanism is referred to as “bulging” or “restricted” flow (EFFC/DFI 2024). If a pile is reinforced, “plug” or “unrestricted” flow cannot occur, no matter the concrete consistence.

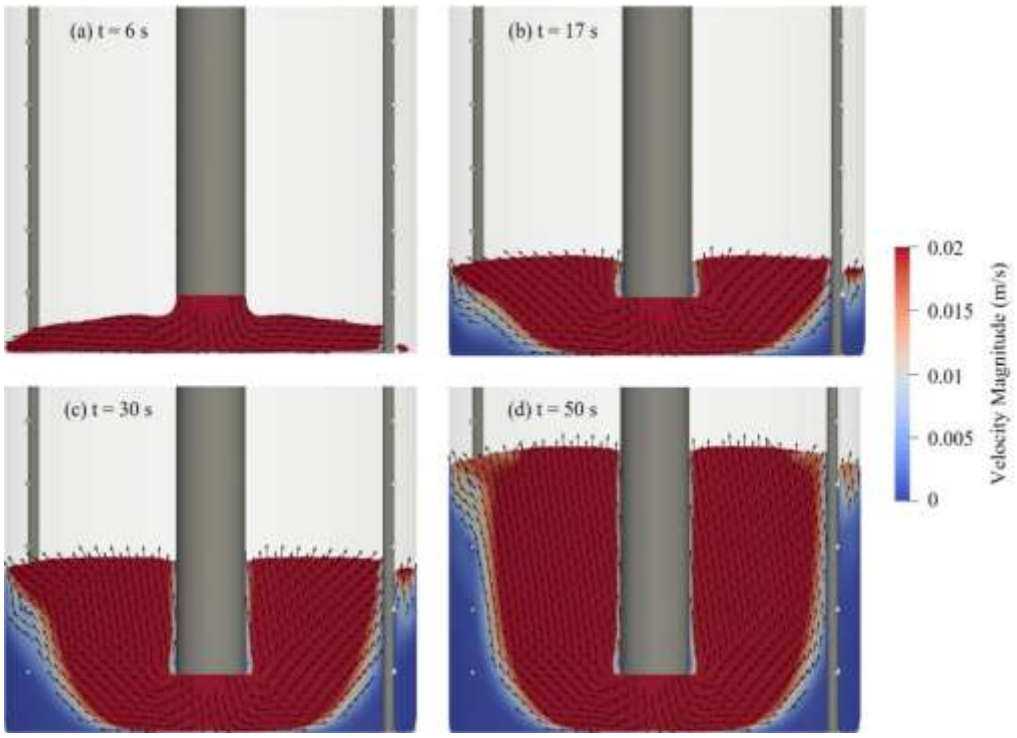


Figure 4. Concrete velocity profile at various times throughout the pouring process – cross-section through the pile centre with SF-590 mm concrete and 75 mm cover zone.

 © DFI International Bruges 2025

Comparison with Industry Defects

Simulation results in Figure 5 (a) and (b) are compared to observations made on a construction site, shown in Figure 5 (c). The exposed bored pile has a significant region of exposed reinforcement where concrete has not filled the cover zone. A cross-section is visible where the cover zone is partially filled, and the angle of the mattressing within the cover zone can be seen to increase with elevation moving up the pile. These mattressing angles are highlighted with arrows for clarity in Figure 5.

This flow phenomenon was observed most prominently in the simulation when a low-consistence concrete, with a slump-flow of 350 mm, was poured into a pile with a cover zone of 25 mm. This case is shown in Figure 5 (a) and (b). The highlighted regions in Figure 5 (a) indicate an increasing mattressing angle as the elevation from the tremie exit increases. In this case, mattressing is observed to form throughout the surface of the pile, leading to exposed reinforcements.

As the concrete level in the pile rises, the angle of the velocity vectors at the reinforcement increases, transitioning from horizontal, shown in Figure 4 (a), to an approximate angle of 50°, shown in Figure 4 (d). This variation in vector angle correlates to the variation in the mattressing angle observed. Mattressing will form in the direction of concrete flow, and concrete flow entering the cover zone transitions from horizontal to angled as the distance between the concrete flow front and tremie exit increases.

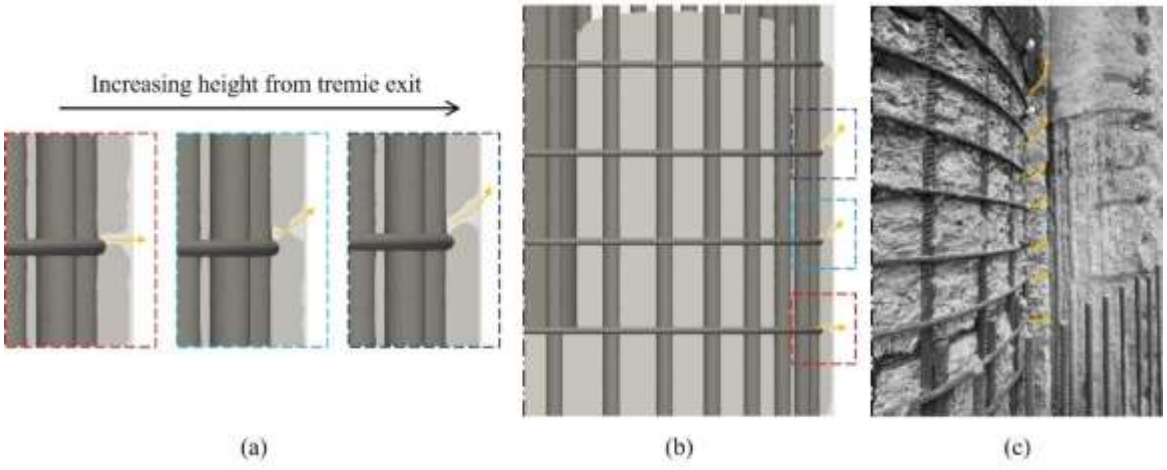


Figure 5. (a) Highlighted mattressing angle variation throughout pile depth. Comparison of (b) simulation results (slump-flow 350 mm and 25 mm cover zone) and (c) defects observed in an excavated bored pile.

Parametric Study

The flow quality within the cover zone is determined by three key parameters: concrete differential, cover zone gradient and mattressing. The concrete differential refers to the difference in the concrete level inside the reinforcement and the cover zone. The cover zone gradient specifies the angle of the concrete surface within the cover zone. Mattressing refers to the cross-hatched surface pattern formed on the pile surface. These quantifications are visualised in Figure 6. An increased concrete differential and cover zone gradient can trap unwanted material such as support fluid, debris or interface layer within the cover zone, increasing the likelihood of inclusions and voids. An undesirable flow feature describes observations of concrete flow directly from simulation results that could increase the possibility of defect generation (e.g. severe mattressing or a sizeable concrete differential). Desirable flow features reflect a low likelihood of defect generation.

Defect severity grids (DSGs) are produced to visualise and qualitatively compare all parametric study simulation results - inspired by the risk maps presented by Wilkes et al. (2024). These grids focus on comparing a specific defect or region of the results across all datasets, displaying qualitative data with

 © DFI International Bruges 2025

a traffic-light system related to the severity of the observed flow feature. Field evidence or testing has not fully validated these results, as equivalent physical parametric studies have not been conducted. However, the observed trends agree with the existing understanding of concrete flow, mechanisms observed in exposed piles have been replicated, and the concrete properties used within this model have been validated by laboratory experiments.

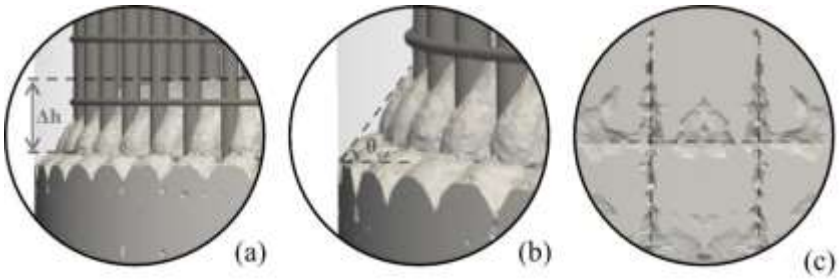


Figure 6. Visualisation of flow features: (a) concrete differential, (b) cover zone gradient, (c) mattressing.

Figures 7 and 8 show the DSGs for mattressing and flow within the cover zone, respectively. The severity of mattressing is determined qualitatively by the depth and thickness of the shadows formed on the surface of the pile. Severe mattressing causes a reduction in the effective cover, producing water paths that can lead to reinforcement degradation and a decrease in the structure's durability.

The results in Figure 7 show that mattressing depends on both concrete workability and cover zone size, but cover zone size has a more significant influence. When the cover zone is sufficiently large (150 mm or 250 mm) mattressing does not form even with very low consistence concrete. However, in the case with the smallest cover zone (25 mm), mattressing is observed to form even with high-consistence concrete. Due to the reduced distance between the reinforcement and pile wall, the relative friction observed by the concrete is more significant, reducing the form-filling ability of the concrete within the cover zone. As such, the pile becomes more sensitive to the creation of defects. The most severe mattressing occurs when low-consistence concrete is used in conjunction with a small cover zone, as both features act as mechanisms to restrict flow. The severity of the observed mattressing is also found to decrease over the elevation of the pile. The purely horizontal flow which occurs during flow initiation at the base of the bile correlates to more severe mattressing. As the pile fills with concrete, the vertical component of flow increases and the severity of mattressing decreases.

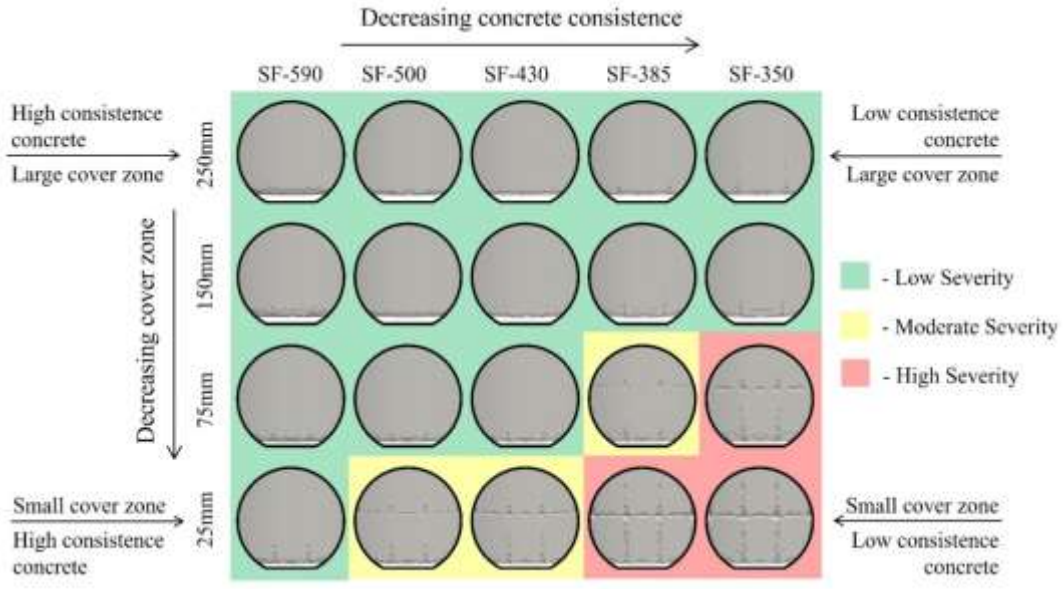


Figure 7. Mattressing Defect Severity Grid.

 © DFI International Bruges 2025

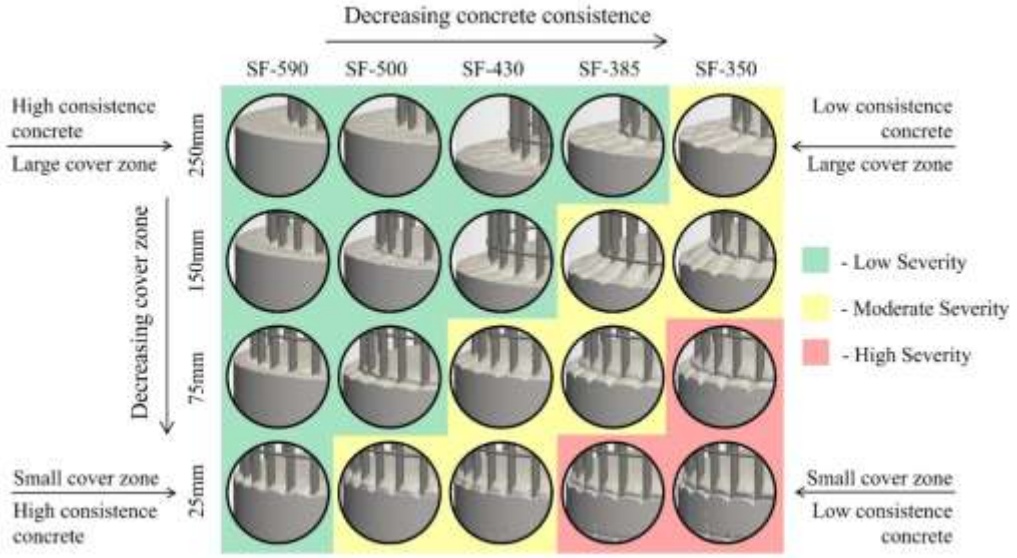


Figure 8. Cover zone Defect Severity Grid.

Figure 8 visualises the quality of concrete flow within the cover zone, which is assessed based on the concrete differential and cover zone gradient. Qualitative data for which is shown in Tables 2 and 3, which is colour-coded to visualise their relative value. The concrete differential decreases with both increased cover zone size and concrete consistence, but concrete consistence has a more significant influence on this value. The cover zone gradient is influenced evenly by both concrete consistency and cover zone size, with a decreasing cover zone size and concrete consistency leading to a more significant cover zone gradient. A large concrete differential, in combination with a significant cover zone gradient, increases the likelihood of inclusions within the cover zone. This occurs when low-consistence concrete is used with a small cover zone.

Based on these results, small cover zones should be avoided wherever possible to prevent undesirable flow features and the increased likelihood of defect generation. If a small cover zone is required in specific regions of the pile design, high-consistence concrete is essential to counteract this restriction to flow.

Table 2. Colour-graded concrete differential values for all cover zone and concrete slump-flow combinations.

Concrete differential (mm)					
CZ \ SF	SF-350	SF-385	SF-430	SF-500	SF-590
25 mm	114.8	93.3	73.6	66.6	51.8
75 mm	106.6	96.2	84.3	52.3	48.8
150 mm	117.9	103.1	66.8	53.2	37.4
250 mm	107.1	91.0	60.8	42.0	33.2

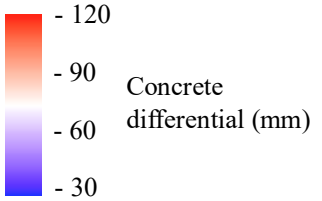
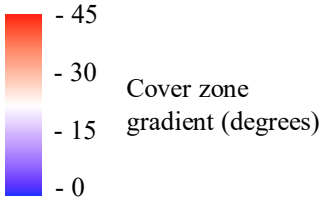


Table 3. Colour-graded cover zone gradient values for all cover zone and concrete slump-flow combinations.

Cover zone gradient (degrees)					
CZ \ SF	SF-350	SF-385	SF-430	SF-500	SF-590
25 mm	41.1	35.8	30.0	28.0	22.7
75 mm	40.6	34.4	25.2	20.6	12.5
150 mm	33.0	26.8	16.1	13.0	6.5
250 mm	22.1	16.1	10.8	6.9	4.1



 © DFI International Bruges 2025

CONCLUSIONS

Numerical modelling is a powerful tool for simulating the flow behaviour of fresh concrete. It offers the ability to conduct a wide range of tests that would not be feasible with physical experimentation and easy access to valuable data, such as velocity vectors, across the whole domain. The parametric study assessed the impact of concrete consistence and cover zone size on fresh concrete flow within bored piles, using industry guidelines and specifications as the baseline for the values investigated. The observed simulation flow features were then linked to the likelihood of defect generation, and Defect Severity Grids were produced to display the qualitative results intuitively.

Decreasing cover zone size and the use of low-consistence concrete both contribute to an increased rate of mattressing, cover zone gradient and concrete differential. These flow features increase the likelihood of debris entrapment, voids and ineffective filling of the cover zone. Small cover zones should be avoided where possible, but if the design requires it, then high-consistence concrete should be used to minimise the chance of defects within such regions.

The variation of mattressing angle observed in exposed piles is found to be caused due to the change in the dominant velocity profile within the concrete as the distance from the tremie exit increases. The severity of mattressing is also observed to correlate to the dominant velocity profile. During concrete flow initiation, purely horizontal flow occurs, leading to more severe mattressing at the base of the pile. As the pile fills with concrete, the vertical component of flow increases, decreasing the severity of mattressing throughout the depth of the pile.

The concrete in this study is modelled as a homogeneous, single-phase, Bingham fluid and thus does not capture aggregate particles. In cases with a very small cover zone, aggregate will contribute to a greater flow reduction due to physical blockage. Therefore, this research should be used to interpret general trends rather than absolute limits on acceptable concrete workability or cover zone size.

FUTURE WORK

Further development of models capable of capturing aggregate particles, such as CFD-DEM, would improve the understanding of aggregates' role in concrete flow. Currently, such models are comparatively inefficient, and thus, simulations are limited to small-scale.

The methodology shown in this paper has been applied to various other pile design features and construction techniques to better understand their direct impact on concrete flow during construction. Mitchell (2024) investigated factors such as reinforcement clear spacing, pile diameter, lap arrangements, tremie embedment, and pile base debris, which will be included in future papers.

ACKNOWLEDGMENTS

The authors gratefully acknowledge support from the Engineering and Physical Science Research Council’s (EPSRC) ICASE grant 2456652 and the financial and technical support from industry partner Arup.

REFERENCES

ACI Committee 301, 2016. ACI SPEC-301-16: Specifications for structural concrete.

Beckhaus, K., Larisch, M., and Alehossein, H., 2011. New performance criteria for fresh tremie concrete. Proceedings of Workshop Performance-based Specifications for Concrete, Leipzig, Germany.

British Standards Institution, 2010a. BS EN 1536:2010+A1:2015: Execution of special geotechnical work. Bored piles.

 © DFI International Bruges 2025

British Standards Institution, 2010b. BS EN 1538:2010+A1:2015: Execution of special geotechnical works. Diaphragm walls.

British Standards Institution, 2019. BS EN 12350-8:2019: Testing fresh concrete – self-compacting concrete, slump-flow test.

British Standards Institution, 2023. BS 8500-1: Concrete. Complementary British Standard to BS EN 206 – Method of specifying and guidance for the specifier.

Brown, D.A., Turner, J. P., Castelli, R. J., and Loehr, E. J., 2018. Drilled shafts: construction procedures and design methods. Technical report, U.S. Department of Transportation.

Fierenkothen, C., 2019a. Numerische simulationen und laborversuche zur ausbreitung von frischbeton in bohrpfählen. PhD thesis, University of Wuppertal.

Fierenkothen, C., and Pulsfort M., 2019b. Investigations on fresh concrete flow mechanisms in bored piles based on CFD simulations. Proceedings from ECSMGE on Soil Mechanics and Geotechnical Engineering, Reykjavik.

Fierenkothen, C., and Pulsfort M., 2016. The spreading of fresh concrete in bored piles – results of large and small scale model tests and numerical simulations. Proceedings of the 19th International Conference on Soil Mechanics and Geotechnical Engineering, Seoul, South Korea.

Flemming, K., Weltman, A., Randolph, M., and Elson, K., 2009. Piling Engineering, Second Edition. CRC Press.

EFFC/DFI, 2024. Guide to Tremie Concrete for Deep Foundations, Third Edition. Joint EFFC/DFI Concrete Task Group.

Institution of Civil Engineers, 2016. ICE specification for piling and embedded retaining walls.

Jeyaraj, J. A., Perez, A., Zayed, A., Mullins, A.G., Tejada-Martinez, A.E., 2023. Computational fluid dynamics modelling of concrete flows in drilled shafts. Fluids. Vol. 9.

Kränkel, T. and Gehlen, C., 2018. Rheology and workability testing of deep foundation concrete in Europe and the US. Research Report No. 20-F-0107, Technical University of Munich.

Larish, M.D., 2019. Concrete defects in bored piles result from insufficient applications of chemical admixtures. Proceedings from The New Zealand Concrete Institute Conference.

Mitchell, T., 2024. Numerical modelling of tremie concrete in deep foundation construction. PhD thesis, Swansea University.

Tettersal, G.H., 1991. Workability and quality control of concrete. CRC Press.

Wilkes, C., Kumar, K., and Biscontin, G., 2023. Investigating the thixotropic behaviour of tremie concrete using the slump-flow test and the material point method. Cement and Concrete Composites. Vol. 143.

Wilkes, C., 2021. Modelling tremie concrete placement in deep foundations. PhD thesis, University of Cambridge.

Wilkes, C., Kanavaris, F., Barker, C., and Nicholson, C., 2024. Practical recommendations for defect avoidance in deep foundations. ACI Materials Journal. Vol. 121.

Yao, H., Ma, L., Duan, Z., and Guo, W., 2024. Reliability analysis of the cast-in-place bored pile with different defects. Frontiers in Built Environment. Vol. 10.

 © DFI International Bruges 2025

QUALIFIED PILE LOAD TESTING CAMPAIGNS AS A KEY ASPECT FOR THE SUSTAINABLE DESIGN OF PILED FOUNDATIONS FOR INFRASTRUCTURE PROJECTS

Christian Moormann, University of Stuttgart, Institute for Geotechnical Engineering, Germany,
+49 (0) 711 685-62437, christian.moormann@igs.uni-stuttgart.de

Axel Ruiken, DEGES Deutsche Einheit Fernstraßenplanungs- und -bau GmbH, Berlin, Germany,
+49 (0) 211 913 491-70, ruiken@deges.de

Olaf Stahlhut, BBI Geo- und Umwelttechnik Ingenieur-Gesellschaft mbH, Hamburg, Germany,
+49 (0) 40 229 468-44, O.Stahlhut@b-b-i.de

ABSTRACT

Qualified pile load testing concepts are an important tool for the technically and economically optimized design of piled foundations and in consequence for a sustainable design of deep foundations with reduced consumption of resources and a reduced carbon footprint. In this context, new and improved measuring devices like fiber optics and ultrasonic instruments can provide a significantly improved knowledge about the bearing behaviour of test piles even for difficult geotechnical conditions. In this paper an exceptional pile load testing campaign for an infrastructure project, a major bridge project in Hamburg, is presented.

Keywords: static pile load tests, bored piles, base expansion, optimization, fibre-optic measurement

INTRODUCTION

For the construction of the 9.7 km long harbour passage in the course of the new A 26 motorway south of Hamburg, Germany, the route crosses the river ´Elbe´ with a major cable-stayed bridge. In conjunction with the adjoining elevated road and the foreland bridges, this approximately 5 km long section will in future form Germany's longest motorway bridge. Due to the challenging subsoil conditions, including thick organic material the foundation of this section is planned with more than 2,000 large bored piles, most of which are planned to be constructed with base expansions. As a basis for a technically and economically optimised design of the pile foundations, a total of 28 large bored piles were constructed as test piles in advance at four locations and static and dynamic axial as well as static horizontal pile loads tests were carried out on these test piles. The targeted variation of only one manufacturing parameter at a time, i.e. per test pile, makes it possible to determine its respective influence on the axial and lateral resistance-displacement pile behaviour. At the same time, intensive instrumentation of the piles, including the use of fibre-optic measurement methods, allows a detailed analysis of the pile load-bearing behaviour. As part of the parameter variation, the influence of different pile diameters and pile lengths, the influence of a cased and suspension-supported execution, as well as the effect of a base widening of different geometries is analysed.

PROJECT

The ´Deutsche Einheit Fernstraßenplanungs- und -bau GmbH´ (DEGES) (German Unity motorway planning and construction company) is planning the construction of the new A26 motorway in Hamburg, Germany, on behalf of the Federal Republic of Germany. Part of the 9.7 km long harbour passage between the existing highways A 7 and A 1 motorways is an approximately 5 km long section designed as a bridge and elevated road, for which deep foundations with more than 1,500 large bored piles, mainly with base expansion, are planned due to the prevailing subsoil conditions. The planning of

 © DFI International Bruges 2025

the deep foundations was initially based on the empirical values of the German ´Recommendation on Piling´ (´EA Pfähle´) (2013) on the basis of the ground investigations carried out.

As a basis for technically and economically optimised planning of the piled foundations, a total of 28 large bored piles were executed in advance at four locations in the area of the ´Süderelbe´ crossing and the elevated highway (Fig. 1) and static and dynamic axial pile test loads were carried out on these test piles. The targeted variation of only one geometric parameter or manufacturing aspect at a time makes it possible to determine its respective influence on the axial resistance-settlement behaviour. At the same time, intensive instrumentation of the piles, including the use of fibre-optic measurement methods, allows a detailed analysis of the pile load-bearing behaviour.

As part of the parameter variation, the influence of different pile diameters and lengths as well as the load-bearing capacity-increasing effect of a base widening of different diameters was systematically investigated. Furthermore, the influence of cased and suspension-supported production on the pile shaft friction was also analysed. In the course of further investigations, the manufacturability and execution quality of a footing expansion to ∅ 2.7 m under suspension support was investigated on inclined piles with an inclination of 1:10 and a length of up to 35 m with a drilling diameter of 1.5 m. In addition, two pile group tests, each on a group of five bored piles was executed aiming to investigate pile group effects; the results will be presented in a further paper. The article presents the results of the extensive field study carried out on a real scale.

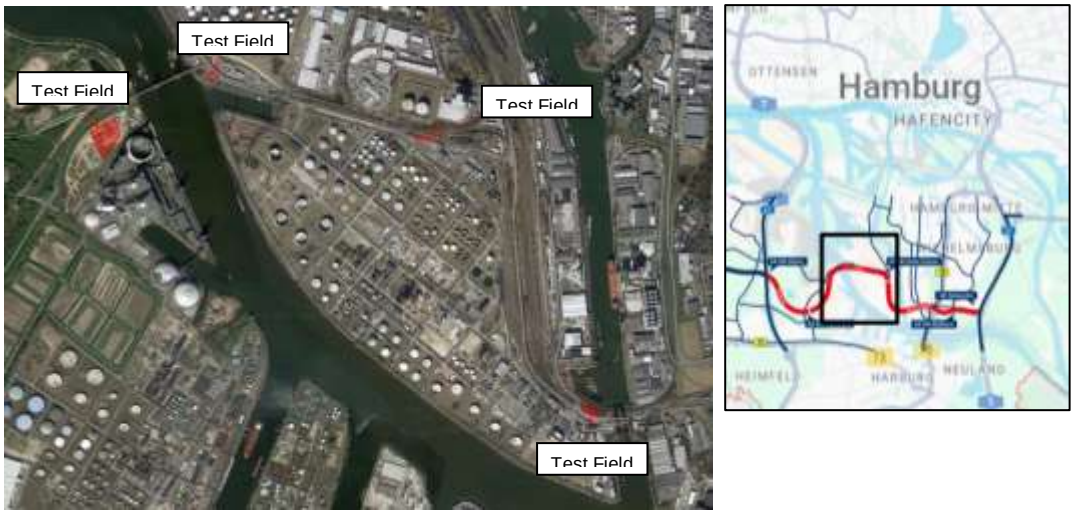


Figure 1. Location of the test fields (© Google Maps, modified)

The locations of the test piles represent the typical subsoil conditions in the area of the future A 26 elevated road. These are characterised by the fact that under a mostly sandy, partly cohesive backfill, usually several meters thick, there are mostly organic soils, which are underlain by at least medium-dense Holocene and Pleistocene sands as well as basin silt and, in deeper areas, basin sands.

Boulder clay and locally occurring basin clay were explored in some areas. The load-bearing subsoil is generally formed by Holocene sands.

EXECUTION OF BORED PILS

A total of 28 test piles with shaft diameters between D_s = 0.88 m and 1.50 m with and without base expansion D_b were executed to carry out static and dynamic test loads. The pile lengths were between 18.5 m and 42.0 m. For the piles with base expansion, the ratio of pile shaft diameter D_s to the diameter of the base expansion D_b was as shown in Table 1.

 © DFI International Bruges 2025

Table 1. Pile load testing campaign: Investigated pile diameters

Large diameter bored piles with base widening		
pile shaft diameter D_s [m]	diameter D_b of the base expansion [m]	ratio D_s / D_b
0.88	1.65	0.55
1.18	2.20	0.55
1.50	2.70	0.56

In addition to the test piles, 50 large bored piles and 80 micropiles were executed as reaction piles.

When producing very long piles with large diameters, the drilling rigs and, in some cases, the additional casing systems used sometimes reach their performance limits due to the high torque required. In these cases, borehole support using bentonite suspension is an alternative to continuous cased production. In the context of suspension support, however, a reduced approach for skin friction is often discussed. Therefore, in the course of the test measure, in addition to fully cased piles, some test piles were only cased in the upper meters and executed with suspension support below the soft layers in order to investigate a possible influence of the execution process on the mobilisable skin friction.

In the case of the piles with base expansion, the borehole was first fully cased and drilled to the final depth under water load, then the water in the borehole was replaced with bentonite suspension, the casing was pulled back over the expansion area and the pile base was successively cut open to the target dimension (Fig. 2). The bottom of the borehole was then cleaned using a drilling bucket with a clearing bar.



Figure 2. Pile base cutter tools used for the test pile campaign.

QUALITY ASSURANCE DURING PILE EXECUTION

Taking the not very common execution of pile base expansions into account, various methods were used to determine the produced borehole geometry and pile integrity as part of quality assurance.

Borehole geometry

Three different methods were used to check the produced borehole geometry and evaluated with regard to their suitability for verifying proper pile and pile base production. These were the following methods:

 © DFI International Bruges 2025

- Koden measurement (ultrasound),
- SHAPE (ultrasound),
- ´pile inspector´ (mechanical scanning).

With Koden and SHAPE measuring devices, the measurement is carried out using ultrasound logging through the bentonite suspension. With the ´pile inspector´ developed specifically for this application, the profile of the borehole wall is scanned mechanically. In principle, the profile of bored piles with base expansion could be recorded using all methods. A detailed explanation and comparative comparison of the methods is given in Lenz et al. (2024), among others.

Pile integrity

To assess the pile integrity and as a basis for converting axial pile strains into pile forces, knowledge of the pile cross-section over the depth is required. For this purpose, all test piles were checked using a low-strain integrity test (PIT). With the aim of being able to make statements about the pile base expansion, all test piles were also checked using thermal integrity testing (TIP) in accordance with Moormann (2020). This method determines the distribution of heat development in the bored pile concrete as a result of hydration. Cross-section reductions or expansions can be inferred from temperature differences. Both point temperature sensors and fibre optic sensors were used to measure the temperature. The main advantage over cross-hole measurements using ultrasound is that information about the pile concrete outside the sensors, i.e. also about pile base expansions, is obtained. Examples of the results obtained using this method are shown in Figure 3.

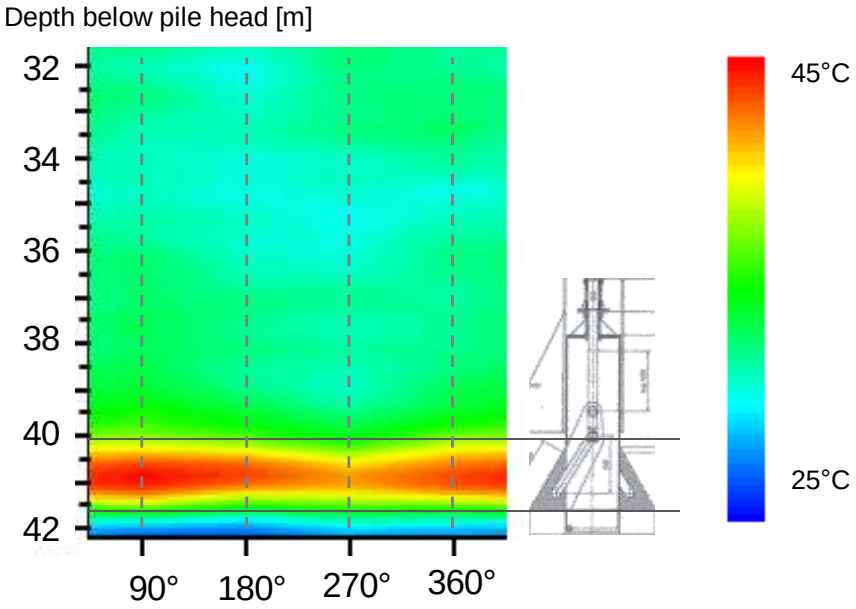


Figure 3. Results of a thermal integrity test in the section of a pile base expansion.

The temperature distribution shown in Figure 3 over the circumference and depth in the area of a pile toe shows, on the one hand, the typically lower temperatures in the pile footing plane. In addition, the increased temperature of around +8 to +10 K as a result of the base expansion and the greater concrete cover is clearly recognisable.

INSTRUMENTATION OF THE PILES

The main aim of the investigations carried out was to determine the pile base and shaft resistances in the in-situ subsoil. For this purpose, all test piles were instrumented with ´sister bars´ (vibrating wire gauges). Depending on the pile length and the respective subsoil stratification, these were installed in up to 14 measuring levels of three (D_s = 0.9 m and 1.2 m) or four (D_s = 1.5 m) gauges per measuring level. In order to position the measuring levels precisely at the level of the transitions between the soil

 © DFI International Bruges 2025

layers along the pile shaft, a CPT-sounding was carried out in advance at each pile location in addition to the drillings in the investigation area.

Furthermore, four high-resolution fibre-optic sensors were installed to selected piles for redundant and continuous determination of axial strains along the piles, distributed around the circumference. The measurements were carried out on the basis of Rayleigh refraction with a spatial resolution of 10 mm. Figure 4 shows an example of an instrumented reinforcement cage instrumented in this way.



Figure 4. Example of an instrumented reinforcement cage

VARIATION OF THE INSTLLATION PARAMETERS

As explained, the installation parameters of the test piles were systematically varied in order to investigate the influence of just one parameter on the axial load-bearing behaviour of the piles at a time. Figure 5 shows an example of the arrangement of test and reaction piles and the parameters analysed in in one of the four realized test fields.

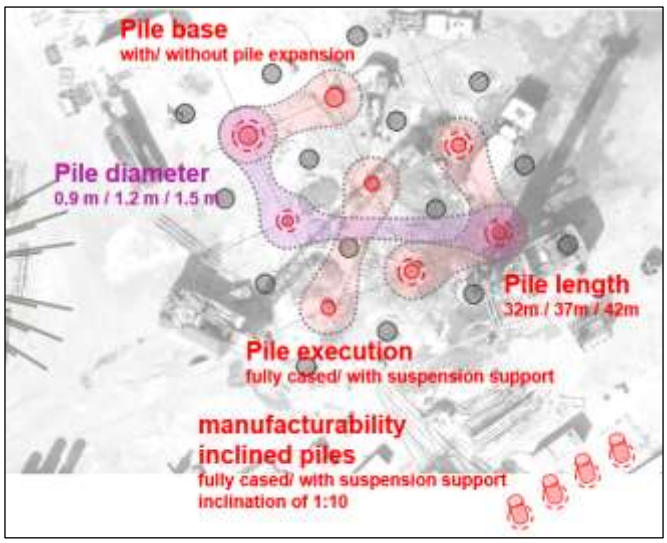


Figure 5. Overview of investigated geometrical and execution parameters in one of the test fields

 © DFI International Bruges 2025

The current foundation concept for the A26 elevated motorway includes a significant number of inclined piles with base expansion. In addition to the test piles, 4 large bored piles were constructed as fully and partially cased inclined piles in order to investigate the feasibility under these special boundary conditions.

EXECUTION OF STATIC PILE LOAD TESTS

The static test loads on the individual piles (Fig. 6) were carried out based on the ´EA-Pfähle´ (2013). The load regime was defined in advance and adapted depending on the resistance-deformation behaviour of the piles on the construction site, for example by extending observation times or reducing load steps.



Figure 6. Example of setup for a static axial pile load test on site

The reaction piles were sufficiently dimensioned so that all the intended test loads could be applied with sufficient safety. However, the loading of the pile with a base expansion to D_b = 2.7 m (D_s = 1.5 m) could not be carried out at loads of up to 35 MN despite press strokes of up to 300 mm due to the deformations in the abutment system (deflection of the crossbeam; stretching of the reaction piles/tension members) without additional relining.

The measurement data were recorded electronically in the performer's system with visualisation of the load-settlement curves. Measured values of the sister bars were only available after completion of the tests. When testing the additionally fibre-optically instrumented piles, the distribution of the distortions could already be viewed during the tests so that the respective status of activation of the pile shaft and pile base resistances could be assessed directly if necessary.

EVALUATION OF STATIC PILE LOAD TEST RESULTS

General

The base resistance and the layer-related skin friction resistances were determined using the measured axial distortions of the test piles. The results of the ground investigations, borehole measurements and integrity tests were also used to evaluate the measured values. With regard to the axial expansion stiffness of the piles, the arrangement of overlap joints and stiffening rings of the pile reinforcement were also taken into account. Due to the large number of test piles, the respective measurement results of one pile could be checked for plausibility on the basis of those of the other piles.

 © DFI International Bruges 2025

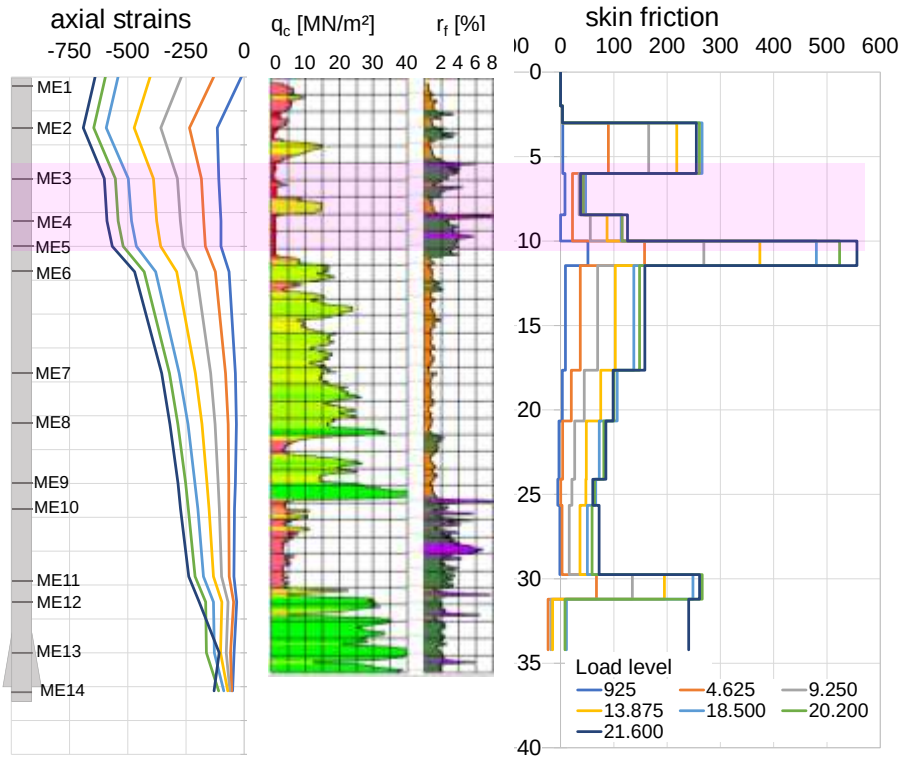


Figure 7. Measured axial strains and corresponding skin friction of a test pile presented related to results of CPT-sounding executed at pile location (example).

Figure 7 shows an example of the measured axial strainqqs for a pile with D_s = 1.18 m and a base expansion of D_b = 2.20 m as well as the derived skin friction at different load levels (925 kN to 21,600 kN) over the pile length. The successive activation of the pile skin friction and of the pile base resistance is clearly recognisable.

Figure 8 shows the results of the measurement of the axial strains in the pile shaft using sister bars and high-resolution fibre-optic sensors as an example for the state of maximum pile head displacement. The results generally show very good agreement. However, the continuous determination of the distortions over the pile length offers an additional possibility of checking the plausibility of measured values, which can contribute significantly to the quality of the test evaluation, especially in the case of conspicuous measurement results.
In addition to greater reliability in test evaluation, which can be particularly decisive with a small number of test piles, fibre optic instrumentation is now often the more economical method even with a single-digit number of measuring levels.

 © DFI International Bruges 2025

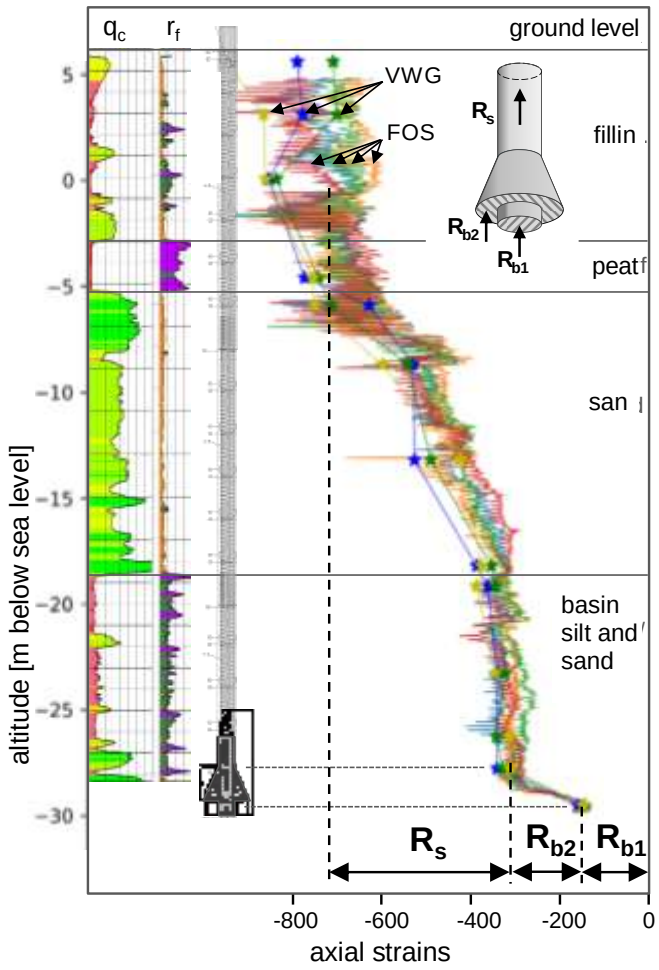


Figure 8. Measurements of axial strains with Sisterbars (VWG) and fibre optic sensors (FOS) at a pile head settlement of s/D_b = 10%.

The results of the high-resolution measurements using fibre optic sensors (FOS) showed that the increased reinforcement content in the area of overlap joints led to a measurably higher axial stiffness of the test piles and correspondingly lower compression. Furthermore, during the successive load increases, the compression of shrinkage cracks could be determined, which occurred in particular at the level of the helical reinforcement and the stiffening rings. If the discrete determination of axial pile strains using sister bars is intended, care should therefore be taken during reinforcement planning to ensure that stiffening rings and overlap joints are not arranged at the level of the measuring planes if possible.

When determining the resistance on the pile base, the instrumentation used made it possible to distinguish between the central base area (R_{b1}) corresponding to the shaft section and the resistance on the lower edge of the ring-shaped base expansion (R_{b2}), which is 0.5 m to 0.9 m higher, depending on the used pile toe cutter.

Pile shaft resistance

The mobilisation of skin friction in the Holocene and Pleistocene sands below the soft layer shall be discussed in more detail. The sands present here are medium-dense to dense, and to a lesser extent very dense (see Figures 7 and 8).

In Figure 9, the empirical values of the ´EA-Pfähle´ (2013) for sands of different densities are shown as vertical lines for orientation. For the present conditions, the skin friction values determined on the basis of the static axial test loads are shown in yellow for the case that the creep criterion $k_s \leq 2$ mm is

 © DFI International Bruges 2025

considered (SLS). In addition, the achieved skin friction when applying the maximum load is shown in red, whereby not all test loads were applied up to a related pile head settlement of s/D = 10%.

Following the static pile load tests, the test piles were tested in addition using dynamic pile load tests. The skin friction determined here was added in blue in Figure 9 for comparison (without reference to s/D_s).

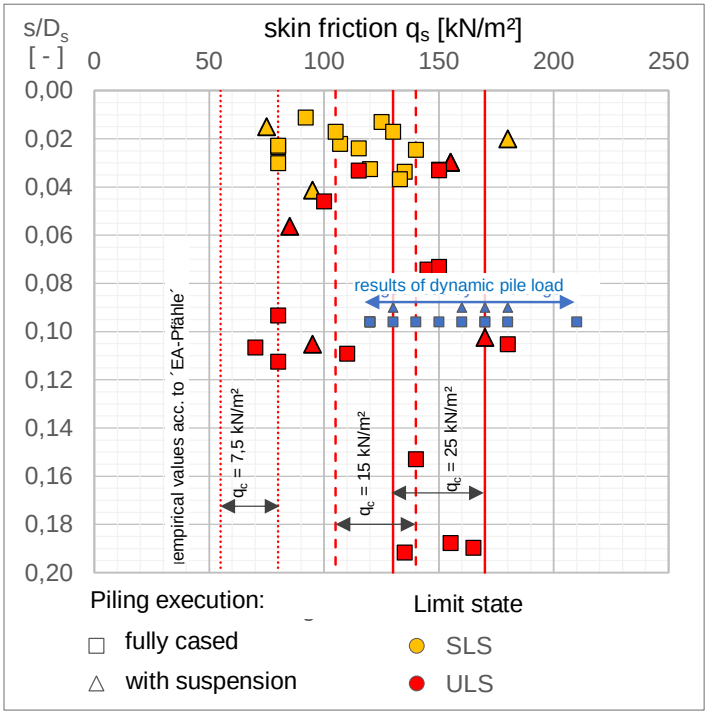


Figure 9. Skin friction mobilised in the sands.

The results show that, in accordance with ´EA-Pfähle´ (2013), the skin friction was generally already fully mobilised at related pile head settlements of s/D_s = 2% to 4%. Furthermore, the determined limit skin frictions show a significant range between $q_{s1,k}$ = 75 kN/m² and 180 kN/m². On the four piles that were produced using the suspension-supported drilling method limit skin friction values could be evaluated being comparable to the values proven using fully cased execution. Therefore, no systematic influence from the pile production (borehole support) could therefore be recognised on the mobilisation of skin friction in sands.

For the predominantly medium-dense conditions of the sands present here, it can be expected on the basis of the empirical values of ´EA-Pfähle´ (2013) and local experience that skin friction values in the order of approx. $q_{s1,k}$ = 120 kN/m² will be achieved. This corresponds to the mean value of the skin friction values determined in the tests.

The skin friction values determined using the dynamic test loads are in the order of $q_{s1,k}$ = 120 kN/m² to 180 kN/m² and therefore in the upper range of the values determined using the static test loads. The individual value of $q_{s1,k}$ = 210 kN/m² does not appear plausible and is therefore not considered further.

In addition to the effects described, a significant load transfer was very frequently observed in the transition from the soft organic layers to the underlying sands. This effect occurred independently of the partially loose density in this upper area of the sands (see Figure 7) and has already been observed in this form elsewhere in the past. Based on the integrity tests carried out, no indications of irregularities in the pile cross-section are recognisable, so that these effects cannot yet be fully explained.

 © DFI International Bruges 2025

Furthermore, a time-variant redistribution of the load transfer from the soft organic layers to the underlying layers was measured during the holding times of individual load stages. This load redistribution requires additional activation settlements and thus leads to increased creep. This results mainly from the layers that are not suitable for permanent load transfer anyway. In order to avoid such negative effects in the future, a constructive decoupling of the skin friction in these layers might be reasonable.

Pile base resistance

The pile tip pressures were determined using the measurements of the axial strains in the pile shaft at the base level. As already described previously, a distinction is made here between the shaft cross-section A_1 and the annular area of the base expansion A_2 arranged above it (Figs. 8 and 10). The area A_1 corresponds to the cross-sectional area of the shaft diameter D_s and is comparable to a pile without base expansion. The corresponding base resistance is labelled R_{b1} and the corresponding tip pressure is labelled q_{b1}. The force and pressure on the annular surface of the base expansion A_2 are labelled R_{b2} and q_{b2} respectively.

Figure 10 shows the tip pressure q_b determined from the static individual pile load tests. To evaluate the results, it is indicated above the diagram whether the pile was constructed with base expansion and whether the borehole was fully cased or partially cased with suspension support. A distinction was made between the shaft area q_{b1} and the base expansion q_{b2} for the specified tip pressures. Experience has shown that the activation of the pile tip resistance is strongly dependent on the pile settlement. To categorise the evaluated tip pressures, the associated maximum pile head settlement in relation to the shaft diameter s/D_s is therefore specified additionally.

The tip pressures q_{b1} determined for the ultimate limit state (s/Ds = 0.1) are in the upper range and in some cases significantly above the empirical values according to ´EA-Pfähle´ (2013). In contrast, the pressures q_{b2} acting on the area of the base expansion A_2 remain significantly lower than the q_{b1}-values. This effect is generally plausible in view of the significantly greater activation settlements required in accordance with $D_b > D_s$. Further effects from the production-related retention of dissolved soil in the expansion area cannot be ruled out. This could also necessitate larger activation settlements.

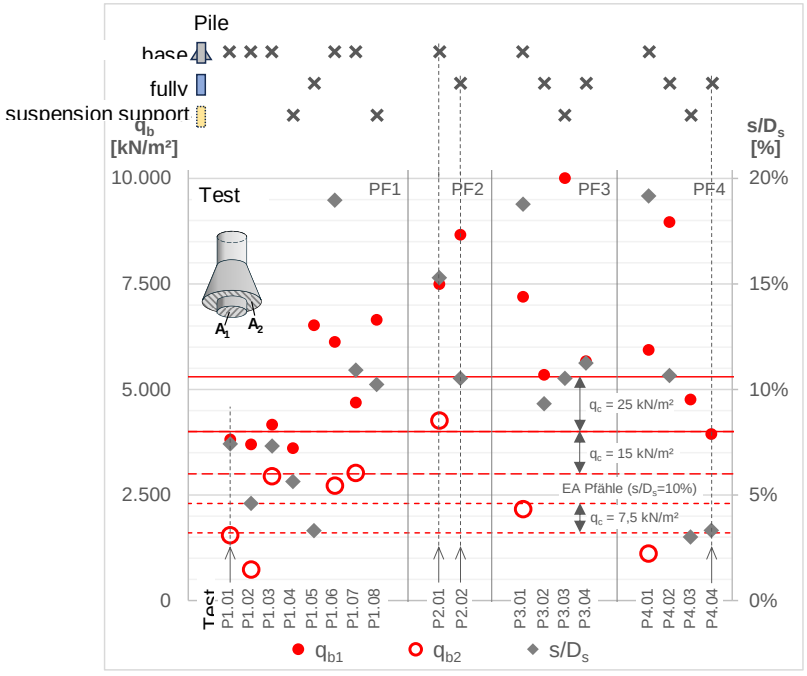


Figure 10. Pile tip pressures q_{b1} and q_{b2} and maximum pile head settlements applied in each case with regard to pile shaft diameter s/D_s.

 © DFI International Bruges 2025

In ´EA-Pfähle´ (2013), this was taken into account by the specification that the empirical values for bored piles with base widening should be reduced to 75%. The specification refers to the entire base contact area A_b. The differentiated consideration of the resistances on surfaces A_1 and A_2 carried out here results in a correspondingly greater reduction for the resistance in the annular area of the widening A_2.

In addition to the previous illustration, Figure 11 shows the determined pile tip pressures q_{b1} of piles with and without base expansion with reference to the respective settlement s/D_s. To categorise the test results determined, the empirical values of the ´EA-Pfähle´ (2013) were again shown.

The tip pressures that were determined taking into account the creep criterion $k_s \leq 2$ mm are shown in yellow. The tip pressures activated up to the application of the maximum load are shown in red. In addition, the results of the dynamic pile load tests are again shown in blue (without reference to s/D_s). It was not possible to differentiate between the proportions q_{b1} and q_{b2} in the dynamic tests, so that only the results of the tests on piles without base expansion are shown here.

With a few exceptions, the test results show that tip pressures corresponding to the empirical values of the ´EA-Pfähle´ (2013) for densely bedded soil are achieved and in many cases exceeded. This is also confirmed by the results of the dynamic load tests.

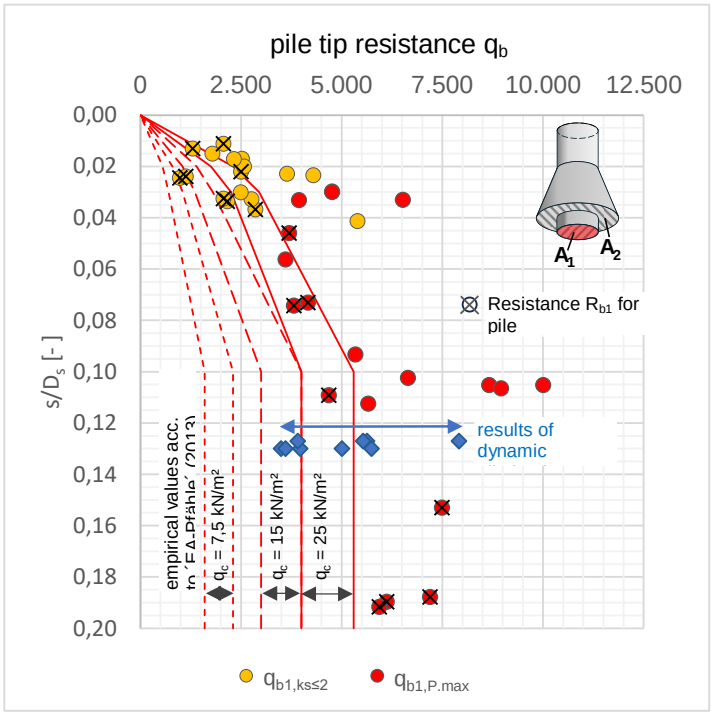


Figure 11. Measured pile tip stresses with consideration of the creep criterion.

For a more detailed examination of the settlement-dependent activation of the pile resistances, these are shown in Figure 12 as an example for a test pile with a pile shaft diameter of 1.18 m and base expansion to 2.2 m. The test results show that the chosen creep criterion $k_s \leq 2$ mm was fulfilled up to a load of 13,125 kN. The further increase in load beyond this up to the maximum load of 20,000 kN was carried out to determine the base resistance with related pile head settlements of up to $s/D_s = 10\%$.

Up to a pile head settlement of 13 mm, the permissible creep criterion of $k_s \leq 2$ mm was adhered to. In this condition, around 80% of the loads are transferred via the pile shaft and around 20% via the pile base. The proportion of pile base resistance increases to around 40% by the end of the load test at a settlement of 90 mm ($s/D_s = 7.5\%$).

The corresponding tip pressures are shown in Figure 13. The respective areas $A_1 = 1.09$ m² and $A_2 = 2.71$ m² were taken into account here. The diagram illustrates the significantly lower activation of the

 © DFI International Bruges 2025

resistances q_{b2} below the annular base widening area A_2 in comparison to q_{b2} activated at base shaft area A_1.

SUMMARY AND CONCLUSION

A total of 28 test piles were installed at four locations in the area of the planned construction of the new A26 motorway elevated road. At 18 of these bored piles axial static and dynamic pile load tests were carried out on single piles. The 10 remaining test piles will be tested by two group load tests (2 x 5 piles). The boreholes were either fully cased or partially cased and suspension-supported. Piles were manufactured with and without base expansion/widening. The different production variants were evaluated with regard to the axial load-bearing behaviour of the piles in order to determine differences and similarities in terms of skin friction and tip resistance.

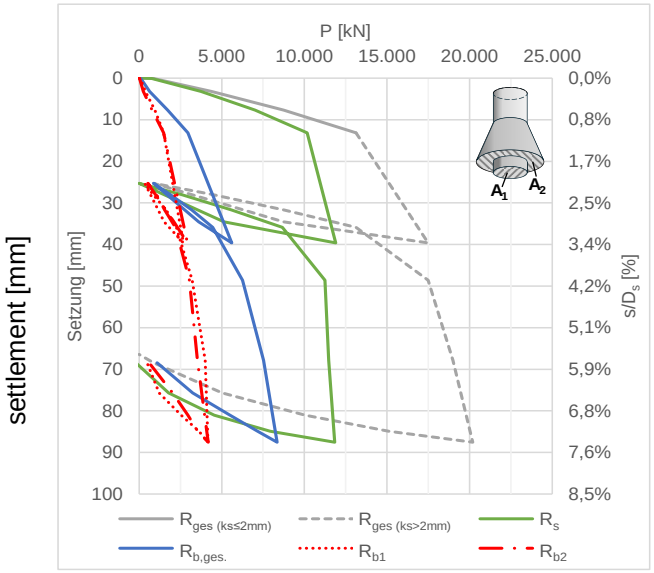


Figure 12. Measured resistance-settlement curve.

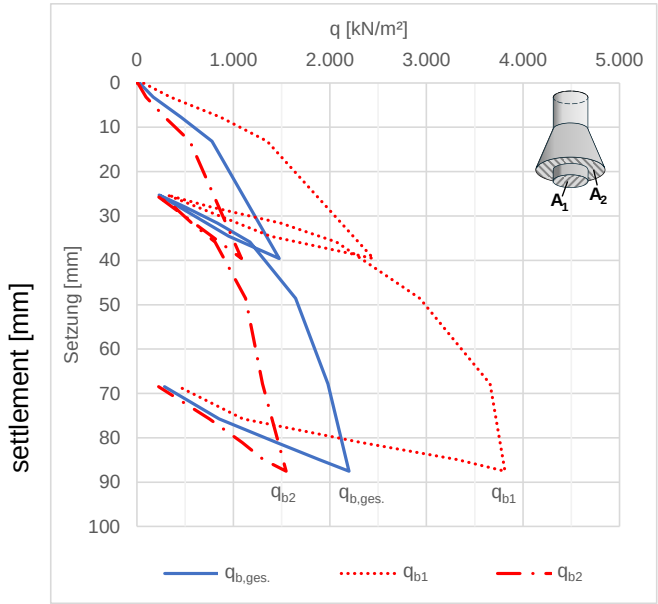


Figure 13. Typical ratio of the pile tip pressures under the shaft cross-section A_1 and under the area of the base expansion A_{2e}.

 © DFI International Bruges 2025

As a result, skin friction was determined in the in-situ Holocene and Pleistocene sands, the mean value of which corresponds to the order of magnitude of the empirical values of the ´EA-Pfähle´ (2013). The determined skin friction of piles that were constructed with suspension support is in the same order of magnitude as that of the fully cased piles. No reduction in skin friction due to the bentonite suspension used could be determined in the in-situ sands.

The determination of the pile tip resistances was differentiated for the contact area A_{b1} below the pile shaft and for the annular area A_{b2} of the base expansion located 0.5 m to 0.9 m higher. The tip pressures q_{b1} determined below the pile shaft cross-section A_{b1} correspond to the upper empirical values of the ´EA-Pfähle´ (2013) for densely bedded soil or are even higher. In most cases, the peak pressures q_{b2} below the annular base expansion A_{b2} are less than half of the mobilisable stresses q_{b1} below the shaft cross-section. Thus, for the situation analysed, a quadrupling of the pile base area approximately (only) led to a doubling of the pile base resistance.

The results of the dynamic load tests carried out on the piles showed skin friction in the range or higher than the values of the static load tests. The results of the static test loads were confirmed with the tip resistances determined.

Further investigations and analyses are currently being carried out. It is planned to carry out a separate analysis of the creep in the soft layers and the underlying load-bearing soil layers.

Both sister bars and high-resolution fibre-optic sensors were used to determine the load transfer in the different soil layers. Comparable values could be determined with both methods. The results of the fibre-optic measurements were also used to determine the influence of the increased degree of reinforcement in the overlap joints of the longitudinal reinforcement on the pile stiffness. If the discrete determination by means of sister bars is aimed at despite economically equivalent methods, the reinforcement should be planned in such a way that there are no discontinuous points at the level of the measuring planes.

REFERENCES

German Piling Committee (2013). Recommendation on Piling (EA-Pfähle). Wiley, Ernst & Sohn, Berlin, 2013, 496 pp.

Franz, S., Künzel, A, Bruns, B. (2023). Innovative Messtechnik bei der Hangsicherung Heuberg (A44). TU Braunschweig: Pfahlsymposium, Mitteilungen Institut für Geomechanik und Geotechnik, No. 113, pp. 369-402 (in German)

Lenz, P., Stahlhut, O., Ruiken, A., Schallert, M., Schneider, N. (2024). Qualitätssicherung bei der Pfahlher-stellung durch Anwendung unterschiedlicher Messmethoden. TU Braunschweig: Messen in der Geotechnik, Mitteilung des Instituts für Geomechanik und Geotechnik, No. 116, pp. 107-127 (in German)

Moormann, Ch. (2020). Jahresbericht 2019 des Arbeitskreises „Pfähle“ der Deutschen Gesellschaft für Geotechnik (DGGT). Bautechnik 97(2), pp. 133–149 (in German)

Schneider, N., Stahlhut, O., Scheffer, J. (2023). Pfahlinspektor, eine Neuentwicklung zur Prüfung von Pfahlfuß-Aufweitungen. TU Braunschweig: Pfahlsymposium, Mitteilung des Instituts für Geomechanik und Geotechnik, No. 113, pp. 513-528 (in German)

Stahlhut, O., Sander, M., Ruiken, A. (2023). Konzeptionierung von Pfahleinzel- und gruppenprobebe-lastungen unter Berücksichtigung von best-estimate Werten. TU Braunschweig: Mitteilung, Institut für Geomechanik und Geotechnik, No. 113, pp. 705-722 (in German)

Stahlhut, O.; Ruiken, A.; Moormann, Ch.(2024). Zum Einfluss von Herstellungsverfahren, Geometrie und Pfahlfußaufweitungen auf das Widerstandsverformungsverhalten von Großbohrpfählen. Vorträge der 38. Baugrundtagung, 25.-28.09.2024, Bremen, DGGT, pp. 212-219 (in German)

 © DFI International Bruges 2025

THE IMPACT OF LONG OPENING TIMES ON SHAFT FRICTION IN COHESIVE SOIL

Duncan Nicholson, Ove Arup and Partners Limited, London, UK, duncan.nicholson@arup.com
João Ferreira, Typsa Limited, London, UK, jferreira@typsa.es
Anton Pillai, Ove Arup and Partners Limited, London, UK, anton.pillai@arup.com
Xiangbo Qiu Ove Arup and Partners Limited, London, UK, xiangbo.qui@arup.com

ABSTRACT

In recent years deep foundations have become deeper and pile diameters and panel thickness have increased. The pile and panel excavation times have increased from less than a day to more than 5 days when allowance is made for weekend work. In addition, rig break downs and construction problems can extend this opening time.

In cohesive soils the clay next to the pile shaft is known to soften and swell with extended opening times. With bentonite support fluids the water flow rate into the clay is so slow that a thick filter cake does not have time to develop.

The results of pile load tests with extended opening times of up to 3 days are summarised to assess the reduction of shaft adhesion factor (α) with time. The softening effect has been extended to diaphragm walls and longer panel opening times by carrying out penetrometer tests in the soil next to the panel surface and comparing the results with tests remote from the panel, see König et al, (2025).

The focus of the paper is the back analysis of the penetrometer tests using numerical modelling of the panel excavation process incorporating the swelling of the adjacent soil prior to concreting. In addition, the horizontal concrete fluid pressures which develop during tremie concreting are considered. Once the concrete sets it forms a rigid boundary at the soil interface. The adjacent soil experiences dissipation of excess pore water pressures and increases in effectives stresses. The final effective stresses and water contents in the adjacent soil are considered and related to the pile shaft friction.

In addition, the changes to the undrained strength at the soil boundary are assessed by extracting the earth and water pressures on a soil element in the model mesh. This mesh element is then subjected to an undrained triaxial stress path to failure. The drop in the undrained strength next to the panel is noted. The model was also used to carry out a numerical panel load test. The results are compared with the adhesion factors from reported pile load tests. This numerical modelling enables the primary, successive and closure diaphragm wall panels to be modelled. The panel construction time was extended well beyond the 3 days pile testing data using this numerical modelling.

Keywords: cohesive soils, diaphragm walls, long opening times, shaft friction, numerical models.

INTRODUCTION

The HS2 railway link into London includes the Victoria Road Crossover Box (VRCB). The plan of this box is shown in Figure 1. The perimeter diaphragm wall comprises a series of arches with end bubbles to form caterpillar-like structure. The box is about 24m deep and the diaphragm wall panels are about 34m deep and 1.5m wide.

The CIRIA C760, (2017) provides guidance on retaining wall design of shaft for pile and barrettes. The shaft friction $\tau = \alpha\ c_u$ where α is the adhesion factor and c_u is the undrained strength. An adhesion factor of 0.3 is recommended to make some allowance for softening. The diaphragm wall specification

 © DFI International Bruges 2025

called for the panels to be constructed within 5 days to minimised swelling and softening of the London Clay. During the diaphragm wall construction work some panels with extended opening times were identified. This paper summaries the studied undertaken to investigate this effect. These studies included:

- Ground conditions and modelling.
- Literature review of pile tests with extended construction time.
- Site investigations using penetrometers to record softening next to the VRCB panel, see König et al, (2025).
- Numerical modelling of diaphragm wall construction process and back analysis of the penetrator tests.
- Extending the modelling to simulate a load test on a diaphragm wall panel.

GROUND CONDITIONS AND SOIL MODEL

The ground conditions at the VRCB site comprise London Clay to a depth of about 80m. The London Clay Units are shown on Figure 2 and the water table is at ground level of 34mOD. An isotropic permeability (k)=10^{-9} m/sec was used for the box design. A lower permeability of k=10^{-10} and 10^{-11} m/sec has been used to test the back analysis of the open panel soften model. This is discussed in more detail later in the paper.

Figure 2 shows the undrained shear strength (c_u) profile, based on Standard Penetration Tests (N), which has been assessed using the correlation of c_u = 5.7N kPa. This is based on a recent review of field data by White et al, (2019). The data from undrained triaxial tests is also shown together with the undrained shear strength design line of c_u= 50 +6z kPa, where z is the depth below 34mOD.

The hardened concrete has been modelled with a density of 24kN/m^3 and a modulus of 28GPa.

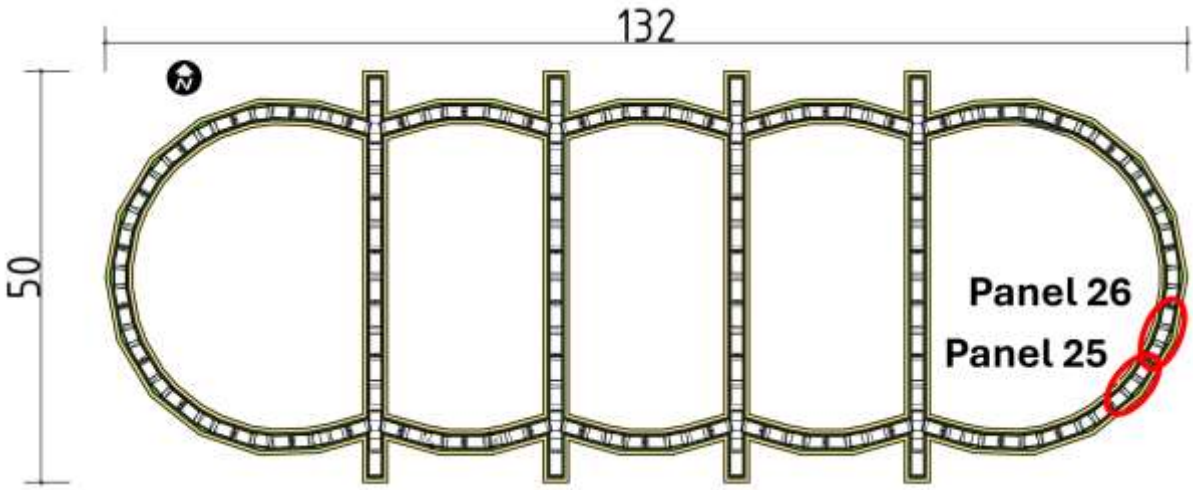


Fig. 1. Site plan

 © DFI International Bruges 2025

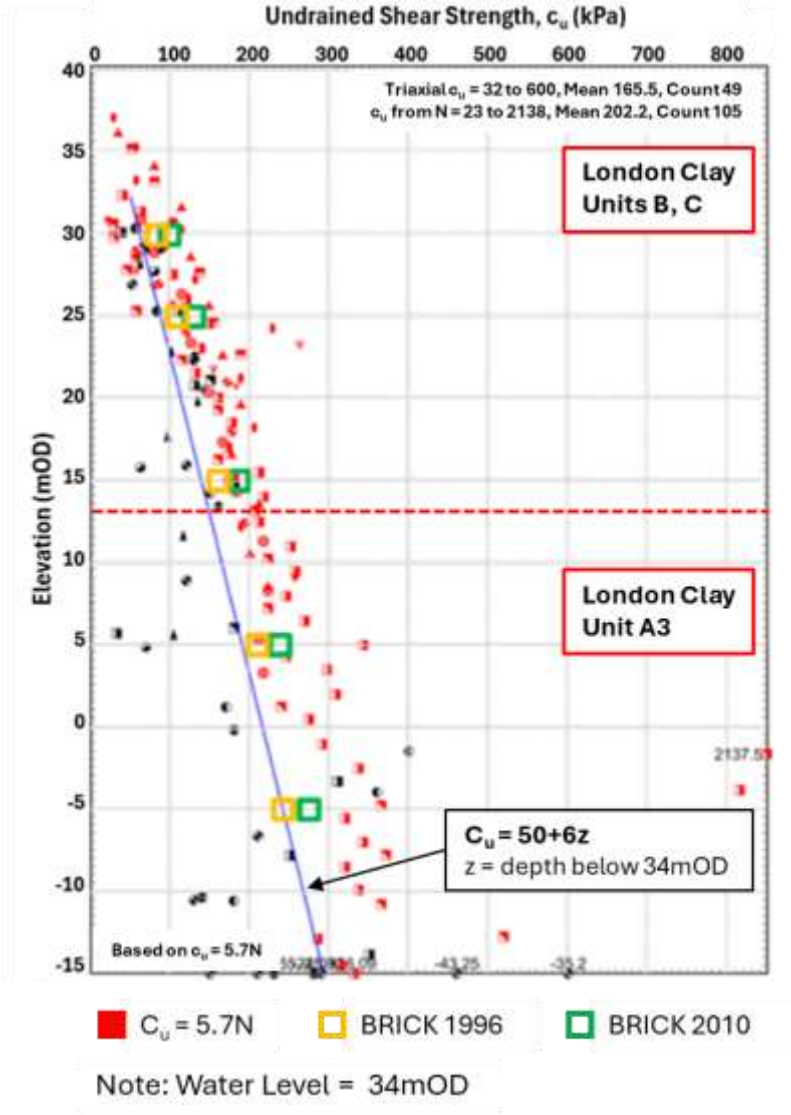


Fig. 2. Undrained shear strength profile – London Clay

Figure 2 also shows the undrained strength profile that has been calculated by the BRICK model 1996 and 2010. The BRICK 1996 has been used to model the diaphragm wall construction process in this paper.

The BRICK model is an advanced non-linear soil model, conceived at Arup by Brian Simpson (Simpson, 1992). It essentially a kinematic yield surfaces model intended to reproduce the full range of soil behaviour from very small strains to failure for normally and over-consolidated (OC) soils. The BRICK model differs from most of the common plasticity models for soils in that the yield surfaces are represented in strain space rather than stress space.

A set of BRICK parameters for London Clay was established by Pillai in 1996 based on laboratory tests conducted from samples on sites across London, together with back analysis of inclinometer wall deflections taken during basement excavation. These parameters were re-visited as part of the SCOUT project (SCOUT, 2007 & 2010). More recent developments of the BRICK model are summarised in Pillai et al. (2023). For design purposes, the 1996 parameters listed in Table 1 are considered to be "characteristic" and the 2010 parameters are "most probable". The 1996 parameters are used in this modelling work.
The 1996 and 2010 BRICK parameters are given in Table 1.

 © DFI International Bruges 2025

Table 1 – 1996 and 2010 BRICK parameters used for simulation of the panel opening study

String length L(b)		Gt /Gmax
1996 parameters	2010 parameters	
0.0000304	0.000030	0.92
0.0000608	0.000075	0.75
0.000101	0.00015	0.53
0.000121	0.00040	0.29
0.00082	0.00075	0.13
0.00171	0.0015	0.075
0.00352	0.0025	0.044
0.00969	0.0075	0.017
0.0222	0.02	0.0035
0.0646	0.06	0

Notes:
1. Pillai (1996), $\lambda^* = 0.1$, $k^* = 0.02$, $\iota = 0.0019$, $\nu = 0.2$, Mu = 1.3, $\beta G = \beta f = 4.0$.
2. SCOUT (2007/10), $\lambda^* = 0.1$, $k^* = 0.01$, $\iota = 0.00175$, $\nu = 0.2$, Mu = 1.3, $\beta G = 4$ $\beta f = 3.0$.

LS-DYNA software was selected for the numerical analysis in this study which is an explicit solver. LS-DYNA is capable of modelling time dependant coupled consolidation with non-linear soil models such as BRICK.

PILE LOAD TESTS ON CLAY SOILS

In over consolidated clay soils the influence of the extended opening times and soften effects for piles is investigated by conducting pile load tests with extended opening times. Data on the reduced adhesion factor for piles with increasing construction time has been reported by Hardy et al, (2019) using a linear time scale. This data has been replotted on a log time scale in Figure 3. In addition, limited barrette load test data has been added. Results from the same site are connected by arrows. This shows the reduction of adhesion factor with time from load tests carried out at the same site. The values reported next to the data points are the average undrained shear strength (c_u) along the pile shaft. A linear trend with log time can be seen. Suggested design lines have been added for piles. A design line for barrettes is suggested based on very limited. It is surprising that this line plots above the bored pile design line. These lines have been extrapolated to 240h using dashed lines beyond the available data. The dashed line for the bored piles has also been extrapolated back to the 1h construction time and an adhesion factor 0.7 can be seen. This is less that the adhesion factor of 1.0 which would be expected from negligible softening. This adhesion factor of 0.7 may be associated with mechanical disturbances on the pile surface during piles excavation. Softening of the pile shaft may occur from this value. A base factor α_0 of 0.7 (König et al, 2025) should therefore be applied to the softened penetrometer readings, see Table 2. Further work is required to carry out pile load tests with short construction times, such as CFA piles, with measurement of penetrometer readings next to the shaft at different levels.

 © DFI International Bruges 2025

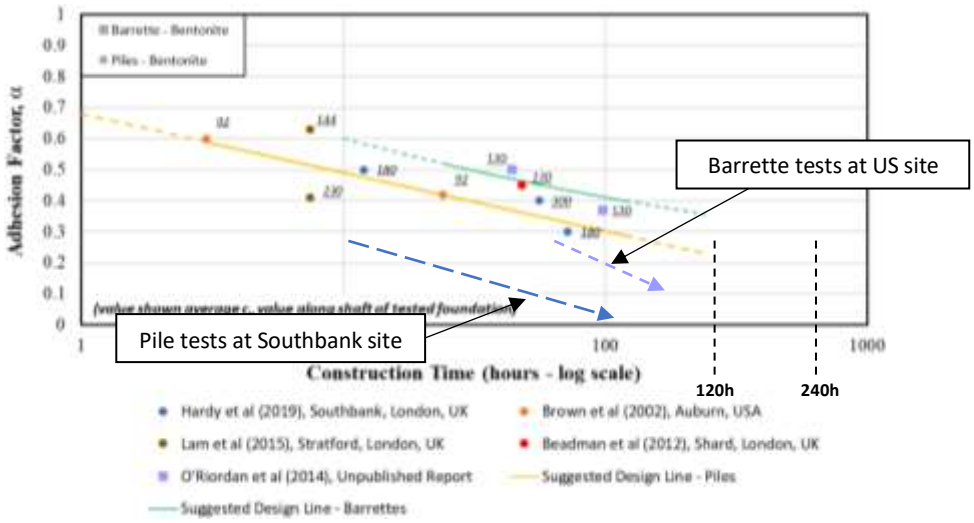


Fig. 3. Pile and barrette load test in clays - log plot

DIAPHRAGM WALL CONSTRUCTION PROCESS

Currently, there is limited load test data for single bites barrettes. These have a rectangular geometry. In the case of diaphragm walls the panels are 7.4m long and 1.5m wide at VRCB. The individual panels were formed by a 2.8m long grab in three individual bites. The end bites being constructed before the central bite was removed. This excavation process leads to a longer construction time compared with bored piles.

Initially, a "primary" panel is constructed, followed by an adjacent "successive" panel. The long panel plan length (7.4m) leads to a large soil arch forming in the adjacent soil in both the horizontal and vertical directions.

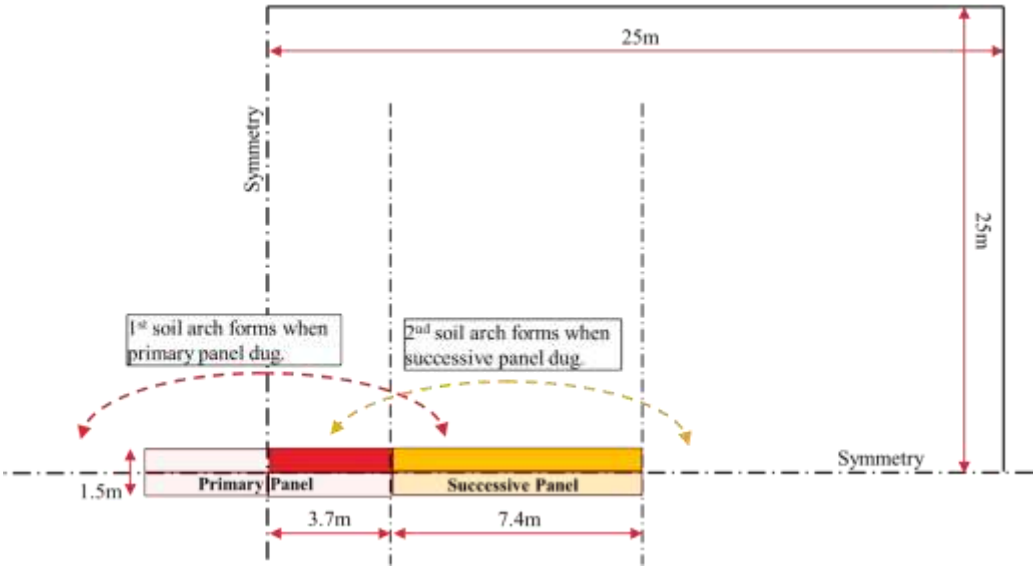


Fig. 4. Panel excavation process showing the horizontal arching effects

Figure 5 shows the initial (k_o) earth pressure profile. The fluid support pressure is also shown and this effectively halves the horizontal total stress on the wall of the panel. Small strain ground movements develop to form soil arch around the open panel.

The concreting stage leads to the application of fluid concrete pressure. Figure 5 shows measurements of the horizontal fluid concrete pressure in a diaphragm wall reported by Lings et al, (1994). These pressures reduce with depth with the onset of thixotropic effects and the concrete setting. It is unclear

 © DFI International Bruges 2025

how long this fluid pressure is applied before the concrete sets. Once the concrete has set it acts as a rigid boundary. For the purposes of this back analysis, it is assumed the concrete is placed rapidly and set immediately with no time to allow for recompression and reconsolidation of the London Clay adjacent to the panel.

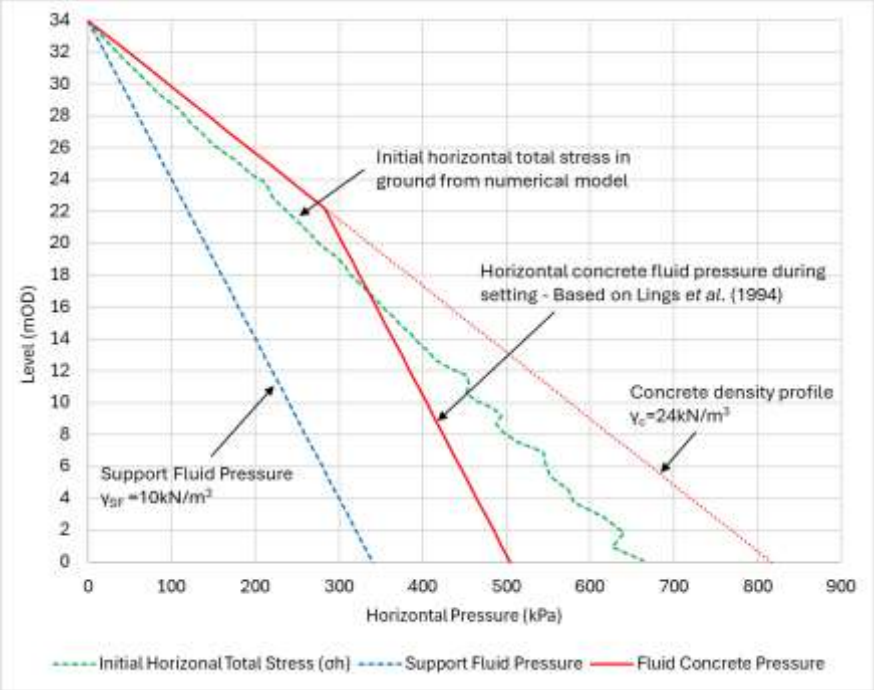


Fig. 5. Comparison of initial horizontal total stress, support fluid pressure concrete fluid pressure

The primary panels were left for about 5 days for the concrete to harden and this allowed for some consolidation to take place near the panel.

Subsequently the successive panel is excavated, and this leads to significant redistribution of earth pressures onto the primary panel as a new soil arch is formed. This enhances the horizontal earth pressure onto the primary panel. This new arch is also shown in Figure 4. The successive panel then follows the same construction process as the primary panel. The London clay is then allowed to consolidate for about 180 days to model Panel 25 and 26.

PENETROMETER TESTS AT VRCB

To investigate the effects of clay softening in the soil adjacent to the panel concrete a series of 6.5mm diameter penetration tests have been carried out during the excavation of the box at a depth of 8m (27mOD). The tests were carried on freshly exposed clay at different distances from the concrete surface. The clay surface was examined, and no filter cake was visible. A smear of bentonite was seen. The penetrometer tests on VRCB successive panels 25 and 26 are reported in the paper by König et al, (2025). These tests were carried out using a digital penetrometer (PCE Instruments, PCE, FM200). In addition, this penetrometer was calibrated against an electronic scale and an analogue penetrometer (Soiltest Inc, CL-700). A template was used to consistently record penetrometer tests results at 1 to 17cm from the wall. Additional tests were taken between 40 and 120cm in undisturbed London Clay. These were located using a tape measure. The panel 25 was open for 62.5 hrs and the panel 26 was open for 157 hrs. The penetrometer tests were carried out 157 days after the panels had been concreted, see Table 2.

The penetrator tests readings on undisturbed London Clay remote from the wall been averaged. This averaged reading has been used to normalise the readings next to the panel concrete, see Figure 6. The soil water contents next to the panel surface are also plotted on Figure 6.

 © DFI International Bruges 2025

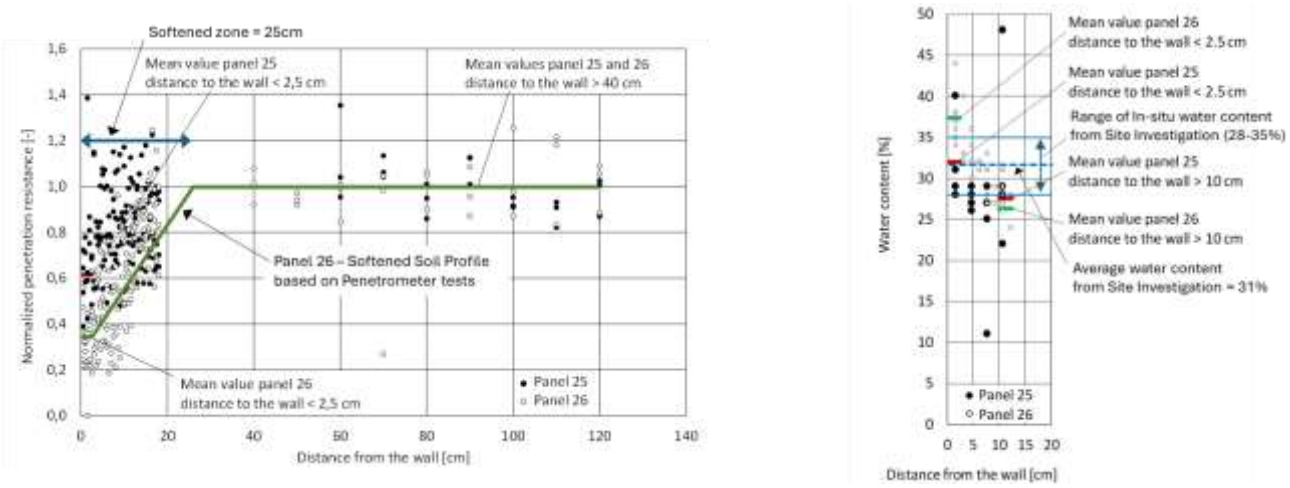


Fig. 6. Normalised penetration resistance and water contents next to the Panels 25 and 26

Table 2 – Normalised penetration resistance and Adhesion Factor (α) from penetrometer tests at 27mOD - König et al, (2025)

Panel ID	Panel opening time (hours)	Normalised penetration resistance	Base Factor α_0	Adhesion Factor α
Panel 25	62.5	0.61	0.7	0.43
Panel 26	157	0.34	0.7	0.24

NUMERICAL MODEL

The construction of a diaphragm wall is a complex modelling problem involving a three-dimensional mesh with both undrained and drained small strain modelling of the London Clay. The model was run using the LS-DYNA program and the panel excavation process is shown in Figure 4. The geometry of numerical model is shown in Figure 7. This model represents a quarter of the primary and successive panel construction process by have two lines of symmetry about the centrelines of the primary panel.

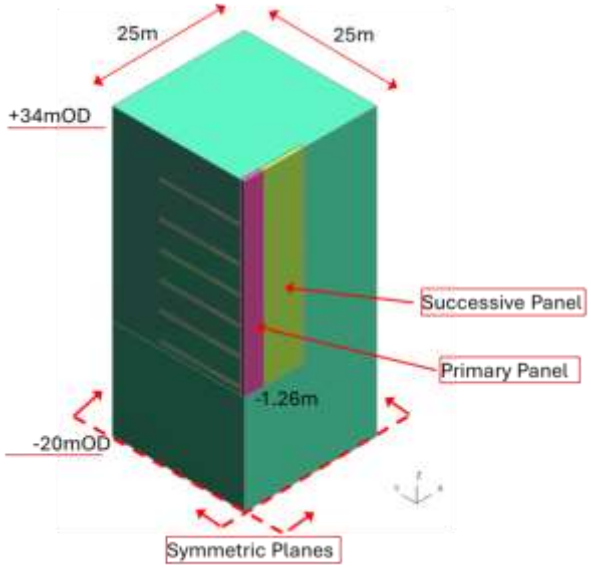


Fig. 7. Numerical model for the construction of primary panel 26 and successive panel 25

 © DFI International Bruges 2025

The diaphragm construction process has been described earlier in the paper. The modelling phases are described in Table 3 for Panel 26 as a primary panel (Phases 1 to 7) and Panel 25 has been considered as a successive panel. (Phases 8 to 17).

During the primary panel construction, the panel excavation under support fluid is Phase 3. The panel is open for 7 days and consolidation is modelled at Phase 4. The application of fluid concrete pressure, Phase 5, was considered but not modelled. Instead, a very short fluid concrete period was considered and the concreted boundary fixed at Phase 6. A consolidation period of 7 days was then modelled allowing the pore water pressures to start to come to equilibrium at Phase 7. The successive panel 25 has then been excavated assuming undrained conditions at Phase 8. The panel is then open for 5 days and some swelling has occurred at Phase 9. The panel was then concreted at Phase 11 (as Panel 26) and pore water pressures allowed to come to equilibrium during phases 12 to 17.

Table 3 – Construction sequence used to model construction of Panel 25 and 26

Model phase	Description	Clay drained/undrained	Construction stage
1	Initialization	Drained	Primary Panel
2	Apply 25kPa surcharge	Drained	Primary Panel
3	Excavate Panel 26, apply slurry pressure	Undrained	Primary Panel
4	Consolidation to 7 days	Consolidation	Primary Panel
~~5~~	~~Apply wet concrete pressure of Panel 26~~	~~Undrained~~	~~Primary Panel~~
6	Fix Panel 26 concrete	Undrained	Primary Panel
7	Consolidate to 7 days	Consolidation	Primary Panel
8	Excavate Panel 25, apply slurry pressure	Undrained	Successive Panel
9	Consolidate to 5 days	Consolidation	Successive Panel
~~10~~	~~Apply wet concrete pressure of Panel 25~~	~~Undrained~~	~~Successive Panel~~
11	Fix Panel 25 concrete	Undrained	Successive Panel
12	Consolidate for 10 days	Consolidation	Successive Panel
13	Consolidate for 30 days	Consolidation	Successive Panel
14	Consolidate for 60 days	Consolidation	Successive Panel
15	Consolidate for 180 days	Consolidation	Successive Panel
16	Consolidate for 1.5 years	Consolidation	Successive Panel
17	Consolidate for 7 years	Consolidation	Successive Panel

NUMERICAL MODEL RESULTS

Figure 7 shows that the panels extend from +34mOD to -1.26mOD. The results are plotted at +15mOD, approximately mid panel level.

Horizontal effective stress during primary panel 26 construction

The horizontal effective stresses in the soil perpendicular to the panel centreline change during the construction of the primary panel 26 are shown in Figure 8 for the Phases 3, 4, 6 and 7. The soil arch can be seen during the excavation of panel 26 in Phase 3. The swelling and effective stress reductions are seen whilst the panel is open in Phase 4. The concreting is at Phase 6 and subsequent consolidation in Phase 7 with the re-establishment of the horizontal effective stresses next the wall.

 © DFI International Bruges 2025

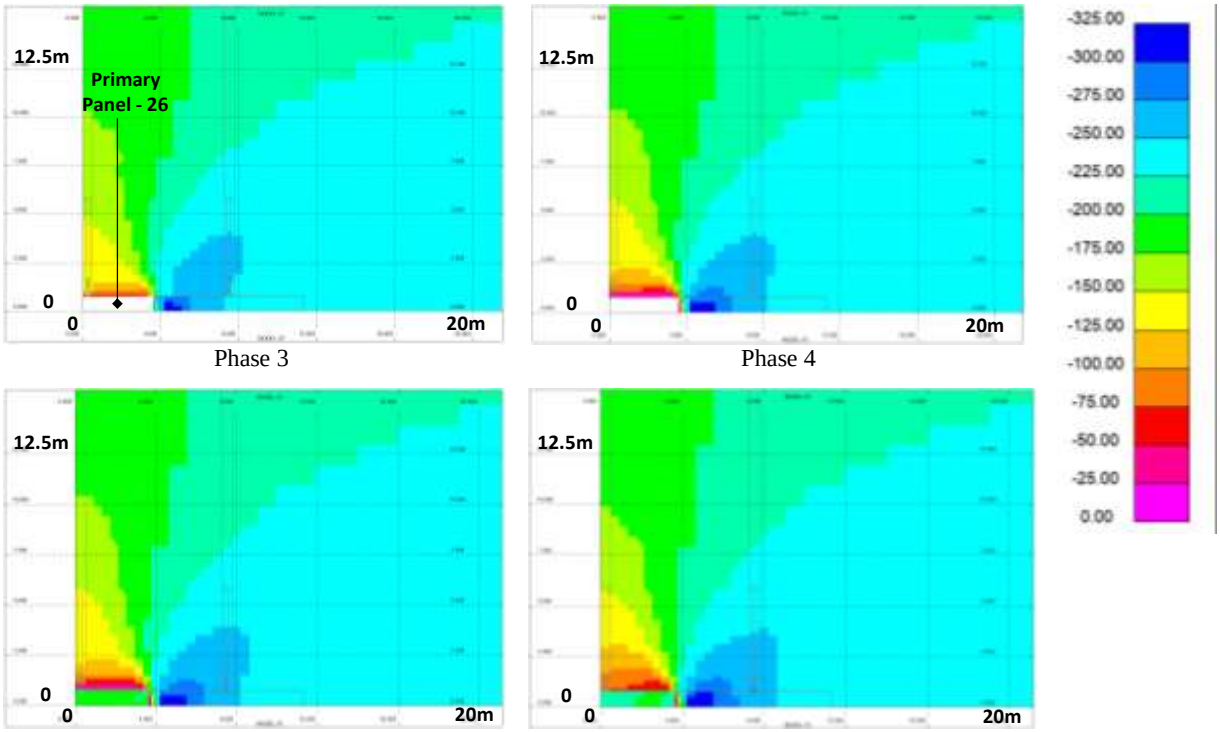
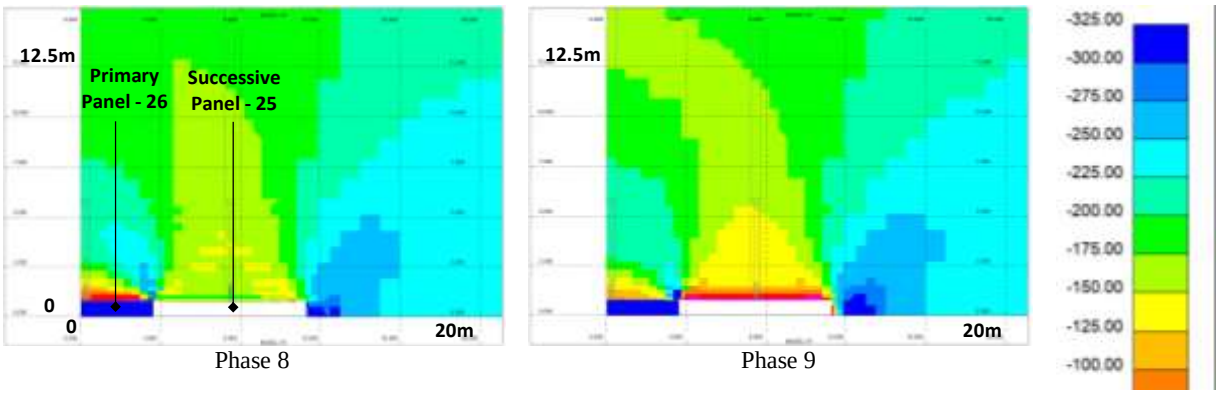


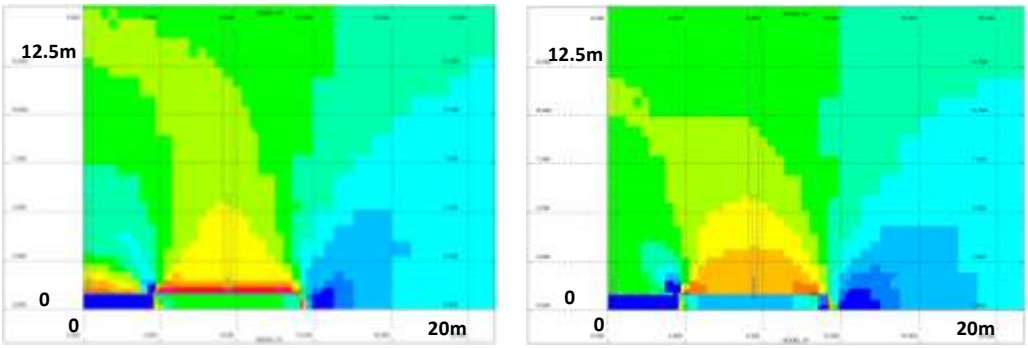
Fig. 8. Horizontal effective stress (kPa) changes during the construction of the primary panel 26 at 15mOD

Horizontal effective stress during successive panel construction

The horizontal effective stresses in the soil perpendicular to the panel centreline also change during the construction of the successive panel 25 are shown in Figure 9 for the Phases 8, 9, 11 and 15. The soil arch can be seen during the excavation of panel 25 with the reduction of effective stresses next to panel 25 and the significant increase at the primary panel 26. The panel 25 is concreted at Phase 11. During the Phase 15 the pore water pressures return to the initial values and the horizontal effective stresses at the primary panel 26 nearly return to the initial conditions, see Figure 9.



 © DFI International Bruges 2025



Phase 11 Phase 15

Fig. 9. Horizontal effective stress (kPa) changes during the construction of the successive panel 25 at 15mOD

Variation of horizontal effective stress and pore water pressures next to the panel

The effects of clay softening are most noticeable adjacent to the panel and therefore the horizontal effective stress and water pressure have been studied at 2cm and 20cm from panel 26 for phases 1 to 17, see Figure 10.

The drop in water pressures at Phase 3 when panel 26 was excavated can be seen. The drop in effective stresses can be seen at Phase 3 and 4. The panel 26 concreting and subsequent consolidation at Phases 6 and 7 show large recovery of effective stress.

The excavation of panel 25 shows corresponding large increases in pore water pressure at Phase 8 at Panel 26, see Figure 10. The concreting of panel 26 and subsequent consolidation lead to relief of excess pore water pressure with associated increase in effective stress.

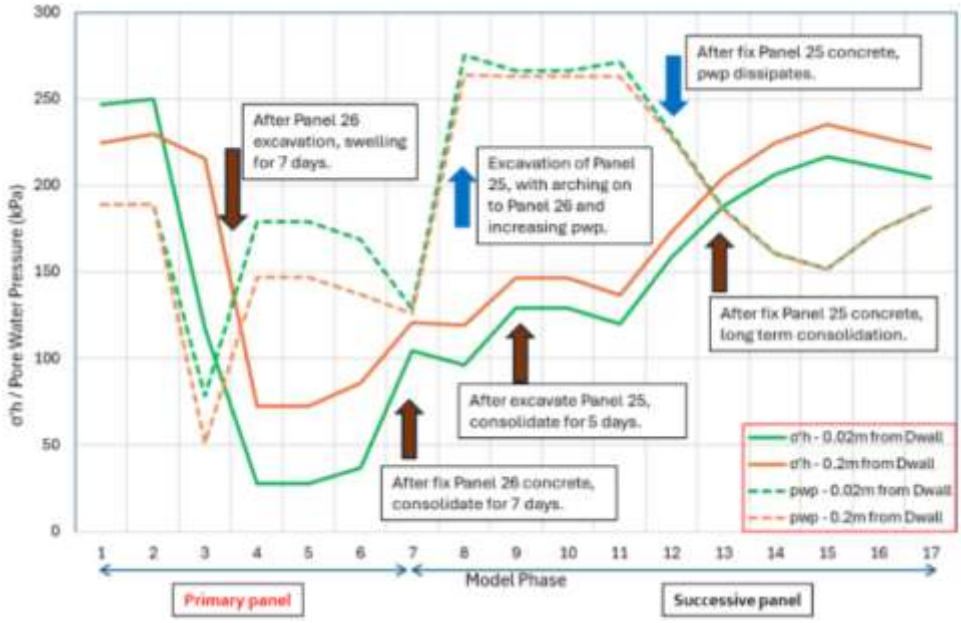


Fig. 10. Changes to the horizontal effective stress and porewater pressure at the centre of the primary panel 26 at 15mOD plotted at 2cm and 20cm from the panel

Variation of undrained shear strength next to the panel 26

The numerical model has been used to assess the undrained strength at 2 and 20cm from panel 26 at 15mOD. This has been done by extracting soil element data from the model at these locations and applying the calculated effective stresses and water pressures to an element of soil. The element of soil is then subjected to a triaxial test, undrained, stress path to determine the undrained shear strengths.

 © DFI International Bruges 2025

The results for these modelled undrained strength tests are plotted in Figure 11 for a location mid-way along panel 26. The drop in undrained strength during the excavation and open time consolidation of panel 26 correspond to Phases 3 and 4. The excavation of successive panel 25 (Phase 8) does not lead to large initial gains in shear strength at panel 26. However, there is a gradual development of undrained strength as consolidation occurs as shown in Figure 11.

Figure 11 also shows that the reductions of undrained strength 2cm from the panel are greater than at 20cm from the panel. The same effect is observed in the penetrator tests, see Figure 6. The right-hand axis on Figure 11 also shows the ratio of softened undrained strength compared with the initial undrained strength.

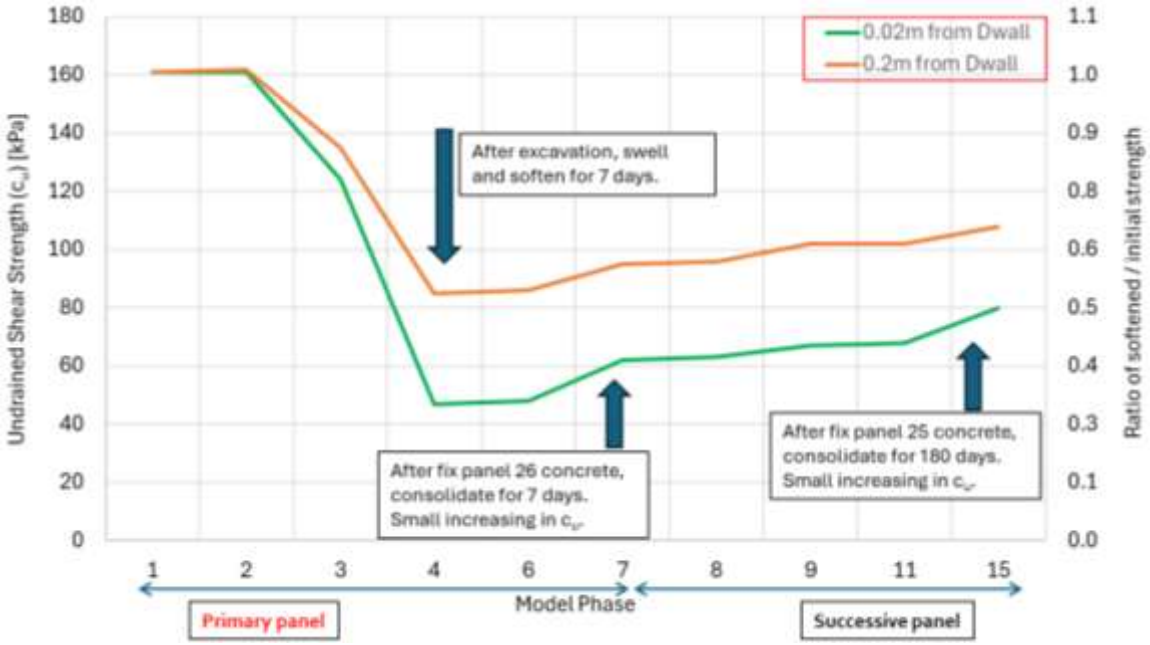


Fig. 11. Changes to the undrained shear strength at the centre of primary panel 26 at 15mOD plotted at 2cm and 20cm from the panel

Comparison with penetrometer tests and influence of London Clay permeability

The variation of the normalised penetrometer tests results with distance from panel 26 is plotted in Figure 6. This shows that softening extends to about 25cm from the face of the panel.

The mean line through the normalised penetrometer data is plotted on Figure 6. This line has been transferred to Figure 12 and calibrated with the calculated undrained strength tests remote from the wall.

A permeability $k=10^{-10}$ m/sec has been used for the calculation presented in Figures 8 to 11. Whilst the softening adjacent to the panel is like the penetrometers, it is observed that the softening extends further into the soil to about 4m. The model was rerun with a permeability of $k=10^{-11}$ m/sec. Good agreement can be seen with penetrometer test mean line.

The water contents adjacent to these panel are also plotted on Figure 6 and the increase in water content associated with the softening can be seen.

The back analysed permeability of $k=10^{-11}$ m/sec is lower than used for the design. It may be associated with the support fluid passing into the clay having a higher viscosity than water.

 © DFI International Bruges 2025

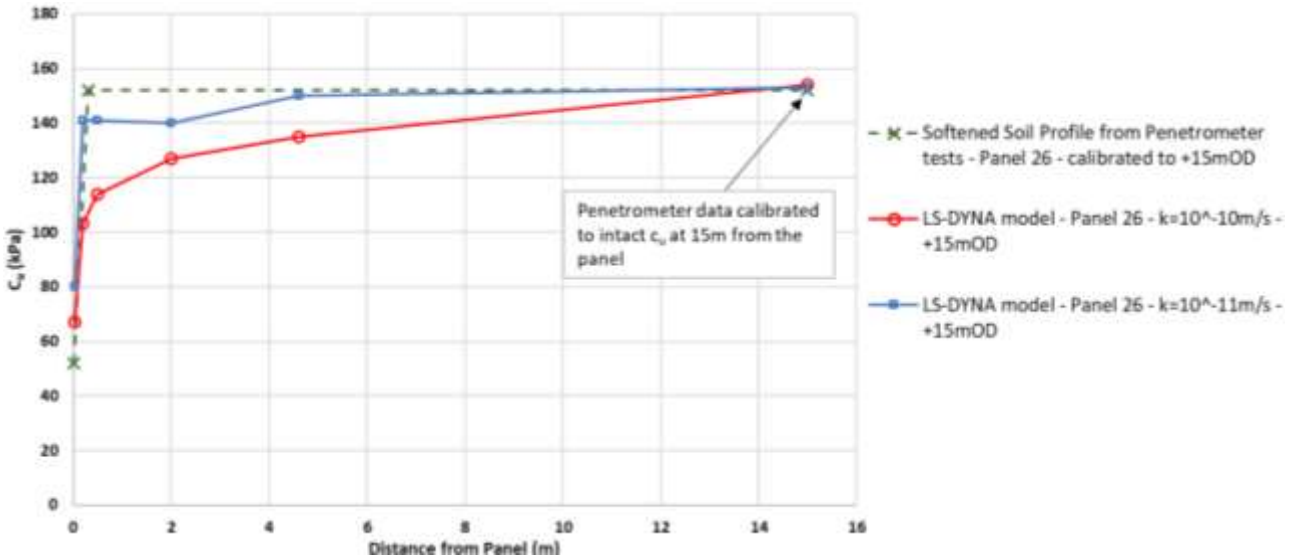


Fig. 12. Variation of undrained shear strength at 15mOD with distance from the centre of panel 26 at Stage 15

Comparison of an individual primary panel (barrette panel) and a primary panel influenced by a successive panel

The diaphragm wall construction has been assessed for two cases:

1) An individual primary panel (Barrette)
2) A primary panel influenced by arching action from a successive panel.

The Figure 13 compares the development of softened undrained strength at 2 and 20cm for these 2 cases. The individual panel (Barrette) achieves a ratio of softened undrained strength compared with initial undrained strength at 2cm from the panel of 0.43 which is about 86% of the primary panel with the successive panel with a ratio of 0.5.

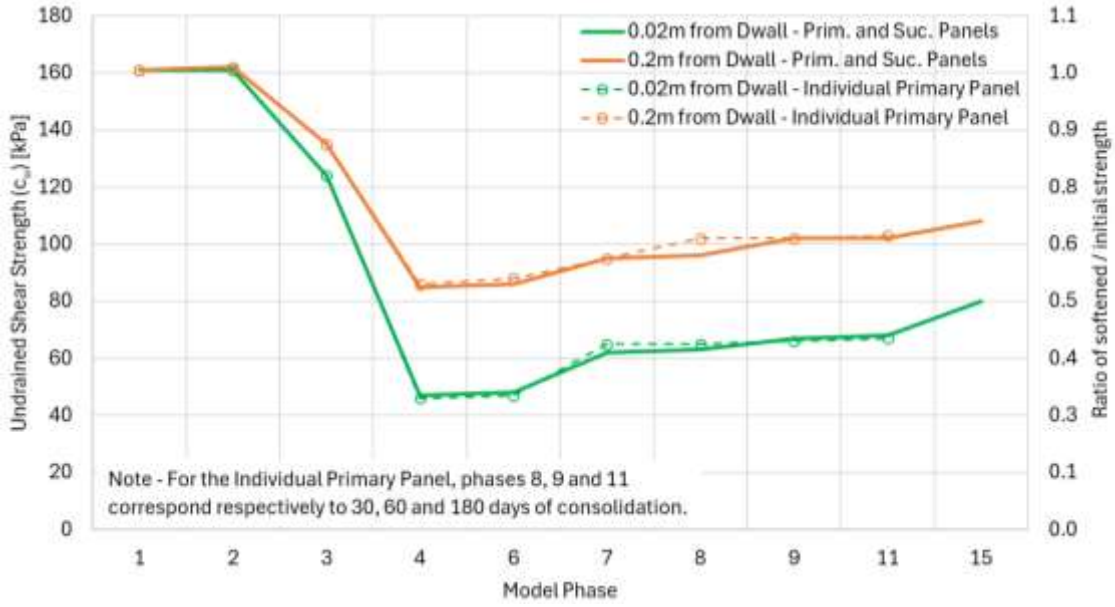


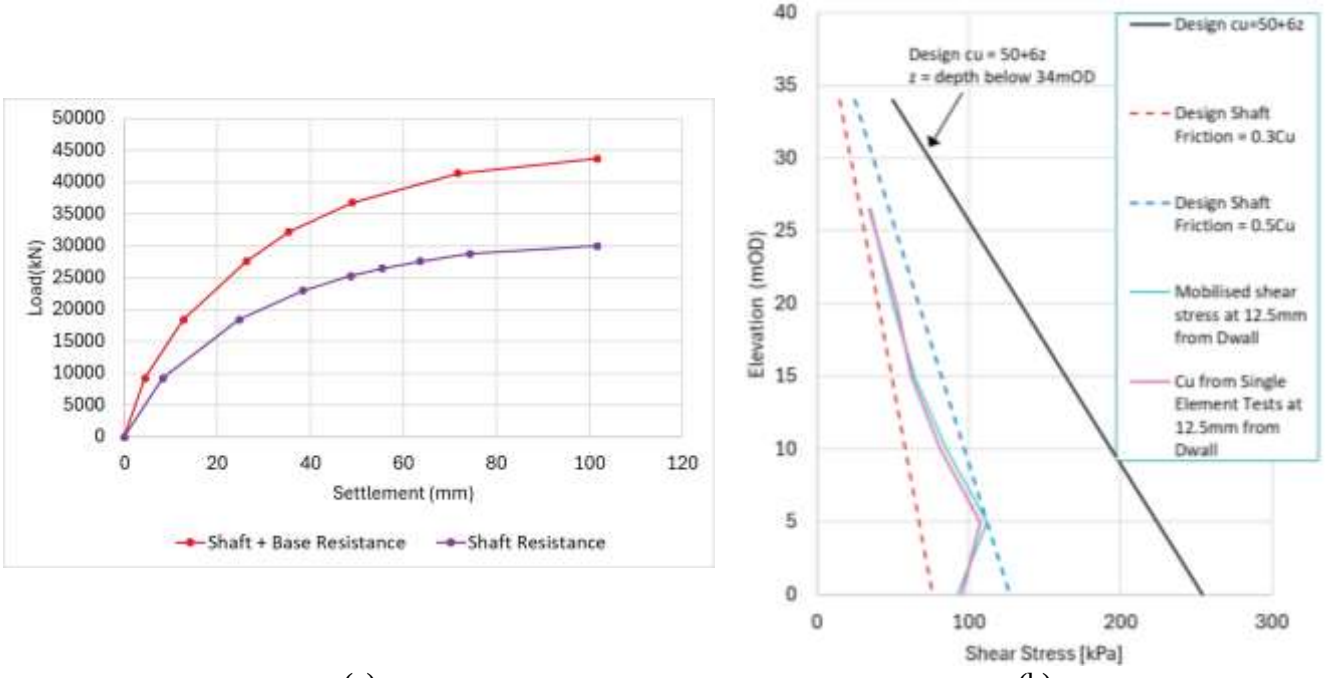
Fig. 13. Comparison of an individual primary panel (Barrette) and a primary panel with a successive panel at 15mOD

Numerical panel load test

The overall load settlement performance of the primary panel influenced by successive panels has been modelled as a numerical panel load test. The shaft resistance only and the combined shaft and base resistances are plotted against settlements on Figure 14a. The panel shaft resistance is given by

 © DFI International Bruges 2025

$Q_s=\alpha \cdot cu_s \cdot A_s$. The undisturbed undrained shear strength (cu_s) at mid depth (15mOD) is 146kPa. The panel shaft area (A_s) is 403m^2. The shaft resistance is 30MN. The calculated adhesion factor (α) from the numerical panel load test is 0.51. The opening times of panels 25 and 26 are summarised in Table 2 and the average opening time is 110h. This information is incorporated in Figure 15.
The design undrained shear strength (c_u) is shown in Figure 14b and increases linearly with depth. The shaft friction (q_s) is adopted as a proportion (α) of the undrained shear strength (c_u). The design shaft friction profiles for α=0.5 and 0.3 are shown in Figure 14b.
The mobilised shear stress for the primary panel (P26) over the depth of the panel at the centreline are plotted on Figure 14b at 12.5mm from the panel. Modelled undrained shear strength tests at the same locations show that the undrained shear strength is fully mobilised. It is noted that the mobilised shear strength increases from 10mOD to 5mOD and then reduces towards the toe of the panel. At the level of the penetrometer tests (27mOD), the mobilised shear stress is about 0.41 based on the modelled undrained shear strength test. This compares with the normalised penetration resistance of 0.34 from the penetrometer tests at the same location, see Table 2. Based on the mobilised shear stress data at the centreline of the panel, the average adhesion factor over the full depth of the primary panel (P26) is about 0.47. This is greater than the mobilised shear stress at 27mOD. This shows that it is difficult to extrapolate the measurements from the penetrometer tests at 27mOD to the performance of the overall panel.



(a) (b)

Fig. 14. Numerical panel load test – a) Load deflection plot for the combined primary and successive panels. b) Mobilised Shear Stress for Panel 26 compared with Design Shaft Friction

Summary of adhesion factors and ratio of softened strength to initial strength
The pile load test data is based on information from Hardy et al, (2019) this has been replotted on a log scale on Figure 3. The suggested design lines from Figure 3 are plotted in Figure 15.

The normalised penetration resistances from VRCB panels 25 and 26 at 27mOD from Figure 6 and Table 2 are plotted on Figure 15.

The numerical modelling for the primary panel 26 with the successive panel 25 at 15mOD gives a ratio of softened undrained strength compared with the initial undrained strength of 0.5 at 20mm from the panel for a panel opening time of 157h. See Figure 11 and 15.

The numerical panel load test was carried out simultaneously on both panels 25 and 26. The average construction time was 110h and the calculated adhesion factor was 0.51. Whereas the average

 © DFI International Bruges 2025

adhesion factor over the full depth of primary panel (P26) with the successive panel (P25) at the centreline of panel 26 is about 0.47, see Figure 15. This is about 8% less than the calculated adhesion factor from the numerical panel load test of 0.51, however, the construction times are different. Note that this numerical model does not include possible effects of mechanical disturbance and remoulding by the excavation tools.

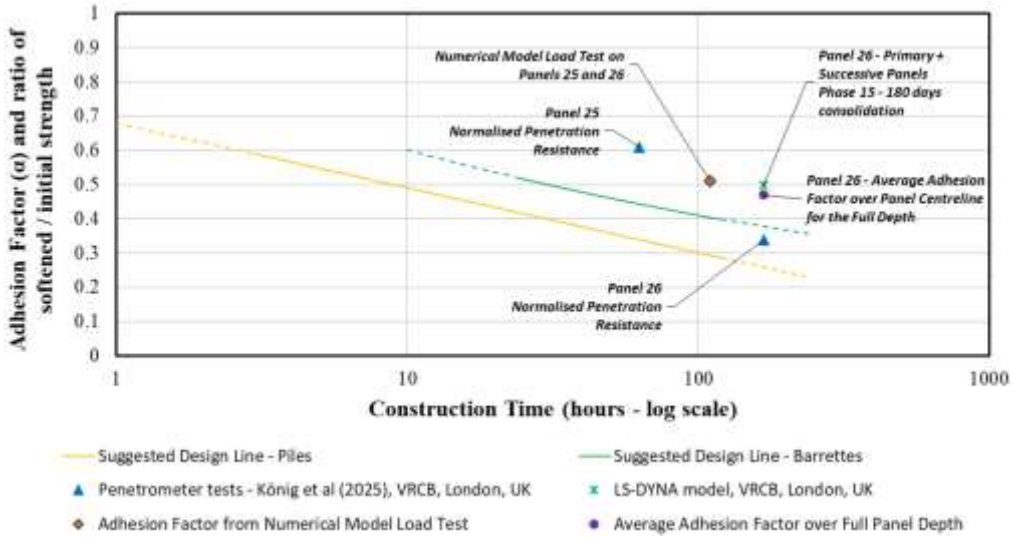


Fig. 15. Comparison of adhesion factors in clay with increasing construction time

CONCLUSIONS

Soil properties

The BRICK small strain soil models 1996 and 2010 were used to make comparisons with the undrained strength profile derived from SPT correlations, see Figure 2. The results from BRICK 1996 are reported in this paper.

The permeability $k=10^{-11}$m/sec was identified during the back analysis. This is a lower permeability than used in the wall design and may be associated with the support fluid entering the soil having a higher viscosity than water which would slow down permeation into the clay. More investigation is needed.

Pile load tests

The reduction in shaft adhesion with increasing pile construction time has been summaries by Hardy et al, (2019). The Figure 3 is based on this work but replotted on log time. In future, it would be useful to carry out additional barrette load tests as well as penetrometer tests adjacent to rapidly constructed dry bored piles and CFA piles.

Panel Construction Process

The diaphragm wall panel construction process involved primary and successive panels with soil arching in both the horizontal and vertical directions, see Figure 4. The effect of mechanical disturbances on the panel shaft during construction has not been incorporated. The fluid concrete applies a horizontal stress reload the soil during concreting, see Figure 5. This study has ignored this effect because of limited data on this effect. In future, additional measurements of fluid concrete total stress and setting time (Lings et al, 1994), should be carried out to assess the effects of reconsolidation of the softened clay next to the panel. This should also be related to the penetrometer tests.

Penetrometer Tests at VRCB

It is very difficult to carry out load tests on large diaphragm wall panels. The assessment of the reduced undrained strength of the clay has been undertaken on panels with long opening times during box excavation to assess the normalised penetration resistance, see Figure 6.

 © DFI International Bruges 2025

Numerical Model
The numerical modelling of the panel construction is complex and a quarter model has been used, see Figure 7. The objective was to back analyse the construction of panels 26 and 25 to replicate the penetrometer results. One weakness of the model is that symmetry about the primary panel centreline focuses increased stress onto the primary panel when the successive panel is constructed.

The Figures 8 and 9 investigate the changes in horizontal effective stress at 15mOD (mid panel depth), during panel construction. The effects on effective stresses and pore water pressures on soil 2cm and 20cm from the primary panel are considered in Figure 10. The changes in undrained strength are plotted in Figure 11. This is related to changes in ratio of softened / initial strength. Comparisons with the penetrometer tests are made in Figure 12.

For comparison, the primary panel 26 has been modelled as a barrette. The ratio of softened / initial strength is found to be about 86% of the combined primary and successive panel case, see Figure 13.

Numerical panel load test
The numerical model has been used to simulate a panel load test and assess the fully mobilised shaft friction, see Figure 14. The calculated adhesion factor (α) from the numerical panel load test is 0.51. At the level of the penetrometer tests (27mOD), the mobilised shear stress of the primary panel (P26) is about 0.41 which compares with the normalised penetration resistance of 0.34 at the same location, see Table 2. The average adhesion factor over the full depth of the primary panel (P26) at the centreline with the successive panel (P25) is about 0.47. This is about 8% less than the calculated adhesion factor from the numerical panel load test of 0.51, however, the construction times are different. Based on this information, it is difficult to extrapolate the penetrometer tests and the modelled undrained shear strength tests at 27mOD to the overall panel performance. Additional work needs to be carried out to model shorter construction times (up to 10h) for panels and also extend the modelling to consider piles.

Summary of adhesion factors
The various methods of assessing pile, barrette and panel shaft adhesion factors are summarised in Figures 3 and 15. Suggested design lines for piles and barrettes are considered as full lines and extrapolation as dashed lines. The barrette design lines are based on limited data.

Recommendations for future penetrometer tests and modelling
Further work is required to establish bored piles and barrettes adhesion factors over a full range of construction times. This should be accompanied by penetrometer tests and numerical modelling. This would help to clarify the adhesion factor of 0.7 from the pile load test at very early construction stages, see Figure 3. The influence of mechanical disturbance and remoulding on the pile shaft resistances and how it relates to softening effects could also be incorporated into the numerical model.

REFERENCES

Lings, ML., Ng, CWW., & Nash, DFT. (1994) The lateral pressure of wet concrete in diaphragm wall panels cast under bentonite. Proceedings of the ICE – Geotechnical Engineering, 107, July, 163 – 172.

Simpson, B. (1992) Retaining structures: displacement and design, Geotechnique 42, No. 4, pp 541 – 576.

Pillai, A. (1996). Review of the BRICK model of soil behaviour, MSc Thesis, Imperial College, London.

Pillai S, Patel B, Hardy S, (2023), Validation of Advanced Soil Constitutive Modelling to Represent London Clay, Ground Engineering, April 2023, pp 25 – 32.

 © DFI International Bruges 2025

SCOUT. (2007 & 2010) D18 Report on Observational Method under the Framework of Eurocodes. European Commission Sixth Framework Programme. Project no: 516290. Re- port ref no: SB.DTTAP-NOT-6.045. Arup Geotechnics.

CIRIA C760, (2017), Gaba, A, Hardy, S, Doughty, L, Powrie, W, Selemetas, D, Guidance on Embedded Retaining Wall Design, London

König D. Nicholson D, Verst R, Harnan C, (2025), Field Investigation on the Characteristics of Clayey Soil close to Diaphragm Walls DFI conference, Bruges, (to be published).

Hardy S, Nicholson D, Srisakthivel S, Oliver L, Disley T, (2019), Preliminary Test Pile Results for the South Bank Place Development. Ground Engineering, Dec 2019, pp 26 – 33.

White F, Ingram P, Nicholson D, Stroud M, Betru M. (2019), An Update of the SPT-cu relationship proposed by M. Stroud in 1974, Proc 27th ECSME.

 © DFI International Bruges 2025

Incorporating distributed fibre optic sensing and machine learning into dry deep mixing

Stefan Ritter, Norwegian Geotechnical Institute and Oslo Metropolitan University, Oslo, Norway, +47 41366217, stefan.ritter@ngi.no (Primary Presenter)
Sølve Hov, Norwegian Geotechnical Institute and Norwegian University of Science and Technology, Trondheim, Norway, +47 45846968, solve.hov@ngi.no
Priscilla Paniagua, Norwegian Geotechnical Institute and Norwegian University of Science and Technology, Trondheim, Norway, +47 94829497, priscilla.paniagua@ngi.no

ABSTRACT

Dry deep mixing (DDM) has frequently been employed as a method to improve the engineering properties of soft soils such as clay and peat. Today's methods to quantify the strength and stiffness of DDM improved ground are limited in terms of their spatial and temporal resolution. This lack of reliable monitoring data often results in uncertainty about the field performance. As a consequence, DDM projects often use overly conservative design solutions which could have negative economic and environmental implications. Recent smart sensing techniques including distributed fibre optic sensing (DFOS), which could provide the required high-resolution data, have, however, not yet been adopted to DDM. Another shortcoming of DDM is that its design relies on resource intensive laboratory and field testing. Advanced methods to predict the properties of DDM improved soils, such as machine learning (ML) techniques, have not yet been sufficiently explored for DDM. This contribution addresses these current gaps in DDM practice by presenting results from the application of DFOS and ML to DDM. The validation of DFOS for DDM improved ground, drawing on data from laboratory and full-scale field trials, is discussed. The obtained results highlight that fibre optical cables installed in DDM improved ground can reliably map the stress-strain response of improved soil columns. Gradient boosting and random forest techniques are utilized to predict the properties of laboratory improved soil for DDM. The application of these ML techniques to existing databases shows that these methods outperform currently used prediction models based on, for example, the water-to-binder ratio. Overall, this contribution presents latest applied research on incorporating digitalization into DDM.

Keywords: dry deep mixing, fibre optic sensing, machine learning

INTRODUCTION

This paper focuses on the dry deep mixing (DDM) technique, which has been widely used in Scandinavia, Japan and elsewhere to improve the properties of soft soils. In the DDM method, dry binders including lime and cement are mixed into the soil using a rotating mixing tool to generate stabilised soil columns of about 0.6 to 0.8 m with depths up to 25 m. Typical applications of DDM are linear infrastructure projects, e.g., road and railway projects, and as part of retaining systems for deep excavations.

Previous research on DDM focused on laboratory studies to substitute traditional binders (i.e., lime and cement) with more sustainable binders (e.g., Åhnberg (2006), Yong-Feng et al. (2017), Hov et al. (2023), López Ramírez et al. (2024)). The main incentive of these studies was to reduce the carbon footprint of DDM. Although the obtained results provide important insight into the performance of alternative binders for DDM, only a limited number of full-scale tests using such alternative binders exist.

Current methods to verify the field properties (e.g., strength and stiffness) of DDM improved soils are core sampling and subsequent element testing, cone penetration tests and column penetration tests. These control methods are limited to providing spatially and temporally restricted information with often considerable uncertainty. Reliable methods to quantify the field performance of DDM improved ground, such as its stress-strain response with depth, are still lacking. Consequently, uncertainty about the field performance exists which frequently results in overly conservative design assumptions.

A widely used strategy to overcome these issues is to conduct full-scale field trials at the beginning of projects to optimize the binder mixture and dosage according to the local ground conditions. Although these field campaigns provide crucial information, they increase the projects costs in both economic and environmental terms. A potential strategy to more reliably define the binder type and content could be to adopt machine learning (ML) methods. Recent research showed the successful application of ML to predict

 © DFI International Bruges 2025

the performance of jet grouting (Tinoco et al. (2011, 2020)) and other ground improvement methods (Das et al. (2011), Eyo et al. (2022), Pham et al. (2021)). However, ML methods have, so far, not been adopted for DDM.

This paper provides an overview of latest research on DDM carried out in the *Green sOil stAbiLisation* (GOAL) project. The first part of this paper provides a brief background about GOAL. Then this paper is concerned with two research focus areas of GOAL: the application of distributed fibre optic sensing and ML for DDM. Finally, a summary, conclusions and recommendations for future research are given.

BACKGROUND

The GOAL project is funded by the Norwegian Research Council (project number 328767). It consists of 10 consortium partners, which are: Bergene Holm AS, Celsa AS, Keller Geotechnic, Lindum, Norske Skog Skogn, Norwegian Geotechnical Institute (NGI), Norwegian University of Science and Technology (NTNU), Technical University of Denmark (DTU), University College Dublin and University of California Berkeley. The project is led by NGI and the project period is from November 2021 to October 2025.

The main objective of GOAL is to transform soil stabilisation technologies using latest sensing and monitoring techniques, automated data-driven design solutions and more sustainable materials. To meet this objective, research is carried out in five work packages, which are listed in Table 1. The first phase of GOAL focused on laboratory investigations to obtain controlled knowledge before upscaling findings to full-scale. For the full-scale field trials, the Norwegian GeoTest Sites (NGTS) were used (L'Heureux et al., 2017). The following section highlights this approach by presenting results from fibre optic sensing of stabilised soil from both the laboratory and subsequent field experiments. A more detailed overview about GOAL including a list of publication can be found here: https://www.ngi.no/en/projects/goal/.

Table 1. Work packages (WP) of the Green sOil stAbiLisation (GOAL) project with description of the specific research objectives.

WP#	WP name	Research objectives
1	Knowledge generation: lab testing	Perform laboratory investigations on soft clay, quick clay and peat stabilised with industry by-products
2	Sustainability: environmental and economic impacts	Quantify the environmental and economic impact of stabilising soils with industry by-products and understand the fate of contaminants in soils stabilised with industry by-products
3	Upscaling: field application	Perform field tests of soil stabilisation with industry by-products including improved digital monitoring
4	Digitalisation and automation: smart soil stabilisation	Validate new monitoring methods to improve quantification of real field behaviour of stabilised soil and translate into an automated design framework
5	Catalysing innovation: enabling sustainable soil	Identify crucial preconditions and stakeholders that enable to utilise industry by-products in construction projects and facilitate knowledge exchange

DISTRIBUTED FIBRE OPTIC SENSING

Several studies showed the successful application of distributed fibre optic sensing (DFOS) in geotechnical engineering. For example, Pelecanos et al. (2018) used DFOS to obtain the stress-strain response of bored concrete piles to axial loading. Other interesting results about the performance of diaphragm walls were reported by, for example, Goeminne et al. (2017). These applications have in common that fibre optical cables can be attached to the reinforcement cages which enables controlled installation of the fibre optical cable. In addition, the stiffness of the fibre optical cables is in good agreement with the reinforcement bars. The application of DFOS for DDM is more challenging because reinforcement is not used and DDM improved soil has a stiffness which is typically orders of magnitude lower than the ones of fibre optical cables (Hov et al. 2025).

Detailed laboratory studies were first conducted to validate DFOS of stabilised soil (Solum, 2023). Both distributed temperature sensing (DTS) and distributed strain sensing (DSS) were tested to obtain information

 © DFI International Bruges 2025

about the integrity of DDM improved soil and the response to loading. The DTS results suggest that zones of lower binder content of only a few centimetres might be reliably detected (Ritter et al., 2024).

Fig. 1 visualises the experimental setup used in the DSS tests, which are a focus of this contribution. Three lime/cement stabilised clay samples with a diameter of 100 mm and height of 200 mm were prepared using Tiller-Flotten clay (L'Heureux et al., 2019), 50 kg/m^3 of dry burnt lime and 50 kg/m^3 of ordinary Portland cement (CEM I 52.5 R). Each sample was prepared by remolding the clay using an ordinary kitchen machine, after which the binders were added. The instrumented lime, cement and clay mixtures were then tampered surrounding a centrally placed fiber optical cable (EpsilonSensor from Nerve-Sensors (2023)), as can be seen from Fig. 2a. Although great care was taken when preparing the samples, some horizontal cracks became apparent after curing (Fig. 2b). An OBR4600 interrogator from Luna Innovations was used for the DFOS measurements, which were carried out with a spatial resolution of 1 cm. The first reading was taken before the unconfined compressive strength (UCS) test started while subsequent readings were taken after displacement increments between 0.1 to 0.4 mm were applied.

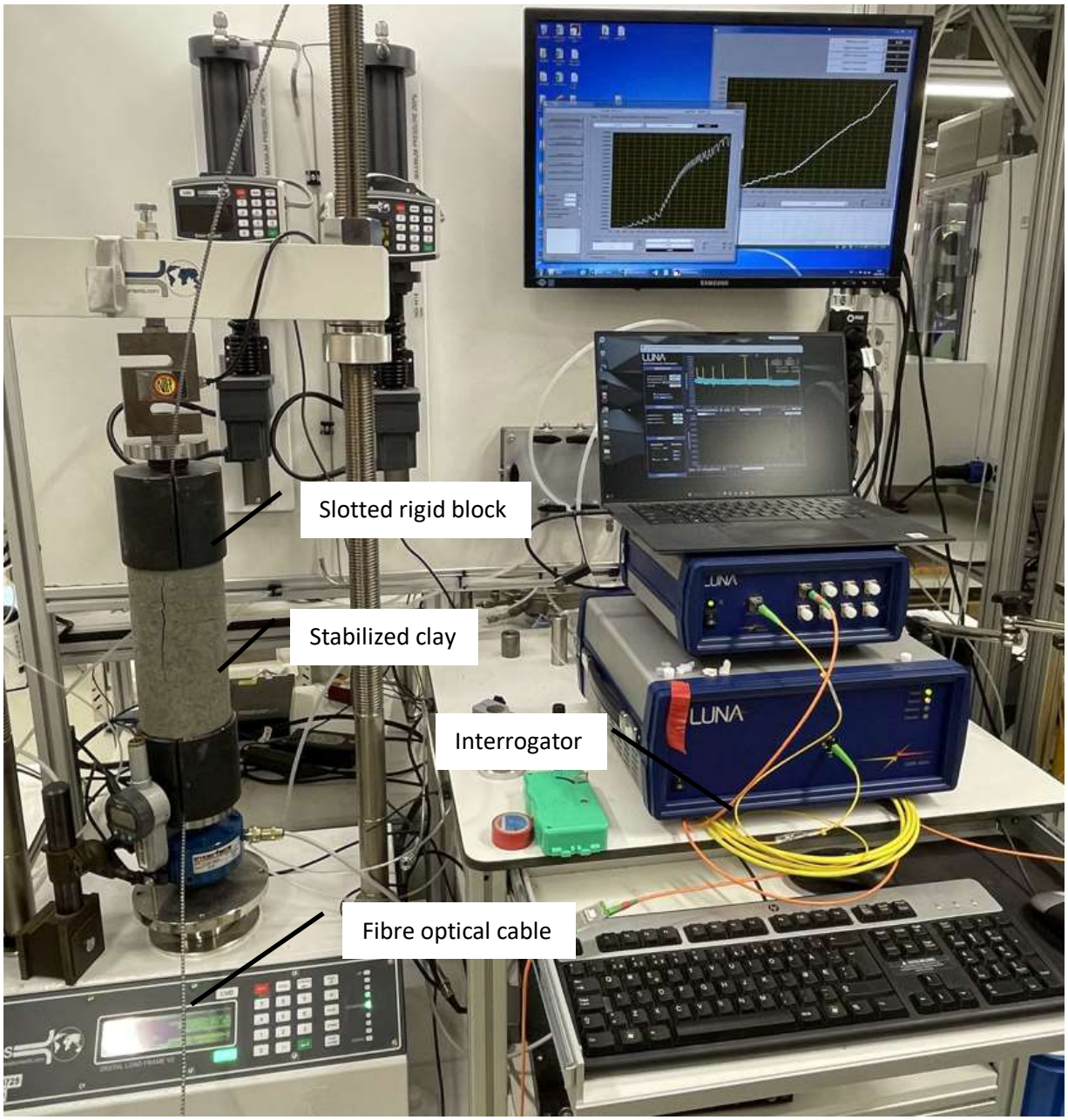
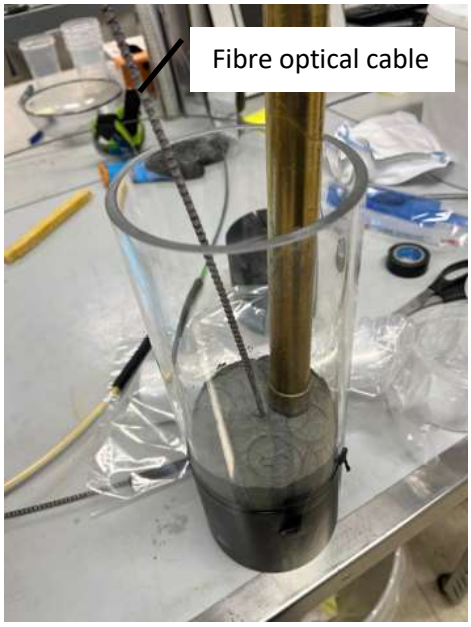


Fig. 1. Experimental setup of the distributed strain sensing. Image source: Solum (2023).

 © DFI International Bruges 2025





(a) (b)

Fig. 2. (a) Preparing a stabilized soil sample instrumented with a fibre optical cable. (b) A sample after curing. Images source: Solum (2023).

The strain along the position of the specimens can be seen in Fig. 3 for the three performed tests. A comparison between the applied strain in the UCS tests, ε_{UC}, and the measured strains indicates that the measured strains were considerably smaller than the applied ones. In addition, the obtained strain profiles with a peak close to the centre of the specimen are different in shape compared to the theoretically expected one (i.e., a constant strain level in the centre region of the specimen; see, for example, Chapeleau & Bassil (2021)). A likely reason for the obtained differences is a too short embedment length of the fibre optical cable, or a too short sample size, to transfer the applied strain to the fibre optical cable. Another reason is the stiffness difference between the fibre optical cable (3 GPa) and the stabilized soil (27 to 54 MPa). Transferring the load from the softer stabilized soil specimen to the stiffer fibre optical cable requires a sufficient bond length which could not be obtained with the 200 mm high specimens. Further laboratory tests are currently being carried out to validate the performance of DFOS in stabilized soil.

Two full-scale field tests were carried out in the GOAL project. The objectives of these tests were to test the performance of alternative binders, such as, wastepaper sludge ash, the impact of different mixing energies on the quality of the stabilized soil columns and different sensing techniques. This contribution focuses on the application of downhole DFOS to measure strains in the stabilized soil columns when experiencing vertical loads.

Figure 4 provides an overview of the field test carried out at the NGTS Tiller-Flotten, which is about 10 km south of Trondheim, Norway. The ground conditions are characterized by marine clays with a thickness exceeding 50 m. The top soil layer is a 2 m dry crust clay, after which a low to medium sensitive clay layer can be found until a depth of about 7.5 m below soil surface. Below 7.5 m, a highly sensitive clay layer with sensitivity values up to 200 follows. This sensitive clay is a typical quick clay with residual shear strengths less than 0.5 kPa. More details about the NGTS Tiller-Flotten are provided in L'Heureux et al. (2019).

 © DFI International Bruges 2025

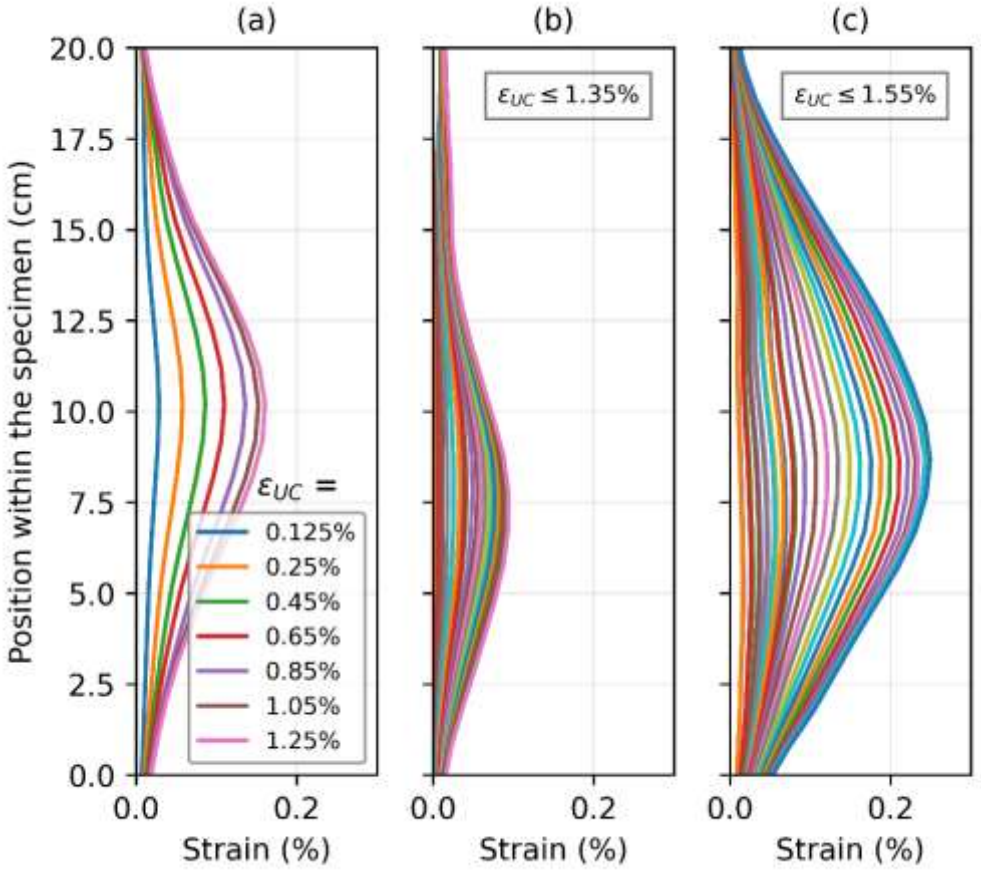


Fig. 3. Strain profiles measured with distributed fibre optic sensing along the position of the specimen for different strain increments, ε_{UC}, applied in the unconfined compressive strength tests. For tests (b) and (c) the applied strain increments were 0.05%. Source: Ritter et al. (2024).

Six stabilized soil columns were instrumented with EpsilonSensors (Fig. 4). The fibre optical cables were installed a short time after performing the DDM using a CPTU rig. Unfortunately, unexpected quick curing of the stabilized soil occurred which resulted in an open cavity; contact between the fibre optical cable and the surrounding stabilized soil was not achieved. For this reason, the cavity was grouted using a cement and bentonite mortar with a water-to-cement ratio of 2. During grouting the fibre optical cable was manually tensioned. The same OBR4600 interrogator as used in the laboratory experiments was adopted for the field measurements. After installation and after taking baseline readings, a 3 m high rock embankment was placed on top of the stabilised soil area.

The DFOS strains in column C4, measured two and four months after applying the embankment load, are plotted in Fig. 5. As expected, the strains increased with time due to a load transfer between the soil and the stabilized soil columns which is caused by consolidation settlements in the clay. With distance from the soil surface, the strains decreased. A comparison between the measured strains and the analytical method by Alén et al. (2005) indicates good agreement. In particular, the measurements after four months fit well with the analytical prediction.

From Fig. 5 it is evident that the DFOS data is not smooth. The noise in the data is likely caused by heterogeneity within the stabilised soil and issues with the bond between the stabilised soil, the grouting and the fibre optical cable. Further studies are required to better understand the interaction between a fibre optical cable and the surrounding stabilised soil. In addition, future investigations on practical methods to install a fibre optical cable in the field are required.

 © DFI International Bruges 2025

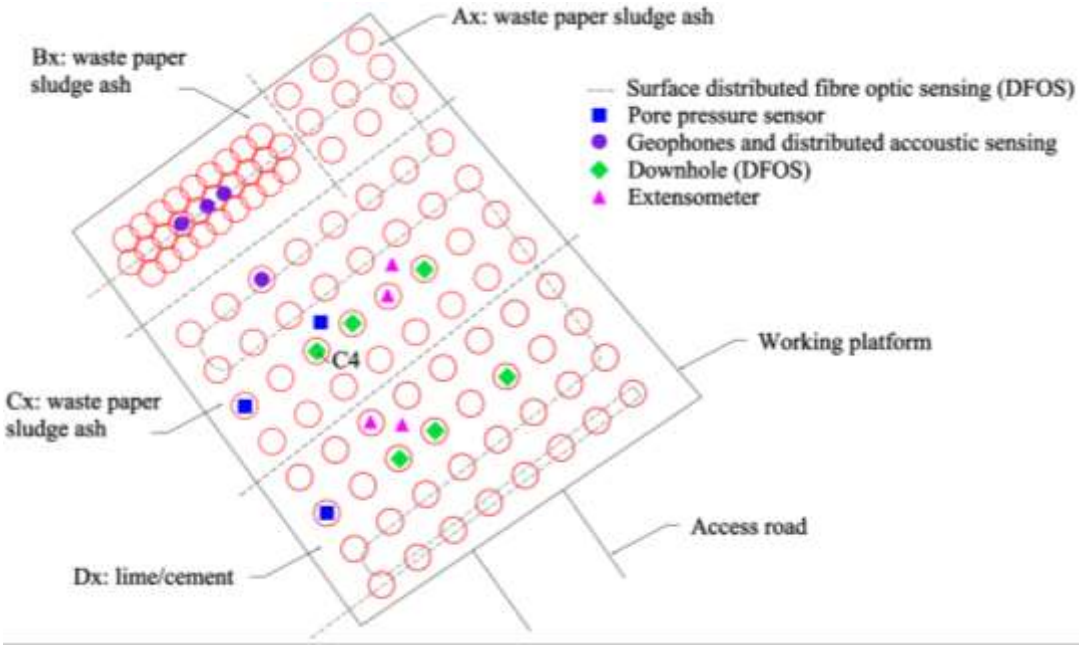


Fig. 4. Full-scale field test at the Norwegian GeoTest Site Tiller-Flotten. Modified from Oberhollenzer et al. (2024).

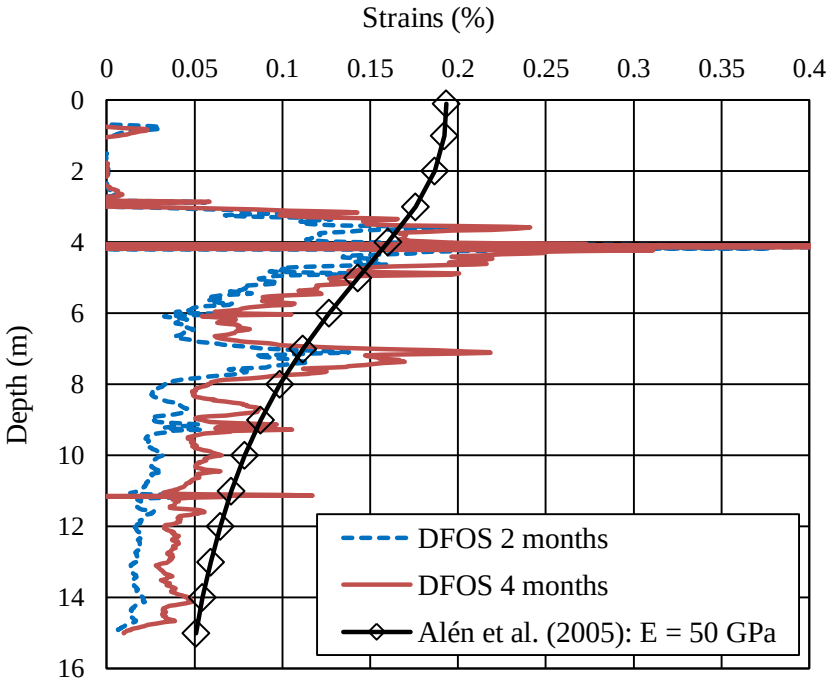


Fig. 5. Strains in column C4 measured by distributed fibre optic sensing and comparison to predictions using Alén et al. (2005).

MACHINE LEARNING

A wide range of machine learning (ML) techniques have been adopted in geotechnical engineering (Zhang et al., 2021). A typical example is the prediction of strength and stiffness of improved ground using ML algorithms such as Artificial Neural Networks (Das et al., 2011; Tinoco et al., 2011) and Support Vector Machine (Das et al., 2011). Although several studies to predict the UCS of stabilised soil exist, there is a lack of studies focusing on DDM with undrained shear strength values frequently between 100 to 500 kPa. This section explores the application of gradient boosting (GB) and random forest (RF) techniques to predict the strength of DDM. GB and RF were adopted because of their abilities to capture complex non-linear

 © DFI International Bruges 2025

relationships between input (i.e., features) and output (i.e., target) variables and to identify features governing the prediction. For both techniques, default hyperparameters were used. Detailed information about these techniques can be found on *scikit – learn* (Pedregosa et al., 2011).

Paniagua et al. (2022) recently presented an extensive database of laboratory-improved Norwegian clays using experimental procedures widely used to guide DDM projects. The database consists of 325 laboratory prepared samples with initial water contents between 20-48%, liquid limits between 20-25%, plasticity indices between 5-20% and soil sensitivity between 2-280. Lime, cement and cement kiln dust were the tested binders. The strength of the laboratory-mixed samples was obtained by UCS tests.

Although widely accepted relations to predict the strength of improved soils, such as between the variation of shear strength with the water-to-binder ratio, were explored in Paniagua et al. (2022), a more detailed investigation of the dataset using ML techniques has, so far, not been carried out. In this initial work, the off-the-shelf ML techniques GB and RF were implemented using *scikit – learn* (Pedregosa et al., 2011) and applied to the Norwegian database. First, the database was pre-processed and only entries including complete data about the following parameters were considered: the natural water content of the soil, w_n, the soil unit weight, γ, the plastic limit, w_P, the liquid limit, w_L, the cement content, C, the lime content, L, the cement kiln dust content, CKD, the curing time, t, and the undrained shear strength at a certain curing time, $c_{u,t}$. Table 2 provides statistical information about the final dataset, which reduced to 185 entries.

Table 2. Features of the database on laboratory-mixed Norwegian clays.

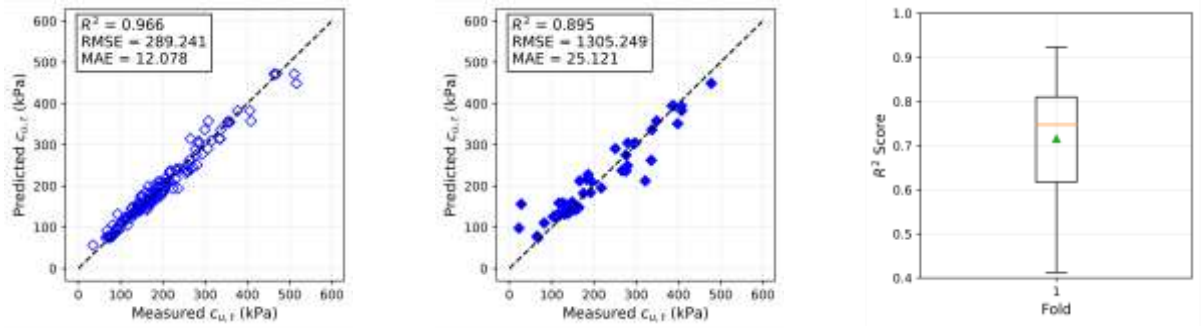
Feature	Count	Mean	Stdv.	Max.	Min.
Natural water content, w_n (%)	185	34.2	7.52	59.0	20.0
Unit weight, γ (kN/m^3)	185	18.7	0.84	20.6	16.9
Plastic limit, w_P (%)	185	20.1	3.84	38.0	15.0
Liquid limit, w_L (%)	185	33.6	9.72	67.5	18.0
Cement content, C (kg/m^3)	185	53.8	11.2	90.0	25.0
Lime content, L (kg/m^3)	185	26.8	24.3	60.0	0.0
Cement kiln dust content, CKD (kg/m^3)	185	20.8	25.1	75	0.0
Curing time, t (days)	185	17.4	11.1	60	0.75
Undrained shear strength at t, $c_{u,t}$ (kPa)	185	198	97.7	517	23.0

The final dataset was subdivided into two subsets: (1) a training subset consisting of 75% of the entire dataset to construct the ML models and (2) a testing subset consisting of 25% of the entire dataset to evaluate the performance of the ML models. After subdivision, the data was normalised in a range [0,1]. The performance of both models was quantified using the mean absolute error (*MAE*), the root means square error (*RMSE*) and the coefficient of determination (R^2). Additionally, 10-fold cross-validation was carried out to assess the overall performance of both ML models. A paired student's t-test with two-fold cross-validation with five repeats using $P = 0.05$ was applied to directly compare the two ML models.

Figure 6 shows the performance of the RF model. Subfigures (a) and (b) present the performance of the model for the training and test subsets, while subfigure (c) provides the result of the 10-fold cross-validation. As expected, the model performed better on the training data (i.e., *MAE* = 12.1, *RMSE* = 289.2, R^2 = 0.966) compared to the test data (i.e., *MAE* = 25.1, *RMSE* = 1305.2, R^2 = 0.895). Note that the performance indicators changed based on how the training and test subsets were randomly split. The 10-fold cross-validation results (Fig. 6c) for the RF model are: a mean cross-validation score of 0.719, a median cross-validation score of 0.762 and a standard deviation of 0.166.

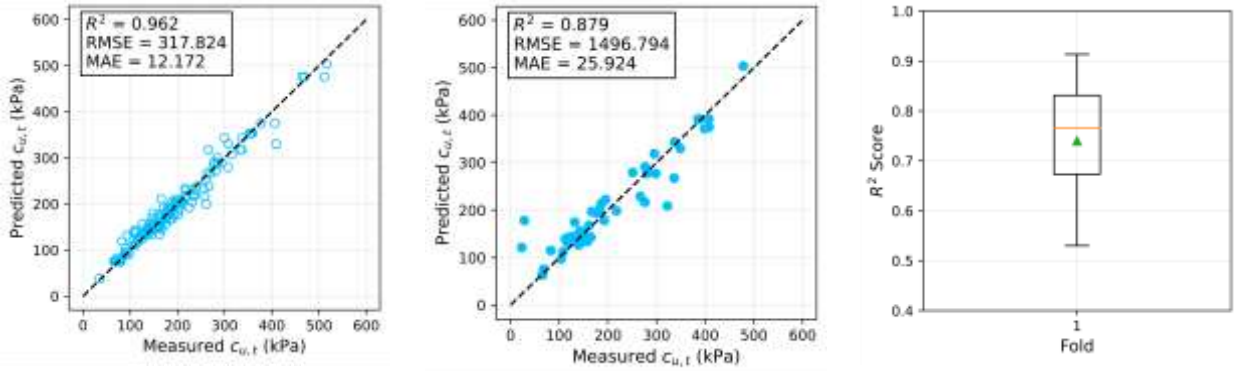
The same types of plots are presented for the GB model in Fig. 7. For the training data MAE = 12.2, *RMSE* = 317.8 and R^2 = 0.962 was obtained, while the test data resulted in *MAE* = 25.924, *RMSE* = 1496.8 and R^2 = 0.879. For the 10-fold cross-validation, a mean cross-validation score of 0.739, a median cross-validation score of 0.770 and a standard deviation of 0.122 was measured.

 © DFI International Bruges 2025



(a) (b) (c)

Fig. 6. Comparison of predicted and measured undrained shear strength with time, $c_{u,t}$, using the random forest technique: (a) training data, (b) test data and (c) cross-validation (orange line = mean, green triangle = median, whiskers based on the 1.5 interquartile range (IQR) value).



(a) (b) (c)

Fig. 7. Comparison of predicted and measured undrained shear strength with time, $c_{u,t}$, using the gradient boosting technique: (a) training data, (b) test data and (c) cross-validation (orange line = mean, green triangle = median, whiskers based on the 1.5 interquartile range (IQR) value).

A comparison between the Fig. 6 and Fig. ***7*** allows one to compare the performance of the RF and GB models. Overall, both models performed similar for the training and test datasets shown in the subfigures (a) and (b). Comparing the boxplots (subfigures (c)), however, suggests that the GB model had a slightly better general performance compared to the RF algorithm. The 10-fold cross-validation showed higher mean and median values for the GB model (i.e., mean R^2 score = 0.739 and median R^2 score = 0.770) compared to the RF model (i.e., mean R^2 score = 0.719 and median R^2 score = 0.762). However, the statistical hypothesis test to directly compare the two algorithms suggests that the RF and GB models perform similarly (i.e., P = 0.4). In other words, a significant difference between the two ML models was not observed.

Overall, both ML models provided predictions of the undrained shear strength with R^2 values exceeding 0.85. Compared to more traditional studies, which relate the strength of laboratory improved soils to the water-to-binder ratio (e.g., López Ramírez et al. (2024), Paniagua et al. (2022), Hov & Larsson (2023)), the ML algorithm predictions may result in notably lower scatter. Incorporating ML into the design of DDM, thus, can result in better estimates of the strength increase.

SUMMARY AND CONCLUSIONS

This contribution focused on latest research to improve the current practice of dry deep mixing (DDM). The work presented was generated in the ongoing research project *Green sOil stAbiLisation* (GOAL). Emphasis was placed on integrating two digital advancements, namely distributed fibre optic sensing (DFOS) and machine learning (ML) techniques in dry deep mixing practice.

The research on DFOS for DDM utilized both laboratory and full-scale experiments. The controlled experiments in the laboratory showed a complicate strain transfer mechanisms between the stabilised soil and the fibre optical cable. A full validation of this technique was found to be difficult based on the used specimen size. Additional experimental studies are currently ongoing using larger specimens to increase the bond length between the fibre optical cable and the improved soil.

 © DFI International Bruges 2025

Results from the full-scale field tests suggest that DFOS can provide strain data with high spatial resolution. In addition, measurements can be taken at different time steps after installation which enables one to better assess the field performance of stabilised soil. A current limitation of this monitoring technique is the reliable installation of the fibre optical cable in the field which requires further studies.

Research on the application of gradient boosting (GB) and random forest (RF) algorithms to predict the undrained shear strength of laboratory-improved Norwegian clays was presented. The two adopted ML models were trained and tested on the dataset presented by Paniagua et al. (2022). Both models performed similar; a significant difference was not found. The results of this investigation suggest that predictions based on the ML models outperform more traditional approaches based on the water-to-binder ratio. This finding is remarkable considering that off-the-shelf ML algorithms were used and, for example, hyperparameter tuning was intentionally not considered. Further research should be undertaken to investigate (1) what features govern the GB and RF outputs, (2) how hyperparameter tuning could improve the GB and RF predictions and (3) the performance of other ML techniques when predicting the strength of DDM soils.

This contribution showed two examples (i.e., DFOS and ML) of integrating digital advancements into DDM. DFOS sheds new light on the field performance of DDM and, thus, provides currently missing data to, for example, better verify the DDM field execution and to improve existing design procedures. The application of GB and RF techniques to DDM opens new possibilities to better predict the performance of DDM which can reduce the amount of initial laboratory and field studies. Consequently, the application of ML to DDM has the possibility to save natural resources and project expenses. In summary, the obtained results combined with ongoing research suggest that both DFOS and ML have the potential to improve the design and execution of future DDM projects.

ACKNOWLEDGMENTS

The authors wish to thank the Research Council of Norway (RCN) to fund the GOAL project (grant number 328767) and MSc Eivind Solum Rørvik and MSc Markus Nikolai Berner for their valuable contribution to this research while working on their MSc theses at NTNU. The collaboration between the consortium members of the GOAL project is greatly appreciated.

REFERENCES

Chapeleau, X. and Bassil, A., 2021. A general solution to determine strain profile in the core of distributed fiber optic sensors under any arbitrary strain fields. Sensors, 21(16), p.5423.

Das, S.K., Samui, P. and Sabat, A.K., 2011. Application of artificial intelligence to maximum dry density and unconfined compressive strength of cement stabilized soil. Geotechnical and Geological Engineering, 29, pp.329-342.

Eyo, E.U., Abbey, S.J. and Booth, C.A., 2022. Strength predictive modelling of soils treated with calcium-based additives blended with eco-friendly pozzolans—A machine learning approach. Materials, 15(13), p.4575.

Goeminne, E., Brutin, M., Benoot, J., Couck, J. and De Vos, L., 2017. Measuring vertical strains and temperature with fiber optics in diaphragm walls. In SMAR 2017-Forth Conference on Smart Monitoring, Assessment and Rehabilitation of Civil Structures.

Hov, S. and Larsson, S., 2023. Strength and Stiffness Properties of Laboratory-Improved Soft Swedish Clays. International Journal of Geosynthetics and Ground Engineering, 9(1), p.11.

Hov, S., Meland, H., Helvacioglu, A., Thurner, R. and Wist Amdal, Å.M., 2025. Distributed Fiber-Optic Strain Sensing in Deep Mixed Columns. Journal of Geotechnical and Geoenvironmental Engineering, 151(2), p.05024015.

 © DFI International Bruges 2025

L'Heureux, J.S., Carroll, R., Lacasse, S., Lunne, T., Strandvik, S.O., Degago, S., Instanes, A., Nordal, S. and Sinitsyn, A., 2017. New Research Benchmark Test Sites in Norway. In Geotechnical Frontiers 2017 (pp. 631-640).

López Ramírez, A., Zhang, Y., Forsman, J. and Korkiala-Tanttu, L., 2024. Stabilization of soft clay with sustainable binders for dry deep mixing design. Geotechnical Testing Journal, 47(1).

L'Heureux, J. S., Lindgard, A., Emdal, A., 2019. The Tiller-Flotten research site: Geotechnical characterization of a very sensitive clay deposit. AIMS Geosciences, 5(4), pp. 831-868, https://www. aimspress.com/article/10.3934/ geosci.2019.4.83

Nerve-Sensors. 2023. EspilonSensor-1. Datasheet. https://nerve-sensors.com/wp-content/uploads/ 2021/04/EpsilonSensor-1.pdf, accessed: 05/07/2023.

Oberhollenzer S., Thurner, R., Helvacioglu, N.Y., Hov, S. and Ritter, S., 2024. Baugrundverbesserung in weichen Böden – Forschungsarbeiten zum Thema Nachhaltigkeit" (Ground improvement in soft soils - research works on sustainability). 38. Christian Veder Kolloquium: Neue Herausforderungen in der Geotechnik – Nachhaltigkeit, Energiewende & Klimawandel, 4-5 April 2024, Graz, Austria (in German.).

Hov, S., Paniagua, P., Sætre, C., Long, M., Cornelissen, G. and Ritter, S., 2023. Stabilisation of Soft Clay, Quick Clay and Peat by Industrial By-Products and Biochars. Applied Sciences, 13(16), p.9048.

Paniagua, P., Bache, B.K., Karlsrud, K. and Lund, A.K., 2022. Strength and stiffness of laboratory-mixed specimens of stabilised Norwegian clays. Proceedings of the Institution of Civil Engineers-Ground Improvement, 175(2), pp.150-163.

Pedregosa, F., Varoquaux, G., Gramfort, A., Michel, V., Thirion, B., Grisel, O., Blondel, M., Prettenhofer, P., Weiss, R., Dubourg, V. and Vanderplas, J., 2011. Scikit-learn: Machine learning in Python. The Journal of Machine Learning Research, 12, pp.2825-2830.

Pham, V.N., Do, H.D., Oh, E. and Ong, D.E., 2021. Prediction of unconfined compressive strength of cement-stabilized sandy soil in Vietnam using artificial neural networks (ANNs) model. International Journal of Geotechnical Engineering, 15(9), pp.1177-1187.

Ritter, S., Rørvik, E.S., Meland, H.J., Hov, S. and Paniagua Lopez, A.P., 2024. Distributed fibre optic sensing of stabilised soil. Proceedings of the XVIII ECSMGE 2024-Geotechnical Engineering Challenges to Meet Current and Emerging Needs of Society.

Solum, E. R. 2023. Distributed Fiber Optic Sensing for monitoring stabilized clay, NTNU MSc thesis, Available at: https://hdl.handle.net/11250/3095069, accessed: 24/09/2023.

Tinoco, J., Correia, A.G. and Cortez, P., 2011. Application of data mining techniques in the estimation of the uniaxial compressive strength of jet grouting columns over time. Construction and Building Materials, 25(3), pp.1257-1262.

Tinoco, J., Alberto, A., da Venda, P., Gomes Correia, A. and Lemos, L., 2020. A novel approach based on soft computing techniques for unconfined compression strength prediction of soil cement mixtures. Neural Computing and Applications, 32(13), pp.8985-8991.

Yong-Feng, D., Tong-Wei, Z., Yu, Z., Qian-Wen, L. and Qiong, W., 2017. Mechanical behaviour and microstructure of steel slag-based composite and its application for soft clay stabilisation. European Journal of Environmental and Civil Engineering, pp.1-16.

Zhang, W., Li, H., Li, Y., Liu, H., Chen, Y. and Ding, X., 2021. Application of deep learning algorithms in geotechnical engineering: a short critical review. Artificial Intelligence Review, pp.1-41.

Åhnberg, H., 2006. Strength of Stabilised Soil-A Laboratory Study on Clays and Organic Soils Stabilised with different Types of Binder, PhD dissertation. Lund University, Sweden.

 © DFI International Bruges 2025

EVALUATION OF VIBRATION MEASUREMENT IN JET GROUTED ELEMENTS

Nikolaus Schneider, GuD Consult GmbH, Berlin, Germany 0049-30-7890890, schneider@gudconsult.de
Elisa Kant, GuD Consult GmbH, Germany, 0049-30-7890890, kant@gudconsult.de

ABSTRACT

Jet grouted seals are an established construction method to build watertight excavation pits in inner city areas. Environmental aspects focus to prevent ground water draw down outside of the construction site by implementing bottom seals for excavation pits. This article introduces a new type of quality monitoring by which the vibrations in the primary columns are read while jetting the secondary columns. The present state of the art focusses on the recording of the execution parameters as applied for the test columns. The new concept refers to recorded signals from installed sensors to evaluate the contact between the primary and secondary columns. Field tests have been carried out in Berlin to explore the influence of the type of construction joints, the relevant distance of sensors to the jetting location and the curing time of the hardened columns. The results allow to develop acceptance criteria for a proper connection of new to old columns.

Keywords: jet grouting, watertight excavation pits, structure borne noise, primary columns, secondary columns

APPLICATION OF JET GROUTING

The support of existing buildings in the vicinity of deep excavation pits in inner city areas demonstrates the versatile application of jet grouting. When applying jet grouting, a high-pressure jet beam with cement slurry or water erodes the adjacent ground and forms a column. This allows to construct a wide range of underground elements, such as:

- Underpinning structures
- Improvement of existing foundation
- Gap closure for sealing purpose
- Bottom seals for excavation pits.

The jet grouting technique has undergone systematic improvements in recent years. A key technique is the implementation of inclinometers inside the drilling rod that allows to read the deviation of the drilling rod while drilling and the recording of structure borne noise in hardened columns triggered by the energy impact of the high-pressure beam.

THEORETICAL BACKGROUND TO THE GEOMETRIC DETERMINATION OF JET GROUTED TEST COLUMNS

The jet grouting process is always associated with energy input into the subsoil. The jet beam cuts through the existing soil and swirls it with the water-cement slurry introduced. If the high-pressure beam meets already hardened jet grouted columns, a force impulse is introduced into the column. Within the column, the induced structure-borne sound essentially propagates in the form of compression waves with a high propagation speed. This physical effect is used to determine the moments at which the jet hits and leaves the column using suitable sensors.

By measuring the structure-borne noise in the hardened column, it is therefore possible to clearly distinguish when the jet beam passes through the surrounding subsoil or hits a jet grouted column. As long as the jet beam cuts through the ground, the resulting ground vibrations are characterized by the fact that the high-frequency components of the signals in particular are strongly attenuated and the amplitudes decrease very quickly. When the jet beam hits the hardened jet grouted column, the structure-borne sound waves propagate in the column in a broadband manner, i.e. in a wide frequency band, due to the higher strength of the column material compared to the ground.

This difference in terms of structure-borne sound propagation in cured jet grouted columns and in the ground is used to detect the overlap of the jet beam with the cured column. The diameter of the cured columns is calculated based on the measured contact time of the jet beam with the cured column and concluded distance of the jet grouting rod to the center of the cured column.

 © DFI International Bruges 2025

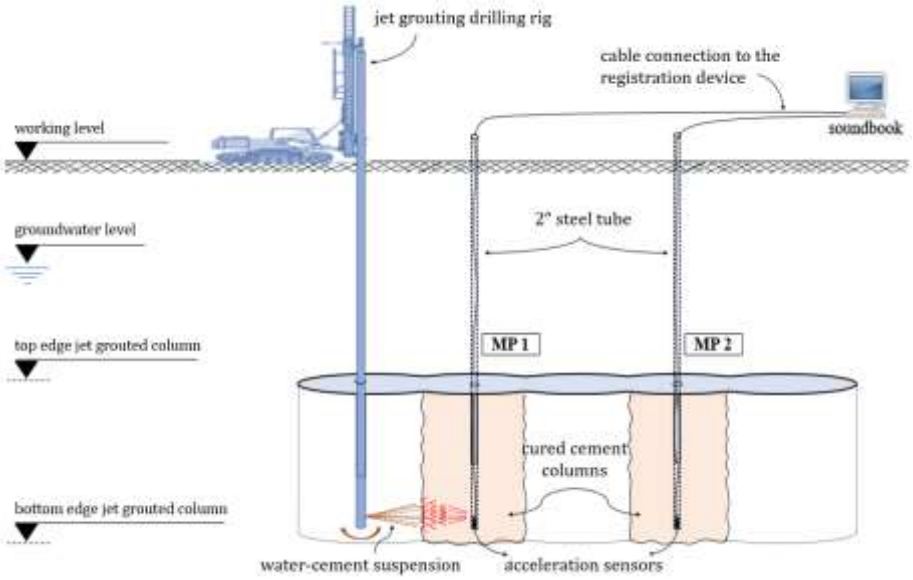


Fig.1: Test arrangement for the test column measurement

DATA ACQUISITION AND EVALUATION

The structure-borne sound in the cured column is recorded using an acceleration sensor. This is placed in the center of the column. To register the relevant frequency components of the signal, the analog signal is digitally sampled at a high sampling rate.

Figure 2 shows a typical acceleration-time curve during a jetting process. The diagram illustrates the rise and fall of the signal and thus the beginning and end of each contact of the jet beam with the column to be measured. In this application example, the signal is repeated approx. every 9 s and has a duration of approx. 2 s. Between the signals attributable to the contact of the jet beam with the cured column, structure-borne sound signals with lower amplitudes are recorded. This reduced vibration excitation is due to the smaller stabilizing nozzle located opposite the main nozzle.

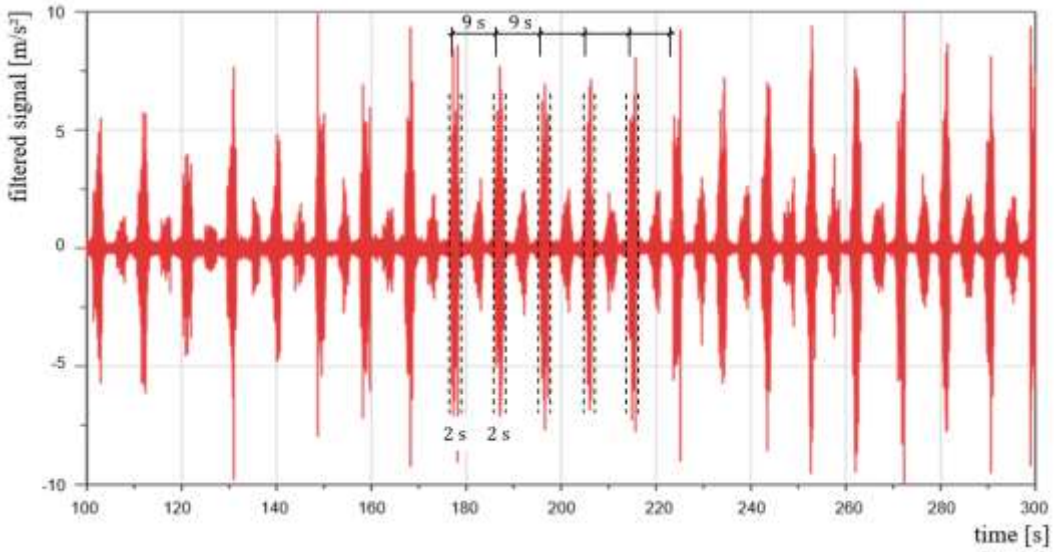


Fig.2.: Time curve of the vibration acceleration in a hardened column

A spectrogram (Fig. 3) can be used to illustrate the time-varying frequency content of the recorded vibration signal. The structure-borne sound components with the highest energy (yellowish) occur during the contact of the jet beam with the column and are generally in a frequency range between 1 kHz and approx. 6 kHz.

 © DFI International Bruges 2025

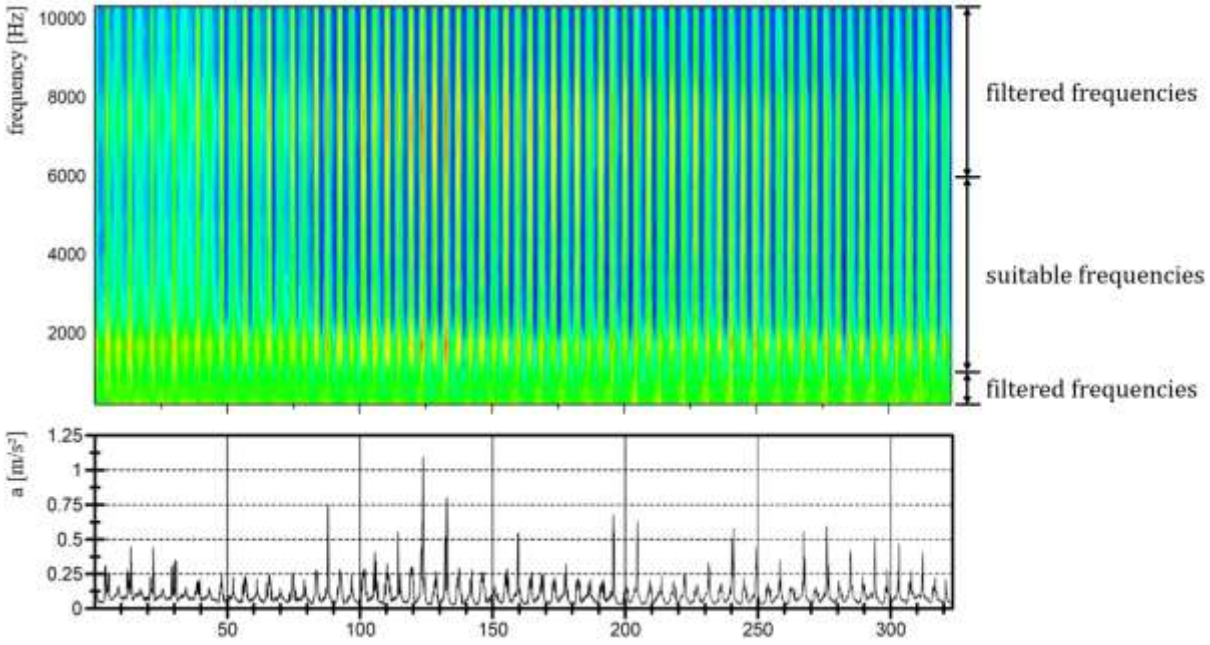


Fig.3: Spectrogram visualizing the time related frequency content of the acceleration signal

Further processing of the acceleration time signal is conducted using

a) suitable bandpass filter in the range of the relevant frequency content (e.g. 1 kHz to 6 kHz);

b) the calculation of moving effective values (RMS values: Root Mean Square) with a suitable time window length (equation 1)

$$a_{RMS} = \sqrt{\frac{1}{\tau}\int_{t_1}^{t_2} a^2(t)} \qquad \text{with } t_2 - t_1 = \tau \text{ (e.g. } \tau = 0.1 \text{ s)} \qquad (1)$$

c) reduction of the RMS- measurement data through classification.

The exact parameters for the limits of the bandpass filter and the sliding time window of the RMS value formation may differ slightly depending on the project or the given boundary conditions. The advantage of using the described bandpass filter is that only the signals that are attributable to the jetting process are included in the further evaluation. Rather low-frequency vibration excitations resulting from general construction site operation - including the motor and drilling operation of the drill itself - are thus filtered out of the relevant signal. The RMS-value formation enables the temporal representation of the energy of the structure-borne sound signal and generally leads to an increase in the significance of the recorded events.

The result are effective values as shown in Figure 4, from which the contact times can be read.

 © DFI International Bruges 2025

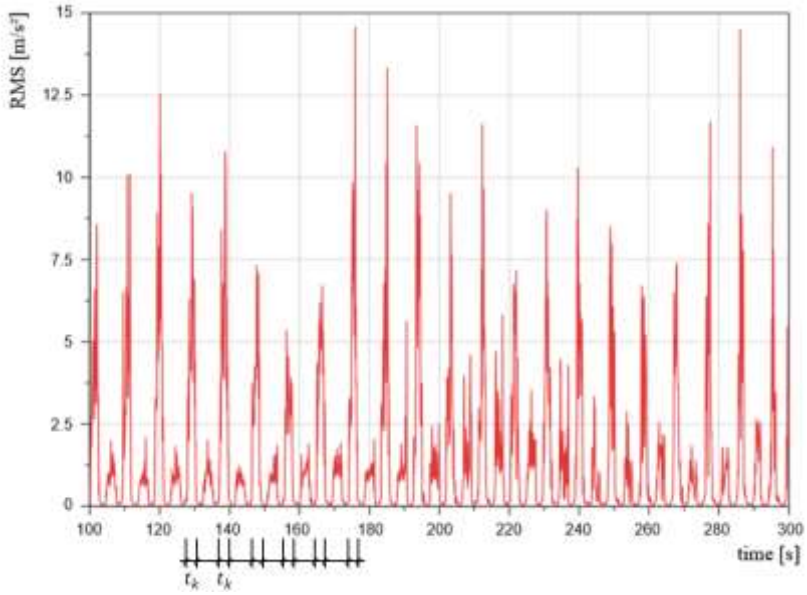


Fig.4: Example of the RMS-values of the filtered signal (1 kHz)

By determining the contact time t_k per rotation, the column diameter can be calculated considering the distance between the drilling rod and the center of the cured column. The basis for calculating the diameter is the application of Thales' theorem (Fig.5). This states that in a circle whose diameter represents the distance between the center of the test column and the agitating jet beam, all angles are perpendicular to the circumference of the circle. The angle between a diameter and any secant of the semicircle is therefore always 90°.

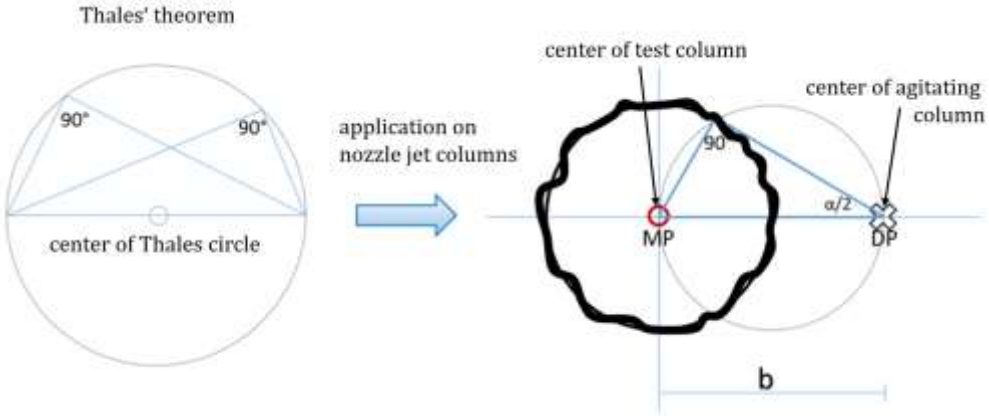


Fig.5: Sketch for calculating the diameter of a cured column

By measuring the contact time of the jet beam with the cured column, the angle at which the right-angled triangle is to be formed in the Thales-circle is determined. The radius of the cured column can be derived from this using simple trigonometric relationships. This conclusion assumes that distance b does not exceed a specified value, as outlined in equation 3.

$b < \frac{D}{\sqrt{2}}$ D = diameter of the excitation column or cured column (3.)

If the distance b is greater, the radius of the hardened column can be determined assuming that both columns have the same diameter (Fig. 6).

 © DFI International Bruges 2025

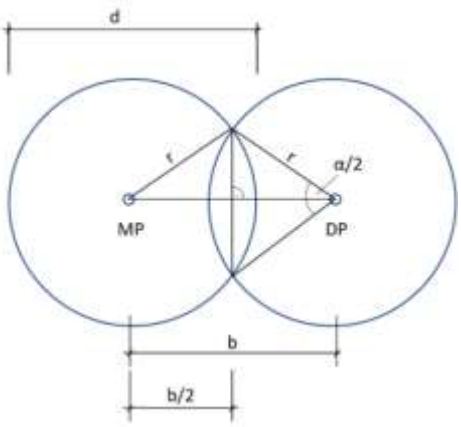


Fig.6: Sketch for calculating the diameter of a cured column with larger distance b

The radius r can then be solved using the trigonometric relationship (see equation 4):

$$\cos(\alpha/2) = \left(\frac{b/2}{r}\right) \quad (4.)$$

Convert equation 4 to the radius r:

$$r = \frac{b/2}{\cos(\alpha/2)} \quad (5.)$$

The diameter d is then obtained by doubling the radius r (see equation 6):

$$d = \frac{b/2}{\cos(\alpha/2)} \times 2 = \frac{b}{\cos(\alpha/2)} \quad (6.)$$

Each contact of the jet beam with the cured column allows conclusions to be drawn about the geometry of the test column. By pulling up the nozzle jet rods when jetting the sample column, contact times are created with each revolution, which can be evaluated. As a result, the test column is made up of discrete disks with corresponding diameters. This results in the 360°-profile of the test column when executed from both sides, as shown in Figure 7.

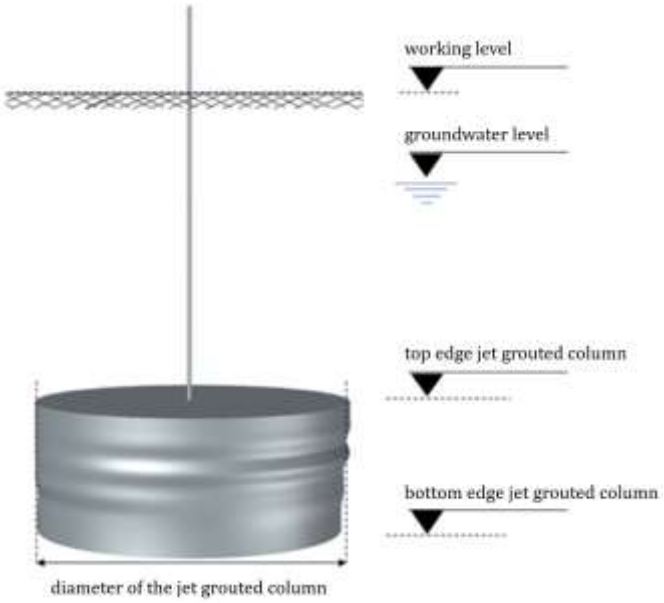


Fig.7: Geometry of the evaluated test column.

 © DFI International Bruges 2025

QUALITY MONITORING IN COMPOSED JET GROUTED STRUCTURES

The structure-borne sound input of a high-pressure jet can also be detected in composed jet grouted structures and evaluated regarding quality assurance. The prerequisite for this is the positioning of structure-borne sound sensors in the primary rows produced. As a rule, jet grouted columns are produced in primary and secondary rows. The production sequence is shown in Figure 12 in green and blue.

The primary rows are cured when the secondary columns are produced. This production sequence makes it possible to monitor the execution of the secondary rows, using the structure borne noise in the cured primary columns. to evaluate them according to defined quality criteria.

The decisive factor for the quality of a watertight seal is the actual connection of the secondary columns to the hardened primary columns. The construction plan, which includes the drilling points of all columns, is usually designed so that the center of the secondary columns is opposite the overlap of the primary rows. The contact of the secondary column with the primary column that occurs at this position during jetting generates a characteristic measurement signal on the sensor of the primary column that is repeated during the production of each secondary column.

FOUR CHARACTERISTICS OF A CONTACT SIGNAL

Following the conclusions of Eberhardt, S.A. (2024), four basic characteristics of a contact signal can be distinguished, which are generated when the secondary columns get in contact with the primary columns:

1. The **standard case** captures both already cured primary columns and reaches the critical point of the gusset as planned with the nozzle jet. This can be seen in the effective value signal of the acceleration (RMS = Root Mean Square) (Fig. 8).

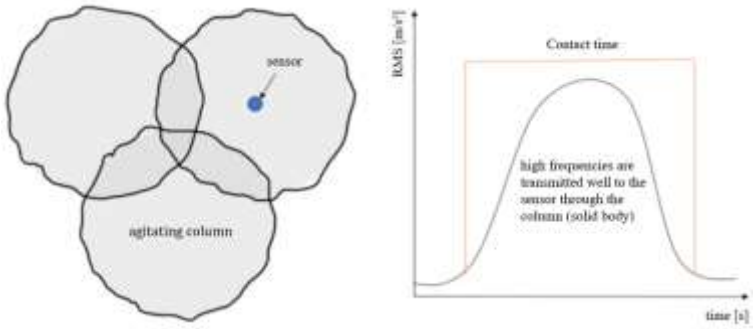


Fig. 8: Expected contact

2. In contrast to the normal case, there is the so-called **gusset defect** (Fig. 9). In this case, the geometrically most distant point (gusset) was not completely eroded. In the recorded signal, it is characterized by a clear amplitude reduction in the RMS-values of the acceleration.

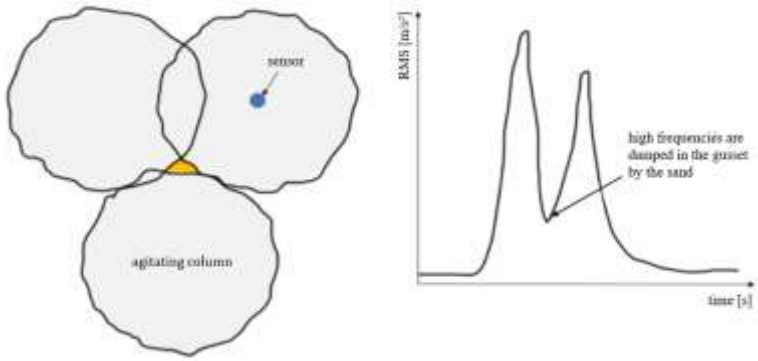


Fig. 9: Gusset error

 © DFI International Bruges 2025

3 If, on the other hand, only one of the two opposing pillars is projected in the case of a **one-sided contact**, this is represented by a one-sided shift in the RMS-acceleration curve (Fig. 10).

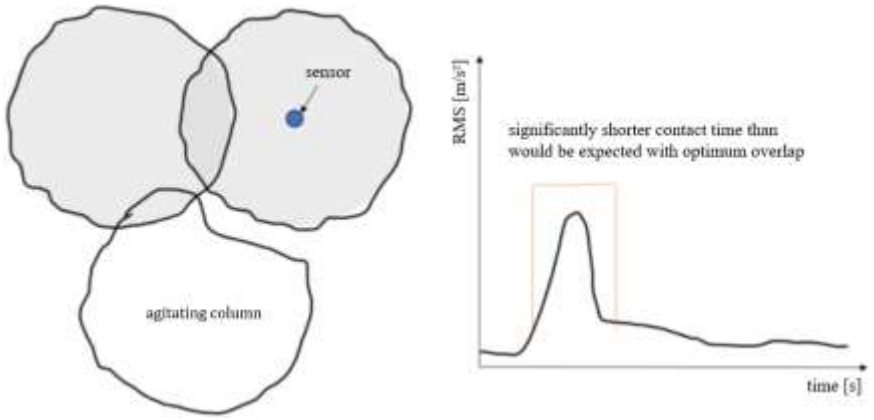


Fig. 10: One-sided contact

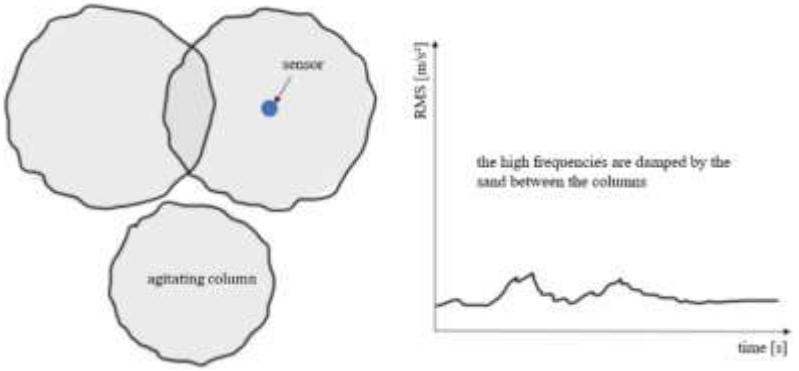


Fig. 11: No overlap

4. If there is **no direct contact** between the nozzle jet and the cured primary rows, the high frequency components of the structure-borne sound signal are strongly attenuated and only transmitted to the primary column to a small extent. The amplitudes of the RMS-values are correspondingly small

These basic signal characteristics represent reference profiles that enable monitoring the connection of the secondary columns to the primary columns during installation.

Recording and evaluating the vibration signals according to these patterns introduces a new form of verification of contact-compliance. The basic test results suggest that the sensors can be positioned up to approximately 7.50 m from the nozzle source and still record sufficiently high-quality structure-borne sound signals in the primary column. It is therefore not necessary to install sound sensors in each primary column for the continuous detection measurements.

These acceptance criteria allow to implement sensors in primary columns in a regular pattern and enable a continuous quality check of the contact of primary and secondary columns. Upgrading every 6th primary column with a sensor in a row provides adequate quality assurance. The sensors are either installed in steel tubes or lost, in case of execution without steel tubes. Reference is the transmission of structure borne noise over 7,50 m from the location of jetting to the location of the sensor.

 © DFI International Bruges 2025

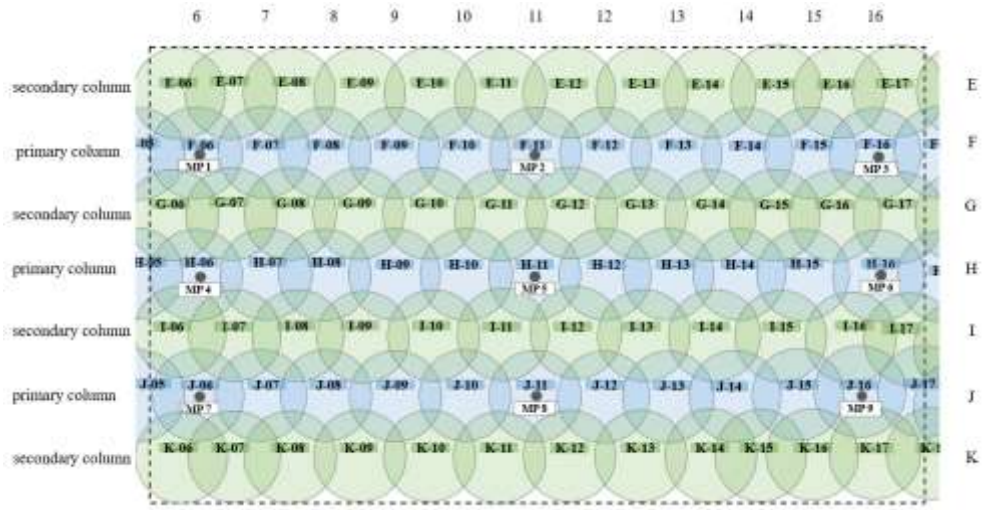


Fig. 12: Systematic location of acceleration sensors in a bottom seal

The influence of the type of construction joint in the grouting sequence was investigated in more detail by Kant, E. (2023) and found to be negligible. The curing of the primary columns within the regular execution times does not play a significant role for the distance grid of the measuring sensors. The diagram in Fig. 13 contains the processing of signals derived from a power density spectrum and shows that meaningful evaluations can still be made even at 7.50 m between the sensor and the nozzle rod.

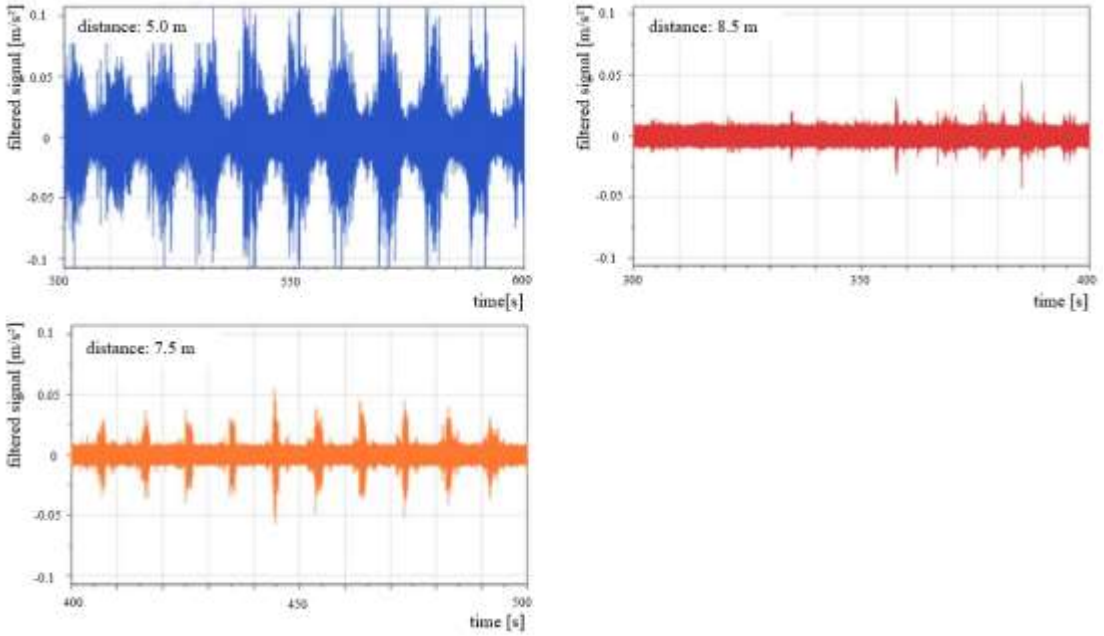


Fig. 13: Distance related signal strength of structure borne noise in primary columns

DETECTION OF UNERODED AREAS

Uneroded areas due to unknown subsoil obstacles contribute a significant project risk. Obstacles in the path of the high-pressure jet block the cutting effect behind it and create interference zones that are larger than the actual obstacle. Such obstacles can be old wells that are not recorded in the as-built documentation, lost exploratory/drilling rods or randomly found boulders. (see Fig. 14).

 © DFI International Bruges 2025

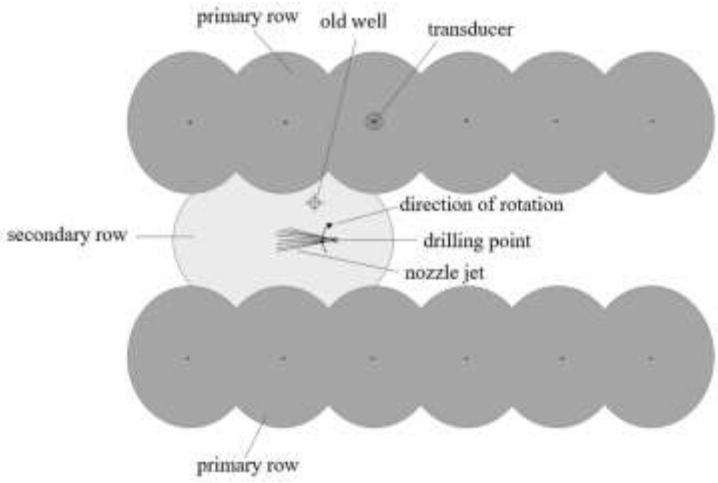


Fig. 14: Site plan of jet grouted bottom seal with uneroded areas caused by an old well

The risk of uneroded areas can be significantly reduced by measuring structure-borne noise in cured primary columns during execution. The structure-borne sound measurement can indicate possible obstructions if the high-pressure beam does not generate the expected signals. Regular disturbances in the signal transmission manifest themselves with every revolution and at all depths. Obviously, the nozzle jet is impaired by an obstacle, which likely leads to uneroded areas. (Fig. 15). If such anomalies are detected during construction, additional columns reduce risk with little effort.

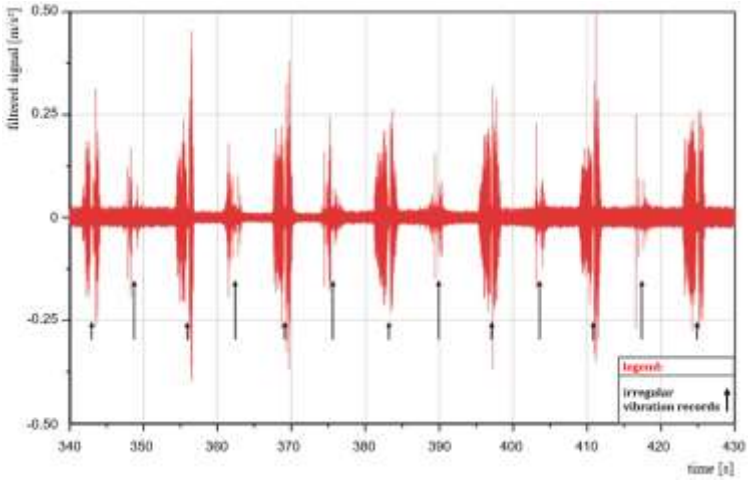


Fig. 15: Signal recordings triggered by uneroded obstacles

SUMMARY

According to the current state of the art, the jetting parameters are verified on test columns and repeated for each column thereafter. This is done under the assumption that the encountered soil conditions are comparable to the ground conditions at the test columns. Jetting against hardened columns with built-in vibration sensors allows to confirm the geometry of the transition between old and new columns by reading the signals of the vibration sensors. This is an immediate control of the jetting parameters.

This technical innovation, adopted for the construction of bottom seals with primary and secondary rows, supports the quality assurance during construction based on contact criteria recorded by vibration sensors. The evaluation of recorded signals allows to monitor the integrity of composed jet grouting structures during construction. In case of unexpected signals, corrective measures like additional columns can be constructed in short-term, while all the equipment is still on site.

 © DFI International Bruges 2025

CONCLUSIONS

The technical success of bottom seals in combination with the watertight retaining walls is usually checked by a test lowering phase inside the trough in which the ground water is lowered prior to the excavation works. Temperature measurements of the groundwater trapped in the bottom sealed excavation pit are carried out during this test phase to identify temperature changes during the lowering of the groundwater in the trough. As a possible result, conclusions about leaks can be drawn in the excavation pit walls or the jet grouted bottom, namely where cold water from outside flows into the warm water in the trough.

In preparation for this test phase, additional tubes are usually drilled in a standard grid and equipped with temperature sensors. This time-consuming localization of possible leakages could be replaced by the structure-borne sound measurements in primary columns described above. The contact between the individual jet columns can already be tested during construction. The implementation of additional tubes and their upgrading with temperature sensors is cost-intensive and requires additional construction time, which can be significantly reduced with structure-borne noise measurements during construction.

Another aspect of more efficiency in the construction process could be the improvement of the transmission width of the structure borne vibration as it is limited. So far, a distance of 7,50 m between stimulator and receiver has been evidenced by site tests. More site tests are recommended to increase this distance by additional elements like selected cement components or steel fibers mixed into the cement slurry.

REFERENCES

[1] DIN EN 12716-2019-03: *Execution of civil engineering works - Jet grouting*. Berlin: Beuth.

[2] DIN EN 12715-2021-01: *Execution of civil engineering works - Injections*. Berlin: Beuth.

[3] Kant, E. (2023) Investigations of jet grouting induced structure-borne noise in primary columns at the Pergamon Museum construction site, considering different distances, curing times and joint formations of DSV columns typical of the process (unpublished master's thesis). Technical University of Berlin.

[4] Eberhardt, A. S. (2024) The evaluation of vibration measurements from construction site tests to derive geometry criteria for jet grouting (unpublished master's thesis). Technical University of Berlin.

 © DFI International Bruges 2025

A CASE STUDY OF UTILISING DIGITALISATION TECHNIQUES TO ACHIEVE EFFICIENCY AND CARBON BENEFITS DURING PILING PROJECTS.

Ian Chong, Author, Ramboll, United Kingdom, ianchong100@gmail.com
Michael Trubshaw, Contributor, Ramboll, United Kingdom Michael.trubshaw@ramboll.co.uk
Kalisha Sejpar, Contributor, Ramboll, United Kingdom, kalisha.sejpar@ramboll.co.uk
Sofia Michelaki, Contributor, Whitby Wood United Kingdom, michelaki.sofia@gmail.com

ABSTRACT

This study demonstrates how digitalisation techniques can be employed to develop a comprehensive database of piling projects specifically focussing on Continuous Flight Auger (CFA) piling, enabling valuable insights into sustainability and cost reduction. These techniques streamline the monitoring of construction progress, and allows designers or contractors to efficiently undertake quality assurance and identify issues during construction, despite the current lack of a standardised data transfer method. Python and Optical Character Recognition (OCR) techniques are used to rapidly extract the relevant data from the site records of 1,092 piles across five historic piling jobs and compile them into a single database. This process is both quicker and less error-prone than traditional manual methods. Insights derived from such a piling database can enhance collaboration between designers and contractors in developing sustainable and cost-effective pile design and construction by reducing on-site material consumption. Increasing the size of the database over time will further benefit the decision-making process and generate actionable insights, enabling greater efficiencies in pile design and reducing the embodied carbon of piled foundations.

Keywords: Sustainability, Digitalisation, Concrete Overbreak, Embodied Carbon

INTRODUCTION

Piling techniques have been extensively utilised in foundation construction and have gained increasing popularity since the nineteenth century. While timber piles existed during Roman times, piling methods evolved to include large-diameter bored concrete piles in the 1950s for high-rise construction (Rutty, 2021). These technologies have continuously advanced to enhance efficiency and meet growing construction demands. This research focuses primarily on analysing construction data related to Continuous Flight Auger (CFA) piling, because unlike traditional rotary bored pile rigs, CFA rigs can automatically record detailed pile construction data. The availability of such automated reports can assist designers and contractors in identifying construction issues in real time and formulating mitigation strategies in collaboration.

Although CFA piling is a well-established technique extensively used by contractors in the United Kingdom and worldwide, there is no standardised format for sharing digital data acquired during the pile's construction. Pile construction data is often published in PDF reports generated by piling rigs. This practice makes analysing pile construction data more time-consuming and challenging. This situation stands in contrast to UK ground investigation data, which is typically shared using the industry-standard Association of Geotechnical & Geoenvironmental Specialists (AGS) format.

The solution is straightforward, there is a need to establish and adopt a digital data-sharing standard for piling information. Encouragingly, efforts are being made in this direction, as discussed in a paper presented at the Piling 2020: Proceedings of the Piling 2020 Conference (Boddy, Pennington, & Chadwick, 2021). In addition, the AGS, has also recently updated their AGS piling roadmap which targets a beta first release in early 2025 (AGS, 2025). However, until an industry-wide standard is formalised, automation tools such as Optical Character Recognition (OCR) and Python programming

 © DFI International Bruges 2025

can be used to convert PDF reports into accessible formats such as Microsoft Excel for easier analysis. This approach is outlined in greater detail in the Methodology section of this paper.

THE BENEFITS OF DIGITALISATION

Standardising digital data transfer for pile construction data offers several key advantages. Firstly, organising the information in a dataset rather than individual pile logs allows designers to visualise the records of all the piles simultaneously while quickly identifying any errors, trends, or outliers. Although it is possible to interrogate the pile logs individually, as often practised, this process might not capture trends or outliers as easily. Such a tool would help designers and contractors during the monitoring of the piling works, providing the opportunity to utilise data analytics to inform potential improvements and mitigations as the construction progresses. These tools and processes will deliver time and material savings, thereby ensuring the project is delivered on schedule and within budget, which will significantly benefit the clients. In addition, this format of data is more easily stored and accessible for future reference, providing valuable insights into risks and opportunities across many different sites. To complement this, machine learning algorithms could be utilised to enable predictive analytics to ensure pile integrity.

The ground engineering industry, particularly foundation construction, contributes significantly to embodied carbon. While structural engineers can accurately estimate material quantities and carbon emissions for superstructures using advanced tools like 3D models and Building Information Modelling (BIM), foundation designs often receive less attention. This oversight can result in inefficient material use, and an increased embodied carbon footprint. Designers and contractors should implement sustainable practices to optimise resource efficiency and reduce embodied carbon for foundation designs. Implementing the digitalisation techniques discussed in this paper enables such practices.

This paper investigates overbreak in piling construction, a critical metric that quantifies the excess consumption of concrete during pile installation. While overbreak has traditionally been viewed as a quality control measure and indicator of pile integrity, it can also serve as a valuable sustainability metric for piling works. If not carefully managed, overbreak can substantially increase carbon emissions. By implementing the digitalisation techniques described in this paper, the extent of overbreak and the associated embodied carbon can be monitored throughout the piling process. These values can then be compared with the embodied carbon estimated during the detailed design phase.

Although overbreak has not been widely studied, several factors are known to influence it. These include piling techniques, pile dimensions, support fluid types, workmanship, and specific ground conditions, such as soft or loose soils, the presence of boulders, cavities, or other obstructions requiring removal. This paper examines the overbreak from different sites across the UK and evaluates associated links with pile dimensions and specific ground conditions. While in the industry the common standard for overbreak target ranges from 15% to 25% (Cruz, 2017); as there are no defined limits, this target is often variable. Similarly, overbreak is commonly measured without yielding any particular actions on process improvements or corrections. The use of digitalisation techniques will support designers and contractors in establishing a more robust range of overbreak targets and enable measured overbreak to be used as an effective indicator of potential problems during construction.

METHODOLOGY

To create the dataset of all the pile logs for a project, the initial procedure involves extracting the individual PDF pile construction data into a spreadsheet. Automation tools such as Python offer clear advantages for this task, reducing the need for repetitive manual input. As demonstrated in this paper,

 © DFI International Bruges 2025

these tools significantly reduce the time spent and minimise human error while enabling analysis of large-scale data.

Two main types of structured pile log PDFs are encountered in this workflow. The first is a PDF where text can be selected and copied relatively easily, allowing for a straightforward conversion process, provided the formatting is consistent. The second type consists of PDFs where the text cannot be selected, either due to file settings or because the PDF is a scanned document. The latter can introduce recognition errors, such as misinterpreting numbers as letters or extracting incorrect information.

For this analysis, the PDFs that can be easily processed by code (i.e., the first type) are converted into unformatted text files using the python library PDFPlumber (pdfplumber, 2024). This conversion occurs line by line, after which each line is split by whitespaces to form rows and columns. Assuming the PDF structure remains consistent, the position of the relevant data can be noted and subsequently extracted for each pile log. It is important to note that because different contractors use slightly varying formats for their pile logs, the process of creating the extraction code will need to be adapted for each project.

For PDFs that cannot be directly read by code, Optical Character Recognition (OCR) must first be applied. OCR converts the PDF into an image file and then detects and converts text or numbers from the image. The accuracy of the output after OCR application depends heavily on the quality of the PDF. Consequently, the rows and columns of different pile logs are highly unlikely to align, making the previous approach unsuitable for this scenario.

There are multiple tools that exist with the purpose of PDF conversion to other formats; one of which is Microsoft Power Automate. This versatile tool includes the functionality of extracting information from PDFs. Notably, it can process scanned PDFs automatically by applying OCR as a first step. To begin the extraction process, users must provide at least five similar PDFs and specify the location of the necessary variables for extraction. According to Microsoft, the tool utilises Artificial Intelligence (AI) and machine learning to accurately extract data directly into a Microsoft Excel file. While there is still potential for errors in the output, Power Automate still offers significant advantages compared to the manual processing of pile logs.

An example CFA log is shown below (see Fig. 1). The green box represents data which can be extracted relatively easily, and has been the focus of this study, while the red box contains data which is challenging to extract. The example output from the extraction process is shown in Table 1.

For this study, piling logs from five sites in the UK have been compiled and processed. This totals 1,092 piles, with diameters ranging from 300mm to 900mm. All the piles analysed were CFA piles. The contractors for all sites were different, except for Sites 5A and 5B, which share the same contractor. Site 5A, 5B, 5C are all located in the same area with similar ground conditions. The details of each site are presented in Table 2.

 © DFI International Bruges 2025

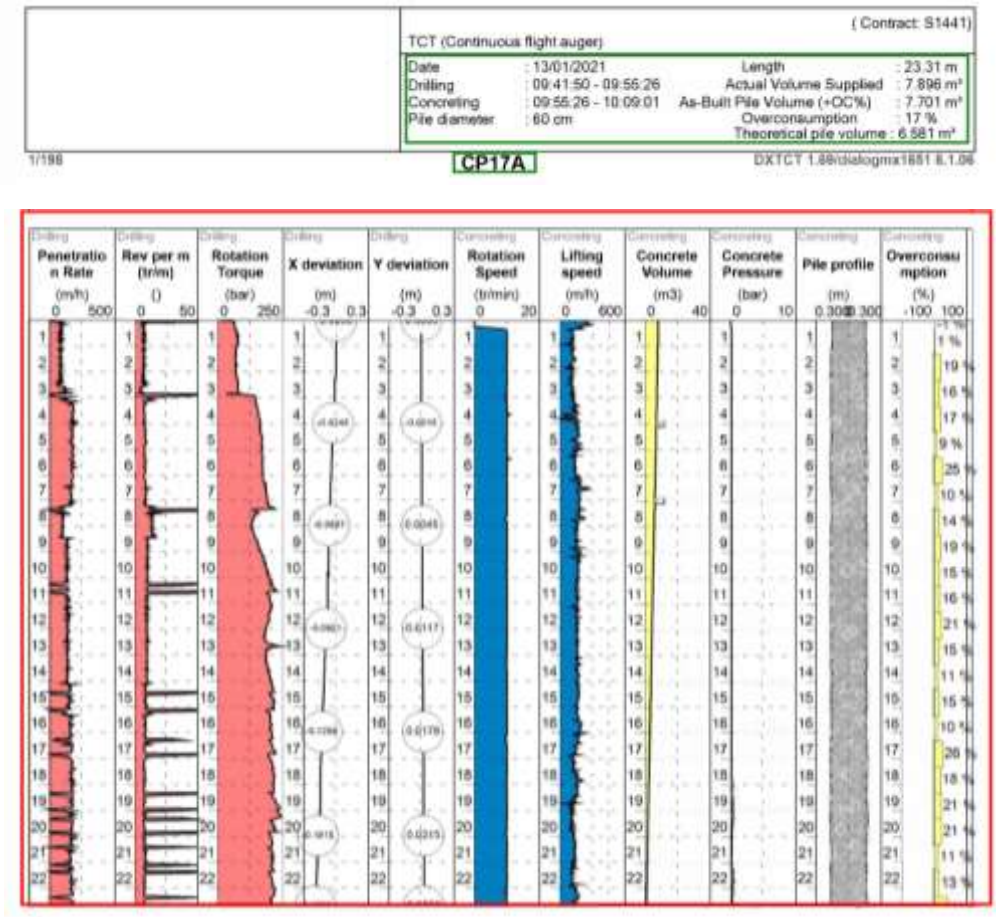


Fig. 1: Example of a CFA log.

Table 1: Example data extraction output from CFA pile logs.

Pile ID	Pile Diameter (mm)	Date	Actual length (m)	Actual concrete vol (m3)	Overbreak (%)
CP17A	600	13/01/2021	23.31	7.896	17
CP18A	600	13/01/2021	20.28	7.896	19
CP19A	600	12/01/2021	22.73	7.938	18
CP20A	600	12/01/2021	20.79	7.77	21

Table 2. Details of each site analysed.

Site	Year	No. of piles	Location	Ground conditions
Site 1	2015	223	Stratford, UK	MG, RTG, LMB, TS
Site 2	2017	228	Wandsworth, UK	MG, KPGR, LC
Site 3	2022	645	Tottenham, UK	MG, ALV, RTG, LC, LMB
Site 4	2022	169	Reading, UK	MG, TG, UCK
Site 5A	2018	102	Camden, UK	MG, LC, LMB
Site 5B	2022	29	Camden, UK	MG, LC, LMB
Site 5C	2022	118	Camden, UK	MG, LC, LMB

(1) MG – Made Ground, RTG – River Terrace Gravels, KPGR – Kempton Park Gravel Member, TG – Taplow Gravels, LMB – Lambeth Group, UCK – Upper Chalk, TS – Thanet Sands.

 © DFI International Bruges 2025

RESULTS AND EVALUATION

The following variables were summarised and compared.

1. The distribution of overbreak for each site (See Fig. 2).
2. The number of piles, average overbreak, and embodied carbon (tCO2e) for each site (See Table 3).
3. The average overbreak percentage for different pile diameters across site (See Fig. 3).
4. Overbreak of embodied carbon normalised by pile length (tCO2e/m) for various pile diameters in each site (See Fig. 4).

The results indicate significant variation in concrete overbreak percentages across the sites, deviating from the typical industry standard range of 15–25%. The maximum average overbreak reaches 34% (See Table 3). However, for Sites 1 to 4 (See Fig. 2), some piles exhibit overbreak levels far exceeding these averages.

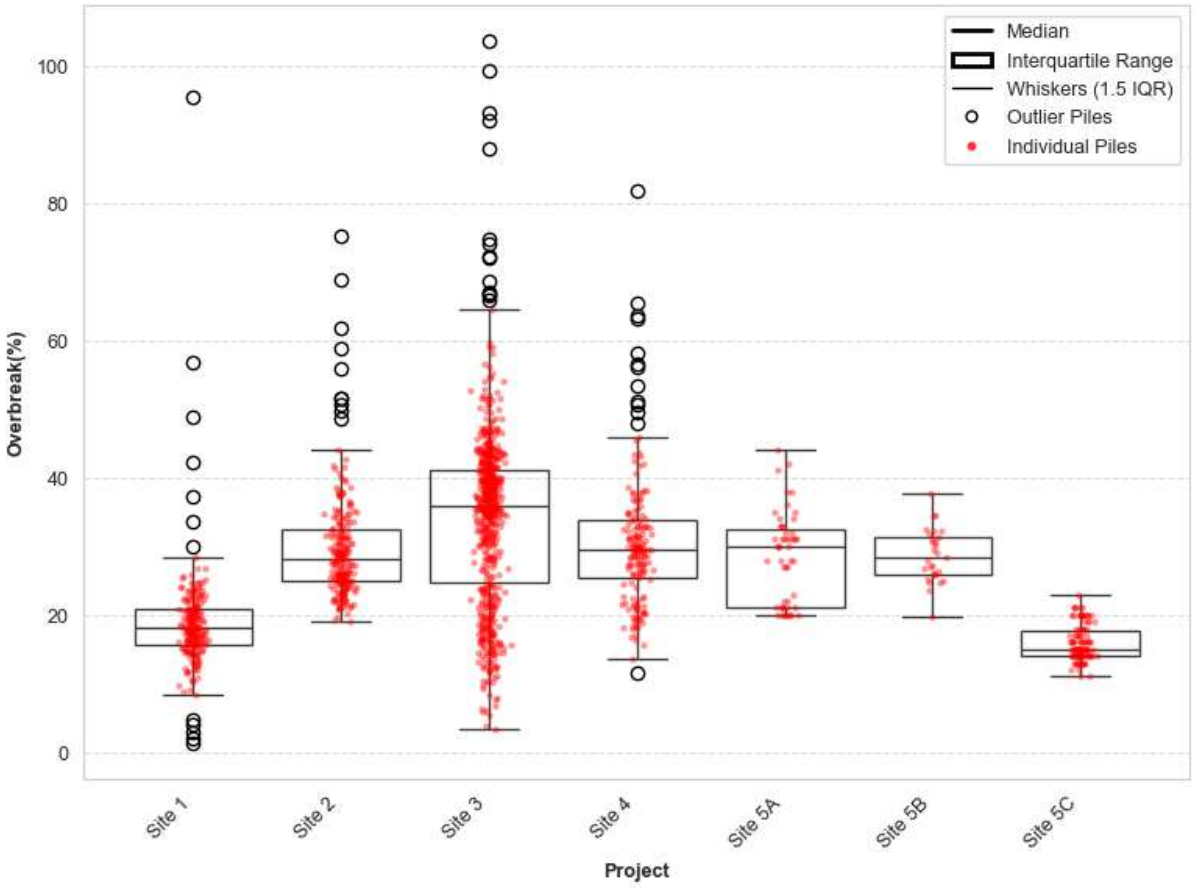


Fig. 2. Distribution of overbreak for each site.

A retrospective analysis of the piling information for Site 2 and Site 3 indicates that both sites encountered challenging ground conditions. The high percentage of overbreak encountered was attributed to potential overflighting of the rig bore. Overflighting occurs when the rotation speed of the auger is excessive relative to its penetration rate, causing excessive removal of the soils. Furthermore, based on the account of the designer, it was noted that the exchange of information between contractor and designer for those two sites was slow and infrequent. Although it is included in the ICE Specification for Piling and Embedded Retaining Walls (ICE, 2017) that piling log information should be provided within 24 hours after construction of the pile, this is often not enforced. However,

 © DFI International Bruges 2025

contractors have generally shown improvement in their practices, typically submitting piling log information in weekly batches.

At Site 2, settlement issues emerged during the pile construction phase. The potential underlying causes were identified as the presence of voids, excessive loading due to large piling rig operation, and overflighting during piling works. Although not a trivial issue to resolve entirely, had this tool been employed during the actual construction, the relatively high levels of overbreak in some piles could have been identified. This supplementary information could have been used to raise concerns, and query potential overflighting issues with the contractor, potentially avoiding costly remedial works. Overflighting issues are usually identified by visually inspecting the graphs in Fig. 1. The current analysis does not yet account for this aspect, which could be a further development of this tool and is discussed in the Limitations section of this paper.

Compared with Sites 5A, 5B, and 5C, the collaboration between contractor and designer was noted to be more apparent based on the account of the designer. This has potentially contributed to better overall workmanship and lower percentages of overbreak achieved. However, although the sites are located in the same area and share similar ground conditions, the average overbreak reported across Sites 5A/5B and 5C varies noticeably (See Fig. 3). This discrepancy could be attributed to differences in contractors and the target overbreak ranges set by each contractor. The absence of a more rigorous and standardised target setting within the industry may further contribute to this inconsistency.

The A1-A3 carbon emissions in tC02e (See Table 3) were calculated based on carbon factors included in the 2022 version of the National Highways Carbon Tool (National Highways, 2022). These factors directly relate to the concrete mix used at each site. The emissions from the reinforcement of the pile cages were not considered.

Table 3. Table summary results for each site.

Site	No. of Piles	Pile length (m)	Average Pile length (m)	Total Carbon (tC02e)	Overbreak Carbon (tCO2e)	Average Overbreak (%)
Site 1	223	21.0 - 28.1	26.9	878.76	165.00	18.8
Site 2	228	10.3 - 29.0	24.1	416.36	116.52	29.8
Site 3	645	13.0 - 21.8	15.6	436.70	148.97	34.3
Site 4	169	12.0 - 26.5	19.1	217.66	64.37	30.8
Site 5A	102	17.2 - 27.8	26.2	410.40	71.33	28.5
Site 5B	29	26.0 - 33.8	31.8	69.72	19.98	28.7
Site 5C	118	21.0 - 28.1	26.9	506.86	79.08	15.9

The percentage of overbreak generally decreases in larger diameters (See Fig. 3). However, the overbreak associated with larger diameters tend to contain more embodied carbon (See Fig. 4). To emphasise the influence of pile diameter, the y-axis in Fig. 4 represents the embodied carbon normalised by the pile length (tC02/m). The data does not provide sufficient evidence to conclude whether using larger diameters contributes to more sustainable construction. However, with additional data, both designers and contractors could potentially optimise pile diameter choices to enhance sustainability by considering the overbreak within carbon calculations and assessments.

 © DFI International Bruges 2025

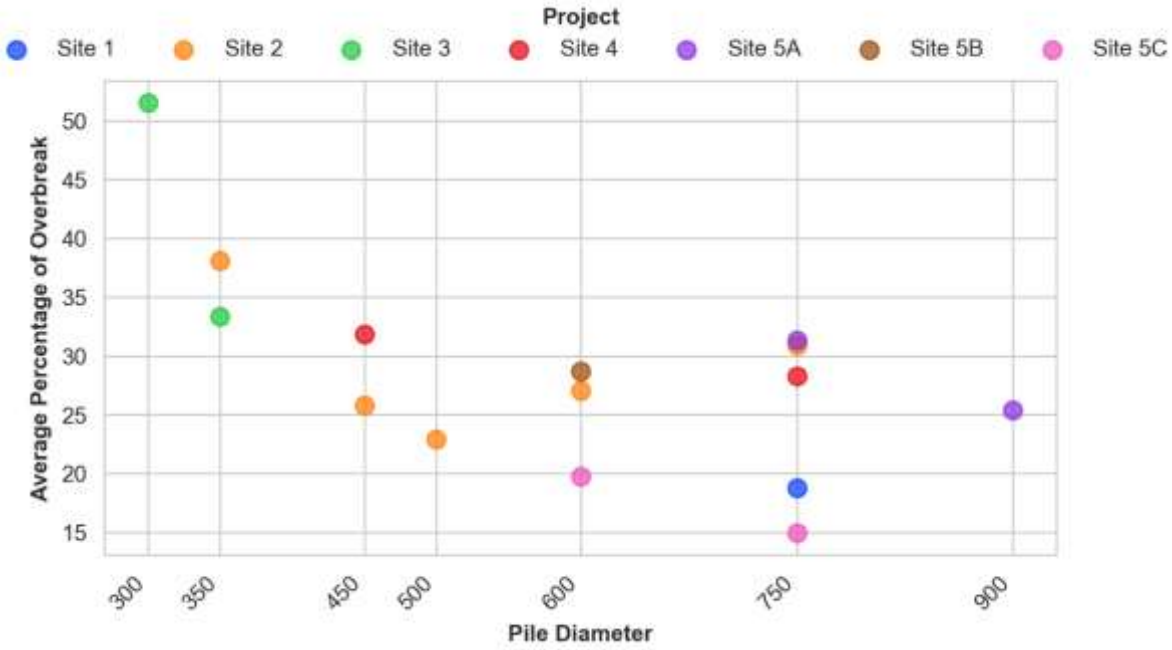


Fig. 3. The average percentage of overbreak by project and pile diameter.

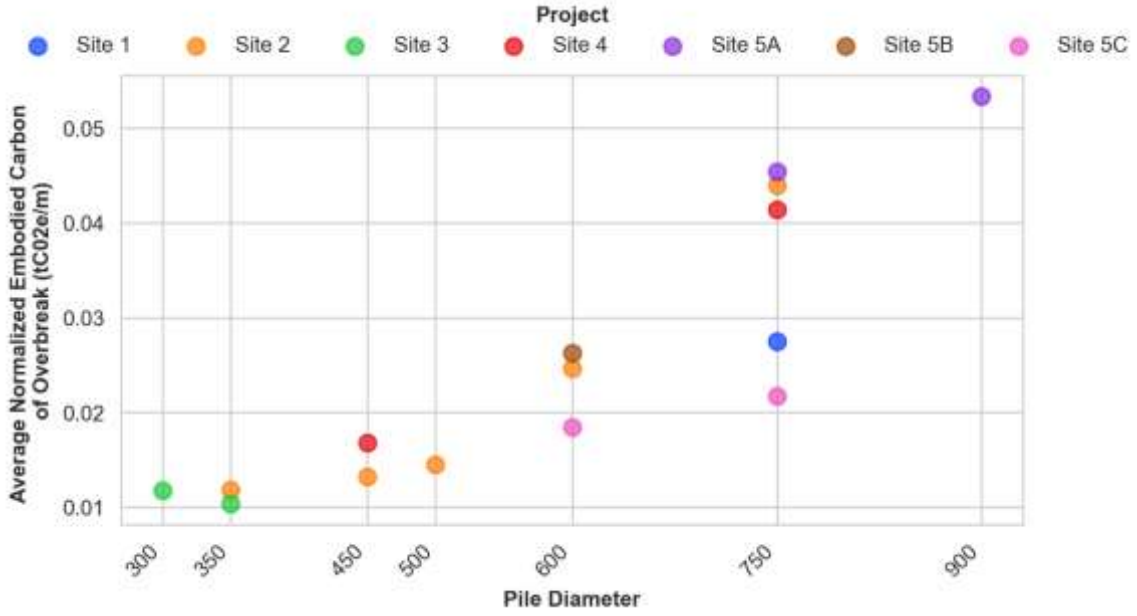


Fig. 4. The average normalised embodied carbon of overbreak (tC02e) by project and pile diameter.

LIMITATIONS

It is known that a single overbreak metric alone is limited in identifying the conditions encountered during pile construction. Overbreak should be analysed in segments to identify regions with the highest overbreak, which may provide more insights into the potential construction issues, as emphasised in a separate study on concrete overbreak (Cruz, 2017). However, due to the complexity involved in extracting data along the pile length based on current pile log formats (as shown in the red box in Fig. 1), this paper does not analyse overbreak in such detail. A future area of development could be to extract the plots in Fig. 1 as raw data, and compare the specific segment depths to the soil

 © DFI International Bruges 2025

description (i.e., “soft” or “loose”) from the ground model stratigraphy developed for the site. This would potentially enable further insights into the relationship between overbreak and the specific ground conditions of the site. Furthermore, the graphs relating to penetration rate and rotation speed in Fig. 1 could be used to identify potential overflighting issues.

Additionally, the accuracy of recorded pile diameters significantly influences the calculation of overbreak. It has been demonstrated by (Cruz, 2017) that even a deviation of 0.02m from the actual pile diameter can lead to a notable difference in overbreak values. However, this difference becomes less significant for larger diameters.

The projects compiled in this paper were accessed with permission from the authors’ company. The author did not directly participate in site supervision for the projects referenced. Any site-specific information or experiences mentioned were obtained through discussions with colleagues involved in those projects and are presented on their behalf.

Neither the author nor the co-authors assume responsibility for the accuracy of the pile data used in this analysis.

CONCLUSIONS

This study highlights the need for improved monitoring, post-processing, and systematic compilation of piling and foundation data. The industry should adopt a standardised data format, similar to the AGS format used in ground investigations, as is currently being proposed. Despite the current absence of such a format, designers can utilise simple scripts and automated processes, as described in this research, to conduct quality assurance through analysis of various piling parameters. To maximise the value and impact of these processes, timely and accurate reporting of key data from contractors is essential.

An analysis of piling data, focusing specifically on concrete overbreak, from seven projects revealed overbreak ranging from 15.9% to 34.3%. Larger diameter piles typically experienced lower overbreak percentages but had higher embodied carbon. Differences in overbreak across sites, particularly at Sites 5A/5B, and 5C, were attributed to inconsistent target setting and control practices of individual contractors.

Early identification of settlement issues, as discussed for Site 2, could have been achieved through analysis of pile logs, allowing designers and contractors to implement timely interventions. Early mitigation steps are critical to avoid potential cost of avoidable remedial works which will benefit both contractor and client.

Overall, effective collaboration among contractors, designers, and other stakeholders is essential in reducing overbreak. Regular site inspection and communication by the designer's resident engineer representative with the contractor is essential, supported by timely exchange of information between all parties. The adoption of digitalisation techniques and real-time data sharing could further strengthen this cooperation, leading to improved process control and more sustainable results for clients and the project.

REFERENCES

AGS. (2025, January). *AGS Piling - Roadmap for development and implementation*. Retrieved from ags.org.uk: https://www.ags.org.uk/content/uploads/2024/11/AGS-Piling-Roadmap_v1-0.pdf

 © DFI International Bruges 2025

Boddy, J. M., Pennington, M., & Chadwick, N. C. (2021). Guidance on the Standardisation of Pile Data Capture. *Piling 2020*. ICE publishing.

Cruz, N. (2017). Concrete Overbreak Estimation And Analysis Errors In Bored Piles. *Deep Foundations Institute.*

ICE. (2017). *Specification for Piling and Embedded Retaining Walls.* London: Thomas Telford.

National Highways. (2022). *National Highways Carbon Tool*. Retrieved from https://nationalhighways.co.uk/suppliers/design-standards-and-specifications/carbon-emissions-calculation-tool/pdfplumber. (2024). *PyPI*. Retrieved from https://pypi.org/project/pdfplumber/

Rutty, P. (2021). Piling In London – A History. *Piling 2020.* ICE Publishing.

 © DFI International Bruges 2025

3D GROUND MODEL NEDER-BETUWE LEVEE REINFORCEMENT PROJECT IN THE NETHERLANDS

N.S. Walrave, Fugro, Utrecht, The Netherlands, n.walrave@fugro.com
M. Hop, Fugro, Utrecht, The Netherlands, m.hop@fugro.com
J. van der Kop, Fugro, Weert, The Netherlands, j.vanderkop@fugro.com
K.M. Hermann, Fugro, Utrecht, The Netherlands, k.hermann@fugro.com
A. Haile, Fugro, Utrecht, The Netherlands, a.haile@fugro.com
E. Ünal, Fugro, Utrecht, The Netherlands, e.unal@fugro.com
J.W.T.A. Schuringa, Fugro (primary affiliation), Leidschendam, The Netherlands; Arup (current affiliation), Amsterdam, The Netherlands, johan.schuringa@arup.com

ABSTRACT

For the Neder-Betuwe levee reinforcement project in the Netherlands, a comprehensive 3D Ground model (Digital Twin) was developed along the entire 20-kilometer length of the levee. This model created using LeapFrog Works software, integrates CPT-data, borehole data and electrical resistivity tomography data. The 3D Ground model serves multiple purposes: it verifies supplied data, generates elevation grids, and produces longitudinal and cross-sections. These outputs are subsequently imported in geotechnical software for further design applications. The 3D Ground model significantly enhances the design process by enabling accurate modelling of the sand section in the levee, facilitating accurate excavation planning and performing detailed 3D settlement calculations. Consequently, it directly supports UN Sustainable Development Goal 15 by promoting the development of a safer, more sustainable and efficient levee reinforcement.

Keywords: 3D ground model, Digital Twin, LeapFrog Works, Geotechnical Design

PROJECT OVERVIEW

The Neder-Betuwe levee reinforcement project is a significant initiative aimed at enhancing the existing flood protection infrastructure for the region. Located in the Netherlands, this project involves strengthening a 20-kilometer stretch of levee to safeguard homes and businesses from potential flooding. The project is a collaboration between Waterschap Rivierenland and the Dijkalliantie Neder-Betuwe consisting of GMB, Ploegam, Dura Vermeer. Fugro has been contracted to conduct the soil- and geophysical investigation, monitoring and make the various geotechnical and geohydrological designs for this project.

This paper presents a comprehensive overview of the development and application of a 3D ground model for the Neder-Betuwe levee reinforcement project. Using LeapFrog Works software (Seequent, 2024), the model integrates CPT data, borehole data, electrical resistivity tomography data and as-built drawings to create a detailed digital twin of the 20-kilometer levee. The paper explores the methodologies used to construct the model, including data classification and interpolation techniques, and discusses the integration of various geotechnical software tools through Python scripting. Key applications of the model, such as settlement calculations, heave calculations, and slope stability assessments, are highlighted, demonstrating how the model enhances geotechnical analysis and design processes.

 © DFI International Bruges 2025

3D GROUNDMODEL

The 3D Ground model has been developed using specialized geotechnical software which allows for the integration of various input datasets to visualize this data and create three-dimensional ground models, also known as digital twins.

The dimensions of the model are as follows:

- The total length of the levee, spanning 20 kilometers, has been reconstructed as one continuous 3D Ground model.
- The model's width is 160 meters, with the center of the levee positioned exactly 80 meters from both ends of the model extensions.
- The height of the model varies between 30 meters to a maximum of 50 meters, depending on the elevation level of the top of the levee.

A visual of a small part (700 meter) of the total model (20 kilometers) is shown in Fig. 1.

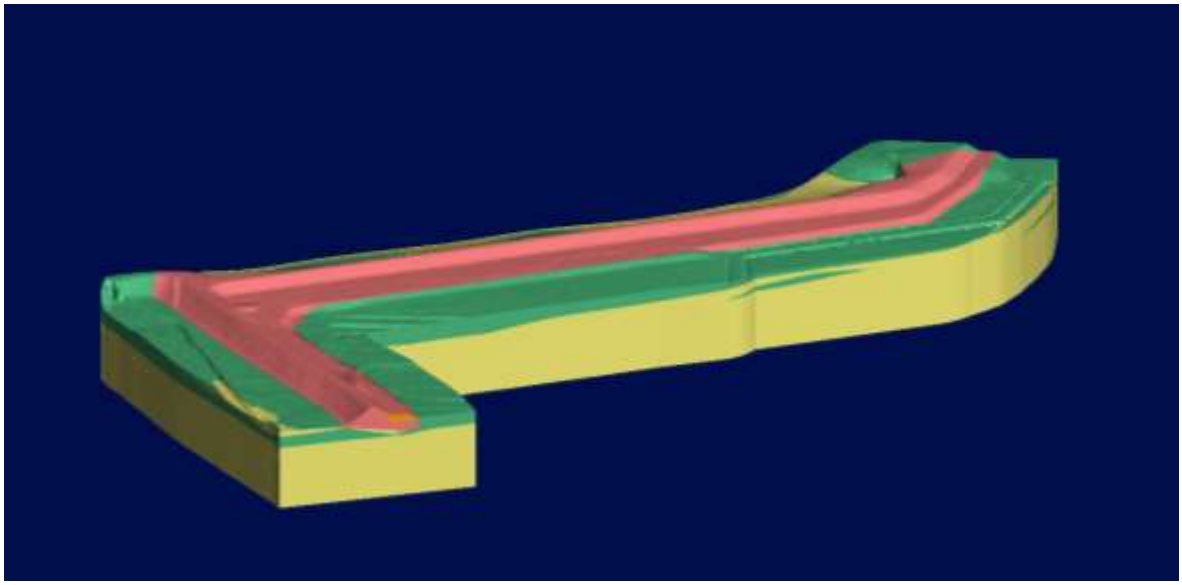


Fig. 1. A visual of a small part (700 meter) of the total model (20 kilometers)

The model has been set up using CPT-data, borehole data and electrical resistivity tomography data. A total of 1265 CPTs and boreholes have been used for this project. These diverse datasets were interpreted by a geotechnical expert to delineate the subsurface layers for the model. In total, seven distinct soil layers have been identified within the scope of the project.

By using and comparing these datasets, including the Robertson (2016) classification from CPTs, assistance from different geotechnical engineers, and previously interpreted CPTs and boreholes, the geotechnical engineer has interpreted the soil layers for all CPTs and boreholes. This process resulted in a total of 8.343 soil layer identifications across all CPTs and boreholes. Figure 2 illustrates the CPT classification process, showcasing just 8 of these soil layer identifications.

 © DFI International Bruges 2025

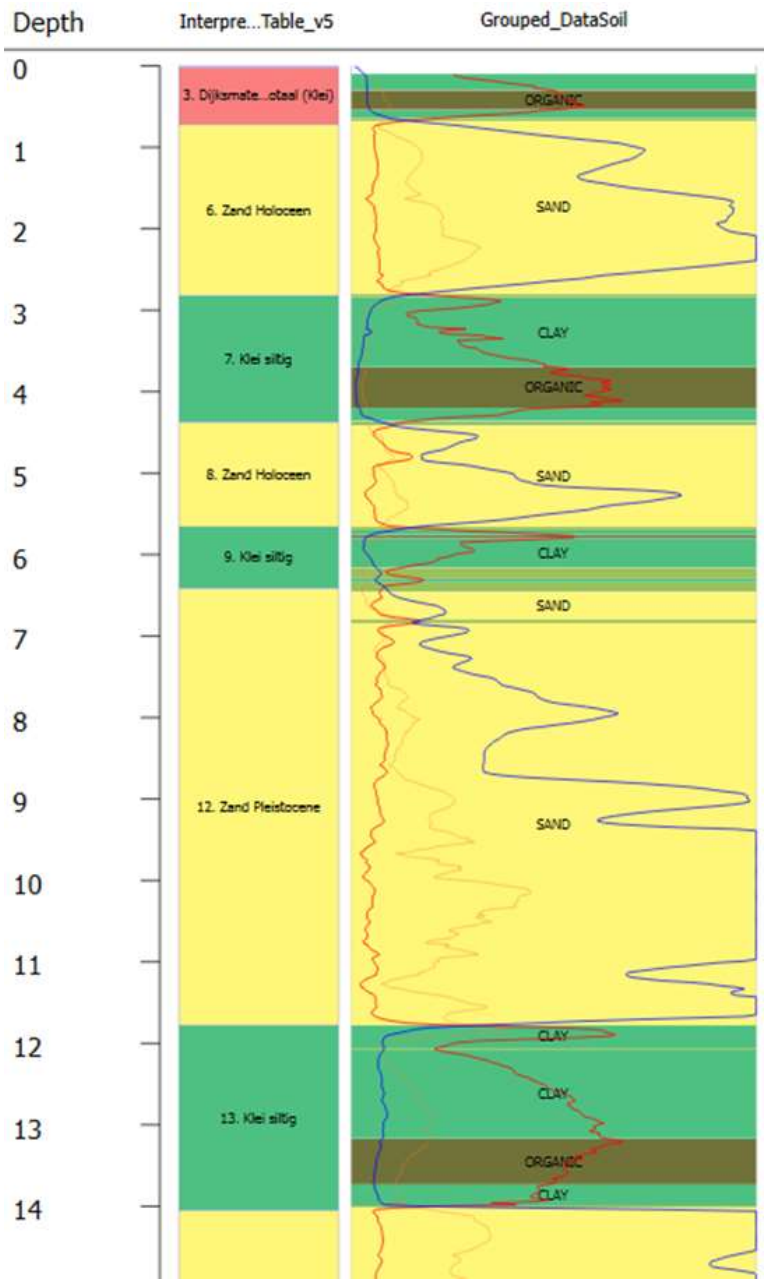


Fig. 2. A visualization of the classification process for the geotechnical engineer. Right shows the CPT data (Cone resistance = Blue, Sleeve Friction = Orange, Friction Ratio = Red) and Robertson (Robertson, 2016) classification, left shows the soil layers as interpreted by the engineer for design purposes

Upon completing the classification process, the identified soil layers were connected to establish the correct layer separations for constructing the model. The interpolation process is largely automated, enabling the geotechnical engineer to correct minor errors found in the interpolation, thereby enhancing the model's accuracy.

Incorporating new data into the current model automatically restarts the interpolation step while retaining the minor adjustments made by the engineer. This allows the engineer to continuously update the model with new data as it becomes available, without the need to reconstruct the model from scratch.

 © DFI International Bruges 2025

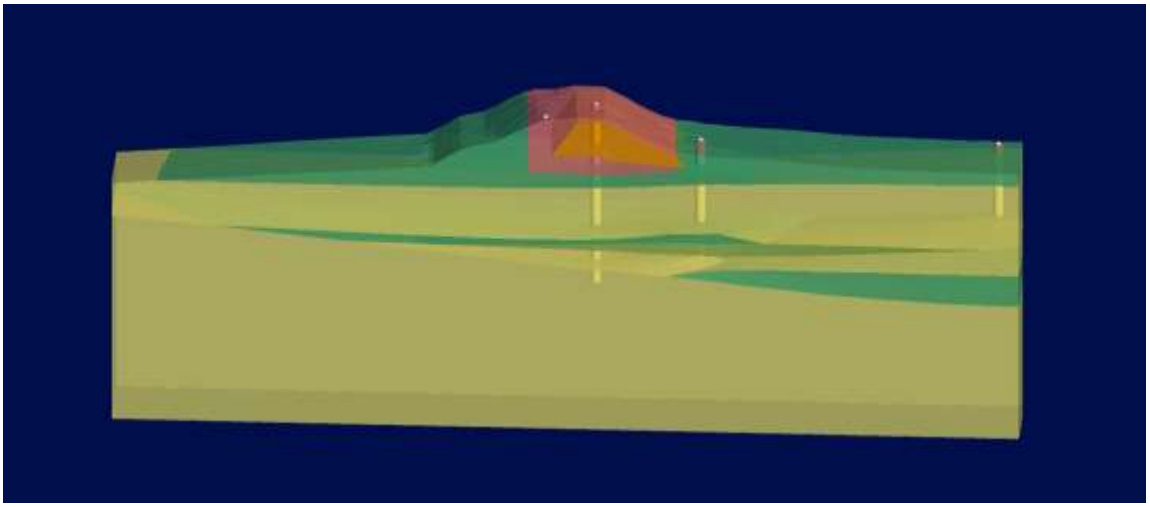


Fig. 3. A visualization of a cross-section of the 3D Ground model highlighting the various soil layers

For the 3D ground model of the levee, new CPTs and boreholes were executed and finalized after the initial model was completed using the available data. The datasets from these newly executed CPTs and boreholes were seamlessly integrated into the existing datasets to enhance the accuracy of the soil layer interpolation, and thereby improving the overall accuracy of the 3D Ground model (see Fig. 3).

To enhance the creation and utilization of the 3D ground model, Python was used to integrate various geotechnical software tools. Custom scripts were developed to automate data transfer between LeapFrog Works and other geotechnical applications, such as settlement calculations and slope stability analysis software (Deltares D-Settlement and D-Stability, respectively). This coupling process not only streamlines the workflow but also ensures consistency and accuracy across different stages of the project. The ability to automate these interactions allows for real-time updates and iterative improvements to the model, significantly enhancing the efficiency of the design processes.

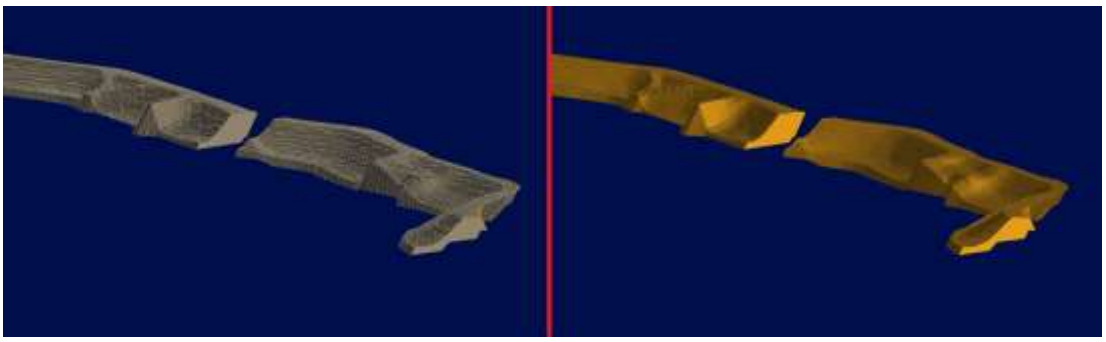


Fig. 4. Original sand layer model in Civil3D (left) vs. modelled sand layer inside levee in 3D ground model (right)

However, CPTs and borehole data alone did not provide sufficient information about the sand layers within the levee. To address this, designers used Civil3D to construct a model of the sand layers using six electrical resistivity topographical profiles and historical as-built drawings (see Fig. 4). These drawings provided critical details that were used to calibrate the model, ensuring it accurately reflected the existing conditions of the levee. This model was integrated into the 3D ground model to understand the exact dimensions of the sand layers. Following a calibration step based on cross-sections with a center-to-center distance of 10 m to verify the sand locations against available soil investigations, the model of the sand layers was updated and integrated into the 3D ground model.

 © DFI International Bruges 2025

This process revealed numerous sand drains within the levee structure, prompting further investigation into the potential for reusing the sand. Consequently, innovative strategies for material reuse were developed, resulting in a remarkable 97.5% reduction in CO2-equivalent emissions. This demonstrates the significant environmental benefits of integrating detailed as-built data into geotechnical modeling and design processes (Hermann et al., 2025).

The comprehensive 3D ground model developed using LeapFrog Works serves as a robust foundation for various geotechnical analyses. By integrating CPT data, borehole data, and electrical resistivity tomography data, the model provides a detailed representation of the subsurface conditions along the 20 kilometer levee. This high-resolution model is instrumental in performing precise settlement calculations, which are critical for predicting and mitigating ground subsidence. Additionally, the model facilitates accurate heave calculations, essential for understanding the upward movement of soil layers due to unloading or other factors. Furthermore, the detailed stratigraphy and soil properties captured in the model enable thorough slope stability calculations, ensuring the levee's structural integrity and safety. These applications, elaborated upon in the following sections, underscore the model's value in supporting geotechnical engineering decisions and enhancing the reliability of infrastructure projects.

APPLICATION OF THE 3D GROUND MODEL FOR SETTLEMENT CALCULATIONS

The 3D ground model is an effective tool for calculating settlements in large infrastructure projects. For the Neder-Betuwe levee reinforcement project, settlements are calculated for 2D cross-sections using the a,b,c-isotache model (Den Haan, 1994) within Darcy's consolidation framework (Deltares, 2023). Settlements are calculated over a period of 50 years. A comprehensive settlement model for the entire levee reinforcement was developed using the following approach:

1. Every 10 meters a 2D cross-section of 120 meters length was generated from the 3D ground model. Load changes due to alterations in the levee's geometry were subtracted from the 3D model to reflect its present state. Hydraulic conditions were derived from the MORIA (Waterschap Rivierenland, 2024) geohydrological model.
2. Settlements were calculated at 10 verticals within the cross-section resembling the levee geometry, and at 2 verticals at the start and end of each cross-section.
3. The resulting settlements were interpolated using a 'natural neighbour' algorithm (Sibson, 1981) to convert the 2D settlements into a surface that covers the entire levee reinforcement.
4. The surface covering settlements are presented in Fig. 5 and Fig. 6**Fig. *6***. By generating the spatial data of the settlements, results can be easily shared among the different disciplines involved in a levee reinforcement project. This detailed analysis provides a reliable estimate of the soil required to compensate for the settlements which can offer financial and logistical benefits. The surface data is also useful for analysing other settlement related issues, such as the relative rotation of the road on top of the levee due to settlements (Fig. 7**Fig. *7***) or the residual settlements after project completion (Fig. 8**Fig. *8***).

 © DFI International Bruges 2025



Fig. 5. Calculated settlements for the western part of the reinforcement where the color scale represents the magnitude of the settlements



Fig. 6. Calculated settlements for the eastern part of the reinforcement where the color scale represents the magnitude of the settlements

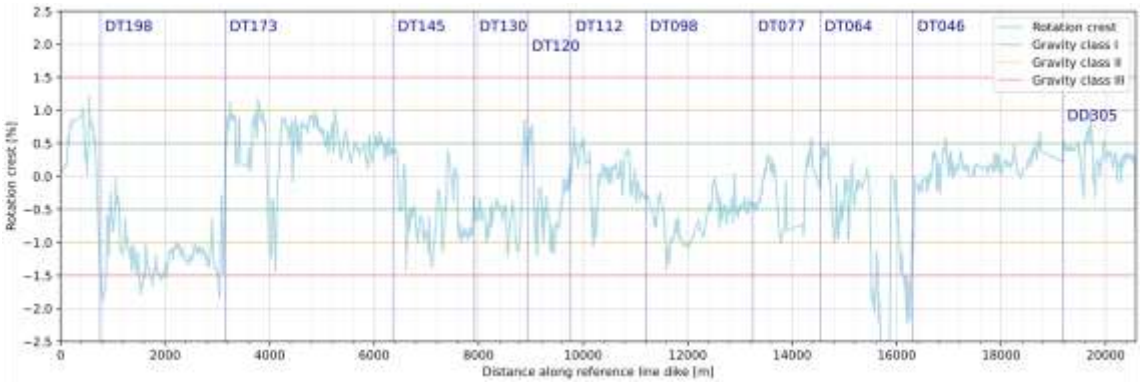


Fig. 7. Relative rotation of the road on the levee reinforcement, showing the rotation between the inner and outer crest due to settlement. The x-axis indicates the distance along the levee from west to east. The dotted lines represent different damage impact classifications based on the severity of the consequences

 © DFI International Bruges 2025

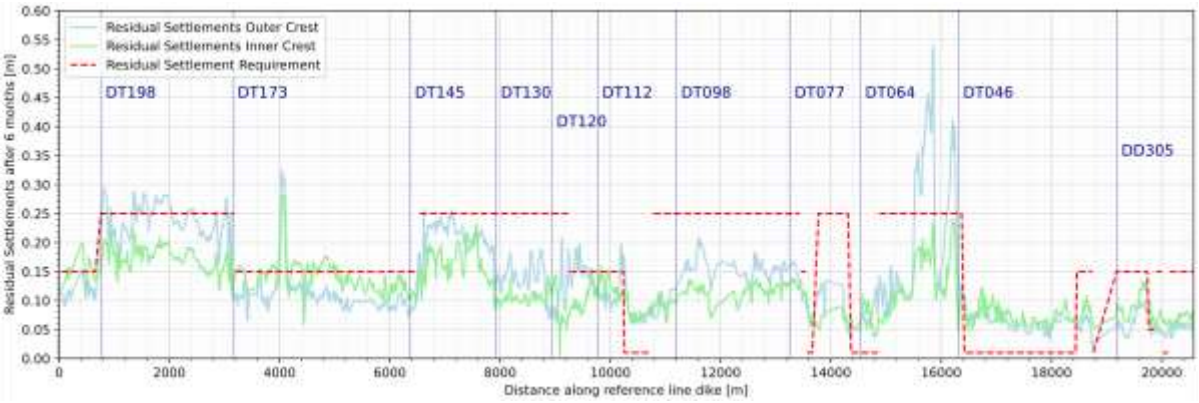


Fig. 8. Residual settlements of the levee reinforcement, occurring 6 months post-reinforcement. The blue line (BUK) shows the outer crest, and the green line (BIK) shows the inner crest. The red dashed line indicates the water board's requirement. The x-axis represents the distance along the levee from west to east

APPLICATION OF THE 3D GROUND MODEL FOR HEAVE

The 3D ground model was applied for two key calculations in the Neder-Betuwe levee reinforcement project. First, it was to design the sheetpile walls to prevent heave, and second, to perform uplift calculations to determine the optimal location of the sheetpile walls within the levee cross-section. Heave and uplift are sub-failure mechanisms within the broader failure mechanism known as piping, which occurs when water flows under the levee, carrying sand and weakening the structure. Piping includes: uplift, heave, and backward erosion. In the case of uplift, increased pore pressures in the aquifer due to the hydraulic head on the river side lift the blanket layer until it ruptures. If the upward force is sufficient, sand grains from the aquifer flow through the uplift channel, creating a fluidized state (heave). This can lead to the development of an erosion channel beneath the blanket layer, known as backward erosion. If this channel reaches the river, the levee is undermined and collapses.

The piping scope included 5.9 km of sheetpile walls for stability and piping, and 5 km solely for piping, totaling 10.9 km. Longitudinal sections were generated from the 3D ground model at the sheetpile wall locations. The scope was divided into segments with similar blanket layer thickness and soil characteristics, and a normative cross-section was taken at the location with the thickest blanket in each segment. These calculations were performed using the flow module of PLAXIS (Bentley Systems, 2023), with geometry and soil characteristics exported from the 3D ground model and imported in PLAXIS via Python scripts. This automation reduced labor time and effort.

To determine the sheetpile wall locations within the levee cross-section, uplift calculations across the entire Neder-Betuwe project area, as shown in

Fig. ***9***. If uplift were to occur on the river side of the sheetpile wall, it cannot protect the levee from heave. Automated uplift calculations were performed on the entire 20 km levee section in a grid of 1 m^2 using the 3D Ground Model. This map was used to determine the optimal locations for the 10.9 km of sheetpile walls within the levee cross-section, between the toe and the crest. This method allowed for a large sum of detailed uplift calculations in a short amount of time and the ability to easily share the results with clients.

 © DFI International Bruges 2025



Fig. 9. Results of the uplift calculations in a high-water situation where green indicates a minimum safety factor of 1.89 and the black line indicates the location of the sheetpile

APPLICATION OF THE 3D GROUND MODEL TO ASSESS SLOPE STABILITY

A total of 5.9 km of levee will be reinforced with sheetpile walls. These walls enable the construction of steep slopes, minimizing the footprint required for the levee. Consequently, they are used in areas where it is essential to preserve buildings in the hinterland. A total of 24 calculations were performed in PLAXIS to determine these locations, which are illustrated in

Fig. **10**.



Fig. 10. Schematic overview of the Neder-Betuwe levee (green) with sheetpiles (red)

The cross- and longitudinal sections from the 3D ground model were used to select the normative cross-sections, which were then exported in the DXF-format. These cross-sections were used by a Python script to automatically set up PLAXIS calculations.

Fig. **12** and 12 show the cross-section of the 3D ground model and the subsequent input for the PLAXIS calculation, respectively. The safety factor against slope failure, the deformations of the sheetpile walls, and their internal forces, as calculated by PLAXIS, were used to optimize the required length of the sheet pile wall, the type of sheet pile wall, and the type of anchor.

 © DFI International Bruges 2025

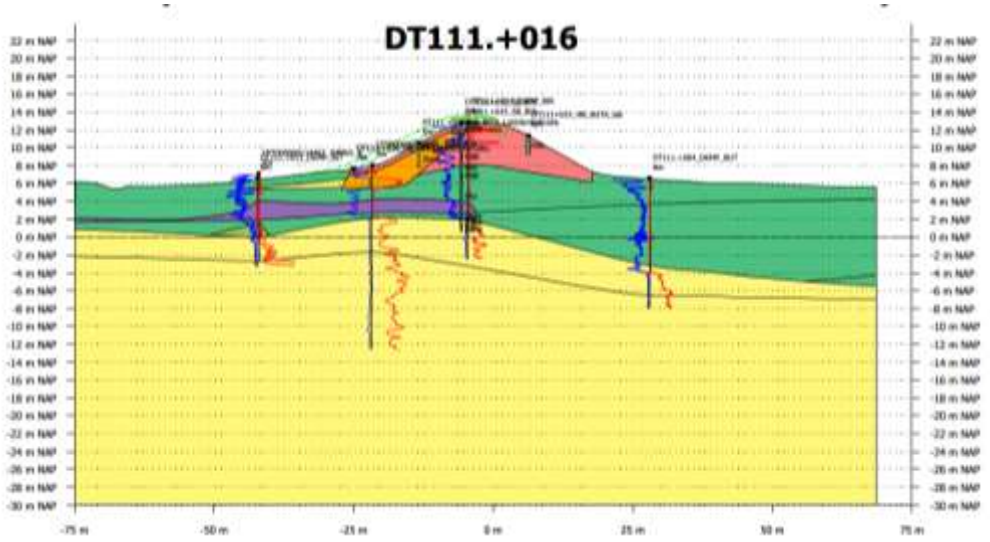


Fig. 11. A schematic overview of a cross-section from the 3D ground model

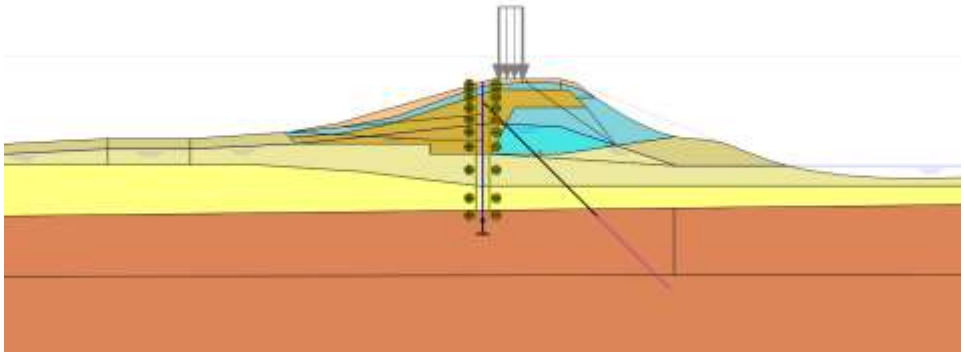


Fig. 12. A cross-section of the resulting Plaxis 2D input

CONCLUSION

The development and implementation of the 3D ground model using LeapFrog Works has proven to be invaluable for the Neder-Betuwe levee reinforcement project. By integrating diverse datasets such as CPT data, borehole data, electrical resistivity tomography data and as-built drawings of the previous levee reinforcement in 2000, the model provides a comprehensive and accurate representation of subsurface conditions. This digital twin facilitates a wide range of geotechnical analyses, including settlement calculations, heave calculations, and slope stability assessments, thereby enhancing the precision and reliability of a design. The ability to perform detailed and tailored georisk analyses enables the engineer to gain deeper insights into potential challenges and optimize engineering solutions accordingly. As a result, the 3D ground model not only improves the overall design process but also contributes to the creation of safer, more sustainable and more efficient infrastructure projects, directly supporting UN Sustainable Development Goal 15. Moving forward, the aim is to further expand the use of Python in integrating additional software tools, further optimizing our geotechnical analysis capabilities and leveraging this approach to support more complex and large-scale projects.

 © DFI International Bruges 2025

ACKNOWLEDGMENTS

The authors would like to thank Waterschap Rivierenland, Dijkalliantie Neder-Betuwe consisting of GMB, Ploegam and Dura Vermeer, and the projectteam for their support.

REFERENCES

Bentley Systems. (2023). Plaxis 2D.

Deltares. (2023). User Manual D-Settlement.

Den Haan, E. J. (1994). Vertical Compression of Soil. Ph.D. thesis, Delft University.

Hermann. K.M., Walrave, N.S., & Hop, M. (2025). The reuse potential and sustainability of locally reclaimed sand in levees. *In proceedings of DFI-EFFC international conference on deep foundations and ground improvement.*

Robertson, P. K. (2016). Cone penetration test (CPT)-based soil behaviour type (SBT) classification system - an update. *Canadian Geotechnical Journal*, 53, 1910–1927.

Seequent. (2024). Leapfrog Works.

Sibson, R. (1981). "A brief description of natural neighbor interpolation (Chapter 2)". In V. Barnett (ed.). Interpreting Multivariate Data. Chichester: John Wiley. pp. 21–36.

Waterschap Rivierenland. (2024). MORIA.

 © DFI International Bruges 2025

Digital measurement technology in foundation works / In-process monitoring to ensure quality

Dr. Patrik Wenzl, Marcus Daubner, BAUER Spezialtiefbau GmbH, Germany

ABSTRACT

In recent years, the topic of digitalization in specialist foundation engineering has been steadily driven forward. With innovative approaches and ideas, the collection, processing, and evaluation of data has been increasingly automated and the collaboration of all project participants more and more digitalized. In addition to the process data from the production of the special foundation engineering elements, which are recorded element-based by the drilling equipment (suspension quantities, verticality, GPS position, etc.), we also record anchor forces, deformations, temperature curves, suspension levels, etc. on our construction sites as required during or after the production of the respective elements. This data is transmitted directly, analyzed and displayed in the dashboard we have developed.

A few case studies of the use of our digital tools during the manufacturing process to ensure the quality of the product demonstrate the practical benefits.
In Feldolling, a cut-off wall was constructed in 2022/2023 using the MIP method (MIP = Mixed in Place) in various construction phases with a scope of around 20,000 m².
As the construction period took place during the winter months, the temperature of the freshly manufactured cut off wall element was monitored during curing for quality assurance purposes on this project

Another special monitoring task was realized on a project in Sweden in 2020. In the immediate vicinity of the Royal Opera House in Copenhagen, a back-anchored excavation pit consisting of 6600 m² of milled diaphragm wall was created for the construction of the "Operaparken" underground car park.
Due to the corona pandemic at the time, it was difficult to deploy personnel on the construction sites. A system was therefore used to monitor the suspension level in the open trench if it was necessary to leave the trench open overnight.

With regard to the monitoring of entire excavation pits, this is currently taking place on a construction project in Cologne. The excavation pit for the construction of a new Centre for Family Health (CEFAM) is being built on the grounds of Cologne University Hospital.
Our customer wanted to continuously monitor the anchor forces in the wall. For this purpose, we installed our monitoring system, which automatically and autonomously displays and monitors the anchor forces in our dashboard via our IoT solution.

This approximately 8,000 m² excavation pit consists partly of a bored pile wall, a mixed-in-place (MIP) wall and a soldier pile wall. The entire excavation wall is anchored back over the height (14 metres) with up to three anchor layers. Up to 32 digital load cells are installed to monitor the anchor forces. The monitoring itself is carried out automatically via the self-sufficient IoT device installed there, which is also solar-powered. The measurement data is sent to the cloud and is displayed and specifically monitored via the dashboard.

Keywords: Monitoring, IoT Device, Dashboard, Anchor, D-Wall, Mixed-in-Place

THE RELEVANT DIGITAL TOOLS

In-house development work on cross-process data utilization in the BIM (Building Information Modeling) context began around 10 years ago. The respective data of the digital (construction) processes in the Bauer Group can be accessed via our digital portal. This portal provides employees and customers with centralized, role-based access to project-relevant information and systems to reduce complexity.

 © DFI International Bruges 2025

The approach of systematic digital recording of all relevant data from planning, production, and quality control, as well as their integral networking and automated evaluation is pursued. Above all, the further utilization of planning data in the manufacturing process and the automated feedback of production data into inventory documentation and invoicing, as well as quality control and targeted monitoring of relevant components are a central concern.

In foundation engineering, digitalization offers systematic data collection (Fig. 1), which undoubtedly offers great potential for optimization for all those involved in construction. This significantly reduces the time and effort required to create and check production certificates for the special foundation engineering elements embedded in the ground. The management of this information and documents requires enormous efforts in terms of documentation and checking activities, especially for trades with a high proportion of individual elements. Up to now, the data has mostly been recorded manually or entered manually in logs.

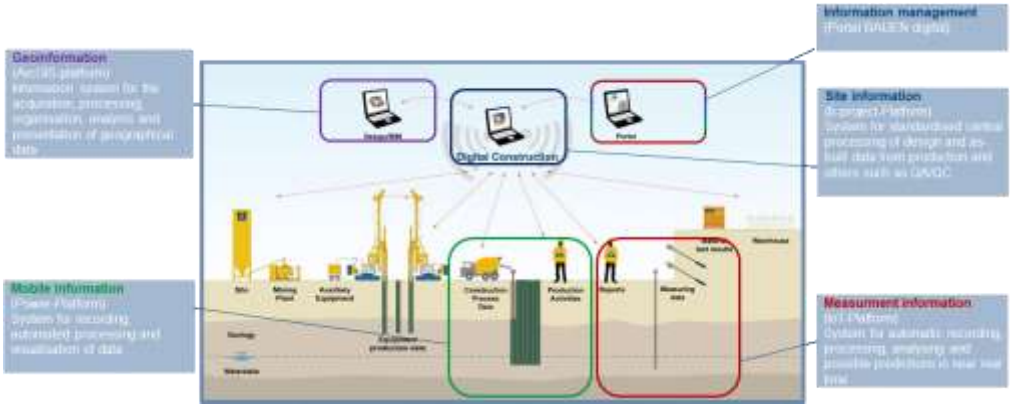


Fig. 1. - Systematic data collection & processing

Once the digital "ecosystem" was in place, further important development steps were and are the recording and utilization of production and quality data during the execution phase, but also in connection with monitoring, e.g. of anchor forces. Applications for mobile devices were developed for recording production and quality data, which allow the relevant data to be recorded immediately by the respective employee. With our own developed construction diary application, for example, all relevant data of the construction process can be recorded independently by the leading employees (foreman, site manager). This data is then merged into a data record and saved.

Individual processes, such as the manufacturing process for anchors (Fig. 2), are also recorded by the device operator using an application. The process data is entered into the application using a mobile device and saved once the manufacturing process has been completed. The data is immediately available for creating the production log and does not have to be transferred from a handwritten record. The advantages are a reduction in the time and effort required to create a production log, the avoidance of transmission errors and the immediate use of the data to analyses the construction process.



Fig. 2. Recording of process data during the production of injection anchors

 © DFI International Bruges 2025

Another important area of digital applications on specialized civil engineering construction sites is the monitoring of relevant process steps during production, such as the suspension level during the production of a diaphragm wall, the measurement of the temperature development of a specialized civil engineering element, but also the monitoring of safety-relevant components such as the anchor force of an injection anchor.
Three case studies for the use of monitoring systems on construction sites are described below.

MONITORING THE SUSPENSION LEVEL DURING DIAPHRAGM WALL PRODUCTION

A special monitoring task was realized on a project in Sweden in 2020. In the immediate vicinity of the Royal Opera House in Copenhagen, an underground car park with 300 parking spaces was built, which disappears completely underground so that its surface serves as a park with trees, ponds and walking paths. For the construction of the "Operaparken" underground car park, we produced a back-anchored excavation pit consisting of 6600 m² of milled diaphragm wall (Fig. 3). The construction task was carried out in compliance with the corona-related measures prevailing at the time. Another challenge was the Copenhagen subsoil with its hard flint layers and the large number of natural and artificial obstacles in the ground. The construction site was also located in the direct neighborhood of Copenhagen's most expensive residential area, which meant that noise and dust levels were also subject to strict requirement.



Fig. 3. Production of the diaphragm wall in Copenhagen

To ensure the high quality of a diaphragm wall, it is important that the slurry level in the trench is at the required level during production. If an excavated slot is left open during the production of a diaphragm wall element, e.g. overnight, a trench watch is required to check the slurry level.
Due to the coronavirus pandemic, this was also difficult to achieve with on-site personnel, so a sensor unit was developed to monitor the suspension level. The relevant components were available in the Construction Technology department and a monitoring system was developed for this measurement task together with the Digitalization and IT departments. The components used here were a level sensor (Fig. 4) for monitoring the slurry level and a unit for transferring data (Fig. 5) directly to the cloud via the mobile phone network.

 © DFI International Bruges 2025



Fig. 4. Sensor for detecting the slurry level



Fig. 5. Installation situation at the trench. Sensor head (left) with transmission unit (right)

A special feature was that the person responsible was called by mobile phone when the level fell below a warning value so that appropriate measures could be initiated.
The monitoring system developed to monitor the suspension level worked without any problems from day one and contributed to the successful completion of this special diaphragm wall project in the center of Copenhagen.

TEMPERATURE MONITORING OF A MIXED IN PLACE (MIP®) WALL

In Feldolling, a cut-off wall was constructed in 2022/2023 using the MIP® method (MIP = Mixed in Place) in various construction phases with a scope of around 20,000 m². One section of this sealing wall was also constructed in the winter months of 2022/2023. The client required a temperature of +10°C to be guaranteed in the freshly constructed sealing wall during production in this period. In order to minimize the measuring effort for the defined measuring ranges on site, it was decided to install an online monitoring system. The monitoring and data transfer were carried out in a similar way to the system mentioned above. The components used here were a LoRaWAN temperature transmitter (**Error! Reference source not found.**) for monitoring the temperature and an outdoor gateway (**Error! Reference source not found.**) for transferring data to the construction site network.



Fig. 6. Device for temperature detection, which is installed in the fresh MIP® element using a measuring tube

 © DFI International Bruges 2025



Fig. 7. Outdoor gateway for receiving data and forwarding it to the construction site network

The measurement data was recorded according to the specified interval and sent to our Cloud via the construction site network. A suitable dashboard was developed to visualize the measurement data, which, in addition to the measurement data itself, was able to display the temperature curve as a diagram and the status information of the IoT devices.

The dashboard (Fig. 8) developed here to display the measurement data was still a prototype and does not represent the current standard of dashboards on our IoT platform. This allowed us to verify the functionality of the measurement setup, the data transmission path and the evaluation of the measurement data. In addition, this form of monitoring helped us to obtain the temperature development data efficiently and promptly and to provide proof for the client.



Fig. 8. Display of the measurement data, the temperature curve and the status information of the IoT device

MONITORING OF ANCHOR FORCES

With regard to the monitoring of entire excavation pits, this is currently taking place on a construction project in Cologne. The excavation pit for the construction of a new Centre for Family Health

 © DFI International Bruges 2025

(CEFAM) is being built on the grounds of Cologne University Hospital. This 8,000 m² construction pit is being excavated to a depth of up to 14 metres and consists partly of a bored pile wall, a MIP® wall and a soldier pile wall (Fig. ***9***). The entire excavation wall is anchored back over the height with up to three anchor layers.



Fig. 9. New CEFAM building site in Cologne in November 2023

The existing buildings of the University Hospital of Cologne adjacent to the new building and the underground car park exit ("spindle") are clearly visible in the lower part of the picture. As these are sensitive building areas, it is important for the client to monitor the anchor forces. Up to 32 digital load cells (Fig. 10) are installed to monitor the anchor forces. The monitoring itself is carried out automatically via the IoT device (Fig. 11) installed there. In this case, the IoT system is operated exclusively via solar power, with two batteries being charged via solar power during normal operation, which allows the IoT device to operate for around two weeks without a new power supply. In the event of longer periods of bad weather without power generation, it is also possible to switch to mains operation without further ado.



Fig. 10. Built-in digital load cell (



Fig. 11. IoT device for transferring data to the cloud

The measurement data is sent to the Cloud (Fig. 12) and displayed and specifically monitored via the dashboard Five measurement cross-sections were defined for this purpose (Fig.13). Access to the measurement data in the cloud is controlled via assigned profiles. Role profiles ensure that the authorized person can either only view the measurement data or can also adjust the dashboard, for example to the alarm values or the measurement interval.

 © DFI International Bruges 2025

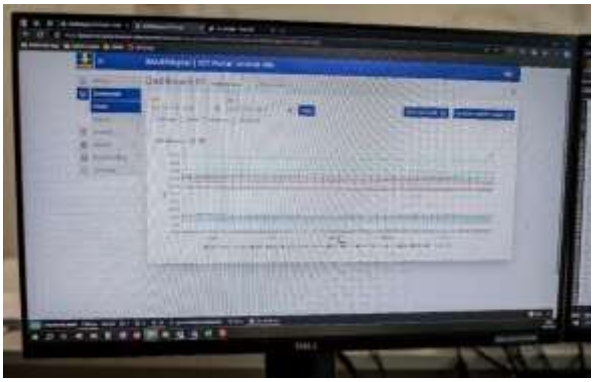


Fig. 12. Dashboard in the IoT portal for displaying the measured value



Fig. 13. Overview in the IoT portal incl. the defined measurement cross-sections

So far, the monitoring system for monitoring the anchor forces is running to our complete satisfaction and shows us that we have been able to develop a stable monitoring system for specialist foundation engineering that is now ready for series production.

SUMMARY AND CONCLUSION

With our management software, a platform has been developed over the last few years with which the structured recording, processing and evaluation of data been increasingly automated, and the collaboration of all project participants has been more and more digitalized.
The recording of data during the production of special foundation engineering elements has been available as standard for some time now with the systems integrated in drilling rigs for determining, for example, suspension quantities, verticality, GPS position, etc. The defined evaluation of this data already makes it possible to analyze the data in a structured manner. The defined evaluation of this data already enables valuable optimizations to be made on our construction sites.
In the meantime, applications for mobile devices have also been developed for recording production and quality data, allowing the relevant data to be recorded immediately by the respective employee.
As a further step, the automated monitoring of product quality during production and product utilization has now been specifically developed with previously non-integrated sensor technology. The three current case studies presented show that we can automatically record anchor forces, temperature curves, suspension levels, etc. on our construction sites during or even after the production of the respective elements as required, transmit them directly, analyze them and display them in a defined dashboard in the IoT platform we have developed.

The structured, centralized storage of information now enables us not only to analyze the manufacturing process itself in a standardized way, but also to monitor product quality in a targeted manner. In addition, efficiency on the construction sites is increased by reducing the workload of the personnel on site, as the relevant data from the production or monitoring of the element is immediately available for the creation of the respective protocol and does not have to be transferred from a handwritten note. This reduces the time and effort involved in generating the report and helps to avoid transmission errors. In addition, we are now able to provide our customers with the required data quickly and transparently online via defined access to the project.

 © DFI International Bruges 2025

UNDERTAKING A LIFE CYCLE ASSESSMENT TO CALCULATE THE ENVIRONMENTAL FOOTPRINT OF REPURPOSED SECONDARY MARKET STEEL TUBULARS FOR FOUNDATIONS (DFI-EFFC25-148)

Author: Bill Baillie, John Lawrie Tubulars, Houston, TX, USA 403.963.2995
bill.baillie@jltubulars.com
Co-authors: Robert W. J. Holdway, Giraffe Innovation Ltd, UK,
r.holdway@giraffeinnovation.com
Mark P. Dowling, Giraffe Innovation Ltd, UK, m.dowling@giraffeinnovation.com

ABSTRACT
The buildings and construction sectors are the largest emitter of greenhouse gases, accounting for 37% of global emissions[1]. With growing pressure on the construction industry to decarbonize building materials and be more resource efficient, material reuse strategies are critical to achieve the world's ambitious target of net zero emissions from the built environment sector by mid-century. This paper describes the method and results for a Life Cycle Analysis conducted by John Lawrie Tubulars (the Company) to determine the environmental impacts by using repurposed mill secondary and oil field surplus steel tubulars in foundations and other structural applications compared to using prime steel tubulars in those same applications. The study showed for repurposed tubulars that the material, collection, and delivery to a distribution yard emitted an average **455kgCO_2eq** per tonne of tubulars. Delivery to project sites added an average **216kgCO_2eq** and installation of the steel as pipe piles added an average **23kgCO_2eq** giving a total carbon footprint of **694kgCO_2eq** per tonne for repurposed tubulars. Using World Steel Association data, this compares to **2800kgCO_2eq** for new mill prime steel equivalent delivered and installed at the same location. The combined material, distribution, and installation carbon footprint of repurposed tubular products has **75% lower** Global Warming Potential (GWP - kgCO_2eq) than new prime mill steel tubulars.

Key words: **Repurposed welded steel tubulars; Environmental impacts; Life cycle assessment; Circular economy; Environmental product declaration; construction driven pipe piling; deep foundation.**

INTRODUCTION
Repurposing steel tubulars for piling in the construction sector demonstrates the innovative cooperation models required to fully realize the potential of the circular economy and meet ambitious decarbonatization goals. Extending the utility of materials through reuse, repurpose, and recycling are key tenants of the circular economy. Repurposing the steel tubulars diverts it from being scrapped or delivered back to steel mills to be processed and re-melted into new steel which would result in releasing more greenhouse gases.

The construction industry in North America is under increasing pressure to quantify the carbon footprint of their prospective projects through required Green House Gas (GHG) reporting and Environmental-Social-Governance requirements. Government legislation, proactive owners, and even employees are demanding GHG data.

The objective for undertaking this Life Cycle Assessment (LCA) was to identify and quantify the potential environmental impacts associated with the use of repurposed mill secondary and oilfield surplus steel tubulars. Then to compare the environmental impacts of using repurposed tubulars versus prime mill steel tubulars in the same deep foundation application throughout their respective lifecycles.

The results of the study could then be used by end customers (project owners, owners' engineers, prime and general contractors) to evaluate the environmental impacts and make cost-benefit decisions for reducing the carbon footprint of construction projects by considering repurposed tubular products for use in their construction projects. This data will help fill in the gaps for construction project Scope 3 GHG data.

[1] United Nations Environment Programme and Yale Center for Ecosystems + Architecture (2023) *Building Materials and the Climate: Constructing a New Future*. Available at: https://wedocs.unep.org/20.500.11822/43293

 © DFI International Bruges 2025

WHAT IS AN LCA?
An LCA is a robust, scientific evidence-based calculation of the environmental impact (GHG emissions and 16 other environmental impacts) of products or activities. International standards like ISO and EN prescribe the methodology, processes and procedures for the analysis. Using an LCA, we can understand the environmental impacts from the creation of a product from raw material and the manufacturing processes through the useful life of the product until the end of life where the product is decommissioned, recycled, or disposed of.

PRODUCT DESCRIPTION – WHAT DID WE STUDY?
Repurposed steel tubulars are sold on the secondary steel market. The tubulars come from steel mills that sell off-spec. OCTG pipe and other bi-product pipe from the start-up process. They can also come from surplus oilfield steel pipe packages that have not been used by the end of a project. **Repurposed tubulars** (shorter name for ease) are collected from across the USA and international sources. These are either collected from project sites or delivered by the seller to the Company's distribution yards. This study models three distribution yards located in Texas, Colorado, and New Jersey in the USA. The steel tubulars are inspected, cleaned (if necessary), and stored onsite at the distribution yards before being delivered to customers' project sites for installation in the ground as a deep pile foundation.

METHOD – HOW WAS THE LCA CONDUCTED?
The Company did not have internal resources qualified in the art of Life Cycle Assessments. The Company engaged an experienced consulting LCA practitioner, Giraffe Innovation Ltd., based in the UK. The scope of the LCA was clearly defined with a phased approach. Phase 1, this LCA, focuses on determining the environmental impacts for repurposed tubulars supplied for driven pipe pile applications in the deep foundation construction market. The scope definition included the operations data required to be provided by the Company.

The technical steps and processes to be followed are prescribed in ISO and EN standards that experienced LCA practitioners are familiar with, and that technical information is provided below for readers that are more familiar with LCA's. LCA practitioners use extensive databases and software for calculating each environmental impact for the various phases (modules) of a product life span.

The study was conducted aligned to the ISO procedural framework for performing LCAs in the ISO14040[2] and ISO 14044[3] standards, which acknowledges the life cycle assessment requirements of key phases beginning with goal and scope definition, inventory, analysis, impact assessment, and interpretation.

The LCA is modelled in accordance with ISO 14025:2006[4] and A1-A5 as per EN 15804:2012+A2:2019/AC:2021, Sustainability of Construction Works - Environmental Product Declarations - Core Rules for the Product Category of Construction Products[5]. The analysis also compares repurposed steel tubulars to prime welded steel tubulars using World Steel Association (WSA)[6,7]data.

The LCA model for this study was developed in Sima Pro version 9.5.01 LCA software (2023)[8] using secondary data from life cycle inventory database ecoinvent v3.9.1 database (ecoinvent, 2023). Primary data was provided by the Company. The analysis was carried out according to Product Category Rules (PCR) for Construction Products, PCR 2019:14, Version 1.3.3.
This LCA is based upon one year's worth of operations data from 2022 provided by the Company, a large supplier of steel tubular products to the construction sector in the USA. Tubulars are procured from steel pipe mills (downgraded pipe that is sold to the secondary market) and from oil field surplus

[2] ISO 14040:2006 Environmental management — Life cycle assessment — Principles and framework
[3] ISO 14044:2006 Environmental management — Life cycle assessment — Requirements and guidelines
[4] ISO 14025:2006 - Environmental labels and declarations — Type III environmental declarations — Principles and procedures
[5] BS EN 15804:2012+A2:2019 Sustainability of construction works. Environmental product declarations. Core rules for the product category of construction products (en-standard.eu)
[6] https://www.worldsteel.org/steel-by-topic/life-cycle-thinking.html
[7] World Steel Association (WSA) global average data. Qualification note: WSA data has been updated to the current ecoinvent data set and CML methodology.
[8] SimaPro: https://www.simapro.co.uk/simapro-9

 © DFI International Bruges 2025

tubular stocks. The tubulars are collected from international sources by ocean freight and from within the USA by truck. The company operates from five distribution yards in the USA. The full year data analysis looked at tubular purchases and sales for sizes ranging from 2 7/8" up to 30" with a weighted average size of 9 5/8" diameter.

SYSTEM BOUNDARY DEFINED

The system boundary of this LCA "Fig. 1" is defined as **"cradle to piling installation" (A1-A5)** as per EN 15804:2012+A2:2019/AC:2021, Sustainability of Construction Works — Environmental Product Declarations – Core Rules for the Product Category of Construction Products. The downstream 'Module B' is not included. There is no decommissioning or recycling at end of life (C1 to C4) due to the long design life of construction projects and the growing efforts to re-use existing foundations that will be more prevalent in 50-75 years[9].

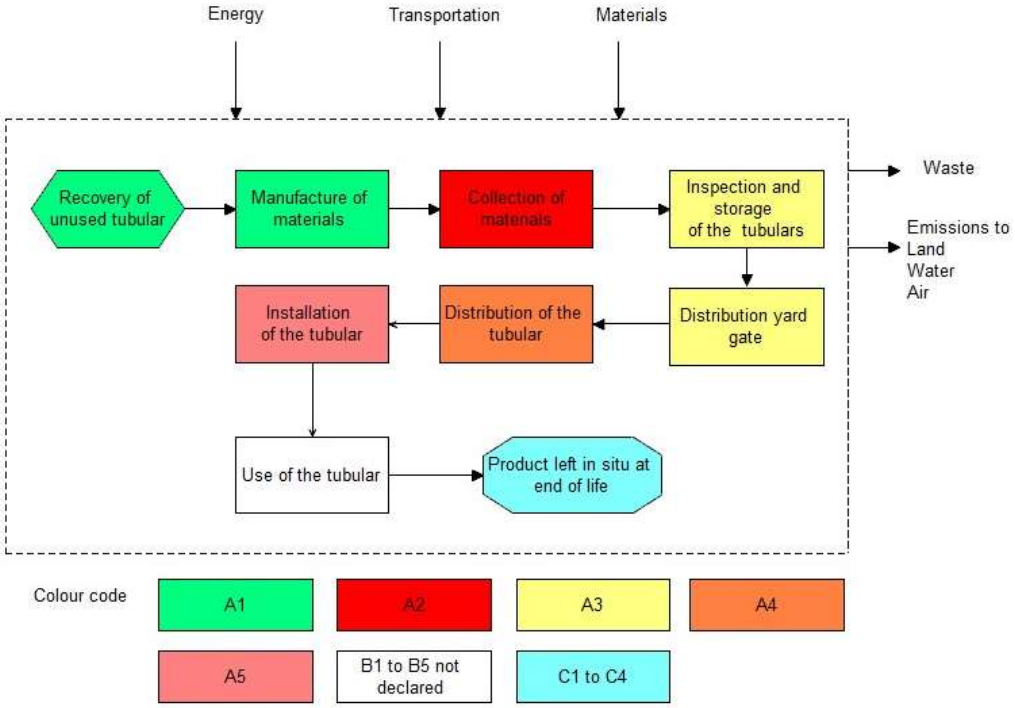


Figure 1. System Boundary

FUNCTIONAL UNIT

The functional unit for this study is **one tonne of repurposed electric resistance welded (ERW) steel tubulars**. From the 2022 data analysis for acquisition of tubulars and sales of repurposed tubulars for driven pipe piling applications, it was determined that the weighted average pipe size was 9 5/8" diameter x 0.352" wall thickness pipe weighing 36 lbs. per foot. One tonne of this pipe size is approximately 60 feet in length, and this became the proxy for the functional unit in the LCA calculations. All the inputs and outputs in the Life Cycle Inventory (LCI) and impact scores produced in the Life Cycle Impact Assessment (LCIA) phase of this LCA study were expressed with reference to this functional unit.

LIFE CYCLE INVENTORY ANALYSIS

The LCI analysis outlines the input/output data regarding the system boundary. Data collection procedures were supplied by the LCA practitioners for the tubulars from cradle (acquisition) to installation in the ground at the project site. This LCI underpins the modelling based on company, operational site, and supply chain specific primary data. The LCA is predicated on the following primary data supplied by the Company:

- Three USA distribution yard locations were selected for analysis – Houston, Pueblo, and Camden.

[9] Foundation Decarbonization and Reuse committee in DFI

 © DFI International Bruges 2025

- Full year data set from 2022 (project started in fall 2023) provided by the Company for repurposed tubulars acquisition and supply to the foundation construction industry for driven pipe pile applications.
- No manufacturing or value-added activities were included for this tubulars volume. Only receiving, quality control, storage, material handling and loading activities were included in the analysis.
- Analyzed the incoming freight by ocean and land to each yard based on purchase origination points for the tubulars to calculate the CO_2eq contributions from the incoming logistics.
- Ship-to locations from all three yards to client project locations were analyzed and mapped for over 1100 transactions. See "Fig. 2".
- Identified clusters of delivery locations and used a weighted average to select five ship-to locations to calculate CO_2eq contributions from the outgoing logistics. See "Fig. 2".
- Houston and Camden had higher volumes of deliveries so a "short" delivery and "long" delivery location were selected for each of these two yards. Pueblo had one main cluster of delivery locations classified as "long" deliveries. See "Fig. 2".
- Installation data was obtained from a major foundation construction contractor, Keller North America, for driven pipe pile installation by averaging estimates from three estimators.
- Next, these emissions were compared to those created by the supply of new mill (prime) steel tubulars from representative pipe mills in the USA through their distribution channels and delivered to the same project sites (client ship-to locations) and installed in the ground.
- Using the average tubulars size of 9 5/8" diameter x 0.352" wall determined in the 2022 data analysis, two representative pipe mills were selected that were located within proximity to the two main ship-to cluster locations identified in the first analysis.
- Using WSA data, the new mill tubulars CO_2eq emissions were determined and then the CO_2eq emissions for transport to the mills' distribution yards, handling, and then delivery and installation at the same locations used in the first analysis, were calculated.
- This provided a direct comparison with the emissions from the LCA data analysis, with the result being substantial savings in CO_2eq emissions by using the repurposed tubulars.

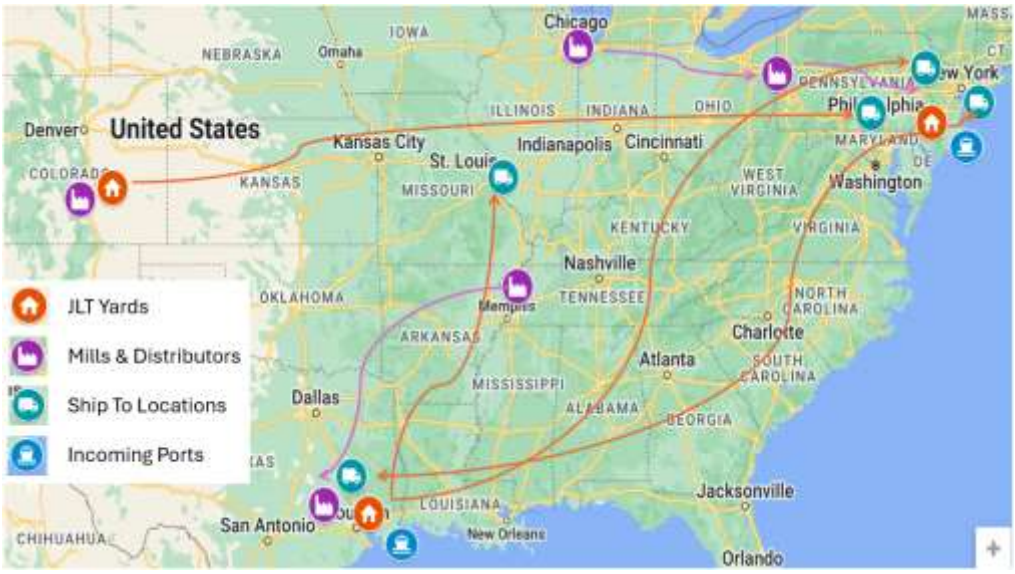


Figure 2. LCA Model – Yard, Mill, and Ship-to locations

DATA QUALITY

Primary and secondary data were collected for all processes within the system boundary and these data form the Life Cycle Inventory (LCI). Primary data was collected for all processes under the operational control of the Company. Secondary data sources included ecoinvent v3.9.1 database (2023) and WSA database. The key sources of data used for LCA modelling were:

- Primary data (material specification, inbound logistics, operations energy, waste, outbound logistics, and installation in the ground) as outlined in the LCI above.

 © DFI International Bruges 2025

- Installation data for 9 5/8" diameter driven pipe pile foundations was obtained from a major foundation construction contractor, Keller North America.
- Ecoinvent v3.9.1database (2023), standard data sets on energy, environmental impacts of materials, material processing and production, waste disposal and recycling.
- WSA data for prime steel tubulars mill data augmented by logistics to the selected outbound locations and installation data used in the primary data model.
- To ensure data quality, checks were completed on key data parameters using data quality indicators (DQIs) which are applied to ensure fit for purpose.
- Exclusions and Cut-off Criteria - when building a life cycle inventory, it is typical to exclude items considered to have a negligible contribution to results.

ASSUMPTIONS AND ESTIMATES

The following assumptions were made:

- Indicative transport modes including typical transport trucks and ship type used for the transportation of the tubular materials.
- The primary energy used for materials was calculated based upon the gross calorific results.
- The environmental burden for the repurposed tubulars using economic value (allocation) was calculated as set out in International EPD Product Category Rules (PCR).
    - As the tubulars are unused oil field stock surplus or downgraded mill pipe secondary stock, they are not environmentally burden free. The burden associated with them is based upon their residual value of **13.2% (economic allocation)** compared to a new (prime steel) welded pipe of the same weight using World Steel Association (WSA) data. Accordingly, the environmental burden from WSA data is allocated at 100% for new mill prime welded steel tubulars for the study. If the mill secondary or oil field surplus pipe was not repurposed, the tubulars could be transported back to a smelter, re-melted, manufactured into new coil, and then transported to a pipe mill to create new tubulars (essentially the original tubulars manufacturing impacts plus the added burden of recycling logistics and handling) resulting in greater environmental impacts.
- General Allocation Procedures - in this study, there were no multi-product processes, and ecoinvent default cut-off allocation was applied to all processes.

LIFE CYCLE IMPACT ASSESSMENT (LCIA)

This step calculates the likely human and ecological effects of material consumption and environmental releases identified during the inventory analysis. Classification and characterization following the ISO14040 guidelines were applied to the inventory data to assess their potential impact on the environment.

In the classification step, the inventory data were grouped into the environmental impacts. In the characterization step, the inventory data that have been classified under each environmental impact category were quantified by its corresponding characterization (or equivalency) factor (provided with the Sima Pro software) to give an indicator result for that inventory item. All indicator results under each impact category were summed to result in an overall impact score (or characterization results) for the impact category. The impact assessment was completed to ensure that the results align with the requirements of EN 15804.

RESULTS AND DISCUSSION

The characterization results for repurposing one tonne of steel tubulars are presented in this section. A comparison is drawn between the material impact, cradle to distribution yard gate (A1-A3), of a repurposed tubular versus that produced from new mill prime steel (A1-A3). Further characterization results are presented for the distribution impacts, cradle to site and installation (A1-A5), using USA yard locations and the selected average distribution data resulting in an average distance of 1,289 miles to project site. Based upon the functional unit, the results are given as site specific, and as aggregated data, based upon tonnes of repurposed tubulars delivered to driven piling project sites from each respective yard.

 © DFI International Bruges 2025

CHARACTERIZATION COMPARISON – CRADLE TO DISTRIBUTION YARD GATE (A1-A3)

The LCA results show repurposed tubulars have a carbon footprint of **455kgCO_2eq** per tonne cradle to distribution yard gate (A1 – A3). The World Steel Association (WSA) welded steel tubulars have a carbon footprint of **2614kgCO_2eq** per tonne (A1-A3). Therefore, repurposed tubulars save **2159kgCO_2eq per tonne** of steel product, an **83% saving** of the carbon emissions of a prime steel equivalent. In other words, the carbon footprint of repurposed tubulars has 17% of the impact of those made from prime steel. The main environmental indicators required under EN15804 are shown below in "Table 1".

Table 1: Cradle to Distribution Yard Gate (A1 to A3) - 1 tonne repurposed tubulars vs 1 tonne World Steel Association (Global average for tubular steel)

Environmental Indicators	Units	Repurposed Tubulars	WSA Prime Welded Tube	Reduction in impact vs prime welded tube (%)
Climate change	kg CO_2 eq	455	2614	83
Ozone depletion*	kg CFC11 eq	1.87E-06	2.35E-12	-7.94E07
Acidification	mol H+ eq	2.29	7.78	71
Eutrophication, freshwater*	kg P eq	0.01	7.43E-04	-1,026
Eutrophication, marine	kg N eq	0.52	1.69	69
Eutrophication, terrestrial	mol N eq	5.58	17.80	69
Photochemical ozone formation	kg NMVOC eq	1.84	6.14	70
Resource use, minerals, & metals	kg Sb eq	4.27E-04	1.41E-03	70
Resource use, fossils	MJ	5401	28,386	81
Water use	m3 depriv.	-927	-7,074	87
Ionising radiation	kBq U-235 eq	975	7,374	87
Particulate matter	disease inc.	2.10E-05	1.14E-04	82
Human toxicity, non-cancer	CTUh	6.56E-06	4.06E-05	84
Human toxicity, cancer	CTUh	2.12E-07	1.24E-06	84
Ecotoxicity, freshwater	CTUe	1,401	3,766	63
Land use*	Pt	1,156	970	-19

**The increase in environmental impact for ozone depletion, freshwater eutrophication and land use are due to the fuel used in collecting and transporting the tubulars to the distribution yards. Note that ozone and freshwater absolute values are extremely small.*

The following chart "Fig. 3" shows the global warming potential (GWP) impact from cradle (material acquisition and burden) to distribution yard gate (A1-A3) for the three different yards in the study, a weighted average based upon annual production output, and WSA welded steel tubulars impacts (A1-A3).

The legends in "Figs. 3 and 4" are aligned with the Product Category Rules (PCR) categories A1 to A3. However, in A3 there is no manufacturing as such, only inspection, material handling, quality control, and storage are accounted for in the analysis.

 © DFI International Bruges 2025

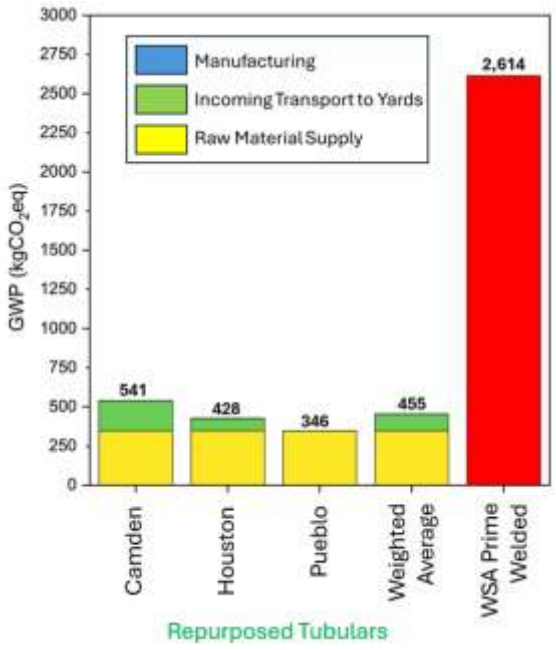


Figure 3. Cradle to gate (A1-A3) GWP of 1 tonne of steel tubulars USA Yards

CHARACTERIZATION COMPARISON – CRADLE TO INSTALLATION (A1-A5)
The weighted average impact across the three sites from cradle to installation (A1 to A5) which includes transport to site and driven pipe pile installation resulted in 75% emissions savings as shown in "Table 2".

Table 2: Weighted average of JLT three sites for Cradle to Installation (A1-A5).

Environmental Indicators	Units	Repurposed Tubulars	WSA Prime Welded Tube	Reduction in impact vs prime welded tube (%)
Climate change	kg CO_2 eq	693	2800	75%
Ozone depletion*	kg CFC11 eq	5.79E-06	3.06E-06	-89%
Acidification	mol H+ eq	2.97	8.32	64%
Eutrophication, freshwater*	kg P eq	0.03	1.48E-02	-103%
Eutrophication, marine	kg N eq	0.71	1.85	62%
Eutrophication, terrestrial	mol N eq	7.63	19.47	61%
Photochemical ozone formation	kg NMVOC eq	2.82	6.92	59%
Resource use, minerals & metals	kg Sb eq	1.02E-03	1.87E-03	45%
Resource use, fossils	MJ	8,846	31,080	72%
Water use	m3 depriv.	-910	-7,061	87%
Ionising radiation	kBq U-235 eq	978	7,376	87%
Particulate matter	disease inc.	3.81E-05	1.28E-04	70%
Human toxicity, non-cancer	CTUh	9.68E-06	4.27E-05	77%
Human toxicity, cancer	CTUh	3.23E-07	1.32E-06	76%
Ecotoxicity, freshwater	CTUe	3,382	5,303	36%
Land use*	Pt	4,388	3,425	-28%

**The increase in environmental impact for ozone depletion, freshwater eutrophication and land use are due to the fuel used in collecting and transporting the tubulars to the distribution yards. Note that ozone and freshwater absolute values are extremely small.*

 © DFI International Bruges 2025

Specific environmental impacts for the Houston site, largest of all the sites, are provided below in "Fig. 4" showing the relative percentages of contribution from each Life Cycle Stage Module (material supply to installation A1-A5).

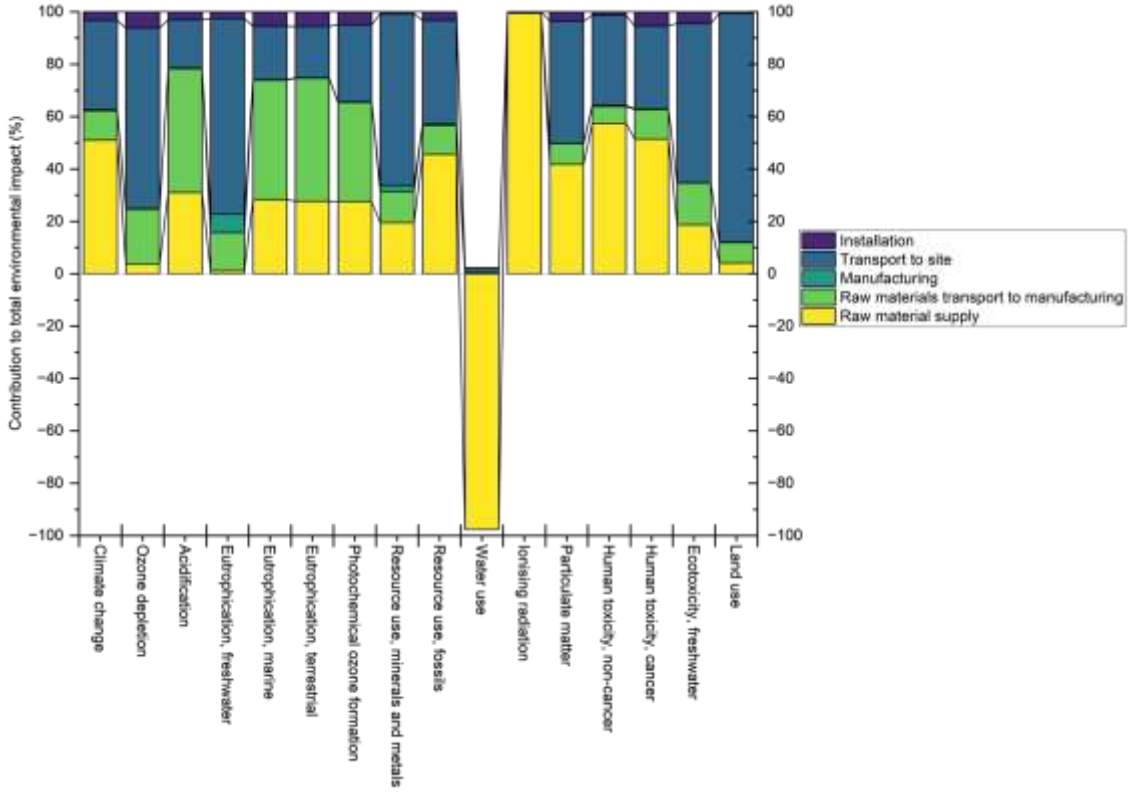


Figure 4. Houston, Texas yard - cradle to installation impacts (A1-A5)

The following chart "Fig. 5" shows the cradle to installation (A1 to A5) total GWP for the three Company yard sites for the long and short delivery distances within the USA compared to an average sourcing, delivering, and installing of prime steel tubulars from a mill.

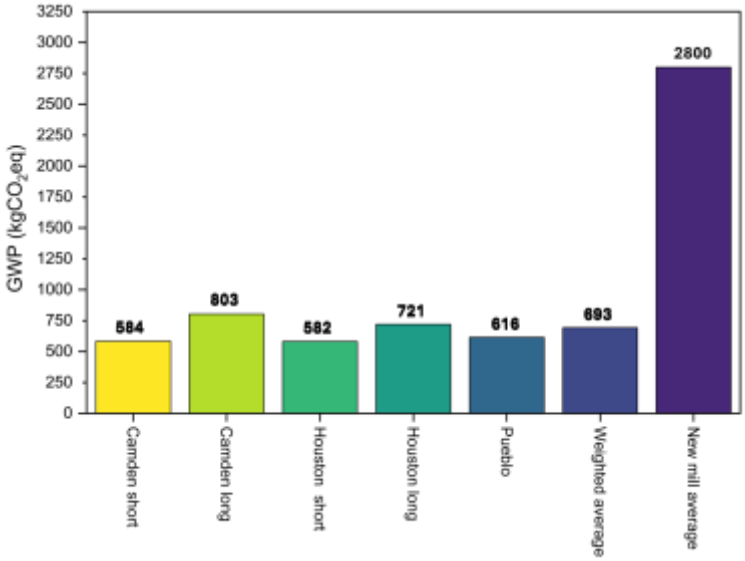


Figure 5. A1-A5 impacts for the Company yard sites (long and short delivery distances within USA) and WSA new mill tube weighted average

 © DFI International Bruges 2025

Further characterization analysis shows the relative contributions of CO_2eq and the percentages from each module in the LCA (A1-A5) in "Fig. 6". The material portion of repurposed pipe has the highest impact.

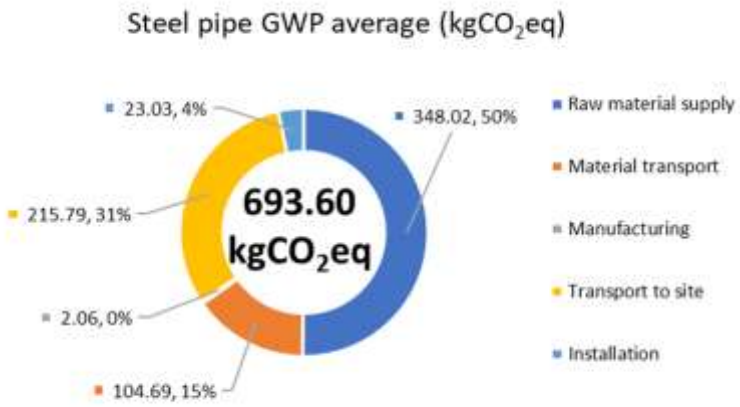


Figure 6. Contributions to CO_2eq Emissions - Cradle to Installation (A1-A5)

CASE STUDY – KELLER NORTH AMERICA NEW HYUNDAI MANUFACTURING PLANT IN ELLABELL, GEORGIA

An example of a major project where repurposed tubulars were supplied to Keller North America to construct the foundation for a new Hyundai manufacturing plant. The deep foundation construction required the use of 72,000 feet of 7 5/8" diameter steel pipe. A total of 1,115 tons of steel was supplied for the project. With the LCA results showing a weighted average CO_2eq savings of 2.107 tons CO_2eq per ton of steel, the project realized an overall savings of 2,350 tons CO_2eq when compared to constructing the foundation using brand new prime mill tubulars. This case study shows valuable environmental information that can now be provided to owners, prime contractors, and general contractors to help make more sustainable materials decisions for major construction projects to reduce the overall carbon footprint and meet sustainability objectives.

CONCLUSIONS

This LCA will allow industry stakeholders to assign evidence based scientific environmental benefits and reduced GHG emissions through the repurposing of mill secondary and oilfield surplus tubulars into structural and foundation end-uses. This data will provide project proponents with environmental data needed to make cost-benefit decisions for reducing the carbon footprint of construction projects.

The LCA described in this study is based upon company and site specific, operational, and supply chain primary data. Average tubular size of 9 5/8" diameter x 0.352" wall was used for volume-based analysis. Secondary data for the new mill prime steel came from WSA databases using the same average pipe size.

The results show **repurposed tubulars save 2,159kgCO_2eq** per tonne of steel product "cradle to distribution yard gate" (A1-A3), which is **83% lower** Global Warming Potential (GWP - kgCO_2eq) when compared to equivalent prime steel tubulars (A1-A3) on a weighted average per tonne basis.

Further analysis which includes distribution logistics to the construction site, and installation of the tubulars for foundation piling (A1-A5) shows **repurposed tubulars save 2,106kgCO_2eq** per tonne, a **75% lower** Global Warming Potential (GWP - kgCO_2eq) when compared to prime steel tubulars (A1-A5) based upon mill distribution chains delivering to the same client locations used by the yard sites in the study and including delivery and installation.

The analysis shows that even with a reduced raw material burden for the repurposed tubulars material CO_2eq contribution, the steel tubulars material itself creates the greatest percentage of emissions with an average of 50% of the overall impact. Transportation of the collected tubulars from origin to the distribution yards creates the second highest impact at 31%, and the delivery to project sites creates

 © DFI International Bruges 2025

the third highest impact at 15%. Yard handling activities and pipe pile installation account for the remaining 4% of emission impacts.

This suggests that for the secondary market pipe distribution industry, having facilities located close to ports and client delivery locations can help reduce environmental impacts significantly. Using repurposed pipe has the greatest savings effects on CO_2eq emissions impacts when it comes to steel tubular foundation construction.

Owners and contractors can be assured that secondary market steel tubulars meet structural requirements with some mill secondary pipe available with MTR's or Independent Test Reports (ITR's) can be arranged by the secondary market pipe supplier.

The results of this LCA have been 3rd Party verified and the EPD is available on the International EPD website (www.environdec.com).

ACKNOWLEDGEMENTS
The authors would like to thank the following people for their contributions:
John Lawrie Tubulars: Andrew Appleton, Jahir Avila, Rhonda Marchal and Michele Broughton
Giraffe Innovation Ltd: Rob Holdway, Mark Dowling and Dr. Rhys Charles
Keller North America: David Kirschner and Chris Meyer

REFERENCES
EN 15804:2012+A2:2019/AC:2021. Sustainability of Construction Works. Environmental Product Declarations. Core Rules for the Product Category of Construction Products.
ecoinvent. https://www.ecoinvent.org/database/database.html
ISO 14044:2006 Environmental Management — Life Cycle Assessment — Requirements and Guidelines
ISO 14040:2006 Environmental Management — Life Cycle Assessment — Principles and Framework
ISO 14025:2006 Environmental Labels and Declarations. Type III Environmental Declarations Principles and Procedures
SimaPro: https://www.simapro.co.uk/simapro-9
Works Steel Association. https://www.worldsteel.org/

 © DFI International Bruges 2025

DOUBLING SUSTAINABILITY OF CONCRETE FOUNDATION PILES THROUGH ENLARGED BASES AND SCREW-IN DISPLACEMENT METHODS

Przemyslaw A. Zakrzewski, Paile Solutions, Brisbane, Queensland, Australia, 0491 621 167
a.zakrzewski@paile.solutions
Stephen Buttling, National Geotechnical Consultants, Brisbane, Queensland, Australia. 0477 717 570
stephen.buttling@ngconsult.com.au

ABSTRACT

This study explores the impact of pile geometry and installation methods on the carbon footprint of concrete cast-in-place piles, focusing on those installed using the screw-in displacement method with an enlarged base. Recently introduced, data-driven installation techniques ensure that these foundations can now be installed in a seamless, efficient, and fully controlled process. Due to the significantly reduced material requirements for piles of the same nominal capacity, and hence less embedded carbon, piles with extended bases are rapidly gaining interest from infrastructure developers, owners, environmentalists, engineers, and commercial managers.

The research aims to quantify the environmental benefits of optimized piling techniques, particularly those with bases designed to maximize vertical bearing capacity, whether through compression or tension. Commercial projects have demonstrated that enlarging, and at the same time preloading, the pile base can significantly reduce the carbon footprint of foundations.

The results presented in this paper show that strategic adjustments in pile design and installation practices can reduce material usage and CO_2 emissions by more than half, while simultaneously lowering risk and reducing installation time.

1 INTRODUCTION

The potential to realise significant CO_2 reduction, project cost savings and minimise risk were the main drivers behind the development of the PAILE technology. PAILE combines existing, proven concepts to facilitate the installation of enlarged base concrete piles, in a single, continuous process.

As described in detail by Zakrzewski and Buttling (2022), the technology minimises ground heave, does not result in induced ground vibration and requires a relatively small piling rig to install. This innovative method increases sustainability and reduces direct installation costs by employing significantly less material and smaller machinery in comparison to standard piling practice, and offers further indirect savings by minimising associated temporary works such as working platforms.

In addition to the construction and sustainability benefits, PAILE also lowers project risk by allowing direct measurement of the resistance being achieved during the construction of each pile. The information this measurement provides is similar to that of a static load test, so the technology adds significantly to the available QA record and offers the opportunity for design adjustments to be made.

2 DESIGN EXAMPLE

To highlight the sustainability benefits of the PAILE system, a comparative study was conducted using a typical soil profile and foundation loads for a two-storey residential building with a single-level basement garage in Australia's Gold Coast region. This smaller-scale project was chosen for its simplicity, though the PAILE method is equally applicable to larger commercial and infrastructural developments.

In the Gold Coast region, including Hope Island, steel helical piles have been the most commonly adopted piling technique for residential projects in recent years, followed closely by CFA piles.

 © DFI International Bruges 2025

Therefore, this study evaluates the PAILE method against both steel helical piles and CFA piles, which are widely used in the area.

A typical residential project for a premium waterfront site has the following parameters:

- The building is a two-storey residence with a single-level basement garage, approximately 35m long by 20m wide in plan.
- Pile working loads specified by a structural engineer are between 50kN to 500kN, with a distribution as shown in Figure 1.

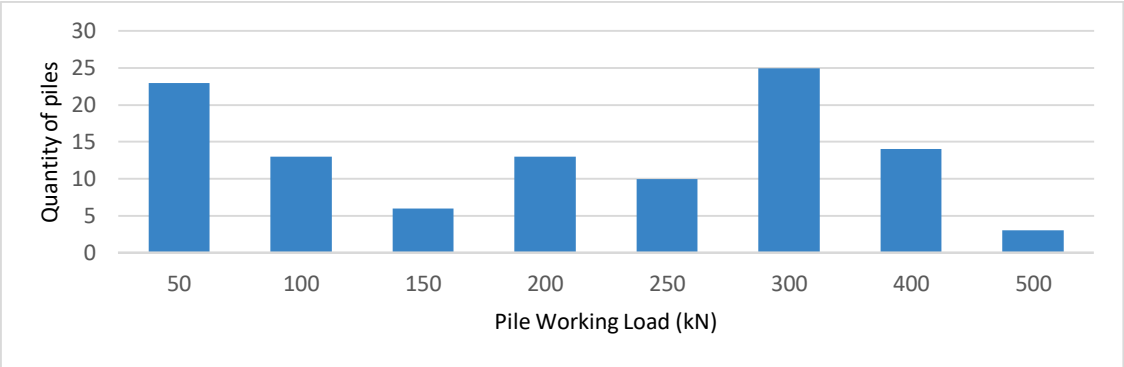


Fig. 1. Required quantities of each pile working load

- The site is located near a seawater canal connected with the Pacific Ocean and as such, it is subject to tidal water fluctuations.
- Subtropical water temperatures north of latitude 30° South in tidal / splash zones require special consideration from a durability design point of view.
- Watertight reinforced concrete basement floor are required, with foundation pile caps and ground beams monolithically connected.

2.1 Pile design methodology

As noted by Kenneth et al. (2021), pile design methods based on CPT data are becoming increasingly popular among engineers across the world. What makes those methods attractive is that they are data-driven, and therefore less prone to errors due to subjective interpretation.

Bearing capacity factors for helical pile design have been adopted based on Bittar et al (2023) and for CFA design using the LCPC1984 method after Bustamante and Gianeselli (1982).

With regard to PAILE foundations, full scale intrumented loads tests carried out in similar ground conditions, demonstrated by Zakrzewski and Buttling (2025) that the base capacity factor for PAILE foundations ranges between 0.50 to 0.60. For this study, a lower bound value of the base capacity factor as determined from the static tests has been assumed (see Table 1). Note that the assumed base capacity factor for the PAILE base bearing is the same as recommended for drilled displacement cast-in-situ piles as per Bustamante and Gianeselli (1982).

Table 1. Bearing capacity factors

Pile Type	Base capacity factor α_b	Shaft capacity factor α_s
Steel Helical Piles in sand	0.20	1/230
CFA piles in sand	0.30	1/100
PAILE method piles in sand	0.50	1/100

 © DFI International Bruges 2025

2.1.1 Steel Helical Piles

The design methodology adopted for the pile design follows the CPT-based method proposed by Bittar et. al (2023). The design process is iterative and typically includes the following steps for each pile:

- STEP 1: Select pile shaft diameter d_s, helix diameter d_b and founding depth L_p
- STEP 2: Calculate average CPT tip resistances q_{cs} and q_{cb}.
- STEP 3: Calculate pile capacity R_g and installation torque T using equations [1] and [2], respectively.

$$R_g = \alpha_s \, q_{cs} \, A_{shaft} + \alpha_b \, q_{cb} \, A_{base} \quad [1]$$

$$T(kNm) = \left[1/230 \;\; q_{cs} \, A_{shaft} + 0.15 \, q_{cb} \, A_{base}\right] \cdot 0.4 \, d_s^{0.92} \quad [2]$$

Where R_g = pile capacity, α_s = pile shaft capacity factor, q_{cs} = average CPT q_c along shaft length, A_{shaft} = pile shaft area, α_b = base bearing capacity factor, q_{cb} = average CPT q_c within pile base influence zone, T = installation torque in kNm, d_s = shaft diameter in m.

- STEP 4: Verify pile geotechnical and structural capacitates considering necessary safety factors as per equations [3] and [4].

$$N \leq R_g / SF_g \quad [3]$$

$$T \leq T_u / SF_T \quad [4]$$

Where N = pile load, SF_g = geotechnical safety factor, T_u = pile shaft structural torque capacity, SF_T = structural safety factor.

- STEP 5: If geotechnical capacity is insufficient, go back to STEP 1 and increase the helix diameter and/or change installation depth until the condition [3] is satisfied.
- STEP 6: If structural torque capacity is insufficient, go back to STEP 1 and increase shaft diameter, wall thickness and/or steel grade.
- STEP 7: Verify the axial and lateral capacity of the pile shaft.
- STEP 8: Select and verify helix thickness.
- STEP 9: Verify durability requirements.

The above procedure can be easily programmed in an Excel spreadsheet for quick and efficient design.

2.1.2 CFA Piles

The CFA piles were designed considering the following:

- All piles are to have a diameter of 450mm.
- Geotechnical capacity has been calculated in accordance with LCPC1984 method, using bearing capacity factors as shown in table 1.
- 40MPa concrete has been assumed for durability.

 © DFI International Bruges 2025

- 0.5% reinforcement rate has been assumed over a minimum length of 4.5m (10 D), or pile length, whichever is shorter.

2.1.3 Concrete PAILE system

The design process for piles installed using the innovative PAILE method follows a similar process to Helical Piles:

- STEP 1: Select pile shaft diameter d_s, helix diameter d_b and founding depth L_p
- STEP 2: Calculate average CPT tip resistances q_{cs} and q_{cb}.
- STEP 3: Calculate pile capacity R_g using equation [1].
- STEP 4: Verify pile geotechnical and structural capacitates considering necessary safety factors as per equations [3] and [4].
- STEP 5: If geotechnical capacity is insufficient, go back to STEP 1 and increase the helix diameter and/or change installation depth until the condition [3] is satisfied.
- STEP 6: Carry out the structural design of the pile shaft to determine reinforcement and concrete grade requirements need to resist the axial and lateral loads.
- STEP 7: Verify durability requirements.

The main advantages of the PAILE method have been described in detail by Zakrzewski and Buttling (2022). In summary, the benefits include:

- Much better verified pile-bearing capacity factors, leading to significantly higher geotechnical capacity and better load/settlement behaviour under working load conditions (refer to Table 1).
- Installation torque is much less of a limiting factor because the PAILE tool shaft can be made much stronger to cater for higher installation torque. Note that the tool shaft is reusable, not left in the ground. As such, pile reinforcement can be designed for the building loads only, and not for installation torque as is the case for steel helical piles. This leads to a much lower utilisation of steel, thus leading to a much lower carbon footprint of the pile foundation system.
- Concrete used to form pile shafts provides excellent compressive resistance and protection against corrosion of the reinforcement. There is no need to allow for sacrificial steel thickness to fulfill durability requirements.
- The enlarged base is thick, rigid and not prone to corrosion, as shown in Figure 2 below. This provides better confidence, especially when piles are to be installed in corrosive environments.
- Potential helix damage during installation is verified after each installation, unlike in the case of helical piles, where the steel helix is left in the ground and impractical to inspect, as it would require removal of the pile from the ground.

 © DFI International Bruges 2025



Fig. 2. Photo of an excavated PAILE foundation.

2.2 Ground Conditions

A soil profile similar to the profile found at the PAILE trial site has been adopted for this comparative study. The soil layers have been characterized by the average CPT cone resistance within each layer, as shown in Table 2 below. Note that only soil layers below the basement excavation level have been considered.

Table 2. Ground conditions adopted in the example

Soil Description	Depth to top of layer (m)	CPT q_c (kPa)
Very Loose to Loose SAND interbedded with layers of Firm CLAY	0.0	1000
Loose to Medium Dense SAND	1.5	5000
Medium Dense SAND	2.5	10000
Medium Dense to Dense SAND	4.0	14000
Very Stiff Silty CLAY	9.0	3000

2.3 Pile sizes

2.3.1 Steel Helical Piles

Design calculations for the Steel Helical Piles have been carried out and pile dimensions have been selected considering the following assumptions and requirements:

- 350MPa steel grade has been adopted.
- To ensure sufficient stiffness and strength, helix thickness has been selected to satisfy equation [5] below.

$$t_h \geq (d_h - d_s)/20 \qquad [5]$$

Where t_h = helix plate thickness, d_h = helix diameter, d_s = shaft diameter.

 © DFI International Bruges 2025

- To ensure sufficient durability to satisfy 50-year design life requirements, the cores of all helical piles are required to be filled with concrete. Additionally, cathodic protection or specialized coating is deemed required.
- The number of different pile types has been reduced to three (3) to limit the risk of construction errors.
- A geotechnical safety factor of SF_g = 2.25 has been adopted.
- A structural installation torque safety factor of SF_T = 1.40 has been adopted.

Table 3 below summarises the adopted helical pile sizes and quantities deemed appropriate for the project.

Table 3: Steel Helical Pile sizes adopted

Maximum safe working load (kN)	Pile shaft diameter and wall thickness (mm)	Helix diameter and thickness (mm)	Pile length (m)	Pile Quantity
100	CHS 88.9 x 5.5	310 x 11	5.0	36
250	CHS 168.3 x 7.1	570 x 20	5.5	29
500	CHS 219.1 x 8.2	710 x 25	5.5	42

2.3.2 CFA Piles

Table 4 below summarizes pile sizes adopted using the CFA method.

Table 4: CFA pile sizes adopted

Maximum safe working load (kN)	Pile shaft diameter (mm)	Base diameter (mm)	Pile length (m)	Pile Quantity
250	450	450	3.5	65
400	450	450	4.0	39
500	450	450	6.5	3

2.3.3 Concrete PAILE system

Design calculations for the piles installed using the innovative PAILE method have been selected considering the following assumptions:

- 40MPa concrete grade, to ensure 50yr durability requirements are satisfied.
- 500MPa grade reinforcing steel, designed to cater for 60% of compression loads, with the remainder of the compressive load to be resisted by concrete.
- Reinforcing steel in the form of a single central bar has been adopted.
- One-size PAILE tooling was adopted, to simplify logistics and limit construction errors on site.

Table 5 below summarizes pile sizes adopted using the alternative PAILE method.

Table 5. PAILE method pile sizes adopted

Maximum safe working load (kN)	Pile shaft diameter (mm)	Base diameter and thickness (mm)	Pile length (m)	Pile Quantity
200	220	600 x 400	2.5	55
400	220	600 x 400	3.5	49
500	220	600 x 400	5.0	3

 © DFI International Bruges 2025

2.4 Carbon Footprint comparison

The CO_2 emissions associated with concrete production are a significant environmental concern, particularly in the context of deep foundation piles. The emission levels vary based on the type of concrete used, influenced by material composition, cement content, and supplementary materials.

The emitted carbon dioxide budget is directly linked to the amount of material used and indirectly to the CO_2 emitted during the installation process. Although the emissions of the larger piling equipment are not irrelevant, this study focuses on the direct impact on the structure sustainability related to the material used. Justification for this can be found in De Melo et al (2024), where it is shown that the embedded carbon impacts from materials alone were about 91% of the total impact for driven steel piles and 81% for driven concrete piles.

To compare the embodied carbon footprint of the three foundation systems considered, the parameters suggested by Hammond and Jones (2011), as shown in Table 6 have been adopted:

Table 6. Embodied carbon footprint rates adopted

Construction material	Embodied Carbon $kgCO_2/kg$	Embodied Carbon $kgCO_2/m^3$
40 MPa concrete	0.13	312
Steel	2.70	N/A

In the calculation of the carbon footprint of concrete piles, the overbreak and/or waste need to be considered. Based on the authors' experience, the typical concrete overconsumption for CFA piles ranges between 20% to 40%, depending on the ground conditions and skill level of the construction team.

In the case of the PAILE system, based on the authors' experience, the overconsumption is slightly higher than for CFA piles. This is due to the volume of concrete lost by filling the space created by helical plates cutting through the soil during the extraction of the auger.

For this study, an average concrete overbreak of 50% and 30% has been assumed for the PAILE and CFA methods, respectively.

Figure 3 illustrates the total embodied carbon footprint of all three systems. As expected, the Helical Piles system exhibits the highest overall carbon footprint, with 56,828 kg of CO_2 from steel and an additional 3,199 kg of CO_2 from concrete, summing up to a total of 60,087kg. The CFA piles have about half of that, with 9,639 kg of CO_2 from steel and an additional 25,984 kg of CO_2 from concrete, totalling 35,623 kg. In contrast, the PAILE method demonstrates a significantly lower carbon footprint, with 11,059 kg of CO_2 from concrete and 3,792 kg of CO_2 from steel, resulting in a total of 14,851 kg of CO_2.

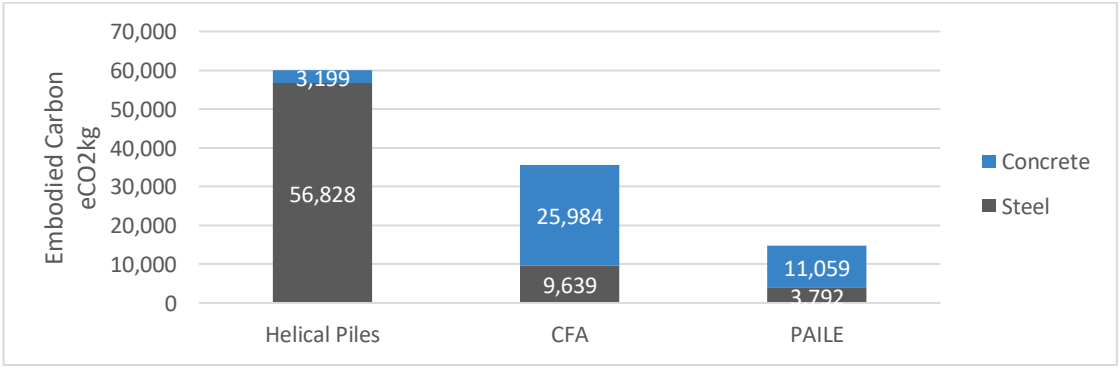


Fig. 3. Total embodied carbon footprint.

 © DFI International Bruges 2025

The PAILE system achieves substantial carbon savings, primarily due to its optimized pile shape, which reduces the volume of material required while maintaining the structural integrity of the foundation. This results in a reduction of material use, particularly steel, which has a much higher embodied carbon per kilogram compared to concrete (as shown in Table 6).

For this project, the number of different pile geometries was intentionally limited to three types to minimize the risk of on-site errors. This design constraint resulted in several piles being overdesigned, particularly those with lower specified loads. When assessing the design capacity using the same metric as De Melo et al. (2024), which expresses carbon footprint in terms of kg of CO_2 per kN of pile capacity, the PAILE method demonstrates a significantly lower global warming potential compared to the other pile types (Figure 3).

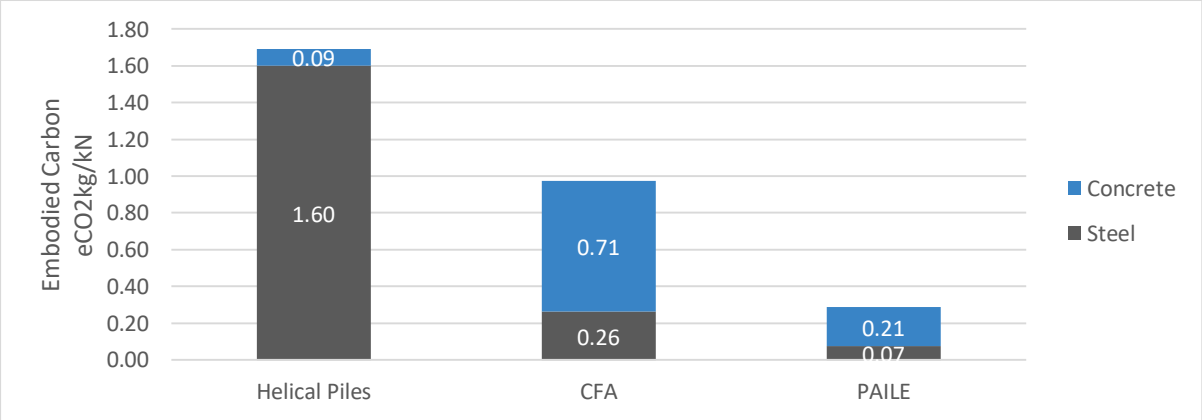


Fig. 4. Embodied carbon footprint per 1kN allowable pile capacity.

Table 7: Material consumption and embodied carbon footprint of different foundation options

	Concrete (m^3)	Steel (kg)	eCO_2kg	eCO_2kg / kN
Helical Piles	10.3	21,048	60,027	1.69
CFA	83.3	3,570	35,623	0.97
PAILE	35.4	1,404	14,851	0.29

The ideal pile shape and installation method should be compatible with any type of concrete and contribute to CO2 reductions beyond material selection. By incorporating a slender column with an extended base (as shown in Figure 2), the pile's optimized design reduces material volume while maintaining structural performance. This design innovation leads to substantial carbon savings across the entire project lifecycle.

3 CONCLUSIONS

By evaluating various aspects of pile designs and installation techniques, it has been identified that PAILE technology provides several competitive features ensuring its sustainability and cost-efficiency.

The method provides optimal material consumption by use of a slender shaft with an enlarged and precompressed base. As a result, the method achieves lower CO_2 emissions linked directly to the reduced quantities of materials consumed, whether steel or concrete. For example, when making a direct comparison with helical steel screw piles and CFA piles for a notional typical housing project, the embedded CO_2 was reduced by factors of approximately 4 and 2 respectively. Additional factors that drive the method adoption and therefore contribute to the sustainability impact include:

- High load/settlement stiffness due to preloading of the pile base
- Simple and continuous installation process in one pass

 © DFI International Bruges 2025

- Minimised ground heave due to high capacity-to-pile volume ratio
- No induced ground vibrations during pile installation
- Use of cost-effective building material (reinforced concrete)
- Requires comparatively small and manoeuvrable piling equipment

4 REFERENCES

AS 2159:2009, Australian Standard, A. S. 2159-2009 Piling-Design and Installation.

Bittar, E., Lehane, B.M., Blake, A., Richards, D., White, D., Mahdavi, S., & Cerfontaine, B., 2023. CPT-based design method for helical piles in sand. Canadian Geotechnical Journal, 61(1), 102-117.

Bühler, M M., 2016. White Paper: Shaping the Future of Construction, Insights to Redesign the Industry. http://www3.webforum.org/docs/WEF_Shaping_Future_Construction.pdf.

Bustamante, M, and L Gianeselli., 1982. Pile Bearing Capacity Prediction by Means of Static Penetrometer CPT. Proceedings of the 2nd European Symposium on Penetration Testing, 493–500.

De Melo, D.L., DeJong, J.T., Kendall, A and Leane, B.M., 2024. Life-cycle-based considerations in design of driven piles in sand. Proceedings of the Institution of Civil Engineers – Engineering Sustainability. https://doi.org/10.1680/jensu.23.00099

Hammond, G., Jones, C., Lowrie, E.F. and Tse, P., 2011. Embodied carbon. The inventory of carbon and energy (ICE)

Gavin, K., Kovacevic, M.S., & Igoe, D., 2021. A review of CPT based axial pile design in the Netherlands. Underground space, 6(1), 85-99.

Zakrzewski, P.A. and Buttling, S, 2022. A novel ground improvement and deep foundation system using PAILEs. DFI-PFSF Piling & Ground Improvement Conference.

Zakrzewski, P. A. and Buttling, S., 2025. Field trials and load tests of the PAILE system of expanded base piles. (Paper in review)

PAILE is a registered trademark. Patent pending. http://paile.solutions

 © DFI International Bruges 2025

The Tremie Guide – about Concrete Performance and Sustainability

Rabea Barhum, BAUER Spezialtiefbau GmbH, Germany
Karsten Beckhaus, BAUER Spezialtiefbau GmbH, Germany
Chris Harnan, Ceecom Geotech, United Kingdom

ABSTRACT

When the first standards on concrete were written, far more than five decades ago, concrete technology was relatively simple. Modern "high-performance" concrete is far more complex. Specifying the essential criteria for successful placement of concrete in submerged conditions using tremies at depths in excess of 100 m is a major challenge. A joint task group of EFFC and DFI (European Federation of Foundation Contractors and Deep Foundations Institute) has brought together a broad church of industry experts to find a common understanding on this topic. The group is presently updating the 2nd edition of the EFFC/DFI Guide to Tremie Guide for Deep Foundations, and edition 3 has been released in late 2024. It also highlights the need for sustainability, to which the Tremie Guide contributes with its performance-based concept to design concrete, giving all options to materialize a lower-carbon concrete without diminishing quality aspects. Future approaches may be founded on lessons learned from numerical modelling which is a key to better understanding the complex interactions governing concrete flow mechanisms. The task group continues its work to validate simulations to justify new requirements, e.g., a reduction in workability retention for long pours. It is hoped that the recommendations in the Tremie Guide will become contractually binding norms to make them broadly applied in practice, resulting in a higher quality reliability in quality and optimised sustainability.

Keywords: Fresh concrete, performance, quality, sustainability

HISTORY

The very first meeting of the EFFC/DFI Concrete Task Group (CTG) took place on 23rd of January 2014 in Amsterdam. It was initially set up by the European Federation of Foundation Contractors (EFFC) that had discussed, in their annual general meeting in October 2013, the quality of geotechnical works in the light of concrete quality. It was decided that a broad group of experts should discuss the lack of suitable test methods and sufficient testing of relevant properties of fresh concrete for placement in deep foundations and provide a state-of-the-art report. The CTG, presently comprising 15 full members, has been working in a very trustful and target-oriented atmosphere for more than 10 years. With a constant overall target to reduce defects in deep foundations, see
Fig. **1**, caused directly by inadequate workability or stability of concrete, or indirectly by a lack of consideration of related parameters effecting the flow of concrete and/or proper filling of the excavation.).
The CTG decided from the very start to invite consultants to join the group to bring their technical views on these complex and exclusively quality-related topics. A group of corresponding members, consulting the group and reviewing status papers and drafts, was also established as well as a group of academics to give scientific advice.
The major focus has always been on the specification and testing of fresh concrete as the core of a "Tremie Guide". It was intended to use the Australian tremie handbook [CIA Z17, 2012] as a start-off, which was created in the same sense to give updated recommendations better suited for modern tremie concrete. Given the fact that the CTG chairman was also a member of the Australian working group it was guaranteed that all relevant information beyond the published recommended practice was considered in its entirety.
The basic scope and structure of the "EFFC/DFI Guide to Tremie Concrete for Deep Foundations" (Tremie Guide) set out in the 1st Edition (2016) was repeated in the 2nd Edition (2018) and will remain the same for the 3rd edition. To the core of the fresh concrete specification and testing, other topics were added including design, execution, and the need or benefit of monitoring the quality by non-destructive test method. The 1st edition also contained recommendations on support fluids. The task of supporting open boreholes and trenches using support fluids is a complex subject which cannot be adequately covered in a simple sub-section. A separate support fluid task group was therefore

 © DFI International Bruges 2025

established, and a guide was issued in 2019. This group is currently working on the 2nd edition, implementing lessons learned from a field research study that is ongoing. That same approach had been applied for the evolution of the Tremie Guide.



Fig. 1. Schematic representation of support fluid bored pile production

Based on a comprehensive study of international standards and literature the CTG acknowledged the demand for a detailed test program for fresh concrete properties. By that time, colleagues representing the Deep Foundation Institute from America joined the Group. Meetings attended by up to 20 full members took place in European cities, as well as the USA.

A big step forward occurred when approximately €150,000 was received from industry sponsors. The money was used to carry out an extensive test program in the laboratory and in the field, in Europe and the USA. This was contributed to by specialist contractors opening their construction sites for a detailed investigation of the concrete used. Researchers from the Technical University in Munich and from the Missouri University of Science and Technology collected data for multiple concrete mixes, reflecting also their technical boundary conditions of application, for later interpretation and assessment of results, with the main findings merged into the 2nd Edition 2 of the Tremie Guide.

Finally, it was already decided for the preparation of the 2nd Edition to add a chapter on Numerical Modelling Methods for backing up the Group's understanding of tremie flow and cross-checking reasonable conclusions regarding flow mechanisms within an excavation during casting. A sub-group with mainly academics was established and worked separately on what computer programs can and cannot prove without exceeding their limited capabilities to deliver reliable simulations.

 © DFI International Bruges 2025

After the 2nd Edition had been released – again for free download from the homepages at effc.org and dfi.org – the Group was silent for a period of 4 years until it met again during the DFI/EFFC Conference on Deep Foundations and Ground Improvement in Berlin in May 2022. It was decided to produce a 3rd Edition, in order to: -

- emphasise the need to reduce greenhouse gas emissions,
- strengthen the recommendations regarding acceptance criteria with respect to testing,
- add new findings from numerical modelling,
- update individual sections where users had asked for clarifications.

2 THE TREMIE GUIDE EDITION 3

As the name suggests, the Guide to Tremie Concrete for Deep Foundations is limited to the application of the "tremie method" to install cast-in-situ elements like bored piles, diaphragm walls or elements, for which a typical set-up is shown in Fig. 2. The Guide defines the tremie method as follows:
„*Concrete pouring method by use of a tremie pipe in order to prevent the concrete from segregation or contamination by the fluid inside the excavation, where the tremie pipe – after the initial placement – remains immersed in previously poured, workable concrete until the completion of the concreting process.*"

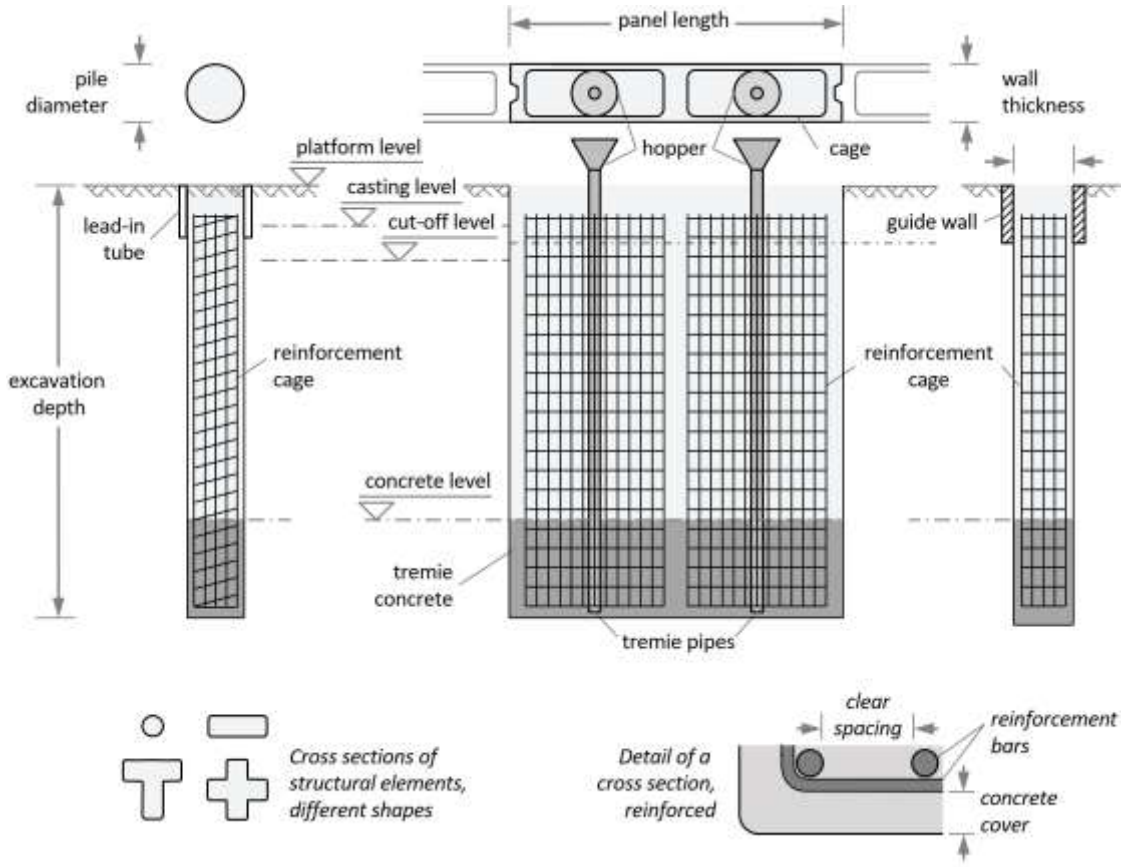


Fig. 2. Examples of deep foundations

2.1 GENERAL

The background has been presented by the history of the Concrete Task Group founded to reduce defects in deep foundations.
The primary purpose of the Guide to Tremie Concrete for Deep Foundations (Tremie Guide) is to give guidance on fresh concrete characterisation with respect to its performance, the concrete mix design process, and the methods used to test the fresh concrete. The principles of this Guide apply to tremie concrete for deep foundations but may also be applied for other forms of deep foundations (e.g., continuous flight auger piling).

 © DFI International Bruges 2025

Figure 3 summarises how the demanding and often conflicting requirements should be considered throughout the development of a concrete mix. The Guide highlights the important areas that require careful consideration in order to minimise the potential risks, including the appropriate structural detailing and the use of state-of-the-art execution methods.
It is strongly believed, and that's why the Tremie Guide is addressing all stakeholders, that getting the mix right can only be achieved via a joint approach between the Constructor, the Structural Designer, and the Concrete Supplier.

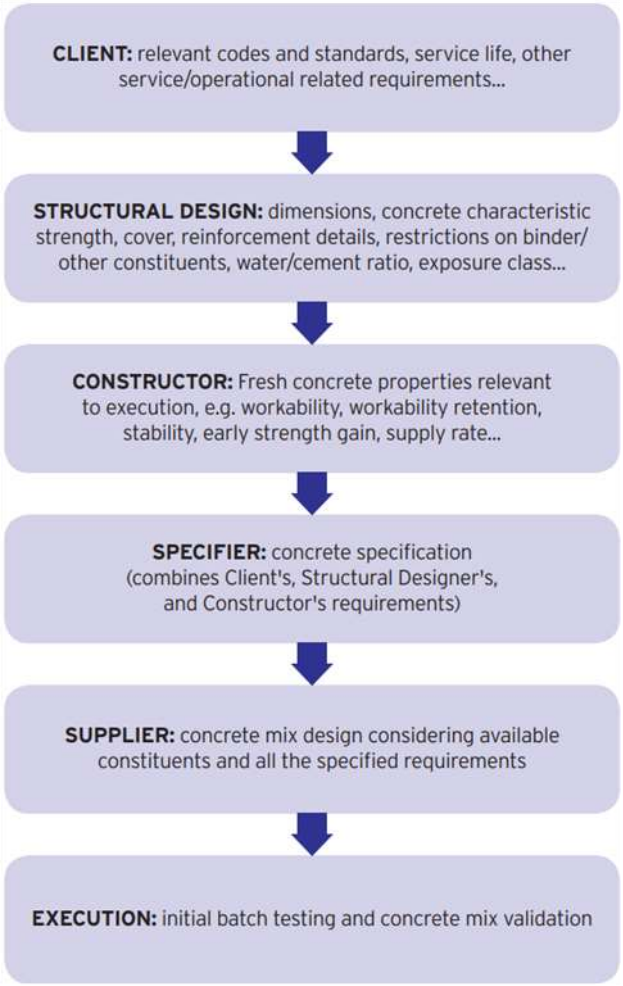


Figure 3: Typical evolution of concrete mixes

2.2 DESIGN CONSIDERATIONS IMPACTING CONCRETE FLOW

The structural design of deep foundations is a specialist subject requiring both structural and geotechnical input, as it must also consider the conditions for the execution of the deep foundation works. However, within the context of the Tremie Guide, the recommendations are limited mainly to the detailing of the reinforcement cages.
It is obvious that the reinforcement bars, in their longitudinal (usually vertical) and transversal combined configuration present a considerable obstruction to flow. The main criteria to obey are subsequently enough clear space for the concrete to flow through „windows", and the concrete cover to allow complete filling of the excavation and embedment of the reinforcement. It should be recognised that the required minimum cover for execution cmin,execution for ensuring concrete placement is independent from the structural need for a minimum cover to ensure bond or durability. The designer should consider specifying a minimum clear spacing and a nominal cover respecting both demands.
Figure 4 summarises these main recommendations, which are explained in more detail in the Tremie Guide. It should also be noted that for the concrete placement in deep foundations a larger clear

 © DFI International Bruges 2025

distance in relation to the maximum grain size of concrete aggregate D_{max} is needed to avoid blocking, and that for practicable reasons the outer dimensions of the cage need to include a tolerance, Δd_c for its installation into the excavation with a nominal dimension equal to that of the excavation tool.

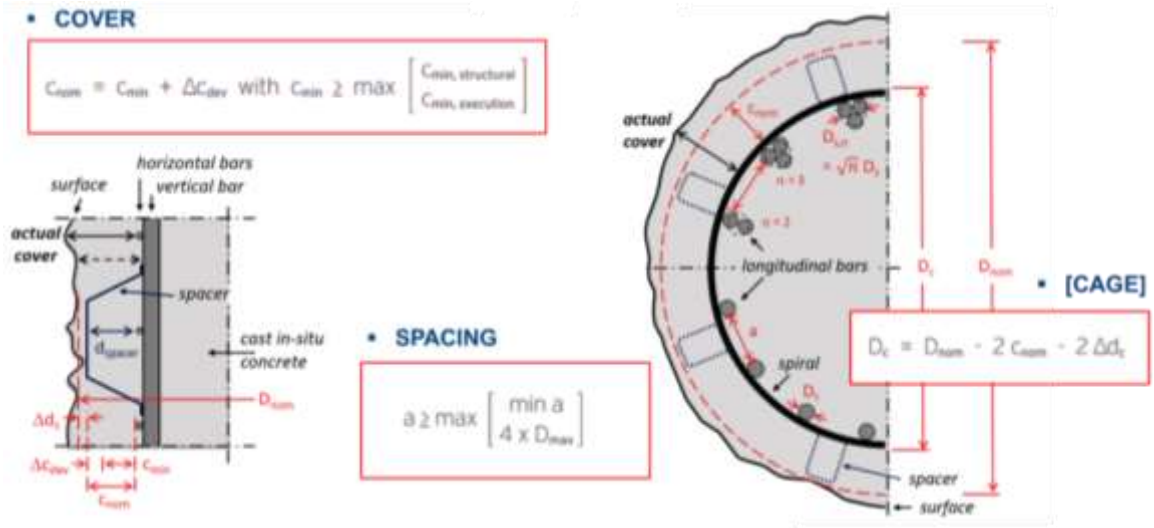


Figure 4: Considerations for detailing a reinforcement cage in deep foundations (also applicable to rectangular)

2.3 PROPERTIES OF TREMIE CONCRETE

It has already been explained that a principal task for the CTG has been to consider modern concrete technology. There was a consensus to focus on the right performance of fresh concrete, driven by the rheology of the bulk concrete mix, but also – on a microscale – of the paste where inter-particle mechanisms and chemical actions become relevant. In this context, the principle – normative – requirements for self-levelling, self-compacting by gravity, and filling the excavation, are all governed by the concrete's workability characteristics. Stability characteristics must avoid the negative effects of segregation, bleeding or filtration. A sufficient control of stiffening (with time) is a matter of workability retention.

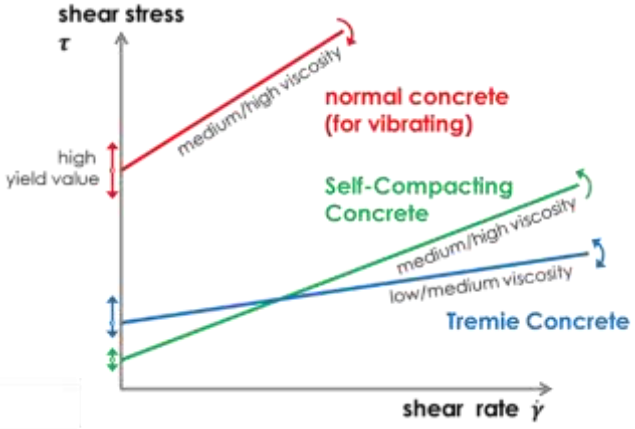


Figure 5: Qualitative comparison of rheology for different types of concrete

Figure 5 explains Tremie Concrete performance in simple rheology terms, and gives evidence why Tremie Concrete should not be mistaken with a self-compacting or self-consolidating concrete, often referred to as ‚SCC'. In comparison to normal concrete that is vibrated to overcome the yield value to initiate flow, Tremie Concrete and SCC both have a much lower yield and a much lower viscosity, which is the resistance to flow, once started. However, Tremie Concrete does need a significantly higher yield than SCC mainly in order to control stability e.g., avoid segregation over often long workability retention times, achieved by retarding admixtures (that are seldom used for SCC). At the same time, the viscosity of Tremie Concrete is significantly lower than for SCC, mainly to ease

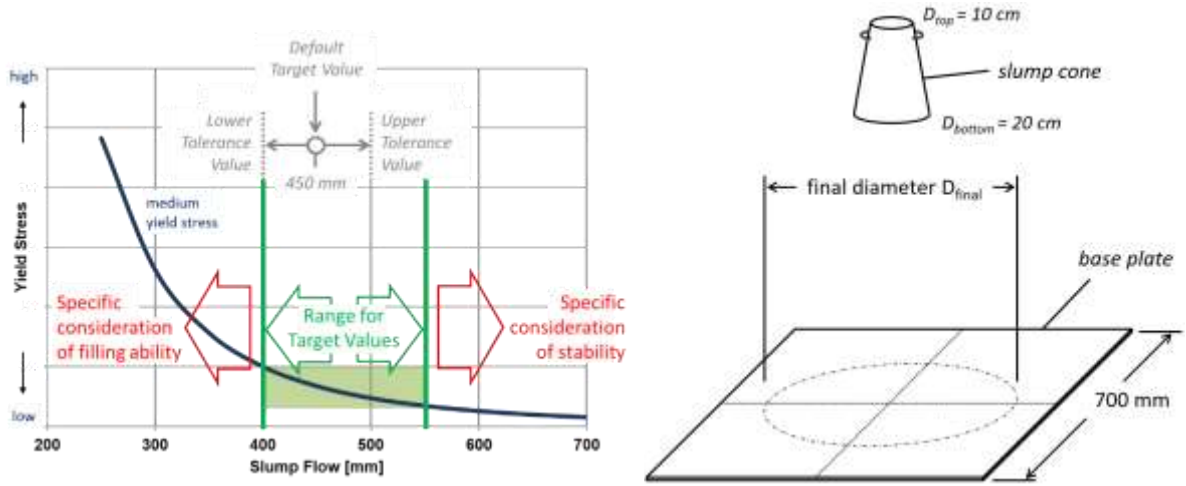
distribution and to limit the time to empty a truck i.e., to reduce total pouring times, which in turn limits the time for any segregation to occur.

2.4 CONCRETE MIX DESIGN

The right concrete mix design has to be based on a good general knowledge of concrete technology. The section just highlights typical steps in developing a concrete mix design for deep foundations and assumes that suppliers have a sufficient range of established concrete mix designs. However, as the Tremie Guide also presents non-normative test methods to better characterise fresh Tremie Concrete, additional considerations on mix design, constituents, and proportioning might be useful also for concrete technology generalists.

2.5 SPECIFYING AND TESTING OF CONCRETE, AND QUALITY CONTROL OF CONCRETE PRODUCTION, AND SUSTAINABILITY

In this central section of the Tremie Guide, "A New Approach to Specifying Fresh Concrete" is presented.
As indicated in the sections above, fresh tremie concrete cannot be described by a single measure of consistence (workability) only. As stated in the Guide, the consistence of a concrete is the best characterisation for its ability to fill the excavation and to "squeeze" through openings in the reinforcement cage. However, more characterisation, and testing, is needed to ensure good performance.
The EFFC/DFI research program has clearly revealed that for fresh Tremie Concrete, the Slump Flow (SF) test is much more sensitive than the widely used slump or flow table tests. Figure 6 comprises a preferred range for a SF target value to be specified as recommended in the 2nd Edition of the Guide that will be narrowed down to a default value for typical applications in the 3rd Edition.



Figures 6 & 7: Slump Flow curve related to yield stress and recommended range for tremie concrete, and (to the right) test equipment for combined slump flow, slump flow velocity and VSI test

In combination with the Slump Flow test, it is literally no extra effort to also get an indication of the concrete's viscosity and stability, two more important characteristics. As the test equipment for this "triple test" is the standard slump test equipment, as shown in Figure 7, plus a stopwatch, there should be no issue at all to implement such testing on a regular basis i.e., also on site for standard acceptance testing if specified.
In fact, the Slump Flow test not only shows the initial workability but also, by repeated testing, its development over time. The workability retention test validates the end of workability that occurs after placement, see Figure 8.
In the context of necessary workability retention, the decisive question to answer is, how long the concrete load is being moved or displaced before finally cast. This could happen, for example for the first load, before the pour is completed. And Numerical Modelling can help to better understand dependencies, as explained in section 2.9.

 © DFI International Bruges 2025

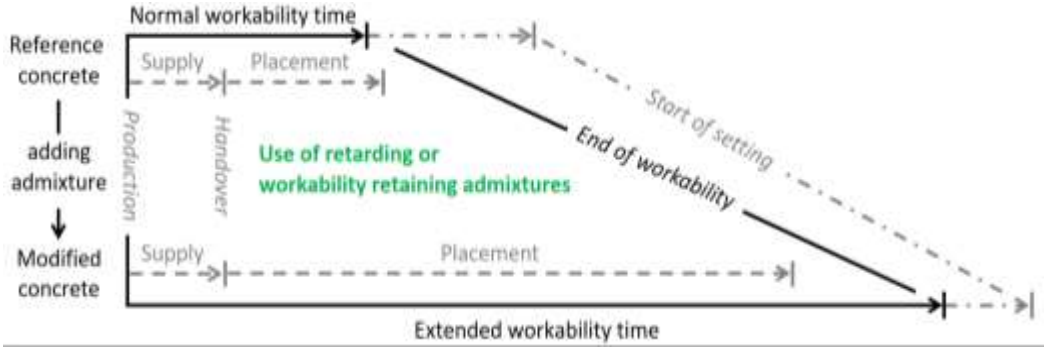


Figure 8: Extension of workability time

2.6 EXECUTION

Techniques and methods used prior to concreting and for the actual tremie pouring operation are clearly within the scope and responsibility of the specialist contractor. However, a quality control inspection & test plan may vary according to country or region. As European, American and International Standards and Codes of Practice vary, the Guide limits its recommendations to what is considered good practice, without scrutinising individual state-of-the-art practices. Execution parameters contribute greatly to a successful concrete placement and will have influence on the final distribution of concrete in a completed element.

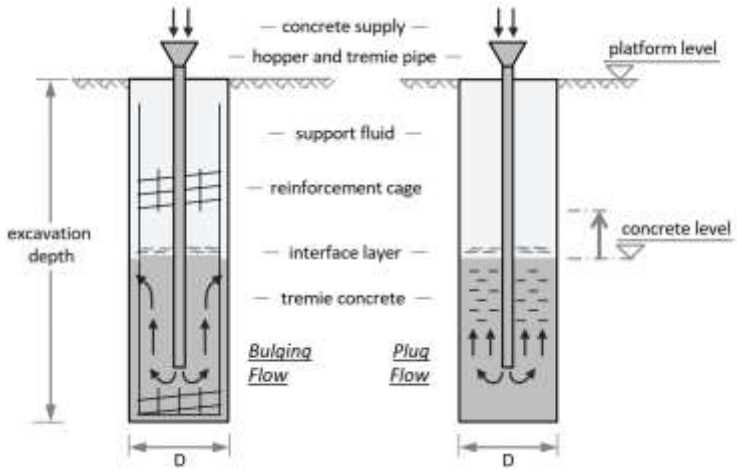
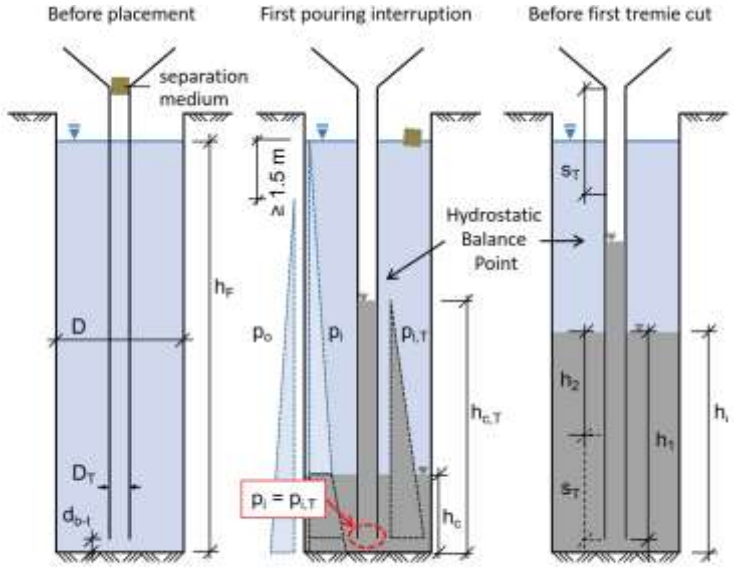


Figure 9: Schematic of bulging and plug flow

Consensus in the Group was built on a principle of understanding concrete flow mechanisms. Based on experience and observations on many tremie concrete pours, and backed up by numerical modelling, there are two extremes of how fresh concrete displaces earlier poured concrete and distributes through an excavation. Figure 9 shows, in a simplified schematic, the bulging flow path in the case of maximum friction at the outsides of the excavation e.g., by a reinforcement cage, and the plug flow in case of literally no friction restricting the flow at the outside.

The most critical step in the tremie concreting process is attributed to the initial placement. The first batch or batches of concrete have to be continuously poured until a safe embedment of the open tremie pipe is achieved, by a concrete level in the excavation affecting an outside pressure at the outlet (equal to the inside hydrostatic pressure in the tremie pipe (levelled after the dynamic flow downwards), high enough to let the concrete level in the tremie pipe above the outside concrete level. This stage is shown in the centre of Figure 10. Other relevant parameters are discussed in detail in the Tremie Guide.

 © DFI International Bruges 2025



Where:

h_F	Fluid level in excavation
D_T	Diameter of tremie pipe
D	Dimension (diameter or thickness) of excavation
d_{b-t}	Distance from bottom of excavation to tremie pipe outlet
h_c	Concrete level in excavation
$h_{c,T}$	Concrete level in tremie pipe (= hydrostatic balance point)
h_1/h_2	Embedment of tremie pipe before (1) / after (2) tremie pipe cut
s_T	Section length of tremie pipe section to cut, with: $h_2 \geq 3$ m [10ft]
p_o/p_i	Hydrostatic pressure outside (o) / inside (i) of excavation
$p_{i,T}$	Hydrostatic pressure inside the tremie pipe

Figure 10: Phases in the tremie pour sequence

2.7 FULL SCALE TRIALS

This brief section in the Tremie Guide emphasises the potential of full-scale trials to identify problematic conditions and address these before commencement of the permanent works. These might not be obvious before starting a new project. The extent and scope should be proportionate to the project size.
The components to be tested should be selected from a review of:

- the design and detailing,
- the fresh concrete performance,
- the constructor's placement methods, overall experience and capability, and
- the experience in the given ground properties.

Any extra time and costs needed for such trials must be recognised by the client at an early stage and specified in detail in the tender documents. In any event, it is recommended to perform on-site conformity testing to verify or allow adaption of the concrete mix design usually developed in the supplier's laboratory.

2.8 QUALITY CONTROL OF COMPLETED WORKS

It is essential that the Constructor complies with relevant standards for quality assurance and control, and that the production process is supervised and undertaken by competent persons with suitable training, qualifications and experience.
Some imperfections of the hardened concrete of the deep foundation element are possible even though good practice construction methods were applied by the Constructor. Quality control requirements for the completed works should therefore make allowance for acceptance of some imperfections where

 © DFI International Bruges 2025

these are not significant with regard to the structural performance and durability of the completed works. To support efficient and consistent inspection and acceptance, acceptable imperfections should be clearly identified in work procedures and inspection and test requirements. Optional non-destructive testing methods might assist, and their use should be planned upfront in detail. To give one example with relevance to execution: testing pipes are usually pre-installed in the excavation by attaching them to the reinforcement cage, and their configuration must obey the same rules as for the reinforcement bars to ensure the required clear spacing for concrete flow.

2.9 NUMERICAL MODELLING OF CONCRETE FLOW

This section is the most dynamic regarding reaction on consideration of the latest developments. To cope with the new knowledge generated at a scientific level, it requires time to publish the validated results.
A 4th Edition of the Tremie Guide is planned which will present further modelling results once completed. This will allow a better understanding of concrete flow mechanisms and the sensitivity to changes in various parameters such as concrete rheology, clear spacing, cover thickness, volume and height of the open excavation to be filled.
It should be noted that numerical modelling is used to understand principal interrelations resulting in flow patterns. It has not been, and will not be, intended to use a numerical model as a realistic digital twin. To do so, the methods would need to allow realistic simulations not only of bulk flow but also for stability issues like concrete segregation which in turn would affect the workability and filling ability of the fresh concrete in a real and usually very complex situation.

3 FUTURE

A key objective of the CTG was to translate the Tremie Guide's approach to applying the performance concept to the design and testing of tremie concrete into standards. A significant step has been to move away from a descriptive minimum cement content, which is required in the older generation execution standards for Bored Piles and Diaphragm Walls (EN 1536 and EN 1538) in Europe. New, performance-related, but also more specific regulations not only improve the quality of completed works, but also make it possible to improve sustainability by reducing cement and thus the carbon footprint of foundations.
In favour of a clear assignment of concrete topics to the relevant European standard EN 206 on Concrete – Specification, performance, production and conformity, concrete related regulations were copied and pasted from the standards for the execution of special geotechnical works (EN 1536, EN 1538, EN 12699 and EN 14199) without any harmonisation, let alone a revision of the content in the context of modern concrete technology and modern execution aspects.
Subject to the formal approval of CEN, Figure 11 shows the relationship between the future EN 206-3 and the relevant execution standards for concrete placement. For bored piles and diaphragm walls produced in accordance with EN 1536 and EN 1538, tremie concrete is standardised due to the applied excavation method, amongst others.
It should also be noted that EN 206 defines tasks for the specifier, the producer and user in its parts -1 and -3 which are relevant for concrete in general and for tremie concrete in particular. This establishes the mutual endeavour of all parties involved to work together, as is also defined in the scope and purpose of the Tremie Guide. The right concrete will never be a product that is blindly taken off the shelf in future either. But the new EN 206-3 paves the way for specifying and testing the required performance in the respective area of application more precisely. Engineering assessment and concrete-technology expertise remain essential.
EN 206-3 not only opens up the standard for plastic concrete to cover applications that may go beyond load-bearing structures, but also prescribes the Slump Flow test method for tremie concrete as the future main criterion. The relevant clause states that "Tremie concrete shall be specified by slump flow, by a target value, based on a detailed engineering assessment." The standard allows to choose the actual target value from the range from 400 to 550 mm or to set to 450 mm, with a maximum tolerance of +/- 50 mm, as recommended in the Tremie Guide.
Regarding all three main characteristics of fresh concrete (workability, workability retention and stability), EN 206-3 refers to normative and non-normative test methods based on the Tremie Guide, which are described in an informative annex. This informative annex will become superfluous once the

same test methods have become normative. Standardisation within the EN-12350 series for fresh concrete test methods has been applied for at corresponding task group under the umbrella of CEN/TC 104 for Concrete and Related Products.

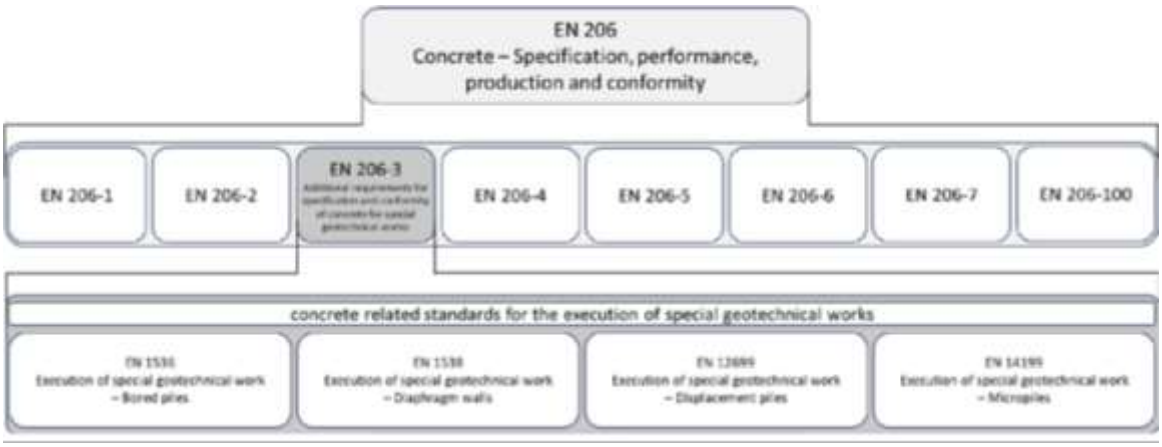


Figure 11: Relationship between EN 206-3 and concrete related standards for the execution of special geotechnical works

4 CONCLUSIONS

Up to date, in a 10-year period, the joint EFFC/DFI Concrete Task Group has made great efforts to establish a Guide to Tremie Concrete for Deep Foundations in its 3rd Edition published late 2024. A 4th Edition is already in preparation, which will incorporate the last validated findings from Numerical Modelling.

Already from the 1st Edition in 2016, the Guide has focused on improving the quality throughout the whole process of in-situ casting of deep foundations. To do so, the Guide has always been intended as a practical addition to existing standards, not a substitute. Project specifications, standards and codes should always take precedence.

However, the Guide assists individuals and corporations involved in the procurement, design, and construction of bored piles and diaphragm walls including Owners/Clients, Designers, General Contractors and Specialist Contractors.

ACKNOWLEDGEMENTS

The author is grateful for the continuous and extraordinary support provided by the members of the EFFC/DFI Concrete Task Group and wishes to express his sincere thanks to all experts and sponsors who have contributed to the Tremie Guides.

REFERENCES

CIA Z 17 (2012). Recommended Practice, Tremie Concrete for Deep Foundations, Concrete Institute of Australia.

EFFC/DFI (2018, 2024). Guide to Tremie Concrete for Deep Foundations, European Federation of Foundation Contractors and Deep Foundation Institute, draft for 3rd Edition from 2024, based on 2nd Edition from 2018.

 © DFI International Bruges 2025

INVESTIGATION, TRIAL AND USE OF CEM VI (C VI) CONCRETE FOR A SUSTAINABLE DEEP FOUNDATION FUTURE

Chris Barker, Ove Arup & Partners Ltd, London, United Kingdom
Fragkoulis Kanavaris, Ove Arup & Partners Ltd, London, United Kingdom
Titusz Tomor, Bachy Soletanche Ltd, Lancashire, United Kingdom
Jonathan Ly, Canary Wharf Group, London, United Kingdom

ABSTRACT

The ready-mix concrete supply chain in the United Kingdom is actively innovating to provide piling concrete with lower embodied carbon emissions. The recent BS 8500-2: 2023 Concrete - Complementary British Standard to BS EN 206 update now allows multicomponent cements to support a more sustainable future. This paper presents the composition of low-emission multicomponent combination C IV equivalent to CEM VI cement that was investigated for piling. Portland cement was replaced with 61% of other cementitious components comprising limestone (LL) and granulated blast furnace slag (GGBS). This C VI multicomponent cementitious combination has an embodied carbon of 199 kgCO2e per cubic metre of concrete. This is a significant reduction from a typical C/CEM IIIA piling concrete with 228 kgCO2e per cubic metre of concrete. The concrete testing results obtained confirmed the feasibility of the use of ground limestone in cement composition for piling. This supports the supply chain to reduce demand for granulated blast furnace slag where there is limited market availability. Durability characteristics of concrete (carbonation susceptibility, chloride ion permeation, water penetration) made of C VI multicomponent cementitious combination are also presented. Results of a field trial showed successful concrete placement in a CFA pile and subsequent installation of reinforcement cage. Following the trial, two permanent marine piles were successfully constructed with 200m^3 of CVI concrete.

Keywords: concrete, piling, embodied carbon, sustainability, ternary mix, multicomponent cements

INTRODUCTION

Ground granulated blast furnace slag (GGBS) is a co-product of the iron and steel industry. It is obtained by water-cooling and grinding blast furnace slag that is formed in the blast furnaces that create iron out of iron ore. It has been used as a supplementary cementitious material (SCM) in concrete around the world since the end of the nineteenth century due to its technical properties, such as improving the concrete's durability.

More recently the increased use of GGBS as a supplementary cementitious material has gained popularity to reduce embodied carbon emissions within foundation concrete and meet project targets. While for piling concrete 40 to 50% of the total cementitious material is now commonly GGBS, this has on some UK projects been increased up to 70% for piling or even 95% for unreinforced secant piles. The significant differences in carbon emissions in cementitious materials can be seen with The Concrete Centre, MPA (2019) published indicative 'cradle to factory gate' CO2e values of Portland Cement CEM I 800 kg/tonne, GGBS 35 kg/tonne and limestone fines 8.0 kg/tonne.

A review undertaken by Arnold et al. (2023) indicates that the cement industry's global clinker production is currently 8 to 12x higher than global GGBS production and will remain at this order of magnitude to 2030 and beyond. It was found that around 90% of all iron slag is already processed into GGBS each year by the iron and steel industry. The review found no significant usable GGBS stockpiles, noting that air-cooled slag stockpiles are unlikely to be suitable and that water-cooled slag material loses reactivity over time if it comes into contact with moisture. The Arnold et al. (2023) review demonstrates that GGBS is a limited and constrained resource that is

 © DFI International Bruges 2025

almost fully utilised globally. Any increase in its use in one location is highly likely to result in a reduction in use elsewhere, balancing each other out overall.

GGBS should continue to be used where required technically. Beyond this, it may still be specified where well-established supply chains exist, but it should not be used in high proportions in the hope of reducing global greenhouse gas emissions. It should also be noted that very high proportion mixes can lead to a need to increase total binder content if not managed through the project programme. Alternative options exist for reducing clinker usage and thus reducing global emissions, and designers should work with the supply chain to identify the best way to do this on each project. Concrete buyers and specifiers should recognise these issues and decide how best to align their ambitions to reduce emissions both on-site and globally.

In November 2023, the British Standards Institution published the much-awaited update to BS 8500 Concrete - Complementary British Standard to BS EN 206 Part 1 and 2. The purpose of this update was to introduce the possibility of specifying ternary cements containing GGBS, fly ash, or limestone. While such ternary mixes might have been used in few regions in Europe, limestone-containing ternary cements were not permitted in the UK. In any case, although such mixes were included in the European norms, their industry adoption is not common, especially for high CEM I replacement levels, due to uncertainties with concrete performance. While limestone fines have been used in small quantities as fillers in piling concretes, significantly increasing the amount of limestone fines inclusion as cementitious material is still not widely adopted due to aforementioned performance-related issues.

In this study, a combination of relatively high contents of GGBS and limestone fines is considered for piling applications in ternary formulations with 35% CEM I, 45% GGBS and 20% ground limestone, which is the maximum ternary replacement permitted by BS 8500 Parts 1 and 2 and EN 197-5:2021. This has been the first application, known to authors, of such mixes for piling concrete in the UK and quite possibly in Europe.

Limestone fines have been considered for incorporation in concrete and cement production for several decades, particularly in certain parts of Europe. This includes the addition of limestone fines in the production of cement which leads to cement designations CEM II A-L, which is a relatively popular cement type across Europe containing up to 20% limestone and CEM II B-L, which is less popular, containing up to 35% limestone. Studies have indicated that limestone powder becomes inefficient when it exceeds 15% by mass in blended cement Bentz et al. (2015). Beyond this percentage, it has been reported that the dilution effect can significantly reduce the concrete's physical properties, such as compressive strength Wang et al. (2018); Kim et al. (2018).

Limestone fines have been used in small quantities as fillers in piling concretes in the UK and globally. However significantly increasing the amount of limestone fines and accounting for their contribution to cementitious properties when combined with other supplementary cementitious materials brings obvious uncertainty in the performance of such concretes. The development of ternary concrete mixes with GGBS and limestone has been previously reported in other studies, such as Palm et al. (2019); Król et al. (2020) where laboratory-prepared mixes were tested for fresh and hardened behaviour. These studies indicated that it is possible to produce ternary concrete mixes with GGBS and limestone for structural applications. Nevertheless, there has been limited research on the applicability of GGBS limestone combinations in deep foundation concrete mixes, which are known to be susceptible to concrete-related defects.

RESEARCH SIGNIFICANCE AND METHODOLOGY

With the increasing need to step away from concrete mixes which utilize high volumes of conventional SCMs, such as fly ash and GGBS. The reliance on GGBS in particular for producing lower carbon concretes of acceptable performance can be reduced through the incorporation of ground limestone powder in the mix to form a ternary binder combination.

 © DFI International Bruges 2025

Over the past years, particularly for piling concrete, utilizing GGBS in the concrete mix has become a relatively common practice. However, there is a knowledge gap with regard to the development and performance of ternary mixes containing CEM I, GGBS and limestone fines as binder (CEM VI or C VI combination). This is particularly important for piling concretes which need to exhibit certain fresh and hardened behaviour in order to be acceptable on site and demonstrate decreased proneness to defects.

It is known from the authors' experience that adding limestone fines to concrete beneficially decreases concrete bleed but it also can make the fresh concrete 'sticky' for which additives are important to maintain satisfactory workability.

Several properties relevant to piling concretes with ternary mixes containing CEM, GGBS and limestone fines have not yet been investigated which potentially hinders the wider adoption of such mixes in piling applications. Therefore, this paper evaluates certain key concrete properties of ternary mixes with CEM I, GGBS and limestone fines which are pertinent to piling applications, aiming to increase confidence on using such mixes for piling concrete. This is done here through reporting results from mix development, experimental investigations on key concrete properties as well as observations and monitoring results from the first trial of a cast in-situ bored CFA pile with a ternary mix in the United Kingdom. Site compliance results are then also presented for 200m^3 of CVI concrete placed in two permanent marine piles.

CEM VI (C VI) CONCRETE MIX

Historically, piling concrete mixes have been CEM IIIA with about 40 to 50% of the total cementitious material being GGBS. During the course of piling at the North Quay project in Canary Wharf, London, the opportunity was jointly taken by the developer, consultant and contractor to investigate, trial and use a CEM VI concrete mix recently permitted by the update to BS 8500: 2023. On site, a CEM IIIB concrete mix was being used for 900mm diameter CFA piles up to 29m deep and tremie concreting of 1500mm and 1800mm diameter rotary bored piles up to 38m deep and allowed a comparison to be made. Both of these mixes are detailed in Table 1 together with a reference CEM IIIA mix recently used on another project. The workability for this CFA piling CEM IIIB mix was specified as a flow of 600mm ± 60mm. In accordance with BRE (2005), the design chemical class for the site was DC-2. The proposed CEM VI mix was developed to be compliant with DC-2 design chemical class, conforming to D1 Combined Performance Category as CEM VI (S-L)+SR in BS 8500-1. For this mix category, the minimum GGBS content is 36% and the maximum limestone fines content is 20%. The workability for this CEM VI mix was specified as a flow of 620mm ± 60mm. It is worth clarifying that due to the particularities of concrete batching in the UK, e.g., concrete binders mixed at the batching plant rather than using factory blended cement, the mix produced was an equivalent combination denoted C VI(S-L)+SR to BS 8500-1. Nevertheless, as the C VI+SR designation is not that popular Europewide, the designation CEM VI (S-L)+SR is used throughout the paper for simplicity.

The aim of the proposed CEM VI mix was to reduce the quantity of GGBS while compensating the loss of this cementitious material with an increase in limestone fines. It was expected that these changes would affect the workability retention and that the performance of the additives would be critical to also achieve the 5-hour retention being used for the CEM IIIB mix. During the investigation and trials, the amount of CEM VI additives was optimised, these mixes noted as Mix 1 to 3 in Tables 3 to 6. The CEM VI constituents remained otherwise unchanged. Achieving the specified C32/40 concrete strength at 28 days was also required.

 © DFI International Bruges 2025

Table 1. Concrete Mix Designs

C32/40 Concrete Constituents	CEM IIIA	CEM IIIB	CEM VI
CEM I 52,5N	221.25	126.00	163.80
GGBS	153.75	294.00	193.20
Betacarb 80ST Limestone - cementitious	-	-	89.00
4/10 Washed Conc. SS Limestone	803.00	795.00	797.00
0/4 Conc. Sand MP Blended	982.00	975.00	977.00
Betacarb 80ST Limestone - filler	-	30.00	-
Admixtures (various)*			
Water (Cold)			
A/C Ratio	4.8	4.2	4.0
Actual WCR	0.55	0.44	0.41
% Fines	55.0	55.1	55.1
% GGBS	41.0	70.0	43.3
Total Cementitious (kg/m^3)	375	420	446
Total Embodied Carbon A1-A4 (kgCO2e)	228.3	187.0	199.0

*Admixtures comprised: Super Plasticiser, Consistence Retaining Admixture and Retarding Admixture.

The key complication with adopting a ternary mix with GGBS and limestone fines stems from reducing the reactivity of the combined cementitious material. CEM I is highly reactive, while GGBS is latent hydraulic and contributes significantly to the cement hydration reaction in a comparable behaviour to a pozzolan. However, ground limestone is generally considered to be inert, thus replacing GGBS with limestone in the mix was not expected to significantly impact the reactivity of the binder and the strength gain. It is worth noting that while ground limestone is regarded as an inert material for concrete, it can still contribute to cementitious properties specifically through the “filler effect”, pore filling with increased surface area powders as discussed by Oey et al (2013).

From the supplier Environmental Product Declarations (EPD) Table 2 shows the embodied carbon values for the Life Cycle product stage (A1-A3) for comparison. The values exclude carbon offsetting, which was not undertaken, and the GGBS value includes economic allocation. European directive no longer considers GGBS as waste but as a by-product of the steel industry. Economic allocation allocates the impacts of the ironmaking process to granulated blast furnace slag in proportion to its value compared to pig iron. Prior to including economic allocation GGBS had an embodied carbon value of only around 76 kgCO2e / tonne. Nevertheless, the ability to reduce embodied carbon with GGBS and ground limestone fines remains advantageous.

Table 2. Product stage (A1-A3) embodied carbon values

C32/40 Concrete Constituents	kgCO2e / tonne	Life Cycle Modules
CEM I 52,5N	723	A1-A3
GGBS	168	A1-A3
Betacarb 80ST Limestone	43	A1-A3

TEST METHODS AND RESULTS

Several tests were carried out as part of the performance evaluation of the mixes. Those tests focus on the fresh behaviour and volume stability, strength and durability characteristics of the investigated concretes.

 © DFI International Bruges 2025

Fresh properties and volume stability

Evaluating the fresh behaviour of piling concrete is of paramount importance in order to obtain an indication of potential risks associated with concrete flowability, stability of the mix in terms of segregation issues and avoidance of post construction defects. As such, specifically, the bleed rate (ASTM C232), Bauer filtration (ICE Specification 2017, EFFC 2018), segregation resistance (ASTM C1610), visual stability index (VSI) (ASTM C1611) and hardened visual stability index (HVSI) (AASHTO PP 58-12) were performed for the mixes and are shown in Table 3.

A CEM IIIB mix (70% GGBS) was kept as reference and this was a mix of known, and compliant with the specifications, performance. The ternary CEM VI developed appeared to exhibit acceptable fresh behaviour, with negligible bleeding for the investigated timeframe (4-6 hours). An increased Bauer filtration value was observed for the ternary CEM VI mixes compared to the CEM IIIB, however, that was still well below the specification limit. Segregation resistance was improved for the ternary CEM VI mix and this can be attributed to the increased mix cohesiveness from the addition of finely ground limestone Wang et al. (2018). Finally, VSI and HVSI indicated no segregation and good volume stability for the investigated mixes.

Table 3. Pre-construction Concrete Stability Test Results

C32/40 Concrete Mixes	Bleed Rate (mL/min)	Filtration (mL)	Segregation (%)	VSI	HVSI
Specification limits:	≤0.1	≤22	≤10	0/1	0/1
CEM IIIB	0.00	9.0	4.2	0	0
CEM VI (Mix 1: Initial site trial)	0.02	9.0	0.9	0	0
CEM VI (Mix 2: Repeat site trial)	0.00	14.0	1.6	0	0
CEM VI (Mix 2: CFA pile trial)	0.00	12.0	0.0	0	0
CEM VI (Mix 3: Marine piles)	0.07	11.0	4.9	0	0

Workability and workability retention are also fundamental properties of fresh concrete for piling applications as it governs how efficiently the mix can be cast on site. Table 4 contains results from different workability tests, namely, slump, flow table, slump-flow and slump-flow velocity. It appeared that the ternary CEM VI mixes developed resulted in comparable, or even, higher workability properties which can be attributed to a higher target and quantity of superplasticizer and the presence of limestone fines. Slump test yielded high results for CEM VI, i.e. outside of an S4 mix 200mm ± 50mm and this was also observed from the flow and slump-flow results.

Table 4. Pre-construction Concrete Workability Test Results

C32/40 Concrete Mixes	Slump (mm)	Flow Table (mm)	Slump-Flow (mm)	SF Velocity mm/sec
CEM IIIB	210	580	-	-
CEM VI (Mix 1: Initial site trial)	260	675	570	21.1
CEM VI (Mix 2: Repeated site trial)	260	640	540	18.7
CEM VI (Mix 2: CFA pile trial)	230	650	460	32.5
CEM VI (Mix 3: Marine piles)	240	640	590	38.4

Figure 1 shows the results from workability retention tests with the CEM VI flow table acceptance range shaded. As mentioned previously, the target flow was designed 20mm higher for the CEM VI mixes compared to the CEM IIIB mix. The initial CEM VI (Mix 1) flow retention showed a relatively abrupt loss of workability 4 hours after mixing. This indicated that CEM VI mix required attention towards achieving the required workability retention time. Following the initial

 © DFI International Bruges 2025

trial, the quantity of retarding admixture was increased for the repeat and CFA pile trials (Mix 2) showing a successful increase in retention time beyond 5 hours. The CEM VI admixtures were optimised again for the subsequent marine piles to achieve a 7-hour retention time.

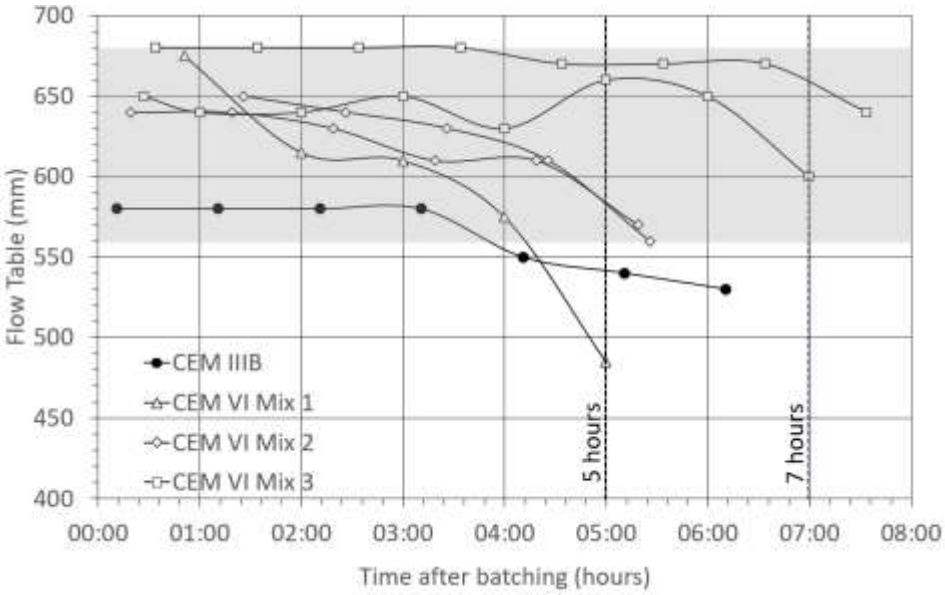


Fig. 1. Pre-construction fresh concrete workability retention (flow table)

Compressive strength and durability properties

Further tests were performed on hardened concrete in order to evaluate key properties. These were the compressive strength development of the investigated mixes, as well as certain durability properties of the developed CEM VI mix.

The compressive strength development of the investigated mixes is shown in Figure 2. It is demonstrated that CEM VI mixes can develop strength characteristics similar to CEM IIIB mixes and well above the 28-day 40MPa design strength, therefore, from a strength development perspective no major adjustment could be expected from adopting CEM VI mixes more widely.

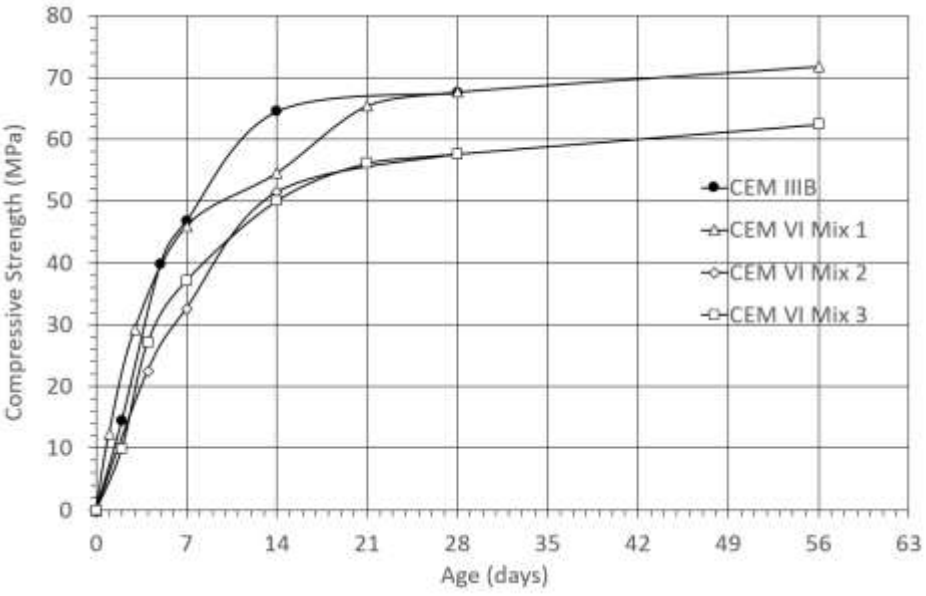


Fig. 2. Pre-construction concrete compressive strength test results

 © DFI International Bruges 2025

Durability properties were also measured, namely, chloride migration coefficient (FIB 34), inverse carbonation resistance (FIB 34), water absorption (BS 1881: Part 122) and depth of water penetration under pressure (EN 12390–8:2000) with results being shown in Table 6.

Table 6. Concrete Durability Test Results

C32/40 Concrete Mixes	Chloride Migration Coefficient (28-day) (m^2/s)	Inverse Carbonation Resistance (28-day) $(m^2/s)/(kg/m^3)$	Water Absorption (%)	Water Penetration (28-day) (mm)
CEM IIIA (typical)	$3.0\text{-}8.0x10^{-12}$	$0.5\text{-}2.0x10^{-12}$	0.5-2.0	-
CEM IIIB (typical)	$1.5\text{-}3.5x10^{-12}$	$1.0\text{-}4.0x10^{-12}$	0.5-2.0	-
CEM VI (Mix 1: Initial site trial)	$3.8x10^{-12}$	$1.6x10^{-12}$	0.8-0.9	4

Generally, the durability properties of CEM VI appeared to be similar to CEM IIIA and CEM IIIB typical values. Carbonation resistance is relevant to carbonation-induced corrosion, a commonly encountered deterioration mechanisms in concrete, often reported as inverse carbonation resistance. The inverse carbonation resistance of the investigated CEM VI was at the lower end of the spectrum in terms of what is expected for CEM IIIB and CEM IIIA which can be attributed to the relatively low water/cement ratio of the mix. It was also at the lower end of the spectrum for water absorption and penetration measured properties, that indicate the permeability characteristics of the concrete, which are directly relevant to durability. The addition of limestone, however, appeared to affect the chloride migration characteristics which also dictate the vulnerability of reinforced concrete to chloride-induced corrosion. Normally, CEM IIIB mixes do encompass good resistance to chloride penetration, followed by CEM IIIA mixes. The addition of limestone combined with a reduction of GGBS in a ternary CEM VI system seemed to bring the chloride migration coefficient towards the higher end of the spectrum of what would be expected for CEM IIIB and more in line with the typical chloride migration coefficients for CEM IIIA. However, conditions which require lower than $3x10^{-12}$ (28-day) (m^2/s) chloride migration coefficient are mostly relevant to marine structures and structural elements exposed to saline water as well as parts of structures exposed to de-icing salts, which is not the case for the investigated piles.

In 2022, the VDZ (German Cement Association) initiated a project on the durability of concretes with clinker-efficient cements CEM II/C and CEM VI supported by the Federal Ministry of Economic Affairs and Climate Action (VDZ, 2025). This follows research from the same organization on ternary mixes with GGBS and limestone which indicated that concretes with 50% CEM I, 20% limestone and 30% GGBS are suitable for producing structural concretes with admissible durability properties, with the exception of the freeze-thaw resistance. The research also found that while it is possible to increase limestone content to 50%, it is so with inferior durability properties (Palm et al. 2019).

 © DFI International Bruges 2025

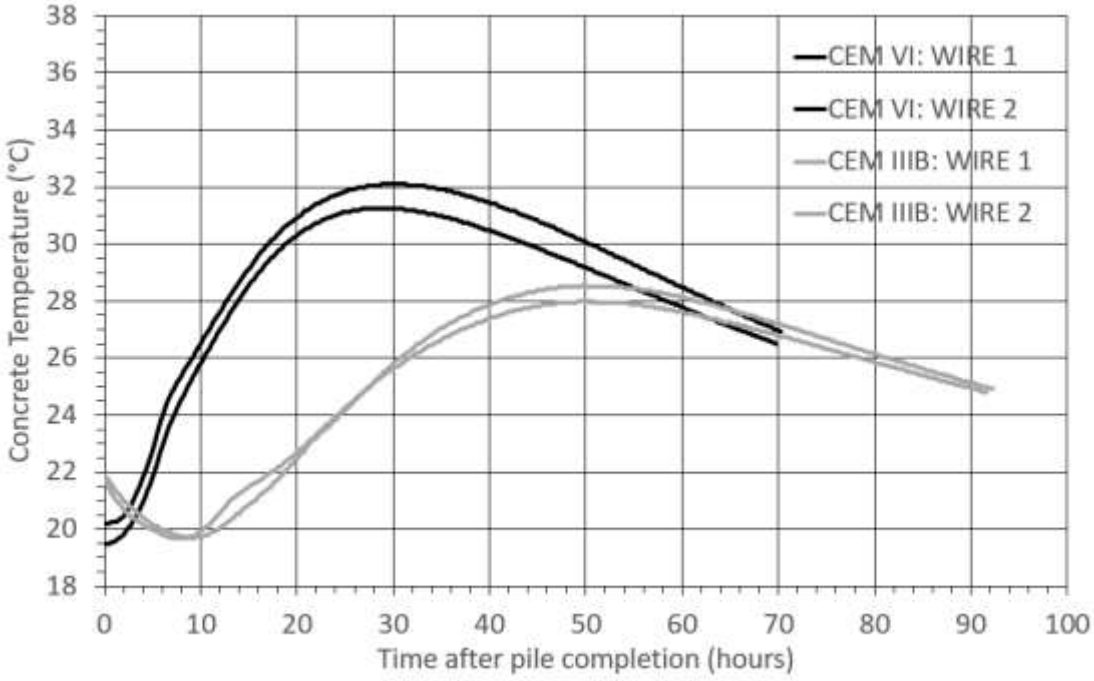


Fig. 3. CFA piles concrete temperature development at -9.34mOD

The concrete temperature development was measured in situ using the thermal integrity testing method during the CFA pile trial. Two thermistor cables were attached to the reinforcement cage and in the case of the CEM VI pile, a third cable attached to the central bar. The maximum temperatures reached over all sensors was 33.6°C at -1.82mOD for CEM IIIB and 37.9°C at -0.81mOD for CEM VI. Typical temperature development plots measured from thermistor cables attached to the reinforcement cage for both concretes at the same depth in the ground are shown in Figure 3. At this depth of -9.34mOD, the piles are in granular soil below the water table. Measuring concrete temperatures during curing can provide useful insight and indication on the hydration characteristics, setting and hardening rate Schlicke et al. (2019). Measured temperatures indicated that the rate of temperature increase of the CEM VI mix was higher compared to that of the CEM IIIB. This can be attributed to the CEM VI mix containing 38 kg/m^3 more CEM I and approximately 100kg/m^3 less GGBS than the CEM IIIB mix. As such, the higher and lower CEM I and GGBS, content respectively in the CEM VI mix contributed to an acceleration of the hydration reaction. Regardless, the peak temperatures recorded for both mixes were well below the limiting temperature of 70 °C often suggested by corresponding guidance documents and standards (BS8500-1; ACI 207.1-21).

CONCRETE TEST PERFORMANCE SUMMARY

The CEM VI mix developed exhibited similar behaviour to a CEM IIIB mix. While strength, flowability and certain durability properties of CEM VI were measured to be comparable or even better than the control CEM IIIB mix, particular attention might be required towards workability and its retention time, and chloride penetration resistance of CEM VI mixes which is relevant to structures exposed to saline water and groundwater as well as de-icing salts.The temperature development of CEM VI was more rapid reaching a peak 2°C higher and about 20 hours sooner than the CEM IIIB concrete.

CFA TRIAL

To fully evaluate the workability, stability and retention of the concrete mix a trial CFA pile construction was undertaken on Saturday 14th September 2024. The CEM VI (Mix 2) concrete was batched in three 7.50m^3 loads between 07:57am and 08:30am and when arrived on site was tested

 © DFI International Bruges 2025

and then discharged into the agitator, see Figure 4, for pumping into the concrete lines using a Putzmeister BSA 1409 concrete pump ready to commence piling.



Fig. 4. CEM VI CFA trial concrete



Fig. 5. CEM VI CFA trial pile cage

From a piling platform level of -0.3mOD, a Casagrande B360 XP2 piling rig drilled a 900mm diameter 25.1m deep pile commencing augering at 09:23am and withdrawing the auger above platform level at 10:13am (2 hours 15mins after first batching. The plunging of the 444kg 10m long cage (10no. B25 + B10@275mm) commenced at 10:20am with the plunging of the 18.5m long 46mm diameter central bar completed at 10:35am, 2 hours 38mins after first concrete batching, see Figure 5. The thermal integrity testing data loggers were then connected.

The concrete pumped well without any issues and remained stable without bleeding. The cage plunged freely under its own weight for half its length and then was assisted with 3 tonne steel cage static tamp to its final level with the subsequent central bar plunged under its own weight and was trapped off.

PERMANENT BRIDGE PILES

After the CFA trial, the mix was approved for use in the construction of two 2.1m diameter marine piles for the Eden Dock bridge. In November 2024, with additives adjusted to achieve a 7-hour retention time, 200m^3 of the CEM VI mix (Mix 3) was successfully placed by tremie under support fluid. This is believed to be the first use of CEM VI concrete in deep foundations in the UK.

The frequency of compressive testing was increased to investigate the variability of 28-day concrete strength. From the results of the sixteen 28-day compressive strength cube tests the mean was 54.9 MPa, minimum 48.7 MPa, maximum 61.9 MPa and standard deviation of 3.3 MPa. All results were well above the specified 40 MPa design strength and continuing to gain strength. Figures 6 and 7 below show the results of the CEM VI (Mix 3) compressive cube strength testing. The results were favourable and allow further future optimisation of CEM VI concrete mix design to be made in reducing the CEM I content to reduce the total cementitious material.

 © DFI International Bruges 2025

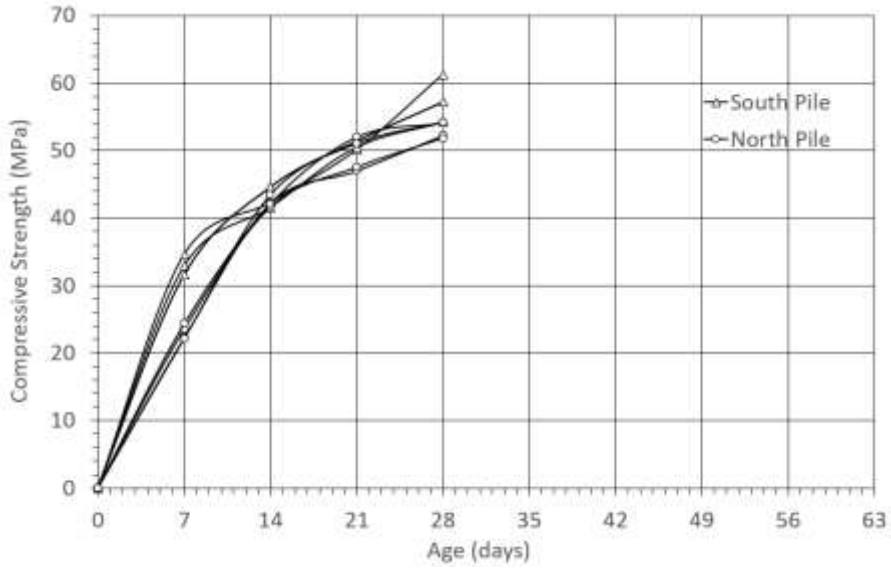


Fig. 6. CEM VI (Mix 3) compressive concrete cube strengths

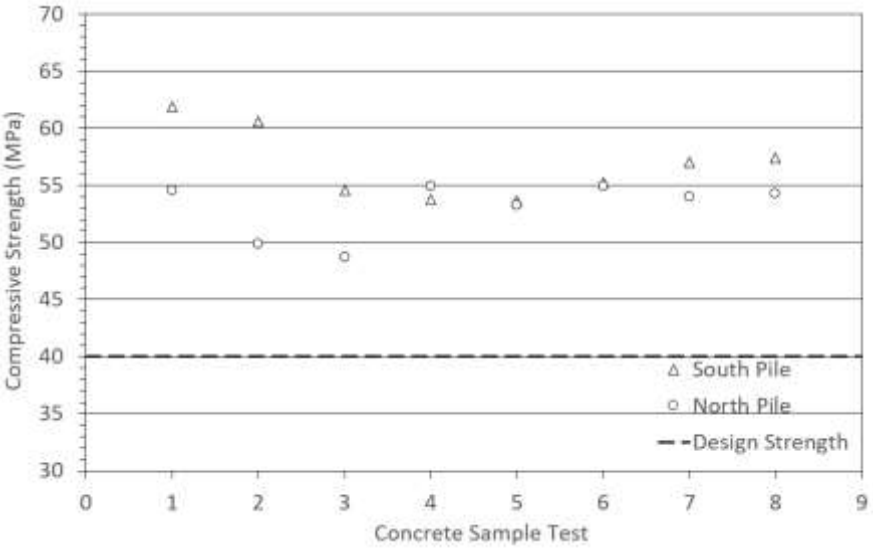


Fig. 7. CEM VI (Mix 3) compressive concrete cube strengths at 28 days

CONCLUSIONS

It is usually a challenge to introduce new materials into construction, particularly for deep foundations where there are inherent risks with construction in the ground. Projects that want to lead with new techniques or materials sometimes struggle to find solutions that can be trusted. The risks associated with adopting a new material can be considered either too high or can be overlooked and can result in serious consequences. This case study demonstrates a successful investigation, trial and implementation of a CEM VI concrete mix.

A series of tests were undertaken to evaluate the CEM VI mix for pile construction. The CEM VI mix trialed demonstrated satisfactory results for workability, retention, stability and bleed while significantly exceeding the required hardened strength. The two biggest challenges of concrete mixes during CFA pile installation are concrete pumping and cage plunging. During the CEM VI trial, both the concrete pump and piling rig used performed successfully. Also, the reinforcement installation was successful with no differences in installation methodology compared to the CEM IIIB mix.

 © DFI International Bruges 2025

The CEM VI concrete mix trialed reduced the amount of GGBS by 100kg/m^3 and successfully increased the amount of limestone fines by 59kg/m^3 compared to the CEM IIIB concrete being used with comparable embodied carbon. In conclusion, it is considered that CEM VI mix can be successfully used in deep foundations.

The compressive strength achieved was significantly above the specified target and therefore gives opportunity to further optimize the CEM VI design mix to reduce the total cementitious material. The investigation and results presented in this paper provides a basis for others in the industry to develop their own CEM VI mixes conforming to the new BS 8500 parts 1 and 2 published in 2023.

ACKNOWLEDGMENTS

The authors would like to acknowledge and thank Canary Wharf Contractors Ltd for supporting the trial and permission to publish this paper. The authors would also like to thank London Concrete Ltd for their technical support during the trial and to Socotec UK Ltd for the concrete thermal measurements.

REFERENCES

ACI PRC-207.1-21: Mass Concrete - Guide, 2022. American Concrete Institute.

Arnold, W., Astle, P., Drewniok, M., Forman, T., Gibb, I., Kanavaris, F., Khosravi, N., Martin, B., Mulholland, A., Munro, I., Scrivener, K., de Silv, M., Wake, G. 2023. The efficient use of GGBS in reducing global emissions: an appraisal of the global availability of ground granulated blast furnace slag. The Institution of Structural Engineers, United Kingdom.

Bentz et al. 2015. Multi-scale investigation of the performance of limestone in concrete. Construction and Building Materials. 75. Pp. 1-10.

BRE, 2005. Special Digest 1 Concrete in aggressive ground. 3rd Edition. United Kingdom.

BSI, 2023. BS 8500-1: 2023 Concrete - Complementary British Standard to BS EN 206 - Method of specifying and guidance for the specifier. British Standards Institution. United Kingdom.

BSI, 2023. BS 8500-2: 2023 Concrete - Complementary British Standard to BS EN 206 - Specification for constituent materials and concrete. British Standards Institution. United Kingdom.

EFFC/DFI, 2024. Guide to Tremie Concrete for Deep Foundations 3rd Edition, European Federation of Foundation Contractors / Deep Foundation Institute.

Kim, Yoo-Jae, Ryno van Leeuwen, Bum-Yean Cho, Vedaraman Sriraman, and Anthony Torres. 2018. "Evaluation of the Efficiency of Limestone Powder in Concrete and the Effects on the Environment" Sustainability 10, no. 2: 550.

MPA, 2019. Fact Sheet 18. Embodied CO2e of UK cement, additions and cementitious material. MPA The Concrete Centre, United Kingdom.

Oey et al. 2013. The Filler Effect: The Influence of Filler Content and Surface Area on Cementitious Reaction Rates. J. Am. Ceram. Soc., 96 [6] 1978–1990.

Palm S., Müller C., Proske T., Rezvani M. and Graubner C.A. 2019. Concrete application of clinker-efficient cements. Advances in Cement Research 31(5): 225–234,

 © DFI International Bruges 2025

Schlicke, D., Kanavaris, F., Lameiras R. and Azenha, M. 2019. On-site monitoring, Book chapter in: RILEM State-of-the-art report in cracking mitigation in massive concrete structures, Springer (edited by E. Fairbairn and M. Azenha).

VDZ. 2025. Durability of concretes with clinker-efficient cements CEM II/C and CEM VI. Durability of concretes with clinker-efficient cements CEM II/C and CEM VI [Accessed 15/01/2025].

Wang, D., Shi, C., Farzadnia, N. Shi, Z. and Jia, H. 2018. A review on effects of limestone powder on the properties of the concrete. Construction and Building Materials. 192, pp. 153-66.

 © DFI International Bruges 2025

EVALUATING ENVIRONMENTAL IMPACTS OF DEEP FOUNDATIONS: A LIFE CYCLE APPROACH FOR SUSTAINABILITY

André V. A. Borgatto, CONSTRUCT, Faculty of Engineering, University of Porto, Porto, Portugal and Federal Rural University of Pernambuco, Recife, Brazil, andre.borgatto@ufrpe.br
Guilherme A. F. Silva, Environmental Engineering, University of Porto, Porto, Portugal
Belmira Neto, LEPABE/ALiCE. Laboratory for Process Engineering, Environment, Biotechnology and Energy and Associate Laboratory in Chemical Engineering, Faculty of Engineering, University of Porto
Castorina S. Vieira, CONSTRUCT, Faculty of Engineering, University of Porto, Porto, Portugal, cvieira@fe.up.pt

ABSTRACT

This study presents a comprehensive Life Cycle Assessment (LCA) of four deep foundation systems—Steel H-Section Piles (SHP), Continuous Flight Auger Piles (CFA), Bored Piles (BP), and Precast Concrete Piles (PCP)—used in a 19-story residential building in Natal, Brazil. The objective is to quantify the environmental impacts of each system and compare these results with technical and economic factors to evaluate overall sustainability. Using ABNT ISO NBR 14040/44 standards and a cradle-to-site boundary, the LCA assesses emissions and resource use during material manufacturing, transportation, and installation stages. The results reveal that while CFA piles are the most economically viable, PCP piles offer the best environmental performance in terms of greenhouse gas emissions. SHP piles, due to the steel production process, exhibited the highest environmental impacts. These findings highlight the importance of integrating environmental factors in foundation design and contribute to the growing body of knowledge aimed at reducing the environmental impacts of construction practices.

Keywords: life cycle assessment, deep foundations, sustainable construction

INTRODUCTION

The construction industry is a major contributor to global carbon emissions, resource depletion, and environmental degradation. Among the various stages of construction, foundation systems represent a significant portion of the overall environmental impact due to the extensive use of energy-intensive materials such as concrete and steel (Sandanayake et al., 2017). As sustainability becomes increasingly important in civil engineering and geotechnical practices, it is imperative to assess the environmental implications of foundation systems and explore ways to improve their performance in line with sustainability goals.

While carbon footprint calculators are widely used to estimate greenhouse gas emissions, they often provide only a partial picture of a construction project's environmental impact. Carbon footprints focus primarily on CO_2 emissions, overlooking other critical environmental factors such as depletion of natural resources (e.g., raw materials, fossil fuels, and minerals), water use, land degradation, and ecosystem impacts. For foundation systems, in particular, the environmental impacts extend far beyond carbon emissions, as material extraction, production processes, transportation, and installation all contribute to a much broader range of environmental consequences (Pujadas-Gispert et al., 2021). Thus, limiting environmental assessments to carbon footprint calculations can result in underestimating the true environmental impacts of foundation systems (Giri and Reddy, 2014).

Expanding environmental studies through Life Cycle Assessment (LCA) allows for a more comprehensive evaluation of a construction project's environmental performance. LCA not only accounts for carbon emissions but also evaluates impacts across multiple environmental categories, including resource consumption, water usage, energy depletion, and pollution. This is particularly relevant for deep foundation systems, which consume significant amounts of steel, concrete, and other materials, each of which has its own distinct environmental footprint (Sandanayake et al., 2016). By expanding beyond carbon-centric evaluations, LCA provides a more nuanced understanding of the sustainability of foundation systems and helps identify opportunities for reducing environmental impacts across a broader spectrum (Lee and Basu, 2022).

 © DFI International Bruges 2025

Research has demonstrated that the choice of foundation system significantly influences environmental emissions during the construction phase. For example, steel and concrete are highly carbon-intensive materials, and their use in foundation systems can result in considerable greenhouse gas emissions and resource consumption (Pujadas-Gispert et al., 2021). Moreover, the specific foundation method employed must balance structural performance, cost, and environmental impact, making it a complex decision-making process (Li and Zheng, 2020). Integrating LCA into foundation system evaluation enables engineers and decision-makers to identify the most sustainable solutions for minimizing the environmental impact of construction projects.

This study conducts a detailed LCA of four commonly used deep foundation systems: Steel H-Section Piles (SHP), Continuous Flight Auger (CFA) Piles, Bored Piles (BP), and Precast Concrete Piles (PCP). The objective is to provide a comprehensive assessment of the environmental impacts of each system, covering material manufacturing, transportation, and construction. In addition to the environmental analysis, the study integrates geotechnical and economic evaluations, offering a holistic approach to foundation selection for high-rise buildings.

This research is based on a case study of a 19-story residential building in Natal, Brazil, with sandy soil conditions and no groundwater up to 18 m. The LCA follows ABNT ISO NBR 14040 (ABNT, 2014a) and ABNT ISO NBR 14044 (ABNT, 2014b) standards using a cradle-to-site boundary, covering material production, transportation, and installation stages. The study evaluates four foundation systems: SHP piles, which are strong but carbon-intensive; CFA piles, which are cost-effective but emit more during installation; BP piles, with moderate environmental impact; and PCP piles, which reduce emissions due to prefabrication. Environmental impacts are assessed using ReCiPe 2016 Midpoint (H) (Huijbregts *et al.*, 2017) for a broad analysis and IPCC 2021 GWP100 (IPCC, 2021) for greenhouse gas emissions.

The primary objectives of this research are to: (1) quantify the environmental impacts of four deep foundation systems using LCA, (2) compare these impacts with technical and economic factors for a comprehensive sustainability evaluation, and (3) identify opportunities to reduce environmental impacts, promoting more sustainable construction practices. By aligning foundation design with circular economy principles, this research supports the construction industry's shift towards resource-efficient, low-emission practices.

This study enhances existing knowledge of the environmental performance of deep foundation systems and offers practical recommendations for minimizing the environmental impacts of foundation construction in large-scale projects. By integrating LCA with geotechnical and economic evaluations, the findings provide a robust framework for selecting foundation systems that balance both structural and environmental considerations, guiding more sustainable decision-making in foundation design.

METHODOLOGY

Case Study Overview

This study builds on the technical and economic comparison of four deep foundation systems previously conducted by Diógenes (2022) for a 19-story residential building. The building includes a basement level, a ground floor, 15 typical floors with two apartments per floor, a roof level, and an upper floor for housing the water reservoir. The total constructed area amounts to approximately 3,800 m^2, comprising 30 apartments.

The local geotechnical conditions, typical of Natal/RN, Brazil, primarily consist of sandy soil profiles. The geotechnical investigation involved twelve Standard Penetration Test (SPT) boreholes, which revealed the following stratigraphy: the first two meters consist of fine to medium loose sand with light gray organic matter. From two to six meters, the soil is composed of light brown to yellowish fine to medium sand with compaction levels ranging from loose to moderately compact. From six to ten meters, the soil transitions to yellowish silty fine sand with moderate compaction. No groundwater was detected up to 18 meters below ground, the maximum depth of the boreholes.

The foundation systems for the four deep foundation alternatives studied—SHP, CFA, BP, and PCP—were designed in accordance with the criteria established by ABNT NBR 6122 standard (ABNT, 2019), ensuring compliance with geotechnical and structural performance requirements.

 © DFI International Bruges 2025

The design process accounted for the most unfavorable soil profile (lowest SPT values) and the demands specified in the structural project. The required pile lengths were determined based on the ultimate limit state (ULS) design approach, considering the characteristic loads and geotechnical conditions. The final design accommodated a total compression load of 71,600 kN, distributed across 22 columns.

The technical specifications of the deep foundation alternatives are summarized in Table 1, which presents key parameters such as load-bearing capacity, required pile quantity, cumulative pile length, total concrete volume, and total steel weight for each foundation type.

Table 1. Technical Specifications of Deep Foundation Alternatives

Pile Alternative Terminology [a)]	Load-bearing Capacity (kN)	Required Pile Quantity (units)	Cumulative Pile Length (m)	Total Volume of Concrete [b)] (m^3)	Total Mass of Steel [b)] (kg)
P-C40-33-12 (PCP) [c)]	895	85	1,020	52	5,171 [d)]
S-HP-250x62-17 (SHP)	1,344	58	986	-	70,302 [e)]
C-C30-60-14 (CFA)	1,280	62	868	295	2,872 [d)]
B-C25-60-13 (BP)	807	93	1,209	376	2,198 [d)]

a) Pile alternative terminology: Type of pile (PCP, SHP, CFA, BP) - Pile Concrete Strength (C25/30/40) or Steel Section (HP) - Pile Dimensions (mm) – Unit pile length (m).
b) Quantities include an allowance for material wastage.
c) Precast hollow circular pile
d) Rebar cage.
e) Steel H-Pile.

Beyond the technical and economic analyses, this study incorporates an environmental perspective by applying a LCA to the selected foundation alternatives. This approach enables a more comprehensive evaluation of sustainability factors, guiding foundation selection towards environmentally responsible choices.

Life Cycle Assessment

The LCA methodology follows the guidelines of ABNT ISO NBR 14040 (ABNT, 2014a) and ABNT ISO NBR 14044 (ABNT, 2014b). The assessment includes goal and scope definition, life cycle inventory (LCI), life cycle impact assessment (LCIA), and interpretation. This structured approach enables a detailed environmental evaluation of four deep foundation alternatives, complementing technical and economic assessments for a comprehensive sustainability analysis.

This LCA quantifies and compares the environmental impacts of four deep foundation systems for a 19-story residential building, complementing technical and economic evaluations to support sustainable decision-making.

The system boundaries of this LCA follow a cradle-to-site approach, in accordance with EN 15978 (European Committee for Standardization, 2011), focusing on the manufacturing stage (A1). This includes the production of materials such as ready-mix concrete, steel H-sections, and steel rebar cages. The processes involved in the extraction and refining of raw materials (e.g., iron ore, limestone, and clinker for cement production) are excluded, as the study begins with the production of materials to be used at the manufacturing facilities.

During the manufacturing stage (A3), concrete is produced at batching plants, and steel products are fabricated through processes such as steelmaking, casting, shaping, and rebar fabrication. These materials are then transported to the construction site, covering the transportation stage (A4), which accounts for the energy and fuel consumed in delivering materials and equipment to the site. The transportation stage (A4) is informed by the distances used for calculating environmental impacts, as shown in Table 2.

 © DFI International Bruges 2025

Table 2. Transport Distances Used for Calculation

Item	Transportation		One-Way Distances (Km) [a]
	From	To	
Ready-mix Concrete	Concrete Batching Plant	Construction Site	15
Steel Rebar Cage	Rebar Fabrication Shop	Construction Site	20
Precast Concrete Piles	Precast Concrete Plant	Construction Site	25
Steel H-Section Piles	Structural Steel Supplier	Construction Site	20
Pilling Equipment	Storage Yard	Construction Site	55
Debris & Excess Soil	Construction Site	Landfill Site	30

a) based on the locations of main suppliers, contractors, municipal landfill and the construction site.

Once materials arrive at the site, the construction stage (A5) covers the primary activities involved in installing the foundation systems. This includes pile driving, drilling, material handling, and concrete pouring, along with the energy and fuel consumption of machinery and equipment. The fuel consumption and estimated operating hours for pile installation equipment are shown in Table 3.

Table 3. Fuel Consumption and Operating Hours Estimated for Pile Installation Equipment

Equipment	Diesel Consumption Rate [a]	Estimated Operating Hours (h) [b]			
	(liters/hour)	PCP	SHP	CFA	BP
Hydraulic Pile Driver	40	680	464	-	-
Drilling Rig	50	-	-	-	744
Auger Drilling Rig	75	-	-	496	-
Concrete Pump	20	-	-	10	-
Concrete Mixer Truck	30	-	-	10	15
Crane Truck	20	34	23	25	37
Backhoe Loader	20	21	15	16	23
Hydraulic Pile Cutter	15	85	-	62	93

a) based on manufacturer specifications and industry standards.
b) based on local subsurface conditions, pile type, and an 8-hour daily work schedule.

However, certain activities fall outside the system boundaries of this assessment. These exclusions include site grading, load testing, pile cap construction, and site restoration. Other tasks, such as pile splicing, performance testing, and post-installation quality control, are also beyond the scope. The system boundaries for this study are clearly illustrated in Fig. 1, showing the life cycle stages considered in this LCA.

This study does not consider the operational phase of the building, as foundation systems typically do not consume energy or resources during this phase. Furthermore, the end-of-life stages, including demolition, recycling, or disposal of materials, are beyond the scope of this LCA. Therefore, the assessment focuses solely on the environmental impacts up to the point where the foundation systems are fully installed and ready for building construction, as noted by Lee and Basu (2022).

The functional unit used for environmental impact comparison is defined as the 'foundation system required to support a 19-story residential building with a total compression load of 71,600 kN, distributed across 22 columns, designed in accordance with the limit state design criteria established by ABNT NBR 6122 (ultimate and serviceability limit states)".

The LCI for this study utilizes data from the Ecoinvent v3.10 (Ecoinvent, 2024) database. Brazilian-specific datasets were applied wherever available to ensure regional relevance. For materials and processes where, localized data were not accessible, global datasets were used. This approach ensures consistency in modeling all materials and processes involved in the manufacturing, transportation, and installation of the foundation systems.

 © DFI International Bruges 2025

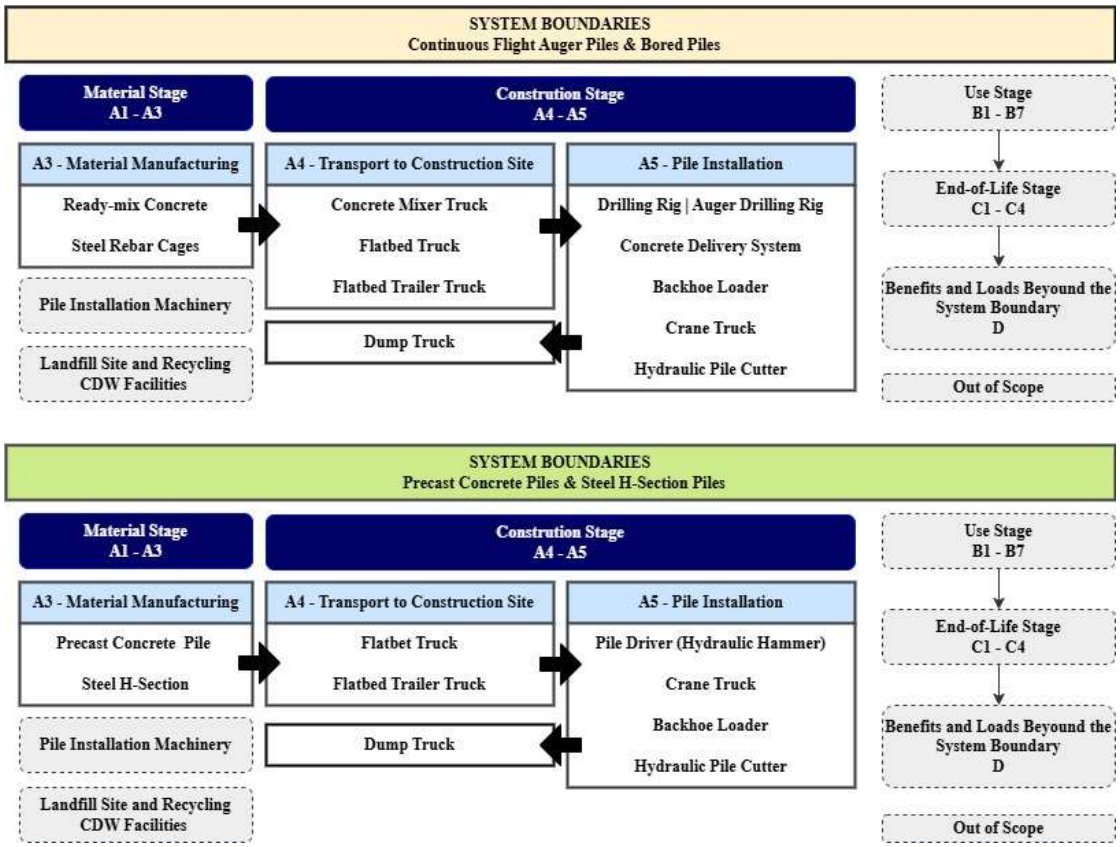


Fig. 1. System Boundaries for the Life Cycle Assessment of Deep Foundation Alternatives

In the LCIA stage, environmental impacts were assessed using SimaPro v9.6.0, applying two complementary methods: ReCiPe 2016 Midpoint (H) (Huijbregts et al., 2017) and IPCC 2021 GWP100 (IPCC, 2021). The ReCiPe method was chosen for its broad coverage of environmental categories, offering insights into impacts like climate change, acidification, and eutrophication. It operates at the midpoint level, quantifying impacts through characterization, which converts emissions into common units (e.g., CO_2-equivalents). The IPCC 2021 GWP100 method focuses specifically on climate change, assessing the Global Warming Potential (GWP) of emissions over a 100-year period. This method provides a focused view on climate impacts, while ReCiPe offers a broader analysis for distinct environmental impacts. Together, these methods provide a well-rounded assessment, enabling decision-makers to evaluate both general environmental performance and specific climate-related concerns for a comprehensive understanding of the foundation systems' environmental trade-offs.

The final stage of the LCA—interpretation—will adhere to regulatory standards and will be discussed in the next section.

RESULTS AND DISCUSSION

IPCC 2021 GWP100 Method

Using the IPCC 2021 method, the total GHG emissions for the four foundation systems were assessed across the life cycle stages of manufacturing (A1-A3), transport to site (A4), and pile installation (A5). The analysis showed considerable variation in emissions, with SHP generating the highest emissions and PCP showing the lowest, as illustrated in Fig. 2.

 © DFI International Bruges 2025

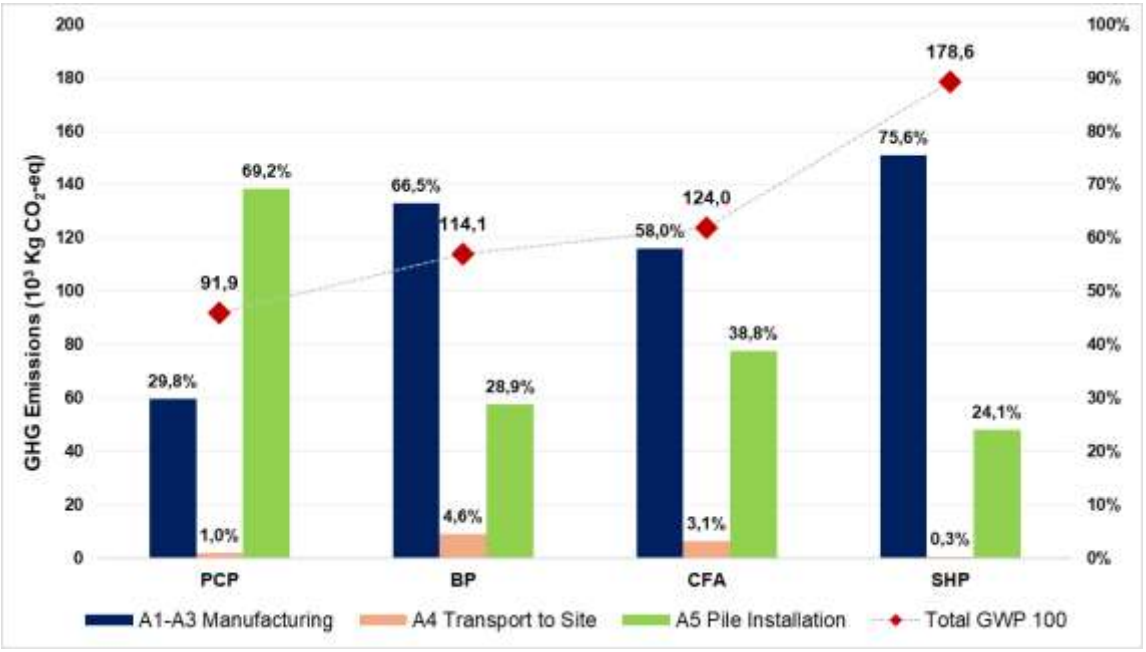


Fig. 2. GHG Emissions by Life Cycle Stages for the Deep Foundation Alternatives Studied

SHP generated the highest total emissions of 178,631 kg CO_2-eq, with an emissions rate of 181.17 kg CO_2-eq/m, primarily due to the carbon-intensive nature of steel production, which contributed 75.6% of the total emissions. In terms of GHG emissions efficiency, SHP exhibited the highest emissions per unit of compression load (2.50 kg CO_2-eq/kN), significantly exceeding the values observed for the other foundation types, making it the least environmentally favorable option. PCP had the lowest total emissions, with 91,876 kg CO_2-eq and the lowest emissions rate per meter at 90.07 kg CO_2-eq/m. They also had the most efficient emissions per unit of compression load at 1.28 kg CO_2-eq/kN, making them the best-performing system environmentally in terms of GHG emissions. BP emitted 114,110 kg CO_2-eq, with an emissions rate of 94.38 kg CO_2-eq/m, resulting in 1.59 kg CO_2-eq/kN per unit of compression load. This balanced performance positions them as a moderate option in terms of emissions. CFA produced 123,976 kg CO_2-eq, with an emissions rate of 142.83 kg CO_2-eq/m and 1.73 kg CO_2-eq/kN per unit of compression load, indicating a relatively higher environmental impact in terms of GHG emissions, as shown in Table 4.

Table 4. Technical Specifications of Deep Foundation Alternatives

Pile Alternative	Total GHG Emissions (kg CO_2-eq.)	Emissions Intensity per Meter of Pile (kg CO_2-eq./m)	Emissions Intensity per Unit of Total Compression Load (kg CO_2-eq./kN)
PCP	91,876	90.07	1.28
BP	114,110	94.38	1.59
CFA	123,976	142.83	1.73
SHP	178,631	181.17	2.50

The results reveal clear trade-offs between material use, pile length, and CO_2 emissions. PCP require higher-strength concrete, increasing cement use and CO_2 emissions, but their smaller cross-section reduces the overall concrete volume, reflected in their low emissions per meter. However, the need for additional steel reinforcement partially offsets these gains. In contrast, BP and CFA use less steel, lowering their emissions from steel production, but rely heavily on concrete, leading to higher emissions from cement production. SHP have the highest emissions overall due to energy-intensive steel production, making them the least favorable in terms of environmental performance.

When comparing these results with existing literature (Luo et al., 2019), it becomes evident that PCP perform better in this study, with emissions of 90.07 kg CO_2-eq/m, which is lower than the 107.46 kg CO_2-eq/m reported in the literature. Similarly, BP align with typical values reported in the literature but still outperform those numbers. The installation phase plays a critical role, especially for PCP,

 © DFI International Bruges 2025

contributing nearly 70% of total emissions, while (S) and BP show a more balanced split between material production and installation.

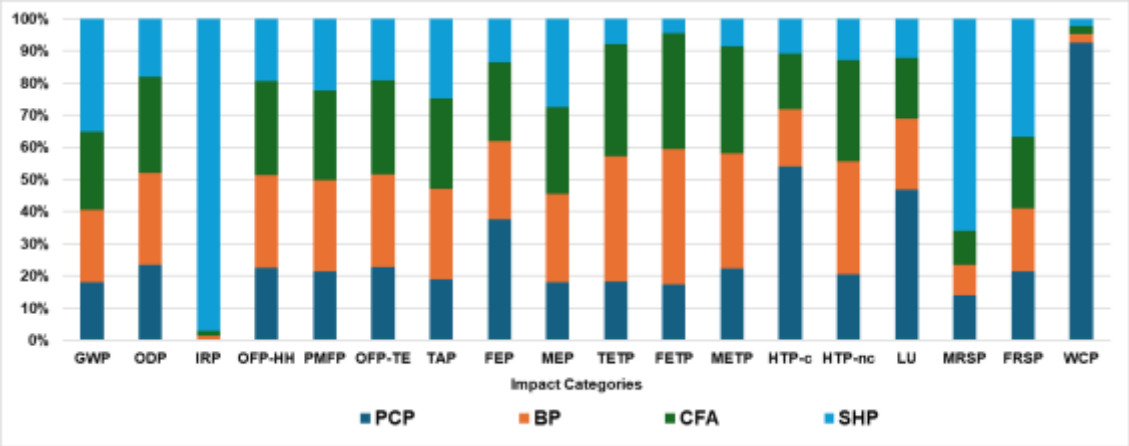
ReCiPe Midpoint (H) Method

The ReCiPe 2016 method evaluated a broader range of environmental impacts, such as Global Warming Potential (GWP), Fossil Resource Scarcity (FRSP), Water Consumption (WCP), and Human Health Impacts (HHI). The foundation systems' performance was assessed across the life cycle stages of manufacturing, transport, and installation.

GWP was again the highest for SHP, with 115,672 kg CO_2-eq, driven by energy-intensive steel production. This is notably higher than the 93,591 kg CO_2-eq recorded for PCP. Normalization contextualized the global significance of these results, showing SHP contributing 22.746 normalized units of GWP—nearly double that of PCP at 11.693 units. The focus here should be on improving steel production's energy efficiency and increasing the use of recycled materials to mitigate these emissions.

In terms of Fossil Resource Scarcity (FRSP), SHP emerged as the most resource-intensive system, with 44.067 normalized units, reflecting the energy demand in raw material extraction and steel processing. PCP, although lower at 25.779 normalized units, also showed significant impacts due to concrete production.

Figure 3 illustrates the characterization analysis results for the deep foundation alternatives under study, showing how each pile system performs across multiple environmental impacts categories. This visualization highlights the distribution of impacts, providing a clearer view of how each system contributes to various environmental challenges.



Impact Categories: Global Warming Potential (GWP), Stratospheric Ozone Depletion (ODP), Ionizing Radiation (IRP), Ozone Formation-Human Health (OFP-HH), Fine Particulate Matter Formation (PMFP), Ozone Formation-Terrestrial Ecosystems (OFP-TE), Terrestrial Acidification (TAP), Freshwater Eutrophication (FEP), Marine Eutrophication Potential (MEP), Terrestrial Ecotoxicity Potential (TETP), Freshwater Ecotoxicity Potential (FETP), Marine Ecotoxicity Potential (METP), Human Carcinogenic Toxicity Potential (HTP-c), Human Non-Carcinogenic Toxicity Potential (HTP-nc), Land Use (LU), Mineral Resource Scarcity Potential (MRSP), Fossil Resource Scarcity Potential (FRSP), Water Consumption (WCP).

Fig. 3. Percentage Contribution of Environmental Impact Categories by Deep Foundation Alternatives

WCP was highest for PCP, with 25,361 m^3 consumed, mainly from water-intensive fabrication and concrete curing. CFA and BP consumed far less water (663 m^3 and 725 m^3, respectively). Normalized results emphasized this discrepancy, with PCP contributing 95.156 units, far exceeding the water use of SHP (2.399 units) and CFA (2.490 units). The high-water demand of PCP highlights the need for water-efficient technologies, particularly in water-scarce regions.

Human Carcinogenic Toxicity (HCT) impacts were most severe for PCP during installation, contributing 291.210 normalized units, mainly due to diesel-powered equipment emissions. SHP also showed high impacts in this category, with 58.408 normalized units. Reducing emissions from

 © DFI International Bruges 2025

installation activities, especially by adopting cleaner equipment, could mitigate these health-related risks.

Terrestrial Acidification Potential (TAP) was another major concern for PCP, contributing 240.16 kg SO_2-eq during installation. Normalization results emphasize this further, with 33,201.815 normalized units attributed to PCP, compared to BP and CFA, which each contributed around 8.7 normalized units. This impact is primarily linked to emissions from diesel engines and the fabrication of the piles, highlighting the need for cleaner installation and production processes.

Final Insights from IPCC 2021 GWP100 and ReCiPe 2016 Methods

The combination of the IPCC 2021 and ReCiPe 2016 methods provides a comprehensive understanding of the environmental trade-offs between deep foundation systems. The IPCC GWP100 method focuses on GWP, offering detailed insights into GHG emissions, while the ReCiPe Midpoint method expands the analysis to include resource use, water consumption, and human health impacts.

The results reveal that SHP are the least sustainable in terms of GWP and FRSP, but their low water consumption makes them viable in water-scarce areas. PCP, though performing well in terms of GWP, face challenges in water consumption and terrestrial acidification, especially during manufacturing and installation. CFA and BP offer a more balanced profile with moderate impacts across most categories, but the reliance on diesel during installation still presents significant health and environmental risks.

Ultimately, the choice of foundation system should consider both emissions efficiency and resource use, with a focus on optimizing construction practices to mitigate impacts across all stages of the life cycle. This dual-method approach underscores the need for comprehensive environmental evaluations when selecting foundation systems, ensuring that both global and regional environmental impacts are considered in decision-making processes.

SUMMARY AND CONCLUSIONS

This study conducted a comprehensive LCA for a case study involving the foundation system of a 19-story residential building in natal, Brazil. The analysis aimed to integrate environmental considerations with the technical and economic evaluations already performed, providing a holistic approach to foundation selection based on local availability and conditions.

The LCA analysis showed marked differences in environmental impacts across foundation systems. SHP had the highest impact, driven by the carbon-intensive steel production process, contributing significantly to GWP and resource consumption. While PCP and BP exhibited moderate impacts, CFA, despite being the most economically viable, showed higher environmental impacts, particularly in GWP and fossil resource consumption, compared to PCP.

These findings underscore the importance of balancing economic and environmental factors. Local geotechnical conditions, such as soil profiles and groundwater presence, directly affect foundation selection and environmental outcomes, which may vary across different sites. Alternative engineering designs could also lead to different environmental outcomes. Local factors, such as transportation distances, material sourcing, and equipment use, greatly influence environmental performance. The system boundaries used in this study reflect the specific conditions of the project site, and different locations or supply chains could lead to varying results.

In conclusion, this case study demonstrates the importance of integrating environmental considerations into foundation engineering as the construction industry moves toward a circular economy. By evaluating the full life cycle of foundation systems, decision-makers can make more informed, sustainable choices. Future studies should prioritize the use of local life cycle data, implement cleaner installation techniques, and further investigate how specific local geotechnical conditions affect both technical performance and environmental sustainability in foundation engineering.

 © DFI International Bruges 2025

ACKNOWLEDGMENTS

This work was financially supported by Base Funding - UIDB/04708/2020 (DOI: 10.54499/UIDB/04708/2020) and Programmatic Funding - UIDP/04708/2020 (DOI: 10.54499/UIDP/04708/2020) of the CONSTRUCT - Institute of R&D in Structures and Construction, funded by national funds through FCT/MCTES (PIDDAC). Additionally, this work was supported by national funds through FCT/MCTES (PIDDAC) via LEPABE, UIDB/00511/2020 (DOI: 10.54499/UIDB/00511/2020) and UIDP/00511/2020 (DOI: 10.54499/UIDP/00511/2020), and ALiCE, LA/P/0045/2020 (DOI: 10.54499/LA/P/0045/2020). We also thank the Federal Rural University of Pernambuco (UFRPE-UACSA) for the financial support that enabled the first author to carry out this work.

REFERENCES

ABNT NBR ISO 14040, 2014a. Environmental management - Life cycle assessment - Principles and framework. Brazilian Association of Technical Standards, Rio de Janeiro, RJ, 21p. (in Portuguese)

ABNT NBR ISO 14044, 2014b. Environmental management - Life cycle assessment - Requirements and guidelines. Brazilian Association of Technical Standards, Rio de Janeiro, RJ, Brazil, 46p. (in Portuguese)

ABNT NBR 6122, 2019. Design and Execution of Foundations. Brazilian Association of Technical Standards, Rio de Janeiro, RJ, Brazil, 91p. (in Portuguese).

Diógenes, N.J.S., 2022. Technical and financial analysis of pile types: Dry bored pile, continuous flight auger pile, precast concrete pile, and steel pile in sandy soil of Natal/RN. Federal University of Rio Grande do Norte. Available at: https://repositorio.ufrn.br/handle/123456789/46172. Accessed on August 12, 2024. (in Portuguese)

ECOINVENT, 2024. Ecoinvent Version 3.10. Available at: https://support.ecoinvent.org/ecoinvent-version-3.10. Accessed on: 24 Jul. 2024.

European Committee for Standardization EN15978, 2011. Sustainability of construction works. Assessment of environmental performance of buildings. Calculation method. European Committee for Standardization (CEN), Brussels, 2011.

Giri, R.K. and Reddy, K.R., 2014. LCA and Sustainability Assessment for Selecting Deep Foundation System for High-Rise Buildings. In: International Conference on Sustainable Infrastructure, 5 Nov. 2014. ICSI 2014, Long Beach, California: American Society of Civil Engineers, 2014. p. 621–630. https://doi.org/10.1061/9780784478745.057.

Huijbregts, M.A.J. et al., 2017. ReCiPe2016: A harmonized life cycle impact assessment method at midpoint and endpoint level. The International Journal of Life Cycle Assessment, [*S. l.*], vol. 22, no. 2, p. 138–147, 1 Feb. 2017. Available at: https://doi.org/10.1007/s11367-016-1246-y. Accessed on: 31 Jul. 2024.

IPCC, 2021. Climate Change 2021: The Physical Science Basis. Contribution of Working Group I to the Sixth Assessment Report of the Intergovernmental Panel on Climate Change. Cambridge University Press, Cambridge, United Kingdom and New York, NY, USA, 2391 pp. https://doi.org/10.1017/9781009157896.

Lee, M. and Basu, D., 2022. Life Cycle Assessment of Drilled Shafts. DFI Journal the Journal of the Deep Foundations Institute, [*S. l.*], vol. 16, no.2, p.1–24, 2022.

Li, X.-J. and Zheng, Y., 2020. Using LCA to research carbon footprint for precast concrete piles during the building construction stage: A China study. Journal of Cleaner Production, vol. 245, p. 118754, Feb. 2020. ISSN 0959-6526, https://doi.org/10.1016/j.jclepro.2019.118754.

Luo, W.; Sandanayake, M. and Zhang, G., 2019. Direct and indirect carbon emissions in foundation construction – Two case studies of driven precast and cast-in-situ piles. Journal of Cleaner Production, vol. 211, p. 1517–1526, Feb. 2019. https://doi.org/10.1016/j.jclepro.2018.11.244.

Pujadas-Gispert, E.; Vogtländer, J.G. and Moonen, S.P.G.(Faas), 2021. Environmental and Economic Optimization of a Conventional Concrete Building Foundation: Selecting the Best of 28 Alternatives by Applying the Pareto Frontier Sustainability, vol. 13, no. 3, p. 1496, Jan. 2021. https://doi.org/10.3390/su13031496.

 © DFI International Bruges 2025

Sandanayake, M. et al., 2016. Environmental Emissions in Building Construction – Two Case Studies of Conventional and Prefabricated Construction Methods in Australia. *In*: Fourth International Conference on Sustainable Construction Materials and Technologies, 2016. P.1637–1644. Available at: http://www.claisse.info/2016%20papers/M104.pdf.

Sandanayake, M. et al., 2017. Estimation and comparison of environmental emissions and impacts at foundation and structure construction stages of a building – A case study. Journal of Cleaner Production, vol. 151, p. 319–329, May 2017. https://doi.org/10.1016/j.jclepro.2017.03.041.

 © DFI International Bruges 2025

COMPARATIVE ANALYSIS OF CARBON FOOTPRINT BETWEEN PILE FOUNDATION TYPE: A PERSPECTIVE ON THE CONSTRUCTION PROCEDURE

Ricardo B. Born, Bornsales Engineering, Brazil, ricardo@bornsales.com.br
Luis F. P. Sales, Bornsales Engineering, Brazil, luis@bornsales.com.br
Renan E. Cordeiro, Bornsales Engineering, Brazil, renan@bornsales.com.br
Marcus V. A. Belloli, Bornsales Engineering, Brazil, marcus@bornsales.com.br
Gabriel M. Corrêa, Bornsales Engineering, Brazil, projetos@bornsales.com.br

ABSTRACT

The environmental perspective on civil construction and its impacts is not a new topic, yet it remains relevant due to the increasing energy consumption driven by population growth and the challenges imposed by increasingly taller buildings. In this context, Born et al. (2024) present a database of material consumption in 100 pile foundation projects in southern Brazil, analyzing the carbon footprint per type of pile, considering buildings between 60 and 270 meters high. This paper aims to further the discussions on carbon footprint in foundation design by assessing the carbon emissions generated from different construction methods. Foundation execution times, type of drilling rig, and additional inputs materials for Continuos Flight Auger (CFA),Bored Piles (BRD) and Micropile (ROOT) were evaluated. In the end, the results from the database are presented, identifying the foundation solutions with the lowest impact on carbon emissions.

Keywords: carbon footprint; carbon emission; deep foundation; pile foundation; tall building foundation.

INTRODUCTION

For decades, governments have deliberated on global climate conditions and pursued agreements with specific targets for reducing carbon emissions and implementing other practices aimed at slowing climate change. Agreements like the Kyoto Protocol, signed in 1997, were later replaced by the Paris Agreement in 2015. According to BNDES (2018), Brazil committed to lowering greenhouse gas emissions, setting targets for 2025 and 2030.

Among the gases with the most negative environmental impact, carbon dioxide has the highest emission levels, with China, the USA, and Russia as the main emitters. In this context, Vital (2018) and THE INTERNATIONAL ENERGY AGENCY; UNITED NATIONS ENVIRONMENT PROGRAMME (2018) present the construction industry as having an important role in CO_2 emissions. Although the construction sector has seen advancements in cleaner materials and processes, Zhang et al. (2019) and Mazurana (2019) point out that concrete remains one of the most used materials in the sector, with the cement industry playing an important factor in the carbon footprint.

As global population grows and urban land scarcity increases, CTBUH (2024) reports a worldwide trend toward taller buildings. This trend escalates the challenges faced by foundation designers in ensuring comfort and safety. Optimized foundation designs, aligning foundation performance with structural performance, offer opportunities to reduce carbon emissions and create a greener buildings.

Born et al. (2024) assessed the carbon footprint caused by material consumption in a database of 100 foundation projects. Thus, this paper aims to expand the discussions on environmental impact by also considering the carbon footprint of secondary sources for Continuous Flight Auger (CFA) piles, Bored piles (BRD), and Micro-piles (ROOT) for 70 buildings developed in Balneário Camboriú City, Brazil.

 © DFI International Bruges 2025

GROUND CONDITION

Balneário Camboriú is a coastal city located in the south of Brazil, with a population of 148,000 and an area of 45 km² (IBGE, 2022). The projects are concentrated near the beachfront, where the soil investigation campaigns were carried out through Standard Penetration Tests, Cone Penetration Tests, and Rotary drilling procedures. The extensive in-situ tests performed improve the understanding of the local stratigraphic profile, which can be defined as a marine sedimentary deposit, with variations between clayey and sandy soil layers. The granite bedrock varies in depth from 8 meters to 55 meters. The granitic rock mass was categorized based on its integrity as sound (A1), cohesive (C1), and slightly fractured (F2-F3). The active groundwater table is located near the surface.

DATABASE

The database was developed from 70 projects, designed between 2019 and 2024 by the authors of this paper. The foundation designs were organized to contribute to the development of the objectives of this research.

The database accumulates a total of 1,582,313 m² of built area, where the smallest development has 9,998 m² and the largest development has 74,202 m². The towers range in height from 95 m to 238 m, with a slenderness ratio varying between 1:3 and 1:16.

The distribution of building heights in the database is presented in Fig. 1.

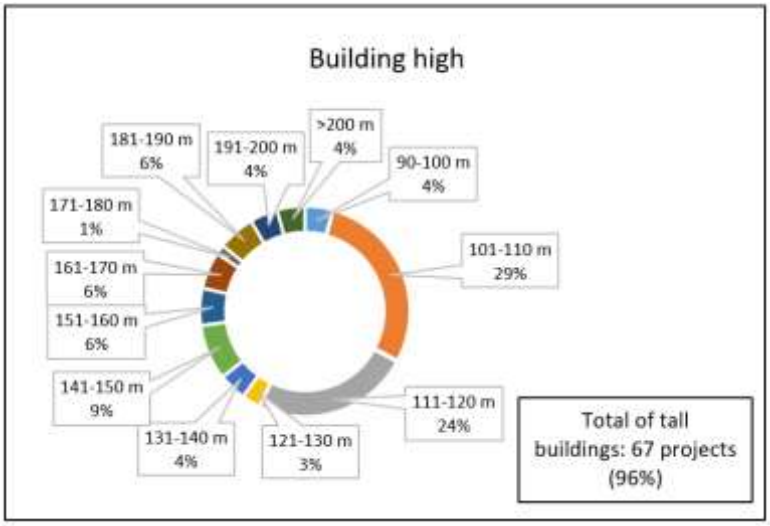


Fig. 1: Distribution of building heights in the database.

The projects were organized by 3 different pile foundations: CFA, BRD and ROOT.

As shown in Fig. 2, CFA piles have a higher representation in the database. This is due to the fact that it is a suitable solution for the local soil and generally meets technical and productivity requirements more effectively.

 © DFI International Bruges 2025

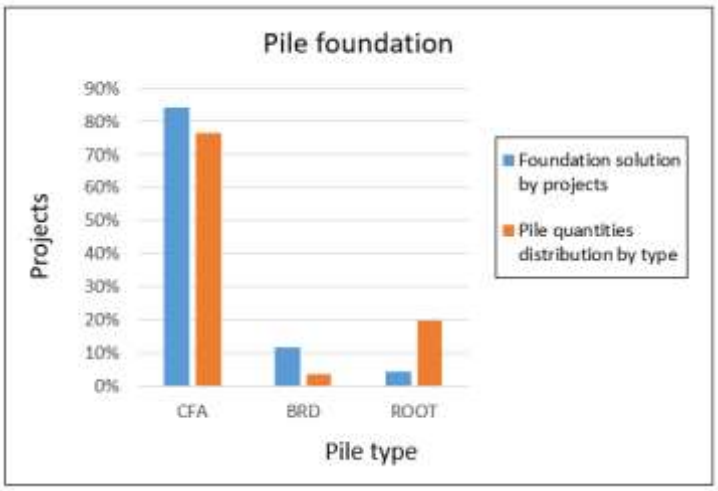


Fig. 2: Distribution of pile foundation by projects.

The database contains a total of 16,615 piles, representing 508,834 m of total length, distributed by diameter, as shown in Table 1.

Table 1. Distribution of piles by diameters and foundation solution.

Pile type	*Diameter (m)*							
	0.35	***0.40***	***0.45***	***0.50***	***0.60***	***0.70***	***0.80***	***1.00***
CFA	-	2%	-	12%	84%	2%	-	-
BRD	-	-	-	-	-	-	-	100%
ROOT	8%	26%	-	54%	-	-	-	-

Fig. 3 presents the distribution of piles by length.

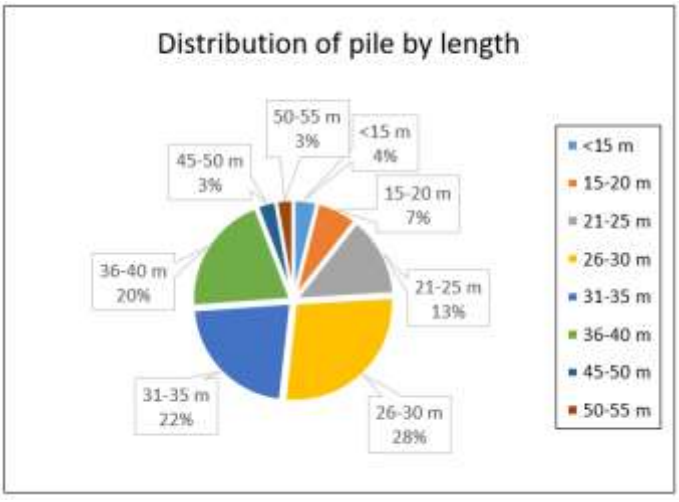


Fig. 3: Distribution of piles by length.

with the average length for CFA, BRD, and ROOT being 32 m, 51 m, and 22 m, respectively.

Fig. 4 provides a visualization of the distribution of piles by length and foundation's type.

 © DFI International Bruges 2025

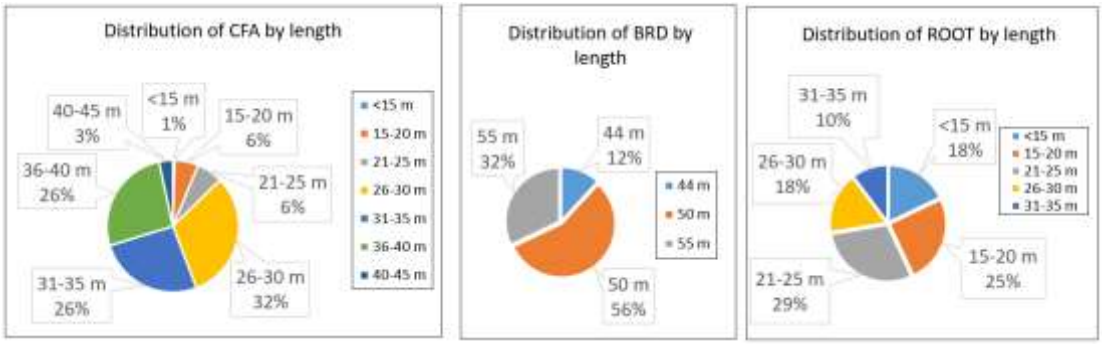


Fig. 4: Distribution of piles by length and foundation type.

CARBON CALCULATION METHOD

For this study, the methodology proposed by the European Federation of Foundation Contractors (EFFC) and the Deep Foundations Institute (DFI) was used, specifically through the EFFC-DFI Carbon Calculator tool. According to Lasne et al. (2015), this tool was developed by integrating best practices from various methodologies. By separating CO_2 emissions into primary and secondary categories, the EFFC-DFI Carbon Calculator provides a comprehensive assessment of a project's carbon footprint, calculated by summing up emissions from both sources.

According to Lasne et al. (2015), primary sources consider the carbon embodied in the inputs associated with the manufacturing of materials (cement, steel, sand, aggregates, etc.) and the consumption of energy from sources such as diesel, gasoline, and the electricity grid during construction. Secondary sources are calculated considering the transportation of people to the site, equipment transportation, waste transport, waste treatment, and CO_2 emissions related to the manufacturing of heavy equipment used in the project.

As stated by Zhang e Whang (2016) and EFFC-DFI (2014), the carbon footprint is obtained through the multiplication of the material quantity (A_i) and its associated emission factor (EF_i), as presented in equation 1.

$$Carbon\ footprint = \sum_{i=1}^{n} A_i \times EF_i \quad [1]$$

Concrete – CO_2 emission factor

To assess the carbon footprint of concrete used in the projects, the methodology proposed by Lima (2010) was adopted. Lima's study evaluated various concrete mixes commonly used in Brazil and established a carbon emission factor. Considering the inherent uncertainties in such calculations, an average value of 225 kg CO_2/m^3 ± 43 kg CO_2/m^3 was proposed for Brazilian concrete. By incorporating the uncertainties presented in Table 2, the carbon footprint of the concrete used in the database was calculated.

Table 2. Emission factors ranges.

Materials	*Carbon factor emission uncertainties*	*Quantity uncertainties*
Cement	± 8,4%	-
Sand	± 50%	± 10%
Coarse Aggregate	± 50%	± 10%

 © DFI International Bruges 2025

To obtain the emission factor for concrete used in CFA and BRD, as well as to determine the emission factor for the grout of the ROOT piles, the following mixes were used:

Table 3. Concrete and grout mixes.

Material	***CFA ; BDR***	***ROOT***
Cement	400 kg/m³	625 kg/m³
Sand	900 kg/m³	972 kg/m³
Coarse Aggregate	834 kg/m³	0 kg/m³

Therefore, a differentiated approach was proposed to define the carbon footprint of concrete, based on the mix design specified in the projects and differentiating between CFA, BRD, and ROOT piles, as indicated in Table 4.:

Table 4. Carbon footprint of concrete/grout mixes.

Solução	***Pegada de carbono ($kgCO_2/m^3$)***
HCM	249.36 – 315.50
Escavada	249.36 – 315.50
Raiz	379.42 – 455.57

Consequently, for the purposes of this paper, an emission factor of 268 kg CO_2/m³ was adopted for both CFA and BRD concrete. This value aligns with the range provided in Table 4 and is consistent with the values used in the EFFC-DFI Calculator. For the root pile grout, an emission factor of 417 kg CO_2/m³ was applied.

Steel – CO_2 emission fator

In order to determine the parameters for steel, Costa (2012) developed a Method for Quantifying CO_2 Emissions. This method calculates emissions generated by the steel sector at a basic level using the following equation:

$$Carbon\ footprint = QT \times LF \times (EF_{AC} + EM_{EN}) \quad [2]$$

Where QT = material quantity (t), LF_j = steel loss factor, EM_{EN} = CO_2 emissions due to energy consumption for transportation, extraction, and steel production, EF_{AC} = CO_2 emission factor resulting from chemical reactions.

The results of the calculation of the emission factor for the steel sector are shown in Table 5:

Table 5. Estimation of CO_2 emissions from the steel industry. (Adapted from Costa, 2012).

Description	**Value**
CO_2 from energy consumption (tCO_2)	45,659,777.84
Steel production (ton)	26,506,000.00
Carbon emission factor from energy consumption (tCO_2/t steel)	1.7226
Carbon emission factor from steel transportation (tCO_2/t steel)	0.0154
Carbon emission factor from chemical reactions (tCO_2/t steel)	0.1072
Steel emission factor (tCO_2/t steel)	**1.8452**

 © DFI International Bruges 2025

Other CO_2 emission factors

As described by Lasne et al. (2015), to use the EFFC-DFI Calculator, it is necessary to define other emission factors involving primary and secondary sources of CO_2 emissions. Table 6 presents the reference emission factors used in this paper.

Table 6. Emission factors considered in this paper.

Primary Sources	Materials			
	- Concrete (CFA ; BDR)	$kgCO_2/m^3$	268	Lima (2010) ; Costa (2012)
	- Grout (ROOT)	$kgCO_2/m^3$	417.5	Lima (2010) ; Costa (2012)
	- Steel	tCO_2/t	1.8452	Costa (2012)
	- PVC pipes	$kgCO_2/t$	615	Costa (2012)
	- Synthetic Polymer Slurry	$kgCO_2/m^3$	3,325	EFFC-DFI Calculator
	- Energy (diesel)	$kgCO_2/l$	2.671	MMA (2011)
Secundary Sources	Transportation			
	- Car	$kgCO_2/vkm$	0.27	Costa (2012)
	- Rigid > 17t	$kgCO_2/vkm$	1.21354	EFFC-DFI Calculator
	- Articulated > 33t	$kgCO_2/vkm$	1.1348	EFFC-DFI Calculator
	- Assets (Machines)	$kgCO_2/t$	5,500	EFFC-DFI Calculator

Calculation premises

This paper is a study based on a database of foundation projects developed between 2019 and 2024. None of the works in this database were under construction during the preparation of this paper. Therefore, for study purposes, it was necessary to estimate some variables required for the development of the methodology, such as transport distances and productivity of each solution. Similarly, it was decided to consider the composition of machinery and professionals as presented by ABEF (2022). For the calculation of waste transport, the use of 17t rigid truck was considered. For workers' trips, individual vehicular transport was considered, with 8 roundtrips per day. For the transport of heavy machines, the use of 33 t articulated truck was considered. The productivity of the CFA pile foundation was considered to be 8 piles per day. For BRD, it was considered 1 pile per day. And for ROOT, it was considered 1.5 piles per day. For the daily consumption of diesel during the execution of the piles, 300 liters was considered for CFA, 250 liters for BRD, and 220 liters for ROOT.

Tabela 7. Equipe e maquinários utilizados por tipo pile foundation (ABEF, 2022)

Equipment	CFA	BRD	ROOT	Work team	CFA	BRD	ROOT
Foundation drilling rig	1	1	1	Civil engineer	2	2	2
Concrete mixer truck	1	1	1	Foreman	1	1	1
Concrete pump truck	1	1	1	Crane operator	1	1	1
Excavator	1	1	1	Slurry expert		2	
Rigid truck 17 t	1	1	1	Drill operator	1	1	1
Recirculation pump		1	1	Excavator operator	1	1	1
Polymer slurry mixer		1		Truck driver/operator	3	3	3
Tower/Mobile Crane	1	1	1	General laborer	3	3	4

 © DFI International Bruges 2025

RESULTS

The results presented below were derived from the EFFC-DFI Calculator, incorporating the specified emission factors and the relevant calculation assumptions.

Concrete's carbon emission *vs* Steel's carbon emission

This study found that concrete consumption generated a significantly higher carbon footprint than steel consumption. The accumulated data showed that concrete accounted for 55,111,481 $kgCO_2$ in emissions, while steel contributed 9,280,443 $kgCO_2$. This represents a 17% contribution from steel compared to concrete. Fig. 6 visualizes the relative carbon footprints of steel and concrete across various foundation types

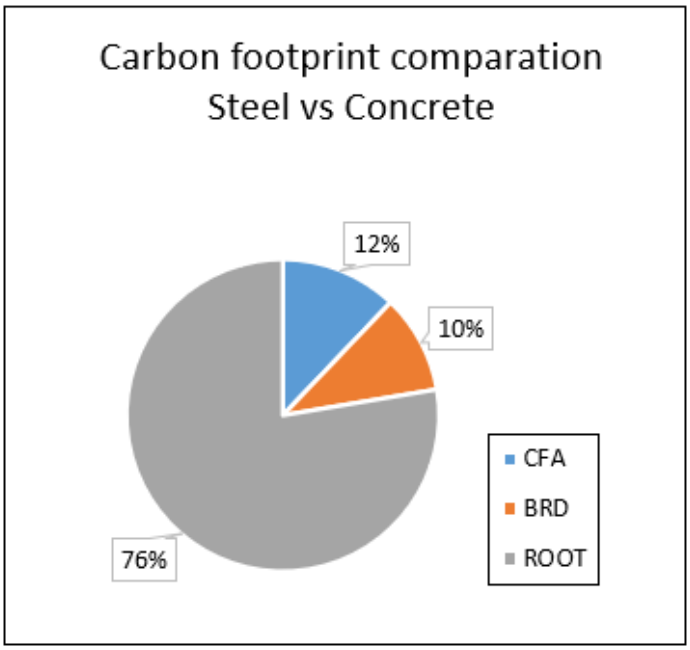


Fig. 6: Carbon footprint comparative: Steel *vs* Concrete

Fig. 6 shows that steel contributes 10% and 12% of the CO_2 emissions compared to concrete for CFA and BRD solutions, respectively. This proportion is lower for BRD due to its larger diameter and average length compared to CFA. For ROOT, the proportion is higher due to its shorter length and smaller diameter, which results in lower grout consumption, along with its higher load capacity and full reinforcement, leading to higher steel consumption.

Carbon emission by diesel fuel consumption *vs* Carbon emission by material consumption

In addition to concrete and steel, energy use during foundation construction also significantly contributes to CO_2 emissions. The database showed 2,966,762 $kgCO_2$ from diesel consumption, compared to 64,391,924 $kgCO_2$ from steel and concrete. This means diesel accounted for 5% of the total emissions. Fig. 7 below shows the proportion of the carbon footprint from diesel relative to the combined footprint of steel and concrete, by foundation type.

 © DFI International Bruges 2025

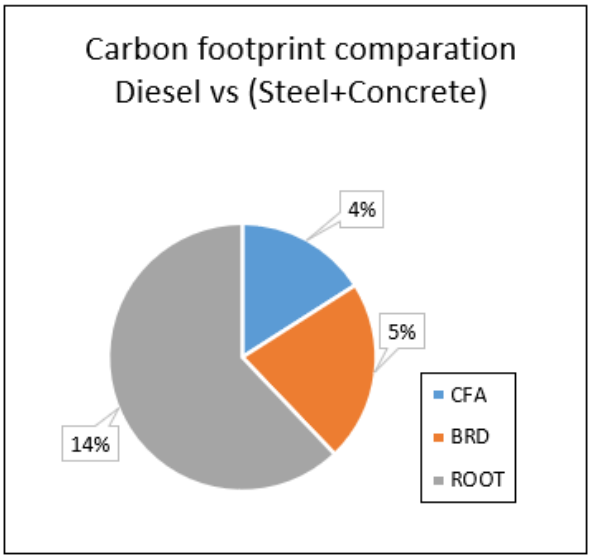


Fig. 7: Carbon footprint comparative: Diesel *vs* (Steel+Concrete)

As shown in Fig. 7, diesel consumption contributes 4% and 5% of the total CO_2 emissions associated with material use for CFA and BRD solutions. While ROOT is more productive than BRD, its material consumption is considerably lower than BRD pile foundation..

Carbon emission by primary sources *vs* Carbon emission by secondary sources

By calculating the carbon footprint from various sources, we can assess the relative contribution of secondary sources compared to primary sources. The database showed that the primary source accounted for 67,462,904 kg of CO_2 emissions, while the secondary source contributed 5,470,289 kg. As a result, the secondary source represented only 8% of the total emissions. Fig. 8 illustrates the proportion of carbon emissions from the secondary source relative to the primary source for different foundation types.

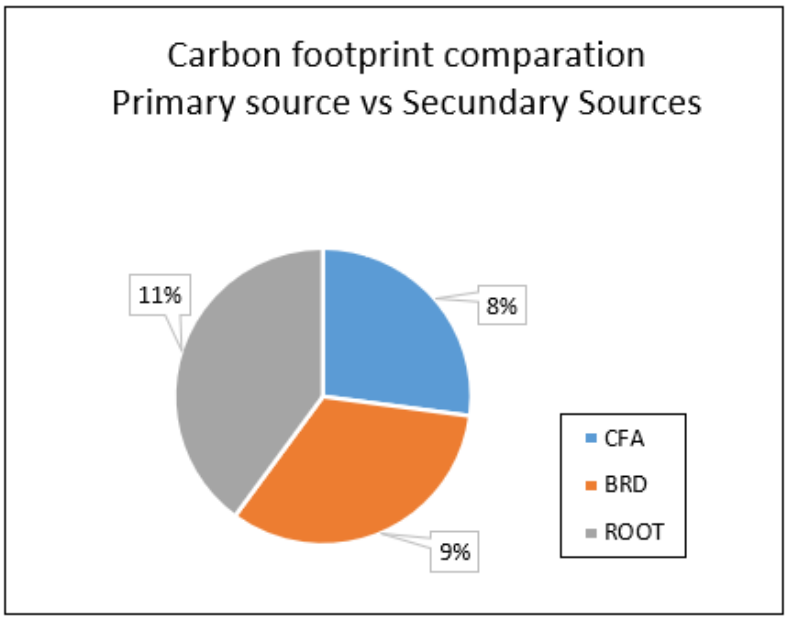


Fig. 8: Carbon footprint comparative: Primary *vs* Secundary sources

 © DFI International Bruges 2025

Benchmark

To provide a preliminary assessment of carbon emissions ($kgCO_2$) for new foundation projects, Born et al. (2024) suggested a method that considers the combined effects of loads, built area, and building height. This approach is visualized in Fig. 9.

Once the foundation design is finalized, engineers can compare their design with the database from Born et al. (2024) by calculating the carbon emission efficiency index (i_{CEE}) using equation 3.

$$i_{CEE} = \frac{\sum_{i=1}^{n}(kgCO_2)_i}{\left(\frac{\sum_{i=1}^{n} Q_i\,(kN)}{built\ area\ (m^2)}\right)} \quad [3]$$

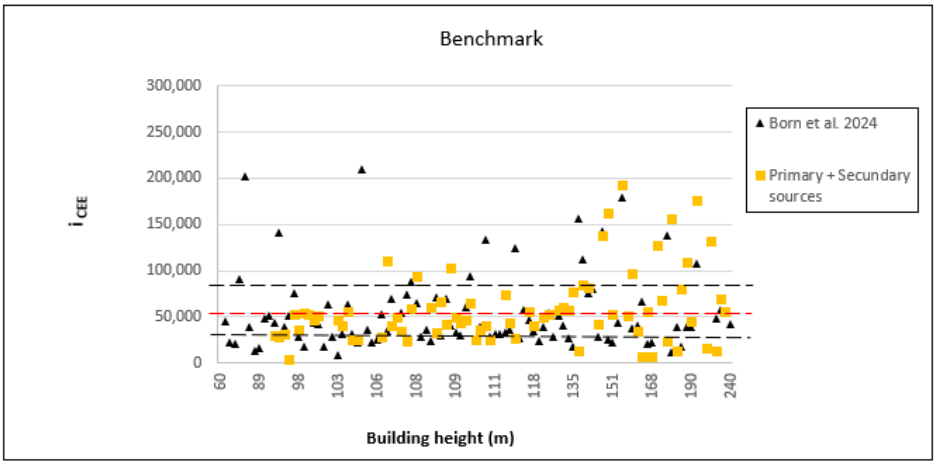


Fig. 9: i_{CEE} (Born et al., 2024) *vs* i_{CEE} (primary + secondary sources of emissions).

It is important to note that Born et al. (2024) present the i_{CEE} based exclusively on CO_2 emissions from steel and concrete consumption. The range represents values considering both the mean and standard deviation of the database.

Fig. 9 also presents the comparison between the proposal presented by Born et al. (2024) and the database analyzed in this paper, considering both primary and secondary carbon emission sources.

According to the i_{CEE} calculations for the pile foundations in this database, the average i_{CEE} values ($kgCO_2/MPa$) are as follows : $i_{CEE\ (CFA)}$: 61,466; $i_{CEE\ (BRD)}$: 122,736; $i_{CEE\ (ROOT)}$: 71,604.

CONCLUSION

This paper presents a database of 70 foundation projects, including 67 high-rise buildings over 100 meters tall, aimed at assessing the carbon footprint using the methodology employed in the EFFC-DFI Calculator, considering both primary and secondary emission sources for three different foundation pile solutions: CFA, BRD, and ROOT.

The database is based on projects from 2019 to 2024, located on Brazil's southern coast. Given the specific characteristics of the local soil profile, sounding quality, and load cases, the analyzed projects feature a wide range of foundation designs, varying in diameter, depth, and steel content.

Through the development of this paper, it was possible to compare the carbon footprint of various emission sources across different foundation solutions, such as: Steel vs Concrete carbon footprint, Energy vs Materials carbon footprint, and Primary vs Secondary carbon footprint.

 © DFI International Bruges 2025

Finally, the Carbon Emission Efficiency Index (i_{CEE}) was calculated and compared with the results from Born et al. (2024). As shown in Fig. 8, the secondary sources represents a small percentage of the carbon footprint compared to steel and concrete consumption, with most projects falling within the range proposed by Born et al. (2024), as illustrated in Fig. 9.

Based on the i_{CEE} calculation, it can be inferred that CFA solutions typically demonstrate a lower carbon footprint among the analyzed projects. It is important to highlight that the database is predominantly composed of CFA pile projects. Therefore, caution should be exercised when using i_{CEE} for BRD and ROOT as a reference in future studies.

REFERENCES

Born, R.B., Sales, L.F.P., Cordeiro, R.E., Belloli, M.V.A.B., Corrêa, G.M., 2024. Carbon footprint database of tall buildings foundation in southern Brazil. 17th Pan-American Conference on Soil Mechanics and Geotechnical Engineering (XVII PCSMGE). La Serena, Chile.

Costa, B.L.deC., 2012. Quantification of carbon dioxide releases generated by the production of Building materials in Brazil. Master dissertation. Federal University of Rio de Janeiro, Departament of Civil Engineering. 190 p.

CTBUH, 2024. Ranking of the tallest buildings in Brazil. Council on Tall Building and Urban Habitat. https://www.skyscrapercenter.com/country/brazil. Access in: 10/08/2024.

EFFC, DFI, Carbone 4, 2014. EFFC DFI Carbon calculator methodological & user guide – V2.2

Instituto Brasileiro de Geografía e Estatística (IBGE), 2022. Brazilian demographic census.

https://cidades.ibge.gov.br/brasil/sc/balneario-camboriu/panorama . Acess in: 08/10/2024.

International Energy Agency, 2018. Global status report: Towards a zero-emission, efficient, and resilient buildings and construction sector. United Nations Environment Programme. 71 p.

Lasne, M., Large, M.E., Bruni, L., 2015. EFFC-DFI Geotechnical carbon calculator project. 11 p.

Lima, J.A.R., 2010. Avaliação das consequências da produção de concreto no Brasil para as mudanças climáticas. Doctoral thesis. São Paulo University, Departament of Civil Engineering. 129 p.

Manual de Execução de Fundações: Práticas Recomendadas, 2022. Second Edition. Associação Brasileira de Empresas de Engenharia de Fundações e Geotecnia (ABEF), São Paulo, Brazil, 448 p.

Mazurana, L., 2019. Captura de CO_2 em argamassa de revestimento através da carbonatação natural. Master dissertation. Federal Technological Univ. of Paraná, Departament of Civil Engineering. 119 p.

Ministério do Meio Ambiente (MMA), 2011. Inventário nacional de emissões atmosféricas por veículos automotores rodoviários.

Vital, M.H.F., 2018. Global warming: international agreements, CO_2 emissions and the emergence of carbon markets in the world. BNDES, Department of the Environment and Management of the Amazon Fund, Rio de Janeiro, v. 24, n. 48, 167-244 p.

Zhang, X. and Wang, F., 2016. Assessment of embodied carbon emissions for building construction in China: Comparative case studies using alternative methods. Energy and Buildings, v. 130, p. 330-340.

Zhang, Y., Luo, W., Wang, J., Wang, Y., Xu Y., Xiao J., 2019. A review of life cycle assessment of recycled aggregate concrete. Construction and Building Materials, v. 209, p. 115-125.

 © DFI International Bruges 2025

LIMESTONE FILLER IMPLEMENTATION IN GEOTECHNICAL CONCRETE MIXES

Hugo Chapin, Soletanche Bachy International, Birmingham, United Kingdom, +44(0)7 805 792878, hugo.chapin@soletanche-bachy.com

Christophe Justino, Soletanche Bachy International, Montereau-Fault-Yonne, France, +33(0)6 07227439, christophe.justino@soletanche-bachy.com

Sivilay Sayavong, Bachy Soletanche Ltd, Camberley, United Kingdom, +44(0)7 891 835594, sivilay.sayavong@bacsol.co.uk

ABSTRACT

Bachy Soletanche Balfour Beatty Ground Engineering Joint Venture (SB3) is a geotechnical subcontractor on a high-speed railway project in the U. K. West Midlands. SB3's scope includes 4,500 linear meters of diaphragm walls, 19,000 piles for deep foundations and retaining walls, and 85,000 rigid inclusions, requiring over 600,000 m³ of concrete. In May 2023, SB3 successfully integrated limestone filler into the concrete mix design after extensive trials. These new mixes resulted in a 5-7% reduction in embodied CO_2, leading to a 761-tonnes reduction in CO_2 emissions from June 2023 to end of January 2025. Although the percentage reduction appears modest, the project's scale amplifies its impact. Additionally, limestone filler is recognized within the concrete industry for improving the quality of fresh concrete in deep foundations by reducing common issues such as segregation and bleeding. Its fine particle size and non-reactive nature enhance the density of the concrete paste, effectively preventing these issues.

Keywords: limestone filler, geotechnical concrete mix, CO_2 reduction

PROJECT INTRODUCTION

SB3, a joint venture incorporating Bachy Soletanche Ltd (BSL) and Balfour Beatty Ground Engineering, is delivering the geotechnical works required for a major railway project in the United Kingdom, spanning over 90km. The scheme will provide a new high-speed rail connection between London and Birmingham as well as connections to the North.

The works comprises over 150 individual assets with the following key metrics:

- Circa. 5km of Diaphragm Walls with approximately 110,000 m³ of concrete and over 17,000 tonnes of reinforcement
- 18,800 piles with a total length of approximately 335 km, 385,000 m³ of concrete and over 50,000 tonnes of reinforcement
- 85,000 ground improvement Rigid Inclusions with a total length of approximately 950 km *(the same distance as from London to Gijon in the North of Spain)*
- Additional scope includes plunge columns, tension piles, ground anchors and soil nails.

The scheme is a key infrastructure project that will reduce carbon emission and help the UK fight against climate change, while providing better connectivity and creating greater capacity for local services and freight on existing lines.

 © DFI International Bruges 2025

HISTORY OF LIMESTONE FILLER IN CONCRETE

Introduction of limestone filler

Limestone filler is a very fine natural product obtained from crushed limestone rocks and is available as a dry product (powder) or in an aqueous suspension (slurry). Its physical and chemical characteristics for use in concrete are described in BS 7979 and BS EN 12620. The mains characteristics are:

- The purity of the limestone, expressed in percentage of $CaCO_3$ must be above 75%;
- The percentage passing on a 0.063 mm sieve must be at least 70%.

Other chemical and physical properties are also investigated to ensure that the limestone filler does not negatively impact the properties of concrete in either its fresh or hardened state. In the concrete industry, limestone filler is mainly used in the production of the CEM II/A/B-L or recombined directly at the concrete plant as a CII/A/B-L, as a substitution for the Portland cement. More and more, it is also used as a mineral addition for its filler effect for self-compacting concrete. The filler effect allows the optimization of the granulometry by filling all the voids left by the lack of fine particles, meaning a better compacity. This optimization gives the concrete a better workability and thus allows a water reduction, finally making possible an increase of the concrete strength.

Another advantage of the limestone filler over CEM I and other minerals additions is its very low carbon dioxide footprint of 8 $kgCO_2eq/ton$, 10 times less than Ground Granulated Blastfurnace Slag (GGBS) and more than 100 times less than Portland cement CEM I, according to Mineral Products Association Fact Sheet 18 from 2019.

Effect of limestone filler on the fresh and hardened concrete properties

The most common issues with fresh concrete in the deep foundation industry are bleeding of the concrete and concrete segregation. To fully understand how limestone filler helps prevent these problems, it is important to remind the underlying mechanisms behind these phenomena:

Bleeding of concrete: To ensure the required workability, there is usually an excess of water compared to the voids in the granulometry of the concrete. Once the pour is complete, the granular skeleton of the concrete tends to settle under its own weight, pushing out this excess of water. It then rises to the top of the poured element through percolation, leading to concrete bleeding. This phenomenon is also linked to the height of the element, the deeper the pile (or diaphragm-wall, Fig.1) is, the greater the settlement will be (Josserand, 2002). Mild bleeding will not affect the quality of the element and can provide a thin layer of water on top of it, assuring a satisfactory cure of the concrete. However, severe bleeding can be detrimental to the quality of the element, the worst case being a washing out of the concrete paste and the fine elements as the water is rising, leading to voids within the deep foundation element. EFFC/DFI Guide to tremie concrete discloses suitable test to evaluate concrete bleeding behavior through static bleed test and pressure filtration test. The most used test is described in different standards such as ASTM C232 and NF XP P18-468 and in the yet to be published prEN 12350-13.

Concrete segregation: aggregates in the fresh concrete usually have a higher density than the concrete paste, however there is no separation of the constituents due to the high yield value of the concrete paste, preventing aggregates movements. However, it may not be always the case due to an excess of water or superplasticizer for example, especially for high workability concrete such as in the deep foundation industry as they require a low yield value to be self-levelling. This will provoke the heavy aggregates to go down and the concrete paste up within the element. This will create a heterogeneous concrete, with different durability and mechanical properties locally situated. The most used standards for testing the segregation resistance of a concrete mix are the static segregation column defined in

 © DFI International Bruges 2025

ASTM C1610, or the sieve test as per EN 12350-11, however these methods might not be practical on a construction site. The Visual Stability Index (VSI), as described in ASTM C1611, can be practical to identify segregating concrete on-site as the appreciation is done at the same time as the consistency test (Fig 2) and based on visual observation. The concrete is considered stable if the index is 0 or 1 and unstable for indexes 2 and 3.



Fig. 1. Example of bleeding channels on a diaphragm-wall head



Fig. 2. Categories of VSI to identify concrete segregation after the consistency test

Within the available scientific literature, very few publications are explaining the mechanisms of the limestone filler on the bleeding and segregation resistance of the fresh concrete. However, its impact on these issues is well documented, mainly to improve self-compacting concrete behavior.

Ahmed et al. (2018) demonstrated the 'filler effect' in their studies. The authors compared different concrete mixes where Portland cement was partially replaced by limestone filler, while keeping the other constituent proportions fixed. The density of the fresh concretes increases as the filler quantity increases and replaces the Portland cement, reaching a maximum of 15% before decreasing. This increase in density is attributed to the limestone particles filling the small voids in the concrete's granulometry. It is also correlated by the strength results, as the strength of the concrete also peaked at 15% filler content, despite a reduction in cement. This highlights that the compaction of the granular skeleton plays an important role in the development of the strengths. It is also worth noting that the setting time decreases with the filler implementation. This is due to the limestone particles participating in the hydration process as a support to the cement hydrates, improving the kinetic of the reactions.

 © DFI International Bruges 2025

Similar results were reported by O. M. A. Daoud et al. (2021), who confirmed the results observed by Dr. Hamed Ahmed on the strengths behavior with the filler implementation. O. M. A. Daoud et al. also investigated the fresh concrete properties and the segregation resistance with a similar method than described before. It shows that the consistency of the concrete increases to a maximum as the filler content increases with the same water content, meaning that the water content can be reduced for the same consistency if the filler is introduced. The study also shows sieve segregation test, as per BS EN 12350-11, is decreasing as the filler content augments, meaning a better segregation resistance. The density and the strengths are also reaching a maximum with 20% of replacement, while it was 15% for Dr. Hamed Ahmed. This shows that the optimal filler content is dependent on the granulometry of the concrete rather than the replacement percentage.

Finally, Hafez E. Elyamany et al. (2014) studied the filler effect on the bleeding of fresh concrete, on the segregation resistance, and on the strengths. The results for the strengths and the segregation resistance are similar to the two previous studies, showing consistency of the studies. Regarding the bleed, the study shows that the bleeding of the concrete decreases while the filler content increases. It is interesting to note that the non-pozzolanic fillers (limestone filler, granite dust, ect) allows a better bleeding reduction than the pozzolanic fillers (fly ashes, metakaolin). The authors concluded their studies that the reactive nature of the pozzolanic fillers prevents and inhibits the bleeding phenomenon, as they will chemically react with the water of the concrete.

Bibliography conclusion

Concrete segregation and concrete bleeding are two of the most common issues with fresh concrete in the deep foundation industry. The mechanisms behind these issues are known and solutions exist to prevent them from happening, such as optimizing the granulometry of the concrete by introducing limestone filler. However, the mechanisms of action for the filler are not fully described within the studies. The first one is the filler effect, allowing an optimization of the granulometry of the concrete and a reduction of the water content for the same required consistency. This reduction of water also allows a reduction of concrete segregation and bleeding, as they are linked to the water content of the concrete.

On the other hand, it is likely that the filler plays an active role in the bleeding inhibition and the segregation reduction. The inert and small particles of the filler can effectively block the percolation channels, preventing the concrete from bleeding. As the limestone filler is inert in water, it is not dissolved like the usual cements are. It is helping to improve the yield of the concrete paste and, hence preventing concrete segregation.

On another hand, Appendix D of the BS EN 206 is specific to geotechnical concrete and gives specification on concrete composition on concrete mixes for such works. It indicates a minimal cement content of 325 kg/m^3 (or 375 kg/m^3 for concrete placed under submerged condition) and a minimal fines content of 400 or 450 kg/m^3 depending on the aggregates – fines being particles with a size less than 0.125 mm and includes cements and additions. In most cases, minimum fines content requirement is complied by adjusting the cement content. Hence, adding filler to the mixes allow to reduce the cement content by achieving the minimum fines content with the use of limestone filler.

 © DFI International Bruges 2025

LIMESTONE FILLER IN SB3 WORKS

SB3 filler mixes implementation

Since the start of the project, SB3 has consistently encouraged the concrete suppliers to implement limestone filler in the geotechnical mixes if it was not already introduced. Two of the three concrete suppliers lacked filler available at their plants, which occasionally led to mild bleeding issues. SB3's main objectives in promoting the use of filler were to replace cement by filler to reduce the CO_2 footprint of the mixes and to lower the likelihood of mild bleeding occurring in the mixes.

SB3 used three main concrete mixes for its works:

- Mix A: 20 mm aggregates, CIII/B cement, minimum cement content of 380 kg/m^3, maximal water/cement ratio of 0.40 and DC-4 according to BS 8500-1. This mix is used for diaphragm-walls, foundation piles and rigid inclusions.
- Mix B: 10 mm aggregates, CIII/B cement, minimum cement content of 400 kg/m^3, maximal water/cement ratio of 0.40 and DC-4 according to BS 8500-1. This mix is used for diaphragm-walls, foundation piles and rigid inclusions.
- Mix C: 20 mm aggregates, CIII/C cement, minimum cement content of 300 kg/m^3, maximal water/cement ratio of 0.55 and DC-4 according to BRE IP 17/05. This mix is used for firm piles in secant piles walls.

All the mentioned mixes are designed for a flow consistency target of 600 mm +/- 60 mm as per BS 8500-1, and have criteria on bleed test, Bauer filtration test and consistency retention of four or six hours.

Once the concrete supplier agreed to implement the filler, the mixes were modified as follows with the help of the supplier expertise:

- Mix A: replacement of 25 kg/m^3 of cementitious materials by 30 kg/m^3 of filler;
- Mix B: replacement of 40 kg/m^3 of cementitious materials by the same amount of filler;
- Mix C: replacement of 30 kg/m^3 of cementitious materials by the same amount of filler.

The new mix designs were thoroughly tested before their implementation with extensive laboratory trials. Once the laboratory trials were satisfactory, the mixes were then tested at the concrete plants to ensure their behaviors are similar at the plant than at the laboratory. It is noted that the fresh and hard properties criteria were the same for the filler and non-filler mixes. Finally, the mixes were reviewed and approved by all the relevant parties and the greenlight was given for the use in the permanent works early June 2023.

Plant trials results and comparison

As discussed previously, the filler mixes have been tested at the concrete plant and compared to the non-filler mixes.

 © DFI International Bruges 2025

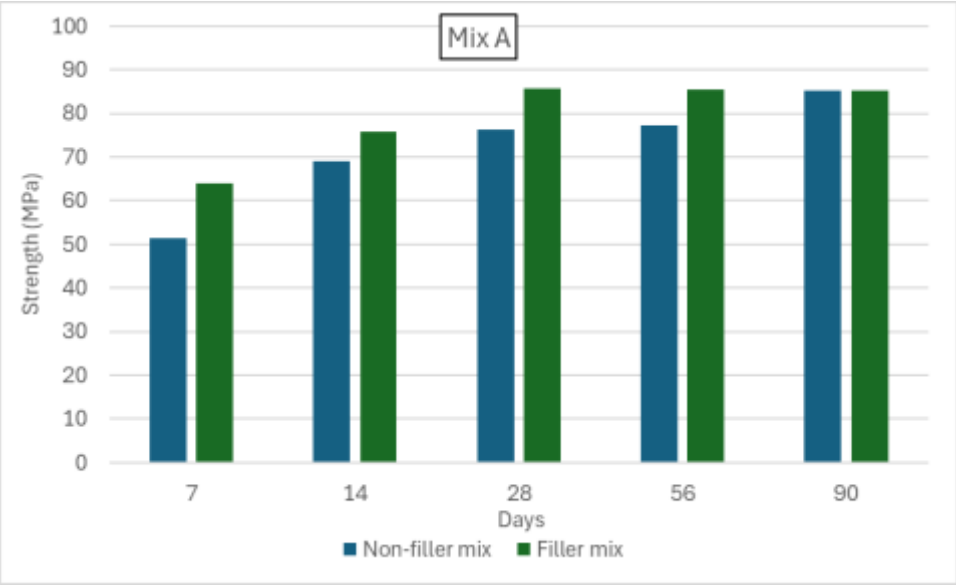


Fig. 3. Strengths comparison between filler and non-filler mixes for mix A

The bleed rates have also been compared:

- 0.01 mL/min for mix A without filler;
- 0.01 mL/min for mix A with filler.

As shown in Fig. 3, the long-term strengths are similar for the non-filler and the filler mixes, even though the filler mix have a lower cement content and higher water/cement ratio, 0.39 against 0.37 for the non-filler mix. The water contents are the same for both mixes. These strengths results are showing the filler effect discussed within the bibliography section. There is no impact on the bleed rate as the bleed rates are the same. These results are showing that the limestone filler implementation in mix A does not have negative effects on the fresh and hard properties of the concrete.

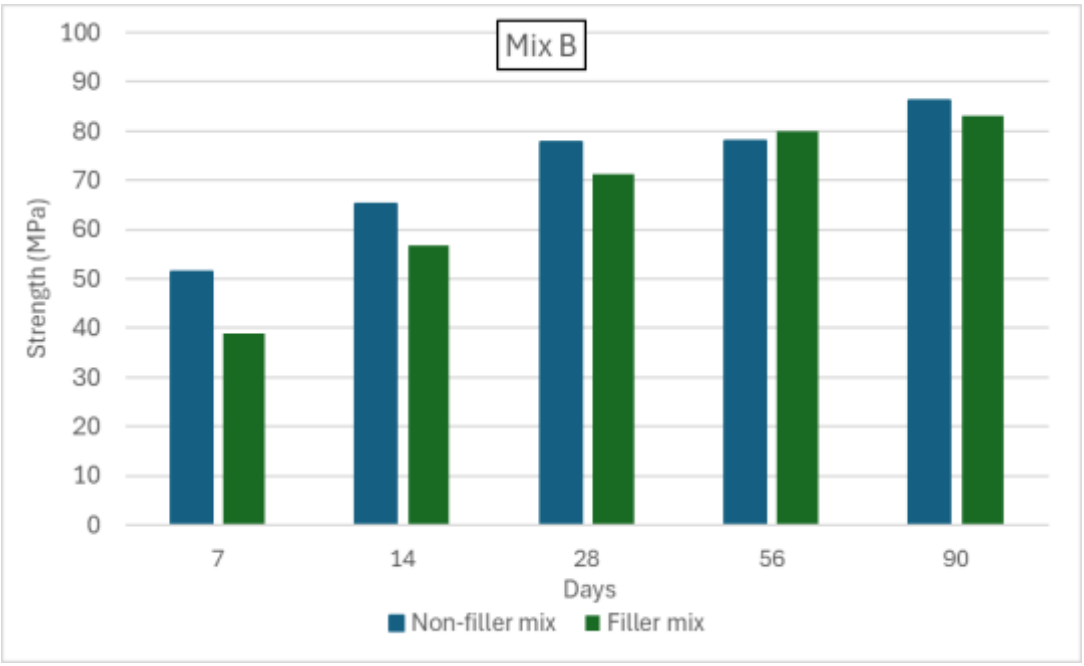


Fig. 4. Strengths comparison between filler and non-filler mixes for mix B

 © DFI International Bruges 2025

The bleed rates have also been compared:

- 0.04 mL/min for mix B without filler;
- 0.05 mL/min for mix B with filler.

As shown in Fig. 4, the long-term strengths are similar for the non-filler and the filler mixes, even though the filler mix have a lower cement content and higher water/cement ratio, 0.39 against 0.36 for the non-filler mix. These strengths results are showing the filler effect discussed within the bibliography section. There is no impact on the bleed rate as the difference is marginal. All these results are showing that the limestone filler implementation in mix B does not have negative effects on the fresh and hard properties of the concrete.

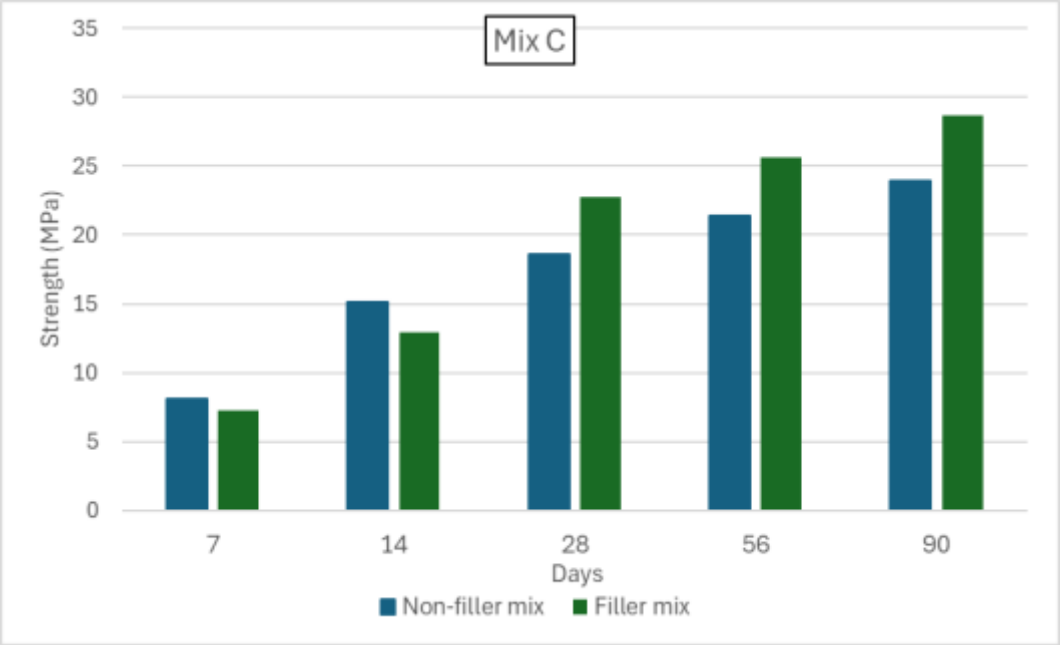


Fig. 5. Strengths comparison between filler and non-filler mixes for mix C

As shown in Fig. 5, the long-term strengths are similar for the non-filler and the filler mixes, even though the filler mix have a lower cement content and lower water/cement ratio, 0.54 against 0.50 for the non-filler mix. The water contents are similar for both mixes. These strengths results are showing the filler effect discussed within the bibliography section. These results are showing that the limestone filler implementation in mix C does not have negative effects on the hard properties of the concrete.

Effect of the filler mixes on the quality and the environment

Since June 2023, the frequency of mild bleeding events has widely decreased, with no reports of bleeding from any sites. The concrete is also tested routinely on the Bauer filtration test and the bleed test, no out-of-specification results have been recorded during this period.

The biggest gain is probably for the carbon reduction potential. All the carbon footprints for the concrete mixes have been calculated using the EFFC-DFI Carbon Calculator, which accounts for nearly all CO2 emission sources. An additional 10 $kgCO_2eq/m^3$ has been added to consider the energy consumption of the mixer, the concrete plant vehicles movement and the treatment of the grey water coming from the washing of the trucks. This is summarized in Table 1:

 © DFI International Bruges 2025

Table 1. Emissions factors for each type of mix in $kgCO_2eq/m^3$

	Without limestone filler	With limestone filler	Percentage difference
Mix A	174	165	5.2%
Mix B	190	176	7.4%
Mix C	88	83	5.7%

Considering that the mixes already had low carbon emissions before the limestone filler implementation, the difference is also low, from 5 $kgCO_2eq/m^3$ to 14 $kgCO_2eq/m^3$. However, due to the extensive scope of the project and the large volume of concrete being placed, the overall carbon savings amount to hundreds of tons. The data presented in Table 2 is from June 2023 to the end of January 2025.

Table 2. Volume of each filler mix placed and CO_2 savings

	Difference between non filler and filler mix ($kgCO_2eq/m^3$)	Total volume placed (m^3)
Mix A	9	46,341
Mix B	14	22,634
Mix C	5	5,405

Total CO_2 savings: 761 tons

As the project is still on-going, the savings are continuously increasing. With more than 761 tons saved since its implementation, there is the potential to reach 1,000 tons of savings at the completion of the project.

CONCLUSION

As highlighted previously, the use of limestone filler in geotechnical concrete mixes offers several benefits. Firstly, it effectively addresses common fresh concrete issues such as segregation and bleeding. Due to its particles size and non-reactive nature, it helps to increase the yield of the concrete paste and to block the bleeding channels. Moreover, it can also be used to substitute cementitious materials to reduce the CO_2 footprints of the concrete mixes. Although specific data on limestone resources in the United Kingdom is not available, it is abundantly present, constituting roughly 15% of the Earth's crust. SB3 has encouraged their concrete suppliers to implement limestone filler for these reasons, leading to improved concrete mixes for geotechnical applications and environmental benefits. Each cubic meter poured results in a CO_2 reduction compared to the original mix design, with a total saving of 761 tons so far, which corresponds to 380 travels from London to New York – considering 2 tons per passenger for a return flight. Although the reduction appears to be modest in percentage, every little amount of CO_2 counts for the Global Warming fight.

Limestone filler as replacement of the total binder (cement and supplementary cementitious materials) has been used successfully in this project to proportion concrete with the total fines content necessary

 © DFI International Bruges 2025

to achieve the concrete stability requirements. There is no impact from the limestone filler on the fresh and hard concrete properties. This allowed us to reduce binder content and CO_2 emission compared to standard practices in the U. K. for geotechnical works. Further reduction could be envisaged, by revising actual standards (ICE SPERW and Annex D of BS EN 206-1). Revision should include to specify minimum cement (binder) content for durability purposes (according to BS 8500-1 standard) and minimum fines content as sole prescriptive parameter to ensure stable concrete is designed. Using other fines like limestone filler as replacement to cement to achieve the minimum fines content will allow for further CO_2 reduction. The stability of the concrete can be assessed by performance tests already in place and mentioned in this paper.

REFERENCES

Ahmed, Dr & Alshahwany, Rana & Mohammed, Zena.Adel. (2018). Influence of Limestone Powder as Partial Replacement of Cement on Concrete and the Effect of High Temperature on It

ASTM C232:2010, Standard Test Methods for Bleeding of Concrete

ASTM C1610:2021, Standard Test Method for Static Segregation of Self-Consolidating Concrete Using Column Technique

ASTM C1611/C1611M-21, Standard Test Method for Slump Flow of Self-Consolidating Concrete

BS EN 197-1:2011, Cement - Composition, specifications and conformity criteria for common cements

BS EN 206:2013+A2:2021, Concrete. Specification, performance, production and conformity.

BS 7979:2016, Specification for limestone fines for use with Portland cement

BS 8500-1:2023, Concrete. Complementary British Standard to BS EN 206 - Method of specifying and guidance for the specifier

BS EN 12350-11:2010, Testing fresh concrete - Self-compacting concrete. Sieve segregation test

Building Research Establishment, Information Paper 17/05, Concretes with high ggbs contents for use in hard/firm secant piling, 2005

Daoud, Osama & Mahgoub, O. (2021). Effect of limestone powder on self-compacting concrete. FES Journal of Engineering Sciences

EN 12620:2013, Aggregates for concrete

Hafez E. Elyamany, Abd Elmoaty M. Abd Elmoaty, Basma Mohamed, Effect of filler types on physical, mechanical and microstructure of self-compacting concrete and Flow-able concrete, Alexandria Engineering Journal, Volume 53, Issue 2, 2014, Pages 295-307, ISSN 1110-0168.

ICE SPERW 3rd Edition 2016

Le grand livre des bétons, Laetitia D'Aloia-Schwartzentruber, Jean-Michel Torrenti, Editions Le Moniteur, 2014

Mineral Product Association Cement, Fact Sheet 18, Embodied CO2e of UK cement, additions and cementitious material

NF XP P18-468, Béton – Essais pour béton frais - ressuage

 © DFI International Bruges 2025

COMPARISON OF PROPAGATION EFFICIENCY BETWEEN TUBE-A-MANACHETTE AND MULTI-STRAINER CHEMICAL GROUTING METHODS IN GRANULAR SOILS

S.-H. Cheng, National Taiwan University of Science and Technology, Taipei, Taiwan, email: shcheng@mail.ntust.edu.tw
Ricky K.-N. Wong, SANSHIN CORPORATION, Taipei, Taiwan, email: ricky_wong@sanshin-corp.co.jp
Isaac T.-Y. Wong, SANSHIN CORPORATION, Taipei, Taiwan, email: isaac.sanshin@gmail.com
H.-W. Cheng, SINOTECH engineering conculants, Ltd., Taipei, Taiwan, email: chenghw@mail.sinotech.com.tw
K. Imakura, Taoyuan Rapid Transit Green Line GC03 Civil Construction Turnkey Project, Taoyuan, Taiwan, email: imakura.kazuhiko@obayashi.co.jp
H.-M Huang, Department of Rapid Transit Syetems, Taoyuan, Taiwan, email: 10009814@mail.tycg.gov.tw

ABSTRACT

The Tube-A-Manchette (TAM) grouting method has been used in Taiwan for several years, particularly in underground construction projects such as tunneling boring mechanisms (TBM) tunnels and cross-passage construction. While the TAM grouting method is effective, the 33 cm grouting intervals and limited grout outlets can present challenges in areas with surface obstacles, raising concerns about infiltration reliability. To address this issue, this study adopted the multi-strainer (MS) grouting method, which features 100 cm grouting intervals and additional grout outlets for improved soil penetration. The study compares the TAM and MS grouting methods in a TBM tunnel construction case, evaluating their effectiveness using data recorded during the grouting process.

Keywords: propagation efficiency, Tube-A-Manachette grouting, multi-strainer grouting, granular soils

INTRODUCTION

The Tube-A-Manchette (TAM) grouting method is a type of chemical grouting that uses chemical substances to improve soil structure and control water flow. It typically stabilizes granular soils by permeating the spaces between soil particles, binding them together, and increasing the soil's bearing capacity, all without affecting the surrounding structures. While in cohesive soils, it infiltrates fissures, with compaction and solidification improving soil strength. In addition to its effectiveness, cost reduction is a key priority. However, in areas with surface obstacles, such as cable conduits, achieving the standard grout hole spacing of 1.0 to 2.0 m can be challenging, raising concerns about infiltration reliability. This study adopts the multi-strainer (MS) grouting method, a modified version of TAM grouting, to ensure effective soil improvement in such conditions. We present the application of both TAM and MS grouting methods for the cross-passage and cutter head maintenance of tunneling boring mechanisms (TBM) in granular soils. The study evaluates their effectiveness and analyzes feedback based on grouting parameters recorded by dataloggers.

CHEMICAL GROUTING METHOD

Tube-A-Manachette (TAM) grouting method

TAM grouting offers the unique advantage of being compatible with any grouting material and applicable to any grouting hole. Once the grouting zone, grouting hole locations, and grouting amount are determined, grouting pressure control or grouting volume control can be employed. However, due to the non-uniform and anisotropic nature of soil, controlling grouting volume typically enhances grouting efficiency more than controlling grouting pressure. This is especially true when the absolute value of grouting pressure is less important than its relative changes. The relevant construction procedures are illustrated in Fig. 1. The TAM method offers several advantages, including the ability to perform repeated injections at specific depths, control grout volume at each injection point, apply sequential injections of different grout materials, and adjust the shape and direction of the outlet on the TAM pipe. In TAM grouting, the diameter of the TAM pipe determines the radius of the spherical permeation source. Simply increasing the grout volume may raise the flow rate but does not necessarily improve permeation efficiency. Fig. 2 presents the TAM grouting pipe layout, structure, rubber valve design, and a water injection test demonstration.

 © DFI International Bruges 2025

Multi-Strainer (MS) grouting method

The equipment, grout materials, and grouting process of the MS grouting method are similar to those of the TAM grouting method. However, in the MS method, each grouting stage covers approximately 100 cm, with increased grout intervals. The grout material is injected through cylindrical permeable sources, allowing it to spread outward. Despite the increased intervals, the flow rate remains unchanged even with a higher grout volume. As a result, a larger volume of grout can be injected into the ground compared to the TAM grouting method, corresponding for wider grout penetration. Fig. 3 illustrates the layout and structure of the MS grouting pipe, including the rubber valve, and demonstrates a water injection test (SANSHIN CORPORATION, 2022).

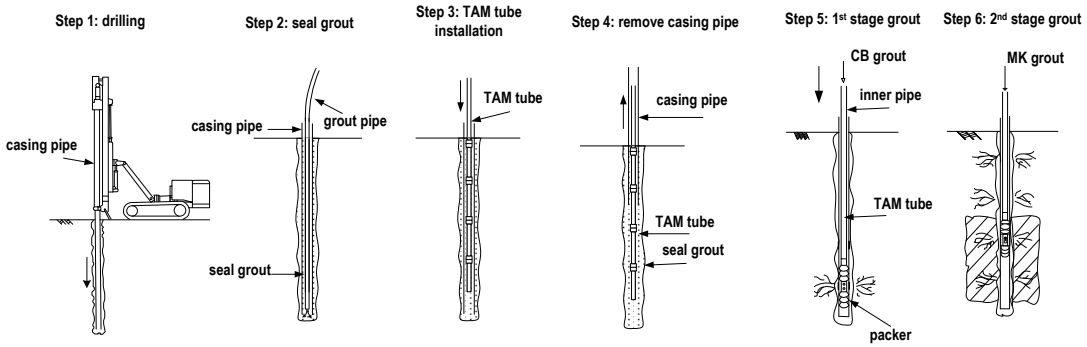


Fig. 1. TAM grouting procedure

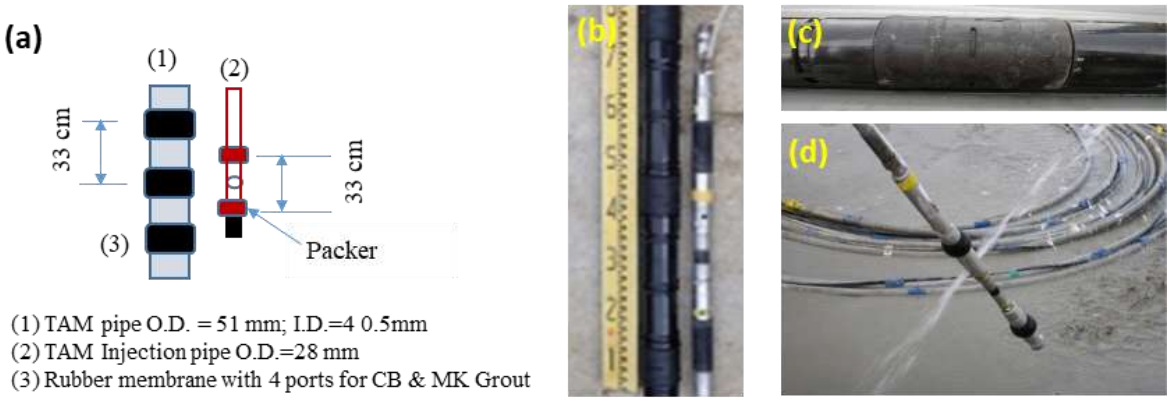


Fig. 2. (a) structure layout of TAM pipe, (b) photo of TAM pipe and grouting pipe, (c) rubber valve of the TAM pipe, and (d) water injection condition of TAM grouting pipe



Fig. 3. (a) structure layout of MS pipe, (b) photo of MS pipe and grouting pipe, (c) rubber valve of the MS pipe, and (d) water injection condition of MS grouting pipe

 © DFI International Bruges 2025

SITE CONDITIONS AND GROUTING WORKS

Fig. 4 shows the location and geological conditions of the study site. Due to the narrow and congested space between Stations G07 and G12, cross-passages could not be installed when TBM tunneling was used. Instead, a circular tunnel with an internal diameter of 7.5 m was constructed, incorporating emergency escape routes. Under these conditions, overlapping tunnels were bored using a medium circular shield tunnel machine (Earth Pressure Balance, EPB) with a diameter of 8.36 m and a length of 15.53 m. However, ground improvement work was required at the TBM cutter head near Station G09 (route G09+448) to facilitate cutter maintenance and prevent sand and water ingress during construction. To address this, measures were taken to enhance impermeability and stabilize the soil through grouting operations using both the TAM grouting and MS grouting methods (Fig. 5).

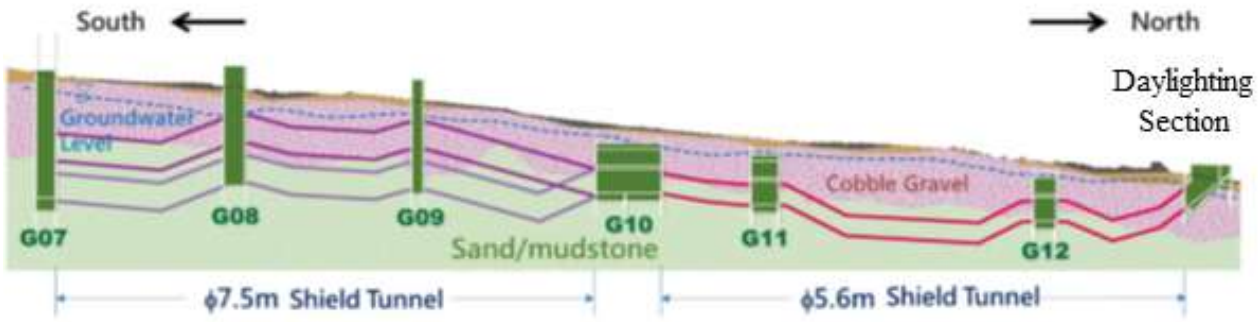


Fig. 4. Route of study case and geological profile

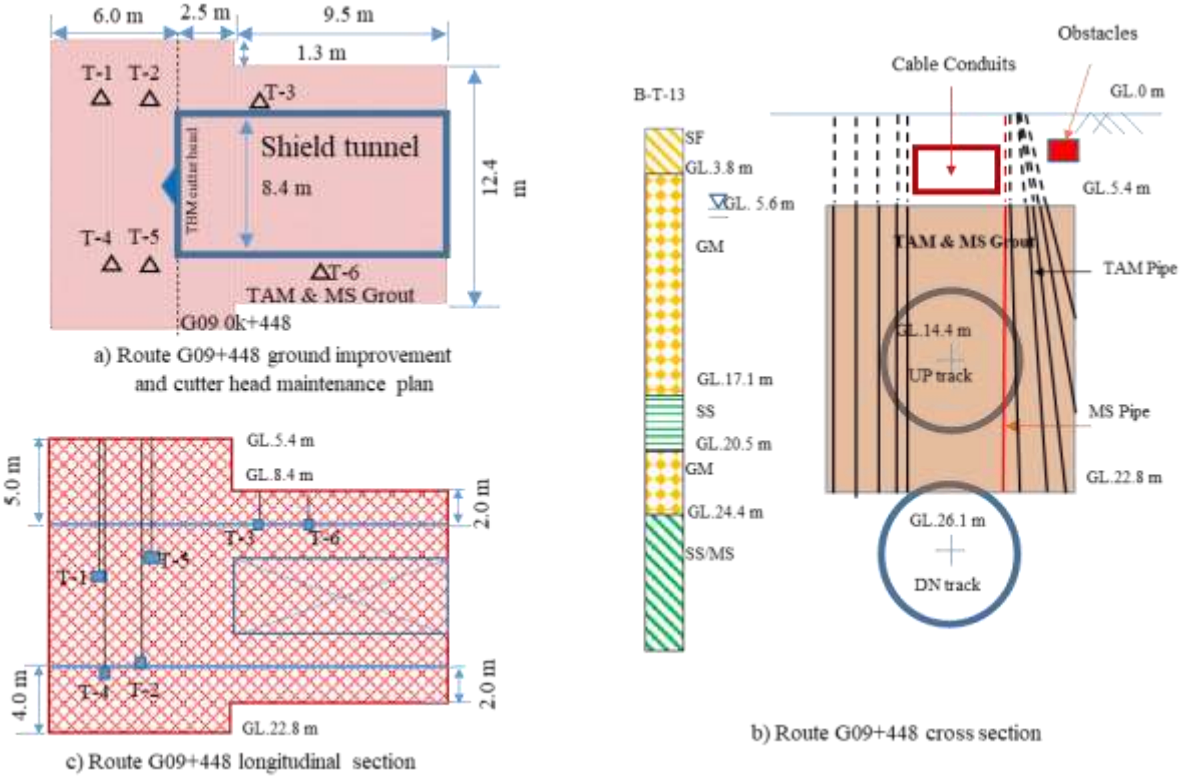


Fig. 5. Plan and cross-section of ground improvement works to facilitate TBM cutter maintenance near route G09+448

The soil formations along the medium circular tunnel and cross passage section of route G09+448 can be broadly classified into fill soil (SF), clay layer (CL), granular layer (GM), and sandstone/mudstone layer (SS/MS). The groundwater table is typically located 4.5 m below the ground surface.The granular layer is very dense, with an average SPT-N value greater than 50. Its gravel content ranges from 40% to 80%, with a maximum gravel particle size of approximately 60 mm. The sandstone/mudstone layer primarily consists of gray sandstone (SS) and gray mudstone (MS), with an average SPT-N value greater than 50, exhibiting slightly to moderate weathering. Table 1 shows the simplified soil parameters for route G09+448. The TAM/MS grouting is primarily applied to the gravel and sandstone/mudstone layers. The effective particle size of grouting soils, D_{10}, ranges from approximately 0.1 mm to 0.8 mm. The coefficient of permeability (k)

 © DFI International Bruges 2025

is calculated using the Hazen formula, ranging from $4.9X10^{-3}$ cm/s to $6.89X10^{-1}$ cm/s, with an average value of k=$3.4X10^{-2}$ cm/s.

Typically, chemical grouting employs quantitative management, with grouting pressure serving as a key reference for oversight. During quantitative grouting, both the grouting volume and pressure are monitored post-injection and compared to surrounding pressures. If significant deviation are observed, additional grouting may be required. There is a relative relationship between grouting flow rate and pressure. When the flow rate is fixed, grouting pressure becomes the primary management parameter. The grouting process follows a quantitative approach—once the maximum grouting pressure is reached, the stage is considered complete, and operations proceed to the next stage. Grouting pressure is influenced by various factors, including geological conditions, material properties, gelling time, grouting method, duration, and flow rate. Current practices rely on comprehensive assessments of geological and environmental conditions, as well as historical grouting records, to evaluate pressure and flow rates as key management indicators. Based on grouting experience, the parameters for the TAM and MS grouting methods are summarized in Table 2, while Table 3 presents the mixing proportions of grout materials used in this study (SANSHIN CORPORATION, 2022).

Table 1 Typical Geotechnical Parameters of the route G09+488

Layer	Soil Type	Depth(m)	SPT-N Values	γ_t (t/m^3)	Wn (%)	φ' (°)	c' (t/m^2)	N (%)
1	Fill (SF)	1.0	7	1.9	--	28	0	--
2	Clay (CL)	3.5	4	2.0	--	29	0	--
3	Gravel (GM)	24.0	/50	2.1	13.1	37	3	30
4	Rock (SS/MS)	48.0	/50	2.1	22.1	34	5	38

Table 2 Grouting parameters adopted in the study case

Item	TAM Method	MS Method
Injection type	1 shot	1 shot
Injection step	0.33 m/step	1.0 m/step
Range of influence (Sandy soil)	1.0 ~ 2.0 m	2.0 ~ 4.0 m
Grout ratio	Gravel：35%	Gravel：35% + 5%（Inspection）
	Sand Stone /Shale：15%	Sand Stone/Shale：15%
Injection flow rate	4 ~ 15 L/min	10 ~ 30 L/min
Allowable injection Pressure, P	P < 20 kg/cm^2	P < 30 kg/cm^2
	(P > P_i (Initial) + 0.5~2.0 kg/cm^2)	(P>P_i（Initial）+ 0.5~2.0 kg/cm^2)
Material: 1st Grout	CB	CB
2nd Grout	MK	MK

Table 3. Mixing proportions and grouting parameters of the grouts

Cement-bentonite grout (CB grout)		Silicate grout (MK grout)	
Cement (kg)	150	Sodium silicate (liter)	250
Bentonite (kg)	50	MK reagent (kg)	50
Water (liter)	The rest	Water (liter)	700
∑ = (liter)	1000	∑ = (liter)	1000
Gel time (min)	-	Gel time, grout itself (min)	60
		PH	1.4~2.0

QUALITY CONTROL AND GROUTING RESULTS

Limit injection test

Before grouting, the optimal grout flow rate must be determined to ensure effective grouting. When the soil profile is uncertain, field tests can be conducted to establish the optimal grouting rate for effective grout propagation. Mori et al. (1993) proposed a method to determine the critical injection rate (q_{cr}) and introducted an on-site limit injection test for penetration grouting. As shown in Fig. 6, the limit injection test consists of two stages: the first stage involves permeation, while the second stage includes both permeation

 © DFI International Bruges 2025

and fracturing. Fracture grouting occurs when the critical injection rate is exceeded, as confirmed by the q_{cr} test, which identifies the appropriate injection rate for the specific soil conditions. Injection rates below the critical velocity facilitate permeation grouting, whereas rates exceeding this threshold the grouting mode to fracturing. This results in a drop in pressure and an expanded improvement zone due to fracturing effects. The algorithm for calculating effective injection pressure based on empirical equations is as follows:

$$P = P_0 - P_r + \gamma_w h \quad [1]$$

where P is effective injection pressure (kgf/cm²), P_0 is pressure value measured by the flow meter during grouting (kgf/cm²), P_r is the pressure inside the pipe (kgf/cm²), h is height difference between the grouting depth and groundwater level (m), and γ_w is unit weight of water (MN/m³). Limit injection tests were conducted at route G09+488, as shown in Fig. 7. The optimal injection flow rates, determined from q_{cr} tests at various soil layer depths, indicate that the effective q_{cr} for the TAM and MS grouting methods in gravel and rock (SS/MS) layers ranges from 13 to 16 L/min. The q_{cr} values for the MS grouting are slightly higher than those for the TAM grouting.During grouting operations, the grout flow rate can be adjusted based on test results, with a reference standard of below 13 L/min for the optimal grout flow rate.

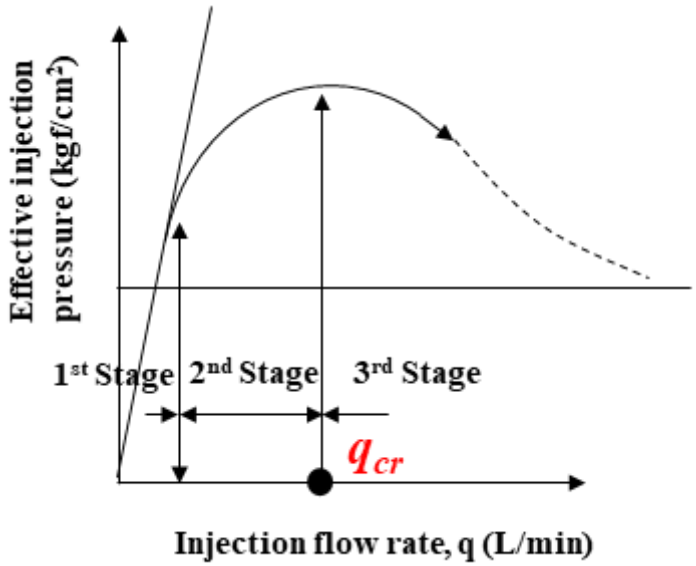


Fig. 6. P-Q curve of chemical grouting (after Mori et al. 1993)

Estimate radius of penetration grout of gravel

The propagation zone of chemical grouting in soil is influenced by various factors, including grout materials, grouting pressure, grout viscosity, gelation time, soil type, permeability coefficient, soil porosity, and drilled hole diameter. Magg's theoretical equation, based on Darcy's law, assumes homogeneous soils, a static state of grout injection, constant viscosity of grout, and spherical flow during grout penetration (Shimada 1972; 1974). Under these assumptions, the permeation theory is illustrated in Fig. 8, and the derived equation is as follows:

$$R = \sqrt[3]{\frac{3k \times H \times \gamma \times t}{n \times \mu}} \quad [2]$$

$$r = \sqrt{\frac{d \times Ch}{4}} \quad [3]$$

where R is the radius of penetration (cm), k is soil permeability (cm/s), n is soil porosity, $\mu = \mu_g/\mu_w$ is the relative viscosity of grout in centipoises (μ_g of MK grout = 3 cp, μ_w of water = 1 cp), H is the injection pressure head(cm), and r is radius of spherical injection source (cm). For a cylindrical injection source of length Ch, Ch = 33 cm for Tam grouting and Ch = 100 for MS grouting. The drill hole diameter is d =11 cm, and t represents the time (in sec) for the grout to penetrate to radius R.

 © DFI International Bruges 2025

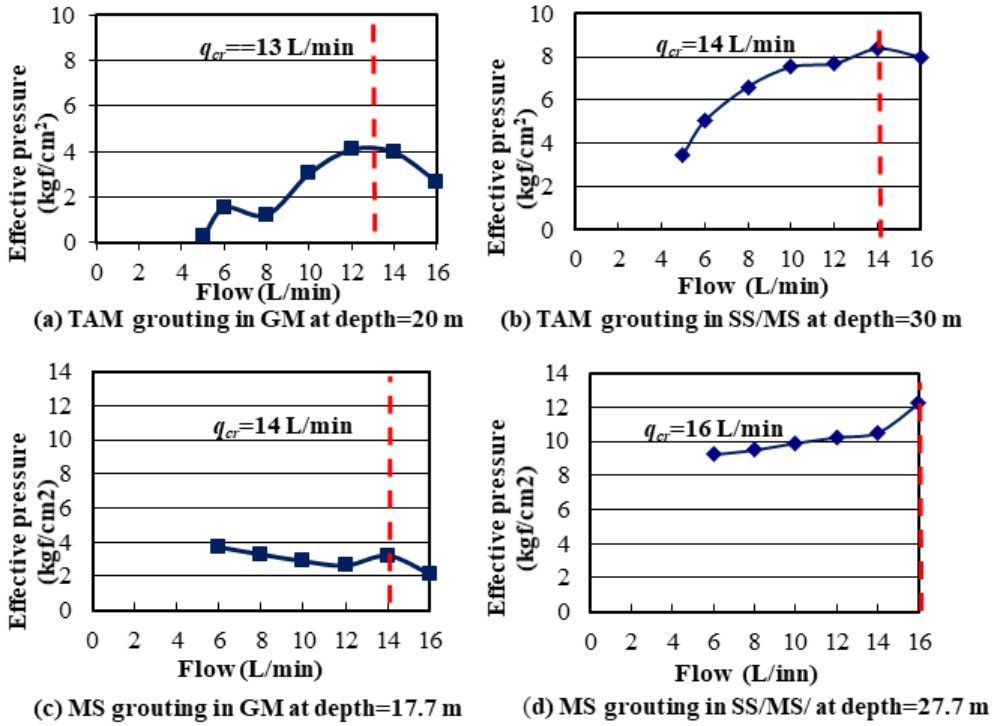


Fig. 7. Results of limit injection tests for TAM and MS grouting methods

As shown in Fig. 5, grouting data was used to calculate the grout penetration radius in the granular layer. According to the site investigated reported that the soil porosity (n) of the granular layer is 30%, and the permeability is k = 1.4 X10^{-1} cm/s. Based on the grouting parameters in Table 3, 33 TAM grouting holes and 5 MS grouting holes were selected for penetration radius calculations. For the granular layer treated with CB grouting, the estimated R-value for TAM grouting was 186 cm, while for MS grouting, it was approximately 253 cm. In the GM layer treated with MK grouting, the R-value was calculated to be 326 cm for TAM grouting and approximately 553 cm for MS grouting.

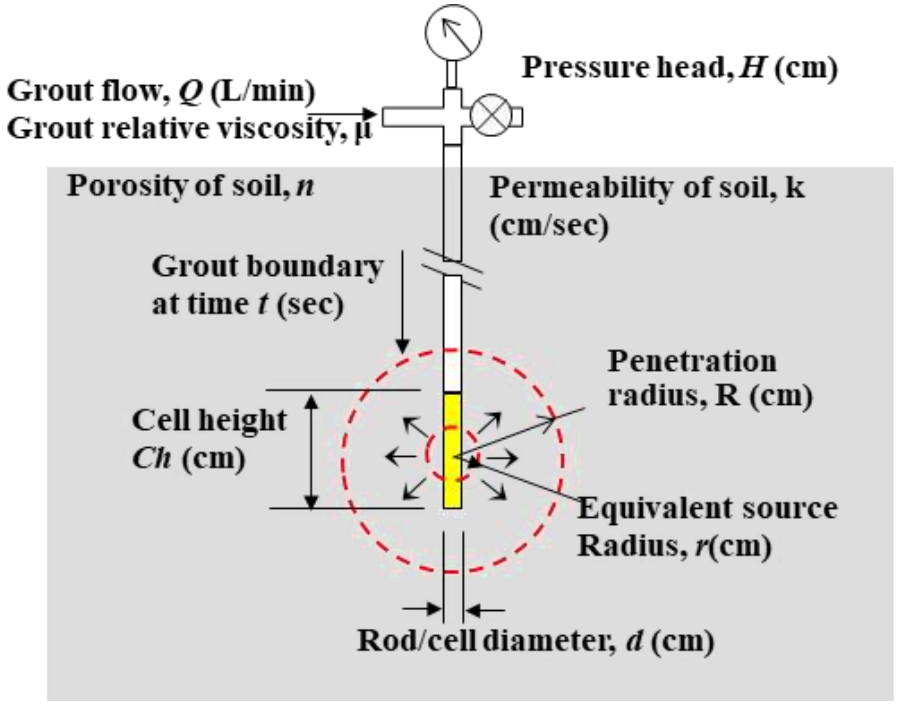


Fig. 8. Maag's penetration grouting theory (Shimada 1972; 1974)

 © DFI International Bruges 2025

Permeability and cutter head maintenance in grouted zone

Falling head permeability test is usually single-pipe. It can be used in verified partial improvement area. This study operates falling head permeability test by sigle hole in each grouted zone. A total of six tests were conducted at different location and depth, as shown in Fig. 5. The coefficients of permeability (k) measured after grouting using the falling head test ranged from $2.2X10^{-6}$ ~ $4.7X10^{-7}$ cm/s, meeting the designed requirement (< 1 $X10^{-5}$ cm/s) and significantly lower than the in-situ gravel layer's permeability (=1.4 $X10^{-1}$ cm/s) before grouting, as shown in Table 4.

The maintenance task for route G09+488 involved replacing the roller bits. As shown in Fig. 9a, a sleeve pipe was embedded in the gravel layer in front of the shield machine, indicating that the granular surface was moist and no groundwater leakage occurred. After inspecting the roller bit conditions, a total of 19 roller bits required replacement. Fig. 9b illustrates the application of sprayed concrete at the open face, while Figs. 9c and 9d show the replacement of the damaged roller bits inside the earth chamber. After completing the roller bit replacement and backfilling the earth chamber with grout, subsequent tunneling operations proceeded as planned.

Table 4 Permeability tests in grout zone after completion of grouting at G09 0k+448

Test hole	Depth of tests (m)	Ground water depth (m)	Permeability (k, sec/s)
T-1	10.7~11.7	4.20	$1.37X10^{-7}$
T-2	16.7~17.7	4.20	$4.73X10^{-8}$
T-3	8.3~9.3	4.20	$1.46X10^{-7}$
T-4	18.3~19.3	4.85	$5.26X10^{-6}$
T-5	12.3~13.3	4.85	$2.19X10^{-6}$
T-6	9.8~10.8	4.85	$4.22X10^{-6}$



Fig. 9. Route G09+448 ground improvement works and roller bits replacement: (a) sleeve pipe in grouted zone; (b) sprayed shotcrete; (c) damaged roller bit; and (d) replaced new roller bit

CONCLUSION

Thanks to TAM and MS grouting methods used for ground improvement, no groundwater leakage occurred during the roller bit replacement on the G09+488 shield machine route. After spraying concrete on the open face and replacing the damaged roller bits inside the earth chamber, the chamber was backfilled with grout, allowing subsequent tunneling to proceed without issues. The permeability coefficients (k) measured from the grouted zone using the falling head test ranged from $1X10^{-6}$ to $1X10^{-7}$ cm/s, fully meeting the design requirement (i.e., < $1X10^{-5}$ cm/s) and significantly lower than the in-situ granular soil permeability before grouting ($1.4X10^{-1}$ cm/s). Moreover, the MS grouting method has proven to be a cost-effective, high-productivity technique, particularly suitable for large borehole spacing and space-constrained construction sites. Based on the findings of this study, the following conclusions were drawn:

1. It allows grout to propagate over large distances about 3 m. By injecting grout from discrete injection points, a pre-defined zone can be uniformly stabilized.
2. The MS grouting method incorporates features of TAM grouting, enabling repeated injections of different grout materials at the same injection point, even after the initial grouting is completed.

 © DFI International Bruges 2025

REFERENCES

SANSHIN CORPORATION, 2022. TMRT green line contract G03, G08, G09 station ground improvement report (Ver. 0A), SANSHIN CORPORATION, Taipei, Taiwan. (In Chinese)

Mori, R., Tamura, M., Komine, H., and Ogawa, Y., 1993. Determination method of limiting injection rate considering penetration and solidification in chemical grouting. Journal of the Japanese Geotechnical Society, Vol. 33, No. 3, pp. 159-169. (In Japanese)

Shimada, S., 1972-1974. Chemical grouting methods for field engineers. Construction Journal, Vol. 10, No. 1 - Vol. 12, No. 10. (In Japanese)

 © DFI International Bruges 2025

SIMPLIFIED CIRCULARITY ASSESSMENT MODEL FOR SOIL MIXING APPLICATIONS

Brian J Freilich, PhD, PE, Keller, Houston, Texas, USA, bjfreilich@keller-na.com
Kimberly K Martin, PhD, PE, Keller, Ottawa, Ontario, Canada, kimberly.martin@keller-na.com

ABSTRACT

Soil mixing is a versatile ground improvement technique that involves blending soils in-situ with a designed cementitious slurry to create stabilized geometries for foundation, earth retention and groundwater control solutions. As a design-build solution, practitioners can adapt the soil mixing process to the unique project requirements and site-specific geologic conditions, allowing for cost-effective and sustainable alternatives to traditional deep foundations and earth retention systems. While soil mixing requires less material than traditional solutions, resulting in an overall less carbon intensive product, cement is still typically required as part of the mixing process. Therefore, with the increased focus on sustainability in the construction industry, soil mixing practitioners must continue to reduce (and even eliminate) cement usage to further reduce embodied carbon while still providing a cost-effective and quality product. The following paper provides an example of a circularity assessment model for soil mixing to exemplify several ways practitioners can make the mixing process more environmentally sustainable. Included are several innovative ideas that practitioners have used to reduce embodied carbon and improve participation in the circular economy. The objective is to illustrate a simple method to track the evolution and compilation of innovative ideas, lessons learned, and implemented processes that make soil mixing more efficient, cost-effective, and, most importantly, a more sustainable solution.

Keywords: Sustainability, Soil Mixing, Carbon Reduction, Embodied Carbon, Circular Economy

INTRODUCTION

As the geotechnical construction industry focuses on implementing environmentally sustainable processes and methods, practitioners are tasked to provide lower carbon solutions that still satisfy project criteria. Soil mixing provides a unique geotechnical solution in which purpose-built tools are used to blend cementitious binders into problematic soil profiles (creating soil-cement elements, or soilcrete), providing a cost-effective than can be a less carbon intensive solution as compared to other deep foundation and earth retention solutions. Our challenge as soil mixing practitioners is to continue innovating to provide a more environmentally sustainable solution. However, the mixing process requires diesel fuel and cement, both of which contribute to carbon emissions (cement production alone accounts for about 8% of the world's total carbon emissions, IAE 2017). In a study of five case histories, Lemaignan and Wilmotte (2014) reported that carbon emissions associated with fuel and cement usage accounted for about 93% of the total embodied carbon from soil mixing (Table 1). Thus, any effort to reduce fuel and cement consumption will yield the highest reduction in embodied carbon for soil mixing applications.

Table 1. Soil Mixing Carbon Emissions Contributions (Adapted from Lemaignan and Wilmotte 2014).

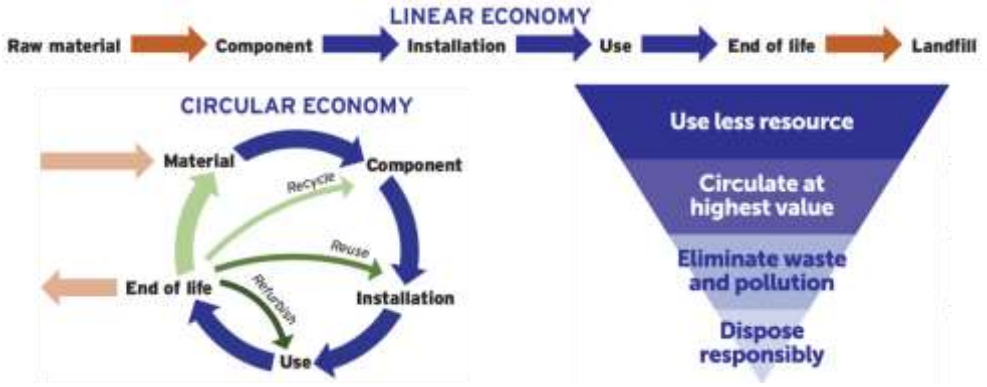
Scope	Source	Data type	Percent Contribution
1	Equipment fuel	Fuel quantity	16%
1	Freight	Distances and truck types	2.70%
1	Mob/demob	Distances and truck types	1.90%
2	Energy	Grid energy	0%
3	Materials	Quantity of materials	77%
3	Assets	Equipment weight, use, and lifetime	1.50%
3	People transportation	Commute distance and type	0.70%
3	Waste transport	Waste volume and truck type and dis	0.10%

While tools are available to help calculate the embodied carbon of various geotechnical solutions (the European Federation of Foundation Contractors (EFFC) and Deep Foundations Institute (DFI) developed a carbon calculator for the geotechnical industry), there is sparse guidance on how project

 © DFI International Bruges 2025

teams can use better planning and innovative ideas to reduce carbon emissions. Therefore, it is up to the soil mixing community to continue innovating to develop more efficient designs, build partnerships with new suppliers to use less carbon intensive materials, and manage our mixing processes to reduce carbon emissions and waste materials.

Navigating sustainable development can be an intimidating and oftentimes difficult process. Fortunately, there are models that can be used to guide practitioners in developing sustainable processes within their teams. In this paper a Circular Economy model (Fig. 1a, EFFC 2023) will be used to illustrate this collaborative process. The circular model is a closed-looped system that encourages partnerships throughout project development, construction, and lifecycle to develop sustainable processes founded on the Circular Economy Hierarchy (Fig. 1b, EFFC 2022). These circular models, whether prepared on a global scale or focused solely on a single process (as used in this paper), rely on each participant within the economy to find (and implement) ways to recycle existing infrastructure and supplies, improve processes to use less materials and energy, and to distribute resources efficiently. By moving from the standard linear economy and ultimately creating a circular system, soil mixing practitioners can reduce their impact on the environment.



(a) Linear and Circular Economy Models (EFFC 2023)

(b) The Circular Economy Hierarchy (EFFC 2022, adapted from IEMA 2022)

Fig. 1. Global Circular Economy and Circular Economy Hierarchy Models (From EFFC).

We start by developing a circularity assessment model focused on foundations and ground improvement (including soil mixing) that reflects the goals of the circular economy and hierarchy. This sector-specific model (Fig. 2) covers the building lifecycle from foundation materials and construction process (A1-A3 and A4-A5), skips the use stage and end of life (B1-B5, C1-C4), and closes with the circularity model (O1a-O1b). The areas considered in the circularity model, which are project phases that result in carbon emissions from foundation construction, are highlighted. Considering these circular economy models and lifecycle stages, the resulting circularity assessment model can illustrate the planning, engineering, and operational aspects of the project that allow for reduced costs, faster schedules, and (most importantly) a lower carbon and circular solution.

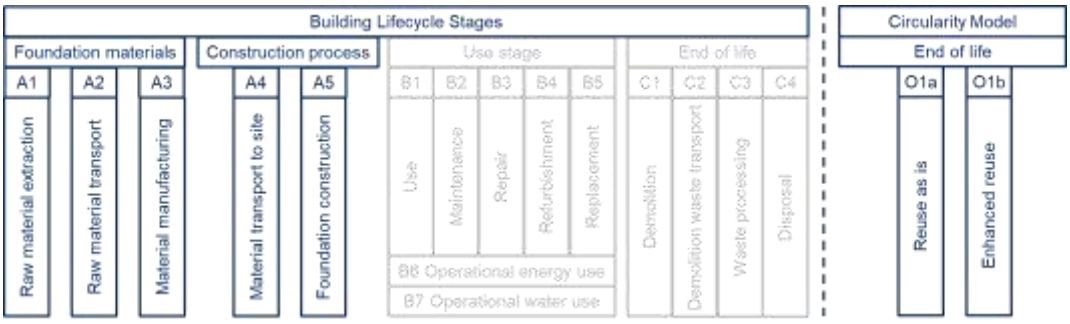


Fig. 2. The Building Lifecycle Stages Modified from BS EN 15804 (2019).

 © DFI International Bruges 2025

SIMPLIFIED CIRCULARITY ASSESSMENT MODEL FOR SOIL MIXING

As project teams focus on innovations to reduce carbon emissions and work within the circular economy, it becomes evident that sustainable development with the construction industry requires cooperation between many different parties. Thus, the simplified circularity assessment model includes the decision-makers for the project (owners, engineers, and regulators), the suppliers that provide the input materials, fuel, and equipment, the project managers that track the materials and fuels consumed, and onsite operations that perform the work and track excess materials produced during the process.

The simplified circularity assessment model for soil mixing is shown in Fig. 3, which is based on the "butterfly diagram" by the Ellen MacArthur Foundation (EMF) (www.ellenmacarthurfoundation.org) and the associated lifecycle stages depicted in Fig. 2. Each path (arrow) within the model represents the participation of the various project team members to implement innovative ideas at each project phase, including design, operations, and procurement. Implemented in this way the negative impacts, particularly with respect to carbon emissions, can be greatly reduced and supports the goal of reusing the ground improvement solution in the future.

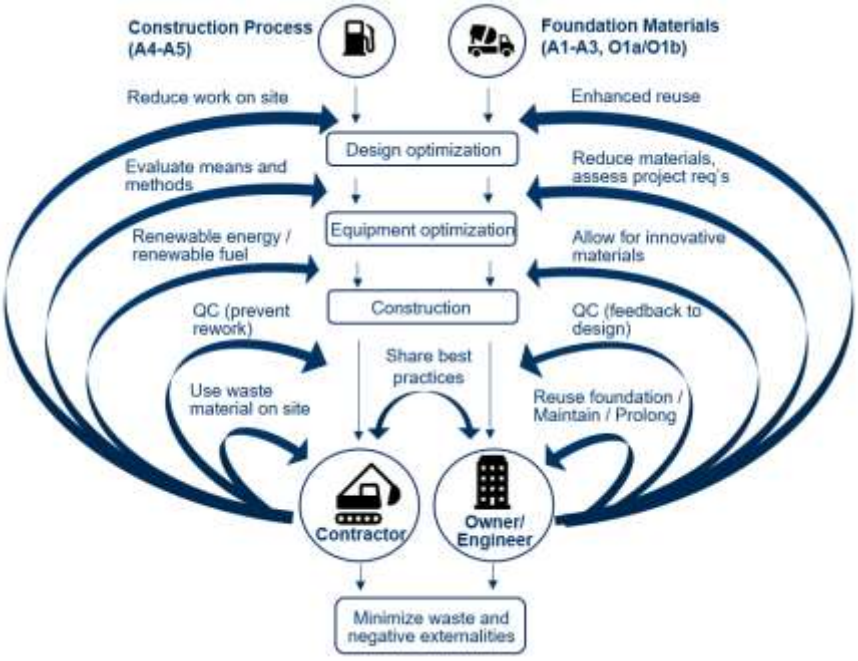


Fig. 3. The Simplified Circularity Assessment Model for Soil Mixing Applications.

The right flow of the model represents technical aspects of the project, such as developing project specifications, using innovative design to reduce project scope, working with suppliers to locate lower carbon alternatives, and finding means to use renewable energy. The left flow of the model represents the operational aspects of the projects, such as developing improved processes to reduce input materials and waste, optimizing equipment to reduce fuel consumption, and using renewable fuel alternatives. Both sides of the model include quality control (QC) processes to ensure the final soil mixing product meets design requirements, ensures rework is minimized or eliminated, and confirms that teams are using proper processes and materials to achieve design goals.

Suppliers, engineers, project and operational managers, regulators, and owners all play important roles in the circular system as they each have control and expertise in different areas. Considering each team member as a partner allows for challenges to be solved in a collaborative nature, resulting in the most cost effective and sustainable solution. The circular flow of the model also supports the three principles as outlined by the EMF: (1) eliminate waste and pollution, (2) circulate products and materials, and (3) regenerate nature.

 © DFI International Bruges 2025

There are many participants and factors that must be considered in sustainable development, which makes participation in the circularity model seem complex. However, practitioners continually implement innovative ideas throughout the project lifecycle to work with owners and suppliers to reduce embodied carbon and participate within the circular economy. Several of these examples are presented in the following sections to illustrate how innovations follow the circularity assessment model.

DESIGN OPTIMIZATION TO REDUCE PROJECT SCOPE

As a design-build solution, soil mixing practitioners are involved throughout the planning and construction process represented through several paths on the left and right sides of the circularity model. This collaboration allows practitioners to share their best practices to optimize the soil mixing scope, and work with suppliers to find alternative materials to provide the most efficient and environmentally sustainable solution. A case study presented in Selvaraju et al. (2023) highlighted how this collaboration was used to quickly identify simple innovations during Design Optimization phases that led to reduced scope and lower embodied carbon. During an evaluation of the project scope, in which deep soil mix columns were required to create a bottom seal for excavation support, the contractor suggested using a larger column diameter (switching from 1.8m to 2.2m) to increase production by 10% (*Reduce Work on Site / Evaluate Means and Methods paths in Fig. 3*). The contractor also worked with suppliers to locate a CEM III/A cement blend with 65% granulated ground blast furnace slag (slag) that would achieve the project requirements (*Allow for Innovative Materials path*). These simple changes resulted in a reduction of about 4,200 tonnes of embodied carbon (tCO_2e, Fig. 4), equivalent to the carbon savings of driving an average car around the equator 380 times (US EPA 2024). This collaborative effort shows the project team participating within the **Use Less Resource,** **Circulate at Highest Value**, and **Dispose Responsibly** phases of the circular hierarchy (Fig. 2b) with relative ease.

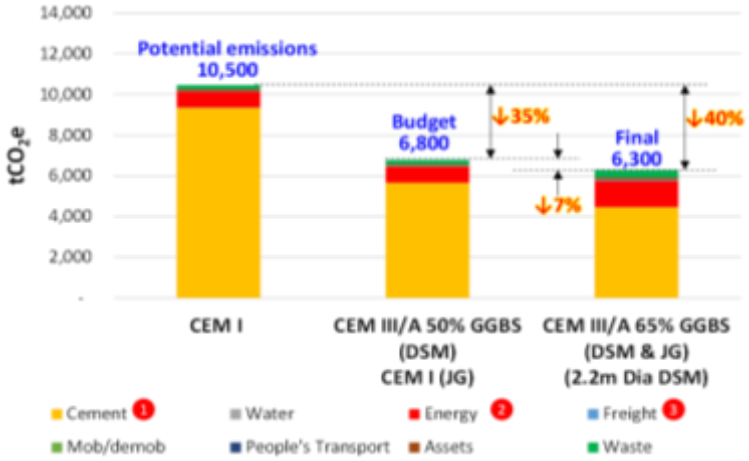


Fig. 4. Total Embodied Carbon Reduction Through Value Engineering and Alternative Materials (Selvaraju el at. 2023).

Another simple approach that can quickly reduce cement usage and carbon emissions is the application of soilcrete cure factors in the engineering analysis of the soil mix system (Bruce et al. 2013, Eq. 1). A common example is in seismic regions, engineers noted that soilcrete strength used in design (typically unconfined compressive strength, UCS_{28}) was tested at a 28-day cure time as verification during the project construction phase, yet the application of the peak load (an earthquake) could statistically happen years after construction. Boulanger and Shao (2021) discussed the use of empirical cure factors to relate the higher soilcrete strength requirements at the time of the seismic event (UCS_t at time t) to a lower 28-day soilcrete (UCS_{28}) measured during the project quality control program.

 © DFI International Bruges 2025

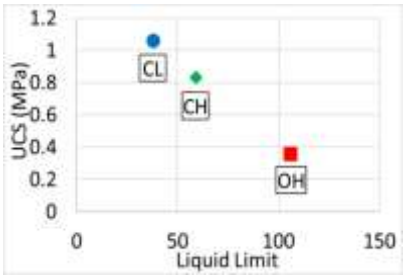
Soilcrete Strength Curing Factor, $f_C = 0.187 \cdot \ln(t) + 0.375$

Soilcrete Strength at Time "t" $= UCS_t = f_C \cdot UCS_{28}$ [Eqs. 1]

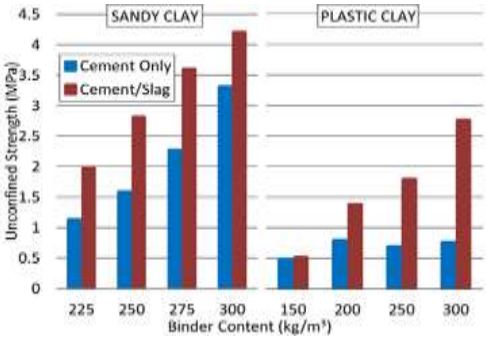
The use of long-term strengths has been validated through various case histories providing evidence of the continued increase in soilcrete strength with time after soil mixing activities (Kitazume et al. 2003, Takahashi et al. 2018). Even for static loading conditions, a long-term construction phase may push maximum loading conditions to months after soilcrete installation. On one project the use of a 90-day cure factor allowed the project team to reduce the cement usage (*Reduce Materials path*), resulting in a 10% reduction in cement usage for the project and a potential carbon reduction of over 1,900mt CO_2e.

ALTERNATIVE CEMENTITIOUS MATERIALS IN SOIL MIXING APPLICATIONS

Cement contributes the highest portion of embodied carbon in soil mixing applications, and thus project teams have been working with suppliers to identify alternative binders that can provide better quality soilcrete while reducing embodied carbon. During the Design and Equipment Optimization phases, practitioners can use laboratory (bench scale) testing to evaluate how different alternative binders react with the soils to achieve the most effective and environmentally sustainable mixing process (*Evaluate Means and Methods / Allow for Innovative Materials paths*). This initial phase of the quality control program is critical in optimizing the binders used in the soil mixing process, as illustrated by Freilich et al. (2022). Samples of different soil stratum were blended with the same grout slurry to show the reduction in soilcrete UCS with increasing soil plasticity (Fig. 5a). Working with suppliers, project teams have found innovative ways to incorporate slag as a replacement for cement in soil mixing applications and, by replacing a high percentage of cement with slag (up to 90 percent), achieve higher soilcrete strengths as compared to cement only grouts (Fig. 5b), even in highly plastic and organic clays.



(a) Impact of Clay Plasticity on Soilcrete Strength (Freilich et al. 2022).



(b) Soilcrete UCS for Samples Mixed with Ordinary Portland Cement and Slag/Cement Blends (Freilich et al. 2024).

Fig. 5. Soilcrete Strength Results from Laboratory (Bench) Scale Testing Programs.

Utilizing slag has allowed soil mixing practitioners to use less grout (due to higher strengths) and, because these materials are considered waste, provide a significant reduction in embodied carbon and close the reuse materials loop for our suppliers (**Circulate at Highest Value** and **Dispose Responsibly** in the hierarchy). The performance and sustainability benefits of using low carbon alternative binders has motivated practitioners to work with suppliers to quicky bring these new materials into soil mixing work. For a project in the Northeast United States, the project team used laboratory testing to evaluate slag/cement and ground glass pozzolan/cement blends for a large soil mixing project. The use of blended grouts results in a 42% to 54% reduction in embodied carbon (Fig. 6). Both options provide viable opportunities to reduce the project embodied carbon simply by supplementing the cement used in the grout slurry with a waste material.

LOWERING CARBON EMISSIONS THROUGH ONSITE PROCESS OPTIMIZATION

Once onsite the contractor can include non-production test elements (*Evaluate Means and Methods and QC paths*) to verify the grout design evaluated in the laboratory, and set the mixing parameters

 © DFI International Bruges 2025

for production. Oftentimes our best quality control tool during this process (and thus the best way to reduce embodied carbon) is our ability to observe the mixing process and resulting soilcrete material. For highly plastic clays encountered in Texas (liquid limits ranging between 80 to 110), contractors found that increasing the water/cement ratio of the grout slurry provided a more fluid and easily mixable soil-cement element (Fig 7a). Increasing the added water during the mixing process resulted in a less viscous soilcrete material and increased production up to 40%. This quick change resulted in a potential fuel savings of over 82,000 liters of diesel and avoided up to 280 tCO_2e of carbon emissions. This is equivalent to the amount of carbon sequestered by 4,600 tree seedlings grown for ten years.

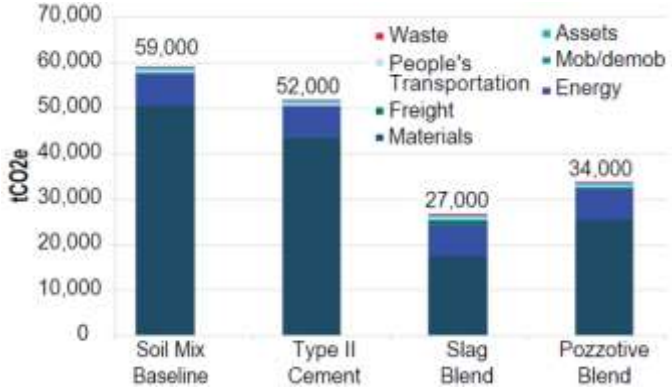
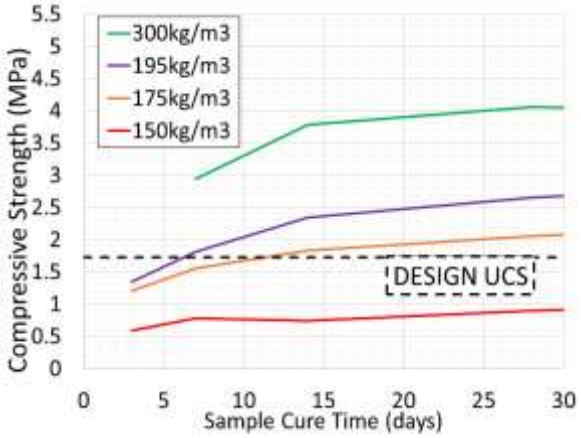


Fig. 6. Total Embodied Carbon of Different Grout Slurry Blends for a Deep (Wet) Soil Mixing Project.

(i) Low W/C Grout (ii) High W/C Grout



(a) Excess Soilcrete Materials Observed During Test Column Installation.



(b) Soilcrete Strength Results from Test Columns Installed at Various Binder Contents.

Fig. 7. Example Quality Control Results from Deep (Wet) Soil Mixing Test Columns, (a) Visual Observations from Excess Materials and (b) Unconfined Strength Results for Various Binder Contents.

Test columns also allow contractors the opportunity to trial different binder dosages and water/binder ratios to further adjust the cement usage for the project. This final adjustment to the grout design has allowed project teams to reduce cement consumption in the range of 20 to 40%. Practitioners in California tested various grout slurry designs in a sandy clay profile (Fig 7b) and found that with continued refinement to the grout design they could reduce cement usage by up to 30%, with a potential cement reduction of 950 mt and a carbon reduction of 800 tCO_2e.

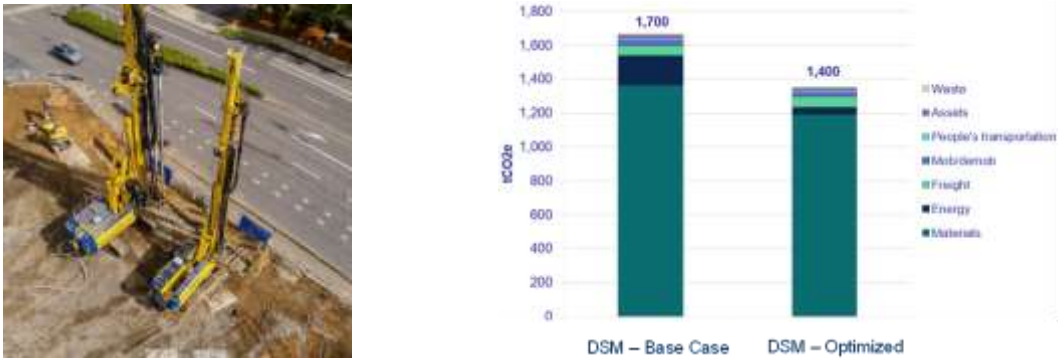
IMPLEMENTING RENEWABLE FUELS INTO PRODUCTION

Working with suppliers to replace petrochemical diesel, which accounts for about 16% of the embodied carbon from soil mixing, with renewable diesel reduces life cycle carbon and nitrogen

 © DFI International Bruges 2025

oxide emissions without having to modify site operations (*Renewable Energy path*) (US DOE 2024). Verifying that the renewable diesel feedstock is waste products is key to realizing all the benefits from renewable diesel as a transition fuel before other zero-emission fuels come online in the future.

On a quad-axis soil mixing project in North America (Fig. 8), the project team worked with local suppliers to implement two optimizations to reduce the carbon footprint. The first was to modify the grout design to include Type IL cement (*Allow for Innovative Materials path*), resulting in a 171 tCO_2e reduction as compared to straight Portland Cement. Secondly, the operation managers were able to source renewable diesel for the onsite equipment. After discussions with the fuel refiner (Neste) the project team was able to use renewable diesel that had 75% lower lifecycle carbon emissions than petrochemical diesel, saving an additional 132 tCO_2e for the project. The switch to renewable diesel required no changes to the fueling process or site operations, making it an easy way to cut emissions and participate in the circular economy for fuel.



(a) Quad Axis Project Site Photo (b) Carbon Calculation Results

Fig. 8. Quad-Axis Deep (Wet) Soil Mixing Case History (Photo Courtesy of Keller).

PROCESS ADJUSTMENTS TO REDUCE WASTE

Soil mixing is a volumetric process, adding water and binders during the installation process results in excess soilcrete at the surface (in some areas considered a hazardous waste) that requires significant effort and costs to dispose. Rather than dealing with this costly disposal process, contractors found that including predrilled cavities in the soil mixing process (Fig. 9) not only reduced the mixing length (and amount of cement required), but it also reduced (or eliminated) excess materials during the mixing process (*Reduce Work On Site / Evaluate Means and Methods / Reduce Materials paths*). Balancing the mixing length and expected soilcrete volume has allowed operations teams to eliminate 10% to 30% of the cement consumption while still creating the required element geometry (in line with the **Use Less** and **Eliminate Waste** in the hierarchy).



(a) (b)

Fig. 9. Pre-Drilled Cavities Used for Excess Soilcrete Handling on a (a) Triple Axis Soil Mixing Project and a (b) Cutter Soil Mixing Project (Photos Courtesy of Keller).

 © DFI International Bruges 2025

SOIL MIXING APPLICATIONS TO REUSE EXISTING STRUCTURES

Thus far we have focused on how project teams work within the circularity model to develop the most efficient soilcrete solutions while reducing carbon emissions. However, owners and engineers working through the technical aspects of the project (the right side of the model) can also utilize soil mixing as a tool to rehabilitate and reuse existing infrastructure to extend their service life and eliminate the need for carbon intensive new construction (following the *Enhance Reuse path* and **Circulate at Highest Value** in the circular hierarchy). Several recent examples of using soil mixing applications to rehabilitate or improve existing structures are provided in Fig. 10.

Although the exact carbon savings from reusing the existing infrastructure are unknown, soil-mixing solutions can play a crucial role in increasing circularity in the foundation industry, and thereby reducing overall impact on the environment.



(a) Dry Column Soil Mixing for Shear Panel Stabilization of Existing Levee.



(b) Deep (Wet) Soil Mixing Columns and Panels for Bulkhead Stabilization and Slab Remediation.



(c) Deep (wet) Soil Mixing Columns for New Equipment Foundations Within Existing Warehouse.



(d) Mass Soil Mixing for Additional Slab Bearing Support Within Existing Warehouse.

Fig. 10. Soil Mixing Applications to Rehabilitate Existing Structures for Continued Use (Photos Courtesy of Keller).

 © DFI International Bruges 2025

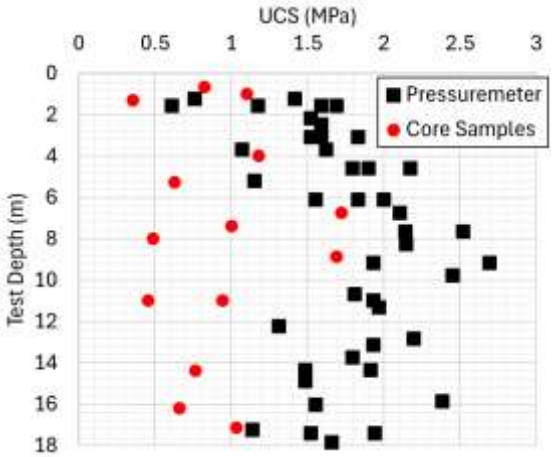
CONSIDERATIONS FOR THE REUSE OF SOIL MIXING ELEMENTS

As existing structures are demolished and sites prepared for new construction, owners and contractors need to consider how to reuse the existing soilcrete elements left over from previous site development (*Reuse Foundations path*). This provides a cost benefit to the owners, reduces embodied carbon for the project, and most importantly follows the **Circulate at Highest Value** of the circular hierarchy. If available, project teams can rely on previous (and new) geotechnical information and design submittals to evaluate the capacity of existing soil mixed systems, and review past performance to confirm the adequacy of the system. However, existing details can be difficult to obtain and, in some cases, may not contain installation deviations from original drawings. Therefore, the soil mixing reuse cycle will ultimately require that contractors rely on QC methods to verify the condition of the soilcrete.

While load testing of soil mixed elements is an option to test both the geotechnical and structural capacity, this can be difficult and expensive for larger diameter elements, or for grids/wall panels. Thus, traditional mechanical coring could be used to collect samples from soilcrete elements for compression testing (to verify soilcrete strength) and allow direct access to soils below the element for additional soils testing to estimate geotechnical capacity (such as cone penetrometer testing). The open hole also provides an avenue to utilize downhole cameras to provide a full depth visual inspection of the element for better verification of the soilcrete condition (Fig 11a).



(a) Downhole Camera for Visual Observation of Installed Soilcrete Elements (Photo Courtesy of Keller).



(b) Shear Strength Values from Pressuremeter Test Results for Soil Mix Columns.

Fig. 11. In-Situ Verification Options for Soilcrete Elements.

Open core holes can also be used for additional in-situ testing to verify structural capacity of the soilcrete. Electronic pressuremeter testing (PMT) is an option for verification of the soilcrete strength (Fig 11b) that is widely available within the geotechnical community. The instrument is lowered into the open borehole and tests performed at various depths to correlate with existing soilcrete strength data (such as the previous wet grab and core sample strengths). The PMT results are a quick verification of the soilcrete consistency that can be used to verify that the elements can be reused.

Project teams can also use geophysical methods to assess the quality of existing elements. Geophysical testing requires a highly specialized skillset as results can be misinterpreted if an expert is not used. This method is least likely to help in achieving a full reuse of the existing elements but may be beneficial in supplementing other testing/verification methods.

A proposed flowchart is provided in Fig. 12 illustrating how project teams can evaluate existing soilcrete systems for reuse. Based on this proposed flowchart, one of the most important contributions owners, engineers, and construction teams can do to enhance circularity in the future is keep meticulous records and anticipate the need for access to some elements by future users.

 © DFI International Bruges 2025

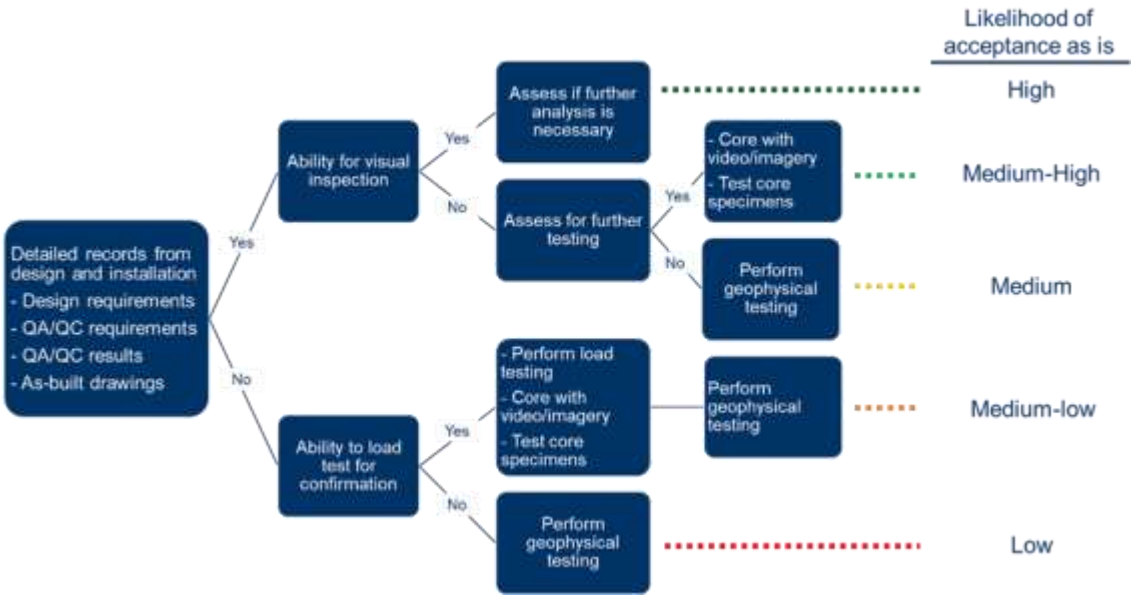


Fig. 12. Proposed Flowchart for Predicting Likelihood of Soilcrete Acceptance for Reuse.

CONCLUSIONS

Soil mixing has become a robust geotechnical solution utilized around the world to solve challenging geotechnical problems at lower costs and with reduced embodied carbon. However, as communities require continued carbon reduction efforts and move towards a circular economy, soil mixing practitioners need to better understand their project lifecycle to more effectively participate in the circular economy. For this purpose, a simplified circularity assessment model was presented illustrating the various ways soil mixing can provide lower carbon solutions and participate within the global circular economy.

Developing the model itself is an important step in the sustainable development of soil mixing applications. However, it also assists practitioners in identifying the numerous examples of how soil mixing is continually being improved to reduce embodied carbon through value engineering, implementing low carbon alternative binders, and using quality control programs to manage cement usage. The examples presented herein highlighted how teams are already participating in the circularity model through implementing better processes and collaborative optimization. As project teams further refine the mixing processes and implement new low carbon materials, the circularity model can be modified to reflect how soil mixing applications can continue to fit within the global circular economy. Practitioners should anticipate the needs of future projects to reusing soil mix solutions, which allows for eventually closing the lifecycle loop.

ACKNOWLEDGEMENTS

The authors would like to thank Daniel Alford, Claude Berard, Dennis Boehm, Gabriel Guzman, Ryan Thamm, Dustin Walkenhorst, Konstantinos Tzavaras, and Brian Wilson for providing the valuable case history data and photos shared in this paper.

REFERENCES

Boulanger, R.W., and Shao, L. (2021) Liquefaction Mitigation with Deep Mixing. Proceedings of Deep Mixing 2021 – Best Practice and Legacy. DFI. Online Conference, pp. 1146-1202.

Bruce, M., Berg, R., Collin, J., Filz, G., Terashi, M., and Yang, D. (2013) Deep Mixing for Embankment and Foundation Support. Federal Highway Administration Report No. FHWA-HRT-13-046.

 © DFI International Bruges 2025

British Standard Document BS EN 15804:2012+A2:2019. (2019) Sustainability of construction works. Environmental product declarations. Core rules for the product category of construction products.

European Federation of Foundation Contractors. (EFFC) Sustainability Guides for Foundation Contractors, 2022. Guide No. 1, Carbon Reduction, First Edition 2022.

European Federation of Foundation Contractors. (EFFC) Sustainability Guides for Foundation Contractors, 2023. Guide No. 2, Circular Economy, First Edition 2023.

Freilich, B., Boehm, D., and Rogers, C. (2022) Laboratory and Field Verification of Soil-Cement Strength from Deep Mixing in Highly Plastic Cohesive Soils. Proceedings of the 6th International Conference on Grouting and Deep Mixing. DFI. New Orleans, LA, USA.

Freilich, B., Martin, K., and Boehm, D. (2024) Sustainability in Practice: A Brief History of Innovation in Deep Soil Mixing. Proceedings of Deep Mixing 2024. Yokohama, Japan.

International Energy Agency (IEA). (2017) Energy Technology Perspectives 2017; Müller, N. and Harnisch, J. (2008) A Blueprint for a Climate Friendly Cement Industry. WWF International. http://awsassets.panda.org/downloads/englishsummary__lr_pdf.pdf.

Institute of Environmental Management and Assessment (IEMA). (2020) Pathways to net zero: Using the IEMA GHG Management Hierarchy, https://www.iema. net/resources/reading-room/2020/11/26/pathways-to-net-zero-using-the-iema-ghg-management-hierarchy-november-2020

Kitazume, M., Nakamura, T., Terashi, M., and Ohishi, K. (2003) Laboratory tests on long-term strength of cement treated soil. Proceedings of the 3rd International Conference on Grouting and Ground Treatment. ASCE, Reston, VA, USA, vol. 1, pp. 586–597.

Lemaignan, B. and Wilmotte, J. (2014). EFFC DFI Carbon Calculator Methodological & User Guide, https://www.effc.org/content/uploads/2020/10/EFFC-DFI-methodological-and-user-guide-v2.2.pdf.

Selvaraju, S., Tang, C., and Raj, D. (2023) Effective Ways to Reduce Carbon Footprint in a Deep Soil Mixing Solution, Proceedings of the 2nd Annual Conference on Foundation Decarbonization and Re-Use. KIVI and DFI. Amsterdam, Netherlands.

Takahashi, H., Morikawa, Y., Fujii, N., and Kitazume, M. (2018) Thirty-seven-year investigation of quicklime-treated soil produced by deep mixing method. Proceedings of the Institution of Civil Engineers – Ground Improvement. 171(3).

US DOE. (2024) Alternative Fuels Data Center – Renewable Diesel. Alternative Fuels Data Center: Renewable Diesel

US EPA. (2024) Greenhouse Gas Equivalencies Calculator. Greenhouse Gas Equivalencies Calculator | US EPA

 © DFI International Bruges 2025

PILE GROUP SETTLEMENT ANALYSIS FOR WEAK ROCK FOUNDATION SOCKETS DESIGNED USING A MODIFIED CORELATION FACTOR

Sujatha Manoj, Beca, Sydney, NSW, Australia, +61 456 814 829, sujatha.manoj@beca.com
Harry G Poulos, Tetra Tech Coffey, Sydney, NSW, Australia, harry.poulos@tetratech.com

ABSTRACT

Deep foundations in weak rock have traditionally been designed as friction elements, and most of the published correlations estimate the frictional capacity using shaft frictional resistance (f_s) calculated from the unconfined compressive strength (UCS) of rock. Heavily loaded foundations in weak carbonate rocks have historically been designed using conservative correlations, and settlements are often overpredicted when conservative deformation parameters are used, even with advanced numerical modelling techniques. This paper presents a review of a revised correlation factor to estimate f_s from UCS of the weak carbonate rocks, developed by back-analysis of a 44-test dataset of high-capacity foundations with test loads in the range of 100 to 320MN, and presents a case study where settlement calculations using 3D finite element modelling are compared against the load test results to check whether serviceability limits are met when the revised correlation coefficient is used to design the foundations. The case study uses the revised correlation and ground stiffness parameters based on the small-strain modulus from geophysics (E_d), resulting in an overall saving of about 30 to 35% of concrete volume, and thus resulting in a reduction of foundation cost and a reduction of the carbon footprint and its potential effects on climate change.

Keywords: Bearing capacity, friction, piles, carbon footprint

INTRODUCTION

Deep foundations such as barrettes and large diameter piles are common types of foundations for structures including tall and super tall buildings where heavy loads are required to be carried through sockets in weak. Rapid urbanization in recent decades has resulted in a surge in construction of such tall buildings and heavy structures, and the geotechnical design of deep foundations to carry several tens of mega newtons of load has become a major challenge. The traditional methods of design have been developed for relatively short piles carrying much smaller loads, and applying those methods to heavily loaded deep foundations can often result in very conservative designs. With the increasing demand to use sustainable and only moderately conservative design practices, geotechnical engineers are more inclined to use state of the art design methods to arrive at safe and sustainable designs. With advanced testing methods such us the bi-directional load cell tests and the availability of testing information from such load tests, and also with the availability of advanced numerical modelling tools, it is now possible to optimize these traditional methods.

Foundations for tall towers in the Middle East region are typically designed as frictional elements deriving strength from sockets in weak rock, with “weak rock” being defined by a lower bound UCS of 0.6MPa (CIRIA 181) and an upper bound UCS of 3 MPa. The pile capacity is estimated from shaft frictional resistance (f_s) calculated from the unconfined compressive strength (UCS) of rock. and the design depth derived using the typical correlations commonly used in the region (Table 1) varies significantly. Most of these correlations are developed based on load test results conducted on relatively short piles with low load capacity, and several of these tests are conducted in different geological conditions not necessarily similar to the weak carbonate rocks. These methods, when used to estimate ultimate friction (f_s) for high-capacity deep foundations in the weak carbonate rocks for heavily loaded large diameter piles and barrettes, can result in a large variation in design depths. The typical design methods adopted in the Middle East region, especially for deep foundations of tall and supertall towers, tend to be rather conservative, mainly due to a lack of previous similar cases of such deep rock socket designs in the region. (Manoj et al. 2020, Latapie et al. 2018, Alrifai 2007, Ibrahim et al. 2009). With the availability of load test results from these initial designs, it has been subsequently possible to revise, and develop more efficient design correlations.

Manoj et al (2023) presented the results of a study based on 44 high- capacity load tests on barrettes and piles supporting tall towers in weak rock, with UCS in the range of 1.25-3 MPa. A new correlation factor was recommended for use to estimate rock socket friction from UCS in weak carbonate rock formations, and a design chart was proposed on this basis. The 2023 paper however did not include the checks for serviceability limits when the revised correlation is used to design pile groups. The design checks for

 © DFI International Bruges 2025

serviceability limits in terms of settlements when the revised correlation is used for estimating pile and barrette length, are presented in this paper. The deformation modulus derived from geophysical tests, E_d has been used in the finite element model to estimate pile group settlements.

DESIGN OF ROCK SOCKETS – TRADITIONAL METHODS

Rock socketed piles transfer applied load to the bearing ground by shear, end bearing or by a combination of both. The initial transfer of shaft load through shear stresses on the interface may be described as an elastic process, and for rock socketed piles the roughness will also play a major part in the shear load transfer. When the rock sockets are relatively small, end bearing may also contribute to pile capacity, however, the foundations discussed in this paper consist of deep rock sockets, and are generally designed as friction elements, ignoring any contribution from end bearing. For deep foundations in weak rock or Intermediate Geo material (IGM), general design guidance is provided in CIRIA 181 (Gannon et al. 1999), FHWA (2010) and EN 1997-1. The methods previously in practice for calculating shaft shear strength and end bearing strength of piles and barrettes in weak rock in the United Arab Emirates are presented Table 1, which also presents the conditions for which these equations are developed. Most of these use a correlation factor applied to the square root of the UCS, which varies from 0.15 to 0.8, and the upper and lower bound relationships vary almost 4 times.

Table 1 : Correlations of UCS to skin friction based on various equations in published literature

Author	Year	Skin Friction (f_s) correlation based on UCS	Condition for which the correlation is developed
Charif, et al.	2010	$0.18(UCS)^{0.5}$	Carbonate rocks in the Middle East region
Carter and Kulhawy	1987	0.15(UCS)	
Horvath et al.	1983	$(0.20 \text{ to } 0.30)(UCS)^{0.5}$	Interpreted from load tests in Shale/Mudstone. Factor of 0.2 to 0.3 for smooth to rough socket
Horvath and Kenney	1979	$(0.20 \text{ to } 0.25)(UCS)^{0.5}$	Shale and Mudstone Factor of 0.2 to 0.25 for smooth to rough socket
Meigh and Wolski	1979	$0.22(UCS)^{0.6}$	
Manoj et al	2023	$0.52(UCS)^{0.5}$	Develop for weak rock sockets using 44 load test results (up to 370MN) for high-capacity piles and barrettes
O'Neill and Reese	1999	$\alpha\phi(UCS)$	Intermediate Geo Material
Reese and O'Neill	1988	$00.15 \text{ to } 0.2(UCS)^{0.5}$	
Rowe and Armitage	1987	$00.45(UCS)^{0.5}$	Regular surface Interpreted from load tests
Rowe and Armitage	1987	$0.60(UCS)^{0.5}$	Rough Surface Interpreted from load tests
Rosenberg and Journeaux	1976	$0.375(UCS)^{0.515}$	Interpreted from load tests for weathered and soft rocks
Williams and Pells	1981	$\alpha\beta*(UCS)$	Sandstone, Shale and Mudstone
Zhang and Einstein	1998	$0.40 \text{ to } 0.8 (UCS)^{0.5}$	Smooth to Rough interface. Based on load test results from various locations take from literature

These correlations are not validated with site specific data in several cases. Since rock characteristics play an important role in development of such correlations, it is desirable to develop and validate these equations depending on regional geology. Kullhawy et al. (1993) also highlighted the relative lack of sophistication in these methods and commented that the UCS values used in developing these correlations were not average values along the test depths and may not be representative of actual conditions around the test location. Developing site specific correlations of UCS with shear wave velocity (Poulos 2021) and point load test results, can help in arriving at a more representative and reliable UCS profile to be used in the design. A

 © DFI International Bruges 2025

brief overview of the tall tower foundations in the middle east region based on a literature survey, is presented in Table 2.

Table 2 Foundations of tall towers in Dubai – an overview

Building name	Structure details	Foundation details	Depth of foundation	Design details
Burj Khalifa, Dubai Poulos and Bunce (2008); Poulos (2009)	160 story 828m	3.7m thick raft, 1.5m dia. piles	50m deep	Design by Horvath and Kenney (1979); Maximum load 35 MN; 61 to 85mm predicted settlement; 45 mm measured; design using $fs=0.25(q_u)^{0.5}$
Entisar Tower Pereira et.al. 2017		1.5x2.8 barrettes	57-68m	55 to 58MN load, design using $fs=0.2(q_u)^{0.5}$
Nakheel Tower, Dubai Haberfield et al. (2008)	›1300m tall	Barrette 1.5x2.8m &1.2x2.8m; 2.5m to 4m/6 to 8m thk raft	55 to 79m	Settlement predictions of 75 to 85mm; Osterberg Cell Testing of the Barrettes to 327 MN.
The Emirates Towers Poulos and Davids (2005)	355m	1.20m dia. piles raft thickness 1.50m	40 to 45m	18 load combinations; E modulus from Seismic data; End Bearing and Friction and Support from raft considered; load tested to 30MN; ultimate load capacity 23MN; Actual settlements only 25% of predicted, after 12 months of construction. design using $fs=0.2(q_u)^{0.5}$
La Maison Manoj et al. (2020)	380m	Barrettes 1.5 x 2.5m and 3 m raft	Initial 48m revised to 42m	Initial Design by Horvath and Kenney (1979); Maximum load 53 MN. Load test to 163 MN., design revised using $fs=0.4(q_u)^{0.5}$

Most of these tower designs in the early years were performed adopting the equation recommended by Horvath et al.1983. The conservatism in design of these towers is understood as there was previously no similar heavily loaded foundation designs or load test data available for the region. However, with the availability of load test results on heavily loaded foundations, especially with the bi-directional load cell test methods which made such high load tests possible, and also with the advanced numerical modelling techniques, it is now possible to modify these correlations to develop geology-specific and more reasonable and efficient designs, as discussed in the following section.

MODIFIED CORRELATION FACTOR FOR WEAK ROCK SOCKETS

Manoj et al. (2023) presented a modified correlation factor between ultimate skin friction and the unconfined compression strength of rock for the design of socket in weak rocks, using load cell test results of 44 load tests conducted on barrettes and large diameter piles, collected from 18 locations in Dubai in the UAE. The barrettes in the data set were 2.8mx0.8m to 2.8x2m in size and the piles were 0.75m to 2m in diameter. It is also noteworthy that the data set used in this study is one of the largest data sets used in any such study for weak rocks, with highest test loads in the range of 100 to 320MN and the depth of foundations mostly in the range of 20m to 87m below ground level.

 © DFI International Bruges 2025

Results from bi-directional load cell tests of large diameter piles and barrettes, along with the UCS profiles within the test zone, have been used in this study to analyse the test results, and back-analyse and calibrate the data, and arrive at appropriate correlation between skin friction in rock and UCS test results in the region. It is noteworthy that in most of these load tests, the loading did not reach close to the geotechnical failure, even close to the load cells. The actual friction measured closest to the load cell locations are considered conservatively as ultimate values, while developing these correlations. The rock sockets are supported by the rock mass and not the intact rock, and therefore using the frictional resistances measured from a bi-directional static load test is considered to take into account the effect of discontinuities in the rock and its stress state. Fig. 1 presents the correlation between UCS values and corresponding mobilized skin friction.

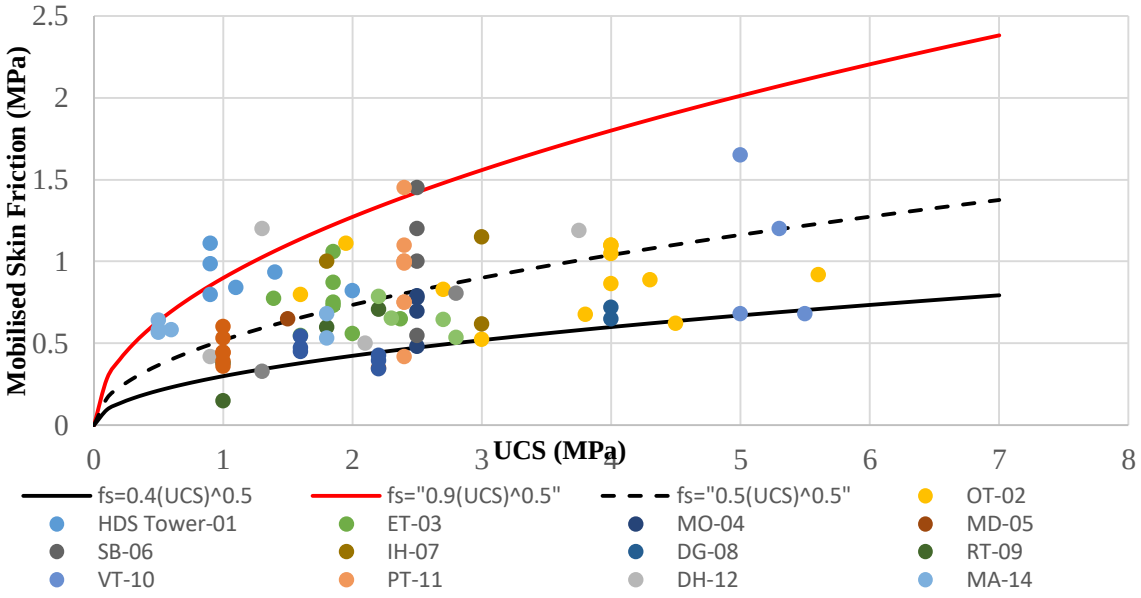


Fig. 1 UCS to Ultimate skin friction for Barrettes and Piles (Manoj et al. 2023)

The graph is plotted for all the 44 load test results incorporating pile load test results as well as barrettes. A regression analysis was done to establish the best fitting relationship between UCS of the rock and f_s, which shows a coefficient of 0.52 between mobilised friction and square root of UCS as the best fit with a minimal residual standard error 0.2924 and multiple R-squared of 0.8791, which means 87.91% variation in mobilized skin friction can be explained by this regression. Based on the results of this study, the following equation has been recommended to calculate ultimate skin friction for barrettes and large diameter piles in weak carbonate rocks with UCS values in the range of 1 to 3 MPa.

$$\text{Ultimate skin friction } f_s = 0.52(UCS)^{0.5} \qquad [1]$$

The paper also recommends that preliminary load tests should be conducted by bi-directional load tests to validate the capacity when the above equation is used in design. When preliminary load tests are not proposed, the paper recommends using a lower bound factor of 0.4 instead of 0.52, in equation 1. The next section of this paper presents the revised design of the La Maison tower (Manoj et al. 2020) using this modified correlation, and presents design checks for serviceability limits.

FOUNDATION DESIGN OF LA MAISON USING THE REVISED CORRELATION

In order to check whether the revised design using equation 1 satisfies the serviceability limits, the La Maison tower design (Manoj et.al 2020) is revised by re-calculating the barrette length using the new correlation factor of 0.52 as presented in equation 1.

The original design barrette length of 48m, calculated using a factor of 0.3 and for design load of 54MN, is revised to 35m for the same design load, using the factor 0.52 as in equation 1. A typical subsurface profile at the La Maison tower site in Business Bay, Dubai, used for the design, is presented in Fig 2.

 © DFI International Bruges 2025

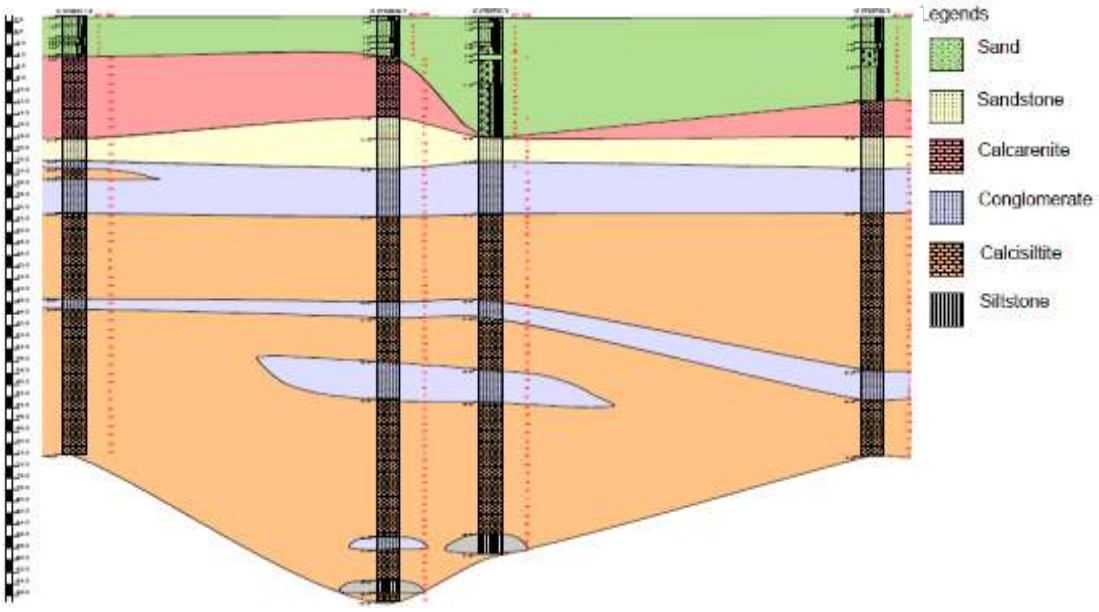


Fig 2 Typical subsurface profile at La Maison tower site

Design parameters and use of small-strain stiffness modulus from geophysics tests

The ground model under the tower was selected based on the boreholes and geophysics data within the tower footprint area, as presented in Figure 2. Geotechnical design parameters representative of the site conditions have been estimated based on data obtained from drilled boreholes and through in-situ testing, laboratory testing and other established correlations. The foundation design of tall structures also must consider vertical displacements under serviceability limit state conditions, for the given critical load combinations. Differential settlements, both within the tower core area, and between tower core and podium areas, must be within allowable limits. Pile and barrette group analysis methods, and methods for the prediction of settlements, also vary widely, and the deformation modulus values used for design require careful consideration. It is important to use ground stiffness parameters at appropriate strain levels, to predict settlements realistically. Several previous case studies presented load test results (for example Russo et al, 2013) have indicated that the measured settlements were less than the predicted values. Alzaylaie (2018), in his PhD thesis, back-calculated the elastic modulus from Osterberg cell testing for sedimentary rocks in the Dubai region, and concluded that the stiffness parameters used in design based on pressuremeter and laboratory tests result in conservative settlement predictions and so need to be revised.

Manoj et al. (2020) demonstrated, using load test data from the La Maison Tower, that the ground stiffness back-analysed from load tests was 2.5 to 15 times higher than that from typical laboratory tests. It was also demonstrated by back-analysis of load test results that the use of 0.2 times the small-strain stiffness modulus from geophysics tests (E_d) in settlement predictions, as recommended by Poulos (2017), gave results close to those from the load test results. The ratio of 0.2 is used in accordance with recommendations by Poulos (2009) and Haberfield (2008). Referring to the representative stiffness degradation curves for soft rocks (Haberfield, 2008), it is noteworthy that $E=0.2E_d$ corresponds to strain levels in the order of 10^{-5} (Fig. 3).

Based on the above, the secant Young's modulus used in the finite element model for settlement prediction in the ground model presented below, was therefore estimated from down-hole seismic test data as 0.2 times the E_d Poulos (2017). The design parameters used in the model are presented in Table 3 below for a Mohr Coulomb constitutive model.

 © DFI International Bruges 2025

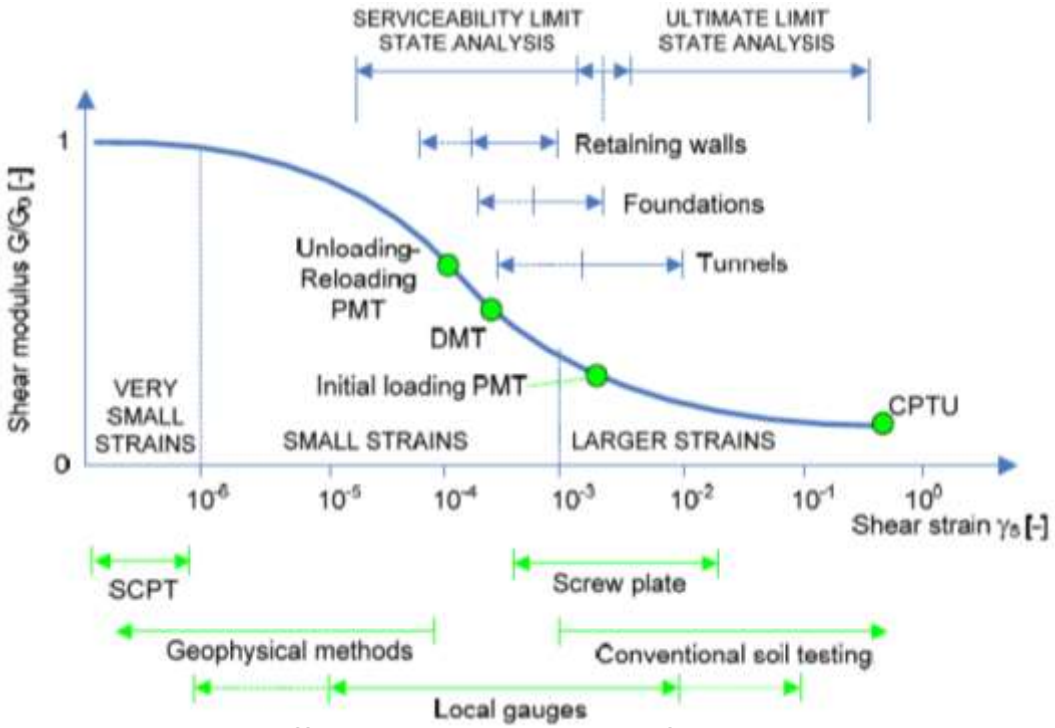


Fig. 3 Characteristic stiffness-strain behavior ranges for typical geotechnical structures different tests (Atkinson and Sallfors, 1991)

Table 3 Design parameters used in the numerical model for La Maison Tower

Strata Description	Elevation(mDMD)		Thickness	Unit Weight	RQD	UCS	Φ'	c'	$0.2E_d$
	Top	Bottom	m	kN/m^3	%	MPa	Degree	MPa	MPa
Gravelly sand[2]	2.88	-10.00	12.88	18	-	-	32	-	40
Calcarenite	-10.00	-14.20	4.20	20	95	2.20	39	0.20	185
Sandstone	-14.20	-23.00	8.80	20	95	0.75	41	0.07	300
Conglomerate 1	-23.00	-28.00	5.00	22	100	4.00	44	0.39	400
Conglomerate 2	-28.00	-31.00	3.00	22	100	2.50	44	0.24	400
Calcisiltite 1	-31.00	-47.00	16.0	20	70	1.17	37	0.08	640
Conglomerate 3	-47.00	-50.00	3.00	20	100	1.05	44	0.10	700
Calcisiltite 2	-50.00	-60.50	10.5	22	70	1.10	37	0.08	800
Conglomerate 4	-60.50	-63.80	3.30	20	100	1.15	43	0.11	900
Calcisiltite 3	-63.80	-90.00	26.2	22	70	1.30	37	0.08	960
Calcisiltite 4	-90.00	-100.0	10.0	20	70	1.50	37	0.10	960

Acceptable limits for pile group settlements

In the Serviceability Limit State (SLS), the design vertical displacements under serviceability limit state conditions are assessed and checked against certain pre-set requirements (allowable settlements) which are usually defined by local authorities or local practices, depending on the structure and its serviceability limit states. The overall settlements and differential settlements between the core of tall towers and the relatively smaller podium structures, need to be within the specified limits. For the design of tall buildings, the following acceptance limits for serviceability has been adopted from Poulos 2009 as presented in Table 4 below.

 © DFI International Bruges 2025

Table 4 Settlement and Deformation Limits for group behavior (Poulos, 2009)

Criterion	Limit (service stage)
Total Settlements	80 mm
Differential Settlement along the raft	1/500

Group modelling and settlement predictions

The total barrette group settlement and serviceability conditions for the La Maison tower were checked using a finite element model in PLAXIS 3D. Barrettes were modelled as beam elements in the group model and the raft was modelled via plate elements. 35m long 1.2 x 2.8m barrettes with a raft of 4m thickness at the core were modelled. Loads were applied as nodal reactions on top of the barrettes. The shoring system (wall) to model excavation stages and the excavation wall, were modelled as a 2D shell, with all other elements modeled (including soil mass and plates) as 3D elements. A rigid interface R_{inter} of 1 was defined to consider the interaction between the barrettes and rock. The interface factor R_{inter} represents the interface between two different materials, to consider the soil structure interaction, and is defined using the standard stiffness approach available in Plaxis. The maximum vertical settlement at the core of the building was obtained as 40mm, as presented in Figures 4a.

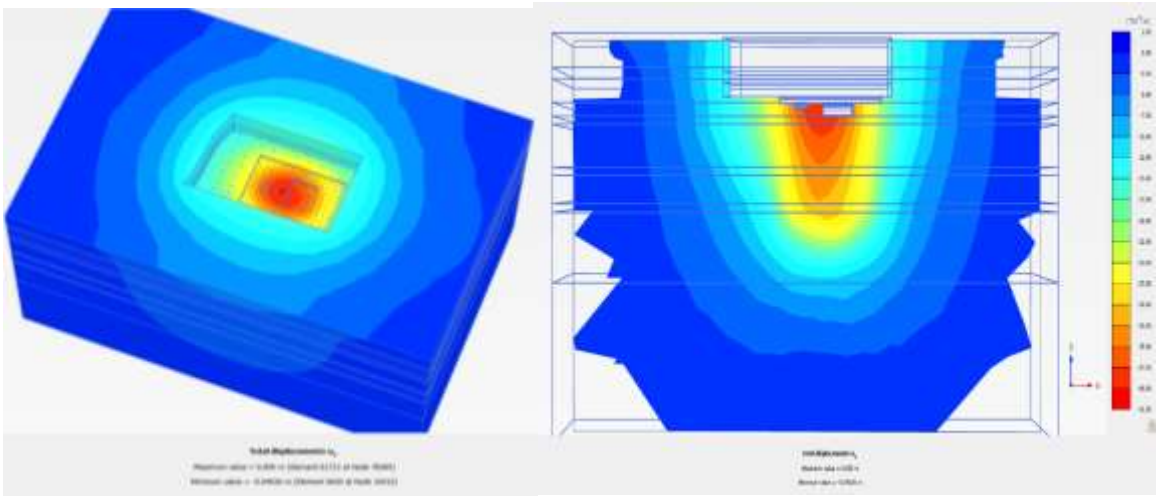


Fig. 4a. Settlement analysis for barrette group with 35m length from cutoff level, designed using a UCS to skin friction correlation factor of 0.52, at the La Maison tower

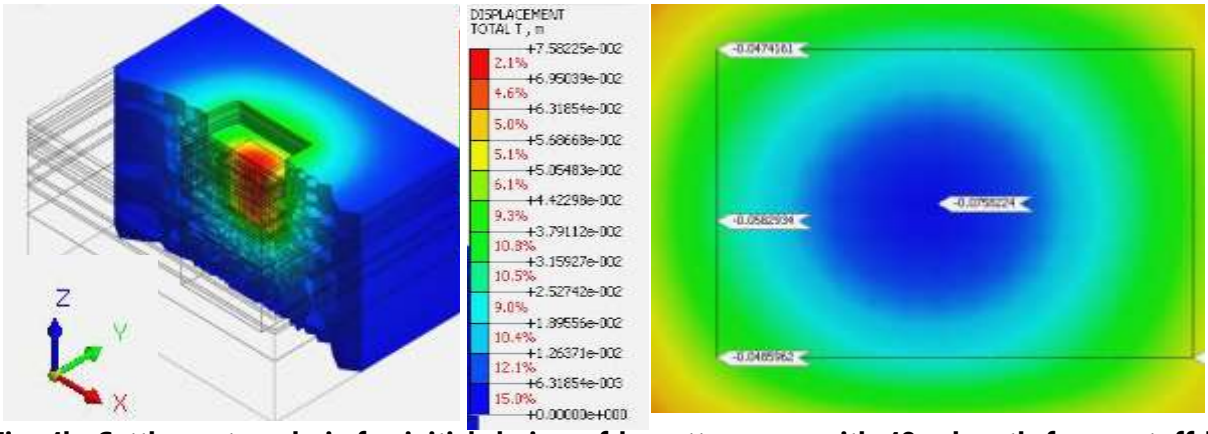


Fig. 4b. Settlement analysis for initial design of barrette group with 48m length from cutoff level, designed using a UCS to skin friction correlation factor of 0.3, at the La Maison tower

The maximum settlement calculated for the initial design with 48m barrettes and using E modulus from Pressuremeter tests and lab tests, was about 75mm (Fig,4a) whereas the maximum settlement from a group barrette FEM model with a barrette length of 35m, (Fig 4b) as estimated using equation 1 is 40mm, well

 © DFI International Bruges 2025

within the limits of 80 mm which is generally accepted as a permissible group settlement for tall towers (Poulos, 2009). This exercise demonstrates that the barrette or pile design with the revised equation for calculating ultimate skin friction from UCS values as $f_s = 0.52(UCS)^{0.5}$, and using a modulus equal to $0.2E_d$, provides a more reasonable estimate for serviceability limits.

It is noteworthy that the final design of La Maison tower was actually approved for construction based on calculations using ultimate skin friction from UCS values as $f_s = 0.4(UCS)^{0.5}$, and using a stiffness modulus equal to $0.2E_d$, which resulted in a design barrette length of 42m thereby reducing the barrette length by about 11% as compared to the original design length of 48m (Manoj et.al.2020). The factor 0.4 is adopted in final design of La Maison tower conservatively, as it is the lower bound value from the correlations presented in Figure 1. The lower bound value of 0.4 is also recommended to be used as the correlation factor when the results cannot be validated by a preliminary load test. The decision to adopt barrettes as a more efficient foundation system for the tower core, and value engineering using O-cell test results, resulted in an overall saving of 7466 m^3 of concrete for the project. This translates to a significant saving in terms of money and time, but it has also contributed to reducing cement and concrete consumption and thereby reducing carbon emission and the carbon footprint of the tower.

REDUCTION IN CARBON FOOTPRINT OF THE LA MAISON TOWER

The average CO_2 emission for the steel industry is 1.9 tons of CO_2 per ton of steel produced. The manufacturers of cement produce about 0.9 tons of CO_2 for every ton of cement. According to the World Business Council for Sustainable Development (WBCSD www.WBCSD.org), the CO_2 produced in the manufacture of structural concrete (using ~14% steel) is estimated at 0.410 ton/m^3.

Based on the above estimates, with the savings of about 7466 m^3 of concrete and about 586 tons of steel, the carbon footprint reduction of the building amounts to a total reduction in carbon emission of 4170 tons. The reduction of carbon emissions by reduced construction equipment and operations will be in addition to this, which is a significant positive impact on the environment. Application of similar savings in building projects can bring down the net carbon emissions due to foundation construction significantly helping mitigation of climate change.

CONCLUSIONS AND RECOMMENDATIONS

The design of rock socketed friction piles has historically been done using traditional design methods which have been developed based on pile load test data from non-similar geological conditions and for much smaller test loads and smaller pile depths, and which may under-predict capacities to a significant extent. Based on back-analysis of a data set of bi-directional load cell tests, Manoj et al. (2023) developed a modified correlation between ultimate skin friction and UCS. In this present paper, the serviceability limits in terms of total barrette group settlements are checked by finite element modelling and the results are presented to demonstrate that when the piles and barrettes are designed using the modified correlation, the computed settlements are also within the specified serviceability limits.

The main conclusions and recommendations are summarized as follows.

- The ultimate skin friction in weak rock sockets can be estimated using the equation $f_s = 0.52(UCS)^{0.5}$ The results should however be validated by a preliminary load test.
- The modified design using the above correlation is validated in this paper for a tall tower in Dubai and group settlement analysis, with the revised design length of barrettes, have been checked and found to be well within the allowable limit of 80mm.
- It is recommended that serviceability limits and pile group settlements are to be checked using an appropriate finite element model. It is important to use characteristic design parameters which are representative of the ground conditions at the project site. Ground stiffness parameters at appropriate strain levels shall be used in the model for analysis.
- It is recommended to adopt a secant Young's modulus of $0.2E_d$ (a value of 20% of E_d) where E_d is the small-strain Young's modulus from geophysical tests. This value is considered to represent the ground stiffness at appropriate strain levels.

 © DFI International Bruges 2025

The modified design should result in significant savings of concrete, in turn resulting in a reduction in the carbon footprint for the structure and further carbon reduction due to savings during installation of the barrettes. Such design optimization, using state of the art methods, can help reduce carbon emissions with more sustainable foundation designs, and with a significant benefit in terms of the impact of climate change on the environment.

REFERENCES

Alrifai L (2007) Rock socket piles at Mall of the Emirates, Dubai. Proceedings of the Institution of Civil Engineers – Geotechnical Engineering 160(2): 105–120, https://doi.org/10.1680/geng.2007. 160.2.105.

Alzaylaie M (2018) Stiffness and Strength of Dubai Sedimentary Rock. PhD thesis, Technische Universitat Darmstadt, Darmstadt,Germany. See https://tuprints.ulb.tu-darmstadt.de/id/eprint/8153

Atkinson, J.H., Sallfors, G.,1991. "Experimental determination of soil properties"; Proceedings of the 10th European Conference on Soil Mechanics and Foundation Engineering, Florence, 3, 915–956.

BS EN 1997-1:2004: Eurocode 7: "Geotechnical design. General rules"; BSI, London, UK.

Carter JP and Kulhawy FH (1987) Analysis and Design of Foundations Socketed Into Rock. Geotechnical Engineering Group, Cornell University, Ithaca, NY, USA, Res. Rep. 1493-4.

Charif KH and Najjar SS (2010) Side friction along drilled shafts in weak carbonate rocks. In The Art of Foundation Engineering Practice (Hussein MH, Anderson JB and Camp WM (eds)). ASCE, Reston, VA, USA, pp. 190–204.

FHWA-NHI-16-064 (2016) GEC 012 "Design and Construction of Driven Pile Foundations – Comprehensive Design Examples", NHI Courses No. 132021 and 132022

Gannon, J. A., Masterton, G. G. T., Wallace, W. A., and Wood, D. M. (1999). "Piled foundations in weak rock". Construction Industry Research and Information Association CIRIA, 181 (*ISBN 0860174948*), UK

Haberfield CM, Paul D and Ervin M (2008) Case history – geotechnical; design for the Nakheel tall tower. ISSMGE Bulletin 2(4): 5–9.

Haberfield CM (2013) Tall tower foundations – from concept to construction. In Advances in Foundation Engineering (Phoon KK (ed.)). Research Publishing, Chennai, India, pp 33–65.

Horvath RG and Kenney TC (1979) Shaft resistance of rock-socketed drilled piers. In Proceedings of Symposium on Deep Foundations. ASCE, Reston, VA, USA, pp. 182–214.

Horvath RG, Kenney TC, Kozicki P (1983) Methods of improving the performance of drilled piers in weak rock. Can Geotech J 20(4):758–772

Ibrahim K, Bunce G and Murrells C (2009) Foundation design for the Pentominium tower in Dubai, UAE. Proceedings of the Institution of Civil Engineers – Civil Engineering 162(6): 25–33, https://doi.org/10.1680/cien.2009.162.6.25.

Latapie B, Rhea A, Michelle A, Marwan A and Joyshwin S (2018) A review of piling industry practices in Dubai, UAE: proposed UCS-based correlations. Geotechnical Research 6(2): 103–129, https://doi.org/10.1680/jgere.18.00021.

Kulhawy FH and Phoon KK (1993) "Drilled shaft side resistance in clay soil to rock- Designand Performance of Deep Foundations: Piles and Piers in Soil and Soft Rock",ASCE New York:(38),172–183.

Meigh AC and Wolski W (1979) Design parameters for weak rock. In Proceedings of 7th European Conference on Soil Mechanics and Foundation Engineering, Brighton. British Geotechnical Society, London, UK. vol. 5, pp. 59–79.

 © DFI International Bruges 2025

O'Neill MW, Reese LC (1999) "Drilled shafts: Construction procedures and design methods"; FHWA-IF-99-025. FHWA

Manoj S, Choudhury D and Alzaylaie M (2020). "Value engineering using load-cell test data of barrette foundations - La Maison, Dubai", Proceedings of the Institution of Civil Engineers - Geotechnical Engineering, ICE, London, U.K., (doi: https:// doi. org/ 10. 1680/ jgeen. 19. 00246)

Manoj, S., Choudhury, D., Poulos, H. *et al*. Friction to Unconfined Compression Strength Correlation for Evaluating Capacity of Weak Rock Foundation Sockets. *Geotech Geol Eng* **41**, 2153–2171 (2023). https://doi.org/10.1007/s10706-022-02361-w

Poulos HG (2009) Tall buildings and deep foundations – Middle East challenges. In Proceedings of the 17th International Conference on Soil Mechanics and Geotechnical Engineering (Hamza M, Shahien M and El-Mossalamy Y (eds)). IOS Press, Amsterdam, the Netherlands, vol. 4, pp. 3173–3205.

Poulos HG (2010) High-rise building foundations – a limit state design approach. In The Art of Foundation Engineering Practice. ASCE, Reston, VA, USA, pp. 501–516.

Poulos HG (2017) Tall Building Foundation Design. CRC Press, Boca Raton, FL, USA.

Poulos HG and Bunce G (2008) Foundation design for the Burj Dubai – the world's tallest building. International Conference on Case Histories in Geotechnical Engineering 14.

Poulos HG and Davids AJ (2005) Foundation design for the Emirates Twin Towers, Dubai. Canadian Geotechnical Journal 42(3):716–730.

Poulos HG (2022). *Use of Shear Wave Velocity for Foundation Design*, Geotechnical and Geological Engineering 40(2)

Pereira G, Lam P, Jeanmaire T , Poulos H.G., Bergere A (2017), "Deep foundation systems of ultra-high-rise buildings: the Entisar tower in Dubai", Proceedings of the 19th International Conference on Soil Mechanics and Geotechnical Engineering, Seoul 2017

Rowe RK, Armitage HH (1987) "Theoretical solution for axial deformation of drilled shaft." Can Geotech J Ottawa 24:114–125

Reese LC and O'Neill MW (1988) Drilled Shafts: Construction Procedures and Design Methods, U.S. Department of Transportation, FHWA-HI-88-042, Dallas, TX, USA.

Rosenberg P and Journeaux NL (1976) Friction and end bearing tests on bedrock for high-capacity socket design. Can. Geotech. J., Ottawa 13, 324–333.

Russo G, Poulos HG, Small JC (2013) "Re-assessment of foundation settlements for Burj Khalifa, Dubai"; (ISSN 1861–1125). Acta Geotech 8:3–15. https:// doi. org/ 10.1007/ s11440- 012- 0193-4

Williams AF and Pells PJN (1981) Side resistance rock sockets in sandstone, mudstone, and shale. Canadian Geotechnical Journal 18(4): 502–513.

Zhang L and Einstein HH (1998) End bearing capacity of drilled shafts in rock. Journal of Geotechnical and Geoenvironmental Engineering 124(7): 574–584.

 © DFI International Bruges 2025

The application of CO_2-fixed recycled fine aggregate as filler of sand compaction piles

Sho NISHIIE, Takenaka Corp., Inzai, Chiba, Japan, +81 476-47-1700, nishiie.shou@takenaka.co.jp
Takao KONO, Takenaka Corp., Inzai, Chiba, Japan, +81 476-47-1700, koono.takao@takenaka.co.jp
Ryohei ISHIKURA, Kyushu Univ., Fukuoka, Fukuoka, Japan, +81 92-802-3382, ishikura@civil.kyushu-u.ac.jp
Adel ALOWAISY, Kyushu Univ., Fukuoka, Fukuoka, Japan +81 92-802-3378, a.adel@civil.kyushu-u.ac.jp

ABSTRACT

The sand compaction pile (SCP) method improves the bearing capacity of the ground and prevents liquefaction by constructing compacted sand columns on the ground. Natural sand is usually used as a filler in this method. In this study, the applicability of carbonated recycled fine aggregate (RFA) as a filler for SCP is investigated to reduce CO_2 emissions. RFA can fix approximately 5% of CO_2 by mass by reacting CO_2 with cement hydrates adhered around sand particles to form calcium carbonate. To verify the applicability of carbonated RFA, particle size distribution, soil compaction, permeability, triaxial CD, and hexavalent chromium elution tests are performed. RFA has a particle size distribution suitable for SCP; the optimum water content is 20.8% and the maximum dry unit weight is 14.79 kN/m^3. The hydraulic conductivity, cohesion, and internal angle of friction at the optimum water content are 3.1×10^{-5} m/sec, 27.7 kN/m^2, and 34.8 °, respectively. Additionally, by adding 1% iron (II) sulfate, the dissolution of hexavalent chromium in the carbonated RFA is reduced to less than 0.01 mg/L. We concluded that carbonated RFA can be used as an eco-friendly filler for SCP.

Keywords: carbon capture and utilization, recycled fine aggregate, sand compaction piles,

INTRODUCTION

The sand compaction pile (SCP) is a ground improvements method in which compacted sand columns are constructed on the ground (Fig. 1), and is applicable to both loose sandy and soft clayey ground. For loose sandy soils, this method is mainly used to prevent liquefaction, whereas for soft clayey soils, it is used to promote consolidation through the drainage effect. The SCP method was put into practical use in Japan in the 1950s, and natural sand was widely used as a filler material. In recent years, concerns over the depletion of natural resources and their environmental impacts have increased, and several alternative filling materials have been proposed. An alternative filler material is iron–steel slag, a byproduct of the steel industry that has been reported to provide higher-strength compacted piles than natural sand (Takahashi et al., 2014). Another method involves using construction waste soil modified with quicklime as a filler instead of natural sand (Yabe et al., 2024).

In this study, the applicability of recycled fine aggregate (RFA) as an SCP filler material was investigated to reduce its environmental impact. RFA is produced from crushed waste concrete. Therefore, its application reduces the use of natural resources. Furthermore, cement hydrates adhere to the sand particles of the RFA, and calcium carbonate ($CaCO_3$) is produced when CO_2 reacts with the cement hydrates; hence, RFA is a carbon capture and utilization material, and the use of this material could lead to ground improvement methods with negative CO_2 emissions. Several methods have been proposed for its reaction with CO_2 (Nishioka et al., 2023; Liu et al., 2023); however, the optimal method has not yet been determined.

Suitable filler materials for SCP are granular materials with low fine particle content, a maximum particle diameter of 50 mm or less, and no particle crushing by compaction (Kitazume, 2005). When SCP is used to promote the consolidation of clayey soils, they should be highly permeable. In this study, we confirmed that RFA has these properties through soil tests and verified its applicability as a filler material for SCP.

 © DFI International Bruges 2025

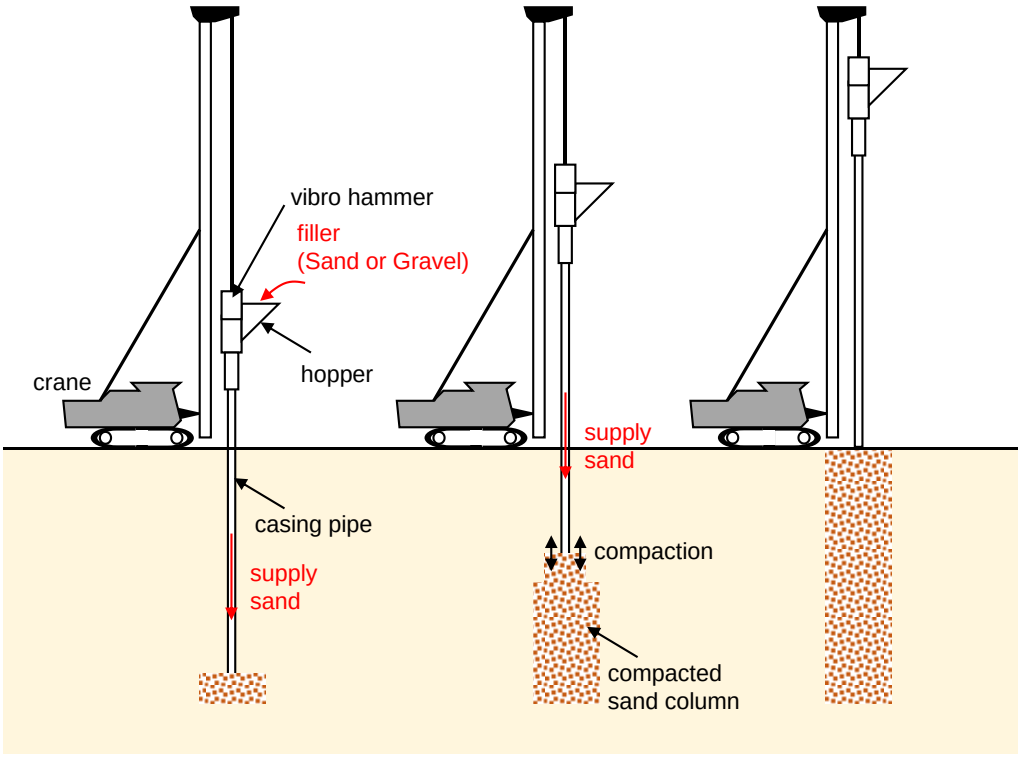


Fig. 1. Schematic diagram of SCP method

CARBONATION OF RFA

The RFA used in this study was produced from concrete with a compressive strength of 30 MPa, using graywacke as a fine aggregate. The dry carbonation method was used to react RFA to CO_2. Fig. 2 shows the dry carbonation system used in this study, which maintains a constant temperature, humidity, and CO_2 concentration in the chamber. The RFA was stored in a chamber and carbonated for seven days at a temperature of 20 °C, 60% relative humidity, and 10% CO_2 concentration, which are typical conditions for dry carbonation of cement paste fine powder (Kadota et al., 2022). The amount of CO_2 emitted from the process of crushing concrete to produce RFA and the carbonation equipment was 0.37% of the mass of RFA.

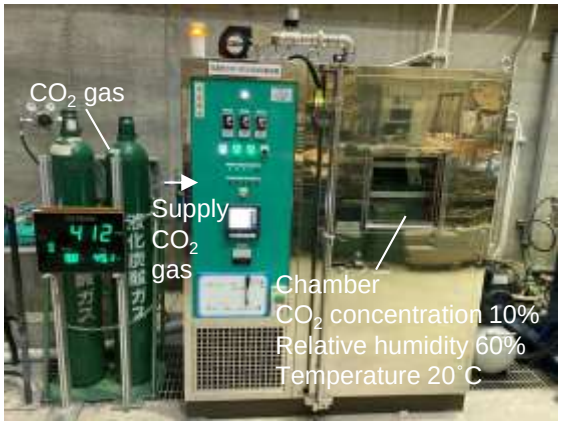


Fig. 2. Dry carbonation system

The amount of CO_2 fixed in RFA was estimated from the weight loss and temperature obtained by thermogravimetry differential thermal analysis (TG/DTA). A previous study reported that the thermal

 © DFI International Bruges 2025

decomposition reaction of $CaCO_3$ occurs between 450 and 900 °C, based on TG/DTA test results of carbonated cement paste (Wu & Ye, 2015). In this study, the same temperature range was adopted, and weight loss occurred at temperatures from 450 to 950 °C owing to the decomposition of $CaCO_3$ of dry carbonated RFA. The percent weight loss in this temperature range was the mass percentage of fixed CO_2. Because the decomposition reaction of $CaCO_3$ does not occur below 450°C, mass reduction below 450°C is not considered. Fig. 3 shows the TG/DTA results for RFA before and after carbonation. Even before carbonation, a mass loss of 2.51% was observed in the temperature range of 450 – 900°C. This is because the RFA used in this study was approximately one year old after manufacturing and contained $CaCO_3$ before carbonation owing to the reaction of the cement hydrates in the RFA with CO_2 in the air. After carbonation, a mass loss of 5.09% was observed in the same temperature range, and the CO_2 fixation capacity of the RFA used in this study was approximately 5% of its mass.

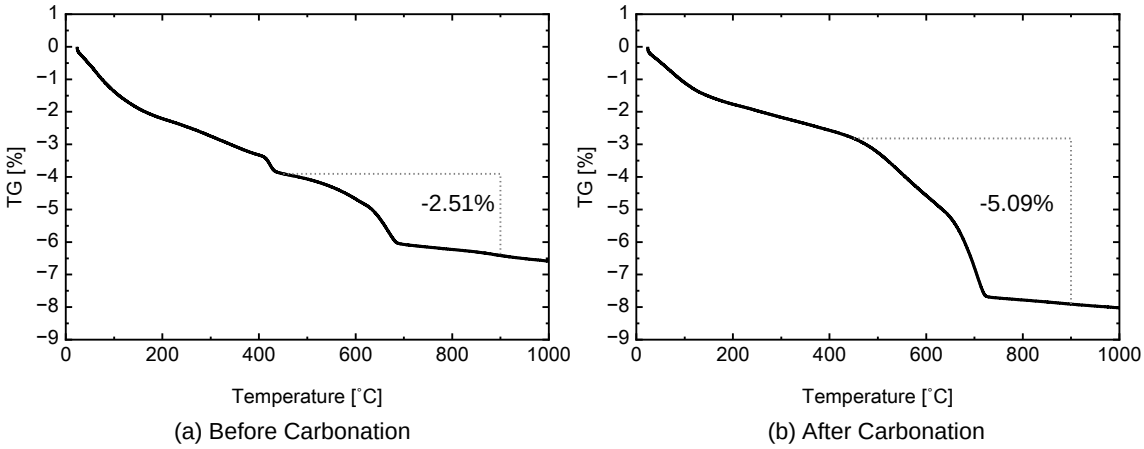


Fig. 3. TG/DTA results

GEOMECHANICAL PROPERTIES OF RFA

Fig. 4 shows the grain size accumulation curves of uncarbonated and carbonated RFA, and the dashed lines in the figure indicate the range of grain sizes suitable for the SCP method. Slight differences in the grain size distribution are observed before and after carbonation; however, the grain size distribution is within the range suitable for SCP.

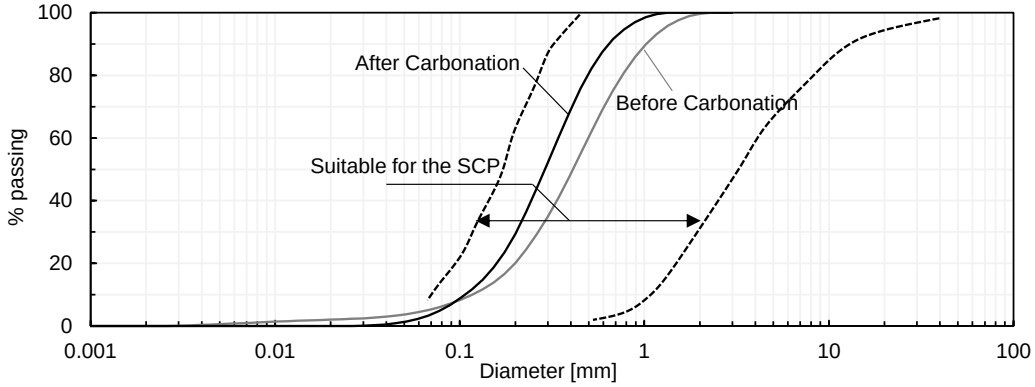


Fig. 4. Grain size accumulation curves

Fig. 5 shows the compaction test results for carbonated RFA. Compaction tests were performed in accordance with the Japanese Geotechnical Society standard (JGS 0711) using a mold with an inner

 © DFI International Bruges 2025

diameter of 100 mm, without repeated use of the sample. The test results demonstrated that the optimum water content of the carbonated RFA was 20.8% and the maximum dry density was 15.1 kN/m^3. Compared with natural sand, RFA has a slightly higher optimum water content; however, it has a similar maximum dry density, along with compaction properties applicable to SCP.

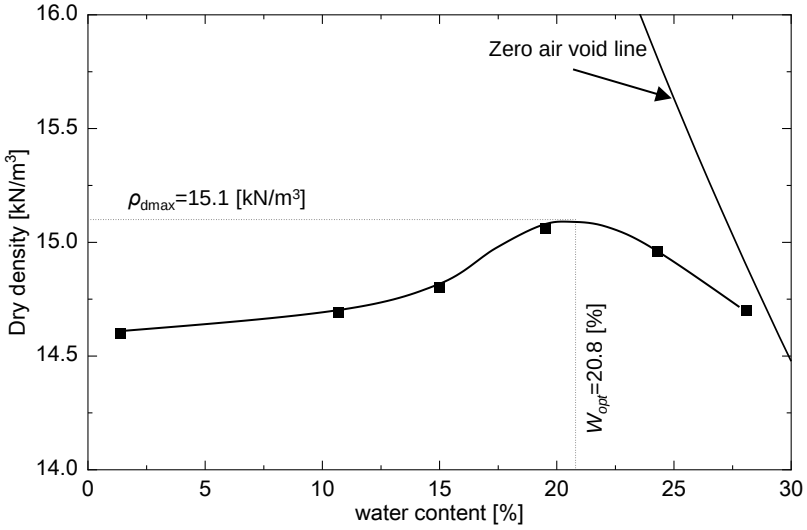


Fig. 5. Compaction test result

Fig. 6 shows the triaxial shear test results. The test was performed under consolidated drained (CD) conditions, and the test specimens were prepared using a compaction method with a water content of approximately 18%. Triaxial test results demonstrated that cohesion c_d and internal friction angles ϕ_d were 27.7 kN/m^2 and 34.8 °, respectively, indicating that the carbonated RCF has the internal friction angle equivalent to that of natural sand. Carbonated RFA has $CaCO_3$ crystals on its surface and surface angularities compared with natural sand. These surface characteristics are considered to result in relatively higher apparent cohesion values compared with natural sand. In addition, the permeability test results revealed that the permeability of the compacted specimens at the optimum water content was 3.08×10^{-5} m/s, indicating that it has the permeability to be used as a drain material.

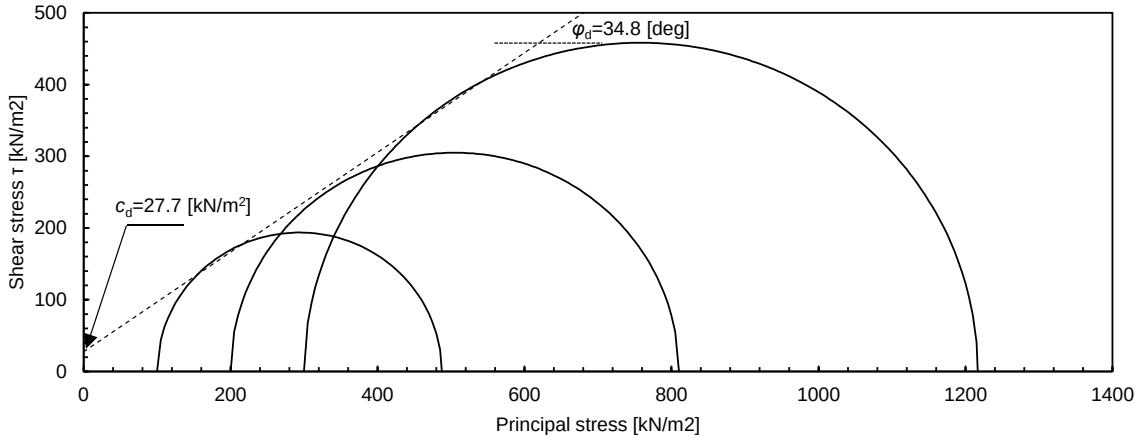


Fig. 6. Triaxial shear (CD) test result

HEXAVALENT CHROMIUM DISSOLUTION

The leaching of hexavalent chromium (Cr^{6+}) from carbonated RFA is a concern. Before carbonation, Cr^{6+} is fixed in cement hydrates, however after carbonation, Cr^{6+} leaching can increase because the

 © DFI International Bruges 2025

cement hydrates decompose by reacting with CO_2. The decomposition of cement hydrates has been reported to increases the leaching of Cr^{6+} (Kuroda & Koshiishi, 2010). Fig. 7 shows the relationship between the amount of fixed CO_2 and Cr^{6+} leaching in RFA. Elution tests were performed in accordance with the standards of the Japanese Ministry of Environment. In this test, the sample was placed in a solvent nine times its mass and shaken for 24 h, and the concentration of Cr^{6+} in the solvent was measured. The Japanese environmental standard for the concentration of Cr^{6+} in this solvent was 0.05 mg/L or less. Cr^{6+} leaching increased in proportion to the amount of fixed CO_2. The amount of Cr^{6+} leached from the fully carbonated RFA was approximately five times that specified in the Japanese regulations.

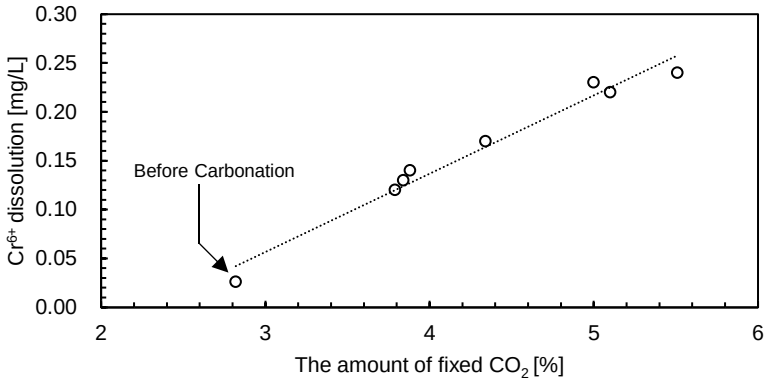


Fig. 7. Relationship between amount of fixed CO_2 and dissolution of Cr^{6+}

Cr^{6+}, in contrast, is an unstable substance that is easily reduced and reacts with reducing agents to form non-toxic trivalent chromium (Cr^{3+}). In this study, iron (II) sulfate ($FeSO_4$) was mixed with carbonated RFA as a reducing agent to investigate changes in hexavalent chromium leaching. Eq. [1] describes the reaction in which Cr^{6+} is reduced to Cr^{3+} by Fe^{2+}. Fig. 8 shows the relationship between the amount of $FeSO_4$ mixed with naturally dry carbonated RFA and the amount eluted Cr^{6+}. The addition of $FeSO_4$ significantly reduced the amount of Cr^{6+} eluted. Adding 0.1% $FeSO_4$ to the mass of RFA reduced the amount of Cr^{6+} eluted to below the Japanese regulations and adding 1% or more resulted in almost no hexavalent chromium being eluted. Because the amount of $FeSO_4$ addition was small compared with the mass of carbonated RFA, the compaction characteristics are considered not to change with or without the addition.

$$Cr_2O_3^{2-} + 6Fe^{2+} + 6H^+ \rightleftarrows 2Cr^{3+} + 3H_2O + 6Fe^{3+} \quad \#[1]$$

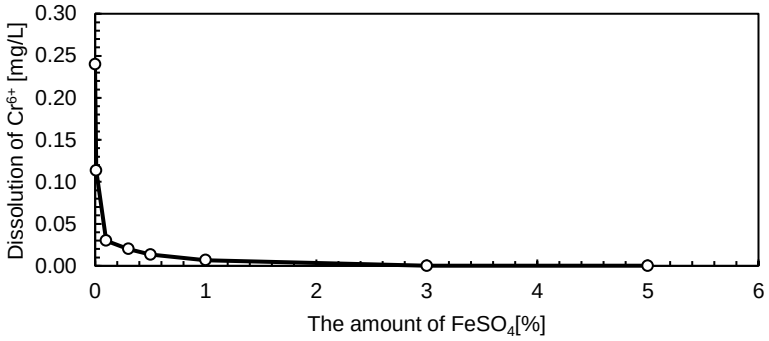


Fig. 8. Relationship between amount of iron (II) sulfate and dissolution of Cr^{6+}

 © DFI International Bruges 2025

CONCLUSION

This study investigated the applicability of CO_2-fixed RFA as a filler for SCP. RFA could fix approximately 5% CO_2 by mass, and carbonated RFA had a particle size distribution suitable for SCP filler, and compaction properties, internal friction angle, and permeability comparable to those of natural sand. The elution of Cr^{6+} was below the Japanese regulations with the addition of a small amount of $FeSO_4$ as a reducing agent. Based on these test results, we conclude that carbonated RFA can be used as a filler for SCP. Although natural sand commonly used in SCP currently emits 0.3% of its mass in CO_2 during mining and transportation, RFA can absorb approximately 5% of its mass in CO_2. Equipment for mass production of carbonated RFA is currently under development, however, the cost of carbonated RFA is approximately twice that of natural sand. Because SCP consumes a large amount of filler material, further cost reduction in the manufacturing and carbonation process of RFA and complete replacement of natural sand with RFA are expected to significantly reduce CO2 emissions.

ACKNOWLEDGMENTS

This paper is based on the results of “Development of Materials, Manufacturing Methods and Quality Control System on Innovative Carbon Negative Concrete”, JPNP21023, commissioned by the New Energy and Industrial Technology Development Organization (NEDO).

REFERENCES

Kadota, H., Ikeo, Y., Nara, T., Kojima, M., 2022. CO_2 sequestration of cement paste fine powder and recycled fine powder by wet and dry carbonation and evaluation method of fixed amount of CO_2. Cement Science and Concrete Technology, Vol.76, pp.503-511. (In Japanese)

Kitazume, M., 2005. The sand compaction pile method. CRC Press, pp. 19-31.

Kuroda, Y., Koshiishi, N., 2010. Influence of various factors on leaching of hexavalent chromium from cement concrete. The Architectural Institute of Japan’s Journal of Structural and Construction Engineering, Vol.75, No.650 pp. 715-722. (In Japanese)

Liu, Q., Tang, H., Chen, K., Sun, C., Li, W., Jiao, S., Tam, V., 2023. Improving industrial drying process of recycled fine aggregates as a means of carbonation to improve the mechanical properties and plastic shrinkage of self-leveling mortar, Construction and Building Material, No.403, 133001.

Nishioka, Y., Eguchi, K., Tsuji, D., Nara, T., Ikeo, Y., Kojima, M., 2023. CO_2 sequestration by wet carbonation treatment of recycled fine aggregate and recycled fine powder and application to concrete. Proceedings of RILEM 2023.

Takahashi, H., Morikawa, Y., Shinozaki, H., Kinoshita, H., Maruyama, K., 2014. Ground improvement method by reusing solidified iron-and-steel slug. Geo-Congress Technical Paper. pp. 3713-3720.

Wu, B., Ye, G., 2015. Development of porosity of cement paste blended with supplementary cementitious materials after carbonation. Proceedings of the 14th International Congress on the Chemistry of Cement.

Yabe, H., Takeuchi, H., Ogata, F., Harada, K., 2024. Sand compaction pile method utilizing recycled material. Proceedings of IC-CREST 2023, pp. 267-280.

 © DFI International Bruges 2025

INFLUENCE OF ANCHORING SYSTEMS AND THEIR MANUFACTURING PROCESSES AND HIGH-STRENGTH STEELS ON CO_2 REDUCTION

Andreas Schiller, Stahlwerk Annahuette, Hammerau, Bavaria, Germany, +49 8654 487 413,
andreas.schiller@annahuette.com

ABSTRACT

The influence of the CO2 footprint of geotechnical anchoring systems can be derived from several influencing factors. Of course, the amount of raw materials used, i.e. steel and cement in particular, plays a role, but so does the amount of CO2 produced as a result of the respective manufacturing process. In addition, the choice of the anchoring system has an influence on the amount of steel and cement used, which in turn has a significant impact on sustainability. Rarely considered, but the choice of steel grade can also make a positive contribution to CO2 reduction. High-strength steels can make a significant contribution to this. In addition to the advantages of high-strength steels in terms of handling and occupational safety, the consequential economic benefits such as lower freight costs, and the up to 85% reduction in CO2 compared to iron ore-based products should also be emphasized. High-strength steels are not an invention of today. Strands in ground anchor systems have been used in geotechnical engineering since the 1960s. Today, high-strength reinforcing steels make their contribution in high-rise construction. And geotechnical engineering will also continue to use high-strength steels, and not only in ground anchor systems.

Keywords: sustainability, geotechnical anchoring systems, influencing factors, CO2 reduction

INTRODUCTION

„Sustainability is not just an option. It is a necessity“. This quote from Ban Ki-moon says that if we do not adopt sustainable practices, we will deplete our planetary resources and damage the environment. This will lead to a number of negative consequences, including climate change, pollution and food shortages. The construction industry including geotechnics will also be called upon to play its part.

One of the main tasks of geotechnical engineering is to secure slopes, excavations, rock faces etc. with anchoring systems or to safely transfer loads from structures into the building site. Depending on the initial building site situation and the requirements of the structure, geotechnical engineers have various tie-back systems at their disposal. The most common systems include grouted anchors, soil nailing and micropiles. In the past, the choice of anchoring system and associated components was primarily determined by technical expediency and cost-effectiveness. In fact, for various reasons, the issue of 'sustainability' is increasingly coming to the fore as a major third decision parameter.

Apart from the generally recognized need to reduce CO2 emissions, the reasons on the part of users range from pure conviction to increasing cost pressure due to CO2 pricing to pure economic sense due to the lowest resource consumption of a construction product. This article will look at the factors that influence the CO2 footprint of geotechnical anchoring systems and how this can be optimized with the help of new, high-strength steel grades.

MATERIAL COMPONENTS OF COMMON ANCHORING SYSTEMS

The usual geotechnical anchorage types are generally the following systems:

Ground anchors acc. to EN 1537:
Ground anchors are used as anchoring elements, usually as prestressed anchors, when, for example, a retaining structure needs to be anchored, the stability of slopes, cuttings and tunnels needs to be achieved, uplift forces acting on supporting structures need to be resisted, slippage or tilting needs to be prevented or tension cables need to be anchored. This involves introducing a tensile force into a load-bearing soil or rock formation.

 © DFI International Bruges 2025

Soil nailing acc. to EN 14490:
Soil nailing is a composite supporting structure. A monolithic body is created in the loose soil by the arrangement of soil nails, which safely absorbs the earth pressure forces of the subsoil. The surface is sealed using shotcrete, which is designed to withstand the earth pressure forces. In the rock, the nails act as dowels that prevent rock wedges from slipping or tilting.

Micropiles acc. to EN 14199:
Micropiles are pile foundations. Micropiles are used as foundation elements in all types of soil and rock if the subsoil has a low load-bearing capacity or if tie-backs are possible without prestressing. Depending on the building site conditions, micropiles can be a particularly economical option for transferring forces from overlying structures or from uplift forces into the subsoil.

What the systems have in common is that they generally consist of a steel supporting element that is filled with cement suspension inside a borehole. Rarer designs such as those consisting of fibre glass load-bearing elements will not be considered here.

Most common steel load-bearing elements are:

- Solid bars, mainly consisting of a coarse thread steel.
- Hollow bars, mainly used as self-drilling load-bearing members.

Cement grout has two functions:

- In temporary and permanent systems: Transferring the load from the steel load-bearing member to the subsoil (≙ ultimate limit state)
- Only for permanent systems: Ensuring corrosion protection, if necessary in combination with an additional plastic coating for double corrosion protection (≙ serviceability limit state)

The requirements for cements for permanent systems are regulated in the relevant design standards. CEM I (Portland cement) must always be used for double corrosion protection in accordance with EN 1537 or when using prestressing steel for micropiles in accordance with EN 14199. Double corrosion protection in accordance with EN 1537, on the other hand, must always be used for permanent grouted anchors and in accordance with EN 14490 for soil nailing with steel grades with fy > 600 MPa. Cement mortar within corrosion protection coatings or cement mortar in contact with prestressing steel in corrosion protection coatings must comply with EN 447 and therefore consist of CEM I (Portland cement). A comparison of the CO2 emissions of common types of cement shows that there is considerable potential for optimization in the use of cement.

The cement industry will have to make efforts to use cement types with low CO2 emissions in production that prove their suitability in combination with steels for geotechnical anchoring systems. First and foremost, suitability means achieving properties for standard cements in accordance with EN 197-1 or properties for cements with special properties in terms of compressive strength, solidification, hydration resistance, volume stability, density and grinding fineness. This applies in particular to systems with simple corrosion protection in which the steel comes into direct contact with the hardened cement paste covering.

Table 1. Potential of CO2 reduction of different cement types acc. to Schwenk (2023)

Cement type and manufacturing plant	Global Warming Potential net [kg Äq. CO2/to cement]	CO2-reduction compared to CEM I average Germany [%]
CEM I Portland cement (average Germany)	665	-
CEM I 42,5 N (Allmendingen)	508	24
CEM II/B-M (V-LL) 42,5 N (Allmendingen)	401	40
CEM II/C-M (V-LL) 42,5 N (Allmendingen)	348	48
CEM II/C-M (S-LL) 42,5 N (Mergelstetten)	400	40
CEM II/C-M (S-LL) 42,5 N (Karlstadt)	317	52
CEM III/A 42,5 N (Bernburg)	361	46

 © DFI International Bruges 2025

INFLUENCE OF THE STEEL PRODUCTION PROCESS

In most cases, the main components of a geotechnical anchoring system are steel and cement. Of course, the following applies to both manufacturing processes: the less CO2 produced, the more sustainable the product. With regard to the steel component, there are two main manufacturing processes:

- Production of steel from the blast furnace (BOF, blast oxygen furnace)
  Iron ore is melted in a blast furnace using coke or, in some cases, renewable fuels. The pig iron obtained in this way is then melted in the steelworks with additional alloying elements and scrap in a converter with the addition of oxygen to produce steel.
- Production of steel from the electric arc furnace (EAF)
  In an electric arc furnace, recycled steel, i.e. scrap, is melted in an electric arc using electrodes and steel is recovered in this way together with additional alloying elements.

The differences between the two manufacturing processes in terms of CO2 emissions are considerable. While the blast furnace route (BOF) can be expected to emit around 1750 - 2500 kg of CO2 per tonne of steel produced, steel production in the electric arc furnace (EAF) only produces around 625 - 790 kg/t.

Current efforts to achieve CO2-reduced steel production via the blast furnace route through the use of hydrogen are considerable and noteworthy. At the same time, however, they are very challenging due to the high demand for CO2-neutral hydrogen. In addition, the advantage of using scrap in the electric arc furnace is that the supply of CO2-neutral primary energy in the form of electricity from sustainable energy sources can be switched relatively quickly - no structural changes are necessary. The current figures for CO2 emissions from EAFs using green electricity are around 260 - 630 kg/t CO2, depending on the depth of processing.

Table 2. Global warming potential in steel production

EAF, today's conditions	[kg CO2-Äq]	260 – 625
EAF, ideal conditions	[kg CO2-Äq]	625 – 790
BOF, integrated metallurgical plant	[kg CO2-Äq]	1750 – 2450

Furthermore, in its study ‘Securing Germany's sovereignty - resilient supply chains for the transformation to climate neutrality in 2045’ (2023), the Climate Neutrality Foundation concludes that a stronger supply of domestic secondary raw materials (i.e. scrap) is the best insurance against import dependencies in the steel sector too.

Unfortunately, the user of the anchoring system is generally not aware of the type of steel production. An Environmental Product Declaration (EPD) can provide information on the actual amount of CO2 produced. If sustainability is currently seen as an aspect when considering the planning, the only option currently available to those involved in the project is to make individual enquiries with the manufacturer of the anchoring system. While an EPD is already a common requirement in some Northern European countries, it is voluntary elsewhere. However, the voluntary nature is changing. With the introduction of the new Construction Products Regulation in 2024, the publication of sustainability values will gradually become mandatory in Europe. The aim is not only to increase transparency, but also to influence tenders, particularly in the public sector. Users of geotechnical anchoring systems will be forced to deal with the corresponding values.

INFLUENCE OF ANCHORING SYSTEM

As described in the chapter 'Material components of common anchoring systems', most commercially available geotechnical anchoring systems consist of a steel support member embedded in cement

 © DFI International Bruges 2025

mortar in a borehole. The two common steel load-bearing members are solid bars, which are produced by means of a simple borehole in good geological conditions or a cased borehole if there is a risk of borehole collapse.

Table 3. Corrosion protection systems for permanent geotechnical anchoring systems

Anchoring system	Ground Anchor	Soil nail	Micro pile
Execution standard	EN 1537	EN 14490	EN 14199
Corrosion system fy ≤ 600 Mpa	DCP[1)] acc. EN 1537	acc. approval	acc. approval
Corrosion system fy > 600 Mpa		DCP[1)] acc. EN 1537	
Cement type Inner grout (DCP[1)])	CEM I Portland cement acc. EN 447		
Cement type Outer grout (DCP[1)])	no direct specification		
Cement type SCP[2)] (one mortar layer)	not provided	Cements with special properties and cements according to EN 197-1, taking into account the corresponding exposure class	
Cement cover Inner grout (DCP[1)])	≥ 5 mm (0.2 in)		
Cement cover Outer grout (DCP[1)])	≥ 10 mm (0.4 (in)		
Cement type SCP[2)] (one mortar layer)	not provided	acc. approval or ≥ 10 (0.4 in) mm for DCP[1)]	≥ 25 mm (1.0 in) [3)] or acc. approval or ≥ 10 mm (0.4 in) for DCP[1)]

[1)] DCP: Double corrosion protection (= cement coating with additional cover)
[2)] SCP: Standard corrosion protection (= single cement cover)
[3)] the specifications of EN 14199 apply; in any case, expansion body tests are recommended to determine the crack width development of the system used

Single or double corrosion protection is available as a (simultaneously load-transmitting) corrosion protection system. While solid bar systems offer a choice between single corrosion protection consisting of a single layer of cement paste covering (= standard corrosion protection or SCP for short) or double corrosion protection (= DCP), the corrosion protection of a hollow bar system can consist of only one or, alternatively, self-drilling hollow bars, which can only be equipped with single corrosion protection.

The cement stone covering is determined by two factors:

- Required borehole size to achieve the necessary skin friction for load transfer
- Required concrete cover for corrosion protection

For reasons of corrosion protection alone, a higher concrete cover is generally required for self-drilling systems with single standard corrosion protection consisting of a single layer of cement paste cover compared to solid bar systems with double corrosion protection. This assumes that the geology permits small borehole diameters with the same load. Smaller borehole diameters per se lead to less drilling work and a reduction in the amount of cement used.

 © DFI International Bruges 2025

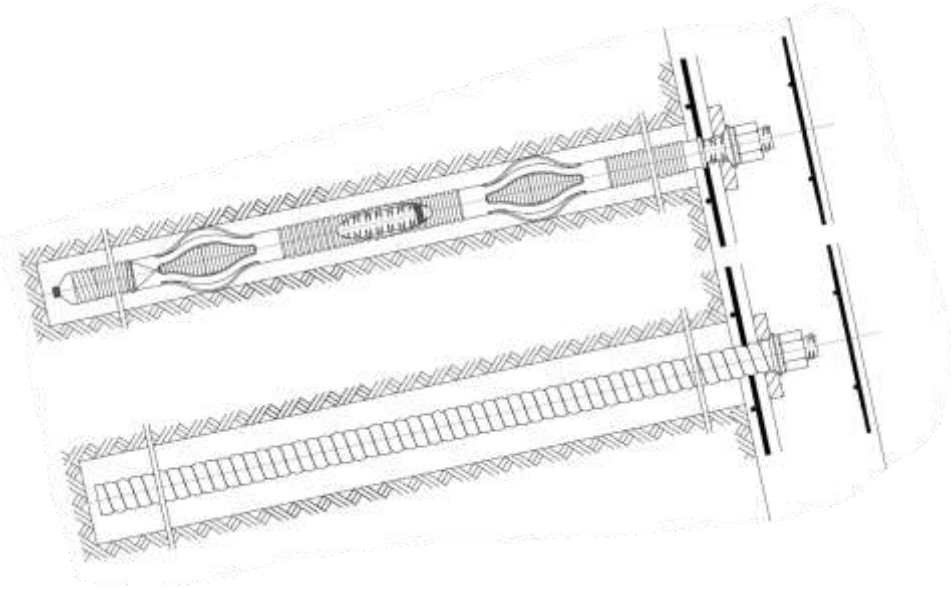


Fig. 1: Soil nail system, top solid bar system with double corrosion protection (DCP), below hollow bar system with standard corrosion protection (SCP)

Approved permanent soil nail systems that use a coarse threaded bar as a load-bearing element are provided with double corrosion protection in accordance with DIN EN 1537. This consists of a 5 mm thick cement stone cover over the load-bearing element and a plastic ribbed sheathing on top, which is usually manufactured in the factory.

On the one hand, the plastic sheathing creates redundancy, and, on the other hand, the ribbed design of the plastic ribbed pipe leads to very favorable crack formation. A cement stone covering at least 10 mm thick must be provided on site over the ribbed pipe. The advantage of this redundant system is that the borehole diameters can be kept to a minimum. A cased borehole in combination with suitable spacers also guarantees that the required concrete cover is guaranteed over the entire length.

Permanent soil nail systems that use a hollow bar as a load-bearing element do not allow the use of a plastic casing and are therefore provided with an increased cement paste cover as corrosion protection, simply for reasons of redundancy. The thickness of the increased cement stone covering required, which of course influences the size of the borehole and subsequently the cement consumption, depends on the thickness of the supporting member. Alternatively, with hollow bars it is possible to optimize the cement stone covering by increasing the steel insert with corresponding load reserves.

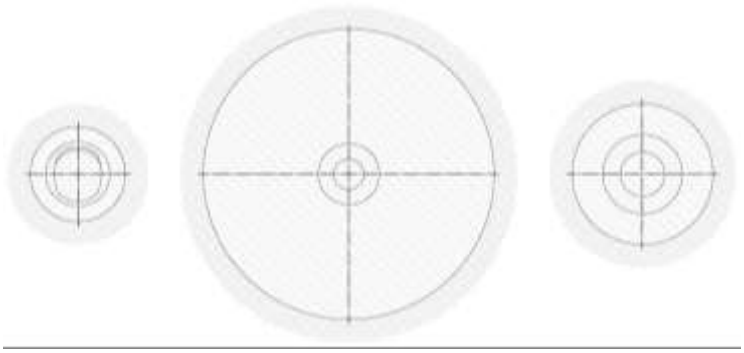


Fig. 2: Scaled minimum cross-sections of a 400 kN micropile system for corrosion protection (without consideration of a minimum cross-section for load transfer taking into account the geology), left: solid bar DCP; center: hollow bar SCP with low steel insert; right: hollow bar SCP with high steel insert

 © DFI International Bruges 2025

Regardless of the choice of supporting element, it should be noted that a flushing and supporting fluid made of cement mortar should be used for the installation process of hollow bars. the water-cement ratio should generally be around w/c ≈ 0.4 - 0.7. On the one hand, this serves the stability of the borehole itself. On the other hand, a cement stone body that binds into the construction thread should be produced as a stable anchoring body in the ground. Once the base depth has been reached, the flushing and support fluid must be completely replaced by cement mortar with a water/cement ratio of w/c ≈ 0.4 - 0.5. The consumption of cement during drilling and for the production of the supporting body must be taken into account accordingly in the sustainability assessment.

For prestressed ground anchors, the choice of anchoring system is specified by standards: Strand or solid bar systems with double corrosion protection in accordance with EN 1537.

In the case of soil nailing, relative displacements mobilize shear stresses between the nails and the adjacent soil, which lead to tensile stresses in the nails.



Fig. 3: (inner) sliding surface as a form of failure of a soil nailing system

According to the Federal Association of Test Engineers (Bundesvereinigung der Prüfingenieure für Bautechnik, Germany, 2016), undesirable bending stresses occur during soil nailing due to the necessary deformations in the ground transverse to the nails. These lead to an increase in crack widths and unacceptable damage to the corrosion protection. For this reason, it is necessary to ensure double protection against corrosion. From a formal point of view, the use of a system with double corrosion protection not only makes technical sense, but is also a formal requirement for use in Germany. Consequently, only approvals for solid bars with double corrosion protection exist in Germany for permanent nailing systems.

In general:

The assessment of the ideal anchoring system in terms of sustainability will therefore have to be based largely on the combination of geology (stability of the soil and exposure class) and the resulting corrosion protection measures required.

 © DFI International Bruges 2025

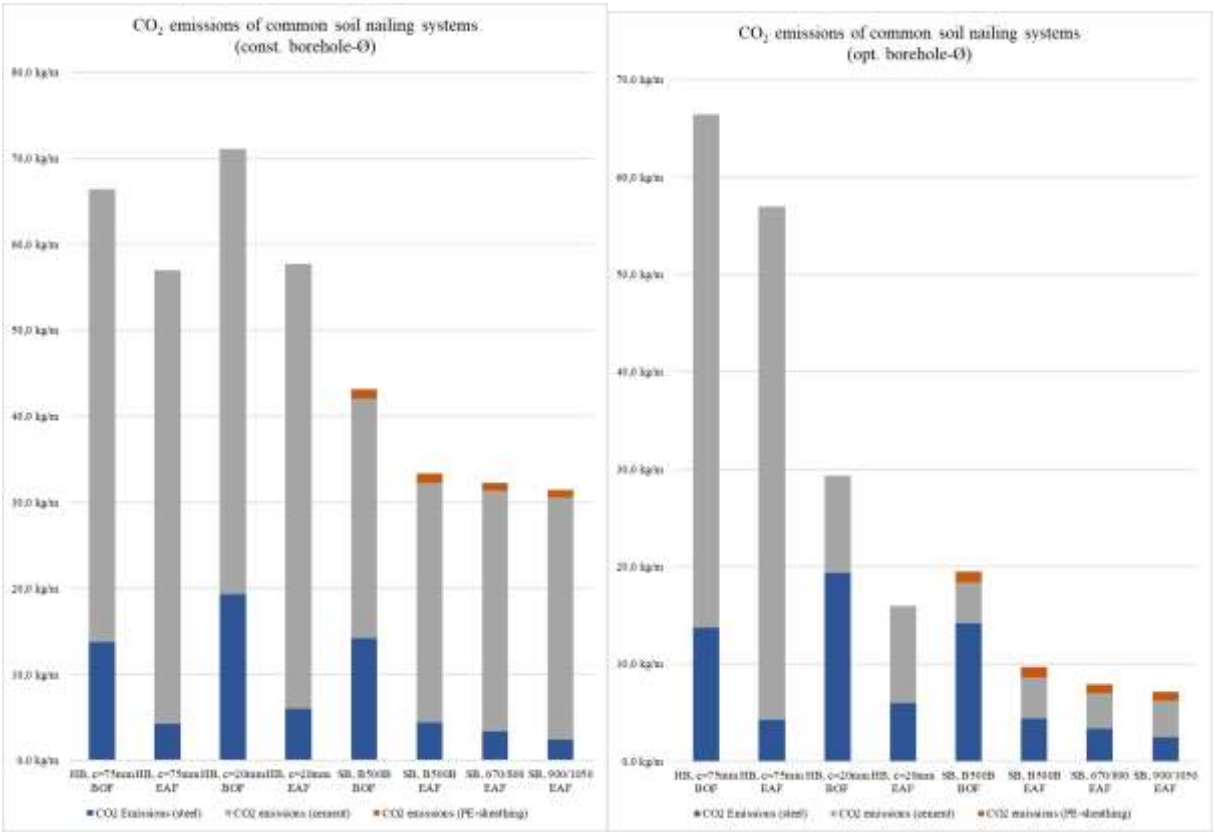


Fig. 4: CO2 emissions of geotechnical anchoring systems per metre through production (without installation); left: assuming the same borehole diameters, right: assuming optimized borehole diameters (HB: hollow bar system, SB: solid bar system)

Table 4. Calculation assumptions	**Unit**	**Identical drill hole Ø**	**Optimized drill hole Ø**
CO2 equivalent cement grout	[kg CO2/t]	600	600
CO2 equivalent cement grout, inner cover of DCP	[kg CO2/t]	500	500
CO2 equivalent steel production via BOF	[kg CO2/t]	2250	2250
CO2 equivalent steel production via EAF	[kg CO2/t]	700	700
CO2 equivalent PE-sheathing	[kg CO2/t]	3110	3110
Characteristic yield force	[kN]	400	400
Borehole-Ø Hollow bar system, low use of steel	[mm/in]	190/7.5	190/7.5
Borehole-Ø Hollow bar system, high use of steel	[mm/in]	190/7.5	92/3.6
Borehole-Ø Solid DCP bar system	[mm/in]	190/7.5	56/2.2 resp. 50/2.0

Figure 4 thus shows that the influencing parameters are diverse and the differences are considerable. The user will therefore have no choice but to determine the ideal system for each individual building project in terms of statics, serviceability and sustainability.

Note: the figures for the CO2 footprint are subject to constant adjustment as a result of many optimization efforts. The assumptions on which Figure 4 and Table 4 are based are largely taken from Schwenk (2023), Fraunhofer Institute (2016) and the German Steel Federation (2024).

 © DFI International Bruges 2025

USE OF HIGH-STRENGTH STEELS – YESTERDAY, TODAY AND TOMORROW

High-strength steels are considered a "wonder weapon" in automotive engineering. In terms of reducing fuel consumption and CO2 emissions, the trend towards ever lighter vehicles is a foregone conclusion. This saves fuel, reduces CO2 emissions and protects the climate, while at the same time providing an impressive level of occupant protection without making the body heavier. Despite all the engineering skill, the car must remain affordable and must be able to score points ecologically in the holistic assessment of the materials used. The trend in automotive engineering has already partially penetrated the construction industry.

From a technical point of view, however, the use of high-strength steels is not a matter of course. Prestressing steels developed in the seventies showed a high susceptibility to stress corrosion cracking and led to corresponding cases of damage. In particular, high-strength steels with high yield strength and tensile strength - this applies to both bars and strands - showed a much higher susceptibility. The general consensus is that sensitivity to hydrogen embrittlement can be assumed from a strength of around 800 MPa. In his investigations, Professor Nürnberger (1980, 1995) came to the conclusion that the service life L in the stress corrosion cracking test decreases with the 3rd power of the stress σ and the 9th power of the strength R_m:

$$L = \frac{C}{\sigma^3 \cdot R_m^9}$$

The findings from damage cases in the seventies to nineties flowed into the development of more resistant steel grades from the Stahlwerk Annahütte. Today it can be seen that the maxims of early prestressing steel development based on the motto 'higher, faster, further' have reached their limits. This applies in particular to the parameters of susceptibility to corrosion and fatigue. With today's steels from the Asian region, it can be seen that development began at a later point in time and has yet to be continued. From today's perspective, we know that limiting strength is generally preferable. However, other parameters such as the selection of the right alloying elements or the setting of residual compressive stresses at the edge of a bar cross-section also lead to good-natured high-strength steels.



Fig. 5: Residual compressive stresses at the edge of a steel bar

In his many years of research and experience in cases of damage to geotechnical anchors, Professor Wichter (2018) has also come to the conclusion that damage to the corrosion protection during installation is the main cause of subsequent failure. The following three examples are intended to show how high-strength steels have been and are being used sensibly in the construction sector while maintaining comparable technological properties and reducing CO2 emissions, how the use of high-strength steels can be technically successful and how high-strength steel can successfully contribute to reducing CO2 emissions.

Example of ground anchor made of prestressing steels

The use of high-strength steels as ground anchors dates back to 1958, when the excavation pit for the headquarter building of the Bavarian broadcasting in Munich was constructed by Bauer Spezialtiefbau

 © DFI International Bruges 2025

(Mayer, 2006). The invention was created in an almost desperate situation on the construction site. The Bavarian Broadcasting Corporation required an open excavation pit without any obstructive support elements. Shafts were sunk around the excavation pit, into which anchors were to be drilled and fixed. However, the Munich gravel threw a spanner in the works - the boreholes deviated and did not hit the shafts. The original idea was to leave the difficult-to-retract drill pipes in the ground as a supporting element. The result is well known. Prestressing steel was pushed into a cased borehole, the casing was pulled out and at the same time grouted with cement mortar. Tensile tests after 5 days confirmed the birth of the ground anchor.

Ground anchors in combination with high-strength steels not only help with the stability of structures such as slope stabilization or construction pits, they also help to reduce CO2 emissions, both through the use of optimized steels and in the optimization of structures (for example, by using prestressed ground anchors instead of heavyweight retaining walls).

Example of high-strength reinforcement as steel supporting member

The use of high-strength reinforcing steel was proposed and tested by Leonhardt as early as 1972. As a substitute for conventionally designed columns reinforced with BSt 500 S, up to 25 % of the reinforcement area can be saved with the same dimensions and full utilization of the SAS 670 (≙ grade 97). If the focus is on increasing the usable area, the column dimensions can even be significantly reduced by utilizing the maximum possible reinforcement ratio. Due to the large diameters of up to 63.5 mm and the socket connections, high reinforcement ratios of up to 15% are unproblematic.

The same steel has long been used in geotechnical engineering. Grade 670/800 as a load-bearing member for micropiles, single-bar anchors or soil nails. In the case of geotechnical systems, the saving on the steel supporting element is easy to put into perspective. The savings for the steel load-bearing member are simply determined by the ratio of the yield strengths, e.g. B500B is replaced by 670/800, resulting in a saving of -34%.

Example of high-strength tunnel anchors

As part of efforts to optimize materials, Stahlwerk Annahütte came up with the idea of using high-strength steel grade R_e/R_m 900/1050 as an SN anchor as a substitute for commercially available SN anchors made of reinforcing steel B500B - hence the steel grade SAS 900/1050 SN. The high-strength SN anchor proved its suitability first in practice during the excavation of the Bleßberg Stollen on the high-speed rail line Erfurt - Nürnberg.

An SN anchor is a fully bonded anchor. In terms of design, the method of improving the rock mass properties (commonly: by increasing the cohesion) is used for fully bonded anchors. The only decisive factor when using fully bonded anchors is the anchor load that can be absorbed, which is characterized by the yield strength or tensile strength and the cross-sectional area of the load-bearing member. In other words, only the yield load and/or breaking load are decisive for the load-bearing capacity. If one compares the yield loads of the high-strength SN anchors with those of commercially available SN anchors made of B500B, there is a weight reduction per se and an associated minimum reduction in CO2 emissions during production of 44%, not including savings due to the potential reduction of the drill hole.

The new high-strength SN anchors offer the user above all easy handling resulting from a 44% weight saving compared to conventional SN anchors with the same static properties. In addition to the advantages in handling and occupational safety, there are of course also the consequential economic

 © DFI International Bruges 2025

advantages such as lower freight costs, the potential possibility of faster drilling by reducing the borehole diameter, the possibility of carrying out different work steps in parallel and thus ultimately optimizing the rate of advance.

The relationship between radial tunnel anchoring and floor nailing is given. So, the next step can only be to transfer these savings to soil nailing systems. Especially with temporary systems, the savings potential would be considerable.

CONCLUSION

The parameters influencing the sustainability of geotechnical systems are manifold. The following framework parameters were considered:

- Selection of the ideal manufacturing process for the basic construction materials (steel and cement)
- Selection of the optimal geotechnical system with regard to statics, serviceability and sustainability
- Choice of innovative building materials such as high-strength steels and their influence on sustainability

It is obvious that the choice of sustainable systems is not a question of the future. Even today, there are many ways for users to take sustainability into account.

The use of resource-saving building materials and anchoring systems seems to be primarily the preserve of manufacturers, contractors and building owners. In fact, however, it is not only those directly involved in the construction process who are called upon to optimize their environmental impact. Legislators, who as public clients are certainly also one of the largest building owners, will also be obliged to enshrine sustainability in planning as a third pillar alongside load-bearing capacity and serviceability. Some countries are already playing a pioneering role here. Europe has taken its first step with the introduction of the new Construction Products Regulation.

REFERENCES

EN 1537:2013; *Execution of special geotechnical works - Ground anchors*

DIN EN 14199:2015; E*xecution of special geotechnical work - Micropiles*

DIN EN 14490:2010; *Execution of special geotechnical works - Soil nailing*

Schwenk; *Der Weg zur Klimaneutralität von Zement und Beton; https://www.schwenk.de/der-weg-zur-klimaneutralitaet-von-zement-und-beton/;* August 2023

Bundesvereinigung der Prüfingenieure für Bautechnik e.V.; *Korrosionsschutz bei Dauernägeln, Festlegung der Prüflasten bei Bodenvernagelung*; April 2016

Fraunhofer-Institut für Umwelt-, Sicherheits- und Energietechnik Umsicht; *Technische, ökonomische, ökologische und gesellschaftliche Faktoren von Stahlschrott* ; November 2016

Wirtschaftsvereinigung Stahl; *Regelbuch für das Klassifizierungssystem im Low Emission Steel Standard (LESS);* April 2024

U. Nürnberger; *Analyse und Auswertung von Schadensfällen bei Spannstählen*; Forschung, Straßenbau und Straßenverkehrstechnik 308, 1980

 © DFI International Bruges 2025

U. Nürnberger; *Korrosion und Korrosionsschutz im Bauwesen*; Bauverlag, 1995

L. Wichter; *Schäden und Schadensmöglichkeiten bei Verankerungen*; Juli 2018

F. J. Mayer; *Bauer - Geschichte und Geschichten*; 2006

Leonhardt, Teichen; *Druckstöße von Bewehrungsstäben und Stahlbetonstützen mit hochfestem Stahl St 900, DAfStb Heft 222*, 1972

 © DFI International Bruges 2025

A LOOK INTO THE FUTURE OF SELF-HARDENING SLURRIES IN A DE-CARBONIZING WORLD

Gilbert R. Tallard 434 9890 2182, Mclean VA, gtallard@liquidearthsupport.com
Gregory E. Thomas 973 997 5970, Wayne, NJ USA, thomascabin1955@gmail.com

ABSTRACT

The authors examine future options when modernization of steel production worldwide will cause the disappearance of slag cement as a primary ingredient for Self-Hardening Slurries (SHS). The general adoption of the carbon calculator and carbon content pricing will also change the economic equation of the use of Portland cement in this use. The Ca/Si ratio of the Portland cement Calcium Silica Hydrate (C-S-H) (main strength contributor) is between 1.6 and 2.0. Studies for concretes with the water/cement (W/C) ratio between .35 and .5 show significantly better results may be obtained with a Ca/Si ratio closer to one. In this study the W/C ratio varies between 5 and 10, as typical for a SHS. With essential focus on strength and hydraulic conductivity, test results for selected formulations are given over a relatively long aging period up to one year. A narrowing of suitable options became apparent offering as a conclusion a direction for further research for future mixes with a significantly lower Portland cement content and thus potential reduction of the mix carbon footprint.

KEY WORDS: cement bentonite (CB), self-hardening slurry (SHS), ground blast furnace slag cement (GBFSC), cutoff wall, hydraulic barrier, Portland cement (OPC), Calcium /Silica ratio (Ca/Si), hydraulic conductivity (K), Perlite, perlite ore, pumice, Read Lake Earth, calcium and sodium bentonite, Kaolin, Attapulgite, carbon footprint.

INTRODUCTION

Stable grouts made of Portland cement suspension in a hydrated bentonite slurry are at the origin, sixty years ago, of cement bentonite slurries allowing the construction of hydraulic barrier or cutoff walls in a single phase, the fresh slurry acting as a trench support fluid during excavation and becoming the end-product body upon setting and curing in place. In Europe during the Seventies using ground blast furnace slag as a Portland cement replacement became common, and in some cases compulsory, in underground workings. Along with many other construction technologies imported from Europe, slag cement became progressively used in underground works, including cutoff walls. Depending on location and local resources, other ingredients such as fly ash and powdered limestone have also been used as partial replacement for Portland cement. But only slag cement was capable of 100% Portland replacement in a self-hardening slurry (Tallard 1996). Regarding bentonite, other clays such as sepiolite and attapulgite have broadened the performance possibilities for cutoff wall construction [US Pat. No. 4726713] with slag cement SHS technology for cutoff wall construction for hazardous waste mitigation with hydraulic barriers of very low hydraulic conductivity (K) combined with superior chemical resistance.

The last three decades have been golden years of cutoff wall construction using SHS with very high slag replacement from 75 to 100%. For a clean ground water situation where a cutoff wall hydraulic conductivity is specified at $<10^{-6}$ cm/s, a typical straight OPC-Bentonite SHS requires at least 22% of binder by weight of water (b.w.o.w.) and a 4-5% bentonite slurry. A blended slag-OPC at 80% slag replacement will achieve better results with only 10-12% binder b.w.o.w.. This provides a reduction of OPC for an equivalent or better result of over 70% (over 5 times smaller carbon footprint for the OPC). Substantial technical and economic benefits have resulted from the use of slag cement. One drawback for slag cement slurries is in areas of high seismicity where the brittle break of slag rich mixes at their limit is in conflict with the difficulty for the engineering community to analyze the potential risk of damage to the cutoff wall during a seismic event.

The latter had led the authors to explore in 2017 the possibility of improving the ductility of high slag-content based mixes by increasing the bentonite content in the formulas. This concept derived from

 © DFI International Bruges 2025

50-year-old information originated by Dr. C. Caron indicating that dosage above 3% of bentonite started to affect negatively the strength of the mix (at the time with 100% OPC). In fact, the conclusion of this exercise was that, contrary to expectations, adding bentonite to the mix did increase the strength of the mix but with no improvement in ductility whatsoever. In view of the future decline of slag cement availability, this old experience connected with the goal of reducing the carbon footprint of everything we use in this business. The modernization of the steel making process is reducing the availability of slag for grinding into slag cement and is a worldwide phenomenon. Becoming harder to find, the price of this commodity is increasing faster than Portland cement with most of the US consumption being imported and prioritized for the concrete ready mix and pre-cast industries.

In a generation or two, blast furnace slag cement will be a thing of the past.

EXPLORATION

As an effort to chart a course for the future of self-hardening slurries in a low carbon environment, an exploration into a minimized carbon SHS successor has been undertaken under the cover of Covid 19 interlude. And who would have imagined a possible U turn back to the original CB, but with a twist!

CALCIUM/SILICA RATIO

The calcium silica ratio (Ca/Si) of hydrating OPC forming C-S-H hydrates varies from 1.6 in Europe to close to 2 in the USA. This has been recognized as an imbalance inherent with the clinker manufacturing process that aims at generating early strength, a must for the conventional concrete construction industry. The SHS industry is not as impatient as the concrete industry and a longer curing curve is generally not an issue in foundation works and often desirable.

Concrete researchers have concluded that a significant increase in strength can be achieved by adding activated silica to the ingredient mix (Kunther et al. 2017), with an ideal Ca/Si ratio near one. Following this precept, in the early seventies, a French researcher in SHS (Portier 1984) investigated whether the same effect could apply to mixes with a W/C ratio ten to twenty time larger than in concrete, as is the case with SHS. He observed that a silica rich natural material such as diatomaceous earth (DE), added in the right proportion to a slag rich-OPC blend, did produce a spike in strength of the SHS. This finding was further verified by the authors in 2017 by comparing a baseline CB slurry (just OPC) with an equivalent solids slurry which replaced a fraction of the OPC by DE, as shown in Fig. 1.

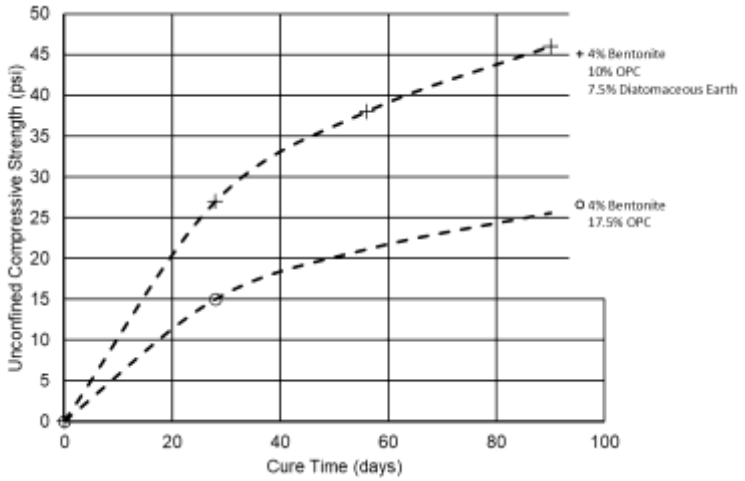


Fig. 1 Impact of Diatomaceous Earth Addition to a basic CB slurry (2017 study)

This experience encouraged conduction of further testing in the same vein. Subsequent exploration of this, shown in Fig. 2, indicated mixes with Diatomaceous Earth provided a phenomenal increase in

 © DFI International Bruges 2025

strength by comparison to a pure CB mix. However, we found little or no improvement in lowering the coefficient of hydraulic conductivity, even with the addition of Kaolin to the mix.

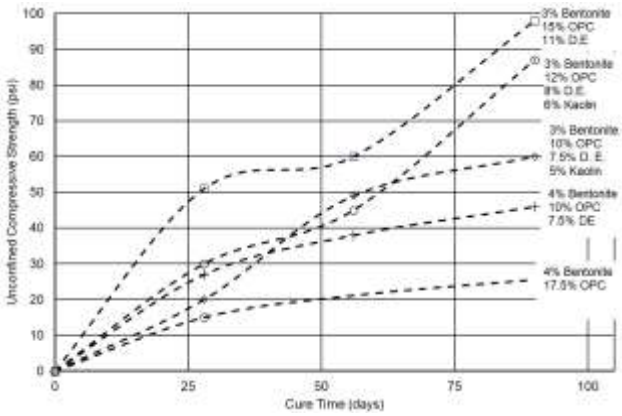


Fig. 2 Results from 2017 and 2021 mixes on impact of added Diatomaceous Earth and Kaolin to a basic CB slurry

MIXES

Mixes Studied

In the search of obtaining a SHS with a hydraulic conductivity coefficient, K, < 10^{-6} cm/s as traditionally required for clean water work, a wider array of silica rich minerals needed to be evaluated. In this vein, as shown in Table 1, a selection of natural materials was evaluated, with silica fume, a waste product being the exception.

TABLE 1. Mineral products used.

Mineral Product	Assumed product SiO2 content for study (%)	Product Added b.w.o.w. (%)	Comments
Diatomaceous earth	80-90	5.4	
Silica fume	90	5.1	
Pumice	76	6.1	
Perlite expanded	72	6.4	
Calcium bentonite	61	7.6	
Attapulgite	60	7.7	
Sodium bentonite	60	6.5	
Kaolin*	58-60	7.7	
Red Lake Earth	50*	7.2	*Assumed
Perlite Ore	50*	11.9	*Assumed
Slag cement (for information)	36		
Baseline OPC	20		
* meta-kaolin was initially also considered but it is processed and onerous for use			

 © DFI International Bruges 2025

For a pure OPC, the target hydraulic conductivity of 10^{-6} cm/s can barely be achieved with a dosage of 22% Portland cement, as used in this study as the base line for comparison. Since the intent was to aim at a drastic reduction of Portland cement required, a goal of Portland reduction by 50% seemed proper for use in this study.

All mixes were prepared based on a hydrated Bara-Kade bentonite slurry dosed at 5% and Portland cement dosed at 11% b.w.o.w, other than the baseline mix with 22% Portland. The mineral additives were added in relation to their assumed SiO2 content to achieve a Ca/Si ratio close to 1, based on the excess Ca in the Portland.

Mixing Method

In traditional cement-bentonite slurry preparation, dry cement is added to the hydrated bentonite slurry. This causes the bentonite to gel in short order which chokes laboratory mixers. Without the addition of a dispersant mixing through the peak of rigidity is not possible. Introducing a chemical additive, the dosage of which may vary from one mix to the next, will skew the results by differentiating their aging curves.

Instead, an alternative mixing preparation was used where the total makeup water required was split between the bentonite and the Portland cement in an 80/20 ratio (Harris, 2021) to obtain a slurry of each. The bentonite slurry was then added into the cement slurry while stirring, which avoided the bentonite gelling and allowed the mixing of a fluid slurry for preparation in the laboratory without additive. It then follows that the test results of all mixes are comparable in regard to time basis. The mineral additives were then added dry to the slurry mix.

Test Schedule

Since these replacement materials would at best exhibit a slow pozzolanic reaction, it was planned to test these mixes starting at 90 days and beyond. Due to unforeseen circumstances, the mixes were first tested past 145 days, with some ultimately at 190 days. Knowing that SHS slurries may take over 12 months to achieve their ultimate characteristics, a final test series was performed on the three most promising mixes at 12 months.

RESULTS

The laboratory test results are summarized in Table 2, where it can be noted that all alternate mixes with 11% OPC have a substantially higher water content and a lower solids content (dry weight) than the baseline cement bentonite mix with 22 % OPC. In addition, in contrast to blast furnace slag cement rich mixes, the strain at rupture in UCS testing is equal or higher than with the base line mix. It follows that from a material weight standpoint alone, lighter mixes may have an added benefit from the supply shipping and reduced carbon footprint.

Unconfined Compressive Strength (UCS) gains for the mixes with OPC replacement, shown in Fig.3, were similar or greater than that of the OPC mix alone. For a number of mixes, in particular those with silica fume, pumice, Red Lake Earth, diatomaceous earth, and perlite ore showed a gain close to 100% over the baseline Portland cement mix. But the hydraulic conductivity (K) of these mixes, as shown in Fig. 4, were above the desired 10^{-6} cm/s except for the perlite ore.

The 22% OPC baseline mix exhibited a K at 200 days was still slightly higher than 10^{-6} cm/s, which confirmed our experience. Once cured, Kaolin clay, attapulgite clay, Bara-Kade bentonite clay, and perlite ore achieved hydraulic conductivities below 10^{-6} cm/s, making them good candidates for cutoff wall construction. With respect to ductility, the strain at rupture of these mixes were equal or higher than that of the 1% failure strain of the base OPC mix.

 © DFI International Bruges 2025

Table 2 Summary of results for mixes studied

MIX/ ADDITIVE	MIX DATE	TEST DATE	CURING PERIOD (days)	WATER CONTENT (%)	TOTAL UNIT WGT. (pcf)	TOTAL DENSITY (Mg/m^3)	DRY UNIT WGT. (pcf)	DRY DENSITY (Mg/m^3)	PEAK COMPRESSIVE STRESS (psi)	STRAIN @ FAILURE (%)	HYDRAULIC CONDUCTIVITY (cm/s)
Diatomaceous Earth	2/12/2022	7/8/2022	146	447.0	71.5	1.15	13.1	0.21			2.7E·06
Diatomaceous Earth	2/12/2022	7/7/2022	145	432.9	68.6	1.10	12.9	0.21	58	1.5	
Silica Fume	2/12/2022	7/7/2022	145	425.7	69.4	1.11	13.2	0.21			3.4E-06
Silica Fume	2/12/2022	7/6/2022	144	415.7	70.8	1.13	13.7	0.22	58	1.4	
Pumice	2/12/2022	7/11/2022	149	410.5	70.7	1.13	13.9	0.22			2.1E-06
Pumice	2/12/2022	7/8/2022	146	406.4	71.1	1.14	14.0	0.22	60	1.2	
Perlite	2/12/2022	7/7/2022	145	402.6	69.4	1.11	13.8	0.22			5.2E-06
Perlite	2/12/2022	7/6/2022	144	394.2	69.7	1.12	14.1	0.23	47	1.3	
Calcium Bentonite	2/12/2022	7/8/2022	146	397.5	70.5	1.13	14.2	0.23			3.3E·06
Calcium Bentonite	2/12/2022	7/7/2022	145	388.0	71.0	1.14	14.6	0.23	24	1.2	
Attapulgite	2/12/2022	7/8/2022	146	397.9	70.4	1.13	14.1	0.23			8.4E-07
Attaputgite	2/12/2022	7/7/2022	145	392.7	70.1	1.12	14.2	0.23	17	1.5	
Barakade Bentonite	2/12/2022	7/11/2022	149	422.0	70.3	1.13	13.5	0.22			1.5E-07
Barakade Bentonite	2/12/2022	7/8/2022	146	420.0	70.2	1.13	13.5	0.22	23	1.4	
Barakade Bentonite	2/12/2022	8/19/2022	188	404.1	69.9	1.12	13.9	0.22	27	1.0	
Barakade Bentonite	2/12/2022	8/22/2022	191	410.8	70.2	1.13	13.8	0.22			1.5E-07
Barakade Bentonite	2/12/2022	2/13/2023	366	417.4	70.2	1.13	13.6	0.22			7.8E-08
Barakade Bentonite	2/12/2022	2/13/2023	366	417.9	70.5	1.13	13.6	0.22	34	1.1	
Kaolin	2/12/2022	7/8/2022	146	351.1	72.0	1.15	16.0	0.26			5.8E-07
Kaolin	2/12/2022	7/7/2022	145	344.9	72.0	1.15	16.2	0.26	22	1.1	
Kaolin	2/12/2022	8/19/2022	188	349.7	71.2	1.14	15.8	0.25	21	1.4	
Kaolin	2/12/2022	8/22/2022	191	353.3	71.6	1.15	15.8	0.25			7.3E-07
Kaolin	2/12/2022	2/13/2023	366	350.2	71.7	1.15	15.9	0.25			5.0E-07
Kaolin	2/12/2022	2/13/2023	366	349.9	71.6	1.15	15.9	0.25	26	1.4	
Red Lake Earth	2/12/2022	7/7/2022	145	399.4	70.2	1.13	14.0	0.22			2.2E-06
Red Lake Earth	2/12/2022	7/6/2022	144	394.2	70.4	1.13	14.2	0.23	53	1.3	
Perlite Ore	2/21/2022	7/11/2022	140	324.4	72.8	1.17	17.2	0.28			3.6E-07
Perlite Ore	2/21/2022	7/8/2022	137	319.3	72.9	1.17	17.4	0.28	59	1.5	
Perlite Ore	2/21/2022	8/19/2022	179	312.1	72.3	1.16	17.6	0.28	59	1.3	
Perlite Ore	2/21/2022	8/22/2022	182	317.3	72.2	1.16	17.3	0.28			6.8E-07
Perlite Ore	2/21/2022	2/21/2023	365	319.1	72.6	1.16	17.3	0.28			4.3E-08
Perlite Ore	2/21/2022	2/21/2023	365	320.1	72.5	1.16	17.3	0.28	81	1.2	
Baseline CB	2/12/2022	7/6/2022	144	297.6	74.0	1.19	18.6	0.30			1.3E-06
Baseline CB	2/12/2022	7/6/2022	144	288.6	73.2	1.17	18.8	0.30	28	1.0	
Baseline CB	2/12/2022	8/19/2022	188	294.4	72.7	1.17	18.4	0.29	31	0.9	
Baseline CB	2/12/2022	8/22/2022	191	295.4	73.5	1.18	18.6	0.30			1.2E-06
Baseline CB	2/12/2022	2/13/2023	366	288.0	73.5	1.18	18.9	0.30			4.8E-07
Baseline CB	2/12/2022	2/13/2023	366	290.7	73.4	1.18	18.8	0.30	32	1.2	

 © DFI International Bruges 2025

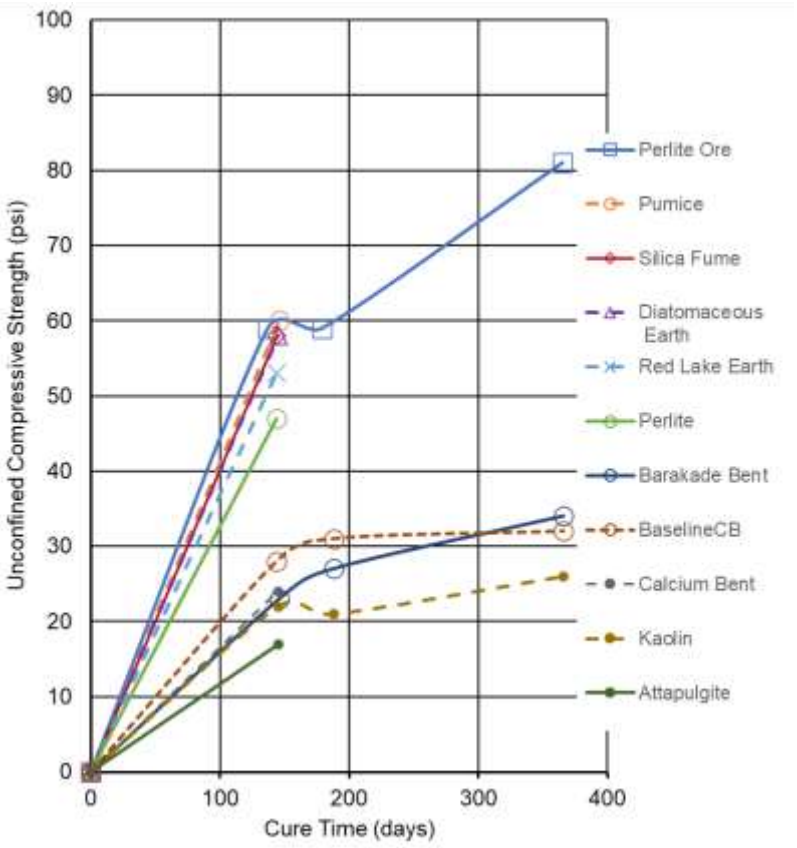


Fig. 3 Unconfined Compressive Strength results up to 1 year

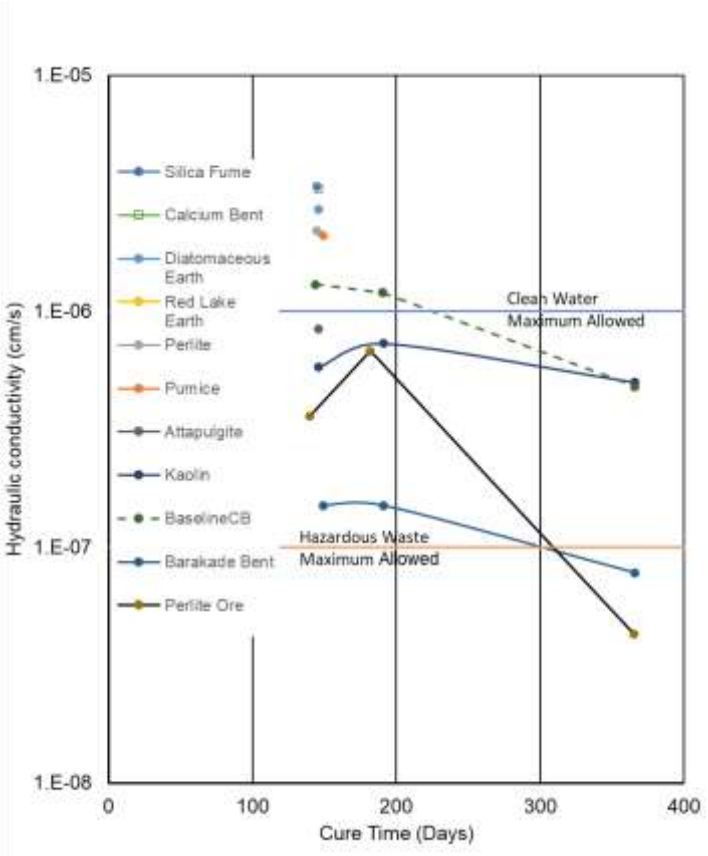


Fig. 4 Hydraulic Conductivity test results

 © DFI International Bruges 2025

SUMMARY AND CONCLUSIONS

The purpose of this self-funded research was to point at a direction for further academic and concerned public agency R&Ds to optimize and enlarge the inventory of possible available replacement products by undertaking further research to plan the future. This study showed that alternatives to Portland cement exist that can provide beneficial results for both strength and hydraulic conductivity.

The disappearance of slag cement being somewhat in the future, there is still time to develop this research. The additives studied can guide designers in the absent slag future to investigate local resources (including recyclable waste like recycled powdered glass) at the regional level to arrive at more diverse cost-effective formulations (Buy local!).
Pricing and taxing of carbon may well arrive well before slag cements complete disappearance and will ultimately influence the re-orientation of SHS formulations.

It was counterintuitive that sodium bentonite, commonly used as a drilling fluid and as a suspension agent for self-hardening slurries for generations, be considered as a potential replacement for Portland cement in this type of work. But so it is with a twist.

Carbon Dioxide Equivalent (CO2e) Emmissions Reduction

The main goal of this study is the reduction of CO2e emissions, better known as the carbon footprint, for self-hardening slurries (SHS) once slag cement becomes a thing of the past. The quantification of the carbon footprint of the various mixes studied consist of adding the respective carbon footprint of each ingredient ex fabrica plus that of the delivery to the jobsite, typically by road freight. Given the wide distribution of Portland cement we assumed that its delivery distance could be 50 miles. For the mineral ingredients, on the principle of finding acceptable local sources, we assumed a shipping distance of 300 miles. Bentonite supply is more complicated depending on required quantities and location, rail freight often combining with road shipping.

Whereas Portland cement footprint is well established at 930 Kg of CO2e per tonne and diesel fuel CO2e emissions is easy to determine for trucks per ton carried based on consumption per mile and average load of 22 tonnes, when we tried to obtain a value of CO2e at the plant exit door from the producers of the mineral resources that were studied, including bentonite, we hit a wall of candid ignorance.

One has to recognize that the US, in contrast to the EU, has no regulatory basis for a generalized evaluation of the carbon footprint for everything produced. This stems from a general laxity on the part of the population as it relates to energy consumption having been blessed with a country of disproportionate energy resources by comparison to most countries. This led the political sphere, the US Congress in particular, to drag its feet on the accounting of carbon, even at a time when it is clear to everyone that we are experiencing the dire consequences of our diletance.

Consequently we failed in figuring a firm percentage of emission reduction value for the minerals replacement considered. Comparing the 930 Kg/tonne for Portland cement versus the 52 Kg per tonne that Slag cement offers today, we are encouraged to find alternative substitutes for slag cement once the latter becomes unavailable.

As an illustration of the weight of CO2e emissions in the cutoff wall industry, the EFFC/DFI Carbon Calculator Tool has determined that materials contribute to 85% of the total emissions for diaphragm and slurry wall construction, which is a fair approximation for SHS cutoff walls.
This experiment was limited in scope and could have been optimized by varying the dosage of replacement minerals for each mix. However, the effort of finding mineral replacement materials of

 © DFI International Bruges 2025

very low carbon footprint permitting the reduction of Portland cement content by 50% to achieve similar performance or better has been successful.
It appears that in this type of construction when strength is the prevalent characteristic for a SHS, certain replacement materials, as indicated above, should be preferred: ground improvement by deep mixing method or incorporation of more of the *in-situ* soil comes to mind; when low hydraulic conductivity is the key criterion, the few replacement materials achieving hydraulic conductivity under 10^{-6} cm/s should be considered.

Test Cure Time

The test results presented show the traditional concrete milestone of the 28 days strength is used abusively when it comes to SHS design and control. Twenty-eight days is barely the age of puberty, not even teenage when it comes to SHS. Adulthood is reached at 90 days and maturity may be achieved at 180 days. It should be understood that pozzolanic reactions are much slower than that of OPC and can continue for over a year. Roman engineers knew that patience was necessary to achieve strength with longevity; had they built their wonderful structures with OPC we would not be able to see today beautiful antique ruins over 2,000 years old.

REFERENCES

Caron C. 1972 La boue auto-durcissable (self-hardening slurry) internal communications

Harris C 2021 SHS Mix Variations and Field Implementations, DFI 46 conf. proceedings

Kunther et al. 2017 Influence of the Ca/Si ratio in C-S-H hydrates, INANO Aarthus U., dk

Portier J.L. 1984 March-April N0. 423 Annales ITBTP conference. Sols & Fondations.fr

Tallard G.R. 1996 Very low Perm. SHS for Permanent Enclosures, FLU St. Petersburg

 © DFI International Bruges 2025

THE INNOVATION OF A NEW PILE SYSTEM TO REDUCE ENVIRONMENTAL IMPACTS: THE PREFABRICATED CONCRETE SCREW PILE

Peter Wardinghus, Centrum Pæle A/S, Vejle, Denmark, +45 2058 3082, pewa@centrumpaele.dk
Paul M. Wiltcher, Aarsleff Ground Engineering, Newark, England, +44 7990 007958, paul-wiltcher@aarsleff.co.uk
Jakob T. Udengaard, Per Aarsleff A/S, Aarhus, Denmark, +45 5144 4925, jau@aarsleff.com
Søren D. Otte, Per Aarsleff A/S, Aarhus Denmark, +45 2212 6399, soren@aarsleff.com

ABSTRACT

In today's fast changing world, expectations for high quality, sustainable and environmentally considerate solutions in every industry are growing and are no longer considered "a nice to have". Foundation design and construction is no different.

Whilst the principles of screw piles are not necessarily innovative, the Prefabricated Concrete Screw Pile (PCSC) combines the benefits of displacement piling and bored piling to reduce CO2 in both the pile design, manufacturing and subsequent installation. The PCSC ensures the benefits of the highest levels of quality control typically achieved with offsite prefabrication of elements. Positive environmental impacts of the PCSC are its vibration free and low noise emissions during installation, zero spoil and that by the very nature of is hollow core, the ability of the pile to accommodate the installation of geothermal loops, now, or in the future.

The paper will discuss the challenges faced during the design of the pile system, the manufacturing process and lessons learned from the trials and testing undertaken to date and how these have impacted the overall development strategy. The paper will conclude with a summary of the commercial challenges associated with bringing a new pile product to market and propose how Engineers and Consultants can collaborate better to achieve greater and faster progress to achieving our collective sustainability and environmental goals. PCSC addresses this as the system combines the advantages of traditional pile systems with its nature of being a prefabricated system with noiseless and vibration free execution.

Keywords: Prefabricated concrete screw pile, full displacement pile, threaded pile, low environmental impact, vibration free, low noise emission, innovation process, sustainable ground engineering

INTRODUCTION

The demand for sustainable and environmentally friendly ground engineering solutions to realize an advancing urbanization, effective infrastructure and other societal developments, continues to rise. Traditional pile systems are challenged to be more effective in reducing their carbon footprint and environmental impact. Still, economic considerations need to be balanced to achieve market acceptance. These outer constraints and expectations define the challenge for the innovating organization.

The PCSC, is an example of a product and concept, which has undergone an innovation management process and successfully being launched to the European ground engineering markets. An understanding of the market demands and potentials, technical possibilities, structural, mechanical and geotechnical design, and considerable trials in the production plant and on site, have challenged and matured the product throughout the process.

The result of the innovation process is a product which meets the original objectives and supplies a more effective, sustainable piling solution with the lowest possible environmental impact on the project surroundings. This paper focusses on the innovation process and its challenges and discusses the results from the production plant and pile installation trials.

 © DFI International Bruges 2025

Prefabricated Concrete Screw Pile (PCSP)

PCSC is a displacement pile under the scope of EN 12699:2015 *Execution of special geotechnical works – Displacement piles*. The pile type is a circular pile with a continuous outer thread. It has a hollow core with keyways for installation with a steel drive rod, see
Fig. 1. The diameter of the core is 377 mm, the height of the threads is 55 mm, and hence the outer diameter across the threads is 487 mm. The pitch of the thread is 250 mm, i.e., 4 revolutions per meter. The standard length is 8 meters per pile segment and piles are mechanically spliced together on site. The bottom pile is mounted with a steel tip.

The pile is installed using a drilling rig with a torque capacity of 280 kNm. During installation, a special drive rod is inserted through the entire length of the pile into the steel tip. Smooth or partially smooth segments (without threads) are produced as required.

The concrete volume of PCSC is 0,088 m^3/m. In comparison, the concrete volume of a circular solid section with an equivalent diameter (508 mm) is 0.203 m^3/m. That is a saving of 0,115 m^3/m or 57 % concrete consumption.



Fig. 1 The prefabricated concrete screw pile during installation: A specially developed drive rod is inserted through the whole length of the pile. Torque from drilling rig is transferred through the drive rod to the pile and pile point via a steel key and a cast keyway in the hollow core of the screw pile

Carbon emissions comparison example

One of the drivers for the pile innovation described in this paper is the saving of materials and hence CO2 emissions. A fictional project with 50 piles of 16-meter length is assumed to calculate the saving in CO2 with the precast PCSC compared to a bored cast-in-situ solution. These piling technologies are compared since they share the advantage of being noiseless and vibration free methods. As a gross assumption, the pile foundation can be realized with either the PCSC or bored piles (CCFA) with a similar diameter (Ø508).

The calculation of CO2-equevalent emission for both pile types is shown in Table 1. The calculation was made with EFFC DFI Project Carbon Calculator v. 5.0 and with EPD data (environmental product

 © DFI International Bruges 2025

declaration) from the pile manufacturer. Emissions from Mob/demob, people's transportation, assets, and waste are not considered.

Table 1 Carbon calculation for fictional project

Pile foundation	Pile design	Assumptions for transportation	Materials + energy + freight [tCO2e]	Total [tCO2e]
Prefabricated concrete screw pile (PCSC)	50 piles, 16 m, Ø487/377	Total pile weight 185 tons Distance from pile factory 250 km	44 + 4 + 3	51
Bored cast-in-situ pile (CCFA)	50 piles, 16 m, Ø508	Concrete C30/37: 178 m^3 (incl. 10% waste) Reinforcement: 18 kg per m pile Distances: - Concrete plant 50 km - Reinforcement supplier 500 km	60 + 7 + 5	72

The calculation of the fictional project shows a saving of 30 % in total tCO2e with PCSC compared to the equivalent bored cast-in-situ solution. Despite the concrete consumption being more than halved with the PCSC, the material emission overall is not. This is primarily attributed to the steel tip and steel pile joints. Further developments of the steel parts to reduce material usage without compromising performance continue.

FROM IDEA TO INNOVATION

An innovative mindset is about managing good ideas; when taking a pipeline perspective, the journey from a first idea to a market launch can be divided into several stages and checking gates. Thereby a cross functional approach must be ensured with thorough internal and external insights within production technology, structural and mechanical design, installation technology as well as marketing.

The motivation: turning weaknesses to opportunities

A strong motivator for innovation is the potential to improve a systems' competitive advantage within its business as well as removing obstacles or even removing system weaknesses. When conducting a SWOT analysis of the market position of the precast concrete driven pile, the rising concern and resistance concerning vibration and noise, represents a considerable threat or weakness of the pile system, particularly as projects are carried out in more and more densely populated areas and increasing urbanization. Therefore, a need to reduce the environmental impact without compromising the qualities of the precast concrete pile system is evident. In that perspective the precast concrete screw pile actually represents an opportunity within the ground engineering market.

When comparing the prefabricated pile system to in situ pile systems, it becomes obvious that each system has advantageous and disadvantageous characteristics. In
Fig. 2 some of the most important characteristics of each system are categorised in a SWOT (Strength-Weakness-Opportunity-Threat) framework. PCSC represents a combination of advantageous characteristics from precast and in situ pile systems and can therefore turn a potential threat to the system into a business opportunity.

 © DFI International Bruges 2025

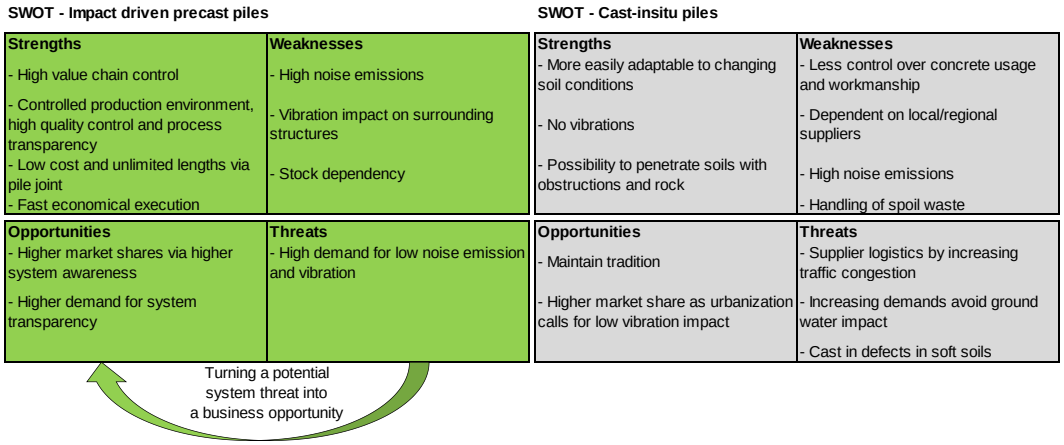


Fig. 2 SWOT turning a weakness of prefabricated concrete piles into an opportunity

Traditionally, in order to avoid vibration caused during the installation of driven precast concrete piles, in-situ pile systems are typically applied, but these are not without their own risks, especially in soft soils. See
Fig. 3 below.



Fig. 3 Typical examples of potential defects with cast in-situ piles. (a) & (b): Reproduced from Felder, 2019, (a) necking and (b) bulging. (c): Photograph of excavated pile wall with typical examples of defects in cast-in-situ piles.

The idea of a precast concrete screw pile

The idea of a prefabricated concrete screw pile is not new. However, prefabricated concrete piles with a continuous thread are not well documented. Motivated by keeping the well-known qualities of precast concrete piles as opposed to occasional challenges for in-situ pile systems (Felder, 2019), is what drives the product and concept development. Attempts have been made in the past to develop a precast concrete screw pile (e.g. Kruijff et al, 1993), but these have failed to establish a foot hold in the market. Relatively high precast production costs and a limited structural torque capacity have been the main barriers to the viability of this pile type. The major development to PCSC is the drive rod and keyway design, that minimizes torsional effects in the pile element during installation.

Due to the outer geometry of the circular threaded cross section, the formwork required is considerably more complicated compared to a traditional square cross section precast pile. Also, the inner hollow core necessitates innovative manufacturing technologies and processes.

 © DFI International Bruges 2025

As the cross section has a limited structural torque capacity, methods of applying the required torque at the top of the pile, have proved the pile cross section to be too weak. Essential for a sufficient inner bearing capacity is an even torque force transmission over the whole length of the pile. With the product development of the prior patent owner, the above-mentioned production and installation issues could be solved to a certain level, at least to serve the Swiss market. In the Bodensee-region of Switzerland, where the soil conditions are dominated by very deep, soft clays, the piles have usually been installed as skin friction piles, requiring relatively low-level torque to penetrate the piles to the design depth.

Identifying essential features: mechanical pile joint

The concept of a joint for prefabricated pile elements, enabling very deep piling and efficient transportation, has been practiced for a longer period of time. In the beginning, pile segments were welded together – a timely and costly process. It was hence identified early on, that the process of pile coupling was a weak link in the pile system. It was essential that an effective system was developed that increased the efficiency of installation whilst also improving pile quality and the health, safety of the workers.

Hence, a new mechanical joint has been developed. This joint represents an inner bearing capacity (Compression, tension and bending moment) corresponding at least to the capacity of the main reinforcement of the pile segment. The new mechanical joint enables quick and safe coupling as well as being cost-effective.



Fig. 4. Mechanical pile joint for the prefabricated concrete screw pile

TRIAL AND TESTING

Manufacturing Trials

Manufacturing trials includes testing components such as the pile joint, pile points and components that are used in the manufacturing of these parts. A major part of manufacturing tests is to prove that the design of pile & accessories can be manufactured in an automated process to ensure high focus on quality, work safety, working environment, energy-, raw material- and production efficiency. Each stage of the manufacturing process has been through several proof-of-concept stages and is thus optimized individually and in combination to prove the production concept.

During the manufacturing trials, various reinforcement combinations, concrete types, pile designs etc. have been tested. The solutions found to be optimum have then been combined and prototypes in scale have been made and tested, followed by full scale factory tests and as a final prove of concept, tested by a full-scale installation trials. After installation, a static load test has been performed followed by the excavation of and removal of the test pile to verify the integrity of the pile post installation.

 © DFI International Bruges 2025

Model testing and industry-academia collaboration

When developing a new pile system, it is necessary to document the load and settlement behaviour in order to gain recognition of the product and its performance. In these efforts, collaboration between industry and academia can be valuable. During the original development of the prefabricated concrete screw pile in Switzerland, centrifuge model testing at scale 1:100 was performed by Lucerne University of Applied Sciences and Arts and TU Delft, Arnold and Askarinejad (2020).

These model tests were conducted in Vingerling-Clay. It was concluded that the screw pile can sustain larger axial loads than a smooth shafted pile with a diameter equal to the outer thread diameter of the screw pile. Furthermore, the screw pile was showing a more robust loading behaviour with some hardening effects compared to the smooth shafted pile. The test also showed that both the smooth shafted pile and screw pile showed the same stiffness as a load-transferring system. The settlement at ultimate limit state of the screw pile corresponded well to 10 % of the diameter, Arnold and Askarinejad (2020).

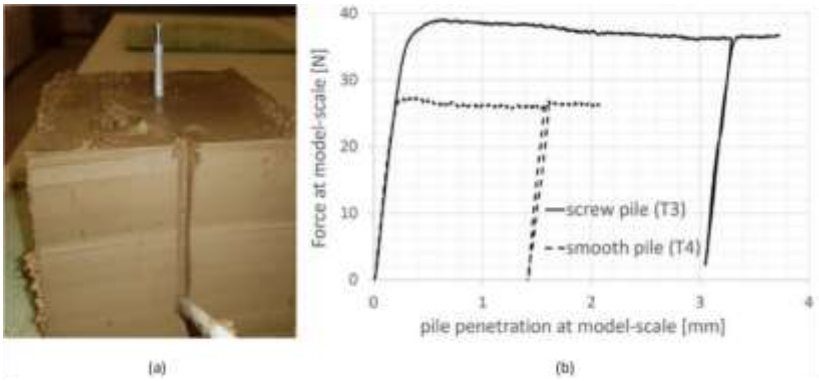


Fig. 5 Reproduced from Arnold and Askarinejad (2020). (a): Vingerling Clay-block after centrifuge test: Backwards: smooth shafted pile; in front: screw pile with the screw profile visible in the pile-soil interface. Model width: 133mm; model length: 200 mm; model depth: 120; pile embedment depth: 80 mm. (b): Load-settlement curves of the screw- and smooth piles tested in the same Vingerling-Clay soil model.

Full-scale Test of the Prefabricated Concrete Screw Pile

At the stage where the product development is sufficiently mature to test at full scale, particular attention for limiting the variables is necessary. The cost for full-scale testing is high, so planning to identify and refine the objectives of the test is essential. In the case of the PCSC, full-scale testing included trial installation with the drilling rig and static load testing.

A test-site with near uniform ground conditions (in the lateral direction) that were representative of those where the intended application of the PCSC would be best suited was identified. The stratigraphy is described in the table below. Depth to ground water level is 2.5 m below ground level.

Table 2. The test site soil profile

Depth (m below ground level)	**Soil type / description**	$\mathbf{q_c}$ [MPa]	$\mathbf{c_u}$ [kPa]
0.0 m to 2.0 m	Sand fill of which the upper 1 m is with organic topsoil	5 to 30	
2.0 m to 4.3 m	Sand fill	2 to 7	
4.3 m to 7.3 m	Loose to medium dense glacial meltwater sand	3 to 8	

 © DFI International Bruges 2025

7.3 m to 15.0 m	Very stiff to hard glacial clay till		150 to 450
15.0 m to 20.0 m	Hard glacial clay till		300 to 700

The site is typical of Danish ground conditions, allowing the test to investigate both the installation and bearing capacities in sand as well as clay till. At 15 meters depth, shear vane tests exceeded values of 450 kPa, characterizing the clay till as very stiff to hard. Hence, the site was ideal for putting equipment and installation possibilities to the test in challenging ground conditions.

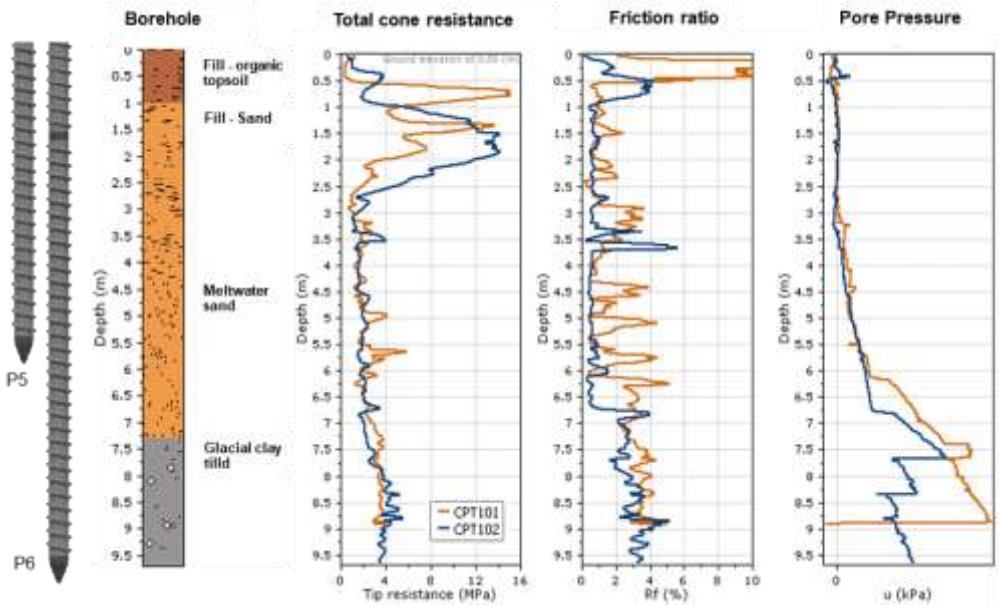


Fig. 6. Test site CPT results

A combination of 15 trial and test piles were installed in lengths between 6 and 16 meters. The longest piles consisted of two 8-meter pile segments. A layout of the piles can be seen in the Fig. 7. The trials were conducted in two phases. In the first phase, learning to install the new pile was the primary focus. This included, training of the rig operator and crew, testing of handling equipment prototypes, pitch, predrilling, and data recording. As expected, there were issues during the first trials with for example handling equipment and newly developed rig software. Hence, some piles were sacrificial, meaning that limited data was gathered that was truly representative of the expected scenarios.

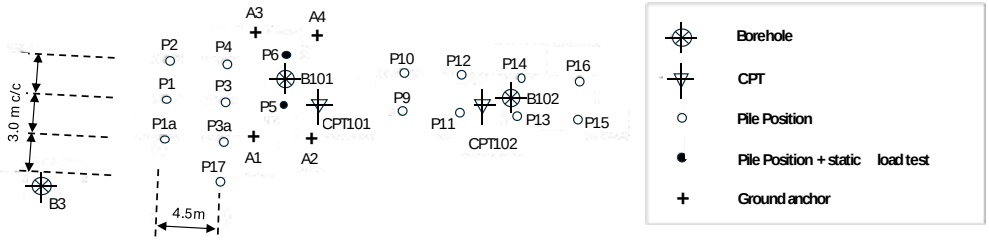


Fig. 7. Layout on the test site.

In the second phase, particular observations made during the first phase were tested further whilst the focus also turned towards how the pile performs in the ground. Two instrumented static load tests were conducted to investigate the geotechnical bearing capacity, settlement behaviour and stiffness. One pile was installed to 5.5 meters depth with its base in the meltwater sand layer, and one pile was in-

 © DFI International Bruges 2025

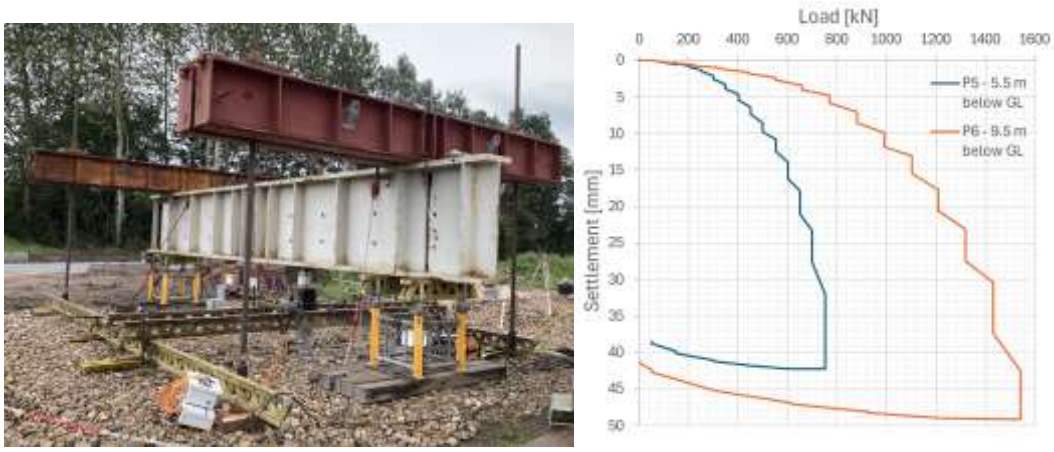
stalled to 9.5 meters depth with base ~2.5 meters into glacial clay till. The piles were instrumented with strain transducers to evaluate base and shaft bearing resistance.

Table 3. Results from full scale static load testing

Pile no.	Base depth	Soil type at base	$R_{ult} = R_{ult,shaft} + R_{ult,base}$	$R_{ult,shaft}$	$R_{ult,base}$
P5	5.5 m below GL	Loose meltwater sand	750 kN	550 kN	200 kN
P6	9.5 m below GL	Very stiff to hard glacial clay till	1540 kN	1140 kN	400 kN

GL = Ground Level

The static load tests were conducted 4 weeks after installation and were performed as a one-cycle maintained load test according to DS/EN ISO 22477-1:2018 Geotechnical investigation and testing – Testing of geotechnical structures – Part 1: Testing of piles: static compression load testing, however with smaller load steps and shorter load holding times to facilitate the strain measurements. The ultimate load was evaluated at a deformation of 10 % pile diameter (= 49 mm). For P5, the load became difficult to maintain after ~42 mm and the test was terminated.



(a) (b)

Fig. 8 (a) Static load testing setup. (b) Load-settlement curves.

An interesting observation from the two static load tests are, that even though they are relatively short with L/D ratios of 12 and 18, both were primarily shaft bearing. This can be contributed to the special shape of the pile that forces the shaft failure slip surface outside of the thread diameter (= 0.49 m) to give a high shaft bearing capacity. This observation is consistent with the findings by Arnold and Askarinejad (2020), that the shaft bearing capacity is higher than a comparable cylindrical pile with the same diameter.

Extraction Test

Another important aspect in innovation is to inform and involve external stakeholders in the work, for example by presenting test results. People outside the innovation team/organization may have a different view on the product and raise questions previously not considered. An example of is, that the nature of the installation process and the shape of the prefabricated concrete screw pile prompted with regard to the integrity of the unreinforced concrete threads. The hypothesis of damaged threads was hence tested by extracting the test pile P5 by means of deep excavation as shown in Fig. 9

 © DFI International Bruges 2025



Fig. 9. Extraction of PCSP after installation and static load test

The extraction of pile P5 after static load testing proved the integrity of the pile shaft and the thread. All threads were intact. Wear on the leading edge of the continuous thread just above the steel pile point was observed as shown in Fig. 10(a). This is regarded to be unavoidable and not detrimental to the general integrity of the pile nor its thread. Furthermore, soil trapped in the space between the threads was highly compacted as shown in Fig. 10(b) and Fig. 10(c), confirming the assumption that the pile can, at minimum, be regarded as a smooth pile with the outer diameter determining geotechnical bearing capacity of the pile shaft.



(a) (b) (c)

Fig. 10 Inspection of extracted PCSP after installation and static load test

CONTINUING INNOVATION CHALLENGES

With the motivation to improve the product further and expand the range of applications of the PCSP, numerous efforts have been initiated. These involve further trials in the fabrication and production of the pile resulting in advancements in the concrete mix design and reinforcement detailing as well as improvement in the installation methodology and instrumentation. As more site trials are completed the data base of static and dynamic pile load test performance data will increase, giving more confidence and verification of the design parameters.

A tangible and for example, area of continuous innovation is the now patented asymmetric cast keyway design to ensure an even transmission of force from the driving rod steel key. This development considers more precisely the differences in torsional deformation between the concrete pile cross section and the steel drive rod. Multi-purpose applications will also be investigated, for example, utilising the hollow core for the extraction of geothermal energy from the surrounding soil and for structural inserts for mast connections. These and other efforts are supported with information and marketing campaigns, involving plant and site demonstrations, aimed towards relevant educational institutions,

 © DFI International Bruges 2025

consultants and clients about the innovation and continuous learning process that has led to the development of the PCSP.

As with every pile system, thorough and adequate soil investigation is crucial for an effective pile foundation design, and installation. However, changes in ground conditions can still occur and might call for correcting actions. As installation data (torque, pull down pressure and pitch control) is recorded in real time, this allows a comparison to the invested soil profile to be made quickly and the selection of the correcting solution to be made more efficiently.

If the issue is with the ability of the pile to reach the required (design) bearing layer underneath a hard to penetrate upper layer, the first measure that can be applied is predrilling with an auger and allowing a low pitch (less than 25 cm penetration per rotation). Following predrilling of the upper hard layer and as the CPSP reaches the bearing layer, the pitch of 25 cm per rotation must be maintained to ensure the required interaction with the surrounding soil is achieved.

If the planned pile depth cannot be reached and the pile has effectively achieved refusal, the surplus pile length can be cut off and, in some cases, it could be used as an upper pile element for the following piles. This is possible since pile sections are fabricated as (i) bottoms with a pile tip and (ii) tops with a joint at each end. Examination of the installation data of a refused pile against the soil profile will determine whether load tests are necessary to verify the required bearing capacity, or to determine if an additional remedial pile is the right solution.

As with rotary bored augers, there are many different configurations of auger head to with deal with a variety of hard and soft, cohesive and non-cohesive ground condition. The same applies to the auger tip of the PCSP. Whilst several different auger tips have already been developed, further developments will be made as more installation experience, in a wider range of ground conditions is gained. These developments will be driven by a philosophy of continuous improvement and a constant desire to improve operational efficiency.

SUMMARY AND CONCLUSIONS

The paper presents the development and market introduction of the PCSP, as a sustainable alternative to traditional in-situ pile systems within the field of ground engineering. This innovation addresses the growing demand for environmentally friendly piling methods by reducing material consumption and limiting noise and vibration impacts while retaining the advantages of precast concrete piles:

- PCSP combines the advantages of traditional pile systems with its nature of being a prefabricated system with noiseless and vibration free execution.
- High quality precast concrete pile shaft with guaranteed pile cross section.
- Full displacement pile type: no spoil, no soil excavation and a stiff load-settlement behaviour
- Suitable to use and install in contaminated soil (no soil excavation).
- Being prefabricated there is no chemical interaction with soil and ground water.
- Segmented pile installation with the advantages of normal transport conditions, easier and safe logistics on site.

An experimental campaign has been performed with scaled laboratory tests, installation tests in full scale and static load testing on full scale piles. Additionally, one of the load tested piles was excavated after installation and testing to soil rupture to observe its integrity. The key findings of the experimental campaign showed that the PCSP performs similar to other displacement pile types, and that the pile and its unreinforced thread remains intact after installation and loading to soil rupture.

The innovation journey involved solving technical challenges in manufacturing and installation, particularly regarding the pile's complex design and torque transmission. Key breakthroughs include the development of a mechanical pile joint ensuring structural integrity and installation efficiency. Exten-

 © DFI International Bruges 2025

sive trials, including model and full-scale testing, demonstrated the screw pile's competent load-bearing behaviour. Ongoing innovations aim to further enhance the pile's production process and expand its applications, including the potential for geothermal energy harvesting. The prefabricated concrete screw pile represents a significant advancement in ground engineering, offering both environmental benefits and robust performance, positioning it as a competitive solution for future urbanization challenges.

The innovation and marketing of the PCSP must deal with considerable commercial challenges as large strategic investments are necessary combined with uncertainties. A longer-term perspective expects an economy of scale, but the volume is relatively low on the short term. Also, the always very competitive market environment, especially towards slim diameter in situ pile systems, pressures the business case.
For the system innovation and the basis for the strategic business case, the collaboration between internal and external stakeholders is essential. In this case, the very early involvement of many different professionals was well facilitated allowing effective synergies. In that spirit, further developments are strived for to stabilize and increase a sustainable competitive advantage of the PCSP system and thereby meet the demands for more sustainable ground engineering solutions.

REFERENCES

André Arnold and Amin Askarinejad. (2020), "Behaviour of prefabricated concrete screw piles under axial loading." Proceedings of the 4th European Conference on Physical Modelling in Geotechnics

Felder, Hans-Peter (2019). “Vorfabrizierte Schraube statt Ortbeton” Der Bauingenieur 3.

H.de Kruijff, B. Kuiper, T.J.N Vinks (1993). “Europaal, Erste toepassing europaal bij NS-viaduct te Utrecht”, Cement Issue Nr. 2 1993, 6-14

 © DFI International Bruges 2025

TOWARDS SUSTAINABLE GROUND IMPROVEMENT: A LIFE CYCLE ASSESSMENT OF STONE COLUMNS AND DRY SOIL MIXING IN NORWEGIAN CLAYS

Nejla Y.H., Keller Grundläggning AB, Kungsbacka, Sweden, nejla.helvacioglu@keller.com
Simon O., Norwegian Geotechnical Institute, Oslo, Norway, simon.oberhollenzer@ngi.no
Robert T., Keller Grundläggning AB, Kungsbacka, Sweden, robert.thurner@keller.com
Vincent W., Keller Grundbau Ges. mbH, Vienna, Austria, vincent.winter@keller.com

ABSTRACT

In Scandinavia, the most commonly used ground improvement method is dry soil mixing that typically uses lime and cement as the stabilizing binders which consumes large amounts of cement and thus contributing to the global warming potential of construction projects - typically quantified in terms of carbon dioxide equivalents (CO_2-eq). Vibro replacement is a widely adopted ground improvement method aiming to increase the stiffness and strength of the soil by installing stone columns. The research project VIBE (VIBro-rEplacement) funded by RFF Oslo and initiated by Keller and NGI investigates possibilities and limitations of the vibro replacement method in Norwegian clays. Primary and secondary (recycled) aggregates were used for the stone column installation at a full-scale test site Onsøy.

This paper presents a comprehensive Life Cycle Assessment of the executed soil improvement work using the European Federation of Foundation Contractors (EFFC) carbon calculator and a modified approach using CO2-eq representative for Scandinavia. In the second step the calculated carbon footprint is compared to an alternative ground improvement method, namely dry soil mixing. Therefore, the CO_2 emissions were estimated for a fictional construction site by assuming an equivalent ground improvement stiffness. It is shown that vibro replacement leads to significantly smaller CO_2 emissions compared to dry soil mixing if an adequate improvement factor is assumed. Emissions can further be decreased during the stone column installation when using secondary aggregates (instead of primary aggregates) and assuming no extensive processing of the material. The findings offer valuable insights in a more sustainable ground improvement, showing great potential for Scandinavian clays.

Keywords: sustainability, soil improvement, vibro-replacement, Scandinavian clay

INTRODUCTION

The construction industry accounts for approximately 40% of annual consumption of mineral resources and 38% of global CO_2 emissions (Kedir et al. 2021). At the same time, the demand for ground improvement in construction is steadily growing and is estimated to reach a volume of around US $40 billion in 2029 (Global Soil Stabilization Market, 2023). Currently, resource- and emissions-intensive methods, like dry soil mixing (DSM), are predominantly used to improve soft soils in Scandinavia. The research project “VIBE - Sustainable Ground Improvement Solution for Oslo” was initiated by Keller and Norwegian Geotechnical Institute (NGI) to investigate a more sustainable soil improvement method – namely vibro replacement – for Norwegian soft soils.

In the first part of the paper both ground improvement methods, namely dry soil mixing and vibro replacement, are shortly described. In the following section, large-scale investigations executed within VIBE at the Norwegian-Geo-Test-Site (NGTS) Onsøy are described.

The second part of this paper presents a comprehensive Life Cycle Assessment of the executed soil improvement work using the European Federation of Foundation Contractors (EFFC) carbon calculator and a modified approach using CO_2-eq representative for Scandinavia. The calculated

 © DFI International Bruges 2025

carbon footprint is further compared to an alternative ground improvement method, namely dry soil mixing.

GENERAL SOIL CONDITION IN NORWAY

It is necessary to get an understanding of the Norwegian ground conditions to discuss the used soil improvement techniques. Figure 1 summarizes the location of surficial deposits in Norway (NGU, 2024) and further indicates the location of the test site VIBE (VIBro-rEplacement) in Onsøy.

Most of Norway's geology is characterized by bedrock and a moraine layer with various thicknesses, with only around 25% of the surface covered by soil deposits (Löfroth et al., 2010). These deeper soil deposits are primarily found in lowland areas, valley floors, and a narrow strip along the coastline. Below the highest shoreline, the geology is dominated by clay and silt, with some locations featuring glaciofluvial deltas composed mainly of gravel and sand, along with finer materials. In most cases, the bedrock is overlain by glacial tills. At higher elevations along the shoreline, soil deposits tend to be thinner than in lowland regions, with the geology consisting largely of glacial tills, glaciofluvial sediments, or dead-ice deposits from retreating glaciers. Lacustrine clays or silts are relatively rare in these areas (Löfroth et al., 2010).

The soft, sensitive and partly quick clays can pose different geotechnical challenges in populated areas (e.g., landslides, bearing capacity failures, bearing capacity and settlement problems due to frost susceptible soils, large deformations during deep excavations, large total and differential settlements) (Löfroth et al., 2010). These fine-grained soils are characterized by low shear strength and high compressibility, especially when the pre-consolidation pressures are exceeded. High water contents and low permeabilities lead to a time-dependent behaviors (i.e., creep effects, secondary compression). (

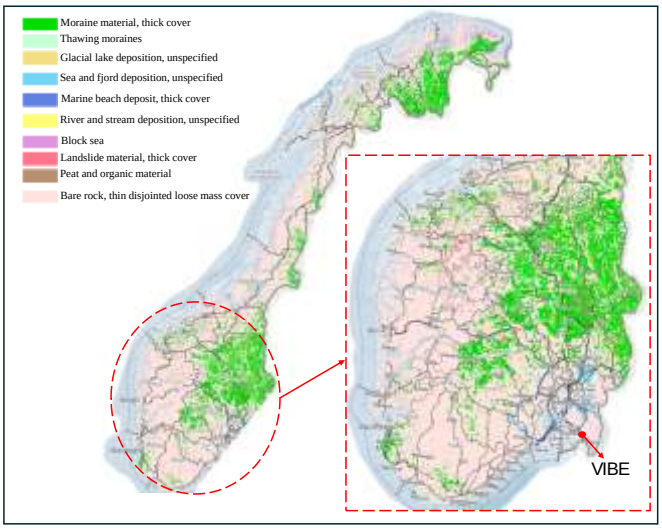


Figure 1. Surficial deposits of Norway with a zoomed in view to show the project area (Retrieved from NGU website, 2024)

GROUND IMPROVEMENT METHODS IN NORWEGIAN CLAYS

Dry deep soil mixing (DDSM)

Dry soil mixing is a ground improvement method used to enhance the properties of soft soils, high-moisture clays, peats, and other weak soils by mechanically blending them with a dry cementitious binder. This technique is particularly effective in high groundwater conditions where the chemical reaction between the soil and the binder occurs even when the binder is introduced in its dry form.

 © DFI International Bruges 2025

The method is commonly used to reduce settlement in structures or to increase the bearing capacity of the ground (e.g., for the foundation of structures and embankments, stabilization of slopes, and excavation pits).

In the initial phase of the dry deep mixing method, a drilling rod equipped with a rotating mixing tool is driven into the ground. As the mixing tool with radial blades penetrates the soil, it shears the surrounding soil. Once the target depth is reached, the binder is pneumatically delivered through the drilling rod to the mixing tool, where it is blended with the soil as the rod is withdrawn. This process facilitates the formation of individual columns as well as overlapping columns or block-like elements. The diameter of these columns can range from 0.6 to 1.0 meter, and depths generally range between 20 and 25 meters (see Figure 2). The process is relatively quiet and generates low vibration. To ensure quality, the dry soil mixing process is closely monitored through installation protocols for each column, which are detailed logs that include the information such as column id, equipment, mixing tool specification, mixing depth and time, binder dosage, BRN (blade rotation number), rotation speed and mixing/penetration rate. There are two main quality control techniques used in Scandinavia, namely the predrilled column test -FKPS and reverse column test -FOPS (SGF, 2000).

There are ongoing research activities for optimization of the amount of binder as well as more sustainable binder alternatives. By using environmentally friendly binders, CO_2 footprint can be reduced significantly. This approach further opens the possibility of discovering new, innovative materials that are both cost-effective and eco-friendly.

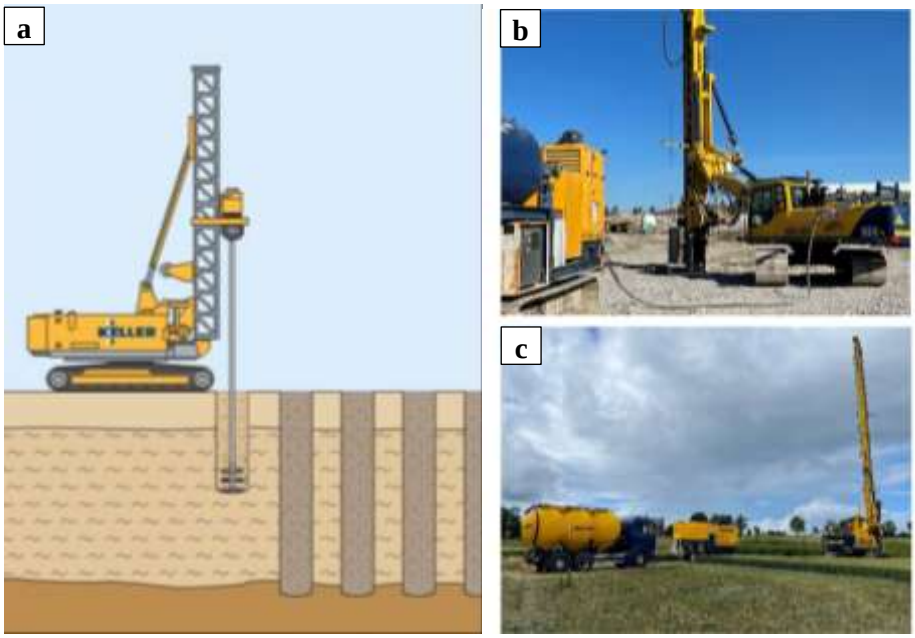


Figure 2. Dry deep soil mixing execution (a, b) and site setup photo (c)

Vibro-replacement (Stone columns)

Vibro-replacement is a widely adopted ground improvement technique used globally. This method involves the creation of columns made of gravel, crushed stone or recycled materials arranged in a defined grid pattern. It aims to reduce building settlements, enhance soil bearing capacity, improve soil permeability or stabilize cut slopes and embankments in mixed or fine-grained soils.

A bottom feed process is commonly used for installing vibro-replacement columns. Keller has developed the Vibro-cat base rig to enhance the effectiveness of this process. The process utilizes a bottom-feed vibrator (see Figure 3: Penetration) that penetrates fine soils such as clay, silt, and fine to medium sand and delivers the coarse granular material to the vibrator's tip (supported by pressurized

 © DFI International Bruges 2025

air). The vibrator fills the created space with coarse-grained material which is compacted by the vibrator in a single compaction step (see Figure 3: Compaction). As a result, a stone column remains in the ground (see Figure 3: Finishing).

Electronic devices are used at all vibro techniques to ensure and automatically record consistent high-quality work. Time, depth, speed, force, and power consumption during penetration and compaction are recorded and shown graphically and can be printed out for each column (see Figure 4).

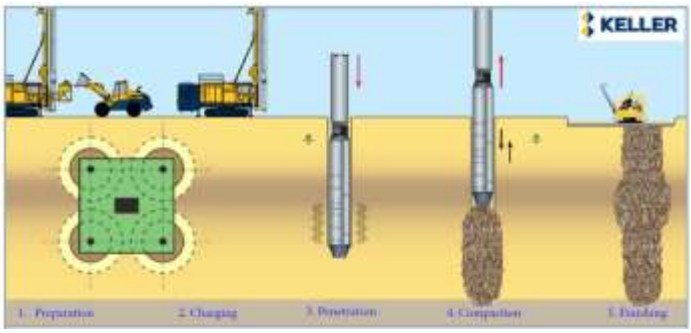


Figure 3. Application of stone columns in stages

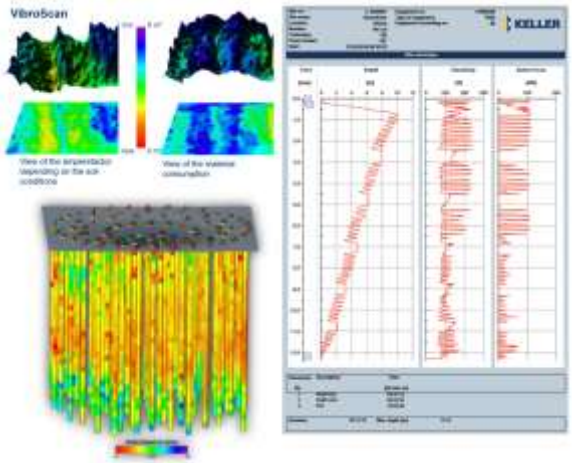


Figure 4. Keller data recording and processing systems for stone columns

LARGE SCALE TEST SITE IN ONSØY - VIBE

The VIBE is a research project focused on developing a sustainable ground improvement solution for Oslo, Norway. The project was partly funded by Regional Research Fund of Oslo and Keller Geoteknikk AS. NGI is also part of this project as research and development partner. The main goal of the project was to generate the essential but currently missing full-scale field data of vibro-replacement with both primary and secondary aggregate in soft soils (e.g., clays) typical to Oslo and to assess the environmental impact of the technique by evaluating the role of secondary aggregate use as a stone column material.

The test field is located in Onsøy in southern Norway, west of Fredrikstad. It was one of the test fields of NGI where extensive soil investigation tests such as soil sampling, pressure sounding, CPTu, seismic and flat dilatometer tests were performed previously to characterize the properties of the clay at the site. Those investigations were 50-70 meters away from the location where stone columns were planned to be installed. Based on these soil investigations the clay at the site was identified as having low sensitivity (S_t < 8) and low to medium strength (Oberhollenzer et al., 2024). Based on the investigations, the test field was selected for the field trials of VIBE. Bedrock was encountered at 9 to 16 meters depth at the VIBE test field. The groundwater table was about 1 meter below the ground

 © DFI International Bruges 2025

surface. During the installation of the stone columns (see Figure 5), unexpected soil conditions were encountered and later investigated as highly sensitive clays (S_t = 24-91) encountered at greater depths, contrary to the original concept, indicating the presence of highly sensitive clays (so-called quick clays) in the test area. Significant challenges were encountered due to these unexpected soil conditions, such as soil liquefaction and softening during the penetration and vibration process.



Figure 5. Photos from VIBE test field during trial phases

The project highlighted the importance of a well-distributed sampling strategy, even in small working areas, particularly when dealing with Norwegian soft clays. This approach is essential for capturing soil variability and ensuring accurate assessments which directly impact the success of soil improvement techniques like vibro-replacement. Detailed investigation on the remolded shear strength and/or soil sensitivity are essential for evaluating the applicability of the vibro replacement method. It should be further mentioned that the collected data from an advanced monitoring set-up (including real-time measurements of piezometers, ShapeArrays™, earth pressure cells, vibration sensors) provided valuable insights into soil behavior during the work of which the comparative calculations of CO_2 emissions are presented in subsequent sections.

The utilization of secondary aggregates for stone columns has demonstrated potential for enhancing soil stability, after appropriate postprocessing at the quarry (e.g., reduction of fines using sieving). Furthermore, it should be mentioned that the transport distance (of secondary aggregate) is crucial for managing both, CO_2 emissions and project costs.

LIFE CYCLE ASSESSMENT

The importance of sustainability in geotechnical projects has gained significant attention through recent advancements in the field, particularly in ground improvement techniques. Basu et al. (2015) categorized sustainability research in geotechnology into two areas: studies that promote global sustainability by using alternative materials and innovative methods, and those focused on developing frameworks for assessing sustainability. This paper falls into the first category, demonstrating the effect of using alternative technologies for ground improvement together with alternative eco-friendly material to ensure more sustainable geotechnical practices.

Calculation method

Life cycle assessment (LCA) of vibro-stone columns is performed for the test site VIBE using the (i) European Federation of Foundation Contractors (EFFC) carbon calculator and (ii) modified carbon calculator, assuming CO_2-equivalents more representative for Scandinavia. Transport distances, material usage and fuel usage were documented during the test execution to enable representative calculations. In the following analyses only emissions until completion of the soil improvement work are considered (i.e., emissions that occur after the vibro work are excluded). Total emissions (tCO_2) and emissions per improved square meter ($kgCO_2/m^2$) will be documented and further subdivided into the scopes of transport (machinery, material, people), material usage and fuel usage.

 © DFI International Bruges 2025

The used CO_2-equivalents are summarized for both calculators (EFFC carbon calculator, modified carbon calculator for Scandinavia) in Table 1. While CO_2-equivalents of the EFFC carbon calculator are considered representative for Europe, CO_2-equivalents were defined for Scandinavia based on a literature review (Kedir et al., 2021). Table 1 shows that CO_2-equivalents used by the EFFC carbon calculator are on average slightly higher compared to the modified carbon calculator. It is further noted that no equivalents are reported for secondary aggregates and lime production by the EFFC carbon calculator.

Table 1. Summary of CO_2 equivalents used for the life cycle assessment based on the EFFC carbon calculator and modified carbon calculator (Scandinavia).

Position		**Unit**	**CO_2 equivalent - (EFFC) carbon calculator**	**CO_2 equivalent - Modified carbon calculator (Scandinavia)**
Transport machinery Transport material	Mega trailer	g/km	1130 #1	854.1 #2
	Trailer	g/km	950 #1	696.9 #2
	Truck	g/km	740 #1	861.7 #2
Transport people	Car	g/km	200 #1	148.59 #3
	Plane	g/km	160 #1	298 #4
Material usage	Primary aggregates	kg/t	4 #1	6.18 #5
	Secondary aggregates	kg/t	not defined	3.7 #6
	Lime production	kg/t	not defined	750 #7
	Cement production	kg/t	860 #1	600 #8
Fuel usage	Diesel	kg/l	3.3 #1	2.66 #9

#1 Neil (2020), #2 Global Soil Stabilization Market (2023), #3 Hoff Sekkelsten (2024), #4 The European Federation of Foundation Contractors (2023), #5 European Automobile Association (2020), #6 Statistisk sentralbyrå (2016), #7 Jörgen and Anneli (2022), #8 National Stone Sand & Gravel Association (2021), #9 Lei et al. (2022)

The CO_2 emissions at the test site VIBE are summarized and discussed in following section. The documented quantities for transport of machinery, material and people as well as material usage and fuel usage are summarized in Table 2 (see column Vibro replacement – as built). It should be noted that the vibro-cat, container and rods were transported from Austria to Norway (documented distance: 1850 km). The compressor was transported to the site from Drammen (Norway). The material for the working platform and primary aggregates were transported from a quarry in Fredrikstad to Onsøy (one way: 9 km, total distance: 360 km and 504 km for working platform and primary aggregates, respectively). Tunnel excavation material was first transported from Oslo to the quarry Fredrikstad (one way: 100 km) for sieving. Subsequently, the sieved material was transported to the site and used as secondary aggregates (total distance: 1854 km). Two construction workers travelled from Austria to Norway by plane (total distance: 2780 km) and two cars were used during the test execution (total distance: 88 km). The material quantities for the working platform, primary aggregates and secondary aggregates are summarized in Table 2. Secondary aggregates were installed at only one location, amounting to 39.3 tons. 1843 liters of diesel were consumed by the machineries during test execution. Vibro work was executed on an area of 129.6 m^2.

In a second step, the emissions of vibro replacement works are compared to dry soil mixing for a fictional example. This comparison intends to represent a more realistic scenario for the comparison of both methods as the transport distances are significantly reduced. To enable a comparison of both methods the same soil improvement factor and modified CO_2 equivalents (Scandinavia) are considered. It is assumed that only secondary aggregates are used for vibro work, which are transported from the quarry in Fredrikstad to Onsøy without postprocessing (i.e. no additional sieving required). The required machinery for both soil improvement methods is transported from Goteborg to Onsøy. The construction workers have the same travel distance. For a summarized overview of the quantities, please refer to Tab. 2 (see columns Vibro replacement - fictional case and Dry deep soil mixing - fictional case).

 © DFI International Bruges 2025

Table 1. Summary of quantities used for the life cycle assessment: CO_2 equivalents used for the life cycle assessment based on the EFFC carbon calculator and modified carbon calculator (Scandinavia).

Scopes		Vibro replacement - as built	Vibro replacement - fictional case	Dry soil mixing - fictional case
Transport machinery *	Vibro-cat (transport by mega trailer)	1850	200	-
	Container and rods (transport by trailer)	1850	200	-
	Compressor and generator production (transport by trailer)	119	200	-
	Shuttle (transport using a trailer)	-	-	200
	Rig (transport using a trailer)	-	-	200
	Silo (transport using a trailer)	-	-	200
Transport material*	Working platform (transport by truck)	360	360	360
	Primary aggregates (transport by truck)	504	-	-
	Secondary aggregates (transport by truck)	1854	551.5	-
Transport people*	Car	88	488	444
	Plane	2780	-	-
Material usage**	Working platform (0-63mm)	444.4	444.4	444.4
	Primary aggregates (new material)	416.1	-	-
	Secondary aggregates (recycled material)	39.3	455.3	-
	Lime	-	-	12
	Cement	-	-	28
Fuel usage***	Diesel for vibro work	1843	1843	700
distance (km)*, quantity (t) and quantity (l)***				

Emissions at the test site VIBE

The estimated CO_2 emissions of the work, executed at the test site VIBE (vibro stone column installation) are summarized in Table 3. It is shown that the total emissions and emissions/m^2 are in good agreement based on $kgCO_2/m^2$ for both carbon calculators. Consequently, the differences in CO_2 equivalents (between the two calculation methods) have no significant influence on this calculation. Table 3 and Figure 6 illustrate that the largest emissions are related to the transport of the machinery, material usage and fuel usage which cover approximately 80 to 85 % of the total emissions. Transport of people and material ranges between 15 and 20 %.

Table 2. Summary of CO_2 equivalents (total emissions: tCO_2, emissions per m^2: $kgCO_2/m^2$) for test site VIBE using the EFFC carbon calculator and a modified carbon calculator (CO_2 equivalents Scandinavia).

Positions	(EFFC) carbon calculator		Modified carbon calculator (CO_2 equivalents Scandinavia)	
	tCO_2	$kgCO_2/m^2$	tCO_2	$kgCO_2/m^2$
Transport Machinery	4.0	30.6	3.0	22.8
Transport Material	2.0	15.5	2.3	18.1
Transport People	0.5	3.6	0.8	6.5
Material Usage	3.4	26.6	5.5	42.2
Fuel Usage	6.1	46.9	4.9	37.8
Total Sum	16.0	123.2	16.5	127.4

 © DFI International Bruges 2025

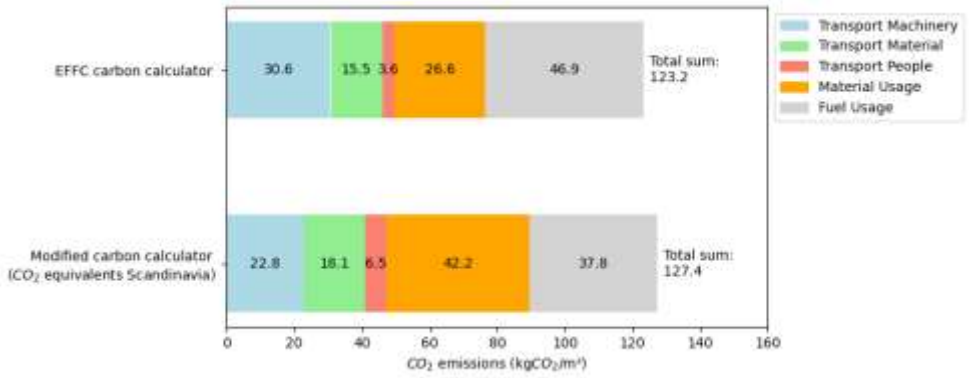


Figure 6: Summary of CO_2 emissions ($kgCO_2/m^2$) for test site VIBE using the EFFC carbon calculator (upper row) and a modified carbon calculator, assuming CO_2 equivalents for Scandinavia (lower row).

Comparison of emissions for the vibro-replacement method and dry soil mixing

In the next step we assume that machinery and people are transported from Gothenburg to Onsøy and only secondary aggregates (without postprocessing, i.e. sieving) are used for the vibro-replacement method. The CO_2 emissions, derived from the modified carbon calculator (CO_2 equivalents Scandinavia) amount to 9.5 tCO_2 and 73.7 $kgCO_2/m^2$ (see Table 4). Due to the shortened transport distance and the use of secondary aggregates (no postprocessing assumed), emissions can be reduced by approx. 40% compared with the test site VIBE (see section with Table 3).

The estimated emissions for dry soil mixing are summarized in Table 4 and amount to 31.2 tCO_2 and 240 $kgCO_2/m^2$ according to the modified carbon calculator. The emissions by DSM per m^2 increase by a factor of 3.3 compared to the vibro-replacement method, assuming the same improvement factor. This significant increase in the emissions can mainly be attributed to the high CO_2 equivalents of the lime and cement production (see Table 1 and Table 4). The significant increase in CO_2 emissions due to dry soil mixing is further shown in Figure 7. It is important to note that the assumed CO_2 equivalent of 3.7kg/t is conservative for the preparation of secondary aggregates. If we would assume no emissions for the preparation of secondary aggregates, dry soil mixing would lead to emissions by a factor 5 higher compared to the vibro replacement method (based on the modified carbon calculator).

Table 3. Summary of CO_2 equivalents (total emissions: tCO_2, emissions per m^2: $kgCO_2/m^2$) using the modified carbon calculator (CO_2 equivalents Scandinavia): Comparison of vibro replacement and dry soil mixing.

Positions	**Vibro replacement method (secondary aggregates only without postprocessing are assumed)**		**Dry soil mixing**	
	tCO_2	**$kgCO_2/m^2$**	**tCO_2**	**$kgCO_2/m^2$**
Transport Machinery	0.4	3.5	0.4	3.2
Transport Material	0.8	6.1	0.3	2.4
Transport People	0.1	0.6	0.1	0.5
Material Usage	3.3	25.7	28.5	220.3
Fuel Usage	4.9	37.8	1.9	14.4
Total	**9.5**	**73.7**	**31.2**	**240.8**

 © DFI International Bruges 2025

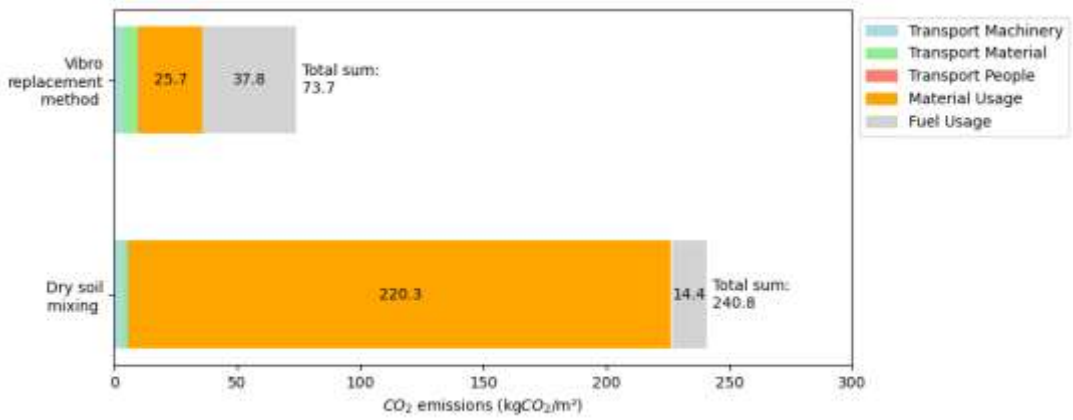


Figure 7. Comparison of CO_2 emissions ($kgCO_2/m^2$) for vibro stone columns (upper row) and dry soil mixing (lower row) using the modified carbon calculator (CO_2 equivalents for Scandinavia).

CONCLUSION

The research project VIBE investigated the potential and of the vibro replacement method, as a sustainable ground improvement method in soft, Norwegian clays using both, primary and secondary aggregates. It was aimed to collect high-quality field data at the Norwegian Geo-Test Site (NGTS) Onsøy and to assess environmental impact of this technique.

The field tests were conducted in high-sensitive clays, a condition not anticipated as no prior documentation had reported such soil characteristics. Although the installation of stone columns was unsuccessful due to unfavorable soil conditions, which caused significant softening around the vibro points, the study was able to achieve two key outcomes: (i) collecting valuable data through a real-time monitoring setup during the installation process, and (ii) evaluating the Life Cycle Assessment (LCA) of vibro stone columns.

The assessment was done using two carbon calculators: the EFFC carbon calculator (representative for Europe) and a modified version tailored for Scandinavia. This assessment includes emissions from transport, material usage and fuel consumption. It was shown that the use of secondary aggregates can significantly reduce the environmental impact compared to primary aggregates. However, emissions due to transportation (of material and people) can have a big impact on the overall emissions.

It was further shown that CO_2 emission of the vibro replacement method is significantly smaller compared to dry deep soil mixing, assuming the same soil improvement factor. Based on our calculations, CO_2 emission ($kgCO_2/m^2$) for ground improvement with DSM increases by a factor of greater than 3 compared with vibro replacement method.

Additionally, the comparison between the EFFC calculator and the modified carbon calculator revealed that the differences between the two are relatively minor. Therefore, it is assumed appropriate to utilize the EFFC calculator in Norway.

REFERENCES

Basu, D., Misra, A., Puppala, A.J., & Chittoori, C.S. ,2015. Sustainability in Geotechnical Engineering: Perspectives and Review. Canadian Geotechnical Journal 52, pp. 96-113.

Data Bridge Market Research, 2024. Global Soil Stabilization Market – Industry Trends and Forecast to 2029. https://www.databridgemarketresearch .com/reports/global-soil-stabilization-market. 350 p. Accessed 05-02-25.

European Automobile Association, 2020. CO_2 emissions from heavy-duty vehicles, Preliminary CO_2 baseline (Q3-Q4 2019) estimate. https://www.acea.auto/files/ACEA_preliminary_CO2_baseline_ heavy-duty _vehicles.pdf. Pp. 5-5. Accessed 05-02-25.

 © DFI International Bruges 2025

European Environmental Agency, 2016. EMEP/EEA air pollutant emission inventory guidebook. https://www.eea.europa.eu/publications/emep-eea-guidebook-2016/download. 28 p. Accessed 05-02-25.

Hoff Sekkelsten, N., 2024. Vibro replacement - sustainable solution for ground improvement - An analytical, numerical and environmental evaluation of the vibro replacement method in Norwegian soft clay conditions. Master's thesis. Norwegian University of Science and Technology. 146 p.

Jörgen, L., Anneli, K., 2022. Metodrapport för www.klimatsmartsemester.se Version 3.0. Chalmers Tekniska Högskola. https://research.chalmers.se/publication/519162/file/519162_Fulltext.pdf. Pp. 7-7. Accessed 05-02-25.

Kedir, F. and Hall, D.M, 2021. Resource efficiency in industrialized housing construction - A systematic review of current performance and future opportunities. Journal of Cleaner Production, Vol.286, p.125443.

Larsson, S., 2021. The Nordic dry deep mixing method: Best practice and lessons learned. DFI Deep Foundation Institute. 30 p.

Lei, B., Yu, L., Chen, Z., Yang, W., Deng, C., Tang, Z., 2022. Carbon Emission Evaluation of Recycled Fine Aggregate Concrete Based on Life Cycle Assessment. *Sustainability*, 14 (21):14448.

Löfroth, H., Sandven, R., Bonde, C., Halkola, H., 2010. Regional Report for the Nordic Countries. 2nd International Symposium on Cone Penetration Testing, Huntington Beach, CA, USA.

Miljødirektoratet, 2022. Utslippsfaktorer i klimagassregnskap for Norge. https://www.miljodirektoratet.no/ansvarsomrader/klima/ klimagasser-utslippstall-regnskap/ utslippsfaktorer-klimagassregnskap. Accessed 05-02-25.

National Stone Sand & Gravel Association, 2021. The Aggregates Industry Greenhouse Gases: Low Emissions, High Resiliency. https://www.nssga.org/sites/default/files/2021-05/NSSGAGreenhouse GasEmissionsReport04-26-21.pdf. Accessed 05-02-25.

Neill, P., 2020. Construction industry accounts for 38% of CO_2 emissions. Environmental Journal. https://environmentjournal.online/articles/emissions-from-the-construction-industry-reach-highest-levels/. Accessed 05-02-25.

NGU, Geological Survey of Norway, 2024. https://geo.ngu.no/kart/losmasse_mobil/?lang=eng. Accessed 05-02-25.

Oberhollenzer, S., Thurner, R., Yildiz-Helvacioglu, N., Hov, S., Ritter, S., 2024. Baugrundverbesserung in weichen Böden - Forschungsarbeiten zum Thema Nachhaltigkeit. *Christian Veder Kolloquium 24*, Graz, Austria.

Statistisk sentralbyrå, 2016. Drivstofforbruk og utslipp per kjørte kilometer for et utvalg av trafikksituasjoner og kjøretøygrupper. https://www.ssb.no/318322/drivstofforbruk-og-utslipp-per-kjorte-kilometer-for-et-utvalg-av-trafikksituasjoner-og-kjoretoygrupper.2016.g-km. Accessed 05-02-25.

Svenska Geotekniska Föreningen (SGF), 2000. Kalk- och kalkcementpelare. https://svenskageotekniskaforeningen.se/wp-content/uploads/Publikationer/SGF_Rapporter/2000_2_Kalk_%20kalkcementpelare.pdf. Accessed 28-03-25.

The European Federation of Foundation Contractors, 2014. EFFC DFI Carbon Calculator Methodological & User Guide. https://www.effc.org/content/uploads/2020/10/EFFC-DFI-methodological-and-user-guide-v2.2.pdf. Accessed 05-02-25.

The International Energy Agency, 2023. Cement. https://www.iea.org/energy-system/industry/cement. Accessed 05-02-25.

 © DFI International Bruges 2025

COORDINATION OF COMPLEX GEOTECHNICAL WORKS AT A TIDEWAY SITE IN CENTRAL LONDON

Sophie Vicard & Sivilay Sayavong
CVBJV *sivilay.sayavong@tideway-east.london*

Adrian Bugea
Bachy Soletanche (previously Wentworth House Partnership), *adrian.bugea@bacsol.co.uk*

Vasileios Papastathis & David Kwong
Wentworth House Partnership, *vasileios.papastathis@wentworth-house.co.uk*

ABSTRACT

The Thames Tideway Tunnel is one of the largest current infrastructure projects in the UK: upgrading London's Victorian sewer network and extending over 25km across the city. The Tideway construction site at the Earl Pumping Station raised several technical, managerial, logistical and environmental challenges. At this 'postage stamp' sized site, a 52m deep drop shaft intercepting a 6.45m TBM-dug tunnel, a combined sewage overflow chamber and other ancillary structures have been constructed within heavily contaminated ground, immediately adjacent to the live Thames Water pumping station serving the local South London community. Solutions developed between the joint venture of Costain, Vinci Grands Projets & Bachy Soletanche (CVBJV) and its partners, required extensive geotechnical works including: a diaphragm wall installed using a hydrofraise, Cased Continuous Flight Auger (CCFA), rotary bored and Sectional Flight Auger (SFA) piling, deep soil mixing (both panels and columns), and grouting (as jet, chemical and cementitious permeation). This paper discusses the approaches to reviewing the challenges, risks and key lessons learnt on and off site, with the aim of showcasing the cohesive implementation and integration of complex schemes within the very congested site space and challenging delivery programme.

Keywords: infrastructure, urban, project management, complexity, coordination, environment, lessons learnt

INTRODUCTION

The Thames Tideway Tunnel, along with the Lee Tunnel, forms London's current sewage network upgrade, required as the city's population reaches 9 million, more than double the capacity for which the Victorian network was designed.

The tunnel works stretch across the capital from Acton in the west to Abbey Mills in the east, where the Thames Tideway Tunnel connects to the Lee Tunnel reaching Beckton. The 7.2m diameter, 25km long tunnel connects critical pumping stations where during heavy rain periods, sewage overflows into the river Thames occur an average of once a week all year round. The tunnel is to form both a transport route of the combined rainwater and sewage (as the current system cannot differentiate) and work as a storage tank, allowing the treatment plant to process the stored volume. The cost of the Tideway project, currently standing at £4.5 billion, along with the sheer size of the works, make the project one of the largest infrastructure endeavours in the UK.

Due to the innate nature of the environment, with the project located in one of the most developed European cities, the sites are limited in size, facing challenges on technical, managerial and sustainability levels. Whilst some are located on the Thames' river bank and temporary cofferdam solutions managed to increase the site area, some others are located within the city, with little room to spare.

One such 'postage stamp' sized site in southeast London is Earl Pumping Station (Figure 1). With a footprint of approximately 50x65m, the site is occupied on the north and north-east by the live

 © DFI International Bruges 2025

pumping station, whose main building was constructed in the 1940s, extending east with an underground 7.6x6.7m penstock chamber and supported by a piled substation located central to the site. Further west, a deep structure, the Dry Weather Flow chambers, was added in the 1970s, intercepting and diverting the sewage for treatment during dry periods.



Figure 1. Aerial view of the Earl Pumping Station site during geotechnical works

The main building is a single basement level, single storey (above ground level) masonry building. The foundations and buried walls are made of mass concrete cast against a masonry interior. On its western end, the penstock chamber descends to a depth of approximately 10.50m, connecting with a suction culvert running underneath the pumping station, feeding the pumps during the overflow periods (Figure 2).

The Dry Weather Flow chambers are split in two halves: a deep founded inlet (at the northern end of the structure) and pump chambers, located at depths between 11 and 3m below ground level and within a diaphragm wall box of 800mm panels of varying length, and a shallow founded motor room overlaying the outlet chamber.



Figure 2. Historical photos during the construction of the pumping station (views from the penstock chamber – eastward on the left, and towards southeast on the right)

SCOPE AND ENVIRONMENT CONDITIONS

Within this very limited area, the following main items have been constructed:

- An 18.8m internal diameter shaft descending to 52m below ground level (Figure 3). The shaft facilitates the transportation of the sewage, allowing it to drop into the tunnel below;

 © DFI International Bruges 2025

- Works to accommodate the Tunnel Boring Machine's (TBM) passage through the previously installed shaft, as it constructing the Greenwich Connection Tunnel, linked with the main tunnel;
- Interception (Combined Sewage Overflow – CSO) chamber with Air Treatment Unit (ATU), located between the penstock and the DWF chambers, 30m long, 6 to 8m wide and 12m deep;
- Other works: mains diversions and removal, landscaping, mechanical and electrical works, etc.



Figure 3. Aerial view at the Earl Pumping Station site during diaphragm wall installation

These permanent works required enabling works design and assessments, carried out by Wentworth House Partnership (WHP), as a temporary works specialist. Further on, agreement and approvals from the client, Tideway and ultimate assets holder, Thames Water Utilities, were needed ahead of the works.

The temporary works covered:

- Working platforms across the site for various scopes – hydrofraise, piling and ground improvement rigs, crawler cranes;
- Ground treatment to mitigate contaminants transportation prior to shaft diaphragm wall installation;
- Temporary foundations for diaphragm walls and bentonite farm silos;
- Mains diversion with shoring/trenching works;
- Shaft infill with lean concrete mix and water to facilitate TBM passage;
- Piling works to form the retaining structures for the CSO chamber and its ATU building;
- Ground improvement to cut-off groundwater within the CSO excavation;
- Ground improvement to underpin existing structures;
- Overall support to the site team throughout the construction stages.

The ground conditions on site comprised uncontrolled infills following the construction of the pumping station buildings, alluvial deposits made of soft silty sandy clays, River Terrace Deposits in both loose to medium dense and very dense condition, overlaying compact Thanet Sands, Bullhead deposits, Seaford and Lewes Chalk.

One can note that although this represents almost a typical Thames basin stratigraphy, the London Clay and cohesive Lambeth formation are lacking, leading to two aquifers only. The upper Terrace Deposits and Thanet Sands on one hand, and the lower Seaford and Lewes chalk layers on the other, separated by the Bullhead deposits and the putty weathered chalk.

 © DFI International Bruges 2025

Since the pumping station was constructed, the site has been subjected to extensive hydrocarbon contamination, located within the upper aquifer. Therefore, from the outset, the Environment Agency (EA) demanded that any contaminants transportation from the upper into the lower aquifer must be completely mitigated, forbidding the typical approaches such as extensive active dewatering. Any extracted volume must be remediated before being disposed of in the drainage system.

Despite of the best of efforts in identifying all the features of the adjacent historical assets using archive drawings and photos, and state-of-the-art survey techniques, certain details of the existing structure remained unknown during the design and preparation phases, with potential high risks for the scheme.

Also in the mix were the effects of a heavy-duty site within the middle of a residential area, as well as working in the immediate adjacency to live assets serving the community and ensuring a considerate and careful approach to all works, trying to limit disruption to everyday life.

THE SOLUTIONS

The shaft was formed by installing 26no. 61.5m deep, 1.00m thick diaphragm wall panels. The panel excavation was carried out using the hydrofraise, Bachy Soletanche proprietary equipment, to ensure productivity targets were achieved in both soils and rock. The shaft was designed to withstand soil and rock pressures in both permanent and temporary case including a uniform 20kPa blanket at ground level and groundwater pressures in temporary condition only. The secondary lining deals with the water pressures in permanent conditions, as the construction method allows for better quality control to ensure waterproofing.

Due to the contamination issue, in agreement with the EA and the rest of the stakeholders, ahead of the panels' installation, 2no. concentric circles of Deep Soil Mixing (DSM) were installed to the top of the chalk (located at 20m depth), using Cutter Soil Mixing (CSM) (Figure 4). This was to trap the contaminants in their current location and prevent a drawdown of contamination withing the Chalk Lower Aquifer.

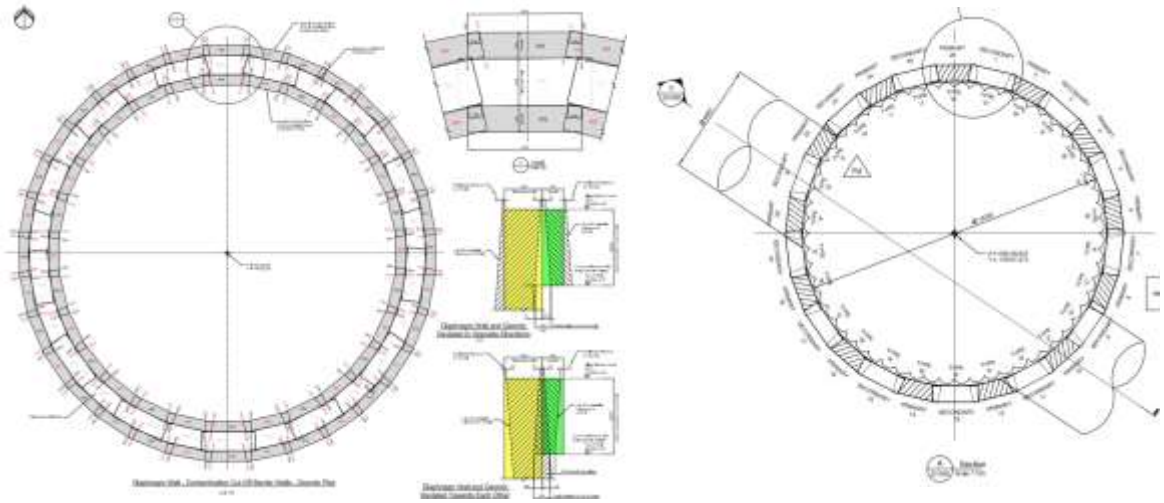


Figure 4. CSM layout (left, marked with grey hatch) installed around the shaft diaphragm wall layout (right)

From design to execution, site constraints have been driving the team to constantly innovate. Plant and equipment have been carefully chosen to minimise mobilisation and demobilisation, adapting one piling rig to undertake ground improvement and different piling techniques. The cranage was reduced to a minimum and a dolly system designed and trialled at the cage manufacturing yard to replace the

 © DFI International Bruges 2025

need of a second crane – needed for the tandem lift of the six 14m long cage part of the panel reinforcement.

An onsite one way system during the works allowed a smooth concrete delivery and muckaway removal, as the site has a limited stockpile capacity. Out of the five shafts across the project, the EARPS diaphragm wall was constructed using polymer as digging fluid as opposed to bentonite, due to the presence of heavy contamination. As a result, the moisture content of the spoil has been higher than expected and additives were used to allow safe transportation offsite.

As part of the work phasing, extensive co-activity had to be managed to accommodate the secondary lining of the shaft while working on the CSO chamber construction. Access to the Thames Water asset for maintenance and emergency had to be granted during the works, overnight and during weekends, further restricting plant movement within the already reduced working space. A transparent communication channel was established during the duration of the works, giving confidence to the Third Party Assets.

During the excavation of the shaft and up to the completion of the base slab – a domed 3.0 (at the centre) to 1.20m (at the edge) thick reinforced concrete raft doweled into the diaphragm wall, passive relief wells carried out groundwater control at limited abstraction rates. This was possible due to the diaphragm wall managing to cut-off the main local fissure and cracks systems within the shaft footprint. This is an important aspect, as on other sites, rock fissure grouting was necessary to support controlling the water flow.

The CSO excavation was supported using secant pile wall segments installed between the existing assets using Cased Continuous Flight Auger (CCFA) or Cased Secant Piling using Auger (CSP) method to ensure remaining within stringent verticality limits due to the adjacency to various underground assets. The piles of 880 and 600mm diameter, reached the top of the chalk, reinforced over 18.70 out of the drilled 21.00m.

At the interior, the secant walls were supported by 5no. levels of struts (Figure 5). By making use of the available surveys and historical data, WHP in collaboration with CVBJV and MML (permanent works designer), managed to reduce the levels and numbers of members supporting the excavation by identifying ‘strong points’ on the existing underground assets, able to withstand the loads the props would attract from the opposite side and coordinating installation and removal sequences to the permanent works.



Figure 5. Propping system installed in the CSO chamber

Slightly offset to the piling works programme-wise, an extensive stabilisation scheme has been carried out, mixing existing ground with grout to form a continuous basal plug (Figure 6). Due to the

 © DFI International Bruges 2025

existence of the DWF-to-penstock chambers connection sewer, on the northern side of the future excavation the plug had to be formed using Jet Grouting (JG), as the method allows for inclined drilling, used around the pipe to reach underneath it. Across the central and southern end, the plug has been formed by mechanical mixing, using 1.20m diameter interlocked columns (Deep Soil Mixing).

JG columns have been used to seal the ends of the secant pile wall segments to the adjacent existing assets, seal and underpin areas where the new excavation descended below the formation level of the adjacent structures and provide additional support (underpin) to the shallow DWF motor room/outlet chamber.

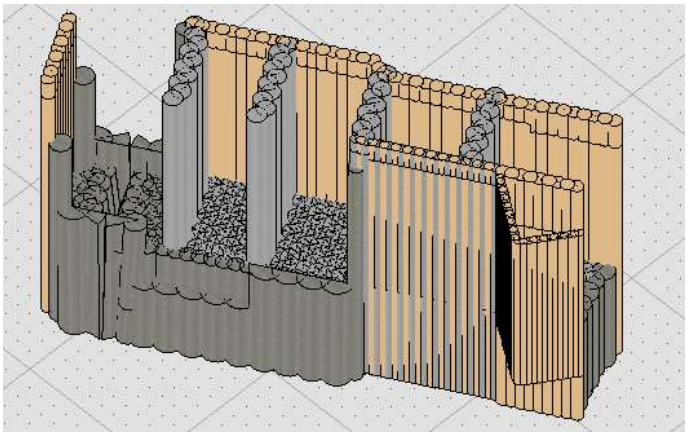


Figure 6. Isometric overview of the designed stabilisation works: piles in orange, stabilised soil columns in grey

Small diameter secant piles have been installed on the side of the western CSO secant pile line, south of the DWF motor room/outlet chamber, using Sectional Flight Auger (SFA) method cutting into previously formed Jet Grouting columns (Figure 7), to support the ground and asset behind during the excavation required for the ATU duct.

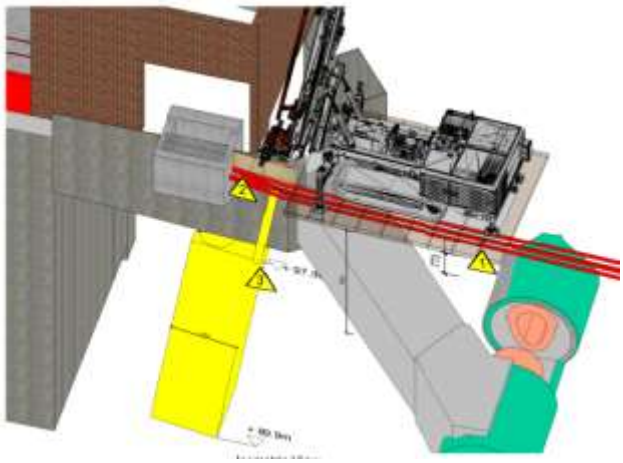


Figure 7. 3D model of the jet grouting rig located adjacent to the DWF chamber

IMPLEMENTATION AND CHALLENGES

Due to the task complexity and limited room for error, significant geotechnical, geophysical, intrusive structural and topographical surveys were undertaken to provide thorough information on ground conditions and the assets' geometry and structural state (Figure 8). When compared to/cross-checked with the historical information, the results aligned well, building confidence in the proposed scheme.

 © DFI International Bruges 2025

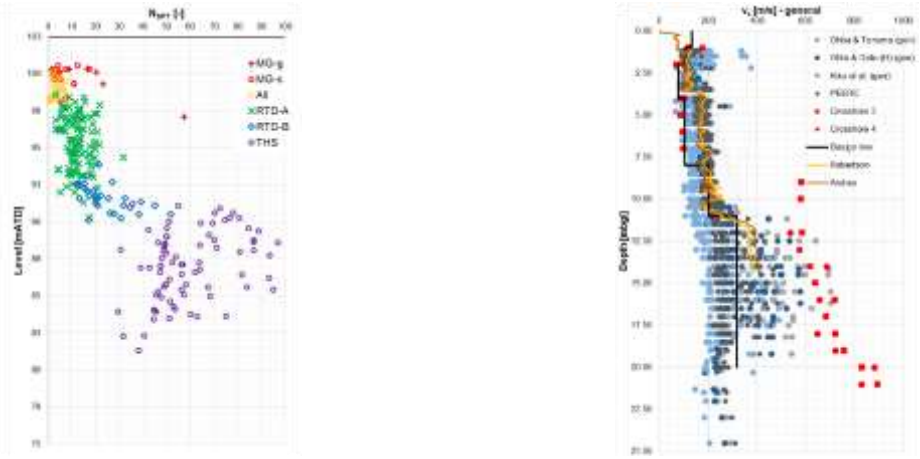


Figure 8. SPT diagram (left); SPT and CPT correlated to secondary wave velocity overlapped to cross hole results (right)

The adjacent assets' structural capacities have been assessed to ensure no damage will occur as they will be loaded differently to current conditions by the temporary condition, especially with the propping system concentrating loads at specific locations and providing more limited support should the two underground structures flood during excavation works.

Due to the complexity and risks of the proposed works, the design used a multitude of methods – from hand calculations to validate feasibility and principles, to 2D and 3D Finite Element methods to detail the various temporary and permanent stages (Figure 9).

To ensure that the proposed FE modelling is as correct as possible, back-calculations and calibrations were carried out following the shaft excavation, with focus on the upper soil layers, leading to refining the measured and correlated soil and rock parameters. This was critical for assessing the condition of the live assets, which were designed under old regulations and shown not to be compliant with the current codes.

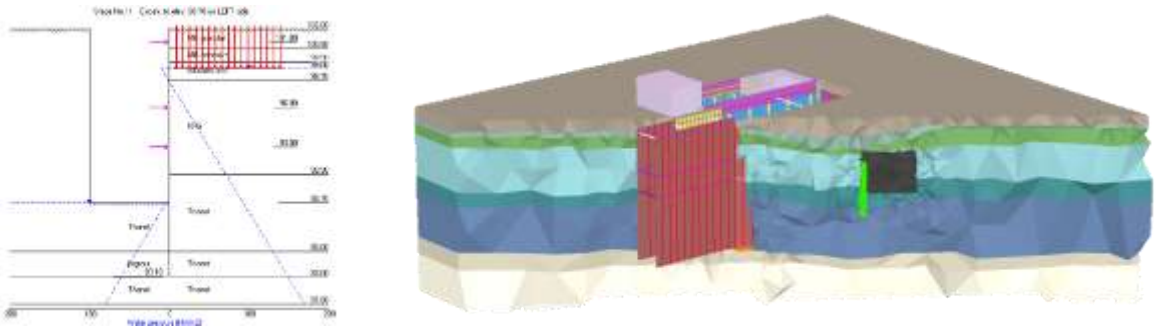


Figure 9. Various calculation models adopted throughout the design phase of the CSO excavation works

Given the sheer scale of the works to be addressed by the Ground Movement and Combined Potential Damage Assessment, independent FE models have been produced, separately addressing the various items such as shaft installation and excavation, tunnelling, CSO and ATU chambers excavation and construction (Figure 10). This needed the design team to confirm the proposed model's efficiency through calibration using the shaft excavation as reference. New tools and methods have been developed to correctly identify and sum the effects of each activity and correctly add them to the baseline defined using site monitoring.

The temporary works engineer identified a potential overstressing of the DWF chamber's capping beam, so an internal propping system has been designed and installed, providing support to the pump

 © DFI International Bruges 2025

room's side walls: 12m long and up to 10m plates, cantilevering in two directions. These were removed once the permanent CSO chamber structure was installed.

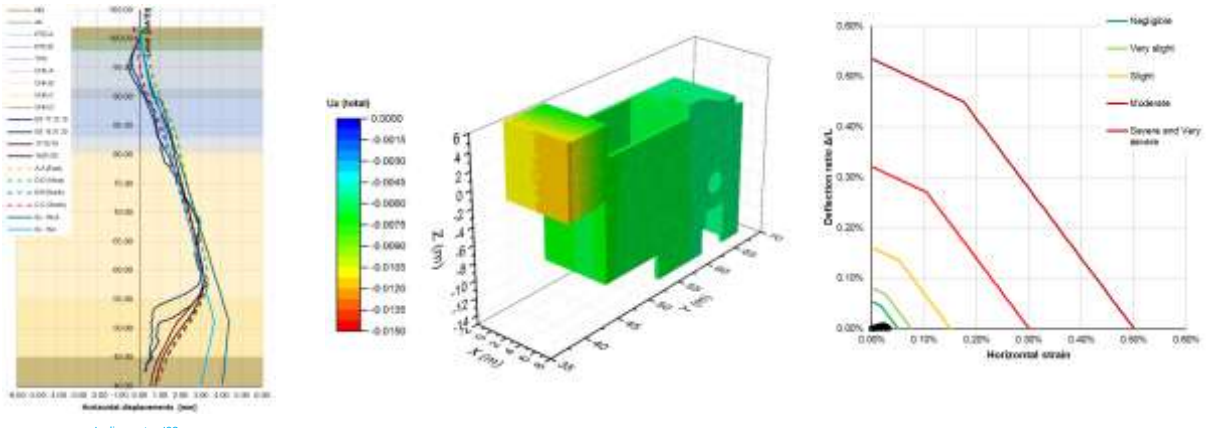


Figure 10. Potential Damage Assessment main stages: model calibration (left), output processing (centre) and damage assessment (right)

These designs and assessments have been thoroughly scrutinised by both industry and academia before approvals were obtained and works began. This required close control from the project management team through coordination discussions with the design, check and review teams on all sides, to ensure that the final submission deadlines were achieved.

From an operational management perspective, complex works were completed within a very limited footprint, as existing buildings and ongoing activities occupied a significant part of the site. On site deliveries were scheduled well in advance with vehicle movements outside peak hours wherever possible.

During the ground improvement scheme installation, given the criticality to seal the base and sides of the excavation and reach required strength to withstand approximately 18m water head pushing upwards from the underside of the plug with no pressure relief wells to mitigate the uplift risk, a thorough continuous review was carried out by the designer (WHP) and the site team (CVBJV) to ensure the works were of the highest quality (Figure 11). Post installation verticality measurements using shape array accelerators in conjunction with topographical survey, all plotted in 3D CAD identified gaps in the plug, located at depth as the tool deviated, which required additional columns.

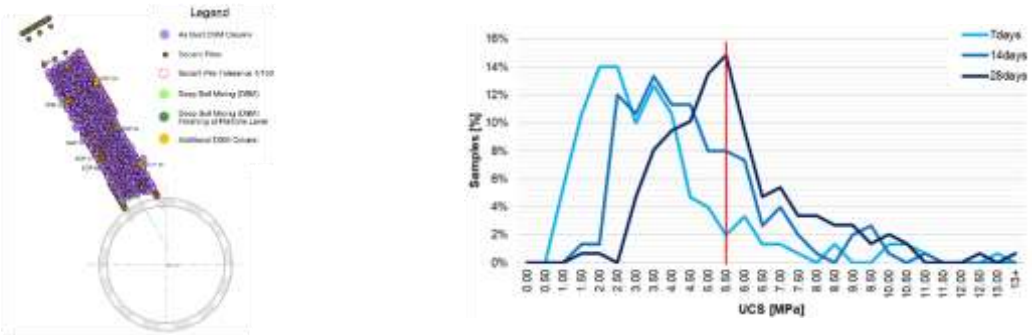


Figure 11. Horizontal section through the basal plug showing as built positions of columns (left) and Unconfined Compressive Strength analysis of wet samples (right)

As the excavation progressed, strut load, assets deformation (settlement, inclination, and joints opening) and groundwater level monitoring was continuously reviewed by the designer, ensuring that the design assumptions were representative of the current situation and the expected behaviours developed.

 © DFI International Bruges 2025

As a risk mitigation measure, the progress rate on the northern end of the CSO excavation was more limited following the uncovering of the historical sheets, to allow for survey and assessment. Nonetheless, the risk of the toe being higher than the target excavation level remained and within the later stages of digging, it manifested as bursts, with granular material being washed into the excavation and the enclosure flooded. The areas through which the seepage occurred were injected underwater using divers, and once successfully completed, the excavation drained and civil works resumed.

Subsequent ground investigations showed a weakened River Terrace Deposits (RTD) layer, deprived of the finer parts, leaving behind clean uniform gravels needing remediation. This has been assumed to be due to the water flow high velocity developed leading to piping within the medium dense layer.

The strengthening works were carried out in parallel to the construction of the CSO and ATU buildings, consisting of permeation grouting using Tubes-a-Manchette (TAMs) (Figure 12, left) targeting the pumping station subgrade and the remaining areas identified as being affected by the piping. Extensive Cone Penetration Test (CPT) based investigations confirmed the efficiency of the treatment (
Figure **12**, right).

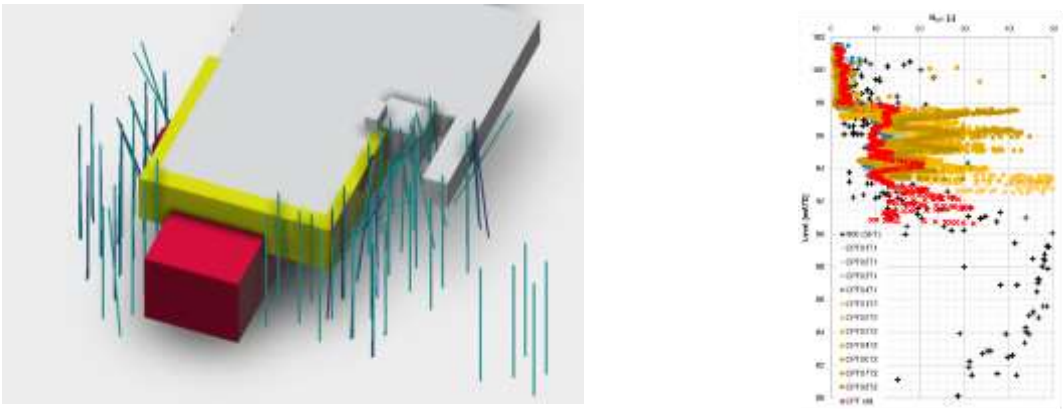


Figure 12. TAMs layout (left) and strengthened RTD layer

CONCLUSIONS

At Earl Pumping Station site, a series of challenges:

- Environmental, due to high ground contamination;
- Technical, due to lack of information and works complexity;
- Managerial, due to a very confined environment and programme availability;
- Social, working adjacent to residential area and near live assets serving the community,

led to adopting a significant variety of methods and techniques in both design and on site. Through extensive coordination between the design, site, checker, asset owners' and stakeholders' teams, a coherent and efficient scheme has been defined and installed, able to overcome the challenges.

Despite additional ground related technical challenges during the CSO chamber excavation, the main works have been successfully completed the first half of 2024, with Mechanical, Electrical, Instrumentation, Control and Automation (MEICA) works following. The end of the project is currently predicted for the end of 2025, with the commissioning phase currently in progress.

ACKNOWLEDGEMENTS

The authors would like to thank the wider teams for the support and dedication they showed throughout the development and construction of the works at Earl Pumping Station (and wider Tideway project), especially K. Cranfield, A. Chaizemartin, M. Stanley and M. Griffiths (CVBJV), A.

 © DFI International Bruges 2025

Brucy, A. Prugnaud, F. Mathieu (SBI), A. Carvalho, L. Ellis, G. Swanson, G. Mowatt (BSL), Y. Zhao and, S. Vaughan (WHP). Further thanks are extended to the Mott MacDonald, Tideway and Thames Water teams, and all the external checkers and reviewers who took part in the project.

REFERENCES

A. Carvalho, D. Hard, S. Sayavong, M. Stanley, R. Talby, P. Rutty, G. Pereira, T. Newman, M. Hanscomb, Design of geotechnical structures for Thames Tideway Tunnel East Section, 2022, 20th International Conference on Soil Mechanics and Geotechnical Engineering proceedings, Sydney, pp. 4683-4688

J.B. Burland, C.P. Wroth, Settlement of Buildings and Associated Damage, 1974, Conference on the Settlement of Structures proceedings, Cambridge, pp. 611-654, British Geotechnical Society

M.D. Boscardin, E.J. Cording, Building Response to Excavation-Induced Settlement, 1989, Journal of Geotechnical Engineering, Volume 115, Issue 1 pp. 1-21, American Society of Civil Engineers

G.W. Clough, Construction Induced Movements of In Situ Walls, 1990, Specialty Conference on Design and Performance of Earth Retaining Structures proceedings, pp. 439-470, American Society of Civil Engineers

R.J. Finno, J.T. Blackburn, R.F. Roboski, Three-dimensional effects for supported excavations in clay, 2007, Journal of Geotechnical and Geoenvironmental Engineering, Volume 133, Issue 1, pp. 30-36, American Society of Civil Engineers

E. Leca, B. New, Settlements induced by tunneling in soft ground, 2007, Tunnelling and Underground Space Technology, Vol.22, No.2, pp. 119-149

T. Schwamb, M.Z.E.B. Elshafie, K. Soga, R.J. Mair, Considerations for monitoring of deep circular excavations, 2016, ICE Proceedings Geotechnical Engineering Vol. 169, No. 6, pp. 1-17, Institution of Civil Engineers

 © DFI International Bruges 2025

ANALYSIS OF THE LATERAL PRESSURE OF WET CONCRETE ON NEIGHBORING FOUNDATIONS

Amira Chouikh, Soletanche Bachy, Paris, France, 0758492368, amirachouikh@yahoo.com
Stéphane Guérineau, Soletanche Bachy, Paris, France
Cristophe Justino, Soletanche Bachy, Paris, France
Maxime Fonty, Soletanche Bachy, Paris, France

ABSTRACT

Engineering constructions are done in the core of Urban area, when constructing deep foundations approximate to the existing ones, it is well known that it is very important to investigate the effects of the construction process. In France, on the banks of the Seine, a deep diaphragm wall was constructed near a quai made of sheet pile. The issue of wet concrete pressure on the sheet pile during wall construction arose, therefore specific monitoring was carried out. The objective of investigating the pressure of wet concrete, is to gain a better understanding of the potential effects of building a diaphragm wall on surrounding soil and foundations. Accordingly, this paper performs an extensive literature survey on wet concrete's pressure and provides a description of the observational method implemented in an example project. This paper also provides analysis of the results given by instrumentation and proposes the focus and direction for follow-up work.

INTRODUCTION

The construction of a diaphragm wall (Fig. 1) involves three distinct phases. First, three bites are excavated, creating a panel, a left/right bite measuring typically 2.8 m, and a center bite, while using support fluid simultaneously (usually a mix of water and bentonite or, water and a blend of bentonite and polymer, or more seldomly water with soluble polymer only). Second, during excavation, a total desanding mechanism is put in place to purify the bentonite and assure a constant density inferior to 1.15 kg/cm^3. Finally, water stops are placed on the edge of the excavated panel, two prefabricated cages are placed between the water stops, and concrete is poured into the excavation.



Fig. 1. Diaphragm wall construction procedures

The first panel is called primary panel, the second one is also primary but must be done from a safe distance, the other panels are called running panels, and the final one is called the closing panel.

In real-life projects, in specific circumstances, such as building close to an existing foundation, we take precautionary measures because the impact of pouring concrete is not standardized and therefore difficult to assess. Worldwide researchers have conducted theoretical analysis on the lateral pressure of wet concrete (Stivaros & Kevin, 2004; CIRIA, 1965; Omran & Khayat, 2010; DIN18218, 1980; Duca, 2001; Poineau, et al., 1997). This paper discusses the analytical methods used by the norm, as well as Soletanche Bachy laboratory, to calculate the lateral pressure exerted by wet concrete. It also examines the impact of wet concrete on adjacent soil, incorporating real-world monitoring data and linear elastic

 © DFI International Bruges 2025

calculations to illustrate the key factors influencing soil displacement assessment. The findings offer valuable recommendations for future applications.

BIBLIOGRAPHY ON CONCRETE PRESSURE

Wet concrete acts as a liquid and, as the concrete sets, the pressure is reduced. The horizontal pressure changes hydro-statically until it reaches a certain depth, known as critical depth. Wet concrete exerts constant pressure beyond the critical depth (experimental observations have even shown that there is a slight decrease in pressure after critical depth (Poineau, et al., 1997). The researchers agree on the form of the diagram (Fig. 2), however, the evaluation of the maximum value of pressure is a subject of disagreement.

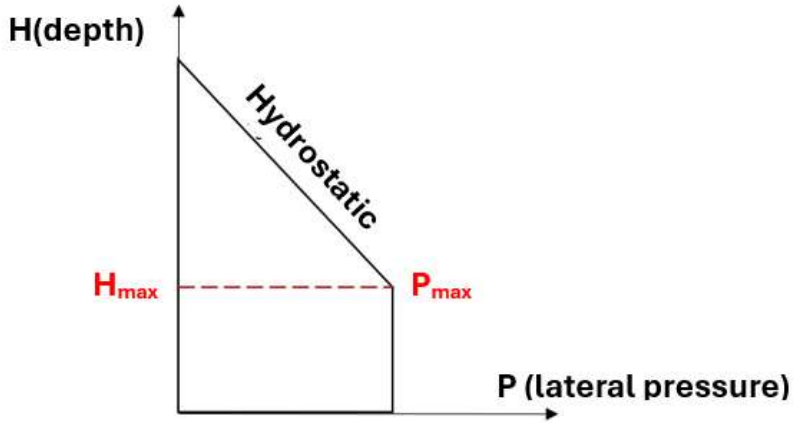


Fig. 2. Concrete pressure diagram

The theoretical models propose a formula for calculating the maximum pressure as a function of several parameters:

Table 1. Bibliographic references

Author	Formula
ACI(USA)	min (p_1, p_2, p_3) (Table 1)
CIRIA(ENG)	$G[C1\sqrt{R} + C2Kt\sqrt{H - C1\sqrt{R}}\,]$
DIN1828 (GER)	$GxC_3xK_Tx(0.48R+0.74)$
NFP 93-350 (FREN)	3m hydro pressure

G: unit weight (minimum 24 kN/m^3) ;
C_1 = 1 for walls and 1.5 for barrettes ;
C_2 = 0.3 for normal concrete, 0.45 for retarded one ;
C_3 : adjuvant coefficient ;
K_T : $\frac{145-3T}{100}$;
R: ascension speed in m/h ;
$K_t = \left(\frac{36}{T+16}\right)^2$;
T: temperature in °C ;
H: depth of wet concrete in m ;

 © DFI International Bruges 2025

Table 2. Theoretical recommendations by ACI

	R(m/h)	H(m)	p1(kPa)	p2(kPa)	p3(kPa)
wall (slump < 175 mm) (horizontal dimensions >2m)	<2,14	<4,2	$7.2 + \frac{785R}{17.8+T}$	24H	96
	2,14<<4,5	>4,2	$7.2 + \frac{785R}{17.8+T} + \frac{244R}{17.8+T}$		
	>4,5	-	-		
Column (Slump < 175mm) (horizontal dimensions < 2m)	-	<5,5	$7.2 + \frac{785R}{17.8+T}$		144

Assumptions:

The equations used by ACI in Table 2 are mainly elaborated for form-work designs and are limited by slump value, depth, and ascension speed.

The CIRIA equation in Table 1 is only available when the depth (H) is greater than the depth affected by vibration and workability $C1\sqrt{R}$).

For DIN18218, the ascension speed is not more than 7m/h. If the consistency class is F1 to F4 the equation is only used for a maximum of 10m depth. The equation is defined for concrete cast at T = 15°C, if during placing concrete cast is below 15°C, the maximum pressure is to be increased 3% for each degree below 15° and vice versa (DIN18218, 1980).

We have come to the conclusion that the technical recommendations relating to fresh concrete in formwork are not appropriate for the situation of delayed-setting fluid concretes poured quickly at great depths and with no vibration.

SOLETANCHE BACHY EXPERIENCE

The French standard precises a minimum pressure only for a wall of small depth and does not offer any guidance on how to calculate the maximum value depending on depth. To compare the equations used above and to specify equations for our future projects, we conducted multiple tests.

Used theory

Using the N.Roussel LCPC (Roussel & Ovarlez, 2005), we aim to calculate the maximum pressure reached during concreting and pressure distribution on the panel walls. Which requires a characterization of the fresh concrete, by measuring:

- SLUMP during pouring phase: by doing the Abrams cone test, outlined in standard NF P 18-451 and detailed in (Rebitzer & Breson, 1999), used to evaluate the consistency of concrete and its capacity to deform under its own weight. This test is unsuitable for very dry concrete or excessively fluid concrete. The procedure involves manually shaping a standardized truncated cone and, after removing the mold, measuring the slump caused by the concrete's own weight. A larger slump indicates a more fluid concrete (AFGC & BAP, 2008).

- volume mass of concrete ρ

- Thixotropix coefficient A_{thix}: by measuring the threshold rigidity (shear maximal stress) evolution of a material at rest over time. A vane test is used with a blade size adjusted to take account the heterogeneity of the material and the size of the rigid inclusion.

 © DFI International Bruges 2025

- Quantity of trapped air in concrete (φ): our different study cases suggest that the spherical fraction of trapped air (φ) is approximately 2%.

The following equations are taking from Roussel research (Roussel & Ovarlez, 2005). Using MORI TANAKA, we can calculate Poisson coefficient of concrete:

$$\vartheta = \frac{6 + \varphi}{12 + 11\varphi} \quad [1]$$

Threshold without thixotropy evolution:

$$\tau 0 = \frac{\rho\left(25.5 - Slump(cm)\right)}{17.6} \quad [2]$$

Threshold with thixotropy evolution:

$$\tau 0app = \tau 0 + A_{thix}t \quad [3]$$

Ratio (K) between horizontal and vertical stress:

$$K = \frac{\vartheta}{1 - \vartheta} \quad [4]$$

For traditional concrete and in static conditions the reduction occurs because a portion of the material's weight is supported by the walls, resulting in the mobilization of shear stress that is less than or equal to the concrete's yield strength. While it is generally negligible during the pouring of short elements, it can be significant when dealing with deeper elements. An adaptation can be performed as shown in eq [5] incorporating the material's yield strength and the geometry of the formwork.

$$\sigma_{max}(z) = \rho g K((H - H_{tube})\left(1 - \frac{2\tau_0}{\rho g}\left(\frac{1}{L} + \frac{1}{e}\right)\right) + H_{tube}) \quad [5]$$

Knowing that L : panel length, e : thickness of the panel , H_{tube} : depth of the mixing tube (typical value : 3m). For walls deeper than 50m, the impact of the mixing tube can be deleted and the equation to be used is :

$$\sigma_{max}(z) = \rho g K H\left(1 - \frac{2\tau_0}{\rho g}\left(\frac{1}{L} + \frac{1}{e}\right)\right) \quad [6]$$

This equation shows that it's better to pour thin panels and to increase as possible the threshold of concrete. For nontraditional concrete, where thixotropy is significant, the expected value of fresh concrete is smaller than the one calculated with only concrete threshold. For our typical cases, we take the hypothesis of constant ascension speed and the fact that shear stress in all points (except in the areas where concrete is flowing) increases with thixotropy as shown in eq [7]. The equation to be used is:

$$\sigma_{max}(z) = \rho g K H\left(1 - \left(\frac{2\tau_0}{\rho g} + \frac{A_{thix}H}{R\rho g}\right)\left(\frac{1}{L} + \frac{1}{e}\right)\right) \quad [7]$$

Note: the impact of the immersion tube is not taken into account.

 © DFI International Bruges 2025

As cited in N.Roussel report (Roussel & Ovarlez, 2005), we can distinguish 3 types of thixotropy where concrete is considered : Non thixotropic for structuring taking over 20 minutes ; Semi-thixotropic for structuring between 5 and 20 minutes ; Thixotropic for structuring taking less than 5 minutes

In order to show the two types of thixotropy, we took the following hypothesis:

Semi thixotropic concrete (Roussel & Ovarlez, 2005):

We can consider a characteristic structuring time of 80 minutes. In this case, the rate of structuring would be approximately 360 Pa/h. This approach is conservative. It does not consider the reinforcements that reduces pressure and assume a minimum level of thixotropy.

Thixotropic concrete (Roussel & Ovarlez, 2005):

It is conceivable that there could be concrete mixtures that maintain their rheological properties for a few hours while exhibiting slightly enhanced thixotropic behavior. In that case, a test must be conducted to justify the values calculated using the equation [7]. Their rate of hardening would be approximately 1400 Pa/h. The maximum pressure shown in Fig. 4 is no longer located at the bottom of the trench. The weight of the material is significantly supported by vertical transfer to the wall, and the increase in lateral stress caused by the pouring of the upper layers is less than the increase in pressure transfers due to hardening. It is important to contextualize the relevance of modeling the lateral stress at the bottom of the formwork at the end of the pouring process. The concrete in this area is nearly 10 hours old and may have set. To predict this transition, it is generally necessary to know the setting time of the material, and thixotropy alone rarely suffices to explain the evolution of lateral stresses (AFGC & BAP, 2008)

- ⇨ Considering only thixotropy ensures a conservative estimate of the maximum lateral stress reached during the operation.

When it becomes necessary to study the effect of fresh concrete pressure on an existing structure, it is useful (Brest Radoub, Quai Issy Les Moulineaux) to use a simplified diagram as in Fig. 3.

$$\begin{cases} P(z) = \gamma_{concrete}\, z & \text{if } z <= z_{cr} \\ P(z) = P_{cr} + 11z & \text{if } z > z_{cr} \end{cases}$$

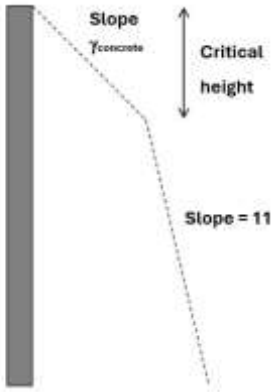


Fig. 3. Wet concrete pressure design by SBF

The design is adopted by SBF and is based on experimental measurements conducted by LCPC (test on tremie Pasteur, Rouen, France), which indicates that the concrete pressure in diaphragm walls differs from that in formworks. The critical height is approximately one-quarter of the height of the panels, with a slope corresponding to the concrete density (24 kg/m³). Beyond this point, the pressure evolves with a slope equivalent to 11 considering concrete maturing and arching effect. Three types of

 © DFI International Bruges 2025

foundations, characterized by the attributes listed in Table 3, are analyzed using the cited theories and compared to the hydrostatic pressure of concrete, as illustrated in Fig. 4,Fig. 5 and Fig. 6.

Table 3. Characteristics of the used concrete

Foundation type	Unit weight (kN/m3)	Slump (cm)	Ascending speed (m/h)	Rate (m3/h)	Temperature (°C)	Thickness (m)	Length (m)	depth (m)	A_{thix} (Pa/h)	
Diaphragm wall	24	20	6	40	15	1	7	70	1400	360
Barrette 1			7,4			1,5	3,6			
Barrette 2			11			1	3,6			

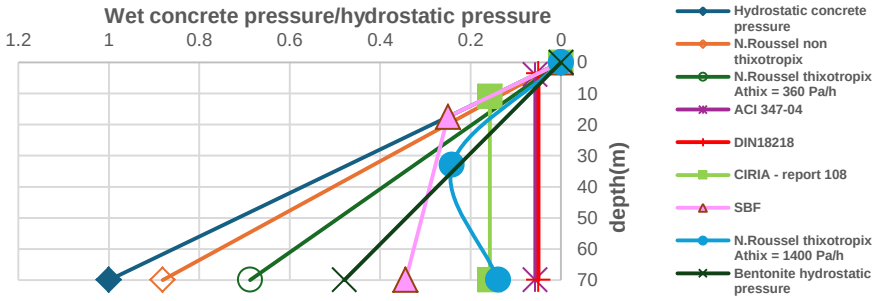


Fig. 4. Wet concrete comparison for wall type 1m x 7m

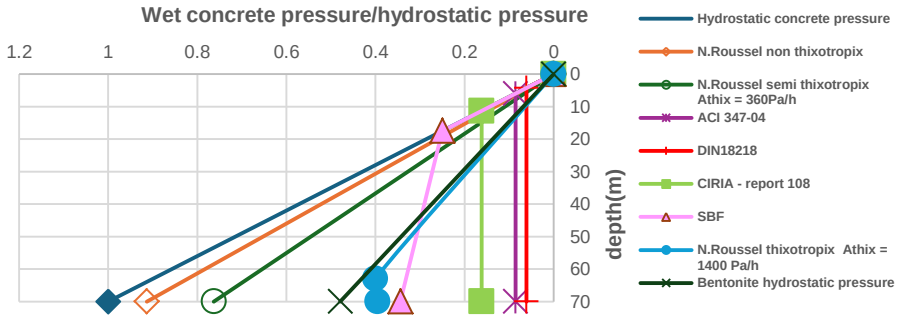


Fig. 5. Wet concrete comparison for barrette type 1.5m x 3.6m

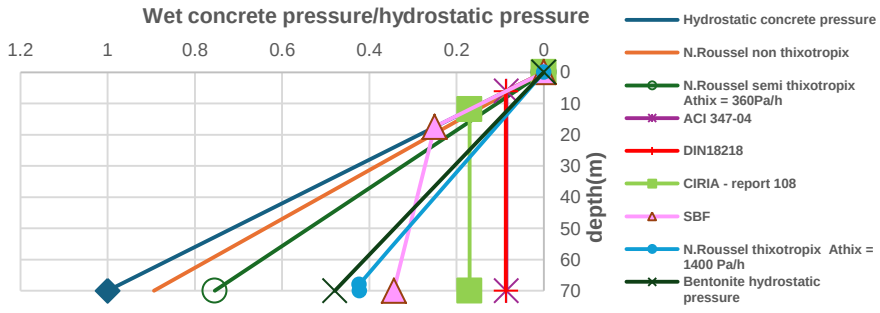


Fig. 6. Wet concrete comparison for barrette type 1m x 3.6m

Based on the results shown by the three Fig. 4,Fig. 5 andFig. 6, it is likely to conclude : There seems to be a systematic underestimation (CIRIA, 1965; DIN18218, 1980; Stivaros & Kevin, 2004) in all current recommendations regarding the pressure exerted on formwork, particularly in the case of very tall formwork or deep panels, when compared to N. Roussel's approach. The hypothesis proposed by SBF suggests using a design (Fig. 3) that acts as an envelope for low depths and aligns between N. Roussel's non-thixotropic and thixotropic models for greater depths.

 © DFI International Bruges 2025

It is also noted that the ascension speed ($R = \frac{concrete\ flow(m3/h)}{section\ of\ panel}$) plays a role in eq [7], where the term $\frac{1}{R}\left(\frac{1}{L}+\frac{1}{e}\right)$ positively influences the stress.

Theory vs real life measures

Laboratory tests:

The N.Roussel theory was tested and confirmed in experimental real life projects in Canada, Montreal (Roussel & Ovarlez, 2005), where various placement rates and self-consolidating concrete mixtures of different thixotropy properties were used (Fig. 7).

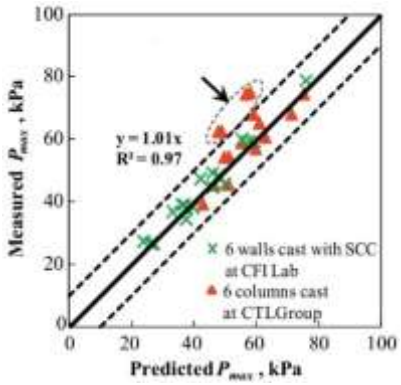


Fig. 7. N. Roussel theory applied on walls/barrettes (Roussel & Ovarlez, 2005)

Another trial was also conducted by the laboratory of soletanche bachy while working on a diaphragm wall project in London gateway. The trial took place in the dedicated shed on the site of Montereau. Where a 800 L tank was placed in a heated shed (15 to 20°C). The tank was equipped by SOLDATA with one horizontal pressure gage, one vertical pressure gage and one piezometer (pore pressure gage). The results of pressure evolution over time were calculated taking into account thixotropy and measured in two different depths (CPT 6 is at 30cm and CPT 4 is at 85cm) as shown in Fig. 8:

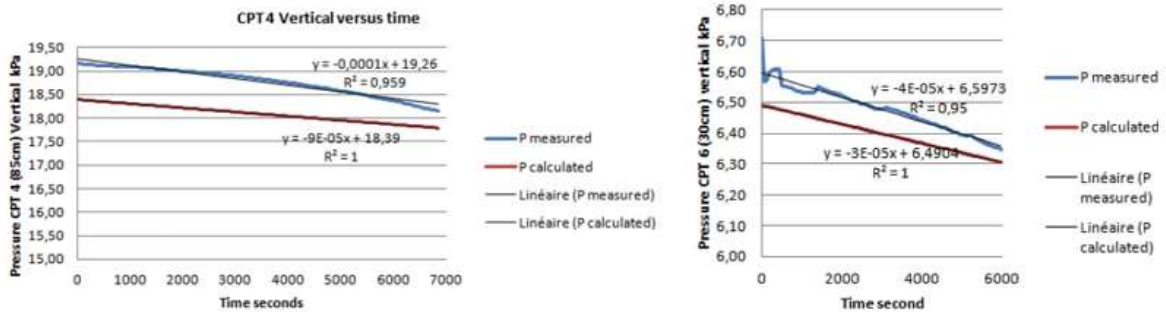


Fig. 8. Measured/predicted pressure vs time (CPT4&6)

The results suggest that the developed equations offer a reliable estimation, with values closely matching the measured data. Additionally, the thixotropy coefficients are very similar.

 © DFI International Bruges 2025

Real life projects monitoring:

Some of the researchers like in (Dong, 2024; Merifield, et al., 2012; Papadopoulou & Comodromos, 2013) have done finite element modeling showing the impact of the entire process of building a wall panel on neighboring foundations. The primary focus of this research is on settlements caused by the construction of diaphragm walls. Fresh concrete's effects are also studied, but they are not frequently monitored. Soletanche bachy has participated in the construction of a circular diaphragm wall (total depth: 59m) very close to the quai of the seine (total depth: 15m). Inclinometers were put close to two panels (P05 and P03) since they are done simultaneously. The seine quai which is a pile sheet wall was equipped by extensometers to evaluate the felt pressure in each phase of the construction.

The panel P05 is the closest to the existing wall and is to be done after P03 and P02. An observational method was implemented. Based on the monitoring results during the construction of P03, a reinforcement of the existing wall was planned, potentially prior to the construction of P05. To minimize the impact of concreting on the sheet pile, lightweight concrete was applied along the height of the sheet pile, in conjunction with a specific concreting procedure involving frequent concrete column cuts. The measuring devices has shown the following results (Fig. 9):

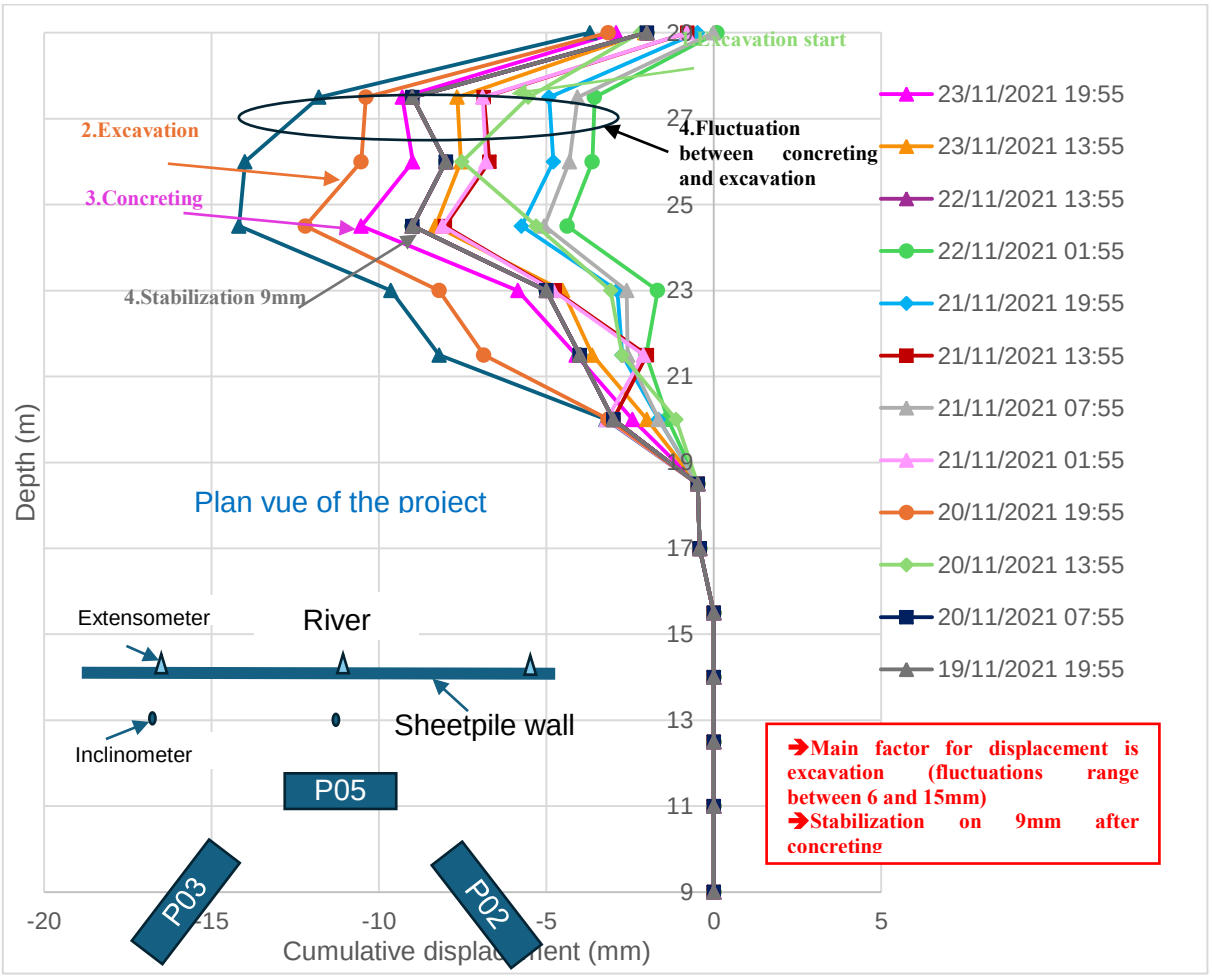


Fig. 9. Measured displacement while concreting P05

For the construction of P03: it was observed (via the inclinometer) that a bulge is manifesting in the direction of the seine following the concreting of P03 (1mm). However, the extensometer has shown no stress ➔ Following these observations, the reinforcement was deemed unnecessary.

 © DFI International Bruges 2025

For the construction of P05, stress on the existing retaining wall has manifested showing a bulge formed, reaching up to approximately 15 mm, then stabilized around 9 mm. Stresses in the sheet pile wall reached approximately 20 MPa.

Discussion:

In this project, the concrete monitored stress was found to be lower than expected, which allowed to not reinforce the existing structure. It is noteworthy that the monitored phase of excavation produced higher pressure than the concreting phase (Fig. 9), further supporting the observation that the actual pressure of wet concrete is lower than the hydrostatic pressure of bentonite (Fig. 4Fig. 5 and 6) As expected, the only impact of concreting came from the closest panel to the existing wall. It is also interesting to note that the pressure exerted on one panel is only felt by the inclinometer that is facing it.

The added stress of concreting depends on so many factors, such as distance between the existing wall and the panel, the type of soil, the dimensions and strength of the existing foundation, etc. In the following paragraph, we will discuss how to forecast the impact on the surrounding soil.

Suggestion of a simplified path

Complex elastoplastic models are commonly used in articles to predict the impact of lateral pressure on surrounding soil. A simpler approach could be searching for the radius of impact by using the cavity expansion theory. The expansion of the cavity generates complex stress distributions in the surrounding material, leading to possible plastic deformation close to cavity.

The soil surrounding the cavity initially undergoes elastic deformation, followed by plastic yielding once the yield condition is met. As the cavity expands, the pressure continues to rise progressively until the soil reaches its critical state. Beyond this point, further expansion of the cavity walls does not lead to any increase in pressure (Frikha & Bouassida, 2007; Carter, 1986).

Analytical methods were developed by multiple researchers depending on the laws assumed on the surrounding soil, such as linear elastic, nonlinear elastic, elastic perfectly plastic without volume variation or with variation (Chen, 2022; Xiao, et al., 2021). The type of soil has also played an essential role on the methodology used in calculating the expansion of cavity, as an example purely cohesive soil, purely frictional soil and cohesive frictional soil (Frikha & Bouassida, 2007; Carter, 1986).

For our case study, it is more appropriate to model the rectangular panel as a cylindrical cavity rather than a spherical one. The panel section is approximated to a circle inscribed within the rectangle (Fig. 10), $R_1 = \frac{length\ of\ panel}{2}$, this value can be discussed and seems to be conservative.

This paper covers only typical cases where the soil is considered homogenous, isotropic, linear elastic perfectly plastic and infinite. The soil behaves elastically and obeys Hooke's law until the onset of yield which is determined by the Mohr coulomb criterion. For special cases, elastoplastic behavior may be described by the large strain theory and cam clay (Xiao, et al., 2021), or non-associated Mohr coulomb (Chen, 2022). Some articles like in (Hu & Zhang, 2013) deal with a closed form solution (limited soil). At this stage, we assume that the soil remains within the elastic domain.

The model we are referring to is presented in Fig. 10, where P_0 is the pressure of soil at rest ($K_0.\sigma_v$). R_1 is half length of a panel and R_2 represents the radius of the concreting impact on the soil, which is considered infinite in this case.

 © DFI International Bruges 2025

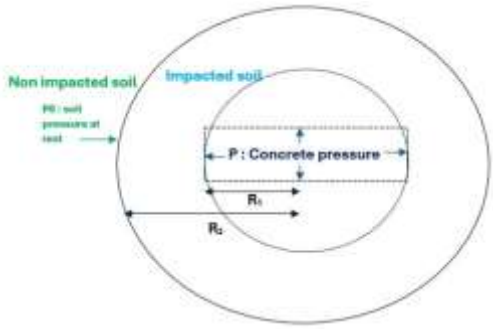


Fig. 10. The considered stress field

The following elastic law and the equilibrium equation are used: Injecting the elastic law in the equilibrium equation gives the following displacement and stress equations:

$$u(r) = \frac{p - p_0}{2G\left(\frac{1}{R_1} - \frac{1}{R_2}\right)}\left[\frac{1-2\vartheta}{R_2^2}r + \frac{1}{r}\right] \quad [8]$$

$$\sigma_r(r) = -\frac{p_0 R_2(r^2 - R_1^2)}{r^2(R_1^2 - R_2^2)} - \frac{pR_1(R_2^2 - r^2)}{r^2(R_1^2 - R_2^2)} \quad [9]$$

$$\sigma_\theta(r) = -\frac{p_0 R_2(r^2 + R_1^2)}{r^2(R_1^2 - R_2^2)} + \frac{pR_1(R_2^2 + r^2)}{r^2(R_1^2 - R_2^2)} \quad [10]$$

Where:

$$G = \frac{E}{2(1+\vartheta)} \quad [11]$$

$$\lambda = \frac{2\vartheta G}{1-2\vartheta} \quad [12]$$

Knowing that E is Young's modulus, ν is Poisson coefficient, $\sigma_r = p$ when $r = R_1$ and $\sigma_r = p_0$ when $r = R_2$. As explained in (Frikha & Bouassida, 2007) beyond R_2 we assume that the cavity expansion does not generate any significant stress component. The stress field is independent of elastic properties. When R_2 is considered infinite (limitless impact of cavity expanding), we can use the following equations:

$$u(r) = \frac{(p - p_0)}{2G}\left(\frac{R_1}{r}\right)^2 \quad [13]$$

$$\sigma_r(r) = p_0 - (p_0 - p)\frac{R_1^2}{r^2} \quad [14]$$

$$\sigma_r(r) = p_0 + (p_0 - p)\frac{R_1^2}{r^2} \quad [15]$$

In order to explore these equations, we presented the evolution of radial stress and displacement in Fig. 11:

 © DFI International Bruges 2025

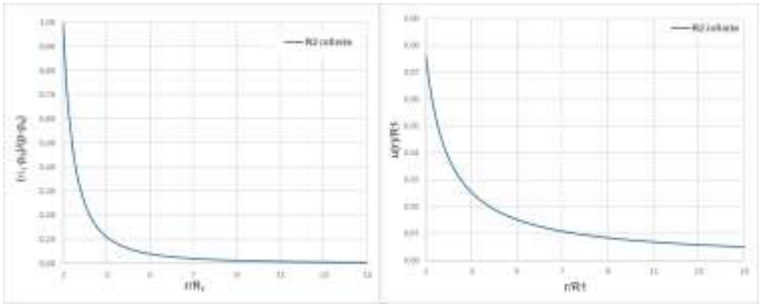


Fig. 11. Normalized displacement/stress against radius of impact

Discussion:

The determination of the impact radius using cavity expansion theory is not always beneficial, particularly because the predicted radius giving no significant impact on elastic yield, strains, and displacements can be significant.

While this approach can be effective, it is constrained by yield conditions. For an example, for cohesive soil when there is little cohesion in the soil, the limit yield pressure is relatively low and can easily be exceeded by the internal pressure applied in cavity. In scenarios where the soil begins to plastify, the stress filed should be coherent with the Mohr coulomb strength criteria as detailed in (Frikha & Bouassida, 2007) and further development is required.

CONCLUSION

This study has provided a comprehensive overview of the existing literature on the pressure exerted by fresh concrete during the construction of diaphragm walls. It has been demonstrated that current recommendations are inadequate, particularly for walls and barrettes applications. The method proposed by N. Roussel appears to be a practical approach, showing greater reliability when compared to site measurements and inspections.

In the subsequent section, we focused on quantifying the effects of this pressure on the adjacent soil using the cavity expansion method, a well-established analytical technique essentially made for predicting soil characteristics in pressiometre trial or for studying tunnel support. This method proved effective for estimating the stress distribution around the diaphragm wall and its influence on the adjacent soil layers. However, while the cavity expansion method offers a simplified and computationally efficient approach, its applicability is limited in more complex scenarios, specifically, the method assumes idealized soil behavior and linear-elastic conditions, which may not accurately reflect real-world situations where soil exhibits non-linear, plastic deformation under high loads which can be easily the case for deep walls.

To overcome these limitations, it becomes necessary to explore more detailed analytical approach (dos Santos, 2020; Frikha & Bouassida, 2007) like finite element (FEA), a more sophisticated method capable of capturing the complex, non-linear/plastic behaviors of the soil.

ACKNOWLEDGEMENTS

We extend our deepest gratitude to Nicolas ROUSSEL for his valuable expertise and feedback that have greatly enriched our understanding of the issues related to the pressure exerted by fresh concrete during the construction of diaphragm walls. We also wish to express our sincere appreciation to Benoît GIRARD for providing the data of the mentioned worksite.

 © DFI International Bruges 2025

BIBLIOGRAPHY

AFGC & BAP, 2008. Recommandations pour l'emploi des bétons auto-plaçants. *AFGC64,* pp. 1-64.

Carter, J. P., 1986. Cavity expansion in cohesive frictional soil. *Geotechnique* .

Chen, S. L., 2022. "A Graphical Theoretical Framework for Cylindrical Cavity Expansion in Mohr Coulomb Geo materials. *Department of Civil Environmental Engineering Louisiana State University.*

CIRIA, 1965. "the pressure of concrete on formwork". In: Construction industry Research and information Association. pp. 1-42.

DIN18218, 1980. frishbeton auf lotrechte (pressure of concrete on vertical formework).

Dong, Y. P., 2024. Effect of diaphragm wall construction process on the performance of braced excavation. *Technical University of Denmark, Kgs Lyngby,* pp. 176-181.

dos Santos, A. L., 2020. Determination of soil shear modulus at low strain level using an innovative pressuremeter probe : Application to cyclic pile design. *Université Paris-Est,* pp. 35-68.

Duca, v., 2001. *Etude experimentale des composantes normales des contraintes totales en laboratoire et in situ,* Paris: Ecole des Ponts ParisTech.

Frikha, W. & Bouassida, M., 2007. "Extreme pressure due to expanded cylindrical and spherical cavity in a limitless medium: applications in soil mechanics. *Acta Geotechnica.*

Hu, X. & Zhang, C., 2013. A new closed-form solution for circular openings modeled. *Computers and Geotechnics.*

Merifield, R. S., Li, A. J., Lin, H. D. & Lyamin, A. V., 2012. *A case study of ground response due to diaphragm wall installatione.* New Zealand, s.n.

NFP93-350, 1995. Banches industrialisées pour des ouvrages en béton. *Norme française* .

Omran, A. f. & Khayat, K. H., 2010. State of the art review of form pressure exerted by self consolidating concrete. *Sherbrook university,* pp. 1-141.

Papadopoulou, M. C. & Comodromos, E. M., 2013. *Effects on adjacent buildings from diaphragm wall installation.* s.l., s.n.

Poineau, D., Vié, D. & Durot, M., 1997. Poussée du béton fluidifié. *matériaux,* pp. 19-30.

Rebitzer, C. & Breson, J., 1999. Essai de maniabilité sur béton frais.. *CERIB.*

Roussel, N. & Ovarlez, G., 2005. A physical model for the prediction of lateral stress exerted by self-compacting concrete on formwork. *Materials and Structures,* 08.pp. 1-10.

Stivaros, P. C. & Kevin, W. L., 2004. Guide to formwork for concrete. *ACI Committee 347,* pp. 3-31.

Xiao, S., Zhai, Z., Zhang, Y. & Li, T., 2021. Undrained Elastoplastic Solution for Cylindrical Cavity Expansion in Structured Cam Clay Soil Considering the Destructuration Effects. *Appl. Sci.*

 © DFI International Bruges 2025

DEWATERING WITH ARTIFICIAL RECHARGE FOR THE CONSTRUCTION OF A MULTIFUNCTIONAL COMPLEX

Nicolas Denies, Buildwise, Limelette, Belgium, 0032 2 655 77 11, nicolas.denies@buildwise.be
Griet Goossens, Embuild Vlaanderen, Brussel, Belgium, griet.goossens@embuild.be
Bert Creve, G Smeyers, Zandhoven, Belgium, bert.creve@gsmeyers.be
Eric Leemans, Soetaert, Oostende, Belgium, eric.leemans@soetaert.be

ABSTRACT

The multifunctional complex “HOF VAN SAEYS” was built in 2022 in Dendermonde. The complex includes a parking lot consisting of two underground levels with nine elevator shafts. Due to the sensitivity to settlement of the underground and the adjacent abbey garden, the groundwater lowering was carried out within retaining walls (soilmix walls). No ground layer with a very low permeability was accessible at an economically reasonable depth. The groundwater lowering was therefore carried out with deep wells and artificial recharge wells: 22 submersible pumps pulled the groundwater out from the construction pit. These submersible pumps then pushed the groundwater to 22 artificial recharge wells that reinjected it into the ground.

The artificial recharge wells were located immediately behind the partial retaining walls. The soilmix walls were not embedded in a ground layer with a very low permeability. This method allows groundwater to be pumped out of the excavation and reinjected, forming a closed water cycle. This significantly reduces the amount of water pumped and discharged into the city's wastewater system and the risks of settlement. This project demonstrates the effectiveness of recharge techniques combined with retaining walls for construction projects in sensitive areas, enabling sustainable and environmentally friendly management of groundwater resources.

Keywords: dewatering, artificial recharge, partial retaining walls, soil mixing

INTRODUCTION

A new multifunctional complex was built in 2022 on Dijkstraat in Dendermonde. The complex includes a parking garage with two underground levels and nine elevator shafts. The complex is built in the historic center of the city (see Fig. 1). The objective of the project, led by the project developer Uplace and carried out by the general contractor Cordeel Group, was to build an entirely new neighborhood in an already densely populated urban center with the rational use of underground space. This had to be achieved while considering the immediate environment of the construction site in terms of construction techniques and minimizing the impact of dewatering on the surrounding area.

HYDROGEOLOGICAL CONTEXT AND DIMENSIONS OF THE CONSTRUCTION PIT

Figure 2 illustrates the excavation plan. The dimensions of the excavation were approximately 114 x 70 square meters. The ground level at the site is assumed to be at an elevation of +5.45 m TAW (the reference elevation against which height measurements in Belgium are expressed).

Figure 3 illustrates a cross-section of the soilmix walls with the excavation performed to the level of the foundation slab (-2.05 m TAW). The original groundwater level varies between approximately +3.30 and +3.40 m TAW, with partially free and partially confined groundwater. The excavation needed to be carried out to -2.05 m TAW for the foundation slab and -2.35 m TAW for the foundation footings. The elevator shafts needed to be excavated deeper to the level of -2.75 m TAW. The groundwater needed to be half a meter lower than the excavation, which corresponds to levels of -2.55 m TAW, -2.85 m TAW, and -3.25 m TAW, respectively. The base of the soil mix wall (55 cm thick), built with secant panels using the cutter soil mix technique, is at -15.5 m TAW.

The Quaternary formations encountered throughout the vertical profile of the excavation and along the soilmix walls are a succession of sandy, loamy, and clayey layers, which do not provide a natural impermeable bottom for the excavation. Typical results of cone penetration test for the site are given in Fig. 4.

 © DFI International Bruges 2025



Fig. 1. Project location of the multifunctional complex "HOF VAN SAEYS" in the historic center of the city of Dendermonde



Fig. 2. Excavation plan including the 22 (red) deep wells and the 22 (blue) artificial recharge wells just behind the soilmix walls

 © DFI International Bruges 2025

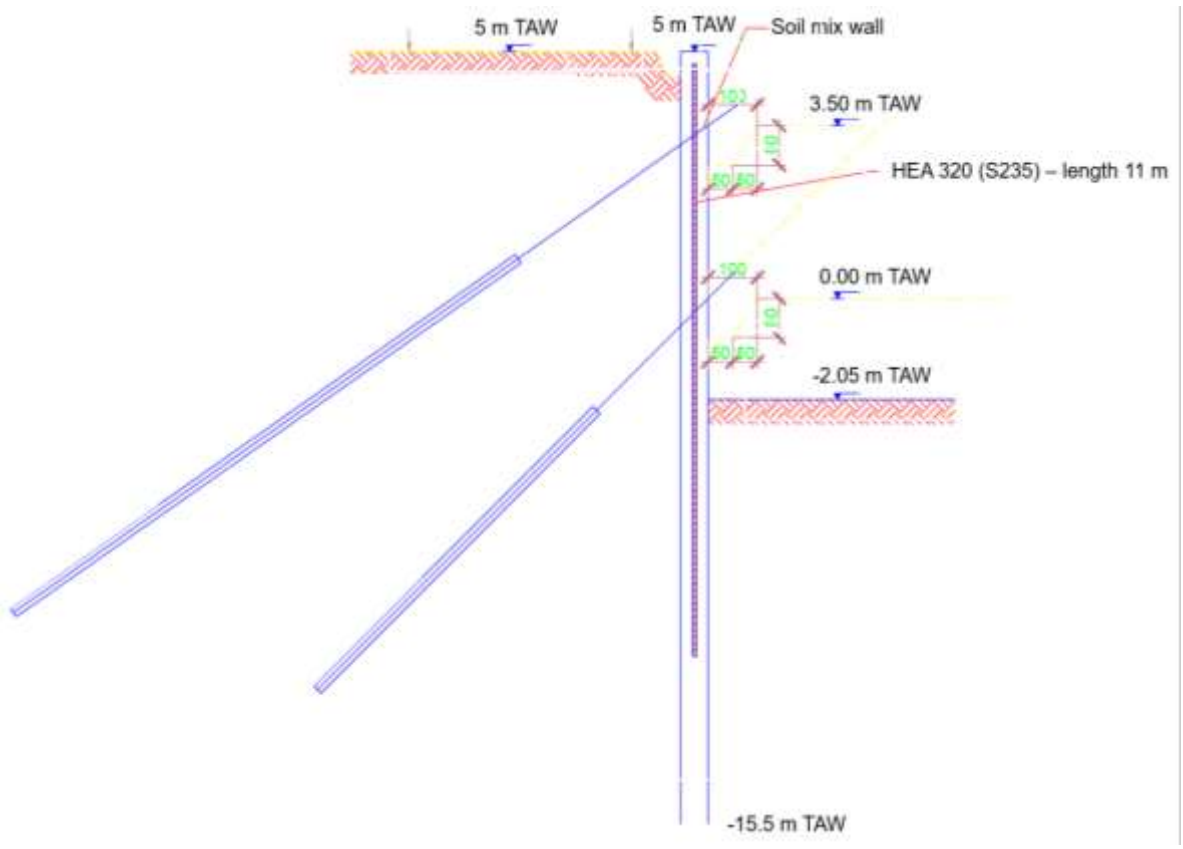


Fig. 3. Cross-section 6 (see Fig. 2 for the location) of the construction pit: anchored soilmix walls reinforced with HEA-beams to resist the bending moments

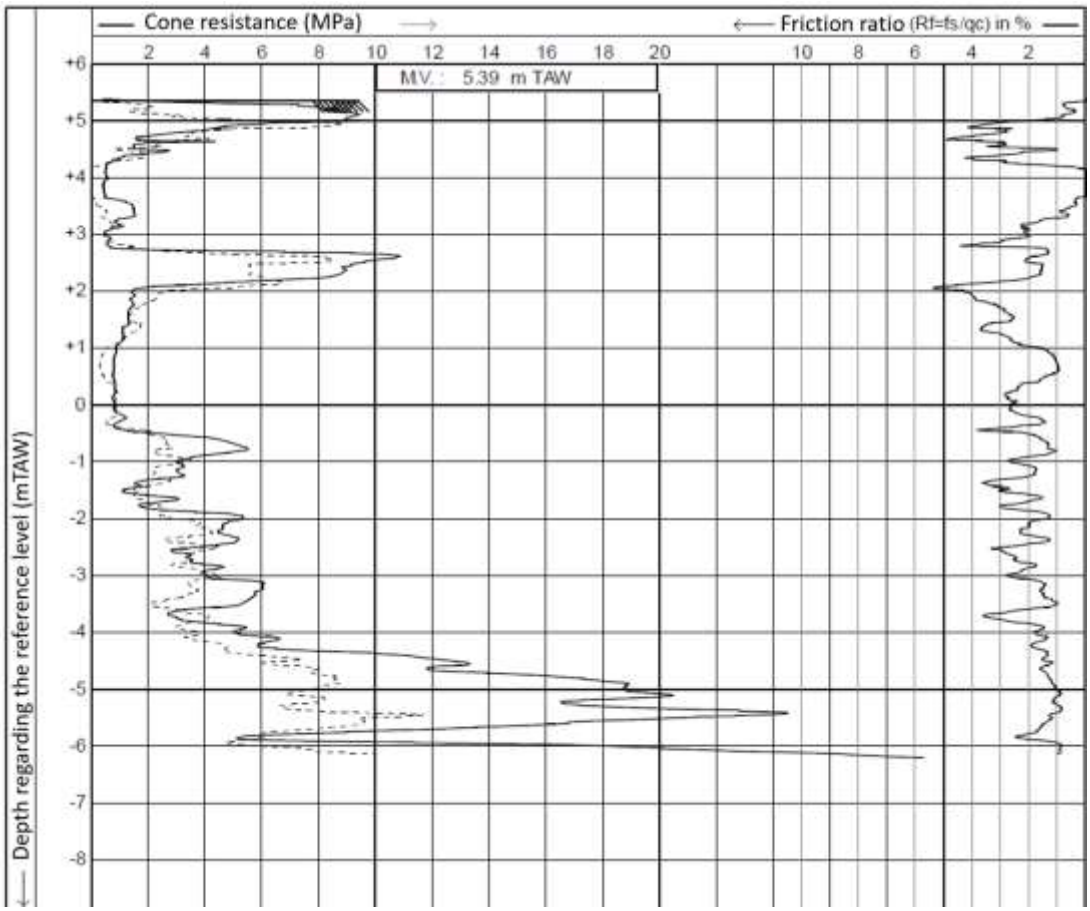


Fig. 4. Results of the cone penetration test (CPT-E type with base area of 15 cm²) performed at the location of the cross-section 6 identified in Fig 2

 © DFI International Bruges 2025

From a hydrogeological perspective, the underground is modeled considering 6 main layers. The following permeability values are assigned to the different layers:

- Layer 1: Ground surface to +2.27 m TAW, sandy clay: k_{hor} = 0.1 m/day and k_{vert} = 0.03 m/day;
- Layer 2: +2.27 m TAW to -0.38 m TAW, clayey sand: k_{hor} = 2.0 m/day and k_{vert} = 0.2 m/day;
- Layer 3: -0.38 m TAW to -3.92 m TAW, sandy clay: k_{hor} = 0.01 m/day and k_{vert} = 0.01 m/day;
- Layer 4: -3.92 m TAW to -12.55 m TAW, gravelly sand: k_{hor} = 12.0 m/day and k_{vert} = 4.0 m/day;
- Layer 5: -12.55 m TAW to -15.55 m TAW, loamy sand with sandstone banks: k_{hor} = 6.0 m/day and k_{vert} = 1.0 m/day;
- Layer 6: -15.55 m TAW to -35.50 m TAW, sand: k_{hor} = 6.0 m/day and k_{vert} = 2.0 m/day.

Figure 5 illustrates the construction pit after excavation. The water leakages through anchor holes indicates a high water table behind the soilmix walls.

In order to carry out the excavation, it was actually necessary to design a dewatering system taking into account the absence of a ground layer with a very low permeability at an achievable depth and the presence of settlement-sensitive soil around the construction site. This aspect is addressed in the following paragraph.



Fig. 5. Construction pit after excavation during the foundation works: the water leakages through anchor holes indicates a high water table behind the soilmix walls

GROUNDWATER LOWERING WITH ARTIFICIAL RECHARGE

Due to the settlement-sensitive soil under adjacent existing buildings and the adjacent abbey garden (visible in Fig. 1), the dewatering was being carried out within retaining walls (soilmix walls). No ground layer with a very low permeability was accessible at an economically depth. Therefore, dewatering was being carried out with deep wells and artificial recharge wells: 22 submersible pumps pulled the groundwater out from the construction pit. The submersible pumps then pushed the groundwater to 22 artificial recharge wells that re-injected it into the ground. There were no submersible pumps in the recharge wells. The artificial recharge wells were installed immediately behind the partial retaining walls: actually, the soilmix walls were not embedded in a ground layer with a very low permeability. This method allows groundwater to be pumped out of the excavation and reinjected, forming a closed water cycle. This significantly reduces the amount of water pumped and discharged into the city's wastewater system and the risks of settlement.

Figure 6 gives the typical configuration of the deep wells and artificial recharge wells for this site. The location of the deep wells and the artificial recharge wells around the construction pit are represented in Fig. 2.

 © DFI International Bruges 2025

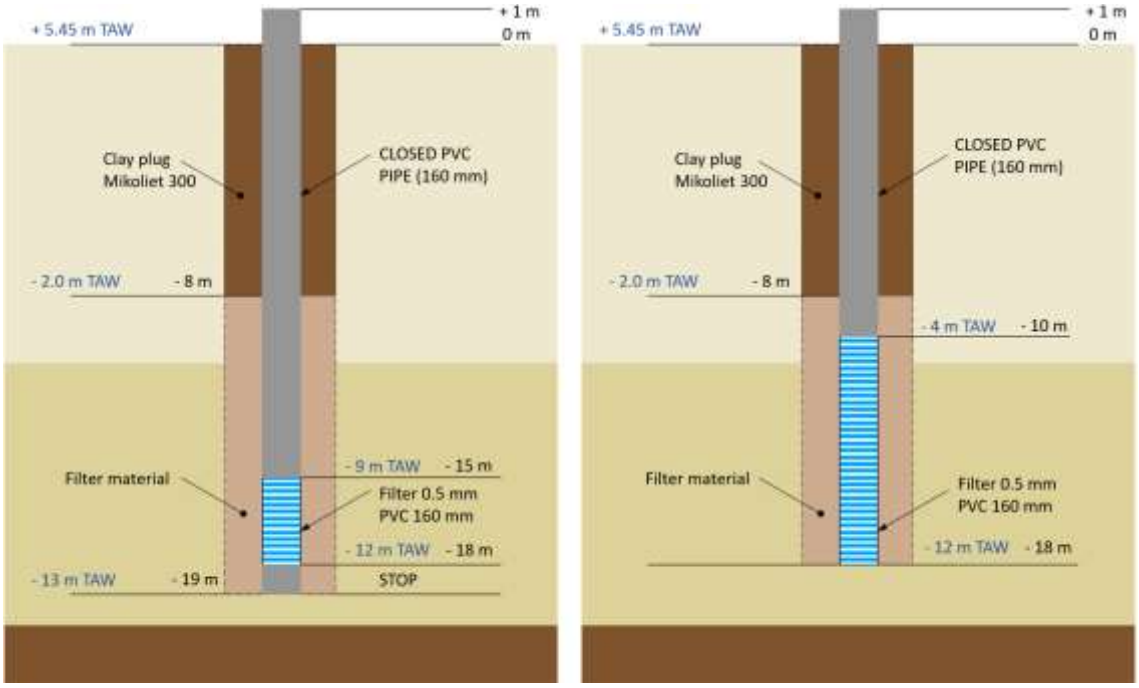


Fig. 6. Configuration of the deep wells and artificial recharge wells for the site

Figure 7 illustrates the head of a typical deep well as installed in the construction pit. Figure 8 illustrates the head of an artificial recharge well located in the vicinity of the construction pit. The drilling of the wells was carried out with clear water without additives and with a diameter of 38 cm.

Figure 9 shows the construction pit during the construction of the underground infrastructures. The dewatering pipelines were installed at the top of the retaining walls (visible on the right). The abbey gardens are visible on the left side of the image.



Fig. 7. Head of a deep well, equipped with a submersible pump, as installed in the construction pit

 © DFI International Bruges 2025



Fig. 8. Head of an artificial recharge well connected to the recharge pipelines



Fig. 9. View of the construction pit during the construction of the underground infrastructures

ARTIFICIAL RECHARGE - MAIN CHALLENGES

An artificial recharge well operates in the same way as a deep well used for groundwater extraction, only the direction of the flow is reversed. A recharge well must ensure that water can flow into the aquifer with minimal hindrance. However, recharging water in the underground is more difficult than pumping it out.

 © DFI International Bruges 2025

A deep well is essentially self-cleaning, because all loose particles (or particles in suspension) are removed from the well by the flow. In contrast, a recharge well is 'self-clogging': even if the water being pushed into the recharge pipes is of high quality, suspended particles or gas bubbles will become trapped in the well (or in the aquifer just outside the well), leading to a certain loss of efficiency and even clogging of the artificial recharge well over time.

There are various mechanisms that can lead to the clogging of recharge wells. Relevant information can be found in Pyne (1995), Martin et al. (2013) and Cashman and Preene (2021). To ensure the efficiency of the artificial recharge wells throughout the duration of the works, there are two approaches: avoiding or minimizing clogging (with strict management of the quality of the recharge water) on the one hand, and accepting clogging and thus planning the regeneration of the recharge wells on the other. Many of the practical problems with artificial recharge stem from water quality issues that lead to the clogging of recharge wells.

To avoid clogging of the artificial recharge wells, it is necessary to:
- Correctly design, develop and regenerate the deep (extraction) wells to minimize the amount of suspended solids (soil particles, algal matter, rust, or limescale deposits from pipes, etc.) present in the recharge water.
- Effectively develop the artificial recharge wells before the beginning of the dewatering operations and periodically regenerate them. As the permeability around the recharge well can decrease due to the rearrangement of loose particles around this recharge well caused by the flow of recharge water, the development and regeneration of the recharge well ensure that the flow rate of the recharge can be maintained despite this rearrangement.
- Carefully seal the pipe connections and minimize aeration of the recharge water. Degassing equipment can be installed on the piping to tap any gas before it enters the recharge wells.
  The worst enemy of the artificial recharge is the aeration of the pumped water. Aeration of the groundwater causes the precipitation and the deposition of calcium carbonate and iron or manganese oxides, on the one hand, and biological growth, as some bacteria are aerobic, on the other hand. These two phenomena can lead to clogging of filters and wells.
- Minimize temperature and pressure change of the water during recharge, as these changes can lead to precipitation of the aforementioned components.

In Flanders, the following measures can be found in the VMM guidelines (2021) to control the quality of the artificial recharge process:
- The amount of suspended solids in the recharge water can be determined by measuring the Membrane Filter Index (MFI). The Membrane Filter Index (MFI) is a measure of the amount of suspended solids. It is measured by pumping water under constant pressure through a standardized filter and timing how long it takes to pump a fixed volume through the filter. VMM (2021) provides values to be met to ensure a minimum water quality.
- To avoid gas (air) bubbles, a minimum pressure of 0.5 bar (shallow extraction) to 1.5 bar (deeper extraction) must be provided over the entire length of the pipelines. High flow rates can cause local under-pressures. Therefore, the flow rate in the entire piping system must be limited to a maximum of 2 m/s.

The recharge wells must be equipped with an injection pipe that extends below the groundwater level and is fitted with a control valve or adapted device to manage both the flow rate and the injection pressure.

The continuous monitoring of the parameters of the artificial recharge wells (injection pressure, injection flow rate, water level in the well, etc.) allows for ongoing tracking of each well's performance. This enables the detection of the progressive clogging of a recharge well and the planning of well regeneration.

For the regeneration of the recharge wells, air lifting is often used. With air lifting, a column of water in a pipe or borehole is transported or pushed to the surface by injecting compressed air at the bottom of the water column. This technique is faster than redevelopment using a pump.

 © DFI International Bruges 2025

ARTIFICIAL RECHARGE – DESIGN ASPECTS

For the design of artificial recharge wells, numerical modeling is necessary to study the influence of the groundwater lowering and recharge system. The reliability of such a model will be greater the more adequately it has been calibrated.

Conducting a preliminary dewatering test is ideal. This type of test allows for determining the local hydrogeological properties of the underground at a real scale, taking into account the site's history (e.g., previous dewatering operations that may have led to soil consolidation) and any underground obstacles or cavities (e.g., old, perforated sewer pipes that may act as preferential flow paths for the pumped groundwater). This type of large-scale test is very useful for calibrating the numerical model used to design the artificial recharge system and for measuring settlements of adjacent structures during the test, but it is unfortunately not always feasible in practice.

When designing a dewatering system in an urban environment, especially in a city center, it is important to recognize that the underground is not entirely composed of soil. It is often a complex area where old temporary retaining walls, which no longer serve a structural function, or underground structures (such as underground parking garages, tunnels, pipes, cellars...) define the hydrogeological model to be designed and the behavior of the groundwater once it is pumped and reinjected as much as, or even more than, the properties of the soil itself.

If there is an intention to reinject the pumped water into the ground through artificial recharge wells, a recharge test allows for verifying that the flow rate intended for the artificial recharge can be achieved/imposed considering the properties of the soil layers encountered. If this test is maintained for a specified period, it is even possible to get an idea of the maintenance schedule for the recharge wells by observing the progressive clogging of the well(s) during the test.

Whether a dewatering and recharge test has been conducted or not, it is anyway recommended to start progressively the artificial recharge system in phases so that the numerical simulations can be checked and updated at each stage. Preliminary calculations with a numerical model only provide indicative values of the expected water levels. It is always necessary to calibrate the hydraulic parameters of the model and its boundary conditions based on the measured water levels. The pumping curves recorded during the first general lowering of the groundwater are also relevant for the determination/adjustment/verification of the hydraulic parameters.

In an artificial recharge system, the impact of (temporary or permanent) changes in water pressure on existing (underground) structures must be assessed. The same considerations apply to recharge wells as to deep extraction wells. Where it is necessary to reach a certain lowering depth for dewatering, a minimum (recharge) groundwater level must be maintained for artificial recharge. Considering the reduction in the efficiency of the recharge system over time, it is advisable to reduce the capacity of the recharge wells in the numerical model by conservatively estimating (lowering) the permeability. It is also important to limit the length of the filter element of the deep (extraction) wells. Above the filter element, a minimum saturated height must be maintained to prevent aeration and thus the precipitation of oxidation products.

One must consider that the position and length of the filter elements of the artificial recharge wells are often different from those of the deep extraction wells (see Fig. 6). It is essential that the filter element of the recharge well extends over the entire height of the aquifer to compensate for the influence of dewatering over the full height of the aquifer.

If the recharge wells are located in the immediate vicinity of a vertical retaining wall, this wall must be installed sufficiently deep. This is necessary to avoid a too-direct hydraulic short-circuit between the deep extraction wells and the artificial recharge wells. Such a hydraulic short-circuit could lead to excessive water flow into the excavation, which cannot be pumped out. Especially in this case, where the soilmix walls are not embedded in a ground layer with a very low permeability. The depth of the retaining walls should be determined using a numerical model.

In any case, a potential increase in the extraction rate due to the artificial recharge must be considered in the design.

 © DFI International Bruges 2025

ARTIFICIAL RECHARGE – RESULTS AND CONCLUSIONS

Given the importance of water preservation, the use of an artificial recharge system offers the significant advantage of not discharging the extracted groundwater into the sewer but rather reinjecting it directly into the aquifer (preferably the same one from which it was pumped). In this way, the influence of the dewatering on the environment is significantly limited.

As shown in Fig. 10, in this project, the installation of artificial recharge wells allowed for the reinjection of 80% of the extracted water: 80 m³/h were reinjected into the ground for every 100 m³/h of extracted water. On the project, it was planned to preserve more than 720 000 m³ of water.

The purpose of an artificial recharge system is not to maintain the groundwater level itself but to prevent side effects (such as settlements or limitations for industrial water users) from reaching unacceptable proportions. Groundwater levels naturally vary in response to seasonal fluctuations and industrial pumping operations. An artificial recharge system that results in absolutely no lowering of the groundwater level would not be realistic. However, it is possible to define in advance the minimum groundwater levels that must be respected in the piezometers (these levels can vary spatially). Knowing that groundwater levels around a construction site can naturally vary over time and that this variation does not cause adverse side effects, the seasonal minimum is often set as the lowest acceptable groundwater level in a piezometer (Cashman and Preene, 2021).

Sometimes it can also be useful to specify a maximum groundwater level for certain piezometers. This reduces the risk of overfill, which could cause groundwater levels to exceed the seasonal maximum, potentially leading to problems like flooded basements. By establishing both minimum and maximum allowable groundwater levels for each piezometer (with at least 0.5 meters between the maximum and minimum levels), the manager of the dewatering system has some flexibility to adjust the system. In the present case, combining soilmix walls and artificial recharge, the groundwater lowering outside the excavation site was limited to 0.55 to 0.75 meters to mitigate the risk of settlement, as illustrated in Fig. 11.

As a general rule, more artificial recharge wells than deep extracting wells are often installed because it is more difficult to reinject water into the ground than to pump it out. However, thanks to the experience of the dewatering manager and attentive, continuous monitoring of the recharge system, an equal number of deep wells and artificial recharge wells were installed in this project, resulting in significant cost savings.

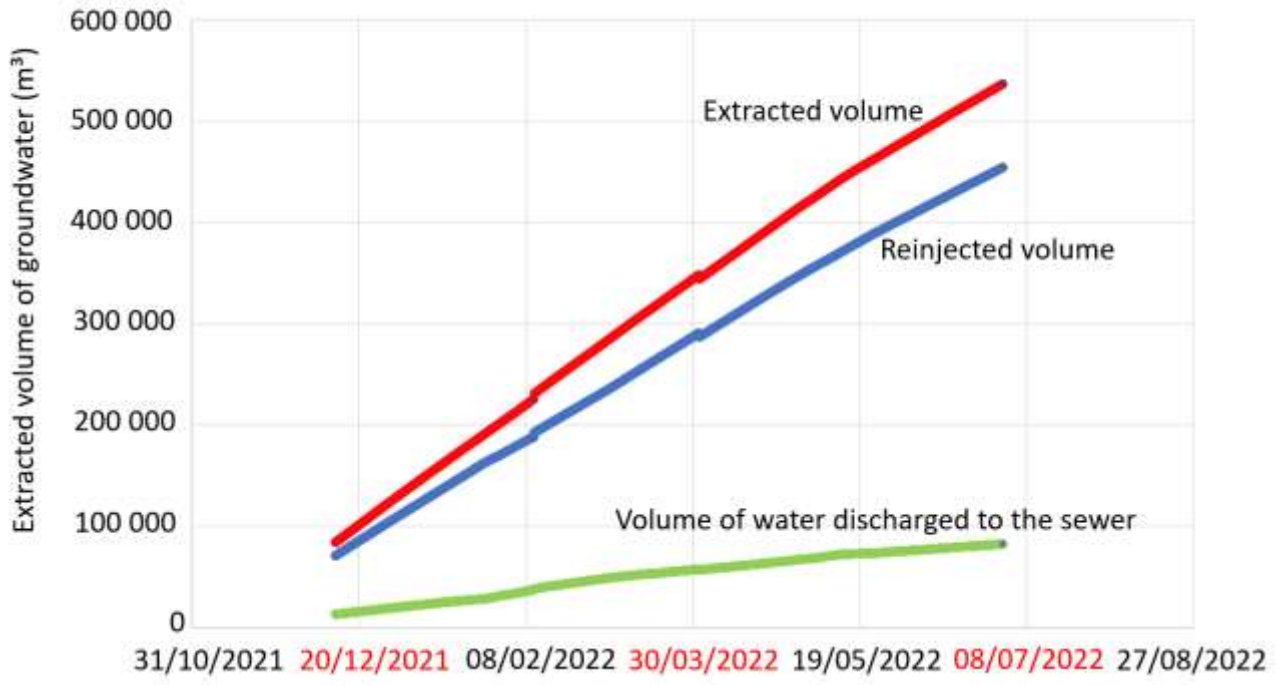


Fig. 10. Water preservation on the project versus time

 © DFI International Bruges 2025

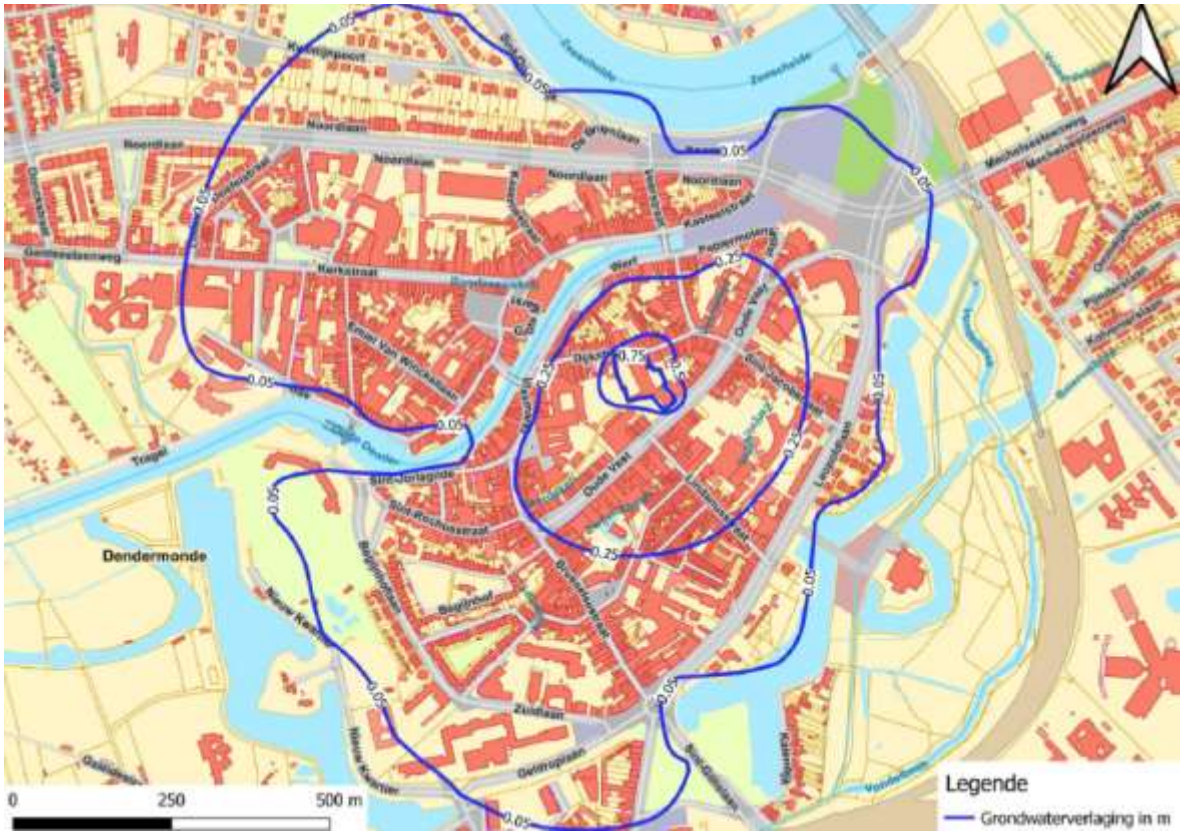


Fig. 11. Groundwater lowering (in meter) around the construction pit as a result of the combination of the soilmix cut off walls and the artificial recharge

REFERENCES

Cashman, P. M. and Preene, M., 2021. Groundwater lowering in construction. A practical guide to dewatering. CRC Press, 3rd Editon.

Martin, R. (ed.), 2013. Clogging issues associated with managed aquifer recharge methods. IAH Commission on Managing Aquifer Recharge, Australia.

Pyne, R. D. G., 1995. Groundwater recharge and wells. A guide to aquifer storage recovery. CRC Press.

VMM, Vlaamse MilieuMaatschappij, 2021. Richtlijnen bemalingen ter bescherming van het milieu.

 © DFI International Bruges 2025

SERVICEABILITY LIMIT STATE DESIGN: BASE RESPONSE OF SCREW INJECTION PILES

Kevin J. Duffy, Delft University of Technology, Delft, South Holland, The Netherlands, k.duffy@tudelft.nl
Ken G. Gavin, Delft University of Technology, Delft, South Holland, The Netherlands

ABSTRACT

Screw injection piles are a type of screw displacement pile that use grout injection to displace soil around the pile tip and to reduce the installation resistance on the pile. The process results in lower noise and vibrations compared to a driven pile, whilst creating displacement mechanisms considered beneficial to the pile's capacity. Yet while these benefits have increased the uptake of screw injection piles in the industry, divergences in design standards means there is no consensus on the axial response of these piles, particularly with regards to their load-displacement response for serviceability limit state design. This paper takes two settlement prediction methods for sandy soils and compares their performance to instrumented load tests on screw injection piles from two different sites. In summary, the results suggest that screw injection piles develop little to no prestressing around the pile base during installation into sand, and a stiffness-based formulation could accurately estimate the pile displacement at both test sites. The formulation presents an effective way of predicting pile displacement, allowing for more benefit to be gained out of proof load tests and providing an efficient means of validating the in-situ pile capacity after installation.

Keywords: screw displacement, drilled displacement, cone penetration testing, pile testing, serviceability limit state

INTRODUCTION

Design according to Eurocode 7 must comply with both ultimate limit state (ULS) and serviceability limit state (SLS) criteria. ULS pertains to the pile's maximum bearing capacity which, if exceeded, may lead to severe economic losses, environmental damage, and human casualties. On the other hand, SLS focusses on the pile's displacement before ULS is reached, ensuring deformations remain within acceptable limits throughout a structure's service life.

While ULS design of screw displacement piles is generally well-defined, SLS design is often not codified (Allani and Huybrechts 2020). Engineers therefore face considerable uncertainty in predicting the load-displacement response of a screw displacement pile, compounded by the lack of fully instrumented field tests. Moreover, recent research (Duffy et al. 2024b) suggests that screw displacement piles mobilise base capacities more comparable to a soil-replacing, bored pile as opposed to a full-displacement, driven pile. Given the fundamental differences in how bored piles and driven piles affect soil stresses around the pile base, the findings can have important implications for SLS design.

To consider this further, this paper looks at a subset of screw displacement piles known as screw injection piles. Screw injection piles combine a push-in force and torque with fluid injection (typically grout) from the pile tip, reducing the installation resistance and increasing the pile stiffness upon curing. The pile's adaptability to different soil conditions and the low noise and vibrations it generates during installation, means they are becoming increasingly common in the deep deltaic soil deposits of the urbanised lowlands of the Netherlands and Belgium (Bottiau and Huybrechts 2019).

As part of a Dutch research programme on the axial capacity of piles in sand, two full-scale field tests were performed at Amaliahaven in the Port of Rotterdam and in Delft. Using the base resistance measurements, this paper evaluates the performance of the Dutch code and compares it to an alternative stiffness-based formulation to reduce the uncertainty designers face with SLS design.

SERVICEABILITY LIMIT STATE DESIGN

Pile settlement is often assessed using the load-transfer method, modelling the pile-soil interaction as a series of one-dimensional springs. These springs, known as *t-z* and *q-z* curves, describe the shaft and base resistances as a function of the local displacement. Their shape depends on the installation method and soil conditions, making them virtually unique to every pile.

 © DFI International Bruges 2025

A variety of approaches are available to estimate the *t-z* and *q-z* springs (Allani and Huybrechts, 2019; Bohn et al. 2019; Bateman, 2022). One of the few codified methods for screw displacement piles appears in the Dutch National Annex to Eurocode 7 (NEN 9997-1): the method prescribes "type-curves" (Fig. 1), where the curve is selected based on the pile type and soil conditions. For screw injection piles, a stiff response akin to a full-displacement pile is assumed and so Curve 1 is used. For soil-replacement piles, like bored or auger piles, Curve 3 is usually used and so a softer base response is modelled.

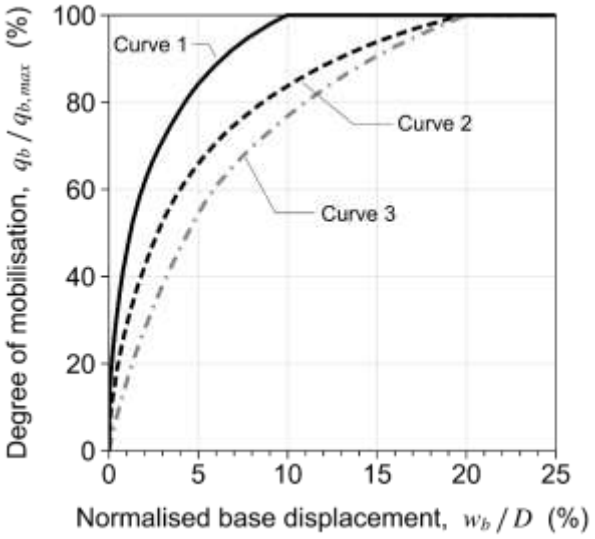


Fig. 1. Type-curves prescribed by the Dutch design method NEN 9997-1

Nevertheless, the rate at which a pile mobilises its full capacity is fundamentally dependent on the in-situ soil stiffness (Fleming, 1992; Atkinson, 2000). Recognising this, Fleming (1992) proposed a stiffness-based equation to evaluate the pile base displacement w_b:

$$\frac{w_b}{D} = \frac{q_b(1-\nu^2)\left(\frac{\pi}{4}\right)}{E_{b,eq}} \quad [1]$$

where D pile diameter, $E_{b,eq}$ is the equivalent stiffness beneath the pile base and ν is the Poisson's ratio which is approximately 0.2 for drained loading in sand (Mitchell and Soga 2005).

This same formulation was later adapted by Gavin and Lehane (2007) to assess both driven and bored piles, and Flynn (2014) later extended this to driven cast-in-situ piles (colloquially known as "vibro piles"). The adaptation assumes a linear stress-strain response upon initial loading of the pile. After reaching a certain yield displacement, w_{by}, the base response is expressed as a parabola of the form:

$$q_b = k\left(\frac{w_{by}}{D}\right)^{1-n}\left(\frac{w_b}{D}\right)^{n} \quad [2]$$

where n is related to the base capacity at $w_b = 0.1D$, and k represents the initial stiffness response of the piles. A detailed description of the approach is given in Gavin and Lehane (2007).

PILE TEST SITES

At Amaliahaven (Duffy et al. 2024a), three screw injection piles with a permanent casing (*Tubex* piles, maximum diameter of 850 mm) were installed, as well as three 400 mm square, driven closed-ended piles. At Delft (Duffy et al. 2024b), two screw injection piles with a removable casing (*Fundex* piles) were installed along with three Tubex piles (Fig. 2), with both sets of piles having a maximum diameter of 470 mm.

The base mobilisation of all piles was relatively comparable at both sites and so for brevity, this paper presents just three screw injection piles:

1) Pile SI1: Amaliahaven, with permanent casing (D = 850 mm; L = 37 m).
2) Pile F1: Delft, with removable casing (D = 470 mm; L = 20 m).
3) Pile T2: Delft, with permanent casing (D = 470 mm; L = 20 m).

 © DFI International Bruges 2025

To compare the mobilisation rate of a screw displacement pile to a full-displacement pile, one of the driven closed-ended piles at Amaliahaven (DP2; L = 32 m) has also been included.



Fig. 2. The conical tip of a screw injection pile with a permanent casing (*Tubex* pile)

Ground conditions

The test piles at both sites were founded at least five pile diameters into a sand formation known as the Kreftenheye Formation. The Kreftenheye Formation is a fluvially deposited coarse sand found across all of the western Netherlands, colloquially known as “the Pleistocene sand”. At Amaliahaven, the formation was characterised by its very high relative density, with CPT cone resistances q_c measuring 40 MPa on average (Fig. 3) and occasionally reaching peaks of 80 MPa. At Delft, the cone resistances were much lower, averaging around 12 MPa.

Ideally, the initial in-situ stiffness modulus E_0 of sand is derived from shear wave velocity measurements, such as geophysical surveys or seismic CPTs. In the absence of such data, E_0 can also be approximated by correlations to CPT q_c data, such as that defined by Rix and Stokoe (1991) :

$$K_G = \frac{G_0/q_c}{Q_{tn}^{-0.75}} \quad [3]$$

where Q_{tn} is the stress-normalised cone tip resistance and G_0 is the initial shear modulus, related to E_0 by the equation $E_0 = 2G_0(1+\nu)$.

At Amaliahaven, a geophysical survey (multichannel analysis of surface waves, MASW) was performed alongside the test piles, penetrating three metres into the Kreftenheye Formation. The survey yielded mean G_0 values of 125 GPa which, when compared to the CPT data (Fig. 4), showed that a K_G value of 215 gave a good fit to the measurements and consistent with values for young, uncemented sand (Schneider and Moss 2011). No shear stiffness measurements were made beyond three metres into the Kreftenheye Formation at Amaliahaven nor at the Delft test site. However, since the sand formation at both sites is geologically identical, the same K_G was assumed for both sites. Within two pile diameters from the pile base, G_0 ranged from 125−200 MPa at Amaliahaven and from 70−100 MPa at Delft.

 © DFI International Bruges 2025

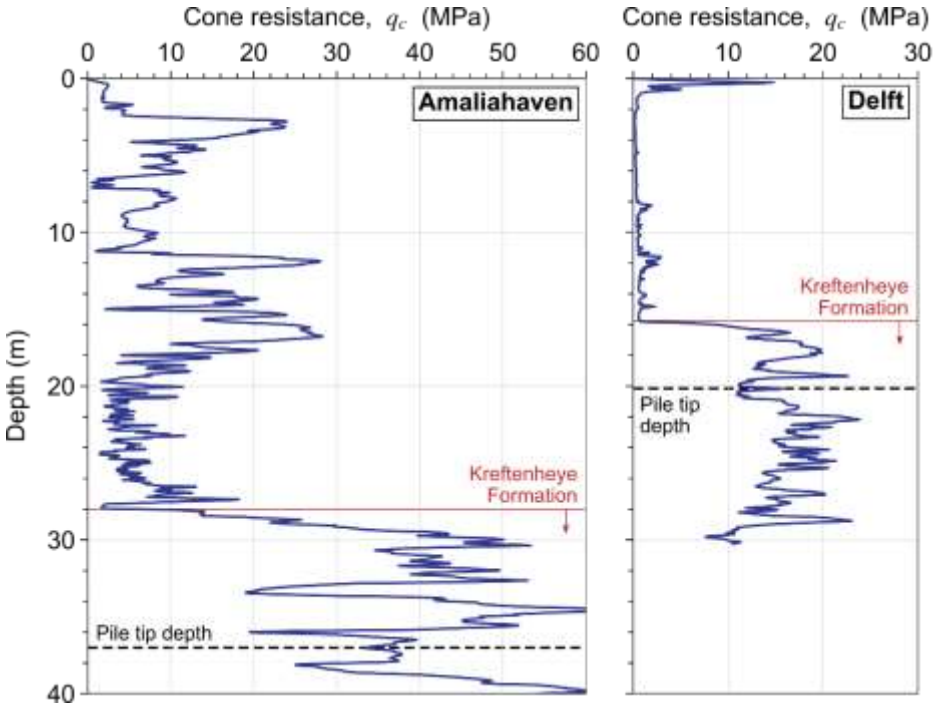


Fig. 3. CPT cone resistances at Amaliahaven and Delft

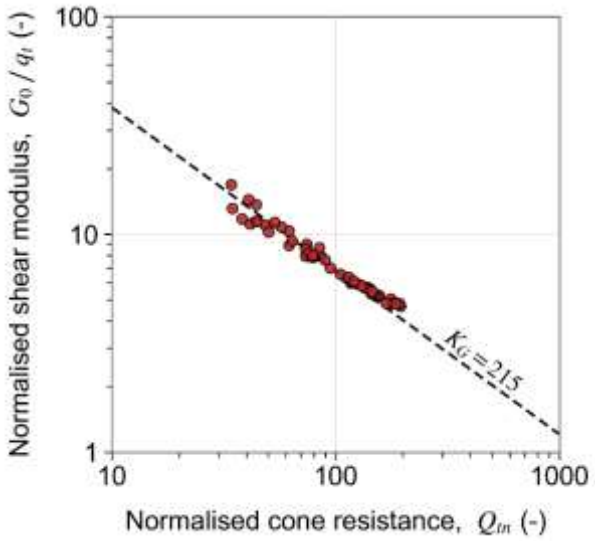


Fig. 4. Results of the MASW survey at Amaliahaven compared to CPT measurements

Pile installation

Compared to the Delft site, the penetration speed was much slower in the very dense sand of Amaliahaven. This is shown in Fig. 5 by the advancement ratio, colloquially known as the "scrape factor". The advancement ratio normalises the vertical displacement in one full pile rotation by the helical pitch of the screw tip. The pullup force was not measured at Delft and so the pulldown force in Fig. 5 can be seen as the maximum downward force on the pile. The pulldown force varied across all three piles, because of the different installation procedures for each pile as well as differences in relative densities at the two sites.

Grout with a water-cement ratio of 1.5 to 2.0 was injected at 200 L/min from the pile tips for most of the installation. Towards the end of installation, the piles were installed "in-the-dry"—a typical practice where the grout injection is turned off towards the end of penetration to avoid destructuration of soil around the pile base. At Delft, the piles penetrated an additional 25 cm without grout injection whereas at Amaliahaven, the very dense sands meant only one additional rotation of the pile was possible without grout injection.

 © DFI International Bruges 2025

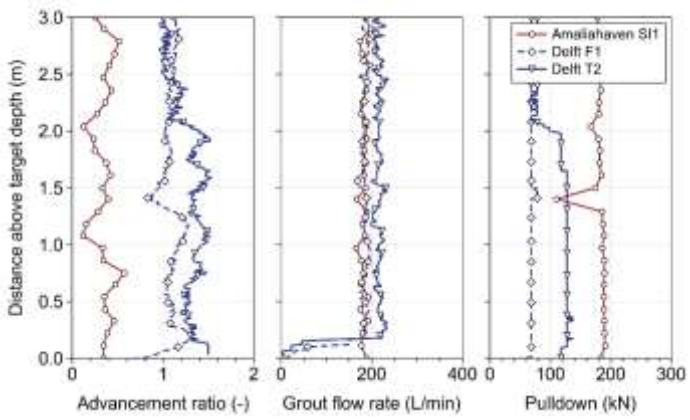


Fig. 5. Comparison of installation performance towards the end of installation

STATIC LOAD TEST RESULTS

All piles were instrumented with distributed fibre optic sensors along their entire length, affixed to either the permanent casing or to the reinforcing cage. Each pile was loaded incrementally under axial compression until a base displacement of around 0.1*D*, giving clear insights into the shaft and base capacity of each pile.

Measured base mobilisation curves

Fig. 6 compares the mobilised base resistances at both test sites. To account for the variation in soil strength around the pile base, the base resistances have been normalised by $q_{c,filter}$ using the spatial filtering algorithm by Boulanger and DeJong (2018). At Amaliahaven, SI1 mobilised its full resistance much more gradually compared to DP2, with the base stress continuing to rise as it approached a normalised displacement of 10%. In contrast, DP2 mobilised most of its resistance within a displacement of just 3%. In the medium dense sand of Delft, piles F1 and T2 behaved much stiffer than SI1: both piles mobilised most of their resistance within a displacement of 5%, showing a clear plunging failure beyond this point whereby further displacement mobilised little additional base stress.

At a base displacement of 0.1*D*, all three screw injection piles mobilised normalised base stresses $q_b/q_{c,filter}$ of around 0.28. By comparison, the driven closed-ended pile DP2 mobilised twice as much base capacity, including the residual stresses developed during the process of pile driving.

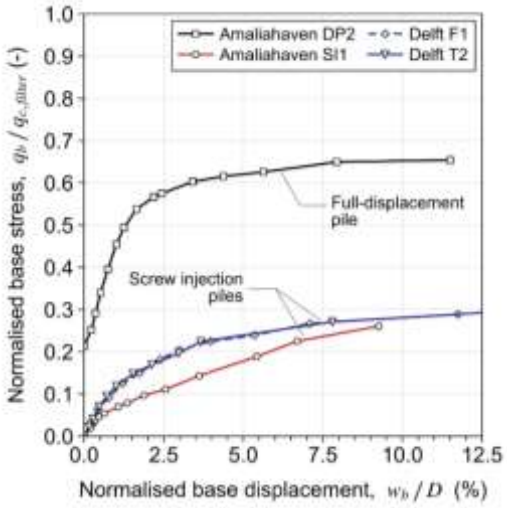


Fig. 6. Mobilised base resistances at Amaliahaven and Delft

Equivalent linear base stiffness

Using Equation 1, the base response can be interpreted as a stiffness degradation response (Fig. 7). Since field tests focus on large-scale movements, very small displacements (< 0.5mm) could not be accurately resolved with the fibre optic instrumentation. Notwithstanding, the initial stiffnesses of the screw injection

 © DFI International Bruges 2025

piles generally aligned with the in-situ G_0 values. By contrast, the driven closed-ended pile DP2 showed much higher initial stiffnesses, likely because of the large amount of prestressing created by the installation process.

This same prestressing has also been shown (Gavin and Lehane, 2007) to affect when stiffness degradation occurs (i.e. w_{by} from Equation 2). For the screw injection piles, stiffness degradation begins at normalised displacements of 0.3−0.6%. By comparison, stiffness degradation occurs later in DP2, at a displacement of around 0.8%. From this point, the stiffness degrades much more rapidly in DP2 compared to the screw injection piles.

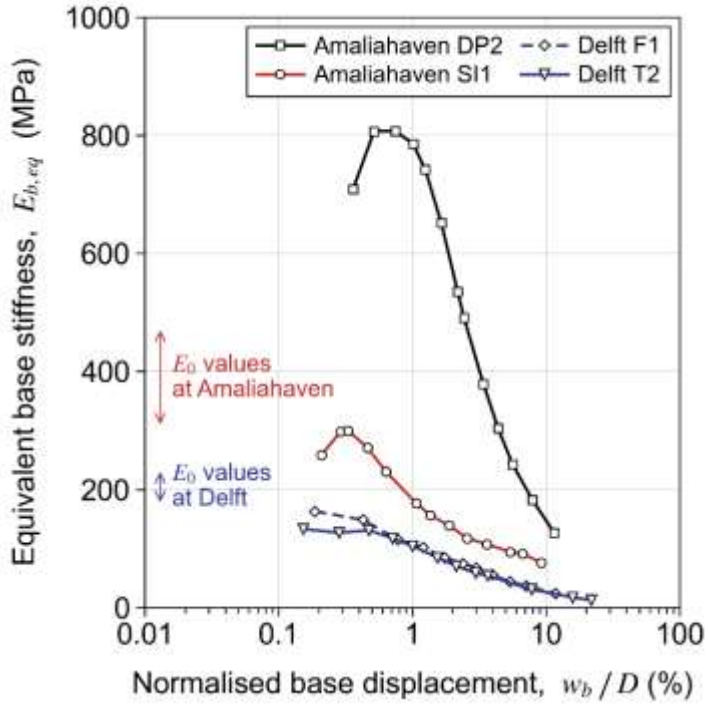


Fig. 7. Stiffness response of the test piles under static loading

Prediction of the base mobilisation curves

Fig. 8 compares the predictions of Equation 2 to the NEN 9997-1 type-curves. Both methods were calibrated using a normalised base stress $q_b/q_{c,filter}$ of 0.28, as indicated by the measurements in Fig. 6. The methods therefore converge to the same base stress at a normalised displacement of 10%, that is, the pile base capacity for ULS design.

The type-curve predictions align well with the measurements at Delft—a site whose geotechnical conditions (soft clay overlying medium dense sand) are relatively representative of most of the western part of the Netherlands. The stiffness-based method performs similarly to the type-curves, accurately predicting the base mobilisation for pile F1 and slightly underestimating the displacement for pile T2.

However for Amaliahaven SI1, the type-curve overestimates its initial stiffness by nearly a factor of two at a normalised displacement of 3%. In contrast, this response is captured well by the stiffness-based approach. This agreement comes in spite of the observed installation differences shown in Fig. 5, suggesting that the in-situ soil stiffness governs the base response of screw injection piles over other installation effects, within the range of installation parameters considered.

 © DFI International Bruges 2025

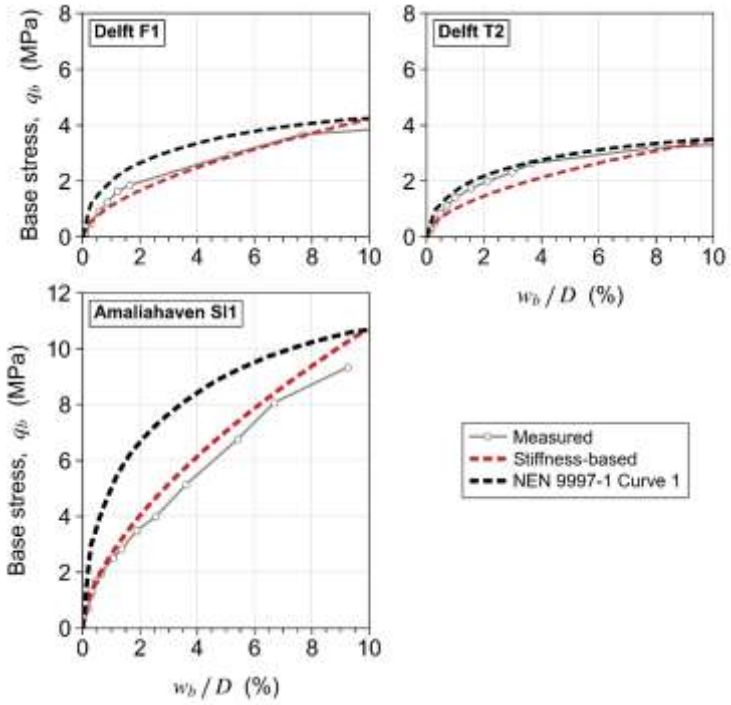


Fig. 8. Prediction of the base mobilisation curves

CONCLUSION

Measurements from screw injection piles at two test sites have been used to investigate how screw injection piles mobilise their base resistance in sandy soils. Considering the measurements in terms of an equivalent base stiffness, it was shown that stiffness degradation in screw injection piles begins at much lower displacements compared to an equivalent driven closed-ended pile. Comparing this equivalent stiffness to the in-situ soil stiffnesses before pile installation suggests that screw injection piles create little to no prestressing around the pile base, leading to a softer response under loading compared to a driven pile.

This behaviour was well captured by a load-transfer method that directly incorporates the in-situ soil stiffness into the formulation. By defining the input parameters directly from site investigation data, the approach is more generalisable to sand layers of different relative densities, improving on existing formulations prescribed in design standards for screw displacement piles. Ongoing research is focussing on understanding the site-specificity of CPT-based small-strain stiffness correlations, although it's recommended that geophysical measurements are used directly in order to give more confidence in stiffness-based SLS design.

ACKNOWLEDGEMENTS

This research is part of the STABILITY (Sustainable Circular Life Extension Strategies for Inner-City Bridges and Quay Walls) project, funded by the Dutch Research Council (NWO, NWA.1431.20.004). The authors are also grateful for the financial support of the Port of Rotterdam and the Ministry of Infrastructure and Water Management of the Netherlands (*Rijkswaterstaat*) for the Amaliahaven and Delft pile test sites respectively.

REFERENCES

Atkinson, J.H., 2000. Non-linear soil stiffness in routine design. ICE Publishing, Géotechnique, 50(5), pp. 487–508.

Bateman, A.H., Crispin, J.J., Vardanega P.J., and Mylonakis, G.E. 2022., Theoretical *t-z* curves for axially loaded piles. American Society of Civil Engineers ASCE, Journal of Geotechnical and Geoenvironmental Engineering, 148 (7), 04022052.

 © DFI International Bruges 2025

Bohn, C., Lopes dos Santos, A., and Frank, R., 2017. Development of axial pile load transfer curves based on instrumented load tests. American Society of Civil Engineers ASCE, Journal of Geotechnical and Geoenvironmental Engineering, 143 (1), 04016081.

Bottiau, M., and Huybrechts, N., 2019. Recent advances in pile design, construction, monitoring and testing. Proceedings of the 17th European Conference on Soil Mechanics and Geotechnical Engineering, Reykjavik, Iceland, ICSMGE.

Boulanger, R.W., and DeJong, J.T., 2018. Inverse filtering procedure to correct cone penetration data for thin-layer and transition effects, Proceedings of the 4th International Symposium on Cone Penetration Testing (CPT'18), CRC Press, pp. 24–44.

Duffy, K.J., Gavin, K.G., Korff, M., de Lange, D.A., and Roubos, A.A., 2024a. Influence of the installation method on the axial capacity of piles in very dense sand. American Society of Civil Engineers,ASCE, Journal of Geotechnical and Geoenvironmental Engineering, 150 (6), 04024043.

Duffy, K.J., Gavin, K.G., de Lange, D.A., and Korff, M., 2024b. Base resistance of screw displacement piles in sand. American Society of Civil Engineers, ASCE, Journal of Geotechnical and Geoenvironmental Engineering, 150 (8), 04024070.

Fleming, W.G.K., 1992. A new method for single pile settlement prediction and analysis. ICE Publishing, Géotechnique, 42 (3), pp. 411–425.

Flynn, K.N. 2014. Experimental investigations of driven cast-in-situ piles. PhD Thesis. Galway, Ireland: NUI Galway.

Gavin, K.G., and Lehane, B.M., 2007. Base load-displacement response of piles in sand. NRC Research Press, Canadian Geotechnical Journal. 44 (9), pp. 1053–1063.

Mitchell, J.K., and Soga, K., 2005. Fundamentals of soil behaviour. Chichester, United Kingdom: John Wiley & Sons Ltd.

NEN (Dutch Standardisation Institute), 2017. Geotechnisch ontwerp van constructies–Deel 1: Algemene regels [Geotechnical design of structures–Part 1: General rules]. [In Dutch.] NEN 9997-1+C2. Delft, Netherlands: NEN

Rix, G.J., and Stokoe, K.H., 1991. Correlation of initial tangent modulus and cone penetration resistance. Proceedings of the First International Symposium on Calibration Chamber Testing (ISOCCT), New York, USA: Elsevier, pp. 351–362.

Schneider, J.A., and Moss, R.E.S., 2011. Linking cyclic stress and cyclic strain based methods for assessment of cyclic liquefaction triggering in sands. ICE Publishing, Géotechnique Letters, 1 (2), ICE Publishing, pp. 31–36.

 © DFI International Bruges 2025

THE ROLE OF MECHANIZED SHAFT SINKING WITH VSM IN INNER-CITY APPLICATIONS

Stefan Frey and Julian Binder
Product Management Business Unit Utility Tunnelling
Herrenknecht AG, Schwanau-Allmannsweier, Baden-Wuerttemberg, Germany
Phone : +49 7824 302 7865, Email: frey.stefan@herrenknecht.com

1 ABSTRACT

Space on the surface is becoming increasingly scarce and expensive. Safe and economic construction of underground infrastructure in steadily increasing depths requires mechanized tunnelling and shaft sinking solutions. Shafts are needed for tunnelling operations, sewer systems, storage or for ventilation and rescue purposes in traffic tunnels.

The Vertical Shaft Sinking technology (VSM) is a mechanized approach developed to overcome challenging mixed-ground conditions with high groundwater tables, and safety or economic limits of conventional methods. Since 2004, far more than 100 circular shafts have been sunk with VSM, to depths of up to 115 meters and an inner shaft diameter range from 4.5 to 12 meters. The VSM is remote-controlled from the surface, thus, it is a completely unmanned sinking procedure without personnel required in the shaft during the sinking process. It meets the key requirements for shaft construction in inner cities: no groundwater lowering, maximum production accuracy and safety, and flexible arrangement of jobsite equipment. Due to the electrified operation of the overall VSM equipment with the possibility to be powered by the local grid, the CO_2 footprint and noise emissions can be considerably reduced compared to conventional construction methods. When using prefabricated concrete segments, shaft sinking with VSM requires up to 40% less concrete for the shaft structure. This paper will present the VSM technology, with international project references in urban infrastructure projects.

Keywords : Mechanized shaft sinking, VSM, foundation shafts, tunnelling shafts

2 INTRODUCTION

Almost all tunnelling projects require shafts, either as launch and reception shafts for the tunnelling process or for inspection, ventilation, and rescue purposes. Also, a current trend towards infrastructure installations in growing depths can be observed. It is driven, among other things, by deep sewer construction projects that aim to avoid pumping stations as well as the need to build new installations below existing infrastructure.

In addition to shafts required for tunnelling projects, foundation structures on- and offshore can be designed as shafts, safely built by mechanized solutions in order to use the space underneath a building, or to build harbor or bridge foundations. A foundation designed as a shaft can even enable buildings to be constructed where the ground itself is not stable enough.

The Vertical Shaft Sinking Machine (VSM) was developed and named by Herrenknecht AG. Its original purpose was the mechanized construction of deep launch and reception shafts for microtunneling projects. The goal was to overcome existing challenges in deep vertical shaft construction while enhancing safety and project reliability for all stakeholders. Beginning with design and testing in early 2004, the first VSM equipment was successfully deployed in Kuwait and Saudi Arabia in 2006.

Unlike conventional or competitive technologies, which require lowering the groundwater table and can cause settlement or structural damage to surrounding areas, the VSM is designed to operate entirely underwater. The slurry system functions exclusively within the water, ensuring stability and minimizing environmental impact. This makes the VSM particularly effective in urban environments and challenging geological conditions where conventional construction methods are impractical or pose significant risks.

Another key design advantage of the VSM is its adjustable working diameter through the extendable cutting drum, allowing it to cover a range of shaft diameters. This flexibility makes the machine more economical by reducing the need for additional machineary equipment. Additionally, VSM technology offers exceptional accuracy in shaft construction, ensuring precise alignment and minimal deviation.

 © DFI International Bruges 2025

The machine concept, fully remote-controlled from the surface, as well as its implementation on site proved to be an efficient solution right from the start for the safe and fast construction of shafts especially in difficult, inner-city environments without lowering the groundwater table.

The latest application was the construction of two shafts for the first U-Park® system in Nanjing, China, with on OD of 12.8 m and a depth of 65 m each. U-Park® is an underground car parking system ideal for cities with high-density populations, like London or Paris, where the availability of parking places is limited and therefore expensive. A VSM shaft might even be used as a underground parking space as well as a permanent statical foundation simultaneously, not only for buildings above surface, but also for bridges and other near-shore construction foundations relying on the principle that deeper soil layers are often more stable than surface layers. By excavating the shaft into these stable layers, the structure's weight is evenly distributed, ensuring a stable foundation. Also, the friction between the shaft walls and surrounding soil provides extra support, further reducing stress on the ground and enhancing stability.

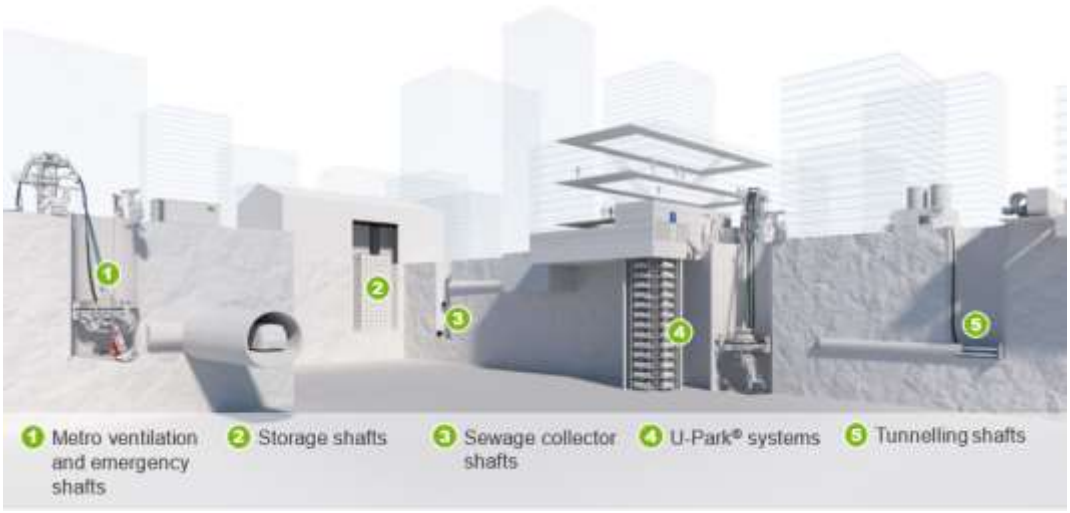


Figure 1. Overview of VSM application fields in inner-city surroundings

3 MECHANIZED SHAFT SINKING WITH VSM

3.1 Benefits of VSM Technology

The VSM technology overcomes the main challenges associated with shaft sinking: inner-city shaft structures demand safe working conditions for surrounding buildings and the environment, especially regarding potential ground settlement. There is an increased requirement to avoid the lowering of groundwater during the construction of shafts in order to avoid subsequent settlement, which can affect a wide, inner-city area and the surrounding buildings. Deep shaft construction companies often encounter difficult geological conditions such as high groundwater pressure combined with layers of hard and soft material. In addition, deep shafts need special attention for the safety of the operating personnel.

3.3.1 Cost and Time Benefits

Simultaneous excavation and ring building facilitate high advance rates and shortened overall project duration. At the same time, continuous performance ensures overall high planning reliability for all stakeholders.

The lining of a VSM shaft consists of either precast segments or cast-in-situ concrete. As the lining installation is completed on the surface, high quality installation can be accomplished, leading to greater accuracy of the shaft structure. In most cases, a secondary, time-consuming lining is not required, resulting in a reduced wall thickness of the shaft and, thus, less soil excavation.

 © DFI International Bruges 2025

The possibility of combining the two lining methods provides the flexibility of having the best structural and functional configuration at different depths, this characteristic allows for greater efficiency from both the technical and economic point of view of the projects.

Furthermore, each VSM type is very flexible as its excavation diameter can be adjusted within a specific range. A VSM12000 (named after the maximum shaft diameter of 12 meters), for example, can cover an inner shaft diameter range from 7 meters to 12 meters and is, therefore, a one-time investment for multiple use cases.

3.1.1 Construction and Occupational Safety Benefits

As the water level in the shaft is maintained close to the groundwater level outside the shaft, water inflow is prevented which otherwise could cause ground movement and lead to a high risk of settlement. The VSM can be utilized below groundwater with a high hydrostatic pressure and in heterogeneous soil and hard rock with compressive strength up to 140 MPa in intermediate layers.

All installations, including the lining erection, are remotely controlled from the surface. No personnel have to enter the shaft until it has reached the final depth and is fully secured. In general, mechanized shaft sinking requires less personnel and machinery on site, which leads to minimized risk exposure.

3.1.2 Environmental Benefits

Measures for groundwater lowering are not necessary, as the VSM machine concept is designed for operation under groundwater. As the VSM technology applies a high degree of accuracy of shaft construction, the shaft lining thickness can be reduced to a minimum, which reduces the amount of excavated soil and therefor reducing the construction cost.

3.2 VSM Machine Components

The VSM consists of two main components (Figure 2): the excavation unit and the lowering unit. The excavation unit systematically cuts and excavates the soil and consists of a cutting drum attached to a telescopic boom that allows excavation of a determined overcut. The lowering unit on the surface stabilizes the entire shaft construction against uncontrolled sinking by holding the total shaft weight with steel strands and hydraulic jacks. When one excavation cycle is completed, the complete lining can be lowered uniformly and precisely.

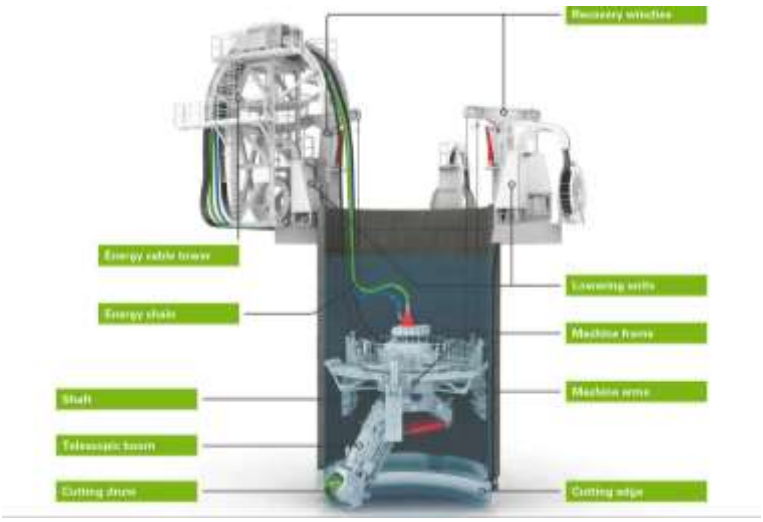


Figure 2. VSM components of equipment

A slurry discharge system removes the excavated soil and a submerged slurry pump is located directly on the cutting drum casing. It transports the water and soil mixture through a slurry line to a separation plant on the surface. The whole operation takes place from the surface and is controlled by the operator from the control container on the surface. All machine functions are remote-controlled without the necessity to view the shaft bottom or the machine. Power supply for the submerged VSM is secured by the energy chain. After reaching its final depth, the VSM is lifted out of the shaft by the recovery winches and the jobsite crane.

 © DFI International Bruges 2025

3.3 Jobsite arrangement in inner-city conditions

Depending on the space conditions on site, the VSM components can be positioned flexibly to suit local circumstances (Figure 3). As most sites are located in heavily built-up urban areas, access for logistics (e.g. trucks, ring segment stock, or soil disposal) is limited. Special concepts to relocate components such as the separation plant already exist for this purpose and can be discussed if required. The advantage of modular and flexible arrangement of the system makes the VSM perfect for urban shaft applications where space is limited.

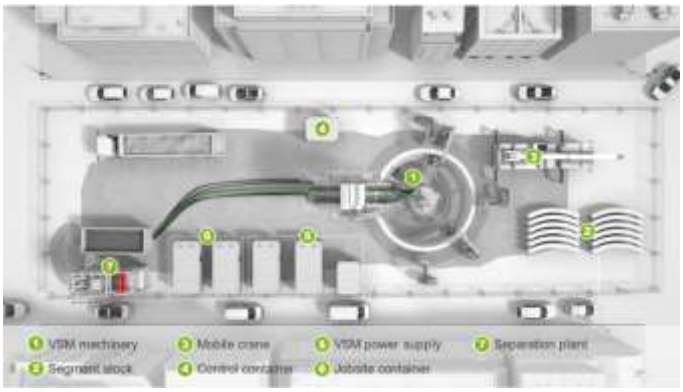


Figure 3. Layout of a VSM jobsite in dense urban area

3.4 Installation of VSM Equipment

The excavation unit arrives on site in three parts: the telescopic boom with the cutting drum, the machine main body, and the adapter parts to the required shaft internal diameter. The lowering unit consists of the strand jacks and the coiled steel strands on a drum. The number of strands depends on the total predicted weight of the shaft including the machine weight and the estimated buoyancy and friction forces. The strand jacks are bolted to the ring foundation by anchor bolts. Coming from the strand drum, the strands are fed through the strand jack, lowered through the outer annulus of the shaft wall, and connected to the cutting edge. When all strand jacks are installed and connected to the cutting edge the strands can be tensioned and carry the loads.

Now, the preassembled excavation unit can be lifted into the start section. The VSM is secured by hydraulically activated locking bolts. When the VSM is in place, the recovery winches are installed and connected to the three arms of the machine. The recovery winches are used to recover the VSM for required maintenance or for final machine recovery.

Next, the energy chain system is installed, and the excavation unit is connected to the hydraulic and electrical supply as well as to the feed and discharge lines. The energy chain tower with its winch has bolted connections for easy assembly. As a final step, all the electrical and hydraulic connections are made, and the equipment is now ready to operate. Before starting the excavation, a calibration of the VSM in reference to the projected alignment of the shaft is required to ensure the accurate action of the cutting boom.

3.5 VSM Operation – Shaft Sinking Procedure

Excavation is remote-controlled from the operator cabin at the surface. Stored data, together with the position of the cutting boom, is shown on a graphic display, giving the operator full control of the excavation and sinking process. The cutting arm moves radially from the center to the outside of the shaft with an additional telescopic extension. With a rotation of +/-190° the cutting boom covers the whole cross section of the shaft. The cutting speed and the movement of the boom can be varied to achieve the best excavation rate.

 © DFI International Bruges 2025

During the excavation and sinking process, the shaft is kept full of water to balance the level of the groundwater table in the surrounding geology. The cutting drum cuts and crushes the material to a granular size that can be handled by the discharge pumps. A slurry circuit transports the excavated material from the shaft to a separation plant on the surface.

The excavation unit can be operated in three different overcut options. The respective annulus should be stabilized by a bentonite-water suspension in soft ground conditions. In addition, each segment can be equipped with bentonite nozzles for lubrication, which can also later be used to grout the annulus. Within the standard installation bentonite lubrication is only installed in the start section of the shaft.

In contrast to horizontal tunnelling procedure, excavation and ring building are taking place simultaneously. Therefore, the lowering units hold the already assembled shaft structure in place until the subsequent excavation cycle is finished. Then the shaft structure is lowered to the next position and excavation can start again. The stabilization of the annulus, together with the controlled sinking of the shaft by the lowering units, minimizes the risks of settlement.

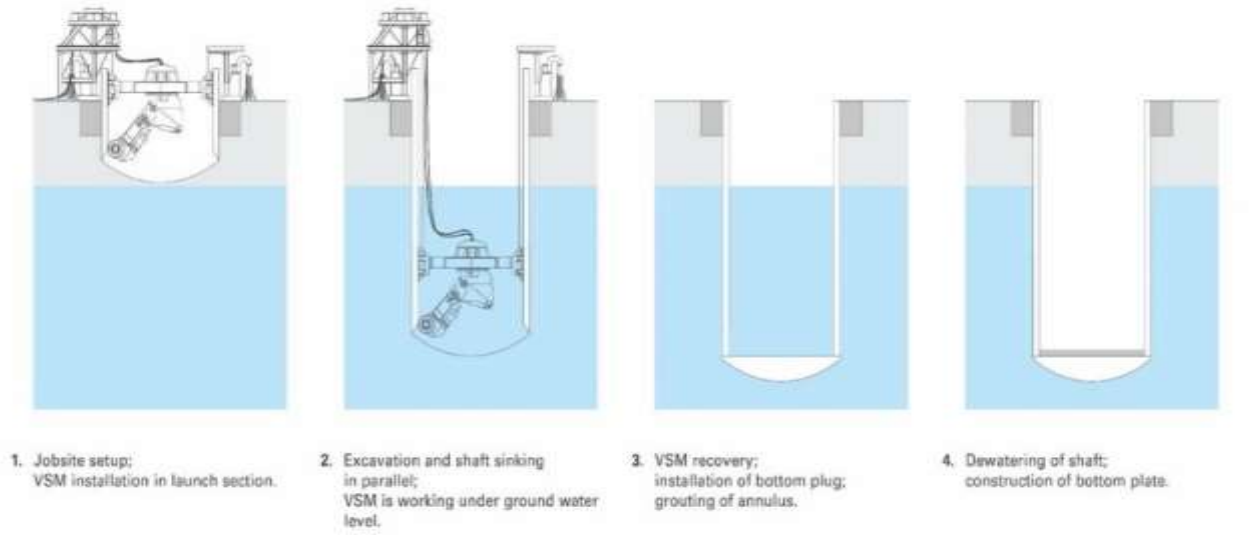


Figure 4. Installation steps of mechanized shaft sinking with VSM

3.5.1 Shaft lining

In most cases, the shaft lining consists of precast concrete segments installed at the surface. This so-called “ring building” is comparable to segmental lining in tunnelling. The ring is built at the surface by a crane. The number of segments depends on the shaft diameter. Ring building work includes the proper connection of the rings by anchors and bolts, which can be handled from outside the shaft. The excavation process of the VSM is not affected by the ring building process, which increases the shaft sinking performance significantly.

Alternatively, in-situ concrete casting of the shaft walls is another solution, especially for larger shaft diameters where segment handling becomes more difficult. In this case, the progress of shaft construction is slowed down by the necessary time to build the formwork and the setting time of the concrete structure. The benefit of in-situ casing is the "continuous" structure without joints and the possibility to integrate entire entry and exit structures (e.g. for microtunnelling activities in the shaft walls).

As mentioned previously, there is the possibility of combining the two lining methods, allowing for the best structural and functional configuration at different depths within one shaft.

 © DFI International Bruges 2025

3.6 Completion of the shaft

After reaching the required shaft depth, the bottom plug must be installed. Usually, the VSM is used to perform the required over-excavation for the bottom plug. When this final excavation is done, the VSM can be disconnected, recovered by the recovery winches, and lifted to the surface and out of the shaft by a crane. The bottom plug is cast with underwater concrete. Following final excavation, the shaft annulus is grouted through the lubrication lines to stabilize and anchor the shaft to the surrounding geological formation(s). Finally, the shaft water can be pumped out and the shaft is completed. Personnel access is now possible.

4 VSM IN INNER-CITY PROJECTS

4.1 Grand Paris Express, France

The Grand Paris Express is currently the largest infrastructure project in Europe with 200 kilometers of track on four new, fully automated subway lines with 68 stations and seven technical centers. The metropolitan area of the French capital is getting an additional network of routes, designed with sustainability in mind, whose main task is connecting the municipalities surrounding the city with each other more efficiently. Since August 2018, a VSM has been in operation for the first time in France on Line 15 Sud (T3C). Until end of November 2019, the VSM12000 had sunk four emergency and ventilation shafts for the Line 15 South tunnels, excavated by a tunnel boring machines. The shafts are up to 48 meters deep with inner diameters between 8.3 to 11.9 meters. So far, the respective outer diameter of 12.8 meters is the largest diameter ever installed by VSM technology with prefabricated concrete segments, even if larger diameter machine concepts already exist.

4.1.1 Large-Diameter Shaft Construction

In mechanized construction of large diameter shafts, the flexible use and setup options of all VSM components is a major benefit of the VSM technology. Within a given jobsite surface, in extremely restricted inner-city conditions, all components can be arranged according to the available space conditions, enabling the construction of a large diameter shaft at the same time. Nevertheless, detailed planning of the jobsite logistics and organization of the overall process is mandatory prior to the arrival of the equipment onsite. With growing diameter, the ring arrangement and related number of segments must be adapted. For the large inner diameter of 11.9 meters in Paris, 6 segments have been used for the construction of the shaft lining. The in-time delivery of the large and heavy precast segments required detailed planning and adaptation to the sinking progress during construction. Figure 5 shows the jobsite layout for the first shaft.



Figure 5. View on shaft sinking jobsite in inner-city conditions, Paris, France

 © DFI International Bruges 2025

4.1.2 Noise Emissions

Furthermore, the client and contractor considered the significantly lower level of noise emissions as a further decisive benefit of the VSM technology compared to conventional shaft construction methods. During shaft construction, the main components of the VSM equipment work underwater and are supplied with electrical power. Instead of using diesel generators, the electrical power for the VSM jobsite was provided by the municipal power grid. Thus, a considerable reduction in noise emissions was achieved.

4.1.3 Reduced CO_2 emissions

The VSM machine offers significant environmental advantages, particularly in reducing CO_2 emissions. Its innovative design and efficient construction process help minimize the environmental footprint of construction projects. The VSM enables much faster installation on construction sites due to modularity of the jobsite equipment. By speeding up the process, the machine reduces overall operating time and, consequently, the energy consumption associated with prolonged site activities. This not only improves construction efficiency but also lowers CO_2 emissions. Secondly, the VSM's shaft lining doubles as the permanent shaft lining, eliminating the need for additional concrete work. Concrete production and transportation are major sources of CO_2 emissions in construction, so reducing the amount of concrete required has a direct and significant impact on the overall carbon footprint of the project. Finally, the VSM machine and related equipment (e.g. powerpacks and separation plant) are powered entirely by the public electricity grid, eliminating the need for combustion engines to run the site and reducing greenhouse emissions. In regions where the electrical grid increasingly relies on renewable energy, the environmental benefits are even more pronounced. By integrating faster processes, reducing material consumption, and relying on cleaner energy sources, the VSM machine provides a forward-thinking solution for environmentally friendly construction, aligning efficiency with sustainability.

4.1.4 Mobility

Due to the inner-city locations of the different shaft construction sites, a quick and smooth mobilization and demobilization of all VSM components and detailed logistics planning was required, not only before the construction start of the first shaft, but also for disassembly, transport and installation of the VSM equipment on subsequent locations. After completion of the shaft, disassembly and assembly of the equipment at the next location took place simultaneously, because of the flexibility and compact design of the VSM equipment. A duration of three weeks from the recovery of the machine on one shaft until ready-to-bore on the next location was a remarkable performance of the jobsite and logistics crew.

4.1.5 Soil Conditions

Challenging geological conditions due to changing strata ranging from very cohesive clay to limestone with a compressive strength of up to 100MPa required continuous monitoring, adaptation of excavation parameters, and correction of the shaft position at any time. Due to the swelling clay expected, the overcut around the shaft lining had to be adapted flexibly to avoid getting the shaft structure stuck. The cutting tools have been adjusted regularly, according to the ground conditions, to achieve optimal performance rates. Furthermore, a high-pressure nozzle system has been used to clean the cutting drum during excavation in sticky soil conditions in order to maintain production rates. The modular design of the separation equipment provided the ability to adapt to soil and space conditions at each shaft location, and for flexible use of coarse and fine screens, different cyclone stages, and a centrifuge.

4.2 Other tunnelling shafts built with VSM in Europe

4.2.1 Napoli, Italy

Constructing subway tunnels beneath the historic city center of Naples, a UNESCO World Heritage Site, demands precise planning and cutting-edge technology. A crucial element in this project is the use of the Vertical Shaft Sinking Machine (VSM), which played a central role in ensuring the successful and efficient completion of key infrastructure components.

 © DFI International Bruges 2025

The VSM was tasked with drilling vertical shafts from the surface down to the tunnel level, for ventilation and to serve as emergency exits. Over the course of the project, the machine drilled ten shafts each with a diameter of 4.5 meters and depths of up to 45 meters. The technology and design of the VSM proved effective, particularly given the narrow streets and limited space in Naples. Its compact footprint made it ideal for urban environments, and the reduced noise disturbance ensured that the surrounding residents were only mildly affected by the work.



Figure 6. VSM construction for ventilation shaft in Napoli

The VSM offered further advantages with its daily production rates, advancing nearly five meters each day. This speed was possible due to the simultaneous drilling and construction of the shaft, using prefabricated concrete segments to ensure stability as the machine advanced. Additionally, the tight construction site conditions required a space-efficient solution, making the VSM the preferred approach over conventional methods. Unlike conventional methods, which demand large work areas and extensive ground preparation measures, the VSM's compact and modular design allowed for efficient operation in a highly constraint urban environment. Once a shaft was completed, the VSM's modular design allowed for quick disassembly and transportation to the next site, further optimizing the workflow.

While two Earth Pressure Balance (EPB) Tunnel Boring Machines (TBMs) were also working underground to bore the twin subway tunnels, the VSM's visible work at the surface was instrumental to the overall optics of the project with the public, showcasing a modern and efficient approach to underground construction in a highly sensitive and historic area.

4.2.2 Barcelona, Spain

With speeds of up to 350 km/h, high-speed trains on the AVE line connect Spain's major cities, Madrid and Barcelona, to the French border. A significant portion of the route runs underground, requiring the installation of escape routes and ventilation shafts. For this purpose, two Vertical Shaft Sinking Machines (VSMs) were deployed to excavate a total of six shafts along the Montcada to Trinitat section of the track, demonstrating the capabilities of VSM technology in challenging environments.

The first shaft was particularly demanding, passing through varying geological conditions, from very soft to extremely hard, down to a depth of 56 meters. The top 15 meters consisted of loose sand and gravel, while the remaining 42 meters required penetrating 200 MPa hard quartz slate rock. This was achieved using the VSM equipped with two specialized cutting wheels designed for the variation in ground conditions. The main challenge in this densely populated area was to avoid ground settlements during shaft construction, a task for which the VSM was designed.

 © DFI International Bruges 2025



Figure 7. VSM construction for ventilation and emergency shaft in Barcelona

During the construction of the first shaft, a daily progress of 3,5 meters was achieved with a 16-hour, two-shift operation. By simultaneously sinking and lining the shaft with precast concrete segments (tubings), the project advanced swiftly and safely, with the first shaft completed on October 2, 2009. A follow-up shaft was completed by mid-2012.

In 2015, a second VSM was deployed to construct an additional shaft for the high-speed rail line. The machine continued its work in 2019, drilling three more shafts for the project, demonstrating continuing reliability and efficiency of the VSM in delivering critical infrastructure for Spain's high-speed rail network.

VSM technology was chosen specifically due to the dense network of existing underground infrastructure, which required highly accurate shaft installation. The proximity of buildings above ground also demanded a solution that could minimize the risk of settlements to avoid structural damage. Unlike conventional methods, the VSM enabled precise and settlement-free shaft construction, making it the logical choice for this complex urban project.

While tunnel boring machines (TBMs) handled the underground sections, the VSMs installed the necessary safety infrastructure, demonstrating the effectiveness of the method and equipment in large-scale urban projects.

5 CONCLUSION

The current and worldwide trend in inner-city environments is to construct more and more underground infrastructure, which has resulted in a growing demand for the construction of shafts. In challenging ground conditions with high groundwater levels and increasing shaft depths, conventional methods reach their technical and economical limits. The mechanized construction approach with VSM has many benefits in terms of budget, construction time, and occupational safety, which has led to a total of more than 111 VSM projects where shafts have been successfully constructed in dense, urban surroundings. These ongoing technological advancements significantly expand the potential applications of vertical shaft sinking machines, enabling projects at increasing depths and with considerably larger shaft dimensions. For future urban development, underground storage of goods and sustainable energy generation concepts will be major considerations that require safe, economical, and ecological shaft construction approaches. VSM technology has the potential to play a key role in enabling vertical underground applications, such as hydrothermal energy storage, underground food production, or logistical hubs for urban supply chains. By providing highly accurate and space-efficient shaft construction, VSM opens new possibilities for future-proof, sustainable infrastructure in dense metropolitan areas.

 © DFI International Bruges 2025

FIRST EXPERIENCES OF A NEW GENERATION OF TRENCH CUTTER – CONTRIBUTING TO REDUCING CARBON EMISSIONS

Franz-Werner Gerressen, BAUER Maschinen GmbH, Schrobenhausen, Germany, Franz-Werner.Gerressen@bauer.de
Alexander Blatt, BAUER Maschinen GmbH, Schrobenhausen, Germany, Alexander.Blatt@bauer.de
Joao Nunes, NGE Fondations, Issy Les Moulineux Cedex, France, jnunes@ngefondations.fr

ABSTRACT

Diaphragm walls are known as underground structural elements commonly used as retention systems for excavation pits and shafts and permanent foundation walls or elements. It can be anticipated that global urbanization and increasing demands on environmental considerations will need to be accommodated in underground space in the future. These trends show an increasing requirement for diaphragm walling in even more complex conditions, especially in inner-city applications with limited space. For the construction of one of the iconic stations on the Toulouse metro Line C, notable for its exceptional dimensions and the critical scheduling challenges associated with its construction, a new generation of D-wall equipment was launched for the first time in Europe to contribute to the success of this jobsite. Usually, trench cutters are mounted on multi-functional duty-cycle cranes. For those who do not require a multi-functionality equipment but needs equipment that is specially optimized for trench cutting, the extended portfolio will become an alternative. The special design combines proven technology with a vast variety of other useful features as well as the necessary design and construction functions that meet the latest transport requirements. Easier and faster assembling, disassembling and reduced number of transports provide a more cost effective and efficient solution. This contribution and the future possibility to run the system using an electric driven power pack will reduce the local carbon emissions. For that reason, the development can contribute to zero emission sites, which will be in demand in the future. This paper will describe the first finalized project using the equipment, including the construction of the 53-meter deep and 1.5-meter-thick walls of La Vache station at the Toulouse metro line C. In addition, it will give a general outlook on future developments.

Keywords: Diaphragm wall, Trench Cutter

INTRODUCTION

The history of the trench cutter technology started in the early 1960's with a kind of suction cutter as well as reverse circulation concepts. These can be seen as the predecessor of today's hydraulically driven trench cutter technology. Usually, these trench cutters are mounted on multi-functional duty-cycle cranes. For anyone who doesn't require this multi-functionality but needs equipment that is specially optimized for trench cutting, the newly developed Cutter Systems BCS 185 offers an alternative solution. This new generation is capable of cutting trenches up to a depth of 90 m. In addition, the special design of BCS systems combines proven technology with a vast variety of other useful features necessary to meet current strict transport requirements and standards. With this features, the number of transports can be reduced thus contributing to a reduction of carbon emissions of each jobsite.

THE WORKING PRINCIPLE

Construction sequence

The working steps follow a pre-defined sequence. The main steps are shown in Fig. 1. After the pre-excavation, which is necessary to allow starting the suction pump installed in the cutter frame, the excavation of a primary panel starts. Most common is to install multiple bite primaries as shown in

 © DFI International Bruges 2025

Fig. 1. After finishing several primary panels, the installation of secondary, single bite panels takes place while overcutting the adjacent primary panels. The Overcut Joint System is a well proven way for the installation of diaphragm walls using the trench cutter system. In confined conditions the use of special auxiliary equipment (e.g. for installation of reinforcement cages) might become necessary. During excavation the open trench is stabilized by supporting fluid.

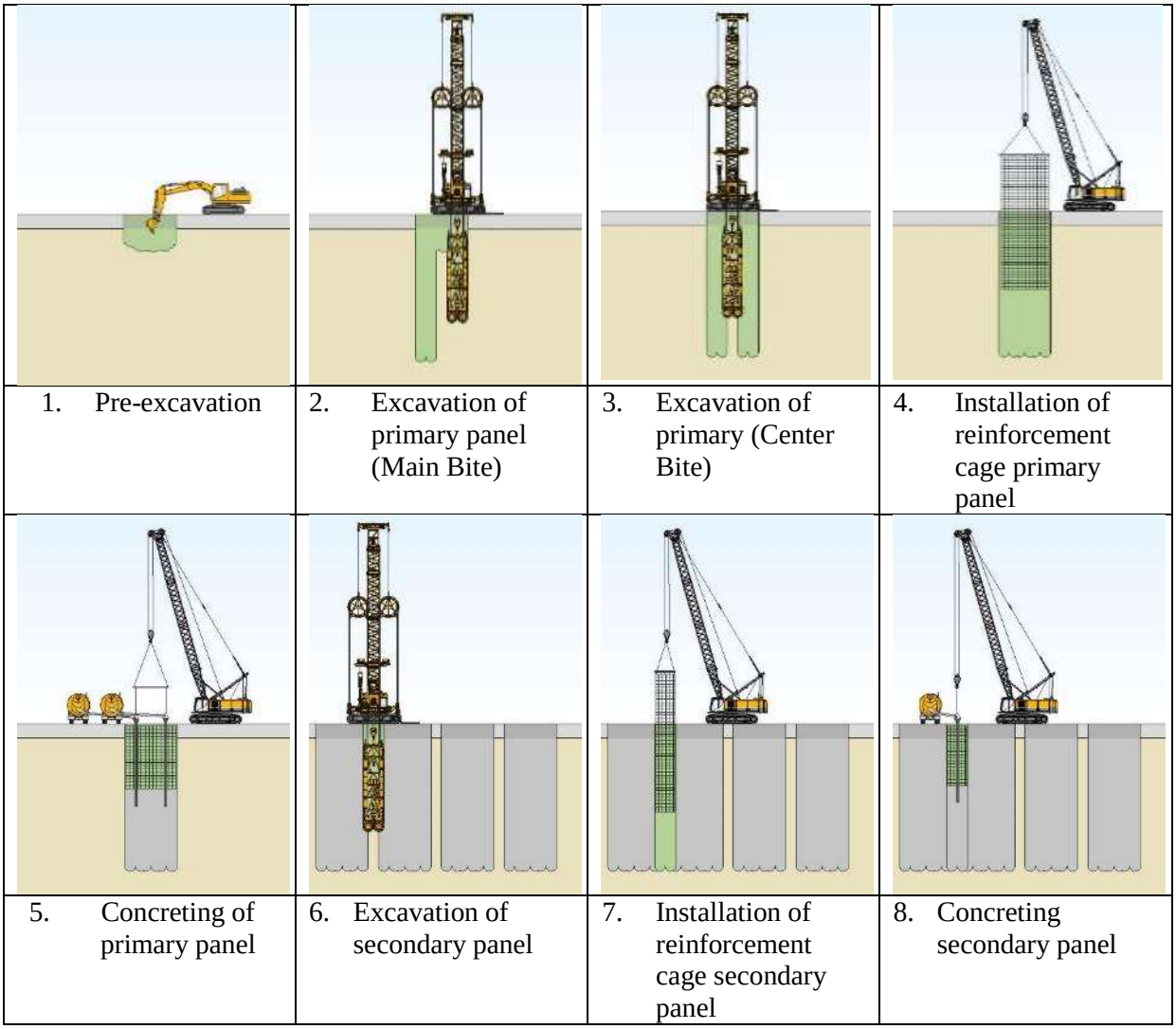


Fig. 1: Construction sequence

To meet tight schedules and avoid cost explosion of a project, the quality of the product is of utmost importance for success. Real time operation and quality control is state of the art and fast and effective data transfer and analysis will become more relevant in the future.

THE NEW CUTTER SYSTEM

The main difference of the new cutter system BCS 185 compared to the well-known systems is the base carrier as shown on the right side in Fig. 2. One will notice the arrangement of the hose drums inside the lower boom section, so that the cutter system delivers a highly streamlined impression overall. For this system, mud hose drum and hydraulic hose drum are placed in one line to optimize the width and consequently the dimensions of the entire unit. The 30-ton winch was specifically designed for use in the mid-sized range. With the maximum hook load of 43-ton, the BCS 185 can be equipped with a wide range of cutters allowing trench widths of up to 1,500 mm for depth up to 90 m. In addition, proven technology like the turning device allows the cutter to be twisted within a range of

 © DFI International Bruges 2025

-50 to +95 degrees from its normal position which allows this cutter to work in extremely confined construction sites and will still be able to cut the corners.



Fig. 2: Multi-purpose carrier cutter system (left), “New” Single purpose carrier cutter system (right)

With its modularity, the new system provides benefits for transport situations as well as for assembly/disassembly. The number of transports required as well as the assembly/disassembly time is reduced from 6 for a standard system to 3-4 for the new system, which leads to cost savings and reduction in carbon emission. In a next step the carrier will be equipped with an electric driven hydraulic power pack. A further contribution to local emission reduction which is going along with an 50% noise reduction, another important demand especially for inner-city use.

REFERENCE PROJECT

Toulouse Metro Line C

The construction of Toulouse's new Metro Line C is driven by several key objectives aimed at significantly enhancing the city's urban mobility and addressing its growing transportation needs. One of the primary goals is to improve connectivity across Toulouse, particularly by linking the western and eastern parts of the city, including neighborhoods that are currently underserved by public transport. Additionally, the new line is expected to play a crucial role in reducing traffic congestion, especially in the city center and along major roads. By offering a fast, efficient alternative to car travel, Line C will help to ease the burden on the city's road network.

The new line is designed to improve access to new residential, commercial, and industrial areas, thereby fostering economic growth in the region. In line with Toulouse's environmental goals, the project also emphasizes sustainability. By encouraging greater use of public transport, the new line aims to reduce carbon emissions and promote more environmentally friendly travel. Moreover, the new line is set to enhance the overall commuter experience by offering faster travel times, more frequent service, and modern amenities, making public transport a more attractive option for residents and visitors alike. Finally, the construction of Line C is part of a broader strategy to prepare for future population and economic growth, ensuring that Toulouse's transportation infrastructure can meet the foreseen increase in demand.

 © DFI International Bruges 2025

In summary, Line C reflects the city's commitment to developing a robust, sustainable, and user-friendly public transport system that supports its long-term growth and improves the quality of life for its citizens.

The Toulouse region is characterized by complex and varied geology, which is particularly significant for deep foundation construction. The reference projects, La Vache and Fondeyre stations, are located in an urban environment where geology plays a crucial role in determining the design and construction methods for diaphragm walls, as well as the need for compact equipment suitable for urban development.

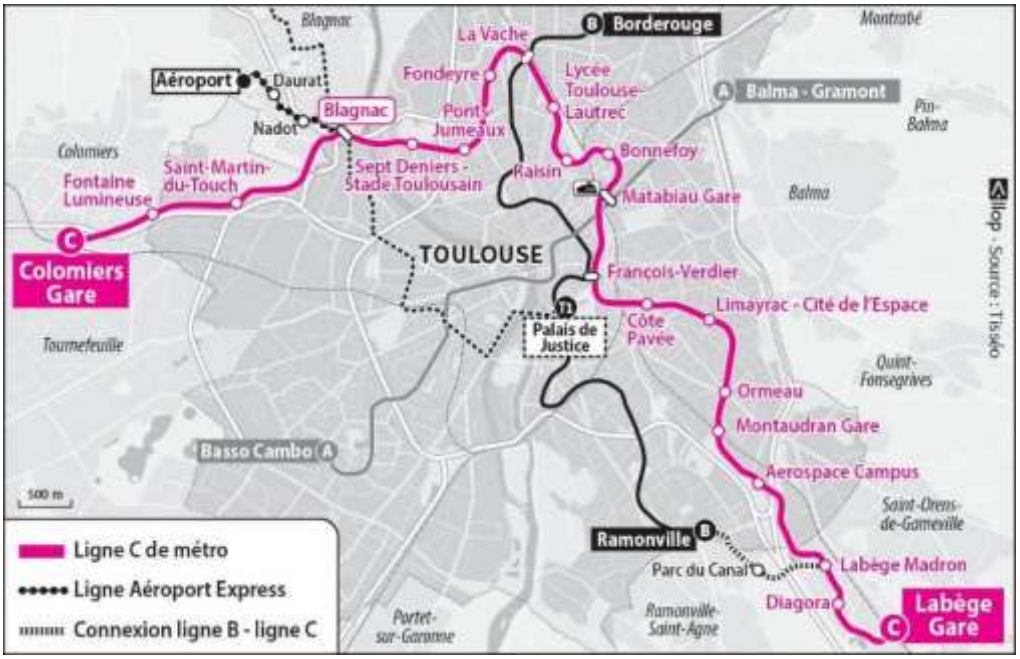


Fig. 3: Toulouse Metro Line C overview

Geology

The Toulouse region is characterized by complex and varied geology, which is particularly significant for deep foundation construction. The reference projects, La Vache and Fondeyre stations, are located in an urban environment where geology plays a crucial role in determining the design and construction methods for diaphragm walls, as well as the need for compact equipment suitable for urban development.

The surface topography common to both job sites is relatively flat, typical of the Toulouse metropolitan region, which lies within the larger Garonne River basin. The region's geological history has been shaped by fluvial processes, resulting in a landscape predominantly composed of alluvial deposits. These alluvial soils generally consist of varying layers of gravel, sand, silt, and clay, with the composition and thickness of these layers differing across locations. These heterogeneous layers are locally known as “molasses.”

The subsurface stratigraphy encountered is primarily made up of alluvial deposits overlying older Tertiary formations. The stratigraphy can be broadly divided into the following layers:

- **Alluvial Layer:** The uppermost layer consists of recent alluvial deposits, typically comprising fine sands, silts, and clays. These materials can present challenges in terms of stability and groundwater management. Deposited by the Garonne River and its tributaries, the thickness of these sediments varies across the site, with an average thickness of 4 meters.

 © DFI International Bruges 2025

- **Gravel and Sand Beds:** Below the alluvial deposits, more consolidated layers of gravel and coarse sands are encountered. These layers vary widely in their silty or clayish content and are often water-bearing, requiring special consideration for dewatering during excavation. The alternating gravel and coarse sand layers, along with the silty or clayish layers, resemble a "mille-feuille"—a typical French pastry—with each layer varying in thickness from 1 to several meters.
- **Tertiary Clayey Formations:** At greater depths, the site is underlain by Tertiary clay formations. These clays are more competent than the overlying alluvial deposits but can be prone to swelling or shrinkage, depending on moisture content.
  These formations were not intercepted at the project depth.

Based on the geotechnical data available at an early-stage phase, the presence of several layers were identified potentially too hard to for cable grab operation only. The respect of tolerance in terms of verticality requirements also influenced the choice of cutter excavation. Below as summary with the geotechnical mechanical parameters, valid for both stations.

Table 1. Geotechnical mechanical parameter

Terrain	Abbreviation	Thickness (m)	γ (kN/m^3)	EM (MPa)	pL (MPa)
Backfill	NA	2	20.0	5	0.5
Alluvial	Ag	4	22.0	16	2
Altered Gravel and Sand Bed	Mf,Alt+Mg	7	20.5	50	3
Silty sand and gravels	Mf+Mm	10	21.5	115	6
Gravel and coarse sand	Mg	2	21.0	134	6
Silty sand and gravels	Mf+Mm	15	21.5	156	6
Gravel and coarse sand	Mg	1.5	21.0	172	6
Clayish sand and gravels	Mf+Mm	7.5	21.5	180	6
Gravel and coarse sand	Mg	2	21.0	187	6
Clayish sand and gravels	Mf+Mm	>10		190	6

The hydrogeological conditions are characterized by the presence of a shallow groundwater table, influenced by the proximity to the Garonne River. Groundwater levels can fluctuate seasonally, posing a significant challenge during excavation. The presence of water-bearing gravel layers necessitates efficient dewatering systems to maintain stability and control seepage.

Toulouse Metro Line C - La Vache Station

Scope of work

Construction of a metro station consisting of a main central box with two lateral sub-superficial boxes for access and technical services. The main box is formed by 24 panels, each with a thickness of 1,052 mm and a depth of 52.90 meters. The lateral boxes consist of 10 and 15 panels, respectively, each with a thickness of 1,020 mm and a depth of up to 22.10 meters.

 © DFI International Bruges 2025

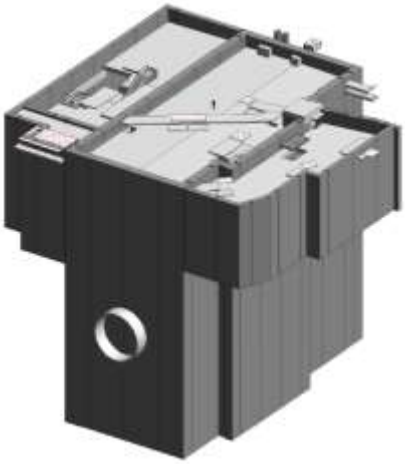


Fig. 4: La Vache Station BIM modeling

Execution

The mobilisation of personnel and equipment started on the beginning of July 2023 until the 2nd of August.
Two trench cutters were mobilised – a MC cutter system and a BCS cutter system, this last coming straight from Germany – as well its respective desanders – 2 full BE550 units – complemented by 2 additional smaller desanding units to treat continuously the bentonite in the pools.

Due to the geological conditions, two excavation cranes equipped with cable grabs were also mobilised, with the first equipped with 1.02 meters grab, allowing the construction of the lateral boxes in parallel to the main box construction and the second equipped with 1.52 meters grab, allowing the excavation of the softer soil layers, and thus optimizing the usage of both cutters for the harder and deeper layers.

The production lasted for around 3 months, in double shifts (6h – 22h) from Monday to Friday (Fig.5.), with more than 70 specialized workers and 10 engineers and supervisors fully mobilised on site. The “full power” mobilisation allowed the completion of works in line with a very tight schedule once this station would be also a starting point for one of the 3 TBM used for the tunnel construction of Sections 1 and 2.



Fig. 5: La Vache Station production

 © DFI International Bruges 2025

The demobilisation of resources and equipment from La Vache Station lasted from the mid-November to mid-Decembre, with most of the equipment mobilized to Fondeyre Station. The remaining equipment were sent either to a 3rd jobsite starting at the Toulouse Metro project or to the Plant Department warehouse for the equipment that were not going to be needed on these sites.

Toulouse Metro Line C - Fondeyre Station

Scope of work

Construction of a metro station consisting of a main box with one lateral sub-superficial box for access and technical services. The main box is formed by 28 panels, each with a thickness of 1,020 mm and a depth of 31.90 meters. The lateral box consists of 11 panels, each with a thickness of 620 mm and a depth of up to 15.00 meters.

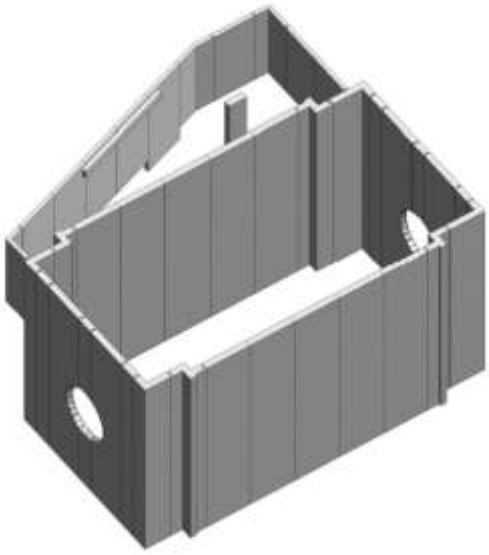


Fig. 5: Fondeyre Station BIM modeling

Execution

The mobilisation of resources to the Fondeyre Station lasted from the 13th of November until the 11th of December.

For this project, only one cutter – BCS cutter system – and a cable grab equipped crane were used for excavation. And it was on this transfer from site-to-site that the BCS cutter system showed one of its main advantages compared to a standard MC cutter system: its modularity allows an optimised transport configuration, especially for low distance travels, demanding only 2 transports to be done – one for the BC48 cutter itself and a second one for the base machine, with its mast and hose drums still attached on it. For reference, a MC cutter system demands at least 5 transports, no matter the distance between jobsites. Saying that, 40 % of the transport costs could be saved, going along with related savings in CO2.

Another greatly appreciated advantage of the new BSC cutter system compared to the MC cutter system it's its assembly simplicity – moreover that the BCS cutter system doesn't need to be fully disassembled for transport. This feature allows to reduce the installation time from one week to simply 2 days, with fewer people and fewer usage of additional equipment – namely a service crane, that is required in almost full time for a MC cutter system assembly.

 © DFI International Bruges 2025

The production phase started on the 12th of December end lasted up to the 1st of March 2024, in double shifts as the previous jobsite, with one cutter – BCS cutter system – and his desanding unit – BE550 – with an additional smaller unit for permanent bentonite pools treatment. An excavation crane equipped alternately in 0.62 meters – for the lateral box – and in 1.02 meters – for the main box – was also mobilised, allowing the excavation of superficial and softer layers, leaving the deepest and hardest layers for the trench cutter, optimising in this manner its usage.

At the completion of the production phase of these two jobsites where the BCS cutter system was used, the advantages of using it compared to a MC cutter system were evident – more than on the production rates, that were quite similar in both systems, it was BCS simplicity of assembly and transportation that was impressive. I addition, fuel saving of approx. 10 % could be achieved as well.

For the following jobsites carried on the Toulouse Metro project no cutter was used. Shallower excavation depts and softer soils allowed the completion of the project using only cable and hydraulic grabs.

In overall, NGE Fondations constructed 5 Station, 2 service shafts and 1 train reversal facility, all completed over a 12-month period.

CONCLUSION

With an increasing number of people, moving into urban and inner-city areas, the demand for new infrastructure will also soar in the future. Existing buildings and structures as well as high prices for areal spread and new restrictions that will set the modalities for these new infrastructures. In addition, environmental standards will become more stringent and will raise the questions for new strategies. The impact of these demands will further influence the construction processes and the design of new equipment to meet the challenges.

In the future, further developments of powerful equipment and methods to work within confined space are to be expected. Further, efforts to reduce noise and fuel emissions will take place to prepare the equipment for wider spread of inner-city applications. New thinking of advances and innovations in systems will help birth compact and smart equipment to meet the anticipated needs in matured built environment, the type that are not easily available today to make these targets attainable.

With its modularity, this new system provides efficient transportation benefit as well as ease of assembly/disassembly. The number of transports required is reduced from six for an MC to 3-4 for a BCS system. The assembly/disassembly time is reduced by min. two days, which leads to cost savings and reduction in carbon emission.

The new system proofs that developments to achieve sustainability goals are possible without losing performance and quality in the production process.

REFERENCES

Gerressen, F.-W.; Blatt, A.; 10th Anniversary Conference on Deep Foundation Technologies for Infrastructure Development in India, November 2020; Confined space and inner-city projects – future challenge and opportunity for diaphragm walling

 © DFI International Bruges 2025

REMEDIAL WORKS TO ARREST THE DIFFERENTIAL SETTLEMENT OF FOUNDATIONS OF SABIC BUILDING

Haytham T. S. Hamdan, Executive Manager, Bullivant Arabia Ltd. Riyadh, KSA.

ABSTRACT: *This paper presents the remedial works performed to seize the active settlement of raft foundation of East wing of SABIC Building in Al-Jubail, Saudi Arabia. The expansion joint between the East Wing and the main building was reported to have continuous movement over the past few years. The opening of the expansion joint was in the range of 150 mm at the top roof level. Several possible causes that may have led to the opening of Expansion joint such as spreading of the ground towards the sea, differential settlement and Seasonal thermal expansion/contraction of buildings.*

A Micropiling support system consisting of 103 piles, 225 mm diameter grout body, 25.5 meters long under the soffit of the raft was installed to stabilize the East Wing framing system and limit the applied soil pressure under the raft to the recommended allowable soil capacity. The installed Micropiling system at the East Wing was stabilized from outside to avoid service disruption of the building functionality.

KEYWORDS:

Micropiling, Differential Foundation settlement, Pile load test, Foundation strengthening.

INTRODUCTION

All structures settle under load and naturally take up their new positions over months or years after construction. Further settlement of foundations is caused by stresses generated in the sub soils, or movement related to desiccation. Settlement only becomes problematical when it becomes excessive, or irregular. In case of granular/fine sub soils, settlement under loading tends to be very rapid.

The SABIC Building in Al-Jubail Industrial Area is a multi-story reinforced concrete structure, consisting of basement, ground floor, six typical floors, and a penthouse. The main building has three Expansion joints extending from the raft foundation to the top roof level. Hence, all the building parts are supported on a continuous raft foundation. The expansion joint between the East Wing and the main building was reported to have continuous movement over the past few years. The opening of the expansion joint was in the range of 150 mm at the top roof level.

The structure is founded on a 900 mm thick raft foundation built on an improved soil by means of stone columns. The soil under the structure consists of light brown to light gray, medium dense to very dense, fine to very fine sand, with traces of silt, extending from the ground level to a depth of 20 m. A sandwich layer of gray, very loose to loose, fine to medium, silty sand encountered at depths from 3 to 6 m. The structural design drawings state that the foundation was designed for an allowable bearing capacity of 1.0 kg/cm^2.

A comprehensive study, including visual inspection, NDT testing, crack and tilt monitoring, structural analysis and design was performed to come up with a design of Micropiling support system to resist the applied loads on the raft in the East Wing. In order to minimize the service disruption of the interior of the building, the Micropiling system was limited to the exterior part of the raft foundation.

 © DFI International Bruges 2025

A pile load test to check the bearing capacity of the pile and to investigate the load-settlement behavior of the pile was performed. The tested pile had a drill hole diameter of 175 mm, grout body of 225 mm diameter, reinforced with steel hollow rod 53/29, and the tested pile extends 25.5 m below the soffit of the raft foundation. The Micropile service load capacity was calculated from pile load test result to be 500 kN, with an associated settlement of 4 mm. Hence, the spring's constant of the pile was found to be 125,000 kN/m.

PROBLEM STATEMENT

The expansion joint between the East Wing and the main building was reported to have continuous movement over the past few years. The opening of the expansion joint was in the range of 150 mm at the top roof level. From initial structural analysis and estimation of loads, it was found that the applied soil pressure was at least double the recommended soil bearing capacity specified in the site geotechnical reports.

The raft was constructed at the lower level of the basement of the main building and extended towards the East and West wings. Hence, a need to backfill all of the areas that do not have basement in the building was required. The thickness of the soil fill above the raft foundation in the East Wing was around 3.5 m, and it was noted that the fill was not engineered properly.

Several possible causes that may have led to the opening of Expansion joint were examined. The following are the potential aboveground and underground reasons for the movements considered in this study.

Potential aboveground causes for separation:

- Thermal movement
- Moisture movement
- Lack of lateral restraint
- Excess loading or change in loading patterns.

Potential underground caused for movements:

- Creep of local pockets of Sabkha soils
- Soils collapsible due to wetting
- Lateral spreading of reclaimed land
- Geological faults and subsidence due to buried utilities such as (broken drains)

The following were the potential mechanisms that could explain fully or partially the observed movements. These mechanics were observed via monitoring by installing crack measurement gauges, inclinometers, tiltmeters etc. The movements were potentially a combination of three mechanisms summarized below.

- Localized differential settlement and resultant tilting towards southeast corner of building.
- Seasonal thermal expansion/contraction of buildings
- A larger areal spreading of the ground towards the sea

 © DFI International Bruges 2025



Fig. 1: SABIC Headquarter Building in Al-Jubail



Fig. 2: Opening of Expansion joint between Main Building and East Wing

 © DFI International Bruges 2025

DESIGN AND DETAILS OF FOUNDATION SUPPORT

The following remedial measure was designed and executed to prevent further settlement and tilting of raft foundation of SABIC Building's East wing.

Structural analysis and design software was used to construct a 3-D model of the structure and the raft foundation was modelled as a Slab-on-Elastic Springs. In addition, the piles were modeled as multi-linear phase springs, in which the nonlinear phase of the pile was introduced to the system based on the information gathered from the pile's load test. The effect of stone columns in the soil was ignored and considered completely deteriorated.

A major variable in the system was the coefficient of subgrade reaction of the virgin soil under the raft [K-value in kN/m^3]. The adopted K-value for the soil in its current conditions was derived by an iterative numerical analysis of the structure, so that the tilting in the analysis model matches the reported tilt in the East Wing.

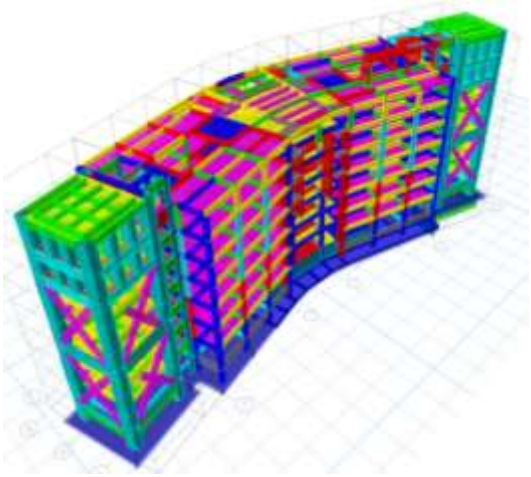


Fig. 3: 3-D model of the building structure

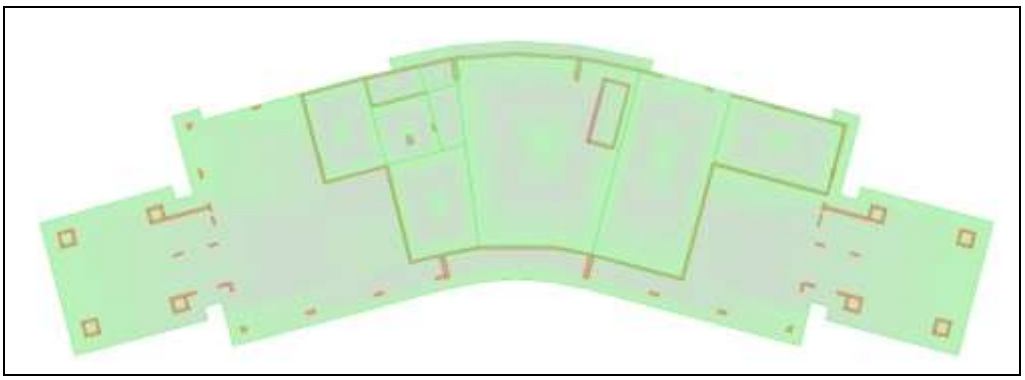


Fig. 4: 2-D model of the Raft foundation

 © DFI International Bruges 2025

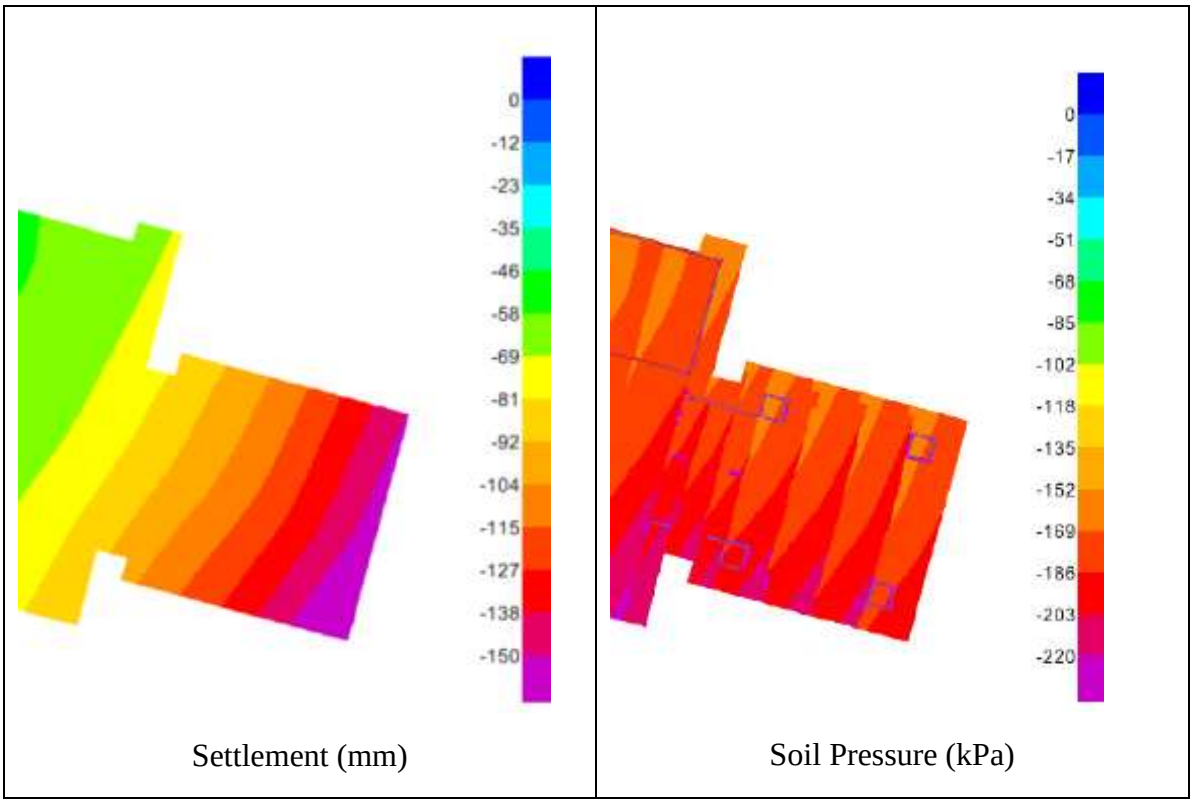


Fig. 5: Settlement and Soil Pressure (kPa) before installation of Micropiles

PILE LOAD TEST

The compressive geotechnical capacity of micropile was calculated by considering the grout to ground bond strength of 120 kN/m^3 [1] with a factor of safety of 2.5. The calculated geotechnical capacity of 785 kN (80 Tons) was considered as design load to perform pile load test. The pile was tested for a test load of 1570 kN (160 Tons) 2.0 times the design load and then increased to a maximum load of 2.5 times the design load, i.e., 1962 kN (200 Tons).

The gross settlement at design load (2nd Cycle) of 80 tons was 7.25 mm whereas net settlement after completing unloading was 3.65 mm. During 3rd Cycle, settlement at design load of 80 tons was 7.065 mm. Load was further increased to 1.30 times design load (104 tons) (for checking creep effects as per FHWA -039) and corresponding settlement was 9.39 mm. This load was maintained for 10 minutes, and recorded settlement was found to be 9.78 mm. The difference in settlement at 1.3 times Design Load is 9.78 – 9.39 = 0.39 mm maintained for 10 minutes was less than 1 mm. Therefore, pile qualifies creep criteria at 1.3 times design load.

 © DFI International Bruges 2025

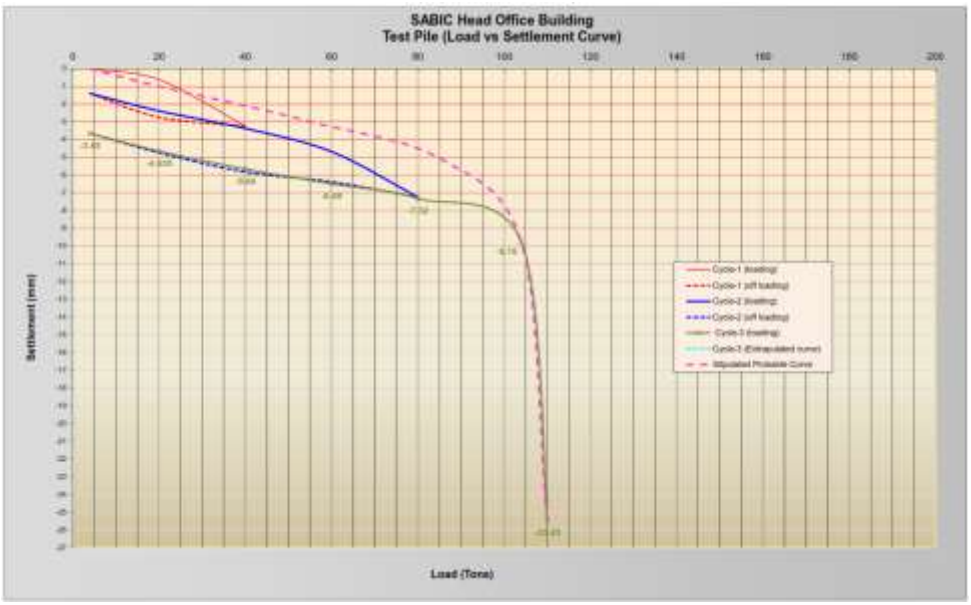


Fig. 6: Pile Test Results – Load vs Settlement Curve

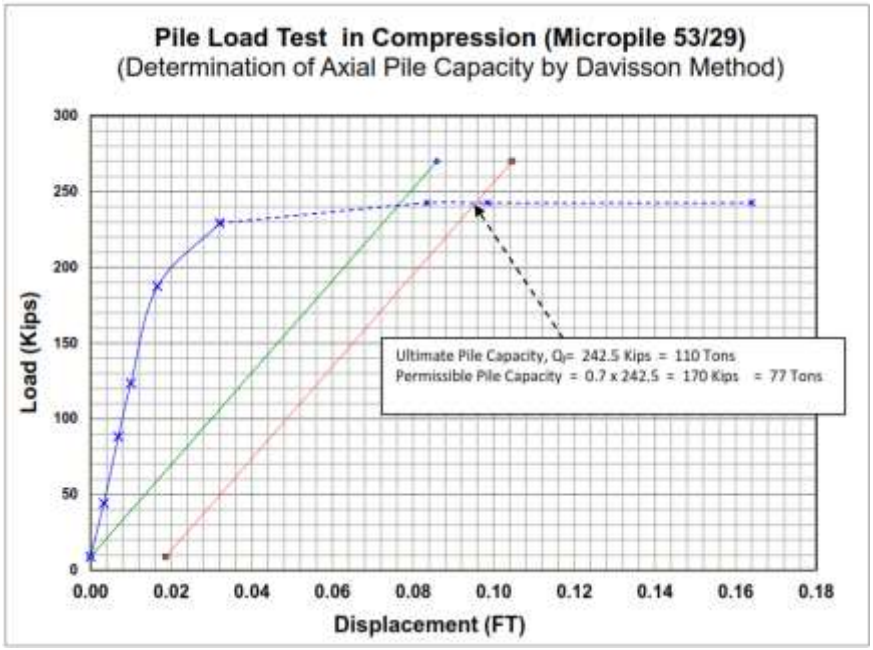


Fig. 7: Pile Test Results – Load vs Displacement Curve

The maximum geotechnical load capacity of the pile was found from the pile load test to be 755 kN (77 Tons), considering a resistance factor of 0.7 as per AASHTO Table 10.5.5.2.5-1 [2]. The pile's structural capacity was checked for the maximum recorded axial load during the pile load test, which was 104 tons (1020 kN). This assumption was made to cover any loading conditions where the load in the pile could reach the maximum tested load of 1020 KN. To limit the immediate settlement of pile to 4mm, the maximum

 © DFI International Bruges 2025

permissible load capacity of pile was factored to be 50 Tons, and this value was used to determine the number of micropiles required to support the building foundation.

MICROPILE FOUNDATION SUPPORT

A Micropiling system consisting of 103 piles, with steel hollow rod 53/29, 175 mm drill hole, 225 mm grout body, 25.5 m long under the soffit of the raft was found to be adequate to stabilize the East Wing framing system and limit the applied soil pressure under the raft to the recommended allowable soil capacity of 100 kPa. Utilizing three-dimensional Nonlinear analysis of the Micropiling system, it was concluded that the East Wing is feasible to be stabilized from outside and avoid service disruption of the building interior.

The pile cap was designed and checked for punching, shear, bond and bending forces. All piles were under compression with no tension in any of the considered load combinations. The existing reinforcement in the raft was found to satisfy the strength requirements for loading conditions. The thickness of the raft was also found to be adequate to resist the applied forces.

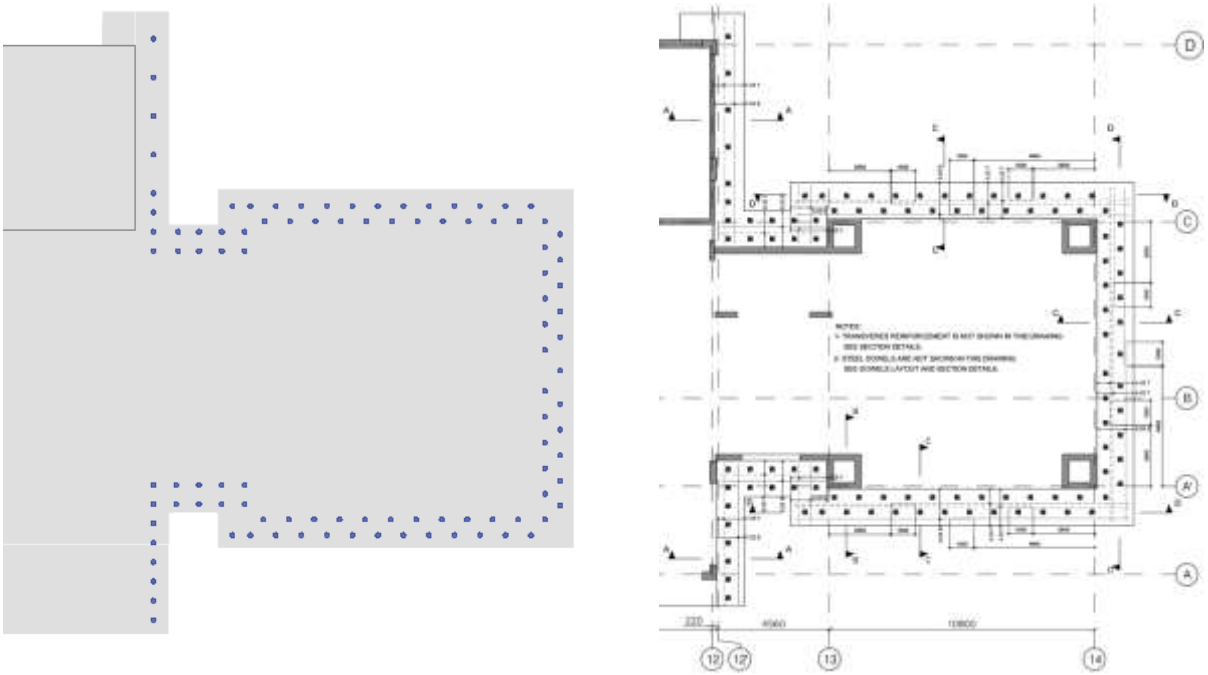


Fig. 8: Micropiling layout for East Wing Raft Foundation

 © DFI International Bruges 2025

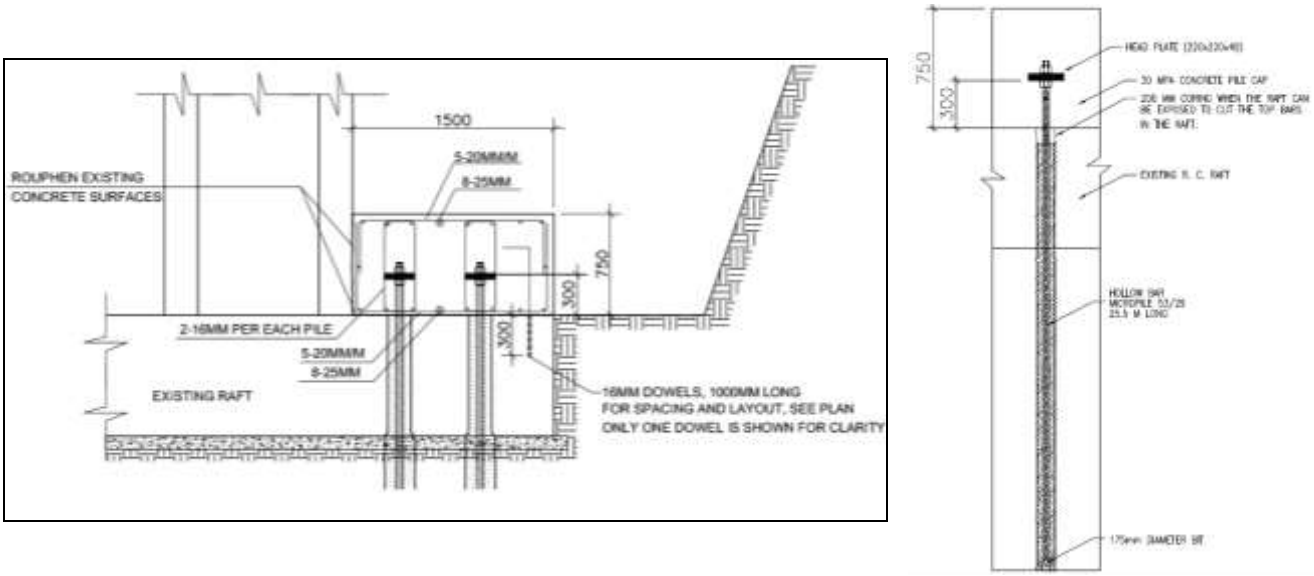


Fig. 9: Micropiling detail for East Wing Raft Foundation

MICROPILE INSTALLATION PROCESS

Hollow bar pressure grouted Micropiles best suited the site conditions. A small diameter hollow steel bar with a coarse thread along its entire length acts as a drilling and injection bar during the installation and as a reinforcement element. The cementitious grout is injected under pressure, simultaneously as the drilling is advanced. During installation a bond is created between the grout body and the surrounding soil layers. The high tensile steel hollow bar becomes the reinforcement element of the pile while the grout body surrounding the bar provides bearing capacity by transferring the tensile, compression and cyclical loads to the ground through the high bond values achieved between the grout and soil because of the use of pressure during grouting and because of the irregularity of the sides of the micropile which creates mechanical friction compared to straight sided micropiles.

After marking the pile locations on the raft foundation, 250mm diameter cores were drilled to start the micropile installation process. Initially a lean grout with 0.7 water-cement ratio was used as flushing grout during drilling process till the target depth is reached. A final grout designed with a water-cement ratio of 0.34 to achieve compressive strength of 42 MPa at 28 days was pumped under 0.5 bar pressure through the hollow bar to replace the flushing grout.

A square steel head plate of 220mm having 40mm thickness was attached to each micropile. Steel reinforcement was anchored into the raft foundation to fix a steel cage for casting pile caps as shown on Fig. 9.

 © DFI International Bruges 2025

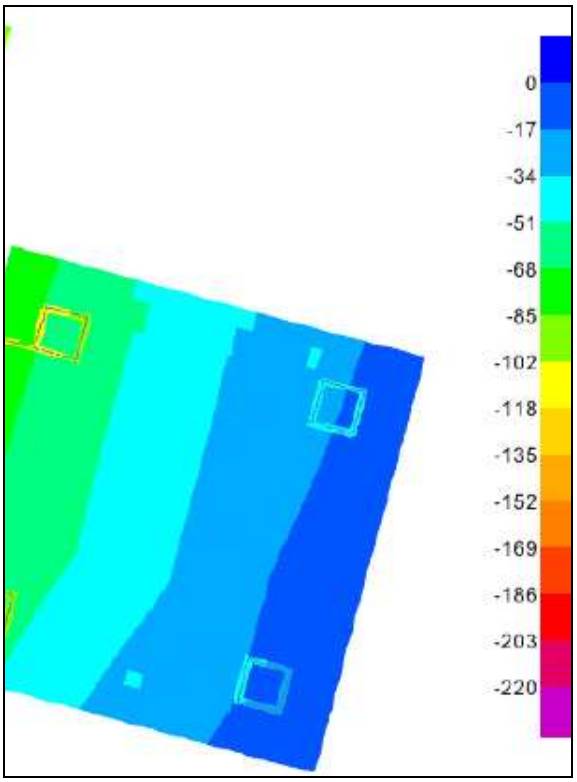


Fig. 10: Soil Pressure (kPa) after installation of Micropiles



Fig.11: Site Photographs for construction of Micropiles and Pile caps

 © DFI International Bruges 2025

CONCLUSIONS:

The main conclusions that can be drawn from this project case study are as follows:

1. The recommendations provided by geotechnical consultants for soil improvement and design basis for foundations should be rechecked. The soil should be retested after the improvement process is completed. The structural engineer should consider the recommended geotechnical parameters to design foundations.
2. The main cause of the V-Shape opening in the expansion joint between the East Wing and the main building was due to excessive differential settlement of the soil. The applied soil pressure was found to be at least double the recommended soil bearing capacity in all available site geotechnical reports.
3. A micropiling system designed to support the raft foundation was found to be adequate to stabilize the East Wing framing system and limit the applied soil pressure under the raft to the recommended allowable soil capacity.

References

1. Federal Highway Administration. Micropile Design and Construction. Reference Manual-2005; NHI Course No. 132078; National Highway Institute, U.S. Department of Transportation.
2. AASHTO LRFD BRIDGE DESIGN SPECIFICATIONS 2012, Section 10.9 – Micropiles.
3. ASTM D1143-07 “Standard Test Methods for Deep Foundations under Static Axial Compressive Load.

 © DFI International Bruges 2025

REMOVEABLE GROUND ANCHORS USING PYROTECHNICS – INNOVATIVE, SUSTAINABLE AND SAFE

Florian Hude, DSI Underground Austria GmbH., Pasching, Austria, +4366488155846, florian.hude@sandvik.com

ABSTRACT

This paper explores the development and application of removable ground anchors using pyrotechnics. Ground anchors are essential in various civil engineering projects to stabilize structures, support excavation sites, and anchor retaining walls. Ground anchors can also be used permanently (e.g. retaining walls) but this paper concentrates on temporary use only. Temporary anchors are used to provide a retaining for a certain timeframe (mainly less than 2 years). In this case anchors may be required to be removed after its end of use. This study introduces a novel approach utilizing pyrotechnic technology to enable the removal of ground anchors efficiently and effectively. The proposed method aims to provide a practical solution for temporary anchoring applications, reducing environmental impacts and project costs.

Keywords: removeable ground anchor, pyrotechnics, temporary construction

INTRODUCTION

Temporary anchors play an important role in geotechnical engineering, providing essential support during the construction of various structures such as retaining walls, deep excavations, and excavation shoring. These anchors are designed to stabilize soil and rock masses temporarily, allowing for safe and efficient construction processes in complex and challenging environments. Unlike permanent anchors, temporary anchors are designed for short-term use, with a focus on efficiency and cost-effectiveness.

Once their purpose is fulfilled, they either remain in the ground or can be (partially or fully) removed. At a minimum they should be unloaded [1]. Remaining steel elements in the ground may cause issues for later constructions as they may not corrode completely.
Over the last 30 years different types of removable anchors were developed: Use of steel elements with a predetermined breaking point, use of ductile iron anchoring elements, use of a breaking cone for the bonding zone and various other creative solutions that have seen attempted implementation (see also [2]). The need for a fast, completely removable anchoring solution which is cost effective has prompted research into innovative methods to consistently accomplish this goal.

This paper gives an overview of steel tendons used for ground anchors, describes different methods for partially and fully removeable anchors and investigates the use of pyrotechnics to develop removable ground anchors which are viable for temporary applications and enhance sustainable construction practices. It aims to provide a comprehensive overview of the design, application, and performance of temporary removable anchors in geotechnical applications.

GROUND ANCHORS: MATERIALS AND METHODS

Ground anchors comprise a bonded section, an unbonded section and the head structure. The tension load is applied via the anchor head and is transferred through the anchor tendon to the surrounding soil or rock via friction, adhesion, and bearing mechanisms. The load transfer occurs in the bonded length of the anchor, which is the section embedded into the ground. This portion is encased in grout to enhance the interaction between the tendon and the ground. The remaining length of the anchor, known as the free length, is unbonded, allowing for the transfer of load from the structure to the bonded section.

 © DFI International Bruges 2025

Steel tendons used for ground anchors

Steel tendons are the primary load-bearing components in ground anchors, responsible for transmitting tensile forces from the structure (head) to the ground (bond length). They are typically made from high-strength steel to ensure durability and the capacity to withstand significant loads while minimizing the cross section and therefore the required drilling diameter. The choice of tendon type depends on the specific application, required load capacity and the overall length of the anchor. The three most common types of steel tendons used in ground anchors are strands, threaded bars, and hollow bars. Additionally helical tieback anchors can be used. Each has unique characteristics and advantages that make them suitable for different ground conditions and installation methods. (see also [3])

1. Strands

Post-tensioning strands, made of 7-wire prestressing steel, are the most common steel elements for ground anchors due to their flexibility and high tensile strength. They can be coiled, transported, and installed in complex geometries, with lengths exceeding 100 meters. Their multi-wire structure provides superior load-bearing capacity, which can be increased by adding more strands. These qualities make them ideal for deep anchors in retaining structures, dam stabilization, and narrow sites where rigid tendons cannot be inserted.

2. Threaded Bars

Threaded bars are solid steel rods with a continuously threaded surface, enabling secure tensioning and anchoring with nuts and plates. Their continuous ribs enhance bond strength with surrounding grout. Unlike strands, threaded bars are rigid, allowing for easy, direct installation into boreholes with greater stiffness. Their threaded design enables precise tensioning and load adjustment using nuts and bearing plates at the anchor head. Threaded bars are ideal for shorter ground anchors, applications requiring minimal anchor slip, and situations where anchors need to be re-tensioned or released.

3. Hollow Bars

Hollow bars, or self-drilling anchors, are tubular steel bars with a hollow core that allows them to serve as both the drill rod during installation and the tendon once in place. Their self-drilling capability enables direct drilling into the ground while grout is pumped through the hollow core to stabilize the borehole and bond the anchor. This simplifies installation by eliminating separate drilling, installation, and grouting operations, making them ideal for sites where speed is critical. Hollow bars are commonly used for temporary or permanent ground anchors in hard-to-access locations or where rapid installation is required.

4. Helical Systems

Helical systems are advanced foundation and anchoring solutions that use screw-like steel shafts with helical plates to provide structural stability in various soil conditions. Typically, thread bars or other steel reinforcement bars serve as the free length of a helical anchor, which is screwed directly into the ground, offering immediate support without curing time. These systems do not require grouting or fluid injection, making them an efficient and clean solution. Installation is simplified with lightweight equipment, reducing labor costs while allowing minimal excavation, immediate load-bearing capacity, and easy length adjustments. Commonly used for both temporary and permanent ground anchors in suitable soil conditions with moderate load requirements, helical anchors can also be fully removed by unscrewing, though this method is not further considered in this paper.

Installation methods

The installation of ground anchors typically involves drilling a borehole, placing the tendon, and then grouting the tendon to secure the anchor. The installer can choose between cased and uncased drilling methods depending on ground conditions and on the chosen steel tendon. Cased drilling uses a temporary steel casing to support the borehole walls during drilling, which is essential in loose, collapsing, or waterlogged soils. The casing stabilizes the borehole, preventing it from collapsing

 © DFI International Bruges 2025

during anchor installation. After the tendon is placed the casing is removed during the grouting process. All above mentioned steel tendons can be used with cased drilling methods.

Uncased drilling, on the other hand, is performed in more stable soils or rock, where the borehole can maintain its shape without external support. In this method, the borehole is drilled without casing, and the tendon is inserted directly, followed by grouting. Uncased drilling is faster and less costly, but it is only suitable for solid ground conditions that can resist collapse, or when a self-drilling anchor (see above) is used.

The choice between the drilling method depends on site-specific geotechnical conditions and on the chosen anchor system. Removable ground anchors using pyrotechnics can only be installed with cased drilling.

REMOVEABLE GROUND ANCHORS: CONCEPTS AND METHODS

Removable ground anchors are designed for temporary applications where the anchors need to be extracted after their purpose is fulfilled, such as in temporary retaining structures or temporary tiebacks on a construction site. These anchors come in two main types: partially removable and fully removable. For both types, only the steel tendon will be removed whereas the grouting or other bonding agent will remain in the ground. Removing the steel tendon is mandatory to allow unobstructed future use of the site. Grout does not affect any future building activities and fills the drill hole. Hence a removal of grout is not required and could be disadvantageous.

Partially removable anchors allow for the removal of the tendon in the free length while leaving the bonded section in place. This is typically achieved by disrupting, unscrewing or heating the tendon in the free length, leaving the bonded length within the ground. Partially removable anchors are simpler to remove, but they leave a portion of the system permanently underground, which may affect future site use.

Fully removable anchors, on the other hand, are designed so that the full length of the tendon can be completely extracted from the ground. This is often achieved by destroying the grouting body or by unscrewing/unlocking the tendon at the back of the borehole. Fully removable anchors are ideal for projects with strict environmental or land-use requirements, as they leave no permanent steel tendons in the ground. However, fully removable systems tend to be more complex and costly than their partially removable counterparts.

Partially removeable anchors

These anchors provide a practical balance between performance and ease of removal, allowing the free length to be extracted while leaving the bonded section in place. This concept reduces environmental impact and prepares the site for future use as the anchor is unloaded and the bonded section left in the ground is usually short compared to the total length of the anchor. There are three primary methods for removing the tendon in the free length for a partially removable anchor: the disruptive method, unscrewing method, and heating method. Each approach has specific advantages, safety requirements, and technical considerations.

1. Disruptive Method

The disruptive method was a widely used approach in the past where a predefined breaking point in the transition zone between free and bonded section was generated. This was achieved by a localized inductive heating during the production process. Depending on the induced heat the ultimate strength of the steel tendon was reduced by approx. 20 %. This reduction allowed the tendon to break mechanically by applying sufficient axial force in the defined breaking zone to cause a rupture of the tendon.

 © DFI International Bruges 2025

This method is favored for its simplicity and cost-effectiveness. The procedure can be completed using relatively straightforward equipment, requiring a jacking system to generate the required force. However, this method comes with certain risks and several uncertainties. Excessive force can lead to potential damage to the surrounding ground or adjacent structures, especially in sensitive environments or densely populated urban areas. Furthermore, the pulling jack and the disrupted tendon must be shielded, so that they cannot cause any harm to the surrounding environment and/or construction personnel. The rupture causes dangerous and excessive wear and tear on the whole of the equipment and the entire process has a high safety risk.
Additionally, the strength reduction from the inductive heating process has a very large allowable variation. This reduces the allowable stressing force for the design of the anchor requiring larger and/or more anchors increasing the cost of this method.

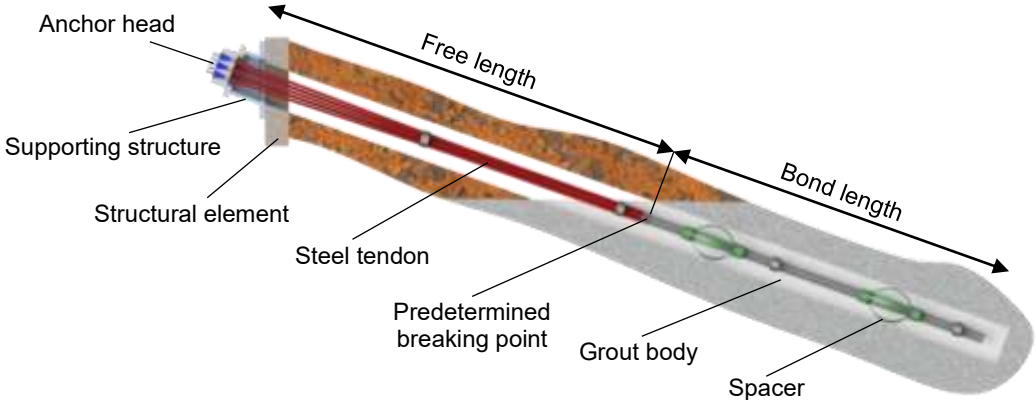


Fig. 1. Partially removable anchor, disruptive method

2. Unscrewing Method

The unscrewing method offers a more controlled means of tendon removal by incorporating a threaded connection in the transition zone so that the free length can be unscrewed from the bonded section after its service life. In this method, the tendon is coupled at the transition zone, and it must be ensured that the free length can be rotated along its axis. The coupling device is locked to the bonded section and will remain in the ground. After the load-carrying phase of the anchor is complete, the anchor must be unstressed and then the free length can be removed by rotating and unscrewing it from the coupler, leaving the bond length intact and in ground.

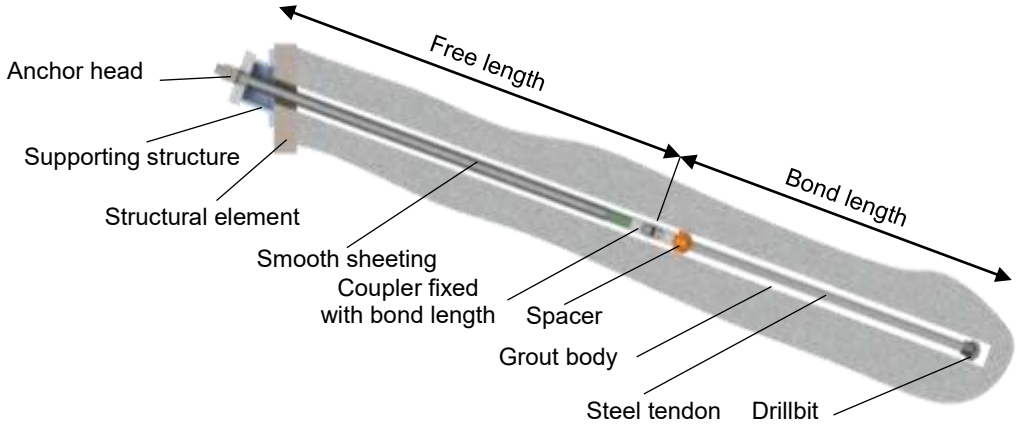


Fig. 2. Partially removable anchor, unscrewing method

One of the main advantages of this method is the minimal disruption it causes to the surrounding soil or rock. By simply rotating the tendon the unscrewing method requires much less force than the disruptive approach, reducing the risk of damage to nearby structures. Additionally, this method

 © DFI International Bruges 2025

ensures that the grouted section remains stable, making it suitable for environments where maintaining the integrity of the surrounding ground is crucial.

However, the unscrewing method requires precise installation, including the use of specialized coupler/threaded connection and equipment capable of applying the necessary rotational force. As a result, it may be more labor-intensive and time-consuming compared to the disruptive method. This technique is used in projects requiring quiet and safe removal.

3. Heating Method

The heating method is a newly developed and highly effective technique for removing the free length. This method involves an in situ separative element (e.g. “easy out-element [4]) which applies heat to the tendon through induction heating, to degrade the steel and forces a rupture. This element can be located anywhere along the free length. This means, the anchor can simply be unloaded (when the separative element is located just behind the anchor head) or the free length can be removed (when the separative element is in the transition zone between free and bond length). By carefully heating the tendon, any damages of the surrounding ground or construction is avoided.

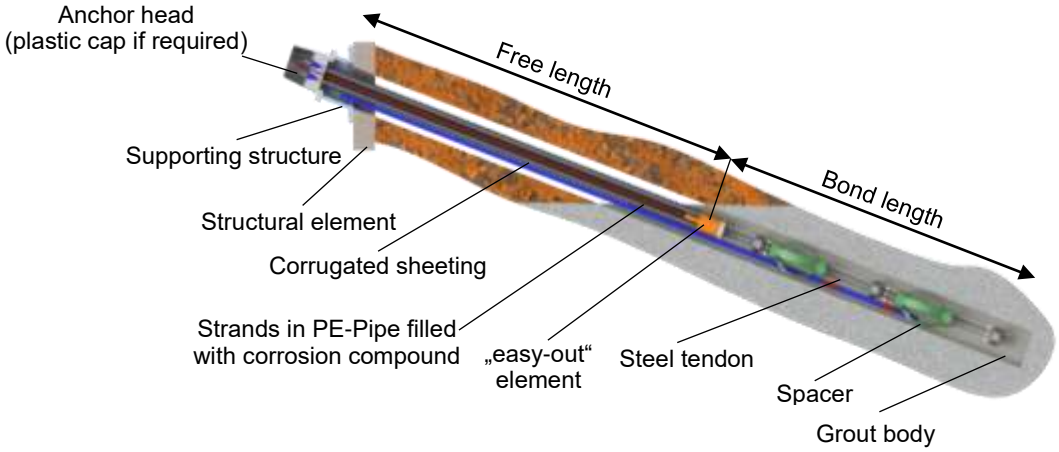


Fig. 3. Partially removable anchor, heating method

Usually, this method is used for strand anchors. For an easy removal the individual strands are covered in a greased smooth pipe and a corrugated sheeting is used as a casing for the complete anchor in the free length. This allows an easy pulling of the strands after heating.

The anchor must be stressed to a minimum of 40 % of its ultimate load so that the tendons will break due to heating.

This method is particularly useful in sensitive environments or in projects where conventional pullout forces could lead to excessive structural damage. Additionally, there is no noise or vibration using this method. The tendon can be used up to its full capacity because the tendon is heated after the load-carrying phase. However, the heating method requires specialized equipment, and the equipment must be applied to the steel prior to the installation of the anchor. It is best suited for projects in sensitive locations and all projects where an easy and fast removal is required.

Fully removable anchors

Fully removable ground anchors are designed for temporary applications where both the free length and the bonded section must be completely extracted from the ground once their purpose is fulfilled. Unlike partially removable anchors, where the bond length remain in the ground, fully removable anchors leave no permanent steel tendons behind (in the unscrewing method, the unscrewing box and the compression body remains in the ground; however, it does not pose an obstacle to further

 © DFI International Bruges 2025

construction activities), making them ideal for projects where future construction, environmental, or land-use constraints require clean removal. The three primary methods for achieving full removal of the anchor system include the unscrewing method, the pull-out cone method, and the pyrotechnic method. Each method offers unique technical solutions depending on ground conditions, structural requirements, and project constraints.

1. Unscrewing Method

The unscrewing method for fully removable anchors is an extension of the partially removable unscrewing approach. The anchor consists of the anchor head, the steel element (debonded over the full length), a steel plate with a coupler at the bottom of the borehole and compression elements which transfer the load from the tendon into the ground. In this technique, the tendon is unscrewed at the bottom of the bore hole after use. The tendon is threaded at its bottom, allowing for its disengagement from the steel plate. The compression elements are fully grouted into the ground and can transfer compression load only. They usually consist of short steel elements which do not interfere with possible future construction projects.

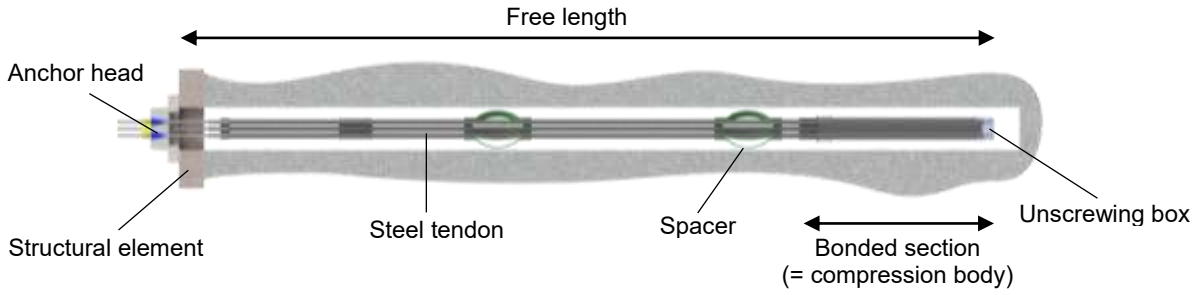


Fig. 4. Fully removable anchor, unscrewing method

In fully removable unscrewing anchors, the tendon is first rotated to disengage it from the bonded section, which is typically a compression element. The tendons are then removed, and the compression body is left in the ground. The compression body consists of casted steel tubes with a ribbed surface to enhance bonding properties. Each tube has a length of 0.5 to 0.8 meter. They are placed in a continuous row depending on the required force to be transferred. The compression body and the unscrewing box are short blocks so they do not pose an obstacle to further construction activities nevertheless steel is left behind in the ground.

This method is frequently used in temporary construction projects where precise control over the removal process is required, minimizing disruption to the surrounding ground.

The unscrewing method offers the benefit of complete tendon removal without causing excessive mechanical disruption to the borehole. It is highly controllable and allows for safe extraction in dense urban areas. However, it requires specialized tendons and grouting techniques which increases installation complexity and costs. Additionally, grout can accidentally flow into the coupling area making unscrewing impossible.

2. Pull-Out Cone Method

The pull-out cone method only works for strand anchors. It involves using an additional strand with a mechanical cone at the base of the tendon, which can be pulled through the grouted section, destructing the grout body of the bonded section. This method provides a robust and reliable mechanism for complete tendon removal without the need for a complex detachment process.
When the anchor is ready to be removed, the strand with the attached cone is pulled upward, causing the cone to break the grouted section and destroy the bond between grout and the tendons. As the tendon is pulled through the entire bonded length the tensioned strands can be removed from the ground. The force required to pull the cone and the strand is significant and requires hydraulic jacks,

 © DFI International Bruges 2025

but it results in the full removal of the anchor system. For an easier removal after reaching the free length, the strands are covered by a corrugated sheeting.

This method is well-suited for projects where the anchor is embedded in softer soils or weak rock, allowing for easier displacement of the grouted section by the cone. It is commonly used where future construction will take place and where no residual steel can be left behind.

The pull-out cone method is highly effective for full removal of the anchor system, ensuring no residual steel elements remain in the borehole. It is also relatively simple to implement, making it cost-effective for certain temporary applications. However, this method requires significant pulling force and is very time consuming, so its not suitable for tight schedule projects.

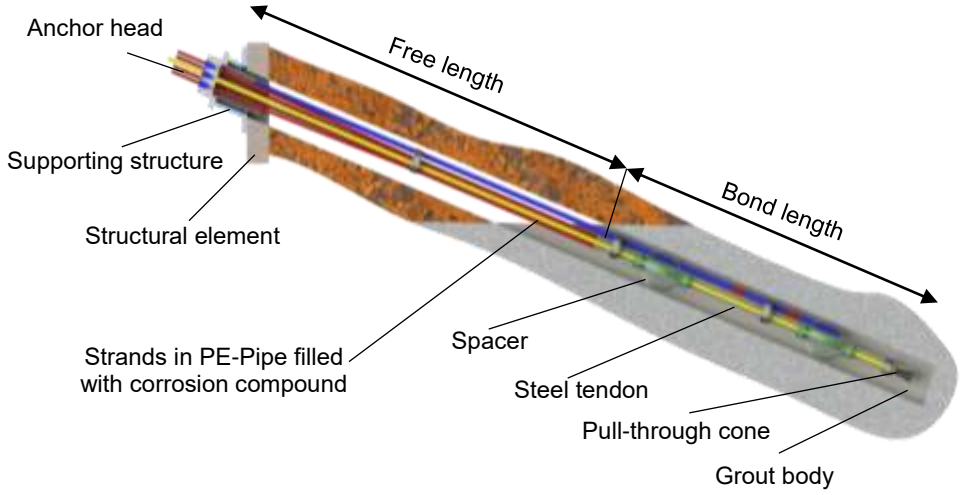


Fig. 5. Fully removable anchor, pull-through method

3. Pyrotechnic Method

The pyrotechnic method is an advanced technique for fully removing ground anchors by using a pyrotechnic induced deflagration to break apart the grouted section. This method allows for complete removal by fracturing the bond between the tendon and the grout.

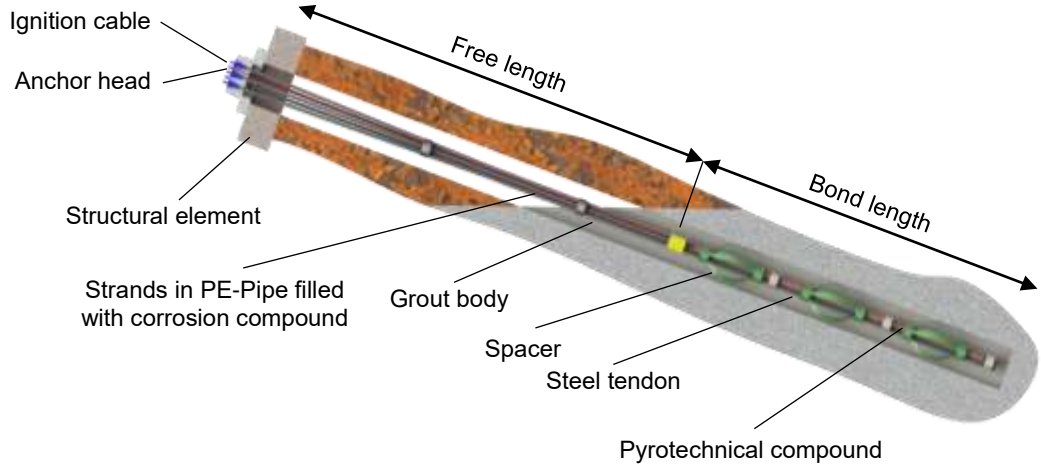


Fig. 6. Fully removable anchor, pyrotechnic method

In the pyrotechnic method, a pyrotechnic device is embedded within or around the tendon along the bonded section during installation. When the anchor is no longer needed, the device is activated,

 © DFI International Bruges 2025

breaking the bond between the steel and the grout. The fractures created by the deflagration separates the ground and the steel and the tendon can be easily pulled from the borehole.

The pyrotechnic method enables complete removal of the anchor system with minimal residual material left behind. However, the material cost of employing pyrotechnic techniques can be higher compared to other methods but the time savings make the method overall very economical. A more detailed description including results from projects is given in the next section.

REMOVEABLE GROUND ANCHORS USING PYROTECHNICS

As described above, pyrotechnical devices can be used to break up the grouting body and destroy the bond between the steel element and the grout. This method works with all three above mentioned steel elements. However, strand anchors are the most typical anchor type used for temporary applications where the steel element must be removed. That's why the following chapter will concentrate on strand anchors although the same principals can be applied to threaded bar and hollow bar anchors.

Principle description of pyrotechnical devices

Blasting explosive can be defined as "a product that is intended to release energy in the event of arbitrarily triggered chemical changes of state…" [5]. Pyrotechnical devices cannot be arbitrarily triggered and hence they are not considered as blasting explosives.

The principal function of a pyrotechnical device is to generate a controlled and rapid release of energy through a chemical reaction, typically combustion or deflagration, to produce a specific physical or mechanical outcome. In many engineering applications, including the removal of ground anchors, this reaction is harnessed to create a localized explosive force that can disrupt or break apart materials in a precise and efficient manner. The chemical compounds within a pyrotechnical device undergo a rapid exothermic reaction when ignited, releasing gases and heat that cause an instantaneous pressure increase. This pressure can fracture materials when the pyrotechnical device is fully embedded in this material. A pyrotechnical device would not cause any harm or damage when it is activated without containment, as it will not cause a shock wave. The reaction velocity is 800 – 1000 m/s whereas an explosion has a reaction velocity of 2000 m/s or more.

Pyrotechnical devices for removeable anchors

The pyrotechnical device involves a PE-pipe which is sealed on both ends against water intrusion, an electric detonator, and a pyrotechnical compound (nitrocellulose and aluminum nitrate). The electric detonator is activated with a blasting machine. The ignition cable is routed from the anchor head to the electric detonator.

In ground anchor systems, pyrotechnical devices are strategically placed within the bond length, and when detonated, they create fractures in the grout, effectively reducing the bond to the anchor tendon. This allows for the removal of the tendon.

The precision and controllability of pyrotechnical devices are crucial for their function. These devices are designed to deliver a targeted amount of force. The deflagration does not cause shock waves as a blasting explosive would do. Therefore, it affects only the intended materials without causing widespread damage to adjacent structures or the surrounding ground.

The PE tube is made of food safe material and the deflagration of the pyrotechnical compound produces hydrogen, nitrogen and carbon dioxide which are all naturally occurring in the ambient atmosphere. Hence the pyrotechnical device is suitable also for conservation areas and other environmentally critical sites.

 © DFI International Bruges 2025

Fully removeable anchor using a pyrotechnical device

A temporary anchor where the entire steel element can be removed after its intended use consists of following parts:

Anchor head: The anchor head of a strand anchor includes
- an anchor plate for the load transfer to the ground (typically concrete),
- a wedge plate, which rest on the anchor plate and holds the wedges,
- wedges, which secure the strands,
- corrosion protection, typically a plastic cap filled with grease.

Tendon: The tendon can comprise two or more strands which
- consists of the tail, free and bond length,
- are not coated in the protrusion and bond length,
- covered by a plastic pipe (PE or PVC) to allow stretching in the free length,
- may be covered in grease within the plastic pipe to ease the removal process.

Injection pipe: The anchors has
- one or more injection pipes where at least one goes from the head to the bottom of the anchor to grout the entire anchor length and
- one or more post grouting pipes depending on the ground conditions.

Pyrotechnical device: The pyrotechnical device is
- assembled along the entire bond length,
- has an ignition cable, which must be shielded in a pipe,
- must be handled with care.

Examples of use

Removeable anchors using pyrotechnics were used in different building sites. One of those sites will be shown here.

An office and residential building complex was built next to a train track and train station in Tirol (Austria). The foundation was approximately six meters below the track surface. The excavation was secured by bore piles and shotcrete walls (see sketch below). The anchors had a total length of 11 m and a bond length of 6 m and were made of two strands. The initial loading was 300 kN. In total 27 anchors were installed.

The railway authority demanded a complete removal of the steel tendons so that they would not cause any obstructers during future construction work. The schedule was very tight, and the removal process was scheduled in two stages with one day each.

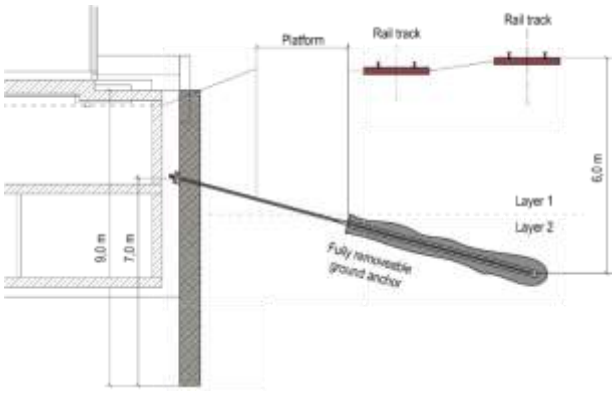


Fig. 7. Cross section of the Spaced pile-curtain wall

 © DFI International Bruges 2025

The anchors were installed in April 2024 and removed in July and August 2024, following the standard installation process for temporary anchors, with an added check of the ignition cable's electrical resistance. Removal occurred after excavation and the first basement floor was built, with 13 anchors removed in the first stage and 14 in the second. A conventional system would have required approximately 108 hours (2 hours per anchor with 2 workers), whereas the pyrotechnic system completed the removal in just 9 hours (3 hours with 3 workers), significantly reducing time. Additionally, the process was completed without disrupting other construction activities.

Results

Experimental results and site usage demonstrated the effectiveness of the pyrotechnic-enabled removable ground anchors. It was proven that the anchors maintained their load-bearing capacity during installation and use, comparable to traditional ground anchors. Upon activation of the pyrotechnic charge, the anchors were successfully de-bonded from the grout, allowing for easy removal with minimal time consumption. The pyrotechnic charge was found to be reliable and safe, with controlled activation ensuring that the surrounding soil and structures were unaffected. These results indicate that the proposed system meets the required standards for temporary anchoring applications, providing a balance between performance and removability.



Fig. 9. Anchors: during installation - before activating – after activating – after removal

DISCUSSION

The implementation of pyrotechnic technology in ground anchors presents several advantages and challenges. One significant advantage is the reduction in environmental impact, as the anchors can be removed cleanly without extensive excavation or disturbance. This approach also offers cost savings in site restoration and material reuse. However, challenges include ensuring the safety and reliability of the pyrotechnic charges, particularly in varied soil conditions and depths. Further research is needed to optimize the system for different geotechnical environments and to develop guidelines for safe operation and disposal of the pyrotechnic components.

CONCLUSION

This study summarizes available ground anchor tendons (strands, threaded bars, and hollow bars) and current removable anchor types (partially and fully removable). Removability applies only to the steel elements, with grout remaining in place. The preferred method for partially removable anchors is the heating method (easy-out [4]), where a heating device is pre-installed, allowing the anchor to be fully loaded and later relaxed or partially removed without special equipment or trained personnel. For fully removable anchors, a novel pyrotechnic approach has been introduced and validated through experiments and job site trials. This method aligns with sustainable construction practices and offers an efficient alternative to labor-intensive removal processes. While results are promising, further development and site testing are needed to refine the technology and ensure reliability.

 © DFI International Bruges 2025

REFERENCES

[1] Smith, Matthew W., Lindsay C. Flangas, and Daniel P. Ciani. "Case History: Investigating the Risks Associated with Allowing Temporary Tiebacks to Remain Stressed." *Earth Retention Conference 3*. 2010.
[2] Bogdan, Lucian, and Patrick Wörle. "Innovations in Removable Post Tensioned Strand Ground Anchors." *IFCEE 2018*. 2018. 33-42.
[3] PTI: “Recommendations for Prestressed Rock and Soil Anchors”, 2014
[4] Spantec: „Ausbaubare Litzenanker SPANTEC „easy out“ (temp + dauer)”, https://spantec-gmbh.de/export/shared/documents/pdf/spantec/SPANTEC-EASY-OUT.pdf (28.9.2024)
[5] Austrian Parlament: “Sprengmittelgesetz 2010”, §3, https://ris.bka.gv.at/GeltendeFassung.wxe?Abfrage=Bundesnormen&Gesetzesnummer=20006570 (28.9.2024)

 © DFI International Bruges 2025

FIELD MEASUREMENT OF AIRBORNE NOISE EMISSION DURING IMPACT PILEDRIVING ON LAND AND THE EFFECT OF REDUCED STIFFNESS AT THE IMPACT INTERFACE

Maarten in 't Veld[1], Jort van Wijk[2]

[1]*IQIP, Lead engineer piling and noise, The Netherlands*
[2]*IQIP, Manager Discipline Engineering, The Netherlands*

ABSTRACT

Impact piledriving is the most common method for pile driving on land. Hydraulic impact hammers are known for their high efficiency due to a very stiff impact with the pile, especially in the case of steel tubular piles, leading to a relatively large impact force and a small impact duration. Pile vibrations during driving are the main source of airborne noise. As noise limits become stricter in the built environment, there is a need for mitigation measures.

In this paper we investigate the effect of reduced contact-stiffness of the impact interface on the noise levels in air. To this end, a 90-kJ hydraulic impact hammer is equipped with a novel technology between the hammer ram and the anvil on top of the pile, that consists of a hydraulic spring element. This element reduces the impact force while it lengthens the impact duration. Due to the reduced stiffness, the introduction of the stress wave in the pile is smoother, which is beneficial for noise reduction.

The 90-kJ hammer with and without the new technology was used for installation of steel tubular piles, during which the pile driving was monitored, and airborne noise was measured. The noise measurements show significant reduction of the equivalent noise level and of the peak noise level when piling with the reduced contact-stiffness, compared with conventional impact piling.

Keywords: impact piledriving, reduced stiffness, airborne noise.

1. INTRODUCTION

The effect of construction noise on human health is a growing problem, with increasing city population the need for construction rises along with it, as well as the number of people affected by it (Mir et al., 2022). Pile driving contributes amongst the highest levels of construction noise, both for residents in the area and construction workers themselves (Li et al., 2016).

 © DFI International Bruges 2025

The source of the piling noise finds its origin in the hammer impact upon the pile, creating a stress wave in the pile which transmits noise to its surroundings. One method to reduce noise is therefore to encapsulate the pile, thereby reducing the noise emitted, this is however a costly and laborious method. In this work the option of smoothing the transmission of hammer energy to the pile by adding a hydraulic spring, reducing peak forces and elongating impact duration is investigated. The results of noise emission registered during driving of identical piles, under comparable conditions, with and without spring element will be discussed.

2. THEORY

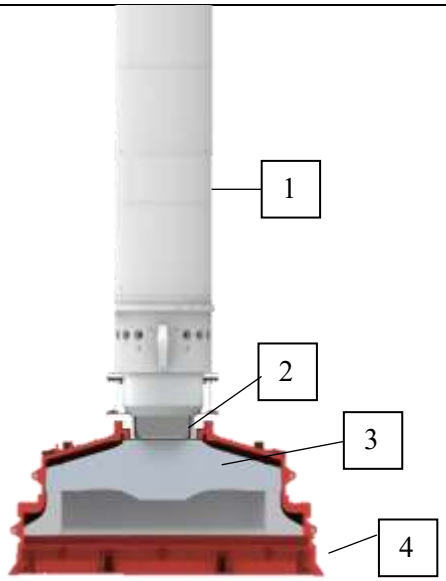
The energy transfer from an impact hammer to the pile takes place in a short time span. For impact piling with a hydraulic hammer the impact duration typically is in the order of 10 ms, during which the pile top is compressed, and a stress wave starts propagating downward to the pile toe. The sudden impact causes accelerations and vibrations in the entire pile, which become a source of airborne noise.

There is a strong relation between the impact characteristics of a hammer-anvil-pile system and the noise levels. The impact characteristic is described as the force and velocity at the pile top as a function of time, resulting from the collision of the hammer (ram) with the anvil and the successive transfer of the stress wave to the pile top. With the use of commercially available stress wave equation solvers for pile driving, such as GRL WEAP, impact characteristics can be generated and their influence on pile driveability evaluated.

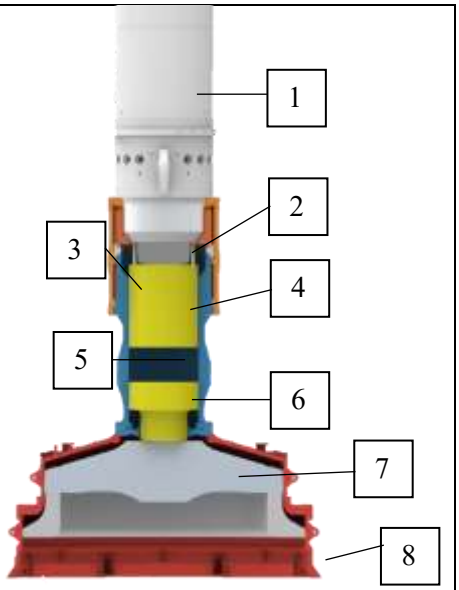
In case of steel-to-steel contact as occurring in the driving of steel piles with hydraulic impact hammers, the energy is introduced in a short time span. This results in excellent driveability performance, however noise levels are relatively large. Modification (reduction) of the stiffness at the location of impact would lead to a gentler introduction of energy and is expected to generate less noise and limit fatigue of the pile.

The stiffness at the impact interface can be reduced by placing a spring element. In this study, a hydraulic spring element is used (the IQIP Pulse technology) combined with a 90 kJ Hydrohammer. Figure 2.1 schematically shows the hammer configurations.

 © DFI International Bruges 2025



a. Lower part of the hammer (1) with the ram (2) protruding the housing and resting on the anvil (3), which sits in the sleeve (4). The sleeve slides over the pile top.



b. Lower part of the hammer (1) with the ram (2) resting on the upper piston (4) of the hydraulic spring element. The lower piston (6) rests on the anvil (7) which sits in the sleeve (8). The housing of the spring (3) connects the hammer to the sleeve. The space in between the pistons (5) is filled with fluid, and the distance between the pistons together with the fluid properties determine the spring stiffness.

Figure 2.1. The Hydrohammer hydraulic impact hammer in two configurations, without and with hydraulic spring element.

In GRL WEAP, the hydraulic spring can be modelled as the stiffness of the helmet. This one-dimensional stiffness depends on the mechanical stiffnesses of the different components in the assembly: the upper piston, fluid volume and lower piston:

$$K = \left(\frac{1}{K_{up}} + \frac{1}{K_{fluid}} + \frac{1}{K_{lp}}\right)^{-1} \quad [1]$$

With K the stiffness of the hydraulic spring, K_{up} the stiffness of the upper piston, K_{fluid} the stiffness of the fluid volume and K_{lp} the stiffness of the lower piston, all in N/m. These component stiffnesses depend on their geometry (cross section area A in m^2, length L in m) and elastic properties (Young's modulus E in Pa), hence for N discrete cylindrical elements Eq. 1 can be rewritten to:

$$K = \left(\sum_{i=1}^{N} \frac{L_i}{E_i \cdot A_i}\right)^{-1} \quad [2]$$

Reducing the stiffness will result in an elongated and smoothened introduction of the force into the pile, which in turn can reduce noise emission (Klages et al., 2021).

 © DFI International Bruges 2025

3. PROJECT DESCRIPTION

In this project three steel tubular piles (P1, P2 and P3) were installed using an IQIP Hydrohammer S-90 with 90 kJ of maximum impact energy. Pile P1 was installed with the S-90 only, while piles P2 and P3 were installed with the S-90 + Pulse. An impression of the site is given in Figure 3.1. Throughout the project, the hammer energy was kept 80 kJ at maximum. The piles have dimensions OD = 509 mm and wall thickness of 25.4 mm. They were driven in segments of ~12.3 m each, welded onto the previous. The total pile lengths after cutoff were 85.3 m for P1, 84.4 m for P2 and 86.3 m for P3 respectively.

Welding typically took 1 – 2 hrs per weld, hence during driving multiple driving stops were required. During these stops the soil strength will partly recover, and more energy is required to continue driving afterward. No detailed soil information was available at the start of the project, hence any anomalies should be inferred from post-piling data. Piling energy and blow count per 0.25 m of penetration were recorded during driving, records are shown in Figure 3.2.

For all three piles, energy is varied to keep the blow count in the range of 30 – 50 blows/0.25 m as per the regular piling procedure for the hydraulic impact hammer used. As the pile penetrates further to 40-50 m, the hammer energy was increased to the maximum impact energy of 80 kJ and was kept at that level until end of driving. The blow count is seen to increase to a maximum of >100 blows/0.25 m at the end of driving of P3.

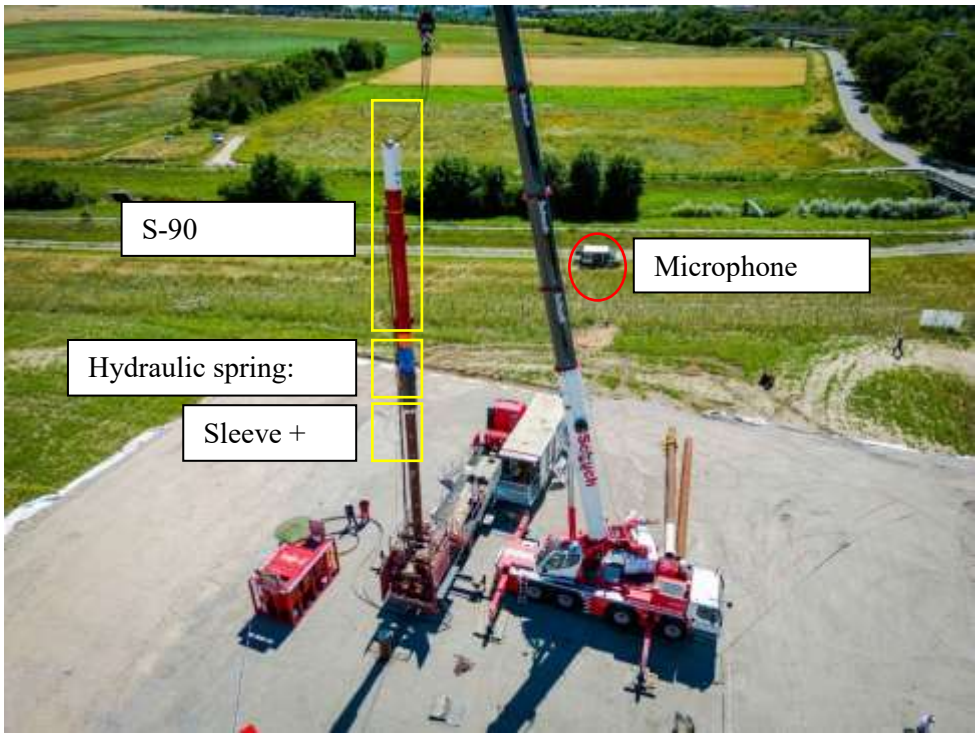


Figure 3.1. The S-90 Hydrohammer with the hydraulic spring element placed on top of the OD 509 mm pile. The microphone was placed in the marked area just outside the construction site, with no obstructions.

 © DFI International Bruges 2025

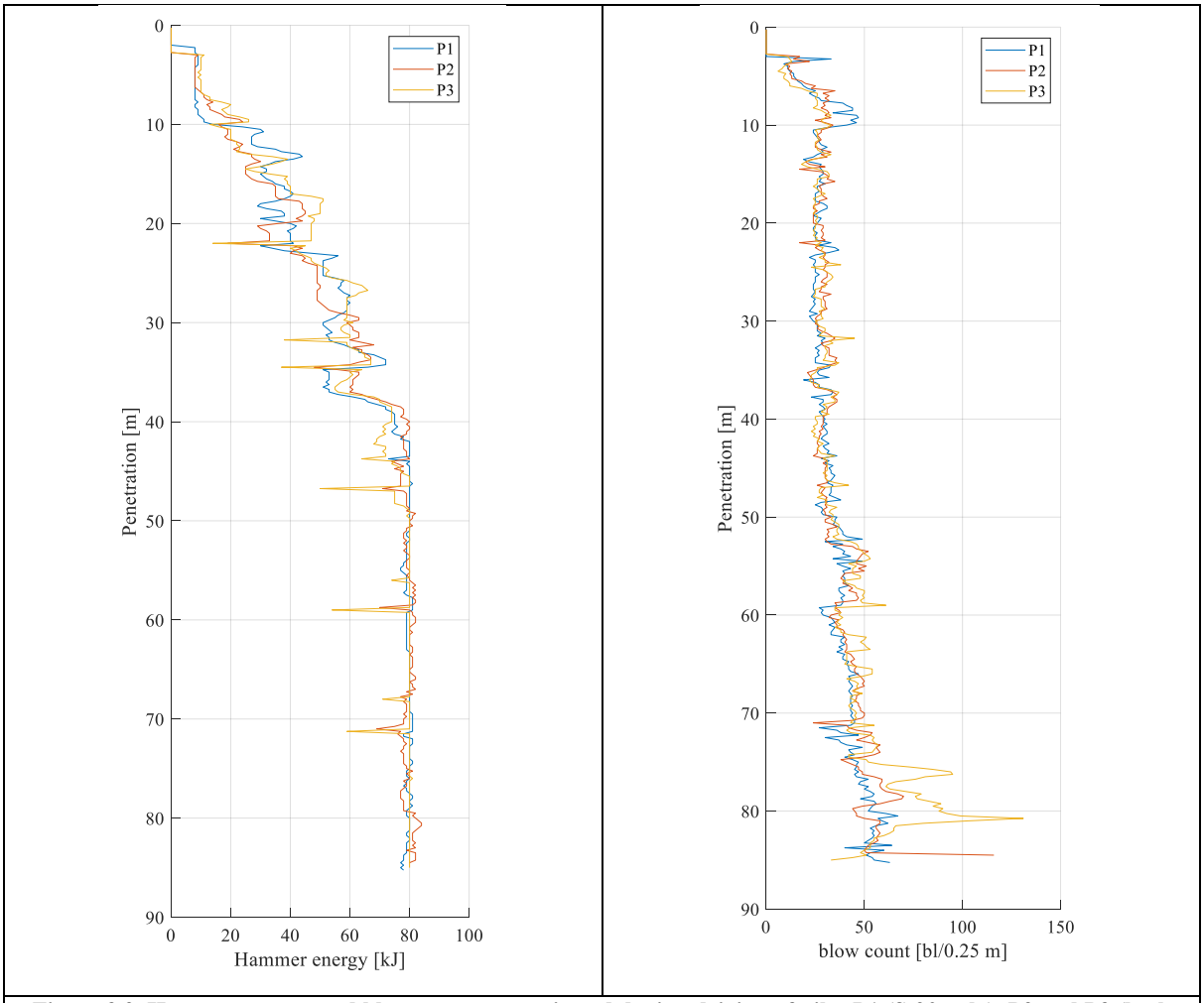


Figure 3.2. Hammer energy and blow count as monitored during driving of piles P1 (S-90 only), P2 and P3 (both with Pulse). The overall picture of the three installations is very comparable, suggesting that the soil resistance at the three locations is comparable. The higher blow count near final penetration of P3 can be explained by the presence of the hydraulic spring element at its maximum setting, which results in a lower ENTHRU energy. Pulse at pile P2 was switched back to zero during the final meters.

4. AIRBORNE NOISE MEASUREMENT SETUP

For the driving of pile P1 (without Pulse) and P2 (with Pulse) noise measurements were taken at a distance 41.5m from the pile, the microphone was positioned at a height of 5 m from the ground. To account for the different positions of the pile the microphone as shown in Figure 3.1 was moved to keep the distance identical.

The noise measurements were performed with a Norsonic 1225 Free-field microphone, the data of which was processed with a Norsonic 140 Precision Sound Level Analyser. The wind velocities were registered with a Testo 410-2 Anemometer.

 © DFI International Bruges 2025

For each segment the A-weighted equivalent continuous sound level expressed in 1/3 Octave bands ($L_{Aeq,\ Oct}$) was determined for the driving of the whole segment. The single A-weighted equivalent continuous sound level (L_{Aeq}) value (not in octave bands) was logged with a frequency of 1 Hz.

During measurements the relative humidity varied from 23 to 70%, temperatures varied from 17°C to 32°C and wind velocities ranged from <0.1m/s up to 4.0 m/s. Given the relatively short distance of the microphone from the pile (<10 times minimum pile height) meteorological effects and effects such as ground attenuation are neglected.

During installation, the setting (height) of the liquid column in the Pulse unit was registered as a function of pile penetration, as well as the hammer impact energy and the blow count (records of the latter two are presented in Figure 3.2).

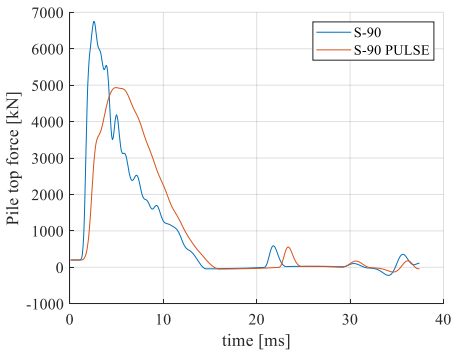
5. RESULTS AND DISCUSSION

The impact characteristics have been simulated using GRL WEAP which is commercial software for one-dimensional wave equation analysis of pile driving. Sufficient pile length (the full ~80 m) above soil level is modelled to avoid reflections from the pile toe showing in the impact diagrams. The pile is modelled in terms of length, cross section area (385.1 cm^2), Young's modulus (210 GPa) and material specific weight (77.5 kN/m^3). The helmet weight is 3.43 kN, which is the weight of the anvil used on the project. The helmet stiffness is set to infinite with a coefficient of restitution of 1 in case of direct steel-to-steel piledriving. With Pulse, the helmet weight 15.3 kN and the stiffness is calculated with Equations 1 and 2, using the geometry of the Pulse system, resulting in K = 696 kN/mm for Pulse maximum. The impact hammer S-90 is taken from the GRL WEAP library with an efficiency of 1 for the sake of comparison.

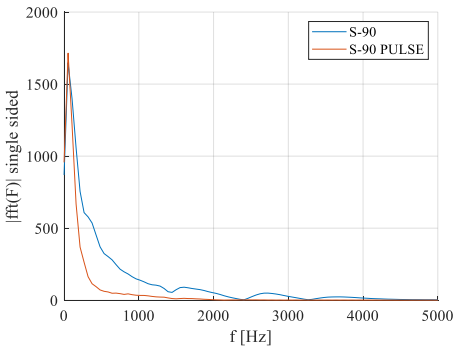
It can be seen that the addition of the Pulse element smoothens the introduction the force and velocity. The Fourier Transformation shows that force is reduced for all frequencies above 70 Hz and velocity is reduced for all frequencies above 120 Hz, as shown in Figure 5.1.

During driving the L_{Aeq} was measured continuously, the data clearly shows the effect of changing exposed pile length (surface area), each new segment results in a jump in emitted noise, which gradually reduces as the pile penetrates further as can be seen in Figure 5.2. For driving with Pulse this effect is less pronounced due to changes in Pulse settings during penetration of the segment.

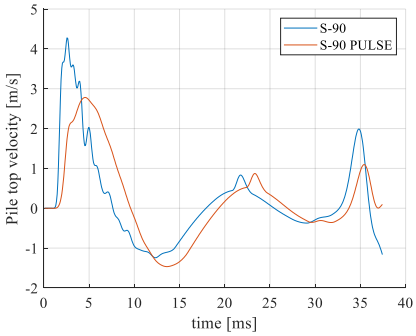
 © DFI International Bruges 2025



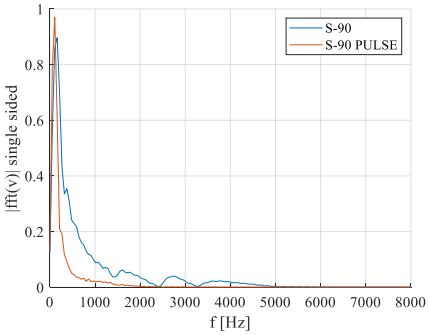
a. Pile top force calculated with GRL WEAP.



b. Single-sided FFT of the force signal.

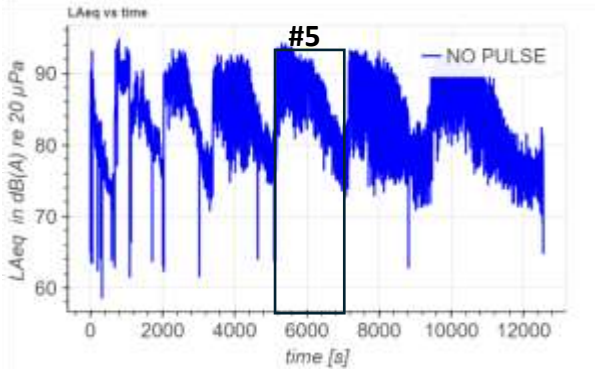


c. Pile top velocity calculated with GRL WEAP

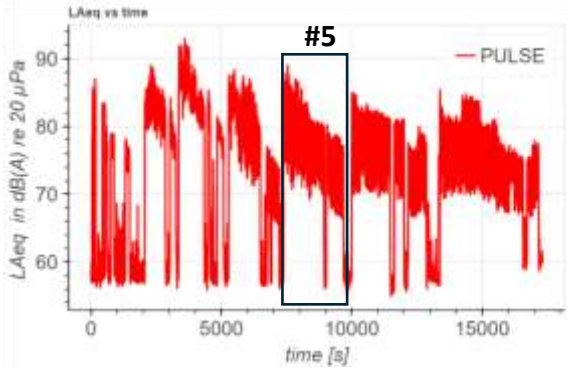


d. Single sided FFT of the velocity signal.

Figure 5.1. Impact characteristics and their dominant frequency content, analysed for the S-90 on an OD = 509 mm pile. When using Pulse, most energy is contained in the lower frequencies compared to impact piling without Pulse. This will have a positive effect on the noise emission.



a. Noise emission during driving of P1 (without Pulse)



b. Noise emission during driving of pile P2 (with Pulse)

Figure 5.2. Noise emission during driving of pile P1 (left) and P2 (right), dominating factor is the addition of new segments on the pile, resulting in additional exposed surface area.

Since the blow count (number of blows per 0.25 m) varied over time, the driving of the fifth segment of pile P1 was selected for comparison with the fifth segment of pile P2 (with Pulse). For these

 © DFI International Bruges 2025

segments the blow count was stable around 40 blows/0.25m. The stiffness of the Pulse unit was constantly at 840 kN/mm during the driving of segment 5 of P2. The lowest possible stiffness of the Pulse unit is 696 kN/mm. Whereas the highest stiffness with the lowest expected noise reduction is 2896 kN/mm.

To investigate the influence of the exposed surface area, a scaling law as in Equation 3 can be applied (in 't Veld et al., 2023). The distance from source to receiver also influences the noise levels registered.

$$L_{Aeq,i} = L_{Aeq,0} + 10 \cdot \log_{10} \frac{E}{E_0} + 10 \cdot \log_{10} \frac{S}{S_0} + 20 \cdot \log_{10} \frac{r}{r_0} \quad [3]$$

With $L_{Aeq,0}$ the reference sound level, E the impact energy in kJ, E_0 the reference energy, S the exposed pile surface area in m^2, S_0 the reference surface area, r the distance from the source and r_0 the reference distance.

The difference in L_{Aeq} between start of driving a segment and the end of driving with constant energy and constant Pulse setting (or no Pulse) is 12 dB(A). If one applies the scaling laws as in Equation 4, this means that the exposed height is reduced by a factor of 16, which would be 0.8 m. This 0.8 m is an effective exposed height, deduced from the noise data. In reality the exposed pile height at the end of driving is higher, however a large part of this is shielded by the installing vehicle, therefore the effective height of 0.8 m will be used for further calculation.

The L_{Aeq} is influenced by each blow, for which the conditions change during driving (reduced surface area and changing impact energy), the relation between the L_{Aeq} over a longer period and the individual blows can be calculated according to Equation 4.

$$L_{Aeq,tot} = 10 \cdot \log_{10} \left(\frac{1}{T} \sum t_i \cdot 10^{\frac{L_{Aeqi}}{10}} \right) \quad [4]$$

With T the total duration of the combined events, t_i the integration time used for each individual blow (typically 1 s) and $L_{Aeq,i}$ the equivalent sound pressure level of each individual blow.

In order to derive the expected noise emission for one individual blow at maximum hammer energy (80 kJ), 50% of exposed surface area (6 m exposed pile height) and at 41.5m distance, Equation 3 and 4 can be combined as shown in Equation 5.

$$L_{Aeq,tot} = L_{Aeq,80\ kJ,6m} + 10 \cdot \log_{10} \left(\frac{1}{T} \sum t_i \cdot \frac{L}{6} \right) \quad [5]$$

Applying Equation 5 results in a $L_{Aeq,\ 80kJ,6m,NoPulse}$ of 88.3 dB(A) and a $L_{Aeq,\ 80kJ,6m,NoPulse}$ of 80.1 dB(A)

It can be seen in Figure 5.3. that, for the whole driving of the fifth segment of both piles, the noise was reduced over the whole frequency range, except for the noise at 20 Hz (the lowest registered

 © DFI International Bruges 2025

frequency). The L_{Aeq} over the whole driving period ($L_{Aeq,tot}$) of the segment with Pulse was 8.2 dB(A) lower than without Pulse.

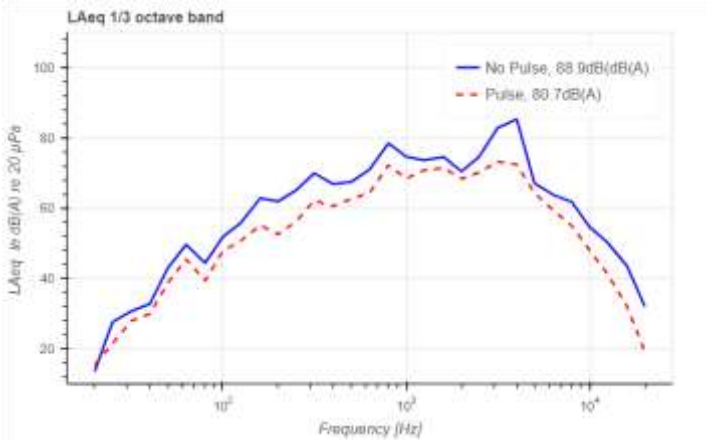


Fig.5.3. LAeq in the frequency domain for driving one segment of 12.3 m with and without Pulse unit. P1 (without Pulse) was driven with an average blow count of 37 blows/0.25 m and a hammer energy of 79 kJ for a duration of 2050 s. P2 (with Pulse) was driven with an average blow count of 39 blows/0.25m and a hammer energy of 82 kJ for a duration of 2200 s. Blow frequency was around 1 Hz for both piles.

During driving it can occur that the stiffness of the Pulse unit needs to be increased, to be able to reach final penetration. In order to investigate the effect of changing settings during driving, three hypothetical cases have been calculated for which driving was started with Pulse and finished without. The results have been calculated by combining the noise data from segment 5 of pile P1 with the noise data from segment 5 of pile P2 with the use of Equations 3 and 4. The results of which are listed in Table 5.1.

Table 5.1. Expected noise emission for driving with and without Pulse for driving partly with and without Pulse. Hammer energy was constant around 80 kJ.

Scenario	L_{Aeq}	Δ dB
100% no Pulse (measurement)	88.9	0
25% Pulse, 75% no Pulse (hypothetical)	86.8	2.1
50% Pulse, 50% no Pulse (hypothetical)	84.6	4.3
75% Pulse, 25% no Pulse (hypothetical)	82.3	6.6
100% Pulse (measurement)	80.7	8.2

6. Conclusion

Noise data from piledriving with and without reduced stiffness at the impact interface has been presented. It shows noise reduction for all frequencies above 20 Hz. Resulting in a total L_{Aeq} reduction

 © DFI International Bruges 2025

of 8.2 dB(A) when a hydraulic spring element with a stiffness of 840 kN/mm is added. If there are driving conditions where the reduced stiffness is not applicable over the whole driving range noise reduction can still be significant, considering the fact that driving conditions at the beginning of driving have the highest exposed pile surface but typically the lowest required driving energy. Whereas at the end of driving, soil resistance is likely to be harder, but exposed pile surface will be lower.

For future research it is recommended to perform a detailed analysis of the relation between the smoothing of the forcing function (impact characteristic), and the noise reduction due to decreased stiffness at the impact interface. Such an analysis specifically is to be performed in the frequency domain.

The relation between the noise reduction in the frequency domain and the introduction of force in the frequency domain can be investigated to provide more insight in the ability to predict specific noise reducing effects.

Acknowledgements

The authors thank Wagenborg Foxdrill for facilitating the test and measurement campaign. Measurements were conducted by the specialist engineering firm Krebs und Kiefer, Germany, and their work is gratefully acknowledged. The authors also thank our colleagues Matteo Ambrosi, Mirko Mento, Griedo Bel and Jonathan Stolk for witnessing and organizing the test campaign. The work published in this paper is funded by IQIP, The Netherlands.

References

Klages, Elin. Lippert, Stephan. Estorff, Otto van. (2021) A noise-reduced impact hammer for offshore pile driving. 6th Underwater Acoustics Conference and Exhibition

Mir, M., Nasirzadeh, F., Bereznicki, H., Enticott, P., Lee, S., Mills, A., 2023. Construction noise effects on human health: Evidence from physiological measures. Sustainable Cities and Society 91, 104470.

Li, X., Song, Z., Wang, T., Zheng, Y., Ning, X., 2016. Health impacts of construction noise on workers: A quantitative assessment model based on exposure measurement. Journal of Cleaner Production 135, 721–731.

Veld, M in't. Roest A and Wijk, J. van. (2023) Airborne noise emission measurement during near-shore monopile installation in The Netherlands. 9th International SUT OSIG Conference "Innovative Geotechnologies for Energy Transition"

 © DFI International Bruges 2025

SUPPORT FLUIDS FOR PILING IN URBAN AREAS: PREPARATION, OPERATION AND SPECIFICATION

Stephan A. Jefferis, Environmental Geotechnics Ltd, Oxfordshire, UK, envgeot@gmail.com
Chris Barker, Ove Arup & Partners, London, UK,
Daniel P. McNamara, University of Oxford, Oxford, UK,
Brian B. Sheil, University of Cambridge, Cambridge, UK.

ABSTRACT

Developments on urban sites often require the installation of large diameter deep foundation piles (drilled shafts). Typically these will require the use of an excavation support fluid. The paper considers some of the properties of, and operational and logistical issues associated with, synthetic polymer fluids and bentonite slurries in the field which may favour the use of one fluid system over the other – no one system can be suitable for all applications. It then goes on to consider how specifications for support fluid management should be drafted given the present state of knowledge and experience with fluids based on synthetic and natural polymers.

Keywords: bentonite slurry, polymer fluid, soil dispersion inhibiting polymers, water treatment, specifications.

INTRODUCTION

This paper is concerned with excavation support fluids for piling (drilled shafts) though it also may be applied to support fluids used for diaphragm walling, horizontal directional drilling, slurry tunnelling and borehole drilling. It will focus on experience gained in the field with bentonite slurries and polymer fluids contrasting the behaviours of the two systems. However, it is first necessary to define some terms as used in this paper.

Bentonite slurry: A water based fluid containing bentonite clay. It may contain other products including polymers, for example, to modify fluid loss, rheology etc. Bentonite slurries do not inhibit the dispersion of soil from the excavation into the slurry.

Polymer fluid: a support fluid system based on a solution of a polymer in water. When considering the general behaviour of polymers, it is necessary to distinguish between polymers derived from natural gums and those based on high molecular weight synthetic polymers. These two types of polymer have distinct properties which must be respected when specifying, preparing using, and maintaining them.

Soil dispersion and soil dispersion inhibiting polymers (SDIPs)**:** Native soils from an excavation will tend to disperse in water based excavation support fluids so that, in use, dispersed soil may build up in the fluid if the soil has a significant fines fraction. The resulting fluid may become effectively just a soil-water slurry, unacceptably dense, viscous and gelling. This build-up can be expected in clay based systems such as bentonite or attapulgite based slurries. For these slurries it is usually necessary to employ soil-slurry separation plant to maintain acceptable fluid properties and/or to dispose of substantial quantities of dense slurry during the works and replace it with fresh slurry – an increasingly expensive and environmentally undesirable practice.

Excavation soil also can be expected to disperse in support fluids based on natural gums or modified natural gums such as xanthan, guar and carboxymethyl and hydroxyethyl cellulose (CMC and HEC). In soils with fines some soil-slurry separation equipment will be necessary with these polymers.

Synthetic polymers may be formulated to inhibit soil dispersion. In this paper these polymers will be referred to as SDIPs (soil dispersion inhibiting polymers). Currently, the polymers used to prepare support fluids for piling are typically based on high molecular weight partially hydrolysed polyacrylamides (referred to as PHPAs in the civil engineering literature also, and more logically,

 © DFI International Bruges 2025

known as hydrolysed polyacrylamides, HPAMs in the chemical literature as any hydrolysis is necessarily partial since full hydrolysis yields polyacrylates (PAs) though they would not be manufactured by such a route. High molecular weight polyacrylates have been used as support fluids when there were concerns about polyacrylamide. High molecular weight PHPAs and PAs inhibit soil dispersion and if properly managed do not require the use of soil-slurry separation plant. Indeed they cannot be used with conventional soil-slurry separation plant as they can sheet over fine screens (i.e. flow across them but not through them). Also there would be excessive damage to the polymer molecules in the high shear environment of hydrocyclones. For small urban sites the inhibition of soil dispersion is the most important property of these polymers as soil-slurry separation plants can be eliminated. More generally, if soil dispersion can be inhibited the support fluid remains as a polymer-water system without its properties being compromised by dispersed soil. Additives can be employed to impart other properties as required.

In the oil-well-drilling industry there are many products offered to stabilise shales/stop them swelling. The term SDIP is proposed to distinguish polymers such as PHPAs and PAs from the often complex oil-industry inhibitive mud systems.

WHY USE POLYMER FLUIDS?

Synthetic polymer solutions have become the support fluid of choice for constrained urban sites because, when appropriately managed, they offer the following benefits in terms of fluid properties and management, plant required, operations and excavated soil management:

- In some, soils polymer fluids can give better shaft resistance than bentonite slurries with the potential for shorter piles and so reduced excavation, less excavated soil to be managed and importantly less concrete;
- The required concentration of polymer will be of the order of one fortieth of that of bentonite. Consequently, vehicle movements to deliver polymer will be less than for bentonite;
- The much smaller quantities mean that there is no need for storage silo(s) though a dedicated area will be required for the storage of polymer tubs/bags;
- There is no need for a high shear mixer with weigh batching. Because of the small quantities involved, polymer can be dosed by simple manual systems;
- The hydration time for polymers is much shorter than for bentonite. There is no need for hydration tanks;
- The fluid can be maintained as polymer-water system with minimal dispersed soil so there is no need to manage/dispose of heavily soil-laden slurry during the works;
- It follows that the soil-slurry separation plant and its associated fluid storage tanks which are required for bentonite slurries and other non-SDIP fluids can be eliminated. These are items of plant with significant site footprint, substantial operating and maintenance costs, and demands on personnel. For polymer fluids, soil suspended in the fluid should be allowed to settle in the bore prior to concreting. If necessary, this settlement can be accelerated with additives proprietary to the polymer supplier. If the operational programme does not permit settlement time then the fluid in the bore should be replaced prior to concreting and the used fluid routed back to the polymer plant via a settling tank;
- Disposal of the used polymer fluid is simpler and cheaper. Disposal should be required only at the end of the works. PHPA and PA polymer fluids can be broken to low viscosity to meet the local sewage undertaker's requirements for discharge to sewer or in some jurisdictions, for environmentally compliant polymers, for direct discharge to the environment. In contrast the solids in bentonite slurries will preclude their disposal to sewer without prior treatment by centrifuging or filter pressing.
- Drier soil arisings – the excavated soil can be drier and so easier to stockpile, transport and reuse;
- As a consequence of drier soil arisings, somewhat reduced water usage; the fluid can be systematically reused, with additional polymer being added to the fluid after each use.

 © DFI International Bruges 2025

SUPPORT FLUID PREPARATION

Mix water treatment

The first step in the preparation of a support fluid will be to study the mix water chemistry. Typically the mix water will be drawn from public mains and chemical data should be available from the supply company. For bentonite slurries mains water may be suitable for use as supplied, though contractors may choose to treat some waters to optimise bentonite consumption.

For synthetic polymer systems pre-treatment of the water is normally undertaken as PHPA and PA polymer systems are sensitive to ionic salts in the mix water, even at the ionic concentrations typical of many tap waters. For example, Lam (2011) reported a four-fold lower viscosity for a PHPA fluid prepared with Oxford, UK tap water (treated with sodium carbonate to pH 10) compared with distilled water. Appropriate treatment of mix water to optimise polymer fluid performance is therefore important. For PHPA and PA fluids, the divalent ions calcium and magnesium are expected to be the most troublesome of the ions commonly found in tap waters. However, total dissolved solids also is an issue (strictly ionic strength, the sum over all ions: Molar concentration x Ionic charge^2). Water treatments that reduce calcium and magnesium but significantly increase the ionic strength may be of marginal benefit.

Calcium can be precipitated as calcium carbonate by addition of sodium carbonate. However, many natural waters contain significant concentrations of dissolved inorganic carbon (DIC) species (dissolved carbon dioxide, carbon dioxide, bicarbonate ion and carbonate ion). The speciation of the DIC will depend on the water chemistry and especially its pH. Below pH 9, the situation for most tap waters, there will be effectively no carbonate ion. However, if the pH of a water containing DIC is raised to pH>9, for example, by adding sodium or potassium hydroxide then the DIC will be progressively converted to carbonate ion which will, in turn, react with any calcium ions present to precipitate calcium carbonate. DIC is seldom reported in water analyses but it can be assessed, by calculation, from alkalinity data (acid neutralising capacity) which are usually included tap water analyses.

By way of example, the effect of adding sodium hydroxide and sodium carbonate (common name: washing soda) on the calcium and magnesium ion concentrations in a water with the chemistry shown in Table 1 (a London type tap water) are plotted in Fig. 1a. In Fig 1b the concentrations (on a log scale so that low concentrations can be seen) are plotted against the pH of the resulting solution.

The concentrations of sodium, potassium, chloride, and sulphate ions are shown in Table 1 for information. They are unaffected by the addition of sodium hydroxide but they do contribute to the ionic strength of the water.

Table 1. Properties of example water

Parameter	Concentration: mg/litre	Parameter	Concentration: mg/litre
pH	7.85	Chloride	38
Calcium	100	Nitrate	28
Magnesium	5	Sulphate	51
Sodium	28	Alkalinity, as $CaCO_3$*	202

* Alkalinity is usually expressed as the equivalent amount of calcium carbonate with the same acid neutralising power as the water; expression as equivalent calcium carbonate does not mean that calcium carbonate is present in the water. In many tap waters the alkalinity is dominated by bicarbonate ion.

From Fig. 1a it can be seen that calcium ion starts to precipitate as soon as alkali is added. From Fig 1b it can be seen that for sodium hydroxide there is little further calcium ion precipitation above pH10, at this point the calcium ion concentration <1 mg/litre. For sodium carbonate a slightly lower

 © DFI International Bruges 2025

pH of 9.5 is sufficient as the added carbonate helps with calcium ion precipitation (the common ion effect) whereas for sodium hydroxide it is necessary to rely in the dissolved inorganic ion species in the water. Fig 1a shows the masses of sodium hydroxide and sodium carbonate added in mg/litre. Had the data been plotted in terms of moles of alkali added the quantities would have been equal for calcium treatment but not magnesium.

Magnesium cannot be precipitated as a carbonate as the solubility of magnesium carbonate is too high, over 100 mg/litre giving magnesium ion concentrations in excess of 28 mg/litre. However, magnesium hydroxide is less soluble at about 10 mg/litre giving a magnesium ion concentration of 4 mg/litre and this can be further reduced by increasing the pH beyond that of saturated magnesium hydroxide solution (10.6), that is, by increasing the hydroxyl ion concentration. For the dissolution of magnesium hydroxide, $Mg(OH_2)$:

$$[\mathrm{Mg}][\mathrm{OH}]^2 = K_{\mathrm{sp}} \qquad [1]$$

Where [Mg] and [OH] are, respectively, the concentrations (strictly the activities, these are used in the modelling described below) of magnesium and hydroxyl ions in moles/litre and K_{sp} is the solubility product of magnesium hydroxide which is constant at any fixed temperature and pressure. Increasing the pH increases the hydroxyl ion concentration and so reduces the magnesium ion concentration for constant K_{sp} (an example of the common ion effect, note the hydroxyl ion concentration is squared).

From Fig. 1b, it can be seen that to reduce the magnesium ion concentration to <1 mg/litre it is necessary to raise the pH of the water to pH>11.0. This can be done by adding caustic alkalis such as sodium or potassium hydroxides. Figures 1a,b also show the performance of sodium carbonate as a water treatment agent as it may be preferred over caustic alkalis on health and safety grounds. However, whilst it is effective for calcium precipitation, it is not effective for magnesium. Very large doses would be required to raise the pH sufficiently high for magnesium precipitation and the associated increase in overall ionic strength would counteract any benefit from magnesium ion precipitation.

For the unusual situation of waters low in alkalinity relative to calcium ion, a combination of sodium carbonate for calcium treatment and sodium hydroxide for magnesium may be employed. Advice is needed from polymer suppliers as to acceptable ionic concentrations in mix water and especially the magnesium ion concentration as its removal requires rather high pH.

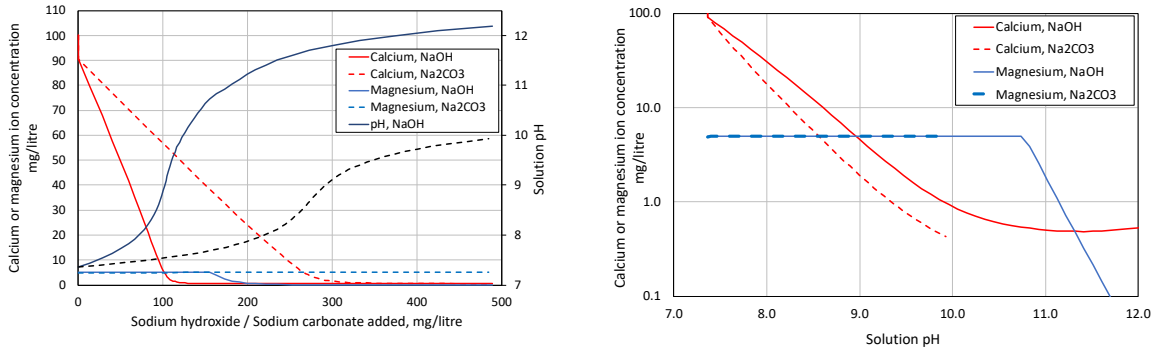


Fig. 1a and b Effect of sodium hydroxide / sodium carbonate addition on the calcium and magnesium ion concentrations in a London mains water .

Notes to Figs. 1a,b: Results were modelled using the Aqion software (Aqion.de, 2024) which uses the numerical solver of the widely used free software PHREEQC developed by the U.S. Geological Survey: see https://wwwbrr.cr.usgs.gov/projects/GWC_coupled/phreeqc/ and Parkhurst et al. 1999.

 © DFI International Bruges 2025

The water was initially slightly super saturated with respect to calcite, hence the immediate drop in calcium concentration before the addition of any alkali. For the sodium carbonate, the above figures relate its anhydrous form. If sodium carbonate decahydrate (Na_2CO_3:10H2O, washing soda) is used then the concentrations shown in Figs. 1a,b must be multiplied by 2.7.

Water treatment requires rather precise pH measurement – greater precision than is required for the in-field management of either bentonite slurries or polymer fluids. Water treatment schemes should be developed using a properly calibrated electronic pH meter with sufficient resolution, perhaps in the laboratory rather than on site. Once a treatment scheme has been developed and deployed, it should be necessary only to check the pH of the site treated water to confirm that there has been no change in the supply water chemistry, there can be seasonal and other changes and/or monitor chemical data from the water supplier.

The required doses of water treatment chemicals will be specified as mass of treatment chemical per cubic metre of water. However, weighing scales are unlikely to be available on site and even if scales are available, weighing takes precious time. In practice, water treatment chemicals and indeed the polymer system components themselves will be dosed by volume, using bulk volume as a surrogate for mass. Appropriately calibrated and labelled/colour coded dispensing containers must be provided to site, a container for each product to be dispensed. These containers should be calibrated so that the mass of product dispensed per container is known and can be recorded.

Management of water treatment precipitates

Calcium carbonate and perhaps magnesium hydroxide can be slow to precipitate so it may be beneficial to leave the precipitated solids in the water treatment tank to act as seed crystals for further precipitation, so avoiding significant supersaturation. It follows that, in principle, it will be preferable to have separate tanks for water treatment and polymer mixing. However, this will be at the expense of an extra tank, pipework and increased plant footprint. If a single tank is used then the precipitated solids will mostly remain in suspension in the polymer fluid and be lost from the tank as seed crystals. Furthermore, if the magnesium hydroxide precipitate remains in suspension in the fluid, it may tend to re-dissolve if the pH drops as often happens whilst support fluids are in use in an excavation. It is also possible that calcium may re-dissolve from calcium carbonate precipitates and be taken up on PHPAs and PAs tending to cause them to coil up. However, the effects of any re-solution may be much less than those of ions released from the soils and the groundwater in the excavation. Whether a separate mix tank is essential currently remains an open issue. It is to be preferred but space on site may dictate.

Preferred pH for polymer fluid performance and pH measurement

In addition to the benefit of calcium and magnesium precipitation, suppliers of PHPA based polymer systems typically advise that the pH of the mix water should be raised to at least 10 as high pH tends to promote stretching of the molecules (or perhaps the inverse is more correct – low pH allows coiling of the molecules as also occurs if calcium or magnesium ions are present). Longer chains give higher viscosity and so better performance as a support fluid. However, it has been suggested that pHs over 12 may cause hydrolysis of PHPAs and so loss of properties. There also will be health and safety concerns at high pHs. Overall a maximum pH of 11.5 for the treated water seems appropriate if magnesium is to be precipitated (the pH at which magnesium precipitates is relatively insensitive to its concentration but the quantity of alkali required to precipitate it will, of course, increase with its concentration). It may be noted that the magnesium ion concentration in the tap water shown in Table 1 is just 5 mg/litre. It is questionable whether it is worth treating magnesium at such a concentration, especially as magnesium may have less impact on PHPA coiling than calcium (pers. comm. Sorbie, K., 2025). If magnesium ion in the mix water is not an issue, a limit of pH 10 to 10.5 may be adopted subject to advice from the polymer supplier.

 © DFI International Bruges 2025

Support fluid preparation – process and procedures

Bentonite slurries usually will be prepared in self-contained mixing plant with automatic weigh batching of the bentonite as quantities are relatively large for manual handling – typically 30 to 50 kg bentonite per cubic metre of slurry – the concentration will depend on the source of the bentonite and the application. Once mixed, the slurry will be pumped to hydration/storage tanks. The required hydration time will depend on factors including the source and type of bentonite and the mixer. Some settlement of bentonite solids can occur in the hydration tanks after mixing so recirculation of the slurry through these tanks will be beneficial. Bentonite slurries will be delivered to the excavation by centrifugal pumps. These may be set to recirculate the slurry through the storage tanks when it is not being drawn off for use so counteracting any tendency for solids settlement and improving the dispersion of the bentonite clay particles though at the cost of extra energy usage. Fig. 2 shows a schematic of the slurry circuit for excavation under bentonite slurry. Only the basic elements of the process are shown in the figure. Details of the plumbing interconnections are not shown, these can be complex, nor are the pumps shown. The volume of slurry storage required will depend on the maximum volume of excavation open at any time with an allowance for losses to the ground, especially sudden large volume losses and the volume lost directly with the excavated soil and that separated from the slurry in the soil-slurry separation plant.

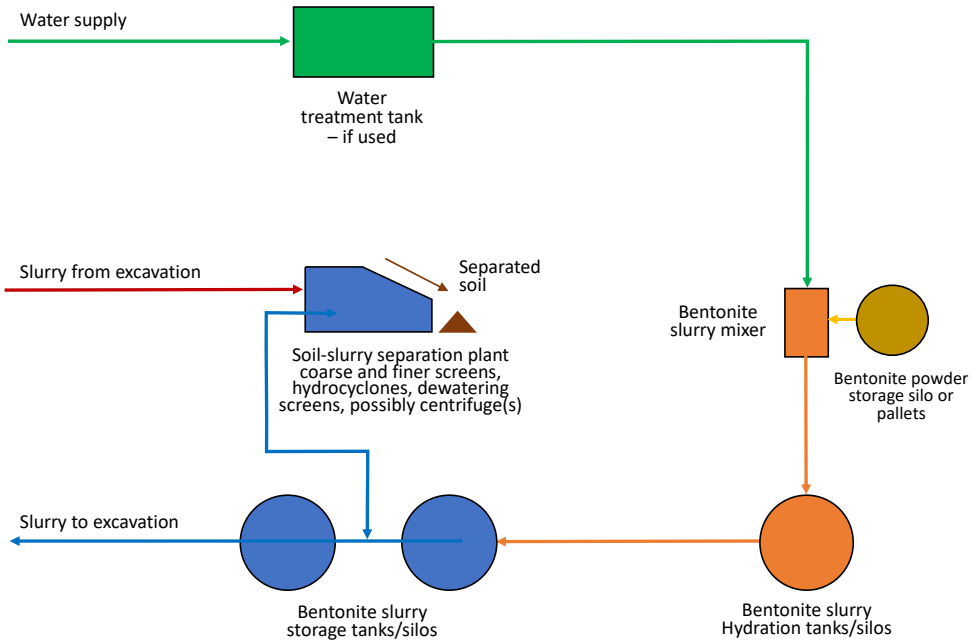


Fig. 2 Schematic flow chart for bentonite slurry operations

For synthetic polymer fluids based on PHPAs, mix concentrations typically will in the range 0.6 to 1.6 kg/m^3 depending on the product and the soil(s). For PAs concentrations can be expected to be 2 to 3 times higher. For powdered polymers (as opposed to emulsions), to avoid undissolved polymer, mixing must be done in two stages: initial wetting out of the polymer grains which requires their dispersion into a vigorous flow followed by their dissolution which requires a gently agitated tank. The grains must be wetted individually otherwise they will clump. For small volumes, the polymer may be manually sifted onto a splash-plate over which mix water is flowing. For larger volumes, a venturi eductor may be used but experience is mixed, eductors are easily blocked if the polymer in the eductor headworks is inadvertently wetted. A compromise system of a funnel discharging polymer powder onto a splash plate has been used (a ball or convex disc beneath the funnel will help to spread the powder over the splash plate). Vortex mixers as used in the oil industry may yet prove preferable. Supplier's advice should be sought with regard to the addition of any additives for their polymer

 © DFI International Bruges 2025

system (components in addition to the base polymer). Some additives may be best added as pre-prepared solutions rather than powders.

For the dissolution stage, typically polymer mixing tanks will be agitated by air bubbling (as will the water treatment tank). The bubbler bars should be set to induce circulation in the tanks to homogenise the mix and to ensure that there is no build-up of undissolved polymer at the base of the tank or fish-eyes of undissolved polymer in the fluid. Undissolved polymer is wasted polymer. Mechanical, in-tank, stirrers are not recommended as they would have to be slowly rotating to avoid shear damage to the long chain polymer molecules and so several could be required in a single tank. Figure 3 shows the basic circuit for a polymer fluid operations.

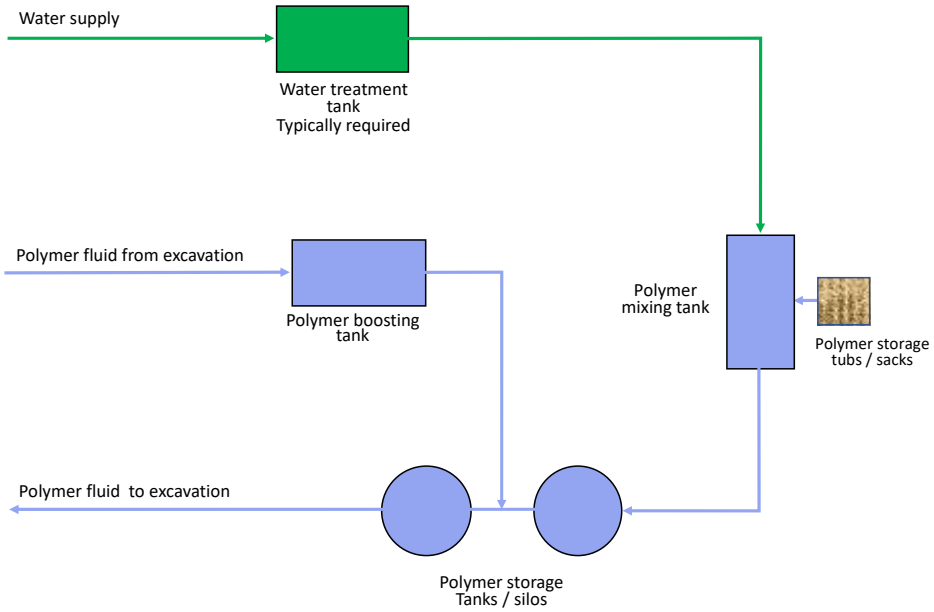


Fig. 3 Schematic flow chart for polymer fluid operations

Air contains carbon dioxide, an acid gas at about 412 ppm by volume, and thus continued bubbling will, over time, reduce the pH of the fluid in the mixing and storage tanks though the effect is likely to be quite limited unless bubbling is extended over days. Bubbling lines need not be run continuously provided good mixing can be assured by regular sampling and testing to prove the system set-up and operation. Bubbling of the water treatment tank will add carbon dioxide which, in the alkaline environment will be converted to carbonate ion which will contribute to calcium precipitation but the benefit is likely to be small; the reduction in pH will be the greater effect.

DELIVERY OF THE SUPPORT FLUID TO AND RETURN FROM THE EXCAVATION

The long-chain molecules of high molecular weight PHPA and PA polymers can be damaged by shearing in centrifugal pumps, especially if re-circulation is employed (see Lam et al. 2010). Air operated diaphragm pumps were recommended for polymer fluids as they impose lower shear and stop when the discharge valve is closed so avoiding the need for recirculation or an operator to switch the pump on and off. For higher fluid volumes, peristaltic (hose) pumps are now being adopted.

During concreting of an excavation, the support fluid will be returned to the fluid farm. For SDIP systems this fluid will be depleted in polymer as a result of sorption onto soils. Sorption is undesirable as regards polymer consumption but fundamental for the inhibition of soil dispersion. It is therefore essential that after each use, fresh polymer is added to the fluid to return its properties to those of the original mix. Typically this is assessed by Marsh funnel time which can be used as a surrogate for polymer concentration for polymer fluids with small suspended soil contents.

 © DFI International Bruges 2025

DISPERSION OF EXCAVATED SOIL INTO SUPPORT FLUIDS

Excavated soil will tend to disperse into a support fluid increasing its density, degrading its rheological properties, increasing filter cake thickness due to the extra solids and potentially giving rise to problems during concreting. For bentonite slurries the build-up of soil will be managed with a soil-slurry separation plant (see Fig. 2) which will have coarse and finer screens, hydrocyclones, dewatering screens and possibly centrifuges or occasionally filter presses. Soil-slurry separation plants have a large site footprint and power demands. A soil-slurry separation plant is not required for properly managed SDIP fluids (see Fig. 3) as there should be minimal solids in suspension. Indeed fine screens cannot be used with SDIP fluids as they will flow in sheets over screens. Nor can hydrocyclones be used as the high shear in them will damage the polymer.

The effect of soil dispersed into a polymer fluid during excavation will be even greater than for bentonite slurries as the polymer is sorbed onto soils and so removed from solution. Figure 4 shows a plot of the ratio of soil content to polymer content (both by dry mass) against polymer fluid density. The soil has been assumed to saturated with a grain specific gravity 2.65 and bulk density 2000 kg/m^3. It is assumed that all the water from the dispersed soil is incorporated in the fluid and so dilutes the polymer. From Fig. 4 it can be seen that there is a near linear increase in the soil: polymer ratio with fluid specific gravity. For example, if dispersed soil has raised the fluid specific gravity to the SPERW (2017) *ready for re-use* limit of 1.02 g/ml (see Table 2) there will be 33 times as much soil as polymer in the fluid. At the SPERW provisional *during digging* maximum of 1.05 g/ml there would be 85 times as much soil. Should the specific gravity rise to 1.1 g/ml as could occur with a non-SDIP polymer then there would be 178 times as much soil. Can a polymer have any useful effect on the properties of such soils-laden fluids, for example during concreting? Non-SDIPs may retain useful fluid loss control properties when soil is dispersed into them but that is a separate matter.

As SDIPs bind to soils, the active polymer concentration in solution will reduce as the amount of soil exposure increases a result of sorption onto the soil. Loss of polymer will reduce dispersion inhibition so promoting soil dispersion, exposing yet more soil surface area to polymer and so yet more sorption. Ultimately the fluid will become just muddy water but to the untrained eye this may not be apparent. In the 1990's, lack of active polymer was responsible for failures on a diaphragm wall project in the UK. When the wall was exposed many fluid filled voids were found. This set back the use of polymer fluids for diaphragm walling in the UK for tens of years. Control of density and boosting polymer concentration are key to polymer performance on site. To use SDIPs at low concentration is a false economy.

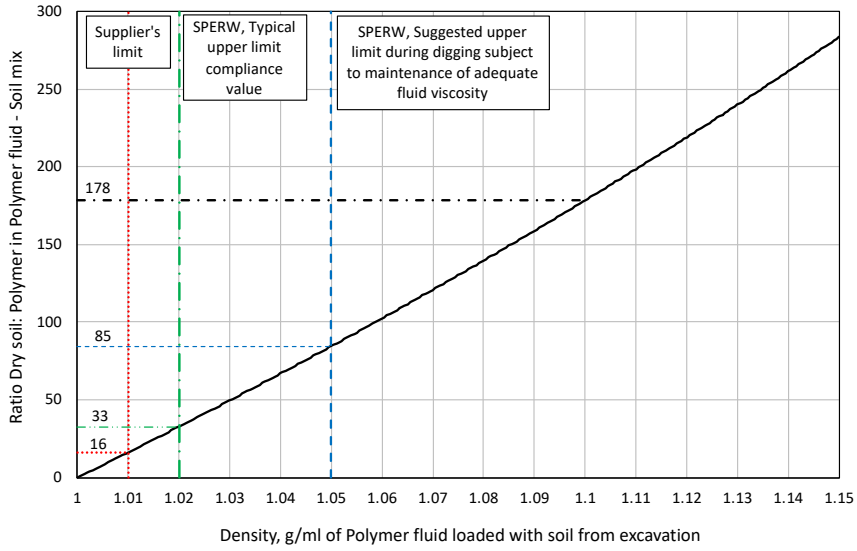


Fig. 4 Effect of soil suspension in a polymer fluid, Soil to Polymer ratio - fluid specific gravity

 © DFI International Bruges 2025

SPECIFIC GRAVITY DATA FROM SITES

On site all fluid density measurements are calibrated against water which is assumed to have a density of 1.000 g/ml. In reality water has this density only at 4°C, while at 25°C it has a density of 0.997 g/ml. It is therefore more correct to refer to site data in terms of specific gravity rather than density. The difference is small but avoid concerns about temperature corrections to reported results when considering site data for polymer fluids which will have density very close to that of water. In this section specific gravity is used in place of density.

$$Fluid\ Specific\ gravity\ at\ temperature, T = \frac{Mass\ of\ fluid\ at\ T}{Mass\ of\ equal\ volume\ water\ at\ T} = \frac{Density\ of\ fluid\ at\ T}{Density\ of\ water\ at\ T} \quad [2]$$

Figure 5 shows specific gravity data for polymer fluid supported piling works on two projects. Projects A and B. Both involved large, deep piles bored under polymer fluid. Polymers from different suppliers were used on the two sites; both are understood to have been based on high molecular weight PHPAs.

The data shown for Project A are for the polymer fluid from middle and base of the piles during excavation, that is they are worst case (highest) fluid specific gravities. Also shown is the SPERW (2017) provisional maximum specific gravity for polymer fluids during digging. This figure was proposed to ensure that the polymer was not exposed to excessive amounts of soil with so much lost by sorption as to be ineffective as an SDIP. As each pile was concreted the fluid was boosted by the addition of polymer powder at the boosting tank (see Fig. 3). It can be seen from Fig. 5, that the polymer fluid was well managed and the maximum recorded specific gravity of 1.017 was well below SPERW provisional maximum 1.05.

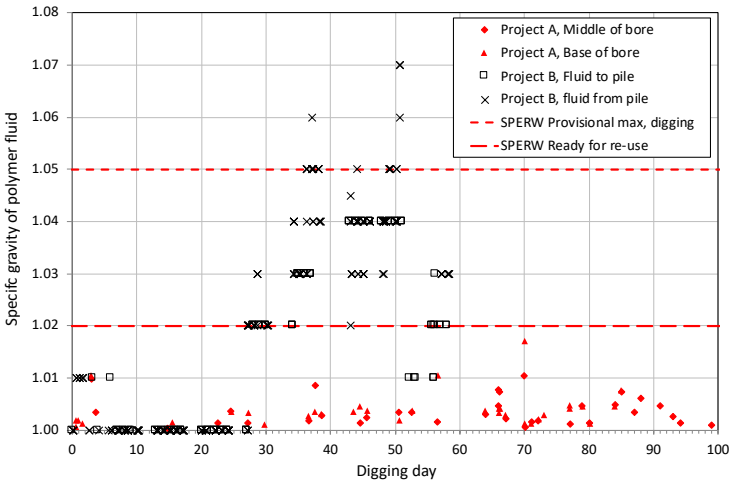


Fig. 5 Example of Polymer fluid specific gravity during digging on two pile projects

For Project B the specific gravity data presented are for polymer fluid supplied to the pile during excavation and pumped from the pile after excavation. Also shown in Fig. 5 is the SPERW typical control value for the maximum specific gravity for fluid supplied to the pile. Initially the management of Project B was in line with that for Project A, that is fluid specific gravities were low as supplied to the bores and after excavation. However, part way through the project there was a change in the fluid management strategy, fluid specific gravities were allowed to rise, a rise not necessitated for bore stability. The rise in amount of suspended soil led to concerns about base cleaning and measures had to be put in place. Also it seems that it proved impracticable to return the fluid specific gravities to low values by increasing the polymer concentrations. It is very probable that working at high specific gravity increased the amount of polymer used because of the amount of polymer sorbed onto the

 © DFI International Bruges 2025

dispersed soil. Furthermore, the soil suspended in the fluid will have been fine and, at the higher fluid specific gravities it will have increased the Marsh funnel time, giving false confidence that the polymer concentration was sufficiently high. A caution from this experience is that once a polymer fluid has become soils-laden, it can be difficult and costly to recover the situation.

To show the much higher permissible fluid specific gravities for bentonite slurries, Fig. 6 shows the data for a site using bentonite slurry. The data are for a digging slurry. On this site, excavation was done with a digging slurry which was completely replaced, before concreting, by a concreting slurry. It can be seen that the specific gravity of the digging slurry was much higher than for polymer fluids and without the use of soil-slurry separation plant, after each pile, continual spoil entrainment into the bentonite slurry would have led to unworkably dense fluids.

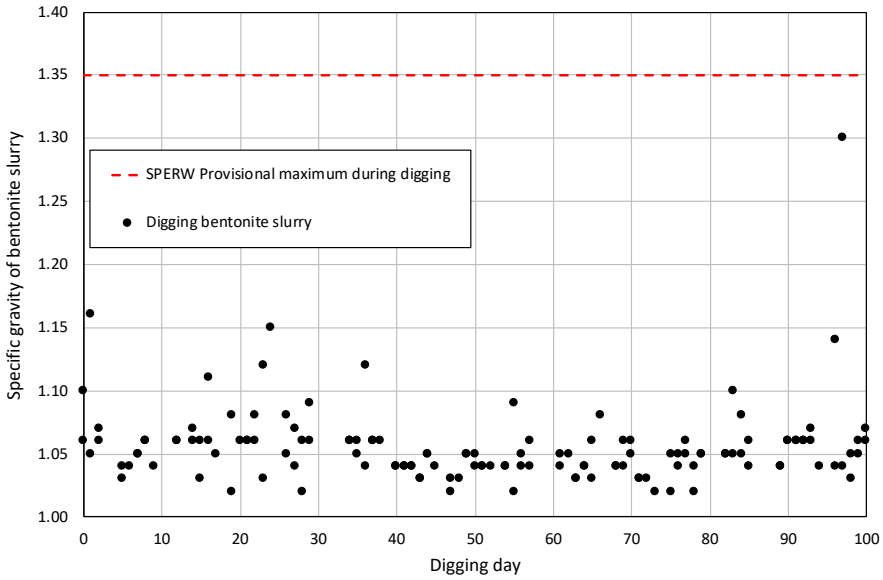


Fig. 6 Example of Bentonite slurry specific gravity during digging on a bentonite project

SALINE GROUNDWATERS – GROUNDWATER SPECIFIC GRAVITY

The specific gravity of freshly mixed polymer fluid will be 1.00 and as shown in Table 2, except during digging the specific gravity of the fluid should be less than 1.02 and indeed at least one polymer supplier recommends a maximum in-use specific gravity of 1.01.

It is important to consider the groundwater specific gravity when digging under support fluid in saline soils. The specific gravity of an average seawater is 1.025 and so, for example, a 40 m head of seawater will be equivalent to a 41 m head of fresh water or fresh polymer fluid. A pile taken to a depth of 40 m below a seawater groundwater will require an extra 1 m head of polymer to prevent inflow of the saline groundwater at the base (over and above the recommended minimum head for excavation stability, 2 m in SPERW giving a minimum total head above groundwater level of 3 m). In more saline soils such as can occur in hot climates the impact will be greater. Designers and main contractors should allow for this extra head when selecting piling platform levels. Too often, even with fresh groundwater, there is uncomfortably limited head for excavation stability unless substantial casing upstands are used. The cost-benefit balance should be considered if there are plans to reduce a site working platform level. A reduced level may save excavation and concrete but compromise hole stability and put the quality of the final foundation element at risk.

It is suggested that when working in saline or chemically contaminated soils, the electrical conductivity of the support fluid is monitored and compared with the conductivity of the fresh fluid. If the conductivity increases/continues to increase during the works, the underlying causes should be

 © DFI International Bruges 2025

investigated. Note: on record sheets, electrical conductivity should be recorded not one of the derived parameters such as total dissolved solids or salinity as these depend on the conversion factors used.

SPECIFICATIONS FOR SUPPORT FLUIDS

A headline on the Arts page of the Financial Times, 15 July 2024, ran:

'*If you make a show for everyone, you make it for no one*'.

For specifications, one could adapt this headline to:

'*If you make a specification for everyone, you make it for no one*'.

The dilemma is simply this, specifications have both technical and financial implications and no company will offer or support a specification that could put it at risk of technical constraints or financial risks. It is therefore of fundamental importance to identify what a specification is seeking to achieve. For example, BS EN 1536:2010+A1:2015, *Execution of special geotechnical works – Bored Piles* (BSI, 2015), and BS EN 1538:2010+A1:2015 *Execution of special geotechnical works – Diaphragm walling* (BSI, 2015) both state at Clause: 6.2.1.3:

> '*Other than in special circumstances (see Notes), the fresh bentonite suspension shall meet the conditions shown in Table 1 and the "re-use" or "before concreting" bentonite suspension shall meet the conditions shown in Table 2*'.

The combined requirements of Tables 1 and 2 of the Standards are shown in Table 2 below. There is no equivocation in these two standards, the fluid *shall meet*. This is an absolute requirement except in *special circumstances* – which are narrowly defined. To use such words requires that those developing standards have the absolute confidence that the numbers they are proposing are correct but what do we mean by correct in this context? Given the accompanying technical and financial risks the temptation is to set wide/high limits to minimise the risk of an out of range result – *a specification for everyone* and so *a specification for no one*.

Table 2. BS EN 1536 and BS EN 1538: *Characteristics for bentonite suspensions*

Property	Fresh slurry	For reuse	Before concreting
Density in g/ml	<1.10	EN 1536: not applicable; EN 1538: <1.25	<1.15
Marsh value in s	32 to 50	32 to 60	32 to 50
Fluid loss in ml	<30	<50	not applicable
Filter cake thickness in mm	<3	<6	not applicable
Sand content in % volume		not applicable	<4
pH	7 to 11	7 to 12	not applicable
Estimated solids content, kg/m^3 at maximum permitted density	*161*	*402 at density 1.25*	*241*
Ratio maximum total solids to typical as supplied bentonite content of 45 kg/m^3	*4*	*9.9*	*6*

Notes to Table 2: figures in *italics* are not included in the standards. They have been estimated from the specified density figures and have been calculated assuming that the increase in density is the result of dispersing a saturated soil of density 2000 kg/m^3 in a slurry initially containing 45 kg/m^3 bentonite powder at an 'as supplied' moisture content of 11%.

To consider just one parameter in Table 2, fluid density, the figures shown in italics have been calculated from the specified densities (for a discussion of other test parameters see, Jefferis, 2020 and for field test facilities, Jefferis and Ouyang, 2020). It can be seen that at all the operational stages of fluid supported excavation work at the limit values the amount of other solids would vastly outweigh the amount of bentonite. Furthermore, it is difficult to understand how even for a fresh slurry could

 © DFI International Bruges 2025

have a density 1.10 g/ml with an implied total solids content of over 160 kg/m^3. At the specified density limits for *re-use* and *before concreting* fluid will not be bentonite slurries but a slurries of soil solids. Such fluids should not be expected to behave as bentonite slurries. A valid question is therefore: are the specified values of any use in managing excavations under bentonite slurries? Will they promote good workmanship and ensure a quality final product? Experts may know how to constrain fluid properties but what of those new to the area? Does compliance with the Tables 1,2 of BS EN 1536 or 1538 bring a false sense of security to those learning to use bentonite slurries?

Polymer fluid typical test and compliance values from SPERW (2017)

In the UK the third edition of the Specification for Piling and Embedded Retaining Walls (SPERW, 2017) provides, for the first time, 'typical compliance values' PHPA polymer fluids (see Table C20.2 which is reproduced as Table 3 below). Previous editions have provided values only for bentonite slurries. Experience with polymer fluids has continued to develop since 2017.

Table 3. ***Typical tests and compliance values for support fluid prepared from polyacrylamide polymer polymers for use in bored piles*** **as shown in Table C20.2 of SPERW (2017)**

Property	Freshly mixed	Ready for reuse	During digging	Prior to concreting
Density, g/ml	1.01	<1.02	<1.05	<1.02
Solids content kg/m^3	*16*	*<32*	*80*	*<32*
Fluid loss, ml at 30 mins	n/a	n/a	n/a	n/a
Filter cake thickness, mm at 30 mins	*	*	*	*
Marsh funnel time, s	>90	60-120	60-120	90-120
Sand content	0	<2%	<5%	<1%
pH	9-11	9-11.5	9-11.5	9-11.5
Shear strength (10 min gel strength) N/m^2	n/a	n/a	n/a	n/a

Footnotes to Table C20.2 in SPERW, 2017 include:
** if filter cake thickness is specified it should be for a fixed volume of fluid (400 ml) as all fluid may drain from the cell during the test.*
The maximum Marsh funnel time of 120 s for 'ready for reuse fluid' is a typical value. It may be revised if appropriate experience exists or if the polymer supplier recommends other values.
The minimum Marsh funnel time of 60 s for digging fluid is again a typical value. A higher value may be used if recommended.

COMPARISON OF THE CONCEPTS IN EN1536/EN1538 AND SPERW

In the UK, since 2017, SPERW has successfully provided 'typical compliance values' for bentonite slurries and PHPA polymers (earlier editions considered only bentonite slurries). It is important to recognise that SPERW avoids the EN 1536:2015 and EN 1538:2015 wording such as '*bentonite suspension shall meet the conditions'*. SPERW does not specify but gives examples of *typical tests and compliance values*. This approach whilst allowing specifiers/contractors to adopt other values, guides them to realistic values and does not imply that results at the extremes may be acceptable in everyday operations. There is less risk of false confidence as a result of compliance with overly-wide specified *shall meet* ranges.

SPERW (2017) provides values only for PHPA based polymers. If other polymers types are to be included in specifications/standards it will be essential to draw a distinction between natural polymers and synthetic SDIPs. Natural polymers, modified natural polymers and gums such as CMC, xanthan, and guar are regularly used as additives to bentonite slurries. However, there is much less experience of their use as simple solutions without bentonite. They do not inhibit soil dispersion to the extent that PHPAs do, if they inhibit it at all. How does soil dispersion affect their behaviour in the field? Guidance has been developed for the management of synthetic SDIPs. It is questionable whether there

 © DFI International Bruges 2025

is currently sufficient industry-wide field experience of non-SDIP polymers amongst contractors, consultants and field technicians to set and validate useful control limits that these fluids *shall meet*.

The use of polymer fluids is developing rapidly but maybe stalled if failures flow from specification values which are over-widely drawn without sufficient guidance text. Polymer fluids like all support fluids require careful use supervised by those with the necessary training and experience. Specified *shall meet* limits carry with them the implication that provided these limits are met all will be well. When overly-wide limits are set, field experience tells us otherwise.

POSSIBLE UPDATES TO THE TYPICAL COMPLIANCE VALUES IN SPERW, 2017

From field experience and further research, the authors suggest the following updates to SPERW Table C20.2 *Typical tests compliance values for support fluid prepared from polyacrylamide polymers*:

a) In the title of Table C20.2 *polyacrylamide* should be corrected to *partially hydrolysed polyacrylamide*;
b) The word *density* should be replaced by *specific gravity*. For a discussion of support fluid density measurement and achievable density resolution, see Jefferis and Lam, 201).
c) The specific gravity of the fresh polymer fluid should be revised to 1.00. The figure shown in the table, 1.01 g/ml was to allow for measurement error and the table should have read <1.01 g/ml. Precision measurements have now shown that to two decimal places the specific gravity of the most concentrated PHPA based polymer fluid used in the field is unlikely to exceed 1.00 g/ml;
d) The *Ready for re-use* and *During digging* upper limits on Marsh funnel time should be removed. There is no need for an upper limit during these stages of piling work. Practical handling of the polymer fluid will set the limit which may be over 400 s; an inconveniently long time for any test in the field – always provided specific gravity limits are achieved;
e) The lower bound Marsh funnel time for *Ready for re-use* and *During digging* should be increased from 60 s to 80 s – depending on the polymer system in use;
f) The *Prior to concreting* Marsh funnel time could be decreased to perhaps 80 s to though, again, this will depend on the particular polymer system in use;
g) The upper pH limit for the freshly mixed fluid should be increased to 11.5 to allow for the precipitation of magnesium if this is necessary. This will bring it into line with the pH at other stages of the work;
h) McNamara (McNamara et al. 2024a and b) has shown that for clean polymer fluids, the API fluid loss is controlled by the pore size of the filter and the viscosity of the fluid at the shear rate of the flow in the pores of the paper. However, even for filter papers drawn from the same batch the variation in results from paper to paper is such as to make the results useless for control purposes. The API fluid loss test is marked as not applicable in SPERW (2017) and must remain so.

SUMMARY AND CONCLUSIONS

This paper has set out some recommendations based on recent experience with support fluids and in particular polymer support fluids and then develops the discussion to consider specifications. Polymer fluids are now widely used, a situation that has changed dramatically over the last 25 years, moving from proscribed by at least one company to prescribed on some projects. However, wide adoption does not ensure success. All support fluids require careful management by trained and experienced site staff. The EFFC/DFI Support fluid guide (2019), an excellent document provides a baseline. We now need a training document for site staff, a draft has been prepared by the Oxford research group (McNamara at al., 2024c).

It is hoped that those involved in drafting future standards will recognise that a *specification for everyone is a specification for no one* and avoid specifying overly wide operational ranges that key control parameters *shall meet*. Overly wide ranges bring false confidence and promote the falsehood: *my field results are within the specification limits so all will be well*. The SPERW approach,

 © DFI International Bruges 2025

recommending *typical compliance values* will do more to promote good practice and successful outcomes. The SPERW (2017) values for PHPA polymer fluids were developed from experience, consultations and substantial research. They have now been successfully used for over 7 years. From further experience the authors recommend the edits shown in items (a) to (h) above. The authors do not recommend any changes to the in use fluid specific gravity limits; any relaxation of these would have to be based on substantive field data.

Currently there is insufficient industry-wide field experience of the use of non-SDIPs such as CMC, guar and xanthan as simple solutions without bentonite to set and validate useful control limits that these fluids *shall meet*. Specifications can be developed later as experience develops.

REFERENCES

Aqion, 2024. Hydrochemistry software tool, www.aqion.de and https://en.wikipedia.org/wiki/Aqion. Accessed 03-02-2025.

BSI (British Standards Institution), 2015. BS EN 1536:2010+A1:2015. Specification for special geotechnical works – Bored piles. BSI, London, UK.

BSI (British Standards Institution), 2015. BS EN 1538:2010+A1:2015. Specification for special geotechnical works – Diaphragm walls, BSI, London, UK.

EFFC/DFI Support Fluids Task Group, 2019. Guide to Support Fluids for Deep Foundations, First Edition.

Financial Times, 2024. Arts Pages, 15 July, London, , p19.

Institution of Civil Engineers, Specification for piling and embedded retaining walls (SPERW), 2017. Third edition, ICE Publishing, Thomas Telford, London, UK.

Jefferis, S.A. and Lam, C., 2018. Using density to determine the solids content of construction slurries, Proceedings of the 19th International Conference on Soil Mechanics and Geotechnical Engineering, Seoul, pp1695-1698.

Jefferis, S.A., 2020. Rationalising specifications for bentonite slurries and polymer fluids excavation support fluids. British Geotechnical Association Conference, Piling 2020.

Jefferis, S.A. and Ouyang, E., 2020. Laboratory facilities for the field testing of excavation support fluids. British Geotechnical Association Conference, Piling 2020.

Lam, C., 2011. Properties and Applications of Polymer Support Fluids in Geotechnical Engineering, DPhil Thesis, University of Oxford.

Lam, C., Jefferis, S.A. and Goodhue, K.G. Jr., 2010. Observations on viscosity reduction of PHPA polymer support fluids. Proceedings of the GeoShanghai 2010 International Conference, Geotechnical Special Publication No. 205, American Society of Civil Engineers, 184-191.

McNamara, D., Sheil, B., Jefferis, S.A. and Barker, C., 2024a. Analysing the suitability of the American Petroleum Institute filter press test for polymer support fluids. Proceedings of the 5th International Conference on Geotechnics for Sustainable Infrastructure Development, pp. 477–486.

McNamara, D., Sheil, B., Jefferis, S.A., Barker, C. and Nicholson, D., 2024b. An investigation of the behaviour of polymer fluids in the American Petroleum Institute filter press, Geotechnique, https://doi.org/10.1680/jgeot.23.00209.

McNamara, D., Sheil, B., Jefferis, S.A. and Barker, C., 2024c. A Guide to the preparation and use and re-use of polymer support fluids for the site team, Revision 3, February.

Parkhurst, D.L. and Appelo, C.A.J., 1999. User's Guide to PHREEQC (version 2), a computer program for speciation, batch-reaction, one-dimensional transport and inverse geochemical calculations. USGS Water-Resources Investigations Report 99-4259.

U.S. Geological Survey, 2024. PHREEQC, https://wwwbrr.cr.usgs.gov/projects/GWC_coupled/phreeqc/.

 © DFI International Bruges 2025

REIMAGINING FOUNDATION DESIGN IN THE ELECTRIC POWER TRANSMISSION INDUSTRY

Peter Kandaris, Gannett Fleming, Gilbert, AZ, USA, 480.273.9445, pkandaris@gfnet.com
Prasad Yenumula, Principal Engineer, Duke Energy, Raleigh, NC, USA, 919.546.5017, prasad.yenumula@duke-energy.com

The electric power infrastructure is rapidly growing and changing, driven by the need for more energy and a broad-based conversion from traditional generation to more sustainable sources. Managing this change has resulted in the need to streamline and modernize transmission line foundation design practices. Current industry approaches are fragmented and inconsistent, impeding change. Guide documents developed by various utilities and engineering societies describe general design methodologies for foundation types used in the electric power industry, but their application, relevance and approach vary significantly from utility to utility.

Industry transmission line and foundation engineers have come together under the DFI's Electric Power Systems Foundations (EPSF) Committee to document the state of the practice in overhead transmission line foundation design and construction, delineate the shortcomings in these practices, and provide recommendations for the future development of consistent guidelines. This paper presents the scope and findings of the committee's 2024 state of the practice report that identifies foundation design and construction best practices, the type and scope of guidelines needed to streamline design, and research needed by the industry to advance the practice.

The DFI EPSF Committee report has been followed by the formation of an ASCE subcommittee whose goal is to develop foundation design guidance through a comprehensive manual of practice (MOP) for overhead power lines and substations. This paper presents high level insight from the current draft of the MOP. The new document will offer the opportunity for other industry sectors to understand how the power industry applies classical geotechnical design approaches for the foundation design of electric system structures.

Keywords: transmission line, foundation, design, guidelines, state-of-the-practice

INTRODUCTION

The electric power infrastructure is rapidly growing and changing, driven by the need for more energy and an ongoing broad-based conversion from traditional generation to more sustainable sources. The US Department of Energy's 2022 clean electricity study identifies the need to build 91,000 miles of new high voltage interregional transmission lines by the year 2035 (Denholm et al. 2022). But past history is not promising, as projects in the US from 2014 through 2021 have only resulted in a yearly US average of just under 1,000 miles of new lines (USDOE 2023). Federal monies through grid resilience and infrastructure programs to upgrade existing transmission lines may help supplement needed expansion, but innovation, new technology, and process improvements will be essential to accelerate new line construction.

The World Economic Forum recently stated that expanding the world's electric power transmission grid is essential to combat climate change (WEF 2023). As the report notes, new renewable energy capacities that are coming up across the world will serve little purpose without the power transmission grids to connect the green energy produced in renewable rich areas to the renewable deficit corners of the country (Figure 1). According to a recent *BloombergNEF* report (2023), staying on track for net zero will require annual expenditure on world's electricity grids to jump more than threefold over the coming decades.

Change expected over the next decades related to demand and climate requires a more responsive system for adapting designs to meet needs. Current design practices lack flexibility in responding to changing climatic load conditions – there is a need to create more agile standards.

 © DFI International Bruges 2025

Managing this change has resulted in the need to streamline and modernize transmission line foundation design practices. As late as 2017, there are over 3000 US utility companies (USEIA 2019), all with varying needs, financing, goals, and rules. But unlike the commercial building and transportation sectors, the electric transmission industry does not have a unified engineering manual or code that explicitly covers design and construction of the various foundation types currently utilized to support electrical structures. There is no overarching professional group that leads this effort. As such, existing design guidance is fragmented and based on experience, with application, relevance, and approach varying significantly from utility to utility.

There is great room for improving the transmission line foundation design process. Empirically, transmission line foundation design can be considered conservative (with the exception of some prescribed approaches) since few design-caused failures have been documented (Grigsby 2012). Statistically, there should be some situations where applied structure loads exceed assumed design values. The lack of failures is also a likely result of the lack of consensus in the design process, encouraging the compounding of safety factors by (a) owners specifying design requirements, (b) structural engineers and their code load cases, (c) geotechnical consulting firms not understanding the basis of the design models to be used by transmission line foundation designers, and (d) foundation designers not fully understand the sources of data and loads they are provided.

This conservativeness can be seen in a recent article in T&D World (Cisko et al. 2020) in their assessment of the design-bid-build process often used for transmission lines in the US. The article notes that each participant in the process sequentially adds their own safety factors and contingencies to design to account for the same unknown conditions such as geotechnical resistance, installation materials quality, and construction methodology. The resulting compounded conservatism leads to foundations being overdesigned, with potential cost and schedule efficiencies left on the table.



Figure 1. To bring on line new wind turbine and solar farms, transmission lines must be constructed from challenging, remote terrain to congested urban areas.

APPROACH

DFI's Electric Power Systems Foundations (EPSF) Committee was organized to identify common goals, develop guidelines, and aligning standards of practice for transmission structure foundations to improve their overall design and construction in North America. The committee provides an industry-wide forum to address issues related to deep foundation design, construction, economy, risk, safety, and quality in the electric power industry. This collaboration connects electric power industry professionals with contractors, consultants, researchers/academics, and manufacturers/suppliers.

 © DFI International Bruges 2025

This group was formed in 2013 when DFI agreed to sponsor a working group to better understand the deep foundation needs of the electric power industry. At its first meeting, the working group created a task force to study the state of the practice for transmission structure foundation design. The ad hoc task force was comprised of experienced individuals from the electric power industry, utility consultants, and academia with the following goals:

- Compile and review relevant published literature,
- Perform a survey of industry practices,
- Identify critical elements needed for uniform processes and guidelines, and
- Prepare a state-of-the-practice report to advance the development of industry design and construction standards.

The challenge for the task force was to first catalog the broad range of geological and geotechnical practices required to develop new overhead transmission lines and upgrade or maintain existing facilities. These efforts stretch from the early planning phases and route selection process to the operation and maintenance of lines under the pressure of ongoing development around them, through to the foundation needs of upgrading of aging infrastructure.

Survey results were published as a conference paper (Kandaris & Davidow 2015) that summarized the working group efforts to date. The paper also presented discussions of existing design and code documents as they relate to electric transmission line foundations, and elements needed in a guide document to improve the efficiency and reliability of electrical transmission line foundation design.

STATE OF THE PRACTICE REPORT

Based on the task force survey, the working group (DFI's EPSF Committee starting in 2018) moved forward with the preparation of an industry report. This document's purpose was to summarize the state of practice for the design and construction of electric system transmission lines and serve as the basis for future development of guidelines and standards for the industry. The committee report titled, "Design and Construction of Deep Foundations to Support Electric System Transmission Lines" was finalized and presented to the DFI in October 2024. The report had been prepared over an 8-year period, researched, drafted, edited, and reviewed by over 20 professionals both within the DFI and the wider utility industry. In general,

- The report presents the broad range of foundation types used in the power industry, describing the multiple foundation options available to support electric systems structures. Commonly, foundation selection is not part of the planning process or is done relatively late in the overall transmission line design stage, limiting opportunities for optimization and often extending construction schedules to remedy challenging conditions (Figure 2). This aspect of the report was developed to aid in understanding appropriate and economical foundations for transmission line projects in differing terrain, subsurface conditions, and locations.
- Background information is presented to give an understanding of structure load cases that are outside the control of the foundation engineer and how to contend with them for foundation design. The report provides great detail on how these load cases (ranging from deterministic to probabilistic to operational) impact the safety, cost, reliability, and resilience of the foundation system. Other types of loads (fluvial, seismic, etc.) that affect foundations only are traditionally outside structure design codes and need to be incorporated to address extreme and changing climatic conditions.
- Rational threshold criteria (foundation rotation, deflection and settlement) are identified to better evaluate safe and economical transmission line foundation performance. Criteria are needed since transmission line structure codes do not directly provide service load cases.

 © DFI International Bruges 2025

- The report summarizes current subsurface investigations practice. Methods used by utilities are highly variable and are often based on local or regional practices instead of focused on the unique aspects of electric system foundations or system reliability needs.
- By cataloging the state of the practice, the report shares best practices performed by US utilities.

One of the most important aspects of the report is the delineation of industry design needs and deficiencies to focus future guideline development and research efforts. There is a need to provide unified approaches or comprehensive state of the practice guidelines for the design of electric transmission line foundations to meet current and future challenges to rapidly build and upgrade transmission lines. The report notes that the electric power utility industry lacks consistent processes relating to foundation design approach, compatible load and strength factors and/or safety factors, reliability levels, performance parameters, dynamic and/or static load testing methods, and design elements.

TRANSMISSION LINE FOUNDATION DESIGN SHORTCOMINGS

The following highlight of the report's findings relates to industry shortcomings where standardization and guidance is needed to provide better performance with greater economy for transmission line foundation design and construction.

Design Models and Methodologies

Little consistency is seen in foundation engineering practice for the selection of transmission line foundation design methodologies. This is due to the lack of comprehensive guidance and proliferation of regional design practices. Foundation design should be based on factors mostly under the control of the utility and its design team. Guidelines, therefore, are needed to identify which models best fit the type of foundation for the specific design. In practice, some designers rely heavily on models that they are familiar with, software that they have purchased, or methods (including empirical approaches) as dictated by internal standards, possibly irrespective of applicability to the conditions, loads, or limits.

Self-supporting poles are the dominant structure type used for transmission line construction (either a single deep foundation for monopoles or double deep foundations for H-frame type structures). Different assumptions regarding foundation rigidity and fixity points are incorporated into the various lateral load models. But most designers often do not check or even consider this important aspect when choosing a model. Guidance is needed for proper model selection and use.

Model abuse: Foundation design models are stretched beyond tested limits as transmission line structures become larger and result in higher base reactions. Few prototype transmission line reinforced concrete drilled shafts greater than 6 feet in diameter and 30 feet in depth have ever been full-scale lateral load tested for the model calibration. Yet designers commonly use these models for production shafts up to 15 feet in diameter and 100 feet in depth. More testing and research are needed to assess the appropriateness of this approach.
Design guidance needs to be modernized for direct embedment pole foundations that are used throughout the power industry. Designers often determine embedment depth for a variety of laterally loaded direct embedment poles by prescribed methods traditionally developed for the lower class wood monopoles. These prescribed methods (often referred to as "rule of thumb" design, or 10 percent of the pole's overall length plus 2 feet of additional embedment) have remained nearly unchanged for over 100 years, yet substantial research has been done to provide improvements. Guidance is needed to modify prescribed design methods when using higher class wood, concrete, and steel monopoles and to axially loaded H-frames and similar types of structures.

Some direct embedment pole foundation design models neglect the effect of backfill on axial and lateral resistance. Only a few models consider the backfill geotechnical properties.

 © DFI International Bruges 2025



Figure 2. Design guides will aid in the growth of innovative transmission line foundation design approaches.

The interactions between the pole, backfill, and native soil are more complex, and there is not much test data available on direct embedment pole foundations under axial loads to validate some of these simplified theoretical models. Guidance related to the use of direct embedment models is needed to ensure proper application where backfill materials and placement could result in poor foundation performance.

Codes and Load Standards

Although there is substantial guidance for determining transmission structure loading, current codes offer little direction on how these load cases should be applied to the foundation system. Most codes simply advise that foundations should provide resistance equal to or higher than the structure loads. Very little guidance is provided in terms of factors that should be used in developing subsurface material resistance that are compatible with structure load cases (mixing deterministic structure loads with probabilistic geotechnical resistance). Unlike other infrastructure sectors, the electric power industry gives no methodology for integrating design load cases and factors developed by civil code organizations for reinforced concrete foundation design with load factors for the transmission structure.

Most utilities deterministically require loads applied to foundations to be greater than the structure to prevent foundation failure prior to structure loss (IEEE 2001). But there are no consistent methods to ensure uniform load increases for foundations as opposed to structure capacities. Additionally, transmission line load cases do not include service loads related to everyday structure performance to assess equivalent foundation performance under these conditions. Concerns regarding the use of current structural load cases for foundation design are illustrated in the following examples.

 © DFI International Bruges 2025

- A typical design practice is to envelope worst case foundation reactions components, shear, axial, and overturning moment, across all structural loading combinations into an unrealistic foundation loading condition, exacerbating the conservative nature of current design practices.
- Everyday load cases are likely to be of great use in the development of service limit state design. But there is a lack of consensus on how these would be determined and how the structure's performance would be impacted by foundation service limit deflection, rotation, and settlement. More work is also needed to evaluate combined structure and foundation movement displacement. Direction is needed on how this can be done and integrated into the development of service loads.

Code load cases relate only to forces imposed by the above-grade structure to the foundation at ground line. The additional effect of non-structure load conditions on the foundation by the surrounding environment can result in both ground resistance loss and increased load. Load or resistance reduction sources are generally related to foundations subject to flowing water including scour, bank loss, fluid forces, and flowing/expanding ice forces. Design considerations related to ground motion include liquefaction-induced ground resistance loss and subsidence, lateral spread, and downdrag. Landslides can both reduce resistance and increase foundation load. Common transmission line design codes do not directly address these conditions and leave it up to the designer to decide if or how to approach the problem.

There are no industry guides for compatible probabilistic load factors and load cases for evaluation of transmission foundations subject to non-structural environmental events such as flowing water and ground motion. More guidance is needed in the development of load cases that incorporate the simultaneous occurrence of multiple extreme load events. Approaches used by the transportation industry may provide a useful framework for establishing compatible load factors and cases.

Design Approaches

An Electric Power Research Institute (EPRI) study (DiGioia 2012) found two-thirds of responders use traditional deterministic (safety factor) approaches for design of transmission line foundations, with safety factors ranging upwards of 4.0 (depending on the structure type, foundation type, and design model). The EPSF Committee survey showed about half of the electric system foundation professionals using traditional methods and just under 40% using probabilistic design approaches.

Probabilistic design methods should result in improved foundation economy and reliability and allow the industry to be more agile in adjusting to future climate-related load changes. Deterministic approaches, though, are still far too entrenched in the industry. The report details some of the challenges for moving the industry toward greater use of reliability-based methods.

- There is a lack of guidance for consistent approaches to both allowable strength (ASD) and reliability-based (RBD) foundation design methods. EPRI has proposed an approach to RBD, but its use is not widespread nor uniformly accepted.
- There is no consistent or agreed upon reliability level for load and resistance probability distributions using standard reliability methodologies. This includes the selection of a target reliability index (beta). This value varies throughout the published literature from 2.33 to 3.5, relating to return periods for design varying from less than 100 years to hundreds of years (Ghosn, 2003). This problem, in turn, has resulted in a variety of strength factors used in the industry with different bases. A uniform approach is needed to develop strength factors for the industry's foundation models.
- ASD and RBD methods rely on using characteristic geotechnical design parameters. But the selection of geotechnical properties is often done by a consulting sampling and testing firm

 © DFI International Bruges 2025

with little understanding of the model(s) to be used for foundation design due to the lack of guidance. Consultant reports often provide low bound parameters that are not consistent with the safety or strength factors being used by the foundation design model. Overly conservative characteristic values are typical and result in conservative designs and increased costs.

Limit States and Movement

The establishment of performance criteria for the design of safe and economical transmission line foundations is important, but are poorly understood. Too often, performance criteria for laterally loaded foundations are set at the point where failure of the structure is imminent. Most industries evaluate foundation performance where differential settlements may result in warping of the structure, inducing unanticipated loads in the structural members or creating difficulties in functional operations. As discussed earlier, little work has been done to quantify the load levels related to damage limit displacements for transmission line structures.

The report notes that utilities often assign performance limits tied to maximum loads cases or ultimate load conditions. This is not done in other civil engineering sectors as most would expect significant foundation movement at geotechnical failure. This practice can result in individual and combined steady-state and transient loads unrealistically controlling foundation geometry. As such, there is no agreement on how much foundation movement is acceptable or how movement affects transmission structure function and operation.

There is a lack of understanding on how rotation and lateral deflection are interrelated with laterally loaded structures supported by deep foundations such as reinforced concrete drilled shafts and direct embedment pole foundations. This is especially important with the rigid foundations that dominate industry use where the two performance parameters are dependent variables. Over half of the engineers responding to the DFI survey noted that the standards used do not consider this dependency, with overly restrictive lateral deflection limits paired with incompatible rotation limits.

Similarly, there is a lack of understanding on how vertical movement mobilizes axial resistance in terms of side shear and end bearing. Very little side shear is required to reach full mobilization, yet (except in bedrock) a much greater compressive movement is nearly always needed to achieve full end bearing. Guidance is needed so that designers use strain-compatible axial resistance values.

Site Conditions and Investigation

Current codes relating to transmission line design offer little guidance in evaluation of conditions other than lines and structures (and their associated loads) that potentially can impact foundation resistance. Though standard industry codes recognize that variations in ground conditions can influence design, specific direction is lacking. Exploration programs are left to the judgment of practitioners, where they vary widely (Figure 3). When included in analysis, designers most often borrow approaches from other engineering sectors such as the highway design and building industries to develop reasonable approaches toward dealing with these conditions.

Near-surface soil conditions are not handled in a consistent manner and often are not compatible with the load model used for design. Most designers assume some resistance reduction is prudent. But often this condition is simplified by ignoring the existence of some depth of upper subgrade. One would expect, though, that soil resistance reduction for axially loaded foundations, where the ground and foundation may not be in intimate contact due to near surface desiccation, should be evaluated differently that with laterally loaded foundations where foundation rotation will most certainly keep good ground contact on at least half of the foundation. The report outlines several methods used by practitioners that could be adopted as guidelines.

 © DFI International Bruges 2025



Figure 3. Comprehensive geotechnical investigations for transmission line projects will improve project economy and provide better subsurface information for construction .

Many utility design standards and industry practices do not consider ground loss due to transient conditions such scour and bank erosion from flowing water or ground motion induced liquefaction (similarly, downdrag forces on foundations from earthquake induced settlement is often not assessed). Review of the history of transmission line foundation failures shows that most are the result of scour and embankment ground loss during extreme water flow events. The literature suggests liquefaction or downdrag due to ground motions as the most likely seismic events that would impact transmission line foundation design and performance, and should be routinely included in foundation assessments.

Obtaining sufficient data for transmission line foundation design is very challenging since these facilities are often constructed in remote areas in difficult terrain with poor access. This is especially true during the site investigation phase since road construction often waits until just prior to transmission line construction. Industry surveys show little consistency in investigation program approaches. Ideally, testing would be done at each transmission structure location. But most transmission line projects provide limited funding for investigations that often extend many miles and through a variety of subsurface conditions. Guidelines for transmission line geotechnical engineering investigations are needed. The report identifies various challenges and strategies to be considered for future guidelines.

- Often, test locations are selected based only on existing road access points along the transmission route, irrespective of subsurface conditions or local anomalies. The report identifies best practices for selecting the location and type of field/lab testing to be done for transmission line foundation design that combine access considerations with the subsurface geology. Traditionally boring and sampling should be augmented with geophysical surveys that can better reach remote sites.
- Field testing should maximize the use of cone penetrometer testing where feasible to better understand the full subsurface profile and develop geotechnical design parameters. Drilling and sampling via auger rig with SPT soundings are used far too often because it is cheap and has always been the way investigations were conducted. The industry must modernize.
- Investigation budgets should be sufficiently robust to allow mobilizing equipment for coring in bedrock and sampling in other hard ground conditions that adversely affect foundation construction costs. Refusal SPT soundings provide little insight for, and can slow down construction.
- It is important that geotechnical reports provide detailed information regarding likely excavation and ground stabilization conditions to reduce unexpected construction costs. Too often, the recommendations in consultant reports avoid needed detail due to concern of potential litigation for changes in conditions.

 © DFI International Bruges 2025

Design Considerations Related to Foundation Construction

Foundation design for transmission line structures includes aspects that are unique to the practice. As such, there is a need to create a comprehensive catalog of design options and alternatives. The practice is fragmented on these design elements and vary from utility to utility, and region to region. This creates unnecessary cost and confusion for those constructing foundations. Guidance is needed.

- Loss of ground support where foundations are constructed on slopes or near embankment tops needs to be addressed. The report provides methods used by some utilities and approaches published by the transportation industry.
- Reinforced concrete design: There is no general agreement on how to use common design codes (such as ACI 318) and how best to apply good practices to electric system foundations. Transmission line laterally loaded reinforced concrete drilled shaft foundations typically have very little axial load but high overturning (bending) reactions. Also, their diameter is controlled by the pole structure, not geotechnical conditions. Current codes provide some guidance, but EPRI and others in the electric industry have developed modifications to code design that provide good economy and more rapid construction while not sacrificing performance. A comprehensive design approach is needed.
- Direct embedment pole annulus backfills: There is a lack of standards for compacted material, poor understanding of the impacts of slurry materials, and few studies/guidelines on best practices. Recent study findings discussed in the report should be incorporated into design guidelines, with a renewed effort on applied research in this area.
- Foundation integrity testing: Although commonly used in the transportation industry, this type of testing is, at best, fragmented in the utility industry. Utility practices range from not performing any testing to not knowing when to test. Report recommendations are provided on best practices.
- There is no available guideline for the type and/or number of load tests to be performed at substation sites or along transmission lines for small diameter pile type foundations such as micropiles, helical piles, and driven piles. These foundations are becoming increasingly used in the industry, but the lack of testing guidance is slowing their acceptance.
- Foundation quality assurance and quality control (QA/QC): Like concerns seen with integrity and load testing, there is a wide variance in QA/QC approach and scope. There are few broadly used construction specifications developed specifically for transmission line foundations, as most are borrowed specifications from other industries. There is a lack of consistent QA/QC programs for the various foundation types used in the transmission industry.

NEXT STEPS

Done as part of industry outreach, several papers preceded the completion and publication of the committee report (Kandaris et al. 2017; Kandaris et al. 2018). The American Society of Civil Engineers (ASCE) through the Structural Engineering Institute is sponsoring a manual of practice (MOP) to establish an industry guidance document based on the recommendations and best practices in the EPSF Committee report. The MOP titled “Design of Overhead Power Line and Substation Foundations” is drafted and in ASCE Blue Ribbon Panel review.

The MOP presents a summary of current foundation design best practice for overhead power lines and substation structures and equipment, providing information for foundation engineers to use in making informed decisions on projects. It is intended to provide useful and comprehensive information to foundation engineers with varying experience levels. A wide range of best practice guidance with

 © DFI International Bruges 2025

detailed discussions are presented in this +750-page document. This comprehensive manual is comprised of 18 chapters with foundation design guidance on the following topics:

- Basics of overhead power line and substation structure foundations and associated loading
- Foundation type selection
- Development of foundation loads from structural load cases and foundation design philosophy
- Subsurface geotechnical exploration program
- Geotechnical parameter development
- Design and construction methods/considerations for various foundation types (drilled shafts, direct embed poles, large diameter open pipe piles, grillages, spread footings, micropiles, driven piles, helical piles, auger cast piles, tension anchors)
- Other topics (special design considerations, seismic design, evaluation of existing foundations, etc.)

There are also four appendices in this MOP covering the results of a new ASCE industry survey of design foundation practices, basics of below grade foundation corrosion, concrete and grout materials and placement, and anchoring to concrete for transmission line and substation foundations. A few of the specific MOP sections relevant to aiding rapid industry growth and change are as follows:

- Chapter 3 outlines a rational process for the selection of appropriate foundation types for various project and jobsite conditions. A generalized process is presented that includes various steps the foundation engineer should take to work through the project-specific conditions and considerations in an organized manner. This process is meant to provide a consistent method to use in the selection of foundation type for transmission line projects.
- Chapter 4 presents a comprehensive discussion on reliability-based design philosophy for electric utility foundations, a summary of foundation design strength factors, threshold criteria for drilled shaft foundation design, and a balanced design approach for drilled shafts to optimum cost.
- Chapter 5 includes a formal process for the development of a comprehensive transmission line geotechnical investigation focused on needs specific to the industry. Consideration is recommended for unique features of the equipment and locations of the structures related to varying environmental settings, boring layout, depth of borings, sampling method and elevations where samples need to be collected, type of sampling, and type of laboratory tests required.
- Chapter 18 gives guidance for evaluating existing transmission line foundations for reuse or modification where system upgrades are planned to increase line ampacity without constructing a new line that could result in increased loading on structures and foundations. This approach can result in cost savings, reduced time to increase power flow within existing corridors, and reduced outage needs.

The EPSF Committee recently established two subcommittees tasked to develop guideline documents focused on topics ranked by power industry engineers as of greatest need to the industry. The first subcommittee is developing guidance on load case combinations for transmission line foundations related to external conditions such as seismicity, liquefaction, scour and ice flow. The second subcommittee is developing guidelines for the use of pile groups to support electric transmission structures. These guide documents are expected to be published in late 2025 and early 2026.

 © DFI International Bruges 2025

CONCLUSIONS

Comprehensive foundation design guidance is needed to support the rapid growth of electric transmission lines in the US that is essential to adapting to climate change and bringing on line sustainable generation sources. This paper summarizes work by the DFI's Electric Power Systems Foundations Committee in the development of its 2024 state of practice report titled, "Design and Construction of Deep Foundations to Support Electric System Transmission Lines." The objective of the report is to advance the development of industry design and construction standard practices and guidelines. This paper presents important report conclusions related to industry design needs and deficiencies to focus future efforts toward both guidelines and research. The report has already resulted in the drafting of an ASCE guidance manual of practice titled "Design of Overhead Power Line and Substation Foundations." The report provides a blueprint for continued streamlining and modernization of transmission line foundation design practices.

Engineers cannot be expected to control or have significant influence on climate change and sustainable power development policies. Engineers do have the key role in helping society adapt to change as objective technologists facing these realities head on and constructively. Engineers are recognizing their role with incorporating change into design. An example can be seen in London's Thames Barrier designed to protect from tidal changes and cope with future sea level rises. ASCE continues to assess how its current design guides can be modified to adapt to changing (more intense) wind and storm conditions. This is a complex process that will require tools such as comprehensive guidelines to allow for long-term change. Engineers continue to integrate adaptation into practice. Stony Brook University College of Engineering and Applied Science (2024) has established an Engineering Adaptation to Climate Change team that highlights this challenge:

> "Our climate is not only changing, resulting in numerous changes in our environment, but is doing so in a discontinuous and in many ways impossible-to-predict sense, due to the overwhelming complexity of our global natural and engineered systems. In light of this, sustainability means. . . . also finding new ways to adapt our society and civilization . . ."

REFERENCES

Bloomberg/NEF. 2023. T*he New Energy Outlook: Grids.* Report. Bloomberg, New York.

Cisko, R., B. Wallis and S. Davidow. 2020. "The foundation for design success." T&D World, February 3.

Denholm, P., P. Brown, W. Cole, T. Mai, B. Sergi. 2022. Examining Supply-Side Options to Achieve 100% Clean Electricity by 2035. Golden, CO: National Renewable Energy Laboratory. NREL/TP6A40-81644

DiGioia, A. M. Jr., 2012. Transmission structure foundation design guide. EPRI, Palo Alto, CA. 1024138.

Grigsby, L.L., 2012. Electric power generation, transmission and distribution. 3rd, Ed. (Chapter 23), Taylor and Francis, Boca Raton.

Ghosn, M., Moses, F., and Wang, J., 2003. Highway bridge design for extreme events. National Cooperative Highway Research Program, NCHRP Report 489.

Institute of Electrical and Electronics Engineers (IEEE), 2001. IEEE guide for transmission structure foundation design and testing. New York, NY. Standard 691-2001.

 © DFI International Bruges 2025

Kandaris, P.M. and S. Davidow. 2015. Study of electric transmission line deep foundation design. In Electrical Transmission and Substation Structures 2015: Technical Challenges and Innovative Solutions in Grid Modernization, Branson, MO, pp. 577-587.

Kandaris, P.M., S. Davidow and A.E. Evans. 2017. Framework for risk-based electric system deep foundation design

Kandaris, P.M., S. Davidow and A.E. Evans. 2018. Groundwork for developing comprehensive transmission line foundation design guidelines, Proc: Electrical Transmission and Substation Structures Conference 2018, Atlanta, Georgia, November 4-8, pp. 84-93.

Stony Brook University College of Engineering and Applied Sciences. 2024. Vertically integrated projects program: EACC, Viewed on 9/22/2024: https://www.stonybrook.edu/commcms/vertically-integrated-projects/teams/_team_page/team_page.php?team=Engineering%20Adaptation%20to%20Climate%20Change%20(EACC)

United States Energy Information Administration. 2019. *Annual electric power industry report*. Viewed on 9/22/2024: https://www.eia.gov/todayinenergy/detail.php?id=40913#:~:text=According%20to%20the%20U.S.%20Energy,the%20United%20States%20in%202017.

US Department of Energy. 2023. *National Transmission Needs Study*. Washington D.C.

World Economic Forum. 2023. *Why embracing power transmission is key to tackling climate change*. webforum. Viewed on 9/22/2024: https://www.weforum.org/agenda/2023/09/why-embracing-power-transmission-is-key-to-tackling-climate-change/

 © DFI International Bruges 2025

DESIGN OOSTERWEEL LINK WITH PRESERVATION OF A HISTORICALLY PROTECTED BUILDING SAMGA SILO A

Bart Rombauts, Sweco Belgium, Antwerp, Belgium, +32473562122, bart.rombauts@swecobelgium.be
Ramses Verachtert, Sweco Belgium, Antwerp, Belgium, +32475825070, ramses.verachtert@swecobelgium.be

ABSTRACT

This paper presents a comprehensive stability analysis of the historic masonry structure, Samga Silo A, located in Antwerp, Belgium, in the context of the Oosterweel Link construction project in its vicinity. The research details a series of calculations aimed at estimating potential settlement and subsequent crack formation in the Samga building due to nearby construction activities. Various Plaxis models were utilized to simulate these activities, with a particular focus on the construction of a tunnel, which extends over 20 meters below ground level and is situated less than 15 meters from the building's corner—representing a significant engineering challenge. Additional construction tasks include the erection of a temporary quay wall and the stabilization of an adjacent dock. To further assess the potential impacts of construction, a piling test was conducted to evaluate settlement and vibration effects. A finite element model using Diana was developed to predict the cracking and deformation responses of the masonry structure due to anticipated settlements. Furthermore, the Plaxis models were employed to assess various settlement mitigation strategies. Continuous monitoring of the predicted settlements will be undertaken throughout the construction phase to refine and calibrate the models, ensuring the structural integrity of the Samga building is maintained.

Keywords: settlements, foundation, tunnels, masonry, Diana, Plaxis, Oosterweel connection

INTRODUCTION

Building description

The Samga Silo A is a historically significant masonry structure located in the northern part of Antwerp, Belgium, adjacent to the America-dock, as shown in Fig. 1. Constructed in 1895 by the Société Anonyme des Magasins à Grains d'Anvers (SAMGA), this monumental building measures 100 meters in length, 25 meters in width, and stands 32.5 meters tall from the soil level. It features a shallow foundation that extends 6 meters below the surface.

The internal layout of the building consists of a grid of silos, which are separated by slender masonry walls and reinforced with steel trusses at the corners. The foundation is made of unreinforced concrete, with a thickness ranging from 1.0 to 1.1 meters. During World War II, the structure suffered partial demolition due to bombings in Antwerp but was subsequently rebuilt. The top floor was reconstructed with two large expansion joints to accommodate structural integrity, as can be seen in Fig. 2. The company used the building until the early 2000s.



Fig. 1 (left) Location and (right) 3D-rendering of the Samga-building (source: Google Maps).

 © DFI International Bruges 2025

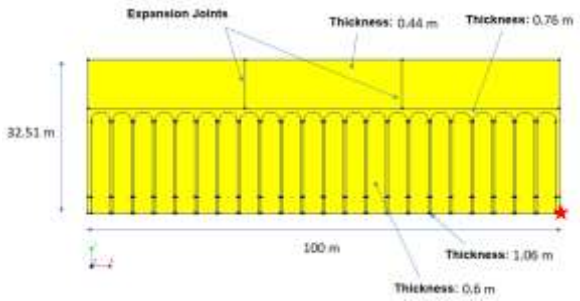


Fig. 2 Illustration of the building with the location of the expansion joints.

Samga Silo A is situated near the future Oosterweel Link a major infrastructure project designed to complete the ring road around Antwerp, as shown in
Fig. 3, through the construction of bridges and tunnels. Notably, a tunnel is planned to be built approximately 15 meters from the southeast corner of the building. Given its location and protected status, Lantis, the governmental body overseeing the Oosterweel Link construction, has acquired the building, and is exploring options for its repurposing following the project's completion. Unfortunately, two other similar structures, Samga Silo B and C, were demolished due to conflicts with the tunnel's planned location.



Fig. 3 Oosterweel Link

Because of the proximity to the construction works and the sensitive nature of the building, Lantis and Rinkoniên (the contractor consortium) conducted several analyses to assess the influence of the construction works on its surroundings and the stability of the Samga building. The most important activities investigated are shown in Fig. 4 and include the filling of the adjacent Samga-dock (necessary for the future construction of the tunnel), the construction of a temporary quay for transporting and storing construction equipment and materials over the channel (Samga-plateau), heavy construction transport, and the construction of the tunnel itself. Additionally, the influence of smaller activities such as pile driving and dewatering was also examined.

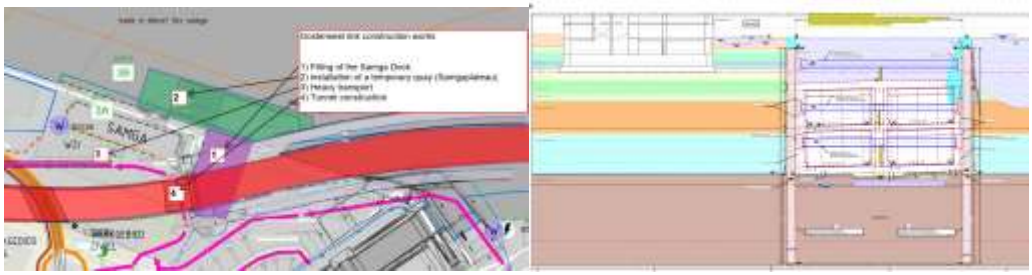


Fig. 4 (left) Location of the construction activities and (right) cross section of the tunnel to be constructed near the Samga building.

 © DFI International Bruges 2025

Soil layering of the site

The soil layering near the Samga building is well understood, although it presents challenges for modeling. The geotechnical profile utilized in the tunnel design near the Samga building is depicted in Fig. 5.

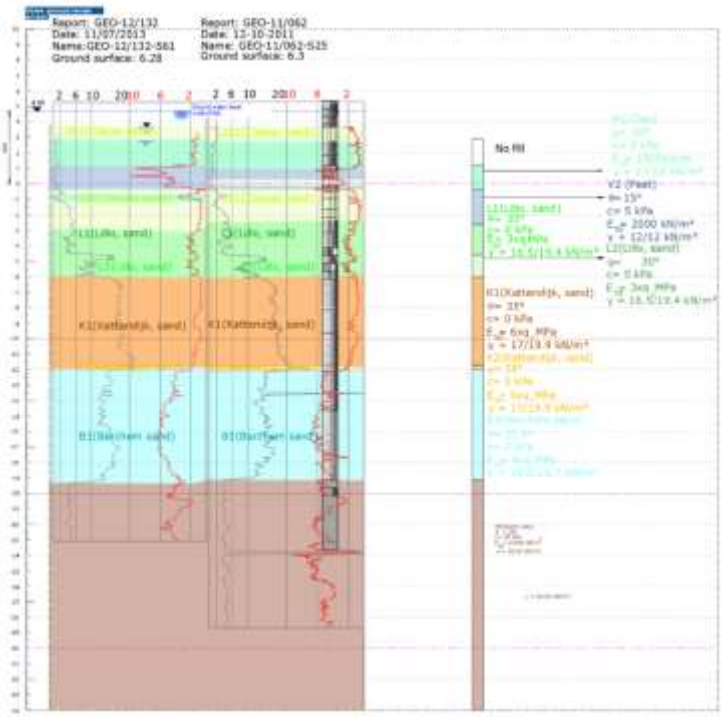


Fig. 5 Soil layering near Samga building.

The typical soil layering in the Antwerp region is characterized by a highly heterogeneous quaternary layer, primarily composed of sand and clay at the surface. The phreatic water depth ranges from 2 m to 3 m below the surface (surface level = 6.30 mTAW). Beneath this, there is polder clay rich in peat, which contains an aquifer fed by the Scheldt River. Below these quaternary layers, a series of very stiff tertiary sand layers can be found, starting with the Lillo sand at approximately -2 mTAW and concluding with the Berchem sand at -18 mTAW. Below -18 mTAW lies the well-known overconsolidated Boom clay layer, which exceeds 30 m in thickness. The presence of this clay layer allows for excavation in a dry building pit after the installation of diaphragm walls that extend into the Boom clay and are supported by steel struts,.

The Boom clay also introduces significant design challenges due to its swelling behavior post-excavation. This swelling can persist for years following project completion. To address this, a box-in-box design has been adopted for the tunnels. The building pit is fully excavated first, followed by the bottom-up construction of the tunnels, which do not rely on structural connections between the retaining diaphragm walls and the tunnel itself, resulting in an auto-stable tunnel design. The final weight of the tunnel is less than that of the excavated soil, ensuring the tunnel's stability without dependence on the diaphragm walls.

Given the extensive scale of the Oosterweel project and its substantial impact on the surrounding area, precise geotechnical modeling is essential for achieving an economical and stable design. To ascertain soil characteristics, a comprehensive field campaign was commissioned by Beheersmaatschappij Antwerpen Mobiel (BAM), now known as Lantis, as reported by Couck et al. (2015). This campaign involved excavating an octagonally shaped building pit with a depth of 24 m, a surface area of 402

 © DFI International Bruges 2025

m², and sheet pile walls measuring 29.65 m in length, stabilized with five layers of struts, from January 2014 to April 2015. After a monitoring period of four months, the pit was refilled in September 2015. The results from this measurement campaign, along with a pq-analysis of the tertiary layers conducted by Vanhaekendover et al. (2021), were used to determine the various soil characteristics for the Finite Element (FE) Plaxis model. Key characteristics related to the in-situ CPT results include stiffness, drained friction angle, cohesion, and self-weight. For the Boom clay, hydraulic permeabilities were also assessed to estimate its swelling behavior. The determination of Boom clay characteristics and guidelines for modeling it in this project are documented by Van Zegbroeck et al. (2021). It was found that the top 5 m of the Boom clay on the excavated side of the retaining walls behaves as if it were drained, while the deeper Boom clay behaves undrained. This results in different soil characteristics of the top 5 m, with notably larger permeabilities and lower stiffness.

ANALYSES

In situ investigations

Over the years, Lantis, Rinkoniên, and other parties conducted several in situ investigations to evaluate the dimensions, foundation, and condition of the Samga building. They performed an in-situ excavation to verify that the building is founded on a concrete plate rather than on piles, a fact later confirmed when the original plans were located in a city archive. Pelser Hartman executed a 3D scan of the building, which was utilized to create 2D measurement plans, shown in Fig. 6. Additionally, Sweco developed a 3D model based on this scan. Rinkoniên carried out a pile driving test adjacent to the building to assess the impact on building vibrations and settlement, following the guidelines from the SBR and CUR166. KULeuven collected masonry samples to test and evaluate the characteristics of the masonry used in the models.

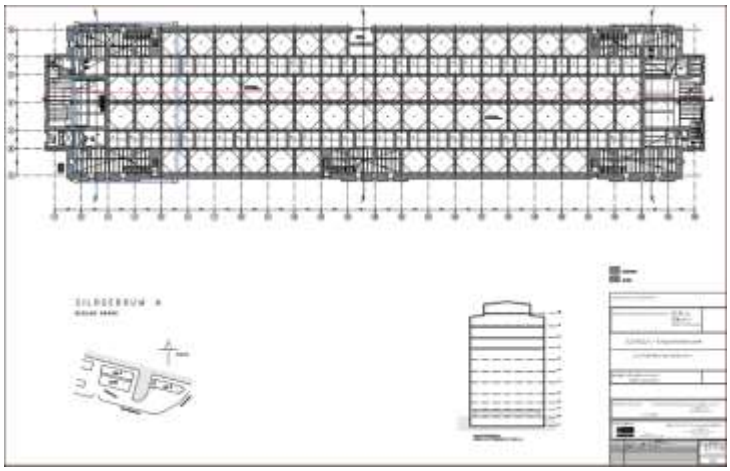


Fig. 6 Measurement plan based on 3D-scan performed by Pelser Hartman.

Plaxis

Plaxis 2D was utilized to estimate the deformations of the Samga building resulting from various construction activities. Multiple variants for some activities were investigated to minimize deformation as much as possible. The calculated settlements and deformations for each activity are shown in Fig. 7. These settlements were superimposed linearly to estimate the total deformation of the building, which is considered a conservative assumption. The expected crack formation due to this settlement was predicted through a Diana model.

 © DFI International Bruges 2025

The construction activities included damping of the Samga-dock, construction of a quay at the north side (Samga-plateau), driving of sheet piles next to the Samga building, demolishing the existing quay east of the building, removing piles under the existing quay wall east of the building, and excavation and installation of the tunnel at the southeast of the building. Each of these activities contributed to the overall expected settlement of the building.

The Plaxis models provided crucial insights into the deformation behavior of the building due to the anticipated construction activities, allowing for the evaluation of different settlement mitigation measures.

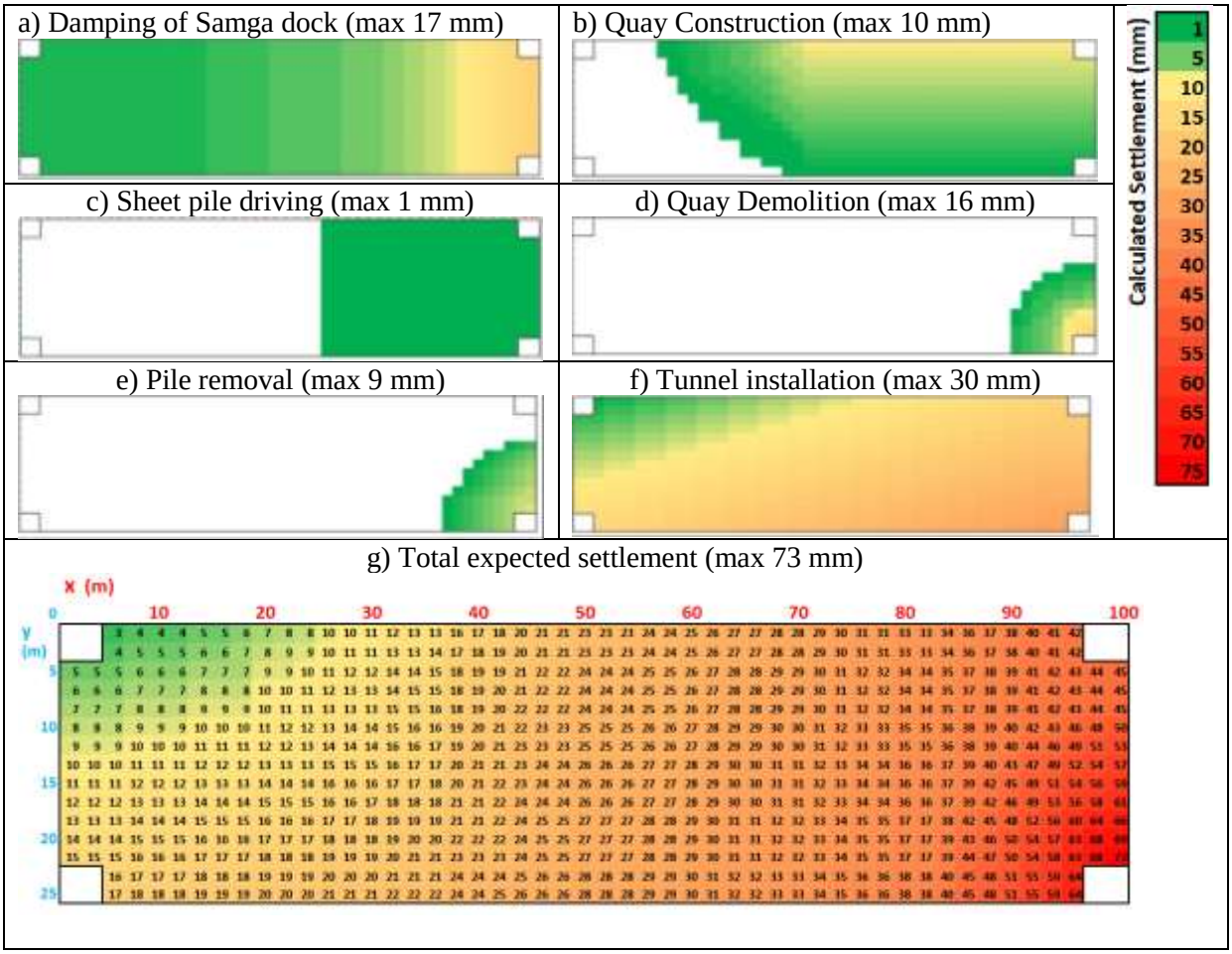


Fig. 7 Estimated vertical deformation (in mm) due to construction activities: a) damping of Samga-dock; b) Construction of quay at north side (Samga-plateau); c) Driving of sheet piles next to the Samga-building; d) Demolishing of the existing quay east of the building; e) removal of the piles under the existing quay wall east of the building; f) excavation and installation of the tunnel at south-east of the building; g) total expected settlement).

Settlements caused by the construction of the nearby tunnel

The settlements caused by the construction of the nearby tunnel will significantly impact the Samga building. This is due to the excavation reaching a depth of -19mTAW, which penetrates the Boom clay. To manage the soil pressures and stabilize the diaphragm walls, three layers of steel struts are necessary. The Boom clay layer at the bottom of the building pit is relatively soft compared to the stiffer sand layers above it. As the sand layers are excavated, the horizontal stresses must be supported by both the steel struts and the Boom clay. The large width of the excavation pit in combination with

 © DFI International Bruges 2025

increased stresses, results in substantial deformation of the clay layer and, consequently, significant deformations in the diaphragm wall. This process causes the soil outside the diaphragm walls to relax and move horizontally, leading to vertical settlement at the surface and, ultimately, settlement of the Samga building. To determine the settlements of the Samga, caused by the construction works of the tunnel, a Plaxis 2D model was constructed, based on the soil layering presented in Fig. 5. The complete Plaxis model of the tunnel and foundation of the nearby Samga building, as performed by Verachtert et al. (2024), is shown in Fig. 8.

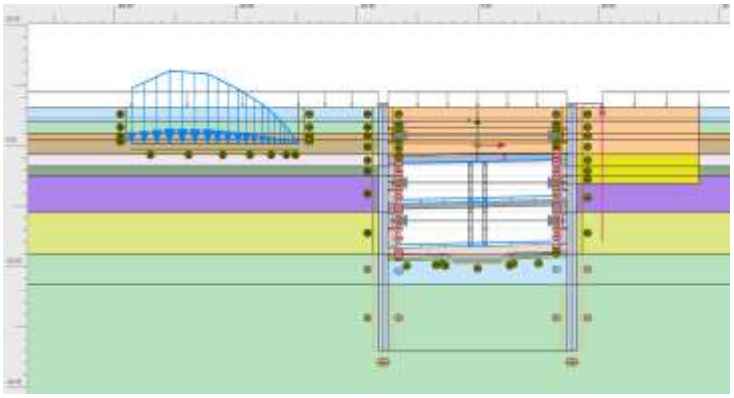
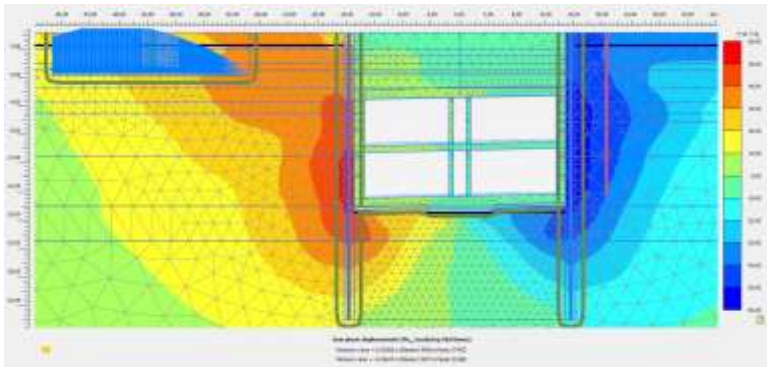


Fig. 8 Plaxis 2D model of the tunnel nearby the Samga building.

The final soil displacements are illustrated in Fig. 9, where the horizontal and vertical soil displacements after the tunnel is fully constructed are shown for the final design, adopted at the date of writing the paper.

a)



b)

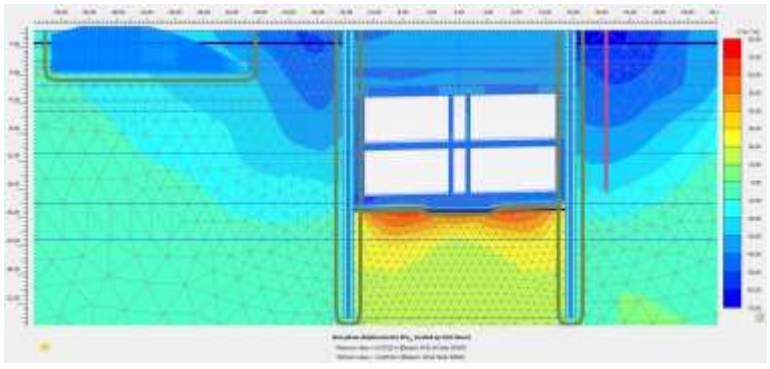


Fig. 9 Final a) Horizontal and b) vertical soil displacements after construction of the tunnel near Samga for the final design.

To mitigate these settlements, various countermeasures were proposed and evaluated for their technical and economic viability. These countermeasures included:

 © DFI International Bruges 2025

1) **Optimization of strut positions, drainage, and excavation steps**: While not strictly a countermeasure, these design considerations significantly influence the results but do not achieve sufficiently small settlements within the design constraints.
2) **Use of T-panels:** This method aimed to enhance the bending stiffness of the diaphragm walls, allowing for more effective mobilization of the Boom clay between the walls, though it proved to be inefficient.
3) **Deeper diaphragm walls**: Increasing the depth of the diaphragm walls enhances the thickness of mobilized clay, making it an effective but costly solution.
4) **Reducing the final excavation step**: Introducing a fourth row of struts was considered, but it was impractical due to varying floor levels of the tunnel and did not significantly help as the bottom strut's position, which has the largest impact on the settlements, could not be lowered.
5) **Increasing diaphragm wall thickness** Raising the thickness from 1.20 m to 1.50 m improves bending stiffness, similar to using T-panels but easier to execute, but this measure alone is insufficient and should be combined with other strategies.
6) **Trench shoring:** This method involves installing a "wished-in-place" concrete strut at the depth of the Boom clay to enhance horizontal stiffness, effectively reducing horizontal deformation of the diaphragm wall and the settlement of the Samga building. However, it requires manual excavation, impacting the project timeline.
7) **Transversal diaphragm walls**: Similar to trench shoring, this technique increases the stiffness of the Boom clay layer and has a lesser impact on planning since it can be executed simultaneously with the retaining walls. However, it is an expensive option that necessitates demolition during excavation.
8) **Underwater excavation** This method provides additional horizontal support and reduces strain in the Boom clay, but it presents numerous challenges and safety concerns, while also significantly affecting the contractor's planning due to the different execution techniques to be used.
9) **Prestressing steel struts**: This cost-effective technique aims to minimize settlements during excavation steps, though its efficiency is limited and should be combined with other measures.

During the design, different countermeasures were 'in the running' for the final design, with changing boundary conditions, such as the planning of the contractor, final excavation depths, nearby loads, reduced settlements due to other activities, etc. changing the design continuously. The impact of the countermeasures on the reinforcement ratio in the diaphragm walls was also an important aspect.
In the final design, the overall most economical solutions, having the smallest impact on the planning of the contractor (and thus on the planning of the complete Oosterweel project) and requiring the least different design methods were implemented. This included increasing the thickness of the diaphragm walls, increasing the foundation depth of the diaphragm walls, and optionally prestressing the struts. At the moment of writing this paper it was finally decided not to use prestressed struts.

Diana

The deformation of the soil below the building will affect the building and potentially cause crack formation. To estimate the consequences of this deformation, a Diana model was created, as shown in Fig. 11 Diana Model with (left) imposed deformation and (right) expected crack formations. This model includes the transverse walls and the expansion joints, as these elements significantly influence the building's stiffness and the locations where cracks are likely to occur. A dummy layer beneath the building serves as support, and the calculated deformation from the Plaxis models is applied to this layer. The deformation is not directly imposed on the building to ensure that the soil does not exert direct pulling forces on it; instead, it allows the building to deform solely due to its self-weight. The material model used for modeling the masonry is the Total Strain Crack Model (TSCM), which can be used for brittle materials like stone, concrete and masonry. KULeuven did a separate analysis where the influence of the Engineering Masonry Model (EMM) and a hybrid model (EMM-TSCM)

 © DFI International Bruges 2025

was also checked, but the TSCM was ultimately used in the analysis, since this gave the most stable and logical results concerning crack widths and locations. The masonry tests performed by the KULeuven confirmed that the material-parameters used in the model align with the test results. The masonry test sample and results of the compression-strain diagram can be seen in
Fig. 10.

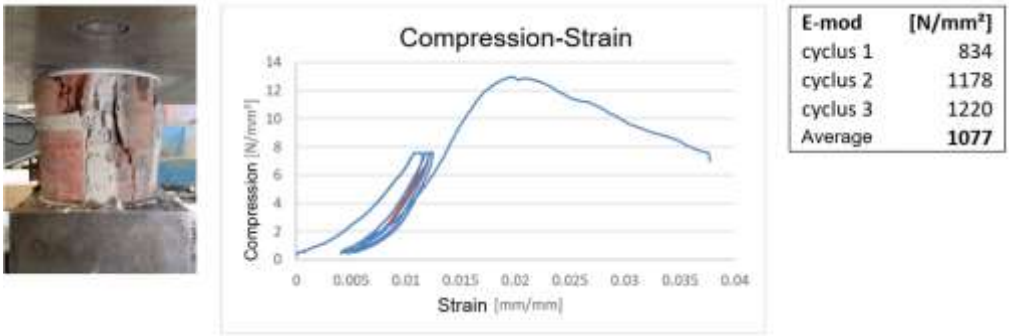


Fig. 10 Masonry test performed by KULeuven (left) test setup; (center) Compression-strain-diagram; (right) Test results E-modulus).

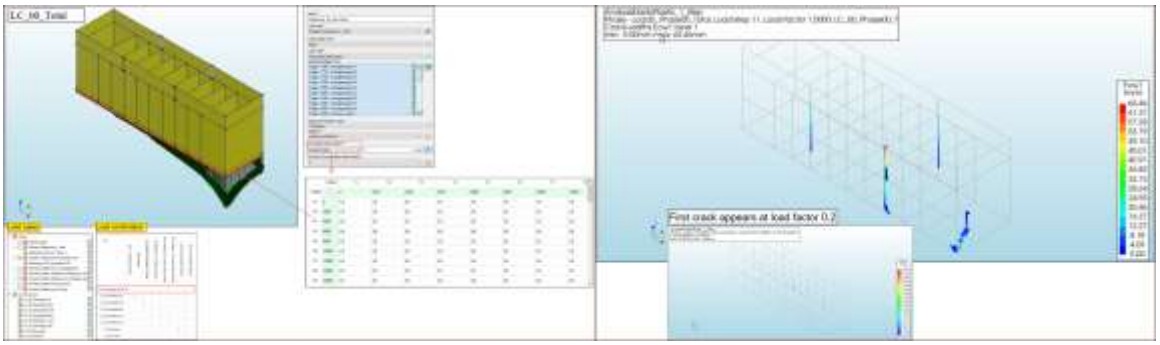


Fig. 11 Diana Model with (left) imposed deformation and (right) expected crack formations.

Results, monitoring and possible measures

According to the model results, significant cracks, approximately 65 mm in size, are anticipated beneath the expansion joints. However, quantifying the uncertainty of this prediction is challenging due to various assumptions regarding the impact of construction activities, soil and building deformation, and the masonry's behavior, each carrying its own uncertainties. Therefore, monitoring the settlements and crack widths is crucial.

To mitigate deformation during the demolition of the quay wall, the execution method for some activities was modified. For example, instead of creating a building pit and demolishing the entire quay, localized drilling was performed in the existing quay wall at the future diaphragm wall's location, depicted in Fig 2. The remaining quay will be demolished during the excavation between the diaphragm walls.

 © DFI International Bruges 2025

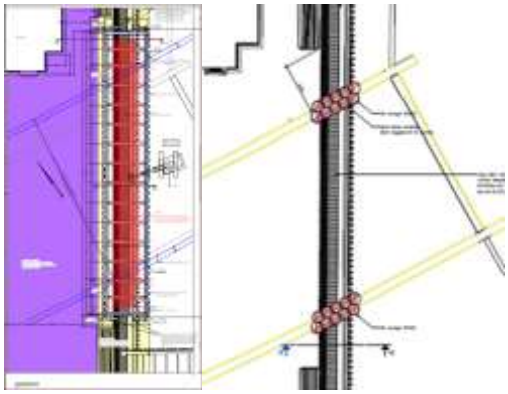


Fig. 12 Existing quay wall demolishing - Change of execution method (left) old method with building pit; (right) new method with locally drilling through the quay.

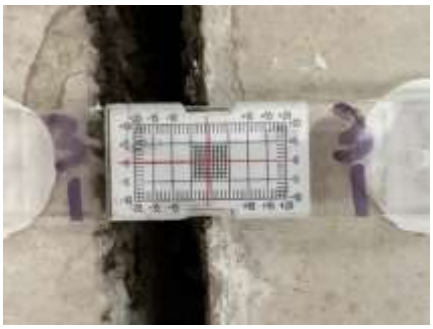


Fig. 13 Strip for measuring the joint deformation at the expansion joints on the top floors.

As of the writing of this paper, construction activities around the building have commenced. Given the uncertainties and the gradual nature of the deformations expected over several years, Lantis and Rinkoniên have chosen to minimize deformations within the design without implementing large preventive measures at this stage. Continuous monitoring of the building's state will occur throughout the construction period. This includes tracking deformations, vibrations, and crack widths at critical locations (with strips comparable to the strips shown in Fig. 13). These results will be used to refine models or determine necessary interventions. If significant deformations or cracks arise, potential remedial actions include repairing cracks, placing steel rebar in joints to distribute cracks over a larger area, or using compensation grouting to counteract building deformation by injecting grout under high pressure to lift the building back to its original position. The latter two are depicted in Fig. 14.

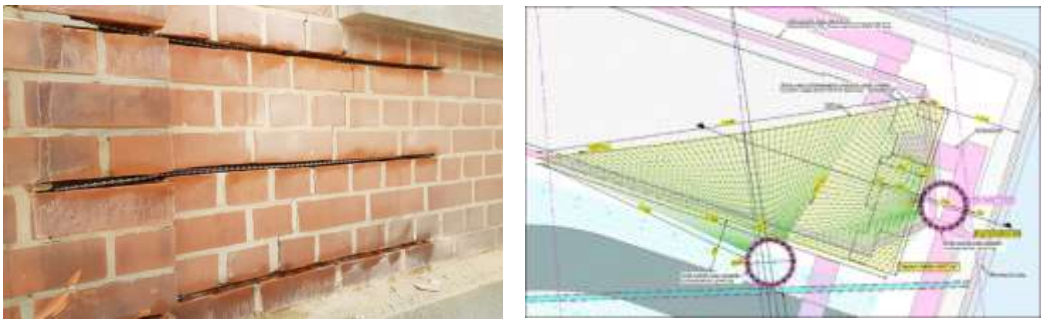


Fig. 14 Possible mitigating measures: (left) providing rebar in the masonry joint; (right) compensation grouting below the building foundation).

 © DFI International Bruges 2025

SUMMARY AND CONCLUSIONS

The Samga building (Samga Silo A) is situated in a critical area due to the ongoing construction activities for the Oosterweel Link. Given its historical and protected status, Lantis and Rinkoniên conducted various tests and utilized Plaxis and Diana models to assess the impact of these activities on the building's stability. The models predict potential settlement and crack formation in the Samga building, and the effectiveness of various countermeasures was evaluated. Efforts were made to adapt the design and execution methods to minimize deformation. Continuous monitoring of the building will occur over the coming years during the Oosterweel Link construction, focusing on deformation, vibrations, and cracks. This monitoring will inform management strategies and necessary repairs or counteractions if significant damage occurs.

ACKNOWLEDGEMENTS

We like to acknowledge Rinkoniên and Lantis for making the design of the Oosterweel link possible and giving permission to publish these results. We would also like to acknowledge KULeuven for assistance with the Diana-model and performing the masonry-tests.

REFERENCES

Couck, J., Van Royen, K, Janssens, B., de Nijs, R., Van Lysebetten, G. 2015. Proefcampagne voor de Oosterweelverbinding in Antwerpen. Geotechniek 2015, Special Geotechniekdag 10-19

Rombauts, B., Vandemeulebroecke, S. 2023. Invloed werkzaamheden Oosterweelverbinding op Samga silo A. OWRA-02796-LAN-NOT-W66-000001 110p.

Vanhaekendover, H., Van Es, T., Van Zegbroeck, B., Kiekens, A., Van Riel, W. 2021. Analyse triaxiaalproeven pq-analyse – tertiaire lagen. OWRO-00ALG-LAN-RAP-W65-000002 38 p.

Van Zegbroeck, B., Van Riel, W., Kiekens, A., Janssens, B. 2021. Aangaande de modellering van de Boomse klei, notitie expertencollege i.v.m. modellering van de klei voor grond en waterkerende constructies overheen de hele Oosterweel verbinding. OWRO-00ALG-LAN-NOT-W65-000001 59 p.

Verachtert, R., Deblauwe, B., Paul, M. 2024. EWP2 gestapelde tunnel rekennota dwarssnede G05. OWRA-05982-RNK-REK-W60-000003 547 p.

Verstrynge,E. Katholieke Universiteit Leuven, Departement Burgerlijke Bouwkunde, Laboratorium Reyntjens, PV 31765/22 – deel A Numerieke studie van het zettingsgedrag van een historisch industrieel metselwerkgebouw (SAMGA site, Antwerpen)

Vrijdaghs R. Verstrynge,E. Katholieke Universiteit Leuven, Departement Burgerlijke Bouwkunde, Laboratorium Reyntjens, PV 31765/22 – deel B Experimentele studie van het metselwerk van een historisch industrieel gebouw (SAMGA site, Antwerpen)

 © DFI International Bruges 2025

Elephant and Castle Town Centre Development - Engineering within the Harwich Formation in close proximity to tunnels

Tony P. Suckling, A-squared Studio Engineers Ltd, London, United Kingdom,
+44(0)2076202868, contact@a2-studio.com
Sajjad R. Peima, A-squared Studio Engineers Ltd, London, United Kingdom,
+44(0)2076202868, contact@a2-studio.com

ABSTRACT

The excavation for the new ticket hall is above the London Underground Ltd (Transport for London TfL) Bakerloo Line tunnels and comprises up to ~18m of excavation to form the basement and associated transfer beams of the eastern half of the new Integrated Ticket Hall. The Harwich Formation layer is approximately 8m below the general basement formation level (and ~5m below the transfer beam trench formation) and is known to be water bearing due to its coarse-grained nature and therefore of high permeability. The project team had to assess the basement formation stability in this area, which is founded within the London Clay but is subject to the hydrostatic uplift pressures from the Harwich Formation below. Satisfying the EC7 UPL requirements would not limit movement induced damage to the underlying tunnels. Any technical solution had to also consider the difficult site logistics.

Keywords: Harwich Formation, UPL, Ground Movement Assessment

INTRODUCTION

The authors have worked on the Elephant and Castle Town Centre Development from 2021 until 2024, employed by A.J Morrisroe & Sons (Morrisroe). The project involves the redevelopment of the Elephant & Castle Shopping Centre in the London Borough of Southwark. Elephant and Castle has been an important junction into London since Roman times. The Old Kent Road and Newington Causeway, two of the main roads which converge at the Elephant, generally follow the path of two Roman routes; Watling Street and Stane Street, which led into Londinium towards an early incarnation of London Bridge. Bombing destroyed much of the area during the Second World War. As part of the post war redevelopment in the 1960s the Elephant and Castle shopping centre was built, the first of its kind in Europe. The shopping centre, along with the elephant statue which stood outside, was one of the neighbourhood's defining landmarks for many decades. It was demolished after ~60 years as part of this development in 2021.

The site has an area of approximately 1.8 hectares. Adjacent to the site is a railway brick viaduct, Elephant and Castle railway station, Elephant and Castle underground station, and heavily trafficked roads including purportedly the busiest roundabout in London. The existing centre is being replaced by a new shopping centre, including three residential towers ranging from 20- storeys to 32storeys (inclusive of 4 storeys of podium) to provide ~1000 new homes, and a 12-storey University of Arts building. Car parking will be provided in a two-level basement. Part of the development includes a new five-level excavation which will form a new Integrated Ticket Hall (ITH) that will be adopted by Transport for London / London Underground Ltd (LUL).

The site before demolition in 2021 is shown in Fig. 1 and the final development is illustrated in Fig. 2.

 © DFI International Bruges 2025



Fig. 1. Site Before Demolition



Fig. 2. Illustration of the Project within a Wider Redevelopment (highlighted by the red circle)

There were many geotechnical hazards associated with the works on this project. This paper will describe one of these hazards which was associated with the excavation stability of six large reinforced concrete 3m deep transfer beams to support part of the ITH and the above ground University of Arts building. The excavation in this particular area is above the LUL Bakerloo Line tunnels and comprises ~18m of excavation to form the three level basement and associated transfer beams of the eastern half of the new ITH. The Harwich Formation layer is ~8m below the general basement formation level in this area (and hence ~5m below the transfer beam trench formation).

The slab level of the ITH on the eastern side is -10.65mOD with the crown of the Bakerloo Line tunnel (which varies in diameter due to a cross-over) being, at its shallowest depth, at -15.25mOD. The invert level of the tunnels is at around -21.5mOD. The six transfer beams are supported to the east by a contiguous piled wall, and to the west by a secant piled wall which also enabled excavation of the five level basement outside of the tunnel exclusion zone. The general arrangement in this area is illustrated in Fig. 3.

 © DFI International Bruges 2025

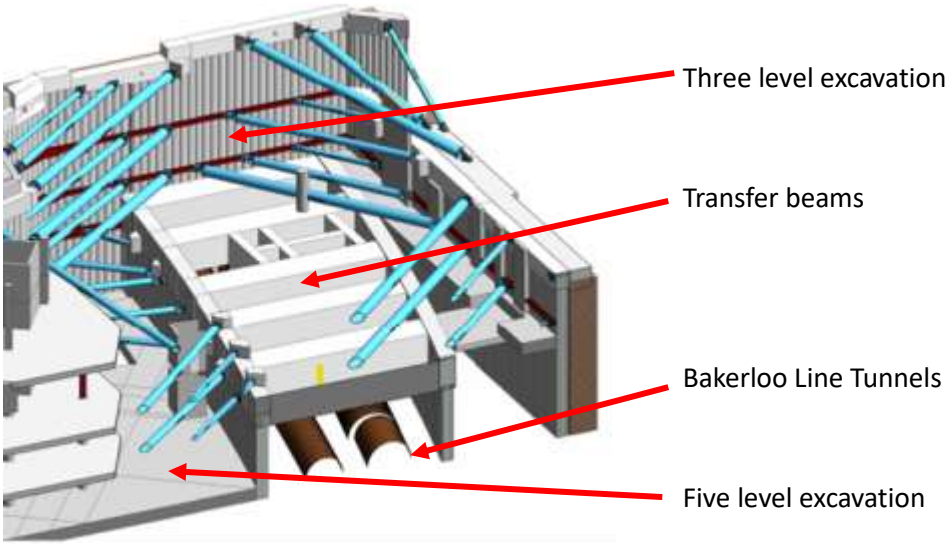


Fig. 3. 3D Illustration of the Transfer Beams to be Excavated over the Bakerloo Line Tunnels

GROUND CONDITIONS

Two phases of ground investigation were undertaken on the site during 2018 and 2019 under the supervision of Principal Designer WSP UK Ltd. The geological sequence encountered can be summarised as:

Made Ground of variable thickness; overlying,
River Terrace Deposits; overlying,
London Clay and Harwich Formation; overlying,
Lambeth Group Formation; overlying,
Thanet Sand Formation; overlying,
Chalk.

Figure 4 reproduces the ground model produced by WSP in their Ground Investigation Report;

Table 4 – Summary of the Geological Profile on Site (Phase 1&2 and BGS logs on-site)*

Stratum	Elevation of Upper Surface (mOD)	Average Upper Elevation (mOD)	Typical range of thickness (m)	Average Thickness (m)
Hardstanding and Made Ground, MG	+3.7 to -4.4*	+0.8*	0.8 to 3.9	2.0
Alluvium, Al	+2.1 to -0.3	+1.0	0.1 to 1.4	1.0
River Terrace Deposits, RTD	+1.3 to -1.0	-0.0	1.7 to 7.0	3.7
London Clay, LC	-2.2 to -6.9	-3.9	14.9 to 17.8	16.2
Harwich Formation	-18.1 to -21.8	-19.8	0.5 to 3.0	1.6
Lambeth Group - Clay	-19.2 to -23.3	-21.4	11.0 to 12.6	11.6
Lambeth Group - Sand	-31.0 to -34.4	-33.2	5.3 to 6.8	5.9
Thanet Sands	-37.5 to -39.9	-38.9	7.7 to 12.0*	9.8
Chalk	-47.2 to -50.9	-48.5	NP	NP

* Concept Phases 1 & 2 (Table 1); BGS logs on-site: TQ37NW 1783, TQ37NW 799, TQ37NW 796, TQ37NW 800.

Fig. 4. Ground Model (reproduced from WSP GIR)

 © DFI International Bruges 2025

A detailed review of the individual boreholes indicated that the Harwich Formation varied in thickness across the site footprint but was also not encountered in some boreholes. A review of the arisings from the well borings in the vicinity of the ITH where the transfer beams were to be excavated confirmed its presence.

A pumping test undertaken on the site in 2021 indicated that the Harwich Formation had the expected high horizontal permeability.

HARWICH FORMATION

The Harwich Formation is part of the Thames Group and underlies the London Clay Formation, also overlying the Lambeth Group. It is normally encountered as a layer of thickness <1m up to 5m. The Harwich Formation comprises three distinct different members each with different characteristics; Swanscombe Member, Oldhaven Member and the Blackheath Member. This project site is underlain by the Blackheath Member.

The Blackheath Member normally comprises flint gravel in a sandy matrix with lenses of sand and thin clay bands. Local shell-rich beds can be present. A typical example is shown in Fig. 5.



Fig. 5. Typical Example of the Blackheath Member (not from this project site)

The Harwich Formation has long been of concern to engineers and particularly to tunnellers, and is generally associated with the following geotechnical risks; variable deposits, irregular cementation, high permeability, raised groundwater pressure and poor stability.

ANALYSES AND TECHNICAL RECOMMENDATIONS

Morrisroe had previously excavated elsewhere on the site down to a similar depth within the London Clay as would be required for the transfer beams. An uplift verification (UPL) in accordance with BS EN 1997 indicated that a suitable factor of safety would be present for the excavation stability. However, as described below, it was found that the excavations for the transfer beams would likely cause movement induced damage to the underlying tunnels without additional measures.

With the slab level of the ITH on the eastern side being -10.65mOD this meant that the underside of the slab excavation was at -11.25mOD and the underside of the transfer beam excavations was at -14.25mOD. This can be compared with the crown of the Bakerloo Line tunnel being in this area at -15.25mOD and the top of the Harwich Formation being at -19.4mOD.

 © DFI International Bruges 2025

It is important to note that the secant pile walls either side of the tunnels penetrated through the Harwich Formation into the underlying Lambeth Group (clay). However the secant pile walls that crossed over the tunnels to the north and south founded ~1m above the crown of the tunnels within the overlying London Clay. Thus the Harwich Formation was in global hydraulic continuity outside the site to the north and to the south of the ITH station box. This meant that the presence of a deep filled hollow feature near to the site would likely have had a hydraulic connection continuously replenishing the Harwich Formation with groundwater.

A detailed review of the well borings indicated that the Harwich Formation stratum on site represents a less common lateral development of the Blackheath Member composed mostly of sand. This historically has been logged as part of the Lambeth Group or confused with the Oldhaven Member (J. Edgar pers. comm; article in prep.). The average thickness recorded in this area was >1m and can generally be described as a grey slightly silty fine to medium SAND with occasional lignite fragments/debris, dispersed shells/shell fragments and locally rare black rounded fine-coarse flint gravel at the base. This can be seen in Fig. 6.

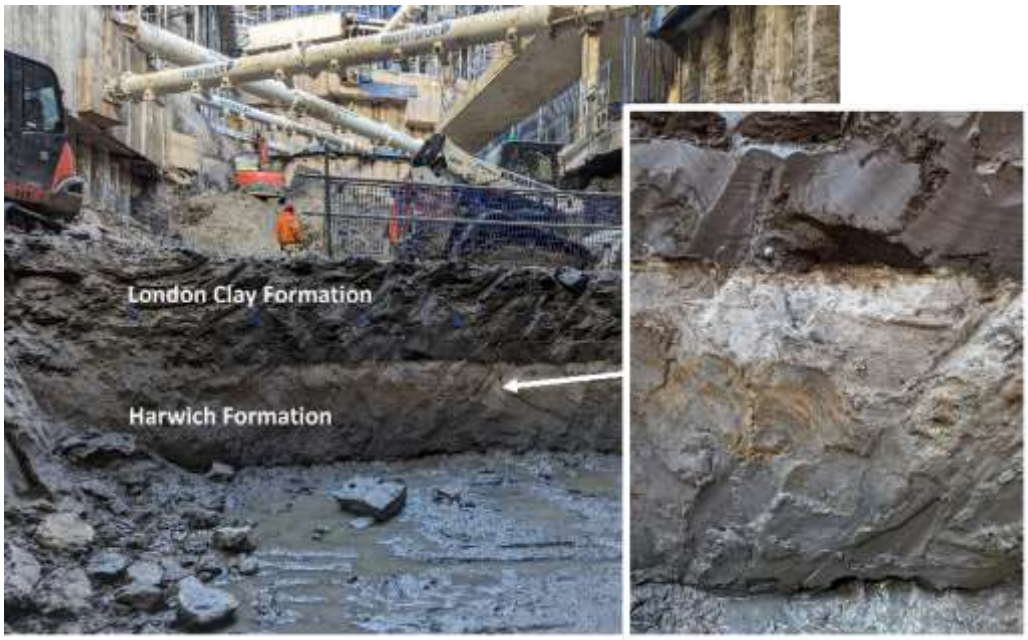


Fig. 6. Exposure of the Harwich Formation during the Excavation of the Western Side of the ITH

In addition, the construction of the Bakerloo Line tunnels and associated station in the late 19th century and early 20th century may have disturbed the London Clay around these assets and there are no available records how the groundwater within the Harwich Formation was controlled during their construction.

During the excavation of the transfer beams the upward groundwater pressure within the Harwich Formation acting on to the underside of the London Clay is resisted by the vertical total stress exerted by the mass of the London Clay block above. In addition, frictional stresses will exist between the London Clay block and the piled walls along the perimeter and these will also contribute to the vertical resistance to uplift. From a global equilibrium perspective, the excavation formation will become unstable should the total force exerted on the underside of the London Clay block exceed the sum of the block's total weight + frictional resistance at the sides.

In February 2023 the first well boring was installed to determine the specific level of, and the real groundwater pressure within, the Harwich Formation. This borehole found the Harwich Formation at a level of -19.4mOD and the groundwater was found to rise immediately to -6mOD. The water level

 © DFI International Bruges 2025

then subsequently rose over the following days and was observed to be at -4mOD 7 days later implying an actual pressure of around 154kPa at the London Clay/Harwich Formation interface.

A three-dimensional soil-structure interaction simulation was then undertaken, using Plaxis 3D, which included the LUL Bakerloo Line tunnels, the piled walls either side and to the ends of the eastern ITH box and a representative zone surrounding them. The model encompassed a zone of approximately 65m x 70m in plan and contained approximately 70,000 10-node tetrahedral elements (soil volume). Two-dimensional plates were used to model thin shell-like structures, i.e. tunnel linings and embedded retaining walls. Plates are composed of 6-node triangular, linear elastic elements and were modelled with a low stiffness so that the ground movement predictions in this Ground Movement Analysis (GMA) did not rely on constraints by the tunnel linings. The analysis replicated the proposed sequence that the six transfer beams would be excavated and constructed in pairs, and that those pairs were sequenced such that the distance between excavations is maximised. A selected 3D model illustration is provided in Figure 7.

The results of the analyses can be summarised as;

- A much higher factor of safety of 2 on uplift was required to limit the uplift of the tunnels to the accepted magnitude that would not cause damage to them. This factor of safety was based on a conventional calculation but calibrated to the vertical uplift movement predicted by the 3D model.
- The groundwater head in the area of the eastern ITH box within the Harwich Formation needed to be reduced to around -10mOD in order to achieve this stability factor of safety of 2. This equated to reducing the groundwater pressure within the Harwich Formation from 154kPa to 100kPa.

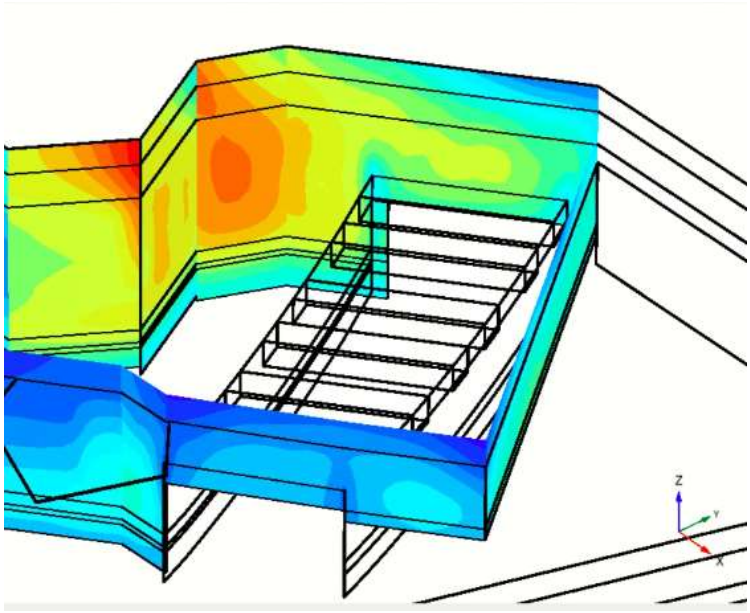


Fig. 7. View of part of the 3D model

APPLICATION ON SITE

The technical recommendations were adopted by the project team and the following additional measures were implemented on site by Morrisroe:

- 6no wells installed to de-pressurise the Harwich Formation and to log the arisings by a geologist

 © DFI International Bruges 2025

- Submersible pumps running 24 hours 7 days per week
- Constant checking of pumping system (plus competent persons on 1 hour call out)
- 4no back up pumps on site (assuming all 6no pumps within the wells would not all fail at once)
- Back up generator on site
- Increased monitoring of the tunnels and the alert/response system upgraded
- Inspection of the transfer beam subgrade by a competent person
- Reduced construction time using additional shifts to work 24 hours 7 days per week
- Ground improvement provision in place if required
- Arisings stored for emergency backfill if required.

The six transfer beams were successfully excavated and constructed. The de-pressurising of the groundwater within the Harwich Formation was successful during the required period until enough of the substructure and superstructure had been constructed to overcome any destabilising forces. On one occasion a pump failed and following the emergency preparedness plan this pump was extracted and replaced before any damage could occur. Monitoring of the tunnels indicated that the induced movements were within the predictions. Selected progress photographs are provided in Figures 8 to 12.

At the time of writing all structural below ground works have now been successfully completed, and the above ground structural works are near to completion.



Fig. 8. The Transfer Beams Could Only be Excavated from the Side, not from Above due to Propping.

 © DFI International Bruges 2025

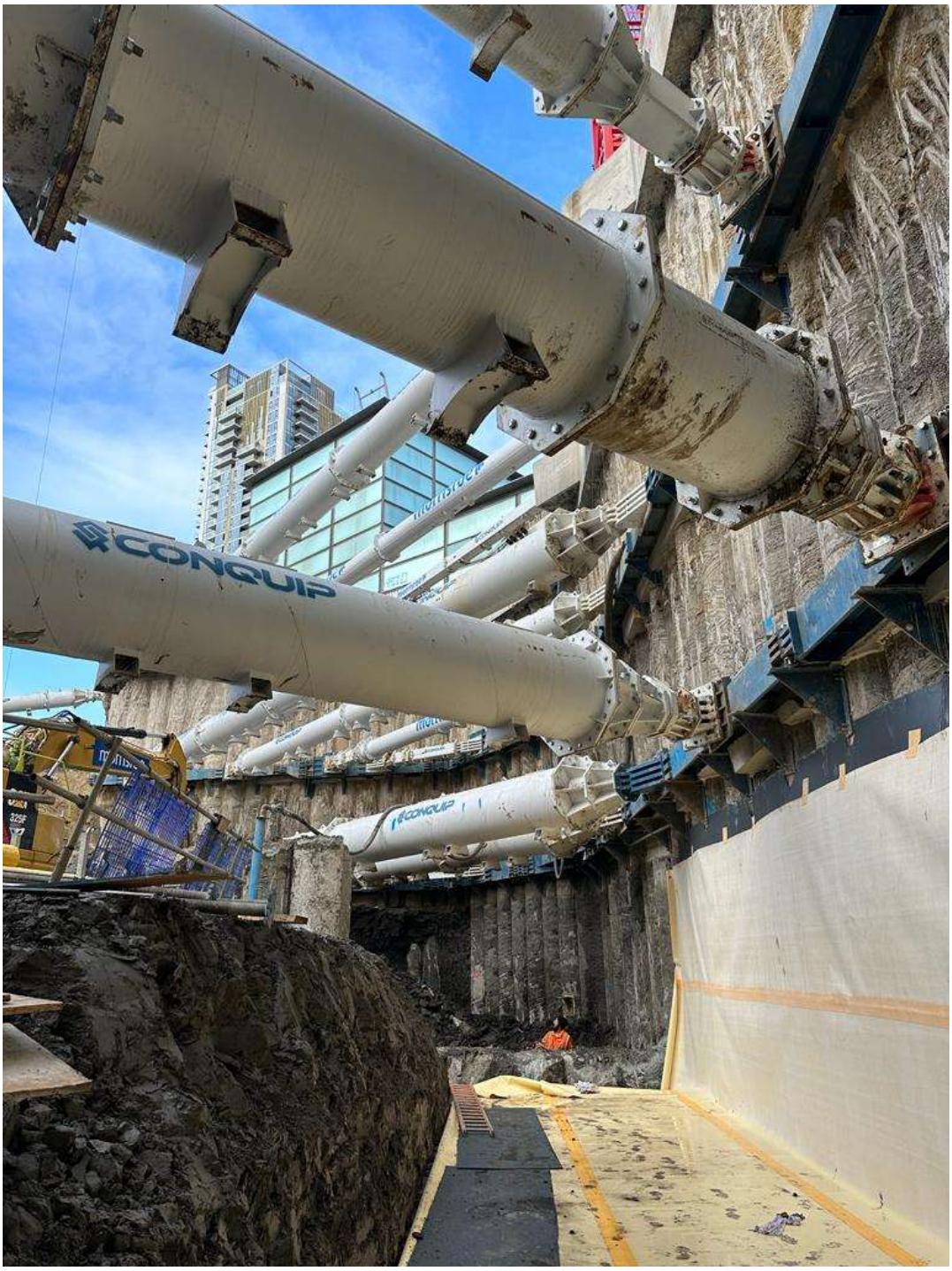


Fig. 9 Excavation of Transfer Beam Closest to Secant Pile Wall and Closest to Bakerloo Line Assets

 © DFI International Bruges 2025



Fig. 10. Inspection of Transfer Beam Subgrade



Fig. 11. Transfer Beam Reinforcement being Placed by Hand

 © DFI International Bruges 2025



Fig. 12. Removal of Spoil required Handling Several Times before Removal from the Work Area

SUMMARY AND CONCLUSIONS

There were many geotechnical hazards associated with the works on this project. One of these hazards was associated with the excavation stability of six large reinforced concrete 3m deep transfer beams. This example shows that satisfying the BS EN 1997 UPL requirements did not limit movement induced damage to the tunnels underlying the excavation. It was necessary to introduce additional measures so that a much higher factor of safety of 2 on uplift could be provided to limit the uplift of the tunnels to the accepted magnitude that would not cause damage to them. This meant that the groundwater head within the Harwich Formation needed to be reduced from 154kPa to 100kPa. Measured uplift movements within the Bakerloo Line Tunnels were comparable to the predictions from the Plaxis 3D model.

ACKNOWLEDGMENTS

The authors would like to acknowledge the collaboration and support we received from the project teams at A.J. Morrisroe & Sons Ltd, Multiplex Europe Ltd, WSP UK Ltd, Transport for London, and Dewatering Services Ltd. In particular the authors appreciate the significant contribution of Mark Wadsworth of A.J. Morrisroe & Sons Ltd and the expertise of Dr Justyna Edgar of A2 Site Investigation Ltd.

REFERENCES

The Harwich Formation in London – The legacy of Chris King, J. Skipper and J. Edgar, Proceedings of the Geologists' Association 131 (2020) 474–485

 © DFI International Bruges 2025

INNOVATIVE APPLICATIONS OF SHORING TECHNIQUES FOR DEEP EXCAVATION IN DOWNTOWN SAN FRANCISCO

Sam Yao, Ph.D., P.E.,
Senior Principal, Simpson Gumpertz & Heger, Oakland, CA, USA, +1 (510) 457-4452,
sxyao@sgh.com
M. Ali Naeem, P.E.,
Senior Technical Manager, Simpson Gumpertz & Heger, Houston, TX, USA, +1 (713) 265-6450,
manaeem@sgh.com

ABSTRACT

The Salesforce Tower is currently the tallest building in San Francisco CA, and the tower foundation construction involves the deepest excavation ever in downtown San Francisco. The foundation excavation utilized five shoring methods in three different construction stages:

- Cement deep soil mixing (CDSM) soldier pile shoring walls, with 4-levels strut-wale internal bracing in the Phase I excavation, which allows the excavation down to 66 ft (20m) below the street level.
- Twelve (12) reinforced jet grout shafts in the Phase II excavation that extends from the bottom of the Phase I excavation.
- A 137 ft (42 m) diameter secant pile ring as excavation shoring in Phase II excavation, which extends down from the bottom of the Phase I excavation and provides shoring for excavation to 95 ft (29 m) down from the street level.
- A three-level tieback system allows excavation in the Plaza area in Phase III of the project.

The presentation focuses on the use of innovative uses of several shoring techniques to meet significant challenges in the excavation under difficult circumstances, such as very tight shoring deflection limits for deep excavation in the dense urban area, risk of base heaving due to artesian pressures, risk of differential settlement in adjacent building due to the excavation, design of a new shoring system within a braced shoring that was already in place, interfacing with adjacent shoring system and ongoing construction, innovative uses of jet grouting and secant piles as shoring methods in complex soil conditions, and complex construction logistics with multiple construction trades interfacing with shoring and excavation. The innovative shoring design allows the complex and demanding deep excavation project to be successfully completed without a hitch.

Keywords: braced CDSM shoring, secant pile shoring ring, jet grout shoring ring, tieback shoring

INTRODUCTION

The Salesforce Tower is a 1,070 ft (326 m) tower in downtown San Francisco, California. The tower is part of the San Francisco Transbay redevelopment plan. The redevelopment plan is centered around the Salesforce Tower and the Transbay Transit Center (TTC) which accommodates high-speed rail transport. The Salesforce Tower is situated in a dense urban setting with the TTC directly adjacent to the south. Figure 1 shows the Salesforce Tower, TTC and their surroundings during excavation construction and on completion. The shoring system shared a Cement Deep Soil Mixing (CDSM) soldier pile wall with the adjacent TTC under construction (Fig. 2). The interactions between the Salesforce Tower excavation and TTC construction had been checked for each construction stage.

The Salesforce Tower is supported on cast-in-place load bearing elements (LBE) that were installed from the existing grade down to the bedrock. Excavation and shoring were required to construct the below grade. A braced shoring system was initially designed for Phase I excavation to a depth of 64 ft (20 m). Soon after installation of the shoring, concrete anomalies were identified in the top portion of LBEs. To repair the concrete anomalies, the Tower excavation had to be deepened from 64 ft (20 m)

 © DFI International Bruges 2025

to 95 ft (29 m) in Phase II excavation, which required a new shoring within an installed shoring. An innovative reinforced secant pile ring and jet grout rings were designed and constructed within the initial shoring in order to perform the Phase II excavation below the Phase I excavation. The final phase involved a tieback shoring system to excavate and build the below grade levels beneath the plaza. The three phases of the excavation construction are illustrated in Fig. 2.



Fig. 1: Salesforce Tower and TTC during excavation and on completion of construction

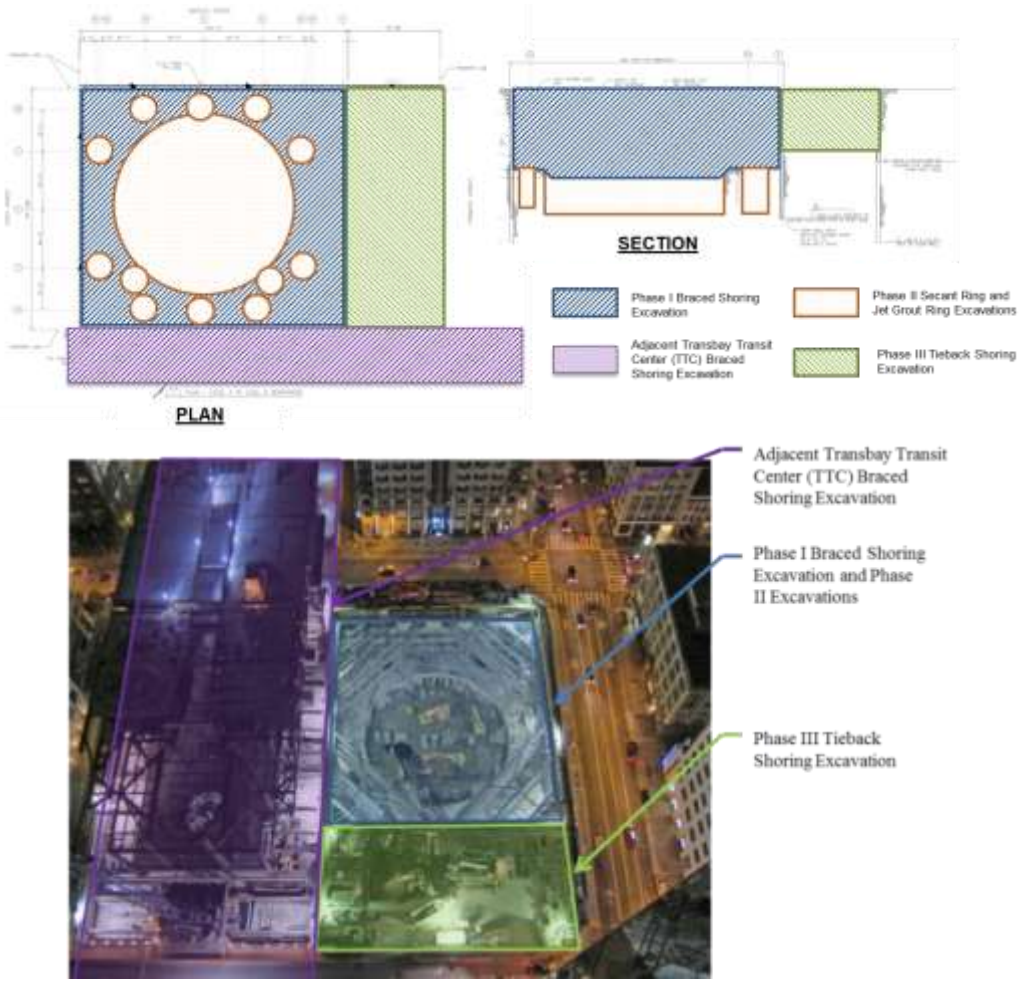


Fig. 2: Three interacting shoring systems: (top left) Schematic plan view, (top right) Schematic section view, (bottom) Aerial view

 © DFI International Bruges 2025

PHASE I BRACED SHORING EXCAVATION

The Tower excavation measured 205 ft (62 m) by 184 ft (56 m). The perimeter shoring wall consisted of Cement Deep Soil Mixing (CDSM) columns with soldier piles placed every 4 ft (1.2 m). Three exterior perimeter walls were constructed on the east, north and west sides. The soldier pile length varies between 98 ft (30 m) and 110 ft (34 m) while the CDSM wall extends deeper to effectively create a cut-off wall. An interior perimeter CDSM wall was also constructed to allow excavation and build-out of the tower while the plaza remained unexcavated and available for staging. A triple auger soil mixing rig was used to build the soil mixed columns and a support crane with a vibratory hammer was used to "wet set" the soldier pile reinforcement to depth. Additional loads considered in the design included seismic and surcharge loads from construction and traffic.

On the south side, the shoring system braced against the TTC excavation, which was also a CDSM solider pile with 4-levels internal bracings shoring system. The TTC site was to be excavated, and the below-ground structure was to be constructed simultaneously with the Tower excavation and with a shared shoring wall. To minimize construction risks and avoid overstressing the shared shoring wall, the Tower shoring level elevations were carefully selected to allow build-out of the below grade levels while being within 3 ft (0.9 m) vertically offset from the adjacent TTC shoring levels. Figure 3 shows an elevation of the shared wall with strut elevations from both excavations.

At the onset of the Salesforce Tower shoring design, it was expected that the adjacent TTC struts would be in place when the Tower excavation proceeds. Due to project delays, the TTC excavation was at an advanced build-out stage with final floors being built and temporary struts being removed. The Tower shoring system and shared wall design had to account for numerous TTC build-out stages. Figure 4 shows the 3-dimensional finite element analysis model used to evaluate the shoring system and shared shoring wall for their interaction with the various TTC build-out stages.

The Tower bracing system consists of four bracing levels with walers and diagonal struts. The 40 in. (1 m) deep walers, distributed the lateral pressures from the soldier piles to the struts. The 36 in. (0.9 m) diameter diagonal struts were installed and pre-loaded to minimize wall deflections. The struts framing into the shared south wall had to be jacked to a higher pre-load (about 80% of design load) to resist the TTC shoring forces. Struts were also braced by pin piles and secondary bracing. The strut installation and pre-load forces were closely monitored in the field to minimize wall deflections without overstressing the shoring system. The wall was observed to move back 0.1 in. to 0.5 in. (2.5 mm to 13 mm) due to strut pre-loading. Levels B-D were installed with grout packing whereas Level A was installed with a longer steel pack. The longer packing between the CDSM wall and the waler at Level A allowed construction of the permanent wall without removing or re-bracing the Level A shoring system. The packing at the shared south wall was replaced with a sliding bearing to prevent in-plane wall forces and adverse impact on the TTC construction.

The braced shoring was installed by first excavating below the strut level, installing the walers and struts and finally pre-loading the struts. This sequence was repeated for all four shoring levels. For the build-out sequence, the permanent floors below strut levels B-D were built before removing the struts. Level A was installed with a gap between the CDSM wall and the waler to allow the permanent wall to be cast without removing the shoring system. The Level A struts were removed after the ground level slab was built. The entire internal bracing installation was installed under a very stringent schedule using two off hauling locations (the plaza and a trestle on the other side of the excavation).

The shoring system had to meet stringent deflection limits due to the proximity and impact of the excavation on adjacent structures. The shoring deflections were monitored with inclinometers and conventional surveys on a weekly basis. Figure 5 plots the deflection measurements in this project in comparison with shoring deflections reported in publications over decades (Peck 1969, Goldberg 1976, Clough et al. 1990). The shoring deflections in this project were at or below the lower bound of the shoring deflections among many past projects. In this project, modern shoring technologies

 © DFI International Bruges 2025

undoubtedly provided much stiffer lateral responses than the published data in the past shoring projects.

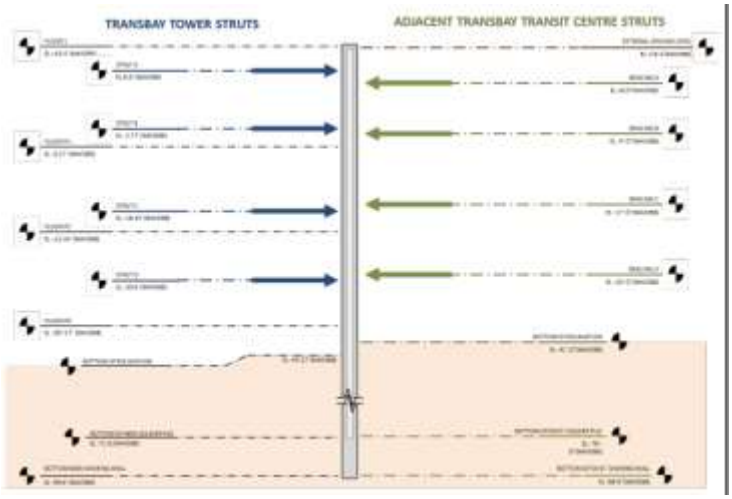


Fig. 3: Interaction of two braced shoring system sharing a common shoring wall

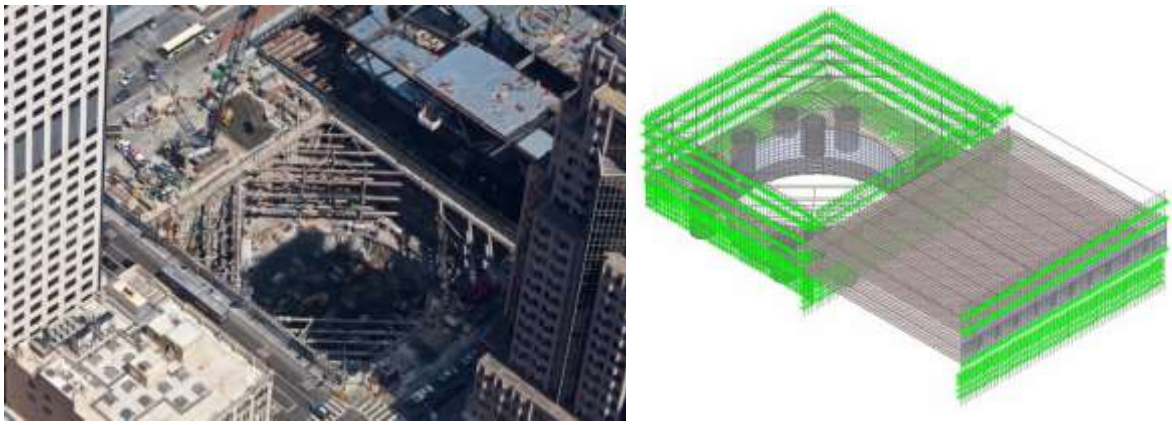


Fig. 4: Phase I & II excavation and finite element analysis model to simulate construction of Salesforce Tower and Transbay Transit Center at different stages

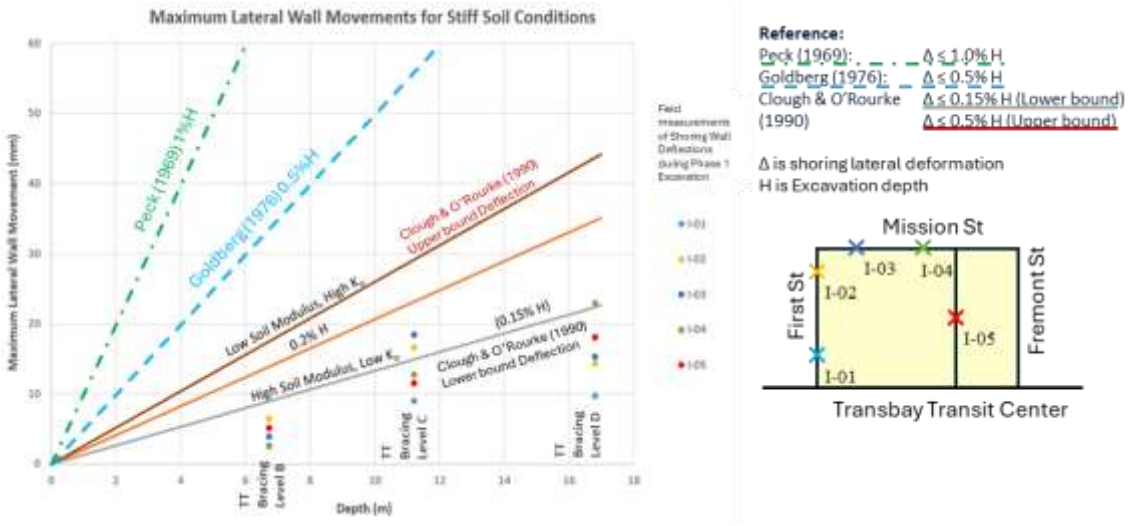


Fig. 5: Shoring deformation during Phase I Excavation of Salesforce Tower compared against commonly accepted practice guidelines

 © DFI International Bruges 2025

PHASE II EXCAVATION

The Salesforce Tower is supported on forty-two (42) reinforced concrete load bearing elements (LBE). Each LBE is 5 ft by 10 ft (1.5 m by 3.1 m) in size and extends approximately 270 ft (82 m) down to a socket in bedrock. Figure 6 shows the tower foundation and LBE layout. Soon after the Phase 1 shoring system was being installed, crosshole sonic loggings identified concrete anomalies in the top portion of the LBEs. Figure 7 illustrates the extent of the concrete anomalies in LBEs.

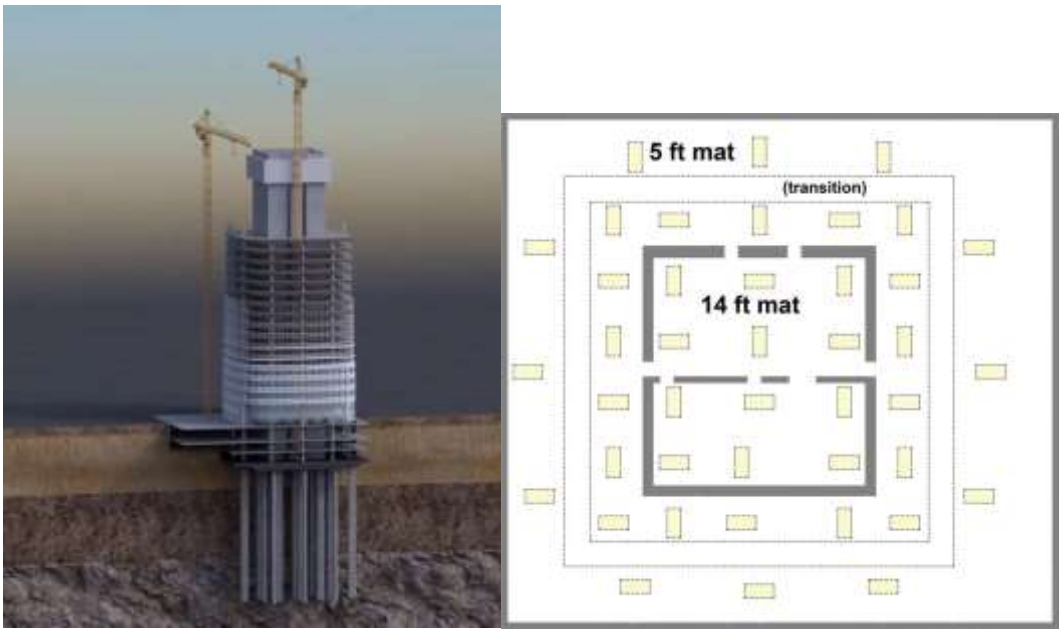


Fig. 6: Tower foundation and LBE layout



Fig. 7: Phase I & II excavation shoring and extent of concrete anomalies in LBEs

To inspect and, if needed, repair the concrete anomalies, further excavation in the range of 5 ft to 30 ft (1.5 m to 9 m) beyond the initial plan was required. The engineering challenge was to design a shoring system for deeper excavation within a shoring that had already been installed, while

 © DFI International Bruges 2025

maintaining ground stability and controlled ground movement in a dense urban area. The shoring systems were modeled in the finite element software PLAXIS 3D (See Figure 11). The analysis model was used to evaluate forces, deflections, and stresses on the various shoring systems due to their complex interaction. Furthermore, the interaction of the additional excavation on the shared wall and the adjacent TTC shoring system was analyzed in a combined 3D SAP2000 model (see Figure 4).

After several iterations of analysis and evaluation of multiple shoring design concepts using both PLAXIS 3D and SAP 2000 models, the final shoring design implemented a large secant pile ring with additional jet grout rings. This design was proven to be ideal for constructability, reliability, and rigidity against lateral deflections. The shoring design plan are shown in Fig. 8 and discussed below.

A secant pile ring was installed with a 137 ft (42 m) diameter and 50 ft (15.2 m) depth. The additional excavation within the central secant pile ring was 30 ft (9.1 m). The individual 4 ft (1.2 m) diameter secant piles were cast-in-place with 5000 psi (34.5 MPa) concrete and reinforcement in every alternate pile (secondary piles).

In areas located under the internal bracing, twelve local excavations and LBE repairs were completed using jet grout rings as the shoring system. To maximize the headroom available under the struts the jet grouting rings had to be installed before the fourth level of bracing was in place. Each jet grout ring was built using overlapping jet grout columns of 6 ft (1.8 m) diameter to create an 18.5 ft (5.6 m) diameter ring. The excavation within the jet grout rings ranged between 10 ft to 25 ft (3 m to 7.6 m). The jet grout column tip extended approximately 10 ft (3 m) below the bottom of the Phase I excavation. The lateral pressures on the jet grout rings and secant pile ring vary depending on the excavation depths and proximity to the perimeter CDSM walls. The lateral pressures on a typical jet grout shoring ring are shown in Fig. 9. The design calculations concluded that reinforcement was required due to this unbalanced loading on the shoring rings. Each jet grout column was reinforced with a 12 in (0.3 m) diameter steel pipe to resist vertical bending due to unbalanced loads. An extensive test program of the jet grout was performed before the jet grout production. Four test columns were installed with different jet grout parameters and then locally excavated to verify the actual column diameters. The target jet grout strength of 900 psi (6.2 MPa) was verified using a combination of wet grab samples and cores. Due to the tight schedule, three jet grouting drill rigs and two separate jet grouting set-ups (plants and high-pressure pumps) were used to build (241) jet grout columns.

After the completion of the jet grouting rings, the equipment was removed, the fourth level of bracing was installed, and the entire excavation was lowered another 10 ft (3m). A guide wall was then installed for the secant piles installation and a floor of crane mats was placed throughout the remainder of the site. During this time, a 40 ft tall concrete placement boom was installed in the center of excavation. Then the drills for the secant piles were lowered into the excavation. There were three large piling drills to install the 181 secant piles. At peak time there were 11 major pieces of equipment simultaneously in operation within the excavation site. Some of the main logistical challenges on the project were the space constraints and the low headroom. All secant piles successfully passed the Crosshole Sonic Logging (CSL) tests to verify concrete integrity.

A 24 in. thick reinforced concrete mat slab was built at the interface of the planned Tower excavation and the additional local shoring systems. This slab was designed as a diaphragm to tie the secant pile ring and the jet grout rings together and provide stiff support to the CDSM perimeter shoring walls. Once the excavation proceeded down to 66 ft (20 m) below the grade, the slab was constructed to tie the secant pile rings and jet grout rings together before the additional excavation started below the slab.

The geotechnical investigation identified a thin sand seem layer of 5 to 20 ft (1.5 to 6.1 m) in thickness between the Old Bay Clay stratum and the Valley Deposits (Fig. 10). The sand layer is hydraulically connected to the ground water up to 200 ft (46 m) above the layer. The initial design check showed the factors of safety against hydrostatic uplift within the excavation area would be less than 1.0, implying

 © DFI International Bruges 2025

the bottom of the excavation will be unstable against a base heave failure. Base heave of an excavation occurs when the weight of the block of soil behind the excavation support wall displaces the soil at the base of the excavation inside the excavation support wall. This results in a bearing capacity failure of the underlying soil and heaving of the bottom of the excavation.

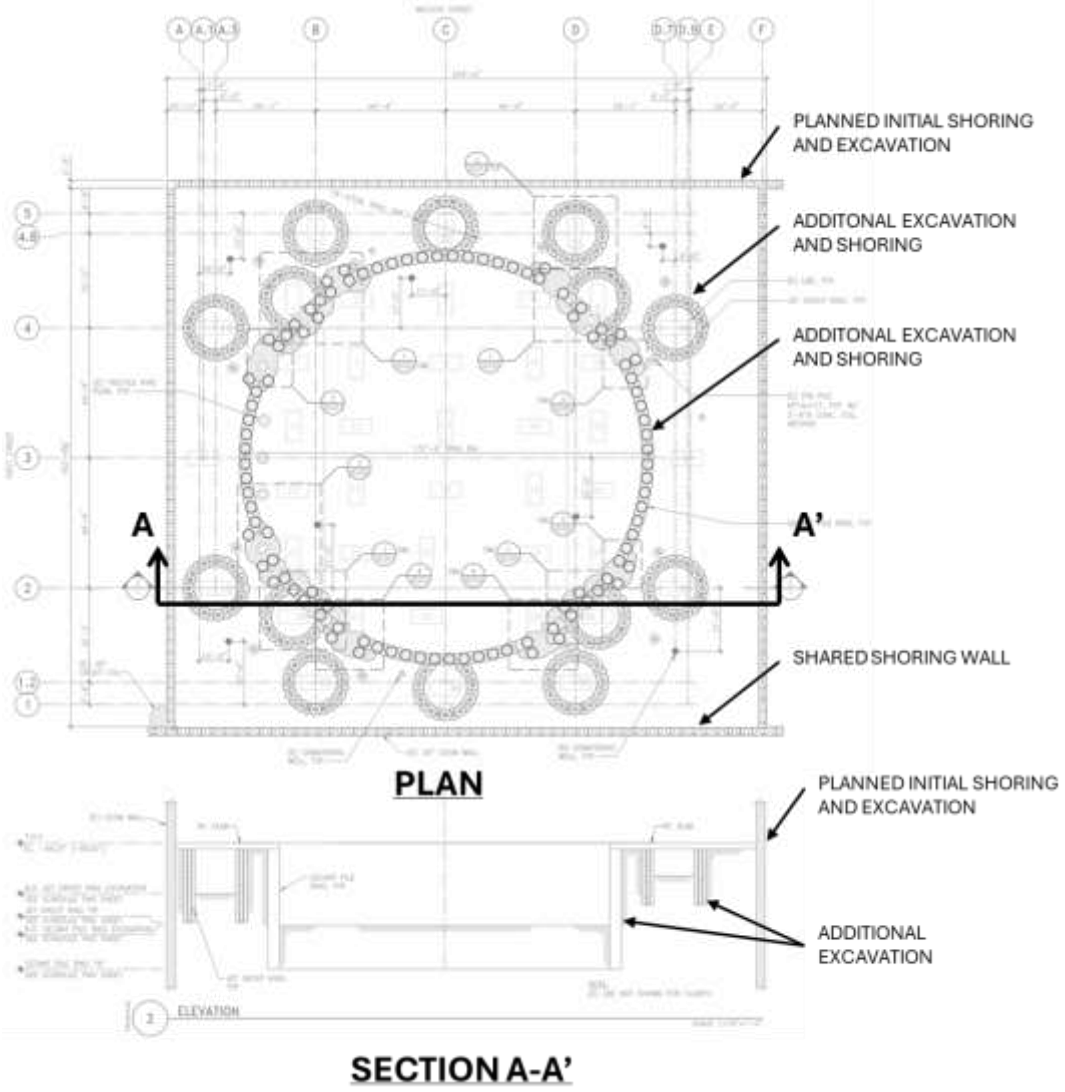


Fig. 8: Shoring system for deeper excavation within the installed shoring

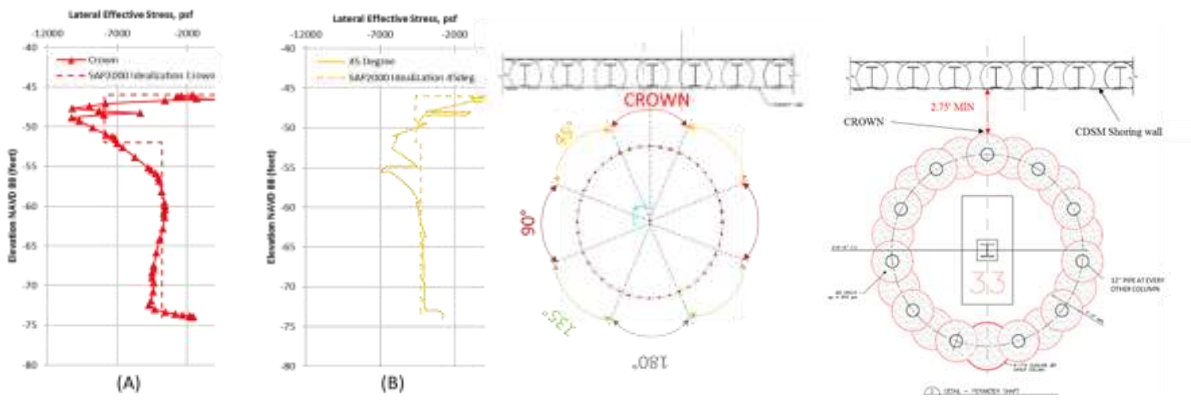


Fig. 9: A typical jet grout shoring ring and lateral pressure plots from finite element analysis

 © DFI International Bruges 2025

Further engineering evaluation was performed to account for the "stitching" effect of the LBEs, i.e., the LBEs with rock socks in Franciscan Formation act as tension piles to hold down the clay soil mass above the sand layer, as illustrated in Fig. 10. The 3-dimensional PLAXIS analysis and SLIDE analysis with consideration of the LBEs were performed to evaluate the excavation base stability. The soil profile contains a layer of free draining sand and gravel that is overlaid by clayey soils. The depth of this free draining layer is 140 ft to 200 ft (42.6 m to 61 m) below the ground level. Base heave due to the additional excavation is resisted by shear in the soil plug and tension in the LBEs. The analysis including effects of the LBEs concluded that the factor of safety against base heave increases to greater than 1.5. Figure 11 shows the analysis results.

A deep settlement marker system (Sondex system) was installed at the center of the excavation area. The settlement or heave readings were recorded daily during the excavation. The field measurements indicated no measurable base heave, primarily due to the beneficial stitching effects of the LBSEs.

Figure 12 shows repair of LBEs in the Phase II excavation to 95 ft (29 m) below the grade and within the secant pile ring. Figure 13 shows the inclinometer reading of the shoring wall throughout the excavation, indicating the maximum lateral defections were within the allowable limit of 1.5 in (3.8 cm). There was no damage or reported adverse effects to the adjacent structures and roadways during the excavation and backfilling.

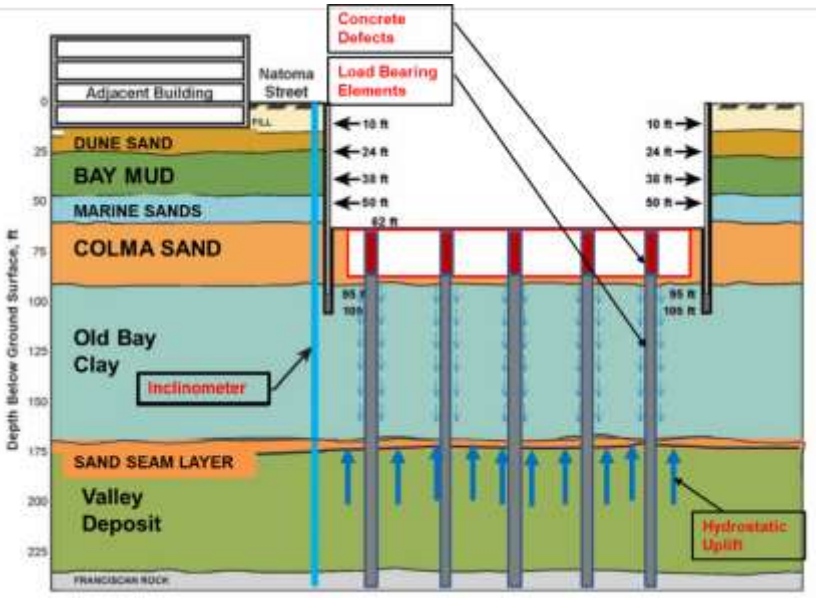


Fig. 10: Hydrostatic uplift and excavation base stability

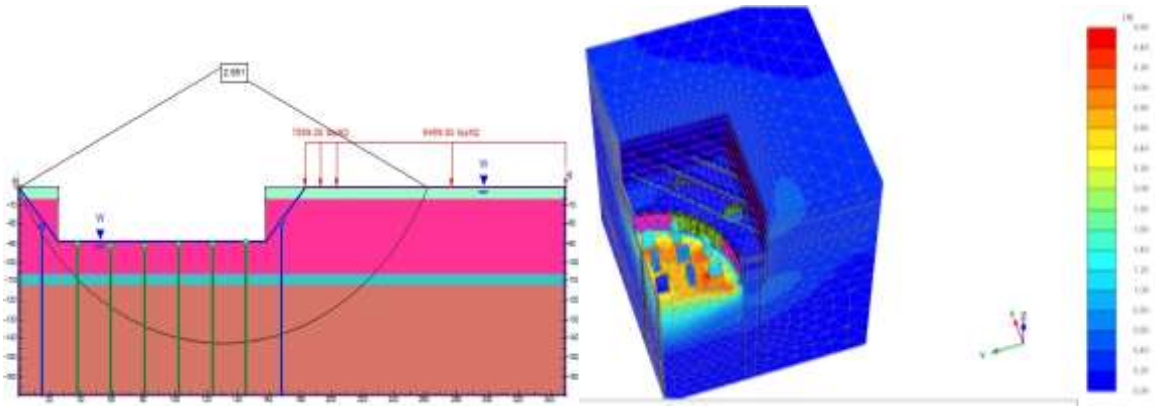


Fig. 11: Evaluation of excavation base stability using Plaxis 3D

 © DFI International Bruges 2025



Fig. 12: Repair of LBEs within the secant pile ring

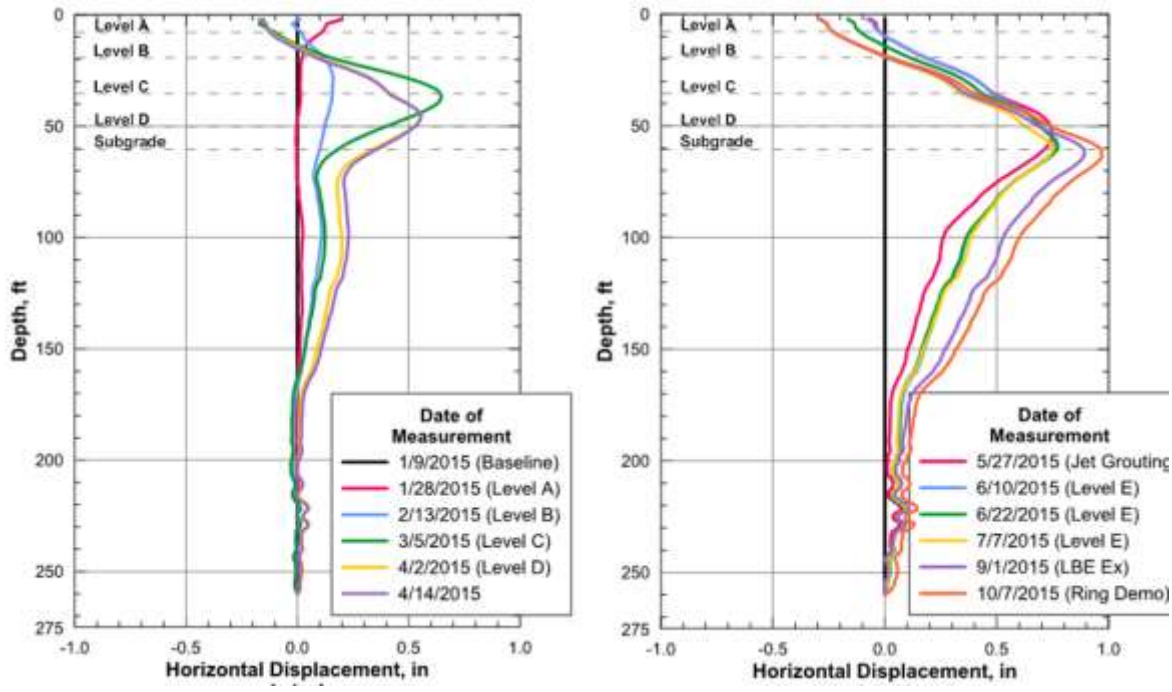


Fig. 13: Inclinometer readings of lateral deflections of shoring during Phase I & II excavation

PHASE III TIEBACK SHORING EXCAVATION

The plaza shoring is located to the East of the Tower excavation and footprint. The plaza is separated from the main excavation with an intermediate CDSM soldier pile wall. The plaza excavation is 74 ft (22.6 m) wide by 184 ft long (56 m) and 43 ft (13.1 m) deep. The plaza area was excavated after the below-grade Salesforce Tower and TTC permanent below-ground structures were completed. The plaza shoring system consists of three levels of tiebacks. The tiebacks extend below Fremont St. on the south and Mission St. on the North and are setback 10 ft (3 m) from the adjacent property lines.

Several different tieback options were considered including strand systems and threaded bars. Hollow Geo-Drill Threaded bars were the preferred option due to their greater stiffness and effectiveness in limiting wall deflections. The Williams Geo-Drill bars were grouted with a 6 in. (152 mm) diameter

 © DFI International Bruges 2025

outside the active wedge zones and each tieback was proof tested to 120% of the design load to ensure adequate bond length. The tiebacks at the top level are spaced at 8 ft (2.4 m) with a waler system whereas second and third tieback rows were installed at 4 ft (1.2 m) spacing through pre-installed steel sleeves on the soldier piles. The waler option for the top level allowed for flexibility and adjustment to avoid interference with underground utilities and obstructions. A construction staging analysis was performed in SAP2000 to account for the various installation stages and the wall movement was assessed for each incremental excavation and tensioning phases (Fig. 14). The excavation was completed with small lateral ground movement and no reported adverse effects on the adjacent buildings and roadways.

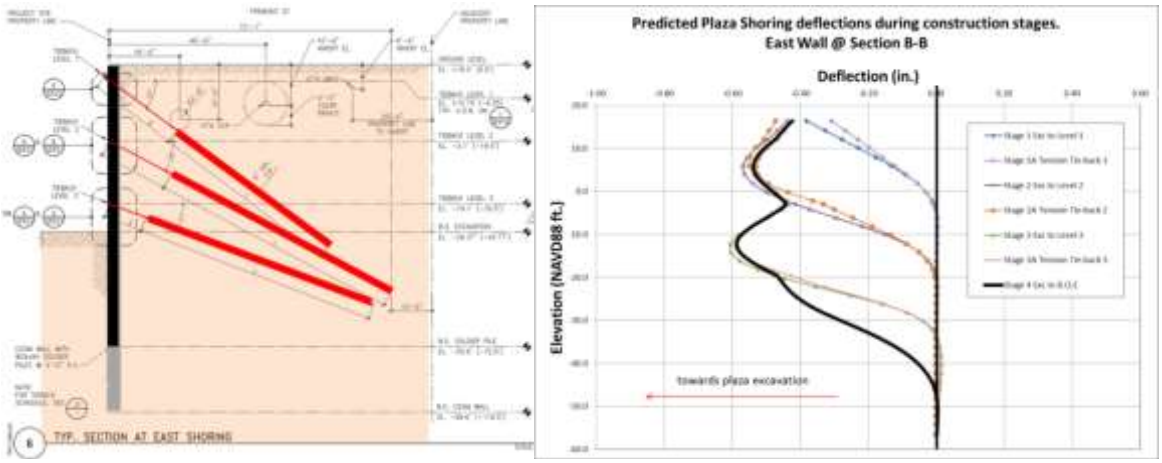


Fig. 14: Tieback layout and shoring deflections at different excavation stages

SUMMARY

The Salesforce Tower excavation presented unique challenges due to proximity of the adjacent Transbay Transit Center excavation, stringent deflection limits and the unforeseen need for 30 ft (9 m) of additional excavation. The challenges were overcome by conventional waler and pre-loaded strut shoring systems in the Tower excavation and hollow core tieback systems to limit wall deflections.

Due to unanticipated requirements for repairing the LBEs, further excavation below the bottom of the initial excavation was necessary, thereby requiring a shoring system within the CDSM shoring that was already installed. An innovative approach was implemented to use a 137 ft (42 m) diameter secant pile ring and twelve smaller 18.5 ft (5.6 m) diameter jet grout rings. These shoring systems allowed for the additional of 30 ft (9 m) excavation without compromising the waler and strut shoring system and limiting wall deflections within the project requirement (approximately 1.5 in).

Phase III excavation in Plaza was accomplished with CDSM wall with 3-level tiebacks that also met stringent lateral deflection limits. The entire excavation shoring work was successfully completed with any reported adverse effects on the project and on the adjacent structures.

REFERENCES

Clough, G.W. and O'Rourke, T.D., 1990. Construction Induced Movements of Insitu Walls, ASCE, Proc. Of Design and Performance of Earth Retaining Structures, GSP #23, 439-469.

Goldberg, D.T., 1976. Lateral Support Systems and Underpinning. Reports. Federal Highway Administration, FHWA-RD-75-128 to 131, Vols 1-4.

Peck, R.B., 1969. Advantages and limitations of the observational method in applied soil mechanics. Ninth Rankine Lecture, Geotechnique 19, No. 2, 171-187.

 © DFI International Bruges 2025

COMPARING THEORETICAL PREDICTIONS AND GUIDELINES AGAINST PILE TEST DATA FOR CFA PILES IN GLAUCONITIC SANDS IN BELGIUM

Grégoire Dawans, Jan de Nul, Belgium gregoire.dawans@jandenul.com
Olgu Orakci, KU Leuven, Bruges & The University of Melbourne, Australia olgu.orakci@kuleuven.be
Hannes Claes, KU Leuven, Geology, Leuven, Belgium hannes.claes1@kuleuven.be
Hanne Vanhaekendover, FUGRO, Belgium h.vanhaekendover@fugro.com
George Anoyatis, KU Leuven Bruges, Belgium. george.anoyatis@kuleuven.be

ABSTRACT

Assessing the axial bearing capacity and load-settlement response of pile foundations in glauconitic sands by means of engineering practice tools can encounter limitations. Glauconite, an iron potassium phyllosilicate mineral with a characteristic green color, forms dark green rounded aggregations that often resemble sand grains. In geotechnical context, glauconitic sand presents challenges due to its tendency to transform from coarse-grained material into fine-grained material through particle crushing and can impact pile foundation installation and performance. Such complexities can make accurate pile settlement prediction and design challenging. This study assesses the predictive power of past and current guidelines in Belgian practice, as well as a t-z approach, to predict the load-settlement response of piles in glauconitic sands. For this purpose, the theoretical predictions are further compared against data from CFA pile tests conducted in Belgium. A systematic parametric analysis investigates how the selection of model parameters impacts the pile load-displacement response. The findings emphasize the need for careful parameter selection to accurately represent the properties of glauconitic sands and achieve reliable outcomes.

Keywords: pile foundations, axial bearing capacity, CFA piles, glauconitic sands, guidelines, full-scale tests

INTRODUCTION

In piling engineering design, the analysis of pile settlement has long been a subject of extensive research. Various methods, such as boundary element solutions (Davis & Poulos 1968, Banerjee & Davies 1978), finite element methods (Ottaviani 1975, Syngros 2004), and simplified *t-z* models (API 2014, DNV-GL 2016 guidelines), have been developed. However, traditional pile design methodologies, based on the behavior of conventional sandy or clayey soils, fall short when applied to glauconitic sands. Often referred to as 'greensand,' glauconitic sand poses significant challenges for foundation installation and performance. The available methods, mostly relying on empirical formulas from Cone Penetration Tests (CPTs), do not account for the unique characteristics of glauconitic sands, leading to potential inaccuracies in bearing capacity and settlement predictions, and risking the reliability and safety of pile foundations. Glauconitic sands, known for their distinctive green color, are commonly found in marine environments such as the continental shelves of the Atlantic Outer Continental Shelf (OCS) in the U.S., the Mediterranean Sea, and the North Sea. These sands impact geotechnical projects, particularly offshore wind farm installations, due to their friability and tendency to crush under pressure, altering soil behavior and complicating pile driving. Onshore, glauconitic sands are notably found in regions like New Jersey (US) and parts of Belgium. These sands pose significant challenges for geotechnical projects due to their friability and tendency to crush under pressure, which can alter soil behavior and complicate foundation design.

Glauconitic sands, characterized by their greenish iron-bearing granules, predominantly consist of the mineral glauconite. This mineral forms in marine sands, where aluminosilicate gels solidify into grains that replicate the internal structure of microfossils, influencing the sands' unique geotechnical behavior (Van Alboom et al. 2012). Laboratory tests reveal a broad range in particle size gradation and high specific gravity. Glauconite's composition includes potassium, sodium, iron, magnesium, aluminum, silicon, oxygen, and hydroxide, endowing it with significant iron content and high cation exchange

 © DFI International Bruges 2025

capacity. This facilitates the adsorption of heavy metals like arsenic and chromium, impacting soil behavior in construction projects (Westgate et al. 2022). While glauconitic sand displays high strength when intact, it degrades into a clay-like material under moderate disturbance, increasing plasticity, reducing shear strength, and inducing strong thixotropic behavior. This transformation necessitates specialized handling and analysis techniques in engineering projects (Westgate et al. 2022a, 2022b).

A significant geotechnical challenge is high pile auger resistance, characterized by high tip resistance at the pile head in granular soil and increased side friction along the pile shaft in fine-grained soil due to particle crushing. Its crushable nature causes it to transform from a stiff, high-permeability coarse-grained material to a weak, low-permeability fine-grained material. Glauconitic grains are softer and more compressible than quartz sand grains, making them more susceptible to deformation and crushing under mechanical stresses. This can compromise the pile's designed bearing capacity, necessitating specific construction methods, such as choosing suitable auger blades for Continuous Flight Auger (CFA) piles to counter the soil's stickiness and ensure adequate pile embedment depth (Timbremont & Siemens, 2009). Further complications include early pile driving refusal due to high friction and reduced pile capacity with depth, arising from the crushing of glauconite particles, which increase fines content and plasticity. Research on glauconitic sands, particularly from the Flanders region of Belgium, focuses on the Berchem and Diest formations, characterized by significant glauconite content (Adriaens et al. 2014). This research emphasizes the need to adapt geotechnical practices to the distinct characteristics of glauconitic sands, ensuring the structural integrity and longevity of pile foundations under these challenging conditions.

Motivated by observed discrepancies between theoretical predictions and test data, this research addresses the problems in pile design in glauconitic sands encountered in Belgium. This study aims to bring attention to piles in glauconitic sands by critically evaluating the existing design methodologies. The objectives include: 1) reviewing the geotechnical properties of glauconitic sands and the problems posed to foundation design, 2) investigating the predictive power of current Belgian practices in bearing capacity and settlement estimations, and 3) proposing a methodology with updated empirical factors derived from vertical static load tests and theoretical analysis to improve the design.

METHODS

This section employs a systematic approach to evaluate the effectiveness of different predictive models in assessing the load-settlement behavior of piles in glauconitic sands. The methodology encompasses theoretical prediction models - both past and current guidelines used in Belgian practice - and a t-z approach, with subsequent validation against empirical data obtained from CFA pile tests conducted in Belgium. To rigorously explore the influence of model parameters on load-displacement outcomes, a parametric analysis is conducted. The following subsections provide a description of each predictive model, the testing procedures. The next section presents the results from the parametric analysis and the comparisons between the different methods and the field test data, to evaluate their performance and sensitivity.

Design of piles according to the Belgian Practice: axial capacity and settlement

Historically, Belgium lacked formal national standards for pile design, leading various owners and engineers to develop their own specifications. The situation shifted in 2005 with the adoption of Eurocode 7 (NBN EN 1997-1: 2005) as a Belgian standard, providing a unified approach. In 2009, WTCB-CSTC (now Buildwise) published the first guideline for designing axially loaded compression piles using CPT, which became a Belgian reference in the Eurocode 7 national annex. A revised version of this guideline, approved in 2016, addresses additional factors like tension loads and negative skin friction. Complementary standards for pile execution, covering displacement, bored, and micropiles, have been published, along with datasheets detailing the characteristics and installation requirements for various pile types to align with the Belgian design guide.

 © DFI International Bruges 2025

Currently, pile design in Belgium follows the most recent guidelines as outlined in Huybrechts & De Vos (2020). This document serves as a primary reference in Belgian geotechnical engineering, incorporating local soil characteristics and construction practices into the Eurocode framework. In particular, this guideline provides a structured framework for geotechnical design in Belgium, specifically for axially loaded foundation piles and micropiles, aligning with Eurocode 7 standards. The document outlines the methodology for ultimate limit state (ULS) design, ensuring that pile foundations meet both structural safety and serviceability requirements under extreme loading conditions. Based on static cone penetration tests (CPTs), it offers detailed recommendations on assessing soil-structure interactions, deriving pile load capacities, and determining settlement responses. The guideline is designed to unify national practice, providing standardized procedures for engineers to ensure safety, reliability, and compliance with Belgian construction standards.

In the guideline for axial pile capacity based on the Eurocode 7 framework, the ultimate axial pile capacity is typically calculated as the sum of the pile shaft resistance R_s and the pile base (tip) resistance R_b. The tip resistance R_b is determined using the following formula (Huybrechts & De Vos 2020)

$$R_b = a_b \, \varepsilon_b \, \beta \, \lambda \, A_b \, q_b \tag{1}$$

where q_b is the unit base resistance is calculated using the De Beer method (De Beer E 1971-1972); a_b is an empirical installation factor that accounts for the influence of the pile installation method in a specific soil type, and values are obtained from pertinent tables, ε_b is a parameter that accounts for the scale effect on the shear resistance due to soil cracking, obtained from a simple algebraic equation which takes into account the CPT conus diameter and the pile base diameter, differentiating between tertiary clay and the rest of the soil types; β is a shape factor that accounts for the influence of a non-circular or non-square pile base; λ is a reduction factor for piles with an enlarged base, where the enlarged pile base causes a relaxation of the soil around the pile shaft during pile installation; and A_b is the cross-sectional area of the pile base.

The friction resistance R_s is determined using the following formula (Huybrechts & De Vos 2020)

$$R_s = \chi_s \sum \left(a_{s,i} \, a_{D,i} \, h_i \, q_{s,i} \right) \tag{2}$$

where the subscript i denotes the i-th soil layer and h_i its thickness, $q_{s,i} = 1000 \, \eta_{p,i} \, q_{c,m,i}$ is the unit friction resistance in [kPa], calculated as a function of the average cone resistance along the $q_{c,m,i}$ and an empirical factor that indicates the ratio between the unit friction resistance of layer $q_{s,i}$ and the cone resistance q_c; χ_s is the pile shaft perimeter, $a_{s,i}$ is an empirical installation factor which takes into account the influence of the pile installation method in a specific soil type as well as the roughness of the pile shaft; and $a_{D,i}$ is an enlargement factor for the pile shaft diameter for the i-th layer. It is worth mentioning that when a Technical Approval (Technische Goedkeuring, ATG) with certification or an equivalent document exists for the relevant pile type, applicable values for both R_b and R_s should be obtained from that document. In such cases, these values take precedence over those provided in the guidelines and may be used exclusively for design purposes.

Given that values for η_p, a_b and a_s are not currently reported in the guidelines for glauconitic sands (Table 4 and 5, Huybrechts & De Vos 2020), this investigation seeks raise awareness by analyzing available data from pile tests executed in Belgium and highlight the needs for identifying a suitable methodology for determining these critical parameters.

In Belgian practice, the calculation of axial pile settlements does not currently have dedicated guidelines established by Buildwise. Therefore, this study will refer to earlier work published by De Cock (2008), which outlines methodologies for estimating axial pile settlements. By utilizing De Cock's framework, we aim to analyze and apply relevant principles that can capture the settlement behavior of piles, in glauconitic sands. In particular, De Cock used hyperbolic functions to back-analyze pile load-settlement curves; the graphical inverse slope method, introduced by Chin (1970),

 © DFI International Bruges 2025

effectively fits curves of measured load (Q)-settlement (s) data, facilitating the extrapolation of load-settlement curves to estimate ultimate pile resistance. The method is based on a semi-graphical approach, allows for transforming the basic equation $Q = s/(a + b\ s)$ into a straight line of the form $(s/Q) = a + b\ s$. The transfer functions for base resistance R_b and shaft resistance R_s are obtained as:

$$R_b = \frac{s_b}{K_b + {s_b}/{R_{bu}}} \tag{3}$$

and

$$R_s = \frac{s_s}{K_s + {s_s}/{R_{su}}} \tag{4}$$

where s_b amd s_s are the corresponding base and shaft settlements, R_{bu} and R_{su} are the ultimate base and shaft resistances and can be obtained from Equations (1) and (2), respectively. K_b and K_s base and shaft flexibility factors can be obtained from the following equations:

$$K_b \approx \frac{0.54}{D_b\ E_u} \tag{5}$$

and

$$K_s \approx \frac{M_s\ D_s}{R_{su}} \tag{6}$$

where M_s is a flexibility factor and E_u is the secant modulus of the soil under the pile base, for which a range of values are presented as a function of cone resistance (De |Cock 2008): $E_u = (4 - 6\ )\ q_c$, for bored piles in NC-sands, $E_u = (6 - 8)\ q_c$, for bored piles in OC-sands, $E_u = (8 - 12)\ q_c$, for screw piles, $E_u = (15 - 20\ )\ q_c$ for driven piles. For cohesive soils (stiff OC-clays) it was found from back-calculation of screw piles in clay that $E_u = (50 - 80)\ q_c$ or $E_u = (750 - 1000)\ c_u$. Note that according to De Cock (2008) the ultimate base and shaft resistances are mobilized at specific displacement ratios, typically around 10 % of the pile diameter. In this study the R_{bu} and R_{su} values are calculated according to (Huybrechts & De Vos 2020, Dimensioneringsmethode nr. 20). The base and shaft transfer functions are then applied to calculate the load-settlement curves.

Load-settlement response of piles using t-z curves

The t-z method is a widely used approach for assessing pile settlements, offering a relatively simple way to model the interaction between the pile and surrounding soil. This method characterizes the relationship between axial load (t) and settlement (z) through (semi-)empirical or analytical curves (i.e., vertical springs), allowing for a detailed representation of the load transfer mechanism along the pile shaft. This study employs axial curves and calculates deformations under static loading within a finite element method framework, as detailed in Orakci et al. (2023). Computations are performed using Python and the non-linear solver library OpenSees (Zhu & Scott, 2018). By defining t-z curves based on site-specific soil properties, the load-settlement behavior of piles can be effectively predicted. This study adopts the t-z curves proposed by Allani & Huybrechts (2022), which are based on an extensive database of instrumented pile load tests available at the WTCB (Scientific and Technical Centre for the Construction Industry) in Belgium.

The transfer functions take the following form for the response at the shaft and at the pile base, respectively:

$$t = \frac{z}{\frac{1}{k_{si}} + \frac{z}{t_{max}}} \tag{7}$$

and

$$q \approx \frac{z_b}{\frac{1}{k_b} + \frac{z_b}{q_{max}}} \tag{8}$$

where t_{max} [kPa] is the maximum shaft resistance, k_{si} [kN/m³] is the stiffness of the soil along the shaft layer i, q_{max} [kPa] is the maximum pile base resistance and k_b [kN/m³] is the stiffness of the soil at the pile base. The maximum resistances t_{max} and q_{max} can then be calculated using the expression of hyperbolic transfer functions

 © DFI International Bruges 2025

$$t_{max} = t_{10\%}\,(1 + 10\,M_s) \tag{9}$$

and

$$q_{max} \approx q_{b,10\%}\left(1 + \frac{\beta}{M_b\,\frac{d_b}{10}}\right) \approx q_{b,10\%}\left(1 + \frac{4.55}{M_b}\right) \tag{10}$$

where $t_{10\%} = \alpha_{s_i}\,q_{s,i}$ and $q_{b,10\%} = R_b/A_b$ can be calculated from Huybrechts & De Vos (2020) (Dimensioneringsmethode nr. 20). The sum of both components gives the total bearing capacity of the pile and corresponds, by definition, to a mobilized pile resistance at a pile base settlement equal to 10% of the pile base diameter. Indicative values for the dimensionless flexibility factor M_s and the ddimensionless stiffness factor M_b are proposed in Allani & Huybrechts (2022), as a function of soil and pile type (Table 1 and Table 2 in Allani & Huybrechts 2022), in which no specific reference is made for glauconitic sands.

FIELD & PILE TEST DATA

Fig. 1 shows the test site and the exact locations of the CPT's conducted in June, 2021 (Fugro 2021). Information from boreholes and test pits are also available (Fugro 2008a).

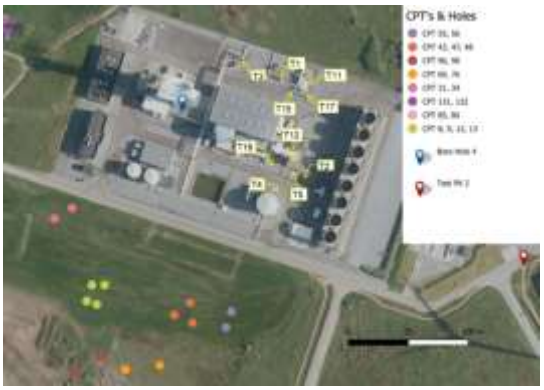


Fig. 1 Pile test location.

The soil layer, under the surface layer of made ground, includes weathered glauconitic sands designated as sandy silt. The rest of the soil layers consist of glauconite, with increasing cone tip resistance q_c from 8 MPa to 16 MPa and a friction ratio R_f of 4 % to 8 % with depth. Layers 2, 3, and 4 are glauconitic sands with an average glauconite content of 30% (Diest formation). The soil stratigraphy, as identified by the piling contractor is summarized in Table 1, in which the glauconitic layers are identified as sand, yet using lower q_c values than those obtained from the CPT tests.

Table 1. Stratigraphy (Timbremont D., 2009)

layer	level [m TAW]	q_c [MPa]	material
1	+24.5 to +21.5	2	sandy silt, no skin friction
2	+21.5 to +17.5	8	medium-dense sand
3	+17.5 to +2.50	12	dense sand
4	> +2.50 to	14	dense sand

The piles installed are CFA PCS piles with a diameter of 0.6 m (Table 2). Augering in glauconitic sand proved to be challenging, as installation crushed the glauconitic sand, resulting in a sticky clayey soil. This disturbed glauconitic sand sticks to the blades and stem of the auger, considerably impacting the pile installation. The R_{cm} values shown in Table 2 are obtained from the static load tests (SLT) and correspond to the maximum value its pile was subjected to. Note that, although the standard practice is to evaluate capacity at a settlement equal to 10 % of the pile diameter, these values were obtained at smaller settlements because the tests were stopped earlier, indicating the complex behavior of the

 © DFI International Bruges 2025

material. In particular, for piles P11, P12, P15 and P17 the loads have been measured at pile head settlements of 17.65 mm, 25.64 mm, 21.94 mm and 6.04 mm, respectively.

Table 2. Pile characteristics (Fugro, 2008)

Pile	Working level [mTAW]	tip [mTAW]	L [m]	R_{cm} [kN]
P11	25.2	0	25.2	5000
P12	25.2	-0.1	25.3	4500
P15	25.2	0	25.2	4500
P17	25	10.2	14.8	3000

RESULTS & DISCUSSION

Table 3 shows the predictions of axial pile capacity following the Belgian practice (Dimensioneringsmethode nr. 20), for CFA PCS piles in terms of R_b and R_s values evaluated using base and shaft capacity coefficients $a_b = 0.5$ and $a_s = 0.4$ according to Belgian practice and Huybrechts & De Vos (2020).

Table 3. Axial bearing capacity predictions according to Belgian practice (Dimensioneringsmethode nr. 2, Huybrechts & De Vos 2020)

Pile no.	Length L [m]	R_b [kN]	R_s [kN]	R_{cm} [kN]
P11	25.2	1408	3592	5000
P12	25.3	1394	3106	4500
P15	25.2	1408	3092	4500
P17	14.8	791	2209	3000

Table 4 shows the back-calculated values for the parameter η_p^* (Equation 2, and $q_{s,i} = 1000\ \eta_{p,i}\ q_{c,m,i}$) per soil layer and pile, based on the SLT data and the stratigraphy as estimated by the piling contractor. From Table 4 it is evident that there is a good agreement between the η_p value proposed for the long piles namely Piles 11, 12 and 15, while a different set of values seems to better capture the capacity for the short Pile 17. Note that, following the Belgian practice, no skin friction is considered and thus the contribution of this layer to R_s is omitted.

Table 4. Back-calculated η_p^* (Eq 2) values

pile no.	q_s [kPa]	layer no.	q_{cm} [MPa]	η_p	pile no.	q_s [kPa]	layer no.	q_{cm} [MPa]	η_p^*
P11	222	2	8	1/36	P12	191	2	8	1/42
		3	12	1/54			3	12	1/63
		4	14	1/63			4	14	1/73
pile no.	q_s [kPa]	layer no.	q_{cm} [MPa]	η_p	pile no.	q_s [kPa]	layer no.	q_{cm} [MPa]	η_p
P15	191	2	8	1/42	P17	259	2	8	1/31
		3	12	1/63			3	12	1/46
		4	14	1/73			-	-	-

 © DFI International Bruges 2025

Figs. 2, 3, 4 and 5 show results for the load-settlement curves obtained from the method proposed in De Cock (2008), using the shaft and base capacities as included in the Belgian practice following the report titled "Dimensioneringsmethode nr. 20" by Huybrechts & De Vos 2020 (proposed approach in this work), and the *t-z* method following the formulations proposed in (Allani & Huybrechts 2022).

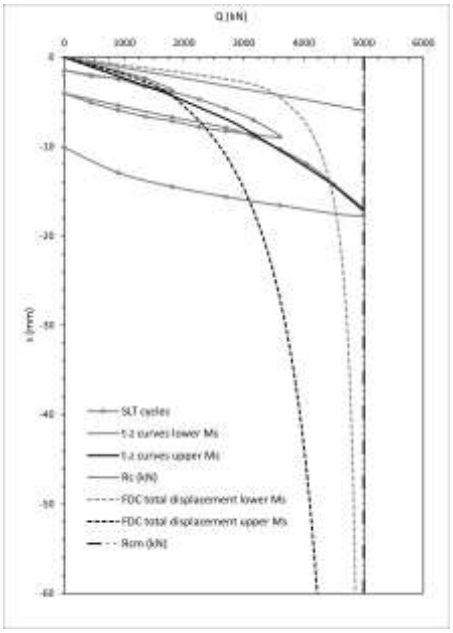


Fig. 2 Comparisons of load-settlement curves obtained from different methods, against pile data for P11

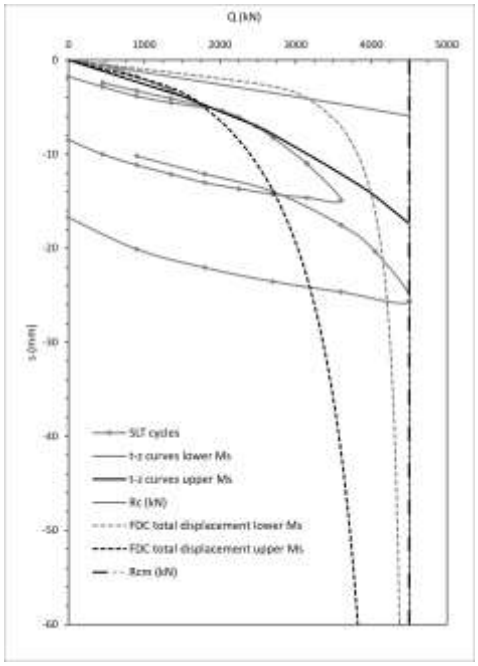


Fig. 3 Comparisons of load-settlement curves obtained from different methods, against pile data for P12

Results from the joint De Cock (2008) method and Dimensioneringsmethode nr. 20 (Huybrechts & De Vos 2020) are shown in Figs.2-4, for pile settlements up to 60 mm (10 % of pile diameter). The secant modulus E_u in Equation (5) is calculated using the expression $E_u = (50 - 80)\, q_c$, where $q_c =$ 14 MPa for piles P11, P12, P15 and $q_c = 12$ MPa for pile P17 (shorter pile). For E_u a value of 50 q_c

 © DFI International Bruges 2025

was considered. For calculating the load-settlement curve, this study uses M_s values as proposed by Allani & Huybrechts (2022), in which M_s range from 0.003 to 0.026 for replacement piles in clays and sands. To investigate the effect of M_s on the response, herein two set of load-settlement curves are plotted for $M_s = 0.003$ proposed for clays (blue dashed-dotted curves), and $M_s = 0.026$ proposed for sands (red solid curves). This allows us to capture the upper and lower bounds of the predicted settlement behavior. A practically perfect agreement between the predictions for the high M_s value and the test data is observed for loads up to approx. 2000 kN. For higher loads, the results seem to overpredict settlements and fail to capture the behavior at large loads (axial capacity). On the other hand, it is observed that the results which correspond to the low M_s value underpredict settlements up to an axial load of approximately 4000 kN for pile P11 and 3000 kN for piles P12, P15 and P17. For higher loads, the approach seems to overpredict settlements and potentially strongly underpredict the piles' axial capacity (yet the experimental data are limited to relatively small settlements, below 10 % of the pile diameter). For the analysis using *t-z* curves, the following ranges of values for the dimensionless flexibility factor $M_s = 0.003 - 0.026$ and stiffness factor $M_b = 5 - 60$ are investigated. For piles P11, P12, and P15 in Fis. 2, 3 and 4, respectively, the load-settlement prediction is made using $M_s = 0.026$ and $M_b = 60$ (solid green curves in Figs. 2-5). The predictions using the aforementioned parameters seem to be in almost perfect agreement with the data for pile P11 along the entire loading (Fig. 2), and up to an axial load of approximately 3500 kN for piles P12, P15 and P17 (Figs. 3, 4, 5). For higher loads the theoretical predictions give adequate estimated of the pile settlements up the maximum load investigated in the pile tests. Results for $M_s = 0.003$ and $M_b = 60$ (yellow dash-dotted curves in in Figs. 2-5), seem to represent a much stiffer behavior and underpredict settlements along the entire range of experimental data, indicating that higher M_s value is more realistic for the problem at hand.

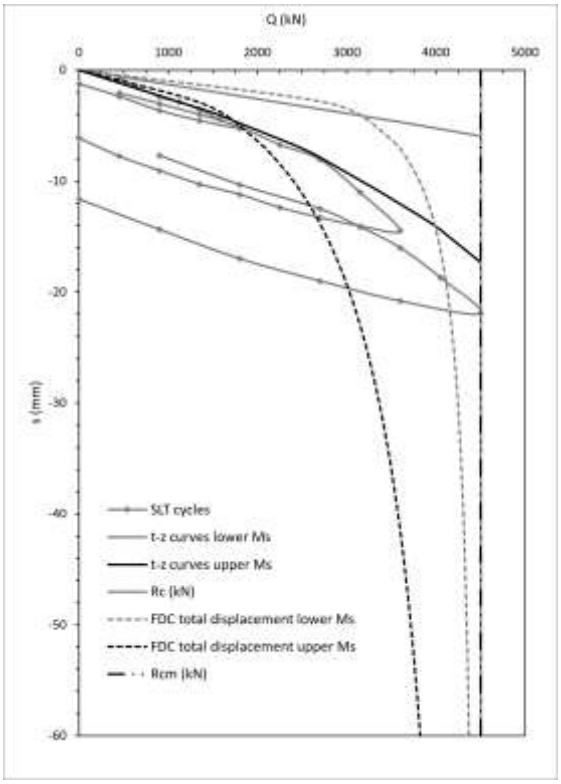


Fig. 4 Comparisons of load-settlement curves obtained from different methods, against pile data for P15

 © DFI International Bruges 2025

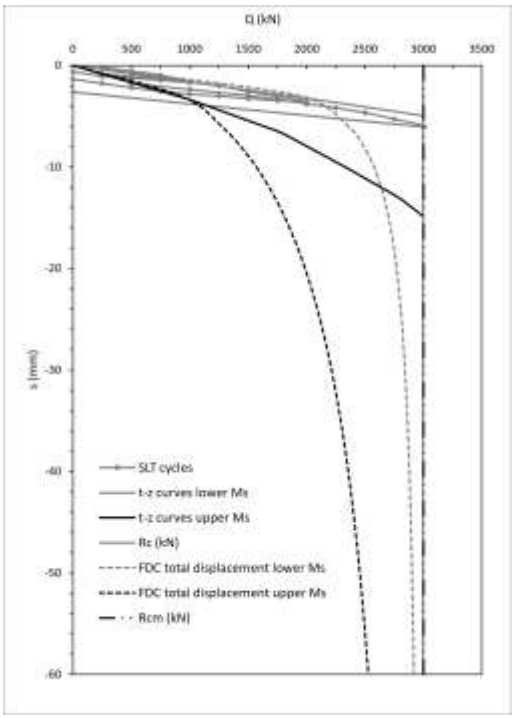


Fig. 5 Comparisons of load-settlement curves obtained from different methods, against pile data for P17

CONCLUSIONS

Assessing the axial bearing capacity and load-settlement response of pile foundations in glauconitic sands presents significant challenges due to the unique properties of glauconite. This mineral, commonly forming green, sand-sized grains, often undergoes particle crushing under load, transforming from a coarse- to fine-grained material. Such behavior complicates accurate settlement predictions, as current predictive tools and guidelines - including those established in Belgian practice - may not account fully for the impact of glauconite on pile foundation performance. The study's findings underscore that while existing guidelines and the *t-z* curve approach offer valuable insights, they may fall short when applied to glauconitic sands due to limitations in parameter calibration. For instance, Belgian guidelines for axial capacity (with parameters such as a_s, a_b, η_p) are based on an extensive testing campaign in non-glauconitic sands, thus lacking direct relevance for glauconitic soils. The challenge of determining realistic values for these and other parameters such as those governing *t-z* curves i.e., M_s and M_b that should ideally align with the physical characteristics of glauconitic sands, highlights the need for expanded testing. A perhaps more robust predictive framework for settlements of piles in glauconitic sands would require a broad, systematic testing campaign involving various pile geometries and embedment depths, combined with an in-depth analysis of glauconitic sand properties, such as glauconite content. This campaign should also allow for the separate evaluation of shaft and base resistance, which is critical to calibrating models accurately. Given the limited number of pile tests available in this study, drawing solid conclusions or proposing concrete improvements remains a challenge. However, the *t-z* method appears to offer an attractive alternative, and further exploration of the pertinent M_s and M_b values specific to glauconitic sands may provide a promising path forward. Ultimately, further research is essential to refine design parameters and methods specifically for CFA piles in glauconitic sands, with potential adaptations for other pile types as well.

ACKNOWLEDGEMENTS

We would like to express our sincere gratitude to Dimitri Timbremont, previously engineer at Fugro and currently Senior Commercial Area Manager at Soetaert, for their invaluable insights and guidance

 © DFI International Bruges 2025

throughout Grégoire Dawans' master's thesis at KU Leuven Campus Bruges. Their support played a pivotal role in the successful completion of this research.

REFERENCES

Adriaens, R., Vandenberghe, N., & Elsen, J. (2014). Natural clay-sized glauconite in the Neogene deposits of the Campine Basin (Belgium). *Clays and clay minerals*, *62*(1), 35-52.

Allani, M., & Huybrechts, N. (2022). Pile settlement under vertical static load: SLS design method based on Belgian experience. In Rahman, M., & Jaksa, M. (Eds.), Proceedings of the 20th International Conference on Soil Mechanics and Geotechnical Engineering (pp. 3165-3170). Australian Geomechanics Society. Sydney, Australia. ISBN 978-0-9946261-4-1.

API, 2014. RP2GEO: Geotechnical and Foundation Design Considerations. American Petroleum Institute.

Chin, F. K. (1970). Estimation of the ultimate load op piles from tests not carried to failure. Proc. 2nd Southeast Asian Conference on Soil Mech. and Found. Eng. Singapore: 81–92.

Davies, T. G., & Banerjee, P. K. (1978). The displacement field due to a point load at the interface of a two layer elastic half-space. *Geotechnique*, *28*(1), 43-56.

Davis, E. H., & Poulos, H. G. (1968). The use of elastic theory for settlement prediction under three-dimensional conditions. *Geotechnique*, *18*(1), 67-91.

Dawans, G. (2024) *Pile Design in Glauconitic Sands* (Master's thesis, KU Leuven)

De Beer E (1971-1972). Methoden om het grensdraagvermogen van een geheide paal uit de resultaten van diepfunderingen af te leiden. Brussel, Tijdschrift der Openbare Werken van België, volume 72, nr. 4 (p. 191-268), nr. 5 (p. 321-353) en nr. 6 (p. 351-405).

De Cock, F. A. (2008). Sense and sensitivity of pile load-deformation behaviour. In Deep Foundations on Bored and Auger Piles-BAP V (pp. 35-56). CRC Press.

DNV-GL, 2016. Support structures for wind turbines. Offshore Standard DNVGL-ST-126.

Huybrechts, N., & De Vos, M. (2020). Richtlijnen voor de toepassing van de Eurocode 7 in België volgens de NBN EN 1997-1 ANB. Deel 1: het grondmechanische ontwerp in de uiterste grenstoestand (UGT) van axiaal belaste funderingspalen en micropalen op basis van statische sonderingen (CPT's) (Dimensioneringsmethode No. 20). Belgium: Buildwise.

Orakci, O., Huvaj, N., François, S., & Anoyatis, G. (2023). Probability of unsatisfactory performance of monopile foundations for offshore wind turbines considering variations in seabed properties. *Ocean Engineering*, *277*, 114335.

Ottaviani, M. (1975). Three-dimensional finite element analysis of vertically loaded pile groups. *Geotechnique*, *25*(2), 159-174.

Syngros, K. C. (2004). *Seismic response of piles and pile-supported bridge piers evaluated through case histories*. City University of New York.

Timbremont, D., & Siemens, M. B. (2009). SIEMENS T- Power Tessenderlo-Belgium Method Statement Status.

 © DFI International Bruges 2025

Van Alboom, G., Dupont, H., Maertens, J., & Haelterma, K. (2012). Geologische context.

Westgate, Z., McMullin, C., & DeGroot, D. (2022a). Glauconite Sand Challenges for US Offshore Wind Development. In *International Conference on Offshore Mechanics and Arctic Engineering* (Vol. 86618, p. V001T02A002). American Society of Mechanical Engineers.

Westgate, Z. J., McMullin, C., Zeppilli, D., Beemer, R., & DeGroot, D. J. (2022b). Geological and Geotechnical Characteristics of Glauconitic Sands. In *Geo-Congress 2022* (pp. 113-121).

Zhu, M., McKenna, F., & Scott, M. H. (2018). OpenSeesPy: Python library for the OpenSees finite element framework. *SoftwareX*, *7*, 6-11.

 © DFI International Bruges 2025

RE-EVALUATION OF THE DESIGN DURING CONSTRUCTION WITH MONITORING DATA AND UTILIZATION OF THE OBSERVATIONAL METHOD IN SHORING WORKS

Cihat A. Author, Zetaş Zemin Teknoloji A.Ş., İstanbul, Türkiye, cihat.asci@zetas.com.tr
Önder A. Contributor, Zetaş Zemin Teknoloji A.Ş., İstanbul, Türkiye, onder.akcakal@zetas.com.tr
Nuray İ. Ç. Contributor, Zetaş Zemin Teknoloji A.Ş., İstanbul, Türkiye, ipek.calim@zetas.com.tr
Canberk A. Contributor, Zetaş Zemin Teknoloji A.Ş., İstanbul, Türkiye, canberk.acar@zetas.com.tr
Numan V. Contributor, Zetaş Zemin Teknoloji A.Ş., İstanbul, Türkiye, numan.velioglu@zetas.com.tr

Monitoring studies provide an opportunity to compare the target performance of a shoring project during the design phase with its actual behavior during excavation. This data allows for a timely response to discrepancies between estimated and actual conditions. Either an increase or decrease in the support elements can be considered depending on the necessary action. Two shoring projects located in Istanbul were reviewed as examples in this study. These projects employed different shoring techniques, such as diaphragm walls and soil nailing, and monitoring data enabled a re-evaluation of the design during excavation. Displacements were monitored using inclinometers and reflectometers throughout the gradual excavation process. Load cells were utilized to monitor anchor loads during excavation steps. In one project, it was necessary to strengthen the support system, while in the other, monitoring allowed for optimization of the remaining applications. These shoring projects were back-analyzed to verify the soil properties assumed in the design phase. A comparison study was also conducted to evaluate the impact of employing the observational method during the design phase. The design process of the observational method in shoring works was described, and its effects on cost, duration, and environmental impact were discussed.

Keywords: observational method, monitoring, shoring

INTRODUCTION

Monitoring is a critical phase of a shoring project that allows the performance of the application to be tracked during excavation. Beyond safety purposes, a well-designed monitoring scope enables valuable evaluations of shoring performance and comparisons with early-stage considerations. When performance targets are clearly defined for all steps of the application, it is possible to estimate final performance values by comparing calculated and monitored values at intermediate steps. By examining shoring applications in this manner, project revisions can be made during implementation to mitigate potential failures caused by unaccounted parameters in the design phase. Additionally, monitoring can lead to cost savings in overdesigned projects. In conjunction with field tests conducted before implementation, using the actual performance of the shoring section as data can lead to cost-effective, faster, and more environmentally friendly solutions. This study examines two case studies from Istanbul within this scope.

CASE STUDIES

Two examples of monitoring applications and design revisions made during excavation are presented below.

Case 1 – A diaphragm Wall Shoring Project

Within the scope of the project, a basement excavation reaching a maximum depth of 13.30 m was required in an area measuring 78 x 80 m. There were no adjacent structures to the site. Borehole investigations revealed predominantly clay layers with thin rock interlayers. The groundwater level

 © DFI International Bruges 2025

was approximately 1.5 m below the surface. The soil properties and soil models are presented in Table 1.

Table. 1. Soil Properties

Layer	Soil Model	γ (kN/m³)	Ø' (°)	c' (kN/m²)	E (kN/m^2)
Fill	Hardening Soil	18	28	0	6000
Clay-1	Hardening Soil	18	26	2	6000
Clay-2	Hardening Soil	18	28	5	16000
Breccia	Hardening Soil	19	34	5	150000
Clay-3	Hardening Soil	19	30	10	40000
Clay-4	Hardening Soil	19	30	15	56000
Clay-5	Hardening Soil	19	30	20	80000

The shoring system was determined as diaphragm wall and prestressed anchor, and tubular steel supports were considered at the corners. The layout plan of the shoring system and the section of the anchored part are given in Fig. 1.

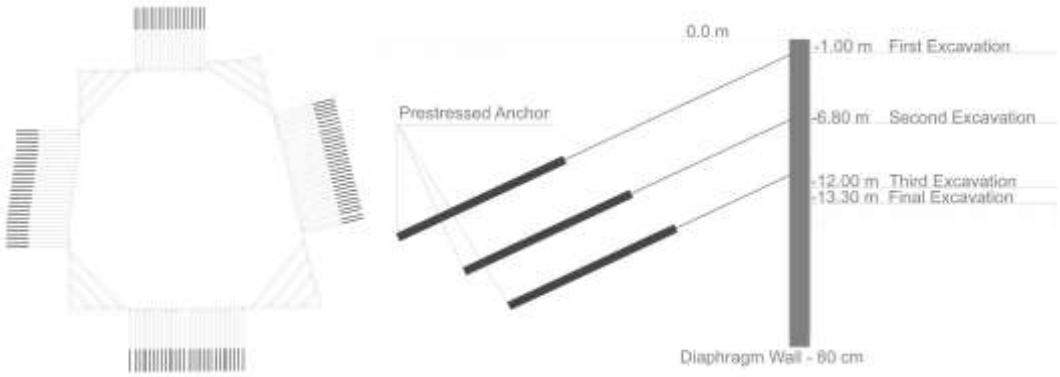


Fig. 1. The layout and section of the shoring system

The shoring section was modeled in Plaxis 2D software (Fig. 2), diaphragm wall, anchors and steel struts were calculated and designed accordingly. Settlements and horizontal displacements were calculated and compared with the limits given in the codes.

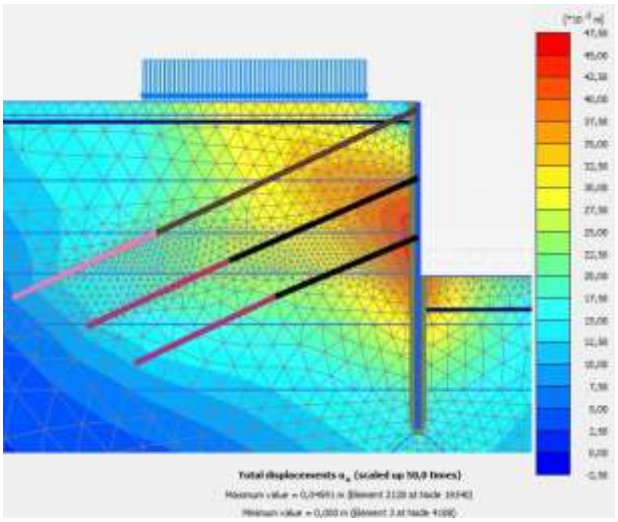


Fig. 2. Plaxis 2D - displacement results

 © DFI International Bruges 2025

The displacements are calculated for the different stages of the anchored shoring section and they are listed in Table 2.

Table. 2. Displacement corresponding to excavation depth

Excavation Stage	Depth (m)	Calculated Disp. (mm)	Occurred Disp. (mm)
First Excavation	1.20	1.8	1.0
Second Excavation	6.80	20.7	10.0
Third Excavation	11.30	40.6	12.5
Final Excavation	13.30	45.9	15.5

During implementation, horizontal displacements of the shoring system were monitored using inclinometers and a total station (Fig. 3). Anchor loads were measured using installed load cells. The inclinometer results of the most critical anchored section are illustrated in the figure below.

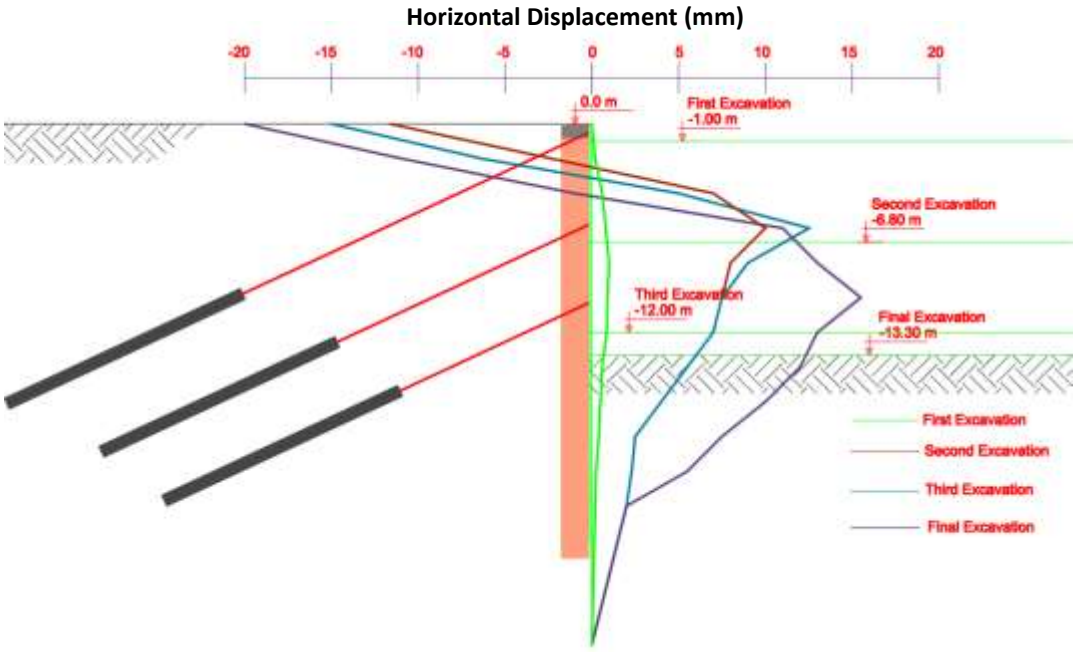


Fig. 3. İnclinometer readings

The displacement values increased to 1 mm, 10 mm, 12.5 mm, and 15.5 mm at the end of the excavation stages, aligning with the inclinometer readings (Fig. 3). The maximum displacement in the reflector readings was recorded as 21 mm. At the final excavation stage, the displacement was observed to be 12 mm. Since reflector readings are not as sensitive as inclinometer readings, the data were used to validate the inclinometer results.

 © DFI International Bruges 2025

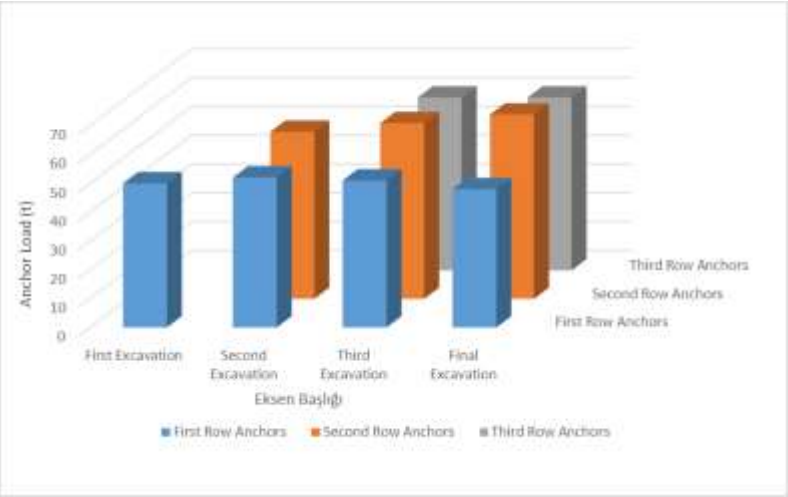


Fig. 4. Loadcell readings corresponding to excavation levels

Two loadcells were placed in each anchor row. The load change of the placed loadcells depending on the excavation stages is given in the graph below. The anchor load of the first row increased slightly with the second excavation, and then negligible decreased as the excavation continued (Fig. 4). The second row anchor loads increased by 12% at the final excavation level (Fig. 4). The anchors in the third row retained their loads (Fig. 4).

The development of horizontal displacements after the 2nd row anchor excavation was compared with the values calculated at the design stage as follows and it was determined that they were much lower than the estimated values.

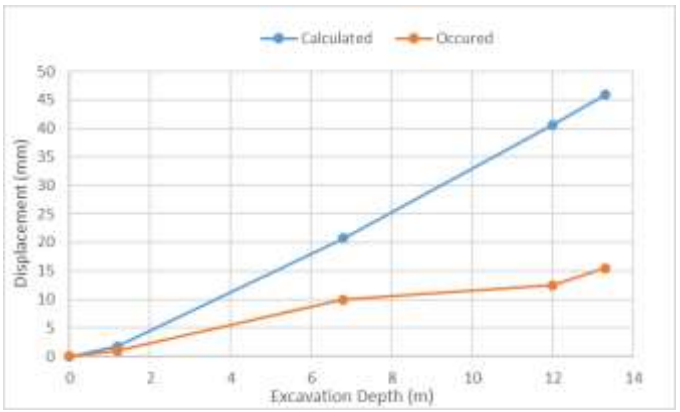


Fig. 5. Calculated displacement versus occured displacement

When Figure 5 is examined, it is seen that the displacements occurring in the field are lower than the calculated displacements. The section was back-calculated considering the occurred displacement and the soil parameters were re-estimated (Fig. 7). And it was determined that the horizontal displacements would remain within the displacement limits in case the application was completed without the 3rd level of anchors were applied. In this context, the alternative without the last row of anchors was evaluated. Shoring section was recalculated with the estimated soil parameters and structural elements were checked accordingly. Figure 6 shows the construction of the last remaining façade.

 © DFI International Bruges 2025



Fig. 6. Prestressed Anchor Applications on the Site

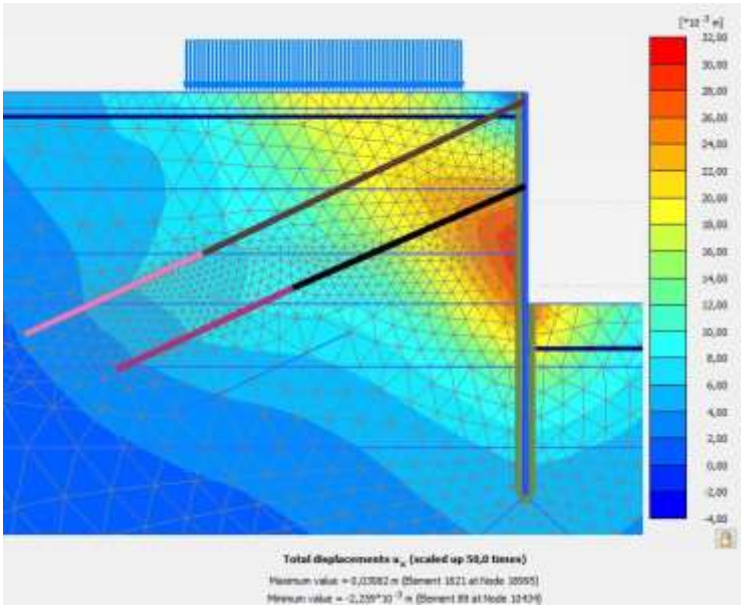


Fig. 7. Plaxis 2D - back calculation result

Table. 3. Comparison of different shoring systems

Shoring System	Budget	CO2 Emissions	Time of Completion
3 Rows Anchor	100%	2430 tons	15 weeks
2 Rows Anchor	97%	2300 tons	12 weeks

Table 3 shows the project budget comparison, duration and CO2 emission changes in case the last row anchor is not constructed. Saving in the total cost of the project is only 3% however this revision could provide a reduction in completion time (20%) and also 5% decrease in CO_2 emissions.

Case 2 – Soil Nailing Wall

A shoring system was planned for an industrial building construction with variable excavation depths and different shoring techniques. The soil nailing section of the project was evaluated in this study as an example of monitoring data utilization in design. The excavation depth of this section was 23.00 m, with a perimeter of approximately 110 m. Borehole investigations revealed predominantly clay layers and weathered rock. No groundwater level was reported in the soil investigation report. The soil properties and models are presented in Table 4. The shoring system was determined as soil nailing wall in the beginning of the project. The section of the shoring system are given below. The shoring section was calculated Plaxis 2D (Fig. 8).

 © DFI International Bruges 2025

Table. 4. Soil Properties

Layer	Soil Model	γ (kN/m³)	Ø' (°)	c' (kN/m²)	E (kN/m^2)
Fill	Hardening Soil	19	29	5	5000
Completely Weathered Arkose	Hardening Soil	19	30	10	35000
Intermediate Weathered Arkose	Hardening Soil	21	35	20	100000

During the application, horizontal displacements of the shoring were monitored with an inclinometer. The inclinometer results are shown in the Table 5. Since the measured displacement value exceeded the calculated displacement value at the 8th excavation stage, additional piles and prestressed anchors were taken into consideration in order to increase the shoring safety (Fig. 8).

Within the scope of the local standards in Türkiye, the monitoring of excavation displacements and the precautions to be taken are examined in 3 categories. A red alert was given because the displacements in the site were 50% more than the maximum model displacement. And it was decided to take precautions for the shoring system.

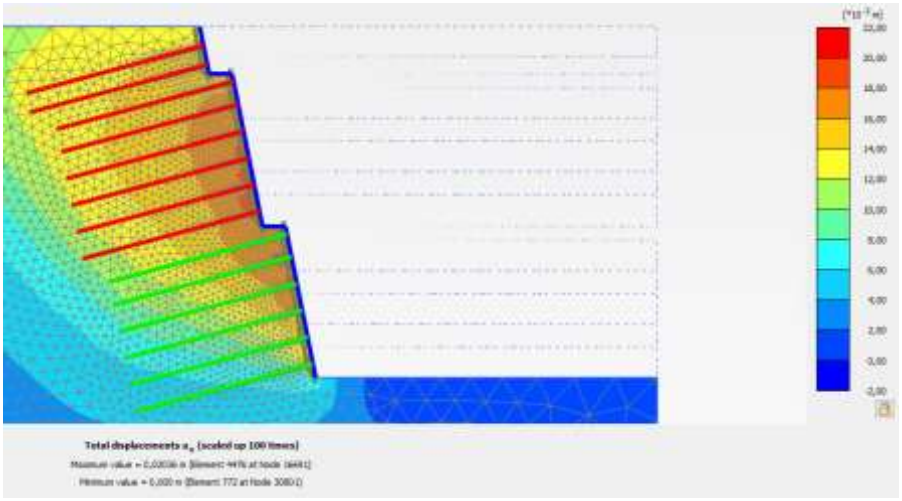


Fig. 8. Plaxis 2D - soil nailing solution

Table. 5. Displacement corresponding to excavation depth for soil nailing

Excavation Stage	**Depth (m)**	**Calculated Displacement for Soil Nailing (mm)**	**Occurred Displacement (mm)**
First Excavation	2.00	0.3	3.7
Second Excavation	3.10	0.5	5
Forth Excavation	6.00	1.0	13
Sixth Excavation	9.50	2.3	15.5
Eighth Excavation	13.10	6.3	20*
Tenth Excavation	16	7.7	29**
Twelfth Excavation	19,5	12.4	30**
Fourteenth (Final) Excavation	23	20.4	31**

* Two additional rows of anchors were added.

**The remaining excavation part was executed with bored piles and 3 rows of anchors.

 © DFI International Bruges 2025

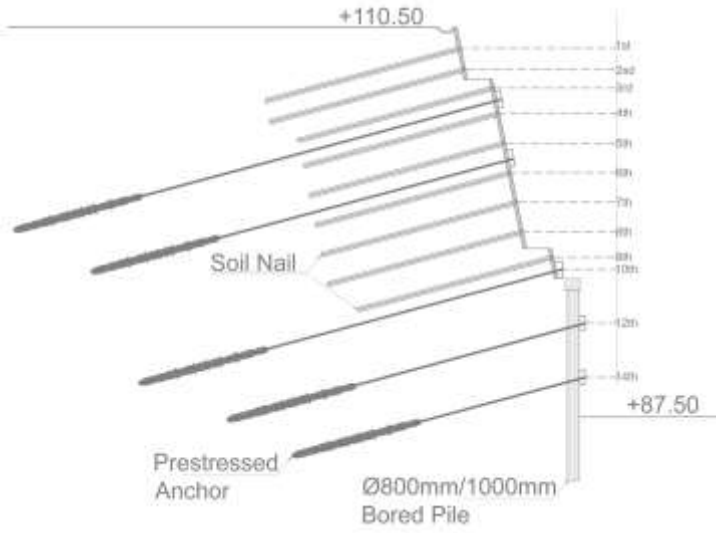


Fig. 9. Shoring system after revision

Initially, soil nailing was chosen as a cost-effective solution over bored piles and prestressed anchors. However, as monitoring data indicated excessive displacements, additional piles and prestressed anchors were incorporated to enhance the shoring system's safety (Fig. 9). If the section had been designed solely with an anchored bored pile system from the beginning, the cost would have been significantly higher. However, by employing this methodology, project cost, duration, and carbon emissions were optimized. The cost, duration, and carbon footprint comparison between the initially planned and revised shoring systems is presented in Table 6. Figure 10 shows the shoring system completed after the project revision.



Fig. 10. The shoring system completed after the revision

Table. 6. Comparison of different shoring systems

Shoring System	Budget	CO2 Emissions	Time of Completion
Anchored Bored Pile	100%	1,400 tons	20 weeks
Applied Mix System	92%	1,400 tons	16 weeks

Budget comparison, duration and CO2 emission changes between the cases if the anchored bored pile section was applied in the beginning or the applied case which mixed section with both soil nails and short bored piles were applied. Saving in the total cost of the project is approximately 8% however this

 © DFI International Bruges 2025

revision could provide a reduction in completion time (20%), carbon emissions were calculated approximately same between the cases in this project.

Observational Method – As a Cost Effective And Green Approach

The selection of characteristic values for geotechnical parameters must be based on laboratory and field test results, as well as the engineer's experience. Characteristic values of geotechnical parameters can be selected within a range of values considering the risk level. The BS EN 1997-1:2004 standard states that when geotechnical behavior is difficult to predict, it may be appropriate to apply the 'observational method,' wherein the design is reviewed during construction. Spross and Johansson (2017) explained that the observational method can be applied by determining acceptable behavioral limits based on the preliminary design. This method can provide both environmental and economic benefits by optimizing the design.

In this study, shoring design was developed based on displacement tracking to provide more economical solutions. At the project phase, it was planned to analyze shoring systems with different soil parameters and initiate construction using the optimal target. If model displacement values were exceeded, predefined additional measures could be implemented promptly. If model displacement values were not exceeded, a transition to a more economical and environmentally practical shoring system would be possible. A sample implementation scheme for the observational method is given in Fig. 10.

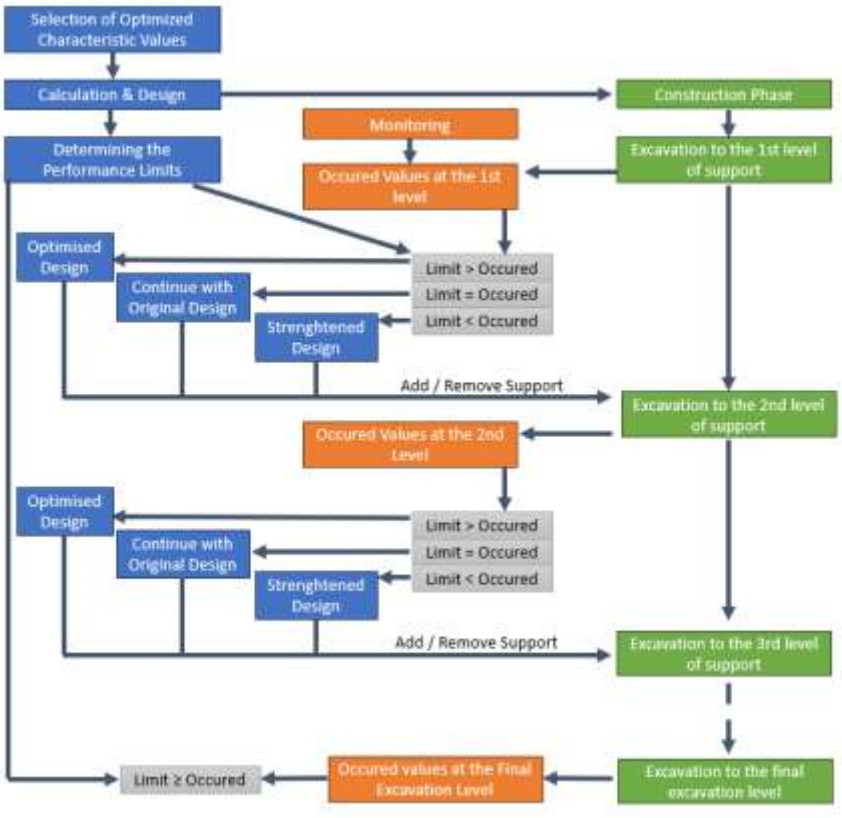


Fig. 10. Example of observational method scheme

 © DFI International Bruges 2025

SUMMARY AND CONCLUSIONS

A well-planned monitoring system allows for the re-evaluation of the design during excavation. Two case studies were presented in this paper, demonstrating design optimization possibilities.

- In the first case, a diaphragm wall shoring system initially designed with three rows of anchors was optimized by eliminating the last row based on monitoring data.
- In the second case, monitoring data indicated that the soil nailing solution was under-designed, and additional support measures were implemented to complete the excavation safely.

These cases highlight how the observational method can optimize support systems while also reducing total costs, project duration, and environmental impact. The observational method can be preferred in similar projects to achieve timely, cost-effective, and environmentally friendly solutions.

REFERENCES

British Standards Institution. (2003) BS 1997-1:2004. Eurocode 7: Geotechnical design - Part 1: General rules. London, British Standards Institution.

Spross, Johan, and Fredrik Johansson. "When is the observational method in geotechnical engineering favorable?" Structural safety 66 (2017): 17-26.

 © DFI International Bruges 2025

BORED PILES IN ROCK: RECENT DESIGN LESSONS LEARNED

Paul Axtell, P.E., BC.GE, Dan Brown and Associates, Overland Park, Kansas, USA, +1-816-210-1954, paxtell@dba.world

ABSTRACT

Over the last two decades, widespread implementation of bi-directional axial load testing has resulted in a wealth of data from full-scale load tests of rock-socketed bored piles. Accordingly, valuable insights are now available to help advance the state of practice with respect to both design and construction, making it practical to achieve satisfactory performance economically. Demonstrated behavior indicates when good design, construction, and quality assurance/quality control (QA/QC) procedures are followed, the design of bored piles in rock can be controlled by structural considerations, even in rock that is often characterized to have very poor quality.

Specifically, this paper will describe in detail the following lessons learned: 1) Rock socket side resistance and base resistance are mobilized at very small displacements (*i.e.*, immediately) and at compatible displacements. 2) What is often characterized as poor or very poor bedrock is often capable of providing axial geotechnical resistance in excess of the axial structural resistance of the reinforced concrete cross section, particularly when considering the contributions of both side and base resistance in a rock socket (see lesson 1). In such cases, the structural strength controls the axial design. 3) Construction controls the performance of bored piles and as an extension, design and construction of bored piles are inseparably linked.

This relatively new body of knowledge, when appropriately applied, has allowed the optimization of bored pile design and construction, reducing required rock socket sizes. Such optimizations are beneficial not only for project cost and schedule but also reduce the carbon footprint and risks associated with the construction of bored pile foundations in rock.

Keywords: Bored piles, rock, design, lessons learned, risk, optimize, carbon

INTRODUCTION

Bored pile rock socket excavation can be expensive and risky. Depending on the composition and integrity of the bedrock, drilling can be time consuming and can accelerate the wear of drill tooling when hard or abrasive bedrock exists. Or, in some more favorable instances, drilling bedrock can be relatively easy, especially with recent advancements in drill rig capabilities. Given the evolution of design requirements and equipment capabilities, design demands are increasing as are bored pile lengths and diameters necessary to resist the increased demand. When practical, socketing the bored piles into rock is desirable from both a design and performance perspective.

Over the past few decades, several valuable lessons have been learned regarding the behavior of bored piles socketed into bedrock. Unfortunately, in many cases, those hard-learned lessons are not currently being employed in current foundation designs, often resulting in:

1. uneconomical bored pile solutions;
2. increased and unnecessary exposure to construction risk;
3. increased and unnecessary exposure to performance risk;
4. avoidable post-construction anomalies and subsequent schedule and cost issues; and
5. larger carbon footprint.

Prior to the 1990s, full-scale axial load tests on bored piles with rock sockets were prohibitively expensive. The advent and implementation of bi-directional axial load testing has resulted in a wealth of data from full-scale load tests of rock-socketed bored piles. Accordingly, valuable insights have been gained to help advance the state of practice with respect to both design and construction, making

 © DFI International Bruges 2025

it practical to achieve satisfactory performance economically and with reduced exposure to construction risks. Demonstrated behavior indicates when good design, construction, and quality assurance/quality control (QA/QC) procedures are followed, the design of bored piles in rock can be controlled by structural considerations, even in rock that is characterized to be very poor quality. Some specific conditions warrant additional consideration, such a karstic bedrock, but these instances are now known to be the exception rather than the rule.

This paper details the following lessons learned with respect to bored piles with rock sockets:

1. rock socket side resistance and base resistance begin to mobilize immediately upon receiving load and at compatible displacements;
2. what is often characterized as poor or very poor bedrock is often capable of providing geotechnical axial resistance in excess of the axial structural resistance of the reinforced concrete cross section, particularly when considering the contributions of both side and base resistance in a rock socket (see lesson 1). In such cases, the structural strength controls the axial design; and
3. construction controls the performance of bored piles and as an extension, design and construction of bored piles are inseparably linked.

To support the lessons learned, a recent state of the art paper will be summarized, recent full-scale load test results will be presented, and a comparative summary of load test results spanning two decades on a single project will be discussed. This relatively new body of knowledge, when appropriately applied, has allowed the optimization of bored pile design and construction, reducing required rock socket sizes. Such optimizations are beneficial not only for project cost and schedule but also reduce the carbon footprint and risks associated with the construction of bored pile foundations in rock.

BACKGROUND

The lessons learned that are described below rely on certain fundamental practices of sound geotechnical and foundation engineering that have been augmented with recent advancements in technology. First, a thorough and comprehensive understanding of the geology and subsurface conditions is required. This is not unique to bored pile design and construction but should be a given on any geotechnical project. Physical boundaries between various strata as well as all pertinent engineering properties of the soil, bedrock, and groundwater regime must be understood; it is not possible to optimize foundation design otherwise. The nature and magnitude of the site investigation program must therefore be sufficient to adequately characterize the subsurface conditions. While this should go without saying in engineering practice, many projects still progress with insufficient site characterization at their own peril.

Second, appropriate design methodologies need to be utilized. Old “rules of thumb” without sufficient empirical support, or which were developed for construction techniques that do not apply, should be discarded in favor of more up to date methods developed using the sufficient body of evidence available following the advent of bi-directional load testing. The adage “that’s the way we’ve always done it” is often based on one instance of poor performance experienced some time in history and likely as a result of violating one of the fundamental necessities described herein.

Third, appropriate construction methodologies need to be utilized. This goes beyond drilling a hole and includes consideration of the entire process. This may involve constantly maintaining an adequate positive head above adjacent groundwater or artesian head prior to encountering the groundwater and until achieving initial set of the concrete. Cleaning both the base of the bored pile after drilling as well as the slurry fluid with an airlift or other means of suction at the base of the bored pile is necessary. Often, for bored piles placed in the wet, a cleanout bucket alone is insufficient as the sole means of cleanout. Careful consideration and implementation of the reinforcing cage pick and placement is necessary. A deformed cage or placement of the cage that

 © DFI International Bruges 2025

compromises the cleanliness of the excavation or the alignment of the cage within the excavation should be avoided. Proper methods for concrete placement, particularly when performed in the wet, are essential and excellent guidance on the topic is available in EFFC/DFI (2024). Note that the appropriate construction techniques briefly summarized above are all considered good practice even for routine bored piles.

Finally, although often under- or mis-used in current practice, valuable inspection tools exist to reliably evaluate the condition of bored pile excavations, even under water or slurry. Devices such as the mini-SID, SQUID, DID, SoniCaliper, SHAPE, etc., are capable of accurately evaluating the size, shape, alignment, and cleanliness of bored pile excavations prior to placement of the reinforcing cage and concrete. The additional time and cost of verifying the cleanliness of the excavation is insignificant compared to the effort required to address integrity or performance issues that may result from inadequate inspection. We have the tools at our disposal; we should use them to our advantage.

The lessons below are appropriate for bored piles founded in rock when proper design, which includes sufficient site investigation, construction, and inspection/verification are performed. These fundamental principles of foundation engineering are well established and are required prerequisites. Detailed information and guidance on these topics have been developed by the Federal Highway Administration (FHWA) and are available in Brown, et. al. (2018).

LESSON ONE

Rock socket side and base resistance mobilize immediately and at compatible displacements. A prevalent misconception exists within the industry regarding "strain compatibility" with respect to mobilization of the side and base resistance in rock sockets. This misconception likely stems from unfavorable axial load test performance during initial implementation of bi-directional testing technology in the early 1990's and 2000's. The poor results are probably a result of insufficient construction, cleaning, and inspection/verification or some combination thereof. The deleterious material remaining at the base of the socket due to lack of adequate cleaning and inspection result in unnecessarily large displacements necessary to engage and mobilize the available base resistance of the rock socket. These few and currently avoidable bad experiences appear to have shaped a mindset for subsequent decades.

The Deep Foundations Institute (DFI) recently published a consensus document (Axtell, et. al, 2022) encouraging the use of both side and base resistance in bored pile rock socket design. An excerpt from that paper's summary is provided below:

> For properly designed, constructed, and inspected rock-socketed shafts, this evidence shows that in the vast majority of cases, side and base resistances are mobilized at small, compatible displacements that are within the settlement tolerance of most structures. While there are specific rock formations found in select regions that warrant further consideration, rock socket behavior and design for these unique conditions should not be generalized to all cases.
>
> A key behavior illustrated by the load test data presented herein is that for cases in which the base of a rock socket excavation is properly cleaned and verified to be clean, significant base resistance mobilizes at small displacements on the order of 25 mm or less. Considering the drill tooling and inspection technologies currently available, a clean base can be achieved and confirmed, and base resistance can be relied upon with proper verification. Notably, the authors are unaware of any cases in which a rock socket that was cleaned and verified to be clean exhibited a "soft bottom" condition.
>
> Designs that disregard rock socket side or base resistance without a justified reason add significant cost to the project. Drilling in rock, especially large-diameter sockets

 © DFI International Bruges 2025

in very hard rock, can be one of the most challenging and expensive construction items on a project. Furthermore, increasing the length of a rock socket when it is not warranted increases the risk of encountering difficulties and problems during construction. Moreover, when base resistance is disregarded and thus procedures for cleaning and verifying a clean excavation base are not prescribed, geotechnical side resistance can be adversely impacted and the likelihood of concrete anomalies near the base of the shaft increases because sediment at the base is displaced outward and upward into the concrete during the pour.

In summary, the recommended best practice for design of rock-socketed drilled shafts is to account for both side and base resistance unless there is a valid documented reason to disregard one or the other on a project-specific basis.

The seemingly prevalent misconception that side and base resistance don't mobilize at compatible displacements or that excessive deformation is necessary to mobilize any substantial base resistance in rock sockets is definitively dispelled, as shown below in Figures 1 and 2 for properly constructed and inspected rock sockets. Both figures show results of bi-directional load tests, with displacement on the vertical axis versus bi-directional load on the horizontal axis. Positive displacement represents upward movement of the top of the bi-directional cell to mobilize side resistance. Negative displacement represents downward movement of the bottom of the bi-directional cell to mobilize base resistance. Figure 1 includes results from five sites with diameter ranging from 0.9 to 1.2 m.

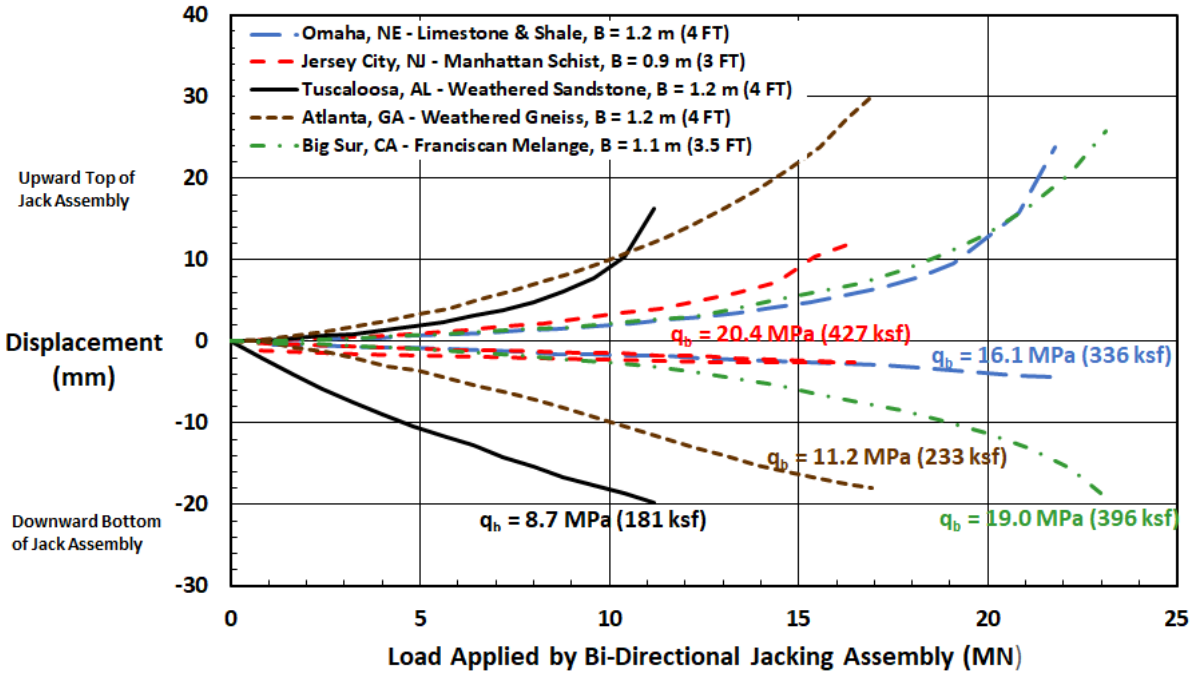


Fig. 1. Representative bi-directional load test results on rock sockets, diameter range 0.9 m to 1.21 m (*reproduced from Axtell, et. al., 2022*)

Figure 2 includes results from five sites with diameter ranging from 1.5 to 3.4 m. Results in both figures, from all ten sites, offer strong support for the consensus document recommendation to account for both side and base resistance in properly executed rock sockets.

 © DFI International Bruges 2025

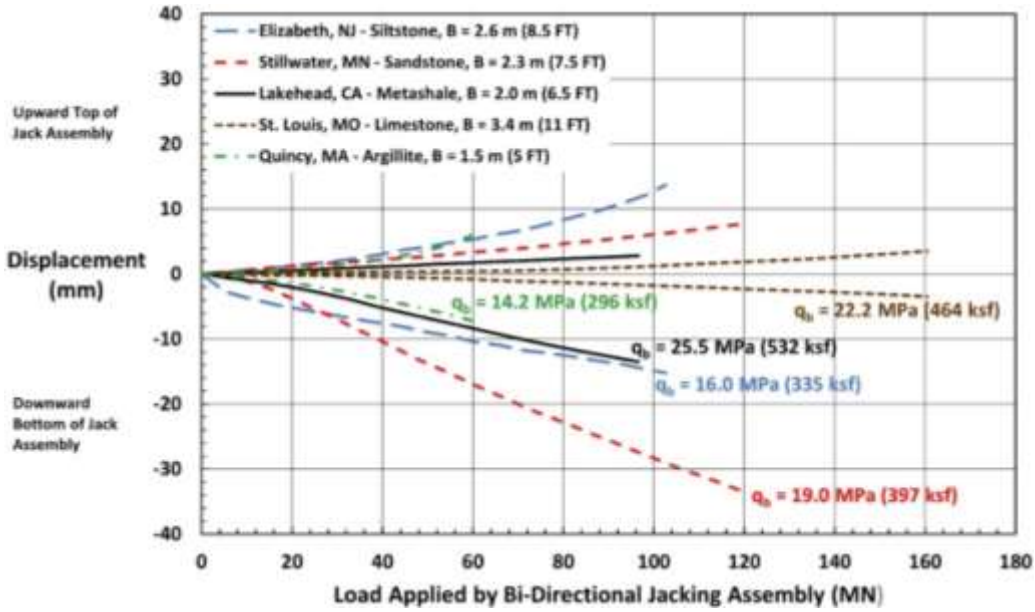


Fig. 2. Representative bi-directional load test results on rock sockets, diameter range 1.5 m to 3.35 m (*reproduced from Axtell, et. al., 2022*)

LESSON 2

What is often characterized as poor or very poor bedrock is often capable of providing geotechnical axial resistance in excess of the axial structural resistance of the reinforced concrete cross section, particularly when considering the contributions of both side and base resistance in a rock socket (see lesson 1). In such cases, the concrete strength controls the axial design of bored piles with rock sockets. This concept has been known for some time in highly competent bedrock conditions, as documented in Axtell and Brown (2011) as an example. Several recent bridge projects have included large diameter bored piles with rock sockets and subsequent axial load testing in bedrock conditions that are so poor that no recovery of cored samples could be obtained during the site investigation despite diligent efforts to do so. Results of the load tests, which were conducted on properly designed, constructed, and inspected/verified bored piles, indicate geotechnical axial resistance is available in these poor rocks exceeding what the structural engineer can apply to the column.

The following example is provided for a project from 2024 in Lansing, Iowa. Every attempt coring the sandstone bedrock during the site investigation failed to recover any samples. Two different borehole drilling subcontractors familiar with the regional and local geology made attempts with various bedrock coring tools, including double- and triple-tube systems. Regardless of the driller or the tooling, no core recovery was obtained in the sandstone bedrock of the Upper Cambrian Series and the Elk Mound Group. Since no core recovery was achieved, Standard Penetration Testing (SPT) was performed by both drilling agencies in the bedrock. The reported values of blows per 0.3 m (N) from one of the drilling agencies ranged from 44 to 77 with an average of about 59. The other drilling agency's measured and reported N values were all at refusal, ranging from 50 blows per 5 cm to 50 blows per 0 cm. Because no bedrock core samples could be obtained, no strength testing in the laboratory was possible.

To support the design and reduce uncertainty, a full-scale axial static load test using the bi-directional method was conducted on a sacrificial demonstration bored pile. The test bored pile included a 37.3-m long permanent casing through the soil overburden and embedded into the top of bedrock. The rock socket as measured beneath the tip of the permanent casing was 9.4-m long and 2.6 m in diameter. The base diameter of the test rock socket was reduced by casting a 1.83-m diameter, 5-cm thick steel plate attached to the bottom of the bi-directional cell test assembly into the bored pile. This effectively reduced the bearing area upon which the base resistance was acting, thereby

 © DFI International Bruges 2025

increasing the applied unit end bearing stress. The bi-directional test results are provided in Figure 3 by means of a butterfly chart, which presents the upward and downward displacement of the test assembly versus load. Note that the test assembly was located at the very base of the bored pile rock socket.

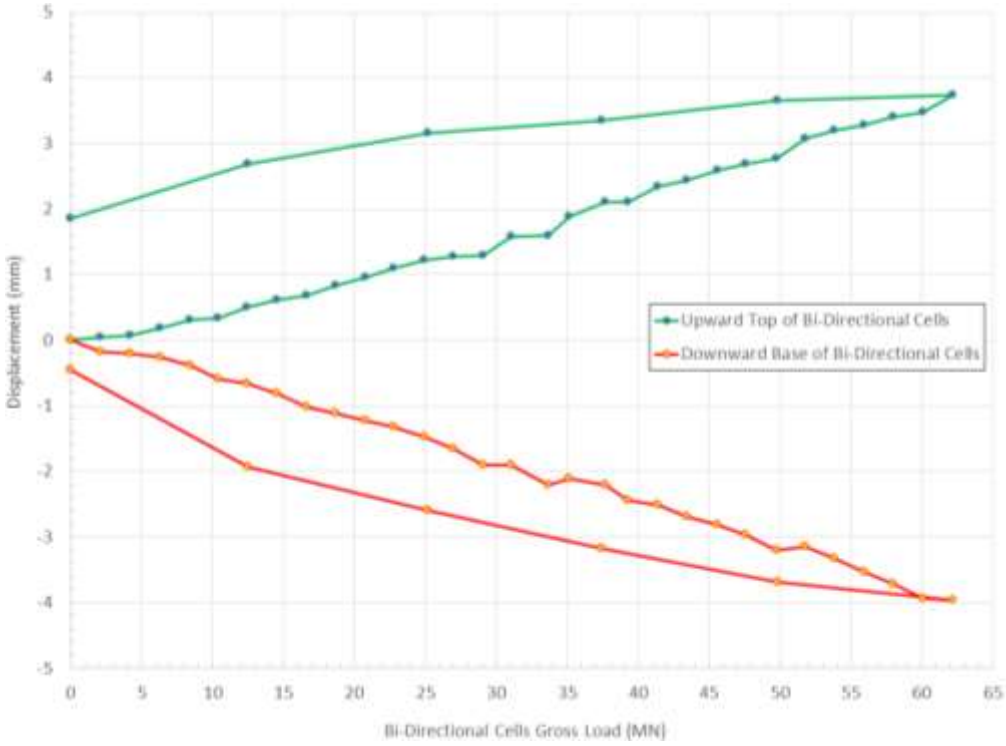


Fig. 3. Bi-Directional Test Butterfly Curve from Project in Lansing, Iowa (*reproduced from LoadTest, 2024*)

Tremendous load is being resisted both in side resistance above the cells and base resistance below the cells. Multiple levels of vibrating wire strain gages were installed in the bored pile, including the rock socket. Unit side resistance values inferred from the strain gage data indicate an average unit side resistance of 0.79 MPa was mobilized along the length of the socket during the test. Note that the maximum upward displacement above the cell assembly was only 3.7 mm. Therefore, a strength limit state was not attained and the nominal side resistance available in the socket is likely much greater than that demonstrated during the test. However, the test was terminated once the bi-directional cells reached 150 percent of their rated capacity, i.e., there was no more ability to impart additional load into the test pile even though it was capable of resisting more.

The mobilized unit base resistance was 21 MPa at a displacement of only 4 mm. Similar to the side resistance, a strength limit state was not achieved. Accordingly, the mobilized value is less than the nominal value, likely by a wide margin based on inspection of the base curve in Figure 3 which demonstrates mostly elastic behavior. Despite the limitations of the testing apparatus, the following facts are apparent:

1. the load is resisted immediately and at compatible displacement (see Lesson 1);
2. the displacements are very small and well within the acceptable tolerance of practically every civil engineering structure; and
3. despite not "failing" the pile to obtain the actual nominal values of side and base resistance, 124.4 MN of force was resisted at the location of the test assembly.

Given these facts, what is often characterized as poor or very poor bedrock can produce axial resistance on par with values traditionally only assigned to strong, competent bedrock. Bored pile

 © DFI International Bruges 2025

rock socket design, when properly designed, constructed, and inspected/verified can be controlled by the concrete strength for axial purposes, even in rock that is too weak to core or sample. When significant lateral loads resulting from seismic demands, vessel collision, wind, ice/debris, and/or scour are applicable, the diameter and the length of the rock sockets are usually, but not always, controlled by the required flexural strength and the minimum embedment to prevent geotechnical overturning.

LESSON 3

Construction controls the performance of bored piles, particularly for those founded in rock, and as an extension, design and construction of bored piles are inseparably linked. A unique opportunity to assess the influence of bored pile construction on rock socket behavior under axial load occurred relatively recently in Stillwater, Minnesota and is documented in Axtell, et. al. (2013). In that publication, the authors detail the observed profound differences in load test behavior between a bored pile rock socket constructed in 1995 and another constructed at the same site by the same contractor in 2012. Pertinent bi-directional load test results in terms of measured unit resistance values are shown below in Figures 4 and 5. The tested rock socket sizes, both in terms of diameter and length, are different, so direct comparison of the top-down load-settlement behavior is not directly applicable. The 1995 test was conducted on a 1.2-m diameter socket that was 8.5-m long. The 2012 test was conducted on a 2.3-m diameter socket that was 14.3-m long.

The mobilized unit side resistance measured in 2012 was approximately 60 percent greater than in 1995, and at approximately one-sixth the displacement, indicating substantially stiffer response. The mobilized unit base resistance measured in 2012 was five times that in 1995. However, the initial stiffness of the unit base resistance curves is similar, so it is possible the base resistance of the 1995 shaft would have been similar to that of the 2012 shaft if sufficient side resistance and testing capability had been available during the 1995 bi-directional test to demonstrate additional base resistance. An inability to maintain pressure in the bi-directional jacking apparatus was noted during later stages of the 1995 load test, suggesting some form of plumbing leak in the hydraulic lines, which may have limited the ability of the testing apparatus to mobilize additional base resistance, assuming it existed. It is noted that the bi-directional test method was still in the early stages of development in 1995.

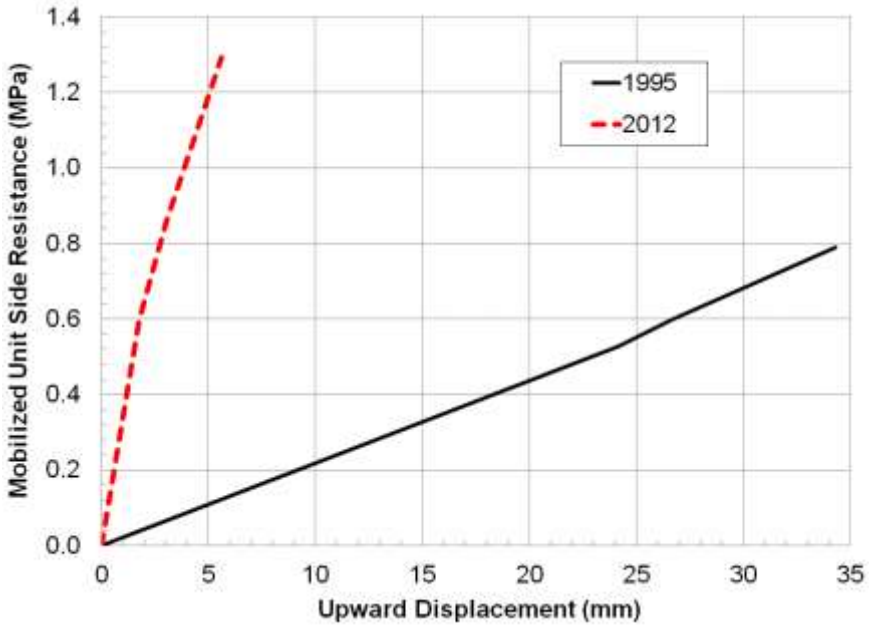


Fig. 4. Average measured unit side resistance in Stillwater, MN rock sockets (*reproduced from Axtell, et. al., 2013*)

 © DFI International Bruges 2025

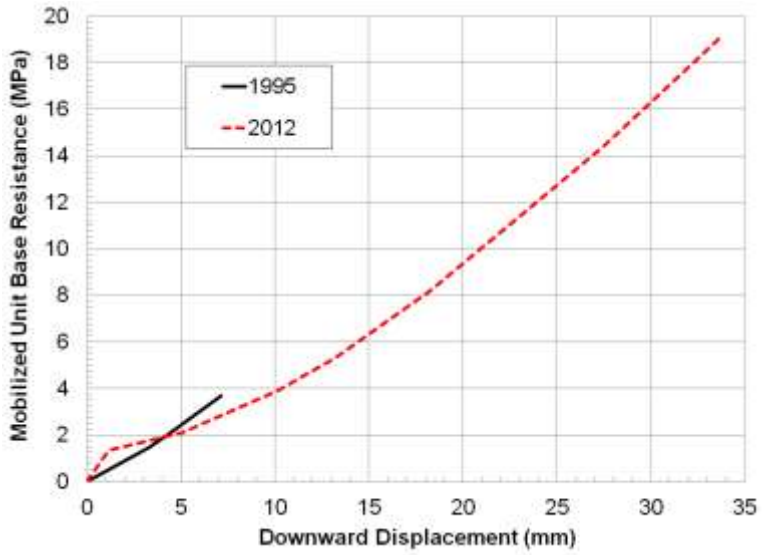


Fig. 5. Measured unit base resistance in Stillwater, MN rock sockets (*reproduced from Axtell, et. al., 2013*)

While the same contractor used essentially the same drilling method and in the same weak bedrock, careful attention was paid to the design and construction details in the 2012 test. Some of the notable differences in construction and inspection, along with anticipated influence on the respective test results as they may relate to measured side and base resistance from the two load tests, are provided below:

1. The use of polymer slurry in 2012 versus water in 1995. Studies have shown that the use of polymer slurry can be beneficial in preserving the integrity of some relatively poor bedrock materials, particularly as it relates to side resistance. The use of polymer slurry may or may not have influenced the base resistance response depending on Item 2 below.
2. Continuous maintenance and documentation of a positive slurry head within the casing at all times in 2012. Although unknown, it is possible, and suspected by the author, that a sufficient positive head was not maintained at all times during construction of the 1995 test. If so, both the side resistance and base resistance could have been negatively affected due to hole instability and potential basal heave. Presumably, maintaining a positive head of polymer slurry (2012) would have been easier than maintaining a positive head of water (1995).
3. Imposed time limitations regarding the duration in which the rock socket can be open upon both starting the socket and completing the socket in 2012. The potential for additional stress relief, degradation of the bedrock, and difficulty to continuously maintain a sufficient positive head for the extended duration of the 1995 test could all negatively impact the measured side resistance.
4. Final cleanout with an airlift in 2012 versus a one-eyed cleanout bucket in 1995. While the initial stiffness of the mobilized base resistance is similar in both tests, suggesting a clean base, airlifting has the added benefit of cleaning the drilling fluid. Suspended sediment in dirty drilling fluid that precipitates out of suspension with time can negatively impact both side and base resistance. The influence on base resistance is obvious if the sediment accumulates at the base prior to concrete placement. The influence on side resistance is less obvious if the sediment precipitates out of suspension during concrete placement, as discussed in Item 5 below. It is noted that use of a one-eyed cleanout bucket may re-introduce solid particles back into suspension in the drilling fluid as the bucket is withdrawn.

 © DFI International Bruges 2025

5. Sufficient cleaning of the drilling fluid to remove suspended solids that would otherwise precipitate out of suspension after cleanout but prior to/during concrete placement. As stated above in Item 4, the initial base response does not suggest a dirty base, but the effect on side resistance is uncertain.
6. Continuous inspection by qualified foundation engineers familiar with the design assumptions and with bored pile construction in 2012. Due to the complex and critical nature of bored pile construction, particularly in the wet, constant and vigilant inspection by qualified individuals is a necessity. The author can attest with certainty that sufficient inspection was performed in 2012 but is not aware of the level of effort in 1995. This could influence either the mobilized side resistance, mobilized base resistance, or both.
7. Application of the mini-SID to visually inspect the cleanliness of the base of the socket in 2012 versus weighted tape measurements in 1995. While this was a notable difference between the two tests, the initial response of the mobilized base resistance does not indicate the presence of a soft bottom in 1995. Presumably, there would be no effect on side resistance. Regardless, the author considers it good practice to verify the cleanliness of the socket base with more refined tools such as the mini-SID or similar, which are readily available in today's market.
8. Use of a sufficiently workable, flowable, stable concrete mix that also possessed adequate workability retention in 2012. While a relatively workable mix based on high slump was used in 1995, the stability, flowability, and workability retention of the mix are unknown. If quality concrete is not in intimate contact with the socket wall, after flowing through the reinforcing cage and remaining uncontaminated/unsegregated, the side resistance could be negatively affected. It is also noted that slump is not a reliable indicator of fresh concrete properties when it exceeds 15 cm.

Based on results from the 1995 and 2012 load tests, careful attention to quality during construction likely had a substantial influence on the side resistance, while the impact on base resistance could not be sufficiently evaluated due to testing limitations in 1995. While no single factor can be definitively identified from the 1995 test that lead to the lower demonstrated resistance, we can confidently conclude, in aggregate, improvements in methodology and process produced much better results in 2012 in the same bedrock. Informed and vigilant attention to details during the design and construction of bored piles with rock sockets leads to superior performance of the foundation element as demonstrated by side-by-side full scale load test results. As an extension, considerations of bored pile constructability should begin at the onset of the design process and should run concurrently through the entire process. Similarly, bored pile construction should be observed by informed engineers familiar with, and responsible for, the foundation design.

SUMMARY

The advent of bi-directional load testing has advanced the state of the practice with respect to bored piles founded in rock. Testing has confirmed that proper design, including sufficient site characterization, construction, and inspection/verification of bored piles founded in rock can produce geotechnical axial resistance similar to if not exceeding the structural resistance. An appropriate body of knowledge has been obtained over the past three decades that produces sufficient evidence to support the following lessons learned:

1. Rock socket side and base resistance mobilize immediately and at compatible displacements in most cases. Exceptions do exist, but they are considered the exception rather than the rule. Unless a rational, documented reason exists, both side and base resistance should be relied upon in design.
2. What is often characterized as poor or very poor bedrock is often capable of providing geotechnical axial resistance in excess of the axial structural resistance of the reinforced concrete cross section, particularly when considering the contributions of both side and base resistance in a rock socket (see lesson 1). In such cases, the concrete strength controls the axial design.

 © DFI International Bruges 2025

3. Construction controls the performance of bored piles, particularly when founded in rock, and as an extension, design and construction of bored piles are inseparably linked.

The necessary tools exist to reliably design, construct, and inspect/verify bored piles founded in rock, even those constructed in the wet. Using these tools to our advantage is becoming increasingly more necessary as drill rig equipment continues to increase in size, power, and capability. Finally, in addition to cost, schedule, and risk reduction benefits, optimization is required to protect our depleting natural resources.

ACKNOWLEDGEMENTS

Many colleagues have contributed to this effort by imparting knowledge, guidance, and valuable experience. David Graham, P.E., John Turner, Ph.D, P.E., and Dan Brown, Ph.D, P.E., to name a few individuals, have been instrumental in the work and these lessons learned would not have been possible without their involvement. My friend Andy Boeckmann, Ph.D., P.E., was kind enough to provide much needed editorial review and comment and for that I'm grateful. Many of the bi-directional tests used to inform these lessons learned have been conducted by Bill Ryan and his associates at Fugro Loadtest. The DFI Drilled Shaft Committee has also been a productive voice in attempting to advance the state of the art of bored pile design and construction.

REFERENCES

Axtell, P.J. and Brown, D.A. (2011) "Foundations for the New Mississippi River Bridge, St. Louis," *J. of Deep Foundations Institute*, Vol. 5, No. 2, pp. 3-15.

Axtell, P.J., Brown, D.A., Lamb, R.A., Graham, D.S., and Ryan, W.G. (2013) "St. Croix Bridge, Minnesota: The Influence of Construction on the Axial Resistance of Drilled Shaft Foundations in Weak Sandstone," *Proceedings: Deep Foundations Institute 38th Annual Conference*, pp. 125-133.

Axtell, P., Turner, J., Turner, B., Jacobs, S., McIntosh, K., Vega, B., Hertlein, B., and Gomez, J. (2022) "Combined Side and Base Resistance in Rock-Socketed Drilled Shafts – A State of the Art Consensus," *J. of Deep Foundations Institute*, Vol. 16, No. 2, pp. 1-9.

Brown, D.A., Turner, J.P., Castelli, R.J., and Loehr, J.E. (2018) "Drilled Shafts: Construction Procedures and Design Methods," U.S. Department of Transportation, Federal Highway Administration, Publication No. FHWA-NHI 18-024, FHWA GEC 10, September 2018.

EFFC/DFI Joint Concrete Task Group, (2024) "Guide to Tremie Concrete for Deep Foundations," Third Edition, revised December 2024.

LoadTest (2024) "Report on Drilled Shaft Load Testing (Osterberg Cell® Method), TS-1 _ IA 9 Mississippi River Bridge Project Allamakee County, IA," February 20, 2024.

 © DFI International Bruges 2025

PILE LOAD TESTING AND DATA COLLECTION ADVANCES IN THE LAST TEN YEARS AND THE CASE FOR DESIGN OPTIMISATION

Zoe Baldwin, Cementation Skanska, Doncaster, UK, zoe.baldwin@skanska.co.uk

Anthony Fisher, Cementation Skanska, Doncaster, UK, Anthony.fisher@skanska.co.uk

ABSTRACT

There have been significant developments within ground engineering over the past ten years in terms of pile load testing, however opportunities relating to scheme optimisation and performance based design are not being realised in most cases. Static load tests of up to 50MN have been carried out in the UK and the ability to test piles up to 30MN is readily available. Alongside this, advances in measuring real time strain along the length of the pile and displacement mean that piles are being tested to higher loads and higher quality meaningful data is being collected. This in turn gives us a better understanding of pile behaviour both at serviceability limit state and ultimate limit state, alongside improved data on the strength of the soils that we are installing piles into. However, even though this data is incredibly meaningful, project programme pressures and lack of Client buy-in means that this data is usually being used for design validation rather than optimisation.

This paper will set out examples of where high quality data has been obtained in the UK in the last ten years, how these advances can better be embraced to impact design optimisation and why this should be considered in the early stages of design development.

KEYWORDS: deep foundations, piling, embodied carbon, design optimisation, sustainability, value engineering, design, geotechnical design, net zero.

INTRODUCTION

Design optimisation and value engineering are critical processes in ground engineering projects. Not only are they often used as comparators in a competitive bidding situation by Clients when assessing which contractor to award a contract, they are also critical for the reduction of embodied carbon in construction projects. However, projects often struggle for the essential buy-in from Clients that allows the full process for design optimisation to be realised, with most projects falling short. Within the UK, the ground engineering sector size for the 2023 financial year was approximately £2,565M with £1,754M being the turnover for 50 of the biggest ground engineering contractors in the UK (GE Top 100, 2024). A significant portion of the costs of a ground engineering project is materials and based on the size of the ground engineering contractor turnover in the UK, active and intentional design optimisation could provide significant savings to Clients as well as impact the embodied carbon in projects. There is often the *expectation* that value engineering and design optimisation will happen, but projects are rarely set out at the initial stages with this as a clear *intention*.

For design optimisation to take place there needs to be the buy-in from stakeholders early in the project realisation process, whereas the reality is often that it is a late add on from a Client or Principal Contractor who wants to try and make a cost or programme saving too far into the procurement process for it to fit into planning and programme requirements. As a result, it is often not considered early enough in the project to allow for sufficient consideration in cost and programme to allow it to take place. There seems to be several factors which contribute to lack of early engagement specific to piling contracts within the UK, these include:

 © DFI International Bruges 2025

1. Lack of understanding and intention in the early stages of project planning and design
2. No consideration in initial cost planning stages
3. Lack of ground engineering specialist input in very early stages
4. Unwillingness of the Client to pay upfront costs with no guarantee on exact value of savings
5. Unwillingness of ground engineering contractors to engage with a Client prior to contract award to carry out up front proposals for efficiencies as these would be undertaken without compensation on a "goodwill basis" and without commercial protection ensuring that these proposals are not given to others in a competitive market to drive further perceived efficiencies/value
6. Lack of understanding in how to engage a ground engineering contractor in the earlier stages of design development
7. Lack of understanding in how to engage a ground engineering contractor in a pre-construction services agreement (PCSA) contract or similar
8. Perception that early engagement of a ground engineering contractor doesn't provide good value as the Client is choosing a contractor too early in the process to result in prices being driven down in a competitive environment
9. Size of project vs upfront monetary and programme requirements may not be viable (e.g. for smaller, domestic projects)
10. Principal contractor doesn't have their contract in place with the Client sufficiently in advance of the piling contract so they can't action a PCSA. In this instance the PCSA needs to come from the Client, who in many cases, is unwilling to do this (see items 4 and 5)

This paper discusses the advances in instrumentation and load testing over the last ten years within the UK and specific to projects undertaken by Cementation Skanska Ltd, and provides project examples of where more up front engagement could have resulted in programme, cost and carbon savings for the project.

CURRENT SITUATION

Within the UK, the procurement and award of ground engineering projects are generally undertaken in a competitive bidding environment where the scheme design is sufficiently progressed to allow foundation elements to be quantified and a cost plan put in place for the Client and other stakeholders for the overall project. This is then put out to competitive tender, usually by a Principal Contractor who is also bidding for the project. In the experience of most ground engineering contractors, the design stage at which the initial bidding takes place is usually between RIBA stage 2 and RIBA stage 3. Once a contract has been awarded, the design information will then move to RIBA Stage 4.

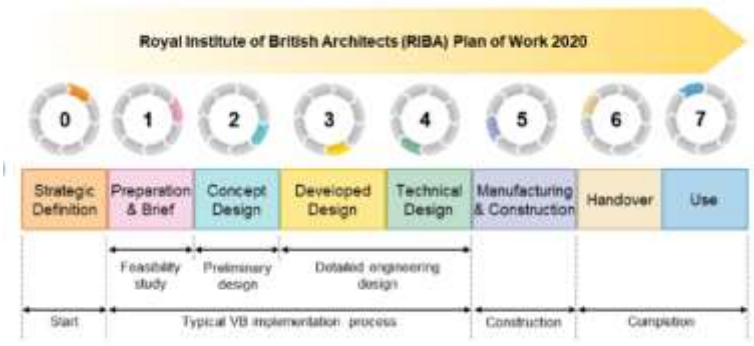


Figure 1 – RIBA plan of work (2020) including design stages

 © DFI International Bruges 2025

Although early engagement with a ground engineering contractor with the UK doesn't require any sort of framework agreement and despite RIBA Stage 3 including pre-contract services agreements (PCSA) within the procurement route, these are seldom used or implemented on projects, and yet they are arguably key to being able to deliver design optimisation on projects. A PCSA or similar agreement with a ground engineering contractor provides a sense of safety where a contractor will be compensated for the time and work put into understanding Client needs, including risks and programme, it promotes a collaborative approach between all the stakeholders and allows direct collaboration with the scheme designer. Without this collaborative approach, the full extent and benefits of design optimisation within ground engineering projects is not going to be achievable.

THE GROWTH OF INSTRUMENTATION AND LOAD TESTING

Load testing

Over the last ten years the market for sophisticated instrumentation being installed into ground engineering elements such as piles, micro piles and diaphragm walls has increased significantly. The capability of piling rigs to install deeper and bigger piles has meant the demand to test piles to higher loads in order to understand pile performance, reduce factors of safety following load tests and implement design efficiencies has also increased. This is further compounded by the development of urban sites which have already had multiple phases of use meaning that foundation congestion in redeveloped urban sites often now requires a greater load to be taken by fewer piles.

The need to test piles to higher loads is also driven by the requirement to improve our understanding of the behaviour of highly loaded foundations. Only through testing them to failure will it be possible to understand their performance and improve the efficiency of their design, resulting in both economic and carbon related savings. With the exception of the bi-directional load test, which can be an effective means of testing in appropriate ground conditions, the UK's testing capacity has been limited to the availability of suitably sized reaction frames. As a result, test loads have often been limited to 30MN and, where this is insufficient, additional measures such as slip liners and reduced diameter testing have had to be employed. The other alternative has been to build bespoke testing frames such as that used on the 21 Moorfields Project in London (undertaken by Cementation Skanska in 2015) where piles were tested to a maximum load of 50MN.



Figure 2 – bespoke load test frame at 21MF, courtesy of Robert Bird Associates

Recently, responding to this need, Cementation Skanska have developed a modular reaction system capable of carrying out static load tests of up to 60MN, which to date has been used to test piles in

 © DFI International Bruges 2025

excess of 30MN. This reaction system will enable tests to be carried out at full scale and without other compromising features which make the interpretation of results more complicated.

Instrumentation

Over the last ten years, the instrumentation that Cementation Skanska has installed into foundation elements has increased significantly. This instrumentation has included thermal cable for integrity testing (CemOptics™), vibrating wire strain gauges (VWSGs), extensometers and distributed fibre optic sensing cable (DFOS) for strain.

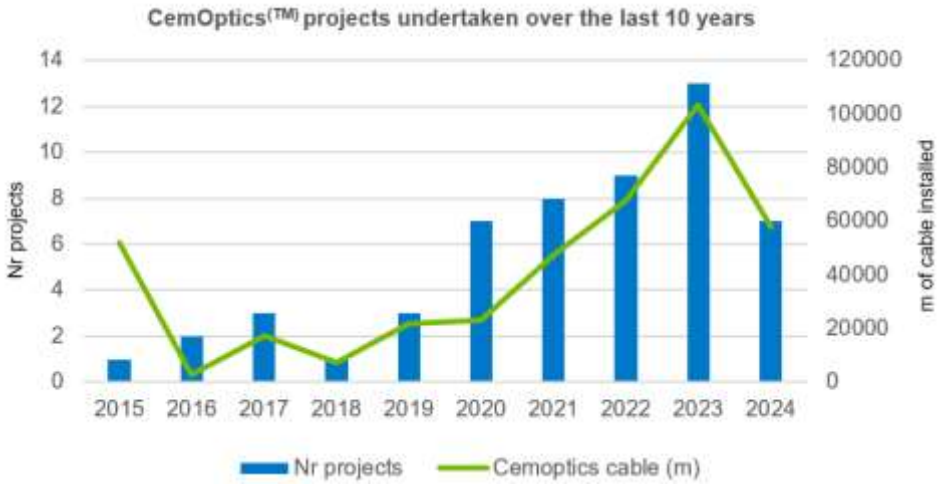


Figure 3 – Number of projects and length of thermal fibre optic cable installed for CemOptics™ testing over the past ten years.

VWSGs have been used in infrastructure and ground engineering to measure strain as part of both short term and long-term monitoring strategies for several decades but the use of DFOS to measure strain is relatively new. Distributed Fibre Optic Sensing (DFOS) works using the principal of optical time domain reflectometry where laser light propagating along the fibre optic cables is reflected or back scattered due to varying properties in the glass itself. Frequency analysis of this backscatter yields information about temperature and strain at the point from which the reflection originated. The benefits to piling and other ground engineering projects is the ability to determine the strain along the length of the pile as one long continuous measurement rather than at discrete intervals as with VWSGs. This allows for a better understanding of strain and load along the pile shaft and base. It can provide much more detailed information about the shaft friction and end bearing in layered stratigraphy compared to VWSGs.

 © DFI International Bruges 2025

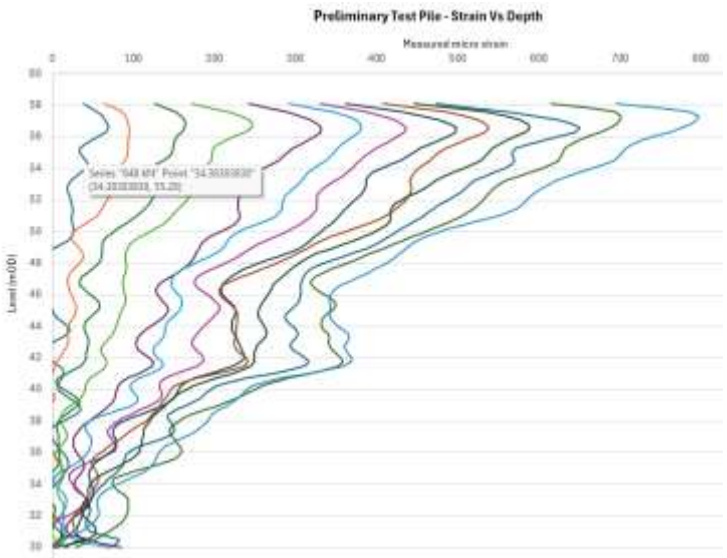
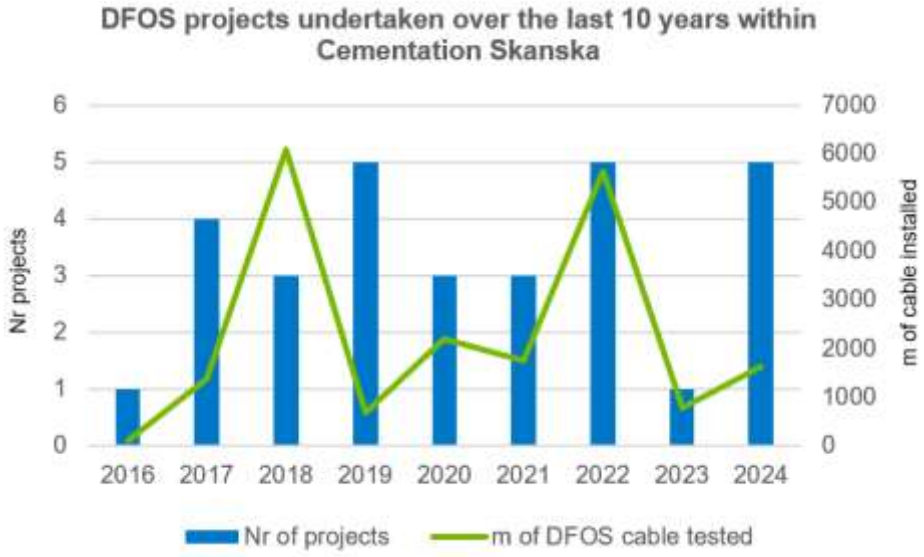


Figure 4 – measurement of strain with depth (mOD) in a 30m long CFA preliminary pile test

Cementation Skanska utilized DFOS in a preliminary micro pile test at the Broadgate development project in London in 2012. One of the earliest major projects (if not the first) to commercially adopt DFOS in the UK was at Farringdon Station in London, under the C435 contract for new ticket halls and tunnels for the Crossrail development in 2013.This contract was undertaken by Cementation Skanska and involved the installation of 26nr large diameter, base grouted rotary bored piles and a single bi-direction static load test using Osterberg load cells. The DFOS cables were used for the measurement of strain during the load test.

Since these initial contracts, the number of projects and the amount of DFOS cable Cementation Skanska has installed and utilised has increased significantly (Figure 5). Alongside this, the capability of installation of DFOS into continuous flight auger (CFA) piles has progressed significantly with cable frequently being installed into CFA piles up to 30m in depth.



Draft figure 5 – Number of projects and length of DFOS cable tested the past ten years.

 © DFI International Bruges 2025

The installation of DFOS as part of a design optimisation strategy has significant benefits in terms of providing a strain profile over the entire length of the pile which can then be converted to force, allowing interpretation of measured shaft friction long the length of the pile. This can then be compared against design parameters, allowing the design to be reviewed and potentially optimised using a combination of measured parameters and geotechnical strength testing, rather than parameters wholly interpreted from strength correlations and testing in the ground investigation.

This allows for huge scheme optimisation potential and even if measured shaft friction and end bearing fall below those values expected, this can still have added project benefits as it would allow early understanding of the ultimate geotechnical strength of materials which could be incorporated into the design before it significantly impacted the project. Historically this realisation would have happened when working test piles might have underperformed, however with early instrumentation and pile load testing, any implications for increased settlement profiles can be reviewed and incorporated into the scheme designer's model before project commencement. Thus it is also a potential tool to understand the ground in much more detail and deal with unknown ground risk before projects commence on site.

EMBODIED CARBON

The climate emergency is now a priority when it comes to the built environment with public bodies, professional bodies, Clients and stakeholders trying to achieve net zero carbon in line with the 2015 Paris Agreement (emissions reduced by 45% by 2030 and net zero by 2050) and aligning their values with the UN goals for sustainable development.

The key influence of ground engineering projects on whole life carbon emissions is through embodied carbon (emissions from making, placing, transporting and disposing of construction materials) rather than operational carbon. Operational carbon is generally reducing with the decarbonisation of energy sources so embodied carbon is becoming a larger percentage of the whole life carbon of projects.

It is generally accepted that the earlier carbon is considered in a project, the more impact it can have This aligns with the early involvement of contractors collaborating on projects to maximize the impact on design optimization, risk management, cost efficiency, scheduling, and embodied carbon reduction.

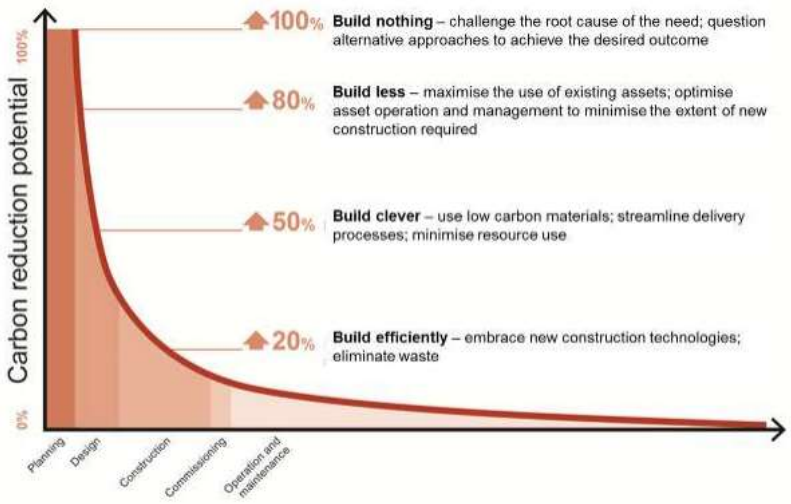


Figure 6 – The carbon reduction curve, taken from The Green Construction Board, Infrastructure Carbon Review Technical Report (2013)

 © DFI International Bruges 2025

In line with the need to impact carbon emissions, design optimisation continues to be a key element in realising this and reaching net zero.

CASE STUDY EXAMPLES

Below there are two case studies that Cementation Skanska were awarded the piling contract for. In both instances preliminary test piles were undertaken in advance of the main piling works, but there was insufficient early engagement to allow design optimisation to be undertaken, instead the preliminary test piles were used to validate the design, rather than offer any savings to the scheme.

	Project 1	**Project 2**
Type of project	Large commercial	Large industrial
Dates undertaken	2021-2022	2023-2024
Piling works	CFA piles of 600mm, 750mm and 900mm diameter Rotary piles of 650mm and 900mm diameter 4nr preliminary test piles and 15nr working test piles	CFA piles of 600mm, 750mm and 900mm diameter Rotary piles of 1180mm diameter 4nr preliminary test piles and 16nr working test piles
Piling programme	20 weeks	25 weeks
Total build programme	36 months (~140 weeks)	38 months (150 weeks)

Table 1 – Case study information for two projects undertaken by Cementation Skanska

Design validation

For both projects, preliminary test piles were installed around four weeks in advance of the main piling works commencing and all main works permanent bearing piles were designed and installed using reduced factors due to preliminary and working pile tests being carried out. For both projects DFOS and VWSGs were installed into four preliminary test piles.

Unfortunately, the four week period in advance of the main works may have been acceptable for traditionally installing and testing preliminary test piles for design validation, but it did not give sufficient time to review and interpret the strain data collected before the main piling commenced and it did not allow for any design optimisation based on the preliminary test piles. As a result, the test piles validated the design approach but no further benefit was taken.

Optimisation benefits

With hindsight, and reviewing both these projects, the potential benefits if earlier contractor engagement happened would have included:

- Optimisation of pile lengths and diameters based on measured data alongside geotechnical test data and current industry guidance
- Increase in design values for shaft friction of up to 30%. Note that these values still sit within current industry guidance
- Reduction in material costs
- Reduction in embodied carbon emissions
- Cost saving to the Client

 © DFI International Bruges 2025

	Project 1	Project 2
Cost savings against original scheme	Concrete 16.6% saving on concrete volume 6% cost saving >£200k as a value Rebar 8% saving to rebar tonnage 2.5% cost saving >£150k as a value	Concrete 19.2% saving on concrete volume 9.3% cost saving >£300k as a value Rebar 11.3% saving to rebar tonnage 3% cost saving >£100k as a value
Carbon savings against original scheme	19.2% on concrete 8% on rebar	19.3% on concrete 11.3% on rebar

Table 2 – Indicative savings that could have been realised from design optimisation early contractor engagement. Comparisons of carbon are based on concrete mix CIIIB - 28/35 MPa with embodied carbon taken from the ICE database – embodied carbon database. Reinforcement embodied carbon is based on CARES and BRE industry average.

Note that in this instance, and is likely for a lot of ground engineering contracts, the most embodied carbon is in concrete rather than the rebar due to the ratio of steel to concrete in a pile

Advances in test loads

For Project 1, the maximum load that was applied to 600mm preliminary test pile was 7.8MN, which at the time was considered a high load to apply to relatively small diameter piles. However, based on experience on this project, 600mm PTPs were again installed for Project 2, but the load was pushed even further to 12.1MN as a maximum test load, in addition to this, a 750mm rotary test pile had a maximum load of 13.5MN applied. Based on these applied loads, none of the piles were pushed to their ultimate capacity with maximum displacements of less than 40mm in all instances and in some cases less than 20mm. Had earlier engagement been in place, there may have been the opportunity to test the piles to higher loads and gain insight into ultimate shaft friction acting on the piles as well as how much end bearing was contributing to the pile capacity.

Early engagement costs – a piling contractor perspective

If ground engineering contractors are to be engaged earlier to undertake value engineering and design optimisation there is a cost for the contractor's time and effort. Based on current projects where Cementation Skanska are proposing earlier engagement, a simplified process with an upfront programme and cost has been submitted to Clients. Generally the programme is a 12 week upfront period which includes collaborative working with stakeholders whilst preliminary test piles are being installed and tested. Following testing, further review, collaboration and agreement occurs with the Cient and scheme designer, followed by full design release by the piling contractor.

 © DFI International Bruges 2025

	Weeks											
	1	2	3	4	5	6	7	8	9	10	11	12
Install test piles and reaction piles												
Test piles curing												
Stage 3 RIBA information available												
Initial design and collaboration based on RIBA 3												
Load tests undertaken												
Review and interpretation of test piles												
Collaboration and review of pile tests												
RIBA Stage 4 released												
Finalisation of pile design and release												

Figure 6 – proposed programme for early piling contractor engagement for design optimisation

The programme and process represented in Figure 6 is an idealised programme and some flexibility may be required in order to meet specific deadlines, however as an intention, it proposes a relatively small amount of time and resource up front compared to both the overall project build time and as a percentage of the piling cost. Based on Project 2 in the case studies section (used as it is the most recent), the programme time required represents 8% of the total build time and just 1% of the total piling contract cost. Compare this to the percentage savings on the piling contract cost detailed in Table 2 and there is significant reason to engage ground engineering contractors early in project planning and the design stages.

PROPOSALS FOR THE FUTURE

If Clients expect design optimisation and value engineering to be an important part of the design phase of their project, they need to engage ground engineering contractors as early as possible to realise cost and carbon benefits. There needs to be better understanding of the ways in which Clients can engage, compensate and create a collaborative working environment to allow contractors to understand project needs, Client requirements, the scheme design and project risk. Early stage project costing and proposals need to include allowances for PCSA type contracts in project programmes and costs and these need to be communicated to the Client to engage them and gain their buy-in as early as possible. If value engineering and scheme optimisation is an expectation, then projects and contracts should start out with this as a clear intention.

CONCLUSIONS

Pile load testing and sophisticated instrumentation capabilities have progressed significantly in the last ten years, providing data on the ground and pile performance. These advances should be utilised on projects as much as possible to provide information to allow design optimisation and value engineering to be carried out, not just design validation.

The two project case studies have shown that with relatively minimal programme and cost impact, there are significant savings to be made in both cost and carbon with early contractor engagement. An increase in cost of 1% to a piling contract is almost insignificant compared to the savings of around 10% on cost and almost 20% saving on carbon for some materials.

As an industry, if we are to remain at the forefront of sustainability by design for the built environment and to reach the net zero goals required to prevent the climate emergency, then Clients and project stakeholders should be prioritising early contractor engagement and design optimisation on all their projects.

 © DFI International Bruges 2025

AKNOWLEDGMENTS

The authors would like to thank Andrew Bell at Cementation Skanska for his support with the case studies in this paper and the technicians within Cementation Skanska's testing business stream that have spent significant time and effort installing instrumentation and gaining high quality, meaningful data in the past ten years.

REFERENCES (DRAFT)

Baldwin et al, 2015, Proceedings of the 16th European Conference on Soil Mechanics and Geotechnical Engineering. Innovative use of micro-pile groups to replace hand dug under ream piles at 5 Broadgate, London.

Broadbent 2015, Base Grouting, Osterberg Cell Test and The Use of Fibre Optics in Large Diameter Rotary Board Piles, Crossrail learning Legacy

Kechavarzi (2016). Distributed Fibre Optic Strain Sensing for Monitoring Civil Engineering Infrastructure: APractical Guide. Authors: Cedric Kechavarzi, Kenichi Soga, Nicholas de Battista, Loizos Pelecanos, Mohammed Z E B Elshafie and Robert J Mair Published 2016.

Lam and Jeffries (2011). Critical assessment of pile modulus determination methods, Carlos Lam and Stephan S. Jeffries, Canadian Geotechnical Journal, 2011, 48 (10), pp. 1433-1448.

Ouyang Y et al, 2015, Proceedings of the 16th European Conference on Soil Mechanics and Geotechnical Engineering, 'The use of fibre optic instrumentation to monitor the O-Cell load test on a single working pile in London'

GE100 2024, The leading Ground engineering Firms in the UK, Ground Engineering Magazine, 23rd September, 2024

Embodied Carbon – The Inventory of Carbon and Energy (ICE database)

RIBA Plan of Work 2020 Overview - Royal Institute of British Architects.

Infrastructure Carbon Review Technical Report, 25th November 2013 – The Green Construction Board

 © DFI International Bruges 2025

EXECUTION OF BORED PILES UNDER POLYMER FLUID SUPPORT – SUSTAINABLE AND FLEXIBLE CONCEPT FOR A MEGA PROJECT

Rabea Barhum, BAUER Spezialtiefbau GmbH, Germany, +49 (8252) 97-3854,
rabea.barhum@bauer.de
Rowena Verst, vorm. Bergische Universität Wuppertal, verst@igw-geotechnik.de
Karsten Beckhaus, BAUER Spezialtiefbau GmbH, Germany, karsten.beckhaus@bauer.de

ABSTRACT

Polymer-based support fluids are increasingly becoming an international standard construction method for the production of deep bored piles. At the same time, regulatory implementation is in its early stages. However, the knowledge regarding the specific properties of polymer solutions and the advantages or limitations of their use in special foundations is, at least in Europe, still uncertain for those involved in the construction process.

This article aims at explaining the current state of knowledge of theory and established practice for (synthetic) polymer-based support fluids using the example of a mega project. These will be categorized with regards to the mechanisms of action of the support fluids distinct to the more-known bentonite suspensions.

In particular, the comparatively simple application in the construction process will be demonstrated and questions regarding environmental compatibility will be answered.

Keywords: Polymer Support Fluid, Long-chain Polymer, Bored Piles, The-line

INTRODUCTION

Buildings are getting higher, loads to be transferred are becoming greater, and “good” soil is often already used. The higher the loads, the deeper and larger the foundations. Bored piles are typical foundations that meet these demanding geotechnical boundary conditions.

Temporary support for the open borehole, which is crucial for successful pile production, is usually provided by a temporary casing. This is installed into the ground - alternating with the excavation - and withdrawn during concreting. At greater drilling depths, the required torque can become the limiting element, which can make using support fluid necessary. However, an "uncased borehole" can also be chosen for economic reasons.

In an uncased situation, the borehole support (for soil and water pressure) is created by the hydrostatic overpressure of a support fluid, which is initially controlled by the pressure head and the density of the support fluid “Fig. 1”.

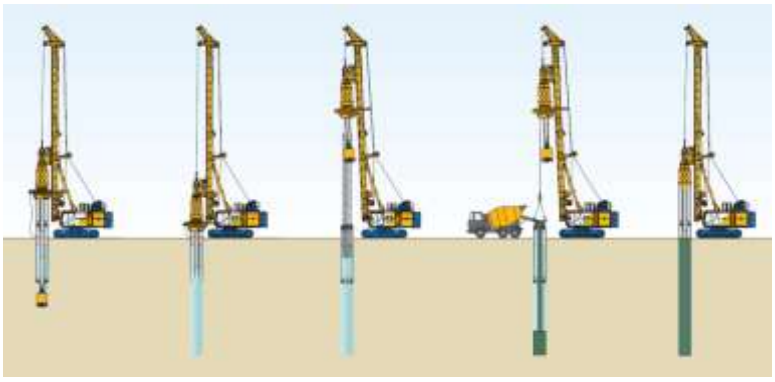


Fig. 1. Schematic representation of fluid-supported bored pile production

 © DFI International Bruges 2025

The support pressure mobilization takes place either A) by transferring shear stresses to the grain structure of the in-situ soil along the penetration depth of the support fluid or B) via normal stresses (membrane effect through the formation of a filter cake / a thin colmation zone) at the fluid-soil boundary.

In the first case, the maximum penetration depth must be limited, primarily against the background of an economical use of the supporting liquid, e.g. by reducing the penetration speed (due to a high "viscosity" of the fluid compared to water) or, in the limiting case, by stagnation ("yield point"). Bentonite suspensions do not have high viscosity, but a pronounced yield point. The opposite is true for the polymer solutions commonly used; see. Fig. 2.

.

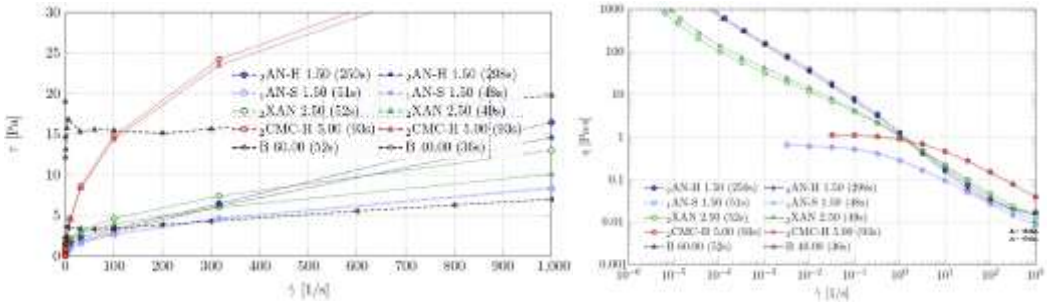


Fig. 2. Shear stress mobilization of different polymer solutions ("AN"/"CMC"/"XAN") in the rheometer (so-called "bulk rheology") in comparison to bentonite suspensions ("B") (left) as well as tensile stress viscosity ($\eta = \Delta\tau/\dot{\gamma}$) with indication of Marsh times (right); Verst, 2021

In the second case, the filter cake can be formed either by the particles in the support liquid (e.g. bentonite), by other generally granular additives (mineral or polymer-based) or by natural loading with fine grains, which can enable an "effective" colmation with quasi-stagnation of the support liquid. The effectiveness of the filter cake thereby depends on the grain distribution of existing subsoil and loaded particles. For "pure" bentonite suspensions without fines loading, DIN 4126:2013 contains a differentiation into the mechanisms of action A) or B) depending on the yield point τ_F of the fluid and the effective grain diameter d_{10} (grain diameter at 10% sieve passage) of the in-situ soil (as an indication of permeability). For common polymer solutions, a corresponding connection was found with the grain diameters at 30% (d_{30}) or 50% (d_{50}) sieve passage, characteristic to a specific polymer type (Verst, 2021). Due to the much smaller size of polymers compared to bentonite particles, filter cake formation in polymer solutions can generally only occur through loading with fines. However, filter cakes of bentonite suspensions also consist mainly of fine particles from the excavation; see also Verst et al., (2022).

For a more detailed description of the failure mechanisms to be considered and the mode of action of mineral support fluids, please refer to further literature (DIN 4126:2013; Haugwitz and Pulsfort, 2018; Verst, 2021; Idda and Beckhaus, 2022).

Due to the mixing of excavated material with the support fluid, the use of a bentonite suspension results in additional costs for the removal and disposal of the excavated material compared to bored pile production with casing. In addition, these suspensions are not stable in all ground conditions and therefore cannot be used reliably. This is another reason polymer solutions have been used in specialist foundation engineering - with an increasing trend - especially in Asia and America since the 1970s, as discussed by Lam and Jefferis (2018).

The term polymer is not a synonym for plastic, but simply for a substance consisting of high molecules made up of many repeat units (Greek: poly = many, meros = part). Very different properties and structures can result depending on the composition and order of the repeat units. These can form viscosifiers, i.e. water-soluble, comparatively large, thin linear chain polymers, or hydrogels, i.e. swellable grains (pore blockers). The polymer category therefore includes a variety of products for a wide range of chemical boundary conditions. Typical viscosifiers used in practice are acrylamide-

 © DFI International Bruges 2025

acrylate copolymers (AN/PHPA), a group of synthetic polymers with specifically modifiable properties (chain length, charge distribution, etc.) as well as polymers of natural origin. These include Na-carboxymethylcellulose (CMC) and xanthan gum (XAN), which are known and approved as food additives E466 and E415. CMC and XAN are considerably more complex in their structure than AN polymers; Verst, (2021). A detailed discussion on the comparison of two polymer solutions, long-chain and short-chain synthetic polymers, based on two different projects, can be found in Barhum et al. (2024).

Due to their special structure, polymers with usual concentrations of 0.5 to 3 kg/m^3 are much more productive than bentonite in suspension as a support fluid. In clayey soils, long-chained synthetic polymers have the advantage of effectively inhibiting sensitive (clayey) soil layers. Due to the lack of a pronounced yield point, the solid particles in a polymer solution can settle comparatively quickly and, thus, the cleaning of the support liquid in preparation for concreting can be completed faster and easier. In some cases, slurry handling and separation systems can therefore be dispensed.

An overview of the practical handling of polymer solutions in construction is given below, based on the mega project NEOM The-Line.

NEOM – THE LINE – THE PROJECT

The world's largest construction site is currently under construction in the Saudi desert. Covering an area of around 26,500 km², THE LINE “Fig. 3”, a "city of the future" is one of a total of four NEOM projects. 200 m wide, 170 km long and with a height of 500 m above sea level, the megacity is to be powered by 100% renewable energy and 95% of the land is to be preserved as natural land (NEOM.com).

The piling work, which started in Q3/2022, is the largest piling project in the world to date with a peak rate of >60 piles per day “Fig. 4”. The construction work in Module 43 “
Fig. *5*”, consisting of 1365 large bored piles, was awarded to Saudi BAUER Foundation Contractors Ltd, a company of Bauer Spezialtiefbau GmbH.



Fig. 3. The Line, Animation (NEOM.com)



Fig. 4. Pile work for module 43 (BAUER)

 © DFI International Bruges 2025



Fig. 5. Foundation work for THE LINE

GEOTECHNICAL BOUNDARY CONDITIONS

The 1365 pile holes drilled by BAUER to date have a length of up to 74 m and a diameter of 1.5 m or 2.5 m. The geological description of the in-situ soil with the corresponding depths is shown in “ Fig. ***6***”. The soil below the medium-dense, silty sand is generally characterized by narrowly graded sand, fine sand and clay/silt layers.



Fig. 6. Typical soil profile in module 43; Factual Geotechnical Report (2022)

The soils described are well suited for hydraulic support with a pure polymer solution due to their low permeability and the requirement for a clay-inhibiting medium. In addition to the conditions of the polymer solution given in the specifications, further internal quality aspects were tested and adjusted. As part of preliminary tests, the polymer concentration was determined based on the required functions of the support fluid listed below:

- Clay-inhibition and stabilization against softening or/and swelling to reduce the risk of borehole instability.
- Fastest possible settling of any loaded clayey/silty or sandy soil particles.
- Limited penetration speed into the soil.

One of the main challenges was to control viscosity, which increases when "loaded" with clayey or silty particles as well as sand content in the working slurry, in order to remain within the technical limits (Table 1). A synthetic water-soluble polymer “in-House” product, a long-chain acrylamide-acrylate copolymer (PHPA) in granular form, was selected for the effective stabilization of the clayey soil.

 © DFI International Bruges 2025

PLANT FACILITIES

There is generally a greater variety of mixing systems available for polymer solutions than for bentonite suspensions.; EFFC/DFI Guide to Support Fluids for Deep Foundations, (2019).

A comparatively simple and effective mixing system was selected for mixing the long-chain, high molecular wight polymers. The main mixing process consists of fine granulate slowly being “spread” onto a flat plate “Fig. 7” and then distributed into the mixing tank via a water jet.

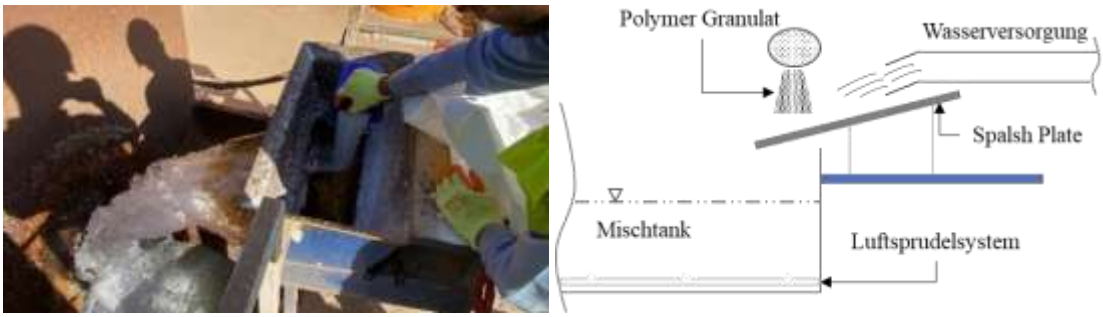


Fig. 7. Gravity spread of polymer granulate into a water jet

The polymer solution is further homogenized with an additional "air bubble system" in the mixing tank. This takes place in fixed mixing batches of 60 m³ each, which enables the dosing of the added polymer quantity (mix design) to be controlled. The fresh polymer solution is then transferred to two further tanks for final homogenization “Fig. 8, left”, which are also equipped with an air bubble system. Subsequently, after quality inspection, the polymer solution is pumped into vertical silos for storage and is ready for use “Fig. 8, right”.



Fig. 8. Mixing and fresh polymer solution tanks (left) and vertical silo storage tanks (right)

Polymer-friendly pumps (here: peristaltic pump from the HP series) were used to keep the polymer solution in motion as well as for the transfer activities (mixer, tanks, pile drilling, storage). The peristaltic pump is preferable especially for the long-chained synthetic polymer solutions used here, which are very sensitive to shear stress. In the case of continuous circulation with unsuitable pump systems, a considerable deterioration in the properties of this type of polymer solution is likely, as was shown by Lam et al. (2010) and Jefferis and Lam (2013).

SPECIFICATION AND QUALITY CONTROL - GENERAL

As with bentonite suspensions, ensuring the required quality of a polymer-based support liquid is not solely a function of the correct selection of polymer raw materials.

Depending on the chemical composition and ingredients of the mixing water (e.g. due to impurities or different water treatment) or ground conditions (chemically contaminated groundwater, soil

 © DFI International Bruges 2025

replacement, contaminated soil, etc.), the properties of the support fluid can be influenced. The preparation of the polymer solution and the treatment of the support fluid, which may be "charged" with fines, may also play a role depending on the local conditions (Lam and Jefferis, 2018; EFFC/DFI Guide to Support Fluids for Deep Foundations, 2019; Verst, 2021).

MIXING WATER

The pre-treated (using ion exchanger filter cartridges) mixing water delivered to The Line construction site is tested. The parameters: electrical conductivity (from 50 to 5000 µS/cm at 25°C), calcium (83 to 390 mg/l), chloride (12 to 1100 mg/l) and magnesium (0.6 to 85 mg/l) were subject to a large variation. As a measure to prevent the risk of the polymer solution suffering a considerable drop in viscosity (undesirable change in chain conformation) and thus impact the support function, an extended quality tests were carried out and additional treatment of the mixing water on site was required.

By using certain additives, the total solids content could be controlled and adjusted to the desired limit (<800 ppm) and the pH-value to the appropriate range (9 to 10.5). These measures significantly improved the performance, robustness, and service life of the polymer solution.

POLYMER SOLUTION

The properties of the polymer solutions were continuously monitored as standard during the pile drilling process. In particular, testing included Marsh viscosity, density, sand content and water release time. Generally, preparation and control of the polymer solution for the bored pile work in The Line “Table 1” was carried out on the basis of the target parameters according to the "ICE Specification for Piling and Embedded Retaining Walls" (in short: "SPERWall").

Table 1: Conditions to be complied with for the polymer solution for The-Line construction site

#ID	Type of solution	Density g/cm^3	Marsh-Value s	Sand Content %	pH-Value
A	Fresh polymer	≥ 1.01	> 90	-	9 – 11
B	For re-use	< 1.02	60 – 120	< 2	9 – 11.5
C	Working polymer solution	< 1.05	60 – 120	< 5	9 – 11.5
D	Concreting solution	< 1.02	90 – 120	< 1	9 – 11.5

The polymer solutions used were also tested for classification using a rheometer. The results show clear properties of a long-chain synthetic polymer “Fig. 9”.

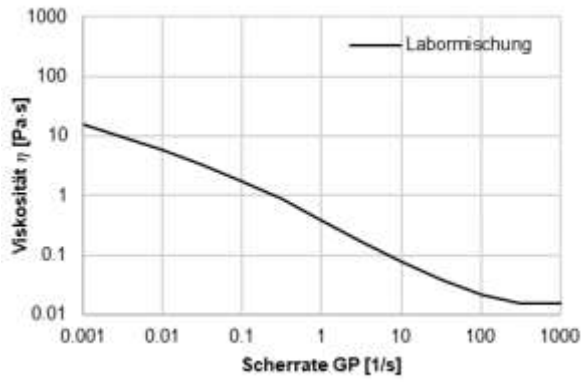


Fig. 9. Rheometer results for the polymer solution used

 © DFI International Bruges 2025

ENVIRONMENTAL SUSTAINABILITY AND DISPOSAL

The economic advantages of using polymer solutions include not only low overall consumption, but also technically simple mixing, immediate usability (without "pre-swelling times"), short waiting times due to fast "settling rates" and simple disposal. In summary, low overall treatment costs and low disposal costs (for low volumes). Moreover, the synthetic polymer solution used in the above-mentioned project has also shown pronounced robustness with regard to maintaining its properties against physical charging (suspended soil material) and possible chemical reactions (biological stability). This robustness and the associated low effort required to "refresh" the support fluid are some reasons for the significantly longer and therefore – operation-related – more sustainable use of this support fluid concept.

At present, there is no standardized and therefore reliable approval process for the use of polymer solutions. Internationally, various project examples like Neom show that relevant authorities either allow the use and disposal of polymer products, e.g. on project level, or, as the lowest imaginable hurdle, do not have any legal restrictions. However, many countries differentiate with regards to the potential effect on the environment, and request approval processes to go through.

In Germany, for example, water permits must generally be issued by the local water authority, in accordance with the German Federal Water Act (in German: Wasserhaushaltsgesetz). However, if there is no sufficient expertise or existing framework rules on how to proceed for the permission of the use of certain polymer solutions and under specified boundary conditions, no reliable planning (and therefore no serious calculation) for the use of polymer solutions as support fluids is feasible. With early consideration by the project planners, i.e. before the contract is awarded, the conditions for approval could be known in good time. Another alternative, which is also conceivable, is that "building authorities" approve individual polymer products, which is expressly approved in the tender, for certain areas of application.

Moreover, monitoring measures and supplementary inspections, e.g. recurring analyses of groundwater quality (organic parameters: TOC, acrylamide; and bacteriological parameters: Enterococci, Escherichia coli, coliform bacteria, colony count at 22°C) in the inflow and outflow of a construction site could be stipulated and thus standardized.

In The Line, the use of polymer solutions is currently not subject to approval. However, the depth of the piles (up to 74 m) was planned to reach the aquifer, and the construction work was not allowed to influence the water quality of the aquifer. In particular, a contamination of the groundwater should be prevented. This was ensured by minimizing the penetration depth of the polymer solution by specific product selection (see above) and continuous monitoring of the physical properties (especially viscosity) of the solution.

The environmental impact of polymer support fluids – whether composed of synthetic or natural polymers – is generally low and controllable. This is due to their limited penetration depth, effective separation through settling, and already low initial concentrations. Existing research reviews (e.g., Verst, 2021) indicate that the long-chain structure of polymers restricts their mobility in soil after construction is completed, with degradation occurring over time and distance. Furthermore, if the polymer solution has low viscosity or its chains are broken, synthetic polymers become even less detectable due to significant dilution, which depends on both time and distance from the point of introduction in the borehole (Beckhaus et al., 2015). For further discussions on polymer mobility and degradation, see Lesemann (2010), Lam and Jefferis (2018), and Verst (2021).

The loaded polymer solution is stored in separate tanks (or small earth basins) for disposal and then treated with a flocculant made from hydrogen peroxide (H_2O_2). This solvent accelerates the natural decomposition of the polymer. Carbonic acid (soda) is dissolved, and water, oxygen and carbon are

 © DFI International Bruges 2025

produced. The amount of carbon introduced is minimal and the TOC value (Total Organic Carbon) is hardly affected. The settled polymers, which remained as residue at the bottom of the earth basin, were transferred to an inert waste landfill. In other European projects, the polymer solution cleaned of fines could be disposed of as gray water in the sewer system, as discussed by Lam and Jefferis (2018).

SUMMARY AND CONCLUSION

The use of a polymer solution as a support fluid for executing large-scale bored piles may allow for both technical and economic advantages. Polymer solutions, especially long-chain polymer types with high molecular weight, have the unrivaled advantage of effectively inhibiting sensitive (clay-containing) soil layers.

Especially for the long-chain synthetic polymer products in use, the distribution of fine particles in the support fluid during excavation can be kept to a minimum. This effect subsequently reduces the effort required for fluid regeneration (also in preparation for concreting), among other things resulting in a high efficiency of these types of polymer solutions.

The use of polymer-based support fluids has long been established in practice for geotechnical solutions. The simplified cleaning process for the used polymer and the short waiting times for the necessary settling of sand before the final cleaning of the borehole base in preparation for concreting also generally have a positive effect on the construction process. To generate these advantages, however, the "polymer site" must be prepared accordingly. The approval process must therefore be known in the early planning stage of such a construction project to enable a reliable calculation of costs and time for the appropriate equipment and, of course, for the procurement of suitable polymers.

With the approval process, the requirements for the product to be used, but also for disposal, must be known. Various bodies around the world are working on incorporating generally applicable correlations into regulations. However, the current state of the art already provides a sufficient basis for decision making for the responsible authorities and independent expert offices can provide support with appropriate objectivity.

REFERENCES

Barhum, R., Chropen, J., Verst, R., 2024. Tiefe Gründungspfähle mit Polymerstützung - am Beispiel Bratislava, Culenova Office 1 und NEOM, The Line. 14. Österreichische Geotechniktagung. Vienna, Austria.

Beckhaus, K., Lesemann, H. and Quillfeldt, M.v., 2015. Bauweisen im Untergrund und ihre Auswirkungen auf das Grundwasser, Vorträge zum 11. Hans Lorenz Symposium, Berlin; Veröffentlichungen des Grundbauinstituts der TU Berlin, Heft 43.

DIN 4126, 2013. Nachweis der Standsicherheit von Schlitzwänden.

EFFC/DFI Guide to Support Fluids for Deep Foundations, 2019. First Edition.

Factual Geotechnical Report, 2022. NEOM Prototype Ten Tower-SO-001, Rev “A”.

Haugwitz, HG., and Pulsfort, M., 2018. Pfahlwände, Schlitzwände, Dichtwände. By Karl Joseph Witt. 8. German. Wiley Online Library, pp. 823-907.

Idda, K., and Beckhaus, K., 2022. Planung und Umgang mit Risiken bei der Stützung offener Schlitze im Spezialtiefbau. 13. österreichische Geotechniktagung. Tagungsband. Wien Österreich.

Jefferis, S., and Lam, c., 2013. Polymer support fluids: use and misuse of innovative fluids in geotechnical works. Proceedings of the 18th International Conference on Soil Mechanics and Geotechnical Engineering, Paris, Vol. 4, pp. 3219-3222.

 © DFI International Bruges 2025

Lam, C., and Jefferis, S., 2018. Polymer support fluids in civil engineering. London: ICE-Publishing.

Lam, C., Jefferis, S. A., Goodhue, K., G., 2010. Observations on viscosity reduction of PHPA polymer support fluids. Geotechnical Special Publication Geotech Spec. American Society of Civil Engineers. pp. 184-191

Lesemann, H., 2010. Anwendung polymerer Stützflüssigkeiten bei der Herstellung von Bohrpfählen und Schlitzwänden. Dissertation. Technische Universität München.

Verst, R., 2021. Stabilisation mechanisms of polymer solutions in the context of temporary earth-wall support – Stabilisierungswirkung von Polymerlösungen bei der Stützung von Erdwänden. Dissertation. Bergische Universität Wuppertal.

Verst, R., Blumenthal, A., Du, J., Koenig, D., Pulsfort, M., Wichtmann, T., 2022. Systematic laboratoryand field study on the shear resistanceof the soil-concreteinterface of diaphagm wallsand bored piles. DFI-EFFC International Conference on Deep Foundations and Ground Improvement: Smart Construction for the Future, Berlin.

 © DFI International Bruges 2025

ACCEPTANCE CRITERIA TO OPTIMISE THE FOUNDATION DESIGN AND INSTALLATION

Marcel W. Bielefeld, Allnamics Geotechnical & Pile Testing Experts, The Netherlands
Eelco van der Sloot, Grondgrip, The Netherlands
Rob F. van Dorp, Allnamics Geotechnical & Pile Testing Experts, The Hague, The Netherlands

ABSTRACT

In traditional pile design and installation processes, the design phase sets the parameters for installation. However, practical considerations take centre stage once the project is handed over to the contractor and piling contractor. Incorporating those considerations during the design phase is essential to optimise pile foundations and reduce cost, carbon footprint, and raw material consumption. This process can be expanded even further by including factors such as (preliminary) pile load results, which help determine shaft friction unit values and the contribution of the pile toe to the total resistance.

The paper illustrates the interaction between design and construction-related aspects for a project in The Netherlands where precast prestressed concrete piles were installed. The Cone Penetration Tests (CPTs) performed to investigate the soil profile showed refusal within less than 0.5 m into the bearing stratum. Consequently, the designer and piling contractor anticipated hard driving and possible pile damage, but they also expected to achieve sufficient capacity at shallow penetration into the bearing stratum. By utilising the results from pile driving prediction (PDP) before installation, pile driving analysis (PDA, HSDT) during installation of trial piles and subsequent signal matching to establish the mobilised static pile capacity for single blows, acceptance criteria for pile installation were established. This approach ensured that the objectives of both the piling contractor (limiting driving stresses and installation times) and the designer (sufficient pile capacity) were met effectively.

Keywords: drivability, SRD, PDP, PDA/DLT, HSDT, driving protocol, case study

INTRODUCTION

The construction of a 110 kV High Voltage Substation for Tennet in Bolsward, The Netherlands, is designed on a foundation using precast piles. Applying the standard foundation design codes resulted in a required penetration depth, which was 1.5 to 3.25 meters into a very dense sand layer, depending on the site variation.

The very dense sand layer showed CPT tip values exceeding 50 MPa just 0.50 m into this layer, and even causing an early refusal of the CPT during the initial and additional soil investigation program, which resulted in a lack of data beyond the deepest recorded reading. The Dutch design code requires an investigated depth of at least 8 times the pile diameter below the toe level. In this case, that level had not been reached, even not in the additional soil investigation program. Therefore, the foundation could not be designed based on the results of the soil investigation. The high CPT values in that particular part of The Netherlands do not always lead to high pile resistances, when the sand layer has high horizontal soil stresses.

 © DFI International Bruges 2025

The high resistance values raised the question whether precast piles could be driven into the dense sand layer. If the blow counts were excessive, a heavier ram or hammer could be used, but this would lead to increased pile stresses with the potential for pile damage during installation. On the other hand, reducing the hammer impact would reduce the risk of high stresses, but also increase the blow count, leading to longer installation times or even early refusal. This presented a dilemma for the foundation design of this project, mainly reaching the required penetration depth. However, CPT results indicate that to achieve the required pile capacity, there seems no need to penetrate the bearing layer more than just one or two 'tocht' (the Dutch term to describe pile penetration as a result of 30 blows).

General relationships between blow counts and capacity (driving formulae) are never valid for a specific site. Since the 'Hollands Heiformule', the Dutch Piling Formula, from the 19th century, hundreds of relationships have been developed worldwide (Fig. 1).

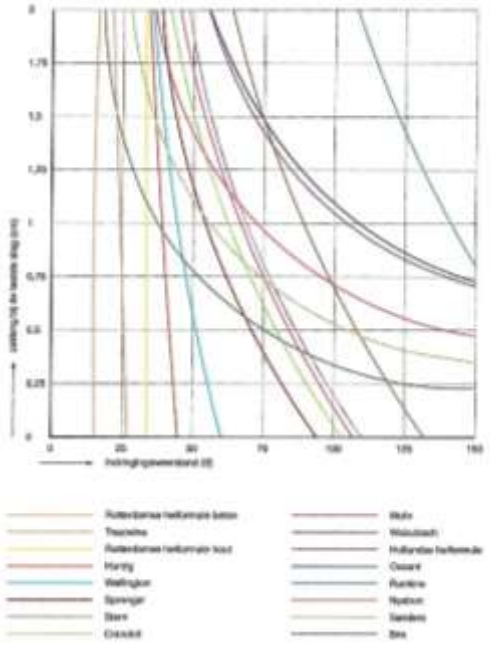


Fig. 1. Relationship between capacity and blow count (here as set per blow at the vertical axis) for a couple of driving formulas (Bolderman et. al. 1998). A blow count of 25 blows/0.25 m (set of 1 cm per blow) leads to a scatter in results from 150 to 1400 kN (15 to 140 tf)

SOIL STRATA AT THE PROJECT SITE

Fig 2. shows the results of a typical soil investigation at the project site. The soil profile can be described (somewhat simplified) as follows:

1. Ground level at approximately NAP +0.80 m (as a fill is yet to be placed)
2. A fill made of sand and crushed debris down to approximately NAP -0.20 m
3. Soft peat and clay layers down to approximately NAP -5.50 m.
4. Moderately compact sand and silty sand layers down to approximately NAP -13.50 m.
5. Stiff, silty clay down to approximately NAP -19.50 m.
6. Dense to very dense sand down to the maximum explored depth (around NAP -30.00 m)

 © DFI International Bruges 2025

The design pile foundation level is planned at NAP -20 m to NAP -22 m (depending on the soil variability), i.e., 1.5 to 3.25 meters into this dense to very dense sand layer with CPT cone tip resistance values exceeding 50 MPa just a few decimeters into this layer.

During the soil investigation, it was found that this sand layer is locally so hard that the Cone Penetration Test (CPT) encountered refusal above the intended pile installation depth. As a result, it was expected that very heavy pile driving would be required during pile installation, and there was a possibility that (some of) the piles may not be driven to the desired depth ("early refusal"), or if they were, that it could cause damage to the piles. At the same time, piles encountering early refusal were expected to have more than sufficient compression bearing capacity. However, the calculation and design method Koppejan requires that the piles are sufficient penetrated in the bearing layer.

In consideration of this, a pile test program was established to design the piles and pile toe level, assess the driveability of the piles, and the determination of the capacity of the piles in case of an early refusal, along with a protocol to follow in such cases.

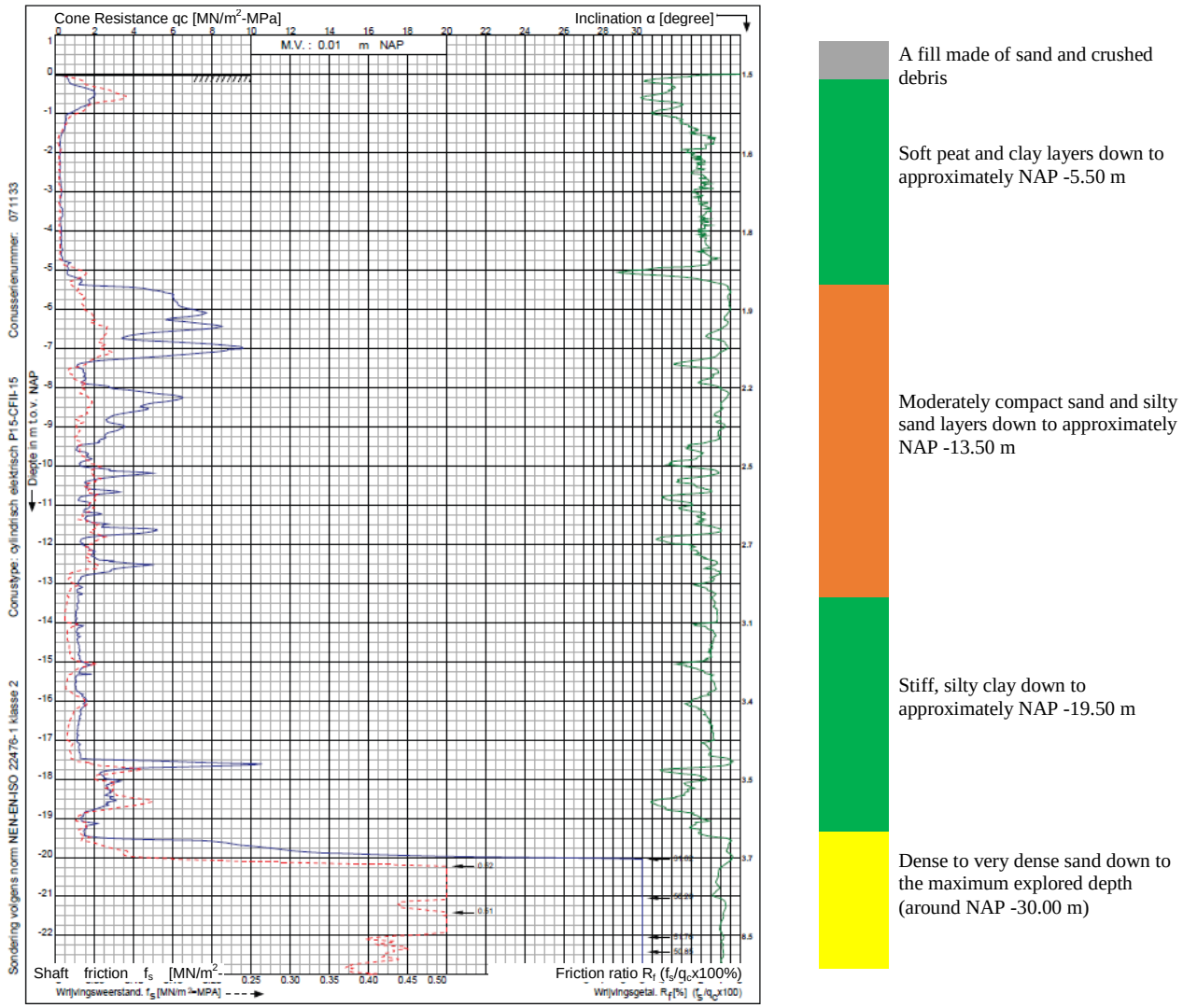


Fig. 2. Relevant soil investigation result shows the (very) dense sand layer starting at -19.5 m NAP and Qc values exceeding 50 MPa almost immediately

 © DFI International Bruges 2025

PILE TEST SETUP

The setup for the pile test, designed to meet the objectives outlined above, consists of the following components:

A. Conducting pile driveability predictions to assist in the selection of the hammer for the test and to verify expected driving stresses. Based on the outcome, an initial forecast of the acceptance criteria (i.e., the minimum required blow count as a function of the achieved toe depth and the hammer used) would be derived.
B. Performing PDA measurements while installing two test piles at the site. These measurements would provide field results regarding hammer energy effectively transferred to the pile, blow counts, and soil resistance.
C. Determining the mobilized static pile capacity through Signal Matching on the measured signals. This would allow the mobilized static pile bearing capacity to be determined at the final depth achieved.
D. Performing post-predictions to adjust and refine the soil resistance to driving (SRD) curves. This step would calibrate the dynamic soil model used in Part A based on the field results, enabling the final determination of the acceptance criteria, i.e. the combination of the minimum required penetration depth and minimum blowcount, as a function of applied nominal hammer energy.

The acceptance criteria can then be used by the piling crew and site engineer during the production pile installations to assess whether or not pile driving can be stopped because sufficient pile capacity has been achieved.



Fig. 3. Performing the monitoring on the pile with the Allnamics PDA system

TEST PILES

For the pile test, two different precast, prestressed concrete piles were selected: one with a side length of 290 mm and another with a side length of 320 mm. Both piles, which were

 © DFI International Bruges 2025

23.5 meters long, were situated between the planned production piles. The hammer used was a Junttan HHK7A with a ram weight of 7.000 kg, and a maximum nominal energy of 84 kNm.

DRIVEABILITY RESULTS

In a pile driving prediction based on hammer specifications, pile data, and soil investigation results, a forecast is made for factors such as driving resistance, effective blow energy, blow count, and pile stresses as a function of penetration depth.

For creating an SRD curve, the prediction is used in a somewhat reversed direction: instead of predicting what blow count is expected at a given depth based on soil resistance, the SRD curve predicts the soil resistance (i.e., pile bearing capacity) at the same depth as a function of the blow count.

The predicted soil resistance can then be compared with the pile bearing capacity required by the design. This allows determination of the minimum blow count that must be achieved to ensure sufficient bearing capacity, given the soil conditions and the hammer being used.

PDA FIELD MEASUREMENTS

For the PDA measurements, the piles were equipped with strain and acceleration sensors positioned on opposite sides of the pile at 1 to 2 times the pile diameter below the pile head. The measurement signals provide information on various factors, including the hammer energy transferred to the pile, the stresses within the pile, and the soil resistance during driving.

For this project, the PDA/DLT field monitoring was performed using the Allnamics PDA system with the wireless PDR data acquisition unit. The sensors were combined, which simplified the mounting of the sensors on the pile (Fig. 4).

The Allnamics-PDADLT software package was used to acquire and process PDA/DLT measurement data and generate input signals for signal matching. Fig. 5 presents some of the monitored results.

Table 1 summarizes the results of the test. Both piles were driven to a depth of (almost) 22.0 m – NAP. The final blow count was about 60 blows/0.25m, and the compression stresses in the pile exceeded 37 and 40 MPa, respectively. That was above the allowable stresses, even though the piles had been manufactured using high-grade concrete (compressive strength at 28 days of at least 55,0 MPa and prestressed at 4,5 MPa).

For both piles, the compression stresses are far above the allowable stresses. In the case of high toe resistance, pile stresses at the toe can be even higher than measured at the top. That is because of the stress wave phenomenon, leading to the superposition of downward and upward traveling waves. Without a test setup and test pile, the installation would have stopped at a higher penetration level (early refusal).

 © DFI International Bruges 2025



Fig. 4. Allnamics PDA/DLT is based on wireless data transmission from the data acquisition unit PDR to the monitoring computer. Right, the combined sensors for simplified mounting.

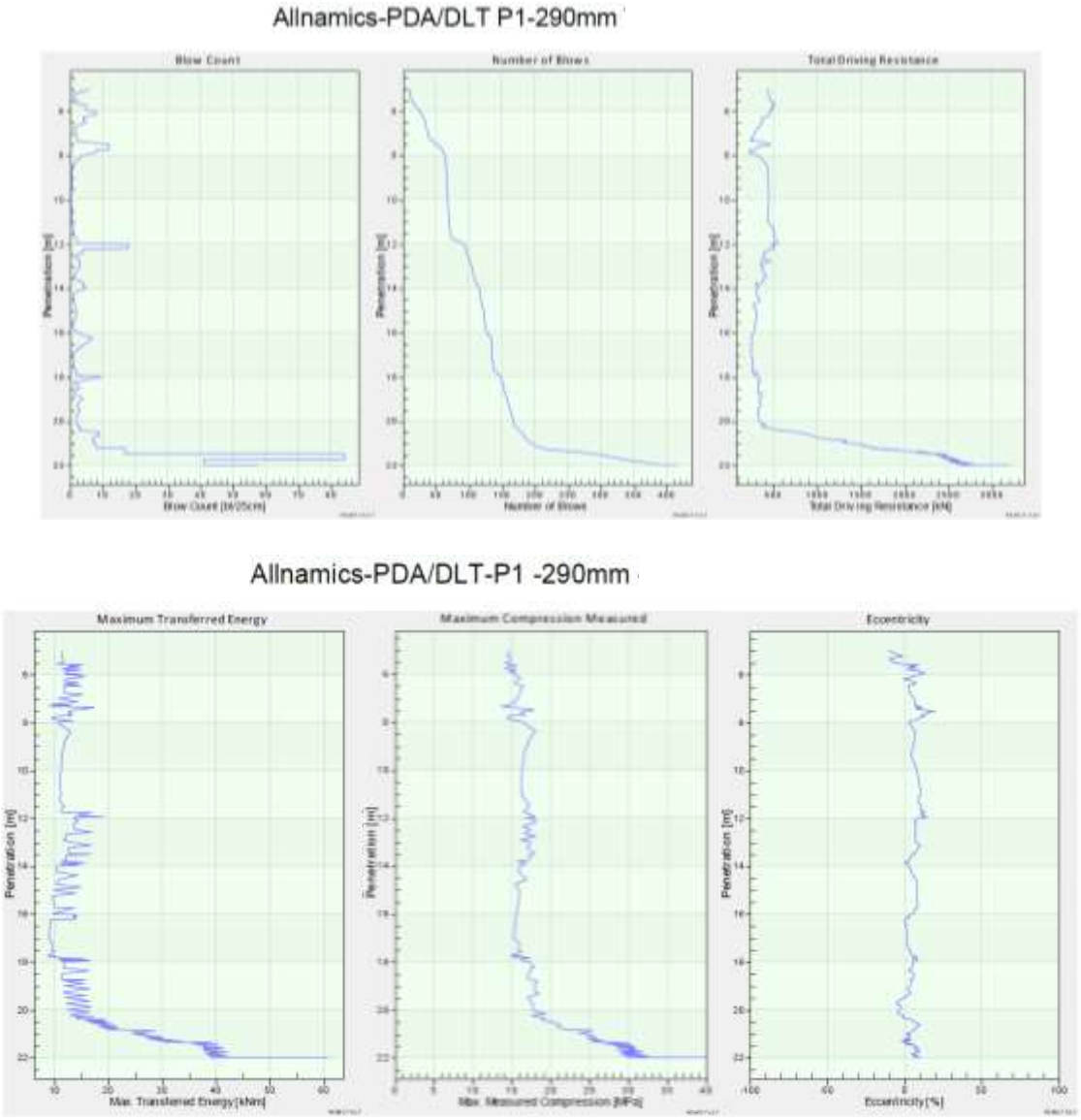


Fig 5. Results of the PDA test on the 290 mm test pile

 © DFI International Bruges 2025

Table 1. Main results of the measurements during installation of the test piles

Pile number	Penetration depth end [m – MV]	Final blow count [bls/0.25m]	max comp. stresses [MPa]	max. tensile stresses [MPa]	max. driving resistance [MN]	max enthru energy [kNm] [%]
P1	-22.0	58	40.3	0.6	3.22	60 [71%]
P2	-21.8	65	37.0	0.5	4.66	64 [76%]

SIGNAL MATCHING FOR DETERMINING PILE CAPACITY

Through signal matching on a specified hammer blow, it is possible to estimate the mobilized static bearing capacity using the theory of one-dimensional wave propagation. This assesses the bearing capacity at the measurement time, corresponding to the toe depth of the selected hammer blow. This process is often indicated as a Dynamic Load Test (DLT), or High Strain Dynamic Testing (HSDT).

The wave analysis has been performed on one of the last blows at the end of driving (EOD). When evaluating a blow during pile driving or at the end of installation, the soil fatigue is at its maximum, allowing for a conservative estimate of the long-term bearing capacity.

Signal Matching was carried out for this project using the AllWave-DLT software package. This software is based on the method of characteristics, which is applied to one-dimensional wave propagation theory (Josselin de Jong 1956, 2022, Middendorp 2022).

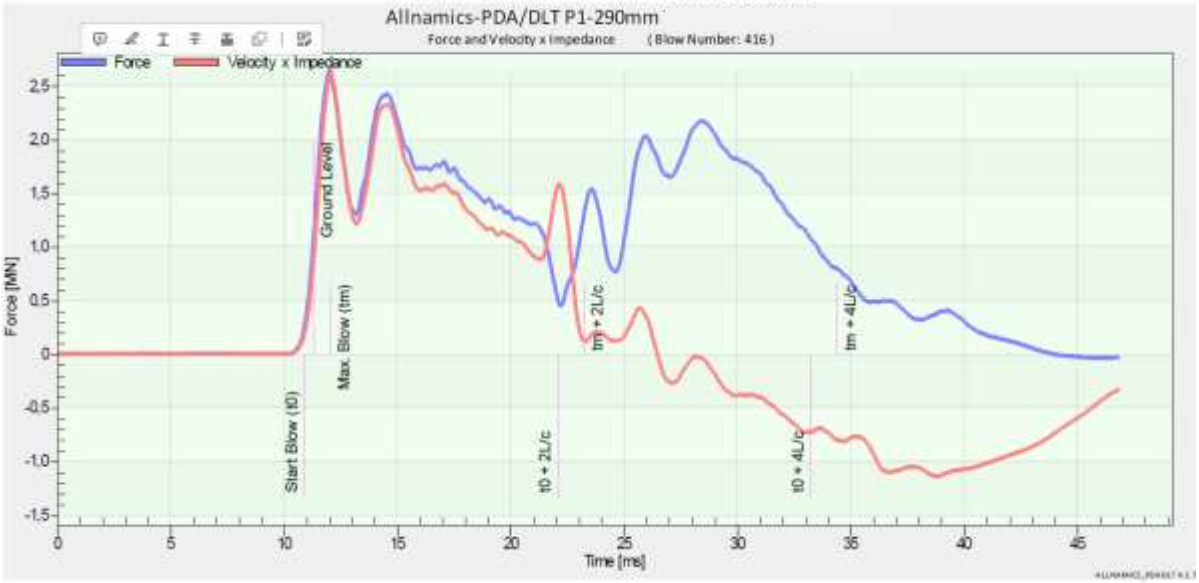


Fig 6. Measured signals for Force and Impedance times velocity; blow nr 416 at penetration depth of 22,0 m

 © DFI International Bruges 2025

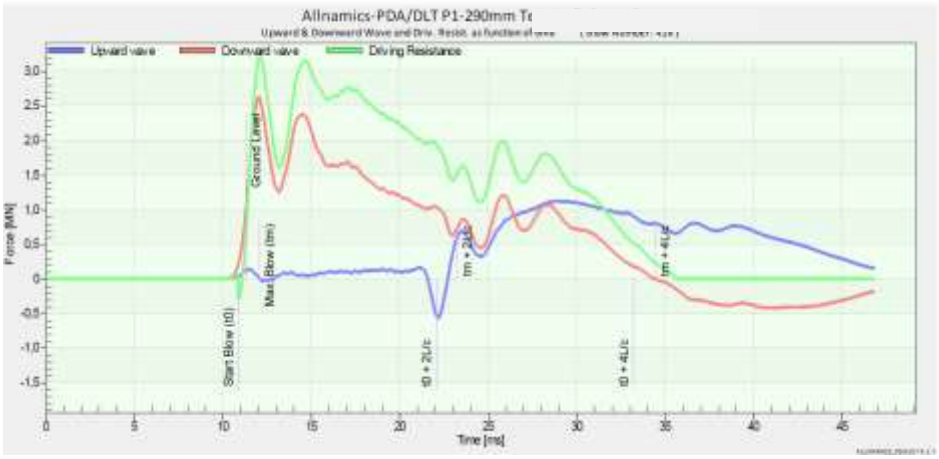


Fig 7. Measured signals for downwave, upwave and driving resistance; blow nr 416 at penetration depth of 22,0 m

SIGNAL MATCHING RESULTS

During Signal Matching a specific hammer blow is analyzed using the F-Z·v diagram, where F represents force, and Z·v represents velocity multiplied by the pile's impedance Z. From these signals, two key wave components are extracted: the downward traveling force wave (the Downwave $F^{\downarrow}$) and the upward traveling force wave (the Upwave $F^{\uparrow}$). These components are separated based on the one-dimensional stress wave theory. See the Fig. 7.

The upward traveling wave is particularly important, providing information about the mobilized soil resistance as a function of depth below ground level, as shown in Fig. 8. Shaft friction causes reflections during the passage of the downward traveling wave caused by the hammer impact. (Similarly, impedance changes in the pile cause reflections as well.) To interpret the resistance, the pile and surrounding soil are modeled using the analysis software. The properties of the model are determined by the soil investigation results and the pile's specific characteristics.

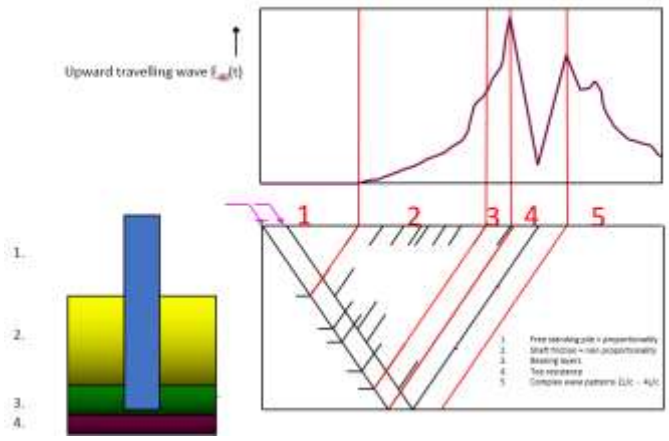


Fig. 8. Soil resistance at both the shaft and toe generates reflections. These upward traveling waves carry valuable information about the resistance encountered at deeper levels. The process of Signal Matching involves analyzing these upward waves to estimate the distribution of shaft friction along the pile and the resistance at the pile toe.

 © DFI International Bruges 2025

The process begins by inputting the measured force of a selected hammer blow into the dynamic soil-pile model. The software then simulates the stress wave propagation and calculates the upward traveling force wave (upwave) based on this input and compares it to the actual measured upwave. Through iterative adjustments of the model parameters, the calculated upwave is aligned with the measured one—this process is referred to as the "signal match".

The results of the Signal Match, the simulated and measured signals as a function of time, are presented in Figures 9 and Table 2.

Additional consistency checks ensure that the calculated driving energy and pile head displacement correspond to the measured values and that the soil parameters are within the physical limits of the actual soil strata (validated signal matching, Verbeek et al. 2022). Once a satisfactory signal match is achieved, the soil model is accepted as describing the soil strata on site. This model then provides insights into the mobilized static resistance and its distribution between the pile toe and shaft friction along the pile's length. The result is the simulated static load-settlement diagram, as presented in Fig 10.

While signal matching is a powerful tool, it is important to note that no unique solution exists (Verbeek and Bielefeld 2022, Viana da Fonseca 2008). The complexity of the soil-pile interaction model, coupled with numerous adjustable parameters, allows for multiple combinations of variables that can produce an acceptable signal match. As a result, the final outcome is user-dependent. This inherent variability makes signal matching less consistent and accurate than the other testing methods: Static Load Testing and Rapid Load Testing.

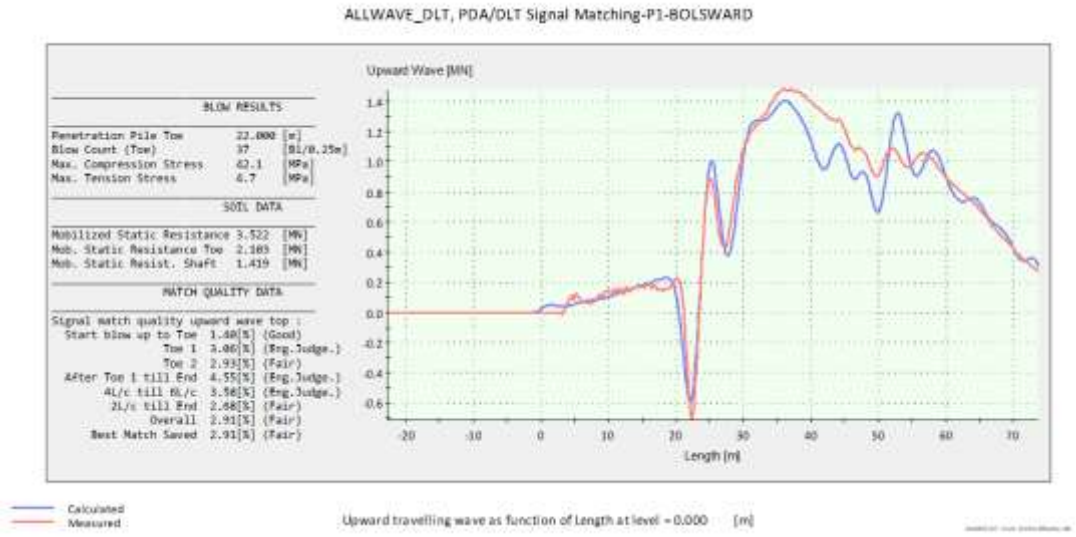


Fig 9. Results of the Signal Matching process: calculated and measured results for the upwave (upward travelling force wave)

 © DFI International Bruges 2025

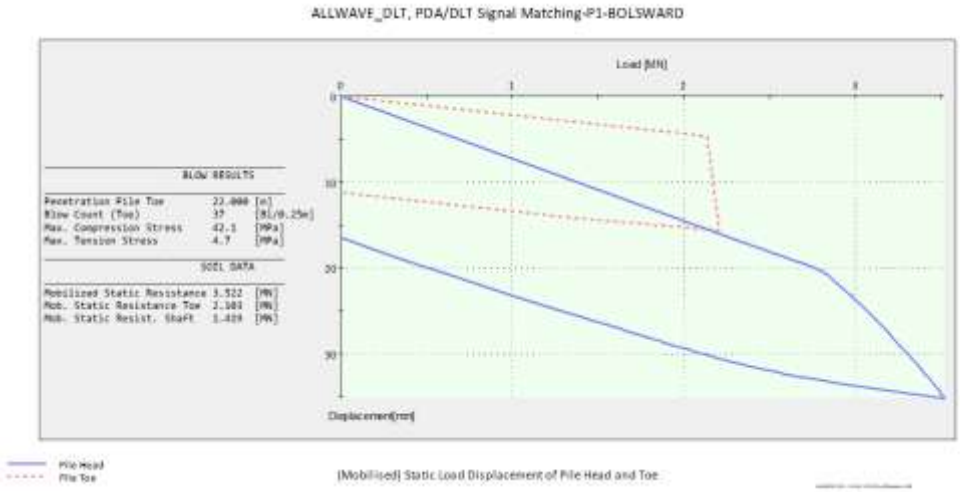


Fig 10. Results of the Signal Matching: The static load settlement diagram (pile top and toe)

POSTDICTIONS TO ESTABLISH DRIVING PROTOCOL

The actions performed have been the basis for determining site-specific SRD Curves. With the relationship between blow count and pile capacity, Acceptance Criteria can be established.

The driveability simulations had slightly different parameters than were utilized during pile installations. At the maximum penetration depth of NAP -21.2 m, the effective energy transferred to the pile (E_{transf}) was measured to be 60 kJ (pile 1) and 64 kJ (pile 2). The signal matching results showed the mobilized static pile bearing capacity was 3.522 kN (pile 1) and 3.965 kN (pile 2), corresponding to the observed final blow counts of approximately 70 (pile 1) and 80 (pile 2).

In the first step, the performance of the hammer in the simulations is set equal to that which was measured on site. That is done by an iterative adjustment of the hammer model. The hammer configuration (hammer block – helmet – helmet cushion) is iteratively adjusted so that the calculated transferred energy corresponds as closely as possible to the PDA measurement results for the applied maximum nominal impact energy. Once the hammer model shows comparable impacts as measured on-site, the next step is to adjust the soil model. The modeled soil behavior is iteratively adjusted to match the mobilized static bearing capacity as closely as possible with the signal matching results. This is primarily achieved by adjusting the unit values for toe resistance and shaft friction. Other dynamic model parameters were iteratively adjusted to ensure that the calculated blow count corresponds as closely as possible with the observed final blow count. In this case, the damping and the so-called quake values for both the shaft and the toe were primarily adjusted.

Now the model for hammer, pile and soil are giving similar results as the measured signals at final penetration depth. The final step is to perform SRD Runs using that model for hammer, pile, and soil. The SRD runs are performed using AllWave-PDP, predicting the mobilized static bearing capacity as a function of the blow count for the same hammer blow (transferred energy) and at the same toe depth. A higher blow count should correspond to higher soil resistance (i.e., pile bearing capacity) and a lower blow count to less resistance.

 © DFI International Bruges 2025

Table 2. Results of the Signal Matching

Pile	Blow nr	Penetration depth	Transferred energy	Displacement pile top max	Resistance Shaft	Resistance Toe	Resistance Total
Nr		[m tov NAP]	[kNm]	[mm]	[MN]	[MN]	[MN]
P1	416	-21.2	60	15.4	1.419	2.103	**3.522**
P2	200	-21.0	64	11.7	0.381	3.584	**3.965**
Mobilised capacity is more than the required capacity of 850 kN							

DRIVING PROTOCOL AND ACCEPTANCE CRITERIA

Now a relationship between blow count and capacity has been set for this site, the SRD curve (Fig. 11) had to be converted into a design value for allowable pile loads according to Dutch code NEN 9997-1 (according to table 11A of the code) by dividing the loads by a partial safety factor ξ_6 = 1.50. On top of that the values had to be reduced by $2 \cdot F_{s,nk}$ to account for the negative skin friction expected in the design calculations.

$$R_{c;d} = \frac{R_{mob,test}}{\xi_6} - 2 \cdot F_{s,nk}$$

The design values for the negative skin friction was specified as $F_{s,nk}$ = 65 kN (for the pile 290 mm) and $F_{s,nk}$ = 72 kN (for 320 mm).

Once this is done, the minimum required blow count can be determined based on the design value of the (maximum) design load, which was set by the structural engineer at 850 kN, see Table 3. From this, it was inferred that, when using the same driving configuration and drop heights as in the pile driving test, a blow count of ≥ 20 blows per 0.25 m is already sufficient to reach required pile capacity.

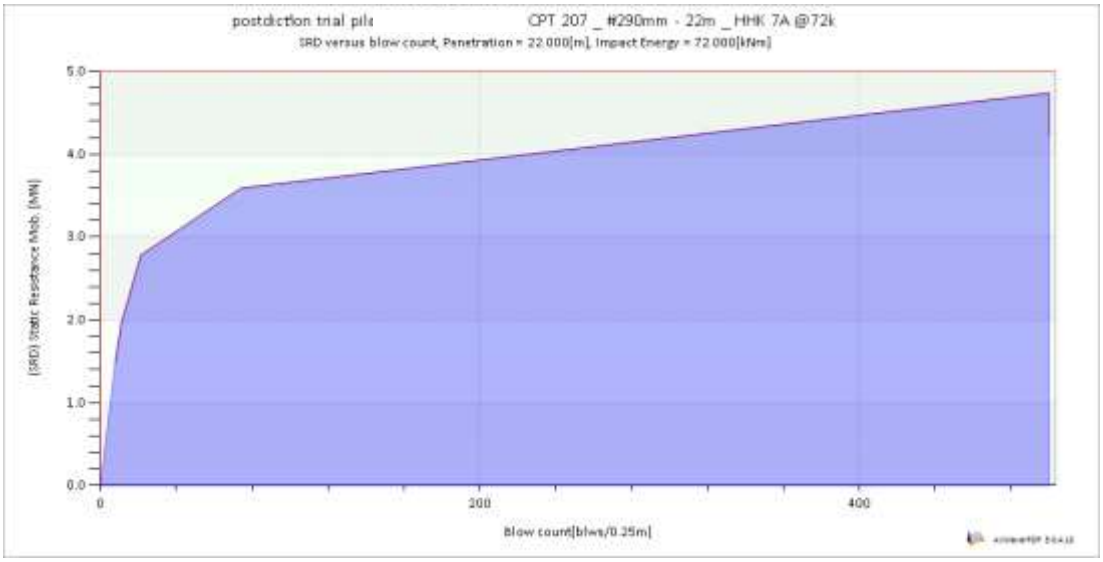


Fig. 11. Determined SRD diagram

 © DFI International Bruges 2025

Table 3. Results of the relationship between capacity and expected blow count (SRD), based on the results of the post-dictions

Paal nummer	Penetration depth [m – MV][1]	Heiblok	Nominal hammer energie [kJ]	Blow count [bls/0,25m]	Mobilized capacity [kN]	*Allowable pile load*[1] *kN*
P1 # 290mm	< -21.2	HHK-7A	72	**20**	**2.600**	*1.603*
				40	**3.050**	*1.903*
				60	**3.350**	*2.103*
				80	**3.590**	*2.263*
				100	**3.650**	*2.303*
P2 #320mm	< -21.0	HHK-7A	78	**20**	**2.990**	*1.849*
				40	**3.350**	*2.089*
				60	**3.700**	*2.323*
				80	**3.990**	*2.516*
				100	**4.050**	*2.556*

[1]: based on negative skin friction $F_{s,nk}$ = 65 kN (#290mm), resp. $F_{s,nk}$ = 72 kN (#320mm),

CONCLUSIONS

By performing simulations and measurements, a site-specific relationship between blow count and pile capacity can be derived, serving as a valuable tool during the pile installation process. In this case, the established relationship not only expedited the pile driving process but also prevented potential pile damage during installation.

Had the pile been driven to its original design depth without considering this approach, significant issues during execution could have occurred, such as decreased production and mitigation measures required for piles with early refusal and/or pile head damage. These issues might have led to troubleshooting, legal complications, and significant delays. By identifying potential problems in advance, a practical set of acceptance criteria was developed, and agreed upon by the piling contractor (in terms of blow counts), the pile manufacturer (ensuring pile stresses during driving were manageable), and the structural engineer (confirming pile capacity).

The total number of hammer blows per pile is reduced by setting a maximum blow count instead of requiring a fixed penetration depth. Consequently, this approach helps lower carbon emissions on-site (Scope 1 and 2). The exact reduction in emissions is difficult to quantify, as the total number of blows required to reach the originally planned penetration depth remains unknown. However, it is essential to note that the final meter of penetration typically demands significantly more energy, time, and effort, making this adjustment an effective strategy for minimizing environmental impact.

In this case, the precast piles were already manufactured. Had the soil and the pile test campaign has been set up in a earlier stage, the pile length could have been optimized, reducing carbon emissions and raw materials even more.

It is important to note that these results are correlated to the specific hammer configuration (hammer type, ram weight, helmet, cushioning, restriction of drop height) used during the pile driving test. If a different configuration is employed for the production piles, new predictions must be made to generate adjusted SRD curves and corresponding acceptance criteria.

 © DFI International Bruges 2025

LITERATURE

ASTM D4945, Standard Test method for High-Strain Dynamic Testing of Deep Foundations

Allnamics' PDA Monitoring / PDR

Bolderman, R., Bielefeld, M.W., Van Klarenbosch, C., Schmittmann, B., Van Oudenallen, T.C.G., Brons, K.F., 1998, Handboek Paalfunderingen, deel 3, De installatie van geprefabriceerde betonnen heipalen, Prepal

Josselin de Jong, G. de. (1956). Wat gebeurt er in de grond tijdens het heien? (What happens in the soil during pile driving?), in Dutch, De ingenieur 68e jaargang no. 25

Josselin de Jong, G. de. (2022, September 20). What happens in the soil during pile driving?, 11th International Conference on Stress Wave Theory and Design and Testing Methods for Deep Foundations (SW2022), Rotterdam, The Netherlands.
https://doi.org/10.5281/zenodo.7143118

Middendorp, P. (2022, September 20). More than 80 Years of Experience with the Method of Characteristics – from Graphical Analyses to Advanced Driveability Analyses by Scripts. 11th International Conference on Stress Wave Theory and Design and Testing Methods for Deep Foundations (SW2022), Rotterdam, The Netherlands.
https://doi.org/10.5281/zenodo.7148669

Verbeek, G.E.H., Bielefeld, M.W., Moscoso, N. (2022, September 20). Validated signal matching to analyze HSDT data. 11th International Conference on Stress Wave Theory and Design and Testing Methods for Deep Foundations (SW2022), Rotterdam, The Netherlands.
https://doi.org/10.5281/zenodo.7148219

Verbeek, G.E.H., Bielefeld, M.W. (2022, September 20). Alternative facts in pile testing. 11th International Conference on Stress Wave Theory and Design and Testing Methods for Deep Foundations (SW2022), Rotterdam, The Netherlands.
https://doi.org/10.5281/zenodo.7148281

Viana da Fonseca, 2008, International Prediction Event Behaviour of CFA, Driven and Bored Piles in Residual Soil Experimental Site, ISC'2, September 2008 / 240×170 / 688 pages
ISBN: 978-972-752-104-3 ISBN: 978-98995625-1

 © DFI International Bruges 2025

OPTIMIZING FOUNDATIONS BASED ON CSM PANELS USING RAPID LOAD .

Marcel W. Bielefeld, Allnamics Geotechnical & Pile Testing Experts, The Hague, The Netherlands
Rob F. van Dorp, Allnamics Geotechnical & Pile Testing Experts, The Hague, The Netherlands
Jurgen Houben, H4D Raadgevend Ingenieurs, The Netherlands
Oskar H.J. de Kok, BodemBouw, The Netherlands
Frits Huijbrechts, Geosonda, The Netherlands

ABSTRACT

This paper describes the foundation system for apartment buildings at Cosun Park in Breda, The Netherlands. This ambitious urban development project is transforming a former office site (the former headquarters of the Suikerunie) into a residential area with six residential buildings and underground parking. Since a Cutter Soil Mixing (CSM) rig would already be present to construct the required retaining walls at the site, it was decided to use CSM barrettes for the building foundations as well.

However, the current design codes limit the maximum loads on CSM panels, increasing the number of panels required under each pile cap. Moreover, the current calculation methods appear to overpredict settlements under working loads, resulting in unnecessary overdesign of these panels to meet the settlement (serviceability) limits.

To address this, the load-bearing capacity of the CSM panels was tested in advance. Rapid Load Testing was conducted in accordance with the Dutch pile testing code, NPR 7201, to assess the capacity and stiffness of the CSM panels. The testing showed minimal settlement at a load of 9 MN, demonstrating that CSM barrettes had a substantially higher load-bearing capacity than indicated by the design standards. Consequently, this led to a significant optimisation, reducing both the number and size of CSM panels.

These findings raise the question of whether the current method of calculating the capacity for these CSM barrettes is appropriate and whether the standard design values from the Dutch codes are correct for design for this type of foundation element. Further research is needed to obtain more economical foundation designs using CSM panels.

Keywords: rapid load tests, Statrapid, CSM, panes, case study, re-use of foundations, design codes

INTRODUCTION

When constructing with the materials steel and concrete, the engineer can ensure that the material properties, such as strength and stiffness, closely meet those that are required. That is impossible with the construction material ‘soil’, which basically has to be taken as it is, and even after soil improvement the properties can only be changed to a limited extent. Thus, the soil properties have to be discovered through soil investigation and to address the likely variability of the soil properties, factors of uncertainty (often erroneously indicated as factors of safety) have to be applied. This variability becomes even more critical in the design process when existing foundations are part of the design of a new superstructure.

This was the case for a project in Breda, in the South of the Netherlands, where a 6 stories condo building had to be built at a location with an existing foundation of a (never finished) building. The existing Continuous Flight Auger (CFA) piles interfered with the new design, and the capacity of the new deep foundations elements was affected by the subsoil disturbance due to the construction of these CFA piles. In situations like that, as is frequently the case when existing foundations are re-used, the design process has to be re-considered to include preliminary pile tests. Such tests can not only show higher pile capacities, but also allow the use of project or location-related factors instead of general factors given in the design code.

 © DFI International Bruges 2025

THE CASUS

Cosun Park in Breda is an ambitious urban development project that transforms a former office site into a residential area. At the site of the former Suikerunie headquarters (a company producing sugar from beets), six residential buildings with underground parking are being constructed. CSM panels are used as the foundation elements after testing their load-bearing capacity during the design phase.

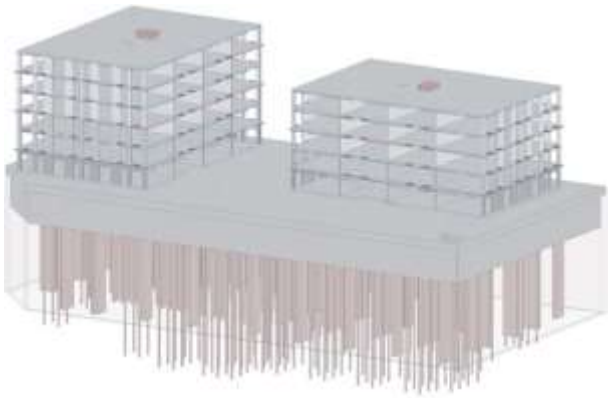


Fig. 1. Structural model of Cosun 4 and 5, with a transparent representation of the load-bearing CSM wall surrounding the building, and within it, the CSM barrettes under the column structure, screw injection piles as tension elements, and existing CFA piles

STRUCTURAL DESIGN

The Cosun 4 and 5 residential buildings have five and six floors respectively, on a two-story underground parking garage. This garage extends beyond the footprint of both buildings. It will feature a roof garden on its deck. The superstructure is designed as an unbraced framework using the wall-wide slab construction method. Stability along the building's length is provided by rigid joints between the walls and floors, while in the transverse direction, the shear strength of the walls is utilized. Starting from the basement deck, the wall structure rests on a column structure within the basement. On levels 0 and -1, the basement structure consists of wide-slab floors combined with beam bottoms and cast-in-place concrete columns.

DESIGN OF THE EXCAVATION AND FOUNDATION

The two new residential buildings are located on the former Cosun 4 and 5 sites, which were never entirely constructed except for the foundation. At that time, ground-replacing continuous auger piles (mortar screw piles) were installed at both shallow and deep pile toe levels. The pile toe level of the shallow piles was more or less at the same level as the basement that is now being constructed, allowing these piles to be removed during the construction. The toe level of the deep piles reached below a water impermeable clay layer into a dense sand layer. CPT results indicated that the ground around these existing piles was disturbed during their installation, so a shallow slab foundation combined with soil improvement was not viable. Reusing the existing piles gave insufficient confidence and were therefore been replaced by the CSM barrettes. Every barrette exist of 1 or more rectangular CSM panels as deep foundation elements.

 © DFI International Bruges 2025



Fig. 2. CSM rig

For the construction of the basement, an anchored CSM wall was installed (fig 2). This CSM wall extends into the dense sand layer, below the water impermeable clay layer, creating a sealed excavation pit. CSM walls were preferred over diaphragm walls for affordability. The CSM method utilizes the soil in place without the need to truck concrete or remove soil. Sheet piles were also ruled out due to cost, as well as concerns about potential noise and vibrations during installation and removal. With the CSM rig already on site, it was decided to use CSM deep foundations as piling system. One system could be used for the sealed excavation pit and the foundation of the building

Under the column structure in the basement, several CSM barrettes, consisting of 1, 2 or more adjacent panels of app 2400 x 600 mm, with 100 mm spacing were used. The load transfer ranges between 2000 and 7500 kN per column. Footings are provided as part of the basement floor on these CSM barrettes, which evenly distribute the column load over the CSM surface, see Fig 3 for a two panel barrette.

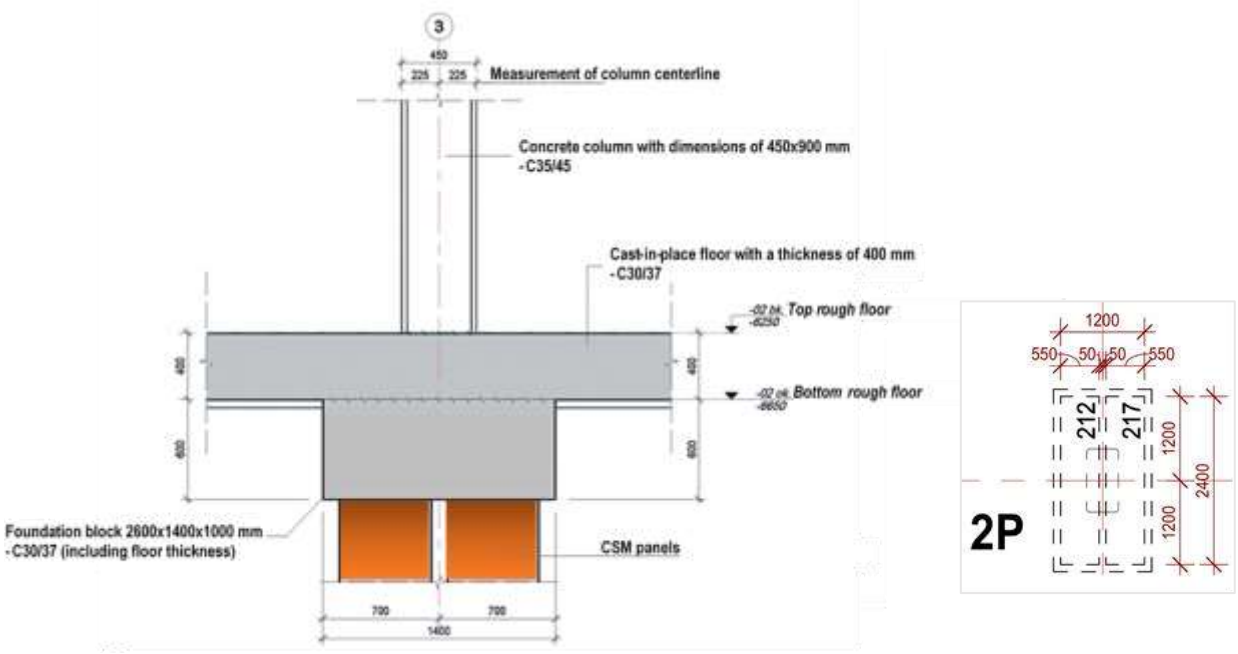


Fig. 3. Cross section and plan of the column, pile cap or footing and (in this case) 2 CSM panels.

 © DFI International Bruges 2025

LOAD-BEARING CAPACITY AND SETTLEMENT BEHAVIOR

To determine the load-bearing capacity of these CSM barrettes, the Dutch geotechnical standard NEN 9997-1+C2 was followed. Design calculations were made based on the results of the cone penetration tests (see a typical CPT in Fig. 4). The barrettes were constructed with a 100 mm gap between the CSM panels. For the CSM panels and the barrettes, the following factors from the Soilmix Walls Handbook [1] can be applied.

- Pile class factor for shaft compression: $\alpha_S = 0.006$
- Pile class factor for toe: $\alpha_p = 0.35$
- Load-settlement curve 3 (according to NEN 9997-1, fig. 6)

The pile's maximum capacity is considered when the settlement (displacement) of the pile reaches 20% of the equivalent pile toe diameter D_{eq}. The equivalent diameter D_{eq} corresponds with the same cross-sectional area as that of a square or rectangular pile, in this case app. 1300 mm.

Based on these assumptions, design calculations for the load-bearing capacity of the barrettes showed that every barrette should be constructed out of 3 to 4 CSM-panels. And even then, significant pile toe displacements at working load conditions were calculated, which the structure could not absorb. The design results, indicating both a limited load-bearing capacity (strength) and the considerable displacements of the pile (serviceability) were considered unrealistic. Therefore, it was decided to conduct load tests in advance on several two-panel barrettes.

PILE TEST CAMPAIGN

The method of Rapid load testing (RLT) was used for testing the CSM piles. This method determines the behavior of the pile by determining its load-settlement diagram and, therefore, the load-bearing capacity of pile foundations and the resulting deformations at working loads. This relatively fast method has been applied for decades as a replacement for and in addition to Static Load Testing (SLT).

For the execution and interpretation of the results, ISO 22477-10 [2], NPR 7201 [3], and CUR report 230 [4] were used. These standards clearly describe how the measurement data should be processed and assessed.

STATRAPID

StatRapid is a method used for conducting Rapid Load Testing (RLT) for testing individual piles, pile groups en foundation blocks. See the test setup in Fig. 5. The principle of StatRapid involves dropping a weight onto a specially designed spring system. Through an advanced combination of the mass of the falling weight and the relative soft stiffness of the spring system, the load duration is such that the pile behaves quasi-statically. In other words, unlike dynamic load tests, the entire pile moves simultaneously in the same direction, eliminating the need to model and consider complex stress wave interference patterns.

The StatRapid device has a built-in hydraulic lifting mechanism, allowing the drop height to be adjusted. The weight is then hydraulically released, and once it rebounds from the spring system on the pile head, it is caught again, preventing the weight from impacting the pile head a second time. This allows for a simple cyclic test with progressively increasing load steps. For the next load step, a higher fall height is set.

During the test, the pile head's force, displacement, and acceleration are measured. The data can be used to derive the pile stiffness, load-settlement behavior, and maximum mobilized static bearing capacity in accordance with the Unloading Point Method (UPM), which is described in ISO 22477-10.

 © DFI International Bruges 2025

For this project, a configuration with a 40-ton mass was used, allowing for test loads up to 10 to 12 MN.

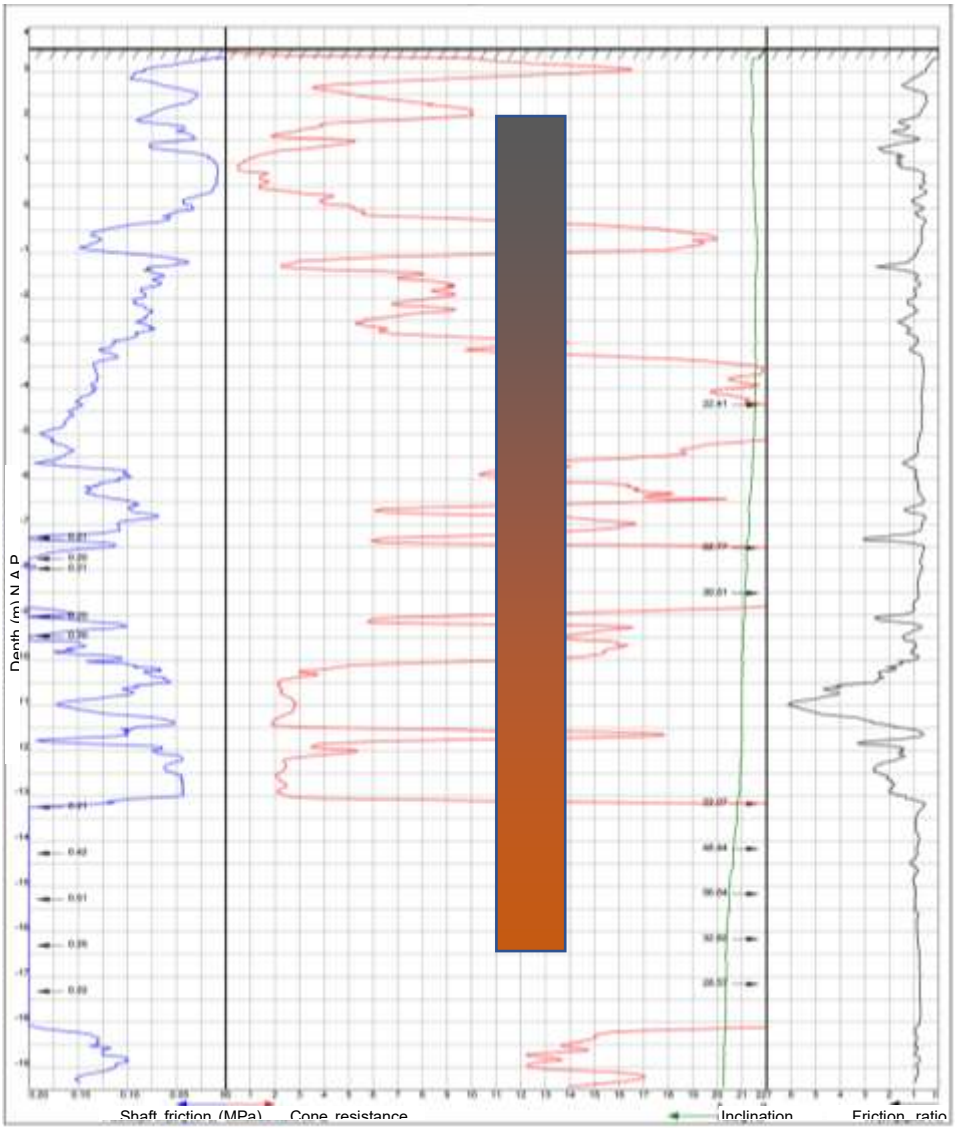


Fig. 4. Typical result of the CPT on this site

For the tested barrette with 2 panels with a design load of 3.300 kN, the required test loads were 5.450 kN. To prepare the foundation for future excavations works, the required test loads on the two panel barrettes were determined between 6.370 and 9.140 kN.

Load duration

The load on the pile is considered to meet the criteria for a Rapid Load Test if it satisfies the following equation (ISO 22477-10):

$$10 < \frac{T_f}{L/c_p} \leq 1000 \qquad [1]$$

Where T_f is the duration of the load, L the length of the pile, and c_p the wave propagation speed in the pile material.

In this case, the panels of 1200x2400 mm had a length of 18.5 m, so the duration of the load had to be at least 90 ms.

 © DFI International Bruges 2025



Fig. 5. The StatRapid device ready for testing a two panel barrette

EXECUTION OF LOAD TESTING ACCORDING TO NPR 7201

Since 2017, the Dutch guideline NPR 7201 has been available for conducting foundation load tests. This guideline defines five classes (A1, A2, B, C, and D) for the setup and execution of the tests, as outlined in Table 1 of the guideline. At Cosun Park, Class C was followed and the philosophy of this class can be summarized as follows:

- The foundation design predicts the minimum available load-bearing capacity based on a specific combination of shaft dimensions and pile toe level.
- A test is conducted to verify whether this load-bearing capacity is available. For this, at least three representative piles are tested.
- A positive test result is obtained when the test piles exhibit load capacity greater than the design loads. In that case, the design method (on a project basis) is confirmed, meaning the calculation method used accurately predicts the minimum available load-bearing capacity for all piles.

NEN 9997-1+C2 assumes that for displacement pile systems, the maximum pile load-bearing capacity is reached when the maximum pile toe displacement equals 10% of the (equivalent) pile toe diameter. For replacement piles, like in this case, is that a value of 20%.

This maximum pile toe displacement is generally equated to the residual pile head displacement after unloading (definition 1: serviceability). However, geotechnical failure only occurs when the load on the pile head can no longer be increased due to rapidly increasing settlement of the pile (definition 2: ultimate capacity). This is where the load-settlement curve transitions from a curve to a vertical line,

 © DFI International Bruges 2025

but such a failure point is not always easy to determine. It is therefore often selected as the intersection of the tangent before and after the trend break.

TEST MONITORING EQUIPMENT

To determine the bearing capacity with StatRapid, the monitoring setup of Fig 6 is prepared. The labels in the figure are indicated below:

- The force is measured using calibrated load cells (A).
- The load cells are mounted on a steel plate (E) to distribute the force to the barrette evenly.
- Acceleration is measured using a sensitive accelerometer (D), and the displacement is derived through numerical integration.
- The load cells and accelerometer are connected to the Allnamics PDR system (F), the data acquisition system.
- The displacement of the pile top is measured during the test by the reflector plate mounted at the pile, monitored by the self-calibrating optical measuring device Reyca (C).



Fig. 6. Monitoring setup and data acquisition system PDR of the StatRapid device

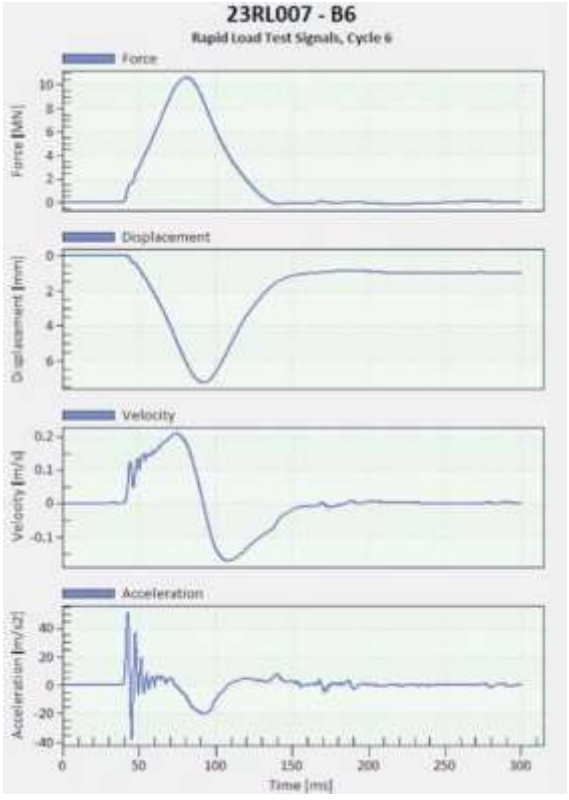


Fig. 7. Example of graphical field results from one load cycle. From top to bottom: measured force, displacement, velocity, acceleration.

 © DFI International Bruges 2025

TEST RESULTS

The graphical field results from one load cycle are presented in Fig 7.

Fig. 8 provides an example of the directly measured 'raw' load-displacement curves from all load cycles of the same panel, along with the derivation of the static load-settlement diagram. These results were derived according to NEN-EN-ISO 22477-10:2016 using the Unloading Point Method (UPM). First, they were corrected for inertia forces (blue, correction 1), and then for the loading rate effect (red, correction 2, applying $\eta = 0.85$), see Fig 8b.

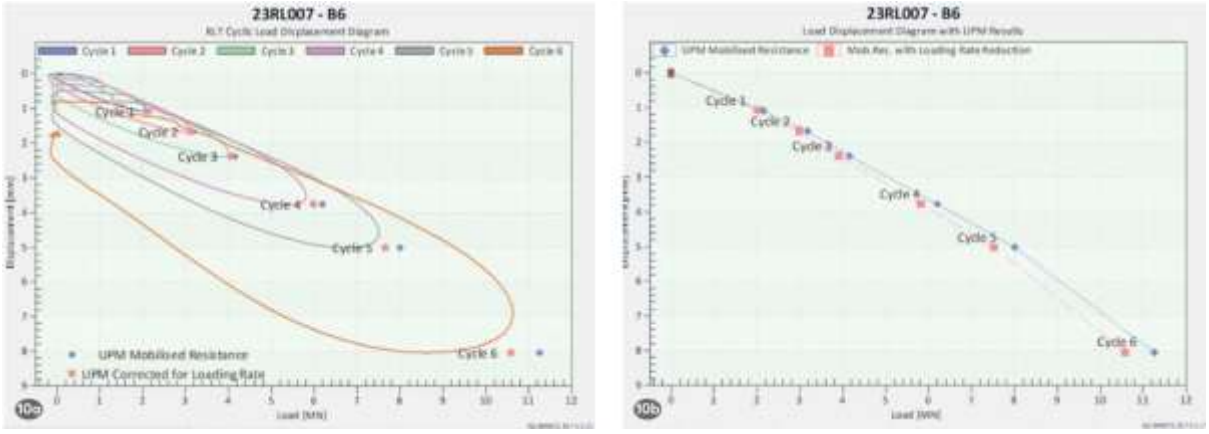


Figure 8. 'Raw' load-settlement curves per cycle (a) and the derived static load-settlement diagrams (b), panel B6

Table 1. Test results Pile Tests class C on 6 double panel barrettes

panel#	target F_{RLT} [kN]	actual F_{RLT} [kN]	Cyclus	Max. displacement cumulatief [mm]	permanent displacement cumulatief [mm]	Check minimum load time	result Class C
as B/as 3	9.140	11.669	6	8,2	1,7	ok	**OK**
as B/as 6	9.140	11.262	6	8,0	1,7	ok	**OK**
as C/as 7	6.370	6.732	5	6,2	2,5	ok	**OK**
as E/as 2	9.140	10.528	6	7,5	1,6	ok	**OK**
as G/as 6a	6.370	6.630	5	5,3	2,0	ok	**OK**
as G/as 6b	6.370	6.977	5	4,8	0,6	ok	**OK**

Table 1 overviews the key test results for six double panels.

In all load tests, the load duration met the required RLT minimum, and the target test load was achieved without exceeding the load-bearing capacity according to definition 1 or geotechnical failure according to definition 2.

Thus, all piles considered have met the test criteria according to Class C.

CONCLUSION

The results of the load tests showed that a load of 9 MN resulted in minimal pile head displacement. This demonstrates that a higher load-bearing capacity can be assigned to the CSM-barrettes than initially calculated according to the calculation with the standard design values for CSM panels in the Dutch code, and that their load-settlement behavior is much stiffer.

 © DFI International Bruges 2025

Due to the results of the Class C tests, the piling plan has been optimized, significantly reducing the number of required CSM panels. Even at higher penetration levels, sufficient bearing capacity can be mobilized. The number of CSM panels under a barrette came down from 3-4 to 1-2. A significant cost saving, and savings in time, carbon footprint and reduced usage of raw materials.

This case demonstrates that additional field testing can reduce costs, time, and emissions. For future projects utilizing CSM panels, load tests can be integrated into the design process to determine site-specific characteristic values for design factors. In this case, the cost of testing, which should be seen as an investment, is offset by the subsequent savings in overall costs, time, and environmental impact. With more test data from various sites, the pile class factors and load-settlement curves for CSM panels could be further refined and optimized, leading to more economical foundation designs using CSM panels.

LITERATURE

Cement 3 2024 (in Dutch) Funderen op CSM-panelen na proefbelastingen

CUR Report 230 - Guidelines on the Interpretation of Rapid Load Testing on Piles.

Handbook Soilmix-walls – Design and Execution, CROW.

ISO 22477-10:2016 - Geotechnical Investigation and Testing – Testing of Geotechnical Structures, Part 10: Testing of Piles: Rapid Load Testing.

NPR 7201:2017+A1:2020 nl - Geotechnics - Determination of the axial bearing capacity of foundation piles by pile load testing

 © DFI International Bruges 2025

ASSESSMENT AND MITIGATION OF CROSSHOLE SONIC LOGGING ANOMALIES IN LARGE DIAMETER BORED PILES

Patrick Casey, Ove Arup & Partners Ltd, Belfast, United Kingdom.
Chris Barker, Ove Arup & Partners Ltd, London, United Kingdom.

ABSTRACT

When the results of integrity testing of pile foundations identify anomalies in the readings, assessment by the designer is required in order to determine if the geotechnical and/or structural performance of the pile is compromised and if remediation measures are required. This paper presents a case history where crosshole sonic logging (CSL) was used on large diameter rock socketed bored piles constructed with tremie concrete methods. Anomalies were identified in the results and then subsequently investigated by excavating around the pile to the anomaly level with significant inclusions within the concrete being observed. The potential for common methods for investigating CSL anomalies to accept piles with defects is discussed. The risks to the performance of bored pile foundations through incorrect identification of the defects of this nature is illustrated through results from a fully instrumented load test pile exhibiting similar CSL anomalies where structural failure observed at a load significantly lower than the design capacity. The time dependant nature of CSL data and discussion on when to undertake these tests after concreting a pile is also included and illustrated through a series of repeat tests at 7, 11, 53 and 87 days after casting.

INTRODUCTION

Eighty-five bored piles were constructed to carry the four foundations for a new river bridge. The balanced cantilever bridge construction methods resulted in significant variation in the design loading across the pile groups. Maximum tension and compression loads in the piles of 3MN and 10MN respectively, were calculated under accidental load case scenarios. The structural form of the piers and superstructure meant that pile cap rotation and the redistribution of loading amongst the pile group was a critical consideration in the overall design of the foundations.

The piles ranged in diameter from 1050mm to 1350mm and the design required a 4.5m long rock socket. The design did not include reliance on end bearing in the rock. Piles ranged in length from 41.0m to 48.0m as rock level varied across the site. The piles were drilled with polymer support fluid. Reinforcement extended the full depth of the pile and concrete was placed using tremie methods.

Integrity testing by crosshole sonic logging (CSL) was carried out on 100% of the piles. In response to anomalies apparent in the CSL results, a methodology is set out describing further analysis that was carried out to assess the potential impact of the anomalies on pile and foundation behaviour. This methodology significantly reduced the extent of remedial works required on the project. Important observations are also discussed for the interpretation and mitigation of CSL anomalies in bored piles taking into consideration the age at which the pile is tested and the impact of interruption to the placement of tremie concrete.

GROUND CONDITIONS

Typical stratigraphy encountered at the site is presented in Table 1. The piles were designed to extend 4.5m into the sandstone bedrock. Groundwater was encountered in the alluvial deposits, hydraulically linked to river water levels, and within the sandstone and glacial deposits. The groundwater in the

 © DFI International Bruges 2025

sandstone and glacial till layers was under artesian pressure at several of the foundation locations due to geological local lowering of existing ground level in forming the current broad river channel at the site. The groundwater pressure was measured at a level 5m above surrounding ground levels during the site investigation.

Table 1 Typical stratigraphy at foundation locations

Stratigraphy	Top Level (mOD)	Thickness (m)
Construction platform	14.0	up to 3.5
Alluvial deposits / Raised Marine Deposits*	10.5	1.0
Upper Glacial Till (firm sandy CLAY)	9.5	4.5
Glacial Till (stiff sandy gravelly CLAY)	5.0	15
Granular Glacial Till	-10.0	13 – 16
Sandstone	-23 to - 26	Unproven

*Where encountered across the site, the alluvial deposits generally coincide with the absence of the raised marine deposits through erosion.

The glacial till deposits typically have 50 to 60% sand and gravel sized particles, with this increasing to 70 to 90% in localised zones. The glacial till plots as a low plasticity clay on Atterberg charts and is heavily over consolidated with typical natural moisture contents of 10%.

CONSTRUCTION PROCESS

The piles were drilled using Casagrande B300 XP2 piling rigs. A typical pile construction sequence was as follows:

Day 1:

a. Install temporary casing into upper glacial till
b. Add polymer support fluid
c. Excavate to one to two meters above design toe level within the rock

Day 2:

a. Complete excavation to design toe level
b. Hold period and polymer testing
c. Carry out base inspection
d. Install reinforcement cage
e. Install tremie pipe and concrete pile and remove temporary casing

The piles were constructed using a partially hydrolysed polyacrylamide polymer support fluid. Samples of polymer were recovered from the top, middle and toe of the pile during drilling and prior to placement of reinforcement cages. The tests and compliance values adopted by the piling contractor are shown in Table 2.

Table 2 Polymer compliance values

Property	Fresh	Excavation / Concreting
Density by Mud Balance (g/ml)	<1.01	<1.02
Marsh Funnel Viscosity (sec)	>90	90 – 120
Sand content (%)	0	<1%
pH	9 - 11	9 – 11.5

 © DFI International Bruges 2025

Density results were generally 1.004 to 1.005 g/ml. Viscosity results were generally within the compliance limits with occasional high values (up to 180 sec.) during drilling. Sand content results were within the compliance limits and rarely exceeded 1.5% during drilling. pH results were all between 9 and 11.

Following completion of base cleaning, the pile base hardness was assessed. A semi-quantitative assessment was carried out in accordance with the classification system described in Table 3. Base hardness tests were typically Grade 2 or 3. A continual rain down of fine debris was noted on some piles with significant accumulation of material (>50mm) recorded after placement of reinforcement cage and ahead of tremie concreting.

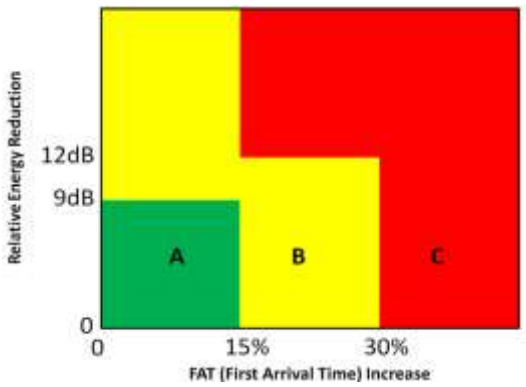
Table 3 Base hardness classification (ICE, 2016)

Grade	Description
1	Hard, sudden impact
2	Sudden impact felt but some damping (<25mm) of impact vibrations
3	Distinct base detected with slight embedding (<50mm) of weight into soil
4	Significant embedding of weight (<100mm) detected, making definitive base difficult to detect
5	Weight sinks slowly into base, making definitive base very difficult to detect

Slump testing on the concrete showed results of 200mm to 240mm

INTEGRITY TESTING

Integrity testing by crosshole sonic logging, (CSL) was specified on all piles. The tube arrangement consisted of steel CSL tubes evenly spaced around the reinforcement cages. Four tubes were used on the 1.05m diameter piles and 5 tubes on the 1.35m diameter piles. The evaluation criteria applied for the CSL test was as described in DFI (2019) and a graphical representation of the rating criteria used is reproduced in Figure 1.



Class A: Acceptable CSL test result,
Class B: conditionally acceptable CSL test result,
Class C: Highly abnormal CSL test result.

Fig. 1. Graphical representation of the CSL rating criteria (DFI, 2019)

CSL testing began on site 7 – 10 days after casting and potential anomalies were observed after one third of piles had been cast. A change in the relative energy signal was observed at the toe of the piles with a reduction of more than 12db frequently recorded. An increase in the first arrival time was usually recorded along side the drop in energy. One set of profiles showing typical FAT and relative energy anomalies recorded at the pile toe level is shown in Figure 2 with a reduction in relative energy of > 12db and an increase in FAT of >20% resulting in a Class C classification. The potential anomalies recorded typically affected bottom 1.5m to 4.5m of the rock socket. While construction continued on the foundation, and in advance of engineering evaluation and identification of a cause of

 © DFI International Bruges 2025

the anomalies the decision was taken with the contractor to increase the length of the rock socket of the piles. This meant adding extra length to the bottom of the piles as a precaution, in case future CSL tests showed similar issues.

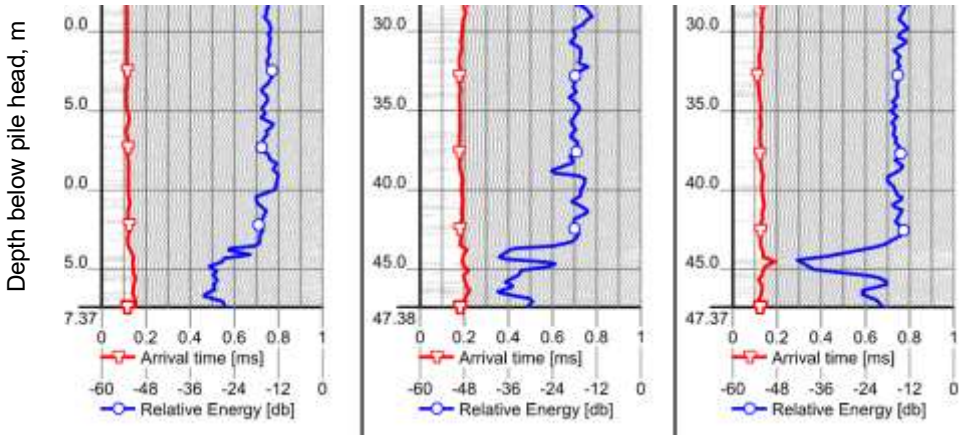


Fig. 2. Typical FAT and relative energy anomalies recorded at pile toe level

ASESSMENT OF POTENTIAL IMPACT ON DESIGN

The anomalies recorded at the toe of the piles could indicate the absence of sound concrete over the affected length. This in turn could result in the absence of adequate pile to rock bond and consequently no proper load shed over this length of the rock socket. Along with reducing the ultimate capacity of the pile, the higher contact stress over the remaining length of the pile could also potentially result in a greater settlement in the affected piles. Approximately half of the overall pile capacity was calculated to come from the rock socket and loss of some of, or all of, the rock socket on a pile could significantly change the load shed from the pile into the till over the shaft above the rock. This increase in contact stress between the pile and the till could lead to some piles moving more under load compared to those with a sound rock socket.

The potential impact of the anomalies on the foundation was accounted for in the analytical model by a 50% reduction in the vertical stiffness of individual piles within the overall group. This was done to mimic a soft pile within the group that would have a lower resistance compared to piles with no anomalies present. The amount of reduction was quantified considering piles with a fully formed rock socket to be almost fully rigid (at the toe) and piles with significant anomalies in the rock socket to behave as friction piles supported in the till. The subsequent redistribution of loads within the pile group were reviewed to identify any piles which had become overloaded by picking up load from weak piles.

The assessment method adopted involved looking at risk scenarios with bespoke capacities and loads on each individual pile within the group. The process followed is summarised in the flowchart shown in Figure 3.

Where redistribution of the pile loads due to application of a reduced stiffness in some piles resulted in overloading of piles, a further iteration was undertaken with a reduced stiffness also adopted for those overloaded piles. When compatible geotechnical loading was achieved, the new structural forces envelopes were reviewed against the original design envelopes and reinforcement. The overall pile cap rotations were also reviewed to assess the risk of movements outside what could be accommodated by the design of the pier and other elements of the bridge.

 © DFI International Bruges 2025

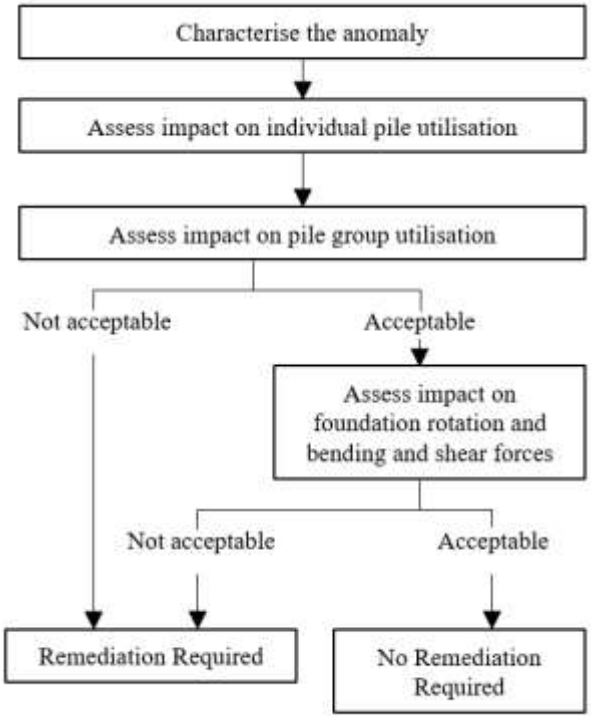


Fig. 3. Assessment Flowchart

REMEDIAL MEASURES

Where the risk management methodology adopted for this scheme indicated there was a potential risk to the geotechnical capacity of the group, further remedial measures were recommended.

The use of tomography was reviewed and the potential to determine a 3D image of the anomaly to allow further refinement and better quantification of the risk. Potential scenarios that the tomography work could lead to included; elimination of the anomaly with no further work recommended (considered to have a low possibility at the time), quantification of the amount of affected concrete showing that the remaining sound section was adequate to transfer the load to the pile below the anomaly and quantification of the amount of affected concrete showing the remaining section was not sufficient to transfer the to the pile below the anomaly. This last scenario would lead to a need for repairs such as drilling and grouting with further testing to validate the success of the repair work. An alternative remedial measure reviewed was construction of additional piles to bring the overall group capacity and foundation behaviour back within what could be tolerated with in the design.

As with every major construction project, programme is a critical element. The potential delay to completion of the foundation works and commencement of the follow-on pier works which could have arisen from further investigation through tomography followed by drilling and grouting was considered to large compared to the more readily quantifiable delay and cost from installation of additional piles. After careful review, construction of additional piles was the remedial option adopted on the project.

Of the 85 piles in the original design, the capacity of 41 piles were down rated due to the presence of anomalies, with 13 of these piles assessed as having no effective rock socket. After following the process set out in this paper, only 5 additional piles were required to mitigate the potential risk to the performance of the foundations.

 © DFI International Bruges 2025

FURTHER OBSERVATIONS ON SITE

Visual Examination of Anomalies

A CSL anomaly showing a 15% increase in FAT and a 15dB reduction in relative energy was recorded in one pile at a depth of 3m below the pile cut off level. These figures classify the anomaly as borderline Class B to C following the DFI system. The contractor took the decision to excavate around this pile and expose the surface for visual examination. On excavation significant concrete inclusions were noted in the cover zone and around the reinforcement. Figs. 4 a - d illustrate what was found. It is noteworthy that these inclusions were localised to the reinforcement and cover zone with the affected concrete noticeable weaker than the concrete above, below and also within the core of the pile. Tomography analysis of these defects may not have identified the full extent of the inclusions within the cover zone and surrounding the reinforcement. Coring the centre of this pile would likely have recovered sound concrete possibly resulting in this pile being passed without further remedial work. This example highlights the limitations of traditionally investigating CSL anomalies through tomography and coring.









Figs. 4a – d, concrete inclusions in cover zone. 4a shows inclusions around the reinforcement spacer skid, 4b shows the general extent of inclusions, 4c shows inclusions around the CSL reservation tube and 4d shows the extent of inclusion s in a piece of concrete recovered from the cover zone.

 © DFI International Bruges 2025

Change in CSL readings over time

In line with typical specifications for this work, the piles were required to be tested at a minimum of 7 days after casting. It was found that, for these piles, a time of 12 – 14 days after casting was typically required for CSL readings to stabilise and to produce a reliable result from which to assess the integrity of the piles.

The temperature in the concrete varies during curing. Figure 5 shows the temperature measured in the pile in strain gauges during curing with temperature changes of approximately 5 deg. C recorded in the piles between 7 and 14 days after casting. Taking the reduction in temperature as being inversely proportional to the increase in density then the data in Figure 5 also indicates large changes in concrete density in the piles after 7 days.

The first arrival time measured in an CSL is a function of the wave speed velocity of the sonic impulse through the concrete. The wave speed velocity is, in turn, a function of the density of the concrete and therefore the temperature changes, even after 7 days, may affect the CSL readings obtained. It is proposed that consideration of curing temperatures and curing time is necessary in specifying a minimum time after casting for CSL readings to be taken.

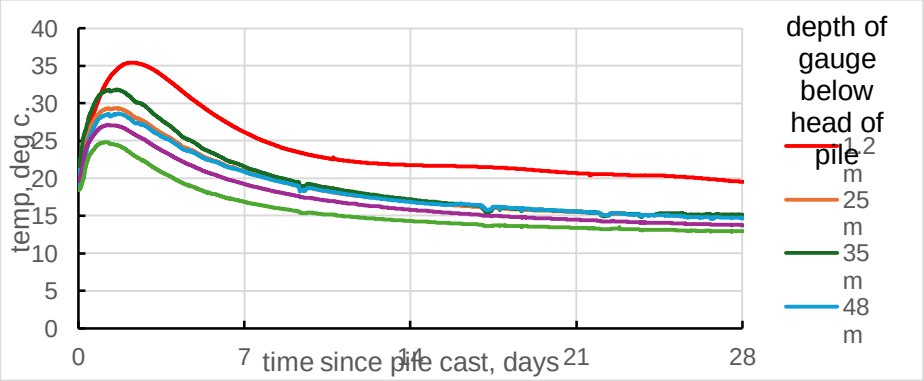


Fig. 5. Concrete curing temperature over time

This project also allowed repeated CSL readings to be obtained from individual piles at different ages. Fig. 6 shows FAT and relative energy readings taken in the same pile 11, 53 and 87 days after casting.

Figure 6a shows the average FAT over the depth of the pile decreasing by 10 – 15% between day 11 and day 53, with little change between day 53 and day 87. This is consistent with an assumption that the concrete will gain in strength and density up to 60 days after casting, with little noticeable change thereafter. While the arrival time decreases over time, the shape of the FAT plot over the depth of the pile remains broadly constant.

Figure 6b shows a noticeable change in the relative energy reading from day 11 to day 87. It should be noted that Figure 6b shows only shows a 20m long segment of the pile, while Figure 6a shows the full 54m length of the pile. Compared to the average reading, a reduction in relative energy of around 20dB was recorded at day 11 at a distance of 42m above the base of the CSL tube. This changed significantly to a reduction of around 10dB on day 53 and around 5dB on day 87.

In this instance, the day 11 reading would be categorised as Class C, (increase in FAT of close to 30% and reduction in relative energy of 20dB). The day 87 readings however, would be categorised as Class B, with a much lower energy reduction, and could be classified as borderline Class A depending on how exactly the average FAT is determined.

 © DFI International Bruges 2025

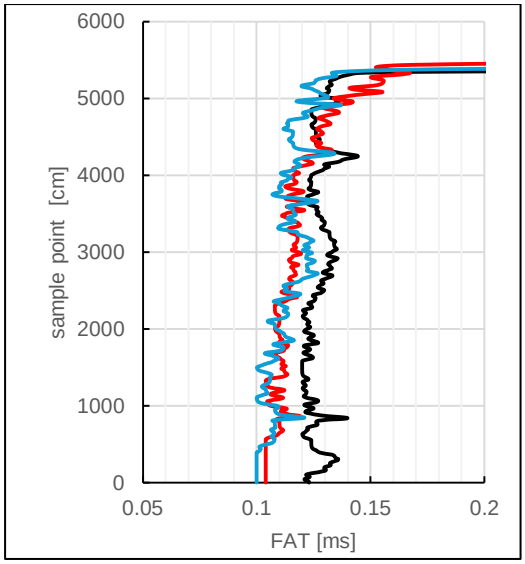


Fig. 6a

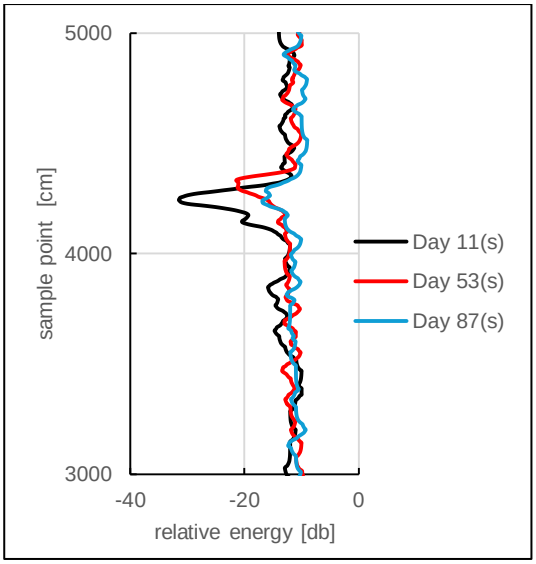


Fig. 6b

Fig. 6a – b, Change in FAT and relative energy records 11, 53 and 87 days after casting

Review of concrete records and tremie records

Review of the concrete records alongside the CSL logs for the piles suggest that an anomaly was more likely to be present in the CSL logs at a depth in the pile where there was an interruption to the concreting process or a change in the consistency of the concrete between one batch and the subsequently placed batch. Inclusions such as those shown in Fig. 4 may have arisen due to debris carried up from the base of the pile becoming trapped in the cover zone between batches of concrete. Artesian groundwater may also have contributed. In light of these observations, the importance of careful and rigorous control of the pile construction and the concreting process cannot be overstated.

Explanation of the anomalies recorded at the base can only be based on theory and interpretation as there was no way to physically examine these areas. Current research by Mitchell (2024) using CFD modelling of the flow of concrete placed via tremie in reinforced piles shows that the presence of debris at the base of the pile can become mixed into the concrete and that this concrete flows around the reinforcement and up through the cover zone. If this debris becomes lodged around the reinforcement, inclusions such as were shown in Fig. 3 could arise. Construction of piles under support fluid through fine grained material will bring fine grained material into suspension within the support fluid. This fine gained material may be silt and clay sized and will require more time to fully settle out of suspension than would be required for sand sized particles. Depending on project specifics, an overall better outcome may be achieved by adopting a full fluid exchange at the lower part of the pile to mitigate the build-up of fine-grained debris at the pile toe prior to concreting.

EFFECT OF SHALLOW ANOMALY IDENTIFIED THROUGH CSL ON PILE LOAD CARRYING CAPACITY

A static load test was carried out on a 0.88m diameter pile in which CSL integrity testing showed the presence of a Class B anomaly 2m below the head of the pile with a reduced energy of >12dB and an increased first arrival time of < 30%. The pile was instrumented with vibrating wire strain gauges and multi-point extensometers. This pile was constructed without a rock socket and was expected to generate its resistance through a combination of shaft and toe resistance.

 © DFI International Bruges 2025

Review of the pile head movement during the test at first appeared to show expected behaviour, with the shape of the load-movement curve suggesting the test had managed to fully mobilise the shaft resistance and engage the toe resistance of the pile. Subsequent, detailed analysis of the instrumentation data however highlighted a number of issues with this interpretation. Strain gauge results over the lower half of the pile showed negligible load getting to the toe of the pile. This was corroborated by extensometer data which also showed negligible compression of the lower half of the pile. Figure 7 shows the strain gauge data for two opposite gauges located 1.55m from the head of the pile with individual readings diverging at a pile head load of c. 5MN. This divergence can be attributed to a pile undergoing bending, with one side of the pile compressing more than the opposite side.

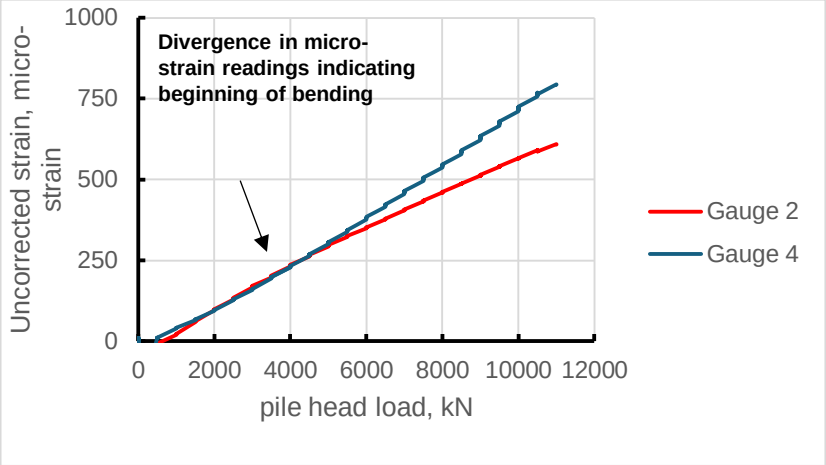


Fig. 7. Micro strain readings on opposite gauges 1.55m below pile head

This was confirmed on excavation of the pile when significant cracking was evident at the depth of the CSL anomaly as shown in Fig. 8.

 © DFI International Bruges 2025



Fig. 8. Pile damage observed on excavation after load testing

This test pile was reinforced with 12No. B32 bars with 40MPa concrete. At an axial force of 5MN, this reinforcement would give a bending resistance of 1500kNm. This bending moment resistance should have been far higher than any potential induced moment in the pile, (through inclination or off-centre application of the jack) at that point in the test.

Inclusions of the type shown in Fig. 4a-d would reduce the effective reinforcement in the pile and also the bending moment resistance of the pile. Assuming a reduced reinforcement the pile equivalent to 8 B16 bars shows that cracking would begin at a moment of 200kNm. For this moment to be induced I the pile the verticality would need to be outside what is typical for bored piles, or the jack set up several cm's off centre, or a combination of both of these.

In the case of the test pile, a Class B SCL anomaly may have resulted in a 80 to 90% reduction in the bending moment resistance of the pile.

SUMMARY AND CONCLUSIONS

Results from CSL carried out on large diameter bored piles recorded anomalous readings indicating potential risks to the load carrying behaviour of the piles within the foundation from the presence of poor concrete at the pile toe and along the shaft. This risk was assessed through iterative reanalysis of the overall foundation behaviour by including for soft piles within the group. This resulted in a changed load distribution among the pile group arising from weaker load settlement behaviour in the affected piles. By considering the individual loads, (after iterative redistribution) and the as-built capacity of each pile this approach was able to demonstrate that many of the affected piles were suitable for inclusion in the foundation without further investigation or remedial works.

Excavation of a pile with CSL anomalies at a shallow depth below the pile head showed significant inclusions around the reinforcement and in the cover zone. The depth of the inclusions into the pile was restricted to the zone around the reinforcement. Investigation of the anomalies through coring the pile would likely have recovered sound concrete, potentially allowing a defective pile to be accepted.

 © DFI International Bruges 2025

It is interesting to consider if thermal integrity testing would have shown anomalous readings in this cover zone.

Load testing of an instrumented test pile which showed a CSL anomaly in the shaft close to the head of the pile resulted in bending and cracking of the pile at an applied load far below the calculated bending moment capacity of the pile. It is proposed that inclusions in the concrete in the cover zone and around the pile reinforcement rendered the reinforcement almost entirely ineffective due to loss of bond leading to the failure of the pile.

These two observations together highlight the potential for the presence of a Class B anomaly to significantly reduce the structural capacity of a bored pile. The potential for coring of a pile to result in a defective pile being accepted through the presence of sound concrete inside the reinforcement zone is also highlighted.

The CSL data collected from for some piles at different ages showed changes in the results over time. The first arrival time generally decreased uniformly over time, consistent with the concrete density increasing over time. This project presented an opportunity to gather CSL data over an extended period of time with data recorded 11, 53 and 87 days after casting. The changes in the FAT results over time were generally consistent with the concrete density increasing over time. However, where an anomaly in the FAT was recorded, the magnitude of the anomaly generally didn't change over time, resulting in an increase in the % change in the FAT reading. Generally, little change in the relative energy was observed over time. A significant change in the decrease in relative energy at the location of an anomaly was observed with a Class C anomaly reducing to a Class B anomaly from day 11 to day 87.

This work shows that CSL readings, and classification of anomalies, can change over time. CSL anomalies were also more likely to be observed at a depth in the pile where there was an interruption to the tremie process and artesian groundwater may also have contributed. There is risk in the strict use of numerical boundaries alone to classify anomalies and to determine the appropriate course of action. The use of coring alone as an investigation method for CSL anomalies without the assistance of tomography should also be carefully reviewed.

This highlights a need to consider anomalies recorded in CSL as indicative of a potential problem that need to be considered further alongside a full understanding of the pile construction methodology and in particular the concreting process.

REFERENCES

Deep Foundations Institute (2019) Terminology and Evaluation Criteria of Crosshole Sonic Logging (CSL) as applied to Deep Foundations.

Institution of Civil Engineers (2016) Specification for Piling and Embedded Retaining Walls, 3rd ed. ICE Publishing, London, UK

Mitchell, T., 2024. Numerical modelling of tremie concrete in deep foundation construction. PhD thesis, Swansea University.

 © DFI International Bruges 2025

PILING FOR SOLAR FARMS

John R. Davie, Ph.D., P.E., M.ASCE, Sr. Principal Geotechnical Engineer, G&HES, Bechtel Corporation, Reston, VA, jdavie@bechtel.com
José L.M. Clemente, Ph.D., P.E., BC.GE, F.ASCE, Manager of Geotechnical Engineering, Geotechnical & Hydraulic Engineering Services (G&HES), Bechtel Corporation, Reston, VA, jlclemen@bechtel.com

ABSTRACT

Solar farm projects require the installation of pile-supported solar panel arrays and depending on the planned electric power output the number of required piles could be in the six-figure range. Because the installation cost of piles tends to represent a significant percent of the total project installed cost, pile design combined with load testing and installation time must be optimized for cost effectiveness. Consequently, viable sites need to present favorable subsurface conditions to allow for the use of piles that consist of small size steel W-sections pushed/vibrated into the ground. This paper presents and discusses experience with pile design, testing and production installation at solar farms under construction or recently completed in the United States.

Keywords: pile, piling, solar, array, farm

INTRODUCTION

Energy transition projects have rapidly multiplied in the United States because of the on-going push for decarbonization. A large number of these projects involve electric power generation using photovoltaic (PV or solar) panel arrays, popularly known as solar farms. These projects require the installation of pile-supported solar panel arrays, with each array containing multiple PV panels, as illustrated in Fig. 1 (photo).

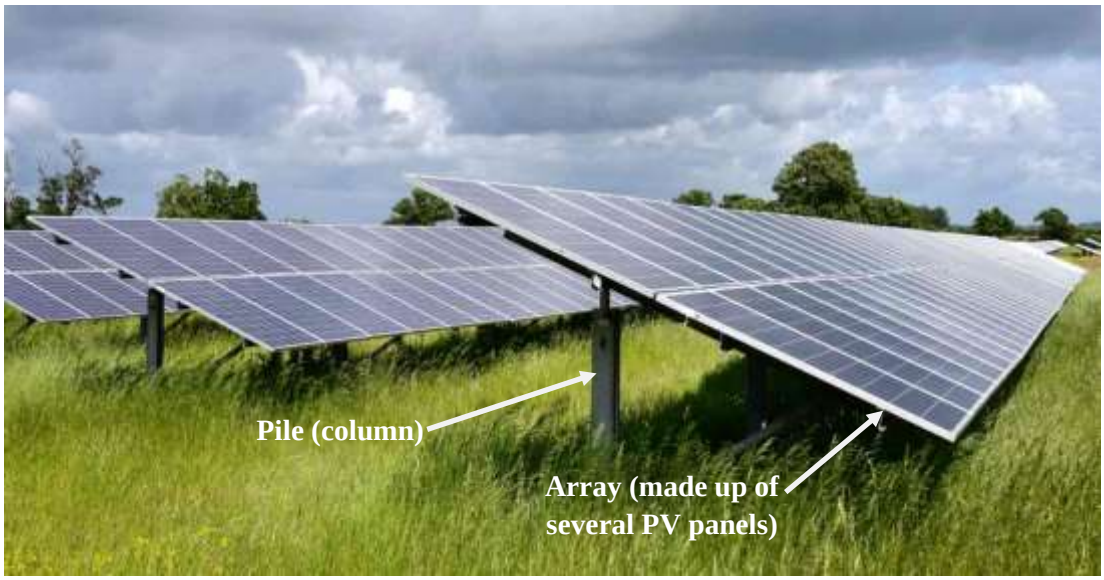


Fig. 1. Illustration of solar panel array

Depending on the planned electric power output, the number of required piles could be in the six-figure range. A 360-megawatt (MW) solar farm project under construction required about 173,000 piles for support of the solar arrays and a total of about 800,000 PV panels. A typical 200 MW alternating current (AC) PV project may use 80,000 to 90,000 piles. A recent prospect aims to install solar panel arrays to generate 6 gigawatts of electric power, which will require millions of piles. Thus, a cost-effective design and installation of piles is essential for project success because the cost of piles

 © DFI International Bruges 2025

represents up to about 10% of the total project installed cost. A cost-effective design requires not only good quality and sufficient subsurface data, but importantly, pile load testing data.

Typically, small size steel W-sections such as W 6x8.5* up to W 6x25* used for solar farm piling are pushed/vibrated to depths typically ranging from about 2 m to 4 m below the ground surface. Assuming a 3-m depth, this represents about 60 MN of steel for a 200 MW AC PV project. Thus, adding margins and allowances in installed pile lengths can be expensive. For example, 0.3m of extra length on each installed pile may cost over $750,000 for a 200MW project, excluding costs associated with a possible productivity reduction. Installed pile lengths must strictly comply with design requirements to avoid cost escalation.

*These sizes are in U.S. customary units (ASTM 2022c). The first number (6) represents the section height in inches (h in Figure 3) and the second number represents the section weight in pounds/foot (lb/ft). Thus, a W 6x8.5 section has a height of about 6 inches (150 mm) and weighs 8.5 lb/ft (124 N/m).

The next sections of this paper present and discuss experience with pile design, testing, and production installation at solar farms that are under construction or recently completed in the United States at sites designated A through F. Note that the discussions that follow apply to piles supporting panel arrays only. Solar farms often include ancillary structures and equipment, such as inverters and the solar cable management systems that hold the electrical cables that run alongside and between the arrays. Ancillary structures and equipment require their own piling systems. Inverters often require larger sizes or deeper piles than the panel arrays.

DESIGN CONSIDERATIONS

One important feature of solar projects discussed here is that the solar panel arrays use tracker systems to follow the sun, i.e., they are not fixed arrays. Consequently, load combinations vary depending on the position of the arrays. Piles are normally designed to support a combination of lateral loading caused by wind or earthquakes. Compressive loads tend to be small, but tension loads caused by wind can impact pile design.

The presence of frost-susceptible soils can result in ad-freeze, and swelling soils can generate tension forces on the upper portions of the pile section, impacting the uplift pile design and requiring additional pile length. Near-surface rock can require predrilling with major impacts to cost and schedule. Another important consideration at some sites is corrosion protection. The presence of salt flats at a prospective site requires the consideration of alternative fiber reinforced pipe piles. The next subsections discuss specific design considerations.

Typical pile geometry

Piles for solar panel arrays typically stick up above the ground surface by 1.4 m to 2.3 m, depending on site topography. The center of rotation of the solar panel is typically 150 mm to 230 mm above the top of the pile, or a distance h above the ground surface, as illustrated in Fig. 2.

Solar farm piles used in the U.S. are typically the steel W section illustrated in Fig. 3. The 6x9 wide flanged beam is the most commonly used pile. Dimensions for this section, provided in Table A2.1 of ASTM (2022c), are flange width, $w \approx 100$ mm, depth, $h \approx 150$ mm, flange thickness, $t_f \approx 5.5$ mm and web thickness, $t_W \approx 4.3$ mm. Pile size can increase to as large as W 6x20 or even W 6x25 when stick-up is high and the pile is located in an exterior row where wind exposure is greater. W 8 section piles have been used but are less common. The W 8x10 pile has a section modulus on the strong axis of almost 40% more than the W 6x9, increasing the lateral capacity of the pile by more than the 10% increase in the weight of steel used. It is noted that the section modulus (and moment of inertia) is much higher with respect to the strong axis (X-X') than the weak axis (Y-Y') of the W section. Table A2.1 of ASTM (2022c) lists properties of W-section piles in U.S. customary units.

 © DFI International Bruges 2025

Typical pile loads

Loads applied by the panel arrays are transferred to the ground surface by the piles/columns, as illustrated in Fig. 2, and R_D, R_L, and M_G are used for pile sizing. The downloads shown in Table 1 (described below) are combined, resulting in compressive axial loads on the piles.

Table 1 illustrates the magnitude of unfactored loads applied to piles at the ground surface at Site A. This example is for a project site in a coastal area with no snow loading, negligible earthquake loading, and significant wind load caused by a 3-second gust at 210 km/h (hurricane force wind loading). The loads in Table 1 are maximum loads occurring when the solar panels are set at 52° to the horizontal (their maximum angle), and the wind is perpendicular to the panels. As suggested by the values in Table 1, pile design is generally governed by lateral loading caused by wind or an earthquake. Axial compressive loads resulting from wind tend to be larger than applied dead loads. Ad-freeze loading, discussed later, can be more significant than wind loads for pile uplift.

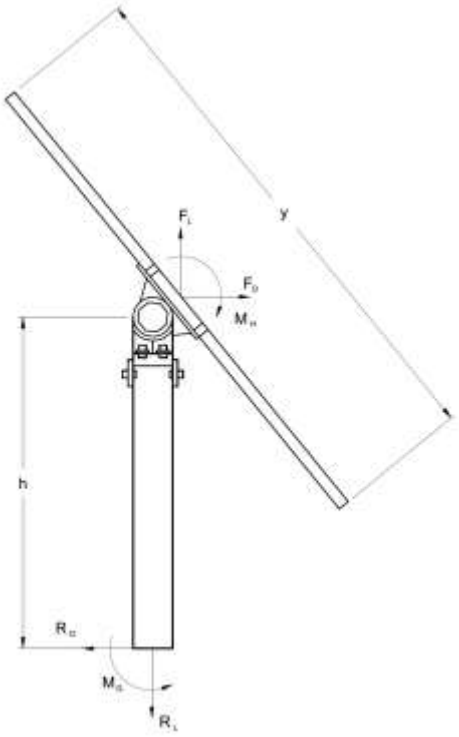


Fig. 2. Typical pile geometry (above grade)

Allowable stress design (ASD) is typically used for lateral load analysis, and ASD, or load and resistance factor design (LRFD), can be used for axial loading. ASCE 7 (ASCE, 2017) provides a factor of 0.6 for lateral wind loading. Factored tension loads due to wind typically range from about 7 kN to 9 kN while factored compression loads, with the dead weight of trackers and solar panels added, can reach over 13 kN.

Factored lateral loads on the pile can range from about 7 kN to 10 kN. Pile design for lateral loads is often performed based on the ground-line moment, which is the lateral load times the distance from point of application to the ground (M_G in Fig. 2), plus the hinge moment, which is the moment created by the solar panel rotating about the torque tube (M_H in Fig. 2).

 © DFI International Bruges 2025

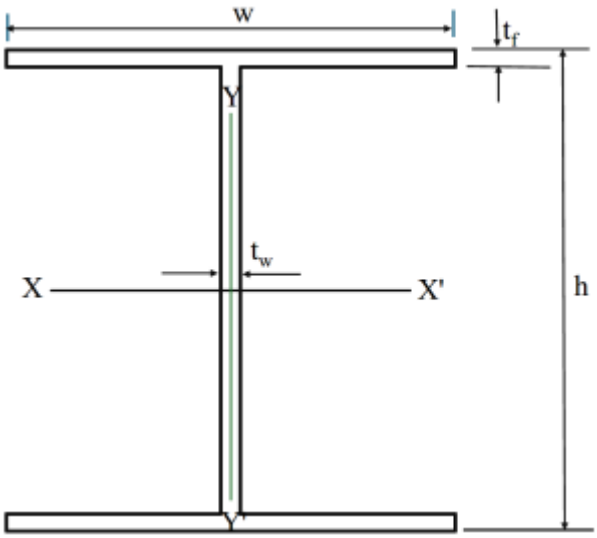


Fig. 3. W-section geometry

Table 1. Typical pile loads at Site A

Loading Type	Height (h*, m)		
	2.1	**1.8**	**1.5**
R_D (wind lateral), kN	13.3	13.2	13
R_L (wind vertical up), kN	10.6	10.4	10.3
R_L (wind vertical down), kN	-8.6	-8.4	-8.4
R_L (snow vertical down), kN	0	0	0
M_G (ground-line), kN-m	353.1	305.9	260.5
Estimated Dead Weight, kN	-1.8	-1.8	-1.8
*Refer to Fig. 2. Note that h is influenced by site topography to accommodate movements of the solar arrays.			

Note that during design wind events, the panels are stowed at their maximum angle to the horizontal, typically 50° to 55°, thus maximizing the wind loading on the piles. If the panels are stowed in a horizontal position, vortices are created that can cause extensive damage.

Earthquake loading on the piles, even in high seismic areas, is relatively small because of the light weight of the arrays. Since ASCE 7 (ASCE, 2017) does not have the design wind and earthquake loading occurring at the same time, earthquake loading does not impact the pile loading on the strong axis. However, earthquake loading can be significant on the weak axis of the pile where the section modulus is much lower, e.g., less than 20% of the strong axis modulus in a W 6x9 pile. Typically, only the center pile and the piles on each side of the center pile in a row (consisting of anywhere from 12 to 20 piles) carry loads parallel to the row, i.e., all the seismic loading for the row is carried by these piles. A similar loading occurs when the row is on sloping ground parallel to the direction of the row. The component of the total weight of the array parallel to the ground is carried on the weak axes of the 3 piles.

Axial load analysis

Axial load analysis (compression and tension/uplift) is carried out using conventional approaches, such as those outlined in NAVFAC (1982) with geotechnical parameters developed from site-specific

 © DFI International Bruges 2025

subsurface test data. Because the cross-sectional area of the steel W-sections are small, tip resistance is often ignored in calculations of compressive axial loads (unless piles are installed to refusal in a hard/dense layer). Tension/uplift axial load analysis is similar to compression analysis, except that a 0.67 (2/3) reduction factor is applied to calculated tension loads (Poulos & Davis, 1980). Piles are often protected against corrosion by a hot-dip galvanized (HDG) coating. Any increase in pile section size due to an HDG coating or reduction due to corrosion is small, and it can be neglected in axial load analysis. Note that the discussion in this paragraph is related to geotechnical capacity. As previously discussed, compression/tension loads on piles for solar farms are small. Structural capacity of piles under these loads can be checked for completeness.

Ad-freeze can occur when the pile is in frost susceptible soil, frost depth is significant (more than 0.9 m), and the water table is high, allowing ice lenses to form in the soil. The icy soil is frozen against the pile and when the soil heaves, it can take the pile with it with a heave of several inches possible. Typical ad-freeze uplift forces being assumed for a W 6x9 pile are in excess of 27 kN, which is significant for these small piles as evidenced by the typical loads listed in Table 1. If the piles are in strong soil, the depth of penetration, typically governed by lateral loading, may be sufficient to resist or withstand the ad-freeze forces. However, in weaker soils, the amount of extra depth required can be prohibitive, and alternative measures are needed. One is to replace the frost susceptible soil around the top of the pile with non-frost susceptible soil (clean coarse sand or pea gravel). Since the cost of pile installation is closely linked to the time of installation, this process adds considerably to the cost per pile. Helical piles and blade piles can have significantly higher uplift resistance and may be a viable alternative.

Where the near-surface soils are expansive (e.g., CH clays), they have the potential to pull up the pile with them when they expand. Typically, surface clays are not strong, and the adhesion between the clay and the pile may vary from about 10 kPa to 24 kPa. For a 0.9-m deep expansive zone, this gives a maximum uplift force on a W 6x9 pile of less than about 16 kN, considerably less than for the ad-freeze.

Note that the uplift force due to wind should not be added to the uplift due to expansive or ad-freeze soil. Once the pile tries to move due to the wind pullout forces, the uplift stress system will be reversed, and the soil causing uplift of the pile will resist the wind uplift force.

Possible soil scour from surface runoff needs to be carefully evaluated and considered in the axial as well as lateral load analyses.

Axial (and lateral) load analyses using site-specific geotechnical parameters need to be validated by the results of load tests that are routinely conducted for these projects, as discussed later in this manuscript.

Lateral load analysis

Lateral load analysis involves estimates of pile deflection at the ground surface based on applied lateral load, pile cross-section, load direction, (against strong or weak pile axis) and soil resistance. Loads used in these analyses are illustrated in Fig. 2. Lateral load analysis can be performed considering the lateral load applied perpendicular to the strong axis (X-X' in Fig. 2) or to the weak axis (Y-Y' in Fig. 2).

Lateral load analyses are commonly performed using the LPILE software (Ensoft, 2019), but the simplified characteristic load method (CLM) (Clarke and Duncan, 2001) can also be used in some cases. Free-head conditions are considered in these analyses. LPILE analyses provide lateral deflections, shear forces, and bending moments along the pile depth. CLM analyses provide the lateral deflection at the ground surface and the maximum moment. Allowable lateral loads are typically selected based on a maximum horizontal deflection of 15 mm at the ground surface. Note that there is

 © DFI International Bruges 2025

no pile standard developed specifically for solar farm applications. However, paragraph 1810.3.3.2 of ICC (2021) states that "The resulting allowable (lateral) *load* shall not be more than one-half of the (lateral) *load* that produces a gross lateral movement of 1 inch (25 mm)." A common interpretation of this requirement is that the allowable lateral load corresponds to a gross lateral movement of 12.5 mm. However, because the lateral load vs. lateral movement is non-linear, a slightly higher lateral movement, e.g., 15 mm is typically justified. Note that if actual pile load tests are used, then adjustments may be required.

Lateral loads generate bending moments on the pile that require an evaluation of the allowable stresses of the pile. Typically, Grade 50 steel is used with a minimum yield point of 345 MPa (ASTM, 2021). The allowable stress in bending can be obtained by applying a factor of safety of 1.67 to the minimum yield point of the steel member. Thus, typically the allowable steel stress is about 210 MPa. The maximum stress on the pile that is compared to and must be less than the allowable steel stress is calculated from $M \cdot y/I + P/A$, where:

M = maximum bending moment from lateral load analysis
y = half of the beam depth (but including fractional decrease due to corrosion)
I = moment of inertia
P = applied axial load
A = cross-sectional area (including decrease due to corrosion)

Because the web and flange thickness are small (about 5 mm for the W 6x9 pile), corrosion over the lifetime of the plant (typically 35 years) can be a significant issue. Extensive field electrical resistivity testing is typically performed during the geotechnical investigation for the plant. Electrical resistivity values over 100 ohm-m indicate mildly corrosive soil, and little action is required. Lower values of electrical resistivity, especially below 20 ohm-m, indicate corrosive soil, and preventative measures are required. This typically takes the form of 0.08 mm to 0.13 mm of HDG plus an allowance for loss of steel from the pile, typically anywhere from 0.25 mm to 0.75 mm per face over the life of the plant, depending on the corrosiveness of the soil.

The flange and web thicknesses are reduced to about 3.5 mm for 0.75 mm of corrosion per face. This loss of area can have a significant effect on the lateral capacity, both on the deflection and stresses in the pile due to the reduction in section modulus. The loss of area will increase the axial stresses on the pile, but these stresses are low because of the low axial loads and are typically in the 7 MPa to 10 MPa range for an allowable stress of 210 MPa in the steel. Maximum bending stresses due to lateral loading can often exceed the 210 MPa allowable stress and result in an increase to the next larger section (a W 6x9 pile would increase to a W 6x12).

On a site for a planned solar farm, the measured electrical resistivity was so low (0.15 ohm-m to 0.2 ohm-m) that steel piles would require such a large corrosion allowance that it would render them impractical. Piles made of fiber reinforced polymer were recommended as a substitute.

TESTING CONSIDERATIONS

Extensive pile load testing is typically performed during the initial stages of the project. Testing is often performed concurrently with the subsurface investigation with piles driven to different depths. Table 2 provides the numbers of pile load tests performed at six solar farm sites. As expected, the focus is on tension/uplift and lateral load testing.

Pile load testing follows procedures contained in ASTM standards for axial compression (ASTM, 2020), axial uplift (ASTM, 2022a) and lateral (ASTM, 2022b) load tests (quick test). However, considering the small size of these piles and small loads applied to them, approximate load test setups are often used in the field. Fig. 4 illustrates the use of equipment available on site to perform pile load tests. Note that all of the lateral pile load tests in Table 2 were performed on the strong axis of the pile. Piles are installed to resist wind loads along their strong axis. Testing along the weak axis is

 © DFI International Bruges 2025

seldom performed because the lateral resistance along the weak axis can be calculated from the results of tests on the strong axis. Loading on the weak axis only becomes significant if the arrays are on sloping ground and/or in a high seismic area.

Table 2. Number of pile load tests at six solar farm sites

Site	Number of pile load tests			Notes
	Compression	Uplift	Lateral	
A	30	102	84	2 adjacent Sites
B	6	91	58	2 adjacent Sites
C	38	230	230	3 adjacent Sites
D	9	47	42	
E	10	20	20	
F	11	30	30	



(a)



(b)



(c)

Fig. 4. Pile load testing illustrations at Site E (a) compression; (b) tension; (c) lateral

Fig. 5 illustrates the results of twenty lateral load tests performed at Site E. Note that different colors are used for clarity. As previously discussed, the allowable lateral load corresponds to a 15-mm deflection at the ground surface. For the example shown in Fig. 5, the allowable load ranges from about 12 kN to 23 kN. These pile load test results are typically back analyzed using the computer program LPILE (Ensoft, 2018) to simulate the load test results and develop p-y parameters for subsequent analyses. Note that uncorroded pile sections are used in these back analyses and FS_{min} = 1.5, or maximum lateral deflection at the ground equal to 15 mm, are sought. The p-multiplier feature of LPILE is used to fine tune the LPILE load deflection curve to match the lower bound pile load test

 © DFI International Bruges 2025

curve. Considering that overall the pile design is very “lean” and lateral loading drives the design, it is reasonable to match the lower bound pile load test curve. If the LPILE deflection curve matched the median of the load test results, then half of piles designed using that curve could be considered to be under-designed.

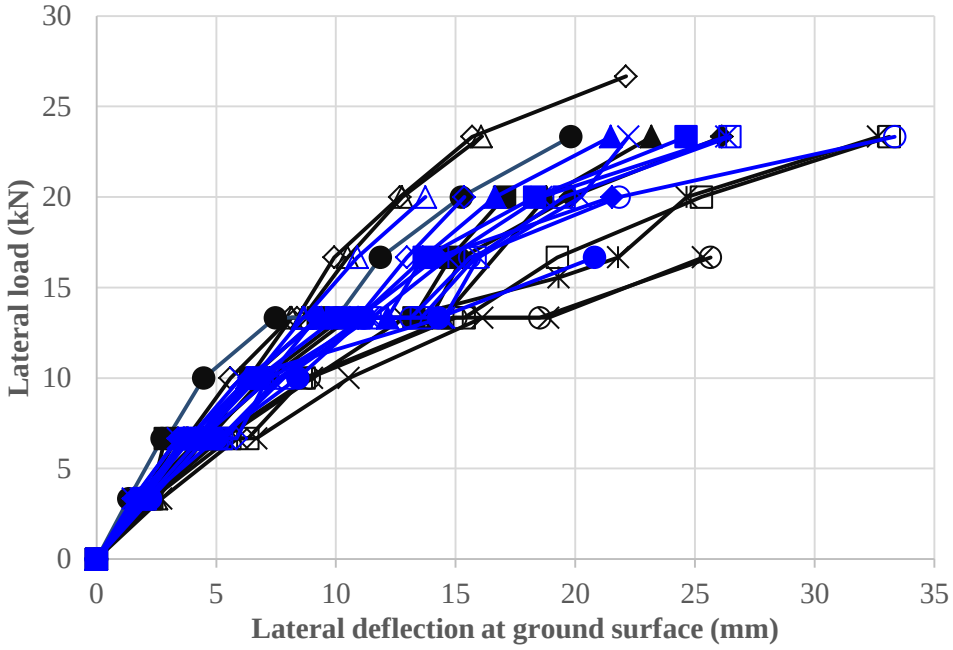


Fig. 5. Lateral pile load test results at Site E

PRODUCTION INSTALLATION CONSIDERATIONS

Piles are typically installed by a small, tracked rig such as the one illustrated in Fig. 6. These rigs are typically Gayk HRE 4000 or Vermeer PD10. They are used for pre-production pile installation and testing as well as for production installation once construction gets under way. Because of the considerable number of piles involved, multiple rigs are used during construction.

Pile driving time varies with the depth of pile penetration and soil conditions and is a reasonably accurate predictor of the pile performance. For one of the previously mentioned sites (Site A) where the soils are stiff high plasticity clay, the drive times for 16 test piles driven to a 1.8 m depth ranged from 31 seconds to 64 seconds, with an average of 42 seconds and a coefficient of variation of 0.21. For 16 test piles driven to 2.7 m depth, drive times ranged from 75 seconds to 137 seconds, with an average of 101 seconds and a coefficient of variation of 0.17. These results show relatively uniform soil conditions.

More variable driving was encountered in predominantly sand Site D. The drive times for 48 test piles driven to 2.4 m depth ranged from 12 seconds to 62 seconds, with an average of 29 seconds and a coefficient of variation of 0.35. For 48 test piles driven to 3.7 m depth, drive times ranged from 16 seconds to 117 seconds, with an average of 68 seconds and a coefficient of variation of 0.38.

The small rig has its limitations. If a hard soil layer is encountered (dense gravel, very dense sand, caliche, etc.), the pile will reach refusal. This may require verification that the pile as installed meets the design requirements, and if it does not, abandoning the pile and installing replacement piles possibly using a bigger rig and/or pre-drilling Also, the maximum total length of the pile that can be handled is normally limited, typically to 6 m to 7.5 m.

 © DFI International Bruges 2025



Fig. 6. Pile installation rig at Site E

As stated in the Introduction, adding margins and allowances to design pile lengths can be expensive. Incorrect installation can further drive up cost and schedule. Automation tools have been developed to use the following items as inputs: design pile information, terrain, flood elevations for the site, tracker geometry, project-specific ground clearance, and flood freeboard. Pile installation data are determined using these factors and transferred to a file that is loaded into the pile driver control software. This allows driving the piles to within less than an inch of the correct location and height. Such tools must be validated and verified through comparison with hand calculations. The use of such tools can be highly successful in improving the accuracy and speed of installing piles to the design heights, thus minimizing rework related to pile installation.

SUMMARY AND CONCLUSIONS

Recent design, testing, and installation experience with piles for solar farms is presented. Because of the considerable number of the small size piles used for these projects, it is important to develop economical design with minimal margin and allowances. This requires adequate geotechnical information and pile load testing that is usually performed at the same time as the geotechnical investigation for the project. Pile installation control is critical to avoid extra pile lengths and associated additional installation time.

Because of the very large number of piles installed for solar farms (often in excess of 100,000), the driving characteristics of the pile can have an outsized impact on the economics of the project. Having one or two piles take 10 minutes to drive under a typical structure or reach early refusal is not a game changer. However, having 5,000 piles on a solar farm experience this can have a crucial impact on schedule.

REFERENCES

ASCE (2017). Minimum Design Loads and Associated Criteria for Buildings and Other Structures. *ASCE/SEI 7-16*, American Society of Civil Engineers, Reston, VA.

 © DFI International Bruges 2025

ASTM [ASTM International] (2020). Standard Test Methods for Deep Foundation Elements Under Static Axial Compressive Load, *ASTM D1143/D1143M-20*, West Conshohocken, PA.

ASTM [ASTM International] (2021). Standard Specification for High-Strength Low-Alloy Columbium-Vanadium Structural Steel, *ASTM A572/A572M-21*, West Conshohocken, PA.

ASTM [ASTM International] (2022a). Standard Test Methods for Deep Foundation Elements Under Static Axial Tensile Load, *ASTM D3689/D3689M-22*, West Conshohocken, PA.

ASTM [ASTM International] (2022b). Standard Test Methods for Deep Foundation Elements Under Static Lateral Load, *ASTM D3966/D3966M-22*, West Conshohocken, PA.

ASTM [ASTM International] (2022c). Standard Specification for General Requirements for Rolled Steel Bars, Plates, Shapes and Sheet Piling, *ASTM A6/A6M-22*, West Conshohocken, PA.

Clarke, A.C. and J.M. Duncan (2001). Revision of the CLM Spreadsheet for Lateral Load Analysis of Deep Foundations, Virginia Polytechnic Institute and State University, Blacksburg, VA.

Ensoft, Inc. (2019). "Technical Manual for LPILE, Version 2019-11.001," Austin, TX.

ICC [International Code Council] (2020). *2021 International Building Code*, Country Club Hills, IL.

Naval Facilities Engineering Command (NAVFAC) (1982). *Foundations & Earth Structures*, Design Manual 7.02, Alexandria, VA.

Poulos, H.G, and E.H. Davis (1980). *Pile Foundation Analysis and Design*, John Wiley & Sons, New York, NY.

 © DFI International Bruges 2025

DEEP FOUNDATIONS DIFFICULTIES SOLVED BY CUSTOMISED GROUTING

Russell J. Denny, Wagstaff Piling Pty Ltd, Queensland, Australia, +61419031265, r.denny@wagstaffpiling.com.au

David Martel, Wagstaff Piling Pty Ltd, Queensland, Australia, +6141732457, d.martel@wagstaffpiling.com.au

ABSTRACT

Customized drilling and grouting techniques solve many challenging deep foundation problems that arise on projects. Consider that deep foundations are themselves a way to construct in difficult conditions, and conventional deep foundation techniques have their risks and limitations. Beyond the conventional construction limits, aid is provided by use of grouting techniques for ground improvement. A wide range of grouting techniques are possible and often a combination of techniques may is required. Improvement is achieved firstly using an initial primary approach, but then further improvement requires deliberate adjustment of the initial technique in response to early improvement and changed ground conditions. Extreme ground difficulties can be resolved if an observational and open-minded approach is adopted on the project. This paper provided project examples including grouting for the recovery of an open-faced hard rock TBM bogged in soft soils, and grouting in overburden mine waste to permit trench cutter diaphragm wall construction. Customized grouting techniques are done often as temporary works to provide improvement and reduce the risks in a tricky construction situation. Customised techniques are not a pre-defined textbook category solution. These are applications where the approach is variable, maybe a hybrid solution, although with lateral thinking the most unexpected and challenging conditions can be overcome.

Keywords: Compaction Grouting, Permeation Grouting, Jet Grouting, Cement, Bentonite, Sodium Silicate

INTRODUCTION

Problems arise frequently in deep foundations, many issues both expected and unexpected, particularly regarding ground stability and ground water. More regularly, new projects are built on sites with more challenging subsurface conditions. The degree of difficulty is always an increasing trend, and cost constraints mean calculated risks are forever present. Grouting provides many possible ways to improve the conditions either ahead of the main foundation construction technique, or retrospectively as a remediation, repair, or for a rescue and problem-solving solution.

Grouting techniques are widely varied, depending on soil conditions, rock conditions, groundwater, hydraulic gradient. Textbook categories of grouting are as follows;

- Jet Grouting - Mono, Double, Triple fluid
- Pressure Grouting - down stage, up stage, etc.
- Permeation Grouting - via end of casing, via drill rods, or via down hole packers
- Compaction Grouting – via end of casing
- Packer grouting, TAM grouting, etc.

 © DFI International Bruges 2025

Many of these systems can be used alone in a predictable and homogeneous situation, or in combination, as 'special' customised techniques to suit the requirement. These customised techniques are often overlapping hybrids, particularly in heterogeneous less predictable conditions. Customising the grouting with built in flexible approach on difficult sites, is a good way to deal with uncertainty and changing conditions. This paper gives some insight into a few special grouting projects using Part A and Part B grout combinations for control of grout mobility, viscosity, and gel set times. This method is used to resolve challenging and uncertain conditions, as the project examples demonstrate.

SPECIAL GROUTING METHOD – PART A AND PART B INJECTION

The method involves use of part A and part B fluids, combined by parallel pumps in a manifold at the back of the drill rig, and delivered to the location downhole via the drill string or casing (various ways to do this). Part A typically comprising cement, bentonite, and water, and part B comprising activator Sodium Silicate diluted in a bentonite and water slurry. The ability to vary the activator dose in real time allows the injected grout to be changed between high and low mobility very quickly. Grout properties can therefore be adjusted to suit unpredictable and/or variable downhole conditions. Textbook terms 'compaction' grouting, at the low mobility end of the range, and 'permeation' grouting at the high mobility end of the range. Real time oscillation between high and low mobility is the key to solving difficult problems with flowing ground water, artesian pressures, voids, cavities, karstic conditions, and the like. This technique is predominantly a 'single shot' technique, although a 'double shot' process can be used if required.

SINGLE VS DOUBLE SHOT TECHNIQUE

The single shot process is the combination of part A and part B fluids by parallel pumps prior to injection, which is the preferred technique, although difficult to manage, the fluids are certainly combined in known proportions. Double shot process (similar to the original Joosten Process) involves multiple passes, the injection of part A, followed by separate injection of part B in the same drill hole.

The original double shot Joosten Process can be very usefully modified with a partially activated initial injection, followed by a more focussed 2nd pass injection. This hybrid double shot process can be used quite effectively, such as in jet grouting. An example is a pre-cutting pass of jet grout using a sodium silicate fluid, activated with a minor dose of cement. The activated sodium silicate initially gels in position close to the drill string, and then on the 2nd pass of higher energy jetting using cement rich grout, remixing for a final mixture which is more rapid gelling, lower mobility, and more resistant to ground water movement/ingress, etc. This method can be used in the most challenging circumstances, such as in artesian conditions.

The same approach may be applied to other grouting techniques, and very effectively in mechanical soil mixing. Project examples are used to show how special grouting can be used effectively, these are unusual cases, including as follows;

- TBM Recovery Sinkhole Grouting - Snowy Hydro, NSW
- Pretreatment Grouting of waste rock for Diaphragm Wall construction – Lihir, PNG

 © DFI International Bruges 2025

TBM RECOVERY

An open faced TBM of 11m diameter had been launched in an adit portal for the main headrace tunnel on major project. The TBM was a convertible machine, which had been set up in open faced mode for rock drilling, although was able to be converted to slurry shield mode, for conditions expected later where slurry would be required. After its launch and initial drive through low strength rock, a sink hole formed in an unknown faulted and fractured zone where the rock was completely weathered, coinciding with a buried gully with substantial subterranean water flow. The TBM began to dip steeply in the completely weather and saturated conditions, with collapsing material above reeling into the open face of the machine, opening a sink hole to surface. The machine could not progress, was not able to be steered, and in open face mode the material above would collapse in with any machine movement, causing the sink hole to increase. A series of investigations were done including horizontal boreholes alongside from adjacent to the adit launch, inclined boreholes from above, geophysical MASW seismic lines from above, forward investigation holes from the 2 drill rigs inside the TBM. The situation indicated by figure 1, shows the sinkhole relative to the shield of the TBM.

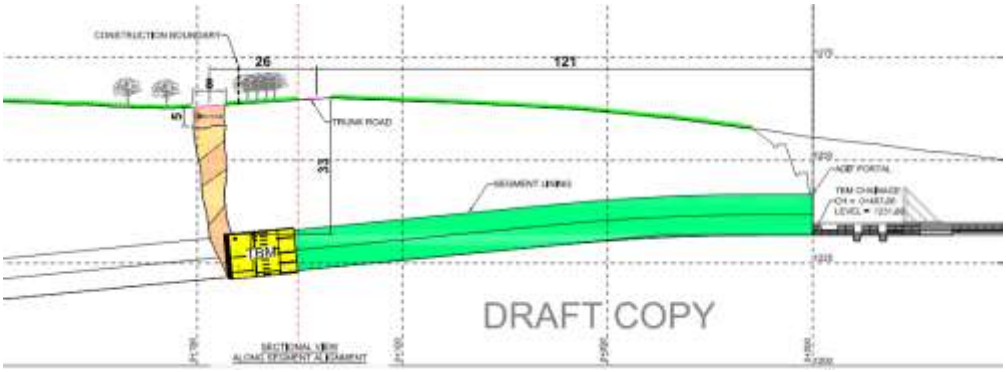


Figure 1: Elevation (from uphill) – General Arrangement of the stranded TBM

An investigation of subsurface conditions by MASW geophysical methods, specifically measurement of compression wave speeds, and the relative location of the stranded TBM, 33m deep to the crown of the cutting head, is shown in figure 1. These sectional views are from uphill, with the flowing water passage across the TBM face from left to right (i.e. into the page).

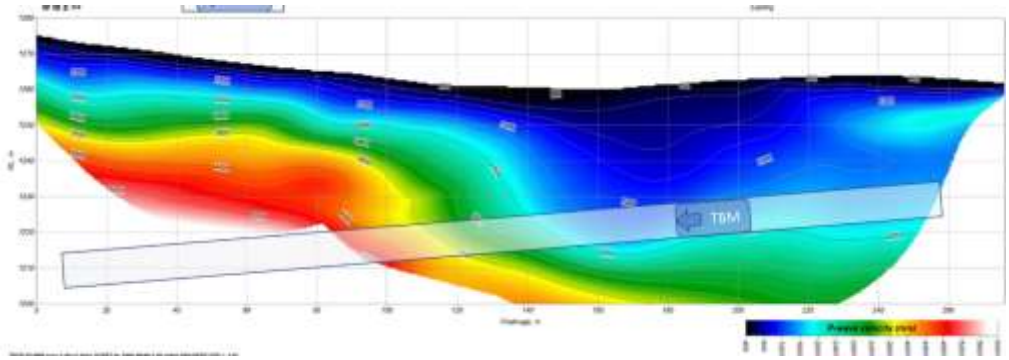


Figure 2: Geophysical Sub-surface conditions around the TBM

 © DFI International Bruges 2025



Figure 3: Duplex Drilling rig set up for stabilization grouting, Snowy Mountains NSW, Australia

EQUIPMENT AND METHODOLOGY

A Comacchio MC22 duplex drilling rig was used, with 152mm dia. outer casing rotating left and inner rods rotating to the right with interchangeable drill bits. The drill holes extended from 45m to 60m at varying sub-horizontal angles in a canopy above and around the TBM's cutting head under the sink hole, and in front of the cutting face to reach the sound rock head forwards of the TBM location. Following air flush drilling to the toe level, the inner drill rods were extracted, and the pressure grouting would then be conducted via the end of the casing, as the casing was slowly withdrawn.

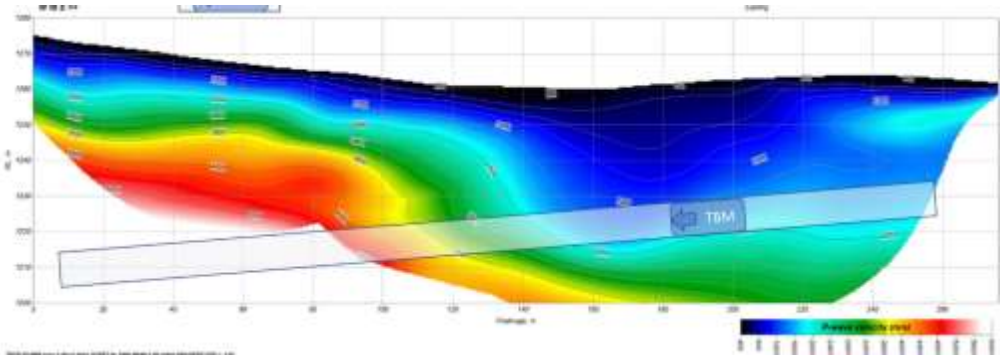


Figure 4: Elevation - Geophysical Interpretation of Subsurface Conditions

A series of 152mm dia holes in the improvement zone would be drilled and grouted, with the variation of the grouting properties analysed, including delivery pressures, flow rates and volumes. A general target sequence was developed involving primary holes followed by secondary infill holes. However as early works commenced the sequence was soon re-developed in response to the observations of the early grouting performance. Primary holes generally provided a baseline of the performance, and later holes indicated considerable ground improvement. Comparison of flows, back pressure, volumes, and connectivity to the TBM itself, led to necessary viscosity adjustments, and hole sequencing adjustments.

 © DFI International Bruges 2025

Methodology and hole sequencing was found to be critical, as the early drilling and grouting was used to investigate in more detail the sink hole geometry, via the drilling and grouting performance. Connection through to the TBM proved an issue for the TBM personnel, who were concerned about the TBM getting locked in position, and the work required in cleaning when grout connected through to the TBM. The open faced TBM was driven forward occasionally during the 6-month grouting program, to check it was free, and to gauge grouting effectiveness. Unfortunately, the premature TBM drives most likely had a detrimental effect on the grout canopy, casing damage, and most likely prolonging the entire grouting campaign. After every TBM drive, grout would connect through to the TBM again. Ongoing injection eventually led to sufficient improvement in front of the TBM to allow thrust on the face to reinstate the ability to steer the machine A sufficient stabilized canopy had been provided above the machine to drive ahead without unstable ground reeling into the machine. Now with stability at the face, the machine could be converted to closed face slurry mode. Once in slurry mode, the TBM could progress into through the unstable interface zone, and drive into stable rock, where normal operation was possible.

DRILL TOOLS

Tooling for air drilling – Both completely weathered soil and hard rock existed around TBM and sink hole, so hole support and tooling was important. Fully cased system was adopted with under-reaming DTH hammer (Odex), and other drill bits such as PDC, and conventional blade bits. Air flushing was the early approach to drilling, although drilling with self-hardening slurry would later become an effective method. Shortening the gel time of the slurry is an effective way to pack the anulus of the drill hole, allowing for the development of pressure and to promote grout penetration. The slurry properties, made up of cement, bentonite, and sodium silicate, would be modified in real time to fill and block up-hole escape, allowing down hole grout pressures to be developed at around 12bar, allowing for permeation grouting in the case of high mobility grout, or compaction grouting in the case of low mobility grout. Using the system with real-time adjustment between high and low mobility, allowing real time oscillation from high mobility to low mobility.

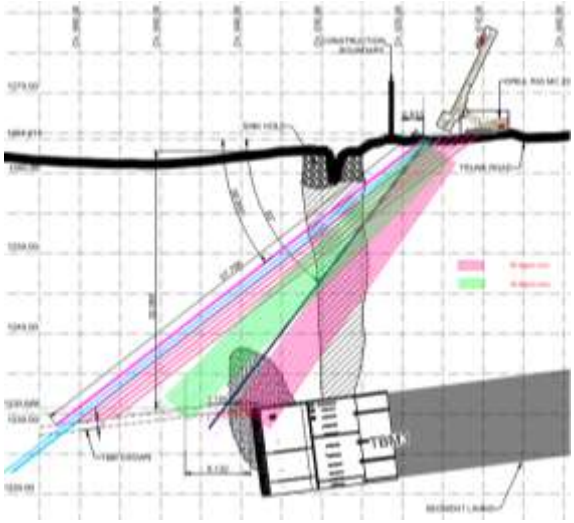


Figure 5: Elevation during later stages of the recovery project showing sub-horizontal drill angles and target zones for grouting above and ahead of the TBM, also showing the sinkhole position.

 © DFI International Bruges 2025

THERMAL PROFILES

Further verification of grouting effectiveness was also undertaken by continuously logging the heat of hydration using thermal strings i.e. thermal profiling (TIP). Strategically placed thermal strings were a sophisticated approach, also with very promising results. Figure 3 indicates the thermal behaviour showing an overlay of temperature performance of a series of adjacent grout locations. The temperatures shown are the peak values, and note that the higher temperatures certainly do co-incide with the zones targeted from grouting, where we used our range of techniques to achieve highest possible grout take, thereby filling, compacting, permeating, squeezing, etc.

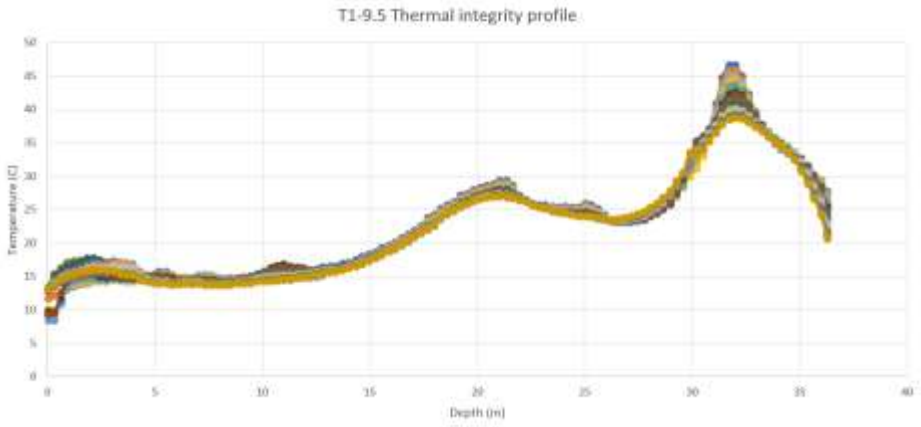


Figure 6: Thermal Profile Overlay of peak temperatures - Note that the temperature peaks co-incide with the zones targeted from grouting.

TBM RECOVERY GROUTING - SUMMARY DISCUSSION

Key technical aspects from this emergency grouting project are summarised as follows;

1. Use a pressure grouting approach with part A and part B components in a single shot system for rapid set, allows for a completely flexible grouting approach, able to be adjusted in varying ground conditions and short notice;
2. This grouting method allows the ability to vary grout properties in real time, so as to alternate between high mobility permeation grouting, and low mobility compaction grouting. The ability to fluctuate the grout properties in real time provides a unique ability to respond to material chaotic nature.
3. Ongoing adjustment of the drilling and grouting procedures - Early grout holes and their performance are effectively diagnostic investigation holes, which lead to on to continuous revisions of the ongoing methodology.
4. Grouting Sequence – This case of a sink hole is typical of emergency grouting, with the most successful sequence being to build from least voided zone towards most voided zone. Starting at the edges, effectively squeezing towards the more voided zone, the grout can flow, push, compact, etc. travelling towards the more voided formation. Client expectation in this case was very much the opposite, expecting us to place grout in the most voided zone as if a “hole in one” could be achieved. Analogous to building bridge ridge across a river, the idea it to progress outwards from the stable river bank.
5. Verification of Success – Grout flows and pressures studied over time (pressure and flow response) being the most useful verification technique. Beyond this, observing the occurrence of

 © DFI International Bruges 2025

grout connection to the TBM, and other techniques such as Thermal Profiling of grout holes proved very useful. A combination of all these things is most useful in determining the degree of improvement over the duration of the grouting campaign.

PRETREATMENT GROUTING - LIHIR PNG

The feasibility study of the Seepage Barrier at the Lihir Gold Mine required a full scale Cut-off Wall trial, using a 1.2m thick diaphragm wall through 45m of mine overburden waste rock, which had been dumped onto the sea bed, with the wall socketed in Volcanic Breccia to around 65m. A BC40 Trench Cutter was to be used, although importantly Pretreatment Grouting was needed to sufficiently stabilise and reduce the porosity of the rockfill, prior to trench cutter use under bentonite. The end dumped mine waste was known as the Harbour Waste Platform (HWP), and had been constructed over 20 years or so. The ground conditions presented a significant risks during excavation in terms of slurry losses and stability of a bentonite slurry filled open trench, also with the high risk that loose oversize boulders would collapse onto the trench cutter itself, which would have serious consequences.

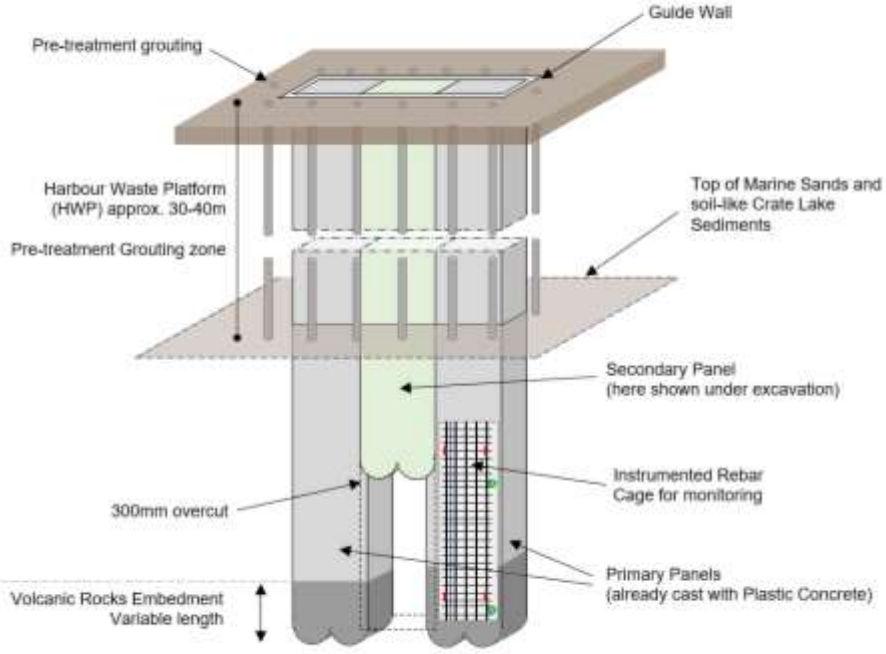


Figure 7: Trial Cut-off wall panel showing pretreatment grouting

The need for ground improvement of the HWP to stabilise the material in close vicinity to the Cut-off Wall alignment was identified and first grouting trials were carried out from December 2018 to April 2019, and the geology is shown in figure 8.

 © DFI International Bruges 2025

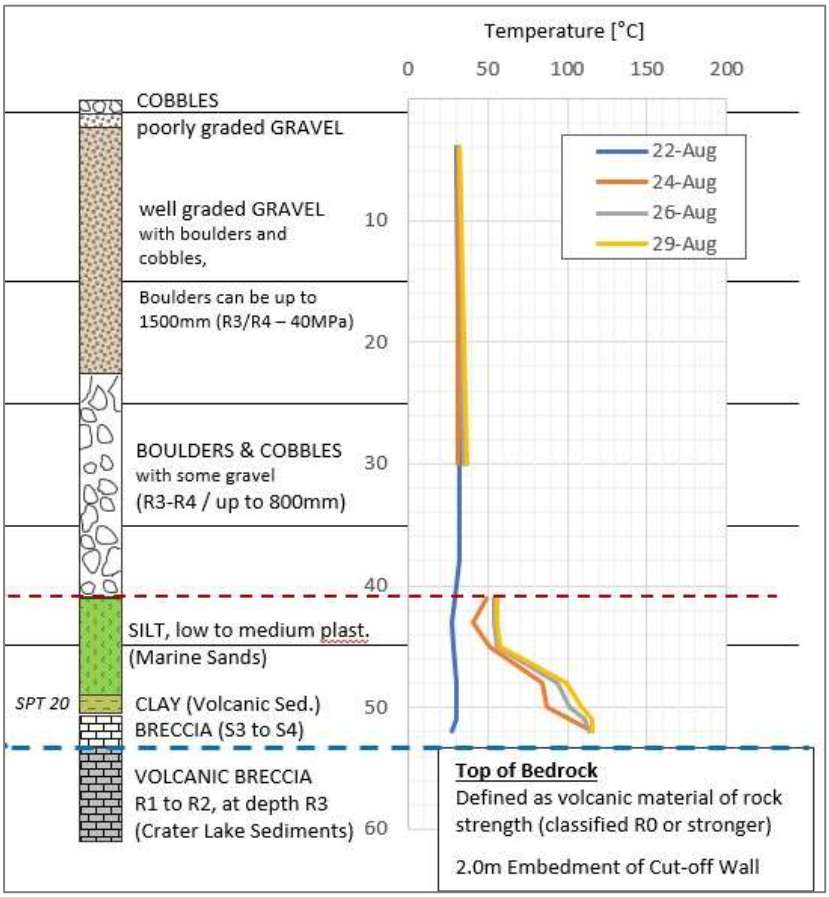


Figure 8: Geology at the cut-off wall location

GROUT SYSTEM - TECHNICAL PROPOSAL

The Pre-Treatment Grout consist of two components, a Cement-Bentonite Slurry (Part A) and a Sodium Silicate Solution diluted in Bentonite (Part B).

Cement, bentonite and sodium silicate were combined in a sequence, firstly with bentonite and water mixed and transferred to a holding tank for hydration. Part A and Part B of the final mix were then prepared and held in separate circulation tanks, as follows;

- Part A - Sodium Silicate was added to hydrated bentonite/water. This mix was not yet reactive, so could be held for long periods, including overnight, etc.
- Part B - Cement and water was then mixed at w/c=0.75, and combined with the hydrated bentonite/water mix in equal parts by volume. This mix was prepared just prior to use.

From the two holding tanks, Part A and Part B components are supplied to the drilling rig where they are combined and mixed in a manifold at the drill rig prior to injection. The proportions of Part A and B can be adjusted in real time, in response to observations and down hole behaviour.

MIX DESIGN

A typical mix combination is shown in Figure 9.

 © DFI International Bruges 2025

Part A Mix expressed per 1m3			
	kg	SG	Litres
C	575	2.95	195
B	21	2.2	9.4
W	796	1.0	796
	1391		1000

Part B mix expressed per m3			
	kg	SG	Litres
SS	275	1.375	200
B	36	2.2	16
W	784	1.0	784
	1095		1000

Part A + Part B Final mix summary 1m3			
	kg	SG	Litres
C	438	2.95	148
B	24	2.2	11
SS	66	1.375	48
W	793	1.0	793
	1321		1000

SG = 1.32

w/c = 1.81

Figure 9: Mix Combinations

TYPICAL INSTALLATION PROCEEDURE

At the completion of the drilling using a duplex system with under-reaming DTH (air) hammer, the rods and hammer are removed, leaving behind the outer casing.

Top head entry swivel - Grout is injected through the top head swivel via the drill string which connects to the top of the casing via a top plug which seals the system, so that grout can be delivered under pressure.

Grouting will be done either with or without rotation and progressively in line with lifting the casing incrementally, while grout is delivered via the end of casing. During this operation the pressure at the swivel was monitored and typical variation was from lows of 2-3 bar, up to around 12 bar, depending on the formation conditions, and the grout properties at the time of grouting i.e. viscosity.

As the grout volume and pressure vary, decisions on the rate of extraction were determined, with the grout injected continuously as the casing was extracted. Monitoring of the grout pressures and flow rates at the top of the hole is a key feature of the system. As the pressures increases, indicating filling of cavities, the casing was lifted and the pressure then reduces until the flow is resumed and cavities further filled, with low mobility grout squeezing into the formation.

Performance indicated by grout pressure and flow will be expected to vary from primary to secondary, and then to tertiary holes, as more cavities are filled, and the monitoring of these aspects is important to understand the effectiveness of the grouting.

DISCUSSION AND CONCLUSIONS

1. The 2 project examples given are entirely different, one being an emergency recovery operation with voided ground, absent of water table but with zones of fast flowing subterranean water. The second example was a planned pre-treatment grouting campaign in overburden waste rock dumped into the ocean, so high water table in voided rockfill. The same style of grouting was successfully utilised in both cases;

 © DFI International Bruges 2025

2. A valuable benefit of this type of grouting is the ability to oscillate the grout properties in real time. The variation of the grout mobility allows for both Permeation and Compaction grouting in the same hole and/or adjacent locations. This can be achieved by controlling the proportions of the components part A and part B;
3. A rapid gel or a slower gel can be used, which is significantly beneficial in these circumstances, and allows for a completely flexible grouting approach, able to be adjusted in the varying ground conditions and in real time;
4. Verification of Success – Grout flow and pressure response observed as the works progress are the most useful verification technique, and provide real time feedback which in turn allow decisions and adjustments to be made progressively during the grouting campaign;
5. Verification is progressively achieved with the comparison of the pressure and flow performance between earlier and later holes.

DEFINITIONS

Sodium Silicate – N grade, $Na2SiO^4$
Cement – Ordinary Portland Cement.

ACKNOWLEDGEMENTS

The author would like to acknowledge the co-operation, support and contribution of all involved parties. The comments and views in the paper are those of the authors and not necessarily those of other parties.

REFERENCES

1. Method Statement - Pre-Treatment Grouting (carried out by Wagstaff Piling), Bauer Engineering PNG, 23 August 2020.
2. Snowy 2.0 Geotechnical Baseline Report – Geological Summary
3. Snowy 2.0 Tantangara Geotechnical, Description of ground conditions in the TBMs alignment, 15th February 2023.

 © DFI International Bruges 2025

BARRETTE BI-DIRECTIONAL PRELIMINARY LOAD TEST UP TO 148750 kN

Federico Fanti, Trevi SpA, Cesena, Italy, ffanti@trevispa.com
Claudio Asioli, Trevi SpA, Cesena, Italy, casioli@trevispa.com
Davide Benvenuto, Swissboring Overseas Piling Corp. LTD, Dubai, UAE, dbenvenuto@trevispa.com

ABSTRACT

TREVI-SWISSBORING executed an unconventional bi-directional preliminary static load test on a 2.8 x 1.2 m barrette element. A very high load of 148750 kN, corresponding to 2.5 times the maximum working load, was reached to verify the ultimate bearing capacity of the element. The test was carried out in Dubai for a project located in Business Bay (Burj Khalifa district), where a tower founded on barrettes will be erected. The barrette tested was 52.5 m long with a cut-off level 8 m below the actual ground level and was executed using a hydromill with polymeric supporting fluid. The soil consisted of calcarenite and sandstone, with UCS varying from 0.1 to 10 MPa. Eight hydraulic jacks, each with a 10000 kN capacity, applied the load at 32.5 m below the cut-off level to achieve the theoretical resistance balance. In addition to the jacks, the steel reinforcement cage was equipped with 12 strain gauge levels to measure the skin friction between the soil and the barrette. The paper presents and discusses the bi-directional load test results, comparing the skin friction values achieved in the load test with those assumed in the design.

Keywords: barrette, load test, hydromill,

PROJECT DESCRIPTION

The project consists of a residential tower to be constructed in Dubai Business Bay on a square plot with a 30.5 m dimension. The tower consists of a basement, a ground floor, 88 upper floors, and a rooftop with residential apartments. The foundation system is composed by a 5 m thick slab supported by 56 barrettes having dimensions 2800 mm by 1200 mm. Due to the presence of one basement, the effective length of all the barrettes is 52.5 m, starting from 8.0 m below ground level.

TREVI-SWISSBORING was awarded the project's design and build. The barrettes were executed from June to November 2023 by SC-130 Soilmec Hydromill equipment (Fig.1). As per the project specifications, the drillings were executed by adopting a polymeric supporting fluid.



Fig. 1. Barrettes' execution

 © DFI International Bruges 2025

Given the high barrette density (average centre-to-centre distance of 4 m) and the relevance of the foundation systems of such a structure, the design considered both vertical and horizontal group effects to account for the mutual interaction between the single barrette elements.
From the performed analyses, the maximum characteristic working load applied on top of barrettes turned out to be equal to 59500 kN.

It was planned to verify the barrettes' ultimate bearing capacity, hence, in addition to the 56 working barrettes, a preliminary load test was carried out on a trial barrette executed inside the tower footprint area, as shown in Figure 2. The selected test load was equal to 148750 kN, reaching at least 2.5 times the maximum working load. This very high load led to choice as testing method a bi-directional static load test in which the load is applied to the element by sacrificial jacks installed in the reinforcement steel cage at a well-defined position. Such a loading method is widely used for piles for a long time, but its application to rectangular barrette elements is somewhat more unusual.

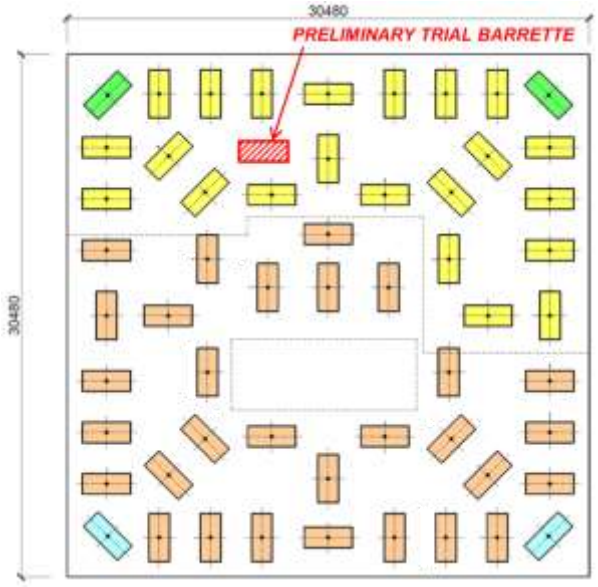


Fig. 2. Barrettes' Layout

SOIL PROFILE AND BEARING CAPACITY DESIGN PARAMETERS

The site subsoil conditions are quite uniform with an uppermost medium dense Sand layer down to the depth of 5.0 to 7.5 meters (hence above barrettes top level) followed by a very weak to weak massive Calcarenite/Sandstone stratum, unweathered to partially weathered characterised by an average UCS from 0.1 to 5.0 MPa. Beneath these layers down to the maximum investigated depth, subsoil consists of weak to moderately weak massive fine-grained Siltstone/Calcisiltite, slightly to moderately weathered, with a UCS range from 0.15 to 10.1 MPa. The design groundwater level was 1.5 m below ground level.

Although cavities were not encountered in any available boreholes up to the drilled depth, the base capacity of the barrettes was disregarded for safety reasons, according to the project specification.

Concerning the ultimate lateral skin friction, the local values of the barrette-soil limit adhesion "τ" in the weak rock were assumed according to the following relationship proposed by Williams and Pells (1981):

$$\tau = 0.5 \times \beta \times (UCS)^{0.5} \quad [1]$$

 © DFI International Bruges 2025

Where β is the friction reduction factor, assumed to be equal to 0.67, depending on the ratio between rock mass modulus and the modulus of intact rock.

The UCS values for each layer, as provided by the geotechnical consultant, reflect the average values measured in the two 80 meters deep boreholes available within the area. The barrette-rock limit adhesion adopted in the design is summarised in Table 1 while a graphical representation is provided later in Figure 9.

Table 1. Barrette-rock limit adhesion adopted in the design

Depth below Ground Level (m)		Unit Weight	UCS	$\tau_{LIM_COMPRESSION}$
From	To	(kN/m^3)	(kPa)	(kPa)
8.0	32.0	22	1000	325
32.0	37.0	22	350	192
37.0	60.0	22	1650	417
Below 60.0		22	3000	563

LOAD APPLICATION SYSTEM AND JACKS' POSITION

The load application system comprised eight hydraulic jacks, each with a maximum capacity of 10000 kN. This provided a maximum total force equal to 80000 kN applied both in the upper and lower portion of the barrette, assuring a maximum test capacity of 160000 kN.

Above and below the jacks, two 50 mm thick distribution rectangular plates were present assuring a uniform load application. To allow the passage of the tremie pipes, of the concrete flow during pouring operations and the jacks' hoses connection passage, some holes were present in the plates. The assembly of jacks and plates was installed in the barrette reinforcement cage in the design position by welding the vertical bars to the plates, as shown in Figure 3. In correspondence with the top plate, additional steel bars were installed in the reinforcement to guide the two tremie pipes passing through their reservation holes.

 © DFI International Bruges 2025



Fig. 3. Load application system and its installation in the reinforcement cage

To maximise the load that can be mobilised during the test, the position of the loading jacks was defined by balancing the capacity of the upper and lower parts of the barrette. The lateral skin friction provides the resistance of the upper part, while the resistance of the lower part is given by both lateral and base capacity of the barrette. Although the design did not account for the base capacity of the barrettes, it was considered in the test as no cavities were found in the boreholes assuming a unit limit base capacity equal to 5000 kPa. The balance resulted at a depth of 32.5 m below the cut-off level, with a calculated resistance of 83500 kN for both the upper and lower parts.

MEASUREMENT EQUIPMENT DESCRIPTION AND LOAD TEST PROCEDURE

Eight displacement transducers (two per each level) were used to measure all movements at the designated points. The barrette toe, top plate and bottom plate movements were measured using displacement transducers connected to telltale rods against a reference beam at working platform level. The top of the barrette was measured using displacement transducers directly installed at the platform level. Adopted reference standard was ASTM D8169-18.

To evaluate the load trend along the barrette and define the load transfer curves between the barrette and soil, the reinforcement cage was instrumented with twelve levels of vibrating wire strain gauges by adopting four elements per level. The upper barrette portion was equipped with eight strain gauges level with approx. 4.3 m spacing, while in the portion below jacks, four levels at 5.8 m spacing were installed, with the last one placed 0.5 m above the base.

During the load test two dataloggers (one for pressures and displacement and one for strain gauges) recorded data at an interval of one minute.

 © DFI International Bruges 2025

The test was executed by adopting four loading-unloading cycles, as shown in Figure 4. In the first cycle the working load was applied in four steps and maintained for six hours. In the following cycles, a load equal to 1.5, 2.0 and 2.5 times the working load was applied by keeping it for at least one hour. Between each load cycle, the barrette was completely unloaded for at least one hour.

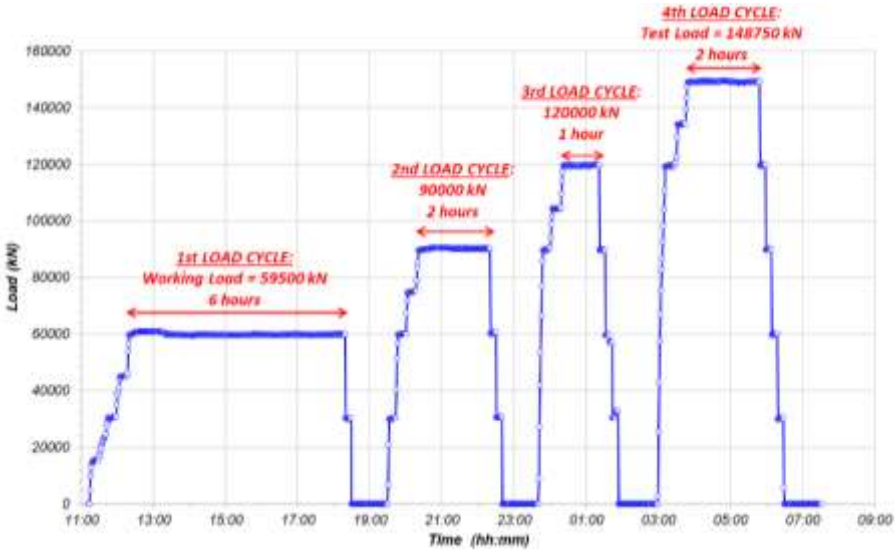


Fig. 4. Load vs Time recorded data

LOAD TEST RESULTS AND DATA INTERPRETATION

At the maximum applied load of 148750 kN, the barrette top movement was 9.4 mm and the upward movement at the jack assembly was 15.3 mm, while the maximum downward movement was 10.9 mm and the barrette toe displacement was 7.5 mm. Figure 5 shows the displacements measured versus the effective bi-directional applied load respectively for all load cycles and only for the last fourth cycle.

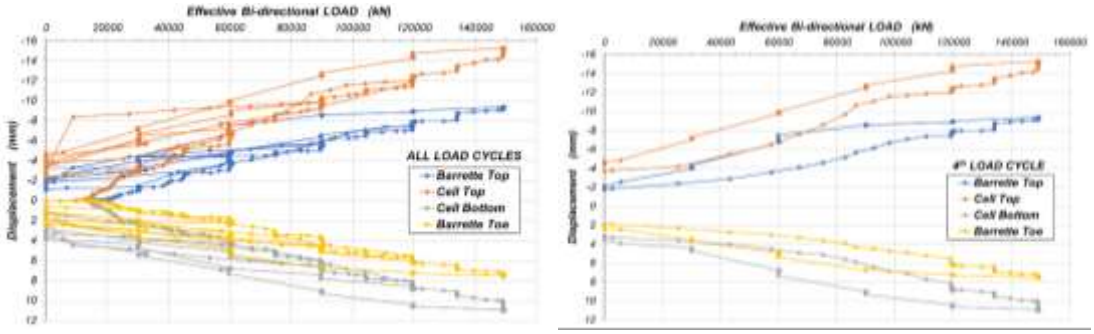


Fig. 5. Displacement vs Load for all cycles and only for the 4th cycle

From the measured displacements, the equivalent load-settlement curves at the top of the barrette shown in Figure 6 have been obtained, achieving a total settlement of 35 mm at the maximum load, corresponding to approximately 1.7 % of the barrette's equivalent diameter.

 © DFI International Bruges 2025

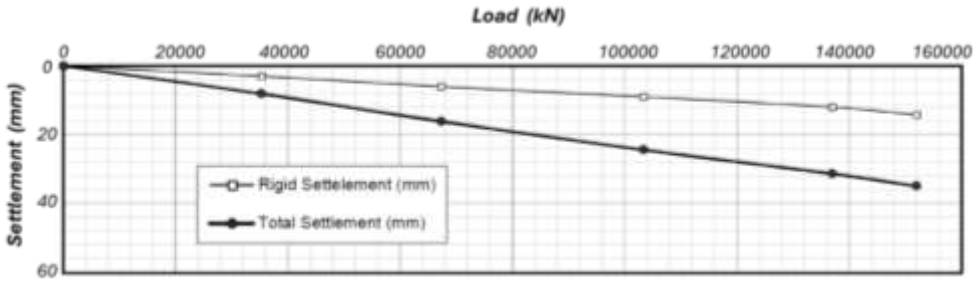


Fig. 6. Equivalent Load vs Settlement curve at the top of the barrette

The test showed that even at the maximum test load the barrette behaviour was practically elastic, without achieving a clear failure. This means the actual barrette resistance should be much higher than the maximum applied load.

Figure 7 shows the load trend along the shaft of the barrette obtained by processing the strain gauge readings. It can be noted that the load transferred to the base of the pile results in just 5220 kN, while a load equal to 8800 kN is registered at the cut-off level. This last value, reduced by the weight of the barrette, corresponds to the skin friction in the upper eight meters, from working platform to the cut-off level.

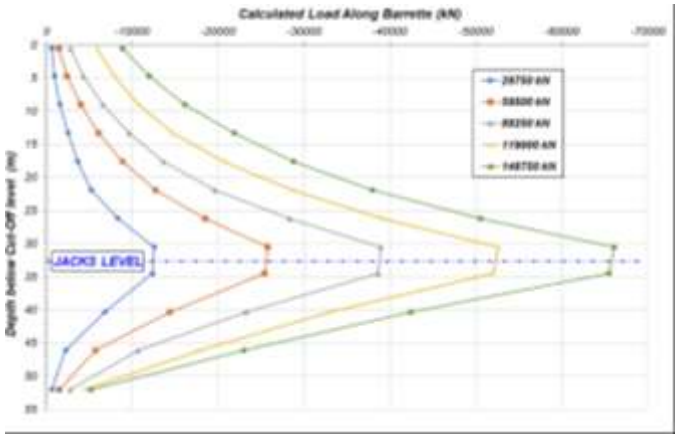


Fig. 7. Calculated load trend along barrette shaft and achieved barrette-rock adhesion values

The load obtained at each strain gauge level allowed us to calculate the barrette-soil adhesion registered at each instrumented sector and the unit base capacity at each load step. Figure 8 shows the obtained load transfer curves for lateral friction (dashed lines refer to the lower barrette portion) and for unit base capacity, while Table 2 the indicates the maximum adhesion achieved. All the curves show an almost linear behaviour and the limit resistance was never achieved in the instrumented sections.

Table 2. Barrette-rock limit adhesion adopted in the design

UPPER PORTION			LOWER PORTION		
Strain Gauge Level (m)		$\tau_{LIM_COMPRESSION}$	Strain Gauge Level (m)		$\tau_{LIM_COMPRESSION}$
From	To	(kPa)	From	To	(kPa)
SG-1	SG-2	93	Jack	SG-9	557
SG-2	SG-3	121	SG-9	SG-10	497
SG-3	SG-4	166	SG-10	SG-11	418

 © DFI International Bruges 2025

SG-4	SG-5	200
SG-5	SG-6	268
SG-6	SG-7	365
SG-7	SG-8	453
SG-8	Jack	516

SG-11	SG-12	377

The achieved unit base capacity of 1550 kPa is quite lower than the estimated ultimate base capacity because of the very small settlement of the bottom of the barrette.

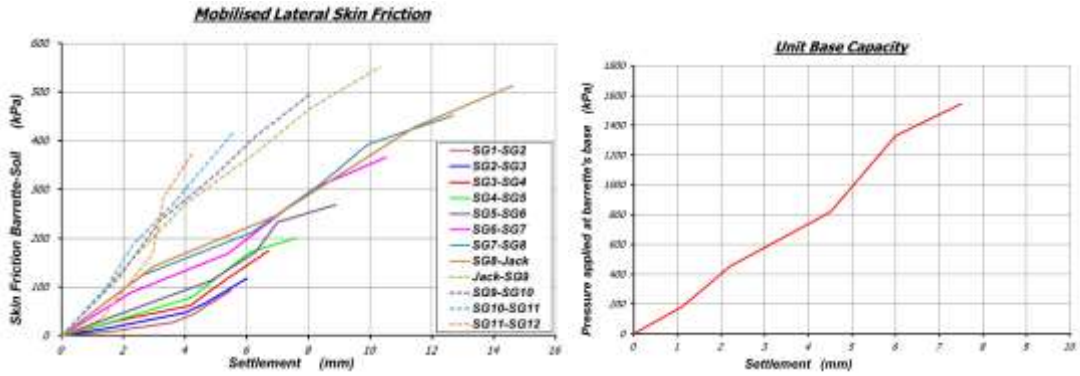


Fig. 8. Mobilised lateral skin friction and unit base capacity

COMPARISON BETWEEN ESTIMATED AND ACHIEVED PARAMETERS

The obtained lateral skin friction values along the barrette shaft were compared with those estimated at the design stage, as Figure 9 shows. Achieved friction for both barrette top and bottom portions have a similar trend, with higher values in correspondence of the Jacks position, which gradually decreases moving to barrette extremities. This result is related to the fact that limit friction values have never been reached, and the measured friction decreases because the load gradually decreases.

From the barrette cut-off level up to 22.5 m depth and in the lowest 6 m above the base, achieved values are lower than those assumed in the design. Out of these sectors, achieved values are always higher or equal to those considered in the calculation, without evidence of skin friction reduction between 24 and 29 m below the cut-off level as expected based on the boreholes' information. Since all results show almost elastic behaviour without achieving the failure, recorded values cannot be considered ultimate limit values.

 © DFI International Bruges 2025

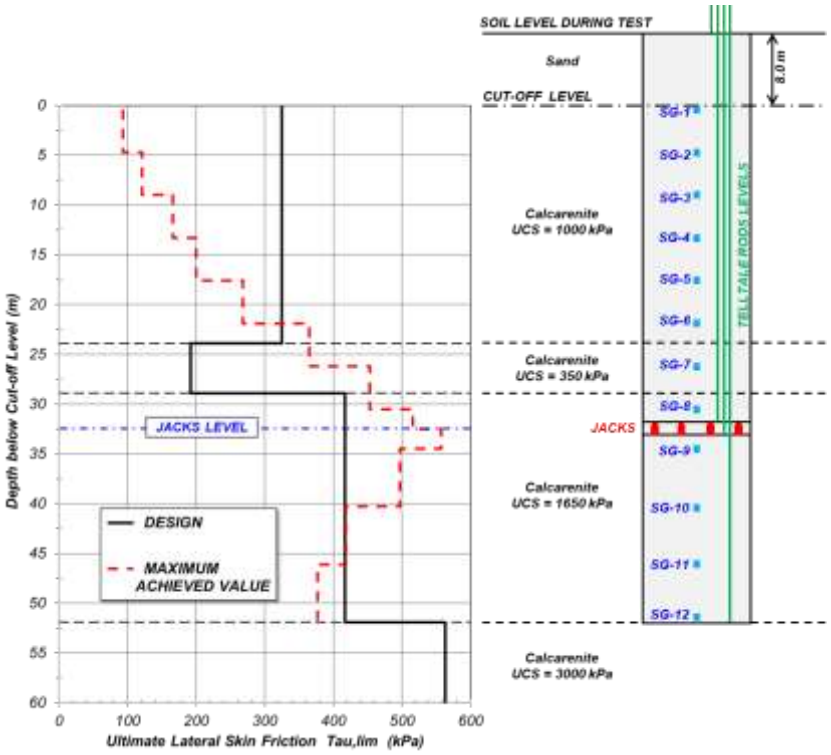


Fig. 9. Comparison between achieved and estimated lateral skin friction

CONCLUSIONS

The performed load test obtained very good results reaching the maximum test load with a very rigid behaviour, suggesting a much higher failure load than expected. Even the result interpretation showed a linear behaviour in all the instrumented sections, and the limit resistance values were not reached in any portion of the barrette.

Very high lateral skin friction values ranging from 90 kPa up to 550 kPa were recorded. These values are equal to or higher than those estimated in the lower portion of the barrette (below 22.5 m depth from the cut-off level). In the remaining upper portion, obtained values were lower than the estimated ones, but this does not affect the design assumptions since results far from failure were obtained.

REFERENCES

Williams A.F. and Pells P.J.N., 1981. Canadian Geotechnical Journal, Vol. 18.

ASTM D8169-18, Standard Test Methods for Deep Foundations Under Bi-Directional Static Axial Compressive Load.

 © DFI International Bruges 2025

FOUNDATION ARCHITECTURE: A NEW APPROACH FOR REALIZING INFRASTRUCTURE FROM THE GROUND UP.

Boyoung Yoon, Georgia Institute of Technology, Atlanta, GA, USA, byoon39@gatech.edu
Morgan NeSmith, Berkel and Company, Atlanta, USA, mnesmith@berkelandcompany.com
Anna C. Frost, Staycity, Dublin, Ireland, annafrost.archi@gmail.com
J. David Frost, Georgia Institute of Technology, Atlanta, GA, USA, david.frost@ce.gatech.edu

ABSTRACT

The universal principles of good architecture are durability, utility and beauty. As practiced today in the development of many structures, they tend to be implemented in the following sequence: a) beauty as dictated by an architect; (b) utility as interpreted by a structural engineer; and (c) durability as demanded from the foundation engineer. While there are many examples of how this approach has served society well where the architect desires are driven down through the structural engineer to the foundation engineer, this has likely led to the construction of foundations that are substantially overdesigned in many cases compared to what might be achieved if the order of input into the overall design process were different. There are also many examples of how this beauty-first approach had resulted in failure. What if however, a new approach to the realization of buildings were to emerge? Think for example if the foundation engineer, based on their knowledge of the subsurface, were to identify a family of foundation types that could work at an existing site and then these alternatives were provided to the structural engineer who could propose alternative structural systems that could perform optimally with each of these different foundation systems. In the same way that building heights are limited by wind loads and roof pitches are fortified against snow loads, foundations could be another design-lever that is pulled in the scoping of possibilities. Finally, the range of combinations and foundations would be provided to the traditional architect so they could then explore alternative aesthetically appealing structures that could complement the existing surrounding environment of man-made and natural spaces. This paper will expand on these ideas which might be regarded as seeking to turn the design process of structures “upside down” but which could also revolutionize the materials, designs and techniques for foundation construction. This new approach would be termed *Foundation Architecture – building structures from the ground up.* As our planet prepares for the onslaught of climate change and how it can impact infrastructure and materiality, taking a bottom-up approach can yield foundations that are adaptive and capable of meeting the challenges of the next few centuries.

Keywords: Foundation, Architecture, construction design, foundation design

INTRODUCTION

The word architecture is inherently associated with the portion of a structure that is visible above ground. This is both a misnomer and a missed opportunity to recognize that the foundation of a structure can contribute as much, if not more, to the realization of a structure. As our planet faces significant challenges due to climate change effects such as sea-level rise, elevated temperatures, increased precipitation, and severe wind events, the importance of considering the architecture of a structure foundation is likely to become even more important when the consequences of climate change (drought, wildfires, landslides, debris flows, floods, glacial lake outflows, and tsunami amongst others) are considered. Indeed, increased usage of underground space and more strategic design of foundations may have a critical role in helping society adapt to and survive climate change stressors that are at best ill-defined and poorly understood at this stage.

 © DFI International Bruges 2025

HISTORICAL ROLE OF ARCHITECTURE IN INFRASTRUCTURE CONSTRUCTION

Architects require parameters to work effectively. It is known that even the most primitive of architecture was the result of requirement for shelter against adverse conditions, both predatory and environmental. Existing landforms and robust monoliths would have been used in the selection of safe and sturdy shelters. As early as 4000 BC, builders were digging holes of varying depths in which to lay stones of different heights upright so that the resulting post-and-lintel superstructures were horizontally planar. While the geotechnical characteristics of the soil would have inadvertently affected where and to what level of difficulty excavation could be completed, the superstructure was driving the intent for the plan beneath the soil surface. In some cases, where excavation would have been either impossible given the tools available or futile given the dynamic landscape, such as in bedrock or sand, subterranean structures would have been forgone. Stone pedestals and vast plinths would have provided no meaningful mechanics other than to position a column or compositionally make the superstructure appear more substantial. Again, the superstructure took precedent.

While the evolution of architecture began above ground, becoming virtuous through The Renaissance, and being catapulted through The Industrial Revolution to Postmodernism, beauty in architecture was not always necessarily conventional or pleasing to the eye. In the case of The Eiffel Tower or The Centre Pompidou – two iconic buildings which were famously protested and vilified at the time they were realized – the design was a celebration of new tools or innovative techniques of the time. Today geotechnical and atmospheric research advancements have shown that the unpredictability of natural events will define the next epoch of architecture. It is natural to think that new techniques that develop from an aforementioned scarcity in materiality and geotechnical uncertainty could be and ought to be celebrated as well. Through Foundation Architecture, a new style of architecture predicated not on self-expression or industry but on the certainty of the “immovable” earth could look entirely different from what has been developed to date. Designing the superstructure to showcase the substructure can only be meaningful if the foundation is given attention from the start of the project.

CURRENT FOUNDATION ENGINEERING PRACTICE

Since the appearance of mankind on Earth, the act of occupying land through construction has continued to this day, causing a shortage of construction sites. The exterior design of a building may depend on the purpose of the building and designer’s preferences; however, the design and construction of the foundation should be preceded to construct the buildings. Despite this essential prerequisite, the role of the geotechnical engineers in charge of foundation design has always been hidden and unseen, just like the foundation itself, which is constructed underground. This can be assured from the basic construction process generally conducted, as summarized in Fig.1.

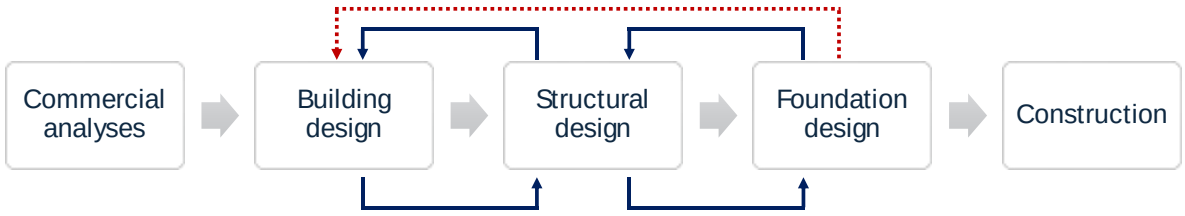


Fig. 1. Current general construction process

Fig. 1. shows one aspect that is very questionable from a geotechnical engineering point of view: the lack of interaction between the geotechnical engineer and the structural engineer or architect, compared to the close collaboration between the architect and the structural engineer. Though the design and construction of the foundation is a prerequisite for successful completion of building

 © DFI International Bruges 2025

construction, geotechnical engineers are usually introduced at the end of the design process. However, it is the 'soil risk' that mostly causes time delays, modifications in construction process, and damages occurring after construction (Katzenbach et al. 2016). Tam et al. (2007) highlighted that the abnormal ground conditions are considered a high-risk factor for both architects and engineers. Since the ground conditions affect both the bearing capacities and shape of foundations, changes in foundation design due to unexpected ground conditions can lead the entire design changes of structures, which can be a major cause in time-delay of construction projects (Aziz and Abdel-Hakam 2016; Gebrehiwet and Luo 2017). Many construction projects suffer from unanticipated ground conditions and subsequent time-delay. For example, while constructing Burj Khalifa, the excavation work was expected to be completed over 5 months, however, it actually took more than a year (McLaughlin and Davies 2024).

With the help of relatively good ground conditions and advanced technology, it would not have been a big burden for geotechnical engineers to find an optimized method to satisfy both architects and structural engineers. However, as people demand more advanced infrastructure, geotechnical engineers will be forced to face the challenge of dealing with poor conditions/problematic soils in limited space. In addition, the value of "sustainability", which have emerged from concerns about rapid environmental change and resource depletion, is also a value that the construction industry should pursue in the future.

Aligning with these changes in both environment and construction paradigms, a new infrastructure design concept should now be introduced, and accordingly, the role of geotechnical engineers should change starting from unseen to visible and ultimately to leading. With this idea in mind, the authors propose a new paradigm called **"Foundation Architecture".**

CHALLENGES IN CURRENT FOUNDATION ENGINEERING PRACTICE

In many respects, there has never been a more interesting time to design foundation systems for structure support. In the past 25 years, there has been a wide introduction (some would argue re-introduction) of ground improvement techniques along with process and equipment improvement for existing deep foundations that continue to expand the potential for a foundation designer to maximize economy without sacrificing safety or utility. The increase in consideration of ground improvement techniques in particular has led to a more global or holistic approach to foundation design that has begun to trickle into deep foundation design as well.

This should likewise be an exciting time for an owner / developer or facilities designer, as these foundation approach options provide a broad opportunity to maximize overall structure efficiency, improve sustainability, conserve energy, and improve resilience. However, the basic construction process summarized in Figure 1 limits the opportunities to implement all of the options that might be available.

At some point between the Commercial Analysis and Foundation Design, a site characterization is performed and (usually) general foundation recommendations are made, which are then incorporated in the Structural Design and Foundation Design. Given the breadth of options available, there are essentially too many options for the "site characterization specialist" to be fully aware of, much less to be an expert in, to properly evaluate all of their potential uses for a given combination of site location and structure to be built.

Because of the specialist systems that now exist, much of the knowledge base of foundation design and construction now resides with the installers. However, these installers are typically only engaged somewhere between the Foundation Design and Construction steps in Figure 1. Often, the project team considers this too far along in the schedule, or requiring too much of a change to a portion of the already completed Structural Design to incorporate suggestions for economy or sustainability that may be recommended by various installers. Thus, the significant opportunities to maximize overall structure efficiency are often being missed in the current process. In particular, multi-functional

foundations and energy foundation systems as discussed in this paper require inclusion in the overall structure design concept from the outset to maximize their usefulness or even be included at all as foundation options.

TOWARDS FOUNDATION ARCHITECTURE

According to the dictionary provided by Oxford Languages, 'Architecture' is defined as 'the art or practice of designing and constructing a building'. Then what does the 'designing a building' indicates? Again, in terms of language definition, it says, 'process of planning and creating the physical structure or facility while taking into consideration various factors such as functionality, aesthetics, safety, sustainability, and cost-effectiveness'. Since the foundation is mostly constructed underground, the 'aesthetic' is not an essential option to consider for geotechnical engineers, while other stated options can be adopted and applied to develop foundation design. In other words, since geotechnical engineers are designing the foundation only considering factors of safety and cost-effectiveness, the conventional foundation design process can also be referred to as "Foundation Architecture". However, with the emerging socio-economic-environmental conditions with limited construction areas available and depleted resources, the authors would like to propose the adoption of "Foundation Architecture" with expanded functionality and sustainability of foundations, could see foundation engineers leading the entire construction design process.

In most cases, foundations faithfully perform their fundamental role of supporting the structural loads while being invisible to the public by being located beneath the ground. For some cases, the foundations are designed to provide additional spaces with additional functions such as insulation. These kinds of foundation include basement foundation, garage foundation, concrete masonry units – those applied to home building and commercial buildings (Fig. 2). Although these foundations provide functions other than load bearing, the foundation design is performed in compliance with the external and structural requirements of the building that were performed/determined prior to the foundation design.



Fig. 2. Examples of foundation usage after construction

But what if the buildings were to be designed in the reverse order? Instead of the traditional sequence of exterior design – structural frame – foundation, imagine designing in the opposite order: foundation – structural frame – exterior. By providing architects and structural engineers with a variety of essential and optional methods for utilizing empty sites assessed by geotechnical engineers, they could design buildings/structures within a given envelope that also considers the subsurface options. This concept is visualized in Fig. 3. Compared to Fig.1, the process illustrated in Fig. 3 shows that the construction design process starts with foundation design and moves towards the superstructure considering the very active interactions between architects and structural engineers. Moreover, the foundation design is further divided into two steps: site investigation and foundation design. The aim of 'Foundation Architecture' is not to deny the traditional construction design process, but to broaden and highlight the role of foundation engineers in the construction design.

 © DFI International Bruges 2025

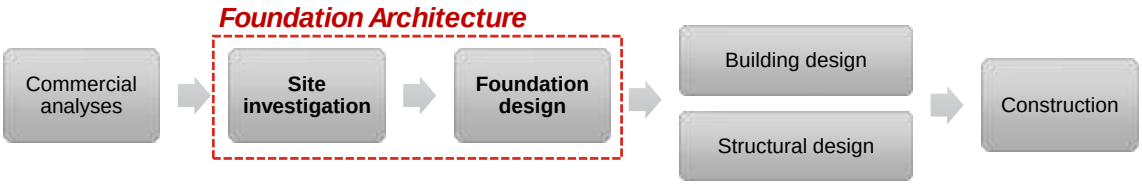


Fig. 3. Suggestion of novel construction process: Foundation Architecture

The 'foundation design' in Fig. 3 differs fundamentally from that in Fig. 1, as it incorporates the role of geotechnical engineers in providing judgement and evaluation on whether a given site can be built on and how the project should be initiated. The following examples can help to understand what Foundation Architecture aims to achieve.

Example of Foundation Architecture: *InterContinental Wonderland Hotel, Shanghai*

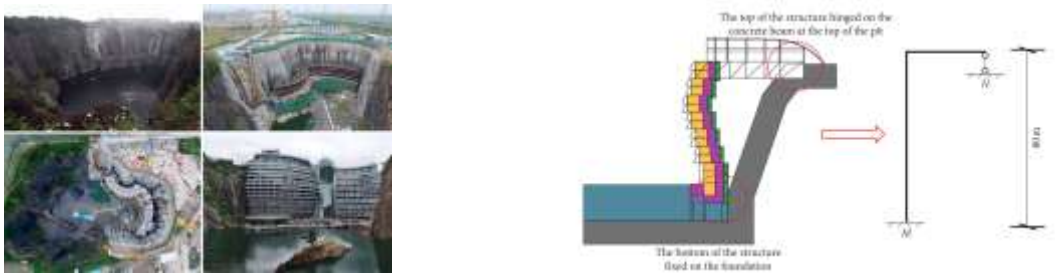
InterContinental Shanghai Wonderland, located in Songjiang District (Shanghai, China), is the world first underground hotel constructed on an abandoned quarry pit (Fig. 4 (a)). The architects designed to celebrate the quarry, so that the cliff, the green hills, and lakes became part of the building's design. The stiffness, depth and size of the pit (88m depth with side slope inclination angle of 80°) presented engineers with several challenges, including the difficulty of transporting equipment to the construction site and satisfying dynamic stability issues. Nonetheless, the engineering team patented more than 41 different engineering methods for the purpose of this project, and the InterContinental Shanghai Wonderland finally officially opened in November 2018, 12 years after the project began.

The construction design did not start from geotechnical engineering as proposed in Fig. 2. However, the focus of the foundation engineers was on providing practical solutions so that the structure could be constructed in the end, under challenging but innovative conditions. The InterContinental Shanghai adopted a new type of two-point support structure: (1) a block box foundation that is used to fix the tip of main building to the weakly weathered bedrock at the bottom of the pit; and (2) a vertical steel truss, that is connected to the bedrock at the top of the pit wall by hinged bearings (Fig. 4 (b)). This system is very interesting in that it transposed the concept of the foundation, which is usually located vertically beneath the base of a structure (i.e., substructure), to a horizontal application. Meanwhile, the frames that acts as foundation become integrated into the upper floors of the building, acting as bridges that connect the cliff and the building entrance. Additionally, this design supports sustainability by preserving and utilizing the existing conditions of the site: the quarry face.

Example of Foundation Architecture: *Multi-functional foundations*

Fig. 5 shows two types of system/foundation: (a) base isolation systems, that are a widely used method to protect the buildings from seismic hazards (Ramallo et al. 2002; Sheikh et al. 2022); and (b) buoyant foundations, that causes buildings to temporarily float on the surface of floodwater and lower back into original position after the floodwater recedes (English 2009; English et al. 2021). As they were developed under different conditions, the specific requirements and limitations for each foundation system should be very different from each other. However, they share one common concept, which is to let the foundation adapt to the given applied conditions, rather than controlling them through supplementary systems. Therefore, the foundation system at each case not only withstands the structural loads, but also provides resilience to natural disasters.

 © DFI International Bruges 2025



(a) (b)

Fig. 4. (a) Construction of InterContinental Shanghai and (b) adopted two-point support system

The authors propose the category of 'multi-functional' foundation to classify foundations that perform other functions in addition to resisting structural loads. This multi-functional foundation can also be one of the components that describe the Foundation Architecture, as it allows geotechnical engineers to effectively utilize the given conditions that will be encountered in the future. In other words, it will allow the design and construction of structures to adapt to the changing natural environment.
These foundation systems also share a design concept of 'separation' between the superstructure and the substructure (foundation or substructure). Similar to a ball bearing, the 'separation' is the functionality because it allows for dynamic movement which preserves the structures integrity. Designing the joint between the structural blocks and the foundation blocks is another issue, however, this approach provides additional opportunities in foundation design that will be discussed in the next section.



(a) (b)

Fig. 5. (a) Base isolation system and (b) buoyant foundation (English et al. 2019)

FUTURE OPPORTUNITIES

Previous engineers may not have prioritized sustainability or considered construction in poor soil conditions, not because of a lack of intention, but because of the technical limitations of the time. However, as the engineering team of the InterContinental Shanghai proved, modern engineers can solve problems by introducing new technologies when existing technologies are not immediately applicable. Similarly, future construction projects will continue to require innovative solutions and from geotechnical engineers, challenging us to overcome current limitations and advancing the field.

The repetitive challenges and solutions will ultimately empower foundation engineers to persuade architects and structural engineers by saying "We can design foundations capable of supporting a structure of a certain scale on this challenging site. Is there anyone who can complete an attractive and structurally sound superstructure?". This mirrors the traditional construction design started from architects saying, "Who can construct this type of building at this location?". In this respect, the basic of Foundation Architecture presented in Fig. 2 should be understood to suggest the value creation for both the site and structures begins with foundation engineers, contrasting with the conventional

 © DFI International Bruges 2025

process where this value creation begins with the architect. To perform this role, foundation engineers must explore the utility of the given soil conditions and surrounding environment. Developing multi-functional foundations could offer an innovative and appealing solution.

Furthermore, extending the 'separation' approach between foundation and structural components provides an opportunity to explore the ultimate design process to which Foundation Architecture could eventually evolve. Imagine a construction methodology where foundations and structural components are no longer tightly constrained by one another. Instead, they could be treated as separate modular components that are each designed, optimized, and constructed independently. Then they are seamlessly combined to be an entire structure.

In this scenario, the foundation components and structural components would be developed using their own design criteria, materials, and methods, which are optimized for their respective roles. For example, the foundation may be constructed to satisfy the particular soil conditions, loads, and environmental factors without being influenced by the structural design above. Conversely, the superstructure could be engineered for maximum efficiency, performance, or aesthetics without having to strictly adhere to foundation limitations. Certainly, a key prerequisite for this approach is the ability to create robust joints that connect two components. However, the specifics of these joint solutions will not be addressed here. Assuming the successful development of joints between the structure and foundation, the final Foundation Architecture approach offers several potential benefits, as outlined below.

Degree of Freedom: By decoupling the structure and foundation, architects and engineers can gain greater design flexibility. This flexibility may allow engineers to solely focus on optimizing them for their respective conditions.

Enhanced maintenance and repairs: Since the foundation and superstructure are separate, problems in one area can be addressed without significant disruption to the other. For example, the excessive foundation settlement can be managed without disrupting the building above, by reinforcing the independent foundation system.

Adaptability and resilience: Structures designed with this approach could be effectively adapted to changes over time. If the superstructure needs to be modified or replaced, this can be done without affecting the foundation, and vice versa. This flexibility can extend the life of the building, allow for partial or complete reconfiguration of the buildings, increase the ground utilization, and reduce construction waste.

Hybrid Structures: This approach could encourage development of hybrid structures, in which different part of the building are optimized for specific purposes: the foundation could be designed for resilience to natural disasters, while the superstructure could be optimized for energy efficiency or aesthetic appeal.

Engineered Thermal Transition Zone Foundations: Existing thermal foundation systems have evolved from adopting a structural foundation pile member and incorporating some additional elements to fulfill the thermal function. With an improved approach, superior designs can be achieved if both structural and thermal functions are considered, ab initio rather than the current approach of adapting a structural member to a structural member with added thermal functionality that will likely be limited by the initial structural design factors.

Enhanced Capacity Oriented Foundation: The design loadings of concern to a structure are not always those occurring above-ground. Indeed, in seismic zones, the critical loading scenarios typically come from ground motions which can have directionality and thus yield preferential orientations. If the original structure design and layout is predicated only on above-ground factors, then it is likely that more damaging load conditions can result. By designing foundations is seismic regions recognizing the directionality of ground motions, it may be possible to reduce seismic impact on structures.

 © DFI International Bruges 2025

Expanding the Envelope of Foundation Applicability: As architects and structural engineers expand the envelope of superstructures being realized, an implicit assumption has been made that traditional foundation types and approaches will still be viable. A number of recent and ongoing poor performance or even foundation failures are questioning this assumption. For example, the ongoing tilting of the slender Seaport Tower in New York or the Millenium Tower in San Francisco are an illustration of this concern and suggest that such issues and failures might be avoided if a Foundation Architecture paradigm were adopted,

CONCLUSIONS

With increasing challenges in construction site conditions, the novel approach of Foundation Architecture has been suggested. This design concept emphasizes the role of geotechnical engineers in leading the construction projects to create the value of the given site. With help of continuous evolution of construction techniques and engineering methods, this idea may become a practical reality, allowing us to build structures that are sustainable and adaptable to future needs.

ACKNOWLEDGEMENTS

This work was supported in part by the National Research Foundation of Korea (NRF) through the Korean Government under Grant RS-2023-00214321 and Higginbotham Professorship at Georgia Tech.

REFERENCES

A Case Study and Lessons Learned: Retaining Wall Design and Construction of the Maid of the Mist Winter Storage Facility, IFCEE 2015, pp. 442-456.

Aziz, R.F., Abdel-Hakam, A.A., 2016. Exploring delay causes of road construction projects in Egypt. Alex. Eng. J. 2(55), 1515-1539.

English, E., 2009. Amphibious foundations and the buoyant foundation project: Innovative strategies for flood resilient housing, International Conference on Urban Flood Management sponsored by UNESCO-IHP and COST Action C, pp. 25-27.

English, E., Chen, M., Zarins, R., 2019. An innovative strategy to increase the resilience of flood-vulnerable communities while reducing risk of population displacement and psychological trauma. 8th ICBR Lisbon Book of Papers, 278.

English, E.C., Chen, M., Zarins, R., Patange, P., Wiser, J.C., 2021. Building Resilience through Flood Risk Reduction: The Benefits of Amphibious Foundation Retrofits to Heritage Structures. International Journal of Architectural Heritage 7(15), 976-984.

García Gamallo, A. M. (2003). The evolution of traditional types of building foundation prior to the first industrial revolution. In S. Huerta (Ed.), *Proceedings of the First International Congress on Construction History* (pp. 943-956). I. Juan de Herrera, SEdHC, ETSAM, A. E. Benvenuto, COAM, F. Dragados.

Gebrehiwet, T., Luo, H., 2017. Analysis of Delay Impact on Construction Project Based on RII and Correlation Coefficient: Empirical Study. Procedia Engineering (196), 366-374.

Jiang, P., Yu, S., Luan, W., Chen, X., Qin, Y., Li, Z., 2020. The Key Construction Technology Research on the Intercontinental Shanghai Wonderland. Adv. Civ. Eng. 1(2020), 8890282.

Katzenbach, R., Leppla, S., Weidle, A., Choudhury, D., 2016. Aspects regarding management of soil

 © DFI International Bruges 2025

risk. Forensic Geotechnical Engineering, 343-356.

McLaughlin, K., Davies, R., 2024. Burj Khalifa: Everything You Need to Know About the Tallest Building in the World Architectural Digest.

Ramallo, J.C., Johnson, E.A., Spencer, B.F., 2002. “Smart” Base Isolation Systems. Journal of Engineering Mechanics 10(128), 1088-1099.

Sheikh, H., Van Engelen, N.C., Ruparathna, R., 2022. A review of base isolation systems with adaptive characteristics. Structures (38), 1542-1555.

Tam, V.W.Y., Shen, L.Y., Tam, C.M., Pang, W.W.S., 2007. Investigating the intentional quality risks in public foundation projects: A Hong Kong study. Building and Environment 1(42), 330-343.

 © DFI International Bruges 2025

DEEP MIXING METHOD FOR STABILIZATION OF COAL COMBUSTION RESIDUAL MATERIAL

Raffaella Granata, Trevi S.p.A., Cesena, Italy, rgranata@trevispa.com
Lorenzo Faedi, Treviicos Corp., Charlestown MA, USA, lfaedi@treviicos.com
Mohamed Elgouhary, Treviicos Corp., Charlestown MA, USA, melgouhary@treviicos.com

ABSTRACT

The paper describes the activity performed nearby a large coal-fired power station (sited in the South-Eastern USA) for the stabilization of Coal Combustion Residual (CCR). Two retaining walls were designed to provide structural stability to the landfill during the excavation works. The two retaining walls were constructed by installing soil-cement columns with the deep mixing method. The columns were partially overlapped and arranged in a grid manner, to create cells providing lateral support to the industrial landfill material. The paper describes the solutions developed both during the pre-construction and construction phases, to address the variable behavior of the CCR when treated by deep mixing. The paper deals also with the Environmental impact of the Project, which was reduced by (1) selecting a technology that mixes the soil in situ rather than replacing it, (2) using eco-friendly binders like cement type ASTM-IL (CEM-IIL) and ground granulated blast furnace slag, (3) taking advantage of the CCR pozzolanic activity, to reduce the binder content.

Keywords: Deep Mixing Method, Coal Combustion Residual, Fly Ashes, Environmental Impact

PROJECT DESCRIPTION

Scope and background

The Coal-fired Power Station is sited in the South-Eastern USA. For decades, the power station conveyed the Coal Combustion Residual (CCR) material via wet sluicing methods in dedicated ash-basin lying on an impervious layer of saprolite. In the late 1980's, the plant was converted with dry ash handling system, and the ash basin was converted to landfill for dry ashes. The landfill was positioned mostly on top and within the footprint of the existing ash-basin, which was permitted and constructed without liners, as per standard practice for those times.

In recent times, confinement works were required to stop the risk of leachate migration out of the landfill perimeter. The design foresaw excavation works to remove the ashes deposits along the two segments of the landfill perimeter, which were not actually confined by the saprolite layers.

Two retaining walls were designed to provide structural stability to the landfill during the excavation works. The consolidation works were also conceived to allow the construction of safe basins to allocate
the new ashes produced by the same power plant in the next future. The two retaining walls, namely the East Wall) and the West Wall, were to be constructed by the Deep Mixing Method (DMM), installing soil-cement columns, partially overlapped and arranged in a grid manner, embedded in the saprolite impervious stratum.

As shown in Fig. 1, the East Wall covers a rectangular area of about 2582 m^2 (0.64 acres) whereas the West Wall has an irregular "S" shape that covers about 25,336 m^2 (6.26 acres).

 © DFI International Bruges 2025



Fig. 1. Ash Basin and DMM East and West

Subsoil Profile

A supplemental soil investigation campaign was conducted to verify the soil profile and properties provided based on previous campaigns. The soil campaign consisted of seven (7) rotary boreholes and four (4) sonic continuous cored holes to retrieve sufficient material for the Bench Scale Testing. Standard Penetration Tests were conducted within the rotary bore holes, as well as collection of Shelby tubes samples for laboratory testing.

The subsoil profile is composed by a variable thickness layer of Coal Combustion Residuals (CCR) overlying the Native soil (aka Residual soil), before encountering the gneiss bedrock. The CCR is composed of fly ashes and bottom ashes in variable percentages, resulting from the power plant coal combustion process. The fly ashes are silty-sized particles whereas the bottom ashes are more associated to a fine sand grain size distribution. The CCR was placed by sluicing method on top of the Residual soil (Saprolite), thus resulting in little to no consolidation, and high moisture content. The topmost 4.5-6.0 m (15-20 ft) of CCR were placed and compacted by mechanical methods, thus resulting in a highly consolidated layer with low moisture content.

The Residual Soil layer originates from the weathering and decomposition of gneiss bedrock. This layer is typically 1.5 to 3.0 m (5 to 10 ft) thick and performs as a high plasticity clay with low moisture contents (Consistency Index of 1.70 on average). Underlying the residual soil is the Partially Weathered Rock (less degraded than the residual soil) and the Bedrock. The typical properties of CCR and Residual Soil resulting from the supplemental soil investigation are presented in Table 1.

Table 1 - Typical Properties of CCR and Residual Soil

Soil Type	Average NSPT	Natural Moisture	Consistency Index CI	Wet Unit Weight	Dry Unit Weight	Specific Gravity	Organic Content
Consolidated CCR	16	33%	0.59	103 pcf 1.65 g/cm^3	78 pcf 1.25 g/cm^3	2.36	1.8%
Sedimented CCR	1	50%	-	92 pcf 1.47 g/cm^3	60 pcf 0.96 g/cm^3	2.17	2.0%
Residual Soil	34	19%	1.70	121 pcf 1.93 g/cm^3	102 pcf 1.62 g/cm^3	2.73	1.3%

The typical facies of CCR and Residual soil are shown in Fig. 2.

 © DFI International Bruges 2025



Fig. 2. Left: Compacted CCR (Sonic sample). Center: Sedimented CCR (SPT sample). Right: Transition between Sedimented CCR and Residual Soil (SPT sample)

DMM Treatment Requirements

Treviicos was awarded the Contract in May 2022, starting the production in October, and completed the works in January 2024, ahead of schedule.

The Contract included the installation of 4613 DMM Columns over a total area of about 28,000 m2 (6.9 acres), to construct the stability features supporting the industrial landfill during excavation and removal of Coal Combustion Residuals (CCR) material in the Ash Basin.

The DMM stability feature consists of two separate segments (Fig. 1). The west segment (West Wall) is to support the landfill during excavation of the adjoining ash basin; the east segment (East Wall) is to support the landfill during excavation of the extension impoundment.

The East Wall (Fig. 3) has a planimetric rectangular shape measuring 18.3 m x 145 m (60 ft x 475 ft) with a maximum retained height of approximately 11 m (36 ft), before a berm of shot rock is placed in front of the DMM wall, to provide long-term stability.

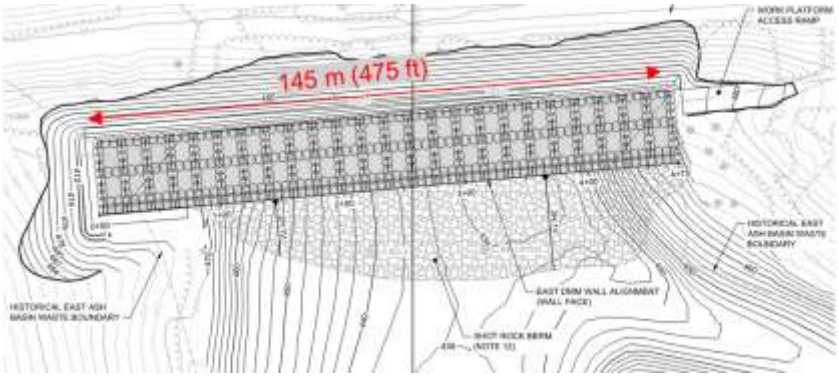


Fig. 3. East DMM Wall Layout (contour lines after excavation, in feet)

 © DFI International Bruges 2025

The West Wall (Fig. 4) has an S-shape, with a front face 817 m (2680 ft) long, and 15 to 45 m (50-150 ft) wide. The excavation to expand the ash basin will be done in front of the West Wall, down to the top of the residual soil, creating a maximum retained height of approximately 24 m (78-ft).

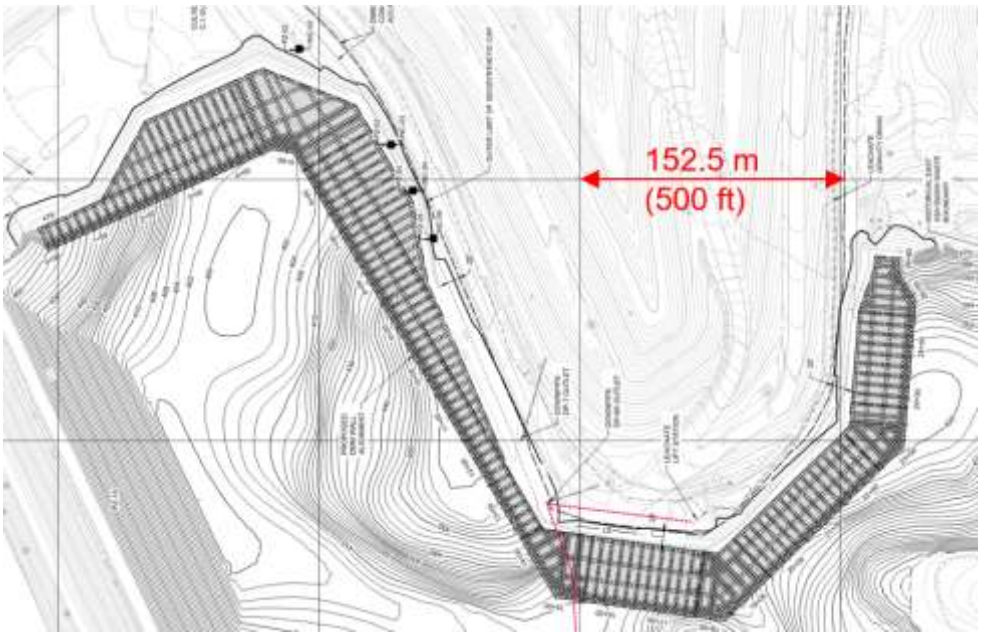


Fig. 4. West DMM Wall Layout (contour lines after excavation, in feet)

The Design required the installation of DMM columns, 2.4 m (8-ft) in diameter, partially overlapped and arranged in a grid manner (e.g. Fig. 5) to create cells and provide lateral support to the industrial landfill material. The columns were to be embedded at least 1.5 m (5-ft) in the impervious residual soil (saprolite), to grant the proper confinement. To this aim, they were to be installed to a max depth of 26 m (85-ft). As per technical specifications, the DMM was designed to provide UCS not less than 1.4 MPa (200 psi) and a permeability lower than $1x10^{-7}$ m/s.

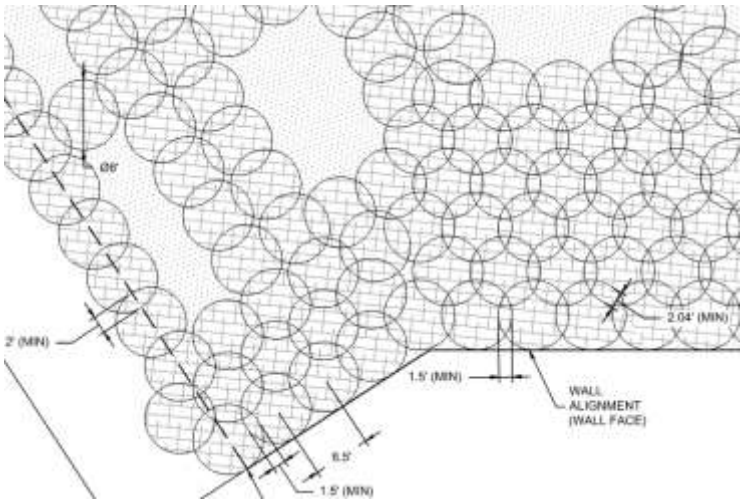


Fig. 5. DMM Column Arrangement –Detail at one of the Corner

The material to be treated was mainly composed of CCR (i.e., bottom and fly ashes), for which very limited background experiences were available. In addition, the CCR was characterized by a certain degree of pozzolanic activity, extremely variable from place to place. Hence, an extensive pre-

 © DFI International Bruges 2025

construction process was needed to define the installation parameters, involving a soil investigation campaign, two bench scale tests, and several stages of field validation.

PRECONSTRUCTION TESTS

Bench Scale Test Program

The Bench Scale Test (BST) program started after completion of the subsoil investigation. During the BST, the three main types of soil and CCR types were individually mixed with a cementitious grout in different proportions, to define a range of parameters that can produce a treatment in compliance with the specification's requirements.

During the BST, a wide range of Binder Factor was tested to study the mechanical and permeability performances. The binder included Cement and Blast Furnace Slag, in ratios ranging between 25/75 and 50/50. The cementitious grout was prepared utilizing Water/Binder ratios between 1.0 and 1.25.

Both cement type ASTM-I/II and type ASTM-IL were tested (ASTM, 2008). The aim was to investigate the performances of the ASTM-IL (which contains 5-15% of limestone additions and is relatively new in the US market) versus the ASTM-I/II (for which more background information is available).

The step-by-step procedures for the bench scale testing in the lab followed the industry standards (Hodges et al., 2008).

The results of the BST showed that:

- The BF in the lower value was sufficient to successfully treat Compacted CCR and Residual Soil;
- The BF in the upper value was required to treat the Sedimented CCR to obtain the required target UCS;
- A Water/Binder of 1.0 was adequate to obtain a homogeneous mixture in the CCR material, whereas a higher amount of water was necessary to obtain a homogeneous mixture in the Residual Soil;
- The mixes with the cement ASTM-IL yielded lower strengths compared with similar mixes prepared with cement ASTM-I/II.

Field Validation Program

Prior to production, a test section was installed on both the East and West to verify that the proposed equipment, procedures, and mix design were suitable to uniformly mix the onsite materials and achieve the product requirements according to the acceptance criteria. As per technical specifications, at least three columns were to be installed, each column extended from the ground surface to a minimum of 5 feet into the residual soil below the CCR or Refusal.

For this Field Validation Program (FVP), Treviicos planned to use the same Binder Factor range tested during the BST, installing five (5) clusters (each one with three overlapping columns), two (2) of which on the east side, and three (3) on the west side of the Project as shown in Fig. 6.

During the installation of the columns in the first cluster in the West Wall, utilizing the Binder Factor selected based on the results of the bench sale test, it was noticed a high and unexpected initial strength gain of the DMM material. This high strength made the installation of the secondary overlapping column more difficult, causing unacceptable deviations from the vertical alignment. The

 © DFI International Bruges 2025

strength behavior was confirmed by the UCS tests on wet grab samples performed at the age of 2-4 days, that yielded strengths higher than 1.4 MPa (200 psi, the 28-day target).



Fig. 6. Foreseen FVP layout at West (left) and East (right) Walls

Consequently, it was clear that the behavior of the in-situ CCR material mixed with the cementitious grout was different than what observed in the laboratory testing: the pozzolanic reaction of the fly ashes composing the CCR would sensibly increase the performance of the treatment. Based on this finding, reductions of the BF were attempted in Cluster 2 and 3, to define the minimum dosage necessary to meet the Project requirements, avoiding excessive UCS at early ages. Nevertheless, the sole reduction of the BF was not sufficient to mitigate the high early strength development. For this reason, a final fine-tuning was performed, enriching the grout with pre-hydrated bentonite and admixture, to delay the strength gain development and provide a sufficient time window to allow the proper installation of the overlapping secondary/tertiary/quaternary columns.

Following West FVP Clusters 1, 2, 3, the East FVP clusters were installed with a BF lower than the one planned after the Bench Scale Test. In the East Wall area, the pozzolanic activity of the in-situ CCR was not as strong as in the West Wall area, therefore the use of bentonite slurry and admixture was not implemented.

 © DFI International Bruges 2025

Eventually, a total of eleven (11) clusters (each one with 3 to 6 DMM columns, Fig. 7) were installed as part of the West and East Field Validation Program to define the mix design, so as to produce a compliant treatment in terms of UCS and permeability, concurrently allowing the installation of the overlapping columns within the allowed verticality tolerances. All the FVP columns were installed within the treatment cells, thus not interfering with the future production columns.

During the installation of the FVP columns, it was noticed that a high resistance to penetration was offered by the topmost layer of the Compacted CCR. This behavior was due to the high density and low moisture content characterizing this layer of CCR. For this reason, before the treatment with cementitious grout, a pre-cut stage was performed by drilling and withdrawing the tool while injecting water. This pre-cut stage allowed to maintain a constant penetration rate throughout the DMM treatment.

Furthermore, the saprolite layer into which the columns were to be embedded was characterized by a high plasticity index. Therefore, a tip-treatment was performed by re-stroking the bottommost 5-ft of all columns, while injecting the cementitious grout. This additional mixing increased the BRN (blade rotation number), enhancing the uniformity of treatment.

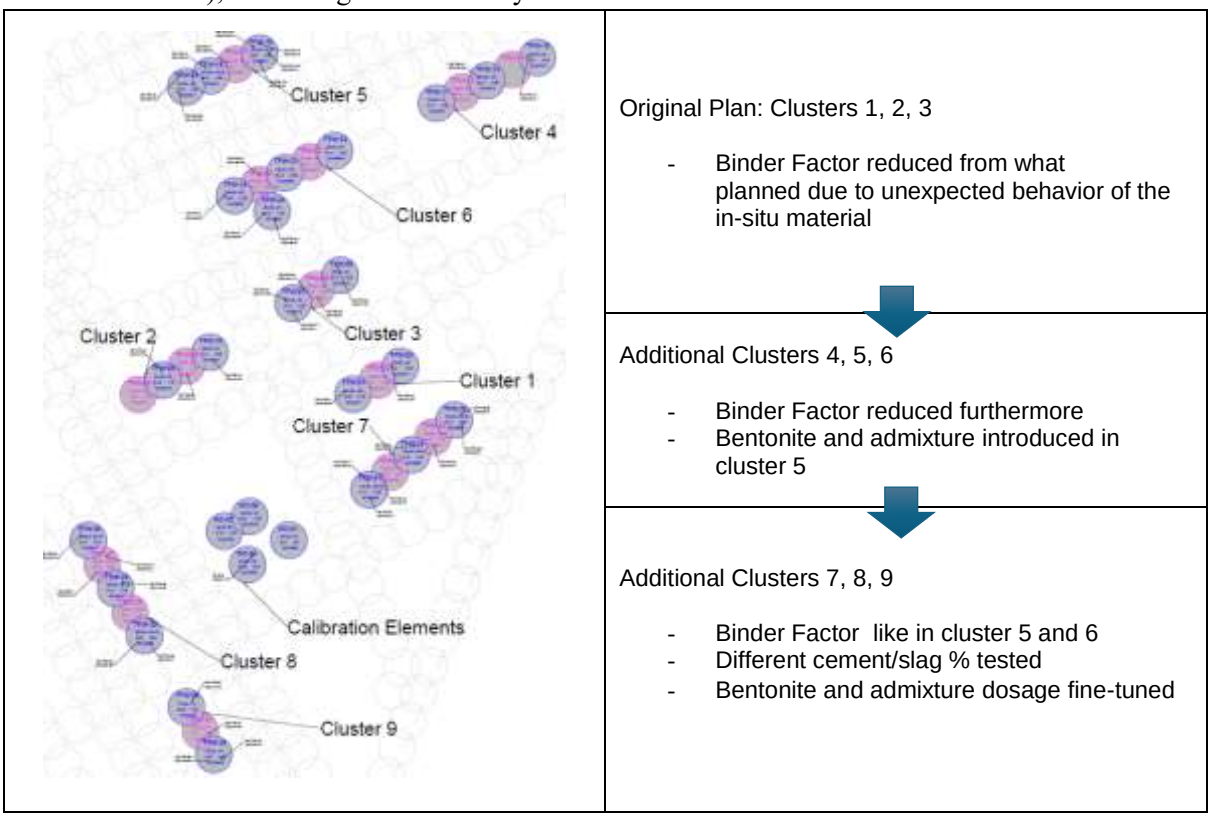


Fig. 7. Field Validation Program Final West Layout and Summary

CONSTRUCTION PHASE

After elaborating the results of the East and West FVP, the production stage commenced. The General Contractor provided a stable work platform, mainly composed of compacted CCR material, to allow the safe travel and operations of the DMM rigs. Treviicos used timber crane mats to provide additional stability to the DMM rigs and spread their load on a wider area (Fig. 8).

Three DMM rigs were used to install the columns at site (Fig. 9). The configuration of the mixing tools was improved throughout the FVP and the production phase, with a constant interaction between

 © DFI International Bruges 2025

field and design teams, to enhance the verticality and penetration speed of the treatment, in particular for the secondary/tertiary/quaternary columns.



Fig. 8. Soilmec SR125 rigs on timber mats



Fig. 9. Deep Mixing activity

The DMM columns were arranged in cells with overlaps between columns typically between 0.45-0.60 m (1.5–2.0 ft). The front face of each wall was characterized by three rows of overlapping columns whereas the intermediate and backside alignments, as well as the transverse buttresses, were typically composed of single rows. Some corners had a more congested arrangement with several rows of overlapping columns, to provide extra mass treatment and stiffness to these areas (Fig. 5).

The treatment parameters and the grout composition to be used for the production elements were defined based on the results of the FVP. It was noticed that the fly ashes composing the CCR layers had different level of pozzolanic activity in the East and the West areas; therefore, different grout compositions and BF were used for production in the different areas. In addition, while installing the columns in the West Wall, the UCS tests showed that the pozzolanic activity varied also within the different sectors of the West Wall. Accordingly, it was necessary to make a continuous adjustment of the installation parameters throughout the production, based on the monitoring of the strength of the columns already installed.

QUALITY CONTROL AND VERIFICATION TESTING

The Soilmec rigs were equipped with a proprietary data acquisition system (DMS®) to allow the monitoring and control of the installation parameters in real-time. The verticality was measured on all the installed columns utilizing the Jen Lutz PRAD® deviation sensor. A data management system was implemented to allow prompt visualization and elaboration of the recorded data.

 © DFI International Bruges 2025

The Quality Control of the DMM treatment consisted of a combination of wet grab samples (WGS) and verification corings (VC). A total of 235 verification boreholes were drilled (32 in East Wall, 203 in West Wall). The core samples retrieved from the VC were analyzed to verify the homogeneity of the treatment and to confirm a good contact at the base with the residual soil or the weathered rock (where the residual soil thickness was less than the target embedment depth).

UCS tests were performed on core samples collected at different depths (each 3 m – 10 ft spacing) and cylinders prepared with the WGS retrieved at three different depths (top, middle, bottom). Fig. 10 presents photos of core sample taken at the base of the columns, with evidence of treatment at the contact with the weathered rock or residual soil. Fig. 11 and Fig. 12 presents the UCS results obtained at the West Wall.

A total of 1288 UCS tests were carried out on cored samples; a total of 3749 tests were carried out on WGS (at different curing times). Based on the comparison between the UCS results from the WGS and the ones from the core samples (retrieved from the same columns at similar depths), it was noticed that in general the core samples yielded UCS much higher than the WGS ones. A total of 1017 WGS specimens were also tested by ASTM-D5084, to confirm the compliance with the designed hydraulic conductivity.



Fig. 10. Typical Coring of treated material and contact with the residual soil/weathered rock

All the records from multiple sources were uploaded in the data manager system specifically developed for the Project, which ultimately produced the as-built for each column. Based on the as-built and verticality measurements, it was possible to detect any deviation from the acceptance criteria, e.g. the overlapping between adjacent columns to be within acceptable values.

Thanks to the continuous analyses of the data, subsequent adjustments of the treatment parameters, and improvement of the drilling tools, the acceptance criteria were met in all the areas. Only four additional columns were required to remediate the few detected deficiencies.

 © DFI International Bruges 2025

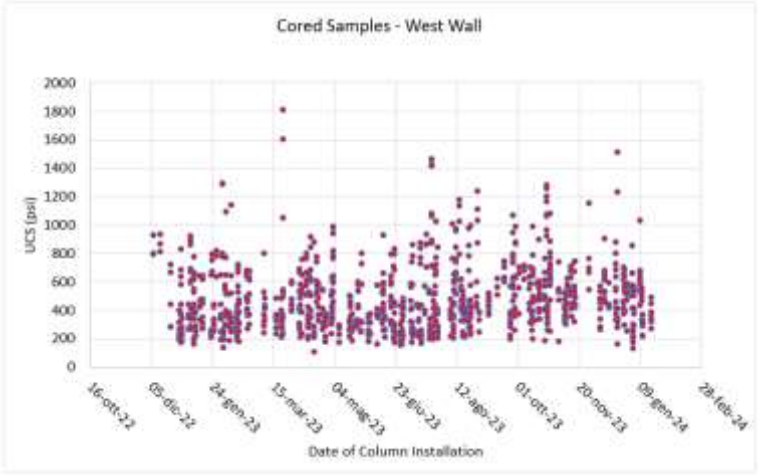


Fig. 11. UCS results (vs. time) on samples cored at the West Wall (1119 tests)

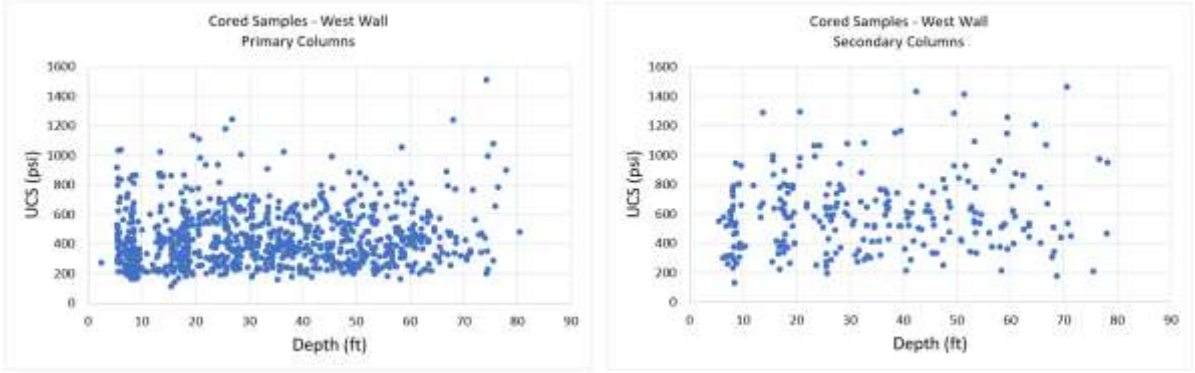


Fig. 12. UCS results (vs. depth) on samples cored at the West Wall (1119 tests)

SUMMARY AND CONCLUSIONS

The DMM technology was successfully implemented to treat the in-situ materials. The required characteristics were always achieved, even if the variable behavior of the in-situ CCR at different locations required adjustment of the installation parameters throughout the duration of the Project.

Treviicos was able to minimize the carbon footprint of the project by taking advantage of the pozzolanic activity of the fly ash at the site to sensibly reduce the dosage of binders in the grout mix. We further minimized the carbon footprint utilizing cement type IL and GGBFS in the preparation of the grout, thus using a total recycled material content exceeding 50% of total binder.

The DMM turned out to be a very efficient technology to treat the CCR in place with their minimal removal and consequent handling. This had the positive effect of reducing the volume of spoil produced.

Almost all the in-situ CCR remained in place, within the DMM columns. The small amount of spoil generated was partially re-used for the top-off of the DMM columns. Indeed, several columns experienced a drop (i.e. lowering of the surface level), the day after installation.

The DMM spoil could have been used for other purposes, such as embankment construction, with further reduction of Project footprint.

 © DFI International Bruges 2025

REFERENCES

American society for testing and materials (2008), ASTM C595-08a: Standard Specification for Blended Hydraulic Cements

European Committee for Standardization (2006), EN 14679:2005a - Execution of special geotechnical works. Deep mixing.

Federal Highway Administration (2013) – FHWA Design Manual: Deep Mixing for Embankment and Foundation Support, Publication no. FHWA-HRT-13-046

Holz, K., Filz, G., Weatherby, D, (2008) - Laboratory Mixing, Curing and Strength Testing of Soil-Cement Specimens Applicable to the Wet Method of Deep Mixing. Published by Virginia Polytechnic Institute and State University

 © DFI International Bruges 2025

THREADED DISPLACEMENT PILES – A COMPARISON WITH CONTINUOUS FLIGHT AUGER PILES IN CORK, IRELAND

David Hard
Bachy Soletanche Ltd, Camberley, UK +44 1276 674 940, david.hard@bacsol.co.uk
Kevin McDonnell
McDonnell Piling & Foundations, Cork, Ireland +353 214613131,
kevin.mcdonnell@mcdonnellpiling.ie

ABSTRACT

The use of threaded displacement piles can offer a more sustainable and geotechnically efficient alternative to traditional bored piles, and in particular, Continuous Flight Auger (CFA) piles. This paper presents the results of static load testing on preliminary test piles installed by McDonnell Piling and Foundations (as a sister company to Bachy Soletanche Ltd) in the centre of Cork City, Ireland using the proprietary "Screwsol" threaded displacement pile system, developed by Bachy Soletanche Ltd. The tests were carried out alongside standard CFA test piles to allow direct comparison of the two techniques. The paper discusses the design approach and enhancement of capacity developed through the use of the threaded displacement system and compares the load-settlement behaviour of the two different pile types. In addition to the technical aspects, the environmental benefits of the reduced concrete and spoil volumes in Screwsol piles compared to CFA piles are presented.

Keywords: threaded, displacement, carbon savings

INTRODUCTION

The use of Continuous Flight Auger (CFA) piles to form the foundations for structures in the middle of Cork city is well established. The piles can be founded on the underlying rock or within the overburden above. Developments in piling techniques resulted in large displacement piling becoming an option in the right ground conditions using the same machines as for CFA piles. These create minimal spoil and a degree of soil compaction during the drilling process, with concreting during extraction of the tool.

As a further refinement to the technique, Bachy Soletanche Ltd have developed a large displacement cast in situ pile that has the addition of a helical thread which is formed as the drilling tool is extracted during the concreting process. The thread increases the effective geotechnical diameter of the pile, but with less concrete than the equivalent full section displacement or CFA pile. This pile, named Screwsol for promotional purposes, has been widely used in England, Hungary, Poland and Romania but until now has not been used in Ireland.

The introduction of the threading on the pile allows the geotechnical capacity to increase, therefore maximising the structural capacity of the piles, which is not normally the case for friction CFA piles.



Figure 1. Location of test sites.

 © DFI International Bruges 2025

GROUND CONDITIONS

The centre of Cork is built on a floodplain that was originally a series of estuarine channels and islands. Over hundreds of years the land has been reclaimed and the levels raised to create the topography of the modern city. The floodplain is narrow, ranging from between 500m to 750m, beyond which the underlying rock outcrops to form ridges to the north and south of the river. This has left a deep valley infilled with glacial and interglacial granular deposits.

The soil profile at the specific sites comprises a varying depth of made ground over a thin layer of alluvium, underlain by a mixture of sand and gravel deposits. The alluvium is typically a mixture of silt and clay. The sand and gravel have been deposited in a steep sided valley cut into the underlying rock. Near the river the glacial deposits can extend to depths of over 60m. The gravels are not homogenous with varying densities being encountered and a layered profile being identified in the ground investigation for each site.

The three sites showed broadly similar in situ testing results, with a middle layer where the 'N_{SPT}' values are constant but slightly lower than the strata above. At depth we can note a return to a denser layer, with increasing SPT values. There are slight differences between the two sides of the river but the general trends remain the same. Table 1 summarises the stratigraphy at the three sites. The individual plots for each of the sites are displayed in Figure 2.

The groundwater was encountered between elevations of -2.0mOD and +1.0mOD and is influenced by the tides, but with a delay in response and a reduced range of variation.

Table 1. Geological profile at test sites

Strata	Horgan's Quay (mOD)	Albert Quay (mOD)	Kennedy Quay (mOD)
Made Ground	+3.50	+3.00	+3.50
Alluvium	-1.00	-1.00	-0.50
Sandy Gravel	-3.00	-2.00	-2.00
Sand	-8.00	-8.50	-6.50
Sandy Gravel	-14.00	-14.00	-14.00
Rock	-24.00	-19.00	Not identified

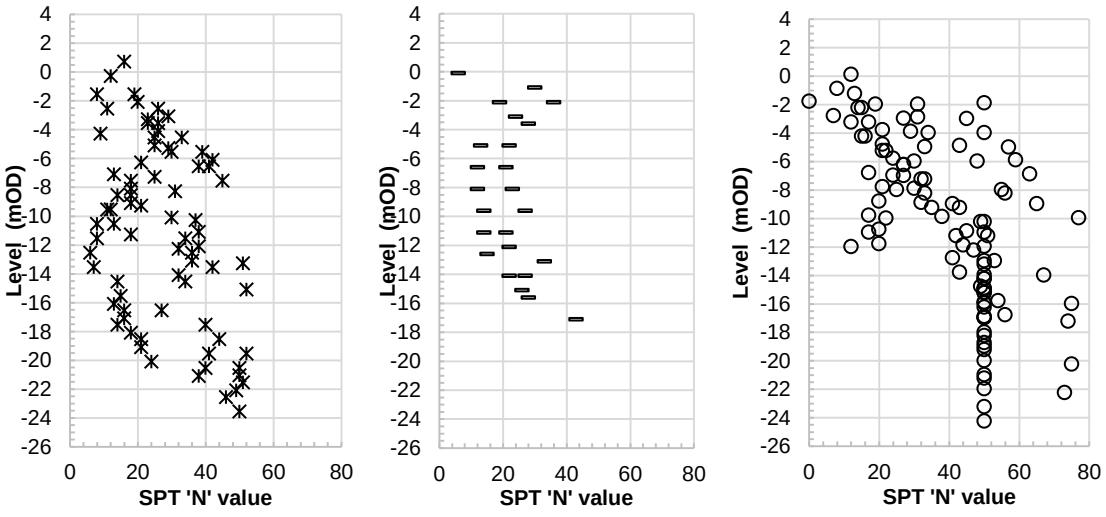


Figure 2. SPT "N" plots for each site (L-R): Horgan's Quay, Albert Quay, Kennedy Quay.

 © DFI International Bruges 2025

TEST PILES

To progress with the introduction of a piling technique new to Ireland, McDonnell Piling (MDP) undertook the installation and testing of sacrificial Screwsol piles alongside traditional CFA piles on sites located on both sides of the river in Cork (Figure 1).

The test piles were installed on three separate sites, all embedded within the deep granular deposits immediately adjacent to the river. The same Llamada P105 rig was used to drill all the test piles, increasing the consistency of the installation between the different sites. A range of loads and depths was considered. The Screwsol test piles were installed with two different diameter tools (Figure 3) to gather information on how practical it is to install a larger displacement pile into the denser materials. Dynamic tests were carried out on separate piles in addition to the static testing on two of the sites.



Figure 3. Screwsol drilling tools (L-R) 430/600mm diameter and 330/500mm diameter.

The first piles were installed and tested on the Horgan's Quay site, with the piles at Albert and Kennedy Quay following the load test results review. This allowed for the refinement of the design approach to maximise the information gathered. Tables 2 and 3 summarise the details of the test piles and loads for the Screwsol and CFA piles respectively.

Table 2. Screwsol Test Pile details

Test Pile	Diameter (mm)	Depth (m)	SWL (kN)
Horgan's Quay (HQ1)	430/600	15.00	1700 (SLS2)
Horgan's Quay (HQ2)	330/500	15.00	1350
Kennedy Quay (KQ_DTP1)	330/500	18.00	1800 (SLS1)
Kennedy Quay (KQ_DTP2)	330/500	17.00	1400 (SLS3)
Albert Quay (AQ_DTP1)	330/500	18.00	1700

Table 3. CFA Test Pile details

Test Pile	Diameter (mm)	Depth (m)	SWL (kN)
Horgan's Quay (HQ TP1)	600	20.30	1800 (SLS1)
Kennedy Quay	-	-	-
Albert Quay (AQ_STP1)	900	22.30	3000 (SLS4)

The CFA pile installed at Albert Quay was drilled to the underlying rock to supply information on the capacity of piles taken to this stratum. This was in anticipation of the piles for the core of the proposed building requiring high load capacities that would not be achievable structurally with the diameter of the Screwsol piles. The information gained in the first stages of the static load test still allowed a comparison of the mobilised friction in the CFA pile compared to the Screwsol piles. The CFA pile at Horgan's Quay was founded within the granular deposits above the rock but was dimensioned on the basis of a traditional design for a CFA pile in this type of ground.

 © DFI International Bruges 2025

INTERPRETATION OF RESULTS

The Screwsol piles are designed geotechnically using the diameter at the outside of the thread, and structurally considering the smaller diameter of the core. The process of displacement during the initial drilling to depth with the tool, followed by the formation of the thread during extraction, creates a compaction effect in the soil around the pile. The shape of the thread around the pile creates an interlocking effect in the ground, increasing the friction above that which would be found with a smooth pile, whether it was a displacement or CFA pile.

The shaft friction on a bored cast in place pile in granular soil is classically calculated as shown by Equation 1:

Unit shaft friction, $q_{us} = k_s \cdot \tan(\delta) \cdot \sigma_v'$ [1]

Where k_s = coefficient of horizontal soil stress, δ = average angle of friction between the soil and the pile, and σ_v' = effective vertical stress.

The use of the Screwsol piles within the Soletanche Bachy group has been ongoing since its first implementation in 2000, with thousands of piles installed across several different countries in Europe. The back analysis of test piles from these countries has allowed a design approach to be developed for the Screwsol piles, which models the enhanced shaft friction observed in the results. It has been found that the simplest method to model this interaction is through the adoption of an enhanced k_s value when calculating the shaft friction developed on the pile. Typically, this enhanced value lies between 1.20 and 1.40 depending on the nature and density of the material the piles are built in. This value is comparable with the values used for traditional design of driven piles.

The curves presented in Figure 4 are based on the results of 125 different static load tests carried out on Screwsol piles. These tests have provided a data set covering piles of differing lengths in varying ground conditions. The soils have been predominantly granular, to suit the technique, but covering a range from silty sand up to sandy gravels. In each case, the design was based on a site-specific site investigation to ensure the most accurate modelling of the ground and an accurate assessment of the degree of enhancement that has been observed in the value of k_s.

The results of the specific test pile results carried out in Cork are shown in Figure 4, plotted against the other European wide test results. These show that the performance was in line with those results, with a similar shape to the load-settlement curves. They represent upper bound curves, which is most likely linked to the nature of the ground compared to some of the other sites – the stiff and relatively high shear strength sandy gravels, further improved by the densification during pile installation, provide the pile a very good bearing capacity and a stiff load-settlement behaviour. Both the comparison to the wider acquired data, and the review of the testing in absolute terms give the confidence that the adopted design approach is valid and can be successfully used in the ground conditions encountered in Cork.

In line with good practice, the design at each of these sites in Cork has relied on project specific site investigation supplemented by the preliminary static load tests to verify the design assumptions. Going forward it is suggested that this same approach adopted to supply further data on the use of the technique in Cork ground conditions. The data sets presented in Figure 4 provide a benchmark against which designs can be checked but the individual characteristics of each site need to be addressed on their own terms.

 © DFI International Bruges 2025

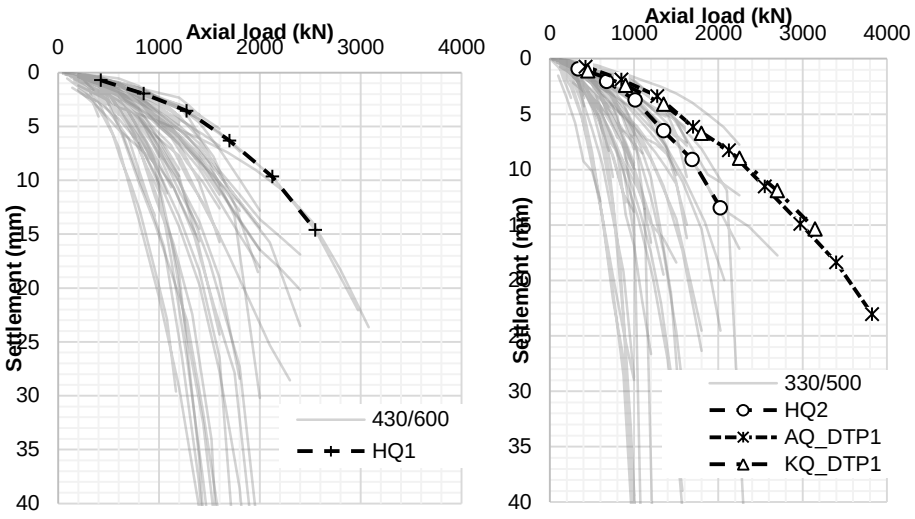


Figure 4. Comparison of Cork data with other European sites.

The results of the static load tests on the three Cork sites are presented in Figure 5, together with predictions for the two different design loads considered. These predictions were made using the design approach with enhanced skin friction.

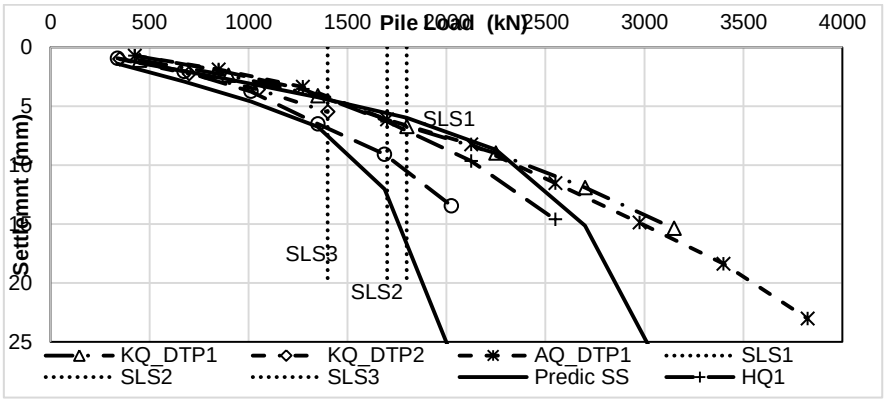


Figure 5. Load settlement plots for Screwsol test piles.

The results of the tests show good correlation with the predictions up to the service load. Beyond this load the piles continue to perform well, with less settlement than predicted. This may indicate that although the shaft stiffness and resistance have been well estimated as they mobilise first under limited displacements and low loads, the end bearing should be further studied.

The equivalent load-settlement plots for the CFA piles are presented in Figure 6. These piles were designed using traditional design values for the calculation of shaft friction, where the value of k_s is in the range of 0.9 to 1.0. These results also show good correlation between the predicted and observed settlements up to the service load, and a slightly better than estimated performance at higher load stages.

It is likely that the improved performance observed at higher loads for both the Screwsol and the CFA piles is due to a greater base capacity than was allowed for in the design calculations. However, there is more of a discrepancy in the behaviour at higher loads between the Screwsol piles and the CFA piles. The prediction for the CFA piles, using a moderately conservative approach, is still in line with the observed results, whereas the Screwsol piles show an improvement over the prediction as the test progresses. This implies that the while the shaft capacity for both pile types has been accurately

 © DFI International Bruges 2025

predicted, the displacement piles have significant additional base capacity from improvement in the soil beneath the toe of the piles that has not been fully accounted for in the design approach. The observed improvement in the mobilised base capacity in the Screwsol piles is most likely due to the design being based on an Nq value in line with normal CFA. This does not include for compaction effects that will occur due to the displacement installation technique. Although this is a conservative assumption, it does not raise the design toe level of the piles as this is chosen in line with maintaining a minimum factor of safety on shaft capacity alone. This approach is used to control settlements and remove the risk of relying on the condition of the material below the toe of the pile in serviceability conditions.

The comparison of the unit shaft friction and total shaft friction is presented in Figures 7 and 8 respectively. The only difference in the unit shaft friction capacities is the different values of k_s which results in the same line but offset higher for the Screwsol piles. When this is carried across into the calculation of the ultimate shaft friction with depth in Figure 5, the effect of the diameter also becomes a factor. It can be seen that the 330/500mm diameter Screwsol returns almost the same shaft capacity as the 600mm diameter CFA pile, whilst requiring far less concrete to form the pile. If the larger 430/600mm diameter Screwsol pile is adopted, there is an increase above that of the 600mm diameter CFA, but still without the same volume of concrete in the section, allowing for a potential shortening of the pile if targeting the same capacity.

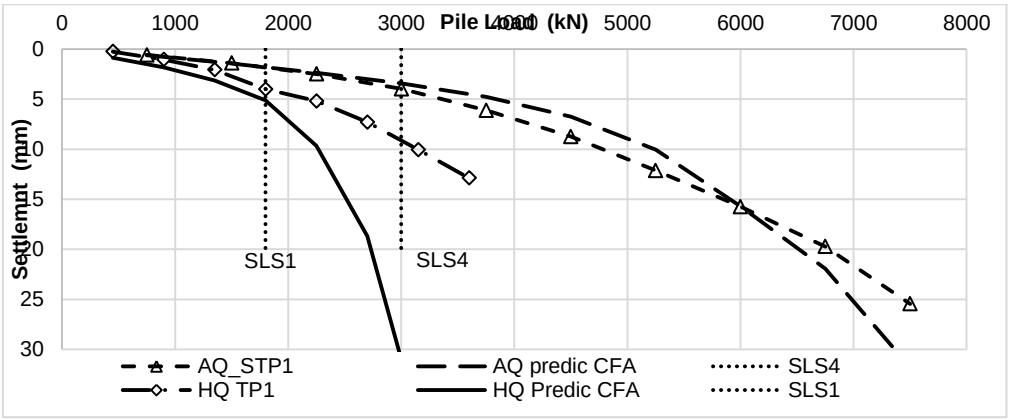


Figure 6. Load settlement plots for CFA test piles.

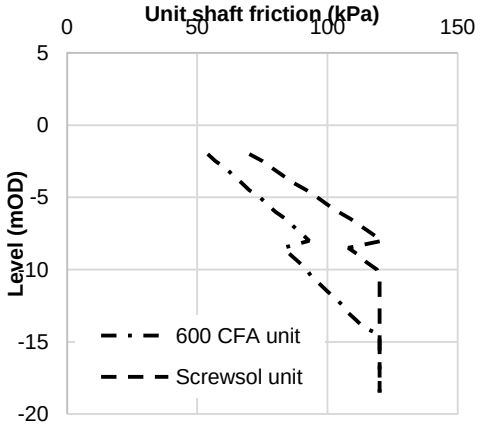


Figure 7. Comparison of unit shaft fiction.

 © DFI International Bruges 2025

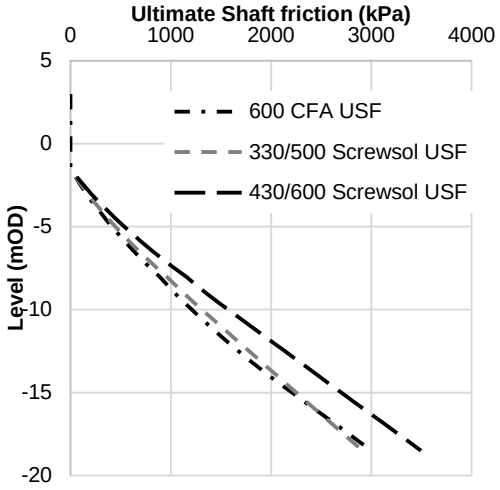


Figure 8. Comparison of total shaft fiction.

ENVIRONMENTAL BENEFITS

The use of the threaded displacement piles has been compared to the traditional CFA ones. This demonstrates significant environmental benefits. The bored displacement pile can be installed without the vibration and noise associated with other driven displacement techniques, which can be a source of problems in urban environments. The use of a displacement technique reduces the spoil for each pile to a negligible level, ensuring less handling of the arisings. The enhanced friction through the use of the threaded pile increases the efficiency of the concrete section, by balancing the geotechnical and structural capacities, which historically has not been the case.

The carbon savings can be classified in two groups: the direct reduction in quantities of concrete, and then the second being the indirect savings such as the reduced numbers of truck movements required, with positive effects on the surrounding non construction traffic movements. In addition, as the soil is displaced rather than extracted, any stored carbon within the soil is left in-situ. In the case of brown field sites where contaminated spoil exists, the use of the Screwsol pile eliminates the requirement to remove and dispose of the contaminated ground.

The savings in quantities can be simply evaluated by considering the volumes of concrete and spoil involved in the Screwsol piles compared to the CFA pile to carry a similar load. For the purposes of the comparison the 1800kN pile will be used, with either a 430/600mm Screwsol pile or a 600mm diameter CFA pile (see Table 4). There is also no spoil to be removed with the use of the Screwsol pile due to the adoption of a displacement technique.

Table 4. Comparison of Screwsol and CFA volumes & lengths – SLS = 1800kN

Pile Type	Diameter mm	Length m	% saving	Volume m^3	% saving
CFA	600	20.30	-	5.74	-
Screwsol	430/600	18.00	11	3.26	43

An assessment of the carbon savings the above volumes represent has been made using the DFI-EFFC Carbon Calculator. This has used a C35/45 grade concrete in the Screwsol piles and a C32/40 grade for the CFA piles. Despite the higher cementitious material in the Screwsol mix ,there is still an indicated saving around 380kgCO2 per pile, which is a saving of approximately 24% of the total impact of the CFA technique.

CONCLUSIONS

The use of threaded displacement piles to replace the traditional CFA piles is a viable option in the granular deposits in central Cork with observed benefits in terms of load carrying capacity. The load-settlement behaviour of the piles is well within the normal industry accepted values, confirming their fitness for purpose. The design approach with an enhanced value of k_s (as is common practice in

 © DFI International Bruges 2025

driven pile design) to model the effect of the thread has been shown to be applicable, with back analysis of the piles justifying this approach.

The implementation of the Screwsol technique offers significant potential environmental savings over standard CFA piles. This is created through the lower carbon impact of the reduced quantities of concrete and spoil used. The more efficient use of the installed section allows more load to be carried in the ground compared to CFA piles. The installation process does not have the negative implications of noise and vibration associated with driven solutions but allows the benefits of a displacement technique in terms of reduced spoil and improvements in the ground properties.

ACKNOWLEDGEMENTS

The authors would like to thank the staff of McDonnell Piling, especially Ian McCarthy and Vinny O Flynn. The work of Adrian Bugea is also acknowledged for his analysis of the results from Screwsol static load tests across Europe, as well as the support from SBR and HBM in providing historical data on pile testing.

REFERENCES

DFI-EFFC Carbon Calculator, 2023, version 5
Kaltenbacher, T., Sata, L. and Deli, Á., The applications of the Screwsol soil displacement piling solution, 2008, Közúti és Mélyépítési Szemle (Roads and Engineering Review) vol.58 nr. 9, Budapest, pp. 34 – 37
L. Sata, S. Manea, The threaded displacement piling system technical and economical efficiency leading to sustainable foundations solutions, 2024, Proceedings of the 18th European Conference on Soil Mechanics and Geotechnical Engineering, Lisbon, pp. 2621 – 2624

 © DFI International Bruges 2025

BEARING CAPACITY OF PILE GROUPS UNDER GENERALIZED LOADING CONDITION

Raffaele Di Laora, Università della Campania 'Luigi Vanvitelli', Aversa, Italy, raffaele.dilaora@unicampania.it
Raffaele Cesaro, Università della Campania 'Luigi Vanvitelli', Aversa, Italy, raffaele.cesaro@unicampania.it
Chiara Iodice, Università della Campania 'Luigi Vanvitelli', Aversa, Italy, chiara.iodice@unicampania.it
Maria Iovino, Università di Napoli 'Parthenope', Napoli, Italy, maria.iovino@uniparthenope.it
Luca de Sanctis, Università di Napoli 'Parthenope', Naples, Italy, luca.desanctis@uniparthenope.it
Alessandro Mandolini, Università della Campania 'Luigi Vanvitelli', Aversa, Italy, alessandro.mandolini@unicampania.it

ABSTRACT

Recently new criteria have been proposed to assess the failure envelopes of the foundation in the force space which are referred to as interaction diagrams. For vertical eccentric loads, these can be constructed using an exact solution based on the theorems of the limit analysis accounting for the direction of the resulting moment vector. In case of horizontal loads, the available approximate solution is derived from the limit equilibrium method and incorporates the dependance of the yielding moment of the pile concrete cross-section from the axial force acting at its head. When compared with conventional criteria, these recent methods offer undeniable advantages in the design of pile foundations. Nevertheless, the interaction between the horizontal and moment components has not yet been properly implemented in routine design and may lead to an overestimation of the collapse load when the sectional moment capacity of the piles is not negligible. To fill this gap, an approach based on the limit equilibrium method to construct the collapse domains in the force space is proposed, in which the interaction mechanisms between the components of the resulting load are fully addressed. An application to the case study of a real pile group is also presented.

Keywords: pile groups, bearing capacity, interaction domains, numerical analyses

INTRODUCTION

Following a standard design approach for pile groups, the vertical capacity is assessed as the combination of axial and moment loads (Q, M) that the foundation can withstand when the axial capacity of the outermost pile is reached (e.g. AASHTO). However, identifying the capacity of the group as that of the single pile neglects the ductility of the system since reaching the axial failure in one pile only marks the beginning of yielding. Although recent codes, including Eurocode 7 and the Italian building code, recognize this conservatism by defining the group failure with reference to the whole foundation, they lack specific design methods. With respect to the pile lateral capacity, this is often evaluated neglecting the dependency of the yielding moment of the pile concrete cross-section on the axial force acting at its head, and treating the horizontal component, H, as if applied alone. It can be therefore stated that current design practice implicitly refers to interaction diagrams like those presented in grey lines in Fig. 1 for the case of 4 equally spaced identical piles.

An exact solution for the failure envelope in the Q-M plane that accounts for the ductility of the foundation system was proposed by Di Laora et al. (2019) using the theorems of limit analysis. Assuming the piles are hinged to the cap, they demonstrated that the moment capacity of the foundation, M_N (solid black lines in Fig. 1), always exceeds the moment capacity of the yielding domain derived using the conventional design approach. Additionally, they showed that an increase in the ultimate moment for a given axial load is possible due to the cross-sectional capacity of the pile heads, M_S, which adds to M_N (dashed black lines in Fig. 1). The vertexes of the failure envelope are defined by closed-form expressions and represent load distributions where all piles in the group achieve their axial capacities N_u (in compression) or S_u (in uplift), which are the only parameters

 © DFI International Bruges 2025

required for the construction of these domains. Note that the equations by Di Laora et al. (2019) are an exact solution for a moment vector perpendicular to an axis of symmetry otherwise they represent an upper bound. For situations where the moment vector does not meet this condition an exact solution based on the theorems of limit analysis was later provided by Cesaro et al. (2024).

Recent works (Iovino et al., 2021; Di Laora et al., 2022; Gorini and Callisto, 2022) have extended the above domain to include the horizontal component by introducing an incremental algorithm for assessing the lateral capacity of the pile group under any combination of (Q, M), in the hypotheses of M_S negligible compared to M_N and postulating a double-hinged failure as for long fixed-head piles (Broms 1964a, 1964b). These studies consistently found that the interaction between H and M is minimal while the lateral capacity is significantly affected by the axial load on the foundation. In the Q_u-H_u plane Di Laora et al. (2022) suggested the use of a linear approximation of the domain (trapezoid shown in Fig. 1) which can be determined by only two additional parameters, the horizontal capacities of the single pile under N_u and S_u. Consequently, the H_u-M_u domain is rectangular.

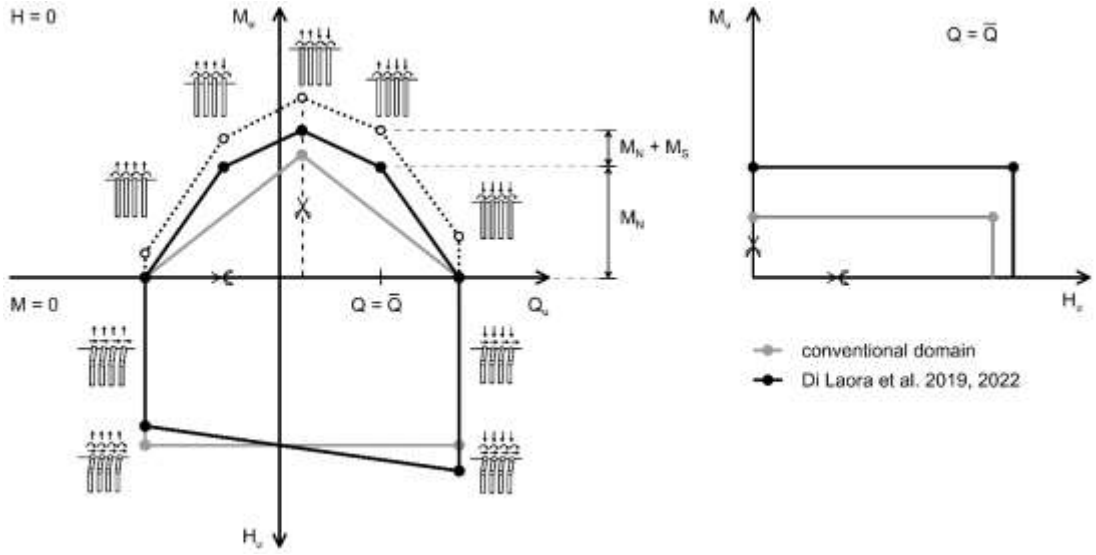


Fig. 1. Comparison between conventional and new criteria for safety assessment of a pile group.

Despite these remarkable achievements, the interaction between H and M when M_S is non-negligible compared to M_N may lead to an overestimation of the collapse load. In this regard, a pioneering effort is found in the work by Sakellariadis and Anastasopoulos (2022, 2024), which however requires a numerical implementation. In this work an approach based on the limit equilibrium method to construct the collapse domains in the force space is proposed in which the H_u-M_u domain of the foundation under any axial load Q is identified by a few points whose coordinates can be easily determined by hand calculation. A straightforward procedure is also proposed to assess the safety of the foundation using a simple plot. A case study of a real scale pile group is also presented to highlight the benefit of the innovative design approach.

PROPOSED INTERACTION DIAGRAM

The interaction diagram in the H_u-M_u plane depicted in Fig. 2 is constructed for a row of 4 equally spaced identical piles, by considering a certain external vertical load upon the group. In particular, the selected Q corresponds to that at which the ultimate moment is maximum, and the load distribution is such that all the piles' heads have achieved M_y with two piles failing in compression (i.e., $N = N_u$) and two in tension (i.e., $N = -S_u$). This situation corresponds to points 1 and 2 on the H_u-M_u interaction diagram under the assigned Q, representing the moment at failure in absence of horizontal load (Fig. 2). The coordinates are (0; $[M_N + \Sigma M_y(N_i)]$) and (0; - $[M_N + \Sigma M_y(N_i)]$) for point 1 and 2, respectively. Note that the sum is extended to the p piles belonging to the group (in this case $p = 4$).

 © DFI International Bruges 2025

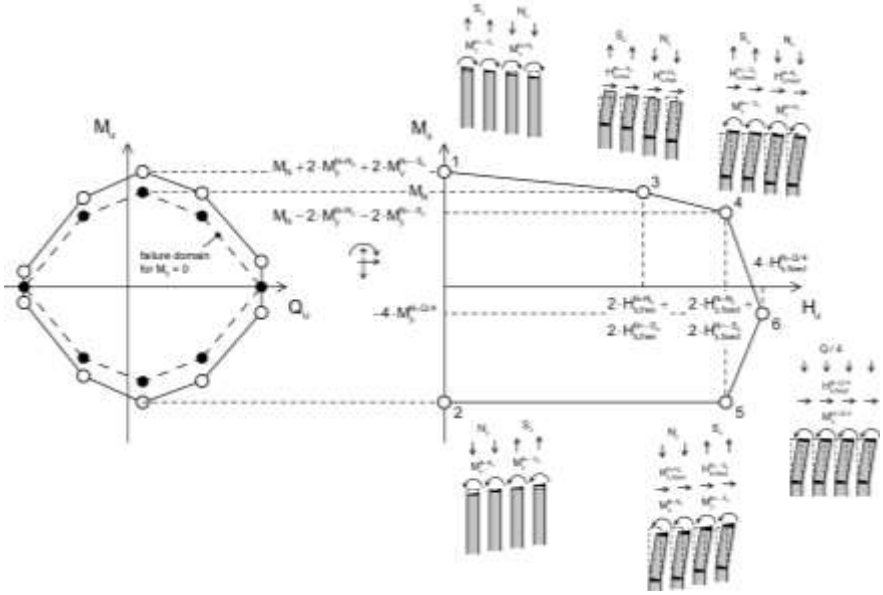


Fig. 2. Construction of the proposed H_u-M_u interaction diagram at failure.

From point 1 the application of a positive horizontal force is possible decreasing the external moment since maintaining it constant would induce a moment larger than M_y along the piles, thus violating the failure criterion of the pile cross-section. A possible load distribution is represented by point 3 in Fig. 2 of coordinates ($\Sigma H_{s,free}(N_i)$; M_N) in which piles have no head moment (as if they are hinged to the cap) and the horizontal bearing capacity corresponds to the free-head condition with no eccentricity and 1 plastic hinge developed at some depth. Nevertheless, failure by a double-hinge mechanism (fixed-head piles) is still possible if a counterclockwise M_y at piles' top is considered. This corresponds to point 4 of coordinates ($\Sigma H_{s,fixed}(N_i)$; $[M_N - \Sigma M_y(N_i)]$). In contrast with point 1, from point 2 the application of a positive horizontal force is possible under same external moment since in this case the moment along the pile decreases with depth until the formation of the second plastic hinge. It follows that, a new point can be detected, point 5, of coordinates ($\Sigma H_{s,fixed}(N_i)$; $-[M_N - \Sigma M_y(N_i)]$).

It is worth noting that the maximum horizontal load the pile group is able to carry for continuously non-homogenous soil is given by point 6 of coordinates ($p \cdot H_{s,fixed}(Q/p)$; $- p \cdot M_y(Q/p)$). This load scenario is possible considering, under the same vertical load Q, a positive horizontal translation applied while imposing zero rotation. In this case, piles are subjected to some vertical load, supposed to be $N = Q/p$ upon each pile, and will fail through a double-hinge mechanism with the same counterclockwise yielding moment $[-M_y(Q/p)]$. In this scenario, the rotational equilibrium is satisfied owing to a negative external moment equal to the sum of pile head yielding moments. Note that when M_S is negligible compared to M_N, the constructed domain reduces to the rectangular domain proposed by Di Laora et al. (2022). The above procedure can be applied for any intermediate value of the external axial load. This way, the 3D domain is obtained connecting the so derived points by straight lines (Fig. 3). For a straightforward application of the proposed domain in the Ultimate Limit State, ULS, design of pile groups, point 6 can be safely neglected (highlighted in red in Fig. 3) and thus the resulting interaction diagrams are obtained by directly connecting points 4 and 5.

 © DFI International Bruges 2025

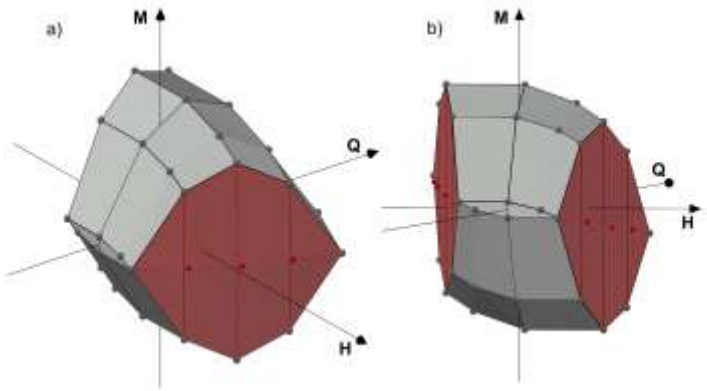


Fig. 3. Proposed 3D failure locus.

IMPLICATION IN DESIGN

Although the proposed framework allows to plot any planar section of the generalized failure surface at a very low computational cost, the safety of the foundation can be still assessed from the plot discussed in Fig. 1 (black continuous lines) by adding only one supplementary condition, provided that, as in most design scenarios, horizontal load and moment have the same sign. For each load combination, the points in the Q_u-M_u and Q_u-H_u planes can be plotted. Points that fall within the blue shaded area of Fig. 4, where $M \leq M_N$ and $H \leq H_{free}$, represent a safe state for the foundation while those located in the yellow zone, with $M_N \leq M \leq M_N + M_S$ and $H_{free} \leq H \leq H_{fixed}$, indicates an unsafe state for the foundation. There might also be points in the green areas, corresponding to (1) $M_N \leq M \leq [M_N + M_S]$ and $H \leq H_{free}$ or (2) $M \leq M_N$ and $H_{free} \leq H \leq H_{fixed}$; under these circumstances it is sufficient to impose the conditions (1) or (2) in Fig. 4.

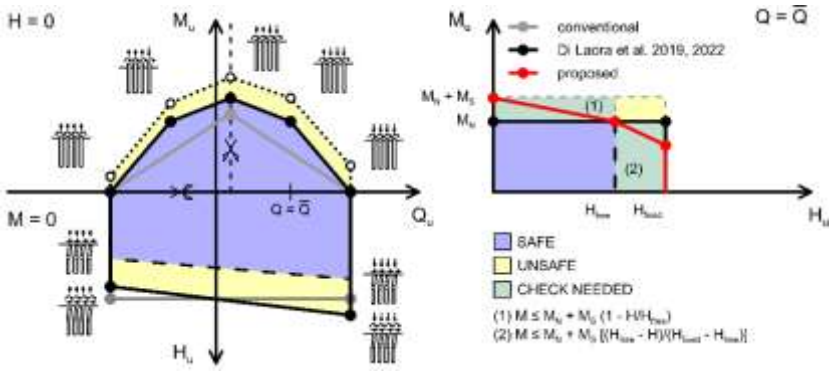


Fig. 4. Simplified design framework for ULS checks.

APPLICATION TO A CASE STUDY

The case study involves doubling a railway section in Italy to enhance passenger and freight transport efficiency along the Adriatic route. This project includes running parallel to an existing line featuring a viaduct built in the early 1990s, originally designed with provisions for future double tracks. Additionally, the project features a new plan-altimetric variant featuring an 1175 m viaduct with 47 spans of prefabricated prestressed reinforced concrete box girders with a 25 m span length between expansion joint axes. Each deck module measures 13.7 m in length. The substructure includes 46 piers with heights varying from 5 m to 7 m. These piers have a pseudo-rectangular 10.40 m x 3.20 m hollow shaft with a solid section cap. The bicellular cross-section maintains 40 cm thick walls, except for a 50 cm thick central web. Each pier's foundation is a 12 m x 12 m rectangular footing supported by nine piles, each 1.5 m in diameter and of varying lengths (Fig. 5). The deck is also supported by one abutment with fixed bearings and one with expansion bearings. The stratigraphy of the area was

 © DFI International Bruges 2025

reconstructed by integrating data from available bibliographic sources and site-specific investigations. Geological surveys conducted in 2001, 2012, and 2017, along with seismic microzonation, provided characterization of the geological and soil conditions. Soil characterization relied on the following methods: Standard Penetration Tests carried out in boreholes, Cone Penetration Tests with pore pressure measurement, laboratory tests on undisturbed and remolded samples, and seismic investigations including Down-Hole, Multi-channel Analysis of Surface Waves and Refraction Microtremor tests.

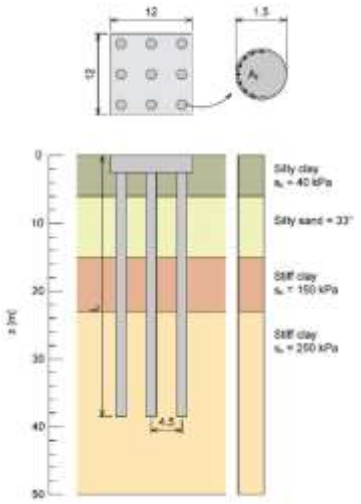


Fig. 5. Soil stratigraphy and foundation system for the considered case study.

This study analyzes a recurring foundation-soil system within the viaduct, as depicted in Figure 5. The design will include evaluations of pile length (L), reinforcement (the number of reinforcement bars, n, and their diameter, Φ) and geotechnical Ultimate Limit State (ULS) verifications using conventional and recent approaches to assess the practicality and economic feasibility of these last methods, considering potential benefits beyond mere rationality. The design adheres to Italian building code Italian building code (NTC 2018 hereafter).

Pile group capacity under vertical and moment loading

In the limit state design framework, the maximum compressive design load that is possible to apply upon pile head, N_{ud}, is obtained as the sum of its base and shaft capacities (P_d and S_d, respectively) and deducting pile weight W_p which represents an action. When subjected to tensile loading, it is assumed that the pile resistance, S_{ud}, is solely due to shaft friction, as the base is lifted away from the underlying soil. The following expressions hold:

$$N_{ud} = P_d + S_d - W_p = \frac{P_k}{\gamma_b} + \frac{S_k}{\gamma_s} - \gamma_F W_p = \frac{1}{\xi_3}\left(\frac{P_{cal}}{\gamma_b} + \frac{S_{cal}}{\gamma_s}\right) - \gamma_F W_p = \frac{1}{\xi_3}\left(\frac{\pi d^2}{4\gamma_b} b + \frac{\pi d}{\gamma_s}\int_0^L s(z)dz\right) - \gamma_F W_p$$

$$S_{ud} = S_d + W_p = \frac{S_k}{\gamma_{st}} + W_p = \frac{S_{u,cal}}{\xi_3 \gamma_{st}} + \gamma_F W_p = \frac{\pi d}{\xi_3 \gamma_{st}}\int_0^L s(z)dz + \gamma_F W_p$$

(1)

Here, W_p is the weight of the pile, b and s(z) are the unit base and shaft strengths, ξ_3 is a correlation factor depending on the number of profiles of tests and is used to determine the characteristic values of base and shaft resistances (P_k and S_k), γ_F is the partial safety factors on actions, and γ_b, γ_s and γ_{st} are partial factors for pile base and shaft capacities.

Unit shaft resistance is calculated as:

 © DFI International Bruges 2025

$$s = \begin{cases} \alpha s_u & (\text{layers } 1, 3, 4) \\ k\sigma'_v \tan\varphi' & (\text{layer } 2) \end{cases}$$

(2)

where α is a coefficient depending on the pile installation technique and the undrained shear strength, s_u, k is the horizontal earth pressure coefficient, σ'_v is the effective overburden stress at the depth under consideration and φ' is the soil friction angle. For values of $s_u \leq 150$ kPa, α can be assumed as 0.55, whereas for $s_u \geq 250$ kPa, α can be set to 0.45, according to O'Neill & Reese (1999). For large-diameter bored piles, the parameter k can be taken equal to 0.7, as recommended by Viggiani (1993).

Unit base strength is evaluated in undrained conditions in terms of total stress through the following equation:

$$b = N_c s_u + \sigma_{vL}$$

(3)

where σ_{vL} is the total overburden stress at the depth L of the pile base and N_c is a bearing capacity factor, which can be set to be 9 (Skempton 1951).

Design approach 2 of the Italian building code, along with the partial factors from the Italian national annex ($\gamma_F = 1.30$, $\gamma_b = 1.35$, $\gamma_s = 1.15$, $\gamma_{st} = 1.25$, $\xi_3 = 1.40$), was employed to calculate the values of N_{ud} and S_{ud} for three different pile lengths: L = 36, 29 and 31 m, as detailed in Table 1. A group efficiency factor under vertical compressive loads, η, of 0.9 has been considered.

Table 1. Pile group resistance under compressive and tensile loads.

L [m]	P_{cal} [MN]	S_{cal} [MN]	W_p [MN]	N_{ud} [MN]	S_{ud} [MN]
36	5.28	13.94	1.59	8.72	9.55
29	5.04	10.22	1.28	6.84	7.12
31	5.11	11.29	1.32	7.42	7.77

It can be shown that a length of 36 m is necessary according to the conventional approach, while a reduction in length of about 20%, i.e. L = 29 m suffices to satisfy ULS checks for the proposed design framework (Fig. 6a). Note if the additional strength supplied by yielding moments at the top of piles is considered, the same design action is well within the boundary of the domain accounting for the extra capacity offered by the sectional strength.

Pile group capacity under vertical and horizontal loading

To assess the horizontal load-bearing capacity of piles, Broms (1964a) proposed a widely used theory in routine design, assuming rigid-plastic behavior for both pile and soil. The maximum lateral load a pile can withstand occurs when the soil yields around it. In soil with constant undrained shear strength, Fleming et al. (2009) provided a generalized relationship for ultimate lateral pressure, p_l, increasing linearly from $2s_u$ at the surface to $11s_u$ below a depth of $3d$. In cohesionless soil, p_l increases linearly with depth and can be approximated as $p_l = 3k_p\gamma\sigma'_v$ (Broms 1964a), where k_p is the passive earth pressure coefficient and γ the soil unit weight. The calculation of the geotechnical horizontal load-bearing capacity also involves the selection of an appropriate cross-sectional size that meets the moment capacity requirement. In concrete piles, this includes detailing the reinforcing steel.

In the limit state design framework, safety is defined by a coefficient, γ_T, which applies to the lateral resistance of the pile, H_{sd}, without any factors on the material resistances (concrete and soil):

 © DFI International Bruges 2025

$$H_{\mathrm{sd}} = \frac{H_{\mathrm{sk}}}{\gamma_T} = \frac{H_{\mathrm{s,cal}}\left(d, p_l, M_y\right)}{\xi_3 \gamma_T}$$

(4)

In standard practice, it is presumed that fixed-head piles, except those with extremely low slenderness ratios, fail in the 'long' mode. This involves the formation of two plastic hinges: one at the head and another at a depth of approximately 5 to 10 pile diameters, where the bending moment reaches its maximum capacity M_y (= moment capacity of the pile) and shear force is zero. Here, the horizontal capacity of the pile, H_{sd}, depends on pile diameter d, soil resistance p_l and M_y. This moment is usually calculated for a zero axial load at the pile head, despite being affected by this load. Instead of this approach, Di Laora et al. (2022) proposed using a trapezoidal shape for the interaction domain in the (Q, H) plane, which is easily determined by assessing the horizontal capacity of the foundation for a scenario where all piles in the group are subjected to N_{ud} or S_{ud}. The relationship between M_y and N_{ud} or S_{ud} can be easily accounted for by utilizing the closed-form expression proposed by Di Laora et al. (2020) for axial force-moment interaction diagrams of circular reinforced concrete cross-sections.

Design approach 2 of the Italian building code, along with the partial factors from the Italian national annex (γ_T = 1.30, ξ_3 = 1.40), was employed to design the reinforcing steel (the number of reinforcement bars, n, and their diameter, Φ) for the considered pile group configurations, with L = 36, 29 and 31 m, as detailed in Table 2. The table also includes the bearing capacities of the group, $H_{\text{cd-fixed}}$, $H_{\text{cd-free}}$ and $H_{\text{td,fixed}}$, $H_{\text{cd-free}}$ (considering a group efficiency factor, η, of 0.9) for the scenario where all piles are subjected to N_{ud} or S_{ud}, respectively.

In the case of L = 36 m (conventional approach in Table 2), the ULS checks for horizontal loads are satisfied using a steel reinforcement of 54 Φ 28 (Fig. 6b). From Figure 6b it can be noted that ULS checks are still fulfilled if pile length and reinforcement are reduced to L = 29 m and 36 Φ 28 (Solution 1 in Table 2), respectively, since in this case the design action falls within the domain by Di Laora et al. (2022), in which the interaction between H and M is neglected. Nevertheless, this design action is out of the proposed domain (red line in Fig. 6b); in particular, it falls in the green zone (2) of Figure 4. A possible design solution (Solution 2 in Table 2) is to select L = 31 m with a steel reinforcement of 48 Φ 28 (Fig. 7b).
Although the simplified method by Di Laora et al. (2022) represents a significant advancement over the conventional approach, in circumstances lying beyond the declared range of applicability of the method (i.e. when yielding moments' contribution to the overall moment capacity is not negligible compared to the moment coming from axial forces), it may lead to an overestimation of the foundation bearing capacity due to the unfavorable interaction between H and M components.

Table 2. Pile group resistance under lateral loads.

Approach	L [m]	n	Φ [mm]	N [MN]	$H_{\text{cd-fixed}}$ [MN]	$H_{\text{cd-free}}$ [MN]	$H_{\text{td-fixed}}$ [MN]	$H_{\text{td-free}}$ [MN]
Conventional	36	54	28	0	14.01	–	14.01	–
Solution 1	29	36	28	S_{ud} N_{ud}	16.01	9.52	5.45	3.19
Solution 2	31	48	28	S_{ud} N_{ud}	18.34	10.90	8.48	5

 © DFI International Bruges 2025

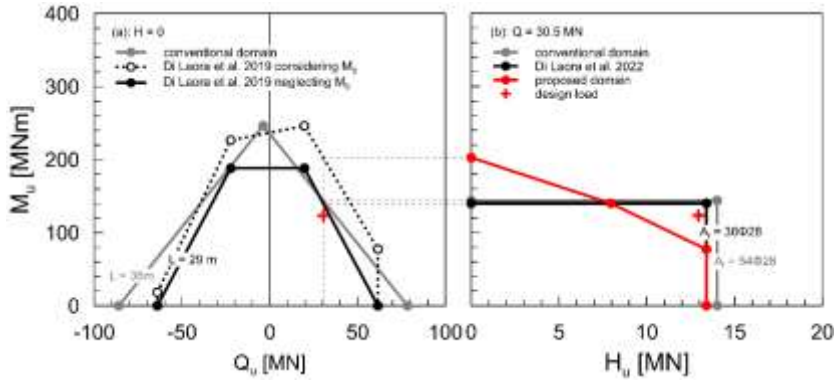


Fig. 6. Conventional and innovative design approaches for Solution 1.

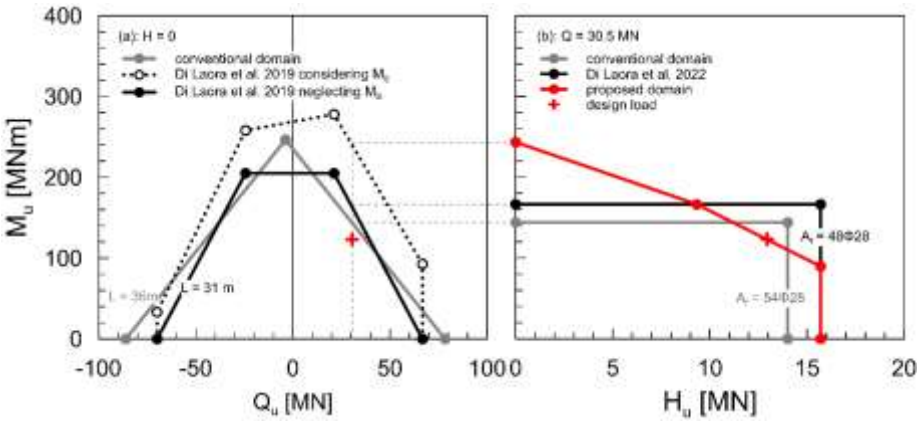


Fig. 7. Conventional and innovative design approaches for Solution 2.

CONCLUSIONS

A new approach for the evaluation of the interaction domain in the horizontal load – moment plane has been proposed by considering the interaction between the horizontal and moment forces acting on the pile group when the moment capacity of the concrete cross-section of piles is not negligible compared to the moment generated by the axial loads at pile heads. The approach is based on limit equilibrium and requires only the coordinates of 6 points in the H-M plane. These are function of the axial and horizontal capacity of the piles in compression and uplift, and of the cross-sectional yielding moments. These quantities are already required in routine design and can be simply derived by hand calculation.

The application of the proposed approach in the ULS design of pile groups is straightforward. Neverthelss, a simple procedure is presented allowing for ULS check by plotting only the *Q*-*M* domain for $H = 0$ and the *Q*-*H* domain for $M = 0$.

An application of the proposed framework to the case study of a real pile group is presented. It is shown that a reduction of the pile length or steel reinforcement (or a combination of the two) is possible, confirming that a more rational approach, considering the ductility of the system and the interaction between the load components in a proper manner, helps avoiding the conservativims inherent in the conventional design.

References

AASHTO, 2012. AASHTO guide specifications for LRFD seismic bridge design, 2nd edn. American Association of State Highway and Transportation Officials, Washington, D.C.

 © DFI International Bruges 2025

Broms, B. B., 1964a. Lateral resistance of piles in cohesive soils. Journal of the soil mechanics and foundations division, 90(2), 27-63.

Broms, B. B., 1964b. Lateral resistance of piles in cohesionless soils. Journal of the soil mechanics and foundations division, 90(3), 123-156.

CEN, 2003. (pr)EN 1997-1. Eurocode 7: geotechnical design—part I: general rules. European Committee for Standardization Technical Committee 250, Brussels, Belgium.

Cesaro, R., Di Laora, R., Iodice, C. and Mandolini, A., 2024. Interaction domains for capacity- and performance-based design of pile groups. Acta Geotech.

Di Laora, R., de Sanctis, L. and Aversa, S., 2019. Bearing capacity of pile groups under vertical eccentric load. Acta Geotech. 14 (1), 193–205.

Di Laora, R., Galasso, C., Mylonakis, G., and Cosenza, E., 2020. A simple method for N-M interaction diagrams of circular reinforced concrete cross sections. Struct Concr 21(1):48-55.

Di Laora, R., Iodice, C. and Mandolini A., 2022. A closed-form solution for the failure interaction diagrams of pile groups subjected to inclined eccentric load. Acta Geotech. 17, 3633–3646.

Fleming, K., Weltman, A., Randolph, M., and Elson, K., 2009. Piling engineering. CRC press.

Gorini, D. N. and Callisto L., 2022. Generalised ultimate loads for pile groups. Acta Geotech. 17, 2495–2516.

Iovino, M., Maiorano, R. M. S., de Sanctis, L. and Aversa S. (2021). Failure envelopes of pile groups under inclined and eccentric load. Géotech. Lett. 11, No. 4, 247–253.

NTC 2018. Norme Tecniche per le Costruzioni - Decreto Ministeriale 17-01-18.

O'neill, M. W., and Reese, L. C., 1999. Drilled shafts: Construction procedures and design methods, Publication No. FHWA-IF-99-025, Federal Highway Administration, Washington, DC, 758 p.

Sakellariadis, L. and Anastasopoulos I., 2022. On the mechanisms governing the response of pile groups under combined VHM loading. Géotechnique.

Sakellariadis, L. and Anastasopoulos, I., 2024. Analytical 3D failure envelopes for RC pile groups under combined loading: A generalised design approach. Soil Dynamics and Earthquake Engineering, Vol. 181.

Skempton, A. W., 1951. The bearing capacity of clays. Selected papers on soil mechanics, 50-59.

Viggiani, C., 1993. Fondazioni. Cooperativa Universitaria Editrice Napoletana.

 © DFI International Bruges 2025

THE EFFC/DFI SUPPORT FLUID TASK GROUP FIELD RESEARCH STUDY

Christophe Justino, Soletanche Bachy International, France, Support fluid Task Group Chair,
+33607227439, christophe.justino@soletanche-bachy.com

Chris Harnan, Ceecom Geotech Limited, UK, Support fluid Task Group Chair
+447720444713, chris.harnan@ceecom-geotech.com

ABSTRACT

The European Federation of Foundation Contractors (EFFC) and the Deep Foundations Institute (DFI) Support Fluid Task Group developed a field research study (FRS) with the aim of enhancing industry knowledge and good practice on the support fluid management in geotechnical works. The FRS and associated academic research commenced in 2020 and is still ongoing. The FRS covers a large range of deep foundation elements from piles to diaphragm walls excavated under either bentonite-based support fluid or polymer-based support fluid at depths greater than 30 m and in different ground conditions. The Paper presents analysis and findings on different aspects of the support fluid management. The Paper focuses on fluid samplers' performance, support fluid monitoring, relevance of standard and non-standard testing, base quality evaluation, interaction between support fluid and concrete, sustainability and environmental considerations. New features and key topics to be addressed in Edition 2 of the "EFFC/DFI Guide to Support Fluids for Deep Foundations" are also discussed in the Paper.

Keywords: Support fluids, site testing, bentonite, polymers

INTRODUCTION

The European Federation of Foundation Contractors (EFFC) and The Deep Foundations Institute (DFI) have set up a Task Group to compile a Support Fluid Guide for Deep Foundations. The First Edition of this Guide was published in April 2019. The aim of the Guide is to improve existing support fluid design, testing and practices for deep foundation elements (drilled shafts or piles, load bearing elements and diaphragm wall panels). This Guide has identified areas of support fluid performance where research and development will benefit the industry. Before the Second Edition of the Guide can be published it was proposed to carry out an extensive Field Research Study (FRS) which is being funded by EFFC, DFI, contractors, consultants and suppliers.

The Field Research study program was developed by the working group to improve the industry understanding of support fluid interaction with ground, excavation methodology and concrete. A detailed method statement presents the content of the field research study. FRS program and first findings were previously presented. As program is reaching completion, this paper gives an update of the results obtained. This paper focuses on presenting sites details, describing the specific test and preliminary analysis of the results. A discussion is proposed on how these results can be used as guidance for the industry.

SCOPE OF THE FRS

The field research study covers a full range of special foundation works. 17 sites across Europe and the US have been selected to develop testing at different stages of deep foundation element construction. Sites selection allowed to cover piles excavated with auger and buckets, diaphragm wall excavated with grab and cutter (hydromill) where either bentonite or polymer support formed part of the support fluid mix design.

 © DFI International Bruges 2025

Figure 1 presents the different stages of a deep foundation element construction that are involved in the testing program. The testing program is divided in six sections covering the production of support fluid (focus on materials), the monitoring of support fluid during excavation, the quality of the base at end of excavation and support fluid desanding, the quality of the base before concreting, the concreting process and the sampling of the interface layer near the concrete cut-off level at the end of the cast-in place.

The first stage (A) of the program is the batching of the support fluid. Fresh fluid mixing procedure and equipment were recorded. Incoming water quality was tested for pH, electrical conductivity, total dissolved salts and hardness. Fresh fluid properties including density (measured following ISO 10414-1 procedure and alternative method with electronic scale and volume calibrated jar), Marsh Viscosity, API filter volume and cake, pH and additional test described below were measured.

Additional test selected for the FRS are listed below:

- Apparent viscosity, plastic viscosity and yield value according to ISO 10414-1
- Shear strength Ball Harp test according to DIN 4126
- Electrical conductivity and Total dissolved salts (TDS)
- Total solid content (derived method from sand content test) for polymer fluid only

During the second stage (B) of the program, support fluid in the trench was sampled at different depth, after the excavation process (of a pile, barrette, panel or bite – primary or secondary in case of multi bites panel) was near completion (circa 2 meters above base design depth). When excavation (pile, barrette, panel or bite - primary or secondary in case of multi bites panel) is about 2 meters above design depth, site specialist will proceed with a series of tests involving lowering in the excavation monitoring equipment and fluid samplers. A reference sampler was used (3-part sampler) for the fluid properties profile over depth. Alternative samplers were used at a single depth to compare fluid properties (Marsh viscosity, density and sand content) from different samplers' setup.

The third stage (C) started after standard desanding and base cleaning procedure. The fourth stage (D) started after cage installation. At those stages, a sample of support fluid was obtained from 50 cm above the base and whenever possible an inspection of the base debris and sediment was done with DID and base hardness test. It was initially the objective to monitor base debris over time, but this part of the program revealed difficult to implement in the sites' conditions.

The fifth stage (E) covered the concrete placement. During the pour, concrete level measurements were taken before and after breaking the tremie at one break approximately at mid pour. Several concrete depth probes were tested to compare and assess if this empirical concrete sounded was reliable or should be improved compared.

At the end of the pour, special tools were used to investigate the interface layer between fresh fluid, contaminated blend of support fluid and concrete and sound concrete (stage F)

 © DFI International Bruges 2025

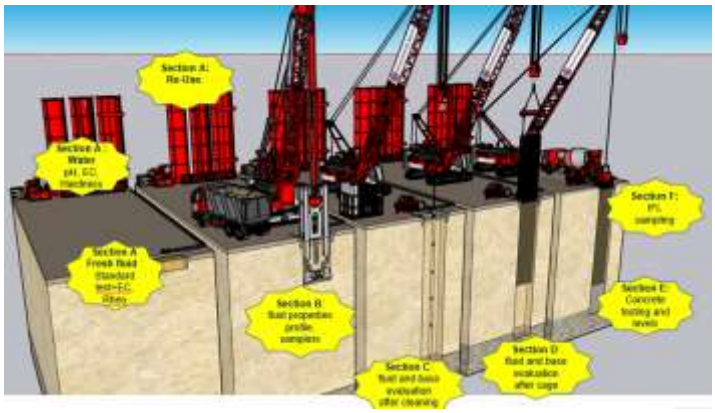


Figure 1: Typical layout of the Diaphragm wall project and FRS program stages

SITES DETAILS AND METHODS

Sites details are presented in table 1. Deep foundation element type, support fluid type, depth and ground conditions were the defined criteria to select the sites. It was intended to have both piles and diaphragm wall at depth greater than 25 m with bentonite and polymer support fluid. For each site bentonite and polymer materials were sampled. Except EU6, where a natural modified polymer was used, all sites, where the chosen support fluid type was polymer, were using partially hydrolysed polyacrylamide (HPAM) also referred in the article as synthetic polymer, long chain polymers or PHPA. For Diaphragm wall elements width ranged from 0,90 m to 1,5 m. Piles diameter ranged from 0,90 m to 3,05 m. Ground conditions were mainly fine sand, silty sand and clay, except for EU7 consisting in sand and gravel.

Table 1 : Site main details

Site reference	Support fluid	Depth m	Depth ft	Volume m^3	Volume yd^3	Excavation Method	Main soil types
Diaphragm Walls							
EU2	Bentonite	32	105	290	380	Grab	Fine sand
EU7	Bentonite	40	130	270	350	Grab	Sand & Gravel
EU9	Bentonite	27,5	90	190	250	Grab	Sand
US1	Bentonite	30	100	240	315	Grab & Hydromill	Sand & Silty Sand
US3	Bentonite	48	158	300	390	Hydromill	Clay & Sand
US4	Bentonite	40	130	340	450	Grab & Hydromill	Silts & Shale
US6	Polymer (Natural modified)	50	170	300	390	Grab & Hydromill	Clay & Sand
Bored Piles							
EU1	Bentonite	70	230	180	235	Bucket & Auger	Clay
EU3	Polymer (HPAM)	35 - 45	115 - 150	80	105	Bucket & Auger	Clay & Fine Sands
EU4	Polymer (HPAM)	45	150	115	150	Bucket & Auger	Clay & Sand
EU5	Polymer (HPAM)	35 - 50	115 - 165	30 - 45	52 - 59	Bucket & Auger	Sand & Silty Sand
EU6	Polymer (HPAM)	53	175	150	196	Bucket & Auger	Sand & Soft Clay
EU8	Bentonite	75	245	180	235	Bucket & Auger	Sand & Clay
US2	Bentonite	30	100	220	290	Bucket & Auger	Clay & Sand
US5	Polymer (HPAM)	50	170	350	460	Bucket & Auger	Clay & Sand
US7	Polymer (HPAM)	28	90	50	65	Bucket & Auger	Clayey Silt
US8	Polymer (HPAM)	55	175	230	300	Bucket & Auger	Clay & Silt

pH, electrical conductivity and total dissolved salts were measured with HI98130 pH & EC combo meter from Hanna Instruments calibrated before each site for pH and electrical conductivity. Calcium hardness was measured with Simplex strips (ppm of $CaCO_3$) and Baroid strips (ppm of Ca). Marsh viscosities were measured using a Marsh Funnel in conformity with API 13B and ISO 10414-1 and calibrated with water to 26 +/- 0,5 s. Unit weight or density were measured with a mud balance calibrated with water to 1 +/- 0,01 g/cm^3. An alternative method was implemented to measure density by means of an electronic scale with reading at 0,01 g and spring bottles with a volume capacity between 1 and 2 liters (calibration with water to 1 +/- 0,005 g/cm^3). Plastic, apparent viscosity, yield value and gel strength were measured using a Fann Viscosimeter model 35SA in accordance with API 13 and ISO 10414-1.

 © DFI International Bruges 2025

Different samplers device were investigated based on market availability however 3-part sampler was considered to allow the most representative samples and used to recover samples every 5 m for elements depth lower than 30 m and every 10 m for elements depth lower than 75 m. Support fluid properties were tested right after sampling whenever possible or at later stage after being stored in sealed containers. All support fluid testing were done on stirred samples. Comparison between samplers was only done for samples taken at the base of the excavation.

Base inspection was done with Ding Inspection Device (DID) where possible and compared to base hardness test and site weighted tape evaluation of the base depth.

Figure 2, Figure 3 and Figure 4 shows the concrete level probes used to evaluate reliability of the concrete level measurement during the casting of the elements.



Figure 2: Rebar weighted tape



Figure 3: Plastic bottled filled with tremie concrete.



Figure 4: Teardrop shape probe (large teardrop on the left / cover zone teardrop on the right)

MAIN RESULTS AND DISCUSSIONS

Samplers' comparison

In order to allow comparison, the 3-part sampler was assumed to give the most representation sample. The properties of the 3-part samples were therefore compared with the properties of other samplers at similar depths. A designed "heavy" 3-part sampler was used for EU1 to EU5, to ensure penetration in dense fluid and in the interface layer. Given the practical difficulties of using "heavy 3-part sampler, requiring an electric winch mounted on a lift frame, a lighter 3-part sampler was used on EU6 to EU9.

 © DFI International Bruges 2025

Reliability of the sample taken with the 3-part sampler was assessed during EU9 site and results are displayed in table 2 and table 3.

Table 2 : Marsh viscosity: mean, standard deviation and coefficient of variation of the three-part sampler for a bentonite support fluid sampled three times at same location and depth (13 m) by three different operators.

Property	Marsh Viscosity					
Operator	Sample 1	Sample 2	Sample 3	Mean	Std deviation	CV
1	43,4	44,6	45,3	44,4	1,0	2,2%
2	44,1	44,3	44,3	44,2	0,1	0,3%
3	44,3	44,8	45	44,7	0,4	0,8%

Table 3 : Density: mean, standard deviation and coefficient of variation of the three-part sampler for a bentonite support fluid sampled three times at same location and depth (13 m) by three different operators.

Property	Density (electronic scale)					
Operator	Sample 1	Sample 2	Sample 3	Mean	Std deviation	CV
1	1,198	1,191	1,195	1,195	0,004	0,3%
2	1,196	1,196	1,185	1,192	0,006	0,5%
3	1,200	1,186	1,188	1,191	0,008	0,6%

The results obtained from this reliability test are within the variability of the Marsh Funnel Viscosity that was evaluated in a laboratory by one single operator for 11 repetition of the test (see table 4) on a bentonite support fluid, and within the precision of the scale for density.

Table 4 : Repeatability test on a bentonite support fluid taken from a site and tested by a single operator for 11 times (fresh density = 1,03 / Excavation = 1,33 / Ready for reuse = 1,11)

Property	Marsh Viscosity		
Testing n°	Fresh fluid	Excavation fluid	Ready for reuse
1	35,32	45,84	35,63
2	34,78	44,94	35
3	34,47	45	34,92
4	34,97	44,13	34,64
5	34,34	43,19	34,31
6	35,32	43	35,28
7	34,37	44	34,72
8	34,47	43,47	34,22
9	34,43	42,75	34,6
10	34,39	41,97	35,21
11	34,35	43,06	34,75
Mean	34,66	43,76	34,84
Std deviation	0,38	1,15	0,42
CV	1,10%	2,62%	1,21%

The overall trend is that most of the values measured on samples obtained with the three-part sampler are similar or higher compared to the other samplers. Highest variations were observed on samples showing extreme values compared to standard acceptance value as it shows on figure 5 for bentonite support fluid, with more variation between samplers with increasing density (above 1,25) and

 © DFI International Bruges 2025

viscosity (above 50 s). Polymer fluid data seemed to be influence by the high viscosity of some fluid samples as observed on table 5 and figure 7.

Table 5 : Repeatability test on a PHPA polymer support fluid taken from a site and tested by a single operator for 10 times.

Testing n°	1	2	3	4	5	6	7	8	9	10
	74,83	69,16	71,28	64,78	64,06	64,67	63,09	60,01	60,47	60,13
Property			**Mean**	65,25						
Marsh Viscosity			**Std dev**	5,02						
HPAM Fresh fluid			**CV**	7,69%						

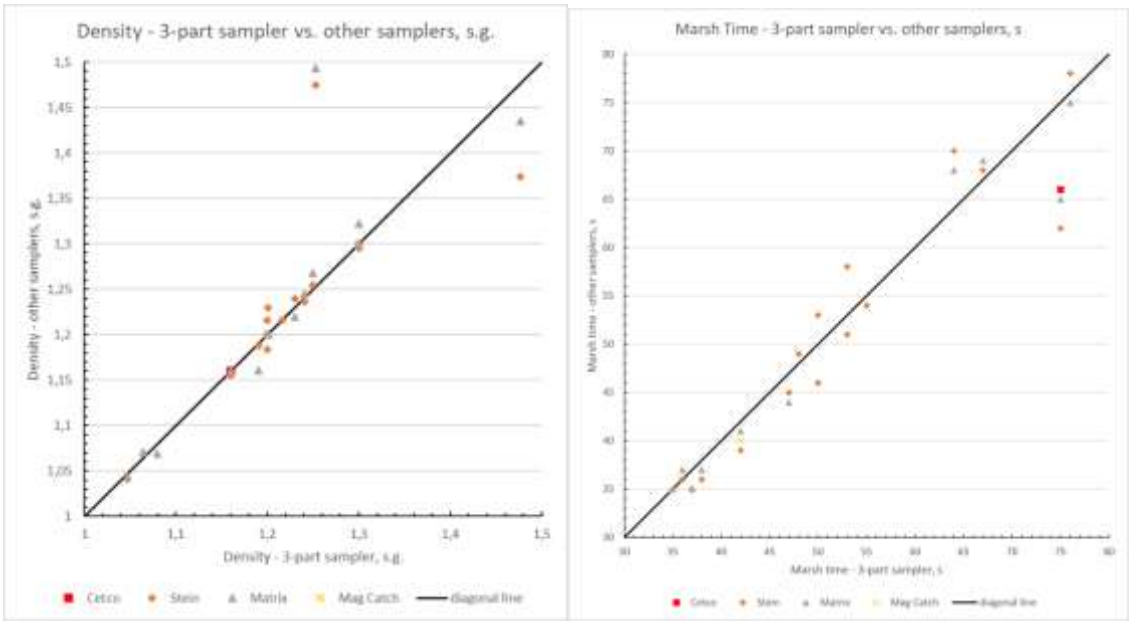


Figure 5: Bentonite support fluid sites

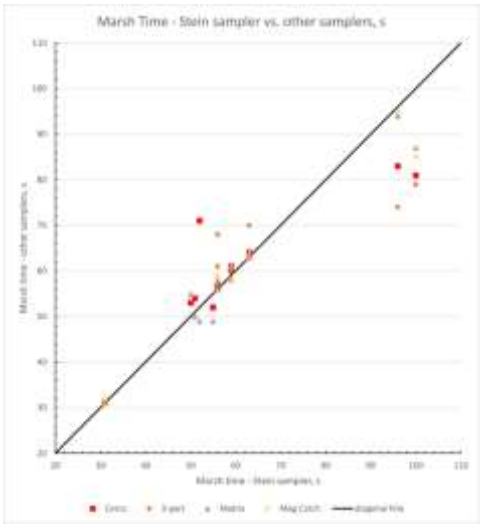


Figure 6: Polymer support fluid sites

Support fluid monitoring

Support fluid characteristics over depth from all sites were obtained, giving a wide range of densities, Marsh Viscosity and sand content values depending on support fluid type, excavation method and

 © DFI International Bruges 2025

ground conditions as illustrated in figure 7 and 8. For example, with bentonite support fluids, higher fluid densities were obtained in sand dominated soils excavated with a grab and in clayey soils excavated with a cutter. On the other hand, PHPA support fluids are predominantly working with Marsh viscosities above 60 seconds in piling or D-Wall with grab and maintaining lower densities compared to bentonite fluid system. This was found to be validated for PHPA polymer considered as soil dispersion inhibitors but not in the case of US6 where a natural modified polymer was used as main component of the support fluid mix design.

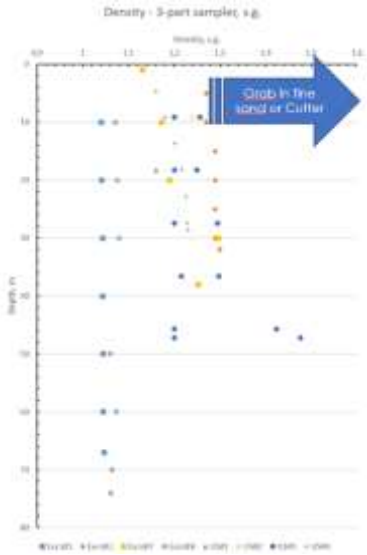


Figure 7: density profile with depth for bentonite support fluid

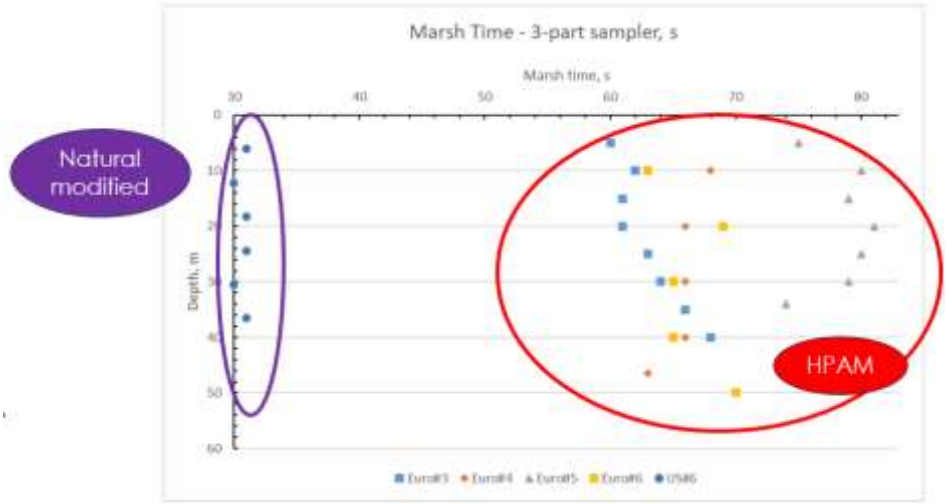


Figure 8: density profile with depth for polymer support fluid

Nonstandard test

Density measured by mean of an electronic scale offers higher accuracy on the results compared to mud balance which could be found useful for PHPA support fluid.

 © DFI International Bruges 2025

Measurement of apparent viscosity for bentonite support fluid ranged from 7,5 to 37,5 mPa.s for Marsh Viscosity ranging from 30 to 76 s and for polymer support fluid ranged from 10 to 70 mPa.s for Marsh Viscosity ranging from 31 to 87 s.

Measurement of electrical conductivity showed good correlation with total dissolved salt content and no direct correlation with support fluid density as shown in figure 9.

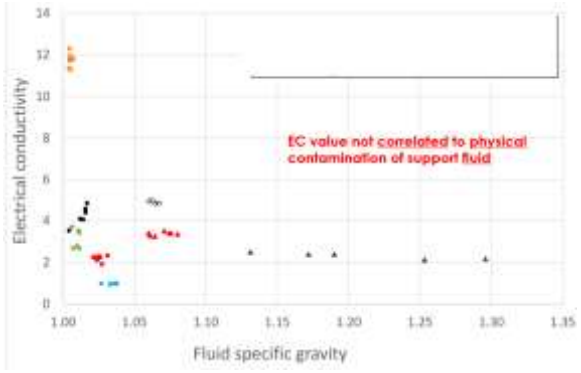


Figure 9: Electrical conductivity from different sites measurement on support fluid compared to fluid density.

Total solid content measured on polymer support fluid was measured as well as sand content. Results showed no direct correlation between total solid content and sand content nor when comparing total solid content to estimated solid volume calculated from density measurement.

Base evaluation and interface layer (IFL)

Although base evaluation was not easy to assess on all sites. Results obtained allow to draft preliminary findings linking the base sediment value measured by DID device to base hardness test. As an example, sediment thickness of 60 mm to 180 mm were classified as grade 3 to 4.

Sampling of interface layer was also challenging, and the sampling methodology was improved during the FRS testing phase. IFL was successfully sampled at EU2 with the “heavy 3-part sampler”. Results are presented in table 6.

Table 6 : description of the interface layers

Sample	Photo	Physical parameters	Description
Euro 2 # (1)		density 1,11 Cohesion 0,26 kPa w% 480%	Low consistence structured mud)
Euro 2 # (2)		d 1,16 Cohesion 20 kPa	compact mud (trace gravel and cement)
Euro 2# (3)		d 1,46	Hydrated grout (green color typical of GGBS) too weak to obtain core sample
Euro 2#(4)		d 1,88 UCS ~ 16 MPa	Segregated concrete (only mortar phase remaining)
Euro 2#(5)		d 2,25 UCS ~ 47 Mpa	Concrete

 © DFI International Bruges 2025

PERSPECTIVE AND CONCLUSION

This paper presents a part of the main results obtained during the FRS. It is expected that the EFFC/DFI Support fluid will improve edition 2 of the Support fluid guide based on findings from this study. This paper does not present academic works that is also followed by the support fluid task group.

Among, the main findings that will bring value to second edition, the sampler comparison will serve to provide further guidance and procedure for fluid sampler use. 3-part sampler, heavy sampler like Stein and flap sampler are more suited for bentonite support fluid. Lighter samplers like the CETCO and Magnetic catch will be more suited to PHPA support fluid. All samplers (except the heavy 3-part sampler) are losing on reliability with fluid density above 1,25 which is the limit recommended for reuse of bentonite support fluid.

Monitoring of bentonite support fluid showed a good agreement in general with accepted values in European execution standard whereas for polymer PHPA, the data showed more scattered value but generally in the range of 60 s up to 190 s for fresh fluid showing that lower bound of the ACI and FHWA specs could be considered low compared to field experience whereas ICE SPERW specifies higher requirement than what was observed in practice. Analysing further these data could help in a proposal for acceptance value for polymer support fluids based on PHPA chemistry or considered as soil dispersion inhibiting polymers.

In the non-standard suit of test implemented in the FRS, it appeared useful to use electrical conductivity to assess both batching water quality and support fluid chemical contamination by salts in addition to pH measurement. Testing rheology didn't appear as improvement to routine QA/QC testing realized with Marsh Funnel however it could be interesting to keep those tests for specific case, for example when troubleshooting process is necessary to solve issues with support fluid performance.

Interface layer was successfully sampled and analysed on one site. Visual evaluation of the IFL was suggesting that IFL was generally showing a gradient profile from pure support fluid, contaminated support fluid with cement and fines, grout, segregated concrete to sound concrete. Results from EU2 IFL samples tended to confirm this assumption.

There is still data to review to finalize the FRS conclusions. It is expected that results from FRS and academic research (not discussed in this paper) will contribute to upgrade edition 2 in improving the support fluid flow mechanism comprehension, giving guidance on support fluid routine controls and specific test to be implemented in preparation of a project. Section 5 of the support fluid guide will also be improved based on the findings of the FRS with improved guidance on the different steps of the execution, as an example, it appears important to insist on base cleaning procedures. The FRS was also the opportunity to demonstrate how important it is to acquire relevant data from support fluid properties which can only happen if projects allow sufficient budget for the site laboratory equipment and facility as well in the training of plant foremen.

The authors want to acknowledge the special contributions of Pr. Stephen Jeffries, Duncan Nicholson, and all the members of EFFC/DFI Support fluid task group.

REFERENCES

Joint EFFC/DFI Support fluid task group, 2019. Guide to support fluids for deep foundations edition 1

Justino, C., Harnan, C., 2022. The EFFC/DFI guide to support fluids for deep foundations, Proceedings of the DFI EFFC International conference on deep foundations and ground improvement: Smart construction for the future, Berlin.

Ding, J.Z. and al. 2015. New device for measuring drilled shaft bottom sediment thickness, DFI Journal of the Deep Foundation Institute, 9(1):42-47

 © DFI International Bruges 2025

EVALUATION OF SLUMP FLOW AND SLUMP FLOW VELOCITY TEST METHOD FOR DEEP FOUNDATION CONCRETE

Christophe Justino, Soletanche Bachy International, France,
+33607227439, christophe.justino@soletanche-bachy.com

ABSTRACT

Specifications for concrete in deep foundations have evolved toward an increase in durability and strength requirements demanding lowering water / cement ratios. This evolution is leading to mix designs with rheological properties controlled by admixture chemistry. Simultaneously, concrete mix designs optimised to reduce carbon footprint are following the same pattern. Consistency test methods are not always adapted to characterise the fluid consistency of concrete mixes that are not designed to be true self-compacting concrete. The EFFC/DFI Guide to tremie concrete recommends slump flow in the range of 400 to 550 mm and slump flow velocity as the most suitable test method to characterise concrete workability. NF EN 12350-8 for Europe and ASTM C1611 in North America do not provide precision and bias for these test parameters. Slump flow velocity has no standard test method to help in specifying on projects. The authors find that there is a standard gap in the use of slump flow test method in the recommended range of the EFFC/DFI guide with the limitation expressed in the EN 206 concrete standard. This paper presents results of a different method to evaluate slump flow with repeatability tests measured with invert Abrams cone according to the NF P18-469 standard and gives technical background data to validate the use of the slump flow method for concrete used in deep foundations.

Keywords: tremie concrete, consistency, slump flow, viscosity

INTRODUCTION

The specification of tremie concrete for deep foundations elements requires consideration of the need for suitable workability and stability. The Abrams cone slump test (EN 12350-2) is the most widely used concrete control test in France, but it appears to be a non-discriminatory test for flowable, non-self-compacting concrete (SCC) (i.e. slump flow not allowing class SF1 to SF3 to be achieved according to EN 206). Anomalies or defects may occur despite meeting the limit values specified in Annex D of EN 206:2013. The flow table test (EN 12350-5) commonly specified in UK appears to be more appropriate compared to the slump test however the test procedure does not reflect the placement condition of tremie concrete. In addition, implementation as an identity test on site requires additional tools and test duration.

The EFFC/DFI Guide Tremie Concrete for Deep Foundation (Tremie Guide), in its 2018 version (Second Edition), introduced a new approach to specifying fresh properties with the main target to ensure requirements for self-levelling, passing, filling ability and stability control are met. Following two academic studies led by the Technical University of Munich (TUM)[1] and the Missouri University of Science and Technology[2], the slump flow test for fresh concrete was identified as the most appropriate test to capture the rheological properties of tremie concrete governed by its yield and viscosity. The concept of Slump flow velocity was introduced to assess apparent viscosity. According to the Tremie Guide, slump flow should be specified by a target value in the range of 400 to 550 mm (depending on parameters such as element size, elements reinforcement detailing, concrete stability risk assessment, etc…) with a tolerance to the target value of plus or minus 50 mm.

Testing tremie concrete using the slump flow method (according to EN 12350-8 or ASTM C1611) appears to be a suitable test method for identifying concrete mix design with a potential for anomalies, however according to EN 206 standard, the slump flow test to EN 12350-8 is only recommended for slump flows between 550 mm and 850 mm. Applicability would then fall within the ranges of (SCC)

 © DFI International Bruges 2025

that are not generally required for tremie concrete. It is important to understand correlation between test methods and verify their reliability in the range of 350 mm to 600 mm.

This paper presents a wide range of data using slump flow for tremie concrete and a discussion on slump flow test methods. A comparative study of the slump flow testing procedures with flow table testing is discussed. Slump flow testing procedures using EN 12350-2 and NF P18-469 standards were evaluated during a round robin test involving seven different entities (five contractors, one concrete supplier and one concrete testing laboratory).

TECHNICAL BACKGROUND

This section presents test results correlations between concrete consistency test procedures from various sources:

- EFFC/DFI Concrete task group R&D program led by Technical University of Munich (2018)
- EFFC/DFI Support fluid group Field Research Study (2019 - 2024)
- Soletanche Bachy site trials and identity testing in France and UK
- Soletanche Bachy International material department laboratory testing on tremie concrete mix design (2019 – 2024)
- FNTP material committee slump flow test procedure research (2023-2024)

This article presents slump flow test results from three different test methods:

- EN 12350-8: Abrams cone in the normal position is filled with concrete in one layer without compaction.
- EN 12350-2: Abrams cone in the normal position is filled with concrete in three layers, each compacted 25 times.
- NF P18-469: Abrams cone in the inverted position is filled with concrete in one layer compacted 25 times. This procedure is mentioned in the EFFC/DFI tremie guide, appendix A for the flow time measurement.

Figure 1 presents the comparison between slump (EN 12350-2) and slump flow (EN 12350-8), Flow table (EN 12350-5) and slump flow, Flow table and slump from TUM R&D program.

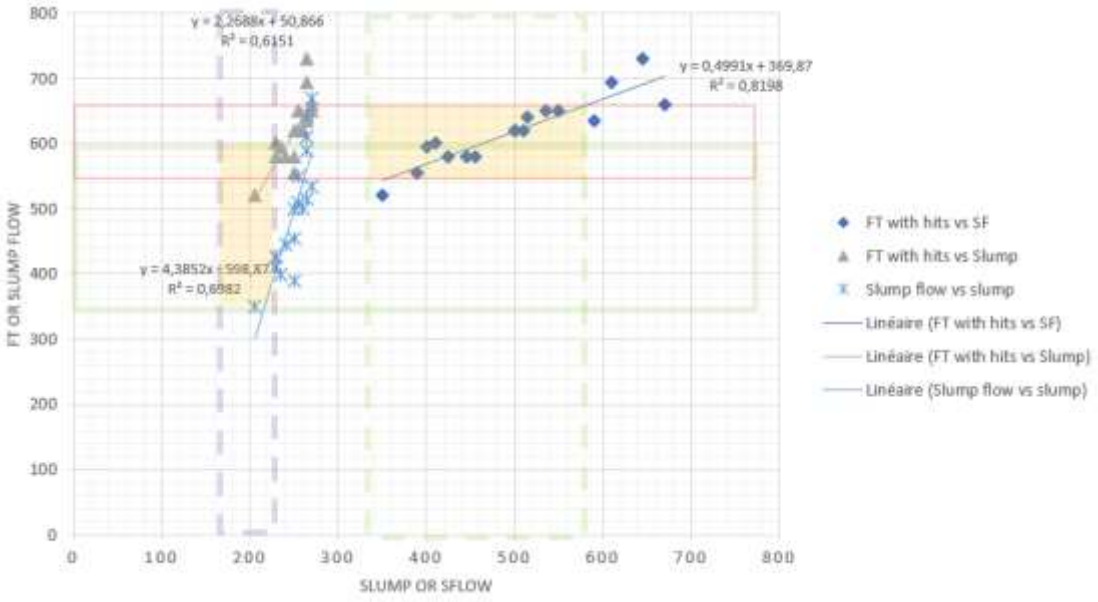


Figure 1 : Concrete consistency plotted results showing EN 206 targets for slump range (purple), Flow table range (red) and EFFC/DFI Tremie guide Slump flow range (green)

 © DFI International Bruges 2025

The results reported by the University of Munich illustrates the lack of sensitivity of the slump test compared to the slump flow test and provide a first correlation between the slump flow test and the flow table test.

The slump flow test is recommended by the EFFC/DFI Tremie Guide as the most relevant test method for tremie concrete. However, this test is generally used for SCC with a specified slump flow class described in EN 206 as SF1 to SF3. The SF1 class starts at 550 mm and ends at 650 mm of slump flow. The Tremie Guide is also very clear on the risks of specifying true SCC for deep foundation elements, regarding stability and bleed potential of such mix design. It is therefore important to highlight that the Tremie Guide recommends specifying the consistency of tremie concrete using the slump flow test method in the 350 to 600 mm range, which is not the same range as SCC. Following the publication of the second edition of the Tremie Guide, Soletanche Bachy's materials department started to evaluate concrete during trials and site acceptance testing using the former testing method (flow or slump depending on site location) and slump flow test according to EN 12350-8.

Figure 2 shows comparison between flow and slump flow (EN 12350-8) from different tremie concrete mix design.

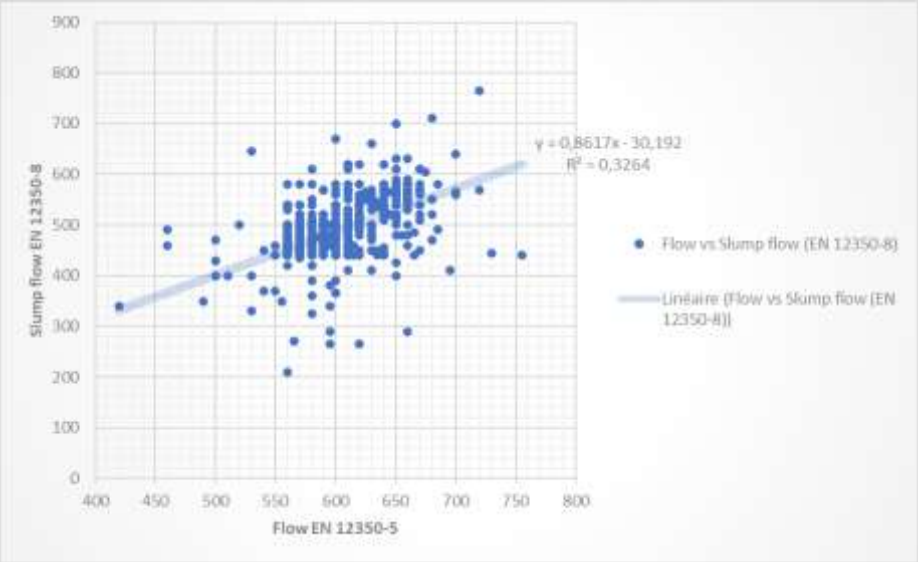


Figure 2 : Flow table (x-axis) vs Slump Flow (y-axis) test results from TUM (2019), Thames Tideway d-walls (2018), HS2 Old Oak Common d-walls (2021-2022), Clichy circular shaft (2024), Soletanche Bachy lab trials (2019-2024) and FNTP/SB slump flow test campaign (2023-2024)

Analysis of these correlations shows that the relationship between flow table and slump flow is more scattered than what was observed from the TUM results. This scatter has led to questions on the reliability of the slump flow test method and the possible correlation between flow test and slump flow test.

Few data are available to correlate slump flow velocity with flow time from invert cone. Results available from EFFC/DFI FRS are showing that SF velocity in the range 18 to 26 mm/s correspond to flow time through invert cone in the range of 2,7 to 6 s.

Figure 3 and 4 show additional correlations between alternative slump flow test methods and the EN 12350-5 flow test method.

 © DFI International Bruges 2025

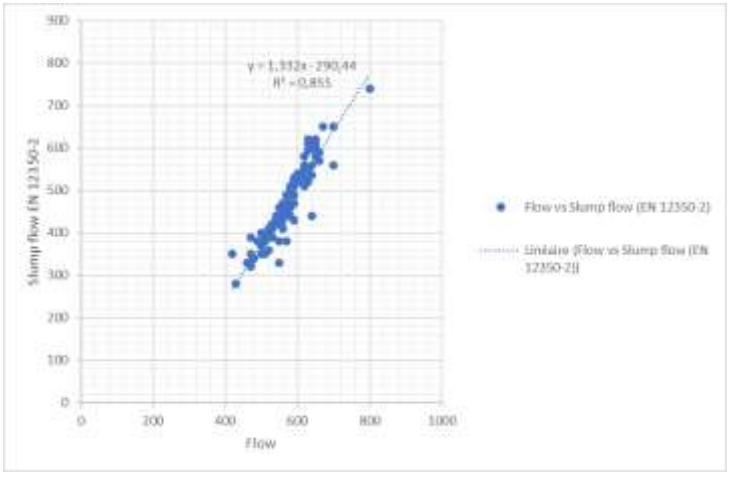


Figure 3 : Flow table (x-axis) vs Slump Flow (y-axis) measured after EN 12350-2 test from Toulouse metro project dwalls (2024) and Soletanche Bachy lab trials (2019-2024) and FNTP/SB slump flow test campaign (2023-2024)

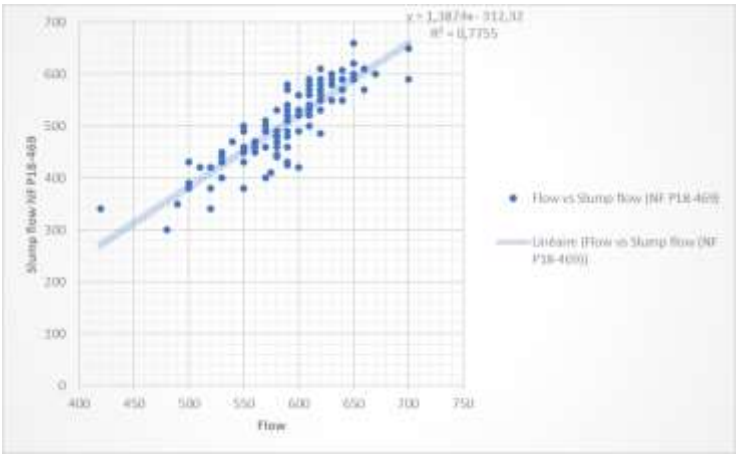


Figure 4 : Flow table (x-axis) vs Slump Flow (y-axis) measured after NF P18-469 test from Toulouse metro project dwalls (2024) and Soletanche Bachy lab trials (2019-2024) and FNTP/SB slump flow test campaign (2023-2024)

Figure 5 shows a correlation between the spread diameter obtained from the ASTM C1611 slump flow test using method A and method B (inverted cone).

The slump flow test recommended in the EFFC/DFI Tremie Guide appears to be more sensitive to concrete rheological properties. The lack of a standard recommendation in Europe and the dispersion between former testing procedure (such as flow) require further investigation to propose a suitable test and improve standards for easier specification of tremie concrete between contractors, suppliers, and specifiers. Figures 3 and 4 show a promising correlation between alternative slump flow test method and flow for concrete specified as per the Tremie Guide. At the same time, use of the invert cone to measure spread compared to normal slump flow test is well correlated according to figure 5. Based on this technical background further studies were undertaken by the FNTP Materials Committee with the aim of providing technical data for an update of the standard procedure or an alternative procedure for slump flow in the range of 350 to 600 mm.

 © DFI International Bruges 2025

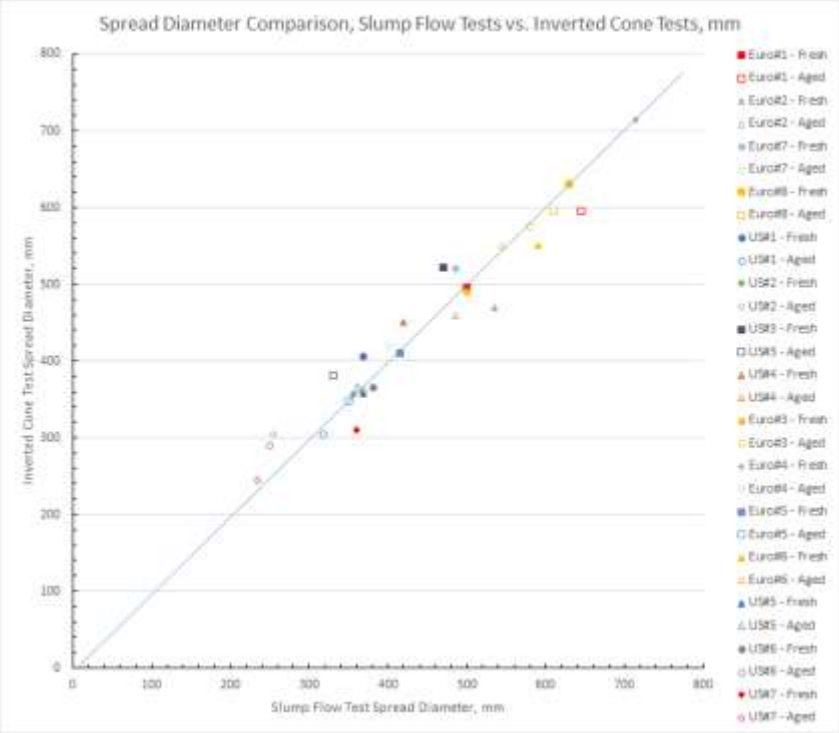


Figure 5 : Comparision between Inverted cone slump flow test and slump flow test, data from EFFC/DFI Support fluid field research study.

EXPERIMENTAL INVESTIGATION LABORATORY TRIAL PHASE

Materials and mix designs

The concrete mix design used in the laboratory trial phase are the same as the mix C1 and C4 used in a previous study to develop a concrete pressure filter test using Baroid filter press[3] (table 1).

Water content was varied for C1 mix to achieve flow (EN 12350-5) in the range of 600 plus or minus 50 mm.

Table 1 : Concrete mix design

Constituents	G2	G4
Cement, kg/m^3	385	330
Fine Sand, kg/m^3	190	-
Sand, kg/m^3	690	800
Coarse aggregate, kg/m^3	930	1040
perplasticizer, $\%_{w\ of\ cement}$	2,00%	1,40%
Retarder, $\%_{w\ of\ cement}$	0,20%	0,20%
Effective water, kg/m^3	168	182
Water/Cement ratio, -	0,44	0,55
tal fines at 125µm, kg/m^3	530	496
Coarse aggregate / Sands ratio	1,06	1,30

Methods

For each batch, the consistency of the concrete was tested immediately after being batched with flow method (EN 12350-5) and with slump flow method (EN 12350-2, EN 12350-8 and NF P18-469) once by four different operators.

 © DFI International Bruges 2025

NF P18-469 is the French standard for measuring the invert cone flow time, which is an evaluation of concrete viscosity. The test procedure consists of filling the Abrams cone in an inverted position with a single layer of concrete and then compacting the entire layer with a rod 25 times in the same manner as for EN 12350-2. Once the cone has been filled and compacted, the operator lifts the cone in one to two seconds at a height of 30 cm and starts the chronometer. When the cone is emptied, the chronometer is stopped. The test is carried out on a metal plate similar to the slump flow test (EN 12350-8) which allows the spread diameter of the concrete to be measured after the test.

Results and discussion

Figure 6 shows the variation of flow and slump flow (three methods) with variation of C1 mix water. Figures 7 and 8 show the comparison between operators for C1 mix design with varying water content to achieve a flow of 620 – 640 mm (figure 6) and a flow of 540 – 560 mm. In the flow range of 620 – 640 mm the coefficient of variation between operators is respectively 0,88%, 3,91% and 3,09% for NF P18-469, EN 12350-2 and EN 12350-8 respectively. In the flow range of 540 – 560 mm, the coefficient of variation between operators is respectively 4,98%, 5,07% and 2.29% respectively for NF P18-469, EN 12350-2 and EN 12350-8 with a non-representative value for EN 12350-2 of 470 mm which if eliminated brings coefficient of variation for EN 12350-2 method to 1,35%.

From this laboratory trial phase, 3 test methods appear to be reliable but do not give the same range of results for a given flow. The three test methods for slump flow have the same response to water variation of the concrete mix.

Additional observation can be made from this testing phase with C4 mix. NF P18-469 appears to overestimate slump flow compared to other methods which can be linked to the test method and the height of the cone lift. This test method is interesting because it is easier to perform (the cone is stable during the filling process), and a single test provides both yield and viscosity evaluation. EN 12350-2 and EN 12350-8 show similar results but during the trial phase it was observed that the use of EN 12350-8 use may be limited when the concrete is in the lower range of the EFFC/DFI tremie guide specification. EN 12350-2 could be relevant to identify segregating concrete in the upper range of the guide specification as shown in figure 9.

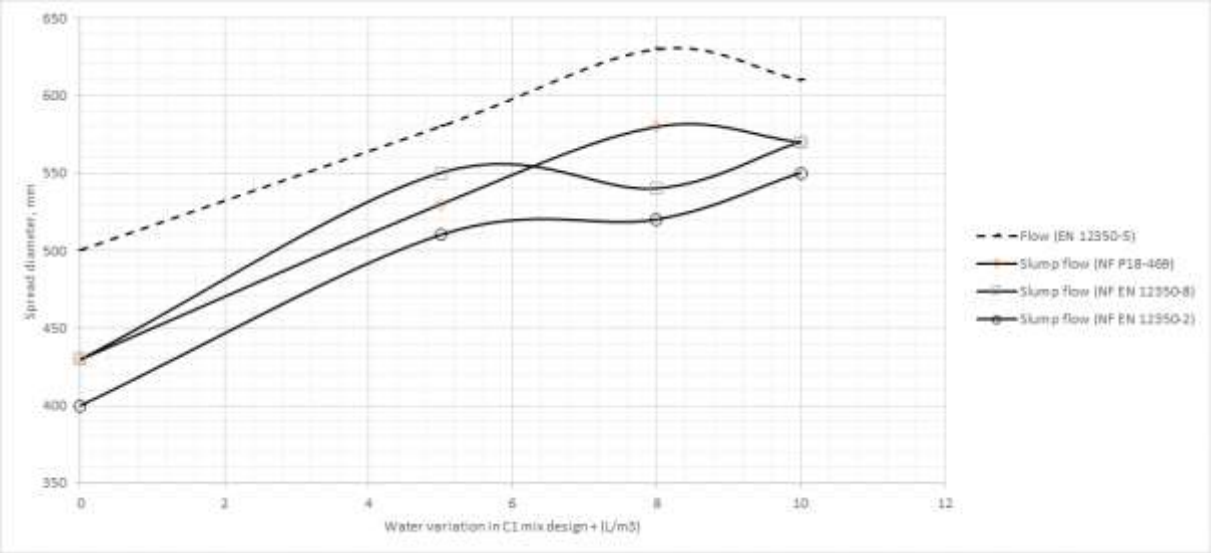


Figure 6 : evolution of flow and slump flow (three methods) with water in C1 mix design

 © DFI International Bruges 2025

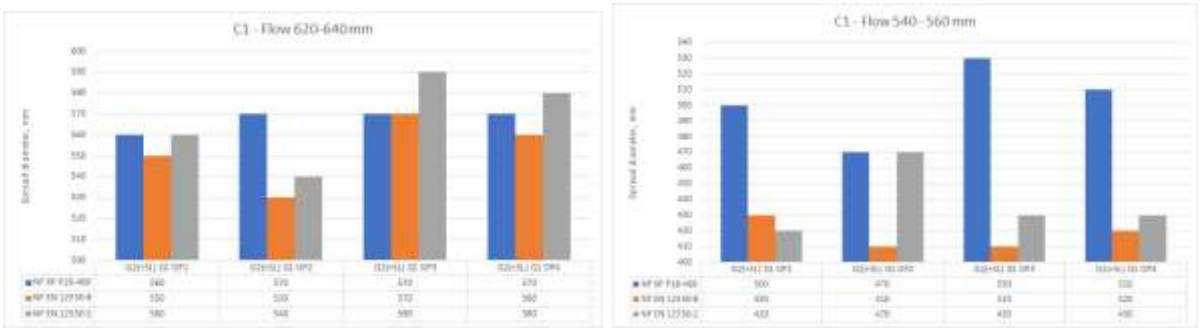


Figure 7 and 8: Slump flow methods with 4 different operators

Following laboratory trials investigation, FNTP materials committee decided to organize a round robin test to evaluate more in detail the EN 12350-2 and NF P18-469 test methods for slump flow evaluation.

EXPERIMENTAL INVESTIGATION PLANT TRIAL PHASE

Materials and mix designs

The round robin test was organised with the help of CEMEX ready-mix supplier in Toulouse. The concrete mix design selected was the concrete supplied by CEMEX for the Toulouse Metro project line 4 for the construction of diaphragm walls with a workability retention of seven hours. Table 2 presents the C35/45 mix design. A CEM III/B cement, limestone filler and siliceous aggregates are used in the mix.

Table 2 : Concrete mix design

Constituents	C35/45 XA1
Cement, kg/m^3	340
Limestone filler, kg/m^3	90
Sand, kg/m^3	855
Coarse aggregate, kg/m^3	895
Superplasticizer, $\%_{w\ of\ cement}$	1,14%
Retarder, $\%_{w\ of\ cement}$	0,44%
Effective water, kg/m^3	159
Water/Cement ratio, -	0,47
Total fines at 125µm, kg/m^3	470
Coarse aggregate / Sands ratio	1,05

Methods

Seven operators participated in the round robin test. Each operator was provided with a full inspected Abrams cone kit and metal plate. The metal plates were all new, identical and supplied by CEMEX. Two batches of concrete were produced. The first batch was produced in the morning to achieve high flow, and the second batch was produced early in the afternoon to achieve a flow in the middle range. On delivery of the concrete, the flow was measured by the concrete supplier's technician in accordance with EN 12350-1 and EN 12350-5. After the flow value was validated by the observer, the concrete was remixed in the truck and poured into static containers of sufficient volume to allow the testers to sample the concrete according to EN 12350-1, perform two measurements of slump flow according to EN 12350-2 and also two measurements of slump flow according to NF P18-469. Figure 9 presents the round robin test set up.

 © DFI International Bruges 2025



Figure 9: Round robin test setup

Results and discussion

The first truck of concrete was batched at 7:54am and arrived at the test site at 8:30am. The flow was measured at 630 mm and the concrete was left mixing in the truck mixer at slow agitation for one hour to ensure a stable concrete flow. The flow was tested again at 620 mm after one hour. The test phase was carried out between 9:30 and 11:30 for a total of 3 slump flow measurements with each method.

Figures 10 and 11 show the slump flow results for the two retained testing methods.

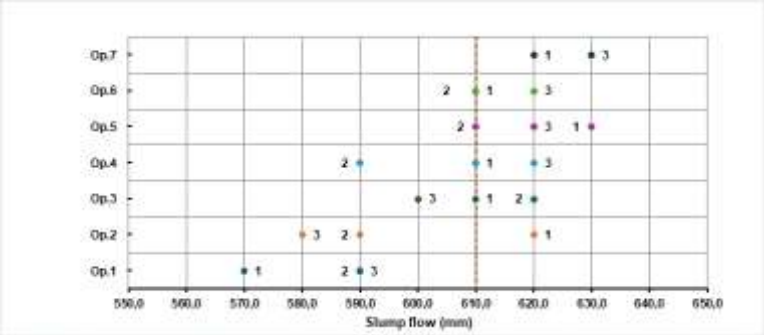


Figure 10: Slump flow (EN 12350-2) for a flow of 620 mm

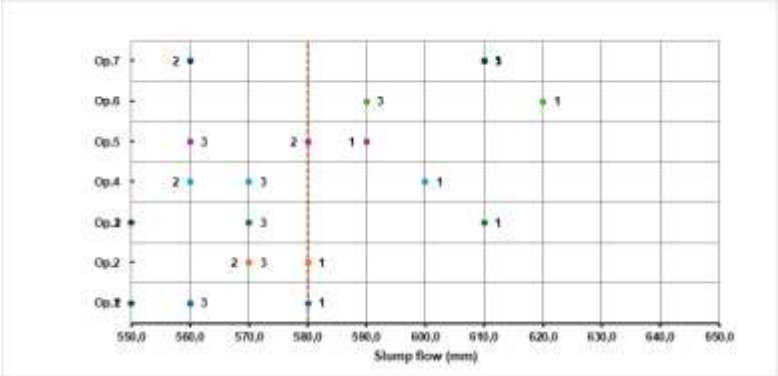


Figure 11: Slump flow (NF P18-469) for a flow of 620 mm

 © DFI International Bruges 2025

The second truck of concrete was batched at 12:08 and arrived at the test site at 13:30. The flow was measured at 530 mm and concrete was left mixing in the truck mixer at slow agitation for one hour to ensure a stable concrete flow. The flow was tested again at 590 mm after one hour. The test phase was carried out between 14:20 and 15:10 for a total of 2 slump flow measurements with each method.

Figures 12 and 13 show the slump flow results for to the two retained test methods.

Tables 3 and show the results of the statistical analysis according to ISO 5725-2.

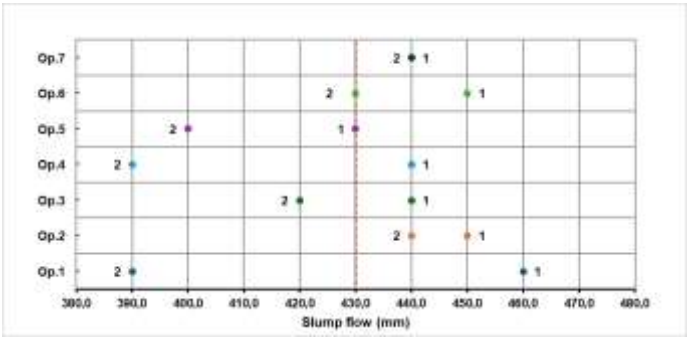


Figure 12: Slump flow (EN 12350-2) for a flow of 590 mm

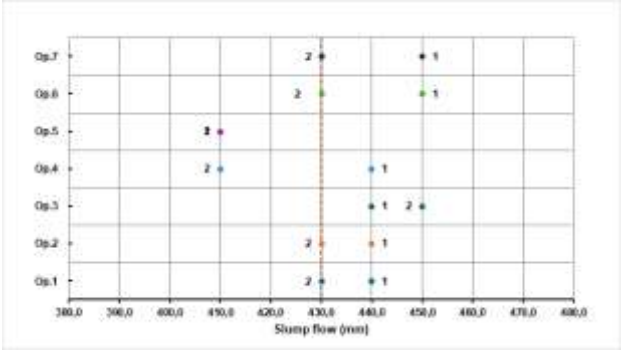


Figure 13: Slump flow (NF P18-469) for a flow of 590 mm

Table 3 : Precision data for slump flow according to EN 12350-2

Flow (mm)	Average value (mm)	Repeatability conditions		Reproductibility conditions	
		Sr (mm)	r (mm)	S_R (mm)	R (mm)
620	610	14	40	21	59
590	430	24	68	24	68
-	430 - 610	19	54	22	63

Table 4 : Precision data for slump flow according to NF P18-469

Flow (mm)	Average value (mm)	Repeatability conditions		Reproductibility conditions	
		Sr (mm)	r (mm)	S_R (mm)	R (mm)
620	610	25	71	27	76
590	430	12	34	15	42
-	430 - 610	19	52	21	59

CONCLUSION

This paper presents correlations between flow test and slump flow test according to different test methods found in slump test, slump flow and flow time standards. Technical data obtained from

 © DFI International Bruges 2025

construction sites confirm the relevance of slump flow for the evaluation of tremie concrete, as a more sensitive measure of concrete rheological parameters. The lack of precision data for SCC slump flow method is addressed in this paper with proposed reliability values for alternative slump flow test method. The use EN 12350-2 or NF P18-469 could be advantageously utilised to evaluate the slump flow of tremie concrete and, more generally, high slump flow concrete not designed as SCC. Precision data are provided for further evaluation. Slump flow velocity testing is not standard and additional data will be required in the near future to correlate the slump flow velocity and the flow time through the invert cone.

ACKNOWLEDGEMENT

The authors would like to thank the financial support of FNTP, the members of FNTP technical materials steering committee, the EFFC/DFI Support fluid and Concrete task group members and all the participants for the precision study (Vinci Construction, Cemex, NGE, Ginger CEBTP, Eiffage Genie Civil, Soletanche Bachy International and Soletanche Bachy France)

REFERENCES

[1] Kraenkel, T, and al, 2018: Rheology and workability of Deep Foundation Concrete in Europe and the US, Technical University of Munich

[2] Feys, D., and al 2018: Testing Concrete for Deep Foundations – Progress Report, Missouri University of Sciences and Technology

[3] Holder, T, and al 2022: Test method using pressure filtration cell to evaluate bleed in tremie concrete, EFFC/DFI Berlin conference (2022)

 © DFI International Bruges 2025

HIGH MODULUS WALLS IN UPDATED EN 12063

Antti J. Perala, SSAB Europe Oy, Turku, Finland, antti.perala@ssab.com

ABSTRACT

High modulus wall, a pile wall consisting solely of so-called primary piles, is becoming a more popular solution as a retaining wall in challenging conditions. This has now also been recognized in standardization and the new updated version of EN 12063, the execution standard for pile walls, considers this type of a pile walls more broadly. This has led also to a change in the name of the standard "*Execution of special geotechnical work. Sheet-pile walls"* to "*Execution of special geotechnical work - Sheet pile walls, combined pile walls, high modulus walls"*. The new updated standard also includes an informative Annex K on the installation of tubular piles by percussive drilling with a Down-The-Hole (DTH) hammer, which over the past 15 years it has been the most used technique for installing tubular steel piles by drilling. Percussive drilling with a DTH hammer ensures efficient installation of high modulus walls in ground conditions where soft soils, hard soils and boulders need to be penetrated and the piles need to extend all the way into the bedrock. Updating of the standard was needed and responded to the needs of the industry by bringing the standard into the 21st century.

Keywords: EN 12063, high modulus wall, DTH drilling

UPDATING OF EN 12063

The updating of the EN 12063 started back in 2017 and was a normal periodical update for the standard. After the publishing of an EN standard, there is a normal review process which is done at 5-year intervals (European Committee for Standardization CEN, 2024). During each review, the national committees of the CEN member states review the standard and check to see if there are needs for updating. Even though the review process is quite frequent, the old version of the standard had been approved as long ago as in October 1999, which made it almost 20 years old at the time the updating was started.

During those 20 years there had been lots of changes and improvements in the pile walls themselves, execution techniques, safety regulations, etc. Naturally many the other related standards referred to had been updated. Beside this, the ongoing process for updating all the Eurocode design standards meant there was a need to update EN 12063. The new updated version of the standard was approved in May 2024 and released shortly after.

TYPES OF STEEL RETAINING WALLS COVERED BY THE STANDARD

In the past, the coverage of the EN 12063:1999 (1999) had been considered to mainly involve only the execution of sheet pile walls. This relates clearly to the name of the old standard - "*Execution of special geotechnical work. Sheet-pile walls*" - even though the scope also included the execution of combined pile walls. Due to changes in pile walls actively available on the market, it was decided to change the name of the standard. The new name is "*Execution of special geotechnical work - Sheet pile walls, combined pile walls, high modulus walls*". Other types of steel retaining walls than sheet pile walls were also given more attention in the actual text.

Figure 1 shows three types of steel retaining walls covered by EN 12063:2024 (2024). Sheet pile walls on the left are the most common type. Sheet pile walls are mainly made of hot-rolled U or Z piles which consist of interlocks in both edges and a bent sheet part in between. Combined pile walls are combinations of primary piles, either tubular piles or H piles, and sheet piles acting as secondary piles in between the primary piles. High modulus walls consisting solely of piles similar to the primary piles of combined walls.

 © DFI International Bruges 2025

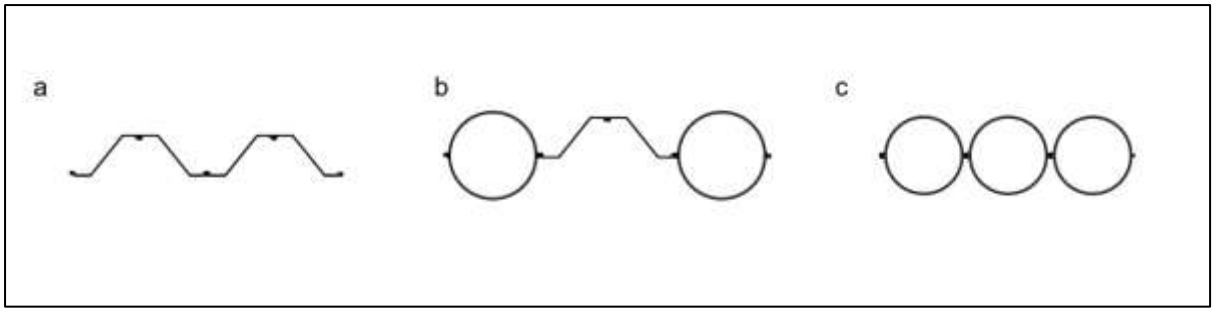


Figure 1. Examples of different steel retaining walls covered by EN 12063:2024, a) sheet pile wall b) combined pile wall c) high modulus wall.

Both EN 12063:2024 (2024) and FprEN 1993-5:2024 (2024) define a high modulus wall as a retaining wall formed by interlocking or connecting primary steel elements that have the same geometry. The old EN 12063:1999 (1999) didn't mention high modulus walls at all and EN 1993-5:2007 (2007) doesn't mention primary elements, only elements with the same geometry. The piles used in high modulus walls are most often either tubular piles or H piles as shown in
Figure 2. Other cross-sections, for example box piles, are also possible as long as the piles in the wall have the same geometry.

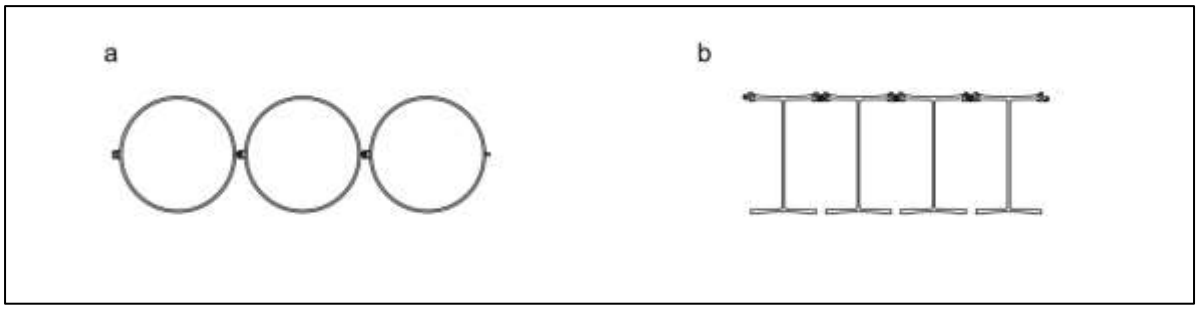


Figure 2. Typical high modulus walls made of a) tubular piles and b) H piles.

The name high modulus wall clearly refers to the high section modulus of the wall. The basis for this can be found in the default design method for combined walls according to Clause 5.5.1(2) of EN 1993-5:2007 (2007). In this method, only the primary piles are considered as retaining elements against the earth and water pressure, and the function of the secondary elements is solely to fill the gap between the primary elements and transmit the loads to the primary piles. With high modulus walls, the bending stiffness and resistance of the wall naturally increase when there are only primary piles in the wall. On the other hand, the size of the piles used in high modulus walls can sometimes be quite small. In some cases even d = 219.1 mm piles have been used in situations where the wall has been installed in a cramped space below an existing bridge or in a basement. Use of these small piles makes the section modulus of the wall much smaller than with many commonly used sheet pile profiles. During the updating of EN 12063, the naming of high modulus wall was discussed, but was not changed in order to maintain similar terminology with EN 1993-5:2007 (2007).
Besides higher section modulus, due to having only primary piles in the wall, the structure of high modulus walls also offers another benefit compared to combined pile walls. In combined pile walls the secondary elements direct the forces from earth and water pressures to primary elements via connecting devices, the connectors. The effect of these introduction forces on the resistances of tubular primary piles should be taken into account according to procedure given in Annex D.2 of EN 1993-5:2007 (2007). The introduction forces from secondary elements and the internal forces and moments in shell bending are shown in Figure 3. Since all the piles in high modulus wall are primary piles, there are no such introduction forces and thus no reduction in cross-sectional resistances of tubular piles.

 © DFI International Bruges 2025

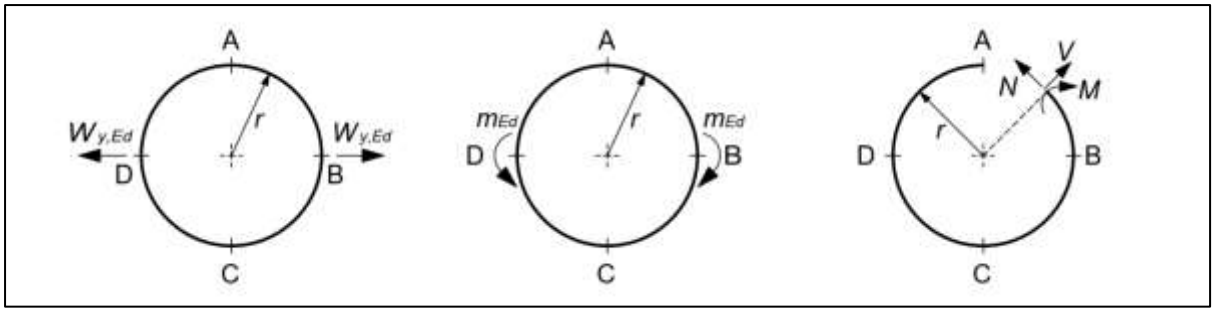


Figure 3. Local shell bending due to introduction forces from secondary elements, reproduced from Table D-1 in EN 1993-5:2007 (2007).

INSTALLATION METHODS OF HIGH MODULUS WALLS

As mentioned, high modulus walls are like combined pile walls without secondary elements. The lack of secondary elements also results in the installation of the high modulus walls differing from the installation of primary piles of combined walls. In combined pile walls, the primary piles are most often installed first and the infilling secondary elements are installed in between the already installed primary piles. Since high modulus walls consist solely of primary piles, installation is done consecutively. The differences in installation sequences are shown in Figure 4.

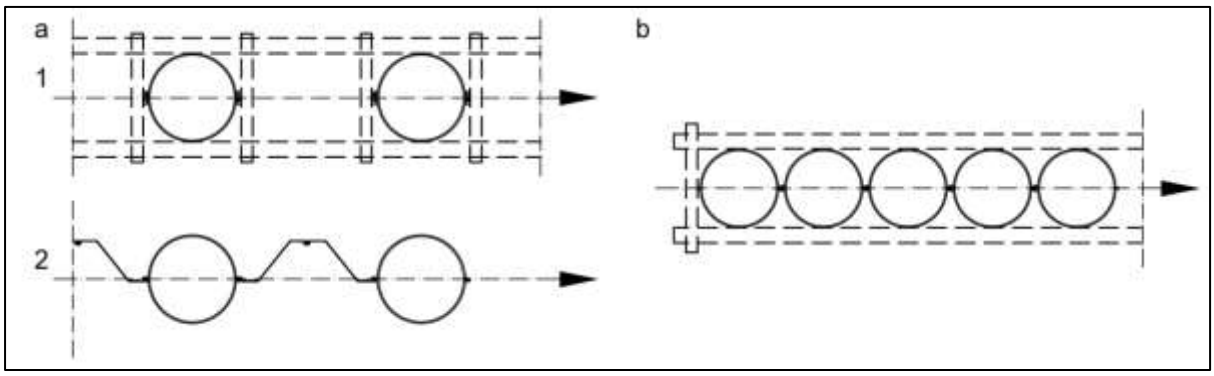


Figure 4. Examples of installation sequences of a combined pile wall and a high modulus wall, a) combined pile wall with 2 phases; 1) installation of primary piles and 2) installation of secondary piles, and b) high modulus wall with only one installation phase. A guide frame is shown with dashed lines.

Steel retaining walls are most often installed by driving. Driving as a term includes several methods, i.e. impact, vibrating, pressing, resonance and screwing. The two main driving methods for sheet pile walls and combined pile walls are vibrating and impact driving. The piles of high modulus walls are often quite large and impact driving may require high impact forces. These high impact forces can damage the connectors since a pile is always connected to the previous pile. This means impact driving is not as recommended an installation method for high modulus walls as vibrating.

Percussive drilling

Use of tubular piles in high modulus walls offers also a possibility to use percussive drilling as an installation method. Percussive drilling is a very efficient installation method which allows piles to be penetrated through hard and stony soils strata, boulders and even embedding the piles into the bedrock. Basic information on percussive drilling as an installation method for tubular piles was added to EN 12063:2024 (2024) in the form of an informative Annex K. The most common technique used for percussive drilling of large diameter tubular steel piles is Down-The-Hole (DTH) drilling.

 © DFI International Bruges 2025

In DTH drilling, the percussive power is generated with a hammer, which is inside the pile, just above the drill bit. This enables efficient direction of the percussive power to the soil and rock without absorption by the drill string. Figure 5 shows the main components of percussive drilling and the principle of DTH drilling.

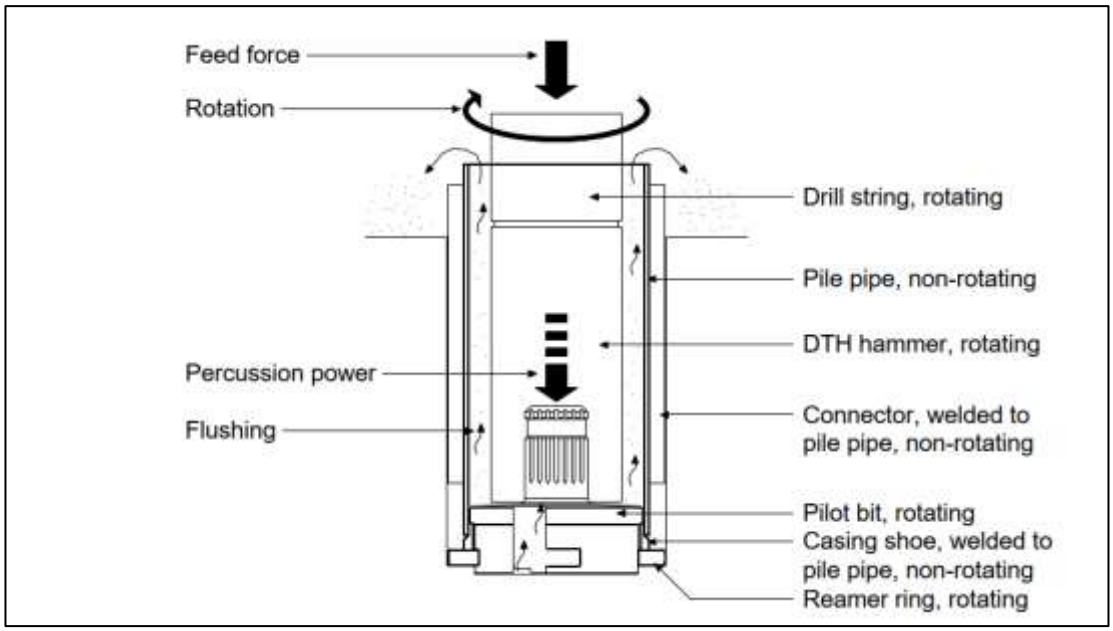


Figure 5. Percussive drilling, main components on left and principle of DTH drilling on right.

Annex K of EN 12063:2024 (2024) also considers an important topic related to high modulus walls, where the piles are installed by percussive drilling. Since the piles in high modulus walls are installed consecutively and the pile is always connected to the previous pile via connectors during installation, the diameters of the reamer rings and the widths of the connectors need to be adjusted to work together. Figure 6 shows the basic principle of adjusting connectors and reamers.

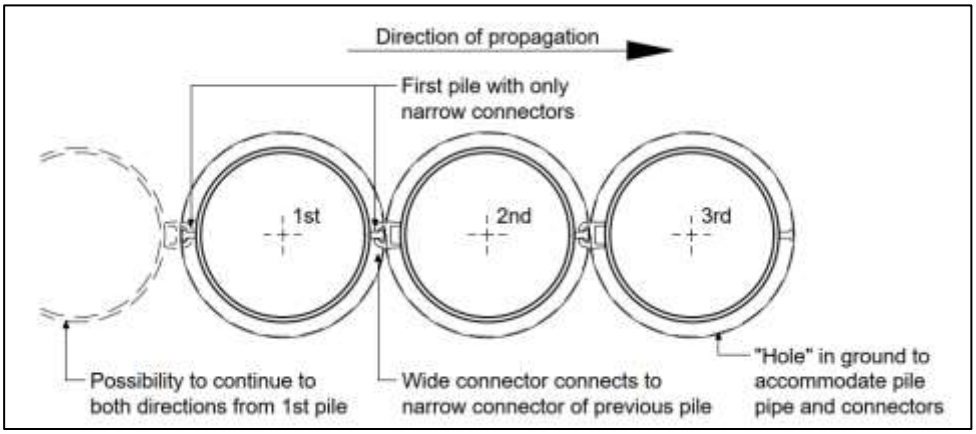


Figure 6. Adjusting connector widths when using DTH drilling to install a high modulus wall.

The connectors in the first installed pile need to be “narrow” ones and fit into the “hole” made by the reamer. The “hole” is not an empty space between the pile and surrounding ground. The “hole” is filled with drill cuttings, but the soil is softened, any boulders and rock are penetrated to enable the connector to embed into the ground. In next pile, the connector which connects to the previous pile is a “wide” one. Part of this connector extends to the “hole” made during the drilling of the previous pile. Any other connectors in the next pile are narrow ones similar to those in the first pile.

 © DFI International Bruges 2025

EXECUTION CLASSES

Under Annex C of EN 1993-1-1:2005+A1:2014 (2014), it is mandatory to select an appropriate execution class for every steel structure already at the design phase. The execution class can be specified for the execution of the works as a whole, of an individual component or of a detail of a component. This means there may be different execution classes for different structures and details of a structure in a project. The basis for the requirement is given in EN 1990:2002+A1:2005+AC:2010 (2010), where different consequences classes and reliability classes are defined in order to obtain the required reliability for the completed works.

In general, the requirements given in EN 1090-2:2018 (2018) are followed in the execution of steel structures. But in the case of piling, EN 1090-2:2018 (2018) states very clearly in its scope, that piling is executed in accordance with relevant standards EN 12063, EN 12699 and EN 14199. EN 1090-2:2018 (2018) applies only to the execution of waling, bracing and connections. The reasons for this are the installation methods of piles (i.e. impact driving, vibrating, drilling, etc.), which are not included in EN 1090-2:2018 (2018). Since the execution of piling is not within the scope of EN 1090-2:2018 (2018), the requirements of EN 1090-2:2018 (2018) are not considered in piling unless the relevant execution standard for piling works refers to EN 1090-2. There are no references to EN 1090-2 in EN 12063:2024 (2024) and due to this, the requirements on EN 1090-2:2018 (2018) are not followed on manufacturing and installation of piles for high modulus walls.

In EN 12063:2024 (2024) the execution classes are considered only in the execution of pile welds. The execution classes are not considered for example in pile installation or in the supervision or testing of the installed piles. The different requirements for example on quality levels of the welds, type and extent of testing of the welds are given in Tables 1 to 3 of EN 12063:2024 (2024).

CASE HISTORIES OF HIGH MODULUS WALLS INSTALLED BY DRILLING

Mall of Tripla, Pasila, Helsinki, Finland

Mall of Tripla in the Pasila district of Helsinki, Finland is a building complex which includes a shopping centre, railway station, hotel, offices, etc. It was built in 2016 to 2019. An excavation pit at a depth of 18 to 21 metres and size of approx. 225 metres x 128 metres, total area of 2.3 hectares, was needed to accommodate an underground car parking facility of up to five storeys. The retaining walls had to be able to penetrate through fill layers of variable thicknesses, soft clay and silt layers, as well as a hard moraine layer, and to achieve required water tightness the walls had to be embedded into the bedrock. To enable all this, a high modulus wall of tubular steel piles installed by DTH drilling, known as an RD® pile wall, was chosen. (Tyynelä, 2016)

The majority of the piles in the retaining walls, a total of 760 piles and 16.7 kilometres in length, were of size RD700/14.2 (711x14.2) and steel grade S440J2H. Part of the retaining walls, a total of 60 piles and 1.3 kilometres in length, were of size RD400/12.5 (406.4x12.5) of steel grade S440J2H. The reason for smaller pile size was installation below an existing railway bridge, which reduced the piling rig size and therefore also the pile size. (Mara, 2016) All RD700/14.2 piles were installed as one element, with maximum length of 33.5 metres. Approximately 21-metre long RD400/12.5 piles were installed from several 4-metre long elements due to low headroom. (Mara, 2017) The photo in Figure 7 shows the drilling of RD400/12.5 piles under the bridge.

 © DFI International Bruges 2025



Figure 7. Installation of RD400/12.5 piles below an existing railway bridge.

The northern pile wall of Pasila Tripla had four anchor levels and two waling levels for each anchor level. The bedrock surface was partly well below the excavation level and partly above. The bedrock above the excavation level was removed by blasting. Figure 8 shows the northern wall and also drilled RD1200 (1220.0x12.5 and 1220.0x14.2) piles for the frame of the building.



Figure 8. Northern pile wall of Mall of Tripla, Pasila, Helsinki.

Piles were installed through soft soil layers of peat, gyttja soil and clay as open ended piles by vibrating. An auger was used to remove the soil from the piles. The pilot bit, DTH hammer and drill string were lowered inside the empty piles and the piles were drilled through the friction soils and embedded approximately 1.5 metres into the bedrock (SSAB, 2016). Installation into soft soil by vibrating is fast and can cause connectors to heat due to friction. It was noticed in the project that whereas the use of bitumen-based sealant reduced friction significantly, the connectors were cooled

 © DFI International Bruges 2025

by spraying water to prevent damage. Out of a total of 760 piles, the connectors from only two piles, approx.. 0.3 % of the total number of piles, had broken during installation. Breaking was probably due to vibrating too deep into the friction soil (Vunneli, 2017).

The project had also placed special demands on the pile walls. The design service life of the pile walls was 200 years and due to the layers of peat and gyttja soil, the corrosion values were high. The corrosion reduction used was 12 mm for the 200 years of service life. The corrosion reduction was higher than the total material thickness of the connectors, which lead to the special design shown in Figure 9 to maintain the water tightness. Water tightness in the final stage was achieved by welding a steel plate in front of the connectors and by grouting the gap with a concrete grout. (Tyynelä, 2016) A bitumen-based Pertex sealant was successfully used in the connectors to enable water tightness against approx. 20 metres of water pressure in the construction phase (Vunneli, 2017).

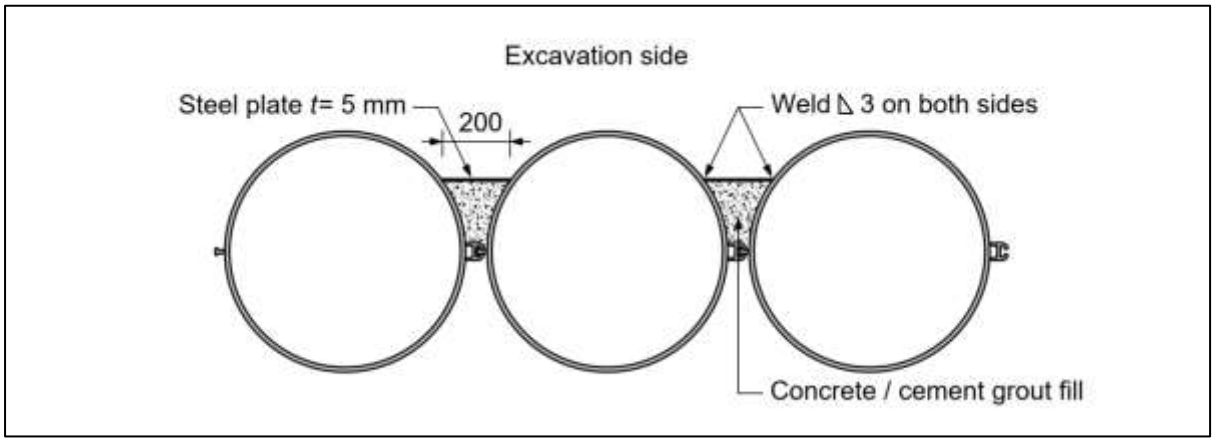


Figure 9. Special design to maintain water tightness for 200 years of design service life at the locations of the connectors (reproduced from (Tyynelä, 2016)).

Peterhead harbour, Scotland

The Inner Harbour Redevelopment Project of the Peterhead harbour in Scotland included strengthening the existing quay walls with new piled walls and generally deepening the harbour by 3 metres to level of -6.5 metres. The new pile walls were installed from old existing quay walls by using DTH hammer and a wing pilot. The piles were installed below sea water and drilled 7.5 metres into the bedrock to depth of -10.5 metres. The bedrock was granite rock with an approx. UCS value from 10 to 20 MPa. (Brennan, 2017)

The pile walls consisted of 960 RD600/12.5 (610.0x12.5) piles and 102 RD600/16 (610.0x16.0) piles of steel grade S440J2H. The lengths of the piles varied from 10.6 metres to 20.0 metres with total length of 15.5 kilometres. The piles were fitted with RM/RF connectors and casing shoes at the mill. (van Breukelen, 2017)

The initial solution for the project was a secant pile wall of concrete. Installation of cast-in-situ concrete piles into the water would have required a temporary fill in front of the existing quay to prevent fresh concrete from washing away. The need for a temporary fill was avoided by using a retaining wall of steel piles. The requirement to install the piles into the bedrock was achieved by using tubular piles and DTH drilling.
Figure 10 shows an illustration comparing the methods. (Brennan, 2017) The use of sheet pile walls or combined pile walls was naturally not possible due to the requirement to embed the piles into the bedrock.

 © DFI International Bruges 2025

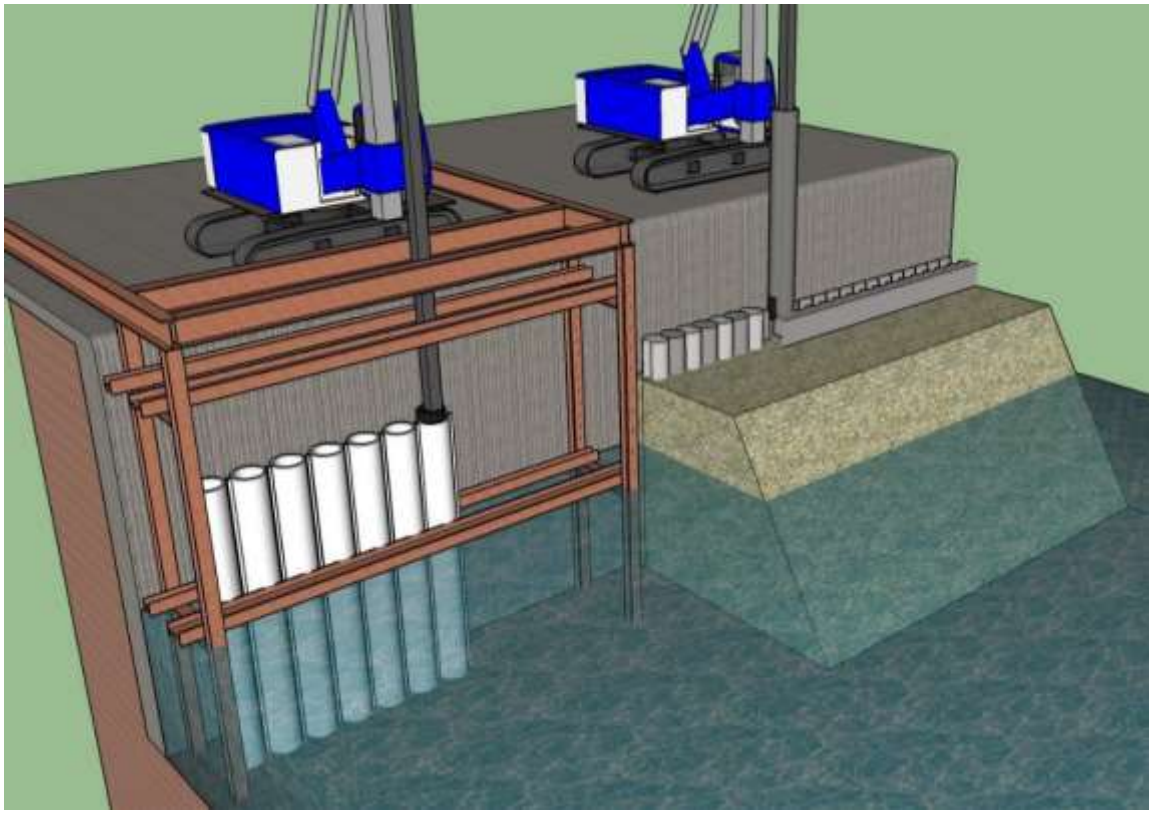


Figure 10. Illustration showing the installation of pile walls from the existing quay, the high modulus wall of steel piles (left) and the secant pile wall of concrete (right) (Brennan, 2017).

Melo dam, Nokia, Finland

The Melo dam is an earth dam which is part of the Melo hydropower plant in Nokia, Finland. Construction of the first parts of the dam started back in 1950s, but the actual dam was completed in the early 1970s. The difference in water levels at the dam is 19.7 metres. The leaking of the dam was noticed in 2005. Different injections and sheet pile walls had been used to seal the dam, but without sufficient success. A decision was made to properly seal the earth dam using a pile wall of drilled tubular steel piles. (Mincon Group, 2023)

The soil conditions at the dam are challenging for installing a pile wall. At the very bottom the dam has a “Benoto pile wall”, a secant pile wall of concrete. On top of the secant pile wall is the dam core, which is made of compacted moraine and surrounded with layers of different types of gravel. The outermost layers of the dam are blasted rock, some layers are compacted and some not. The design was to make the new sealing pile wall on the upstream side of the old dam core by drilling the piles all the way through the layers of blasted rock, natural soil layer at the bottom and a sufficient length into the bedrock. (Hakanen, 2023)

The total number of piles was 193 and the total length was 8,400 metres. Most of the piles, a total of 7,950 metres, had a diameter of 508.0 millimetres and the remainder, 450 metres, had a diameter of 273.0 millimetres. The piles in the project were extremely long. The longest pile had length of 67 metres. This naturally meant that the piles had to be lengthened by welding at the site. The piling rig limited the maximum element length to 18 metres. The longest pile had 4 elements and 3 splice welds in it. The length of the piles also resulted in the use of two different wall thicknesses in piles. With the longest piles, the bottom element had a wall thickness of 14.2 mm and the above elements had a wall thickness of 12.5 mm. Figure 11 shows the Melo dam site.

 © DFI International Bruges 2025



Figure 11. The Melo dam site.

Since water tightness was the key issue in the Melo dam project, the connectors were filled with a bitumen-based sealant material at the mill. Besides sealing the connectors, also the connection between the pile toes and the bedrock was sealed. This was done by grouting through the injection channel in the RF connector. The bottom end of the injection channel was blocked and the channel was fitted with valves on both sides as shown in
Figure 12. The functioning and opening of the valves was tested with water pressure before the actual grouting was done with mixture of water and cement.



Figure 12. Bottom end of RF connector with valves at sides.

CONCLUSIONS

Periodical reviewing and updating of standards is needed. Technological development and changes in different requirements and legislation means there is a need to also keep the standards up to date. The old EN 12063 dating from 1999 had become obsolete and was no longer fit for purpose. The new updated version of the standard is far more in line with modern requirements and techniques used at construction sites.

Use of high modulus walls made of tubular piles has increased a lot during last 15 years. Mainly high modulus walls installed by percussive drilling are used in the Nordic countries, where the bedrock is hard and the bedrock surface is also relatively close to the ground level. But there are suitable projects across Europe and around the world. In many projects, the need to be able to embed the piles into the bedrock is clear. The updated version of EN 12063 contains much more on the execution of high modulus walls using percussive drilling and also clarifies the use of execution classes as well as the roles of EN 12063 and EN 1090-2 for pile walls made of steel piles.

 © DFI International Bruges 2025

REFERENCES

Brennan, G. (2017, 03 09). Peterhead Harbour Redevelopment Project. *Presentation at PIANC seminar: "So you think you know what's going on down there?" - Piling for Maritime Works*. London, United Kingdom.

CEN. (1999). EN 12063:1999. *Execution of special geotechnical work. Sheet-pile walls*. Brussels: European Committee for Standardization CEN.

CEN. (2009). EN 1993-5:2007+AC:2009. *Eurocode 3. Design of steel structures. Part 5: Piling*. Brussels: European Committee for Standardization CEN.

CEN. (2010). EN 1990:2002+A1:2005+AC:2010. *Eurocode. Basis of structural design*. Brussels: European Committee for Standardization CEN.

CEN. (2014). EN 1993-1-1:2005+A1:2014. *Eurocode 3: Design of steel structures. Part 1-1: General rules and rules for buildings*. Brussels: European Committee for Standardization CEN.

CEN. (2018). EN 1090-2:2018. *Execution of steel structures and aluminium structures. Part 2: Technical requirements for steel structures*. Brussels: European Committee for Standardization CEN.

CEN. (2024). EN 12063:2024. *Execution of special geotechnical work - Sheet pile walls, combined pile walls, high modulus walls*. Brussels: Europen Committee for Standardization CEN.

CEN. (2024, 07 23). FprEN 1993-5 as submitted to FV. *Eurocode 3 - Design of steel structures - Part 5: Piling*. Brussels: European Committee for Standardization CEN.

European Committee for Standardization CEN. (2024, 08 22). *Review of European Standards*. Retrieved from https://boss.cen.eu/maintenance/reven/pages/

Hakanen, T. (2023, 06 01). Melo dam - drilled pile wall. *Presentation at Stålpeledagen 2023*. Oslo, Norway.

Mara, J. (2016, 01 21). Pasila Tripla - Yhteenveto ja RD-paaluseinän materiaalitoimitukset (in Finnish). *Presentation at Teräspaalupäivä 2016*. Helsinki, Finland.

Mara, J. (2017, 01 19). Pasila Tripla, paalutoimittajan näkökulma (in Finnish). *Presentation at Teräspaalupäivä 2017*. Helsinki, Finland.

Mincon Group. (2023, 01 19). *Sealing the Melo earth dam with the world's deepest drilled interlocked pipe pile wall*. Retrieved from YouTube.com: https://www.youtube.com/watch?v=HsBi4uOaZDI

SSAB. (2016, 02 17). *RD pile wall - Pasila Tripla/Retaining wall for underground car park*. Retrieved from YouTube.com: https://www.youtube.com/watch?v=Zebd7Dmz9FI

Tyynelä, P. (2016, 01 21). Case Tripla Suunnittelijan Näkökulmasta (in Finnish). *Presentation at Teräspaalupäivä 2016*. Helsinki, Finland.

van Breukelen, P. (2017, 01 19). Redevelopment of Peterhead inner harbours. *Presentation at Teräspaalupäivä 2017*. Helsinki, Finland.

Vunneli, J. (2017, 01 19). Tripla by YIT (in Finnish). *Presentation at Teräspaalupäivä 2017*. Helsinki, Finland.

 © DFI International Bruges 2025

PIV ANALYSIS OF THE GROUND BEHAVIOR AT PILE TIP BY VERTICAL LOAD TEST OF MODEL PILES WITH AND WITHOUT EXPANDED BOTTOM AS A VARIABLE

Kazuto K. Author, Nihon University, Narashino, Chiba, Japan, +81 70-4140-6952, cikz24002@g.nihon-u.ac.jp
Shuichi S. Contributor, Nihon University, Narashino, Chiba, Japan, shimomura.shuichi@nihon-u.ac.jp
Yasuhiro G. Contributor, NISHIMATSU Construction, Tranomon, Tokyo, Japan, yasuhiro_gunji@nishimatsu.co.jp
Toshiaki A. Contributor, NISHIMATSU Construction, Tranomon, Tokyo, Japan, toshiaki_arai@nishimatsu.co.jp
Kenta K. Contributor, NISHIMATSU Construction, Tranomon, Tokyo, Japan, kenta_kumada@nishimatsu.co.jp

ABSTRACT

In evaluating the vertical bearing capacity of cast-in-place concrete piles, there are many findings for straight piles, but few for expanded bottom piles. Since the group pile effect is a phenomenon in which adjacent piles interact with each other through the ground, it is important to understand the behavior of the ground during loading, which may be affected by the pile geometry near the pile tip. In this study, the behavior of the ground at the pile tip during vertical loading tests of a single pile and two piles in a group was investigated based on the results of PIV analysis using a pressurized tank test apparatus that can observe the ground behavior, with the parameters of the overburden pressure and pile shape. The results showed that the distribution of vertical and horizontal displacement of the ground between the piles varied depending on the overburden pressure, pile geometry, and pile spacing because oblique downward ground displacement occurred from the corner of the pile tip surface regardless of the pile geometry, and the ground inside the group pile interfered with each other.

Keywords: belled pile, group pile, piv analysis, vertical bearing capacity, ground behavior

INTRODUCTION

Straight piles have been extensively investigated in studies pertaining to the group-pile effect on the vertical bearing capacity of piles under narrow pile spacing. In Japan, significant progress has been realized in the development of construction methods for belled piles (Fig. 1), which are cast-in-place concrete piles whose tip diameter exceeds the shaft diameter. These piles are being used widely as pile foundations for buildings. Additionally, they may reduce both the distance between piles and the ground near slopes during vertical load action as well as the earth pressure[1)]. Notably, the group-pile effect may be different from the straight-pile effect. The group-pile effect is a phenomenon in which adjacent piles mutually affect one another via the ground. Therefore, the behavior of ground surrounding pile tips must be determined in identifying the relationship between pile geometry and the group-pile effect.

In recent years, particle image velocimetry (PIV) and other forms of PIV analysis have been used in various studies to visualize ground behavior in model tests of pile foundations. Aoyama, et al.[2)] performed two-dimensional group-pile model testing and reported the differences in the ground deformation mode before and after the yield point of the load-sinking relationship based on PIV analysis. Additionally, Kiriyama, et al.[3),4)] used a centrifugal loading device to analyze ground behavior during the pull-out and push-down loading of piles placed in dense sandy ground. However, previous studies have targeted straight piles, and no findings have been reported for group piles comprising belled piles.

In this study, we conduct vertical loading experiments of straight and belled piles using a circular pressurized tank with an observation window and PIV[5)]. Additionally, we observe the ground behavior in the vicinity of the pile tips of single and group piles.

 © DFI International Bruges 2025

EXPERIMENTAL METHOD

Experimental equipment and model ground

Figs. 2 show the experimental equipment. The pressurized tank is half a steel cylinder with an inner diameter and a clear height of 600 mm, and is equipped with an acrylic window for observing the ground behavior during pile loading, as shown in Fig. 3. Grease and Teflon sheets were attached to the inner circumferential surface of the tank to reduce friction between the tank side walls and the ground.

Two types of model piles (Fig. 4) were used: straight and belled piles. They were made of stainless steel and measured 450 mm long (240 mm embedded length). Additionally, the model piles were cut in half to be observed via the window. As shown in Fig. 5, felt was attached to the cut surfaces to prevent sand from entering in between the acrylic surface and model piles. Additionally, Toyoura sand was blown at the surfaces where the model piles were in contact with the ground to prevent slipping between the pile-body surfaces and ground. The compression of the pile bodies due to vertical loading was extremely low.

We used dried Toyoura sand for the ground and mixed it with colored Toyoura sand at a ratio of 5:5[6)] to ensure the accuracy of PIV analysis; a relative density of 90% was achieved. After releasing the sand via air pluviation until the height of the pile-tip surfaces while consistently maintaining the release height from the sand rainer nozzle, as well as after placing the model piles, we released the sand until the height of the ground surface. This ground preparation method simulates the method for the on-site construction of cast-in-place concrete piles. Overburden pressure on the ground was applied using three hydraulic jacks pushing vertically downward on a rigid pressure plate placed on the ground surface. The loading rate of the model piles was 1 mm/min. The loading displacement was 35 mm, i.e., the same as the pile-tip diameters. In the experiments, we measured the vertical load and displacement of the pile head.

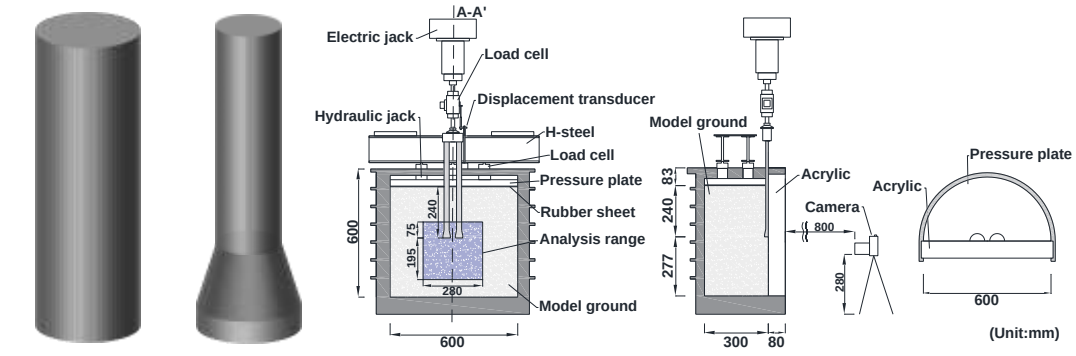


Fig.1. Straight piles and Belled Pile



Fig.3. apparatus of vertical

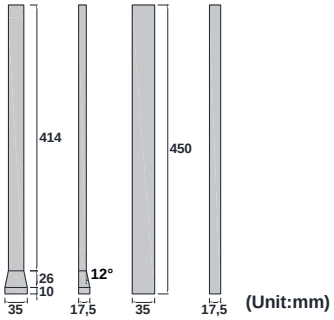


Fig.4. Model pile



Fig.5. Photo of model

 © DFI International Bruges 2025

Experimental cases

Table 1 shows the experimental cases. The experimental parameters were number of piles, overburden pressure, and pile spacing. Pile-spacing GM is a guideline for the minimum spacing of pile cores that considers the workability of piles (shaft diameter d + enlarged base diameter d_1), pile-spacing GN is a pile spacing that is 0.7 times pile-spacing GM, and GW is the maximum pile spacing that can be implemented using the experimental equipment.

PIV ANALYSIS METHOD

We used a single-lens reflex camera (approximately 61 million pixels) to capture photographs for PIV analysis. As shown in Fig. 6, the camera was placed inside a dark room with an observation window at the front. Photographs were captured every 0.2 mm until the pile-head displacement reached 35 mm. The scope of the PIV analysis is shown in Fig. 2. The PIV analysis method, as shown in Fig. 7, was to set track points in a grid pattern within the analysis range for all continuously captured images, The track points were arranged in the center of a reference frame and contained information regarding the luminance values and coordinates within the reference frame. For example, we acquired the distribution of luminance values within each reference frame of Scene (N). Subsequently, by detecting luminance values altered by ground displacement in Scene (N+1) and detecting the coordinates of track points having the most similar luminance values within the search range, we were able to record changes in the coordinates of track points between scenes. By sequentially performing this process while updating the distribution of luminance values within reference frames in all scenes, we were able to continuously visualize the ground behavior during pile loading. We analyzed the size of the reference frames, among others, and the values are shown in Fig. 7.

Table.1. Conditions of pile loading tests

CASE	Pile geometry	Number of piles	σ'v (kPa)	Shaft Diameter d (mm)	Base Diameter d_1 (mm)	Ratio of Pile spacing	Symbol
B-S100	Belled pile	1	100	24	35	–	S
B-S300			300			–	S
B-GN100		2	100			1.17d_1	GN
B-GM100						1.67d_1	GM
B-GW100						2.74d_1	GW
B-GN300			300			1.17d_1	GN
B-GM300						1.67d_1	GM
B-GW300						2.74d_1	GW
S-S100	Straight pile	1	100	35	–	–	S
S-S300			300			–	S
S-GN100		2	100			1.17d	GN
S-GM100						1.67d	GM
S-GW100						2.74d	GW
S-GN300			300			1.17d	GN
S-GM300						1.67d	GM
S-GW300						2.74d	GW



Fig.6. Photo of Inside the darkroom

 © DFI International Bruges 2025

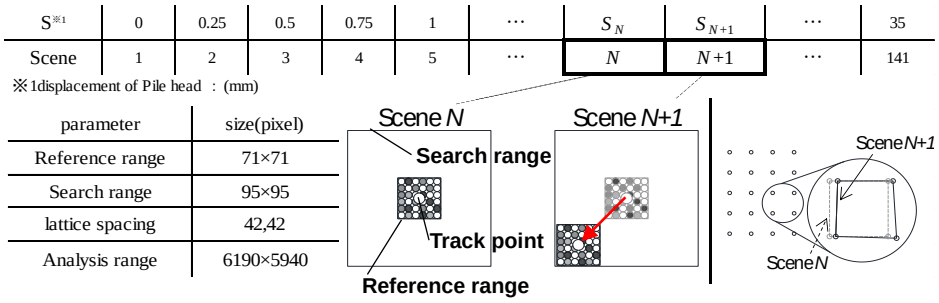


Fig.7. PIV Analysis Overview

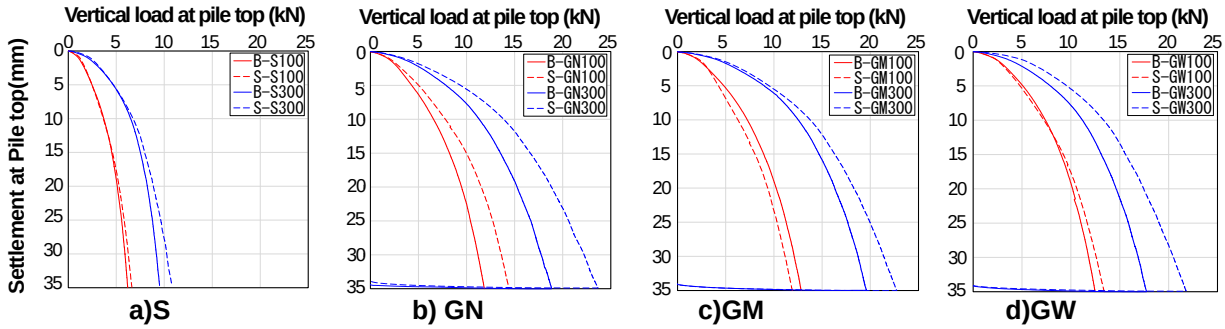


Fig.8. Load-settlement curves

LOAD–DISPLACEMENT RELATIONSHIP OF SINGLE AND GROUP PILES

Fig. 8 shows the relationship between the pile-head loads and displacements for both single and group piles. Specifically, Fig. 8a) shows the results for single piles. When comparing the differences in pile geometry based on the same overburden pressure, the belled piles exhibited a smaller pile-head load than the straight piles under the same pile-head displacement, regardless of the magnitude of the pile-head displacement. Additionally, the difference in the pile-head load between the belled and straight piles under the same displacement increased with the pile-head displacement. Figs. 8b) to d) show the relationship between the pile-head load and displacement of the group piles per pile spacing. At an overburden pressure of 300 kPa, similar to the case of single piles, the belled piles exhibited a smaller pile-head load than the straight piles under the same pile-head displacement, regardless of the pile spacing. Meanwhile, at an overburden pressure of 100 kPa, the belled piles exhibited a larger pile-head load than the straight piles beginning from 3 mm of pile-head displacement for pile-spacing GM, and beginning from 13 mm for pile-spacing GW. Additionally, although the difference in the pile-head load between the straight and belled piles under the same displacement increased with the pile-head displacement, the magnitude of this difference differed depending on the pile spacing and overburden pressure.

SHEAR STRAIN OCCURRING IN PILE-TIP GROUND

During single-pile loading

Fig. 9 shows the distribution of the maximum shear strain γ_{max} at subsidence ratios S/D of 0.0143, 0.0286, and 0.1 normalizing the pile-head displacement S during single-pile loading by the pile-tip diameter D. Additionally, Fig. 10 presents a schematic diagram of the shear strain. In S-S300 and B-S300, when S/D = 0.0143, bulbous shear strain (γ_{max}①and γ_{max}②in Fig. 11) occurred almost symmetrically directly below the tip surfaces of both the belled and straight piles. As S/D increased, γ_{max}①and γ_{max}②gradually expanded vertically downward and γ_{max}③occurred symmetrically directly below the pile-tip corners. We confirmed that the ground failure region was determined by S/D = 0.1,

 © DFI International Bruges 2025

and that the strain value at the same position increased thereafter. In fact, the shear strain shown in Fig. 10 was reported previously in vertical loading experiments on straight piles[7].

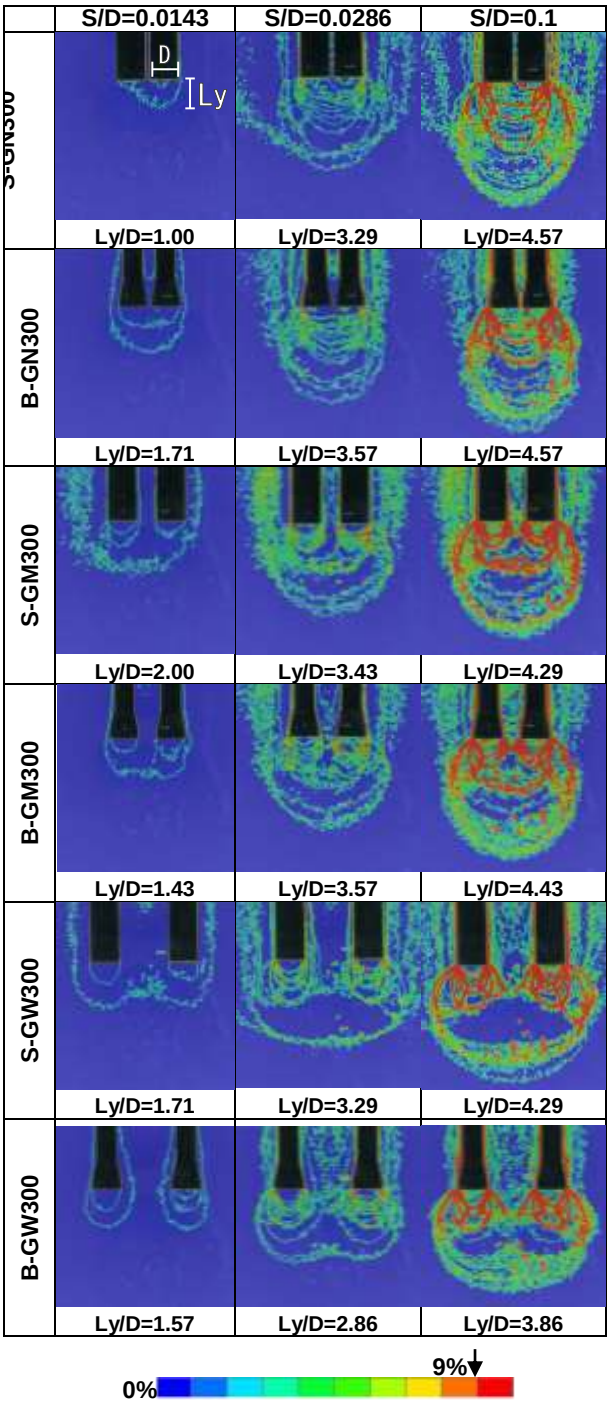


Fig.9. Distribution of maximum shear strain in a single pile

Additionally, Fig. 9 shows the distance Ly from the pile-tip surfaces to the maximum depth where the maximum shear strain occurred (normalized by the pile-tip diameter D) as an index reflecting the size of the ground resistance area. Comparing the Ly/D values for B-S300 and S-S300, although they differed during initial loading, as S/D increased, the same degree of Ly/D was attained, and definite differences could not be ascertained based on the pile geometry.

Next, when comparing B-S300 and B-S100, γ_{max}③ occurred at S/D = 0.0143, and γ_{max}③was more widely distributed in B-S100 than in B-S300, regardless of S/D. Additionally, B-S100 indicated a

 © DFI International Bruges 2025

larger Ly/D value than B-S300. We discovered that the smaller the overburden pressure, the more significant was the pile-load effect.

During group-pile loading

Fig. 11 shows the distribution of the maximum shear strain γ_{max} of the ground at S/D values of 0.0143, 0.0286, and 0.1 during group-pile loading. The ground overburden pressure was 300 kPa. At S/D = 0.0143, similar to the case of single piles, bulbous shear strain ①② (γ_{max}①and γ_{max}②in Fig. 10) occurred directly below the tip surfaces of each pile for both the belled and straight piles. Meanwhile, γ_{max}①occurred individually directly below the tip surfaces of each pile with pile-spacings GM and GW, and was confirmed to occur with pile-spacing GN in two piles, as if they were a single pile with a larger diameter. Additionally, γ_{max}②occurred individually for only B-GW300, encompassing each pile. γ_{max}①, γ_{max}②, and γ_{max}③occurred for all pile spacings beginning from S/D = 0.0286. At S/D = 0.1, shear strain (γ_{max}④ in Fig. 10) occurred at pile-spacings GM and GW, which connected the pile corners; however, this was not observed at pile-spacing GN as it was narrow. The group-pile results showed a failure mode superimposing the failure modes of single piles; apparently, the overlapping changed depending on the pile spacing, thus resulting in different strain-occurrence trends. Notably, similar results were obtained for the strain-occurrence trend shown in Fig. 10, including PIV-analysis results[3),4)] from previous group-pile vertical loading experiments using a semicircular soil tank.

Next, similar to the single piles, Ly/D increased with S/D, and Ly/D differed depending on the pile spacing at the same S/D. When comparing Ly/D based on the same pile spacing at S/D = 0.1, Ly/D reached the same value for both B-GN300 and S-GN300. However, we confirmed that when the pile spacing was widened, Ly/D differed depending on the pile geometry.

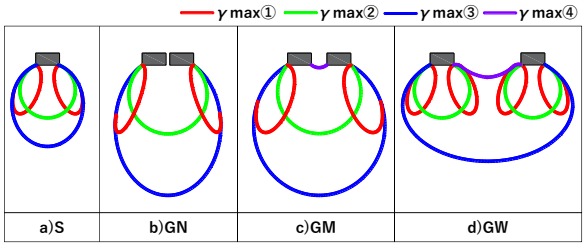


Fig.10. Illustration of main shear strain

BEHAVIOR OF GROUND SURROUNDING PILE TIPS

During single-pile loading

Figs. 12 and 13 show the ground-displacement vectors at S/D = 10%. In Figs. 12 and 13, the overburden pressures shown are 100 and 300 kPa, respectively. In general, we can confirm that displacement occurred until depths of approximately 2.5D to 3D from the pile tips regardless of the pile geometry or overburden pressure. Focusing on the area around the pile tips, we observed a wedge-shaped area directly below the pile-tip surfaces, where a relatively large vertical downward displacement occurred regardless of the pile geometry or overburden pressure. At depths of 0.5D to 1D or more from the pile-tip surfaces, displacement occurred diagonally downward outside the wedge-shaped area. This trend is consistent with the finding of previous study that modeled vertical loading with straight piles[7)]. Apparently, lateral movement occurred simultaneously with downward compressive deformation at the base of the piles. Comparing the differences in pile geometry in Fig. 12, the downward diagonal displacement from the tip of the wedge-shaped area occurred at a slightly deeper position for the straight piles than for the belled piles. As shown in Fig. 13, the depth at which downward diagonal displacement from the tip of the wedge-shaped area occurred was closer to the pile-tip surfaces compared with the case at 100 kPa, and no difference in pile geometry was observed at that depth compared with the case at 100 kPa.

Fig. 14 shows a comparison of the ground horizontal displacement at S/D = 10% in terms of the pile geometry and overburden pressure. This figure shows the displacement of track points in the PIV analysis extracted at intervals of D/4 in the horizontal direction, and the displacement amount is magnified by 10× for both the horizontal and vertical displacements. Ground horizontal displacement

 © DFI International Bruges 2025

occurred at depth of 1.5D to 2D from the pile-tip surfaces, within a range of 1D from the pile side surfaces regardless of the pile geometry and overburden pressure. In Figs. 14a) and 14b), we could not confirm a significant difference in the overburden pressure based on differences in the pile geometry. In Figs. 14c) and 14d), differences in the overburden pressure were observed in the horizontal displacement at depths of 0.5D or more from the pile-tip surfaces for the belled piles, and at depths of 1D or more for the straight piles. The horizontal displacement was larger at lower overburden pressures. Additionally, the depth at which the abovementioned differences occurred differed depending on the pile geometry.

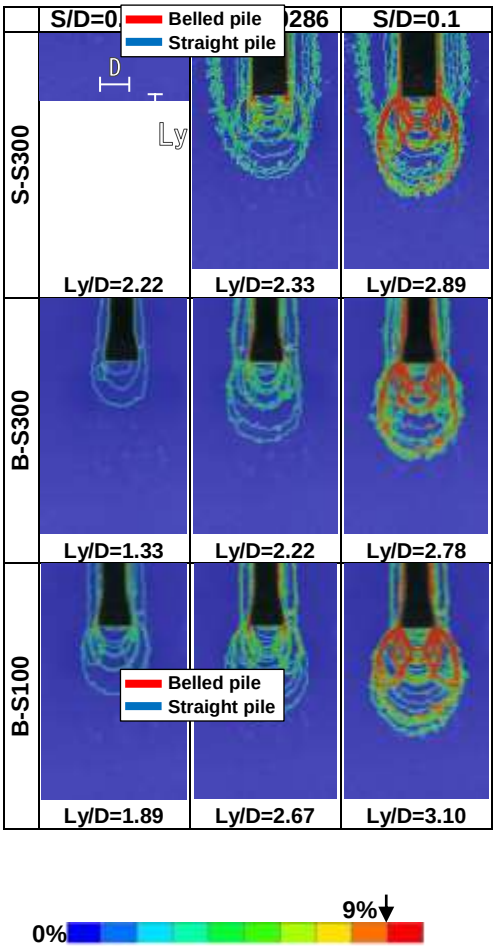


Fig.11. Distribution of maximum shear strain in group pile

Fig. 15 shows a comparison of the distributions of the ground vertical displacement at S/D = 10% in terms of the pile geometry and overburden pressure. The visualization method of the figure is the same as that of Fig. 14. Vertical displacement occurred in the ground at depths of approximately 2.5D to 3D from the pile-tip surfaces, within a range of 1D from the pile side surfaces. For the vertical displacement, the difference in depth and magnitude due to differences in the pile geometry and overburden pressure was insignificant.

During group-pile loading

Figs. 16 and 17 show the ground displacement vector at S/D = 0.1. Specifically, Figs. 16 and 17 show the cases for belled and straight piles, respectively, at the same overburden pressure of 300 kPa. Directly below the pile tips, a wedge-shaped area where a relatively large vertical downward displacement occurred was observed regardless of the pile geometry. In the GN series, owing to the narrow pile spacing, the wedge-shaped area was formed as a single large pile by the group piles, and outside the area, displacement occurred diagonally downward relative to the pile-tip surfaces. Similarly, diagonal downward displacement occurred at pile-spacings GM and GW, and at the ground in the middle of the group piles, it changed to a mutually interfering downward displacement. In

 © DFI International Bruges 2025

previous study[8], it was analyzed from the results of image analysis during three-pile loading that the horizontal displacement generated just below the pile tip face interferes with the ground in the middle of the group piles, increasing the lateral confining pressure of the ground below the piles in the center of the group piles and increasing their stiffness, which in tur increases the tip bearing capacity of the center pile. Although most of the previous experiments were conducted on straight piles, horizontal displacement like that of straight piles was observed in the ground inside the group piles for expanded bottom piles. However, as shown in Fig. 16, oblique downward displacement interference was also observed for the diagonal piles, and there was no significant difference in the depth of displacement interference due to pile geometry.

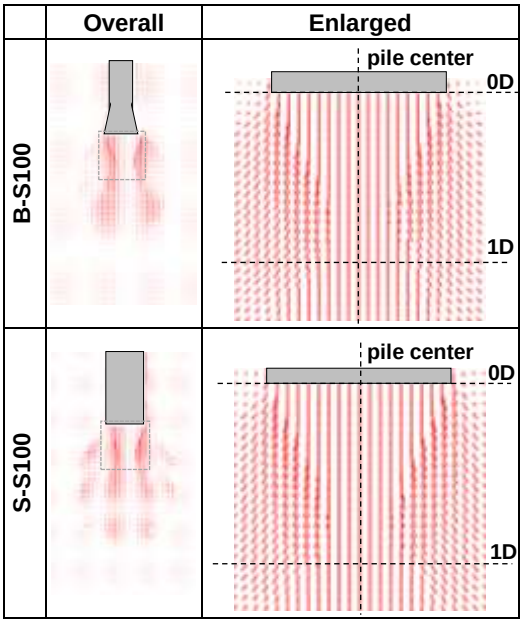


Fig.12. Behavior of the ground at S/D=0.1 (σ'v=100kPa)

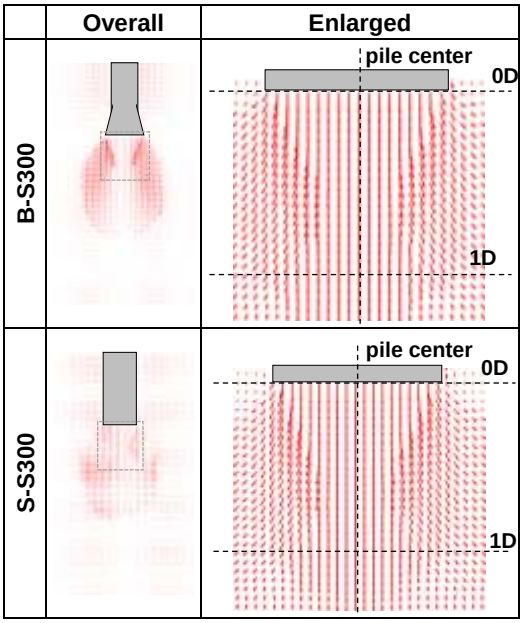


Fig.13. Behavior of the ground at S/D=0.1 (σ'v=300kPa)

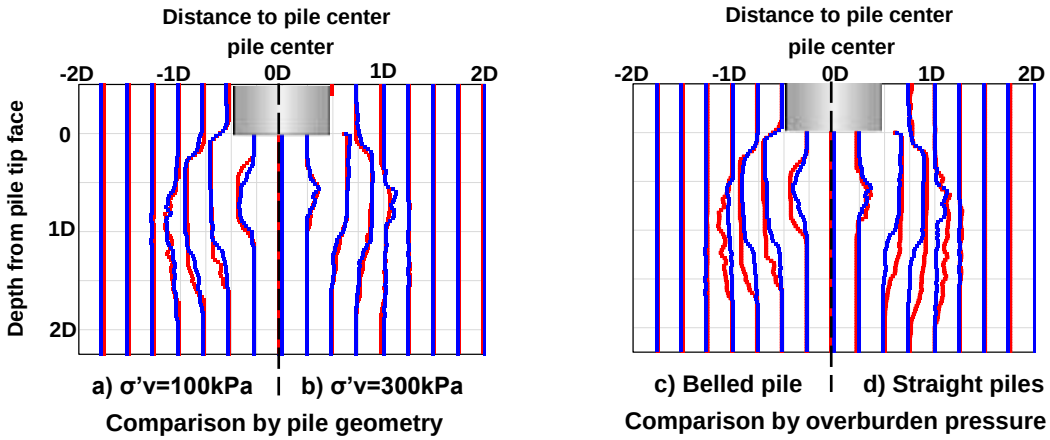


Fig.14. Distribution of horizontal displacement in single pile (S/D=0.1)

Fig. 18 shows the distribution of horizontal displacement of the ground at S/D = 10% during group-pile loading per pile spacing. The ground overburden pressure was 100 kPa. As shown in the figure, regardless of the pile spacing, displacement occurred within a range of 1D horizontally from the pile side surfaces outside the group piles, and within 2D to 2.5D deep from the pile tips. Additionally, no significant difference due to pile geometry was observed between outside the group piles and the ground directly below the pile cores. Meanwhile, in the ground inside the group piles, no

 © DFI International Bruges 2025

ground horizontal displacement was observed for B-GN100 and S-GN100, as shown in Fig. 18a). However, in the cases of pile-spacings GM and GW shown in Figs. 18b) and c), horizontal displacement occurred in the ground inside the group piles, and this horizontal displacement was larger for the belled piles than for the straight piles; additionally, the pile geometry differed even under the same pile spacing. In the case of pile-spacing GN, the pile base surfaces horizontally restrained the ground below the pile-tip surfaces owing the narrow pile spacing, which was speculated to have inhibited the occurrence of horizontal displacement.

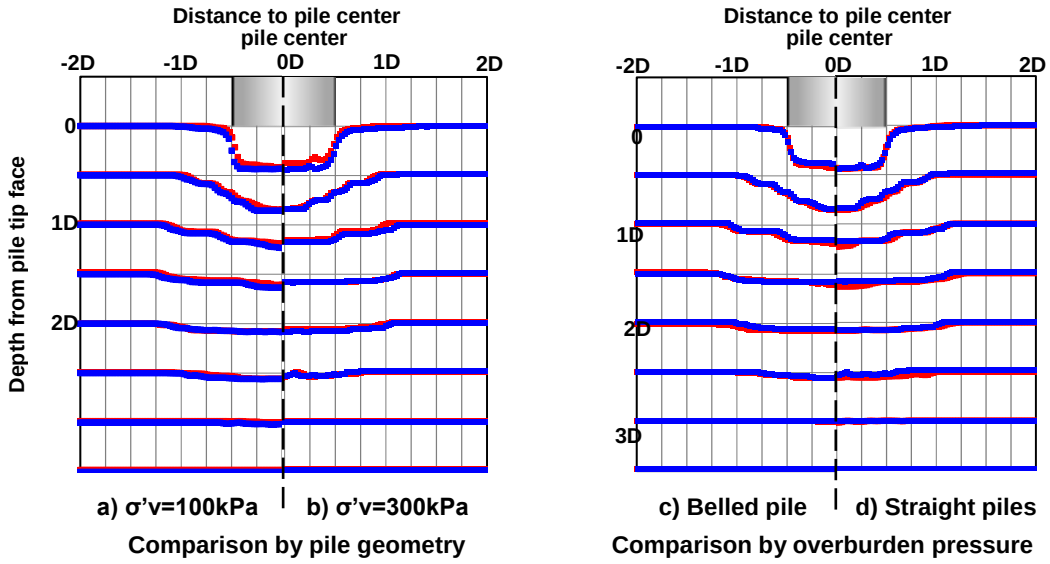


Fig.15. Distribution of vertical displacement in single pile (S/D=0.1)

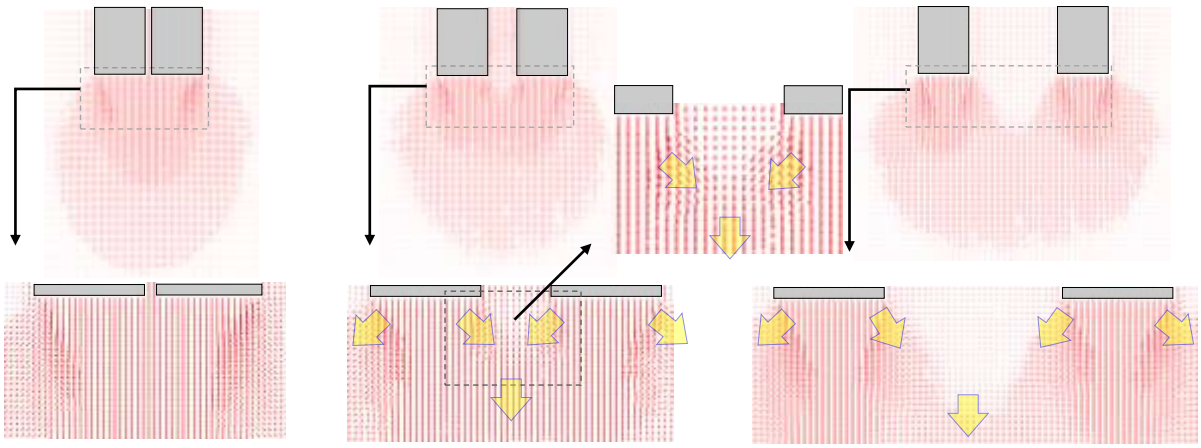


Fig.16. Behavior of the ground in group of straight piles (S/D=0.1, σ'v=300kPa)

Fig. 19 shows the distribution of ground horizontal displacement at S/D = 10% during group-pile loading per pile spacing. The ground overburden pressure was 300 kPa. Based on Figs. 19b) and c), when comparing the ground horizontal displacement inside the group piles for the belled and straight piles, the difference was insignificant compared with the case when the overburden pressure was 100 kPa. Additionally, the smaller the overburden pressure, the greater was the difference in the horizontal displacement depending on the pile geometry.

Fig. 20 shows the distribution of ground vertical displacement at S/D = 0.1 for the group piles per pile

 © DFI International Bruges 2025

spacing. The ground overburden pressure was 100 kPa. The vertical displacement extended to a depth of approximately 4D from the pile-tip surfaces regardless of the pile geometry or pile spacing, and no differences due to pile geometry could be confirmed. The trend was the same as that under a ground overburden pressure of 300 kPa.

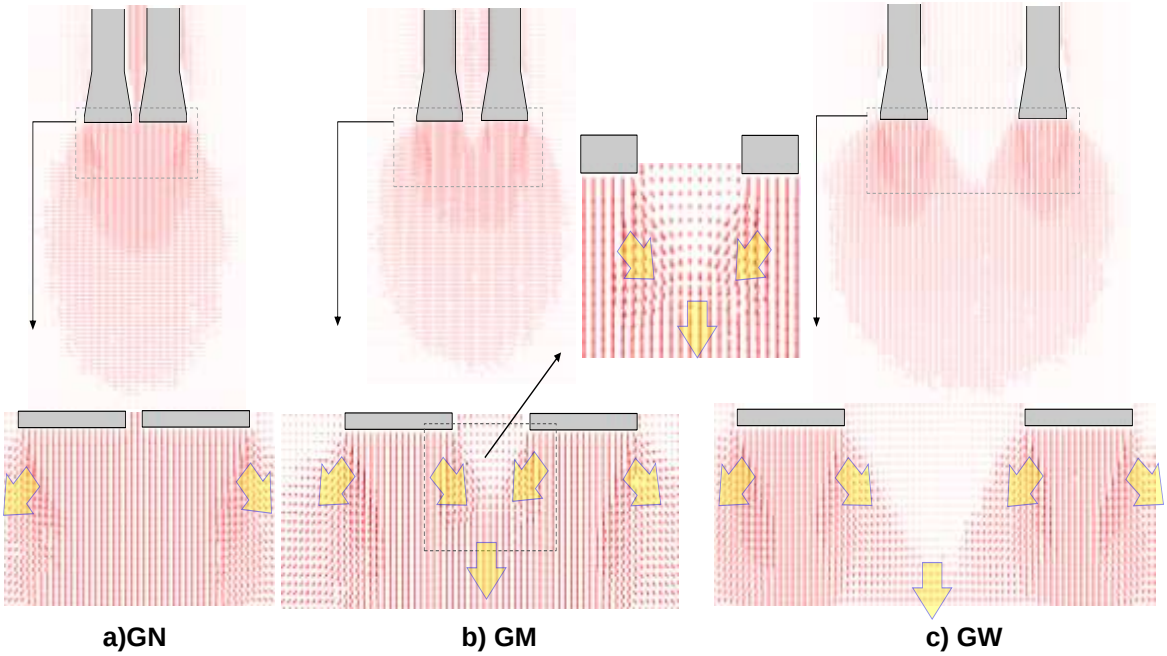


Fig.17. Behavior of the ground in group of belled piles (S/D=0.1, σ'v=300kPa)

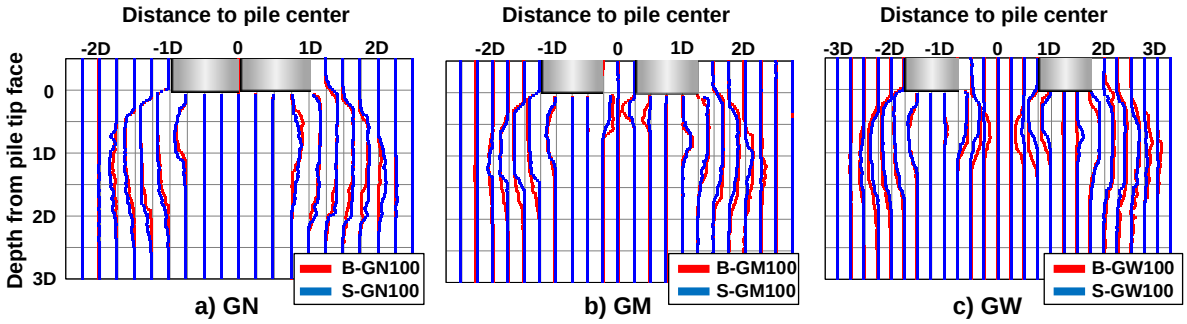


Fig.18. Distribution of horizontal displacement in group piles
Comparison of pile geometries at the same pile spacing (S/D=0.1, σ'v=100kPa)

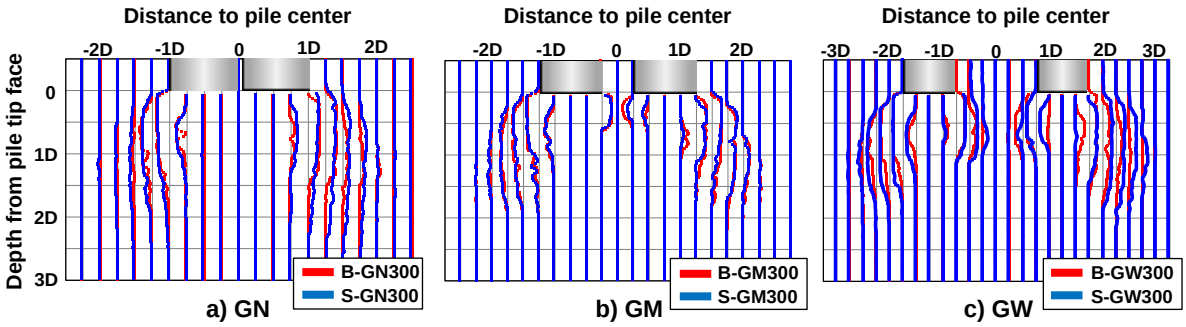


Fig.19. Distribution of horizontal displacement in group piles
Comparison of pile geometries at the same pile spacing (S/D=0.1, σ'v=300kPa)

 © DFI International Bruges 2025

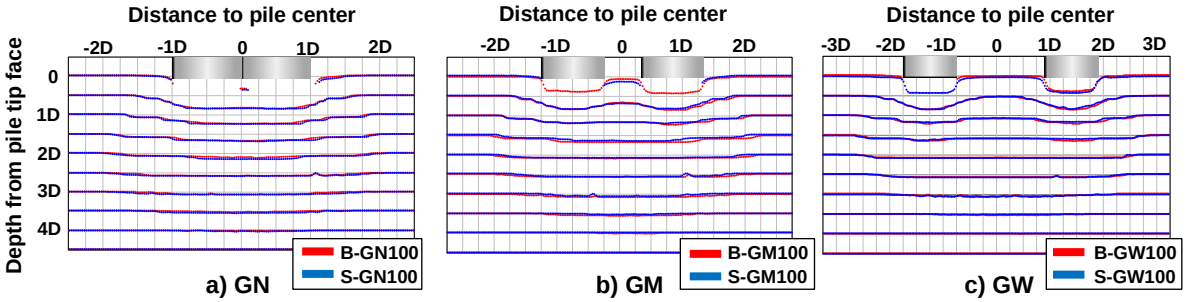


Fig.20. Distribution of vertical displacement in group piles
Comparison of pile geometries at the same pile spacing (S/D=0.1, σ'v=100kPa)

Based on the above, no difference in the ground horizontal distribution during group-pile loading due to pile geometry was indicated between the outside of the group piles and the ground directly below the pile cores. However, differences due to pile spacing and pile geometry were observed on the inside of the group piles. By contrast, no differences were observed in the distribution of vertical displacement due to pile spacing or pile geometry.

CONCLUSION

In this study, we observed the distributions of ground shear strain and displacement for pile tips during group-pile loading. Differences due to pile geometry were confirmed based on the magnitude of horizontal displacement in the ground inside the group piles under the same pile spacing. In cases of narrow pile spacing, no horizontal displacement occurred in the ground inside the group piles. However, when the pile spacing was widened, horizontal displacement occurred in the ground inside the group piles, where the horizontal displacement of belled piles was larger than that of straight piles. Furthermore, the lower the ground overburden pressure, the greater was the difference in horizontal displacement between the straight and belled piles. In previous study[8)] in which three straight piles were loaded, it was analyzed that the interference of the horizontal displacement of the ground in the center of the group piles increased the lateral confining pressure of the ground under the piles in the center of the group piles, increasing the stiffness of the center pile and thus the bearing capacity at the tip of the center pile.
Therefore, the difference in horizontal displacement due to pile geometry observed in this study suggests that the group pile effect differs between belled piles and straight piles.
In the future, we plan to conduct experiments with different number of piles and pile diameters, and with model piles in which the pile head load can be separated into tip resistance and circumference skin friction, to study the effect of the difference in horizontal displacement due to pile geometry on the group pile effect in more detail.

REFERENCES

1) Kuwabara, F. 1991. Mechanism and bearing capacity of pile tip support of expanded bottom cast-in-place piles. The foundation engineering & equipment, 19(12), 9-15
2) Aoyama, S., Danaridli, L., Bangan, L., Goto, S. and Towhata, I. 2012. Study of the interaction of the group pile by applying the PIV to the pictures of ground deformation during the loading, 9th Kanto Branch Conference of the Japanese Geotechnical Society
3) Kiriyama, T., Zhou, Y., Odagiri, M. and Asaka, Y. 2024. Ground failure patterns of dense sand layer in foundation loading by Digital Image Correlation. The Japanese Geotechnical Society, 59th Japan National Conference on Geotechnical Engineering
4) Kiriyama, T., Zhou, Y., and Asaka, Y. 2022. Observation of ground behavior during pile loading test in centrifuge by particle image velocimetry (PIV). Korean Geotechnical Society (KGS), International society for soil mechanics and geotechnical engineering 2022, Korea, 881-884
5) Fast Pattern Matching, Shark, User manual, 2023. Library co., Ltd, 14p.

 © DFI International Bruges 2025

2D-Motion Analysis, Move-tr/2D, User manual, 2023. Library co., Ltd, 122p.
2D-Strain Analysis, Strain-mp User manual, 2023. Library co., Ltd, 26p.
6) Miyamoto, S., Miyata, Y. 2022. Experimental Investigation on Ground Displacement Measurement in Geotechnical Physical Modeling using PIV Technique. Japanese Journal of Japan Society of Civil Engineering, SER.A2 Applied Mechanics, 78(1), 1-10
7) Takano,A. and Kishida,H. 1979. Failure Mechanism of Soil Mass under Base of Non-displacement Pile in Sand, Transactions of the Architechtural insutitute of Japan, No.285, 51-62
8) Report on the Activities of the Committee for the Empirical Study of Group Pile Behavior and the Committee for the Empirical Analysis and Review of Group Pile Behavior, 2015. Japanese Geotechnical Society, 384p.

 © DFI International Bruges 2025

Investigation of soil reaction curves extracted from 3D FE models.

A. Kheffache
Ghent University, Ghent, Zwijnaarde 9052, Belgium.

B. Stuyts
Ghent University, Ghent, Zwijnaarde 9052, Belgium.

ABSTRACT: Monopiles are the preferred type of support structures for offshore wind turbines due to their technical and economical suitability. Monopiles have been designed for a long time using recommendations drawn from the Oil and Gas industry such as the API/DNV guidelines, which were shown to be unreliable for the design of large diameter piles, as the recommendations have been formulated for much slender ones. New design methodologies have since then been developed, namely the PISA methodology in which in situ testing and advanced simulations were carried out on piles having a comparable aspect ratio *L/D* as monopiles used in the offshore wind industry.

In this paper, the soil reaction curves are extracted from a 3D Finite Element model of the monopile and the surrounding soil, using lateral pushover analysis. The soil is modelled using advanced sand and clay constitutive models which were calibrated using laboratory as well as in situ test results. The extracted reaction curves are compared to the input rule-based PISA and API RP2 GEO reaction curves used in 1D monopile beam-column models. The results are discussed and conclusions are drawn.

Keywords: reaction curves, finite element method, beam-column, offshore wind turbines

1 INTRODUCTION

The evolution of offshore wind turbine sizes (increase of mass and length) is leading to a decrease of their natural frequency f0 (typically in the range of 0.2-0.3 Hz) towards the wave-forcing frequency range (typically 0.1-0.2 Hz) as shown in Figure 1, raising concerns about any possible dynamic amplification of the structural response due to resonance. The need for models that can accurately predict the stiffness of offshore wind turbines is now more critical than ever.

Monopile foundations have for a long time been designed using methodologies drawn from the Oil and Gas industry, such as the API RP2 GEO (API, 2011) and DNV (DNV, 2014) recommendations, in which the pile is simulated as a 1D beam-column and the soil response is captured using nonlinear lateral springs; the so called *p-y* reaction curves. The first version of the p-y curves was developed empirically using lateral loading test results on piles that were 610mm in diameter and 21m in penetration depth, setting the slenderness ratio *L/D* of the tested pile to 34.4 (Cox et al., 1974). At the same time, the wind turbine monopiles have slenderness ratio values between 4 and 6, which falls outside of the range of applicability of the API RP2 GEO/DNV *p-y* curves. Moreover, these curves do not take into account the extra components to the overall lateral stiffness and strength of monopiles.

Following the mismatch between the measured and predicted natural frequency of the wind turbine structure, new design methodologies that are more adapted to large-diameter piles have been developed. The joint industry PISA project (Burd et al., 2020; Byrne et al., 2020) developed new design methodologies for monotonic-laterally loaded piles in sands and clays. The PISA methodology introduced new sets of reaction curves on top of the *p-y* ones (
Figure **2**) which are:

- Base shear H_B-y
- Base moment M_B-θ
- Distributed moment m-θ

 © DFI International Bruges 2025

Kheffache et al. (2024) carried an investigation on the bending moments of five monopile-supported offshore wind turbines using 3D FEM models, 1D beam-column models using API RP2 GEO and PISA reaction curves, as well as monitoring data. They also compared the different modeling approaches and concluded that the bending moment profiles were sensitive to the lateral stiffness of offshore wind turbines, 3D FEM models resulted in closer bending moment profiles compared to the monitored ones, due to a higher stiffness. The PISA models were less stiff than the 3D FEM ones while the API RP2 GEO exhibited the least amount of stiffness. The reason behind the different stiffness values is investigated in this paper.

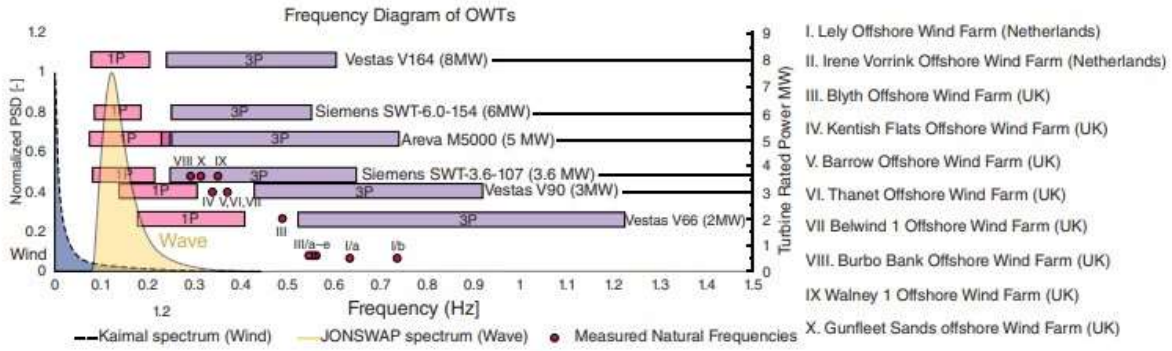


Figure 1. Evolution of wind turbines frequencies across multiple wind farms (Bhattacharya, 2019)

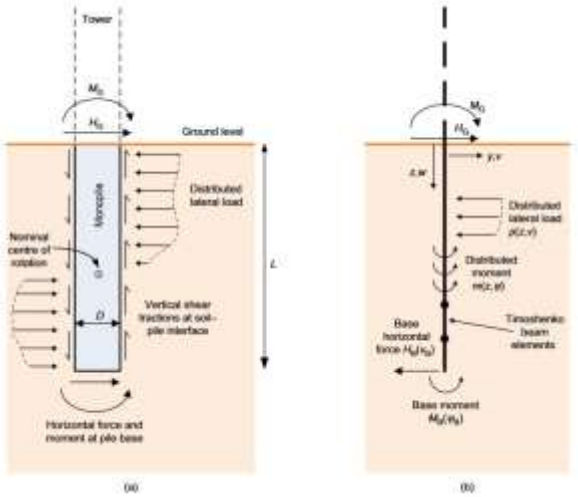


Figure 2. Representation of the PISA reaction curves applied on (a) laterally loaded pile (b) 1D beam-column model

2 SITE CONDITIONS

2.1 Monopile

The studied monopile is located in the Belgian North Sea. It has been monitored using Fiber Bragg Gratings (FBGs) which record the strains along the monopile. The monopile's geometry details are given in **Table *1*** where *h* is the stick-up length, *L* is the penetration length, *t* is the wall thickness, and *D* is the diameter. The position of the FBGs is shown in

 © DFI International Bruges 2025

Figure **3**.

Table 1. Monopile geometry

h (m)	L (m)	t (mm)	Water depth (m)	D (m)
37	29.9	57-95	32	5

2.2 Soil conditions

The monopile is embedded in a two-layered soil medium where the first 8m is a medium-dense quaternary sand, the lower soil part is made of overconsolidated tertiary clay, that may include a descent amount of sandy layers. This layering is typical in the Belgian North Sea, the top layer sand tends to increase in thickness in the north-east, while the clay layer rises to the mudline level towards the south-west direction. The piezocone penetration test (CPTu), soil profile at the wind turbine's location is shown in
Figure **3**.

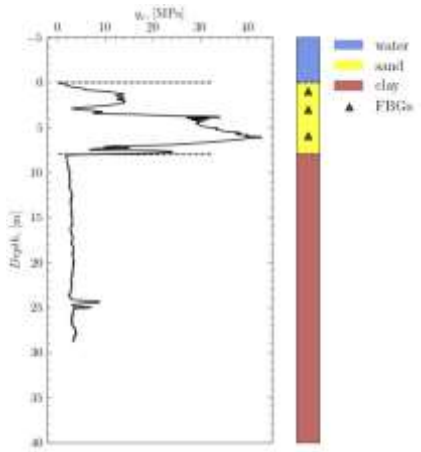


Figure 3. CPT, FBGs and soil layering at the wind turbine's location.

3 FE MODELLING

The 3D finite element model of the pile and soil is shown in
Figure ***4***. The size of the model was selected iteratively, until limited effects on the results were observed.

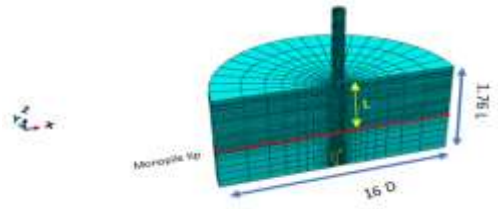


Figure 4. 3D FEM model showing the pile and soil parts

 © DFI International Bruges 2025

3.1 *Soil*

The soil sand and clay layers are modelled using the hypoplastic models (Mašín, 2013; von Wolffersdorff, 1996). The constitutive models have been previously calibrated (Kheffache et al., 2024), the calibration is not repeated here for brevity. The constitutive models are first calibrated using the available laboratory test data, performed on soil samples that were extracted from boreholes close to the wind turbine location. The calibration is then optimized using in-situ test data that consists of Seismic (SPCTu) and CPT measurements around the wind turbine location. The measured and calibrated G_{max} profiles are shown in
Figure ***5***, the values below 30m (depth at which the CPT data stops) were extrapolated from nearby borehole-CPT which can go up to 60m depth.

The soil stress was initialized using a K0 initial stress state, where K0 is the coefficient of earth pressure at rest, calculated using the following equation:

$$K \quad (1 \qquad)OC \qquad [1]$$

Where φ_c is the critical state friction angle and OCR is the overconsolidation ratio, interpreted using oedeometer tests. The sand initial void ratio was established using water content measurements. The calibrated soil stiffness profile is shown in
Figure ***5***.

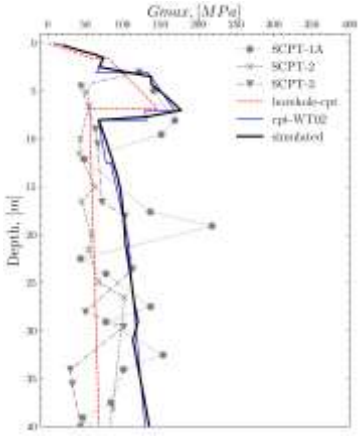


Figure 5. Calibrated Gmax profiles (Kheffache et al., 2024).

3.2 Monopile

The monopile is modelled using C3D8I mesh elements which are incompatible 3D continuum 8 noded fully integrated linear brick elements, recommended for solid elements subject to bending (Abaqus, 2011). A comparative study was done by comparing C3D8I elements to S4R (shell) bending moments, negligeable differences were observed.

3.3 Boundary conditions

Only half of the model is modelled, taking advantage of symmetry. The symmetry plane is fixed in the normal direction (horizontal). The outer model is fixed in all directions except the vertical. The model is fixed in all directions at the bottom.

 © DFI International Bruges 2025

3.4 Interface

The tangential interface behaviour is modelled using a Mohr-Coulomb friction coefficient μ. The calculated values for the sand and clay layers were between 0.3 and 0.5, a sensitivity analysis was performed on μ values which indicated that this parameter had no effect on the computed bending moments. An uniform value of μ=0.5 was adopted along the monopile. The normal contact behaviour was modelled using the 'hard' contact pressure overclosure relationship.

4 RESULTS AND DISCUSSION

4.1 Validation of the 3D FEM model

The developed 3D FEM model is validated using centrifuge tests on two laterally loaded piles, performed by Wang et al. (2021). The model scale piles were instrumented with strain gauges (SGs), the centrifuge acceleration was set to 100g. the size of the scale and prototype piles are given in the following table:

Table 2. Geometry of the prototype and scale piles in the centrifuge test.

	Diameter (m)	Length (m)	L/D
Scale pile	0.04-0.06	0.6	15-10
Prototype pile	4-6	60	15-10

The slenderness L/D ratios of both piles are of 15 and 10, which is slightly higher than the common slenderness ratio of monopiles that are currently used (L/D < 10). The piles were embedded in a Toyoura sand which was compacted to a relative density of 65%. The Toyoura sand hypoplastic parameters were previously calibrated by Hong et al. (2017), and are used in this analysis. The force-displacement results are shown in Figure 6 (a). It can be seen that the simulated piles closely replicate the behavior of the tested ones, however, small discrepancies are noted for the pile with 6 m diameter at larger displacements. The simulated and recorded bending moments for the 4 m diameter pile are shown in Figure 6 (b), where a good match can be seen under two different load levels. The lateral reaction curves were then extracted by differentiating the bending moment at each depth twice, according to the following equation:

$$p = -\frac{d^2M}{dz^2} \quad [2]$$

Where M is the bending moment at depth z. It should be nothed that this method might not be suitable for large diameter piles, as both lateral and vertical shear influence the bending moment. The numerical reaction curves were extracted by integrating the stresses on the soil elements in contact with the pile. The results are shown in Figure , it can be seen that the numerical reaction curves are also in close agreement with the computed ones at each depth.

 © DFI International Bruges 2025

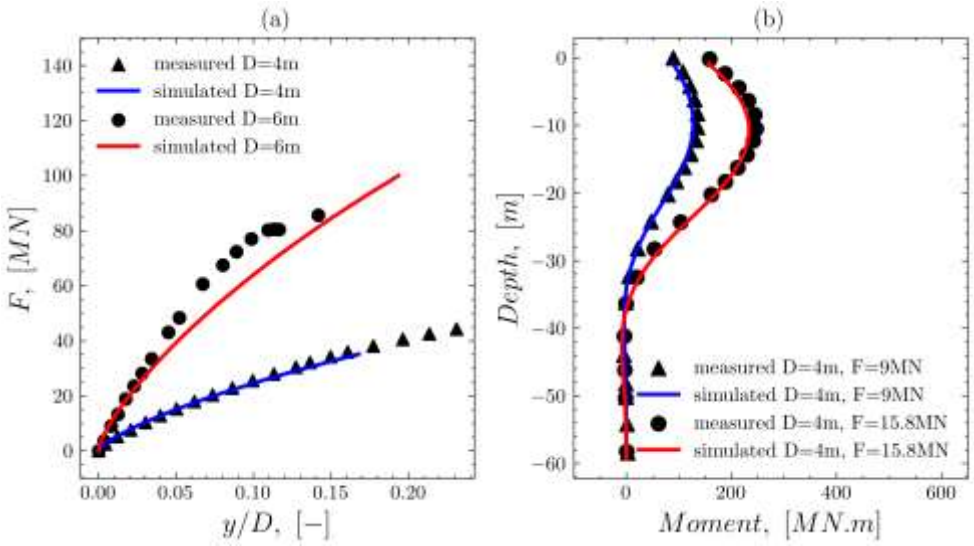


Figure 6. Comparison between the simulated and measured: force-displacement curves (a), bending moments (b), Kheffache et al. (2024)

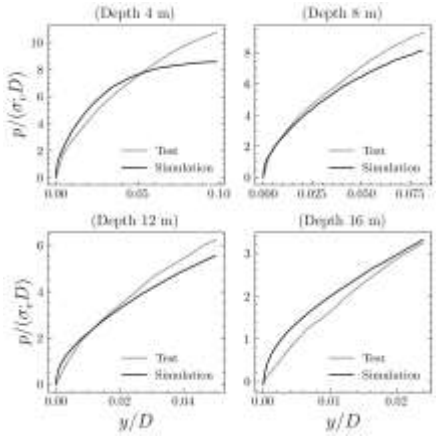


Figure 7. Comparison between the simulated and measured reaction curves in the centrifuge test, on the 4m prototype pile.

4.2 Extraction of reaction curves from 3D FEM models

The monopile model is subjected to lateral load at the head level until failure, which is generally assumed to be characterized by a mudline displacement of 0.1D, where D is the monopile's diameter. The pushover analysis results are shown in Figure 8, where it can be seen that the FEM capacity curve is stiffer than the 1D-PISA and API ones. The PISA capacity curve is comparable to the FEM one, while for the API curve, the same ultimate load as for FEM and PISA is reached at around 2m of displacement at the mudline level, exceeding the conventional 0.1D limit, which was not reached by the FEM and PISA curves. The pile-soil total contact forces (CTF) which are a combination of normal and shear contact forces (CSF and CNF respectively) are extracted from each segment, the soil resistance *p* is calculated by summing the forces acting on a segment and multiplying them by two (due to symmetry), then dividing the total by the segment's thickness, resulting in a soil resistance in units of *kN/m.* The extracted p-y reaction curve from the 3D FEM model as well as the rule based PISA and API RP2 GEO p-y curves are shown in

 © DFI International Bruges 2025

Figure **9** at a depth of 0.15D. It can be seen that out of all the curves, the FEM based reaction curves are stiffer and can mobilize more soil pressure *p*, however, the critical (post-peak) value of *p* from the FEM models seems similar to the PISA one. It should be that the PISA reaction curve formulation explicitly ignores the peaks, and sets the ultimate resistance to the critical one (at larger displacements). Due to the dynamic nature of offshore wind turbines, a stiffer behavior has direct implications on the dynamic stability of such structures. In fact, monopile-supported offshore wind turbines were seen to be stiffer (in the monitoring data) compared to the simulations. This mismatch can be due to several reasons, one of them being the use of methodologies that poorly capture the soil-monopile interactions, leading to a soft numerical response compared to reality.

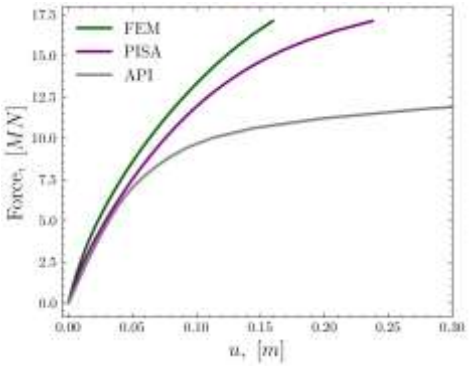


Figure 8. 3D FEM Pushover analysis, load applied at the top of the monopile

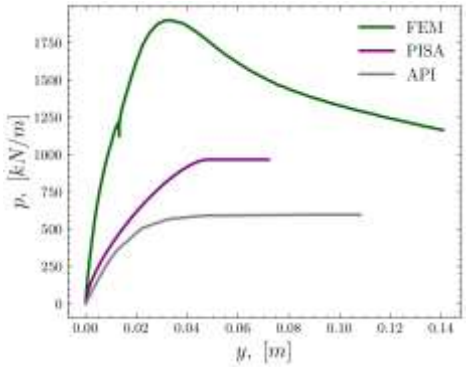


Figure 9. p-y reaction curve extracted from the 3D FEM model and the 1D beam-column using PISA and API guidelines, at a depth of 0.15D.

 © DFI International Bruges 2025

In Figure 10, the initial stiffness of the p-y curves *k* is shown along the normalized depth *z/D* obtained from different models. It can be seen that the 3D FEM p-y curves are generally stiffer than both the PISA and API RP2 GEO ones along the monopile depth (in both sand and clay layers). In terms of soil pressure *p*, the results obtained by the 3 approaches are generally in agreement at shalow levels (from 0 to 0.22L, where L is the monopile's length), all the lateral resistance is fully mobilized in this depth range, in all 3 models. At deeper levels (below 0.2L), the soil pressure is fully mobilized in the API model, which explains the lower lateral pile capacity observed in

Figure **8**. The pressure mobilization in both the 3D-FEM and 1D-PISA approaches are almost identical, even closely replicating the zero pressure at the depth of 0.6L, characteristic of the rotation point location.

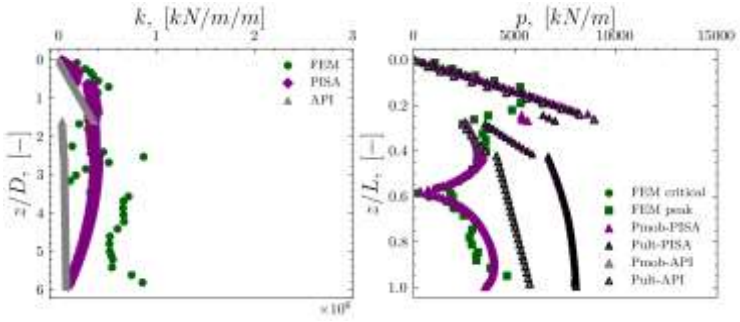


Figure 10. p-y curves initial stiffness k and pressure p

5 CONCLUSIONS AND RECOMMENDATIONS

In this work, the different stiffness values exhibited during the simulation of laterally loaded wind turbine monopiles, using different approaches, namely 3D FEM and 1D beam-column models using the API RP2 GEO and PISA rule-based nonlinear springs, are investigated. The following conclusions are drawn:

- The extracted 3D FEM *p-y* curves have a higher stiffness than the API RP2 GEO and the rule-based PISA ones along the monopile depth, and can generally mobilize more soil resistance due to the peak behavior.
- The PISA rule-based curves can be recalibrated to match the 3D *p-y* curves, which would enhance the 1D beam-column modeling of offshore wind turbines, as the increase in p-y curves stiffness and capacity would lead to a better agreement with the monitoring data (bending moments and resonance frequencies).
- The scour protection surrounding the monopiles are suspected to be the reason between most of the mismatch between simulations and monitoring, studying their effect on the lateral response of monopiles (effect on p-y curves) is needed.

In future work, the PISA *p-y* curves are going to be recalibrated to match the 3D FEM ones. Moreover, the other reaction curves (m-θ, M_b-θ and H_B-θ) are also going to be re-evaluated.

ACKNOWLEDGEMENTS

The authors would like to acknowledge the support of the Belgian Ministry of Economic Affairs through the EFT project WINDSOIL project. The Support of VLAIO through the De Blauwe Cluster SBO SOILTWIN project is also acknowledged.

 © DFI International Bruges 2025

REFERENCES

Abaqus, G. (2011). Abaqus 6.11. Dassault Systemes Simulia Corporation, Providence, RI, USA, 3.

API. (2011). API RP2 GEO Geotechnical and Foundation Design Considerations.
Bhattacharya, S. (2019). Design of Foundations for Offshore Wind Turbines (1st ed.). Wiley. https://doi.org/10.1002/9781119128137

Burd, H. J., Taborda, D. M. G., Zdravković, L., Abadie, C. N., Byrne, B. W., Houlsby, G. T., Gavin, K. G., Igoe, D. J. P., Jardine, R. J., Martin, C. M., McAdam, R. A., Pedro, A. M. G., & Potts, D. M. (2020). PISA design model for monopiles for offshore wind turbines: Application to a marine sand. Géotechnique, 70(11), 1048–1066. https://doi.org/10.1680/jgeot.18.P.277

Byrne, B. W., Houlsby, G. T., Burd, H. J., Gavin, K. G., Igoe, D. J. P., Jardine, R. J., Martin, C. M., McAdam, R. A., Potts, D. M., Taborda, D. M. G., & Zdravković, L. (2020). PISA design model for monopiles for offshore wind turbines: Application to a stiff glacial clay till. Géotechnique, 70(11), 1030–1047. https://doi.org/10.1680/jgeot.18.P.255

Cox, W. R., Reese, L. C., & Grubbs, B. R. (1974). Field testing of laterally loaded piles in sand. Offshore Technology Conference, OTC-2079. https://onepetro.org/OTCONF/proceedings-abstract/74OTC/All-74OTC/46408

DNV. (2014). DNV-OS-J101 Design of Offshore Wind Turbine Structures.

Hong, Y., Koo, C. H., Zhou, C., Ng, C. W. W., & Wang, L. Z. (2017). Small Strain Path-Dependent Stiffness of Toyoura Sand: Laboratory Measurement and Numerical Implementation. International Journal of Geomechanics, 17(1), 04016036. https://doi.org/10.1061/(ASCE)GM.1943-5622.0000664

Kheffache, A., Stuyts, B., Sastre Jurado, C., Weijtjens, W., Devriendt, C., & Troch, P. (2024). Advanced simulations of monitored wind turbine monopiles located in the Belgian North Sea under operational quasi-static loading. Ocean Engineering, 311, 118914. https://doi.org/10.1016/j.oceaneng.2024.118914

Mašín, D. (2013). Clay hypoplasticity with explicitly defined asymptotic states. Acta Geotechnica, 8(5), 481–496. https://doi.org/10.1007/s11440-012-0199-y
von Wolffersdorff, P.-A. (1996). A hypoplastic relation for granular materials with a predefined limit state surface. Mechanics of Cohesive-Frictional Materials, 1(3), 251–271. https://doi.org/10.1002/(SICI)1099-1484(199607)1:3<251::AID-CFM13>3.0.CO;2-3

Wang, H., Wang, L., Hong, Y., Mašín, D., Li, W., He, B., & Pan, H. (2021). Centrifuge testing on monotonic and cyclic lateral behavior of large-diameter slender piles in sand. Ocean Engineering, 226, 108299. https://doi.org/10.1016/j.oceaneng.2020.108299

 © DFI International Bruges 2025

LESSONS LEARNT FROM BACK-ANALYSIS OF OFFSHORE MONOPILE LATERAL RESPONSE

Bruno Stuyts, Vrije Universiteit Brussel (OWI-Lab), Brussels, Belgium, bruno.stuyts@vub.be
Wout Weijtjens, Vrije Universiteit Brussel (OWI-Lab), Brussels, Belgium, wout.weijtjens@vub.be
Christof Devriendt, Vrije Universiteit Brussel (OWI-Lab), Brussels, Belgium, christof.devriendt@vub.be
Carlos Sastre Jurado, Vrije Universiteit Brussel (OWI-Lab), Brussels, Belgium, carlos.sastre.jurado@vub.be

ABSTRACT

Monopiles are a widely used foundation type for offshore wind turbine structures. They support the tall and slender superstructure and have an impact on the dynamic behavior of the entire structure. The thrust loads generated by the wind on the wind turbine blades and tower and the loads due to wind, waves and current on the submerged part of the structure lead to cyclic loading, with oscillating bending moments in the monopile. These bending moments are absorbed by the soil surrounding the monopile and the lateral pile-soil interaction governs the magnitude of the bending moments below the ground level.

The dynamic behavior of the wind turbine structure and the resulting fatigue stress cycles govern the design of offshore wind turbine structures. Hence, it is important to accurately predict the natural frequency of the wind turbine structure and the influence of the pile-soil interaction on the dynamics. To validate existing theoretical models, the WINDSOIL research project was set up to back-analyze pile-soil interaction stiffness and wind turbine structure natural frequency across all the structures in an offshore wind farm. The project made use of in-situ monitoring of natural frequencies for benchmarking the natural frequency estimates.

The approach followed in the WINDSOIL project can be applied to other types of piled foundations or retaining structures where accurate predictions of displacement or dynamics is required. This paper describes the more accurate soil stiffness modelling which was carried out based on the results of in-situ tests and shows how the small-strain stiffness of the soil influences leads to more accurate estimation of the pile dynamics. The importance of modelling surcharges around the pile (scour protection in this case) is also highlighted.

Keywords: monopile, offshore, lateral

INTRODUCTION

Offshore wind energy is rapidly emerging as a cost-effective renewable energy alternative to fossil fuels (WindEurope, 2024). Compared to onshore wind energy, the offshore environment allows larger structures to be transported and the power of a single offshore wind turbine exceeds 10MW at the time of writing. The growth in turbine sizes imposes higher stresses on the support structure which in turn requires larger and heavier foundations. The majority of offshore wind turbines are supported by monopile foundations; large-diameter tubular piles which are installed by impact driving. To reduce the cost of offshore wind energy, the dimensions of the monopile (diameter and wall thickness) need to be optimized while still meeting the design requirements.

The thrust load on the rotor and the environmental loads acting on the structure impose a large overturning moment at the seabed. The lateral support provided by the soil surrounding the monopile needs to be sufficient to absorb these moments while keeping the monopile tilt within acceptable limits. Moreover, the lateral stiffness provided by the pile-soil interaction is an important contributor to the dynamic response of the structure (Weijtjens and Devriendt, 2019). In this paper, the limit states of concern for monopile design are reviewed first.

The structural and geotechnical design of offshore wind turbine monopiles is generally performed using semi-empirical beam-column models calibrated to a limited number of instrumented onshore field tests. The available pile-soil interaction models are presented in the third section of the paper. The geotechnical properties used in these models are also discussed. While such controlled tests

 © DFI International Bruges 2025

provide valuable insights, the monopiles installed in the field are larger than the piles used in the field tests. Therefore, there is value in evaluating the in-field response of the full-scale structures using data from a monitoring system. **Fig. 1** shows an instrumented offshore wind turbine structure with strain gauges and accelerometers installed above the water level. Below the water level, an optical fiber with Fiber Bragg Gratings (FBGs) is used to measure the strains in the pile. To measure stresses and pore pressures in the soil, pore pressure and earth pressure sensors can be installed on the monopile below the mudline (Stuyts et al., 2023). Finally, a SCADA system measures the wind speed and the operational parameters of the wind turbine.

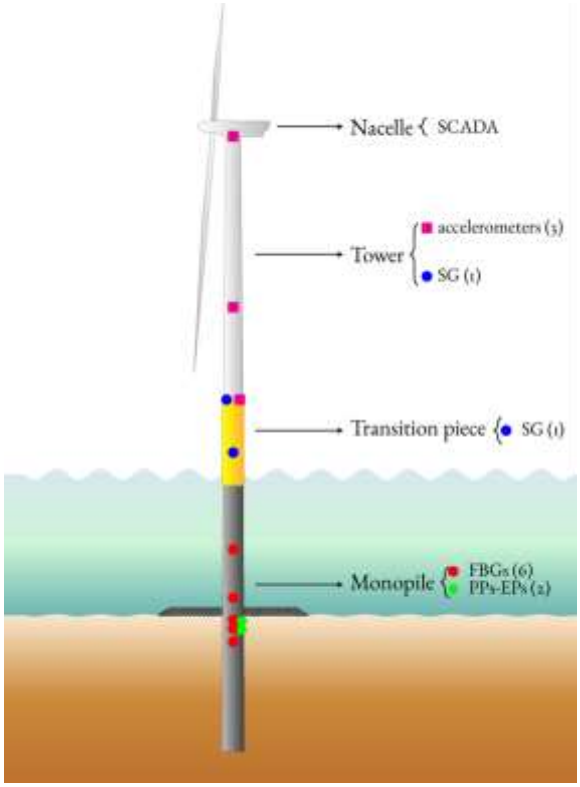


Fig. 1. Instrumented offshore wind turbine monopile

Based on the in-situ monitoring data captured with the sensors, the behavior of the offshore wind turbine structure can be back-analyzed and the geotechnical models for the pile-soil interaction can be fine-tuned. In this contribution, the dynamic behavior of a fleet of offshore wind turbine structures is back-analyzed in terms of the first natural frequency of the structure. The impact of the pile-soil interaction modelling on the first natural stiffness is investigated and the influence of the scour protection system is quantified.

GOVERNING LIMIT STATES FOR OFFSHORE WIND TURBINE MONOPILES

Ultimate limit state

The ultimate limit state (ULS) received the most attention for the design of offshore Oil & Gas platform jacket piles. Jacket structures transform much of the lateral loading on the topside to axial loads on the piles and as a result, the lateral loading during the lifetime of the piles is limited. The lateral loading during extreme storms governs the design in most cases and as a result, the design methods developed for lateral loading of Oil & Gas platform piles tend to provide conservative predictions.

For offshore wind turbine structures, the highest bending moments are imposed on the monopile when the turbine blades have the highest exposed area to the wind. This condition happens at a wind speed when the turbine reaches it rated power. For higher wind speeds, the blades are pitched out of the wind and the thrust load reduces while the rated power can be maintained. During extreme storms, the bending moments due to thrust loading are therefore not at their

 © DFI International Bruges 2025

maximum. This leads to the ULS not generally being the governing limit state in the design of monopile foundations.

Serviceability limit state

The turbine operation requires the tilting of the monopile to stay within acceptable limits. According to the DNV standards (DNV-ST-0126, 2021), the monopile and tower need to be installed with a maximum tower axis tilt of 0.25°. A total allowable tilt of 0.5° is proposed in the standard allowing for permanent deformations of the soil around the monopile to develop if they do not lead to more than 0.25° tilt. Cyclic loading is a concern in this respect as soil stiffness degradation could lead to additional displacements. Cyclic ratcheting was also observed during laboratory measurements (Liu et al., 2021). Cyclic soil testing can be combined with advanced constitutive models to perform 3D finite element analysis of the effects of cyclic loading on the accumulated tilt. These models often make the conservative assumption of fully undrained conditions during cyclic storm loading. Monitoring data at a wind turbine with a clean sand at the surface has revealed that this assumptions does not hold true, even during severe storms (Stuyts et al., 2023). Moreover, no studies have been found which reveal tilting problems for monopiles, which shows that the serviceability limits state (SLS) is also not the governing limit state.

Fatigue limit state

Offshore wind turbines are tall and slender structures with a heavy top mass which leads to a dynamic response of the structure. The structural steel is subject to millions of load cycles of varying amplitude during the lifetime of the structure and therefore the fatigue limit state (FLS) is often the governing limit state. To allow for a detailed calculation of the accumulated fatigue damage, the dimensions of the structure, the masses of the structural components and the stiffnesses of the structure itself and the pile-soil interaction stiffness need to be known. The geotechnical response of the soil surrounding the monopile is known to be non-linear and this complicates the definition of the pile-soil interaction stiffness in linearized structural models. Moreover, given the uncertainty on geotechnical parameters, an accurate definition of pile soil interaction stiffness is not straightforward and undue conservatism should be avoided as this would lead to an underestimation of the natural frequency of the structure. Indeed, the natural frequency needs to be assessed as accurately as possible as an under- or overestimation would bring the natural frequency closer to the range of excitation frequencies (1P, 3P, wind and wave frequencies).

LATERAL PILE-SOIL INTERACTION ANALYSIS

Pile-soil interaction analysis methods

There are several approaches available for analyzing the interaction of large-diameter monopiles with the surrounding soil. These are summarized below and shown graphically in **Fig. 2**:

- Lumped stiffness matrix: The entire pile-soil interaction is lumped into a set of (non-linear) springs located at the mudline (interface between soil and water) (Arany et al., 2016). A lateral and rotation spring as well as coupling terms are defined. While this approach has the advantage of being simple, it ignores the depth-dependence of soil stiffness and cannot take the layered nature of soils into account. While it can be a useful screening tool, this approach is generally not used for detailed design;
- Distributed springs: 1D beam-column models where the pile-soil interaction is modelled as a set of non-linear springs attached to the submerged pile nodes is the most widely used approach for monopile foundations design. The models are relatively quick to calculate and allow a large number of load combinations to be evaluated. The main challenge is in a fit-for-purpose definition of the non-linear response curves from measured geotechnical parameters. The available response curve models are discussed further in this section;
- Continuum models: 3D finite element models with advanced constitutive stress-strain relations provide the most insight in the stress and deformation pattern in the soil surrounding the monopile. However, calibrating the constitutive models can be

 © DFI International Bruges 2025

challenging due to the limited amount of advanced laboratory tests available. 3D FEA is often performed for a limited set of load cases and serves to benchmark the 1D beam-column models.

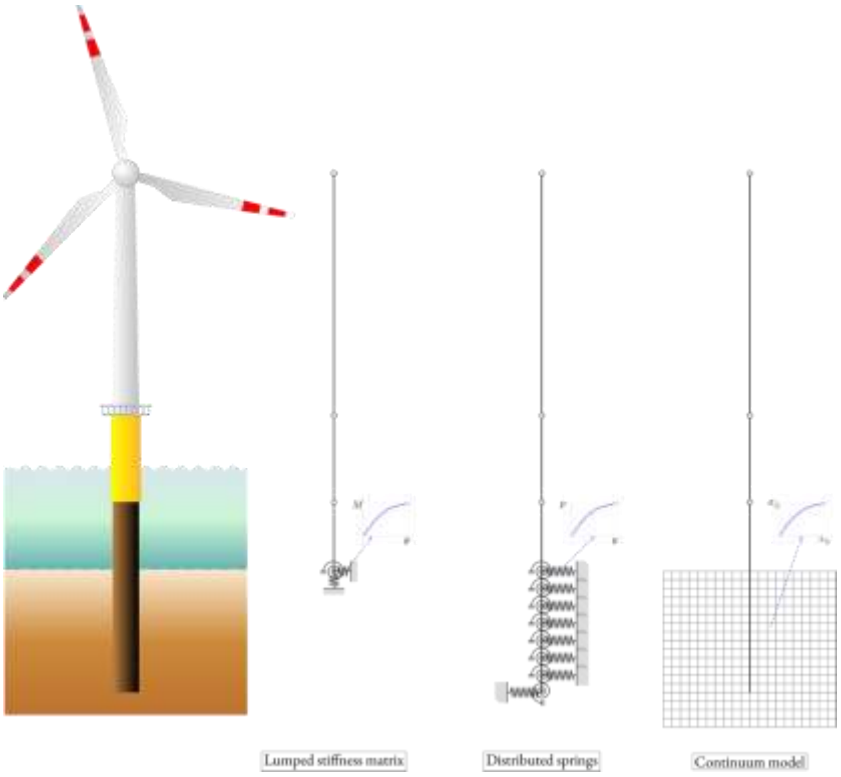


Fig. 2. Modelling approaches for offshore wind turbine monopile soil-structure interaction

API RP2 GEO method

The API RP2 GEO method was developed to define non-linear relations between pile deflection and lateral soil resistance (so-called *p*-y curves) based on onshore tests piles of up to 0.8m in diameter (Matlock, 1970). The method is aimed at providing design guidance for offshore Oil & Gas platform piles and therefore has some conservatism built into the method. Devriendt et al. (2014) and Kallehave et al. (2015) observed a underestimation of the natural frequency of offshore wind turbine structures designed using the API RP2 GEO method.

A detailed description of the *p-y* curve definition is beyond the scope of this paper, but the methods makes use of geotechnical parameters associated with the soil's ultimate strength (friction angles for sand and undrained shear strengths for clay). For an offshore wind turbine monopile, the majority of the loading is far below the ultimate strength. Due to the non-linearity of soil stiffness, higher stiffnesses are expected for low-amplitude loading, which explains the observations of Devriendt et al. (2014) and Kallehave et al. (2015). Kallehave et al. (2012) proposed a modification to the API RP2 GEO curves for sand to better capture the initial stiffness.

PISA method

The observed mismatch of the monitored and designed natural frequencies led to additional field testing and numerical analysis on larger diameter piles. Byrne et al. (2017) describe onshore field testing of driven tubular piles up to 2.5m in diameter in sand and clay profiles. Based on the results of these tests and numerical analysis with advanced constitutive models, the PISA rule-based method was defined (Burd et al., 2020) which provides guidance for *p-y* curves but also moment-rotation springs along the monopile and non-linear curves describing the shear and moment resistance mobilization at the pile toe. Because of the large diameter of offshore monopiles, these additional response curves are required.

 © DFI International Bruges 2025

While a detailed discussion of the PISA response curves is beyond the scope of this paper, the method uses the small-strain stiffness G_{max} of the soil as the main input parameter. The strain-dependent stiffness reduction is then incorporated in the non-linear response curve construction. An accurate characterization of the soil stiffness is therefore an important objective of the windfarm geotechnical investigation.

Integrated structural modelling

To allow an assessment of the natural frequency of the offshore wind turbine structure, an integrated model of the structure needs to be built in which the dimensions, masses and stiffnesses of the structural components need to be defined. Moreover, the pile-soil interaction needs to be defined through a series of springs, but these springs must be linear. This requires a linearization of the response curves. This linearization is performed by running a lateral monopile response analysis at the expected load level for a given metocean condition and turbine operational condition. The pile deflections obtained from this analysis are then used to define the linearized stiffness. A calculated natural frequency is therefore only valid for the conditions used in the linearization step. The integrated model used in this study was implemented in the OpenSees software (McKenna et al., 2010). Jurado et al. (2024) describe the development of the integrated model. Such models could also be developed for other geotechnical structures such as onshore wind turbine foundations or retaining walls.

GEOTECHNICAL PROPERTIES FOR PILE-SOIL INTERACTION CALCULATIONS

Strength properties

As shown in the section above, the strength properties of the soil need to be defined for the API RP2 GEO *p*-y curve calculation method. For the wind farms studied in this paper, the strength parameters were derived based on correlations with cone penetration tests (CPTs) and direct measurements of friction angle and undrained shear strength performed in the geotechnical laboratory. The geotechnical profiles at the investigated monopile locations consisted of overconsolidated sands and clays with varying thicknesses. Location-specific parameter profiles for the API RP2 GEO method were defined based on the available geotechnical tests.

Stiffness properties

The definition of geotechnical parameter profiles for the PISA rule-based method required the selection of small-strain stiffness G_{max} at each foundation location. While this parameter can be derived from direct measurements of the shear wave velocity V_S with the seismic CPT (S-PCPT), such measurements were not available at every foundation location. Therefore a CPT-based correlation for V_S had to be defined. Several published correlations can be found in the literature, each developed based on a specific dataset combining V_S measurements and CPT data. Stuyts et al. (2024) evaluated several published correlations for application in the Southern North Sea and proposed a stress-dependent relation between V_S and the soil behavior type index I_c (Equation 1). This relation was used to define site-specific stiffness profiles.

$$V_S = 10^{2.075-0.213\cdot I_c} \cdot \left(\frac{\sigma'_{v0}}{1\ kPa}\right)^{0.77-0.25\cdot\log_{10}(2.075-0.213\cdot I_c)} \quad [1]$$

It should be noted that using this correlation introduces a transformation uncertainty. Sensitivity studies on the shear wave velocity and the corresponding shear modulus are recommended.

Scour protection properties

During the back-analysis of natural frequencies for a monopile-supported offshore substation, an important effect of the scour protection on the natural frequency was observed (Winkler et al., 2023). The scour protection can influence the pile-soil interaction stiffness in three possible ways:

- The weight of the scour protection system increases the effective stresses in the soil surrounding the monopile. This effect is most pronounced for the shallow layers. As the

 © DFI International Bruges 2025

scour protection layer has a limited lateral extent, the effective stresses in the soil can be calculated using elastic stress solutions.

- The increased effective stress in the shallow layers lead to an increased stiffness of those layers (increased G_{max}) which has an influence on the pile-soil interaction stiffness.
- The scour protection layer itself provides lateral restraint to the monopile. Given the blocky natural of the scour protection system, this resistance is hard to quantify, and *p-y* curves developed for sand may not be applicable. Nevertheless, response curves for this layer were modelled assuming dense sand behavior in the scour protection layer.

Three modelling approaches were defined for modelling the scour protection as shown in **Fig. 3**. Natural frequencies were calculated for each scenario to check which modelling scenario gave the best correspondence with the monitored natural frequencies.

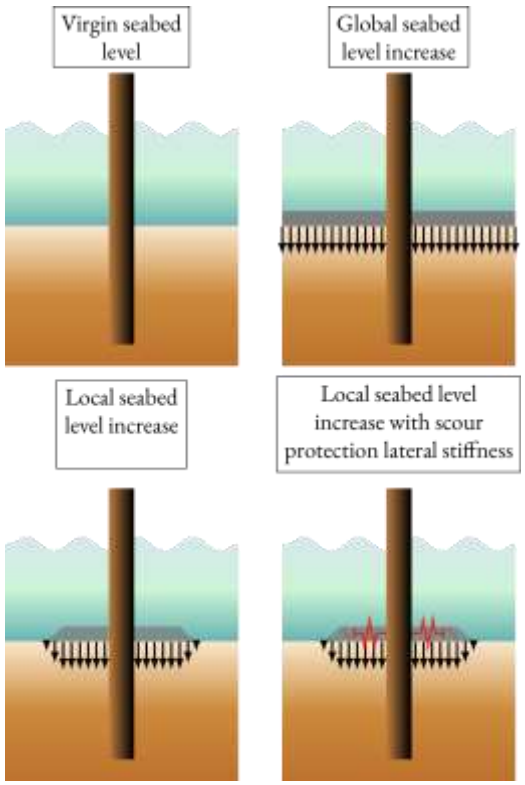


Fig. 3. Modelling approaches for scour protection

NATURAL FREQUENCY MONITORING

Natural frequencies were monitored at two Belgian offshore wind farms using a mobile measurement system. All measurements were taken during periods with calm weather. The monopile diameters ranged between 5m and 7.8m and the stratigraphy at the wind turbine locations showed varying proportions of sand and clay. The scour protection systems had thicknesses between 0.7m and 1.7m. Given the variations in the water depth, structural dimensions, geotechnical properties and scour protection, the objective was to reach an integrated model of the wind turbine structure which could produce reliable estimates of the first natural frequency.

BACK-ANALYSIS RESULTS

The results of the back-analysis of the first natural frequency in the side-side direction (perpendicular to the turbine axis) were evaluated by calculating the relative error (percentage difference) between the calculated and measured natural frequency at 73 offshore wind turbine locations and making a combined boxplot and violin plot from the data.

Fig. 4 shows the effect of the response curve method on the distribution of the relative errors. The known underestimation of the first natural frequency with the API RP2 GEO method is clearly

 © DFI International Bruges 2025

observer from the data. While the corrections made by Kallehave et al. have a positive effect on the mismatch between measured and calculated natural frequencies, there are a number of clay-dominated locations on which the corrections have no effect (these are shown as outliers in the figure). Overall, the PISA method leads to the closest match with the measurements although an underestimation is still observed, with the mean relative error being -1.48%.

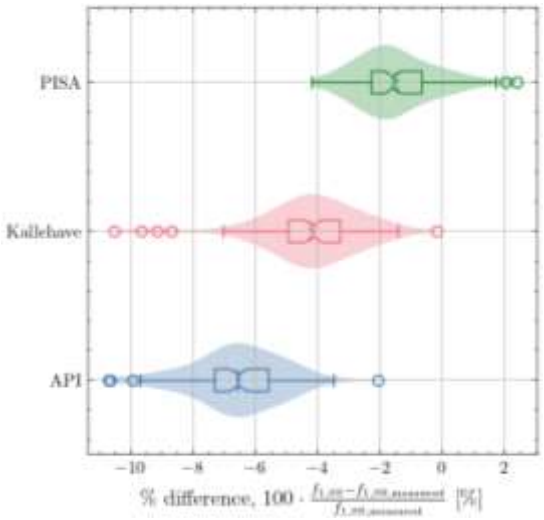


Fig. 4. Distribution of the relative errors between measured and calculated natural frequencies for different response curve methods

Fig. 5 shows the effect of modelling the scour protection using the different approaches from **Fig. 3**. The estimation is most accurate when all three effects (increase effective stress and stiffness in the shallow layers and lateral fixity provided by the scour protection layer) are modelled. The combined effect of modelling the scour protection brings the mean of the distribution of the relative errors to -0.51% and a standard deviation of 1.30%. Overall, the results show that both the pile-soil interaction and the scour protection system need to be modelled accurately to get a close match between the observed and calculated natural frequencies.

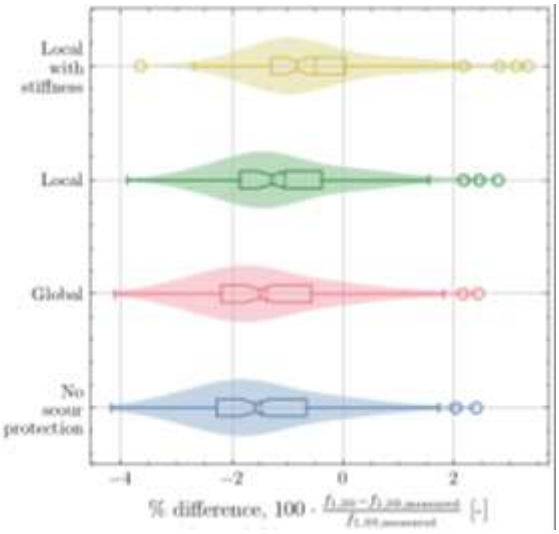


Fig. 5. Distribution of the relative errors between measured and calculated natural frequencies for different scour protection modelling approaches

CONCLUSIONS AND RECOMMENDATIONS

This study shows the development of a workflow for the natural frequency prediction for monopile-supported offshore wind turbine structures. Given the importance of the fatigue limit state, an accurate predication of the natural frequency needs to be made, omitting undue

 © DFI International Bruges 2025

conservatism in the workflow. This requires a good understanding of both the pile-soil interaction, the loading conditions on the structure and the structural properties of the wind turbines.
Achieving a close match between measured and calculated natural frequencies is only possible when all components of the integrated model of the structure are optimized to lead to a modelling approach which is as realistic as possible. The requirement for accurately quantifying the soil stiffness across the range of expected load levels stands out as a pre-requisite for getting realistic predictions. Methods focused on the ULS will underestimate the stiffness in most cases and lead to unrealistic lateral pile deflections. This does not only apply to offshore wind turbine monopiles. Onshore piles and retaining walls also mobilize the resistance of the soil to a greater or lesser extent and thus the strain-dependent stiffness of soil will also play an important role when back-calculating monitored lateral deflections.

The monitoring data also revealed a need for modelling the scour protection installed around the monopile foundation. This layer appears to contribute significantly to the lateral response of the structure. However, due to the blocky nature of the scour protection layer, further research is required to accurately quantify this effect.

REFERENCES

Arany, L., Bhattacharya, S., Macdonald, J.H.G., Hogan, S.J., 2016. Closed form solution of Eigen frequency of monopile supported offshore wind turbines in deeper waters incorporating stiffness of substructure and SSI. Soil Dynamics and Earthquake Engineering 83, 18–32.

Byrne et al, 2017. PISA: New design methods for offshore wind turbine monopiles, in: Proceedings of the 8th Int. Conf. on Offshore Site Investigation and Geotechnics. Presented at the OSIG 2017, pp. 142–161.

Devriendt, C., Weijtjens, W., El-Kafafy, M., De Sitter, G., 2014. Monitoring resonant frequencies and damping values of an offshore wind turbine in parked conditions. IET Renewable Power Generation 8, 433–441. https://doi.org/10.1049/iet-rpg.2013.0229

DNV-ST-0126, 2021. Support structures for wind turbines.

Fallais, D.J.M., Winkler, K., Jurado, C.S., Weijtjens, W., Devriendt, C., 2022. Farm wide sensitivity assessments of resonant frequencies of integrated offshore wind turbine finite element models. Proceedings of Torque 2022 15.

Jurado, C.S., Weijtjens, W., Stuyts, B., Winkler, K., Fallais, D., Devriendt, C., 2024. Benchmarking Measured Eigenfrequencies: A Case Study of a North Sea Offshore Wind Farm.

Kallehave, D., LeBlanc, C., Liingaard, M.A., 2012. Modification of the API P-Y formulation of initial stiffness of sand, in: Integrated Geotechnologies - Present and Future. Presented at the SUT OSIG, London, pp. 465–472.

Kallehave, D., Thilsted, C.L., Troya, A., 2015. Observed variations of monopile foundation stiffness, in: Frontiers in Offshore Geotechnics III. Oslo, Norway, pp. 717–722.

Liu, H., Kementzetzidis, E., Abell, J.A., Pisanò, F., 2021. From cyclic sand ratcheting to tilt accumulation of offshore monopiles: 3D FE modelling using SANISAND-MS. Géotechnique 1–45. https://doi.org/10.1680/jgeot.20.P.029

Matlock, H., 1970. Correlations for design of laterally loaded piles in soft clay. Presented at the Proceedings Offshore Technology Conference - OTC 1204, pp. 577–594.

McKenna, F., Scott, M.H., Fenves, G.L., 2010. Nonlinear finite-element analysis software architecture using object composition. Journal of computing in civil engineering 24, 95–107.

Stuyts, B., Weijtjens, W., Gkougkoudi-Papaioannou, M., Devriendt, C., Troch, P., Kheffache, A., 2023. Insights from in-situ pore pressure monitoring around a wind turbine monopile. Ocean Engineering 269, 113556. https://doi.org/10.1016/j.oceaneng.2022.113556

Stuyts, B., Weijtjens, W., Jurado, C.S., Devriendt, C., Kheffache, A., 2024. A Critical Review of Cone Penetration Test-Based Correlations for Estimating Small-Strain Shear Modulus in North Sea Soils. Geotechnics 4, 604–635. https://doi.org/10.3390/geotechnics4020033

Weijtjens, W., Devriendt, C., 2019. Stiffness and damping of offshore wind-turbines and its impact on design.

 © DFI International Bruges 2025

WindEurope, 2024. Wind energy in Europe: 2023 Statistics and the outlook for 2024-2030. Brussels, Belgium.

Winkler, K., Weil, M., Sastre Jurado, C., Stuyts, B., Weijtjens, W., Devriendt, C., 2023. Quantifying the effect of rock armour scour protection on eigenfrequencies of a monopile supported OHVS, in: Journal of Physics: Conference Series. p. 012039. https://doi.org/10.1088/1742-6596/2626/1/012039

 © DFI International Bruges 2025

FIELD INVESTIGATION ON THE CHARACTERISTICS OF CLAYEY SOIL CLOSE TO DIAPHRAGM WALLS

Diethard König, Ruhr-Universität Bochum, Bochum, Germany, diethard.koenig@rub.de
Duncan Nicholson, ARUP, London, United Kingdom, duncan.nicholson@arup.com
Rowena Verst, IGW Ingenieurgesellschaft für Spezialtiefbau mbH, Wuppertal, Germany, verst@igw-geotechnik.de
Chris Harnan, Ceecom Geotech Ltd, Strood Green, United Kingdom, chris.harnan@ceecom-geotech.com

ABSTRACT

During excavation of a diaphragm wall panel soil is supported by a support fluid, which is often a bentonite suspension. Generally, the support fluid pressure is smaller than the initial stress state in the soil. Due to this the soil tends to deform into the excavated panel. In water-saturated overconsolidated clayey soil this behaviour is related to a decrease of pore water pressure. Simultaneously the bentonite suspension or only the water from the suspension may penetrate the pore space of the clay. This may lead to a softening of the clay while the panel is open prior to concreting. After concreting the panel a zone of softened clay may remain close to the wall. Such a zone, with lower shear strength, would influence the transfer of shear stress between the wall and the soil which has an impact on the magnitude of active and passive earth pressure as well as on the vertical bearing capacity of the diaphragm wall. To date, this phenomenon has not been proved by field measurements.

Site investigations were performed during the excavation phase of construction pits at two sites that were formed by diaphragm walls in clayey soil. The penetration resistance of the soil was measured using a pocket penetrometer at different distances from the wall, and samples were taken to determine water contents. The investigations were performed at two panels on each site, one with short opening time (time between start of excavation and beginning of concreting) and one with long opening time. Test results indicate a clear reduction of penetration resistance and an increase of water content close to the walls. These effects decrease with increased distance from the wall and are more pronounced at the panels with long opening time. From the strength reduction, adhesion factors are derived, and these are compared to reported adhesion factors observed during installation of bored piles.

Keywords: diaphragm wall, soil wall interface, clay, softening

INTRODUCTION

Earth pressure load acting on retaining walls, bearing capacity, and load settlement behaviour of barrettes or bored piles are all connected to the transfer of shear forces along the soil/wall or soil/pile interface. The characteristic properties of the interface are influenced by the construction procedure. The construction of diaphragm walls and bored piles without casing requires temporary fluid support to stabilize the open trench or bore before concrete placement. Bentonite suspension is often used as the support fluid. The pressure transfer from the fluid to the grain skeleton of the soil depends on the composition of the support fluid and the soil. In coarser soils the bentonite suspension penetrates the pores of the soil and, depending on the grain size distributions of the solids in the suspension and in the soil, a filter cake forms at the soil surface. This often comprises excavated soil particles held in suspension in the support fluid. In fine grained soils, especially clay, penetration into the pore space of the soil is not possible, because solid particles within the suspensions are often larger than the pores of the soil. In general, the volume of fluid flowing into the fine grained soil is so small that a significant filter cake does not develop on the soil surface.

 © DFI International Bruges 2025

Two other effects may arise in such soils. First, the fluid pressure is smaller than the initial stress state in the soil especially in overconsolidated clay. Due to this the soil tends to deform into the excavated panel. In water saturated clayey soil this deformation is related to a decrease in pore water pressure. With time the decrease of pore pressure is compensated either by take-up of water from the bentonite suspension or by flow of water from more distant areas of the soil. In both cases the water content and void ratio closer to the wall increase leading to a softening of the soil close to the wall and to a reduction of the shear strength of the soil/wall interface (macroscopic effect).

Second, a physical chemical interaction between the support fluid and the nearby soil leads to swelling of the soil within a thin zone close to the interface. This swollen and softened layer remains after concreting between the diaphragm wall and the soil (microscopic effect).

A number of studies (e.g. Verst et al., 2022) on the pressure transfer from the support fluid to the soil, on filter cake development in more coarse soils (silt, sand, gravel) and characteristics on the interface between soil and diaphragm wall exist but investigations on the behaviour of clays close to a diaphragm wall panel are rare. Within this paper the influence of the diaphragm wall construction process in overconsolidated clayey soils on the characteristics of the soil close to the wall are studied by site investigations.

Site investigations were performed during the excavation phase of two construction pits supported by diaphragm walls in clayey soil. The soil strength was determined at different distances from the wall by measuring the penetration resistance using a pocket penetrometer, and samples were taken to determine water contents. The investigations were performed at two panels on each site, one with short opening time (time between start of excavation and beginning of concreting) and one with long opening time. Test results indicate a clear reduction of soil strength and an increase of water content close to the wall. These effects decrease with increased distance from the wall and are more pronounced at the panels with long opening time.

Bearing capacity of bored piles in overconsolidated clayey soil tends to decrease with production time. In design practice this decrease is considered by a reduced adhesion factor α and by this a reduced skin friction. The reason for decreasing bearing capacity (probably reduced skin friction) of bored piles with production time may be the same as softening of the nearby soil as observed at the diaphragm wall panels. In this paper, investigated strengths adjacent to the diaphragm wall panels are used to develop adhesion factors and these are compared to adhesion factors observed from pile load tests.

FIELD STUDY SITE 1

Description of the construction site

The Victoria Road Crossover Box (VRCB) is part of the high-speed train HS2 project in the UK and is located close to Old Oak Common station in the north of London. The structure is designed as a “caterpillar” (Figure 1), consisting of five intersecting circular cells made of two-phase-diaphragm walls, each with a 20.75 m radius, to form a box with a total length of around 130 m (HS2 2021). The diaphragm walls have a thickness of 1.5 m and a depth from platform level of 35.5 m. The panels were excavated using a grab. Soil conditions are characterized by the stratigraphy of the London clay (Table 1, HS2, 2021).

Panels 25 and 26 were selected, located at the east end of the pit (Figure 1). Both panels have a length of 7.38 m and were excavated in 3 bites (HS2, 2022). Excavation started at +34 m OD. To support the panels, a bentonite suspension with 40 kg Bentonite / m³ was used. The properties of the suspension at different stages of the excavation are given in Table 2. The total time the trench is stabilized by the

 © DFI International Bruges 2025

support fluid (opening time) is defined as the time from the beginning of the excavation until the start of concreting. Because the start of the excavation of each bite is different the opening time varies from bite to bite (Figure 1).

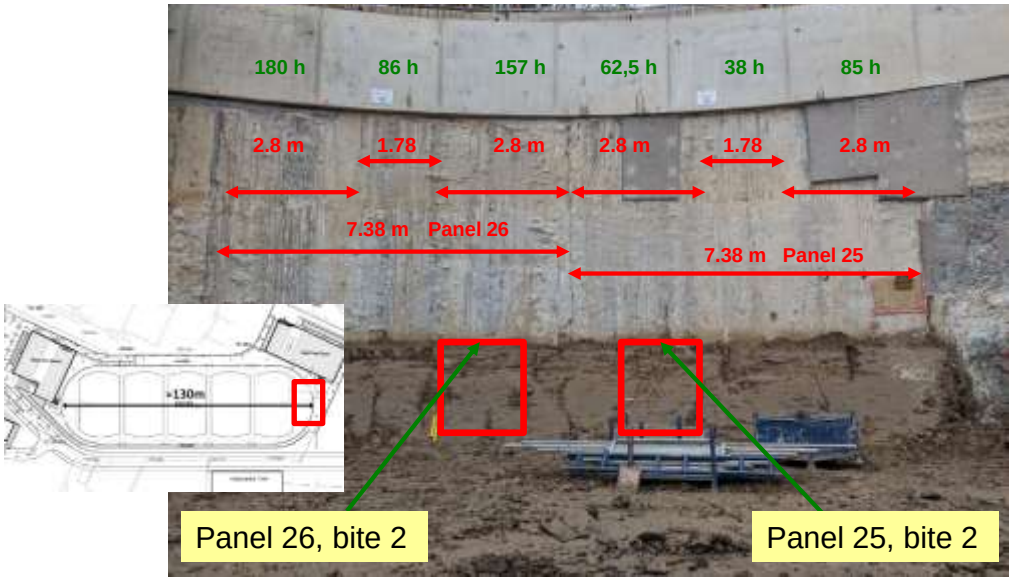


Fig. 1. Site 1, Victoria Road Crossover Box S2, east end, locations of site investigations (red squares) at panel 25, bite 2 and panel 26, bite 2. On top (green) opening time of each bite, in the middle (red) length of each bite, at the bottom (red) length of both panels. Overview on the left from HS2 (2021)

Table 1. Site 1, soil conditions close to panel 25 and panel 26 (HS2, 2021)

Depth below ground level	Soil type	w	c_u	k	w_P w_L PI	Grain Size Distribution			
						< 0.002 mm	0.002 mm to 0.063 mm	0.063 mm to 2 mm	> 2 mm
m		%	kPa	m/s	mm	%	%	%	%
0	London clay unit A and B	32 - 38	50	$1 \cdot 10^{-9}$	22 – 31 58 – 83 45	45 - 60	30 - 50	0 - 25	< 3
21		23 - 30	180						
21 to 49	London clay unit A3	23 - 30	180						

Table 2. Site 1, Properties of the bentonite suspension at different construction stages of panel 25 and 26 (HS2, 2022)

	Density[1]		Marsh funnel flow time[2]		Fluid loss[3]		Filter cake thick-ness[3]		ph-value[4]		Sand content		Shear strength[5]		Tempe-rature	
	g/cm³		s		ml		mm		-		%		N/m²			
Panel number	25	26	25	26	25	26	25	26	25	26	25	26	25	26	25	26
Freshly mixed	1.04	1.09	33	34	11	12	1	1	9.5	9.7	0.01	0.01	8.4	8.4	15.2	15.6
During digging	1.05	1.09	34	34	10	12	1	1	9.6	9.7	0.2	0.01	8.4	8.4	16.4	15.6
During digging	1.09	1.09	38	39	10	11	1	1	n/a	10	1.05	1.25	11.8	12.3	16.5	17.2
After regeneration	1.05	1.03	34	32	11.5	11	1		9.4	10	0.05	n.A.	8.4	8.4	15.3	14.5
Prior concreting	1.04	1.03	31	31.8	11	10	1	1	9.4	10.2	0.01	0.1	8.4	12.3	16.6	13.2

[1] Mud balance, [2] Marsh cone, [3] Low temperature fluid loss test, [4] Electrical pH-meter to BS 3445, [5] Fann viscosimeter

 © DFI International Bruges 2025

Testing and sampling

The excavation at panels 25 and 26 had reached a depth of 7 m below ground level (+27 m OD) when site investigations were performed. A berm (Figure 2a) of about 1.5 m height was left in front of the wall. Within this berm soil was carefully removed by an excavator (Figure 2b). The last 40 cm of soil towards the wall was removed by hand. During removal of soil close to the wall, soil conditions and possible filter cake were inspected visually. Soil strength was measured by a digital penetrometer (PCE Instruments, PCE FM, 200, Figure 3a). The tip of the penetrometer was flat, and the diameter was 6.3 mm. A load on the tip is shown on the digital display in N.

After reaching the wall. the side and bottom faces of the handmade cut were carefully levelled. After this a positioning plate was placed on a side or bottom face in a manner that its rear edge was in contact with the wall (Figure 3b). The template of the positioning plate defines positions for testing the strength of the soil by the digital penetrometer in fixed distances from the wall. A thin metal sleeve was used to mark the positions of the testing points through the holes of the positioning plate on the soil surface and the plate was removed. The tip of the penetrometer was pushed into the soil at the marked positions up to a penetrating depth of about 6 mm. Additional measurements were taken at distances of 40 cm to 120 cm from the wall.



a) *b)*

Fig. 2. Site 1, removing the soil towards the wall first by excavator (a) and then by hand (b)



a) b) c)

Fig. 3. Site 1, digital penetrometer (a), handmade pit in front of the wall with (b) positioning plate to mark the positions for penetrometer testing and (c) metal grid for taking samples for determination of water content

 © DFI International Bruges 2025

In order to obtain samples for water content measurement at fixed distances from the wall a metal grid was pushed into the soil (Figure 3c) and later carefully separated from the soil. The soil within each cell was used to determine water contents at exact distances from the wall.

Results

Figure 4 shows the interface between the concrete surface of the wall and the clay for both panels at the side and at the bottom of the handmade pit. The clay stuck directly to the wall. No filter cake was visible and no layer of soil with divergent colour or obviously divergent liquidity could be identified.

Penetration resistances (minimum, maximum and mean values) measured by the digital penetrometer at distances between 40 cm to 120 cm and between 0 and 2.5 cm from the wall are shown on the left side of Table 3. Penetration resistances at distances between 40 cm and 120 cm are similar for panel 25 and 26. Resistances at distances between 0 and 2.5 cm from the wall are significantly lower. This reduction is more pronounced for panel 26 with long opening time. Assuming penetration resistance at a distance greater than 40 cm from the wall is not influenced by the diaphragm wall construction, the penetration resistance is normalized by the mean value calculated from all measurements taken at a distance from the wall greater than 40 cm (72 N for panel 25 and 64 N for panel 26). Figure 5a shows the normalized penetration resistance versus distance from the wall for both panels. With distances closer than 40 cm to the wall normalized penetration resistance is decreasing. This decrease is more pronounced for panel 26. Mean values of normalised penetration resistance related to distances up to 2.5 cm from the wall are 0.61 for panel 25 and 0.34 for panel 26.

Water content (minimum, maximum and mean values) measured at distances between 10 cm to 12.5 cm and between 0 and 2.5 cm from the wall are shown on the right side of Table 3. All data are shown in Figure 5b. Water contents at distances between 10 cm to 12.5 cm are similar for panel 25 and 26. Water contents at distances between 0 and 2.5 cm from the wall are significantly higher. This increase is more pronounced for panel 26 with long opening time.

The significant decrease of normalized penetration resistance and increase in water content of panel 26 compared to panel 25 at closer distance to the wall may be related to the longer opening time of panel 26. The opening time of panel 26 (bite 2) was 94,5 h longer than panel 25 (bite 2) (Figure 1). All other boundary conditions like soil properties, support fluid characteristics and excavation process were similar.

FIELD STUDY SITE 2

Description of the construction site

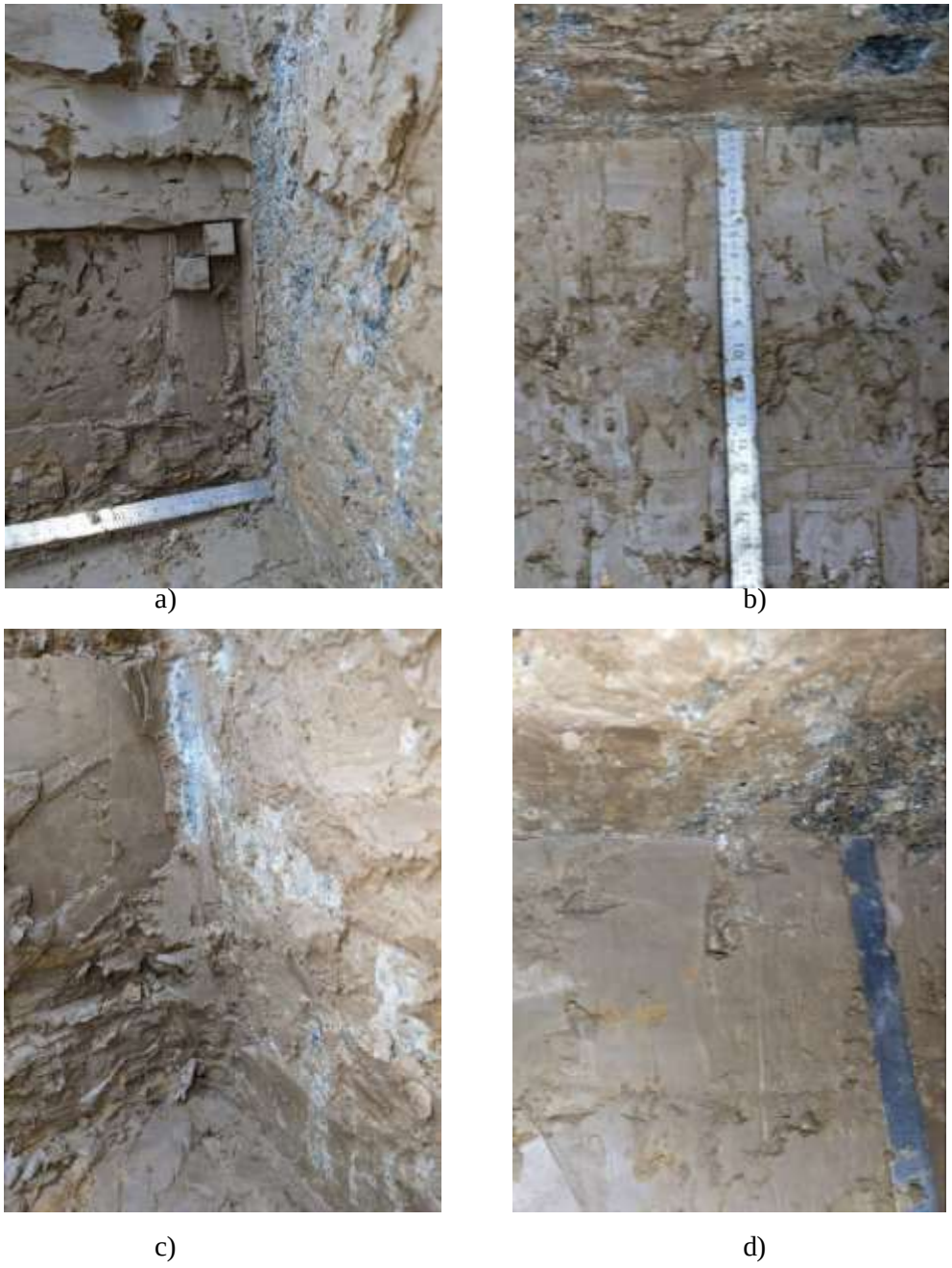
Birmingham is connected to the HS2 high speed railway track by the Bromford Tunnel. The eastern portal of the tunnel is reached by a concrete-lined cutting close to Water Orton. The cutting is supported by diaphragm walls (Figure 6). At about chainage 164+750 panels N008 and N009 of the north wall were investigated. These diaphragm walls are 1 m thick and have a depth of 21 m (HS2, 2023). The trenches were excavated in five bites. The left, central, and right bites were excavated up to a depth between 13 m and 15 m by grab and from there on by hydromill. The switch from grab to hydromill took place at a depth of about 5 m to 8 m for the middle left and middle right bites. Properties of the bentonite suspension are given in Table 4.

Up to a depth varying between 4 m and 10 m, there was made ground (reworked Mercia Mudstone) comprising sandy and gravely clay varying from soft to stiff followed by firm to stiff sometimes slightly sandy, sometimes slightly gravely clay (Fugro, 2022). At larger depths, soil conditions changed to weathered mudstone (extremely weak to weak) and siltstone (weak to medium strong).

 © DFI International Bruges 2025

Table 3. Site 1, penetration resistance and water content measured and panel 25 and panel 26

Distance from the wall	Panel	Penetration resistance			Distance from the wall	Panel	Water content		
		min	max	mean			min	max	mean
cm		N	N	N	cm		%	%	%
40 to 120	25	59	98	72	10 to 12.5	25	22	29	26
	26	54	81	64		26	26	31	28
0 to 2.5	25	21	62	44	0 to 2.5	25	28	40	32
	26	12	41	22		26	34	44	37

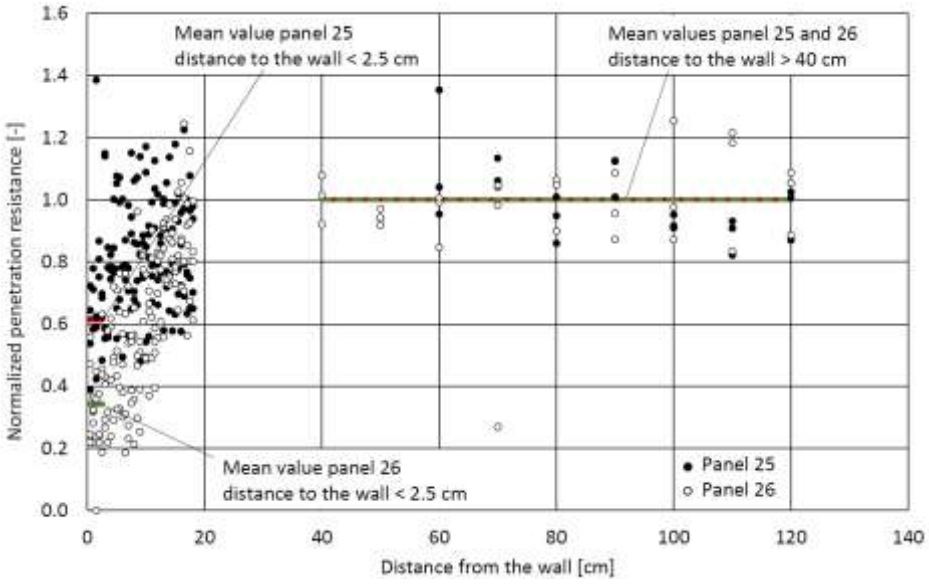


a) b) c) d)

Figure 4: Site 1, interface between concrete wall and soil at panel 25 (a, b) and panel 26 (c, d) on the left side of the handmade pit (a, c) and at the bottom of the handmade pit (b, d)

 © DFI International Bruges 2025

a)



b)

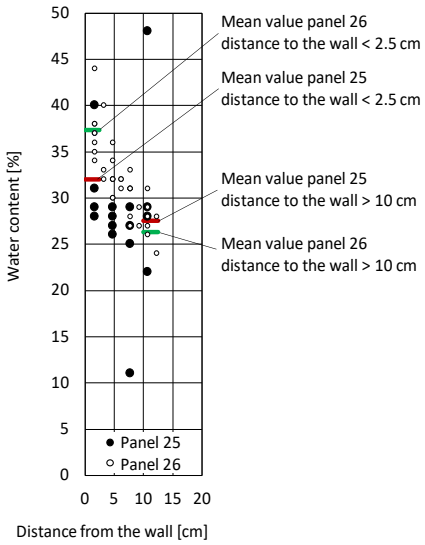


Figure 5: Site 1, normalized penetration resistance (a) and water content (b) versus distance from the wall for panel 25 and panel 26

Testing and sampling

Testing and sampling were performed after bulk excavation reached a depth of 4 m to 5 m below ground level. A small pit was excavated close to the joint between panel N008 and N009 in a distance of about 40 cm of the diaphragm wall. Remaining soil towards the wall was carefully removed by hand and investigations were performed in a same manner as described above for site 1. Undrained shear strength was determined by vane shear test in a range of 50 kPa to 104 kPa.

Results

Figure 7 gives an impression of the interface between the soil and the wall for panel N008 (a) and panel N009 (b, c). Soil conditions were inhomogeneous. Reddish-brown and grey clayey soils were unevenly distributed horizontally and vertically. A very soft to liquid layer of reddish-brown fine-grained material

 © DFI International Bruges 2025

with a maximum thickness of 5 mm was visible directly on the wall. This layer was significantly softer than the nearby soil, which showed a mostly firm to stiff liquidity. It is difficult to say whether this layer was formed as a filter cake from a filtration process or whether it is softened nearby soil. The layer was not continuous and was more pronounced in panel N009 than in panel N008. Visually, it consisted exclusively of the reddish-brown fine-grained soil present in the nearby soil. In the laboratory, it was shown that this material tends to dissolve quickly when water is added.

Measured penetration resistances are shown in Table 5. At distances between 40 to 120 cm from the wall penetration resistances at panel N008 and N009 are similar. At distances between 0 and 2.5 cm penetration resistances are significantly lower compared to those measured at distances between 40 to 120 cm. Normalized penetration resistance is plotted versus distance from the wall in Figure 8. It is obvious that penetration resistance is decreasing with decreasing distance from the wall. This reduction is more significant for panel N009 (left bite) where opening time was 217 h longer compared to panel N008 (right bite). Mean values of the normalized penetration resistance for a distance closer 2.5 cm to the wall are 0.48 for panel N008 and 0.29 for panel N009.

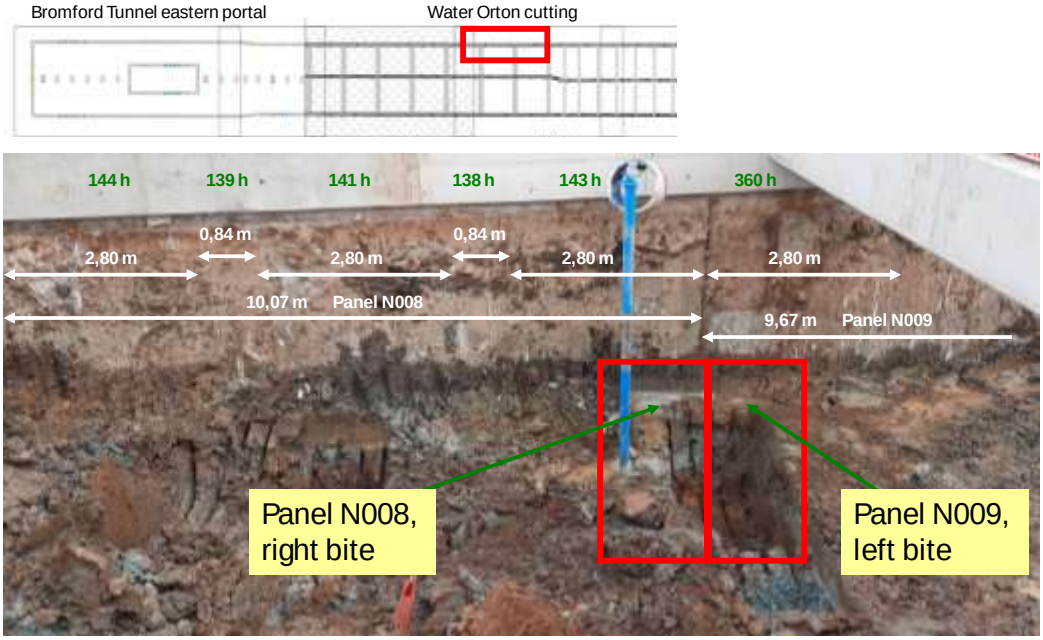


Figure 6: Site 2, Water Orton cutting, north wall, locations of investigations (red squares) at panel N008, central bite and panel N009, left bite. On top (green) opening time of each bite, in the middle (white) length of each bite, at the bottom (white) length of both panels. Overview from HS2 (2023)

Table 4. Site 2, characteristics of the bentonite suspension at different construction stages of panel N008 and panel N009 (HS2, 2023)

	Density		Marsh funnel flow time[1]		Fluid loss[2]		Filter cake thick-ness[3]		ph-value[4]		Sand content		Shear strength[5]		Tempe-rature	
	g/m³		s		ml		mm		-		%		N/m²			
Panel number	008	009	008	009	008	009	008	009	008	009	008	009	008	009	008	009
Freshly mixed	1.03	1.03	37	40	12	13	0.5	0.5	7	7	-	-	-	-	11	11
Before start HM	-	1.2	-	35	-	20	-	2	-	7	-	-	-	-	-	14
Prior concreting	1.03	1.03	39	39	13	14	0.5	0.5	7	7	0.5	0.5	-	-	11	14

[1] Marsh cone, 946 ml, [2] 30 min

 © DFI International Bruges 2025

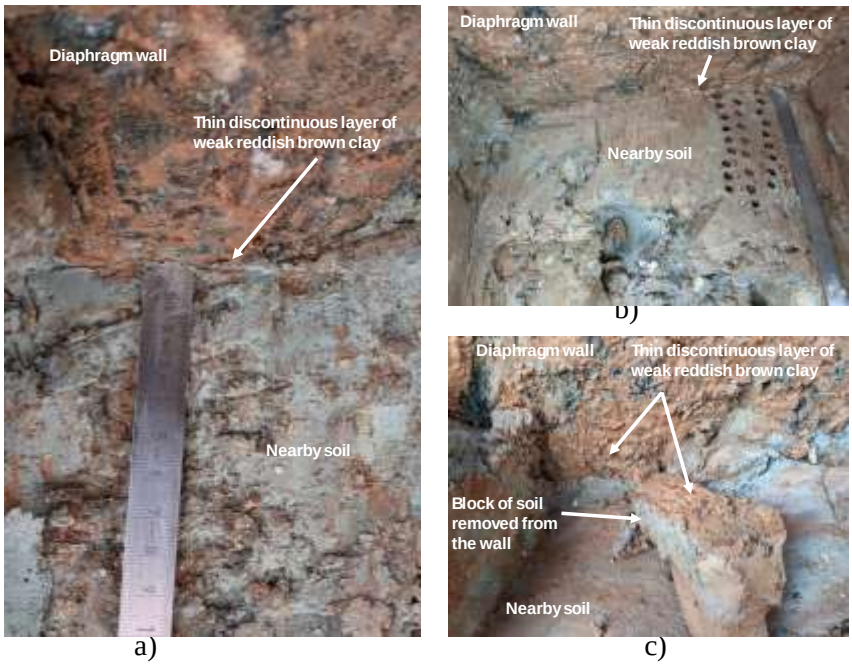


Figure 7: Site 2, interface between concrete wall and soil at panel N008 (a) and panel N009 (b, c)

Table 5. Site 2, penetration resistance measured at panel N008 and panel N009

Distance from the wall	Panel	Penetration resistance		
		min	max	mean
cm		N	N	N
40 to 120	N008	35	46	39
	N009	30	41	35
0 to 2.5	N008	18	21	19
	N009	5	16	10

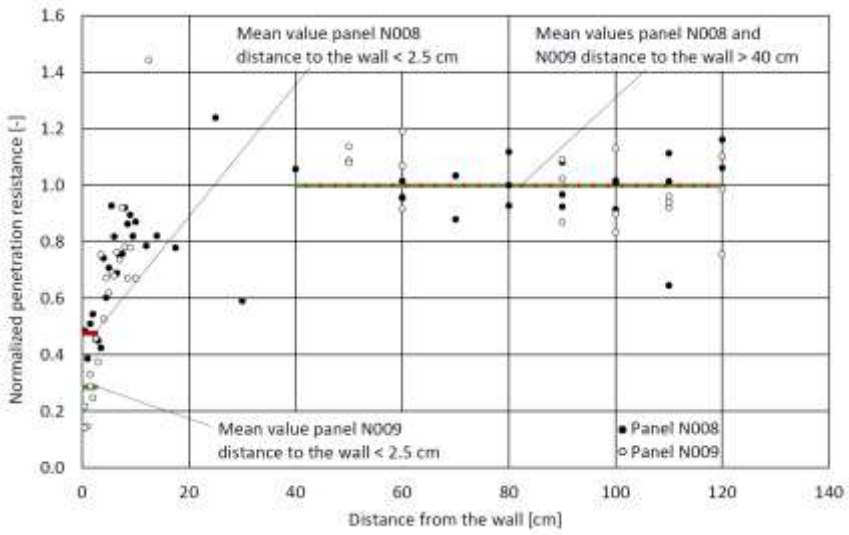


Figure 8: Normalized penetration resistance versus distance from the wall for panel N008 and N009

 © DFI International Bruges 2025

CONCLUSION

Soil conditions adjacent to diaphragm walls were investigated. Soil strength at different distances from the walls were determined by measuring penetration resistance with a digital pocket penetrometer. Test results indicate a clear reduction of penetration resistance and an increase of water content close to the wall. These effects decrease with increased distance from the wall and are more pronounced at the panels with long opening time. This indicates a soil softening caused by the excavation of the panels which is more significant with longer opening time.

Hardy et al. (2019) derived adhesion factors α from own pile tests and pile tests documented in the literature assuming the relation $q_s = \alpha \cdot c_u$, where q_s is the unit shaft friction of the pile and c_u is the average undrained shear strength of the soil along the pile shaft. He plotted the observed adhesion factors α versus the construction time. The undrained shear strength of the soils related to the different piles ranged between 92 kPa and 300 kPa. These data are redrawn in Fig. 9 with logarithmic time scale (Nicholson et al., 2025). A trend line shows a decrease of adhesion factor α with increasing construction time. Generally, the adhesion factor α is linked to the undrained shear strength and is often assumed to values below 1 for overconsolidated soils. Extrapolating the trend line to short construction time leads to an adhesion factor α of 0.7. It is assumed, that this factor is valid for short construction times and is named as base factor α_0.

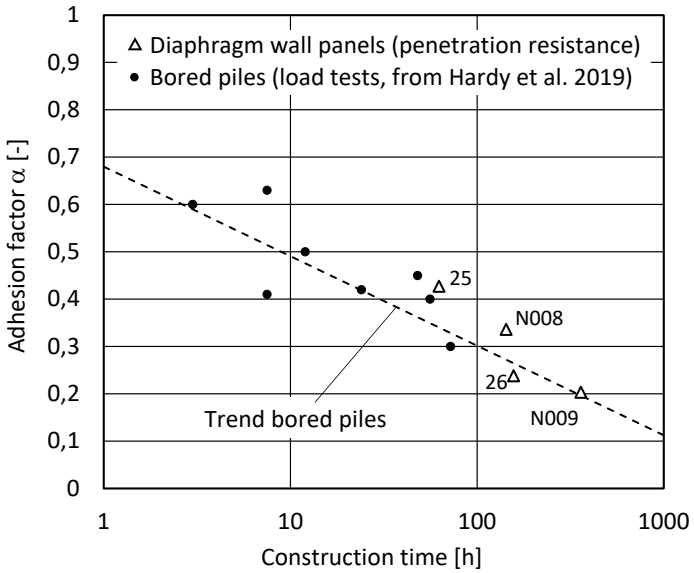


Figure 9: Adhesion factor α calculated for panels 25 and 26, site 1 and N008 and N009, site 2 plotted versus construction time (opening time) together with results on bored piles from Hardy et al. (2019)

Table 6. Calculation of adhesion factors α for panels 25 and 26, site 1 and N008 and N009, site 2

Site	Panel	Opening time	Base factor α_0	Normalized penetration resistance distance to the wall < 2,5 cm	Adhesion factor α
		h	-	-	-
1	25	62.5	0.7	0.61	0.43
	26	157	0.7	0.34	0.24
2	N008	143	0.7	0.48	0,34
	N009	360	0.7	0.29	0,20

 © DFI International Bruges 2025

The diaphragm wall panels investigated within this study (Field studies site 1 and site 2) were excavated in soils with c_u between 50 kPa and 180 kPa. Due to this it is assumed that the base factor $\alpha_0 = 0.7$ derived above seems also valid for the diaphragm wall panels. The effect of the construction time is considered by multiplying the base factor α_0 with the normalized penetration resistance observed close to the wall (distance < 2.5 cm) as shown in Figures 5 a and 8 reaching to adhesion factors α for each panel. The values are summarized in Table 6.

The calculated adhesion factors α of the four panels are added to the factors from Hardy at al. (2019) in Figure 9 assuming opening time can be interpretated as construction time. The dependency of adhesion factors α of the four panels on construction time fits well to the trend observed on the piles by Hardy et al. (2019).

ACKNOWLEDGEMENT

We thank the Clients and Contractors of the sites for allowing site visits and for sharing information on the sites. The support of Sophie Danowski and Gordon Kempkes is gratefully acknowledged.

REFERENCES

HS2 (2021) Ground Investigation Report - VRCB. Doc. 1MC04-SCJ-GT-REP-SS04-000003, Rev. C04.

HS2 (2022) Prod. Sheets VRCB Panels 25, 26. Doc. 1MC04-SCJ-QY-PKG-SS04-000014, Rev. C01.

HS2 (2023) SL DELTA Quality Record, Package Water Orton Cutting, D-Wall Panel N008 and N009. 1MC09-BBV_BSJ-QY-PKG-NS04_NL11-000008 and -000009.

Fugro (2022) Reports of site investigation borings BS164-CR415A and BS164-CR414.

Hardy S, Nicholson D, Srisakthivel S, Oliver L, Disley T, (2019) Preliminary test pile results for the South Bank Place development. Ground Engineering, Dec 2019, pp26 – 33.

Verst, R., v. Blumenthal, A., Du, J., König, D., Pulsfort, M., Wichtmann, T. (2022). Systematic laboratory and field study on the shear resistance of the soil-concrete interface of diaphragm walls and bored piles. Int. conf. on deep foundations and ground improvement – smart construction for the future. DFI/EFFC. Berlin.

Nicholson DP, Ferreira J, Pillai A, Qui X. (2025) The Impact of Long Opening Times on Shaft Friction in Cohesive Soils. DFI-EFFC, Int. Conf. on Deep Foundations and Ground Improvement - Geotechnics Reimagined. Bruges.

 © DFI International Bruges 2025

SYSTEMATIC LABORATORY AND FIELD INVESTIGATIONS ON THE SOIL-CONCRETE INTERFACE OF DIAPHRAGM WALLS AND BORED PILES WITH FOCUS ON THE INFLUENCE OF WALL ROUGHNESS

Rowena Verst, IGW Ingenieurgesellschaft für Spezialtiefbau mbH, Wuppertal, Germany, verst@igw-geotechnik.de
Diethard König, Ruhr-Universität Bochum, Germany, diethard.koenig@rub.de
Jiarui Du, Ruhr-Universität Bochum, Germany, jiarui.du@rub.de
Achim von Blumenthal, Ruhr-Universität Bochum, Germany, achim.vonblumenthal@rub.de
Matthias Pulsfort, Bergische Universität Wuppertal and IGW Ingenieurgesellschaft für Spezialtiefbau mbH, Wuppertal, Germany, pulsfort@uni-wuppertal.de
Torsten Wichtmann, Ruhr-Universität Bochum, Germany, torsten.wichtmann@rub.de

ABSTRACT

The construction of diaphragm walls and bored piles requires temporary fluid support to stabilise the open trench or borehole before concrete placement. During excavation, a filter cake may develop remaining between the hardened wall and soil. The effect of formed filter cake and influencing factors are currently controversially discussed, especially with respect to responsibility as well as economic and design efficiency.

First results from an R&D project on this soil-cake-concrete interface have been published covering the evaluation of the shear resistance of the interface between diaphragm walls and soils. This paper summarises the remaining findings of this project considering laboratory and field results on the influence of wall roughness, long fluid exposure times and a detailed investigation of penetrated soil characteristics depending on the support fluid constitution. Wall roughness was found to increase the shear strength of the interface. This was proven even for the case of sandy soils and a filter cake thickness larger than the roughness depth of the concrete surface by direct shear tests. For fine-grained soils, the wall roughness depth exceeds the filter cake thickness, as shown by site investigations, and thus dominates the shear strength of the interface. Field observations on diaphragm walls in gravel confirmed a very rough concrete surface. Wall roughness and coarse grains in the soil lead to direct contact between concrete and soil. Prolonged fluid exposure times did not consistently affect filter cake thickness, though effective regeneration processes led to filter cakes with higher bentonite content. Future research is needed to better understand the interplay between wall roughness, filter cake properties, and support fluid types, particularly in cohesive soils.

Keywords: filter cake, friction, bentonite, polymer, diaphragm wall, wall roughness, soil-concrete interface

INTRODUCTION

The construction of diaphragm walls and bored piles without casing requires temporary fluid support to stabilise the open trench or borehole before concrete placement. The support fluid is generally either bentonite- or polymer-based and may contain various additives to enhance certain fluid properties (EN 1536:2015; EN 1538:2015; EFFC/DFI 2019). Regardless of the type of slurry, construction under fluid support is assumed to reduce the mobilisable shear stresses at the interface between soil and final concrete structure (e.g., EFFC/DFI 2019). This assumption is linked to the formation of a filter cake of certain thickness, for which reduced frictional properties compared to the native ground are assumed, especially for long open times of the trench or borehole. The effect of formed filter cake and influencing factors are currently controversially discussed, especially with respect to responsibility, economic impact and design efficiency of the final structure compared to other types of construction.

 © DFI International Bruges 2025

Internationally, whether reduction factors are taken into account and, if so, according to which criteria, differs between countries as well as type of construction, i.e. bored pile or diaphragm wall, despite all being formulated for excavation under fluid support, i.e. with long duration of contact between fluid and soil. Moreover, historically, international standards and guidelines have been developed around clay-based support fluids. Only in recent years have polymer solutions been introduced into practice and into the first guidelines for deep excavations. Polymer solutions, however, are known to behave quite differently rheologically compared to bentonite suspensions (small yield stress at rest, but high shear-dependent viscosity). That is, their penetration behaviour and consequently the driving mechanisms at the fluid-soil interface can be markedly different (Lam and Jefferis, 2018; Verst, 2021; Verst et al., 2022).

The first findings of an R&D project evaluating the shear resistance of the interface between diaphragm walls and soils for non-cohesive soils based on laboratory and field investigations were summarised in Verst et al. (2022). In Verst et al. (2022), special focus was placed on a realistic representation of the filter cake constitution. It was concluded that the filter cake – in addition to the influence of the adjacent soil permeability – rather depends on the grading of the suspended fines forming the filter cake and thus influencing its residual permeability. In silty and sandy soils, during panel excavation, bentonite suspensions show sand contents up to 10 % and more before regeneration and in many cases after regeneration 1 % to 2 %. The investigations in these conditions showed that the filter cake mainly consists of silt and sand grains with diameters ≤1 mm and that bentonite contents of filter cakes generally range below 20%. For polymer solutions, a comparable filter cake development was not observed. Depending on the composition of the polymer solution and type of upload, a solidification of the soil surface through bonding was even observed increasing the shear strength in the contact zone.

The results so far support the view that shear stress transfer in the soil-concrete interface can be described by a wall friction angle in a range of 25° to 30° for bentonite suspensions and between 35° and 40° for polymer solutions in non-cohesive soils. Current regeneration systems lead to sand contents in the regenerated bentonite suspension of well below 1 %. The influence of such low sand contents, combined with long opening times, on the composition of the filter cake has not been conclusively clarified yet. Recent studies show higher bentonite content in the filter cake when the sand content of the suspension falls below 1% after regeneration, especially when the opening time is long and regeneration begins early, e.g., immediately after excavation.

Evidently, these findings cannot immediately be transferred to diaphragm walls (or bored piles) excavated under fluid support in cohesive soils, as distinctly different mechanisms of action are taking place. Field investigations on interface characteristics in clayey soils are addressed in König et al. (2025). Filter cakes were not found in such soils, which is in agreement with earlier observations (König & Schröder, 2017). However, the investigations show a significant increase of water content and decrease of undrained shear strength of the soil close to a diaphragm wall panel excavated in overconsolidated clayey soil under bentonite suspension support, resulting from migration of water. Swelling through negative pressure from relief is one reason that can be substantiated numerically, e.g., by Nicholson et al. (2025).

With this background, this paper summarises the remaining laboratory and field results of the R&D project on wall roughness, fluid exposure time and modified adjacent soil characteristics. These findings are embedded into a general overview of respective driving mechanisms (penetration and interface behaviour in cohesive vs. non-cohesive soil) and supplementary influencing parameters, differentiated depending on the support fluid constitution and the characteristics of the native ground.

 © DFI International Bruges 2025

MECHANISMS OF INTERACTION BETWEEN FLUID AND SOIL

Bentonite suspensions and polymer solutions are chemically different fluids (suspension vs. solution). The suspended bentonite lamellas from bentonite slurries may filter out at the interface leaving filtrate water to penetrate the ground. Polymer solutions (without granular load) are chemically more stable and do not tend to filter in this way. Therefore, experience with bentonite suspensions cannot and should not be transferred directly. Additionally, the presence of granular load, either taken up from the excavated ground or added artificially, in both cases, also influences the modes of interaction at the interface, complicating differentiation.

However, general mechanisms of interaction between fluid and soil may be differentiated independently of the type of support fluid as a basis for classification. Here, four groups may be differentiated, influencing in different ways the fluid-soil and subsequently the concrete-soil interface:

1. Migration of water (very slow flow) (low-permeable / cohesive ground)
2. (Bulk) Fluid flow (non-cohesive ground)
3. Surface clogging ("clogging") (non-cohesive ground)
4. Deep clogging (deposition and accumulation) (non-cohesive ground)

Mechanism 1 can generally be associated with cohesive or comparatively impermeable ground conditions and can be differentiated distinctly relative to mechanisms 2-4, which address penetration mechanisms in non-cohesive more permeable ground. While it is known that migration of water occurs in certain cases resulting in a degradation of the soil surface or a softening effect and decrease in stiffness in the contact area, this mechanism is considered not to be well understood up to now by the authors. Driving mechanisms can be differentiated, but the complex interplay between variables complicates easy predictions. Thermodynamically formulated, migration of water is caused by differences in the total energy level, expressed by potentials or gradients, e.g. a hydraulic gradient (overpressure or negative pore pressure from stress relief) or a physicochemical gradient (diffusion, osmosis, hydration) (Verst, 2021). Soil swelling or softening driven by differences between fluid pressure and horizontal stresses in the soil is often mentioned and studied (Lam and Jefferis, 2018; König et al., 2025; Nicholson et al., 2025). While it is mostly addressed and found with clayey materials, other types of soils such as silt or marl may also be affected. Water in all cases may originate from both sides of the interface, from the support fluid or from the surrounding soil. Overconsolidated clayey soils show an increased potential for stress relief and some types are sensitive to mineralogy-driven water uptake (König et al. 2025). Support fluids such as bentonite suspensions and especially polymer solutions may slow down the process of water uptake by the ground, e.g., by reducing the availability of water from one side (water retention capacity) (Verst, 2021).

With regards to the penetration-related mechanisms 2-4, the following images illustrate key differences in penetration and pressure transfer differing between these mechanisms at specific times t_i and penetrations depths $s_i(t_i)$. The support fluid (yellow), which can be "clean" or "dirty", displaces pore water (blue). Grains (brown) can be e.g. mineral or polymeric (aqueous). The graphs depict characteristic pressure drop curves along penetration depth s at time steps t_1 and t_2 (and t_3) between pore water head (p_w) and support fluid overall fluid head (p_F) at a given depth z.

In (bulk) fluid flow (Fig. 1), penetration behaviour is driven by the base fluid's rheology and soil permeability. Small additives do not significantly interact with the soil matrix, though granular load may affect flow properties Penetration velocity depends on overhead pressure, penetration depth, and fluid rheology.

 © DFI International Bruges 2025

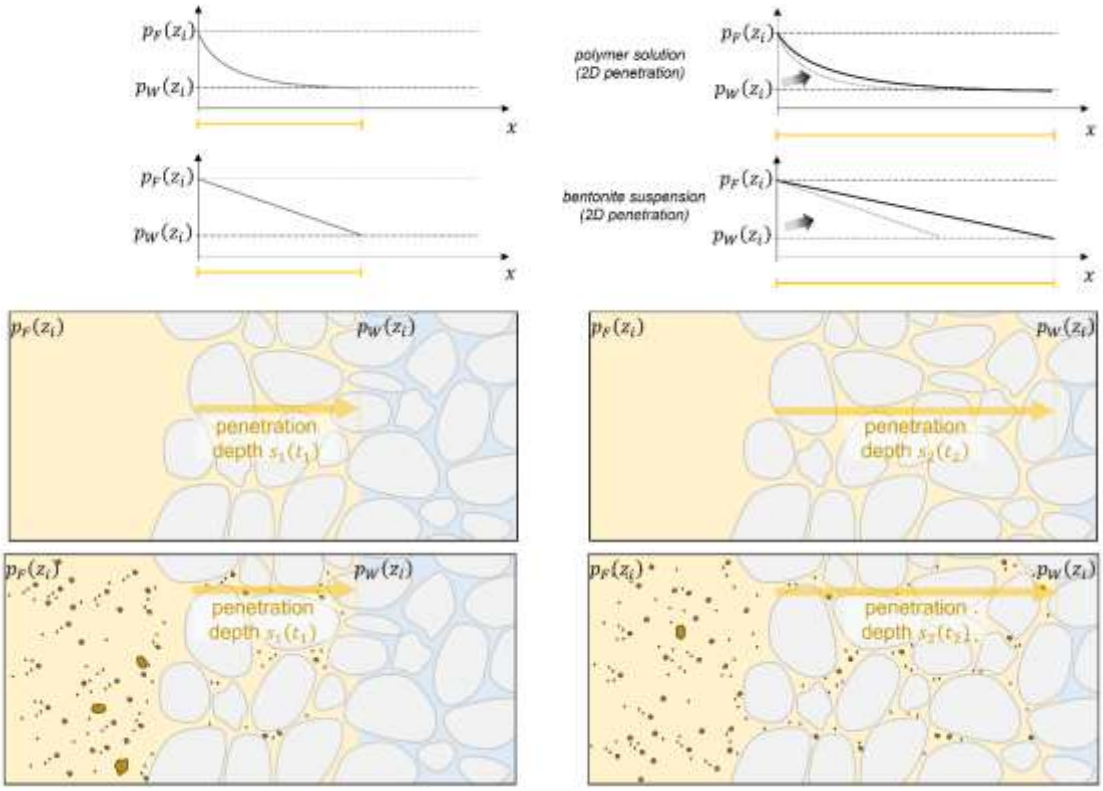


Fig. 1. (Bulk) Fluid flow and rheological blocking – "clean" (top) vs. "dirty" fluid (bottom)

The flow behaviour of the fluid within the permeable soil matrix ("in-situ" rheology) may differ from flow behaviour measured in the context of other geometric boundary conditions (e.g. rheometer). The applied overpressure transfers to the soil matrix through shear forces mobilised along the penetration depth, causing the pressure drop curve to align with the penetration depth. Penetration velocity decreases with progressing penetration under constant overpressure and/or with increasing viscosity, potentially reaching a sufficiently low level, so that the time-dependency of the penetration depth can be neglected as the maximum penetration depth can be estimated (function of soil permeability, fluid rheology and fluid overpressure). Additionally, with a certain characteristic fluid rheology, if a minimum shear stress is required to initiate flow (e.g., in Bingham fluids like bentonite suspensions), penetration may stagnate due to a balance between shear strength and overpressure (Verst, 2021).

Any form of penetration will start with (bulk) fluid flow. Surface clogging (mechanism 2) will then occur in the case of the availability of larger grains for clogging of the soil pores at the fluid-soil interface (Fig. 2). The effectiveness of the filter cake in transferring pressure and stopping penetration depends on the interaction between granular load (diameter, grading) and the (residual) permeability of the soil surface. Clogging by means of fines can occur as long as transportability of the fines is ensured, i.e., that the sinking velocity of the relevant grain fractions is lower than the remaining penetration velocity of the fluid transporting the fines. Moreover, the clogging material in the relevant sizes should be available for deposition and not be held back by the fluid (poor dispersibility). Well-graded material is needed to effectively clog the pores.

 © DFI International Bruges 2025

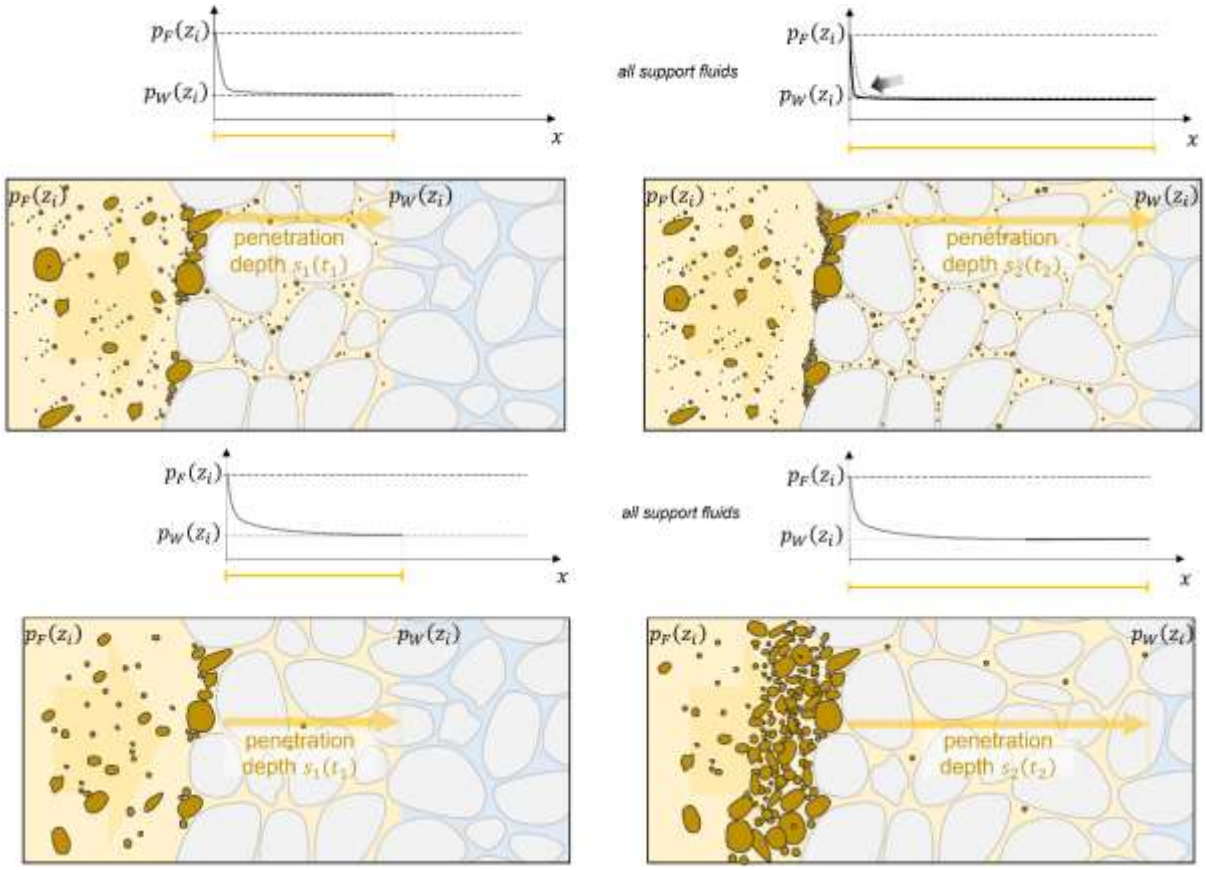


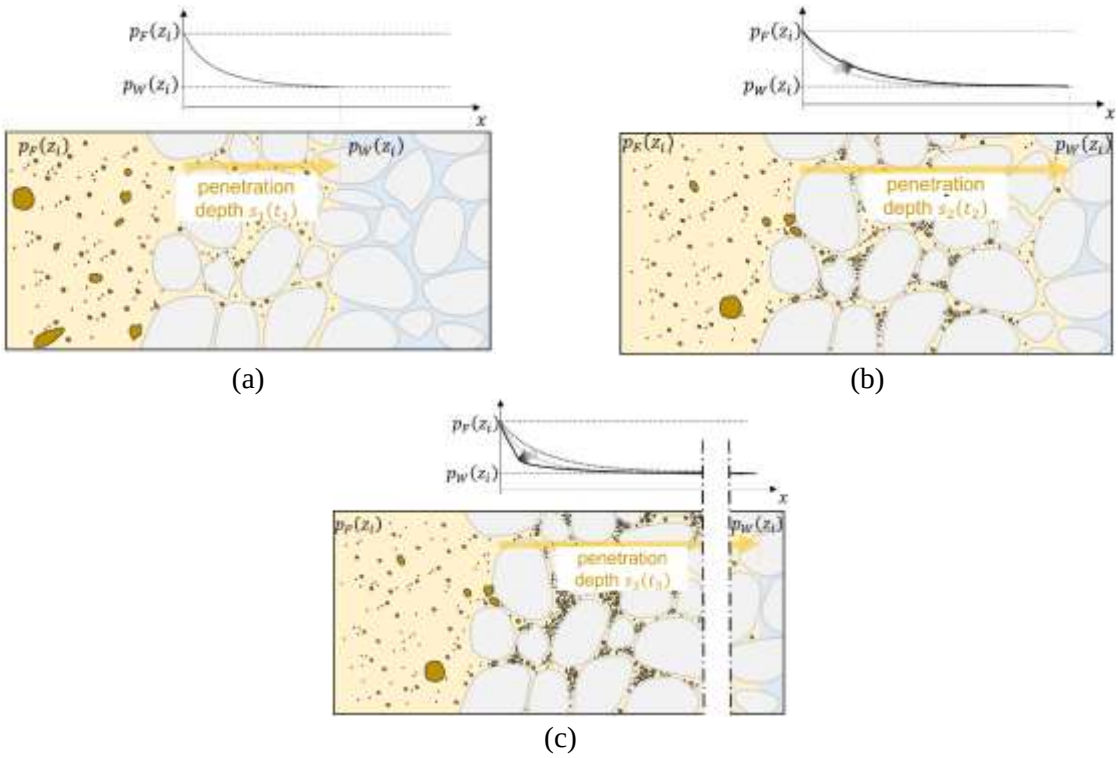
Fig. 2. Surface clogging – "effective" clogging (top) vs. incomplete clogging with growing outer filter cake (bottom)

Complete surface clogging with full pressure transfer was found to correlate with a reduction of the residual penetration velocity to below around $1 \cdot 10^{-6}$ m/s for different types of support fluid (Mianji et al., 2020; Verst, 2021) and is only possible if the smallest fines fraction is available or if other means of fine clogging are possible (opposite: incomplete clogging). For granular material to clog, fluid penetration is necessary so that material can filter and accumulate at the contact zone. The Terzaghi filter criteria (mechanical criterion $d_{max} = d_{15,F}/4$), inverted drainage criterion $d_{min} = d_{15,s} < d_{15,F}/4$) are a safe-side indicator for surface clogging. A higher fines concentration requires less fluid penetration for the same degree of pore blocking, i.e. a high concentration of fines is favourable for this effect. The residual penetration velocity through the filtered zone is primarily controlled by the residual permeability (permittivity) of the contact zone and bulk fluid rheology. A cake can grow on the clogged zone if the permittivity of the filter cake surpasses the sinking velocity of the loaded grains (Verst, 2021).

Deep clogging (mechanism 4,

Fig. 3) may be regarded as a gradual overall reduction of soil permeability through deposition and accumulation of fine granular material within the soil body. In contrast to surface clogging, the fine particle sizes are too small to immediately effectively successively clog soil pores as the larger fines fractions are missing. They are still deposited along the penetrated zone because of winding flow paths and consequently local variations in flow velocity and thus transportability of loaded fines. A marked accumulation of fines in the soil matrix can influence the ratio of grain sizes in the soil matrix to such an extent that pressure-transferring "effective" clogging may become possible with smaller fines fractions at the soil-fluid contact zone. Deep clogging needs significantly higher amounts of fines than the mechanisms created by surface clogging to stop penetration and ensure full pressure transfer at the contact zone, regardless of time.

 © DFI International Bruges 2025



(a) (b) (c)

Fig. 3. Deep clogging with progressing penetration depth s_1 (a) → s_2 (b) → s_3 (c) resulting in a small (b) vs. marked (c) influence on the pressure drop curve (curve displayed exemplarily for an initially non-linear pressure drop curve)

INTERFACE CHARACTERISTICS AND INFLUENCING PARAMETERS

Filter cake thickness and wall roughness represent two opposing factors with influence on mobilisable shear in the contact zone between soil and concrete under bentonite-based fluid support. The extent of their influence and their interplay are again influenced by other factors such as soil type, excavation method, and fluid exposure time. In fine-grained soils with usually negligible filter cake thickness and low intrinsic soil roughness, e.g., trails from the excavation tool create an increased wall roughness exceeding filter cake thickness. This relationship can be reversed with increased filter cake thickness in more permeable ground such as sand. At some point, the grain size of the adjacent soil may become the decisive factor determining the roughness and thus shear resistance of the contact zone, creating entrapped pebbles and/or unconnected spots of filter cake. In this regard, laboratory experiments by Lam et al. (2014) were able to show that filter cake growth over time only creates a reduction in shear stress transmission once the filter cake thickness has covered the roughness of the concrete surface to a minimum of 50% of the total contact area.

König & Schröder (2015), e.g., describe roughness values R_t (as differences between the highest and lowest point of the profile line; wall roughness depth) of 15 – 25 mm up to 50 mm along measurement lengths of ~1 m. More recent investigations of the authors (unpublished) confirm these findings. Additional field and laboratory investigations carried out within the scope of this R&D project to study the interplay of these influencing factors are described hereinafter.

Field investigations: filter cake thickness vs. wall roughness

Investigations on field samples covered the exploration of three diaphragm wall construction sites A, B and C during pit excavation under bentonite suspension. All panels were excavated using a grab. Soil conditions varied from marine clay (Klei), silt and sand to gravel. Wall roughness for all sites was measured by using a profile gauge at different positions The difference between the highest and lowest point of the profile line is defined as roughness depth R_t (

Fig. 4).

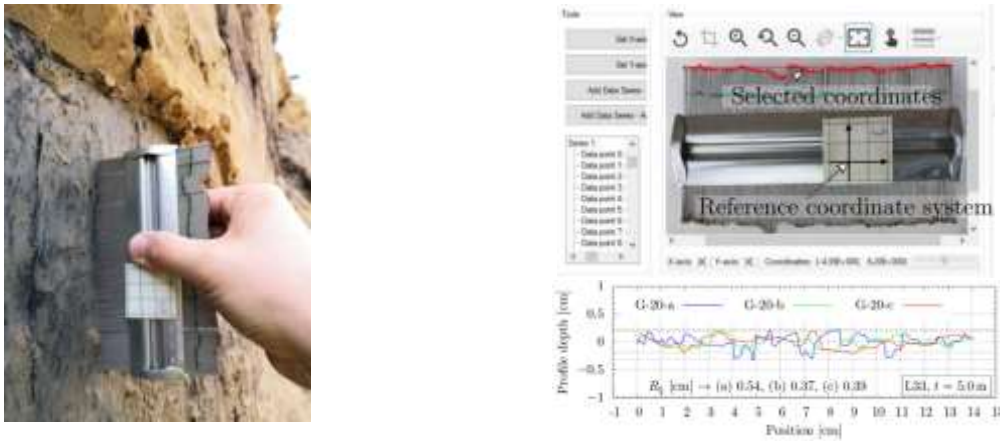
 © DFI International Bruges 2025

Silty sand dominates the soil stratum at site A. The panels were supported by a suspension with a bentonite content of 50 kg/m³. Filter cake thickness was 0.3 to 3 cm in more silty sand and 0.5 to 3 cm in less silty sand. Water content for filter cakes in both soil strata was 40 % and bentonite content about 9 %. Wall roughness R_t was 0.36 cm in more silty sand and 0.53 cm in less silty sand, meaning that filter cake thickness exceeds wall roughness.

At site B, excavation took place mainly in gravel underlaid by gypsum keuper. Suspension was used with bentonite contents of 60 kg/m³. A filter cake was found to be continuously formed over the wall surface with a thickness of 4 cm to 6 cm, water contents of (average) 80 % and bentonite contents of (average, taking into account mineralogy of the nearby soil (von Blumenthal et al., 2021)) 20 %. Wall roughness R_t was about 0.94 cm. In this case, it was concluded that high bentonite contents of the fresh suspension may lead to a small penetration depth with water flow out of the suspension through the filter cake, which exhibited relatively high water content and high permeability. This appears to favour filter cake growth. Filter cakes observed at other diaphragm walls excavated in gravely soils were not formed continuously and direct contact between gravel grains imbedded in the filter cake and wall was observed. In all these cases, bentonite content of the fresh suspension was about 50 kg/m³ (König & Schröder, 2015, and unpublished site reports). It may be concluded that the high bentonite contents in the fresh suspension led to the prominent filter cake at site B.

Investigations on site C took place at panels 1 & 2. In the sand stratum, filter cake development was significantly different for both panels, with panel 1, 0.5-1.5 cm and panel 2, 3.0-6.0 cm, despite similar fluid exposure times (panel 1: 27 hrs, panel 2: 26 hrs) and bentonite content of the fresh slurry (50 kg/m³). The filter cakes taken at panel 1 showed water contents about w = 123-145 % (dry density ρ_d = 0.6 g/cm³) and bentonite contents of b $\leq$ 16 %, compared to panel 2 with w = 68-80 % (ρ_d = 0.9-1.0 g/cm³) and b $\leq$ 10 %. Following the installation protocols, density (ρ_f) and sand content (SC) of the suspension differed between panels 1 and 2 as fresh suspension (panel 1: ρ_f = 1.02 g/cm³, panel 2: ρ_f = 1.1 g/cm³) and before concreting (panel 1: ρ_f = 1.03 g/cm³ / SC = 0.8 %, panel 2: ρ_f = 1.15 g/cm³, / SC = 2.5 %). These differences can be attributed to modifications during regeneration resulting in a much more effective regeneration process for panel 1. The low concentration of soil particles in the bentonite suspension caused by the effective regeneration process (panel 1) lead to a reduction in thickness and an increase of the bentonite content of the filter cake. The higher bentonite content is related to a higher water content, because the bentonite holds the water. In this case, the bentonite particles clogged the pores of the soil together with the remaining more fine soil particles in the bentonite suspension forming a filter cake with low permeability (Fig. 2, top). Both phenomena, reduction of thickness and increase of bentonite content of the filter cake, have a different effect on the shear strength of the soil - cake - wall interface. Thinner filter cakes may increase, higher bentonite contents reduce the interface shear strength. For panel 2 with higher concentration of soil particles, incomplete clogging (Fig. 2, bottom) has probably led to the growth of the filter cake consisting of sand and silt particles, mainly, which indicates higher shear strength. Wall roughness at site C was about 0.3 cm, which is smaller than the filter cake thickness observed for both panels. In additions, the panels of site C partly passed the stratum of marine clay (Klei), where no filter cake was observed. Wall roughness at these locations was small (R_t = 0.18 cm), but high enough to provide interlocking between wall and soil.

 © DFI International Bruges 2025



(a) (b)

Fig. 4. Profile gauge used to measure wall roughness (a), measurement process (b, top) and profile plot with evaluation of roughness depth R_t (b, bottom)

The investigations support the assumption that wall roughness exceeds filter cake thickness in fine grained soils such as Klei, while in silty and sandy soils, filter cake thickness exceeds wall roughness. For gravel soils, wall roughness, discontinuous filter cake and gravels embedded in the filter cake with direct contact to the wall could be expected. These findings are in agreement with König & Schröder (2017). Extremely high bentonite contents of the bentonite suspension may lead to thick filter cakes preventing any contact between soil and soil particles with the wall.

Field investigations: filter cake properties vs. fluid exposure time

The influence of opening time on the filter cake characteristics was examined on sites A and B. Opening times on both sites ranged between 24 hrs to 30 hrs and 72 hrs to 78 hrs. Neither filter cake thickness (short opening time / long opening time: 1.4 cm / 1.3 cm (A) and 3.5 cm / 3.8 cm (B)) nor bentonite (5.7 % / 5.2 % (A) and 26.7 % / 21.5 % (B)) content were found to show a systematic or significant influence from the opening time.

Laboratory investigations: roughness vs. mobilizable interface shear strength

The effect of the wall roughness on the increase of the shear strength of the interface was studied by means of direct shear tests with prefabricated concrete plates and sandy soil.
Fig. 5 (a) shows the concrete plates used. Two types of concrete plates with no profiled surface (series 1 and 4) (R_f = 0.17-0.2 cm) were compared to a plate with a stepped offset of 4 mm (series 2, the offset was oriented perpendicular to the shear direction, R_f = 0,45 cm) and a plate with regular circular elevations of 5 mm in diameter and height (series 3, aluminium rods) (R_f = 0.65 cm). The roughness values were determined by measuring the profile of the concrete plate's surfaces with a profile gauge (
Fig. 4) at several locations. The roughness values calculated from the different profiles were averaged to an average roughness depth. The plates were placed in the lower part of a shear box, with filter cake material placed on the concrete plate. Medium sized sand was poured on the filter cake material. The filter cake and soil were consolidated in two steps up to 80 kPa.

 © DFI International Bruges 2025



(a) (b)

Fig. 5. Samples from series 1, 2, and 3 (a) and respective results of the shear tests on the interface between concrete, filter cake and soil (b)

The thickness of the filter cake material after consolidation was about 10 mm, i.e., filter cake thickness exceeded the roughness of the concrete plates in all cases and no direct soil plate contact occurred. Shearing was performed with a displacement rate of 0.005 mm/min. The shear plane was located in the middle of the filter cake (series 1 and 4), in the level of the upper part of the concrete plate (series 2) and in the level of the upper and of the elevations (aluminium rods) (series 3). Filter cake material was a mixture of bentonite (7 m-%, “Aktiv-Bentonit Ibeco S”), fine sand (58 m-%, “Siligran S90”) and water (35 m-%). For series 4, two other filter cake materials were used: medium-sized sand instead of fine sand and original filter cake material taken from construction site C.

Fig. 5 (b) shows the results of the direct shear tests in terms of determined peak friction angle and average roughness depth. The trend line shows an increase in friction angle from about 27° to 31° with increasing roughness (without direct contact between soil and concrete), i.e. increasing confinement of the shear plane with increasing roughness.

MODIFIED SOIL CHARACTERISTICS

Non-cohesive soil: Penetration testing, filter cake, and soil stability

Aside from filter cake formation, support fluid penetration may also influence the adjacent ground it penetrates. Small-scale soil penetration testing with different support fluids with a modified Bauer filter press set-up unit (FP) as shown in Fig. 6 was found to relatively easily show the effect a penetrating support fluid may have on sandy soils. The findings obtained as part of this R&D project are summarised here.

The tests were performed with two types of soil (medium and coarse sand), two types of base fluid (bentonite suspension at 45 g/l and CMC-H (high-viscosity carboxy methyl cellulose) solution at 5 g/l) and under 0.5 bar overpressure. The fluids were prepared with different gradings of mineral load to form filter cakes and limit penetration. After stagnation, the penetrated soil samples with formed filter cakes were carefully removed from the press and running water was rinsed on all filter cake and soil samples to test the stability of filter cake and penetrated soil, as shown exemplarily in Fig. 7.

 © DFI International Bruges 2025

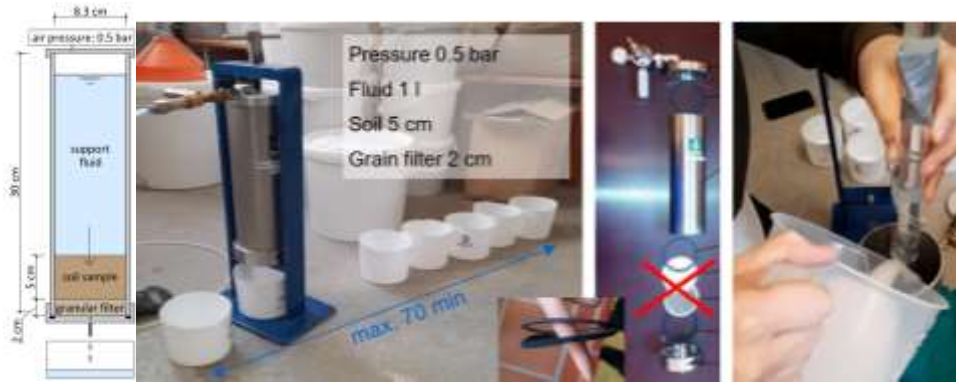


Fig. 6. Bauer filter press modified set up for soil penetration testing



(a) (b)

Fig. 7. Bauer filter press evaluation with bentonite suspension at 45 g/l (a) vs. CMC-H solution at 5 g/l (b) with mineral load, soil: medium sand 0/2 mm

Overall, it could be seen that the formed filter cake differs depending both on the nature of the granular additives and on the base fluid. With bentonite suspension, water rinsing on filter cake and soil showed no significant bond / cohesion of the filter cake in medium or coarse sand. The coarse sand seemed slightly more cohesive resulting from larger amounts of actual penetration of clay suspension. With medium sand, bentonite particles were filtered out at the interface forming the filter cake, leaving mainly residual water filtering into the ground and the ground properties undisturbed (
Fig. 7a). With CMC-H, in medium sand, the filter cake was seemingly formed from mineral load and a polymeric network, which was found to be more cohesive and stable against water placement or manual scraping. Evidently, the polymer solution is able to stabilise not only the filter cake but also the penetrated medium sand (
Fig. 7b). This effect was less pronounced in coarse sand. This shows that the polymer chains in these ground conditions are not only able to not diminish stability-related interface properties in the contact zone but stabilise or improve these properties.

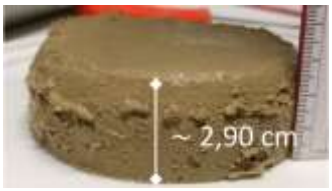
Cohesive soil: soil swelling and shear tests

The FP test set-up (Fig. 6) was also used to exemplarily study the influence of different types of support fluid (water, bentonite suspension or CMC-H solution) on clayey ground and under realistic overpressure levels and long contact between the support fluid and soil (24 hrs). Three FP tests were performed with an artificially prepared and Proctor-consolidated soil sample ("Calcigel" bentonite and sand at 1:1, initial water content 9%). Outflow was measured and heave and soil consistency were examined afterwards. The top ~1 cm of the contact zone was then placed into a small direct shear device and sheared under a normal pressure of 80 kN/m². Selected support fluid properties are ranked as follows:

- Water activity water > bentonite suspension > CMC-H solution > soil sample
- Viscosity water < bentonite suspension << CMC-H solution

 © DFI International Bruges 2025

Fig. 8 gives an overview on the test results. The results indicate that the polymer solution least affects the soil sample in terms of fluid uptake, stiffness, consistency, and shear strength. The bentonite suspension performs poorer than the CMC-H solution, but still markedly better than pure water. This may be explained by the individual water retention capacity of the original fluid (indicated by their water activity) – water is most strongly bound by the CMC-H solution – and its viscosity (general deceleration).



- soil: soft
- heave: $\Delta h/h_0$=0.45
- outflow volume: 200 ml
- $\tau_{max} = 22$ kN/m²

(a) water



- soil: kneadable
- heave: $\Delta h/h_0$=0.30
- outflow volume: 10 ml
- $\tau_{max} = 54$ kN/m²

(b) bentonite suspension



- soil: stiff
- heave: $\Delta h/h_0$=0.15
- outflow volume: 0 ml
- $\tau_{max} = 81$ kN/m²

(c) CMC-H solution

Fig. 8. Test results FP swelling tests with different support fluids after 24 hrs of fluid contact

This small test regime does not sufficiently reflect all mechanical, mineralogical and other boundary conditions found in the field, which may influence the swelling behaviour of different soils. König et al. (2025) show that some soils do not swell or degrade as much in the field owing to specific interplays of soil and excavation conditions. However, these tests do show the effect different fluid properties may have on otherwise fixed circumstances and may be used as a first conservative estimate.

CONCLUSIONS

The construction of diaphragm walls and bored piles under fluid support presents unique challenges in terms of shear stress transfer at the soil-concrete interface. Understanding the effects of interface mechanisms, especially filter cake formation, but also the influence of wall roughness is crucial for optimizing design and ensuring structural integrity.

The interaction between support fluids and soil varies depending on soil permeability and the rheological properties of the fluid. Bentonite suspensions and polymer solutions behave differently at the interface, influencing filter cake formation and penetration depth, which in turn affect shear strength. Wall roughness and filter cake thickness are key factors influencing the shear resistance at the soil-concrete interface. The balance between these factors depends on soil type and fluid exposure time as well as on excavation conditions (tools, fluid regeneration, etc.). The field and laboratory investigations confirm that even in the presence of a filter cake, roughness continues to influence shear resistance, with rougher surfaces providing better performance. Furthermore, the findings show that extended exposure times to support fluids were found to not consistently affect filter cake thickness or composition. However, more effective and early fluid regeneration processes with bentonite support fluids can lead to thicker filter cakes with higher bentonite content, negatively influencing shear strength. Additionally, laboratory testing shows that the penetration of support fluids can modify the adjacent soil characteristics, affecting the stability and mechanical behaviour of the soil near the interface. Different fluids, such as polymer solutions, can enhance soil stability, which may improve interface performance.

Overall, this research highlights the variety of interaction parameters positively or negatively influencing the shear strength at the soil-concrete interface. Further studies could refine these findings, especially for cohesive soils, to refine design recommendations and improve construction practices.

 © DFI International Bruges 2025

REFERENCES

v. Blumenthal, A., Lieske, W., König, D., Wichtmann, T. (2021). Quantification of the bentonite content in diaphragm wall filter cakes based on cation exchange capacity. Geotech. Test. J. 44 (6) 20200095.

EFFC/DFI (2019). Guide to support fluids for deep foundations. First edition.

FHWA-NHI-18-024:2018 (2018). Drilled shafts: construction procedures and design methods. United States. Federal Highway Administration.

König, D., Nicholson, D., Verst, R., Harnan, C. (2025). Field investigations on the characteristics of clayey soil close to diaphragm walls. EFFC/DFI. Int. Conf. on Deep Foundations and Ground Improvement, Bruges.

König, D., Schröder, T. (2015). Zusammensetzung des Filterkuchens an Schlitzwandlamellen mit kurzer und langer Standzeit. Bauingenieur 90 (2) 60-70.

König, D., Schröder, T. (2017). Zur Beschaffenheit des Filterkuchens und der Kontaktfläche Boden-Wand bei Schlitzwänden. Tagungsband zum 8.RuhrGeo Tag 2017. Essen, pp. 127–146.

Lam, C., Jefferis, S.A., Martin, C.M. (2014). Effects of polymer and bentonite support fluids on concrete-sand interface shear strength. Géotechnique 64 (1) 28-39.

Lam, C., Jefferis, S.A. (2018). Polymer support fluids in civil engineering. ICE Publishing.

Mianji, P., Baille, W., Wichtmann, T., Verst, R., & Pulsfort, M. (2021). Influence of mineral or polymeric modification on bentonite-based tunnel face support. Geotechnical Aspects of Underground Construction in Soft Ground (pp. 796-803). CRC Press.

Nicholson, D., Ferreira, J., Pillai, A., Qui, X. (2025). The impact of long opening times on shaft friction in cohesive soils. DFI-EFFC, Int. Conf. on Deep Foundations and Ground Improvement, Bruges.

Verst, R. (2021). Stabilisation mechanisms of polymer solutions in the context of temporary earth-wall support. PhD thesis. Bergische Universität Wuppertal.

Verst, R., v. Blumenthal, A., Du, J., König, D., Pulsfort, M., Wichtmann, T. (2022). Systematic laboratory and field study on the shear resistance of the soil-concrete interface of diaphragm walls and bored piles.
EFFC/DFI International Conference on Deep Foundations and Ground Improvement. Berlin.

 © DFI International Bruges 2025

PERFORMANCE AND LOAD DISTRIBUTION IN STABILIZED SOIL AS SUPPORT FOR AN EXCAVATION IN MARINE CLAY

Marit S. Løyland, Norwegian Geotechnical Institute, Oslo, Norway, +47 415 06 645, marit.skaug.loyland@ngi.no
Egil J. Monsås, Norwegian Geotechnical Institute, Oslo, Norway, +47 954 16 823, egil.monsas@ngi.no
Anders G. Nore, Asplan Viak AS/NTNU, Norway, +47 917 90 476, anders.nore@asplanviak.no
Ana P. Paniagua, Norwegian Geotechnical Institute, Trondheim, Norway, +47 948 29 497, priscilla.paniagua@ngi.no

ABSTRACT

Urban development and progressive growth of the construction industry requires geotechnical activities under difficult conditions. In Norwegian practice, ground improvement by lime-cement stabilization (LCS) is often used to achieve the required safety level and to reduce deformations on support walls for deep excavations in marine clay. Despite previous studies and research on LCS, there are still uncertainties regarding the quality, performance and load distribution in the stabilized soil volume which influence the design of such excavations.

The research project CURIOUS (Campus Ullevål: Research and Instrumentation Of Underground Structures) was initiated to study and improve the design of deep excavations in sensitive marine clays supported by sheet pile walls (SPW) and LCS. A six-meter-deep excavation pit in Oslo was equipped with an enhanced monitoring system to gain a better understanding of the performance of the SPW and the stabilized soil during the different stages of construction.

The paper presents results of the monitored horizontal displacements of the stabilized soil volume and assesses the performance of the LCS soil during the excavation. The results are compared with the numerical design analyses in 2D and 3D finite element analyses and subsequently used to evaluate design procedures for deep excavations supported by SPW and LCS.

Keywords: marine clay, deep excavation, ground improvement, lime-cement, load distribution.

INTRODUCTION

Background

Urban development and progressive growth of the construction industry requires geotechnical activities under difficult conditions, such as sensitive marine clays. Ground improvement by lime-cement stabilization (LCS) is often used to achieve the required safety level and to reduce deformations on support walls for deep excavations in these conditions. Despite previous studies and research on LCS, there are still uncertainties on the quality, performance and load distribution in the stabilized soil volume which influences the design of such excavations.

Norwegian Geotechnical Institute (NGI) is, together with Aspelin Ramm AS, building a new office building at Ullevål in Oslo, Norway. As part of this project, NGI initiated a research project SP CURIOUS (Campus Ullevål: Research and Instrumentation Of Underground Structures). This project was initiated to further study and improve the design of deep excavations in sensitive marine clays supported by sheet pile walls (SPW) and LCS. The excavation pit in Oslo was equipped with an enhanced monitoring system to gain a better understanding of the performance of the SPW and the stabilized soil during the different construction stages. The monitoring system consists of strain sensors, inclinometers, load cells and geodetic points on the SPW, and will be described further in the

 © DFI International Bruges 2025

article. Monsås et al. (2024) evaluates the performance of the SPW during excavation, whereas this research evaluates the performance of the stabilized soil.

Problem Formulation

In Norway, LCS has been widely used to enhance the safety of construction pits and slopes and reduce displacements and settlements (Karlsrud et al. 2005, 2015). In the Scandinavian countries, LCS is predominantly implemented with the deep dry mixing (DDM) method. In Norway, LCS in the passive zone is a common technique for reducing deformations behind retaining structures, lowering structural forces, and increasing resistance against basal heave failure. In recent years, its application has also grown in Sweden, resulting in increased research on the topic (Ignat et al. 2016, 2020; Larsson et al. 2012).

Often, the measured strength and stiffness of the stabilized soil is higher than is allowed in commonly used Norwegian design guidelines. In excavation pits, LCS is recommended to be installed in panels perpendicular to the sheet pile wall (SPW). Between the LC-panels there is untreated soil. Norwegian design practice is to calculate the design based on an average strength and stiffness of the stabilized volume (Norsk Geoteknisk Forening 2012, Statens Vegvesen 2012). In this article a study of the load distribution in the LC-panels in a PLAXIS 3D model will be evaluated and compared to normal design practice of a PLAXIS 2D model, and also compared with data from the excavation pit in Oslo. Evaluating design methods which could lead to optimization of the LCS could be beneficial to both environmental impact, construction time and costs.

GROUND CONDITIONS AND EXCAVATION

Ground Conditions

The site is located at Ullevål in Oslo, Norway. The site borders a national road in the north, pile foundations for a pedestrian bridge north and east of the excavation pit, an office building to the south and an allotment to the west. The terrain is relatively flat, with an elevation above sea level between +97.1 to +98.3. The ground investigations on the site consisted of total soundings, a Norwegian developed sounding for finding the soil layering and depth to bedrock (Kolstad 1987), CPTu-tests and collection of undisturbed samples in two boreholes.

The soil conditions are characterized by an upper layer of dry crust and fill material with a thickness of around 1-2 m, followed by a 6-7 m layer of low-sensitive marine clay with an undrained shear strength of 40 to 45 kPa. Below lays a layer of quick clay down to the bedrock, located between 20 to 45 m below the original terrain level. The soundings indicate sand and silt layers with thickness from a few cm to 2 m.

Pore pressure measurements show the groundwater level at about 1.5 m below the terrain. The index properties for the clay are presented in Fig. 1. The clay has an average unit weight, γ, of 19.3 kN/m^3 in the upper 15 m, decreasing with depth. The water content, w, of the clay is approximately 30 %, and the soil is highly sensitive, $S_{t,}$ from 7 m depth. The shear strength, c_u, profile is evaluated from interpretations of cone penetration tests (CPTu) and from consolidated anisotropic undrained active (CAUA) triaxial tests. The soil layering is interpreted as in Fig. 1.

 © DFI International Bruges 2025

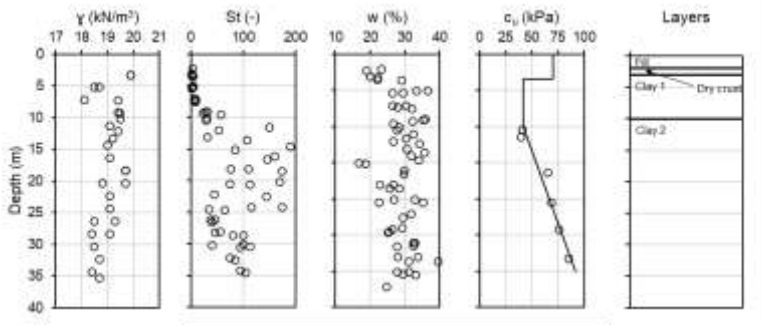


Fig. 1. Index properties of the clay at the Campus Ullevål site

Excavation sequence

Due to location in an urban environment and close to existing structures, a retaining wall was designed and installed to support the excavation. The retaining wall was designed as a floating SPW, supported by LCS and internal struts to a concrete slab. Excavation was planned to an elevation of level +91.4, a total excavation depth of up to 6.8 m. To ensure global stability during all phases of the excavation, the excavation was carried out in an order as indicated below and illustrated in Fig. 2.

1. First sheet piles of the type AZ 17-700 were installed to 14.5 m below the original terrain.
2. LCS was installed in double ribs perpendicular to the sheet pile. The LC-panels were installed to a depth of approx. 20 m from the original terrain level and in a width of 20 m from the sheet pile.
3. Excavation in the center of the construction pit. A berm with a 4 meter wide plateau and a slope of 1:1.5 down towards the excavation floor was left to support the sheet pile wall and to reduce deformations.
4. Installation of inclined struts against a work platform of reinforced concrete.
5. Excavation of the berm carried out in sections of approximately 6 m width at the same time as the work platform was cast toward the sheet pile.
6. When the concrete slab was extended to support the SPW, the inclined struts were removed, and the sheet pile was supported by the LC-panels and the concrete slab.

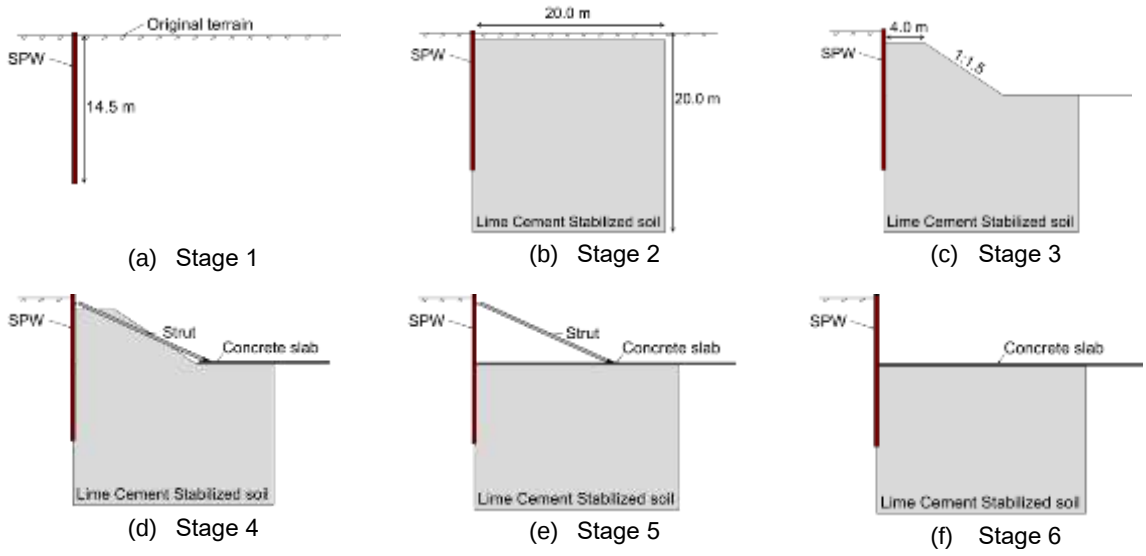


Fig. 2. Excavation sequence of the excavation pit for Campus Ullevål.

 © DFI International Bruges 2025

SOIL STABILISATION WITH LIME CEMENT/NORWEGIAN PRACTICE

Design of Deep Dry Mixing

DDM is widely used in Scandinavia (Porbaha, 1998, Broms, 2004). A rotating mixing tool is mounted on a machine. The tool penetrates the soil while remolding the clay. When reaching the design depth, dry substance/binder is mixed with the soil as the tool rotates and is pulled up. The binder is typically a mixture of lime and cement, or Multicem and cement, which reacts with the clay. The result is a stabilized column with increased strength and stiffness.

Design of LCS in Norway is based on theory and experience summarized in the LCS-handbook published by Norsk Geoteknisk Forening (2012) and in the handbook from Statens Vegvesen (2012). The characteristic design strength of the stabilized soil volume is based on a weighted average of the strength of the soil and the strength of the stabilized soil as in equation 1.

$$\tau_m = a \cdot \tau_p + (1 - a) \cdot \tau_k \quad [1]$$

Where τ_m = Average shear strength in the stabilized soil volume, τ_p = Shear strength in the stabilized material, τ_k = Shear strength in the surrounding soil, and a = Coverage of the stabilized area (the ratio of stabilized soil to non-stabilized soil)

For LC-panels consisting of double ribs of LCS the coverage of the stabilized soil is calculated proposed in equation 2.

$$a = \frac{1.6 \cdot d}{c} \quad [2]$$

Where d = diameter of the column, and c = the center-to-center distance between the LC-panels. For sufficient soil structure interaction, it is not recommended that the width of untreated soil between two panels exceeds 3.0 m. For double ribs, the maximum design strength, according to Statens Vegvesen (2012) of the stabilized material is 175 kPa.

Parameters of the Installed Lime Cement Columns

In the Campus Ullevål site, the LC is installed in panels perpendicular to the SPW. The center-to-center distance between the panels is on average 3.5 m. Preferably the panels would be distributed evenly along the sheet pile wall, but due to pile driving the LC-panels had to be adjusted to avoid future pile foundations.

Installation of the columns was performed using the deep dry mixing method. Dry binder, Multicem and cement, was mixed with the clay. The binder amount per unit of volume for completed columns was 30 kg/m^3 above the excavation floor and 50 kg/m^3 below the excavation floor. The LC-panels consisted of two rows of columns with a diameter of d = 0.6 m. The columns overlapped 20 %. The panels were installed to an elevation of +77.0, approximately 20 m below the original terrain. The length of the panels was 20 m.

The amount of binder was based on a test field at the site executed before the construction project started. Different ratios between Multicem and cement and binder amounts were tested. The strength of the LC-columns was tested with reverse column penetration test (FOPS) and column penetration test (FKPS).

 © DFI International Bruges 2025

INSTRUMENTATION

Instrumentation Plan

After the SPW and LCS were installed, and before excavation started, instrumentation was installed. Inclinometers were installed in eight locations in the section presented, fiber optic strain gauges were attached to the SPW and three geodetic points were established on the top of the SPW for monitoring. For the layout of the instrumented section, see Fig. 3. In this paper, the results from the inclinometers are of greatest interest. The inclinometers are used to evaluate the deformation behavior of the SPW, the terrain behind the SPW and deformation in a LC-panel and between two LC-panels. Information about the inclinometers is listed in Table 1.

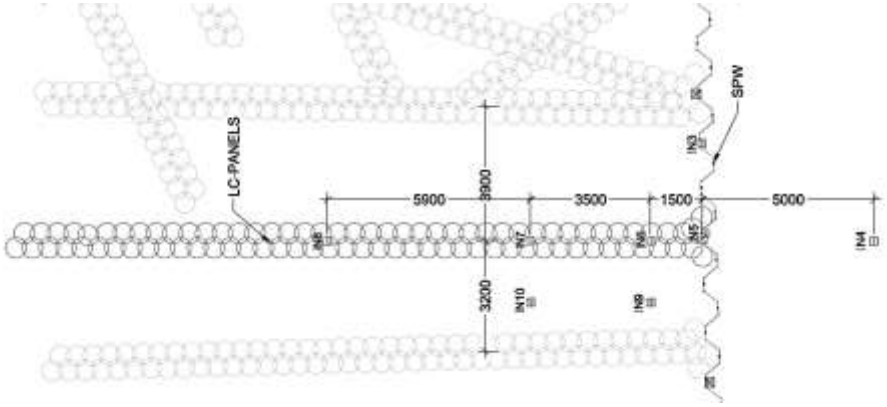


Fig. 3. Layout of instrumented section

Table 1. Inclinometer Summary

Name	Type	Distance from SPW (m)	Comments
IN3	Inclinometer uniaxial	0.0	Installed behind the sheet pile wall
IN4	Inclinometer, biaxial	-5.0	Installed on the active side, behind the sheet pile wall
IN5	Inclinometer, biaxial	0.0	Installed behind the sheet pile wall and a LC-panel
IN6	Inclinometer, biaxial	1.5	Installed in a LC-panel
IN7	Inclinometer, biaxial	5.0	Installed in a LC-panel
IN8	Inclinometer, biaxial	10.9	Installed in a LC-panel
IN9	Inclinometer, biaxial	1.5	Installed between two LC-panels
IN10	Inclinometer, biaxial	5.0	Installed between two LC-panels

* All inclinometer readings were at 2.0 m intervals in the vertical axis, except for IN5 for which readings were at 0.5 m intervals

Results

Figure 4 shows the measured displacements of the inclinometers for four construction stages. The solid lines show the deformations after SPW is installed, from stage 1 in Figure 4, the long dashed lines show excavation in the central part of the excavation pit, also referred to as stage 3. The dotted lines show the deformation in stage 6, after the concrete slab is cast to the SPW and the struts are removed. The black lines represent deformations in a LC-panel and the grey lines represent deformations in the soil volume between two LC-panels. From the measurements, it is seen that most of the displacements below the excavation floor occur when excavating in the central part of the excavation pit.

Two of the inclinometers, IN7 and IN9, show a kink at the depth just below the installed sheet pile wall. There is uncertainty whether these are real measurements or whether the measuring equipment may be faulty, as removal and reinstallation of the instruments between excavation stages may have

 © DFI International Bruges 2025

introduced anomalies in the data. Apart from this, it nevertheless appears that there is somewhat more deformation in the soil volume between two ribs than in the inclinometers placed in an LC-panel.

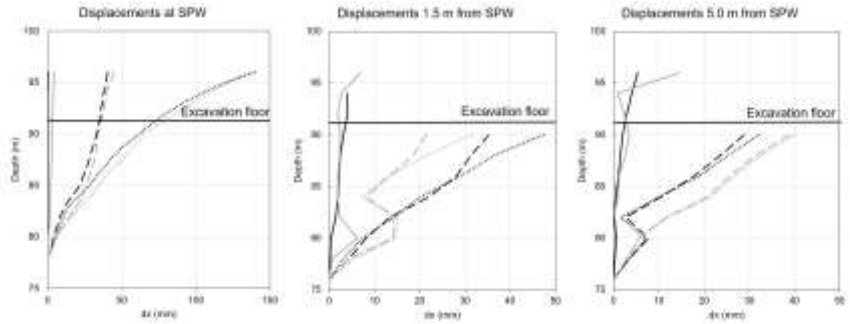


Fig. 4. Results from instrumentation. Grey lines show data from between two LC-panels and the black data shows data from inclinometers installed in a LC-panel.

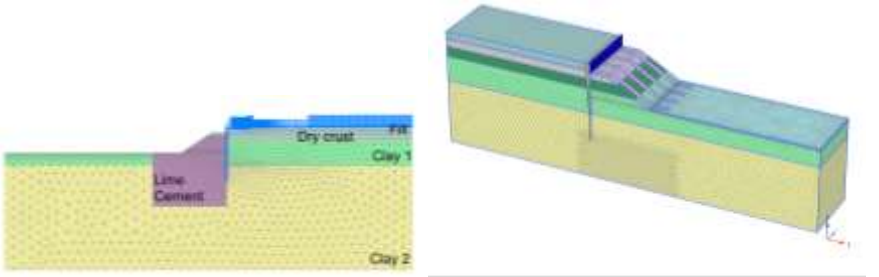
NUMERICAL MODELLING OF LIME CEMENT STABILISED SOIL

Modelling in PLAXIS

Soil parameters used in the calculations are summarized in Table 2. Model geometry and layering for the models in both PLAXIS 2D and PLAXIS 3D are shown in Fig. 5. In PLAXIS 2D, the stabilized volume is calculated with a weighted average strength and stiffness of the stabilized soil and the untreated soil inbetween, while in PLAXIS 3D, LC-panels are modeled with the correct strength and stiffness according to the requirements in the guideline (Statens Vegvesen, 2012).

Table 2. Soil parameters as input in PLAXIS-calculations

	Unit	Fill	Dry crust	Clay 1	Clay 2	LC-2D	LC-3D
Material model		Hardening soil	NGI-ADP	NGI-ADP	NGI-ADP	Mohr-Coloumb	Mohr-Coloumb
Unsaturated unit weight, γ_{unsat}	(kN/m^3)	19	19.3	19.3	19.3	19.5	19.5
Saturated unit weight, γ_{sat}	(kN/m^3)	22	19.3	19.3	19.3	19.5	19.5
Young's Modulus, E	(kN/m^2)	20 000	-	-	-	25 540	75 000
Posson's ratio, ν'	(-)	0.2	0.495	0.495	0.495	0.495	0.499
Undrained shear strength, s_u	(kPa)		70	42	42+2.5·z	88	175
NGI ADP-factors, $[s_u^A, s_u^{DSS}, s_u^P]/s_u^A$ (Grimstad et al., 2012)			[1,0.63,0.35]	[1,0.63,0.35]	[1,0.63,0.35]		
Effective friction angle, φ'	(°)	35	0	0	0	0	0



(a) PLAXIS 2D-model (b) PLAXIS 3D-model

Fig. 5. Layout of the instrumented section as calculated in PLAXIS

The results from the calculations in PLAXIS are shown in Fig. 6. It is plotted for the same phases as for the results from the inclinometers, stage 1, 3 and 6. Displacements at the SPW, 1.5 m from the SPW and 5.0 m from the SPW are shown. Results from the 3D calculations are shown in black and

 © DFI International Bruges 2025

gray, where black shows displacements from the center of a LC-panel and gray shows displacements between two LC-panels. Red shows results from 2D calculations where the strength and stiffness of the LC-columns and the surrounding clay are converted to a weighted average. Figure 7 shows the data from the inclinometers plotted together with the results from the calculation in PLAXIS 3D.

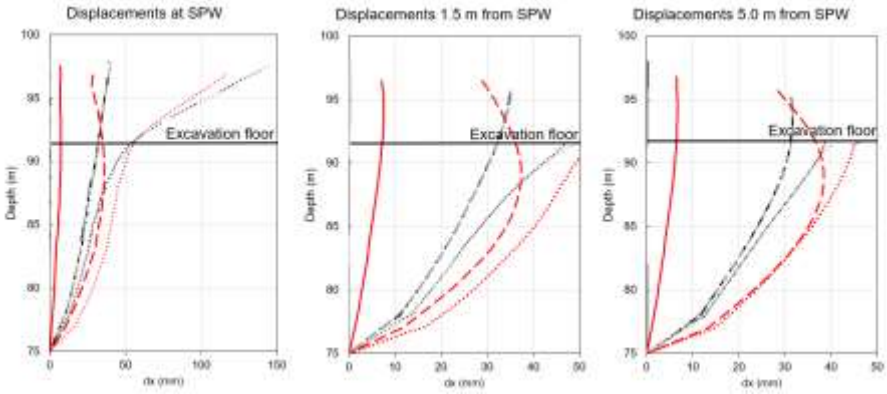


Fig. 6 Displacements calculated in PLAXIS. Grey lines show data from between two LC-panels and the black data shows data from inclinometers installed in an LC-panel. The red lines show data from PLAXIS 2D.

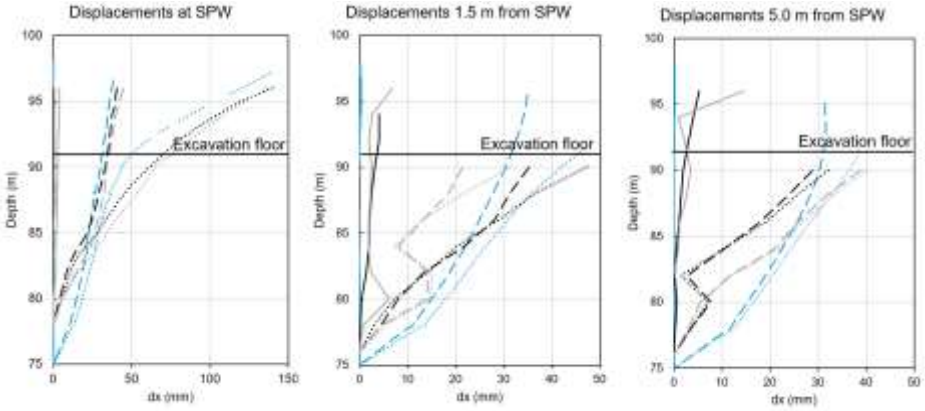
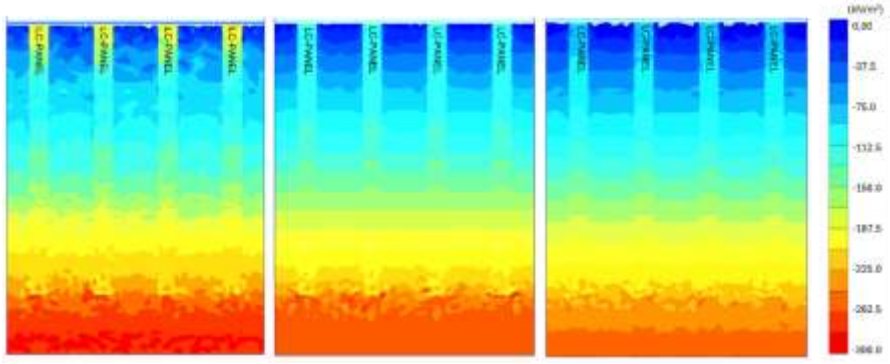


Fig. 7. Comparison between measured displacements and displacements calculated in PLAXIS 3D. Blue lines show calculated data from inside an LC-panel.

From the PLAXIS 3D calculations, normal stresses have been extracted in three cross sections, 1.5 m, 5.0 m and 10.0 m from SPW. The results are shown in Fig. 8.



(a) 1.5 m from SPW (b) 5.0 m from (c) 10.0 m from SPW

Fig. 8. Effective normal stress distribution (σ'_N) at three distances from SPW.

 © DFI International Bruges 2025

DISCUSSION

The results from the 3D calculation agree relatively well with the results measured at Campus Ullevål. When comparing horizontal displacements at a specific depth and distance from the SPW, the results from the inclinometers show tendencies that there are somewhat greater horizontal displacements in the unstabilized soil volume compared to in the LC-panel. There is also a small increase in horizontal displacements in the unstabilized soil volume in the 3D calculations. This indicates that there is not full interaction between the LC-panels and the untreated soil. In this case the deviation is too small to affect the construction, but for larger distances between two LC-panels this should be considered.

The results from the 2D calculation seem to overestimate the deformations below the excavation floor, while it underestimates the deformations for the actual cantilever on the SPW. The horizontal displacements are overestimated and is assumed to come from the fact that the weighted stiffness and strength of the LCS material in the average soil volume is estimated based on design strength values, which results in a lower calculated strength and stiffness than in reality.

The inclinometers are installed to bedrock, but the bottom is not fixed. This can lead to the measured displacements being underestimated compared to reality.

As shown in Ignat et al. (2016), there are clear indications on the Campus Ullevål project that LC-panels act as supporting struts against the SPW. The calculations in PLAXIS 3D show that the earth pressure on the SPW is transferred to the LC-panels. The distribution of the normal stress with depth is uniform with depth, both in the stabilized volume and the untreated soil volume. In the top of the LC-panels, close to the excavation floor, normal stress in the LC-panels is higher than in the stabilized volume. The load is transferred to the ribs due to their high stiffness and strength. With depth, this difference decreases, and the stress distribution between the stabilized and unstabilized material becomes more even.

CONCLUSION

Extensive instrumentation has been carried out in connection with the SP CURIOUS research project. The project focused on the load distribution and deformations in and between LC panels on an excavation in marine clay. The results have also been evaluated and compared with numerical modelling in PLAXIS 2D and 3D.

There is a difference between the measured horizontal displacement in the stabilized panel and in the untreated soil between. This indicates that there is not full interaction between the LC-panels and the untreated soil. For large distances between two LC-panels, this should be considered.

Numerical simulations in 3D give a more accurate representation of the load distribution in the LC-panels compared to numerical simulations in 2D. The 3D model has the ability to give a representation of complex 3D effects and the load distribution in the LCS-pattern which is not possible in the 2D models. Due to the underestimation of the strength and stiffness in the stabilized volume, the numerical simulations in a 2D model overestimate the deformations in the LCS, proving that the normal practice is conservative.

ACKNOWLEDGEMENTS

Parts of this work were funded by the basic funding to NGI from The Research Council of Norway. The authors would also like to make an extended thank you to the contractor, Skanska Norge AS together with E-service and DmixAB. The work would also not have been possible without the

 © DFI International Bruges 2025

excellent work from the instrumentation section at NGI. The work is also based on a master's thesis written in collaboration with Norwegian University of Science and Technology (NTNU) with the great supervision from Dr. Yutao Pan.

REFERENCES

Broms, B., 2004. Lime and lime/cement columns. In Ground Improvement. Eds. Moseley M.P. and Kirsch K., Spon Press, Second Edition.

Ignat, R., Baker, S., Karstunen, M., Liedberg, S., and Larsson, S., 2020. Numerical analyses of an experimental excavation supported by panels of lime-cement columns. Computers and Geotechnics. https://www.sciencedirect.com/science/article/pii/S0266352X1930360X

Ignat, R., Baker, S., Liedberg S., and Larsson S., 2016. Behavior of braced excavation supported by panels of deep mixing columns. Canadian Geotechnical Journal, Research Press. https://cdnsciencepub.com/doi/10.1139/cgj-2016-0137

Grimstad, G., Andresen, L., Jostad, H.P., 2012. NGI-ADP: Anisotropic shear strength model for clay. International Journal for Numerical and Analytical Methods in Geomechanics. https://doi.org/10.1002/nag.1016

Karlsrud, K., & Andresen, L., 2005. Loads on braced excavations in soft clay. International Journal of Geomechanics, Vol. 5(2), p. 107-113.

Karlsrud, K., Eggen, A., Nerland, O., 2015. Some Norwegian Experiences Related to Use of Dry-Mixing Methods to Improve Stability of Excavations and Natural Slopes in Soft Clays. In Proceedings of the Deep Mixing 2015 Conference, San Francisco.

Kolstad, P., 1987, Totalsondering. Systembeskrivelse og resultatvurdering. NGI report number 57600-10. Norwegian Geotechnical Institute. [In Norwegian].

Larsson, S., Malm R., Charbit B., and Ansell, A., 2012. Finite element modelling of laterally loaded lime–cement columns using a damage plasticity model. Computers and Geotechnics. https://www.sciencedirect.com/science/article/pii/S0266352X12000456

Monsås, E., Oberhollenzer, S., Lande, E.J., Løyland, M.S., 2024. Performance of cantilever sheet pile walls in sensitive clays: Case study Campus Ullevål. Proceedings of the XVIII ECSMGE 2024, 683-688.

Norsk Geoteknisk Forening, 2012. Veiledning for grunnforsterkning med kalksementpeler. Norsk Geoteknisk Forening (Norwegian Geotechnical Society). [In Norwegian.]

Porbaha, A., 1998, State of the art in deep mixing technology: part I. Basic concepts and overview, Proceedings of the Institution of Civil Engineers - Ground Improvement 1998 2:2, 81-92, http://dx.doi.org/10.1680/gi.1998.020204.

Statens Vegvesen, 2012. Veiledning: Grunnforsterkning, Fyllinger og skråninger. Statens Vegvesen (The Norwegian Public Roads Administration). [In Norwegian.]

Wong, D.Y.-C., Sadasivan, V., Isaksson, J., Karlsson, A., and Dijkstra, J., 2014. Trans-scale spatial variability of lime-cement mixed columns. Construction and Building Materials, Elsevier.

 © DFI International Bruges 2025

CPT BASED DESIGN METHOD FOR HORIZONTAL CAPACITY OF PILES INSTALLED BY THE ROTARY CUTTING PRESS-IN METHOD

S.M.K. Pasha, Press-in Technology R&D Center, GIKEN LTD., Tokyo, Japan,
manafi@GIKEN.com
Y. Ishihara, Press-in Technology R&D Center, GIKEN LTD., Kochi, Japan,
ishihara@giken.com
M. Eguchi, Press-in Technology R&D Center, GIKEN LTD., Kochi, Japan,
eguchi@giken.com
Y. Toda, Press-in Technology R&D Center, GIKEN LTD., Kochi, Japan,
toda.y@giken.com

ABSTRACT

The Rotary Cutting Press-in (RCP) method, which combines vertical static jacking and torque, has been developed to extend the traditional press-in technique for use in harder ground conditions. While SPT (Standard Penetration Test)-based methods have traditionally been used to estimate the bearing capacities of RCP piles, CPT (Cone Penetration Test)-based methods are increasingly favored due to their ability to provide continuous, detailed subsurface information. This study proposes a CPT-based method to estimate the horizontal capacity of RCP piles using a lateral soil resistance and displacement model, or p-y analysis. The study's findings reveal that CPT-based models tend to underestimate the horizontal capacity of RCP piles, largely due to their inability to account for installation effects induced by the rotary cutting process. These installation-induced stresses affect soil properties and ultimately influence the pile's load-bearing capacity. Comparisons between CPT-based, API, and SPT-based models showed that the API model predicted higher horizontal capacities, likely due to overestimation of soil parameters such as internal friction angle (φ) and maximum shear modulus (G_{max}). This study suggests that CPT-based models should be refined to better incorporate the effects of pile installation to improve their accuracy in predicting horizontal capacity.

Keywords: Rotary Cutting Press-in; Horizontal Bearing capacity; Vertical bearing capacity; CPT based design method

BACKGROUND

Pile installations can generally be categorized into two methods: displacement and non-displacement. The displacement method involves the use of external forces, either through hammering or static jacking, to drive piles into the ground. Among the various displacement pile installation methods used for constructing structures in both urban and non-urban areas, the press-in piling technique employs hydraulic static forces to drive piles into the ground. In this method, the press-in machine utilizes the reaction forces from previously installed piles, along with their pull-out resistance, to stabilize the machine and drive subsequent piles into the ground. This technology is gaining momentum due to its versatility, as well as its low vibration and noise characteristics, making it suitable for sensitive environments.

However, when applying press-in technology to hard ground or bedrock, where installation using only static hydraulic jacking is not feasible, alternative methods are employed. One such method is the Press-in with Auger (PA) technique, in which piles are installed into the ground using an auger. Another approach is the "Rotating Cutting Press-in" (RCP) method, where a steel pipe pile, equipped with cutting bits, is rotated at the tip. In the RCP method, the pile is driven into the ground while water is injected at its base to aid penetration.

The rotary press-in method is a relatively new technique. Previous studies have shown that displacement piles installed using this method displace the surrounding soil both vertically and radially, generating stresses in the soil. This may result in an increase in the axial capacity and stiffness of the piles compared to non-displacement piles (Hazla, 2013), as well as an enhancement of the horizontal capacity of piles (Ishihara et al., 2021). Therefore, it is essential to assess both the vertical and horizontal capacities of RCP piles.

 © DFI International Bruges 2025

For many years, simplified approaches have been used for designing pile foundations subjected to lateral and vertical loads. These include methods such as the limit equilibrium approach (Dobry and Abdoun, 2001) and the nonlinear Winkler foundation model, where lateral soil-pile interactions are represented by nonlinear springs, often referred to as p-y curves.

Several p-y curve models have been proposed and are well-established for non-liquefied soil conditions. Among the most widely used models are the sand model developed by the American Petroleum Institute (API, 2010) and Matlock's model for clay (Matlock, 1970). A common challenge in applying the API model lies in accurately determining the soil's physical and mechanical properties, such as internal friction angles and cohesion, which are often estimated through correlations based on Standard Penetration Test (SPT) N values.

More recently, there has been growing interest in p-y curves derived from Cone Penetration Test (CPT) data, which utilize cone resistance as a key input. While some of these models have been validated through full-scale pile load tests, many have been developed through Finite Element Method (FEM) analysis. However, the majority of these equations are designed for static or dynamic conditions with reduced resistance.

The primary objective of this study is to evaluate the performance of CPT-based p-y models in predicting the horizontal capacity of piles installed using the Rotary Cutting Press-in (RCP) method. Given the growing use of the RCP method in challenging soil conditions, particularly where traditional press-in techniques face limitations, it is crucial to assess the accuracy of existing predictive models. This study aims to identify the limitations of CPT-based models, particularly their tendency to overestimate or underestimate pile capacity due to installation effects such as soil disturbance and stress changes. Additionally, this study compares the performance of CPT based models with API and SPT-based models, with the goal of determining which method provides the most reliable estimates of horizontal capacity for RCP piles. The findings will inform recommendations for improving the accuracy of CPT-based models, particularly by incorporating the effects of pile installation processes that are currently unaccounted for in the existing frameworks.

TESTING PROGRAM AND SITE CONDITIONS

In this study, field test data from the Moon Project was selected to assess the performance of CPT-based methods. The RCP method was chosen for pile installation due to its applicability across a wide range of ground conditions. Previous studies have explored the performance of the RCP method for pile installation without water injection, a technique typically used in the construction of piles in terrestrial projects.

In this study, a series of small-diameter pipe piles were installed using a press-in machine capable of applying the RCP technique. The test site was chosen from GIKEN testing facilities, where the ground conditions closely resemble the regolith layer found on the Moon. Standard Penetration Tests (SPT) were conducted to reveal the composition and soil profile at the testing site. The ground consisted of loose to medium-dense sandy soil overlying a dense sandy gravel layer. The groundwater level was approximately 7 meters below the ground surface (**Fig. 1a**)

A total of 10 tests were conducted, as shown in Table 1, which summarizes the pile type (closed-ended or open-ended) and the type of loading test (horizontal or vertical). The J2203 test series aimed to evaluate RCP installation without water injection, using both closed-ended and open-ended piles. The J2301 series focused on assessing the effects of load limits during RCP installation with open-ended piles (**Fig. 1a and b**).

The test procedure involved the following steps: (1) installation of reaction piles using the RCP, (2) positioning of the press-in machine on the reaction wall, (3) installation of the test pile using the RCP, (4) conducting the static loading test (vertical or horizontal), and (5) extracting the test pile.

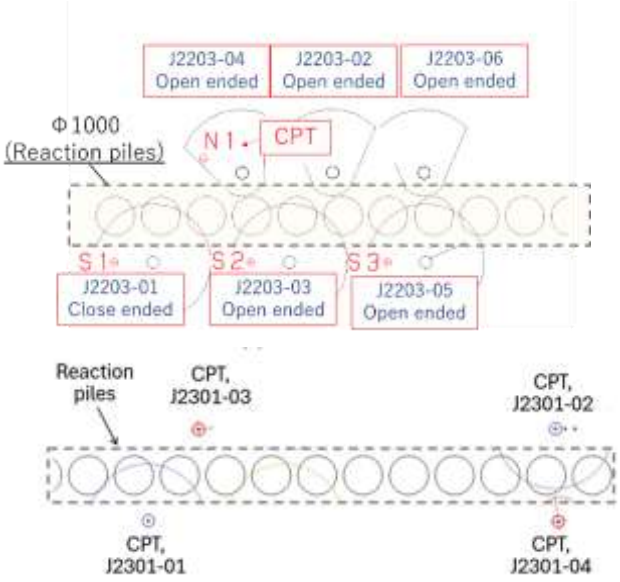
In some tests, an upper limit for the press-in force (Q'_{UL}) was applied. During "surged installation" (or "installation with surging"), the pile was inserted by repeating cycles of penetration and partial extraction. In each cycle, the penetration distance (l_d) was greater than the extraction distance (l_u), ensuring net downward movement. When the press-in force (Q') reached the upper limit (Q'_{UL}), the pile was extracted slightly after

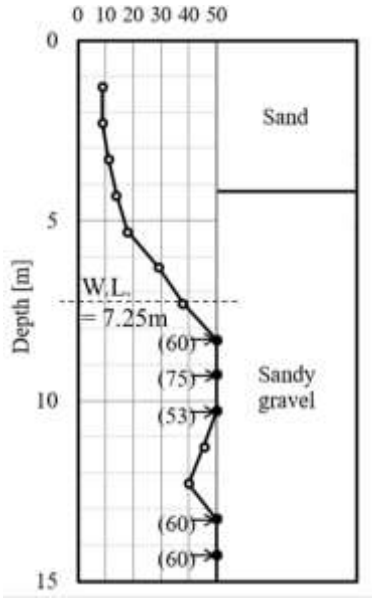
 © DFI International Bruges 2025

each cycle. This meant the installation was displacement-controlled when the force was below Q'_{UL}, and it became load-controlled when the force reached Q'_{UL}.

Two types of test piles were used: closed-ended and open-ended pipe piles. The closed-ended pile had an outer diameter (Do) of 318.5 mm and an inner diameter (Di) of 297.9 mm, with a steel plate closing the base. The open-ended pile had the same Do and Di, but with a base ring equipped with cutting teeth.

Vertical and horizontal static loading tests were performed using either a hydraulic jack or the press-in machine. The time between installation and the start of the loading test was 7 days for all tests. The horizontal loading tests were applied 0.15 m above the ground surface.





(a) (b)

Fig. 1. (a) SPT N values and Soil profile at testing site (b) Field tests and CPT tests locations

 © DFI International Bruges 2025

Table 1. Summary of field tests

Test case	Pile	Q'_{UL} [kN]	Loading Test
J2203-01	Close ended	200	Vertical
J2203-02	Close ended	200	Horizontal
J2203-03	Open ended	200	Vertical
J2203-04	Open ended	200	Horizontal
J2203-05	Open ended	200	Vertical
J2203-06	Open ended	200	Horizontal
J2301-01	Open ended	100	Vertical
J2301-02	Open ended	No limit	Vertical
J2301-03-2	Open ended	100	Horizontal
J2301-04	Open ended	No limit	Horizontal

OVERVIEW OF NUMERICAL ANALYSIS
OVERVIEW OF EXISTING P-Y CURVES

p-y springs in the Winkler Spring model are commonly developed for specific sites using either full-scale pile load tests or, alternatively, through 3D Finite Element (FE) analyses. Over the years, numerous p-y models have been proposed, one of the most prominent being the API method. Originally introduced by Reese et al. (1974) following field tests on small-diameter piles (D = 0.61 m) with large aspect ratios (L/D = 34.4), the method was subsequently refined by O'Neill & Murchison in 1983 and is now part of the API guidelines (API, 2011). This approach has since become the industry standard for estimating lateral pile deflections in cohesionless soils.

The API method, however, estimates soil strength using an equation that incorporates the internal friction angle (φ'), which is typically derived indirectly through empirical correlations based on in-situ tests like CPT or SPT. The high sensitivity of the API method to the chosen empirical equation for φ' introduces considerable uncertainty in p-y curve predictions. To address the challenges in selecting appropriate strength parameters, p-y models based on cone penetration test (CPT) data, specifically using cone resistance (qc), have been developed. A summary of the CPT-based p-y models utilized in this study is presented in Table 2.

Although models proposed by Dyson & Randolph (2001) and Li et al. (2014) provide useful insights, they were not developed from a wide range of Pile Load Tests (PLTs) that represent both flexible and rigid piles. While Li et al. (2014) accounted for variations in pile aspect ratios and rigidity, their tests were limited to dense siliceous sands and included only six tests. On the other hand, the work of Suryasentana & Lehane (2014; 2016), which employed 3D FEM modeling, explored relative densities ranging from 28% to 97%, enhancing the broader applicability of their methods.

In the Table 2, p represents lateral soil resistance per length of pile, and y is deflection φ' represents internal friction angle, D represents pile diameter, q_c represents the cone resistance, while σ_v denotes the total overburden stress. Pa stands for atmospheric pressure, $\acute{\sigma_v}$ symbolizes the effective stress and γ soil unit weight. G_{max} is the small strain shear modulus.

Table 2. API- and CPT-based p-y methods used in this study

p-y model	p-y expression	Notes
API (2011)	$\frac{p}{p_u}$=A×tanh($k \times z/A \times p_u \times y$) , p_u=min[p_{us}; p_{ud}] p_{us}=(C_1×z+C_2×D) ×$\acute{\gamma}$×z p_{ud}=(C_3×D×$\acute{\gamma}$×z) $C_1 = (\tan\beta)^2 \times \tan\alpha/\tan(\beta-\varphi) + K_0(\tan(\varphi)\times\tan\beta/\cos\propto\times\tan(\beta-\varphi) + \tan\beta\times(\tan(\varphi)\times\sin\beta - tan\alpha))$ $C_2 = \tan\beta/\tan(\beta-\varphi) + K_a$ $C_3 = K_a((\tan\beta)^8 - 1) + K_0 \times \tan(\varphi) \times (\tan\beta)^4$ $K_0 = 0.4$, $\alpha = \frac{\varphi}{2}$, $\beta = 45 + \frac{\varphi}{2}$ and $K_a = (1-\sin\varphi)/(1+\sin\varphi)$	-Submerged dense fine sands, Mustang Island - D= 0.61m, L/D= 34.4

 © DFI International Bruges 2025

Dyson & Randolph (2001)	p=2.84×D×($\acute{\gamma}$×D) ×$(\frac{q_c}{\acute{\gamma}\times D})^{0.72}\times(\frac{y}{D})^{0.64}$	-CPT, centrifuge tests (N=160), small scale PLT, D= 13mm, L/D=26.15 -Driven piles, free headed
Li et al. (2014)	p=3. 6×D×($\acute{\gamma}$×D) ×$(\frac{q_c}{\acute{\gamma}\times D})^{0.72}\times(\frac{y}{D})^{0.66}$	- CPT based Length (L): 2.20 m to 7.00 m L/D Ratio Range: 6.5 to 20.6
Suryasentana & Lehane (2014)	p=2.4×D×($\acute{\sigma_v}$) ×$(\frac{q_c}{\acute{\sigma_v}})^{0.67}\times(\frac{z}{D})^{0.75}\times$ [1-exp(-6.2×$(\frac{z}{D})^{-1.2}\times(\frac{y}{D})^{0.89}$]	-CPT cavity expansion, CPT, 3D FEM -D=0.5-5m, L=21m, L/D= 42-4.2
Suryasentana & Lehane (2016)	p=4.5×G_{max}×y, $\frac{y}{D}$<0.0001 (a) p =2.4×D× ($\acute{\sigma_v}$) ×$(\frac{q_c}{\acute{\sigma_v}})^{0.67}\times(\frac{z}{D})^{0.75}\times$ (b) [1-exp(-8. 9×$(\frac{z}{D})^{-1.25}\times(\frac{\sigma_v-u_g}{\acute{\sigma_v}})^{0.5}\times(\frac{y}{D})$]<$q_c$×D, $\frac{y}{D}$>0.01 Interpolation between equations (a) and (b) for 0·0001<$\frac{y}{D}$<0·01.	-CPT cavity expansion analogue, CPT, 3D FEM, field study - D=2, L/D=20

The internal friction angle (φ') and the distribution of the small-strain shear modulus (G_0) were calculated using the following equations, which play a crucial role in interpreting the test results.

$$\varphi' = 17.6 + 11\log[(q_t - \sigma_{v0}/P_a)(P_a/\sigma'_{v0})^n] \quad [1]$$

$$G_0 = (\gamma/g)\left((10^{0.55I_c+1.68})(q_t - \sigma_{v0}/P_a)\right)^{0.5} \quad [2]$$

In this context, q_t represents the corrected cone resistance, while σ_{v0} denotes the total overburden stress. Pa stands for atmospheric pressure, σ'_{v0} symbolizes the effective stress, g is the gravitational acceleration and γ soil unit weight. Additionally, I_c refers to the soil behavior type index.

1D FINITE ELEMENT ANALYSIS OF LATERALLY LOADED PILES

a series of 1D finite element analyses on laterally loaded piles using the Winkler model were performed. The soil profile was divided into 5 layers, each 1m thick, to enhance accuracy. The pile was modeled using beam elements supported by p-y springs, as illustrated in Fig. 2. The piles were fixed in the X direction (alongside the pile axis).

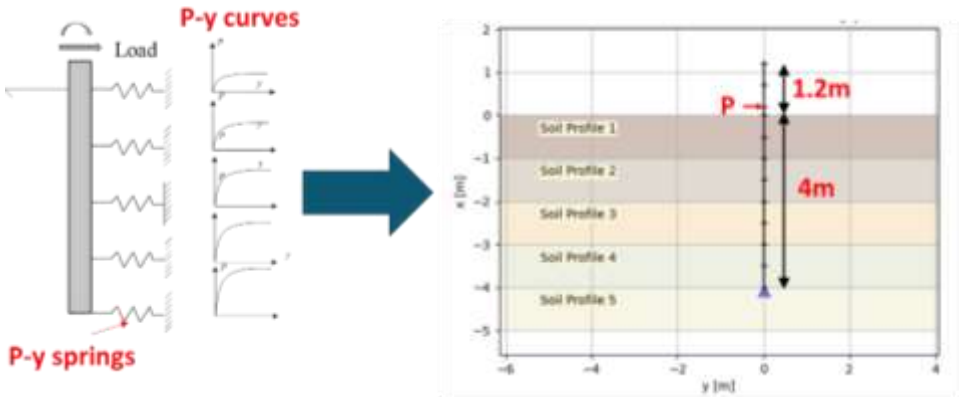


Fig. 2. Schematic diagram of 1D FEM of Laterally loaded pile

RESULTS OF FIELD TESTS

Fig. 3 presents the results of the CPT tests, showing both the cone resistance (qc) and cone friction resistance.

Fig. 4 illustrates typical results from the installation of RCP piles without water injection. Both open-ended and closed-ended piles were successfully driven to a penetration depth of 4 meters. The measured head load (Q) and head torque (T) account for the effects of the chuck's weight and mechanical friction during installation. The results of the horizontal loading test are presented in Fig. 5, where the horizontal axis

 © DFI International Bruges 2025

represents the horizontal displacement at the loading height. The horizontal capacity (P_f) obtained in each test is defined as the load applied when the horizontal displacement of the pile at the loading height reaches 15 mm. These values are summarized in Table 3.

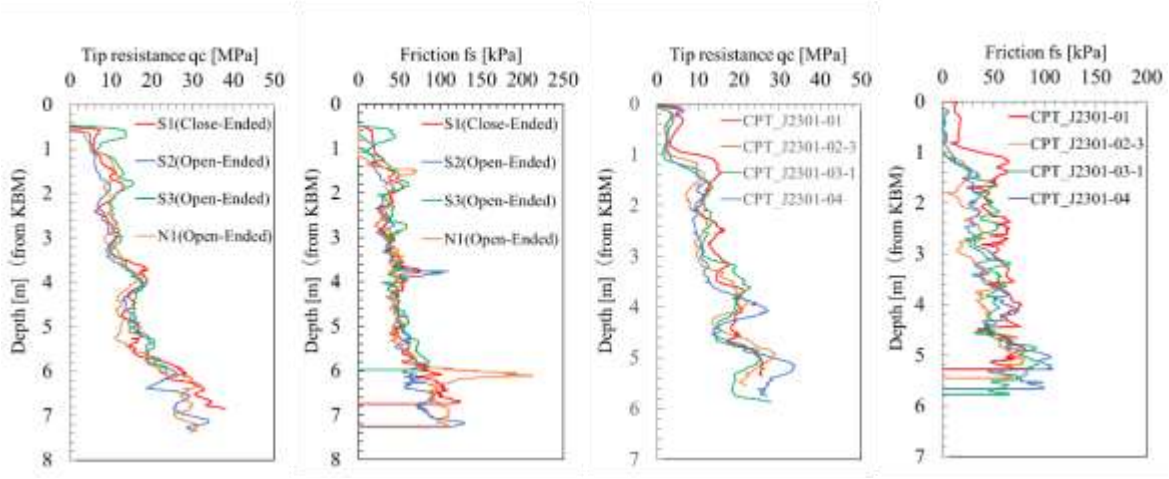
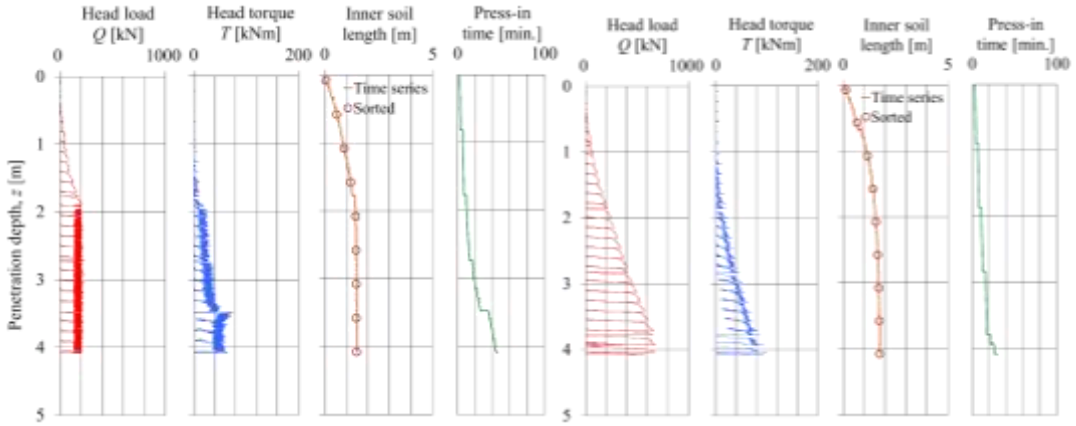


Fig. 3. CPT Test results



(a) J2301-03-2 (b) J2301-04

Fig. 4. Piling data obtained in RCP installation without water

In the J2203 test series, the horizontal capacity (P_f) of the closed-ended pile was slightly greater than that of the open-ended pile, though the difference was marginal. Conversely, the results of the J2301 test series indicated that P_f was only minimally influenced by the load limit. This limited influence can be explained as follows: P_f is more dependent on the horizontal resistance of the soil at shallower depths than at deeper ones. At shallow depths, the load limit had little effect because the head load required for pile installation was lower than the load limit itself.

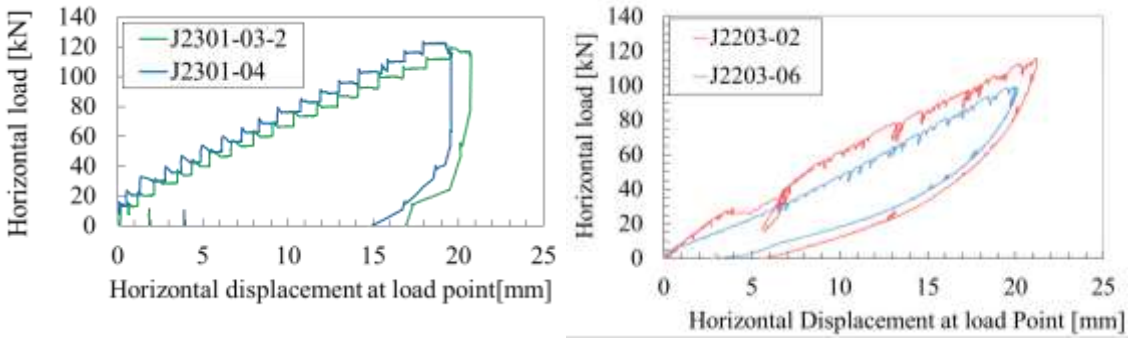


Fig. 5. Results of horizontal loading test

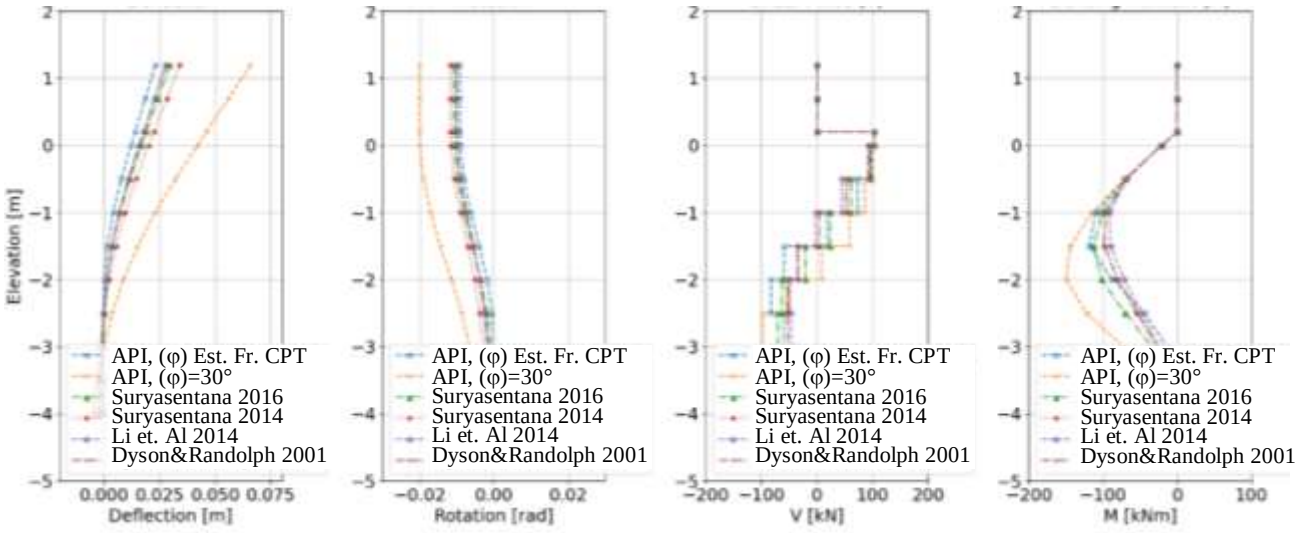
 © DFI International Bruges 2025

Table 3. Measured horizontal capacity

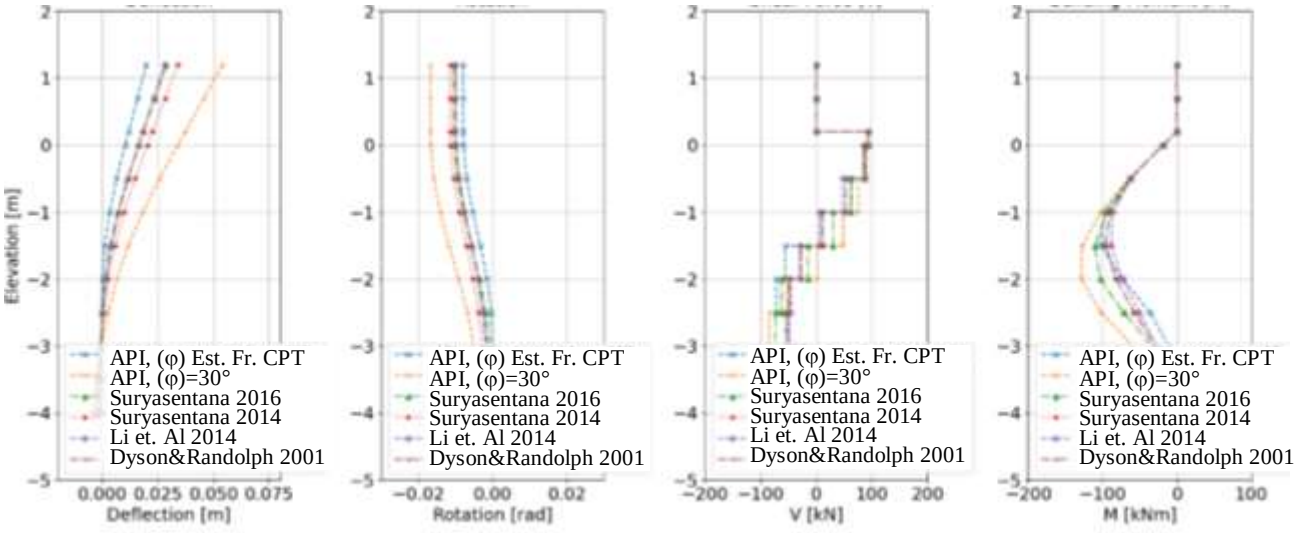
Test case	Pile	Measured horizontal capacity, P_f [kN]
J2203-02	Close ended	78
J2203-04	Open ended	75
J2203-06	Open ended	65
J2301-03-2	Open ended	93
J2301-04	Open ended	103

RESULTS OF 1D FEM ANALYSIS

Fig. 6 presents the predicted load-deflection, shear forces, and bending moments of the pile for several test cases at the maximum horizontal capacity. In addition, Fig. 7 illustrates the load-horizontal displacement curves, calculated using various CPT-based p-y models, and compares them to the results from field tests. The analysis revealed that most of the existing p-y models, including those based on CPT data, tend to underestimate the load-horizontal displacement response. This underestimation is particularly evident in test cases J2301-03-2 and J2301-04, which were specifically designed to evaluate the effect of the load limit used during the RCP installation of open-ended piles.

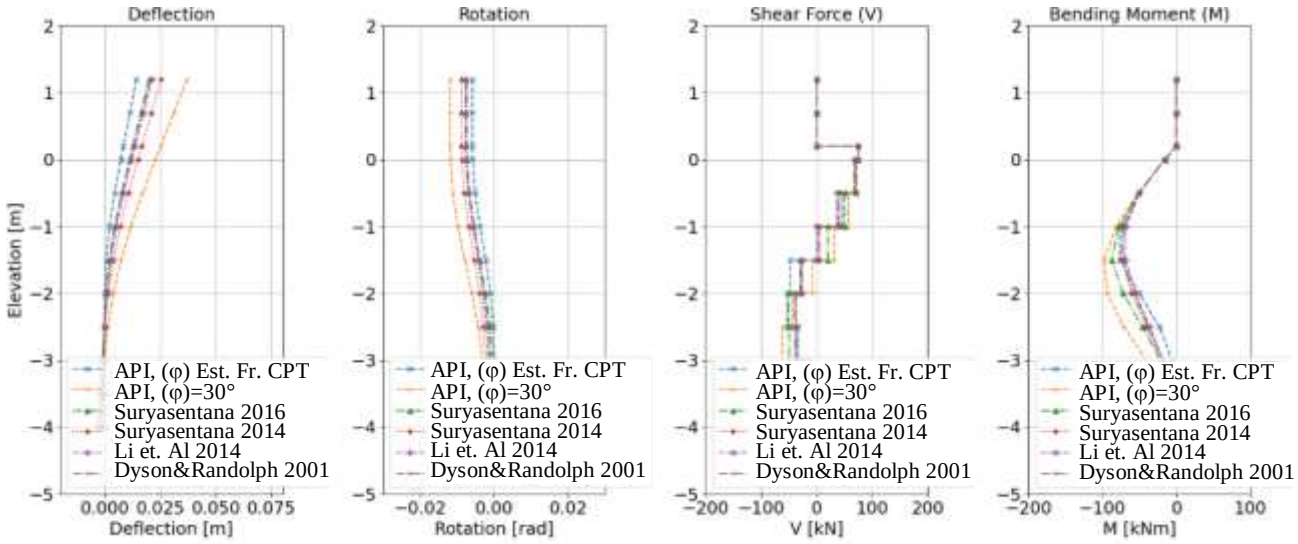


(a) 2301-04



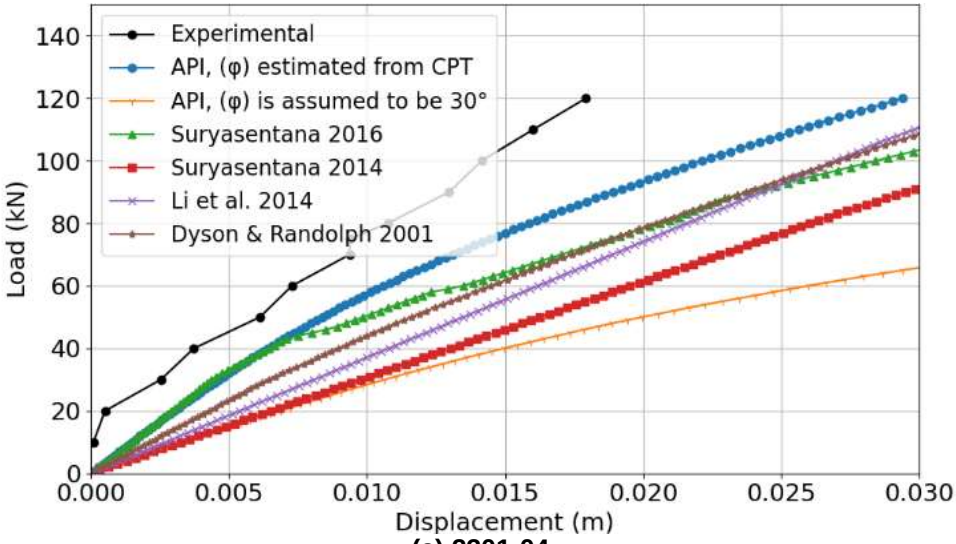
(b) J2301-03-2

 © DFI International Bruges 2025

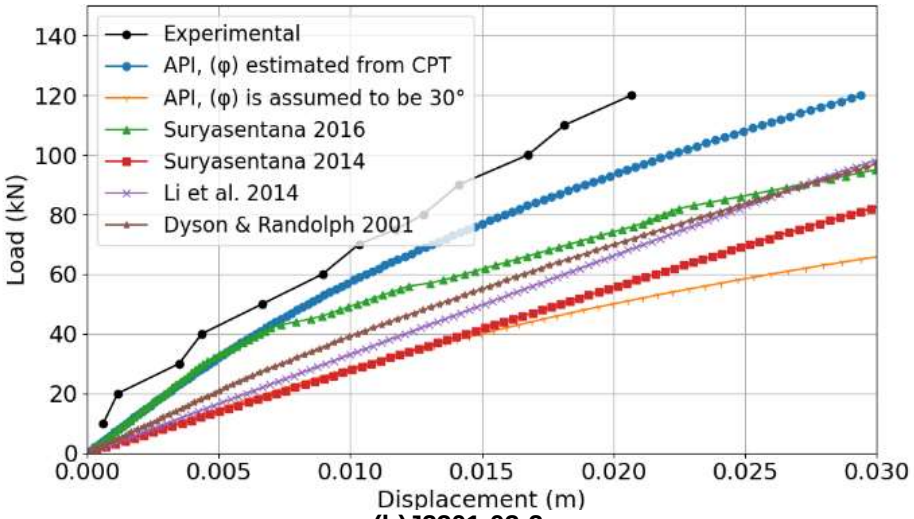


(c) J2203-04

Fig. 6. Predicted pile response using API and CPT based p-y models

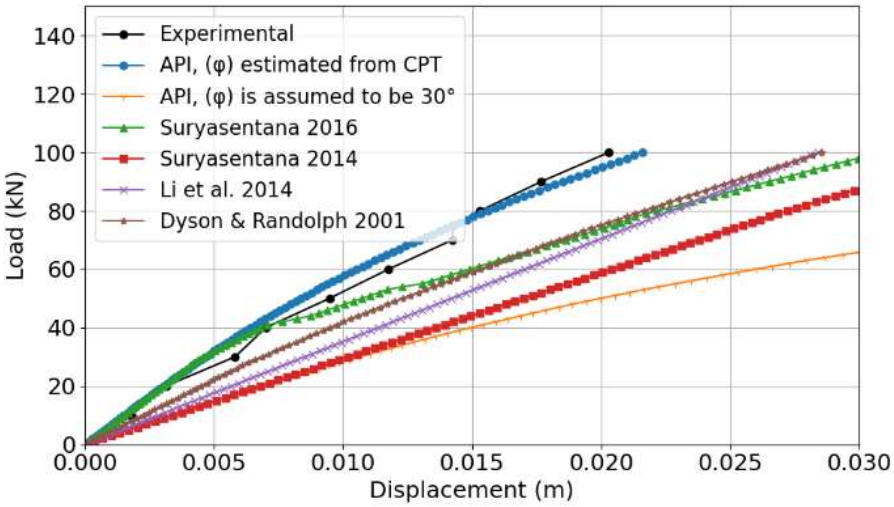


(a) 2301-04



(b)J2301-03-2

 © DFI International Bruges 2025



(c)J2203-04

Fig. 7. Predicted Load displacement results vs field test results

The results from this study indicate that CPT-based models tend to underestimate the horizontal capacity of piles installed through rotary cutting methods. This observation aligns with findings from recent studies which show that these models often fail to account for the stress changes and soil disturbance caused during installation, particularly those induced by rotary or jacked methods (Xiong et al. 2024). These stresses significantly alter the surrounding soil properties, which impacts the pile's load-bearing capacity. For instance, Xiong et al. (2024) found that the horizontal capacity of jacked piles was enhanced due to soil compaction and stress redistribution induced during the installation process . Given that rotary cutting similarly involves both jacking and rotation, it is likely that these stress effects contribute to the underestimation seen in CPT-based models.

A comparison between API and CPT-based models for estimating horizontal capacity showed that API predictions were generally higher. However, the higher values provided by the API model do not necessarily indicate more accurate performance. As suggested by this study, the discrepancy may arise from overestimations of soil parameters, such as the maximum shear modulus (G_{max}) and internal friction angle (φ), which are derived from CPT data. While these parameters are useful for initial analyses, they often require further validation through element testing methods, such as triaxial or resonant column tests, to improve accuracy.

SUMMARY AND CONCLUSIONS

In this study, the performance of CPT-based p-y models and the API model was assessed using 1D FEM analysis by comparing them with the results obtained from field tests data of rotary cutting piles (RCP). The results demonstrated that CPT-based models tend to underestimate the horizontal capacity of piles in general, primarily due to the underestimation of soil stiffness. More specifically, these models lack the ability to account for the effects of pile installation by the rotary cutting process.

As discussed, the pile installation process, particularly the combination of jacking and rotation in RCP piles, induces significant soil compaction and stress redistribution. These installation-induced stresses affect the surrounding soil properties, potentially increasing the pile's load-bearing capacity over time. The inability of CPT-based models to incorporate these installation effects is a key reason for their underestimation of horizontal capacity. Therefore, it is recommended that these models be modified to better account for the impacts of pile installation and consolidation effects.

Additionally, this study highlighted the sensitivity of the API model, and potentially the approach discussed by Suryasentana & Lehane (2016), to parameters such as the internal friction angle (φ) and the maximum shear modulus (Gmax), which are often derived from CPT test data. The API model's better performance in predicting horizontal capacity may be due to an overestimation of these soil parameters, rather than the

 © DFI International Bruges 2025

inherent accuracy of the model itself. This indicates that the API model, too, is sensitive to the accuracy of input parameters, particularly those related to soil stiffness and strength.
In conclusion, while the API model provided higher predictions for horizontal capacity, this is suggested to due to the be overpredictions of φ and Gmax from CPT data, further emphasizing the need for careful validation of these parameters. The findings suggest that CPT-based models, in their current form, require modification to improve accuracy by incorporating the effects of pile installation, while the API model should also be used with caution, particularly in cases where soil parameters are derived solely from SPT or CPT data.

REFERENCES

AIJ, 2001. Recommendations for design of building foundations. Architectural Institute of Japan, Japan.

Almeida, M.S.S., Fernando, A.B.D., and Lunne, T., 1996. Use of the piezocone test to predict the axial capacity of driven and jacked piles in clay. Canadian Geotechnical Journal, 33(1), 23–41.

API, 2014. Recommended practice for planning, designing, and constructing fixed offshore platforms - working stress design. American Petroleum Institute, USA.

Dou, J., Chen, J., Liao, C., Sun, M., and Han, L., 2021. Study on the correlation between soil consolidation and pile set-up considering pile installation effect. Journal of Marine Science and Engineering, 9(7), 705. https://doi.org/10.3390/jmse9070705

Dyson, G.J., and Randolph, M.F., 2001. Monotonic lateral loading of piles in calcareous sand. Journal of Geotechnical and Geoenvironmental Engineering, 127(4), 346–352.

EN1998-5, Eurocode 8, 2004. Design provisions for earthquake resistance of structures – foundations, retaining structures, and geotechnical aspects.

Ishihara, Y., and Haigh, S., 2018. Cambridge-GIKEN collaborative working on pile-soil interaction mechanisms. Proceedings of the First International Conference on Press-in Engineering, Kochi, 23–45.

Ishihara, Y., Eguchi, M., Brown, M., and Koseki, J., 2021. Comparison of penetration resistance and vertical capacity of short piles installed by Standard Press-in in loose sand. Paper presented at Second International Conference on Press-in Engineering, Kochi, Japan, p. 208.

Ishihara, Y., Eguchi, M., Mori, A., and Toda, Y., 2024. Use of press-in piling data for construction on the moon: Estimating subsurface information and pile capacity. Proceedings of the 3rd International Conference on Press-in Engineering, Singapore.

Kulhawy, F.H., and Mayne, P.W., 1990. Manual on estimating soil properties for foundation design.

Li, W., Igoe, D., and Gavin, K., 2014. Evaluation of CPT-based p–y models for laterally loaded piles in siliceous sand. Géotechnique Letters, 4, 110–117.

Madabhushi, G., Knappett, J., and Haigh, S., 2009. Design of pile foundations in liquefiable soils. Imperial College Press, 1st Edition, ISBN-13: 978-1848163621.

NEHRP, 2009. Recommended seismic provisions for new buildings and other structures.

Randolph, M.F., 2003. Science and empiricism in pile foundation design. Géotechnique, 53(10), 847–875.

Robertson, P.K., 2009. Interpretation of cone penetration tests—a unified approach. Canadian Geotechnical Journal, 46(11), 1337–1355.

Smith, T.D., 1983. Pressuremeter design method for single piles subjected to static lateral load. (Volumes I and II), Texas A&M University.

 © DFI International Bruges 2025

Suryasentana, S., and Lehane, B., 2016. Updated CPT-based p–y formulation for laterally loaded piles in cohesionless soil under static loading. Géotechnique, 66(6), 445–453.

Suryasentana, S.K., and Lehane, B.M., 2014a. Numerical derivation of CPT-based p-y curves for piles in sand. Géotechnique, 64(3), 186–194.

Toda, K., Mori, A., Ishihara, Y., Eguchi, M., Tamboura, H.H., and Pasha, S.M.K., 2024. Investigation into geotechnical parameters of liquefied sand by static pile load tests, cone penetration tests, and pressuremeter tests. Proceedings of the Third International Conference on Press-in Engineering, International Press-in Association.

Xiong, W., Li, Z., Hu, D., and Li, F., 2024. Performance analysis of pile group installation in saturated clay. Applied Sciences, 14, 8321. https://doi.org/10.3390/app14188321

 © DFI International Bruges 2025

NEW CONCEPTS FOR SUSTAINABLE APPLICATION OF DEEP VIBRATORY COMPACTION

K. Rainer Massarsch, Geo Risk & Vibration Scandinavia AB, Stockholm, Sweden, +46707286663, rainer.massarsch@georisk.se

ABSTRACT

Although more powerful and efficient compaction equipment has become available, the full potential of deep vibratory compaction has not been used. The main parameters that govern the vibratory compaction process are discussed: shear strain, number of vibration cycles, and horizontal stress variations. An important parameter for efficient and cost-effective soil treatment is the vibration frequency. Deep vibratory compaction is frequently used to reduce settlements in granular soils. The tangent modulus method is briefly described, and how the input parameters can be derived from cone penetration tests. Another important aspect of vibratory is the horizontal stress increase, which results in a horizontal prestressing effect. The results of recent studies have demonstrated that vibratory compaction at the resonance frequency of the operating system enhances soil compaction and reduces energy consumption, independent of the compaction method. Finally, concepts are presented which make it possible to optimize the compaction process during project execution.

Keywords: compaction, frequency, penetration test, resonance, strain, settlement, vibration,

INTRODUCTION

Different foundation methods are available for supporting structures to be constructed on soil deposits that do not meet structural requirements. Pile foundations are widely used as geotechnical engineers have extensive experience regarding their design and execution. Pile foundations can be designed on existing standards and executed on a routine basis by a variety of contractors. However, this is not the case for ground improvement, where the number of experienced designers and specialist contractors is often limited. In the case of structures to be founded on loose to medium-dense granular soils, usually, two design considerations prevail: a) reduction of total and differential settlement and b) mitigation of liquefaction hazard. However, for the design and execution of ground improvement methods, the involvement of geotechnical engineers during all phases of the project is important. Unfortunately, only a limited number of geotechnical designers are familiar with, and have experience from deep vibratory compaction projects. Therefore, such alternatives are frequently discarded at the design stage as geotechnical engineers have limited experience regarding the calculation of settlements in granular soils or the mitigation of liquefaction.

The most cost-effective solution is, if the designer can demonstrate that ground improvement or deep foundations are unnecessary. Should the prevailing soil conditions not meet the design requirements, deep vibratory compaction (DVC) can be a competitive and sustainable alternative to pile foundations. In the recent past, more powerful and sophisticated vibrators have become available, which can be operated and controlled electronically and can make the application of DVC more effective and sustainable. In this paper, concepts are described that can be used in practice during the planning, design and execution of DVC projects. The most common vibratory compaction method uses depth vibrators that are inserted in the ground and compact granular soils. In the case of horizontally oscillating depth vibrators, the term “Deep horizontal vibratory compaction” (DHVC) is used. The DHVC method, also called “vibroflotation,” is extensively described in the geotechnical literature (Kirsch and Kirsch, 2016). Soil compaction is achieved during the extraction and re-penetration of the compaction probe and is usually combined with water jetting. DHVC projects are generally designed and executed by specialist foundation contractors using proprietary equipment (Kirsch and Bell, 2012). The European standard EN 14731:2005 provides guidelines regarding the application of ground treatment by DVC and includes depth vibrators and top-mounted vibrators. In the case of top-mounted vibrators, a purpose-built probe is inserted in the ground and excited by a vertically oscillating vibrator. There are fundamental differences between the application of depth

 © DFI International Bruges 2025

vibrators and top-mounted vibrators. Therefore, Massarsch and Fellenius (2019) introduced the term "Deep vertical vibratory compaction" (DVVC). A vertically oscillating vibrator with variable frequency is attached to the top of a purpose-built compaction probe. The compaction probe emits vibrations in the vertical and horizontal direction (Massarsch, 2024a) along the entire length of the probe. Vertical vibrations – but also horizontal vibrations are transferred to the surrounding soil.- A special case of DVVC is when the vibrator-probe-soil system is excited at its resonance frequency. At resonance, ground vibrations are amplified, especially in the vertical direction along the entire soil deposit (Massarsch, 2024a). This method is called resonance compaction (DVVCR). However, DVVCR requires the use of a vibrator with variable frequency and vibration monitoring. When DVVCR is carried out in water-saturated loose to medium dense sands, during initial compaction, spontaneous liquefaction occurs (Massarsch et al. 2021).

IMPLEMENTATION OF DEEP VIBRATORY COMPACTION

The efficient planning and execution of DVC requires competence by the designer and experience on the part of the contractor. Also, the project owner and his representative (site engineer) are essential in the cost-effective project execution. The design process includes the following steps:

1. **Stipulate performance requirements for the structure to be constructed:** for foundations on granular soils, total and differential settlements and/or liquefaction hazard are primary design considerations.
2. **Calculate settlements for initial conditions:** decide whether – or to what degree – ground improvement is required. Analyses should be based preferably on in situ tests such as cone penetration (CPT) or flat dilatometer (DMT) data.
3. **Quantify improvement requirements:** calculate settlements in an iterative process by gradually increasing soil stiffness until the design requirements are met. Express compaction specifications in terms of CPTU and/or DMT.
4. **Select suitable ground improvement method and process**: in granular soils, DVC is generally the most efficient ground treatment solution. Equipment and process should be chosen based on the initial ground conditions and the required degree of improvement.
5. **Perform compaction trials:** an important aspect of DVC is the selection of the optimal treatment process (compaction grid spacing, duration of compaction, number of compaction passes, vibrator operating parameters such as frequency and hydraulic pressure, vibration response of the ground, etc.).
6. **Monitor and document the compaction work:** DVC is a repetitive process that needs to be monitored and documented by recording different performance parameters.
7. **Verify the achieved compaction:** demonstrate that the prescribed compaction requirements have actually been met.

EFFECTS OF VIBRATORY TREATMENT

Although DVC has been used extensively to improve the geotechnical and cyclic properties of granular soils, the soil densification process is still misunderstood. In the past, soil particle acceleration and the dynamic force generated by the vibrator were considered to cause efficient soil densification. In a frequently referenced paper by Kirsch and Kirsch (2016) it is proposed that: "*the stability of the structure of granular soils is destroyed by dynamic stresses when a critical acceleration of more than 0.5 g is reached. With increasing accelerations, the shear strength of the sand decreases until it reaches a minimum between 1.5 and 2 g. At this point, the soil is fluidized, and a further increase of acceleration causes dilation."* However, acceleration is not important for the vibratory compaction process. Youd (1972) commented on using acceleration as the primary reason for compaction: *"Unfortunately, this approach has not led either to a clear understanding of the compaction process or to adequate methods for predicting compaction in situ.*" In the following paragraphs, the main factors controlling the vibratory compaction process are discussed.

 © DFI International Bruges 2025

Shear Strain

The importance of shear strain on soil densification and liquefaction has been discussed by several authors. Brumund and Leonards (1972), Seed and Silver (1972), and Youd (1972), have demonstrated that shear strain is the most important parameter that controls the rearrangement of soil particles. Soil densification is triggered when a critical cyclic shear strain is exceeded (Dobry and Abdoun, 2015, 2017). Youd (1972) summarizes his findings regarding the significance of shear strain, based on a literature review and experimental data, as follows:

1. "Fundamental concepts and published data show that shear strain is the primary factor causing compaction of granular materials.
2. The rate of compaction (volume change) increases with shear strain amplitude.
3. Compaction is not significantly affected by values of vertical stress for strain amplitudes exceeding 0.05 %.
4. No significant behavioral differences were detected between samples tested dry and similar samples tested in a saturated but completely drained condition.
5. The field density profiles predicted from analytically estimated in situ shear strain data and laboratory samples shear tests are consistent with published data from studies of static, vibratory, and seismic compaction."

The shear strain amplitude can be determined from seismic measurements. The following relationship can be used to estimate shear strain from vibration measurements during DVC, but is strictly valid only for plane waves,

$$\gamma = \frac{v}{c_s} \qquad [1]$$

Where γ = shear strain, v = particle velocity measured perpendicularly to the wave propagation direction, and C_S = shear wave speed. C_s can either be measured in the field or estimated with sufficient accuracy empirically. The densification (reduction of pore volume) of granular soils starts when a shear strain level of approximately 0.01% is exceeded. With increasing shear strain levels, the structure of granular soils changes, which causes settlement (Seed and Silver, 1972) or can induce liquefaction (Dobry and Abdoun, 2015). As shear strain is directly related to soil densification, the magnitude of the vibration velocity in the ground is an important parameter controlling densification (Youd 1972). Thus, vibration measurements in connection with DVC can provide valuable information regarding the soil compaction effect (Massarsch, 2024a).

Number of vibration cycles

Another important parameter that affects soil densification is the number of vibration cycles. Vibratory compaction is typically performed at about 25 to 30 Hz for 4 minutes in the vicinity of a soil layer; thus, approximately 6,000 to 7,000 cycles will be generated. Thus, the duration of compaction is an important parameter affecting soil densification. Seed (1976) applied the "*cumulative damage hypothesis*" to convert random motions to equivalently damaging uniform cyclic motion. Green and Terry (2005) developed more sophisticated concepts for liquefaction analyses, considering the dissipated energy of random and uniform motions. As a rule of thumb, it can be assumed that 100 vibration cycles at about 30 % of the peak vibration velocity, have an equivalent densification effect as one peak cycle, v_{max} (Massarsch, 2024a).

Horizontal Stress Increase

During vibratory compaction, many vertical and horizontal vibration cycles are emitted from the probe/vibrator to the soil. The permanent increase in horizontal effective stress has been observed on various vibratory compaction projects. To better understand the compaction process, ground vibrations were measured in connection with DVVC (Massarsch 2002, 2024a). Vibration sensors (geophones) were installed on and below the ground surface. The vertically oscillating probe generated strong vertical and horizontal ground vibrations. The measurements showed that due to cyclic loading, the horizontal stress pulses compacted the soil. Extensive field measurements were also performed by Gasser et al. (2022) during DHVC. At two test fields with different compaction

 © DFI International Bruges 2025

grids, a novel method, the "inclinodeformeter," was used to measure horizontal stress changes. Additionally, conventional compaction control techniques (dynamic probing and cone penetration tests) were performed. The field investigations confirmed the effect of horizontal prestressing due to DHVC. Besides the qualitative development of the stress change over depth, the influence of the compaction grid spacing could be documented. Based on these and other observations of horizontal stress changes, a conceptual description of the stress path in the soil during vibratory compaction can be developed as illustrated in Fig. 1.

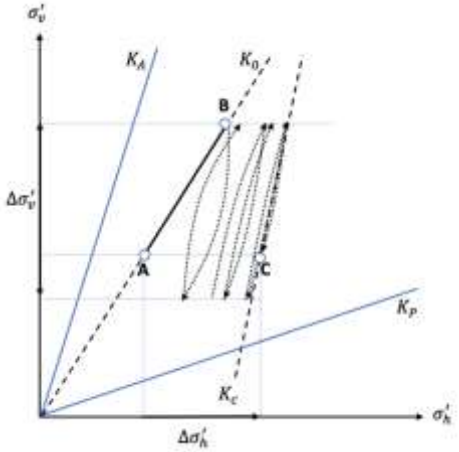


Fig. 1. Conceptual representation of stress path during vibratory compaction: stress before compaction (A), maximum stress level during cyclic loading (B), and state of stress after repeated loading cycles (C)

The initial stress conditions are indicated by (A). During initial loading, the stress path follows the direction of active earth pressure, K_0. During compaction, the ground is subjected to many vertical and horizontal loading and unloading cycles, causing stress variations between (B) and (C). It should be noted that with an increasing number of vibration cycles, the initial loop due to the first unloading-reloading cycle becomes gradually smaller; it can be concluded that due to compaction, the soil becomes more elastic. At the end of compaction, horizontal stresses have permanently increased from (A) to (C) while the vertical stresses remain essentially unchanged. Note that the stress relationship at the end of compaction, K_C, has changed compared to the initial loading, K_0.

As a result of vibratory treatment, horizontal effective stresses increase, as indicated by Fig. 1, but the pore volume also decreases. The relationship between void ratio, *e*, and mean effective stress, *p'*, in the case of vibratory compaction is shown in Fig. 2.

The conditions at the start of treatment are indicated by (A). Assuming the soil is normally consolidated (*NC*), the stress state at the end of the first loading is (B), with a soil stiffness M_0. Following compaction, the void ratio, *e*, decreases, and the mean effective stress, *p*', increases due to horizontal stress changes, to (C). The critical state line, *CSL*, separates consolidated from the overconsolidated soils. It can be concluded that due to compaction, the soil has become overconsolidated (*OC*). Accordingly, also the soil stiffness increased from M_0 to M_1. The stress state at (C) corresponds to overconsolidated conditions. Rowe (1954) has earlier proposed that compaction could be interpreted as the repeated application and removal of static surcharge cycles. Fig. 2 suggests that vertical vibratory compaction results in a preloading effect similar to that of static preloading. This important aspect is not generally appreciated in geotechnical design, as will be discussed in the following sections.

 © DFI International Bruges 2025

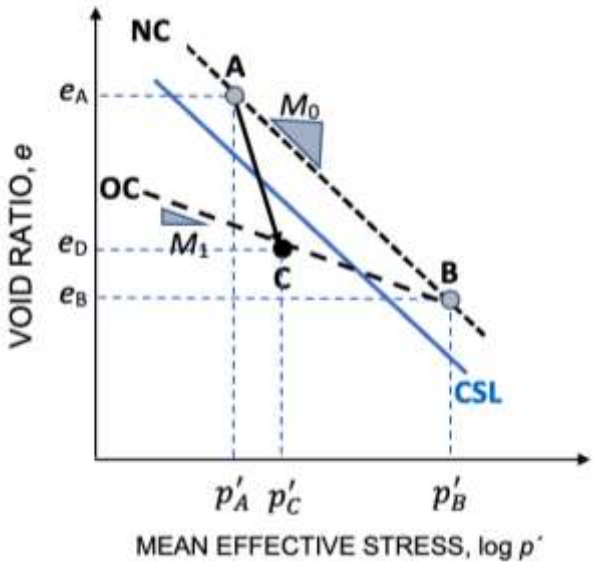


Fig. 2. Conceptual relationship during vibratory compaction between void ratio, e, mean effective stress, p', and soil stiffness, M: different stress states are indicated (normally consolidated: NC; overconsolidated: OC). The critical state line, CSL, separates normally consolidated from overconsolidated soils

IN SITU INVESTIGATION METHODS

In granular soils undisturbed samples can usually not be obtained, and the designer must rely on field investigations. The most widely used in-situ tests used in connection with deep vibratory compaction projects are the cone penetration test (CPT), with pore water pressure measurement (CPTU), the seismic cone penetration test (SCPT), and the Marchetti dilatometer (DMT) or the seismic dilatometer (SDMT). The CPT and the DMT have the advantage that changes in horizontal stress can be determined, which is not the case when dynamic penetrometers such as the Standard Penetration Test (SPT) or heavy dynamic penetrometer (HDP) are used. The Menard Pressuremeter (PMT) has the capability of measuring soil stiffness and horizontal stresses. However, the performance of the PMT is relatively complicated in granular soils and can only be carried out at selected levels. Therefore, only limited experience is available from horizontal stress changes caused by vibratory compaction.

The increase in horizontal stresses can be measured from the relative increase in CPT sleeve resistance f_s, or the DMT horizontal stress index, K_D (Massarsch et al. 2020). In the case of ground improvement, it can be conservatively assumed that prior to treatment, the soil deposit is close to being normally consolidated. This is a conservative assumption. In normally consolidated granular soil, the horizontal stress coefficient, K_0, can be estimated from the following simplified relationship proposed by Jaky (1948)

$$K_0 \sim 1 - sin(\phi') \qquad [2]$$

Where ϕ' = effective friction angle. In uncompacted granular soil ($\phi \approx 33°$), a typical value of K_0 = 0.43 can be assumed. The change in horizontal stress can be calculated from the increase in sleeve resistance from the following relationship,

$$\frac{K_1}{K_0} = \frac{f_{s1}}{f_{s0}} \frac{tan(\phi'_0)}{tan(\phi'_1)} \qquad [3]$$

Where K_0 = earth pressure coefficient before compaction; K_1 = earth pressure coefficient after compaction; f_{s0} = sleeve resistance before compaction; f_{s1} = sleeve resistance after compaction; ϕ'_0 = friction angle before compaction; ϕ'_1 = friction angle after compaction. It can be assumed that due to compaction, the friction angle increases by approximately 5°. This effect can be considered by the introduction of a correction factor (0.85)

 © DFI International Bruges 2025

$$\frac{K_1}{K_0} \cong 0.85\ \frac{f_{s1}}{f_{s0}} \qquad [4]$$

Immediately after compaction, the increase in horizontal stresses is highest close to the center of treatment and decreases with distance. The distribution of horizontal stresses is initially uneven but does equalize with time (Massarsch and Fellenius, 2019). This equalization can, at least to some extent, explain the time-dependent increase in penetration resistance.

PRE-LOADING EFFECT

It is common practice to evaluate the effectiveness of ground improvement by measurement of the cone resistance, q_c, "before" and "after" treatment. This practice, although valid from the standpoint of drained shear strength. However, the cone resistance does not fully show the increase in horizontal stress, as shown in Eq. 4. Neglecting the increase in sleeve resistance can grossly underestimate the benefits of stress changes with respect to settlements. As has been shown above, the permanent increase of horizontal stresses after vibratory compaction has a major effect on the in-situ stress conditions of the soil deposit. The stress conditions are changed from normally to overconsolidated, as illustrated by Fig. 2. An important paper by Leonards and Frost (1987) presented a conceptual framework for understanding the effects of overconsolidation on reducing soil compressibility. Calibration chamber test results were used to determine the dilatometer moduli. A framework for understanding the effects of overconsolidation in reducing the compressibility of all types of soils was presented. Although the concepts used to account for horizontal stress changes are at present limited in scope, it is better to use approximate correction factors than to ignore this effect entirely.

The results of in-situ tests (CPT or DMT) can be used to estimate the increase of the pre-loading (overconsolidation) effect. The overconsolidation ratio, *OCR*, is defined by the following relationship

$$OCR = \frac{\sigma'_p}{\sigma'_{v0}} = \frac{\sigma'_{v0}+\Delta\sigma'}{\sigma'_{v0}} \qquad [5]$$

Where σ'_{v0}= vertical effective stress; σ'_p= preloading stress and $\Delta\sigma'_p$ = preloading margin ($\sigma'_p - \sigma'_{v0}$). The value of *OCR* is based on the ratio of effective vertical stress prior to and after loading/compaction. Based on extensive laboratory tests by Mayne and Kulhawy (1982), the following relationship can be used to estimate the relationship between the increase in horizontal stress and *OCR*

$$\frac{K_1}{K_0} = OCR^{\beta} \qquad [6]$$

Where K_0 = earth pressure coefficient at rest (normally consolidated); K_1 = earth pressure coefficient (preloaded); β = empirical stress exponent from one single loading-unloading cycle. Using Eq. 4, it is possible to estimate the change in horizontal stress from sleeve resistance measurements. In the literature (Massarsch and Fellenius, 2002), values of the stress exponent, β, have been proposed for different soil types, ranging between 0.30 and 0.48. The relationship given in Eq. 6is based on results from different investigations as shown in Fig. 3 (*PI*: 1 -10; ϕ: 30 – 40 degrees, density index: I_D = 50 %) and β = 0.42). For practical purposes, it is recommended to choose an *OCR* value in the lower range (e.g., Schmertmann). As has been shown in Fig. (1), the width of the unloading-reloading stress loop becomes gradually smaller as the number of stress cycles increases. This aspect of cyclic loading needs to be further investigated. However, at present, it is recommended to estimate OCR from

$$OCR = \left(\frac{K_1}{K_0}\right)^{1/\beta} \qquad [7]$$

Also, the results of DMT investigations can be used to assess the relative increase in horizontal stress. The pre-loading effect can then be determined from the change in the horizontal stress index, K_D. Massarsch and Fellenius (2018) suggested a stress exponent, β = 0.48, which yields the following relationship (1/0.48 = 2.1)

$$OCR = \left(\frac{K_{D1}}{K_{D0}}\right)^{2.1} \qquad [8]$$

 © DFI International Bruges 2025

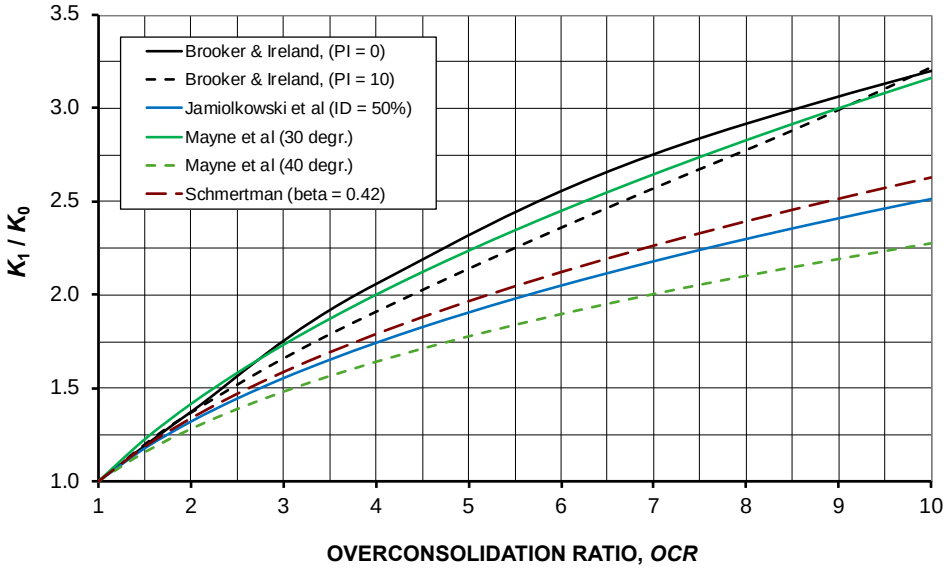


Fig. 3. Relationship between OCR and increase in horizontal stress ratio due to pre-loading

Where K_{D0} = horizontal stress index before compaction; K_{D1} = horizontal stress index after compaction. As has been discussed above, neglecting the overconsolidation effect caused by static or cyclic preloading significantly underestimates the beneficial effect of vibratory compaction (Leonards and Frost, 1988; Schmertmann, 1986; Massarsch, 1994).

COMPACTION REQUIREMENTS BASED ON CPT

An important task in connection with DVC projects is formulating realistic compaction requirements. Usually compaction specifications are usually based on penetration test results, particularly CPT results. Unfortunately, even on large and important projects, compaction specifications are frequently based on rules of thumb or experience from past projects without taking into account the project-specific settlement requirements. For the execution of sustainable and cost-effective ground improvement projects, compaction requirements need to be transparent and based on geotechnical principles. Vibratory compaction is primarily used to reduce total and differential settlement. Another important application is the mitigation of liquefaction hazards. In this presentation, the focus is on how settlements can be estimated based on cone penetration tests. A detailed description of settlement analysis of granular soils after vibratory treatment has been given by Massarsch and Fellenius (2019).

The CPT - and variations thereof, such as the CPTU (with pore water pressure measurement) or the SCPT (with seismic downhole test) - is today the most widely used field investigation method on vibratory compaction projects. The CPT is standardized, thereby reducing the risk that equipment and operation affect the measured parameters (ISSMGE, 1999, ISO 22476-1:2012). The CPT has the advantage of generating geotechnical information at low cost in most soils suitable for compaction. An additional important advantage of the CPTU is that it measures three independent parameters: cone stress, q_c, sleeve resistance, f_s, and pore water pressure, u.

Settlement Analysis based on Tangent Modulus Method

The tangent modulus method for settlement analysis has been described in the literature, for instance, in the 2nd and 3rd editions of the Canadian Foundation Engineering Manual, CFEM (1985) or Massarsch and Fellenius (2019). The tangent modulus is defined by

$$M_t = \frac{d\sigma}{d\varepsilon} = m\,\sigma_r \left(\frac{\sigma'_v}{\sigma_r}\right)^{(1-j)} \qquad [9]$$

 © DFI International Bruges 2025

Where M_t = tangent modulus, $d\sigma$ = change of stress, $d\varepsilon$ = change of strain, m = modulus number (dimensionless), σ_r = reference stress (equal to 100 kPa), σ'_v = vertical effective stress, j = stress exponent. An important step in the application of the tangent modulus concept is to define the modulus number, m. Integrating Eq. 9, yields the following general relationship for calculating the strain, ε, of a soil layer due to an increase of stress.

$$\varepsilon = \frac{1}{m}\left[\left(\frac{\sigma'_{v1}}{\sigma_r}\right)^j - \left(\frac{\sigma'_{v0}}{\sigma_r}\right)^j\right] \qquad [10]$$

Where σ'_{vo} = vertical effective stress prior to loading, σ'_{v1} = vertical effective stress after loading. The most important aspect when applying the tangent modulus method is the selection of realistic input parameters, that is, the stress exponent, j, and the virgin and re-loading modulus numbers, m and m_r,. Typical values of the stress exponent, j, for granular soils can be found in the literature (CFEM, 1985).

The re-loading modulus number, m_r, applies to stress increase at the overconsolidated condition. Prior to compaction, it can be assumed that the untreated soil deposit is normally consolidated, which is a conservative assumption. Janbu (1985) updated typical values of the modulus number, m, for normally consolidated silt and sand (j = 0.5), which categories are of interest in regard to settlement analyses for soil compaction. In Fig. 4 the modulus number, m, derived by Janbu (1985), is shown as a function of void ratio, e, for silt and sand and different degrees of density. Also indicated is the approximate range (and lower/upper boundaries) of modulus numbers for the respective soil category (sand and silt),

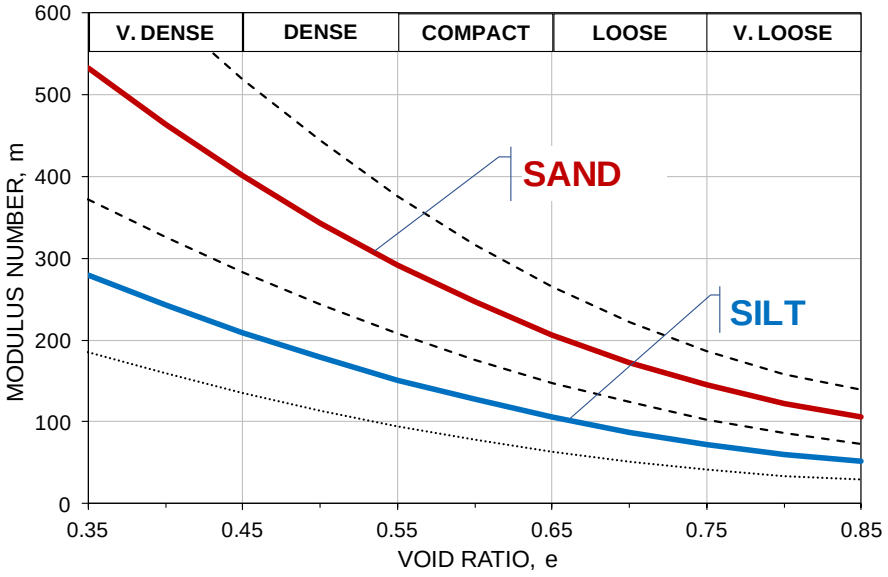


Fig. 4. Typical values of modulus numbers for normally consolidated sand and silt with upper and lower boundaries for silt (lower heavy line) and sand (upper heavy line). Data derived from Janbu (1985)

The values of modulus number, m, shown in Fig. 4 can be used as guidelines for preliminary settlement assessment. However, in the case of soil compaction it is preferable to derive m directly from CPT. Massarsch (1994) proposed a method for estimating the modulus number, m, from the cone resistance, q_c, later refined by Massarsch and Fellenius (2019). The modulus number can be derived using a stress-adjusted cone resistance, q_{CM}

$$m = a\left(\frac{q_{cM}}{\sigma_r}\right) \qquad [11]$$

Where a = empirical modulus factor and σ_r = reference stress (100 kPa). The modulus factor, a, which reflects soil type, is shown in ***Table 1***. The empirical modulus factor, a, can be related to the soil behavior index, I_c, according to the Soil Behavior Type (SBT) chart, Robertson (2010).

 © DFI International Bruges 2025

Table 1. Soil classification according to the SBT chart (Robertson, 2010) and comparison with empirical modulus factor, a.

Soil Classification	SBT Zone	SBT Index I_c	Modulus factor, *a*		
			Loose/Soft	Compact	Dense
Gravelly sand	7	$I_c < 1.31$	35	40	45
Sands - clean to silty	6	$1.31 < I_c < 2.05$	22	28	35
Silty sand/sandy silt	5	$2.05 < I_c < 2.60$	20	22	28
Clayey silt/silty clay	4	$2.60 < I_c < 2.95$	12	15	20
Clay	3	$2.95 < I_c < 3.6$	-	-	-

The stress-adjusted cone resistance, q_{CM}, can be determined from the following relationship

$$q_{CM} = q_c \left(\frac{\sigma_r}{\sigma_0'}\right)^{0.5} \quad [12]$$

Where q_c = cone resistance, σ'_0 = mean effective stress. Thus, it is possible to calculate settlements using the tangent modulus method based on CPT results.

Importance of Stress History

The stress history of the soil deposit affects settlements. Therefore, it is essential to estimate the preloading stress, σ_p', either based on geological information or by empirical methods. As it is difficult to obtain undisturbed soil samples, different empirical correlations between in situ tests and preloading stress can be used. Mayne et al. (2009) proposed, for natural soils, including sands, silts, clays, and mixed soil types, the following relationship to estimate the preloading stress, σ'_p

$$\sigma_p' = 0.33\ (q_t - \sigma_v)^{m'} \quad [13]$$

Where q_t = stress-corrected cone resistance, σ_v = vertical total stress, and m' = grain size parameter (not to be confused with the modulus number). The grain size parameter, m', increases with fines content and decreases with mean grain size (clean quartz sands: $m' \approx 0.72$, silty sands: $m' \approx 0.8$, clays: $m' \approx 1.0$). Although Eq. 13 gives only an approximate estimate of the preloading stress, it is recommended to use an approximate value rather than completely neglecting the preloading effect.

The modulus number increases as a result of pre-loading as has been discussed in detail by Massarsch (2024b). Fig. 5 shows the relationship between the modulus number ratio, m_u/m, and the modulus number, m, at virgin loading (normally consolidated), where m_u is the modulus number determined from the unloading test (Ohde 1951). The increase in the unloading modulus number is most significant at low values of the modulus number (loose sands). The correlation between the m_u/m ratio and m at virgin loading shown in Fig. 5 can be expressed by the following relationship:

$$\frac{m_u}{m} = 225\ m^{-0.76} \quad [14]$$

Equation 14 can be used to estimate the unloading modulus for different values of the virgin modulus number. For example, in loose sand ($m \sim 100$), the unloading modulus ratio $m_u/m \sim 7$. In the case of an initially denser sand (m ~ 300), the unloading modulus ratio is lower, $m_u/m \sim 3$. When the virgin modulus increases towards $m \sim 1250$, the m_u/m-ratio approaches 1. Thus, the increase in the m_u/m ratio is more pronounced in loose granular soils than in dense soils. The constrained modulus at

 © DFI International Bruges 2025

unloading and reloading is typically about 5 to 8 times higher than the virgin loading modulus (Janbu 1985). The information in Fig. 5 is thus in good agreement with experience.

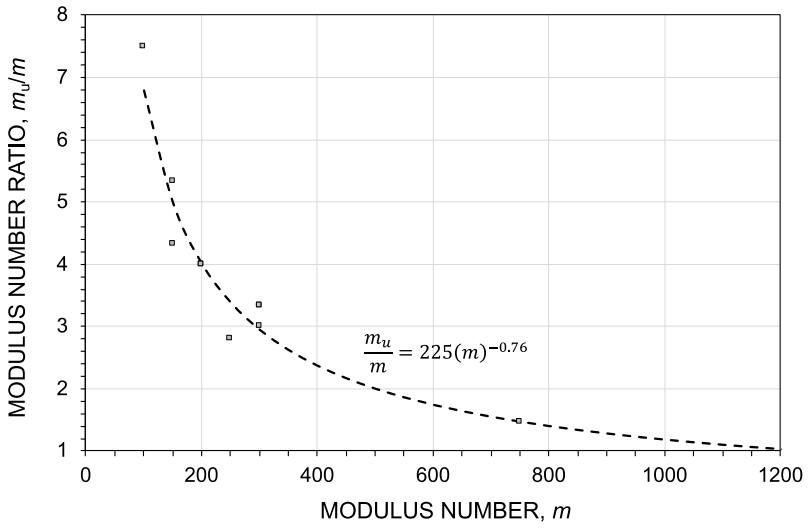


Fig. 5. Unloading modulus number ratio as a function of modulus number for virgin loading (Massarsch, 2024)

Specification Process for Compaction Projects

In the design of vibratory compaction projects, compaction specifications are frequently based on settlement criteria. It is conservative to assume that prior to treatment, the soil deposit is normally consolidated. It is recommended to use the tangent modulus method for the calculation of total and differential settlements. Prior to the start of the project, settlement analyses shall be based on average CPT records to determine whether compaction with respect to settlements is required at all. If the allowable settlements are exceeded, it is then possible by an iterative process to gradually increase the cone resistance until the design requirements have been met. The effect of horizontal stress increase and preloading should be considered in the analysis as outlined above. Based on the settlement analyses it is then possible to formulate rational compaction specifications. Note that several different cone resistance profiles can meet the settlement requirements.

Once the required degree of compaction has been established, compaction trials should be used to determine the different compaction parameters, such as compaction grid spacing, duration of treatment, extraction and re-penetration steps, and vibrator operating parameters. Within a representative trial area, a sufficient number of soil investigations (preferably CPTU) should be performed before and after treatment. After the first compaction pass, which could be at a larger point spacing, CPTUs should be carried out at the diagonal between the treatment points. Thereafter, the second pass should be performed in the intermediate points, after which the second set of penetration tests can be used to verify whether the required compaction effect has been achieved.

OPTIMIZATION OF THE COMPACTION PROCESS

An important aspect of cost-effective and sustainable vibratory compaction is to avoid overcompaction. Also, the treatment process should be carried out as efficiently as possible. Modern compaction equipment is powerful, and its performance can be optimized using monitoring and process control systems (MPCS). These aspects will be discussed in the following paragraphs.

Vibrator Operating Frequency

A parameter, the importance of which is frequently neglected, is the operating frequency of the vibrator. However, the use and adjustment of the vibrator operating frequency during the compaction process has a significant influence on the compaction effect but also on the project economy (energy

 © DFI International Bruges 2025

consumption and wear of bearings). The importance of the vibration frequency has not been studied until recently (Wehr, 2005). Pistrol et al. (2024) showed that in the case of horizontally oscillating vibrators, it is necessary to gradually adjust the operating frequency. They found that a higher compaction effect was achieved when the vibration frequency was significantly reduced.

Wersäll (2016) studied the performance of vibratory rollers for the improvement of embankments. Full-scale tests were conducted using a vibratory soil roller on a test bed of crushed gravel. The results showed that resonance can be utilized by vibratory rollers and compaction plates and that the optimum compaction frequency is at, or slightly above, the coupled compactor-soil resonant frequency. Since vibratory rollers typically operate far above resonance (about 30 to 35 Hz), the compaction frequency can be significantly reduced (to about 15 to 20 Hz), resulting in a considerable reduction in fuel consumption, environmental impact, and machine wear. The compaction effect is at least as high or better at resonance than at conventional vibration frequencies.

Large vibratory plates can be used to treat granular soil to a depth corresponding approximately to the side length of the plate, which is typically 3 to 4 m. This is a depth interval at which conventional vibratory compaction is not effective. Extensive field trials were performed using a large-scale compaction plate, shown in Fig. 6, (Wersäll et al. 2023).



Fig. 6. Field trials using a vibratory compaction plate to investigate the influence of vibration frequency and other compaction parameters (Wersäll et al., 2023)

Compaction tests were conducted at a site consisting of medium-dense, partially saturated sandy silt and silty sand with a 40.5-ton HVP compactor. The geotechnical conditions were characterized as difficult for vibratory compaction, requiring longer compaction times. In addition, the dynamic characteristics of the vibrator were judged to be too small for the optimum dynamic response of the compactor. Although the required compaction time was longer compared to previous studies on coarser material, the silty sand and sandy silt could be compacted significantly, showing that the

 © DFI International Bruges 2025

technique is also applicable on silty soils. It is important that the vibrator can provide sufficient centrifugal force to cause disconnection between the plate and the soil.

Deep vertical vibratory compaction using resonance amplification (DVVCR) has been successfully used on a variety of projects (Massarsch and Vanneste 1988, Massarsch 1991a, Massarsch 1991b, Choa et al. 2001, Massarsch and Fellenius 2005, Liu and Cheng 2012, Cheng and Liu 2013, Massarsch et al. 2017, Massarsch and Fellenius, 2017 and Massarsch et al. 2021b). The compaction machine is shown in Fig. 7.



Fig. 7. DVVC machine with a variable frequency vibrator and flexible double-Y probe

Monitoring and Process Control

A vibrator with variable frequency is mounted on a purpose-built compaction probe with openings that reduce its mass and increase the interaction with the surrounding ground. To achieve optimal vibratory compaction, a suitable treatment process must be chosen (Massarsch and Fellenius, 2005). The probe is inserted at a high frequency (typically above 30 Hz), during which the shaft resistance is reduced significantly, and the vibration energy is consumed as heat along the shaft of the probe.

During the compaction phase, the vibration frequency is gradually lowered to the vertical resonance frequency of the vibrator-probe-soil system. At resonance, the probe oscillates in phase with the surrounding soil, which enhances the transfer of vibration energy. Also, the probe penetration speed decreases, and vertical ground vibrations increase. Thus, the probe acts as an antenna for transferring vibration energy from the vibrator to the surrounding soil.

For the efficient implementation of resonance compaction, several machine parameters and the dynamic ground response need to be measured (Massarsch and Wersäll, 2019). For this purpose, a monitoring and process control system (MPCS) was developed, which makes it possible to measure a variety of performance parameters (Massarsch, 2024). The different sensors are mounted on the compaction machine and on the ground as shown in Fig. 8. The measured parameters are recorded by an on-board computer and the data transferred by wireless connection to the project office. At the same time, measurements are displayed to the machine operator in real time, making it possible to manually adjust the compaction process.

 © DFI International Bruges 2025

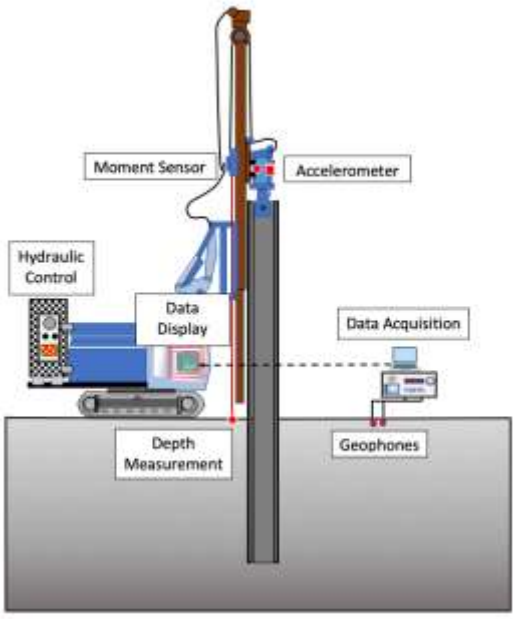


Fig. 8. Principle of Monitoring and Process Control System (MPCS), showing sensors mounted on the rig and ground surface (Massarsch and Wersäll 2019)

An important parameter in the application of DVVC is the ground vibration velocity, which is related to shear strain, and the vibration frequency, which controls system resonance. Vibration measurements can be performed by a geophone placed at a lateral distance of about 4 m from the insertion point, Fig. 9. Geophones can also be installed at different depths below the ground surface (Massarsch 2023a).



Fig. 9. Tri-axial geophone for measurement of resonance frequency at 4 m distance from compaction probe

The system resonance frequency is affected by several parameters, such as the dynamic characteristics of the compaction machine (mass of probe, eccentric moment of vibrator, centrifugal force etc.) and the dynamic properties of the soil (shear modulus), which change with strain levels and frequency. Estimating the system resonance frequency of a vibrating system is challenging (Guangyin et al. 2012). However, it is relatively simple to measure the dynamic ground response and system resonance on-site by a vertical geophone. The results of a resonance test are shown in Fig. 10, where the following parameters were measured: a) vibration frequency, b) vertical ground vibration velocity, c) hydraulic pressure. The effect of changing the vibrator frequency on the vertical ground vibration velocity and vibrator performance is illustrated by an MPCS record in Fig. 10.

 © DFI International Bruges 2025

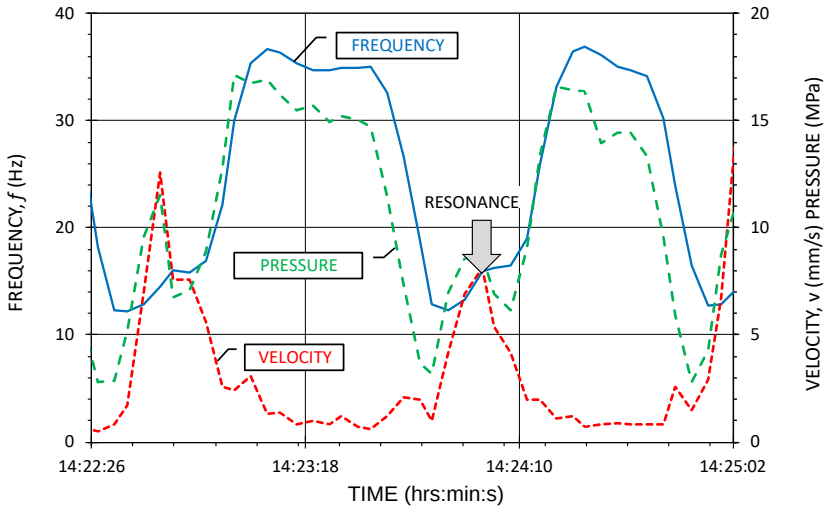


Fig. 10. Dependence of hydraulic pressure and vertical ground vibration velocity (RMS) as a function of frequency (Massarsch et al. 2021)

At a probe penetration frequency of 38 Hz, ground vibrations are low (less than 3 mm/s RMS). When the frequency is reduced to 12 Hz, corresponding to system resonance, ground vibrations are amplified by a factor of 5 to 10. Also note the reduction of hydraulic pressure when the frequency is reduced, which implies that the energy consumption is significantly reduced. The MPCS can be programmed to automatically optimize the different stages of resonance compaction.

Probe Penetration Speed

A parameter that is unique to the DVVC system is the probe penetration speed. During the insertion of the compaction probe at high frequency, the shaft resistance is effectively reduced and most of the resistance is generated by the toe of the probe. The penetration speed is high and is inversely related to the cone penetration resistance. When penetrating dense layers, the probe penetration speed is low but increases in looser layers. Thus, when operating at a constant, high frequency, the probe can be used as a large-scale soil investigation tool similar to a penetrometer. Site-specific correlations can be established during the trial phase between the required cone resistance and the corresponding probe penetration speed.

To achieve efficient compaction, the frequency of the vibrator is reduced to the resonance frequency of the vibrator-probe-soil system, and the probe oscillates “in phase” with the surrounding soil. Ground vibrations are high, and the probe penetration speed becomes slow. The probe penetration speed can be used as an indicator of soil strength.

The following three parameters can be used to optimize the compaction process: ground vibration velocity, vibrator frequency, and probe penetration speed. Ground vibration velocity is an indicator of shear strain in the soil; vibration frequency is used to enhance the compaction process; and probe penetration speed reflects the increase in soil stiffness. The penetration speed measurement is an important parameter for determining on-site when the required soil resistance has been achieved.
A site-specific relationship can then be used to correlate the required probe penetration speed with respect to the compaction requirements. The maximum allowable probe penetration speed can now be programmed into the MPCS and displayed to the machine operator.

CONCLUSIONS

At present, the full potential of deep vibratory compaction as an alternative to deep foundations, such as piles is still not realized in spite of the availability of powerful and more sophisticated equipment. However, there exists a lack of understanding of which parameters cause soil densification. The most

 © DFI International Bruges 2025

important parameters for vibratory compaction are shear strain and the number of vibration cycles. Shear strain can be derived if the ground vibration velocity is measured.

Deep vibratory compaction is frequently used to reduce total and differential settlements. However, many geotechnical engineers are not familiar with how to estimate settlements in granular soils although reliable analytical methods such as the tangent modulus concept are available. A concept is presented that illustrates how the soil modulus number, which is an important input parameter, can be derived from cone penetration tests (CPT). Another important aspect that should be taken into consideration in geotechnical design is the horizontal pre-stressing effect. A stress path diagram shows that due to the increase in horizontal stresses, the compacted soil becomes overconsolidated. Sleeve friction measurements from CPT, performed before and after soil treatment, can be used to quantify the increase in horizontal stresses. A concept is presented which can be used to assess the pre-consolidation effect (OCR).

An important parameter that affects the efficiency and energy consumption of vibratory compaction is the vibration frequency. Independent of the method of treatment, a reduction in vibration frequency to the resonance frequency of the operating system results in reduced energy compaction and enhance soil improvement. This aspect of vibratory compaction has major practical importance but is still not fully recognized.

Modern electronic systems can be used to optimize soil compaction during project execution. Deep vertical vibratory compaction using a powerful vibrator with variable frequency can be used to optimize the compaction process. Different machine parameters and vibration measurements on the ground can be used to adjust the compaction process to achieve maximum soil densification at a minimum of compaction energy. One example is the resonance compaction process that uses the vibration amplification effect to enhance soil improvement. The compaction process can be monitored and adjusted by using the optimal vibration frequency during different phases of the compaction process. A useful parameter is measuring the probe penetration speed at a controlled frequency to determine when the required densification has been achieved.

REFERENCES

Brumund, W.F., and Leonards, G.A. 1972. Subsidence of Sand Due to Surface Vibration. Journal of the Soil Mechanics and Foundation Division, Proceedings ASCE, Vol. 98, 27 – 42.

Canadian Foundation Engineering Manual (CFEM) (1985) Canadian Geotechnical 3rd Edition. BiTech Publishers Ltd., 460 p.

Cheng, Y., and Liu, S.Y. 2013. Application of Resonant Vibro-Compaction in Treatment of Liquefiable Sites. Chinese Journal of Geotechnical Engineering, 352): 83–87.

Choa, V., Bo, M.W., and Chu, J. 2001. Soil Improvement Works for Changi East Reclamation. Ground Improvement. Vol 5, no 4, 141-153.

Dobry, R., and Abdoun T. 2015. Cyclic shear strain needed for liquefaction triggering and assessment of overburden pressure factor Ks." ASCE. Journal of Geotechnical and Geoenvironmental Engineering. Vol 141, no 11, 18 p.

EN 14731:2005. Execution of special geotechnical works. Ground treatment by deep vibration. European Committee for Standardization (CEN), Effective 2010, AC:2010.

Gasser D., Marte, R., and Tschuchnigg, F. 2022. Horizontalverspannung nicht bindiger Böden durch die Rütteldruckverdichtung mit Tiefenrüttler – Experimentelle und numerische Untersuchungen (Horizontal stress state of non-cohesive soils due to deep vibro compaction with depth vibrator –

 © DFI International Bruges 2025

Experimental and numerical studies). Geotechnik 45, H. 1, S. 16–30. https://doi.org/10.1002/gete.202100008

Green, R.A., and Terri, G.A. 2005. Number of Equivalent Cycles Concept for Liquefaction Evaluations—Revisited. Journal of Geotechnical and Geoenvironmental Engineering 131(4):477-488, DOI: 10.1061/(ASCE)1090-0241(2005)131:4(477).

Guangyin, D., Changhui, G., Songyu, L., et al. 2021. Resonance Vibration Approach in Soil Densification: Laboratory Experiences and Numerical Simulation. Earthq. Eng. Eng. Vib. 20, 317–328 (2021).

ISSMGE (International Society for Soil Mechanics and Geotechnical Engineering Technical Committee 16). 1999. International reference test procedure (IRTP) for the cone penetration test (CPT) and the cone penetration test with pore pressure (CPTU). In Proceedings of the XIIth ECSMGE (de Cock F, Legrand C and

Jáky, J. 1948. Pressure in silos. In Proceedings of the 2nd ICSMFE, Rotterdam, the Netherlands, vol. 1, pp. 103–107.

Janbu, N. Soil models in offshore engineering. Rankine Lecture. Géotechnique 1985, 35, 241–281.

Kirsch, K., and Bell, A. (2012). Ground improvement. Eds: CRC Press. 3 Ed., 511 p.

Kirsch, K., and Kirsch, F. (2016). Ground improvement by deep vibratory methods. CRC Press. 2nd Ed, 234 p.

Leonards, G.A. and Frost, J.D. 1988. Settlement of shallow foundations on granular soils. Journal of Geotechnical Engineering, Vol. 114, No. 7, July, 1988. ©ASCE, ISSN 0733-9410/88/0007-0791/$1.00 + $.15 per page. Paper No. 22591.

Liu, S.Y., and Cheng, Y. 2012. Resonance Compaction Method for Highway Ground Improvement at Liquefaction Site. China J Highway Transport 2012;25(6): 24–9.

Massarsch, K.R. (1991a). Deep Soil Compaction Using Vibratory Probes. ASTM Symposium on Design, Construction and Testing of Deep Foundation Improvement: Stone Columns and Related Techniques, Robert C. Bachus, Ed. ASTM Special Technical Publication STP 1089, Philadelphia, 1990, 297-319.

Massarsch, K.R. (1991b). Deep Vibratory Compaction of Land Fill using Soil Resonance. Proceedings, Infrastructure ´91, Intern. Workshop on Technology for Hong Kong´s Infrastructure Development, December 1991, 677 - 697.

Massarsch, K.R., and Vanneste, G. 1988. Tri Star Vibrocompaction Annacis Island, British Columbia, Canada. Franki Technology International (FIT) Internal Report, Liège, 108 p.

Massarsch, K.R. 1994. Settlement analysis of compacted fill. Proceedings, 13th ICSMFE, New Delhi, January 5-10, Vol. 1, pp. 325-328.

Massarsch, K.R. 2002. Effects of Vibratory Compaction. TransVib 2002 – International Conference on Vibratory Pile Driving and Deep Soil Compaction. Louvain-la-Neuve. Keynote Lecture, 33 – 42.

Massarsch, K.R., and Fellenius, B.H. (2002). Vibratory compaction of coarse-grained soils. Canadian Geotechnical Journal 39(3) 695 - 709.

Massarsch, K.R. and Fellenius, B. H. 2005. Deep vibratory compaction of granular soils. Chapter

 © DFI International Bruges 2025

19, in Ground Improvement-Case Histories, Geo-Engineering Series Volume 3, Elsevier (UK), B. Indraratna and Chu J. (Editors), pp. 633 – 658.

Massarsch, K.R., and Fellenius, B.H. 2017a. Evaluation of resonance compaction of sand fills based on cone penetration tests. Ground Improvement. Proceedings of the Institution of Civil Engineers. Paper 1700004, Volume 170, Issue 3, August 2017, 149-158.

Massarsch, K.R., and Fellenius, B.H. 2017b. Liquefaction assessment by full-scale vibratory testing. Proceedings of the 70th Annual Canadian Geotechnical Conference, Paper 147, Ottawa, October 1 - 3, 7 p.

Massarsch, K.R., and Fellenius B.H. 2018. In situ tests for settlement design of compacted sand. Proceedings of the Institution of Civil Engineers – Geotechnical Engineering, https://doi.org/10.1680/jgeen.18.00046, 11 p.

Massarsch, K.R. and Fellenius, B.H. 2019. In situ tests for settlement design of compacted sand. Proceedings of the Institution of Civil Engineers – Geotechnical Engineering, Volume 172, Issue 3, June, 2019, pp. 207-217.

Massarsch, K.R. and Wersäll, C. 2019. Monitoring and Process Control of Vibratory Driving. Geotechnical Engineering Journal of the SEAGS & AGSSEA Vol. 50 No. 3 September 2019 ISSN 0046-5828; pp. 1 – 10.

Massarsch, K.R., Wersäll, C., and Fellenius, B.H. 2020. Horizontal stress increase induced by deep vibratory compaction. Proceedings of the Institution of Civil Engineers – Geotechnical Engineering 173(3): 228–253, https://doi.org/10.1680/jgeen.19.00040

Massarsch, K.R., Wersäll, C. and Fellenius, B. 2021. Liquefaction induced by deep vertical vibratory compaction. Proceedings of the Institution of Civil Engineers – Ground Improvement. Volume 174 Issue 3, August 2021, pp. 194-205.

Massarsch, K.R. 2023a. Application of deep vertical vibratory compaction using resonance Amplification. Geotechnical Engineering Journal of the SEAGS & AGSSEA Vol. 54 No.1 March 2023, ISSN 0046-5828, pp. 1-7.

Massarsch, K.R. 2023b. Applications of deep vertical vibratory compaction. Geotechnics for Sustainable Infrastructure Development - Geotec Hanoi 2023, Phung (Edt), pp. 3-23.
Massarsch K.R. 2024. Monitoring and Process Control of Deep Vertical Vibratory Compaction Using Resonance Amplification. International Journal of Geoengineering Case Histories, Volume 8, Issue 1, pp. 22-38, doi: 10.4417/IJGCH-08-01-02.

Mayne, P.W., and Kulhawy, F.H. 1982. K_0 – OCR Relationships in soil. ASCE Journal of the Geotechnical Engineering Division108(GT6) 851–872.

Mayne, P.W.; Coop, M.R.; Springman, S.M.; Huang, A.-B. 2009. Geomaterial behavior and testing. Theme Lecture. In Proceedings of the 17th International Conference on Soil Mechanics and Geotechnical Engineering, Alexandria, Egypt, 5–9 October 2009; Volume 4, pp. 2777–2872.

Ohde, J. Grundbaumechanik (Ground Engineering Mechanics), 27th ed.; A. V. Hütte: Berlin, Germany, 1951; pp. 886–902.

Pistrol, J. Kopf, F., Adam, D. and Kummerer, C. 2024. Deep Vibrocompaction at the Natural Frequency of the Soil Response. J. Geotech. Geoenviron. Eng., 2024, 150(9): 04024076

 © DFI International Bruges 2025

Robertson, P.K. 2010. Soil behavior type from the CPT: an update. International symposium on cone penetration testing, 2, CPT'10, Huntington Beach, CA, May 9-11, 2010. Proceedings, Vol. 2, pp 575-582.

Rowe, P.W. 1954. Stress-strain theory for cohesionless soil with applications to earth pressures at rest and moving walls. Geotechnique 4(2), 70 - 88.

Seed, H.B. 1976. Evaluation of soil liquefaction effects on level ground during earthquakes. ASCE Annual Convention and Exposition, Liquefaction Problems in Geotechnical Engineering. Philadelphia. 1 – 104.

Seed, H.B., and Silver, M.L. 1972. Settlements of Dry Sand during Earthquakes. Journal of the Soil Mechanics and Foundation Division, Proceedings ASCE, Vol. 98, 381 - 396.

Schmertmann, J. H. 1986. Dilatometer to compute foundation settlement. Proc. ASCE Specialty Conf. on Use of In-Situ Tests in Geotechnical Engineering, Blacksburg, Va., 303-321.

Wehr, J. 2005. Variation der Frequenz von Tiefenrüttlern zur Optimierung der Rütteldruckverdichtung (Variation of frequency of depth vibrators for the optimization of deep vibratory compaction). Thesis, Mitteilungen des Fachgebiets Grundbau und Bodenmechanik, 67–77. Berlin: Technische Universität Berlin.

Wersäll, C. 2016. Frequency Optimization of Vibratory Rollers and Plates for Compaction of Granular Soil. Royal Institute of Technology (KTH), Civil and Architectural Engineering, Soil and Rock Mechanics., 40 p. ORCID iD: 0000-0002-7361-0729

Wersäll, C., Massarsch, K.R. and Spross, J. 2023. Heavy vibratory plate compaction of silty sand: A field study. Soils and Foundations, 62 (2022) 101208, https://doi.org/10.1016/j.sandf.2022.101208, pp. 1 – 17.

Youd, T.L. 1972. Compaction of Sands by Repeated Shear Straining. Journal of the Soil Mechanics and Foundation Division, Proceedings ASCE, Vol. 98, 709 – 725.

 © DFI International Bruges 2025

ENHANCEMENTS TO THE COUPLED HYDRO-MECHANICAL HYPOPLASTIC MODEL FOR UNSATURATED SOILS

Shanujah Mathuranayagam, School of Engineering, Design and Built Environment, Western Sydney University, Australia.
William Fuentes, School of Engineering, Design and Built Environment, Western Sydney University, Australia.
Samanthika Liyanapathirana, School of Engineering, Design and Built Environment, Western Sydney University, Australia.

ABSTRACT

The conventional design of geotechnical structures adheres to the principles of saturated soil mechanics. However, these conventional practices often overlook the impact of matric suction associated with alternating wetting and drying scenarios within the unsaturated zone. Recognizing the importance of this factor, developing a constitutive model becomes crucial for designing geotechnical structures in unsaturated soils. This paper introduces an enhanced version of the coupled hydro-mechanical hypoplastic model proposed by Tafili and Machaček (2023). The reference model can simulate volumetric collapse upon wetting and incorporates suction effects on stiffness and strength. Its mechanical constitutive equation links Bishop's effective stress with strain and suction. This paper introduces two advancements to the reference model: (i) improvement in the bulk modulus (K) to account for the influence of the degree of saturation and (ii) accurate projection of the overconsolidation ratio (OCR) dependency of the unsaturated soil. The model's performance is analyzed through the back-calculation of three experimental studies: (i) variation of bulk modulus during the wetting-drying process for Bonny silt, (ii) shearing at different suction and mean net stress for Loess and (iii) wetting at different mean net stress for Lower Cromer Till. The results confirm that the proposed model has significantly improved the predictive capability of the experimentally observed hydro-mechanical behaviour of unsaturated soils.

Keywords: unsaturated soil, soil matric suction, volumetric collapse and constitutive models

1. INTRODUCTION

Understanding the behaviour of unsaturated soils, common in natural settings, is crucial for accurate analysis and effective design in geotechnical engineering and environmental science. The constitutive model for unsaturated soils is essential for characterizing the hydraulic and mechanical behaviour (Fredlund, 2000; Liang and Zhao, 2019). Over the last few years, there has been a strong emphasis on improving and developing constitutive models to accurately capture the stress-strain behaviour of unsaturated soils.

Most constitutive models involve in coupling two components: one that governs the mechanical behaviour of the soil and another that describes the hydraulic behaviour of the water within the void structure of soils. Alonso et al. (1999) introduced the first comprehensive strength-deformation model for unsaturated soils, framed within the general principles of elastoplasticity. They integrated the effects of partial saturation into a Cam-clay type elastoplastic model by accounting for net stress and a yield surface size dependent on suction. This development was quickly followed by a series of models within the elastoplastic framework that incorporated the hydraulic variables suction (s) and degree of saturation (S_w) (Loret and Khalili, 2002; Wheeler et al., 2003; Wray et al., 2005; Fredlund, 2006; Sun et al., 2007; Yang et al., 2008; Buscarnera and Nova, 2009; Zhou et al., 2012; Hu et al., 2014; Lloret-Cabot et al., 2017; Gholizadeh and Latifi, 2018; Duan et al., 2019; Rotisciani et al., 2021; Khalili et al., 2022; Liu et al., 2022; Li et al., 2023).

Hypoplastic models have emerged as a significant alternative in constitutive modelling, using smooth tensorial functions and avoiding the loading-unloading conditions typically used in elastoplastic models. Gudehus (1995) was the first to apply hypoplasticity theory to model unsaturated soil behaviour. He employed the effective stress concept and adapted Bishop's scalar factor χ in the basic

 © DFI International Bruges 2025

equation. However, hypoplastic models have not been widely used for simulating unsaturated soil behaviour in the literature (Gudehus, 1995; Niemunis, 2003; Bauer et al., 2007; Mašín and Khalili, 2008; Khalili and Zargarbashi, 2010; Fuentes and Triantafyllidis, 2013a; Mašín, 2019; Grandas Tavera et al., 2022; Tafili and Machacek, 2023).

This paper introduces an improved version of the hydro-mechanically coupled hypoplastic constitutive model proposed by Tafili and Machaček (2023). Their model is formulated based on the model by Fuentes and Triantafyllidis (2013) by extending it to a three-dimensional generalized stress space. The reference model incorporates Bishop's stress as the constitutive stress, with the Bishop parameter defined as the effective degree of saturation $\chi = S^e$(Alonso et al., 2010; Lu et al., 2010). Recent numerical simulations using the reference model have demonstrated that compression paths subjected to variations in the degree of saturation allow stress states beyond the normal consolidation line, which may result in numerical instabilities. This paper introduces two key improvements to the model: (i) an enhanced bulk modulus (K) that reflect the effect of the degree of saturation, and (ii) the inclusion of overconsolidation ratio (OCR) effects in unsaturated soil behaviour as discussed in the following sections.

2. PROPOSED ENHANCEMENT TO THE REFERENCE MODEL

The selected reference model by Tafili and Machacek (2023) is a coupled hydromechanical hypoplastic model for unsaturated soils to a three-dimensional generalized stress space. Under isotropic conditions, the selected reference model behaves similar to the one proposed by Fuentes and Triantafyllidis (2013). The hydraulic component of the reference model is based on the approach proposed by Fuentes and Triantafyllidis (2013), which can capture the hysteretic behaviour of soil during the wetting and drying processes.

The Normal Consolidation Line (NCL) of unsaturated soils depends on the degree of saturation S_w (Fuentes and Triantafyllidis, 2013). Previous studies have observed that the slope of the NCL increases as S_w decreases, leading to a multiple number of NCLs for varying S_w. These lines eventually converge at higher pressures (Wheeler and Sivakumar, 2000; Sun et al., 2007b; Baille et al., 2023) with an intersection point defined as p_{ref} and e_{ref} as shown in Fig. 1(a). Beyond this intersection point, the NCL does not depend on the degree of saturation and follows the NCL of the saturated soil. The compression index of an unsaturated soil (λ_u) can be written as:

$$\lambda_u = \lambda_{sat} r_s \quad [1]$$

where λ_{sat} is the compression index for saturated soil and $r_s \geq 1$ is a scalar function defined by:

$$r_s = 1 + (r_{s0} - 1)(1 - S_w)^{n_s} \quad [2]$$

where r_{s0} and n_s are material parameters. According to the definition provided, λ_u remains constant during the compression for a specific S_w. However, in hydromechanical models, both variables e and S_w change simultaneously during the isotropic compression under constant suction. As a result, a variable compression index for unsaturated soil λ_u emerge along the compression path. This phenomenon is clearly illustrated in Fig. 1(a). To address this behaviour during the compression, we re-examined the equation for the Bulk modulus K in the reference model. The given equation for bulk modulus is as follows:

$$K = \frac{(1+e)\,p}{\lambda^u (1-Y_0)} \quad [3]$$

where ν is the Poisson's ratio and $Y_0 = (\lambda_u - \kappa)/(\lambda_u + \kappa)$ is the isotropic value of the degree of nonlinearity where κ is the swelling index.

Consider the equation describing the normal consolidation line:

 © DFI International Bruges 2025

$$e_i(p) = e_{ref} - \lambda_u \ln\left(\frac{p}{p_{ref}}\right) \quad [4]$$

where e_{ref} and p_{ref} are the reference void ratio and reference mean effective stress, at which all NCLs for different S_w intersect. Differentiation of Eq. [4] with respect to p is shown below:

$$\dot{e}_i(p) = -\dot{\lambda_u} \ln\left(\frac{p}{p_{ref}}\right) - \left(\frac{\lambda_u}{p}\right)\dot{p} \quad [5]$$

where $\dot{\lambda_u}$ can be derived by differentiating the Eq. [1] with respect to the degree of saturation:

$$\dot{\lambda_u} = \lambda_{sat}\left(\partial r_s / \partial S_w\right)\left(\partial S_w / \partial \varepsilon^v\right)\dot{\varepsilon}^v \quad [6]$$

The well-known constitutive equations under isotropic states and constant suction are as follows:

$$\dot{p} = K(\dot{\varepsilon}^v - \dot{\varepsilon}^p) \quad [7]$$

$$\dot{e} = (1+e)\dot{\varepsilon}^v \quad [8]$$

where $\dot{\varepsilon}^v$ is the volumetric strain rate and $\dot{\varepsilon}^p$ is the hypoplastic volumetric strain rate. By solving Eqs. [5], [6], [7] and [8], the modified equation for the Bulk modulus reads:

$$K = -\frac{(1+e)pB}{\lambda_u\,(1-Y_{0m})} \quad [9]$$

where B is a scalar factor which depends on p, e, S_w, given by:

$$B = 1 + \frac{\lambda_{sat}\left(\partial r_s / \partial S_w\right)\left(\partial S_w / \partial \varepsilon^v\right)}{(1+e)} \log\left(p / p_{ref}\right)\left(1 / OCR\right)^{n_u} \qquad (\text{for } e = e_i). \quad [10]$$

where $B = 1$ for $S_w = 1$ and $B < 1$ for unsaturated states $S_w < 1$. The previous studies found that the effect of suction or degree of saturation can be neglected for overconsolidated states $\mathrm{OCR} > 1$ (Estabragh and Javadi, 2008; Yao et al., 2014; Wu et al., 2019; Liu et al., 2020). Therefore, an additional factor $\left(1/OCR\right)^{n_u}$ is introduced to control the effect of factor B in the Bulk modulus equation for the over-consolidated state. The OCR defined in Eq. [10] can be described using the projected stress p^+ on the isotropic axis ($q = 0$) following the bounding surface equation $F_b \equiv 0$, as shown in Fig. 1(b):

$$\mathrm{OCR} = p_{max} / p^+ \quad [11]$$

where p^+ is the projection of p on the $p - q$ space for the current bounding factor, f_b.

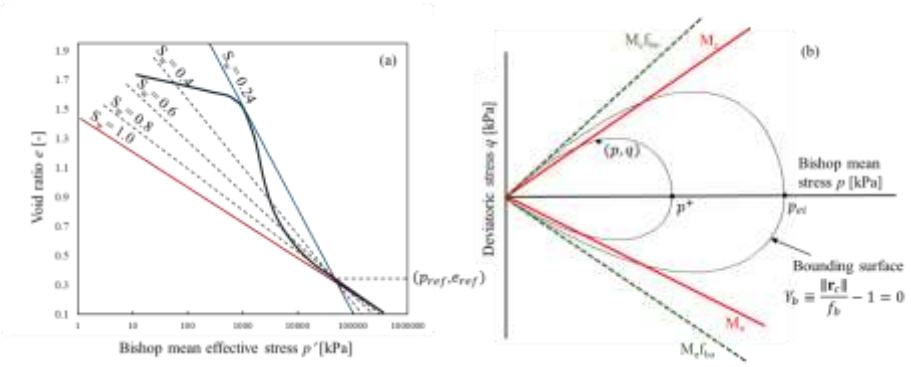


Fig. 1. (a) Variation of degree of saturation S_w during compression, initial state at (e=1.7, S_w = 0.2 and s = 150 kPa) and (b) Projection of p^+ using the bounding surface function $F_b = 0$

 © DFI International Bruges 2025

3. VADILATION OF THE PROPOSED MODEL

The proposed model comprises eighteen parameters, with nine for the hydraulic component and nine for the mechanical component. Hydraulic parameters are calibrated with the use of water retention curves (IWRC) across varied soil densities, while mechanical parameters undergo calibration using triaxial tests on both unsaturated and saturated samples. The detailed calibration procedure of the parameters used for the mechanical model and hydraulic model can be found in Tafili and Machacek (2023) and Fuentes and Triantafyllidis (2013), respectively. The proposed model was coded in FORTRAN in the format of User Defined Material subroutine (UMAT) given by the ABAQUS finite element program. Notably, the temperature inputs are assumed as suction parameters within this framework. Furthermore, the numerical simulations were performed with *INCREMENTAL* DRIVER (Fuentes and Triantafyllidis, 2013a; Niemunis, March 2008).

The accuracy of the proposed model in simulating the hydraulic and mechanical behaviour of unsaturated soils is validated against the experimental data for various stress state conditions: (i) variation of bulk modulus during the wetting-drying process for Bonny silt (Khosravi et al., 2016), (ii) shearing at different suction and mean net stress (P_{net}) for Loess (Garakani et al., 2015)and (iii) wetting at different mean net stress (P_{net}) for Lower Cromer Till (Maswoswe, 1985). The mechanical and hydraulic parameters of each selected soils are dipicted in Table 1 and Table 2, respectively.

Table 1 Mechanical parameters of Bonny silt, Loess and Lower Cromer Till

κ [-]	ν [-]	λ_{sat} [-]	e_{ref} [-]	φ_c [-]	f_{bo} [-]	p_{ref} [MPa]	r_{s0} [-]	n_s [-]	n_u [-]	Soil type
0.02	0.3	0.10	0.35	27	1.3	10	8	3.7	0.7	Bonny silt
0.012	0.35	0.115	0.13	29	1.2	10	3.4	3.7	0.9	Loess
0.015	0.3	0.15	0.15	30	1.3	3.58	4.0	3.7	0.7	Lower Cromer Till

Table 2 Hydraulic parameters of Bonny silt, Loess and Lower Cromer Till

S_{wo}^d/S_{wo}^i [-]	α^d/α^i [-]	n^d/n^i [-]	m_e [-]	κ_w [-]	n_w [-]	Soil type
0.01/0.01	0.045/0.1	1.6/1.7	2.0	0.05	3	Bonny silt
0.085/0.085	0.03/0.035	1.45/1.6	1.5	0.05	3	Loess
0.05/0.05	0.09/0.095	1.4/1.6	1.5	0.05	3	Lower Cromer Till

Variation of bulk modulus during the wetting-drying process

Khosravi et al. (2016) conducted a series of drying and wetting tests at different constant net stresses to investigate the anisotropic shear stiffness of unsaturated Bonny silt specimens. They employed the Resonant-Column Test device to measure the small strain shear modulus during the drying and wetting process at constant P_{net} of 125 and 225 kPa. The matric suction of each sample was initially increased to 70 kPa, followed by a wetting process that reduced the suction to 0 kPa. The experiment results were normalised to compare the simulations with the proposed model ($K/K_{ref} = G/G_{ref}$).

 © DFI International Bruges 2025

Figure 2 (a) and (b) present the Soil Water Characteristic Curve (SWCC) of Bonny silt at p_{net} of 125 and 225 kPa, respectively. The simulation produced by the proposed model adequately predicts the hysteresis behaviour observed in the SWCC, indicating that the hysteresis size is smaller for specimens subjected to higher p_{net} of 225 kPa. Figure 3(a) and (b) illustrate the variation of normalised bulk modulus (K/K_{ref}) at very small strains with suction during drying–wetting cycle at p_{net} of 125 and 225 kPa, respectively. The experiment results reveal a non-linear variation of normalised bulk modulus with suction, with higher normalised bulk modulus observed at the higher p_{net} (225 kPa) compared to lower p_{net} (125 kPa). Additionally, there is a hysteresis behaviour of the normalized bulk modulus with matric suction during the drying and wetting cycles, similar to that observed in the SWCC. Interestingly, the proposed model satisfactorily predicts the characteristics observed in the experiment.

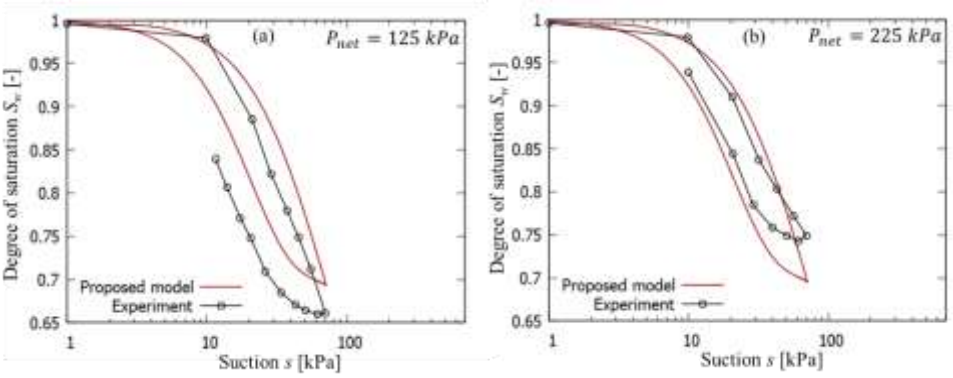


Fig. 2. SWCC of Bonny silt during drying–wetting at constant p_{net} of (a) 125 kPa and (b) 225 kPa

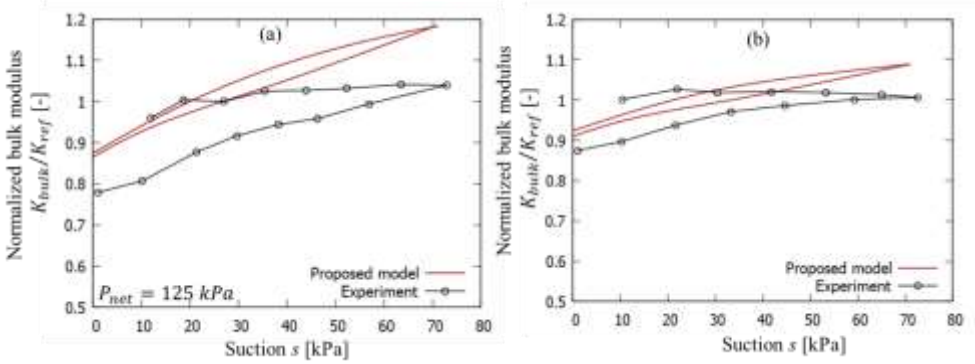


Fig. 3. Variation of normalized bulk modulus (K/K_{ref}) at very small strain with suction during drying–wetting at constant p_{net} of (a) 125 kPa and (b) 225 kPa

Shearing at different suction and mean net stress (P_{net})

Garakani et al. (2015) carried out several collapse tests followed by shearing tests on Loess using a modified triaxial test apparatus. This paper focuses on two shearing tests performed after a wetting-induced collapse test. The initial matric suction of the sample was 750 kPa. To begin, the samples were isotropically compressed to the desired P_{net} of 200 kPa and 400 kPa, and their matric suction was reduced to 0 (saturated state) and 50 kPa by wetting. Consequently, each sample was sheared under these specific stress states. Figure 8 presents the results of the shearing test conducted on Loess, after a wetting process. It also includes the model simulations with different p_{net} of 200 and 400 kPa under a saturated state and a suction level of 50 kPa. It is evident from Fig. 8 that the deviatoric stress q increases with axial strain ε_{axial} at different constant p_{net}, with higher q values observed at higher p_{net}. At a constant p_{net}, the maximum deviatoric stress q for the saturated sample is lower than that

 © DFI International Bruges 2025

of the sample at a suction level of 50 kPa. These results indicate that the proposed model effectively captures the experimental observations.

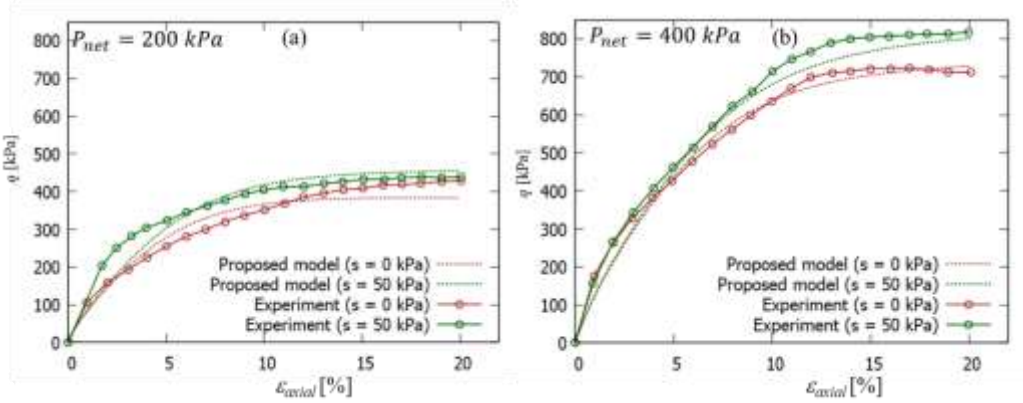


Fig. 4. Variation of deviator stress *q with* axial strain ε_{axial} during the shearing after the wetting process at constant p_{net} of (a) 200 kPa and (b) 400 kPa

Wetting at different mean net stress (P_{net})

The oedometer tests conducted by Maswoswe (1985) on Lower Cromer Till were selected to validate the model under wetting at different P_{net} values. This study considers five oedometer test results, which showed an average initial void ratio of 0.65 and a degree of saturation of 0.45, subjected to wetting at different P_{net} levels of 60, 110, and 220 kPa. Figure 5 shows the volumetric collapse of Lower Cromer Till at different isotropic net stresses together with the predicted simulations using both the proposed model and the reference model. Both models are capable of reproducing the increasing volumetric collapse with increasing P_{net}. However, the proposed model provides more reliable predictions than the reference model.

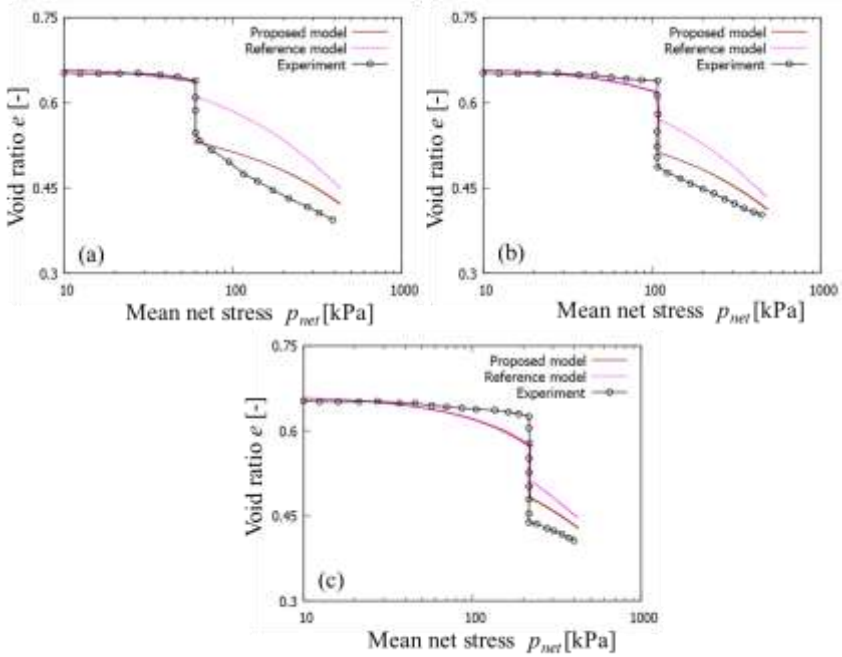


Fig. 5. Volumetric collapse during the wetting process under different isotropic p_{net} of (a) 60 kPa, (b) 110 kPa and (c) 220 kPa

 © DFI International Bruges 2025

4. CONCLUSIONS AND RECOMMENDATIONS

This paper presented an enhanced version of the hydro-mechanically coupled hypoplastic constitutive model proposed by Tafili and Machacek (2023) for the simulations of unsaturated soils at three-dimensional generalized stress space. Two significant advancements were proposed to the model: (i) an improved bulk modulus (K) to account for the effect of the degree of saturation, and (ii) a modification to the overconsolidation ratio (OCR) dependency of the soil. The validation of the proposed model was achieved through experimental results encompassing various stress paths for three different types of clay soils. The simulations revealed that the advancements made in the proposed model enhance the predictive capabilities compared to the reference model. However, some limitations were observed in the proposed model. For instance, small strain effects are not accounted for in the constitutive relations, and residual states of the hydraulic model, such as residual water and air entrapment, are not included in the hydraulic component of the model.

5. REFERENCES

Alonso, E. E., Pereira, J.-M., Vaunat, J., & Olivella, S. (2010). A microstructurally based effective stress for unsaturated soils. *Geotechnique*, *60*(12), 913-925.

Baille, W., Jebeli, A., Tafili, M., Machaˇcek, J., & Wichtmann, T. (2023). Experimental and numerical

investigation of wetting-induced settlements in sandy deposits of open-mine cast. *In: submitted.*

Bauer, E., Tantono, S. F., Cen, W., Zhu, Y., & Kast, K. (2007). Hypoplastic modeling of the disintegration of dry and saturated weathered broken rock. Theoretical and numerical unsaturated soil mechanics,

Buscarnera, G., & Nova, R. (2009). An elastoplastic strainhardening model for soil allowing for hydraulic bonding–debonding effects. *International Journal for Numerical and Analytical Methods in Geomechanics*, *33*(8), 1055-1086.

Duan, X., Zeng, L., & Sun, X. (2019). Generalized stress framework for unsaturated soil: demonstration and discussion. *Acta Geotechnica*, *14*, 1459-1481.

Estabragh, A., & Javadi, A. (2008). Critical state for overconsolidated unsaturated silty soil. *Canadian Geotechnical Journal*, *45*(3), 408-420.

Fredlund, D. G. (2006). Unsaturated soil mechanics in engineering practice. *Journal of Geotechnical and Geoenvironmental Engineering*, *132*(3), 286-321.

Fuentes, W., & Triantafyllidis, T. (2013). Hydro-mechanical hypoplastic models for unsaturated soils under isotropic stress conditions. *Computers and Geotechnics*, *51*, 72-82.

Garakani, A. A., Haeri, S. M., Khosravi, A., & Habibagahi, G. (2015). Hydro-mechanical behavior of undisturbed collapsible loessial soils under different stress state conditions. *Engineering Geology*, *195*, 28-41.

Gholizadeh, E., & Latifi, M. (2018). A coupled hydro-mechanical constitutive model for unsaturated frictional and cohesive soil. *Computers and Geotechnics*, *98*, 69-81.

Grandas Tavera, C. E., Nitsch, A., & Machaček, J. (2022). A 1D Hypoplastic constitutive model for expansive soils. *Acta Geotechnica*, *17*(10), 4313-4331.

 © DFI International Bruges 2025

Gudehus, G. (1995). A comprehensive concept for non-saturated granular bodies. PROCEEDINGS OF THE FIRST INTERNATIONAL CONFERENCE ON UNSATURATED SOILS/UNSAT'95/PARIS/FRANCE/6-8 SEPTEMBER 1995. VOLUME 2,

Hu, R., Liu, H.-H., Chen, Y., Zhou, C., & Gallipoli, D. (2014). A constitutive model for unsaturated soils with consideration of inter-particle bonding. *Computers and Geotechnics*, *59*, 127-144.

Khalili, N., Romero, E., & Marinho, F. A. (2022). State of the Art Report. Advances in Unsaturated Soil Mechanics: Constitutive modelling, experimental investigation, and field instrumentation. *Proceedings of the 20th ICSMGE-State of the Art and Invited Lectures—Rahman and Jaksa, Sydney, Australia*, 1-5.

Khalili, N., & Zargarbashi, S. (2010). Influence of hydraulic hysteresis on effective stress in unsaturated soils. *Geotechnique*, *60*(9), 729-734.

Khosravi, A., Salam, S., McCartney, J. S., & Dadashi, A. (2016). Suction-induced hardening effects on the shear modulus of unsaturated silt. *International Journal of Geomechanics*, *16*(6), D4016007.

Li, X., Lu, D., Lin, Q., Dong, X., & Du, X. (2023). A hydro-mechanical constitutive model for unsaturated soils over a wide saturation range. *Computers and Geotechnics*, *159*, 105475. https://doi.org/https://doi.org/10.1016/j.compgeo.2023.105475

Liu, W.-h., Li, W.-g., Zhang, H.-y., Lin, X.-y., Kong, G.-q., Wang, L., & Hu, P. (2022). A critical state constitutive model for unsaturated structured soils. *Computers and Geotechnics*, *152*, 104993.

Liu, W., Yang, Q., & Sun, X. (2020). Hydro-mechanical constitutive model for overconsolidated unsaturated soils. *European Journal of Environmental and Civil Engineering*, *24*(11), 1802-1820.

Lloret-Cabot, M., Wheeler, S. J., & Sánchez, M. (2017). A unified mechanical and retention model for saturated and unsaturated soil behaviour. *Acta Geotechnica*, *12*, 1-21.

Loret, B., & Khalili, N. (2002). An effective stress elastic–plastic model for unsaturated porous media. *Mechanics of Materials*, *34*(2), 97-116.

Lu, N., Godt, J. W., & Wu, D. T. (2010). A closed-form equation for effective stress in unsaturated soil. *Water Resources Research*, *46*(5).

Mašín, D. (2019). Modelling of soil behaviour with hypoplasticity. *Springer Series in Geomechanics and Geoengineering, Ó Springer Nature Switzerland AG, https://doi. org/10*, *1007*, 978-973.

Mašín, D., & Khalili, N. (2008). A hypoplastic model for mechanical response of unsaturated soils. *International Journal for Numerical and Analytical Methods in Geomechanics*, *32*(15), 1903-1926.

Maswoswe, J. (1985). Stress paths for a compacted soil during collapse due to wetting. *ph. D. Thesis, University of London*, 1-484.

Niemunis, A. (2003). *Extended hypoplastic models for soils* (Vol. 34). Inst. für Grundbau und Bodenmechanik Vienna.

Niemunis, A. (March 2008). *Incremental Driver, user's manual*. University of Karlsruhe KIT, Germany.

 © DFI International Bruges 2025

Rotisciani, G., Desideri, A., & Amorosi, A. (2021). Unsaturated structured soils: constitutive modelling and stability analyses. *Acta Geotechnica*, *16*(11), 3355-3380.

Sun, D., Sheng, D., Cui, H., & Sloan, S. (2007). A density-dependent elastoplastic hydro-mechanical model for unsaturated compacted soils. *International Journal for Numerical and Analytical Methods in Geomechanics*, *31*(11), 1257-1279.

Sun, D. a., Sheng, D., & Xu, Y. (2007b). Collapse behaviour of unsaturated compacted soil with different initial densities. *Canadian Geotechnical Journal*, *44*(6), 673-686.

Tafili, M., & Machacek, J. (2023). Generalized hydro-mechanically coupled hypoplastic constitutive model for unsaturated collapsible soils. *Canadian Geotechnical Journal*(ja).

Wheeler, S., Sharma, R., & Buisson, M. (2003). Coupling of hydraulic hysteresis and stress–strain behaviour in unsaturated soils. *Geotechnique*, *53*(1), 41-54.

Wheeler, S., & Sivakumar, V. (2000). Influence of compaction procedure on the mechanical behaviour of an unsaturated compacted clay. Part 2: Shearing and constitutive modelling. *Geotechnique*, *50*(4), 369-376.

Wray, W. K., El-Garhy, B. M., & Youssef, A. A. (2005). Three-dimensional model for moisture and volume changes prediction in expansive soils [Article]. *Journal of Geotechnical and Geoenvironmental Engineering*, *131*(3), 311-324. https://doi.org/10.1061/(ASCE)1090-0241(2005)131:3(311)

Wu, S., Zhou, A., Li, J., Kodikara, J., & Cheng, W.-C. (2019). Hydromechanical behaviour of overconsolidated unsaturated soil in undrained conditions. *Canadian Geotechnical Journal*, *56*(11), 1609-1621.

Yang, C., Cui, Y.-J., Pereira, J.-M., & Huang, M. (2008). A constitutive model for unsaturated cemented soils under cyclic loading. *Computers and Geotechnics*, *35*(6), 853-859.

Yao, Y., Niu, L., & Cui, W. (2014). Unified hardening (UH) model for overconsolidated unsaturated soils. *Canadian Geotechnical Journal*, *51*(7), 810-821.

Zhou, A.-N., Sheng, D., Sloan, S. W., & Gens, A. (2012). Interpretation of unsaturated soil behaviour in the stress–saturation space, I: volume change and water retention behaviour. *Computers and Geotechnics*, *43*, 178-187.

 © DFI International Bruges 2025

BASE CAPACITY DESIGN FOR PILES IN EXTREMELY WEAK TO VERY WEAK MERCIA MUDSTONE

Hiram M. Goncalves, Mott MacDonald Ltd., London, UK, hiram.menezesgoncalves@mottmac.com, +44 (0)20 8774 2000
Michael Vance, Mott MacDonald Ltd., London, UK, michael.vance@mottmac.com, +44 (0)20 8774 2000
Sarah Pye, Mott MacDonald Ltd., London, UK, sarah.pye@mottmac.com, +44 (0)20 8774 2000
Imran Farooq, Mott MacDonald Ltd., London, UK, imran.farooq@mottmac.com, +44 (0)20 8774 2000

ABSTRACT

The Mercia Mudstone Group (MMG) is the bedrock for a large portion of central and southern England, and often the founding material for infrastructure in the area. The High Speed 2 project, a major inter-city high speed railway line connecting London to Birmingham, offered the opportunity to analyse the behaviour of bored piles founded in the MMG under axial loading. The joint venture between Balfour Beatty and VINCI (BBV), with support from design partners Mott MacDonald and SYSTRA, were awarded the delivery of Lots N1 and N2 covering a 90km stretch, south of Birmingham. This paper covers the results from over 25 pile load tests located between Birmingham and Coventry, focusing on the bearing capacity response of the pile toes within the MMG strata. The pile testing schedule encompassed piles of varying diameter/length and different piling techniques, including variation in temporary support measures and pile opening time. The analyses undertaken considered the impact of construction methodology, geology, and rock quality on load-displacement behaviour. Based on the test results, updated methods for calculating pile base capacity are proposed for extremely weak to very weak MMG. These methods serve to broaden the conventional design methodology and provide potential to optimise design to include effects of construction methodology, opening time, base hardness, and Geological Strength Index (GSI) of strata within 5 diameters below the pile toe. Two methodologies are proposed, dependent on the strength of the MMG; the first is the use of an effective stress approach (for materials closer to extremely weak) following on from the methodology proposed in Markvukaj, S. et al (2023) for calculating shaft resistance, and the second an update on the relationship with Unconfined Compressive Strength (UCS) approach, building on the work of Zhang L. and Einstein H.H (1998) (for materials closer to very weak).

Keywords: piles, axial load test, O-cell, bearing capacity, Mercia Mudstone

INTRODUCTION

The delivery of lots N1 and N2 for the High Speed 2 (HS2) railway project in the UK which cover a 90km stretch is being undertaken by Balfour Beatty VINCI (BBV), with support from design partners Mott MacDonald and SYSTRA. The design of the multiple deep foundations for the scheme included a comprehensive pile testing programme, whose data was used in the back analysis and recommendations for the design of piles founded in the Mercia Mudstone Group (MMG), specifically the bearing capacity response of the pile base, presented in this paper. These piles were founded within either Grade II or Grade I MMG.

The available CIRIA guidance on pile design in MMG (Chandler R.K. and Foster, A. 2001), focuses on shaft friction, with limited reference to methods to estimate base capacity. Further work has been developed regarding pile design methodology in MMG since this publication, through large scale pile load test interpretation, such as Omer, J. R et al. (2003) for a viaduct construction near Cardiff. Omer's back analysis uses traditional plasticity theory (equation 1) from both drained and undrained conditions and concludes on the low reliability of the methodology for base capacity of piles toed in MMG.

$$q_{ub} = (cN_c d_c s_c + \eta \sigma_{vb} N_q d_q s_q + 0.5\gamma D_b N_\gamma d_\gamma s_\gamma) \quad [1]$$

Other methodologies to calculate base capacity in rock that have been derived from pile test back analysis include the work by Zhang L. and Einstein H.H (1998) which is based on a correlation with

 © DFI International Bruges 2025

Unconfined Compressive Strength (UCS), although this database does not specifically cover piles founded in MMG (equation 2).

$$qb = 4.8 * UCS^{0.5} \quad [2]$$

A comprehensive method that captures the complex behaviour of MMG with associated varying degree of weathering, interbedded structure, and transitionary soil/rock zones is needed. This paper proposes a methodology for deriving end-bearing capacity for bored piles founded in extremely weak to very weak MMG, building on both traditional bearing capacity factor and effective stress approaches, as well as wider UCS based methods for piles toed in rock, but also goes beyond conventional design methods by exploring the effects of workmanship, rock quality and weathering within the zone of influence below the base.

SUMMARY OF PILE TESTS

The piling test schedule comprised 25 instrumented sacrificial bored piles constructed and tested in 2020, 2021 and 2023, with varying construction methodology and sizing, the majority being 1200mm diameter, 20m-30m in length, constructed with thin wall casing (TWC) and bentonite support fluid, and tested bi-directionally using an Osterberg cell (O-cell). **Figure 1** shows the test pile locations, indicating the piles were founded in the MMG Sidmouth and Branscombe formations, and **Table 1** summaries key construction and testing information.

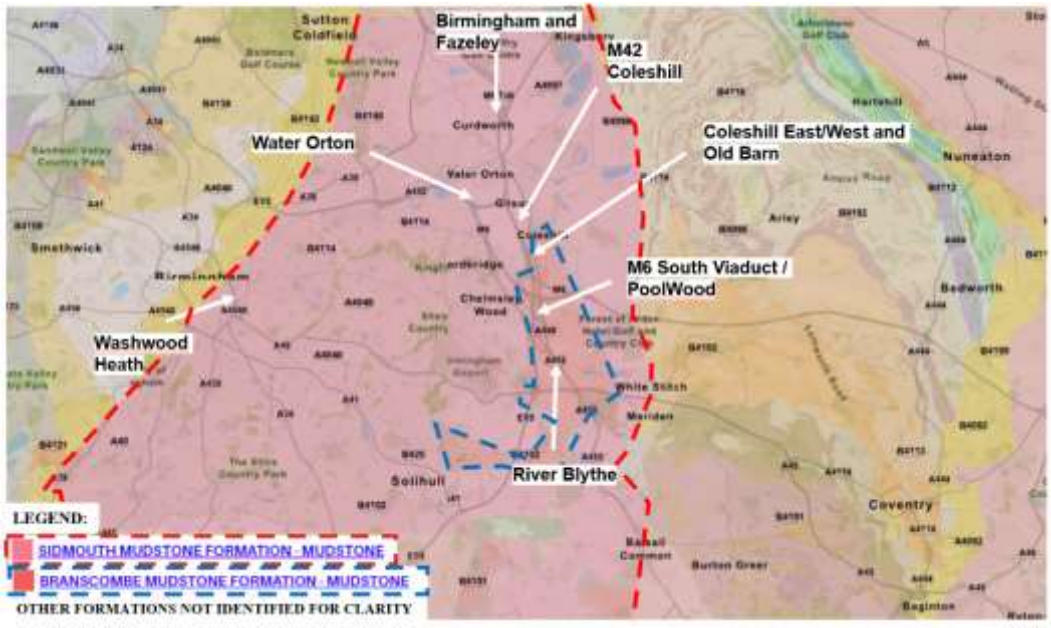


Figure 1. Pile test location (BGS GeoIndex).

Table 1. Summary of test piles

Location		Geometry		Construction				Testing	
Pile ID	Structure	Length (m)	Diameter (mm)	Piling Technique	Temp. support	Base open time (h)	Base hardness	Loading method	Displ. / Pile dia.
WO-03	Water Orton	34.4	1200	Bored	TWC / dry	<12h	1	O-cell	9%
WO-04	Water Orton	32.6	1200	Bored	TWC / dry	<12h	1	O-cell	6%

 © DFI International Bruges 2025

Location		Geometry		Construction				Testing	
Pile ID	**Structure**	**Length (m)**	**Diameter (mm)**	**Piling Technique**	**Temp. support**	**Base open time (h)**	**Base hardness**	**Loading method**	**Displ. / Pile dia.**
GL-01	Coleshill East and West	8.9	900	CFA	N/A	<12h	N/A	Top-Loaded	17%
GL-02	Coleshill East and West	21.3	1200	Bored	TWC / dry	<12h	3	O-cell	17%
GL-03	Coleshill East and West	21.1	1200	Bored	TWC / dry	<12h	2	O-cell	15%
PTP01	Washwood Heath Depot	24.3	1500	Bored	TWC / bentonite	<47h	3	O-cell	5%
M42_04	M42 Coleshill	27.2	1200	Bored	TWC / dry	<12h	1	O-cell	11%
WO-06	Water Orton	28.1	1200	Bored	TWC / bentonite	<46h	1	O-cell	5%
WO-07	Water Orton	27.9	1200	Bored	TWC / water	<22h	1	O-cell	9%
GL_04	Coleshill Old Barn [(2)]	21.0	1200	Bored	TWC / bentonite	<20h	1	O-cell	17%
GL_05	Coleshill Old Barn	21.2	1200	Bored	TWC / bentonite	<44h	1	O-cell	15%
BF01	Birmingham and Fazeley Canal	37.5	1200	Bored	TWC / bentonite	<48h	3	O-cell	17%
BF02	Birmingham and Fazeley Canal	37.0	1200	Bored	TWC / bentonite	<72h	3	O-cell	16%
BF03	Birmingham and Fazeley Canal	37.5	1200	Bored	TWC / bentonite	<24h	3	O-cell	16%
WWH06	Washwood Heath Depot	22.2	1200	Bored	TWC / bentonite	<24h	1	O-cell	4%
A5	M6 South Viaduct	27.7	2100	Bored	TWC / bentonite	<24h	2	O-cell	4%
WWH01	Washwood Heath Depot	11.7	900	CFA	N/A	<12h	N/A	Top-Loaded	17%
WWH02	Washwood Heath Depot	11.7	900	CFA	N/A	<12h	N/A	Top-Loaded	13%
WWH03	Washwood Heath Depot	22.1	1200	Bored	TWC / dry	<12h	1	O-cell	13%
WWH04	Washwood Heath Depot	22.0	1200	Bored	TWC / dry	<12h	1	O-cell	17%
RB-01	River Blythe	8.8	900	Bored	TWC / dry	<12h	1	Top-Loaded	14%
RB-02	River Blythe	8.5	900	Bored	TWC / dry	<12h	1	Top-Loaded	23%
PW_01	Pool Wood	37.8	1200	Bored	TWC / bentonite	<48h	2	O-Cell	4%
PW_02	Pool Wood	37.9	1200	Bored	TWC / bentonite	<24h	2/3	O-Cell	6%
PW_03	Pool Wood	37.8	1200	Bored	TWC / bentonite	<52h	Not available	O-Cell	5%

Notes: Base open time is defined as the time elapsed between final excavation of pile toe and beginning of pile concrete pour. Base hardness test undertaken as per ICE SPERW 2016, prior to concreting.

GEOLOGY, GROUND MODEL AND GEOTECHNICAL PARAMETERS

Geology

The test pile sites are situated within the Knowle Basin, in which the Mercia Mudstone Group forms the upper bedrock unit with a generalised schematic W-E cross section shown in **Figure 2**. The

 © DFI International Bruges 2025

Knowle Basin is a fault bounded basin that developed as part of regional crustal extension and rifting during the late Permian prior to deposition of Permian and Triassic sedimentary infilling.

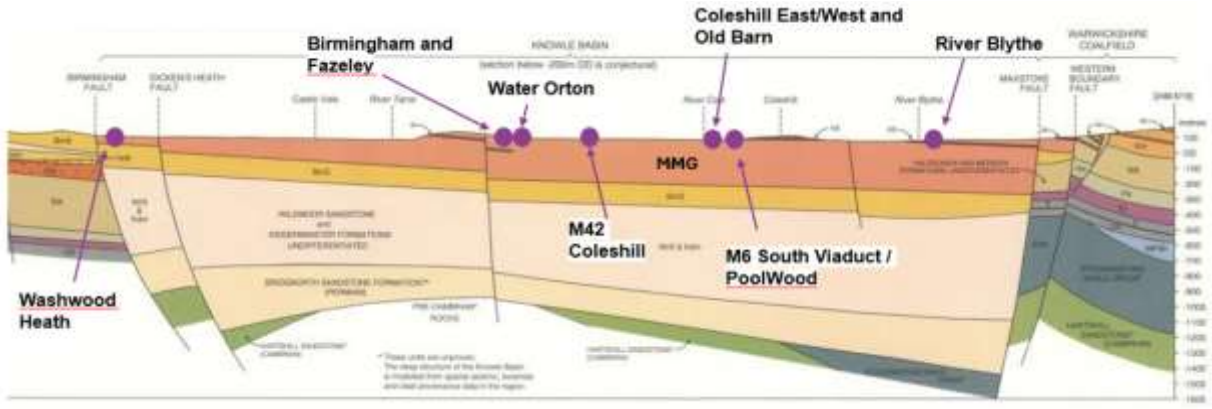


Figure 2. Generalised cross section of geology through the Knowle Basin [British Geological Survey, 1996. Birmingham, England and Wales Sheet 168. Solid and Drift Geology 1:50 000. (Keyworth, Nottingham British Geological Survey)]

The uppermost rock present within the basin is the Mercia Mudstone Group which was deposited through the settling out of clay and silt sized particles in temporary lakes, as sheets of silts/sands from flash floods and as wind-blown dust sticking to mud-flats. These climatic conditions were mainly unchanged throughout the Triassic apart from a sudden change during the late Triassic during which the conditions were much wetter with braided rivers and delta systems leading to the deposition of up to 10m of Arden Sandstone. Drier conditions returned for the remainder of the Triassic period before rising sea levels lead to a marine transgression and deposition of the Penarth Group and Jurassic aged deposits. Chandler, R.J and Forster, A. (2001).

Pleistocene deposits cover much of the Knowle Basin and are a result of at least two periods of glaciation and recession. The glaciation from the older period (Anglian) extends south of the Knowle Basin and the widespread glacial ice cover during the middle Pleistocene resulted in clay rich tills derived of Mercia Mudstone being deposited. A less cold period followed, leading to retreating ice releasing large volumes of water into high energy rivers and onto flood plains. A later cold phase (Devensian) resulted in glaciers extending to approximately the latitude of Birmingham. For the test pile sites, the Devensian deposits are likely to consist of periglacial soils of reworked sands and gravels deposited during the subsequent water release in warmer climate periods. Chandler, R.J and Forster, A. (2001).

All the test pile sites are in Sidmouth Formation of the Mercia Mudstone Group, with the exception of the River Blythe and Pool Wood sites which are founded in the Branscombe Formation. The Branscombe is formed by similar depositional processes to that of the Sidmouth but is slightly younger. The Washwood Heath site is close to the edge of the basin which is more susceptible to lithological variation as well as increased unpredictability of weathering due to faulting. The northern most test site is the Birmingham and Fazeley canal site and, although founded in the Sidmouth Formation, appears to have a different geological setting compared to the other sites, due to thick glacial deposits around the site.

Ground model and Geotechnical parameters

At all pile load test locations site-specific ground investigation and in-situ and laboratory testing were used to define ground models and geotechnical parameters for the pile capacity back analysis. In the

 © DFI International Bruges 2025

specific case of parameters for determining base capacity, the data from the closest borehole to the pile test that was within the zone of influence of the pile toe (5 pile diameters below toe) was considered.

Table 2 summarizes key parameters interpreted, including Unconfined Compressive Strength (UCS), which was either measured directly or correlated from Point Load tests (PLT) (using correlations considering project wide data), and Geological Strength Index (GSI), derived from Rock Mass (RMR_{1989}) (Hoek E. et al 1995). Discontinuity spacing and condition were scored in a discontinuity log whilst the Rock Quality Designation (RQD) was defined from engineering log records. All data sets were validated against field engineering descriptions, core logs and photographs and borehole description. Discontinuity persistence in the horizontal plane cannot be reasonably assessed through core logs, hence were set as a common median rating for 3m to 10m (R=2 rating). This approach puts more influence on other parameters. Groundwater and discontinuity orientation were set to completely dry (R=15) and very favourable (R=0) respectively, as per Hoek E. et al conversion criteria from RMR_{1989} to GSI.

Any relevant variation in strata close to the pile toe was recorded, including hard siltstone/sandstone bands (PTP01), soft clay layers (GL2, BF01, BF03, WWH06, A5, WWH01, WWH02, WWH03), or significant zones of core loss (GL05, RB01, RB02). Moreover, any effect of partial embedment (<3 pile diameters) into the MMG for pile tests GL04 and GL05 was also considered in the back-analysis.

Table 2. Key base capacity parameters

Pile ID	UCS (MPa)	RQD (%)	GSI	Pile ID	UCS (MPa)	RQD (%)	GSI	Pile ID	UCS (MPa)	RQD (%)	GSI
WO-03	3	90-100	60 - 70	WO-07	1	90-100	75 - 80	WWH01	0.8	0-25	40 - 45
WO-04	3	90-100	60 - 70	GL_04	0.6	50-75	40 - 45	WWH02	0.8	0-25	40 - 45
GL-01	0.6	50-75	40 - 45	GL_05	0.6	50-75	40 - 45	WWH03	3.5	25-50	40 - 45
GL-02	0.8	25-50	40 - 45	BF01	2.5	50-75	45 - 50	WWH04	3.5	50-75	40 - 45
GL-03	2	50-75	40 - 45	BF02	2.5	50-75	45 - 50	RB-01	0.6	0-25	35 - 40
PTP01	3	50-75	45 - 50	BF03	2.5	50-75	45 - 50	RB-02	0.6	0-25	35 - 40
M42_04	4	90-100	50 - 55	WWH06	3.5	25-50	40 - 45	PW_01	1.8	25-50	45 - 50
WO-06	1	90-100	75 - 80	A5	2.3	90-100	50 -55	PW_02	1.8	50-75	45 - 50
								PW_03	1.8	50-75	45 - 50

CONSTRUCTION RECORDS AND WORKMANSHIP

The effects of construction methodology and quality of workmanship were assessed based on the information from:

1. pile integrity tests through crosshole sonic logging and Thermal Integrity Profiling (TIP);
2. piling construction records and recorded anomalies;
3. temporary support technique, and support fluid type;
4. base open time;
5. water ingress and borehole collapse (if any);
6. concrete overbreak; and

 © DFI International Bruges 2025

7. base hardness.

None of the test pile construction records recorded any borehole collapses that could increase pile diameter or lead to loose material accumulation at the pile base. The construction records for WO03, WO04, M4204, WO06, WO07, WWH03 and WWH04 recorded significant water ingress, which could lead to a potential softening of the base response; and the records for GL01, GL02, WWH01, WWH02, RB01, and RB02 recorded a concrete overbreak in excess of 20% typically distributed along the pile shaft, with the exception of RB01 and RB02 where an increased diameter was indicated close to the pile toe in the TIP testing.

LOAD VS DISPLACEMENT BEHAVIOUR AND DATA EXTRAPOLATION

The test piles were typically fully instrumented with a load cell, 2 pairs of diametrically opposed strain gauges mounted on the pile cage spaced at regular intervals, and telltales (rod extensometers) installed at multiple levels. The vertical compression pile load testing procedure was a maintained load test, typically undertaken to displacements in excess of 10% pile diameter. Concrete Young's modulus was converted from unconfined compressive strength tests on cube samples (EC2 and ACI correlations), and for O-cell tests also from strain gauges located immediately either side of the O-cell through a method outlined by Fellenius, 2020.

Vertical strain data from both telltales and strain gauges was assessed in terms of reliability, removing defective readings, and used to define load and skin friction distribution curves with depth, as well as the load transferred to the pile base. Displacement vs hold time curves were defined for each load step, and through use of a hyperbolic function, the displacements for infinite load durations were estimated (England M. 2005). The back analysed ultimate pile base capacity was then defined as the load measured at the pile base at a displacement of 10% of the pile diameter, following Eurocode 7 "failure" criterion for piles in compression.

In the case of some of the piles tested using an O-cell, failure was reached for the portion above the loading cell before sufficient movement at the pile base to allow for an interpretation of ultimate base capacity to be undertaken. However, for test piles where a minimum displacement of 4% of pile diameter was reached (but movement had not reached 10% displacement), an extrapolation was performed to estimate the ultimate pile capacity (using Chin-Kondner, Hansen 80%, and Decourt methods from Fellenius B.H. 2020). Extrapolations for movements smaller than 4% of pile diameter were attempted, however the reliability of the methodology for such cases was deemed unacceptably low.

END BEARING BACK ANALYSIS

Figure 3 shows the back analysed pile ultimate base capacity from the test data (qb, testing @10%D) plotted against estimated capacity from UCS data (qb, design UCS) following the Zhang L. and Einstein H.H (1998) formulation (equation 2). A proposed empirical factor (ψ) to account for effects from workmanship, weathering, and rock quality below the pile toe (equation 3) is incorporated on the figure.

$$qb = 4.8 * \psi * UCS^{0.5} \quad [3]$$

Figure 3 can be divided into design "overprediction" and "underprediction" zones, above and below the ψ=1 line, where back analysed test data is lesser or greater than base capacity estimated from equation 2, respectively. Base capacity estimates from equation 3 for ψ=0.5, and ψ=2.0 are also shown to illustrate the range of deviation between test back analysed and UCS estimated base capacity. The data highlights the interpreted GSI range for the MMG strata within the zone of influence beneath the

 © DFI International Bruges 2025

pile toe and is therefore an indication the influence of rock quality on base capacity. The plot also shows base open time between finish of excavation and start of concreting, and base hardness test result recorded, which could signal the potential for any base softening, and provide an indication of the stiffness response of the base.

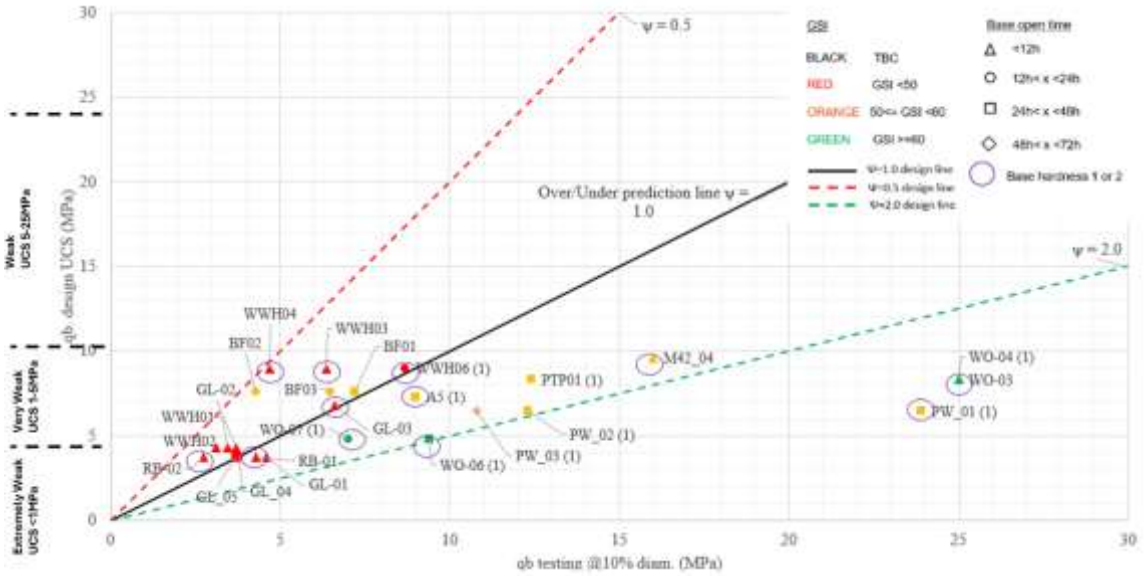


Figure 3. Comparison of design base capacity and back-analysed base capacity

The testing data indicates that for extremely weak MMG the ψ =1.0 design line would be appropriate for estimating base capacity, given good agreement with the design line, and data plots mostly at/near the "underprediction" zone. Significant water ingress and interbedded clay layers below toe at WWH03 and WWH04; large base opening time of >72h at BF02; and the presence of clay layers at/below WWH01 and WWH02 pile toes, could explain the lower base capacities for these test piles when compared with that predicted by design.

The pile load test data for upper range of very weak MMG indicates a modifying factor ψ =1 can considerably underestimate the pile capacity and suggests ψ factors above unity might be applicable. The majority of test data for very weak MMG which plots within the "underprediction" zone relates to GSI>50 and base hardness is 1 or 2 indicating the influence of rock quality, and base stiffness response on the selection of a ψ factor above unity.

Figure 4 shows the back analysed pile ultimate base capacity from the test data (qb, testing @10%D) plotted against estimated capacity using a bearing capacity factor (N_q) and effective stress at pile toe (equation 4). The data suggests that for extremely weak to very weak MMG with UCS<2MPa, an effective stress approach also provides a reasonable estimate of base capacity when using a N_q of 22.

$$qb = N_q * \sigma'_v \quad [4]$$

 © DFI International Bruges 2025

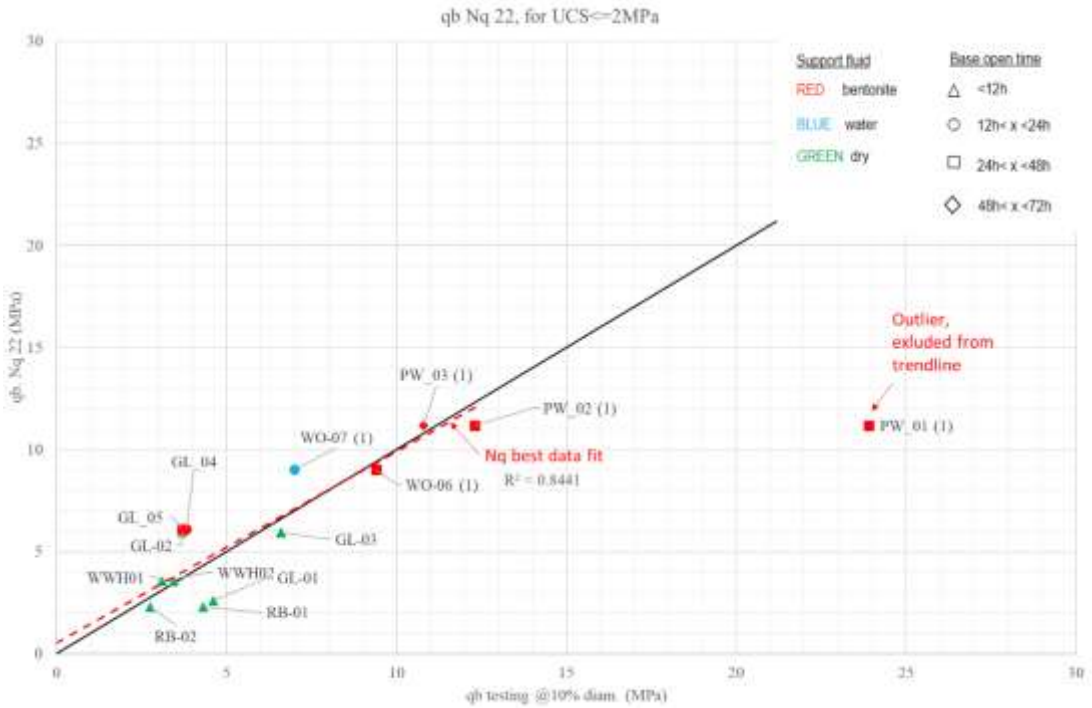


Figure 4. qb design Nq vs qb testing (for MMG at toe with UCS<2MPa)

The methodology detailed by Fleming, 1992 was used to estimate pile loading curves to infinite displacements. **Figure 5** shows the back analysed pile base capacity factor N_q at infinite displacement, plotted against vertical effective stress. The data plots within the range of estimated N_q factors from widely used effective stress-based methodologies: Fleming (2009) and Berezantzev (1961). The data indicates that for very weak to extremely weak MMG with UCS<2MPa, the methodology proposed by Fleming (2009) for a friction angle of $\varphi_{cv}=27^o$ and relative density I_d between 25% and 50% provides a reasonable estimate for pile base capacity at infinite displacement.

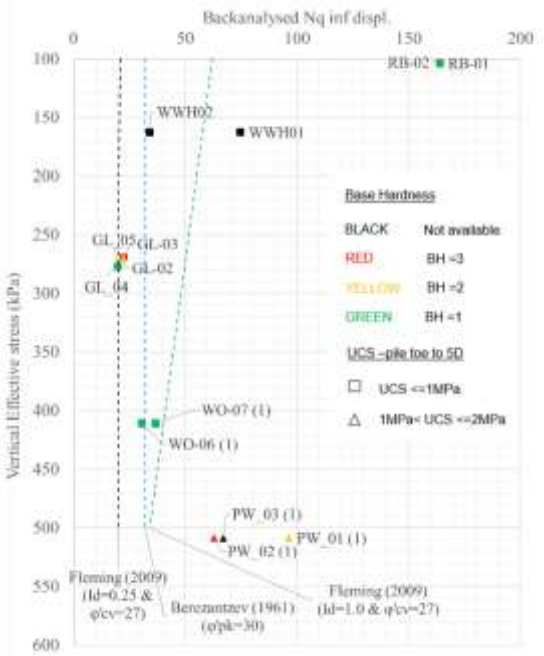


Figure 5. qb Nq backanalysed vs effective stress (for MMG at toe with UCS<2MPa)

 © DFI International Bruges 2025

The data from the pile tests at Poolwood and River Blythe plots within the expected range for pile ultimate base capacity estimates (at 10%D) in **Figure 4**, however, these tests indicate a considerably higher bearing factor N_q for pile capacity at infinite displacement in **Figure 5**, when compared to the whole dataset. These test piles from the schedule are founded in the Branscombe formation, which could indicate a specific behaviour of piles toed within the formation of continuing increase in base capacity with displacements above 10% pile diameter.

The pile test data was also analysed to isolate any effect of the use of bentonite or the longer opening times (compared to standard practice) on base response. **Figure 6** shows the potential effect of bentonite and base opening time on back analysed pile ultimate capacity respectively. These show a possible reduction in base capacity for opening times beyond 48 hours, whereas no significant effect can be identified on base capacity related to the use of bentonite to maintain bore stability.

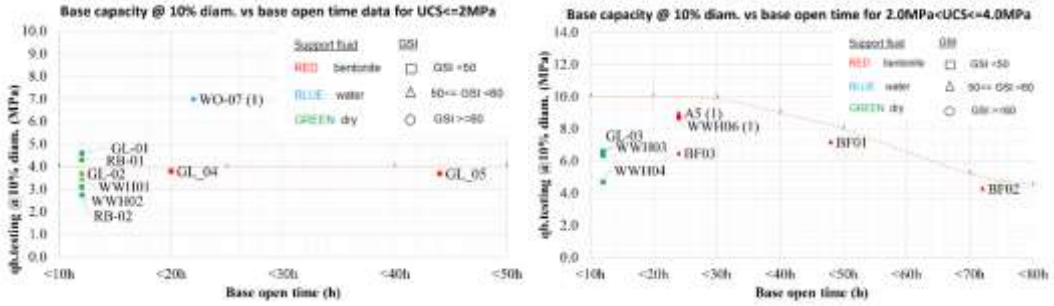


Figure 6. qb, testing vs base open time, for UCS<2MPa (left) ; and 2MPa<UCS<4MPa (right)

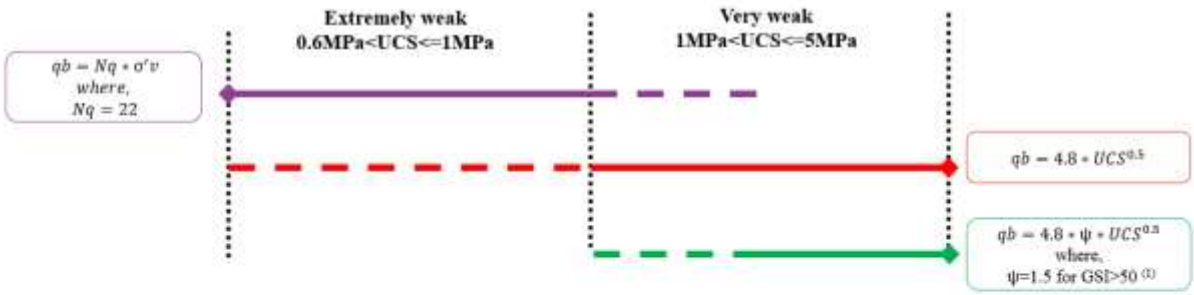
CONCLUSIONS

The following conclusions were reached from the analysis described in this paper:

1) The design Methodology from Zhang L. and Einstein H.H (1998) provides a reasonable but cautious match to observed/back analysed end bearing response, especially for piles founded in extremely weak MMG; and indicates a typical design limit of 10MPa can underestimate pile capacity.
2) Base opening time greater than 48 hours appears to produce some softening of base response and therefore diminishing effect on base capacity. Up to 48h no discernible reduction in base capacity is identified when bentonite is used.
3) The use of bentonite as a support fluid appears (without the influence of opening time) to have either beneficial or limited effect on pile loading performance.
4) The presence of higher quality rock at pile toe, and enforcement of thorough base cleaning indicates a stiffer base response. A modifying factor of ψ=1.5 could be justified if GSI >50%, and base hardness of 1 or 2 is achieved, for piles toed in MMG rock. However, an appropriate GI site indicator that can capture base response needs to be identified.
5) The use of effective stress approach for strata where UCS<2MPa provides reasonable reliability and could be used alongside methods that relate bearing capacity to UCS; in particular, the use of an effective stress approach for extremely weak MMG mitigates against the difficulties in obtaining rock samples that enable UCS testing to be undertaken.

The conclusions above can be summarized in the proposed methodology for base capacity (qb; at displacements of 10% of pile diameter) for extremely weak to very weak MMG I/II:

 © DFI International Bruges 2025



Notes:
1) ψ=1.5 recommendation is based on a well cleaned pile base achieving a 1 or 2 grade in hardness test;
2) Base capacities are for a maximum 48h base open time, beyond which some reduction should be considered;
3) UCS and GSI are defined for strata within zone 5 times pile diameter below pile toe;
4) Vertical effective stress (σ'v) is defined at the pile toe depth for a characteristic groundwater level;
5) The proposed methodology applies only to Mercia Mudstones. The application to other mudstone formations should be validated through extensive pile test data on such formation.
6) Engineering judgment is especially required when defining design qb from UCS and/or effective stress methods, for MMG close to strength classification boundaries, where represented by dashed coloured lines.

ACKNOWLEDGMENTS

The authors would like to thank the Integrated Project Team: SYSTRA, BBV and SB3 delivering the pile testing programme for HS2, and Socotec and Fugro's involvement in pile testing. The contribution of the following Mott MacDonald colleagues who have contributed to the analysis undertaken is also acknowledged: Mubarak Mohammed, Javied Iqbal, and Anthony O'Brien.

REFERENCES

1. Berezantzev, V. G.; Khristoforov, V. S. and Golubkov, V. N. (1961). Load bearing capacity and deformation of piled foundations. In Proceedings of the 5th International Conference of the International Society for Soil Mechanics and Foundation Engineering. Paris: ISSMFE, vol. 2, pp. 11–12.
2. Chandler, R.J and Forster, A. (2001). Engineering in Mercia mudstone. CIRIA C570. 2001.
3. England M. (2005) A Conservative Method of Analysis of test results from bi-directional static load tests
4. Fellenius, B. H. (2020) – Basics of Foundation Design (Red book)
5. Fleming, K.; Weltman, A.; Randolph, M. and Elson, K. (2009). Piling Engineering. 3rd Edition. Taylor and Francis, Oxon.
6. Fleming W. G. K. (1992) – A new method for single pile settlement prediction and analysis. Geotechnique 42, No 3, 411-425.
7. Hoek, E.; Kaiser, P.K.; Bawden, W.F. Support of Underground Excavations in Hard Rock; AA Balkema: Rotterdam, The Netherlands, 1995
8. ICE Specification for Piling and Embedded Retaining Walls (SPERW) , Third Edition, London, UK, 2016.
9. Markvukaj, Stephanie and Farooq, Imran and O'Brien, Anthony and Pye, Sarah and Vance, Michael. (2023). Shaft friction design for piles in extremely weak to weak Mercia Mudstone. High Speed Two (HS2): Infrastructure Design and Construction (Volume 3) (pp. 17-41).
10. Omer, J.R., Robinson, R.B., Delpak, R. et al. Large-scale pile tests in Mercia mudstone: Data analysis and evaluation of current design methods. Geotechnical and Geological Engineering 21, 167–200 (2003).
11. Zhang L. and Einstein H.H, End Bearing capacity of Drilled Shaft in Rock, Journal of Geotechnical and Geoenvironmental Engineering, 1998, volume 124, p574-584

 © DFI International Bruges 2025

DISPLACEMENT PILE GROUP EFFICIENCY ASSESSMENT FOR A TECHNICALLY AND ECONOMICALLY SUSTAINABLE DESIGN OF PILE GROUPS IN NON-COHESIVE SOIL

Felix Mitlmeier, University of Stuttgart, Institute for Geotechnical Engineering, Germany,
+49 (0) 711 685-62071, felix.mitlmeier@igs.uni-stuttgart.de

Christian Moormann, University of Stuttgart, Institute for Geotechnical Engineering, Germany,
+49 (0) 711 685-62437, christian.moormann@igs.uni-stuttgart.de

ABSTRACT

Motivated by field investigations on driven precast piles, this paper presents the results of large-scale physical test series involving a 3 x 3 group of displacement piles with a pile spacing of 3·D in medium-dense sand. Additionally, a comparable single pile test was performed to enable direct comparison under identical conditions. Three of the group piles were equipped with strain gauges to evaluate group effects on the mobilization and distribution of skin friction and tip resistance. Besides, pile head forces were measured to determine the load distribution inside the pile group. Soundings with the dynamic PANDA®-penetrometer in the soil continuum within the pile group were performed to investigate effects due to pile installation like change of void ratio and stress status. Based on the findings from the test program, various types of settlement-related efficiencies for design purposes can be derived, including 3 x 3 pile group efficiency, group pile efficiencies, as well as skin and tip efficiencies.

Keywords: displacement piles, pile groups, group efficiency, axial behaviour, model test, calibration chamber

INTRODUCTION

The axial load-bearing and settlement behaviour of pile groups largely depends on the interaction between the foundation piles. Geotechnical and geometrical boundary conditions, such as soil conditions and pile spacing, significantly influence the pile-pile interaction. Consequently, the settlement-dependent axial resistance of group piles, depending on their position within the group, can differ distinctly from that of an isolated single pile. Unlike bored piles, the group bearing behaviour of displacement pile groups has remained largely unclear. For instance, effects such as changes in status variables like void ratio and stress status caused by pile installation in non-cohesive soils are currently not considered in the design. An important key indicator for the impact on the pile behaviour is the group efficiency η, as defined by Vesić (1969) and Valsangkar & Meyerhof (1983), which is nominally independent of the settlements of both the pile group and the single pile, and is defined as follows:

$$\eta = \frac{Q_g}{n\,Q_s} \qquad [1]$$

where Q_g is the axial resistance of the pile group, n is the number of piles in the group, and Q_s represents the axial resistance of a single pile.

 © DFI International Bruges 2025

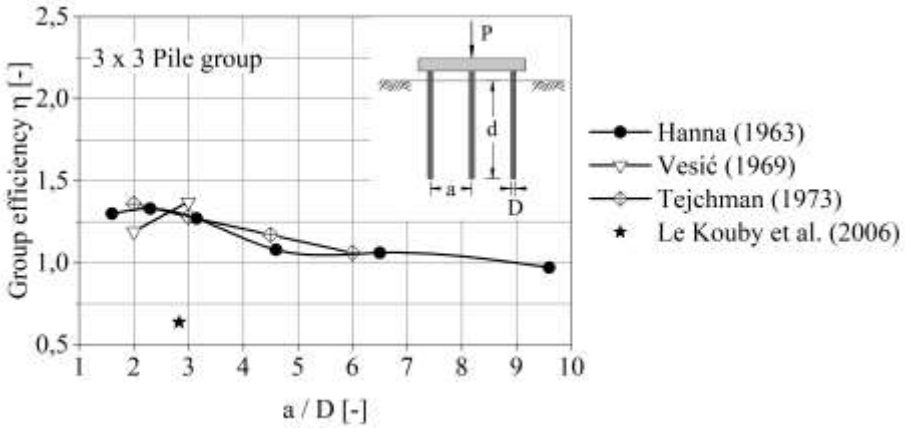


Fig. 1. Group efficiency of 3 x 3 jacked displacement pile groups in medium-dense sands from 1g-model tests

Most findings on the group efficiency of displacement pile groups in non-cohesive soils are based on model tests (e.g. Hanna 1963, Vesić 1969, Tejchman 1973, Le Kouby et al. 2006), field model tests (e.g. Kézdi 1957, Ekström 1989, Phung 1993) or field tests (e.g. Briaud et al. 1989). Figure 1 presents the group efficiency η of 3 x 3 displacement pile groups in medium-dense, non-cohesive soils, all conducted in 1g-model tests of varying scales. Hanna (1963) tested pile groups consisting of round wooden piles (D = 9.8 mm, d = 30 cm) in sand, showing that η consistently exceeded 100 %, with a maximum at a/D = 2.3. Large-scale model tests were performed by Vesić (1969) using round aluminum model piles with a diameter of D = 100 mm and an embedment length of d = 152 cm. Instrumented with strain gauges to enable the separate evaluation of shaft and base resistance, Vesić demonstrated that the higher bearing capacity of displacement pile groups, compared to an equivalent number of single piles, is primarily due to an increase in the skin friction of the group piles, while the tip resistance remains nearly unaffected. In his experiments the group efficiency reaches a maximum value of 1.37 at a spacing of 3·D. Tejchman's (1973) tests with pressed-in square reinforced concrete piles (B = 35 mm, d = 60 cm) confirmed Hanna's (1963) results, showing a maximum efficiency at a/D = 2. In contrast to these researchers, Le Kouby et al. (2006) reported a significantly lower group efficiency of η = 0.64 in a pile group test using metallic model piles (D = 20 mm, d = 50 cm) at a spacing of 2.8·D in a calibration chamber, where the chamber-to-pile ratio ($D_{chamber}$ / D_{pile}) was 26.

Although the overall trend in Figure 1 is clear and derivable, several key questions arise regarding this topic, which are prioritized in this paper:

- What group efficiency can be achieved with a 9-pile group at a pile spacing of 3·D?
- What is the load-settlement behaviour of the respective group piles in comparison to that of a single pile?
- What proportion of the load transfer is due to skin friction and end bearing in group piles compared to individual piles?
- Are there any detectable compaction effects resulting from the installation of group piles?

EXPERIMENTAL SET-UP

The pile group and single pile test were carried out in the IGS Calibration Chamber (Fig. 2), where vertical stress can be applied and controlled. The horizontal boundaries of the test container can be regarded as rigid. Hence, the horizontal stress state is a result of the sand density and applied vertical stress. Conducted in air-dried Berlin Sand, the tests involved medium-dense packing and a vertical surface load of 200 kN/m². The artificially poured sand body measures 1980 x 1980 x 1400 mm³. This sand volume is also used to identify the global soil density. To indirectly determine the soil density after consolidation of the calibration chamber and due to installation of the group piles, soundings are performed using the dynamic cone penetrometer PANDA® (Escobar et al. 2016) with 2 cm² cones.

 © DFI International Bruges 2025

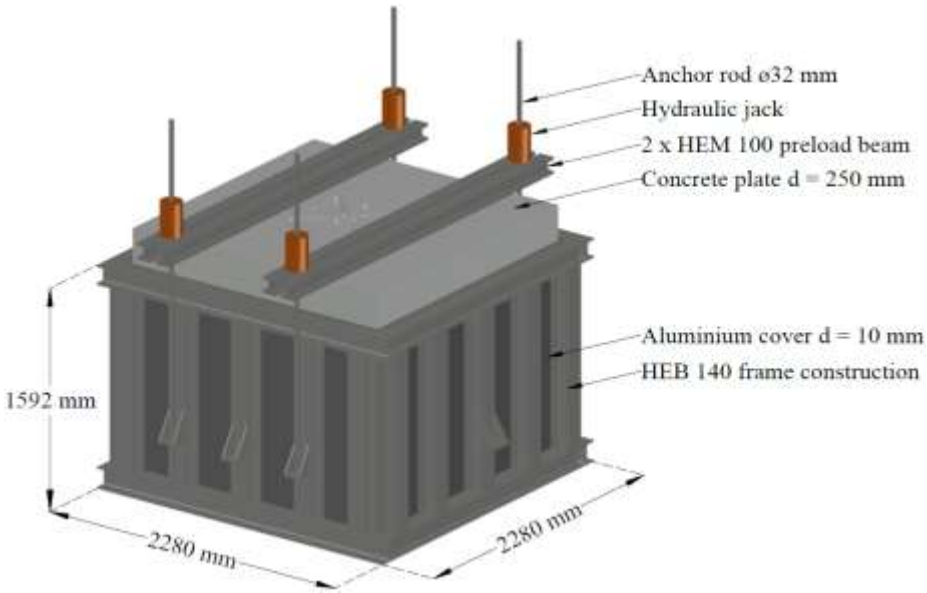


Fig. 2. Composition of the IGS Calibration Chamber (Mitlmeier & Moormann 2024)

Using driven precast piles as prototypes, the model piles have been scaled (Langhaar 1951) to represent both the axial loading behaviour of a pile (Ovesen 1979, Sedran et al. 2001) and the dynamic behaviour of a pile during driving (Alves et al. 2008). The model piles have a circular section, flat tips, are made of aluminum with a smooth surface, and measure D = 40 mm and d = 75 cm. A chamber-to-pile ratio of 50 and a distance of 16·D from the pile base to the chamber bottom are maintained to minimize boundary effects (Foray 1991). The instrumentation of three model piles (center, edge, and corner piles, see Fig. 3 a) with strain gauges enables the separation of the piles' axial resistance into skin friction and tip resistance.

EXPERIMENTAL PROCEDURE

After preparing the medium-dense soil mass (I_D = 38 %) and allowing a dwell time of approximately 18 hours, the soil body is subjected to a corresponding surface load of 200 kN/m². For the pile group and single pile test presented here, the ratio of horizontal to vertical effective stress, measured at mid-height of the calibration chamber, was K_0 = 0.45 ± 0.02. Subsequently, soundings S1 and S2 were performed at a distance of 12·D from the later-installed pile group using a PANDA® probe. The model piles are then hammered, vertically guided, with a theoretical driving energy of 22.5 N·m per blow through holes in the concrete plate into the sand (with a driving weight to pile weight ratio of 2:1). A symmetrical installation order, designated as C1 SYM, comparable to Le Kouby et al. (2016)'s tests with 5-pile groups, was used for the group piles (Fig. 3 b): first the center pile P1 was installed, followed by the four edge piles (P2 – P5), and finally, the four corner piles (P6 – P9). Residual forces from pile driving were negligible in these experiments; thus, after all group piles were installed, the

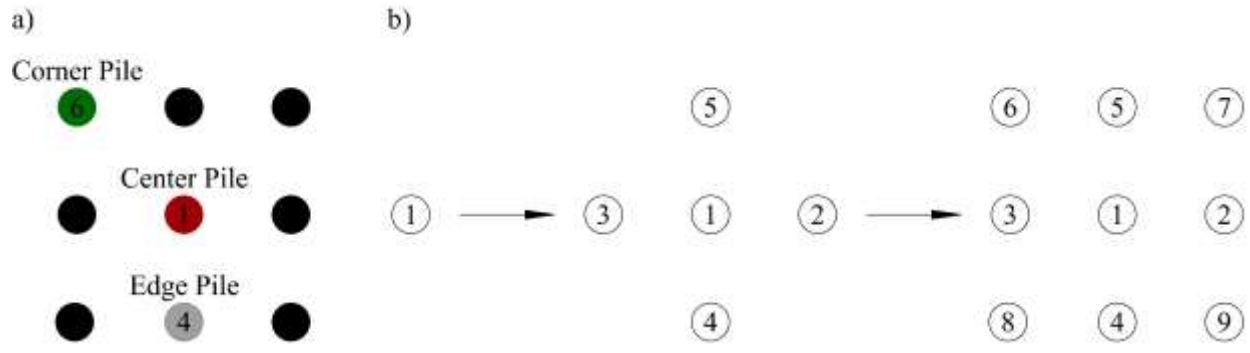


Fig. 3. a) Group pile definition; b) Installation order C1 SYM

 © DFI International Bruges 2025

strain gauges of the instrumented model piles were reset to zero. Then, the load test of the pile group was prepared. Force transducers were mounted on the pile heads, and a rigid pile cap with three vertical and two horizontal displacement sensors was assembled, allowing for the identification of the individual settlement of each group pile.

As recommended by DGGT (2013), two load cycles were applied as part of the loading pattern (see Fig. 4): the first load cycle reaches 50% of the final test load P_p, and after a holding time of 1 hour, unloading and reloading phases follow until the final test load P_p is approached. The load was applied using a force-controlled hydraulic system and a single hydraulic press. The complete set-up during the pile group test is shown in Figure 5. Subsequent to the pile group loading, the pile cap was dismantled, and additional soundings were performed: S3 and S4 at a distance of 12·D from the pile group, aiming to prove – by comparing with S1 and S2 – that no change in soil density occurred due to pile installation in the more distant layers and that there was no influence from the horizontal and vertical chamber boundaries. Soundings S5 to S15 were performed to detect any compaction, loosening, or unaffected zones in the pile group area due to pile installation.

The unaffected single pile was installed and tested in a separate experiment with the same soil properties and subjected to a load of $P_{p,single} = 1/9 \cdot P_{p,group}$.

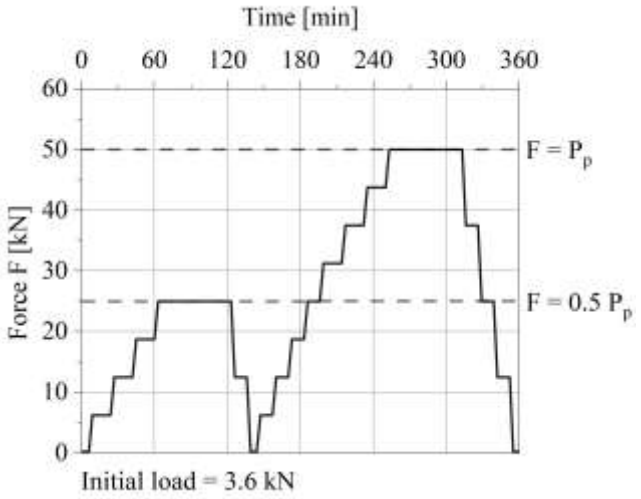


Fig. 4. Static axial load program for the pile group test, following the guidelines of DGGT (2013)

EXPERIMENTAL RESULTS



Fig. 5. Static axial load test of a 3 x 3 displacement pile group with a 3·D pile spacing conducted in the IGS Calibration Chamber

 © DFI International Bruges 2025

The hammer blow count for 5 cm of penetration and the theoretical energy sum for the group piles and the single pile are plotted in Figure 6. Focusing on the theoretical energy sum $\sum W_{theor.}$, a clear trend can be observed: The center pile, installed first, required 2542.5 N·m of energy to reach the final penetration depth. The edge pile, installed second, showed a similar energy requirement of 2632.5 N·m, indicating no significant compaction in the medium-dense sand at a distance of 3·D from the center pile. This hypothesis is supported by the fact that the single pile, installed in a separate specimen, required the same amount of energy as the edge pile (2632.5 N·m). However, the corner pile, which was installed in the influence zone of two edge piles (P5 and P3, see Fig. 3b), required significantly more driving energy (2880 N·m) to reach the final penetration depth. This suggests that the two neighboring edge piles compacted the sand in that area.

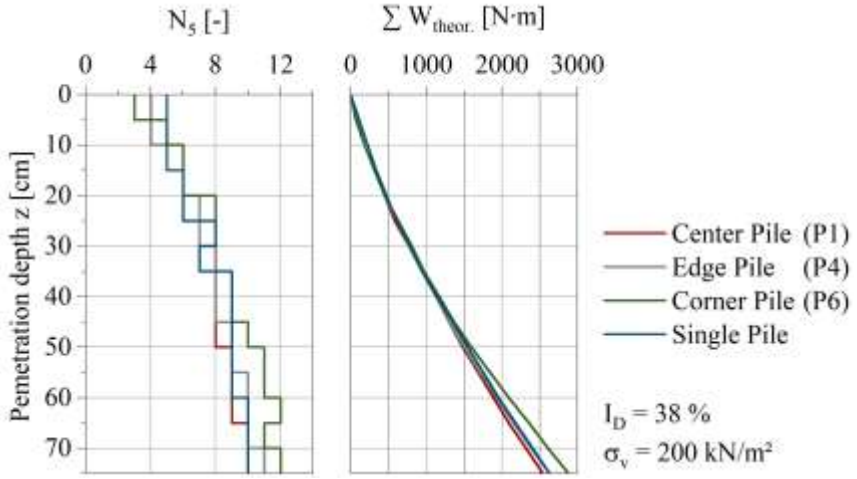


Fig. 6. Drivability versus penetration depth (number of blows, N_5) and theoretical energy sum $\sum W_{theor.}$ versus penetration depth for the center pile, edge pile, corner pile and single pile, $K_0 = 0.45 \pm 0.02$

For the subsequent analysis of the piles' load-bearing behaviour, settlement-related axial resistances and settlement-related group efficiency $\eta(s)$, as defined by DGGT (2013), were used:

$$\eta(s) = \frac{Q_g(s)}{n\, Q_s(s)} \qquad [2]$$

where $Q_g(s)$ is the axial resistance of the pile group at mean settlement, n is the number of piles in the group, and $Q_s(s)$ is the axial resistance of a single pile at mean settlement.

For the Ultimate Limit State (ULS), the axial resistance is evaluated at a settlement s = 0.1·D = 4 mm (DGGT 2013), while for Serviceability Limit State (SLS), a settlement s = 0.025·D = 1 mm is used for the model tests.

Fig. 7 (left) shows the load-displacement curve for both the 9-pile group and nine unaffected single piles, demonstrating a beneficial effect on the load bearing behaviour for the pile group. Under service load conditions, the 9-pile group with η (s = 0.025·D) = 1.08 already shows a positive group effect. At a settlement of s = 0.1·D, the group efficiency increases to η = 1.24, indicating a significantly better bearing capacity for the displacement pile group with a 3·D spacing compared to the equivalent number of single piles. This result shows good agreement with previous research: Hanna (1963) (η = 1.27), Tejchman (1973) (η = 1.26) and Vesić (1969) (η = 1.37).

 © DFI International Bruges 2025

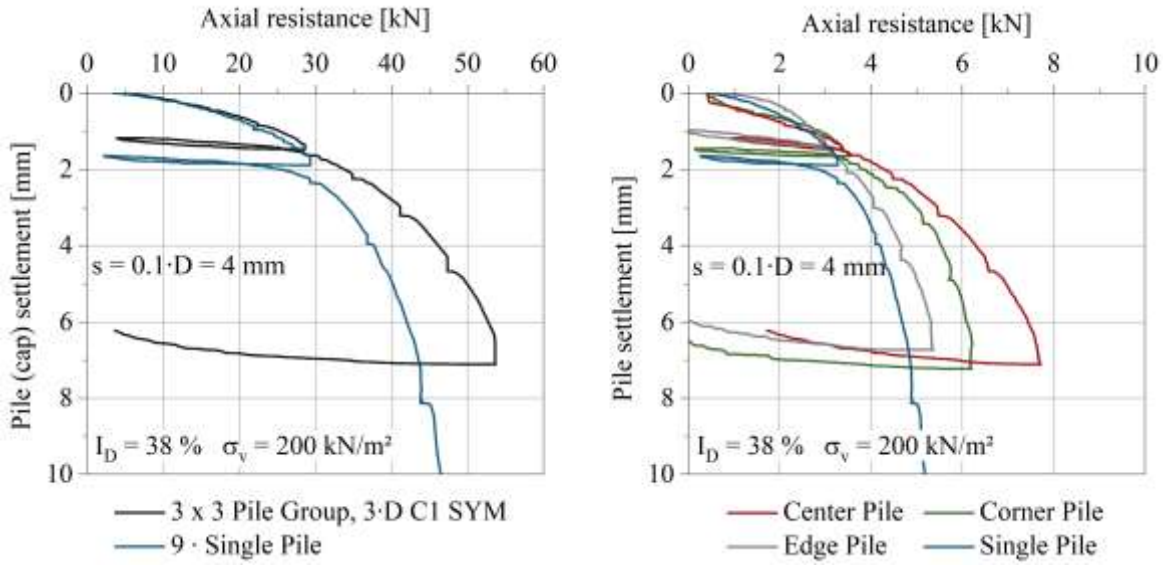


Fig. 7. Pile group resistance compared to the resistance of an equivalent number of unaffected single piles (left) and group piles versus single pile resistances (right) in medium-dense Berlin Sand, $K_0 = 0.45 \pm 0.02$

The axial resistance of the group piles under the pile group test load and the axial resistance of the unaffected single pile are displayed in Figure 7 (right). It is clearly evident that with increasing settlement, all group piles activate more axial resistance than the single pile. The center pile reached an axial resistance of 6.28 kN at the limit settlement of 4 mm, followed by the corner pile at 5.53 kN, and the edge pile at 4.66 kN. In contrast, the single piles' axial resistance was 4.19 kN at s = 0.1·D. The high resistance of the center pile can be attributed to increased soil density due to compaction from surrounding group piles and increased vertical and horizontal effective stress due to the installation and loading of the pile group. The corner pile's resistance in ULS also significantly exceeds that of the edge pile. Based on the installation order (Fig. 3b) and data (Fig. 6), it was concluded that the corner pile was installed in a compacted zone, while the edge pile was placed in conditions closer to the initial state. Although the corner pile's driving displaced sand toward the edge pile, this densification appears to have been less pronounced than that for the corner pile. This hypothesis requires validation through further experiments. Nevertheless, in ULS, all group piles demonstrated positive efficiencies (see Table 1), highlighting the potential for an optimized displacement pile group design when these effects are considered.

Table 1. Pile (group) efficiencies at s = 0.025·D (SLS) and s = 0.1·D (ULS)

Efficiency η	3 x 3 Pile Group, 3·D	Center Pile	Edge Pile	Corner Pile
η (s=0.025·D)	1.08	1.02	1.07	1.11
η (s=0.1·D)	1.24	1.50	1.11	1.32

Another important aspect in clarifying the load-bearing behaviour of displacement pile groups is the load transfer via skin friction and tip resistance of the group piles compared to the unaffected single pile. Figure 8 (left) shows the shaft and base resistance versus pile settlement for the single pile, while Fig. 8 (right) presents the shaft and base resistance versus settlement for the center pile. The single pile's resistance is predominantly mobilized by base resistance, mainly due to the smooth surface of the model piles, which represent real-scale precast concrete piles. The single pile's resistance appears fully mobilized at higher settlements, with the shaft resistance comprising 41% and the base resistance 59% of the axial resistance at s = 0.1·D. The center pile exhibits a higher mobilization of shaft resistance, which primarily drives its increase in axial capacity, though both shaft and base resistance increase with greater settlement. For ULS, the center pile shows efficiencies of η_{shaft} (s = 0.1·D) = 1.92 and η_{base}

 © DFI International Bruges 2025

(s = 0.1·D) = 1.20 (Table 2). It is worth mentioning that the base resistance continues to rise as the settlement increases.

Figure 9 illustrates the shaft and base resistance versus pile settlement for the edge pile (left) and the corner pile (right). The test results show that the increased axial resistance of the corner pile can be attributed to a higher mobilization of shaft resistance. As previously discussed, this may be due to compaction in the area where the corner piles were installed last, and this hypothesis requires further investigation. In contrast, the edge pile shows different behaviour: its shaft resistance appears to be fully mobilized at a relatively small settlement, comparable with the single pile. However, the development of the base resistance is similar to that of the center pile, indicating a positive group effect for base resistance of the edge pile as well.

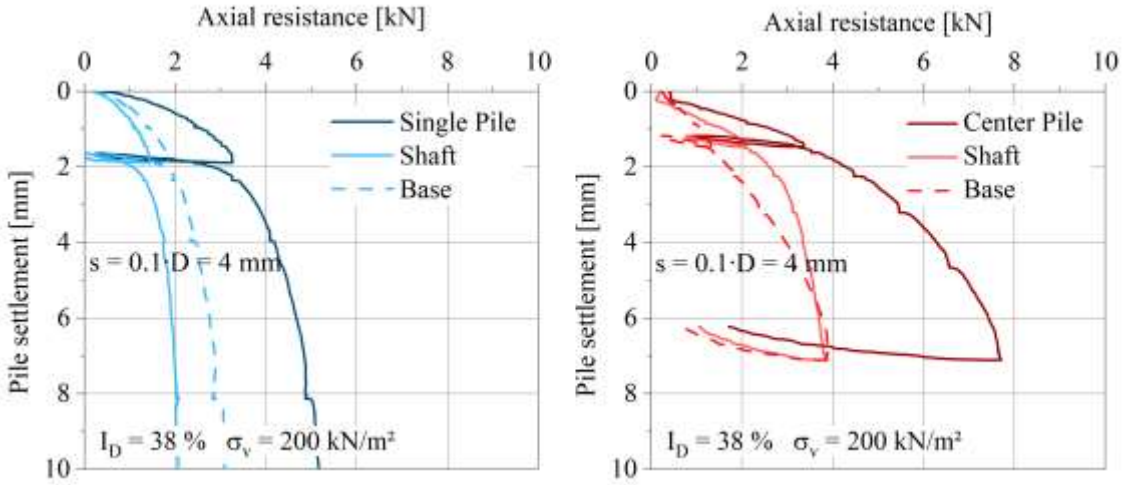


Fig. 8. Axial, shaft and base resistance of the single pile (left) and the center pile (right) in medium-dense Berlin Sand

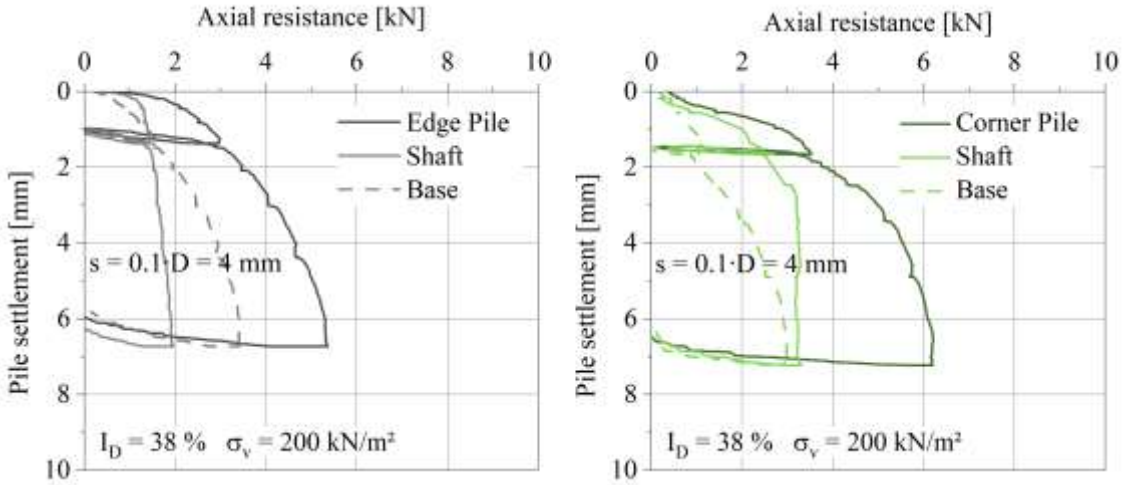


Fig. 9. Axial, shaft and base resistance of the edge pile (left) and the corner pile (right) in medium-dense Berlin Sand

 © DFI International Bruges 2025

Table 2. Shaft and base efficiency of the group piles at s = 0.1·D (ULS)

Efficiency η	Center Pile	Edge Pile	Corner Pile
η_{skin} (s=0.1·D)	1.92	0.99	1.87
η_{base} (s=0.1·D)	1.20	1.20	0.94

To investigate compaction effects between the installed group piles, various soundings were performed using the Dynamic Cone Penetrometer PANDA® in predefined interaction fields. These fields represent zones within the pile group area where the soil is expected to experience different degrees of densification based on the distance from surrounding group piles. The areas are defined according to the number of surrounding piles and their distance (max. 3·D) in terms of pile diameter (D). Figure 10 illustrates the dynamic cone resistance (q_d) versus depth for the soundings conducted.

Soundings S3 and S4, located 12·D from the pile group and executed after the pile group test, show no significant change in dynamic cone resistance compared to S1 and S2, which were performed before pile installation at the same distance as S3 and S4. However, soundings conducted post-test inside the pile group (S5 to S7) clearly indicate that the medium-dense sand has been compacted. Below the pile tips, at a depth of 0.8 m to 1.0 m, the dynamic cone resistance returns to the initial values observed in soundings S1 to S4.

The integral Q_d, defined as

$$Q_d = \int_{0.10\ m}^{1.0\ m} q_d\ dz\ \left[\frac{MN \cdot m}{m^2}\right], \qquad [3]$$

provides a value of $Q_{d,1}$ = 2.50 MN·m/m² for S1 and $Q_{d,6}$ = 5.39 MN·m/m² for S6, indicating that the resistance in the S6 location has increased by a factor of 2.16 from a depth of 0.1 m to 1.0 m. This clearly shows a quantitative increase in soil density. As the distance from the group piles increases (S8 to S15), the dynamic cone resistance decreases, returning to its initial values.

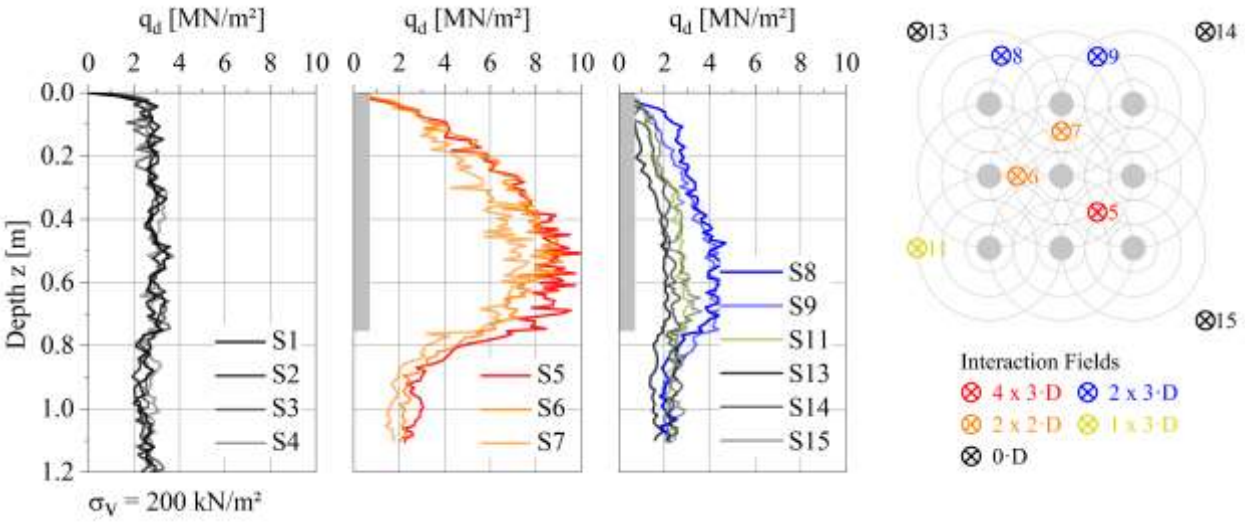


Fig. 10. Soundings conducted with the Dynamic Cone Penetrometer PANDA® to indirectly determine the initial soil density at a 12·D distance from the pile group (S1 and S2 before the installation of the group piles, S3 and S4 after the pile group test), and in various interaction fields within the 3 x 3 pile group (S5 to S15, all after the pile group test) to quantify compaction and stress increase effects

 © DFI International Bruges 2025

SUMMARY AND CONCLUSION

The 3 x 3 pile group test in medium-dense sand, with a pile spacing of 3·D and a symmetrical installation routine, yields a group efficiency of 1.24 for a mean settlement of 0.1·D, which aligns with findings from other researchers. This indicates that the resistance of the displacement piles within the group is in average 1.24 times greater than that of the same number of single piles. For a displacement pile group with a pile spacing of 3·D, both installation effects and group behaviour under load positively influence the load-settlement behaviour. In contrast, for a bored pile group with the same geometric and geotechnical properties, the group behaviour results in a decrease in axial resistance compared to nine unaffected single bored piles. The increase in axial resistance, especially for the center pile, is primarily attributed to the increased shaft resistance (η_{shaft} (s = 0.1·D) = 1.92), while the base resistance is also enhanced (η_{base} (s = 0.1·D) = 1.20), compared to that of a single pile. Additionally, soundings conducted within the pile group clearly show densification effects resulting from pile installation. The efficiencies derived here for the 9-pile group and individual group piles can contribute fundamentally to a more technically and economically optimized – and thus more sustainable – design of groups of displacement piles in the future.

ACKNOWLEDGEMENTS

The soundings herein presented were conducted with the Dynamic Cone Penetrometer PANDA®. The authors would like to acknowledge the provision by Sol Solution and the support from Caroline Forestti-Oliveira and Younes Haddani.

REFERENCES

Alves, A., Lopes, F., Danziger, B. (2008). Dimensional analysis of the wave equation applied to pile driving, Proc. 8th Int. Conf. Conference on the Application of Stress-Wave Theory to Piles, Lisbon, Portugal, pp. 115-121.

Briaud, J.L., Tucker, L.M., Ng, E. (1989). Axially loaded 5 pile group and single pile in sand, Proc. 12th Int. Conf. on Soil Mechanics and Foundation Engineering, Rio de Janeiro, Brazil, pp. 1121-1124.

DGGT (2013). Recommendations on Piling (EA-Pfähle). 2nd ed., John Wiley & Sons.

Ekström, J. (1989). A field study of model pile group behaviour in non-cohesive soils. PhD thesis, Department of Geotechnical Engineering, Chalmers University of Technology Göteborg.

Escobar, E., Navarrete, M.B., Gourvès, R., Haddani, Y., Breul, P., Chevalier, B. (2016). Dynamic characterization of the supporting layers in railway tracks using the dynamic penetrometer Panda 3®. Procedia Engineering, Vol. 143, pp. 1024-1033.

Foray, P. (1991). Scale and boundary effects on calibration chamber pile tests. Proc. 1st Int. Symp. on Calibration Chamber Testing, ISOCCT, Potsdam, New York, U.S.A., pp. 147-160.

Hanna, T.H. (1963). Model studies of foundation groups in sand. Géotechnique, 13(4), pp. 334-351.

Kézdi, Á. (1957). Bearing capacity of piles and pile groups, Proc. 4th Int. Conf. on Soil Mechanics and Foundation Engineering, ICSMFE, London, England, pp. 46-51.

Langhaar, H.L. (1951). Dimensional analysis and theory of models. John Wiley & Sons.

Le Kouby, A., Canou, J., Dupla, J.C. (2006). Group effect on model piles under axial monotonic loading,
Proc. 4th Int. Conf. on Soft Soil Engineering, Vancouver, Canada, pp. 179-187.

Le Kouby, A., Dupla, J.C., Canou, J., Francis, R. (2016). The effects of installation order on the response of a pile group in silica sand. Soils and Foundations, 56(2), pp. 174-188.

Mitlmeier, F., Moormann, Ch., (2024). Axial behaviour of displacement pile groups in sand based on

 © DFI International Bruges 2025

model tests in a calibration chamber, Proc. 18th Eur. Conf. on Soil Mechanics and Geotechnical Engineering, ECSMGE, Lisbon, Portugal, pp. 664-669.

Ovesen, N.K. (1979). The use of physical models in design, Proc. 7th Eur. Conf. on Soil Mechanics and Foundation Engineering, ECSMFE, Brigthon, England, pp. 319-323.

Phung Duc Long (1993). Footings with settlement-reducing piles in non-cohesive soil. PhD thesis, Department of Geotechnical Engineering, Chalmers University of Technology Göteborg.

Sedran, G., Stolle, D.F., Horvath, R.G. (2001). An investigation of scaling and dimensional analysis of axially loaded piles. Canadian Geotechnical Journal, 38(3), pp. 530-541.

Tejchman, A.F. (1973). Model investigations of pile groups in sand. Journal of the Soil Mechanics and Foundations Division, 99(2), pp. 199-217.

Valsangkar, A.J., Meyerhof, G.G. (1983). Model studies of the collapse behaviour of piles and pile groups. In: Developments in Soil Mechanics and Foundation Engineering, Vol. 1, pp. 65-109.

Vesić, A.S. (1969). Experiments with instrumented pile groups in sand. Performance of Deep Foundations, ASTM STP 444, pp. 177-222.

 © DFI International Bruges 2025

MICROPILED PRECAST FOUNDATION DESIGN FOR TRANSMISSION LINE PROJECTS IN AUSTRALIA

Bora Okumusoglu**,** ACCIONA Geotech, Sydney, Australia, bora.okumusoglu@geotech.net.au
Joaquin Sanchez, ACCIONA AED, Adelaide, Australia, joaquin.sanchez@acciona.com
Robin Zeybek, ACCIONA AED, Sydney, Australia, robin.zeybek@acciona.com
Dr Matthew Sentry, ACCIONA Geotech, Sydney, Australia, matthew.sentry@geotech.net.au
Carel Nagel, HumeLink East, New South Wales, Australia, carel.nagel@humelinkeast.com
Pablo Alvarez, ACEREZ ACJV, New South Wales, Australia, pablo.alvarez@acerez-acjv.com.au

ABSTRACT

This paper describes an innovative approach to foundation design and construction for transmission towers, which has been co-developed and successfully implemented at the "HumeLink East" and the "Central-West Orana Renewable Energy Zone" transmission line projects, which are amongst the largest energy infrastructure projects in the state of New South Wales, Australia, encompassing a combination of over 1000 km of new transmission. These projects are crucial for Australia's transition to low-emission energy sources, enhancing grid reliability and sustainability by increasing the delivery of renewable energy across the national electricity grid.
Transmission tower foundations traditionally rely on single cast-in-situ concrete bored piles at each leg. However, these can present logistical and construction challenges when geological conditions are not favourable and in difficult access areas and environmentally sensitive locations.
The micropiled precast foundation design not only meets the structural requirements of transmission towers but also aligns with contemporary environmental and sustainability goals. By broadening the scope of well-established engineering techniques, this solution offers a robust, adaptable, and eco-friendly alternative for transmission tower foundations.

Keywords: energy infrastructure, transmission towers, foundation design, micropiles, precast concrete

INTRODUCTION

As Australia works towards its Renewable Energy Targets (RET) of 33,000 GWh/year for electricity from renewable sources by 2030 (Regulator, 2024), the scale and capacity of renewable projects are growing significantly. Consequently, the urgent need to build transmission infrastructure to connect and distribute clean energy across the nation is as critical as generating clean energy itself. The delivery of national-scale transmission infrastructure required to meet these targets is unparalleled in Australia's history. To achieve these goals, innovative solutions must be developed to address the complex challenges posed by large-scale transmission projects. With numerous transmission line megaprojects under development, coming online, or being constructed, each project faces unique challenges and complexities driven by geographic, geotechnical, or social factors. These challenges must be managed in a socially responsible manner while delivering projects on time and within budget, despite the well-documented tendency for megaproject overruns (Sentry et al., 2024). Currently, two key transmission infrastructure megaprojects, Humelink and the Central-West Orana Renewable Energy Zone, are at the forefront of challenging traditional approaches by developing smarter foundation solutions. In this context, micropiled precast foundations offer an innovative, adaptable, and eco-friendly solution particularly suited for transmission towers in remote or hard-to-access locations. The insights gained from these projects aim to redefine the future of sustainable transmission infrastructure development.

HumeLink

The HumeLink project is a once-in-a-generation investment in Australia's high voltage transmission network and is planned to support the transition to a low emissions generation portfolio. This project is a critical part of Australian Energy Market Operator's Integrated System Plan, connecting a new

 © DFI International Bruges 2025

500kV transmission link through Wagga Wagga, Bannaby and Maragle to the existing transmission network, and supporting large scale renewable energy generation. As shown in Fig. 1, HumeLink will reinforce the transmission network in southern New South Wales (NSW) to improve the flow of electricity from new generation sources in southern and western NSW to major demand centres in the State, and to customers across the National Electricity Market (NEM).

The project will be delivered under two separate contract packages, HumeLink East (HLE) and HumeLink West (HLW) joining to form HumeLink, enabling the project to operate safely, reliably and efficiently as part of the regional network and the whole of NEM. Acciona Genus Joint Venture (AGJV) has been engaged by the regional network manager and operator, Transgrid to deliver the HLE package.



Fig. 1. HumeLink Transmission Lines (Transgrid, 2024)

Starting in late 2024, the scope of HLE includes all works and activities associated with:

- Augmenting the existing Bannaby 500kV substation,
- Delivering a new approximately 227km 500kV double circuit transmission line (471 towers) connecting the augmented Bannaby 500kV substation to the Interface Point where it will connect with HumeLink West,
- Delivering the infrastructure required at the Interface Point to enable the connection of the HLW and HLE transmission line works – including the interface tower and associated infrastructure.

Central-West Orana Renewable Energy Zone

The Central West Orana (CWO) is the first of five regions prioritised by the government of NSW and delivered by EnergyCo, which is a statutory authority established under the Energy and Utilities Administration Act 1987 and is responsible for leading the delivery of the Renewable Energy Zones (REZ) as part of the current energy sector transformation to renewable energy.

 © DFI International Bruges 2025

The CWOREZ includes the construction and operation of transmission line infrastructure, energy hubs, switching stations, and other ancillary works required to connect renewable energy generation projects within the CWOREZ to the existing electricity network.

The project is located within the Warrumbungle, Mid-Western Regional, Dubbo Regional and Upper Hunter local government areas (LGAs) and extends generally north to south from Cassilis to Wollar and east to west from Cassilis to Goolma all as depicted in Fig. 2. The project will enable at 4.5 gigawatts of new network capacity to be unlocked by the mid-2020s and enable renewable energy generators within the CWOREZ.

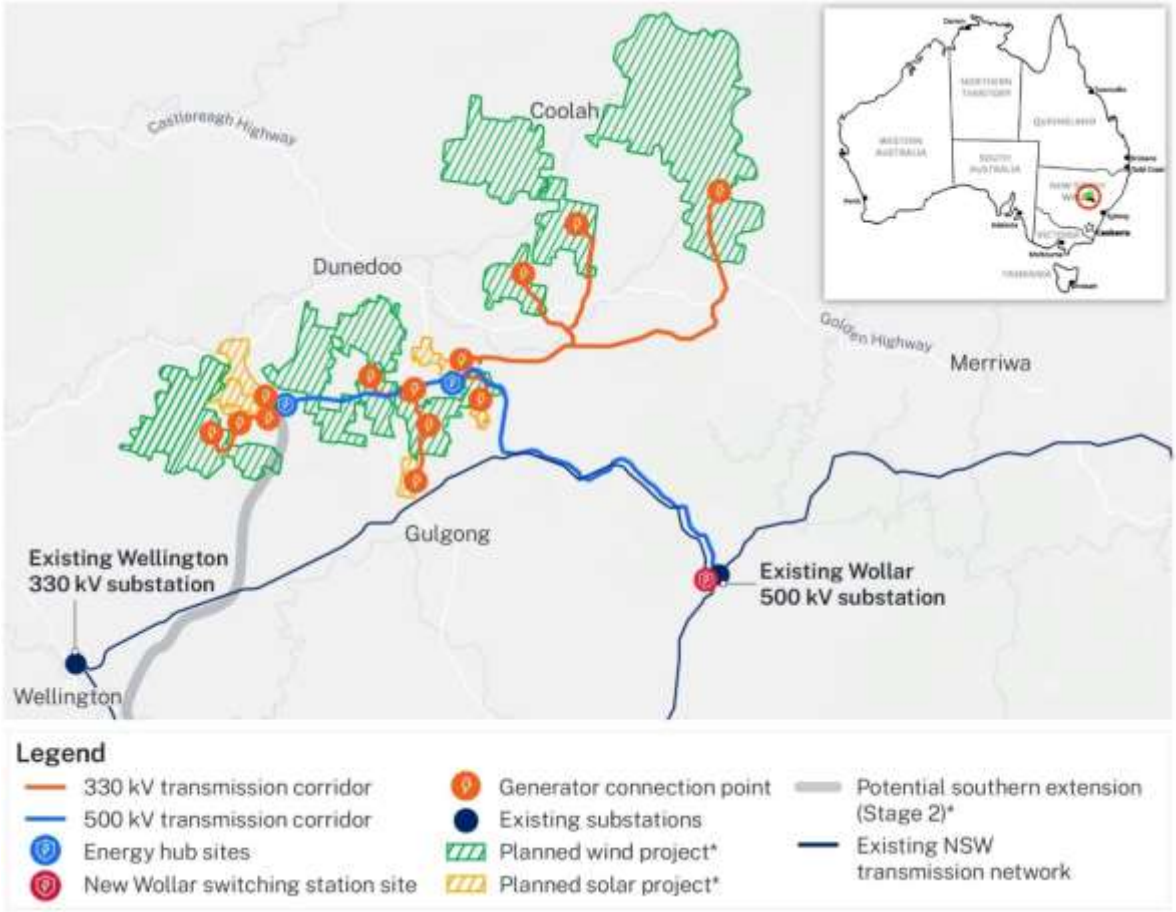


Fig. 2. Central West Orana Renewable Energy Zone (EnergyCo, 2023)

ACEREZ, a consortium by Acciona, Cobra and Endeavour Energy, was selected by NSW government to design, build, finance, operate and maintain the CWOREZ transmission network, which consists of approximately 175km of 500kV transmission lines (395 towers) and 159 km of 330kV transmission lines (467 towers), for a total length of 335km of transmission lines. The transmission line towers are mostly lattice structures with monopole towers in only approximately 80 of the tower locations. Construction works are expected to commence early in 2025. Commissioning and rehabilitation work will extend until second half of 2028.

GROUND CONDITIONS

The overall geological conditions (Fig. 3) of the Central West Orana and HumeLink projects show a predominance of medium to strong rock formations, with isolated occurrences of weaker rock. This mix provides a diverse but generally robust subsurface environment across both project areas.

 © DFI International Bruges 2025

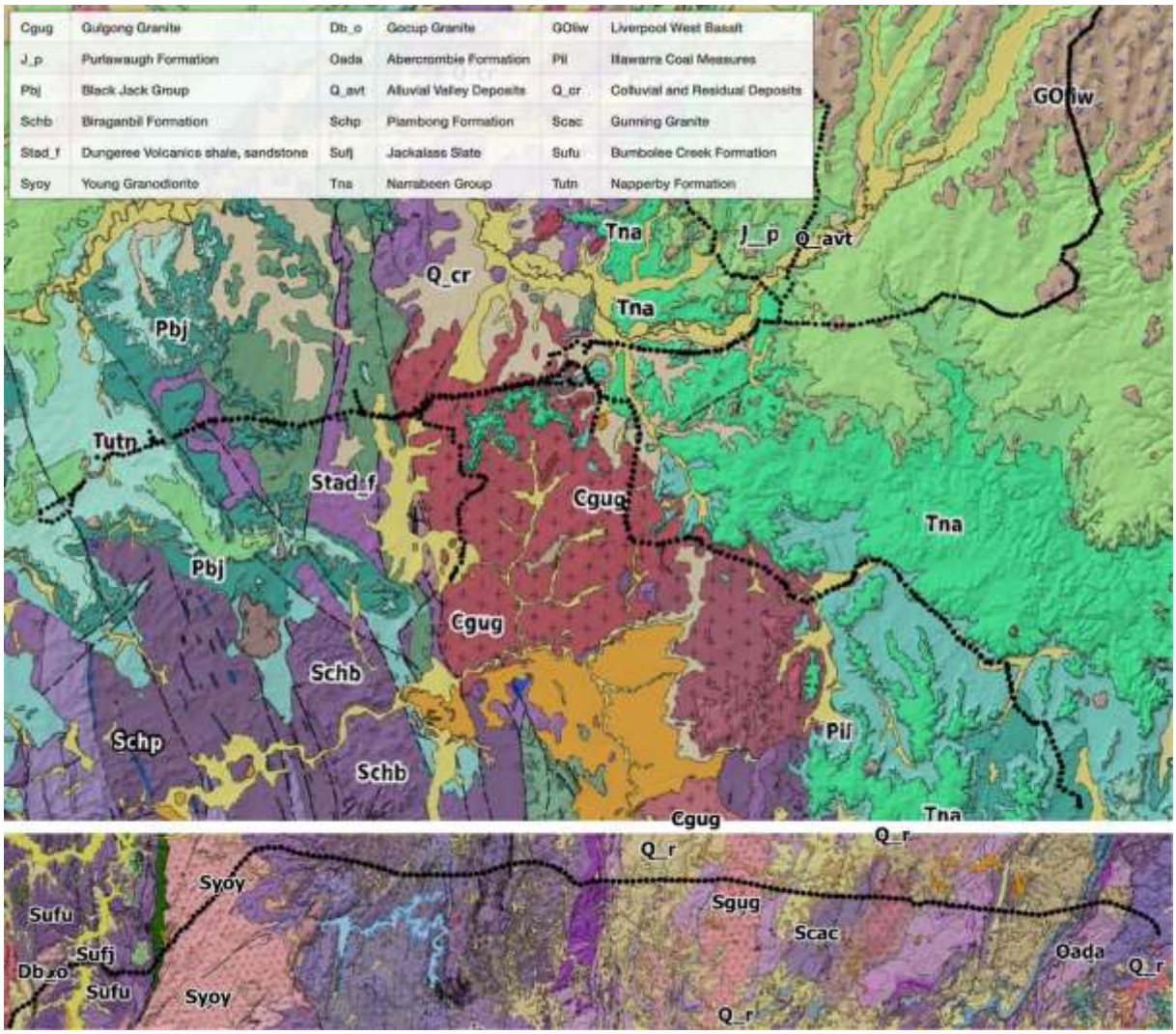


Fig. 3. Geological formations at CWOREZ (top) and HLE (bottom) with dotted lines indicating the alignment of both transmission lines

In both the Central West Orana and HumeLink project areas, rock formations are encountered at an average depth of 5 meters. A range of rock types has been identified, with strength classifications varying from very low to extremely high. Strong rock such as granite and basalt are recognized as the strongest types of rock present. Granite typically exhibits UCS values ranging from moderate to high, with some samples reaching 116 MPa. Basalt shows even higher UCS values, with some tests indicating strengths of over 200 MPa. Medium strength rock, including meta-siltstone, mudstone, agglomerate, sandstone, shale, and siltstone are also widely present. These rock types display UCS values that range from low to moderate, with typical values around 10–20 MPa for rock like mudstone and siltstone, though some sandstone samples can show UCS values up to 75 MPa. Weaker rock, such as breccia, conglomerate, phyllite, and torbanite, are less frequently encountered in the project areas. These rock types tend to exhibit lower UCS values, typically below 10 MPa. Breccia and conglomerate, for example, display UCS values around 9 MPa, while phyllite and torbanite are generally weaker, with values as low as 2–3 MPa.

The overburden soils in the Central West Orana and HumeLink project areas are classified into cohesive and granular types. Cohesive soils, which include hard, very stiff, and stiff soils, are dominant across the depth profile. These soils show a clear trend of increased stiffness with depth,

 © DFI International Bruges 2025

with hard and very stiff soils forming the majority. Softer soils are rarely encountered, suggesting that softer conditions are limited to localized areas.

Granular soils in the project areas are mainly characterized by very dense or dense conditions, particularly as depth increases. The distribution of granular soils indicates that both near-surface and deeper soils are generally well-compacted and therefore most of the areas are mostly composed of dense granular materials.

BORED PILE DESIGN AND CONSTRUCTION

Traditional foundations for transmission towers typically utilize single cast-in-situ concrete bored piles at each leg as illustrated in Fig. 4. However, this method faces significant challenges under unfavourable geological conditions, in remote areas with limited access, and in environmentally sensitive zones as well as:

- Logistical Issues: Transporting heavy equipment necessary for constructing traditional bored piles can be demanding. Restrictions on access and overhead clearance further complicate the process.
- Environmental and Social Impact: The construction process often produces considerable noise and disturbance, which is particularly problematic in areas with noise regulations or near sensitive populations.
- Material and Supply Logistics: Traditional bored piles require large volumes of ready-mix concrete and substantial reinforcement cages, posing additional supply and logistical challenges.

To address these challenges, a value engineering approach was implemented during Stage 2 of the Early Contractor Involvement (ECI) in HLE.

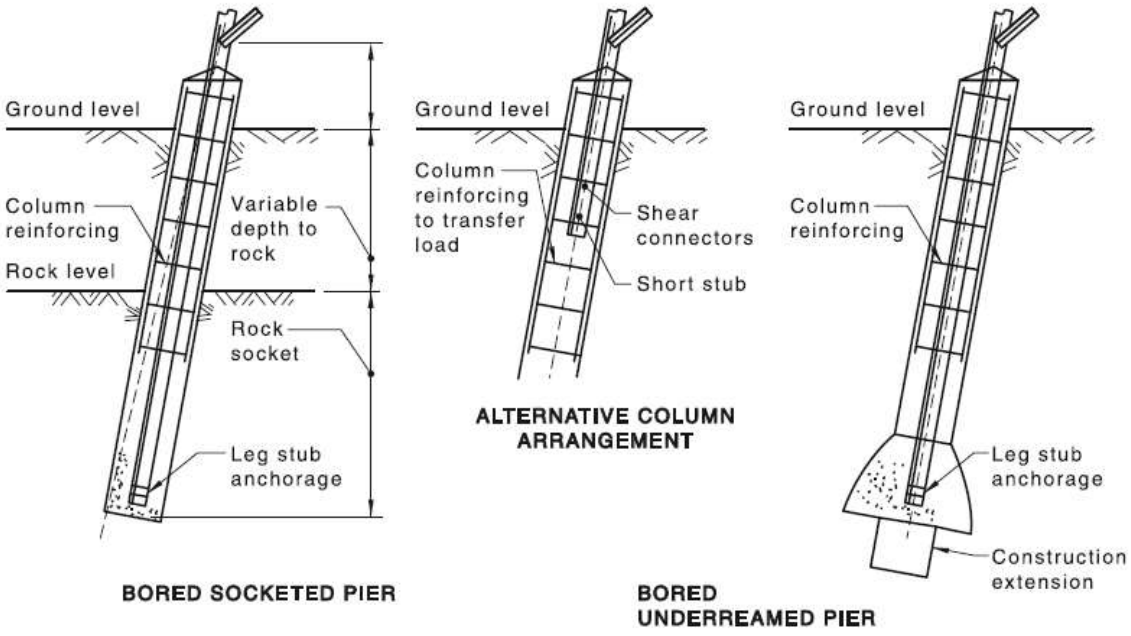


Fig. 4. Typical bored pile foundation for a transmission tower leg from AS/NZS 7000:2016

ALTERNATIVE MICRO PILE DESIGN

The micropile design begins with the positioning of precast pile caps, through which the micropiles

 © DFI International Bruges 2025

are drilled via conical holes. The unique shape of the precast cap allows for 25m of the transmission tower to be erected before any micropiles are installed (Fig. 5), providing flexibility in tower erection, and decoupling the piling works from the project's critical path. The micropiles are reinforced with a single high-strength mono bar, inserted into the drill hole upon achieving the required socket length on-site. This mono bar is then lowered into the hole and grouted to the top of the pile cap.

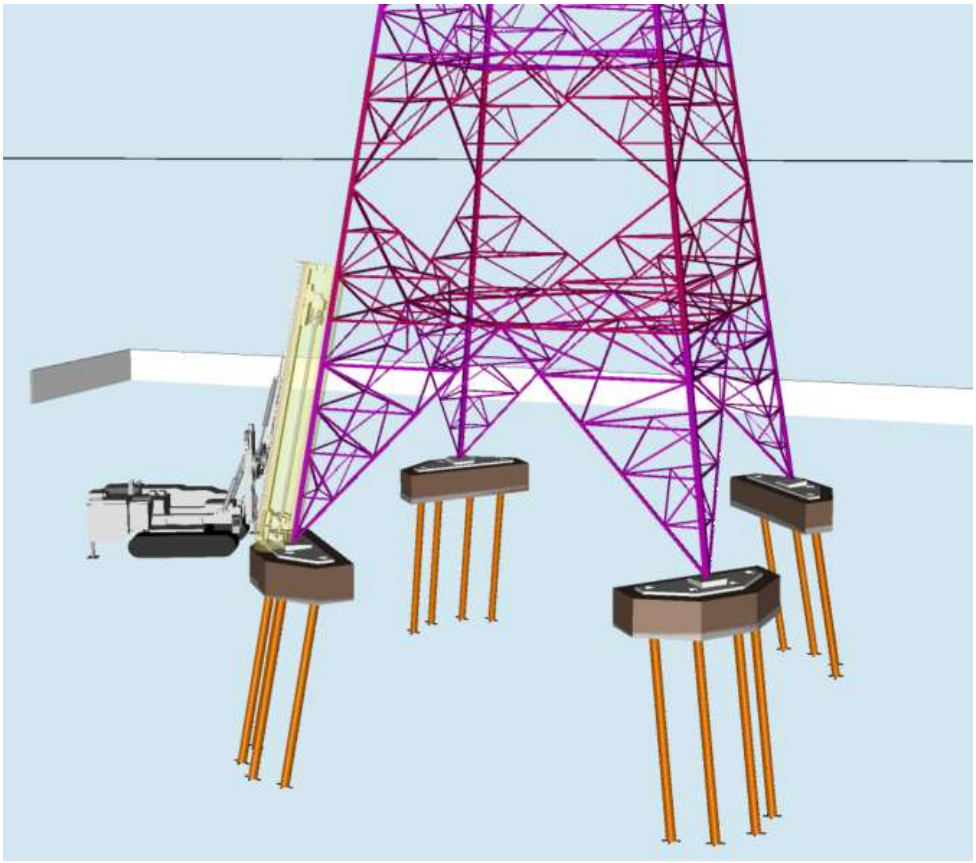


Fig. 5. Alternative micro piled precast foundations for a transmission tower

The micropile design offers several key advantages over traditional bored pile foundations:

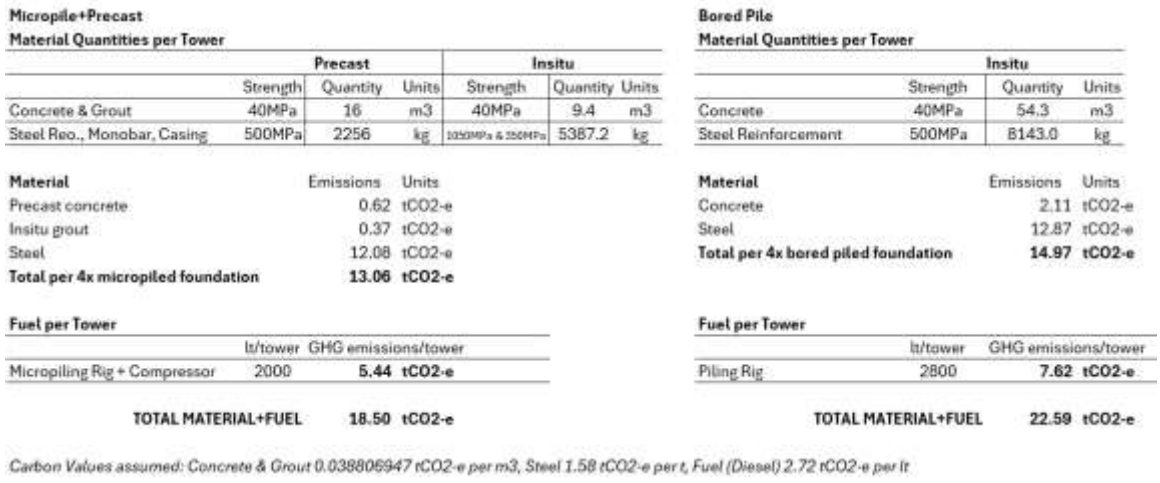
- This alternative design not only reduces the carbon footprint but also increases productivity while maintaining costs comparable to bored piling.
- Micropile construction requires smaller equipment and drill rigs, resulting in significant savings in civil works, as the working platforms and access roads needed for a micropile drilling rig are less onerous compared to those required for a bored piling rig.
- The smaller equipment required for micropile construction results in a much safer work face compared to typical bored pile operations.
- Due to the smaller diameters of micropiles, the environmental impact is considerably lower than that of bored piles.
- The use of a down-the-hole hammer for drilling micropile holes mitigates the risk of slower productivity in high-strength rock formations.
- Micropiles for this project require only a mobile grout truck at each workface, eliminating the need for concrete mixers and reducing the risk associated with concrete retention, which is a significant issue with bored piling in remote locations.
- Geological variations, which might cause delays due to complex cage arrangements in traditional methods, are less problematic with micropiles.
- The use of precast or prefabricated caps significantly reduces on-site manual labour.

 © DFI International Bruges 2025

Typically, in Australia, a stub is cast into an inclined bored pile, with the tower leg connected to the stub. This process is slow and meticulous, requiring jigs to position the stub correctly to ensure that the K-point remains within tolerance. For this alternative design, the precast pile cap design incorporates hold-down bolts cast into the precast pile cap. A base plate with a stub is then positioned on these bolts, to which the transmission tower legs are connected. The benefits of this precast cap design over a cast-in-situ stub include:

- Reduced tolerance issues compared to conventional bored pile stub setups.
- Improved quality control, as manufacturing in a precast factory offers better oversight than in-situ on-site construction.
- Mitigation of safety hazards associated with on-site formwork and reinforcement placement (FRP) activities.

In HLE, the carbon emission calculations showed a 13% reduction in embodied carbon due to decreased material quantities. Additionally, there are substantial fuel savings from reduced construction activities, resulting in a 29% reduction in fuel-associated emissions and an overall reduction of 18%. A summary of carbon emissions estimation is provided in Fig. 6.



Micropile+Precast

Material Quantities per Tower

	Precast			Insitu		
	Strength	Quantity	Units	Strength	Quantity	Units
Concrete & Grout	40MPa	16	m3	40MPa	9.4	m3
Steel Reo., Monobar, Casing	500MPa	2256	kg	1050MPa & 350MPa	5387.2	kg

Material	Emissions	Units
Precast concrete	0.62	tCO2-e
Insitu grout	0.37	tCO2-e
Steel	12.08	tCO2-e
Total per 4x micropiled foundation	**13.06**	**tCO2-e**

Fuel per Tower

	lt/tower	GHG emissions/tower	
Micropiling Rig + Compressor	2000	**5.44**	**tCO2-e**
TOTAL MATERIAL+FUEL		**18.50**	**tCO2-e**

Bored Pile

Material Quantities per Tower

	Insitu		
	Strength	Quantity	Units
Concrete	40MPa	54.3	m3
Steel Reinforcement	500MPa	8143.0	kg

Material	Emissions	Units
Concrete	2.11	tCO2-e
Steel	12.87	tCO2-e
Total per 4x bored piled foundation	**14.97**	**tCO2-e**

Fuel per Tower

	lt/tower	GHG emissions/tower	
Piling Rig	2800	**7.62**	**tCO2-e**
TOTAL MATERIAL+FUEL		**22.59**	**tCO2-e**

Carbon Values assumed: Concrete & Grout 0.038806947 tCO2-e per m3, Steel 1.58 tCO2-e per t, Fuel (Diesel) 2.72 tCO2-e per lt

Fig. 6. Embodied carbon reduction of foundations per tower

STRUCTURAL DESIGN DETAILS

The precast concrete pile cap is a structural element designed to transfer design actions from superstructure to micropiles and eventually to rock strata. Pile caps have been designed to support the superstructure up to 25m during construction without micropiles to provide flexibility in construction programme.

It is a non-flexural member due to its low span to depth ratio and it has been designed following strut and tie design principles. It is approximately a trapezoid on plan which consists of 4 voids, where the micropiles are located, and a pedestal to connect the superstructure. The top face is detailed with 1% slope to prevent water ponding.

Design Challenges and Optioneering Stage

Early design inputs included:

- Weight to be limited to 10t to transfer 2 caps on the same truck.
- Short dimension to be limited to 2.5m for transportation.
- Reinforcement detailing be modular for mass production.
- Pile locations have sufficient clearance to steel tower columns during drilling operations.

Geometrical restrictions have been the main driver of the design from early design development. The first concept design at Optioneering Stage was a rectangular section on plan as shown on Fig. 7.

 © DFI International Bruges 2025

Requirement to have flexibility to install micropiles after superstructure is partially erected while providing clearance for the drilling equipment were main design challenges.

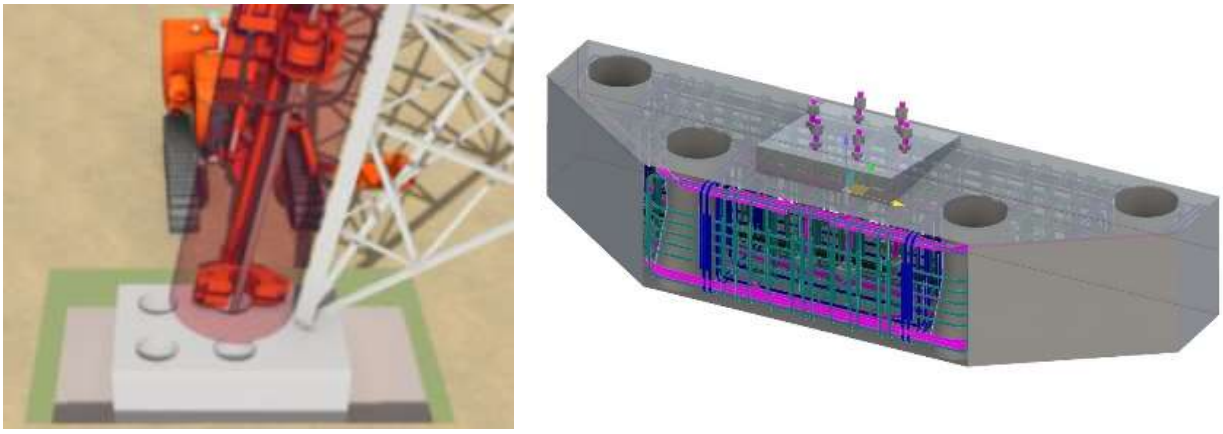


Fig. 7. Rectangular (initial) and Trapezoidal (final) Pile Caps

Rectangular sections would have been easier to fabricate as the reinforcement detailing would be simpler. However, it was found that micropile capacity was the governing element as the system results higher loads in push and pull action. A trapezoidal shape (Fig. 7) on plan was adopted by the end of optioneering stage. The main benefits of this design option include relatively homogenous load distribution between micropiles and reduction in weight.

Load Transfer Mechanism

Having a Span/Depth ratio below 3, this member is categorized as a non-flexural member as per Australian Standards. Therefore, the member is idealized as a truss member where compression members are concrete elements and tension elements are the main reinforcement. Fig. 8 presents Strut and Tie model adopted. The design model is in 3D based on the same principles.

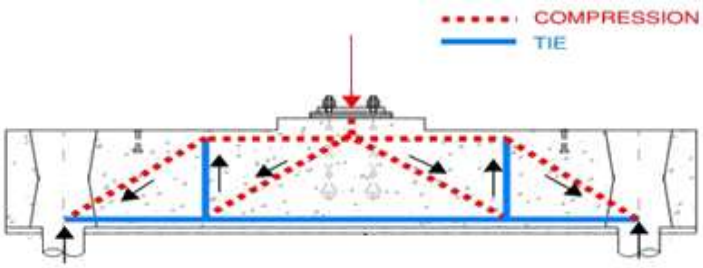


Fig. 8. Strut and Tie Model

Strut and tie idealization is a regular practice for non-flexural members. What differentiates this design from regular practice is the interface between micropiles and the pile cap as shown on Fig. 9:

- Pile cap is designed such that there are 4 conical voids formed to allow micropile construction.
- When transmission tower leg is in compression, pile cap bears on the bottom cones. Cones act as if they are wedged into the pile cap and bear on micropile grout.
- When transmission tower leg is in tension, cones at the top are utilised similar to the compression case and axial force is transferred between anchor plate at the top of the micropile monobar and pile cap eventually pulling the monobar in tension.

 © DFI International Bruges 2025

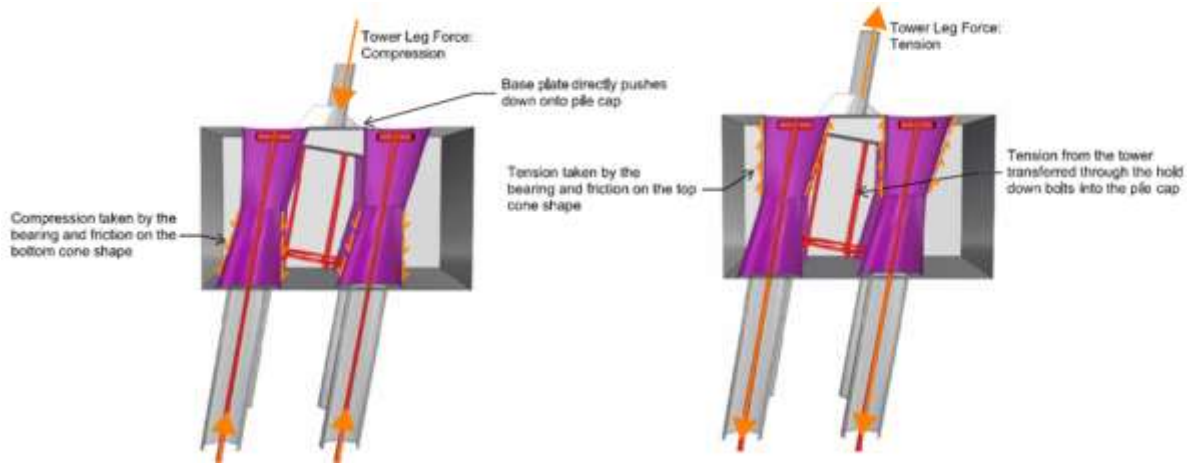


Fig. 9. Force Transfer (Compression and Tension Cases) via Conical Voids

Reinforcement Detailing and Industry Engagement

Detailing a structural element where the main reinforcement is not aligned with orthogonal coordinates presents unique challenges in reinforcement detailing. The main reinforcement is designed to tie conical voids together, while the secondary reinforcement forms a cage around the main reinforcement. This cage provides confinement to the main ties and prevents excessive reinforcement on visible surfaces.

Early industry engagement helped resolve many potential detailing issues and reduced lead times for mass production. By experimenting with different reinforcement arrangements in the workshop, gathering feedback from steel fixers, and addressing these issues during the design phase, a three-stage modular reinforcement detailing approach was adopted. In this method, the bottom cage, main reinforcement, and top cage are placed sequentially in the mould to achieve optimal lead times and the highest quality control. Fig. 10 illustrates the reinforcement detailing from the latest trial, which remains a work in progress at the time of this paper's publication.

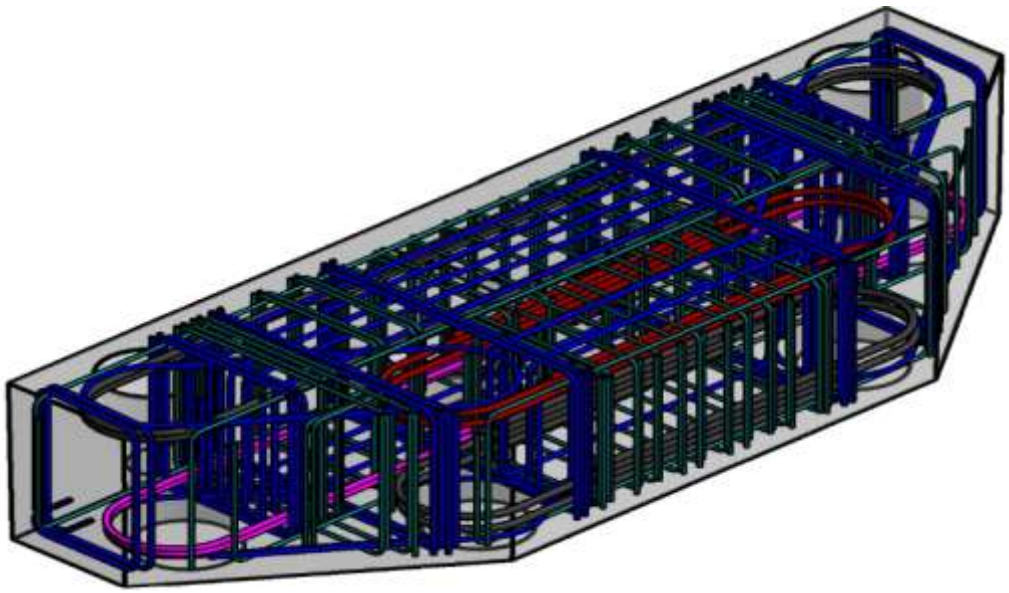


Fig. 10. Reinforcement Detailing

 © DFI International Bruges 2025

GEOTECHNICAL DESIGN DETAILS

The geotechnical design of the micropile foundation was conducted to determine key parameters, including micropile length, micropile stresses, tower settlements, and the bearing capacity and settlement of the pile cap during the tower erection phase, prior to the installation of the micropiles.

The design process adhered to the relevant Australian standards (AS 2159:2009 and AS 7000:2016) and incorporated established geotechnical methods, such as the Brinch Hansen Theory, to calculate the micropile length and the bearing capacity of the pile cap respectively. Additionally, soil structure interaction analysis (SSIA) has been carried out to determine the micropile stresses and settlements during the construction phase using the Finite Element Method (FEM) through the geotechnical software PLAXIS 3D.

Geotechnical Challenges, Dealing with the Unknown

The design of pile and micropile foundations requires the determination of the geological profile along and below the pile, as well as the intrinsic geotechnical parameters of each stratum encountered. These parameters are typically derived from borehole data, in-situ tests, and laboratory tests. While it is common practice to conduct at least one borehole per pile foundation location, in the case of CWO and HumeLink, the number of exploratory holes completed prior to the design stage covered less than 30% of the total number of tower locations.

To address this limitation, the design approach was developed to account for all expected geological scenarios at each tower location, minimizing risks associated with geological variability. This approach included the following key measures:

- Rock Socket Embedment: Micropile foundations are only applied where rock is underlying the foundation and designed with a rock socket embedment of sufficient length to ensure adequate bearing resistance and tension capacity, regardless of ground conditions.
- Conservative Material Assumption: The material above the rock was assumed to consist of stiff clay, a conservative assumption supported by the available ground investigation data.
- Rock Strength Variability: Rock socket lengths were calculated for three distinct rock strength levels: low strength, medium strength, and high strength, ensuring the design accommodates a wide range of geological conditions.
- Comprehensive Analysis: Micropile structural forces and settlements were calculated for 12 different geological sections, accounting for variations in the thickness of the top stiff clay layer (ranging from 2 to 18 meters) and the underlying rock strength (low, medium, or high).

During the construction stage, the geology at each tower location must be confirmed prior to micropile installation. This confirmation is typically achieved through borehole drilling, which penetrates the underlying rock strata. Point load testing (PLT) and unconfined compressive strength (UCS) testing are conducted to determine the strength of the rock. However, the requirement for ground investigation can be waived if an extensive study is carried out to correlate the drilling rate with rock strength for each geotechnical rock unit. In such cases, the rock strength can be determined using the approved correlation during the drilling of each tower leg foundation. This approach not only streamlines the construction process but also ensures the accuracy and reliability of the geotechnical design.

Rock Socket Length

As previously introduced, the foundation solution is composed of 4 micropiles of 254mm diameter, raked in the direction of the tower legs. In order to determine the rock socket length 2 failure mechanisms have been accounted as per AS2159 and AS7000:

a) failure between the ground and the micropile surface, and
b) failure by the mobilization of the rock mass due to tension load.

 © DFI International Bruges 2025

The micropiles are designed to withstand compressive, tensile, and shear forces. Among these, tensile and compression loads are used to determine the rock socket length being the tensile loading the most critical factor. For practical purposes, the final design has only two different socket configurations depending on the strength of the underlying rock: 3 meters (minimum recommended bond length for rock anchorage as per BS8081:1989) for medium to high strength rock and 5 meters for low strength rock.

Soil Structure Interaction Analysis

A Soil-Structure Interaction Analysis (SSIA) was conducted using PLAXIS 3D to determine the forces and movements acting on the micropiles. The micropile section considered in the analysis consists of a 254 mm diameter micropile with a 47 mm diameter bar (DYWIDAG Y1050H 950/1050), including a CHS 219x8.2 steel profile in the upper 3.93 meters.

Model is comprised of only one micropile cap, where pile cap was modelled as a plate element and the micropiles were represented as embedded beams. Embedded beams in PLAXIS 3D (Fig. 11) are structural beam elements positioned within the soil, interacting with it through dedicated interface elements that account for both shaft friction and base resistance. Model accounts for the construction stages and the different combination loads. The analysis included eight load combinations, encompassing compression, tension, and shear forces, which could occur in combination at different load levels and including a 2 degrees deviation. The loads were applied to the plate element as a surface load, corresponding to the area of the tower leg connection. To ensure the pile cap fully transfers the tower loads to the micropiles, the soil beneath the pile cap was slightly lowered in the model. Connection between the plate and the embedded beam has been modelled as pin connection.

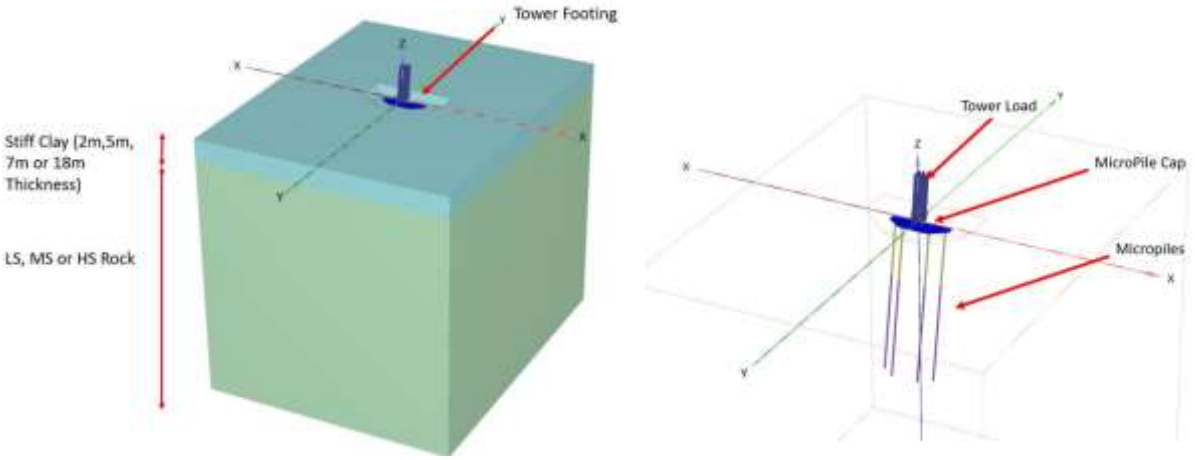


Fig. 11. SSIA, PLAXIS3D model and model elements.

SSIA Results

The Soil-Structure Interaction Analysis (SSIA) yielded the following maximum values across all geological models and load scenarios:

- Compression force: 870kN; Tension force: 711kN; Shear force: 48kN; Bending moment: 44kNm.
- The maximum shear force consistently occurred at the connection between the pile cap and the micropile. The maximum bending moment was observed at approximately 2 meters below the pile cap, diminishing to negligible levels at a depth of 7 meters.
- In terms of settlement, the maximum vertical settlement was less than 3 mm, while the maximum differential settlement of the pile cap was below 2.5 mm.

 © DFI International Bruges 2025

PROTOTYPE TESTING

As an initial step towards the implementation of and final approval for the alternative design with micropiled precast caps, an in-situ trial campaign has been undertaken. This campaign had three objectives:

1. Casting of the precast caps,
2. Dress rehearsals for the installation of the foundation system,
3. Load testing of the connection cone and micropiles.

Casting of the precast caps

In August 2024, a total of 4 precast caps were successfully cast (Fig. 12) at GEOTECH APS (Australian Precast Solutions, a business unit of GEOTECH, an Acciona company) precast facilities in Macksville, NSW. This early casting, done before the final design approval, showcased the viability of the precast cap with its unique reinforcement configuration and concrete form.



Fig. 12. Precast cap cast.

Dress rehearsals for the installation of the foundation system

In September and October 2024, close to the HLE alignment, next to the Transgrid Bannaby 500/330kV Substation, dress rehearsals for precast cap placement and drilling through the precast cap (Fig. 13) were carried out to refine initial methodologies for the foundation system installation. For example, chalk lines – one of which can be seen in the right-hand side photo of Fig. 12 – were implemented to improve the accuracy of precast element placement, ensuring the K-point of the tower is correctly established.

 © DFI International Bruges 2025



Fig. 13. Micropile drilling through the precast caps.

Load testing of the connection cone and micropiles

Three distinct load tests were conducted on the foundation system:

1. Pull-out test on the cone: This test involved a single short micropile installed through one of the precast caps, which was designed to fail geotechnically and start pushing out the cone above it. A custom-designed stressing stool was used to distribute the reaction load away from the cone onto the precast cap, while a hydraulic hollow jack pulled out the mono bar of the micropile.
2. Tension load test on a micropile: This rather routine test was performed on a solo micropile installed without a cap. The test aimed to demonstrate the geotechnical tensile capacity of the micropiles in a similar ground profile to both HLE and CWO: from low to medium strength rock located 5 to 7 meters below ground, overlaid by loose to medium dense to very dense sands, followed by stiff to very stiff clay (residual soil).
3. Compression load test on a micropile: Similar to the tension test, this was conducted on a single micropile to demonstrate the geotechnical compression capability and also aimed at providing additional assurance for the buckling resistance of the micropile at high compression loads.

Following the recommendations of AS2159 Table A1 for compression and Table A2 for tension load testing, two-stage incremental loading and unloading schemes were adopted for all tests. The first stage applied the maximum Serviceability Limit State loads of 331kN (tension) and 379kN (compression), while the second stage applied maximum loads, rounded up from Ultimate Limit State loads, of 1000kN (tension) and 1200kN (compression) per micropile. Test results were graphed and analysed in real time on-site using AnchorTest software (Mothersille and Okumusoglu, 2017) during the presence of technical representatives from Transgrid. Some of the test results, specifically from second stage loading to ULS, are provided in Fig. 14, along with photographs taken during testing.

 © DFI International Bruges 2025

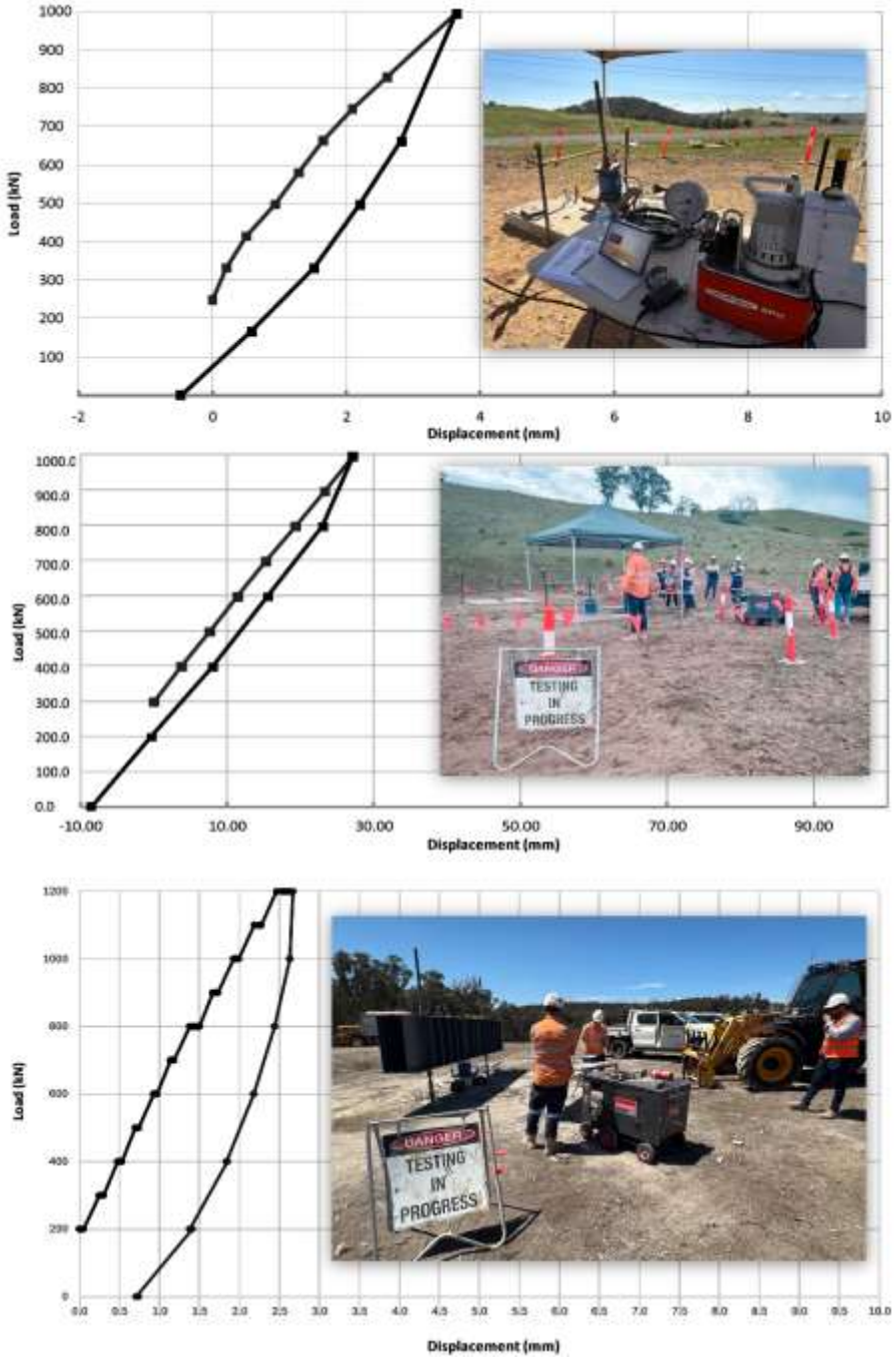


Fig. 14. Load testing (pull-out on cone, tension and compression) of micropiles

SUMMARY AND CONCLUSIONS

An innovative micropiled precast foundation design has been co-developed and successfully implemented in the HumeLink East and Central-West Orana Renewable Energy Zone transmission line projects in NSW, Australia. This alternative addresses the challenges and risks associated with traditional bored pile foundations, especially in difficult geological conditions, and both environmentally sensitive and limited access areas. By utilising smaller equipment and precast caps with conical voids for micropiles, the design reduces environmental impact, enhances safety, and increases efficiency. Prototype testing – including pre-casting, installation rehearsals, and load tests – confirmed the viability and effectiveness of the system. Significant reductions in embodied carbon and fuel emissions were achieved, aligning with contemporary sustainability goals. This robust and

 © DFI International Bruges 2025

highly adaptable solution offers a promising alternative for future transmission tower foundation projects.

ACKNOWLEDGMENTS

The authors express their gratitude to Transgrid and EnergyCo for their support and permission to publish this paper. The HLE and CWOREZ design and construction teams deserve recognition for their commitment in realising this innovative solution, surmounting numerous challenges with unwavering determination. Special thanks are also extended to Nic Morgan, Roseller Oblimar, Gary Nguyen and Andrei Kudalb for their input during the drafting of this paper.

REFERENCES

AS 2159:2009. Piling - Design and installation. Committee CE-018, Piling, Standards Australia.

AS 3600:2018. Concrete structures. Committee BD-002, Concrete Structures, Standards Australia.

AS/NZS 7000:2016. Overhead line design. Joint Technical Committee EL-052, Electrical Energy Network, Construction and Operation, Standards Australia and Standards New Zealand.

BS8081:1989. Code of practice for ground anchorages. British Standards Institution, London.

EnergyCo, 2023. Operational features of the project. Excerpt from an online PDF document. https://www.energyco.nsw.gov.au/sites/default/files/2023-09/cwo-rez-fact-sheet-eis-transmission-infrastructure.pdf. Accessed 25-09-24.

Mothersille, D.K.V. and Okumusoglu, B. 2017. Real-time anchor testing and data management, Deep Foundations Magazine. DFI, Sept/Oct 2017. pp. 65-69.

Regulator, 2024. Clean Energy Regulator, Renewable Energy Target. An Australian Government website. https://cer.gov.au/schemes/renewable-energy-target. Accessed 25-09-24.

Sentry, M., Emin-Petot-Tourtollet, C., Nagel, C., Sanchez Flores, A., Nadarajah, J., & Aziz, M., 2024. Global Risk Management - Suburban Rail Loop Project, MSc Thesis sponsored by ACCIONA. Universidad Poletecnica De Madrid.

Transgrid, 2024. Division of HumeLink East and HumeLink West sections. An online figure. https://www.transgrid.com.au/humelink-east. Accessed 25-09-24.

 © DFI International Bruges 2025

REVIEW OF CPT DIRECT DESIGN METHODS FOR DRIVEN CAST-IN-SITU PILE CAPACITY USING INSTRUMENTED PILE LOAD TESTS TO FAILURE

Packer, M.L., PSM, Brisbane, Queensland, Australia, +61 7 3220 8300, megan.packer@psm.com.au

ABSTRACT

Pile design methods using CPT (cone penetration testing) data have been developed over many decades and are widely used in industry. CPT-based site investigations are economic, efficient and suitable for brownfield sites, as well as spatially restricted environments for applications including reuse of existing deep foundations. Research of CPT-based design has often been focussed on preformed or precast driven piles and, as such, the driven cast-in-situ (DCIS) pile type has received limited attention. DCIS is typically classified as a large displacement pile albeit sharing aspects of its construction with replacement pile types. There are few published case histories of load tests on DCIS piles, let alone instrumented full-scale tests to failure, from which to assess the appropriate CPT design methodology/ies for this pile type.

This paper presents a review of common CPT direct design methods to determine DCIS pile capacities, using results from six load tests taken to failure on sacrificial piles at Avonmouth, England. This case study presents a unique opportunity to evaluate both simplified and advanced CPT design methods as applicable to closed-end driven piles in granular soils, and actively contributes to the publicly available DCIS database to assist with future design and research. The applicability and limitations of using CPT data for pile base capacity determination is discussed.

Keywords: CPT, pile load testing, pile design, case study, back-analysis

INTRODUCTION

This paper presents a critical review of often used CPT direct design approaches to predict total capacity of driven cast-in-situ (DCIS) piles. CPT-based pile capacity design methods have been developed over many decades and are widely used in industry. However, many of these methods targeting driven piles were based upon research using prefabricated (i.e. precast concrete or preformed steel tube) piles. The DCIS pile type has received limited attention with very few published case histories. The intent of this paper is to actively contribute to the already published DCIS database by Flynn *et al.*, 2014.

DCIS piles are a combination between driven displacement and cast-in-situ (replacement) pile types. They offer an economical deep foundation solution suitable for end-bearing dominated piles, and importantly do not generate any spoil (making them more favourable for contaminated brownfield sites).

Six static maintained pile compression tests, loaded to failure, are presented herein to compare both simplified and advanced CPT direct design methods for determination of total pile capacity. The load tests were carried out on sacrificial piles constructed in Avonmouth, England. All six pile tests were loaded to failure which was defined as the applied load at which the measured pile head displacement (settlement) was equivalent to 0.1D (where D = pile diameter). In these cases, 0.1D = 40 mm. Four of the six piles were instrumented, each with four strain gauge levels to determine the distribution of load down the pile length with respect to changing soil stratigraphy.

Avonmouth pile tests

All six test piles (between 6.5 and 9.5 m in length) were driven using a temporary 355 mm internal diameter (20 mm thick) steel installation tube with a sacrificial 415 mm diameter steel shoe fitted to the base of the tube. The installation tube was driven with a Junttan PM26 HHK5ASS hydraulic

 © DFI International Bruges 2025

hammer (5 tonne ram block weight, and 58.5 kJ max. rated energy). Drop height for all test piles was 600 mm. On reaching the target pile depth the hammer was retracted, a full length cage lowered into the tube, and the tube filled with high slump concrete (C35/C40 strength concrete placed using a specialist skip). The tube was then extracted with several downward blows applied to remove concrete voids.

The Avonmouth depositional environment (within the Severn Estuary) consists of extensive Pleistocene and recent estuarine alluvium, dominated by clay and silt deposits. Test piles were driven into normally consolidated very soft to soft alluvial clays and silty clays, overlying a thick body of fluvial sands at depth. The sands are of varying density, depths and character and include interbedded weak layers of silty sands and clayey sands. Table 1, below, summarises pile lengths, embedment below the top of sand founding stratum and strain gauge depths for the four instrumented piles. The top of the sand founding layer was defined where CPT q_c values were > 10 MPa for a minimum of 3 m continuous depth. The instrumented test piles included four levels of strain gauges to determine shaft capacity within different soil stratum and pile toe settlement performance, with respect to pile head displacement.

Table 1. Summary of instrumented test pile construction

Pile ID (m)	Pile length (m)	Pile toe embedment (below top of founding layer)	Strain gauge depths
A1	6.5	-0.3 m	-
A2	9.0	2.2 m	-
A3	7.5	0.7 m	0.4, 1.4, 6.6, 7.4
A4	8.0	0.9 m	0.4, 1.4, 6.5, 7.9
B5	8.0	0.5 m	0.4, 1.2, 5.4, 7.9
B6	9.5	2.25 m	0.4, 5.5, 7.5, 9.4

CPT q_c profiles, soil stratigraphy, pile depths and installation blow counts are presented in Fig. 1. The fluvial sands consist of a top loose sand zone (i.e. reworked sand in Fig. 1), underlain by a medium dense to dense sand layer. Piles A1 to A4 were installed into sands with dense or very dense consistencies from its surface (i.e. below reworked sand layer), whilst piles B5 and B6 were within sands of a more gradational increasing consistency with depth.

Maintained load compression testing

Maintained load compression testing was carried out on all six piles, in accordance with Clause 15.15.3 of the "*Specification for Piling and Embedded Retaining Walls"* (ICE, 2007). Piles were tested to failure; 40 mm pile head settlement in this case. The DVL (Design Verification Load) was assessed as:

$$DVL = SWL + 2*NSF = 990 \text{ kN}$$

Where SWL = Specified Working Load (610 kN); NSF = Negative Skin Friction (190 kN)

The applied loads and corresponding measured pile head displacements are presented in Fig. 2. Each curve is annotated with the respective pile number and embedment length below the top of founding layer identified in brackets. There is a correlation between embedment length and total pile capacity, although local variations in q_c appear to have greater influence. Observations include:

 © DFI International Bruges 2025

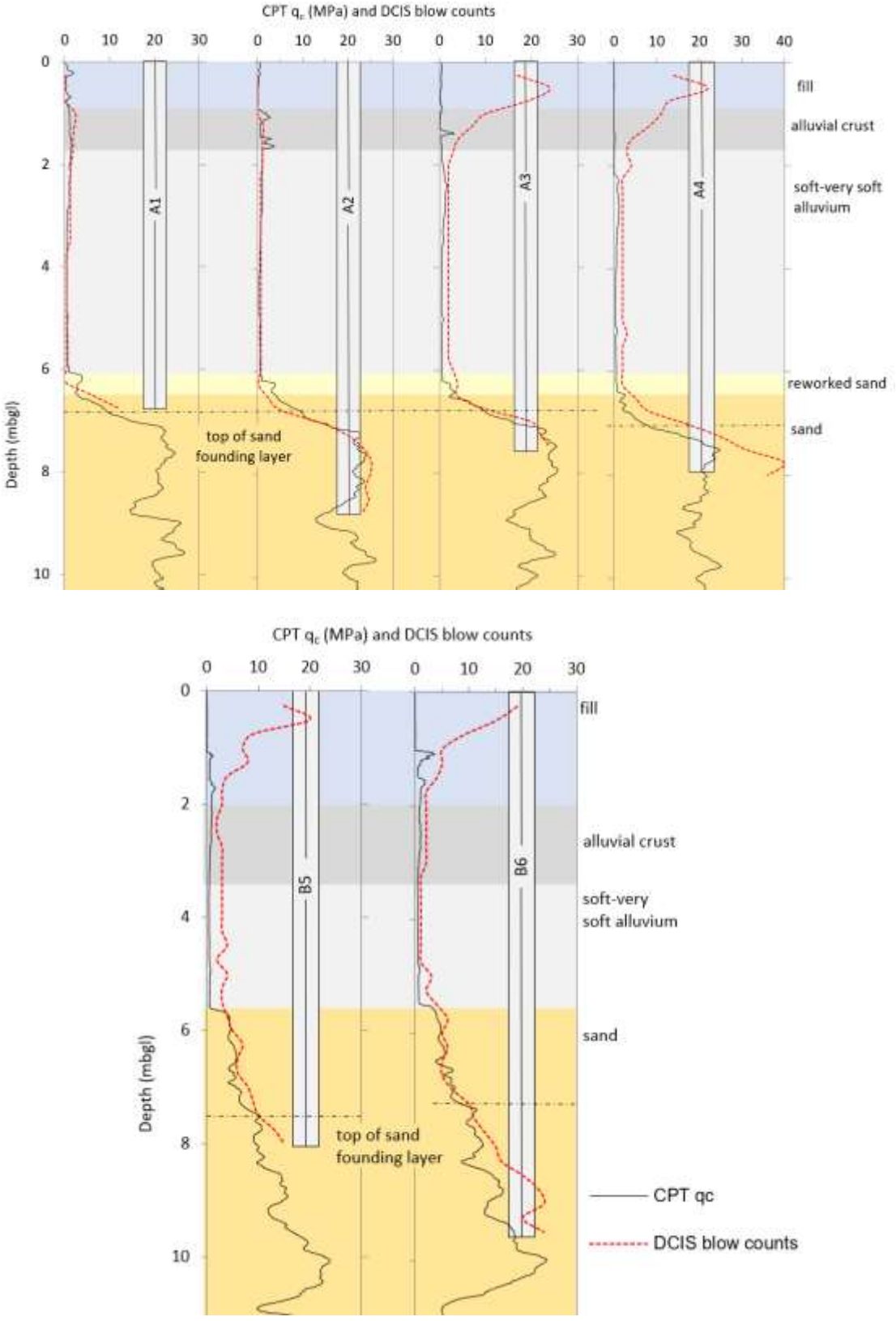


Fig. 1. CPT q_c and installation blow counts for six Avonmouth pile load tests

 © DFI International Bruges 2025

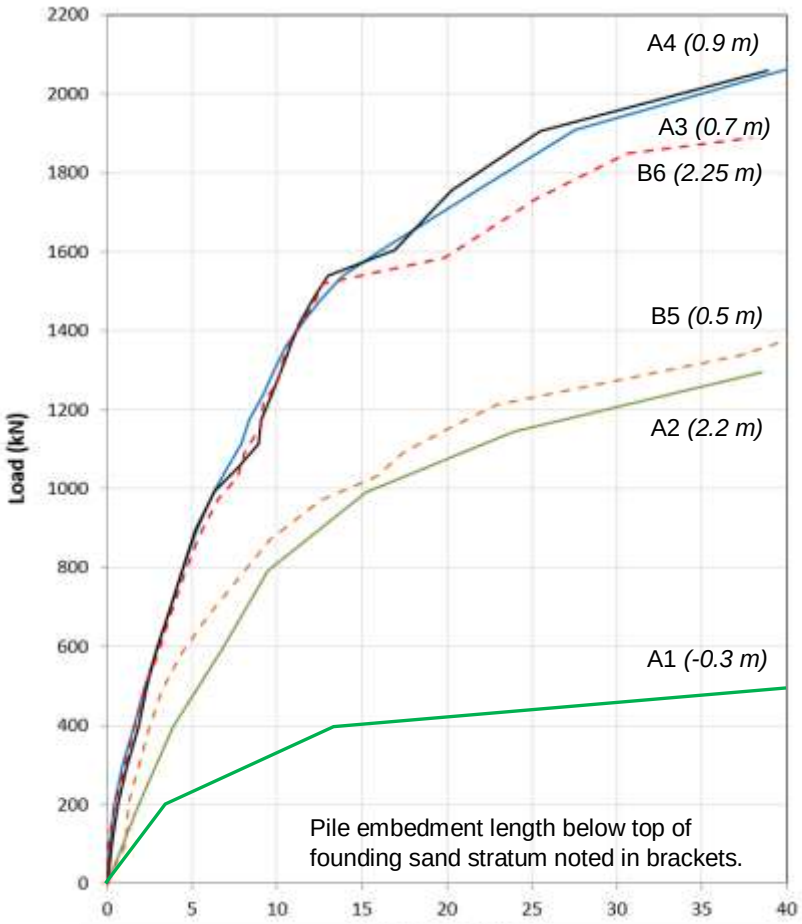


Fig. 2. Results of compression pile load testing

- Despite pile B6 being installed to 2.25 m embedment it recorded a lower total pile capacity than both piles A3 and A4 (with 0.7 m and 0.9 m embedment respectively). As illustrated in Fig. 1, both piles A3 and A4 were driven within a distinct two-layer stratigraphy whereby over a short distance (~0.5 m depth interval) the measured q_c values of the sand increased from 4 MPa to > 20 MPa and remained so for at least 1.0 m below the pile toes. In contrast, over the 2.25 m pile embedment length for B6 the measured q_c values gradually increased from 10 MPa to 18 MPa. Regardless, all three piles mentioned above recorded the highest applied loads at failure (> 1 900 kN).
- The failure load for B5 was considerably less than A3 despite similar embedment lengths, albeit < 2D. This is commensurate with the significantly lower q_c within the embedment length of the founding stratum for B5.
- The failure load for pile A2 (despite 2.2 m embedment) could be attributed to factors including the lower density sand lens underlying the pile toe; potential construction defects such as ground heave; and construction of three adjacent geotechnical boreholes (at 0.5 m, 0.8 m and 1.0 m offsets) possibly causing disturbance of sands at the pile toe. A2 was the only pile with nearby boreholes.

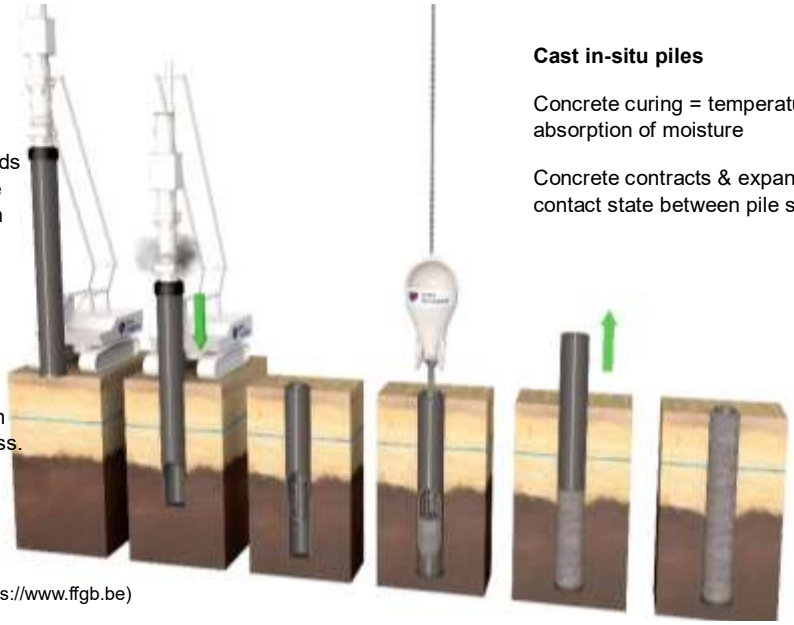
Assessment of the load – displacement curves (including back analysis by curve fitting to the recorded pile load settlement response using CEMSET CEMSOLVE V3; Fleming, 1992) supported that the pile loads were dominantly accommodated by base resistance. Shaft resistance was mobilised first at small displacements and then was observed to asymptote between 260 kN and 500 kN; typically at 380 kN applied load. The base resistance then continued to take load with increasing pile settlement.

 © DFI International Bruges 2025

Driven displacement piles

Compression & rebounds during driving = relative displacements between pile shaft & soils

Stiffness contrast between piles & soil rebounding deformation causing 'locked-in' stress.



Cast in-situ piles

Concrete curing = temperature increase & absorption of moisture

Concrete contracts & expands = changing contact state between pile shaft & soils

All piles

Soil consolidation from:
- excess pore pressure dissipation in cohesive soils
- groundwater drawdown
- surcharge load
-swelling in expansive soils.

Concrete swelling below

(image sourced from https://www.ffgb.be)

Fig. 3. Mechanisms contributing to the development of residual loads

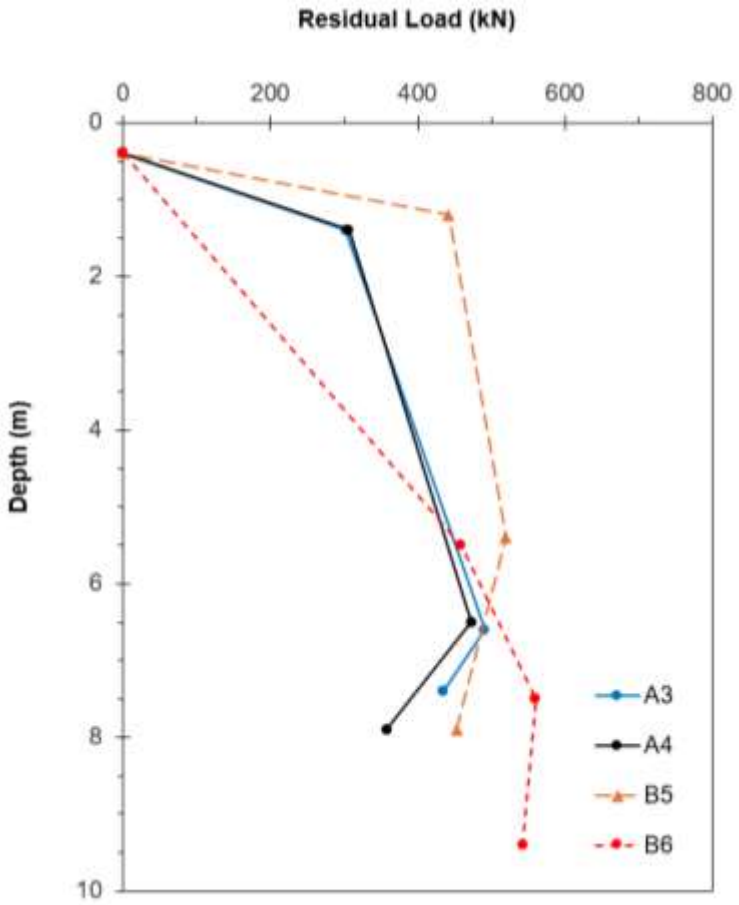


Fig. 4. Assessed residual loads in instrumented piles

 © DFI International Bruges 2025

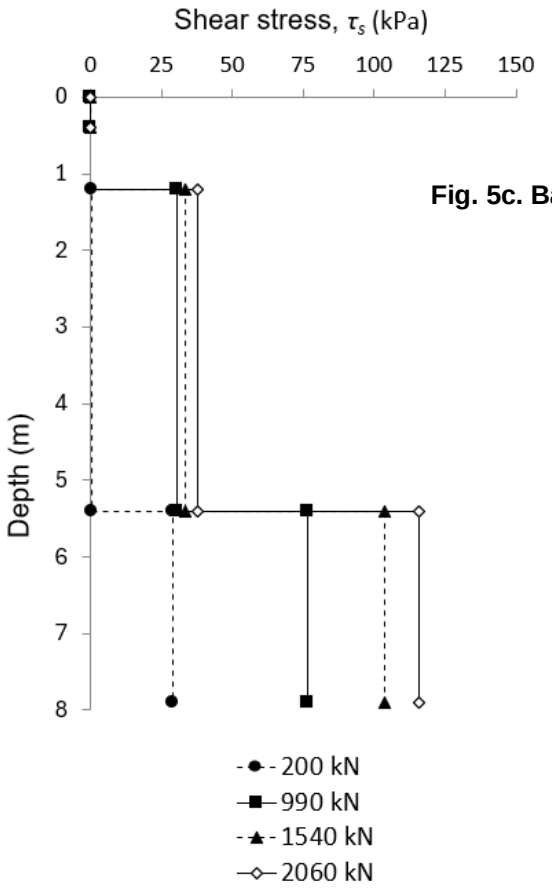


Fig. 5a. Example shaft resistance (pile A3)

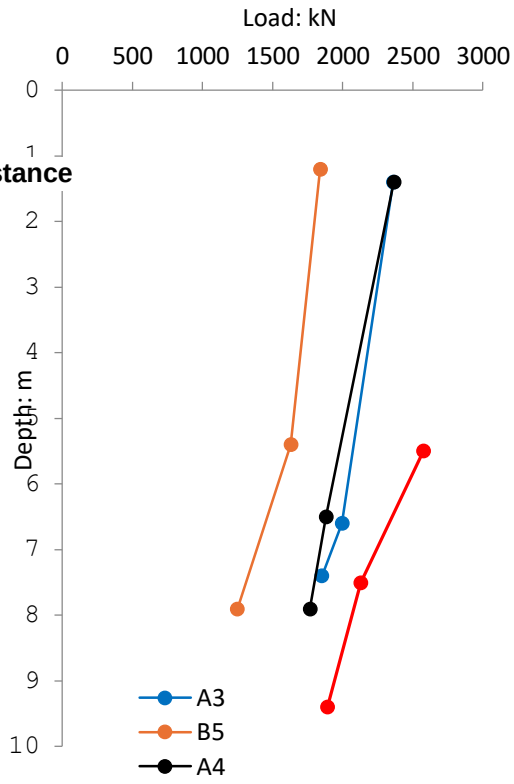


Fig. 5b. Load distribution with depth

Fig. 5c. Base resistance

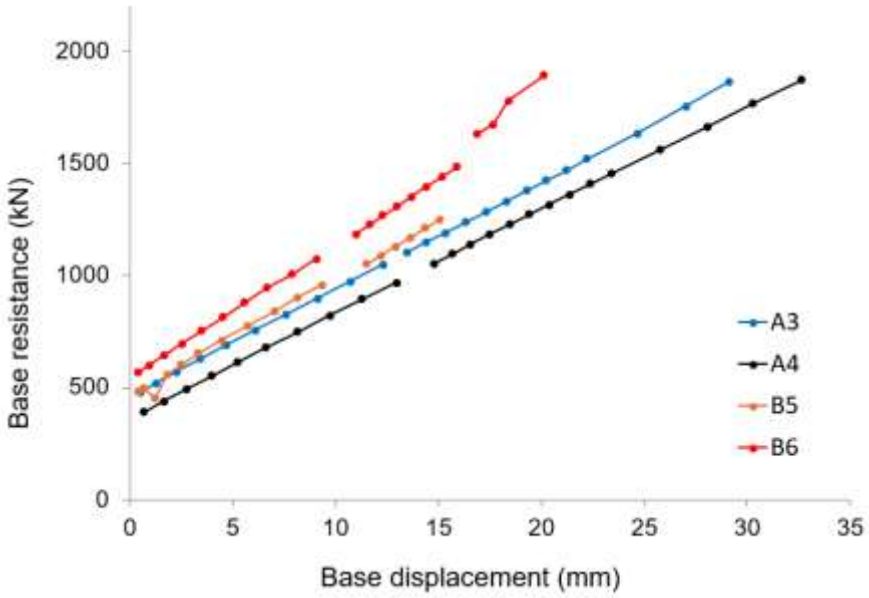


Fig. 5c. Base resistance

 © DFI International Bruges 2025

Residual loads and instrumented pile load tests

Residual loads that develop in the pile during and following construction, but before load testing, arise from a number of factors reflecting the character of this piling method; i.e. part preformed driven displacement and part replacement pile type (Fig. 3). When residual loads are present and not evaluated prior to application of load then the estimate of pile settlement is greater than if these residual loads are known. If residual loads are not recognised when interpreting pile load test results then the shaft resistance may appear greater than the true value and the toe (base) resistance less than the true resistance. The residual loads induce 'pre-stressing' in the pile. For example, with temperature effects during concrete curing the lower pile shaft (below the neutral point) moves downwards relative to the soil partly mobilizing available shaft resistance, and the upper pile shaft may have moved upwards (such that pile loading would have to reverse that shaft resistance).

Assessment of the residual load development in the four instrumented piles discussed herein (A3, A4, B5 and B6) is detailed in Packer (2022) and results shown in Fig. 4. At commencement of test load application the pile bases had already developed a load of 550 kN due to the residual loads produced during construction and curing.

The instrumented load test results were assessed in accordance with the analytical steps set out in Flynn and McCabe (2022). Fig. 5 presents findings including example shaft resistance from pile A3 for increasing applied loads up to final load at failure (Fig. 5a); load distribution with depth (Fig. 5b); and base resistance for all piles (Fig. 5c). Fig. 5a shows that the mobilised shaft resistance within the overlying soft estuarine clays approached ultimate capacity at less than half the total applied load at pile failure. Much of the overall shaft resistance for A3 is generated within the pile interval embedded in the underlying sands (as expected). Fig. 5b indicates that most of the pile load is accommodated in end-bearing. Pile base resistance with displacement (Fig. 5c) for all four instrumented piles show similar gradients of increasing base settlements with applied loads, but piles B5 and B6 exhibit smaller settlements for the same load. Pile toe settlements at failure varied from just 16 mm in B5 to 33 mm in pile A4.

CPT BASED PILE DESIGN METHODS

This section presents several commonly used CPT direct design methods (both simplified and advanced) to determine total pile capacities. The design method formulas and input parameters considered herein (and presented in Table 2) are those applicable to closed end driven piles in granular founding stratum and, for comparison, are those previously considered for DCIS case studies reported by Flynn *et al.*, 2014.

Simplified 'alpha' CPT methods

The simplified methods include LCPC (Butstamante and Gianeselli, 1981), and Unicone (Eslami and Fellenius, 1997). These are methods in which single, empirically derived, alpha coefficients are used to relate cone resistance q_c to local shear stress at failure τ_{sf} and base resistance q_b of a displacement pile in sand (Schneider *et al.*, 2008). The local shear stress at failure is expressed in general form as:

$\tau_{sf} = \left(\frac{q_c}{\alpha_s}\right) \leq \tau_{\text{s,lim}}$ where α_s is the shaft friction coefficient and $\tau_{s,lim}$ is the limiting value of shear stress

The LCPC method recommends α_s values for DCIS piles being double those for precast concrete piles. This implies that for an equivalent q_c the DCIS shaft resistance in sand is half that of the precast concrete pile. The base coefficient α_b varies with q_c for LCPC but is assumed constant at 1 for the Unicone method.

 © DFI International Bruges 2025

Recent advanced methods

Several recent methods (i.e. advanced methods) were developed (predominantly for offshore applications) which improve upon the simplified alpha methods. These advanced methods attempt to account for factors such as the degree of soil displacement and friction fatigue during installation, interface dilation at the pile shaft during loading and reduction in shaft resistance during tensile loading (Flynn, 2014).

The methods considered in this case study include Fugro-05, ICP-05, NGI-05 and UWA-05 (refer to Table 2 for references, formulas and commentary on CPT q_c averaging). Additionally, the White and Bolton (2005) technique applies a correction for partial pile toe embedment in two layered soils (i.e. into a dense founding stratum underlying a significantly weaker material) by weighting q_c. This correction was applied to the ICP-05 method for piles A1 to A4 where a distinct two-layer soil profile is evident (Fig. 1).

Results

Results are presented as ratios of CPT design capacity relative to measured total pile capacity (at failure) and are collated in Table 3. CPT design capacities for shaft and base components are presented in Table 4 and Table 5 respecitvely.

Results presented in Table 3 exhibit a wide range of predicted design capacities. The Fugro-05 method overpredicts total pile capacity for all six tests whilst the remaining methods typically underpredict total capacity, with some CPT methods as low as 40 % of the measured values. The UWA-05 method appears to most consistently predict a total pile capacity close to that measured from the pile tests. The only exception to this is for pile A2, for which the UWA-05 method significantly overpredicts the total capacity. Potential reasons for the failure of A2 have been discussed previously, and thus this pile test result may not appropriately represent actual pile capacity.

Interestingly, when considering the separate shaft and base capacity components (in Table 4 and 5, as assessed from the four instrumented pile tests), the Fugro-05 method most closely predicts both the individual shaft and base components.

Table 2. CPT direct design methods (applicable to closed end driven piles in sand)

Method	**Unit base resistance, q_b**	**Unit shaft resistance, q_s**	**CPT q_c averaging**
Unicone (Eslami & Fellenius, 1997)	$q_b = c_{te} q_{Eg}$ $q_E = (q_{c1}, q_{c2}, q_{c2} \ldots . q_{cn})^{1/n}$ c_{te} = 1.0 for $D \leq 0.4$ m; $\frac{1}{3}D$ for $D >$ 0.4 m	$q_s = c_{se} q_E$ $q_E = q_t - u_2$ c_{se} = 0.3 to 8%	q_{Eg} = geometric mean q_E (= q_t - u_2) values in 8D above and 4D below the pile toe
Fugro-05 (Kolk *et al.*, 2005)	$q_{b0.1} = 8.5 q_{c,avg} \left(\frac{p_{ref}}{q_{c,avg}}\right)^{0.5} A_r^{0.25}$ $A_r = 1$	$\frac{h}{R^*} \geq 4: q_s = 0.08 q_C \left(\frac{\sigma'_{v0}}{p_{ref}}\right)^{0.05} \left(\frac{h}{R^*}\right)^{-0.90}$ $\frac{h}{R^*} \leq 4: q_s = 0.08 q_C \left(\frac{\sigma'_{v0}}{p_{ref}}\right)^{0.05} (4)^{-0.90} \left(\frac{h}{4R^*}\right)$	$q_{c,avg}$ = arithmetic average of q_c values measured of 1.5D above and 1.5D below the pile toe.

 © DFI International Bruges 2025

ICP-05 (Jardine *et al.*, 2005)	$\frac{q_{b0.1}}{q_{c,avg}} = \max\left[1 - 0.5\log\left(\frac{D}{D_{CPT}}\right), 0.3\right]$ $q_{b0.1} = 0.3q_c$ for D > 0.90 m	$q_s = \text{a}\left[0.029bq_c\left(\frac{\sigma'_{v0}}{\rho r_{ef}}\right)^{0.13}\left[\max\left(\frac{h}{R^*}, 8\right)\right]^{-0.38}\right]$	$q_{c,avg}$ = arithmetic average of q_c values measured of 1.5D above and 1.5D below the pile toe.
LCPC (Bustamante & Gianeselli, 1982)	$q_b = k_b q_{c,eq}$ k_b = 0.4 to 0.55 (0.4 where q_c > 12MPa; 0.5 where q_c = 5 to 12 MPa)	$q_s = \left(\frac{1}{k_s}\right)q_c$ k_s = 30 to 150	$q_{c,eq}$ = arithmetic average of q_c values measured of 1.5D above and 1.5D below the pile toe.
NGI-05 (Clausen *et al.*, 2005)	$\frac{q_{b0.1}}{q_{c,tip}} = \frac{0.8}{1 + D_r^2}$ $D_r = 0.4\left[\ln\frac{q_{c,tip}}{22(p_{ref}\sigma'_{vo})^{0.5}}\right]$	$q_s = \left(\frac{z}{z_b\rho_{ref}F_{Dr}F_{sig}F_{tip}F_{load}F_{mat}}\right) \geq 0.1\sigma'_{v0}$ F_{Dr} = 2.1(Dr - 0.1)1.7; F_{tip} = 1.6 (closed-ended pile); F_{load} = 1.3 (compression); F_{mat} = 1.0(steel), 1.2(concrete) $F_{sig} = \left(\frac{\sigma'_{v0}}{p_{ref}}\right)^{0.25}$	
UWA-05 (Lehane *et al.*, 2005)	$\frac{q_{b0.1}}{q_{c,avg}} = 0.15 + 0.45A_{rb,eff}$ $A_{rb,eff} = 1 - FFR\left(\frac{D_i}{D}\right)^2$ $FFR \approx \min\left[1, \left(\frac{D_{i(m)}}{1.5_{(m)}}\right)^{0.2}\right]$	$q_s = \frac{f_t}{f_c}\left[0.03q_c A_{rs,eff}^{0.3}\left[\max\left(\frac{h}{B}, 2\right)\right]^{-0.5}\right]$ $A_{rs,eff} = 1IFR\left(\frac{D_i}{D}\right)^2$ $IFR_{mean} \approx \min\left[1, \left(\frac{D_{i(m)}}{1.5_{(m)}}\right)^{0.2}\right]$	q_b = 0.6q$_{c,avg}$ $q_{c,avg}$ = arithmetic mean of qc value 1.5D above and 1.5D below the pile toe
White & Bolton (2005)	CPT q_c averaging method for partial embedment correction where	$q_{c,corrected} = q_{c,weak} +$	$q_{c,corrected} = q_{c,weak+} \frac{(q_{c,hard} - q_{c,weak})\left(\frac{z}{D}+2\right)}{10}$

Table 3. CPT Design Q_c / Measured Q$_{t0.1D}$

Pile	Fugro-05	ICP-05	ICP-05 (W&B)	LCPC	NGI-05	Unicone	UWA-05
A1	1.93	0.78	0.50	0.86	0.73	0.92	0.99
A2	2.18	1.22	1.05	0.90	0.82	1.25	1.58
A3	1.10	0.80	0.32	0.68	0.66	0.42	1.05
A4	1.03	0.76	0.42	0.59	0.58	0.40	0.99
B5	1.34	0.64		0.59	0.55	0.69	0.82
B6	1.69	0.81		0.57	0.59	0.94	1.01

 © DFI International Bruges 2025

Table 4. CPT Design Shaft Q_{cs} / Measured $Q_{s,t0.1D}$

Pile	Fugro-05	ICP-05	ICP-05 (W&B)	LCPC	NGI-05	Unicone	UWA-05
A3	1.10	0.46	0.13	0.26	0.08	0.76	0.67
A4	1.03	0.52	0.52	0.24	0.08	0.53	0.76
B5	1.28	0.43		0.25	0.08	0.48	0.54
B6	0.94	0.26		0.12	0.03	0.20	0.30

Table 5. CPT Design Base Q_{cb} / Measured $Q_{b,t0.1D}$

Pile	Fugro-05	ICP-05	ICP-05 (W&B)	LCPC	NGI-05	Unicone	UWA-05
A3	0.92	0.77	0.32	0.68	0.71	0.27	0.98
A4	0.90	0.73	0.34	0.62	0.65	0.32	0.93
B5	0.94	0.53		0.55	0.59	0.56	0.68
B6	0.81	0.60		0.49	0.60	0.80	0.77

PUBLISHED DCIS PILE DATABASE

Table 6 presents the six Avonmouth pile tests CPT design method results with published case studies reported by Flynn *et al.* (2014). Only those direct design CPT results from DCIS piles constructed in layered soils and relying primarily on a granular socket base capacity are considered. Additionally, only those load tests taken to failure (pile head displacement = 0.1D) were included. Consequently, the six Avonmouth test pile cases presented herein effectively double the publicly available DCIS database.

Table 6. Results of CPT design methods for DCIS pile capacity

	CPT Design Q_c / Measured $Q_{t0.1D}$					
Site; Pile	Fugro-05	ICP-05	LCPC	NGI-05	Unicone	UWA-05
Avonmouth; A1	1.93	0.78	0.86	0.73	0.92	0.99
Avonmouth; A2	2.18	1.22	0.90	0.82	1.25	1.58
Avonmouth; A3	1.10	0.80	0.68	0.66	0.42	1.05
Avonmouth; A4	1.03	0.76	0.59	0.58	0.40	0.99
Avonmouth; B5	1.34	0.64	0.59	0.55	0.69	0.82
Avonmouth; B6	1.69	0.81	0.57	0.59	0.94	1.01
Erith; E3	1.29	1.10	0.83	1.07	0.95	1.01
Le Havre; A4	1.60	1.17	0.83	1.51	1.20	1.28
Le Havre; C1	1.37	1.01	0.72	1.30	1.04	1.10
Kallo; K5	1.43	1.11	0.88	0.97	1.00	1.04
Kallo; K6[b,c]	0.88	0.66	0.48	0.76	1.01	0.78
Kallo; K7	1.61	1.10	0.83	1.51	0.76	1.28

[a] Unicone method is referred to as EF-97 in Flynn (2014)

When considering total pile capacity using pile head load-displacement relationships for tests taken to failure (defined as pile head settlement = 0.1D), the UWA-05 CPT direct design method more closely (and consistently) predicts the measured pile test results.

The simplified LCPC design method consistently underpredicted the total pile capacity by as much as 50% of the measured result.

CONCLUSION

Observations from this case study include:

- Effects of residual loads and varying degrees of strain-softening can affect the interpretation of pile load tests. Low *apparent* values of base capacity can arise if residual stresses are ignored (White and Bolton, 2005). It is common practice to re-baseline pile instrumentation

 © DFI International Bruges 2025

prior to a load test with the intention to removing influences from pile construction. Consequently, this leads to an underprediction of base resistance and an overprediction of shaft friction.

- Instrumented pile tests allow for determination of shaft capacity at discrete intervals and base resistance with respect to displacement.
- Understanding the basis of design when using CPT correlations for pile design is key as well as identifying ground conditions specific to the pile location and to a sufficient depth below the pile toe. Different CPT design methods consider different depth ranges above and below the pile toe when estimating base capacity. For end-bearing piles such as the Avonmouth test piles presented herein, variations in the inferred pile base influence zone can result in significant differences in base capacity predictions. Additionally, thin lenses of weaker soils below the pile base can have considerable influence on the load-settlement distribution and pile base capacity.
- Similarities between DCIS shaft and base behaviour of the Avonmouth test piles and those of preformed driven piles by Flynn (2014) indicate that the appraisal of preformed pile design methods on a DCIS database is valuable. Flynn (2014) concluded from three simplified and four advanced CPT-based displacement pile design methods that the advanced methods typically gave the best estimates of DCIS total capacity, although capacities tend to be underpredicted by most methods. This may be attributed to enhanced interface friction between cast-in-situ concrete and surrounding soil, compared with preformed piles (although the applicability of this mechanism to DCIS piles is uncertain given that the DCIS driven steel tube is removed causing soil disturbance or remoulding of the adjacent soil).

Comparison of DCIS case studies presented herein suggests that the UWA-05 method most closely predicts total pile capacity at failure (with respect to applied loads at measured pile head displacements equivalent to 0.1D), and the Fugro-05 advanced CPT method best predicts the individual shaft and base components when compared with instrumented pile tests.

REFERENCES

White, D.J. and Bolton, M.D. 2005. Comparing CPT and pile base resistance in sand. Geotechnical Engineering, 158(1) pp. 3-14.

Bustamante, M. and Gianeselli, L. 1982. Pile bearing capacity prediction by means of static penetrometer CPT. In Proc. 2nd European Symposium on Penetration Testing, Amsterdam, The Netherlands. pp. 493-500.

Clausen, C.J.F., Aas, P.M. & Karlsrud, K. 2005. Bearing capacity of driven piles in sand, the NGI approach. 2005. In Proc. 1st Int. Symposium on Frontiers in Offshore Geotechnics, Perth, Australia. pp 677-681.

Eslami, A. and Fellenius, B.H. 1997. Pile capacity by direct CPT and CPTu methods applied to 102 case histories. Canadian Geotechnical Journal 34(6): 886-904.

Fellenius, B.H. (2001). What capacity value to choose from the result of a static loading test. We have determine the capacity then what? Two articles reprinted from Deep Foundation Institute, Fulcrum. Winter 2001, pp. 19-22, and Fall 2001, pp. 23-26.

Fleming, W.G.K (1992) A new method for single pile settlement prediction and analysis. Geotechnique 42, No. 3, 411-425.

Flynn, K.N. and McCabe, B.A. 2022. Instrumented concrete pile tests – part 2: strain interpretation. Proceedings of the Institution of Civil Engineers - Geotechnical Engineering 2022 175:1, 112-135

Flynn, K.N. 2014. Experimental investigations of driven cast-in-situ piles. PhD thesis (in preparation), Department of Civil Engineering, National University of Ireland, Galway, Ireland.

 © DFI International Bruges 2025

Flynn, K.N., McCabe, B.A., Egan, D. 2014. Driven cast-in-situ piles in granular soil: applicability of CPT methods to pile capacity estimation. Proceedings of the 3rd International Symposium on Cone Penetration Testing (CPT ’14), Las Vegas.

ICE, Institute of Civil Engineers (2007) Specification for Piling and Embedded Retaining Walls. Second edition. Institution of Civil Engineers. Thomas Telford Ltd.

Jardine, R.J, Chow, F.C., Overy, R.F. & Standing, J.R. 2005. ICP design methods for driven piles in sands and clays. Thomas Telford, London, UK.

Kolk, H.J., Baaijens, A.E., & Senders, M. 2005. Design criteria for pipe piles in silica sands. In Proc. 1st Int. Symposium on Frontiers in Offshore Geotechnics, Perth, Australia. pp. 711-716.

Lehane, B.M., Schneider, J.A. & Xu, X. 2005. The UWA-05 method for prediction of axial capacity of driven piles in sand. In Proc. 1st Int. Symposium on Frontiers in Offshore Geotechnics, Perth, Australia. pp. 683-689.

Packer, M.L. (2022). Residual load development case study in driven cast-in-situ piles. DFI-EFFC International Conference on Deep Foundations and Ground Improvement: Smart Construction for the Future, Berlin.

Schneider, J.A., Xu, X. & Lehane, B.M. 2008. Database assessment of CPT-based design methods for axial capacity of driven piles in siliceous sands. Journal of Geotechnical and Geoenvironmental Engineering 134(9): 1227-1244.

 © DFI International Bruges 2025

STATE OF PRACTICE FOR QUALITY CONTROL IN DRILLED FOUNDATIONS

George Piscsalko, PE, Pile Dynamics, Inc. Solon, Ohio USA 216-831-6131, gpiscsalko@pile.com
Dr.-Ing. Matthias Schallert, GSP mbH, Mannheim, Germany, +49 621 331361, ms@gsp-mannheim.de
Jon Sinnreich, PE, GRL Engineers, Solon, Ohio, USA 216-831-6131, jsinnreich@grlengineers.com

ABSTRACT

Drilled foundation elements are increasingly being used for deep foundation support. The trend is for larger diameter elements carrying much higher loads. Many of these drilled foundations are cast under slurry, making direct inspection difficult. Some legacy non-destructive testing (NDT) methods are not well suited for the inspection needs of modern drilled foundation elements. The as-built pile shape, pile vertical alignment, pile base cleanliness, cage alignment, concrete cover, and concrete integrity may be important to satisfy the design intent. Additionally, there is a need to demonstrate the capacity of these highly loaded bored piles. Several test methods are available to check these design considerations. Many current test methods are unable to provide all the information needed or do not address all design considerations. There have been several recent advances in bored pile quality control instrumentation and testing. These recent advances in bored pile quality control methods offer owners, engineers, and contractors innovative and powerful tools for quality control and quality assurance of drilled foundations. This paper discusses recent advances in quality control methods for drilled foundation elements and presents field data where these technologies have been successfully used for evaluation of bored piles.

INTRODUCTION

Bored piles are an increasingly popular choice for deep foundation elements due to the large axial and lateral loads that can be supported on the elements. More recently, the trend has been larger diameters to further increase the applied loads. These piles can be cast in a dry condition if the surrounding soils are sufficient to hold the excavation open. If cast in a dry condition, the excavation may be directly inspected prior to concreting, but inspection can become difficult depending upon the pile diameter and length. If the soil conditions are such that support fluid is needed to stabilize the excavation, it is difficult or impossible to inspect these excavations prior to concreting, regardless of length or diameter. Due to the nature of the installation, it is also impossible to visually observe concrete placement. Considering that it is difficult to inspect the excavations prior to concreting and impossible to visually observe concrete placement, the integrity of these piles is often unknown.

Some traditional Non-Destructive Test (NDT) methods are insufficient for many modern foundation designs. New NDT methods are available that can overcome some of the limitations of legacy methods, allowing bored piles to be thoroughly tested to help evaluate that the as-built foundation meets the design intent. These modern NDT methods allow engineers to accurately and easily measure the verticality of the excavation and the cleanliness of the pile base prior to concreting. The integrity and as-built shape including the concrete cover outside of the reinforcing cage after concreting can also be evaluated. Additionally, these large piles are intended for much higher loads than previous, and axial load testing these large capacities is also possible and routinely performed. These methods are described below.

In wet cast installations, the pile sidewalls are frequently profiled to determine the pile shape from the excavated area as well as pile verticality. Mechanical devices have proven to be slow and lack the needed resolution. Today there are devices utilizing ultrasonic pulse to measure the radii along the length of the pile and from this determine the shape of the excavation and the veridicality. The ease of use and speed of testing allow for all piles to be tested to ensure that the piles all meet the required verticality design specifications.

 © DFI International Bruges 2025

The integrity of the as-built pile is another important parameter that needs to be assessed for any successful project. There are various legacy NDT techniques that do not provide all the needed information to ensure that the integrity of the piles is confirmed, but also that the durability is likely to be achieved due to the concrete quality and concrete volume placed outside of the reinforcing cage. When assessing integrity in cast-in-place foundations via the thermal profiling method, many of the limitations of the legacy methods are overcome and the entire cross-section including the area outside the reinforcing cage can be evaluated. The concrete outside the reinforcing cage is especially critical for designs intended for high lateral loads and seismic loads where there is typically large amounts of steel in the reinforcing cage design. The concrete cover, or concrete in the area between the outside of the reinforcing cage and the surrounding soil, protects the steel from groundwater and caustic soils which can deteriorate the steel causing a loss in lateral load capacity.

Finally, with the trend for larger bored piles, the ability to load test these piles have become challenging. A top-down static load test is very costly and time consuming and can be unsafe at these very high loads. Bi-directional load testing has solved these issues as the test is typically faster than a top-down static load test and the jacks are embedded in the pile, so they are much safer, more sustainable and allow the engineers to measure the pile resistance and the toe resistance.

To check that the design intent has been satisfied, the as-built pile shape, vertical alignment, base cleanliness, reinforcing cage alignment, concrete cover, pile integrity, and pile load bearing capacity are all important to evaluate. There are several legacy quality control and load test methods and devices used to evaluate many of these design considerations, but each has limitations that do not allow all aspects of the foundation design to be evaluated. This paper will discuss the limitations of some legacy quality control inspection methods and load testing methods, detail new state-of-practice quality control methods for bored piles and provide field examples where these tests have been successfully employed.

Legacy Integrity Testing Methods and Limitations

There are several legacy integrity testing methods readily available that are commonly used to assess bored piles. The most used legacy methods are the Low Strain Impact Echo test and the Ultra-sonic Cross Hole method. The low strain method is fast and economical, and requires no pre-planning to perform a test, but lacks the precision to identify anomalies located in the top and bottom portion of the pile. The relatively large pulse width (typically greater than 3m or 10 ft.) from the impact hammer can mask an anomaly in the upper portion and the unknown wave speed makes it difficult to identify a soft bottom. Studies have shown that most defects occur in the upper and lower portion of cast-in-place foundations, severely limiting the effectiveness of the low strain method. In case of long and slender piles a reliable assessment of the pile quality in the lower section is often not possible. In typical non-cohesive soils (e.g. sands, gravel), the limitation may be roughly defined at a ratio of diameter to length between 1/20 to 1/30. In stratified and cohesive soils and solid rock this limit is significantly lower. Thus, the Low Strain Impact Echo method is often not suitable for modern foundation designs.

Cross Hole Sonic Logging (CSL) is another legacy method with widescale usage. The CSL test is conducted by lowering transmitter and receiver probes into preinstalled access tubes which are cast into the pile. The probes send a line-of-sight ultrasonic pulse from transmitter to receiver. The timing and the amplitude of these received signals are used to evaluate concrete integrity. The only regions the CSL method scans are those in the direct path of the transmitted signal which completely omits the area outside the reinforcing cage. Additionally, the CSL access tubes can de-bond from the concrete and create received signals that appear to be delayed in time and weak in amplitude, suggesting a severe defect when it is de-bonding due to the differences in the thermal coefficient of expansion for the access tube and the concrete. The CSL method can be susceptible to these and other false positive results which may cause unnecessary delays and costs to projects. However, CSL is not limited by foundation length.

 © DFI International Bruges 2025

State-of-the-Art Integrity Test Methods

The most recent integrity testing method for drilled foundations is the Thermal Integrity Profiler (TIP). The TIP method utilizes the naturally occurring heat of hydration to assess the concrete integrity, concrete cover, and cage alignment. The TIP method uses Thermal Wire® cables attached to the reinforcing cage evenly distributed at a frequency of one wire for each 305 mm (12 inches) of pile diameter and rounded to the nearest whole number. The Thermal Wire cables have digital temperature sensors evenly spaced every 0.3 m (1 foot) along the length of the wire. Once the pile has been cast, the data loggers are attached to the Thermal wires and data collection begins automatically, with samples from each sensor taken once every 15 minutes until the pile reaches peak temperature which usually occurs in 18 to 48 hours after casting is complete. Figure 1 presents a photograph of the Thermal Wire cables attached to the reinforcing cage and extending above the top of a fully cast pile with the end of each cable attached to a data logger.



Figure 1. Thermal wire cables attached to data loggers

There is one data logger (TAP-EDGE™) attached to all but one wire. This last wire is attached to a specific data logger (TAG™) which contains a cellular modem for communicating data from the site to the ATLAS™ Cloud. With the information being sent from the site to the cloud, the site visits from testing agencies are minimized or eliminated. The data are sent in regular time intervals (every 15 minutes) during this early portion of the hydration process. Once peak temperature has been reached in the pile, data collection can end, and the testing agency can immediately start the data analysis. Data transfer using the cloud server reduces data collection costs as well as accelerates data analysis and reporting. Adding the volume placed to the TIP records allows temperature data to be converted to effective radius through the following relationship:

$$\text{Local Effective Radius} = \left(\left(\frac{average_radius}{average_temp}\right) * local_temp\right)$$

 © DFI International Bruges 2025

Knowing the volume and length allows the average radius to be calculated. Temperatures are measured along the length allowing the overall average temperature to be determined. The ability to estimate concrete over the full cross-section along the entire length of the pile allows designers and engineers to have confidence that the as-built piles are meeting their design intent. Evaluating concrete cover is particularly important for laterally loaded piles.

Once the data has been received, the temperature of each sensor on each wire is scanned for local reductions in temperature. This results in a temperature versus depth profile as illustrated in Figure 2 (left). The local temperature reduction near 27.4 m (90 feet) indicates a local anomaly and potential flaw or defect.

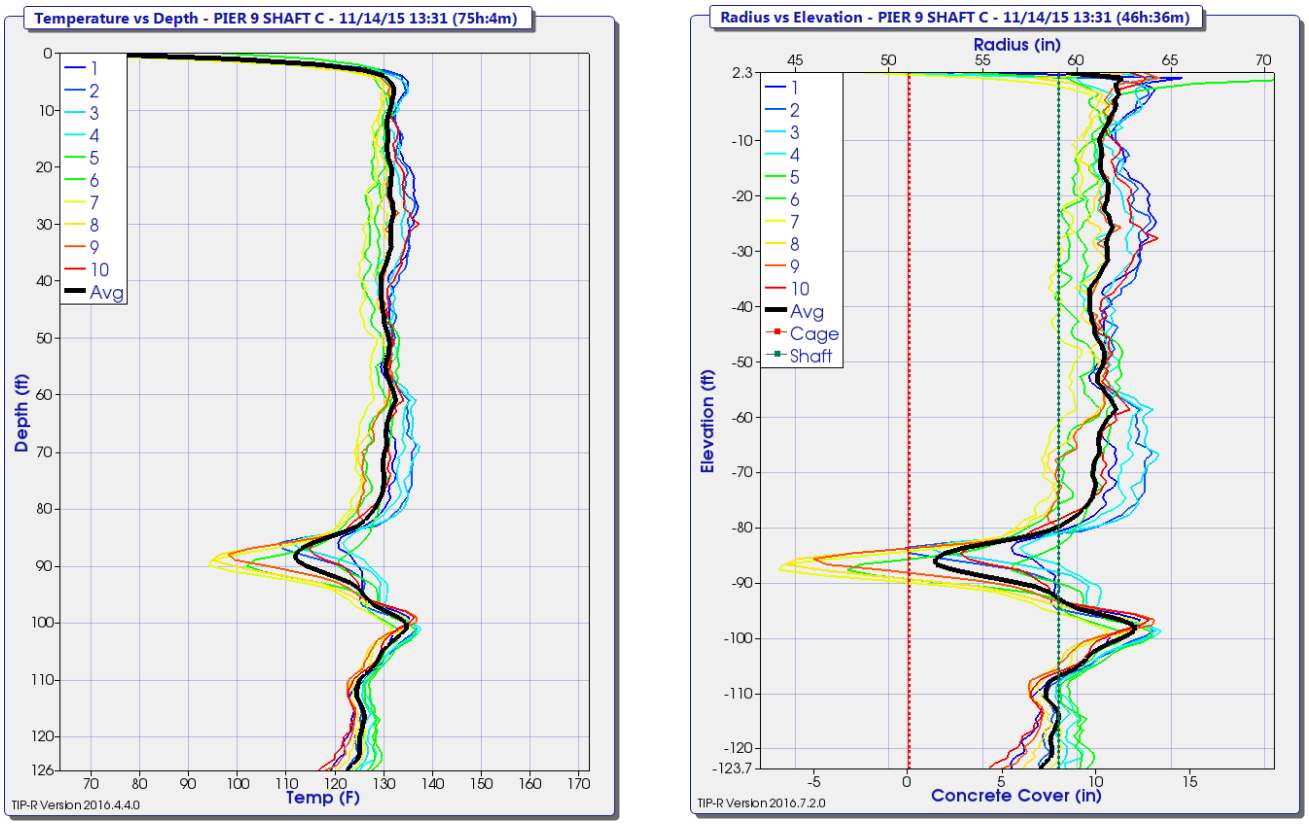


Figure 2. Thermal results of temperature vs depth (left) and radius vs elevation (right) for the same bored pile with a defect at 27.4 m (90 ft.)

Once the volume has been obtained, the above formula is used for the temperature-to-effective-radius conversion. From these radii conversions the effective pile radius along the length of the pile is obtained. Figure 2 (right) presents a plot of the effective pile radius versus depth. Figure 2 (right) also includes the concrete cover versus depth with zero being the point where the reinforcing cage is located. Anything to the left of this zero-cover point indicates that an anomaly may exist inside the reinforcing cage. The individual wires with locations can show the quadrant where the reduction occurs.

In addition to assessing the integrity of bored piles, the TIP method can also detect any eccentricities in the reinforcing cage. This is done by comparing temperature measurements from diametrically opposite locations compared to the average temperature. If a temperature measurement in the first location is warmer than the average while the diametrically opposite location is equally cooler than the average temperature, then this warmer location is closer to the core of the pile while the cooler opposite location is closer to the soil interface.

 © DFI International Bruges 2025

PILE SHAPE EVALUATION METHODS

The shape and verticality of a bored pile is critical in many instances. Several methods have been utilized in the past with varying degrees of success. These range from concrete volume plots and weighted tape measurements to mechanical calipers. All these methods lack the data required to determine verticality and can at best provide a rough concept of the overall shape of the excavation.

The current state of practice in many places is the use of ultrasonic devices to measure the radius as a function of depth. Once all radii along the length have been measured, the verticality of the pile can be determined. The modern devices can be attached to a Kelly bar to both keep test engineers away from the open holes but also to expedite the testing process. One such device, the Shaft Area Profile Evaluator (SHAPE) from Pile Dynamics, Inc., can be lowered at a rate of 0.3 m (1 ft.) per second which allows for even a very long pile to be tested in minutes. This great improvement in the speed of acquiring the data allows concreting to begin in a much shorter time than is possible with other technologies.

The SHAPE device samples eight ultrasonic sensors once per second throughout the testing period. The sensors are equally distributed around the SHAPE body, located 45 degrees apart from the others. The use of eight sensors allows for high resolution in the data acquisition without the need to stop at each measurement location or rotate the device to get sufficient coverage. To compensate for cases when the slurry density changes with depth, there is an integrated self-calibrating feature which automatically adjusts for changes in wave speed with depth, greatly improving the accuracy of the computed radii.

Using this new SHAPE technology allows the test to be easily and accurately completed. The speed and accuracy that the pile radii and verticality can be determined and reported allows the bored pile verification process to proceed efficiently. This allows the concrete to be placed in the excavation quickly, further improving quality control and quality assurance of the bored pile while not delaying the construction schedule.

BI-DIRECTIONAL STATIC LOAD TESTING (BDSLT)

Bi-directional testing was first conceived by various researchers and practitioners perhaps as early as the 1960's (Amir, 1983). More widespread documented use first appeared in the 1980's in Brazil, Japan and the United States, as described by Fellenius (2015). Bi-directional static load testing (BDSLT) is now a common and widespread practice in deep foundation engineering and construction. As of 2018, it has its own American Society of Testing and Materials (ASTM) standard (ASTM D8169/D8169-M-18).

The basic premise of BDSLT is quite straightforward. By embedding the loading apparatus within the foundation element rather than applying load at the element head, the need for an external reaction system is eliminated, and significantly higher loads can be generated safely. The tradeoffs to the traditional static load test method are primarily the loss of sacrificial equipment (hydraulic equipment and instrumentation) and the additional assumptions and more complex analysis of the test data necessitated by the reversed loading of the upper foundation segment. On the other hand, BDSLT provides measurement of the load in the pile that is unaffected by residual force or the effects of nearby reaction piles or a reaction mass, ensuring a greater reliability in the evaluation of the axial load distribution. In recognition of its advantages, BDSLT has grown in popularity worldwide and is accepted by many local, regional and national agencies responsible for overseeing foundations and the construction industry in general globally. Fig. 3 shows the principle of BDSLT.

 © DFI International Bruges 2025

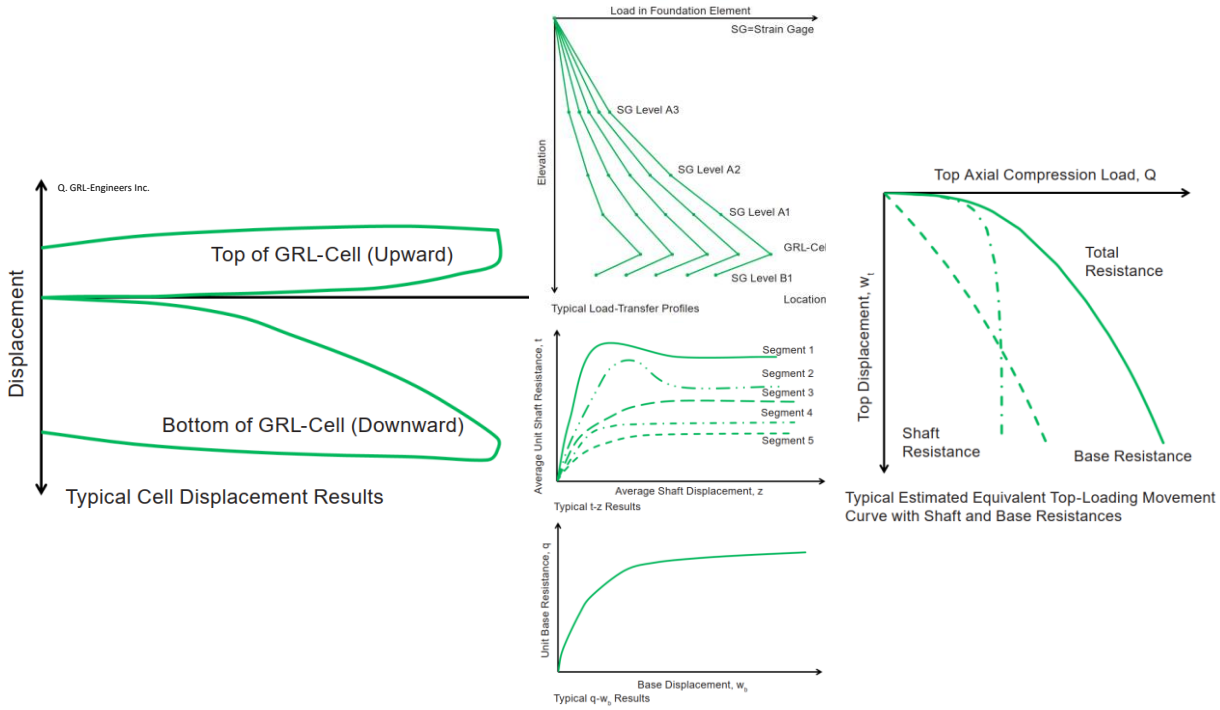


Figure 3. BDSLT schematic principle: left: load-displacement-behavior at GRL-Cell level, middle: strain distribution (top) derived unit pile resistance (center), toe resistance, right: estimated equivalent Top-Loading load-displacement-behavior.

BDSLT testing can typically be carried out for any type of cast-in-place foundation element, including bored piles, augercast grout piles and barrettes. The load test assembly consists of one or more sacrificial hydraulic jacks, connected to the foundation reinforcement steel via horizontal bearing plates and/or vertical gusset plates. Hydraulic hoses connect the jack(s) to the ground surface, so that the jack(s) can be pressurized and the foundation element loaded once the cast-in-place concrete or grout achieves adequate strength (typically 7 to 14 days after casting). Because the size and number of jacks installed in the foundation is only constrained by the available cross-sectional area, significant loads can be generated. In common practice, the pressurizing hydraulic fluid is clean fresh water, since the jacks are one-time use. Because the pressurized hydraulic system is buried deep underground, the method is intrinsically safe. Use of water instead of hydraulic oil makes the method environmentally friendly in case of any spills or leaks.

Field examples

In Southern Hamburg, Germany a new highway is planned to be constructed, connecting two existing highways in the east-west direction. Due to the local ground conditions and existing waterways elevated structures are planned. The bridge across the river Southern Elbe including foreland bridges and other parts of the highway will be founded on a large number of bored piles.

As part of a comprehensive investigation program, test piles with different properties have been installed on several test fields along the planned route. These piles have been tested using various methods. Some of the test piles have been designed with pile toe expansion (bells) up to a maximum diameter of 2.7 m compared to 1.5m regular pile diameter. Extensive investigations were carried out

 © DFI International Bruges 2025

to ensure the pile quality including load tests as a prerequisite for an economical design of the structural piles. The basic objectives were the validation:

- of the pile geometry (with respect to the pile toe expansion) and structural integrity,

- of the bearing capacities (skin and toe resistances) of different pile types and dimensions compared to the assumptions made in pile design calculations based on soil investigation results and local experience.

Different methods were used to determine the borehole geometry and verticality, paying particular attention to the pile sections with pile toe expansion, including the ultrasonic measurements using the SHAPE.

Borehole investigation using the SHAPE:

19 piles total have been investigated using the SHAPE device (fig. 4), one of them battered (10:1), 15 piles with pile toe expansion, 1 fully cased water supported, others bentonite slurry supported.

Figure 5 shows that the arrival of the ultrasonic wave is clearly detected in the water-supported borehole from all of the 8 channels. The result in bentonite slurry drawn below shows a clear result as well. However, interfering influences are also detected in the slurry, i.e. reflections from material present in the suspension. The wave speed calibration pulse also is shown on the bottom of each graph.

Figure 6 shows a result of detected radii vs. depth for a pile of 90 cm diameter and approx. 37 m length. The measured radius in meter is shown on the x-axis for all 8 ultrasonic sensors. The maximum target pile toe diameter was 1.65 m (blue-grey line). With a sand content of 2 % and a marsh funnel time of 37 s, the slurry properties were within the preferred range. The measured maximum toe diameter (dark blue line) was 1.55 m in the selected example. Accordingly, it was concluded the pile toe expansion was built as planned.



Figure 4. SHAPE – Test using the Kelly-bar

 © DFI International Bruges 2025

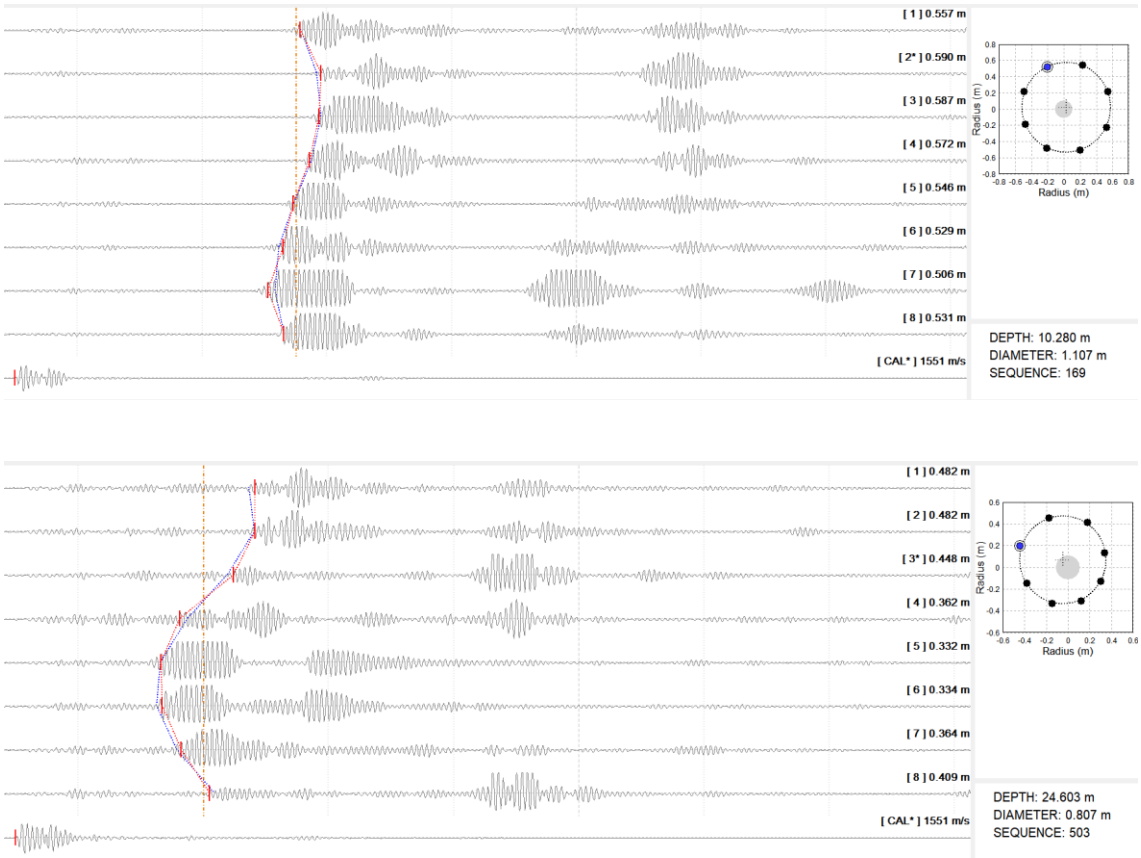


Figure 5. SHAPE-results in water- (top) and bentonite slurry supported borehole (below)

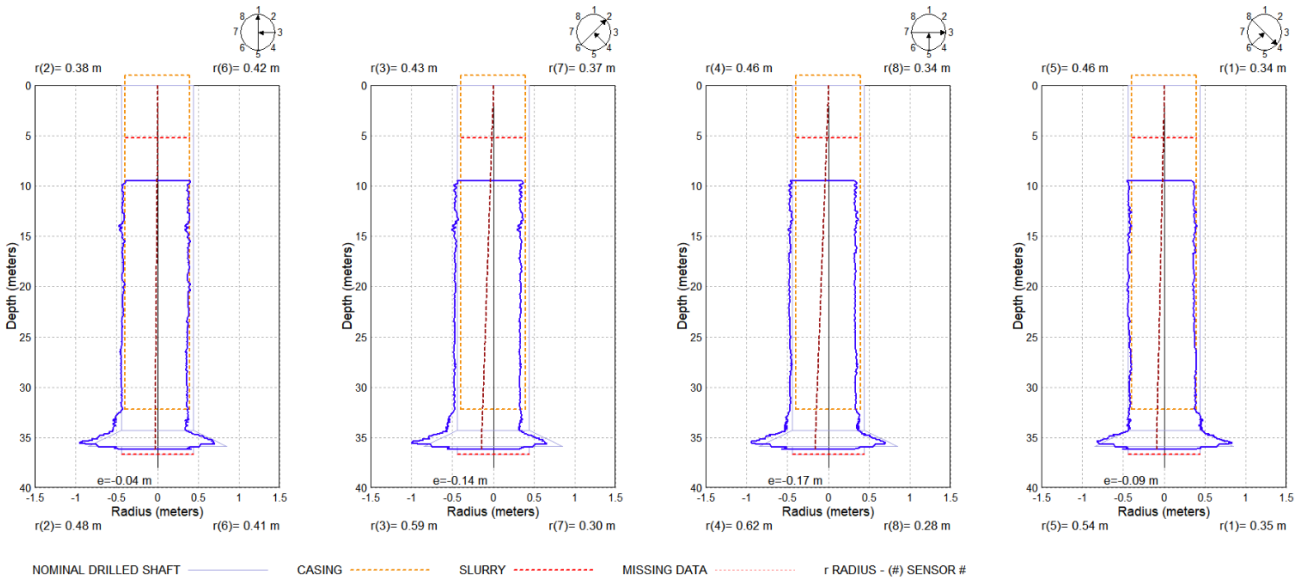


Figure 6. SHAPE-result of a bored pile with pile toe expansion, radii vs. depth

 © DFI International Bruges 2025

Thermal Integrity Testing using the TIP:

In addition, on a few selected piles Thermal Integrity Tests using PDI's TIP-system have been performed. For long piles, as in the example, where the reinforcement cage is assembled from two or more sections, the Thermal Wires® (TW) have been installed at each cage section, then connected by waterproof plug-in connection at the time of assembling the cages to one piece over the borehole (fig. 7). This type of assembly is particularly advantageous for a continuous ongoing construction process without delay.

Figure 8 shows an example of the result of an intact pile without toe expansion. This pile was partially cased up to approx. 12 m below ground level with an outer diameter of 118 cm and below this level it was bentonite slurry supported up to 24 m depth with a diameter of 106 cm. Based on the measurement, this pile has been classified in assessment class A1 according to the guidelines given in German Recommendations on Piling (EA-Pfähle, Moormann 2020). No significant impairment (defect) of pile quality was found based on the TIP-test.

To support this assessment based on the temperature readings, the pile radius was estimated vs. depth using the TIP Reporter software considering the volume used for the pile. The result of this calculation is given in figure 9 and supports the assessment according to EA-Pfähle. Due to an overconsumption of placed concrete of 28% a larger radius as planned has been assessed as plausible.

Based on internationally applied guidelines (Piscsalko 2016), this method can be used to pragmatically evaluate the results with regards to the pile quality, which is very important for the structural engineers involved. Temperature measurements alone do not provide a reliable quantitative estimate of the radius.



Figure 7. Waterproof connection of TW® (left side) and TW® function control before concreting (right side)

 © DFI International Bruges 2025

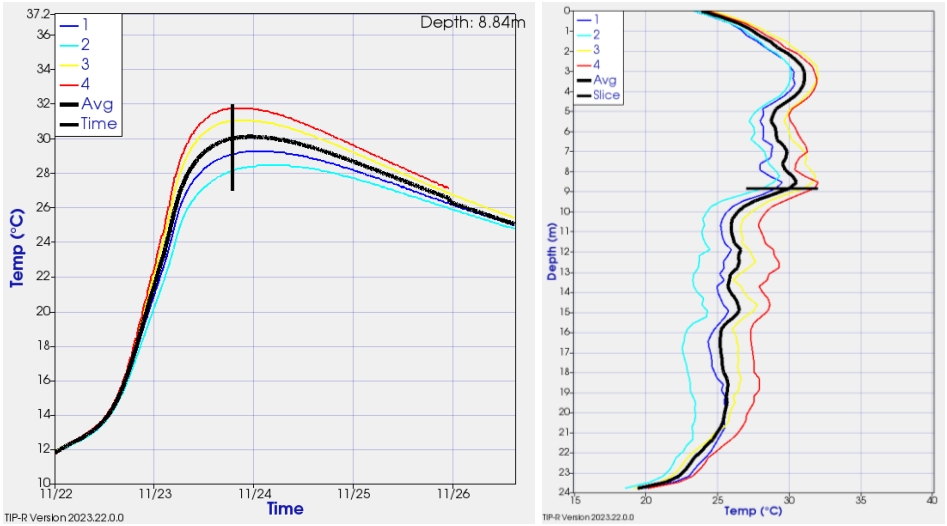


Figure 8. TIP-result – bored pile without pile toe expansion: left side – Temperature vs. Time at a selected depth (8,84 m), right side – Temperature vs. depth at approx. the time of max. Temperature

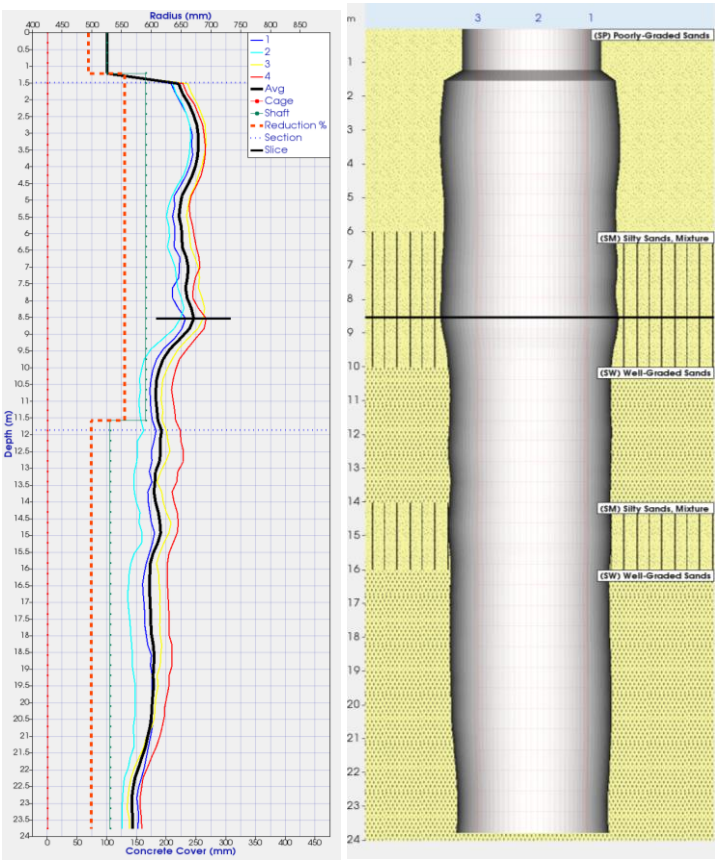


Figure 9. left side – effective radius vs. depth compared to target radius (green), radius of cage (red) and 6% radius reduction indicator (orange), right side - pile profile

 © DFI International Bruges 2025

At another tested pile the SHAPE results showed that the pile toe expansion was not installed successfully in a non-cohesive sand layer. The diameter measured was significantly less than expected and the max. diameter found was located approx. 1 m higher compared to the design. This result has been verified by Thermal Integrity Testing using the TIP system. Only a small increase in temperature was measured and the peak temperature at the pile toe section was found also approx. 1 m above the expected peak value. The maximum average diameter obtained by TIP is 1.5 m. The SHAPE result showed 1.65 m diameter, and the planned diameter was 2.2 m. This result impressively demonstrates the abilities of both quality control methods.

Figure 10 shows the result of the SHAPE recordings. Data starts at approximately 7 m below ground where the device is fully entered in the bentonite slurry (slurry level - red dotted line). Radius vs. depth obtained from TIP recordings after the concrete was placed up to ground level are shown in figure 10 middle and right side.

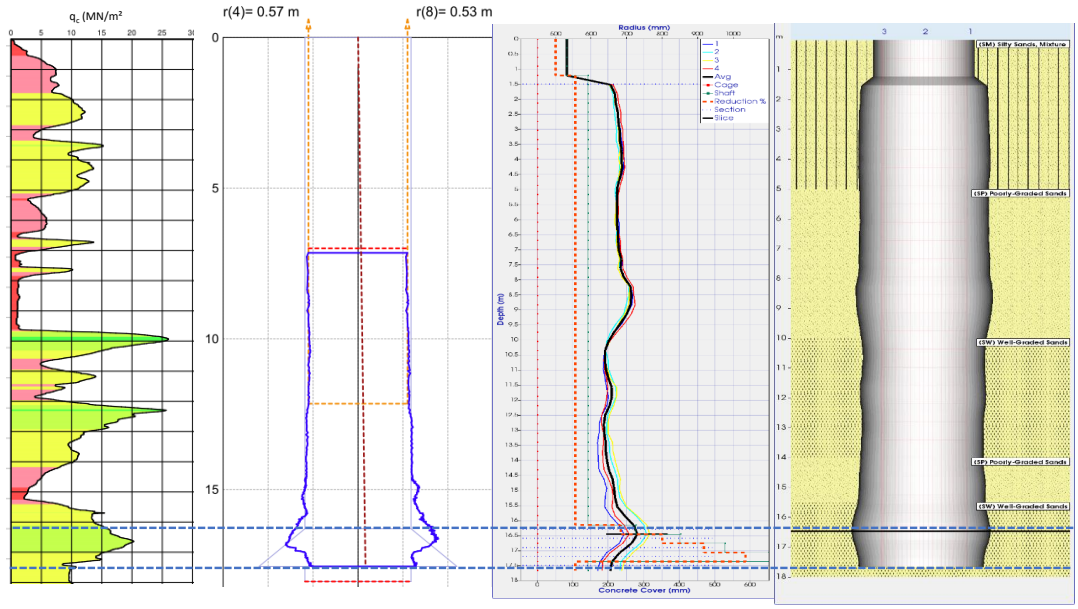


Figure 10. Comparison of SHAPE and TIP results: left side: Ground conditions, CPT-cone tip resistance (MN/m²), middle left: radius vs. depth (SHAPE), max. avg. toe diameter 1.65 m. middle right: radius vs. depth (TIP), max. avg. toe diameter 1.5 m, right: pile profile (TIP).

Verification of piles bearing capacity:

In addition to static instrumented pile load tests, dynamic load tests (DLT, DIN EN ISO 22477-4:2018-07) have been executed using heavy drop masses of up to 50 tons on 16 of the bored piles (Schallert et al. 2024). Depending on the soil conditions and pile dimensions, ultimate bearing capacities of up to 35 MN have been demonstrated by DLT and have been compared to the static load test results by the project involved geotechnical experts (Stahlhut et al. 2024). The DLT of the 16 piles have been carried out in a campaign of only 4 testing days.

BDSLT – Bi-Directional Static Load Tests:

For the construction of a new bridge across a river at a different highway project in central Germany pile load tests were planned and carried out at two locations to determine the actual local soil bearing conditions. Bi-directional static axial compression load tests (BDSLT acc. to DGGT 2013 and ASTM

 © DFI International Bruges 2025

D8169 2018) have been chosen because the static load tests with load application at the pile head have been considered much more complex, time- and cost-consuming in the specific local subsoil.

For the static load tests with load cells embedded in the pile, the pile sections above and below the load cells serve as reaction. The load is applied axially in two directions. No reaction piles or anchors are required for this test, providing a time and cost-efficient method when very high test-loads need to be applied.

At this example project, 1 single-level BDSLT and 2 multi-level BDSLT have been successfully performed by GRL Engineers Inc. with assistance of GSP on 3 piles using GRL load cells (GRL-Cell, www.grlengineers.com). Third parties have been involved for strain and tip pressure measurements.

3 test piles with diameter of 1.2 m were installed with different lengths of embedment in the ground. The single-level test is shown here as an example. The following pictures show impressions of the installation of the GRL-Cells and the pile installation on the construction site.

The load schedule applied during the tests was determined on a project-specific basis in accordance with DGGT (2013) and ASTM D8169 (2018), figure 13 left side. Figure 13 right side shows the upward (blue) and downward (black) displacement components resulting from the single-level test at the various load levels.



Figure 11. GRL-Cell installed and cable management

 © DFI International Bruges 2025



Figure 12. Cage installation for the Single-Level-Test

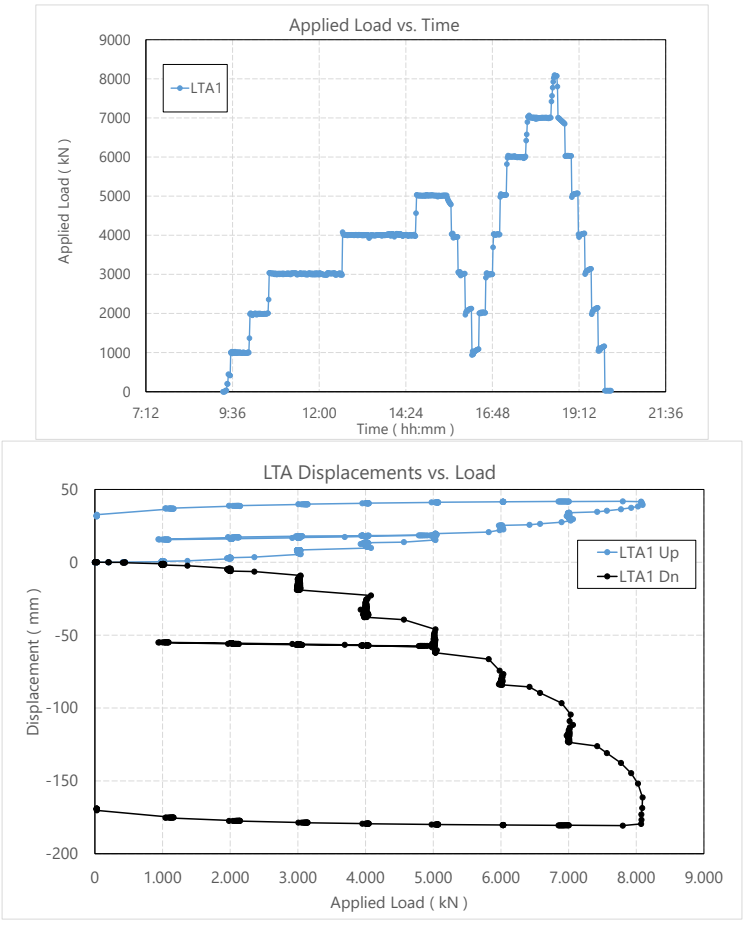


**Figure 13. Applied load vs. time (top),
Load-Displacement curve at the GRL-Cell level (below)**

All 3 BDSLT have been carried out successfully without failure of any installed sensors. An equivalent resistance-settlement curve for the pile head was derived for each pile. The objective of determining meaningful characteristic values of skin and tip resistances for the design of the structural piles was thus achieved.

 © DFI International Bruges 2025

Quality Control Testing

For proof of pile integrity CSL-tests were carried out on this project. The “Cross-Hole-Analyzer” model Champ Q4 from PDI was used for the tests with the associated CHA-W software for data evaluation. The device can be equipped with up to 4 transceiver probes, which are lowered and raised in the measuring tubes at the same height. The height is checked using a depth encoder for each probe. Any height differences between the probes can thus be detected and corrected if needed. The CHAMP allows the visualization of the signals during the test in real time.

Figure 14 shows an impression of the measurements carried out on one of the test piles. Figure 15 shows an example of the results for 3 of the 6 measurement paths. The results were evaluated and assessed in accordance with EA-Pfähle Section 12.3 (DGGT 2013). In addition, the classification system of EA-Pfähle 3rd edition chapter 12 (Moormann 2020) was considered, which is available as the current working version.

A local transit time of the ultrasonic wave that is more than 20% longer than the reference value is considered an anomaly on the corresponding measuring section. The reference value is determined as the average transit time per measurement path in homogeneous concrete in the close range above and below each suspected anomaly.

The GRL-Cell is effectively an “artificial defect” that was detected clearly in all the diagonal paths while the perimeter measurements show increased arrival times at the location of the upper and lower load plates at the GRL-Cell level. Besides this, homogeneous concrete was found, and the piles have been assessed to be intact, assessment class A1 acc. to EA-Pfähle.



Figure 14. CSL-Integrity Test

 © DFI International Bruges 2025

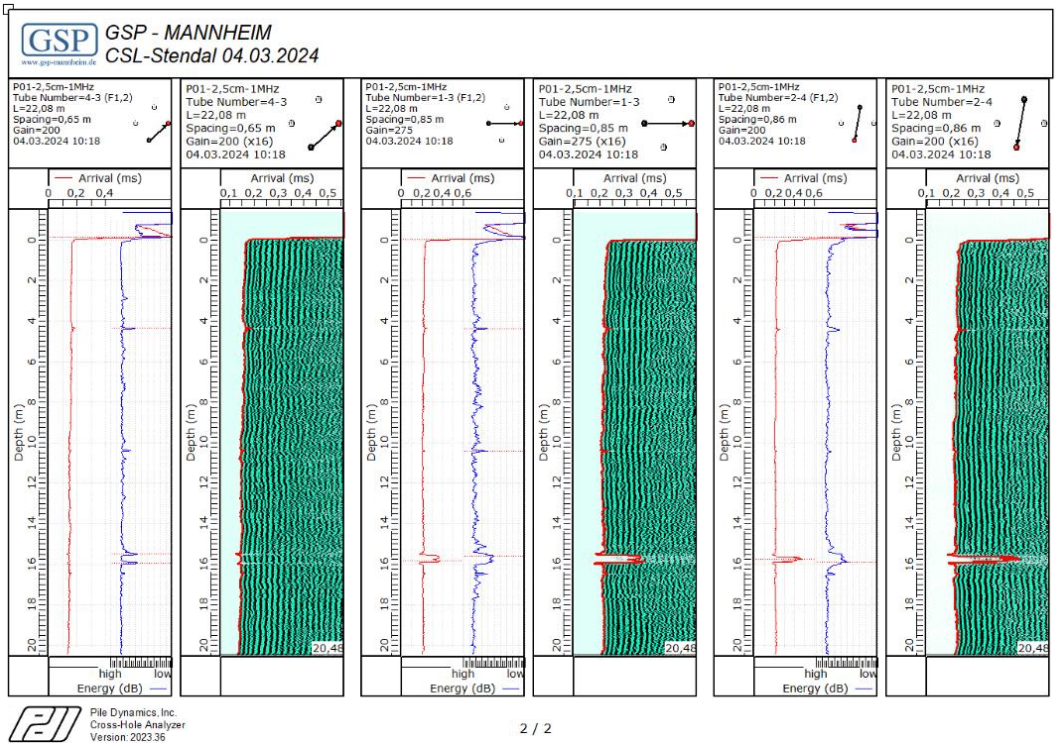


Figure 15. CSL result

Summary and Conclusions

The increase in use of large diameter bored piles within the deep foundations industry continues. This generally allows for much higher loads to be carried by each element. As the size of each foundation element increases and the loads carried by these elements increase, new methods are needed for quality control and quality assurance as well as to demonstrate the axial capacity of these elements. There are new methods for quality control and quality assurance including methods for measuring the overall shape and verticality of a foundation element prior to casting. Additionally, the integrity of foundation elements can be easily evaluated with the thermal method, allowing for accelerated evaluation while providing more information, including estimated concrete cover, than any legacy methods. As the examples show, these new testing methods are easily deployed in the field, can be used individually or together on the same elements to potentially gain further information on the element under test and help to understand the individual data provided from each method, and provide useful information to help the designer assess whether the foundation elements have been constructed as intended. The field example where the shape and thermal integrity testing were both performed on the same element clearly shows that the intended pile toe expansion was not installed as intended, with each method showing that the pile toe had collapsed, and the intended expansion occurred 1 m higher than the design and with an expansion diameter of 1.5 m as built with the intended diameter being 2.2 m. As the loads on these large foundations increase, it becomes impractical to perform a top-down load test. The BDSLT allows the large axial loads to be verified in these large foundation elements. As the example demonstrates, the BDSLT is a practical and economical method to determine meaningful characteristic values for the skin and toe resistances for very large and highly loaded deep foundation elements.

 © DFI International Bruges 2025

REFERENCES

American Society of Testing and Materials (ASTM). (2018). Standard Test Methods for Deep Foundations Under Bi-Directional Static Axial Compressive Load, D-8169/D8169M-18. American Society for Testing and Materials, West Conshohocken, PA.

Amir, J.M. (1983). Interpretation of Load Tests on Piles in Rock, Proceedings of the 7th Asian Regional Congress, SMFE, Haifa.

Brown, D. A., Turner, J.P. and Castelli R.J. (2010). Drilled Shafts: Construction Procedures and LRFD Design Methods, FHWA-NHI-10-016, Geotechnical Engineering Circular (GEC) No. 10. U.S. Dept. of Transportation, Federal Highway Administration, 970 p.

DGGT – German Society of Geotechnics e.V., WG 2.1 „Piles“: Recommendations on Piling (EA-Pfähle), 2. Edition, Berlin, 2013.

Fellenius, B.H. (2015). Analysis of Results of an Instrumented Bidirectional-cell Test, Geotechnical Engineering Journal of the SEAGS & AGSSEA, Vol. 46, No. 2, pp. 64-67.

Moormann, C.: Annual Report 2019 of DGGT WG 1.2 „Piles“, Bautechnik 97 - 2 (2020) Ernst & Sohn, Berlin.

Mullins, A.G., 2010. Thermal Integrity Profiling of Drilled Shafts, DFI Journal Volume 4 No.2, Hawthorne , NJ, pp. 54-64.

Piscsalko, G., Cotton, D., Belardo, D., Likins, G.E., 2015. Using Thermal Integrity Profiling to Confirm the Structural Integrity of foundation applications, Proceedings of The International Foundations Congress and Equipment Expo 2015: San Antonio, TX.

Piscsalko, G.; Likins, G.; Mullins, G.; (2016). Drilled Shaft Acceptance Criteria Based Upon Thermal Integrity, In: DFI 41st Annual Conference on Deep Foundations, New York, NY, pp 1-10, (October 2016).

Schallert, M.; Stahlhut, O.; Kirsch, F. 2024). Effiziente Prüfmethoden zur Tragfähigkeitsermittlung und Qualitätssicherung hochbelasteter Großbohrpfähle (English: Efficient test methods for determining the load-bearing capacity and quality assurance of highly loaded large bored piles), 18. Hans Lorenz Symposium, Advances in Geotechnical Engineering, Technical University of Berlin, Germany, 12.09.2024.

Stahlhut, O.; Ruiken, A.; Moormann, C.: Zum Einfluss von Herstellungsverfahren, Geometrie und Pfahlfußaufweitungen auf das Widerstandsverformungsverhalten von Großbohrpfählen, 38. Baugrundtagung, Bremen, Germany (September 2024).

 © DFI International Bruges 2025

INCORPORATING CYCLIC DEGRADATION INTO PILE DESIGN FOR THE GULL WING BRIDGE, LOWESTOFT

Scott A Reid, Ove Arup and Partners Ltd, London UK, +44 20 77553255, scott.reid@arup.com
Paul J R Morrison, Ove Arup and Partners Ltd, London UK, +44 20 77553545, paul.morrison@arup.com
Cameron J Hughes, Ove Arup and Partners Ltd, London UK, +44 20 77556667, cameron.hughes@arup.com

ABSTRACT

The paper presents the design analysis for the piled support for the rolling bascule Gull Wing Bridge in Lowestoft, England. The nature of the rolling bascule bridge is that individual pile loads within the pile group vary significantly during each bridge opening event. This results in the cyclic degradation of the pile shaft resistance, differing from a conventional static pile design where the resisted variable actions are normally only a small component of the total design actions. The approach has been developed using lessons learned from offshore pile design and modified to be appropriate for the design principles of Eurocodes. An additional capacity reduction factor, as a function of the mean and peak cyclic loading and their resulting cyclic degradation, has been developed and incorporated into the design process. Failure to consider cyclic degradation of the pile shaft capacity would have resulted in the risk of medium to long term settlement being outside the operational limits for the bridge.

Key words: Pile design; Cyclic loading; Shaft resistance; Bridge foundation.

INTRODUCTION

The Gull Wing Bridge comprises a new road bridge crossing over the existing Lake Lothing harbour which bisects the town of Lowestoft in Suffolk, England. The rolling bascule bridge section of the scheme is the largest of its kind with a bascule span of 39.5m, with prefabricated steel J-beams reaching more than 50m above sea level. The bridge came into operation in Summer 2024.

The scheme from south to north includes: a vertically sided reinforced soil embankment up to 7m height, four spans of viaduct over land and then water, the opening rolling bascule bridge span to permit harbour through-traffic, three further spans of viaduct over water and then land, and a battered embankment supported by ground improvement.

This paper describes the design of piled foundations for cyclic loading due to the opening and closing of the rolling bascule bridge span between Pier 4 and Pier 5 of the scheme. The foundation scheme was developed by Ove Arup and Partners Ltd and BAM Nuttall Ltd on behalf of the project's client, Suffolk County Council.

SITE GEOLOGY

The Lake Lothing harbour where the piers were to be laid is underlain by a sequence of up to 4m of compressible silts and clays, about 15m of the Happisburgh Formation of chaotically interbedded sands and clays (becoming clay-dominated with depth), about 45m of the Crag Group of dense silty sands, followed by basal London Clay beyond 70m depth below harbour bed level. Lee et al. (2004) provides more information on the glacial geology of the region.

The Happisburgh Formation and Crag Group are the foundation soils for the piles, with the pile base level chosen to stay several pile diameters above the London Clay (where end-bearing resistance gradually reduces as the clay is approached). With effective stresses governing the design, the Crag Group provides the proportion of geotechnical resistance to piles.

 © DFI International Bruges 2025

The Crag Group is a silty fine to medium grained sand; dense becoming very dense as vertical stresses increase with depth. Shear box testing indicated a peak angle of internal friction ϕ'_{pk} of 28 to 35°, dilating to a constant volume value ϕ'_{cv} of 26 to 33°. Characteristic values of $\phi'_{pk} = 32°$ and $\phi'_{cv} = 30°$ were adopted for pile design purposes.

FOUNDATION CONCEPT FOR OVER-WATER PIERS

Piers 4 and 5 of the structure were located at 1/3rd positions across the 100m wide Lake Lothing harbour and commenced as combi-wall cofferdams for each pier. These steel elements were driven using vibration into the Happisburgh Formation sands, with water level inside the cofferdam remaining in connectivity with the tidal waters of Lake Lothing.

The 1.22m tubular steel piles of the combi-wall cofferdam were used as permanent casings for 22no. 1.08m diameter rotary bored piles at Pier 4 and 20no. piles at Pier 5 to be advanced into the foundation soils to up to 65m below mean sea level. These piles were constructed under a polymer support fluid as described by Wallis-Evans et al. (2023).

Upon completing the piling works the cofferdams were excavated of soft sediments under water and a reinforced concrete plug was tremie placed, displacing the water impounded in the cofferdam. The cofferdam was then pumped dry and the piers were constructed using in-situ reinforced concrete.

DESIGN BASIS

The scheme has a design life of 120 years, with up to ten daily open/close cycles intended during that life. This has resulted in approximately 876,000 peak load changes for the structure to be designed for.

Pile foundation design for the scheme was to British Standard BS 8004:2015, which is complementary to BS EN 1997-1:2004 and its UK National Annex. Collectively these codes take a partial factor approach to the design of piles, reducing the shaft and end-bearing design resistance of piles from a calculated characteristic condition. These codified approaches do not make factor allowances for effects such as cyclic loading, the importance or resilience needed of the structure, or other unusual design or loading requirements, but requires that the design should consider (a) *degradation of the ground strength* and (b) *degradation of ground stiffness* (BS8004, 2015). Due to the piles being constructed over water and 'cut-off' below sea level, load testing would not be possible, requiring the design to take a cautious approach (BS EN 1997-1, Clause 7.5.1(3)).

Earlier revisions of BS 8004 included limited guidance regarding increased factors of safety for piles subject to impact, cyclic, or vibratory loading, however did not go so far as to prescribe a minimum factor of safety for these conditions. *"The factor of safety applicable to single piles should be increased when large impact, cyclic or vibratory loads are expected or the properties of the soil may be expected to deteriorate with time."* (BS 8004, 1986).

Historically geotechnical structures subject to cyclic loading have adopted a global factor of safety in the order of eight to ten (rather than a more traditional two to three) on the ultimate resistance of their piles. These well-reasoned but arbitrary values could however result in uneconomical foundation designs which could call the scheme into question.

CYCLIC TESTING OF SOILS UNDER SHEAR

As described by Tabucanon et al. (1995) and Turner and Kulhawy (1992), monotonic loading in constant normal load (CNL) shear box testing has demonstrated that shear and normal stresses will tend to increase in dense soils that expand when sheared, with the converse apparent in loose soils.

As a foundation is taken through repeated shearing (i.e. cyclic loading), the state of granular soils approaches a constant volume or 'critical' state. The 'constant normal stiffness' condition represented

 © DFI International Bruges 2025

by shear box testing controlled by stiffness rather than stress has been recognised for some time to better represent the reduction of skin friction during cyclic loading (Tabucanon et al., 1995). The loss of frictional resistance in piles under cyclic load depends on several factors including load and displacement magnitude, density (and thus overconsolidation ratio) of the soil, pile roughness, and the soil's stiffness in situ (Poulos, 1989).

Shear box testing with the capability to replicate constant normal stiffness conditions are generally the preserve of academia, and were not accessible to study these cyclic phenomena within the programme available for designing and constructing the Gull Wing Bridge. Similarly, cyclic pile load testing was not practicable within the available design and construction programme.

CYCLIC STABILITY DIAGRAMS – AN ALTERNATIVE TO CONSTANT NORMAL STIFFNESS TESTING

Due to the challenges of accessing CNS test equipment, a design approach was required to account for degradation of pile resistance under cyclic loading. This approach would ideally apportion the degradation and design uncertainty discretely to the partial factors of BS 8004:2015, rather than verify a large global factor of safety as often used historically.

Poulos (1988) presented the concept of a cyclic stability diagram, replicated in Fig. 1, showing the performance of piles under cyclic load degrading progressively from being stable, to meta-stable, to unstable. The cyclic stability diagram space is defined by cyclic load (Pc) (y-axis) and mean (Po) (x-axis) load conditions, each normalised by the static resistance of the pile (Qc).

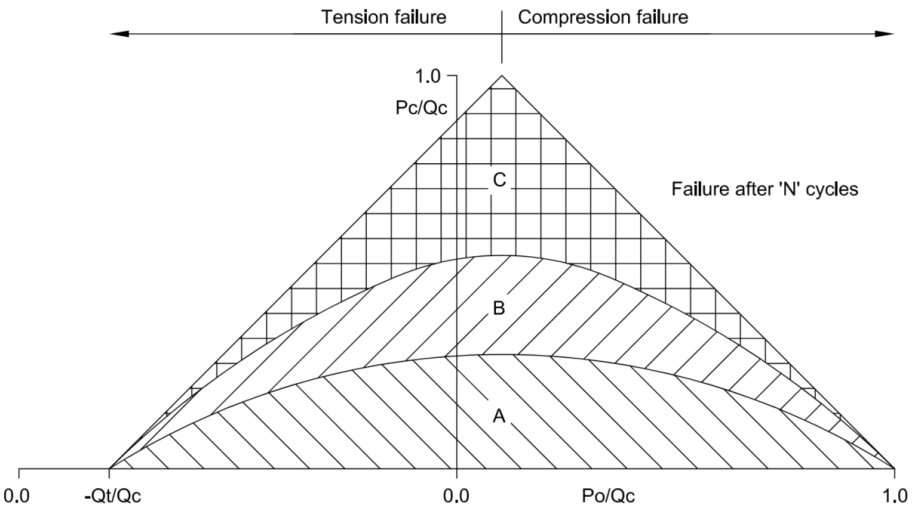


Fig. 1. Main Features of Cyclic Stability Diagrams (Poulos, 1988)

The stable (area A) zone represents loading of low magnitude cyclic load compared to the static geotechnical resistance of the ground, where cyclic loading does not result in a reduction in pile resistance (i.e. cyclic loading has a second order effect only) and pile head displacement remains largely elastic. The meta-stable zone (area B) represents an area where repeated loading gradually reduces the capacity of the ground over a large number of observed cycles, demonstrated by gradual creeping of pile head movement under repeated loading. The unstable zone (area C) represents conditions where pile failure is reached quickly, with pile head movements quickly exceeding a serviceability limit and beyond. Typical responses in these zones for tension loading are presented in Fig. 2 (after Jardine and Standing, 2012). The susceptibility of tension piles to fail in cyclic loading is highlighted in BS EN 1997-1 clause 7.6.3.1(9), with the 'compression only' loading of piles in this scheme unlikely to fail in such a severe manner.

 © DFI International Bruges 2025

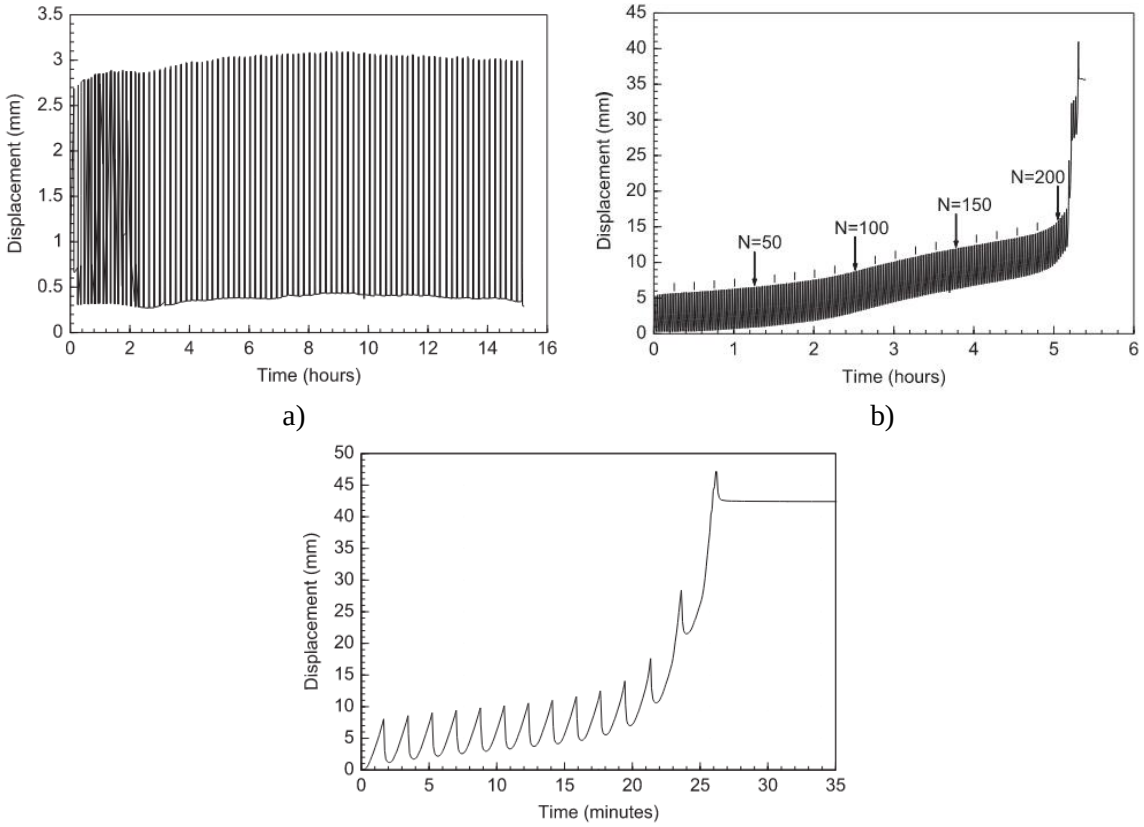


Fig. 2. Displacement performance under cyclic loading (a) Stable, (b) Metastable, (c) Unstable (Jardine and Standing, 2012)

Poulos thereafter presented a framework for an elastic solution for the cyclic response of a pile, combining the static soil stiffness, the static soil/pile resistance, loading rate, accumulated displacement, and independent cyclic degradation parameters for the soil, the pile shaft, and the pile base. These parameters would be interpreted from a range of laboratory, scale model, and field pile tests, which in the case of this project were not practicable.

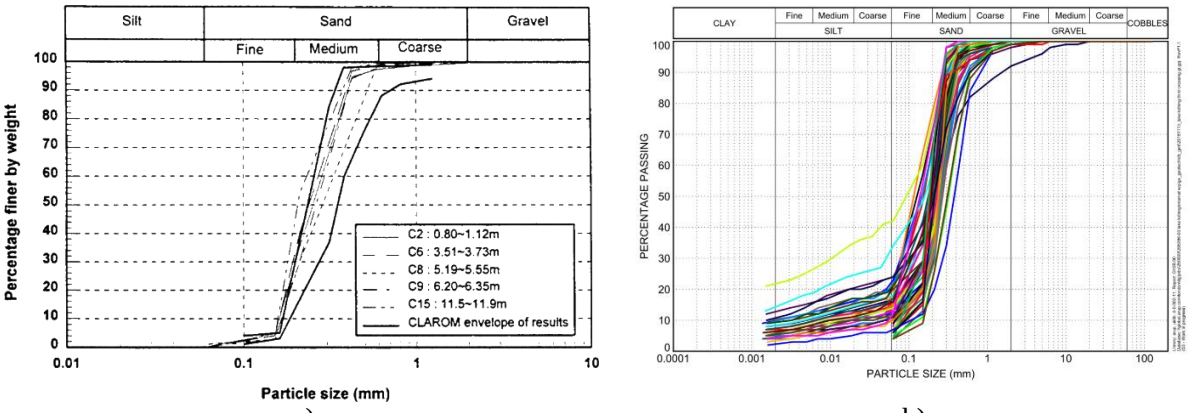
COMPARABLE DATA TO LOWESTOFT CONDITIONS

Jardine and Standing (2012) presented field load tests on driven tubular steel piles loaded in tension in Dunkerque, France, subject to a range of one-way and two-way cyclic loading conditions.

The Flandrian Sand at the Dunkerque site comprised a dense becoming very dense uniformly graded fine to medium grained sand (Chow, 1997), which was considered reasonably comparable to the silty sand found in the Crag Group at Lowestoft. These are presented in Fig. 3.

The drainage influence of the minor silty constituents of the Crag Group were not expected to influence the response of the pile during loading, as the relative permeability of the silty sand at Lowestoft and the clean sand at Dunkerque are similar and the cyclic loading rate is low (ie. excess porewater pressures unlikely to develop).

 © DFI International Bruges 2025



a) b)

Fig. 3. Comparison of (a) Flandrian Sand (Chow, 1997) to (b) Crag Group silty sand at Lowestoft

The load test data from pile load testing in the Flandrian Sand were able to be constructed by Jardine and Standing into a cyclic stability diagram as described by Poulos (Fig. 4), with each test's data representing a failure point within the cyclic stability diagram's space. Accompanying this was a plot (Fig. 5) following the analytical approach described in Jardine et al. (2005) to develop cyclic stability contours, which compared well.

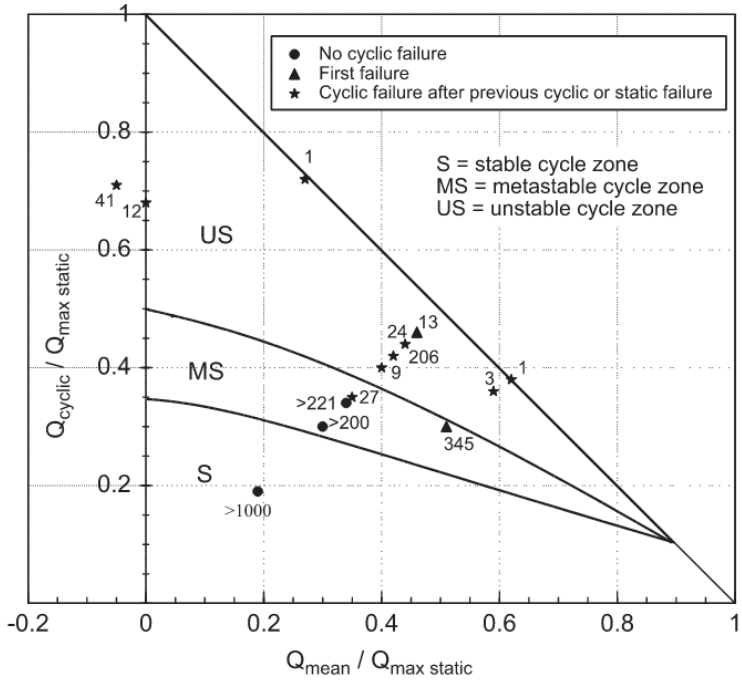


Fig. 4. Data from field cyclic load testing in Flandrian Sand (Jardine and Standing, 2012)

Due to the load tests considered by Jardine and Standing (2012) being subject to tension actions only, the stability results are a cautious estimate of the performance of piles when in compression, where some base resistance should be anticipated.

 © DFI International Bruges 2025

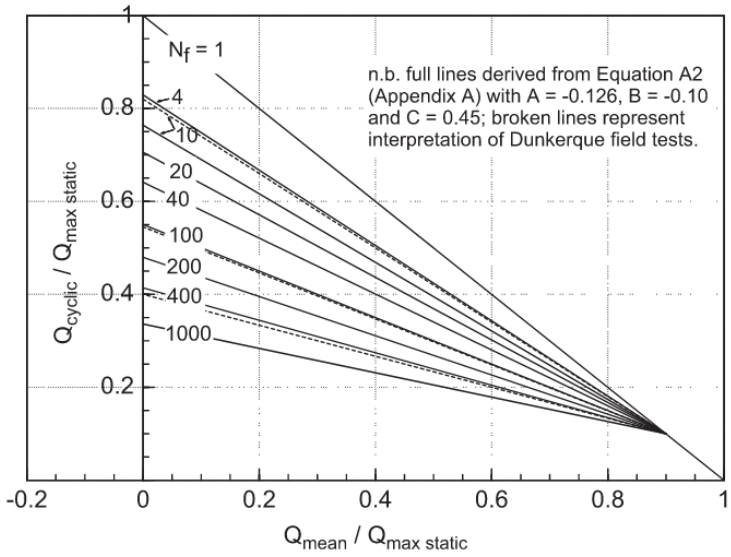


Fig. 5. Analytical estimation of cyclic stability for Flandrian Sand (Jardine and Standing, 2012)

Due to the one-way tension nature of the tests, the presented boundaries between stable and metastable/unstable conditions were postulated to represent the limiting conditions for stable degradation affecting shaft resistance for the piles.

PILE GROUP LOAD CONDITIONS

Pier 4 is supported by a perimeter arrangement of piles installed into the combi-wall tubes, with the group geometry, pile length, and applied group loading resulting in different peak and mean loading for each pile. Piles 1-9 experienced peak compression loading with the bascule closed. Upon opening of the bascule, the loads in piles 1-9 reduce, with piles 10-18 experiencing their own peak compression load.

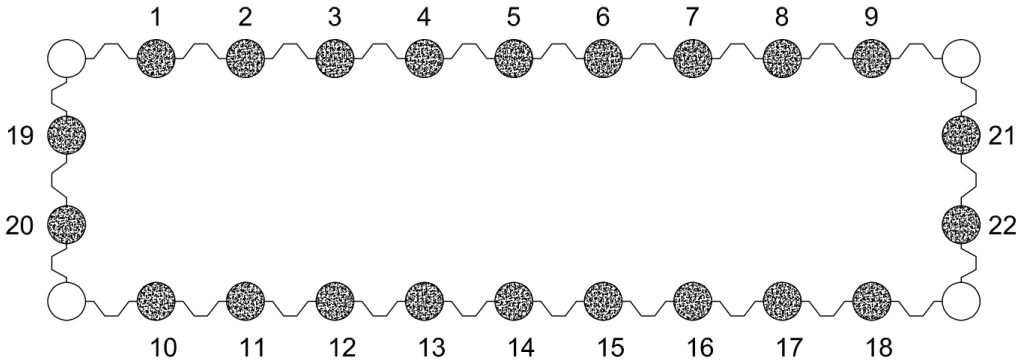


Fig. 6. Pile layout of Pier 4

Piles supporting each pier were grouped into typical load responses which aligned to that presented in Tsuha et al (2012), Fig. 7, where either (a) there was a large cyclic load amplitude with the mean load approximately half of the peak load (called ‘highly cyclic’ hereafter), or (b) where there was a small cyclic load amplitude with the mean load similar to the peak load (‘highly static’ hereafter). Piles 1 to 18 at the extremities of the group were highly cyclic, with piles 19 to 22 having more modest load changes and highly static.

These two typical load responses tend to plot in different locations on a cyclic stability diagram, with the highly static at the maxima of the x-axis, and highly cyclic at the maxima of the y-axis.

 © DFI International Bruges 2025

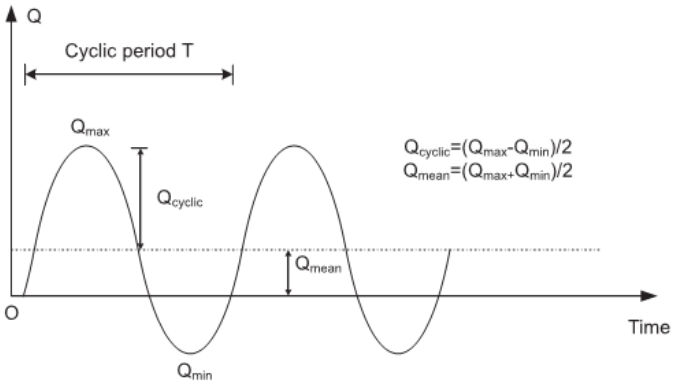


Fig. 7. Tsuha et al. definition of cyclic load conditions

DEVELOPING A CYCLIC CAPACITY REDUCTION FACTOR

The unstable and meta-stable zones estimated by Jardine and Standing represent conditions where performance leads quickly to failure or creeps toward failure under cyclic load, and accordingly the stable zone is prioritised as the suitable stress space for foundations to be designed to perform within.

Evaluation of the cyclic contours and stability boundaries presented by Jardine and Standing, and assuming the stable:meta-stable boundary as a cyclic ultimate limit state (C-ULS) condition not to be exceeded, a framework was developed to reduce pile shaft resistance for cyclic actions. The boundary at the extreme envelope of the diagram was taken to represent the static ultimate limit state (S-ULS), with a comparison of the cyclic and ultimate boundaries a means to estimate the static pile shaft resistance degradation when subjected to a high number of load cycles. This is presented as Fig. 8.

For each pile and its load conditions, the normalised peak cyclic and mean loading (Q'_p and Q'_m respectively) were plotted in the cyclic stability diagram (point 'X'). Extrapolating from the origin through 'X' to 'Y' and 'Z' provides an intercept with the cyclic and ultimate boundary lines respectively. The ratio of the two loading paths from the origin for each pile's loads can be taken as a cyclic capacity reduction factor (whereby stable performance is likely) to be applied to the characteristic shaft resistance of the pile as a pseudo-dynamic reduction when undertaking static calculations.

Figure 9 presents computed responses for the piles in the Pier 4 group, showing the initial load normalised positions for Q'_p and Q'_m to calculate reduction factors for cyclically reduced pile capacity (upon application of which the load ratio position then regresses towards the origin into the 'stable' space as the safety of the design improves). It can be seen that for low amplitude loading conditions such as piles 19 to 22 there is little capacity reduction (which is in agreement with the piles being highly static), but for highly cyclic piles the reduction factor converges to a limiting lower bound value of about 0.35 along the y-axis (i.e. the new "failure" load is 35% of the static ultimate load).

In this way, piles are designed to account for dynamic/cyclic effects. This allows calculations to determine a design pile length after cyclic capacity reduction is applied. The pile group analysis generating individual loads can then be iterated for the revised pile lengths and stiffnesses, revising the Q'_p and Q'_m loading conditions for each pile, moving within the cyclic stability diagram's space and adjusting the cyclic reduction to suit.

 © DFI International Bruges 2025

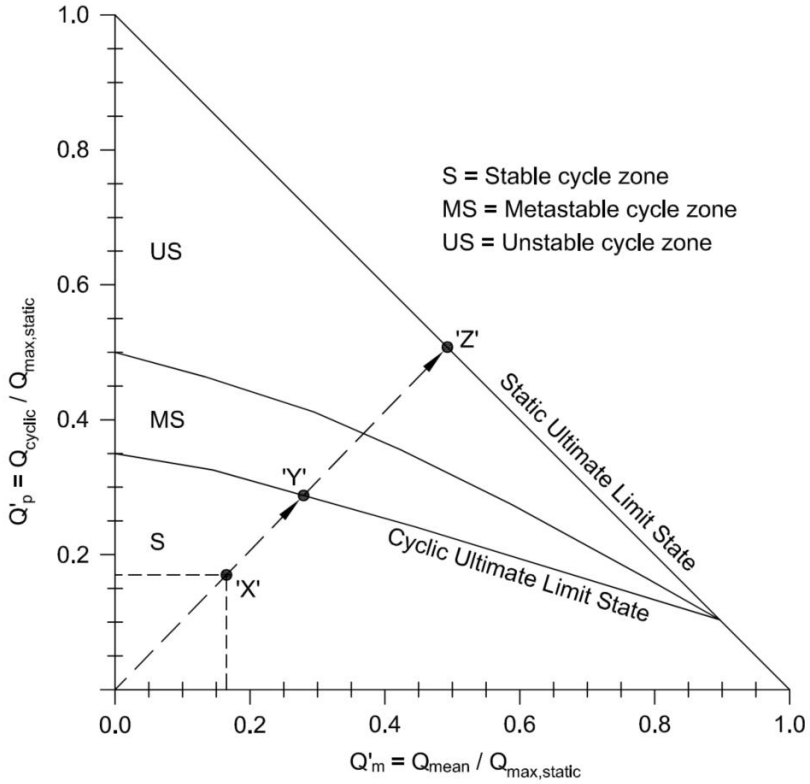


Fig. 8. Cyclic stability reduction factor development

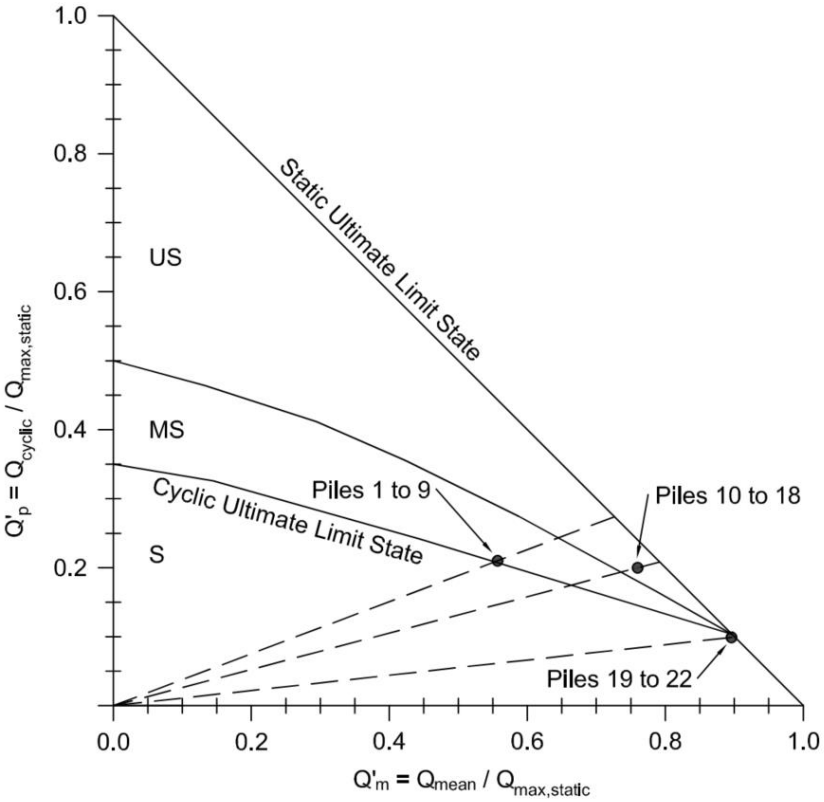


Fig. 9. Initial load ratio positions for Q'_p and Q'_m for pile typologies. Load ratio positions regress along each dashed line as the cyclic reduction factor is applied to the static design.

 © DFI International Bruges 2025

PILE GROUP LOAD DISTRIBUTION AND ITERATION

Developing the pile design length comprised the iteration of pile group stiffness between structural design software (midas Civil™), pile group analysis for pile loads (Geocentrix Repute™), and individual pile capacity calculations (Excel, using the approach described in this paper).

For a given first iteration of pile loading from Repute, each pile in the group was individually designed for its peak and mean cyclic loading conditions. Once converged, the refined pile lengths are then iterated through soil-structure analysis (midas Civil for structural analysis of the group stiffness response to superstructure loading, and Repute for geotechnical load distribution in the group) to derive the next iteration of stiffness-distributed loads upon which the piles lengths can iterate using the cyclic method to again converge.

Table 1. Summary of pile load typologies

Piles	Static DA1C2 load	Loads from cyclic fatigue load cases		Cyclic load amplitude and mean		Initial normalised load ratios*			
	Q_{max} (kN)	$Q_{fat,max}$ (kN)	$Q_{fat,min}$ (kN)	Q_{cyclic}	Q_{mean}	Q'_p	Q'_m	Cyclic Reduction Factor	Length
1 to 9	6,093	4,690	2,185	1253	3438	0.206	0.564	0.76	55m
10 to 18	5,829	5,582	3,252	1165	4417	0.200	0.76	0.83	45m
19 to 22	3,777	3,875	3,111	382	3493	0.101	0.925	1.0	25m

* - initial load ratios are normalised against Q_{max}, and thereafter by the reduced cyclic capacity. This maintains a linear load path from the origin as shown in Fig. 9.

As seen in the table above, the pile loading stays in significant compression throughout cyclic action ($Q_{fat,min}$ >> 0kN); this is effective in minimising the cyclic capacity reduction which is applied to the foundations. The applied cyclic reduction tends to become more significant when minimum foundation loading reduces in low relative compression or moves into tension, so dominant compression in pile groups becomes advantageous.

The degraded shaft resistance is adopted for both ultimate and serviceability limit state calculations. Verifying the serviceability limit state to BS 8004:2015 (clause 6.8.2) for only the degraded shaft resistance allows the full base resistance to remain a component in ultimate limit state calculations.

SUMMARY

The paper presents an approach to cyclic pile capacity reduction, avoiding the need for costly constant normal stiffness shear strength testing and instead following and further developing principles established in offshore pile design.

Experimental load testing data in comparable ground conditions provides a basis for simplified capacity reduction, allowing foundations to be optimised for the loading conditions they are subjected to.
Global factors of safety, as used historically to address uncertainty in cyclic loading conditions, have been improved upon by attributing design uncertainty directly to the resistances which are most affected. The model factor and partial factors on base and shaft resistance in accordance with BS EN 1997-1:2004 remained in place in addition to cyclic degradation to assure safety within the design.

 © DFI International Bruges 2025

ACKNOWLEDGEMENTS

The authors would like to thank Suffolk County Council for their support in this paper being written, and Mr Conor Lavery of Arup for assisting in the preparation of this paper.

REFERENCES

British Standards Institution (1986) *Code of practice for foundations*, BS 8004:1986.

British Standards Institution (2015) *Code of practice for foundations*, BS 8004:2015.

British Standards Institution (2014) *Eurocode 7: Geotechnical design – Part 1: General rules*, BS EN 1997-1:2004+A1:2013.

British Standards Institution (2014) *UK National Annex to Eurocode 7: Geotechnical design – Part 1: General rules*, NA+A1:2014 to BS EN 1997-1:2004+A1:2013.

Chow, F.C. (1997) *Investigations Into Displacement Pile Behaviour for Offshore Foundations*. Ph.D. Thesis. University of London, Imperial College

Jardine and Standing (2012) *Field axial cyclic loading experiments on piles driven in sand*, The Japanese Geotechnical Society - Soils and Foundations 52(4), p. 723-736.

Jardine, R.J., Chow, F.C., Overy, R., Standing, J. R. (2005) *ICP Design Methods for Driven Piles in Sands and Clays*, Thomas Telford.

Lee et al. (2004) *A new stratigraphy for the glacial deposits around Lowestoft, Great Yarmouth, North Walsham and Cromer, East Anglia, UK*, Bulletin of the Geological Society of Norfolk 53, p. 3-60.

Poulos (1988) *Cyclic stability diagram for axially loaded piles*, Journal of Geotechnical Engineering (Aug. 1988).

Puech and Garnier (2017) *Design of piles under cyclic loading SOLCYP Recommendations*, John Wiley & Sons, Inc.

Tabucanon et al. (1995) *Pile skin friction in sands from constant normal stiffness tests*, Geotechnical Testing Journal (Sept. 1995).

Tsuha, C.H.C., Foray, P.Y., Jardine, R.J., Yang, Z.X., Silva, M., Rimoy, S., (2012) *Behaviour of displacement piles in sand under cyclic axial loading*, Soils and Foundations 52, p. 393-410.

Turner and Kulhawy (1992) *Strength changes in sand following cyclic shear*, Geotechnical Testing Journal (Sept. 1992).

Wallis-Evans et al. (2023) *Pile construction using polymer support fluid at Gull Wing Bridge, Lowestoft*, Ground Engineering (May 2023, p. 26-33).

 © DFI International Bruges 2025

HOW EMBRACING ENGINEERING CHALLENGES UNLOCKED THE REDUCTION IN EMBEDDED CARBON AT THE SSTC3 SOIL NAILING PROJECT

Ash Rogers MSc MEng, Technical Director, Aarsleff Ground Engineering Ltd
Cerys Orriss BA PGDip, Sustainability Manager, Aarsleff Ground Engineering Ltd

Commencing in April 2020 and completing in June 2021, Aarsleff Ground Engineering Ltd (a UK subsidiary of Danish construction company Per Aarsleff A/S) undertook the design and installation of soil nailing reinforcement and structural facing for a near 12m high slope inclined at 70° from horizontal. The near 250m length of reinforced slope enabled the excavation for a new highway into the side of an existing slope situated above the old shipyards on the south bank of the River Wear in Sunderland, England. The scheme was developed as an alternative reengineered scheme to the originally specified retaining wall consisting of a combi-sheet pile wall supported by ground anchors.

This paper studies the reduction in embedded carbon achieved with the alternative scheme through the complex design and technical management required to unlock this achievement. The awkward geometry, the unpredictable ground conditions, the coordination between excavation works and soil nailing, the specified design working life of 120 years, relic buried structures, and more; all posed challenges from the outset that could have spelt disaster unless managed correctly. The project was a success, and many learned lessons are discussed herein for the technical management of less conventional geotechnical methods with the benefit of lower embodied carbon.

1. Introduction

Within the design of infrastructure projects, such as the scheme at Sunderland, a low-risk approach is often adopted which can lead to a more emission heavy solutions being implemented than strictly necessary. Historically, the perceived robustness of solutions with high embedded carbon have supported their implementation relative to alternatives available, which negates the spirit of working towards a more sustainable industry. This paper provides embedded carbon calculations for the initial (anchored combi-wall) and the reengineered (soil nail reinforced slope) solutions; and critically, details of the engineering challenges encountered and overcome in the design and construction of the reengineered solution.

2. Initial Scheme Design

The scheme's initial design constituted a vertical combination wall formed by circular hollow section (CHS) steel piles, of 10.5m to 21.5m lengths, positioned behind one in every two 'Z' profile sheet piles of 7.5 to 18.5m lengths. This was supported with up to three rows of ground anchors positioned between the CHS piles. The CHS piles were 1.2m in diameter, the sheet piles were a Z46 section, and ground anchors were a single bore single stage system with either 5nr or 6nr x 15.2mm strands

 © DFI International Bruges 2025

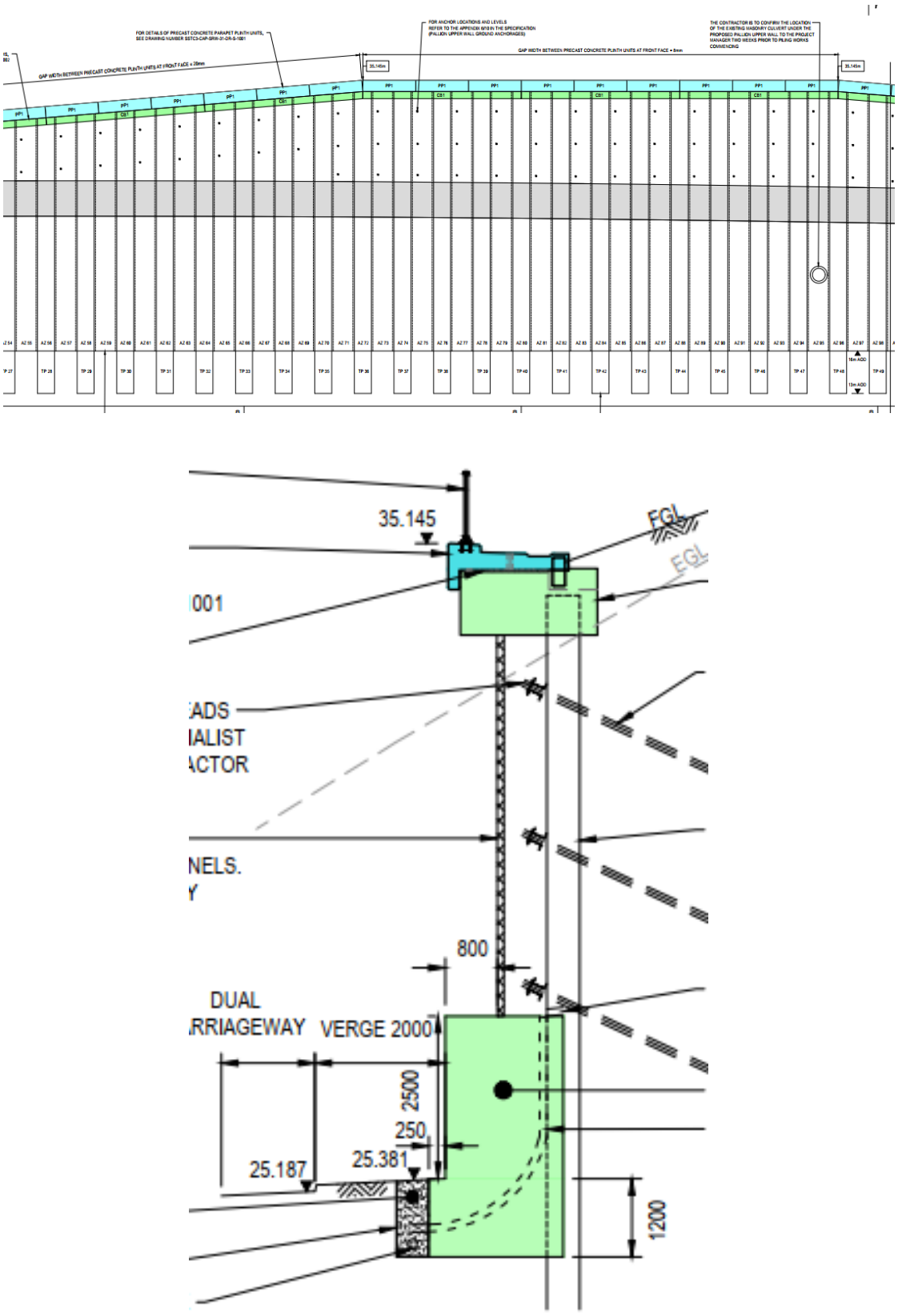


Figure 1a and 1b: extract of the initial design's elevation drawing and cross-sectional detail respectively.

 © DFI International Bruges 2025

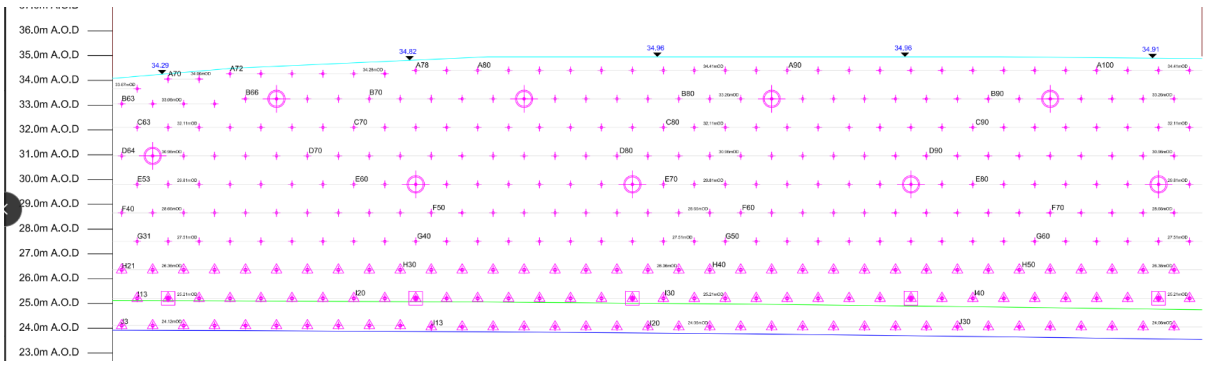
When assessing the landscape of this scheme in particular, an understanding of legislation and standards driving sustainability within the design and build of infrastructure projects helps to provide a backdrop of context to the project's design and build between 2019 and 2021.

The Climate Change Act 2008 mandates significant reductions in transport emissions, influencing highways projects to focus on sustainable construction practices, such as using low-carbon materials and integrating electric vehicle (EV) infrastructure. Furthermore procurement frameworks, such as the Crown Commercial Service (CCS) Construction Works and Associated Services Framework and the Transport Infrastructure Efficiency Strategy (TIES), require that highways schemes incorporate sustainability from the procurement phase. These frameworks emphasize whole-life cost approaches, low-carbon solutions, and innovative construction methods. The Construction Playbook (2020) further guides procurement in highways projects, advocating for modern methods of construction and promoting efficiency, waste reduction, and long-term value. PAS 2080 is a global standard for managing carbon in infrastructure, focusing on reducing greenhouse gas emissions throughout the project's lifecycle. For infrastructure projects, PAS 2080 requires contractors to implement a carbon management strategy from design to construction and operation. Contractors must assess carbon impacts, set reduction targets, and use low-carbon materials and techniques. More recently on industrial projects, BREEAM and LEED are pushing sustainable design, along with the RICS Whole Life Carbon Assessment Version 2 utilising industry standard decarbonisation techniques within their baseline assessments. Examples of this include a standard mix of 70% CEM1 and 30% cement replacements in concrete mixes, and 80% recycled content in steel. Whilst this currently applies to industrial projects in the main, BREEAM Civils is due to launch in 2025 and begin to shape how we manage decarbonisation in civil engineering projects.

This legislative backdrop demonstrates that whilst there was minimal legal need for industrial projects to decarbonise during the project's lifespan, there are a number of frameworks which did encourage more sustainable construction, setting a base understanding across the contractors involved. Fortunately, the circumstances of this project allowed for more sustainable alternatives to be sought, leading to the soil nail reinforced slope solution to be studied and consequently put forward.

3. Reengineered Design

The reengineered solution replaced the retaining wall with a 70° slope that reaches up to 12m in height. The fully hollow bar soil nails are between 32mm and 51mm diameter and were installed using a self-drilled continuously grouted method. The slope face is supported by geotextiles, galvanised steel mesh soil nail head plates. All steel is galvanised to contribute to the long-term durability.



 © DFI International Bruges 2025

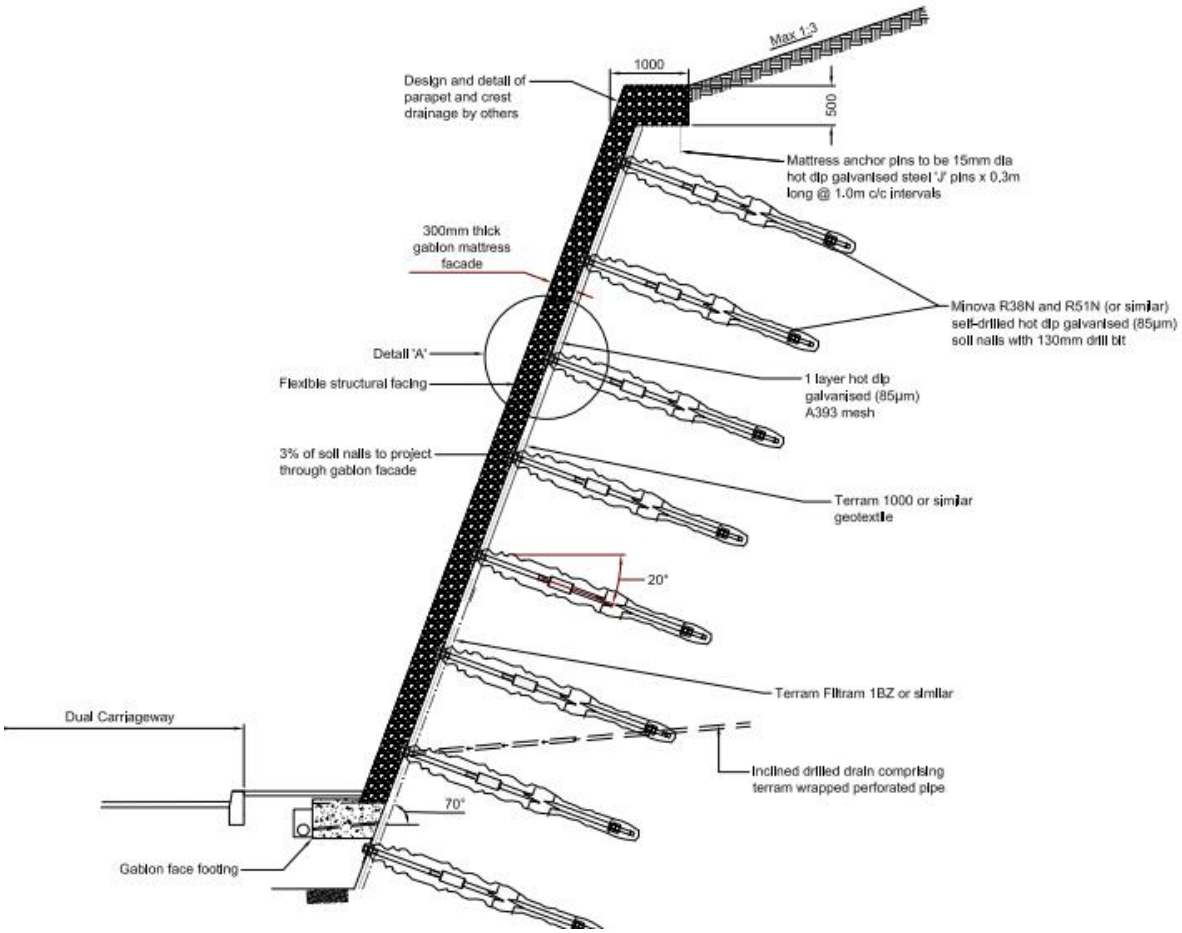


Figure 2a and 2b: extract of the soil nail design's elevation drawing and cross-sectional detail respectively.

Soil nailing is a technique which employs the existing ground as a key element of the system, meaning it is far more sensitive to variations in environmental and ground conditions than the initial scheme would have been. In certain conditions, soil nail reinforcement is even unfeasible. Fortunately, the ground investigation was proportional for the intended works and so ground risks could be assessed and managed in design to a reasonable extent. Since no ground investigation can forecast every hazard and condition, it was concluded that enough was known to implement appropriate supervision and management without the need for additional and excessive investigations to be undertaken. The residual and any unforeseen risks required close engineering supervision during construction to handle any variations or issues encountered. Many of these risks would have had more minor consequences if the initial scheme design had been implemented. The reengineered scheme – and therefore sustainability results – would not have not been possible without a proactive approach to managing the increased risks.

As detailed in the calculations below, the soil nail solution replacing a series of steel elements including sheet piles, CHS piles, and ground anchors has a significant effect on the embodied carbon of the project. Reducing the overall carbon by 74% and saving c.2000 tonnes of CO_2e through both more efficient material usage and a shorter programme, the project is a clear example of how design and sustainability need to be closely examined in tandem. Without the technical expertise of the design teams, the vast reduction in CO_2e through the creative solution to decarbonisation most likely never would have been achieved. However, pure cost focused designers may have never considered the environmental benefits of the reduction without the collaborative effort towards sustainability on the project, delivering vast reductions across the board.

 © DFI International Bruges 2025

3.1 Ground Conditions

Ground investigation reports revealed that the site conditions consisted of Made Ground overlying natural clay, and deeper weathered limestone, though the limestone was not encountered during excavation. The Made Ground, understood to be backfill from the former quarry, consisted of a variety of soil types and man-made materials, leading to a design assumption of soft to firm sandy gravelly clay fill.

While the design identified the clay as the Pelaw Clay Member, it remains unclear if it belongs to the Devensian Glaciolacustrine Deposits, Devensian Till, or a combination of all three. These natural clays were generally firm with medium strength and intermediate plasticity. Additionally, medium dense clayey Glaciolacustrine sand was encountered, though it was not incorporated into the design due to its higher effective shear strength compared to the Made Ground. Given the highly variable ground conditions, particularly with Made Ground and excavation depth, the design model adopted a cautious approach. Sensitivity analyses indicated that using parameters for Made Ground, with a characteristic shear resistance angle of 26° and zero effective cohesion, was more conservative than relying on lower-bound parameters for natural clay.

3.2 Operational Issues

During the setting out of soil nails, it was found that the excavated slope crest was up to 300mm lower than the design specified. This discrepancy likely arose from the design being based on the road verge level, alongside challenges in achieving the correct levels due to the crest's shape and overlying earthworks. To address this, the site engineer conducted an as-built survey and identified non-conforming nail positions, allowing for a redistribution of the soil nails. In areas where nails were too close to the crest (within 100mm), the affected rows were lowered to acceptable levels. This adjustment sometimes required lowering nails in adjacent rows to maintain effective spacing. Despite these modifications, the overall number of rows remained unchanged, ensuring that the soil nail design was unaffected.

Localised face instabilities near the slope crest were observed upon mobilisation to site and during the soil nailing part way through. These issues likely resulted from the deterioration of the slope face, which had been exposed prior to the installation of soil nails and structural facing. In these situations, the collapsed slope would be covered with geotextile and backfilled with site earth for support. Soil nails would be installed through the backfill as designed, using plywood secured by nail head plates to support any sloughed material and serve as a shutter for cavity filling. Cavities were filled using a “letterboxing” method, pumping lightweight grout through slits in the plywood.

Before the contractor mobilised, the earthworks above the slope crest were excavated to a typical gradient of 1:3. These slopes remained unprotected without surface drainage for extended periods, leading to widespread erosion. Significant erosion was particularly noted in two main areas, with water runoff affecting the slope stability. In one area, the slope remained dry until all soil nailing was completed. However, due to rainfall and the site’s topography, water flowed extensively over the earthworks and concentrated at the crest of the soil-nailed slope, primarily from over half of the site's working area. This runoff infiltrated the earthworks, eventually seeping through the slope face. Although site drainage improvements reduced water accumulation at the slope toe, substantial erosion continued until the overlying earthworks were repaired with stone fill and covered with a temporary plastic membrane. Once both toe and crest drainage were completed, water accumulation at the toe was significantly minimised. In another area, extensive erosion likely caused localised bulging of the slope facing, as indicated by monitoring. Despite applying a polymer membrane to the surface, erosion continued at the crest, with material being intermittently removed. Cavities formed beneath the soil-nail zone were backfilled using cavity grout filler, and once completed, no further movement was detected.

 © DFI International Bruges 2025

Numerous buried obstructions were encountered across a significant portion of the site. These obstructions, composed largely of coarse backfill such as brick rubble around buried structures, affected all soil nail installations in this area. There were no consistent patterns to predict the nature or location of the obstructions, complicating drilling efforts. Hard drilling and loss of grout flush often occurred either before reaching or after penetrating the obstructions. Despite efforts to penetrate the obstructions, some soil nails had to be abandoned when achieving the required design length was not possible. In such cases, a replacement nail was immediately attempted adjacent to the abandoned one, with repeated attempts made until the design length was achieved. Loss of grout flush was not exclusively linked to obstructions but was frequently observed in their vicinity. It is unclear whether this was due to the coarse fill surrounding the obstruction or potentially other factors such as buried land drains. The procedure to address this involved continuously pumping grout until a return was achieved or injecting up to 0.75m³ (300% of the theoretical volume of the largest borehole). If no grout return was achieved, the nail was abandoned and a replacement was installed nearby. Subsequent attempts typically encountered fewer issues with grout return due to the grout filling voids during the initial attempt.

Asbestos or asbestos-containing materials (ACM) were encountered within a section of the site, affecting specific areas of soil nail installation. Specialists were engaged to cover the impacted soil face and implement the necessary health and safety precautions. Once protective measures were in place, soil nails were installed through the covered soil face. The grout used during the process successfully suspended and trapped the ACM, which was then safely collected and stored on site before being disposed of offsite in accordance with regulations. Additionally, 31nr drilled drains in the affected area were removed from the design due to the potential risk of creating pathways for asbestos-contaminated water to enter the highway drainage system. The design did not depend on these drains, and their omission was considered a safer option for site operatives.

3.3 Geological observations

Observations on-site were made continuously by a site engineer and periodically by contract managers and design engineers. Made Ground was encountered throughout the western portion of the slope, transitioning to natural soil at the eastern end. The Made Ground was highly variable, consisting mainly of stony clay and clayey granular backfill, with inclusions of sand, ash, clinker, and cobbles of various materials, including brick, concrete, limestone, and sandstone. The distribution of these materials was random, making precise recording impractical. However, visual inspections and field strength tests confirmed that the soil conditions aligned with design assumptions, avoiding extremely weak clay or very loose granular fill.

While sacrificial grout used during drilling prevented inspection of arisings, the drilling team could detect hard and soft areas based on changes in penetration rate and loss of grout flush returns. Spoil arisings from drilled drains were inspected and were generally consistent with the natural soil, confirming that natural soil was encountered at about 2 meters from the slope face in the western half of the site.

Notable observations during excavation included relic retaining walls, poorly compacted fill, historic shipyard foundations, relic drainage channels, and large cobbles or boulders of concrete. Additionally, asbestos-containing materials (ACMs) were identified in a specific section of the slope and addressed with appropriate health and safety measures.

 © DFI International Bruges 2025

3.4 Ground Water Observations

When the site was first mobilised, it was generally dry, including the entirety of the excavated first bench. However, the eastern portion collected rainwater runoff, especially from the excavated bench and the slope above. A potential contributing factor was a major water main burst on Pallion Road, although this is not expected to have significantly affected initial or ongoing groundwater conditions. It remains uncertain whether water contributed to the early collapses of the crest and unsupported slope face, but it is likely to have been a factor.

As the project progressed into wetter months, the lack of site drainage and erosion protection caused deterioration of the earthworks, with erosion rills becoming widespread. Following heavy rainfall events, water would accumulate at the eastern end of the soil-nailed slope, unable to drain from the working bench below. This situation improved as the site earthworks were levelled, allowing water to flow away.

Historical drainage channels were identified in the eastern section of the slope, suggesting prior groundwater management measures. During the latter stages of construction, seepage through the soil face and out of drilled drains was observed in the eastern portion of the slope, particularly after rainfall. This resulted in silt and sand deposits at the toe of the slope, likely caused by water flowing over the crest and through the permeable clayey silty sand soil. Erosion rills and voids formed in the embankment, extending to the back of the soil-nailed face. These issues were mitigated by installing permanent drainage grips, water diversions, and temporary erosion protection, which resolved seepage and surface water flow down the slope.

Throughout the construction works, groundwater was rarely detected, with only isolated instances of perched water seepage, which dissipated quickly. In one case, a dark brown leachate was encountered and chemically analysed. This led to a concrete classification of DC-2 AC-1s, following the guidelines in BRE Special Digest 1.

In conclusion, the pore water pressure ratios used in the design (ru = 0.1 and 0.2 from 4 meters below the final verge level) were validated. This approach corresponds to a groundwater surface approximately 1 meter below the final verge and Pallion Road levels, with steady-state water flow through the reinforced soil zone. Additionally, the drilled drains remained dry, confirming that groundwater was not a significant issue during construction.

4. EFFC-DFI Carbon Calculator

The embedded carbon calculations have been undertaken based on the design schedules and drawings of the anchored combi wall provided by others, and on the final as-built drawings produced by AGE. The calculations are inclusive of building materials, material transport and all plant required to construct the works. Elements that are shared by both solutions such as groundworks and facing have been omitted. Emissions have been calculated utilising the EFFC-DFI Carbon Calculator, with updated 2024 DEFRA figure for diesel. Soil nails, steel tubes, and anchors have been calculated presuming an industry average percentage of recycled steel constituent of 41%. Due to understanding of the market and knowledge of supply, sheet piles have been calculated at 91% recycled steel.

Diesel has been calculated based on idealised programmes shown in figure 3, utilising a 10hour working day and average diesel consumption on all listed plant.

 © DFI International Bruges 2025

1	= AGE sheet piling: 2nr 300tonne craner cranes + 10t hammer + power pack
2	= AGE CHS tube piling: 2nr 300tonne craner cranes + 10t hammer + power pack
3	= AGE Ground anchor: 2nr drilling rigs or excavator mounted drill mast + 2nr grout mixer + 1nr MEWPs
4	= AGE Soil nailing: 2nr drilling rigs or excavator mounted drill mast + 2nr grout mixer + 1nr MEWP
5	= AGE Soil nailing facing: 2nr MEWPs

Working days per week: 5

Ref.	Work Item	Piling Group	Operatves nr	No. Piles	Dia (mm)	Avg Len (m)	Avg piles / rig / day	Days	Start Day No.	End Day No.
	Sheet pile installation	1	1	192			2.5	76.8	1	77
	Crane movements - sheet piling	1	1					10.0	77	86
	CHS pile installation	2	1	96			1	96.0	86	181
	Crane movements -CHS piling	2	1					10.0	181	190
	Ground anchor installation Team 1	3	1	95	220		1	95.0	126	220
	Ground anchor installation Team 2	3	1	34.0	220		1	33.0	190	222
	Soil nailing Team 1	4	1	10624	130	14.3	180.0	59.0	1	59
	Soil nailing Team 2	4	1	10624	130	14.3	180.0	59.0	1	59
	Facing Team 1	5		1065			30	35.5	62	97
	Facing Team 2	5		1065			30	35.5	62	97

Figure 3: Assumed programme adopted for the calculations

Figures 4, 5 and 6 below summarise the weights of materials and their corresponding embedded carbon.

Metrics	Soil nail	Sheet piles	CHS piles	Ground anchors	Capping beam
Steel Tonnage	149	859.3	1213.66	14.29	
Steel tCO2e	302.638	732.74	2278.416	19.776	
CEMII Tonnage	824.93	-		114.652	
CEMII tCO2e	709.44	-		98.601	
Water Tonnage	224.09	-		31.145	
Water tCO2e	0.033	-		0.005	
Diesel Litres	18141.33	45168	55440	15360	
Diesel tCO2e	45.59	113.49	139.31	38.59	
C35/45 XD3 tonnage					14061.6
C35/45 XD3 tCO2e					145.12
B500 rebar tonnage					91.986
B500 rebar tCO2e					127.25
Total tCO2e	961.466	846.23	2,417.726	156.972	272.37

Figure 4: Results of the EFFC -DFI embedded carbon calculations

 © DFI International Bruges 2025

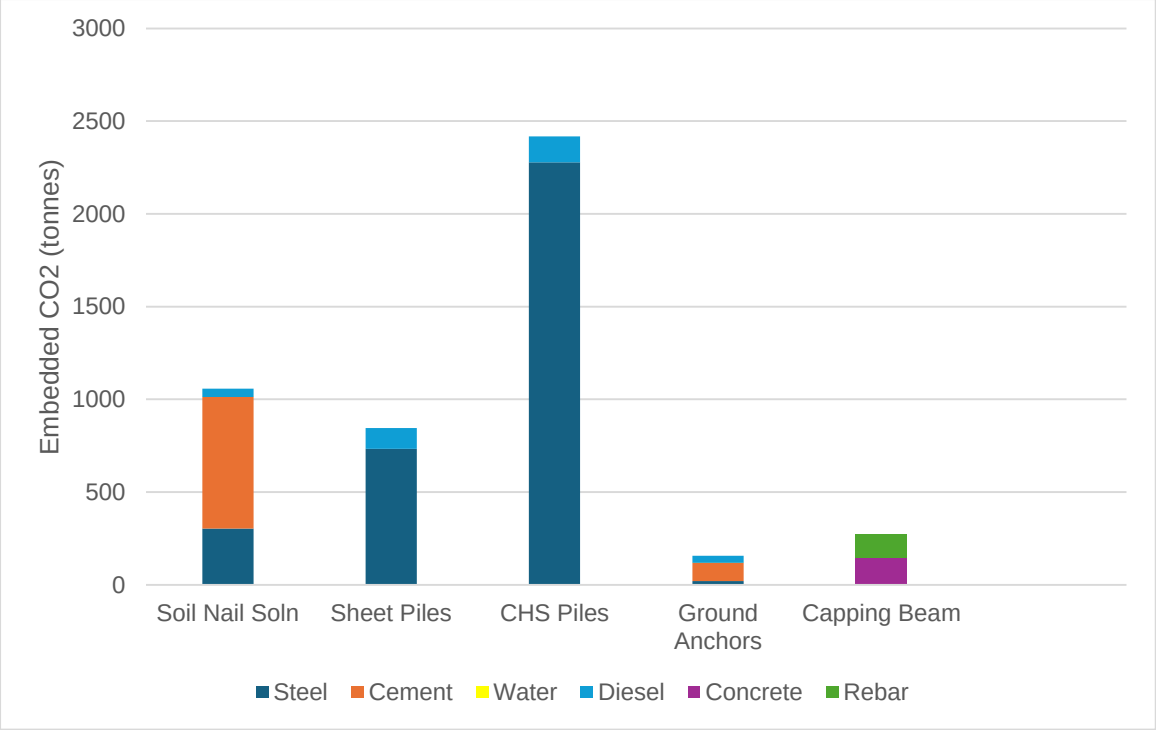


Figure 5: Graph showing constituent break down of each elements CO2 contribution

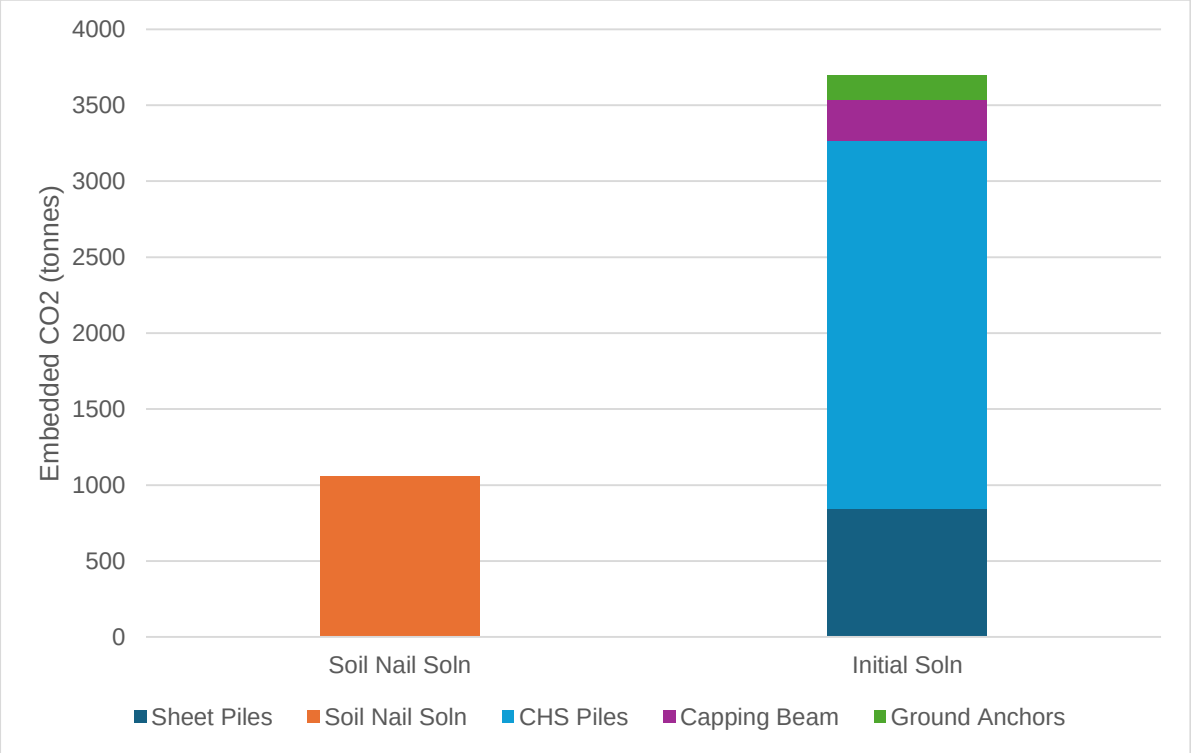


Figure 6: Graphs showing total comparison between the two schemes

Figure 7 below details the main aspect excluded from the calculation and their reasons for exclusion. It is the opinion of the authors that these exclusions have no effect on the overall conclusion, as detailed below.

 © DFI International Bruges 2025

Initial scheme	Soil nail scheme
Excavation and ground work – these are assumed to be equivalent	
Barriers (de minimis)	
Drainage above or below walls (assumed to be equivalent)	
Testing (de minimis)	
Waling beams (lack of information)	Geotextiles (lack of data)
Expanded metal legs facing panels (facing excluded in both schemes)	Gabion facing and its foundation (facing excluded in both schemes)
Special import and transportation of large sheet piles and CHS (lack of data as never ordered)	Drilled drains (lack of data)
Manufacturing of plant (lack of data as never constructed)	
Connection plates and welding between tubes and sheets (de minimis)	

Figure 7: Aspects of construction excluded from carbon calculations

5. Conclusion

In total, the embedded carbon was decreased from an estimated 3,693,300kg in the initial scheme to an estimated 1,057,600kg – a 74% reduction – in reengineering the scheme. Despite these being idealised estimated, this paper clearly demonstrates the significant reduction in embedded carbon achieved on this specific project.

As detailed herein, this significant reduction in the project's emissions could only come through careful management of the geotechnical design risks, and close supervision during construction. Whilst the riskier solution, when considering precedence was selected to be installed, this choice was only made possible by a willingness to adapt and try through the supply chain of the project. Whilst the soil nail solution was proposed by the geotechnical subcontractor, it needed buy-in from the main contractor and end client to ensure that the reduction in carbon could be achieved. When considered with the limited legislative and framework context for infrastructure projects, it is early adoption of more sustainable thinking that can drive carbon reduction in projects today. To mitigate the inefficient use of construction materials yet balance the robustness needed for infrastructure work whilst being committed to more sustainable solutions, engineers must be prepared to face the geotechnical challenges both during the design and construction. Finally, Engineers must not be perturbed from more sustainable solutions on the basis of ground risks without dedicating resources to robustly planning for appropriate risk management.

 © DFI International Bruges 2025

THE SECOND EDITION OF THE EFFC/DFI GUIDE TO WORKING PLATFORMS – DESIGN ASPECTS

Moritz Schleeh, University of Stuttgart, Institute for Geotechnical Engineering, Germany,
+49 711 685-62737, moritz.schleeh@igs.uni-stuttgart.de

Christian Moormann, University of Stuttgart, Institute for Geotechnical Engineering, Germany,
+49 711 685-62437, christian.moormann@igs.uni-stuttgart.de

Peter Faust, DFI, Malcolm Drilling Inc., San Francisco, USA, PFAUST@MalcolmDrilling.com

James De Waele, EFFC, University of Birmingham, GB, jdw@coudrier.uk

ABSTRACT

In 2020 the European Federation of Foundation Contractors (EFFC) and the Deep Foundations Institute (DFI) published the first edition of the *´Guide to Working Platforms´* to enhance safety, simplicity, and productivity in construction under challenging conditions. The second edition published in 2025, is being developed by an international consortium of experts from industry, business, and academia. It addresses critical challenges faced by construction machinery, including drilling rigs and pile drivers, when operating on soft ground. These high weight and elevated center of gravity of these machines require adequately dimensioned working platforms to prevent overturns, mitigating risks of severe accidents, property damage, and operational delays. The new guide focuses on three core areas: field test evaluations (FRS#1), realistic ground pressure distributions beneath crawler tracks (FRS#2), and geotechnical design methods (FRS#3). The Institute for Geotechnical Engineering of the University of Stuttgart, commissioned by DFI and EFFC, has conducted research on FRS#1 and FRS#3. Field tests executed across 40 sites in Europe, the USA, and the UK reflecting significant variability in subsoil conditions, emphasize the necessity for site-specific testing. The guide also compares design methods, revealing significant deviations in required platform thickness and pointing out the importance of an appropriate design approach. The study highlights that the friction angle of granular platform layers and the shear strength of subsoil play a decisive role in determining the required platform thickness, underscoring the need to consider adequate geotechnical input parameters, realistic track pressures, and adequate safety concepts in the design process.

Keywords: Construction Machinery, Working Platforms, Safety, Field Tests, Design Methods, Track Pressure, EFFC, DFI.

INTRODUCTION

Drilling rigs and pile drivers, like other large specialized foundation equipment, have a high weight and elevated center of gravity combined with a limited track footing area. These characteristics make them particularly sensitive to overturning, as improper design is one of the main causes of overturning, especially if the working platform is not properly designed. Overturning incidents involving these heavy machines are among the most severe accidents in the construction industry, and they often result in:

- serious or fatal injuries to project personnel or third parties,
- significant damage to the machinery and surrounding structures,
- project delays and additional costs due to downtime,
- reputational damage for the companies involved in the construction project.

 © DFI International Bruges 2025

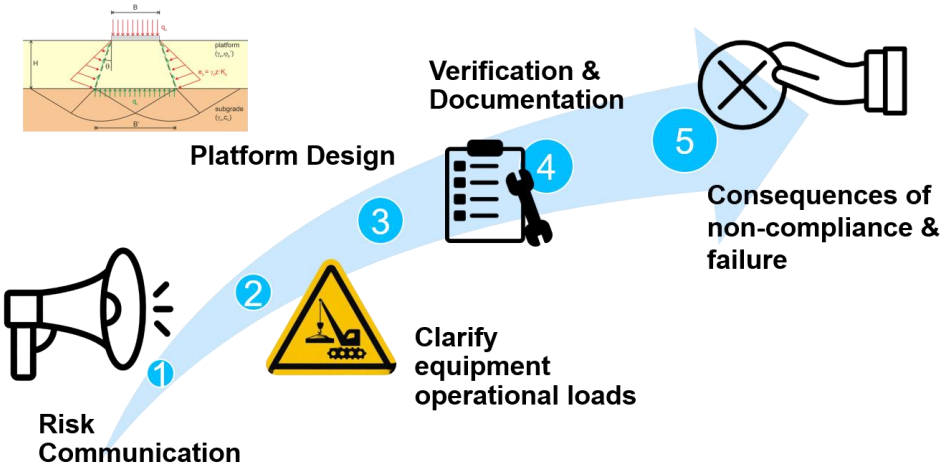


Fig. 1. Key stages in the design and verification process of working platforms.

A study of 75 overturning incidents attributed most accidents to inadequately designed or maintained working platforms (HINZMANN & SIEWERT, 2019). Additional factors contributing to these incidents include the qualifications of the machine operators and construction personnel, site coordination, communication, and control, as well as damage, contamination, softening, and poor maintenance of the working platform (EFFC/DFI, 2020). Mechanical issues and equipment faults were rarely the primary cause of overturns. The proper design and maintenance of working platforms are therefore critical to prevent such accidents. In engineering practice, platform design is often based on experience, but due to the complex interaction between the machine, the working platform and the ground, a more sophisticated geotechnical approach is needed. In the UK, the introduction of the BRE BR470 guideline in 2004 reduced the number of machine overturns by 50% within a year (GILDEA ET AL., 2021). Well-designed and constructed platforms not only improve safety but also enhance productivity by facilitating quicker machine relocation and operations, which ultimately leads to more cost-effective construction processes.

Both unreinforced and reinforced working platforms are considered multi-layer systems from a geotechnical perspective, with layers having significantly different stiffness and strength characteristics. This makes their reliable geotechnical design challenging. To address these challenges, the Deep Foundations Institute (DFI) and the European Federation of Foundation Contractors (EFFC) will release in 2025 the second edition of the *'EFFC/DFI Guide to Working Platforms'*. This updated edition follows a structured process for designing, installing and maintaining platforms, as illustrated in Fig. 1, which outlines the critical steps - from risk communication to platform design and verification - ensuring that all necessary actions are taken before operations begin.

Led by Peter Faust (DFI) and Jim De Waele (EFFC), an international working group has focused on three key research areas:

1. **Field test investigations (FRS#1):** Identification of appropriate field tests to assess the quality and performance of working platforms, focusing on their construction and current condition.
2. **Realistic ground pressure distributions (FRS#2):** Development of methods to determine realistic pressure distributions, especially under tracked construction machinery.
3. **Design methods (FRS#3):** Evaluation and comparison of different calculation methods used for platform design, highlighting the significant discrepancies in the required platform thicknesses and the need for a comprehensive design approach.

The guide aims to provide practical recommendations and calculation methods that can be applied by geotechnicians, engineers, and other construction professionals, offering a reliable framework for the design and maintenance of working platforms. The Institute for Geotechnical Engineering at the University of Stuttgart was commissioned by the DFI and EFFC to carry out research on both field tests (FRS#1) and design methods (FRS#3). Their studies focused on developing more accurate design methods that consider the variability of subsoil conditions and the importance of realistic soil pressure distributions. This research highlights the critical role of factors such as the friction angle of the material of granular platform layers and the shear strength of the subsoil in determining the necessary

 © DFI International Bruges 2025

platform thickness. The new guide provides all stakeholders involved in construction projects with the necessary tools to ensure safe and efficient operations on working platforms for heavy machinery.

CURRENT CHALLENGES IN DESIGN

Despite the critical role of working platforms in ensuring the safety of heavy construction machinery, there is no globally recognized standard for their design. Temporary working platforms, typically made from compacted granular materials, are designed according to different guidelines depending on the region. In the European context, ground investigations must comply with EN 1997-2, and the impacts of construction operations must be calculated following EN 1997-1. In Germany, contractors are responsible for reviewing and flagging any concerns regarding the design or execution as required by VOB/B (DIN 1961).

While some guidelines, such as those provided by the German Construction Industry Association (HDB, 2019), offer basic estimates for soil pressures under typical construction equipment, these values must still be cross-checked against specific machine data. Many standards rely on idealized scenarios that overlook on-site complexities. Real-world conditions, particularly when machines operate on soft ground layers, can cause stress redistribution and plastic deformations in the subsoil, making simple design models inadequate (MEIßNER ET AL., 1992; KUMMETER, 2001; MOORMANN, 2018). Linear-elastic assumptions fail to capture the true interaction between machinery and ground conditions. Current design approaches frequently underestimate the real pressures exerted on working platforms, especially under high-load conditions and when dealing with tracked machinery (LARISCH ET AL., 2021). In fact, studies show that the actual pressure distributions can be higher than predicted (TOPOLNICKI ET AL., 2020). Meeting these basic estimates can lead to underestimations, resulting in incidents of machine overturns. Investing in a well-designed platform may seem costly initially, but it is essential to prevent severe accidents and operational delays. All stakeholders need to factor platform design into the project's overall costs, considering the loads imposed by their equipment rather than relying solely on basic geotechnical solutions. While the installation of safe platforms is a complex process, it is ultimately a necessary investment to reduce risks and ensure operational safety (DE WAELE, 2021).

Traditional approaches like MEYERHOF'S (1974) punching shear model and TERZAGHI & PECK'S (1948) bearing capacity model are still commonly used but face limitations due to their simplified assumptions (Fig. 2). Research by HANNA & MEYERHOF (1980) and BURD & FRYDMAN (1997) has shown that the shear strength of the underlying cohesive soil plays a significant role in determining platform performance, emphasizing the importance of considering both subsoil and platform strength. More advanced methods incorporating geosynthetic reinforcement provide additional stability but are often based on empirical data and may be specific to particular products, limiting their general comparability and applicability (SCHLEEH & MOORMANN, 2023).

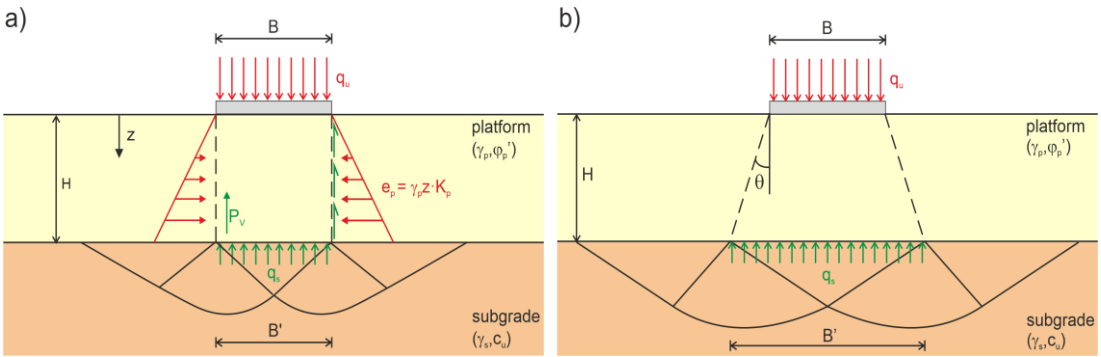


Fig. 2. a) Punching Shear Model (MEYERHOF, 1974); b) Projected Area Model (TERZAGHI AND PECK, 1948).

 © DFI International Bruges 2025

FIELD TEST INVESTIGATIONS (FRS#1)

FRS#1 focuses on the experimental testing and verification of constructed working platforms through global field investigations. These tests are not intended to replace comprehensive geotechnical investigations but rather serve as a secondary verification step. They are performed before and during the operation of heavy machinery on the platforms. Central to these investigations is the practical usability of testing equipment, the reliability of measurements, and how well the data correlates with design approaches. The test methods chosen for these field investigations are selected based on several key criteria:

- ease of use with minimal training,
- efficiency and cost-effectiveness,
- portability and flexibility of equipment,
- reliable measurements despite environmental conditions,
- the usefulness of the collected data for geotechnical design correlations.

From a very large number, the following four testing methods were selected for comprehensive field trials:

1. **Dynamic Probing Light (DPL)** in accordance with EN ISO 22476-2, using a motor-driven compressor and pneumatic hammer with a 5 cm² probing tip.
2. **Panda®-Sonde Light Dynamic Probing with Variable Energy** in line with NF P 94-105, using a handheld or electric hammer with automated data recording, equipped with a 2 cm² probing tip.
3. **Static Plate Load Test (PLT)** as specified in DIN 18134, ASTM D1194-94, AASHTO T222 and ASTM D1196 using a hydraulic hand pump and semi-automated data logging, with a 300 mm plate.
4. **Light Weight Deflectometer (LWD)** according to ASTM E2835 and TP BF-StB Part B 8.3, manually operated with automatic data logging and a 300 mm plate.

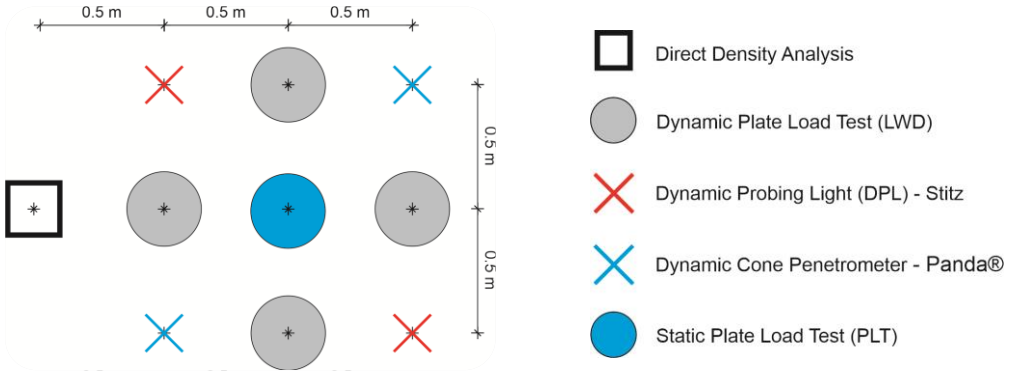


Fig. 3. Configuration of the tests per test location.

Table 1. Observed advantages and disadvantages for each test method.

Test method	Advantages	Disadvantages
DPL	High depth penetration, easy to use, robust, allows multiple tests	Physically demanding, better with two operators, many components, riskier for injuries
Panda®	Short test duration, automatic data logging, high depth penetration, flexible equipment	Challenging with coarse or dense soils, multiple parts, requires power source, needs experienced operators
PLT	Standard equipment, realistic load simulation, direct evaluation	Limited depth range, requires surface prep, heavy, time-consuming, needs counterweight
LWD	High test frequency, light and simple to operate, automatic data logging	Limited depth influence, requires surface prep, needs static PLT calibration, variable results

 © DFI International Bruges 2025

Tests were conducted in a grid pattern (Fig. 3) at multiple locations on each construction site respectively working platform to enhance data correlation.
The tests were carried out on construction sites in various countries under real-world conditions. The field personnel provided feedback on the ease of use and effectiveness of each method. Table 1 summarizes the advantages and disadvantages observed for each test method. Over 40 locations across Europe, the USA, and the UK revealed substantial variations in test results, depending on the test method used and the specific site conditions. These differences were attributed to the variability in the platform layers, subsoil conditions, and testing procedures. Each test method showed different sensitivity to material heterogeneity, with notable inconsistencies even in tests conducted in close

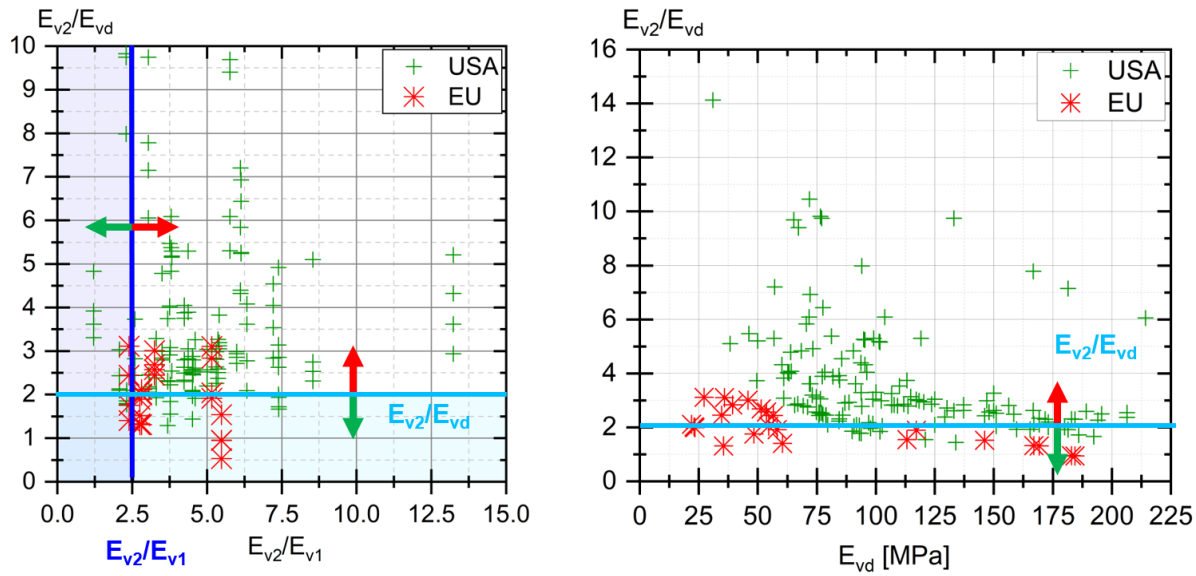


Fig. 4. Selected test results of dynamic and static plate load tests in USA and Europe.

proximity using identical setups.
Fig. 4 presents the normalized results of static and dynamic plate load tests, showing the ratios of E_{v2}/E_{vd} and E_{v2}/E_{v1}, where E_{vd} is the dynamic deformation modulus from LWD, E_{v2} is the reloading static deformation modulus (PLT), and E_{v1} is the first loading static deformation modulus (PLT), for various working platforms in the USA (green) and Europe (red). For each static plate load test (PLT), four lightweight deflectometer (LWD) tests were carried out at 0.5 m distances. BRÄU & VOGT (2020) suggest that the dynamic deformation modulus (E_{vd}) can generally be estimated from the static E_{v2} value using a factor of two, as recommended by ZTV E-StB or FGSV SoB-StB (2020) for compaction control. However, for sands, values around two are expected, while gravel layer may yield ratios exceeding four. The field tests demonstrated that the factor of two does not consistently apply, especially for highly compacted platforms with D_{max} > 63 mm. Nevertheless, the dynamic tests typically produced high E_{vd} values, exceeding the compaction requirements outlined in current guidelines. It is therefore always recommended to calibrate the correlation values of E_{vd} by means of static tests in situ for soil-mechanical scenarios where the mechanical properties differ from a geotechnical perspective. Based on several ZTV guidelines, platforms are considered sufficiently compacted when the deformation moduli reach $E_{v2} \geq 120$ MN/m², $E_{vd} \geq 60$ MN/m², and $E_{v2}/E_{v1} < 2.5$. For thick gravel layers, slightly higher values may be required. Fig. 4 show that while higher E_{v2}/E_{vd} and E_{v2}/E_{v1} ratios can be observed, they do not necessarily indicate inadequate load-bearing capacity. In comparing E_{v1} and E_{vd}, as employed in Switzerland (BODMER ET AL. 2014) and Austria for compaction control, better correlations were observed in some instances than between E_{vd} and E_{v2}.
The 'Panda®-Probe' with its smaller 2 cm² tip, provides detailed measurements of penetration resistance, allowing an accurate in-situ compaction control and soil layer classification. Its ability to vary impact energy and the use of the loosen tip of 4 cm² enhance precision, particularly in softer layers. The DPL, with its smaller 5 cm² tip, was effective in penetrating dense layers but faced

 © DFI International Bruges 2025

challenges in very compacted soils, indicated by higher blow counts. The 'Panda®-Probe' excelled with its automated data recording and cloud-based analysis, making it suitable for more detailed assessments, while the DPL was robust and reliable for rough evaluations in stiffer platform layers. Both methods correlate well with each other and with key parameters, provided the application area permits proper execution

REALISTIC GROUND PRESSURE DISTRIBUTIONS (FRS#2)

Lighter construction equipment can exert similar ground pressures as heavier machinery. Detailed reviews of data and calculations from various equipment manufacturers reveal no clear correlation between factors like machine weight, drilling diameter, or drilling depth and the resulting ground pressure. This variability underscores the importance of evaluating any changes in machine configuration, drilling dimensions, or operational modes during platform design to ensure accurate load

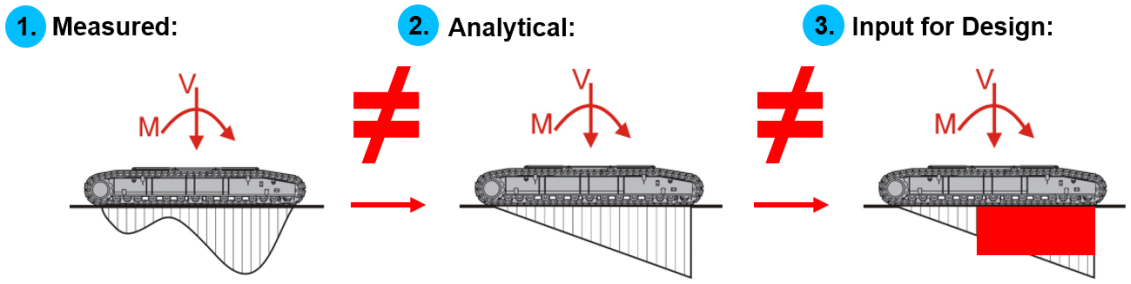


Fig. 5. Chain of errors of transferring realistic ground pressure distributions into design models.

assessments.
Current load models adequately fail to capture real stress distributions, differential settlements, and non-linear effects, all of which present substantial risks in the design process. The EN 16228-1 standard, while widely used, offers a simplified approach that does not fully address these complexities. There is a critical need for further refinement in the interface between load models and computational methods. Field tests using distributed fiber optic sensing (DFOS) demonstrated that actual track pressure distributions deviate significantly from theoretical models like EN 16228-1 (FAUST, 2022). Field results from MOORMANN (2018) and TOPOLNICKI ET AL. (2020) further confirm that pressure concentrations tend to be higher at the edges of crawler tracks, challenging linear assumptions typically used in design. To be utilized in computational models these complex and more realistic pressure distributions must be transformed into a uniform load assumption using methods as MEYERHOF (1953). This transformation introduces a chain of errors (Fig. 5), which can accumulate and directly impact the calculated bearing capacity and the required platform thickness, ultimately influencing the overall safety of the structure.

DESIGN METHODS (FRS#3)

The design process for working platforms involves several key steps, including identifying platform requirements, determining loads, and specifying ground and material parameters. It also includes safety considerations, appropriate calculation models, and in-situ testing to ensure compliance with design specifications.

 © DFI International Bruges 2025

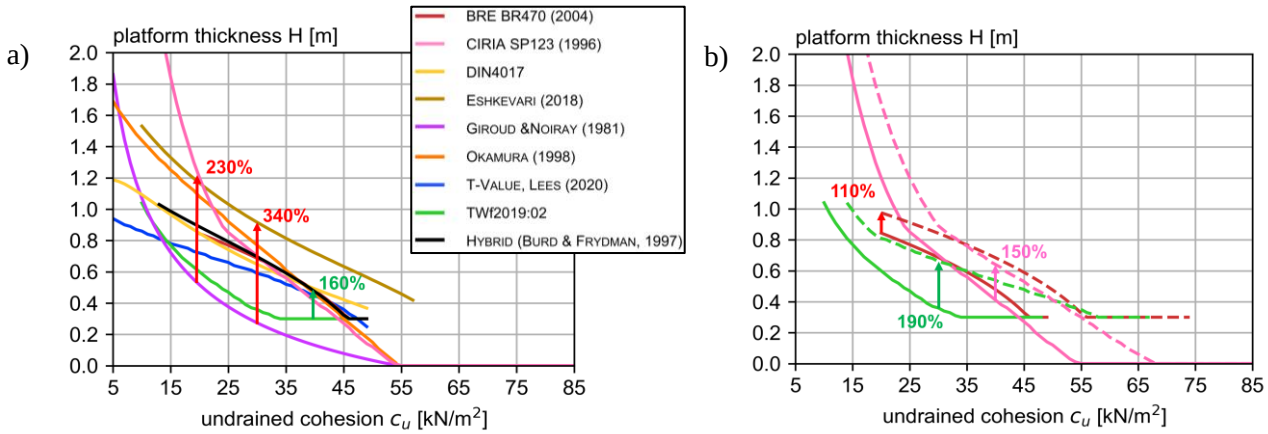


Fig. 6. Platform thickness required for load case a) characteristic values and b) the comparison between characteristic and design values, as determined for the presented calculation scenario using various calculation models.

Benchmark calculations applied common models to assess unreinforced granular platforms thickness using established models such as BRE BR470 (2004), TWf (2019), as well as the more recent methodologies of ESHKEVARI ET AL. (2019) and LEES & ALI (2024) for loosely compacted sand. For the new DIN 4017 standard, the updated VRETTOS & SEIBEL (2023) model is referenced. Different combinations of construction machinery, platform materials, and subsoil conditions were considered. The calculations in this paper focus on a pile driving load case, with a Track width of 0.7 m, equivalent track length of 1.4 m, and a uniform track pressure of 280 kN/m². The study also examined loads of platform configurations with different friction angles.

Fig. 6 illustrates the calculated platform thickness required for load case a) characteristic values and b) the comparison between characteristic and design values, assuming a platform friction angle of φ'_k = 40° and considering various calculation models. As seen in previous comparative studies (SCHLEEH & MOORMANN, 2023), there are significant discrepancies in required layer thickness, with differences of up to a factor of 4, particularly at high bearing pressures and low shear strengths.

Table 2. Safety factors applied by BRE BR470 (2004), CIRIA SP123 (1996) and TWF (2019).

ULS partial safety factors				
	BRE LC 1	BRE LC 2	SP123 (ULS)	EC7 comb. 2 (TWf2019:02)
Permanent loading γ_G	1.60	1.20	1.00	1.00
Variable loading γ_Q	1.60	1.20	1.00	1.30/1.00
Cohesion γ_c	1.00	1.00	1.25	1.40
Shear angle γ_φ	1.00	1.00	1.25	1.25

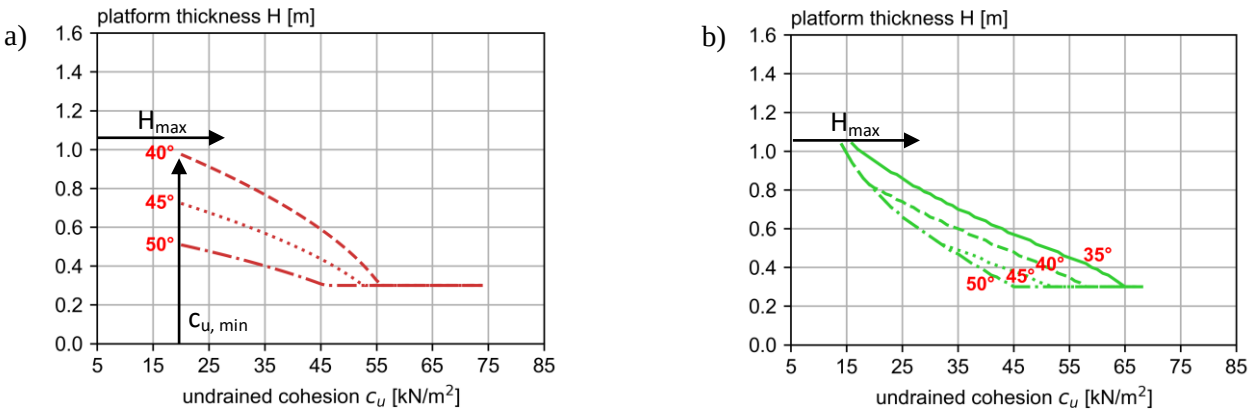


Fig. 7. Platform thickness required according to a) BRE and b) TWf with variation of φ'_k= [35,40,45,50] ° of the working platform material.

 © DFI International Bruges 2025

BRE, TWf, and CIRIA models each employ their specific safety factors (Table 2). For instance, BRE's safety factors are empirically set for different load cases, while CIRIA adjusts shear parameters φ'_k and $c_{u,\ k}$ for worst-case scenarios in ultimate limit state (ULS) calculations. The differences between characteristic and design values in these models significantly affect the required platform thickness (Fig. 6b). If the empirical safety factors from the BRE approach were applied to the TWf calculation method, Fig. 6b shows that this would result in a very low platform height, which would clearly pose a safety risk. Fig. 7 illustratively presents results from the sensitivity analysis, exploring the influence of varying the friction angle φ'_k of the granular working platform material in 5° increments from 35° to 50°. A notable reduction in the required layer thickness - 48% for BRE and over 30% for TWf - is observed when increasing φ'_k from 40° to 50°. The BRE model, as shown in figure 7a, is unable to calculate a required layer thickness for a friction angle of 35° due to its limitations. In contrast, the TWf method, as shown in figure 7b, provides results for a 35° friction angle by applying different safety factors for distinct calculation applications, specifically in this case for the bearing capacity check of the platform material using characteristic values.

For greater platform thickness, failure tends to occur within the platform material rather than by punching shear. Thus, the standard punching shear calculation is unsuitable when H/W > 1.5 (BRE BR 470). In this context, the maximum thickness H_{max} is defined as 1.5 times the track width, yielding H_{max} = 1.05 , ensuring that failure is not limited to the platform itself. BRE is applicable only for undrained shear strengths between $c_{u,\ k}$ = 20 and 80 kN/m², as its underlying failure mechanism assumes punching shear failure. For lower shear strengths, modification parameters from BURD & FRYDMAN (1997) can be applied (MILLER, 2013).

In summary, the calculations reveal significant differences in the required platform thickness for unreinforced platforms over soft soils and loosely compacted sands. Calculation models show discrepancies of up to a factor of four, although safety concepts can reduce these differences by up to one-third. The sensitivity analysis confirms that the platform friction angle is a critical factor in determining the necessary layer thickness, alongside subsoil shear strength. The accurate assumption of friction angle for platform materials is therefore crucial, supporting the need for holistic application of design methods.

CONCLUSION & DISCUSSION

The second edition of the EFFC/DFI *´Guide to Working Platforms´* provides helpful tools and guidelines for safe and efficient heavy construction operations. This updated guide is based on extensive research and field testing, offering practical recommendations to address the complex challenges posed by working platforms. By incorporating findings from global field investigations, the guide highlights the variability in subsoil conditions and emphasizes the importance of site-specific testing and design considerations. The guide can be regarded as a valuable tool and reference for engineers, providing them with the essential knowledge and practical instruments necessary for the effective design and construction of safe and efficient working platforms.

The calculation studies reveal that different design methods result in significant variations in required platform thicknesses, with discrepancies of up to a factor of four. These differences, largely driven by the chosen calculation models and safety factors, underscore the necessity of a holistic design approach. The various design aspects presented earlier must be handled separately and systematically, as improper combinations, or a "pick and mix" approach, are not acceptable. Importantly, the friction angle of the material for granular platform layers and the shear strength of the underlying subsoil are shown to be crucial factors in determining the platform's load-bearing capacity. Sensitivity analyses demonstrate that increasing the friction angle of the platform materials can significantly reduce the required platform thickness, which has both safety and economic benefits.

Field investigations revealed that no single testing method is universally applicable; each method has its strengths and limitations depending on the specific conditions of the site. As a result, a combination of methods and a systematic concept approach is recommended to achieve accurate and reliable results. The findings support the need for continual refinement of field-testing procedures, realistic bearing pressure determination and calculation models to ensure that platforms are designed with both safety and efficiency in mind. The EFFC/DFI guide provides a comprehensive framework for construction engineers and contractors, promoting the use of realistic ground pressure distributions, advanced design

 © DFI International Bruges 2025

methods, and site-specific testing to enhance the safety, efficiency, and reliability of working platforms.

REFERENCES

AASHTO T222. Standard method of test for nonrepetitive static plate load test of soils and flexible pavement components for use in evaluation and design of airport and highway pavements. AASHTO 1981. T222-81-UL.

ASTM D1194-94. Test method for bearing capacity of soil for static load and spread footing. Annual book of ASTM standards: Volume 04.08. October 2003.

ASTM D1196/D1196M − 21. Standard test method for nonrepetitive static plate tests of soils and flexible pavement components for use in evaluation and design of airport and highway pavements. Book of standards volume: 04.03.

ASTM E2835-21. Standard test method for measuring deflections using a portable impulse plate load test device. Annual book of ASTM standards: Volume 04.03. May 2021.

BRE Building Research Establishment (2004/2007). Working platforms for tracked plant: good practice guide to the design, installation, maintenance and repair of ground-supported working platforms (BR 470). IHS BRE Press, Bracknell, Berkshire, ISBN 186081 7009.

Bodmer, P., Byland, H., De Witte, H. (2014). Use of a light weight deflectometer LFG for compaction control of unbound subbase layers. Forschungsprojekt VSS 2002/501 auf Antrag des Schweizerischen Verbandes der Straßen- und Verkehrsfachleute (VSS).

Bräu, G., Vogt, S. (2020). s/v-Wert beim dynamischen Plattendruckversuch. Bericht zum Forschungsprojekt 05.0187. Berichte der Bundesanstalt für Straßenwesen, Reihe S: Straßenbau (143).

Burd, H.J., Frydman, S. (1997). Bearing capacity of plane-strain footings on layered soils. Canadian Geotechnical Journal, No. 34, p. 241–253.

De Waele, J. (2021). Working platforms for specialty geo-construction. GeoStrata Magazine. Volume 25, Issue 3. American Society of Civil Engineers.

DIN 1961:2016-09. German construction contract procedures (VOB) - Part B: general conditions of contract relating to the execution of construction work. Beuth-Verlag Berlin.

DIN 18134:2012-04. German Institute for Standardization. Soil - testing procedures and testing equipment - plate load test. Beuth-Verlag Berlin.

DIN 4017:2006-03. German Institute for Standardization. Soil - calculation of design bearing capacity of soil beneath shallow foundations. Beuth-Verlag Berlin.

EBGEO (2011). German Geotechnical Society. Recommendations for design and analysis of earth structures using geosynthetic reinforcements – EBGEO. 2nd Ed., Berlin: Ernst & Sohn.

EFFC/DFI (2020). Guide to working platforms, 1. edition. Joint EFFC/DFI Working Platforms Task Group.

EN 16228-1:2022-07. Drilling and foundation equipment - safety - part 1. common requirements. German version EN 16228-1:2014+A1:2021. Beuth-Verlag Berlin.

EN 1997-1:2022-10. Eurocode 7 - geotechnical design - part 1. general rules. English version prEN 1997-1:2022.

EN 1997-1:2022-10. Eurocode 7 - geotechnical design - part 2. ground properties. English version prEN 1997-2:2022.

EN ISO 22476-2:2012-03. Geotechnical investigation and testing - field testing - part 2: dynamic probing.

Eshkevari, S., Abbo, A., Kouretzis, G. (2018). Bearing capacity of strip footings on sand over clay. Canadian Geotechnical Journal, Nr. 56, p. 699-709.

Eshkevari, S., Abbo, A., Kouretzis, G. (2019). Bearing capacity of strip footings on layered sands. Computers and Geotechnics, Volume 114.

 © DFI International Bruges 2025

Faust, P., Hubbard, P., Soga, K. (2022). Field measurements of in-situ equipment track pressure and working platform deformation using earth pressure cells and fiber optics. DFI-EFFC International Conference on Deep Foundations and Ground Improvement, 2022 Berlin.

FGSV (2009). ZTV E-StB E. Additional technical conditions of contract and directives for earthworks in road construction. Edition 2009. FGSV. Köln.

FGSV (2020). SoB-StB 20. Zusätzliche Technische Vertragsbedingungen und Richtlinien für den Bau von Schichten ohne Bindemittel im Straßenbau. FGSV. Köln.

Gildea, P.A., Faust, P., Richards T.D. (2021). Working platforms for tracked piling plant - current worldwide practice and guidance for the USA. IFCEE EXPO 2021 – May 10-14.

Giroud, J.-P., Noiray, L. (1981). Geotextile-reinforced unpaved road design. Journal of Geotechnical Engineering Division, Nr. 107 (GT9), pp.1233-1254.

Hanna, A.M., and Meyerhof, G.G. (1980). Design charts for ultimate bearing capacity for sands overlying clays. Canadian Geotechnical Journal, Vol. 17, No. 2, 300.

HDB (2019). Stopp Maschinenumstürze – Merkblatt zur Vermeidung von Maschinenumstürzen im Spezialtiefbau. 1. Auflage 2019. Hauptverband der Deutschen Bauindustrie e.V. (German Construction Industry Association), Bundesfachabteilung Spezialtiefbau, Verein zur Förderung fairer Bedingungen am Bau e.V.

Hinzmann, U., Siewert, D. (2019). Verhinderung von Maschinenumstürzen im Spezialtiefbau. Pfahl-Symposium 2019, Mitteilung des Instituts für Grundbau und Bodenmechanik der Technischen Universität Braunschweig, S. 339-346.

Jewell, R.A. (1996). Soil reinforcement with geotextiles. Construction Industry Research and Information Association, London, CIRIA, Special Publication 123.

Kummeter, B. (2001). Bodenpressung unter Raupenkranen. Tiefbau 6/2001. BG BAU.

Larisch, M.D., Damen, R., Johnstone, G., Attewell, B. (2021). Temporary working platforms – technical guidance on New Zealand good practice. NZGS Symposium 2021, Good grounds for the future, New Zealand.

Lees, A. (2020). The bearing capacity of a granular layer on clay. ICE proceedings of the Institution of Civil Engineers - geotechnical engineering 173, pp. 1-24.

Lees, A., & Ali, A. (2024). The surface bearing capacity of a strong granular layer on weaker sand. ICE proceedings of the Institution of Civil Engineers - geotechnical engineering 2024 177:2, 158-168.

Meißner, H., Becker, A., Geib, S. (1992). Zur Bodendruckverteilung unter Raupenketten hoher Baumaschinen bei Schwerpunktwanderungen. Tiefbau, 8/1992. BG BAU.

Miller, K. S. (2013). Technical note on use of BR470 in soft clay. FPS. Federation of Piling Specialists.

Meyerhof, G G (1953). The bearing capacity of foundations under eccentric and inclined loads. Proceedings of 3rd International Conference on Soil Mechanics and Foundation Engineering, Zurich, vol 1, pp 440–445.

Meyerhof, G.G. (1974). Ultimate bearing capacity of footings on sand layer overlying clay. Canadian Geotechnical Journal, Vol. 11(2), pp. 223-229.

Moormann, C. (2018). Tragschichten für Arbeitsplattformen von mobilen Baumaschinen und für Kranstellflächen. AiF Forschungsnetzwerk Mittelstand – Abschlussbericht. IGF-Vorhaben NR. 18833 N/1 (Research report, in German).

Moormann, C., Schleeh, M. (2022). Ground-supported working platforms for tracked plants and mobile cranes – investigations of interaction effects. DFI-EFFC International Conference on Deep Foundations and Ground Improvement: smart construction for the future, 2022 Berlin.

NF P94-105. Grounds: investigation and testing measuring compaction quality. Method using variable energy dynamic penetrometer. Penetrometer calibration principle and method. Processing results. Interpretation. AFNOR. M. La Plaine Saint-Denis. France. 2012.

Okamura, M., Takemura, J., Kimura, T. (1998). Bearing capacity predictions of sand overlying clay based on limit equilibrium methods. Soils and Foundations 38(1), p. 181-194.

Schleeh, M., Moormann, Ch. (2023). Bearing capacity of un- and reinforced working platforms –

 © DFI International Bruges 2025

verification of different design methods by model tests and field measurements. Proc. 17th Danube European Conference on Geotechnical Engineering (17DECGE) June 7-9, 2023, Bucharest, România.

Terzaghi, K., Peck, R.B. (1948). Soil mechanics in engineering practice. 1st ed. John Wiley and Sons, Inc., New York.

Temporary Works Forum (2019). Design of granular working platforms for construction plant. A guide to good practice. TWf2019: 02. Temporary Works Forum. c/o Institution of Civil Engineers. London. England.

Topolnicki, M., Wäger, J., Schweizer, S., Koller, A., Brzozowski, T., Sołtys, G. (2021). Field test verification of ground bearing pressure under rig tracks and implications for working platform design. Ground Engineering 2021, pp. 26-38.

TP BF-StB Part B 8.3 E. Technical testing regulations for soil and rock in road construction. Part B 8.3. Dynamic plate load testing with the light drop-weight tester. FGSV-Nr.: 591/B 8.3 E.

Vrettos, C., Seibel, E. (2023). Durchstanzen von Fundamenten auf einer Sandschicht über Ton: Berechnungsverfahren und Erkenntnisse aus numerischen Parameterstudien. Geotechnik 46, H. 4, S. 220–236.

 © DFI International Bruges 2025

MEASUREMENT OF PILE SET AND IMPACT VELOCITY FOR DRIVEN PILE ACCEPTANCE

Julian P. Seidel, Construction QA, Melbourne, Australia j.seidel@construction-qa.com
Hossein A. Ahmadi, Construction QA, Melbourne, Australia h.ahmadi@construction-qa.com

ABSTRACT

Traditionally driven pile control has been based on pile driving formulas. These formulas are typically based on an estimation of the potential energy of the hammer, an assumed hammer efficiency (representing energy input) and measurement of the pile set or blow count (representing pile response). In some instances, measurement of the transient movement of the pile during impact (rebound) is also required. Some formulas also include adjustments for losses in the hammer impact process. The advent of dynamic pile testing allowed the energy actually delivered to the pile to be measured, from which an evidence-based hammer transfer efficiency could be computed, and adopted for project control on the 90% or more of untested piles using formulas or simple set or blow count measurements. For diesel hammers, stroke can be inferred from blow rate, and some hammers measure ram impact velocity. However, it is asserted that measurements of stroke or ram velocity are insufficient to predict delivered energy to the pile primarily due to the effect of the helmet and cushion materials between the hammer and pile. This paper discusses why effective project control therefore relies on direct measurements of hammer input and pile response on the pile itself.

Keywords: driven pile acceptance, dynamic pile testing, pile driving formulas

INTRODUCTION

Historically, driven pile projects were controlled by a combination of static load testing and pile driving formulas that interpret pile capacity from simple observations and measurements for each pile at the end of driving. When properly instrumented, static load tests are the definitive method for evaluating the pile load-movement response. However, static load tests cannot logically be used to directly inform the acceptance criteria for piles on the project because, if undertaken at all, static load tests are performed at such low rates (typically 0.5% to 1% of piles) they are rendered statistically insignificant. Furthermore, because they are performed days or even weeks after installation, any soil setup or relaxation will have altered the capacity after initial installation, making correlation with driving criteria complex or impossible.

Pile driving formulas were therefore used historically as the basis for pile acceptance, as observation of the installation process allowed variations in ground conditions across a site to be taken into account. There are numerous pile driving formulas which have been proposed and used over time and in different jurisdictions (Chellis 1951; Groom 2020). These formulas are all based, to varying degrees, on simplistic characterizations of the pile driving process, and accordingly, when used as independent predictors of pile capacity, they are necessarily used with large factors of safety.

These formulas are typically based on an estimation of the potential energy of the hammer, an assumed hammer efficiency (representing energy input), and measurement of the pile set or blow count (representing pile response).

In the particular case of the Hiley Formula, which is preferred in the UK and the Commonwealth countries, measurement of the transient movement of the pile during impact (temporary compression or rebound) is required. This measurement is made by a worker drawing a pencil along a reference beam during pile driving, leaving a characteristic mark on the pile or attached paper from which the permanent and temporary movements can be measured by ruler. Although this may have been normal practice in the past, in most countries, occupational health and safety regulations would now forbid such measurements to be made, so in contemporary practice temporary compression is simply estimated.

 © DFI International Bruges 2025

The Hiley Formula also includes a transfer ratio function based on a so-called *coefficient of restitution* and the relative weights of ram, helmet, and pile, in an attempt to estimate energy delivered to the pile, and therefore available to do work on the pile. Unfortunately, the resulting delivered energy estimates can be wildly incorrect.

Despite such attempts to make pile driving formulas more sophisticated, it remains that they incorrectly model a pile impact event as a Newtonian collision model of lumped masses when in reality the event is dominated by the transmission and reflection of stress waves. Furthermore, the formulas all hold in common that they predict driving resistance rather than static capacity, and to that extent overpredict static capacity by ignoring the additional resistance generated by the motion of the pile against the ground.

Dynamic load testing has become a dominant feature of driven piling control since its commercial advent in the early 1980s (Goble. and Hussein 1994). By measurement of pile-top acceleration and strain, and derivation of the force- and velocity-time responses, a stress wave-based assessment of capacity can be made, separating the static and dynamic components of the impact event. Furthermore, these measurements allow the actual energy, delivered to the tested piles, to be verified.

In practice, dynamic pile testing is typically performed on 3% to 10% of piles, which provides an opportunity for a more statistically significant representation than static load tests, and allows tests to be performed across a project in both time and space. However, this still leaves the 90% to 97% of untested piles requiring some other method of verification. *Project efficiency* demands that these piles be accepted based on fast and simple methods of capacity evaluation.

In contrast to static load tests, dynamic pile tests are undertaken at the exact time of the hammer blow event, which is analyzed to assess capacity. This provides the opportunity to develop correlations between the reference capacity computed from dynamic pile tests and simple pile driving formulas. The correlated formula predictions can then be used to assess the capacity of the untested piles.

Given that it is not possible to safely measure temporary compression of a pile, all such correlations inevitably reduce to verification of the untested piles being based on a hammer transfer efficiency derived from the dynamic pile tests, and the pile set. For diesel hammers, stroke can be inferred from blow rate; for other hammer types, stroke must be assessed visually (with potential inaccuracies), and for some modern piling hammers, velocity measurements are made to confirm hammer stroke and drop efficiency. As referenced in this paper, the overall hammer efficiency is the product of drop efficiency and the hammer transfer efficiency (which is the percentage of kinetic energy which is delivered to the pile).

In practice, overall transfer efficiency is assumed to be constant. However, as will be shown, both practice and research show that it is not. Measurements of stroke or ram impact velocity cannot account for significant variations which occur in the process of delivering energy to the pile through the helmet/cushion system.

THE VARIABILITY OF HAMMER EFFICIENCY

Case 1: Hydraulic hammer with ram impact velocity measurement

Hammer monitoring systems are an excellent way to evaluate the mechanical operation of the hammer, and to confirm the kinetic energy of the ram at impact. Typically, a pair of proximity switches is deployed on the hammer. The switches are separated by known distance along the hammer axis and their purpose is to detect the presence of the ram during the descent of the ram. The time taken for the ram to travel between the switches is precisely measured, and the velocity of the ram at impact (v_{ri}) is computed. The kinetic energy (KE) of the ram is calculated from the mass of the ram (m_r) and its velocity at impact :

 © DFI International Bruges 2025

$$KE = \frac{1}{2} m_r v_{ri}^2 \quad [1]$$

As previously noted, through the measurement of acceleration and strain in dynamic pile testing, and derivation of the pile-top velocity (v) and pile-top force (F) it is possible to compute the energy (E) transferred to the pile as:

$$E = \int F.v\, dt \quad [2]$$

The maximum value of delivered energy (EMX) occurs when the pile-head starts to rebound. The value of EMX is relevant to the assessment of pile capacity.

Flynn and McCabe (2019) undertook a research study in which they simultaneously monitored hammer kinetic energy (KE) and energy transferred to the pile (EMX) for 12 tests on steel pipe piles at five (5) sites. Their results are summarized in Fig. 1, which starkly demonstrates the differences between the kinetic energy, KE, measured using a hammer monitoring system and delivered energy (EMX), measured with dynamic pile testing equipment.

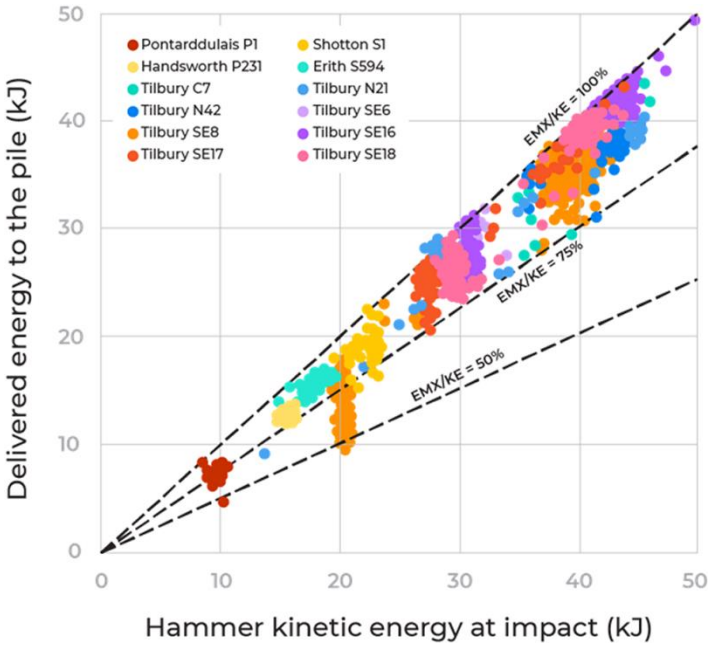


Fig. 1 Comparative measurements of hammer kinetic energy at impact and delivered energy to the pile from Flynn and McCabe (2019)

The x-axis values are kinetic energy, KE, and the y-axis values are EMX. If there were no energy loss, then the data would lie on the 1:1 line (i.e. $EMX/KE = 100\%$). However, the data shows that the ratio typically varies between 75% and 100%, representing a 25% variation in delivered energy over each drive sequence. Some EMX/KE ratios were even below 50%, representing more than a 50% loss below hammer level.

These measurements demonstrate that the delivered energy can be significantly less than the hammer energy. Each of the 12 piles on the five (5) sites was monitored for an extended drive sequence, and each drive sequence is represented here as a unique colour. Stroke height was varied during each drive sequence, and Flynn and McCabe observed that energy transfer ratios were strongly dependent on the hammer drop height, as shown in Fig. 2. Not only is the trend of transfer ratio with stroke height evident, but the variability between blows in the same drive sequence and with the same stroke is

 © DFI International Bruges 2025

shown by the vertical range bars, which typically vary between 5% and 20%, and correspond to plus or minus one (1) standard deviation.

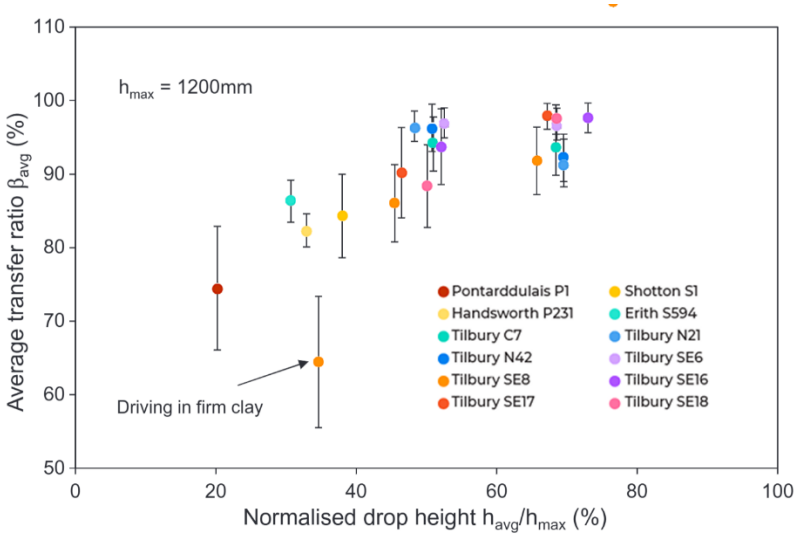


Fig. 2 Effect of stroke height on average transfer ratio from Flynn and McCabe (2019)

Case 2: Diesel hammer with inferred stroke height from blow rate

Diesel hammers are a commonly used hammer in many countries, especially for the driving of steel piles, as these hammers are high stroking, and generate high levels of compression stress. For single-acting diesel hammers, each blow constitutes a diesel cycle – initially the ram is lifted and then dropped; as the ram falls, air inlet valves are closed, and diesel fuel is injected. The air pressure in the chamber progressively increases as the ram descends, and at or around ram impact, an explosion occurs which sends a compression wave into the pile, and simultaneously throws the ram back up the chamber to commence another cycle with exhaust gases being expelled and fresh air being introduced into the chamber. The continuous diesel cycle is self-sustaining, and the hammer stroke varies according to the driving resistance of the pile, with higher strokes resulting from increased resistance.

The approximate hammer stroke can be visually judged by observation of the hammer rings, but stroke is more accurately estimated by measuring the time between blows (i.e., the blow rate). Other than during the compression and expansion phases of the cycle, the ram operates under the influence of gravity alone, with some small frictional losses. Accordingly, Likins and Rausche (1988) proposed that the diesel hammer stroke could be computed by measurement of the rate in blows per minute (BPM), where g is gravitational acceleration of 9.81m/s^2.

$$Stroke\ (m)\ =\ g/8 * (60/BPM)^2 - 0.1 \quad [3]$$

Figure 3 shows the measurement of transferred energy to two (2) tubular steel piles with a diesel hammer with a ram mass of 10 tonne (98.1 kN). For the drive sequences, hammer strokes varied between 1.87m and 3.36m based on the measurements of blow rate applied to Eqn. 3. There is a clear linear trendline for the variation of delivered energy, EMX, with hammer stroke as shown in Fig. 3 and reproduced in Eqn. 4.

$$EMX\ (kNm) = 70 * stroke - 100 \quad [4]$$

The potential energy (PE) of the hammer is the product of ram weight (98.1kN) and stroke height (m):

$$PE\ (kNm) = 98.1 * stroke \quad [5]$$

 © DFI International Bruges 2025

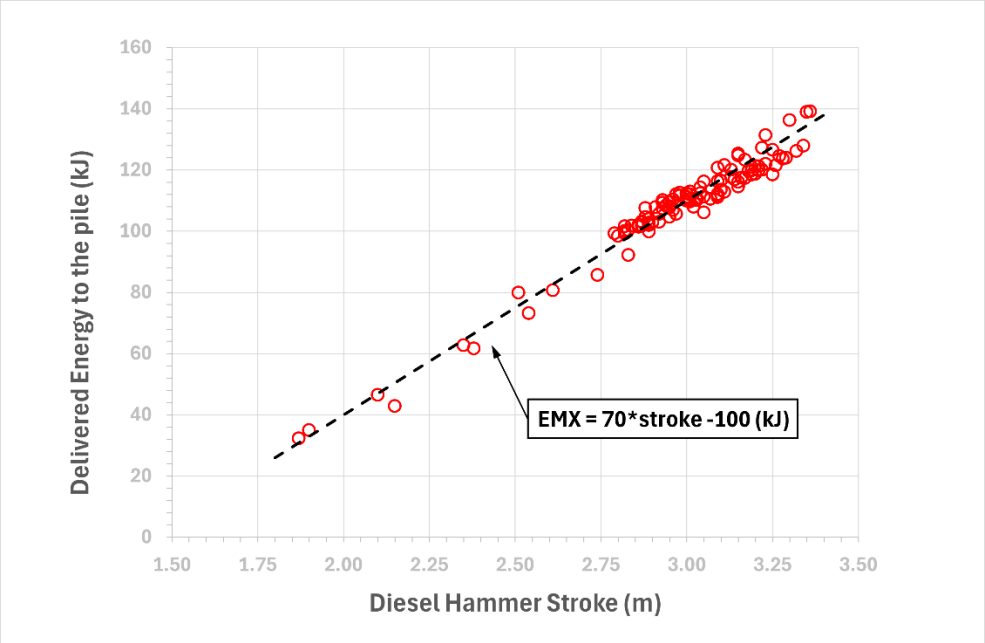


Fig. 3 Variation of delivered energy with hammer stroke for a diesel hammer

The overall hammer efficiency, including drop efficiency and transfer efficiency components, is the ratio of delivered energy and the potential energy given in Eqn. 4 and Eqn. 5, respectively. The variation of efficiency with stroke for the diesel hammer is shown in Fig. 4. At low strokes, the overall efficiency is as low as 17%, but as stroke increases, the efficiency increases to between 39% and 43%.

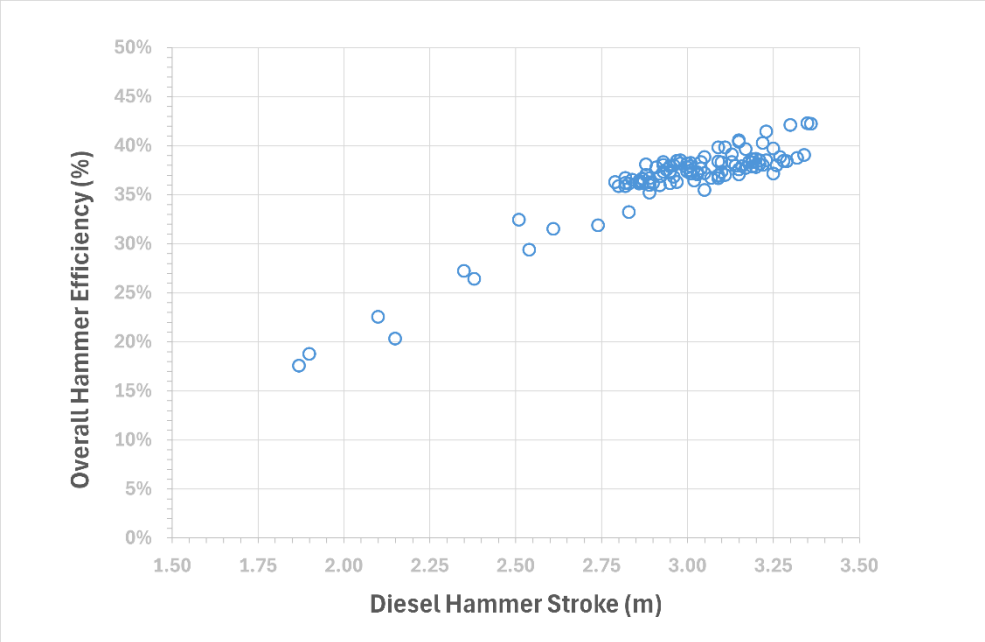


Fig. 4 Variation of overall hammer efficiency with hammer stroke for a diesel hammer

This study shows that losses below the hammer are variable, and that diesel hammer efficiency is not constant, but is strongly dependent on hammer stroke amongst other influencing factors.

 © DFI International Bruges 2025

Case 3: Prestressed concrete pile with hydraulic hammer and fixed stroke

Cases 1 and 2 relate to steel piles with ram impact velocity measurement and with stroke measurement, respectively. It is noted that, in both cases, hammer efficiency is highly variable, and an assumption of constant efficiency is not supported.

Case 3 relates to the driving of a prestressed concrete pile installed with a hydraulic hammer. In this case, all piles were driven with a specified hammer stroke of 0.5m. There was no velocity measurement for this hammer, so strokes were visually estimated by the operator. For concrete piles (unlike steel piles), a pile cushion is used between the helmet and the pile head. The cushion is typically a soft disposable timber, which protects the head of the pile from local overstress and damage. The properties of the cushion can vary considerably depending on the thickness of cushioning introduced, as well as the number of blows to which the cushion has been subjected. The cushion stiffness progressively increases with applied blow. The variability of the pile cushion also potentially results in variable delivery of energy to the pile.

A longitudinal study was undertaken of the variation of delivered energy through the project. A total of 150 piles were dynamically tested, but only the results of the first 52 piles are shown in Fig. 5. It can be seen that delivered energies varied between 37 and 91kNm, for what should have ostensibly been a sequence of tests with constant energy delivery. Based on a ram weight of 16 tonne and a stroke of 0.5m, the overall efficiencies of the hammer varied from 50% to in excess of 100%. The lowest values correspond to those piles tested with fresh and thick cushions. Efficiencies in excess of 100% can only result from the actual stroke exceeding the specified 0.5m.

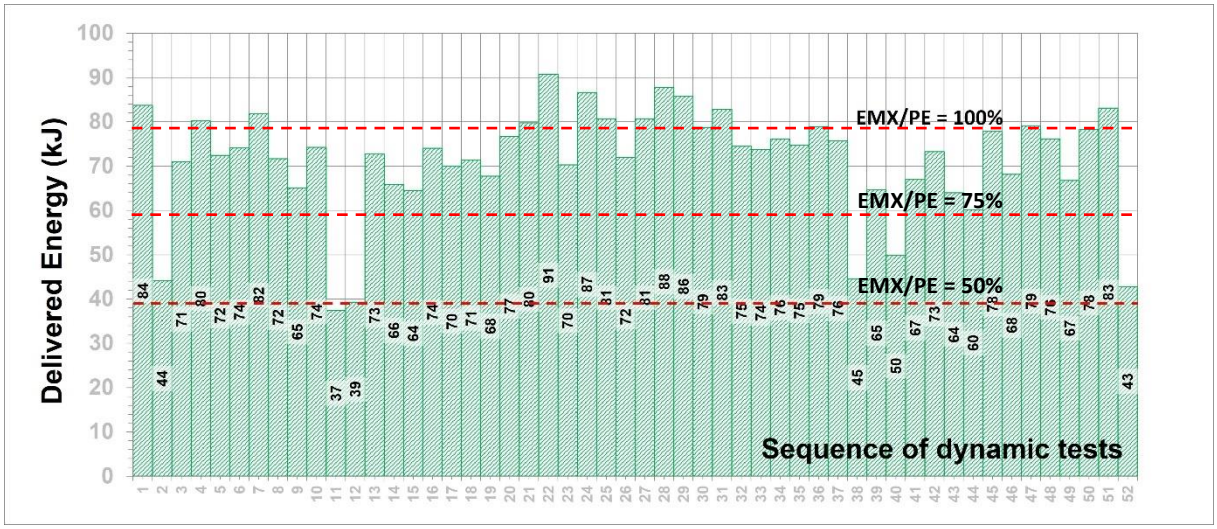


Fig. 5 Variation of delivered energy for a hydraulic hammer on prestressed concrete piles

Case 3 shows that where pile cushions are used, significant variations in delivered energy can occur even in the absence of hammer stroke variations.

DISCUSSION

The three (3) cases detailed above demonstrate that efficiency of pile driving hammers varies considerably, and assuming a constant hammer efficiency is misguided and not supported by a critical review of the available evidence.

Case 1 shows that delivered energy for steel piles driven with a modern hydraulic hammer varies from 45% to 100% of the kinetic energy measured by the hammer monitoring system, depending on the hammer stroke, and the ground conditions. Furthermore, the tests show that even in a drive sequence at

 © DFI International Bruges 2025

constant stroke, the average efficiency range (to plus or minus 1 standard deviation) is as low as 5% but as high as 20%. The range for individual blows is greater.

Case 2 demonstrates that the efficiency of diesel hammers is highly dependent on ram stroke. For the case shown, overall efficiencies varied from 17% at low stroke to as much as 43% for the highest recorded strokes. Delivered energy cannot be computed merely by applying an assumed constant efficiency to the product of ram weight and stroke.

Case 3 shows that the effects of variable energy transfer not only result from variations in hammer stroke but are critically affected by the properties of the pile cushion used for concrete piles. Observed overall efficiencies varied between 50% and 100%, based on the sequence of piles driven with a constant stroke. Although the dominant factor in this case was variations in the properties of the pile cushion, variations in the hammer cushion will also affect the energy transfer.

These cases highlight that neither measurement of hammer stroke, nor measurement of ram impact velocity can provide reliable estimates of energy delivered to the pile.

Pile set is a relative measure dependent on the energy actually delivered to the pile. All current acceptance criteria for the 90% to 97% of piles not dynamically tested are based on measurement of pile set and either hammer stroke or ram impact velocity. Fundamentally, these acceptance criteria assume that (a) the energy transfer ratio is constant, and (b) pile set is an absolute measure. Neither are true.

What logically follows is that acceptance criteria, which take proper account of the critical influence of the hammer stroke and the cushions between the hammer and the pile, must utilize measurements on the pile, both for the input from the hammer and for the response of the pile to that input.

Determination of the energy delivered to the pile, as undertaken in dynamic pile testing, relies on the measurement of both pile-head acceleration and strain. However, dynamic pile testing is too disruptive to the pile installationprocess to be used for the assessment of every pile. Furthermore, pile set still needs to be measured independently, as an accurate set measurement is not provided by dynamic pile testing.

AN ALTERNATIVE AND EFFECTIVE APPROACH TO DRIVEN PILE CONSTRUCION CONTROL

Although pile energy is traditionally used as the representative measure of input from the pile hammer, an alternative approach to construction control is possible by monitoring the peak impact force generated by the hammer at the pile head. One of the key principles of one-dimensional wave mechanics is that the force and particle velocity generated by an impacting compressive wave are related by the impedance of the pile, Z, which is the product of the pile modulus, E, the cross-sectional area, A, and divided by the speed of the wave in the pile material, c. It follows that measurement of peak pile velocity, VMX can be a proxy for measurement of peak impact force, FMX, with Eqn. 6.

$$FMX = Z.VMX \quad [6]$$

If pile displacement is measured remotely by non-contact measurement, the pile set, which is the response of the pile to the applied impact, is directly determined. Additionally, this measurement also allows the temporary compression to be measured directly and safely for use in the Hiley Formula.

If the pile displacement measurement is made at a sufficiently high frequency, then the peak pile impact velocity, VMX, can be computed by differentiating the displacement-time record. As shown by Eqn. 6, this allows the peak pile force, FMX, to be computed.

 © DFI International Bruges 2025

High-speed, remote, non-contact monitoring of pile displacement therefore provides an efficient and effective method of pile driving construction control, which allows both the delivered input from the hammer to the pile and the pile response to be simultaneously measured.

The results from such measurements can be used with any chosen pile driving formula, duly correlated to the results of reference dynamic pile testing. However, a more direct and reliable approach to construction control is possible and recommended, as described below.

Under current practice, dynamic testing is undertaken on some of the initial project piles. The results are analyzed by wave matching technique to confirm pile capacity. A target pile set is then established from the analysis, and subsequent piles are driven to the target set. The deficiencies in this approach have already been elaborated upon.

In the alternative and improved practice, the project should again commence with dynamic pile testing of the initial piles, with wave matching to confirm pile capacity. A target pile set and corresponding minimum impact velocity are established from the wave matching analysis. Subsequent untested piles are driven to the target set *and* corresponding minimum impact velocity, ensuring that any changes in the driving system, including hammer, helmet, and cushions are automatically taken into account.

It is noted that driven pile construction control should always be informed by a sound understanding of the geotechnical subsurface conditions at the site.

CONSEQUENTIAL BENEFITS OF AN EFFECTIVE APPROACH TO DRIVEN PILE CONSTRUCION CONTROL

The current methods of construction control represent a 2-class system for piling acceptance – a high confidence, low risk class for the 3% to 10% of piles which are dynamically pile tested, and a lower confidence, higher risk class for the 90% to 97% of piles accepted using acceptance methods based on the assumption of constant hammer efficiency and an absolute target set.

By implementing advanced and effective methods of construction control, as advocated here, the overall reliability of the foundation can be considerably improved, leading to higher confidence in the completed foundations. This provides an opportunity for designers to be less conservative in their designs, leading to potential savings in foundation sizes and lengths, with consequent benefits to time, cost, and the environment.

CONCLUSIONS

Current methods of driven pile construction control are premised on an assumption that:

(a) hammer performance is consistent,
(b) energy transfer ratios do not vary, and therefore
(c) measurements of hammer efficiency by dynamic pile testing can be applied to every other pile installed, and hence
(d) it is sufficient to drive piles to a target set as the sole criterion to be achieved.

It has been shown that:

(a) hammer performance is not consistent,
(b) energy transfer ratios vary significantly, and therefore
(c) neither measurement of hammer stroke nor ram impact velocity will allow delivered energy to the pile to be reliably estimated, and hence
(d) piles must be driven to a dual criterion, being target set *and* minimum pile velocity, which is a proxy for the pile impact force.

High-speed, remote, non-contact and accurate measurements of pile displacement are able to efficiently provide effective construction control for driven piles.

 © DFI International Bruges 2025

Effective construction control provides greater confidence in the installed foundation system and provides the opportunity for designers to be less conservative, with subsequent benefits to project time, cost, and the environment.

REFERENCES

Chellis, R.D., 1951. Pile Foundations: Theory-Design-Practice. McGraw-Hill Book Company

Flynn, K.N. and McCabe, B.A., 2019. Driven cast-in-situ piles installed using hydraulic hammers: Installation energy transfer and driveability assessment. Soils and Foundations, 59(6), pp.1946-1959.

Goble, G. and Hussein, M., 1994. Dynamic Pile Testing in Practice. Proceedings of the Thirteenth International Conference on Soil Mechanics and Foundation Engineering; New Delhi, 5 - 10 January, 1994

Groom, D., 2020. An Assessment of Dynamic Pile Driving Formulae for use by Military Engineers. Masters Thesis.

Likins, G.E. and Rausche, F., 1988. Hammer Inspection Tools. Third International Conference on the Application of Stress-Wave Theory to Piles, Ottawa, Canada, pp 659-667; 1988

 © DFI International Bruges 2025

DESIGN OPTIMISATION WITH BI-DIRECTIONAL PUSH-OUT LOAD TESTS OF BORED PILES IN ANGOLA

Alberto Silva, Porto, Portugal, +351919325401
Dr. Melvin England, Fugro, Wallingford, United Kingdom, +44(0)1491820700, m.england@fugro.com
Maarten Profittlich, Fugro, Leidschendam, The Netherlands, +31622934237, m.profittlich@fugro.com

ABSTRACT

Terminal Oceânico in Barra do Dande is planned to be the largest storage infrastructure for gas and oil in Angola. It will include a dedicated 1.7 km long pier and two mooring areas to make the export process more efficient. A total of 323 working piles over water, including inclined piles, were designed to serve as foundations for the different structures. Due to uncertainties from the results of soil investigations in the mooring areas, four push-out pile load tests were conducted to validate and optimise the foundation piles. The Ø700 mm cased bored piles, ranging from 31 to 43 metres in length, were built over water and tested using the bi-directional method with the O-Cell® methodology. This eliminated the need for any reaction structure above each test pile, reducing the overall carbon footprint of the foundation testing program in the most efficient, safe, and cost-effective manner. This paper aims to provide a brief overview of the project and the challenges faced during the installation and execution of the four push-out load tests over water. The test results and analysis will be presented including the optimisation of the design of the foundations.

Keywords: O-Cell®, Bi-directional, load test, push-out, deep foundations, design optimisation, over-water

INTRODUCTION

As one of the biggest players in the oil and gas production, the Angolan government commissioned the construction of the Terminal Oceânico da Barra do Dande with the purpose of increasing the existing oil and gas storage capacity and to serve as an exportation port.

The $500 million dollar project involved several activities from the construction of storage tanks to the construction of a pier and mooring areas. The mooring structures involved the construction of several vertical and raking piles to support the various structures. To validate and optimise the foundation design it was decided to execute four static load tests using the Osterberg method (Osterberg 1991). Due to the specifications of the project design, full scale load tests had to be executed as push-out tests. The four tests were divided equally between the two mooring areas.

SITE SUB-SURFACE CONDITIONS

All the tested piles were constructed over-water, with the sea floor at -16.5 metres at the deepest location. The ground conditions below the mudline, where the structural piling work was executed, consists mainly of Limestone, and defined by the client as IGM – Intermediate geomaterial (soft rock). This type of material is difficult to be sampled without disturbances and even more so when sampled over water. For that reason, when tested in the laboratory, the material didn't offer any precise results, with the uniaxial compressive strength ranging anywhere between zero and 6 MPa. The results of the soil investigation and laboratory tests compelled the foundation designers to follow a conservative design approach estimating the skin friction of the foundations. This approach requires the use of a higher safety factor and consequently an increase of the pile's initial design rock socketed length.

 © DFI International Bruges 2025

TEST REQUIREMENTS AND DESIGN

Four O-Cell® loading tests were requested to be executed as push-out tests, as the client desired almost exclusively to observe and evaluate the behaviour of the piles in skin friction. In terms of testing loads specified, the two test piles (TP1 and 2) constructed in the Mooring 1 area were to be tested up to 9 MN and the tests in the Mooring 2 area up to 5.5 MN in one direction (TP 3 and 4).

Based on the client's high load requirements and pile dimensions a decision was made to place the O-Cell® assembly, consisting of a single O-Cell® at the bottom of each test pile. This allowed the upwards load to be directly and precisely measured in the pile section desired. The construction of an additional reaction pile length below the O-Cell ® was required to have sufficient resistance, as described in England (2012).

The construction of the reaction pile below the O-Cell® assembly could not use a standard concrete tremie pipe, as the space between the O-Cell® assembly and the excavation wall was small. The installation and concreting solution applied to the test piles is presented in Section "Test Pile Construction".

Due to the site conditions, the use of anchor piles with reaction frames for full traditional scale load testing from the pile head would be a complicated solution with additional safety measurements. solution. The O-Cell® method has and can easily adapted to these site conditions, as observed in Figure 1 at test pile TP4.



Figure 1 - TP4 during the O-Cell® loading test with the test equipment mounted directly on top of the test pile. (Fugro)

TEST PILES CONSTRUCTION

The piling company began excavating the piles by placing a 914 mm diameter permanent casing to a minimum of 2 metres into the Limestone. Below the casing the excavation was executed with a 700 mm diameter reverse circulation drilling tool to achieve the necessary depth. The excavation was cleaned with an airlift before concreting. This was followed by the placing of the reinforcement cage and then concreting via tremie pipe for the working piles.

 © DFI International Bruges 2025

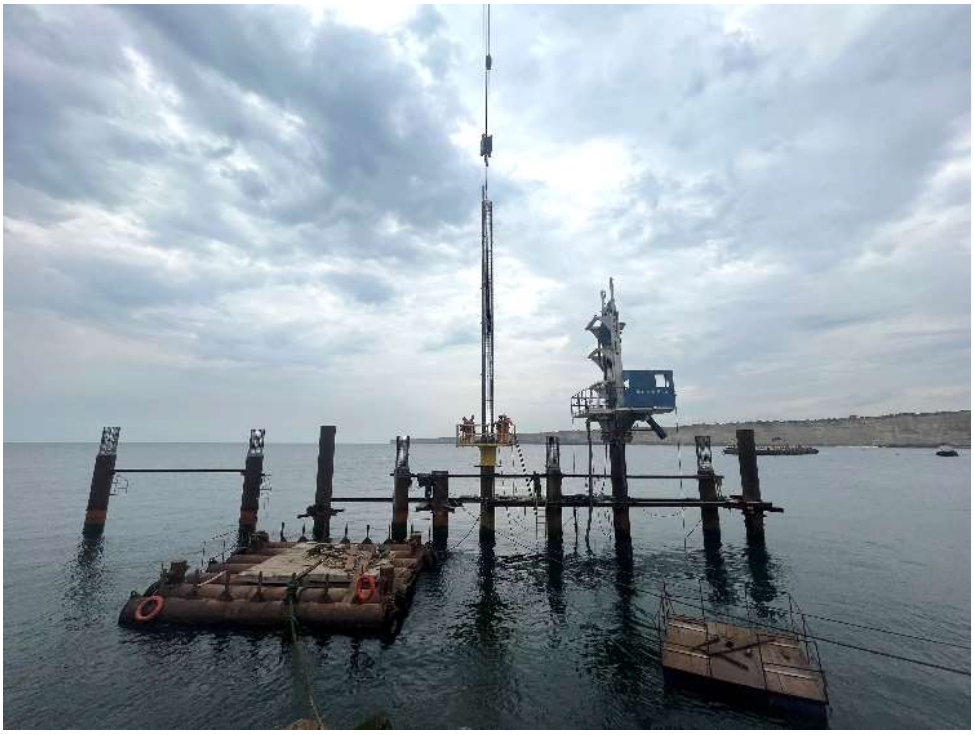


Figure 2 – TP4 cage installation. (Fugro)

The excavation of the dedicated test piles followed the same process described before. However, for the concreting and reinforcement cage installation of the test piles and specifically the additional depth for the reaction pile the following sequence was observed:

1st. Completion of excavation.
2nd. Assembly/installation of the reinforcement cage inside the excavation, including cage splicing and instrumentation connection.
3rd. Complete removal of the assembled cage from the excavation.
4th. Cleaning of the excavation by airlift.
5th. Placing of grout, via tremie pipe, into the excavation up to a predefined depth sufficient to cover the O-Cell® assembly.
*6th. Installation of the assembled cage into the excavation. (*See *Figure 2).*
7th. Plunging of the reinforcement cage into the grout at the bottom of the excavation. The O-Cell® assembly would be completely covered by grout.
8th. Reinsertion of the concrete tremie pipe in the pile. Plunged in the wet previously poured grout.
9th. Concreting of the section above the O-Cell® assembly via tremie pipe and following the normal good practice.
10th. Concreting operation completed with the concrete cut-off level left at the desired elevation.

The four test piles were safely and successfully constructed using the method described above. In Table 1, a summary of the test pile details is presented, TP1 and TP2 located in the Mooring 1 area and TP3 and TP4 in the Mooring 2 area. The grout and concrete strength values after 28 days can be found in Table 2

Table 1- Test Pile details (depths in mCD).

Test Pile	Top of Concrete	TIP of Casing	O-Cell® depth	Pile Toe	Reaction Pile Length (m)
TP1 (E16)	+2.00	-21.86	-31.03	-40.86	9.83
TP2 (E17)	+1.50	-20.80	-34.20	-39.80	5.60
TP3 (E26)	+4.70	-13.36	-21.73	-26.36	4.63
TP4 (E24)	+4.70	-13.41	-21.63	-25.56	3.93

 © DFI International Bruges 2025

Table 2 – Grout and Concrete laboratory strength results after 28 days

Test Pile	Grout (MPa)	Concrete C50/60 (MPa)
TP1 (E16)	63.9	59.1
TP2 (E17)	56.4	57.9
TP3 (E26)	60.1	58.2
TP4 (E24)	58.7	54.4

OSTERBERG CELL TESTING

Pile instrumentation

The test pile instrumentation and assembly were carried out under the direction of Fugro Loadtest with the assistance of the contractor. The loading assemblies for TP1 and TP2 consisted of one 530 mm O-Cell® in each pile and the assemblies for TP3 and TP4 consisted of one 430 mm O-Cell® in each pile. The 530 mm O-Cell®s were calibrated to 15 MN and the 430 mm O-Cell®s to 9 MN and then welded closed prior to shipping by the manufacturer. O-Cell®s were attached to the 530 mm external diameter reinforcement cages with support steel castellations, as shown in Figure 3. This arrangement overcomes the large ratio of O-Cell® diameter to excavation diameter: 0.75 for TP1&TP2 and 0.61 for TP3&TP4.



Figure 3 – Welding of the 530 mm O-Cell®s into the 530 mm outer diameter reinforcement cages. (Fugro)

O-Cell® testing instrumentation included, for each pile, four Linear Vibrating Wire Displacement Transducers (LVWDTs, Geokon Model 4450) positioned between the lower and upper castellations to measure O-Cell® expansion. Two telltale casings were attached to the reinforcing cage, diametrically opposed, extending from the top of O-Cell® to the top of pile to measure the total upper pile compression. Two telltale casings were attached to the reinforcing cage, diametrically opposed, extending from the pile toe to top pile to measure the total pile toe displacement. In TP1 and TP3 Strain Gauges were used to assess the side shear load transfer of the pile above the O-Cell® assembly. In each pile, three pairs of "sister bar" vibrating wire strain gauges (Geokon Model 4911) were installed. All telltale casings were constructed using a nominal 25 mm O.D. steel pipes and 6 mm steel telltale rods. Two lengths of steel pipe were also installed, extending from the top of pile to 1.5 metres below O-Cell®, to vent the break in the piles formed by the expansion of O-Cell®.

 © DFI International Bruges 2025

Test arrangement and data acquisition

Throughout the load tests, key elements of the pile response were monitored using the equipment and instrumentation in the section above. Pile compression and pile toe displacement telltales were measured using Linear Voltage Displacement Transducers (LVDTs) placed at the pile head. Two automated digital survey precision levels, Leica NA3000, were used to monitor the top of pile movement. For the tests in the Mooring 2 area (**Error! Reference source not found.**) the Leica levels were placed on land at approximately 25 metres from the top of pile. While in Mooring 1 area (**Error! Reference source not found.**) the Leica levels were placed at around 10 metres away from the test pile on top of the Dam structure already constructed.



Figure 4 – Leica locations in relation to test pile TP3. (Fugro)



Figure 5 – Leica locations in relation to test pile TP1. (Fugro)

In each test, both a full balance bridge pressure transducer and a vibrating wire pressure transducer were used to measure the hydraulic pressure applied to the O-Cell® at each load interval. The full balance bridge pressure transducer was used for automatically setting and maintaining loads and real time plotting for data analysis. A Bourdon pressure gauge was used for a real-time visual reference and as a check on the transducers. There was a close agreement between the Bourdon gauge and the pressure transducers.

All instrumentation were connected through a data logger (Data Electronics 85g GeoLogger) to a laptop allowing data to be recorded and stored automatically at 30 seconds intervals and displayed in real time, the same laptop synchronised to the data logging system was used to acquire the Leica top of pile data.

Testing procedures

For each test pile, the test begun the test by pressurising O-Cell® to break the tack welds that hold them closed (for handling and for placement in the piles) and to form the fracture plane in the concrete surrounding the base of the O-Cell®. After the break occurred, the pressure was immediately released, and the testing recommenced from zero pressure. Zero readings for all instrumentation were taken prior to the preliminary weld-breaking load-unload cycle.

The O-Cell® tests were conducted as follows: the installed O-Cell®, with their base at the defined depth, corresponding to the bottom of the required test pile, were pressurised in incremental loading steps to assess the skin friction above the assembly using the combined end bearing and skin friction below the assembly as reaction.

The defined loading schedule consisted of 12 loading increments up to the 100% of the desired specified minimum test load (9 MN for TP1 & TP2 and 5.5 MN for TP3 & TP4), however, to obtain

 © DFI International Bruges 2025

further geotechnical information the loading schedules were extended. Table 3 presents a summary of the desired test load required and those applied to each pile:

Table 3 – Load details and mobilised displacements (at the O-Cell ®) at maximum load

Test Pile	100% desired specified minimum test load (MN)	Max Load in each direction (MN)	Upward (mm)	Downward (mm)
TP1 (E16)	9.00	14.86	8.81	5.02
TP2 (E17)	9.00	14.93	3.82	4.36
TP3 (E26)	5.50	8.76	2.79	3.72
TP4 (E24)	5.50	7.34	1.52	1.73

TEST RESULTS AND ANALYSIS

The loads applied by the O-Cell® assembly act in two opposing directions, counteracted by the resistance of the pile above and below. For the purpose of the analysis of the sum of the measured behaviour, it is assumed that the O-Cell® assembly does not impose an upward load until its expansion force exceeds the buoyant weight of the pile above the O-Cell® assembly.

Therefore, *net load*, which is defined as gross O-Cell® load minus the buoyant weight of the pile above, is used to determine skin friction resistance above O-Cell® and to construct the equivalent top load displacement curve.

For the purpose of this case study the test results analyses will focus on TP1 and TP3, the two piles fitted with strain gauges, located in the Mooring 1 and Mooring 2 areas, respectively. The results of the displacements are presented in Figure 6 and Figure 7 for TP 1 and TP3 respectively.

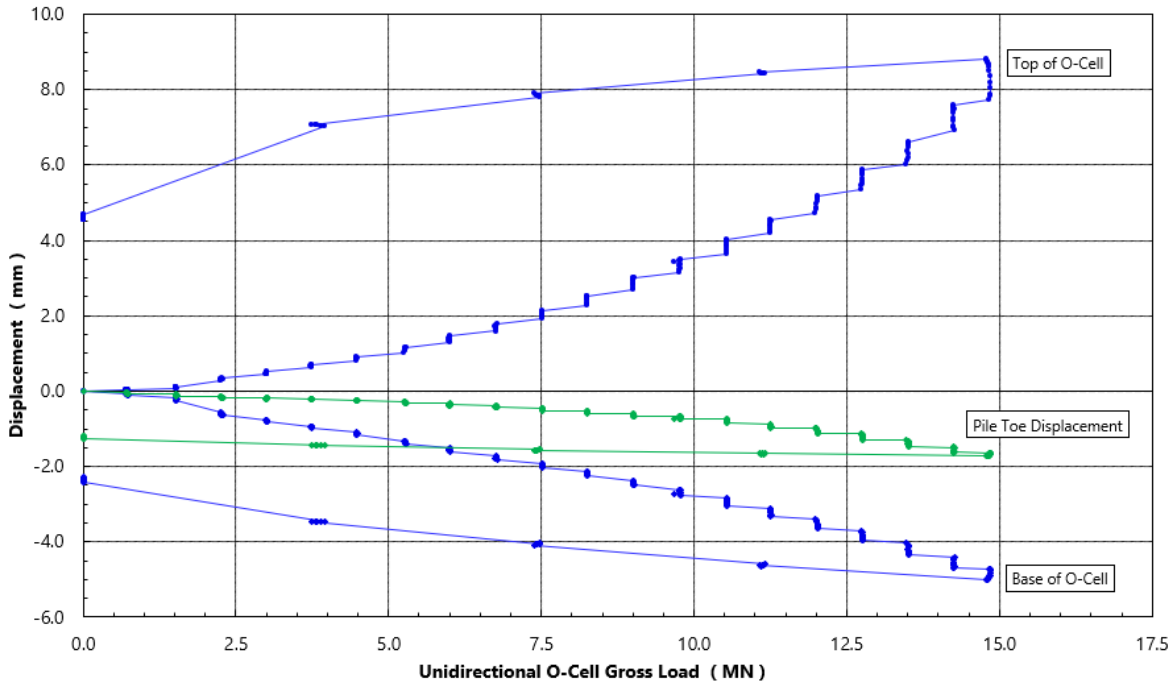


Figure 6 – TP1 O-Cell® Load vs Displacement graph

 © DFI International Bruges 2025

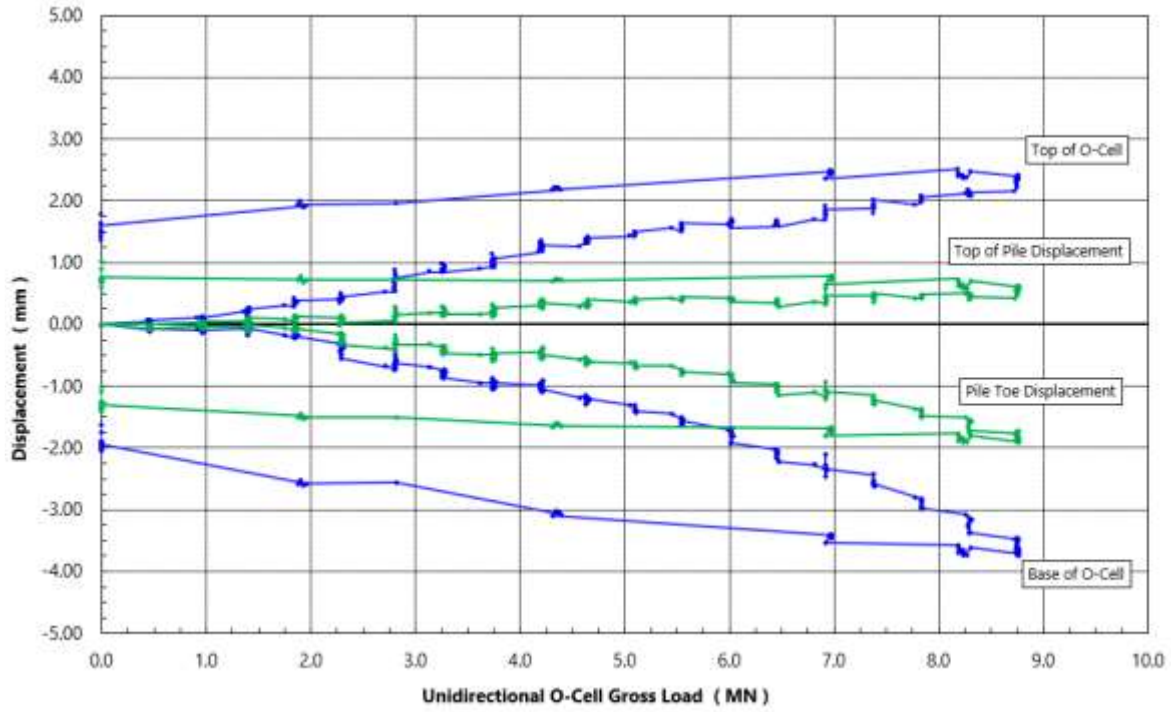


Figure 7 – TP3 O-Cell® Load vs Displacement graph

Strain gauge results

The upward movements of the TP1 and TP3 and the strain gauge micro-strain results have been analysed to determine the mobilised skin friction values, and these are presented in Figure 8 & Figure ***9*** and Table 4.

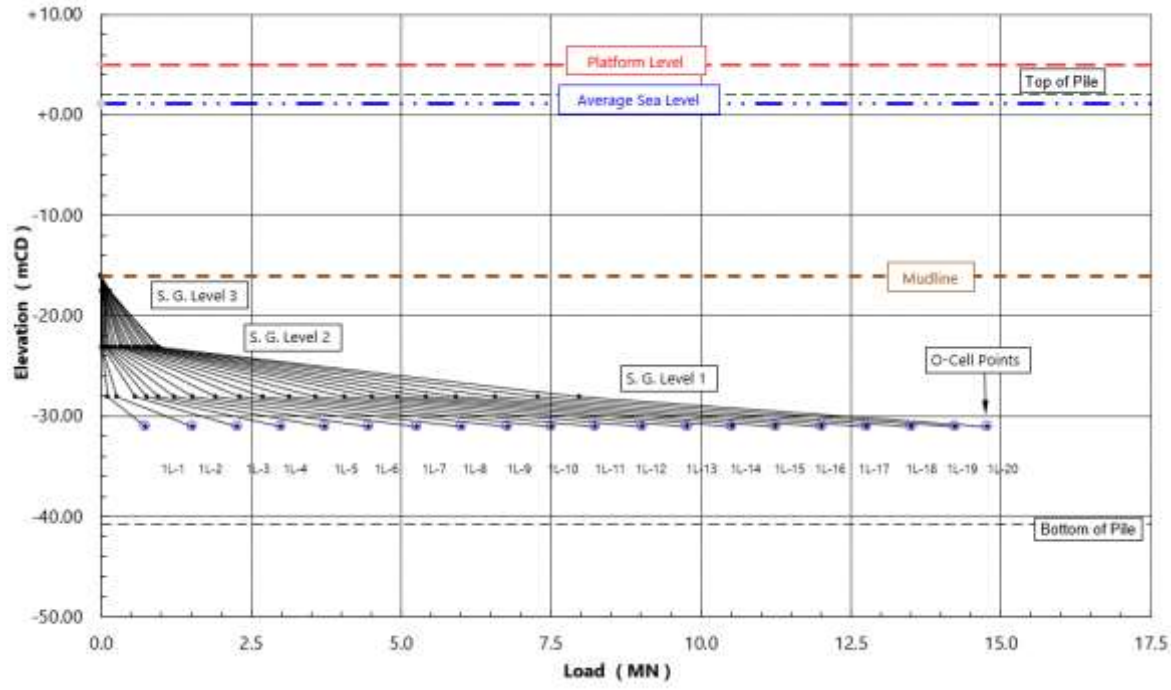


Figure 8 – TP1 Strain gauge load distribution graph for each loading step

 © DFI International Bruges 2025

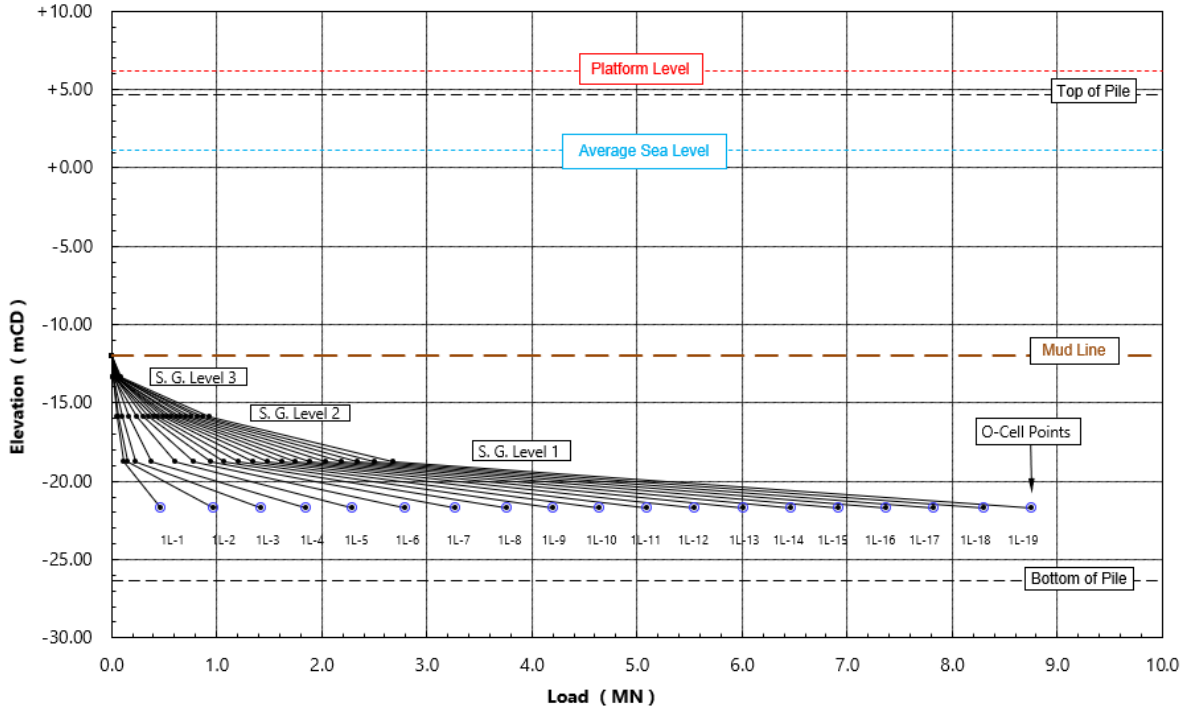


Figure 9 – TP3 Strain gauge load distribution graph

Table 4 – TP1 and TP3 average mobilised net unit skin friction at maximum load

	Test Pile 1		Test Pile 3	
Load transfer zone	Displacement* (mm)	Net unit skin friction (kPa)	Displacement* (mm)	Net unit skin friction (kPa)
Zero Shear to SG3	↑ 0.00	25.6	↑ 0.60	19.6
SG3 to SG2	↑ 0.16	51.5	↑ 0.64	150
SG2 to SG1	↑ 1.94	650	↑ 0.87	275
SG1 to O-Cell®	↑ 6.19	1030	↑ 1.72	920

*average displacement for the zone

Equivalent top-load displacement

Several methods may be used to produce a single load-settlement diagram corresponding to the combination of the measured results from an O-Cell® load test (OLT) upwards and downwards. The method used has been developed by Fugro (Loadtest) and is based on the sum of the measured resistances at equal displacements, plus additional elastic shortening not mobilised during the OLT but which would occur when loading top-down, from the pile head (what applies equally to pull out tests). The technique has been independently evaluated to be a good estimate of the load-settlement curve for the foundation element if the load were applied at the top of the concrete.

The upward skin frictional behaviour, the primary client's goal of this test program, is measured and displayed directly in Figure 6 and Figure 7. The distribution of load mobilised with depth is illustrated in Figure 8 and Figure 9.

In Figure 10 and Figure 11 the equivalent load/displacement diagrams for TP1 and TP3 are shown and, as also experienced with TP2 and TP4, the small pile movements during testing did not allow an assessment of the ultimate capacity. Please note that for the construction of the Equivalent Top Load graphs the reaction pile below O-Cell® level has been included.

 © DFI International Bruges 2025

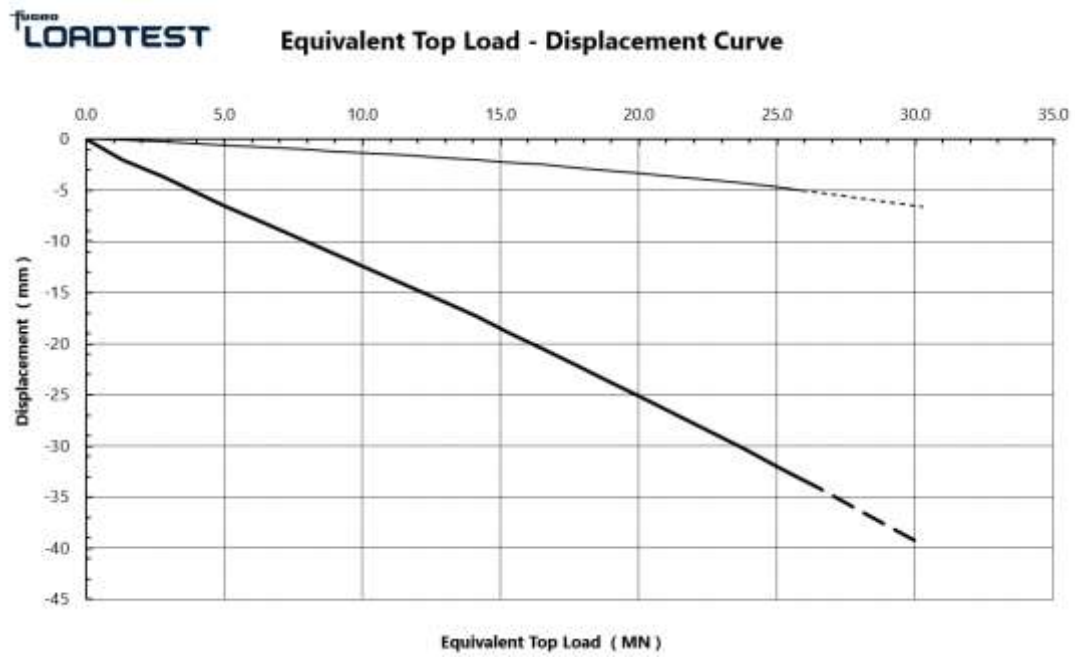


Figure 10 - TP1 Equivalent top load – displacement curve(s)

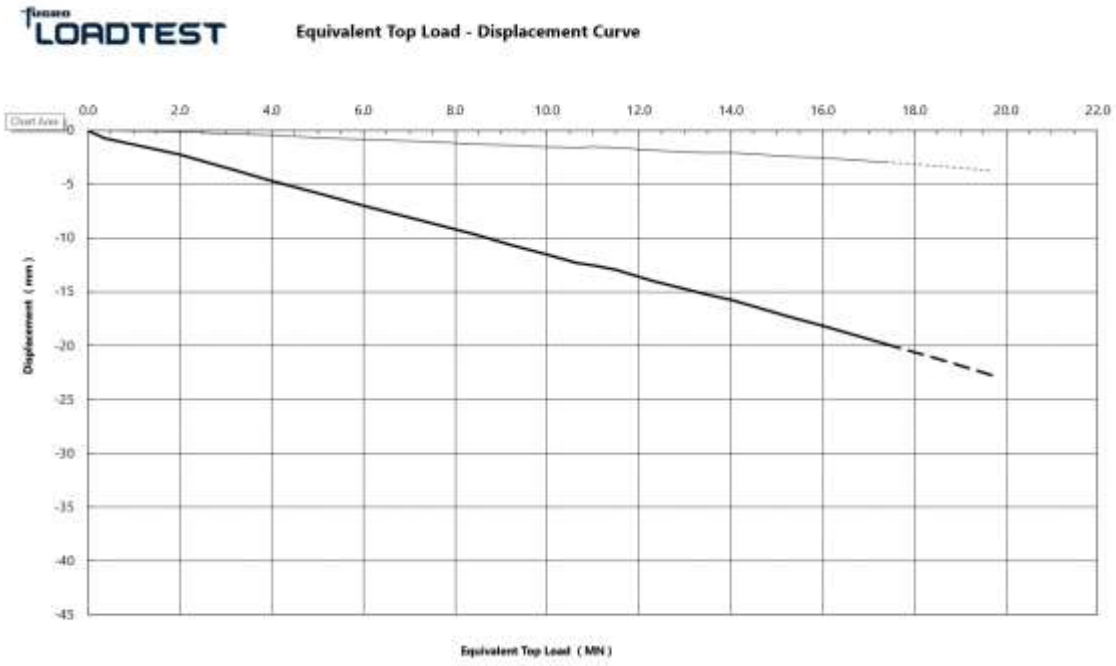


Figure 11 – TP3 Equivalent top load – displacement curve(s)

Note: Equivalent Top Load settlement curve is constructed from the sum of the measured values above and below O-Cell® (Thin solid curve). The thick solid curve includes the additional elastic shortening not mobilised during the O-Cell® test but would occur when loaded from the pile head. The dashed line in the ETL is using estimated hyperbolic curve fit to the upper data.

TEST RESULTS AND ANALYSIS

Based on the obtained test results, the client was able to optimise the rock socket length for the foundation design. It was reported that a considerable reduction of the pile length could be applied to the working piles, some of those reductions were:

 © DFI International Bruges 2025

- Piles E16 to E20 in Mooring 2 area – reduction from 18 to 10 metres
- Piles E10 to E15 in Mooring 1 area– reduction from 14 to 7 metres
- Piles E1 to E4 in Mooring 1 area– reduction from 11 to 6 metres

As observed above, a reduction of the excavated length of approximately 5 metres, more than 40% was applied to some piles. It is important to notice that this reduction applies to the rock socket length, the hardest, slowest and most costly of the boring operations.

Environmental protection

Without referring only to the economical and time savings resultant from the pile design optimisation alone, it is important to also refer to the impact of those changes on the environment. In a conservative scenario, if 161 piles (half of the planned 323 piles) could have their length reduced by 5 metres, around 2 m^3 of concrete could be saved per pile. The total saving could be of 323 m^3 of concrete C50/60. Using the Embodied Carbon value (EC) presented in the ICE database (Inventory of Carbon & Energy) (Hammond 2008) of 0.212 $kgCO_2/kg$ for concrete C50 and an average density of 2300 kg/m^3, a carbon factor of 488 $kgCO_2/m^3$ can be assumed. Assuming the calculated Carbon factor and hypothetically pile length reduction, 157 TN of Carbon dioxide would not be emitted.

CONCLUSIONS

The test program allowed a better understanding of the Limestone strata and offered valuable information that could not be obtain via soil investigation and laboratory testing alone. The O-Cell® method adapted easily to the client's requirements (high load push-out test in a small pile diameter) and to the site conditions (remote area and over-water). All the operations were completed without safety incidents as is characteristic of the O-Cell® bi-directional load testing method. As desired by the client, the loading phase was effortlessly increased to obtain additional geotechnical data. As intended, all the data obtained from the four O-Cell® tests confirmed and allowed an optimisation of the pile foundation design with pile length reductions of 40% in some cases resulting in time, materials and environmental savings.

ACKNOWLEDGEMENT

The authors wish to give a special thanks to all workers and companies involved in this project for the excellent performance of their work.

REFERENCES

England, M (2005). A conservative method of analysis of test results from bi-directional static load tests. X *Baltic Geotechnical Conference, October, Riga, Latvia*

England, M. (2008). Review of method of analysis of test results from bi-directional static load tests. *Deep foundation on bored and auger piles, BAP V, Ghent, pp 235-239*

England, M. (2012). On the subject of piles in tension Geotechnical Special Publication, *GSP 227 Full-Scale Testing and Foundation Design, honors Bengt H. Fellenius ed. Hussein M., Massarsch K., Rainer K., Likins G., Holtz D. pp 680–693*

Hammond, G. and Jones, C. (2008) Inventory of carbon & energy (ICE) Version 1.6a, *University of Bath, UK*

Osterberg, J.O. (1991). A new load testing device innovative approach to load testing of high capacity piles. *Proceedings of the International Conference on Piling and Deep Foundations*, J. B. Burland and J. M. Mitchell (eds.), Balkema, Vol. 1, pp. 409-413.

 © DFI International Bruges 2025

Numerical Simulation of Ground Improvement using Stone Column in Silts

Shivangi Singh, Dayalbagh Educational Institute, Agra, Uttar Pradesh, India,
singh.shivangi3282@gmail.com

Aswathy MS, Central Building Research Institute, Roorkee, Uttarakhand, India,
achuscorpio24@gmail.com

ABSTRACT

Ground improvement techniques are widely employed across various construction sites to address the challenges posed by weak or unstable soil conditions. Such techniques are essential when existing soil properties could result in poor structural performance. Among the many methods available to enhance soft soil characteristics, the use of stone columns stands out as particularly effective. This approach involves the installation of compacted stone pillars to strengthen and stabilize the soil. This study encompasses a comprehensive analysis of raft footing on silty soil reinforced with vibro-stone columns. It evaluates the settlement behavior, and liquefaction potential, providing crucial insights into the performance of these reinforced foundations. Numerical analyses were conducted using the software PLAXIS 3D to evaluate the impact of stone columns**.** The application of stone columns has proven to be highly effective in mitigating soil settlement. This study examines the performance characteristics of stone columns with a diameter of 0.5 meters, each maintaining a length-to-diameter ratio (L/D) of 10**.** After the installation of stone columns, the soil settlement was reduced by 79%. The findings from the parametric study varying the diameter, indicate that by increasing the diameter of stone column from x to y results in a significant reduction in settlement of approximately 48.47%.

Keywords: ground improvement, stone column, settlement, Plaxis 3d

INTRODUCTION

Liquefaction is a geotechnical process that happens when significant ground shaking, usually during seismic events, causes saturated, loosely packed sediments close to the ground surface to lose their strength and stiffness. The sediment's ability to support loads is greatly diminished by this process, which turns the silt into a fluid-like state. Subterranean liquefaction under buildings and other infrastructure can result in considerable structural damage during earthquakes, hence presenting a significant risk to property and human safety. Various ground improvement methods have been documented in the literature to enhance the liquefaction resistance of soil (Bowles et al., 1997).

Field measurements have shown some of the effects of stone column installation. Stone column reduces pore pressure over time this also influencing soil strength and consolidation rates(Castro & Sagaseta, 2012). The field tests confirmed that vibro ground treatment is an effective technique for enhancing foundation performance in areas with variable fill. The use of stone columns significantly reduced settlement under load (Watts et al., 2000).

Over the past few years, the numerical analysis of stone columns has emerged as a primary focus of investigation within the research community. Reduced settlement is generally observed when stone columns are closely spaced and subjected to high embankment loads. The increase in radial stresses, which laterally confine the column, has shown positive outcomes in column installation (Castro et al.,

 © DFI International Bruges 2025

2014). While no model precisely matched the measurements, vertical deformations demonstrated that all models agreed with in-situ data. While the Modified Cam Clay (MCC) and HS-Small models marginally underpredicted settlement, the Hardening Soil (HS) model slightly overpredicted it. The model that best matched the observed settlements was the anisotropic S-CLAY1 model (Karstunen & Leoni, 2009).

The Vibro stone columns enhances drainage efficiency, allowing for swift dissipation of pore water pressure during dynamic loading(Alamgir et al., 1996; Benmebarek et al., 2018; Das et al., 2023; Mohanty & Samanta, 2015; Muzammil et al., 2018; Baez, 1995). An increase in the stiffness of the geosynthetic encasement enhances lateral confinement, facilitating improved load transfer from storage tanks to the geosynthetic-encased stone columns (GESCs). This results in a significant reduction in long-term settlement and lateral deformations. Specifically, settlement decreased by 32% to 55%, while lateral deformations were reduced by 25% to 68% as the encasement stiffness increased from 1,000 kN/m to 10,000 kN/m(Muzammil et al., 2018).Vibro-stone columns are extensively utilized to support embankments, petroleum storage tanks, skyscrapers, and industrial facilities. The Vibro-stone column technique is a widely adopted ground improvement method, primarily used to enhance soil bearing capacity and reduce settlement under vertical structural loads(Adalier et al., 2003; Adalier & Elgamal, 2004; Das et al., 2023; Ng et al., 2021; Remadna et al., 2020).

This study focuses on enhancing the ground stability of silty soil beneath a G+18 residential building through the use of stone columns. Upon reviewing the site conditions, it was found that the presence of a liquefiable soil layer beneath the foundation posed significant challenges. To mitigate this issue, the stone column (SC) ground improvement technique was implemented. The effectiveness of this method was evaluated using a finite element-based numerical analysis, providing insights into the performance of the treated soil.

CASE STUDY

Soil investigation is a critical component of any construction project, as it provides essential data for designing foundations, identifying potential hazards, and assessing site suitability. Accurate soil analysis is fundamental to ensuring the safety and stability of the proposed structures. The properties of the soil layers used in the analysis obtained from the soil investigation report are detailed in Table 1.

The stone columns used have a diameter of 500 mm and extend to a depth of 12 meters from the ground surface. They are arranged in a triangular pattern with a center-to-center spacing of 1.5 meters. A 500mm thick granular blanket was provided above the cutoff level of the stone columns. For the specific properties of the stone columns, please refer to Table 2.

Table 1 Soil Parameters used in Plaxis 3D

SlNo	Depth from Ground Level (m)		Layer thickness (m)	Soil description	Analysis type	Υ_{Sat} (kN/m^3)	C (kN/m^2)	Φ (deg)	E (kN/m^2)
	From	To							
1	0	6	6	Silty Sand	Drained	17.12	1	30	31900
2	6	-7.5	1.5	Low compressibility clay	Undrained	18.55	125	1	125000

 © DFI International Bruges 2025

3	-7.5	-13.5	6	silty sand	Drained	18.65	1	34	98600
4	-13.5	-25.5	12	Low compressibility clay	Undrained	20.22	250	1	250000
5	-25.5	-31.5	6	Silty Sand	Drained	19.14	1	36	87000
6	-31.5	-34.5	3	Poorly graded sand	Drained	19.14	1	38	110200
7	-34.5	-36	1.5	CI/MI*	Undrained	19.53	250	1	250000
8	-36	-50.45	14.45	Low compressibility clay	Undrained	19.96	250	1	250000

*Clay/ Silt of intermediate compressibility

Table 2 Properties of Vibro-stone columns, granular blanket and footing (Das et al., 2023)

Properties of stone for	Material Model	Analysis type	E (kN/m^2)	Υ_{sat} (kN/m^3)	c (kN/m^2)	Φ (deg)	υ
Granular blanket	Mohr-Coulomb	Drained	26000	19.0	0.1	35	0.3
Vibro-stone columns	Mohr-Coulomb	Drained	89142.86	21.0	0.1	42	0.3
Footing	Linear Elastic	Non-porous	27.39×10^6	25	-	-	0.2

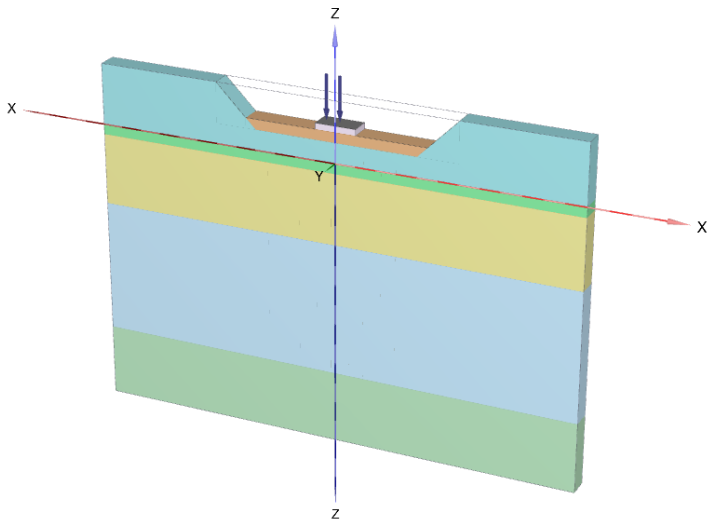
Validation of Numerical Method

The present study has been validated with the work of (Das et al., 2023). Their research focuses on the settlement behavior of soil under two distinct conditions: the natural state of the soil and the application of ground improvement techniques, specifically using Vibro-stone columns. The study employed numerical simulations conducted using PLAXIS 2D software to assess the settlement reduction and enhancement of bearing capacity. Similar to their approach, the results in this study have been simulated in finite element method (FEM) model PLAXIS 3D. The findings, presented in the accompanying Table 3, highlight variations in the results due to the inherent differences in the modeling approaches (2D and 3D). The model is shown in Fig.1 depicting stone column length and corresponding labels. The centre column widens in the bulging zone as a result of the column expanding laterally as the vertical load increases, giving the bulge a barrel-like look. In contrast, the SCs 1 and 2, which are positioned at the right and left sides of the column, exhibit asymmetrical bulging. The bulging on SC 1, 2 and centre are shown in Fig. 2.

 © DFI International Bruges 2025

Table 3 Comparison of results

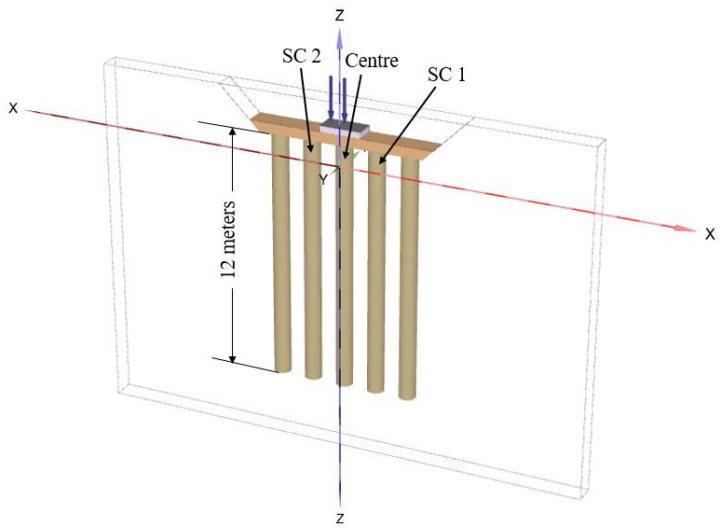
	Das et al., 2023 (using Plaxis 2D)	Present study (using Plaxis 3D)
Settlement before treatment (mm)	456.3	355.3
Settlement after treatment (mm)	44.58	33



a)

b)

Fig. 1 (a) Numerical Model developed in PLAXIS 3D (b) Dimensions and labels of the stone column



 © DFI International Bruges 2025

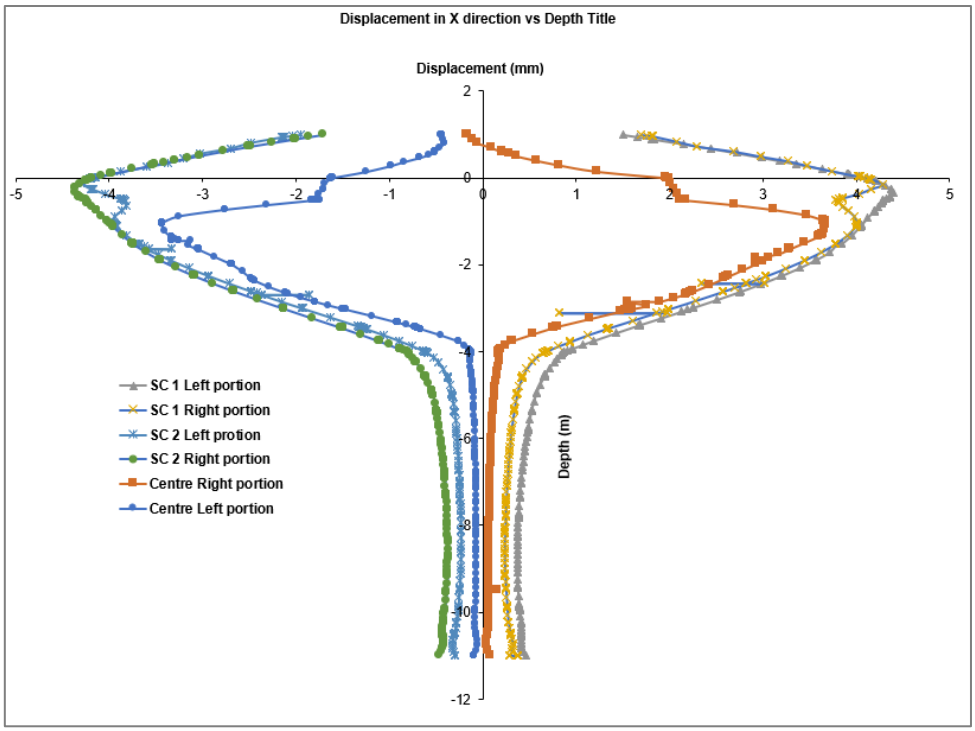


Fig. 2 Bulging in column SC 1, SC 2 and Centre

Parametric Study

This study based on (Das et al.,2023) also evaluated the impact of varying two key parameters: the length and diameter of the stone columns. As the diameter changes, the spacing of the stone columns (twice the diameter) also adjusts accordingly.

The analysis considered five different stone column lengths—8m, 10m, 12m, 14m, and 16m—with the soil strata extended to a depth of 17 meters from the ground level. The results, presented in Table 4, indicate that settlement initially increases with the length of the stone columns, reaching a peak at 12 meters, and then decreases with further increases in length.

Table 4 Settlement on varying Length

Length (m)	Settlement (mm)
8	16.47
10	16.67
12	16.96
14	15.95
16	14.53

For the analysis of different diameters, the study examined stone columns with diameters of 500mm, 600mm, 800mm, 900mm, and 1000mm. The findings, summarized in Table 5, show a linear reduction in settlement as the diameter of the stone columns increases, highlighting the effectiveness of larger

 © DFI International Bruges 2025

diameters in minimizing settlement. This was similar to the studies by Grizi et al., 2022. Also research by Elsiragy, 2021 showed increasing the column diameter from 0.5 m to 1 m resulted in an impressive 80% reduction in settlement, highlighting the importance of optimizing column dimensions for enhanced soil performance.

Table 5 Settlement on varying Diameter

Diameter (mm)	Spacing (mm)	Settlement (mm)
500	1000	19.26
600	1200	17.45
800	1600	15.42
900	1800	13.11
1000	2000	9.925

Liquefaction Potential Analysis of Untreated Subsoil

The liquefaction potential was evaluated utilizing the simplified approach described in IS: 1893 (Part 1)(Bhavan et al., 2002). The liquefaction potential factor of safety (FS) is determined by utilizing the cyclic stress ratio (CSR) and cyclic resistance ratio (CRR) measurements. Earthquake-induced stresses on soil mass are known as CSR and CRR, respectively, are the soil's ability to withstand liquefaction(Bolton Seed & Idriss, 1970; Das et al., 2023; Pestana et al., 2001).

The site is located in Earthquake Zone IV, where the peak ground acceleration for liquefaction analysis is 0.04g. The liquefaction results, summarized in Table 6, indicate that Factor of safety suggests soil is not susceptible. To address this issue, it is essential to implement ground improvement techniques to enhance the soil's bearing capacity and reduce settlement. This study focuses on using vibro stone columns as a method to mitigate the risk of liquefaction.

Table 6 Liquefaction Analysis for top three layers of soil

Layer	Stress reduction factor	CSR	N_{60}	$CRR_{7.5}$	Factor of safety
1	0.980875	0.070231325	11.25	0.124304998	1.769936675
2	0.973225	0.064043737	10.625	0.118670095	1.852953948
3	0.988525	0.062762944	15.625	0.16639703	2.651198592

Numerical Model

In this study, stone columns with a cross-sectional diameter of 500 mm were utilized for ground improvement. These stone columns were spaced at a distance of 3 times their diameter (3D) and arranged in a triangular configuration, a pattern chosen for its superior load distribution and structural efficiency. A 500 mm thick granular blanket was introduced beneath the foundation. The stone columns were installed beneath a raft foundation measuring 35 meters by 20 meters, situated 2.5 meters below the natural ground level. The detailed properties of both the stone columns and the granular blanket are presented in Table 2. For the analysis, the widely used Mohr-Coulomb model was adopted, as it effectively captures the fundamental soil behavior under different stress conditions. A

 © DFI International Bruges 2025

uniform surface load of 150 kN/m² was applied to simulate real-world loading conditions on the raft foundation.

Result and Discussion

The simulated findings of our study, which are presented in Table 7, highlight the significant efficacy of ground improvement methods, especially the application of stone columns. The data clearly shows that the use of stone columns has resulted in a substantial decrease in settlement, with values falling from 298.5 mm to 62.68 mm for load of 150KPa shown in fig. 3 and 4.

Table 7 Settlement before and after treatment

Conditions	Settlement (mm)
Before treatment	298.5
After treatment	62.68

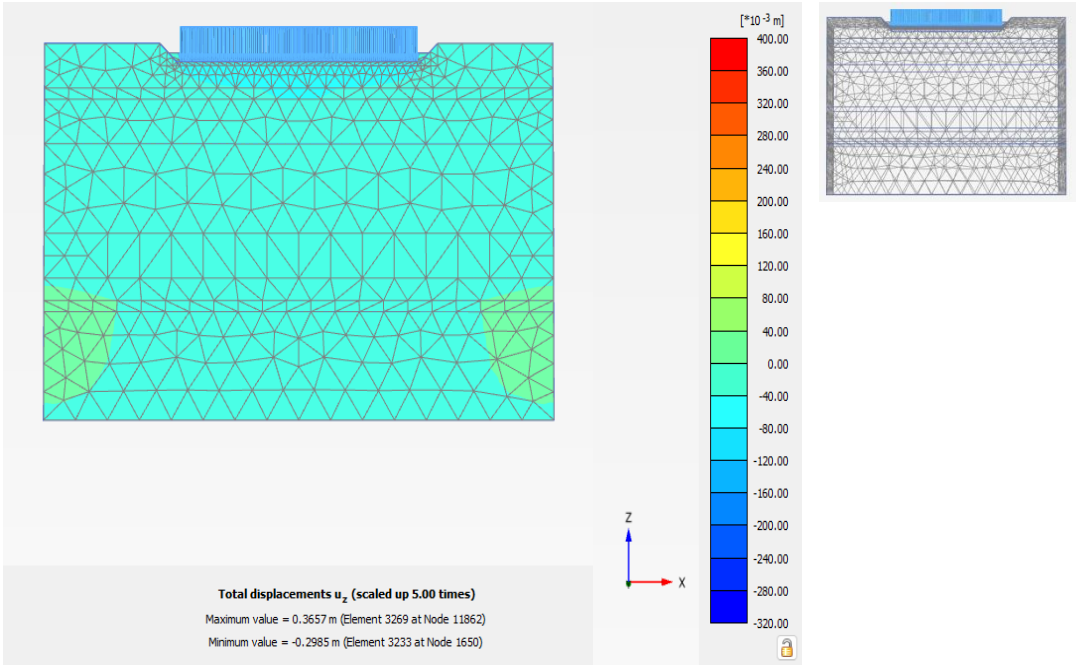


Fig. 3 Settlement before treatment

 © DFI International Bruges 2025

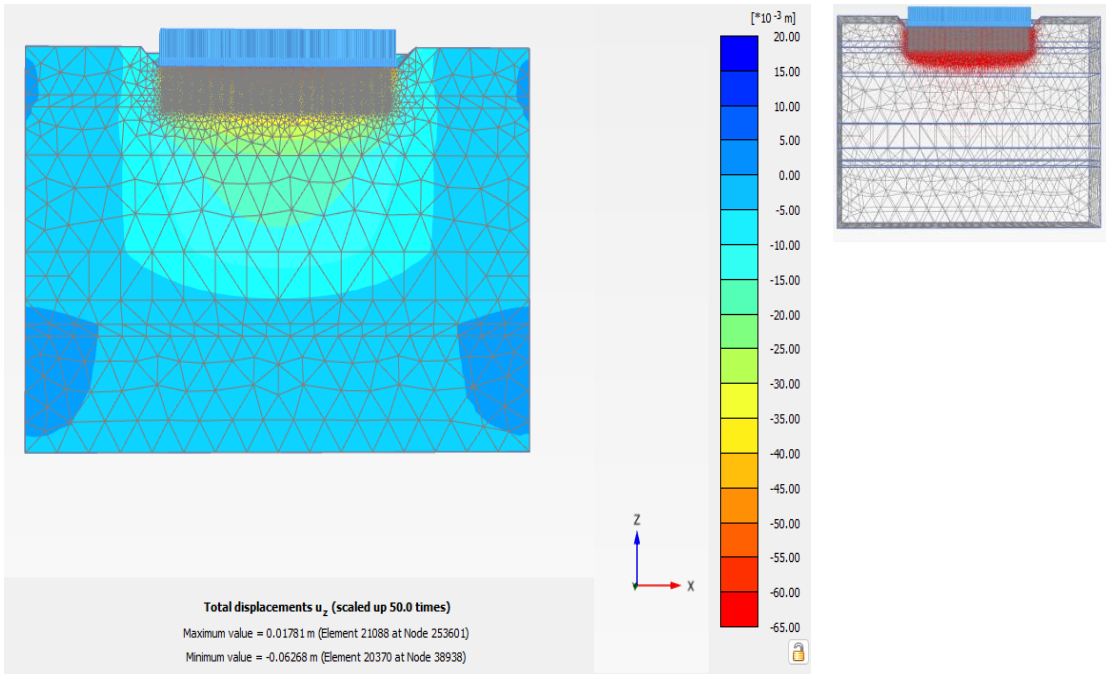


Fig. 4 Settlement after treatment

This diminution signifies a remarkable 79% decline in settlement, underscoring the significant influence of this methodology. Stone columns can improve soil stability and sustain structures more effectively, as evidenced by their success in reducing settlement.

Stone columns help to increase structural integrity and durability by reducing settlement significantly. This can lead to lower maintenance costs and a longer service life for the built infrastructure. This decrease in settlement also raises the foundation's safety and dependability and lowers the possibility of structural problems. Overall, the huge 79% reduction in settlement attained by using stone columns highlights their crucial role in ground improvement projects and verifies their effectiveness, offering substantial long-term benefits in terms of stability, safety, and cost-effectiveness.

CONCLUSION

Numerical simulation, particularly the Finite Element Method (FEM), is a powerful tool for analyzing and predicting the behavior of soil improvement techniques such as Vibro-stone columns. FEM allows for detailed investigation of different parameters, aiding in the optimization of designs for real field conditions. The study demonstrated the effectiveness of Vibro-stone columns in reducing settlement through a real field project in Ghaziabad. Numerical analysis revealed a significant decrease of 79% in settlement when the soil was treated with stone columns for a load of 150KPa.

The parametric study indicated that: .

- Settlement decreases with the increase in diameter of the stone columns, with larger diameter columns being more effective. A notable decrease of 48.47% for an increase in diameter from x to y was observed.
- The stiffness of founding strata is also important in contributing to reduction in settlement. The stone column should be founded on hard strata to effectively reduce settlement.

 © DFI International Bruges 2025

ACKNOWLEDMENT

Gratitude is extended to the CSIR- CBRI (Council of Scientific and Industrial Research – Central Building Research Institute) for their valuable support and resources throughout this study. The provided guidance and technical assistance greatly contributed to the success of this work.

REFERENCES

Adalier, K., & Elgamal, A. (2004). Mitigation of liquefaction and associated ground deformations by stone columns. Engineering Geology, 72(3–4), 275–291. https://doi.org/10.1016/j.enggeo.2003.11.001

Adalier, K., Elgamal, A., Meneses, J., & Baez, J. I. (2003). Stone columns as liquefaction countermeasure in non-plastic silty soils. Soil Dynamics and Earthquake Engineering, 23(7), 571–584. https://doi.org/10.1016/S0267-7261(03)00070-8

Alamgir, M., Miura, " N, Poorooshasbh, H. B., & Madhav', M. R. (1996). Deformation Analysis of Soft Ground Columnar Inclusions Reinforced by. In Computers and Geotechnics (Vol. 18, Issue 4).

Baez J. I., (1995). A design model for the reduction of soil liquefaction by vibro-stone columns. University of Southern California.

Benmebarek, S., Remadna, A., & Benmebarek, N. (2018). Numerical Modelling of Stone Column Installation Effects on Performance of Circular Footing. International Journal of Geosynthetics and Ground Engineering, 4(3). https://doi.org/10.1007/s40891-018-0140-z

Bhavan, M., Shah, B., & Marg, Z. (2002). Indian Standard Criteria for earthquake resistant design of structures part 1 general provisions and buildings (fifth revision) Bureau of Indian Standards.

Bolton Seed, H., & Idriss, I. M. (1970). national technical information service a simplified procedure for evaluating soil liquefaction potential.

Castro, J., Karstunen, M., & Sivasithamparam, N. (2014). Influence of stone column installation on settlement reduction. Computers and Geotechnics, 59, 87–97. https://doi.org/10.1680/j.compgeo.2014.03.003

Castro, J., & Sagaseta, C. (2012). Pore pressure during stone column installation. Proceedings of the Institution of Civil Engineers: Ground Improvement, 165(2), 97–109. https://doi.org/10.1680/grim.9.00015

Das, T., Sharma, M., & Choudhury, D. (2023). Bearing Capacity and Liquefaction Assessment of Shallow Foundations Resting on Vibro-Stone Column Densified Soil in Vallur Oil Terminal, India. Indian Geotechnical Journal, 53(6), 1392–1413. https://doi.org/10.1007/s40098-023-00758-9

El Sawy, O. A. (2001). Redesigning enterprise processes for e-business. Irwin/McGraw-Hill.

Elsiragy, M. (2021). Utilization of stone column for improving seismic response of foundation on soft clay- Numerical study. Journal of Petroleum and Mining Engineering, 0(0), 56–61. https://doi.org/10.21608/jpme.2021.58911.1069

Joseph E. Bowles, RE., S.E(1997). Foundation analysis and design /McGraw-Hill Companies, Inc.

 © DFI International Bruges 2025

Grizi, A., Al-Ani, W., & Wanatowski, D. (2022). Numerical Analysis of the Settlement Behavior of Soft Soil Improved with Stone Columns. Applied Sciences (Switzerland), 12(11). https://doi.org/10.3390/app12115293

Karstunen, Minna., & Leoni, Martino. (2009). Geotechnics of soft soils: focus on ground improvement: proceedings of the second International Workshop on Geotechnics of Soft Soils, Glasgow, Scotland, 3-5 September 2008. CRC Press/Balkema.

Mohanty, P., & Samanta, M. (2015). Experimental and Numerical Studies on Response of the Stone Column in Layered Soil. International Journal of Geosynthetics and Ground Engineering, 1(3). https://doi.org/10.1007/s40891-015-0029-z

Muzammil, S. P., Varghese, R. M., & Joseph, J. (2018). Numerical Simulation of the Response of Geosynthetic Encased Stone Columns Under Oil Storage Tank. International Journal of Geosynthetics and Ground Engineering, 4(1). https://doi.org/10.1007/s40891-017-0122-6

Ng, K. S., Idrus, J., & Chew, Y. M. (2021). Bearing Capacity of Stone Column Reinforced Foundation Subjected to Inclined Loadings. International Journal of Geosynthetics and Ground Engineering, 7(3). https://doi.org/10.1007/s40891-021-00307-5

Pestana, J., Riemer, J. M., Cetin, R. B., & Moss, K. O. (2001). Recent advances in soil liquefaction engineering and seismic site response evaluation.

Remadna, A., Benmebarek, S., & Benmebarek, N. (2020). Numerical Analyses of the Optimum Length for Stone Column Reinforced Foundation. International Journal of Geosynthetics and Ground Engineering, 6(3). https://doi.org/10.1007/s40891-020-00218-x

Saxena, S., Roy, l. b. (2022). Suitability Analysis of Stone Column Materials with PLAXIS_Engineering, Technology & Applied Science Research.

Watts, K. S., Johnson, D., Wood, L. A., & Saadi, A. (2000). An instrumented trial of vibro ground treatment supporting strip foundations in a variable fill.

 © DFI International Bruges 2025

INSTALLATION OF PRECAST REINFORCED CONCRETE PILES AS PART OF THE EXPANSION OF EXISTING INDUSTRIAL BUILDINGS AND TECHNICAL INFRASTRUCTURE

Filip Sokołowski[1]*

Abstract

This paper details the execution of piling works using precast reinforced concrete piles for the construction of the Vestas Wind Turbine Assembly Plant in Szczecin. With the growing shift towards renewable energy in Europe, Szczecin's favorable location offers a strategic advantage in the development of offshore wind farms in the Baltic Sea. The plant, situated on Brdowski Island, will play a crucial role in this multi-stage process, requiring the expansion and adaptation of existing infrastructure, including production halls and a 1400-ton gantry crane. The piling works were carried out in challenging geological conditions, with organic soils up to 7 meters thick across the site, necessitating specialized intermediate foundations. Precast piles were installed for new buildings and also used to reinforce floors in existing halls. Additionally, the expansion of stormwater, sanitary sewage, and water supply networks posed further challenges, as these networks need to accommodate significant loads from vehicle movement during operations, particularly from the transport of heavy wind turbine components. The presentation provides a comprehensive overview of the geological conditions, foundation design, and technical execution of the piling works.

Keywords: precast piles, piling works, soil conditions, offshore wind energy, Baltic Sea

Introduction

Precast technique has gained significant reputation in the construction industry due to improved efficiency and reduced construction waste. Pile foundation is often built through driven precast or cast-in-situ construction technique (Luo et al., 2019). The two types of pile foundations have been widely utilized in various building construction types. The selection of the piling methods has been largely based on the project scope, soil conditions and availability of resources.

[1] Construction Manager in the Precast Pile Department. Aarsleff Ltd. Wyścigowa Avenue 6, 02-681 Warsaw. fso@aarsleff.pl

 © DFI International Bruges 2025

Precast piles are a type of deep foundation system used to support structures by transferring loads to deeper, more stable layers of soil (Pujadas-Gispert et al., 2020). These piles are typically made of concrete, steel, or timber and are driven vertically into the ground to provide enhanced structural support where traditional shallow foundations would be insufficient. Specifically, precast concrete piling involves the use of concrete piles that are manufactured off-site and then transported to the construction site. They are driven into the ground using a piling rig equipped with an impact hammer. This method ensures consistent quality, durability, and strength. As a result, precast piles are widely used for supporting the loads from buildings, bridges and roads. (Sadeghi et al., 2023).

Actions in the field of offshore wind energy development in the Baltic Sea are increasingly becoming a reality (Figure 2). According to the assumptions of Poland's Energy Policy until 2040, the main role will be played by the expansion of the offshore wind energy sector, which is expected to receive investments amounting to approximately EUR 30 billion. The result of this will be, first, a change in the structure of electricity production in Poland, and second, a reduction in CO2 emissions, contributing to the acceleration of the ongoing energy transition in Poland (Figure 2). This transition is of crucial importance from the perspective of environmental protection.

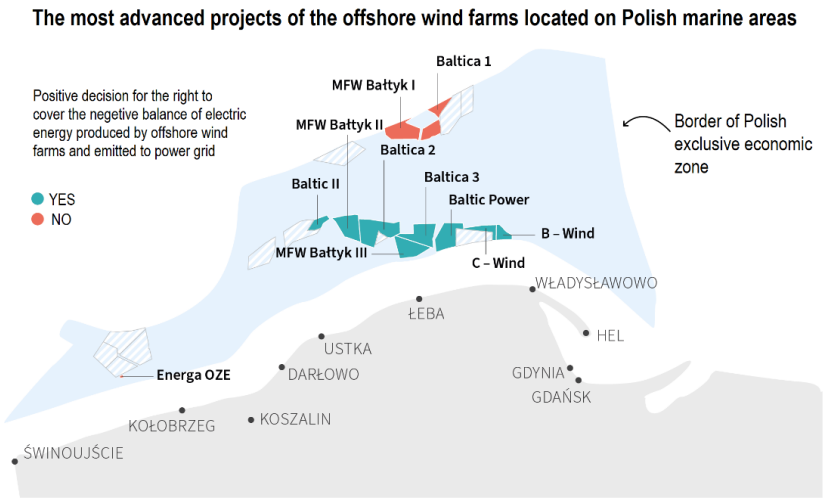


Figure 1. Planned locations of wind farms in the Baltic Sea

 © DFI International Bruges 2025

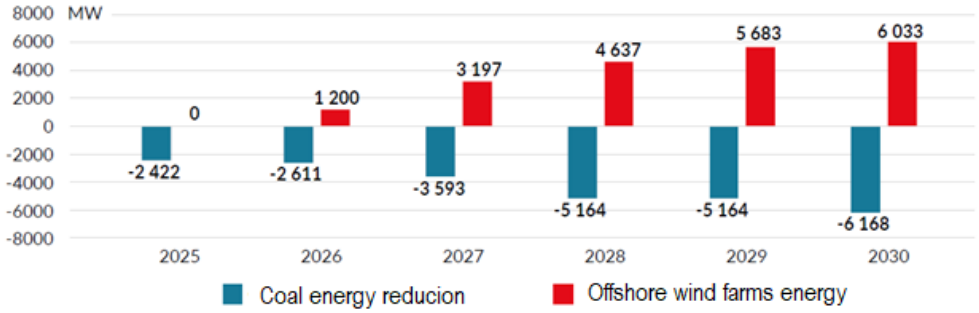


Figure 2. Plan for reducing coal-generated energy capacity and increasing offshore wind energy capacity

The described development directions in the energy sector cannot occur without the construction of infrastructure that will enable the production of offshore wind farm components and their transportation to installation sites. A suitable location for such a facility is the city of Szczecin, situated in the West Pomeranian Voivodeship at the mouth of the Oder River, which flows into the wide Szczecin Lagoon, and then connects with the Świna River, which empties into the Baltic Sea (Figure 3).

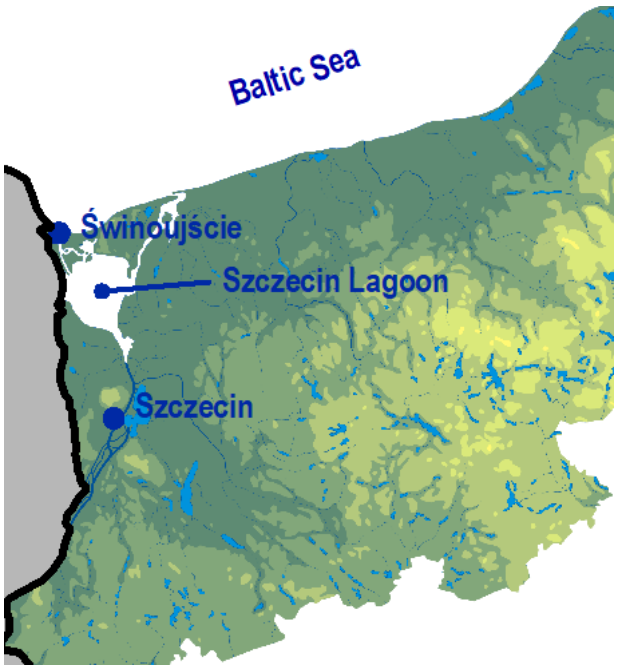


Figure 3. Location of the city of Szczecin

Located in Szczecin, on Ostrów Brdowski Island, is an industrial complex with a gantry crane capable of lifting up to 1400 tons and a wharf, offering a favorable place for producing components for offshore wind farms. However, the size and weight of these elements pose challenges for expanding the existing facilities, which require adaptation to

 © DFI International Bruges 2025

meet future demands. Due to complicated soil conditions, almost all the existing buildings are founded on precast piles installed by Aarsleff company about 10 years ago. After analyzing the soil conditions and the loads that the structures will be subjected to, the designers made several decisions, resulting in the repeated use of precast-driven piles for most of the buildings, both those being expanded and those being newly constructed. For construction of the foundations described in this paper reinforced concrete piles of a 40x40 cm cross-section were used. This type of piles consist of steel rebars manufactured from B500SP steel and C40/50 concrete with fast-setting cement. Reinforced concrete precast piles were designed due to its time-saving advantage comparing to other technologies where the concrete setting is the key factor. It was convenient solution in terms of very tight work schedule. As part of the expansion of the Vestas Wind Turbine Assembly Plant in Szczecin, piling works were carried out, which can be divided into three types, depending on the facility under which the precast piles were installed.

Performed Work

1) Hall H3

The first site for piling work was the newly constructed Hall H3, measuring 177 x 47 m, intended for storing components for the construction of offshore wind turbine gondolas. The eastern wall of Hall H3 was connected to the existing structure of Hall H2. The main factor necessitating the intermediate foundation for Hall H3 was the presence of organic soils in the form of peat and silts, which extended from -2.50 m to -10.50 m below the ground level. Below the organic soil layer, there were medium-dense sands and gravels from river accumulation, reaching thicknesses of up to 10 m.

 © DFI International Bruges 2025

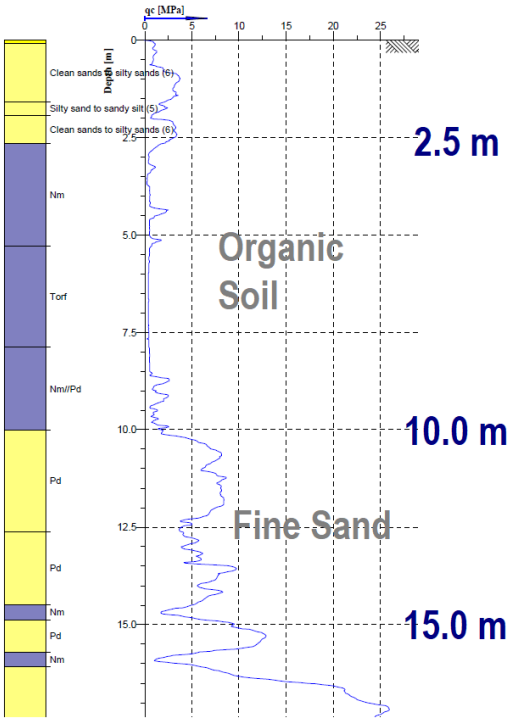


Figure 4. Sample soil profile under the floor of hall H3

In total, approximately 400 precast piles were installed as part of the foundation for the structure, with a cumulative length of over 6500 meters. The floor was supported by about 850 piles with a total length of approximately 15,000 meters. The lengths of the piles ranged from 13 to 22.5 m. To check the load-bearing capacity of the piles, dynamic tests were conducted on both the piles under the foundation of Hall H3 and the area of the floor. This method is quick and easy to execute, not significantly impacting the progress of the piling work while allowing for ongoing verification of design assumptions. A static test was also performed as part of the load-bearing tests. As a result of the dynamic load tests ultimate bearing capacities from 2029 to 3258 kN were recived, depending on the area of the hall. Settlement of a test pile during static load test stabilized on 9,1 mm at compression force of 2425 kN.

 © DFI International Bruges 2025

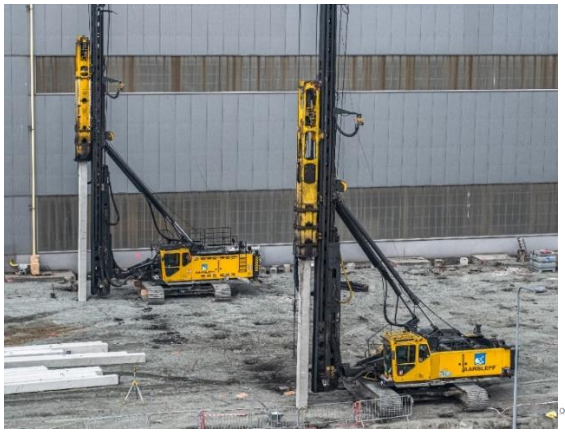


Figure 5. Piling works – Hall H3

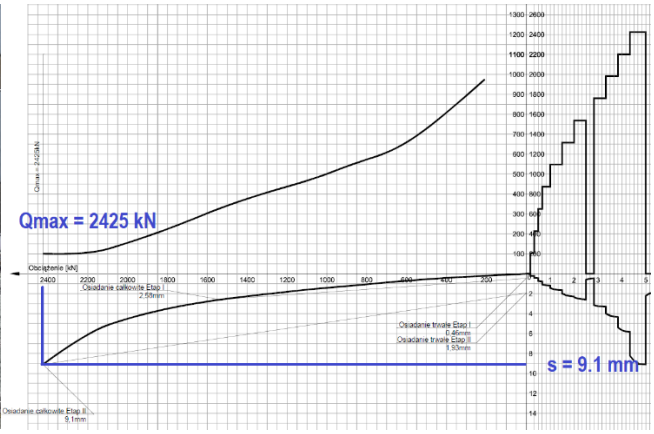


Figure 6. Settlement diagram after SLT

Piling work within Hall H3 proceeded smoothly, as it was a newly constructed facility. This area was free from conflicts with existing underground infrastructure or previously erected foundations, allowing for the free planning of material deliveries based on the current progress of work, unhindered by unplanned exploratory works or inventories of existing structures located below the working platform level. Location of load tests (dynamic and static) were strictly determined in Test Load Desing. Piling works were executed according to predictions so any needs of changes of test piles locations were not necessary.

2) Halls H1 and H2

The existing Halls H1 and H2 were designated as the main assembly areas for wind turbine gondolas to their final shape. Some of the floors, due to increased operational loads, were rebuilt, one element of which was the installation of new precast piles to bear the new loads. To reinforce the flooring, it was necessary first to completely break up the existing floor to then install the piles and re-lay the reinforcement and concrete mix. Due to the risk of damaging the existing piles, separation holes were made to isolate them from the demolished floor (Figure 7).

 © DFI International Bruges 2025

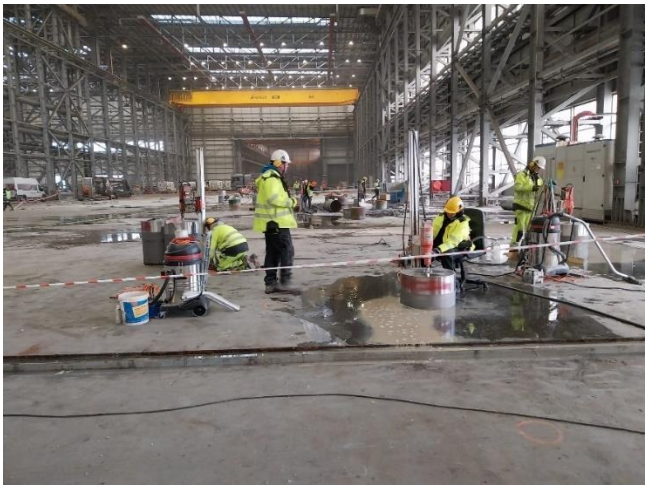


Figure 7. Creating separation holes

Before commencing the main phase of piling work, load-bearing tests were performed to verify the assumed lengths of the precast elements. First, dynamic load-bearing tests were conducted. The newly designed piles were installed in previously drilled holes, while the heads of the existing piles required shape adjustments for the correct installation of sensors for testing and for the application of the impact hammer. The first hole was made to separate the pile from the existing floor, and the sub-base concrete was broken up. Subsequently, after excavating the soil near the pile, its casing was exposed, allowing for the adjustment of the cylindrical shape of the drilled floor to the edge of the pile casing, which guaranteed axial transfer of the hammer's impact and accuracy in conducting the test.



Figure 8. Preparing pile for dynamic load test – Hall H2

 © DFI International Bruges 2025

Furthermore, a static test was prepared in a different manner than usual—steel beams were anchored to the existing concrete floor instead of using anchoring rods for the piles. The existing pile rods were connected to the floor reinforcement during the construction of the halls in 2014. After breaking the heads during the demolition phase, the shape of the rods prevented the anchoring of the static test structure and the correct transfer of the pull-out forces from the anchoring pile. Therefore, a decision was made to anchor eight threaded rods Ø32—in the existing floor of the hall. Chemical anchors were used, assuming the diameter and depth of anchoring provided by the manufacturer based on calculated pull-out forces of approximately 338 kN per rod.



Figure 9. Static test setup

In all tested piles, the ultimate load capacities ranged from 3233 kN to 4400 kN. These results allowed for local optimization of the project in terms of the lengths of newly installed piles, leading to shorter construction times in these areas. During the piling works in Halls H1 and H2, the continuity of the existing piles was also examined, which helped identify potential damages to the piles during demolition works.

 © DFI International Bruges 2025

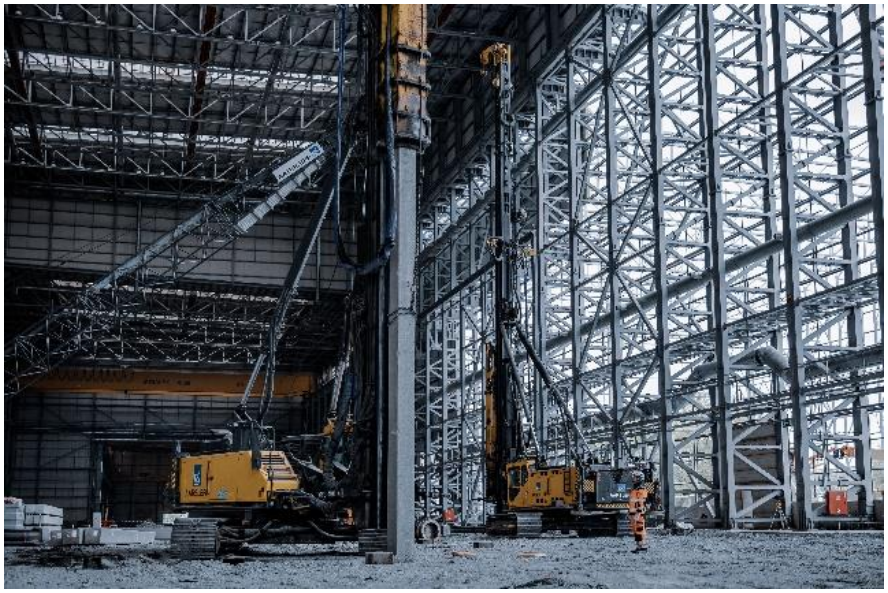


Figure 10. Piling works in Hall H2

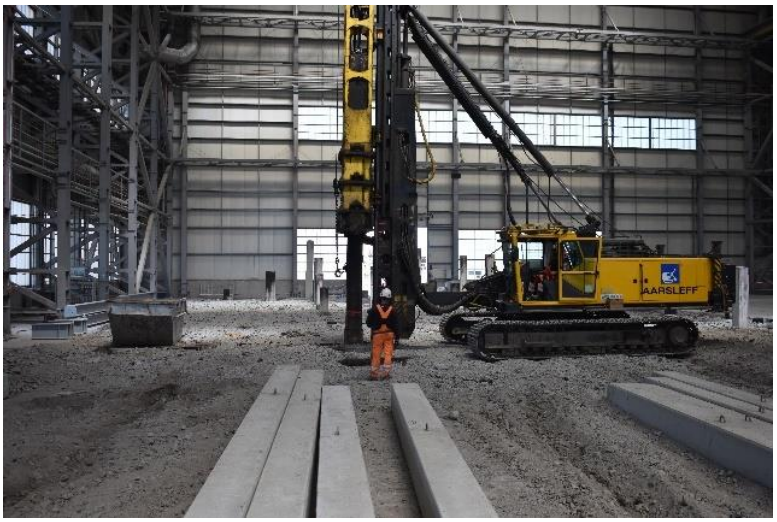


Figure 11. Piling works in Hall H1

The total number of piles installed in Hall H1 was approximately 300, with lengths ranging from 12.5 to 14.0 m, while the work performed for the floor of Hall H2 included around 450 piles with lengths between 13.5 and 15.0 m. Conducting work in the confined spaces of the existing Halls H1 and H2 required increased attention from operators when controlling the hammer to avoid collisions with existing steel structures intended for further use, as well as the floor planned for reuse. Additionally, noise, an inherent aspect of this technology, took on greater significance in this environment. The workers performing the piling operations inside the hall were equipped with protective earmuffs that offered noise

 © DFI International Bruges 2025

reduction up to 38 dB comparing to the type used outside providing reduction of noise approximately 33 dB.

3) Piles under networks

The large-scale elements to be transported between the halls generate significant loads on the ground. On the other hand, the construction of such a large number of production buildings simultaneously required the execution of hundreds of meters of stormwater and sanitary sewer networks, which, due to the heavy loads, required foundation on reinforced concrete bases and piles. The sections of the networks, for which intermediate foundations were designed, were determined based on the areas designated by the Investor for heavy vehicle movement.

Stormwater and sanitary sewer manholes were founded on a minimum of three reinforced concrete piles with a cross-section of 40x40 cm, ensuring their proper stability under any heavy vehicle traffic. The piles under the foundation bases were designed with a maximum axial spacing of 4.0 m. The designed load for piles in the present case ranged from 300 kN to 1600 kN in the areas of heaviest traffic. The lengths of the piles for the underground networks ranged from 14.0 m to 19.0 m, depending on the local geological conditions.

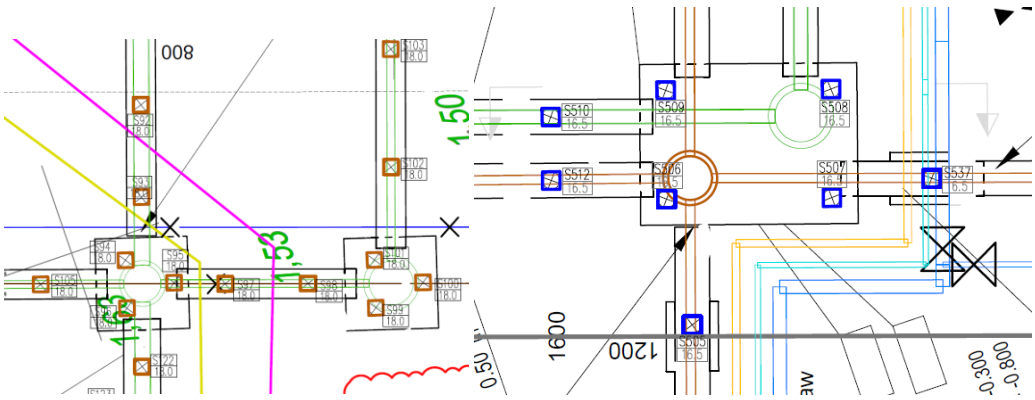


Figure 12. Arrangement of piles under networks

 © DFI International Bruges 2025

Summary and Conclusions

In this work, the use of precast piles has been instrumental in addressing the challenging soil conditions present in the Szczecin area, particularly the presence of organic soils. The consistent quality and strength of precast concrete piles make them an ideal solution for supporting large-scale, heavy structures like those involved in offshore wind energy production. Furthermore, dynamic and static load-bearing tests demonstrated the efficacy of precast piles in supporting both newly constructed and existing structures. The tests allowed for continuous verification of design assumptions, enabling adjustments during the project to optimize pile lengths and reduce construction time. The need to integrate piling work with existing structures, especially in Halls H1 and H2, required innovative solutions, such as the use of separation holes and tailored testing setups. This ensured that the existing piles were not damaged during demolition or reconstruction, safeguarding the integrity of the foundation system.

The presence of Aarsleff in this major investment project, which is part of Poland’s energy transition, underscores the proven reliability of precast pile technology—successfully used once again in the same location. This repetition highlights the trust in the method’s durability and suitability for long-term infrastructure stability. Dynamic and static load tests results confirmed right assumptions and did not reveal any surprises according to load bearing capacity of piles. Major experience of Aarsleff designers in creation of foundation solutions in this particular area of Poland were important to set accurate initial assumptions.

The expansion of wind turbine assembly facilities in Szczecin is a critical step in supporting the future of offshore wind energy in Poland. With planned investments in the sector and the strategic location of the facilities, Szczecin is well-positioned to become a key hub for the production of wind turbine components, aiding in Poland's transition to cleaner energy sources and reducing carbon emissions.

This project demonstrates the vital role of advanced foundation technologies, such as precast piles, in the successful execution of large-scale energy infrastructure projects. The experience gained and solutions implemented here provide valuable insights for future developments in offshore wind energy and similar large-scale projects requiring robust and reliable foundation systems.

 © DFI International Bruges 2025

Acknowledgments

The author would like to extend sincere gratitude to all members of the Aarsleff and Atlas Ward (Main Contractor) teams for their invaluable contributions and support throughout this project. To the Aarsleff team for the commitment to quality in the use of precast piles which provided a solid foundation for the infrastructure. To the Vestas team, for their dedication to advancing wind turbine technology and for supporting the expansion of the turbine assembly plant in Szczecin. This project would not have been possible without the collective efforts of both teams, and the author looks forward to future collaborations.

References

Luo, W., Sandanayake, M., & Zhang, G. (2019). Direct and indirect carbon emissions in foundation construction – Two case studies of driven precast and cast-in-situ piles. *Journal of Cleaner Production*, *211*, 1517–1526. doi: 10.1016/j.jclepro.2018.11.244

Pujadas-Gispert, E., Sanjuan-Delmás, D., de la Fuente, A., Moonen, S. P. G. (Faas), & Josa, A. (2020). Environmental analysis of concrete deep foundations: Influence of prefabrication, concrete strength, and design codes. *Journal of Cleaner Production*, *244*, 118751. doi: 10.1016/j.jclepro.2019.118751

Sadeghi, H., & Singh, R. M. (2023). Driven precast concrete geothermal energy piles: Current state of knowledge. *Building and Environment*, *228*, 109790. doi: 10.1016/j.buildenv.2022.109790

Wu, W., & Editors, H. Y. (2018). China-Europe Conference on Geotechnical Engineering, 2016. In Springer Series in Geomechanics and Geoengineering (Vol. 2).

 © DFI International Bruges 2025

COMPARISON ANALYSIS OF PILE-SUPPORTED LUMPED MASS AND ACTUAL BUILDINGS UNDER DYNAMIC LOADINGS

Sangseom Jeong, Professor, Yonsei University, Seoul, Republic of Korea, soj9081@yonsei.ac.kr
Sumin Song, Post-doctoral, National Taiwan University, Taipei, Taiwan, ssm9780@gmail.com

ABSTRACT

This study investigated the different types of superstructures with soil and pile foundations through 1g shaking table model tests. The emphasis was on analyzing the dynamic interaction of pile foundations with different superstructures in dry sands. The sweep tests were performed to evaluate the dynamic behavior of soil-pile-structures systems. Based on test results, it was shown that lumped mass systems tend to overestimate the resonant frequencies compared to building systems depending on the soil conditions. The pile bending moment of lumped mass systems recorded a smaller than building systems with increasing the magnitude of the input acceleration since the different resonant frequencies of system.

Keywords: Lumped mass, 1g shaking table tests, soil-pile-structure interaction

1. INTRODUCTION

The need for pile structures has increased due to high-rise and large-scale construction projects, necessitating research on the interaction between soil, piles, and structures. According to SEAOC, soil-structure interaction (SSI) under dynamic loading conditions plays an important role in that it can change the design loads or dynamic behavior of building due to these effects: a) period lengthening; b) foundation damping; and c) kinematic interaction. However, conventional structure design methods, ASCE 7-16 or KDS (Korean Design Standard), are mainly separated into two parts, structure engineering and geotechnical engineering (ASCE, 2016; KDS, 2018; KDS, 2019). By expanding from static to dynamic behavior, conventional methods' limitations have been issued.

There is a limitation in conventional seismic designs of soil-pile-building structure systems to calculate accurate dynamic behavior because they analyze the superstructure and soil-pile foundations separately. From the superstructure design, the foundation is assumed to have rigid base conditions, ignoring the deformation of the soil-pile foundations during seismic loading. However, the seismic foundation design conventionally considers only the load transfer from the superstructure to the pile foundation as an equivalent load combination (pseudo-static loads) such as vertical, horizontal, and moments (Jeong et al., 2024; Kim and Jeong, 2019; Ko et al., 2017). However, these methods can cause dissimilar dynamic behaviors during seismic loadings to actual behavior.

Considering the foundation as a rigid base neglects the deformation caused by foundations and soils, resulting in an inability to predict additional horizontal deformations. Moreover, the lack of

 © DFI International Bruges 2025

consideration for irregular stiffness between the building and the soil-pile foundations can lead to stress concentration at the interface between piles and the buildings. Moreover, neglecting the soil and pile foundations can underestimate the natural periods of actual soil-pile-building structure systems due to not considering the whole height of super-substructures. Furthermore, this method is difficult to account for changes in stress resulting from soil deformations like liquefaction.

Therefore, this study aim to investigate the different behavior of SSI systems as different structure type. A series of 1g shaking table experiments were conducted to analyze the dynamic behavior of soil-pile-building systems by using different types of structures. The test results and discussions are investigated including an analysis of the natural periods lengthening and damping ratio changes of SSI system.

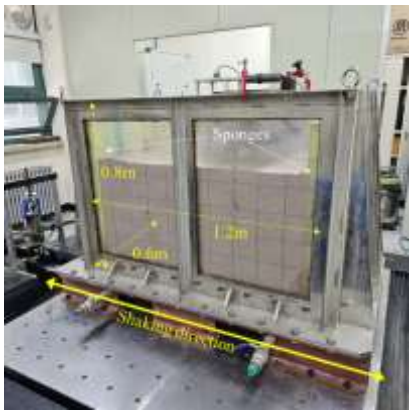
2. EXPERIMENTAL APPROACH

2.1. TEST APPARATUS

In this study, a series of 1g shaking table tests were conducted for the dynamic behavior with different seismic design methods (Fig. 1 (a)). The soil box used in this test has 1.2m width, 0.6m height, and 0.8m depth (Fig. 1 (b)). The lateral sides and the bottom of the model container are constructed with steel plates, while the front and rear sides of the model container are made of transparent polycarbonate (PC) with a thickness of 2 cm for observation during the tests. In addition, 10cm thick sponges were attached on both sides of the container wall to minimize the reflection wave effect caused by soil container walls during shaking tests(Song and Jeong, 2023; Song and Jeong, 2024). The effects on attached sponges in the rigid soil box were studied by Kim et al. (2020), they found that there are almost similar results in input seismic waves between a sponge installed in a rigid soil box and a laminar soil box.



(a) Shaking table devices



(b) Soil box

Fig. 1. Test apparatus

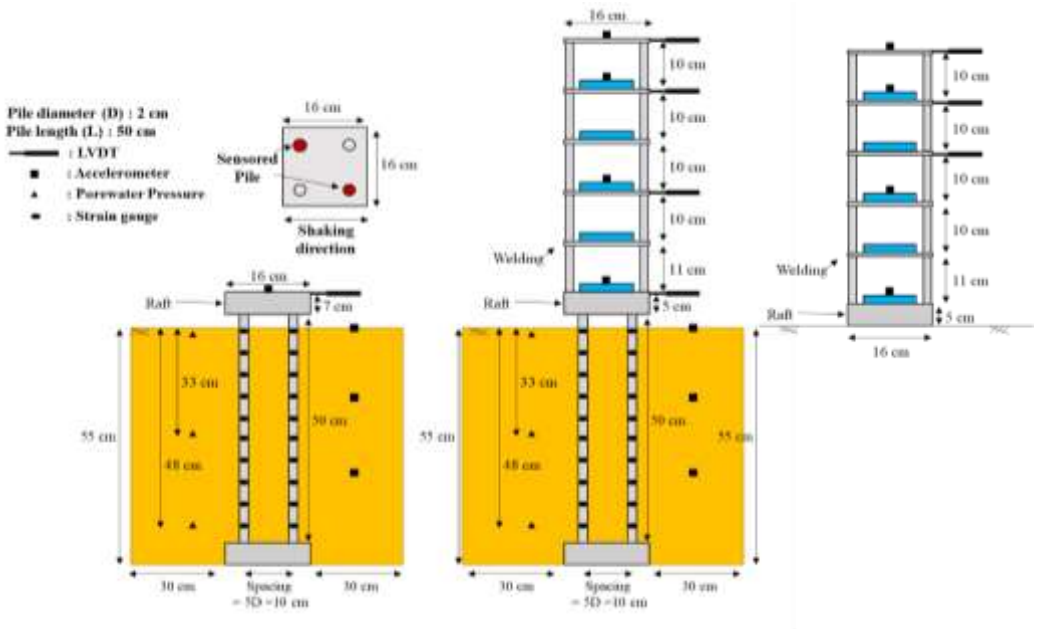
 © DFI International Bruges 2025

2.2. TEST SAMPLES AND MEASUREMENTS

The test soil used in this study was Jumunjin sand. A unit weight of Jumunjin sand with relative densities of 40 and 80 % was used as 14.5 and 15.82 kN/m^3, respectively. Table 1 shows the basic physical properties of the test soils. The testing model piles and structures were uniformly modeled with a scale factor of 25 according to Iai (1989). The prototype pile is a PHC pile with a diameter of 0.5 m, thickness of 0.08 m, and length of 0.5 m. The model piles were made of aluminum (6061-T6). The pile length was selected as 0.5 m to satisfy the long pile condition based on Broms (1964). The model group piles consisted of four piles placed in a 2 x 2 configuration with spacing as 5 times pile diameter (*D*). In addition, piles were inserted into the bottom plate of the soil box at a depth of around 1 *D* to simulate end-bearing pile conditions. To measure the piles' strain, strain gauges were attached to the surface along the pile lengths. A raft, pillars, and slabs in building structures were made of aluminum. It designed for the case of group piles not directly attached to the ground surface. Horizontal accelerometers were installed to measure the acceleration response of the superstructure, and Linear Variable Differential Transformers (LVDTs) were installed to measure the horizontal displacement of the superstructure (Fig. 3).

Table 1 Material properties of test soil

USCS	γ_{max} (kN/m^3)	γ_{min} (kN/m^3)	G_s	D_{10} (mm)	D_{30} (mm)	D_{60} (mm)
SP	16.2	13.6	2.65	0.42	0.54	0.79



(a) Lumped mass **(b) Soil-pile-structure** **(c) Rigid base**

Fig. 3. Schematic view of experiment layout

 © DFI International Bruges 2025

2.3. TESTING PROGRAM

In this study, the experiments were performed by sweep tests (Fig. 4). The sweep tests were conducted to analyze the natural frequency and the dynamic behavior of the soil-pile-superstructure systems. The input acceleration for the sweep test had an amplitude of 0.05 – 0.3g, and the frequency ranged from 1 Hz to 30 Hz during a period of 60 seconds. The test cases are summarized in Table 2.

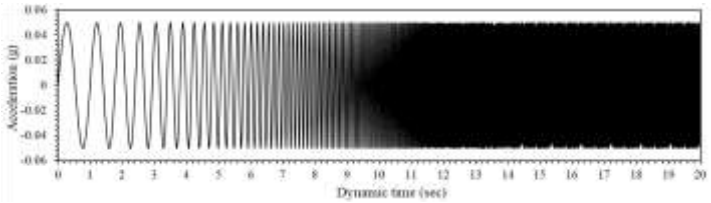


Fig. 4. Typical input acceleration: Sweep tests (1-30Hz)

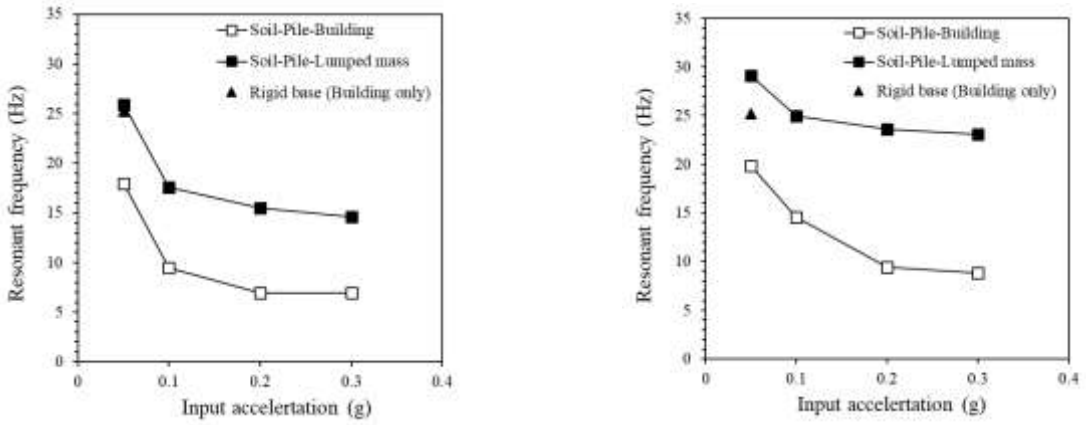
Table 2 Test program – Phase 1

Total case No.	Relative density of soil (%)	Structure condition	Input acceleration (g)	Frequency (Hz)
4	-	Rigid base with 6 stories	0.05, 0.1, 0.2, 0.3	1-30
8	40	2x2 pile groups with 6 stories		
8	80	2x2 pile groups with Lumped mass		

3. TEST RESULTS AND DISCUSSION

3.1. NATURAL PERIOD LENGTHEN

Comparison of resonant frequencies between lumped mass and 6-story buildings with different relative densities are summarized in Fig. 5. The resonant frequencies of lumped mass were higher than buildings in all input acceleration regardless of soil condition. As increasing the magnitude of input acceleration, the resonant frequencies decreased. This was confirmed by the fact that the center of mass of the 6-story building is higher than the lumped mass, resulting in a large horizontal displacement, resulting in a low resonant frequency. Additionally, it was confirmed that the difference between input acceleration of 0.05g and 0.1g was larger in a 6-story building. The resonant frequency of the 6-story building did not show a significant difference between input accelerations of 0.2 g and 0.3 g, while the lumped mass showed a decrease in resonant frequency.

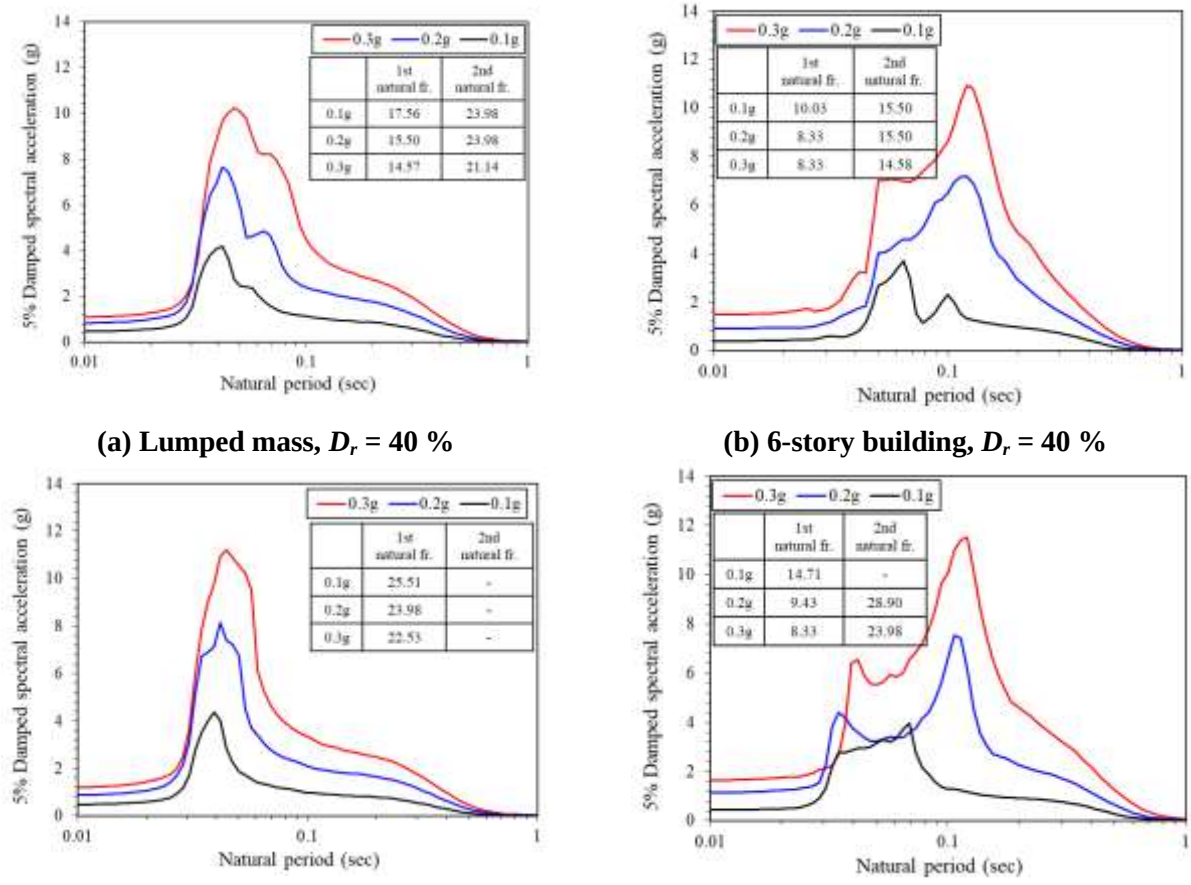


(a) D_r = 40 % **(b) D_r = 80 %**

Figure 5. Comparison of different building conditions on resonant frequencies

 © DFI International Bruges 2025

Fig. 6 shows the 5% damped spectral acceleration (g) of the building under different conditions obtained through sweep tests. The spectral acceleration showed that the natural frequency tends to decrease since the input acceleration was increased. In the lumped mass system, the first and second resonance frequencies were shown when the relative density of soil (D_r) was 40% (Fig. 6 (a)), whereas only the first resonance frequency was observed at D_r = 80% (Fig. 6 (c)). On the other hand, under the 6-story building condition, both the first and second resonance frequencies were observed in all cases except for the 0.1g of input acceleration (Fig. 6 (d)). This indicates that in Fig. 6 (c and d), the second natural frequency is located beyond the observable range limit of 30Hz, resulting in only the first natural frequency being detected. Additionally, it was confirmed that both the first and second natural frequencies tend to change together as the input acceleration increases.



(a) Lumped mass, D_r = 40 %

(b) 6-story building, D_r = 40 %

(c) Lumped mass, D_r = 80 %

(d) 6-story building, D_r = 80 %

Fig. 6. Comparison of different building conditions on resonant frequencies

3.2. DAMPING RATIO VARIATON

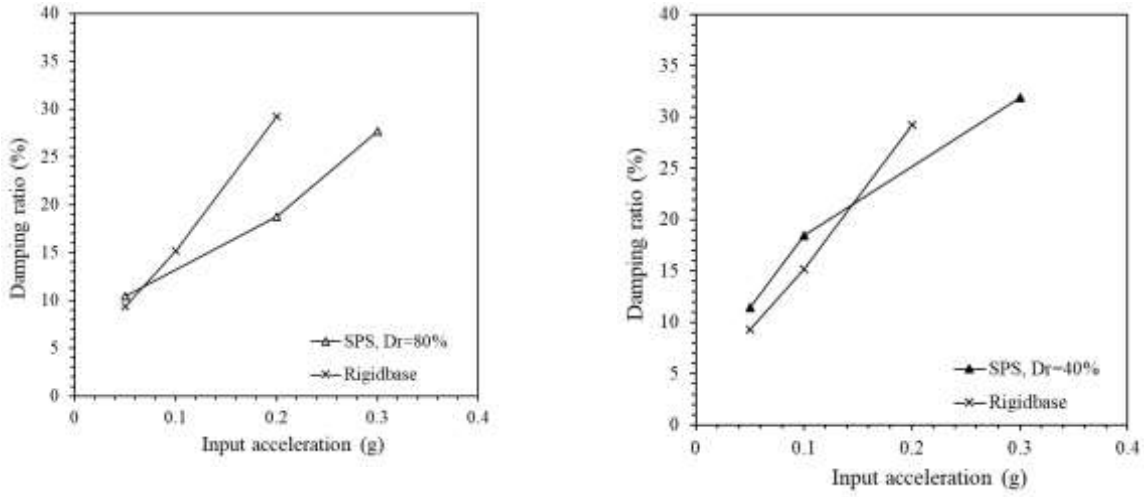
The widely used method to calculate damping ratio is the half-power bandwidth approach. This method calculate natural frequencies by the frequency-response curves. Then it obtains the maximum amplitude at the natural frequency of the system, and gets the two frequencies (f_b and f_a) that have a response amplitude equal to the maximum divided by the square root of two. So, this study used half-

 © DFI International Bruges 2025

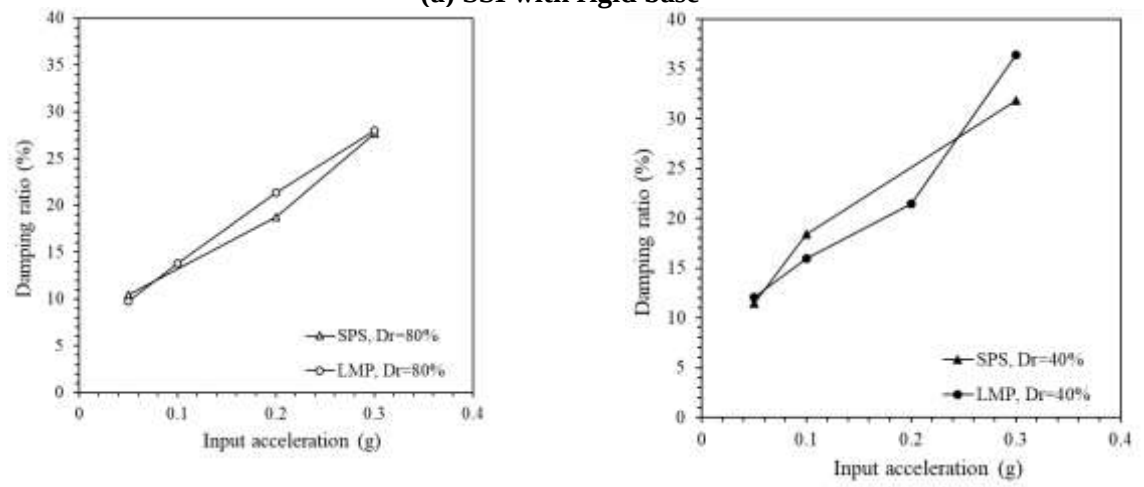
power bandwidth approach to calculate the damping ratio by using period-spectral acceleration curves measured from roof of structure (equation 1).

$$\zeta = \frac{f_b - f_a}{2 f_n} \quad [1]$$

where, ζ is the damping ratio and f_n is the natural frequency. The calculated damping ratio of each test conditions are shown in Fig. 7. It was shown that the soil-foundation-structure embedded in dense soil condition (D_r = 80%) had a lower damping ratio than the rigid base method (Fig. 7 (a)). It was indicated that the damping ratio of the rigid base increases rapidly with increasing of the input acceleration, this result caused by the superposition of the resonant effect occurring at high frequencies due to using the sweep test wave that is artificial sinusoidal wave. It was found that there is not remarkable difference in damping ratios between lumped mass and soil-pile-structure system (Fig. 7 (b)). In all test results, the damping ratio in the dense soil layer (D_r = 80%) recorded lower than the loose sand condition (D_r = 40%) (Fig. 7 (b and c)). This indicated that the hysteric damping increases as the surrounded soil becomes softer, which dissipates more ground motion energy. In addition, it was found that the damping ratio of the lumped mass method did not change significantly compared to the SSI, regardless of the relative density of soil.



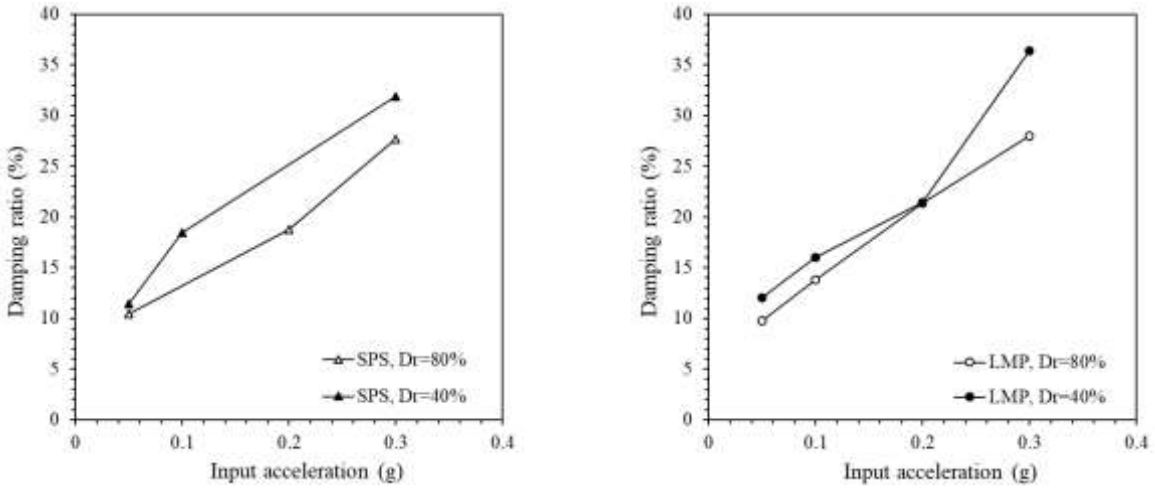
(a) SSI with rigid base



(b) SSI with lumped mass

Fig. 7. Variation of damping ratio with increasing input accelerations (Continue)

 © DFI International Bruges 2025



(c) Effect of different relative densities

Fig. 7. Variation of damping ratio with increasing input accelerations

4. SUMMARY AND CONCLUSIONS

The objective of this study was to evaluate the limitations of the simplified rigid base and lumped mass systems in the context of structural and geotechnical engineering, particularly in their application to dynamic analysis of soil-foundation-structure systems. The key findings from this study are as follows:

1. The rigid base system exhibited a higher natural frequency and the lumped mass system evaluated a lower than the actual soil-foundation-structure system. This discrepancy suggests that the rigid base system may not adequately represent the dynamic behavior of the actual system, particularly under seismic loading.

2. It was found that the damping ratio was affected by the soil and foundation conditions, but was rarely impacted on the lumped mass system.

Acknowledgement

This work was supported by the Basic Science Research Program through the National Research Fund of Korea (NRF) funded by the Ministry of Education (No. 2018R1A6A1A08025348).

REFERENCES

ASCE, 2016. 7-16, Minimum Design Loads for Buildings and Other Structures.

Broms B., 1964. Lateral resistance of piles in cohesive soils, J. Soil Mech. and Found. Division. 90 (2) 27-63.

 © DFI International Bruges 2025

Iai S., 1989. Similitude for shaking table tests on soil-structure-fluid model in 1g gravitational field, Soils and Found. 29 (1) 105-118.

Jeong S., Park J., Chang D., 2024. An approximate numerical analysis of rafts and piled-raft foundation, Com. Geotech. 168 106108.

KDS 17 00 00, 2018. Korea Design Standard, Seismic design code.

KDS 41 17 00, 2019. Korea Design Standard, Seismic building design code.

Kim D., Jeong S., 2019. Comparative study of load distribution ratio of various piled raft foundations based on coupled stiffness matrix, The Struct. Design Tall Special Build. 28 (16) 1669.

Kim H., Kim D., Lee Y., Kim H., 2020. Effect of soil box boundary conditions on dynamic behavior of model soil in 1g shaking table test, App. Sci. 10 (13) 4642.

Ko J., Cho J., Jeong S., 2017. Nonlinear 3D interactive analysis of superstructure and piled raft foundation, Eng. Struct. 143 (15) 204-218.

SEAOC, Blue Book – Seismic Design Recommendations Foundation Modelling, Structure Engineers Association of California, Sacramento, CA.

Song S., Jeong S., 2023. Dynamic analysis of a single pile embedded in SM soil using 1-g shaking table tests, Ocean Eng. 285 115416.

Song S., Jeong S., 2024. Analyses of pile-supported structures with base isolation systems by shaking table tests, Buildings 14 1382.

 © DFI International Bruges 2025

Modeling of vibrations induced by Mecca-Medinah high-speed train and earthquake mitigation analysis

Ahmed M. Taha, University of Prince Mugrin, Al Madinah Al-Munawarah, Saudi Arabia, ah.taha@upm.edu.sa , Tel:920000238
M. Hesham El Naggar, Western University, London, Ontario, Canada, naggar@uwo.ca, Tel: +1 519-661-3942
Ikrema A. Hassan, University of New Brunswick, Saint John, New Brunswick, Canada, ikrema.hassan@unb.ca +1 506-648-5751
Farid Rehimi, Taibah University, Al Madinah, Saudi Arabia, Rehimi_f@yahoo.fr, Tel: +966418618888
Abdulrahman Yussef, Taibah University, Al Madinah, Saudi Arabia, ayussef@taibahu.edu.sa,
Talal Merghelani, Taibah University, Al Madinah, Saudi Arabia, tmergh@taibahu.edu.sa,
Hany El Naggar, Dalhousie University, Nova Scotia, Canada, Hany.Elnaggar@dal.ca, Tel:+1 902-494-3904

ABSTRACT

In the past few years, a new network of high-speed rail (HSR) has been developed to connect the two holiest Muslim cities, Mecca and Medinah. The new HSR traffic induces vibration noise in its surrounding neighborhoods. This study investigates the ground vibration measurements collected at a farm located at the side of the Al-Haramain HSR track. In addition, a three-dimensional finite element model is developed using the program PLAXIS 3D to further elucidate the vibration characteristics and propose a vibration mitigation solution. The model involves a coupled track/soil system with moving axial loads, which simulates a vertical moving load with the same speed of the HSR. The comparison of the numerical and experimental results demonstrates that the numerical model can correctly predict the ground vibration produced by the high-speed train. To explore vibration mitigation schemes, the validated numerical model was used to examine the effectiveness of Tire Derived Aggregate (TDA) barrier in reducing the lateral rail vibration arising from potential earthquakes. The numerical results showed that TDA barrier can effectively reduce the lateral rail vibration.

Keywords: High-speed train, Vibration, Geofoam, Geophones, Modeling, TDA

1. Introduction

Al-Haramain High-Speed Rail Project connects the two holy cities Makkah and Madinah with an electrified passenger railway line, approximately 450 km in length with a commercial operating speed of 320km/h. The project provides safe and fast transportation between the holy cities utilizing a state-of-the-art proven technology. Al-Haramain High-Speed Rail is projected within the parameters of a European high-speed line. The high-speed rails (HSR) industry has seen continuously developing with innovative technologies. However, the high-speed train is still considered a major source of ground vibration noise in the communities located near the HSR lines [2]. Over the past decade, several studies investigated the train-induced ground vibrations and proposed different techniques for its mitigation [3].

2. Literature Review

Modern technological advancements have allowed trains to reach high speeds (over 300 km/hr), which has raised concerns about excessive displacements and track vibrations [4]. Ground vibration is an oscillatory motion, which can be expressed in terms of displacement, velocity, or acceleration [5]. The dynamic load induced due to the movement of a high-speed train on a rail generate vibrations that are transmitted from sleepers to ballast and sub-ballast, and ultimately to the ground [6, 7]. Some researches were conducted to study dynamic properties and behavior of railway tracks [8, 9], while other studies investigated the ballast deformation under cyclic loading [10, 11]. Field instrumentation

 © DFI International Bruges 2025

has been used to study and track substructure behaviour [12]. Sayeed and Shahin [13, 14] have developed an innovative method to design the foundation of ballasted railways to support HSR and heavy axle loads. Recent studies investigated HSR induced vibration using different approaches including field experiments, finite element analyses and modeling and centrifuge experiments. For instance, continuous sinusoidal vertical vibration (20, 40, 60, 80, 95, and 100 Hz) was generated using a mass vibrator operated by a portable power generator [15]. A continuous service system was used to record readings from geophones (0.5 m from each other).

The effect of HSR on different earthwork profiles including at-grade, embankment, cutting and overpass has been investigated [16]. The results showed that vertical vibrations are not always the most dominant and that horizontal vibrations should be considered. It is also found that the lowest vibration was recorded on embankment earthwork while the highest was reported on the cutting. Also, centrifuge tests have been conducted to study and mitigate the vibration induced by HSR [17]. The results showed that the surface waves guide the propagation pattern of ground vibration and double geofoam barrier is more efficient in mitigating vibration than single geofoam barrier. Behavior of ground vibrations induced by trains with rail roughness was investigated. The results showed that at high speed the vibrations are not different in the case of smooth or rough rails [18].

In a previous study, a three-dimensional finite element model was used to simulate multi-layered ground and radiation damping using viscous boundary conditions [19]. The results clearly showed an increase in track deflection with train speed. The material damping model allows a realistic prediction of the track vibration and train body dynamics at high speeds [19]. Feng et al. (2017) [20] developed a three-dimensional track-ground model to study vibrations induced by high-speed trains. The train loads are simplified as a series of moving point loads. Fourier transform is applied to solve the governing equations. The results indicated that the existence of groundwater significantly influences the surface displacement of the ground while the influence on velocity and acceleration is weaker at critical speeds [20]. Also, the loading speed greatly influences pore-water distribution while the influence of drainage conditions is relatively small.

Geofoam materials can be used for thermal insulation, lightweight fill in earthworks, compressible inclusions to reduce earth pressures, vibration and noise damping and drainage [21] [5]. Ground vibrations due to human activity can be reduced by employing geofoam barriers within the soil [21]. Previous experimental results showed that both open air and GeoFoam barriers can effectively reduce the transmitted waves [22]. The beneficial effects of a protective geofoam barrier could be enhanced by increasing barrier thickness only up to a certain limit, beyond which, further increase in thickness did not result in additional reductions [22]. Murillo et al. [23] conducted centrifuge tests to simulate the traffic vibration and to test the efficiency of EPS barriers in ground-borne vibrations. They also conducted a numerical study to investigate the EPS barriers effectiveness based on the dimensionless geometry of the barrier and its location from the source of disturbance. The results showed that the barrier effectiveness is mainly dependent on the barrier depth and its location from vibratory source. Furthermore, the barrier width had a minor influence in the case of deeper barriers and higher frequencies. However, the barrier width had a remarkable influence on the screening effectiveness of low frequency vibration for shallow barriers.

Alzawi and ElNaggar [24] conducted a full-scale field study to simulate the vibration induced by a machine on a foundation and to test the efficiency of various barriers with various geometries in mitigating ground-borne vibrations. They also developed a numerical model using ABAQUS to investigate the barriers effectiveness based on the achieved reduction in soil particle velocities through a parametric study by changing the exciting frequency and the location of the wave barriers. The results showed that the barrier effectiveness is mainly dependent on the normalized barrier depth and its proximity from the vibratory source. Furthermore, the results of the FE model were in good agreement with the experimental observations.

The vibration propagation due to high-speed trains close to vibration-sensitive structures poses a risk to their structural health, especially when the ground vibrations arriving at the structure are amplified

 © DFI International Bruges 2025

through the height of the structure at resonant frequencies [25]. The effect of the presence of alluvium deposit on top of the Basaltic rocks layers on the HSR induced vibration and wave barrier effectiveness has not been investigated in the available literature. Therefore, this paper investigates the ground-borne vibration due to the Al Haramian high-speed rail and evaluates the feasibility of using a vibration barrier to mitigate the induced Earthquake lateral vibrations.

3. Research Methodology

The study involved a field campaign of ground vibration measurements collected at a farm located at the side of the Al-Haramian high-speed trains, and the results were used to validate a three-dimensional finite element model developed using PLAXIS 3D. Multichannel analysis of surface waves (MASW) survey was conducted in the vibration monitoring area and the collected data was analyzed to establish dispersion curves of the generated surface waves, and to establish the shear wave velocity profile of the soil layering. The field campaign of ground vibration monitoring was conducted for several train passages employing an advanced vibration monitoring system comprising three-dimensional field vibration sensors. A numerical model was then developed using the commercial finite element software PLAXIS 3D, which was calibrated and validated utilizing the field measurements. Finally, the numerical model was used to investigate the wave barriers protective effectiveness.

4. Site Investigation and Material Properties

The tests were carried out at a farm area 8 km south of Al-Madinah city adjacent to the HSR line. A borehole investigation was carried out near the railway using a standard penetration test (SPT). The results indicated that the top 1.5 meters below the ground surface consisted of light brown silty clay sand with gravel. Basalt rock was encountered between 1.5 and 3 meters. From 3 to 4.5 meters, the soil was composed of a mixture of light brown materials, including silty sand with gravel, cobbles, basaltic tuff, and basalt rock boulders. This stratigraphy suggests a gradual transition from finer, clayey soils near the surface to coarser materials and rock at greater depths, reflecting varying depositional environments or past geological events. The ballast for the Haramain High-Speed Railway was constructed in accordance with standard EN13450 Aggregates for railway ballast [26]. The embankment soil was classified as AASHTO A-1-b. The soil layering was investigated using the multichannel analysis of surface waves (MASW) method to establish the shear wave velocity profile. In the MASW procedure, a series of 12 geophones placed at a 3 m interval are used to measure and record the seismic surface waves generated by a seismic source. The subgrade measurements were taken near the HSR track embankment while the sub-ballast measurements were taken on the HSR embankment. A series of field measurements of the train-induced vibration was carried out using triaxial 1 Hz seismometers very sensitive to three-dimensional field vibrations.

5. Numerical Model Geometry and meshing

A numerical model was established using the commercial finite element software PLAXIS 3D [27, 28]. Figure 1 shows AutoCAD drawings of the HSR rail embankment, sleepers and track system. Half of the track system was imported to Plaxis3D then a 3D model was generated by expanding the 2D drawing outline as shown in Figures 8a and 8b. The numerical model comprised ten-node tetrahedron elements to simulate the sleepers and soil volumes, and three-node beam elements to simulate the rails. As shown in Figure 1, the HSR embankment dimensions in the PLAXIS 3D model simulate the real constructed embankment. Also, Figure 1a shows that the depth of the embankment is 7.5 m underlain by a 6 m subgrade soil layer simulating the silt clay layer and part of the basaltic rock stratum. The depths of these layers were obtained from the boring log data. The model dimension in the Y axis direction was 70 meters to allow for the estimate of the attenuation behavior of the model surface wave. The model dimension in the X axis was 100 meters to capture the effect of the passage of seven train vehicles and to reduce the calculation time. The target element dimension was 3 meters minimum calculated by substituting the overall 3D model dimensions and a coarseness factor of 0.5 into the following equation:

 © DFI International Bruges 2025

$$l_e = r_e \times 0.05 \times \sqrt{(x_{max} - x_{min})^2 + (y_{max} - y_{min})^2 + (z_{max} - z_{min})^2} \quad [1]$$

The surface Rayleigh wavelength was 29 m estimated from the measured shear wave velocity of the subgrade soil of 501 m/s, using field geophysical exploration, with a model frequency of 20 Hz. The ratio of the element size to the wavelength is 0.13. This ratio is equal to the recommended ratio of 1/8 in finite element simulations. The movement of the train was modelled with a moving load of 88-92 kN with a speed of 50 m/s matching the speed of the train when it passes in front of the research site. During the dynamic analysis, general viscous boundary conditions were imposed around the soil volume to absorb the surface waves and body waves with the default relaxation coefficient C1=1 and C2 = 0.25 [27]. The fastening system which connects sleepers with the rails was modelled with a small vertical beam with dimensions equal to that of the elastomer plate of the fastening system. The vertical track stiffness of the fastening system was 80 kN/mm as per the manufacturer specifications.

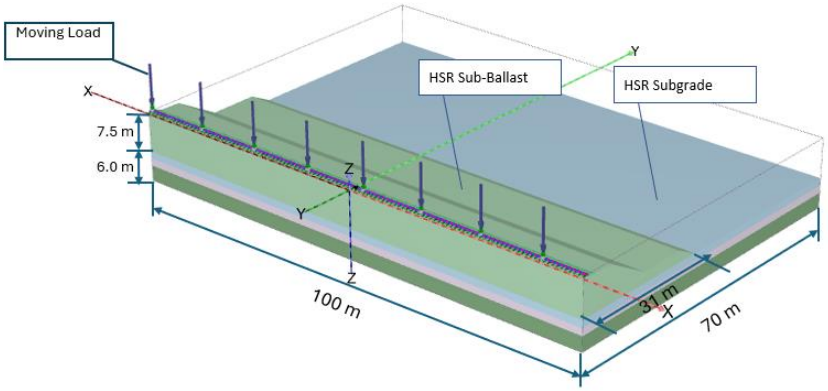


Fig 1a: The Geometry of the numerical model

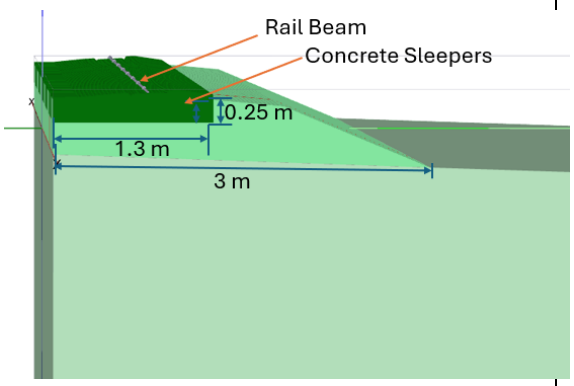


Fig 1b: The Geometry of the sleepers, track and ballast

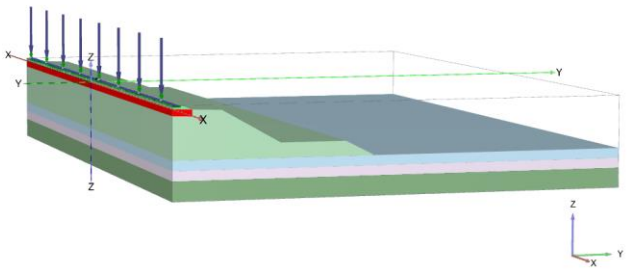


Fig 2: Geometry of the ground vibration barrier

6. Barrier model dimensions:

A model barrier was created to guide future vibration measurement when constructing the barrier in the field. A model barrier was embedded at one location. To investigate its effect on attenuating the lateral earthquake vibration on HSR rail, the barrier models simulate a strip or pad of 100 m long, 3 m wide and 1 m deep. Figure 2 shows the geometry of the barrier. The barrier material parameters were chosen to simulate a TDA barrier.

 © DFI International Bruges 2025

7. Adding the Earthquacke signal procedure:

The present research investigates the effect of a scaled earthquake signal on the HSR track system. The earthquake signal was recorded from an earthquake that hit Al-Ais town in AlMadinah region in year 2009. The acceleration time history of that earthquake was scaled to a stronger earthquake that occurred in Sanaa (southern Arabian Shield) in December 12, 1982 with (Ms = 6.1) [29]. The response spectra of Sanaa earthquake were used as the target spectrum to scale the earthquake signal of AlMadinah region with 5% damping using SiesmoMatch. A sine wave with a maximum velocity and a predominant frequency matching the scaled signal was generated. This sine wave was used to cause the lateral vibration in the Y direction by adding it to the displacement surface at the base of the Plaxis 3D model as shown in Figure 3.

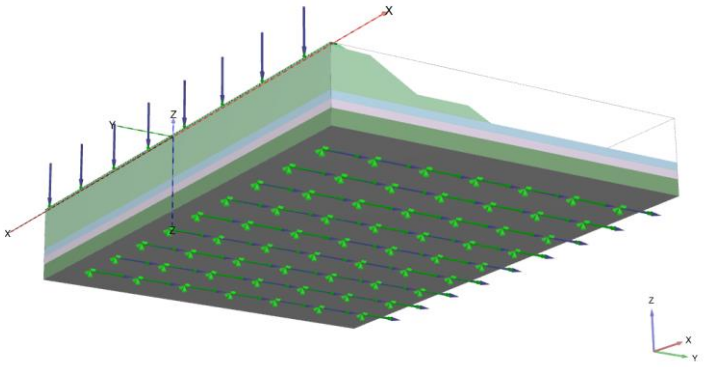


Fig 3: The ground displacement surface attached to the base of model soil layers.

8. Constitutive modeling of the ballast, sub-ballast and subgrade layers

The constitutive behavior of the ballast and TDA was modeled as linear elastic. The sub-ballast and subgrade soils constitutive behavior were modeled using the PLAXIS (HSSMALL) model. This model accounts for the stiffness degradation for different types of soils when subjected to primary deviatoric loading. Simultaneous irreversible plastic strains develop in soils during deviatoric loading causing the yield surface to change in size. In contrast to the elastic perfectly-plastic soil models, the yield surface of the HS model expands due to plastic straining and varies in the principle stress space. Also, the HS model captures the variation of the plastic axial strain with the deviatoric stress by using the theory of plasticity rather than the theory of elasticity and introducing a yield cap [28]. The HSSMALL model parameters in this research were calculated following the methodology adopted by Taha et.al (2015) [30]. The TDA material parameters were taken from the research work by Tandon et.al (2023) [31]. Table 2 shows the material model parameters.

The numerical calculations were executed in four phases: 1. the geostatic equilibrium, 2. construction of rails 3. the application of moving loads and earthquake signal without berries, 4. the application of the earthquake signal with moving loads with barrier.

Damping calculation procedure:

Soil damping ratio is one of the important parameters needed for precise modelling of the dynamic behavior of soil embankment. Ju and Ni (2007) [32] studied they least-squares method to evaluate the Rayleigh damping parameters for the finite element analysis of wave propagation in soils. Using both field experiments and finite element analysis, they found that the least square method is accurate and valid. In this research, the absorption coefficient a was determined using experimental measurements at two different vibration frequencies. The vibration signals were generated using a motor seated on the subgrade. The amplitudes of the induced ground vibration were recorded at 0.5 m and 4.5 m from

 © DFI International Bruges 2025

the motor. After recording two amplitudes 0.04 mm/s and 0.01 mm/s at two frequencies 44 Hz and 20 Hz, the absorption coefficient a was calculated for using the equation:

$$[k][\alpha] = [F]$$

Table 1: Material model parameters

	Rail	Elastomer Plate	Sleepers	Ballast	Sub-Ballast	Subgrade	TDA
Constitutive model	Linear Elastic	Linear Elastic	Concrete	Linear Elastic	HS small	HS small	Linear Elastic
(kN/m^3)	50.6	8E-3	24	17.6	19.5	20	6
(MPA)	210	7.55	25	100	-	-	16.25
	0.25	0.48	0.15	0.35	0.28	0.28	0.3
G (MPA)	-	-	-	37	-		-
^{ref} (MPA)	-	-	-	-	370	255	-
^{ref} (MPA)	-	-	-	-	296	204	-
^{ref} (MPA)	-	-	-	-	1109	764	-
$\gamma_{0.7}$	-	-	-	-	0.058E-3	0.026E-3	-
^{ref} (MPA)	-	-	-	-	4330	2984	-
Velocities	-	-	-				-
(m/s)	-	-	-	144	750	500	101
(m/s)	-	-	-	300	7400	1000	189
Damping	-	-	-				
Rayleigh α	-	-	-	124	19.9	19.9	0
Rayleigh β	-	-	-	2.5E-05	4.41	4.41	0

Accordingly, two damping ratios (D1 and D2) were calculated at the obtained absorption coefficients from the obtained absorption coefficients using the equation:

D = $\sqrt{\quad\quad +(—)}$

Finally, the coefficient was calculated at the damping at two different circular frequencies (ω1 and ω2) using the relation:

$2(D \qquad)/[\pi(\omega \qquad)]$

The damping ratio of the ballast was obtained from Brinji (2016) [33] who studied the mechanical behavior of a railway's ballast using both field experiments and laboratory testing.

9. Results and Discussion

In this study, the influence of the high-speed train on the level of ground was examined using numerical modeling. A coupled finite element model of the track, sleepers and subsoil is employed, adopting a formulation in the moving frame of reference following the high-speed train. Figure 4 compares the wave propagation pattern of the transmitted vibrations measured from the field and calculated from the numerical model. Figure 5 compares the Fourier amplitude and frequency content of the field transmitted vibrations and the calculated frequency content from the numerical model. The

 © DFI International Bruges 2025

general trend of the observed behavior is similar in both cases with respect to frequency content. However, the calculated amplitude falls on the conservative side and it is less than the measured amplitude by around 40%. In general, the model results follow the trend of experimental results, but with slightly higher values at some points and lower values at others [15]. This may be attributed to considering the horizontal homogeneous soil layers in the model, which may not be the case in the field. Previous studies reported discrepancy between field test and finite element model results and that the calculated amplitude falls within the conservative side.

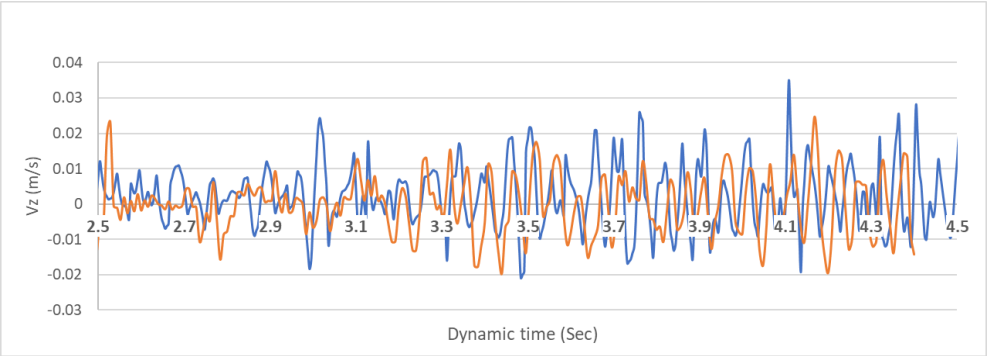


Fig 4: Calculated vs. Measured time history comparison

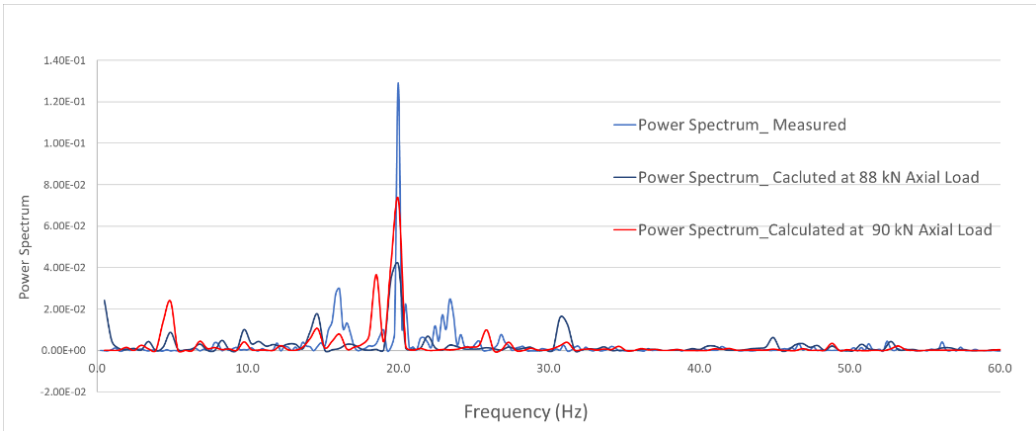


Fig 5: Frequency content comparison: Field vs. model

The calculated attenuation results of the surface wave along a line extending up to 60 meters from the HSR track demonstrate that the numerical model captures the attenuation behaviour of the surface wave as the wave travels farther away from the vibration source. Similar results were obtained by [24] where the recorded vibrations indicated increasing attenuation of the generated surface waves at locations farther from the source of vibration.

Figure 6 compares the model results for the time history of the proposed TDA barrier to isolate vibrations and the same model without isolation. It can be noticed that the FE model captured the amplification effect of the soil layering. Also, the FE model revealed that the TDA pad attenuated the vibration of the rail beam significantly compared to that without activating the TDA pad. In addition, The FE model results suggest that the rail beam vibrates with higher amplitudes and frequency compared to the surface soil layer and sub ballast. This can be owed to the fact that the rail beam is supported by the elastomer plate which adds to it fixability.

 © DFI International Bruges 2025

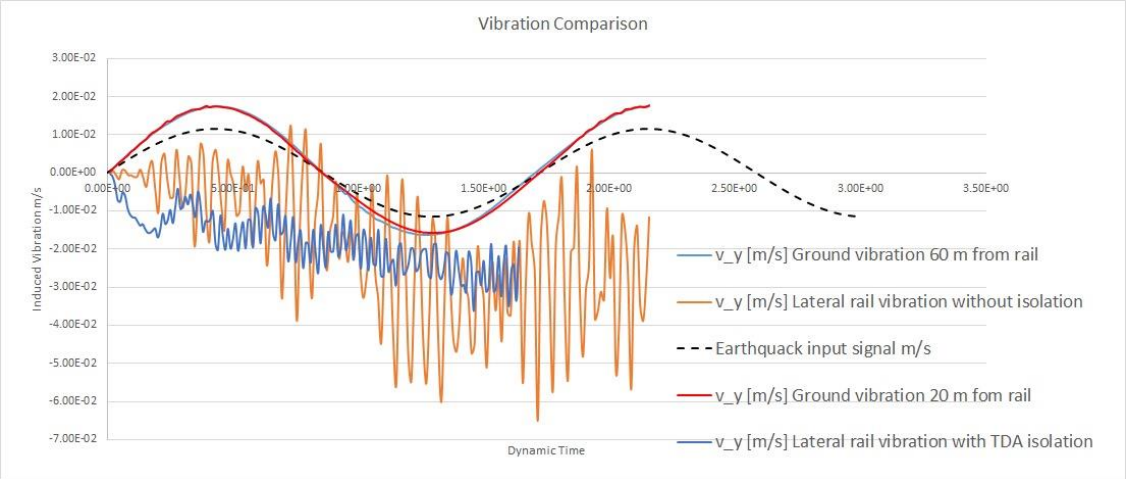


Fig 6: Comparison of the barrier effectiveness considering different barrier materials

10 . Conclusion

Field measurements were conducted to investigate the effect of vibration induced by a high-speed train (Al Haramain train) near Al Madinah Al Munawara, Saudi Arabia. Finite element analysis was used to develop a numerical model to simulate the train vibration. The calibrated model was used to further investigate the effect of adding TDA isolation under the HSR track system. A strong earthquake motion was induced a at the base of the FE model. The main findings can be summarized in the following points.

1. It was observed the FE model was successful in capturing the attenuation behavior in the induced vibration signal and the frequency of the measured vibration but with a lower amplitude. This observation was recorded in previous modelling work [31].
2. The numerical model shows that the FE model was successful in capturing the earthwork amplification effect due to the soil layering.
3. It can be noticed from the FE model that the proposed TDA barrier was effective in isolating the vibrations induced by the earthquake-scaled signal.

11. **Acknowledgements**

The authors also wish to acknowledge Taibah University for funding this research and The Saudi Arabian Railways for all the information and support given during the experimental tests.

References

1. Mahmoud, A.; Siegmann, J. Introducing High-Speed Rail System in Middle East (Kingdom of Saudi Arabia): A Comparison of Past, Current And Future Networks. *Glob. J. Eng. Sci. Res. Manag.* **2017**, *4*, 59–70, doi:10.5281/zenodo.832614.
2. A, H.W. Model Tests on Screening of Surface Waves. *Soil Mech. Found. Eng. 10th Int. Conf. 1981 Vol3* **1981**, 215–222.
3. Woods, R.D. Screening of Surface Wave in Soils. *J. Soil Mech. Found. Div.* **1968**, *94*, 951–979. doi:10.1130/0016-7606(1985)96<817:PMAOTA>2.0.CO;2.
4. Kece, E.; Reikalas, V.; DeBold, R.; Ho, C.L.; Robertson, I.; Forde, M.C. Evaluating Ground Vibrations Induced by High-Speed Trains. *Transp. Geotech.* **2019**, *20*, 100236, doi:10.1016/j.trgeo.2019.03.004.
5. Carl, E.H.; P.E., J.; David, T.; Carl E. Hanson, P.E., Jason C. Ross, P.E., and David A. Towers, P.E. High-Speed Ground Transportation Noise and Vibration Impact Assessment 2012.
6. Ferrara, R.; Leonardi, G.; Jourdan, F. A Contact-Area Model for Rail-Pads Connections in 2-D Simulations: Sensitivity Analysis of Train-Induced Vibrations. *Veh. Syst. Dyn.* **2013**, *51*, 1342–1362, doi:10.1080/00423114.2013.801996.
7. Giovanni, L.; Buonsanti, M. Reduction of Train-Induced Vibrations by Using Barriers. *Res. J. Appl. Sci. Eng. T.* **2014**, *17*, 3623–3632, doi:org/10.19026/rjaset.7.715.

 © DFI International Bruges 2025

8. Gao, Y.; Huang, H.; Ho, C.L.; Hyslip, J.P. High Speed Railway Track Dynamic Behavior near Critical Speed. *Soil Dyn. Earthq. Eng.* **2017**, *101*, 285–294, doi:10.1016/j.soildyn.2017.08.001.
9. Sayeed, Md.A.; Shahin, M.A. Design of Ballasted Railway Track Foundations Using Numerical Modelling. Part I: Development. *Can. Geotech. J.* **2018**, *55*, 353–368, doi:10.1139/cgj-2016-0633.
10. Ngo, N.T.; Indraratna, B.; Rujikiatkamjorn, C. Simulation Ballasted Track Behavior: Numerical Treatment and Field Application. *Int. J. Geomech.* **2017**, *17*, 04016130, doi:10.1061/(ASCE)GM.1943-5622.0000831.
11. Zhang, X.; Zhao, C.; Zhai, W. Importance of Load Frequency in Applying Cyclic Loads to Investigate Ballast Deformation under High-Speed Train Loads. *Soil Dyn. Earthq. Eng.* **2019**, *120*, 28–38, doi:10.1016/j.soildyn.2019.01.023.
12. Boler, H.; Mishra, D.; Hou, W.; Tutumluer, E. Understanding Track Substructure Behavior: Field Instrumentation Data Analysis and Development of Numerical Models. *Transp. Geotech.* **2018**, *17*, 109–121, doi:10.1016/j.trgeo.2018.10.001.
13. Sayeed, Md.A.; Shahin, M.A. Design of Ballasted Railway Track Foundations Using Numerical Modelling. Part I: Development. *Can. Geotech. J.* **2018**, *55*, 353–368, doi:10.1139/cgj-2016-0633.
14. Sayeed, Md.A.; Shahin, M.A. Design of Ballasted Railway Track Foundations Using Numerical Modelling. Part II: Applications. *Can. Geotech. J.* **2018**, *55*, 369–396, doi:10.1139/cgj-2016-0634.
15. Chew, J.H.; Leong, E.C. Field and Numerical Modelling of Sand-Rubber Mixtures Vibration Barrier. *Soil Dyn. Earthq. Eng.* **2019**, *125*, 105740, doi:10.1016/j.soildyn.2019.105740.
16. Connolly, D.P.; Kouroussis, G.; Woodward, P.K.; Alves Costa, P.; Verlinden, O.; Forde, M.C. Field Testing and Analysis of High Speed Rail Vibrations. *Soil Dyn. Earthq. Eng.* **2014**, *67*, 102–118, doi:10.1016/j.soildyn.2014.08.013.
17. Baziar, M.H.; Kazemi, M.; Shahnazari, H. Mitigation of Ground Vibrations Induced by High Speed Railways Using Double Geofoam Barriers: Centrifuge Modeling. *Geotext. Geomembr.* **2019**, *47*, 712–728, doi:10.1016/j.geotexmem.2019.103482.
18. Ju, S.H.; Liao, J.R.; Ye, Y.L. Behavior of Ground Vibrations Induced by Trains Moving on Embankments with Rail Roughness. *Soil Dyn. Earthq. Eng.* **2010**, *30*, 1237–1249, doi:10.1016/j.soildyn.2010.05.006.
19. El Kacimi, A.; Woodward, P.K.; Laghrouche, O.; Medero, G. Time Domain 3D Finite Element Modelling of Train-Induced Vibration at High Speed. *Spec. Issue UK Assoc. Comput. Mech. Eng.* **2013**, *118*, 66–73, doi:10.1016/j.compstruc.2012.07.011.
20. Feng, S.-J.; Li, Y.-C.; Chen, Z.-L.; Chen, H.X. Response of Railway Track Coupled with a Stratified Ground Consisting of Saturated Interlayer to High-Speed Moving Train Load. *Soil Dyn. Earthq. Eng.* **2017**, *102*, 25–40, doi:10.1016/j.soildyn.2017.08.018.
21. Zhang, Z.; Zhang, X.; Qiu, H.; Daddow, M. Dynamic Characteristics of Track-Ballast-Silty Clay with Irregular Vibration Levels Generated by High-Speed Train Based on DEM. *Constr. Build. Mater.* **2016**, *125*, 564–573, doi:10.1016/j.conbuildmat.2016.08.079.
22. De, A.; Morgante, A.N.; Zimmie, T.F. Numerical and Physical Modeling of Geofoam Barriers as Protection against Effects of Surface Blast on Underground Tunnels. *Geotext. Geomembr.* **2016**, *44*, 1–12, doi:10.1016/j.geotexmem.2015.06.008.
23. Murillo, C.; Thorel, L.; Caicedo, B. Ground Vibration Isolation with Geofoam Barriers: Centrifuge Modeling. *Geotext. Geomembr.* **2009**, *27*, 423–434, doi:10.1016/j.geotexmem.2009.03.006.
24. Alzawi, A.; Naggar, M.H.E. Full Scale Experimental Study on Vibration Scattering Using Open and In-Filled (GeoFoam) Wave Barriers. *Soil Dyn. Earthq. Eng.* **2011**, 3, 306–317, doi:10.1016/j.soildyn.2010.08.010.
25. Zhai, W.; Wei, K.; Song, X.; Shao, M. Experimental Investigation into Ground Vibrations Induced by Very High Speed Trains on a Non-Ballasted Track. *Soil Dyn. Earthq. Eng.* **2015**, *72*, 24–36, doi:10.1016/j.soildyn.2015.02.002.
26. Mahdavisefat E; Salehzadeh H; and Heshmati AA. Full-scale experimental study on screening effectiveness of SRM-filled trench barriers. *Geotechnique*. **2018**, 68: 1–14.
27. Brinkgreve RBJ; Kumarswamy S; Swolfs WM, et al. PLAXIS. Netherlands, 2014.

 © DFI International Bruges 2025

28. Brinkgreve RBJ and Vermeer PA. PLAXIS Finite Element Code for Soil and Rock Analysis-Version 7. Rotterdam: Balkema, 1997.41.
29. Al-Malki, M.A., Al-Amri, A.M. (2013). Seismic zones regionalization and hazard assessment of SW Arabian Shield and Southern Red Sea Region. In: Al Hosani, K., Roure, F., Ellison, R., Lokier, S. (eds) Lithosphere Dynamics and Sedimentary Basins: The Arabian Plate and Analogues. Frontiers in Earth Sciences. Springer, Berlin, Heidelberg.
30. Taha, A., El Naggar M., Turan A. (2015).Numerical modeling of the dynamic lateral behavior of geosynthetic-reinforced pile foundation system. Soil Dynamics and Earthquake Engineering, 77: 254- 266.
31. Tandon K; Kumar D; Ayothiraman R; Manna B and Ramana G. Numerical evaluation of tire chips–filled trench barriers for effective vibration isolation. *Journal of Low Frequency Noise, Vibration and Active Control*. **2023**, 42(1): 325–344.
32. Ju, S.-H.; Ni, S.-H. Determining Rayleigh Damping Parameters of Soils for Finite Element Analysis. Int. J. Numer. Anal. Methods Geomech. 2007, 31, 1239–1255.
33. Brinji, Osama Saud M. 2017 "Investigating the Mechanical Behaviour of Railway Ballast." PhD diss., Monash University.

 © DFI International Bruges 2025

METHOD FOR EVALUATING THE IN-PLANE SHEAR STRENGTH OF WALL-TYPE GROUND IMPROVEMENT WITH H-STEEL INSTALLATION

Takao Kono, Takenaka R&D Institute Takenaka Corporation, Inzai, Chiba, Japan, +81-476-47-1700, koono.takao@takenaka.co.jp
Yuki Kageyama, Kyusyu Branch Takenaka Corporation, Fukuoka, Fukuoka, Japan, +81-92-71-1121, kageyama.yuuki@takenaka.co.jp
Jun Hamada, Takenaka R&D Institute Takenaka Corporation, Inzai, Chiba, Japan, +81-476-47-1700, hamada.junji@takenaka.co.jp

ABSTRACT

Wall-type ground improvement techniques are widely used as a countermeasure against liquefaction. During earthquakes, shear forces are concentrated in the wall-type ground improvement, which helps control the shear forces generated in the surrounding soil. When excavation work is carried out in areas with implemented ground improvement to construct foundations or basements, the perimeter of the wall-type ground improvement can serve as a retaining wall and support earth pressure. This approach eliminates the need for additional retaining walls and potentially reduces environmental impact. H-shaped steel can be installed to reinforce wall-type ground improvement. The insertion of H-shaped steel provides reinforcement in the out-of-plane direction. However, the installation of H-shaped steel may decrease the shear resistance in the in-plane direction of the wall due to the low skin friction resistance between the H-steel surface and the ground improvement. As the H-steel section size increases, the liquefaction prevention effect may decrease due to the reduced area of the ground improvement. This paper presents the results of laboratory shear strength tests on wall-type ground improvement with installed H-shaped steel. In these tests, we investigated the effects of H-shaped steel installation, H-shaped steel size, and the roughness of H-shaped steel surfaces with steel bar reinforcement.

Keywords: ground improvement, shear strength, skin friction, earth retaining wall

INTRODUCTION

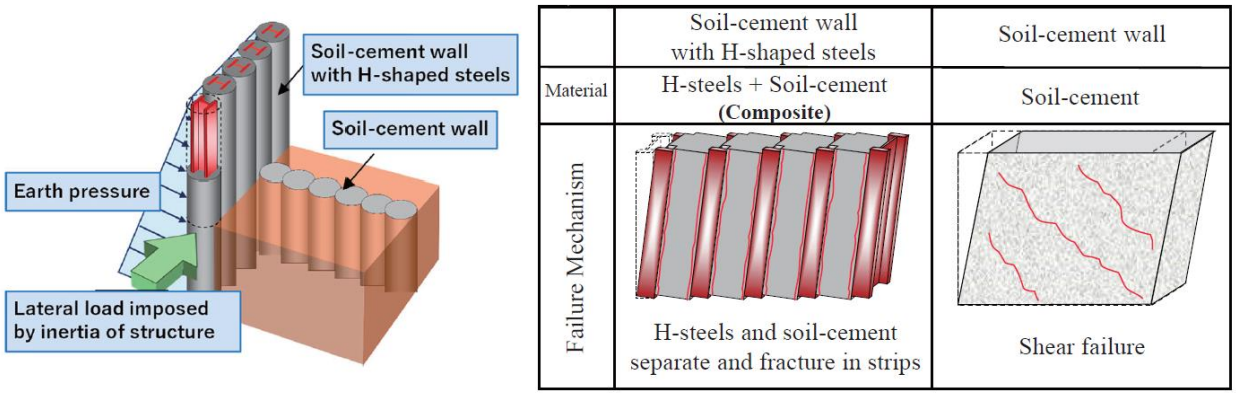
Cement-improvement methods such as the Cement Deep Mixing (CDM) method have been used since the 1970s. The CDM method has been used for various applications, such as retaining walls for excavations and creating embankment slopes. It has been used for preventing liquefaction by constructing grid-form ground improvements with wall-type elements arranged perpendicularly under large earthquake loads (Suzuki et al. (1996)) and is recently being used for piled raft foundations as building foundations (Yamashita et al. (2011)). The perimeter of the wall-type ground improvement can serve as a retaining wall that supports earth and water pressure (see Fig. 1(a)). This approach eliminates the need for additional retaining walls and potentially reduces both environmental impact and costs. H-shaped steel may be installed to reinforce wall-type ground improvement if it cannot independently bear the earth and water pressure.

The insertion of H-shaped steel provides reinforcement in the out-of-plane direction (perpendicular to the surface of the wall-type ground improvement). However, it does not provide reinforcement in the in-plane direction (parallel to the surface of the wall-type ground improvement). Moreover, when H-shaped steel is inserted into a wall-type ground improvement, researchers have observed that rather than overall shear failure of the ground improvement occurring, strip-like failure is possible due to the low adhesion resistance between the H-shaped steel and the ground improvement (Hamada et al. (2024), see Fig.1 (b)). There is a potential for decreased shear resistance in the in-plane direction of the wall-type ground improvement with inserted H-shaped steel.

Experiments on test specimens with soil cement filled between H-shaped steel members have been conducted to understand the in-plane horizontal force resistance of retaining walls. However, there is limited research on the shear strength when horizontal force is applied in the in-plane direction to H-shaped steel installed in ground improvement with relatively large areas. It has been reported through experiments and analysis that the in-plane shear strength of a wall-type ground improvement body with installed H-shaped steel is lower than that of a body without it (Hamada et al. 2022, Okumura et al. 2022). In this paper, H-shaped steel beams with enhanced adhesion were investigated to minimize the reduction in in-plane shear

 © DFI International Bruges 2025

strength of wall-type ground improvement caused by their installation. To enhance the bond strength between the H-beam and the improved ground, reinforcing bars were attached to the web of the H-beam. First, bond tests were conducted to determine the bond resistance between the reinforcing bars and the improved ground. Subsequently, structural shear strength experiments were performed using specimens with H-beams installed in the improved ground. In the experiments, the presence and size of H-beams, as well as the diameter and number of reinforcing bars, were varied to modify the bond strength. Based on the experimental results, we evaluated the in-plane shear strength of wall-type ground improvement with H-shaped steel installation, considering the bond resistance of the H-shaped steel beam web.



(a)Installation status of H-steel beams in wall-type ground improvement **(b) Schematic diagram of shear failure in soil cement**

Fig. 1. Schematic diagram of shear test apparatus for ground improvement (Hamada et al. 2024)

EXPERIMENTAL RESULTS OF ADHESION STRENGTH BETWEEN STEEL BAR AND SOIL CEMENT

To evaluate the structural experiment where reinforcing bars were attached to H-shaped steel to improve the adhesion strength between the H-steel and improved soil, the adhesion between the reinforcing steel bars and the improved soil was investigated. Fig. 2 shows the test specimen. In this test, a tensile test was conducted using a cylindrical improved soil specimen with a height of 10 d and a diameter of 15 d for the reinforcing bar diameter d. Fig. 2 shows the reinforcement arrangement of the test specimen. Half of the reinforcing bars embedded in the improved soil body were friction-cut using curing tape. The specimen was cured vertically and horizontally after fabrication, considering the effect of bleeding on the adhesion between the reinforcing steel and improved soil body. The conditions of the structural experiment conducted in this study are the same as those of the horizontal orientation. The test conditions are shown in Table 1. The vertical condition test was performed on D6, D10, D13, and D16, and the horizontal condition was performed on D13 and D16.

Table 1 and Fig. 3 show the test results and the relationship between reinforcing bar diameter and adhesion. In vertical curing condition, the adhesion remained constant regardless of the reinforcing bar diameter. Conversely, the adhesion strength was lower when in horizontal curing condition than when curing vertically. Furthermore, the larger the reinforcing bar diameter, the smaller the adhesion strength.

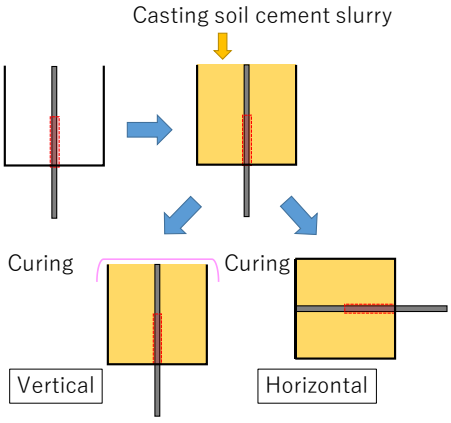


Fig. 2 Casting and curing conditions for adhesion test specimens

 © DFI International Bruges 2025

Table 1. Test conditions of adhesion test

Case	Size of bar	Direction of specimen during curing period	Hight [mm]	Diameter of test specimen of soil improvement [mm]	Area of circumference of bar [mm²]	Curing days during test [day]	Compression strength q_u [N/mm²]	Maximum loads [N]	Adhesive strength [N/mm²]
1	D6	V	60	100	600	15	4.72	1,128	1.88
2	D10	V	100	150	1,500			3,809	2.54
3	D13	V	130	200	2,600			6,391	2.46
4	D13	H	130	200	2,600			3,948	1.52
5	D16	V	160	250	4,000			9,959	2.49
6	D16	H	160	250	4,000			4,016	1.00

V: Vertical, H: Horizontal (see Fig.2)

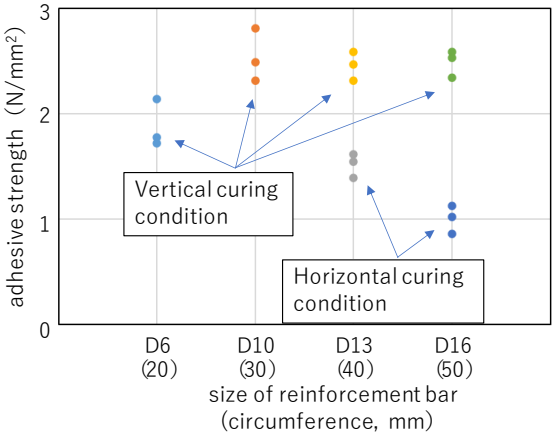


Fig. 3 Adhesion test results

STRUCTURAL EXPERIMENTS

Fig. 4 shows the arrangement of the test specimen and measuring equipment, as well as the experimental setup. As a representative example, the test specimen of Case 4 is shown. For the experiment, we used a beam-shaped ground improvement body with a length of 2,000 mm, width of 400 mm, height of 760 mm, and test section of 700 mm, applied a reverse symmetrical bending moment to the center of the specimen by loading at two points, and confirmed the shear strength using Ohno loading method (Arakawa et al. (1957)) , which generates a uniform shear force in the test section. The shear force acting on the test section in this test is 1/3 of the applied load. Fig. 5 shows the installation status of the H-steel for the test specimen. Tension reinforcing bars were installed at the upper and lower ends of the test section to prevent bending failure of the test section of the specimen. In addition, shear reinforcing bars were installed to prevent shear failure at load application locations and fulcrum locations other than the test section. Table 2 shows the experimental conditions, and Fig. 6 shows the specifications of the H-shaped steel.

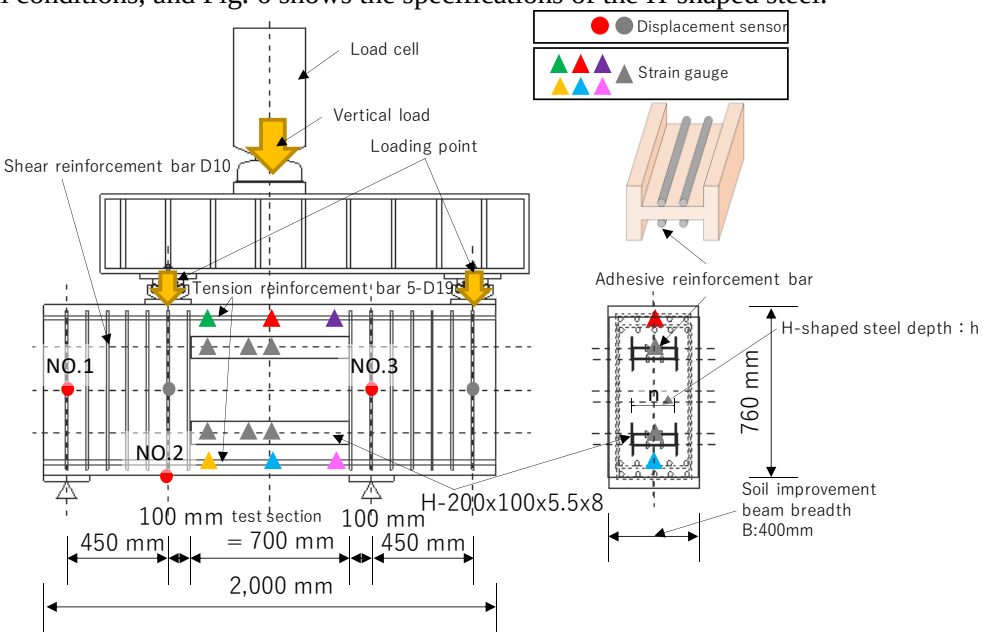


Fig. 4. Schematic diagram of shear test apparatus for soil improvement beam

 © DFI International Bruges 2025

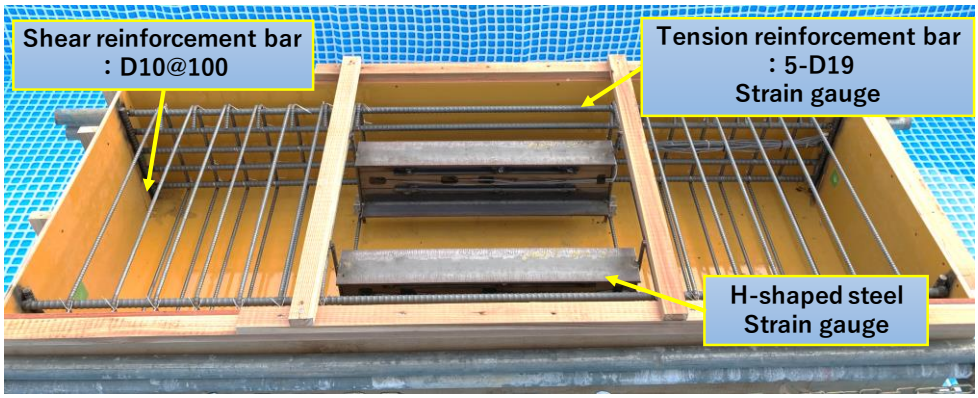


Fig. 5. Photo of Installation status of H-steel and reinforcing bars in test specimens prior to soil cement casting

Table 2. Test conditions of shear test

Case	Size of H-shaped steel	Ratio H-shaped steel depth to soil improvement beam breadth h/B	Adhesive reinforcement bar	Curing period during loading test
1	Non	0.00	Non	16
2	H-200x100x5.5x8	0.50	Non	21
3	H-200x100x5.5x8	0.50	D6 × 1	21
4	H-200x100x5.5x8	0.50	D6 × 2	23
5	H-200x100x5.5x8	0.50	D6 × 3	23
6	H-200x100x5.5x8	0.50	D10 × 2	18
7	H-200x100x5.5x8	0.50	D13 × 2	17
8	H-100x 50x5 x7	0.25	Non	16

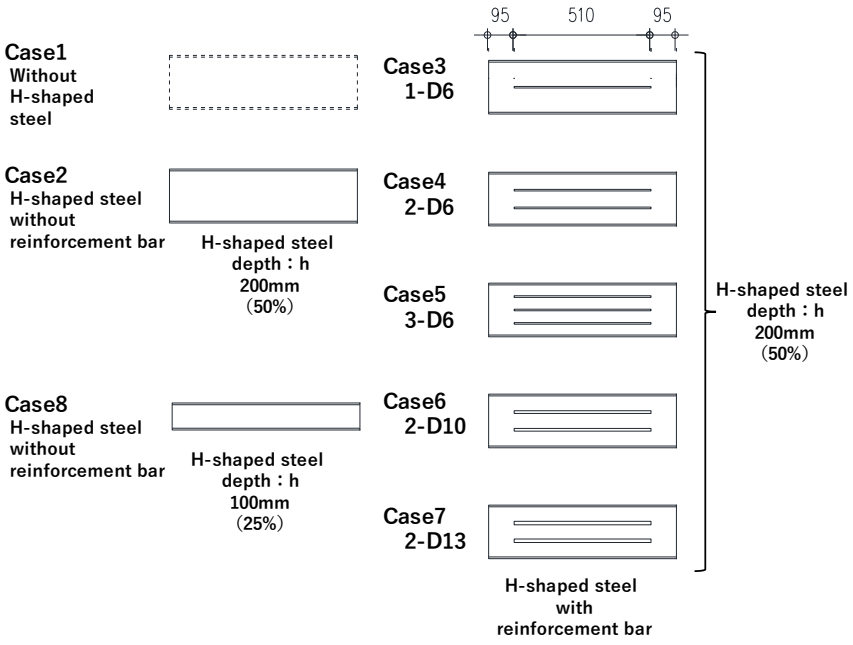


Fig. 6. Details of H-steel to be installed on the test specimens

The experiment involved three types of test specimens: one without H-shaped steel (Case 1), one with H-shaped steel inserted (Case 2), and multiple specimens with H-shaped steel and reinforcing bars for adhesion enhancement (Cases 3 to 7). Fig. 7 shows the installation of adhesion-reinforced reinforcing bars. The reinforcing bars were welded to both sides of the H-shaped steel web. In addition, to evaluate the influence of the H-shaped steel size on the ground improvement body, we conducted a test under conditions where the H-shaped steel had minimal influence (Case 8). In the test, the applied load, vertical displacement of the ground improvement body at both the loading and fulcrum positions, strain of the tension reinforcing bars installed to prevent bending failure, and strain of the H-shaped steel were measured.

 © DFI International Bruges 2025

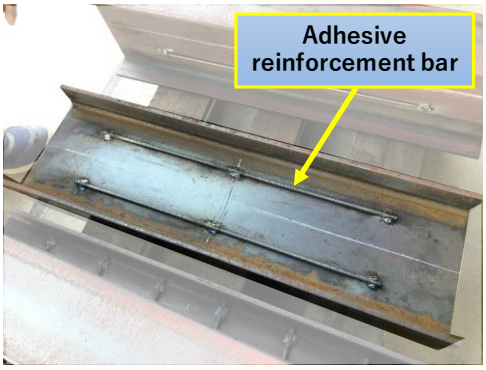


Fig. 7. Photo of details of adhesive reinforcement bar with H-shaped steel

Table 3 shows the estimated compressive strength of the specimens at the time of shear testing. The compressive strength was investigated using core samples taken from the specimens after completing all tests at 25 days of curing (see Table 3). On the other hand, the shear tests were conducted when the specimens were 16 to 23 days old. Therefore, the compressive strength was estimated using Equations 1 and 2, based on the compressive test results (see Table 4 and Fig. 8). The coefficients A and B in Equation 1 were determined to be A = 5.99 and B = -10.7 from the test results of the specimens used for compressive testing.

Table 3. Estimated compressive strength of the specimen for shear test

	Curing period during shear test (day)	Compressive strength of cored sample extract from shear test specimen at curing period of 25 days (N/mm2)	Correction coefficient by equation (1), (2)	Estimated compressive strength of shear test specimen at the date of shear test (N/mm2)
Case1	16	7.52	0.71	5.34
Case2	21	7.56	0.89	6.81
Case3	21	6.07	0.89	5.40
Case4	23	7.31	0.95	6.93
Case5	23	7.29	0.95	6.91
Case6	18	6.93	0.78	5.43
Case7	17	7.41	0.75	5.54
Case8	16	7.13	0.71	5.06

Table 4. Compressive strength of the specimen for compressive test

Curing period(day)	1	4	15	17	21	23
Compressive strength (N/mm2)	0.53	1.73	4.72	5.67	5.65	6.69

$$q_{est} = Alog(MM) + B \quad [1]$$

$$MM = \sum \theta T + 10 \quad [2]$$

Where q_{est} = estimated compressive strength at the date of shear test (N/mm2), A,B = constant calculated from compressive strength of the specimen for compressive test, MM = maturity (℃ day), θ =curing temperature (℃), curing time (day).

 © DFI International Bruges 2025

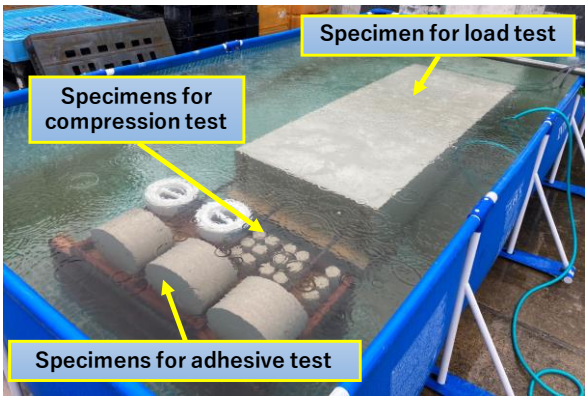
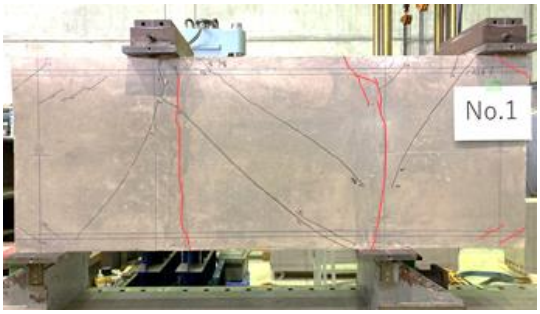
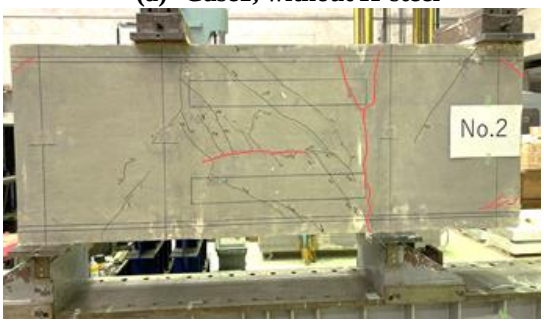


Fig. 8 Photo of curing condition of test specimen

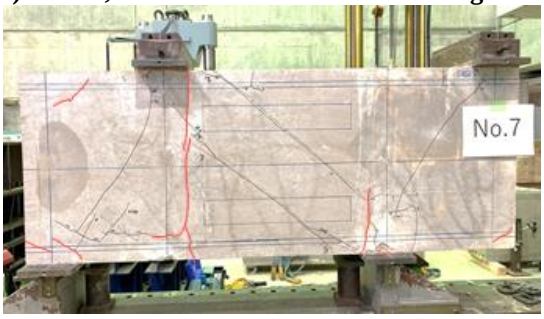
Fig. 9 shows the final failure state from the structural experiment under three test conditions: without H-steel (Case 1), with H-shaped steel without reinforcing steel bar (Case 2), and with H-shaped steel with reinforcing steel bar (Case 7). Cracks that occurred during the loading test are shown in black, and those that occurred before the loading test are shown in red. In Case 1, where H-shaped steel was not installed, cracks occurred in the test section area. In contrast, in Case 2, where H-shaped steel without reinforcing bars was installed, cracks were concentrated in the areas between the H-shaped steel sections, differing from the crack pattern observed in Case 1 without H-shaped steel. In Case 7, where H-shaped steel with reinforcing bars was installed, the crack occurrence pattern was almost the same as in Case 1. Although inserting H-shaped steel into the ground improvement body alters the failure mode, increasing the surface bond resistance of the H-shaped steel can potentially result in behavior similar to that observed in the case without H-shaped steel installation.



(a) Case1, without H-steel



(b) Case2, with H-steel without reinforcing steel bar



(c) Case7, with H-steel with reinforcing steel bar

Fig. 9 Photo of the condition of after test

 © DFI International Bruges 2025

Fig. 10 shows the relationship between the strain of the bending failure prevention steel bar and the shear strain of the specimen. The strain of the bending failure prevention steel bar was measured by strain gauge, and the shear strain of the specimen was determined by calculating the rotation angle of the test piece from the vertical displacement of measurement points No. 1 and No. 3 in Fig. 4, finding the incremental displacement at measurement point No. 2, and subtracting it from the vertical displacement at point No. 2, and dividing by the test section length of 700 mm. Fig. 10(a) shows Case 1 (without H-steel), Fig. 10(b) shows Case 2 (with H-steel, no reinforcement), and Fig. 10(c) shows Case 7 (with H-steel, 2 D13 reinforcing bars attached). The triangular mark (▼) in Fig. 10 is the point at which the compressive strain of the compression side reinforcing bars switches to decrease, which indicates the elastic limit of the test section. In this study, the shear stress ratio at this time is considered as the shear strength of the test specimen.

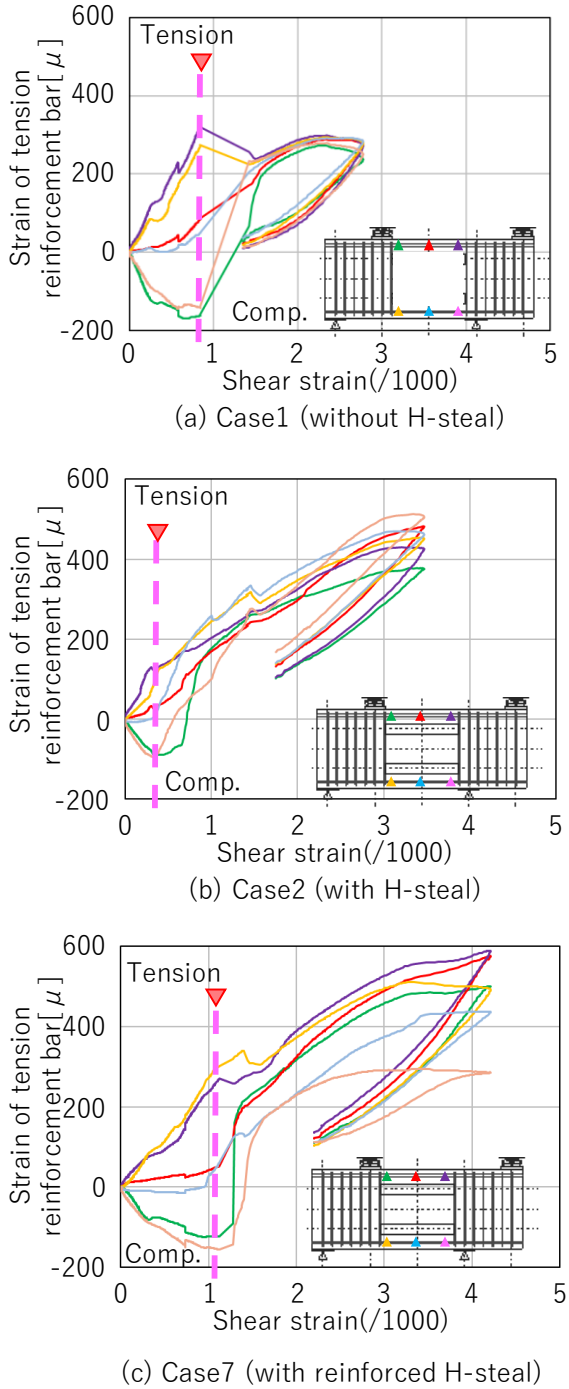
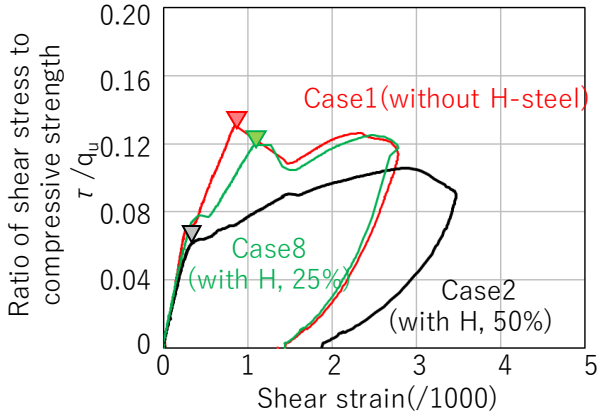


Fig. 10 The relationship between the strain of bending failure prevention steel bar and the strain of specimen during shear test

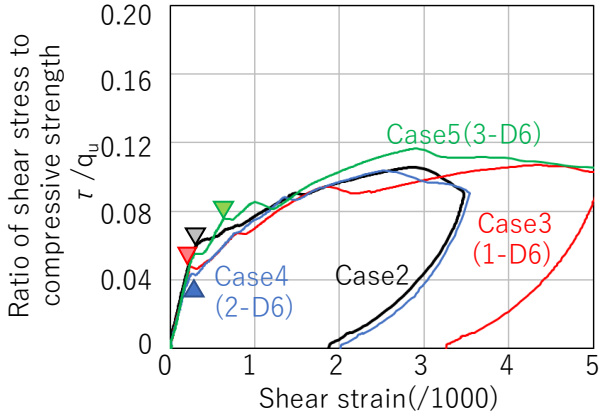
Fig. 11 shows the relationship between the shear stress ratio and shear strain of the test specimen. The shear stress ratio was obtained by dividing the shear force of each case by the cross-sectional area and normalizing it by the estimated compressive strength q at the time of the test (see Table 3). Fig. 11 (a) compares the case

 © DFI International Bruges 2025

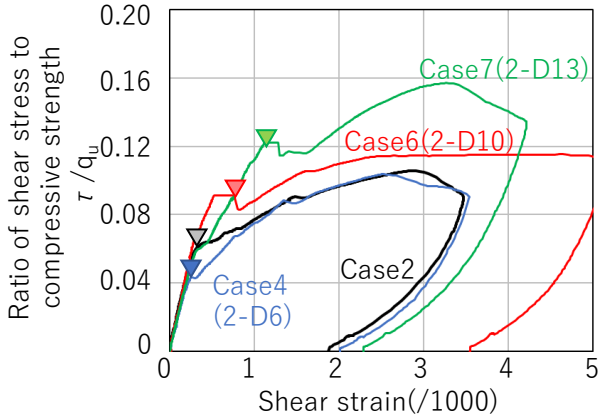
where only the ground improvement body is inserted and H-shaped steel is inserted, and Fig. 11(b) and (c) compare the number and diameter of reinforcing bars used for adhesion reinforcement, respectively. From Fig. 11(a), when H-steel with h/B=0.50 is installed (Case 2), the deformation becomes large when the shear strain is approximately 0.4×10^{-3} rad, and the shear strength is 0.5 times that of Case 1. From Fig. 11(a) and (b), the reinforcing steel strain at the elastic limit in Case 2 was approximately 0.5 times that of Case 1, similar to the shear strength. In addition, as shown in Fig.11 (b), when the adhesion-reinforcing steel was D6, the shear strength was almost the same as Case 2, and approximately 0.5 to 0.7 times that of Case 1. Conversely, as shown in Fig. 11(c), the shear strength when two D13 specimens were installed (Case 7) was comparable to that without H-steel (Case 1). From Fig. 11(a) and (c), both the reinforcing steel strain at the elastic limit and the shear strength in Case 7 were comparable to those in Case 1.



(a) Comparison of the presence and depth of H-steel Beams



(b) Comparison of the number of reinforcing bars



(c) Comparison of reinforcing bar diameters

Fig. 11 Stress-strain relationship of specimen during shear test

Table 4 shows the shear force, the ratio of shear strength to estimated compressive strength, and the ratio of shear strength to Case 1 at the elastic limit. The shear strength in the case of inserting an H-shaped steel without reinforcing bars (Case 2) decreased to approximately half the strength of the case without H-shaped steel insertion (Case 1). This confirms that inserting an H-steel into the ground improvement reduces the in-

 © DFI International Bruges 2025

plane shear strength. In this test, for Case 2, the width of the specimen (B = 400 mm) was about twice the beam depth of the H-steel (h = 200 mm), and the ratio of shear strength reduction was almost the same as the ratio of the specimen width to the H-shaped steel depth. However, in the case of inserting an H-shaped steel with surface reinforcement (Case 7), the shear strength was nearly equivalent to that of the case without H-shaped steel insertion (Case 1). Increasing the reinforcing steel bar of the H-shaped steel web surface prevented strength reduction even when an H-shaped steel was inserted.

Table 4. Shear strength of shear test

	Shear force at the elastic limit Q (kN)	Estimated compressive strength of shear test specimen at the date of shear test q_{est} (Table 3) (N/mm2)	Ratio of shear strength to estimated compressive strength Q/Bhq_{esr}	Ratio of shear strength to Case1
Case1	197	5.34	0.13	1.00
Case2	116	6.81	0.06	0.48
Case3	93	5.40	0.05	0.36
Case4	87	6.93	0.04	0.33
Case5	154	6.91	0.08	0.58
Case6	150	5.43	0.09	0.70
Case7	186	5.54	0.12	0.93
Case8	177	5.06	0.12	0.91

DISCUSSION

Fig. 11 shows the relationship between the ratio of shear strength in the case with H-shaped steel compared to the case without H-shaped steel (Case 1) and the ratio of the shear strength h of the H-shaped steel to the width B of the specimen. In the case where the H-steel occupies 25% of the specimen width B (Case 8) and the case where the H-shaped steel occupies 50% of the specimen width B (Case 2), the shear strength decreases according to the ratio of the width h of the H-shaped steel to the width B of the specimen. This is considered to be because the adhesion between the H-shaped steel and improved soil was smaller than the shear strength, and the adhesion was broken before the shear strength of the improved soil was fully mobilized. Conversely, it has been confirmed that installing adhesion-enhanced reinforcing bars onto the H-shaped steel can prevent a decrease in shear strength.

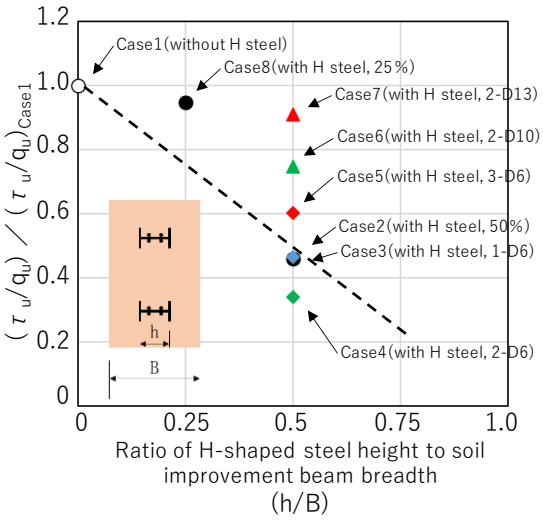


Fig. 11 Reduction ratio of shear strength due to the ratio of H-steel height to specimen width

Figure 12 shows the relationship between shear strength and the normalized perimeter of bond reinforcing bars, comparing cases with and without H-shaped steel. As the perimeter of bond reinforcing bars increases, the reduction in shear strength can be more effectively suppressed. Comparing the bond strength of D13 bond reinforcing bars, the calculated bond strength from the shear test comparison between the case with

 © DFI International Bruges 2025

unreinforced H-shaped steel (Case 2) and the case using two D13 bond reinforcing bars (Case 7) is approximately 1.7 N/mm², which is almost the same as the bond test result of 1.5 N/mm² for horizontal curing condition (see Fig. 3). Furthermore, under these test conditions, it was confirmed that the in-plane shear resistance did not decrease when H-shaped steel was inserted into the ground improvement. This was achieved by installing reinforcing bars on the H-shaped steel web, with a perimeter of approximately 40% of the beam depth (h) of the inserted H-shaped steel.

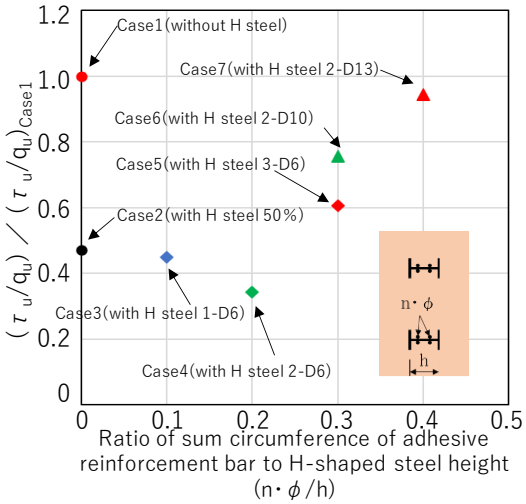


Fig. 12 Effect of rebar reinforcement on H-Steel in enhancing shear strength

SUMMARY

In this study, structural experiments and adhesion tests were conducted to confirm the shear strength of a wall-type ground improvement structure with embedded H-shaped steel. It was found that the shear strength of wall-type ground improvement bodies decreased with the insertion of H-shaped steel. In addition, through the addition of reinforcing bars to the H-shaped steel, it was possible to strengthen the adhesion and suppress the decline in shear strength at the elastic limit. Furthermore, the effect of reinforcing adhesion obtained in the results of this structural experiment may have been reduced due to the influence of bleeding because the direction of curing during specimen preparation differed from field conditions.

REFERENCES

Suguru Arakawa and Kazuo Ohono, 1957. Shear Resistance of Reinforced Concrete Beams: Evaluation Using Novel Loading Techniques, Transactions of the Architectural Institute of Japan, No. 57, 581-584. (in Japanese)

Junji Hamada, Yuji Taya, Takao Kono, Tomio Tsuchiya, Tetus Usami and Hiromitsu Iwasa, 2024. Cyclic Lateral Loading Tests on Soil-Cement Mixing Wall with H-Shaped Steels, Journal of the Society of Material Science, Vol. 73, No.1, 33-38 (in Japanese)

Jyunji Hamada, Yuji Taya, Takao Kono and Hiromitsu Iwasa, 2022. Cyclic lateral loading tests on soil-cement mixing longitudinal wall with H-section steel, Proc. of 57the Japan National conf. on SMFE, 22-6-2-02 (in Japanese).

Yugo Okumura, Hiromasa Sigeno, Takao Kono, Jyunji Hamada and Masamiche Aoki, 2022. experiment and numerical analysis on shear strength of Ground Improvement Wall with H-section Steel, Proc. of 57the Japan National conf. on SMFE, 22-6-2-03 (in Japanese).

Kichio Suzuki, Satoshi Saito, Sadatomo Onimaru, Gen Kimura, Akihiko Uchida and Ryousuke Okumura, 1996. Grid-shaped Stabilized Ground Improved by Deep Cement Mixing Method against Liquefaction for a Building Foundation, Tuti-to-kiso, Vol.43, No.3, 46-48. (in Japanese)

Kiyoshi Yamashita, Junji Hamada and Takeshi Yamada, 2011. Field Measurements on Piled Rafts with Grid-Form Deep Mixing Walls on Soft Ground, Geotechnical Engineering Journal of the SEAGS & AGSSEA, Vol.42, No.2, 1-10

 © DFI International Bruges 2025

SELF-HARDENING SLURRY FILTRATION TEST AND THE END OF THE API TEST DEAD END

Gilbert R. Tallard 434 989 2182, Mclean, VA USA, gtallard@liquidearthsupport.com
Gregory E. Thomas 973 997 5970, Wayne, NJ USA, thomascabin1955@gmail.com

ABSTRACT

Filtrate loss during construction of a slurry wall occurs by a separation of the suspended solids and make-up water under hydrostatic pressure where the permeable ground in the walls acts as a filter, leaving a filter cake behind. For traditional bentonite slurries, this is studied using the API filter press test (API R 13B-1, 2003). For Self-Hardening Slurry (SHS) no simple method is available to either estimate the extent of this loss, the magnitude of the cake, or to assist in the design of the most appropriate mix. This study presents initial results for the development of a modified filter press test for this purpose that eliminates many of the limitations inherent in the API test. The revised test operates at pressures corresponding to realistic hydrostatic heads and duration representative of prior to the setting of the slurry when filtration occurs. Example results are presented for a variety of SHS formulations that indicate both the magnitude of the cakes and of the slurry loss, its variability, and its importance for the wall properties. A discussion on the role of SHS filter cakes in SHS cutoff wall design is provided as well as comments and outlook on future directions of research.

Keywords: Self-Hardening Slurry (SHS), API Filter test, filtration, filter cake, hydrostatic head, suspended solids, slurry density, water content, trenching equipment.

INTRODUCTION

The API filtration test is rarely used in the case of self-hardening trenching slurries (SHS), in contrast to the design of bentonite trenching slurries where the use of the test is common practice for design and QC. Nevertheless, filter cakes resulting from loss of the SHS make-up water through the side walls of the SHS trench do form, are many times thicker than those of a pure bentonite slurry, and are important both for the construction and performance of the wall.

When it came to migrating Design and QC programs developed for pure bentonite slurry trenching to trenching under self-hardening slurry, the use of the American Petroleum Institute (API) filtration test hit a wall: the standard test criterion of running for 30 minutes at a pressure of 100-psi (690-kPa) caused most self-hardening slurries to lose the entire make-up water and allow the pressurizing gas to escape. Not seeing any value in it, the test was not pursued for either design or QC purposes for use for SHS.

The principal limitation of the test apparatus is the height of the API standard cell, typically ~ 3.7-inch (9.3-cm) with a capacity of ~425-ml, while the short duration of the test is not representative of the filtration duration in SHS construction. Attempting to address this gap in design, the authors have considered the limitations and inadequacies of the standard API filtration test and what needed to be modified to develop a valuable testing apparatus leading to a protocol measuring realistic filter cake accumulations. This effort is in line with a general goal to simulate laboratory testing conditions to those occurring in the field with the goal of improving the design of self-hardening slurry cutoff walls (Tallard and Ruffing 2023).

METHODOLOGY

For Tremie concrete quality, the water loss due to bleed and filtration stiffens the mix and changes the rheological properties to higher yield stress and higher viscosity. To study this, a concrete filter press was developed by BAUER as a modification of the standard API apparatus and its use is described in the EFFC/DFI Tremie Concrete Guide (2018). To address many of the same problems seen in

 © DFI International Bruges 2025

filtration tests on SHS, this procedure used a longer cell and a lower test pressure than the API test. Figure 1 shows examples of the BAUER and API test apparatuses.
The BAUER system uses a reservoir cylinder ~12 inches (300-mm) in length. A practical minimum width of a SHS trench is 24-inches (610-mm), so a filter press having a cell 12-inch tall (305-mm) could theoretically represent the half width of this cutoff wall and provide a picture of the complete cutoff wall cross section by mirror image. Its use as a self-hardening slurry filtrate loss apparatus was immediately possible and practical and selected as a base for this study.

Neither the 30-minute API test or the 5-minute BAUER test was representative of the filtration times for SHS, which have by necessity a long workable fluid lifetime. An arbitrary 8 hours test duration was adopted for this program to correspond to a normal workday or shift. Due to the large filtrations found, a partial SHS fluid addition was still required to maintain the sample height over the 8-hour duration and to mimic the long-term filtration exhibited by the SHS mixes.



Fig. 1. BAUER modified filter press and Standard API filter press.

The pressure causing filtration is the hydrostatic head differential between the slurry level and the ground water table; this may correspond to a practical minimum of 1.3-psi (9-kPa), corresponding to the 3-feet (0.9-m) head used to maintain the wall stability, to 65-psi (448-kPa) corresponding to 150-feet head (46-m), an approximate construction maximum such as in the case of a flood control levee. While project test pressures should be selected to match the project, for this exercise we selected 20-psi (138-kPa) as a representative value, which corresponds to about a 46-feet (14-m) differential, for use as a standard testing pressure.

The approach used here to quantify the SHS cake magnitude and its density variation (concentration of ingredients) was to substitute the 12-inch (~300-mm) stainless-steel cylinder with a disposable PVC pipe section of similar dimensions, as shown in Fig. 2. Individual pipe sections were used for filtering a specific SHS formulation for 8-hours including refills to maintain the cell as full as possible. Each section was then capped and cured submerged for 30 days.

 © DFI International Bruges 2025

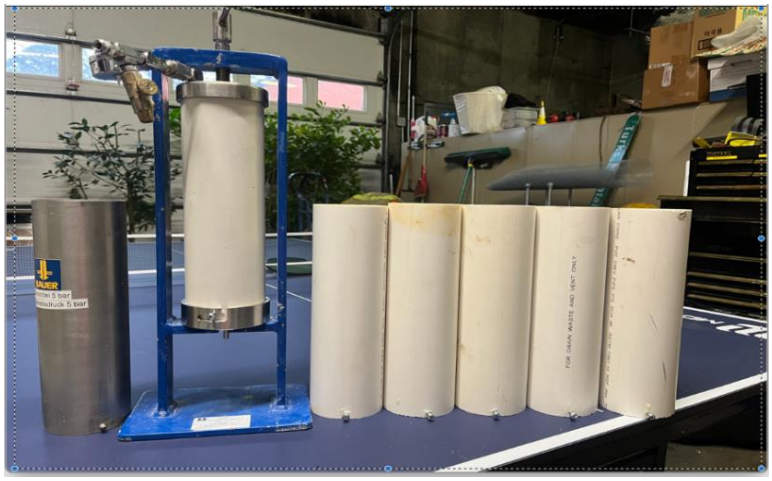


Fig. 2. Filtration test sample cylinders for cake measurement set up with modified BAUER apparatus.

At that point, as shown in Fig. 3, each section was sawed in approximately one-inch slices (25 mm), with each slice weighed, the height measured, and density calculated.



Fig 3. Ten 1-inch slices over 12 inches sample for density testing

MIXES

The following base mixes were studied to reflect the most common SHS mixes used in public and private works, while using full advantage of the benefits of Ground Blast Furnace Slag (GBFS) cement. All mix ingredient quantities are based on use of a 4% bentonite slurry, where only the binder varies:

MIX A: 80% slag, 20% OPC blend, 15% binder by weight of water (b.w.o.w.);
MIX B: 95% slag, 5% OPC blend, 15% binder b.w.o.w.;
MIX C: 100% slag + .5% NaOH (activator), 15% binder b.w.o.w.

Materials Used

Bentonite: CETCO, API 13B, fully hydrated overnight;
Slag: Class 120 Slag cement from Heidelberg Materials, Cape Canaveral FL;

 © DFI International Bruges 2025

OPC: Ordinary Type I/II Portland Cement.
Note: an activator is required to reduce the setting time for the slag. OPC serves this purpose when present but for Mix C, without OPC, a separate activator (NaOH) was needed.
Mix C has not been commonly used, mostly due to the fact that SHS filter cake formation measurement has been unavailable up to now for designs despite the fact it has always been known in deep foundations that OPC contamination significantly increases the filtration of bentonite slurries.

To compare the results on an even plane, no dispersant or retarder was added to the mixes. To make the mixes, an 80/20 split of make-up water between bentonite slurry and binder grout was used to assist in the laboratory mixing process (Harris 2016), but small amounts of Aquafix, a fluidizer, was also added as necessary to make a workable mix when adding suspended solids (mixes A', B' and C').

Since it is well known that fine solids from the excavated soil will become suspended in the SHS during construction, and eventually the gel strength development is sufficient to hold the particles in place, it was realistic to also study added soil particles to the mixes to assess their influence on the cake build-up during filtration. Suspended solids can easily vary from 10 to 25% by bulk volume, which may represent at an average bulk density of 1.76-Mg/m^3 (110-pcf), yielding a 50% to 100 % increase by weight of added load to the mix water (not corrected for possible ground water dilution). For this study a compromise of 15% by volume, (25.5% suspended solids by weight of water) of a silty sand, Virginia loam {SM}) was used for the otherwise corresponding set of mixes, A', B' and C'.

TESTS RESULTS

The results of the tests performed are presented in Figures 4 through 6.
Fig. 4 shows that even at the realistic head pressures used, the SHS filtrate loss for normal mixes such as A and B is on the same order of magnitude as the complete volume (~425 ml) of the standard API filtration apparatus, showing why this system does not work for these materials and has been ignored. This data also shows the importance of having a system capable of estimating this volume, which was on the order of 30% of the initial slurry volume for these tests. This lost volume must be compensated by additional slurry to maintain the hydrostatic head. The increased slurry ingredient concentrations from the loss of water affects the resulting cutoff wall material characteristics and hence must be considered.

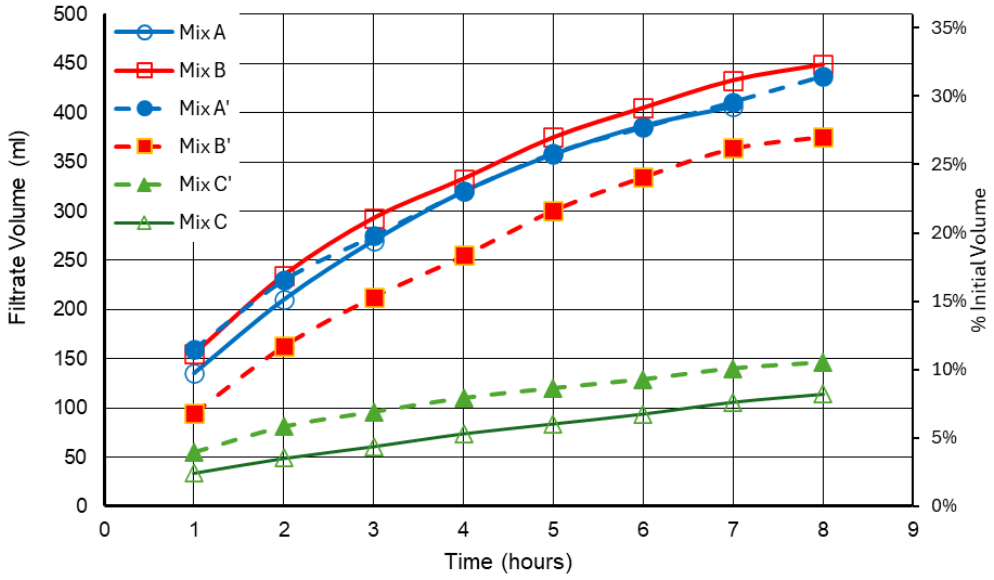


Fig. 4. Filtration curves for the two series of tests under the described conditions

Cutting the samples into 1-inch slices, with some loss due to the cut for each, resulted in up to 10 data points over the 12-inch (300-mm) sample height.

 © DFI International Bruges 2025

The increased solids concentrations due to filtration are not limited to just the cake formed at the ground interface area but also involves the concentration in nearly the entire cross-section of the wall. From the results shown in in Fig. 5, the total cake extended through slices 1 to 7 (covering approximately 7-inches (178-mm)) while a high-density cake was formed primarily in the first 2-3 inches (50-75 mm) from the base interface. The upper portion of the sample had to contend with refills during the test to maintain the original sample volume which distorted this data, and higher densities measured at slices 9 and 10 are not understood at this point.

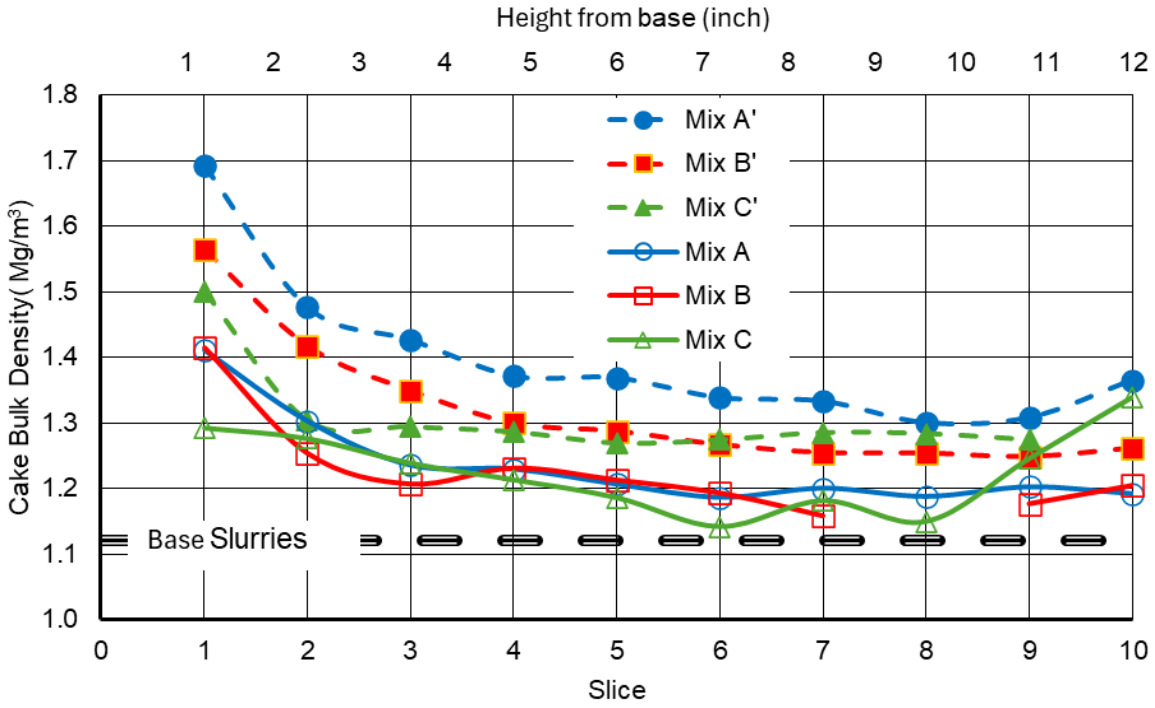


Fig. 5. Profiling of filter cakes per density.

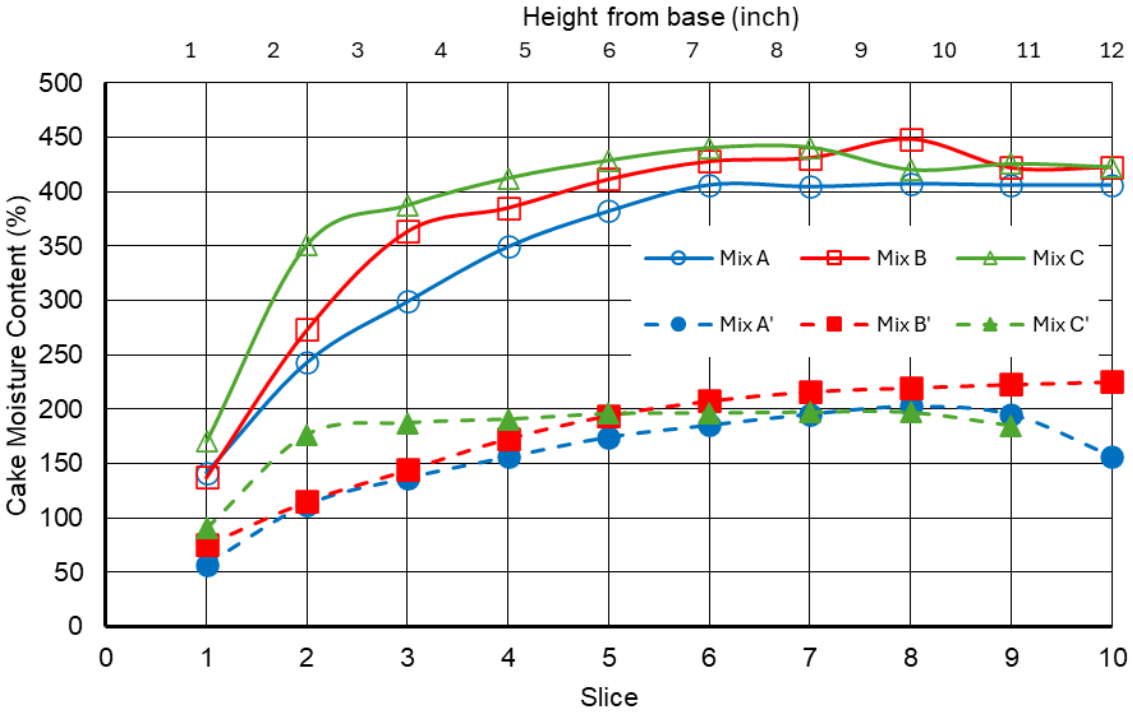


Fig. 6. Profiling of filter cakes per moisture content.

 © DFI International Bruges 2025

It is worth noticing the impact of suspended solids on the filter cake density and W/C ratio reduction will result in a lower permeability and higher strength.

FUTURE SELECTION OF THE INTERFACE MEDIUM

It has been recognized that, for drilling fluids, the standard filter paper in the API filtration test is not representative of field conditions and is often more restrictive than interfaces found in-situ, especially for granular soils, resulting in an underestimation of the filtration. Research (Sorrentino and Biscontin 2023) dealing with drilling fluids of all kinds has looked into the cakes formed both on and in the filter medium. Aside from the different filtration medium, no major change to the API filter press apparatus was considered in their study but shows the importance of the filtrate medium on the estimation of filtrate volumes.

As seen in Fig. 7, where sand was used for the filtrate medium in an additional test for SHS mix A, the filtrate volume was significantly larger. Only the cake formed on the surface of the medium is of interest for SHS studies as the filtrate penetration into the filter medium is minimal for the soils and pressures typical of SHS, as seen Fig. 8.

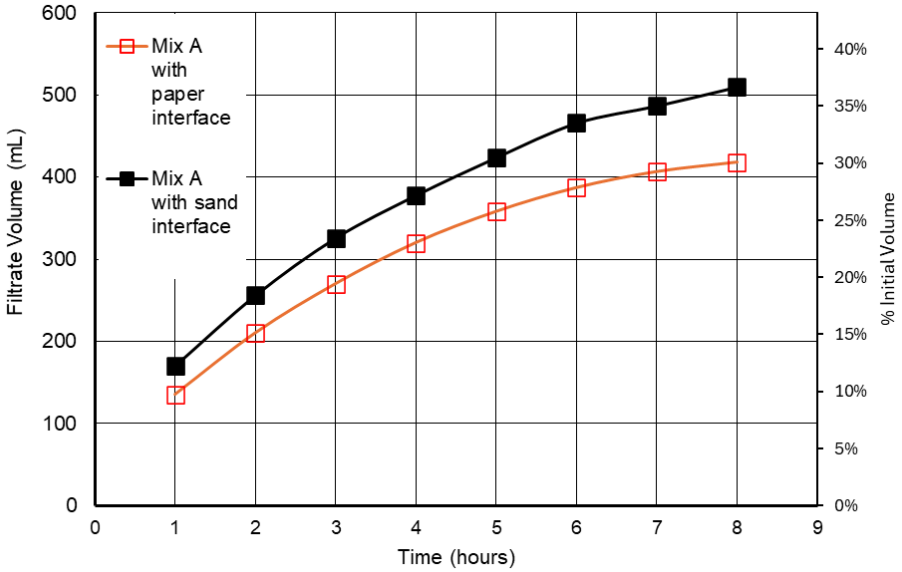


Fig. 7. Impact of paper versus sand filter medium on filtrate loss



Fig. 8. Penetration into sand interface after cake build up at 20 psi (138 kPa) as seen at the interface

 © DFI International Bruges 2025

SUMMARY

This simple study presents filtration results for SHS under conditions closer to *in-situ* conditions than the API filtration test. The filter cakes that developed were on the order of several inches thick and the slurry losses due to this filtration on the order of 30% of the initial volume. This study demonstrated the merit of considering filtration during design and shows its value for use in studying other variables that exist on a project specific basis. It also showed that due to the time required to perform a meaningful test, it is only appropriate for use for design or study purposes, not as a QC test.

Each of the three mixes tested had a distinct setting time, both as pure SHS and when loaded with soil, which affected the long-term filtration profile. Even the extended time (8-hours) that these tests were conducted does not appear to have allowed full development of the cake.

Due to sample height reduction due to filtration, refills were required to maintain the desired height but which then introduced discrepancies in the results at the top of the samples where theoretically densities should have trended towards the base slurry toward the wall center line This shows that the 12-inch (~300-mm) cell used was too short to capture the full cutoff wall half-section, even for a minimal wall thickness of 24-inches and a more typical 3-foot (.91-m) wide cutoff wall would require a much longer sample length.

The filter interface used for testing was shown to influence the tests, with a difference of ~ 20% found in the filtrate volume between the paper and sand interfaces. The test interface used should therefore be representative of the ground interface to obtain the most accurate estimates possible.

CONCLUSIONS

The results show that the restrictions inherent in the API filter test preclude the use of this test to provide meaningful data when testing SHS, and its use for this purpose is limited. They also show that the filtration process affects the overall characteristics of the wall. Consideration of these effects will help lead to the design and construction of SHS walls that reduce construction problems, are more effective for their use, and are more cost effective.

Although the results were unable to fully replicate a walls behavior, they are nevertheless useful at estimating the possible cross-sectional profile of the as-built cutoff wall. The cake thickness obtained here should however be viewed as quite conservative since only a fraction of the time for the filtration process is addressed and filter paper was used as an interface. Hence, the total amount of SHS make-up water loss to the ground cannot be quantified but must be in a multiple of the ones obtained here. To further study the filtration issue, a revised apparatus which is longer and has an appropriate interface is required

Limitations: An impossibility in the laboratory is to replicate the loss of water to the ground during the active trenching excavation phase when cake build-up is prevented by the trenching tool. Only after passing the excavated station can the slurry be at rest and for the filtration to continue, with the SHS thickening until set occurs. Another process that would be difficult to replicate is the constant addition while excavating of fresh slurry to the previous one in place, blending the ages and setting times of the various additions creating the end-product.

COMMENTS

As a lesson learned, as engineers, one should not accept to be hamstrung by standards. Standards follow the technology once the latter is mature. This study is a promising beginning for the development of a standard, half a century after the birth of the self-hardening slurry concept. Using this practical methodology has shown how to measure the filtration potential and cake variable

 © DFI International Bruges 2025

thickness, allowing a more accurate profiling of the SHS wall cross section. By using this simple method, testing various SHS formulations used in the industry, differences in response are exposed and can now be considered in design. These project specific factors, like hydrostatic head, viscosity, dispersion, retardation, temperature, suspended soil particles, and adjacent soil permeability, all affect the magnitude of the loss of water by filtration during the SHS fluid stage until it stops during early set.

While all these factors cannot be integrated in a simple testing program like the one discussed here, this test procedure may open an avenue for studying them. This study's value, despite its limitations, adds to the awareness of the complexity and heterogeneity of what is commonly called a CB wall. Both from a designer's standpoint where the appreciation of the end-product achieved by this construction process is essential and from the specialty contractor, who needs to evaluate the quantity of purchased ingredients required to complete the work per vertical square foot of cutoff wall, typically the single largest pay item in a fixed price contract, the analysis of water loss and filter cake formation is fundamental. Differences between mix designs can be large as shown by Mix C's characteristics with respect to filtration when Portland cement is absent in the formulation.

There are pros and cons related to the presence of filter cakes in the cutoff wall. The benefit of having a densification of the end-product at the interface with the ground confers higher strength and lower permeability. This is beneficial from a structural aspect by increasing shear strength, in shear wall applications for example (Stark *et al.* 2013) or decreasing the risk of dehydration in arid areas. Conversely, and particularly with high dosage of slag cement, the risk of building high internal stresses aggravates the already brittle nature of the end-product with the risk of internal cracking.

The designer should also be informed of the trenching equipment to be used for constructing the cutoff wall when considering filter cake formation. A hydraulic excavator (Backhoe) excavates relatively quickly, the bucket being briefly in contact with the excavation walls which allows the cake formation to accumulate early; further, a good operator can introduce less suspended solids in the slurry (if so instructed). In the case of a clamshell excavator, which is multiple times slower, the repeated travel of the bucket prevents the formation of a thick filter cake until the vertical pass is completed while the repeated opening and closing of the jaws tend to increase the suspended solids content (Axtell et al. 2009). In the meantime, filtration without thick cake build up is taking place. When a hydro-mill/cutter is used for trenching deep SHS cutoff walls, the recirculation process cleans the slurry of most suspended solids but not the ultra-fines. Due to the need for retardation and pumping fluidity, the mix is well dispersed and in constant movement which on one hand impedes a thick cake formation but not the loss of water by filtration and on the other hand the duration of the excavation without extraction of the mill allows for some cake build up.

A personal experience was using a mix similar to the mix C presented in this report with a mill-cutter going down 145-feet (44-m) at the Cannelton Dam Hydro-Electric project on the Ohio River, KY in 2009. The absence of OPC in the pure slag-cement based mix provided a low filtrate loss that limited problems due to the formation of thick cakes and the reduced the added slurry required to maintain wall stability.

The whole cross section of the SHS cutoff wall can be better represented as two filter cakes of variable density (both with densities higher than the base mix) back-to-back to form an average profile quite different from that obtained for the base slurry alone, with a lower permeability and a higher strength. Filtration and cake buildup could then be taken into consideration when designing a SHS cutoff wall to avoid missing the strength brackets and spending more money than necessary on ingredients.

In terms of tolerable suspended solids load, David Kleiner (then with Harza Engineers) as far back as 1977 had established for a conventional CB SHS (Cleveland Cliff Iron Mine) that, if the sand content (as suspended solids) remains below 25% by volume, there was no impact due to suspended solids on the cured CB permeability. Sand content and suspended solids are different things, the role of fines

 © DFI International Bruges 2025

below the fine sand is often ignored but could be major. Past experience (Coughenour et al. 2024) showed that real world SHS densities can be up to 1.7 to 1.8-Mg/m^3 (106 to 112-pcf). Considering that in the present study the suspended fines were added at the rate of 25.5% by weight of water (15% bulk volume) and the SHS density was only 1.245-Mg/m^3 (77.7-pcf), up from 1.12-Mg/m^3 for the pure slurry, the soil mixes may have been on the light side of the in-situ range of occurrences. The question remains on how much suspended solids is desirable, technically and economically.

From a contractor, taxpayer and CO2e emissions standpoints, using more ingredients than necessary for the engineering design is not justifiable and may be detrimental. It may be advantageous to the contractor to cause a maximum of suspended soil particles to mitigate the added concentration of ingredients due to filtration. The design engineer must be aware of this when specifying a laboratory testing program and later writing specifications. Both the increase in binder concentration due to filtration and the presence of granular fines will increase the strength of the end-product, albeit at a later date, compared to the theoretical mix based on the base slurry alone. This is not beneficial when ductility is a desirable characteristic but its study is elusive as it would require long term testing well over the 28 or 56 days typically used for QC/QA.

Outlook

This simple study provides only the partial magnitude of cake formation in SHS cutoff walls but has the merit of advocating it during design and laboratory testing programs using an appropriate apparatus, some still in development and that shows its possibilities for use in studying many other variables.
In order to have a fully consistent filtration test, the original sample must be tested over the SHS full fluid (workable) phase from delivery to the cell after mixing to the occurrence of the set. This implies that filtration tests will need to be caried over a period of 24 hours or more. Further the sample should be allowed to shrink without interference; this implies that the height of the cell must be such that the final sample length once set is at least equal to the half thickness of the cutoff wall. This dimension is governed primarily by the hydrostatic head defining the test pressure. Pressure cells 30 to 40 inches may be required to satisfy this goal under the conditions of this study.
A future series of filtration tests will substitute the filter paper interface with a sand filter like a normalized Ottawa sand or porous stones. Preliminary testing has shown a distinct increase in initial filtration (Fig. 7) despite minimal ingredients penetration (Fig. 8), which is a laboratory inducement in imitating more realistically what happens in-situ with the test.

REFERENCES

API R 13B-1, R., 2003. 13B-1, Recommended practice standard procedure for field testing water-based drilling fluids. Recommended Practice Standard Procedure for Field Testing Water-Based Drilling Fluids pp.12-15.

Axtell, P.J., Stark T.D., and Dillon, J.C. 2009. Strength difference between clam-shell and long-reach excavator constructed cement-bentonite self-hardening slurry walls. GSP No. 187, ASCE, pp. 297-304.

Axtell, P. J., Stark, T. D., and Dillon, J. C.2010. Peak and post-peak shear strength of cement-bentonite. DFI Journal Vol.4 n°1 pp.59-65

Coughenour, N., Ruffing, D., and Evans, J. C. 2024. Recent observations on self-hardening slurries in slurry trenching. IFCEE 2024 Dallas pp. 246-255.

EFFC/DFI, Second Edition 2018. Guide to tremie concrete for deep foundations. free on DFI website

 © DFI International Bruges 2025

Harris, C.R., 2016. Bentonite self-hardening slurry mix variations and field implementation methods. 41st Annual Proceedings of the International Conference on Deep Foundations, Seepage Control and Remediation New York.

Sorrentino G., Biscontin G.: 2023. Improved filtration parameters from modified API filter press. Geoenergy Science and Engineering, Cambridge U. Elsevier B.V.

Stark, T., Walberg, F., Byrne, P., Castro, G., Nicholson, P., Axtell, P., Beaty, M., Dillon, J., Empson, W., Topi, J., Mathews, D., and Bellew, G.. 2013. Soil improvement for seismic retrofit of Tuttle Creek dam. GeoCongress San Diego 2013 2069-2079.

Tallard G. and Ruffing D. 2023. Proposed improvements to laboratory testing programs for the design of self-hardening slurry cutoff walls. 6th International Conference on Grouting and Deep Mixing New Orleans 2023.

 © DFI International Bruges 2025

CPT-based Analysis on Vertical and Lateral Capacity of Steel Sheet Piles Installed by the Press-in with Auger

Tamboura H.H. *, GIKEN LTD., Kochi-shi, Kochi-ken, Japan, +81 (80)-8641-7580, tamboura@giken.com
Ishihara Y., GIKEN LTD., Kochi-shi, Kochi-ken, Japan,
Eguchi M. , GIKEN LTD., Kochi-shi, Kochi-ken, Japan,
Mori, A., GIKEN LTD., Kochi-shi, Kochi-ken, Japan,

ABSTRACT

This study proposes a design method for estimating the vertical and lateral capacity of steel sheet piles installed by the Press-in with Auger (PA) technique using Cone Penetration Test (CPT) results. The research builds upon the work of Ishihara et al. (2024) and investigates the effect of augering on the surrounding ground. Field tests were conducted in two soil types: soft cohesive soil and hard cohesionless soil. The results indicate that the vertical capacity of PA sheet piles can be designed using modified versions of the LCPC method and Eurocode 7, with reduction factors applied to account for installation effects. Lateral capacity can be estimated using Hetenyi's (1946) equations and Bouafia's (2014) subgrade reaction formulations, with appropriate reduction factors. The proposed CPT-based design methods offer a practical approach for estimating PA sheet pile capacities using fresh ground CPT profiles.

Keywords: Sheet Pile; Cone Penetration Test; Lateral Capacity; Vertical Capacity; Press-in with Auger

INTRODUCTION

Steel sheet piles have traditionally been used for temporary retaining structures. Still, their application has expanded to include non-temporary structures such as coastal levees (Ishihara et al., 2020), railway bridge foundations (Kasahara et al., 2018), and architectural buildings (GIKEN, 2016; Kondo et al., 2023). As the use of sheet piles in permanent structures increases, it becomes crucial to accurately assess their performance and design them accordingly. The installation method significantly influences the performance of sheet piles. The Press-in method, a static pile installation technique, has gained popularity in urban construction and challenging ground conditions. One variant of this method, the "Press-in with Auger" (PA), is particularly suitable for hard grounds with SPT N-values exceeding 50. In PA installation, an auger device attached to the front side of the sheet pile penetrates the ground alongside the pile, temporarily lifting surrounding soil to the surface (Fig. 1). After reaching the desired depth, the auger is extracted, and the lifted soil or other material is backfilled. The PA installation process, especially the termination and backfilling conditions, can significantly affect the sheet pile's performance. Ishihara et al. (2024) conducted field loading tests on PA sheet piles and walls, providing valuable insights into their behavior under various conditions. This study aims to build upon the findings of Ishihara et al. (2024) by proposing a design method for estimating the vertical and lateral capacity of steel sheet piles (Fig. 2) installed by the PA technique using CPT results and investigating the effect of augering on the surrounding ground. The research focuses on two soil types: soft



Fig. 1 Auger device used in PA sheet pile

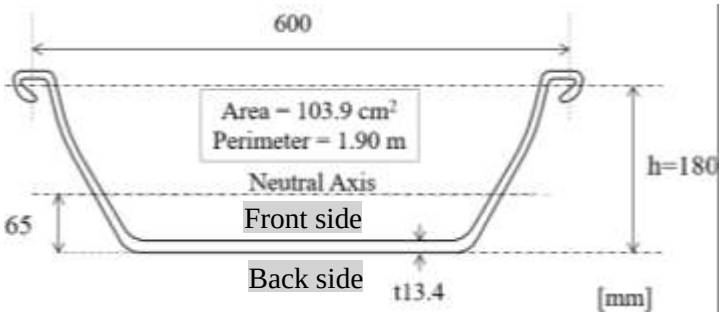


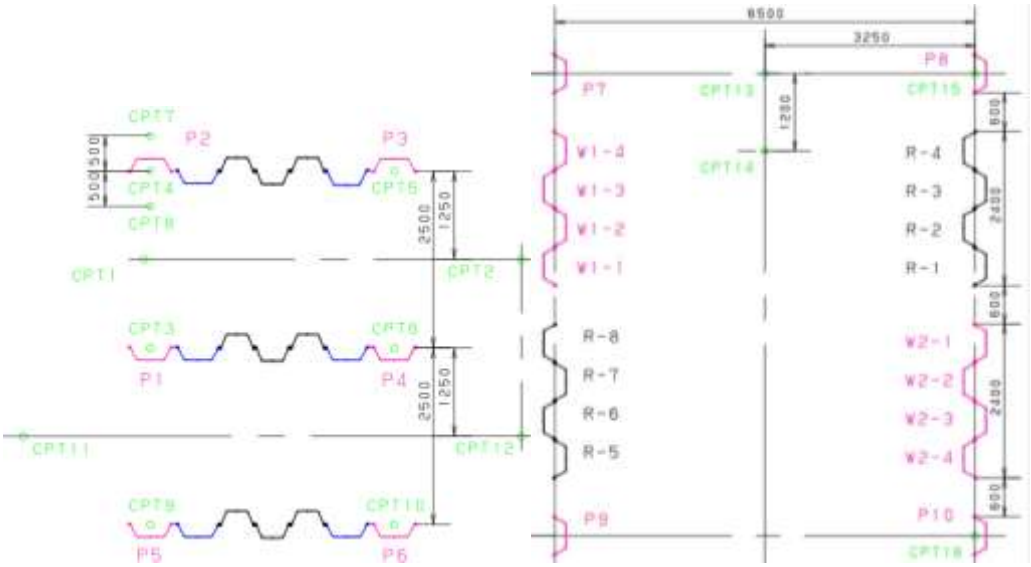
Fig. 2 The geometry of SP-IIIw sheet pile

 © DFI International Bruges 2025

cohesive soil (J2001 test series) and hard cohesionless soil (J2101 test series). By developing CPT-based design methods, this study seeks to provide practical tools for engineers to estimate PA sheet pile capacity using readily available ground investigation data.

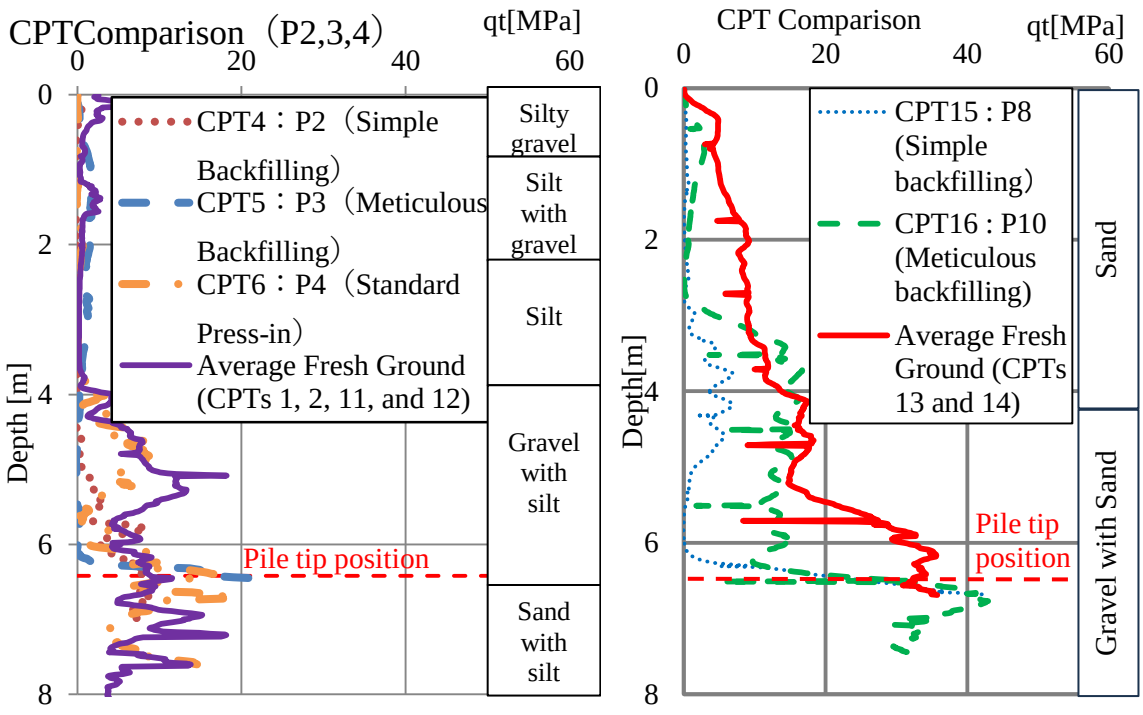
OUTLINE OF THE FIELD TEST

The CPT test layout is presented in Fig. 3. Two series of CPTs were conducted: the J2001 test series in soft cohesive ground (Fig. 3a and Fig. 4a) and the J2101 test series in dense non-cohesive ground (Fig. 3b and Fig. 4b). Sheet piles (P) and sheet pile walls (W) were installed in the test fields, with the sheet pile *P*4 installed by the standard Press-in method, without augering (SP Pile). Some CPTs were conducted before the piling work (CPT1, CPT2, CPT11, CPT12, CPT13, CPT14). These CPTs are used in this study to propose a design based on tests conducted on fresh ground. Other CPTs were carried out after the piling work.



(a) J2001 test series (b) J2101 test series

Fig. 3. Test layout (black piles are reaction piles, and blue piles (near test piles) are not embedded)



(a) (Water level = 1.74m) (b) (Water level = 7.25m)

Fig. 4. CPT results: (a) J2001 test series; (c) J2101 test series

 © DFI International Bruges 2025

The sheet piles used on-site are SP-IIIw sheet piles, Fig. 2. The installation methods for the piles varied. One pile (P4 in Fig. 3a) was a standard SP pile, installed using the press-in method. Some piles were PA piles with simple backfill, installed using the press-in with auger method, where the soil was temporarily lifted by the auger device and then backfilled without additional material or compaction (P1, P2 in Fig. 3a; P7, P8; W1 in Fig. 3b). Other piles were PA piles with meticulous backfill, installed using the press-in with auger method, but the augered soil and device were completely extracted. The void was filled with newly prepared sand (mean diameter D50 = 1.37 mm, uniformity coefficient Uc = 1.78, fine fraction content Fc = 0.4%), which was compacted by the auger's penetration (P3, P5, P6 in Fig. 3a; P9, P10; W2 in Fig. 3b).
Loading tests on all these piles and walls were conducted by Ishihara et al. (2024), and further details on the installation process can be found in their work. Some of the CPT results are shown in Fig. 4.

METHODOLOGY

CPT-Based Estimation of Soil Subgrade Modulus

Ali Bouafia (2014) studied the lateral resistance of single piles based on CPT tests and demonstrated that the soil lateral subgrade modulus, K_h can be correlated with cone resistance q_c and pile characteristics. This relationship is expressed by Eq. (1) at a given depth, where K_E, referred to as the reaction modulus number, and $q^*{}_c$ is the net cone penetration.

$$K_h = K_E . q^*{}_c \quad [1]$$

$q^*{}_c(z) = q_c(z) - \sigma'_{v0}(z)$	$K_E = \begin{cases} \frac{1}{10} K_R{}^{-1.1} & if\ K_R > 2.1 \times 10^{-2} \\ 7.0 & else \end{cases}$	
$K_R = \frac{E_p . I_p}{q^*{}_{ce} . D^4}$	$q^*{}_{ce} = \frac{1}{D_e} \int_0^{D_e} q^*{}_c . dz$	$L_0 = \sqrt[4]{\frac{E_p . I_p}{K_E . q^*{}_{ce}}}$
$E_p . I_p$, and D are respectively the pile flexural stiffness and the pile embedded length. D_e is the effective embedded length of the pile beyond which the pile segments do not deflect defined as $D_e = \min\{D, \pi L_0\}$.		

CPT-Based Estimation of Vertical Bearing Capacity

According to Murad and Hani (2004), among CPT-based methods, the method by Bustamante and Gianeselli (1982) (later updated with minor revisions by Bustamante and Frank (1997)), known as the LCPC Method, yield excellent results in the total pile axial capacity, Q_{ult} as expressed in Eq. (2). Where A_p is pile end area, q_p is the unit end-bearing, A_s is the pile shaft area, and f_p by the unit side friction.

$$Q_{ult} = q_p A_p + f_p A_s \quad [2]$$

$q_p = k_c q_{ca}$	$f_p = \frac{q_c}{\alpha_{LCPC}}$
k_c (end-bearing coefficient), α_{LCPC} (friction coefficient) depend on the type of pile and the piling method. q_{ca} is equivalent average cone resistance (q_c) at the base of the pile, it is the mean q_c value measured along two fixed distances, a (a=1.5D, and D is the pile diameter), above (-a) and below (+a) the pile tip.	

The American Federal Highway Administration (FHWA) in its code FHWA-HIF-07-03 (2007) recommends the LCPC Method to estimate the total axial compressive resistance of CFA piles, with k_c values of 0.15 for cohesionless soils and 0.375 for cohesive soils.
The annex of Part 2 of EN 1997 provides methods to calculate the compressive resistance of a pile from ground test profiles, dividing the ultimate pile capacity into base and shaft components as shown in Eq.

 © DFI International Bruges 2025

(3). In EN 1997, for multiple tests, correlation factors ξ_3 and ξ_4 are applied to the mean and minimum pile resistances to determine the total pile compressive resistance, the base resistances, and shaft resistances.

$$F_{max} = A_{base} \times P_{max;base} + C_p \int_0^{\Delta L} P_{max;shaft;z} dz \quad [3]$$

$P_{max;base} = 0.5\alpha_p \beta S \left\{ \frac{q_{c;I;mean} + q_{c;II;mean}}{2} + q_{c;III;mean} \right\}$	$with\ P_{max;base} \leq 15MPa$
$P_{max;shaft;z} = \alpha_s \times q_{c;z;a}$	

A_{base} is the cross-sectional area of the base. C_p is the circumference of the pile shaft. F_{max} is the maximum compressive resistance of the pile. $F_{max;base}$ is the maximum base resistance. $F_{max;shaft}$ is the maximum shaft resistance. $P_{max;base}$ is the maximum unit base resistance. $P_{max;shaft;z}$ is the maximum unit shaft resistance at depth z. ΔL is the distance from the base of the pile to the bottom of the first soil layer above the base. z is the depth or vertical direction (positive downwards). D_{eq} is the equivalent diameter of the base. α_p is the pile class factor. β is the factor which takes account of the shape of the pile point. S is the factor that accounts for the shape of the pile base. $q_{c;I;mean}$ is the mean of the $q_{c;I}$ values over the depth running from the pile base level to a level which is at least 0,7 times and at most 4 times the equivalent pile base diameter D_{eq} deeper. $q_{c;II;mean}$ is the mean of the lowest $q_{c;II}$ values over the depth going upwards from the critical depth to the pile base. $q_{c;III;mean}$ is the mean value of the $q_{c;III}$ values over a depth interval running from the pile base level to a level of 8 times the pile base diameter above the pile base. α_s is the reduction factor. $q_{c;z;a}$ is the cut-off value of q_c at depth z.

CPT-Based Estimation of Lateral Resistance

A laterally loaded pile can be modeled using the Linear Elastic Method (Pyke and Beikae, 1984), with the lateral deformation governed by the following equation:

$$P = k_h y \quad [4]$$

where *p* and *y* are lateral pressure and deflection respectively, and k_h is the coefficient of lateral subgrade reaction. The coefficient of subgrade reaction (k_h) and the subgrade modulus (K_h) are often used interchangeably in practical engineering. In this paper, k_h is considered as the average value of K_h ($k_h = \frac{1}{Z}\int_0^Z K_h(z)dz$). From distributed load versus moment relationships,

$$pB = \frac{d^2M}{dz^2} = -E_P I \frac{d^4y}{dz^4} \quad [5]$$

where B is the width of the pile and $E_P I$ is the pile stiffness.
Then the equation governing the lateral deformation can be expressed as:

$$E_P I \frac{d^4y}{dz^4} + Bk_h y = 0 \qquad \text{with} \qquad \beta = \left(\frac{k_h D}{4E_P I}\right)^{1/4} \quad [6]$$

$1/\beta$ is also known as the non-dimensional length. Broms (1964a,b) showed that a laterally loaded pile acts as an infinitely stiff member when β is less than 2. When β L ≥ 4, it behaves as an infinitely long member, failing when the bending moment exceeds the pile's yield resistance. For constant k_h along the pile depth, Hetenyi (1946) derived closed-form solutions. For lateral deformation due to lateral load *H* on a free-head pile, the following expression gives the lateral displacement. The influence factors $K_{\Delta H}$, are given in Table 1 as functions of β L and z/L (the ratio of depth below the surface to total length).

Lateral displacement: $\Delta = \frac{2H\beta}{k_h d} K_{\Delta H}$ [7]

Table 1: Influence factor for linear solution.

β*L*	**Z/L**	**K(ΔH)**	**β*L***	**Z/L**	**K(ΔH)**	**β*L***	**Z/L**	**K(ΔH)**	**β*L***	**Z/L**	**K(ΔH)**
2.0	0	1.1376	3.0	0	1.0066	4.0	0	1.0008	5.0	0	1.0003
2.0	0.25	0.6015	3.0	0.25	0.3515	4.0	0.25	0.1979	5.0	0.25	0.0901
2.0	0.5	0.1838	3.0	0.5	0.0164	4.0	0.5	-0.059	5.0	0.5	-0.0671
2.0	0.75	-0.1288	3.0	0.75	-0.0861	4.0	0.75	-0.0505	5.0	0.75	-0.0197
2.0	1	-0.3999	3.0	1	-0.113	4.0	1	0.0038	5.0	1	0.0167

 © DFI International Bruges 2025

RESULT AND DISCUSSION

Effect of augering on the ground

The effect of augering was investigated by calculating the ratios of q_t from augered soil to fresh ground. Two ratios were considered: r_b, the ratio around the pile base, and r_s, the ratio along the pile shaft. For r_b, the LCPC method's average q_t (q_{ca}) was used, while for r_s, q_t was integrated over the pile's embedment length. The results in Table 2 show that augering affects the soil along the pile more than at the base.
For meticulous backfilling, ratios depend on the strength difference between the backfill material and local ground. A higher strength backfill results in larger ratios, as in the J2001 series, where r_b values were higher. The r_b values are directly related to end-bearing capacity and act as a reduction factor. In the J2001 series, average r_b values of 0.785 and 1.09 were found for simple and meticulous backfilling, respectively.

Table 2: Effect of augering and backfilling on the ground

		Name	q_{ca} (base) [kPa]	$\int_0^{6.45} q_t$ (Shaft) [kPa]	r_b	r_s
J2001 Series (Soft cohesive soil)	Fresh ground	Average CPT1; 2; 11; 12	8264	2150304	1	1
	Simple Backfill	CPT3	5817	103334	0.70	0.05
		CPT 4	7220	526215	0.87	0.24
	Meticulous Backfill	CPT5	8102	712599	0.98	0.33
		CPT10	9918	510447	1.20	0.24
J2101 Series (Dense non-cohesive soil)	Fresh ground	Average CPT13; 14	33877	8318952	1	1
	Simple Backfill	CPT15	19781	1198095	0.58	0.14
	Meticulous Backfill	CPT16	24578	4892551	0.73	0.59

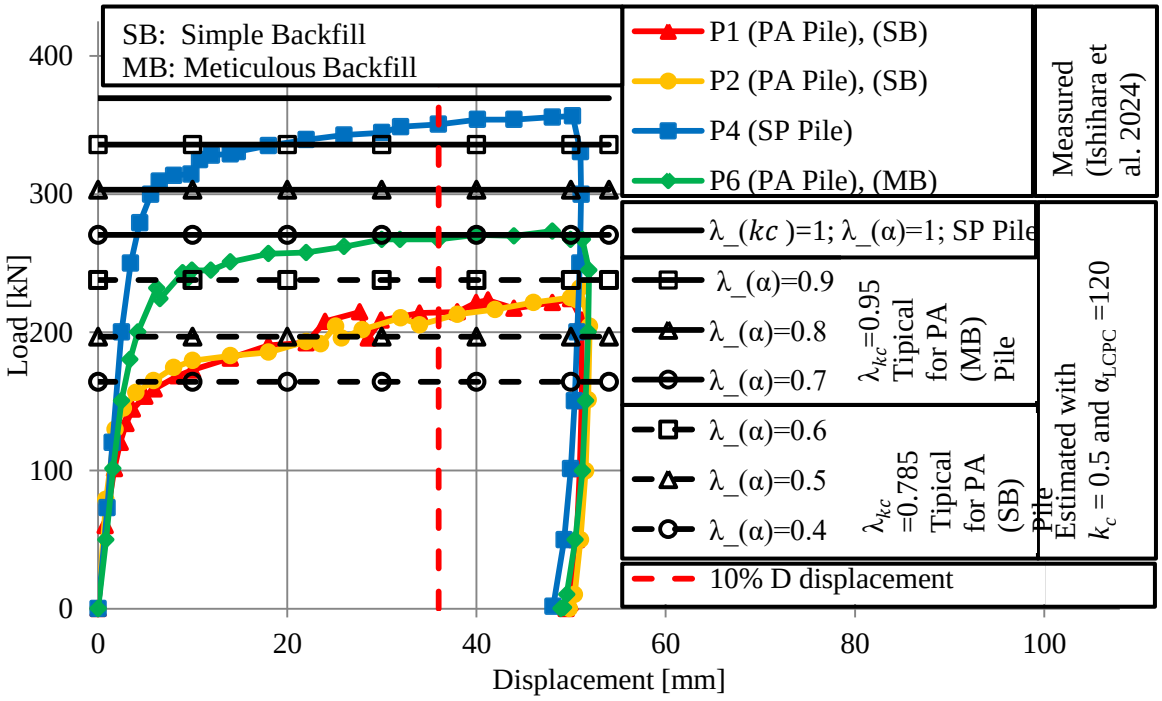
Vertical bearing capacity

Vertical capacity is defined as the head load at a pile head displacement of $0.1D_{o,eff}$, where $D_{o,eff}$ is the equivalent tubular pile diameter (36 mm for SP-IIIw).
For the LCPC method (Eq. 2), average q_t values of CPT on fresh ground were used. For Piles installed with standard pilling methods like the standard press-in method, without augering (SP Pile) (P4 in Fig.3a and Fig.4a), the method suggests the coefficients k_c = 0.5 and α_{LCPC} = 120 for soft cohesive soil (J2001 series, q_t = 1 to 12 MPa), and k_c = 0.4 and α_{LCPC} = 200 for dense cohesionless soil (J2101 series, q_t > 12 MPa).
For the EC7 method (Eq. 3), the q_t from CPT1, CPT2, CPT11, CPT12, CPT13, CPT14 were used and the corresponding correlation factors ξ_3 and ξ_4 were applied. The corresponding coefficients α_p and α_s for SP piles in J2001 series are α_p=1 and α_s = 0.025; in J2101 series, they are α_p = 1 and α_s = 0.012.
No values of the coefficients k_c and α_{LCPC} of LCPC method and α_p and α_s of EC7 are available for the design of PA piles (Pressed-in Piles with auger). This study proposes to design PA piles by applying reduction factors λ_{k_c}, λ_{α}, λ_{α_p}, and λ_{α_s} to the values of the coefficient k_c, α_{LCPC}, α_p, and α_s respectively.
The average values of r_b in Table 2 are considered as values of λ_{k_c} and λ_{α_p}, in the case of the J2001 series, for simply backfilled ground the average value r_b = 0.785 is considered, but for meticulously backfilled since the average value is higher than 1 the minimum value r_b= 0.95 is taken. The values of λ_{α} and λ_{α_s} can be back analyzed using the loading test results.
The estimated results for the J2001 series are compared with Ishihara et al. (2024) in Fig. 6 and the estimated results for the J2101 series are in Table 3 for SP piles only.
Figure 6 shows that SP piles can be designed using the LCPC method and EC7 ($\lambda_{k_c} = \lambda_{\alpha} = \lambda_{\alpha_p} = \lambda_{\alpha_s} = 1$). However, for PA piles, the values of reduction factors depend on the backfilling method. Table 3 shows results for SP piles; for PA piles in the case of J2101 series, r_b and r_s from Table 2 can be referenced.

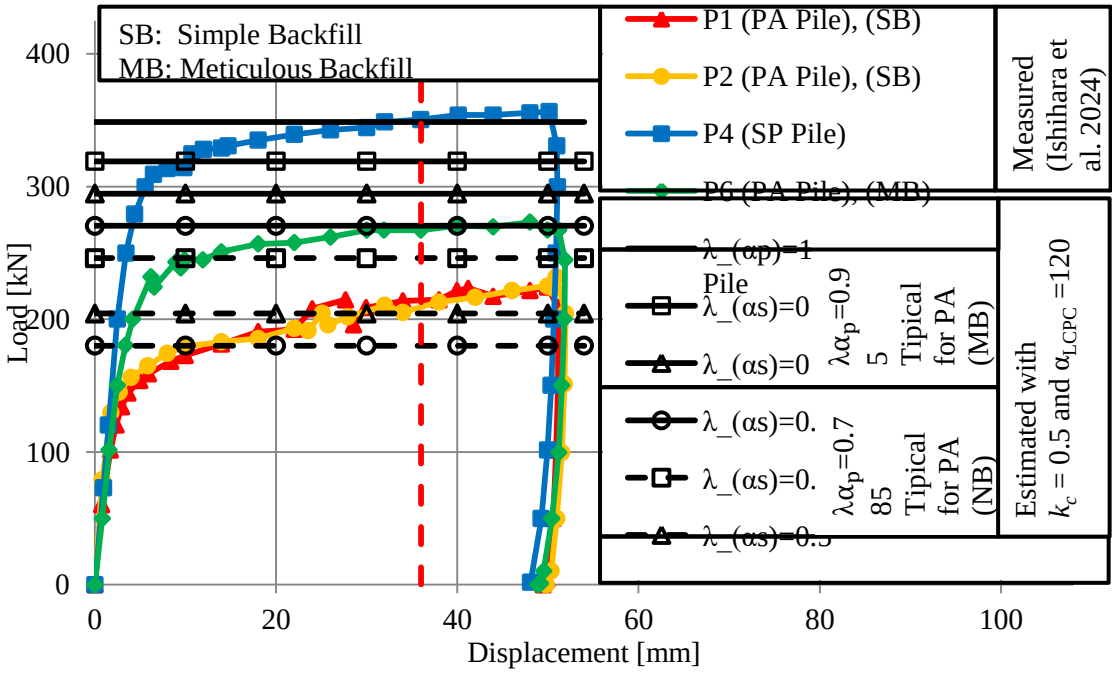
 © DFI International Bruges 2025

Lateral resistance

The lateral capacity was analyzed using the linear elastic method. The coefficient of lateral subgrade reaction (k_h) was taken as the average value of the subgrade modulus (K_h) which was determined using the method from the "CPT-Based Estimation of Soil Subgrade Modulus" section. The variations with depth of K_h for both the J2001 and J2101 series are shown in Fig. 7 along with the k_h values. These k_h values were used in Eqs. 4-7 and Table 1 to assess pile lateral capacity with a pile embedment of 6.45 m and pile mechanical properties as listed in Table 4. The lateral displacements, in the case of SP piles, are shown in Fig. 8.



(a) LCPC Method



(b) Eurocode 7 method

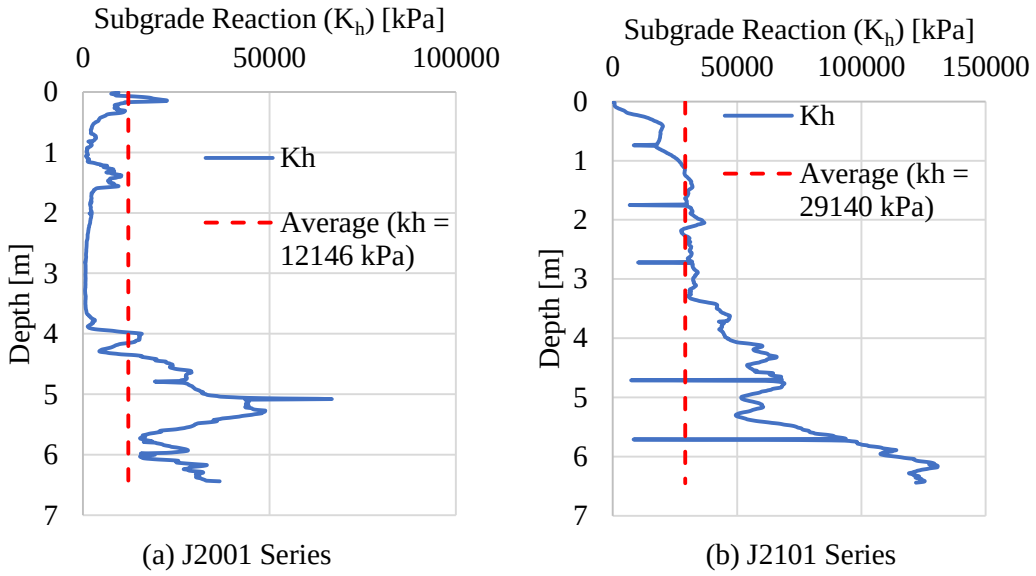
Fig. 6 Vertical capacity results for the J2001 test series and comparison with Ishihara et al 2024

 © DFI International Bruges 2025

Table. 3 Vertical capacity results for J2101 test series (SP Piles)

Method	Base Capacity (kN)	Shaft Friction (kN)	Total Capacity (kN)
LCP method	166.79	797.61	964.40
EC7	279.93	569.73	849.66

Load-displacement curves were extracted and compared with Ishihara et al. (2024), as shown in Fig. 9. For estimation of the capacity of PA piles reduction factor λ_{k_h} are applied to k_h.
Unlike vertical loading, where capacity is often based on 10% of the pile diameter displacement, lateral capacity is more serviceability-sensitive and governed by smaller displacements.
From Fig. 9a, the lateral capacity of the SP pile is accurately estimated (λ_{k_h} = 1). For the J2101 test series, all load tests are on PA piles. Fig. 9 shows that PA pile capacity can be estimated by applying a reduction factor λ_{k_h} to k_h, ranging from 0.9 to 0.2. The values of λ_{k_h} highly depend on the backfilling method.

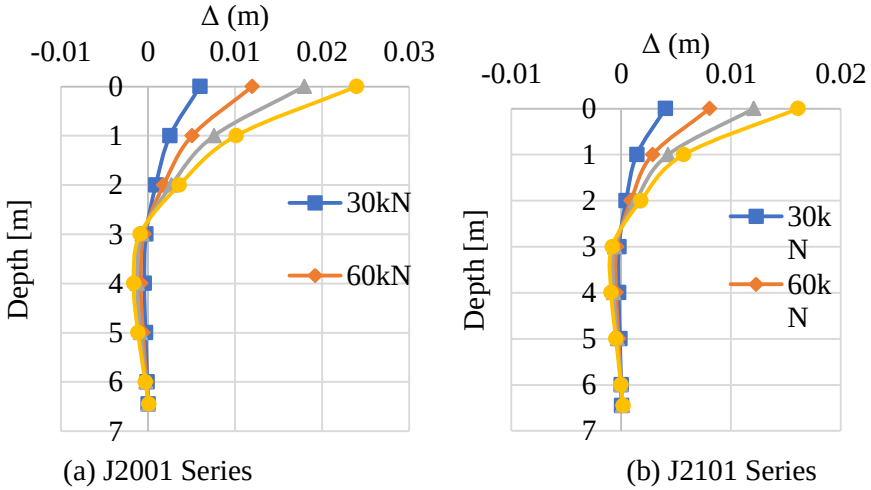


(a) J2001 Series (b) J2101 Series

Fig. 7: CPT-based determination of lateral subgrade modulus

Table 4. Mechanical Properties of SP-IIIw sheet pile

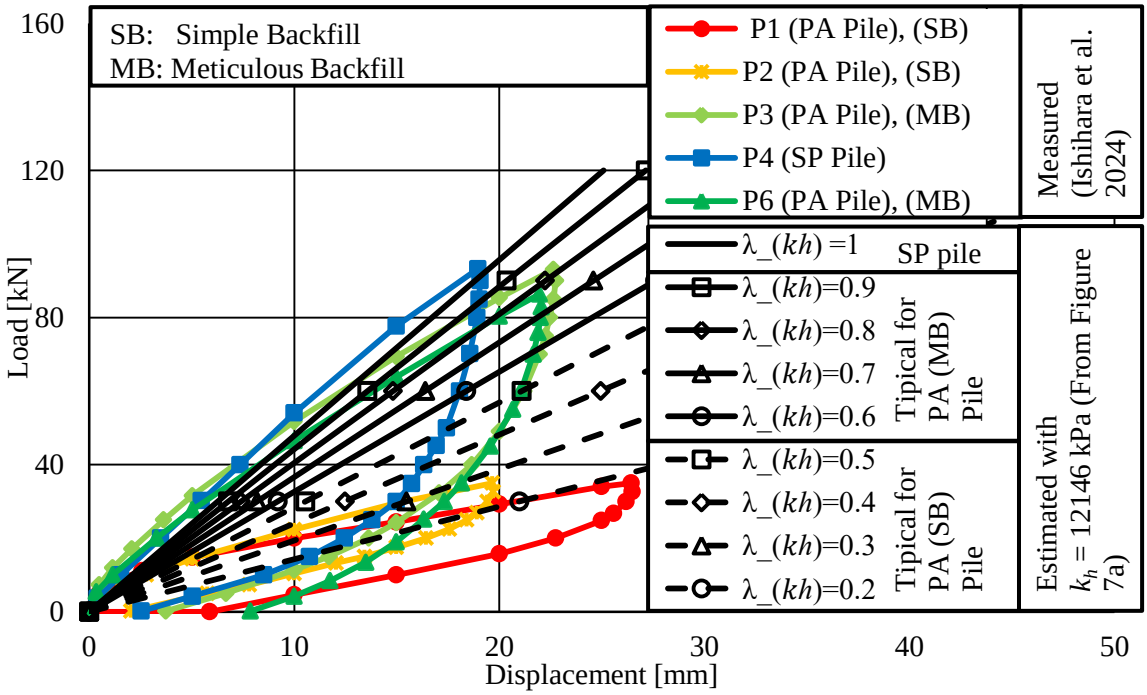
Yield Stress [kPa]	Section Modulus [m^3]	Yield Moment [kN.m]	Elastic Modulus [kPa]	Inertia (I) [m^4]	Stiffness (EI) [$kN.m^2$]
295000	0.000376	110.92	205000000	5.22E-05	10701



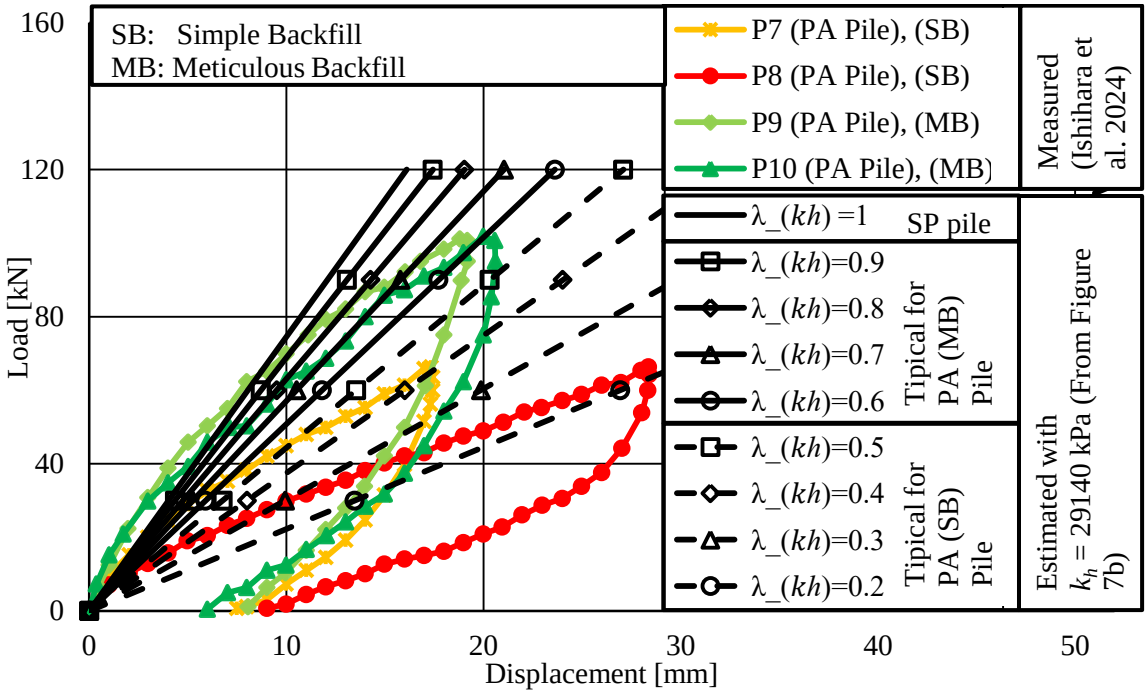
(a) J2001 Series (b) J2101 Series

Fig. 8: Lateral displacement of SP pile

 © DFI International Bruges 2025



(a) J2001 test series



(b) J2101 test series

Fig. 9 Comparison of load-displacement curves for lateral capacity

Proposition of design methods for PA sheet piles and PA sheet pile walls.

Based on the discussion above, the following equations are proposed for estimating the vertical and lateral capacities of pressed-in sheet piles.

Equation for unit end bearing capacity based on the LCPC method, q_p:

$$q_p = \lambda_{k_c} \times k_c \times q_{ca} \quad [8]$$

Equation for unit side friction based on the LCPC method, f_p:

$$f_p = \lambda_\alpha \times \frac{q_c}{\alpha_{LCPC}} \quad [9]$$

 © DFI International Bruges 2025

Equation for the maximum base resistance based on Eurocode 7, $P_{max;base}$:

$$P_{max;base} = 0.5 \times \lambda_{\alpha_P} \times \alpha_p \times \beta S \times \left\{\frac{q_{c;I;mean} + q_{c;II;mean}}{2} + q_{c;III;mean}\right\} \; with \; P_{max;base} \leq 15MPa \qquad [10]$$

Equation for the maximum shaft resistance based on Eurocode 7, $P_{max;shaft;z}$:

$$P_{max;shaft;z} = \lambda_{\alpha_s} \times \alpha_s \times q_{c;z;a} \qquad [11]$$

Equation for the lateral subgrade modulus based on Bouafia (2014), K_h; since $k_h = \frac{1}{Z}\int_0^Z K_h(z)dz$,

$$K_h = \lambda_{k_h} K_E . q^*_c \qquad [12]$$

The coefficient λ_{k_c}, λ_α, λ_{α_P}, λ_{α_s}, and λ_{k_h} are given in Tables 5 and 6 for various backfilling methods.

Table 5. Reduction factors for vertical capacity of pressed-in sheet piles in soft cohesive ground.

	Based on the LCPC Method		Based on Eurocode 7	
	λ_{k_c}	λ_α	λ_{α_P}	λ_{α_s}
SP-Standard Press-in	1	1	1	1
PA pile with Simple Backfilling	0.785	0.5	0.785	0.5
PA pile with Meticulous Backfilling	0.95	0.7	0.95	0.7

Table 6. Reduction factors for lateral capacity of pressed-in sheet piles

λ_{k_h}			
Press-in in soft cohesive ground		Press-in in dense cohesionless ground	
SP- Standard Press-in	1	PA pile (Simple Backfill)	0.2-0.5
PA pile (Simple Backfill)	0.2-0.5	PA pile (Meticulous Backfill)	0.6-0.9
PA pile (Meticulous Backfill)	0.6-0.9	-	

As lateral capacity is more sensitive to serviceability and governed by smaller displacements, the reduction factors in Table 6 are presented as intervals, leaving the exact value to the reader's discretion. These reduction factors are applied not to the bearing capacity itself but to the coefficient of lateral subgrade reaction.

CONCLUSION

This study developed CPT-based methods to estimate the vertical and lateral capacities of steel sheet piles installed using the Standard Press-in (SP) and the Press-in with Auger (PA) technique. The methods adapt existing approaches, with adjustments for PA-pile's specific characteristics.

For vertical capacity in soft cohesive ground, LCPC and Eurocode 7 methods can be modified by applying reduction factors (0.785 to 0.95) to the end resistance and by applying reduction factors (0.5 to 0.7) to the shaft resistance, depending on installation methods.

A method for estimating the lateral capacity of PA piles was proposed, combining Hetenyi's (1946) and Bouafia's (2014) equations with reduction factors applied to the coefficient of lateral subgrade reaction ranging from 0.9 to 0.2.

These CPT-based methods enable accurate and efficient design of PA sheet piles. Future research could expand validation, examine long-term performance, and develop advanced numerical models.

REFERENCES

Bouafia, A. 2014. P-Y curves from the CPT test for laterally loaded single piles in sand, Proceedings of the 3rd International Symposium on Cone Penetration Testing, Las Vegas, Nevada, USA - 2014.

Broms, B., 1964a, Lateral resistance of pile in cohesive soil, Journal of Soil Mechanics Foundation

 © DFI International Bruges 2025

Division, ASCE, 90(SM3):27–56.

Broms, B., 1964b, Lateral resistance of pile in cohesionless soil, Journal of Soil Mechanics Foundation Division, ASCE, 90(SM3):123–156.

Bustamante, M., and Gianeselli, L. (1981). “Portance Réele et Portance Calculée des Pieux Isolés Sollicités Verticalement,” Revue Francaise de Geotéchnique, No. 16, Presses de l’ ENPC, France.

Bustamante, M., and Gianeselli, L. (1982). “Pile Bearing Capacity by Means of Static Penetrometer CPT,” In Proceedings of the 2nd European Symposium on Penetration Testing. Amsterdam, pp. 493–500.

E N 1997-1: 2004. Eurocode 7: Geotechnical design. Part 1: General rules. CEN.

E N 1997-2: 2004. Eurocode 7: Geotechnical design. Part 2: Ground investigation and testing. CEN.

Federal Highway Administration (FHWA). 2007. Geotechnical Engineering Circular No. 8 Design and Construction of Continuous Flight Auger (CFA) Piles, Report no. FHWA-HIF-07-03, Washington, DC, USA

GIKEN. (2016). Load Bearing Steel Intensive Basement - Press-in Method and Thorough Inspection Technique, Case Study, 28p.

Hetenyi, M., 1946, Beams on Elastic Foundations, University of Michigan Press, Ann Arbor, MI.

International Press-in Association (IPA). (2016). Press-in Retaining Structures: a Handbook, First edition 2016, 520p.

Ishihara, Y., Yasuoka, H. and Shintaku, S. (2020). Application of Press-in Method to coastal levees in Kochi Coast as countermeasures against liquefaction. Geotechnical Engineering Journal of the SEAGS & AGSSEA, 10p.

Ishihara, Y., Okada K., Eguchi M., Mori A., Miyanohara T. (2024). Field tests on vertical and lateral resistance of steel sheet piles installed by the Press-in with Auger. Proceedings of the XVIII ECSMGE 2024, Lisbon Portugal.

Kasahara, K., Sanagawa, T., Nishioka, H., Sasaoka, R. and Nakata, Y. (2018). Seismic reinforcement for foundation utilizing sheet piles and soil improvement. Proceedings of the First International Conference on Press-in Engineering 2018, Kochi, pp. 555-562.

Kondo, Y., Sato, K., Nishimori, Y., Nakagawa, D. (2023). Giken Research Building: challenge for structure using sheet piles (part 2). Steel Technology, pp. 34-43. (in Japanese).

 © DFI International Bruges 2025

REDUCING THE CARBON FOOTPRINT OF PILE CONSTRUCTION: THE IMPACT OF INNOVATIVE TECHNOLOGIES

Mario A. Terceros H., Executive Director INCOTEC S.A. Santa Cruz, Bolivia, math@incotec.cc.

Mario Terceros Arce; Director INCOTEC S.A. Santa Cruz, Bolivia, mta@incotec.cc.

Walter Paniagua Paniagua, President PILOTEC S.A. Ciudad de México, México, wpaniagua@pilotec.com.mx.

Antonio Marinucci. President ADVANCED FOUNDATION SOLUTIONS LLC Nueva York, United States of America (USA), antmarinucci@gmail.com.

ABSTRACT

Integrating advanced technologies such as Smart Cell and Expander Body in drilled pile foundations represents a significant step forward in reducing the carbon footprint of construction projects. These innovations optimize load-bearing capacity by pre-mobilizing tip resistance and improving load transfer mechanisms, resulting in more efficient use of materials and energy. By reducing the required number of piles, minimizing concrete volumes, and decreasing the excavation and transportation of soil, these technologies substantially reduce greenhouse gas (GHG) emissions. This paper highlights the environmental and operational advantages of adopting Smart Cell and Expander Body technologies, offering practical evidence of their contribution to sustainable construction practices.

Keywords: Carbon footprint, QA/QC, innovation, deep foundations, Expander Body, preloading cell, tip injection, optimization.

INTRODUCTION

This paper discusses key aspects related to reducing the carbon footprint in deep foundation projects by implementing available technologies such as Expander Body and Smart Cell, which enhance the preload and pre-deformation of pile toes. These are complemented by technologies increasingly adopted, including continuous monitoring of construction processes and full displacement piles.

The construction industry is responsible for approximately 40% of global CO2 emissions and other greenhouse gases, GHGs, expressed in this paper as CO2 equivalents. These emissions stem from various sources, including the production of construction materials, manufacturing of equipment, transportation of materials and waste, use of machinery, energy consumption during construction, and indirect resources required for project execution. Reducing the carbon footprint in construction has thus become a critical objective to address climate change and promote sustainability to maximize the efficient utilization of natural resources while minimizing their depletion.

The experience of the authors shows that for a wide range of geotechnical conditions, the technologies analyzed herein lead to reductions of approximately 50% in concrete consumption and up to 90% in the transportation of excavated soil for deep foundations. Moreover, these technologies significantly reduce construction timelines, thereby decreasing the use of drilling machinery and achieving substantial fuel savings. As an additional benefit, the monitoring of construction processes, required as part of these systems, ensures a high level of quality control.

Over time, various technologies have been introduced to reduce the carbon footprint in the deep foundation industry. While most were initially developed to optimize costs and construction schedules, their contribution to CO2 emission reduction has been significant. Some technologies, however, have been designed specifically with greenhouse gas reduction as their primary focus.

Technologies contributing to carbon footprint reduction include:

 © DFI International Bruges 2025

- **Full displacement cast-in-situ piles**, which compact the surrounding soil and increase the piles' lateral resistance.
- **Automatic control systems for the installation of deep foundations**, enabling the optimization of adopted solutions.
- **Quality control systems for cast-in-situ piles**, active before, during, and after concreting.
- **Increased use of loading tests**, both for design purposes and quality control.
- **Devices for enhancing pile toe response**, which increases resistance, reduce deformations, and shorten construction schedules. Systems such as Expander Body and Smart Cell fall under this category.
- **Electric construction equipment**.
- **Energy piles**.

All these technologies optimize the design and construction of deep foundations, achieving lower energy consumption and reduced use of reinforced concrete. Consequently, they deliver both direct and indirect benefits regarding carbon footprint.

This paper evaluates the carbon footprint of cast-in-situ pile technologies incorporating Expander Body or Smart Cell systems, compared to traditional solutions without any of those devices. Furthermore, it highlights real project examples where these technologies were successfully implemented, demonstrating their substantial capability to reduce the carbon footprint in deep foundation construction. The proper combination of these technologies stands out as an effective and promising strategy for driving more sustainable and environmentally friendly construction, while also delivering inherent economic benefits.

BRIEF DESCRIPTION OF THE EXPANDING DEVICES TECHNOLOGIES: EXPANDER BODY AND SMART CELL

Expander Body

The Expander Body (EB) consists of a folded cylindrical steel body installed at the tip of a pile or anchor and expanded by injecting mortar or cement grout. After 24 hours from the initial injection, a secondary post-injection is carried out at the base of the body, increasing the system's stiffness and reducing settlements. The expansion process results in a density increase of the surrounding soil within a distance of approximately three times the diameter of the expanded EB. This phenomenon is analogous to the expansion of a spherical cavity, and its behavior is theoretically governed by the cavity expansion theory.

While the pressuremeter test is the geotechnical investigation tool that most closely replicates the behavior of an EB, common geotechnical investigations utilize SPT and CPTu tests to evaluate its performance. Building on over 30 years of expertise, more than 40,000 EBs have been successfully installed in all types of soil conditions and for a wide range of projects. The typical range of service load increase provided by EBs is between 30 tons and 150 tons, depending on the site’s geotechnical conditions and the specific type of EB utilized. Figure 1 illustrates the complete expansion process.

 © DFI International Bruges 2025

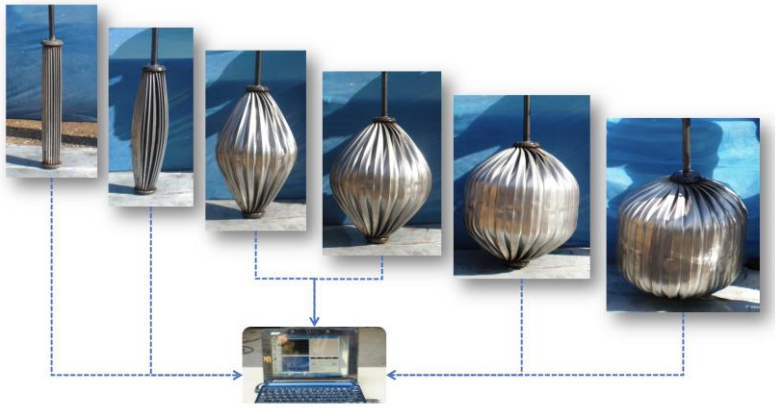


Figure 1: The complete expansion process of the Expander Body and its corresponding record

Smart Cell

The Smart Cell (SC) is a closed-type cementitious grout injection device attached to the lower part of the steel reinforcement cage in cast-in-situ piles. It functions similarly to a hydraulic jack in bidirectional static load tests. The system is instrumented with tell-tales to monitor movements during injection, allowing the generation of a load-movement curve for 100% of the piles. It acts as a preloading and pre-deformation cell. As axial compressive load is applied to the top of a drilled pile, the pile moves downward relative to the in-situ soil, where axial resistance is first mobilized as shaft resistance and then as toe resistance. Conventional drilled piles (i.e., without toe injection) cannot achieve maximum optimized resistance because full shaft resistance is attained with small vertical displacements (∂<10mm), while total toe resistance is achieved with relatively large vertical displacements (typically >4%D). This system optimizes pile resistance by matching deformations and increasing stiffness at the pile toe level.

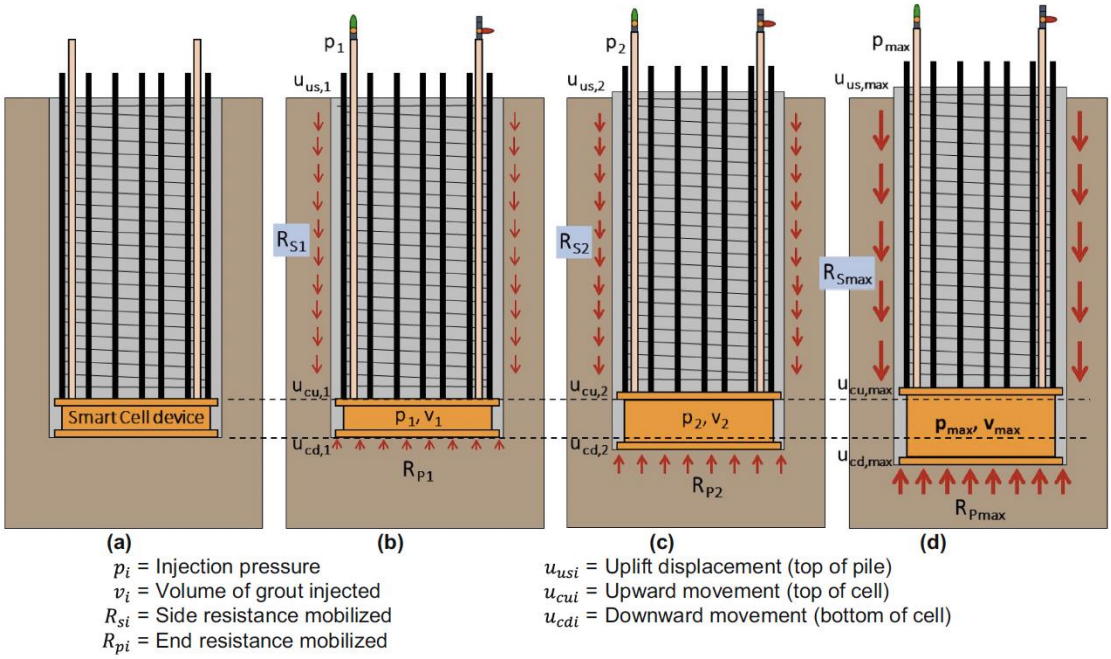


Figure 2: Schematic of the Smart Cell

 © DFI International Bruges 2025

GENERAL ASPECTS OF CO2 EMISSIONS ANALYSIS

Greenhouse gas (GHG) generation can be broadly classified into input-based, product-based, and process-based categories, depending on the environmental impact. Both direct and indirect emissions generated during the construction phase contribute to these diverse impact categories.

According to our measurements and specialized publications, the selection and use of materials and construction processes, as well as the embedded emissions from materials and the emissions arising from the operation and transportation of construction equipment, directly influence the design and construction of deep foundations.

In this analysis, we use direct CO2 generation categories, while indirect emissions are summarized as an equivalent of electricity consumption encompassing all tasks and their associated construction support and management components.

Emission factors and assumptions

As the focus of this article is the comparison of different in-situ cast deep foundation solutions, the following inputs used in this evaluation are outlined below:

1. Production of ready-mix concrete (m^3)
2. Cement content for concrete (t/m^3)
3. Aggregates for concrete (t/m^3)
4. Transportation and placement of concrete (h/m^3)
5. Reinforcement steel (t)
6. Placement of reinforcement steel (equipment hours)
7. Pile drilling and concreting (equipment hours)
8. Transportation of excavation waste (equipment hours)
9. Expander Body steel (t)
10. Cement for Expander Body injection (t)
11. Smart Cell steel (t)
12. Cement for Smart Cell injection (t)
13. Injection equipment (kW)
14. Indirect emissions expressed as electricity consumption (kW)

Based on these criteria, the equivalent CO2 generation can be expressed as follows:

$$E_{total} = \sum_{i=1}^{n} (E_{dir\,i} + E_{indir}) \quad [1]$$

Where E_{total} = total emissions, $E_{dir\,i}$ = direct emissions, E_{indir} = indirect emissions

All are expressed in kg CO2 equivalent.

While there are very complete and sophisticated methods for accurately calculating CO2 emissions in deep foundation projects, for this article, simplified criteria are presented. It is also noted that while some activities can be optimized, such as various transportation activities, that optimization would be the same for all compared cases. As a result, conservative values are considered in these categories, as the change in construction technology implies significant variations in the amount of material to be transported (incoming inputs and outgoing waste).

Using the prior values, Table 1 shows the amount of CO2 equivalent produced to execute 1 m^3 of in-situ cast pile.

 © DFI International Bruges 2025

Table 1: CO2 equivalent produced in each construction activity for 1 m³ of in-situ cast pile, including emissions for EB or SC

Item	Unit	Quantity	CO2 Emitted	CO2 Total/Unit
Concrete Production	m³	1,05	0,216	0,2268
Concrete Transport	h	0,1	0,0536	0,00536
Reinforcement Steel	t	0,08	1,6	0,128
250HP Construction vehicle	h	1	0,0536	0,0536
350HP Drilling Machine	h	0,125	2,68	0,335
150HP Support Equipment	h	0,015	2,68	0,0402
Electric Consumption	kW	25	0,005	0,125
TOTAL CO2/m³ OF CONCRETE PLACED IN THE PILE (t)				**0,91396**
Item	**Unit**	**Quantity**	**CO2 Emitted**	**CO2 Total/Unit**
EB Steel	t	0,03	1,6	0,048
SC Steel	t	0,03	1,6	0,048
EB Cement	t	0,03	0,9	0,027
SC Cement	t	0,005	0,9	0,0045

Specific Data

Table 2 shows specific results for different types of cast-in-situ piles, their typical service loads for the soils of Santa Cruz, Bolivia, and the incidence of tons of CO2 per ton of service load. It should be noted that the data were obtained from quaternary sandy-silt saturated soils with heterogeneous stratification.

Table 2: CO2 emissions analysis for different types of piles

Item	Amount of CO2 per Unit	Piles 1, Ø 1 m, L = 20 m	Piles 2, Ø 1 m, L = 20 m with SC	Piles 3, Ø 0.40 m, L = 12 m	Piles 4, Ø 0.40 m, L = 12 m with EB	Piles 5, FDP (Full Displacement pile) Ø 0.36 m, L = 12 m	Piles 6, FDP (Full Displacement pile) Ø 0.36 m, L = 12 m with EB	Piles 6, DCFA (Partial Displacement CFA) Ø 0.50 m, L = 24 m	Piles 6, DCFA (Partial Displacement CFA) Ø 0.50 m, L = 24 m with EB
Diameter(m)		1	1	0.4	0.4	0.36	0.36	0.5	0.5
Length(m)		20	20	12	12	12	12	18	18
Theoretical Volume + Overconsumption (m³)	m³	19.635	19.635	1.885	1.885	1.368	1.368	4.064	4.064
CO2 EMISSIONS (t)									
Concrete Production	m³	4.453	4.453	0.428	0.428	0.310	0.310	0.922	0.922
Concrete Transport	h	0.105	0.105	0.010	0.010	0.007	0.007	0.022	0.022
Steel	t	1.508	1.508	0.014	0.014	0.014	0.014	0.014	0.014
Transport Truck 250 HP	h	0.158	0.158	0.015	0.015	-	-	0.022	0.022
Drilling Machine 350HP	h	2.680	2.680	0.168	0.168	0.084	0.084	0.335	0.335
Support Equipment 150 HP	h	0.080	0.080	0.010	0.010	0.006	0.006	0.040	0.040
Electricity Consumption	kW	2.454	2.454	0.236	0.236	0.171	0.171	0.508	0.508
EB Steel	t				0.048		0.048		0.048
SC Steel	t		0.192						
EB Cement	t				0.027		0.027		0.027
SC Cement	t		0.018						
Total CO2 (t)		11.439	10.292	0.880	0.955	0.592	0.667	1.863	4.283
Normalizing CO2 Value Relative to Pile 1		1.000	0.900	0.077	0.084	0.052	0.058	0.163	0.374
Service Load (kN)		3500	7000	450	1100	750	1500	2000	3000
t of CO2/kN Service		0.00327	0.00147	0.00196	0.00087	0.00079	0.00044	0.00093	0.00143
Normalized t/CO2 Value Relative to Pile 1		100.00%	44.99%	59.86%	26.58%	24.17%	13.61%	28.50%	43.68%

It is important to highlight that the unit values of CO2 produced by each activity are considered for typical transportation distances and urban-type equipment in optimal working conditions. These tables intend to show the difference between technologies. As shown in Table 2, the CO2 emissions range from 5,8% to 100% per resisted ton, depending on the technology.

 © DFI International Bruges 2025

This analysis can also be performed in terms of costs per ton resisted; however, since prices vary by location, this would lead to confusion.

CASE HISTORIES

New Bridge over the Piray River – Mario Foianini 2

Figure 3 shows the geotechnical profiles show the bridge's construction line.

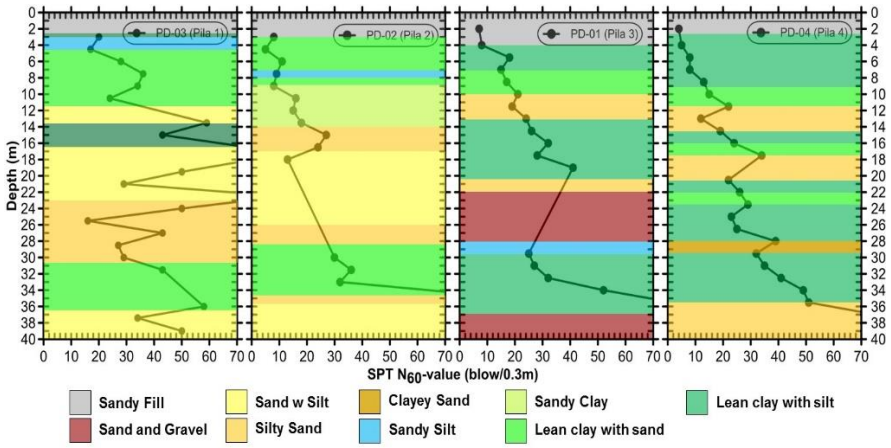


Figure 3: Geotechnical profiles of the bridge's implementation line

As shown in Figure 3, there is a clear heterogeneity in the distribution of layers.

Thirty-four piles were constructed with Smart Cell according to the following layout:

- 4 piers – 7 piles each, 30 m long. Tip in stiff lean clay.
- 2 abutments – 3 piles each, 25 m long. West abutment – Tip in silty sand; East abutment – Tip in lean clay.
- Design load per element: 4800 kN.

Load measured with head-down static tests: >8000 kN (Figure 4) Tests were stopped at deformations of less than 10 mm because of the high resistance obtained. The allowable project deformation was 25 mm. The piles have a resistance over 8.000 kN for less than 10 mm.

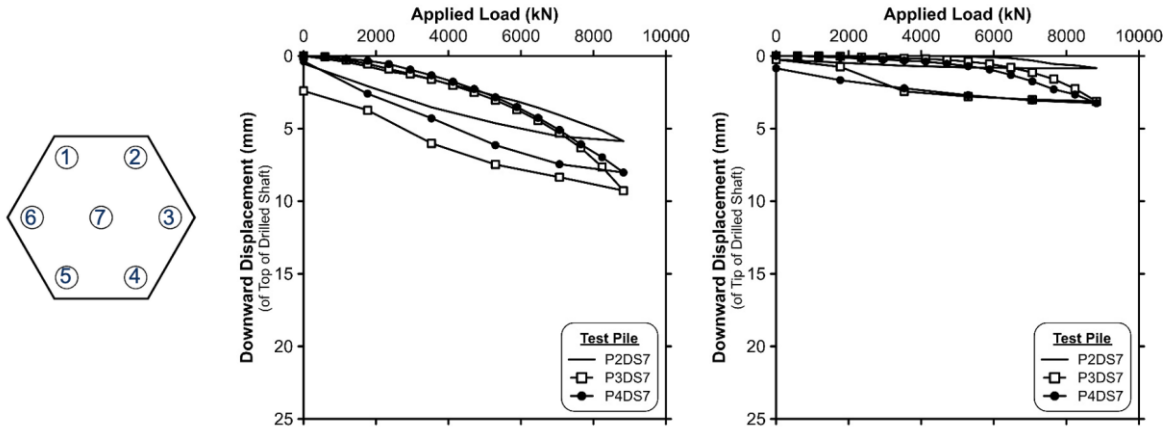


Figure 4: Load-movement curves measured at the head and at the tip of P2, P3 and P4 piles

With this data, the piles with Smart Cell have a CO2 production of 51,7% compared to the original design pile (without SC), meaning a 48,3% reduction in emissions. If the designer had conducted a

 © DFI International Bruges 2025

load test for the design using Smart Cells, these foundations would have been more economical and quicker to construct, as instead of 7 piles per pier, only 4 could have been constructed, saving 12 of the 34 piles, i.e., 36%.

Experimental Field B.E.S.T

In 2017, an experimental field for piles was constructed near the city of Santa Cruz, Bolivia, where more than 20 different types of piles were tested. The geotechnical investigation comprised SPT, CPTuS, DMT, DPSH, PMT, MASW, and REMI. Almost all the piles were bidirectionally and head-down tested.

The geotechnics of the site show low to medium-resistance soils composed of fine sands, silts, and clays. All the information can be found in http://www.cfpbolivia.com/web/page.aspx?refid=113. Figure 5 shows a compilation of 15 CPT tests and 5 SPT.

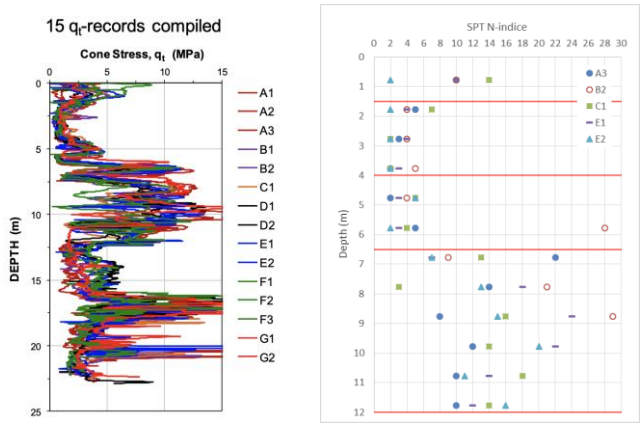
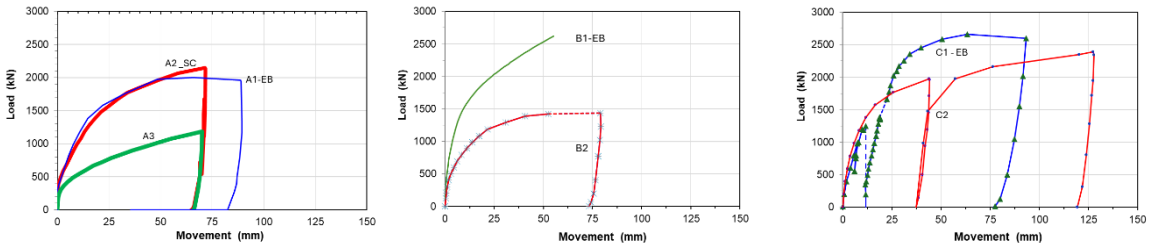


Figure 5: CPT and SPT compilations

The data of the seven piles of the B.E.S.T., analyzed for this paper, are presented in Table 3, as well as the results of the loading tests for the seven piles constructed with different methods and toe improvement devices are presented in Table 3 and Figure 6.

Table 3: Data for 7 piles constructed in the B.E.S.T. experimental field

Pile Code	Pile Type	Diameter(mm)	Length(m)	Concrete Type	Pile Toe Accessory	25 mm Movement Load (kN)
A-1	Drilled with Slurry	620,00	9,50	H-30	EB800	1580
A-2	Drilled with Slurry	620,00	9,50	H-30	SC	1578
A-3	Drilled with Slurry	620,00	9,50	H-30	NO	785
B-1	CFA	450,00	9,50	H-30	EB600	2030
B-2	CFA	450,00	9,50	H-30	NO	1240
C-1	FDP	450,00	9,50	H-30	EB600	2023
C-2	FDP	450,00	9,50	H-30	NO	1767



6.a: Drilled with slurry **6.b: CFA** **6.c: FDP**

Figure 6: Loading test results of piles at the B.E.S.T. experimental site

 © DFI International Bruges 2025

Conducting the same analysis as in Table 2, Table 4 shows values of ton of CO2 per kN of service load at 25mm deformation are obtained.

Table 4: CO2 generation analysis for each type of pile

Pile	Service Load (kN)	CO2 Per Pile (t)	CO2/Kn of Service (t/kN)	Normalized kN Service/tCO2 Value Relative to Pile A3 (Simple Bored)
A-1	1580	3.732	0.002362	54.31%
A-2	1578	3.714	0.002356	54.19%
A-3	785	3.414	0.004349	100.00%
B-1	2030	2.090	0.001029	23.67%
B-2	1240	1.639	0.001322	30.40%
C-1	2023	1.557	0.000770	17.70%
C-2	1767	1.270	0.000791	18.19%

In this case, the improvement in terms of CO2 generation and economy in full displacement piles (FDP) with EB is significant. These results are quite similar in the Santa Cruz area, where more than 150 projects were already built.

ENVIRONMENTAL IMPACT AND CARBON FOOTPRINT REDUCTION

One of the most significant advantages of integrating Smart Cell and Expander Body technologies into drilled pile foundations is their contribution to reducing the carbon footprint of construction projects. Traditional foundation methods, which often require substantial quantities of concrete and steel, are major contributors to greenhouse gas emissions due to the energy-intensive processes involved in the production, transportation, and handling of these materials. By enhancing the performance of drilled piles through these innovative technologies, several critical environmental benefits are achieved.

These technologies optimize the load-bearing capacity of piles by pre-mobilizing toe resistance, enabling the use of smaller pile diameters and reducing the overall number of piles required. This optimization directly translates to a substantial decrease in the volume of concrete needed. As concrete production is one of the largest sources of CO2 emissions in construction, minimizing its usage significantly mitigates environmental impacts. Case studies have demonstrated reductions in concrete usage ranging from 10% to 50%, resulting in a notable decrease in carbon emissions associated with foundation projects.

The enhanced load transfer capabilities provided by Smart Cell and Expander Body technologies facilitate more efficient utilization of materials. By achieving higher load capacities and structural stability with reduced material quantities, the consumption of key raw materials such as cement, aggregates, and reinforcing steel is significantly diminished. This efficiency not only alleviates the environmental burden of resource extraction and processing but also reduces energy demands related to material transportation and handling on-site.

The application of these technologies leads to measurable energy savings throughout the construction lifecycle. With fewer piles and reduced material handling requirements, the energy consumption for on-site operations is significantly reduced. Furthermore, the increased efficiency of the foundation system accelerates construction schedules, thereby lowering the energy demand for heavy machinery and equipment. These factors collectively reduce the overall environmental impact of the project.

As the construction industry intensifies efforts to reduce its environmental footprint, the adoption of advanced technologies like Smart Cells and Expander Body plays a critical role in driving sustainable development. By illustrating the clear benefits of these technologies in lowering the carbon footprint of foundation construction, this discussion advocates for their broader adoption as a cornerstone of

 © DFI International Bruges 2025

sustainable practices in the sector. The case studies include herein provide compelling evidence that Smart Cells and Expander Bodies not only achieve sustainability objectives but also maintain and enhance performance and safety standards.Tables 5 and 6 provide a summary of the concepts analyzed herein.

Table 5: Comprehensive Benefits of Expanding Devices Technologies

Category	Benefit
Economic	- Reduced material costs due to smaller pile diameters and fewer piles. - Lower overall project costs through optimized material usage and faster construction times.
Construction Timeline	- Accelerated project timelines due to improved efficiency in pile performance. - Faster installation and load testing processes
Carbon Footprint Reduction	- Significant reduction in concrete usage, leading to lower CO2 emissions. - Reduced energy consumption during construction and transportation of materials.
Quality Control	- Enhanced monitoring and real-time adjustment capabilities during installation. -Improved consistency and reliability in load-bearing performance.
Load Measurement	- Accurate measurement of pile resistance through pre-mobilization of toe resistance. - Reliable data for load tests and performance assessments.
Long-Term Durability	- Increased structural stability and longevity, reducing the need for maintenance or repairs. - Sustained performance over the lifespan of the structure.
Environmental Sustainability	- Contribution to sustainable construction practices by minimizing resource usage and emissions. - Support for green building certifications and environmental goals

Table 6: Comparison of Piles with Smart Cell or Expander Body vs. Conventional Piles

Parameter	Piles with expanding devices (Expander Body or Smart Cell)	Conventional Piles without expanding devices (Expander Body or Smart Cell)
Axial strength	Greater resistance mobilized with less displacement	Skin and tip resistance are mobilized separately
Vertical Displacement	Lower displacement required to achieve full resistance	Greater displacement required to mobilize tip resistance
Materials	Lower volume of concrete and steel required	Increased concrete and steel consumption
QA/QC	Real-time monitoring during injection	Depends on the quality of the installation process
Construction time	Significant reduction in construction times	Longer construction times due to the need for greater deformation control
Carbon footprint reduction	Significant reduction in CO2 due to reduced use of materials and machinery	Higher costs due to increased material quantity and lead time
Total costs	Lower total costs due to resources optimization	Higher costs due to increased material quantity and lead time
Load capacity	Load capacity increased by 50% or more depending on soil conditions	Load capacity limited by strain incompatibility

CONCLUSION

Smart Cell and Expander Body technologies represent a significant advancement in cast-in-situ deep foundation engineering, offering a dual benefit of improved structural performance and reduced environmental impact. By pre-mobilizing tip resistance and harmonizing deformations, these innovations optimize load-bearing capacity, minimize vertical displacements, and reduce the number and size of piles required. This leads to substantial reductions in the consumption of concrete, steel, and other materials, and lower emissions associated with material production, transportation, and handling.

Case studies demonstrate that these technologies can achieve up to a 90% reduction in the carbon footprint per ton of load resisted, setting a new standard for sustainability in foundation engineering.

As demand for environmentally responsible solutions grows, these technologies are poised for broader adoption. Future research should focus on optimizing their implementation and exploring applications

 © DFI International Bruges 2025

across diverse soil conditions and project types, ensuring continued advancements in both performance and sustainability.

REFERENCES

FHWA, Evaluation and Guidance Development for Post-Grouted Drilled Shafts for Highways (2017)

Broms, B.B. And Nord, B, 1985. Axial Bearing Capacity Of The Expander Body Pile. Soils And Foundations Vol. 25, No2, June 1985. Japanese Society Of Soil Mechanics And Foundation Engineering. Pp. 31-44

EFFC/DFI Carbon Calculator https://www.effc.org/how-we- operate/eco%e2%82%82-foundations/

Fellenius, B.H. 2013. Report On A Pile Prediction Event. 1° CFPB, Santa Cruz, Bolivia

Fellenius, B.H. and Terceros, M.H. Response to load for four different bored piles. Proceedings of the DFI- EFFC International Conference on Piling and Deep Foundations, Stockholm, May 21-23,

Gang Guo ,Zhong Liu, Aiping Tang, Yibing Deng, Jiqiang Zhang: Model, Test Research on Bearing Mechanism of Underreamed Ground Anchor in Sand. Hindawi Mathematical Problems in Engineering Volume 2018, Article ID 9746438, 14 pages

IEA-UN 2019 Global Status Report for Buildings and Construction

Loehr, J.E., Marinucci, A., Hagerty Duffy, P., Gómez, J., Robinson, H., Day, T.J., Boeckmann, A.Z., and Cadden, A.W. (2017). Evaluation and Guidance Development for Post-Grouted Drilled Shafts for Highways, Report No. FHWA-HIF–17-024, *Federal Highway Administration*

Massarsch, K.R., Execution, supervision and quality control of anchors. 1994. Proceedings of the 13th International Conference on Soil Mechanics and Foundation Engineering, New Delhi,India

Marinucci, A., Mario Terceros H., Mario Terceros A., Tip Post-Grouting and Premobilization of Resistance of Drilled Shafts using Smart-Cells at Two Bridge Structures in Bolivia.

Marinucci, A., Mario Terceros H., Mario Terceros A., Increased Resistance of Small-Diameter Piles and Ground Anchors by using an Expander Body.

Mullins, G. (2015). "Grouting Effectiveness – Construction QA/QC of Post-grouted Shafts." *Presentation delivered at FHWA/Caltrans Workshop on Quality Assurance for Post- grouted Drilled Shafts. April 15-16.* Oakland, CA.

Murillo, T., Design, and Construction of Cast-in-situ Piles Using Toe- Grouting Cell. Application in Bolivian Rivers.) Proceedings 3, CFPB (Congreso Internacional de Fundaciones Profundas de Bolivia)

Randolph, M., Considerations in the design of piles in soft rock,

Fellenius, B.H., Massarsch, K.R., Terceros H., M. 2018. A study of the augmenting effect of equipping piles with an Expander Body. DFI-EFFC

Proceedings of the 17th Pan-American Conference on Soil Mechanics and Geotechnical Engineering (XVII PCSMGE), La Serena Chile, 2024.

CONTEXT AND CHALLENGES OF DEEP FOUNDATIONS IN URBAN ENVIRONMENTS: A CASE STUDY

Adrien Dumont, Franki Foundations Belgium, Saintes, Belgium, +32 (0) 2 391 46 46, adrien.dumont@ffgb.be

Grégory Laurent, Franki Foundations Belgium, Saintes, Belgium, +32 (0) 2 391 46 46, gregory.laurent@ffgb.be

Thomas Wulleman, Franki Foundations Belgium, Saintes, Belgium, +32 (0) 2 391 46 46, thomas.Wulleman@ffgb.be

ABSTRACT

This article presents an innovative construction project located in the center of Brussels, involving the use of kelly-bored piles approximately 50 meters deep in a highly confined space. The project concerns the construction of a hotel and is distinguished by the adoption of advanced techniques such as polymer-supported drilling and the use of recycled aggregate concrete, tailored to the specific constraints of a dense urban environment.

Kelly boring with polymer support was chosen to stabilize the walls of the deep boreholes, minimizing disruptions to surrounding structures and ensuring site safety. Additionally, the use of recycled aggregate concrete demonstrates the project's commitment to sustainable and economical practices, while ensuring high performance in terms of durability and strength.

The results show that despite space constraints and technical challenges, it is possible to install long piles efficiently and sustainably. The innovative techniques employed have overcome the physical limitations of the site while ensuring high structural quality. This project provides valuable recommendations for engineers and designers working in similar urban environments, highlighting the importance of adapting construction methods to the specific conditions of the site.

In conclusion, this project illustrates how advances in drilling techniques and the use of recycled materials can be successfully integrated into complex urban construction projects, paving the way for more sustainable and environmentally friendly practices.

Keywords : bored piles, polymer, recycled aggregates, design

INTRODUCTION

Urban environments today are often densely packed, leaving minimal space for new construction projects. Consequently, buildings frequently undergo expansions or renovations within their current locations, which requires careful consideration of soil properties and the constraints posed by adjacent structures. These projects become increasingly complex due to intricate building designs and foundational requirements, including limited basement space for large structures and cantilevered designs.

In crowded urban spaces, planning and organizing construction is challenging due to limited workspace. The reduced space available for the works has a considerable influence on the technical and logistical choices made at every stage of the project. In these environments, environmental and ecological nuisances are all the more critical. This is specifically the case for the execution of the deep foundations. This was exemplified in the extension of the Palace Crowne Plaza hotel in Brussels. We

 © DFI International Bruges 2025

explain below the choices we made together with the general contractor and consultants on this particular project in the hyper Centre of Brussels.

EXTENSION OF THE PALACE CROWNE PLAZA HOTEL IN BRUSSELS

The context



Figure 1 - Extension of the Palace Crowne Plaza Hotel – Place Rogier- Brussels

The project to extend the Palace Crowne Plaza hotel in Brussels, the foundations of which were completed by Franki Foundations in 2023, is a good illustration of these challenges. Located in the heart of the Belgian capital, around 1 km from the Grand Place (Figure 1), this complex project is set in a dense urban environment, surrounded by a pedestrian zone, a pavement, an underground metro and the existing five-star hotel, which remained in operation during the works (Figure 2).

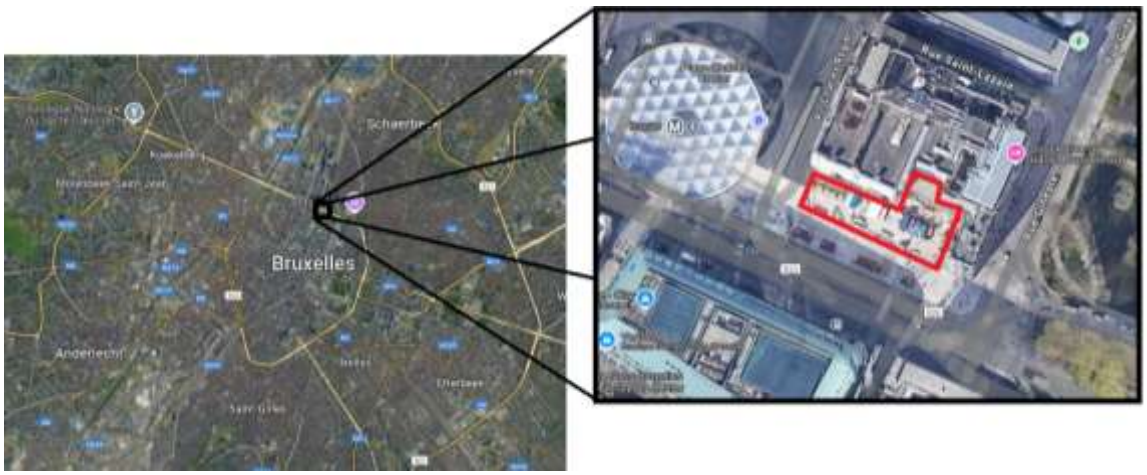


Fig. 2 - Project Location

This context had two major consequences for the design and execution of the deep foundations. Firstly, specific constraints were imposed on the dimensioning of the foundations, in particular due to the immediate proximity of the hotel and the underground metro which leads to a cantilevered structure of the new hotel. These aspects are detailed in the next section. Secondly, the work area was extremely tight: the work platform was only 900 m² and the storage and circulation area 500 m², equivalent to only 20% of the surface area of a football pitch. These restrictions dictated crucial choices for the organization of the site, which will be explained in more detail below. Furthermore, the project was

 © DFI International Bruges 2025

guided by a commitment to minimize the carbon footprint, implementing various initiatives that will be elaborated on later.

GEOTECHNICAL CONDITIONS

The subsoil in Brussels is made up of three main geological layers: a sandy fill, a compact Ypresian sandy clay and clayey sand layer 30 to 40 meters thick, and very compact Landes sands with a high cone resistance (qc greater than 25 MPa) (Figure 3).

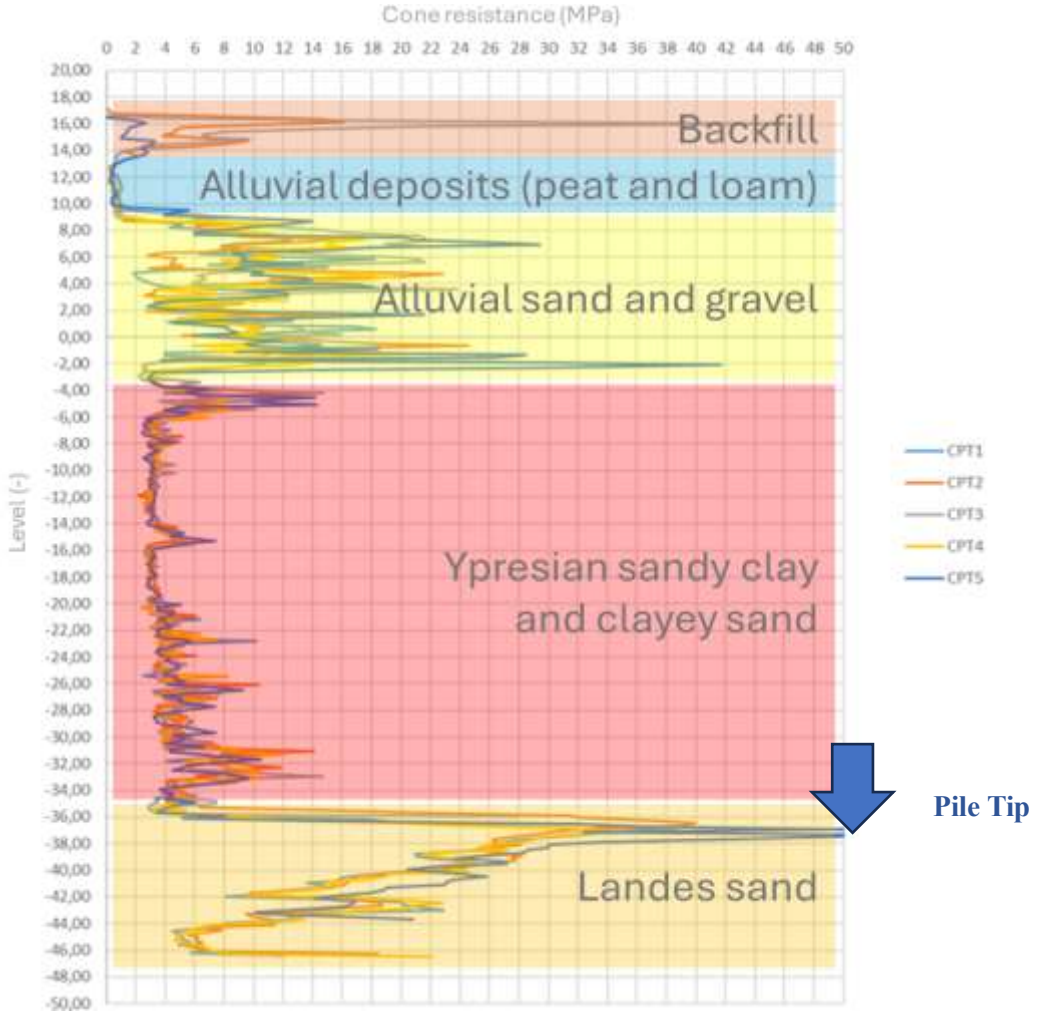


Figure 3 – CPT Diagram

DIMENSIONING THE FOUNDATIONS: A MAJOR TECHNICAL CHALLENGE

As explained above, the new wing of the hotel is bounded to the north by the existing hotel and to the south by an underground railway.

To the north, the existing hotel has a cellar level and sits on wooden piles. Underpinning the hotel's foundations with jet grout columns (Figure 4) was adopted to limit the risk of differential settlement of the existing building during earthworks for the new section.

 © DFI International Bruges 2025

To the south, the presence of the metro beneath the construction site drastically limited the footprint of the new foundation, leading architects to cantilever the building over the metro to avoid reducing the surface area of the new building (Figure 4 and Figure 5).

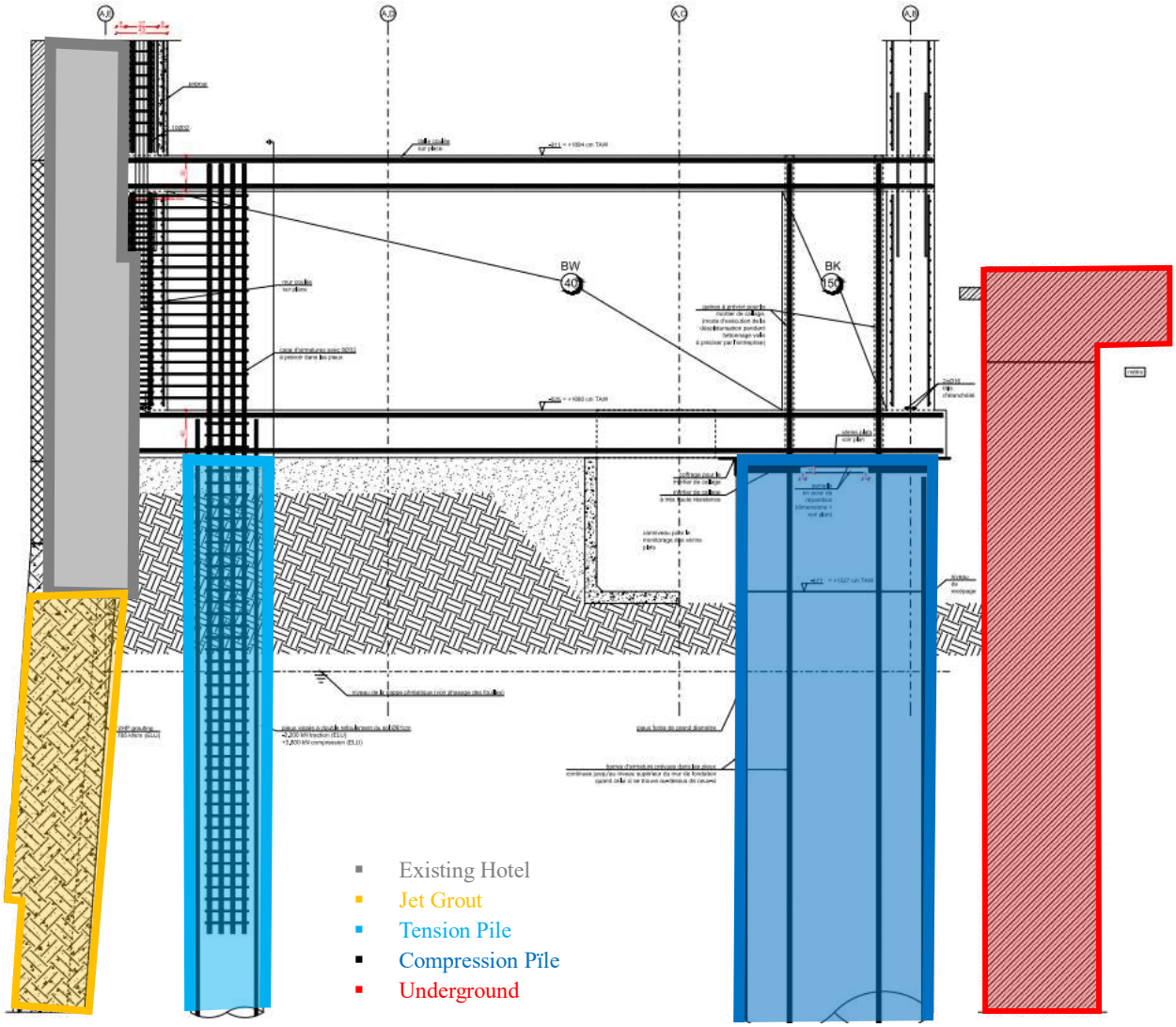


Figure 4 - Foundations solution for the new hotel

 © DFI International Bruges 2025

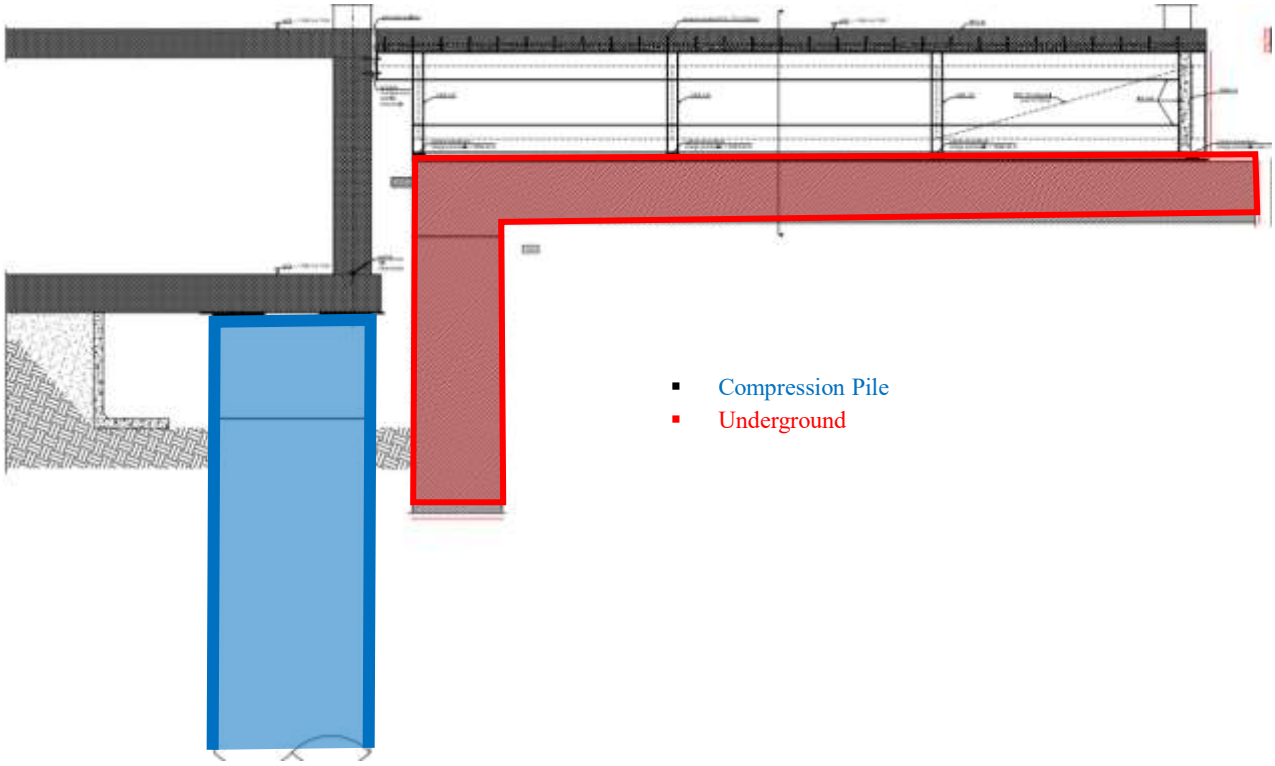


Figure 5 – Cantilever structure above underground

The final ultimate loads are distributed over large-diameter bored piles, ranging from 1,500 (max 13 000kN per pile) to 2,000 mm (max 17 000kN per pile), as well as 559/680 mm injected tubed screw piles (max 3 800kN per pile), as shown in Figure 6.

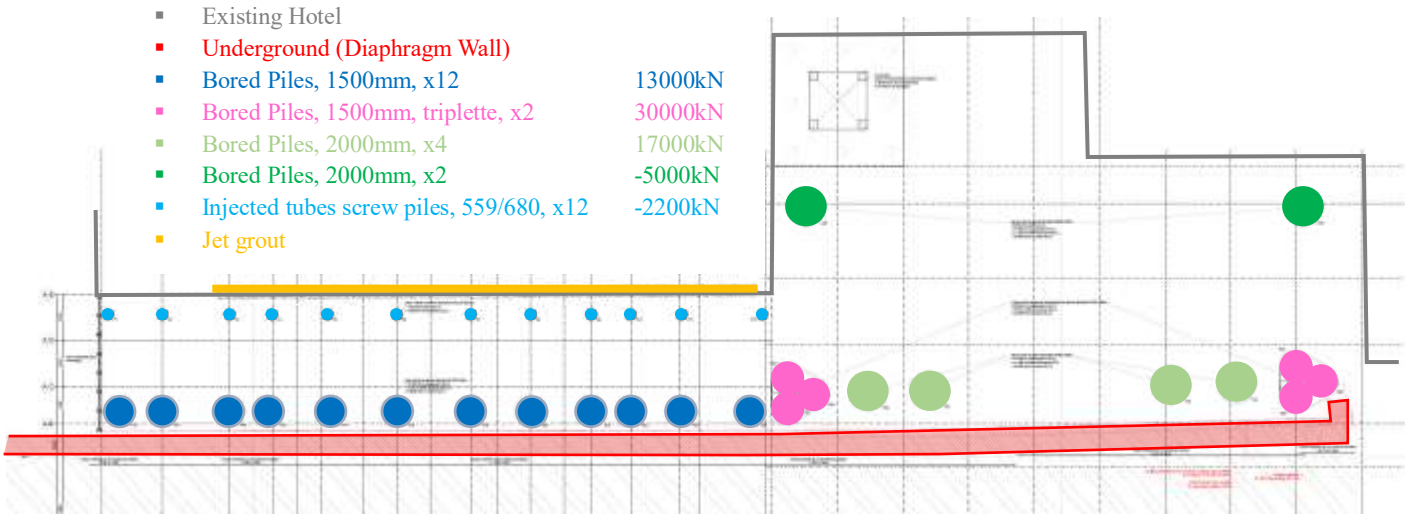


Figure 6 - Piles details

For the highest loads (30 000kN incl. safety per unit) of the border columns, a triple pile solution was necessary. The maximal diameter of 2.00m didn't ensure the requested bearing capacity. The use of double piles was a possibility, but this solution had a negative influence on the eccentricity of the structure. The final setup is a compromise between the number of piles and their diameter. Three piles of 1,50m were defined to reach the necessary bearing capacity and the requirements for the geometry.

 © DFI International Bruges 2025

For the piles close to the D-wall of the metro, a calculated reduction in pile diameter was applied up to the level of the D-wall base to take account of potential friction loss. The same principle was used for the piles located very close together (Figure 7).

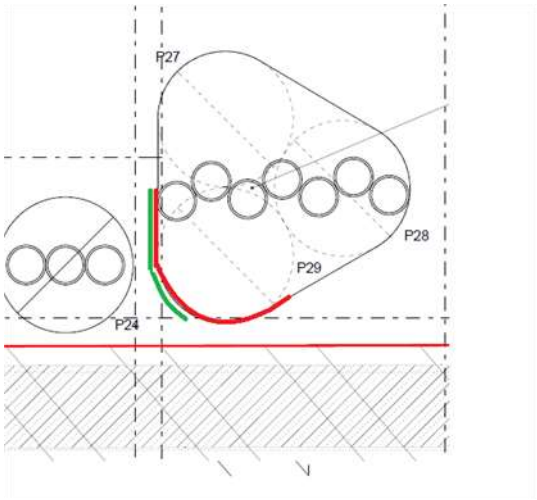


Figure 7 - Reduction of the diameter of the triple-pile solution

The bored piles, 50 meters long, were set 1 meter in Landes sands and were partially reinforced. To prevent the ground between the piles and the D-wall from collapsing as distance between them was about 40cm, the piles were cased to a depth of 1 meter below the base of the walls. This distance is very challenging concerning the relaxation of ground during the execution influencing the bearing capacities of the existing deep foundations. This limits also the risk of concrete contact between the hotel's foundations and the walls of the metro and therefore limits the direct transmission of vibrations from the metro to the hotel.

The challenge for this type of hyperstatic and hypersensitive structure is the management of the settlement during the construction. Flat jacks were installed on the head of the piles to compensate for the settlement during the construction.

DRILLING PROCESS

The piles were drilled under partial casing and under stabilizing fluid (see further). The rig was a Bauer BG 39 with the technical characteristics summarized in Table 1.

Table 1 - Technical characteristics of BG39

Rotary Drive	Torque (nominal) at 350 bar	389 kNm
	Speed of rotation (max)	46rpm
Crowd winch	Crowd force push and pull, effective/nominal	460 / 590 kN

The piles were about 50m and cased on 20m in the Ypresian clayey sand due to execution and design requirements (see previous section). Drilling occurred using buckets instead of auger to increase the recovery of soil in the stabilizing fluid. It was a sand bucket with 2 entries to limit deviation of the tool under the casing.

At the end of the drilling process, a waiting period was implemented to allow the suspended particles to settle. A flocculant additive was used to minimize this time. The pile tip was then cleaned with a cleaning bucket, and samples of drilling fluid were taken from three different levels of the pile (top,

 © DFI International Bruges 2025

middle, and bottom) to check the parameters, including sand content. Some of the piles were partially reinforced with a cage approximately 17 meters long, installed before concreting. To prevent the reinforcement from sinking during the casing removal process, a trial lift of the cage was conducted to ensure sufficient friction to keep the cage in place within the fresh concrete.

SUSTAINABLE INNOVATIONS

Polymers

Carrying out the large-diameter bored piles in a restricted working area was a major challenge. Drilling required a stabilizing fluid to guarantee the stability of the walls during digging. The use of water as support fluid was ruled out because of the potential presence of pockets of saturated sand under pressure in the clay layers, a phenomenon well known in Brussels. Drilling under polymer fluid was chosen.

Drilling under polymer is not so common in Belgium. Most of the bored piles are fully cased, which is often the best solution because of limited depths. When piles are long (exceeding 35 m), bentonite is often used as stabilizing fluid. However recent ecological or space considerations drive the use of alternatives such as biodegradable polymers.

In this case, the choice was made on a synthetic polymer from Geosoil (Polymud), which is a synthetic long chain anionic polyacrylamide polymer with high molecular weight and charge density that generates a high viscosity slurry. Polymer allows suspended particles to precipitate out, eliminating the need for sand removal and reducing the drilling cycle time. This method also reduces the amount of space required on site, as there is no need for a de-sanding installation. Under NBN EN 1536, the maximum value for the verification of sand content is 4% per unit volume of support fluid. To increase the self-cleaning effect of the polymer, the additive MicroBond was used as a flocculant to speed up the sedimentation of particles. This additive strengthens the anionic and associative groups of the polymer's matrix and is also used as a catalyst for the different sedimentation and cleaning process.

The drilling was a success, the quality and the productivity were reached but the polymers was more a mitigation of risks measure and a execution requirement.



Figure 8 – Partially cased bored piles under polymer fluid were installed

 © DFI International Bruges 2025

Additionally, recent Brussels legislation classifies bentonite sludge as waste to be treated, thereby increasing disposal costs. The biodegradable polymer used in this project, in agreement with an environmental consultant, could be discharged into the sewage system after limited treatment and checks on certain parameters (temperature, pH, viscosity, suspended matter and matter extractable with petroleum ether). During execution, the viscosity and pH had to be adjusted before discharge.

CONCRETE MADE FROM RECYCLED AGGREGATES

As part of its commitment to environmental innovation, Franki Foundations decided to use concrete made from recycled aggregates for this project. This project marks the first large-scale trial in Belgium of this type of concrete for deep foundations, a choice that is part of a sustainable development strategy. This application was developed in close cooperation with our concrete supplier, with the objective to comply with the Belgian BENOR-certification system. Depending on the application of the concrete, a maximum substitution rate for natural aggregate is imposed in the standards. These substitution rates should certainly be revised upwards in the future, and recycled sands should also be considered for performance concretes. In this case, 30% of the natural aggregates were replaced by recycled concrete aggregates which comply with category A+, for which high technical requirements are imposed in standard NBN B15-001. The pile concrete mix meets all the requirements of Annex D of standard NBN EN 206 and was supplied with BENOR inspection and with the following specification: C-Green Recypile Engi WE C30/37 EE1 20 S5.

In addition, the additional requirements from Table 2 had been specified, according to the DFI/EFFC guidelines for tremie concrete.

Table 2 – Additional requirements for concrete

Test	Standard	Criterium
Slump-flow test	EN 12350-8	500 ± 50mm
Slumpflow velocity test	EN 12350-8	40 ± 5mm/s
VSI	ASTM C1611	0-1
Bauer test	EN ISO 10414-1	≤22ml
Bleeding test	EN 480-4	≤ 10%
Workability		4 hours

 © DFI International Bruges 2025



Figure 9 – Pouring of concrete with recycled aggregates

Given the large diameter of the bored piles (up to 2 metres), the application of a low-heat cement from CCB was opted for: CEM V/A 42.5N LH HSR LA. The quantity of fine particles and granule skeleton were fine-tuned to obtain a stable and robust composition so that the different requirements of fluidity and water separation limitation could be combined. Use of recycled granulates has a negative impact on initial fluidity and workability over time due to higher water absorption and more angular and porous nature of the granules. By adapting the mixing time, storing the concrete aggregates with continuous water saturation, adapting the recipe with sufficiently fine particles and mixing additives (superplastifier and rheology extender), a good initial fluidity could be obtained on the one hand and processability could be maintained for 240 minutes on the other.

CONCLUSION

Renovations or extensions of existing buildings in crowded urban environments challenge the capacities of developers, consultants and contractors, pushing the limits of standard construction methods.

On the other hand, recent technological advancements help foundation contractors to meet high standards of architectural and structural requirements while adhering to new environmental regulations. These advancements include both construction technologies and materials. New standards are being developed to encourage and integrate innovative technologies.

In this context, the Crowne Plaza Hotel extension is a prime example of how these complex challenges of deep foundations in urban environments can be addressed, showcasing innovative and adaptive solutions to geotechnical constraints, spatial limitations, and environmental demands.

ACKNOWLEDGMENTS

We want to recognize the excellent collaboration between all the stakeholders to this challenging project: our client, the JV Socatra-Denys, the consulting engineers UTIL, and our suppliers Geosoil (polymer) and CCB (Concrete).

 © DFI International Bruges 2025

DEVELOPMENT AND IMPLEMENTATION OF AN AI-BACKED HUMAN DETECTION SAFETY SYSTEM FOR PILING RIGS AND CRANES

Andrew Bell, Technical Director, Cementation Skanska
David Fowle, Electrical Supervisor, Cementation Skanska
Jason Dobson, Spillard Safety Systems

ABSTRACT

Contact with moving plant is one of the most significant health and safety hazards on modern construction sites. This risk can be exacerbated when employing specialist geotechnical equipment with restricted operator visibility. To help reduce this risk, an AI backed human form detection and recognition camera system has been development and installed on piling rigs and cranes. The system recognises people or objects if they enter designated configurable exclusion zones and automatically suspends high risk operations of the machine, such as tracking and slewing. The system uses a combination of operator aids and audible and visual exterior warnings dependant on the detected situation.

This paper will present the authors experience of the evolution of rig/crane operator aid technology over the last 20 years, starting with simple reversing cameras to the first use of 360 degree camera systems, culminating in the latest AI backed human detection system currently undergoing development and trials by Cementation Skanska in the UK, developed in conjunction with Spillard Safety Systems.

The paper will provide an overview of the new system and share some of the key challenges in its development and incorporation on to specialist geotechnical plant. It will also discuss the human behavioural challenges that such systems have to overcome to ensure they are fully supported and adopted by the end user.

INTRODUCTION

The human to construction plant interface is one of the top fatality risks identified in the construction industry. Based on some research carried out in 2017[(1)], over the preceding five years there had been 217 fatal accidents on UK construction sites, 10% of which were due to workers being struck by moving vehicles and plant. There was also many more major injuries and near misses during this period involving the human-plant interface that also had the potential for fatal injury.

Unfortunately, things have not improved in the UK since 2017. In 2023/24, 51 UK construction workers were killed by fatal injuries on site and it remains by far the worst industry in terms of number of fatalities, over 10% was attributed to contact with plant or vehicles.

The interface between humans and construction plant remains one of the highest risks to health and safety on modern construction sites. Whilst the development of autonomous plant and vehicles may, in the future, remove the need for humans on, or at least in certain areas of the construction site, this will not be possible for many years if indeed ever. Modern construction plant has been available with remote operation capability for a number of years, examples include small drilling or piling rigs where removable remote controls are fitted. Whilst this may reduce the risk of plant contact with the operator, additional risks of operator visibility of the working area may be created.

Development and trial of semi or fully autonomous vehicles continue for more general construction and mining plant, such as autonomous quarry trucks, but very little development is taking place in the specialist geotechnical plant sector and projects are typically fully reliant on human piloting of the plant and human management of the working area surrounding the machine.

Whilst it is important to consider and support the development of autonomous construction plant, this paper will focus on advancements in technology that have allowed currently available construction

 © DFI International Bruges 2025

machinery, specifically specialist geotechnical plant and cranes, to be retrofitted with systems that significantly improve the safety of the working zone around such equipment.

The paper will concentrate on the authors personal experience and acknowledges that there may be other initiatives and systems under development globally that could improve the safety of the human-plant interface.

EVOLUTION OF THE HUMAN-PLANT INTERFACE SAFETY SYSTEMS

The easiest way to reduce or indeed eliminate the risk of plant-human contact related incidents is to remove humans from the risk zone entirely.

For specialist geotechnical works, with current technological advancements, it is impossible to remove humans from the working area as there are multiple tasks in and around the machines that only humans can carry out. This would include simple operations such as checking a pile depth with a tape measure during drilling, or inspection of spoil arisings from the bore. There are many parts of the works process that require humans to enter the danger zone, for varying periods.

If left unmanaged, the human-plant interface zone presents a significant risk. The image below shows an extreme example of such an interface with no active or passive safety systems in place.



Figure 1.0 Graphical representation of high risk human-plant interface

The following section summarises currently available systems and processes that are used to manage the human-plant interface, sharing the latest state of the art system currently under development.

The Banks Person (also known as Rig Attendant)

The use of a banks person to manage the danger zone at the pile-human interface is well known and widely adopted. This relies heavily on the individual responsible for managing the zone to keep it clear of humans and remain in regular contact and visibility with the plant operator.

This system can be improved with regular training and competence assessment of the banks person, often complimented by health surveillance to ensure the human is both competent and capable of carrying out the task. This is applicable to both the banks person and the plant operator.

Whilst this paper describes a number of other systems, basic and sophisticated, physical and digital that can reduce the human-plant contact risk, the authors recommend the continued use of a banks person to compliment the ongoing development of any advanced, potentially autonomous safety system.

Physical barriers

As mentioned previously, removal of the human element of the human-plant interface is the easiest way to reduce or eliminate the risk of contact. Whilst not possible for all aspects of any specialist geotechnical works, good segregation of humans and plant, as much as practical, is essential.

 © DFI International Bruges 2025



Figure 2.0 photo: typical good quality site segregation barriers

The photo above shows a good example of human-plant segregation, whilst this may be appropriate for fixed site access and walkways such a system is not easy to adopt to ensure a physical exclusion zone around, for example, piling plant, given the need for the machinery to constantly move in location and orientation and for multiple human activities needed close to the plant.

The authors acknowledge that there are many circumstances when such physical segregation is not possible and thus this paper describes a number of other safety measures and systems than can be considered.

Plant specific barriers

Over the last 20 years Cementation Skanska have trial a wide range of physical barriers to isolate the plant from humans and create a suitable exclusion zone. For specialist geotechnical works, there remains a need for humans to work in the exclusion zone for tasks such as checking casing alignment, dipping pile depths etc. Attendant plant, such as cranes, are more easily segregated with an enclosed barrier system.

Cementation Skanska currently utilise a pole and cone system, as shown in the photos below. This has been found to be very effective and combines a highly visible physical barrier with the ability to easily move the system. It is recognised that this mobility is also one of the weaknesses of the system and robust processes and consistent behaviours are needed to ensure its effectiveness.



Figure 3.0 photo of barriered exclusion zone with operative working within the zone, in full view of the rig operator. In this case to check casing verticality.

 © DFI International Bruges 2025



Figure 4.0 photo of static barriered exclusion zone around a supporting crane and a close up of the pole and cone system.

The above photos are used to demonstrate why physical barriers may be particularly appropriate for some general construction plant such as supporting cranes, that do not move in location much, but specialist geotechnical plant.

In 2021, the UK Federation of Piling Specialists (FPS) published a guidance document 'Plant Restricted Zones' [(2)], providing clear guidance on planning and managing the human-plant interface on specialist geotechnical sites. Whilst an excellent document covering a broad range of ground engineering works, this focused on the use of physical barriers and did not consider the adoption of advanced technology to further improve safety on site. It is recommended that this paper be read in conjunction with the FPS guidance.



Figure 5.0: Extract from FPS guidance

Piling plant and crane specific technological advancement

This section of the paper describes the authors experience with incorporation of additional technology to existing specialist geotechnical plant, such as piling rigs, that has reduced the risk of human-plant contact. In all cases such systems were used in conjunction with both the banks person and physical barriers, wherever possible.



Figure 6.0: Rope winch camera & reversing camera

 © DFI International Bruges 2025

Winch and reversing cameras (early 2000's)

Cementation Skanska began fitting reversing cameras and winch cameras to their geotechnical plant and cranes in the early 2000's. It was broadly recognised that these systems improved safety on sites by improving the rig operators visibility and eliminating a key blind spot at the rear of the plant.

The drawback of such systems is it relied fully on the rig operator monitoring a camera output monitor. This could also create an additional distraction to the operator.

Most large modern specialist geotechnical plant has these systems fitted as standard by the manufacturer now.

Quadview TSS2 (Early 2010's)

Cementation Skanska were the first company in the UK to introduce a 360 degree quadview camera system to its specialist geotechnical plant. This system provide a view of the complete rig perimeter and displayed this on a 'quad view' screen inside the operators cab.

Whilst a significant improvement on the reversing/rear camera system in terms of visibility, the system still relied fully on the operator to watch the screen and look out for humans entering the danger zone, then act accordingly. There remained the distraction risk associated with another screen being added to the existing cab instrumentation and controls.



Figure 7.0 Operators view of the quadview screen

The system also recorded all camera footage as this could be useful to support any incident investigations and help with sharing lessons learnt and drive behavioural improvements.

Spillards object detection incorporation into Quadview (2017+)

It was around 2017 that Cementation, working closely with Spillard Safety Systems, developed an active CCTV based system that could identify when a human entered a defined exclusion zone. Specific forms could be identified and the system then alerted the operator to the presence of a human entering the exclusion zone. This was a huge improvement on the previous system, with the need for the operator to constantly monitor the camera eliminated. The system allowed a virtual exclusion perimeter to be set that surrounding the plant. Once activated, an alarm would sound and the operator would need to actively 'acknowledge' this, by pressing a button on the system. This was to ensure the operator looked at what had activated the system and intervened if necessary, by, for example, stopping an operation. This was a 'passive' system and still relied fully on the operator to intervene when warned that a human had entered the exclusion zone.



Figure 8.0 Details of the hardware attached to a typical piling rig and the cab screen display. Yellow box denotes detection of human crossing the exclusion zone.

 © DFI International Bruges 2025

Current 'State of the Art' Smart Human-Plant Interface System

CSS (Cementation Skanska Spillard) Live AI human form detection system (2024)

The latest system under development now offers a significant improvement on previous CCTV based system in the form of active intervention.

This is the latest system that has been developed by Cementation Skanska in conjunction with Spillard Safety Systems.

Detection

An evolution of the previous CSS Live system, this latest system combines a 360 degree camera system with sophisticated AI assisted human form recognition to detect the presence of humans in defined and customisable zones around the machine. The system recognises humans and objects, differentiating between the two, and can intervene with defined actions such as stopping tracking or slewing. Such an integrated system is believed to be a first in the UK for Specialist Geotechnical Plant.

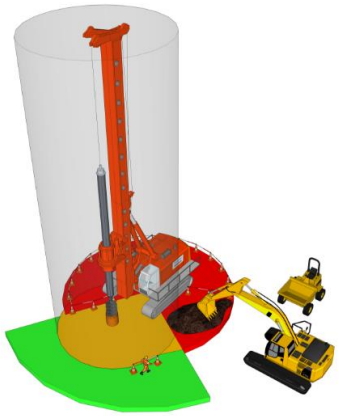


Figure 9.0 – Schematic of exclusion zone colour and terminology

The system is incredibly customisable, with the ability to set various exclusion zones and permit or allow access into each zone on a bespoke basis. Figure 9.0 shows the exclusion zones in a colour format, red, amber and green. This terminology will be used throughout the paper.

The red zone is an area where there should never be any human entry during operation of the specialist geotechnical plant.

The amber zone denotes a potential danger zone but is where authorised personnel need to enter for specific tasks, such as the banks person.

The green zone, or safe zone, is that which is outside of the risk of human plant contact. The interface between green and amber/red zones should be segregated using physical barriers wherever possible and managed by the banks person.

If any human enters the red zone, audible and visual alarms are triggered both internally and externally and the system immediately intervenes, stopping tracking or slewing. Entry to the amber zone activates the same alarms but with no intervention to warn the operator and banks person that this zone has been entered.

The system has so far been integrated into a number of piling rigs and refinement of the 'zone' orientation and extents has been carried out following full scale trials. Zone optimisation is summarised below.

The originally zone perimeter from the piling rig was set at radius of, 'Amber' 3.5m, 'Red' 2.0m

 © DFI International Bruges 2025

Careful consideration of the plan geometry and orientation of the amber zone is essential, initial geometry was selected as follows.

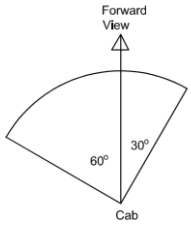


Figure 10.0– original shape of the ‘Amber’ zone

From extensive full scale trials, on live construction sites, it was found that the amber zone was too narrow with the system intervening when planned and safe operations were taking place, it was optimised to the following.

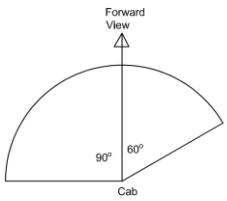


Figure 11.0 Optimised amber zone

The radius at which the exclusion zone was also optimised was, ‘Amber’ 2.5m, ‘Red’ 1.5m.

It should be noted that the system is ‘always on’ during plant operations and cannot be disengaged by the operator. The only way to switch the system off is with a rig specific key held by the site supervisor. This can only be used after consultation between a number of key site personnel with any additional safety measures agreed and applied.

The system uses AI technology, the results of over two years research and development by Spillard Safety Systems, to enable it to identify human forms entering a virtual exclusion zone and intervened accordingly.

External Hardware

Cameras

The system incorporates high definition cameras mounted externally around the machine which create a 360 view for the operator. These live images are stored and processed on a cloud based system.



Figure 12- Examples of the high definition external cameras

On triggering of the system external ‘warnings’ are activated, both prerecorded verbal voice warnings eg. ‘you have entered a restricted zone, please leave…’ and visual ‘red’ no entry led warnings as below.

 © DFI International Bruges 2025

Visual ‘green’ thumbs up are given by the operator to the banks person on entering the amber zone and the person should only continue once given the ‘thumbs up’ to signify that the operator is aware of their location.

Alerts



Figure 13 – Green ‘thumbs up’ led signalling safe to proceed and red ‘no entry’ warning

Internal Hardware

Insite the cab, the operator has an additional display screen that provides a 360 degree view surrounding the rig. The display is configured to provide a ‘bird eye’ type view rather than the previous four screen quad view system.



Figure 14 – Internal screen and ‘parking radar’ type display.

The system also incorporates a ‘parking radar’ type display under the screen that provides a simple and effective warning of when and where someone enters the exclusion zones. This is combined with an audible alarm eg. ‘human detected on your left’.

An additional control panel has also been created to incorporate a few key controls needed to manage the system, the controls also use the ‘zone’ colour system and adopt simple tactile push button and switches that need to be actively engaged. These controls have been intentionally kept to a minimum.



Figure 15 - Simple/basic additional in cab controls – kept to a minimum

The latest system has been integrated into a number of piling rigs now and following extensive plant yard trials has now been deployed on a number of live construction projects. The following section shares some of the challenges encountered to date and feedback received.

 © DFI International Bruges 2025

Data Protection

One of the challenges that had to be overcome was the use of CCTV cameras on sites and the storage and processing of the images.

In Europe, the introduction of the General Data Protection Regulations (GDPR) provides a clear framework and strict rule for the collection and processing of personal data. Compliance with this was essential for the new system and required robust business processes and even assessment and training of individuals who would need access to live or stored footage. Cementation Skanska now has all the necessary processes and procedures in place to ensure the new system complies with all relevant regulations. Some useful guidance on the use of CCTV systems is provided in the UK by the Information Commissioner's Office.

https://ico.org.uk/for-organisations/uk-gdpr-guidance-and-resources/cctv-and-video-surveillance/

Findings

One unexpected benefit was that the system was found to be very useful when placing safety barriers at the correct location using the system sensors and external warnings. Operatives simply have to walk towards stationary plant and use the audible or visual warnings to advise where to place the barriers. This is particularly useful on projects where the plant is constantly moving.

The 'Human Form' detection system was not faultless, and on occasions confused a high visibility jacket hung on the rig handrails with a human form. This was useful in driving behavioural changes in terms of where to hang PPE to support such a system. It was also found that dumpers driving very close to the exclusion zone could activate the system. Again this helped inform the early development of the system and management of dumper routes.

Feedback from plant operators and site operatives (positive and negative) had been instrumental in developing and refining the system and Cementation Skanska have seen improved safety behaviours driven by the systems interaction with site teams.

Noise from the system could become a 'nuisance' to neighbours and other site workers and must be considered when using these safety systems

Whilst the system actively intervenes without the driver needing to monitor another screen, the additional display may still present a distraction to unfamiliar operators not trained in the use of an integrated CCTV safety system. See images below.

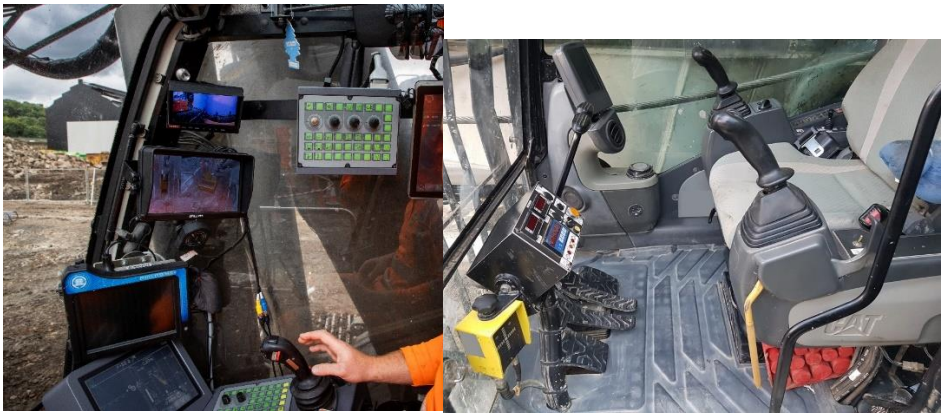


Figure 16 – Left image shows a modern piling rig with multiple displays including the CSS Live system. Right image shows the 'basic' rig controls.

One of the key challenges in incorporating this system into Cementation Skanska entire plant fleet, which is the intention, is that the interfaces across various plant manufacturers and rig types makes integration complicated. For example a Soilmec rig requires hydraulic systems disabled to intervene, whilst a Bauer rig requires intervention via an electronic system.

 © DFI International Bruges 2025

When tracking across site the system can stop plant suddenly if activated and may invariable increase risks when, for example, tracking down a ramp. The extensive yard and site trials have been invaluable in identifying such situations and developing a solution. The supervisor can disable the system with a bespoke key for special circumstances that can be managed by human support and intervention or exclusion zones (such as tracking). This is only done when an agreed methodology is finalised and briefed accordingly'.

Lastly, as with all camera based systems, there is the simple risk of dirt on the camera lens causing the system to become 'blind' and either ineffective or causing a false alarm to be raised. Again, through the extensive and ongoing trial process, such occurrences have been identified with the aim of the system learning to distinguish any false alarms so that it can become more efficient and less prone to errors.

Summary

The key question is, have the systems described in this paper, in particular the very latest system developed by Cementation Skanska and Spillers Safety Systems, improves site safety.

With the latest system in place, Cementation Skanska have seen a behavioural shift due to more accountability on site. Feedback from site personnel and observations is that safety related behaviours have generally improved and there have been more challenges to unsafe behaviour from peers on site. During extensive testing the system intervened on numerous occasions and whilst a small number of these interventions were related to false alarms many related to actual human entry to a danger zone and stopped a potential incident. The system continues to be refined taking account of human feedback and analysis of the incident data collect, the current iteration minimises false alarms.

All incident data is collected and part of ongoing analysis to both improve the system and also demonstrate the system has significantly reduced the risk at the human-plant interface. Whilst there have been numerous system interventions in 2024, there have been no human-plant safety incidents where the latest CSS Live has been used.

There does still remain too many 'false' alerts eg. dirt on a camera lens and there is work underway now to review all incidents to refine the system and reduce or ideally eliminate such false alerts.

Cementation Skanska, working closely with Spillard Safety System is now developing the system for incorporation into all of its specialist geotechnical plant, including small mini piling rigs and ground engineering rigs.

Whilst delivering tangible safety improvements to the high risk human plant interface zone, the system should still be considered a secondary safety device and used in conjunction with a competent banks person and physical barriers. All site personnel must still remain vigilant around plant operations.

This paper concludes with a quote from a rig operator who has recently operated a CFA piling rig with the new CCS Live system fitted.

"It's good for raising awareness as it tells people there is a danger, instructing them to move away. Barriers are not enough because people can bypass them. It's great because the system doesn't rely on you as an operator to activate it – reducing the risk of distractions. You can get on with the job, knowing that there is an added layer of safety."

References

(1) Skanska UK plant people interface initiative, 2017
(2) Federation of Piling Specialists, Plant Restricted Zones, 2021, UK, www.fps.org.uk

 © DFI International Bruges 2025

THE USE OF THE ENVIRO-WALL-MAT COMBINATION IN SOFT SOIL CONDITIONS FOR MARSHALLING AREAS, CRANE HARD STANDS AND LAY DOWN AREAS

J.W.R. Brouwer, Geobest BV, Vianen, The Netherlands, +31650740785, roel.brouwer@geobest.nl
H.W.H. Engelen, Geobest BV, Vianen, The Netherlands, +31628521605, hugo.engelen@geobest.nl

ABSTRACT

This paper presents the study towards a new foundation concept, named ”the Enviro-Wall-Mat combination”. This concept is based upon the successfully adopted Enviro-Mat horizontal soil stabilization, combined with vertical trench formed walls.

The Enviro-Mat is realised by in situ mixing of (local) soil, cement and a stabilizing additive that promotes stronger bonds between the soil and cement particles. In this way a stabilised layer is created with a low carbon footprint as local soil is used. The Trench Formed Wall is created by means of a deep trenching machine, that creates a trench with a maximum depth of 15 m. The outcoming soil is transported to ground level and the trench can be simultaneously filled with a low strength slurry that is mixed on surface level.

By combining both techniques, a fully supported stabilised layer can be created that is capable to withstand high and irregular loads even in very compressible soils. The Enviro-Walls act therefore as a deep foundation for the Enviro-Mat.

The concept has first been analysed by means of finite element calculations with program Plaxis 3D. The conclusion was that the concept should be feasible. Based on these positive results, it was decided to perform a full scale load test. This test was performed in August 2021. This paper describes the initial Plaxis analyses and the results of the field test.

Keywords: soft soil, stabilization, wall, mat

PREAMBLE

For almost 10 years now, the Enviro-Mat concept has been successful as a pavement option in heavy duty loading projects. By means of in-situ mixing of local soil, cement, water and the Geosta additive at ground level, a stabilized layer is created. Although in certain load cases the Enviro-Mat can be used in soft soil conditions, it remains sensitive for excessive differential settlements. In order to try and make this concept work reliably in very soft soil conditions, the Enviro-Wall-Mat is developed.

STABILISATION PRINCIPLE

Geosta is a mixture of inorganic salts, that in combination with hydraulic binders such as Portland cement or lime, is applied in soil stabilisation. By adding Geosta to the cement a noticeable improvement of the soil stabilisation is realized (Omotosho, 2005), especially in flexibility and load spreading behaviour. Geosta is a mixture of zeolites, oxides (aluminium, magnesium, and silicon oxide) or chlorides (magnesium, sodium, potassium and calcium chlorides). Geosta stabilised soil is applied as a hardstand foundation for several wind farms in the Netherlands (Brouwer and van der Veer, 2021).

A typical recipe for the Enviro-Mat consists of 150 kg Portland cement and 1.5 kg Geosta additive per cubic meter. This recipe was first tested under laboratory circumstances in 2017 with different soil types as base material. From each base material, three separate samples are prepared and subsequently tested on compressive strength. Results are presented as average values in Table 1.

 © DFI International Bruges 2025

Table 1. Typical compression strength values of Enviro-Mat in different soils

Base material	Compressive strength		
	7 days MPa	14 days MPa	28 days MPa
Peat	0.5	1.0	1.5
(River) clay	0.8	1.2	2.0
Silt	1.8	3.0	3.8
(River) sand	2.1	3.7	5.4
Crushed rubble	3.8	5.6	8.7
(River) gravel	3.9	5.9	8.9

In cases where the stabilization involves clayey soil, pre-treatment with lime (2 – 3%) is a good option to achieve strength values that are comparable with granular materials. Clay particles tend to exhibit a delayed and often incomplete chemical reaction with cement and lime. Pre-treating the clay with lime leads to a more effectively stabilized product. This is attributed to the chemical interactions between and clay particles.

As a light-weight alternative, foam glass mixed with soil can be used as a base material. This method is described in Brouwer et al. (2024).

PRINCIPLE ENVIRO-WALL-MAT COMBINATION

The Enviro-Wall-Mat is a combination of the Enviro-Mat and trench formed walls. Trench formed walls are created using a deep trenching machine, that is able to create trenches with a maximum depth of 15 m. The outcoming soil is transported to ground level and the trench can simultaneously be filled with a low strength concrete slurry that is mixed on surface level.

The principle is shown in figure 1 and corresponds to the actual design used in two field tests conducted in Zeewolde (2021). Walls with a length of 5 m were applied for this project. The elevations in the figure are related to NAP (Nieuw Amsterdams Peil), which is the standard reference level in the Netherlands.

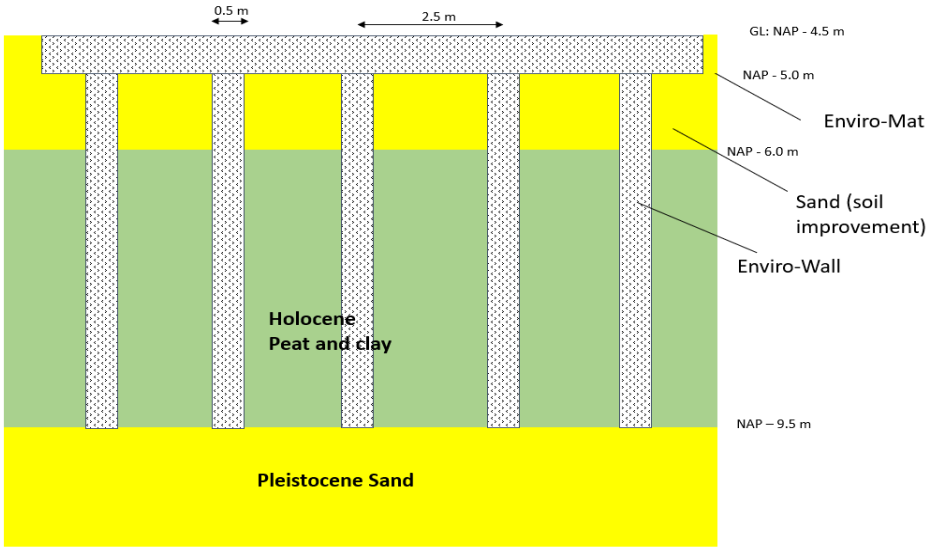


Figure 1: Principle of Enviro Wall-Mat as tested in Zeewolde (NL) in 2021

By combining both techniques, a fully supported stabilised layer can be created that is capable to withstand high and unevenly distributed loads even in very compressible soils. The trench formed

 © DFI International Bruges 2025

walls act therefore as a deep foundation for the Enviro-Mat with the tip elevation in a sufficiently dense sand layer. As an alternative, a somewhat higher tip elevation may be chosen in the softer layers. In this case, the walls act as a settlement reducing solution, that can be compared to a raft foundation. In the latter case, the whole structure may settle more than in the first option, but considerably less than without walls.

The original application of the Enviro-Wall-Mat combination was expected to be in the field of onshore wind energy in The Netherlands as wind turbines are predominantly placed in areas with soft, virgin soils.

Due to the increase in size and capacity of offshore wind farms, the demand for high bearing capacity marshalling areas where monopiles and transition pieces can be stored has also increased. The Enviro Wall-Mat can be an effective foundation solution for these storage areas where large bearing capacities in combination with small settlements are required.

DESIGN

The soil conditions at the Zeewolde site consisted of very soft Holocene clay and peat layers until a depth of 5 meters below ground level, followed by medium dense Pleistocene sand layers. A typical CPT is presented in Figure 2. The blue line represents cone resistance, the red the line sleeve friction. The orange line on the right represents friction ratio. The elevations in the figure are related to NAP.

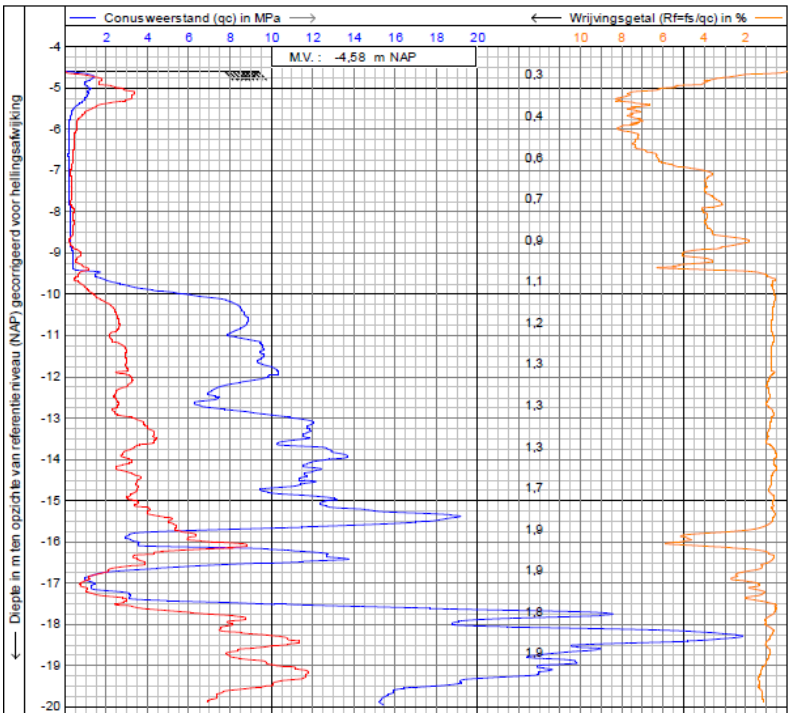


Figure 2: Typical CPT at project location

The Enviro-Wall-Mat design has been explored by means of a complete finite element analysis performed using Plaxis 3D. In 2019 multiple Enviro-Mat field tests are conducted in Zeewolde. As a result to the post-analysis of these tests, a Plaxis 3D model with an accurate soil stratigraphy with corresponding strength and stiffness parameters was available. By adding the Enviro-Wall-Mat to this Plaxis 3D model, both the modelling of the concept could be elaborated whilst at the same time the deformations could be compared to the interpretation of the Enviro-Mat field tests.

The configuration consisted of five trench formed walls with a width of 0.5 m and a length of 5.0 m (tip level at approx. NAP – 9.5 m). The centre-to-centre distance was 2.5 m. The Enviro-Mat with a

 © DFI International Bruges 2025

thickness of 0.5 m was constructed on top. The Enviro-Mat is modelled directly on top of each trench formed wall to ensure direct contact between the Enviro-Mat and the trench formed walls.
For the compression strength of the Enviro-Mat and the walls, a value of 4 N/mm^2 was adopted, given the fact that a sand layer is installed prior to the installation of mats and walls. The Enviro-Mat is made with this sand as base material.

The Plaxis 3D modelling of the Enviro-Wall-Mat is presented in Figure 3.

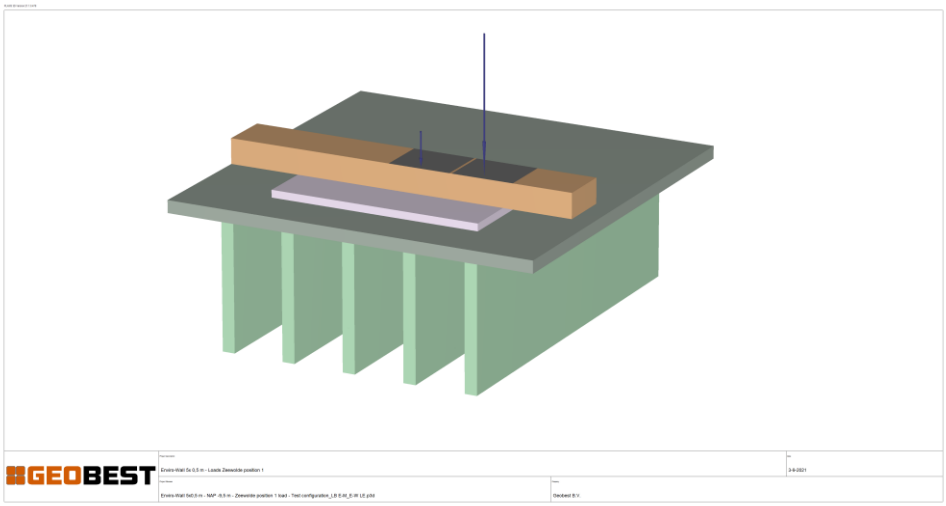


Figure 3: Plaxis 3D modelling Enviro-Mat-Wall

Loads correspond to a single crawler load that is common for onshore wind turbine construction.

Calculated deformations (maximum value approximately 15 mm) are given in Figure 4 and reflect the behaviour of the Enviro-Wall-Mat under fully undrained circumstances (short-time loading) as is expected during short time crane loading.

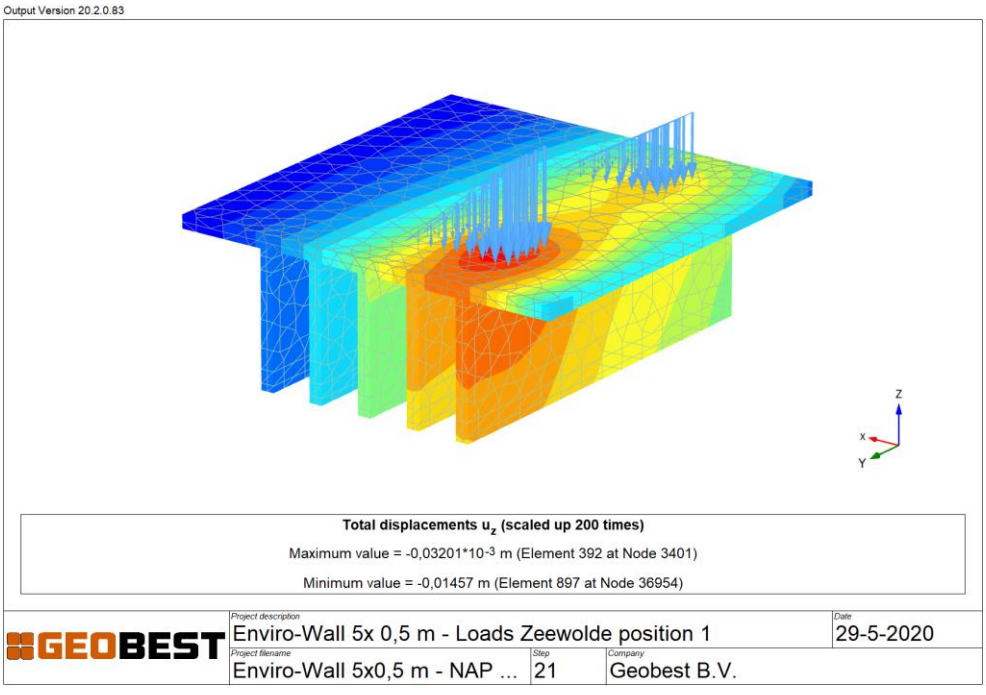


Figure 4: Plaxis 3D - deformations

 © DFI International Bruges 2025

FIELD TESTING

Based on the positive results of the Plaxis 3D design calculations, two field tests were initiated. These field tests were carried out on the same location as used for the Enviro-Mat tests. The two field tests consisted of separate load configurations, based on a single Enviro-Wall-Mat design:

– Test 1: simulating the crane tracks being placed perpendicular to the walls
– Test 2: simulating the crane tracks being placed parallel to the walls.

The test configuration consisted of steel mats with two steel gantry beams on top. Following the load was increased in steps by placing ballast plates up to a total load of approximately 3400 kN. A cross-section of the test configuration is presented in Figure 5.

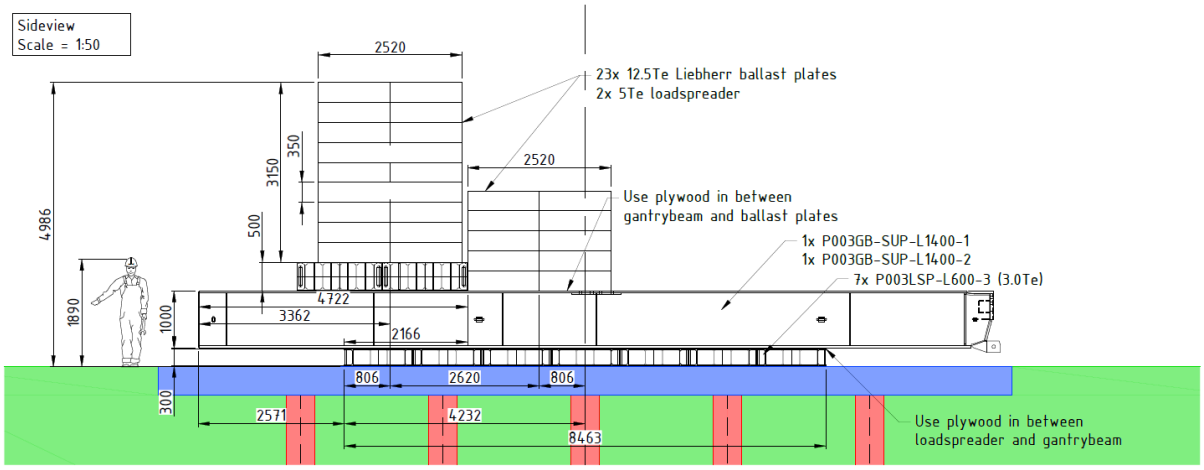


Figure 5: Cross-section Enviro-Mat-Wall and test configuration

The corresponding maximum pressure beneath the gantry beams is at least 270 kN/m^2 (27 T/m^2), depending on the actual load spreading capacities of the steel mats.

The ballast loads were put in place in a period of about 4 hours. The loads stayed in place for a period of about 16 hours. At both load tests the deformation was measured at several locations during loading and unloading.

It is clear that the lay-out from test no. 1 represents a worst-case condition. The centre of the load is placed exactly between two walls and therefore the load on the Enviro-Mat is maximised. The lay-out of test no. 2 gives a much lower load on the Enviro-Mat as the load is perfectly placed on the walls.

An impression of the actual test load is presented in figure 4.

 © DFI International Bruges 2025



Figure 6: The actual test configuration in Zeewolde in 2021

Besides overall stability and bearing capacity, settlement and differential settlement (i.e. rotations) are the main items when considering the suitability of a crane hardstand. It was therefore decided to focus on the deformations (vertical and horizontal) during the load advance in the test by means of automatic total station measurements of deformation prisms.

A time-settlement curve of two governing prisms (at different locations) during test 1 is given in Figure 7. Most deflections occur during the build-up of the load in the first 4 hours (240 minutes). In the following 16 hours, some creep is detected, with an increase in settlement under the constant load.

In general it can be concluded that the measured short-term settlements (15-25 mm) are in the same order of magnitude as the Plaxis 3D prediction under fully undrained circumstances. The application of this solution for longer term loading has to be investigated further by means of a long duration test set-up.

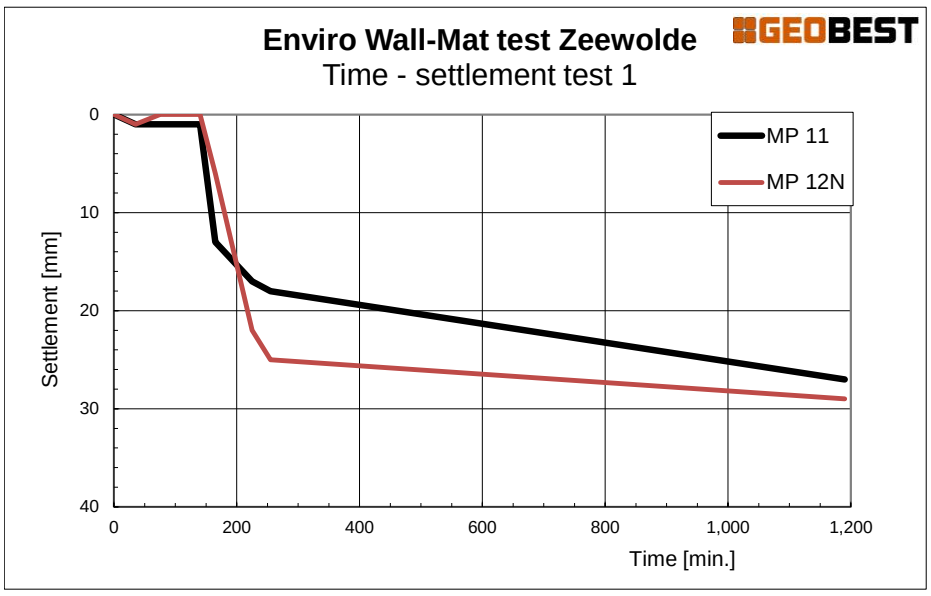


Figure 7: Measured deformations in field test

 © DFI International Bruges 2025

CONCLUSIONS

The Zeewolde field test shows that the concept of the Enviro-Mat supported by Enviro-Walls is a viable method for crane hardstands, laydown areas and marshalling yards in very compressible subsoils. The worst-case load test resulted in small deformations. Two years before the project described here, a load test was performed without supporting walls at a nearby location with comparable soil conditions and loads. During this test, settlements in excess of 250 mm were measured. This leads to a settlement reduction factor of approximately 10 .

The deformation pattern of the Enviro-Wall-Mat can be explained in the Plaxis simulation. The adopted Plaxis model is in line with the field test results.

Additional study may lead to a further optimisation of the concept, especially the material as used in the walls.

On the basis of this study, the Enviro-Wall-Mat combination shows a lot of potential for future heavy duty pavement projects in soft soil conditions. Very often these contracts, especially when dealing with soft soil conditions, comprise an additional full-scale field test. This provides new data that will be very helpful for further study on this concept.

ACKNOWLEDGMENTS

The authors would like to thank Mammoet BV and Heavy Duty pavements BV for their cooperation in realising this article.

REFERENCES

Brouwer, J.W.R., Van Laerhoven, C. (2024), The use of foam glass for a lightweight fill and highway foundation on soft soil conditions, Proceedings of the XVIII ECSMGE 2024, Lisbon.

Brouwer, J.W.R., van der Veer, M.D. (2021) Wind Farm Deil, Solid Foundation for Crane Setup Sites (In Dutch), *Land en Water* 4, April 2021.

Omotosho, O. (2005), Influence of Geosta Addition on cement-stabilised Chioco Mud of the niger Delta., in American Journal of Environmental Science 1 (1), pp 59-63.

 © DFI International Bruges 2025

Bridging Physical and Digital Realms: The Role of Digital Twins in Geotechnical Engineering

Dr. Ehsan Moradabadi, Geostructural Engineering Consultant, Ireland, ehsan@outlook.ie

Abstract

Digital twins, particularly "Asset Twins," serve as virtual replicas of physical assets, continuously synchronised with real-time data. These digital counterparts bridge the physical and digital domains, facilitating real-time insights, accident analysis, workspace optimisation, predictive maintenance, and other functionalities. Their applications extend across various sectors, including smart cities, underground structures, tunnelling, and renewable projects. The global digital twin market is projected to reach USD 195.85 billion by 2030, driven by compound annual growth rates (CAGRs) between 35.7% and 45.1%. This paper demonstrates the application of digital twin models in geotechnical engineering, underpinned by digital simulations of physical assets utilising cloud computing, Internet of Things (IoT) platforms, and machine learning. The development of physics-informed asset models within the digital twin framework involves four key steps: (1) quantifying uncertainty in input variables and propagation, (2) computational modelling (FE/FD modelling), (3) optimisation and surrogate modelling, and (4) Bayesian updating. Since gaining prominence post-2017, particularly in IoT and predictive analysis, digital twins have proven effective in geotechnical projects, enhancing efficiency, safety, and cost-effectiveness. This paper includes physics-informed solutions for two case studies on tunnelling-induced damage and explores applications in geotechnical engineering across various industries, including renewable energy. These examples illustrate how physics-informed modelling in digital twins can address challenges arising from unexpected variations and input parameter uncertainties throughout project stages, thereby enhancing decision-making and overall construction strategies. The paper also reviews the challenges of implementing digital twin frameworks in geotechnical projects and beyond, including the recruitment of skilled experts, management of complex data, overcoming industry conservatism, ensuring information alignment, cybersecurity, and managing cloud computing and data centre costs. Effective leadership, emphasising collaboration and a consultative approach, is crucial for the successful deployment of digital twin projects.

Keywords: Digital Twin, Predictive Analysis, Uncertainty Quantification, Underground Structures

INTRODUCTION

Understanding the behaviour of structures founded on or embedded in the ground is crucial for ensuring safe and effective engineering solutions. Geotechnical designers rely heavily on predicting future ground behaviour. Lambe (1973), a pioneer in this field, extensively discussed various aspects of prediction in geotechnical engineering, categorising them based on the timing and type of information available. These categories distinguish between predictions made before, during, and after an event, with varying levels of known results.

In recent years, the concept of digital twins has significantly advanced the field of geotechnics and beyond. Originating from NASA's space exploration programs in the 1960s and later named by Michael Grieves (2005) as a powerful model for product lifecycle management, the term was further popularised in NASA's 2010 roadmap (Piascik et al. 2010) to describe cosmic twin systems. A digital twin is a virtual replica of a physical compound, asset, system or process that can simulate, predict, and optimise performance in real-time.

A digital twin typically utilises engineering design data such as specifications, drawings, Building Information Modelling (BIM) models, and analysis and operational data from information of things (IoT) feeds, sensors, drones, cameras, and light detection and ranging (LiDAR) scanners. It also incorporates additional information such as asset tags, work orders, and maintenance and inspection

 © DFI International Bruges 2025

records to create a comprehensive visual representation of assets. This is made possible by advances in 3D extended reality, 4D modelling of changes, AI analytics, and machine learning (ML).

This paper explores the application of Digital Twin technology in geotechnical engineering, emphasising physics-informed modelling as the key computational framework for merging the physical and digital realms.

CONCEPT EVOLUTION AND APPLICATIONS

Upon reviewing research papers and geotechnical engineering projects post-2017, a significant increase in the adoption of the digital twin concept in both academic and practical applications has been observed. The Google Trends graph (Fig.1) illustrates a marked rise in interest in digital twins within the scientific community, suggesting that the topic gained popularity only after 2017. Prior to this period, the subject could be explored through related topics such as the Internet of Things (IoT) and predictive analysis.

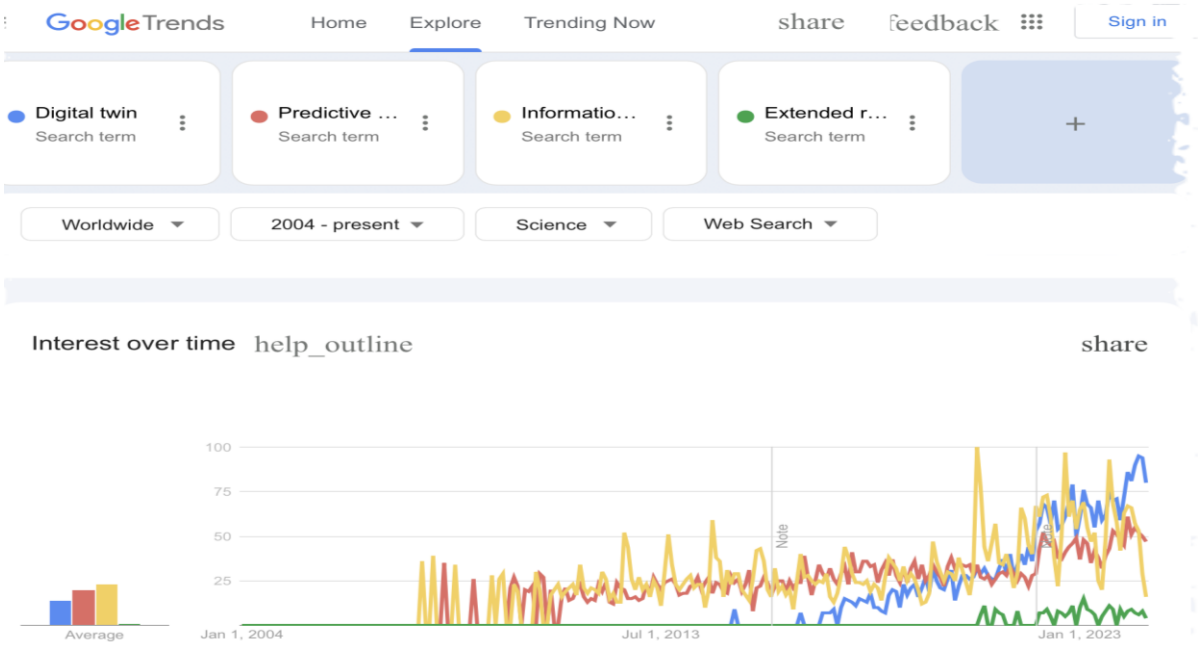


Fig.1. The rise of digital twin technology post-2017 and its comparison with related concepts such as predictive analysis, IoT, and extended reality (Google Trends)

Digital Twin technology is revolutionising Civil Engineering, Construction and geotechnical-engineering-related projects, including tunnels, buildings, bridges, roads, dams, and wind farms (both offshore and onshore), as well as other renewable energy geo-structures such as wave and tidal power generators. The digital twin market is projected to grow significantly, from USD 11.51 billion in 2023 to USD 195.85 billion by 2030, driven by compound annual growth rates (CAGRs) between 35.7% and 45.1%, according to various reliable sources (Grand View Research 2023, Fortune Business Insights 2024).

Comparatively, the global tunnel construction market, as one of the main geotechnical engineering-related project, valued at USD 88.65 billion in 2021, is projected to reach USD 194.064 billion by 2032, with a compound annual growth rate (CAGR) of 7.38% (Business Research Insights 2024). This growth underscores the critical role of digital twins in enhancing the efficiency, safety, and reliability of construction industry including geotechnical-engineering-related projects.

Digital twins enable real-time optimisation and monitoring of physical assets like tunnels and offshore wind farms, without necessitating extensive system modifications (Latif et al. 2023; Haghshenas et al.

 © DFI International Bruges 2025

2023 Tomar et al. 2020 and Zhang et al. 2024). They support Hazard and Operability (HAZOP) and accident analyses throughout tunnel lifecycles by systematically examining processes to identify potential hazards and operability issues (Prabowo et al. 2021; Jafari et al. 2023; Junjia et al. 2024). Furthermore, digital twins enhance workspace optimisation by refining workplace layouts and safety measures through virtual models (Hou et al. 2020).

Augmented reality and digital twins streamline technician training (Robah et al. 2018 and Fan et al. 2021), while financial risk management benefits from simulated economic scenarios for informed decision-making (Ugliotti et al. 2023). Predictive maintenance is enhanced as models forecast equipment failures, enabling proactive scheduling (Robah et al. 2018; Lu et al. 2020; Yu 2020 et al.; Moghaddam et al. 2021; Fahim et al. 2022 and Machado et al. 2024). Supply chain optimisation is achieved by identifying logistics bottlenecks (Lee et al. 2021; Kamble et al. 2022 and Yevo et al. 2023), and energy efficiency is improved through the analysis of energy consumption in asset operations (Francisco et al. 2020 and Kaewunruen et al. 2020).

In smart cities, digital twins inform urban planning decisions in smart grid and transportation system, and in retail and subway stations, they enhance store and spaces layouts and track foot traffic (Kaewunruen et al. 2020; Han et al. 2020; Zheng et al. 2021 and Lehtola et al. 2022). Manufacturing processes benefit from optimised product performance and reduced inefficiencies and defects (Eyre and Freeman 2018; and Li et al. 2022 and Gannouni et al. 2023).

In water management, digital twins aid in drainage design and water and wastewater management (Ramos et al. 2023 and Daneshgar et al. 2024). They simulate mining operations and assess impacts in the mining and exploration sector (Nagovitsyn and Stepacheva 2021; and Hazrathossein et al. 2024).

Digital twins also monitor and analyse the safety, health, and well-being of underground workers, contributing to total worker health (Busollo 2021 et al. and Ye et al. 2023). Simulation-based learning is enhanced with interactive simulations (Nikolaev et al. 2018), and digital twins drive climate change agendas by revolutionising atmospheric and climate sciences (Sahu et al. 2024), improving engineering processes (Wagg et al. 2020), and supporting sustainability efforts by reducing material usage and improving product traceability to minimise environmental waste (Chen et al. 2024).

In the specialised field of geotechnical engineering, digital twins offer a wide array of important applications. They can predict and model ground profiles more accurately than traditional methods (Shi et al. 2022; Shi and Wang 2022 and Jian et al. 2023), aiding in the estimation of risks associated with ground conditions (Moradabadi 2017; Liu et al. 2022; Chen et al. 2023 and Gu et al. 2023). By integrating Building Information Modelling (BIM) with digital twins, geotechnical engineers can create comprehensive models that combine geological and structural data, facilitating better data sharing and collaboration (Hung 2022 and Satyanaga et al. 2023).

Digital twins facilitate comprehensive simulation and analysis of geotechnical processes, including soil-structure interactions, tunnelling, and excavation, under conditions of parameter uncertainty (Moradabadi 2017; Züst et al. 2021; Hu et al. 2023; Shi et al. 2024 and Wang et al. 2024), aiding in visual decision-making and transparent management (Hong et al. 2022).

In offshore geotechnics, digital twins have been employed to simulate geo-structures in renewable energy applications and predict their behaviour under uncertain parameters, including wave power generator structures (Katsidoniotaki et al. and Kim et al. 2023), offshore wind turbines (Abdullahi and Wang 2021; Augustyn et al. 2021 and Jorgensen et al. 2023), and offshore floating wind turbines (Walker et al. 2022, Huang et al. 2023 and Liu et al. 2023).

The subsequent sections provide a general overview of the methodology for creating a digital asset. Additionally, they delve into the core process of bridging the digital and physical realms, with a detailed focus on physics-informed modelling for geotechnical problems.

 © DFI International Bruges 2025

ANATOMY OF A DIGITAL TWIN

To develop a digital twin for an asset, it is imperative to collect project data from various phases of the asset's life cycle, which serves as the foundation for simulation and digital replication. Initially, digital twins are represented as simple 1D or 2D models during the conceptual design phase. These models evolve into complex 3D and 4D representations by the construction stage, utilising data from Internet of Things (IoT) feeds, sensors, drones, cameras, and LiDAR scanners. During the construction phase, the physical asset is integrated with its digital counterpart both horizontally and vertically, thereby enhancing overall system performance. Post-construction, accurate as-built information ensures that the digital twin closely mirrors the real-world asset. These multidimensional twins capture geometry and track behaviour over time, enabling the simulation and optimisation of real-world performance. By leveraging cloud computing, sensor data is efficiently processed through an IoT framework, facilitating behaviour analysis and predictive insights. Continuous updates throughout the asset's life cycle, supported by chronological sensor records, maintain the digital twin's accuracy(Fig. 2).

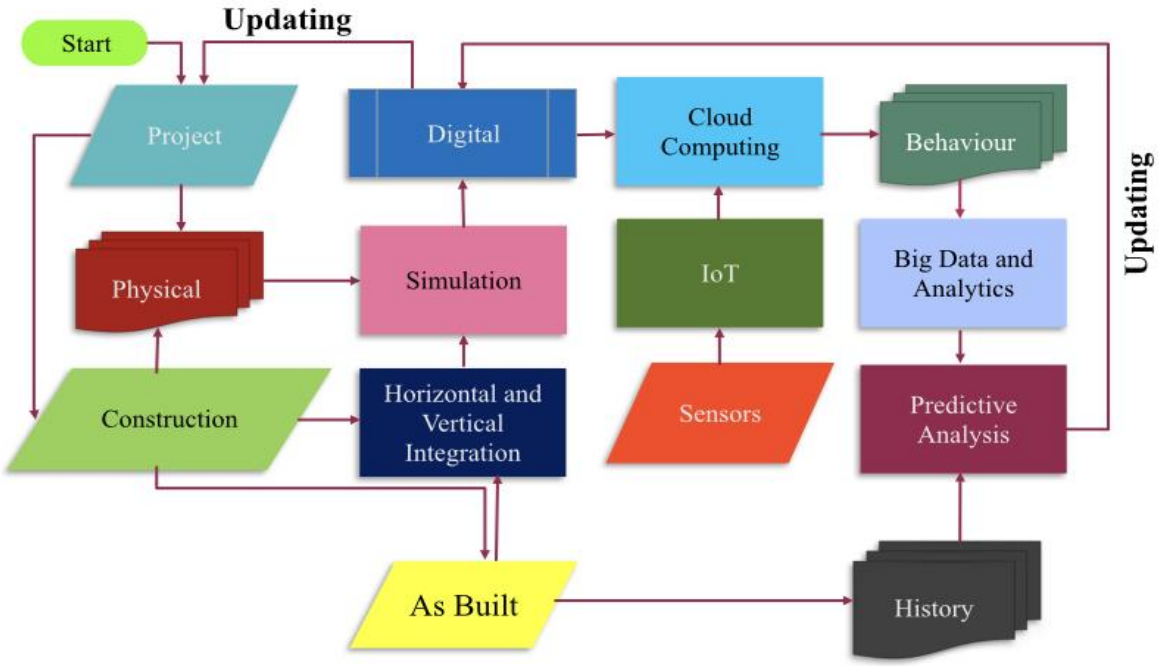


Fig.2. Components required to create a Digital Twin

In the context of digital twin creation, the underlying principles bear resemblance to those of large language models, as articulated by Jeff Bezos. Bezos (2023) has emphasised that large language models often exhibit unexpected capabilities, rendering them more akin to discoveries than inventions. Similarly, digital twin models can be considered discoveries rather than inventions, as they continuously enhance comprehension and bridge the gap between static geometry and dynamic behaviour throughout the project lifecycle. The prediction of an asset's behaviour within a digital twin framework through its life cycle is determined by physics-informed modelling. The following section delves deeper into this context.

PREDICTION OF AN ASSET'S BEHAVIOUR IN DIGITAL TWIN FRAMEWORK

In the context of Digital Twin models, the objective is to create a digital representation that closely mirrors reality. However, mathematically describing system performance is often more complex than classic examples. Typically, there is no neat closed-form solution or well-defined output probability

 © DFI International Bruges 2025

function for the system, particularly when dealing with computational models like Finite Element or Finite Difference methods. Traditionally, sophisticated software packages are employed to computationally model the performance of physical assets under investigation, referred to as the

$$\underset{\sim}{Y}_{ijk} = f_{jk}(\underset{\sim}{X}_i, \underset{\sim}{d}, \underset{\sim}{\ell}) \quad \text{Eq.1}$$

$\underset{\sim}{Y}_{ijk} = \left[Y_{1ijk}, Y_{2ijk}, \ldots, Y_{mijk} \right]$: Vector/Array of Model Prediction

$\underset{\sim}{X}_i = \left[X_{1i}, X_{2i}, \ldots, X_{ni} \right]$: Vector/Array of Model's Uncertain Input

$\underset{\sim}{d} = \left[d_1, d_2, \ldots, d_{n'} \right]$: Vector of Deterministic Parameters

$\underset{\sim}{\ell} = \left[\ell_1, \ell_2, \ldots\ldots, \ell_m \right]$: Vector of Performance Criteria

$\underset{\sim}{Y}_{ijk}$: A Single Sample (Random Sample Number of k) of the General Performance Function with i, Input Parameters of X, and the Random Function of j

"modelling or simulation step" The parametrised model derived from computational modelling functions, where specific input parameters yield corresponding output performance predictions. A general mathematical function to represent the computational process can be expressed as follows:

In highly complex systems, identifying the input and output of each sub-model is not always straightforward. This challenge is exacerbated when input parameters are influenced by various sources of uncertainty, a phase termed "quantifying the source of uncertainty." In this phase, parameters that need to be modelled probabilistically are identified. Advanced computer models and sample-based solutions, even when accelerated using cloud computing, often face the challenge of being computationally expensive or infeasible within a reasonable timeframe. This is where computational optimisation becomes crucial. Efficiency improvements are explored, sometimes through the use of surrogate models—stand-ins for the main computational model—that require less computational power but are less accurate. These serve as cost-effective alternatives.When more reliable information for input and output variables becomes available, Bayesian updating can be employed to adjust these variables accordingly. These procedures are summarised in Figure 3.

The computational steps corresponding to Figure 3 and solving Eq. 1, which are used to predict a geo-structural behaviour as discussed and explored by Moradabadi (2017), are detailed in Figure 4.

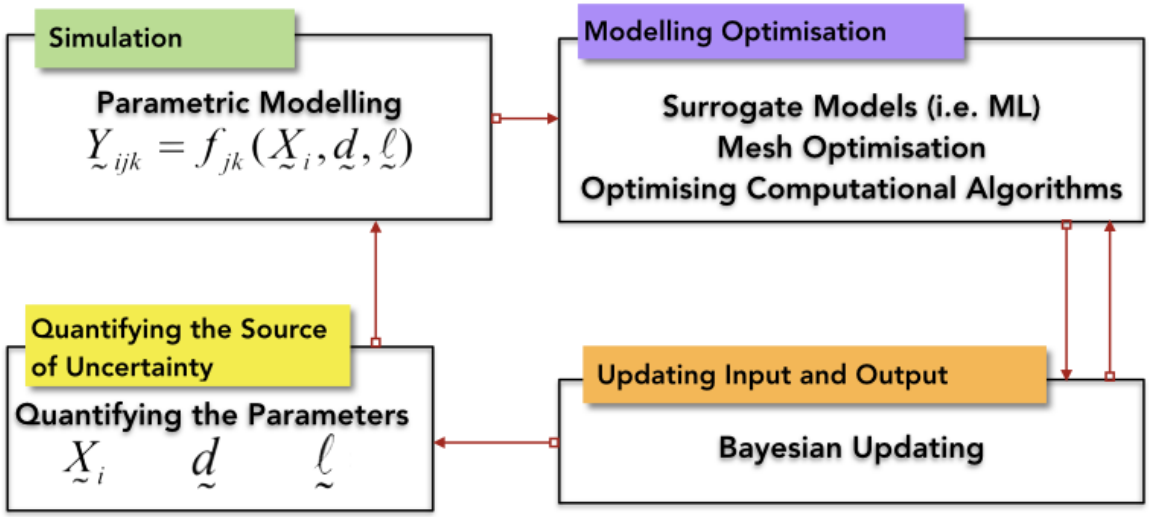


Fig.3. Steps in Physics-informed modelling in the context of Digital Twin

 © DFI International Bruges 2025

A. Statistical analysis to define the distribution function of each important parameters of the problem and to interpret the random field parameters of each layer of the soil profile including distribution functions of characteristic material properties and their correlation structures.

B. Sensitivity analysis To propagate reasonable finite number of random vectors by sampling from uniform distribution functions using Latin Hyper cube sampling or other available efficient smart sampling, and for each generated random vector simulate the following then:

I. Produce finite number of parametric FE models of the problem under investigation, and calculate bellows for each model:

i. Generate discrete random field with the geometry parameters of the problem based on the concept of the random functionality described in section 3.4.2 of the full text (Moradabadi 2017).

ii. Map the random variable of each local domain of random field to the corresponding mesh in the generated FE model.

iii. Execute the model appropriate times to generate a histogram of random finite element model's response (see section 5.5 of the full text (Moradabadi 2017) for how to select an appropriate number).

iv. Construct the weighted histograms from all different types of models (i.e. satisfying equation 3.7 of the full text (Moradabadi 2017))

b. Calculate, the averages, maximums and minimums of the histograms

c. Perform regression analysis, Partial Ranked Correlation Coefficient (PRCC) and Standardised Ranked Regression Coefficient. (SRRC) analysis and to calculate p-values, PRCC and SRRC indexes for each parameter corresponding to the outputs of the previous step

d. Interpret the results to capture the most import input parameters

e. Increase the number of simulations if needed and repeat steps a to d

C. Reliability analysis *

a. Update the uniform density function of each important parameter to non-uniform (if appropriate) and assume a nominal value for the rest.

b. Propagate reasonable numbers of random vectors by sampling from probability distribution functions of important parameters using LHS, and simulate bellows for each generated random vector.

I. Generate finite numbers of parametric FE models of the problem under investigation, and calculate bellows for each model:*

i. Generate discrete random field with the same geometry parameters of the problem based on the concept of the random functionality described in section 3.4.2. of the full text (Moradabadi 2017)*

ii. Map the random variable of each local domain of random field to the corresponding meshes in the FE models generated.*

iii. Execute the model for appropriate finite times to generate a histogram of desired outputs of random finite element models.*

II. Construct weighted probability mass function histograms from all models

III. Fit a known form probability density function to each histogram of the previous step

IV. Calculate reliability curves from the lower bound of each cumulative distribution functions derived from the previous step assuming an appropriate factor as probability of loss

c. Generate the cumulative mass functions of the whole system

d. Fit a known form probability distribution function to each histogram of the previous step to derive the reliability curves

e. Check the limit state functions (i.e. equation 3.15 of the full text (Moradabadi 2017)), assuming an appropriate probability of loss

f. Bayesian updating if needed

I. Construct the likelihood function of the observations, if available.

II. Update reliability curve of system using likelihood functions, if needed

* Reliability analysis can be conducted using either the same Finite Element (FE) Models or surrogate models. To construct surrogate models that accelerates calculations (albeit with potential sacrifices in accuracy), the input and output data from part B (results of FEM with uniform parameters) are utilised to develop an artificial neural network-based prediction model (e.g. Feedforward Neural Networks (FNNs), Radial Basis Function Networks (RBFNs), etc.). In this context, the steps b-C-I.i to b-C-I.iii are replaced with the following two steps::

I.Generate finite numbers of surrogate models of the problem under investigation, and calculate bellows for each :

i. Execute the surrogate model for appropriate finite times for new inputs from non-uniform pdfs to generate a histogram of desired outputs

ii. Fit a known form probability density function to each histogram of the previous step

Fig.4. Computational steps for Physics-informed modelling (Moradabadi 2017)

 © DFI International Bruges 2025

CASE STUDIES

Consider a tunnel project surrounded by diverse geotechnical data. Instead of relying on fixed absolute values, a range of values is dealt with during the design and construction phases. For extended projects, limited borehole data is often available, and its accuracy may be compromised due to human and machine errors. To mitigate risks, increasing parameter values or adjusting design results to ensure safety might be necessary. This conservative approach, however, could lead away from the optimal design solution. As excavation begins, new data is encountered, sometimes revealing values that are less conservative than anticipated. These unexpected variations can significantly influence design decisions and overall construction strategy. Therefore, an approach that accounts for uncertainty at every phase of the project is essential. This involves continuously updating knowledge and refining predictions. The previously discussed digital twin physics-informed model enables consistent and accurate real-time prediction of tunnel performance behaviour, exemplified by a digital tunnelling-induced damage model illustrated in a decision analysis diagram (Fig. 5).

This model facilitates the visualisation and analysis of potential damage resulting from tunnelling activities by incorporating various input variables derived from experience, investigations, and measurements. During the planning stage, input variables are typically estimated based on laboratory and in-situ tests. However, output variables remain uncertain. As the asset progresses through its lifecycle—whether during construction or operation—additional data may be collected to enhance the accuracy of the physical asset model. To reconstruct the geometry of the tunnel and create a virtual reality representation, technologies such as LiDAR scanners, cameras, and drones are employed. IoT sensors are crucial for measuring both input and output variables. Depending on the asset's phase, predictions may need to be updated. Sample-based algorithms, such as Monte Carlo methods and Bayesian updating, are employed to propagate uncertainty for initial predictions and to update these predictions, respectively.

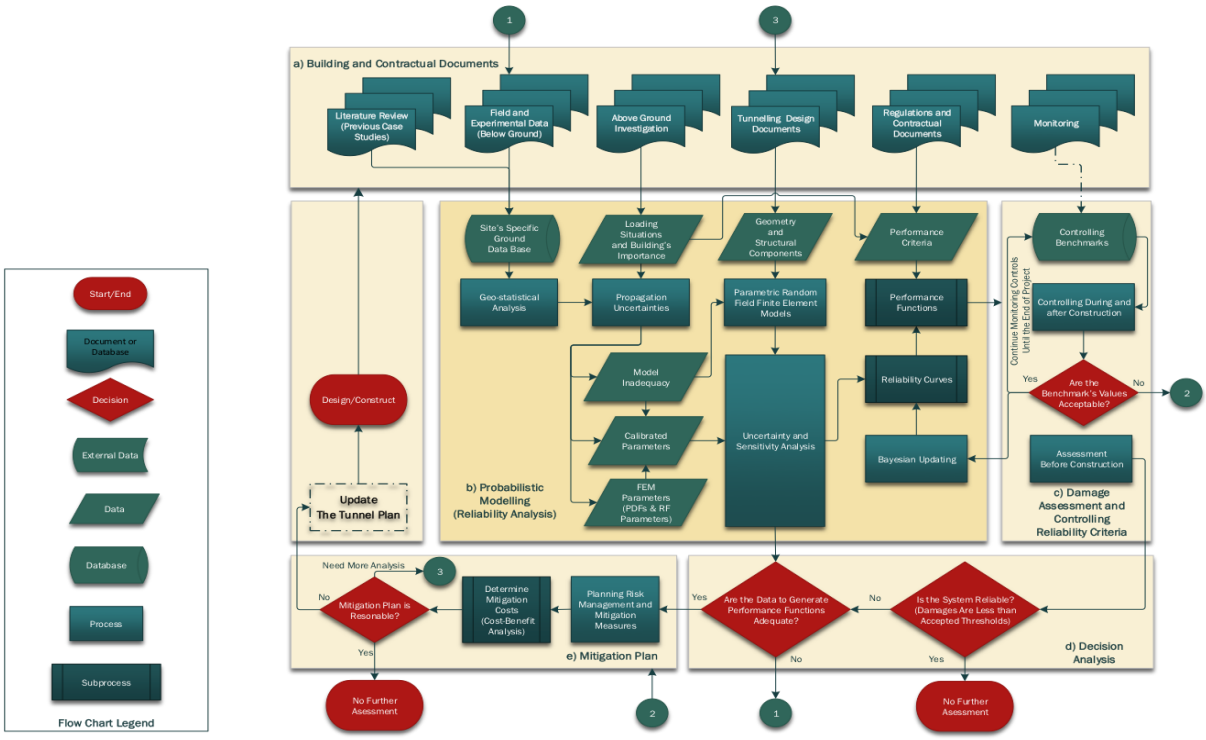


Fig.5. Decision analysis diagram for predicting tunnelling-induced damage (Moradabadi 2017)

In the following, the essential computational steps to achieve a physics-informed model through the context of Digital Twin frameworks for predictive analysis of tunnelling-induced surface settlement during the construction phase are explored through two different case studies in large-scale tunnelling

 © DFI International Bruges 2025

in soft ground. These case studies provide practical insights into the application of the Digital Twin framework for enhancing predictive accuracy and managing uncertainties in tunnelling projects. As discussed subsequently, a Digital Twin model exhibits characteristics analogous to those of an organism. When managing a complex model, the system produces a substantial volume of data. This paper focuses on the methodology and steps for integrating virtual and physical realms. The results and analytical sequences for each case study are depicted in Figures 6 and 7. It is important to note that the presented results are not exhaustive and serve as illustrative examples. For a comprehensive understanding of the assumptions, foundational aspects of model creation, and detailed results, including further descriptions discussions and detail interpretation of the graphs, readers are encouraged to refer to the full text (Moradabadi 2017).

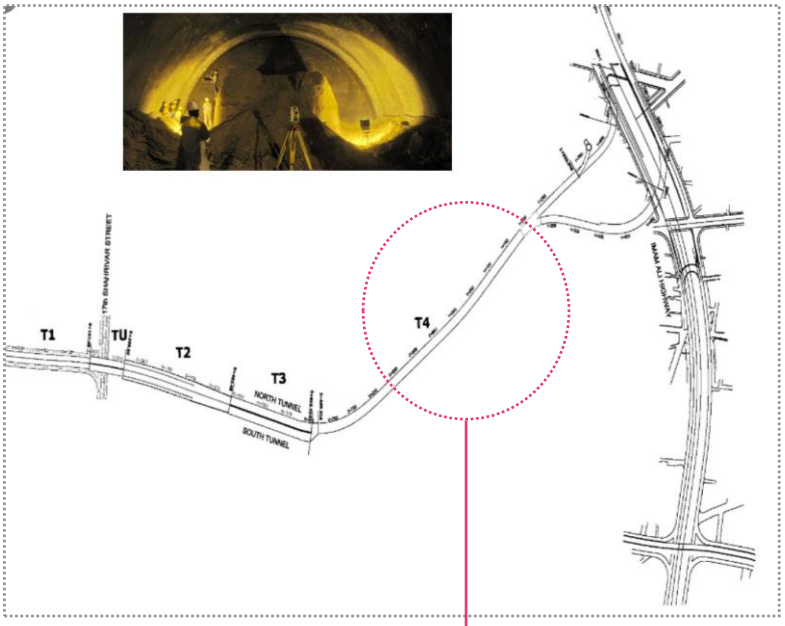
Case Study-1

Figure 6.a illustrates a horseshoe-shaped shallow roadway tunnel situated beneath a densely populated area in southern Tehran. This tunnel extends for 1.5 kilometres and was excavated in soft ground composed of alluvium soil. To analyse the variations in soil parameters along the tunnel, a 3D soil model was developed. Four critical soil parameters, obtained from limited borehole in-situ tests and laboratory experiments, are presented as examples (Fig.6.b). The tunnel construction employed a sequential excavation method. To simulate ground behaviour during excavation, simple parametric Finite Element (FE) models were created, assuming homogeneous ground conditions for simplicity and a Mohr-Coulomb constitutive law for the elastoplastic behaviour of the Alluvium soil. These models incorporates 28 input variables, with a primary objective of estimating surface settlement induced by tunnelling. The simulation aims to construct a reliability curve for the maximum transversal surface settlement and ensure compliance with predefined criteria for the settlement of the road above the tunnel. Initially, a local sensitivity analysis was conducted to verify that the FE models accurately represent the tunnel's behaviour under both nominal and extreme parameter values (Fig.6.c). Subsequently, a global sensitivity analysis was performed using the Monte Carlo-based Latin Hypercube Sampling algorithm (Fig.6.d). All 28 parameters were considered, and approximately 500 simulations revealed that only 10 parameters significantly influenced the results. The uncertainty ranges for the remaining parameters had minimal impact on outcome variations.

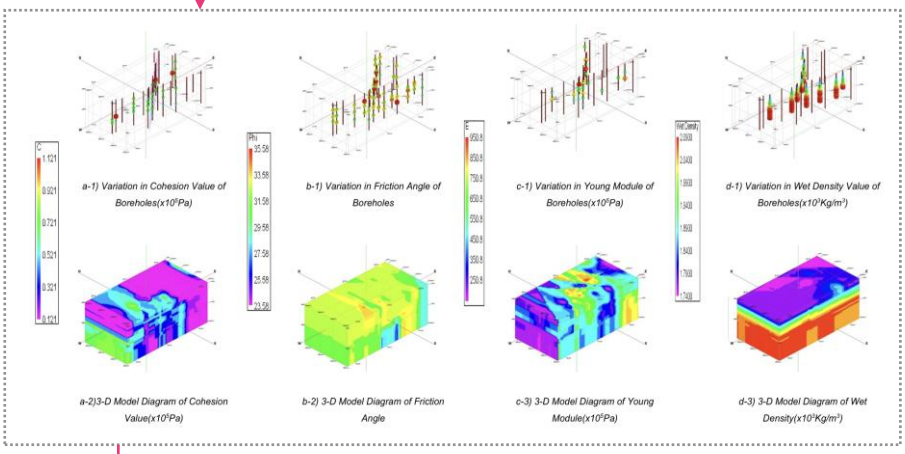
By reducing the model dimension from 28 to 10 (Fig.6.e), computational resources were conserved, and interpretability was enhanced. Regarding computational aspects, these straightforward FE models allowed simulations to be run on an older desktop computer without parallel or cloud computing, with each iteration taking under 5 minutes. With around 1000 iterations of the 10 critical variables, the entire simulation was completed in less than 3.5 days.

However, for more complex 3D models, even with cloud computing, computational costs can become prohibitive. To address this, a surrogate model utilising an Artificial Neural Network (ANN), specifically Feedforward Neural Networks (FNNs), which were found to be sufficient based on fitting results and validation tests, was developed by training on the results obtained from the global sensitivity analysis output (Fig.6f). This approach enabled comparison between the surrogate model and the original FE simulation, as depicted in the accompanying diagram.This comparison demonstrated that, although using surrogate models may reduce the accuracy of predictions, the significant reduction in computational effort makes them a reasonable alternative for more complex and time-consuming models. It is important to note that this study was not conducted during the construction phase. Instead, monitoring data was available, which enabled the updating of predictions using the Bayesian updating method (Fig.6g). This methodology could similarly be applied during construction, allowing for continuous adjustment of input parameters and output results. It is important to note that, the results show that due to the nature of discrete sampling methods, assumptions made in selecting appropriate likelihood functions and the prior distribution for creating the posterior distribution (updated prediction) may affect the results. Consideration is necessary for similar problems to reduce the uncertainty associated with these assumptions and to increase accuracy, warranting further exploration in a new study.

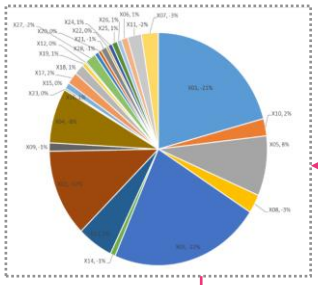
 © DFI International Bruges 2025



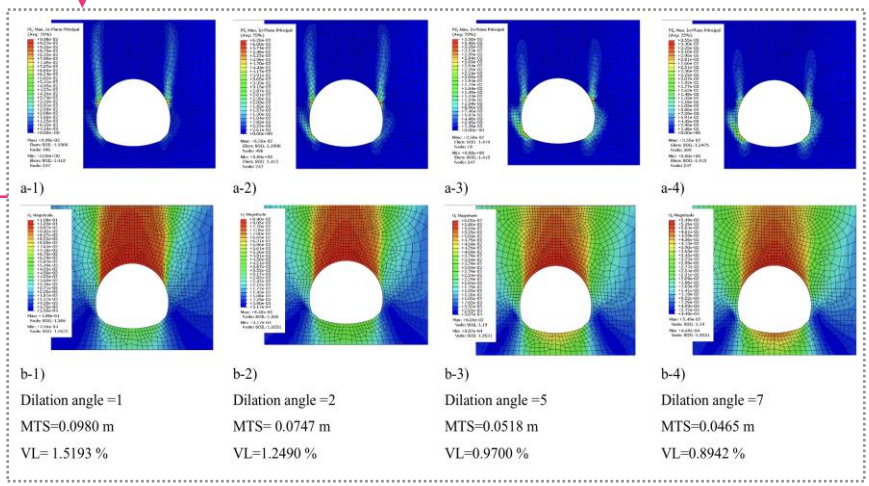
a)T4 section of Amirkabir project



b) Examples of 3D geostatistical analysis through tunnel's length



d) An Example of global sensitivity analysis



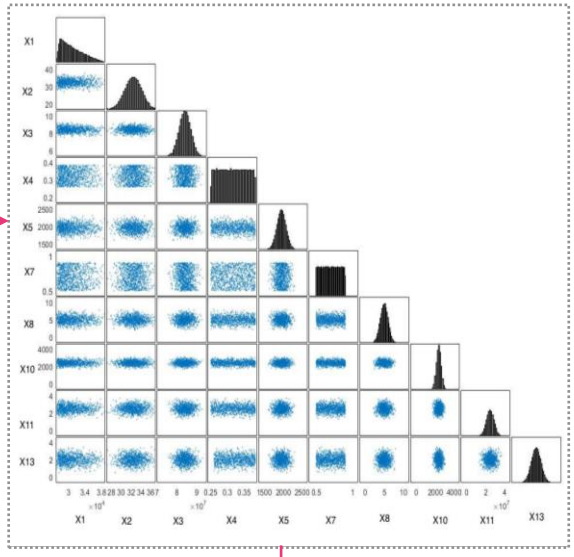
c) Examples of local sensitivity analysis

Fig 6-Part 2-e

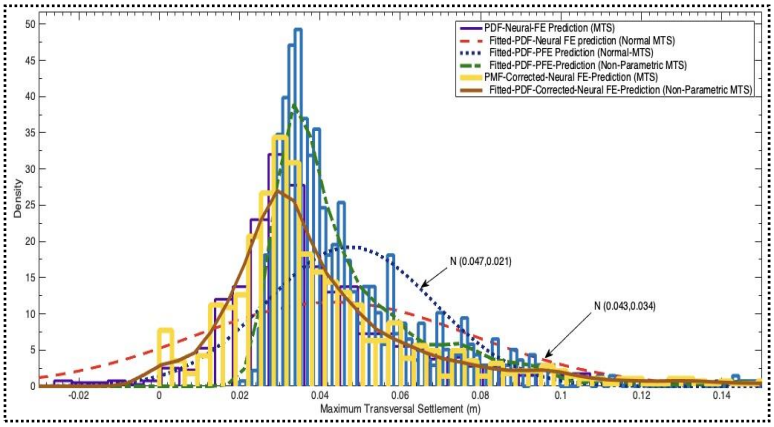
Fig.6 (Part 1). Graphical summary for application of Physics-informed modelling for Case Study-1

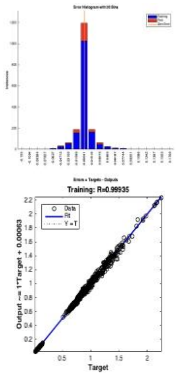
 © DFI International Bruges 2025

Fig 6-Part 1-d

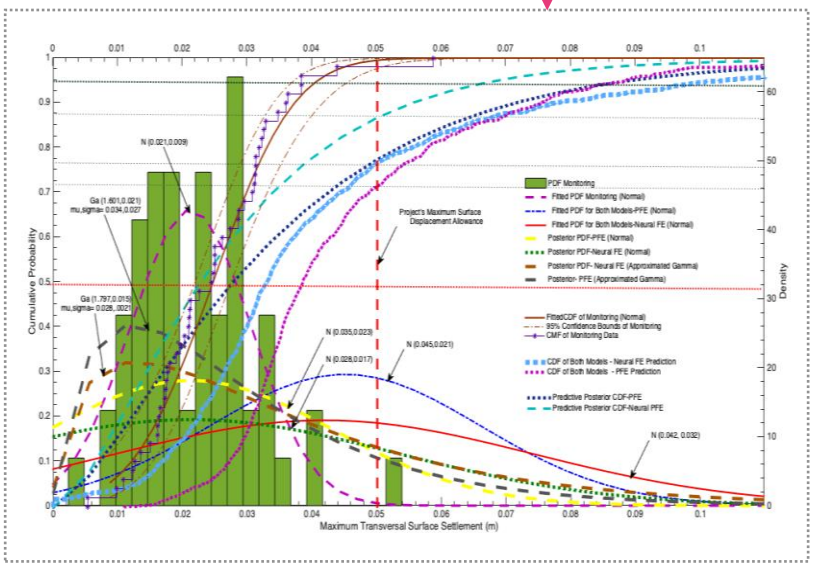


e) Sampling and correlation matrix of prominent parameters after dimensions reduction





f) Examples of pdf results for maximum transversal settlement, with and without



g) Examples of CDF results for maximum transversal settlement, with and without surrogate-modelling, comparison with monitoring data and prediction posteriors using Bayesian updating

Fig.6 (Part 2). Graphical summary for application of Physics-informed modelling for Case Study-1

 © DFI International Bruges 2025

Case Study-2

To explore the application of this method to a more complex problem, the methodology was applied to a more intricate scenario. Fig.7.i shows a cross-section of the Rio Piedras station, part of the Tren Urbano subway tunnel in Puerto Rico, USA. The underground cavern of the station is horseshoe-shaped, measuring 17 meters in width, 16 meters in height, and 150 meters in length, with two 30-meter access shafts at either end, excavated in alluvium soil. To minimise the impact on the structures above, the tunnel was constructed using the stacked drift method, with drifts measuring 3 by 3 meters.

The objective of this case study was to evaluate the method's ability to handle uncertainties in input parameters, such as the spatial variability of soil properties, and to develop a reliability curve for maximum transversal settlement and volume loss. A new geostatistical analysis was conducted to construct a 3D soil model, which provided insights into the spatial variability of the soil.

The mass density function and the fitted probability density functions for different soil characteristics, along with a visualisation of their variation along the tunnel's length, are presented in Fig.7.ii. Similar to the previous case study, a parametric finite element model of the tunnel was developed (Fig. 7.iii.a).

A univariate homogeneous Gaussian discrete random field algorithm was employed to map the spatial variability to the model, creating a random inhomogeneous parametric finite element model (Fig.7.iii.b). In this way, the finite element model was transformed into a probabilistic model, meaning that running the model with the same input variables could yield different results each time. The random field was defined solely for the plastic parameters of the soil, specifically cohesion and effective friction angle, assuming a Mohr-Coulomb constitutive law for the elastoplastic behaviour of the ground

In terms of computational effort, a single simulation of this model takes more than 49 minutes on the same computer that required only 5 minutes for the previous case. Given the probabilistic modelling and the number of variables, running 10,000 simulations for a preliminary sensitivity analysis would take approximately one year on the same computer without cloud computing. To address this, a local sensitivity analysis was performed to identify the influence area of the random field. This approach involves defining a zone where plastic strain in the ground develops. If the in-plane principal plastic strain in an element is zero, it can be assumed that the soil behaves elastically, and defining the plastic parameters are not necessary for that element (Fig.7.iii.c).

The mesh was optimised to reduce computation costs by mapping the random field only to the influence area (Fig.7.iv.a to c). Fig. 7.v. shows the plot of 1000 simulated settlement troughs and its average. This new model ran six times faster. However, this was still insufficient, as each simulation would have taken over a month with two computers, and there was a need to ensure enough simulations to obtain reliable results for the random finite element model.

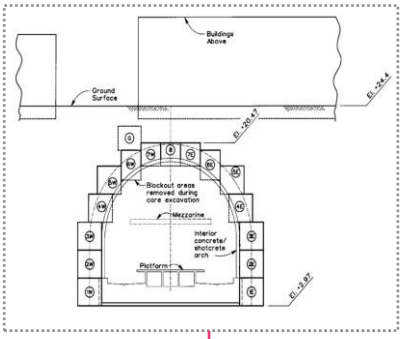
Further optimisation was conducted to determine the effective number of simulations needed. Fig.7.vi illustrates the results for 1,000 simulations with nominal values comparing with the results for 50 simulations, showing maximum transversal settlement versus the number of simulations, indicated that only 50 simulations were sufficiently effective for this model, significantly reducing the number of simulations required for appropriate results. The final sensitivity analysis was conducted with a sample size of 200, equivalent to 10,000 simulations (Fig. 7.vii).

The mentioned case studies highlight the practical challenges associated with the computational effort required to solve these types of problems and offer specific solutions to address these challenges. While interpreting the results is beyond the scope of this paper, further details can be found in the full text of the study (Moradabadi 2017).

As previously discussed, the concept of a digital twin aims to create a digital organism with an intricate anatomy capable of predicting the future behaviour of the asset it represents. These FE models can be considered physics-informed predictive models specifically designed to assess tunnel damage.

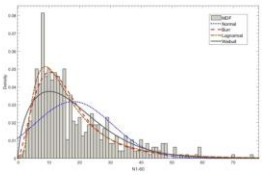
However, a similar approach can be applied to various excavation methods, such as mechanised tunnel excavation, other Architecture, Engineering, and Construction (AEC) simulations, or Hazard and Operability (HAZOP) models when addressing the entire lifespan of a tunnel.

 © DFI International Bruges 2025

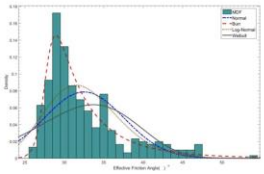


i) Cross Section of Rio Piedras Station

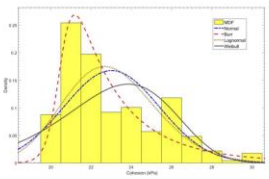
ii) Examples of 3D geostatistical analysis through the length of the tunnel including the MDF and fitted pdf for the main parameters for random field analysis



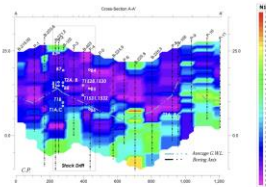
a)$N_1(60)$



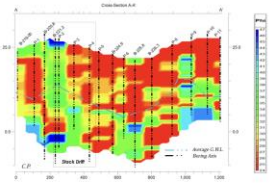
b) Effective Friction Angle



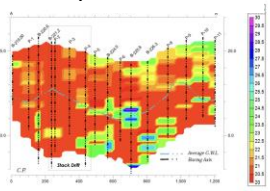
c) Cohesion



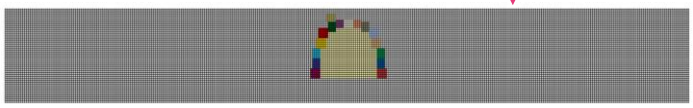
d) Variation of $N_1(60)$



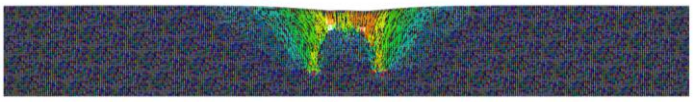
e) Variation of Effective Friction Angle



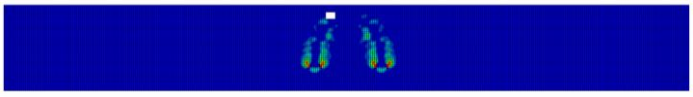
f) Variation of Cohesion



a) Parametric model with fine mesh



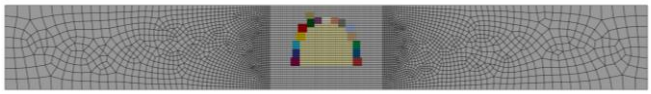
b) An example of results for deformation analysis



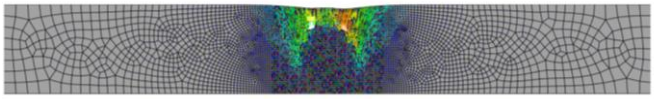
c) An example of result for in-plane principal plastic strain

iii) Random finite element model with homogenised mesh

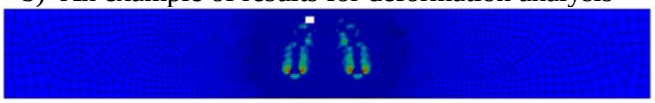
iv)Random finite element model with optimised mesh (finding the influence zone of random field)



a) Parametric model with optimised coarse mesh



b) An example of results for deformation analysis



c) An example of result for in-plane principal plastic strain

Fig 7-Part 2-v

Fig.7 (Part 1). Graphical summary for application of Physics-informed modelling for Case Study-2

 © DFI International Bruges 2025

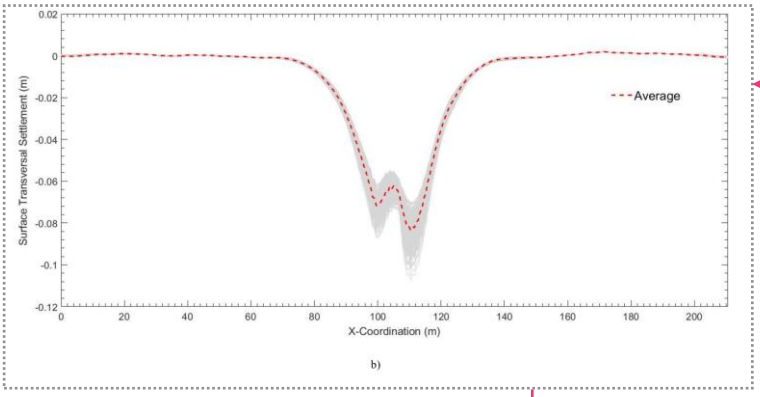
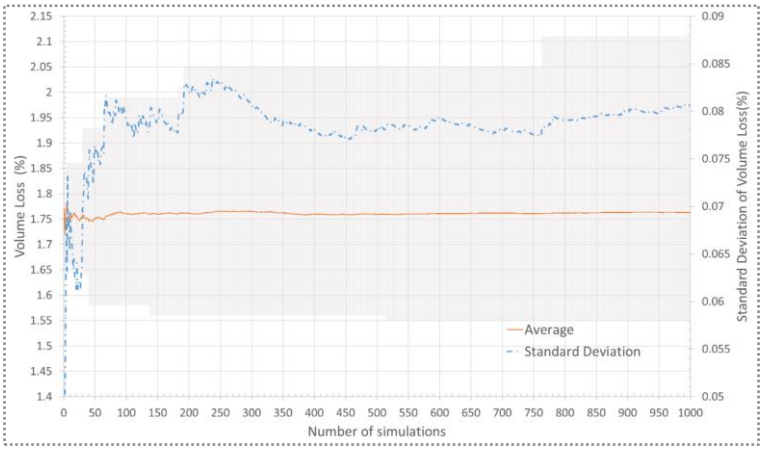
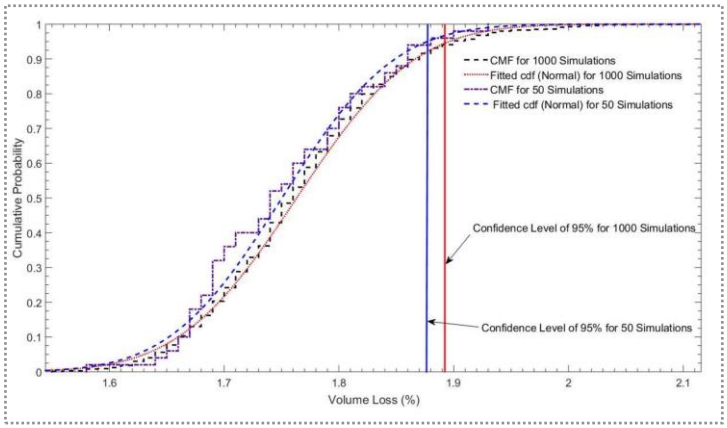


Fig 7-Part 1-iv

v) Effect of number of simulations in settlement troughs of random finite element model: Plot of 1000 simulated settlement troughs and its average for sequence 9

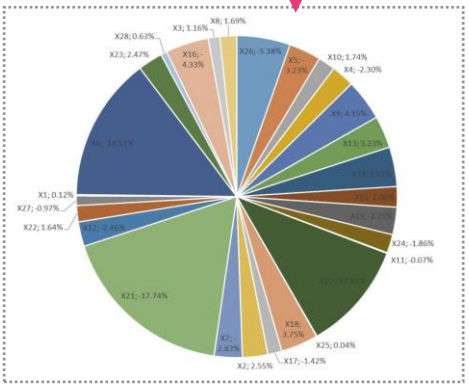
a) Volume loss vs. number of simulations (The grey colour shows the variation of volume loss corresponding to the number of simulations)





b) Comparison of CMF and its corresponding fitted cdf of volume losses resulted from 1000 simulations with CMF and cdf of 50 simulations

vi) An example of results for finding the effective number of simulation



vii) An example of results for sensitivity analysis for finding effective parameters contributing in explanatory power of volume loss

Fig.7(Part 2). Graphical summary for application of Physics-informed modelling for Case Study-2

 © DFI International Bruges 2025

For these models (case studies) to be considered a digital twin, they should be developed during the project's construction phase, utilising chronological data from the project's inception and being updated with real-time data. Additionally, integration with other AEC simulations and Building Information Modelling (BIM) models is crucial.

CHALLENGES IN IMPLEMENTATION

Previously discussed computational challenges inherent in solving physics-informed models highlight the complexities involved. The implementation of Digital Twin frameworks introduces additional challenges. This overview provides a preliminary examination, with each challenge requiring in-depth analysis by domain experts. Ultimately, practical solutions must be customised to address the specific requirements of each project.

Recruiting Experts: The assembly of a project team for Digital Twin implementation necessitates a balanced composition of individuals. The optimal team includes versatile members proficient in managing diverse tasks, integrating various components, and promoting creativity, in conjunction with multidisciplinary experts possessing deep expertise in specific domains (Kober et al., 2022). Enhancing collaboration, networking, and offering targeted training, as well as employing methodologies such as the gamification framework proposed by Bucchiarone (2022), can effectively address the requisite training approaches and the shortage of experts.

Data Complexity and Silos: Infrastructure assets generate vast amounts of data from diverse sources. These data sources often exist in separate silos, complicating management (Malakuti 2021). The solution lies in adopting an open, scalable, and vendor-neutral platform, essential for efficient data management and decision-making (e.g. what suggested by Greif et al. 2020 and Mostafa et al. 2021).

Conservatism in the AEC Industry: The Architecture, Engineering, and Construction (AEC) industry emphasises accuracy and reliability, often leading to a conservative mindset. This conservatism can hinder digital transformation (Sepasgozar et. al. 2023). The solution involves fostering collaboration, breaking down silos, and actively promoting digital transformation initiatives to bridge the gap and embrace technological advancements.

Information Misalignment: Digital Twin relies on Building Information Modelling (BIM) as a powerful tool, but aligning all information can be challenging (Agrawal et al. 2022). The solution is digital alignment, which involves closely monitoring changes and ensuring synchronisation to address this challenge effectively.

Leadership Style and Management System: Successful Digital Twin implementation requires a collaborative approach involving a multidisciplinary team, including visual designers, engineers, building information modellers, architects, and clients. Effective communication among team members, each bringing diverse perspectives, is crucial for aligning with project objectives. Regarding leadership styles, autocratic and paternalistic approaches are ineffective for Digital Twin teams as they create a climate of fear and hinder open dialogue and independent work. Conversely, purely democratic leadership can lead to decision-making paralysis due to conflicting viewpoints. The optimal approach is a consultative leadership style, emphasising task orientation and strong interpersonal relationships within the team. These leaders rely on team members 'expertise and collaborate with external partners to make informed decisions, ensuring adherence to project timelines, budgets, and constraints. ISO 44001 (2017) introduces a novel approach to this type of leadership, emphasising behaviours, organisational culture, and management processes. It acts as a bridge, connecting organisations across borders, enabling sustainable business relationships, and unlocking the advantages of collaborative working. Lastly, the effectiveness of Digital Twin technology relies heavily on high-quality data visualisation during the design and construction phases. Achieving this necessitates comprehensive standardisation across information technology (e.g., ISO 20000 (2018)), data quality (e.g., ISO 8000(2022)), and data supply (e.g., ISO 19158 (2012) and ISO 19650 (2018)).

Cybersecurity: Robust cybersecurity measures are crucial when managing the extensive data involved in Digital Twin applications (Maglaras et al. 2018). These measures protect against unauthorised

 © DFI International Bruges 2025

access, theft, or damage to hardware, software, and electronic data. Implementing a system like ISO 27032 (2023) can ensure effective cybersecurity management.

Interpreting Results for Decision Making: A Digital Twin model functions similarly to an organism, generating vast amounts of data. While AI assists in maintaining constant calibration with physical assets, the critical task of interpreting this data for decision-making ultimately rests with humans. Appropriate, standardised, project-specific indicators are essential to maintain control over the asset, akin to a patient undergoing surgery.

Cost of Building Infrastructure and Energy Consumption: Digital Twin technology and cloud computing infrastructure are interdependent, with improvements in one benefiting the other. Addressing the challenges of cloud computing infrastructure cost and energy consumption involves several strategies (Beri et al. 2010; Zhou et al. 2013 and Teng et al. 2021):

- *Energy-Efficient Data Centres*: Optimise the design of data centres, cooling systems, and hardware, or use renewable energy sources to reduce energy consumption.
- *Resource Consolidation*: Utilise virtualisation and containerisation to better utilise physical servers, reducing the need for additional hardware. Dynamic resource allocation ensures efficient use of computing resources.
- *Energy-Aware Algorithms*: Develop algorithms that consider energy efficiency during resource allocation, workload scheduling, and data movement. Machine learning and heuristics can predict CPU utilisation and optimise VM placement.
- *Edge Computing*: Distribute processing closer to data sources (e.g., IoT devices) to reduce data transfer and central server load, minimising energy-intensive long-distance communication.
- *Energy Monitoring and Management*: Implement real-time monitoring tools to track energy usage and identify inefficiencies. Automated energy-saving policies based on workload demand can be implemented.
- *Green Cloud Providers*: Choose cloud providers committed to sustainability and energy-efficient practices, with some offering regions powered by renewable energy sources.
- *Hybrid Cloud Strategies*: Combine public cloud services with on-premises infrastructure, selectively migrating workloads to the cloud to optimise costs and energy usage.

SUMMARY AND CONCLUSIONS

Digital twins, particularly “Asset Twins,” serve as dynamic virtual replicas of physical assets, continuously synchronised with real-time data. These models bridge the physical and digital domains, enabling real-time insights, accident analysis, workspace optimisation, and predictive maintenance across sectors such as smart cities, tunnelling, and renewable projects. The global digital twin market is projected to reach USD 195.85 billion by 2030.

Integrating digital twins into geotechnical engineering allows for continuous monitoring and updating of models with real-time data, leading to more accurate predictions and proactive management of ground behaviour. This enhances the ability to foresee potential issues and implement timely interventions, ultimately improving the safety and efficiency of geotechnical projects.

This paper demonstrates the application of physics-informed modelling within digital twin frameworks in geotechnical engineering, through two case studies in large-scale tunnelling in soft ground. Key steps include quantifying uncertainty, computational simulation, optimisation, and Bayesian updating.

Additionally, the paper addresses challenges in implementing digital twins, such as recruiting skilled experts, managing complex data, overcoming industry conservatism, ensuring information alignment, cybersecurity, and managing cloud computing costs. Effective leadership and collaboration are identified as crucial for the successful deployment of digital twin projects.

 © DFI International Bruges 2025

REFERENCES

Agrawal, Ashwin, Martin Fischer, and Vishal Singh. 2022. "Digital twin: From concept to practice." Journal of Management in Engineering 38 (3): 06022001.

Augustyn, Dawid, Martin D Ulriksen, and John D Sørensen. 2021. "Reliability updating of offshore wind substructures by use of digital twin information." Energies 14 (18): 5859.

Bezos, Jeff, 2023, "Jeff Bezos on AI: Large Language Models Are Not Inventions, They are Discoveries, Source: MSN," https://www.msn.com/en-us/news/technology/jeff-bezos-on-ai-large-language-models-are-not-inventions-they-re-discoveries/ar-AA1lw6JT.

Bucchiarone, Antonio. 2022. "Gamification and virtual reality for digital twin learning and training: architecture and challenges." Virtual Reality & Intelligent Hardware 4 (6): 471-486.

Busollo, Carlo, Stefano Mauro, Andrea Nesci, Leonardo Sabatino Scimmi, and Emanuele Baronio. 2021. "Development of a Digital Twin for Well Integrity Management in Underground Gas Storage Fields." SPE Annual Technical Conference and Exhibition.

Chen, Gongfa, Xiaoyu Kang, Mansheng Lin, Shuai Teng, and Zongchao Liu. 2023. "Stability prediction of soil slopes based on digital twinning and deep learning." Applied Sciences 13 (11): 6470.

Chen, Xilin, Mengqi Huang, Yu Bai, and Qian-Bing Zhang. 2024. "Sustainability of underground infrastructures." Part 1: Digitalisation-based carbon assessment and baseline for TBM tunnelling." Tunnelling and Underground Space Technology 148: 105776.

Daneshgar, Saba, Fabio Polesel, Sina Borzooei, Henrik R Sørensen, Ruud Peeters, Stefan Weijers, Ingmar Nopens, and Elena Torfs. 2024. "A full scale operational digital twin for a water resource recovery facility: A case study of Eindhoven Water Resource Recovery Facility." Water Environment Research 96 (3): e11016.

Eyre, Jonathan, and Chris Freeman. 2018. "Immersive applications of industrial digital twins." The Industrial Track of EuroVR 2018: 11-13.

Francisco, Abigail, Neda Mohammadi, and John E Taylor. 2020. "Smart city digital twin-enabled energy management: Toward real-time urban building energy benchmarking." Journal of Management in Engineering 36 (2): 04019045.

Gannouni, Aymen, Ali-Emil Naqwi, Hans Aoyang Zhou, Anas Abdelrazeq, Frank Hees, and Robert H Schmitt. 2023. "Experimental Digital Twin of a Tunnel Ring Building Erector." IEEE EUROCON 2023-20th International Conference on Smart Technologies.

Greif, Toni, Nikolai Stein, and Christoph M Flath. 2020. "Peeking into the void: Digital twins for construction site logistics." Computers in Industry 121: 103264.

Grieves, M. 2005. Product Lifecycle Management: Driving the Next Generation of Lean Thinking: Driving the Next Generation of Lean Thinking. McGraw Hill LLC.

Gu, Y, L Zhang, Q Ai, X Jiang, and Y Yuan. 2023. "Digital twin-oriented maintenance: A hybrid finite element and surrogate model approach for predicting the excavation-induced tunnel displacement." In Life-Cycle of Structures and Infrastructure Systems, 600-607. CRC Press.

Haghshenas, Amirashkan, Agus Hasan, Ottar Osen, and Egil Tennfjord Mikalsen. 2023. "Predictive digital twin for offshore wind farms." Energy Informatics 6 (1): 1.

Han, Tianran, Jianming Zhao, and Wenquan Li. 2020. "Smart-guided pedestrian emergency evacuation in slender-shape infrastructure with digital twin simulations." Sustainability 12 (22): 9701.

Hazrathosseini, Arman, and Ali Moradi Afrapoli. 2023. "The advent of digital twins in surface mining: Its time has finally arrived." Resources Policy 80: 103155.

He, Fan, Soh-Khim Ong, and Andrew YC Nee. 2021. "An integrated mobile augmented reality digital twin monitoring system." Computers 10 (8): 99.

 © DFI International Bruges 2025

Hong, Chengyu, Jinyang Zhang, and Weibin Chen. 2022. "An integrated intelligent approach for monitoring and management of a deep foundation pit in a subway station." Sensors 22 (22): 8737.

Hou, Lei, Shaoze Wu, Guomin Zhang, Yongtao Tan, and Xiangyu Wang. 2020. "Literature review of digital twins applications in construction workforce safety." Applied Sciences 11 (1): 339.

Hu, Weifei, Jiquan Yan, Feng Zhao, Chen Jiang, Hongwei Liu, Hyunkyoo Cho, and Ikjin Lee. 2023. "Surrogate-based time-dependent reliability analysis for a digital twin." Journal of Mechanical Design 145 (9).

Huang, Mengqi. 2022. "BIM for Underground Stations: Supporting Decision Making on Lifecycle Stages." Monash University.

Insights, Business Research. 2024a. Tunnel Construction Market Size, Share, Growth, and Industry Analysis, By Type (New Work, Reconstruction, Repairs), By Application (Transportation Tunnel, Utility Tunnel), Regional Insights and Forecast to 2032, Source: https://www.businessresearchinsights.com/market-reports/tunnel-construction-market-109337.

Insights, Fortune Business. 2024b. Digital Twin Market Size, Share & Industry Analysis, By Type (Parts Twin, Product Twin, Process Twin, and System Twin), By Application (Predictive Maintenance, Business Optimization, Product Design & Development, and Others), By Enterprise Type (Large Enterprises and SMEs), By End-user (Aerospace & Defense, Automotive & Transportation, Manufacturing, Healthcare, Retail, Energy & Utilities, Real Estate, IT and Telecom, and Others), and Regional Forecast, 2024-2032, Source: https://www.fortunebusinessinsights.com/digital-twin-market-106246.

International Organization for Standardization. ISO 44001:2017. Collaborative Business Relationship Management Systems — Requirements and Framework. 2017.

International Organization for Standardization. ISO/IEC 20000-1:2018. Information Technology — Service Management — Part 1: Service Management System Requirements. 2018.

International Organization for Standardization. ISO 19650-1:2018. Organization and Digitization of Information about Buildings and Civil Engineering Works, Including Building Information Modelling (BIM) — Information Management Using Building Information Modelling — Part 1: Concepts and Principles. 2018.

International Organization for Standardization. ISO 8000-1:2022. Data Quality — Part 1: Overview. 2022.

International Organization for Standardization. ISO/TS 19158:2012. Geographic Information — Quality Assurance of Data Supply. 2012.

International Organization for Standardization. ISO/IEC 27032:2023. Information Technology — Security Techniques — Guidelines for Internet Security. 2023.

Jafari, Mina, Abdollah Kavousi-Fard, Tao Chen, and Mazaher Karimi. 2023. "A review on digital twin technology in smart grid, transportation system and smart city: Challenges and future." IEEE Access 11: 17471-17484.

Jian, Liu, Zhou Tong, Huang Xianbin, Zhang Keqin, and Zhang Min. 2023. "Inferred Geological Data and Stability Analysis of Tunnel Surrounding Rock by Drilling and Blasting Method Based on Digital Twin." Journal of Civil Engineering and Urban Planning 5 (10): 6-18.

Jorgensen, Jack, Melinda Hodkiewicz, Edward Cripps, and Ghulam Mubashar Hassan. 2023. "Requirements for the application of the Digital Twin Paradigm to offshore wind turbine structures for uncertain fatigue analysis." Computers in Industry 145: 103806.

Junjia, Yin, Aidi Hizami Alias, Nuzul Azam Haron, and Nabilah Abu Bakar. 2024. "Development of a Hoisting Safety Risk Framework Based on the STAMP Theory and PLS-SEM Method." IEEE Access.

Kaewunruen, Sakdirat, Shijie Peng, and Olisa Phil-Ebosie. 2020. "Digital twin aided sustainability and vulnerability audit for subway stations." Sustainability 12 (19): 7873.

 © DFI International Bruges 2025

Kamble, Sachin S, Angappa Gunasekaran, Harsh Parekh, Venkatesh Mani, Amine Belhadi, and Rohit Sharma. 2022. "Digital twin for sustainable manufacturing supply chains: Current trends, future perspectives, and an implementation framework." Technological Forecasting and Social Change 176: 121448.

Katsidoniotaki, Eirini, Foivos Psarommatis, and Malin Göteman. 2022. "Digital twin for the prediction of extreme loads on a wave energy conversion system." Energies 15 (15): 5464.

Kober, Christian, Marc Fette, and Jens Peter Wulfsberg. 2022. "Challenges of digital twin application in manufacturing." 2022 IEEE International Conference on Industrial Engineering and Engineering Management (IEEM).

Lambe, T William. 1973. "Predictions in soil engineering." Geotechnique 23 (2): 151-202.

Latif, Kamran, Abubakar Sharafat, and Jongwon Seo. 2023. "Digital twin-driven framework for TBM performance prediction, visualization, and monitoring through machine learning." Applied Sciences 13 (20): 11435.

Lee, Dongmin, and SangHyun Lee. 2021. "Digital twin for supply chain coordination in modular construction." Applied Sciences 11 (13): 5909.

Lehtola, Ville V, Mila Koeva, Sander Oude Elberink, Paulo Raposo, Juho-Pekka Virtanen, Faridaddin Vahdatikhaki, and Simone Borsci. 2022. "Digital twin of a city: Review of technology serving city needs." International Journal of Applied Earth Observation and Geoinformation 114: 102915.

Li, Siqi, Junfeng Wang, Jin Rong, and Wei Wei. 2022. "A digital twin framework for product to-be-designed analysis based on operation data." Procedia CIRP 109: 179-184.

Liu, Xin, Yu Wang, Raymond CH Koo, and Julian SH Kwan. 2022. "Development of a slope digital twin for predicting temporal variation of rainfall-induced slope instability using past slope performance records and monitoring data." Engineering Geology 308: 106825.

Lu, Qiuchen, Xiang Xie, Ajith Kumar Parlikad, Jennifer Mary Schooling, and Eirini Konstantinou. 2020. "Moving from building information models to digital twins for operation and maintenance." Proceedings of the Institution of Civil Engineers-Smart Infrastructure and Construction 174 (2): 46-56.

Machado, Lucas Bellini, and Marcos Massao Futai. 2024. "Tunnel performance prediction through degradation inspection and digital twin construction." Tunnelling and Underground Space Technology 144: 105544.

Maglaras, Leandros A, Ki-Hyung Kim, Helge Janicke, Mohamed Amine Ferrag, Stylianos Rallis, Pavlina Fragkou, Athanasios Maglaras, and Tiago J Cruz. 2018. "Cyber security of critical infrastructures." Ict Express 4 (1): 42-45.

Malakuti, Somayeh. 2021. "Emerging technical debt in digital twin systems." 2021 26th IEEE International Conference on Emerging Technologies and Factory Automation (ETFA).

Moghadam, Farid K, Geraldo F de S RebouÃ§as, and Amir R Nejad. 2021. "Digital twin modeling for predictive maintenance of gearboxes in floating offshore wind turbine drivetrains." Forschung im Ingenieurwesen 85 (2): 273-286.

Moradabadi, Ehsan. 2017. "Uncertainty Quantification in Tunnelling-induced Surface Settlement." PhD thesis, University College Dublin

Mostafa, Fahed, Longquan Tao, and Wenjin Yu. 2021. "An effective architecture of digital twin system to support human decision making and AI-driven autonomy." Concurrency and Computation: Practice and Experience 33 (19): e6111.

Nagovitsyn, OV, and AV Stepacheva. 2021. "Digital twin of solid mineral deposit." Journal of Mining Science 57 (6): 1033-1040.

Nikolaev, S, M Gusev, D Padalitsa, E Mozhenkov, S Mishin, and I Uzhinsky. 2018. "Implementation of a “digital twin” concept for modern project-based engineering education." Product Lifecycle

Management to Support Industry 4.0: 15th IFIP WG 5.1 International Conference, PLM 2018, Turin, Italy, July 2-4, 2018, Proceedings 15.

Orlov, Pavel, 2023, "What Businesses Should Know About Digital Twins," https://www.forbes.com/councils/forbestechcouncil/2023/04/19/what-businesses-should-know-about-digital-twins/.

Piascik, R, John Vickers, Dave Lowry, Steve Scotti, Jeff Stewart, and Anthony Calomino. 2010. "Technology area 12: Materials, structures, mechanical systems, and manufacturing road map." NASA Office of Chief Technologist: 15-88.

Prabowo, Aditya Rio, Tuswan Tuswan, and Ridwan Ridwan. 2021. "Advanced development of of sensors' roles in maritime-based industry and research: From field monitoring to high-risk phenomenon measurement." Applied Sciences 11 (9): 3954.

Rabah, Souad, Ahlem Assila, Elio Khouri, Florian Maier, Fakreddine Ababsa, Paul Maier, and Mérienne, Frédéric. 2018. "Towards improving the future of manufacturing through digital twin and augmented reality technologies." Procedia Manufacturing 17: 460-467.

Ramos, Helena M, Alban Kuriqi, Mohsen Besharat, Enrico Creaco, Elias Tasca, Oscar E Coronado-HernÃ¡ndez, Rodolfo Pienika, and Pedro Iglesias-Rey. 2023. "Smart water grids and digital twin for the management of system efficiency in water distribution networks." Water 15 (6): 1129.

Research, Grand View. 2023. Digital Twin Market Size, Share & Trends Analysis Report By Solution (Component, Process, System), By Deployment (Cloud, On-premise), By Enterprise Size, By Application, By End-use, By Region, And Segment Forecasts, 2024 - 2030. https://www.grandviewresearch.com/industry-analysis/digital-twin-market.

Sahu, Yamini, and Vaibhav Kumar Upadhyay. 2024. "Environmental Application of Digital Twins: A Review." Environmental Risk and Resilience in the Changing World: Integrated Geospatial AI and Multidimensional Approach: 287-295.

Satyanaga, Alfrendo, Gerarldo Davin Aventian, Yerkezhan Makenova, Aigerim Zhakiyeva, Zhuldyz Kamaliyeva, Sung-Woo Moon, and Jong Kim. 2023. "Building information modelling for application in geotechnical engineering." Infrastructures 8 (6): 103.

Sepasgozar, Samad ME, Ayaz Ahmad Khan, Kai Smith, Juan Garzon Romero, Xiaohan Shen, Sara Shirowzhan, Heng Li, and Faham Tahmasebinia. 2023. "BIM and digital twin for developing convergence technologies as future of digital construction." Buildings 13 (2): 441.

Shi, Anchi, Changhao Lyu, Xuewen Fan, Mingtao Hu, Huanling Wang, and Weiya Xu. 2024. "Prediction of Dam Foundation Displacement due to Excavation Unloading Based on Digital Twin: Case Study of Baihetan Hydropower Project." Journal of Engineering Mechanics 150 (6): 05024001.

Shi, Chao, and Yu Wang. 2022. "Data-driven construction of Three-dimensional subsurface geological models from limited Site-specific boreholes and prior geological knowledge for underground digital twin." Tunnelling and underground space technology 126: 104493.

Teng, Sin Yong, Michal Touš, Wei Dong Leong, Bing Shen How, Hon Loong Lam, and Vítězslav Máša. "Recent advances on industrial data-driven energy savings: Digital twins and infrastructures." Renewable and Sustainable Energy Reviews 135 (2021): 110208.

Tomar, R, J Piesk, H Sprengel, E Isleyen, S Duzgun, and J Rostami. 2020. "Digital twin of tunnel construction for safety and efficiency." In Tunnels and Underground Cities: Engineering and Innovation Meet Archaeology, Architecture and Art, 3224-3234. CRC Press.

Ugliotti, Francesca Maria, Anna Osello, Muhammad Daud, and Ozan Onur Yilmaz. 2023. "Enhancing risk analysis toward a landscape digital twin framework: A multi-hazard approach in the context of a socio-economic perspective." Sustainability 15 (16): 12429.

Wagg, DJ, Keith Worden, RJ Barthorpe, and Paul Gardner. 2020. "Digital twins: state-of-the-art and future directions for modeling and simulation in engineering dynamics applications." ASCE-ASME

 © DFI International Bruges 2025

Journal of Risk and Uncertainty in Engineering Systems, Part B: Mechanical Engineering 6 (3): 030901.

Walker, Jake, Andrea Coraddu, Maurizio Collu, and Luca Oneto. 2022. "Digital twins of the mooring line tension for floating offshore wind turbines to improve monitoring, lifespan, and safety." Journal of Ocean Engineering and Marine Energy: 1-16.

Wang, Xiong, Yue Pan, and Jinjian Chen. 2024. "Digital twin with data-mechanism-fused model for smart excavation management." Automation in Construction 168: 105749.

Ye, Zijian, Ying Ye, Chengping Zhang, Zhiming Zhang, Wei Li, Xuejie Wang, Lei Wang, and Libin Wang. 2023. "A digital twin approach for tunnel construction safety early warning and management." Computers in Industry 144: 103783.

Yevu, Sitsofe Kwame, Emmanuel Kingsford Owusu, Albert PC Chan, Samad ME Sepasgozar, and Vineet R Kamat. 2023. "Digital twin-enabled prefabrication supply chain for smart construction and carbon emissions evaluation in building projects." Journal of Building Engineering: 107598.

Yu, Gang, Shuang Zhang, Min Hu, and Y Ken Wang. 2020. "Prediction of highway tunnel pavement performance based on digital twin and multiple time series stacking." Advances in Civil Engineering 2020 (1): 8824135.

Zhang, Limao, Jing Guo, Xianlei Fu, Robert Lee Kong Tiong, and Penghui Zhang. 2024. "Digital twin enabled real-time advanced control of TBM operation using deep learning methods." Automation in Construction 158: 105240.

Zheng, Hui. 2021. "Research and analysis on the application of digital twin technology in urban rail transit." 2021 IEEE Asia-Pacific Conference on Image Processing, Electronics and Computers (IPEC).

Zhou, Jiehan, Teemu Leppanen, Erkki Harjula, Mika Ylianttila, Timo Ojala, Chen Yu, Hai Jin, and Laurence Tianruo Yang. 2013. "Cloudthings: A common architecture for integrating the internet of things with cloud computing." Proceedings of the 2013 IEEE 17th international conference on computer supported cooperative work in design (CSCWD).

 © DFI International Bruges 2025

HOW GEOTECHNICS CAN SPEED UP DECARBONISATION WITH THE HELP OF CLIENTS

Paul Vidil, Soletanche Bachy, Rueil-Malmaison, France, +33(0)147764262, paul.vidil@soletanche-bachy.com

ABSTRACT

Although foundation contractors have made considerable progress in sustainability over the past few years, decarbonisation is not fast enough on their job sites. How can contractors scale-up their environmental initiatives? Based on past sites, this article describes ten geotechnical issues that are barriers clients (owners, contracting authorities, and prime contractors) can break down before calls for tenders, in the interest of all (economic and environmental), whilst applying standards. Decarbonisation, limitation of dewatering and resource depletion can be amplified if internal and external stakeholders work together, understanding each other's perspectives.

Keywords: geotechnical, decarbonisation, efficiency, clients

INTRODUCTION

Foundation contractors have made considerable progress in sustainability over the past few years, with initiatives such as employee awareness campaigns, training, moving into action, solutions roll-out (e.g. low-carbon concrete, recycled steel, reduction of fuel consumption, etc.), and this, in several lines: acting for climate, optimizing resources thanks to circular economy, preservation of natural environments, etc. But at macroscale, six out of nine planetary boundaries have been breached (Caesar, et al. 2024), and the global average surface temperature is still rising (Copernicus 2025). At contractors' scale, there were a series of improvement, but it appears that it is difficult to continue improving in time. In brief, it looks like decarbonisation is not fast enough in job sites, given the climate emergency. How can contractors scale-up their environmental initiatives?

To understand what prevents contractors from moving forward, one good practice is to make a SWOT analysis at each company level: strengths, weaknesses, opportunities and threats. It makes understand that one way to answer the question of scaling-up is to rephrase it: what prevents contractors from speeding up in their environmental action plans? The biggest levers to change the carbon footprint of sites are not directly reachable for foundations contractors: it is the responsibility of clients, that is to say owners, contracting authorities, prime contractors, etc. that are the real decision makers. First, clients should become aware that some of their decisions have significant carbon cost; contractors are not the only responsible party when it comes to the carbon footprint of a foundation. Clients can break down some barriers, so that foundation contractors can decarbonate as much as possible.

The purpose of this article is to address this issue in the upstream phase of projects, because discussing this with a client during construction phase is often too late, or has less of an impact. The intention is not to point out responsibilities, but to explain to owners, contracting authorities, and prime contractors what could make foundation contractors go further in decarbonisation. It is now time to foster relationships with external stakeholders to unlock issues that prevent contractors from scaling up decarbonisation. The discussion herein goes actually beyond decarbonation; the subject is also to reduce dewatering during excavation inside enclosures.

CONTEXT

When it comes to decarbonisation, the spotlight is put on contractors, whereas it should be put on all project protagonists; it is much too reductive to point the finger at the foundation contractor that pours concrete in the ground: he is carrying out works that he was asked for, trying to be virtuous, on

 © DFI International Bruges 2025

condition that different protagonists allow him to implement his environmental process. Contractors are aware that they are “part of the problem, part of the solution”, but there is a limit to this common saying, because having your hands and feet tied vs. having carte blanche makes a really big difference when it comes to being creative and looking for virtuous alternative solutions. Foundation contractors cannot act on their own to embrace sustainability and reduce CO2 production in foundation design and execution, as they often intervene at the end of decision making.

When answering a call for tenders, ecology sometimes meets economy, because foundation contractors are looking for reduction of quantities (like, concrete, steel, etc.), or clinker substitution in cement composition, because by-products (e.g., blast furnace slag) are cheaper than clinker. To reduce greenhouse gas emissions, the biggest influencer is raw materials. Climate emergency is thus leading to efficiency in terms of construction.
Nevertheless, some requirements in design make contractors implement more than the regulations. As a matter of fact, some specifications are overspecifying.

Finally, some foundations contractors try to innovate and stand out from competition, but clients are often unwilling to change their mainstream solutions. The weighty influence of habits acts like a sharp brake on innovation, although innovation is not a leap into the unknown: it is defined by procedure, investigation, company specifications, monitoring, etc. On certain projects, some foundation contractors want to be proactive, and do not want to limit themselves to being compliant.

OBSTACLES

There are global obstacles, and also foundation contractors know from experience that situations vary a lot, depending on countries, clients, other stakeholders, contract types, etc and that there is no silver bullet solution for decarbonisation.
When it comes to concrete, contractors are aware that in some countries:

- the client supplies concrete, and there is no possibility to reduce carbon content
- low carbon concrete is not common, so that it requires investments and therefore extra cost at the beginning,
- some clients do not want to talk about carbon footprint, or they think that low carbon concrete is greenwashing,
- some sub-contractors use a concrete that is not decarbonized enough,
- there are countries where there is not the opportunity to have the materials needed to make the ideal concrete mix.

It is not because in some cases it is not possible at the moment, that contractors do not have to keep trying whenever it is possible. In any case, in the face of climatic crisis, these subjects will become a priority for everybody sooner or later. Meanwhile, the need to raise awareness among clients is essential. Decarbonisation, limitation of dewatering and resource depletion are in the client interest, not only because it could save him money, and help tackle climate change, but also because he will need to justify his actions to stakeholders (bankers, investment fund, insurers, partners, etc.). European taxonomy for sustainable activities (EU taxonomy for sustainable activities 2025) is a good example of the increasing pressure to progress toward more virtuous projects.
In the next section, more obstacles are mentioned, and it is explained how clients can remove some of them.

POTENTIAL OPPORTUNITIES

Although European taxonomy is beginning to change the behaviour of construction industry protagonists, there is no time to wait for standards that will compel clients (owners, contracting

authorities, prime contractors). Foundation contractors prefer to count on environmental awareness and the cooperation of the stakeholders.
Based on past sites, this article describes ten geotechnics issues, that are barriers clients can break down before calls for tenders, in the interest of all (economic and environmental), while complying with standards. These ten items will not only have an influence on decarbonisation, but also in the limitation of dewatering and resource depletion:

1. Open to alternative solutions
2. Express clearly what the primitive need is
3. Do not limit minimal dimensions where not imposed by applicable standards
4. Do not ask for what is not needed
5. Keep it simple when the project is simple
6. Be consistent in the environmental process
7. Do not underestimate geotechnical parameters
8. Do not disrupt soil mechanics
9. Favour feedback
10. Give more time to answer calls for tenders.

Of course, this list does not fit every country or local market. They are food for thought, nonetheless. It is up to foundations contractors to meet and discuss with their clients in order to understand each other's perspectives, think together, and try to find virtuous solutions; this could be during a conference, exhibition, special event on a particular subject, etc. The following paragraphs give some details of these ten potential opportunities that foundations contractors seek from their clients:

1. *Open to alternative solutions*

Current status: In many project specifications, there is a sentence asking for response only to the conforming scheme, a.k.a. the engineer's scheme or the prime contractor solution, insisting that alternative solutions are forbidden. In other words, answering the call for tenders with another design leads automatically to elimination. With such a directive, the client and his consultants mean well, to spare time and money for everybody, because foundation contractors will therefore spend less energy to study the tender, and the client will spend much less time analysing offers and comparing dozens of alternative projects, before choosing the company that will obtain the contract.
Consequence: Although the refusal of alternative proposals will facilitate the finalisation of the contract, it will also terminate the opportunities and potential savings (carbon, programme, expenditure) that could result from contractor's optioneering. Clients, wherever possible, should try and build in a time allowance for revisions and rewriting of contract documentation, that will permit the full potential of expert, alternative approaches to be achieved. Furthermore, many foundation contractors are special geotechnical works' experts and have feedback of more than sixty years in carrying out diaphragm wall, grouting, piles, deep mixing. Sometimes foundation contractors have even already executed a similar project. They are in the best position to suggest alternative solutions that could be cheaper and maybe faster. Moreover, outside-of-the box solution should not be ignored. Forbidding any alternative solution prevents any potential savings in raw material (e.g., concrete, steel, etc.), water, money, and time, and therefore savings in CO2 and resources. It is even more incomprehensible in public works: the exemplariness of public order should not prevent candidates from suggesting a money saving solution. It should be mandatory in public tenders to authorize money saving alternative proposals.
Opportunity: Authorise alternative schemes in tenders, while giving sacrosanct points that cannot be changed.

2. *Express clearly what the primitive need is*

Current status: Calls for tenders contain results of all previous thoughts on a project, and intervene at the end of decision making. Foundation contractors are therefore forced to price the project outcome, and not the original client need. As an example, being asked to price a 0.80-meter-thick diaphragm

 © DFI International Bruges 2025

wall, for an enclosure 25 meters large, 60 meters long and 15 meters deep, instead of being asked to price a buried car park of 200 places.
Consequence: This approach prohibits foundation contractors from proposing different solutions that might minimize sustainability impacts, such as different techniques, sizes, shapes or structure, etc.
Opportunity: The client does not need a certain volume of cast-in-situ concrete, he only needs 200 places. To know the upstream requirement of a client will allow a foundation contractor to study a solution with different results, why not with a change of shape or depth of the car park within property lines. The aim is to reduce concrete, steel, water flow…
Indicate clearly in the call for tenders file what the ultimate goal of the client is, so that contractors will have the possibility to study different ways to achieve it, whilst also complying to standards and local specificities.

3. *Do not limit minimal dimensions where not imposed by applicable standards*

Current status: The client and their consultants sometimes set minimal geometrical dimensions (e.g., diaphragm wall thickness, piles length, anchors fixed length, etc.) in their specifications, that do not form part of the applicable standards. Answering to a tender with shorter dimensions leads automatically to elimination. And even during the execution process, shorter dimensions will not be tolerated, even if design calculations respect national standards. The client wants to simplify and to prevent contractors from being too aggressive in their design, and later on to prevent unsuccessful bidders from filing a plea.
Another example on a similar subject is the requirement of cement quantities that sometimes goes beyond what is recommended in applicable standards.
Consequence: With such minimal dimensions, contractors cannot implement what is strictly necessary, according to regulations. The best way to reduce carbon is not in concrete mixing but in concrete volume reduction; there is no better ultra-low carbon solution than the one where we do not use as much concrete and steel.
Opportunity: Do not indicate minimal dimensions that do not form part of the applicable standards. Do not over-specify.

4. *Do not ask for what is not needed*

Current status: Client specifications often contain limitations, such as maximum deviation of drilling/excavation tools (e.g., 0.3%), limit horizontal deflection of diaphragm wall (e.g., 2 cm), maximum allowable settlement under roads or adjoining buildings (e.g., 1 cm), etc. Not to mention extreme cases where specifications ask for no deflection at all. Most often, those values do not come from structural sensitivity analyses of surroundings but are copied and pasted from another project. The aim of the client is to make his project safer by imposing limitations.
Consequence: Each limitation has an extra-coast in terms of time, money and CO2. For instance, a limitation in horizontal deflection could lead to a diaphragm wall thickening or the addition of a level of props/ground anchors. Each project is specific, and it is only in occasional cases that limitations are necessary; in most cases, there is no reason to be excessive.
Opportunity: Fix threshold values according to structural sensitivity analysis of adjoining structures.

5. *Keep it simple when the project is simple*

Current status: Even for a simple geotechnical project, the trend is to complicate calculations, with 2D or 3D finite elements models, sometimes with sophisticated soil models, even for first calculations at the upstream stage. Some people are convinced that the more complicated a calculation is, the more precise results are, and the safer a project becomes. It is the same subject when one wants to be absolutely precise in the convergence of a soil-structure interaction model, whereas in geotechnics such a level of precision is wrong and useless.
Consequence: It is not because there is now the possibility to make complex calculations, that they should be applied every time. One part of the engineers' job is to select the appropriate tool to address a particular issue. Beyond time spent, digital technology has a significant carbon footprint (i.e., computers, screen, computing servers, etc.), so demanding complex calculation for a simple project contributes to global warming.

 © DFI International Bruges 2025

Opportunity: Complex calculations must be kept for complex situations. Darcy's law for flows, Frank & Zhao method or Boussinesq formula for settlements, Hamza's approach behind retaining structures, elasto-plastic methods for embedded walls, etc. are often sufficient to make a calculation, and thus to answer the questions raised. Do not ask for complex calculations in client specifications. Let the foundation contractor be the judge of what tool is relevant according to their geotechnical experience.

6. *Be consistent in the environmental process*

Current status: Contracts sometimes contain very specific requirements to reduce the global carbon footprint of a project, e.g., asking for the use of a cement CEM III/C (made from 85% ground blast furnace slag, a hydraulic binder coming from circular economy), while the very same contracts also prevent foundation contractors from reducing concrete quantities. On a recent site, it was an obligation to consider diaphragm walls as temporary works, and not to consider them in the final structure, which leads to the implementation of a thick structural concrete lining wall in addition. It does not make sense to insist on things that indeed have certain impacts, while putting more significant items aside.
Another example is in national standardisation committee when discussing of changing a partial factor from e.g. 1.25 to 1.15, arguing that's a way to get close to efficiency objectives, whereas many specification clauses prevent foundation contractors for optimising or looking for more virtuous solutions etc.
Consequence: Answering such tenders and then executing projects this way, leaves some contractors with a feeling of incompleteness. It is a pity to stop halfway when having the chance to engage stakeholders. It could also demotivate staff, and mainly design engineers who feel powerless to restrain global warming; it is also essential to fight against the loss of motivation of colleagues, that often think that it is not worth trying because the client will certainly reject their proposals. Some contractors eventually may choose not to respond to such calls for tenders.
Opportunity: Take this reasoning to its limit: optimize whatever can be reduced, whilst complying with standards.

7. *Do not underestimate geotechnical parameters*

Current status: Previously to a call for tenders, geotechnical engineering investigations enable foundation contractors to have geotechnical parameters at their disposal, that are inputs to check the engineering calculations, or to design an alternative solution. Extreme caution leads some geotechnical engineering firms to underestimate those inputs, just to be safer, or not to be held responsible in case of extra deflections. Some have noticed that layers of the French Paris basin lose 10 kPa of cohesion every decade! Sometimes it could be more than caution: it deals with risk management policies (fees that are not commensurate with the cost of litigation or repair), or clients unwilling to devote adequate funds for investigations that yield statistically significant data.
Consequence: It comes down to applying a kind of partial safety factor to inputs, that will be added to the safety factors coming from standards. It increases the global safety factor and therefore the quantities of concrete and steel.
Opportunity: Considering realistic cautious geotechnical parameter does not lead to an increase in risk. Characteristic soil parameters should be determined without implicit safety factors, based on field and laboratory tests results, complemented by well-established experience.

8. *Do not disrupt soil mechanics*

Current status: In client specifications, there are sometimes technical requirements that are not aligned to current "state of the practice" in foundation engineering. It is not a question of interpretation of one sentence of a Eurocode or professional recommendation, it is a question of physics. For example, here are some recent demands: consider a constant undrained cohesion on a large height (whereas pressuremeter tests show a clear improvement of geotechnical properties with depth), not considering friction between the soil and the diaphragm wall in the earth pressures' calculation, application of an at rest earth-pressure on the diaphragm wall in all layers (even limestone) at final stage, etc.
Consequence: It is very hard to deal with those requirements, whether it is during the response to a request for proposals, or during the construction design phase, because once it is written down on a client specification, it is nearly impossible to get the client to move back, even with solid technical

 © DFI International Bruges 2025

arguments. Those out-of-the-blue requirements always lead to overdesign in terms of steel and concrete, and therefore do not go in the right direction for reducing the project carbon footprint.
Opportunity: For a specific project, if there is a change to the way geotechnical engineers always design, it must be for a physical reason, and not for an arbitrary decision.

9. *Favour feedback*

Current status: Some engineering and consulting companies do not have the local knowledge of past sites in the vicinity of their future project. They may not have feedback from decades of geotechnical monitoring of structures, pumping tests, anchor investigations, conformity tests, etc., and therefore will design with bibliographic data and abacus from national standards. Yet, there is an example in Europe with the EN1997-1 that brings comparable experience and tests to the forefront, and in the background calculations that are only one way to solve a problem.
Consequence: Bibliographic data and abacus imply big safety factors, and consequently longer anchors, micropiles, etc.
Opportunity: Call for in-situ tests at the very beginning of projects to have a good estimation of geotechnical resistances of foundations and anchors, and favour companies that use their tests databases and nearby feedback to optimise the project. Some foundation contractors have even made post-construction calculations by comparing estimated deflections and stresses from initial calculations, and measured deflection and stresses from geotechnical monitoring during construction (and occasionally beyond); the goal being to find what input parameters should have been considered in initial calculations to get the closest to measured deflections and stresses. In some cases, more realistic geotechnical parameters (e.g., permeability, anisotropy, cohesion, modulus, etc.) are obtained, and can be applied to nearby projects.

10. *Give more time to answer calls for tenders*

Current status: Foundation contractors are compelled to hand over their bidding offer to the client as soon as possible. Some colleagues sometimes price three projects a day. Even for very big projects where there are only three weeks to answer, contractors often face refusal when requesting one or two-week deferrals, whereas the client has studied a project for multiple years.
Consequence: insufficient time leads to an inability to deeply analyse soil reports, take a critical look at characteristic soil parameters, check on similar projects carried out nearby, make some calculations, try to minimize quantities, compare carbon footprints of different solutions, look for an alternative to reduce water pumping etc.
Opportunity: Clients should give more time to answer call for tenders. It's worthwhile, as return on time investment could result in reduction of quantities, risk, pumped water, construction schedule and money.

Through these ten issues, the intention is not to target anybody so that client reaction to this article could only be to justify previous requirements. All parties have to look forward together by becoming aware of huge potentials left in reserve, as they cannot stagnate in the context of climate emergency. Clients, why not try to unlock one of these items in the next call for tenders?

REASONS FOR OPTIMISM

This barriers-to-be-break-down list should not hide the fact that many clients are already aware of the absolute necessity of decarbonation by all manner of means. Most of them are well informed, and obviously do not wait for foundation contractors to push forward their environmental policies:

- not only do some of them take into account the quality of the contractor's environmental offer during the tender analysis; but a percentage of the final marks is sometimes assigned to sustainability criteria: it can be on carbon footprint assessment, life cycle analysis (LCA) or multi-criteria analysis, efficient water management, waste management, preservation of natural environments, nuisance deduction (noise, vibration, dust, etc.).
- but they also ask for contractual commitment on the CO2 tons equivalent spent to build their project, or volume of water extracted from underground during site excavation; this is the case

 © DFI International Bruges 2025

for example for the ongoing design and built contracts for the Line 15 for the Grand Paris Express.

- some of them even help foundation contractors on their disruptive environmental approach; for instance, the constructive attitude of all stakeholders allowed the contractor to implement the first permanent circular diaphragm wall with unreinforced concrete for the Grand Paris Express (Canto, et al. 2022). On another site, a client has agreed to push the requirement for characteristic compressive strength of deep foundations concrete from 28 to 56 days, which allows the contractor to put less cement in the concrete.

Some construction contracts already head in the right direction, e.g., early contractor involvement (ECI), or competitive dialogue procedures. Sometimes it could happen before a call for tenders, during an early dialogue process that allows preliminary discussions with several companies (in France this is called “sourcing”, which is a possibility in public tenders). These types of contracts not only give time for projects improving but also bring more expertise at upstream phase.

CONCLUSION

This article has presented ten examples of barriers that owners, contracting authorities, and prime contractors can break, that will allow foundation contractors to scale up their environmental approach. Thus, decarbonisation, limitation of dewatering and resource depletion can be amplified if internal and external stakeholders work together, understanding each other perspectives. These examples obviously have to be adapted to local context.

A lot of work has to be done, both internally (training colleagues about this global approach) and externally (meet clients, organize seminar, explain things). It will not be easy, and it will take time to become widespread, but little by little clients will try to break through one or several barriers (beginning with one project), and that the economic and ecological success will lead to convince reluctant clients to make a start, as it is a win-win process, and anyway the climate emergency leaves no choice except scaling-up environment action plans. New narratives should not be based on old postures and habits, but on efficiency, that is to say all players efforts to end with what is strictly necessary : enough is better than too much.

REFERENCES

Canto, P., Le Batard, M. and Vidil, P., 2022. A permanent circular diaphragm wall with unreinforced concrete for the Grand Paris Express, DFI-EFFC International Conference on Deep Foundations and Ground Improvement, Berlin

Caesar, L., Sakschewski, B., Andersen, L.S., Beringer, T., Braun, J., Dennis, D., Gerten, D., Heilemann, A., Kaiser, J., Kitzmann, N.H., Loriani, S., Lucht, W., Ludescher, J., Martin, M., Mathesius, S., Paolucci, A., te Wierik, S., and Rockström J., 2024. Planetary Health Check Report 2024, Potsdam Institute for Climate Impact Research, Potsdam

Copernicus, 2025. Global Climate Highlights 2024 report

EU taxonomy for sustainable activities, accessed January 20, 2025. https://finance.ec.europa.eu/sustainable-finance/tools-and-standards/eu-taxonomy-sustainable-activities_en

 © DFI International Bruges 2025

ENGINEERING PEOPLE CENTRIC SUSTAINABILITY

S Briggs-North, Head of Human Resource, Aarsleff Ground Engineering Ltd, Nottinghamshire, United Kingdom, +44 1636 611140, sambriggs@aarsleff.co.uk

ABSTRACT

As societies become more aware of the social, environmental and sustainable impact that businesses have on the world, employers are faced with the fact that employees have an opinion, want to express that opinion and most importantly want it to be listened to. Furthermore, employers are aware that employees are far more likely to make a choice between employers that is based upon the culture and ethics of an organisation rather than just the size of the salary being offered. By weaving sustainability into the employee experience, HR can help shift the perception of ESG as a separate initiative to a central pillar of how the business operates.

The paper will discuss why we have “people” at the top of our sustainability strategy and the initiatives we have taken to give staff from all levels of the company the opportunity to influence the overall employee experience within the organisation. The paper will discuss the various Employee Voice Initiatives within the business.

The paper will also discuss the challenges and successes of an initiative taken to change the traditional and formal annual employee appraisal into a more agile and flexible Micro-Appraisal. It will explain the theory behind the benefit of creating shorter and more regular connections between employees and their line manager. It will demonstrate how this approach gives opportunity for both employer and employee to reflect on current performance, current development needs and summarise how the culture of the business has had to change to one where it is acknowledged and accepted that goals, personal ambitions and development needs can change, and can change quickly.

The paper will conclude with a discussion on the research we are undertaking with a UK University to better understand the barriers to gender diversity in Civil Engineering and to better understand why so many women either do not enter the industry at all or leave shortly after graduating from engineering degree courses.

INTRODUCTION

The paper will discuss why we have “people” at the top of our sustainability strategy and the initiatives we have taken to give staff from all levels of the company the opportunity to influence the overall employee experience within the organisation. The objective is to create a sustainable organisation through consideration of the new generations entering the workforce and adapting our people proposition to meet their needs, support our talent pipeline and ensure sustainability for the future workforce.

This shift towards a people-centric approach is not only re-defining daily work but is actively impacting the future of engineering. Employees play a fundamental role in the strategic success of business; the retention of key skills and experience is more important than ever due to the wider skills shortage and resourcing challenges. As a business, Aarsleff Ground Engineering Ltd recognise the impact that talent have within the business and when considering the sustainability agenda, a large factor in this is ensuring that people are involved in and at the centre of all considerations.

EMPLOYEE EMPOWERMENT THROUGH PIONEERING PROGRESSIVE PEOPLE PRACTICES

With the world of work rapidly changing, there is a growing recognition of the need to put people at the centre of projects. This involves considering human needs and experiences in design and

 © DFI International Bruges 2025

execution, bridging the gap between new to role and experienced engineers, and creating an environment focused on collaboration and innovation.

Every project the business undertakes, from concept to delivery, is a collaborative effort. It is about developing a culture where everyone, from the team to clients, feels valued and empowered. This collaborative approach is twofold, focusing on employee empowerment and integrating sustainability through progressive people practices. Employees are innovators, not just contributors. They approach projects with creativity and efficiency. To ensure people are truly centric, the business has established employee led working groups dedicated to sustainability, the local community and how we can better meet the needs of employees and enhance the employee experience. Integrating sustainability of talent through pioneering progressive people practices enhances satisfaction and retention. Close collaboration with clients ensures solutions meet immediate needs and align with long-term goals.

The adoption of a people-centric approach has multiple benefits including better collaboration, higher employee satisfaction, increased retention, and notably, better project outcomes. Embracing this transformation has enabled effective management of staff shortages while delivering demanding projects.

THE GENERATION GAP AND THE EVOLVING WORLD OF WORK

This paper will now consider into the impact of Generation Z in the workplace and the factors that motivate and engage them. This has resulted in the design of more sustainable retention strategies and HR practices. Improved retention reduces the costs of hiring and onboarding replacement employees and builds a more productive workforce, directly impacting business profitability.

The different generations have been subject to research over the years, however most of this research is now outdated and has focused on the Millennials as the “new” generation at work. Research conducted on the topic of Gen Z is limited due to the recency of Gen Z’s coming of age and entering the workplace, therefore a need to research this topic is evident.

There are currently five generations in the workplace, and they are categorised based on the time periods they were born in and grew up as their lived experiences shape their view of the world. McHenry and Ash (2010) suggest that younger generations use technology in all aspects of life versus the older generations that use the internet more passively.

This difference could potentially impact the effectiveness of communication and work styles within the workplace. Gen-Z’s prefer texts and a style of communication that tends to be rapid and abbreviated. If this style is adopted at work as part of other methods such as email, then it is likely that tensions could arise between different generations.

The world of work is changing too; technological advances affect how we work, communicate, collaborate, and share documentation virtually. Gen-Z are digital natives (Singh & Dangmei, 2016) and only know a world where google can answer any question in seconds, where entertainment can be accessed anytime, anywhere instantly. Society has become centred on instant gratification. Research has found that younger generations do not stay as long with their employers. The transient mindset of the younger generations at work has led to them being titled Generation Quit or job-hoppers, due to their focus on work providing personal fulfilment as well as financial stability.

Gen-Z has experienced vast change and disruption in a short space of time. Hypertechnological advancement, turbulent world politics and recent wars, focus on racial inequality, priority of mental health and the pandemic are all experiences which shape GenZ’s outlook to be vastly different to that of millennials. While many articles have been written about Gen-Z coming into the workplace, most empirical research conducted has focused on millennials. In order to obtain feedback from Gen Z employees in the workplace, at Aarsleff we have conducted surveys and employee forums.

As time passes and Gen-Z continue to enter the workplace, they are subsequently making up a higher proportion therefore enabling better representation of the workforce. Qualitative data has been

 © DFI International Bruges 2025

collected via our employee forum with Gen-Z employees through the to gather initial themes about what is important to them and engages them in the workplace. This would indicate whether the existing HR practices have an impact on retention. Due to this approach, the business has launched the Aarviews Employee Voice campaign which consist of surveys and focus groups where employees can become involved in shaping the people initiatives within the business. Businesses will need to reinvent and adapt their workplaces to appeal to Gen-Z to be seen as an employer of choice.

Gen-Z have grown up in a world of online social interaction, instant gratification and consequently have shorter attention spans. Following a critical review of existing empirical studies into Gen-Z, the author suggests that outdated theories from previous generations have been used as a measure of motivation and engagement factors for Gen-Z and therefore might not fully represent all factors of importance to this new cohort. Gen-Z have also been described as having a unique desire to drive change and not settle for the status quo, to a higher extent than previous generations (Prossack, 2019). Aarviews Employee Voice campaign ensures all employees have a say in how HR practices can be updated to meet their needs and expectations.

AARVIEWS EMPLOYEE VOICE STRATEGY

Aarsleff's Employee Voice strategy, titled 'Aarviews', aims to foster an open, inclusive, and transparent work environment where all employees, including Gen Z feel empowered to share their ideas, concerns, and feedback. By leveraging digital platforms, collaborative initiatives, and leadership engagement, we seek to create a culture where employee voice drives innovation and workplace satisfaction.

The guiding principles of the Employee Voice strategy are Transparency, through open communication channels between employees and leadership, Inclusivity through equal opportunity for all employees to express their opinions, Engagement through encouraging participation through digital and in-person initiatives and Actionability through leadership commitment to acting on feedback where feasible. In order to appeal to a diverse range of employee's, the Employee Voice strategy consists of a suite of communication initiatives, from formal and planned to informal and ad hoc channels, leveraging technology. The planned, formal initiatives include the use of regular anonymous surveys, six monthly Staff Chat's, open communication forums led by the Managing Director, where employees can ask questions directly and real-time polls and feedback mechanisms on company portals.

We have launched Aarviews Forum, an employee led group focused on workplace culture, diversity, and sustainability, this forum encourages employees to lead on initiatives aligned with company values and share their views and shape how things are done within the business. This forum assisted in the design of the Micro-appraisal, which will be discussed later in this paper. The forum has a sub-section of Gen Z employees who have shared their insights on digital trends, workplace expectations, and emerging issues. The views they have shared have been valuable in shaping new initiatives, such as the micro-appraisal concept.

Considering all employee views is important, and it has been recognised that many employees are not comfortable sharing their thoughts, ideas and feedback through open, visible forums. Through the Aarviews Forum, led by employees, a new concept 'Aarviews Open Mic' has been developed. The new Open Mic initiative is an open and anonymous platform for employees to share comments, raise questions, propose ideas of general feedback. The 'Open Mic' name accurately reflects the positioning of the initiative, where anyone is welcome to share and the anonymity provides comfort to employees who might be uncomfortable in an open forum, thus providing an inclusive approach while reflecting diversity. Aarviews Open Mic leverages tech through the use of an app which can be accessed anywhere via a QR code, employees can then add their comments, questions, feedback or suggestions. The Aarviews Employee Voice strategy reinforces our commitment to fostering a workplace where every voice matters. By actively listening to Gen Z employees and all team members, we are building a more engaged, innovative, and forward-thinking organisation.

 © DFI International Bruges 2025

MICRO-APPRAISALS

One example of a HR practice that has been updated as a result of social progress, research into Gen Z and feedback from the Aarviews Employee Voice Forum is the HR practice of conducting annual appraisals. The routine of having one documented performance review per year is outdated and inflexible, it does not reflect modern mindsets or the world of work. Research has shown that people have shorter attention spans, and we live with instantaneous expectations. Research by Sombret (2023), found the shorter attention spans might result in them struggling to adapt to a traditional workplace. Regular performance reviews are critical for nurturing high performing teams and supporting succession planning, but this should be part of the manager's `routine`, not just once a year There is a need for a more flexible, modern and real-time approach which incorporates our values, whilst supporting Operational Excellence and business agility. Modern businesses require a more agile approach to individual objective setting with the capacity to flex during the year due to changing business requirements and the annual appraisal does not support this. A pragmatic approach is required for a lean, fast paced workforce.

In response to these challenges, we have designed and introduced quarterly Micro-appraisals as an update to the one annual appraisal. The Micro-appraisals are conducted quarterly and rather than being paperwork based, these are done digitally on an online form, accessed anywhere by a QR code. This technological development has reduced the need for wasted resources and paperwork, supporting the sustainability agenda by digitalising the process, moving away from physical paperwork and leveraging technology to make the process quicker, more efficient and pragmatic and supporting environmental efforts.

Micro-appraisals facilitate real-time and flexible performance conversations through the concepts of connection and reflection. These are micro check ins whereby objectives can be set and adjusted throughout the year to provide the agility required for a modern and sustainable business. The micro-appraisal format enables greater emphasis on the conversation around support and performance for employees and less on the documentation for documentation's sake. Formal feedback is shared more frequently, supporting younger generational needs for continual feedback, this supports sustainable improvements in communication and wellbeing as feedback becomes part of the daily routine rather than a once yearly event.

Feedback becomes more conversational, regular and real time with objectives being flexed or re-aligned as business needs change. By replacing traditional annual reviews with frequent, constructive evaluations, Aarsleff aim to enhance engagement, skill development, and overall workplace satisfaction.

Following the replacement of annual appraisals by micro-appraisals, the following benefits have been realised. Feedback from employees suggests that there is reduced performance anxiety due to the regularity of feedback, which prevents stress caused from annual reviews. Career progression is encouraged as regular discussions mean employees receive ongoing guidance for skill improvement and career conversations are kept 'living and breathing'. This in turn enhances engagement, which has been seen in survey results which are 18% higher than the industry average, due to continuous recognition boosting motivation and productivity. In turn the micro-appraisal concept is a modern, feedback solution that better aligns with Gen Z expectations, supporting a more sustainable approach to employee satisfaction and loyalty. The introduction of micro-appraisal's reinforces Aarsleff's commitment to fostering a dynamic and responsive work environment. By integrating micro appraisals into the performance management strategy, Aarsleff empower Gen Z employees to grow, innovate, and thrive within the organisation.

GENDER DIVERSITY RESEARCH

As part of the sustainability strategy, Aarsleff are sponsoring a research project with Nottingham Trent University. This research focuses on the retention barriers for female engineers within the civil engineering industry within the UK, with a specific focus on foundation contractors. The aim of the

 © DFI International Bruges 2025

research will uncover and understand any unconscious cultural barriers to the retention of women within the sector, helping to address the gender divide that still exists. The objectives of the research project are as follows:

1. Identify the key barriers to retention for female engineers.
2. Understand the impact of workplace culture on career longevity.
3. Explore the effectiveness of retention strategies in the industry.

Aarsleff have strong links with Nottingham Trent University due to their Civil Engineering focus and the university has proved a valuable talent pipeline for the business. The research project is being conducted by a female final year undergraduate student and is being funded by Aarsleff. The methodology has been co-designed with access to university expertise and the industry involvement ensures the research is relevant. The findings will provide recommendations to support the retention of females within the industry, promoting a sustainable workforce.

There are two parts to this research project, the first has consisted of analysis into secondary data from exit interviews conducted with female employees who have left the business over the past two years. This data has been analysed in order to highlight common themes which has then formed a question set which will be used as part of an interview process with female engineers within the industry. Example questions include the following:

1. What are the primary reasons female civil engineers leave the profession?
2. How do workplace policies and culture affect female engineers' career decisions?
3. What measures can improve retention rates for female civil engineers?

The second stage of the research project will consist of interviews with female engineers within the industry, as well as wider research. The mixed methods approach combines data for broad insights with interviews for deeper understanding, allowing for data triangulation to enhance validity.

The study is still ongoing however key themes which have emerged from early research and analysis include lack of mentorship, work-life balance challenges, and industry bias. The conclusion of the study will provide evidence-based recommendations, such as flexible work policies or mentorship programs.

CONCLUSION

The future of engineering lies in a people centric approach. Empowering employees to contribute to how work is done and HR practices, in order for them to operate at their best is crucial. Sustainable engineering is not just about designing and building structures; it is about building a better world for people and a better world of work. The introduction of the Aarviews Employee Voice campaign has led to a better understanding of what factors engage and retain employees in the workplace, particularly Gen Z, a focus area which is critical for a sustainable talent pipeline. Gen-Z have only ever known a world of instant gratification and have shorter attention spans as a result, might struggle to adapt to a traditional workplace as it currently exists. Therefore, employee empowerment is key to gain insight and enable adaptation of traditional HR practices to better meet the needs and expectations of societal change and future generations entering the world of work. Micro-appraisals are one example of this people centric sustainability focused approach.

The sponsorship of research into the retention barriers for female engineers within the civil engineering industry within the UK furthers this people centric approach and will provide valuable insights to shape policies and practices to support women within the industry and retain their talent, ensuring a diverse, inclusive, and sustainable workforce.

 © DFI International Bruges 2025

REFERENCES

Dwivedula, R. and Singh, P. (2020) What motivates Gen Z at work? An empirical analysis. Journal of Human Resource Management, vol XXIII, 2/2020. Available online: https://web.p.ebscohost.com/ehost/pdfviewer/pdfviewer?vid=1&sid=8a887125-b18f-4b67-a5b3-d8f55ed36bb0%40redis [Accessed 4/7/2024].

Lee, C., Aravamudhan, V., Roback, T. Sook Lim, H. and Ruane, S., G. (2021) Factors Impacting Work Engagement of Gen Z Employees: A Regression Analysis. Journal of Leadership, Accountability and Ethics. Vol. 18(3) 2021. Available online: https://articlearchives.co/index.php/JLAE/article/view/4014 [Accessed 4/7/2024].

McHenry, W., K. and Ash, S., R. (2010) Generational responses to knowledge management and wellbeing through career path and development. Journal of Leadership in Organizations, 2(1). Available online https://ieeexplore.ieee.org/abstract/document/5428463 [Accessed 5/7/2024].

Prossack, A. (2019). Struggling To Retain Millennials and Gen Z? Here Are 4 Reasons Why, Forbes. Available online:https://www.forbes.com/sites/ashiraprossack1/2019/09/30/retain-millennials-genz/#58ed86a7220f [Accessed 15/8/2024].

Singh, A., P. and Dangmei, J. (2016) UNDERSTANDING-THE-GENERATION-Z-THE-FUTURE-WORKFORCE. South Asian Journal of Multidisciplinary Studies 2.246: Volume 3 Issue 3. Available online: https://www.researchgate.net/profile/Jianguanglung-Dangmei/publication/305280948_UNDERSTANDING_THE_GENERATION_Z_THE_FUTURE_WORKFORCE/links/5786a11008aef321de2c6f21/UNDERSTANDING-THE-GENERATION-Z-THE-FUTURE-WORKFORCE.pdf [Accessed 4/7/2024].

Sombret, P. (2023) Gen Z communication style: how to grasp the generation with the briefest attention span. Available online: https://www.deskbird.com/blog/generation-z-communication-preferences#:~:text=In%2Dperson%20communication%20for%20Gen%20Zers,-Growing%20up%20in&text=Therefore%2C%20even%20though%20texting%20is,an%20online%20meeting%20whenever%20possible. [Accessed 15/8/2024].

 © DFI International Bruges 2025

PILE CAPACITY TESTING FOR REUSING THE EXISTING FOUNDATION

Marcel W. Bielefeld, Allnamics Geotechnical & Pile Testing Experts, The Hague, The Netherlands, mbielefeld@allnamics.com
Jeroen C. Beute, Fugro, Leidschendam, The Netherlands, j.beute@fugro.com
Rob F. van Dorp, Allnamics Geotechnical & Pile Testing Experts, The Hague, The Netherlands, rvandorp@allnamics.com

ABSTRACT

Reusing existing foundations is both a sustainable and cost-effective practice, as this approach significantly reduces the carbon footprint and the use of raw materials. But to incorporate existing foundations into new projects, it is essential to know their bearing capacity along with the dimensions, structural integrity, and remaining lifetime of those existing foundation elements.

This paper presents an innovative method whereby an existing foundation, built around 1970, was successfully reused, even though the available information was limited. The original as-built drawings indicated that precast piles with enlarged bases were installed, but the exact dimensions were uncertain. To determine their bearing capacity, rapid load tests were conducted on new precast concrete trial piles with (presumably) the same dimensions and driven near the existing piles into the same sand layer. Instead of testing the existing piles, these trial piles were then load tested. This paper details the execution of these tests and how the results provided valuable insights into the calculated pile bearing capacity and pile-settlement behaviour, enabling the successful reuse of the foundation.

Keywords: rapid load tests, statrapid, case study, re-use of foundations, geotechnical investigations

INTRODUCTION

The role of the modern foundation engineer has become even more challenging. Beyond designing safe and cost-effective foundations, there is now an additional responsibility: ensuring that every foundation is environmentally sustainable or "green." This means minimizing the environmental impact: from reducing noise, vibrations, and disturbances during pile installation to lowering the carbon footprint. Regarding the latter, significant progress has been made in electrifying heavy machinery in the foundation industry, but more effort is required to decarbonize foundations themselves. This includes not just using eco-friendly steel and concrete, as is the common practice in the industry, but also and, even more crucially, reducing the raw material quantities in deep foundations.

One way to achieve this is by optimizing the design—not merely for cost or construction speed, but to minimize the carbon footprint. However, in cases where a new superstructure replaces an old one, reusing the existing foundation should be a logical step. The foundation is already in place and has proven its functionality, so why not incorporate it into the new design? Reuse is especially crucial in densely constructed areas, whether urban environments or industrial plants, where minimizing traffic to transport construction materials to the site and minimizing the footprint of the construction equipment is essential.

However, reusing existing foundations comes with uncertainties. Records of dimensions may be incomplete, the current material quality needs assessment, and the bearing capacity must be re-evaluated using advanced design methods and calculation software, which are (most likely) far more sophisticated than those available when the original foundation was constructed.

This paper presents new methods for evaluating existing structures, exemplified through the reuse of a foundation at a petrochemical plant.

 © DFI International Bruges 2025

THE PROJECT

In the Moerdijk Chemical Plant in The Netherlands, rehabilitation of eight of the sixteen existing furnaces and the connecting piping is under construction. The furnaces are revamped, such that the upper part of the furnaces will be removed and replaced by a new, approximately 30% heavier, superstructure. As the bottom part of the furnaces remain, it was needed to re-use the existing foundation. An overall description of the work was presented by Van Blijswijk et al. (2023).

The existing foundations were constructed in the early 1970s. The combined foundation for each set of two furnaces consists of a 14 x 16 m^2 concrete slab with a 4.5 x 14.5 m^2 "outrigger". A total of fifty piles supports this foundation.

To re-use these foundations, an evaluation of their bearing capacity was required. However, the pile type, pile driving records, pile dimensions, pile penetration, and other structural information could not be retrieved from the archives. From the as-built drawings, precast concrete piles with enlarged bases were expected with possibly different lengths as the depth of the competent sand layer varied across the site. These unknowns necessitated additional investigations, including additional CPTs, to narrow the lack of data.

SOIL STRATIGRAPHY

The original CPTs from this project, dating back to 1971, were available and were supplemented with new CPTs. Based on these combined results, as shown in Fig. 1, the potential bearing layers were identified: either the medium-dense sand layer around NAP -15.0 m or the deeper sand layers below NAP -22.0 m (van Seters et al., 2024).

The soil investigation results revealed variability in the depth and cone resistance (q_c) values of the soil layers between NAP -19.0 m and NAP -22.0 m. It is critical to ensure that the existing piles are not installed with pile toes in between these two potential bearing layers, as the interbedded clay layers found here are compressible and exhibit low cone resistance values. These clay layers are unsuitable as pile tip levels, as they would result in low pile end-bearing capacity and significant settlement.

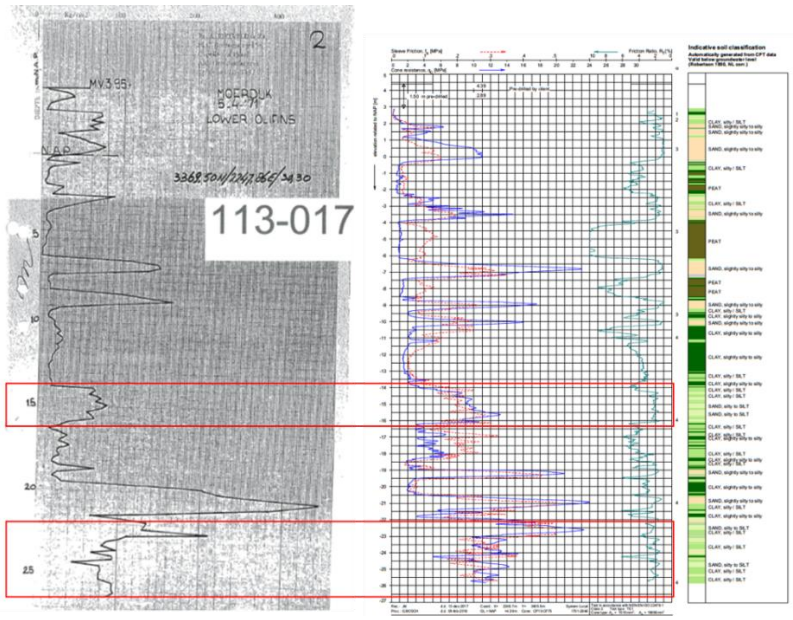


Fig. 1 General soil stratigraphy, possible end bearing layers for pile tip levels indicated with red rectangles. Left CPT from 1971, right CPT from 2017 (van Seters et al., 2024)

 © DFI International Bruges 2025

The investigation also indicated a high degree of negative skin friction on the piles, primarily due to the presence of deep peat layers. This creates an extended zone of negative skin friction, further exacerbated by the man-made sand fill, increasing the negative skin friction effect on the piles.

PILE DIMENSIONS

The construction archive documents provided a preliminary understanding of the foundation under the furnaces. They were driven prefabricated concrete piles with probably a 380 x 380 mm^2 shaft dimension. The pile shafts have been coated with a bitumen coating to reduce negative skin friction. Potentially, these piles could have an enlarged pile tip of 460 x 460 mm^2 over a length of 1 m. The total length of the piles was indicated in the order of 23 m, leading to pile tip levels of about NAP – 20.0 m. However, this did not coincide with the depth of one of the two expected end-bearing layers based on the soil stratigraphy (around NAP – 15.0 m or deeper than NAP -22,0 m).

A magnetometer CPT was performed to assess the pile toe depth of the existing piles. The magnetometer is a module behind the CPT cone that records the disturbance of the earth's magnetic field in 3 directions (X, Y, Z). Ferrous objects present in the subsurface usually cause a local change in the strength of the Earth's magnetic field and can be detected (Elgun et al., 2010). Based on data from the Magnetometer readings, the tip elevation and thus the length of the foundation piles were determined. It should be noted that the magnetometer signal registers the magnetic field and thus indicates the presence (or absence) of the reinforcement in the concrete rather than the concrete itself.

The pile tip can be detected due to a sudden change in magnetic field gradient at NAP – 15.0 m, which coincides with the medium dense sand layer seen in the soil stratigraphy of Fig 1.

Only 7 out of 12 Magnetometer CPTs clearly indicated the pile tip level of NAP – 15.0 m. Nevertheless, based on these results it was concluded that the pile tip level for all piles was at NAP – 15.0 m.

PILE BEARING CAPACITY

The pile tip elevation derived from the Magnetometer CPTs (NAP -15.0 m) was then used as input in the pile bearing capacity calculations. As no conclusive information on the existence of an enlarged toe was found, a continuous pile diameter (380 x 380 mm^2) was assumed. The pile bearing capacity in compression was calculated according to the methodology of NEN9997-1, using the Koppejan method and the applicable regulations for a re-used foundation. Two load cases were distinguished in the pile load calculations: static loading and (dynamic) wind loading.

Even though commonly used calculation methods in accordance with the Dutch standards were used, there remains uncertainty regarding the result. This is best illustrated by the fact that in January 2017, the pile end-bearing factor α_p was re-evaluated and reduced by 30%. This means that it was concluded that the capacity of pile foundations had been overestimated in the past. At the same time, it was agreed that for existing foundations the ‘old’ pile end bearing factor α_p can be used, provided the new foundation loading did not increase by more than 15% of the original value.

Because of the large stiffness of the foundation slab, correlation factors ξ_3 and ξ_4 (correlation factors for foundation capacity calculations based on the number and type of soil investigations) were derived from table A10.b from NEN 9997-1 (stiff foundation slab). To better define the site variability additional CPTs were performed and this soil investigation type as well as the number of investigations resulted in higher pile capacity values.
Negative skin friction was taken into account from the pile head level to a depth of NAP -6.0 m (bottom of the soft peat layer) in case of static/long term loading. Based on the full-scale field tests (Claessen and Horvat, 1974), the negative skin friction was assumed to be reduced by 75 % due to the bitumen coating on the piles, which resulted in a total negative skin friction of 50 kN per 380 x 380 mm pile. However, the bitumen only reduces the shaft friction due to long-term loads; in the case of

 © DFI International Bruges 2025

short-term cyclic loading (e.g., wind), the bitumen will behave stiffly. Therefore, the positive shaft friction in the top layers can be included when determining the bearing capacity due to wind loads and consequently no negative shaft friction was considered in that case.

PILE LOAD TESTING

Given the many uncertainties (pile length, shape, appropriate design factors), it was decided to check the calculated pile bearing capacity with load tests. This test can be categorized as a Pile Load Test according to Class B of the NPR7201 (Van Dorp, 2019).

Instead of testing the existing piles, five newly installed prestressed concrete piles (400 x 400 mm^2) were subjected to a Rapid Load Test utilizing the Allnamics StatRapid device. The piles were installed in similar ground conditions to the original ones at a distance of approximately 100 m from the furnaces. As the endbearing layers at the test location were detected at a slightly higher elevation than at the furnaces, the piles were driven to a tip level of NAP -14.5 m, using a 60 kN hydraulic pile driving hammer.

Table 1 shows the results of the calculations of the bearing capacity (using the factors described above) and the final blow count of these 5 test piles.

Table 1. Calculated bearing capacity and the final blow count of the test piles

Pile	Pile bearing capacity $R_{c;cal;max}$ [kN]	Final blow count [blows/25 cm]
1	2.123	35
2	2.080	50
3	1.973	47
4	1.703	55
5	2.177	53



Fig. 2: StatRapid Tests performed by Allnamics

RAPID LOAD TESTING

The Allnamics StatRapid Load Test is a so-called Rapid Load Test in accordance with Euro Code EN ISO 22477-10, ASTM D7383-10 standard, and Dutch CUR 230 Guideline (Middendorp et al., 2013).

 © DFI International Bruges 2025

StatRapid

The StatRapid 20/40 ton drop mass device is engineered to apply loads to the pile head ranging from 0.2 MN to over 10 to 12 MN. The operating principle of StatRapid involves dropping a weight onto a specially designed modular spring assembly positioned on the pile head. By adjusting the total mass of the drop weight and the spring assembly's stiffness, the load's magnitude and duration can be tailored to achieve quasi-static pile behavior. This combination can be pre-determined using the AllWave-RLT simulation software (Middendorp et al., 2018).

The StatRapid system is modular, enabling easy transport in standard containers. Upon arrival at the site, the device is assembled using a mobile crane. The bottom frame is first positioned over the test pile, connected to its hydraulic power pack, and leveled by adjusting the hydraulic legs. Next, the top frame, which holds the drop weight container, is placed on top of the bottom frame and secured with twist locks. The modular drop weights are then lowered into the container. At this point, the device is ready for testing.

During operation, the device is self-supporting. The hydraulic power pack powers the lifting and catching systems. The catching system captures the drop mass after it rebounds from the springs, preventing unwanted multiple impacts and enabling successive cyclic testing with increasing loads, similar to static load cycle testing.

As per international standards (ASTM, Eurocode), the load duration must be long enough to generate quasi-static conditions. Applying the load in several increasing steps produces load-settlement diagrams similar to those from static load tests. The results from StatRapid tests are presented as load-settlement curves.

Instrumentation and Monitoring

The force, displacement, and acceleration are measured at the pile head during the test. The load is monitored with calibrated load cells, the displacement of the pile head is measured with the Reyca optical system and the acceleration with a dedicated accelerometer (see also Fig. 3, with the labels indicated below):

A. The force is measured using load cells (A).
B. The displacement of a reflector plate (B) mounted to the pile head is measured using the self-calibrating optical measuring system Reyca (C).
C. The self-calibrating Reyca system
D. Acceleration is measured using a sensitive accelerometer (D). The settlement during and permanent settlement after the test is determined with the optical level, the Reyca (C)
E. The load cells are mounted on a steel plate (E) to distribute the force evenly to the pile.
F. The load cells and accelerometer are connected to the Allnamics PDR (F), the data acquisition system.

Load duration condition

An important condition for applying Rapid Load Testing is the minimum duration of the applied load. The duration should satisfy:

$$T_F > (10 * L) / c$$

With T_F = duration applied load, L = pile length, and c = propagation velocity stress wave in pile

Figure 4 shows the graphical field results from one load cycle.

 © DFI International Bruges 2025



Fig. 3: Monitoring setup and data acquisition system PDR of the StatRapid device

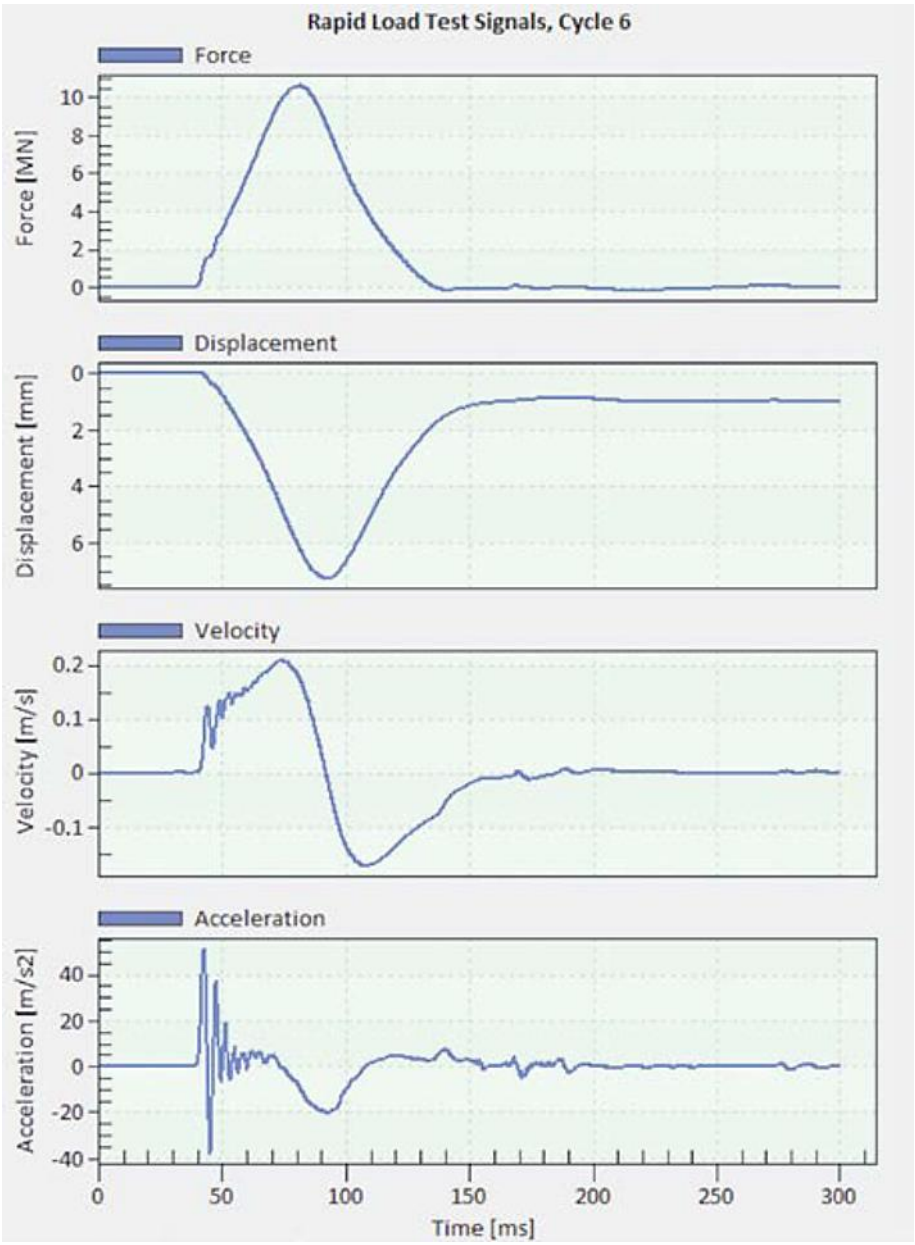


Fig. 4: Example of graphical field results from one load cycle. From top to bottom: measured force, displacement, velocity, acceleration.

 © DFI International Bruges 2025

UNLOADING POINT METHOD (UPM)

During a Rapid Load Test (RLT), stress wave effects are negligible (Middendorp, 1995), and the pile moves as a homogeneous, rigid body. This simplifies the interpretation process, making it user-independent. As prescribed in NEN-EN-ISO 22477, the Unloading Point Method (Middendorp et al, 1992) is used for result analysis.

This method utilizes the moment when the pile velocity reaches zero—known as the Unloading Point—at the peak displacement after load application. Since damping effects are velocity-dependent, the force contribution from damping at this moment is effectively zero.

Consequently, the mobilized pile capacity is independent of the dynamic properties of the soil. Instead, it is determined solely by the force applied to the pile and the acceleration of the pile system (including the loading platform and spring assembly), both recorded during the RLT. By analyzing multiple load cycles, the resulting quasi-static points form a hyperbolic curve, providing an accurate approximation of the pile's load-displacement behavior.

TEST RESULTS

The piles were tested after a setup period of about 4 weeks to allow the porewater pressures introduced by the driving process to dissipate.
The piles were tested up to quasi-static failure load, which coincided with a pile settlement of approx. 45 mm, which is approx. 11 % of the pile size. To achieve this, the test load was increased in 5 to 7 load steps. From the measured RLT data, the static load settlement curve was determined using the above-described Unloading Point Method. The execution of the pile load tests and the subsequent interpretation were performed by Allnamics, with the results for pile 1 shown in Fig. 5. The ultimate bearing capacity observed during the test was 4.463 kN.

The results of the RLT have to be corrected for so-called loading-rate effects. Like any construction material, i.e., concrete and steel, soil has rate effects. That means that the strength and stiffness depend on the rate of loading. Extensive research in the past has led to the EN-ISO22477-10 and NPR7201, which describe how to account for the loading rate effects. The codes describe the application of the loading rate factor η.

$$R_{c;m;g} = \eta_{combined} * R_{c;ic;t}/\xi_{RLT}$$

where:
$R_{c;ic;t}$ = Quasi-static failure load, as measured during the RLT
$R_{c;m;g}$ = Static bearing capacity of the pile based on testing (measurement)
ξ_{RLT} = 1.1

The $\eta_{combined}$ is a combined value for η that takes into account the proportion of the shaft and base resistance (for these piles approximately 75 - 80 % shaft friction and 20 - 25 % end bearing), according to:

$$\eta_{combined} = \frac{R_{c;cal;shaft}}{R_{c;cal;total}} \times \eta_{clay} + \frac{R_{c;cal;base}}{R_{c;cal;total}} \times \eta_{sand}$$

where:
$R_{c;cal}$ = the calculated result from the prediction.

 © DFI International Bruges 2025

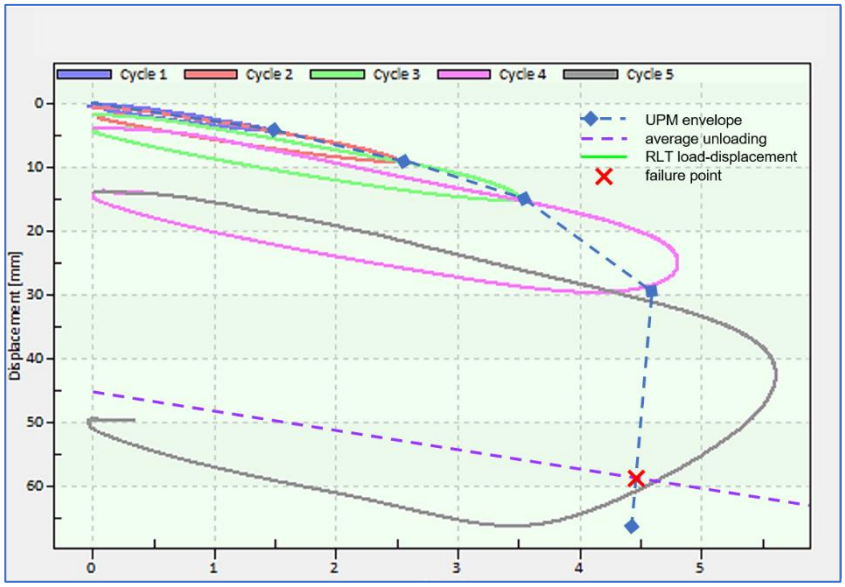


Fig. 5: Resulting Load-Settlement curve for test pile

Although the shaft friction develops in sand and clay layers, the behavior of the clay is dominant, thus for the shaft, the value of η_{clay} of 0.66 was chosen. For the base bearing capacity, the sand layer is governing, resulting in the value of η_{sand} of 0,94 [EN-ISO22477]. The η-values are provided in Hölscher, 2008, 2009. For the combination of shaft and toe a $\eta_{combined}$ of 0,58 to 0,65 was determined. The results after correcting for loading rate effects, are presented in Table 2.
This table presents the test results and the calculated (predicted) capacities based on the Koppejan method in addition to them.

Table 2: Comparison test results and calculation results

Pile	Static bearing capacity from test $R_{c;m;g}$ [kN]	Predicted bearing capacity $R_{c;cal;max}$ [kN]	Difference between prediction and measured [%]
1	2394	2123	+ 13
2	3008	2080	+ 45
3	2494	1973	+ 26
4	2567	1703	+ 51
5	3340	2177	+ 53

From Table 2, it can be observed that the measured bearing capacity exceeds the predicted values by a range of 13% to 53%, with an average increase of 38%. This indicates that significantly higher loads can be applied than initially expected based on the design rules.

The calculated bearing capacity (‘predicted’) of table 2 is based on a design pile toe factor α_p of 1.0, assuming that the tests will proof the correctness of the factor 1.0, instead the standard, reduced factor of 0.7.

Since the test piles were located at a certain distance from the piles intended for reuse, a limited additional capacity was accepted. Specifically, the end-bearing component was increased by 42%, with a design pile toe factor α_p of 1.0 instead of the standard, reduced factor of 0.7. Additionally, shaft friction was increased by 20% to align with the load test results.

 © DFI International Bruges 2025

CONCLUSION

One key uncertainty when reusing existing foundations is determining their actual bearing capacity. Foundation piles that were designed and installed in the past were subject to different design methodologies, design values and factors, and installation techniques compared to modern standards. For example, in the Netherlands, pile toe resistance factors have changed by 30% since 2016, significantly impacting capacity evaluations.

Pile load tests eliminate uncertainty by providing definitive proof of the actual bearing capacity of piles intended for reuse. The StatRapid system, based on Rapid Load Testing (RLT), offers a fast and cost-effective alternative to traditional static load tests. Unlike dynamic load tests, which are influenced by high impact stresses and require user-dependent interpretation, StatRapid ensures a simpler, user-independent analysis method while delivering reliable results.

In this case study, Rapid Load Tests were conducted on newly installed neighboring piles specifically installed for the test program. These tests provided data to validate the assumed bearing capacity of the piles to be reused.

The Rapid Load Tests verified that the assumptions made in the analyses were correct. Moreover, the actual toe resistance could be proven to be designed on the original toe resistance factor, without the 30% reduction. The skin friction might be approximately 20 % higher than on the forehand used in the calculations.

The conclusion is that the existing foundation possessed sufficient hidden safety to withstand the new superstructure's 30% higher loads. All efforts have been made to prove that the hidden safety can be mobilized. The Rapid Load Tests were performed on neighbouring piles, new ones specially installed for the test program. The proven pile-bearing capacity of these newly installed piles proved that the existing foundation was sufficient to carry the increased loads.

LITERATURE

Blijswijk, J.J.A. van, and Cotovanu, B., 2023. Process to accommodate extra loads on the piled foundation plate. Conference on Foundation Decarbonization and Re-use, Amsterdam.

Claessen, A.I.M. and Horvath, E., 1974. Reducing negative friction with bitumen slip layers. ASCE Journal of the Geotechnical Engineering Division 100(GT8) 925-944.

Elgun, S.N., et al., 2010 – Safely uncovering deep foundations and services with magnetometer cone. Proceeding of the second International Symposium on Cone Penetration Testing, Huntington Beach, CA, USA, 8p.

EN-ISO-22476-1:2023 Geotechnical investigation and testing - Field testing - Part 1: Electrical cone and piezocone penetration test.

EN-ISO 22477-10:2016 Geotechnical investigation and testing — Testing of geotechnical structures - Part 10: Testing of piles: rapid load testing.

Hölscher P.; Tol van F. (2009). Rapid Load Testing on Piles, Boek, ISBN 978-0-415-48297-4 ; e-book: 978-0-203-88289-4 , P.1-180 , CRC Press / Balkema.

Hölscher, P., van Tol, A.F., Middendorp, P. (2008). European standard and guideline for Rapid Load Test, 8th Int. Conf. Application of stress-wave theory to piles, Lisbon, P.699

 © DFI International Bruges 2025

Horvath, R.G.; Bermingham, P.; Middendorp, P., 1993, The equilibrium point method of analysis for the Statnamic load testing with supporting case histories, Proceedings of the Deep Foundation Conference, Pittsburgh, Pennsylvania

Middendorp, P, Bermingham P., Kuiper B (1992) Statnamic load testing of foundation piles, 4th International Conference on Stress Waves, The Hague, ISBN 90 54 10 082 6 , P.581-588 , Balkema Rotterdam.

Middendorp, P, Bielefeld, M.W., 1995, Statnamic Load Testing and the Influence of Stress wave Phenomena, First International Statnamic Seminar, Vancouver

Middendorp, P., de Neef, A., van Dorp, R., Lambo (2013) StatRapid ,eine Neuentwicklung für Rapid-Load-Testing, Pfahlsymposium 2013, February 21 and 22th, Proceedings of the Institute for Soil Mechanics and Foundation Engineering, Technische Universität Braunschweig, Germany, , .

Middendorp, P, Bermingham P., Kuiper B, Statnamic load testing of foundation piles. 4th International Conference on Stress Waves, The Hague, Balkema, 1992

NEN 9997-1:2016/C1:2017 Geotechnical design of structures - Part 1: General rules

NEN 8707:2018+C2:2023 Assessment of an existing structure in case of reconstruction and disapproval - Geotechnical structures

NPR 7201:2017+A1:2020 nl Geotechnics - Determination of the axial bearing capacity of foundation piles by pile load testing

Seters, A. van, Beute, J., 2024, Investigations for the re-use of foundations and geotechnical modelling – A case study of the Skyline project, Shell Moerdijk, 1st Conference on Foundation Decarbonisation and Re-use, Amsterdam

Van Dorp, R., Van Delft, M., IJnsen P. (2019) StatRapid used on instrumented piles for optimization of design parameters for high rise building in Den Haag, Proceedings, Pfahl-Symposium 2019, Braunsweigh, 107 , P.285-313 , Institut fur Grundbouw und Bodenmechanik.

 © DFI International Bruges 2025

THE REUSE POTENTIAL AND SUSTAINABILITY OF LOCALLY RECLAIMED SAND IN LEVEES

K.M. Hermann, Fugro, Utrecht, The Netherlands, k.hermann@fugro.com
N.S. Walrave, Fugro, Utrecht, The Netherlands, n.walrave@fugro.com
M. Hop, Fugro, Utrecht, The Netherlands, m.hop@fugro.com

ABSTRACT

The Waalbanddijk levee at the river Waal will be reinforced to prevent failure due to wave overtopping. This levee consists of a clay core with a large sand section at the inner slope, where wave overtopping during a storm may lead to a buildup of excess pore water pressure, potentially causing slope instability. To mitigate this risk, the preliminary design incorporated a drainage construction using high-quality drainage sand. This paper focuses on the sustainable reinforcement of the Waalbanddijk levee at Neder-Betuwe, integrating innovative approaches to material reuse and environmental impact reduction, and supports UN Sustainable Development Goals 9 and 15. The construction of a sand drain and the significant reuse potential of sand were anticipated. To enhance sustainability and feasibility, using locally available sand for the drainage construction was investigated. This involved a numerical modelling study to determine the required permeability and geometry, followed by site investigations and laboratory experiments to characterize the properties of the locally available sand. Compared to the preliminary design, this optimized circular design approach for the sand drain achieved a return on investment and a 97.5% reduction in emissions.

Keywords: design optimization, drain, laboratory tests, sustainability

INTRODUCTION AND PROBLEM STATEMENT

The levee ‘Waalbanddijk’ at the river Waal in the Netherlands requires reinforcement to protect the hinterland from future flooding and meet future safety standards. Originally, the levees were primarily composed of clay, but after the flood waves of 1993 and 1995, it was reinforced with sand on the crest and the inner slope. Sand is a convenient construction material for levee reinforcements due to its workability and low costs. However, wave-overtopping discharge can cause the buildup of excess pore water pressure within the sand section, resulting in slope instability.

The reinforcement design of Neder-Betuwe allows for a maximum wave-overtopping discharge of 10 l/s/m. Initially, wave-overtopping causes water to infiltrate the sand section (1). Over time, as wave overtopping continues, the sand section becomes fully saturated (2). Due to the relatively high permeability of the sand compared to the clay in the levees and the subsoil, the water influx exceeds the efflux, resulting in the buildup of excess pore water pressure. This pressure is highest at the toe of the levees due to gravitational forces (3), ultimately leading to decreased slope stability. These steps (1), (2), and (3) are illustrated in Fig. 1.

 © DFI International Bruges 2025

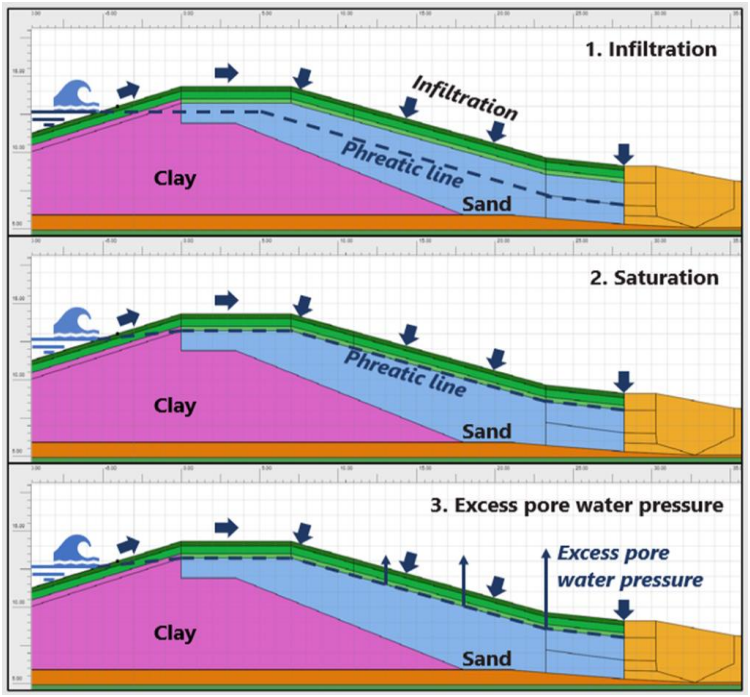


Fig. 1. A visual schematisation of the mechanism by which wave overtopping induces excess pore pressure in a closed sand section.

For the Waalbanddijk at Neder-Betuwe, the interaction between slope stability and excess pore water pressure failed to satisfy the Dutch safety standards as defined for flood protection. Consequently, a solution was required to reduce excess pore water pressures in the sand section.

To mitigate excess pore water pressure buildup, a drainage construction was incorporated into the preliminary design, as illustrated in Fig. 2. This design specifies the use of high-quality drainage sand, which offers the advantage of relatively high permeability, but also presents several drawbacks. Firstly, the sand is not locally available, making the drainage construction both prohibitively expensive (due to external procurement) and environmentally unsustainable (due to substantial import volumes). Secondly, the workability of drainage sand is notably poor, particularly when a compacted clay layer must be constructed on top of it, as is required for the levees at Neder-Betuwe.

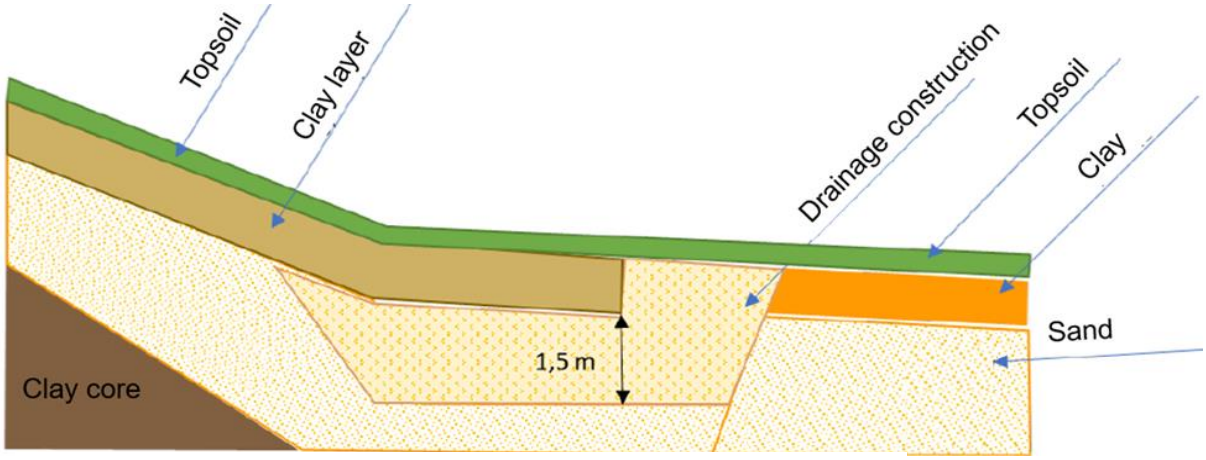


Fig. 2. A visual schematisation of the preliminary drain design

 © DFI International Bruges 2025

Within the larger project team, Fugro is responsible for transforming the preliminary design of the drainage construction into a detailed design. To achieve a more efficient and sustainable design, it was proposed that the design be altered, and local excavated sand used to realize the drainage construction. Therefore, it is imperative to demonstrate that locally reclaimed sand possesses sufficient permeability to function effectively as a drainage construction.

OPTIMIZATION OF DRAIN GEOMETRY BY NUMERICAL MODELLING

A numerical modelling study was performed using the 'Plaxflow module' of Plaxis 2D (v21.01). It is important to note that the infiltration rate plays a substantial role in the saturation process of the sand section. This implies that the contrast between the hydraulic conductivities of the various layers is of paramount importance too. The model simulation comprises three stages:

1. The initial situation with water pressures which are based on field measurements and 2 mm/day precipitation.
2. A flood wave with a gradual increase in water level from reference level +8 m to reference level + 13 m, as illustrated in Fig. 3.
3. 48 hours of wave overtopping at a rate of 10 l/s/m, modelled by applying a head of surface level + 0,10 m across the entire inside section of the levees.

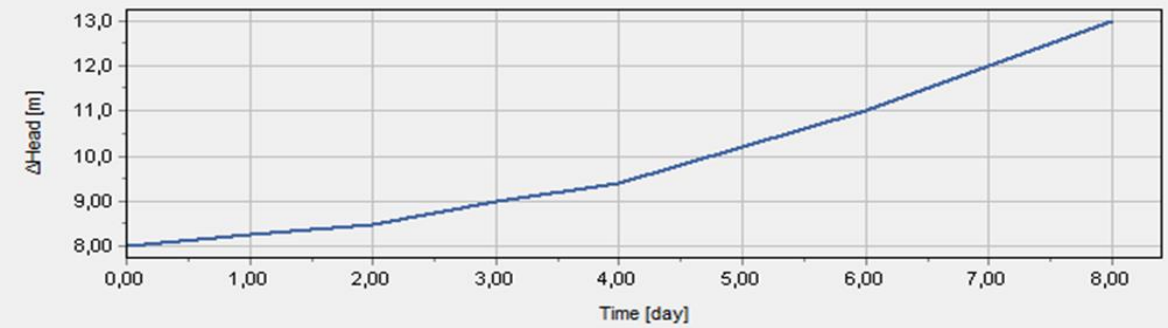


Fig. 3. Modelled rise in water level preceding an extreme storm event

The numerical model, illustrated in Fig. 4 serves two primary purposes. Firstly, to investigate the sensitivity of sand's permeability within both the sand section and the drainage construction. Secondly, to optimise the dimensions of the drainage construction using characteristic permeability values of the locally available sand. The resulting water pressure from the Plaxflow analyses is then used as input for slope stability calculations (considering large slip planes) and cover layer stability (considering small slip planes).

 © DFI International Bruges 2025

In a numerical modelling study, the dimensions of the drain were optimized by varying both the height of the drain and the length of the opening, as illustrated in Fig. 5. The modelling results indicated that the opening size should match the height of the drain, as enlarging either dimension individually had no significant effect. This is likely due to the conservation of mass, where the influx must equal the outflux. An optimal size of 1.2 meters was identified for the drain in this specific configuration. While a larger size could enhance the performance of the drain, its impact on water pressure is minimal. Conversely, smaller sizes could significantly affect water pressure.

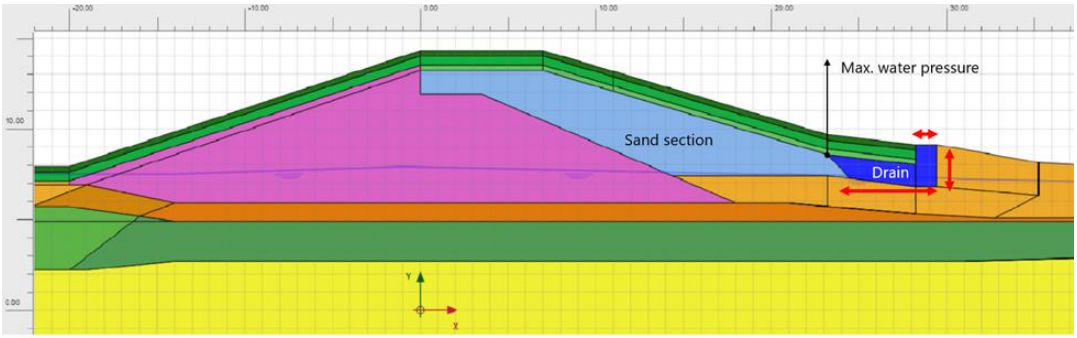


Fig. 4. Schematic representation of the numerical model, showing the dimensions of the drain (indicated by red arrows) and the location where maximum water pressure is measured, serving as an indicator of the drain's performance

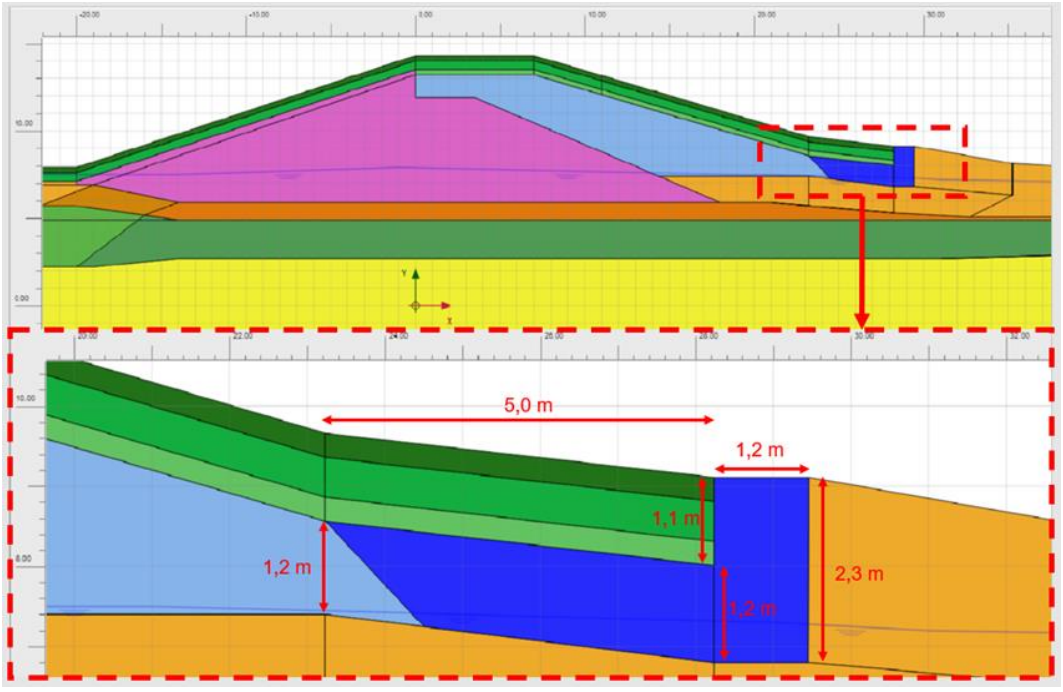


Fig. 5. Overview of optimised drain dimensions for levees with a sand section

 © DFI International Bruges 2025

A sensitivity analysis of the permeability of the sand section and the drainage construction was conducted using the numerical model with the resulting water pressures, illustrated in Fig. 6. The analysis revealed two main effects: higher permeability in the sand section leads to higher water pressures, while higher permeability in the drainage construction results in lower water pressures. Consequently, the required permeability of the drainage construction is dependent on the permeability of the sand section. This figure also suggests that a relationship exists between the permeability of the sand section and the required permeability of the drain, but this is thought to be highly project-specific due to geometry and permeability constraints.

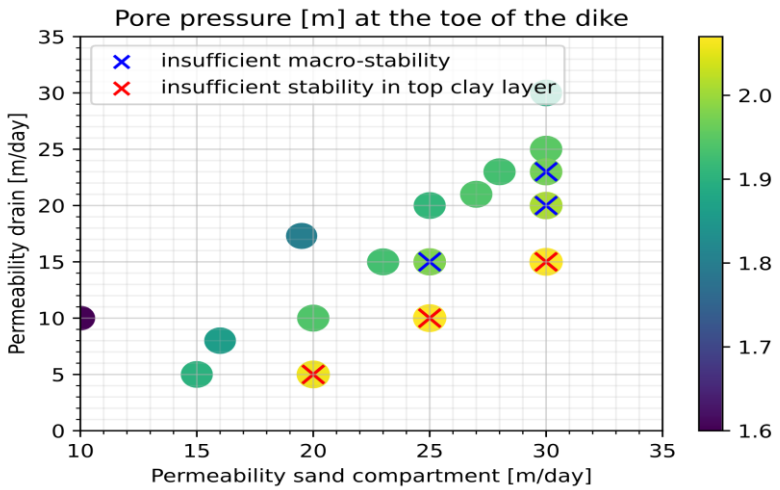


Fig. 6. Sensitivity analysis of permeability of the sand in the sand section and the drainage construction on the resulting water pressure at the toe of the levees

PERMEABILITY ANALYSIS: SITE AND LABORATORY INVESTIGATION

A comprehensive site investigation and laboratory analysis were conducted to address several research questions. To determine the characteristic permeability values of the sand section using the Beyer formula, 104 sieving tests were performed to establish the grain size distribution. To understand the horizontal spatial variability of permeability, samples were collected from five levee sections, with 6 to 10 drillings per section. For vertical spatial variability, both shallow and deep samples were taken from the sand section, illustrated in Fig. 7. To validate the Beyer formula with the Kozeny-Carman formula, additional data were collected, including grain angularity, maximum density, and minimum density for 16 samples, and in-situ density measurements from 29 locations using Cone Penetration Tests (CPT).

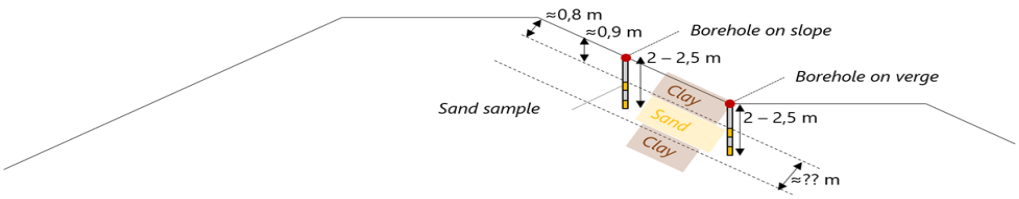


Fig. 7. Locations of drillings in a cross-section of the levee

 © DFI International Bruges 2025

The permeability of the sand within both the sand section and the sand in the drain are sensitive parameters for determining the water pressure in the sand section. The permeability is calculated using two different methods. Firstly, the permeability is determined with Beyer's (1964), which has the advantage of requiring only the grain size distribution as input:

$$k = \beta \times \left(\frac{g}{v}\right) \times LN\left[\frac{500}{d_{60}/d_{10}}\right] \times d_{10}^2, \quad [1]$$

where k = permeability, β = calculation parameter, g = gravitational acceleration, v = kinematic velocity and d_x = the particle fraction at x diameter.

Secondly, the permeability is calculated using the Kozeny-Carman formula (1927 & 1937). While the Kozeny-Carman formula is more accurate, it requires additional input parameters such as particle shape and pore numbers:

$$k = 1{,}96 \times \frac{1}{fS^2} \times \frac{e^3}{1+e}, \quad [2]$$

$$S = \frac{6}{\sqrt{d_1 d_2}}, \quad [3]$$

where k = permeability, f = the grain angularity factor, S = specific surface of the grains, $d_1;d_2$ = the particle fraction being considered and e = porosity of the soil.

The resulting permeability for 15 locations is illustrated in Figure 8. The results indicate that Beyer's formula closely matches the more accurate Kozeny-Carman formula for densely packed sand at this specific location. To verify Beyer's formula's applicability in the project area, cone resistance and relative density of the sand section were analysed in 28 CPTs. In all CPTs, the cone resistance exceeded 5 MPa and the relative density was above 60%. Thus, it was concluded that the sand in the sand section is densely packed, confirming the suitability of Beyer's formula for describing the permeability.

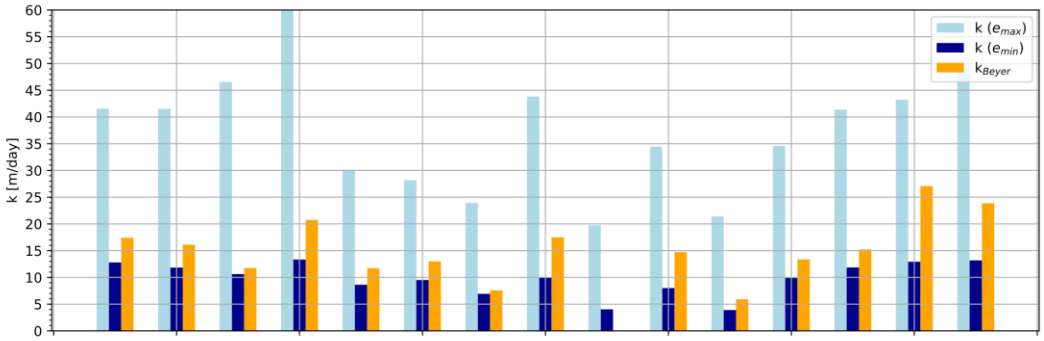


Fig. 8. Permeability of locally available sand based on Kozeny-Carman formula (light and dark blue) and Beyer's formula (orange)

The permeability of the sand, based on Beyer's formula, was analysed using the results of 104 sieving tests, as presented in Table 1. Additionally, the spatial variation of permeability was examined and is shown in Fig. 9. The data indicates that the standard deviation at a given location ranges from 0.9 to 6.3 m/day. Vertically, the average difference in permeability is lower, ranging from 1.3 to 3.9 m/day. However, across the entire levee reinforcement project, the average permeability varies more

 © DFI International Bruges 2025

significantly, between 12 and 26 m/day. Consequently, it was concluded that when determining the required permeability for the drainage construction, local site investigation results should be used rather than a collective value for the entire project area.

Table 1. Overview of permeability parameters based on Beyer's formula

Parameter	Value
Sample size [#]	104
Average [m/day]	18.4
Minimum [m/day]	4.9
Maximum [m/day]	35.4
Standard deviation [m/day]	6.9
Variation coefficient [-]	0.37

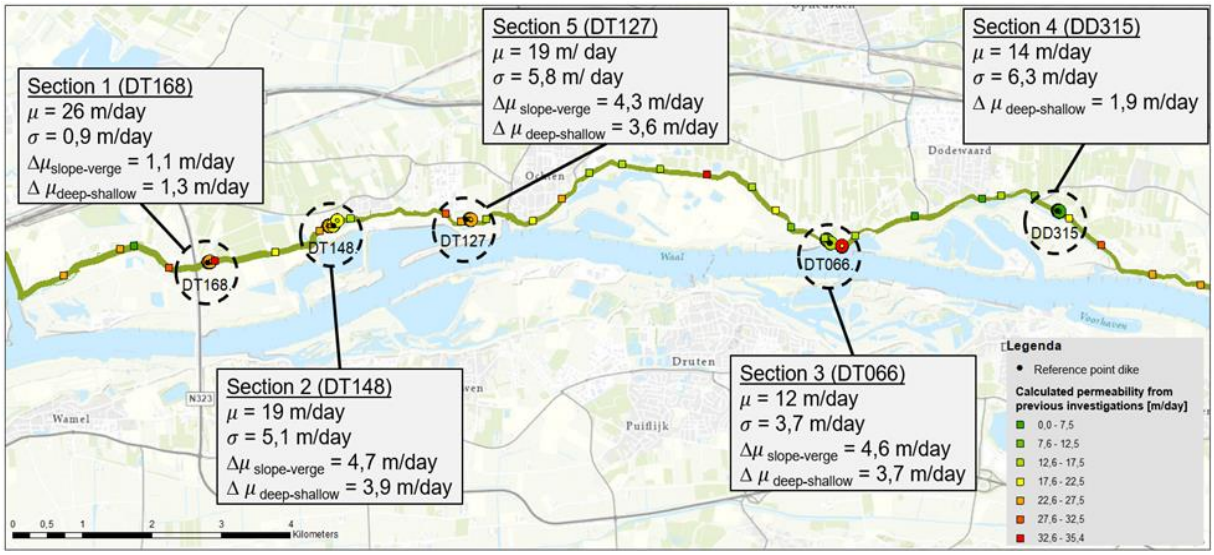


Fig. 9. Overview of statistical results per location

To finalize the design of the drainage construction, the local permeability of the sand section was determined for nine sections. The general statistics per location (see Figure 8) indicate that suitable sand is available for all sections of the drainage construction, as it complies with the minimum necessary permeability characteristics of the drain. Based on the results from Figure 6, a minimum required permeability has been determined for each location and compared with the released sand. Consequently, the drainage construction can be fully realized using locally available sand, thus eliminating the need for importing drainage sand.

LIFE CYCLE ASSESSMENT

The environmental impact of a design optimisation can be quantified using Life Cycle Assessment (LCA) software according to ISO14040/44. In this study, it was opted to use Dubocalc 6.09 and quantify three different design alternatives. Alternative 1 involves the design where entirely new drainage sand needs to be applied, alternative 2 involves reusing the sand from the sand wedge for the drain based on additional soil and laboratory research into the composition of the sand and alternative 3 considers both the reuse of the sand from the sand wedge for the drain and additional computational savings due to reduced drain geometry. The environmental impact of the three variants is shown in Table 2. Reusing the sand results in approximately 96.8% savings in equivalent CO2 impact and Environmental Cost Indicator (ECI) compared to the initial design. The computational savings provide an additional 4% reduction, resulting in a total environmental impact reduction of about 97.5% compared to using entirely new drainage sand.

 © DFI International Bruges 2025

Table 2. Environmental impact per design alternative

Parameter	Design alternative 1: preliminary design	Design alternative 2: preliminary design with reuse	Design alternative 3: optimized design with reuse
Length drain [m]	5970	5970	5718
Volume sand [m^3/m]	9.9	9.9	8.0
Total volume sand [m^3]	59100	59100	45744
Environmental impact [kg CO_2 eq]	1898182	59749	46246
ECI [€]	181780	5907	4573
Saved kg CO_2 eq emissions compared to design alternative 1 [%]	0	96.9	97.6
Saved ECI compared to design alternative 1 [%]	0	96.8	97.5

SUMMARY AND CONCLUSIONS

This study demonstrated that by integrating additional site and laboratory investigations with numerical modelling techniques, significant design optimizations can be achieved for the drainage construction in the Neder-Betuwe levees reinforcement. The locally available sand was found to be sufficiently permeable, making it suitable for reuse in the proposed sand drain design and numerical modelling techniques further improved the dimensions of the drain. This study showed how the geotechnical engineer can exemplify a state-of-the-art approach by promoting a circular and sustainable design while contributing to reduced overall project costs and in turn supporting UN Sustainable Development Goals 9 and 15.

ACKNOWLEDGMENTS

The authors would like to thank Waterschap Rivierenland, Dijkalliantie Neder-Betuwe consisting of GMB, Ploegam and Dura Vermeer, and, the project team for their support.

REFERENCES

W. Beyer. (1964). Zur Bestimmung der Wasserdurchlassigkeit von Kieson und Sanduen aus der Kornverteilung. Wasserwirtschaft Wassertechnik, 14, 165-169.

P.C. Carman. (1937). Fluid flow through granular beds. Transactions, Institution of Chemical Engineers, London, 15, 150-166.

J. Kozeny. (1927). Über kapillare Leitung des Wassers im Boden. Sitzungsber Akad. Wiss., Wien, 136(2a), 271-306.

 © DFI International Bruges 2025

DESIGN VERSUS LOAD TESTING: A CASE STUDY ON 127 LOAD TESTS

Henri de Chaunac, Fondytest, Brussels, Belgium, +32 (0) 2 201 88 88,
henri.dechaunac@fondytest.com

Joachim Clabau, Franki Foundations Belgium, Saintes, Belgium, +32 (0) 51 58 88 81,
joachim.clabau@ffgb.be

Thomas Wulleman, Franki Foundations Belgium, Saintes, Belgium, +32 (0) 2 391 46 46,
thomas.Wulleman@ffgb.be

ABSTRACT

In Belgium, geotechnical pile design is governed by ultimate capacity, and rarely involves the behaviour at service loads. On the other hand, a typical load test campaign focusses on the service settlement, and rarely reaches the ultimate capacity.

This paper presents a case study for which this contrast between design and testing gave rise to a discrepancy in the measured settlements. A total of 5 static load tests and 127 dynamic load tests were performed on screw displacement, continuous flight auger (CFA), and bored piles. The measured settlement at service working loads ranged from 1 to 10 mm, despite a repetitive design made in relatively homogeneous ground conditions.

Although all the piles satisfied the client settlement criteria, some piles did overperform. Therefore, there is room to improve the design in order to reduce, amongst other things, the environmental impact of the foundations.

Keywords: pile, load test

INTRODUCTION

As part of the construction of a new petrochemical plant in the Port of Antwerp, the performance of 127 piled foundations was measured using dynamic and static load tests.

The project consisted of 20 000 piles, with installation techniques encompassing full displacement, partial displacement, and bored piles. The piles were used as foundations for the building, the piperacks, and the tank storage. The project included a large soil investigation campaign, comprised of more than 300 electrical cone penetration tests (CPT-E) and 30 boreholes with laboratory tests. Soil was relatively homogeneous over the entire site, consisting of 11 m of Quaternary sand, interspersed by a 0.5 to 1.5 m thick peat layer, overlying shelly glauconitic Lillo Tertiary sand.

The piles were designed according to the Belgian national application document (NAD) of Eurocode 7 (NBN EN 1997-1, 2005, NBN EN 1997-1/A1, 2014, NBN EN 1997-1 ANB, 2014, CSTC, 2021). Most of the piles of this project were governed by their compressive resistance (R_c), which is conventionally defined in Belgium as being reached for a base displacement of 10% of the pile diameter.

The performance of the pile was controlled using static and dynamic load tests. Five (5) sacrificial piles were tested to 10% base displacement using static load tests, with the aim to verify the ultimate compressive resistance. Alongside the static load tests, 127 piles were tested using dynamic load tests, as a statistical control test of pile performance, after calibration with the static load tests. The shear amount of load tests on one single site allowed us to compare design and actual performance on a representative sample.

 © DFI International Bruges 2025

This paper is organised in six sections. The first and second ones describe the site and the pile design, respectively. The third section introduces the load tests campaign, while the fourth section presents its results. Finally, the fifth section discusses the results and the last section concludes the paper.

SITE DESCRIPTION

The site described herein is located in the Port of Antwerp, in Belgium, which is the second largest seaport in Europe and stands at the estuary of River Scheldt. The site has a surface area of 50 hectares (125 acres) and a relatively flat ground, with an elevation varying between +7.0 and +8.6 m DNG (+23 to +28' above mean sea level).

The ground investigation was in accordance with the project size. There were more than 300 electrical cone penetration tests (CPT-E) conducted and in excess of 30 sample borings with laboratory tests performed. Soil conditions are summarised in Figure 1. Typical soil conditions consist of 6 to 8 m (20 to 26') of silty sand fill and Quaternary soft sand of estuarine origin, followed by a 0.5 to 1.5 m (2 to 5') thick layer of Quaternary peat, which overlies 2 to 4 m (7 to 13') of Quaternary soft sand, and then shelly glauconitic Lillo Tertiary sand. Water is reached at 1 to 3 m (2 to 10') from the ground level.

The project consisted of a total of 20 000 piles, which were installed between early 2023 and the end of 2024. Out of all the installed piles, 92% were cylindrical screw displacement piles, 7% continuous flight auger (CFA) piles, and 1% bored piles. A description of these installation techniques can be found in Bottiau (2006) and Bottiau and Huybrechts (2019). Piles were designed according to the Belgian practice of Eurocode 7, which is described in the next section.

After execution, both the structural integrity and geotechnical performance of the piles was verified. All the piles were examined with a sonic-echo test, which is used to control the integrity of the pile concrete. Alongside, 5 sacrificial piles were tested using static and dynamic load tests, and 122 working piles were tested using dynamic load tests.

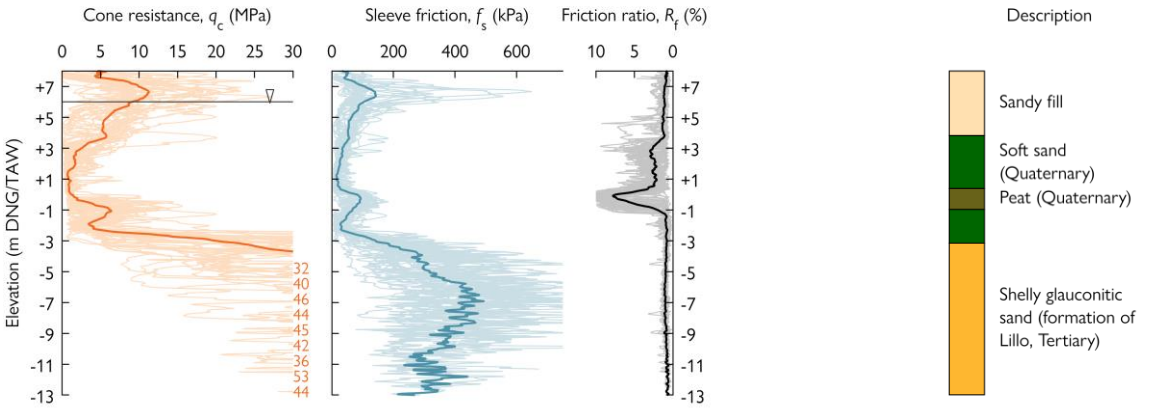


Figure 1 Site typical profile and soil description

PILE DESIGN

Piles were designed according to the Belgian practice, i.e., following Eurocode 7 and the guidelines of the national application document (NAD) of Eurocode 7 (NBN EN 1997-1, 2005, NBN EN 1997-1/A1, 2014, NBN EN 1997-1 ANB, 2014, CSTC, 2021).

 © DFI International Bruges 2025

According to this practice, the piles are designed against their axial compressive geotechnical capacity with the partial factors applied on the actions, and not on the resistance. In other words, the piles are designed against the ultimate limit state (ULS) compressive failure of the ground (GEO), following 'Approach 1, Combination 1' (DA 1.1) of the Eurocode 7. Piles were designed by Franki Foundations Belgium and its partner.

Other design criteria are verified, such as the structural integrity of the pile or the tensile failure of the ground, but these are not presented in this paper.

For piles designed according to their axial compressive capacity, the inequality to satisfy is the following:

$$F_{c,d} \leq R_{c,d} \tag{1}$$

where $F_{c,d}$ is the design value of the pile compressive load and $R_{c,d}$ is the design value of the pile compressive bearing capacity (also named compressive resistance). Both of these are respectively discussed in the two following subsections.

Load

For each pile, the design value of the compressive load ($F_{c,d}$) is given by the project owner. It includes the partial safety factors ($\gamma_{F,c}$), typically 1.35 on permanent actions and 1.50 on variable actions.

Bearing capacity

In Belgium, the pile compressive bearing capacity (R_c) is conventionally defined as the load reached for a pile base displacement of 10% of the base diameter (CSTC, 2021). The design value for the pile compressive bearing capacity ($R_{c,d}$) is obtained by applying a model factor, variability factors and a partial safety factor on the bearing capacity (R_c), which is the addition of the shaft and of the base resistances (R_s and R_b, respectively). These factors depend on the pile type (model factor and partial safety factor), on the stiffness of the construction, on the number of CPTs (variability factors) and on the availability of load tests in similar ground conditions.

The ultimate base resistance (R_b) is computed according to the De Beer (1972) method, which uses a moving average value of the cone resistance (q_c) related to the diameter, and a base installation factor (α_b) which depend on the installation technique. The ultimate shaft resistance (R_s) depends on the cone resistance (q_c), on the soil type, and on a shaft installation factor (α_s) which depends on the installation technique. The factors values are summarised in Table 1.

The nominal diameters varied between 0.51 to 0.88 m (20 to 35"), with lengths ranging from 10 to 34 m (33 to 112'). The design compressive resistance ($R_{c,d}$) ranged between 1100 and 3100 kN for the screw displacement piles, between 2400 and 6000 kN for the CFA piles, and between 6100 and 9700 kN for the bored piles.

All of the piles reached the Lillo sand layer: the screw displacement piles reached 0.5 to 1.5 m of the Lillo sand, while the CFA and bored piles were drilled to deeper depths, reaching from 1 to more than 20 m of Lillo sand.

The next section presents the load test setup used to perform the static and the dynamic load tests.

 © DFI International Bruges 2025

Table 1 Design factor values for the bearing capacity calculation (CSTC, 2021)

	Screw piles	CFA piles	Bored piles
Installation factor for shaft, α_s	1.00	0.40	0.50
Installation factor for base, α_b	0.70	0.50	0.50
Model factor, γ_{Rd}	1.10	1.20	1.20
Variability factor, ξ_3	1.21	1.21	1.40
Variability factor, ξ_4	1.13	1.13	1.40
Partial safety factor for shaft, γ_s	1.00	1.00	1.00
Partial safety factor for base, γ_b	1.00	1.00	1.00

PILE LOAD TESTS DESCRIPTION

Both static and dynamic load tests were performed on the project piles. The static load tests were performed by Buildwise and the dynamic load test were performed by Fondytest.

Static load tests

Static load tests were carried out on five sacrificial piles with the aim to verify the ultimate compression resistance, conventionally defined in Belgium as the load reached at a base displacement of 10% of the base diameter (CSTC, 2021).

On four of the five static load tests, the pile deformation as a function of depth was measured with Fibre Bragg Grating (FBG) sensors. This measuring loop allowed to assess the shaft friction distribution and the base resistance for each step of loading.

A typical photograph of the static load test is depicted in Figure 2a. The force is applied on the pile head thanks to 3 or 4 hydraulic cylinders with a capacity of 1900 kN (427 kips) each. The cylinders are controlled by a high-precision hydraulic unit and the force is measured using a calibrated load cell. The displacement of the pile head is measured with 4 electronic displacement sensors with a precision of 0.01 mm (0.4 thou) and double checked with a total station.

The result of the test is a load-bearing curve per tested pile, as depicted in Figure 4 for 2 of the piles tested.

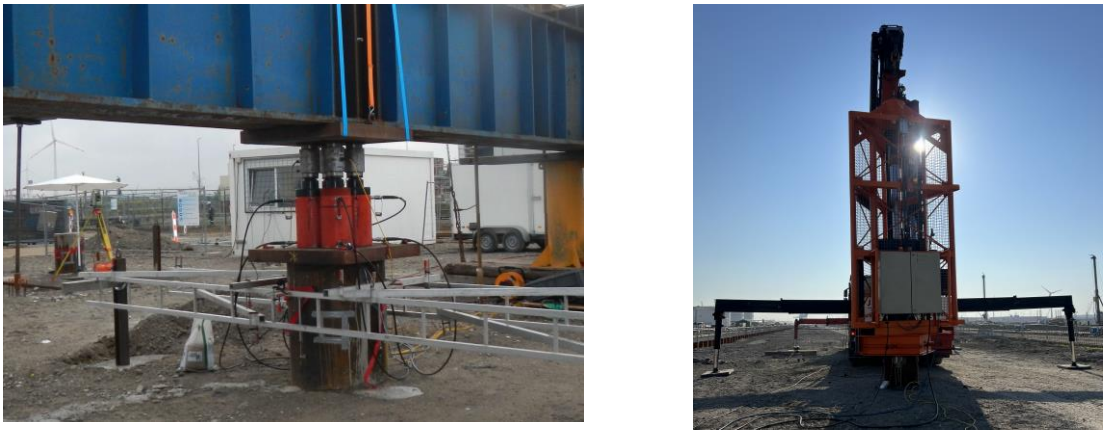
Dynamic load tests

Dynamic load tests were used as statistical control tests of the pile performance on 122 working piles, after calibration with the static load tests on the five sacrificial piles. The working piles were tested to assess settlement under their Service Working Load, which was expected to be inferior to 10 mm (13/32”).

The dynamic load tests were performed according to ASTM D4945-17 (2017) and ISO 22477-4 (2018) using either a 4 or an 11 tonnes (8 800 or 24 250 lb) loading device, capable of dropping its mass accurately onto the pile head from various drop heights (Figure 2b).

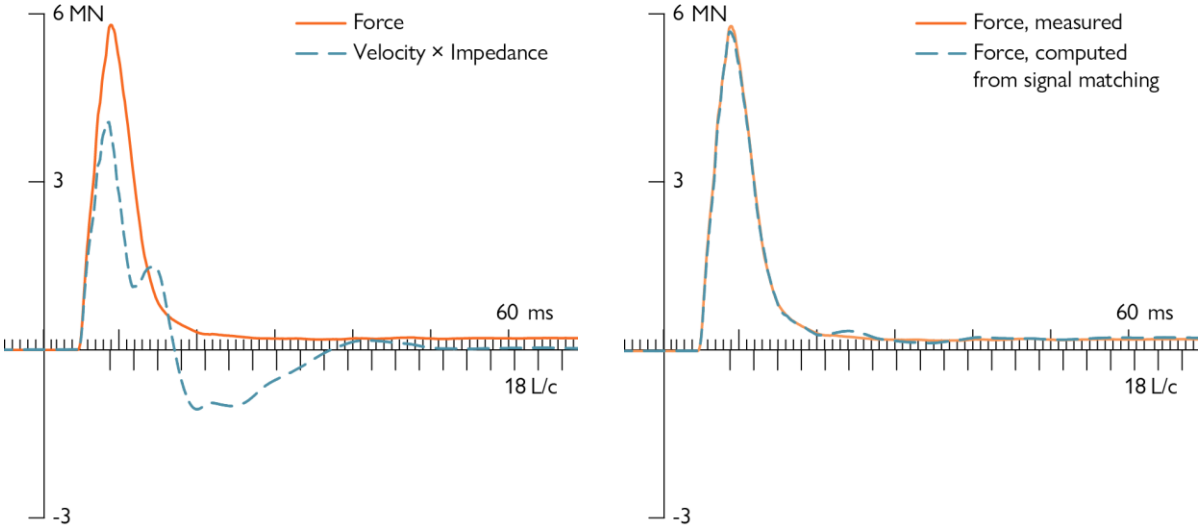
Dynamic monitoring was performed thanks to four accelerometers and four strain transducers connected to a field computer, and a digital surveyor’s level to measure permanent sets. The signals of the four pairs of sensors were individually checked and averaged. The force was evaluated by applying strains measured on the concrete to the relevant section modulus of the concrete head and the velocity by integrating the accelerometer signals. The raw data was monitored on site and stored for subsequent analysis in the office; Figure 3a depicts the signals acquired during one blow of a dynamic load test.

 © DFI International Bruges 2025



(a) (b)

Figure 2 Set-up of the (a) static load test and (b) dynamic load test



(a) (b)

Figure 3 Dynamic load test signals (a) force and velocity and (b) force measured vs signal matching computed force

The dynamic load test data acquired was then used to perform a CAPWAP signal matching analysis, also named ‘inverse analysis’ (CAPWAP, 2006). Signal matching using measured signals enables a rigorous derivation of the soil behaviour around the pile (Goble *et al.*, 1970, Holeyman, 1992). The measured wave down signal is imposed (input) as a boundary condition at the model pile head while soil parameters are adjusted with a view to produce a calculated wave up (output) that closely matches that measured during the impact, as depicted in Figure 3b. Once the wave up match can no longer be improved, static components of the soil model are extracted to evaluate the bearing capacity behaviour of the pile, and in particular the skin friction, the toe resistance, and the downward displacement necessary to mobilise them. The result of the signal matching procedure is a load-bearing curve per tested pile (Figure 4), which is equivalent to the result measured by a static load test.

On the 127 analysed dynamic load tests using CAPWAP signal matching, the average match quality (MQ) of the signal matching procedure was 2.4, with a standard deviation of 0.8.

 © DFI International Bruges 2025

High strain dynamic load testing using signal matching analysis has been used in the industry since over 40 years. Over that time, the validity of the procedure has been extensively covered in the literature, for example against static load tests (Bruno and Randolph, 1999, Likins and Rausche, 2004, Alvarez *et al.*, 2019, Huybrechts *et al.*, 2019), about the influence of the operator (Fellenius, 1988, Buckley *et al.*, 2017), or the rate effects (Rodrígez *et al.*, 2008, Rausche, 2019).

The two main limitations of dynamic load testing are (1) the displacement reached during a dynamic load test is only of the order of the centimetre and (2) the computed load-displacement graphs do not consider long-term creep settlements. The main advantage of a dynamic load test is its efficiency: up to 8 piles can be tested per day. High strain dynamic load testing using signal matching analysis for performance evaluation is justified both economically and technically (Rausche, 2019).

The static and dynamic load tests on the same five sacrificial piles allowed calibration of the dynamic load tests. The comparison for two of the five sacrificial piles, a 610 mm (24") diameter screw displacement pile and a 600 mm (24") diameter CFA pile, is depicted on Figure 4. For these tests, the static load test was first performed, and was followed by the dynamic load test.

Figure 4 confirms that the stiffness measured during the dynamic load test loading is in accordance with the stiffness of the static load test during unloading, or in other words, satisfies the 'calibration' process described in NBN EN 1997-1 (2005). The signal matching procedure of the dynamic load tests was capable of predicting a pile stiffness in the same range as the one measured by the static load test.

Figure 4 also highlights the different objectives of both tests. The static load test is performed until a displacement 10% of the diameter is reached, whilst the load reached during a dynamic load test is inducing a displacement limited to the order of the centimetre. This was in accordance with the objective of both tests on this project.

The following section discusses the results of the dynamic load tests on the 127 piles.

RESULTS

The aim of the load test campaign of the working piles is to assess the settlement of each tested pile at its Service Working Load (SWL), which is compared to the project settlement criteria of 10 mm (13/32") for each pile.

The results of the load test campaign are summarised in Figure 5, which presents, for each pile tested, the settlement at SWL against the SWL. The measured settlements for the 127 pile tests range from 1 to 10 mm (1/32 to 13/32"), with an average of 4 mm (5/32") and a standard deviation of 2 mm (3/32").

 © DFI International Bruges 2025

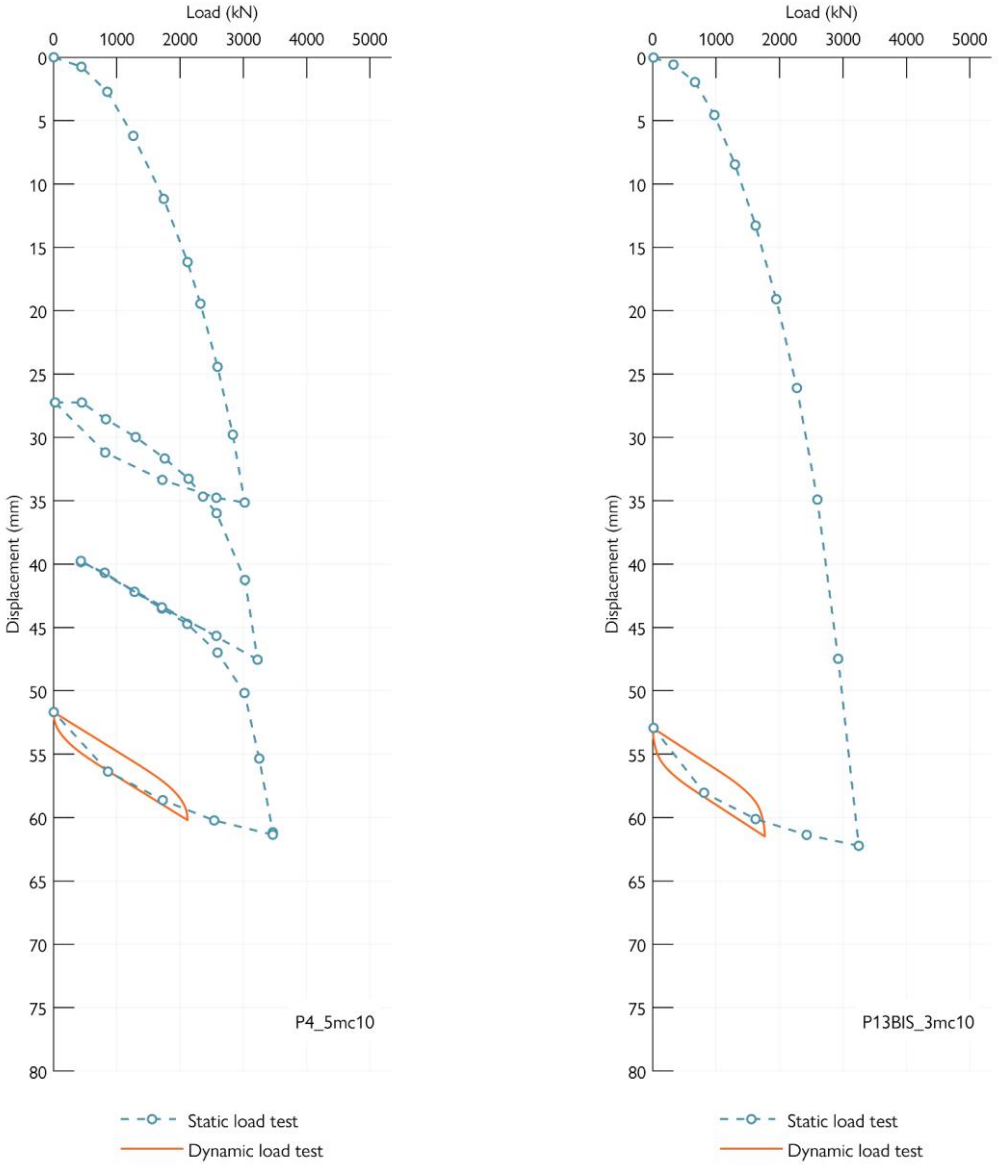


Figure 4 Comparison of static and dynamic load test results on (a) a 610 mm (24”) diameter screw displacement pile and (b) a 600 mm (24”) diameter CFA pile

Out of all the tested piles, several were designed with other considerations than the compressive resistance: tension resistance or lateral loading. Figure 6 highlights this difference by comparing the SWL to the design compressive resistance ($R_{c,d}$). For the piles which have been designed with other design considerations than the compressive capacity, $R_{c,d}$ is significantly higher than SWL. On the other hand, piles for which the compressive strength is governing have a ratio of $R_{c,d}$ to SWL comprised between 1.3 and 1.4. This latter category is of interest to us as it portrays piles with similar load factors; it consists of 57 load tests.

These 57 piles, for which $R_{c,d}$/SWL is comprised between 1.3 and 1.4, are composed of 52 screw piles and 5 CFA piles. The piles have reached a settlement at SWL varying between 2 and 10 mm (3/32 to 13/32”), with an average of 5 mm (7/32”) and a standard deviation of 2 mm (3/32”), as depicted in Figure 7.

 © DFI International Bruges 2025

All of these 57 piles have the same design, are installed in quite homogeneous ground conditions, and are loaded to similar load factors. It was therefore unexpected to measure such a spread in the settlement. The next section investigates these results.

DISCUSSION

This section examines potential aspects which could have influenced the variability in the settlement measured on the 57 piles selected, for which $R_{c,d}$/SWL is comprised between 1.3 and 1.4:

1. Could design aspects have had an effect on the settlement variability?
2. Is the settlement influenced by the location of the piles?
3. Could something during the on-site production of the piles explain the difference in settlement?
4. Could the dynamic load itself test affect the measured performance?

The following four subsections investigate each of these categories.

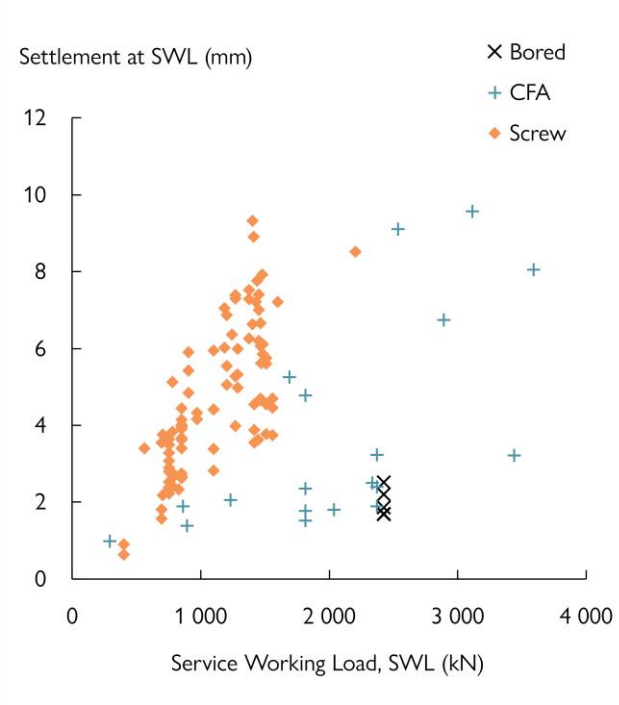


Figure 5 The measured settlement at Service Working Load (SWL) varies between 1 and 10 mm for all piles tested

 © DFI International Bruges 2025

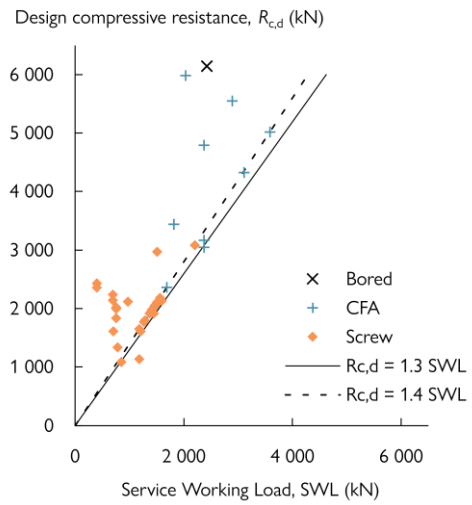


Figure 6 Service Working Load (SWL) vs design compressive resistance ($R_{c,d}$)

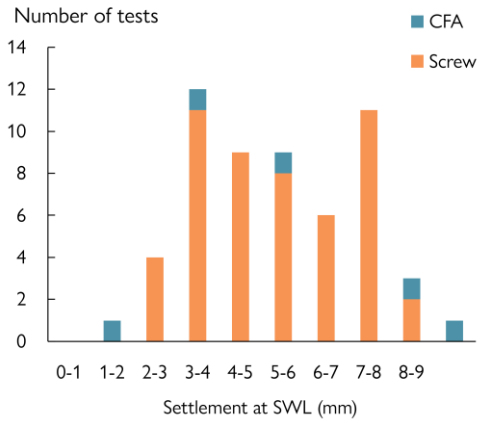


Figure 7 The settlement at SWL of piles for which 1.3 ≤ $R_{c,d}$/SWL ≤ 1.4 varies between 2 and 10 mm (3/32 to 13/32")

Design

In Belgium, the model and installation factors for screw piles are based on a large database of load tests; these factors are commonly regarded as reliable. On the other hand, the confidence for factors used for CFA and bored piles is smaller, as the database for these pile types is smaller.

Out of the 57 piles selected, there were 52 screw piles and 5 CFA piles. These were therefore designed with different factors (defined in Table 1), which are supposed to account for the difference between a full displacement and a partial displacement pile. The average settlement and standard deviation are 5 and 2 mm (8/32 and 3/32") for the screw piles and 6 and 3 mm (8/32 and 4/32") for the CFA piles. The settlement values are similar between screw and CFA, which implies that the design installation factors defined in Table 1 are adequate.

Location

Although the ground conditions are quite homogeneous (Figure 1), we investigated if the location of the pile had an influence on the settlement. The result is illustrated in Figure 8a, which depicts a bubble for each pile, the size of which is proportional to the settlement at SWL, in function of the geographical location of each pile. Figure 8a does not show any settlement trend regarding the position of the piles.

 © DFI International Bruges 2025

Installation

On the 52 screw piles, 7 identified rigs were used, named Rig 02, 06 to 10, as summarised in Table 2. These were similar in design but composed of different teams. Rigs 02 depicts an average settlement at SWL of 3.4 mm (9/64”), which is significantly better than the rest. On the other hand, Rig 14 has the worst measured performance (6.9 mm or 17/64” settlement average).

Furthermore, two types of augers were used, named auger A and B in Table 2. The average settlement for these is respectively 6.1 and 4.1 mm (15/64 and 5/64”). From that data, Auger B surpasses the performance of Auger A by a factor of 1.3.

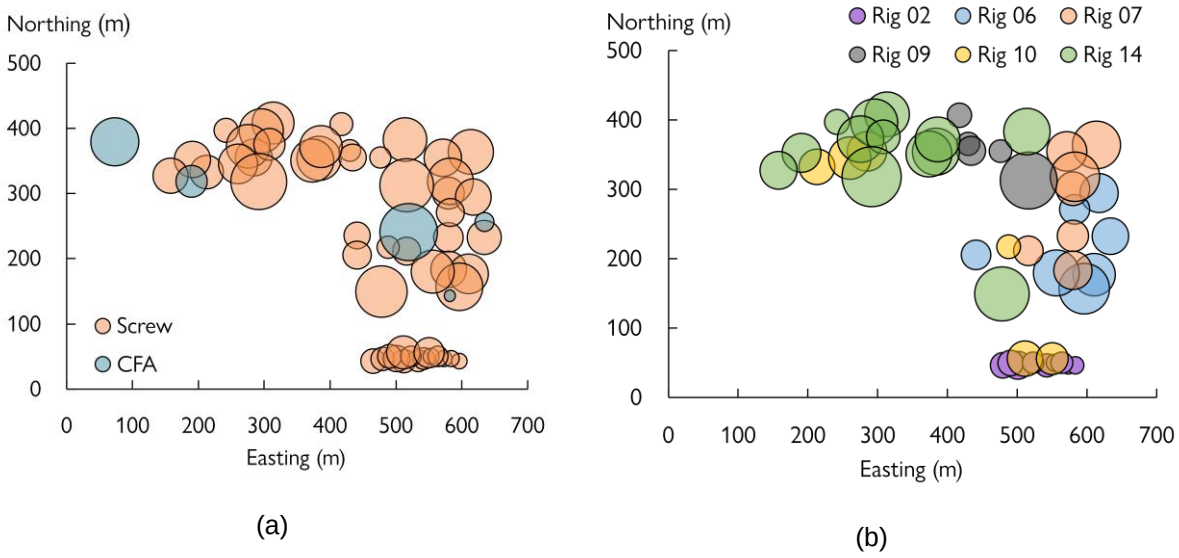


Figure 8 Position of each pile for which 1.3 ≤ $R_{c,d}$/SWL ≤ 1.4with the size of the bubble is proportional to the settlement at SWL, (a) screw vs displacement piles, (b) only screw piles, split per rig

Table 2 Settlement average and standard deviation for each piling rig and auger type (screw piles for which 1.3 ≤ $R_{c,d}$/SWL ≤ 1.4)

Rig	*Settlement at SWL (mm),*		*Number of pile tests*	*Auger*
	Average	*Standard deviation*		
Rig 02	3.4	0.6	9	B
Rig 06	6.1	1.1	7	A
Rig 07	6.2	1.1	8	A
Rig 08	5.4	2.7	6	A
Rig 09	4.9	2.0	5	A
Rig 10	5.5	0.9	6	B
Rig 14	6.9	1.4	12	A
Unknown rig			4	

Testing

Dynamic load test applies a very rapid solicitation, which is undrained in anything else than clear sand. Therefore, if the proportion of low permeability soil differs from one pile to the other, it could be argued that several piles could be loaded as undrained whereas other ones as drained.

 © DFI International Bruges 2025

All the 52 tested screw piles had a toe level between −3.4 and −4.4 m DNG (11 to 14’ below mean sea level), which implies they were roughly encompassed by similar permeability soils, but still had a settlement standard deviation of 2 mm. Therefore, the spread in the measured settlement cannot be explained by the loading rate effects.

CONCLUSION

This paper presents the results of 5 static load tests and 127 dynamic load tests performed on a single site. Ground conditions were relatively homogeneous. Design was conducted following the Belgian practice of Eurocode 7. The dynamic load tests presented in this paper were performed on working piles and their objective was to assess the settlement of each tested pile at their Service Working Load (SWL).

Out of the 127 load tests, we highlighted 57 piles for which the design was governed by the ultimate compressive load and for which the load factor was similar, *i.e.*, the design compressive resistance ($R_{c,d}$) of these 57 piles was comprised between 1.3 and 1.4 times their SWL. For this selection of piles, the settlement varied between 2 and 10 mm (3/32 to 13/32”), with an average of 6 mm (8/32”) and a standard deviation of 2 mm (3/32”).

The paper investigates four potential aspects which could have influenced the settlement variability: (1) pile design, (2) piles’ location, (3) differences in installation processes, and (4) test procedure. No significant influence was highlighted from the pile type, the piles’ location, the piling team used, or the test procedure.

On parameter in the installation process proved to have an influence on the measured performance: of the two different types of augers that were used, one surpassed the performance of the other by a factor of 1.3. This parameter is the only one highlighted that could lead to an improved design.

Finaly, perhaps an average pile settlement of 6 mm (8/32”) with a standard deviation of 2 mm (3/32”) is a spread which is inherent to the uncertainty of geotechnical engineering. This is outside of the scope of this paper but is an open issue for future work.

REFERENCES

Alvarez, C., Sellountou, E.A., and Rausche, F. (2019). *State of the Art Dynamic Load Testing of ACIP Piles in the Americas*, Proceedings of the 10th International Conference on Stress Wave Theory and Testing Methods for Deep Foundations, ASTM STP1611, P. Bullock, G. Verbeek, S. Paikowsky, and D. Tara, Eds., ASTM International, West Conshohocken, PA, 2019, pp. 81-96.

ASTM D4945-17 (2017*). American Society for Testing and Materials (ASTM), Standard Test Method for High-Strain Dynamic Testing of Deep Foundations*, November 2017, 10p.

Bruno, D. and Randolph, M. F. (1999). Dynamic and Static Load Testing of Model Piles Driven into Dense Sand, *Journal of Geotechnical and Geoenvironmental Engineering*, 125(11), 988-998.

Bottiau, M. (2006*). Recent evolutions in deep foundation technologies*, Deep Foundations Institute, 38p.

M. Bottiau, M. and Huybrechts, N. (2019). *Recent advances in pile design, construction, monitoring and testing*, Proceedings of the 17th European Conference on Soil Mechanics and Geotechnical Engineering, 52p.

Buckley, R., Kontoe, S., Jardine, R., Schroeder, F., and Barbosa, P. (2017). *Common pitfalls of pile driving resistance analysis - A case study of the Wikinger offshore windfarm*, Proceedings of the 8th International Conference on Offshore Site Investigation and Geotechnics: Smarter Solutions for Future Offshore Developments, London, UK, Volume: 2, pp. 1246-1253.

 © DFI International Bruges 2025

CAPWAP (2006). *Case Pile Wave Analysis Program, background Report*, Version 2006, Pile Dynamics, 94p.

CSTC (2021). *Directives pour l'application de l'Eurocode 7 en Belgique selon la NBN EN 1997-1 ANB – Partie 1 : dimensionnement géotechnique à l'état limite ultime (ELU) de pieux et de micropieux sous charge axiale à partir d'essais de pénétration statique (CPT) (révision du Rapport n° 19)*, CSTC/BBRI/Buildwise, Report n° 20, 8 April 2021, 56p.

De Beer (1972). *Méthodes de déduction de la capacité portante d'un pieu à partir des résultats des essais de pénétration*, Annales des travaux publics de Belgique, volume 72, n° 4 (p. 191-268), n° 5 (p. 321-353) et n° 6 (p. 351-405).

Fellenius, B.H. (1988). *Variation of CAPWAP results as a function of the operator*, Proceedings of the 3rd International Conference on the Application of Stress-Wave Theory to Piles, Ottawa, May 25-27, 1988, pp. 814-825.

Goble, G.G., Rausche, F., and Moses, F. (1970). *Dynamic Studies on the Bearing Capacity of Piles*, Phase III, SMSMD, Technical Report No. 48, Case Western University.

Holeyman, A. (1992). *Technology of Pile Dynamic Testing, Keynote Lecture*, Proceedings of the 4th International Conference on the Application of Stress-Wave Theory to Piles, The Hague, 21-24 September 1992, pp. 195-215.

Huybrechts, N., De Vos, M., de Chaunac, H., Holeyman, A. E., and Bottiau, M. (2019). *Static versus Dynamic Load Tests on Piles in Sand and Chalk*, Proceedings of the 10th International Conference on Stress Wave Theory and Testing Methods for Deep Foundations, ASTM STP1611, P. Bullock, G. Verbeek, S. Paikowsky, and D. Tara, Eds., ASTM International, West Conshohocken, PA, 2019, pp. 594-610.

ISO 22477-4 (2018). *Geotechnical investigation and testing – Testing of geotechnical structures – Part 4: Testing of piles: dynamic load testing*, International Standard, 1st edition, March 2018, 52p.

Likins, G. and Rausche, F. (2004). *Correlation of CAPWAP with Static Load Tests*, Proceedings of the Seventh International Conference on the Application of Stress-Wave Theory to Piles, Selangor, Malaysia, pp. 153-165.

NBN EN 1997-1 (2005). *Eurocode 7 : Geotechnical design – Part 1 : General rules (+ AC:2009)*, Bureau de Normalisation, 1st edn, January 2005, 203p.

NBN EN 1997-1/A1 (2014). *Eurocode 7 : Geotechnical design – Part 1 : General rule*, Bureau de Normalisation, 1st edn, January 2014, 23p.

NBN EN 1997-1 ANB (2014). *Eurocode 7: Geotechnical design – Part 1: General rules – National annex*, Bureau de Normalisation, 1st edn, January 2014, 25p.

Rausche, F. (2019). *Combining Static and Dynamic Loading Test Results of Piles*, Proceedings of the 10th International Conference on Stress Wave Theory and Testing Methods for Deep Foundations, ASTM STP1611, P. Bullock, G. Verbeek, S. Paikowsky, and D. Tara, Eds., ASTM International, West Conshohocken, PA, 2019.

Rodríguez, J., Alvarez, C., and Velandia, E. (2008). *Load Rate Effects on High Strain Tests in High Plasticity Soils*, Proceedings of the 8th International Conference on the Application of Stress-Wave Theory to Piles, Lisbon, Portugal, pp. 131-134.

 © DFI International Bruges 2025

MODELLING THE IMPACTS OF CLIMATE CHANGE ON GEOTECHNICAL COMPANIES

Luke R. Deamer, Keller Group plc, London, United Kingdom, +44 20 7616 7579, Luke.Deamer@keller.com

Alexander Bridge, Sillion, London, United Kingdom, +44 7927 306 920, Alexander.Bridge@sillion.co.uk

Isis Bliah, Sillion, London, United Kingdom, +44 7415 221 145, Isis.Bliah@sillion.co.uk

ABSTRACT

Climate change already impacts how geotechnical companies operate. The specific impacts of climate change on geotechnical companies can be divided into physical and transition risks / opportunities. Physical risks arise from the physical impacts of climate change, including both acute extreme weather events and longer-term chronic changes in climate. Transition risks arise from moving to a low carbon economy, spanning the products and services we offer, impacts to operations, impacts on our supply chains and reputational changes. Both these risk categories will grow in future, but the rate of increase depends on the pace of decarbonisation across the world.

In this paper, we conduct a full Taskforce on Climate-related Financial Disclosures (TCFD) aligned scenario analysis, modelling multiple climate risks and how they impact a geotechnical company. In terms of transition risks, we look at carbon taxation on materials and the rate of rig decarbonisation required in Europe. In terms of physical risks, we model the impacts of heat, extreme precipitation, wildfires and hurricanes in North America on operations. All these models use the latest International Energy Agency (IEA) scenarios for different climates, applied to how they impact a global geotechnical company. We finish with a look at how some of these climate risks can be mitigated, to safeguard geotechnical companies in the future.

Key words: sustainability, climate change, carbon, risks, opportunities, weather, storms,

INTRODUCTION

The Intergovernmental Panel on Climate Change (IPCC) states that “it is unequivocal that human influence has warmed the atmosphere, ocean and land” (IPCC, 2022). But what does this mean for geotechnical companies, both now and in the future?

Climate change and its mitigation will shape the future markets, designs and operations that geotechnical companies face. If we see further climate change, we will see increased physical impacts. This includes extreme weather events that can impact foundation design and site operations. If the world manages to cut carbon emissions to avoid these physical impacts, we will see more transition impacts instead. These might include carbon taxation on materials or equipment that we use, as governments employ regulation in order to drive emissions reductions.

The framework used to model these risks comes from the Taskforce on Climate-related Financial Disclosures (TCFD). TCFD started as a voluntary scheme to encourage financial companies to cost out the impacts of climate change on their portfolios. However, since 2022, TCFD disclosures have been a legal requirement for UK-listed companies. TCFD also forms part of the foundation of the approach taken with the EU’s Corporate Sustainability Reporting Directive (CSRD), particularly module E1 on climate change. Climate risk modelling, known as scenario analysis, is just one part of an overall TCFD disclosure, that also covers governance, strategies for addressing climate change, risk management and the company’s metrics and targets.

 © DFI International Bruges 2025

Since this modelling is a legal reporting requirement, disclosures have been published by various construction companies. These include reports from Balfour Beatty (2024), Skanska (2024) and Kier (2024). However, none of these are geotechnical-specific, nor do they include metrics to demonstrate the size of these risks. This paper therefore serves the purpose of presenting quantitative, scenario-based modelling of climate risks for geotechnical companies. This paper can also act as an example for other geotechnical companies conducting this modelling. This is increasingly important given the incoming CSRD requirements in the EU.

Whilst this modelling is increasingly a legal requirement in the UK and EU, there are many other reasons for conducting this modelling. The real value comes from being able to use these models to inform purchasing decisions, partnerships and wider strategy. It also helps inform future risks to mitigate and opportunities to realise, across all functions of a company. This paper therefore aims to quantify some of these climate risks, as well as setting out how companies can mitigate these impacts.

DATA INPUTS AND MODELLING

To model future climate or geotechnical markets, we can use social and climate models of the Earth. As of its landmark Sixth Assessment Report (AR6), the IPCC has advanced its climate scenario approach to now focus on five illustrative scenarios, which it created by combining Shared Socioeconomic Pathways (SSPs) and Representative Concentration Pathways (RCPs) (IPCCC, 2022). These IPCC scenarios were used to model physical risks, while IEA scenarios were used for transition risks.

SSPs provide narratives describing alternative socio-economic responses and developments from the global community, and include quantitative assumptions around population and GDP. For example, in one extreme, SSP1, the world moves gradually but in a unified manner towards decarbonisation and sustainability. In the middle pathway, SSP3, policies are pursued in a regional and divided manner, with countries struggling to adapt individually to the impacts of climate change. RCPs, on the other hand, describe the physical reality of different future greenhouse gas concentrations in the atmosphere, with the higher-numbered pathways correlating with higher global surface temperatures and more pronounced physical impacts. For its five scenarios, the IPCC has combined each of the five SSPs with a correlating RCP. Higher SSPs, with more disorganised responses to climate change, are paired with a higher RCP (i.e. ones with more emissions).

IPCC scenarios are accordingly named in the format ‘SSP2-4.5’ – meaning a combination of SSP 2 and RCP 4.5. These scenarios are then applied to earth models to predict climate change impacts in different areas. Whilst this modelling clearly comes with a high degree of uncertainty, the Earth’s response to different emissions is tested on historical Earth climate data and combined with other climate models to improve accuracy. The IPCC, which includes climate scientists from every UN country, has unanimously approved the climate models used in this paper (IPCC, 2022).

Sillion, a UK-based climate transition consultancy, conducted the climate modelling in this paper, using geotechnical knowledge from Keller and standardised climate model data from the International Energy Agency (IEA), and the World Climate Research Programme’s (WCRP) Coupled Model Intercomparison Project 6 (CMIP6). Modelling was conducted in Microsoft Excel and Power BI.

Physical – risk of extreme weather events in North America

One large potential risk to geotechnical contractors is the impact of extreme weather events. These acute events include extreme heat, wildfires, extreme precipitation, hurricanes and storms. These events can delay projects, as equipment is demobilised and remobilised to prevent damage. These events can also cause delays by damaging working platforms or access roads, which need to be repaired before work can restart.

 © DFI International Bruges 2025

Geotechnical projects are often relatively short. For example, Keller conducted over 5000 projects last year, of which the majority lasted less than a month (Keller, 2024). Project lead-in times are also typically short, with most taking less than 6 months to begin site work. As such, it is difficult to determine where future projects are likely to be over the 10-30 year time frames needed for climate modelling. For this reason, we used historical data to capture the spread of geotechnical projects in different markets as a proxy for where future projects may take place. Note that this historical data does not account for any shifts in locations due to changing climate conditions though, so this uncertainty should be factored into risk planning.

On top of these locations, we can then overlay the different climate models for each extreme weather event. We used the SSP2-4.5 scenario to model a 'business as usual' future, and SSP5-8.5 to model as a worst case scenario for climate change. We deemed there was no point in modelling a net zero scenario, because the physical impacts would be the same as those currently faced by geotechnical companies.

Once we know how often each site is likely to be impacted by extreme weather events in each part of the year, we can then overlay assumptions around days delay, time to demobilise and remobilise and opportunity costs. These were determined using interviews with project managers and real-life examples of projects that were delayed due to these events. For example, these included impacts from hurricanes in Florida and the Southeast US where projects were demobilised, then access roads had to be repaired before remobilising after the hurricane. Other projects included those delayed by poor visibility and air quality, as smoke from wildfires paused operations in Canada and Northern USA areas in 2023.

Transition – risk of stranded equipment assets as a result of regulations in Europe

In terms of transition risks to direct operations, we are likely to see a continued rise in legislation restricting emissions and air quality, particularly in urban areas. For example, Oslo is a fossil fuel free city from 2025 onwards. This impacts non-road mobile machinery (NRMM), like diesel piling rigs and grout pumps. Since diesel piling rigs are difficult to retrofit, geotechnical companies will have to purchase lower emission equipment or be unable to operate in certain markets. This may also leave contractors with stranded assets, where they cannot utilise higher-emission equipment.

Scenarios for transition risks are based on potential legislation pathways, rather than the extrapolated climate impacts. This scenario analysis used three of these models from the International Energy Agency: Net Zero Emissions (NZE), Announced Pledges Scenario (APS) and Stated Policies Scenario (commonly known as STEPS). NZE is the most ambitious model, which models what policy makers will have to limit global temperature rise to 1.5°C by 2100. APS looks at what countries have pledged to achieve in terms of net zero or reduction targets, and assumes that all climate commitments made by governments and industries are met in full and on time. This creates an intermediate scenario, resulting in a 1.7°C temperature rise by 2100. STEPS, on the other hand, models the impact of policies that have been enacted or where specific actions have been committed to in the future, and assumes progress towards these commitments based on historical performance. This means STEPS is the most conservative model, showing what would happen if there's no further climate mitigation actions, leading to around 2.4°C temperature rise by 2100.

There is no specific model for the policies on non-road mobile machinery, like drill rigs or excavators. However, there are existing models for vehicles and general heavy machinery which follow a similar legislative path, so we used this as a proxy for legislation of equipment. We also created our own fourth scenario, in addition to the IEA's three scenarios, which was based on known and planned legislation for cities like London and Oslo, which have even more rapid decarbonisation plans.

There were some assumptions to allow for the continued growth in number of rigs, assuming they are servicing a growing business over time. Rigs were not separated by technique they offer, since

 © DFI International Bruges 2025

modelling focused on tailpipe emissions rather than growth or shrinkage in different clients / markets. Modelling was focused on Europe, since this is the area with the most evolved air quality and carbon legislation for vehicles.

Transition – risk of material price changes in Europe

Another key transition risk is carbon taxation on high carbon materials, like cement and steel. A cap and trade carbon taxation system is already in place in Europe and the UK, adding additional cost premiums to materials in heavy foundation projects. If this additional cost cannot be passed on to clients, it can affect project margin. More realistically though, it is more likely that the increased project costs may simply prevent projects going ahead if they're deemed too expensive.

Modelling this risk uses the same approach for transition models and scenarios as the equipment, with a Net Zero Emissions (NZE), Announced Pledges Scenario (APS) and Stated Policies Scenario (STEPS). However, the International Energy Agency has pre-determined and reviewed models for carbon taxation on cement and steel, with many of the future restrictions already written into European law. Therefore, there was less need for additional assumptions around these scenarios.

This modelling was focused where the best available usage data was available, namely Keller Austria. However, since Austria is part of the EU's Emission Trading System, the results are equally applicable to the rest of the EU and the UK.

MODELLING RESULTS AND DISCUSSION

Physical modelling

Impacts were modelled separately for extreme heat, extreme precipitation, hurricanes, wildfires and ensuing smoke (Fig. 1). As this modelling focused on short-lived acute impacts, we look more at the impact on individual projects, rather than overall delays from longer-term climate change.

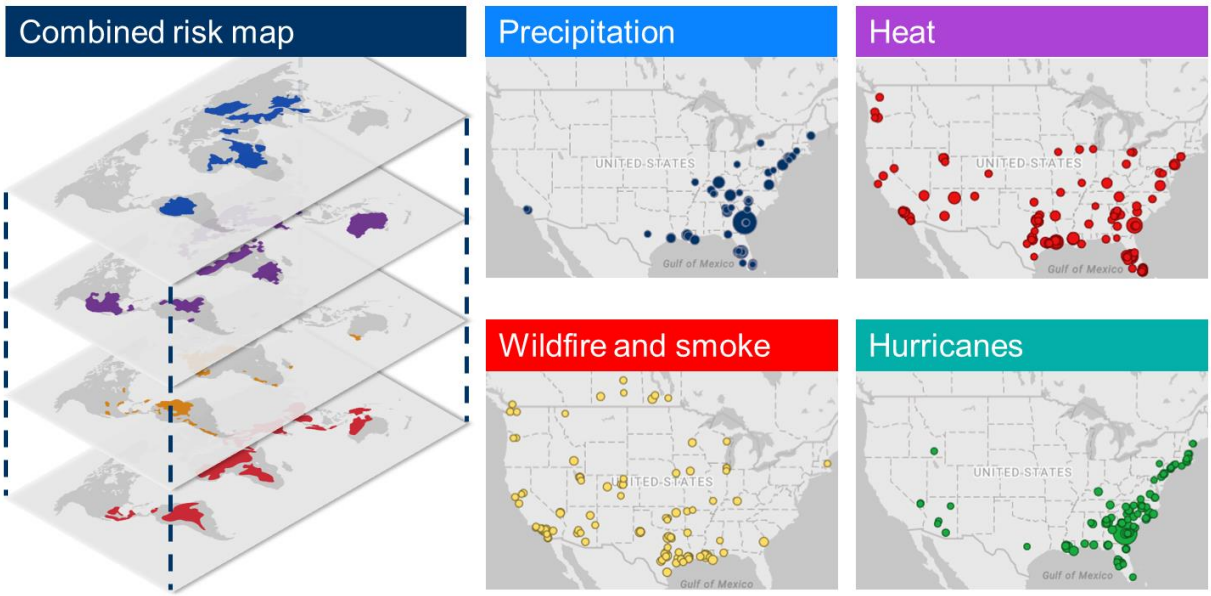


Fig. 1. Maps of each acute physical risk in North America. Each dot is a project that could be impacted by the physical risk in 2050 under an SSP2-4.5, with the size inflated based on the potential cost increases.

The risk of losing equipment to extreme weather events is low. Even in the SSP5-8.5 scenario, most extreme weather events can be forecast a few days out. This means sites can prepare and demobilise to protect equipment and people.

 © DFI International Bruges 2025

Therefore, the greatest cost of extreme weather events comes from the delays to the project from these extreme weather events. There is a risk of potential cost overruns on impacted projects, particularly if the extra days cannot be claimed from the client. Nonetheless, realistically the biggest unabated cost is an opportunity cost; where projects take longer, fewer projects can be carried out. Knock on delays to starting projects can also leave geotechnical companies at risk of contractual costs or losing future work. The opportunity cost becomes a particular challenge during hurricane season or wildfire season.

Both scenarios saw an increase in extreme weather events and delays to operations. However, the greater climate change seen in the SSP5-8.5 scenario leads to more extreme weather events and delays to operations. Although the risk to contract margins is low, the days delay from SSP5-8.5 in 2050 were 1.2x that from SSP2-4.5.

In terms of breaking these impacts down by physical risk, extreme heat has the greatest impact. The final numbers vary depending on union or health and safety thresholds for when outdoor work must stop work. Nonetheless, these risks are greatest in southern states like Florida and Texas, that already see the greatest delays due to extreme heat. By 2030, extreme heat events could result in impacted project days totalling of 80,000 in SSP2-4.5 or 92,000 in SSP5-8.5.

By comparison, wildfires is the next highest risk to operations. Even though actual wildfire locations vary depending on human sources, the risk of wildfires mirrors those geographies at greatest risk from extreme heat. These wildfire impacts are anticipated to lead to 35,000 days delay in an SSP2-4.5 world by 2050, or 45,000 under SSP5-8.5.

Extreme precipitation is relatively a slightly smaller risk, although the risks are more geographically localised compared to extreme heat. Interestingly, there is also more consistency between the scenarios for extreme precipitation, as warmer air holds more moisture. This means that both scenarios result in just under 40,000 days.

Hurricanes cause a lot of disruption to specific states, but their geographical restriction to the Southeast coast of the US means their impacts are limited. Even as warmer seas mean hurricanes can grow larger and can travel further north up the coast of the US, natural drivers like El Nino have far more impact than human-induced climate change. For these reasons, compared to the rest of the physical risks, hurricanes have one of the smallest increases in days delay by 2050.

Across all these risks, we can highlight key geographies that are consistently more at risk of certain extreme weather events. Florida is one of the worst hit, with continued risk of hurricanes, alongside increases in extreme heat, precipitation and wildfire. When coupled with the amount of work done in this state, Florida has three times the days lost compared to the next state. Texas and Georgia are the next most impacted, with delays mostly coming from delays due to extreme heat. Beyond these three, New York, Louisiana and parts of southern Canada like British Columbia, Victoria and Ontario are at the greatest risk of delays due to wildfires, as evidenced by the recent fires and smoke in Southern Canada (Government of Canada, 2024).

Conversely, most of Northern Canada and Alaska and do not see large impacts from extreme heat, precipitation, wildfire / smoke and hurricanes. However, these states and countries may still be impacted by other extreme weather events or more chronic climate change not modelled in this research. For example, sea level rise will impact coastal areas, whilst those areas in Northern Canada will likely be impacted by more chronic climate impacts like permafrost melt. The other challenge is these states have far less current geotechnical work compared to more impacted states.

Transition – equipment modelling for Europe

Broadly, if we see more slow decarbonisation in our markets, like a STEPS scenario, the rate of procurement of non-diesel rigs also is slower. Conversely, if decarbonisation legislation is enacted

 © DFI International Bruges 2025

more quickly to reduce climate change, like a NZE scenario, the market will shift more quickly towards non-diesel equipment (Fig. 2).

Broadly across all the models, there is very limited risk of stranded assets. These would be marked by a sudden drop in the total number of rigs in Fig. 2, where older rigs have to be retired before the end of their life. It was only by running an additional model scaling up the requirements of Scandinavian cities and London to the rest of Europe that the modelling saw any major impairments around 2030 and 2040 as new regulations are scheduled to come in.

However, the risk of stranded assets is very dependent on the assumptions around new electric rigs added to the fleet over time. Given most European countries have a net zero by 2050 target, most rigs operating at this time will need to be non-diesel powered. Given rigs are often in service for up 10-15 years, the models therefore assume any equipment purchased after 2035 or 2040 will be electric or hydrogen powered (see the bottom of Fig. 2). This may mean purchasing electric equipment far sooner than companies initially anticipated. This demand for electric equipment comes with an associated cost premium, as well as changes to site operations, logistics and set up. Nonetheless, even if this alternative equipment is run off of diesel generators in the short-term, it means the rigs can still be used once new legislation and power supplies are introduced.

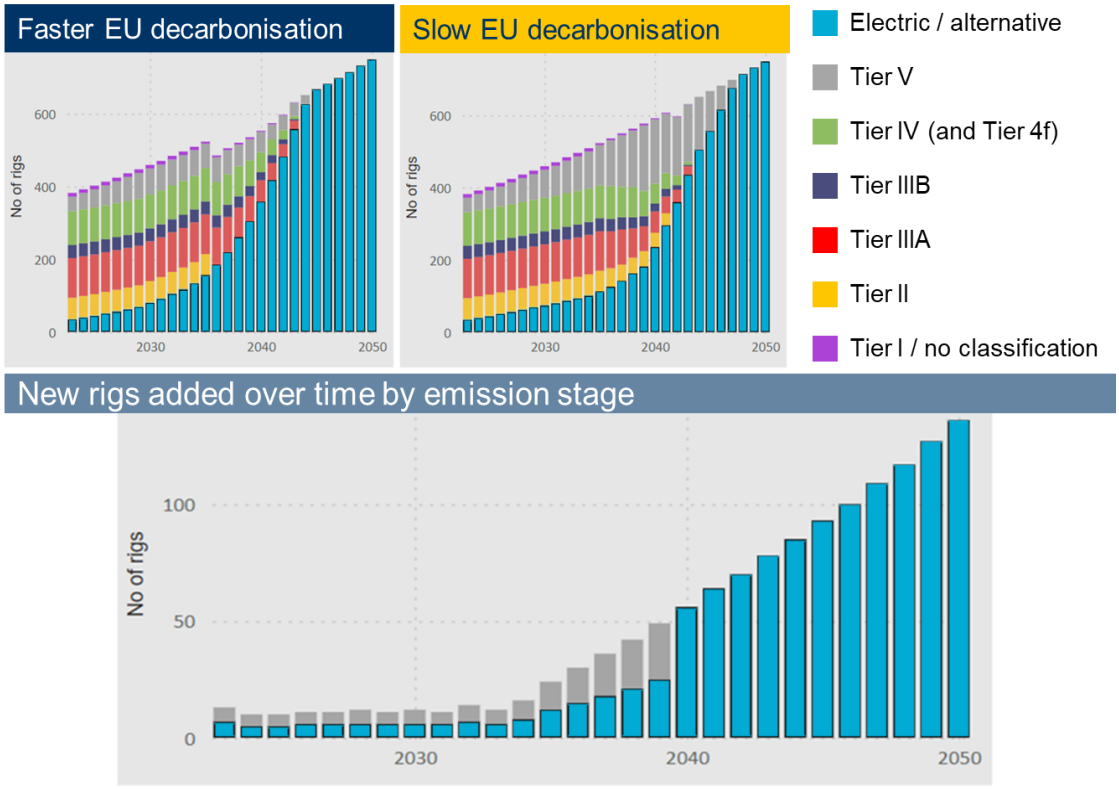


Fig. 2. Rigs by emission stage over time under faster decarbonisation (NZE scenario) and slower decarbonisation (APS scenario)

Transition – materials modelling for Austria

Already, there is a European carbon tax on high carbon materials, including cement and steel, under the Emission Trading System. This also applies to these materials shipped in from outside the EU under the Carbon Border Adjustment Mechanism (CBAM). Therefore, all carbon modelling scenarios begin with some additional cost for cement and steel (Fig. 3).

 © DFI International Bruges 2025

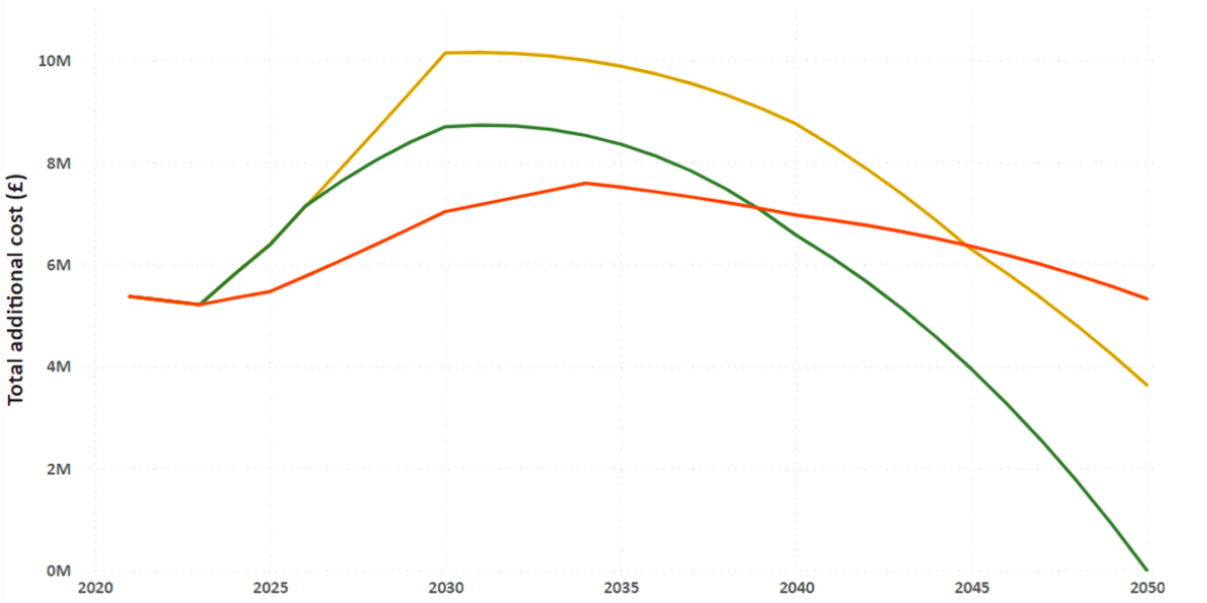


Fig. 3. Example material scenario analysis modelling, with high carbon taxation (NZE) in green, medium (APS) in yellow and business as usual (STEPS) in red.

If we are to get to net zero by 2050, this carbon tax is likely to rise, so we will see initial increases in material costs (see the green NZE model line in Fig. 3). As our suppliers compete to transition towards net zero though, and the legislation ensures everyone has to do this at the same rate, eventually the carbon tax will become zero.

If carbon taxes do not increase on our materials, we will not see an initial increase in material prices. However, as geotechnical companies see increased demand for lower carbon materials, but only certain companies can provide these materials, overall material costs may actually become more expensive in the medium-term (see red STEPS line in Fig. 3).

These price increases are not evenly spread across all geotechnical solutions. All solutions follow a similar trend to the overall one given in Fig. 3, but the size of the additional cost varies. Those solutions that use more cement and steel, like jet grouting or bored piles, are more impacted by carbon taxation than solutions that use lower carbon materials like natural / recycled aggregate (see Fig. 4).

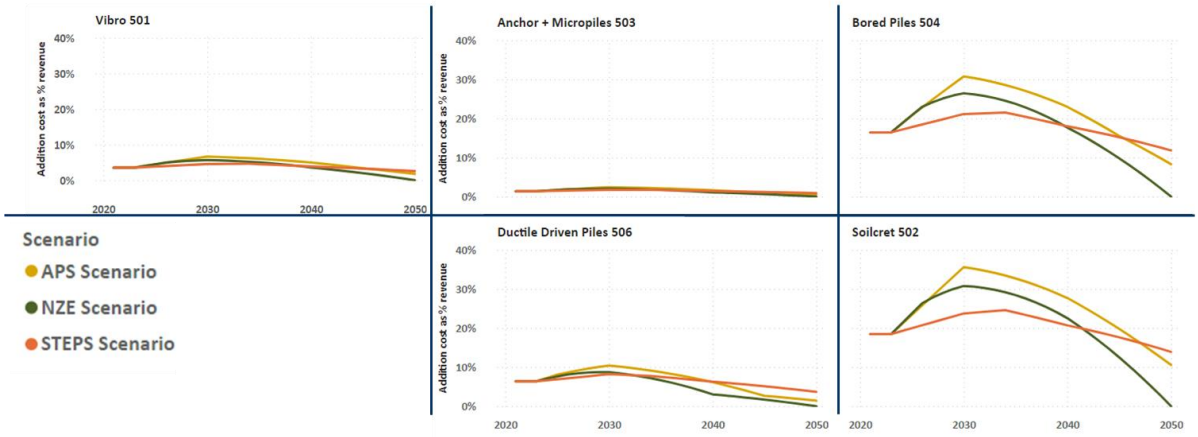


Fig. 4. Additional cost of materials for a solution in different climate scenarios

 © DFI International Bruges 2025

Note these models do not consider large fluctuations in inflation, looking instead at long-term inflation trends. They also refer to additional cost driven by carbon taxation and increased demand, as opposed to local factors such as changes in building policies or government incentives.

MITIGATION DISCUSSION

General mitigation

Once companies know the unmitigated risks associated with climate change, we need to respond to them. Across all three areas, this modelling demonstrates the benefits of starting to measure the current impacts of these risks. This will enable companies to highlight if impacts are increasing over time, as well as highlighting particular locations to prioritise for mitigation.

This modelling cannot be kept separate from other business processes. Given the size of the risks and opportunities, they have to be built into company risk assessments and evaluated alongside project and company considerations. Often these risks are localised, with specific legislation or climate conditions. Only through this integration can climate risks and opportunities be properly realised in company strategy.

In terms of actions, this modelling highlights the need to think long-term. Projects requiring lower carbon equipment and materials will be needed well before the 2040 or 2050 dates modelled in this paper. The same goes for ensuring supply chains are more resilient to extreme weather events. There is no magic switch that turns on these risks in 2050. It is often easier and cheaper for geotechnical companies to embed sustainability into processes now, rather than responding retrospectively once a risk materialises (Deamer, 2023).

On supply chains, geotechnical contractors typically use multiple, localised material suppliers (Deamer et al., 2020). In the future though, securing low carbon materials may only be possible through strategic partnerships with key suppliers. Therefore, establishing these partnerships now offers a competitive advantage, securing supply and quality testing for when there's increased demand in the future. This also applies to collaborating with key suppliers of low carbon equipment, or material suppliers that have supply chains that are more resilient to climate change.

Ultimately though, we will need collaboration to future-proof the sector against these climate risks. Working together, through trade associations and framework agreements, enables geotechnical contractors to better leverage day-to-day suppliers, creating demand for lower carbon or more resilient solutions. Collaboration also ensures a level playing field, so we all include climate risks and opportunities when submitting project proposals.

Physical risk mitigation

Much like the general point on project risk assessments, there is a need to price-in the delays that are likely during a project. Alternatively, geotechnical contractors should be prepared to add contract clauses, like force majeure, that allow us to pass on the cost of delays due to extreme weather events to our clients. This also means accepting we will do less work during hurricane season or during hot summers, and managing our order-books accordingly.

Even in SSP5-8.5, extreme weather events can be forecast days in advance. Therefore sites can prepare for these events and demobilise, reducing the risk to assets and site teams. However, this equipment is often transferred to the local maintenance yard for storage, where it can also be at risk. Therefore, future modelling should include the impacts of climate change on the operations of these maintenance yards. Mitigation work would then focus on making yards more resilient, or relocating to safer areas.

 © DFI International Bruges 2025

Note this modelling does not consider the increase in projects that could come from extreme weather events. An increased risk of flooding could result in more flood defence projects for geotechnical companies. Similarly, an increase in ground desiccation or the melting of permafrost could result in more geotechnical remediation projects. Any modelling of future project demand should therefore reflect these increases, as well as transition changes away from more higher carbon industries.

Transition risk mitigation

On materials, all models see greater costs for cement and steel based solutions, whilst aggregate or other materials remain unimpacted. Therefore, the most obvious response is to reduce the use of these higher carbon materials, using resources like the EFFC-DFI carbon reduction guide (EFFC, 2022). Where we cannot design out cement and steel, there is also a call to price in or pass on carbon prices on materials. Just like the risks of extreme weather events at specific times of the year, this means factoring in these increases in pricing when bidding on projects.

On equipment, there are broadly three key steps to decarbonising machinery and avoiding the risk of stranded assets: efficiency; alternative fuels and alternative equipment. The rate at which companies work through these steps depends on the age / depreciation of their existing equipment and the climate model they think best reflects their local market legislation. Nonetheless, efficiency helps to decarbonise existing equipment right now, saving fuel costs as well as improving air quality. Examples include avoiding fuel use through anti-idling or automatic cut offs, through to 'right-sizing' equipment so it is not overpowered for the task.

From there, we can look at alternative fuels, such as Hydrotreated Vegetable Oil (HVO) or renewable diesel. Whilst not yet available in all countries, these biofuels offer a way to decarbonise existing diesel equipment if a client is willing to pay the associated premium. Providing these are from certified waste stocks, such as used cooking oil, these offer a genuine carbon saving and a potential tailpipe air quality improvement for existing equipment (Department for Transport, 2022).

Finally, it is worth starting to invest in alternative equipment. Right now, alternatives to diesel are typically plug-in electric, battery power or green hydrogen powered rigs (FPS, 2024). Even if these are run off diesel generators in the short-term, it means these rigs can still be used in the future when air quality or carbon legislation is strengthened. If we still need diesel equipment, it may even be better to hire it for the next few years. This way, it can be returned when alternative equipment is needed or developed. Although there is a cost premium to future-proofing equipment, there are often local tax breaks, grants and favourable loans available to help with this transition.

CONCLUSIONS

Overall, climate change has a very real impact on the operations of geotechnical companies. This includes the transition to a low carbon economy, as well as physical impacts of climate change itself.

Of course, the actual impacts and numbers will vary in the future, with many assumptions underlying these current models. However, what really matters is the broad scale of these potential impacts and, more importantly, how we can begin to mitigate them. It is critical to start mitigating these risks now, building them into contracts, purchasing and ultimately strategy decisions.

As more companies begin to model and track these risks, we can also learn from each other. There are plenty of other physical risks that may impact geotechnical companies, including chronic climate changes and changes to ground conditions. On transition risks, there are considerations around future markets as economies decarbonise, as well as things like employee attraction and retention. These are all potential areas for future modelling, either in companies TCFD disclosures or in the upcoming EFFC/DFI climate adaptation and resilience guide, due to be published in 2025.

 © DFI International Bruges 2025

ACKNOWLEDGEMENTS

This paper would not be possible without the work, expertise and time of the Sillion team, led by Isis Bliah and Alexander Bridge. Together with modelling from Benjamin Freas and Glen Sebastian, and more recently the inputs of Pearl Ayem and Marion Betsch, they are central to this paper's modelling and findings.

From Keller, I want to thank all those that contributed their time and effort to this modelling. In particular, Caroline Heath was essential to sourcing good project data and managing the financial impact metrics / assumptions. Silvana Glibota-Vigo advised on the governance of TCFD and helped shape the final disclosures. Warren Bell advised on risks and opportunities costing at a local through to global level. I must also thank all the engineers, procurement and finance teams that contributed their time and knowledge to help quantify how climate risks impact their day-to-day work.

REFERENCES

Balfour Beatty, 2024, Annual Report and Accounts 2023. Available online: https://www.balfourbeatty.com/media/5uubwxhm/balfour-beatty-annual-report-and-accounts-2023.pdf

Deamer, 2023. Supporting the adoption of improved sustainable processes across all functions of a geotechnical company. DOI: https://doi.org/10.15126/thesis.900763

Deamer, L.R., Russell, E. and Lee, J, 2020. Lost in translation: sustainability down the construction supply chain. Article online : https://www.iso20400.org/lost-in-translation-sustainability-down-the-construction-supply-chain/

Department for Transport, 2022. Renewable fuel statistics 2022: Second provisional report. Available online : https://www.gov.uk/government/statistics/renewable-fuel-statistics-2022-second-provisional-report/renewable-fuel-statistics-2022-second-provisional-report

EFFC, 2022. EFFC Sustainability Guides for Foundation Contractors: Guide No. 1 Carbon Reduction. Available online: https://www.effc.org/content/uploads/2022/05/EFFC-Carbon-Reduction-Guide_FINAL.pdf

FPS, 2024. FPS/EFFC Low Carbon Equipment Webinar. Available online: https://www.fps.org.uk/events/low-carbon-equipment/

Government of Canada, 2024. Canada's record-breaking wildfires in 2023: A fiery wake-up call. Available online: https://natural-resources.canada.ca/simply-science/canadas-record-breaking-wildfires-2023-fiery-wake-call/25303

IPCC, 2022: Climate Change 2022: Impacts, Adaptation, and Vulnerability. Contribution of Working Group II to the Sixth Assessment Report of the Intergovernmental Panel on Climate Change. Cambridge and New York, 3056 pp., DOI:10.1017/9781009325844.

Keller, 2024. Annual Report and Accounts 2023. Available online: https://investors.keller.com/~/media/Files/K/Keller-IR/reports/2024rep/keller-ara-2023.pdf

Skanska, 2024. Annual and Sustainability Report 2023. Available online: https://group.skanska.com/493370/siteassets/investors/reports-publications/annual-reports/2023/annual-and-sustainability-report-2023.pdf

 © DFI International Bruges 2025

The Mayor and the Geotechnical Engineer – Challenges Obtaining Approval For Use of Alternative Fill Materials to Accommodate Sea Level Rise in the City of San Francisco

Lori A. Simpson, PE, GE; Langan Engineering and Environmental Services, Inc., San Francisco, California, USA; lsimpson@langan.com; (510) 874-7031

Scott A. Walker, PE, GE; Langan Engineering and Environmental Services, Inc., San Francisco, California, USA; swalker@langan.com; (510) 874-7085

ABSTRACT

Mission Rock is a new waterfront neighborhood in San Francisco. Recently completed, Phase 1 consists of two, 240-foot-tall (80-meter-tall) residential high-rise buildings, a 120-foot-tall (40-meter-tall) and a 210-foot-tall (70-meter-tall) commercial building, a waterfront park, and new public streets and infrastructure. The site is on land owned by the Port of San Francisco. The streets and infrastructure would be maintained by the City and County of San Francisco (CCSF) Public Works and the San Francisco Public Utilities Commission (SFPUC). Approving and permitting agencies consisted of the Port of San Francisco, CCSF Public Works, and the Department of Building Inspection.

The site is located along the San Francisco Bay and was originally below water in a shallow bay, which was reclaimed between 1880 and early 1900's. The future sea level is predicted to rise as much as 66 inches (1.8 meters) by the year 2100, which would submerge the site during a high tide. Raising grades using conventional soil fill to account for future seal level rise was not feasible due to the presence of compressible Bay Mud; the weight from compacted soil would cause as much as 2 feet (0.67 meters) of consolidation settlement. A number of options were considered to allow for raising grades without causing settlement.

Ultimately, the team selected to offset the new loads by overexcavating existing fill and raising grades using lightweight cellular concrete (LCC); however, LCC was not approved for use as fill by the City of San Francisco or the Port of San Francisco. The various stakeholders were uncomfortable with any approach that did not include support of all utilities and roadways in conventional soil. Their concerns included strength, resistance to uplift, performance during an earthquake, excavatability, long-term changes in weight due to saturation, and availability and patent concerns for future replacement. In order to gain approval and prove out the proposed methodology toward constructing a sustainable and resilient new neighborhood, the project owner and design team embarked on a lengthy process, including multiple peer reviews and meetings with the Director of Public Works, the City Engineer, the Chief Harbor Engineer from the Port of San Francisco, and even the Mayor. This paper will present this process, the concerns of the stakeholders and how they were addressed, towards obtaining approval of this non-standard fill material.

Keywords: Sea level rise, lightweight cellular concrete

INTRODUCTION

Mission Rock fronts the San Francisco Bay and McCovey Cove, a channel that separates Mission Rock from Oracle Park (home of the San Francisco Giants), see Figure 1. The site occupies approximately 16.6 acres (6.7 hectares). The Phase 1 Development comprises four new buildings supported on driven steel H-pile, new public infrastructure and streets, and a new shoreline park (see Figure 2 and 3). Mission Rock is on land owned by the Port of San Francisco (POSF), and because the new infrastructure will be in the public right-of-way, approval and oversight was required from many stakeholders: POSF, San Francisco Department of Public

 © DFI International Bruges 2025

Works (SFDPW), the San Francisco Public Utility Commission, and the San Francisco Department of Building Inspection.



Fig. 1. Site Location

With the waterfront location and proximity to major faults, this site is vulnerable to sea level rise and strong shaking from earthquakes. The project developers, the San Francisco Giants and Tishman Speyer, were committed to creating a resilient new neighborhood in San Francisco. Specifically, their criteria were to design for little settlement, which meant that no new loads could be applied to the underlying soils and that seismic hazards would be mitigated.

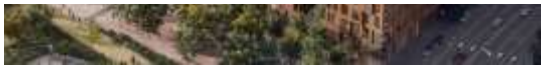


Fig. 2. Phase 1 Development

SITE AND SUBSURFACE CONDITIONS

Originally, the site was below water in a shallow bay known as Mission Bay, as shown in Figure 4. Starting in the 1880s, the bay was reclaimed using various soil materials excavated from construction in San Francisco and from building rubble and debris following the 1906 Great San Francisco Earthquake and Fire. The site was relatively level, generally at elevations ranging from 97 to 101.5 feet (29.5 to 31 meters) Mission Bay Datum, which is approximately 7.6 to 9.6 feet (2.3 to 2.9 meters), mean sea level (MSL). Elevation 100 feet (30 meters) Mission Bay Datum is approximately Elevation 8.6 feet (2.9 meters) MSL.

 © DFI International Bruges 2025



Fig. 3. Overall Mission Rock Development

The subsurface conditions at the site generally consist of approximately 10 to 40 feet (3 to 12.1 meters) of uncompacted heterogeneous fill that varies in density and, in some areas, contains rubble comprised of brick, rock and debris. The fill is underlain by about 40 to 71 feet (12.1 to 21.6 meters) of weak, soft to medium stiff, compressible marine clay, locally referred to as Bay Mud. A layer of dense to very dense sand with varying amounts of fines, known as the Colma formation, underlies Bay Mud and is about 1 to 36 feet (0.3 to 11 meters) thick. It is underlain by an older marine clay, dense to very dense alluvium, and bedrock. There is a dense to very dense sand layer that was encountered at the top of and within the alluvium. The top of the bedrock is about 195 to 255 feet (59.4 to 77.7 meters) below the original ground surface (bgs). Groundwater is shallow, typically at depths of about 5 to 10 feet (3 to 12.1 meters) bgs. Figure 5 shows an idealized subsurface profile.



Fig 4. 1852 Historic Shoreline and Site

 © DFI International Bruges 2025

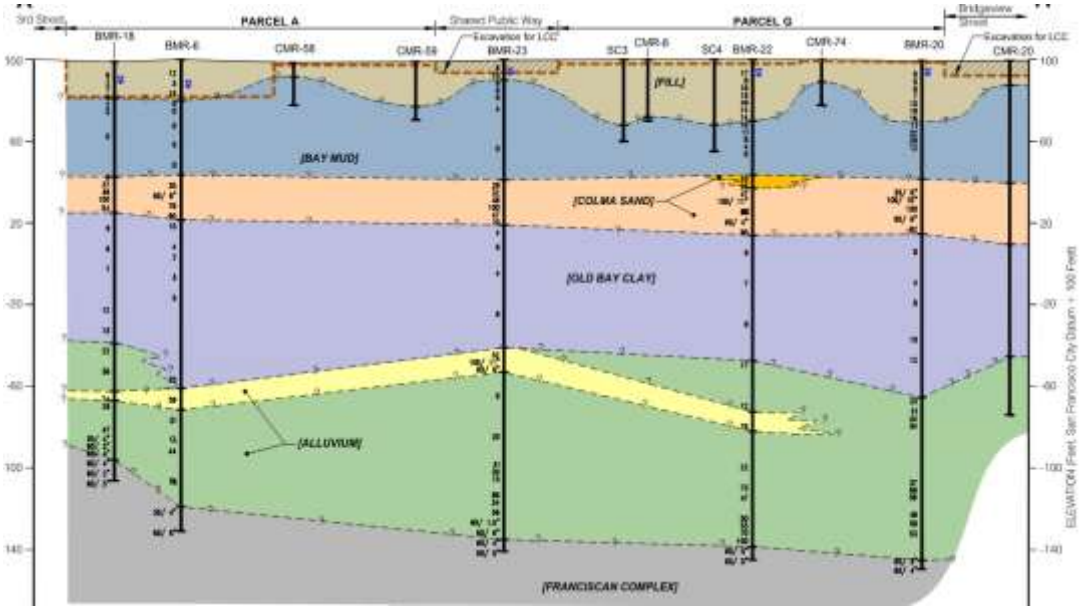


Fig. 5. Subsurface Profile

GEOLOGIC HAZARDS AND GEOTECHNICAL CHALLENGES

Seismicity

The site is between two major earthquake faults: the San Andreas, which is, 12½ kilometers to the southwest and the Hayward fault, which is 13 kilometers to the northeast. During a major earthquake on a segment of one of the nearby faults, strong to very strong shaking is expected to occur at the site. Site specific response analysis indicates a peak ground acceleration of 0.47g during the Maximum Considered Earthquake (MCE_R).

Sea Level Rise

Based on equations from the Federal Emergency Management Agency (FEMA) guidelines, the high estimate of sea level rise by the year 2100 is 66 inches (1.68 meters), which is the level the project sponsors decided to accommodate, as shown on Figure 7. Note that there is no planning or code requirement in San Francisco to mitigate the effects of sea level rise at this time. Given the relatively low elevation of the site and its proximity to the Bay, the site would be flooded at high tide, and groundwater levels would rise consistent with rising sea level. Accordingly, the new streets needed to be raised about 66 inches (1.68 meters) to account for the effects of sea level rise.



Fig. 6. Fault Map

 © DFI International Bruges 2025

Consolidation Settlement

The results of consolidation testing indicate the Bay Mud is no longer settling under the fill placed more than 100 years ago; however, if new conventional soil fill was placed to raise grades, the loads from this fill would start a new cycle of consolidation, causing up to 24 inches (0.61 meters) of settlement due to placement of 66 inches (1.68 meters) of fill. The project team evaluated various options to raise grades at the site without causing settlement, including preloading the site using surcharge and wick drains, pile supporting the streets, and raising grades with lightweight fill.

After reviewing the merits, costs, timing, and complications of the various options, the team determined that using lightweight fill was the most appropriate solution. The team evaluated using geofoam, expanded shale, and lightweight cellular concrete (LCC). Both permeable and non-permeable LCC were considered. Geofoam is the lightest material, but it was presumed that the governing agencies would be least experienced with it and the complications of future maintenance and replacement of utilities and other infrastructure within the geofoam would be make it hard to approve its use. Expanded shale was only briefly considered because of its weight and the need to offset significantly more load. LCC was chosen for its relatively light weight (around 30 pounds per cubic foot [1.4 kPa]), its strength, and the ability to excavate it without the need for shoring when maintaining or installing utilities.

A plan was developed to offset the loads from raising grades and constructing the streetscape elements (pavement, sidewalks, light poles, benches, structural soil sections for trees, etc.) by overexcavating sufficient existing fill, backfilling with LCC, and raising grades using LCC to create at least 10% load offset of overburden on the compressible Bay Mud. An example section of this plan is shown on Figure 8. This plan required overexcavating 5 to 13 feet (1.5 to 4 meters) of existing fill (extending below groundwater in the majority of the streets) and placement of more than 60 thousand cubic yards (46,000 cubic meters) of LCC. However, LCC had only been used for limited applications in the public right-of-way (ROW) in San Francisco and was not an approved material for use as fill.

PATH TO APPROVAL

The site is on land owned by the POSF. The public ROW will be maintained by SFDPW or the POSF. The water utilities will be owned by the San Francisco Public Utilities Commission (SFPUC). The permitting agencies included POSF, SFDPW, and the San Francisco Department of Building Inspection (SFDBI). In addition to these City agencies, the Major of San Francisco relied on the Director of Housing Delivery and the City Engineer to facilitate the process.

Because of the various agencies involved and the lack of a coordinated code or standard for streets, utilities and infrastructure that will be maintained by SFDPW on land owned by POSF, we were referred to a number of guiding documents for design of the project. However, because LCC was not an approved material for use as fill, there were no code requirements or specifications for its use in San Francisco.

History and Precedent of LCC Use in the Public ROW

When asked for approval of the use of LCC, the governing agencies asked for examples of the large-scale use and performance of LCC on public projects. The team was able to provide examples where LCC was utilized, including:

- The California Department of Transportation (Caltrans) approved it for fill to reduce/prevent settlement at the bridge approaches/abutments and lane widening in the California Central Valley.
- City of Oakland utilized LCC to raise grades and act as subgrade at new bridge abutments on 14th Street.
- SFPUC approved LCC for backfill at Crystal Springs Reservoir in San Mateo County.
- City of San Francisco approved LCC for a minor lane widening on Treasure Island.

 © DFI International Bruges 2025

However, the governing agencies indicated the example projects were not sufficiently similar for the application and use because the majority of the example projects did not include the support of significant public underground utilities.

Concerns with use of LCC

A number of concerns regarding the large-scale use of LCC as proposed were raised by the governing bodies:

Strength: the LCC needed to be sufficiently strong to support the repeated use of vehicles, including a hook-and-ladder fire truck (the heaviest of the emergency response vehicles), over the life of the project.

Excavatability: in addition to meeting the strength requirements noted above, the LCC also needed to be weak enough such that it could be "easily" excavated for utility repair and installation by City staff.

Resistance to hydrostatic uplift: standard non-permeable LCC has a closed-cell network of entrained bubbles and is therefore not porous. Because the LCC was planned to be placed below groundwater it will be subject to hydrostatic uplift pressures. At current groundwater levels, there would be sufficient resistance to uplift (with factors of safety over 2). But once sea level rise occurs, hydrostatic pressures would increase and there needed to be sufficient weight to resist the uplift forces. There was much discussion about the appropriate factor of safety (FS) for hydrostatic uplift – other references included using a factor of safety equal to 1.1 under the most critical condition (particularly if conservative assumptions for weights are used in the analyses. However, after much discussion, the team agreed with the governing agencies to the use of a minimum factor of safety of 1.2 when subjected to an increased groundwater level equal to the 66 inches (1.68 meters) of sea level rise. Because the LCC was being approved as a fill material, mechanical methods of resisting hydrostatic uplift, such as some type of anchor, would not be allowed.

Seismic performance: during an earthquake, with the significant volume of pore space in the LCC there was a concern that the LCC would break into pieces or somehow collapse during an earthquake. It needed to be shown that the improvement could still perform adequately if the LCC was damaged, without post-earthquake remediation.

Unit weight increase due to saturation: despite LCC not being porous, it still has the potential to become saturated through the capillaries within the cement lattice; the additional weight of the LCC when saturated needed to be considered in the load offset calculations.

Availability: the agencies were concerned that LCC is not commonly batched by many contractors and there would be a limited pool of bidders for projects, reducing the potential for competition and likely causing higher costs. In addition, the foaming agents (critical to LCC batching) are under various patent provisions, which could prevent the SFDPW from self-performing LCC replacement, even where only small volumes were needed.

Approval Process

Fortunately, there was a shared determination by the developer, the agencies, and the Mayor for this project to proceed. The parties came together to develop a path to approval. The process included convening a Technical Advisory Panel (TAP) and engaging peer reviewers and holding regular meetings with these entities and the stakeholders, the design team, and the developer team. Peer reviewers included an internal reviewer hired by the developer to work collaboratively with the geotechnical engineer and the design team, as well as an external peer reviewer hired by POSF. The TAP was convened by SFDPW and was comprised of experts in the use of LCC manufacturing and testing, a PhD geotechnical engineer with extensive port and near-shore expertise, and a PhD

 © DFI International Bruges 2025

professor in geotechnical and earthquake engineering. Meetings were held almost weekly, and a comment log was maintained. Documents developed and reviewed during the process included a geotechnical investigation report, a white paper describing the purpose and use of the LCC, a specification for the LCC material and placement. Throughout this process research and analyses were performed to address the technical aspects of the use and performance of LCC described above and to close comments on the log.

At one point in this process, it was apparent that some decision makers were missing from the stakeholder group. A meeting was convened at City Hall to present to high level decision makers within the governing agencies to discuss the purpose and benefits of using LCC for this project. However, the meeting did not come to a full resolution or agreement to approve the use of LCC. Besides questions about the technical aspects, some decision makers were concerned about conflicts of interest and lack of multiple bidders for future work, as permeable LCC was not widely used, and the foaming agent was still under patent control by the manufacturer. Conversely non-permeable (closed cell) LCC was more widely used, and the exclusive patent had expired, allowing multiple manufacturers to produce the material. Ultimately, the team decided to use non-permeable LCC.

To help satisfy the outstanding concerns, and with the encouragement of the TAP, the project team elected to build and test a full-scale mock-up section of the future roadway. Constructing and testing the full-scale mockup consisted of:

- Creating a 40- by 40-foot (12.2- by 12.2-meter) excavation about 6 feet (1.8 meter) below grade (Figure 11)
- Clearing the subgrade of debris and loose material
- Installing an impermeable membrane, load cells, and piezometers
- Placing 9 feet (2.7 meters) of non-permeable LCC and street improvements (utilities and backfill, sidewalk, and street section)
- Flooding the mock-up to test for uplift resistance
- Driving a hook-and-ladder fire truck onto the LCC and extending the ladder to create the maximum differential load on the LCC to confirm strength and that LCC would not collapse under load.
- Excavating the LCC to confirm lack of damage from the hook-and-ladder test and excavatability of the LCC.

The mockup was constructed, and tests were completed under the observation of representatives of the governing agencies. All the tests were successful (Figure 12). The technical aspects of the LCC design were published in Brady et al (2023) “Creating a Resilient New Waterfront Neighborhood in San Francisco, Mission Rock Phase 1 Development, San Francisco, California” 2023 DFI Annual Conference Proceedings, 2023.

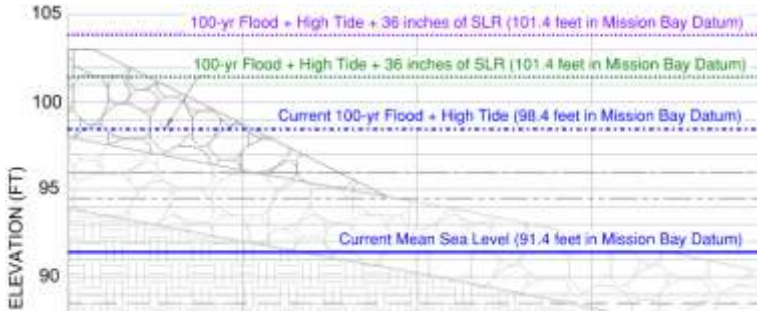


Fig. 7. Sea Level and Tides

 © DFI International Bruges 2025

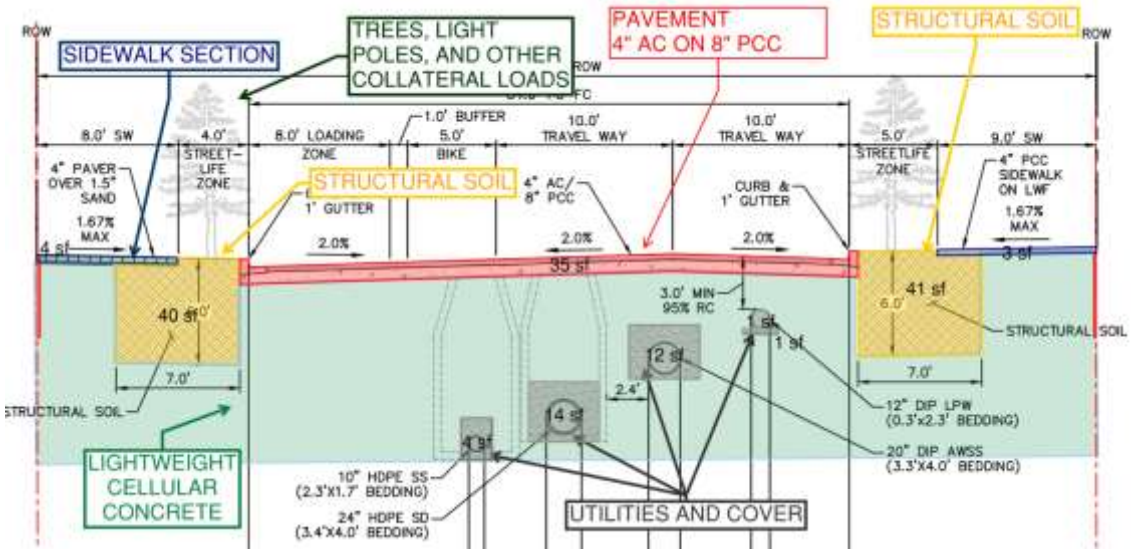


Fig. 8. Typical Street Section



Fig. 9. LCC Excavatability



Fig 10. LCC Placement

 © DFI International Bruges 2025



Figure 11. Constructing the full-scale mock-up



Fig. 12. Hook-and-Ladder Fire Truck on LCC

The Mayor

After lack of approval, a meeting with Mayor London Breed was facilitated. The attendees comprised the Mayor, the Director of Public Works, Chief Engineer of POSF, the City Engineer, the lead developer's representatives, and the Geotechnical Engineer of Record. The developer described the project and the resiliency they were providing the project as a benefit for the City. The GEOR described need for special measures to provide this resiliency and the benefits of using LCC. The Mayor understood the benefits of using LCC not only for this project, but for other projects planned in the City. She noted the far-reaching benefits for San Francisco with approval of the use of LCC and trusted that the technical aspects had been addressed through the process. One by one, she obtained approval from each person there and the team walked out of room with the understanding that the use of LCC would obtain official approval and permits would be issued.

 © DFI International Bruges 2025

Final Steps to Permit

But wait…after the meeting with the Mayor, we still did not have a permit in hand. Final requirements needed to be addressed, consisting of:

- closing open comments in the comment log
- finalizing the specifications
- finalizing quality assurance and quality control (QA/QC) measures
- developing a 10-year monitoring program
- providing step-by-step calculations to allow SFDPW to replicate the load offset calculations
- including additional cross sections in the permit drawings to show load offset where final grades varied
- providing guarantees of the long-term performance of the public ROW.

And once these measures were close to completion, POSF informed the team of a Port Code Procedure needing to be followed for deviations from POSF requirements, codes, or specifications. This procedure requires approval through a document called the Port Director's Orders, which was a document specifying how and where this 'non-standard' material could be utilized on lands controlled by the PSF. This procedure had not previously been communicated to the development team.

After satisfying all these requirements, the governing agencies signed off on the use of LCC, and a construction permit was obtained 22 months after the initial request to use LCC was made. It was a day to celebrate!

CONCLUSIONS AND LESSONS LEARNED

When a new material or technology is proposed, extensive engineering needs to be performed to support its design, application, and performance. It should be expected that extensive technical and peer review be performed. New specifications need to be developed that address the material characteristics, placement or installation, testing, QA/QC, and long-term monitoring. Cost and time for extensive review, testing. QA/QC, and monitoring should be accounted for.

There needs to be public benefits that create the political will for the project to proceed. In this case, the project provides much needed housing in San Francisco, including 40 percent affordable housing, and public space, more of which is always desirable in metropolitan cities, as well as commercial space that would attract corporations to come to San Francisco. The project also created new land and new shoreline spaces that are resilient to sea level rise and future earthquakes. For this project, the dedication of the project sponsor to create this resilient development and their willingness to provide the time and money required to work through the challenging approval process was critical to the success of the project. But it would not likely have been successful without the support of the Mayor's office, which was essential in bringing the governing agencies together to develop and work through the process.

To date, we understand that this in-depth technical evaluation, review, and approval of LCC at Mission Rock has allowed for a more streamlined approval process for use of LCC at two other development sites in the San Francisco Bay Area (one in San Francisco and one in Santa Clara).

 © DFI International Bruges 2025

THE SECOND GENERATION OF EUROCODE 7 – A MODERN BASIS FOR THE DESIGN OF PILED FOUNDATIONS AND GROUND IMPROVEMENT

Christian Moormann, University of Stuttgart, Institute for Geotechnical Engineering, Germany,
+49 (0) 711 685-62437, christian.moormann@igs.uni-stuttgart.de

ABSTRACT

Eurocode 7 is known as the European standard for geotechnical engineering design and is widely considered as a great success story. The second generation of the standard drafted by CEN/TC250/SC7 was recently published and represents a significant step forward towards further harmonization and efficient guidance for geotechnical design. The revision is performed focusing on the user´s need with the main goals of ease-of-use and harmonization, to meet new demands in geotechnical engineering looking at the coming 20 to 25 years. The second generation covers new basic aspects like numerical methods, probability and reliability-based verification, rock on an equal basis as soil, etc. In addition, geotechnical structures like reinforced fill structures, soil nailing and ground improvement were included for the first time. The paper presents an overview of some of the key revisions compared to the first generation of Eurocode, that will affect the practicing geotechnical engineer and explains the application on example of piled foundations and ground improvement. The paper concludes that the 2nd generation of Eurocode will be a modern standard for all kind of geotechnical structures and a useful tool for engineers in practice.

Keywords: Eurocode 7, piled foundation, ground improvement, standards

INTRODUCTION

In 2012, the European Commission decided on the M515 mandate, giving the responsibility to CEN to further develop the Eurocodes. In 2015 the first project teams were established to start the drafting process of the second generation of all structural Eurocodes. The aim has been that the first parts of new generation will be published in 2022 and the last in 2027, a timeline that still applies to this day.
In this context, also Eurocode 7, the basis for the geotechnical design was transferred from first edition to second generation including fundamental reorganisation and extensions. In its 2nd generation the new Eurocode 7 comprises three parts as illustrated in Figure 1. The contents of the existing Eurocode 7, Part 1 ´General rules´ (EN 1997-1:2004) have been split between EN 1990 ´Basis of structural and geotechnical design´, a revised Part 1 (EN 1997-1:2024) ´General rules´; and a new Part 3 (EN 1997-3:2025) ´Geotechnical structures´. The new Part 3 comprises text from Sections 5-9 and 11-12 of 1st generation´s EN 1997-1 together with new clauses on reinforced fill structures, ground reinforcing elements, ground improvement and groundwater control. The reorganization of the second generation of Eurocode 7 is illustrated in Figure 1.

EUROCODE 7 PART 1 – GENERAL RULES

The scope of part 1 has been reduced since the basis of geotechnical design has been moved to EN 1990 and specific considerations for different geotechnical structures has been moved to part 3. However, the table of content has introduced some new concepts, and the strive to include all common topics in part 1, instead of repeating them in each clause in part 3, has given a part with a similar amount of text as in 1st generation.
The concept of the geotechnical category (GC) has been revised so that it is systematically determined with the consideration of the consequence of failure (CC) and geotechnical complexity (GCC). This revised concept is used as the base of classification to achieve geotechnical reliability (Franzén & van Seters 2022).

 © DFI International Bruges 2025

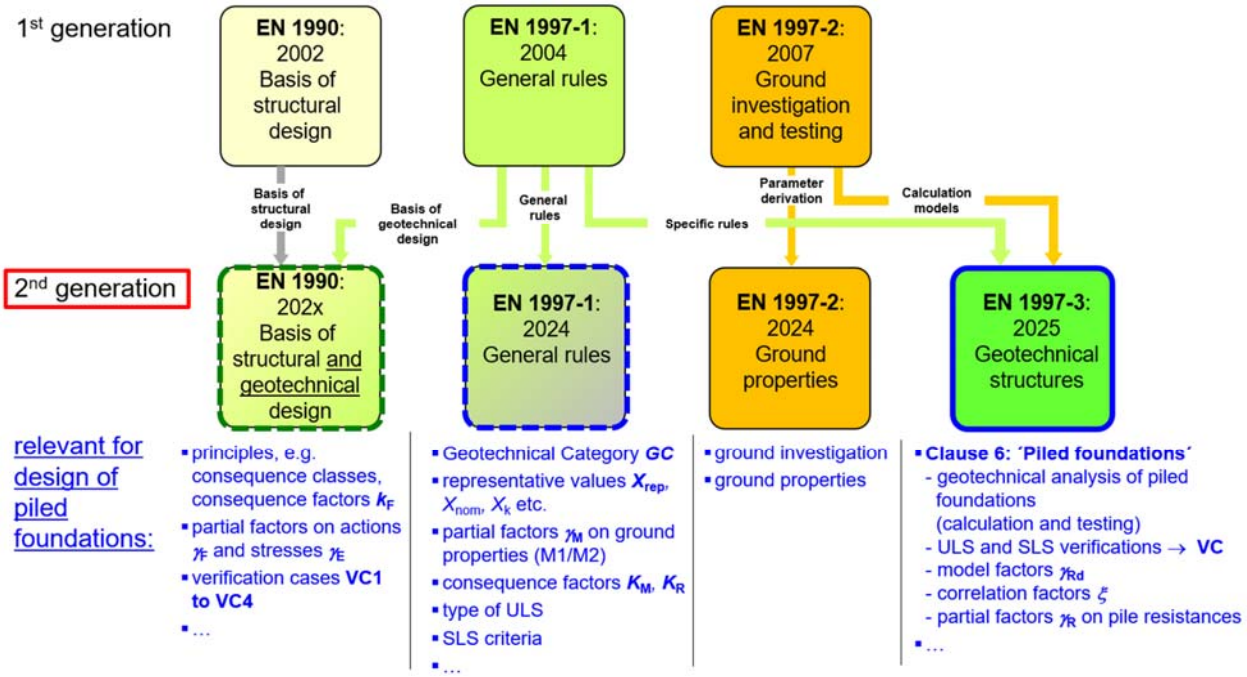


Figure 1. Division and redistribution of the 1st generation of Eurocode 0 and Eurocode 7 into the standards of the second generation (acc. to Bond et al. 2019); at the bottom: contents of these standards being relevant for the design of piled foundations.

The term ´representative value´ is introduced and replace the old characteristic value. The representative value is determined either as a cautious estimate or with a statistical approach.
EN 1997-1:2024 provides further guidance on the four methods for verification of limit states, on the use of numerical methods for design and verification, on the concept of the zone of influence and on the implementation of design during execution and service life focusing on supervision, inspection, monitoring, and maintenance applied to ensure that the design is implemented correctly.

EUROCODE 7 PART 2 – GROUND PROPERTIES

The contents of the existing Eurocode 7, Part 2 ´Ground investigation and testing´ (EN 1997-2:2007) were also being revised to focus in the new Part 2 ´Ground parameters´ (EN 1997-2:2024) on the derivation of design parameters. Thus, while EN 1997-2 was in 1st generation focusing on ground investigation and testing, for the 2nd generation, this part has been turned 90 degrees and is now focusing on the need of the engineer to derive appropriate ground properties as input to the design instead as previous, on the output from ground investigations (Franzén & van Seters 2022).
Calculation models that currently reside in Annexes to EN 1997-2:2007, e.g. on CPT-based calculation of axial pile resistances, have been moved to the new Part 3, as illustrated in Figure 1.

EUROCODE 7 PART 3 – GEOTECHNICAL STRUCTURES

Eurocode 7 part 3 consists of the specific rules for each type of geotechnical structure. General requirements applicable for more than one structure has been moved to part 1. Therefore, the main content for each clause is focused on geotechnical analyses giving the calculation models, ultimate limit state and serviceability limit state.
The chapters known from 1st generation of EN 1997-1. i.e. the clauses on slopes, cuttings and embankments (Clause 4), spread foundations (5), piled foundations (6), retaining structures (7) and anchors (8) were

 © DFI International Bruges 2025

revised. In addition, the following new clauses have been added: on reinforced fill structures (9), soil nailed structures (10), rock bolts and rock surface support (11), ground improvement (12) and groundwater control measures (13). Thus, the range of geotechnical structures covered by the new EN 1997-3 has been increased significantly.

DESIGN OF PILED FOUNDATIONS ACCORDING TO EN 1997-3:2025

In the following the design of piled foundations according to 2nd generation of EN 1997 is presented and explained in detail.

Introduction

Relevant for the design of piled foundations is predominantly Clause 6 ′of EN 1997-3:2025 which was elaborated on basis of Section 7 ′Pile foundation′ of EN 1997-1:2004 whereby the previous regulations were fundamentally revised, improved and supplemented including new resp. additional rules for pile design. Fundamentally, in the second generation pile groups and piled rafts will be covered equivalently to single piles whereby the regulations of the first generation focused solely on single piles. Detailed guidance is provided to consider actions on piles due to ground displacements like downdrag. Revised sets of correlation, model and partial factors were specified. The design approaches for axially and laterally loaded piled foundations were harmonized.

As each Clause of EN 1997-3 follows a common structure, also Clause 6 comprises the following sub-sections which have the same order as the Clauses in EN 1997-1:2024 and which provide structure-specific rules in addition to the general rules specified in Part 1 of Eurocode 7:

6.1	Scope	6.6	Ultimate limit states
6.2	Basis of design	6.7	Serviceability limit states
6.3	Materials	6.8	Execution
6.4	Groundwater	6.9	Testing
6.5	Geotechnical analysis	6.10	Reporting

These sections of Clause 6 provide specific regulations for the analysis and design of piled foundations. In this context the detailed information documented in Clause 6 includes for example the following aspects:

- requirements on the minimum extent of ground investigations;
- analysis of piled foundations due to structural loads and effects of ground displacements;
- design of piled foundations by testing, calculation, prescriptive measures;
- the specification of ultimate limit state (ULS) and serviceability limit state (SLS) verifications for single piles, pile groups and piled rafts including a definition of the verification cases (VC) being relevant for those verifications;
- the specification of the sets of model factors γ_{Rd}, correlation factors ξ as well as partial factors γ_R for the evaluation of the design value of pile resistances.

Besides the structure-specific regulations documented in Clause 6 of EN 1997-3, information needed for the design of piled foundations are provided also by EN 1990 and EN 1997-1 as illustrated in Figure 1.

EN 1990 specifies the principles of classification of structures according to consequence classes and the consequences factors k_F for actions as well as the principles of limit state design and of the verification by the partial factor method including specification of partial factors on actions γ_F and stresses γ_E. EN 1990 also specifies the ′Verification Cases′ VC1 to VC4 being relevant for different design situations like structural resistance, static equilibrium and geotechnical design and the related sets of partial factors. The partial factors can either be applied on material properties, i.e. the ′Material Factor Approach′ (MFA), or to resistances, i.e. the ′Resistance Factor Approach′ (RFA).

EN 1997-1 as well provides relevant specifications and regulations needed for the design of piled foundations. Besides specifications of the Geotechnical Category (GC) which should be determined by a combination of the Consequence Class (CC) of the structure and the Geotechnical Complexity Class (GCC),

 © DFI International Bruges 2025

the evaluation of representative values X_{rep} as well as partial factors γ_M on ground properties and consequence factors both on ground properties k_M and resistances k_R are specified in Part 1 of Eurocode 7.
In the following some of the most relevant modifications for the design of piled foundations according to second generation of Eurocode 7 are presented in more detail.

Ground investigations

In addition to EN 1997-2:2024 which includes fundamental requirements on ground investigation and evaluation of ground properties section 6.2 of EN 1997-3 provides additional specific regulations, e.g. specifications on the minimum depth d_{min} of field investigation on piled foundations (Table 1).

Table 1. Minimum depth of ground investigation for piled foundations.

Application	Minimum depth
Single piled foundation	d_{min} = max (5 m; 3·$B_{n,eq}$)
Pile groups or piled rafts in soils and in very weak and weak rock masses	d_{min} = max (5 m; 3·$B_{n,eq}$; p_{group})
Pile groups or piled rafts in strong rock masses	d_{min} = max (3 m; 3·$B_{n,eq}$)
d_{min} is the minimum investigation depth beneath pile base level. $B_{n,eq}$ is the equivalent size of the pile base, equal to B_b (for square piles), D_b (for circular piles), or p_b/π (for other piles); B_b is the base width of the pile with the largest base (for square piles); D_b is the base diameter of the pile with the largest base (for circular piles); P_{group} is the smaller dimension of a rectangle circumscribing the group of piles forming the foundation, limited to the depth of the zone of influence.	

Verification of axial resistance of single piles (ULS)

For axially loaded single piles the axial (compression) resistance shall be verified using:

$$F_{cd} \leq R_{cd} \tag{1}$$

Thereby, the verification for axial loaded piles (single piles, pile groups and piled rafts) could be harmonized as solely the Resistance Factor Approach (RFA), where the partial factors are applied on the pile resistance, shall be used in combination with Verification Case VC1, where the partial factors are applied on the actions. Thus, the design value of actions is defined as follows:

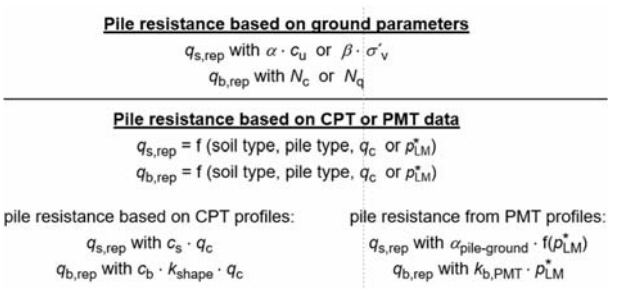
$$F_{cd} = 1.35G_{rep} + 1.5Q_{rep} \tag{2}$$

with Q_{rep} as characteristic value, combination value, frequent value or quasi-permanent value.
The design value of the axial pile resistance is defined as follows:

$$R_{cd} = \frac{R_{c,rep}}{\gamma_{Rc} \cdot \gamma_{Rd}} \quad or \quad \left(\frac{R_{b,rep}}{\gamma_{Rb} \cdot \gamma_{Rd}} + \frac{R_{s,rep}}{\gamma_{Rs} \cdot \gamma_{Rd}}\right) \tag{3}$$

where γ_{Rc}, γ_{Rb}, γ_{Rs} are partial factors for pile resistances and γ_{Rd} is a model factor.
The representative values of the pile resistance in axial compression $R_{c,rep}$ resp. of the base and shaft resistance $R_{b,rep}$ and $R_{s,rep}$ can be obtained by testing, by calculation or by prescriptive rules. The use of prescriptive rules is very rare for piles. For the determination of the axial resistances of single piles by calculation either the ´Ground Model Method´ or the ´Model Pile Method´ can be applied. In case of the Ground Model Method the axial resistance of a single pile is calculated based on ground properties determined from both, field and laboratory tests, accounting for horizontal variability of the ground in the piled area. The Model Pile Method is a calculation method to determine the axial resistance of a single pile based on individual pile resistance profiles determined from correlations with field test results or ground properties from field or laboratory tests. Methods of calculating base and shaft resistance are included in Annex C of EN 1997-3 for ground parameters as well as for cone penetration methods and for pressuremeter methods. Figure 2 provides an overview about these calculation methods.

 © DFI International Bruges 2025



Pile resistance based on empirical tables

Example: Representative values of unit shaft resistance $q_{s,rep}$ for bored piles in soils

Fine soils		Coarse soils	
Undrained shear strength c_u (kPa)	$q_{s,rep}$ (kPa)[a,b]	Mean cone resistance q (MPa)	$q_{s,rep}$ (kPa)[a,b]
60	30-40	7,5	55-80
150	50-65	15	105-140
≥ 250	65-85	≥ 25	130-170

[a] The lower value represents the 10 % quantile and the upper value the 50 % quantile
[b] Intermediate values can be obtained by linear interpolation

Figure 2. Available calculation methods for evaluation of axial pile resistances.

The axial resistance of a single pile at ultimate and serviceability limit state may be also determined from the results of static load tests. Dynamic impact and rapid load tests may be used to determine the ultimate limit state of a single pile in compression.
Table 2 specifies the evaluation of representative values of axial pile resistances from calculated or measured values.

Table 2. Evaluation of representative axial resistances of single piles based on calculation or testing.

Ground Model Method: R_{calc} from ground parameters (c_u, φ' and c', p_{LM}*, q_c, N_{SPT}, etc.)	$R_{rep} = R_{calc}$
Model Pile Method: R_{calc} from N field test profiles (N CPTs, N PMTs, N SPTs, etc.)	$R_{rep} = \min\left\{\frac{R_{calc,mean}}{\xi_{mean}}; \frac{R_{calc,min}}{\xi_{min}}\right\}$
Pile tests: R_{test} from static, dynamic impact or rapid load tests	$R_{rep} = \min\left\{\frac{R_{test,mean}}{\xi_{mean}}; \frac{R_{test,mean}}{\xi_{min}}\right\}$

Figure 3 visualizes the possible procedures to evaluate design values of axial pile resistances from testing and calculation. Tables 3 and 4 document the model factors γ_{Rd} for verification of axial pile resistance assisted by testing and calculations.

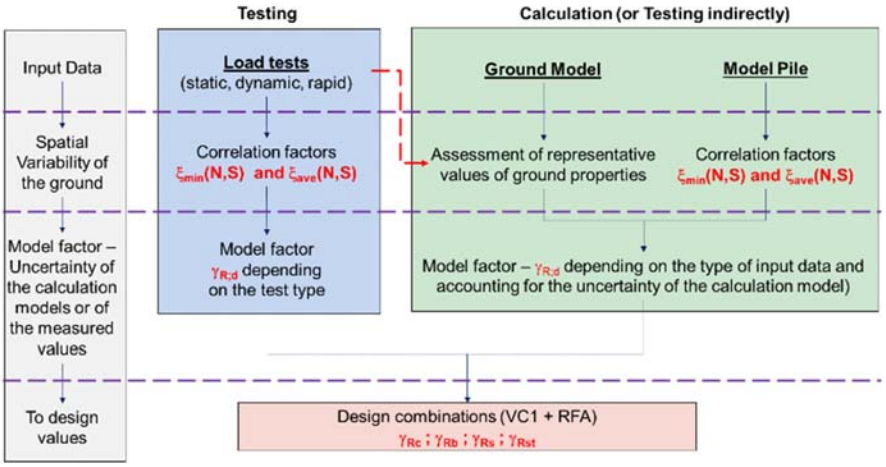


Figure 3. Calculation procedures for piles (acc. to Moormann & Burlon 2024).

Correlation factors ξ allows to consider the spatial variability of the ground alternatively to the selection of the representative values of the ground parameters which is always related to subjective interpretation. Correlation factors ξ as documented in section 6.2.4 of EN 1997-3 continues to be dependent form number

 © DFI International Bruges 2025

of executed pile tests or ground profiles. The correlation factors given reflect an average uncertainty corresponding to a coefficient of variation of about 12%; other approaches are therefore acceptable if spatial variation is lower or higher.
The correlation factors for the Model Pile Method can be adjusted according to the density of the field test profiles (CPTs, PMTs, etc.) considering the ratio of the average horizontal spacing d_{avg} between the N tests profiles located in the area S to a reference distance d_{ref} = 30 m:

$$\xi_{mean}(S) = 1 + \frac{d_{avg}}{d_{ref}}(\xi_{mean} - 1) \quad (4)$$

$$\xi_{min}(S) = 1 + \frac{d_{avg}}{d_{ref}}(\xi_{min} - 1) \quad (5)$$

Table 3. Model factors γ_{Rd} for verification of axial pile resistance assisted by testing.

Verification by		Model factor γ_{Rd} Fine soils	Coarse soils	Rock mass
Static load tests		1.0	1.0	1.0
Rapid load tests (multiple load cycles)		1.4	1.1	1.2
Rapid load tests (single load cycle)		1.4	1.1	1.2
Dynamic impact tests (signal matching)	Shaft bearing	1.5	1.1	1.2
	End bearing	1.4	1.25	1.25
Dynamic impact tests (multiple blow)	Shaft bearing	1.5	1.1	1.2
	End bearing	1.4	1.2	1.2
Dynamic impact tests (closed form solutions)	Shaft bearing	Not permitted	Not permitted	Not permitted
	End bearing	Not permitted	1.3	1.3
Wave equation analysis		Not permitted	1.6	1.5
Pile driving formulae		Not permitted	1.8	1.7

Table 4. Model factors γ_{Rd} for verification of axial pile resistance by calculation.

Verification by	Based on	Model factor γ_{Rd}	
Ground Model Method	Ultimate pile tests	1.15	
	Extensive comparable experience without site-specific control tests	1.3	
	Serviceability pile tests	1.35	
	No pile load tests and limited comparable experience	1.55	
Model Pile Method		Compressive resistance	Tensile resistance
	Pressuremeter test	1.15	1.4
	Cone penetration test	1.1	1.1
	Profiles of ground properties based on field or laboratory tests	1.2	1.2

Verification of axial resistance of pile groups and piled rafts (ULS)

As already mentioned Clause 6 of EN 1997-3:2025 covers not only single piles but equally also pile groups and piled rafts.
Pile group design shall consider that the resistance and load-displacement behaviour of single piles in a group might show significant variation compared to the behaviour of single piles due to pile-pile interaction. Calculation of pile group effects should consider the potential changes in stress and density of the ground resulting from pile installation together with the effects of group behaviour due to the structural loads taking the stiffness of the pile cap and the structure into account. The ultimate vertical resistance of a pile group R_{group} with n piles should be determined from:

$$R_{group} = \min\{\sum_i^n R_i ; R_{block}\} \quad (6)$$

where R_i is the ultimate axial resistance of the i-th pile in the pile group, taking full account of the effects of pile interaction, and where R_{block} is the ultimate vertical resistance of the block of ground bounded by the perimeter of the pile group. The design resistance of a pile group $R_{d,group}$ shall be verified using

 © DFI International Bruges 2025

$$F_{\mathrm{d}} \leq R_{\mathrm{d,group}} \tag{7}$$

with

$$R_{\mathrm{d,group}} = \frac{R_{\mathrm{rep,group}}}{\gamma_{\mathrm{R,group}} \cdot \gamma_{\mathrm{Rd,group}}} \tag{8}$$

where $\gamma_{\mathrm{R,group}}$ is a resistance factor and $\gamma_{\mathrm{Rd,group}}$ is a model factor for the pile group.

The design of piled rafts shall consider beside the pile-pile interaction the pile-raft interaction (Fig. 4). Considering the compatibility of the displacements of the piles and the raft, the ultimate compressive resistance $R_{\mathrm{piled\text{-}raft}}$ of a piled raft should be determined as

$$R_{\mathrm{piled-raft}} = \left(\sum_i^n R_{\mathrm{c,i}} + R_{\mathrm{raft}}\right) \tag{9}$$

where Rraft is the additional bearing resistance from the raft. The design resistance of a piled raft $R_{\mathrm{d,piled\text{-}raft}}$ shall be verified using

$$F_{\mathrm{d}} \leq R_{\mathrm{d,piled-raft}} \tag{10}$$

with

$$R_{\mathrm{d,piled-raft}} = \frac{R_{\mathrm{rep,piled-raft}}}{\gamma_{\mathrm{R,piled-raft}} \cdot \gamma_{\mathrm{Rd,piled-raft}}} \tag{11}$$

where $\gamma_{\mathrm{R,piled\text{-}raft}}$ is a resistance factor and $\gamma_{\mathrm{Rd,piled\text{-}raft}}$ is a model factor for the piled raft.

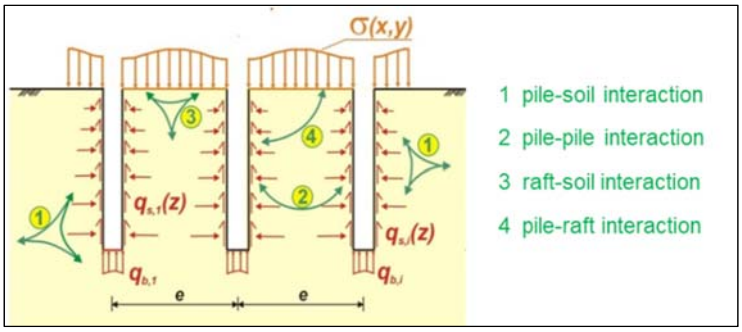


Figure 4. Interaction effects to be considered for the verification of piled rafts according to EN 1997-3, 6.5.6.

For the ULS-verification of axially loaded pile groups and piled rafts EN 1997-3 pretends the application of verification case VC1 in combination with RFA and partial factors of $\gamma_{\mathrm{R,group}} = 1.4$ resp. $\gamma_{\mathrm{R,piled\text{-}raft}} = 1.4$ leading to a comparable equivalent global safety level as for spread foundations or single piles. For combined axial and transversal loaded pile groups and piled rafts both approaches, MFA or RFA, might be used for ULS-verifications.
Verification of limit states for pile groups and piled rafts may be carried out by analytical or empirical, but preferentially by numerical calculation methods.

Pile settlements and SLS verifications

Verification of the serviceability limit state for piled foundations should be based on modelling that accounts for non-linear stiffness of the ground, flexural stiffness of the structure, and interaction between the ground, structures, and piles. The non-linearity of the load-displacement curves of axially loaded piles should be considered for the verification of both geotechnical and structural limit states.
The settlement of a single pile may be determined from load tests or calculated using empirical or analytical methods or numerical modelling.

 © DFI International Bruges 2025

Downdrag (negative skin friction)

The adverse effects of a drag force caused by moving ground shall be included in the verification of serviceability and ultimate limit states of piled foundations when relevant. Thereby the drag force caused by downdrag should be classified as a permanent action. The effects of the downdrag should be modelled by carrying out a ground-pile interaction analysis, to determine the depth of the neutral point L_{dd} corresponding to the point where the pile settlement s_{Pile} equals the ground settlement s_{ground}. This neutral point is different for SLS or ULS conditions as shown in Figure 5 which also illustrates the approach recommended to be used to calculate the neutral point and the dragforce owing to potential downdrag.

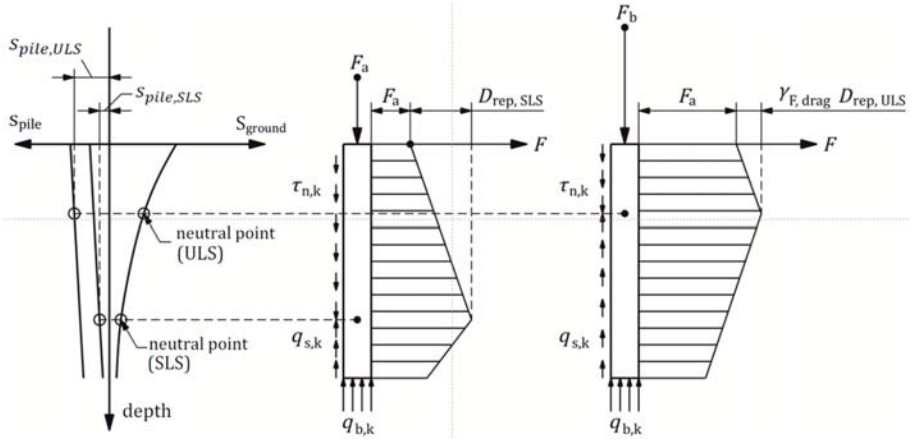


Figure 5. Force distribution for assessment of drag force on a pile subject to downdrag acc. to EN 1997-3, C.9.

The representative drag force D_{rep} should then be determined from

$$D_{rep} = p \int_0^{L_{dd}} \tau_s \cdot dz \quad (12)$$

where p is the perimeter of the pile and τ_s is the (negative) unit shaft friction causing downdrag at depth z. EN 1997-3 provides in its Annex C a simplified approach for calculating the drag force by adopting a depth to the neutral plane L_{dd} that results in an upper value of the drag force.

Transversal loading

Clause 6 of EN 1997-3 provides also guidance on the verification of single piles, pile groups and piled rafts due to lateral loading. In Annex C.12 calculation models, mainly based on p-y curves from undrained and drained soil properties, are provided to calculate the behaviour of transversely loaded single piles. For the verification of the transverse resistance either the MFA or the RFA can be applied.

Buckling

The buckling resistance of a slender pile under compression should be determined by a validated model, either analytic or numerical, according to second order theory considering the support of the soil and initial transverse deflection due to production imperfections, installation etc. EN 1997-3 provides detailed guidance to evaluate the buckling resistance by analytical methods even though other approaches, e.g. by numerical methods can be applied.

Cyclic effects

Cyclic and dynamic actions can result in reduced ground strength and stiffness leading to additional pile displacements and loss of resistance. Therefore, EN 1997-3 requests to consider the adverse effects of cyclic and dynamic actions on the long-term axial and transverse resistance of piled foundations. In Annex C.14 of EN 1997-3:2025 the concept of ´stability diagram´ based on Poulos (1988) is provided.

 © DFI International Bruges 2025

Further aspects

Clause 6 of EN 1997-3 provides guidance to many further aspects being relevant for piled foundations including further calculation and design issues but also execution, testing and reporting. Even aspects of sustainability are addressed as the thermal, geotechnical and structural design aspects of thermoactivated deep foundations are mentioned.

DESIGN OF GROUND IMPROVEMENTS ACCORDING TO EN 1997-3:2025

In its current first generation Eurocode 7 does not cover ground improvement. This will change significantly with the second generation of Eurocode 7 which includes a new clause 12 ´Ground Improvement ´for the design of such geotechnical works. One of the main challenges of including ground improvement works in the code was the wide variety of techniques used for this purpose and considering their specific features as some of them involve soil densification or drainage, while others require installation of various inclusions or treatment of the soil in place using binders. Therefore, it was necessary to establish a comprehensive design methodology that aligns with the philosophy of partial factors in Eurocode 7 and accommodates this versatility (Denies et al. 2024).

Classification of ground improvement

As basis for the design considerations a new classification scheme was developed and implemented in EN 1997-3:2025 which does not consider executional aspects and the specific techniques for carrying out the works but focuses on the bearing behaviour and the calculation model usually applied. Table 5 shows the classification of ground improvement (GI) according to Clause 12 of EN 1997-3:2025, considering the diffused (Classes AI and AII) or discrete (Classes BI and BII) character of the GI and the possibility to measure the unconfined compressive strength (UCS) of the improved ground.

Table 5. Classification of ground improvement according to EN 1997-3:2025, Clause 12.

Class	A - Diffused	B - Discrete
I	**AI – Diffused with no measurable unconfined compressive strength (UCS)** The improved ground has an increased shear strength or stiffness higher than that of the original ground. The improved ground can be modelled as a ground with improved properties.	**BI – Discrete with non-rigid inclusions** Inclusions, installed in the ground, with higher shear capacity and stiffness compared to the surrounding ground. The unconfined compressive strength of the inclusion is not measurable.
II	**AII – Ground improvement zone with measurable unconfined compressive strength** The improved ground is modified from its original natural state, has a measurable unconfined compressive strength and is significantly stiffer than the surrounding ground. Usually, it comprises a composite of a binder and ground.	**BII – Discrete with rigid inclusions** Rigid inclusions, installed in the ground, with unconfined compressive strength and significantly higher stiffness than the surrounding ground. The inclusions can be an engineered material such as timber, concrete/grout or steel or a composite of a binder and ground.

For rigid inclusions (Class BII) which represent structural elements with stiffness and strength both significantly higher than the ground in which they are installed, one of the following conditions should be satisfied in order to clearly distinguish them from conventional piles, as illustrated in Figure 6:

- structural loads are transferred from the slab and spread foundations or embankment through a load transfer platform (LTP) into the improved ground (Fig. 6 A and B);
- in absence of a LTP, there is no structural connection between the rigid inclusions and the slab or spread foundation (Fig. 6 C).

In the absence of a load transfer platform, additional verifications may be considered according to the design situations; further in this situation a single rigid inclusion used to support the foundation shall comply with Clause 6 (´Piled foundations´), except when it is used for settlement reduction only.

 © DFI International Bruges 2025

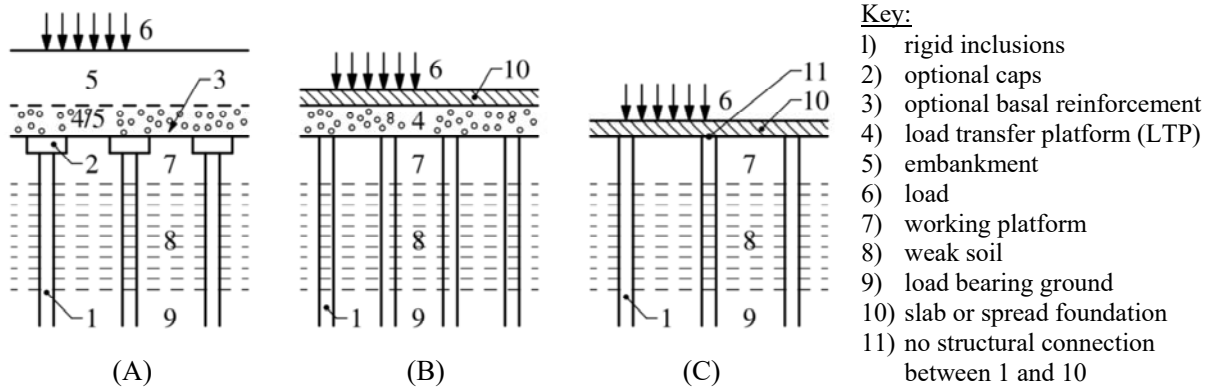


Figure 6. Class BII concepts with rigid inclusions: (A) embankment, (B) slab or spread foundation with a load transfer platform (LTP), (C) slab or spread foundation without a LTP.

In the following the focus will be set on GI used for transfer of predominately vertical loads into the ground, especially by rigid inclusions.

Ground investigations

In addition to considerations on geometrical properties taking acceptable deviations from execution tolerances into account, on actions from structures and due to ground displacements, section 12.2 of EN 1997-3 provides additional specifications on the minimum depth d_{min} of field investigation for ground improvements as documented in Table 6.

Table 6. Minimum depth of ground investigation for ground improvement.

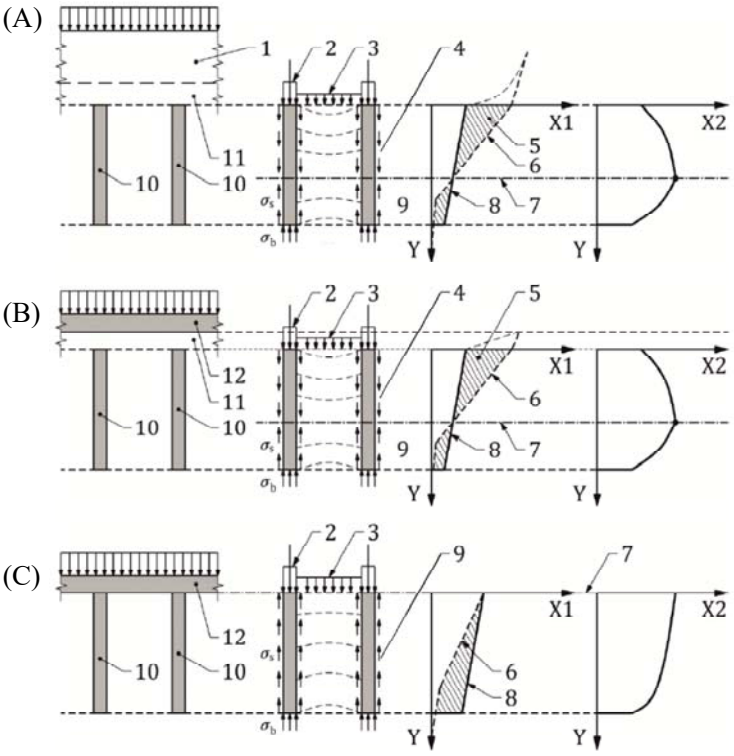
Ground Improvement Class	Minimum depth, d_{min}
AI	treatment depth + 5 m
AII	treatment depth + 5 m
BI	treatment depth + max (5 m; $3 \cdot B_i$)
BII	treatment depth + max (5 m; $3 \cdot B_{ri}$)
d_{min} is the minimum depth of field investigation from the ground surface B_i is the equivalent diameter of a non-rigid inclusion (Class BI) B_{ri} is the equivalent diameter of a rigid inclusion (Class BII) The equivalent diameter of an inclusion is determined from, $B = 2\sqrt{A/\pi}$, where A is its horizontal cross sectional area.	

Geotechnical Analyses and Design Verifications

Analyses of the interaction between a structure, improved ground and ground should be carried out to verify that the ultimate and serviceability limit states (ULS, SLS) are not exceeded, and should take into account the stiffness ratio of discrete inclusions to the surrounding ground. For ground improvement the following ULS shall be verified in particular (Denies et al. 2024):

- failure of the ground improvement inclusion or zone in compression, tension, bending, buckling or shear;
- failure in the ground due to transverse loading of the improved ground zone;
- uplift or insufficient tensile resistance of the ground improvement zone;
- combined failure in the ground and in the ground improvement inclusion or zone;
- bearing resistance failure below the ground improvement inclusion or zone;
- limit states caused by changes in groundwater conditions or groundwater pressure;
- failure at the edges of the improved ground zone.

 © DFI International Bruges 2025



Key:
X1 settlement
X2 inclusion axial force
Y depth
1) embankment
2) load transmitted to the inclusion
3) load transmitted to the ground
4) negative skin friction
5) differential settlement
6) settlement of the ground
7) neutral plane
8) settlement of the inclusion
9) positive skin friction
10) inclusion
11) load transfer platform (LTP)
12) structure (e.g. slab or spread foundation)
σ_s mobilised shaft friction along inclusion
σ_b mobilised tip resistance of the inclusion

Figure 7. Interaction effects of ground improvement with rigid inclusions: (A) embankment, (B) slab or spread foundation with a load transfer platform (LTP), (C) slab or spread foundation without a LTP.

Design of Class A ground improvement is similar to the design of structures without the use of any ground improvement technique, and the resulting improved ground or material properties are used in the verification of limit states for the corresponding geotechnical structure. The behaviour of the improved ground can be conveniently modelled by conventional ground models.

Where Class B ground improvement is used to support or retain a structure, the calculation model shall include:

- the consideration of the interaction effects between the ground, discrete inclusions, and the overlying structure, embankment, or load transfer platform (LTP); and
- for Class BII ground improvement a verification of the structural resistance of the individual inclusions.

Interaction effects for Class BII ground improvement are similar to those relevant for a piled raft, whereby a LTP additionally impacts the load distribution between rigid inclusions and supporting ground, leading to the development of negative skin friction in the upper part of the inclusions (Figure 7: A and B). An appropriate interaction calculation model shall include the derivation of the distribution ratio to determine the proportion of the load applied to individual discrete inclusions and for Class BII ground improvement the derivation of the neutral plane corresponding to the point where the inclusion settlement equals the ground settlement (see Figure 7: A and B).

The design resistance of a Class BI ground improvement $R_{sys,d}$ may be determined from the representative value of the total resistance of the ground improvement system with inclusions $R_{sys,rep}$ using a partial factor $\gamma_{R,sys}$ and a model factor $\gamma_{Rd,sys}$, i.e.:

$$R_{sys,d} = \frac{R_{sys,rep}}{\gamma_{R,sys} \cdot \gamma_{Rd,sys}} \quad (13)$$

Considering the compatibility of the displacements of the inclusions and the gorund, the design resistance of Class BII ground improvement may be determined as:

 © DFI International Bruges 2025

$$R_{\mathrm{sys,d}} = \frac{\sum_i^n R_{\mathrm{ri,i}}}{\gamma_{\mathrm{Rd,ri}} \cdot \gamma_{\mathrm{R,ri}}} + \frac{R_{\mathrm{g}}}{\gamma_{\mathrm{Rg}}} \quad (14)$$

considering the following two components:

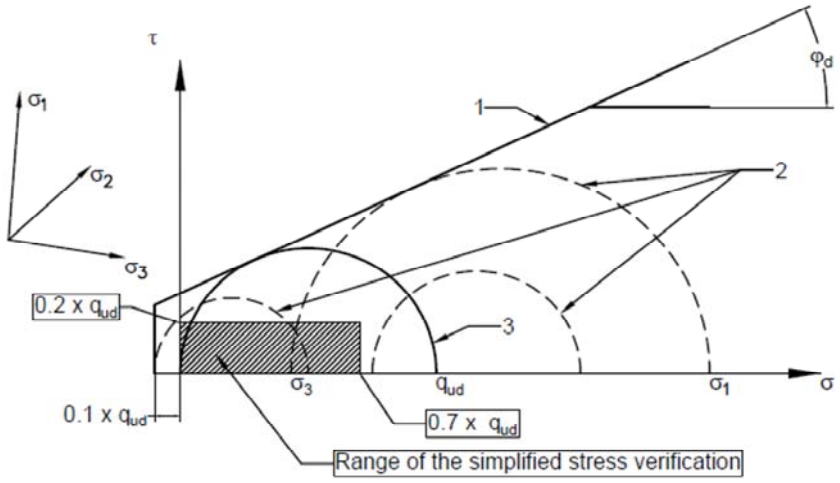
- the sum of the representative values of the vertical resistance of the *i*-th rigid inclusion $R_{\mathrm{ri,i}}$ with a model factor $\gamma_{\mathrm{Rd,ri}}$ and a partial resistance factor for the rigid inclusion system $\gamma_{\mathrm{R,ri}}$, whereby the values of $\gamma_{\mathrm{Rd,ri}}$ and $\gamma_{\mathrm{R,ri}}$ are equal resp. comparable to the values of $\gamma_{\mathrm{Rd,group}}$ and $\gamma_{\mathrm{R,group}}$ for a pile group; and
- the representative value of the vertical resistance of the ground after installation of inclusions R_g with a partial factor γ_{Rg}.

The representative resistance of a rigid inclusion R_{ri} shall be determined as for piles, depending on the installation technique and taking into account group and further interaction effects, as shown in Figure 7. Consequently, the ultimate geotechnical resistance of a group of rigid inclusions is not the same as the sum of that of the individual inclusions.

The verification of geotechnical limit states for individual inclusions may be omitted provided it is verified that the system is able to redistribute loads without itself exceeding an ultimate or serviceability limit state.

Serviceability limit states of geotechnical structures on improved ground shall be verified according to other relevant clauses of prEN1997-3.

In addition, the structural resistance of rigid inclusions needs to be verificed, whereby this resistance shall be verified according to the relevant standard for the material installed. If no such standard exists, for materials of Class II ground improvement, ultimate limit states shall be verified by demonstrating that design effects of actions do not exceed the stress envelope of the material used (Figure 8). When normal stresses and shear stresses are verified separately, the design value of the normal stresses and of the shear stresses shall not exceed $0.7 \cdot q_{\mathrm{ud}}$ and $0.2 \cdot q_{\mathrm{ud}}$, respectively.



Key:
1) envelope for allowed states of stress
2) examples for allowed states of stress σ_1, σ_3
3) state of stress in uniaxial compression test: $\sigma_3 = 0$, $\sigma_1 = q_{\mathrm{ud}}$

Figure 8. Allowable stresses in Class II ground improved material with unconfined compressive strength acc. to Annex I of EN 1997-3:2025.

The buckling resistance subject to compression shall be verified. When one of the following conditions is met, verification of buckling of Class BII inclusions may be omitted:

- inclusion diameter $B_{\mathrm{ri}} > B_{\mathrm{ref}}$;
- thickness of the soft layers, where $c_{\mathrm{u}} < c_{\mathrm{u,ref}}$, is smaller than h_{ref}.

The reference values are: $B_{\mathrm{ref}} = 0.3$ m, $c_{\mathrm{u,ref}} = 15$ kPa and $h_{\mathrm{ref}} = 1.0$ m, unless a National Annex gives different values.

 © DFI International Bruges 2025

The load transfer platform (LTP) and the possible reinforcing elements should be designed to transfer the load from the structure or the embankment to the improved ground. For load transfer platforms over discret inclusion acknowledged calculations methods are the Hewlett & Randolph method (documented in BS 8006-1), the EBGEO method, the Concentric Arches method (details in CUR 226) and the ASIRI method.
ULS verification may be omitted for a LTP where it can be demonstrated that the loads can be redistributed within the confined system, provided that the load transfer platform does not fail at its edges. A confined system can be assumed inside a grid of inclusions in a ground improvement zone (Bohn, 2016).
For reinforced load transfer platforms, the tensile resistance of the reinforcements should be verified according to Clause 9 of EN 1997-3.
In the absence of a LTP, additional verifications may be considered during the design, such as verifications of the stress concentrations at the top of the inclusions and internal forces within the slab or spread foundation.

Testing

Ground improvement should be usually accompanied by testing conducted before or at the beginning of execution. The types of testing should be determined according to the GI technique. The minimum frequency and type of control test should be given by the relevant execution standard or, when no relevant execution standard is available, by the relevant authority or, where not specified, as agreed by the relevant parties for a specific project.
Typical control tests may include for class B ground improvment according to EN 1997-3:

- for Class BI: field testing inside and/or in between inclusions, dummy foundation test on improved ground (individual inclusion and surrounding ground), zone load test on a group of inclusions (group of inclusions and surrounding ground);
- for Class BII: load test on isolated rigid inclusions, zone load test on a group of inclusions (group of rigid inclusions and surrounding ground,) UCS tests of inclusion material.

Clause 12 also provides recommendations on the testing frequency.

CONCLUSION

The second generation of Eurocode 7 is a modern geotechnical standard developed as useful tool for the coming decades. Hence the standard tries to include concepts that are foreseen to be important for the future such as sustainability, robustness, impacts within the zone of influence and climate change. The new structure with a clear division between general rules in part 1, ground properties in part 2 and specific rules for different geotechnical structures in part 3, opens the possibility to add on additional specific clauses, e.g. on tunnels or underground structures, existing geotechnical structures or similar, if ever needed.

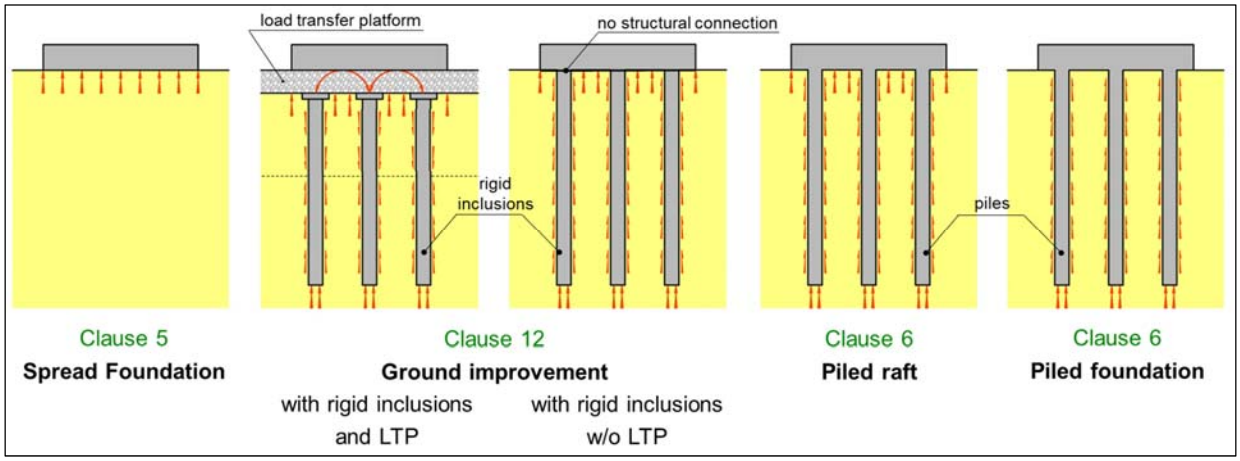


Figure 9. Stringent foundation design and verification concept for all types of foundation acc. to EN 1997-3:2025.

 © DFI International Bruges 2025

The new Eurocode 7 will serve as the commonly agreed standard for the future functioning as a toolbox that fulfil the needs of geotechnical engineers worldwide. Hereby the standard can be easily adopted to national experience as not only all relevant factors like specification of verification cases, partial safety factors, model factors etc. but also basic specifications of geotechnical categories, minimum extent of ground investigation etc. are ´Nationally Determined Parameters´ (NDP) which can be adjusted according to national experiences and standards.
For the design of piled foundations and ground improvement the second generation of Eurocode 7 provides ´state of the art´-guidance including many new design aspects being relevant engineering practice and allows to cover even sophisticated structures. It has to be highlighted that the regulations provided by EN 1997-3:2025 provide a stringent foundation design and verification concept for all types of foundation allowing a smooth transition from spread foundations via ground improvement with and without rigid inclusions and with or without load transfer platforms to piled rafts and piled foundations with comparable equivalent global safety level (see Figure 9).

REFERENCES

ASIRI (2013). Recommendations for the design, construction and control of rigid inclusion. Presse des Ponts, Paris, ISBN: 9782859784706.

Bohn, C. (2016). Serviceability and safety in the design of rigid inclusions and combined pile-raft foundations. PhD thesis, Technical University Darmstadt, Germany.

Bond, A.J., Jenner, C., Moormann, Ch. (2019). Tomorrow's geotechnical toolbox: EN 1997-3: 202x Geotechnical structures. Proc. 17th Europ. Conf. on Soil Mech. and Geotech. Eng., ECSMGE 2019, Reykjavik.

BS 8006-1. Code of practice for strengthened/reinforced soils and other fills.

CEN (2022). Eurocode 0 - Basis of structural and geotechnical design. prEN 1990:2022, The European Committee for Standardization, Brussels.

CEN (2024a). Eurocode 7: Geotechnical design – Part 1: General rules. EN 1997-1:2024, The European Committee for Standardization, Brussels.

CEN (2024b). Eurocode 7: Geotechnical design – Part 2: Ground properties. EN 1997-2:2024, The European Committee for Standardization, Brussels.

CEN (2025). Eurocode 7: Geotechnical design – Part 3: Geotechnical structures. EN 1997-3:2025, The European Committee for Standardization, Brussels.

CUR226 (2016). Design guideline basal reinforced piled embankments (CUR226). van Eekelen, S.J.M. & Brugman, M.H.A. (eds.), CRC press, Delft, the Netherlands (English translation).

Denies, N.; Bohn, C.; Pandrea, P.; Topolnicki, M.; Plomteux, C.; Trybocka, K. (2024). Eurocode 7 – Second Generation – Design of ground improvement works. Proc. 18th Europ. Conf. on Soil Mechanics and Geotech. Eng., ECSMGE 2024, Lisbon, Portugal, CRC Press, Taylor & Francis Group, Balkema, pp. 1566-1571.

EBGEO (2011). Recommendations for design and analysis of earth structures using geosynthetic reinforcements, (English Translation). Deutsche Gesellschaft für Geotechnik, Ernst & Sohn, Germany.

Franzén, G.; van Seters, A. (2022). Eurocode 7 – a toolbox for geotechnical engineering. Proc. 20th Int. Conf. on Soil Mechanics and Geotech. Eng. (ICSMGE), Sydney, Australia, pp. 4753-4758.

Moormann, Ch., Burlon, S. (2024). Eurocode 7 – Second Generation – Piled foundation. Proc. 18th European Conf. on Soil Mechanics and Geotech. Engineering, ECSMGE 2024, Lisbon, Portugal, CRC Press, Taylor & Francis Group, Balkema, pp. 1840-1845.

Poulos, H.G. (1988). Cyclic stability diagram for axially loaded piles. Journal of Geotechn. Eng., Vol. 114 (8), pp. 877-895.

 © DFI International Bruges 2025